

Springer  
Handbook *of*

Power  
Systems

*Papailiou*  
*Editor*

---

**Springer Handbook  
of Power Systems**

---

**Springer Handbooks** provide a concise compilation of approved key information on methods of research, general principles, and functional relationships in physical and applied sciences. The world's leading experts in the fields of physics and engineering will be assigned by one or several renowned editors to write the chapters comprising each volume. The content is selected by these experts from Springer sources (books, journals, online content) and other systematic and approved recent publications of scientific and technical information.

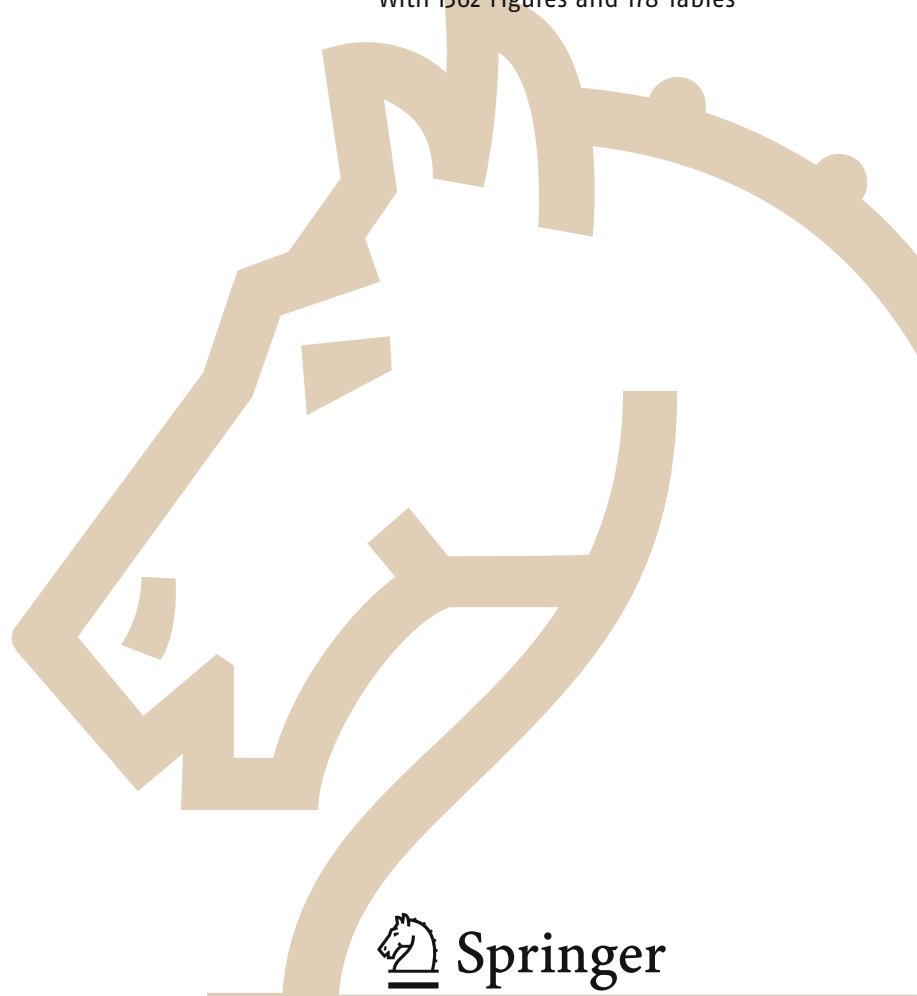
The volumes are designed to be useful as readable desk book to give a fast and comprehensive overview and easy retrieval of essential reliable key information, including tables, graphs, and bibliographies. References to extensive sources are provided.

---

# Springer Handbook of Power Systems

Konstantin O. Papailiou (Ed.)

With 1362 Figures and 178 Tables



---

*Editor*  
Konstantin O. Papailiou  
Malters, Switzerland

ISBN 978-981-32-9937-5 e-ISBN 978-981-32-9938-2  
<https://doi.org/10.1007/978-981-32-9938-2>

© Springer Nature Singapore Pte Ltd. 2021

This work is subject to copyright. All rights are reserved by the Publisher, whether the whole or part of the material is concerned, specifically the rights of translation, reprinting, reuse of illustrations, recitation, broadcasting, reproduction on microfilms or in any other physical way, and transmission or information storage and retrieval, electronic adaptation, computer software, or by similar or dissimilar methodology now known or hereafter developed.

The use of general descriptive names, registered names, trademarks, service marks, etc. in this publication does not imply, even in the absence of a specific statement, that such names are exempt from the relevant protective laws and regulations and therefore free for general use.

The publisher, the authors and the editors are safe to assume that the advice and information in this book are believed to be true and accurate at the date of publication. Neither the publisher nor the authors or the editors give a warranty, express or implied, with respect to the material contained herein or for any errors or omissions that may have been made. The publisher remains neutral with regard to jurisdictional claims in published maps and institutional affiliations.

This Springer imprint is published by the registered company Springer Nature Singapore Pte Ltd.  
The registered company address is: 152 Beach Road, #22-06/08 Gateway East, Singapore 189721, Singapore

## Foreword

It is a great honor to compile the Foreword for this esteemed book on power systems. It is not common to find most of the topics relating to power systems in one book. This book is also unique in that, in spite of the very diverse topics, many authors are well revered and respected members of the CIGRE community. This means that they are respected leaders in their particular fields and recognized by fellow experts.

The book, which is, in fact, a series of books within a book, covers all aspects of electrical power provision from the generator to the meter. Each chapter can be read on its own, and the reader can access all the relevant information on the topic from the particular chapter without necessarily having to refer to other chapters or sections. It is not exclusively a high-voltage or transmission-based book but can be applied to all voltage levels. It can be of value to experienced engineers, as well as to newly graduated engineers, or as a textbook for undergraduates. The chapters themselves provide detailed equations for the design, operation, and maintenance of the grid and the components. The references provided will allow the reader to delve in more depth into a specific topic where necessary.

In order to understand power systems, you need to understand the basics of high-voltage engineering. The chapter on high-voltage engineering covers the theory as well as the application of the theory to power delivery. This provides a well-rounded document for the reader. As mentioned in the chapter “High-voltage engineering is knowledge about power transmission at high voltage and about stress on equipment used in high-voltage transmission systems. The basis for the design of high-voltage equipment is the stress of the insulation by the electric field, whereby the stress magnitude depends on the voltage type. Electric field distribution is given by relative permittivity for AC and by conductivity for DC and homogeneity of the electrode arrangement.” The chapter covers the mathematics and application of the theory to the components of the power grid, such as cables and conductors. The behavior of gases such as air and SF<sub>6</sub>, which are very pertinent to the equipment used on the grid, is given.

The basics of power system analysis cover power flow analysis, short-circuit analysis, stability, power system control, electromagnetic transients, and future network trends covering inverter-based resources. This provides the reader with an in-depth knowledge of all aspects of how the power system behaves under fault

conditions and under certain power system disturbances.

The chapter on switching equipment deals with various HVAC switching equipment. Fundamental interrupting phenomena and switching phenomena related to switching equipment used in power systems are explained. The chapter is very detailed and allows the reader, even one with little experience, to fully understand the components comprising a substation. The latest information on HVDC breakers is also included.

Transformers are explained in great detail from fundamentals, design equations as well as the materials used in construction. The construction of transformers is covered. Different types of transformers are explained. This includes HVDC applications, furnace, traction, and other types. This chapter covers more than most textbooks on the subject of transformer design and theory and will provide the reader with the ability to understand the design, construction, and operation of many types of transformers.

The section on cables covers the history of cables, the involvement of CIGRE in sharing knowledge of cables, as well as the theory, design, maintenance, and operation of cable systems. All cable types are covered, as well as the theory for design of cables. The topic of the upgrading of cable systems is also discussed. The chapter also explains the design and use of superconducting cables and gas-insulated lines (GIL). The reader can also expand their knowledge by studying the additional reading material provided in the last of the 14 sections. Once again, this chapter is a book in its own right, as are most of the other chapters.

The chapter on overhead lines covers all aspects required to understand the design, construction, and maintenance of overhead lines. It covers towers, foundations, insulators, as well as conductor selection and when to use certain tower, foundation, and conductor configurations. The reader can obtain a clear grasp of the concepts of line design, as well as where to apply them. The history of overhead lines and the use of compact line versus conventional line design are covered. The chapter covers the function of the line on the power grid. This relates to the selection of the optimum tower, foundation, and conductor combination. An objective



**Rob Stephen**  
President of CIGRE  
2016–2020

indicator whereby the designer can assess different design options is provided. The design of components from a mechanical and electrical point of view is also discussed. This includes the detailed design of insulators, hardware, towers, and foundations. Construction techniques, foundation testing, and asset management of transmission lines are also explained. Once read, this chapter provides the reader with a full overview of the function, design, construction, and maintenance of overhead transmission lines.

The chapter on substations is, once again, a detailed book in its own right. It covers the concept of substation design, layouts, philosophy, theory, clearances, maintenance, and so on. It provides the reader with a full understanding of the purpose of the substation, as well as which layout or configuration is best suited under which condition. It also includes safety, insulation coordination, surge arrester selection, earth mat design, and other important factors indirectly related to substation design. The chapter is written, as are the others, in such a way that the reader can understand the concepts with little or no prior experience.

The book also covers the generation side of power systems. Types of generation are explained in detail from hydrogeneration and pumped storage to nuclear, thermal, and renewable types. The chapter not only describes the generation type but also includes the equations governing the behavior of the generation. A chapter on rotating machines is also included, covering generator and large motor designs and usage in the power system.

Having read the above chapters, the reader will have an in-depth knowledge of the components and systems relating to the power system generation and delivery of power. The book then includes power system protection and power quality theory and application. The concept and philosophy of power system protection is covered, as well as the types of protection and where to apply them. The chapter on power quality covers the required quality, how to determine power quality, and the issues related to the source of power quality deviations. The reader can then broadly understand the concept of protection, as well as power quality. Optimization of the protection schemes and mitigation power quality issues can also be understood.

The above-mentioned chapters mainly deal with AC transmission. The book would not be complete, however, without a chapter on DC transmission. This chapter explains the purpose and benefits of DC transmission and goes into great detail about the types of pole configuration. Line commutated converters are explained with regard to operation and harmonics. Thyristor operation, characteristics, and valve design are explained. The chapter then looks at different tech-

nologies for converters, such as IGBTs (insulated gate bipolar transistors), VSC (voltage sourced converters), and MMC (modular multilevel converters). The chapter ends with a discussion on the HVDC grid, which was particularly pertinent at the time of writing. Future trends, including cables above 500 kV, power electronic DC circuit breakers, and off-shore DC grids are also covered. The application of DC is growing at all voltages, as the cost of the converter stations is dropping. The ability of VSC technology to allow tap offs provides the benefits of DC to be expanded to areas not possible before. At the time of writing CIGRE was investigating the development of MV and LV DC systems.

The issue of energy is then explained in great detail. This is the content of two chapters. The first deals with the energy fundamentals and covers types of traditional fossil fuels, as well as renewables, such as solar and wind energy. The global use of different types of energy used is also given, as well as emissions of CO<sub>2</sub> per country. The second chapter relating to energy deals with energy storage. The different types of storage are given, from pumped storage and batteries, to flywheels and superconducting magnetic energy storage devices. The uses of each type, as well as where to apply the different types of storage are discussed. This includes fuel cell technologies, as well as the conversion of water to hydrogen and the use of hydrogen in fuel cells. This is important as it could be the next major disruptor in the energy provision field. The reader will have enough information to determine which battery or energy storage device to use in which application.

The issue of markets is then discussed. The concept of markets has been in place for over 20 years at the time of writing this book. The chapter discusses the concept and purpose of markets, the different types of markets, and the application of markets around the world. The case studies of market success and otherwise from different continents and countries, provide the reader with a clear understanding of the pitfalls and successes of markets over the past two decades. Markets distort the power flow, as they affect the generation and use of electrical energy at all voltages. They also determine investment in different generation capacities, ancillary services, and energy provision. Note that inverter-based renewables, such as wind and solar energy provide mainly energy at a very competitive cost. The power grid needs many other components to operate successfully. This includes fault level, frequency support, voltage support, black start capability, and other factors. Markets need to ensure that these can be purchased and put in place when required by the system operator.

The book can be of immense use, not only to university students but also to professionals who have been

in the business of power delivery for a number of years. It provides an excellent overview of the entire industry in one place, which is unique. It is not possible for engineers to be aware of all aspects from markets to transformer design; this book provides a source of valuable information, which can be rapidly referenced and studied.

A further major benefit of the book is that all royalties will be channeled to the development of young engineers via the CIGRE organization ([www.cigre.org](http://www.cigre.org)). This will provide young engineers with the means to meet and discuss with international experts within the CIGRE organization.

I would encourage the reader to study the book and follow up with an in-depth study of the topics covered in

the CIGRE brochures to be found at [www.e-cigre.org](http://www.e-cigre.org). In addition, it is with great pleasure that I can announce that a CIGRE “Green Book”, entitled “Electrical Supply System of the Future” is now available. This book is authored by each of the 16 Study Committees of CIGRE and provides the best possible solutions to enable stakeholders to fully understand the new trends and developments of all components and systems, including markets and regulations that comprise the future grid. This Green Book is an excellent complementary addition to this handbook, and I highly recommend it.

12 August 2020

Rob Stephen  
President CIGRE



## Preface

There is no doubt that writing a book is a stressful endeavor that requires a lot of effort. However, I like comparing the experience of holding a printed copy of the book for the very first time to holding your newborn baby. Being the Editor of a big work like this handbook is at least one level up. Firstly, the work involved takes a considerably longer time than writing a monograph – in our case 5 years – and, secondly, the stress and effort are not limited to birth labor but includes the teething and all the other problems of having a toddler, too. Thankfully, also the pleasure and the proudness of the achievement grow accordingly. In this sense, I am extremely happy and honored to write these lines today, as, evidently, the preface is written a posteriori, i.e., when all the hard work has been done.

I recall the day when Dr Christoph Baumann from Springer asked to have a meeting, during which he placed a heavy, bulky book of the typical Springer red color in front of me. He explained that this was a *Springer Handbook* and asked if I would be interested in becoming the Editor of a new *Springer Handbook of Electrical Power Systems*. My Greek spontaneity took over, and within seconds I agreed. To be honest, despite all imaginable and unimaginable issues that arose during the production of such a major work, and despite my Swiss tendency for perfection, which did not make things easier, I never regretted this decision.

The simplest part was finding the chapter authors. I am extremely proud that my colleagues from academia and industry, the great majority strongly involved in CIGRE, and all of them undisputed leaders in their field, responded positively to my request to become part of this great task. I cordially thank all of them for their strong engagement, which is not self-evident, considering that the writing of the book had to take place in parallel and in addition to their day-to-day work and other important responsibilities. That all authors spontaneously agreed to offer their book royalties to CIGRE in order to support its activities for young engineers is such a clear sign of goodness and generosity for which I can only say: *Chapeau*.

The writing itself proved to be more demanding. To start with, it took some time to decide on the final number, title, and content of the individual chapters, as these should reflect the nature of a Handbook, i.e., the all-embracing coverage of its subject, in this case, electrical power systems. I am confident that the final selection will satisfy our readers.

Then, being a chapter author myself, I realized quite early on that writing a chapter for a handbook is very different from writing a paper or a monograph. While the latter often present new research results, a handbook chapter summarizes established and accepted knowledge for the benefit of the reader. The fact that, by nature, the available space is limited does not make writing any easier – or faster – as the author is continuously trying to find the balance between actuality and tradition, and this as succinctly as possible.

It goes without saying that the high standards of Springer, and also of all authors and the editor, entailed a thorough, strenuous review of each chapter. This would not have been possible if a high number of internationally acclaimed experts had not offered to undertake the task. From my heart, I also thank them for adding immense value to this publication.

To continue in the same vein, unlimited thanks are offered to Dr Christoph Baumann, the initiator of this project, Dr Judith Hinterberg, and her maternity cover, Heather King, for their masterful coordination and management of such a complex undertaking, Dr Werner Skolaut for the skillful language and content editing, Jeanette Krause for the very attractive layout, and all other people involved in the production of this book, in particular those responsible for redrawing all figures and diagrams with such unprecedented quality.

Last, but definitely not least, I would like to thank CIGRE, the great organization that has fostered my scientific and engineering activities, actually my life for the last 45 years, and in particular my good friend Dr Rob Stephen, the CIGRE President, who was kind enough to write the Foreword, and the Secretary General of CIGRE, Philippe Adam, for arranging that CIGRE endorses this Handbook, which I consider a major distinction. And it is a very exciting coincidence that our Handbook will be published in 2021, the centennial year of CIGRE!

No list of thanks would be complete without mentioning my family and, in particular, my wife Margarita, who incidentally I met many, many years back at a CIGRE venue, for always encouraging and supporting my work.

It has been an unforgettable time, *merci!*

Athens, Greece  
July 2020

Konstantin O. Papailiou

---

## About the Editor

**Konstantin O. Papailiou** has spent his entire career of more than 45 years working in the field of power systems and, in particular, overhead lines. He received his doctorate from the Swiss Federal Institute of Technology (ETH) Zurich and his postdoctoral qualification as lecturer (Dr.-Ing. habil.) from the Technical University of Dresden, where he is also Honorary Professor. Until his retirement, he was the CEO of the Pfisterer Group, a company he served for over 25 years. He has held leading positions in various international technical societies and standardization bodies and has authored a number of books and more than 100 papers.

Professor Papailiou is active in power engineering education, teaching courses on high-voltage overhead lines at the University of Stuttgart and the Technical University of Dresden. Since 1976 he has been strongly involved with CIGRE; he has served as Chairman of the CIGRE Study Committee “Overhead Lines” and is the founding Editor-in-Chief of the CIGRE Science and Engineering Journal. In 2020, he was awarded the CIGRE Medal, the organization’s highest distinction.



## About the Authors

### **Pierre Argaut**

Former Chairman CIGRE SC B1  
(Underground Cables)  
Hericy, France  
*pierre.argaut@laposte.net*

### **Math Bollen**

Luleå University of Technology  
Skellefteå, Sweden  
*math.bollen@ltu.se*

### **Alberto Borghetti**

Department of Electrical, Electronic and  
Information Engineering  
University of Bologna  
Bologna, Italy  
*alberto.borghetti@unibo.it*

### **Hartmut Brendel**

Retired Head of Technical Development, ABB  
Transformer Service  
Consultant for Transformers and HV Applications  
Halle, Germany  
*hartmut.brendel@web.de*

### **Valentin Crastan**

Professor emeritus  
Evilard, Switzerland  
*valentin.crastan@bluewin.ch*

### **Alex Cruickshank**

Energy Consulting  
Oakley Greenwood Pty Ltd  
Margate Beach, QLD, Australia  
*acruickshank@oakleygreenwood.com.au*

### **Erli F. Figueiredo**

Electrical Engineering Department  
Rio de Janeiro State University  
Rio de Janeiro, Brazil  
*erliff@uol.com.br*

### **Pavlos S. Georgilakis**

School of Electrical and Computer Engineering  
National Technical University of Athens  
Athens, Greece  
*pgeorg@power.ece.ntua.gr*

### **Ernst Gockenbach**

Schering Institute  
Leibniz University of Hannover  
Hannover, Germany  
*ernst.gockenbach@ifes.uni-hannover.de*

### **Steffen Großmann**

Institute of Electrical Power and High Voltage  
Engineering  
Technische Universität Dresden  
Dresden, Germany  
*steffen.grossmann@tu-dresden.de*

### **Nikos D. Hatzigiorgi**

School of Electrical and Computer Engineering  
National Technical University of Athens  
Athens, Greece  
*nh@power.ece.ntua.gr*

### **Hiroki Ito**

Energy & Industrial Systems Group  
Mitsubishi Electric Corporation  
Tokyo, Japan  
*ito.hiroki@aj.mitsubishielectric.co.jp*

### **José Antonio Jardini**

Energy and Automation Department  
Sao Paulo University  
Sao Paulo, Brazil  
*jose.jardini@gmail.com*

### **George N. Korres**

School of Electrical and Computer Engineering  
National Technical University of Athens  
Athens, Greece  
*gkorres@cs.ntua.gr*

### **Nikolaos C. Koutsoukis**

School of Electrical and Computer Engineering  
National Technical University of Athens  
Athens, Greece  
*koutsoukis@power.ece.ntua.gr*

### **Terry Krieg**

Power Network Consulting Pty. Ltd.  
Willaston, SA, Australia  
*terry.krieg@powernetnetworkconsulting.com.au*

**Oscar Lennerhag**

Independent Insulation Group  
Ludvika, Sweden  
*oscar@i2group.se*

**Fabio Napolitano**

Department of Electrical, Electronic and  
Information Engineering  
University of Bologna  
Bologna, Italy  
*fabio.napolitano@unibo.it*

**Carlo Alberto Nucci**

Department of Electrical, Electronic and  
Information Engineering  
University of Bologna  
Bologna, Italy  
*carloalberto.nucci@unibo.it*

**Konstantin O. Papailiou**

Former Chairman CIGRE SC B2  
(Overhead Lines)  
Malters, Switzerland  
*konstantin@papailiou.ch*

**Mohamed Rashwan**

TransGrid Solutions  
Winnipeg, Canada  
*mrashwan@tgs.biz*

**Colin Ray**

Colin Ray Consulting  
Stratford on Avon, Warwickshire, UK  
*colin@colinray.org.uk*

**Alfred Rufer**

STI-DO  
EPFL, Ecole Polytechnique Fédérale de Lausanne  
Lausanne, Switzerland  
*alfred.rufer@epfl.ch*

**Carlos Samitier**

Pullnet Technology  
Mexico City, Mexico  
*carlos.samitier@smart61850.com*

**Peter Schegner**

TU Dresden  
Dresden, Germany  
*peter.schegner@tu-dresden.de*

**Philip Southwell**

Southwell Power System Consulting  
Shenton Park, WA, Australia  
*phil.southwell.cigre.c1@gmail.com*

**Gregory H. Thorpe**

Executive  
Oakley Greenwood Pty Ltd  
Margate Beach, QLD, Australia  
*gthorpe@oakleygreenwood.com.au*

**Fabio Tossani**

Department of Electrical, Electronic and  
Information Engineering  
University of Bologna  
Bologna, Italy  
*fabio.tossani@unibo.it*

**Peter Werle**

High Voltage Engineering and Asset Management  
(Schering-Institute)  
Leibniz Universität Hannover (LUH)  
Hannover, Germany  
*peter.werle@ifes.uni-hannover.de*

## Contents

<b>List of Abbreviations</b> .....	XXI
<b>1 Energy Fundamentals</b>	
<i>Valentin Crastan</i> .....	1
1.1 Basic Terms, Historical Review .....	1
1.2 Availability of Primary Energy .....	4
1.3 Energy Demand, CO <sub>2</sub> Emissions, Indicators .....	12
1.4 Energy Consumption and CO <sub>2</sub> Emissions in Europe .....	15
1.5 Global Energy Demand .....	21
1.6 Future Development of World Energy Demand .....	32
1.7 CO <sub>2</sub> Emissions and Climate Protection .....	34
<b>References</b> .....	43
<b>2 Power Generation</b>	
<i>Valentin Crastan</i> .....	45
2.1 Hydroelectric Power Stations .....	47
2.2 Hydrological Planning Principles .....	49
2.3 Run-of-River Power Stations .....	50
2.4 Storage Power Stations .....	53
2.5 Water Turbines .....	56
2.6 Dynamics .....	66
2.7 Thermal Power Stations .....	76
2.8 Wind Power .....	93
2.9 Photovoltaics .....	105
2.10 Fuel Cells .....	124
<b>References</b> .....	129
<b>3 High Voltage Engineering</b>	
<i>Ernst Gockenbach</i> .....	131
3.1 Why High-Voltage Engineering? .....	131
3.2 Lightning .....	135
3.3 Electric Field .....	137
3.4 Electric Strength .....	142
3.5 Insulating Materials .....	156
3.6 Test Techniques .....	163
3.7 Measuring Techniques .....	171
<b>References</b> .....	181
<b>4 High Currents and Contact Technology</b>	
<i>Steffen Großmann</i> .....	183
4.1 Current-Conducting Arrangements (Conducting Systems) .....	183
4.2 Current-Carrying Capacity .....	190
4.3 Design Principles .....	194
<b>References</b> .....	271

<b>5</b>	<b>Basics of Power Systems Analysis</b>	
	<i>Carlo Alberto Nucci, Alberto Borghetti, Fabio Napolitano, Fabio Tossani</i> ...	273
5.1	Electric Power System Evolution .....	274
5.2	Mission and Traditional Structure .....	276
5.3	Transmission Line Equations in the Steady State .....	279
5.4	Load Flow .....	285
5.5	Unsymmetrical Fault Analysis .....	300
5.6	Stability .....	319
5.7	Power System Control .....	336
5.8	Propagation of Electromagnetic Transients Along Transmission Lines .....	345
5.9	Electric Power Systems of the Future: Smart Grids .....	360
	<b>References</b> .....	364
<b>6</b>	<b>Rotating Electrical Machines</b>	
	<i>Erlí F. Figueiredo</i> .....	367
6.1	Synchronous Machines .....	368
6.2	Induction Machines .....	415
	<b>References</b> .....	440
<b>7</b>	<b>Transformers</b>	
	<i>Peter Werle, Hartmut Brendel</i> .....	443
7.1	Fundamentals .....	443
7.2	Active Part .....	460
7.3	Testing Power Transformers .....	484
7.4	Types of Transformers .....	497
	<b>References</b> .....	507
<b>8</b>	<b>High Voltage Equipment</b>	
	<i>Hiroki Ito</i> .....	511
8.1	High-Voltage Equipment in Power Systems .....	512
8.2	History and Principles of High-Voltage Circuit Breakers .....	528
8.3	Switching Phenomena in Power Systems .....	542
8.4	Controlled Switching .....	576
8.5	DC Circuit Breakers .....	591
	<b>References</b> .....	608
<b>9</b>	<b>Overhead Lines</b>	
	<i>Konstantin O. Papailiou</i> .....	611
9.1	History and Present Challenges .....	612
9.2	Planning .....	615
9.3	Line Design .....	625
9.4	Conductors .....	640
9.5	Insulators .....	671
9.6	Fittings .....	697
9.7	Supports and Foundations .....	715
9.8	Construction .....	733
9.9	Maintenance .....	740
9.10	Up-rating and Upgrading .....	745
9.11	Conclusions and Further Reading .....	751
	<b>References</b> .....	751

<b>10 Underground Cables</b>	
<i>Pierre Argaut</i> .....	759
10.1 From the First Electric Telegraph to the Foundation of the CIGRE Study Committee on Insulated Cables.....	761
10.2 Current State of Cable Development .....	763
10.3 Basics of Cable System Design .....	772
10.4 AC Cable Theory in Underground Cable System Design .....	784
10.5 Challenges in Cable System Implementation.....	794
10.6 Cable Designs .....	806
10.7 Installation Techniques.....	830
10.8 Testing.....	838
10.9 Maintenance.....	843
10.10 Upgrading and Upgrading .....	848
10.11 Life-Cycle Assessment.....	850
10.12 Superconducting Cables .....	852
10.13 Gas-Insulated Lines .....	854
10.A Appendix.....	858
10.B Further Reading .....	864
10.C CIGRE Technical Brochures to be Published .....	865
<b>References</b> .....	865
<b>11 Substations</b>	
<i>Terry Krieg</i> .....	867
11.1 Overview and History .....	868
11.2 Planning .....	871
11.3 Design .....	886
11.4 Construction and Commissioning.....	908
11.5 Substation Asset Management.....	914
11.6 Secondary Systems .....	921
11.7 Special-Purpose Substations .....	925
11.8 Trends in Substations .....	930
<b>References</b> .....	933
<b>12 HVDC and Power Electronics</b>	
<i>Mohamed Rashwan, José Antonio Jardini</i> .....	935
12.1 History of Power Transmission .....	935
12.2 Applications of HVDC .....	937
12.3 HVDC System Configuration .....	939
12.4 Converter Pole Configuration .....	941
12.5 Line-Commutated Converter (LCC) Fundamentals.....	942
12.6 Voltage-Source Converter (VSC).....	958
12.7 DC Grid .....	969
12.8 Future Trends .....	971
12.9 Further Reading .....	971
<b>References</b> .....	972
<b>13 Power System Protection</b>	
<i>Peter Schegner</i> .....	975
13.1 Background .....	975
13.2 Protection Criteria .....	979
13.3 Requirements on Current and Voltage Transformers .....	987

13.4	General Protection Functions.....	992
13.5	Outlook on Protection Systems .....	1012
	<b>References</b> .....	1013
<b>14</b>	<b>Information Systems and Telecommunications</b>	
	<i>Carlos Samitier</i> .....	1015
14.1	The Role of Information and Communication (ICT) in a Power Grid.....	1016
14.2	Operational Applications .....	1018
14.3	Telecommunications Services .....	1049
14.4	Cybersecurity.....	1084
14.5	Smart Grid .....	1087
14.6	Outlook of Future Technologies .....	1090
14.7	Further Reading .....	1091
	<b>References</b> .....	1092
<b>15</b>	<b>Distribution Systems</b>	
	<i>Nikolaos C. Koutsoukis, Pavlos S. Georgilakis, George N. Korres, Nikos D. Hatziargyriou</i> .....	1093
15.1	Power Distribution Networks.....	1093
15.2	Network Components Modeling.....	1095
15.3	Power-Flow Analysis of Distribution Networks .....	1099
15.4	Active Distribution Networks .....	1103
15.5	Distribution Network Monitoring and Control .....	1107
15.6	Operation of Active Distribution Networks .....	1115
15.7	Distribution Network Planning.....	1120
15.8	Summary .....	1123
15.A	Appendix: Load and Line Data of Distribution Networks .....	1123
	<b>References</b> .....	1126
<b>16</b>	<b>Energy Storage</b>	
	<i>Alfred Rufer</i> .....	1131
16.1	The Context of Use of Energy Storage .....	1132
16.2	General Definitions of Energy Storage .....	1135
16.3	Technical Definitions .....	1138
16.4	Electric Power and Energy Storage .....	1143
16.5	Energy Storage Systems .....	1144
16.6	Storage Systems Based on Physics .....	1144
16.7	Electrical Systems.....	1154
16.8	Electrochemical Systems .....	1156
16.9	Fuel Cells and Hydrogen Storage .....	1163
16.10	System Arrangements and Applications .....	1166
16.11	Examples of Large-Scale Energy Storage Plants.....	1168
	<b>References</b> .....	1169
<b>17</b>	<b>Power Quality</b>	
	<i>Oscar Lennerhag, Math Bollen</i> .....	1171
17.1	Terminology of Power Quality .....	1171
17.2	Harmonics .....	1177
17.3	Other Power-Quality Disturbances .....	1187



---

17.4	Power Quality in Microgrids .....	1199
17.5	Conclusions .....	1200
	<b>References</b> .....	1200
<b>18</b>	<b>Electricity Markets and Regulation</b>	
	<i>Philip Southwell, Gregory H. Thorpe, Alex Cruickshank, Colin Ray</i> .....	1205
18.1	Electricity Industry Structure .....	1207
18.2	Industry Organization .....	1208
18.3	Electricity Markets .....	1209
18.4	Market Models .....	1211
18.5	Market Structures Around the World .....	1215
18.6	Regulation .....	1224
18.7	Regulation Models Around the World .....	1233
18.8	Conclusion .....	1236
	<b>References</b> .....	1237
	<b>Subject Index</b> .....	1239

## List of Abbreviations

1-D	one-dimensional
2-D	two-dimensional
3-D	three-dimensional

### A

AAAC	all aluminum alloy conductor
AAC	all aluminum conductor
AAS	atomic absorption spectrometry
AC	alternating current
ACAR	aluminum conductor alloy reinforced
ACCC	aluminum conductor composite core
ACCR	aluminum conductor composite reinforced
ACE	area control error
ACIM	automated continuous injection molding
ACSE	association control service element
ACSI	abstract communications service interface
ACSR	aluminum conductor steel-reinforced
ACSS	aluminum conductor steel-supported
ADC	analogue-to-digital converter
ADM	add-drop multiplexer
ADMS	advanced distribution management system
ADN	active distribution network
ADNR	active distribution network reconfiguration
ADSS	all-dielectric self-supporting
AFC	alkaline fuel cell
AGC	aerodynamic galloping controller
AGC	automatic generation control
AGM	absorbent glass mat
AGR	advanced gas cooled reactor
AGS	Armor-Grip Suspension
AIS	air-insulated switchgear
Al	aluminum
ALARP	as low as reasonably practicable
AM	accounting management
AMF	axial magnetic field
AMI	advanced metering infrastructure
AMR	automated meter reading
AN	acoustic noise
ANM	active network management
APC	active power curtailment
API	application programming interface
API	arc plasma injector
AR	automatic reclosing
ARP	address resolution protocol
ASE	application service elements
ATCC	automatic tap-change control
ATH	aluminum trihydrate
ATI	appropriate technology index
AVR	automatic voltage regulator
AWM	aircraft warning marker

### B

BAP	basic application profiles
-----	----------------------------

BCM	business continuity management
BCP	business continuity planning
BEM	boundary element method
BER	basic encoding rules
BESS	battery energy storage system
BF	breadth-first
BGP	border gateway protocol
BI	business impact
BIL	basic insulation level
BM	balancing mechanism
BML	business management layer
BMS	battery management system
BO	blocking overreach
BOD	breakover diode protection
BPL	broadband power-line
BPS	bypass switch
BTF	bus terminal fault
BWR	boiling water reactor

### C

C/S	converter station
CAES	compressed-air energy storage
CAIDI	customer average interruption duration index
CAPEX	capital expenditure
CAS	corrugated aluminum sheath
CB	circuit breaker
CBFP	circuit-breaker failure protection
CBM	condition-based maintenance
CC	core clamping
CCC	capacitor commutated converter
CCS	carbon capture and storage
CCUS	CO <sub>2</sub> capture utilisation and storage
CD	combined design
CDC	common data class
CEP	Clean Energy Package
CET	Central European Time
CF	creepage factor
CFC	chlorinated fluorocarbon
CFL	cantilever failing load
CGIC	compressed gas-insulated cable
CGMES	common grid model exchange specification
CHP	combined heat and power plant
CIM	common information model
CIS	component interface specification
CL	corona loss
CL	core lamination
CM	configuration management
COI	center of inertia
CORBA	common object request broker architecture
CPT	cone penetration test
CRM	customer relationship management
CRM	condition reliability maintenance
CSI	current source inverter
CSS	controlled switching systems

CT	current transformer
CUR	contamination uniformity ratio
CVD	capacitive voltage divider
CVM	collection volume method
CVT	capacitive voltage transformer
CWDM	coarse-wavelength division multiplexing

**D**

DAC	damped AC
DC	direct current
DCUB	directional comparison unblocking
DER	distributed energy resources
DFIMG	doubly-fed induction motor generator
DFT	discrete Fourier transform
DG	distributed generation
DGA	dissolved gas analysis
DIL	design insulation level
DL	pressure line
DLL	damage limit load
DM	degraded minute
DMFC	direct methanol fuel cell
DMR	dedicated metallic return
DMS	distribution management system
DNP	distribution network planning
DoD	state of discharge
DP	digital position
DPF	distribution power flow
DR	demand response
DRP	Deutsches Reichspatent
DRS	dynamic rating system
DS	disconnecting switch
DSC	differential scanning calorimetry
DSE	distribution state estimation
DSO	distribution system operator
DSSE	distribution system state estimator
DT	diagnostic test
DTC	distribution transformer controller
DTC	direct torque control
DTOC	definite time overcurrent
DTS	distributed temperature sensing
DTT	direct transfer tripping
DUT	device under test
DVR	dynamic voltage restorer
DWDM	dense-wavelength division multiplexer
DZ	discriminating zone

**E**

EBP	energy balance principle
ECC	earth continuity conductor
ECT	electronic current transformer
EDS	everyday stress
EF	electric field
EGM	electro-geometric model
EHV	extrahigh voltage
EIA	environmental impact assessment
EMC	electromagnetic compatibility
EMF	electromagnetic field

EMF	electromotive force
EMI	electromagnetic interference
EML	element management layer
EMS	energy management system
EMTP	electromagnetic transient
EMTP-RV	electromagnetic transient program
EMU	electromagnetic unit
EP	equilibrium point
EPDM	ethylene propylene diene monomer
EPE	experimental plastic elongation
EPM	ethylene propylene monomer
EPR	ethylene propylene rubber
EPR	European pressurized reactor
ERP	enterprise resource planning
ES	errored second
ES	elastomeric suspension
ES	earthing switch
ESCR	effective short-circuit ratio
ESD	energy storage device
ESDD	equivalent salt deposit density
ESS	energy storage system
ETT	electrically triggered thyristor
EV	electric vehicle
EVT	electronic voltage transformer

**F**

FACTS	flexible alternating current transmission system
FAT	final acceptance test
FC	functional constraint
FC	fast contact
FCAPS	fault, configuration, accounting, performance, and security model
FDM	frequency division multiplexing
FDR	frequency-domain reflectometry
FDS	frequency-domain spectroscopy
FEC	forwarding equivalence class
FEM	finite element method
FEP	tetrafluoroethylen-hexafluoropropylene
FES	flywheel energy storage
FF	fluid-filled
FFT	fast Fourier transformation
FLISR	fault location, isolation, and service restoration
FM	fault management
FMEA	failure mode and effects analysis
FPD	fast protective device
FPI	fault passage indicator
FRA	frequency-response analysis
FRP	fiber reinforced plastic
FTIR	Fourier-transform infrared
FTR	financial transmission rights

**G**

GAMS	general algebraic modeling system
GCD	galloping control device
GDP	gross domestic product

GES	generic eventing and subscription	IE	international efficiency
GF	gas-filled	IEC TS	IEC Technical Specification
GFD	ground flash density	IED	intelligent electronic device
GFP	generic framing protocol	IETF	internet engineering task force
GIC	geomagnetically induced current	IGBT	insulated-gate bipolar transistor
GIL	gas-insulated line	IGCT	integrated gate commuted thyristor
GIS	gas-insulated switchgear	IOP	internet inter-ORB protocol
GITL	gas-insulated transmission line	IMP	intermetallic phase
GOOSE	generic object-oriented substation event	INMR	Insulator News and Market Report
GPR	grid potential rise	IOA	information object addresses
GPS	global positioning system	IOC	instantaneous overcurrent
GRP	glass reinforced plastic	IP	interior point
GRTS	ground return transfer switch	IP	internet protocol
GSSE	generic substation status event	IPS	interphase spacer
GSU	generator step-up	IR	infrared
GtL	gas-to-liquid	IR	insulation resistance
GTO	gate turn-off thyristor	IRLS	iteratively reweighted least squares
GWP	global warming potential	ISWR	inverse standing wave ratio
<hr/>			
<b>H</b>			
<hr/>			
HAES	helically attached elastomeric suspension	ITP	inspection and test plans
HAN	home-area network	ITRV	initial transient recovery voltage
HDD	horizontal directional drilling	ITU-T	International Telecommunication Union telecommunication standardization sector
HDPE	high-density polyethylene	IVT	inductive voltage transformer
HF	high-frequency	<hr/>	
HHPSA	hexahydrophthalic anhydride	<b>J</b>	
HIL	hardware in the loop	<hr/>	
HIS	hybrid-insulated switchgear	JBD	jitter buffer delay
HMI	human-machine interface	<hr/>	
HP	horsepower	<b>K</b>	
HP	high-pressure	<hr/>	
HPFF	high-pressure fluid-filled	KPI	key performance indicators
HPGF	high-pressure gas-filled	KPT	knee-point temperature
HPOF	high-pressure oil-filled	<hr/>	
HSDA	high-speed data access	<b>L</b>	
HSEQ	health safety, environment and quality	<hr/>	
HSGS	high-speed grounding switch	LA	light angle
HT	Hydrophobicity transfer	LAN	local area network
HTLS	high-temperature low-sag	LC	induction-capacitance
HTM	hydrophobicity transfer material	LCA	life cycle assessment
HTR	high-temperature reactor	LCAS	link capacity adjustment scheme
HTS	high-temperature superconductor	LCC	life cycle cost
HTV	high-temperature vulcanized	LCC	line-commutated converter
HV	high voltage	LCD	load control device
HVAC	high-voltage alternating current	LD	logical devices
HVDC	high-voltage direct current	LDAP	lightweight directory access protocol
HVHS	high-voltage, high-speed switches	LDC	line-drop compensation
HVIGBT	high-voltage insulated gate bipolar transistor	LDP	label distribution protocol
HWR	heavy water reactor	LDPE	low-density polyethylene
<hr/>			
<b>I</b>			
<hr/>			
IC	initial cost	LE	linear elastic
ICE	internal combustion engine	LEC	local energy community
ICM	impulse current method	LED	light emitting diode
ICT	information and communications technology	LFP	lithium-iron phosphate
IDL	interface definition language	LI	lightning impulse
IDMT	inverse definite minimum time	Li-Po	lithium-ion polymer
		lidar	light detection and ranging
		LIM	linear induction motor
		LIPL	lightning impulse protection level
		LIWV	lightning impulse withstand voltage
		LLF	long line faults

LLW	live line work
LMR	land mobile radio
LMW	low molecular weight
LN	logical node
LOLP	loss of load probability
LP	linear programming
LP	low-pressure
LPC	last point of contact
LPIT	low-power instrument transformer
LPOF	low-pressure oil-filled
LSA	load shed application
LSP	label-switched path
LSPM	line start permanent magnet
LSR	label switch router
LSR	liquid silicone rubber
LTO	lithium titanate oxide
LTS	low-temperature superconducting
LTT	light-triggered thyristor
LV	low voltage
LVAC	low-voltage AC
LWC	low-weight conductor

**M**

MAP	maximum available power
MCA	maximum credible accident
MCCB	molded case circuit breaker
MCFC	molten carbonate fuel cell
MDCL	maximum design cantilever load
MF	magnetic field
MG	motor generator
MHHPASA	methylhexahydrophthalic anhydride
MI	mass-impregnated
MIF	multi-infeed factor
MIM	multiple impulse method
MJ	megajoule
MM	multimode
MMC	modular multilevel converter
MMF	magnetomotive force
MMI	man-machine interface
MMS	manufacturing message specification
MO	metal oxide
MOS	metal oxide semiconductor
MOSA	metal-oxide surge arrester
MOSFET	metal-oxide-semiconductor field effect transistor
MP	medium-pressure
MPLS	multiprotocol label switching
MPP	maximum power point
MPPT	maximum power-point tracking
MRTB	metallic return transfer breaker
MTBF	mean time between failure
MTBM	microtunnel boring machine
MTS	mixed-technology switchgear
MTTR	mean time to repair
MV	medium voltage
MVA	megavolt ampere
MW	active power

**N**

NBR	nitrile butadiene rubber
NCA	network connectivity analysis
NCI	nonceramic insulator
NCIT	nonconventional instrument transformer
ND	network delay
NE	normal equation
NFB	no-fuse breaker
NIMBY	not in my backyard
NLP	nonlinear programming
NMC	network management center
NMC	nickel mangan cobalt
NML	network management layer
NMS	network management system
NPP	nuclear power plant
NPV	net present value
NS	North and South
NSDD	non soluble deposit density
NSP	nonsalient pole
NSPG	nonsalient-pole generator
NSPL	nonsalient pole
NSPM	nonsalient-pole machine

**O**

OAM	operation, administration, and maintenance
OC	open circuit
OCC	open-circuit characteristic
OD	oil-directed
ODP	open drip-proof
OEE	overall equipment effectiveness
OEL	overexcitation limiter
OF	oil-filled
OF	oil-forced
OHL	overhead line
OHLCD	overhead line corrosion detector
OHS	occupational safety and health
OHVS	offshore high-voltage substation
OIP	oil-impregnated paper
OLTC	on-load tap changer
OMG	object management group
OMS	outage management system
ON	oil-natural
OP	out-of-phase
OPEX	operational expenditure
OPF	optimal load flow
OPGW	optical ground wire
ORB	object request broker
OSI	open system interconnection
OTDR	optical time-domain reflectometry
OV	overvoltage
OW	headwater
OWS	oscillating wave system

**P**

PA	polyamide
PAFC	phosphoric acid fuel cell

PAR	phase-angle regulator
PCB	polychlorinated biphenyl
PCC	point of common coupling
PCE	path computation element
PCI	protocol control information
PCR	price coupling of regions
PD	partial discharge
PD	packetization delay
PDH	plesiochronous digital hierarchy
PDIV	partial discharge inception voltage
PDMS	polydimethylsiloxane
PDU	protocol data units
PE	polyethylene
PED	portable earthing device
PEFC	polymer electrolyte fuel cell
PEM	polymer electrolyte membrane
PF	power frequency
PF	power factor
PFA	perfluoroalkoxy
PFC	power factor corrected
PI	polyimide
PI	polarization index
PI	proportional integral
PICOM	piece of information for communication
PLC	programmable logic controller
PLC	power line carrier
PM	performance management
PM	permanent magnet
PMG	permanent magnet generator
PMR	private mobile radio
PMU	phasor measurement unit
POE	polyoxide ethylene
POTT	permissive overreaching transfer trip
PPA	power purchase agreement
PPA	purchasing-power adjusted
PPL	polypropylene paper laminate
PPL-MI	polypropylene laminate, mass impregnated
PPP	purchasing power parity
PSA	phthalic anhydride
PSS	power system stabilizer
PT	potential transformer
PT	pump turbine
PTFE	polytetrafluoroethylene
PtG	power to gas
PTP	precision time protocol
PU	polyurethane
PUP	permissive underreach transfer tripping scheme
PUTT	permissive underreach transfer tripping scheme
PV	power voltage
PV	photovoltaic
PVC	polyvinyl chloride
PVGIS	photovoltaic geographical information system
PW	pseudowire
PWM	pulse width modulation
PWM-VSI	pulse width modulated voltage source inverter
PWR	pressurized water reactor

---

**Q**


---

QCP	quadratically constrained programming
QoS	quality of service

---

**R**


---

RAS	remedial action scheme
RBAC	role-based access control
RBF	reverse breadth-first
RBM	risk-based maintenance
RBMK	reaktor bolshoy moshchnosti kanalnyy
RBP	resin-bonded paper
RCM	reliability-centered maintenance
RCVD	resistive-capacitive voltage divider
RDDS	rate of decrease of dielectric strength
RDF	resource description framework
REM	raster electron microscope
RES	renewable energy source
RF	radio frequency
RFC	request for comments
RI	radio interference
RIP	resin-impregnated paper
RIS	resin-impregnated synthetics
RIV	radio interference voltage
RML	routine mechanical load
rms	root mean square
RMSLL	RMS line-to-line
RMU	ring main unit
ROCOF	rate of change of the frequency
ROV	remotely operated vehicle
ROW	right of way
RPC	remote procedure call
rpm	revolutions per minute
rps	rotation per second
RRDS	rate of rise of dielectric strength
RRRV	rate of rise in recovery voltage
RSL	residual static load
RSM	rolling sphere method
RSTP	rapid spanning tree protocol
RSVP	resource reservation
RT	routine test
RTM	real-time monitoring
RTS	rated tensile strength
RTU	remote terminal unit
RTV	room-temperature vulcanized
RUSCD	reference unified specific creepage distance
RV	recovery voltage
RVD	resistive voltage divider
RW	regulating winding

---

**S**


---

SA	sunrise
SAIDI	system average interruption duration index
SAIFI	system average interruption frequency index
SAP	service access points
SAS	substation automation system
SBO	select before operate

SCADA supervisory control and data acquisition  
 SCC short-circuit characteristic  
 SCFF self-contained fluid-filled  
 SCiB super-charge ion battery  
 SCL substation configuration language  
 SCL stator overcurrent limiter  
 SCL specified cantilever load  
 SCLF self-contained liquid-filled  
 SCR short-circuit ratio  
 SCSM specific communication service mapping  
 SD separate design  
 SDH synchronous digital hierarchy  
 SDN software-defined network  
 SDU service data unit  
 SE state estimation  
 SEP state equilibrium point  
 SES site equivalent salinity  
 SES severely errored second  
 SFC static frequency converter  
 SFRA swept frequency response analysis  
 SHGM Schwappe–Huber generalized-M  
 SI switching impulse  
 SIL switching impulse level  
 SIL surge impedance loading  
 SIM secondary impulse method  
 SIPL switching impulse protection level  
 SIWV switching impulse withstand voltage  
 SLA service-level agreement  
 SLA sealed lead-acid  
 SLD single-line diagram  
 SLF short line fault  
 SM security management  
 SM single-mode  
 SMES superconductive magnet energy storage  
 SML service management layer  
 SML specified mechanical load  
 SNCP subnetwork connection protection  
 SNMP simple network management protocol  
 SNTP simple network time protocol  
 SOA safe operating area  
 SOA service-oriented architecture  
 SOAP simple object access protocol  
 SoC state of charge  
 SOCP second-order cone programming  
 SOE solid oxide electrolyte  
 SoE state of energy  
 SOFC solid oxide fuel cell  
 SoH state of health  
 SOT standard oil test  
 SPAR single-phase autoreclosure  
 SPE solid polymer electrolyzer  
 SPE simplified plastic elongation  
 SPG salient-pole generator  
 SPM salient-pole machine  
 SPS site pollution severity  
 SPS system protection scheme  
 SR silicone rubber  
 SR switched reluctance  
 SSC series and shunt reactive power compensation

SSC superconductor synchronous compensator  
 SscD separate semiconductive design  
 SSG superconductor synchronous generator  
 SSR subsynchronous resonance  
 ST special test  
 STATCOM static synchronous compensator  
 STLF short-term load forecasting  
 SU sunset  
 SV sampled value  
 SVC static VAR compensator  
 SVL sheath voltage limiter

---

**T**


---

TB technical brochure  
 TBM time-based maintenance  
 TBM tunnel boring machine  
 TCAP thermal capacity factor  
 TCD torsional control device  
 TCO total cost of ownership  
 TCP transport control protocol  
 TCSC thyristor-controlled series capacitor  
 TDD torsional damper and detuner  
 TDD total demand distortion  
 TDM time-division multiplexing  
 TDR time-domain reflectometry  
 TE traffic engineering  
 TEFC totally-enclosed fan-cooled  
 TEM transverse electromagnetic mode  
 TENV totally-enclosed nonventilated  
 TFF transformer-fed fault  
 TGA thermogravimetric analysis  
 THD total harmonic distortion  
 TLF transformer limited fault  
 TMD tuned mass damper  
 TMF transverse magnetic field  
 TMS time multiplier setting  
 TOTEM total energy module  
 TOV transient overvoltage  
 TPHSR three-phase high-speed reclosure  
 TPM total productive maintenance  
 TPSC thyristor-protected series compensation  
 TRV transient recovery voltage  
 TS time slot  
 TSF transformer secondary fault  
 TSO transmission system operator  
 TT type test  
 TV tertiary voltage  
 TVI television interference  
 TW trapezoidal wire

---

**U**


---

UAV unmanned aerial vehicle  
 UCA utility communications architecture  
 UDDI universal description discovery and integration  
 UEL underexcitation limiter  
 UEP unstable equilibrium point

UG	underground
UGC	underground cable
UHF	ultrahigh frequency
UHV	ultrahigh voltage
UHVDC	ultrahigh-voltage direct current
UML	unified modeling language
UPS	uninterruptible power supply
UTP	unshielded twisted pair
UV	ultraviolet
UW	tailwater
UXO	unexploded ordnance

---

**V**


---

VBE	valve base electronics
VBO	breakover voltage
VC	virtual circuit
VC	virtual container
VCAT	virtual concatenation
VFTO	very fast transient overvoltage
VID	VLAN identifier
VL	reference conductor
VLAN	virtual local-area network
VLF	very low frequency
VOLL	value of lost load
VPLS	virtual private LAN service

VPN	virtual private network
VR	voltage reduction
VRLA	valve-regulated lead-acid
VSAT	very-small-aperture terminal
VSC	voltage source converter
VSD	variable speed drive
VT	voltage transformer
VVC	volt/var control

---

**W**


---

WAN	wide area network
WDM	wavelength division multiplexing
WF	water-forced
WG	working group
WLAV	weighted least absolute value
WLS	weighted least squares
WOZ	true local time
WSDL	web services description language

---

**X**


---

XLPE	crosslinked polyethylene
XMPP	extensible messaging presence protocol
XRD	x-ray diffraction
XRF	x-ray fluorescence



# Energy Fundamentals

Valentin Crastan

Fundamentals and the structure of energy supply with primary energy, final energy, energy carriers, reserves and resources, and the potential and use of renewable energy are presented in this chapter.

Past energy demand and CO<sub>2</sub> emissions are illustrated for all regions of the world and for the most important countries. The desired future development with regard to climate protection is discussed and illustrated with the aid of the most important indicators.

1.1	<b>Basic Terms, Historical Review</b> .....	1	1.3.4	CO <sub>2</sub> Emissions and Indicators .....	15
1.1.1	The Energy Sector .....	1	1.4	<b>Energy Consumption and CO<sub>2</sub> Emissions in Europe</b> .....	15
1.1.2	Energy-Usage Processes .....	3	1.4.1	Population and Gross Domestic Product ..	15
1.1.3	Historical Review .....	3	1.4.2	Energy Consumption per Capita .....	15
1.1.4	Perspectives and Problems .....	4	1.4.3	Energy Intensity and CO <sub>2</sub> Emissions, Sustainability .....	19
1.2	<b>Availability of Primary Energy</b> .....	4	1.4.4	Final Energy and Losses of the Energy Sector in the EU-15 .....	19
1.2.1	Non-Renewable Energies .....	5	1.4.5	Countries With More Than 30 Million Inhabitants .....	20
1.2.2	Renewable Energies .....	7	1.5	<b>Global Energy Demand</b> .....	21
1.2.3	Potential and Use of the Main Types of Solar Energy .....	8	1.5.1	Energy Consumption in the Past .....	21
1.2.4	Ecological Problems .....	11	1.5.2	Energy Demand, Population and GDP in 2016 .....	22
1.3	<b>Energy Demand, CO<sub>2</sub> Emissions, Indicators</b> .....	12	1.5.3	Primary and Final Energy and its Distribution 2016 .....	25
1.3.1	General Information .....	12	1.6	<b>Future Development of World Energy Demand</b> .....	32
1.3.2	Final Energy and Losses in the Energy Sector .....	13	1.6.1	Development of the World Population ....	33
1.3.3	Global Gross Energy Demand, Energy Sector .....	13	1.6.2	Increase in GDP (PPP) and Energy Demand .....	33
			1.7	<b>CO<sub>2</sub> Emissions and Climate Protection</b> ....	34
			1.7.1	Climate Protection, Medium and Long-Term Measures .....	34
			1.7.2	Electricity Consumption and Climate Protection .....	35
			1.7.3	Transport .....	38
			1.7.4	Heating .....	39
			<b>References</b> .....		43

## 1.1 Basic Terms, Historical Review

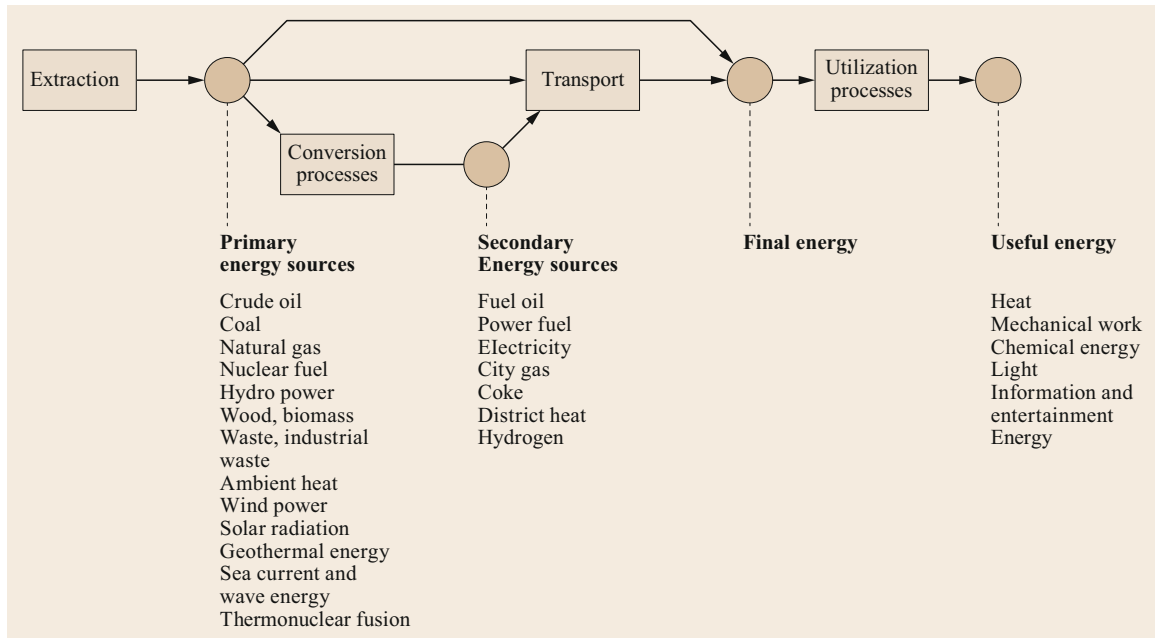
Figure 1.1 represents the structure of the energy industry, showing the energy carriers in use today and the possible future of energy carriers. We distinguish between four energy conversion stages: *Primary energy*, *secondary energy*, *final energy* and *useful energy*.

Companies with activities in the *extraction*, *conversion* and *transport* of energy carriers, form the *energy sector of the economy*. Their task is to provide the *end-*

*user* with energy in the desired form of energy carrier (*final energy*) The consumer converts the *final energy* by means of *usage processes* into *useful energy*.

### 1.1.1 The Energy Sector

*Primary energy carriers* are sources of energy that occur naturally. For the most part, they are not used at



**Fig. 1.1** Forms of energy, and energy conversion stages

the places where they occur, but are first extracted (e.g., mined), then transported and, if necessary, converted into another more suitable form of energy (secondary energy carriers). Coal and natural gas are usually simply extracted and transported to the place of use; oil, on the other hand, is converted into heating oil and motor fuel in refineries; naturally occurring uranium is converted into nuclear fuel; coal, oil, natural gas, water power, wind power, nuclear fuels, solar heat and refuse, generate electricity in power stations.

Fossil fuels, nuclear fuels, hydropower, wind power, solar radiation, geothermal energy, biomass and waste generate electricity and district heating in power plants and combined heat and power plants. A few energy sources, such as solar radiation and ambient heat, but also geothermal heat and wind, can be used in a decentralized way as heat or to generate electricity directly at the place where they arise.

In addition to the most important *secondary energy carriers* that have already been mentioned such as heating oil, motor fuel, electricity and district heat, Fig. 1.1 also shows hydrogen as a secondary energy carrier that could be important in the future (for more details, see [1.1]).

*Extraction*, *transformation* and *transport* are associated with costs, losses and environmental impact.

Under normal conditions and when dealt with correctly and competently, the processes of *mining* and *transport* have only a small adverse environmental impact, but in wartime situations and when there are

accidents with fossil and nuclear fuels, they can have very serious environmental consequences. Some examples are: accidents with tankers, sabotage and fires in conveyor equipment and oil and gas pipelines, accidents in the transport of radioactive fuel elements.

In the *conversion* processes the harm is, above all, the constant environmental pollution from the *burning of fossil fuels* (combustion products, CO<sub>2</sub> that damages the climate). Further localized sources of environmental pollution can be accidents in nuclear power stations, oil storage tanks and refineries.

In addition, the *conversion* of thermal energy from fossil and nuclear fuels into mechanical or electrical energy always produces a high level of *waste heat* for thermodynamic reasons. With appropriate investments, it is possible to use part of this heat (combined heat and power, Chap. 2).

*Final energy* or *final consumption* is the energy actually available to the consumer. *National energy statistics* generally refer to final consumption and/or primary energy, or *gross consumption* (annual consumption of indigenous primary energy carriers plus the import–export difference in primary and secondary energy carriers). The figures differ considerably because of the losses arising in conversion and transport, which includes the energy consumption of the energy sector itself. The *conversion losses* are very high. *Transport losses* arise primarily in the transmission and distribution of electrical energy which, for example in Switzerland, has an overall efficiency of 93%, with the

greatest part of the losses occurring in the distribution network.

### 1.1.2 Energy-Usage Processes

Final energy is converted by the energy-usage processes of energy consumers (households, industry, services, commerce, agriculture, traffic) into *useful energy*, mainly *heat*, *mechanical work* and *light* (Fig. 1.1). A small part is stored in the form of *chemical energy* in end products (steel, aluminum etc.). The amount of this is insignificant, at least in Switzerland. Another small part, but this is likely to increase in the future, is the energy used in *information technology* and *entertainment* (for computers, leisure electronics and communication).

*Energy-usage processes* have very different efficiencies. Whereas, for example, in an electrical heater the electricity is 100% converted into heat, on average only about 20% of the energy in the fuel of a present-day automobile is converted into mechanical energy and a conventional incandescent light bulb converts only about 5% of the electrical energy into light (but at least in winter, the rest of the energy is not lost but contributes to heating the buildings). The energy-usage processes are therefore in some cases associated with large losses of energy; the average efficiency has been estimated, for example for Switzerland in 1997, as 56% [1.2]. Burning fossil heating fuels and motor fuels produces gas emissions, which are *locally* and *globally* (generation of CO<sub>2</sub>) a considerable source of *environmental pollution* (Sect. 1.7).

### 1.1.3 Historical Review

The *uses made* of final energy have changed only little and slowly since the beginnings of human history. Only the range of available energy carriers is much wider, and the technologies of energy conversion and usage have become more varied, efficient and convenient.

#### Mechanical Work

Today, as in previous times, *mechanical work* is used for acquiring and creating goods, for providing services and for transporting goods and people. The muscular efforts of humans and animals were prerequisites for survival in almost all early societies, both for the hunter-gatherers and even more so for the farmers. In ancient times, urban societies could only exist and develop thanks to slave workers. Over the course of time it became possible to make more effective use of muscle power and increase productivity through many mechanical inventions such as the wheel and the lever and, later, all kinds of mechanical devices, and also making use of the natural forces of

water and wind (water-wheel, windmill, sailing ships), in other words to exploit new sources of energy. Much later, starting in the eighteenth century, was the beginning of replacing muscle power by more powerful steam machines. From the end of the nineteenth century, electric motors enabled a big increase in productivity and in the twentieth century, internal combustion engines resulted in greatly increased mobility.

#### Heat and Light

Today, as in earlier times, *heat* and *light* serve to protect from the cold, in the provision of food, increasing security, improving conditions of work, human well-being and thus the development of cultural activities. Energy sources were originally wood, plant waste and dried dung. Hot springs were already in use in ancient times. Coal first came gradually at the end of the seventeenth century and then mineral oil, natural gas and electricity which were not in widespread use for generating heat until the twentieth century.

Heat, mostly at high temperature, was also used for producing various kinds of goods (metals, earthenware, jewelry and art objects). In this connection, we speak today of industrial and commercial *process heat* (in contrast to *heat for cooking and comfort*).

#### Summary

The *structure of making energy available and using it* changed but little for millennia until developments in science from the end of the eighteenth century led to the *age of technology*. The beginnings of this were already present in antiquity and in the Middle Ages. But only in recent times were revolutionary technical means invented for the mechanical use of the heat energy of fuels (steam engines, and later, combustion engines). Success was achieved in creating new (secondary) energy carriers such as town gas and electricity and in distributing them to small-scale consumers. *Electricity* in particular simplified and encouraged the use of energy on a scale previously unknown and, together with *coal*, made the industrial revolution possible. In many countries *water power* gained great significance in generating electricity. Coal, initially the most important primary energy carrier, was to an increasing extent replaced by *mineral oil* after the 2nd World War, i.e., in the 2nd half of the twentieth century, but in many countries it retains a primary position in the generation of electricity. Finally, new primary energy sources were successfully exploited such as *natural gas* and *nuclear fission*.

The structure of the energy industry underwent a fundamental change in the course of a century. The muscle power of humans and animals is still used today (e.g., the bicycle as a means of transport) but is not included in the energy statistics. Wind and water power

are only taken into account to the extent that they contribute to the production of electricity.

### 1.1.4 Perspectives and Problems

The progress of civilization in the twentieth century would have been considerably slower without cheap energy. The *use of energy* in industrialized societies increased by a factor of more than ten in the course of that century. It freed humanity from the burden of heavy manual work and made a decisive contribution to a previously unimaginable mass prosperity. Although this process initially only affected a part of the world, it was the basis for a world-encompassing improvement in the material conditions of life.

An important element of this *progress* was firstly the mechanization of manual labor, and later its replacement by automation. Connected to this are rapid

changes in social structures and a progressive intellectualization of work in general. The social problems that arise from this are a challenge for the socio-economic order, also in the developed world, and cannot be solved simply by an often inadequately thought-out globalization. More of the dark sides of this development became manifest in recent decades with *overloading and poisoning of the biosphere* and *threats to the stability of the climate*.

Attempts are being made to rectify this through political demands for *social and ecological sustainability*. The contribution of the energy industry lies in the implementation of making energy available with the *least possible damage to the environment* and in *environmentally sustainable* usage of energy (Sects. 1.6 and 1.7). In this context, the *rational use* of energy is very important, i.e., the improvement of the efficiency levels of all processes.

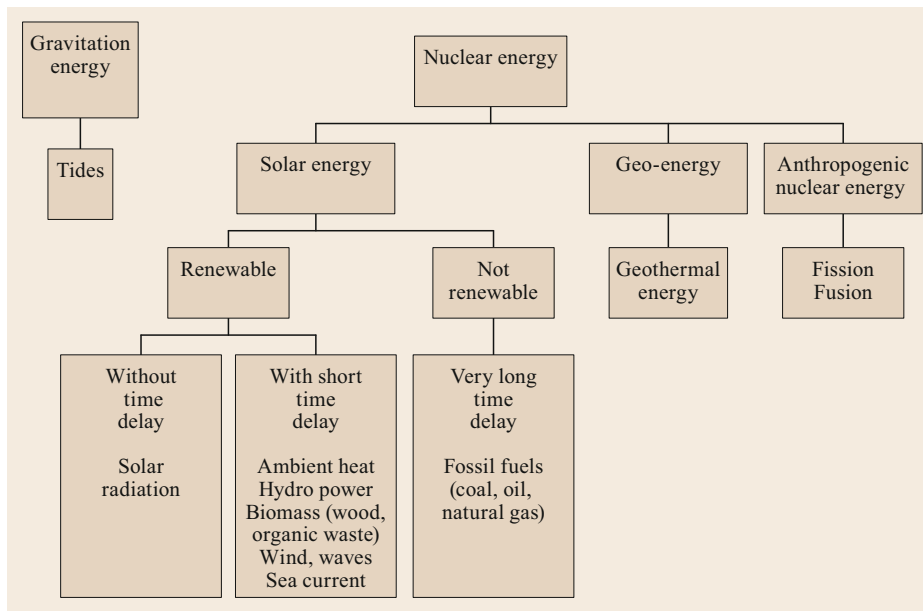
## 1.2 Availability of Primary Energy

All the primary energy carriers listed in Fig. 1.1 can ultimately be traced back to the two principal forms that occur in the universe, *gravitational* and *nuclear energy*, as is shown in Fig. 1.2, with the second being much more significant.

The primary energy carriers can be divided into two large classes that are discussed below:

- *Non-renewable energies*: fossil and nuclear energy carriers
- *Renewable energies*: tidal energy, geothermal energy and above all, direct and indirect solar energy.

Table 1.1 lists and estimates the *energy content* of important energy carriers. Since various units are used in the literature, conversion factors are indicated.



**Fig. 1.2** Origins of available primary energy types

**Table 1.1** Energy content of energy carriers (mean values [1.3]) and conversion factors

Energy carriers		Conversion factors
Oil	10 000 kcal/kg	860 kcal/kWh
Hard coal	6700 kcal/kg	4.19 kJ/kcal
Lignite	4800 kcal/kg	3.6 MJ/kWh
Wood	3600 kcal/kg	31.54 GJ/kWa
Waste	2840 kcal/kg	0.753 toe/kWa
Natural gas	8660 kcal/m <sup>3</sup>	1.12 tce/kWa
Gas from coal and oil (town gas)	4200 kcal/m <sup>3</sup>	1 kWa = 8760 kWh
Uranium 235	20 Tcal/kg	

## 1.2.1 Non-Renewable Energies

### Future Demand

Coal, mineral oil, natural gas, fissile materials (uranium, thorium) are not renewable energy sources. The fusion process has not yet been implemented [1.1, Chap. 11]. In 2016, about 86% of primary energy demand were met from non-renewable energies. According to the older IEA scenarios (International Energy Agency), this share will decline only slightly by 2030 to 86% according to the reference scenario of 2004 and to 83% according to the alternative scenario of 2004; slightly more, namely to around 75%, with the newer 450 scenario of the IEA of 2009 [1.4, Special excerpt] (Fig. 1.3, more details in Sect. 1.6). Less optimistic are the New Policies and Gas Scenario scenarios from

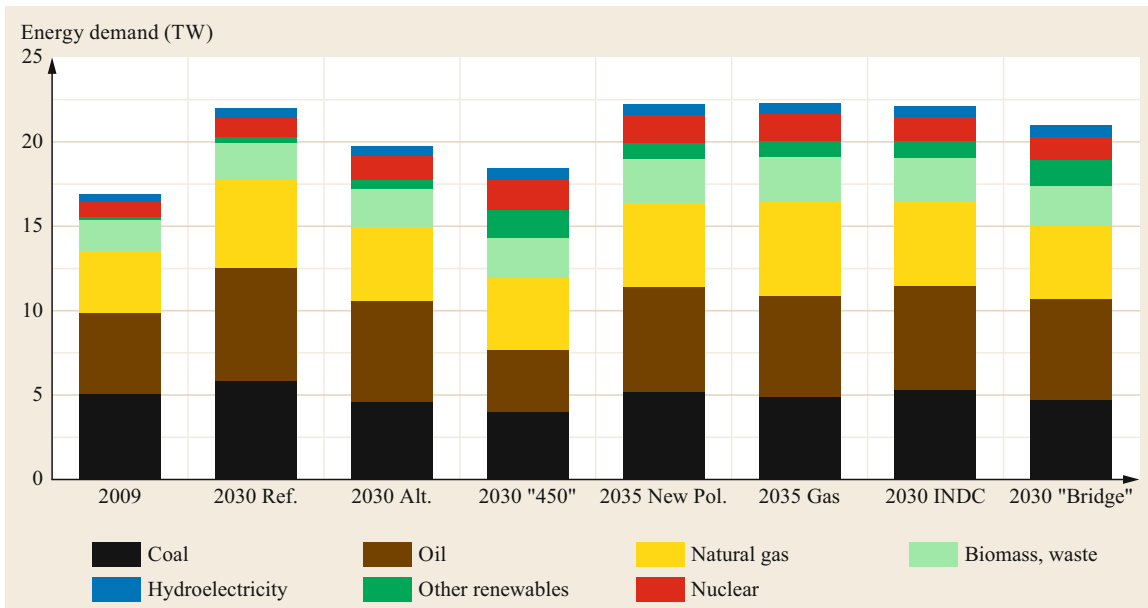
2011, which focus more on CCS (carbon capture and storage). The INDC scenario of 2015 corresponds to the declared contributions of the countries (worldwide); the Bridge scenario of 2015 [1.5] tries to approach the 450 scenario more, but with a lower share of renewable energies (about 15%). The last IEA statistic gives for 2016 a worldwide energy demand of 18.3 TW.

Assuming, for example, that the average energy demand of about 17 TW in 2014 would increase linearly to 20 TW (approx. 15 Gtoe/a) by 2030 and then stabilize by 2050, the cumulative energy demand during this period would be about 710 TWa. The question arises about the *reserves* and *resources* of exhaustible energy sources, whether and how they are able to cover about 80% of this demand, i.e., around 570 TWa. According to the bridge scenario of the IEA (Fig. 1.3), for example, this quantity would be distributed as follows: coal (160 TWa), petroleum (200 TWa), natural gas (160 TWa), uranium (50 TWa).

### Reserves and Resources

*Reserves* are verifiable deposits that can be used at today's market prices and by means of today's technologies. *Resources* are deposits that are known to exist but at present cannot be economically extracted, or those that are assumed and

[...] probably discovered in the future and/or used with technologies yet to be developed and sold at what will then be usual prices. [1.13]



**Fig. 1.3** IEA: World energy demand 2009 and scenarios for 2030 (or 2035), 1 TW = 753 Mtoe/a = 31,54 EJ/a [1.4–7] (Alt: alternative IEA scenario of 2004; New Pol. = New Policies IEA scenario of 2011; INDC = IEA scenario of 2015, corresponds to the declared contributions of countries (worldwide))

**Table 1.2** Reserves and resources of fossil and nuclear energy sources. The duration of the reserves is based on conventional reserves in 2006 [1.8, 9] and on the average consumption of the period 2004–2030 (average forecast IEA)

	Reserves 1980 <sup>a</sup> (TWa)	Reserves 1990 <sup>a</sup> (TWa)	Reserves 1998 <sup>a</sup> 1997 <sup>b</sup> 1996 <sup>c</sup> (TWa)	Reserves 2006 <sup>d</sup> (TWa)	Resources 2006 <sup>d</sup> (TWa)	Range in years of conv. reserves
Petroleum conventional	118	181	185 <sup>a</sup> /203 <sup>b</sup>	216	109	36
Petroleum unconventional	19	68	180 <sup>b</sup>	88	332	–
Natural-gas conventional	89	142	170 <sup>a</sup> /161 <sup>b</sup>	219	250	48
Natural-gas unconventional	–	–	4 <sup>b</sup>	–	1852	–
Coal	647	1005	878 <sup>c</sup>	842 <sup>b</sup> /676	8101	135
Uranium	39	61	63 <sup>c</sup>	85 <sup>e</sup>	98	65

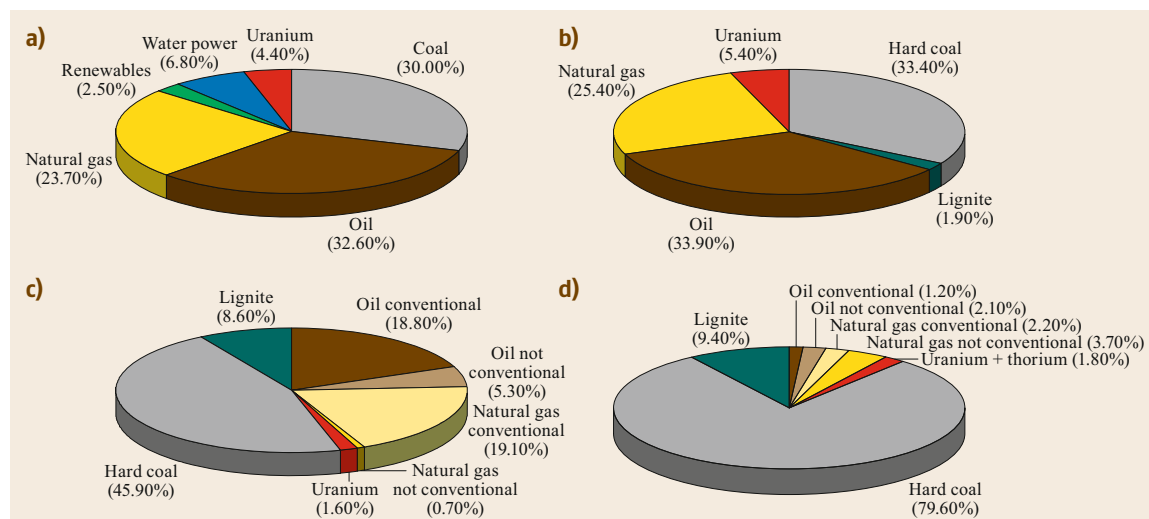
<sup>a</sup> [1.8, 10]; <sup>b</sup> [1.11]; <sup>c</sup> [1.12]; <sup>d</sup> [1.12]; <sup>e</sup> (OECD/IAEA)

The sizes of the reserves and resources are often re-vised upwards, but with differences depending on who collects the statistics, and when (Table 1.2). Resources increase as a result of research and prospecting, that lead to a better understanding of our planet. Resources become reserves when new economically exploitable deposits are discovered, and also as a result of technological progress or higher market prices.

The status of reserves and resources at the end of 2014, as reported by the BGR [1.9], is shown in Fig. 1.4.

The figures of Table 1.2 and Fig. 1.4 show that, thanks to coal, there is no threat of a global shortage in the medium term. The critical energy carrier is mineral oil. The so-called *mid depletion point* (that follows the maximum production point and after which no fur-

ther increase of production is possible) is the date when half the reserves have been used and is estimated by most experts to be 2030–2035. From this date, a large price increase can be expected. The situation is similar for natural gas, with the difference that the reserves are larger and the critical point will not be reached until 2050–2060. There is the possibility of converting coal into liquid and gaseous fuels and of the technology of separating and storing (sequestration) the resulting CO<sub>2</sub>. However, the required industrial processes are still at the stage of development and testing. The outlook as regards technical, economic and ecological aspects is therefore still uncertain. Overall, it seems sensible and sustainable, including from the point of view of the reserves, to reduce the worldwide consumption of fossil energy sources more quickly than the IEA studies



**Fig. 1.4a–d** Worldwide shares of all energy sources in consumption and non-renewable energy raw materials in production, reserves and resources for the end of 2014; (a) Energy consumption: 540 EJ = 17.1 TWa = 12 890 Mtoe; (b) Energy production with non-renewable energy sources: 522 EJ = 16.5 TWa = 12 460 Mtoe; (c) Reserves of non-renewable energy sources: 37 934 EJ = 1202 TWa; (d) Resources of non-renewable energy sources: 551 813 EJ = 17 490 TWa (Source: [1.9])

of 2011 foresee for 2035. The IEA–450 scenario of 2009 and the Bridge scenario of 2015 correspond quite well to this circumstance (Fig. 1.3, see also Sects. 1.6–1.7).

The uranium reserves have been calculated for a marginal price of 130 \$/kg. This is, however, somewhat elastic, as the cost of uranium has little influence on the price of electrical energy supplied by a nuclear power station. With the occurrence of the modest global increase in nuclear power station capacity expected by the IEA, the critical point is likely to occur relatively late towards the end of the century. There is however, no scope for a large-scale substitution of fossil fuels unless alternative concepts are introduced (4th generation breeder technology, high-temperature reactors and thorium – [1.1, Chap. 5.6]). Nuclear fusion is unlikely to play a role until 2050.

#### Ethical Aspects and Environmental Protection

The question of the rate at which these reserves can be allowed to be consumed can be given a good answer from purely economic points of view (Hotelling’s rule and other aspects, e.g., see [1.10]). In addition to these there are ethical considerations and environmental aspects:

- From an ethical viewpoint one must ask whether it is acceptable to extract virtually the whole of this within two or three centuries, the human race’s store of energy, that future generations might be dependent on (emergency supplies, raw materials). This aspect should be relativized to the extent that we do not know today whether future generations will in fact be dependent on this energy. But, is this behavior really responsible?
- The harmful effects of CO<sub>2</sub> emissions on the climate, corroborated by scientific studies (e.g., IPCC), justify political action on a global scale in order to produce a drastic reduction in the output of CO<sub>2</sub> (Sect. 1.7).

*As seen today, it is particularly the second aspect that makes it clearly urgent to correct the economic viewpoint by internalizing the external costs of present and future damage to the climate.*

### 1.2.2 Renewable Energies

Renewable energies (Fig. 1.2) are *natural* energy flows of a certain magnitude that can be tapped using technical means and with a certain economic cost. Most energies are not everywhere, but only available or economically exploitable at favorable locations. The vari-

ous sources will now be considered in respect of their availability.

#### Tidal Energy

Gravitational energy is available to us in the form of *tidal energy*. Tidal friction amounts to about 2.5 TW (i.e., the earth’s rotational energy is reduced by 2.5 TWa each year). It is estimated that only about 9% of this is economically usable [1.12]. For economical use, the tidal range must be at least 6 m. Consequently, in relation to future global energy demands (> 25 TW), tidal energy is of very little significance. For more, details see *Kleemann and Meliss* [1.14], *Kugeler and Philippen* [1.15] and World Energy Council [1.12].

#### Geothermal Energy

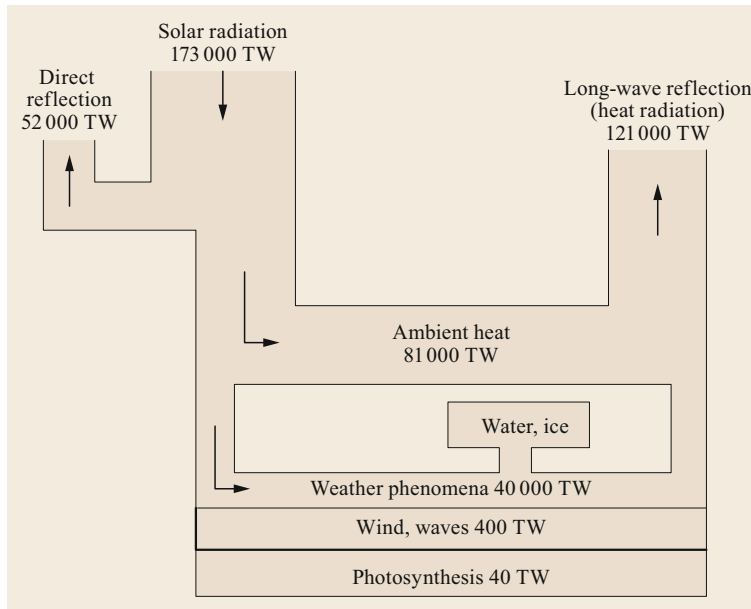
The mean natural flow of heat is very small (about 0.06 W/m<sup>2</sup>). Of this, 30% is from the residual heat of the Earth’s core and 70% from the decay of radioactive isotopes in the earth’s crust. The thermal gradient has a mean value of 1 °C per 30 m. Therefore, it is above all the geothermal anomalies (volcanoes, geysers) that can be economically exploited. In 2005 the world total installed power was about 28 GW, of which 17 GW was *thermal* (main countries: China, USA, Sweden, Iceland) and 9 GW was *electrical* (main countries: USA, Philippines, Indonesia, Mexico, Italy) with annual production rates (mean power) of 6.6 and 6.5 GW. These are almost all *hydrothermal* uses (hot springs). In the future, the *hot dry rock* process may become more significant [1.16–18].

Geothermal energy is a renewable energy, although over relatively long periods (decades to centuries), so *resources* usable in the short to medium term are indicated. The hydrothermal *resources* with high enthalpy levels, > 150 °C, that can be used for generating electricity, amount to about 30 TWa, and the low-enthalpy stocks suitable for heating, about 3200 TWa. How much of this can be called reserves cannot be quantified at present [1.9]. The global installed capacity can presumably be increased to 2 TW (about 100 times the present value), which would cover 5–10% of the future global energy requirement. However, by using the heat pump, this could be significantly greater. In some countries the contribution of geothermal energy is very significant.

#### Solar Energy

Solar is the only renewable energy that is already making a significant contribution to meeting global energy requirements, in the form of water power and biomass (in 2016 about 2.5 TWa).

The supply of solar energy is more than 10 000 times the current global energy demand and it is the



**Fig. 1.5** Solar energy balance of the world

only energy source, possibly together with nuclear fusion, that can meet mankind's energy requirements in the post-fossil age. The problems around the direct use of solar radiation are related to economics and its low density.

As is shown in Fig. 1.5, the flow of solar energy is around 173 000 TW. Of this energy, 52 000 TW are directly reflected back into space as short-wave radiation, while 121 000 TW are absorbed, converted and finally, since the earth is in thermal equilibrium, returned into space as long-wave thermal radiation.

About two thirds of the absorbed radiation is stored in air, water and the ground as *low-temperature heat* and, as such, it can be made use of, e.g., by means of heat pumps.

The remaining third drives the world's weather by evaporating water and creating differences of pressure and temperature; this energy occurs as *potential energy* (water content of clouds, flowing water and glaciers) and as *kinetic energy* (wind, ocean currents, waves).

Only a fraction, about 40 TW, is absorbed by photosynthesis that creates *biomass* and makes life on earth possible.

In view of its importance, the potential and exploitation of solar energy will now be discussed further.

### 1.2.3 Potential and Use of the Main Types of Solar Energy

We distinguish between indirect (delayed) exploitation of:

- Ambient heat (particularly through use of the heat pump)
- Water power (via hydro-electric power stations)
- Wind power, wave power and ocean currents (especially wind turbines)
- Biomass (wood, plants, organic waste) and

direct (immediate) exploitation of:

- Solar radiation (solar architecture, collectors, thermal solar power plants, photovoltaics).

#### Heat Pumps

Heat pumps are a mature technology for making use of low-temperature heat. It enables the temperature to be raised to values suitable for use in space heating and providing hot water. The possible sources of thermal energy are air, ground water, surface water and the interior of the ground. The heat pump makes it possible to use heat from the environment, from waste, and geothermal heat when the source is at least 100–150 m below ground level.

It is the most mature technology for low-temperature applications for substituting fossil fuels with solar heat and geothermal heat. The potential for ambient heat is enormous, as Fig. 1.5 shows. Increased use of heat pumps is being impeded in particular by cheap fossil fuels. Also, the fact that about one third of the generated heat must be obtained from high-value energy carriers (electricity, gas) has an inhibiting effect in countries where a high proportion of electricity pro-



duction is from fossil fuels. For more information about heat pumps, see Sect. 1.7.4 and [1.1, Chap. 6].

### Water Power

The potential of all flowing water in the world is estimated at 6 TWa (average power), of which about 1–1.5 TWa is economically accessible [1.12]. In 2005, 0.334 TWa (hydroelectricity) was used. The development potential is primarily in the developing countries but also in the north (Greenland, Canada). The contribution of water power to *meeting the demand for electricity* was, in 2012, 16.5% worldwide, 13.4% in OECD countries, 61% in South America, 17% in China, 11% in India, 7% in the USA, 11% in the EU-27, 4.4% in Germany, 66% in Austria, 58% in Switzerland and 97% in Norway (more details in Chap. 4, where the use of hydropower is discussed in detail).

### Wind and Ocean Power

The use of wind power has made considerable progress in some countries with favorable wind conditions (Germany, Spain, USA, Denmark) and the associated technology has matured. The economic viability is dependent on the strength and reliability of the wind. Mean wind speeds of at least 5–6 m/s are necessary. These are mainly to be found in coastal regions and some mountainous regions. If it is assumed that 2–5% of wind and wave energy (400 TWa according to Fig. 1.4) can be used economically worldwide, 1–2 TWa are obtained; probably more can be used. In 1996, the installed wind-power capacity worldwide was 6 GW [1.2], but it increased to 20 GW by 2001 and reached 59 GW at the end of 2005 (corresponding to a growth rate of 30%/a). In 2006, the power had reached 75 GW (of which 20 GW was in Germany), which corresponds to an energy output of around 12 GWa (usage factor 0.16). The *offshore* installations (use of wind energy in the sea) have a significantly better utilization factor. At the end of 2014, 370 GW of installed capacity or 86 GWa of generated energy had already been reached worldwide. In Denmark, 1.2 GWa of electricity was already generated by wind in 2012, a third of its total electrical energy consumption, and it is planned to increase this figure to one half by 2030, mainly offshore. In France, 23 GWa of wind energy is expected to be generated in 2040.

If there is a big increase in the energy generated by wind, however, the storage problem must also be solved due to the substantial variability of this form of energy (similar to the somewhat milder variability of hydropower). The corresponding costs must be taken into account when evaluating wind energy.

More information on the technology of using wind energy to generate electrical energy can be found in

Sect. 2.8. For the possible use of waves and ocean currents, see: [1.19, 20].

### Biomass

**Definition.** Biomass consists of materials of organic origin, in other words the material from living beings and organic waste materials (excluding fossil fuels).

**Potential.** The energy in the total biomass of the world is estimated at about 450 TWa [1.18, 21] (1 TWa = 31.5 EJ), with a mean calorific value of about 3500 kcal/kg (referring to fully dry biomass). The growth rate is of particular importance, around 60 TWa/a. The conversion efficiency for solar radiation is, on average, about 0.14%, but higher for forests and fresh water (about 0.5%) and highest of all for tropical forests (up to 0.8%). From the chemical point of view, biomass consists of 82% polysaccharides (cellulose and hemicellulose) and 17% lignin (wood pulp) [1.14].

**Usage.** The technologically exploitable energy potential of biomass in the form of fuels for heating and transport is estimated to be about 6 TW. With a world population of 10 billion people, around 2 TW of this could be obtained from waste. Biomass is thus one of humanity's most significant energy reserves, that could provide about 25% of future demand. Current usage (mainly non-commercial energy) may be (2005) around 1.6 TW. The burning of biomass is CO<sub>2</sub>-neutral only if reforestation is also undertaken.

Technical procedures for use (see details, e.g., in [1.18]):

- **Physical bioconversion:** This includes the *compaction* to biofuels (peat, straw, wood waste → briquettes) and the *extraction* of oils (rape, special oil plants → diesel fuel). If oil plants are cultivated on a large scale, biodiversity is endangered by monocultures.
- **Thermochemical bioconversion:** Methods to mention include in particular: *direct burning* (especially wood) open or in stoves, *gasification/liquefaction* by *pyrolysis*, i.e., the thermal decomposition of high-molecular-weight substances (including used materials, such as waste, old tyres, plastics etc) into smaller molecules, and *methanol synthesis* (for obtaining fuel).
- **Biological conversion:** These are low-temperature processes that use micro-organisms (fermentation). They include *biogas production* and the production of *ethanol* from plants containing sugar (sugar cane), that is used on a large scale for fuel production in Brazil, for example.

### Solar Radiation

**Specific Availability of Solar Energy.** If the 121 000 TW that reaches the earth (Fig. 1.5) is distributed uniformly over the earth's surface, the result for a *horizontal surface* is

$$\begin{aligned}\text{Mean annual power} &= \frac{121\,000\text{ TW}}{510 \times 10^6 \text{ km}^2} \\ &= 237 \frac{\text{W}}{\text{m}^2}.\end{aligned}$$

If we consider only daylight hours (12 instead of 24 h), the result is a doubled mean annual daytime power of 474 W/m<sup>2</sup>. These figures apply to an average latitude, clear weather and at sea level. The effective mean value depends not only on the latitude but also on the climate. In central Europe (often cloudy or foggy), half this figure can be expected, namely 120 W/m<sup>2</sup>.

If we multiply the annual mean power by 8760 h/a, the result is

$$\begin{aligned}\text{Annual mean energy} &= 237 \frac{\text{W}^2}{\text{m}} \cdot 8760 \frac{\text{h}}{\text{a}} \\ &= 2076 \frac{\text{kWh}}{\text{a m}^2}.\end{aligned}$$

For the reasons stated, this annual energy is not achievable at moderate latitudes because it assumes constant sunshine. The value is exceeded (up to over 2200 kWh/(am<sup>2</sup>)) near the equator and in desert climates (Sahara, Arizona, Australia etc.).

**Density of Solar Radiation (Global Radiation).** The earth's cross-section is about 127 × 10<sup>6</sup> km<sup>2</sup>. Outside the atmosphere this gives

$$\begin{aligned}\text{Extraterrestrial radiation density} &= \frac{173\,000\text{ TW}}{127 \times 10^6 \text{ km}^2} \\ &= 1360 \frac{\text{W}}{\text{m}^2}.\end{aligned}$$

This quantity is also known as the *solar constant*. On the earth's surface (sea level) the radiation density (without reflections!) is, on a *surface perpendicular to the rays*

$$\begin{aligned}\text{Radiation density at sea level} &= \frac{121\,000\text{ TW}}{127 \times 10^6 \text{ km}^2} \\ &= 950 \frac{\text{W}^2}{\text{m}}.\end{aligned}$$

In Switzerland the figure of 1000 W/m<sup>2</sup> is usually used. This global radiation contains both a *direct* and a *diffuse* component (diffuse sky radiation). Under the climate conditions of central Europe, the diffuse component is important (Sect. 2.9).

These figures show, on the one hand, that solar radiation has practically unlimited potential, but also make clear the problems that an economical exploitation of solar radiation encounters. The most important methods of use are listed here:

**Solar Architecture.** Designing buildings to exploit solar energy can result in a large reduction in the demand for heating energy. This is an option that should be used and promoted much more than at present. For more information, refer to the special literature and to [1.17, 22].

**Flat Collectors.** Flat collectors can use direct and diffuse radiation. The heat is transferred to a heat carrier (usually water with anti-freeze). High efficiency levels are achieved in low-temperature applications (up to 70% for heating open-air swimming baths, up to 60% for water heating, but only 40–50% for space heating); i.e., the efficiency is strongly dependent on the temperature at which the energy is used. These efficiencies are, however, only achieved for the full irradiation levels and are reduced more than proportionally at lower levels. Collectors are economical at present for heating swimming baths and water heating (especially in summer) (for details see [1.17, 22, 23]).

**Concentrating Collectors.** *Parabolic mirrors* (parabolic cylinders or paraboloids) can be used to concentrate direct radiation (diffuse radiation cannot be used this way). This generates high temperatures that can be used for producing process heat and electricity. The mirrors do need to be moved to track the sun. The heat carrier is usually a special oil. Examples of applications are solar cookers for developing countries, solar farms for producing industrial heat and electricity (solar thermal power stations) by using the usual steam process, see [1.21].

With parabolic cylinders (parabolic troughs) temperatures of 100–400 °C are achieved. The water is heated in a tube placed at the focus of the parabola. For higher temperatures, expensive *paraboloids* or *heliostats* are used, which serve both for generating electricity and for carrying out chemical processes [1.18].

**Solar Thermal Power Stations.** For the production of electricity, one can use *parabolic trough collectors* which concentrate the sunlight on an absorber tube running along the focal axis, or *solar tower systems*; in the latter case, the sun is tracked with the aid of flat mirrors that follow the sun biaxially (the so-called *heliostats*), which concentrates radiation on the top of a tower. A radiation receiver is located here. The heat is transferred to a working medium (e.g., steam, helium, liquid sodium). Temperatures between 500 and 1200 °C can

be reached. This can drive steam or gas turbines that generate electricity in the conventional way.

Solar thermal power plants are particularly suitable for regions with long periods of sunshine and clear skies, as they cannot make use of diffuse radiation. Various pilot plants are in operation worldwide. Three 50 MW parabolic trough power plants have been built in Spain, 100 MW in Abu Dhabi and a total of 350 MW in California; further large-scale plants are planned. Efficiencies of approx. 15% have been estimated. The energy costs for plants of 100 MW are around 20 ct/kWh.

Projects with large installations in the Sahara that could be connected to the European grid by means of HVDC (high-voltage direct current transmission), see [1.24] have been under discussion (Desertec).

### Photovoltaics

Photovoltaics enable the direct conversion of solar radiation into electricity by means of *solar cells*. With *polycrystalline silicon cells*, commercial efficiencies of 15% are achievable today with *monocrystalline*, even as high as around 20%. Crystalline cells have become significantly cheaper in recent years, and the energy-harvest factor (ratio of energy generated to energy required for fabrication) has improved significantly. The technology is quite advanced and the operational experience is good.

Commercial grid-connected photovoltaic plants of over 100 kW output using crystalline cells can today produce electricity at a price of 15 ct/kWh or much less, which approaches or falls below grid parity in terms of household electricity prices in many countries. However, it is often ignored that the fluctuations in the feed-in must also be compensated, as is done with hydroelectrically generated energy with appropriate storage facilities.

For more information on photovoltaics and photovoltaic power plants, Chap. 8.

## 1.2.4 Ecological Problems

The energy industry, together with chemistry and agriculture, is one of the main contributors to the contamination of the biosphere with pollutants. Energy supply and energy use lead to *pollution of the atmosphere* by emissions from the combustion of fossil fuels and biomass and by natural gas losses. Pollution of the sea from tanker accidents is also not negligible. The *main emissions* are:

- Oxides of carbon (CO, CO<sub>2</sub>);
- Oxides of nitrogen;
- Sulfur compounds;

- Methane;
- Ozone.

### Predominantly Localized Effects

Nitrogen oxides, sulfur compounds, CO and tropospheric ozone mainly have regional impacts on health, plant ecosystems and cultural assets, but are sometimes transported over long distances by winds. The harmful effects have been effectively minimized in recent decades in advanced countries through desulphurization and nitrification measures and catalysts.

Stratospheric ozone depletion (the ozone hole) is rather different, and is mainly caused by emissions of chlorinated fluorocarbons (CFCs) and only marginally connected with energy use (for more details see, for example, [1.18]).

### Increasing the Greenhouse Effect

Much more serious consequences for the climate derive from so-called *greenhouse-gas emissions*, and there is an extensive literature on this subject. The fifth IPCC report (Intergovernmental Panel on Climate Change) of 2013/2014 (IPCC 2014) provides a good summary, while other research and reports also support its findings. The report concludes, even more emphatically than earlier reports, that the observed global warming is very probably caused by humans. The most important greenhouse gas is CO<sub>2</sub> which contributes 77% to the strengthening of the greenhouse effect. Further contributions are from methane (15%), CFCs (1%) and N<sub>2</sub>O (7%). The CO<sub>2</sub> concentration in the atmosphere is 380 ppm, i.e., 36% higher than the pre-industrial concentration (280 ppm, practically unchanged over the previous 10 000 a). It increases annually by 1.5–2 ppm. Simulations for the year 2100 give, assuming a doubling of the pre-industrial concentration, and depending on the scenario, an increase in the mean temperature of 2–6 °C (with a probability of 66% for an increase between 2.4 and 4.1 °C). In addition, sea levels could rise by 50 cm or significantly more by 2100 (according to recent studies), and the number and intensity of extreme climatic events could increase. Although the existing uncertainties could have a positive effect, they could also have a much more negative effect, e.g., as a consequence of non-linear feedback. A mean temperature increase of 2 °C corresponds for medium latitudes to a shift of the isotherms about 350 km northwards or of the apparent height above sea of about 350 m, with the possibility of very great regional differences.

The consequences could be even more dramatic in the case of a *tipping point of the climate*. A deflection or slowdown or even a long-term interruption of the Gulf Stream would, for example, have catastrophic consequences for Western Europe.

The consequences of this, in the geological time scale, extremely rapid climate change would undoubtedly be further stress for the already heavily damaged ecosystems (extinction of species, forests). The distribution of water resources and agricultural productivity could be adversely affected world-wide, with increased stress on socio-economic systems, and with particularly great suffering in the regions that are weak and can only adapt slowly or not at all to the changed conditions. Although there may also be winners, the global balance is very negative.

### Sustainable Development

The term *sustainability* has assumed political contours, in particular through the Brundtland Commission's 1987 report, which defined sustainable development as *one that meets current needs without compromising the ability of future generations to meet their own needs* and called for growth that integrates social and environmental aspects into economic considerations, both spatially and temporally.

It is thus a matter of optimizing development in the triangle of economy, society and ecology (the *triple bottom line* of people, planet, profit) and of global and intertemporal solidarity. The main difficulty in implementing this goal is the fact that economic, but also sociopolitical thinking, is too often short-to-medium term, while the ecological requirements, especially in connection with the climate problem, require long-term optimization.

The above paragraph has highlighted the need to vigorously reduce greenhouse-gas emissions world-wide, in particular CO<sub>2</sub> emissions. The costs of this energetic transformation are quite high, but even higher would be the cost of a *laissez-faire* approach. It is not a matter of (purely selfish) adaptation to the consequences of climate warming, but above all, of putting a brake on climate warming, reducing it to the extent that is possible and avoiding the enormous costs of social and infrastructural adaptations, that would linearly increase faster than the increase in mean temperature.

## 1.3 Energy Demand, CO<sub>2</sub> Emissions, Indicators

### 1.3.1 General Information

Prior to a detailed analysis of the energy situation in Europe (Sect. 1.4), in the world (Sect. 1.5) and the prospects in relation to climate-protection requirements (Sects. 1.6–1.7), some basic aspects of energy demand should be presented and indicators defined that are particularly relevant for climate change.

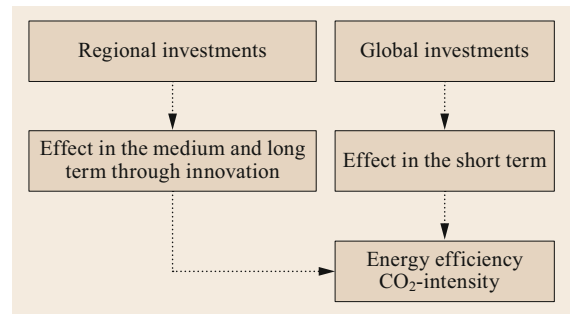
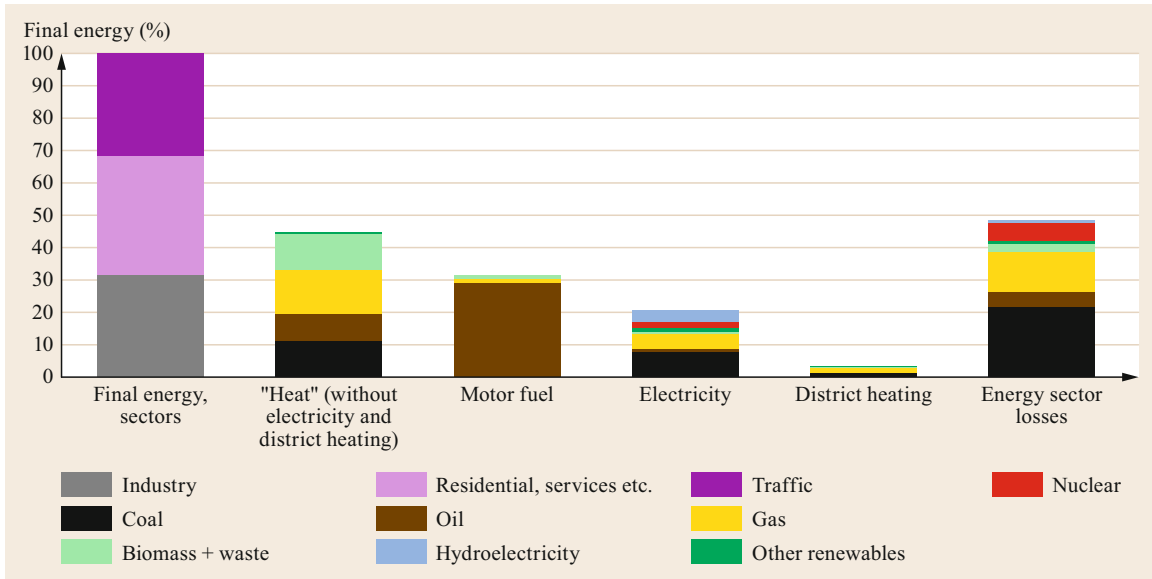


Fig. 1.6 Sustainable investments

Political initiatives are required that aim to internalize current and future external costs, a recipe well compatible with the market economy. In the fight against global environmental damage, it is right in theory to apply capital and knowledge in those areas where the contribution to improving energy efficiency and reduction of CO<sub>2</sub> intensity will be maximized (e.g., via the trading of emission certificates). International co-operation in putting this sensible theory into practice is all too often made problematic by the absence of boundary conditions that steer market forces in the right socio-ecological directions, and by political differences. Sometimes this argument is rather an excuse for doing nothing in one's own region. Both kinds of effort, global and local (Fig. 1.6) are necessary. Although rationalization is suboptimal in terms of global capital spending in the short term, it nevertheless promotes regional innovation in the environmental sector, which will probably pay off globally in the medium and long term (for actions in energy economics see Sect. 1.7).

The results of the UN climate conference COP21 in Paris, December 2015, where for the first time a large number of countries committed to take measures to limit the mean temperature rise of the Earth compared to pre-industrial times to at most 2 °C, and if possible aim for 1.5 °C, provide some hope. See Sect. 1.7 for more details.

Especially for readers unfamiliar with energy demand issues, it can also be useful to review the case of Switzerland's energy demand as an example of a highly industrialized country [1.1, Appendix C]. In particular, the structural aspects of energy demand are illustrated with concrete figures, and the factors that determine their evolution are presented.



**Fig. 1.7** Final energy and energy sector losses worldwide in 2016 (100%  $\hat{=}$  final energy = 8686 Mtoe, together = gross energy consumption = about 150% of final energy)

### 1.3.2 Final Energy and Losses in the Energy Sector

For further considerations, it is useful to distinguish between three areas of the use of final energy [1.25, 26]:

- *Comfort heating and process heat*, predominantly obtained from fossil fuels and partly from renewable energies (geothermal energy, biomass, solar radiation, ambient heat). Heating by electricity is excluded.
- *Propellants* (fuels for transport), mainly fossil, some biomass.
- *Electricity*, all uses, including heating.

Figure 1.7 shows the global importance of each of the three areas as a percent of final energy for 2016 (i.e., heat + district heating: 45% + 3%; transport fuels (motor fuels): 31%; electricity: 21%). The three areas are subdivided into the primary energy carriers.

The bar for final energy (100% = 8686 Mtoe in 2016) also shows the subdivision into the three energy-consuming sectors: industry (32%), traffic (32%) and others (36% residential, services + agriculture).

Finally, the *losses in the energy sector* are shown, attributable to heat losses in power plants and the energy sector's own consumption of energy. The representation of these losses corresponds to the statistics of the IEA (international energy agency), in which hydroelectricity is recorded but not water power. Worldwide,

there are losses of 49% of the final energy. Global gross energy consumption thus amounts to almost 150% of final energy demand or exactly 12 892 Mtoe in 2016.

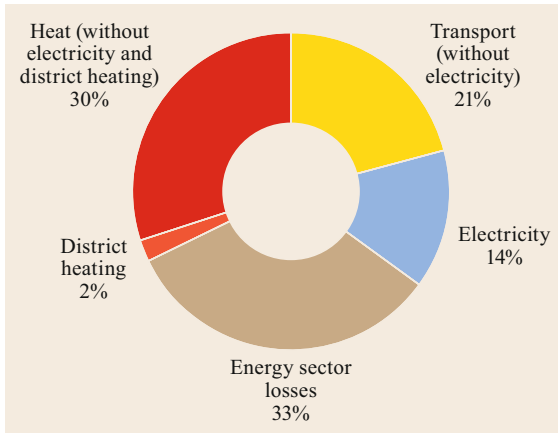
### 1.3.3 Global Gross Energy Demand, Energy Sector

For further analysis, it makes sense to define the *energy sector* as [1.25]:

- The electricity and district heating produced, and
- All losses associated with the conversion of gross energy into final energy.

The global demand for primary energy in 2016 can then be illustrated by Fig. 1.8. It is composed of the energy consumed in the *transport sector* (fuels, excluding electricity), of *heating and process heat energy* (excluding electricity and district heating) required by industry and the other sectors (households, commerce, services, etc.) and of the *energy needs of the energy sector*, which is primarily used for the production and transmission of electricity and district heating, with large losses.

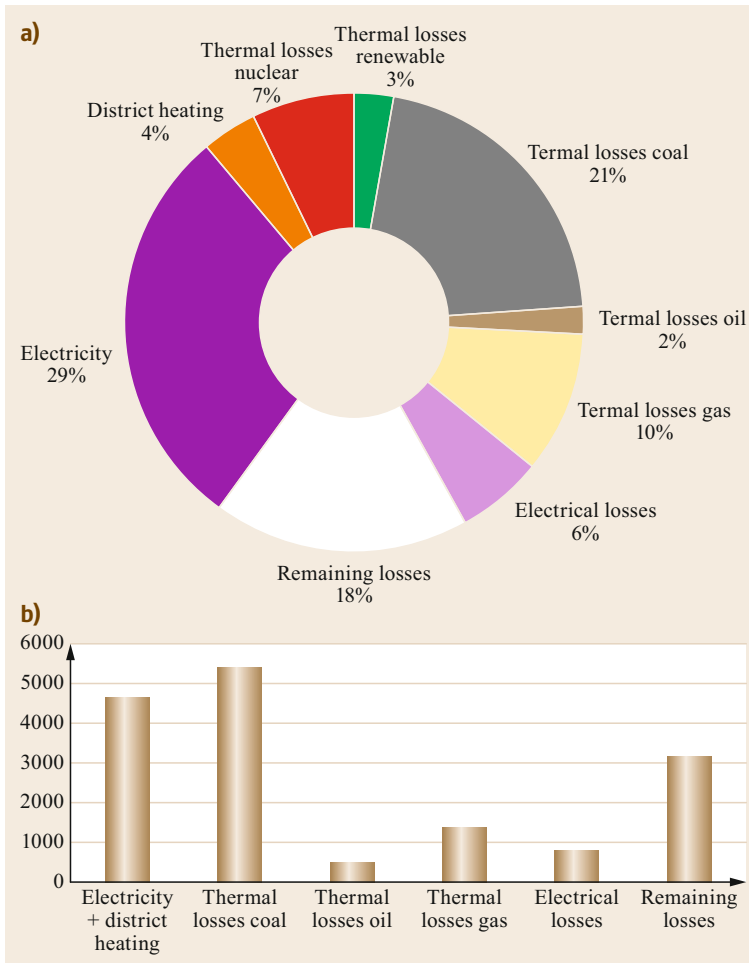
The energy sources with which this total consumption was supplied in the past and will probably be supplied in the future have already been illustrated in Fig. 1.3 (Sect. 1.2); Fig. 1.7 shows the situation in 2016.



**Fig. 1.8** Worldwide consumption of gross energy in 2016 (total 12 892 Mtoe, 1.37 KWh/\$), divided into: transport, heat consumption and energy sector (electricity + district heating + losses)

With 49% of the gross energy consumed worldwide, i.e., around 6300 Mtoe in 2016, the energy sector plays a decisive role for climate protection aims.

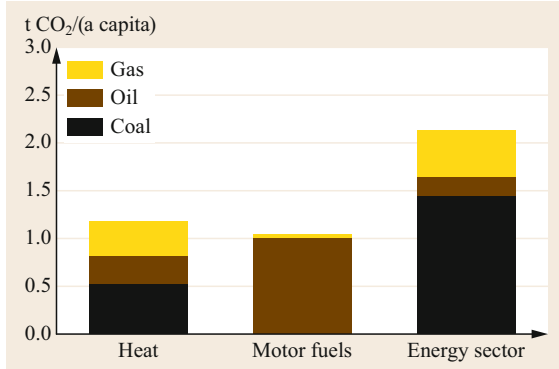
The energy demand of the energy sector can be broken down according to Fig. 1.9. The final energies produced by the energy sector – electricity and district heating – account for 33%. The remaining 67%, corresponding to about 4200 Mtoe, are energy losses or own consumption (difference between the gross consumption of 12 900 Mtoe and the final consumption of 8700 Mtoe). The largest part of these losses are thermal losses in power plants and combined heat and power plants (broken down by type of energy carrier in the figure). Further losses are the electrical transmission losses (in the transmission and distribution networks). Finally, the own consumption and residual losses in pure heating plants and gas works, in refineries and other conversion plants (gasification and liquefaction processes) and in the mine extraction of energy carri-



**Fig. 1.9a,b** World 2016, energy shares of the energy sector (a) Energy sector = final energies electricity and district heating + losses (6283 Mtoe), and corresponding CO<sub>2</sub> emissions, (b) CO<sub>2</sub> emissions = 15 815 Mt

**Table 1.3** Worldwide indicators for 2016 in international dollars from 2010, 1 kW<sub>a</sub> = 8760 kWh = 0.753 toe = 31 540 MJ

2016	$y$ (10 <sup>4</sup> \$/(a capita))	$e$ (kW <sub>a</sub> /(10 <sup>4</sup> \$)) = 1.37 kWh/\$	$k$ (t CO <sub>2</sub> /W <sub>A</sub> ) = 215 g CO <sub>2</sub> /kWh	$\eta$ (t CO <sub>2</sub> /(10 <sup>4</sup> \$)) = 296 g CO <sub>2</sub> /\$	$\alpha$ (t CO <sub>2</sub> /(a capita))
World	1.47	1.56	1.88	2.96	4–35

**Fig. 1.10** Worldwide CO<sub>2</sub> emissions and polluters. 2016, CO<sub>2</sub> emissions = 32.316 Mt, 4.4 t/capita, 296 g/\$ (GDP PPP \$ of 2019)

ers must be taken into account. High residual losses are often a sign of a lack of efficiency in the energy sector.

### 1.3.4 CO<sub>2</sub> Emissions and Indicators

Global CO<sub>2</sub> emissions resulting from the combustion of fossil fuels for 2016 are shown in Fig. 1.10. They amount to a total of 4.4 t/(a capita), and almost 50% comes from the energy sector, with electricity generation from coal being the main polluter.

For further analysis, we introduce the following relationships [1.25, 26]

$$\alpha \left[ \frac{\text{t CO}_2}{\text{a capita}} \right] = k \left[ \frac{\text{t CO}_2}{\text{kW}_a} \right] \times e \left[ \frac{\text{kW}}{\text{capita}} \right], \quad (1.1)$$

where  $\alpha$  = CO<sub>2</sub> emissions per year, per capita,  $k$  = CO<sub>2</sub>

intensity of gross energy,  $e$  = gross energy consumption per capita.

Specific energy consumption  $e$  correlates primarily with gross domestic product (GDP), whereby it is useful for international comparisons to refer to GDP at purchasing power parity (GDP PPP). That's why we can write

$$e \left[ \frac{\text{kW}}{\text{capita}} \right] = y \left[ \frac{10\,000\ \$}{\text{a, capita}} \right] \times \varepsilon \left[ \frac{\text{kW}_a}{10\,000\ \$} \right], \quad (1.2)$$

where  $y$  = specif. gross domestic power (adjusted for purchasing power),  $\varepsilon$  = gross energy intensity.

The CO<sub>2</sub> emissions can then be expressed as

$$\alpha = ke = k\varepsilon y = \eta y$$

$$\begin{aligned} \text{with } \eta \left[ \frac{\text{t CO}_2}{10\,000\ \$} \right] &= k\varepsilon \\ &= \text{CO}_2 \text{ sustainability of energy supply} \end{aligned} \quad (1.3)$$

as a product of *prosperity indicator*  $y$ , energy intensity  $\varepsilon$  and CO<sub>2</sub> intensity of energy  $k$ .

In order to reduce the specific CO<sub>2</sub> emissions per year per capita  $\alpha$ , we must be able to achieve the desired increase of  $y$  (GDP/capita) and compensate it with a considerable reduction of *energy intensity*  $\varepsilon$  and CO<sub>2</sub> *intensity of the energy*  $k$ . The product of these two quantities is defined as the CO<sub>2</sub>-*sustainability indicator*  $\eta$ . The corresponding figures worldwide for 2016 are summarized in Table 1.3. The GDP PPP is expressed in international dollars as of 2010 (sources: IMF, see also [1.25, 27, 28]); we get a worldwide  $\eta = 3.49 \text{ t CO}_2/\$10\,000$  or  $349 \text{ g CO}_2/\$$ . 8

## 1.4 Energy Consumption and CO<sub>2</sub> Emissions in Europe

We refer here to Europe as the EU-28 plus the three Western European countries that are not members of the EU: Iceland, Norway and Switzerland.

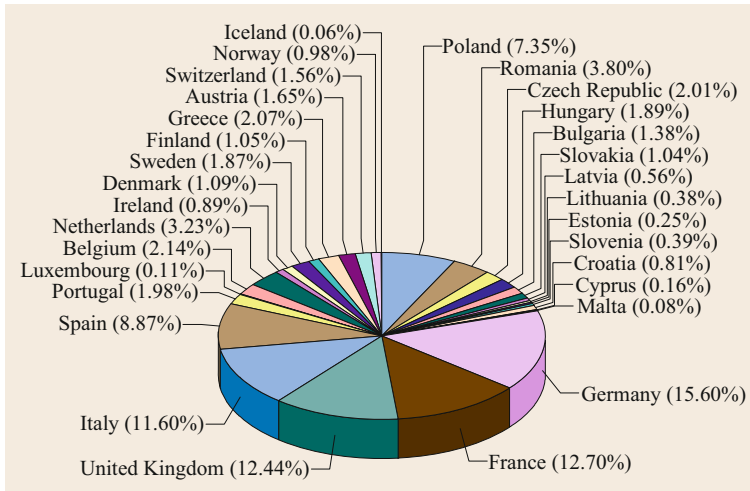
### 1.4.1 Population and Gross Domestic Product

The EU-15 comprises all Western European EU members. Figure 1.11 shows the percentage distribution of the population in 2015. Figure 1.12 shows the

purchasing-power adjusted (PPA) gross domestic product (GDP) per capita of the European countries.

### 1.4.2 Energy Consumption per Capita

Energy consumption per capita depends on the one hand on the level of economic development (measured by GDP/capita, Fig. 1.12) and on the other hand on the efficiency of energy use (measured by energy intensity). Consumption is also influenced

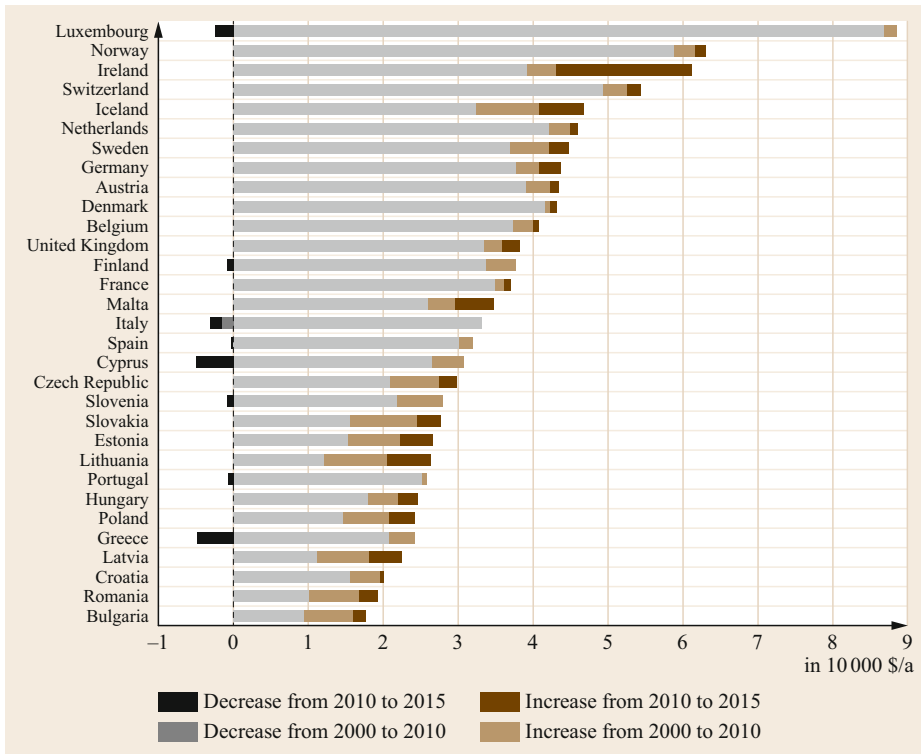


**Fig. 1.11** Percentage distribution of the population of Europe in 2015 (total 524 million): EU-28 + Iceland, Norway, Switzerland

by the climate and depends on the characteristics of the economy of the country in question. Figure 1.13 shows gross energy consumption per capita in 2015 for Western Europe and Eastern Europe (EU 13, only EU members). One notes significant differences. Southern European countries consume less energy than the Scandinavian countries, which is due to climatic conditions and, in some cases, to weaker economic development (Fig. 1.13a). Accord-

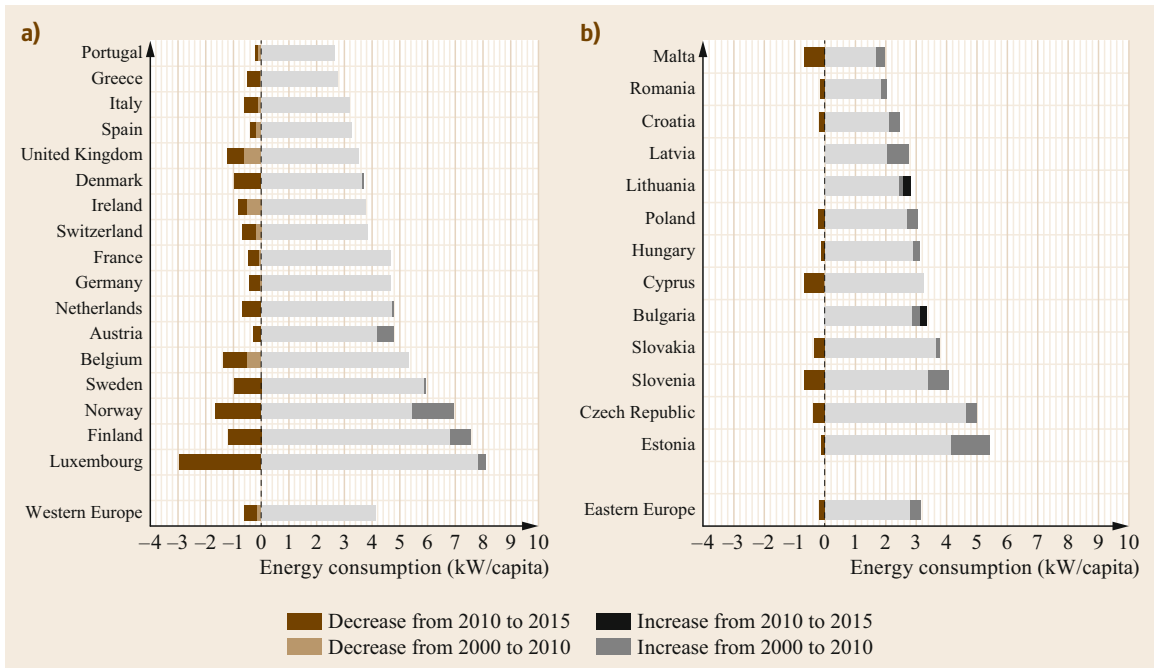
ingly, the figures for Eastern Europe are generally lower (Fig. 1.13b).

Iceland is not included because of the extremely high value of 22 kW/capita, which can be explained by the heavy use of (non-polluting) geothermal energy. For Luxembourg, both in terms of GDP and energy consumption, the distortion caused by the very high proportion of cross-frontier workers must be taken into account (Figs. 1.12 and 1.13a).

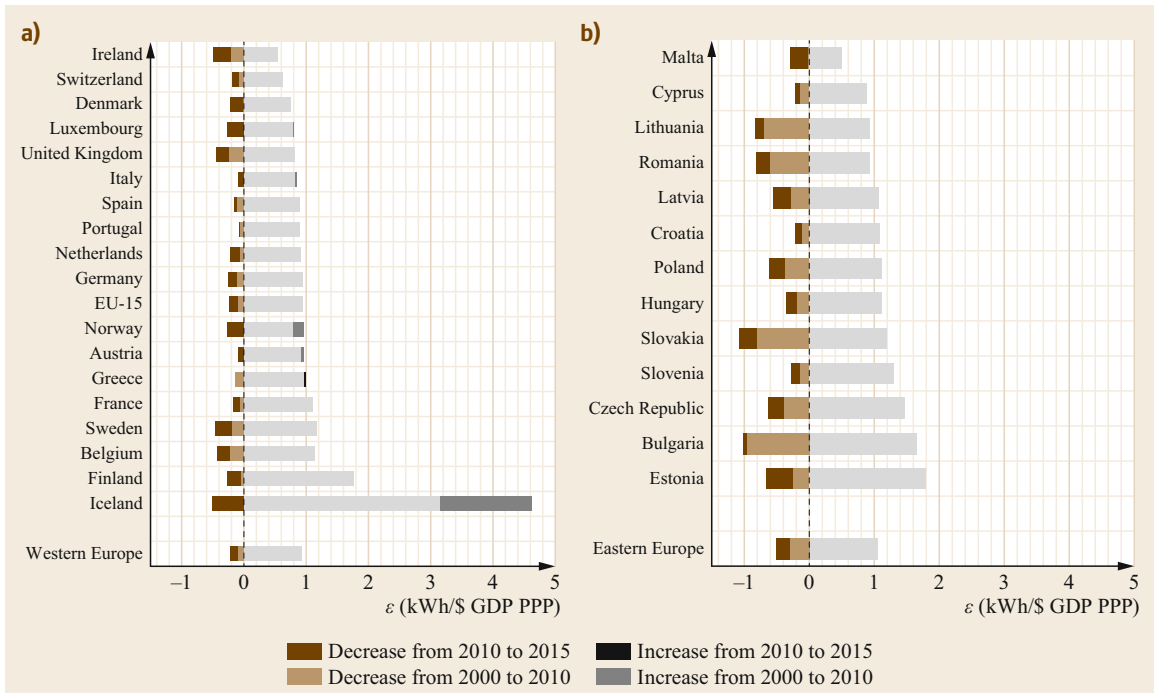


**Fig. 1.12** Per capita GDP (PPP) of the European countries in 2015, in 10 000 \$ (US\$ of 2010)

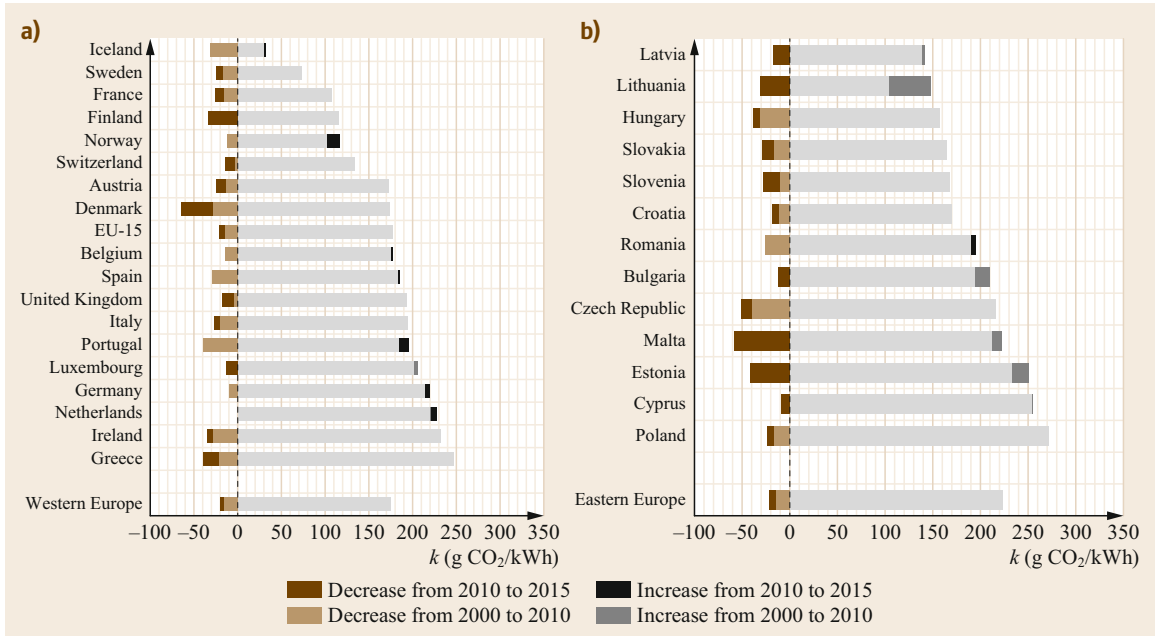




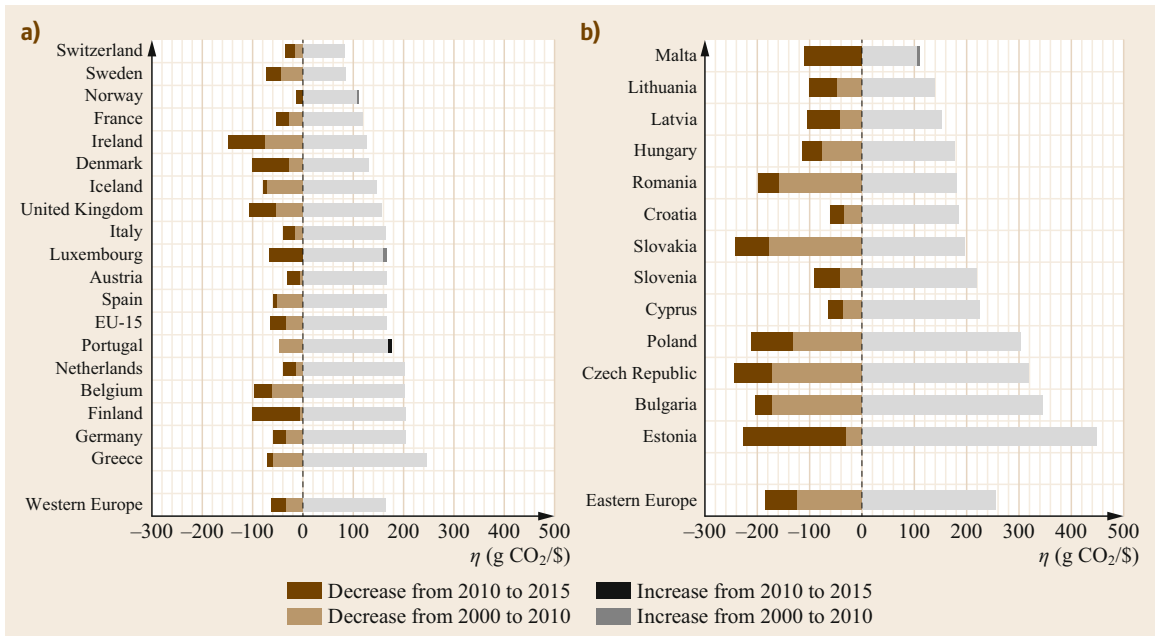
**Fig. 1.13a,b** Per capita energy consumption in Europe [1.5]: (a) Western Europe (EU-15 + Iceland, Norway, Switzerland, all OECD members), (b) Eastern Europe and Malta (only EU-28 members)



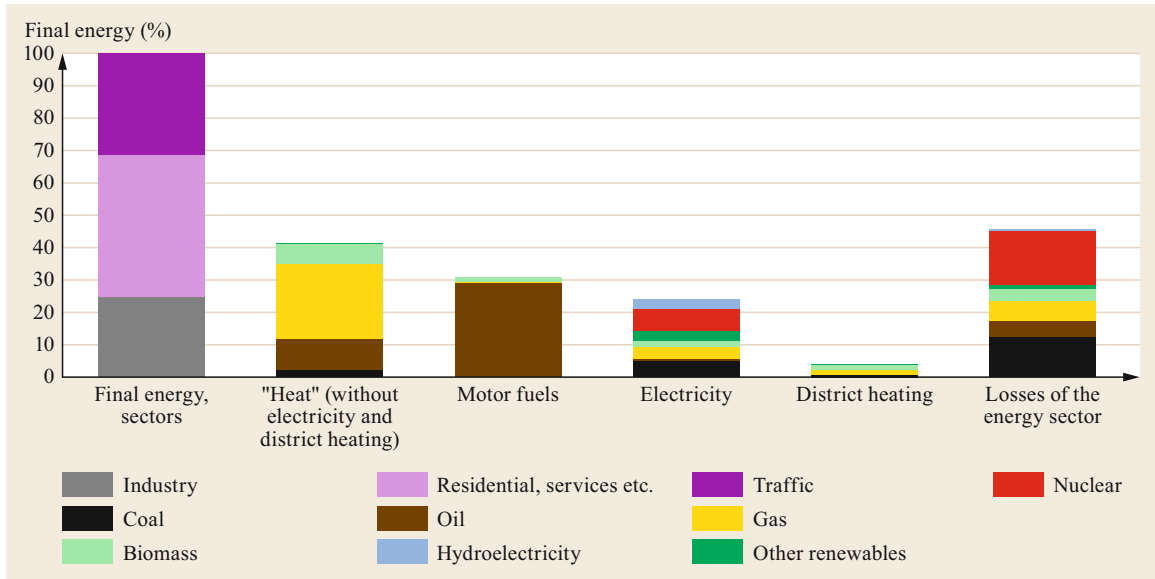
**Fig. 1.14a,b** Energy intensity  $\epsilon$  of the countries of Europe in 2015: (a) Western Europe; (b) Eastern Europe and Malta (GDP PPP in \$ of 2010)



**Fig. 1.15a,b** CO<sub>2</sub> intensity of energy  $k$  of the countries of Europe in 2015: (a) Western Europe; (b) Eastern Europe and Malta



**Fig. 1.16a,b** Indicator of CO<sub>2</sub> sustainability  $\eta$  of the countries of Europe in 2015: (a) Western Europe; (b) Eastern Europe and Malta (GDP PPP in \$ 2010)



**Fig. 1.17** Final energy and losses of the energy sector in the EU-15, 2015. 100%  $\hat{=}$  total final energy = 852 Mtoe (source: IEA statistics)

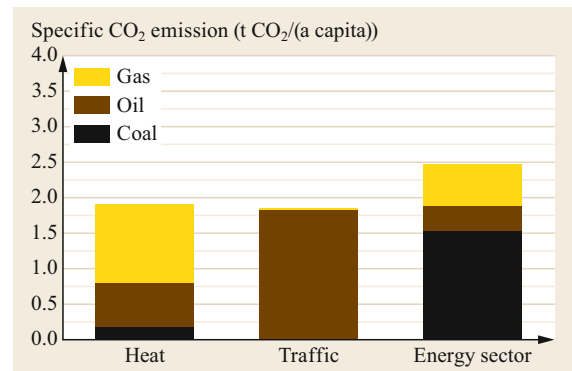
### 1.4.3 Energy Intensity and CO<sub>2</sub> Emissions, Sustainability

The *energy intensity*  $\varepsilon$  of the countries of Europe is shown in Fig. 1.14 for 2015. A low energy intensity basically indicates a rational use of energy. Various factors, such as climate or type of economic performance (services instead of heavy industry) or of electricity generation, also have an impact. Multiplying the energy intensity by the *CO<sub>2</sub> intensity of the energy*  $k$  as shown in Fig. 1.15, gives the *CO<sub>2</sub> sustainability*  $\eta$  of Fig. 1.16 ((1.1)–(1.3)).

Four countries in Western Europe have a *CO<sub>2</sub> sustainability indicator*  $\eta$  below 120 g CO<sub>2</sub>/\$ (Fig. 1.16). These are the countries whose electricity production is predominantly CO<sub>2</sub>-free: Switzerland and Sweden with a mix of hydropower and nuclear energy, Norway with pure hydropower, and France with, in addition to hydropower, predominantly nuclear energy. The remaining EU-15 countries are between 125 and 250 g CO<sub>2</sub>/\$. The countries of Eastern Europe (only EU-28 members) have an average of around 250 g CO<sub>2</sub>/\$ and thus have a clear need to catch up.

#### 1.4.4 Final Energy and Losses of the Energy Sector in the EU-15

The EU-15 comprises the economically strongest countries in Europe. In terms of population, they account for about 400 million inhabitants or almost one third of the population of the OECD-34. Their energy con-



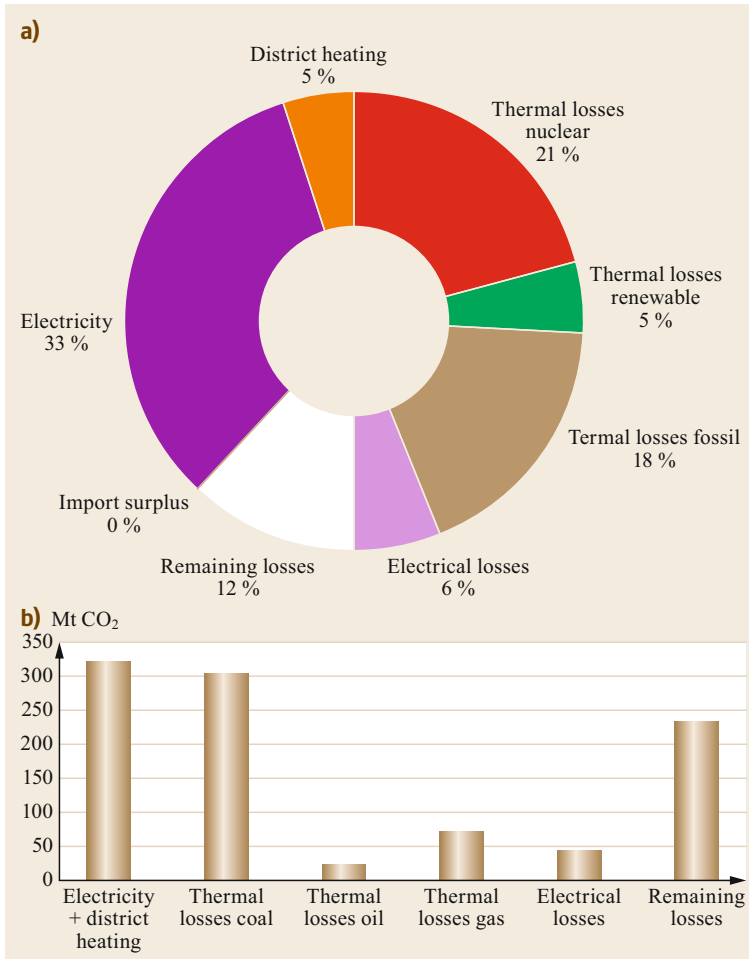
**Fig. 1.18** CO<sub>2</sub> emissions of the EU-15 in 2015 and their distribution. Total emissions = 2517 Mt, 6.2 t/capita, 164 g CO<sub>2</sub>/\$ (GDP PPP in \$ of 2010; Data-source: IEA)

sumption and the associated CO<sub>2</sub> emissions are illustrated in Figs. 1.17 and 1.18, and the characteristic indicators are compared in Table 1.4 with those of Switzerland and Norway. The main difference lies in the energy sector, which has a 40% share of CO<sub>2</sub> emissions (Fig. 1.18).

The electricity production in many EU countries is based mainly on fossil fuels (e.g., in Germany, Italy, Great Britain, Benelux and Denmark). But there are big differences within the EU-15. France and Sweden are structurally similar to Switzerland, thanks to their electricity generation also based on hydro and nuclear power. The structure of the energy sector is shown in Fig. 1.19.

**Table 1.4** Indicators for 2015 for Switzerland, Norway and EU-15.  $\eta = k\varepsilon$ ,  $\alpha = \eta y/100$ 

	$y$ ( $10^4$ \$/(a capita))	$\varepsilon$ (kWh/\$)	$k$ (g CO <sub>2</sub> /kWh)	$\eta$ (g CO <sub>2</sub> /\\$)	$\alpha$ (t CO <sub>2</sub> /(a capita))
Switzerland 2015	5.43	0.62	134	83	4.5
Norway 2015	6.30	0.96	116	112	7.1
EU-15 2015	3.80	0.94	178	167	6.3

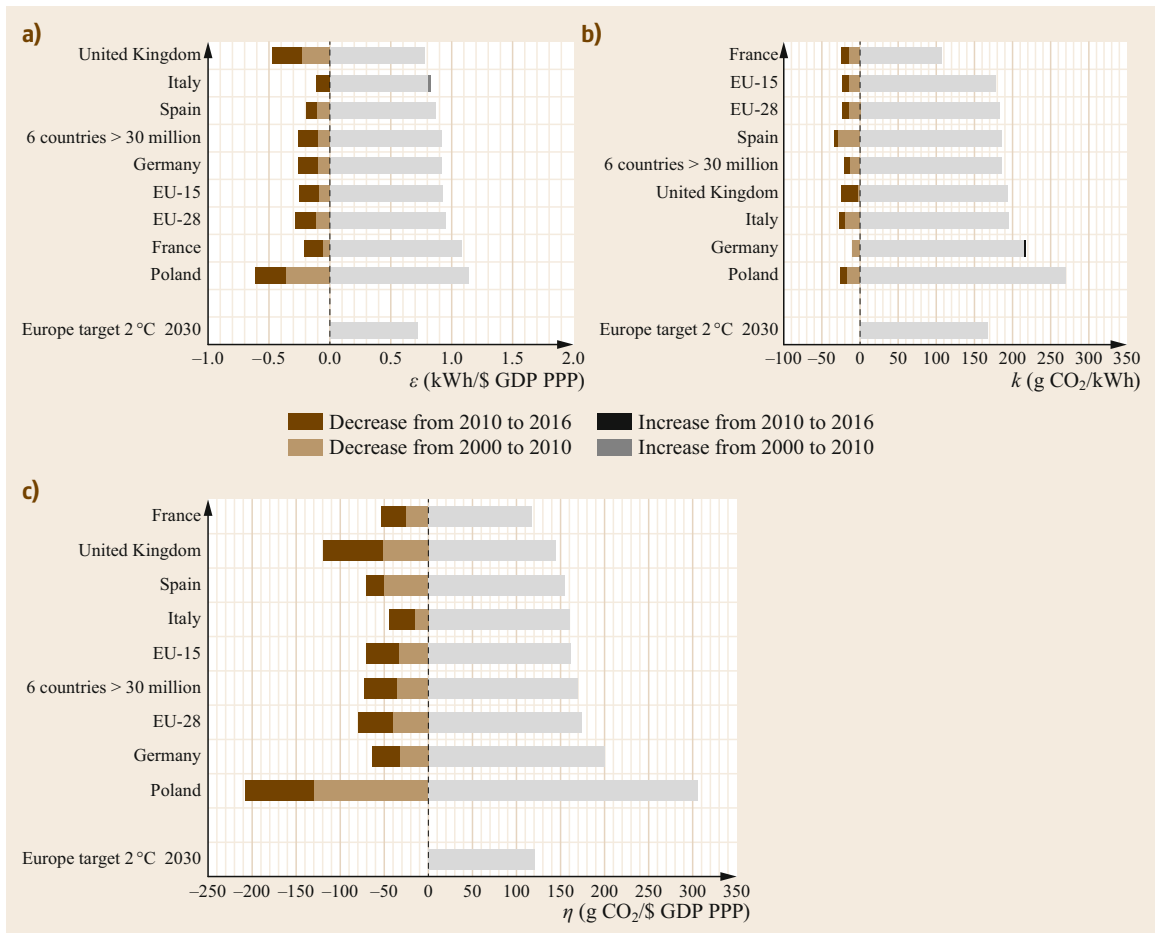


**Fig. 1.19** (a) Structure of the energy sector for the EU-15 in 2015 (627 Mtoe in total): electricity generated and district heating, thermal losses in power stations and cogeneration plants (broken down by type of energy source), electrical transmission losses, residual losses including the sector's own consumption (b) The corresponding CO<sub>2</sub> emissions (1000 Mt in total)

### 1.4.5 Countries With More Than 30 Million Inhabitants

The six European countries with more than 30 million inhabitants: Germany, France, the United Kingdom, Italy, Spain and Poland, accounted for a total of 358 million inhabitants in 2015, and achieved 70% of Europe-wide GDP (PPP). The corresponding energy gross demand was 1100 Mtoe. The detailed energy and emission diagrams of the six countries are given in [1.1,

Annex D] for 2013. Energy intensity, CO<sub>2</sub> intensity of energy and the index of CO<sub>2</sub> sustainability are shown in Fig. 1.20 and compared with the climate protection 2 °C target for 2030 of Europe [1.27, 28]. Thanks to the production of electricity from nuclear energy and thus a low CO<sub>2</sub> intensity of energy, France is closest to this goal at present. Poland has the most catching up to do in terms of both energy intensity and CO<sub>2</sub> intensity. Germany occupies the second-last place.



**Fig. 1.20** (a) Energy intensity  $\varepsilon$ , (b) CO<sub>2</sub> intensity of energy  $k$ , and (c) CO<sub>2</sub> sustainability  $\eta = \varepsilon k$  of the six largest European countries (population > 30 million), for 2016 (GDP PPP in \$ 2010); also given are the average values of the EU-15 and EU-28 in 2016 and the European averages necessary in 2030 for climate protection (2°C target)

## 1.5 Global Energy Demand

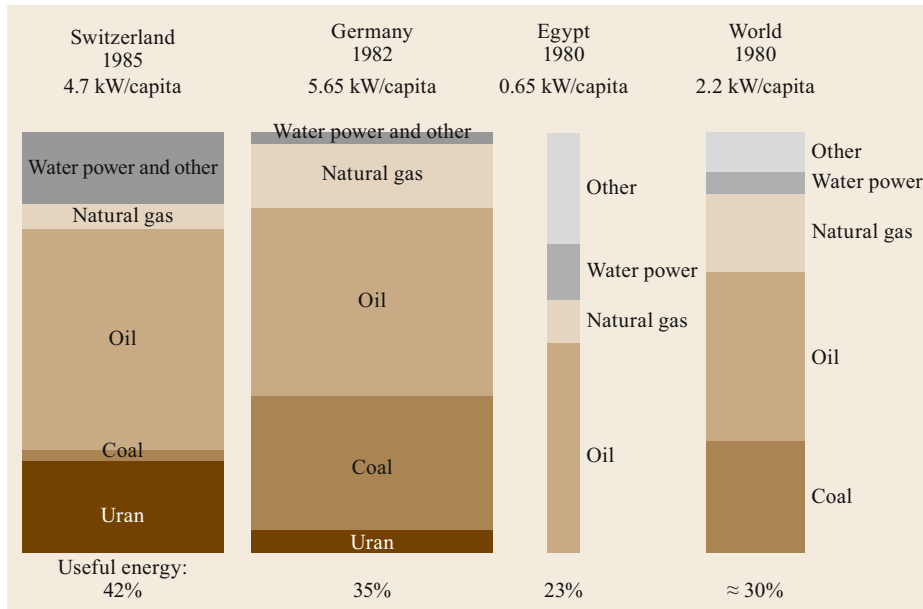
### 1.5.1 Energy Consumption in the Past

Figure 1.21 compares Switzerland's primary energy use and its distribution among energy sources with that of two other countries (the Federal Republic of Germany and Egypt) and the world as a whole [1.29]. The thickness of the column corresponds to the size of the per capita energy consumption.

Per-capita energy demand depends primarily on a country's level of economic development, but it is also influenced by the structural characteristics of the economy and the climate. According to official statistics, Switzerland has a slightly lower specific consumption than Germany, despite a higher gross national prod-

uct per inhabitant. It should be noted, however, that the statistics do not include the so-called gray energy. This is the balance of the energy expenditure for the production of imported minus exported goods or the provision of corresponding services. This import balance was estimated at 23% of gross energy for Switzerland [1.5]. A contrary example is Luxembourg, which has a considerable export balance. For large countries, gray energy is generally not too important.

Figure 1.21 shows Egypt as an example of a developing country. Per-capita consumption in 1980 was about one eighth of that of the developed Western European countries. The degree of utilization of this energy



**Fig. 1.21** Comparison of the primary energy consumption of some countries and the world. *Other* = wood and non-commercial energy sources [1.29]

(useful energy) is also lower. Not to be neglected are the non-commercial energy sources, which still cover a large part of the energy demand in developing countries. They include non-commercial biomass such as wood, vegetable waste, dried manure, etc.

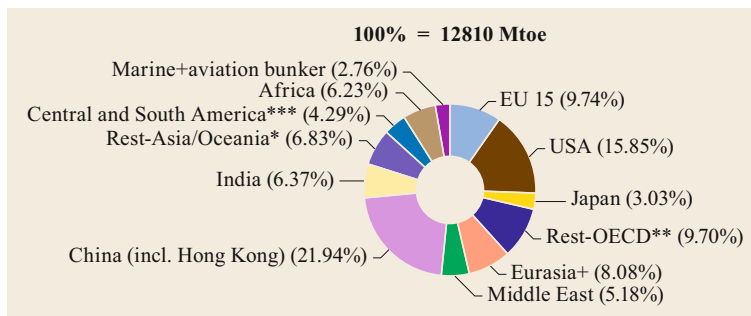
At the end of the century, global specific energy consumption, including non-commercial energy, was still 2.2 kW/capita (thanks to the collapse of the Soviet Union). In Egypt, it increased from 0.65 to 0.95 kW/capita. But there was still a gap between OECD and non-OECD countries. While the former claimed a good 6 kW/capita, the latter had to make do with an average of around 1.4 kW/capita.

Before fire was used, man needed on average 100 W of energy, which he took by means of food. With the use of fire, the amount of energy consumed increased to about 250 W. A sedentary farmer, who performs field work with the help of animals and primitive devices, already needs energy of the order of

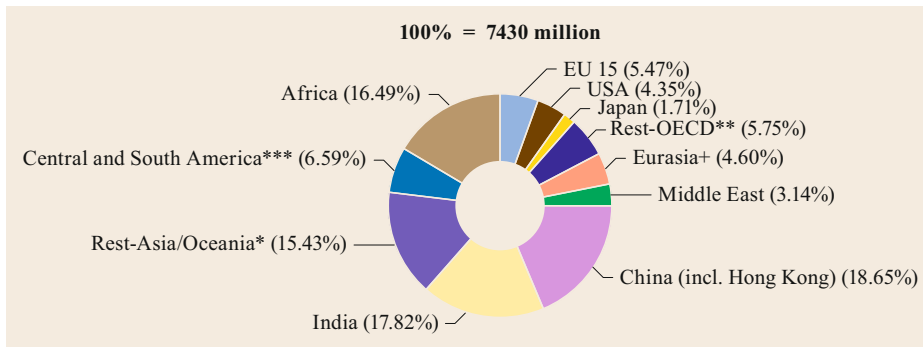
0.5 kW, the climate having a considerable influence on this figure. In Switzerland, per-capita energy consumption of commercial energy amounted to 1 kW in 1910. Due to the mechanization and industrialization process, the increased mobility and the increased demands on comfort, the specific energy consumption rose progressively by 2008 to around 10 kW primary energy in the USA and Canada, and to approx. 4.6 kW gross energy without and 5.6 kW with gray energy in Switzerland, which roughly corresponds to the OECD average and is not far from the Western European average.

### 1.5.2 Energy Demand, Population and GDP in 2016

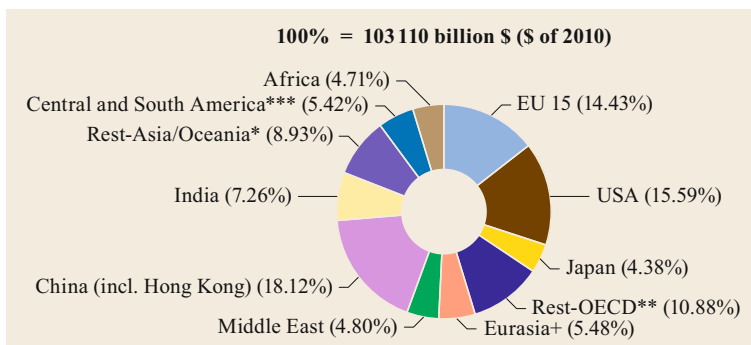
Figures 1.22–1.24 show the distribution of the global gross energy demand (gross domestic consumption) and the two most important influencing factors: popula-



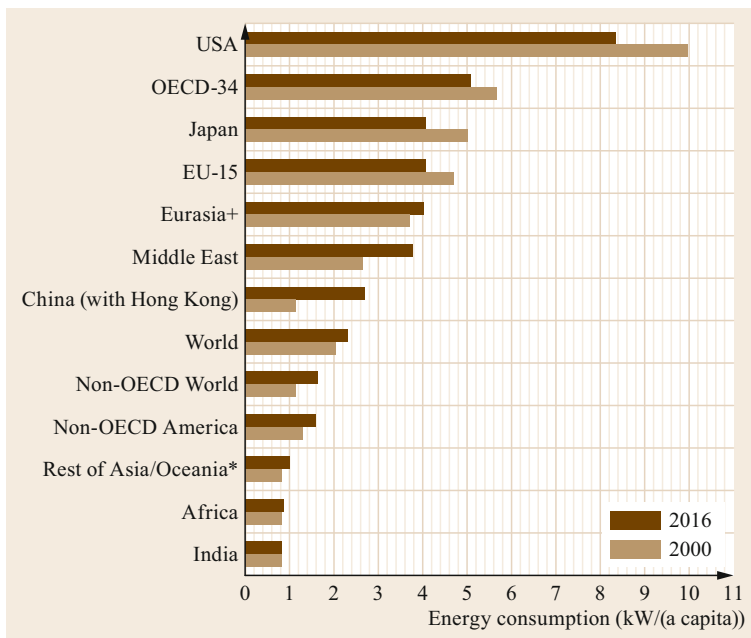
**Fig. 1.22** Worldwide distribution of gross energy consumption 2016; \* without China, India and OECD members, \*\* OECD without USA, Japan and EU-15, \*\*\* without Chile (OECD member)



**Fig. 1.23** World-wide distribution of the world population 2016; \* without China, India and OECD members, \*\* OECD without USA, Japan and EU-15, \*\*\* without Chile (OECD member)



**Fig. 1.24** Worldwide distribution of gross domestic product (adjusted for purchasing power), \$ of 2010; \* without China, India and OECD members, \*\* OECD without USA, Japan and EU-15, \*\*\* without Chile (OECD member)

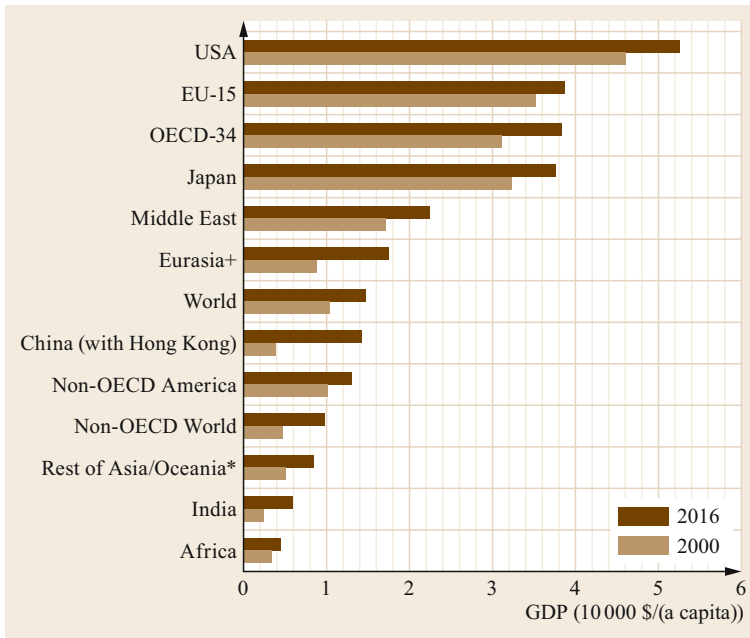


**Fig. 1.25** Gross energy consumption per capita in the world zones, 2000 and 2016, (1 kW/capita = 0.753 toe/(a capita)); \* Asia/Oceania without China, India and OECD members

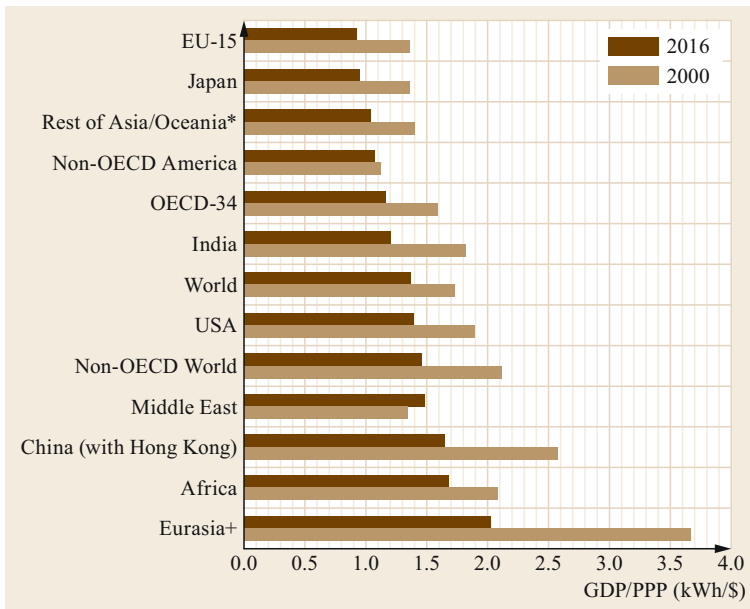
tion and GDP (the latter taking into account purchasing power parity). Figures 1.25–1.29 illustrate, for a number of countries or groups of countries, gross energy consumption per capita, GDP per capita, intensity of gross energy consumption, CO<sub>2</sub> intensity of energy and the CO<sub>2</sub> sustainability indicator.

The world zones considered are:

- EU-15: Germany, France, United Kingdom, Italy, Belgium, the Netherlands, Luxembourg, Austria, Ireland, Spain, Portugal, Greece, Sweden, Denmark and Finland



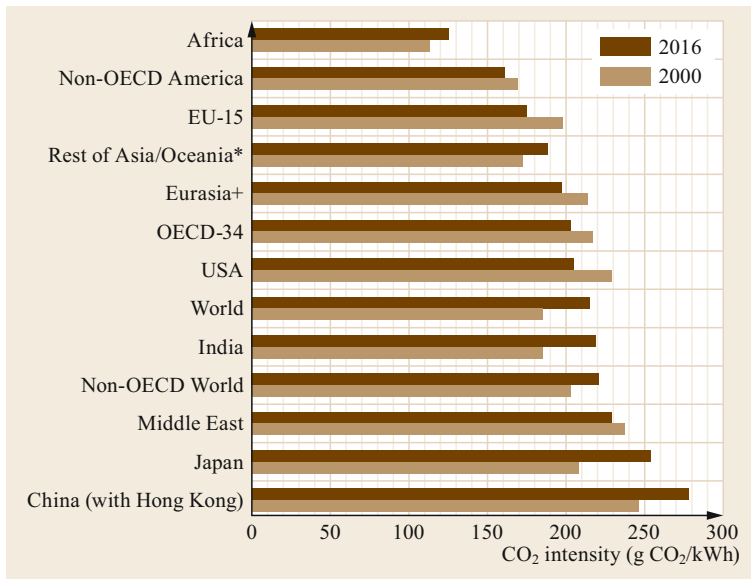
**Fig. 1.26** Gross domestic product per capita, 2000 and 2016 (PPP = purchasing power parity, US\$ of 2010); \* Asia/Oceania without China, India and OECD members



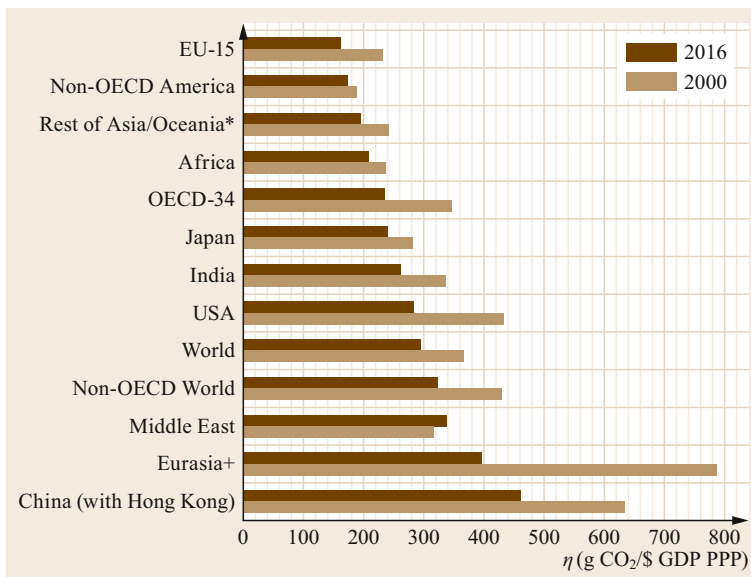
**Fig. 1.27** Energy intensity of GDP PPP (gross energy), 2000 and 2016 (US\$ of 2010); \* Asia/Oceania without China, India and OECD members

- OECD-34: EU-15, Slovenia, Czech Republic, Slovakia, Poland, Hungary, Switzerland, Norway, Iceland, Estonia, Turkey, USA, Canada, Mexico, Chile, Israel, Australia, New Zealand, Japan and South Korea
- Eurasia+: Eurasia (Russia, Ukraine, Belarus, Armenia, Georgia, Kazakhstan, Azerbaijan, Kyrgyzstan, Tajikistan and Turkmenistan and Uzbekistan) and non-OECD Europe (Lithuania, Latvia, Bosnia and Herzegovina, Croatia, Serbia, Kosovo, Montenegro, FYR Macedonia, Romania, Bulgaria, Albania, Cyprus, Malta and Gibraltar)
- China
- India
- Middle East
- Rest of Asia/Oceania (Asia excluding India, China and OECD Asia)
- Non-OECD America (Central and South America excluding Chile)
- Africa.





**Fig. 1.28** Worldwide CO<sub>2</sub> intensity of gross energy, 2000 and 2016; \* Asia/Oceania without China, India and OECD members



**Fig. 1.29** CO<sub>2</sub>-sustainability indicator  $\eta$  (adjusted for purchasing power), 2000 and 2016 (US\$ of 2010); \* Asia/Oceania without China, India and OECD members

The data sources are the reports of the IEA (International Energy Agency) and the IMF (International Monetary Fund) [1.30, 31]. The international \$2010 used corresponds to  $0.895 \times \$2005$  or  $1.087 \times \$2015$ .

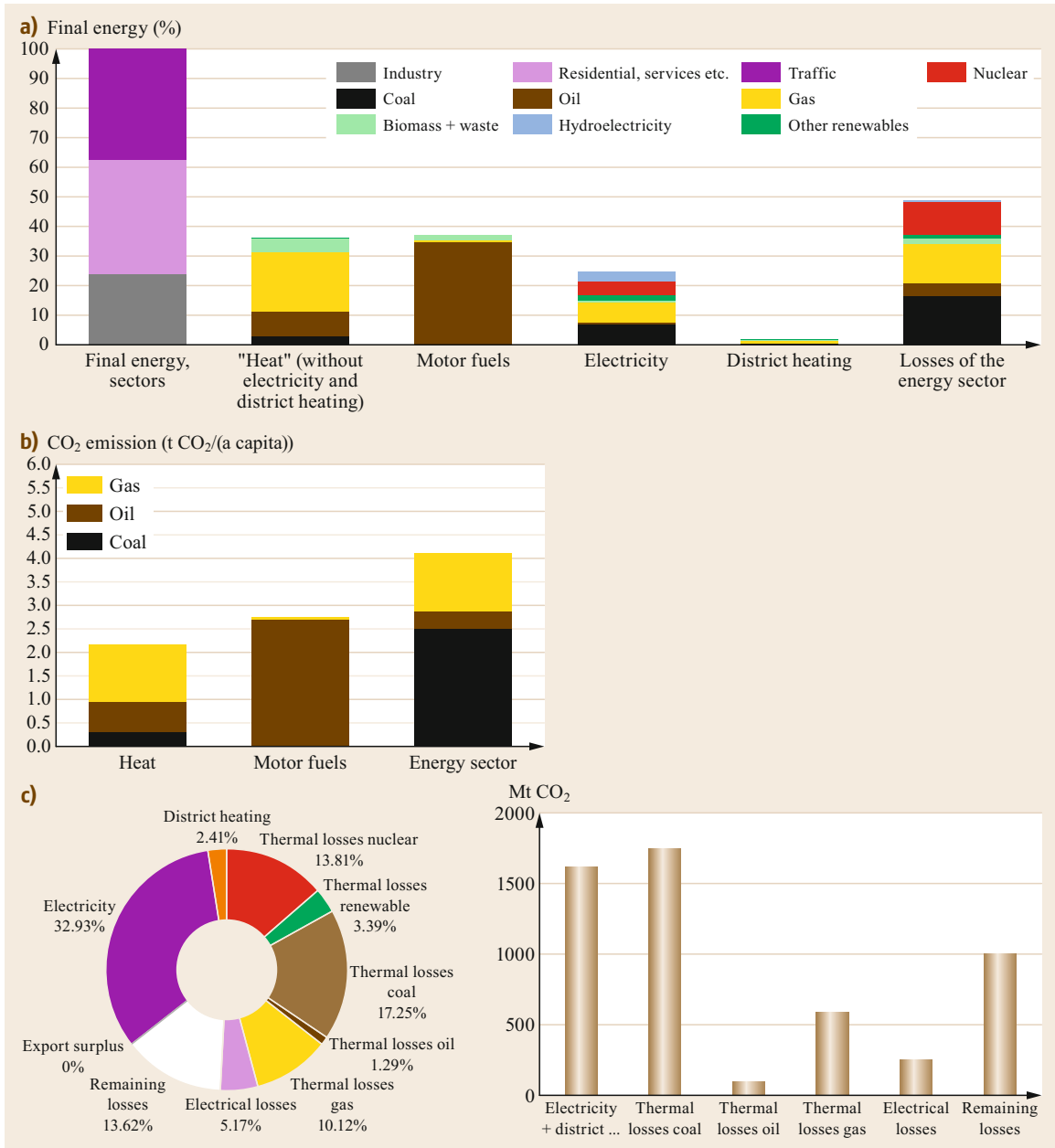
### 1.5.3 Primary and Final Energy and its Distribution 2016

Given the gap that separates the OECD countries from the rest of the world in terms of GDP per capita (Fig. 1.26), it makes sense to analyze the OECD world

and the non-OECD world separately. In addition to the EU-15 already analyzed, other countries or groups of countries within these groups are particularly important and interesting, such as the USA, India, China, the Middle East, Eurasia and Central and South America, which is why we also examine them closely.

#### The OECD Countries as a Whole

The OECD countries accounted for 17% of the world population in 2016 (Fig. 1.23), and consumed 38% of the primary energy (Fig. 1.22). Figure 1.30 illustrates



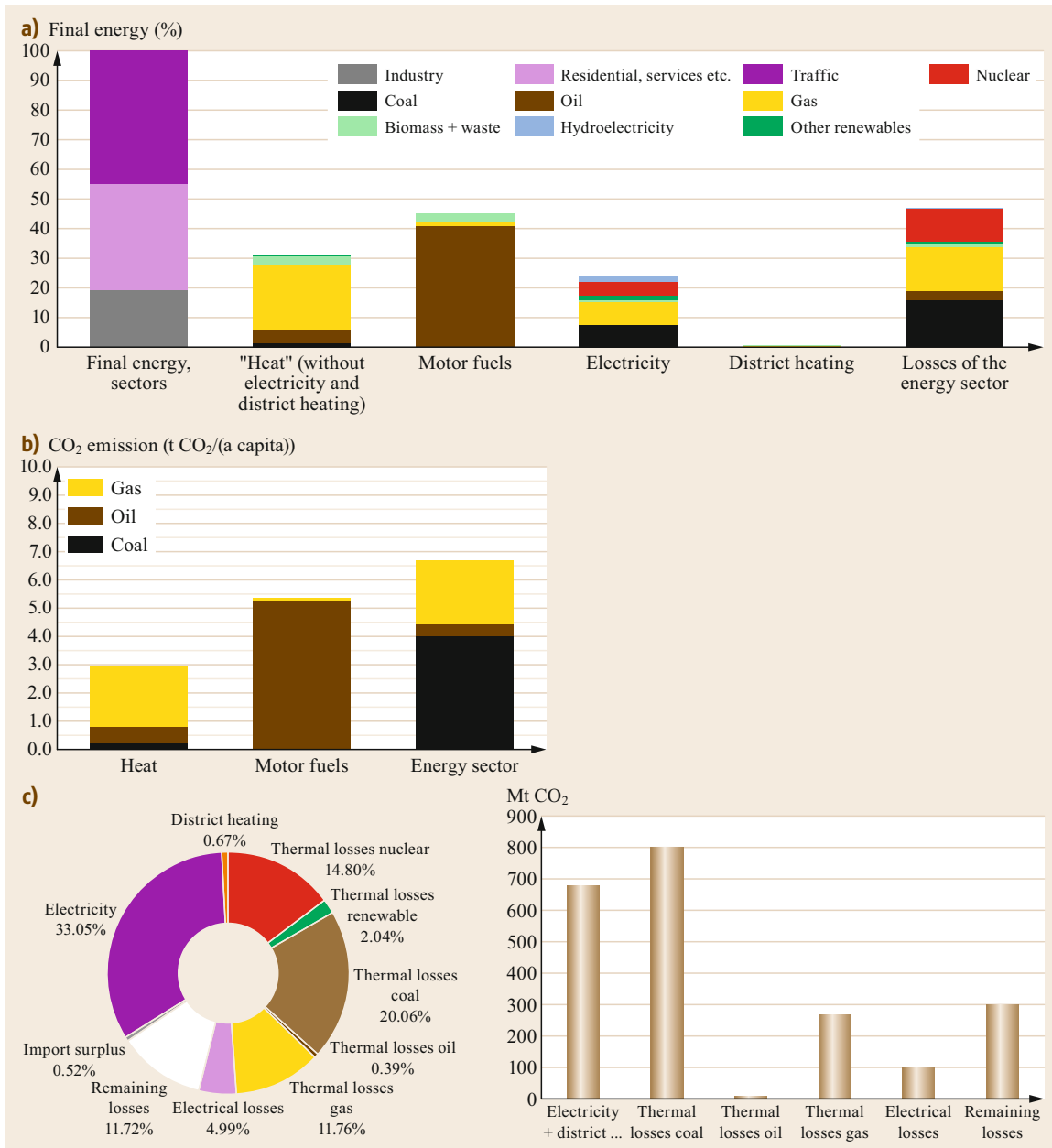
**Fig. 1.30a–c** OECD-34 in 2016: (a) Gross energy as the sum of final energy and losses of the energy sector (100% = final energy = 3303 Mtoe), (b) CO<sub>2</sub> emissions (11 591 Mt in total, 9.0 t/capita, 235 g CO<sub>2</sub>/\$ GDP PPP, US\$ of 2010), (c) Structure of the energy sector (2484 Mtoe in total) and CO<sub>2</sub> emissions of the energy sector (5287 Mt in total)

the energy structure and CO<sub>2</sub> emissions of the OECD area for the year 2016. Figure 1.31 shows the same for the USA (the most important OECD economy).

The structure of energy consumption in the OECD area is comparable to that of the EU 15 (Figs. 1.17–1.19). But although the share of electricity is about the same (just under 25%), it is even more coal-based and

has a lower share of renewable energies; this thus leads to larger coal-heavy losses in the energy sector and is primarily responsible for the poorer CO<sub>2</sub> balance sheet.

**USA.** Since the USA accounts for about 41% of the OECD’s primary energy (and thus just under 16% of the world’s energy demand), its behavior in connection

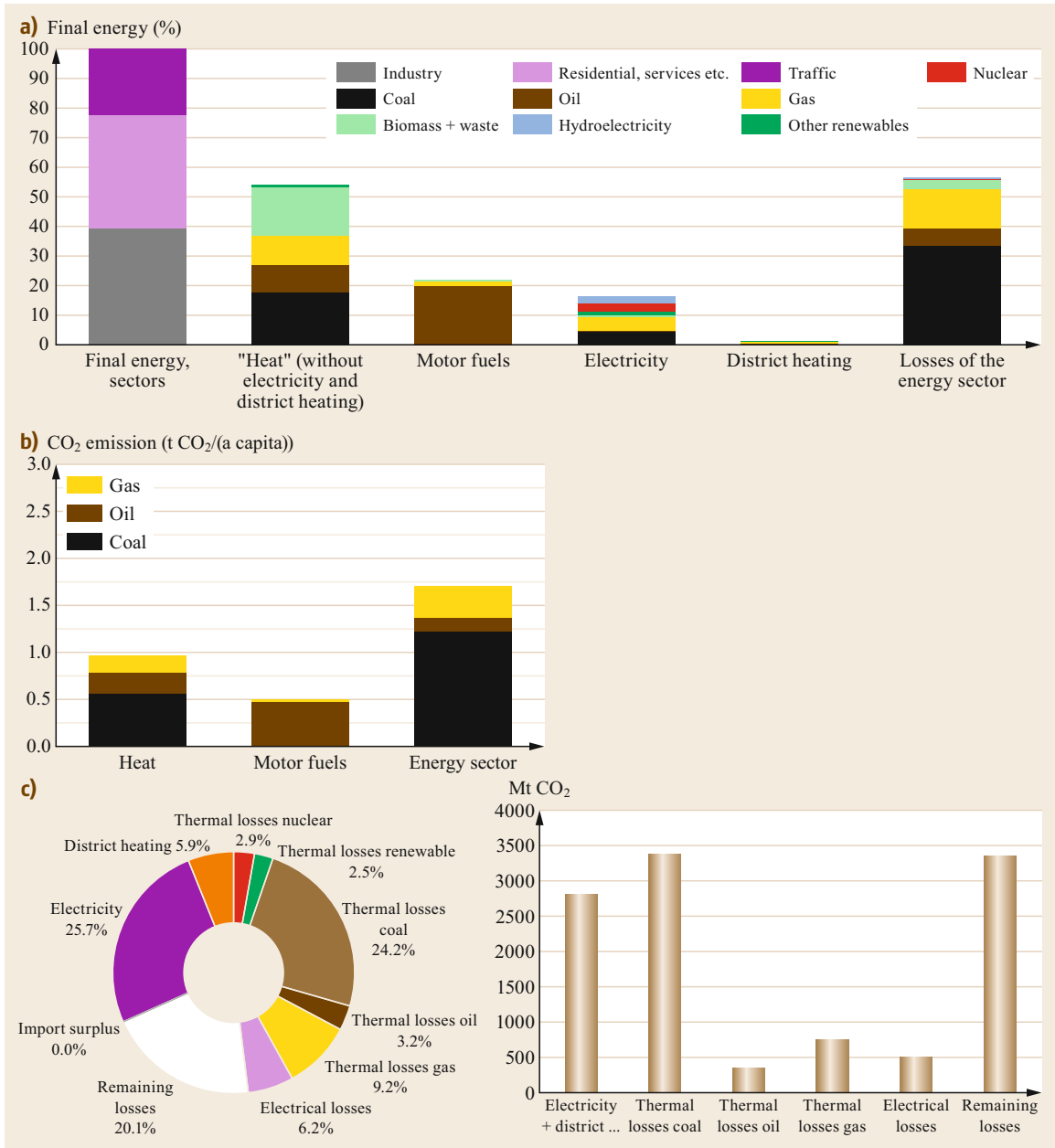


**Fig. 1.31a–c** USA in 2016: **(a)** Gross energy as the sum of final energy and losses of the energy sector (100% = final energy = 1379 Mtoe), **(b)** CO<sub>2</sub> emissions (4833 Mt in total, 14.9 t/capita, 284 g CO<sub>2</sub>/\$ GDP PPP, US\$ of 2010), **(c)** structure of the energy sector (986 Mtoe in total) and CO<sub>2</sub> emissions of the energy sector (2158 Mt in total)

with climate-protection requirements is of paramount importance.

Figure 1.31 shows the structure of energy consumption and the corresponding CO<sub>2</sub> balance sheet. CO<sub>2</sub> emissions per capita are 66% higher than the OECD average; the reasons in 2016 are: 38% higher GDP

per capita (PPP); 20% higher energy intensity; and 1% higher CO<sub>2</sub> intensity of gross energy (Table 1.8). This result is due to the transport sector (with more than 40% of the final energy being more important than the heating sector) and to electricity production, which is still strongly influenced by coal.

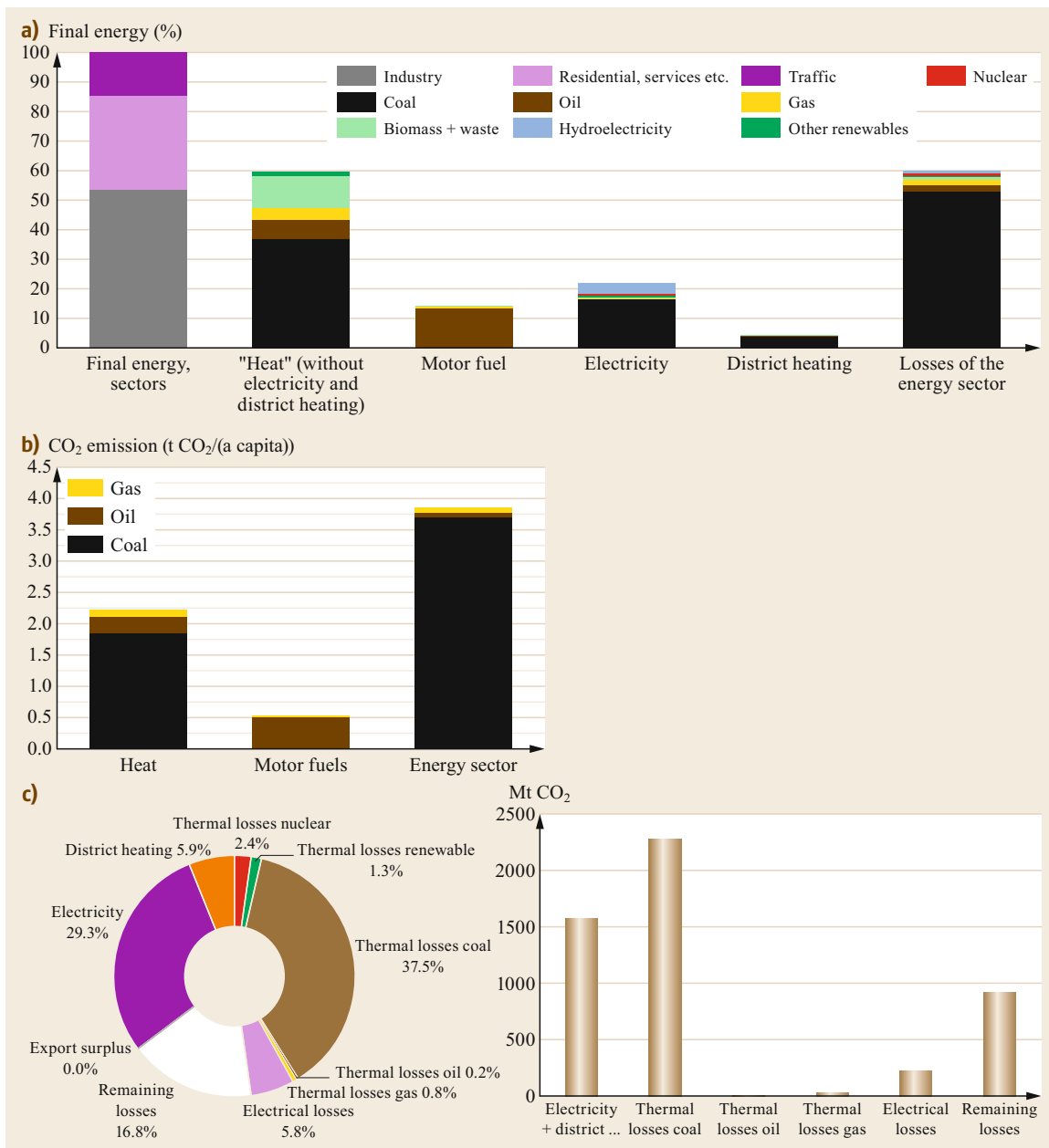


**Fig. 1.32a-c** Non-OECD world in 2016: **(a)** Gross energy as the sum of final energy and losses of the energy sector (100%  $\hat{=}$  final energy = 4985 Mtoe), **(b)** CO<sub>2</sub> emissions (19 485 Mt in total, 3.2 t/capita, 323 g CO<sub>2</sub>/\$ GDP PPP, US\$ of 2010), **(c)** Structure of the energy sector (3800 Mtoe in total) and CO<sub>2</sub> emissions of the energy sector (11 105 Mt in total)

### Non-OECD Countries

The non-OECD countries with a population of 6.15 billion (2016) consume only 51% more energy in total than the OECD countries (1.28 billion inhabitants). The energy structure is completely different, as the comparison between Figs. 1.30 and 1.32 illustrates.

About 55% of the final energy in the non-OECD world is consumed by heat applications. The corresponding CO<sub>2</sub> emissions are relatively small thanks to the high proportion of biomass. This is likely to change unfavourably in the future.

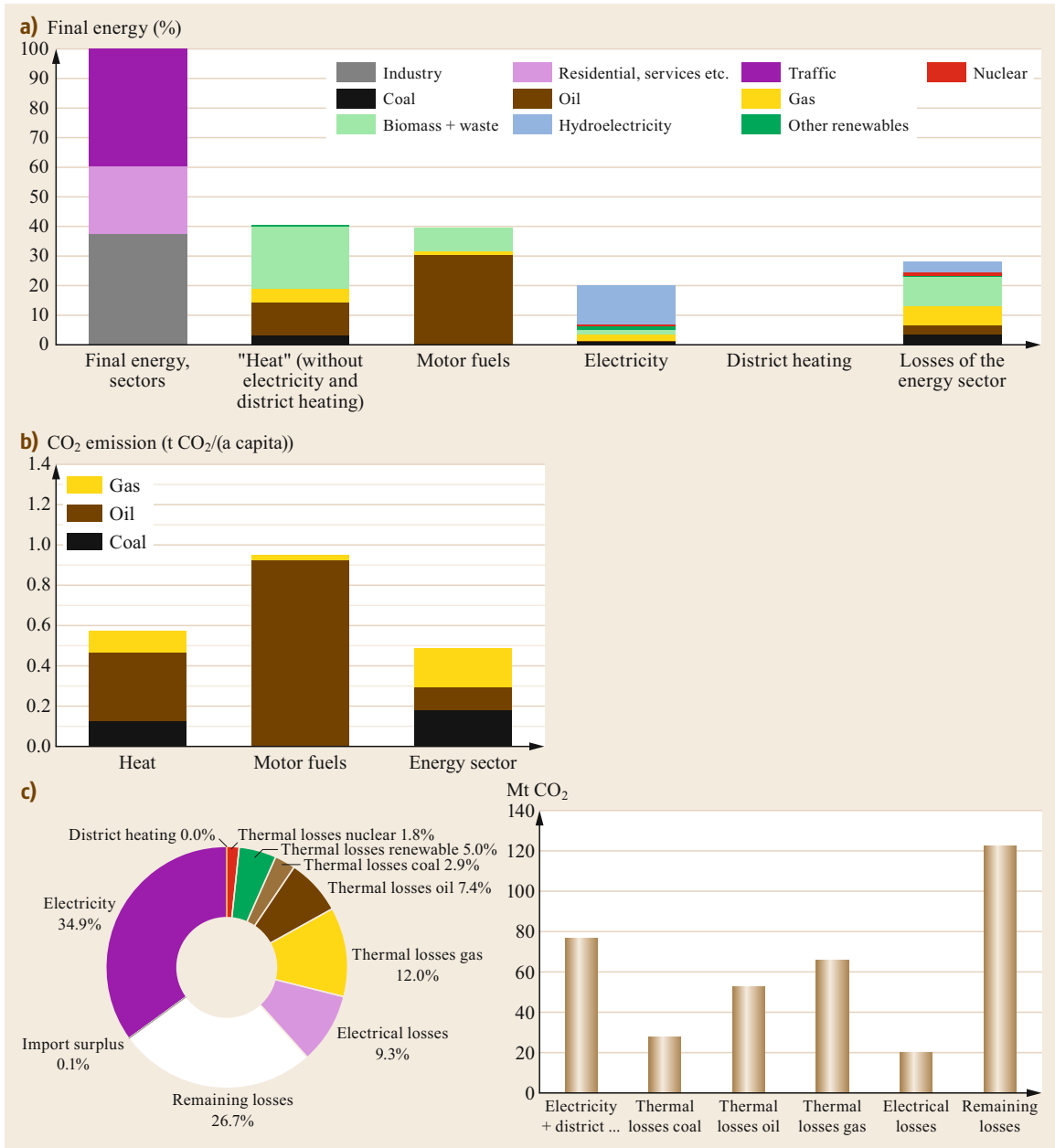


**Fig. 1.33a–c** China (with Hong Kong) in 2016: **(a)** Gross energy as the sum of final energy and losses of the energy sector (100% = final energy = 1816 Mtoe), **(b)** CO<sub>2</sub> emissions (9102 Mt in total, 6.6 t/capita, 461 g CO<sub>2</sub>/US\$ GDP PPP, US\$ of 2010), **(c)** Structure of the energy sector (1533 Mtoe in total) and CO<sub>2</sub> emissions of the energy sector (5084 Mt in total)

The same applies to fuels because mobility is subject to strong growth. The energy sector is coal-heavy, extremely inefficient and responsible for 55% of CO<sub>2</sub> emissions, although electricity accounts for only 21% of final energy.

Figures 1.33–1.35 illustrate in detail the energy consumption structure of the individual non-OECD world regions and the corresponding CO<sub>2</sub> emissions.

*China.* The structure of energy supply and the associated CO<sub>2</sub> emissions are illustrated in Fig. 1.33. China's



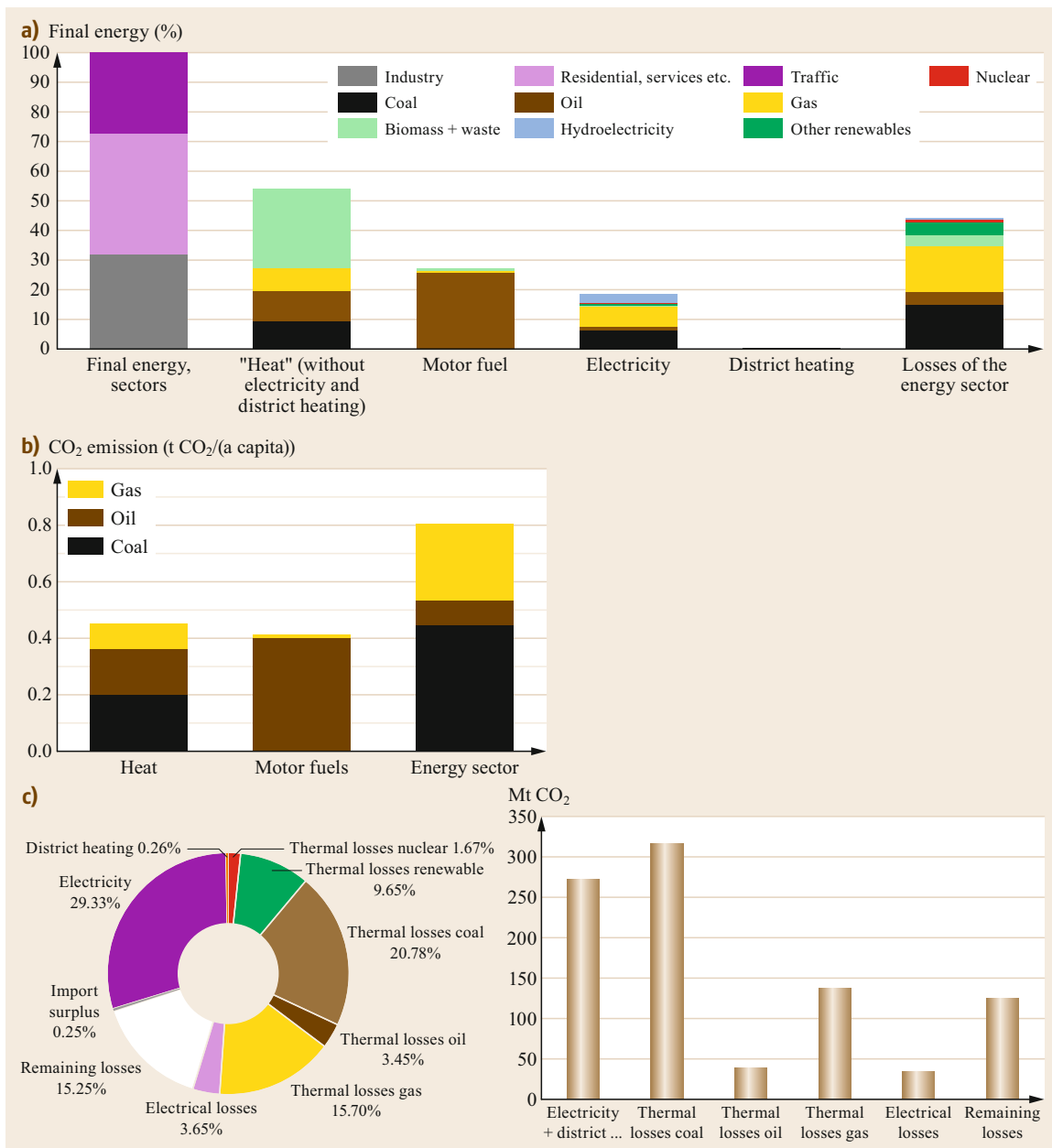
**Fig. 1.34a-c** Non-OECD America in 2016: **(a)** Gross energy as the sum of final energy and losses of the energy sector (100% = final energy = 430 Mtoe), **(b)** CO<sub>2</sub> emissions (1099 Mt in total, 2.2 t/capita, 173 g CO<sub>2</sub>/\$ GDP PPP, US\$ of 2010), **(c)** Structure of the energy sector (240 Mtoe in total) and CO<sub>2</sub> emissions of the energy sector (366 Mt in total)

gross energy demand in 2016 was about 22% of world demand, or 38% of that of non-OECD countries.

The heating requirement in 2016 is 60% of the final energy. The losses of the energy sector are very high and also reach 60% of the final energy demand. The relatively high CO<sub>2</sub> emissions are attributable to the high

consumption of coal (used to produce more than 80% of heat and 68% of electricity).

China ranks last in the CO<sub>2</sub> sustainability list (Fig. 1.29), with around 450 g CO<sub>2</sub>/\$, and is a key factor in the fight against climate change, given its size and increasing economic importance. Efficiency has



**Fig. 1.35a–c** Rest of Asia/Oceania in 2016: **(a)** Gross energy as the sum of final energy and losses of the energy sector (100% = final energy = 606 Mtoe), **(b)** CO<sub>2</sub> emissions (1910 Mt in total, 1.7 t/capita, 195 g CO<sub>2</sub>/\$ GDP PPP, US\$ of 2010), **(c)** Structure of the energy sector (383 Mtoe in total) and CO<sub>2</sub> emissions of the energy sector (922 Mt in total)

improved (Fig. 1.27) but strong efforts are needed to improve and to differentiate the energy sector, which today focuses almost exclusively on a conventional coal economy (Figs. 1.28, 1.29 and 1.33).

#### Characteristic Indicators

The main energy indicators, as defined in Sect. 1.3, are summarized and compared in Tables 1.5 and 1.6 for all groups of countries or countries analyzed and for the world as a whole.

**Table 1.5** Final energy consumption per capita ( $e_f$ ) and gross energy ( $e$ ) as well as total CO<sub>2</sub> emissions for country groups and countries, CO<sub>2</sub> emissions share of the energy sector in %, ordered by increasing  $e$ -value

2016	$e_f$ (kW/capita)	$e$ (kW/capita)	CO <sub>2</sub> (Mt/a)	CO <sub>2</sub> share of the energy sector (%)
India	0.53	<b>0.82</b>	2077	59
Rest of Asia/Oceania	0.70	<b>1.01</b>	1910	48
Non-OECD America	1.17	<b>1.59</b>	1099	33
World	1.55	<b>2.30</b>	32 177	49
China	1.74	<b>2.69</b>	9102	56
Middle East	2.34	<b>3.78</b>	1767	48
Eurasia+	2.40	<b>4.02</b>	2373	61
Japan	2.69	<b>4.06</b>	1147	55 <sup>a</sup>
EU-15 (2015)	2.80	<b>4.07</b>	2544	40
USA	5.77	<b>8.35</b>	4833	45

<sup>a</sup> high value due to the Fukushima incident (March 2011) and the subsequent shutdown of nuclear power plants

**Table 1.6** Worldwide characteristic energy indicators in 2016:  $y$  = GDP (PPP) per capita,  $\varepsilon$  intensity of gross energy,  $k$  = CO<sub>2</sub> intensity of gross energy;  $\eta = k\varepsilon$  CO<sub>2</sub> sustainability indicator (\$ of 2007)  $\alpha = \eta y/100$  = CO<sub>2</sub> emissions per capita; ranked by increasing  $\eta$ -value

2016	$y$ (10 <sup>4</sup> \$/(a capita))	$\varepsilon$ (kWh/\$)	$k$ (g CO <sub>2</sub> /kWh)	$\eta$ (g CO <sub>2</sub> /)\$)	$\alpha$ (t CO <sub>2</sub> /(a capita))
EU-15 (2015)	3.85	0.93	175	<b>164</b>	6.2
Non-OECD America	1.21	1.15	161	<b>173</b>	2.2
Rest of Asia/Oceania	0.85	1.01	188	<b>195</b>	1.7
Japan	3.76	0.95	254	<b>240</b>	9.0
India	0.60	1.20	219	<b>262</b>	1.6
USA	5.26	1.39	205	<b>284</b>	14.9
World	1.47	1.37	215	<b>294</b>	4.33
Middle East	2.25	1.48	229	<b>338</b>	7.6
Eurasia+	1.75	2.02	197	<b>397</b>	6.9
China	1.43	1.65	278	<b>461</b>	6.6

## 1.6 Future Development of World Energy Demand

Predictions in this area are, as the past has shown, difficult and often misleading, even using sophisticated econometric methods [1.10]. However, on the basis of the easily predictable development of the population and certain assumptions about the further development of the economy and the energy intensity of the individual regions of the world, scenarios can be generated that provide an overall picture of possible developments in world energy demand. These scenarios are options that society can choose by means of energy policy, taking into account economic, social and environmental constraints.

Let's start with a few simple considerations. At the turn of the millennium, world energy consumption (primary energy) was 2.2 kW/capita  $\times$  6 billion people  $\approx$  13 TW. During the last 20 years of the previous century, specific consumption has remained almost stable at around 2.2 kW/capita, a level which is mainly due to the collapse of the former Soviet Union in 1989. In 2007, the world energy demand, according to IEA, reached 2.26 kW/capita (with a world popula-

tion of 6.6 billion people, i.e., 15 TW) and increased to 18.2 TW or 2.45 kW/capita by 2016.

In the future, it will not be easy to maintain a value of 2–2.5 kW/capita or even to reduce it to 2 kW/capita (*2000 W-Society*). It is difficult to compensate the strong need to catch up in terms of GDP (PPP) of the developing countries by reducing the energy intensity of the already industrialized world. Scenarios promoting a specific consumption of 2 kW per capita were discussed in the 1980s within the framework of the WEC (then the *World Energy Conference*) in view of the CO<sub>2</sub> problem that was already becoming known [1.29]. In 1996 the World Energy Council predicted a global energy demand of around 3 kW/capita for 2020 [1.2], which would already correspond to a primary energy demand of 24 TW at this point in time for the expected world population of around 7.5 billion people.

The WEO 2006 of the IEA [1.7] envisaged two scenarios for 2030, which have already been mentioned in Sect. 1.2.1 *Future Demand*. The reference scenario, which corresponds to current trends, leads to a global



energy demand of 22 TW or 2.7 kW/capita. The alternative scenario, which requires the political will to reduce CO<sub>2</sub> emissions, leads to a total demand of almost 20 TW or 2.5 kW/capita (Fig. 1.3). Extrapolating this scenario up to 2050, for a world population of 9 billion people, a specific consumption of 2.75 kW/capita and a total consumption of 25 TW are obtained. However, this figure is hardly compatible with climate protection (for a more detailed analysis see Sect. 1.7). This is also the reason why the IEA, in the *Scenario 450* of 2009 for 2030, requires a total global consumption of 19 TW, which corresponds to 2.3 kW/capita. The latest 2015 Bridge scenario is similar, with a good 20 TWa. We start our study with assumptions about the two most important factors influencing the future world energy demand: population and GDP (PPP).

### 1.6.1 Development of the World Population

At the turn of the millennium, the world population was about 6 billion people. This is a doubling since 1960. Of these, approximately 1.5–2 billion people are materially privileged, while the remaining 4–4.5 billion have a long way to go to catch up. Demographic studies are largely in agreement that the world population, as in Fig. 1.36, will increase to at least 8 billion by 2030, and to about 9 billion people by 2050. By 2100, a progressive stabilization to about 10–11 billion people is predicted [1.32]. The population of today’s industrialized countries will grow relatively little, mainly through immigration, and that of the developing countries will increase considerably, even though the current war situation in the Middle-East/Africa shows a different picture.

### 1.6.2 Increase in GDP (PPP) and Energy Demand

Table 1.7 compares GDP for the year 2030 in the OECD, non-OECD countries and the world as a whole, as well as for the US and China: GDP per capita  $y$  (purchasing power adjusted (PPA), in \$ of 2010), intensity  $\varepsilon$  of the gross inland energy demand and the resulting per capita consumption of final and gross energy  $e_c$  or  $e$ . The figures are based on the indicator values required to meet the 2 °C climate target [1.29, 33, 34]. The lower value corresponds to a scenario with a lower CCS input, the upper value to a scenario with a higher CCS input. Both assume the same GDP (PPP), so they assume that the chosen energy policy will not have a major impact on overall economic development. The scenarios demand for coming years a *significant decrease in energy intensity* relative to 2016, anywhere in the world (Fig. 1.27).

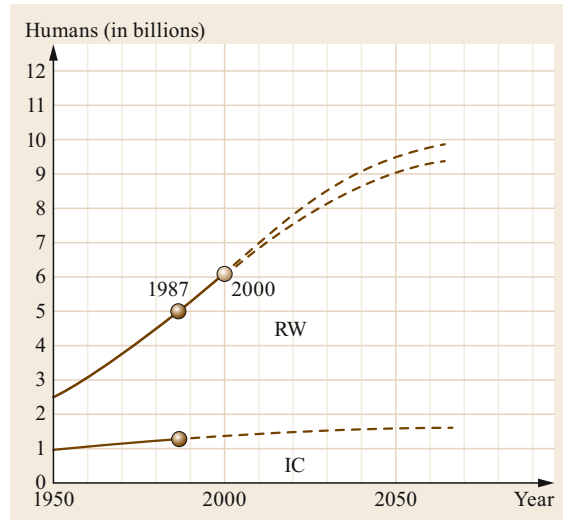


Fig. 1.36 World population growth since 1950 and forecast, IC = today’s industrialized countries (essentially OECD-34), RW rest of the world [1.29]

Table 1.7 Comparison of GDP (PPP)  $y$ , gross energy intensity  $\varepsilon$  and gross energy consumption per capita  $e$  for 2030 according to 2 °C target [1.27]

2030	$y$ ( $\times 10^4$ \$/(a capita))	$\varepsilon$ (kWh/\$)	$e$ (kW/capita)
OECD-34	4.2	0.9–1.0	4.5–4.7
Non-OECD	1.5	1.1–1.2	1.9–2.2
World	1.9	1.0–1.2	2.3–2.6
USA	5.7	1.0–1.1	6.5–7.2
China	2.6	0.9–1.2	2.7–3.2

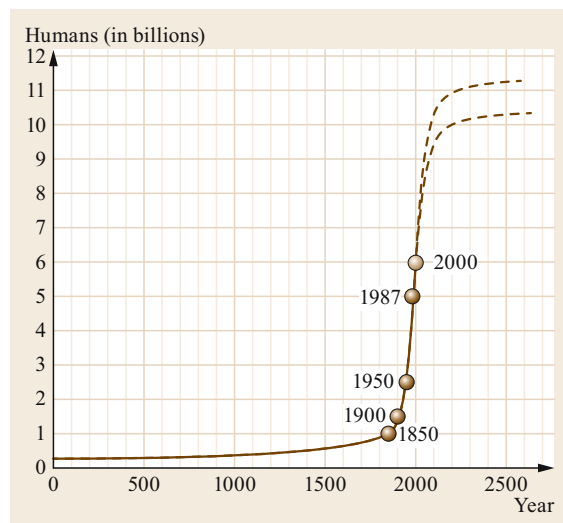


Fig. 1.37 Increase of the world population since the year zero of our time calculation and forecast of further development [1.29]

In the OECD countries, GDP/capita adjusted for purchasing power increases by 9% relative to 2016 and energy intensity decreases by an average of 20%, which essentially suggests a slight decrease in gross energy consumption per capita (−12% on average).

In the rest of the world (non-OECD countries), GDP/capita adjusted for purchasing power increased

by 80% relative to 2016 and an energy intensity decrease by 30%. So the gross energy demand per capita increased by an average of about 10%.

Worldwide, there is an average increase in GDP per capita of 50% and a decrease in energy intensity of just under 25%. The gross energy demand per capita is increasing on average by around 1%.

## 1.7 CO<sub>2</sub> Emissions and Climate Protection

Various climatological studies [1.35, 36] show that for climate protection, the increase in the earth's mean temperature relative to the pre-industrial era must be limited to 2 °C, or even better to 1.5 °C. The emissions reduction by 2100 necessary to reach the 2 and the 1.5 °C targets are shown in Fig. 1.38 [1.27]. To achieve the 2 °C goal, it is necessary to bring CO<sub>2</sub> emissions back to 2010 levels by 2030 (± 10%) and halve them by 2050. The variant *a* is primarily to be aimed at and would also allow a target of 1.5 °C, by a strong decrease gradient from 2030 to zero in 2050.

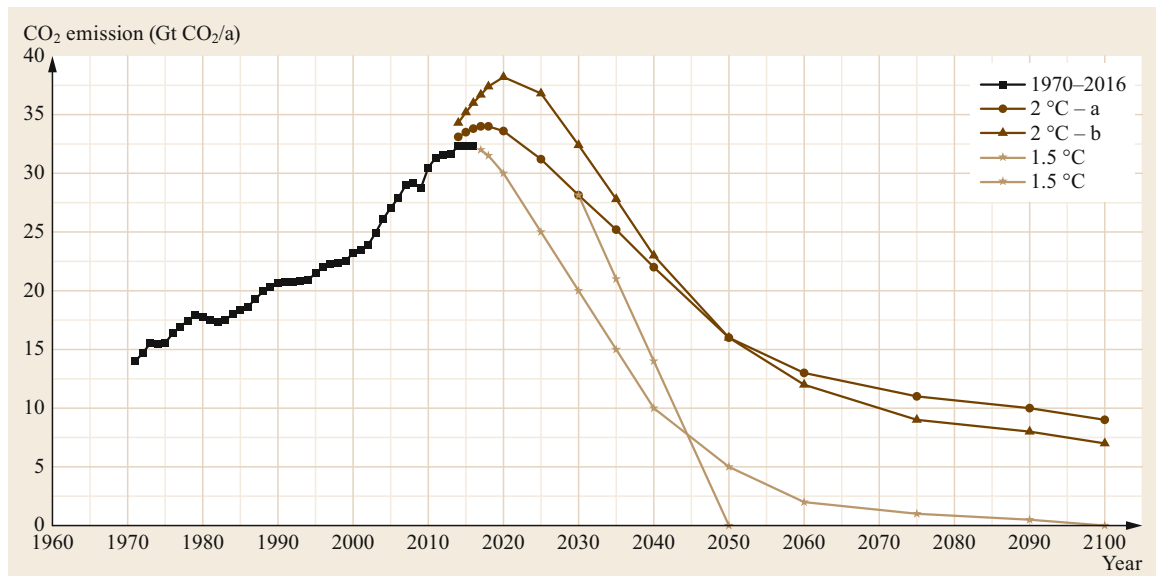
### 1.7.1 Climate Protection, Medium and Long-Term Measures

The most important measure for most OECD and also non-OECD countries, is the reduction of CO<sub>2</sub>-

emissions in the energy sector, which in 2016 accounts for around 50% of total global emissions (Table 1.5) and primarily concerns the generation of electricity. Exceptions are some European countries (France, Norway, Iceland, Sweden and Switzerland) as well as many Central and South American countries with a near CO<sub>2</sub>-free electricity generation. In 2016 their emission of CO<sub>2</sub> was already at or below 120 g CO<sub>2</sub>/\$ (Fig. 1.16). If this advantage is maintained, the efforts of these countries can focus on fuels for heating and transport.

#### Specific Energy Consumption and CO<sub>2</sub> Intensity

The CO<sub>2</sub> emissions per capita and year  $\alpha$  can be expressed as the product of specific energy consumption  $e$  and CO<sub>2</sub> intensity of gross energy  $k$  (Sect. 1.3.4). The gross world consumption in 2016 was around



**Fig. 1.38** Worldwide CO<sub>2</sub> emissions 1970–2016 and climate protection scenarios up to 2100 for 2 and 1.5 °C (cumulative emissions until 2100: 2 °C (< 800 GtC), 1.5 °C (< 550 GtC)); 2 °C scenario with variants *a* and *b*, 1.5 °C scenario with soft variant and hard variant starting 2030 from 2 °C scenario variant *a* [1.27, 28, 34]

**Table 1.8** Target values for gross energy intensity  $\varepsilon$ , CO<sub>2</sub> intensity  $k$  and CO<sub>2</sub> sustainability indicator  $\eta$  for 2030 Var.  $a$  of Fig. 1.38, [1.34]

2030	$\varepsilon$ (kWh/\$)	$k$ (g CO <sub>2</sub> /kWh)	$\eta$ (g CO <sub>2</sub> /)\$)
OECD	0.95	170	160
World	1.05	165	160
Non-OECD	1.1	160	175

2.3 kW/capita, with a factor of around three between the OECD and the non-OECD countries. If the global value is not to exceed 2.3 kW/capita by 2030, an emphatic reduction in the specific value of the OECD countries (2016: 5.1 kW/capita) is required in order to compensate the inevitable increase in that of the non-OECD countries (1.7 kW/capita), which is mainly associated with the expected strong increase in the GDP of this part of the world. An important step towards this is to increase the energy efficiency (reduce energy intensity) in the industrialized countries, but at the same time to make available to the developing and emerging countries, technologies for increasing energy efficiency.

Table 1.8 also shows, however, that increasing the efficiency is not enough for reaching the goals of climate protection set out in Fig. 1.38. It is equally important to achieve a large reduction in CO<sub>2</sub> intensity, that applies equally to OECD and non-OECD countries (Fig. 1.28).

#### The Life-Cycle Cost-Benefit and Grey Energy

These aspects are often brought into the CO<sub>2</sub> balance, making some CO<sub>2</sub>-free energies or energy uses appear to be less favorable. However, as regards the medium and long-term climate protection goals, this is, for the following reasons, not defensible:

**Life-Cycle Cost-Benefit Ratio.** A poor life-cycle cost-benefit factor does have a negative effect on the energy balance (and thus on the economic viability), but not on medium-term climate protection, provided that the energy required for manufacture and transport is also CO<sub>2</sub>-free, which is required in any case for the medium and long-term target.

**Grey Energy.** If the energy used in the manufacture of imported products causes greater emissions of CO<sub>2</sub> than that used for producing exported goods, the CO<sub>2</sub> balance of a country is in theory worsened. However, it does not make sense to include this in the sustainability balance. Each country is ultimately responsible for the energy used in the production of its goods and should

put the required climate protection measures in place using its own efforts or in the context of international agreements or emissions trading. But emissions trading should primarily be seen as development aid.

### 1.7.2 Electricity Consumption and Climate Protection

It has already been pointed out several times that the energy sector (which is largely determined by electricity production) has the main responsibility for global CO<sub>2</sub> emissions (around 50%). The objectives of climate protection can only be achieved if effective measures for CO<sub>2</sub>-free electricity production are brought in.

Figure 1.39 illustrates which energy sources have been used in 2016 to meet global electricity demand. Above all, the large proportion of coal (still 38%) is devastating for the CO<sub>2</sub> balance.

#### Countries With CO<sub>2</sub>-Intense Electricity Production

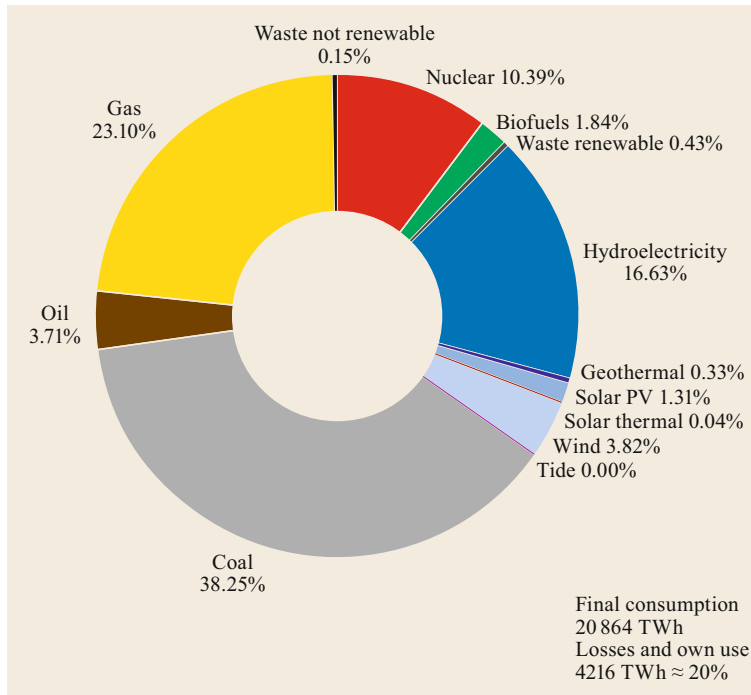
The most important countries in this group are the USA, China, India, Russia, Japan and in Europe Germany, the UK, Poland, Spain and Italy. Their electricity production is essentially dependent on coal (China and India) or heavily on coal and/or oil + natural gas (see also Figs. 1.30–1.35).

Figure 1.40 shows the structure of electricity production in three major countries: the USA, China and Germany.

Turning away from coal and oil as fast as possible or at least from the current way of using them is the *imperative basic requirement for effective climate protection*. The countries of the OECD should be able to achieve this, given the political will, using their own efforts, the emerging economies too with political support, and the developing countries presumably only with international support. This is made more difficult by the fact that the world demand for electrical energy is expected to increase by around 20% between 2016 and 2030.

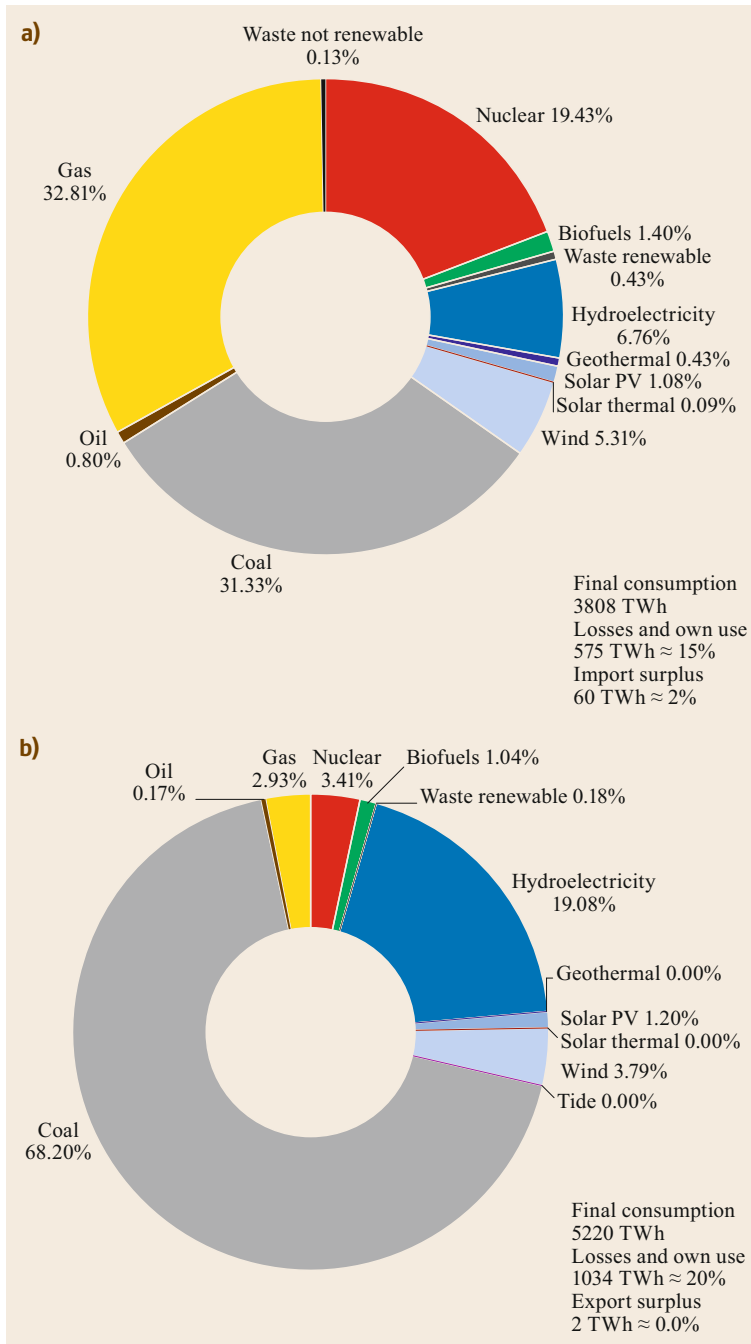
The possible measures and substitutions are as follows (a–h). It should be noted that it makes no sense to play one possibility off against the other in a fundamentalist way. All are necessary and must find their place within the framework of an economic, ecological and also political balance, which can vary from country to country and from continent to continent:

- a) Large reductions in losses in the energy sector by significantly increasing the efficiency of thermal power stations (combined heat and power, combined cycle generation).



**Fig. 1.39** Energy sources used for electricity production worldwide in 2016 (25 0852 TWh in total)

- b) CO<sub>2</sub> capture utilisation and storage (CCUS) in coal and oil-fired power stations; with a significant limitation: The CCS technology is not yet mature, is probably expensive and is not yet fully tested for environmental sustainability. Better is CCU, which allows to produce carbon neutral fuels by hydrogenating carbon exhaust gases with the help of renewables energies. Without CCUS, the 2-degree target, and even more the 1.5-degree target is difficult to achieve.
- c) Use of natural-gas power stations, substitution of coal and oil with natural gas: CO<sub>2</sub> emissions, compared to coal, are reduced to about 55% (compared to oil, to about 75%), with a restriction: worldwide gas reserves are limited. Fracking increases reserves, but its environmental risks have not yet been sufficiently clarified.
- d) Use of nuclear energy: the power stations do not emit CO<sub>2</sub>; restriction: reserves of uranium, used in 3rd-generation reactors, are also limited. Use of fourth generation reactors is possible, but must be well thought out, technically and politically. Nuclear fusion can only be considered in the second half of the century.
- e) Use of all opportunities to generate electricity from water power; restriction: the potential for this is limited.
- f) Use of wind energy: the technology is mature and, where the wind conditions are favorable, cost-efficient. The potential for this is very great. Restrictions: Networks and energy storage require considerable adjustments.
- g) Use of geothermal and biomass energy.  
Limitations: geothermal power stations are only suitable in locations with geothermal anomalies. In several parts of the world, however, the geothermal potential is very high.  
The potential of biomass is limited. Biomass including waste should therefore be used primarily, and provided its use is ecologically acceptable, for fuel in transport and heating, with the exception of local combined heat and power. The production of bio-fuels is often anything but CO<sub>2</sub> neutral
- h) Use of solar thermal energy and photovoltaics. Solar thermal power plants are appropriate only for countries with a low proportion of diffuse light. However, its potential in desert regions (e.g., the Sahara) is very great. HVDC (high-voltage direct-current transmission, see [1.24]) enables connection to consumption centres. Due to its unlimited and capillary exploitable potential, photovoltaics should continue to be promoted purposefully as long as necessary and economically justifiable, including through feed-in tariffs. Here, too, adjustments to the transmission and distribution grids are necessary, as is energy storage (partly also through load control).



**Fig. 1.40a–c** Structure of electricity production **(a)** in the USA (4322 TWh in total), **(b)** China (with Hong Kong) (6256 TWh in total) and **(c)** Germany (649 TWh in total) in 2016

**Remarks.** The great increase in electricity demand expected worldwide by 2030 can hardly be avoided, even by improving efficiency, for various reasons listed below. It is therefore unreasonable to rely only on the latter, however indispensable they may be. The use of natural gas and third-generation nuclear power plants is necessary, but at best does not enable much

more than the maintenance of their percentage shares (Fig. 1.40, worldwide 2016: natural gas 23%, nuclear energy 10%), but hardly the complete replacement of coal and oil-fired power plants (shares 41% and 4% respectively). The same applies to hydropower (17% share). The use of b) must therefore be examined; that of the remaining renewable energies f) to h) is indis-

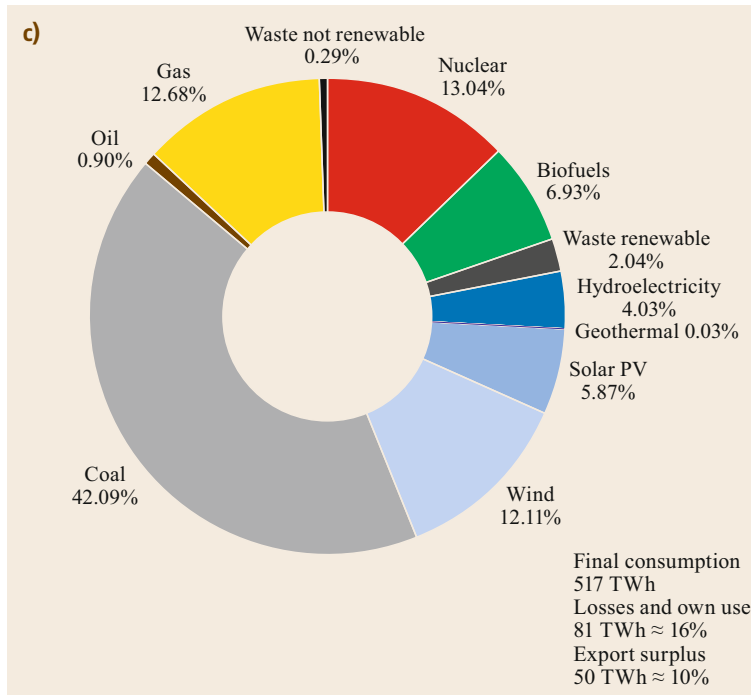


Fig. 1.40 (continued)

pensable and must be greatly increased (share 2016: 6%!). Although electricity from wind energy has multiplied worldwide, at 3.8% it is still a long way from being a significant source of energy.

#### Countries With Nearly CO<sub>2</sub>-Free Electricity Production

These countries have the great advantage of already having solved the most important emissions problem: Switzerland and Sweden with a mix of water power and nuclear energy, Norway with water power, Iceland with water power and geothermal power, France with mainly nuclear energy and Latin America mainly with water power. The first priority is naturally given to maintaining the freedom from CO<sub>2</sub> in the electrical energy sector, which can only be achieved by the measures d) to h). These countries already have the basic prerequisite and so they can be pioneers in the development and application of new technologies for limiting emissions in the areas of transport and heating. The areas will now be analyzed.

### 1.7.3 Transport

Emissions are almost entirely caused by the use of fuels obtained from mineral oil, which accounted for around 22% of world CO<sub>2</sub> emissions in 2016, and is steadily increasing (OECD 23%, non-OECD 15%). In the short

term the increase can be kept within bounds by improvements in efficiency (and the associated reduction of CO<sub>2</sub> emissions per km travelled), by electrification of traffic (electric and hybrid cars) and by partial substitution of petrol and diesel by natural gas and biofuels (for the latter ecological considerations are important and require further examination).

However, in the medium and long term, protection of the climate is possible only with a paradigm shift. The future is likely to belong to electromobility, the *pure electric motor* and the *hybrid solution* with the *electric motor as the primary drive* and an *internal-combustion engine as serial or parallel secondary module* to improve the range before recharging. The latter may, except with petrol or natural gas, be at least partially combined with *biofuels* provided that their production has a good CO<sub>2</sub> balance and is compatible with the food production required worldwide. Secondary operation with *solar gas* (fuel derived from syngas generated with solar energy) is also conceivable.

At least 75% of vehicles are driven for less than 50 km/day. The battery supplying the electric motor can then be charged overnight, which will at least enable urban traffic to be largely CO<sub>2</sub> free. The production of electrical energy in sufficient quantity and as far as possible free of CO<sub>2</sub> together with powerful batteries are the prerequisites for this change which will

therefore not happen immediately, at least not globally.

Using a *fuel cell* to supply the electric motor could also make a significant contribution in the long term; for this, however, hydrogen made using CO<sub>2</sub> free energy is required (Chap. 8).

The change is also imperative from purely economic considerations. The fuel for an efficient mid-range car with a consumption of, for example 6l petrol per 100 km (46 mpg, emissions of about 140 g CO<sub>2</sub>/km) currently costs about 8.4 €/100 km at a price of 1.4 €/l. The energy content of 6l petrol is 52.6 kWh and with an average efficiency of 20% this gives a mechanical power (useful energy) of about 10.5 kWh/100 km. The price of the mechanical drive energy is therefore today already (in Europe) at least 0.8 €/kWh and rising. With an electric motor and including the battery and the power electronics, an average efficiency of at least 65% can be achieved, giving, for the same useful mechanical energy of 10.5 kWh, an electricity consumption of at most 16 kWh/100 km. To achieve the same energy costs as with the combustion engine, the electrical energy from the mains socket for recharging the battery can cost 0.5 €/kWh or more. The corresponding comparison with diesel fuel gives 0.45 €/kWh. Consequently, the mains electricity *fuel* is already much cheaper in most countries than petrol or diesel and the time is not far off when photovoltaic electricity will be cheaper, even from small installations. Even when the extra power required for the heavier vehicle (because of the battery) is allowed for, there is a clear advantage in the energy costs.

The change is also necessary for purely economic reasons. The fuel for a very efficient mid-range car with a consumption of, e.g., 6l of petrol per 100 km (emissions approx. 140 g CO<sub>2</sub>/km) costs, at a price of 1.4 €/l, about 8.4 €/100 km. The energy content of 6l of petrol is 52.6 kWh and, with an average efficiency of 20%, results in a mechanical drive power (useful energy) of 10.5 kWh/100 km. The price of mechanical drive energy is therefore already today (at least in the European environment) at least 80 ct/kWh and is rising.

With the electric motor, together with the battery and power electronics, an average efficiency of more than 65% can be achieved, resulting in an electricity consumption of at most 16 kWh/100 km for the same mechanical drive energy of 10.5 kWh. In order to be on a par with the combustion engine in terms of energy costs, the electrical energy from the socket for charging the battery may therefore cost 50 ct/kWh or more. The analogous comparison with diesel fuel leads to at least 45 ct/kWh. As a result, in most OECD countries

(except the USA), the *fuel* electricity from the grid is already significantly cheaper than petrol or diesel, and the time is not far off when even electricity generated by photovoltaics in small systems will be cheaper. Even taking into account a power supplement for the greater weight of the electric car (battery), there is a clear advantage in terms of energy costs. Although the vehicle price is higher, it can be assumed that technical progress (Chap. 9) and mass production will reduce the price differential.

Whether a primary drive with solar gasoline or solar hydrogen will result in an economically better solution in the medium term is an open question, but is unlikely, due to the following disadvantages:

- The expected high fuel price, probably significantly higher than today's European gasoline price
- The low energy efficiency of the production chain solar energy–mechanical drive power, which will by far not reach that of the mains-operated electric drive.

#### 1.7.4 Heating

Energy for heating (excluding electricity) accounts for 27% of global CO<sub>2</sub> emissions. This applies almost equally to OECD countries (24%) and the rest of the world (30%).

*Heating for comfort* with the lowest emissions possible should not cause particular difficulties, given the appropriate promotion. Suitable means are: solar architecture and good insulation, solar collectors, biomass (wood) and, not least, district heating (combined heat and power) and, above all, the *heat pump* (for using environmental and geothermal heat). For the latter, the restriction applies that the most CO<sub>2</sub>-free electricity possible should be used (in Switzerland, Sweden, Norway and France conditions are almost ideal for this). This gives a new dimension to the importance of an adequate and low-CO<sub>2</sub> production of electricity. With a modern heat pump 25–30% of the heating energy is supplied by the electricity. The importance of the heat pump for heating is explained in more detail in Sect. 1.7.4 *Heat-Pump*.

For *process heat* the contribution from fuels should be reduced in favour of electricity (the most CO<sub>2</sub>-free possible) and the most emissions-free possible in industry by more efficient processes and the use of biomass, above all in the form of waste.

Let it be emphasized again that in the use of biomass, this is not CO<sub>2</sub>-neutral unless woodland clearance is compensated by new growth (preservation of forests and the rain forests in particular).

### Heat-Pump

Technical methods have been known for about 150 a to *pump up* heat by means of work from a low to a higher temperature level. The refrigeration machine has been using these methods for a long time: it extracts heat from the object to be cooled and pumps it up to a temperature slightly above the ambient temperature. Similarly, the heat pump removes heat from the environment and brings it to a temperature necessary for heating purposes.

The refrigeration machine quickly became popular as no other processes were available. The heat pump as a heating system, however, could not compete with conventional heating. Pioneering systems were, in the 1930s, built mainly in the USA and during the Second World War in Switzerland because of the shortage of coal. After the war, however, the heat pump was almost forgotten due to the onset of the oil boom. Only in the USA did it experience a renaissance in the 1950s and 1960s as a year-round air-conditioning unit (about 300 000 in use in 1963).

As a result of the 1973 oil crisis, interest in the heat pump returned everywhere in the second half of the 1970s, and it gradually began to become an alternative heating system.

From an exergy point of view, as well as in terms of energy efficiency, the heat pump clearly has advantages over other heating methods. In terms of sustainability, it is by far the best heating system. The relatively high installation costs compared to a boiler plant and cheap fossil fuels have so far worked against their use. The latter disadvantage should diminish more and more in the future.

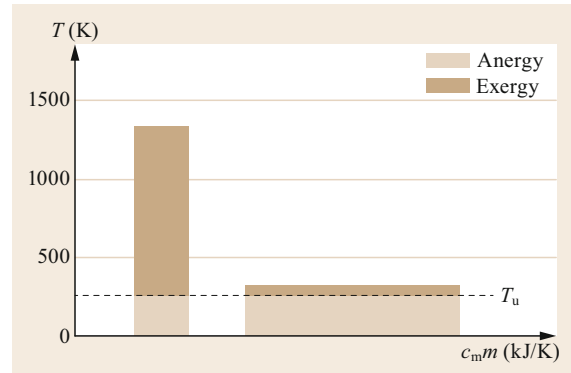
**Exergy Comparison.** The heat energy of a medium is expressed by the following relationship

$$Q = c_m m T \text{ (kJ)} \quad (1.4)$$

with  $c_m$  = average specific heat (KJ/(kg K)),  $m$  = mass (kg),  $T$  = absolute temperature (K).

The heat energy is represented by a rectangle in the  $(c_m m, T)$  diagram (Fig. 1.41), which clearly shows the exergy and anergy components [1.1, in Annex A, Sect. A.2.2] when the ambient temperature is entered. The exergy levels at combustion temperature and at low temperature applications are very different. At low-temperature, a larger mass or greater specific heat is necessary to store the same amount of heat.

In a conventional heating system (Fig. 1.42a), the large exergy content of the fuel is uselessly destroyed during the transition from A to B. The use of fuels



**Fig. 1.41** Heat content at combustion temperature and low temperature

(which have a high potential exergy content) to produce low-temperature heat is thermodynamically very wasteful.

If, for example, the following values are assumed:  $T_0 = 1300$  K,  $T_v = 340$  K and  $T_u = 280$  K and a conversion efficiency of  $\eta = 0.95$  in combustion and heat emission, the following exergy efficiency results

$$\eta_{ex} = \eta \frac{T_v - T_u}{T_v} \frac{T_0}{T_0 - T_u} = 0.21, \quad (1.5)$$

see also the energy flow diagram in Fig. 1.42b.

Heating with a heat pump is quite different. The analogous representation in Fig. 1.43a shows that only that exergy in the form of work is used, that is required for reaching the heating inlet temperature. The energy is supplied by the environment. With reference, e.g., to Fig. 1.43b, the thermodynamically much more favorable characteristic figures result (COP = coefficient of performance),

$$\text{exergetic efficiency: } \eta_{ex} = \frac{\text{useful exergy}}{\text{exergy}} \approx 0.55$$

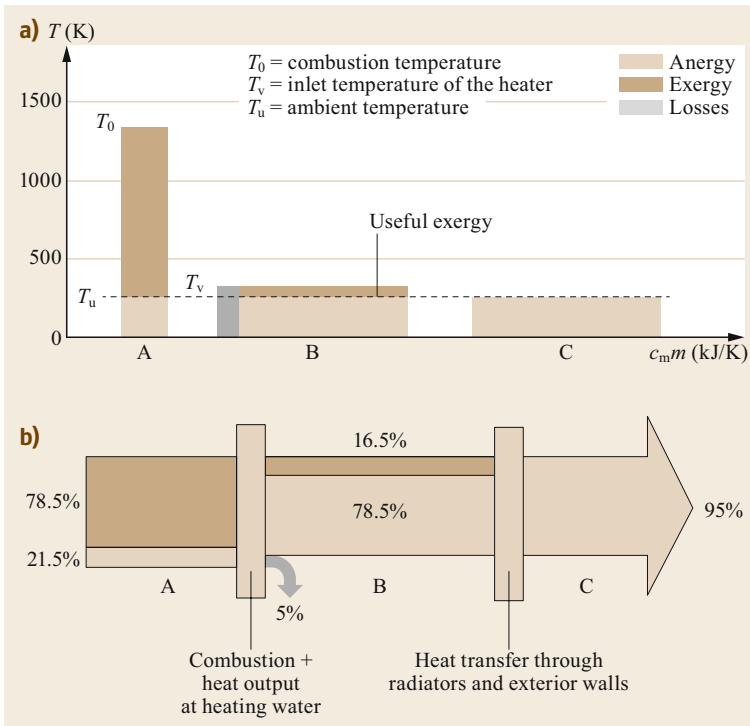
$$\text{COP of heat pump: } \beta = \frac{\text{useful energy}}{\text{work}} \approx 3. \quad (1.6)$$

**Comparison of Energy Utilization Degrees.** To assess the energy utilization degree, assumptions must be made about the origin of the work required to operate the heat pump. The degree of utilization is defined as

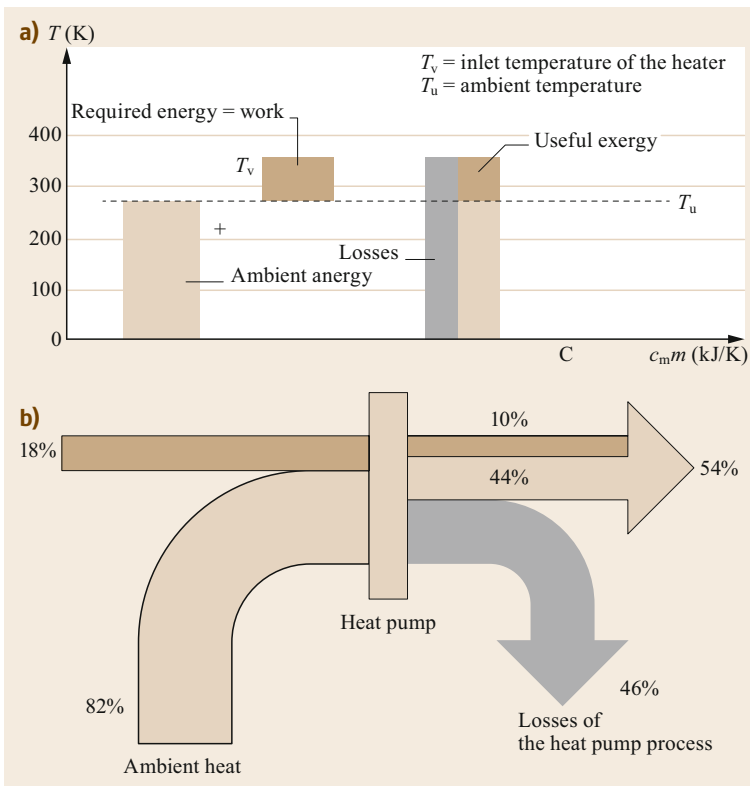
$$\eta_{use} = \frac{\text{useful energy}}{\text{required energy}}. \quad (1.7)$$

In the case of conventional heating, the degree of utilization is always  $< 100\%$  (for example, 95% in

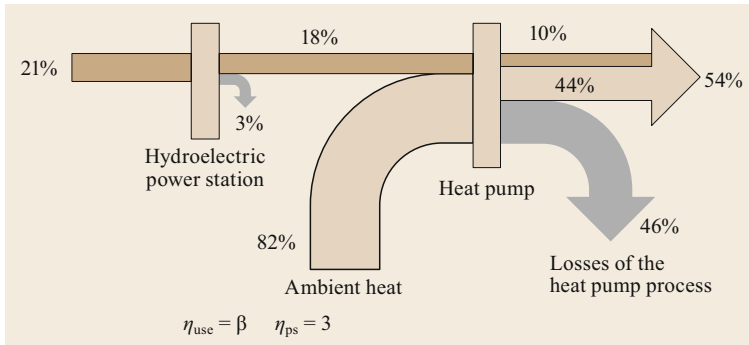




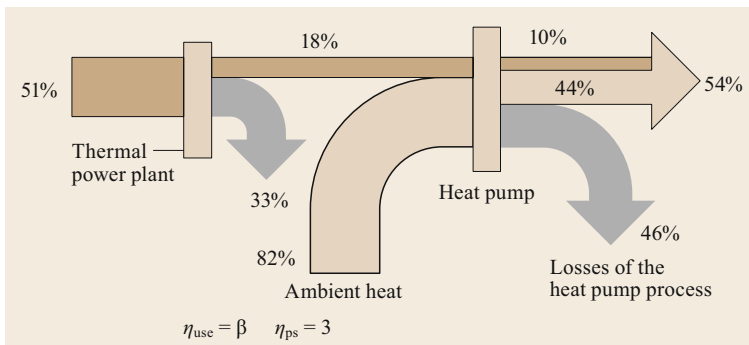
**Fig. 1.42** (a) Heat content, (b) Energy flow in conventional heating. A energy content of the fuel, B heat supplied to the heating system (useful energy), C final state of energy (pure energy)



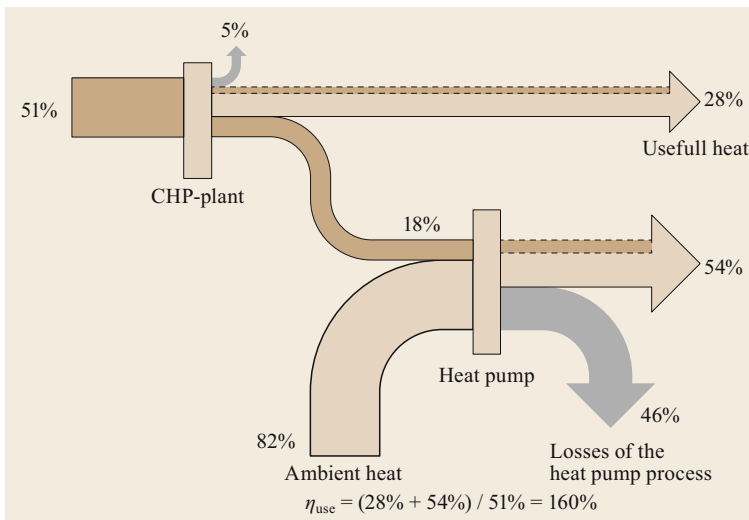
**Fig. 1.43** (a) Heat rectangle, (b) energy flow of the heat pump heating



**Fig. 1.44** Utilization degree of the heat pump heating with hydroelectric energy supply



**Fig. 1.45** Utilization degree of heat-pump heating with energy supply from a thermal power plant



**Fig. 1.46** Utilization degree of heat pump + CHP plant with power balance

Fig. 1.42). In the case of the heat pump, however, utilization rates much greater than 100% are the rule. Here are some examples:

- The electric drive energy comes from a hydroelectric power plant, which works with an efficiency of 85%. Figure 1.44 shows the flow diagram of Fig. 1.43b with a utilization rate of about 250%.
- The drive energy comes from a thermal power plant with an efficiency of 35%. Figure 1.45 then follows with a utilization rate of 105%. If the transmission losses in the network are taken into account, there is no significant advantage over conventional boiler heating.
- The heat pump is operated together with a heat-power cogeneration plant (CHP). Particularly interesting is the case of the *power balance*, in which

the CHP plant generates exactly as much electricity as is required to drive the heat pump. Assuming that the combined heat and power plant has an overall efficiency of 90% and generates 35% electricity, this results in a utilization rate of 160% (Fig. 1.46). With modern gas turbines and combined with district heating the utilization rate can reach 180% [1.1, Sect. 6.1.2])

**Conclusions.** The highest energy utilization degree is achieved with the combination hydropower-heat pump (e.g., small hydro powerplant and heat pump), which is also a very sustainable solution because it is CO<sub>2</sub>-

free. The same applies to the combination: power from another renewable energy (sun, wind)-heat pump.

The combination of heat pumps with conventional thermal power plants operated with fossil energies is pointless. In the case of nuclear energy or biomass, the utilization degree is not higher than that of conventional boiler heating, but the heat produced is CO<sub>2</sub>-free and the contribution to sustainability therefore considerable.

The combination of the heat pump with CHP plants has utilization degrees of well over 150% and therefore, even if it is not CO<sub>2</sub>-free, has a considerable potential for saving CO<sub>2</sub> (but only for countries with a high share of electricity production from fossil energy).

## References

- 1.1 V. Crastan: *Elektrische Energieversorgung 2*, 4th edn. (Springer, Cham 2017)
- 1.2 Swiss Energy Council: Swiss total energy statistics 1997, Bull. SEV/VSE **16** (1998), spec. ed.
- 1.3 Federal Office of Energy: Swiss Total Energy Statistics 2014, Bull. SEV/VSE (2014)
- 1.4 IEA: *WEO-2009 Excerpt: Climate Change* (International Energy Agency, Paris 2009), <https://webstore.iea.org/weo-2009-excerpt-climate-change>
- 1.5 IEA: *World Energy Outlook, Special Report: Energy and Climate Change* (International Energy Agency, Paris 2015), <https://webstore.iea.org/weo-2015-special-report-energy-andclimate-change>
- 1.6 IEA: *Key World Energy Statistics 2010* (International Energy Agency, Paris 2010), <https://webstore.iea.org/world-energy-outlook-2010>
- 1.7 IEA: *World Energy Outlook 2006* (International Energy Agency, Paris 2006)
- 1.8 British Petroleum: *BP Statistical Review of World Energy* (British Petroleum, London 1999)
- 1.9 BGR: *Reserves, Resources and Availability of Energy Raw Materials* (BGR, Hannover 1998)
- 1.10 G. Erdmann: *Energy Economics* (vdf Hochschulverlag, Zurich 1992)
- 1.11 H. Andruleit: *Reserves, Resources and Availability of Energy Raw Materials Study 2015* (BGR, Hannover 2015), [https://www.bgr.bund.de/EN/Themen/Energie/Produkte/energy\\_study\\_2015\\_summary\\_en.html?nn=1548106](https://www.bgr.bund.de/EN/Themen/Energie/Produkte/energy_study_2015_summary_en.html?nn=1548106)
- 1.12 World Energy Council (WEC): Statistics 1996, <http://www.worldenergy.org/wec> (2000)
- 1.13 D. Spreng: *Graue Energie* (vdf Hochschulverlag, Zurich 1995)
- 1.14 M. Kleemann, M. Meliss: *Regenerative Energiequellen [Renewable Energy Sources]* (Springer, Berlin, Heidelberg 1988)
- 1.15 K. Kugeler, P.W. Philippen: *Energietechnik [Power Engineering]* (Springer, Berlin, Heidelberg 1993)
- 1.16 Wikipedia: Geothermal energy, [https://en.wikipedia.org/wiki/Geothermal\\_energy](https://en.wikipedia.org/wiki/Geothermal_energy) (2016)
- 1.17 M. Kaltschmitt, A. Wiese, W. Streicher: *Erneuerbare Energien [Renewable Energies]* (Springer, Berlin, Heidelberg 2013)
- 1.18 A. Wokaun: *Erneuerbare Energien [Renewable Energies]* (Teubner, Stuttgart 1999)
- 1.19 Wikipedia: Marine current power, [https://en.wikipedia.org/wiki/Marine\\_current\\_power](https://en.wikipedia.org/wiki/Marine_current_power) (2016)
- 1.20 Wikipedia: Wave power, [https://en.wikipedia.org/wiki/Wave\\_power](https://en.wikipedia.org/wiki/Wave_power) (2016)
- 1.21 Wikipedia: Biomassepotential, <http://de.wikipedia.org/wiki/biomassepotential> (2016)
- 1.22 A. Goetzberger, B. Voss: *Solar Energy* (Teubner, Stuttgart 1997)
- 1.23 Wikipedia: Solar thermal energy, [https://en.wikipedia.org/wiki/Solar\\_thermal\\_energy](https://en.wikipedia.org/wiki/Solar_thermal_energy) (2016)
- 1.24 V. Crastan, D. Westermann: *Elektrische Energieversorgung 3*, 2nd edn. (Springer Vieweg, Wiesbaden 2018)
- 1.25 V. Crastan: *Global Energy Demand and 2-Degree Target, Report 2014* (Springer, Cham 2014)
- 1.26 V. Crastan: *Weltweite Energiewirtschaft und Klimaschutz [Global Energy Economics and Climate Protection Report]* (Springer, Heidelberg, Berlin 2009)
- 1.27 V. Crastan: *Klimawirksame Kennzahlen*, Vol. I (Springer Vieweg, Wiesbaden 2018)
- 1.28 V. Crastan: *Klimawirksame Kennzahlen*, Vol. II (Springer Vieweg, Wiesbaden 2019)
- 1.29 V. Crastan: *Die Energiepolitik im Spannungsfeld von Ökologie und Fortschritt [Energy Policy in the Field of Tension Between Ecology and Progress]* (Gassmann, Biel 1989)
- 1.30 IMF: *World Economic Outlook Database* (IMF, Washington 2018), <https://www.imf.org/external/pubs/ft/weo/2018/02/weodata/index.aspx>
- 1.31 IEA: *Africa Energy Outlook* (International Energy Agency, Paris 2019), <https://www.iea.org/search/?q=Afrika#gsc.tab=0&gsc.q=Afrika2019&gsc.sort=>
- 1.32 DSW: *World Population, Development and Projections* (German Foundation for World Population, Hannover 2002), <https://www.dsw.org/weltbevoelkerung/>
- 1.33 V. Crastan: Climate change, an analysis of the global energy industry, Bulletin SEV/VSE **19** (2007)
- 1.34 V. Crastan: *Weltweiter Energiebedarf und 2-Grad-Klimaziel [Worldwide Energy Demand and 2-Degree*

- 1.35 *Climate Target*] (Springer Vieweg, Berlin, Heidelberg 2016)
- 1.36 Stocker T (2007) The Earth in a greenhouse, Bulletin SEV/VSE (2007), p. 1
- 1.35 IPCC: *AR5 Synthesis Report: Climate Change 2014* (Intergovernmental Panels on Climate Change, Genf 2014)

---

**Valentin Crastan**

Evilard, Switzerland  
[valentin.crastan@bluewin.ch](mailto:valentin.crastan@bluewin.ch)



Dr-Ing Valentin Crastan is professor emeritus. After practical and managerial work in energy technology companies (Brown Boveri/ABB, Baden, Swiss electricity and transport company (Suisselectra), Basel), he has been appointed professor of energy systems and control engineering at the Bern University of Applied Sciences, Engineering and Computer Science, Biel. He also served as the Dean of the Department of Electrical Engineering/Communications for nine years.

# Power Generation

## 2. Power Generation

Valentin Crastan

The 1.5 °C climate target calls for rapid elimination of coal and oil for electricity production and the progressive reduction of the contribution of natural gas. This demands an enormous effort in the energy sector for the production of electricity using CO<sub>2</sub>-free energy sources. This chapter discusses five ways to generate electrical energy as sustainably as possible. The resulting grid stability problems are briefly outlined.

Hydropower (Sects. 2.1–2.6) is one of the most important sources of energy for generating electricity. It is also ecologically sound (no CO<sub>2</sub> emissions) if the plant construction (river dams, reservoirs) respects nature and human settlements appropriately. In 2016, hydropower installations accounted for 16.6% of global electricity production. This section provides an overview of the planning, engineering and modeling of hydraulic power stations.

The efficiency of power generation from fossil fuels in thermal power plants has risen considerably over time and today reaches almost 60% in natural gas-powered, combined cycle power plants (Sect. 2.7). Nevertheless over 40% of the energy is still lost as waste heat. In *combined heat and power* (CHP), useful heat is produced in addition to electrical energy, thus further increasing overall energy efficiency.

The potential of wind energy (Sect. 2.8) and the prerequisites for its economic use have already been briefly discussed in Sect. 1.2.3. This section deals in more detail with the technical and economic aspects of wind-energy use.

In Sect. 2.9 the basics of photovoltaics (photoelectric effect) and solar cells (structure, types, characteristics, efficiencies) are given. To use them optimally requires knowledge of the radiation intensity and thus the calculation of the apparent movement of the sun relative to the Earth. Photovoltaic is the renewable energy with the highest potential worldwide.

Fuel cells (Sect. 2.10) can be used to convert hydrogen as well as natural gas and other hydrocarbons (e.g., petrol, methanol) or biogas

electrochemically directly into electrical energy. It is predictable that in the course of the next decades this technology will open up a wide range of applications for *mobile* and *stationary* applications.

2.1	<b>Hydroelectric Power Stations</b> .....	47
2.2	<b>Hydrological Planning Principles</b> .....	49
2.3	<b>Run-of-River Power Stations</b> .....	50
2.3.1	Water Management .....	51
2.3.2	Execution .....	51
2.3.3	Design .....	51
2.4	<b>Storage Power Stations</b> .....	53
2.4.1	Daily and Weekly Storage .....	53
2.4.2	Annual Storage (Seasonal Storage) .....	54
2.4.3	Pump Storage .....	56
2.5	<b>Water Turbines</b> .....	56
2.5.1	Pelton Turbine .....	57
2.5.2	Reaction Turbines .....	59
2.5.3	Turbine Selection .....	65
2.5.4	Small Hydropower Plants .....	66
2.6	<b>Dynamics</b> .....	66
2.6.1	Pressure Tunnel .....	67
2.6.2	Surge Chamber .....	67
2.6.3	Rigid Penstock .....	68
2.6.4	Overall Model of the Hydraulic System ...	68
2.6.5	Elastic Pressure Surge .....	69
2.6.6	Overall Model of the Hydraulic System with Elasticity .....	72
2.6.7	Turbine and Hydroelectric Plant Model ..	72
2.7	<b>Thermal Power Stations</b> .....	76
2.7.1	Combined Heat and Power Generation ..	76
2.7.2	Fossil-Fired Steam Power Plants .....	78
2.7.3	Nuclear Power Plants .....	84
2.8	<b>Wind Power</b> .....	93
2.8.1	The Kinetic Energy of Wind .....	93
2.8.2	Wind-Turbine Types and Their Performance .....	95
2.8.3	Horizontal-Axis Wind Turbines .....	97
2.8.4	Modern Horizontal-Axis Wind Turbines ..	99
2.8.5	Other Types of Wind Turbines .....	99
2.8.6	Operation and Control, Design .....	103

2.9	<b>Photovoltaics</b> .....	105	2.10	<b>Fuel Cells</b> .....	124
2.9.1	Physical Basics, Photoelectric Effect.....	105	2.10.1	Structure and Fuel Cell Types.....	124
2.9.2	Photovoltaic Effect, Photocurrent.....	107	2.10.2	Principles and Modeling.....	125
2.9.3	Solar Cell, Overall Efficiency.....	110	2.10.3	Fuel Cells for Stationary Applications...	127
2.9.4	The Sun as a Source of Energy.....	117	<b>References</b> .....		129

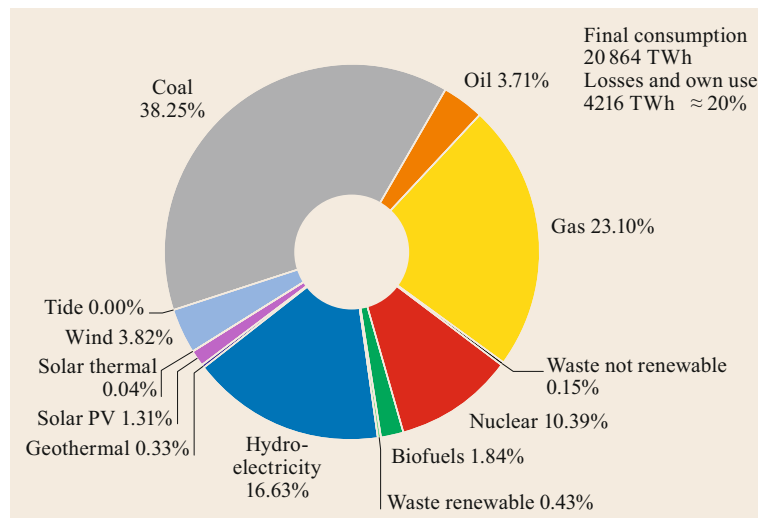
The 1.5°C climate target calls for rapid elimination of coal and oil for electricity production and the progressive reduction of the contribution of natural gas. However, the demand for electricity will continue to increase worldwide, not only because of economic growth, but also because of the increased use of heat pumps for heating buildings, the progressive electrification of mobility and the increasing use of synthetic power to gas (PtG) generation as a natural gas replacement. This requires an enormous effort in the energy sector for the production of electricity using CO<sub>2</sub>-free energy sources. This chapter discusses ways to generate electrical energy as sustainably as possible.

Figure 2.1 shows the current distribution of energy sources used worldwide for electricity production. Due to the high proportion of fossil fuels, electricity production accounts for nearly half of global CO<sub>2</sub> emissions (Fig. 2.2).

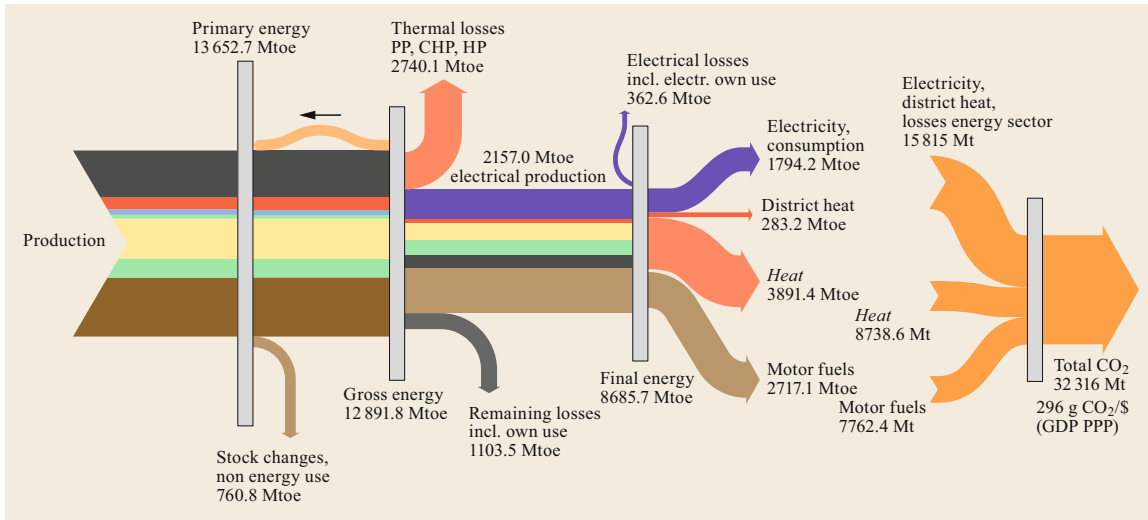
In view of the climate problem, the sections on *hydropower, wind energy and photovoltaics* are paramount. Wind energy and, above all, photovoltaics have enormous potential, but also a temporal *variability*, that represents a big challenge to the control systems for frequency maintenance and grid stability. Because of the bi-directionality of the energy flows, this variability also requires general strengthening of local and transmission grids. *Hydroelectricity* has a very good growth potential in many developing countries and is

indispensable there for primary and secondary regulation of the electricity grid. *Pumped-storage plants* are being used less and less to convert inexpensive nighttime energy into expensive peak energy, as the rising solar energy share reduces the cost of daytime energy, but they remain an essential element for rapid compensation of the variability of wind and solar energy.

Fossil-based *thermal power plants* will be less and less able to take over this work, as their share is likely to be reduced as quickly as possible if climate goals are to be achieved, even if CCS (carbon capture and storage) technology can bring some relief. Combined heat and power generation (CHP) plays an indispensable role in improving efficiency. Although *geothermal or biomass* (wood from forests, waste, landscape maintenance and industrial residues) *power stations* are, or can be, CO<sub>2</sub>-neutral, their capacity is limited, with the exception of certain parts of the world (with big geothermal resources such as Indonesia and certain areas of America). The *power to gas* (PtG) processes for the *synthetic production of CO<sub>2</sub>-free hydrogen or gas* are very interesting for the decarbonization of the transport sector (hybrid long-distance vehicles and air traffic), but also require, due to poor conversion efficiencies, large amounts of electricity that worldwide can only be generated with big photovoltaic systems in sunny regions (e.g., Sahara, Middle East) and require, if local gas production is not appropriate, suitable transmission grids.



**Fig. 2.1** Energy sources used for electricity production worldwide in 2016, 25 082 TWh in total (see Chap. 1)



**Fig. 2.2** Energy flow in the energy sector and total CO<sub>2</sub> emissions from fossil fuels (with marine and aviation bunkers), worldwide in 2016. PP: power plants; CHP: combined heat and power; HP: heat plants; *Heat*: heating and process heat of non-electrical origin, without district heat (may contain non-electrical stationary work, in developed countries usually minimal) (adapted from [2.1, 2])

Since the decreasing use of thermal power stations will reduce their grid control ability, other methods of grid control will be needed. Thus, the importance of the *flexibilization of the load* is constantly increasing. Through appropriate digital controls and intelligent use of storage, the demand for electricity in the field of industry, building technology and mobility can be adjusted in terms of time and be frequency dependent, thus making a contribution to grid stability. Similarly, the supply from *photovoltaic systems and wind turbines* can be adjusted to the grid requirements (smart and micro grids). Above all, *medium and large photovoltaic power plants* (more and more are needed in the evolution to a CO<sub>2</sub>-free en-

ergy supply) can and must replace the inertia of the generators of thermal power plants with a virtual inertia of inverter-to-grid coupling, with *appropriate controllable storage units*, and thus make an important contribution to the primary and secondary regulation of the grid [2.3].

Regulation through *nuclear power plants* has been enforced in France with a flexibilization of the power output (inevitably, because of the very large share of NPPs in power generation), but in principle light-water reactors have, for physical and economic reasons, only limited suitability for primary control within seconds; their flexibility is possible but is associated with disadvantages.

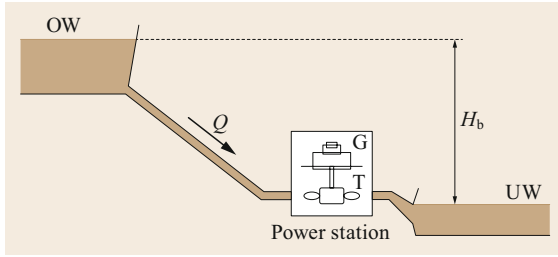
## 2.1 Hydroelectric Power Stations

Hydropower is one of the most important sources of energy for generating electricity. It is also ecologically sound (no CO<sub>2</sub> emissions) if the plant construction (river dams, reservoirs) respects nature and human settlements appropriately.

In 2016, hydropower installations accounted for 16.6% of global electricity production (for Europe see Table 2.1). This section provides an overview of the planning, engineering and modeling of hydraulic power stations.

**Table 2.1** Europe 2016, share of hydroelectric power in electricity production in %

Austria	62.8	Estonia	0.3	Iceland	72.6	Malta	0	Slovakia	17.0
Belgium	1.7	Finland	23.0	Ireland	3.2	Netherlands	0.1	Slovenia	29.0
Bulgaria	10.1	France	11.7	Italy	15.3	Norway	96.2	Spain	14.5
Croatia	55.1	Germany	4.0	Latvia	39.4	Poland	1.6	Sweden	39.8
Czech Republic	3.8	Greece	10.2	Lithuania	24.5	Portugal	28.1	Switzerland	58.1
Denmark	0.1	Hungary	0.8	Luxembourg	69.6	Romania	28.5	United Kingdom	2.5



**Fig. 2.3** Basic diagram of a hydropower plant: OW headwater, UW tailwater,  $H_b$  gross head,  $Q$  water flow, T turbine, G generator

The basic scheme shown in Fig. 2.3 can be used for any hydropower plant, whether it is a run-of-river or a storage power plant.

Due to the stagnation of the water, there is a fall height or gross head  $H_b$  (m) between the upper pool (the headwater) and the lower pool (the tailwater). The gross gradient varies somewhat depending on the amount of water present. The nominal gross head usually refers to the maximum quantity of usable water  $Q$  ( $\text{m}^3/\text{s}$ ) for which the system is dimensioned. The gross power  $P_b$  of the power plant is then

$$P_b = \rho Q g H_b \left( \frac{\text{kg}}{\text{m}^3} \frac{\text{m}^3}{\text{s}} \frac{\text{m}}{\text{s}^2} \text{m} = \frac{\text{J}}{\text{s}} = \text{W} \right). \quad (2.1)$$

Due to friction in the supply and discharge lines, the head is smaller at turbine level; this is known as the effective head  $H$  (m), and is obtained via

$$H = \eta_h H_b, \quad (2.2)$$

where  $\eta_h$  is the efficiency of the hydraulic system or the hydraulic efficiency (which also depends on the amount of water present).

The hydraulic power  $P_h$  that is actually available at the inlet of the turbine is

$$P_h = \rho Q g H. \quad (2.3)$$

The energy of the moving water is converted into mechanical power in the turbine, which is available as a turbine power  $P_t$  on the turbine shaft

$$P_t = \eta_t \rho Q g H, \quad (2.4)$$

where  $\eta_t$  is the turbine efficiency.

The mechanical power is finally converted into *electrical power* in the electrical generator. The net output of the power plant is

$$P = \eta_e P_t = \eta_e \eta_t \rho Q g H, \quad (2.5)$$

where  $\eta_e$  is the efficiency of the electrical device (generator, transformer, own requirements of the power plants).

### Example 2.1

A power plant with a net output of 100 MW and a gross head of 500 m has the following efficiencies:  $\eta_h = 0.92$ ;  $\eta_t = 0.85$ ;  $\eta_e = 0.96$ . Also,  $\rho = 1000 \text{ kg/m}^3$  and  $g = 9.81 \text{ m/s}^2$ . Determine:

- The turbine and hydraulic power
- The effective head and the nominal water flow
- The diameter of the circular feed gallery if the optimal water speed is 4 m/s
- A general expression for the specific energy  $w$  of a kg of water and the value of the specific energy  $gH$  at the turbine entrance.

### Solutions

$$(a) P_t = \frac{P}{\eta_e} = \frac{100}{0.96} = 104.2 \text{ MW}$$

$$P_h = \frac{P_t}{\eta_t} = \frac{104.2}{0.85} = 122.6 \text{ MW}$$

$$(b) H = H_b \eta_h = 500 \times 0.92 = 460 \text{ m}$$

$$Q = \frac{P_h}{\rho g H} = \frac{122.6 \times 10^6}{1000 \times 9.81 \times 460} = 27.2 \frac{\text{m}^3}{\text{s}}$$

$$(c) A = \frac{Q}{v} = \frac{27.2}{4} = 6.8 \text{ m}^2$$

$$D = \sqrt{\frac{4A}{\pi}} = \frac{4 \times 6.8}{\pi} = 2.94 \text{ m}$$

With increasing water speed, the loss costs due to friction increase approximately quadratically, while the investment costs of the tunnel decrease with smaller diameter. Optimizing the total cost results in the optimal speed.

- Since  $\rho Q$  represents the water flow in kg/s, the specific energy  $w$  of the water at the entrance to the turbine is  $gH$ , and can be calculated using (2.3). Therefore, the solution to (d) is:

$$w = \frac{P_h}{\rho Q} = gH, \quad (2.6)$$

$$gH = 9.81 \times 460 = 4.51 \text{ kJ/kg}.$$



## 2.2 Hydrological Planning Principles

Figure 2.4a shows the catchment area of the observation point P of a river.

Concerning the *annual water volume*, as a rule, long-term measurements are available that enable a statistical assessment of the above-ground discharge conditions. If no measured water quantities are available, but rainfall values are available, the mean annual runoff quantity can be used for preliminary studies.  $Q_{ma}$  can be estimated with the following formula

$$Q_{ma} = \beta h_m A \times 10^3 \quad (\text{m}^3/\text{h}),$$

where  $A$  is the catchment area of the observation point P ( $\text{km}^2$ ),  $h_m$  is the long-term average of the precipitation height ( $\text{mm}/\text{a}$ ), and  $\beta$  is the discharge coefficient ( $< 1$  because of evaporation and seepage, dependent on the type of ground and surface, e.g., vegetation).

In addition to the long-term mean values, the maximum values (wet years), as well as the minimum values (dry years) and their frequency, are also of interest.

Measurements at various observation points along the watercourse from the source to the estuary show the *discharge pattern* in Fig. 2.4b.

A part  $Q_a$  ( $\text{m}^3/\text{a}$ ) of the available water at  $P_1$  can be captured and used with the gross head (also gross drop height)  $H_b$ . The corresponding energy potential of the power station (gross energy/a) is

$$W_a = \rho Q_a g H_b \frac{1}{3.6 \times 10^6} \quad (\text{kWh}/\text{a}),$$

( $\rho \approx 1000 \text{ kg}/\text{m}^3$ ,  $Q_a$  ( $\text{m}^3/\text{a}$ ),  $g \approx 9.81 \text{ m}/\text{s}^2$ ,  $H_b$  (m)) and is thus proportional to the area  $Q_a H_b$ .

Several power stations along the watercourse, e.g., a low-pressure power station at  $P_2$ , provide for a more or less complete use of the water body, whose *potential* is shown by the area integral of the diagram in Fig. 2.4b. Figure 2.5 shows an example of an almost complete use of the gradient of a river section on the Rhine.

It is also important for the planning of the power station to take into account the *temporal fluctuations* of the water supply during the year. Figure 2.6a shows the typical behavior of alpine waters (snow melt) and Fig. 2.6b the long-term *duration line* (frequency curve) of the water supply, which serves as the most important planning basis.

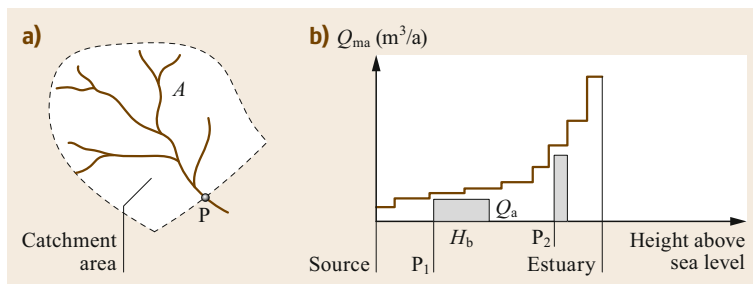


Fig. 2.4 (a) Catchment area, (b) flow rate diagram of a river

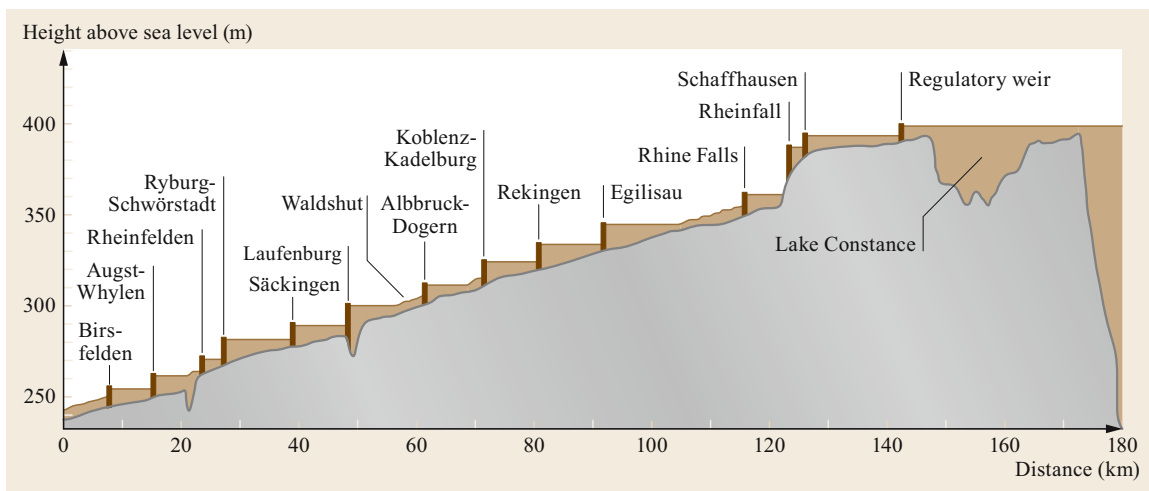
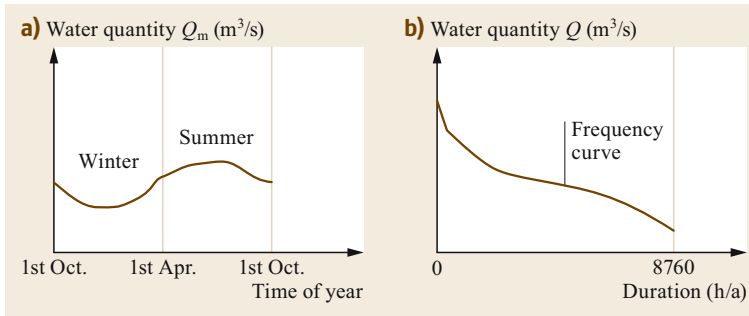


Fig. 2.5 Power station chain on the Rhine between Lake Constance and Basel (adapted from [2.4])



**Fig. 2.6** (a) Typical annual water quantity curve of an alpine water body, (b) annual duration line of the water supply

The construction of a hydraulic power station constitutes an intervention in the natural, constantly renewing water outflow. *Water management planning* must therefore be given priority over the needs of the energy industry. Often other aspects such as irrigation, shipping and flood control [2.5] have to be taken into account. The requirements of *environmental protection* must be taken into account in the broadest sense (drinking and groundwater, fauna, flora, landscape protection). It should not be forgotten, however, that hydropower is a clean, ecologically valuable form of solar energy that can be used as a substi-

tute for more environmentally damaging primary energies.

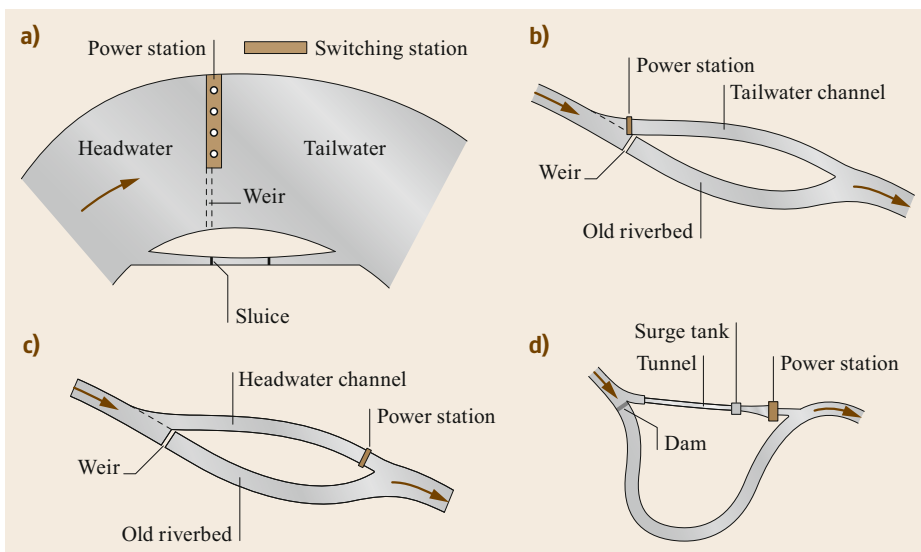
Hydropower plants can be divided into three main categories from an energy-economy point of view, and are discussed below. They are:

- Run-of-river power stations, i.e., power stations without water storage
- Storage power stations with daily and weekly storage
- Storage power stations with annual and multiyear storage.

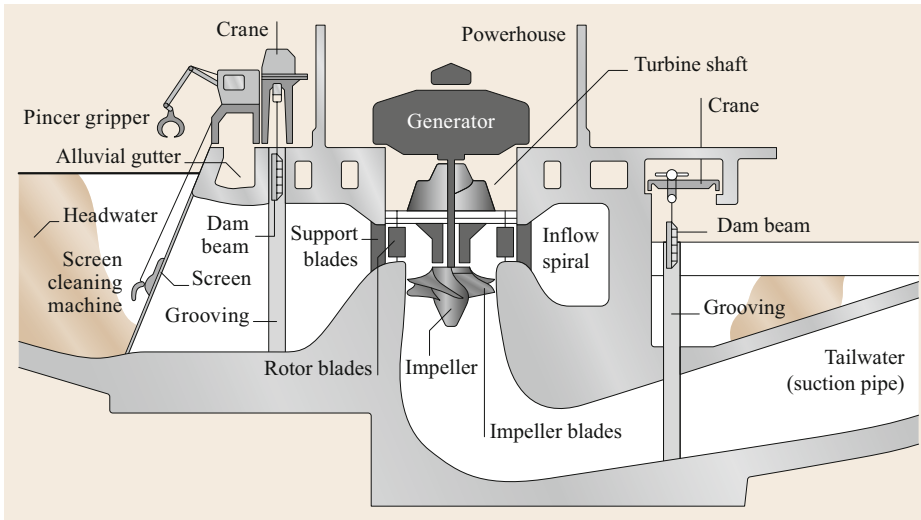
## 2.3 Run-of-River Power Stations

Run-of-river power stations have various *basic forms*:

- If the river has a sufficient gradient, the power station can be placed directly next to the weir (Fig. 2.7a). Full use of the water is then possible. The drop height is usually a few meters.
- A greater drop height is possible if the water is fed to a lower lying tailwater channel (Fig. 2.7b). However, a residual water amount in the river bed is prescribed, so that the full water amount cannot be used.
- The same applies to power stations at the end of an upstream channel (Fig. 2.7c).



**Fig. 2.7a-d** Types of run-of-river power stations: (a) Power station directly at the weir, (b) run-of-river power station with tailwater channel, (c) run-of-river power station with headwater channel, (d) run-of-river power station with upstream water supply through tunnels and pipelines (adapted from [2.4])



**Fig. 2.8** Run-of-river power station with Kaplan turbine (adapted from [2.6])

- With a larger river loop, the drop height can be considerably greater, and the water supply might even require a mountain cutting (Fig. 2.7d).

Due to the normally small drop height, run-of-river power stations are usually *low-pressure systems*. The turbines in question will then be either *Kaplan* (Fig. 2.8) or *bulb turbines* (Fig. 2.10) (see also Sect. 2.5). In special cases with greater drop heights (e.g., waterfalls, rapids and designs as in Fig. 2.7d), *Francis turbines* are also used.

### 2.3.1 Water Management

The natural water inflow is used, i.e., the management usually has no influence on the timing of water use. Sometimes short-term storage (in the hours range, e.g., in the case of hydropeaking [2.8]) is planned, and thus a small contribution to peak energy production is possible.

### 2.3.2 Execution

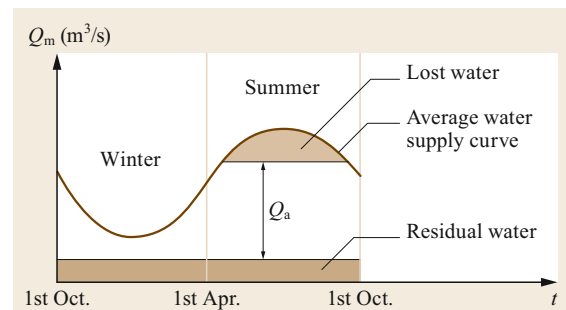
Figure 2.8 shows the section of a run-of-river power station with a *Kaplan turbine*. In order to dam the turbine chamber from headwater and tailwater, dam beams are provided that are inserted with special cranes into the grooves provided for this purpose. The screen prevents coarser items from reaching the turbine. A screen cleaning machine makes it possible to keep the screen free of alluvial material.

The version with a *bulb turbine* (Fig. 2.10a,b) makes practical a low construction method that is well compatible with landscape protection. The bulb turbine can

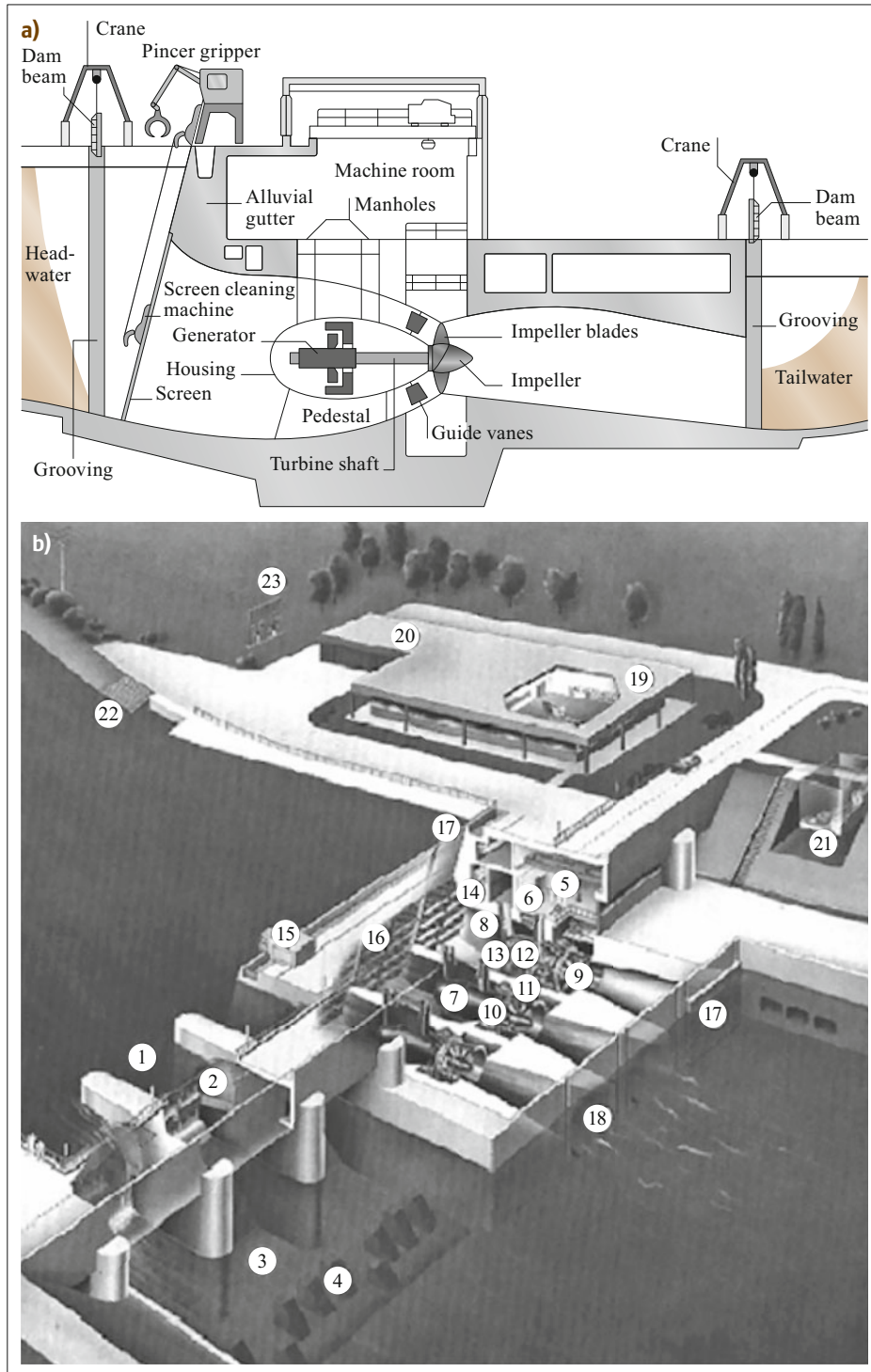
also be used on very small gradients. The inlet spiral is omitted and the generator is located in a watertight housing. Thanks to the favorable hydrodynamics, the efficiency is excellent.

### 2.3.3 Design

If the power plant is designed for the *design water flow rate*  $Q_a$  the hatched area in Fig. 2.9 is lost. The quantity  $Q_a$  is optimized with the following limit value consideration: comparison of fixed capital and operating costs for an additional  $\Delta Q_a$  with the revenue generated by the corresponding increase in energy. This consideration is also decisive in determining the new capacity for power-plant renewals. Note that, with the assumptions in Fig. 2.9, the surplus of energy occurs in summer, i.e., when there is more of an energy surplus in Central Europe and the market value of the energy is low (this is often not true for purely thermal production).



**Fig. 2.9** Selection of the design water quantity  $Q_a$ . Residual water is required if the version includes tailwater or headwater channels

**Fig. 2.10**

(a) Run-of-river power station with bulb turbine (adapted from [2.6]), (b) Low-pressure run-of-river power station: 1 weir system, 2 sluice gate, 3 stilling basin, 4 baffle pier, 5 machine hall, 6 assembly shaft, 7 generator housing, 8 access shafts, 9 turbine runner, 10 guide vanes, 11 guide apparatus, 12 generator, 13 cooler, 14 cable conduit, 15 screen, 16 screen cleaning machine, 17 dam beams, 18 turbine outlet, 19 control and switching building, 20 workshop and garage building, 21 fish ladder, 22 boat stairs, 23 open-air switchgear or energy transport (adapted from [2.7])

## 2.4 Storage Power Stations

### 2.4.1 Daily and Weekly Storage

As a rule, these are river power stations with a higher water level of several tens of meters. The headwater becomes a daily or even weekly storage basin. *Kaplan* or *Francis turbines* are used. A special type of daily storage basin are the *pure pumped-storage plants* (Sect. 2.4.3).

#### Application and Design

The design water quantity  $Q_a$  will be determined on the basis of considerations similar to those set out in Sect. 2.3.3 (Fig. 2.9). However, as more valuable peak energy is produced, it is usually worthwhile to use a larger  $Q_a$ . As long as  $Q_a$ , e.g., for a daily storage plant, exceeds  $Q_m$ , the amount of water available on the day under consideration (Fig. 2.11) energy production can be concentrated on the peak hours.

The quantity

$$k(t) = \frac{V_{\max}}{86\,400 [Q_a - Q_m(t)]} \quad (\text{h/d})$$

can be taken as the daily concentration factor, where  $V_{\max}$  is the daily storage capacity. This factor changes

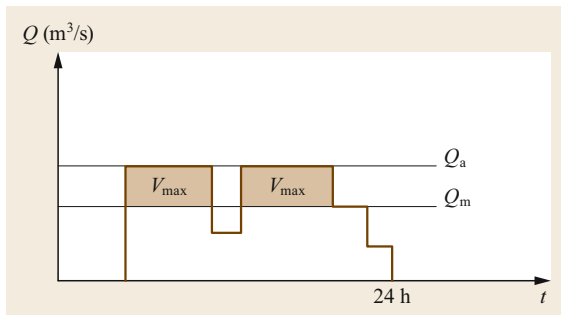


Fig. 2.11 Use of a daily-storage facility

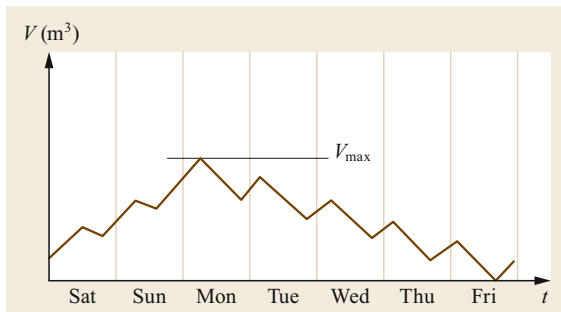


Fig. 2.12 Typical course of the useful content of a weekly storage unit

over the course of the year. The value of the energy increases with the concentration factor. If this dependency is known, the achievable annual revenue can be calculated and compared with the annual costs, and thus the storage capacity and design water quantity can be optimized.

For *weekly storage units*, similar considerations can be made. Figure 2.12 shows the typical course of the useful content of a weekly storage unit. The storage tank is refilled at night and on weekends, while emptying takes place during peak hours, especially on weekdays.

#### Example 2.2

The Schiffenen power plant on the Saane has an installed capacity of 73.2 MW and an average annual production of 136 GWh. The overall efficiency is 0.85. The lake has a useful volume of  $35 \times 10^6 \text{ m}^3$ , and the lake surface area is  $4.25 \text{ km}^2$ . The maximum drop height is 48.2 m. Calculate the following characteristic numbers:

- The storage capacity
- The theoretical draining time at full power
- The theoretical number of cycles per year
- The duration of use of the installed capacity.

What type of power plant and storage facility is it?

Fluctuation of the headwater level is

$$\Delta h = \frac{35 \times 10^6}{4.25 \times 10^6} = 8.2 \text{ m}.$$

The average head is thus approximately 44 m:

- Storage capacity =  $\eta \rho V_{\max} g H_m$  (Ws)  
 $= 0.85 \times 1000 \times 35 \times 10^6 \times 9.81 \times 44 \frac{1}{3600}$   
 $= 3570 \text{ MWh}$
- Theor. draining time =  $\frac{3570 \text{ MWh}}{73.2 \text{ MW}} = 48.8 \text{ h}$
- Theor. number of cycles =  $\frac{136\,000 \text{ MWh}}{3570 \text{ MWh/cycle}} = 38$
- Usage duration =  $\frac{136\,000 \text{ MWh/a}}{73.2 \text{ MW}} = 1857 \text{ h/a}.$

Evidently it is a weekly storage power plant for the production of peak energy.

### 2.4.2 Annual Storage (Seasonal Storage)

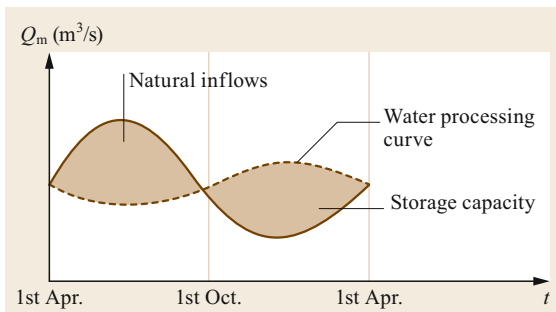
Alpine waters carry considerably more water in summer than in winter. It is an obvious strategy to collect these quantities of water (so-called seasonal water) with the help of annual reservoirs. Since in Switzerland in the winter usually *less running water* is available, a considerable part of the electricity will be generated from *seasonal water*. Accordingly, the water-processing curve in alpine annual storage power stations varies in the opposite direction to the supply curve (natural inflows), as Fig. 2.13 shows. The storage volume is determined by the size of the catchment area and the topographical conditions. Certain legally stipulated quantities of water must also be able to flow down the valley in summer.

The energy content of the stored water is higher when a greater drop height can be selected. Annual storage plants in the high mountains are economical because large amounts of energy can be produced with relatively little water.

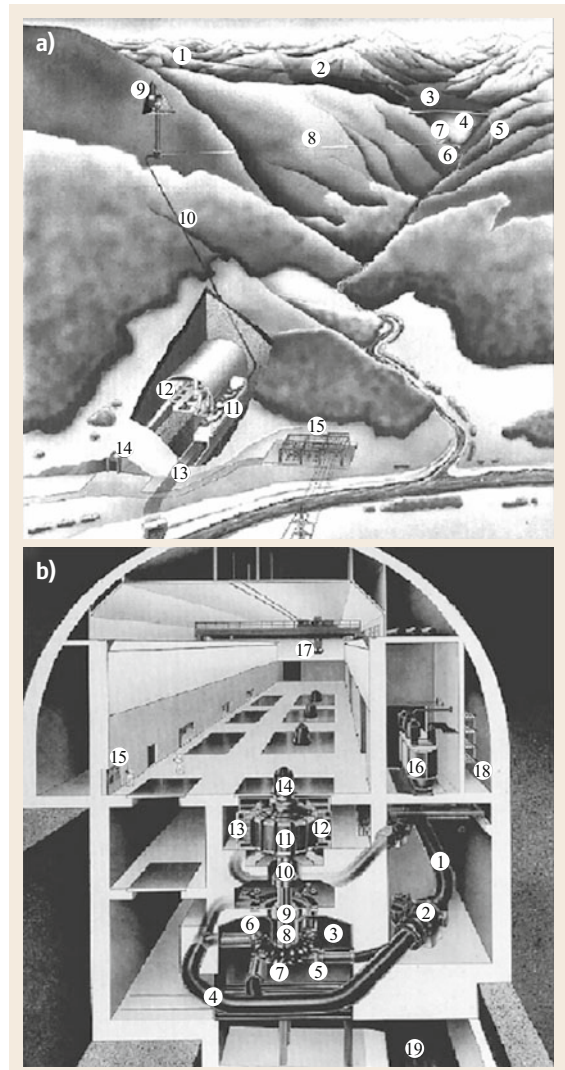
Larger storage volumes of rivers are not possible in Switzerland because of the high population density and for reasons of landscape protection. Worldwide, however, in various cases, rivers have been dammed to form large lakes with annual or even multiyear storage.

The main elements of an alpine annual storage power plant are shown in Fig. 2.14a. The *reservoir-stored water* is transported with an almost horizontal *pressure tunnel*, often over many kilometers to a suitable place, where it is led with a steep *pressure pipe* (or pressure shaft) to the power plant.

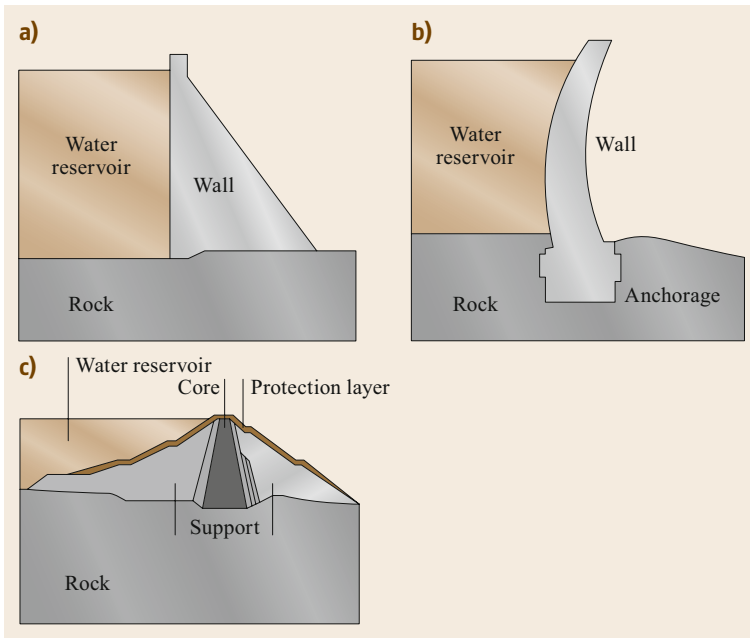
The head can be a few hundred to 2000 m. To provide for this, between the tunnel and the pen stock a *surge chamber* is required. This is an equalizing tank with the task of collecting the water flowing downstream when the turbine closes quickly and thus avoid-



**Fig. 2.13** Typical profile of water supply and water processing in annual storage power plants



**Fig. 2.14** (a) Main elements of an annual storage power plant (1 water catchments, 2 feed tunnel, 3 reservoir, 4 dam wall, 5 overflow, 6 bottom outlet, 7 inflow, 8 pressure tunnel, 9 surge chamber, 10 pressure shaft (or pressure line), 11 ball-valve chamber, 12 machine cavern (or center), 13 underwater tunnel, 14 access tunnel, 15 switching and possibly transformer station), (b) cavern power plant with Pelton turbines (1 distribution line, 2 ball valve, 3 turbine casing, 4 ring line, 5 inlet nozzle, 6 jet deflector, 7 Pelton turbine, 8 turbine shaft, 9 bearing, 10 generator shaft, 11 generator rotor, 12 generator stator, 13 cooler, 14 exciter machine, 15 control panel, 16 transformer, 17 crane, 18 cable gallery, 19 to the underwater tunnel) (adapted from [2.7])



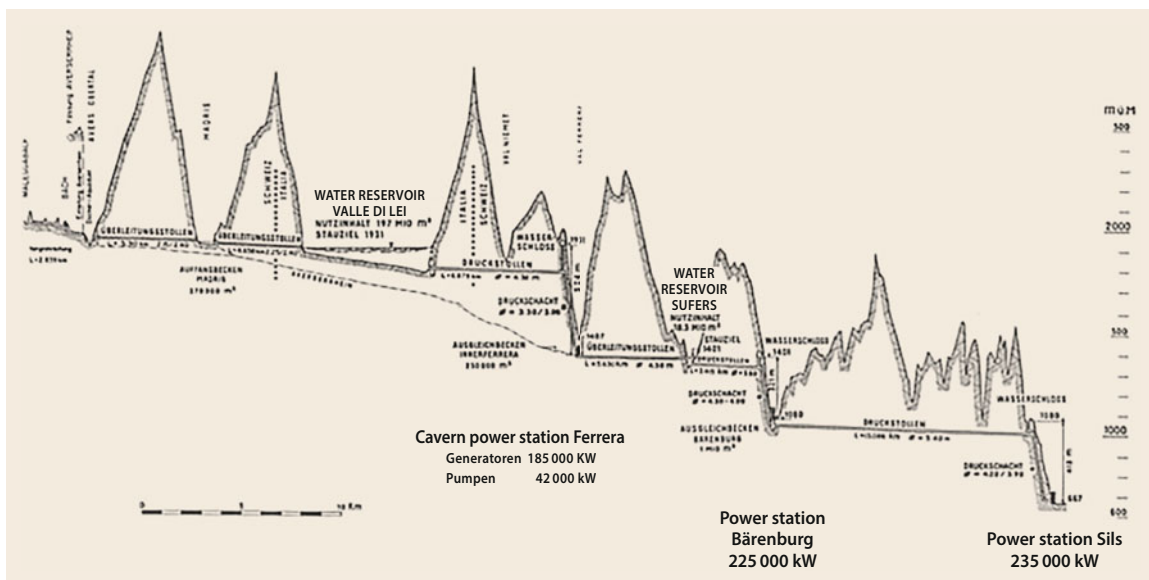
**Fig. 2.15a–c** Types of dam: (a) gravity dam, (b) arch dam, (c) dam (adapted from [2.7])

ing impermissible pressure surges. The power plant is often located in a cavern (Fig. 2.14b).

The types of dams frequently encountered in Switzerland are shown schematically in Fig. 2.15. In a *gravity dam*, the weight of the dam is sufficient to retain the dammed water (example: Grande Dixence near Zion, 285 m high). Particularly elegant and material-saving is the *arch dam* that transmits water forces to the valley flanks through its curved shape (example: Mauvoisin

dam in Val de Bagnes, 237 m high). Another possibility is to use *dams* of soil, clay, gravel or sand (example: Mattmark dam in the Saas Valley, 120 m high).

For the drop heights mentioned, *Francis* and *Pelton turbines* are used (Sect. 2.4). The large drop height can often only be used with the aid of multistage systems. An example of a three-stage system is shown in Fig. 2.16: the total drop height is 1258 m; the individual stages are 524, 321, and 413 m high, with a total output



**Fig. 2.16** Multi-stage plant: Hinterrhein power plants (Switzerland, Canton of Grisons)

of 645 MW. The Ferrera top power station also allows the pumping up of the running water of a side valley (Sect. 2.4.3).

### 2.4.3 Pump Storage

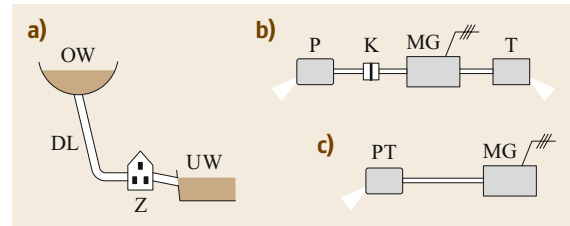
With pumped storage, water is pumped up from a low-lying collecting basin to a higher reservoir. This fulfills two functions:

- Conversion of cheap night or summer energy into expensive peak and winter energy
- Collection of excess running water that would otherwise be lost.

A distinction is made between circulation systems and seasonal pump storage.

*Circulating systems* have a short-term storage, mostly day storage, for the conversion of night into day energy. Recently, they have the function not only of balancing load fluctuations, but also fluctuations of feed-in (wind and solar energy). They are often implemented as *pure pumped-storage plants* without natural inflows; then the turbinated water quantity is equal to the pumped water quantity. In this case, the upper basin is usually artificially excavated (Fig. 2.17a). In other plants, one finds pumped storage sets, combined with normal turbo sets with natural inflow.

The *seasonal pump storage* primarily serves to convert summer run-of-river energy into winter energy. The



**Fig. 2.17** (a) Pure pumped-storage plant with a head of usually 300–700 m: OW headwater (often artificially dredged), UW: tailwater (river or lake), DL: pressure line, Z: control center, (b) separate hydraulic machines (P: pump, T: turbine, MG: motor generator, K: clutch), (c) PT: pump turbine

running water is pumped into a seasonal reservoir at a higher altitude. Seasonal pump storage normally takes place in addition to the turbinating of natural inflows (Fig. 2.16).

There are two design options for the pump-storage units:

- Version with separate hydraulic machines. In turbine operation, the pump is disconnected, while the turbine idles (Fig. 2.17b) in pump operation.
- Version with pump turbine: is often cheaper in terms of investment, but has a lower efficiency. The pump turbine runs as a turbine when water is supplied and as a pump when the direction of rotation is reversed (Fig. 2.17c).

## 2.5 Water Turbines

According to Sect. 2.1, the turbine power is

$$P_t = \eta_t \rho Q g H \quad (\text{W}), \quad (2.7)$$

with  $H$  being the effective head.

The specific work performed by the turbine (per kg of water) is

$$w_t = \frac{P_t}{\rho Q} = \eta_t g H \quad \left( \frac{\text{J}}{\text{kg}} \right), \quad (2.8)$$

where  $gH$  represents the specific utility potential.

In any cross section of a water flow (Fig. 2.18), the specific energy can be expressed as [2.9, Annex A1]

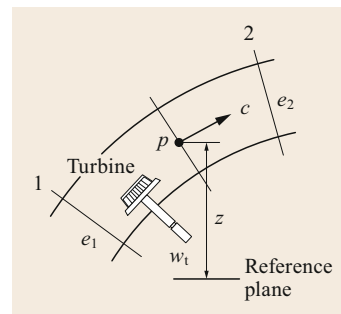
$$e = \frac{p}{\rho} + \frac{1}{2} c^2 + gz \quad \left( \frac{\text{J}}{\text{kg}} \right). \quad (2.9)$$

The *flow energy* is composed of *pressure energy*, *kinetic energy* and *potential energy*.

With reference to Fig. 2.18, let  $e_1$  and  $e_2$  be the energies of cross sections 1 and 2. The flow performs work between points 1 and 2 in a turbine. The mechanical energy supplied by the turbine is in accordance with the principle of energy conservation

$$w_t = e_1 - e_2 - q_f, \quad (2.10)$$

where  $q_f$  are friction losses.



**Fig. 2.18** Water-flow energy ( $p$ : positive water pressure,  $c$ : mean water speed,  $z$ : height coordinates)



If (2.9) is inserted into (2.10), the following applies, namely the *Bernoulli equation* of fluid mechanics

$$w_t = \frac{p_1 - p_2}{\rho} + \frac{1}{2}(c_1^2 - c_2^2) + g(z_1 - z_2) - q_r \quad \left( \frac{\text{J}}{\text{kg}} \right). \quad (2.11)$$

The potential energy  $g(z_1 - z_2)$  plays a secondary role or can even be neglected. Depending on the significance of the two components of kinetic and pressure energy, a distinction is made between action and reaction turbines.

*Impulse turbines* (e.g., Pelton turbine). These are free-jet turbines, where the pressure is equal to atmospheric pressure, and  $p_1 = p_2 = 0$ . In these turbines, *kinetic energy* is converted into *mechanical energy*, and so

$$w_t \approx \frac{1}{2}(c_1^2 - c_2^2) - q_r.$$

*Reaction turbines* (e.g., Francis and Kaplan turbines). Within these turbines, there is a pressure difference ( $p_1 - p_2$ ), and both *pressure energy* and *kinetic energy* are transformed into *mechanical energy*. The *degree of reaction*  $r$  designates the proportion of the pressure energy converted in the impeller relative to the total available pressure energy ( $= gH$ ). The degree of reaction is between 0.3 and 0.8.

### 2.5.1 Pelton Turbine

Figure 2.19 schematically shows a plant with a Pelton turbine. A part of the gross head becomes friction loss  $H_v$  in the feeder lines. The height difference  $H_x$  between the jet level and tailwater level can also not be used. The hydraulic efficiency (Sect. 2.3.3) is thus

$$\eta_h = \frac{H}{H_b} = 1 - \frac{H_v + H_x}{H_b}.$$

The energy conversion of 1 kg of water on its way from the upstream water level to the turbine is illustrated in the energy diagram Fig. 2.20. When descending to the intake of the pressure line, part of the potential energy  $gH_b$  is converted into pressure energy and there partly also into kinetic energy. In the pressure line, the potential energy progressively becomes pressure energy as far as  $H_x$ . The pressure energy available before the nozzle, is converted in the nozzle (Fig. 2.21) into kinetic energy of the water jet.

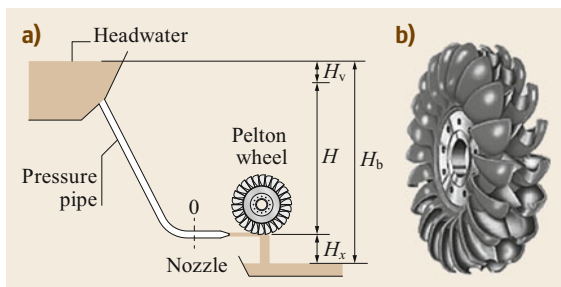


Fig. 2.19 (a) Plant with Pelton turbine, (b) Pelton wheel

Figure 2.21 illustrates the energy conversion within a Pelton turbine (consisting of nozzle and wheel). The Pelton wheel has the diameter  $D$  and rotates at speed  $n$ . The circumferential speed of the wheel is  $u$ . The water jet hits cup-shaped blades and releases its energy. The nozzle needle regulates the jet diameter and thus the amount of water and the power of the turbine. The turbine can also have several nozzles. In the following, we calculate the specific energy in the cross sections 0, 1, and 2.

If the beam plane is selected as the reference plane, the potential energy in this plane is zero. The expression for the specific energy in front of the nozzle (cross section 0) is

$$e_0 = \frac{p_0}{\rho} + \frac{1}{2}c_0^2 = gH. \quad (2.12)$$

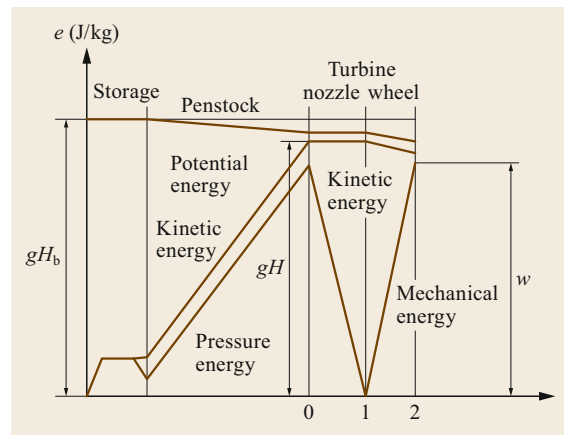


Fig. 2.20 Energy diagram (specific energy  $e$ ) of the Pelton plant

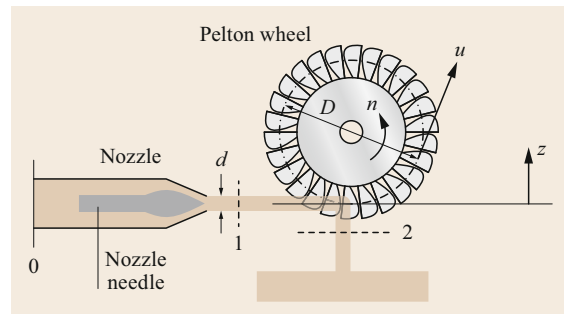


Fig. 2.21 Pelton turbine

The pressure energy in the jet is also zero. For the specific energy after the nozzle (cross section 1), it follows that

$$e_1 = \frac{1}{2}c_1^2 = \eta_D gH, \quad (2.13)$$

with  $\eta_D$  = nozzle efficiency (is a part of  $\eta_t$  and approximately 0.96).

From (2.13), the jet velocity is

$$c_1 = \sqrt{\eta_D 2gH}. \quad (2.14)$$

The jet velocity depends only on the effective head and is therefore independent of the set jet diameter  $d$ .

The specific energy immediately after the wheel (cross section 2) is calculated with the assumption of  $z_2 \approx 0$  to be

$$e_2 = \frac{1}{2}c_2^2,$$

where, for optimally shaped blades,  $c_2 \ll c_1$ .

The specific work and efficiency of the turbine are

$$\begin{aligned} w_t &= e_0 - e_2 - q_r = \eta_t gH, \\ (1 - \eta_t) gH &= \frac{1}{2}c_2^2 + q_r \rightarrow \eta_t = 1 - \frac{\frac{1}{2}c_2^2 + q_r}{gH}, \end{aligned}$$

with friction losses  $q_r$  in nozzle and wheel.

### Jet Diameter and Water Quantity

There is a relationship

$$Q = i \frac{\pi d^2}{4} c_1, \quad i = \text{number of nozzles}. \quad (2.15)$$

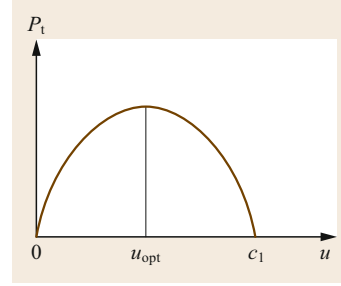
Therefore, the maximum jet diameter corresponding to the design volume of water  $Q_a$  is

$$d_0 = \sqrt{\frac{4Q_a}{i\pi c_1}}. \quad (2.16)$$

### Optimum Circumferential Speed

The relationship between turbine efficiency and wheel circumferential speed for a given amount of water is shown in Fig. 2.22. When the wheel is locked, no power is transmitted. If the wheel speed is equal to the jet speed, the power is also zero, since no power transmission is possible (momentum = 0). The efficiency of the wheel will be greatest at about half the jet velocity. The optimum circumferential speed is thus

$$u_{\text{opt}} = kc_1, \quad \text{with } k \text{ approximately } 0.5. \quad (2.17)$$



**Fig. 2.22** Power yield as a function of circumferential speed

From (2.17), the relationship between diameter and synchronous speed  $n$  (rpm) is

$$D = \frac{60}{\pi n} kc_1. \quad (2.18)$$

### Diameter, Specific Speed

To determine the diameter, a further correlation between diameter and speed is necessary. To find this, the ratio between the maximum jet diameter and the wheel diameter is calculated. From the relationships (2.16) and (2.18), one obtains

$$\frac{d_0}{D} = \frac{2Q_a^{0.5} \pi n}{i^{0.5} \pi^{0.5} c_1^{0.5} 60kc_1} = \frac{Q_a^{0.5} \pi^{0.5} n}{i^{0.5} (\eta_D 2gH)^{0.75} 30k}$$

and finally by introducing the *specific speed of rotation*

$$n_q = n \frac{Q_a^{0.5}}{H^{0.75}} \quad (2.19)$$

and the constant

$$a = \frac{\pi^{0.5}}{(2g)^{0.75} 30k\eta_D^{0.75}} = \frac{0.634 \times 10^{-2}}{k\eta_D^{0.75}} \quad (2.20)$$

we obtain

$$\frac{d_0}{D} = a \frac{n_q}{\sqrt{i}}. \quad (2.21)$$

The specific number  $n_q$  is defined as a *numerical value* with  $n$  in rpm,  $Q$  in  $\text{m}^3/\text{s}$  and  $H$  in m. It characterizes geometrically similar turbines. For the same number of jets and the same  $n_q$ , the ratio  $d_0/D$  that is proportional to the ratio of blade size to wheel diameter is constant. For a mechanically optimal Pelton wheel, this ratio varies only slightly; therefore, the ratio  $n_q/\sqrt{i}$  is for Pelton turbines practically a given. For large turbines and for large water heads (400–1000 m), the ratio  $n_q/\sqrt{i} = 5\text{--}6.5$  can be used. For heads  $> 1000$  m, these values must be corrected downwards (about 3–4 for 2000 m) and for small heads slightly upwards (for more details see [2.10]).

**Example 2.3**

Check the relationships using the Pelton facility depicted in Fig. 2.23. The nominal values are:  $P_t = 167$  MW,  $Q = 46.12$  m<sup>3</sup>/h,  $H = 413$  m,  $n = 180$  rpm.

The hydraulic power and turbine efficiency follow from the data

$$P_h = \rho Q g H = 1000 \times 46.12 \times 9.81 \times 413 = 187 \text{ MW},$$

$$\eta_t = \frac{P_t}{P_h} = \frac{167}{187} = 0.89.$$

From (2.19), one obtains

$$n_q = 180 \frac{46.12^{0.5}}{413^{0.75}} = 13.34,$$

$$\frac{n_q}{\sqrt{i}} = \frac{13.34}{\sqrt{6}} = 5.45.$$

Assuming that  $\eta_D = 0.96$  and  $k = 0.47$ , it also follows from (2.14) and (2.17) that

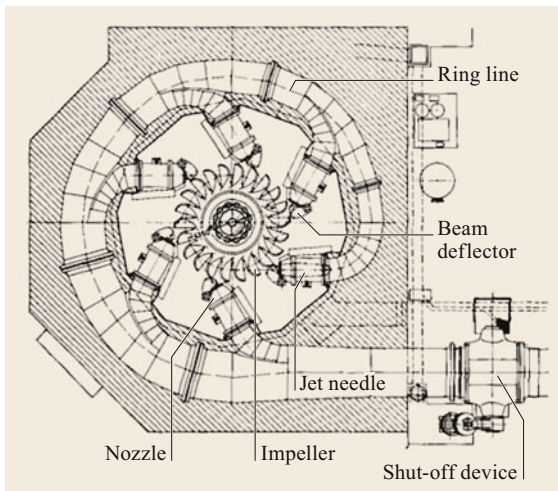
$$c_1 = \sqrt{0.96 \times 2 \times 9.81 \times 413} = 88.2 \text{ m/s},$$

$$u_{\text{opt}} = 0.47 \times 88.2 = 41.5 \text{ m/s}$$

and finally for the wheel diameter from (2.18)

$$D = \frac{60 \times 41.5}{\pi 180} = 4.40 \text{ m},$$

that corresponds well to the real wheel dimensions (4.35 m).



**Fig. 2.23** Six-jet free-jet turbine New Colgate on the Yuba River, California (Voith works drawing) (adapted from [2.4])

The maximum jet diameter determines the blade size. From (2.20) and (2.21), we can see that

$$a = 1.39 \times 10^{-2},$$

$$\frac{d_0}{D} = 1.39 \times 10^{-2} \times 5.45 = 7.58 \times 10^{-2}.$$

The maximum jet diameter is 7.6% of the wheel diameter or 33.4 cm. The guide values apply for the dimensions of blades and nozzle: blade spacing  $0.9d_0$ , blade length and width approximately  $3d_0$ , blade height  $0.3d_0$ , nozzle opening  $1.25d_0$  and nozzle tube diameter  $3d_0$ .

The specific energy at the turbine inlet is

$$gH = 9.81 \times 413 = 4.05 \frac{\text{kJ}}{\text{kg}}.$$

If the penstock diameter at the turbine inlet is estimated as  $d = 2$  m, it follows that

$$c_0 = \frac{4Q}{\pi d^2} = \frac{4 \times 46.12}{\pi 2^2} = 14.7 \frac{\text{m}}{\text{s}}, \quad \frac{1}{2} c_0^2 = 0.11 \frac{\text{kJ}}{\text{kg}}.$$

Using (2.12), the overpressure at the turbine inlet is

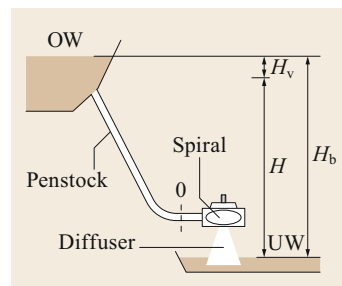
$$P_0 = \rho \left( gH - \frac{1}{2} c_0^2 \right) = 1000 \times (4.05 - 0.11)$$

$$= 39.4 \times 10^5 \frac{\text{N}}{\text{m}^2}.$$

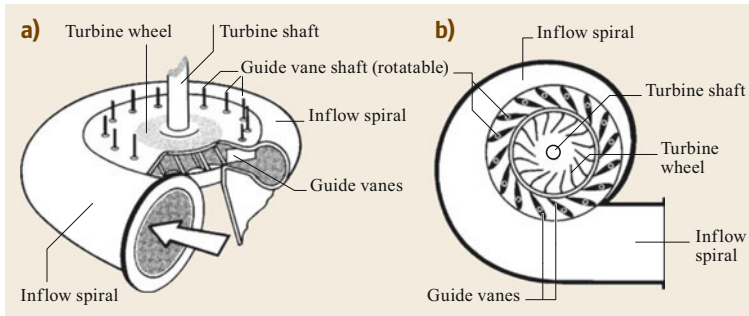
**2.5.2 Reaction Turbines**

Figure 2.24 schematically shows the structure of a plant with a reaction turbine. The water moves from the pressure pipe (or penstock) to the *inlet spiral* and from there by mainly radial movement to the turbine. Thanks to the *diffuser* (or *suction tube*), the entire head to the tailwater level (UW) is used, minus friction losses in the supply lines. The hydraulic efficiency is

$$\eta_h = \frac{H}{H_b} = 1 - \frac{H_v}{H_b}.$$



**Fig. 2.24** Plant with reaction turbine. OW: headwater, UW: tailwater



**Fig. 2.25** (a) Sketch of the volute casing, (b) section through the turbine (adapted from [2.6])

Figure 2.25 shows a sketch of the volute casing and a section through the Francis turbine (adapted from [2.6]).

Francis and Kaplan turbines differ in the shape of the *impellers*. The *Francis turbine* (Figs. 2.26 and 2.31) has fixed rotor blades. The propeller-like *Kaplan turbine* (Figs. 2.27 and 2.32) has rotor blades whose angle of inclination is adjusted as a function of the amount of water in order to improve efficiency at partial load. A *propeller turbine* is the variant with fixed rotor blades and is only appropriate when operation can mainly be at full load.

To describe the energy conversion in the reaction turbine, the specific energy in cross sections 0, 1, 2, and 3 is considered, with the tailwater level being chosen as the reference plane for the potential energy. In cross section 0 in front of the inlet spiral (Fig. 2.24), the

following applies

$$e_0 = \frac{p_0}{\rho} + \frac{1}{2}c_0^2 + gz_0 = gH.$$

The specific energy in cross section 1, immediately after the guide wheel is

$$e_1 = \frac{p_1}{\rho} + \frac{1}{2}c_1^2 + gz_1 = \eta_{SL}gH. \quad (2.22)$$

$\eta_{SL}$  takes into account the losses in the inlet spiral and guide wheel.

The specific energy in cross section 3 (tailwater level) is

$$e_3 = 0, \quad (2.23)$$

because the water velocity and the overpressure are zero here, too.

Some energy is lost in the diffuser due to friction. For the specific energy in cross section 2, immediately after the impeller, the following applies

$$e_2 = \frac{p_2}{\rho} + \frac{1}{2}c_2^2 + gz_2 = q_D, \quad (2.24)$$

where  $q_D$  indicates the friction losses in the diffuser.

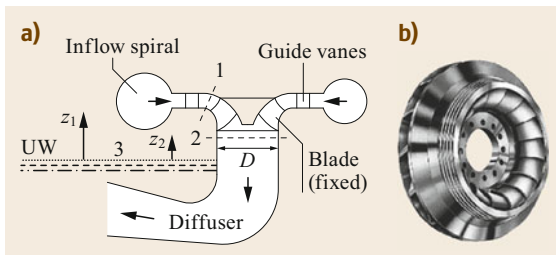
From (2.22) and (2.24), the specific energy available at the turbine shaft follows, in accordance with (2.10) and (2.11)

$$\begin{aligned} w_t &= e_1 - e_2 - q_f = \frac{p_1 - p_2}{\rho} + \frac{1}{2}(c_1^2 - c_2^2) \\ &\quad + g(z_1 - z_2) - q_f \\ &= \eta_{SL}gH - q_D - q_f = \eta_t gH, \end{aligned} \quad (2.25)$$

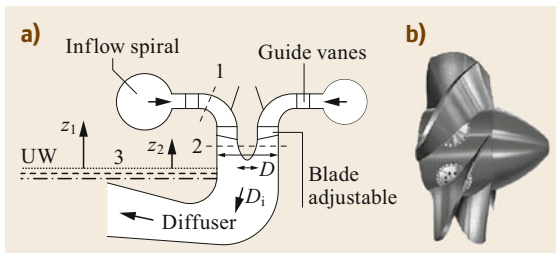
where  $q_f$  = friction losses in the impeller.

Also, from (2.24)

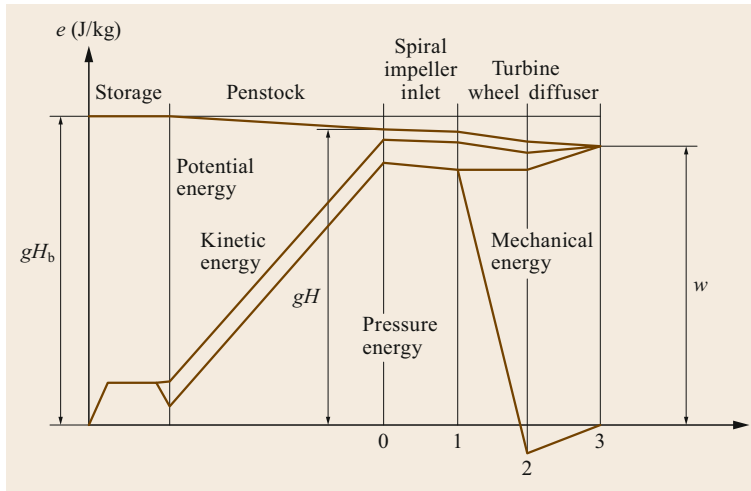
$$\frac{p_2}{\rho} = -\frac{1}{2}c_2^2 - gz_2 + q_D. \quad (2.26)$$



**Fig. 2.26** (a) Schematic representation of the Francis turbine, (b) Francis wheel



**Fig. 2.27** (a) Schematic diagram of the Kaplan turbine, (b) Kaplan wheel



**Fig. 2.28** Energy diagram (specific energy  $e$ ) of a reaction turbine plant

### Cavitation Effects

From (2.26), since  $q_D$  is small, a *negative pressure* results at the exit of the impeller. A too high negative pressure results in steam formation at the usual water temperatures and leads to the *cavitation effect*: implosion-like condensation of steam bubbles that causes noise, vibrations and, above all, corrosion of the blade surface over the course of time [2.11]. Efficiency and service life are reduced. The higher the water velocity  $c_2$ , the greater the negative pressure. Wheels with high rotational speeds are particularly at risk. The cavitation hazard is characterized by a cavitation number (or Thoma number), that is essentially proportional to

$$\frac{2(p_{2\text{abs}} - p_D)}{\rho c_2^2},$$

with  $p_{2\text{abs}}$  absolute pressure ( $= p_2 + \text{atmospheric pressure}$ ) and  $p_D$  vapor pressure (temperature-dependent, for details see [2.11]).

The geometry of the turbine is also determined for the reaction turbine by the specific rotational speed  $n_q$  (2.19) (see also (2.30)). To limit the water speed  $c_2$ , the specific speed may not exceed certain values as a function of the head  $H$ .

To limit the negative pressure, according to (2.26), not only can  $c_2$ , but also  $z_2$  be kept small or even made negative, so that the turbine lies lower than the tailwater level. This measure can be expensive if larger excavations in rocky ground are necessary.

### Energy Diagram

In summary, the energy conversion in a plant with reaction turbines can be illustrated by the energy diagram in Fig. 2.28. In contrast to the Pelton system (Fig. 2.20), the energy at the impeller inlet consists mainly of pres-

sure energy, that is directly converted into mechanical energy. The pressure energy at the impeller output is even negative. The diffusion allows recovering of the remaining kinetic energy (corresponding to  $c_2$ ), and if  $z_2$  is positive to also recover the potential energy, i.e., to convert it back into pressure energy.

### Flow Rate and Pressure Coefficient

In addition to the specific speed (2.19), further characteristic numbers are introduced for the reaction turbine, i.e., the *flow coefficient* and the *pressure coefficient*

$$\begin{aligned} \text{flow coefficient} \quad \varphi &= \frac{c_2}{u}, \\ \text{pressure coefficient} \quad \psi &= \frac{2gH}{u^2}. \end{aligned} \quad (2.27)$$

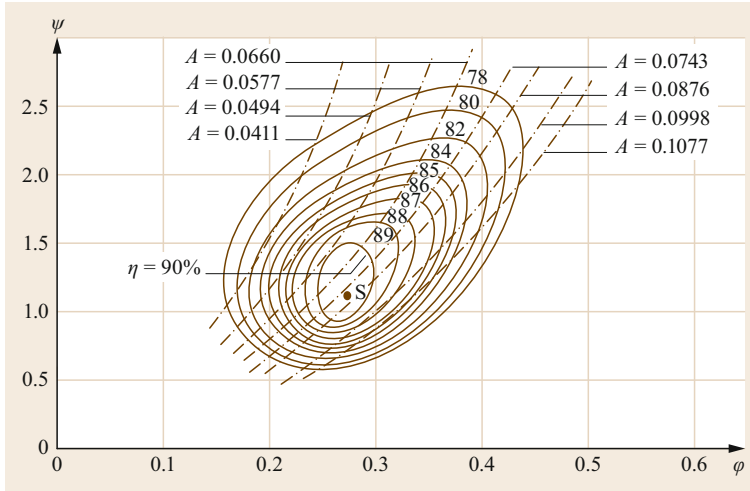
The flow coefficient is defined as the ratio of the water velocity at the outlet cross section 2 and the circumferential velocity  $u$  of the wheel in the same cross section. With reference to the outlet cross section 2, the following applies

$$Q = c_2 \frac{\pi D^2}{4} (1 - \alpha^2) = \varphi u \frac{\pi D^2}{4} (1 - \alpha^2), \quad (2.28)$$

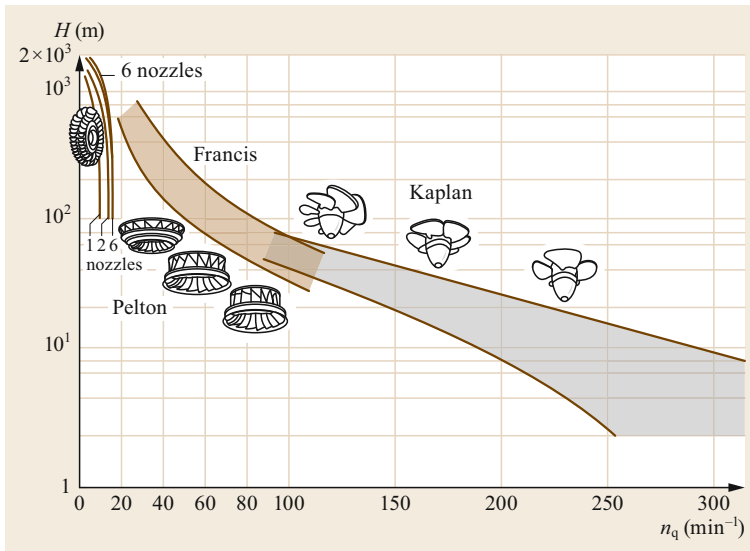
with  $\alpha = D_t/D$ .

The factor  $\alpha$  takes account of the fact that in the Kaplan turbine (Fig. 2.27) the exit cross section is reduced by the propeller body (with diameter  $D_t$ ). With the Francis turbine, this effect can be neglected in a first approximation (Kaplan guide value:  $\alpha \approx 0.4$ , Francis:  $\alpha \approx 0$ ).

For a given turbine, the *flow coefficient* according to (2.28) is proportional to the instantaneous *amount of water*. In order to achieve optimum efficiency at full load (optimum peripheral speed), the flow rate has a certain nominal value  $\varphi_a$ . With increasing specific



**Fig. 2.29** Mussel diagram of a Francis turbine: O: Nominal point, A: opening degree,  $\eta$ : efficiency (adapted from [2.12])



**Fig. 2.30** Relationship between specific speed  $n_q$  and effective head  $H$ . Hatched area: optimum area from experience (adapted from [2.4])

speed, this value is 0.4–0.25 for Francis turbines and 0.2–0.35 for Kaplan turbines.

For a turbine with a given specific rotational speed, there is a so-called *mussel diagram* in the  $(\varphi, \psi)$ -plane (Fig. 2.29), with the curves for constant efficiency and constant guide wheel position (extent of opening).

Since the *pressure coefficient* depends only on the effective head, in stationary operation it has a practically constant value, independent of the output, that corresponds to the maximum efficiency. From the pressure coefficient, the *optimum peripheral speed* follows from (2.27).

**Relationship Between  $n_q$ ,  $\varphi_a$  and  $\psi$**

With (2.27), one can express  $H$  as dependent on  $\psi$ . Using  $H$  and  $Q_a$  (according to (2.28)) in the expression

(2.19) for specific speed, taking into account that

$$D = \frac{60u}{\pi n} \tag{2.29}$$

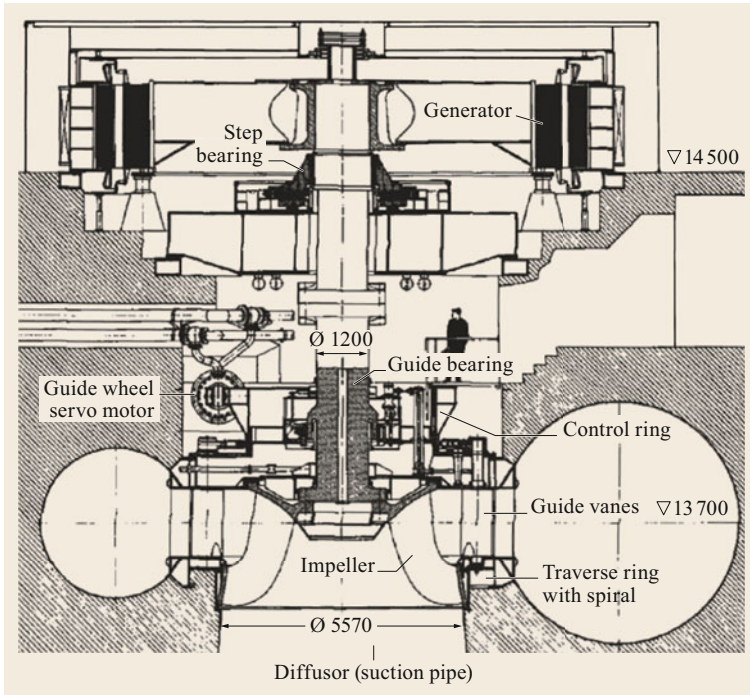
it follows that

$$n_q = n \frac{Q_a^{0.5}}{H^{0.75}} = \frac{60(2g)^{0.75}}{2\pi^{0.5}} \frac{\varphi_a^{0.5}}{\psi^{0.75}} \sqrt{1-\alpha^2}$$

$$\rightarrow n_q = 157.8 \frac{\varphi_a^{0.5}}{\psi^{0.75}} \sqrt{1-\alpha^2} \tag{2.30}$$

**Turbine Design**

When  $H$  and  $Q_a$  are given, the specific speed is first determined according to the effective head so that it lies within range of the diagram in Fig. 2.30 shown by experience to be economically optimal. Within this range,



**Fig. 2.31** Vertical machine set with Francis turbine, Paulo Alfonso at the Rio Sao Francisco, Brazil (Voith work drawing) (adapted from [2.4])

a compromise must be found between two opposing demands:

- A speed (and thus also a specific speed) as high as possible is indeed advantageous for both the turbine and generator for economic reasons.
- But the higher the speed selected, the greater the damage caused by cavitation may be.

Depending on  $n_q$ , the pressure coefficient follows from Fig. 2.30, from Fig. 2.24 the peripheral speed and from (2.29) the diameter of the impeller. Equation (2.30) gives the flow rate for rated operation.

#### Example 2.4

For the Francis turbine in Fig. 2.31, determine the most important parameters without knowing the mus-sel diagram and check the dimensions. The data values are  $H = 87.5$  m,  $Q = 284$  m<sup>3</sup>/s,  $n = 138.5$  rpm,  $P_t = 221$  MW, 60 Hz.

The hydraulic power and turbine efficiency are derived from the data

$$\begin{aligned}
 P_h &= \rho Q g H = 1000 \times 284 \times 9.81 \times 87.5 \\
 &= 243.8 \text{ MW} , \\
 \eta_t &= \frac{P_t}{P_h} = \frac{221}{243.8} = 0.907 .
 \end{aligned}$$

From (2.19), one obtains

$$n_q = 138.5 \frac{284^{0.5}}{87.5^{0.75}} = 81.47 .$$

This number is not far from the lower limit of the optimal range of Fig. 2.30. If the nominal flow rate is estimated at 0.3, the following relationship follows from (2.27), (2.29) and (2.30)

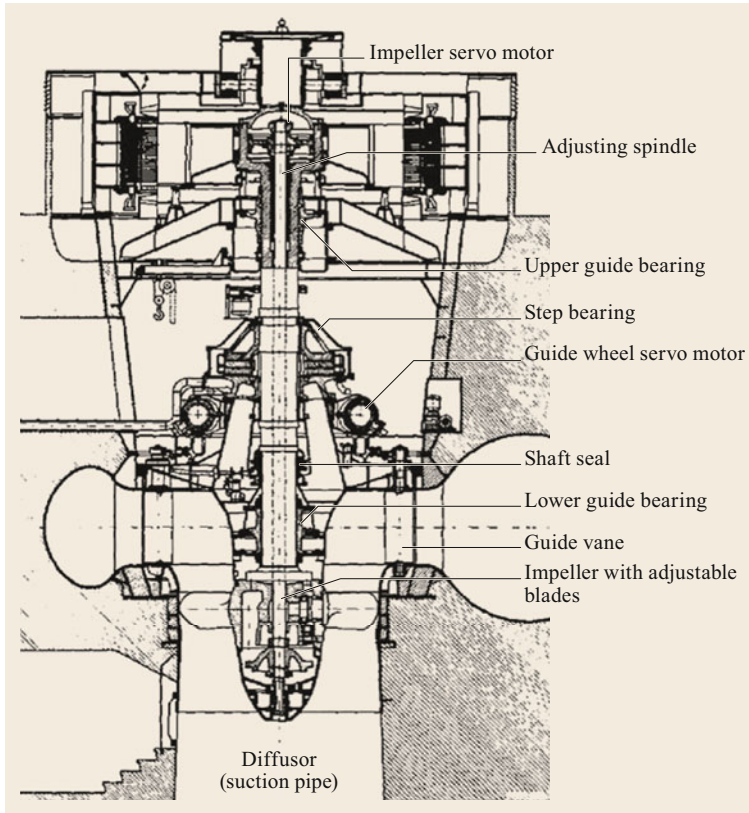
$$\psi^{0.75} = 157.8 \frac{0.3^{0.5}}{81.47} = 1.0609 \quad \rightarrow \quad \psi = 1.082 ,$$

$$u = \sqrt{\frac{2gH}{\psi}} = 39.8 \frac{\text{m}}{\text{s}} ,$$

$$D = \frac{60 \times 39.8}{\pi \times 138.5} = 5.49 \text{ m} ,$$

that is well in line with the real value (5.57 m). Conversely, since the flow coefficient is proportional to  $D^{-3}$ , the actual diameter results in

$$\begin{aligned}
 \varphi_a &= 0.287 , \quad \psi = 1.0505 \\
 \rightarrow u &= 40.4 \frac{\text{m}}{\text{s}} \\
 \rightarrow c_2 &= 11.6 \frac{\text{m}}{\text{s}} .
 \end{aligned}$$



**Fig. 2.32** Vertical Kaplan turbine Rosshaupten am Lech (Voith work drawing) (adapted from [2.4])

If the losses in the diffuser that have a favorable effect are neglected and assuming  $z_2 = 0$ , a negative pressure of 0.67 bar follows from (2.26). The turbine is positioned lower to reduce the negative pressure. For  $z_2 = -4$  m, follows, e.g., that  $p_2 = -0.28$  bar (for details regarding cavitation and permissible negative pressure see [2.11]).

#### Example 2.5

For the Kaplan turbine in Fig. 2.32, determine the most important parameters without knowing the mussel diagram and check the dimensions. The data is:  $H = 38$  m,  $Q = 75$  m<sup>3</sup>/s,  $n = 200$  rpm,  $P_t = 24.8$  MW, 50 Hz.

The hydraulic power and turbine efficiency are derived from the data.

$$\begin{aligned} P_h &= \rho Q g H = 1000 \times 75 \times 9.81 \times 38 \\ &= 27.96 \text{ MW} , \\ \eta_t &= \frac{P_t}{P_h} = \frac{24.8}{27.96} = 0.887 . \end{aligned}$$

Using (2.19) gives

$$n_q = 200 \frac{75^{0.5}}{38^{0.75}} = 113.17 .$$

This number is at the bottom of the hatched area of Fig. 2.30. If the nominal flow coefficient  $\varphi_a$  is estimated as 0.25 and  $\alpha$  as 0.4, (2.27), (2.29) and (2.30) give

$$\begin{aligned} \psi^{0.75} &= 157.8 \frac{0.25^{0.5}}{113.17} \sqrt{1 - 0.4^2} = 0.639 , \\ \rightarrow \psi &= 0.550 , \end{aligned}$$

$$u = \sqrt{\frac{2gH}{\psi}} = 36.8 \frac{\text{m}}{\text{s}} ,$$

$$D = \frac{60 \times 36.8}{\pi \times 200} = 3.51 \text{ m} .$$

The outlet velocity is  $c_2 = \varphi_a u = 9.2$  m/s. From this, the negative pressure can be estimated: for  $z_2 = 0$  and neglecting the diffuser losses, (2.26) gives,  $p_2 = -1.000(0.5 \times 9.2^2) = -0.42$  bar.

#### Types of Reaction Turbines and Rotary Pumps

A reaction turbine, by reversing the direction of rotation, becomes a *rotary pump*. As Table 2.2 shows, the characteristic speed and thus the geometry of reaction turbines and rotary pumps can vary greatly (for the turbines see also Fig. 2.28). A distinction is made be-



**Table 2.2** Specific speed of reaction turbines and rotary pumps

Turbine/pump	$n_q$
Francis slow	20–40
Francis medium	40–65
Francis fast	65–110
Kaplan (propeller)	90–300
Radial pump slow	10–30
Radial pump medium	30–60
Radial pump fast	60–150
Axial pump	110–500

tween *slow runners* (small  $n_q$  suitable for  $H$  large and  $Q$  small, with strongly curved blades), *medium-speed* and *fast runners* (large  $n_q$  suitable for  $H$  small and  $Q$  large, with slightly curved blades). It should be noted that the designations *slow* and *fast* refer to  $n_q$  and not to the effective speed.

The flow direction is radial-axial for Francis turbines and radial pumps and purely axial for Kaplan turbines and axial pumps. Pumps are often *multifluent* (splitting the water quantity into several wheels) and *multistage* (splitting of the pressure onto several wheels) (analogous to parallel and series electrical circuits). The *pump turbine* mentioned in Sect. 2.4.3 is a compromise machine, that has a lower efficiency, but results in lower plant costs.

### 2.5.3 Turbine Selection

The criteria that determine the choice of a turbine are briefly summarized and illustrated here by a few examples. As a rule,  $H$  and  $Q$  are given. The turbine type (specific speed), the speed (generator type) and the dimensions are to be determined. In principle, the speed of the turbine generator group should be chosen as high as possible, as this reduces dimensions and costs.

#### Pelton Turbine

The specific speed varies within narrow limits and can only be increased by the number of nozzles. This practically determines the speed and number of pole pairs of the generator, unless gearing is used. The head determines the jet velocity and thus the optimum circumferential speed. This essentially determines the diameter of the turbine and the blade size.

#### Reaction Turbine

The specific speed should be as high as possible. It has an upper limit because of cavitation (Fig. 2.28). For a specific head, it is therefore determined with narrow limits. From this the speed and number of pole pairs of the generator corresponding to the mains frequency can be found. If the mussel diagram is known, the optimum

value of  $\psi$ , and thus the circumferential speed  $u$  result. This also gives the diameter of the impeller.

#### Number of Groups

The *capacity of the hydropower plant* is determined by hydrological and topographical conditions and by economic considerations. For an optimal *choice of the number of groups* of the power plant, i.e., optimum distribution of the output, the following arguments are decisive:

- If the output is divided into several groups, the dimensions of the plant and thus the investments normally increase. It should be noted that the machines themselves do not necessarily become more expensive because they become faster when the amount of water is reduced.
- However, this disadvantage of higher investments is offset by the advantage that at partial load a better efficiency is achieved by switching off some groups and better utilizing the remaining ones. This is particularly the case for turbines with fixed blades, that exhibit poor efficiency at partial load (Francis and propeller turbines, Fig. 2.33). The loss calculation can be carried out by simulating the intended mode of operation of the power plant.
- The security of the grid feed-in increases with a larger number of groups. However, this argument is only significant in the case of larger outputs compared with the network output.

#### Example 2.6

Determine the turbine and generator types for 50 Hz, assuming a machine efficiency of  $\eta_t \eta_e 0.85$  for the following groups:

- $H = 100$  m,  $P = 30$  MW
- $H = 1000$  m,  $Q_a = 5$  m<sup>3</sup>/s.

According to Fig. 2.28, a Francis turbine with a characteristic rotation speed  $n_q$  of about 70 is chosen. Then,

$$\begin{aligned}
 Q_a &= \frac{P}{\eta_t \eta_e \rho g H} = \frac{30 \times 10^6}{0.85 \times 1000 \times 9.81 \times 100} \\
 &= 36.0 \frac{\text{m}^3}{\text{s}} \\
 n &= n_q \frac{H^{0.75}}{Q^{0.5}} = 70 \frac{100^{0.75}}{36^{0.5}} = 369 \text{ min}^{-1},
 \end{aligned}$$

choose  $p = 8$ ,

$$\begin{aligned}
 \rightarrow n &= 375 \text{ min}^{-1}, \\
 \rightarrow n_q &= 71.15.
 \end{aligned}$$

In order to roughly estimate the dimensions, assume, since no mussel diagram is available,  $\varphi_a = 0.32$ , from this and with (2.30),  $\psi = 1.35$ , with (2.27),  $u = 38.1$  m/s and finally with (2.29), the diameter  $D = 1.94$  m follows. A change in  $\varphi_a$  has a reciprocal effect with the cube root, i.e., relatively little; thus the choice would be  $\varphi_a = 0.25$  and diameter  $D = 2.11$  m.

Only the Pelton turbine is suitable for the 1000 m head. With the number of nozzles  $i = 4$ , and  $n_q = 5.5 \times \sqrt{4} = 11$ , it follows that

$$P = \eta_t \eta_c \rho Q_a g H = 0.85 \times 1000 \times 59.81 \times 1000 = 41.7 \text{ MW}$$

$$n = n_q \frac{H^{0.75}}{Q^{0.5}} = 11 \frac{1000^{0.75}}{50.5} = 875 \text{ min}^{-1},$$

possible solutions are

$$\begin{aligned} p = 4 &\longrightarrow n = 750 \text{ min}^{-1} &\longrightarrow n_q = 9.43, \\ p = 3 &\longrightarrow n = 1000 \text{ min}^{-1} &\longrightarrow n_q = 12.57. \end{aligned}$$

Further solutions are possible by changing the number of nozzles.

The jet velocity is  $c_1 = 137$  m/s (with  $\eta_D = 0.96$ ).

The solution with  $n = 1000$  rpm results in  $u \approx 68$  m/s and  $D \approx 1.3$  m.

### Exercise 2.1

A run-of-river power plant is equipped with bulb turbines with the following parameters:  $H = 13.57$  m,  $Q = 334.8$  m<sup>3</sup>/s,  $P_t = 41.22$  MW [2.8]. Determine the most important parameters and main dimensions of the turbine.

## 2.6 Dynamics

For the investigation of dynamic processes during normal or disrupted network operation, but also for planning studies concerning network stability or network reconstruction, models are necessary that correctly reflect the dynamics of the hydropower plant including the hydraulic part. For example, the speed behavior can be influenced by the characteristics of the hydraulic system. Dynamic calculations of the hydraulic system are also a prerequisite for the optimum design of the

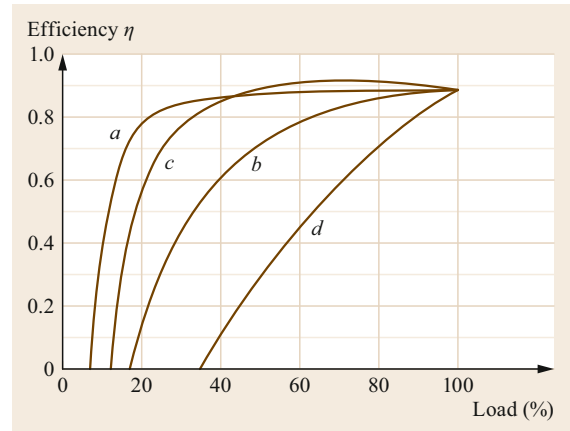


Fig. 2.33 Typical turbine efficiency curve, a: Pelton, b: Francis, c: Kaplan, d: Propeller

### 2.5.4 Small Hydropower Plants

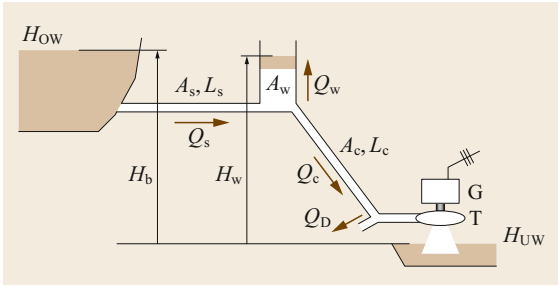
Full exploitation of the hydropower potential requires the construction of small-scale plants, where there are opportunities, often in conjunction with supplying drinking water (in Switzerland, usually < 300 kW). There are also programs to support this [2.13]. The calculations are mostly on the same basis as for a large plant. For the solution of the exercises see [2.9, annex F].

#### Exercise 2.2

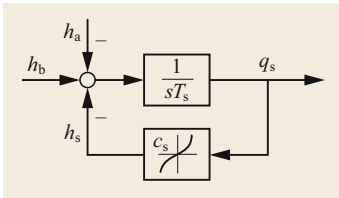
1. A stream continuously supplies a usable water quantity of at least 200 L/s. Without any particular construction problems, an effective head of 10 m can be installed. Which turbine variants are possible and what are their characteristics and dimensions?
2. Which turbine is suitable if the usable water quantity is only 40 L/s, but the usable head can be increased to 50 m?

surge chamber and the pressure line (pressure surge processes, Sects. 2.6.3 and 2.6.5).

In the general case, the system consists, according to Fig. 2.34, of a storage tank, pressure tunnel, surge tank, pressure line and hydro group. The reservoir is usually very large, and the height of the headwater  $H_{OW}$  can be regarded as constant for dynamic processes. For processes that are not too slow, this also applies to the height  $H_{UW}$  of the tailwater. The gross head is  $H_b = H_{OW} - H_{UW}$ .



**Fig. 2.34** Hydropower plant: G: generator, T: turbine,  $Q$ : water flow,  $A$ : cross section,  $L$ : length; indexes: s: pressure tunnel, w: surge tank, c: penstock, D: pressure regulator



**Fig. 2.35** Pressure-tunnel model

### 2.6.1 Pressure Tunnel

The energy balance (specific energy) is

$$L_s \frac{dv_s}{dt} = gH_b - gH_a - gH_s \quad \left( \frac{J}{kg} \right), \quad (2.31)$$

with  $v_s$  = mean water speed,  $H_a$  = effective head at the end of the tunnel,  $H_s$  = loss of height in the tunnel.

The left-hand side shows the acceleration energy of the water masses ( $\int F dx = \int m (dv/dt) dx = m (dv/dt) L$ ). The following is a good approximation of the losses in the tunnel

$$gH_s = K_s Q_s |Q_s|, \quad \text{with } Q_s = v_s A_s. \quad (2.32)$$

Replacing  $v_s$  by  $Q_s$  in (2.31) gives

$$\frac{L_s}{A_s} \frac{dQ_s}{dt} = gH_b - gH_a - gH_s. \quad (2.33)$$

By introducing the *nominal head*  $H_r$  and the *nominal water quantity*  $Q_r$  and dividing (2.33) by  $gH_r$ , one ob-

tains

$$\begin{aligned} h_b &= \frac{H_b}{H_r}, \quad h_a = \frac{H_a}{H_r}, \quad h_s = \frac{H_s}{H_r}, \\ q_s &= \frac{Q_s}{Q_r}, \quad c_s = K_s \frac{Q_r^2}{gH_r}, \end{aligned} \quad (2.34)$$

the *per unit (pu) equations of the tunnel*

$$\begin{aligned} T_s \frac{dq_s}{dt} &= h_b - h_a - h_s \quad \text{with } T_s = \frac{L_s Q_r}{A_s g H_r} \\ h_s &= c_s q_s |q_s|, \end{aligned} \quad (2.35)$$

and the corresponding block diagram Fig. 2.35.

By linearizing the loss equation, the linear model follows as

$$\begin{aligned} T_s \frac{d\Delta q_s}{dt} &= \Delta h_b - \Delta h_a - \Delta h_s, \\ \Delta h_s &= 2c_s |q_0| \Delta q_s = c_{s0} \Delta q_s \end{aligned} \quad (2.36)$$

with the block diagram and transfer function of Fig. 2.36.

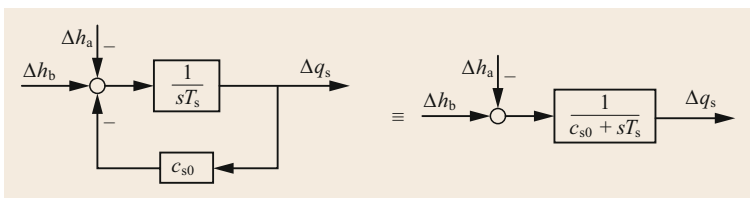
### 2.6.2 Surge Chamber

The exact representation of the surge chamber is quite complex [2.14], but with small oscillations of the water level the energy can be expressed with acceptable accuracy by: Energy  $gH_a$  at the end of the tunnel (or at the base of the surge chamber) is the sum of the potential energy corresponding to the water level  $H_w$  in the surge tank (Fig. 2.34) and the kinetic energy of the water at its base, the latter being assumed, as a good approximation, to be proportional to the square of the water flow in the tunnel [2.12, 14]. Kinetic energy and losses in the surge tank are neglected. Thus

$$gH_a = gH_w + K_w Q_s^2. \quad (2.37)$$

Furthermore

$$\begin{aligned} Q_w &= A_w \frac{dH_w}{dt}, \\ Q_s &= Q_c + Q_w. \end{aligned} \quad (2.38)$$



**Fig. 2.36** Linear tunnel model

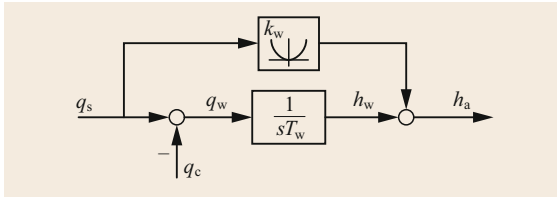


Fig. 2.37 Model of the surge chamber

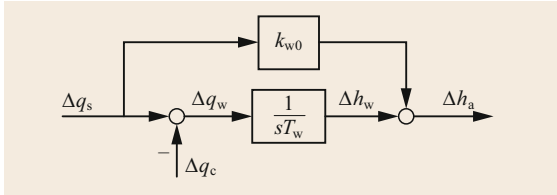


Fig. 2.38 Linearized model of the surge chamber

The introduction of the pu values, and the reference values  $Q_r$  and  $H_r$  analogous to (2.34), yields the pu equations

$$\begin{aligned} h_a &= h_w + K_w q_s^2, & \text{with } K_w &= K_w \frac{Q_r}{H_r}; \\ q_w &= T_w \frac{dh_w}{dt}, & \text{with } T_w &= A_w \frac{H_r}{Q_r}; \\ q_s &= q_c + q_w \end{aligned} \tag{2.39}$$

and the corresponding block diagram (Fig. 2.37). The coefficient  $k_w$  can be determined on the basis of theoretical considerations [2.14] or preferably by experimental identification.

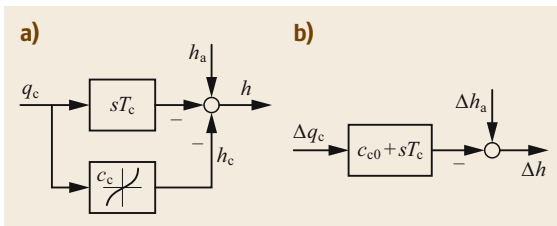


Fig. 2.39 (a) Model of the rigid penstock, (b) transfer function

Linearizing the kinetic energy gives

$$\begin{aligned} \Delta h_a &= \Delta h_w + K_{w0} \Delta q_s, & \text{with } K_{w0} &= 2K_w q_0; \\ \Delta q_w &= T_w \frac{d\Delta h_w}{dt}; \\ \Delta q_s &= \Delta q_c + \Delta q_w, \end{aligned} \tag{2.40}$$

and the linear model in Fig. 2.38, where stationary  $q_{s0} = q_{c0} = q_0$ .

### 2.6.3 Rigid Penstock

With the assumption that water is incompressible and the penstock is *rigid*, the penstock model is identical to that of the pressure gallery (the elastic pressure shock is dealt with in Sect. 2.6.5). If the effective head is denoted by  $H$ , then, instead of (2.35), we have

$$\begin{aligned} T_c \frac{dq_c}{dt} &= h_a - h - h_c & \text{with } T_c &= \frac{L_c Q_r}{A_c g H_r}, \\ h_c &= c_c q_c |q_c|, \end{aligned} \tag{2.41}$$

or by linearizing the losses

$$\begin{aligned} T_c \frac{d\Delta q_c}{dt} &= \Delta h_a - \Delta h - \Delta h_c, \\ \Delta h_c &= 2c_c |q_0| \Delta q_c = c_{c0} \Delta q_c. \end{aligned} \tag{2.42}$$

The block diagram of the rigid pressure pipe (penstock) is shown in Fig. 2.39a, and the transfer function obtained by linearization is shown in Fig. 2.39b. The input variable is the water flow  $q_c$  dictated by the turbine.

### 2.6.4 Overall Model of the Hydraulic System

#### Nonlinear Block Diagram

By bringing together Figs. 2.35, 2.37 and 2.39, the nonlinear block diagram of the hydraulic system results (Fig. 2.40).

#### Transfer Function

From (2.36), (2.40) and (2.42), the linearized relation between the effective energy  $\Delta h$  and the amount of

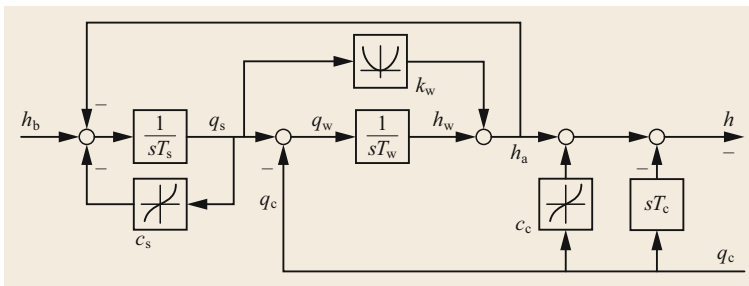
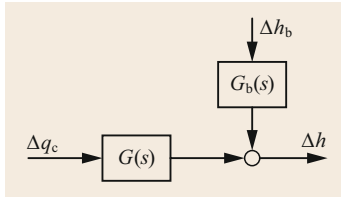


Fig. 2.40 Nonlinear model of the hydraulic system



**Fig. 2.41** Transfer function of the hydraulic system

water  $\Delta q_c$  or the change in the gross head  $\Delta h_b$  can be determined with

$$\begin{aligned}
 G(s) &= G_w(s) + G_c(s) \\
 &= \frac{c_{s0} + sT_s}{1 + s(k_{w0} + c_{s0})T_w + s^2T_wT_s} \\
 &\quad + (c_{c0} + sT_c) \\
 G_b(s) &= \frac{1 + sk_{w0}T_w}{1 + s(k_{w0} + c_{s0})T_w + s^2T_wT_s} \quad (2.43)
 \end{aligned}$$

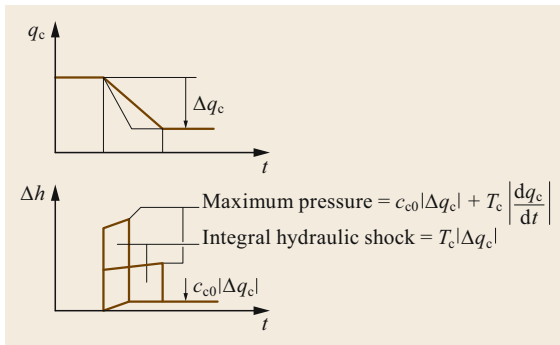
and is represented in Fig. 2.41.

The change of the gross head is usually zero or very slow, so the function  $G(s)$  is of little significance for dynamic processes.

The transfer function  $G_w(s)$  describes the *effect of pressure tunnel and surge tank*. A change of the water flow results in damped oscillations with the properties

$$\begin{aligned}
 \text{resonance frequency } \omega_0 &= \frac{1}{\sqrt{T_wT_s}}, \\
 \text{characteristic frequency } \omega_c &= \omega_0 \sqrt{1 - \zeta^2}, \\
 \text{damping factor } \zeta &= \frac{1}{2} (k_{w0} + c_{s0}) \sqrt{\frac{T_w}{T_s}}. \quad (2.44)
 \end{aligned}$$

For well-damped behavior, the time constant  $T_w$  and thus the cross section of the surge tank (2.39) must be sufficiently large. The period of oscillation is usually in the range of 100–300 s, while  $T_c$  is on the order of 1 s. For slow processes, the effect of the penstock can be neglected and  $G(s) = G_w(s)$  can be used.



**Fig. 2.42** Pressure surge

Conversely, for processes in the seconds range (primary speed control), the height  $h_a$  can be assumed to be constant and  $G(s) = G_c(s)$  can be used. By correctly dimensioning the surge tank, a decoupling between slow and fast processes is achieved.

The transfer function  $G_c(s)$  describes the *effect of the penstock* on the useful energy  $h$ . It is of a differential nature and is illustrated in Fig. 2.42. For large heads,  $h$  is practically the pressure at the lower end of the penstock. A linear decrease in the amount of water required by the turbines results in a pressure surge. If the water flow is restricted quickly, the pressure can assume very high values. An excessively rapid decrease in the water flow in the pressure line must therefore be avoided. To be able to reduce the turbine power quickly despite this (e.g., in the case of sudden load reduction), the Pelton turbine uses *jet deflectors* (Fig. 2.23), while the closing speed of the nozzle needle is limited. In reaction turbines, conversely, the guide wheel is quickly regulated according to the load and the pressure in the penstock is controlled by a *pressure valve* that diverts water upstream of the turbine inlet beyond an adjustable pressure limit (Fig. 2.34).

The preceding description of the penstock disregards the *compressibility of the water and the elasticity of the penstock wall* (together referred to concisely as elasticity). This causes the pressure conditions to be reproduced inaccurately. In Sect. 2.6.5, the elasticity is taken into account.

### 2.6.5 Elastic Pressure Surge

For systems with a large head, elasticity must also be taken into account because it makes it more difficult to stabilize the speed control. This generally applies to heads of approximately 100 m or more.

In any short section of the initially assumed *lossless penstock*, at a distance  $xL_c$  from the beginning of the line, the acceleration energy or acceleration force is

$$\begin{aligned}
 -gdH &= L_c dx \frac{dv}{dt} = \frac{L_c dx}{A_c} \frac{dQ_c}{dt} \left( \frac{\text{J}}{\text{kg}} \right), \\
 -\rho A_c g dH &= \rho L_c dx \frac{dQ_c}{dt} \quad (\text{N}). \quad (2.45)
 \end{aligned}$$

This force causes, in a time  $dt$ , as a result of the elasticity of water and the pipe, a change in the quantity of water per element  $L_c dx$

$$-\frac{dQ_c}{L_c dx} dt = \left( \frac{1}{\varepsilon} + \frac{D}{Ed} \right) \rho A_c g dH \quad (\text{m}^3), \quad (2.46)$$

where  $\varepsilon$  is the elastic constant of the water,  $E$  the modulus of elasticity of the conductor material, where  $D$

**Table 2.3** Analogy between electric cable and pressure line ( $Z_\tau$  = nominal impedance of the electric cable,  $Z_{w0}$  = wave impedance for  $\omega \rightarrow \infty$ ), see also [2.17, Chap. 5]

$U$	$h$
$I$	$q$
$Z_{w0}/Z_\tau$	$2\rho_A$
$\tau$	$\tau$
$CZ_\tau$	$\tau/(2\rho_A)$
$L/Z_\tau$	$T_c$
$R/Z_\tau$	$C_c q_c $ oder $c_{c0}^a$

<sup>a</sup> with linearization of losses

and  $d$  are the diameter and thickness of the pipe. From (2.45) and (2.46) it follows that

$$-\frac{\partial H}{\partial x} = \frac{L_c}{gA_c} \frac{\partial Q_c}{\partial t}$$

$$-\frac{\partial Q_c}{\partial x} = \left( \frac{1}{\varepsilon} + \frac{D}{Ed} \right) \rho_A c L_c g \frac{\partial H}{\partial t} \tag{2.47}$$

These equations are wave equations. Pressure waves (sound waves) propagate in the water with a speed  $a$  defined by

$$\frac{1}{a^2} = \rho \left( \frac{1}{\varepsilon} + \frac{D}{Ed} \right) \tag{2.48}$$

The order of magnitude of  $a$  is 1000 m/s. With the pu values, and the time constant  $T_c$  from (2.41) and the *penstock friction losses*, the following differential equations are finally obtained, where  $\rho_A$  is the *cable characteristic of Allievi*, and  $\tau = L_c/a$  is the *propagation time* of the pressure waves in the penstock [2.15, 16],

$$-\frac{\partial h}{\partial x} = T_c \frac{\partial q_c}{\partial t} + c_c |q_c| q_c,$$

$$-\frac{\partial q_c}{\partial x} = \frac{T_c}{(2\rho_A)^2} \frac{\partial h}{\partial x}, \quad \text{with } 2\rho_A = \frac{T_c}{\tau} \tag{2.49}$$

Equations (2.49) are analogous to Eq. 5.1 of the electric cable in [2.17], if the latter are brought into pu form. The analogous sizes are listed in Table 2.3.

**Penstock Models with Elasticity**  
**Pressure-Wave Model.** A model of the pressure-wave processes results, using the above-mentioned analogy, directly from Equations 5.86 [2.17, Chap. 5] of the distortion-free electric line, which, when rewritten analogously, are (with linearized losses)

$$h_a = h_{ae} + h_{ar},$$

$$h = h_{ae} e^{-(K+s\tau)} + h_{ar} e^{K+s\tau} = h_e + h_r,$$

$$q_c = \frac{h_{ae}}{2\rho_A} e^{-(K+s\tau)} - \frac{h_{ar}}{2\rho_A} e^{K+s\tau},$$

$$q_{ca} = \frac{h_{ae}}{2\rho_A} - \frac{h_{ar}}{2\rho_A} \tag{2.50}$$

The corresponding model is shown in Fig. 2.43;  $h_a$  and  $q_{ca}$  are energy and water flow at the intake, and  $h$  and  $q_c$  are those at the outlet of the penstock. The pressure wave attenuation is taken into account with a block  $e^{-K}$  that corresponds to the block  $e^{-\alpha l}$  of the electrical cable. For  $K$  values, using Table 2.3

$$\alpha l = \frac{R}{2Z_{w0}} \quad \longrightarrow \quad K = \frac{c_{c0}}{4\rho_A} \tag{2.51}$$

In order to include the stationary losses not correctly allowed for by (2.50), an appropriate correction and a non-linear block are introduced. The diagram is simplified if the formation of  $q_{ca}$  is not done and  $q_{ca} = q_c$  is used, i.e., the feedback effect of the fundamental and harmonic components on the sluggish plant on the mountain side is neglected.

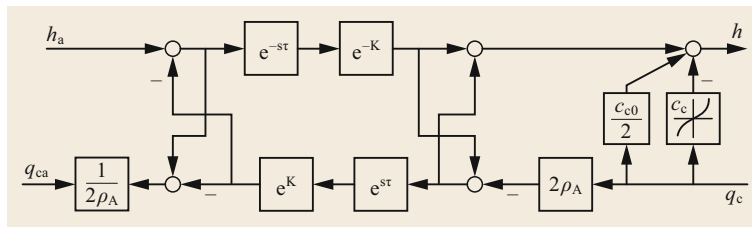
For further analytical considerations, it is useful to write the first of the two-port Equations 5.12 [2.17] by the following analogy

$$h_a = h \cosh s\tau + q_c 2\rho_A \sinh s\tau + h_c, \tag{2.52}$$

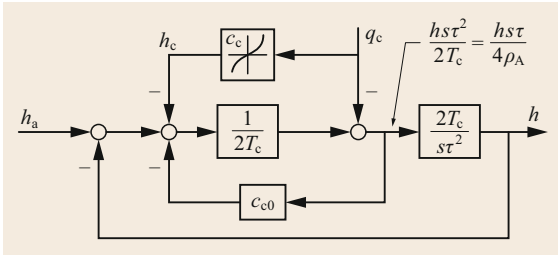
or even

$$h = \frac{h_a - h_c}{\cosh s\tau} - q_c 2\rho_A \tanh s\tau, \tag{2.53}$$

where the equations for the lossless case are written and the losses are dealt with separately.



**Fig. 2.43** Model of the elastic penstock



**Fig. 2.44** Rational approximation to the elastic penstock corresponding to the electrically short line

**Rational Approximations.** Similar to the explanations in [2.17, Sect. 5.6.2] it can be advantageous to replace the transcendental relationships with rational approximations. With the approximation  $\cosh s\tau = 1 + s\tau^2/2$ ,  $\sinh s\tau = s\tau$ , it follows from (2.52) that

$$h_a = h \left( 1 + s \frac{\tau^2}{2} \right) + q_c s T_c + h_c, \quad (2.54)$$

that represents the analogue of the lossless electrically short line. According to this analogy (Table 2.3), by introducing attenuation, the characteristic polynomial  $(1 + s\tau^2/2)$  can be replaced by the characteristic polynomial

$$K(s) = 1 + s\tau \frac{c_{c0}}{4\rho_A} + s^2 \frac{\tau^2}{2}. \quad (2.55)$$

By transformation from (2.54), we have

$$h_a = h + sT_c \left( q_c + h \frac{s\tau}{4\rho_A} \right) + h \frac{s\tau}{4\rho_A} c_{c0} + h_c \quad (2.56)$$

and taking into account that  $2\rho_A = T_c/\tau$ , we have the corresponding block diagram in Fig. 2.44. In this representation,  $q_{ca} = q_c$  is used.

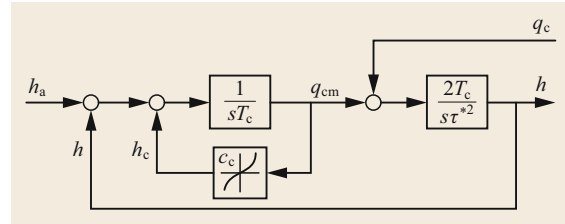
The fundamental oscillation is determined more exactly by the modal reduction analogous to [2.17, Eq. 5.95] with the characteristic polynomial

$$K(s) = 1 + s\tau \frac{2c_{c0}}{\pi^2 \rho_A} + s^2 \tau^2 \frac{4}{\pi^2}, \quad (2.57)$$

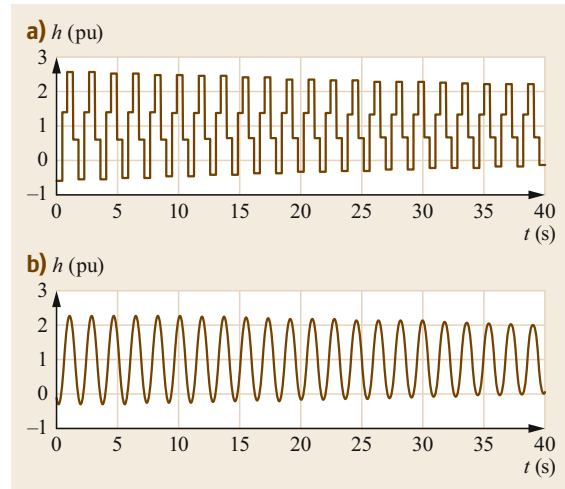
that can be used instead of (2.55). In Fig. 2.44, the propagation time  $\tau$  is then replaced by  $\tau^* = \tau \times 2\sqrt{2}/\pi$ .

A more convenient representation, essentially equivalent to Fig. 2.44, is obtained, if the second of [2.17, Eqs. 5.12] is also used with the somewhat coarser approximation  $\cosh s\tau = 1$ ,  $\sinh s\tau = s\tau$ . The analogy gives

$$q_{ca} = \frac{h}{2\rho_A} s\tau + q_c. \quad (2.58)$$



**Fig. 2.45** Efficient approximation of the elastic pressure line



**Fig. 2.46a,b** Response of  $h$  to a sudden change in  $q_c$ . (a) Model Fig. 2.43; (b) model Fig. 2.45,  $\Delta q_c = 0.2$  pu,  $h_0 = 1$  pu,  $T_c = 1.3$  s,  $\tau = 0.45$  s

By taking this relationship into account, it follows from (2.56) that

$$\begin{aligned} h_a &= h + sT_c q_{cm} + h_c, \\ \text{with } q_{cm} &= \frac{1}{2} (q_{ca} + q_c) = q_c + \frac{hs\tau^2}{2T_c}, \\ h_c &= c_c |q_{cm}| q_{cm}. \end{aligned} \quad (2.59)$$

Equations (2.58) and (2.59) give the model in Fig. 2.45 as a result. The formation of  $q_{ca}$ , that differs from  $q_c$  by only a fundamental oscillation component, and can be dispensed with, as this component has hardly any effect on the sluggish surge-tank-tunnel system. A similar representation can be found in [2.18].

Also in this model, the frequency of the fundamental oscillation is represented more accurately if  $\tau$  is replaced by  $\tau^* = \tau \times 2\sqrt{2}/\pi$ .

Figure 2.46 shows the change in the effective head  $h$  if there is a sudden change in the water flow for the models in Figs. 2.43 and 2.45.

### Transfer Function of the Elastic Penstock

Through linearization of (2.58) and (2.59) and with  $\tau^*$  instead of  $\tau$ , it follows that

$$\begin{aligned}\Delta q_{ca} &= \frac{s\tau^{*2}}{T_c} \Delta h + \Delta q_c, \\ \Delta h_a &= \Delta h + sT_c \Delta q_{cm} + c_{c0} \Delta q_{cm}, \\ \Delta q_{cm} &= \frac{1}{2} (\Delta q_{ca} + \Delta q_c).\end{aligned}\quad (2.60)$$

If  $\Delta q_{cm}$  and  $\Delta q_{ca}$  are eliminated and taking into account the elasticity, the transfer function of the penstock becomes

$$\begin{aligned}\Delta h &= \frac{\Delta h_a - (c_{c0} + sT_c) \Delta q_c}{1 + \frac{c_{c0}\tau^{*2}}{2T_c}s + \frac{\tau^{*2}}{2}s^2} \\ &= \frac{\Delta h_a - (c_{c0} + sT_c) \Delta q_c}{K(s)}.\end{aligned}\quad (2.61)$$

### 2.6.6 Overall Model of the Hydraulic System with Elasticity

#### Transfer Function

The block diagram in Fig. 2.41 is still valid, where for  $G_c(s)$  the following expression is used

$$G_c(s) = \frac{c_{c0} + sT_c}{K(s)}.\quad (2.62)$$

The effect of  $K(s)$  on  $h_a$  (and thus on  $G_w(s)$  and  $G_b(s)$ ) can be neglected because of the inertia of the surge tank.

#### Nonlinear Block Diagram

If in Fig. 2.40 the rigid penstock is replaced by the model of the elastic penstock given in Fig. 2.45, the block diagram Fig. 2.47 is as follows.

### 2.6.7 Turbine and Hydroelectric Plant Model

The behavior of the turbine is statically determined if the mussel diagram in the  $(\varphi, \psi)$ -plane and the two sets

of

$$\begin{aligned}\psi &= f(\varphi, A), \\ \psi &= g(\varphi, \eta_t)\end{aligned}\quad (2.63)$$

are known (2.32). The curves are largely independent of the rotation speed. Let  $A$  be the degree of opening of the control element of the turbine. For analytical treatment, it is advantageous to solve these two equations for  $\varphi$  and  $\eta_t$ . From (2.27) and (2.28), it follows that

$$\begin{aligned}Q &= K_0 \omega \varphi(\psi, A), \\ \eta_t &= \eta(\psi, A), \\ \psi &= \frac{4}{D^2} \frac{2gH}{\omega^2},\end{aligned}\quad (2.64)$$

where  $K_0$  can be determined from (2.28) or experimentally from the mussel diagram for the nominal speed  $\omega_t$  in the  $(Q, H)$ -plane.

For the Pelton turbine ((2.14) and (2.15)), the first line of (2.64) simplifies to

$$Q = K\omega \frac{D}{2} A \sqrt{\psi} = KA \sqrt{2gH}.\quad (2.65)$$

#### Power Equations

The turbine power according to (2.7) is

$$P_h = \rho Q g H, \quad P_t = \eta_t P_h,\quad (2.66)$$

and for the drive torque  $M_t$

$$P_t = M_t \omega.\quad (2.67)$$

The rotation rate is determined by the mechanical equation, which in the simplest case assumes the form

$$M_t - M = J \frac{d\omega}{dt}.\quad (2.68)$$

Here,  $M$  is the load torque and  $J$  is the moment of inertia of the generator group. With the assumption that the

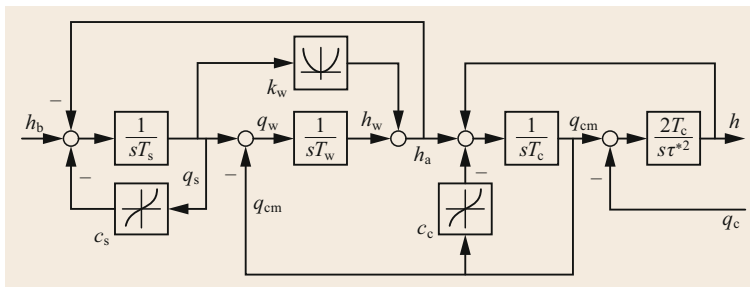
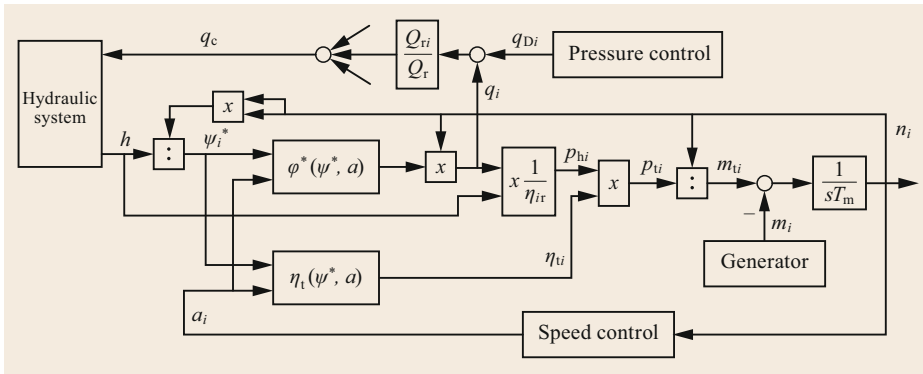
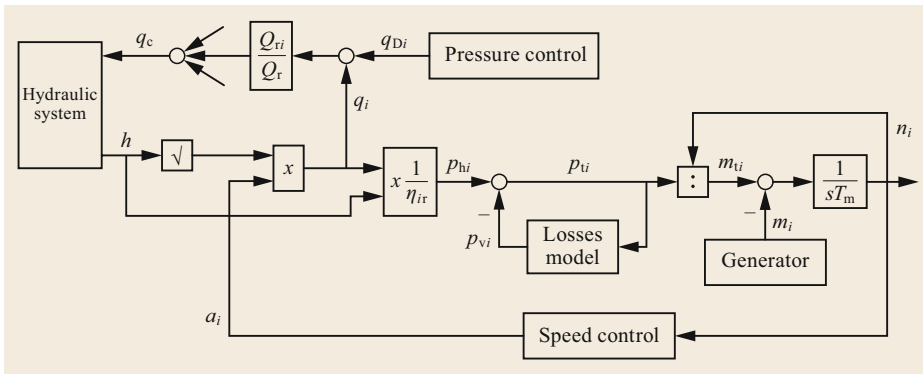


Fig. 2.47 Nonlinear overall model of the hydraulic part





**Fig. 2.48**  
Nonlinear block diagram of the hydropower plant



**Fig. 2.49**  
Simplified block diagram of the hydropower plant

penstock feeds  $m$  turbines and introducing the following reference or nominal values

the following pu system of equations is obtained from (2.64) and (2.66)–(2.68)

$$\begin{aligned}
 \text{Penstock:} \quad & H_r, Q_r = \sum_{i=1}^m Q_{ir}; & q_i &= n_i \varphi_i^*(\psi_i^*) \text{ with } \psi_i^* = \frac{h}{n_i^2}, \\
 \text{Turbine:} \quad & Q_{ir}, \text{ rated speed } \omega_{ir}, & \eta_{vi} &= \eta_i(\psi_i^*, a_i), \\
 & \text{rated efficiency } \eta_{ir}, & p_{hi} &= \frac{1}{\eta_{ir}} q_i h, \\
 & P_{ir} = \eta_{ir} \rho Q_{ir} g H_r = M_{ir} \omega_{ir}^3, & p_{ui} &= \eta_{vi} p_{hi} = m_{vi} n_i, \\
 \text{Pelton turbine:} \quad & Q_{ir} = K_i A_{ir} \sqrt{2gH_r}, & m_{vi} - m_i &= T_{mi} \frac{dn_i}{dt} \text{ with } T_{mi} = J_i \frac{\omega_{ir}}{M_{ir}}, \\
 \text{Reaction turbine:} \quad & Q_{ir} = K_{0i} \omega_{ir} \varphi(\psi_{ir}, a_{ir}), & & \\
 & \text{with } \psi_{ir} = \frac{8gH_r}{D_{ir}^2 \omega_{ir}^2} & & 
 \end{aligned} \tag{2.69}$$

and the corresponding block diagram in Fig. 2.48. For the Pelton turbine, the first equation simplifies to

and as well as the following pu values

$$q_i = a_i \sqrt{h}. \tag{2.72}$$

$$\begin{aligned}
 h &= \frac{H}{H_r}, \quad q_i = \frac{Q_i}{Q_r}, \quad a_i = \frac{A_i}{A_{ir}}, \\
 \phi_i^* &= \frac{\phi_i}{\phi_{ir}}, \quad \psi_i^* = \frac{\psi_i}{\psi_{ir}}, \quad p_{hi} = \frac{P_{hi}}{P_{ir}}, \\
 p_{ui} &= \frac{P_{ui}}{P_{ir}}, \quad n_i = \frac{\omega_i}{\omega_{ir}}, \quad m_{vi} = \frac{M_{vi}}{M_{ir}}, & & 
 \end{aligned} \tag{2.70}$$

A simpler representation results from the assumption that the efficiency depends only on  $a$  or if the losses are modeled instead of the efficiency, where these are usually expressed as a function of the output power. A loss model can be obtained from the efficiency curve for a nominal head and nominal speed. For the Pelton turbine, Fig. 2.49 (without pressure regulator) is appli-

cable. This model is also often used for the reaction turbine, but it should be noted that (2.72) is a rather rough approximation for this turbine [2.12].

### Linearization of Turbine Equations

If we omit the index  $i$  for the sake of clarity, the linearization of (2.71) at the operating point (index 0) yields

$$\begin{aligned}\frac{\Delta q}{q_0} &= K_1 \frac{\Delta h}{h_0} + (1 - 2K_1) \frac{\Delta n}{n_0} + K_2 \frac{\Delta a}{a_0} \\ &\text{with } K_1 = \frac{\partial \varphi}{\partial \psi} \frac{\psi_0}{\varphi_0}, \quad K_2 = \frac{\partial \varphi}{\partial a} \frac{a_0}{\varphi_0}, \\ \frac{\Delta \eta_t}{\eta_0} &= K_3 \frac{\Delta h}{h_0} - 2K_3 \frac{\Delta n}{n_0} + K_4 \frac{\Delta a}{a_0} \\ &\text{with } K_3 = \frac{\partial \eta}{\partial \psi} \frac{\psi_0}{\eta_0}, \quad K_4 = \frac{\partial \eta}{\partial a} \frac{a_0}{\eta_0}, \\ \frac{\Delta p_h}{P_{h0}} &= (1 + K_1) \frac{\Delta h}{h_0} + (1 - 2K_1) \frac{\Delta n}{n_0} + K_2 \frac{\Delta a}{a_0}, \\ \frac{\Delta p_t}{P_{t0}} &= (1 + K_1 + K_3) \frac{\Delta h}{h_0} \\ &\quad + (1 - 2K_1 - 2K_3) \frac{\Delta n}{n_0} \\ &\quad + (K_2 + K_4) \frac{\Delta a}{a_0}, \\ \frac{\Delta m_t}{m_0} &= \frac{\Delta p_t}{P_{t0}} - \frac{\Delta n}{n_0}, \\ \Delta m_t - \Delta m &= T_m \frac{d\Delta n}{dt}.\end{aligned}\quad (2.73)$$

The coefficients  $K_1 - K_4$  can be taken from the musel diagram. In the case of the Pelton turbine, (2.72) is applicable and therefore  $K_1 = 1/2$ ,  $K_2 = 1$ . If the efficiency is only expressed as a function of  $a$ , then  $K_3 = 0$ . If the efficiency is assumed to be constant,  $K_4 = 0$  also.

If, on the other hand, a loss model is used, as shown in Fig. 2.49 with

$$\begin{aligned}p_t &= p_h - p_v(p_t) \\ \rightarrow \Delta p_t &= \Delta p_h - \frac{dp_v}{dp_t} \Delta p_t,\end{aligned}\quad (2.74)$$

the equation for turbine power should be replaced by

$$\begin{aligned}\frac{\Delta p_t}{P_{t0}} &= K_5 (1 + K_1) \frac{\Delta h}{h_0} + K_5 (1 - 2K_1) \frac{\Delta n}{n_0} \\ &\quad + K_5 K_2 \frac{\Delta a}{a_0} \\ \text{with } K_5 &= \frac{1}{\frac{P_{t0}}{P_{h0}} \left(1 + \frac{dp_v}{dp_t}\right)}.\end{aligned}\quad (2.75)$$

Regardless of which assumptions are made, the following generally applies

$$\frac{\Delta p_t}{P_{t0}} = K_h \frac{\Delta h}{h_0} - K_n \frac{\Delta n}{n_0} + K_a \frac{\Delta a}{a_0}, \quad (2.76)$$

where the three coefficients can be obtained from (2.73) or (2.75), depending on the model. Finally, if the electrical power is introduced instead of the torque, then

$$\begin{aligned}\Delta p &= \Delta m n_0 + \Delta n m_0, \\ \text{where } p_0 &= p_0, \quad m_0 = m_0,\end{aligned}\quad (2.77)$$

and the linearized block diagram of the hydro group in Fig. 2.50 results.

The hydraulic system can be described by the following equation, corresponding to Fig. 2.48

$$\begin{aligned}\Delta h &= -G(s) \sum_{i=1}^m \alpha_i (\Delta q_i + \Delta q_{Di}) \\ &= -G(s) \alpha \Delta q + \Delta h_z, \\ \text{with } \alpha_i &= \frac{Q_{ir}}{Q_r};\end{aligned}\quad (2.78)$$

$\Delta h_z$  represents the disturbance caused by the pressure regulator and the change in the water flows of the other turbines fed from the same penstock. For fast processes in the seconds range, as they occur in the primary speed control, we have  $G(s) = G_c(s)$  that is given by (2.62).

### Transfer Function of the Turbine

If the first equations of (2.73) are inserted into (2.78), and (2.78) (or  $\Delta h$ ) into (2.76), one obtains

$$\begin{aligned}\Delta p_t &= G_t(s) \Delta a + G_z(s) \Delta h_z - S_t(s) \Delta n \\ \text{with } G_t(s) &= \frac{P_{t0}}{a_0} K_a \frac{1 - C_2 G(s)}{1 + C_1 G(s)}, \\ G_z(s) &= \frac{P_{t0}}{h_0} K_h \frac{1}{1 + C_1 G(s)}, \\ S_t(s) &= \frac{P_{t0}}{n_0} K_n \frac{1 + C_3 G(s)}{1 + C_1 G(s)}, \\ C_1 &= \frac{\alpha q_0}{h_0} K_1, \quad C_2 = \frac{\alpha q_0}{h_0} \left( K_2 \frac{K_h}{K_a} - K_1 \right), \\ C_3 &= \frac{\alpha q_0}{h_0} \left[ K_1 - (1 - 2K_1) \frac{K_h}{K_n} \right],\end{aligned}\quad (2.79)$$

and the linear block diagram of the hydropower plant as shown in Fig. 2.51, which is suitable for control engineering investigations.

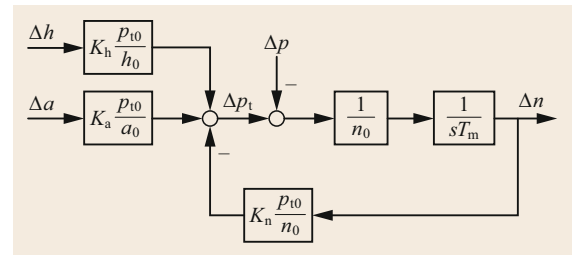
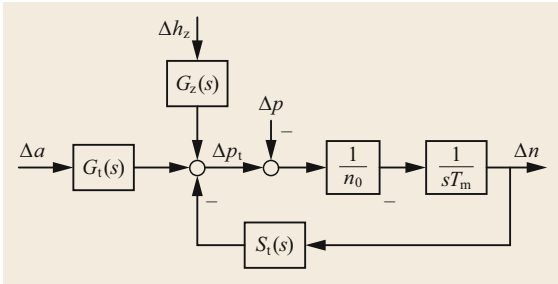


Fig. 2.50 Linearized block diagram of the hydro group



**Fig. 2.51** Linearized block diagram of the hydropower plant

In  $G_t(s)$  is the transfer function of the turbine; it describes the dependence of the turbine power on the degree of opening;  $G_z(s)$  describes the influence of groups fed from the same penstock on the turbine power;  $S_t(s)$  is the *self-regulating function* of the turbine. If it is positive, an increase in speed leads to a reduction in power and thus to a self-regulating effect.

With the *loss model*, the following applies exactly

$$c_2 = \frac{\alpha q_0}{h_0} . \tag{2.80}$$

An approximation of (2.72) is often used, with the exact equation for Pelton turbines, but for reaction turbines this is mostly inadequate, and the following applies

$$K_1 = \frac{1}{2} , K_2 = 1$$

$$\rightarrow C_3 = C_1 = \frac{1}{2} \frac{\alpha q_0}{h_0} . \tag{2.81}$$

The self-regulating function is then reduced to the coefficient  $K_n$ . In the case of the loss model, or if the efficiency depends only on the degree of opening,  $K_n = 0$  and the self-regulation effect is absent, otherwise  $K_n = 2K_3$ .

If even the change in efficiency is neglected, that is exactly correct at the point of maximum efficiency, the following applies

$$K_h = 1.5 , K_n = 0 , K_a = 1$$

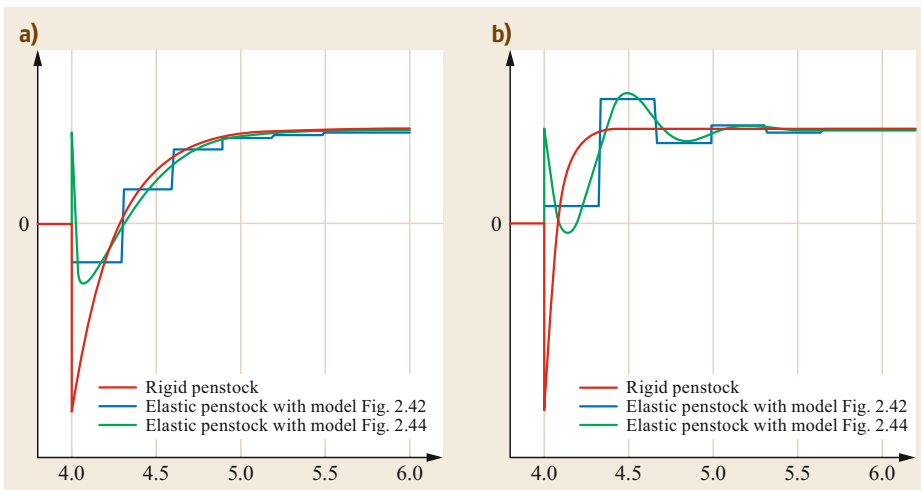
$$\rightarrow G_t(s) = \frac{p_{t0}}{a_0} \frac{1 - \frac{\alpha q_0}{h_0} G(s)}{1 + \frac{1}{2} \frac{\alpha q_0}{h_0} G(s)} , \quad s_t(s) = 0 . \tag{2.82}$$

If  $G(s) = G_c(s)$  is used, corresponding to (2.62), while the elasticity and losses of the penstock are neglected, and the load-dependent effective time constant  $T_{cx}$  introduced, the result is

$$T_{cx} = \frac{\alpha q_0}{h_0} T_c$$

$$\rightarrow G_t(s) = \frac{p_{t0}}{a_0} \frac{1 - sT_{cx}}{4(1 + s\frac{T_{cx}}{2})} . \tag{2.83}$$

Figure 2.52 shows the typical course of turbine power with an abrupt change in the degree of opening. When the elasticity of the penstock is taken into account, damped vibrations are superimposed (if  $\rho_A < 1$ ) with a frequency corresponding to (2.44)  $f_0 = 1/(4\tau) \approx 250/L_c$  Hz ( $L_c$  in m). With a weakly loaded turbine,  $T_{cx}$  and correspondingly, also  $\rho_A = T_{cx}/(2\tau)$ , are small.



**Fig. 2.52a,b** Time course of turbine output  $\Delta p_t/p_{t0}$  in the event of a sudden increase in the degree of opening  $\Delta a/a_0$ :  
**(a)**  $\rho_A = 1.73$ ,  
**(b)**  $\rho_A = 0.433$

## 2.7 Thermal Power Stations

The efficiency of power generation from fossil fuels in thermal power plants has risen considerably over time and today reaches almost 60% in natural gas-powered, combined cycle power plants. Nevertheless over 40% of the energy is still lost as waste heat.

### 2.7.1 Combined Heat and Power Generation

In combined heat and power (CHP), useful heat is produced in addition to electrical energy, thus further increasing overall energy efficiency. In the case of *steam turbines*, this can be done in two ways:

- 1) Through *steam extraction* (as with feed water pre-heating)
- 2) By increasing the condensation pressure (*counter pressure system*).

Variants and combinations of these two basic configurations are possible.

In the case of *gas turbine* with or without a recuperator or downstream steam turbine, the useful heat is recovered from the exhaust gases, with double compression also from the cooler [2.9, Sect. 5.2, Fig. 5.8].

Finally, for small capacities, *diesel systems* are also used, such as so-called *Block unit power plants* or *TOTEM* (total energy modules), whereby heat is extracted from the exhaust gases or the cooling circuit of the engine.

#### Extraction Condensation Circuit

The part  $m'_e$  of the steam mass  $m'$  is extracted at the extraction point G (Fig. 2.53). The corresponding heat is used for a heating system. The *extraction ratio* is defined as

$$\alpha = \frac{m'_e}{m'} \quad (2.84)$$

With reference to the cycle of Fig. 2.53, turbine power  $P_t$ , extracted heat output  $Q_H$  and supplied heat

$Q_1$  are

$$\begin{aligned} P_t &= m' [(h_E - h_G) + (1 - \alpha)(h_G - h_F)], \\ Q_H &= m' \alpha (h_G - h_A), \\ Q_1 &= m' (h_E - h_A). \end{aligned} \quad (2.85)$$

For the *performance figure*  $\varepsilon$  of the extraction condensation circuit, the ratio between the decoupled heat and the reduction of the turbine output is used

$$\varepsilon = \frac{Q_H}{\Delta P_t} = \frac{h_G - h_A}{h_G - h_F}. \quad (2.86)$$

The performance figure is independent of the extraction ratio. If the performance figure is specified (usually  $\varepsilon = 7-10$ ), the enthalpy of extraction  $h_G$  can be calculated from (2.86) and thus the extraction pressure. With the stated values of  $\varepsilon$ , the electrical power is reduced by less than 10% when maximum heat is extracted.

The *power-heat ratio* that indicates the ratio between electrical power and extracted thermal power is

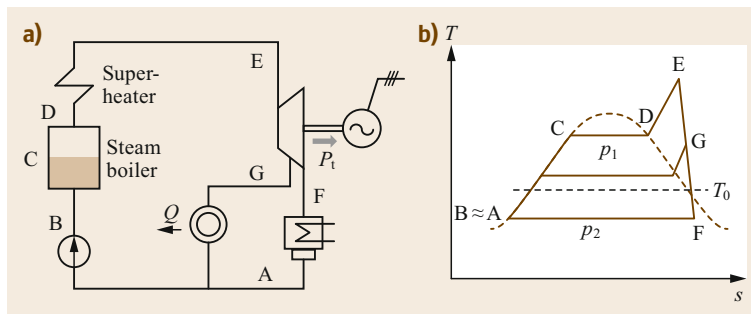
$$\begin{aligned} \sigma &= \frac{\eta_e P_t}{Q_H} = \eta_e \frac{(h_E - h_F) - \alpha (h_G - h_F)}{\alpha (h_G - h_A)} \\ &= \eta_e \frac{(\varepsilon - 1)(h_E - h_F) - \alpha (h_F - h_A)}{\alpha \varepsilon (h_F - h_A)}. \end{aligned} \quad (2.87)$$

The extraction condensation circuit enables a *flexible* adaptation of the heat extraction to the requirements. At full steam extraction ( $\alpha = 1$ ), one obtains the minimum electricity/heat ratio

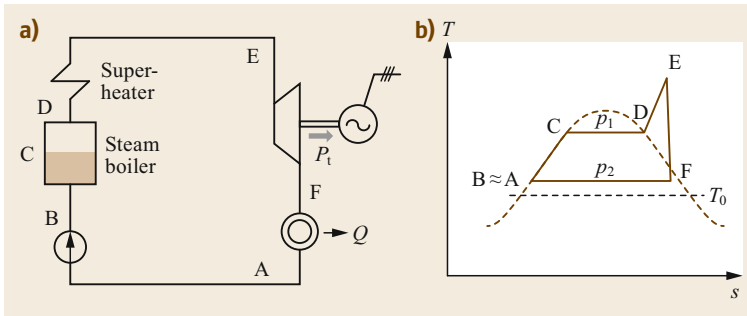
$$\sigma_{\min} = \eta_e \frac{h_E - h_G}{h_G - h_A} = \eta_e \frac{\varepsilon (h_E - h_F) - (h_E - h_A)}{\varepsilon (h_F - h_A)}. \quad (2.88)$$

The *overall energy efficiency* is

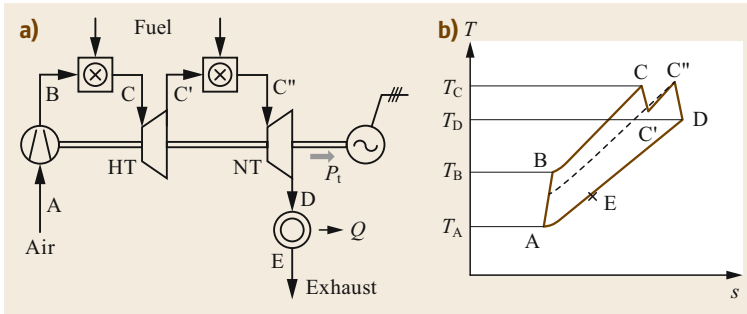
$$\begin{aligned} \eta_{\text{nutz}} &= \frac{\eta_e P_t + Q}{Q_b} = \left( \frac{\eta_e P_t}{Q_H} + \frac{Q}{Q_H} \right) \frac{Q_H}{Q_b} \frac{\eta_e P_t}{Q_b} \\ &= \frac{\sigma + \eta_H}{\sigma} \eta, \end{aligned} \quad (2.89)$$



**Fig. 2.53a,b** Heat-power generation by steam extraction. **(a)** Basic circuit diagram,  $P_t$  = turbine power,  $Q = \eta_H \times Q_H$  = useful heat output. **(b)** Temperature-entropy diagram,  $T_0$  = flow temperature of the heating system



**Fig. 2.54a,b** Combined heat and power with back-pressure system. **(a)** Basic circuit diagram,  $P_t$  = turbine power,  $Q = \eta_H \times Q_H$  = useful heat output. **(b)** Temperature–entropy diagram,  $T_0$  = flow temperature of the heating system



**Fig. 2.55a,b** Gas turbine with sequential combustion and combined heat and power generation. **(a)** Basic circuit diagram,  $P_t$  = turbine power,  $Q = \eta_H \times Q_H$  = useful heat output. **(b)** Temperature–entropy diagram,  $T_0$  = flow temperature of the heating system

where  $Q = \eta_H Q_H$  is the useful heat output,  $Q_b$  the heat content of the fuel and  $\eta$  the efficiency of the power plant without steam extraction. The overall efficiency increases with increasing heat extraction, from  $\eta$  for the process without heat extraction ( $\alpha = 0, \sigma = \infty$ ) up to the maximum value ( $\alpha = 1, \sigma = \sigma_{\min}$ ) according to (2.89).

### Back-Pressure System

In the back-pressure circuit, the turbine outlet temperature  $T_F$  is higher than the inlet temperature of the heating system (Fig. 2.54). This reduces the thermal efficiency of the process, but the full condensation heat is used. The main relationships result from (2.85) that illustrates the extraction condensation circuit for  $h_G = h_F$  and  $\alpha = 1$

$$\begin{aligned} P_t &= m' (h_E - h_F), \\ Q_H &= m' (h_F - h_A), \\ Q_1 &= m' (h_E - h_A). \end{aligned} \quad (2.90)$$

The formula for the *power-heat ratio* is always

$$\sigma = \frac{\eta_e P_t}{Q_H} = \eta_e \frac{h_E - h_F}{h_F - h_A}. \quad (2.91)$$

For the *overall energy efficiency*, it follows that

$$\begin{aligned} \eta_{\text{nutz}} &= \frac{\eta_e P_t + Q}{Q_b} = \eta + \frac{Q}{Q_b} = \eta \frac{\sigma + \eta_H}{\sigma} \\ &= \frac{Q}{Q_b} \frac{\sigma + \eta_H}{\eta_H}, \end{aligned} \quad (2.92)$$

where  $Q$  represents the heat effectively used and  $\eta$  represents the efficiency of electricity generation. The back-pressure circuit does not allow efficient adaptation of the heat extraction for reduced requirements, without a proportional reduction of the electricity production. If electricity production remains constant, the overall energy efficiency decreases in line with the reduction in useful heat efficiency  $\eta_H = Q/Q_H$ .

### Gas Turbines

Gas turbine plants are ideally suited for combined heat and power generation because the waste heat is generated at a high temperature. This also applies to the gas-turbine plant with a recuperator or downstream steam turbine.

With reference to the sequential combustion process of Fig. 2.55, the main relationships ( $m' \approx \text{const.}$  due to the large excess of air in the combustion process) are applicable according to [2.9, Sect. 5.2].

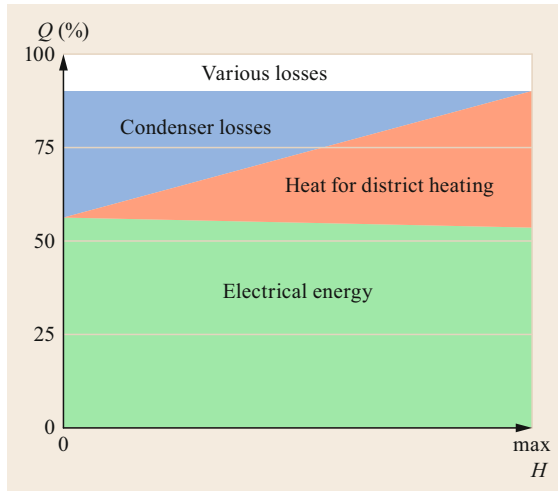
$$\begin{aligned} P_t &= m' c_p [(T_C T_{C'}) + (T_{C''} - T_D) (T_B - T_A)], \\ Q_H &= m' c_p (T_D T_A) \\ Q_1 &= m' c_p [(T_C T_B) + (T_{C''} T_{C'})]. \end{aligned} \quad (2.93)$$

For the power-heat ratio, we have

$$\sigma = \eta_e \frac{(T_C - T'_C) + (T''_C - T_D) - (T_B - T_A)}{T_D - T_E} \quad (2.94)$$

and for the overall energy efficiency

$$\eta_{\text{nutz}} = \frac{\eta_e P_t + Q}{Q_b} = \eta \frac{\sigma + \eta_H}{\sigma}, \quad (2.95)$$



**Fig. 2.56** Energy balance of a combined heat and power plant (gas turbine with sequential combustion and downstream steam turbine) as a function of steam extraction [2.19]

where  $Q = \eta_H Q_H$  is the heat effectively used and  $\eta$  represent the efficiency of electricity generation.

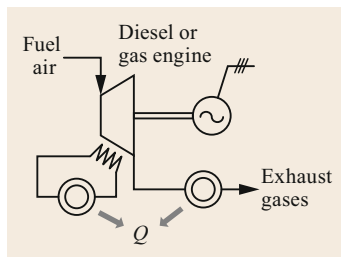
By combining it with a downstream steam turbine and using the heat from the exhaust gases and steam extraction, it is possible to achieve particularly high levels of overall energy efficiency paired with flexible heat extraction. As an example, Fig. 2.56 shows the energy balance of a combined cycle plant in the 100 MW range [2.9, Sect. 5.3, Fig. 5.13], with an overall energy efficiency of up to 85%.

### Block-Type Thermal Power Stations

In a similar way, heat can also be recovered from the exhaust gases and the cooling circuit in diesel- or gas-engine power plants. The basic circuit for this is shown in Fig. 2.57. Units in the power range 50 kW–15 MW are offered, with overall energy efficiencies from 85 to 90%.

### Combined Heat and Power and CO<sub>2</sub> Balance

In countries in which the production of electrical energy is predominantly from fossil fuels (such as Germany),



**Fig. 2.57** Combined heat and power unit

combined heat and power (CHP) enables a much more rational use of fossil fuels and thus contributes to the mitigation of the CO<sub>2</sub> problem (increased greenhouse effect).

In Switzerland, where electrical energy is generated almost exclusively with hydroelectric and nuclear power, the question arises as to whether the widespread use of combined heat and power leads to increased consumption of fossil fuels and thus to the opposite effect, unless biomass is used. The CO<sub>2</sub> balance looks much better when CHP is combined with heat pump technology [2.9, Chap. 6].

## 2.7.2 Fossil-Fired Steam Power Plants

A distinction is made between three main circuits, as illustrated in Fig. 2.58, in which the last two also occur in nuclear power plants:

- Air–fuel–flue gas/ash circuit
- Water–steam cycle
- Cooling water circuit.

### Air–Fuel–Flue Gas/Ash Cycle

The fuel and the air preheated by the flue gases are fed into the combustion chamber. Flue gas cleaning (flue gas treatment) includes, among other things, denitrification, desulfurization and dust removal. An ash extractor is required for coal fired systems. For more information on the combustion process, flue gas treatment and technology of fossil-fired steam generators see [2.20–22].

### Water–Steam Cycle, Losses

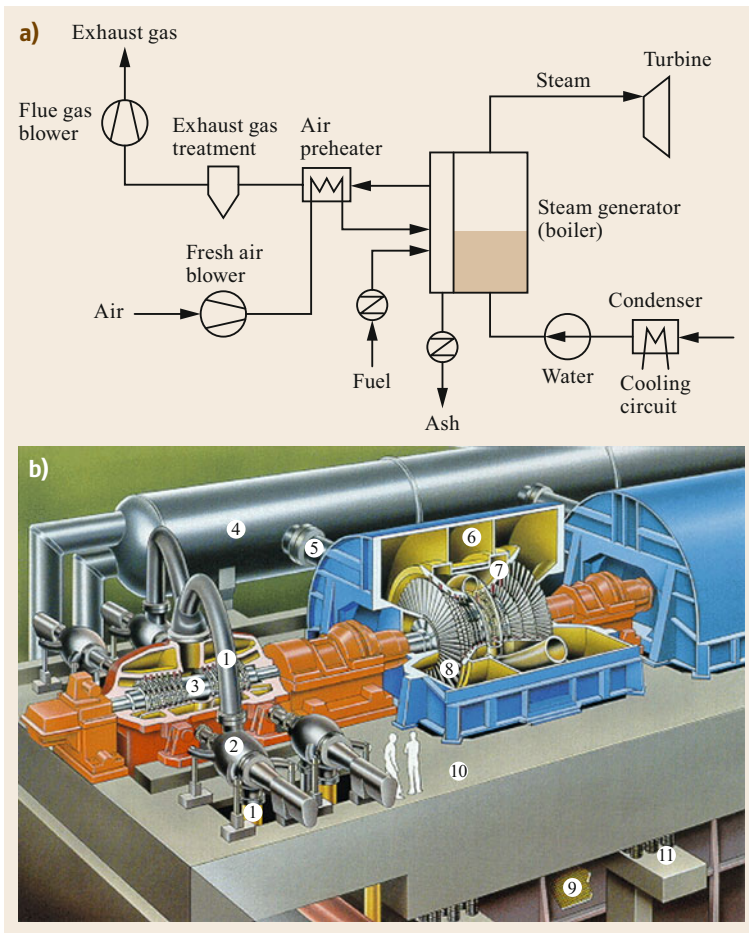
The thermodynamics of the water–steam cycle is described in [2.9, Sect. 5.1]. The main elements are the boiler, including a superheater and intermediate superheater, the turbine, the condenser and a feed-water preheater.

The dimensioning of the *steam generator (cauldron)* is based on the vapor pressure ( $p_1$ ) and the amount of steam required. For the latter, the rough guide value is approximately 3 t/(h, MWe); the exact values can be calculated from the process data (Mollier diagram) and efficiency  $\eta_e$ .

The *steam turbine* is a flow machine that converts the enthalpy difference between inflow and outflow into mechanical energy.

The rotation rate is 3000 or 1500 rpm at 50 Hz (3600 or 1800 rpm at 60 Hz), see also [2.17, Sect. 6.1]. Sometimes higher speeds are also chosen, and then the coupling to the generator is via a gear.

In the *condenser* the condensation heat is extracted from the humid or saturated steam leaving the turbine. Condensation pressure ( $p_2$ ) and temperature are related



**Fig. 2.58** (a) Main circuits in a fossil-fired steam power plant (principle), (b) steam turbine (1 live steam line, 2 stop and control valve, 3 high pressure turbine, 4 water separator/reheater, 5 steam line, 6 low pressure turbine, 7 guide vanes, 8 rotor blades, 9 condenser, 10 support plate, 11 vibration dampers) (adapted from [2.7])

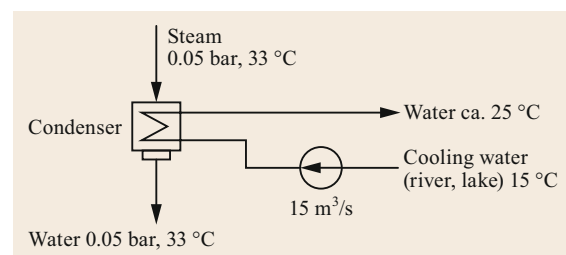
via the vapor-pressure curve. In modern power plants, condensation pressures of 0.04–0.1 bar are usually selected (corresponding to temperatures of 29–46 °C). The choice of condensation pressure strongly influences the efficiency of the cycle, but also the cost of the condenser.

For more information on the technology and design of steam generators, steam turbines and condensers, see [2.22].

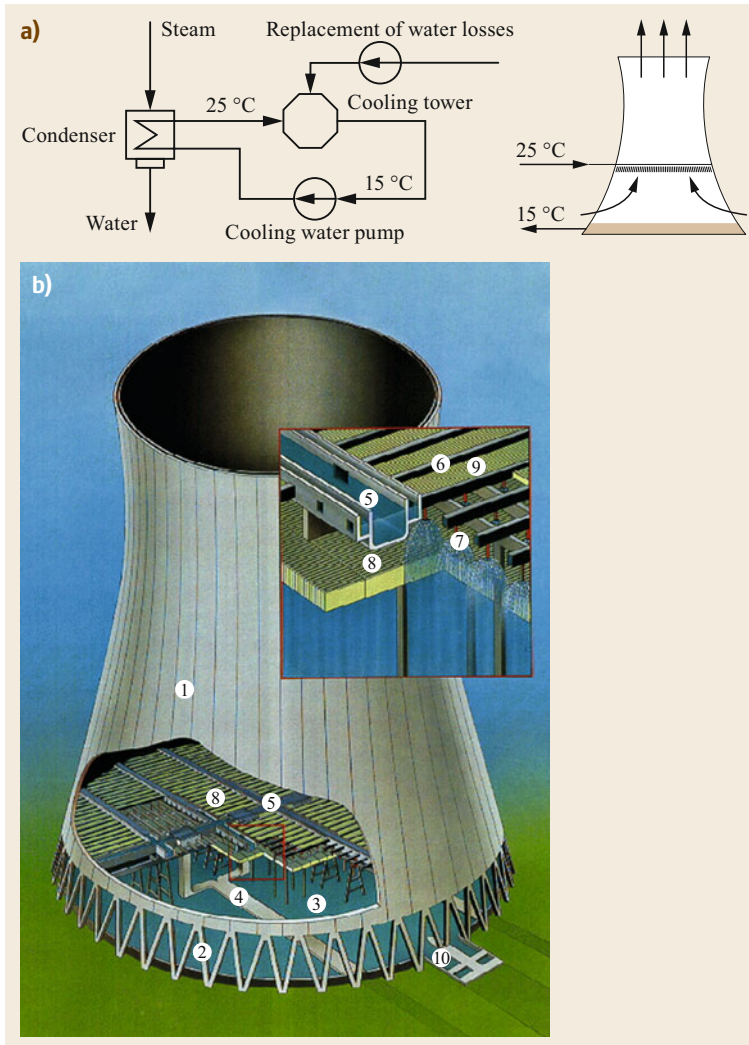
The *losses*, see also [2.9, Sects. 3.2 and 5.1], are the losses of the boilers and the circulation –  $\eta_K$  (guideline value 0.88), the losses of the idealized cycle  $\eta_{\text{threv}}$  (guide value 0.45–0.6 depending on the implementation), turbine losses (guide value 0.85) and generator losses and on-site power  $\eta_e$  (guide value 0.94). The indicated guide give, for example, a power plant efficiency of 31–42%. A small part of the heat loss is released into the environment with the flue gas and at various points in the plant. Most of the *waste heat* is transferred to the cooling water of the *condenser* that emits this heat to the environment via the cooling-water circuit.

### Cooling-Water Circuit

A distinction is made between freshwater cooling and tower cooling. The principle of *freshwater cooling* is shown in Fig. 2.59. The cooling water is taken from a river or lake and the heated water is returned to the source. The necessary cooling water quantity is about 50–70 times the steam weight, if cooling water heating of approximately 10 °C is permitted. For example, for a 300 MW power plant with approximately



**Fig. 2.59** Principle of freshwater cooling, possible values for 900 t/h steam



**Fig. 2.60** (a) Principle of the wet cooling tower, (b) cooling tower (1 shell, 2 supports, 3 basin, 4 water supply lines (from condenser), 5 distribution channels, 6 distribution troughs, 7 spray nozzles with baffle plate, 8 trickle plates, 9 drip catcher, 10 cooling water outlet (to condenser)) (adapted from [2.7])

900 t/h steam, 54 000 m<sup>3</sup>/h or 15 m<sup>3</sup> of cooling water is required. As the river temperature should only rise slightly for ecological reasons (the oxygen content decreases with increasing temperature), large rivers are needed even for these relatively small quantities of water (e.g., the River Rhine near Schaffhausen has a flow rate of around 180 m<sup>3</sup>/s). For this reason, tower cooling is usually used, especially when several power plants are operated on one river. The standard solution used today is wet tower cooling. The principle of *wet tower cooling* is shown in Fig. 2.60. The heated water trickles in a counterflow to the air rising in the cooling tower and partly evaporates. This removes heat, and the cooled water can be recycled. The water losses amount to only 2–3% of the required cooling-water quantity. The air flow results from the natural draught and can be amplified by fans.

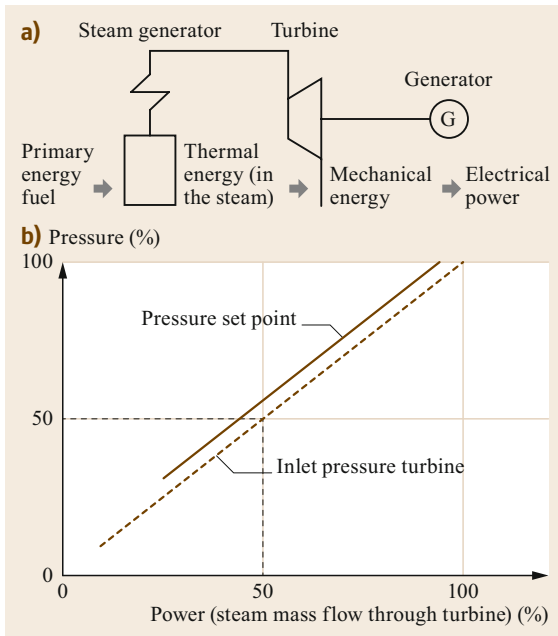
The steam vapors above the tower are disruptive, especially for nearby human settlements. Alternatives that do not have this disadvantage are dry or hybrid cooling towers, that however, have a lower cooling capacity for the same dimensions. For more information on the cooling system and the calculation and performance of wet and dry cooling towers, please refer to the section on the cooling system [2.20–22].

#### Unit Control

The power fed into the interconnected electrical grid by the power-plant units must correspond to the power drawn by consumers.

The grid frequency drops if the consumers draw more electrical power than the power plants feeds in, and increases if more power is fed in than is taken out. By controlling the mains frequency, a balance be-



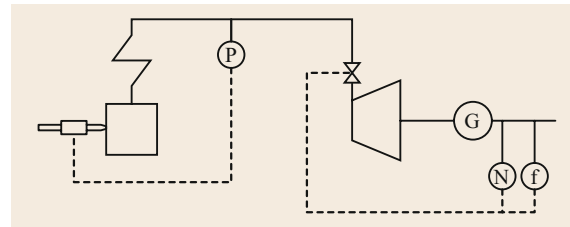


**Fig. 2.61** (a) Energy conversion in a steam power plant. (b) Sliding pressure diagram

tween supply and consumption is established. This is achieved on the one hand by means of fast primary frequency control, in which the power plants involved increase or decrease the output in proportion to the deviation from the target frequency in order to support the grid frequency. On the other hand, the load distributor also specifies power setpoints for the individual power plants so that the grid frequency can be brought back to the desired setpoint (secondary frequency control).

Unit control of a power plant regulates the power setpoint, that is varied with a given load change rate (MW/min) according to the expected power requirements for the grid. Short-term changes in the power drawn from the electrical network are regulated by the primary frequency control. In accordance with the set values (MW/Hz), each power station involved in maintaining the frequency increases or decreases the supplied electrical power proportionally to the deviation of the mains frequency from the set frequency. Further details on primary and secondary frequency control can be found in [2.17, Sect. 6.5.2] and [2.3, Chap. 2].

Figure 2.61 shows the principle of the *energy conversion* in a steam power plant. The thermal energy in the water vapor obtained from the primary energy must be in equilibrium with the electrical energy, taking into account the energy conversion losses. The steam pressure in the boiler falls when more electrical power is consumed than can be generated with the fuel supplied in.



**Fig. 2.62** Unit control principle: *boiler follows*

Unit control is the higher-level load control, that regulates the unit power capacity according to the network requirements and coordinates the interaction between the steam generator and the turbo-generator set of a power-plant unit, taking into account the dynamic behavior of the power-plant unit and the permissible load on the power-plant components.

The electrical output can be changed quickly with the control valves of the steam turbine, whereas firing control and steam generation act slowly. Furthermore, the storage behavior of the boiler can be used to handle short-term load changes of the turbine.

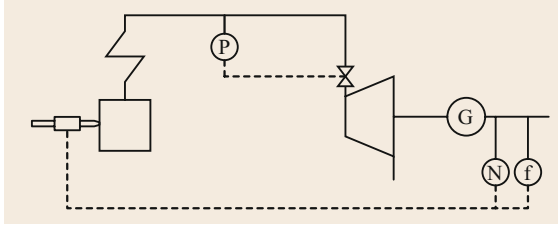
Depending on the plant design, the boiler pressure is set to a fixed set point (fixed pressure control) or to a variable load-dependent set point (sliding pressure). In a condensing turbine, the pressure upstream of the turbine valves and the turbine output are approximately proportional to the steam mass flow. If the steam turbine is operated with fully opened valves (*natural* sliding pressure), the pressure value before the turbine will correspond to the steam mass flow generated by the boiler.

In natural sliding-pressure operation, the turbine output cannot be increased by opening the control valves. Turbine power control is made possible by regulating the boiler pressure slightly above the sliding-pressure characteristic curve determined by the turbine design by means of firing control. This mode of operation is called modified sliding pressure.

In principle, two *types of unit control* can be distinguished [2.23].

In the first case, the steam turbine regulates the electrical power by means of the control valves, and the boiler regulates the steam pressure by means of the firing in order to establish the balance between the electrical power and the corresponding steam production. The steam pressure can be specified as a fixed setpoint or as a variable setpoint for modified sliding-pressure operation. The boiler *follows* the turbine power, as shown schematically in Fig. 2.62.

This procedure allows the boiler storage tank to be used for rapid load changes. If, however, the boiler cannot follow the desired load increase, the steam pressure drops. In order to avoid an inadmissible pressure reduction due, for example, to malfunctions in the steam



**Fig. 2.63** Unit control principle: *turbine follows* or sliding-pressure control

generator, an additional limitation control is applied to the control valves of the steam turbine if the steam pressure falls below the minimum value.

To improve the dynamics of the boiler pressure control, load changes are connected to the fuel control as feed forward control. When operating with modified sliding pressure, it must be taken into account that the boiler pressure must also be increased if the load is increased or reduced if the load is reduced. This type of control enables fast and precise control of the electrical power and requires extra outlay to achieve fuel control that is both sufficiently fast and smooth.

In the second case, the boiler regulates the electrical output, and the steam pressure is regulated by the steam turbine. In this approach, the turbine follows the load changes of the boiler, as schematically shown in Fig. 2.63.

The advantage of this circuit is that the control is stable on its own and also automatically copes with malfunctions in the boiler area. To be able to meet fast performance requirements, the control valves can be operated with some throttling (modified sliding pressure). This increases the steam pressure in the boiler and the stored energy can then be called up for a short-term increase in output before the steam production is adjusted to suit the changed requirements.

A short-term increase in performance can also be achieved by the *condensate-accumulation process*. In

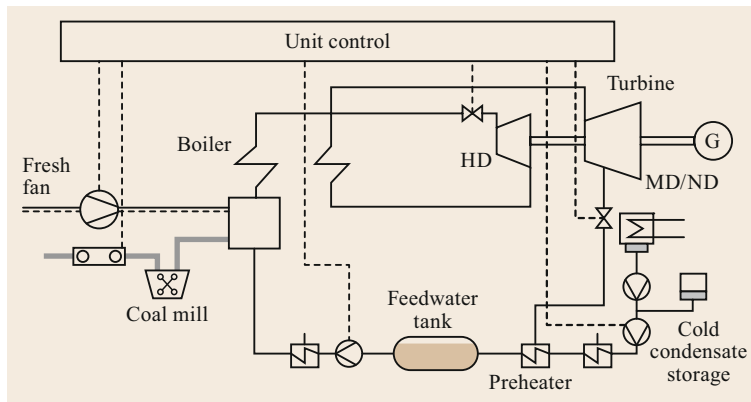
this process, the steam supply to the low-pressure preheaters is temporarily reduced, resulting in an increase in the electrical output of the steam turbine. The condensate supply is reduced accordingly to avoid a drop in the feed-water tank temperature. Depending on the capacity of the feed-water tank and of the cold condensate storage tank, it is thus possible to vary the output for a limited period with almost no reaction before the steam production is adjusted to meet the changed requirements.

Figure 2.64 schematically shows the main intervention points of a unit control with an integrated condensate-accumulation process. The required fuel flow is determined from the required power. Depending on the fuel flow, the combustion air must be adjusted for complete combustion and the feed-water flow set to meet steam production. Fast dynamic-load changes are achieved by the turbine control valves, that are slightly throttled in straight operation, and the extraction flaps for the low-pressure preheaters until the fuel flows again, corresponds to the electrical output.

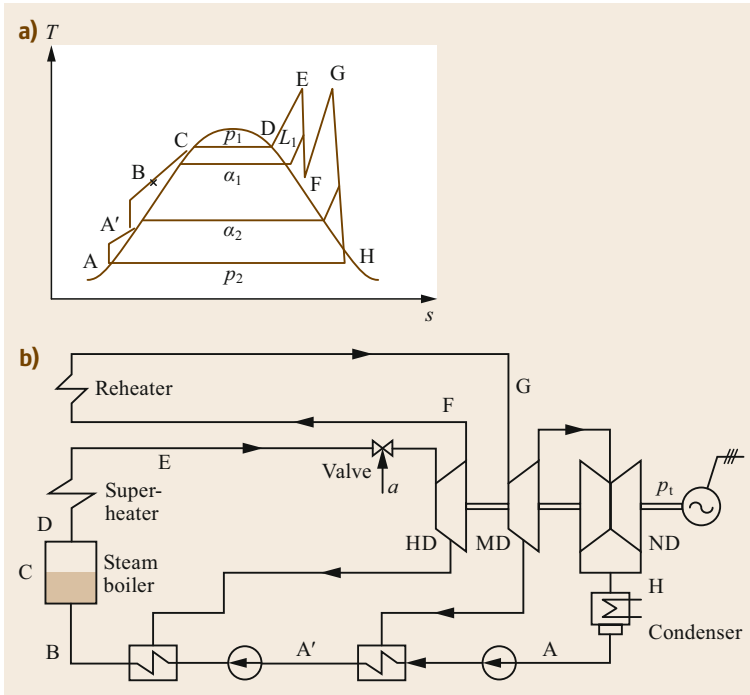
In addition to unit power plants, which serve exclusively to generate electrical energy, there are also power plants that provide process heat in addition to electrical energy (Sect. 2.7.1). Depending on the system configuration, the process steam or process heat extraction can be considered as a disturbance variable in the unit control for the electrical output, so that these power plants can participate in the primary and secondary control of the electrical grid. In many industrial power plants, however, the case occurs where the extracted process heat is the actual main control task, and the electrical output is adjusted according to the required process heat.

### Dynamics

In view of the rich variety and complexity of the steam power plants, only the basic behavior with regards to the reference scheme is described in Fig. 2.65. Although several coordinated valves can be active in a steam turbine, a single equivalent control valve between the



**Fig. 2.64** Unit control with integrated condensate accumulation



**Fig. 2.65** (a) Temperature–entropy diagram. (b) Schematic diagram of a steam power plant with a three-stage turbine, reheating and regenerative preheating

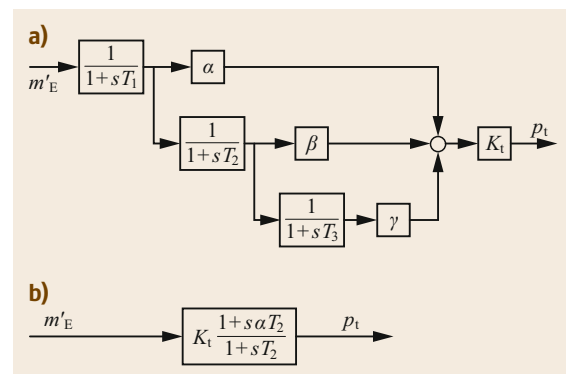
superheater and high-pressure (HP) turbine is assumed for the sake of simplicity. The thermal power available for the conversion at the superheater output E is given by  $P_E = m'_E \times \Delta h$ , where  $m'_E$  is the mass flow and  $\Delta h$  the available enthalpy change. If it is assumed that the subordinate control loops are capable of maintaining the temperature  $T_E$ , the enthalpy change is also constant and thus the power is proportional to the mass flow. This in turn is proportional to the degree of opening of the valve, that is controlled by the primary speed governor [2.3, Chap. 2].

Delays of the mass flow occur due to the volumes of the steam power plant. If we consider the volume  $V$  between two cross sections 1 and 2, then

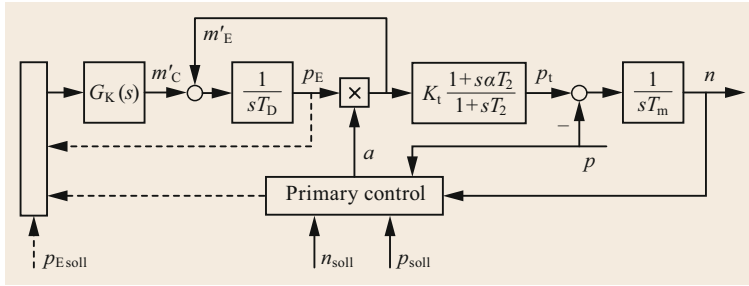
$$\begin{aligned}
 m'_1 - m'_2 &= V \frac{d\rho}{dt} = V \frac{\partial \rho}{\partial p} \frac{dp}{dt} \\
 &= V \frac{\partial \rho}{\partial p} \frac{1}{K} \frac{dm'_2}{dt} = T \frac{dm'_2}{dt}, \quad (2.96)
 \end{aligned}$$

where  $\rho$  represents the mass density. If it is also assumed that the output mass flow is proportional to the pressure, the mass flow  $m'_2$  follows the mass flow  $m'_1$  with the time constant  $T$ , that characterizes the inertia of the steam mass. In the plant under consideration, the largest delay is caused by the *reheater* whose time constant  $T_2$  is of the order of 10 s. Further first-order delays are between the valve and the HP turbine (guide value  $T_1 = 0.3$  s) and between medium-pressure (MP) and low-pressure (LP) turbine (guide value  $T_3 = 0.5$  s).

The relationship between the mechanical pu power  $p_t$  and the pu mass flow  $m'_E$  can be described by the block diagram of Fig. 2.66a. The coefficients  $\alpha, \beta, \gamma$  take into account the shares of the three turbine stages in the total output (with  $\alpha + \beta + \gamma = 1$ ). Stationary power losses can be accounted for with the constant  $K_t$ . Figure 2.66a leads to a third-order transfer function. It can be seen from the above-mentioned reference values that the output of the MP and LP turbines react much slower than that of the HP turbine because of the reheating. In view of the magnitude difference between the three time constants, a first approximation can set  $T_1 \approx 0$



**Fig. 2.66a,b** Transfer function of the steam turbine plant. (a) General third-order schema, (b) first-order approximation



**Fig. 2.67** Dynamic block diagram of the steam power plant ( $p_E$ : live steam pressure,  $p_t$ : turbine power,  $p$ : electrical power)

or  $T_1 \approx T_3 \approx 0$ , with the turbine plant represented approximately by a second- or even first-order transfer function, as in Fig. 2.66b.

Between mass flow in the HP turbine, live steam pressure  $p_E$  and the degree of opening  $a$  of the valve, there is the following pu relationship

$$m'_E = p_E a. \quad (2.97)$$

An increase in valve cross section  $\Delta a$  leads directly to an increase in mass flow and thus to a delayed increase in turbine output as shown in Fig. 2.66. On the other hand, the change in the mass flow causes a drop in pressure and thus, also in the density in the steam generator, that must be compensated by the boiler control. This decrease in pressure can be described by the pu equation

$$T_D \frac{dp_E}{dt} = m'_C - m'_E, \quad (2.98)$$

where  $m'_C$  represents the mass flow generated in the steam boiler. The time constant  $T_D$  can range between several tens of seconds and several hundred of seconds, depending on the type of boiler. The *boiler control* that controls the mass flow  $m'_C$  comprises several control loops that monitor the fuel, fresh air and feed-water supply. For example, it can have the task of maintaining the live steam pressure at the desired setpoint; in this case it is called *fixed pressure control*. In the case of *sliding pressure control*, it is controlled directly by speed or power (Sect. 2.7.2, *Unit Control*).

Figure 2.67 provides a dynamics diagram of the steam power plant, where the turbine is represented by a first-order system (Fig. 2.66b) and the boiler by the transfer function  $G_K(s)$ . The latter includes both the delays caused by heat release and the transfer function of the boiler controller (often a proportional integral (PI) controller).

### 2.7.3 Nuclear Power Plants

Nuclear power plants are essentially (as they are at present) steam-turbine power plants that are operated with nuclear instead of fossil fuel. The furnace is re-

placed by the *reactor*. An additional cooling circuit can be connected between the reactor and turbine ([2.9, Sect. 3.4], Fig. 2.71a).

A distinction is made between the:

- *Primary system*: reactor + in some cases additional cooling circuit and
- *Secondary system*: the other conventional elements of the steam circuit (for which the explanations in Sect. 2.7.2 essentially apply).

#### Energy Generation by Nuclear Fission

Nuclear energy can be released in two ways [2.9, Annex B]:

- By fusion of light atomic nuclei, i.e., from the hydrogen isotopes deuterium and tritium to helium. Industrial application is still a long way off (more details in [2.9, Chap. 11]).
- By splitting heavy atomic nuclei such as uranium, thorium and plutonium into medium-weight nuclei. The current industrial production of nuclear energy is based on the *uranium-fission reaction*. Thorium can be used in high temperature reactors. Plutonium is a by-product of uranium fission. For use in fast breeder reactors, the breeding is required be purified (Sect. 2.7.3).

**Uranium Fission.** Of uranium, 99.3% is the isotope  $^{238}\text{U}$  (238 nucleons, of which 92 are protons and 146 neutrons) and approximately 0.7% is  $^{235}\text{U}$  (with only 143 neutrons), and there are further small amounts of  $^{234}\text{U}$ . Only  $^{235}\text{U}$  can be split, and that is by slow (*thermal*) neutrons. The corresponding reaction is described in a somewhat simplified form in Fig. 2.68: the fission produces two nuclei of medium-weight (e.g.,  $^{137}\text{Ba}$  and  $^{97}\text{Kr}$ ), that have a higher binding energy and are therefore stable, releasing around 200 MeV. The fission of one kg of  $^{235}\text{U}$  results in the amount of energy

$$20 \frac{\text{Tcal}}{\text{kg}} \approx 24 \frac{\text{GWh}}{\text{kg}} = 1000 \frac{\text{MWd}}{\text{kg}}. \quad (2.99)$$

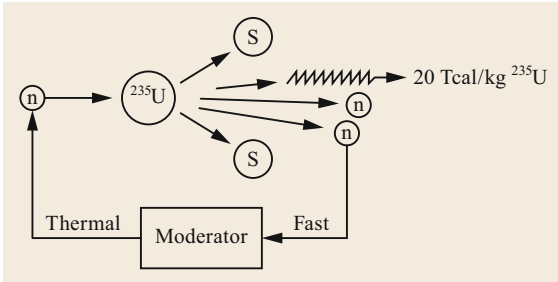


Fig. 2.68 Uranium fission: n: neutrons, S: fission products

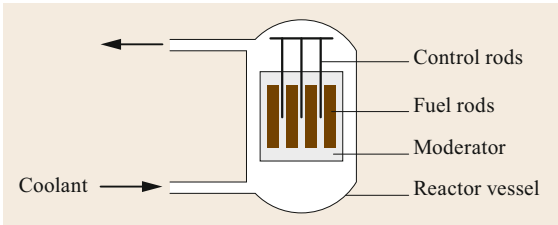


Fig. 2.69 Basic design of the thermal reactor

The fission of  $^{235}\text{U}$  atoms, releases an average of 2–3 neutrons, that have a high kinetic energy (*fast* neutrons). These neutrons are partly absorbed and partly available for further fissions as so-called *fission neutrons*. If on average more than one fission neutron remains, the number of fissions increases like an avalanche, i.e., there is a *chain reaction* with exponentially increasing heat output. With less than one fission neutron on average, the reaction fades out. In a *controlled reaction* it is ensured that just one fission neutron maintains the reaction (Fig. 2.68). The reactor is then *critical*, and the power output is constant.

For the fission neutron to be able to maintain the reaction, however, further conditions must be met. Fast

neutrons with kinetic energies in the range 1 eV to MeV lead much less often to fission of  $^{235}\text{U}$  than thermal neutrons with energies below 0.1 eV. In addition, fast neutrons are more easily captured by  $^{238}\text{U}$  atoms. This has the consequence that, for example, in natural uranium that contains a lot of  $^{238}\text{U}$  and not much  $^{235}\text{U}$ , the reaction ends immediately. The reaction can only be maintained if, with the help of a *moderator*, the speed of the neutrons is reduced to thermal values. Substances that strongly slow down neutrons without capturing them are  $\text{H}_2\text{O}$ , the best  $\text{D}_2\text{O}$  (heavy water) and graphite. Further information on uranium fission can be found in [2.9, Annex B.6].

These physical conditions lead to the basic structure of the *thermal reactor* as in Fig. 2.69. The *fuel rods* containing an uranium compound ( $\text{UO}_2$ ) are surrounded by the moderator. The *control rods* consist of a neutron-absorbing material (e.g., boron), and can be lowered into the reactor to the desired depth, so that the critical state of the reaction can be assured, i.e., the power of the reactor can be regulated. Liquids or gases are used as *coolants* to transport the resulting heat away ( $\text{H}_2\text{O}$ ,  $\text{D}_2\text{O}$ ,  $\text{CO}_2$ , He).

**Conversion Processes.** For each fission reaction of  $^{235}\text{U}$  nuclei, on average, slightly more than two neutrons are generated. One of these is needed to maintain the reaction. The remaining neutrons are absorbed by the moderator, control rods and fuel (without fission) or escape from the reactor core. The neutrons absorbed by  $^{238}\text{U}$  lead in a few cases to the rapid fission of  $^{238}\text{U}$  (that also contributes, to a small extent, to energy and neutron production), but they are mainly absorbed. The resulting  $^{239}\text{U}$  is transformed by electron emission into neptunium  $^{239}\text{Np}$  (atomic number 93) with a half-life of 23 min, as shown in Fig. 2.70. With a half-life

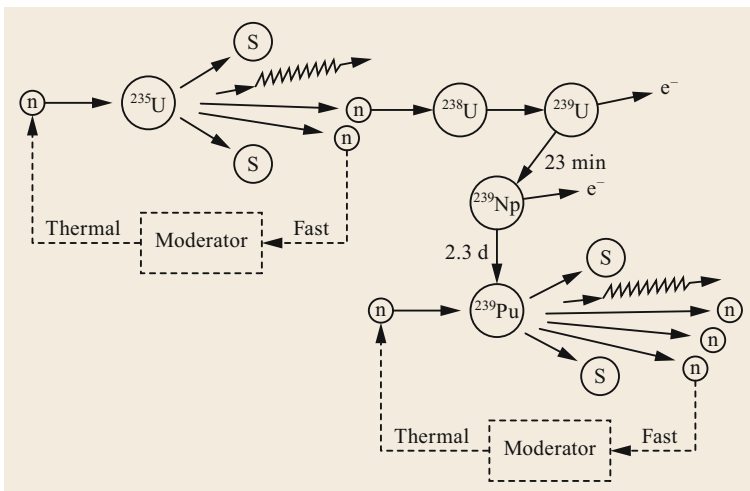


Fig. 2.70 Conversion reaction

of 2.3 days, this unstable element decays into a long-lived isotope *plutonium*  $^{239}\text{Pu}$ , that is fissile and has properties similar to those of  $^{235}\text{U}$  and contributes to energy production (see [2.9, Annex B.5]). Both reactions correspond to the following scheme  $n \rightarrow p^+ + e^-$  ( $\beta$ -radiation).

The conversion factor is the ratio of newly formed  $^{239}\text{Pu}$  nuclei to consumed  $^{238}\text{U}$  nuclei. Depending on the reactor type, it can assume different values, but is always small in *thermal reactors* (reactors in which fission is done by thermal neutrons). The conversion processes only slightly improve the utilization of natural uranium.

The conversion of  $^{238}\text{U}$  can also be triggered by  $^{239}\text{Pu}$  instead of  $^{235}\text{U}$ . Then, starting from  $^{239}\text{Pu}$ , new *Pu* is formed from  $^{238}\text{U}$ . If conversion factors  $> 1$  are reached, this is no longer called conversion, but breeding and breeding factors.

### Reactor Types

The reactors built to date are classed according to the *moderator used*:

- Light water reactors
- Heavy water reactors
- Graphite moderated reactors
- Fast breeder reactors (without moderator).

By far the largest proportion of the reactors used worldwide are *light water reactors* that have gained great importance in the energy sector. The individual reactor types are described briefly in the following, for further details see the relevant extensive technical literature.

**Light Water Reactors (PWR, BWR, EPR).** Normal (light) water is a good moderator, but not an excellent one. The critical state of the reaction therefore cannot be reached with natural uranium as the fuel (contains only 0.7%  $^{235}\text{U}$ ). For this purpose *enriched uranium* is required with a *degree of enrichment* (content of  $^{235}\text{U}$ ) ranging usually from 3–3.5%. For the enrichment natural uranium, available as  $\text{UO}_2$ , is first transformed into the gaseous uranium hexafluoride  $\text{UF}_6$ . This is then centrifuged, using the difference in weight between  $^{235}\text{U}$  and  $^{238}\text{U}$  to separate the enriched and depleted components.

A great advantage of the light water reactors is that the moderator and coolant are identical, namely  $\text{H}_2\text{O}$ . This makes the design very simple and the problem of heat transport can be solved relatively easily.

The achievable steam-inlet temperature of the turbines is significantly lower for all light water reactors than for fossil-fuel fired plants. Correspondingly, the achievable power plant efficiency is generally lower, at approximately 33%.

Light water reactors are built as pressurized water reactors (PWR) and boiling water reactors (BWR). In the pressurized water reactor, the heat is taken to a *separate* steam generator by the pressurized *primary cooling water*. The basic, somewhat simplified structure of the power plant with typical steam data is shown in Fig. 2.71a. The detailed structure of a pressurized water reactor power plant is shown in Fig. 2.71b.

The pressurized water reactor is currently experiencing an upswing as the EPR (European pressurized reactor, French–German financed). A first reactor of this type is under construction in Finland (capacity 1600 MW) and a second one in France (Fig. 2.71). These reactors of the so-called 3rd *generation* have significantly better safety properties. Also the efficiency is said to be better (at 36%).

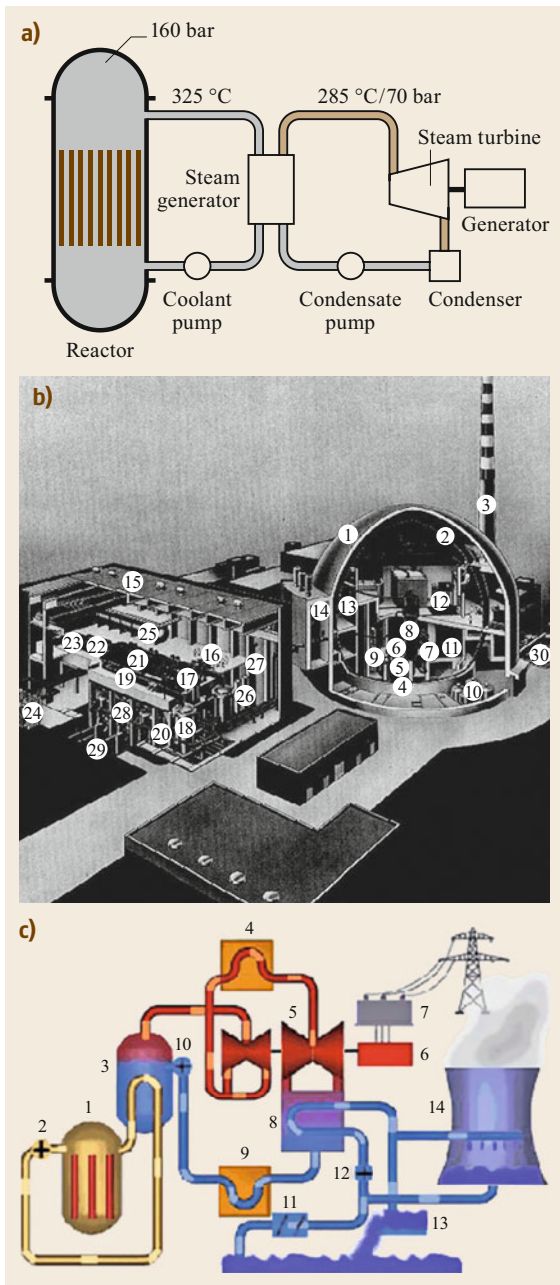
In a *boiling-water reactor*, steam production takes place in the reactor itself. The structure of the power plant and typical steam data are shown in Fig. 2.72.

**Heavy Water Reactor (HWR).** In the heavy water reactor,  $\text{D}_2\text{O}$  (heavy water) is used instead of normal water as the moderator and coolant. The fuel elements are located in pressure tubes that are cooled individually. The heated heavy water transports the heat to the steam generator (as in the pressurized water reactor Fig. 2.71). Since heavy water is an excellent moderator, *natural uranium* can be used as fuel, which is the main advantage of this type of reactor (no enrichment necessary). HWR were developed to industrial maturity in Canada and are used there and in India. The achievable power plant-efficiency is around 32%.

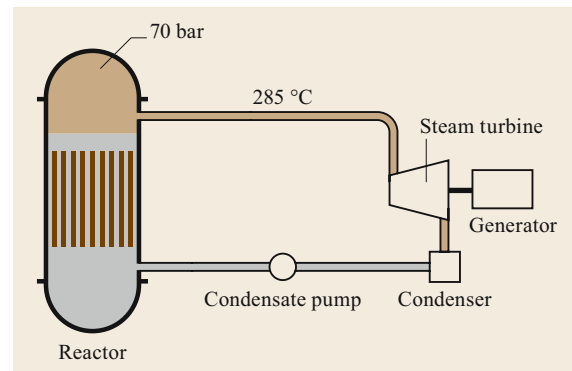
**Graphite-Moderated Reactors.** Various types of graphite-moderated reactors have been developed and used over time.

In the *RBMK (reaktor bolshoy moshchnosti kanalnyy) reactor*, that was developed in the former USSR and is still in operation in the successor countries, the fuel elements are also located in pressure tubes in which  $\text{H}_2\text{O}$  flows (coolant). The pressure tubes are housed in a graphite block. The moderator is  $\text{H}_2\text{O}$  and above all *graphite*. The achievable steam temperatures are comparable to those of light and heavy water reactors. After the accident in *Chernobyl*, the development of this reactor line has been halted.

In the *AGR reactor* (advanced gas cooled reactor), that is being developed and used in Great Britain, the fuel elements in steel tubes are located directly in the graphite. Cooling is done with  $\text{CO}_2$ . The materials used make it possible to reach temperatures of  $550^\circ\text{C}$  and thus implement steam processes with superheating. This increases the power plant efficiency to around 40%.



**Fig. 2.71** (a) Principle of the pressurized water reactor and typical steam and pressurized water data (1 reactor, 2 steam turbine, 3 generator, 4 condenser, 5 condensate pump, 6 steam generator, 7 coolant pump), (b) pressurized water reactor power plant (1 reactor building, 2 safety container (steel shell), 3 exhaust chimney, 4 reactor pressure vessel, 5 fuel elements, 6 control rods, 7 primary coolant pump, 8 steam generator, 9 pressurizer, 10 flood tank, 11 fuel element storage pool, 12 fuel element loading machine, 13 live steam line, 14 safety valves, 15 machine hall, 16 fast-closing and control valves, 17 high pressure turbine, 18 water separator reheater, 19 steam line, 20 steam bypass system, 21 low pressure turbine, 22 generator, 23 exciter, 24 transformer, 25 feed water tank, 26 pre-heater, 27 feed water pipe, 28 capacitor, 29 cooling C pipe (cooling circuit), 30 interim storage facility for radioactive waste (underground)) (adapted from [2.24]), (c) diagram of the EPR power plant under construction in Finland (Areva) (1 reactor, 2 reactor cooling pumps, 3 steam boiler, 4 re-heater, 5 turbine, 6 generator, 7 switchgear, 8 condenser, 9 water preheater, 10 condensate pump, 11 cooling water circuit, 12 cooling water pumps, 13 cooling water system, 14 cooling tower) ◀



**Fig. 2.72** Principle of the boiling water reactor and typical steam data

Since graphite is a better moderator than light water, both reactor types (RBMK and AGR) use fuel elements with a slightly lower enrichment of approximately 2%.

In a *high-temperature reactor* (HTR), graphite and silicon are used as fuel cladding materials and helium as the coolant (nuclear research facility Jülich, Germany, 1970s). This allows coolant temperatures of 700–950 °C to be achieved, enabling the operation of

both superheated steam circuits and gas turbines or combined cycle plants. Accordingly, the power plant efficiencies can reach 40–48% [2.25]. The fuel must have a relatively high enrichment level > 8%. Despite the great advantages of this reactor line, and also the inherent *passive safety* (inherent operational safety), the development towards industrial maturity in Germany is currently blocked. The development of this reactor line, that was to become the *reactors of the so-called 4th generation* is mainly being pursued in China, Japan and South Africa. It also allows thorium (about three times abundant as uranium) to be used as fuel.

**Fast Breeder Reactors.** The fast breeder reactor focuses on the conversion process described in Fig. 2.70 with a conversion factor  $> 1$  (breeder factor). It is not, however, driven by thermal neutrons, but by *fast neutrons* which is why a moderator is not necessary. However, since fast neutrons produce fewer fission neutrons than thermal neutrons, a relatively high enrichment level is necessary. In this respect, plutonium behaves much better than uranium, which is why the reactor core typically consists of an inner *fission zone* with 80% natural uranium and 20% plutonium and an outer *breeding zone* with  $^{238}\text{U}$ . Liquid sodium is used as a coolant because of its non-moderating properties.

Interest in the breeder reactors lies in the far better utilization of uranium, that in thermal reactors is about 1%, while in breeder reactors can be increased 30–50 times. It could therefore solve the problem of limited uranium reserves. This development is stagnating as a result of the risks associated with this reactor line and the resulting lack of acceptance (see also Sect. 2.7.3).

### Steam Cycle and Control

The only difference between a nuclear power plant and a normal fossil steam-power plant is that the reactor replaces the furnace or boiler. The steam cycle of light water reactors is characterized by weak superheating and reheating to temperatures only slightly over the evaporation temperature. Accordingly, as already mentioned, the efficiency is lower than that of fossil-fired plants. Reheating is primarily intended to prevent steam condensation in the turbines.

Nuclear power plants are used as base-load power plants, i.e., they operate at constant power and do not participate in the frequency power control of the grid [2.3, Chap. 2]. In principle, the block diagram in Fig. 2.67 applies to the dynamics of the nuclear power plant, with the reactor control replacing the boiler control. For more information about reactor dynamics and reactor control see, for example, [2.23, 26].

### Reactor Safety and Fuel Cycle

The radiation generated by nuclear fission and the radioactive fission products must be isolated from the environment, for which appropriate safety and disposal measures must be set up. This concerns the nuclear power plant itself and all plants involved in the fuel cycle. [2.27]

**Reactor Safety.** For safety reasons, the primary plant, that comprises the reactor and the primary cooling circuit, is housed in a separate, often spherical building. The fission products produced in the reactor are separated by a graduated *barrier system* isolated from

the environment. The pressure-resistant and gas-tight casings of the fuel elements form the first barrier. A second barrier is the equally pressure-resistant steel shell of the reactor or primary system. Finally, the reactor plants are located in the aforementioned reactor protection building made of steel and concrete, that forms the third barrier. This triple barrier system is intended to provide protection against internal and external influences. Aircraft crashes and earthquakes should be mentioned as external influences. In addition to the radioactive radiation generated during operation, which must be absorbed, the internal influences also includes the increase in pressure or heat build-up occurring in the event of accidents, that in the worst case can lead to core meltdown if the multiple control and shutdown devices fail. During normal operation or in the event of malfunctions, the discharge of contaminated air or water is prevented by suitable *filter systems*.

**Fuel Cycle and Disposal.** The steps involved in the supply and disposal of fuel are shown schematically in Fig. 2.73a.

The *supply* comprises the mining of uranium ore, the extraction of natural uranium and finally the uranium enrichment with subsequent fuel production required for the operation of light water reactors.

After use in the NPP, the spent fuel elements are initially *stored temporarily* in water in the reactor building for about one year and cooled until the residual heat has decayed. Then they are taken into reprocessing or prepared for final storage.

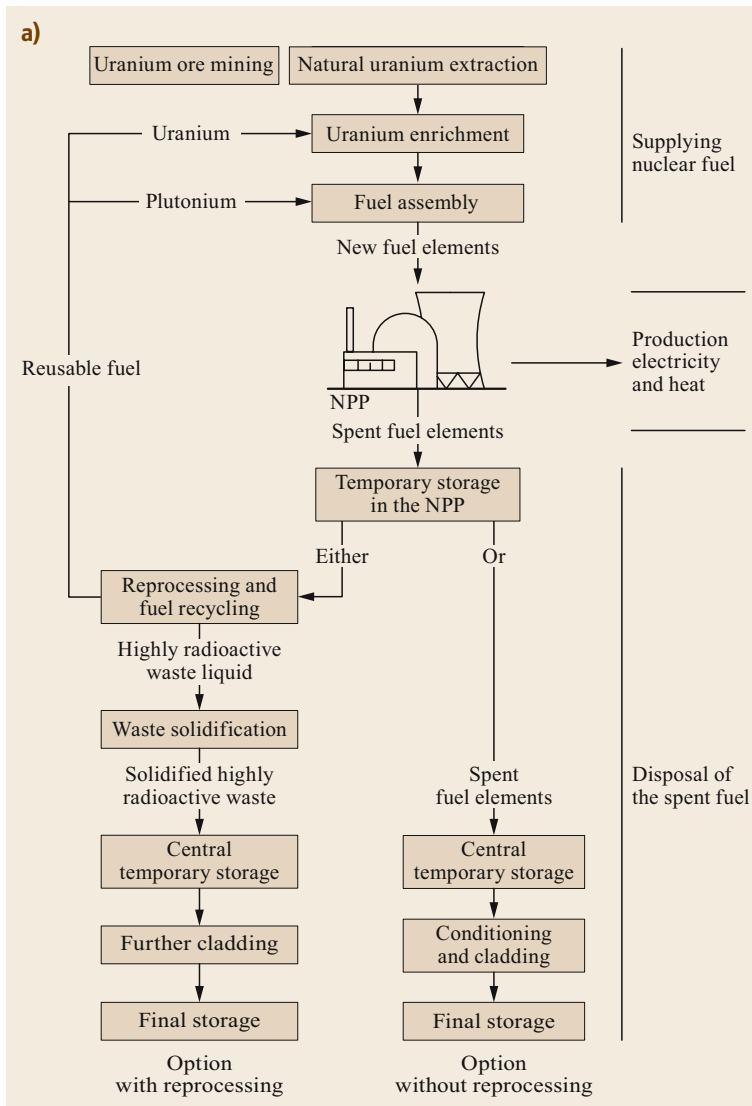
If no reprocessing is planned, the spent fuel elements are temporarily stored centrally for a long time and finally *conditioned*. Conditioning includes vitrification and containment of waste in steel containers. The final storage sites are sealed caverns impermeable to gases and liquids (e.g., salt mines).

During reprocessing, reusable materials such as uranium and plutonium are separated and taken for enrichment or fuel production. Non-usable waste is conditioned and put into permanent storage.

Low and intermediate level waste from power plants is conditioned together with waste from medicine, research and industry (using other processes) and finally disposed of in suitable repositories.

Reprocessing has the advantage that less natural uranium is required and allows the use of plutonium, that reduces the amount of high-level radioactive waste (by a factor of about five). On the other hand, however, the amount of low- and intermediate-level waste increases considerably as a result of the reprocessing process.





**Fig. 2.73 (a)** Fuel cycle of nuclear power plants with light water reactors and associated work steps. The disposal routes for low- and intermediate-level waste are not marked [2.27]. **(b)** Disposal and storage of nuclear waste of high, medium and low activity (adapted from [2.27])

Since civilization with technology produces radioactive waste (not only in nuclear power plants), it is imperative to dispose of it safely. Practical problems arise in democratic, federally organized countries due to the initial lack of regional acceptance of the repositories, which must be achieved through laborious educational work or the centralization of competencies by political means.

Another controversial issue and the subject of technical and political discussion is whether the final disposal of waste should be sustainable, safe and definitively monitored over the long term, and whether the monitoring and maintenance of the repositories should

then be ensured over a long period of time and adapted to the latest technology.

### Hazards of Nuclear Power

Like other processes in our technical civilization, nuclear power has associated hazards. These depend on the state of development of technology that will ultimately decide whether or not nuclear power will continue to play an important role in energy supply in the future. If breeder reactor technology does not prevail, nuclear energy from fissile material will only remain an (albeit important) temporary energy source because of limited uranium and thorium reserves and

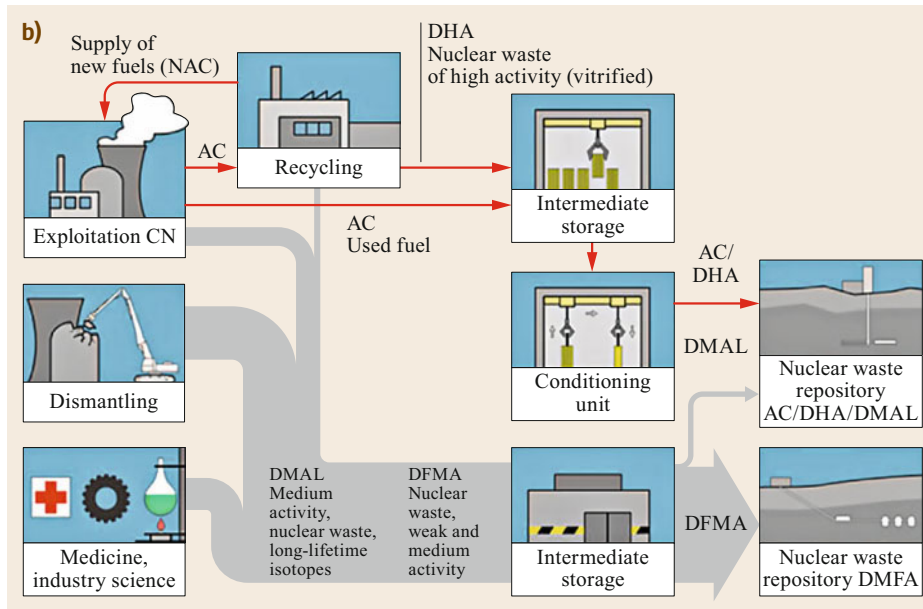


Fig. 2.73  
(continued)

will very probably play a major role only in the 21st century.

Four factors need considering in the hazard discussion:

- 1) Safety during the operation of nuclear power plants
- 2) The possible environmental contamination caused by the fuel cycle
- 3) The safe storage of radioactive waste
- 4) The question of the possible use of fissile material, in particular plutonium, in the manufacture of weapons.

**Safety of the Power Plant.** The *safety measures* taken during planning and construction are described in Sect. 2.7.3 [2.28]. Modern nuclear power plants designed to Western standards offer maximum safety, as demonstrated by the many years of operation of the more than 430 power plants installed and producing energy worldwide, amounting to an experience of more than 10000 man-years. The additional radioactivity level during normal operation in the vicinity of a nuclear power plant is far below that of natural radioactivity.

In the case of a MCA (maximum credible accident), the consequences for man and the environment are not noticeable if the protective devices function correctly, as they are designed to avoid the external effects of such an accident. For a reactor built to Western standards, this also includes the meltdown of the reactor core (the only accident of this kind is Harrisburg 1979, with no consequences for the environment).

If a contamination of the environment occurs (as in Chernobyl 1986), it is referred to as a super-GAU. The

accident at Chernobyl was specifically due to the type of construction used and is not possible in light water reactors. It was also caused by inadequate safety precautions.

In the case of a super-GAU, as in Chernobyl, there is considerable harm to the environment and to people, which must be avoided under all circumstances. In high-standard reactors, such an accident is extremely unlikely, but its probability cannot be reduced to zero. Whether such a loss or risk is acceptable (and insurable) or not is the subject of socio-political debate (a question of assessing a very small probability of a residual risk occurring with major consequences). The ecological benefits of nuclear energy in view of the climate problem must be taken into account and the possible damage must be assessed in relation to that caused each year by other technical facilities (e.g., road and air traffic, chemicals) but tolerated. Section 2.7.3, *Effect of Radioactivity*, considers the hazards of radioactive contamination.

Nuclear technology is also making progress, with (international) efforts moving towards light-water reactors with even greater safety margins (EPRs), with the aim of further reducing the probability of GAUs or super-GAUs [2.25], but also towards an intrinsically safe HTR reactor (China, Japan, South Africa) in terms of both nuclear reaction and heat removal.

**Fuel Cycle.** Concerning the fuel cycle (Sect. 2.7.3), sins have been committed in the past especially in uranium mines and reprocessing. Radioactive contamination can be avoided through high technical and also

ethical standards, which respect the imperatives of social and ecological sustainability, through careful and responsible protective measures during processing and transport as well as through international cooperation. The problem is no more serious than that of other industries (e.g., chemical), where dangerous substances are also used.

**Waste Disposal.** It should be added to the explanations in Sect. 2.7.3 that a distinction must be made between the disposal of low- and intermediate-level waste and that of high-level radioactive waste. The first problem does not only concern nuclear reactors and must therefore be dealt with regardless of whether or not electricity is produced by nuclear power. The technical solutions are in place and the policy is to solve the implementation issues (see Fig. 2.73b).

Concerning the *high-level radioactive waste* that is specific to the nuclear power industry, there are also technical solutions that need to be tested. The problem is the subject of technical and political argument and has not yet been resolved. However, the quantities of high-level radioactive waste to be disposed of are relatively small (see the examples in [2.9, Sect. 3.4]) and not comparable with the enormous amount of climate-damaging CO<sub>2</sub> that results from the combustion of fossil fuels. The latter problem could be much more difficult to solve (see Chap. 1).

**Nuclear Weapons Production.** Highly enriched uranium is required for the manufacture of nuclear weapons. It is feared that the plutonium present in small quantities in spent fuel rods from nuclear power plants could be misused for this purpose. This cannot be completely ruled out, although disposal is subject to strict controls, and recovery is not a simple technical problem. On the other hand, the production of nuclear weapons has been possible in the past independently of the peaceful use of nuclear energy, and will continue to be possible in principle for all those who have gained access to highly enriched uranium or plutonium from nuclear arsenals (USA, former USSR and other countries with nuclear weapons) or are able to operate an enrichment facility. The dangers that this poses are real and are prevented by political measures and appropriate monitoring (non-proliferation agreements). The risks posed by the peaceful use of nuclear energy plants with low-enriched uranium are comparatively low (fast breeders would be somewhat more worrying in this respect).

### Effect of Radioactivity

We will limit ourselves here to a few summary statements. For more details, see [2.28, 29]. Radioactivity

is caused by the decay of *unstable isotopes* [2.9, Annex B.3]. These mainly emit  $\alpha$ -,  $\beta$ - and  $\gamma$ -radiation. The half-life of the isotopes can vary widely. Examples are

$$\begin{aligned} {}^{131}\text{J} &\longrightarrow 8 \text{ d} , \\ {}^{238}\text{Pu} &\longrightarrow 88 \text{ a} , \\ {}^{226}\text{Ra} &\longrightarrow 1620 \text{ a} , \\ {}^{239}\text{Pu} &\longrightarrow 24\,000 \text{ a} , \\ {}^{238}\text{U} &\longrightarrow 4.5 \times 10^9 \text{ a} . \end{aligned} \quad (2.100)$$

The rays have different penetration power.

**$\alpha$ -Radiation.** They do not penetrate deeply; a few cm of air, clothing or a sheet of paper is enough to stop them. If they encounter unclothed body parts, only the skin is affected. However, with their relatively high energy, their biological effectiveness is about 20 times stronger than that of the  $\beta$ -rays. Their energy is usually around 5 MeV.

**$\beta$ -Radiation.** The energy of electrons is most frequently 0.5 MeV, but can also reach a maximum of 1.7 MeV. To reduce their intensity to 37% (defines the range or depth of penetration, exponential characteristic), a few cm of water or a few mm of aluminum are required. In body tissue the radiation penetrates about 2–10 mm deep in the energy range mentioned [2.28].

**$\gamma$ -Radiation.** This high-energy electromagnetic radiation (frequency range  $3 \times 10^{18}$ – $6 \times 10^{21}$  Hz) has an energy of 0.01–20 MeV. Their range in cm (reduction to 37%) is described in Table 2.4. It shows the danger of  $\gamma$ -radiation, that cannot be completely shielded even by layers of lead several cm thick.

**Activity.** The activity of a radioactive substance is defined as the number of decay processes per second. Units are the becquerel (Bq) and the curie (Ci) (formerly)

$$\begin{aligned} 1 \text{ Bq} &= 1 \text{ decay/s} \\ 1 \text{ Ci} &= 37 \times 10^9 \text{ Bq} \longrightarrow 1 \text{ nCi} = 37 \text{ Bq} \end{aligned} \quad (2.101)$$

1 Ci corresponds to the activity of 1 g of radium.

Radioactivity is present everywhere in nature because of radioactive isotopes in the *earth's crust*, but also as a result of the radioactivity arriving from the

**Table 2.4** Penetration of  $\gamma$ -radiation (cm)

	Water	Aluminum	Concrete	Lead
0.1 MeV	6.3	2.3	2.6	0.018
1 MeV	14.3	6.2	6.8	1.36
10 MeV	45.5	15.5	18.6	1.77

*cosmos*. This is called *natural radioactivity*. All living beings are radioactive; human beings have an average radioactivity of 130 Bq/kg through food intake, drinking water and breathing air [2.28]. Building materials, such as concrete, bricks and granite can have several 100 Bq/kg. Wood, on the other hand, normally has a very low level. The radioactive noble gas radon escaping from the earth's interior gives air an activity of approximately 14 Bq/m<sup>3</sup>; in dwellings this value increases on average to 50 Bq/m<sup>3</sup> because of radioactive masonry.

**Radiation Dose.** The energy of terrestrial and cosmic radiation can be measured. The radiation energy absorbed per unit of mass is called the *absorbed dose D*. The unit is the gray (Gy) or (formerly) the rad (rad)

$$1 \text{ Gy} = 1 \frac{\text{J}}{\text{kg}} \quad (1 \text{ Gy} = 100 \text{ rad}) . \quad (2.102)$$

**Equivalent Dose.** The *biologically effective radiation dose* is called *equivalent dose*. It is the product of absorbed dose *D* and quality factor *Q*. The quality factor *Q* indicates the biological effectiveness of the type of radiation. It is  $Q = 1$  for  $\beta$ - and  $\gamma$ -radiation,  $Q = 10$  for neutron radiation and  $Q = 20$  for  $\alpha$ -radiation. Neutron and  $\alpha$ -radiation have much more damaging effects on cell tissue.

The equivalent dose unit is the sievert (Sv) or (formerly) röntgen equivalent man (rem)

$$D \text{ (Gy)} \longrightarrow DQ \text{ (Sv)} \quad (1 \text{ Sv} = 100 \text{ rem}) . \quad (2.103)$$

The biological effect consists of damage to molecules, the fragments of which react chemically and biochemically differently and can impair the functionality of the affected cell. Although living beings possess effective repair mechanisms (since life originated in a radioactive environment), these are not always sufficient, and they can lead to genetic or somatic damage, the latter immediately (early damage) or only after a long time (long-term damage). Many insights have been gained in this respect from the experience with the atomic bomb.

With *single exposure*, the threshold dose above which immediate damage is to be expected in humans is indicated as 200–300 mSv. Embryonic damage can already occur after a single irradiation of 100–200 mSv. A dose of 3–5 Sv is lethal, with a 50% probability.

There is no threshold value for long-term damage, but only the probability of contracting the disease increases with the amount of radiation (e.g., risk of cancer or genetic damage). It is important to note the *cumulative burden* in mSv/a, that can be compared with the natural background radiation. However, as explained

below, there is a large range of fluctuation in background (or natural) radiation.

**Natural Radioactivity.** This consists of cosmic radiation and earth radiation. Cosmic radiation is constant over time (except for large solar flares) and depends strongly on altitude. The annual burden is

$$\begin{aligned} 0 \text{ m a.s.l.: } & 0.30 \text{ mSv/a} \\ 400 \text{ m a.s.l.: } & 0.36 \text{ mSv/a} \\ 800 \text{ m a.s.l.: } & 0.45 \text{ mSv/a} \\ 2000 \text{ m a.s.l.: } & 0.80 \text{ mSv/a} \\ 4000\text{--}5000 \text{ m a.s.l.: } & 2 \text{ mSv/a} \\ & (\text{Mont Blanc} \rightarrow 0.00023 \text{ mSv/h}) , \\ 8000\text{--}9000 \text{ m a.s.l.: } & 15 \text{ mSv/a} \\ & (\text{Mount Everest} \rightarrow 0.0017 \text{ mSv/h}) , \\ 12\,000 \text{ m a.s.l.: } & 40 \text{ mSv/a} \\ & (\text{Aircraft} \rightarrow 0.0045 \text{ mSv/h}) . \end{aligned} \quad (2.104)$$

The Earth's radiation varies from region to region depending on geology and soil conditions. It is relatively strong in granite rocks (the Alps of Europe) and weak in sedimentary rocks (Jura, Swiss central plateau). In Switzerland, it varies between 0.4 and 1.5 mSv/a, on average about 1.2 mSv/a. There are regions in China, Brazil and the Indian subcontinent where 20 mSv/a and much higher are common, with no significant variations observed yet in cancer, malformations, fertility, etc., indicating the effectiveness of biological repair mechanisms. Examples of natural exposure in Switzerland can be found in Table 2.5.

The exposure from food and housing must be added to the natural one. In Germany, it is estimated to be about twice as large as the natural one, that is about 0.8 mSv/a, resulting in a total exposure of 2.4 mSv/a. In addition, there is the radiation exposure due to medical care, that is given as approximately 1.6 mSv/a [2.28, 29]. The accident at Chernobyl in 1986 led to an additional exposure of 0.04 mSv/a in Germany in 1992.

For persons with occupational radiation risk, in Switzerland an exposure limit of 10–50 mSv/a is set, or an accumulated level of 350 mSv over one's entire occupational career.

**Table 2.5** Examples of natural radioactive exposure in Switzerland

City	Cosmic (mSv/a)	Terrestrial (mSv/a)	Total (mSv/a)
Biel	0.37	0.39	0.76
Zurich	0.36	0.83	1.19
Geneva	0.35	0.89	1.24
St. Moritz	0.74	1.1	1.84

## 2.8 Wind Power

The potential of wind energy and the prerequisites for its economic use have already been briefly discussed in Sect. 1.2.3. This section deals in more detail with the technical and economic aspects of wind-energy use.

### 2.8.1 The Kinetic Energy of Wind

An air mass  $m$  moving with speed  $v_0$  has the kinetic energy

$$E_{\text{kin}} = \frac{1}{2} m v_0^2 \quad \left( \text{kg} \left( \frac{\text{m}}{\text{s}} \right)^2 = \text{J} \right). \quad (2.105)$$

For a cross-section  $A$  through which there is an air mass flow with density  $\rho$  and speed  $v_0$ , the air mass  $m'$  per second is

$$m' = A \rho v_0 \quad \left( \text{m}^2 \frac{\text{kg}}{\text{m}^3} \frac{\text{m}}{\text{s}} = \frac{\text{kg}}{\text{s}} \right), \quad (2.106)$$

and the *theoretical wind power* is

$$P_0 = \frac{1}{2} m' v_0^2 = \frac{1}{2} A \rho v_0^3 \quad (\text{W}). \quad (2.107)$$

#### Theoretical Wind Power

The theoretical wind power increases with the third power of the *wind speed* and thus has a strong influence on the economic efficiency.

Another important parameter is the air density. For dry air at normal pressure (1013 mbar) and 0 °C this is  $\rho = 1.292 \text{ kg/m}^3$ . Pressure and temperature influence can be determined from the relationship

$$\frac{P}{\rho} = RT \quad \longrightarrow \quad \rho = \frac{P}{RT} \quad \text{with } R = 287.1 \frac{\text{J}}{\text{kg K}}. \quad (2.108)$$

It should also be noted that the pressure changes with altitude according to the barometric formula ( $P_0$  at 20 °C)

$$P = P_0 e^{-\frac{h-h_0}{a}} \quad \text{with } a = 29.27 \frac{\text{m}}{\text{K}}. \quad (2.109)$$

#### Wind Speed

The relationship between wind force and wind speed is shown in Table 2.6.

Annual mean wind speeds above 5 m/s usually occur only in coastal regions or on free-standing mountain peaks. It should be noted, however, that the mean value, because of  $v_0^3$  (2.107) does not allow a direct statement about the energy content. The wind speed also changes with height, due to ground friction according to the formula

$$\frac{v}{v_0} = \left( \frac{h}{h_0} \right)^\alpha, \quad (2.110)$$

$$\text{where } \begin{cases} \alpha = 0.16 & (\text{sea}), \\ \alpha = 0.17-0.2 & (\text{plain without obstacles}). \end{cases}$$

With obstacles,  $\alpha$  can assume much higher values. An uneven topography can also cause large local differences and alter the altitude profile of the wind. The location of a wind turbine is therefore of great importance.

#### Example 2.7

Calculate the theoretical power per  $\text{m}^2$  of area for  $v_0 = 4 \text{ m/s}$  and  $7 \text{ m/s}$  and the corresponding theoretical power with constant wind conditions:

- For 0 m a.s.l. at standard pressure and 20 °C
- At 2000 m a.s.l. at the corresponding pressure and 10 °C (in % of a))

**Table 2.6** Wind force and wind speed [2.30]

Wind force on Beaufort scale	Wind velocity		Effect of the wind
	(m/s)	(kn)	
0 Calm	0.0–0.2	0–1	Smoke rises vertically
1 Light air	0.3–1.5	1–3	Smoke rises obliquely
2 Light breeze	1.6–3.3	4–7	Draught slightly perceptible
3 Gentle breeze	3.4–5.4	8–11	Leaf movement on trees
4 Moderate breeze	5.5–7.9	12–15	Small tree branches move
5 Fresh breeze	8.0–10.7	16–21	Tree branches move
6 Strong breeze	10.8–13.8	22–27	Large tree branches move; telegraph wires whistle
7 Near gale	13.9–17.1	28–33	Tree movement, wind resistance when walking
8 Gale	17.2–20.7	34–40	Tree twigs break; difficulty in walking
9 Strong gale	20.8–24.4	41–47	Roof tiles disturbed
10 Storm	24.5–28.4	48–55	Trees uprooted
11 Violent storm	28.5–32.6	56–63	Severe destructive effect
12 Hurricane	32.7–36.9	64–71	Walls collapse; general severe damage

c) Assuming that the above speed values apply to a height of 10 m above the ground, how does the power change in % if the wind turbine is installed 20 m above the ground (ground without obstacles)?

$$\begin{aligned} \text{a) } \rho &= 1.292 \frac{273}{293} \\ &= 1.205 \frac{\text{kg}}{\text{m}^3} \begin{cases} 4 \frac{\text{m}}{\text{s}}: P_0 = \frac{1}{2} 1.205 \times 4^3 = 38.6 \frac{\text{W}}{\text{m}^2} \\ 7 \frac{\text{m}}{\text{s}}: P_0 = \frac{1}{2} 1.205 \times 7^3 = 207 \frac{\text{W}}{\text{m}^2} \end{cases} \end{aligned}$$

$$\begin{aligned} \text{b) } p &= p_0 e^{-\frac{2000}{29.27283}} = p_0 0.7855 \\ \rightarrow \rho &= 1.205 \frac{293}{283} \times 0.7855 = 1.205 \times 0.8133, \end{aligned}$$

The power is reduced by almost 19%.

$$\text{c) } \left(\frac{v}{v_0}\right)^3 = \left(\frac{20}{10}\right)^{3(0.17 \dots 0.2)} = 1.424 \dots 1.516$$

The power increases by 42–52%!

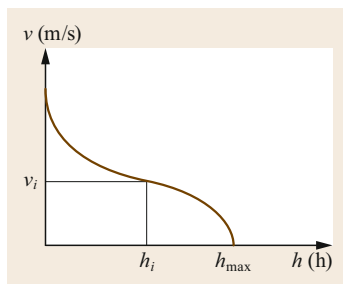
### Energy Supply

In order to be able to evaluate the potential wind-energy supply of a site, long-term measurements must be available or measurements using anemometers must be carried out over a lengthy period. The measurement results can be displayed in the form of a duration curve (Fig. 2.74). The duration curve indicates during how many hours  $h_i$  in the period under consideration a certain wind speed  $v_i$  is reached or exceeded. From the duration curve of the wind, the duration curve of the theoretical power can be calculated with (2.105), and from this, taking into account the operating limits and the efficiency of the wind turbine, the effective available energy can be determined.

Experience shows that working with 10 min mean values is a good basis for the design of the wind turbine. To learn about the influence of the superimposed wind turbulence see [2.31].

### The Weibull Distribution

Analysis of wind statistics has shown that in very many cases the wind distribution can be described with ade-



**Fig. 2.74** Wind duration curve (mean values of 10 min)

quate approximation by the Weibull distribution. This is defined by the following cumulative frequency (duration curve)

$$\frac{h}{h_{\max}} = S(v) = e^{-\left(\frac{v}{c}\right)^k} \quad (2.111)$$

The distribution is thus given by the two parameters  $c$  (position parameter, proportional to the mean speed) and  $k$  (scattering parameter).

The wind frequency is obtained by differentiation of the cumulative frequency

$$f(v) = -\frac{dS(v)}{dv} = \frac{k}{c} \left(\frac{v}{c}\right)^{k-1} e^{-\left(\frac{v}{c}\right)^k} \quad (2.112)$$

and is generally represented by Fig. 2.75.

The following quantities can be determined from position and scattering parameters

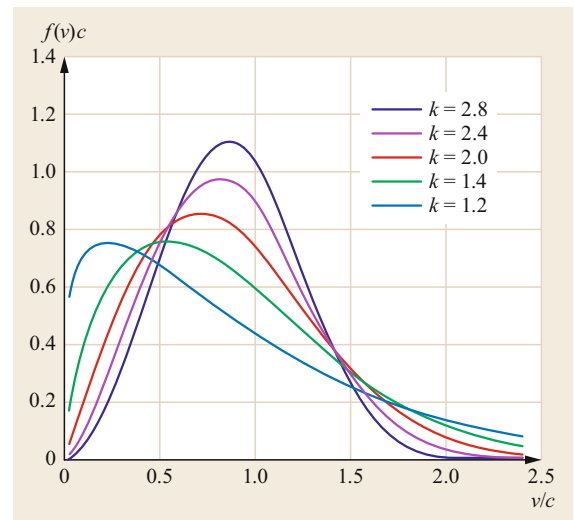
$$\begin{aligned} \text{mean wind speed } v_m &= c \Gamma\left(1 + \frac{1}{k}\right), \\ \text{and energy factor } K_E &= \frac{\Gamma\left(1 + \frac{3}{k}\right)}{\Gamma\left(1 + \frac{1}{k}\right)}, \end{aligned} \quad (2.113)$$

where

$$\Gamma(x) = \int_0^{\infty} e^{-t} t^{x-1} dt \quad (2.114)$$

represents the gamma function evaluated in [2.1, Annex E].

The energy factor  $K_E$  is the ratio between the supply of wind energy at variable wind speed and the supply at



**Fig. 2.75** Weibull wind frequency

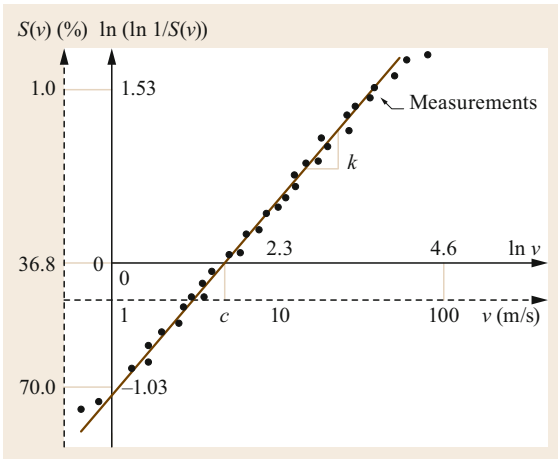


Fig. 2.76 Wind measurements and their evaluation

constant mean wind speed. The theoretical wind energy potential of a site is then

$$W_0 = 8.76 \frac{1}{2} \rho v_m^3 K_E \left( \frac{\text{kWh}}{\text{m}^2 \text{a}} \right). \tag{2.115}$$

To calculate this potential, the parameters  $c$  and  $k$  are first determined from the measured values. For this pur-

pose, (2.111) is written with double logarithms as

$$\ln \left( \ln \frac{h_{\max}}{h} \right) = \ln \left( \ln \frac{1}{S(v)} \right) = k(\ln v - \ln c) \tag{2.116}$$

and the measured values  $\ln[\ln(1/S(v))]$  are plotted as a function of  $\ln v$  (Fig. 2.76). If the measured values in the range  $S(v) = 1-70\%$  lie on a straight line, the assumption of a Weibull distribution is justified. The slope of the straight line is  $k$  and  $c$  is the intersection with the abscissa.

From  $c$  and  $k$ , with the help of the gamma function with (2.113), the mean wind speed and the energy factor are obtained. The two values are listed in [2.1, Annex E] as a function of  $k$ . The air density is derived from pressure and temperature ((2.108) and (2.109)) and the wind-energy potential is finally derived from (2.115).

### 2.8.2 Wind-Turbine Types and Their Performance

Figure 2.77 shows the most important wind turbine types. A distinction is made between wind turbines that

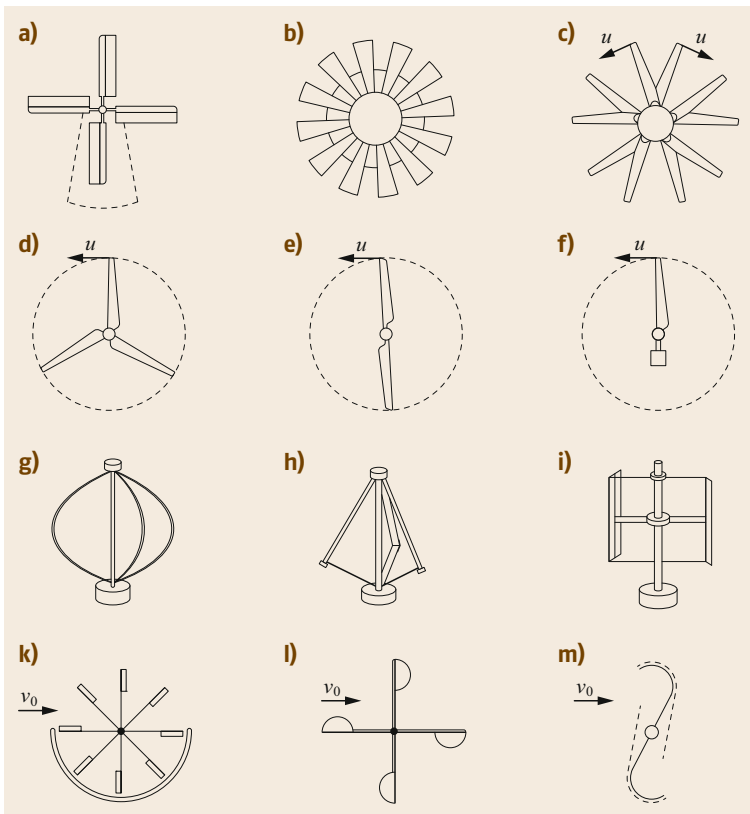
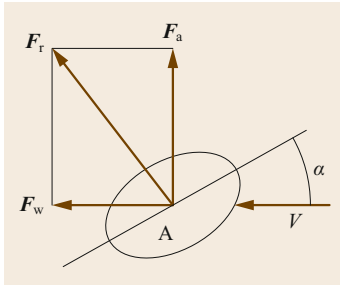


Fig. 2.77a-m Wind turbine types: (a) La Cour wind turbine, (b) American wind turbine, (c) 2 x 5-blade rotor, (d) three-blade rotor, (e) two-blade rotor, (f) one-blade rotor, (g) three-blade Darrieus, (h) Δ-Darrieus, (i) H-Darrieus, (k) semi-shielded drag rotor, (l) cup cross, (m) Savonius rotor (dotted line: divided rotor); (a-f) horizontal axis, using lift; (g-i) vertical axis, using lift; (k-m) using drag



**Fig. 2.78** Drag and lift force

operate predominantly on the *principle of resistance* (drag-type) and those based on the *lift principle* (lift-type).

Every surface of area  $A$  exposed to the wind, experiences a force  $F_w$  in the wind direction (Fig. 2.78) and a force  $F_a$  perpendicular to it.

$$\begin{aligned} F_w &= c_w \times 0.5\rho Av^2, \\ F_a &= c_a \times 0.5\rho Av^2. \end{aligned} \tag{2.117}$$

The drag and lift coefficients  $c_w$  and  $c_a$  depend on the shape (profile) and position of the surface (angle  $\alpha$ ) relative to the wind direction. They can be calculated numerically or determined by tests, e.g., in a wind tunnel [2.31].

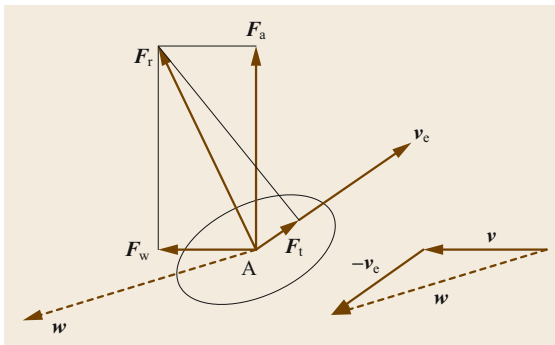
The resulting force on the surface is  $F_r$ .

If the surface moves with speed  $v_e$  (Fig. 2.79), the relative wind speed in (2.117) is  $w$  instead of the absolute  $v$

$$w = v - v_e. \tag{2.118}$$

If the resulting force  $F_r$  gives a positive component  $F_t$  (driving force) in the direction of motion, the motion is increased (Fig. 2.79); in the opposite case it is retarded.

This most important wind turbine types are discussed in the following sections. For more details see [2.31, 32] and for the construction of wind turbines



**Fig. 2.79** Forces on moving wind turbine

see [2.33].

Theoretical power of the wind turbine:  $P_{th} = c_p P_0$ ,

$$\text{Effective power: } P = \eta_t P_{th} = \eta_t c_p P_0 = c_p' P_0. \tag{2.119}$$

$P_0$  is the theoretical wind power according to (2.107). Added terms are:

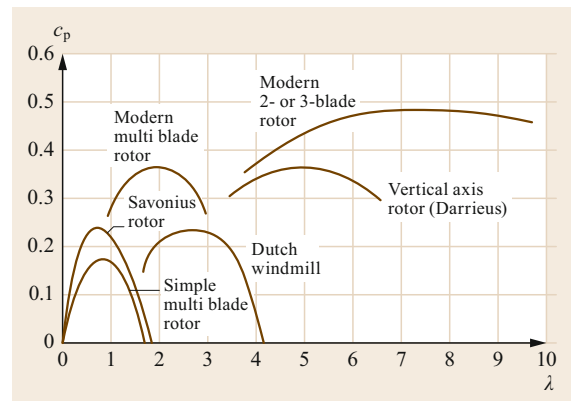
- $c_p$  ideal power coefficient of the turbine (always  $< 1$ )
- $\eta_t$  efficiency of the turbine (relative to loss-free operation)
- $c_p' = \eta_t c_p$  effective coefficient of power.

$c_p$  determines the upper power limit, that cannot be exceeded for physical reasons (even without friction losses). It can be shown that  $c_p$  (and therefore also  $c_p'$ ) are dependent on the *tip speed ratio*  $\lambda$  of the wind turbine (Sect. 2.8.3)

$$\lambda = \frac{u}{v_0}, \tag{2.120}$$

where  $u$  represents the *peripheral speed* of the turbine blade and  $v_0$  the *absolute wind speed* before the turbine. Figure 2.80 shows the ideal power coefficients of some wind turbines. For all wind turbines,  $c_p$  has a maximum for a certain (optimal) tip speed ratio  $\lambda_{opt}$ . For optimal operation, the speed of the wind turbine would have to be adapted to the wind speed. For reasons of cost, this is often dispensed with, but in modern systems it is increasingly done, thanks to cheaper power electronics (see Sect. 2.8.3, *Airfoil Theory*).

Wind turbines are classified as slow-speed or high-speed turbines according to the optimum tip speed ratio. The last category includes Darrieus rotors and 1–3-blade horizontal-axis rotors. In practice, horizontal-axis



**Fig. 2.80** Ideal power coefficient  $c_p$  of various rotors as a function of the tip speed ratio  $\lambda$



rotors have become established and account for by far the largest share of all wind turbines worldwide.

### 2.8.3 Horizontal-Axis Wind Turbines

#### Betz's Law

With reference to Fig. 2.81, consider the wind mass  $m$  passing through the wind-turbine section  $A$ . The wind speed before the turbine is  $v_0$ . The wind is slowed down by the turbine, so that the wind speed after the turbine is  $v_1 < v_0$ . In the turbine itself, the wind speed is  $v$ .

If ideal lossless conditions are assumed, the difference between the kinetic energies ( $W_0 - W_1$ ) is fully converted into mechanical energy and appears as the theoretical power  $P_{th}$  on the turbine shaft

$$W_0 - W_1 = \frac{1}{2}mv_0^2 - \frac{1}{2}mv_1^2 = \frac{1}{2}m(v_0^2 - v_1^2).$$

The mass flow per time unit through the turbine is  $m' = \rho Av$ . The theoretical power is therefore

$$P_{th} = \frac{1}{2}\rho Av(v_0^2 - v_1^2). \quad (2.121)$$

On the other hand, using the momentum equation, the force follows as momentum change per s

$$F = m'(v_0 - v_1) = \rho Av(v_0 - v_1).$$

The power from the wind is therefore

$$P_{th} = Fv = \rho Av^2(v_0 - v_1). \quad (2.122)$$

Comparison of (2.121) and (2.122) provides

$$v = \frac{v_0 + v_1}{2}. \quad (2.123)$$

From (2.122), the power is

$$P_{th} = \frac{1}{4}\rho A(v_0 + v_1)(v_0^2 - v_1^2), \quad (2.124)$$

and for the ideal power coefficient

$$\begin{aligned} c_p &= \frac{P_{th}}{P_0} = \frac{\frac{1}{4}\rho A(v_0 + v_1)(v_0^2 - v_1^2)}{\frac{1}{2}\rho Av_0^3} \\ &= \frac{1}{2} \left(1 + \frac{v_1}{v_0}\right) \left(1 - \frac{v_1^2}{v_0^2}\right). \end{aligned} \quad (2.125)$$

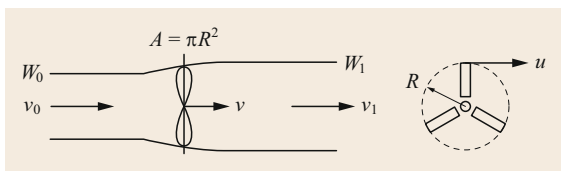


Fig. 2.81 Horizontal axis wind turbine, Betz's law

Replacing  $v_1$  by  $v$  (see (2.123)), then (Fig. 2.82)

$$c_p = 4 \left(\frac{v}{v_0}\right)^2 \left(1 - \frac{v}{v_0}\right). \quad (2.126)$$

The maximum value is  $c_{p,max} = 16/27 = 0.593$  and is achieved for  $v/v_0 = 2/3$  or  $v_1/v_0 = 1/3$ . There is a fixed relationship between the speed  $v$  and the rotational speed of the turbine or the tip-speed ratio, that depends on the *blade solidity* (completeness) and the *profile shape* of the blade (see airfoil theory). The completeness increases with the number and width of the blades. A distinction is made between two extreme versions:

1. Low speed rotors  
(Example: American wind turbine, Fig. 2.77). Due to the high blade solidity, the optimum speed  $v$  is reached at low speeds ( $\lambda_{opt}$  small).
2. High speed rotors  
(Example: two-blade rotor, Fig. 2.77). The blade solidity is small, the optimum speed  $v$  requires high rotational speed and precise design of the blades ( $\lambda_{opt}$  large).

The power supplied by the turbine is calculated according to (2.119)

$$P = \eta_t c_p P_0 = c'_p P_0. \quad (2.127)$$

The overall efficiency can reach for  $\lambda_{opt}$  a value  $c'_p = 0.45$  (Fig. 2.84), that corresponds to a turbine efficiency  $\eta_t = 0.76$ .

#### Airfoil Theory

Consider the blade element  $dr$  (Fig. 2.83a), that is moving at the speed  $u_r$ . With the wind speed  $v$  in the axial

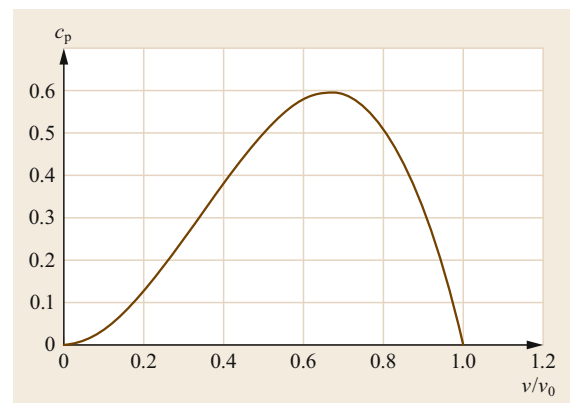
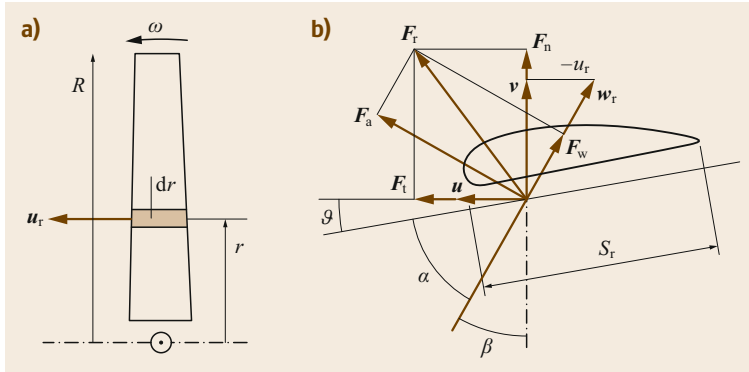


Fig. 2.82 Curve of the ideal power coefficient of horizontal-axis wind turbines



**Fig. 2.83a,b** Speeds (a) and forces (b) of a wing element

direction, the relative wind speed is  $w_r$  (Fig. 2.83b).

$$\begin{aligned} w_r &= v - u_r, \quad \text{with } u_r = \omega r, \\ w_r &= \sqrt{v^2 + u_r^2} = v \sqrt{1 + \left(\frac{u_r}{v}\right)^2}, \\ \cos \beta &= \frac{v}{w_r} = \frac{1}{\sqrt{1 + \left(\frac{u_r}{v}\right)^2}}. \end{aligned} \quad (2.128)$$

The blade profile has an adjustable angle  $\theta$  relative to the normal to the wind direction. This angle is often a function of  $r$ . The angle of attack  $\alpha$  is the angle between the profile and the relative wind speed (Fig. 2.83b). Thus

$$\alpha = 90^\circ - (\theta + \beta). \quad (2.129)$$

The forces acting on the wing element (Fig. 2.83b) are:

- $F_a$  Lift, perpendicular to  $w_r$
- $F_w$  Drag, direction  $w_r$
- $F_r$  Resultant force  $F_a + F_w$
- $F_t$  Driving force, direction  $u_r$
- $F_n$  Normal force, perpendicular to  $u_r$

For the area  $dA = s_r dr$  of the blade element, the following apply, according to (2.117)

$$\begin{aligned} dF_w &= c_w \times 0.5 \rho s_r dr w_r^2 \\ dF_a &= c_a \times 0.5 \rho s_r dr w_r^2, \end{aligned} \quad (2.130)$$

where  $c_a$  and  $c_w$  are profile-dependent, wind-tunnel measurable and thus known functions of the angle of attack  $\alpha$ .

For tractive force and normal force, Fig. 2.83b shows

$$\begin{aligned} dF_t &= dF_a \cos \beta - dF_w \sin \beta \\ dF_n &= dF_a \sin \beta + dF_w \cos \beta \\ \longrightarrow dF_t &= \frac{1}{2} \rho s_r dr w_r^2 (c_a \cos \beta - c_w \sin \beta). \end{aligned} \quad (2.131)$$

The torque generated by the blade element  $dr$  is thus

$$dM = dF_t r = \frac{1}{2} \rho s_r r dr w_r^2 (c_a \cos \beta - c_w \sin \beta). \quad (2.132)$$

If  $z$  is the number of blades, the total torque is then

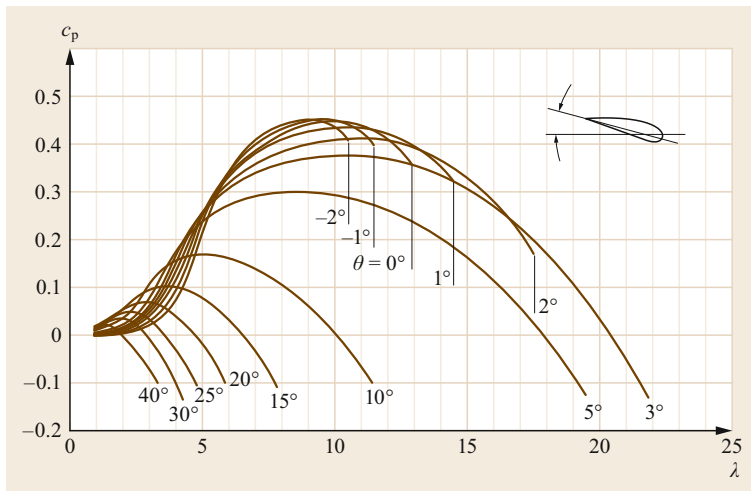
$$\begin{aligned} M &= z \int_{R_{\min}}^R dM \\ &= \frac{1}{2} \rho z \int_{R_{\min}}^R s_r r w_r^2 (c_a \cos \beta - c_w \sin \beta) dr. \end{aligned} \quad (2.133)$$

Finally, the theoretical power is  $P_{th} = M\omega$ , from which the ideal power coefficient can be calculated as a function of tip speed ratio and orientation angle. In particular, the optimum tip speed ratio  $\lambda_{opt}$  follows from this. Figure 2.84 shows the typical curve for a high-speed machine.

### Exercise 2.1

- a) A horizontal three-blade rotor ( $\lambda_{opt} \approx 8$ ) should deliver an effective output of 15 kW at an optimal wind speed of 6 m/s. The efficiency of the turbine  $\eta_{opt}$  is 0.72. Estimate:
  - The radius of the blades (assumption  $\rho = 1.2 \text{ kg/m}^3$ )
  - The optimum rotation speed of the rotor
  - The specific power in relation to the wind turbine area.
- b) Repeat the calculation with  $v_{0, opt} = 8 \text{ m/s}$ .
- c) Same calculations for an American wind turbine of the same power, if  $\eta_{opt} = 0.5$  and  $\lambda_{opt} \approx 1$ .

The solution can be found in [2.9, Annex F].



**Fig. 2.84** Power coefficient  $c_p$  of a high-speed turbine as a function of tip speed ratio  $\lambda$  and pitch angle  $\theta$

### 2.8.4 Modern Horizontal-Axis Wind Turbines

The vast majority of modern wind-power plants use horizontal-axis, high-speed turbines with three rotor blades. An even number of rotor blades have disadvantages in terms of dynamic stability, and the (cheaper) solution with a single rotor blade is also mechanically unfavorable for reasons of dynamic balance.

The investment costs of large plants (output in the MW class up to 5 MW) today are about 860 €/kW. At an average wind speed of 6 m/s and a rated speed of 15 m/s (corresponding to  $P_{\max}$  = rated power), the annual usage time is 1767 h/a from (2.107) and (2.115) assuming an energy factor of 0.7 [2.9, Annex E] and an average power coefficient of 0.45. With an 8% annual return the energy costs are 3.9 ct/kWh. These costs do not take into account the expenses for operating and transporting the energy. Wind energy is a base-load energy like that of hydraulic run-of-river power plants, but much more irregular; it must therefore be compensated by other rapidly controllable energy supplied by hydroelectric or gas turbine-power plants, or used or stored locally.

A greater tower height allows a better energy yield thanks to stronger wind, but increases the costs. The optimum height is usually about 1–1.5× the diameter of the rotor.

Large wind farms, consisting of a large number of wind turbines, are most common near the sea. The distances between the turbines in the wind direction must be approximately 5–9 rotor diameters; 3–5 rotor diameters across the wind direction are sufficient. For details, see Wind Power [2.34] (<http://www.windpower.dk/en>).

In the mountains, the requirements for measurements and modeling in the planning phase are particularly high [2.35].

For the future, large *offshore installations* (installations anchored in the sea) are planned. This avoids the often serious aesthetic problems associated with coastal locations; in addition, the energy potential increases considerably. The problems associated with anchoring (floating systems) are currently being investigated. A coupling with *tidal-power plants* is quite conceivable ([https://en.wikipedia.org/wiki/Marine\\_current\\_power](https://en.wikipedia.org/wiki/Marine_current_power); [https://en.wikipedia.org/wiki/Wind\\_power](https://en.wikipedia.org/wiki/Wind_power)).

### 2.8.5 Other Types of Wind Turbines

We shall consider two types of vertical-axis wind turbine. The first type, the Darrieus rotor, belongs to the high-speed category and works on the lift principle; the second, the Savonius rotor, is a low-speed rotor and works on the drag principle (Figs. 2.77 and 2.80).

#### The Darrieus Rotor

This rotor was invented in the 1920s by the Frenchman Georges Darrieus, but it was not used in practice until around 1970. Since then, rotors up to approximately one MW have been built. The rotor usually consists of two or three blades attached at their ends to a co-rotating vertical axis (Fig. 2.77g). If we rotate a rope instead of the wings, it would take the shape of a troposkein (skipping-rope curve). If the blade is given such a shape, only tensile forces occur, which is mechanically ideal. In practice, the troposkein is approximated by an arc and a straight line. The airfoil profiles are generally symmetrical. Compared to the horizontal-axis

rotor, the Darrieus rotor has the following advantages and disadvantages:

- **Advantages**
  - The Darrieus Rotor is independent of wind direction. This means that no mechanism for wind tracking is necessary, no alignment units, such as wind vanes, auxiliary rotors or servomotors, are required.
  - The power plant with gearbox, generator and control unit is located on the ground. Therefore, no complex tower constructions are necessary, and maintenance is easier.
- **Disadvantages**
  - The torque pulsates because of the variable angle of attack (resulting in mechanical problems).
  - The lower height above the ground leads to weaker wind in the lower parts of the rotor blades, that has a negative effect on the power coefficient.
  - A starting aid is necessary (motor, Savonius) as the angle of attack is not adjustable.

**Rotor Geometry.** The troposkein is approximated by circle and straight line, with the data values  $R$ ,  $R_0$  and  $H$  (Fig. 2.85). From this the auxiliary variables are as follows

$$\begin{aligned} x_0 &= R - R_0, \\ \gamma_0 &= \pi - \gamma_1 - \gamma_2, \\ r_0 &= x_0 + R_0 \cos \gamma_0, \\ z_0 &= R_0 \sin \gamma_0, \end{aligned} \quad (2.134)$$

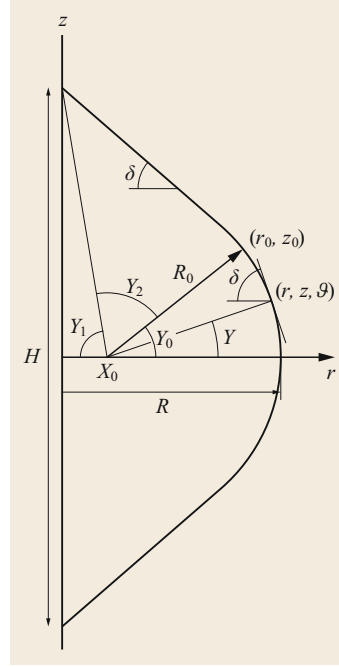
where

$$\begin{aligned} \gamma_1 &= \arctan \left( \frac{H}{2(R - R_0)} \right), \\ \gamma_2 &= \arctan \sqrt{\left( \frac{H}{2} \right)^2 + R^2 - 2RR_0}. \end{aligned}$$

If  $(r, z, \vartheta)$  denote the general coordinates of a blade element; this results in the following equations for the circle and the straight line (with  $z$  as a parameter):

Circle equations for  $-z_0 < z < z_0$

$$\begin{aligned} \gamma &= \arctan \left( \frac{z}{\sqrt{R_0^2 - z^2}} \right), \\ r &= x_0 + R_0 \cos \gamma, \\ \sin \delta &= \frac{r - x_0}{R_0} = \cos \gamma. \end{aligned} \quad (2.135)$$



**Fig. 2.85** Geometry of the Darrieus rotor

Straight line equations for  $z > z_0$  and  $z < -z_0$

$$\begin{aligned} m &= \frac{H/2 - R_0 \sin \gamma_0}{x_0 + R_0 \cos \gamma_0}, \\ r &= \frac{H/2 - |z|}{m}, \\ \sin \delta &= \frac{m}{\sqrt{1 + m^2}} \end{aligned} \quad (2.136)$$

( $m$  being the slope).

**Forces on the Wing Elements.** For the elementary wind tube (Fig. 2.86), the following applies

$$dA = r d\vartheta \sin \vartheta dz. \quad (2.137)$$

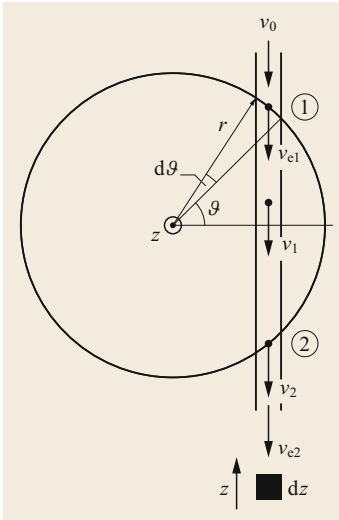
The wind meets the blade profiles at 1 and 2. The mean force at 1 results from the momentum equation (analogous to Sect. 2.8.3)

$$d^2 F_{1m} = dm' (v_0 - v_1) \quad (2.138)$$

Set according to (2.123),  $v_1 = 2v_{e1} - v_0$ , gives

$$\begin{aligned} d^2 F_{1m} &= dm' 2 (v_0 - v_{e1}), \\ \text{with } dm' &= 2\rho r d\vartheta \sin \vartheta dz v_{e1}. \end{aligned} \quad (2.139)$$

This force acts on the rotating blade element only for a short time (during the angle  $d\vartheta$ ). Using  $dF_1$  as the



**Fig. 2.86** Forces on the Darrieus blade

element  $dz$  has the inclination  $\delta$  to the horizontal and has the surface area

$$dA_p = \frac{sdz}{\sin \delta} \tag{2.143}$$

The forces acting on the blade element (2.117) are

$$\begin{aligned} dF_a &= \frac{1}{2}c_a\rho dA_p w_1^2 \text{ (lift) ,} \\ dF_w &= \frac{1}{2}c_w\rho dA_p w_1^2 \text{ (drag) ,} \end{aligned} \tag{2.144}$$

where  $w_1$  represents the relative wind speed, the components of which are against the direction of motion  $u$  and normal to the blade and given by (Fig. 2.87)

$$\begin{aligned} w_1 \cos \alpha &= u + v_{e1} \cos \vartheta , \\ w_1 \sin \alpha &= v_{e1} \sin \vartheta \sin \delta , \end{aligned} \tag{2.145}$$

force actually acting on the profile element, the relationship is

$$d^2F_{1m} = dF_1 \frac{Nd\vartheta}{2\pi} , \tag{2.140}$$

where  $N$  is the number of blades.

From (2.139) and (2.140),

$$dF_1 = \frac{1}{N}4\pi\rho r \sin \vartheta dz v_{e1} (v_0 - v_{e1}) . \tag{2.141}$$

The same consideration for position 2 leads to

$$dF_2 = \frac{1}{N}4\pi\rho r |\sin \vartheta| dz v_{e2} (v_0 - v_{e2}) , \tag{2.142}$$

where  $v_2 = 2v_{e2} - v_1$ .

**Airfoil Theory.** The blade element in position 1 (Fig. 2.86) should be examined more closely with regard to resistance and lift force (Fig. 2.87). The vertical

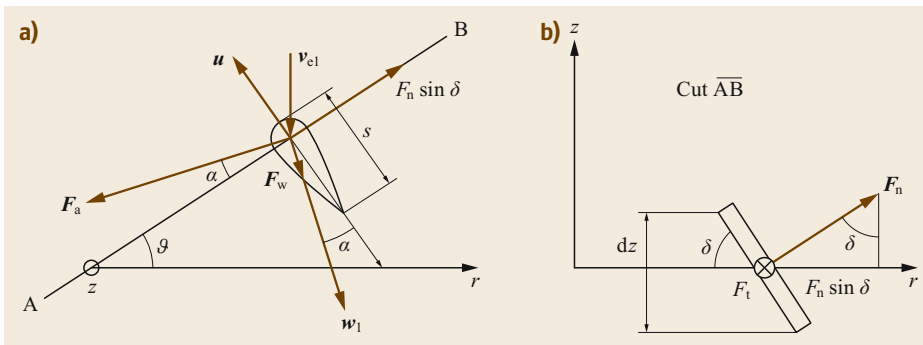
where  $\alpha$  is the angle that  $w_1$  makes with the direction of motion.

**The Savonius Rotor**

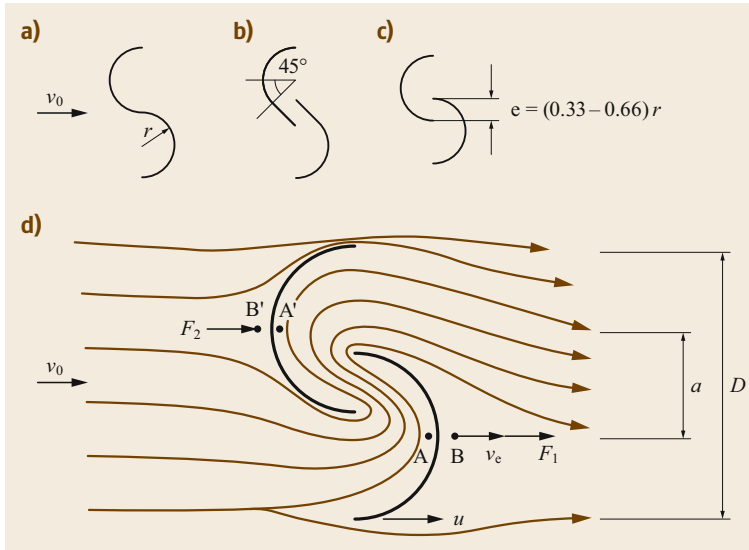
The Savonius rotor will be considered more closely as an example of a low-speed rotor that works predominantly according to the principle of drag. As Fig. 2.80 shows, power coefficients of 0.2–0.25 are achieved, i.e., at best 25% of the maximum theoretical wind power.

**Structure.** The vertical-axis Savonius rotor originally consists of two semi-circular cylinders as shown in Fig. 2.88a and is then a pure drag-type rotor. The split Savonius rotor (Fig. 2.88b,c) achieves a better power coefficient due to the contribution of the lift forces, that are also effective.

Fig. 2.88d shows the airflow in the split rotor. Due to the different resistance coefficients,  $F_2 < F_1$  and setting  $F = F_1 - F_2$ , the torque is  $M = F - a/2$ . Splitting the rotor gives a higher value  $F$  than in the case of the undivided rotor.



**Fig. 2.87a,b** Depiction of the airfoil theory of the Darrieus rotor. (a) Airfoil of the Darrieus rotor. (b) Cut  $\overline{AB}$



**Fig. 2.88a–d** Savonius rotor (a) pure drag turbine, (b) and (c) improved variants with drag and lift (split Savonius), (d) airflow path for rotor (c)

**Power Output.** The power can be expressed by

$$P = M\omega = M \frac{2u}{D} = M \frac{2v_c}{a} = Fv_c. \quad (2.146)$$

Using (2.117) and (2.118), the force is

$$F_{th} = c \frac{1}{2} \rho A (v_0 - v_c)^2, \quad (2.147)$$

where  $A = DH$ , with  $H$  = effective height of the rotor. In the case of the drag-type rotor (Fig. 2.88a),  $c = c_w$ , with  $c_w = 2.3$  for the concave and  $c_w = 1.2$  for the convex side [2.30, 35], that results in a total of  $c_w = 1.1$ .

For the theoretical power,

$$P_{th} = F_{th}v_c = c \frac{1}{2} \rho \frac{1}{2} \rho A v_c (v_0 - v_c)^2, \quad (2.148)$$

and, for the *ideal coefficient of power*

$$\begin{aligned} c_p &= \frac{P_{th}}{P_0} = \frac{c \frac{1}{2} \rho A (v_0 - v_c)^2}{\frac{1}{2} \rho A v_0} \\ &= c \frac{v_c}{v_0} \left( 1 - \frac{v_c}{v_0} \right)^2. \end{aligned} \quad (2.149)$$

The speed ratio  $v_c/v_0$  can be expressed as a function of the tip speed ratio using the geometry factor  $\beta$

$$\beta = \frac{D}{a} = \frac{u}{v_c}, \quad \rightarrow \quad \frac{v_c}{v_0} = \frac{u}{v_0} \frac{v_c}{u} = \frac{\lambda}{\beta}. \quad (2.150)$$

Thus it follows that (Fig. 2.89)

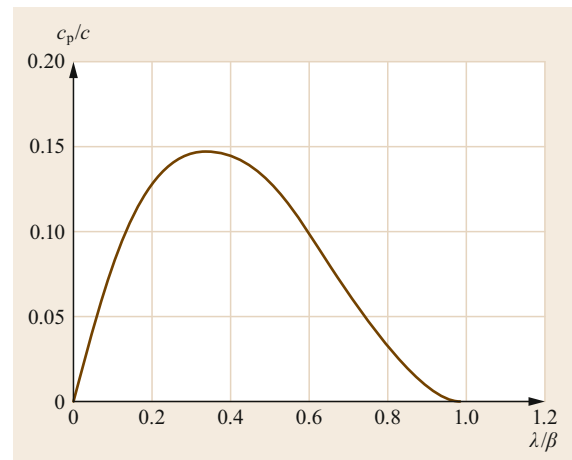
$$c_p = \frac{\lambda}{\beta} \left( 1 - \frac{\lambda}{\beta} \right)^2. \quad (2.151)$$

The optimal value is  $\lambda = \beta/3$  with  $c_p/c = 4/27 = 0.148$ . For the rotor in Fig. 2.88a,  $\beta = 2$  and therefore  $\lambda_{opt} = 0.67$ . In rotors like that in Fig. 2.88c, it is more likely that  $\beta \approx 2.5 \rightarrow \lambda_{opt} \approx 0.83$ . The Savonius rotor clearly belongs to the slow-speed category.

The effective power is

$$P = \frac{c_p}{c} c \eta_t P_0 \quad \rightarrow \quad P_{max} \approx 0.15 c \eta_t P_0. \quad (2.152)$$

With good design and build,  $c \eta_t$  is approximately 1.5.



**Fig. 2.89** Ideal power coefficient of the Savonius rotor

**Torque.** From the power,

$$M = \frac{P}{\omega} = P \frac{D}{2u} = P \frac{D}{2\lambda v_0} = \frac{c_p}{c} c \eta_t \frac{D}{\lambda 2 v_0} P_0$$

$$\rightarrow M = \left(1 - \frac{\lambda}{\beta}\right)^2 M_A, \text{ with } M_A = c \eta_t \frac{D}{\beta 2 v_0} P_0, \quad (2.153)$$

where  $M_A$  is the starting torque ( $\lambda = 0$ ).

An advantage of drag-type rotors is that they have a high starting torque and are therefore able to start up and produce electricity even in weak winds.

### Exercise 2.2

Configure a Savonius rotor for an output of 300 W at the optimum wind speed of 6 m/s. Choose  $\beta = 2.5$ ,  $\rho = 1.2 \text{ kg/m}^3$ ,  $c \eta_t = 1.5$ .

- Find the following:
  - The specific power per  $\text{m}^2$  at 6 m/s
  - The diameter and height of the rotor
  - The rated rotation speed of the system.
- From what wind speed  $v_{0\min}$  is power supplied? What is the starting torque at  $v_{0\min}$ ? Draw the power as a function of wind speed  $v_0$  at rated rotation speed.

A solution can be found in [2.9, Annex F].

## 2.8.6 Operation and Control, Design

### Performance and Operating Modes

Fig. 2.90 shows the power actually produced by a given wind turbine with area  $A$  as a function of wind speed:

*Curve a:* Theoretical wind power

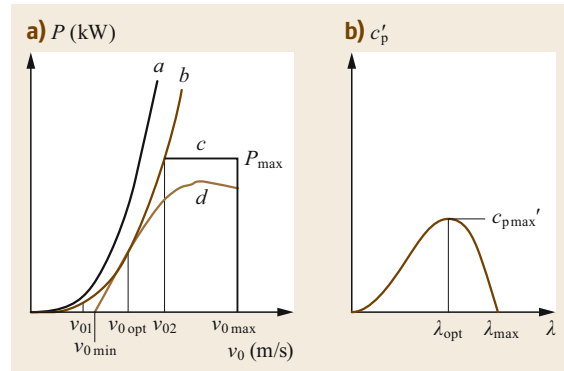
$$P_0 = \frac{1}{2} \rho A v_0^3. \quad (2.154)$$

*Curve b:* Wind-turbine power at maximum efficiency

$$P = c_{p\max}' P_0. \quad (2.155)$$

*Curve c:* Effective wind-turbine power when operating at optimized rotation speed. At the minimum wind speed  $v_{01}$ , the power plant begins to supply energy. Between  $v_{01}$  and  $v_{02}$ , rotation speed control ensures optimum adaptation to the wind speed

$$\omega_{\text{opt}} = \frac{\lambda_{\text{opt}}}{R} v_0, \quad (2.156)$$



**Fig. 2.90** (a) Power of the wind power plant: *a* theoretical wind power, *b* wind-turbine power at maximum efficiency, *c* effective power at optimized speed, *d* effective power at constant speed. (b) Effective power coefficient as a function of the tip speed ratio

that complies with (2.155). For  $v > v_{02}$  the maximum allowable power  $P_{\max}$  is reached and power control is implemented, so that  $P = P_{\max}$ . The speed  $v_{02}$  is usually approximately 15 m/s in modern plants. If the maximum permissible wind speed  $v_{0\max}$  is exceeded, the power plant is switched off (mechanical safety).

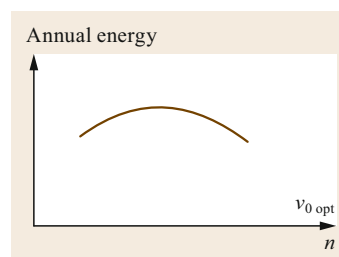
*Curve d:* effective wind turbine power at constant rotation speed operation. At the freely selected optimum wind speed  $v_{0\text{opt}}$ , the maximum efficiency is achieved. The corresponding rotation speed is ( $R =$  radius of the wind turbine)

$$\omega = \frac{v_{0\text{opt}} \lambda_{\text{opt}}}{R}$$

$$\rightarrow n = 30 \frac{\omega}{\pi} = 30 \frac{v_{0\text{opt}} \lambda_{\text{opt}}}{\pi R}. \quad (2.157)$$

For other wind speeds, the power decreases according to  $c'_p(\lambda)$ . The wind turbine delivers energy from  $v_{0\min}$  according to the tip speed ratio  $\lambda_{\max}$ .

For a given location with a given wind frequency distribution, the annual energy produced reaches a value



**Fig. 2.91** Optimum wind speed or rotation speed

that depends on the choice of the optimal wind speed, as illustrated in Fig. 2.91. For a certain value of  $v_{0opt}$ , this energy becomes maximum. Whether this value also represents an economic optimum depends on the cost figure as a function of the selected rotation speed (gearbox investment and losses, rotor blade strength, etc.).

### Power Regulation

A distinction is made between systems with *stall control* and systems with *pitch control* (blade angle control) [2.35, 36]. In horizontal-axis rotors, the power factor at a given rotation speed depends not only on the wind speed but also on the angle of attack of the profile (blade angle), as illustrated in Fig. 2.84.

In stall-controlled systems, the blade angle is fixed over the entire speed range up to  $v_{0max}$ . The power limiting is effected by the geometry of the rotor blade, that is aerodynamically designed in such a way that, on reaching the speed  $v_{02}$ , turbulences arise, leading to a stall. Thus a power curve is achieved approximately similar to curve *d* in Fig. 2.90. Stall control avoids the relatively complicated blade-angle control mechanism. Approximately two-thirds of the installed systems have stall control [2.35] (<http://www.windpower.dk/en>). The stall control is called active if the rotor blades have several fixed positions that are selected according to the wind speed.

The blade angle control automatically searches for the optimum angle of attack at a given wind speed, as shown in Fig. 2.84. This enables the power coefficient at the given speed to be maximized with the appropriate outlay. When the maximum permissible power  $P_{max}$  is reached, the power is kept constant. The maximum possible power coefficient corresponding to curve *c* in Fig. 2.90 can only be obtained with variable rotation speed.

### Grid Operation

The electricity produced is fed into the power grid. The simplest and cheapest scheme is shown in Fig. 2.92. The wind turbine drives an asynchronous generator via a gearbox. The power supplied to the grid is

$$P_c = \eta_c \eta_m P = \eta_c \eta_m c'_p P_0. \tag{2.158}$$

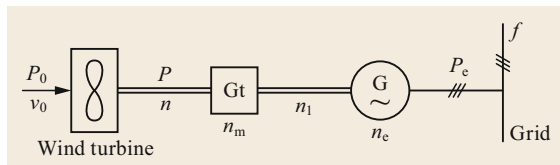


Fig. 2.92 Simplest wind energy system (Gt: gearbox, G: generator)

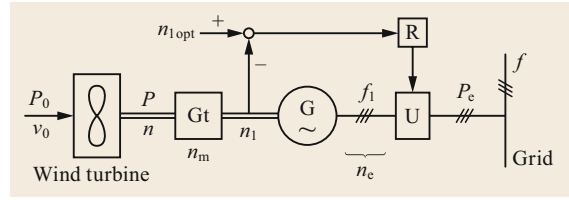


Fig. 2.93 Wind energy system with optimized speed (Gt: Gearbox, G: Generator, U: Converter, R: speed governor)

Asynchronous generators are inexpensive and robust, but they cannot deliver reactive power without the use of capacitors. For higher powers, therefore, a synchronous generator is preferred. In both cases

$$\begin{aligned} \text{Generator speed } n_i &= 60 \frac{f}{p} \\ (p &= \text{number of pole pairs}), \\ \text{Gear ratio } \ddot{u} &= \frac{n_1}{n} = \frac{2\pi f R}{p v_{0opt} \lambda_{opt}} \end{aligned} \tag{2.159}$$

and the delivered power corresponds essentially to curve *d* in Fig. 2.90, the rotation speed being constant (dictated by the grid frequency).

Power according to curve *c* in Fig. 2.90 is possible, but requires the use of a frequency converter, e.g., as shown in Fig. 2.93. By controlling the frequency conversion, the rotation speed is kept optimal. The higher energy yield must be earned through higher investments. It should also be noted that the energy gain from the higher average efficiency of the wind turbine is somewhat reduced by the losses in the converter (lower electrical efficiency).

In addition to the solution shown in Fig. 2.93, solutions with wound-rotor asynchronous machines are also available, in which the converter changes the frequency of the rotor current. The converter power required for this is considerably smaller [2.35, 37].

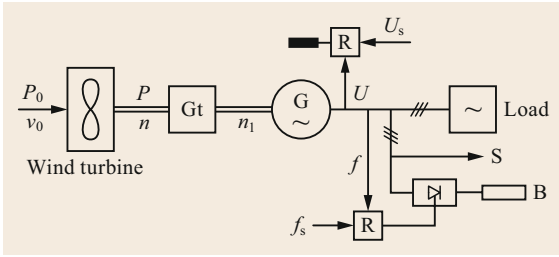
### Island Operation

Normally, the consumer requires a constant frequency and a constant voltage (exception: heating resistors). The most suitable generator is then a synchronous generator, that allows voltage regulation via the excitation [2.3, Sect. 1.1]. An asynchronous generator with regulated capacitor battery is also possible.

Since wind energy supply is very variable, storage facilities and/or ballast resistors must be provided for frequency control (Fig. 2.94). The rotation speed changes according to

$$M - M_b = J \frac{d\omega}{dt}. \tag{2.160}$$

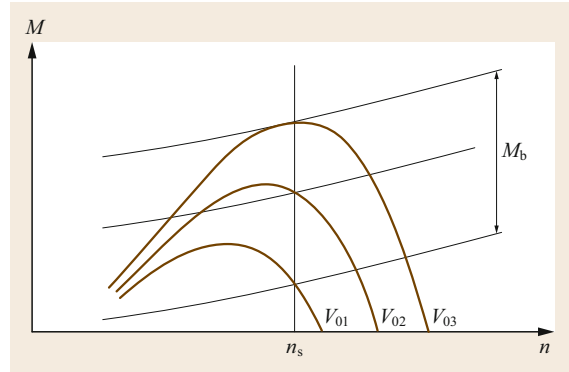




**Fig. 2.94** Wind energy system in island operation: Gt: Gearbox, G: Generator, R: Regulator, S: Storage (flywheel, pump storage, accumulator), B: Ballast resistor (sewage treatment plant, storage heating)

The graph of the drive torque  $M$  as a function of rotation speed and wind speed is shown in Fig. 2.95 ( $n_s =$  synchronous rotation speed).

The load torque  $M_b$  must be adjusted accordingly. Its value depends on the nature of the load and on



**Fig. 2.95** Torque characteristic of a wind turbine  $M = f(n, v_0)$

the voltage–frequency characteristic. Operation with optimized rotation speed is also possible with a converter.

## 2.9 Photovoltaics

In this section, the basics of photovoltaics (photoelectric effect) and solar cells (structure, types, characteristics, efficiencies) are given. To use them optimally requires knowledge of the radiation intensity and thus the calculation of the apparent movement of the Sun relative to the Earth.

### 2.9.1 Physical Basics, Photoelectric Effect

The behavior of semiconductors and insulators can be well explained by the *energy-band model* [2.38, 39]. For the photoelectric effects, only the *valence band* with upper energy level  $W_V$  and the *conduction band* with lower energy level  $W_L$  play a role (Fig. 2.96a). The two bands are separated by a band gap  $\Delta W = W_L - W_V$  that is, e.g., 1.12 eV for silicon. The density of states  $Z(W)$  of the electron energy  $W$  within the bands is described by a parabola. According to Pauli’s exclusion principle, the probability of occurrence of an energy state results from multiplication with Fermi–Dirac statistics (Fig. 2.96b)

$$F(W) = \frac{1}{1 + \exp\left(\frac{W - W_F}{kT}\right)}, \quad (2.161)$$

where  $W_F$  is the Fermi energy and  $k$  is the Boltzmann constant

$$k = 8.62 \times 10^{-5} \frac{\text{eV}}{\text{K}} = 1.30805 \times 10^{-23} \frac{\text{J}}{\text{K}}. \quad (2.162)$$

Integrating over the conduction band gives the electron density [2.38, 40]

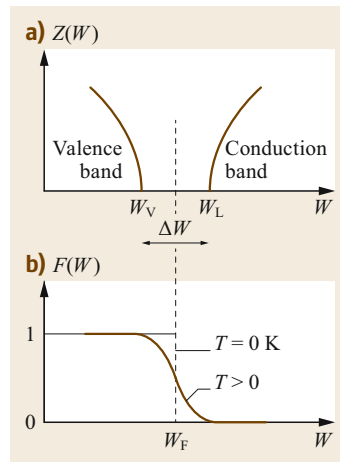
$$n = \int_{W_L}^{\infty} F(W)Z(W)dW \approx N_L \exp\left(-\frac{W_L - W_F}{kT}\right)$$

$$\text{with } N_L = 2 \left(\frac{2\pi m_n kT}{h^2}\right)^{\frac{3}{2}} \quad (2.163)$$

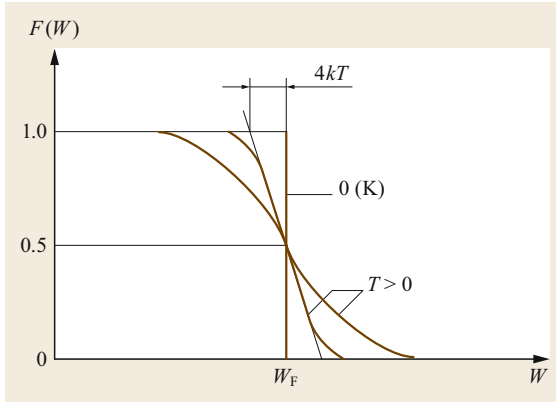
and

$$h = \text{Planck’s constant} = 6.6256 \times 10^{-34} \text{ J s}$$

$$m = \text{electron mass} = 0.9109 \times 10^{-27} \text{ g}. \quad (2.164)$$



**Fig. 2.96a,b** Band model of the semiconductor. (a) Density of possible energy states within the valence and conduction band,  $\Delta W =$  band gap (forbidden zone), (b) Fermi–Dirac statistics for the probability of occurrence of an energy state



**Fig. 2.97** Influence of temperature on the Fermi–Dirac distribution

The effective mass  $m_n$  of the electron differs somewhat from the rest mass due to the effect of the potential of the solid-state lattice  $m$  [2.39]. While the band gap  $\Delta W$  is of the order of 1 eV for semiconductors, it is significantly larger for insulators. The Fermi level is located in the middle of the forbidden zone.

For  $T = 0$  K,  $n = 0$  according to (2.163), that is, there are no electrons in the conduction band (sharp Fermi level). The higher the temperature, the more the Fermi level becomes blurred (Fig. 2.97). At room temperature, a few electrons get into the conduction band. At 20 °C, for example,  $4kT \approx 0.1$  eV, and for silicon with  $\Delta W = 1.12$  eV, (2.163) gives  $n = 5.7 \times 10^9$  electrons/cm<sup>3</sup>. At first sight this may seem a lot, but silicon has a density of 2.33 g/cm<sup>3</sup> and an atomic weight of 28. Thus, the number of atoms per cm<sup>3</sup> is (Avogadro)

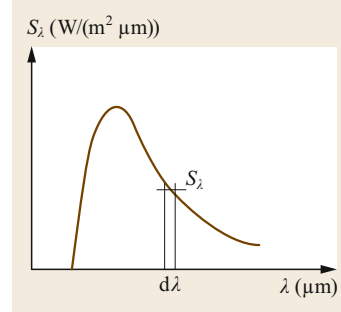
$$6 \times 10^{23} \frac{2.33}{28} = 5 \times 10^{22} \frac{\text{atoms}}{\text{cm}^3} \left( \frac{\text{atoms g/cm}^3}{\text{mol g/mol}} \right).$$

Thus, only about one electron in  $10^{13}$  silicon atoms is in the conduction band. Accordingly, the *intrinsic conductivity* of silicon at 20 °C is very low.

### Photoconductivity

When light falls on a thin semiconductor wafer of surface area  $A$  and thickness  $d$ , the energy level of electrons is raised by the absorption of photons (light quanta) and, as long as the photons have an energy of  $hf > \Delta W$ , electrons from the valence band are lifted into the conduction band. In *direct* semiconductors [2.40], such as GaAs, layers of only a few  $\mu\text{m}$  are needed to completely absorb the radiation. In *indirect* semiconductors, such as crystalline silicon, on the other hand, several hundred  $\mu\text{m}$  (200  $\mu\text{m}$  for 90% absorption) are required.

The electrons of the conduction band move freely in the crystal and form the negatively charged electron



**Fig. 2.98** Spectral intensity  $S_\lambda$  of solar radiation

flow. This makes it possible to convert radiant energy into electrical energy (photoelectric effect). Gaps (holes) remaining in the valence-band can also move by the movement of neighboring electrons that forms the positive current. The *recombination* of electrons with holes, counteracts the proliferation of conduction band electrons, so that an equilibrium state is established. The number of electrons in the conduction band increases according to the law

$$\frac{dn}{dt} = \eta \varphi_q \frac{1}{Ad} - \frac{n}{\tau}, \quad (2.165)$$

where:

$\varphi_q$  photon flux (photons/s)

$\eta$  quantum efficiency

$\tau$  recombination time of electron–hole pairs.

The stationary solution of this differential equation is

$$n = \eta \varphi_q \frac{\tau}{Ad} \left( \frac{\text{electrons}}{\text{m}^3} \right). \quad (2.166)$$

From the spectral intensity  $S_\lambda$  of the radiation falling perpendicular to the surface (Fig. 2.98), the photon flux can be calculated

$$S_\lambda d\lambda \left( \frac{\text{W}}{\text{m}^2} \right) = \frac{d\varphi_q}{A} hf \left( \frac{\text{photons}}{\text{m}^2 \text{ s}} \frac{\text{W s}}{\text{photons}} \right). \quad (2.167)$$

Since  $f = c/\lambda$  ( $c$  = speed of light),

$$d\varphi_q = \frac{A}{hc} S_\lambda \lambda d\lambda. \quad (2.168)$$

If photons of wavelength  $\lambda$  have an efficiency  $\eta_\lambda$ , then

$$\eta \varphi_q = \frac{A}{hc} \int_0^\infty \eta_\lambda S_\lambda \lambda d\lambda. \quad (2.169)$$

Inserting this into (2.166), leads to the *intrinsic conductivity* of the irradiated semiconductor.

### The p-n Junction

By implanting foreign atoms (*doping*), the conductivity of the semiconductor can be influenced. This is known as *impurity conduction*.

If the valence electron number of the foreign atoms is greater than that of the semiconductor material (e.g., pentavalent P in tetravalent Si), the excess electrons in the crystal can detach themselves from the impurity and increase the conductivity of the semiconductor. The foreign atoms in this case are called *donors*. The semiconductor doped in this way has *n-conductivity*, i.e., the electrons are majority carriers, the holes minority carriers.

Conversely, if the foreign atoms have fewer valence electrons (e.g., trivalent boron), then we speak of *acceptors* and of *p-conductivity*, the number of holes being increased. The holes are majority carriers and the electrons minority carriers.

If a p-n junction is formed according to Fig. 2.99a, then, as consequence of the different concentrations of the charge carriers, there is a *diffusion of the majority carriers*, i.e., of the electrons from n to p and of the holes from p to n. In the boundary layer, the now ionized donors and acceptors remain behind, forming a potential barrier that stops the diffusion current. This produces the diffusion voltage  $U_D$  (Fig. 2.99c), with the

value (for further details see [2.30, 39, 40])

$$U_D = \frac{kT}{e} \ln \frac{n_n}{n_p}, \quad (2.170)$$

where:

$n_n$  density of the n-majority carriers  
 $n_p$  density of the p-minority carriers  
 $e$  electron charge ( $1.6021 \times 10^{-19}$  A s).

In terms of energy, the bands on the n-side are lowered by  $eU_D$ , as shown in (Fig. 2.99b), with

$$eU_D = \Delta W - \delta_n - \delta_p, \quad (2.171)$$

where  $\delta_n$  and  $\delta_p$  are the distances between the conduction and valence bands and the Fermi level. With increased doping, these distances become smaller and smaller, and in the case of high doping, we get

$$U_D \approx \frac{\Delta W}{e}. \quad (2.172)$$

The thickness of the space charge zone is [2.40]

$$x = \sqrt{\frac{2\varepsilon U_D (n_D + n_A)}{en_D n_A}}, \quad (2.173)$$

where  $n_D$  and  $n_A$  are the densities of donors and acceptors.

### 2.9.2 Photovoltaic Effect, Photocurrent

When an external voltage  $U$  is applied, a p-n junction acts as a diode (Fig. 2.100a). The result is the characteristic curve in Fig. 2.100b. For  $U < 0$ , the potential barrier is increased and the diffusion is reversed. The diode blocks the flow of current. The thermally generated electrons are sucked off and generate the saturation current  $I_s$  in the reverse direction [2.38]

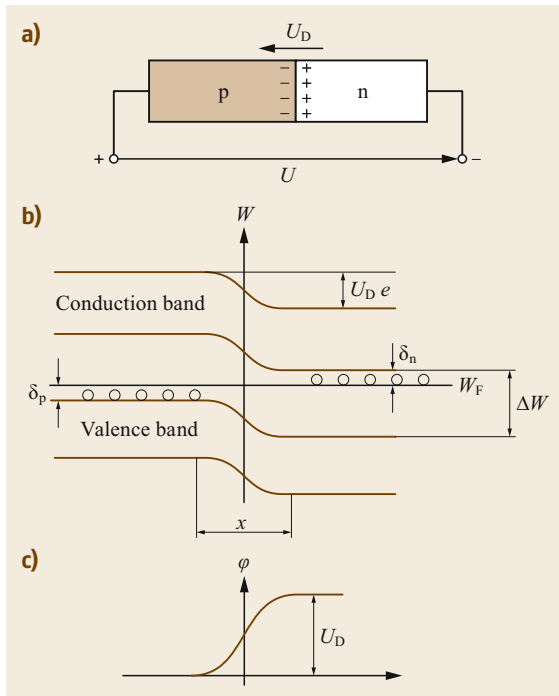
$$I_s \propto T^3 \exp\left(-\frac{U_D}{U_T}\right). \quad (2.174)$$

For  $U > 0$ , the potential barrier is reduced, diffusion is favored and the current flows, where

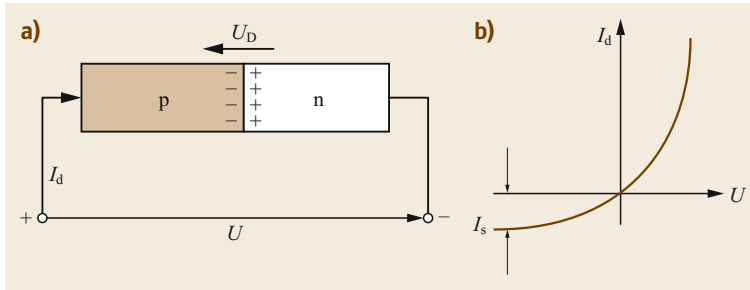
$$I_d = I_s \left[ \exp\left(\frac{U}{U_T}\right) - 1 \right]$$

$$U_T = \frac{kT}{e} = \text{thermodynamic voltage}$$

$$= 25.7 \text{ mV at } 25^\circ \text{C}. \quad (2.175)$$



**Fig. 2.99** (a) p-n junction, (b) energy-band scheme, (c) potential curve



**Fig. 2.100** (a) p-n junction as diode, (b) characteristic current–voltage curve

If the p-n junction is irradiated with photons with  $hf > \Delta W$  (Fig. 2.101), electrons jump from the valence band into the conduction band. Since there is a potential gradient in the space charge zone, the electrons migrate via the external electrical connection to the positive pole (n-region) and the holes to the negative pole (p-region). This results in an opposite flow to the diffusion flow, the *photocurrent*. However, only the electron–hole pairs directly formed in the boundary layer contribute to the photocurrent, since the others recombine before they can be separated by the potential gradient. The radiation must therefore be brought as close as possible to the boundary layer (Fig. 2.101). For details on the structure of the solar cell, see [2.39, 40].

The resulting photocurrent  $I_{ph}$  is *proportional to the irradiance*. From (2.175), the total current in the conducting direction of the diode is

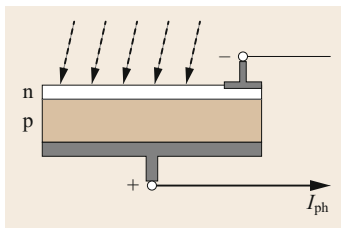
$$I^* = I_s \left[ \exp\left(\frac{U}{U_T}\right) - 1 \right] - I_{ph} .$$

The diode characteristic decreases by  $I_{ph}$  as illustrated in Fig. 2.102. In the 4th quadrant, the arrangement works as a *generator* (solar cell). The current generated by the *solar cell* is  $I = -I^*$

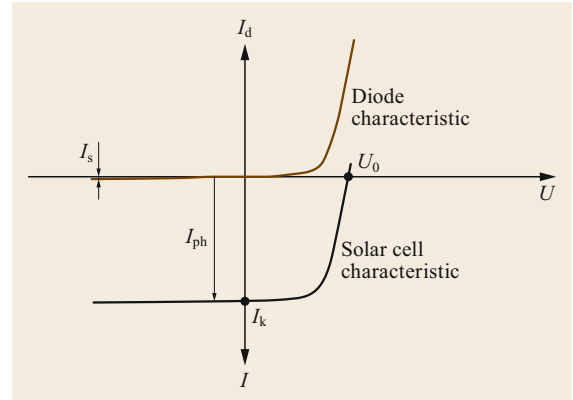
$$I = I_{ph} - I_s \left[ \exp\left(\frac{U}{U_T}\right) - 1 \right] . \tag{2.176}$$

*Short-circuiting* the solar cell ( $U = 0$ ), gives, in the ideal case

$$I = I_k = I_{ph} . \tag{2.177}$$



**Fig. 2.101** Irradiated solar cell

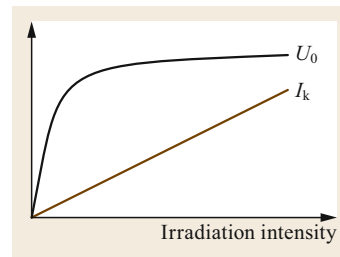


**Fig. 2.102** Formation of the solar-cell characteristic curve by irradiation of the p-n junction

With *no load* ( $I = 0$ ), (2.176) yields

$$U = U_0 = U_T \ln \left( 1 + \frac{I_{ph}}{I_s} \right) . \tag{2.178}$$

The short-circuit current is equal to the photocurrent and thus proportional to the irradiance, while the open-circuit voltage has a logarithmic curve as a function of the irradiation (Fig. 2.103). Through  $U_T$  (2.175) and  $I_s$  (2.174) the temperature has a big influence on the open-circuit voltage in such a way that it decreases with increasing temperature. Rising temperature thus reduces the performance of the solar cell. The short-circuit current, on the other hand, is only slightly influenced by the temperature (Fig. 2.110).



**Fig. 2.103** Dependence of short-circuit current and open-circuit voltage of the solar cell on irradiation intensity

### Calculation of the Photocurrent

For spectral intensity  $S_\lambda$  as in Fig. 2.98 and according to (2.168), the photon flux for wavelengths between  $\lambda$  and  $\lambda + d\lambda$  is

$$d\varphi_q = \frac{A}{hc} S_\lambda \lambda d\lambda \left( \frac{\text{photons}}{\text{s}} \right). \quad (2.179)$$

The number of electrons contributing to the photocurrent is smaller, because of the losses.

$$dn = \eta_\lambda d\varphi_q = \frac{A}{hc} n_\lambda S_\lambda \lambda d\lambda \left( \frac{\text{electrons}}{\text{s}} \right). \quad (2.180)$$

The efficiency  $\eta_\lambda$  takes into account that:

- *Photons are lost* through reflection, transmission and thermalization.
- Some of the generated electron–hole pairs *recombine* before they are separated by the potential gradient.

The photocurrent is then

$$dI_{\text{ph}} = edn = en_\lambda d\varphi_q = \frac{e}{hc} A \eta_\lambda S_\lambda \lambda d\lambda \quad (\text{A}),$$

and the photocurrent density

$$dJ_{\text{ph}} = \frac{e}{hc} n_\lambda S_\lambda \lambda d\lambda \quad \left( \frac{\text{A}}{\text{m}^2} \right).$$

Integrating over the whole spectrum, the photocurrent density is obtained as

$$J_{\text{ph}} = \frac{e}{hc} \int_0^\infty \eta_\lambda S_\lambda \lambda d\lambda \quad \left( \frac{\text{A}}{\text{m}^2} \right). \quad (2.181)$$

The power density of the radiation is, on the other hand,

$$P_s = \int_0^\infty S_\lambda d\lambda \quad \left( \frac{\text{W}}{\text{m}^2} \right). \quad (2.182)$$

The spectral response of the solar cell is defined as

$$\varepsilon = \frac{J_{\text{ph}}}{P_s} = \frac{\int_0^\infty n_\lambda S_\lambda \lambda d\lambda}{\int_0^\infty S_\lambda d\lambda} \quad \left( \frac{\text{A}}{\text{W}} \right). \quad (2.183)$$

Overcoming the band gap  $\Delta W$  is only possible for radiation with

$$hf = h \frac{c}{\lambda} > \Delta W.$$

The radiation is therefore only effective if

$$h < \frac{hc}{\Delta W} = \lambda_{\text{max}}, \quad (2.184)$$

$\lambda_{\text{max}}$  depends on the semiconductor material. For example, for silicon, it is, e.g.,  $\Delta W = 1.12$  eV, from which  $\lambda_{\text{max}} = 1.11 \mu\text{m}$ . For  $\lambda > \lambda_{\text{max}}$ ,  $\eta_\lambda = 0$  because the photons do not provide enough energy to overcome the band gap. The corresponding energy is thermalized. Therefore

$$\int_0^\infty \eta_\lambda S_\lambda \lambda d\lambda = \int_0^{\lambda_{\text{max}}} \eta_\lambda S_\lambda \lambda d\lambda,$$

and the spectral response can also be expressed as follows

$$\varepsilon = \frac{e}{hc} \frac{\int_0^{\lambda_{\text{max}}} S_\lambda d\lambda}{\int_0^\infty S_\lambda d\lambda} \frac{\int_0^{\lambda_{\text{max}}} \lambda S_\lambda d\lambda}{\int_0^{\lambda_{\text{max}}} S_\lambda d\lambda} \frac{\int_0^{\lambda_{\text{max}}} \eta_\lambda S_\lambda \lambda d\lambda}{\int_0^{\lambda_{\text{max}}} \lambda S_\lambda d\lambda}, \quad (2.185)$$

or written in shorter form as

$$\varepsilon = \frac{e}{hc} \eta_1 \lambda_0 \eta_3. \quad (2.186)$$

Discussion of the individual factors: The first factor is a constant

$$\frac{e}{hc} = 0.807 \frac{\text{A}}{\text{W} \mu\text{m}}. \quad (2.187)$$

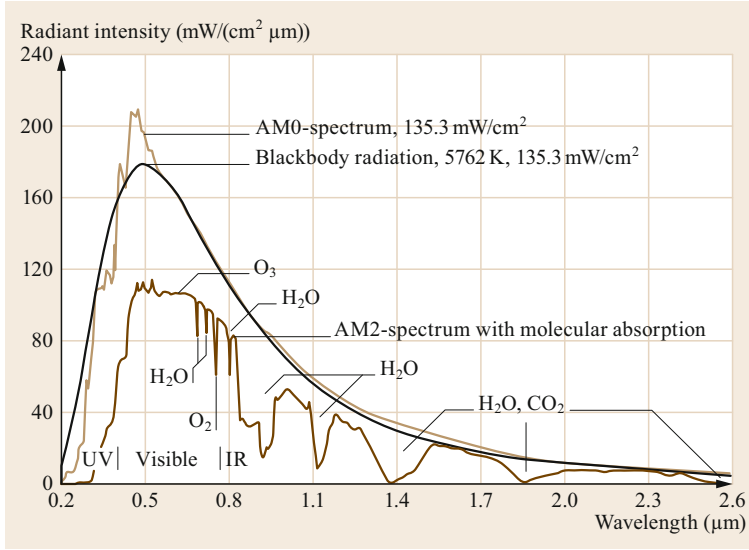
The efficiency parameter  $\eta_1$  takes into account losses for  $\lambda > \lambda_{\text{max}}$  (*thermalization* of the corresponding photon energy). It is a function of the solar spectrum and the band gap of the semiconductor material. It increases with decreasing band gap. The guideline value for silicon is  $\eta_1 \approx 0.75$ , i.e., around 25% of the solar energy lies in the wavelength range above  $\lambda_{\text{max}}$ . With monochromatic light of wavelength  $\lambda_{\text{max}}$ , it would be  $\eta_1 \approx 1$ .

The wavelength  $\lambda_0$  is proportional to the ratio between the number of photons in the range  $0 - \lambda_{\text{max}}$  and the corresponding radiation energy ((2.181) and (2.182)). For  $\lambda = \lambda_{\text{max}}$ , the photon energy is just enough to overcome the band gap and is fully transferred to the electrons. For  $\lambda < \lambda_{\text{max}}$ , it is too large, and the excess energy is *thermalized*. The corresponding losses can be represented by the efficiency factor  $\eta_2$

$$\lambda_0 = \eta_2 \lambda_{\text{max}},$$

$$\longrightarrow \int_0^{\lambda_{\text{max}}} \lambda S_\lambda d\lambda = \eta_2 \lambda_{\text{max}} \int_0^{\lambda_{\text{max}}} S_\lambda d\lambda,$$

$$\text{thus, } \varepsilon = \frac{e}{hc} \lambda_{\text{max}} \eta_1 \eta_2 \eta_3. \quad (2.188)$$



**Fig. 2.104** Spectral radiation distribution of sunlight. AM0: Radiation characteristic outside the Earth's atmosphere; AM2: Radiation characteristic with atmosphere ( $2\times$  atmosphere thickness at the equator, with the sun at zenith and 0 m altitude); the calculations mostly refer to AM1.5 ( $1.5\times$  atmosphere thickness) (adapted from [2.39])

If the solar cell were irradiated with monochromatic light of wavelength  $\lambda_{\max}$ , this would give  $\eta_2 = 1$ . With the solar spectrum AM1.5 (Fig. 2.104), the guide value for monocrystalline silicon is  $\eta_2 \approx 0.66$ . This means that for silicon  $\eta_1\eta_2 \approx 0.49$  so 51% of the solar energy cannot be used because of the spectral composition of sunlight. The product  $\eta_s = \eta_1\eta_2$  is therefore also called the spectral efficiency of the solar cell.

The efficiency  $\eta_3$  is proportional to the ratio between useful electrons and photons in the range  $0-\lambda_{\max}$  according to (2.179) and (2.180). It therefore takes into account *photon losses* and *recombination losses*. This efficiency depends on the state of solar cell technology. For silicon solar cells with an overall efficiency of 15%, it is likely to be  $\eta_3 \approx 0.75$ . Theoretically, the limit is one, so that a further increase can be expected if the technology is improved.

With monochromatic light of wavelength  $\lambda_{\max}$  and  $\eta_3 = 1$ , the theoretically maximum attainable spectral response would be

$$\varepsilon_{\max} = \frac{e}{hc}\lambda_{\max} = \frac{e}{hf_{\min}} = \frac{e}{\Delta W} \quad (2.189)$$

It is therefore inversely proportional to the band gap energy  $\Delta W$ . For silicon, one obtains  $\varepsilon_{\max} = 0.89 \text{ A/W}$ . The equation can finally be written as

$$\varepsilon = \varepsilon_{\max}\eta_1\eta_2\eta_3 \left( \frac{\text{A}}{\text{W}} \right) \quad (2.190)$$

With the reference numbers mentioned, e.g., for crystalline silicon

$$\varepsilon \approx 0.89 \times 0.75 \times 0.66 \times 0.75 = 0.33 \frac{\text{A}}{\text{W}} \quad (2.191)$$

From the spectral response, the photocurrent density and photocurrent of the solar cell are

$$\begin{aligned} J_{\text{ph}} &= \varepsilon P_s \left( \frac{\text{A}}{\text{m}^2} \right) \\ I_{\text{ph}} &= \varepsilon P_s A \quad (\text{A}), \end{aligned} \quad (2.192)$$

where  $P_s$  is the radiation power ( $\text{W/m}^2$ ) and  $A$  is the active semiconductor area ( $\text{m}^2$ ).

Since  $\eta_3$  can theoretically be increased to one, the upper limit of the spectral response for silicon when irradiated with the AM1.5 solar spectrum is  $\varepsilon_{\text{th}} \approx 0.44 \text{ A/W}$ .

Figure 2.105 shows the maximum possible current density ( $\eta_3 = 1$ ) with an AM0 and AM1.5 spectrum and  $P_s = 1000 \text{ W/m}^2$  as a function of the band-gap energy of the semiconductors

$$J_{\max} = \varepsilon_{\text{th}} P_s = \varepsilon_{\max} \eta_s P_s \quad (2.193)$$

The spectral efficiency is derived from (2.193) as

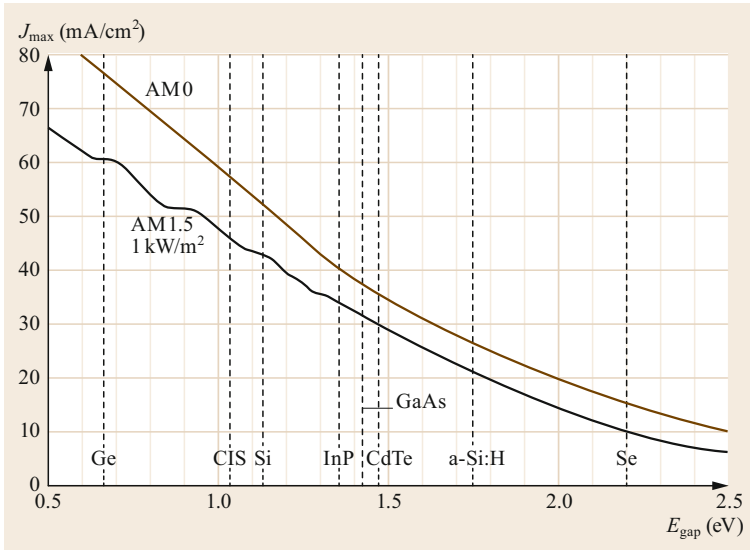
$$\eta_s = \frac{J_{\max}}{\varepsilon_{\max} P_s} = \frac{J_{\max} \Delta W}{P_s e} \quad (2.194)$$

It is shown in Fig. 2.106 as a function of band gap energy for irradiation of semiconductors with AM0 and AM1.5 and  $1000 \text{ W/m}^2$ .

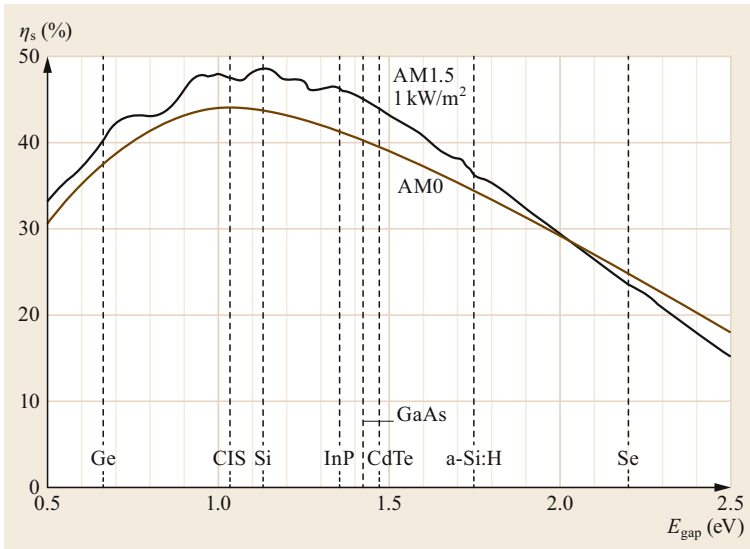
### 2.9.3 Solar Cell, Overall Efficiency

#### Characteristic Curve and Equivalent Circuit

The characteristic curve of the solar cell and how it arises are shown in Fig. 2.102. Figure 2.107 shows a typical *real* (measured) characteristic curve for a cer-



**Fig. 2.105** Maximum current density as a function of the band gap ( $\eta_3 = 1$ ) [2.41]



**Fig. 2.106** Spectral efficiency as a function of band gap (adapted from [2.41])

tain radiation intensity with the most important characteristic values. The maximum power is reached at point P. The solar cell should therefore be operated as close as possible to this point (MPP) by adjusting the load resistance.

The characteristic curve can be well described qualitatively with the equivalent circuit of Fig. 2.108, which is analyzed in the following. More accurate models are discussed in [2.9, Sect. 8.5.5].

The photocurrent is proportional to the irradiation intensity, and is simulated by a current source. According to (2.176), the difference between the photocurrent and diode current is theoretically the useful current of the solar cell. The equivalent circuit also takes into account that leakage currents cannot be avoided (parallel

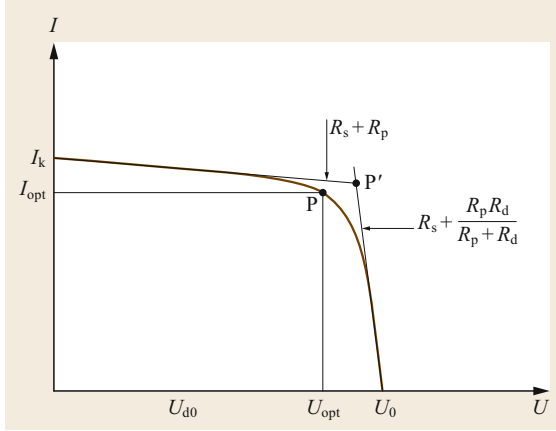
resistance  $R_p$ ) and that ohmic losses occur at transition points and in the contacts (series resistance  $R_s$ ).

The size and effect of the two resistors on the characteristic curve of the solar cell can be determined by idealizing the diode characteristic curve with  $U_{d0}$  and  $R_d$  as in Fig. 2.109. It has proved useful to define the diode resistance as the differential resistance at half the photocurrent.

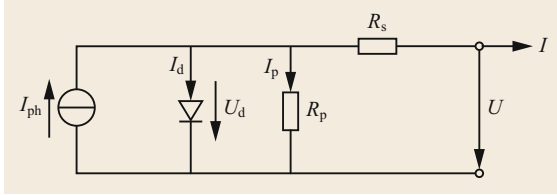
From (2.175), for  $I_d \gg I_s$  and with  $A =$  ideality factor (2.198)

$$U_d = AU_T \ln \left( \frac{I_d}{I_s} \right)$$

$$R_d(I_{ph}) = \left( \frac{dU_d}{dI_d} \right)_{I_{ph}/2} = \frac{2AU_T}{I_{ph}}. \quad (2.195)$$



**Fig. 2.107** Real characteristic curve of a solar cell ( $U_0$ : open-circuit voltage,  $I_k$ : short-circuit current, P: point of maximum power (MPP maximum power point),  $R_p$ : parallel resistance,  $R_s$ : series resistance,  $R_d$ : diode resistance)



**Fig. 2.108** Equivalent circuit diagram of the solar cell (single-diode model)

The *no-load range* of the solar cell (diode conducting) can then be approximated by the straight line

$$U = U_0 - \left( R_s + \frac{R_p R_d}{R_p + R_d} \right) I$$

with  $U_0 = \frac{R_p}{R_p + R_d} (U_{d0} + R_d I_{ph})$ . (2.196)

The corresponding resistance line is shown in Fig. 2.107.

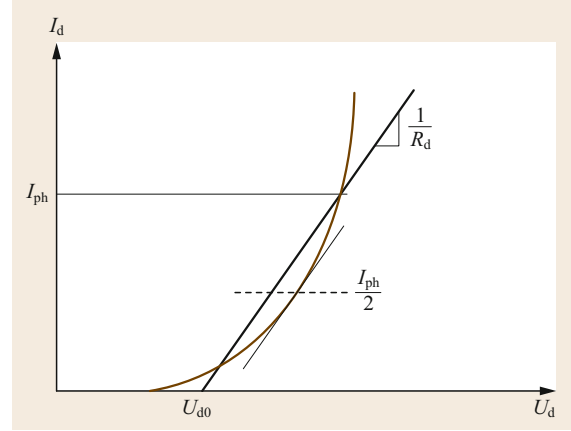
For the *short-circuit range* of the solar cell (diode blocking), the idealized characteristic curve follows, since  $U_d \leq U_{d0}$  and  $I_d = 0$ , giving

$$U = (R_p + R_s) (I_k - I)$$

with  $I_k = \frac{R_p}{R_p + R_s} I_{ph} \approx I_{ph}$ . (2.197)

The corresponding resistance line is also shown in Fig. 2.107. The two resistance lines intersect at P'. The values  $R_s$  and  $R_p$  can be calculated from the experimentally determined characteristic curve.

Figure 2.110 shows the typical characteristic curves of a silicon cell as functions of radiation intensity and



**Fig. 2.109** Diode characteristic curve and its idealization

temperature. Noteworthy for the control of the solar cell is that the optimum voltage (MPP) weakly depends on the irradiation and the optimal current weakly depends on the temperature.

From the equivalent circuit in Fig. 2.108 it follows, by also adding a parallel capacitance, a dynamically satisfactory simulation circuit for the solar cell, that is described by (2.198). The values  $I_{ph}$ ,  $I_s$  and  $U_T$  are temperature-dependent, and also the temperature dependency of  $R_s$  and  $R_p$  can be taken into account. The diode characteristic curve is described more accurately by introducing the ideality factor  $A$  (usually  $A = 1-1.5$ )

$$I_{ph} = I_d + I_c + I_p + I,$$

$$I_d = I_s \left( \exp \left( \frac{U_d}{A U_T} \right) - 1 \right),$$

$$I_c = C \frac{dU_d}{dt},$$

$$U_d = R_p I_p,$$

$$U = U_d + R_s I. \quad (2.198)$$

### Open-Circuit Voltage

From (2.174), (2.116) and (2.122), for  $I_{ph} \gg I_s$

$$U_0 = U_T \ln \left( 1 + \frac{I_{ph}}{I_s} \right) \approx U_T \ln \left( \frac{I_{ph}}{I_s} \right)$$

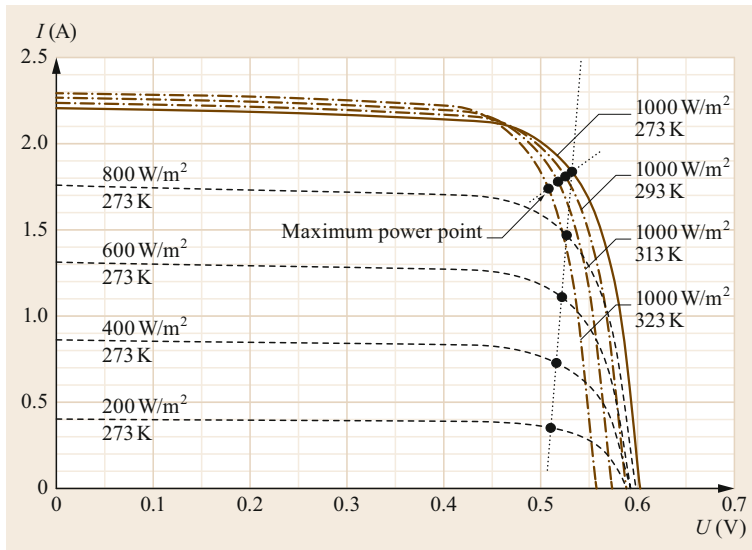
$$I_s = K_s(T) \exp \left( -\frac{U_D}{U_T} \right) \quad \text{with } U_D = \frac{\Delta W}{e}$$

$$\rightarrow U_0 = \left[ 1 - \frac{U_T e}{\Delta W} \ln \left( \frac{K_s(T)}{I_{ph}} \right) \right] \frac{\Delta W}{e}$$

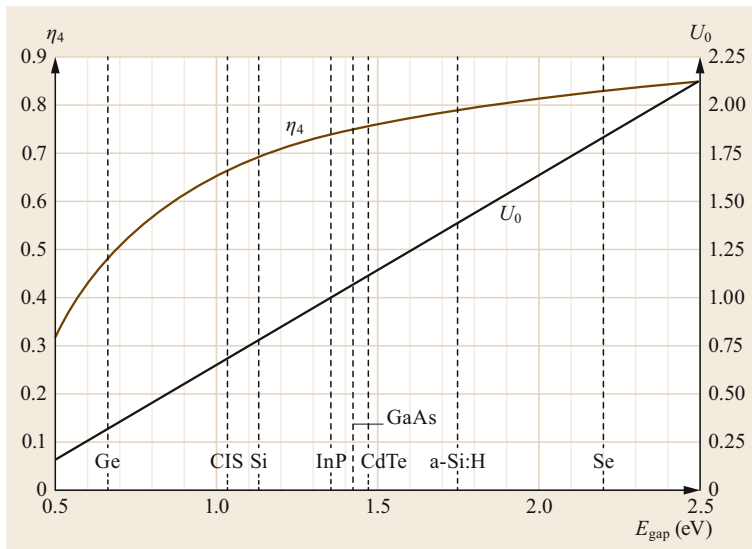
$$= \eta_4 \frac{\Delta W}{e} = \frac{\eta_4}{\varepsilon_{\max}}. \quad (2.199)$$

Fig. 2.111 shows the open-circuit voltage  $U_0$  and the efficiency  $\eta_4$  (also called the voltage factor) as a function of the band gap for 25 °C and for an ideal solar cell.





**Fig. 2.110** Typical current–voltage characteristics of a silicon solar cell as a function of irradiation and temperature (adapted from [2.36])



**Fig. 2.111** Open-circuit voltage  $U_0$  and efficiency  $\eta_4$  (voltage factor) of an ideal solar cell as a function of the band gap for 25 °C (adapted from [2.41])

The open-circuit voltage  $U_0$  can theoretically reach at most the value of the diffusion voltage, that corresponds to the band gap at a high doping level according to (2.172). In reality, for a real cell or module, the open-circuit voltage is slightly lower. The efficiency  $\eta_4$  is strongly dependent on irradiation intensity and temperature. With the assumptions (2.174) and (2.178) for silicon (with  $\epsilon_{\max} \approx 0.89$  A/W), the dependency is shown in Fig. 2.112. With an irradiation of 1000 W/m<sup>2</sup> and a temperature of 25 °C, an efficiency of  $\eta_4 = 0.54$  was assumed ( $U_0 = 0.6$  V, according to Fig. 2.110).

Concentrating the radiation by a factor of 100 (concentrator cells [2.40]) would increase the efficiency by about 20% (relative), provided the cell temperature

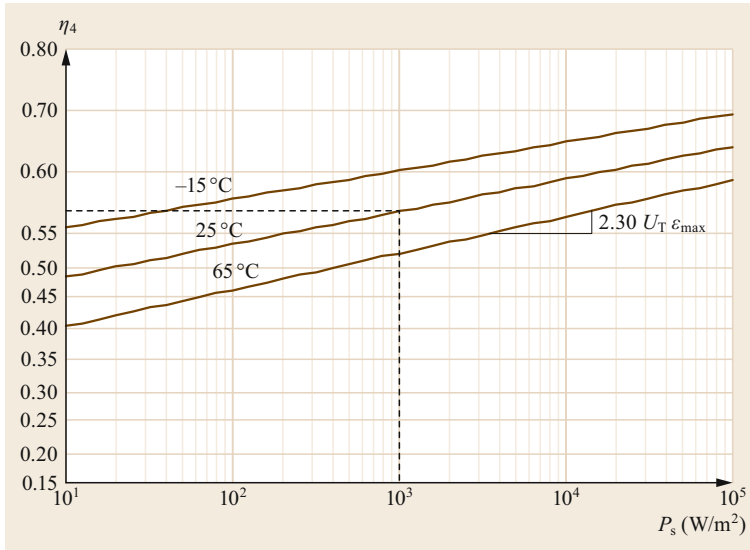
remains the same. A temperature increase causes, as already mentioned, the open-circuit voltage to drop and accordingly reduces the efficiency by approximately 0.3% (relative) per °C.

#### Fill Factor

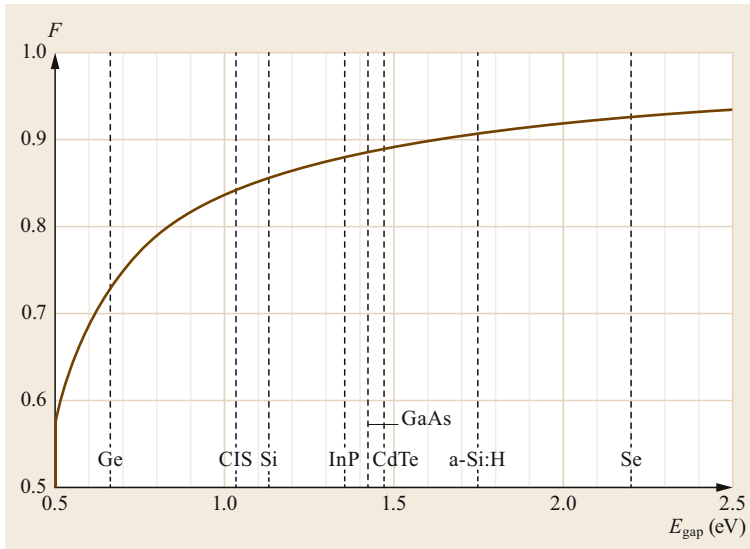
The *fill factor*  $F$  is the ratio between the product of voltage and current at the optimum point (MPP) and the product of open circuit voltage and short-circuit current

$$F = \frac{U_{\text{opt}} I_{\text{opt}}}{U_0 I_k} \quad (2.200)$$

If  $P$  is replaced by  $P'$  (Fig. 2.107), from the theoretical characteristic curve and with the following generally



**Fig. 2.112** Dependence of  $\eta_4$  (voltage factor) on radiation intensity  $P_s$  and temperature (crystalline silicon) for a solar module



**Fig. 2.113** Idealized fill factor  $F$  of various semiconductors (adapted from [2.41])

good approximation for high irradiation levels,

$$R_s, R_d \ll R_p, \quad R_0 = \frac{U_0}{I_k}, \quad (2.201)$$

the following can be written

$$F < F_{\text{th}} \approx 1 - \frac{R_s + R_d}{R_0} - \frac{R_0 - 2(R_s + R_d)}{R_p}. \quad (2.202)$$

Finally, we introduce the partial efficiency

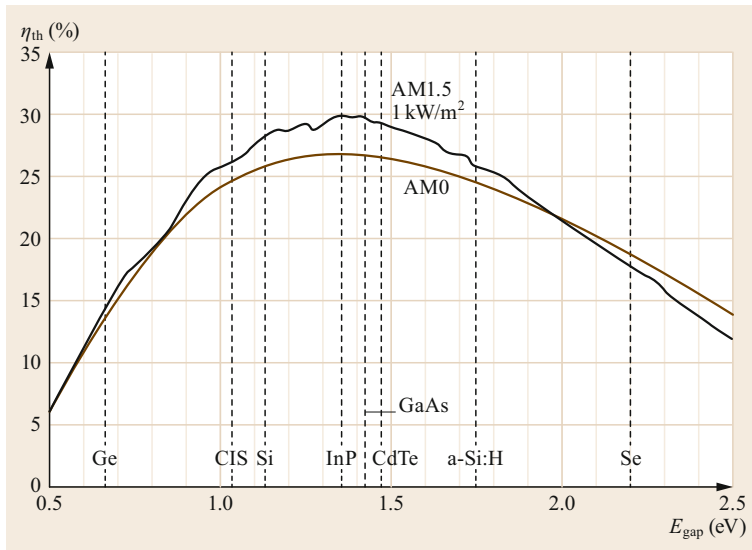
$$\eta_5 = \frac{R_p}{R_p + R_s} F, \quad (2.203)$$

that takes into account *leakage currents* and *ohmic losses* of the diode and contacts. For good silicon modules, the standard value of  $\eta_5 = 0.75$  can be expected. It is theoretically possible to approach 1. Figure 2.113 shows the idealized fill factor  $F$  (with  $F < F_i$ ) as a function of the bandgap of the semiconductor.

### Overall Efficiency

The efficiency is defined as the ratio of power at the optimal point P (MPP) and radiation power

$$\eta = \frac{U_{\text{opt}} I_{\text{opt}}}{A \int_0^\infty S_\lambda d\lambda} = \frac{U_{\text{opt}} I_{\text{opt}}}{A P_s}. \quad (2.204)$$



**Fig. 2.114** Theoretical maximum efficiency of solar cells (adapted from [2.41])

Introducing the fill factor (2.200) and considering (2.197), as well as the photocurrent (2.192), gives

$$\eta = \frac{R_p}{R_p + R_s} F U_0 \varepsilon . \quad (2.205)$$

According to Sect. 2.9.2 and, in particular, (2.190), the spectral response is

$$\varepsilon = \varepsilon_{\max} \eta_1 \eta_2 \eta_3 .$$

If, in addition, the open-circuit voltage according to (2.199) and the fill factor according to (2.203) are used, the five-factor formula is obtained

$$\eta = \eta_1 \eta_2 \eta_3 \eta_4 \eta_5 . \quad (2.206)$$

With the indicated guide values for silicon modules at  $1000 \text{ W/m}^2$  and  $25^\circ\text{C}$ ,  $\eta \approx 0.75 \times 0.66 \times 0.75 \times 0.55 \times 0.75 = 0.15$ , that corresponds approximately to the efficiency of today's good commercial solar cells. With the assumptions  $\eta_3 = \eta_5 = 1$  the theoretical maximum efficiency is

$$\eta_{\text{th}} = \eta_1 \eta_2 \eta_4 . \quad (2.207)$$

Figure 2.114 shows this efficiency as a function of the bandgap for different semiconductors for AM0 and AM1.5 solar spectrum. For crystalline silicon, the theoretical maximum value is  $\eta_{\text{th}} = 0.28$ . In the laboratory, efficiencies up to approximately 21% or even 23–24% [2.40] have been achieved.

### Possibilities for Improving Efficiency

An increase in efficiency is of great importance from an economic point of view, as it reduces the required area and thus considerably lowers the costs of the photovoltaic system. It can also be allowed to incur a further cost (but not too much). The previously defined theoretical maximum efficiency

$$\eta_{\text{th}} = \eta_1 \eta_2 \eta_4$$

cannot be exceeded and is scarcely achievable with affordable costs. For crystalline silicon at  $1000 \text{ W/m}^2$  and  $25^\circ\text{C}$ , it is approximately 0.28 as mentioned before. To approach this value, the efficiencies  $\eta_3$  and  $\eta_5$  whose product today for commercial modules is approximately 0.56, must be further improved. For this, primarily the *electrical losses* from *recombination* and *ohmic resistance* (there is a good analysis of this in [2.40]) have to be reduced as well as the *leakage losses*. The efficiency  $\eta_3$  is also reduced by *optical losses* (photon losses) in the range  $\lambda = 0 - \lambda_{\max}$ . Antireflection coatings and texturing of the surface (pyramidalization of the silicon surface) reduce reflection and light scattering as much as possible (on the textured surface), reflection on the rear of the solar cell also improves absorption [2.40, 41].

There is the further question of the possibility of increasing the low theoretical efficiency  $\eta_{\text{th}} = \eta_1 \eta_2 \eta_4$  of approximately 28%.

**Radiation Concentration.** The efficiency  $\eta_4$  can be improved by *concentration* of the radiation (Fig. 2.112).

Theoretically, this efficiency increases logarithmically with the radiant power, only to flatten out to one at a very high concentration. With a hundredfold concentration, e.g., at 25 °C,  $\eta_4$  increases from 0.54 to approximately 0.65, but only the *direct radiation* can be used (Sect. 1.2.3, Solar Radiation); this technology therefore only makes sense for sites with a low diffuse-light component. With lens and mirror concentrators, concentration factors up to over 1000 can be achieved.

However, the improvement in the overall efficiency of the solar cell is usually less than expected for the following reason: as can also be seen from Fig. 2.112, the improvement only occurs if the temperature remains constant. Since the concentration of the energy causes more heating, cooling would have to be provided, incurring more costs. In this context, it should be noted that the temperature increase negatively affects not only the efficiency  $\eta_4$ , but also  $\eta_5$  (the temperature dependency of  $R_p$ ).

This difficulty, as well as the additional costs associated with tracking and concentration, despite the reduction of the active area, have led to the fact that the coupling of focusing mirror devices with conventional silicon cells has not yet been successful. One solution could be special *concentrator cells* implemented as point contact cells [2.39, 42].

**Improving the Use of the Solar Spectrum.** The product  $\eta_1\eta_2$  is determined by the spectral distribution of the effective radiation and the semiconductor material. With AM1.5 (1.5 atmosphere lengths, see Fig. 2.104) it is approximately  $0.75 \times 0.66 = 0.49$  for crystalline silicon. Other semiconductors are also no better (Fig. 2.106). A significant improvement can only be achieved with *tandem* or *multiple cells*. This means the combination of various semiconductors, whereby each semiconductor absorbs as far as possible that part of the spectrum whose wavelengths are directly below its own  $\lambda_{\max}$  (for  $\lambda = \lambda_{\max}$ ,  $\eta_1\eta_2 = 1$ ). In practice, there are difficulties with the choice of the circuit. The simple series circuit is commonly used, but it has the disadvantage that the worst solar cell determines the current. With parallel connection, problems arise with the contacts and the necessary transparent intermediate layers. Either way, tandem cells require a more complex technology, which implies a considerable additional cost [2.40]. Accordingly, this technology, although promising, has not yet been commercially successful, except for aerospace cells, where it has achieved efficiencies over 30% which are quite common. Tandem cells are also used for thin-film cells (Sect. 2.9.3). More information about tandem and triple cells can be found in [2.41].

### Solar-Cell Types

The most successful solar cell for power applications to date is clearly the *monocrystalline* or *polycrystalline* silicon cell. Virtually all photovoltaic systems today are based on this technology, that is accordingly well-developed, even if it is too expensive by a factor of five for grid applications. The efficiencies of the commercially available modules today are in the range of 12–18% (the laboratory record for a single solar cell is 24.7%). A major handicap of this technology is that more than 50% of the costs are accounted for by the solar cell itself, not least because of the large amount of material required (cell thickness of 200  $\mu\text{m}$  for 90% absorption).

**Thin-film Solar Cells.** For this reason, on the one hand, efforts are being made to reduce the cell thickness of silicon cells to approximately 100  $\mu\text{m}$  (or less) to minimize the cost of materials. On the other hand, attempts are being made to bring actual thin-film solar cells to commercial maturity. An initial area of research is:

- *Thin-film cells made of crystalline silicon* whose thickness is up to about 5  $\mu\text{m}$  (e.g., on glass) and therefore they have considerable advantages in terms of material use (and costs). To achieve the necessary absorption of the radiation, the light is reflected several times (optical confinement). For details, see [2.40, 43].  
It was mentioned in Sect. 2.9.1 that there are semiconductors with much greater absorptive power than crystalline silicon. Research efforts have led to the development of various types of solar cells. The most important are:
- *Amorphous silicon solar cells* With layers of < 1  $\mu\text{m}$ , it is possible to build solar cells that have become widely used in the low-power range (pocket calculators, watches, etc.). For higher powers, the stabilized efficiency achieved is approximately 6% for modules and max. 13% in the laboratory. Although the initial efficiencies are higher, they are reduced to the stated values due to light-induced degradation.
- *Gallium arsenide (GaAs) solar cells.* This crystalline material enables 90% absorption at 2  $\mu\text{m}$ . The band gap of 1.42 eV is also very favorable. With AM1.5, efficiencies of up to 24.5% are achieved in the laboratory. The price (at present) and above all environmental aspects (toxicity of Ga and As) stand in the way of the spread of these cells. Cells of GaAs are being developed for space applications and as concentrator cells. With these cells, higher

efficiencies can be achieved, particularly in the configuration of tandem and multiple cells (see above). However, such cells are very expensive.

- **Solar cells made of cadmium telluride CdTe.** These thin-film cells are very much under discussion today (the laboratory record is 16.5%, modules probably at 6% approximately). Problems are that cadmium is toxic, and tellurium is not sufficiently available. Minimal production costs.
- **Solar cells made of copper indium diselenide CuInSe<sub>2</sub>.** For this arrangement of polycrystalline material, also known as *CIS solar cells*, a layer of approximately 2 μm is sufficient to absorb the radiation. The slightly less favorable band gap of 1 eV can be increased to the optimum of 1.4 eV by adding Ga to the In. In this way, efficiencies of 18.8% have been achieved in the laboratory. However, commercial modules have an efficiency of approximately 9%. The development potential is assessed as good. A disadvantage could be the limited availability of indium.
- **Dye-sensitized cells (Grätzel cell).** This is a cell that uses organic dyes to convert light energy into electrical energy. Among the organic cells, it provides one of the best efficiencies, up to 12%. Significantly higher efficiencies can be achieved according to more recent research. Significant progress has also been made in terms of service life, and mass production is now within reach. Its flexibility makes it particularly suitable for building integration.

Thin-film solar cells are particularly suitable for *tandem structures*. In particular *micromorph solar cells*, that combine microcrystalline and amorphous solar cells, open up new perspectives here [2.44, 45]. Many production facilities for micromorph modules are currently being planned; commercial module efficiencies are slightly above 8% (with hopes for achieving 10% soon). The manufacturing costs and the cost of materials are significantly lower than for classic crystalline silicon cells.

### 2.9.4 The Sun as a Source of Energy

About five billion years ago, at a certain point of the Milky Way, the fusion reactor called the Sun was formed by local compression of the original gas mass of the universe (consisting of about 75% H and 25% He), that led to the critical temperature of about  $12 \times 10^6$  K. Possibly a supernova explosion was the cause of the compression. Over the past five billion years, radiation intensity has probably increased by about 25%. The Sun will continue to burn hydrogen to helium in the same way for another five billion years, and its radiation in-

tensity will continue to increase slightly. Then it will enter into a kind of energy crisis and inflate into a *red giant*, collapse later and continue to shine as a *white dwarf*, finally burning out slowly and ending its star career as an invisible sphere.

Today the Sun is a gas ball with the following dimensions

$$\begin{aligned} \text{Radius: } & 696\,000 \text{ km } (109 \times \text{Earth}) \\ \text{Volume: } & 1.412 \times 10^{27} \text{ m}^3 \\ \rightarrow \text{Surface: } & 6.087 \times 10^{18} \text{ m}^2 \\ \text{Density: } & \frac{1.41 \text{ t}}{\text{m}^3} \left( \frac{1}{4} \text{ of Earth} \right) \\ \text{Mass: } & 2 \times 10^{27} \text{ t } (\text{Earth: } 6 \times 10^{21} \text{ t}). \end{aligned} \quad (2.208)$$

The total radiation is  $380 \times 10^{12}$  TW; referred to the surface, that has a temperature of 5900 K; this is about 62 TW/m<sup>2</sup>.

The radiated energy is  $12 \times 10^{33}$  J/a and the corresponding mass loss according to the relation  $E = mc^2$  is  $\Delta m = 133 \times 10^{12}$  t/a. Approx.  $20 \times 10^{15}$  t/a of hydrogen is burned. In five billion years, it will be about  $10^{26}$  t, that is about 10–15% of the original amount.

#### Extraterrestrial Radiation Intensity

The Earth's orbit around the sun is slightly elliptical. The distance between the Earth and the Sun is

$$\begin{aligned} d_{\max} &= 152 \times 10^6 \text{ km: at the beginning of July,} \\ d_{\min} &= 147 \times 10^6 \text{ km: at the beginning of January,} \\ d_m &= 149.5 \times 10^6 \text{ km: at the beginning of} \\ &\quad \text{April/October.} \end{aligned} \quad (2.209)$$

This can be used to calculate the average *extraterrestrial radiation intensity* (outside the atmosphere, but near the Earth)

$$D_0 = \frac{380 \times 10^{14}}{4\pi d_m^2} = 1353 \frac{\text{W}}{\text{m}^2} = \text{solar constant}; \quad (2.210)$$

The minimal value at the beginning of July is 1310 W/m<sup>2</sup>, while the maximal value at the beginning of January is 1400 W/m<sup>2</sup>.

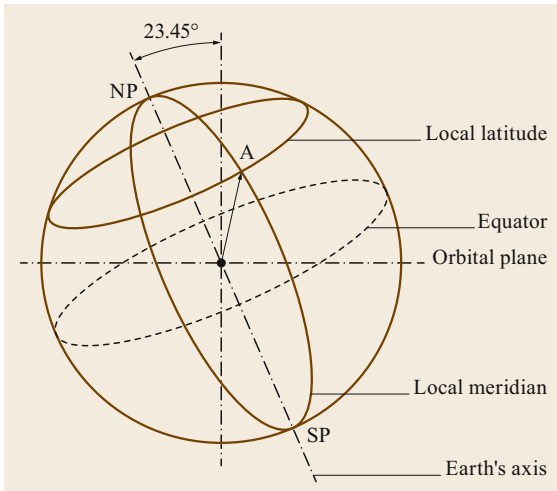
The total radiant power on Earth can be calculated from this, taking into account the Earth's radius of approximately  $6.38 \times 10^6$  m (incl. the atmosphere). The average radiant power is

$$1353\pi(6.38 \times 10^6)^2 = 173 \times 10^{15} \text{ W} = 173\,000 \text{ TW}. \quad (2.211)$$

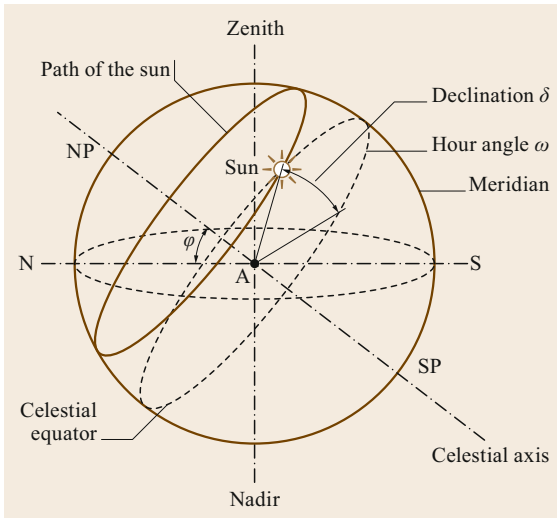
Between July and January, it changes from 167 000 to 179 000 TW.

**Apparent Solar Motion Relative to the Earth**

Figure 2.115 shows the Earth's coordinate system (longitude and latitude) and the inclination of the Earth's axis of rotation at  $23.45^\circ$  from the perpendicular to the orbital plane. Projection onto the celestial sphere, gives the so-called celestial-equator system for the location under consideration (Fig. 2.116). Because of the small size of the Earth's radius, location A is practically at the center of the system. The direction of the celestial axis is determined by the latitude of the location. At the equator, the celestial axis is horizontal; at the poles it corresponds to the nadir–zenith axis.



**Fig. 2.115** Coordinates of location A on the Earth (longitude, latitude)



**Fig. 2.116** Apparent motion of the Sun, for the latitude  $\phi$  obtained by projecting the coordinates of the location onto the celestial sphere. Position of the Sun is given by declination  $\delta$  and hour angle  $\omega$  (adapted from [2.46])

The Sun appears to describe a circular orbit around the celestial axis. This orbit is shifted by the declination  $\delta$  (given as an angle) relative to the celestial equator. The shift depends on the time of year because of the inclination of the rotation axis of the Earth in the orbital plane. It varies between  $-23.45^\circ$  and  $+23.45^\circ$  and is zero at the spring and autumn equinoxes (Fig. 2.117). The declination can be calculated using the following formula ( $n_d$  = daily index, starting on January 1)

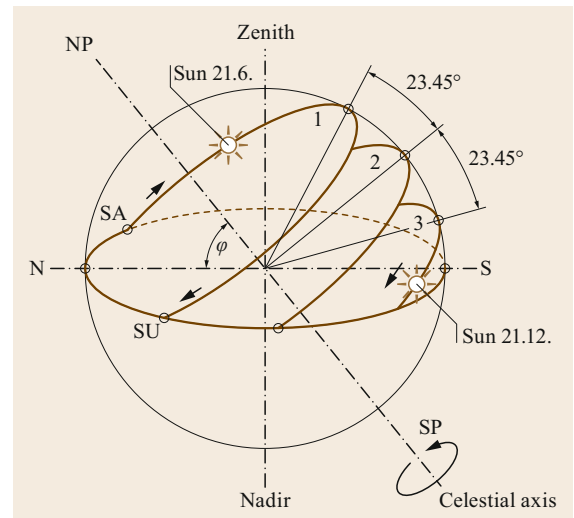
$$\delta = \arcsin \left[ 0.398 \sin \left( 360^\circ \frac{n_d - (79 - 79.75)}{365.25} \right) \right] + 0.026 \sin \left( 360^\circ \frac{n_d - 173}{365.25} \right). \quad (2.212)$$

The second term is a consequence of the elliptical orbit of the earth and differs from zero only for  $173 < n_d \leq 366$ . In the first term

$$\left. \begin{array}{l} n_d - 79 \quad \text{for leap years,} \\ n_d - 79.25 \\ n_d - 79.50 \\ n_d - 79.75 \end{array} \right\} \text{for the next three years.} \quad (2.213)$$

The exact position of the Sun during the day is given by the hour angle, measured from the celestial meridian (relative to the South Pole). When the Sun is due south, the true local time (solar time)  $TS = 12.00$  h. The hour angle (angle deviation from true south) is then

$$\omega = (TS - 12) \times 15. \quad (2.214)$$



**Fig. 2.117** Path of the Sun at: 1 summer solstice, 2 spring and autumn equinoxes, 3 winter solstice; SA: sunrise, SU: sunset (adapted from [2.46])

It should also be kept in mind that the effective local time (*zone time* TL) is not the same as TS. The world is divided into 15 zone times. In the general case

$$TS = TL + \frac{L - L_0}{15} + ET \quad (2.215)$$

where:

$L$  longitude of the location ( $L > 0 \rightarrow$  longitude east)

$L_0$  longitude of the normal-time location (where  $TS = TL - ET$ )

ET correction term, (2.217).

For Western European or Greenwich Time (England, Portugal),  $L_0 = 0^\circ$  (Greenwich or zero meridian, London).

For central European time (CET, valid for most European countries)  $L_0 = 15^\circ$ ; for Eastern European Time or Moscow Time  $L_0 = 30^\circ$  etc. For Switzerland and most European countries the following therefore applies

$$\begin{aligned} \text{Winter: } TS &= CET + \frac{L - 15}{15} + ET, \\ \text{Summer: } TS &= SUT - 1 + \frac{L - 15}{15} + ET, \end{aligned} \quad (2.216)$$

where summer time  $SUT = CET - 1$ .

The term ET is a consequence of the elliptical orbit of the Earth, whose solar orbital velocity is not constant according to Kepler's laws. With sufficient accuracy for solar applications (but not for nautical applications), one can write

$$ET(h) = \sum_{k=1}^3 a_k \cos(kN) + b_k \sin(kN), \quad (2.217)$$

with  $N = \frac{360}{365.25} n_d$  ( $n_d$  = current day number),

$$\begin{aligned} a_1 &= 0.072, & a_2 &= -0.0528, & a_3 &= -0.0012, \\ b_1 &= -0.1229, & b_2 &= -0.1565, & b_3 &= -0.0041. \end{aligned}$$

The behavior of the correction term ET in minutes over the year is shown in Fig. 2.118.

### Calculation of the Position of the Sun

The position of the Sun is defined by the *elevation angle*  $h$  (above the horizon) or the *zenith angle*  $z = 90^\circ - h$  and the *azimuth*  $a$  (deviation from south).

With the help of theorems of spherical trigonometry (sine and cosine theorem), for the spherical triangle

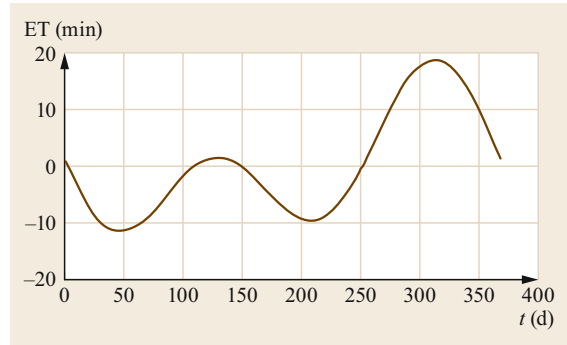


Fig. 2.118 Correction term ET

north-pole-zenith-solar position ( $\varphi > 0$  for the northern hemisphere)

$$\begin{aligned} \sin h &= \cos z \\ &= \sin \varphi \sin \delta + \cos \varphi \cos \delta \cos \omega, \end{aligned} \quad (2.218)$$

$$\begin{aligned} \sin a &= \frac{\cos \delta \sin \omega}{\cosh}, \\ \cos a &= \frac{\sin \varphi \sin h - \sin \delta}{\cos h \cos \varphi}. \end{aligned} \quad (2.219)$$

Both equations (2.219) must be obeyed because of the ambiguity. For the *theoretical sunrise* or sunset (with a flat horizon)

$$\begin{aligned} h = 0 &\rightarrow \sin \varphi \sin \delta = -\cos \varphi \cos \delta \cos \omega, \\ \cos \omega_0 &= -\tan \varphi \tan \delta, \\ \cos a_0 &= -\frac{\sin \delta}{\cos \varphi}. \end{aligned} \quad (2.220)$$

### Calculation of Radiation Intensity

The extraterrestrial radiation intensity  $D_0$  varies according to (2.210) by a good 3% around the mean value and can be expressed as a function of the declination. If  $D_1$  is the effective incoming radiation, the radiation intensity on a *horizontal surface* is

$$D = D_1 \sin h \quad (2.221)$$

as shown in Fig. 2.119.

For an *inclined surface*, with inclination relative to the horizontal given by the angle  $\psi$  and with orientation given by the azimuth  $a$  (Fig. 2.120), the plan view in Fig. 2.121a is considered with the vertical sections in

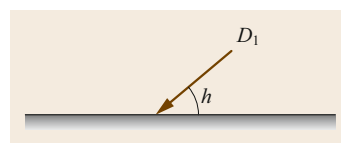


Fig. 2.119 Radiation on a horizontal surface

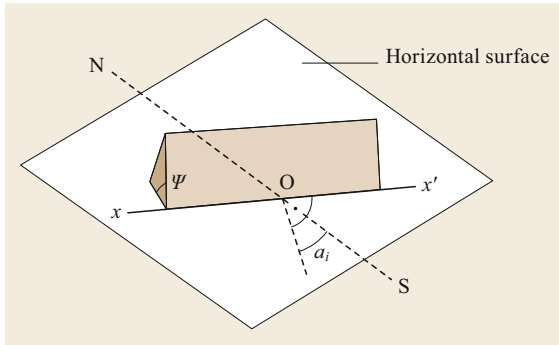


Fig. 2.120 Inclined surface in any direction

Fig. 2.121b,c. The vertical radiation component  $D$  acting on the surface results in then

$$\begin{aligned}
 D &= x_1 + x_2 \\
 \text{with } y_1 &= D_1 \sin h \tan \psi, \\
 y_2 &= D_1 \cos h \cos (a - a_i) - y_1, \\
 x_1 &= \frac{D_1 \sin h}{\cos \psi}, \quad x_2 = y_2 \sin \psi. \quad (2.222)
 \end{aligned}$$

From (2.222), with substitutions and rearrangements

$$D = D_1 [\sin h \cos \psi + \cos h \sin \psi \cos (a - a_i)]. \quad (2.223)$$

The special case of (2.221) follows for  $\psi = 0$ . If the surface is traced around a vertical axis of the Sun, so that  $a = a_i$ , this gives  $D = D_1 \sin(h + \psi)$ . Finally, if the surface is also rotated about a horizontal axis corresponding to the position of the Sun, so that  $\psi = 90^\circ - h$ ,  $D = D_1$  results.

### Radiant Energy per Day

The radiation density  $D_1$  is not constant during the day because of the effect of the atmosphere and the weather, and the effective daily radiation energy is therefore not readily accessible for calculation and can only be obtained empirically and statistically. As the highest guide value, with  $D_1 = D_0$ , the extraterrestrial daily sum (irradiation without atmosphere) can be given as:

#### Horizontal Surface.

$$W_d = \int_{SA}^{SU} D dt = D_0 \int_{SA}^{SU} \sin h dt. \quad (2.224)$$

If the time is replaced by the hour angle according to (2.214),

$$dt = d\omega \frac{24}{2\pi}, \quad (2.225)$$

where the integration limits for a flat horizon can be replaced by  $\pm\omega_0$  according to (2.220), and using (2.218),

$$W_d = D_0 \int_{-\omega_0}^{\omega_0} (\sin \varphi \sin \delta + \cos \varphi \cos \delta \cos \omega) \frac{24}{2\pi} d\omega.$$

For the location and day in question,  $\varphi$  and  $\delta$  are constant, and finally

$$W_d = \frac{24}{\pi} D_0 (\sin \varphi \sin \delta \omega_0 + \cos \varphi \cos \delta \sin \omega_0) \left( \frac{\text{kWh}}{\text{m}^2 \text{d}} \right). \quad (2.226)$$

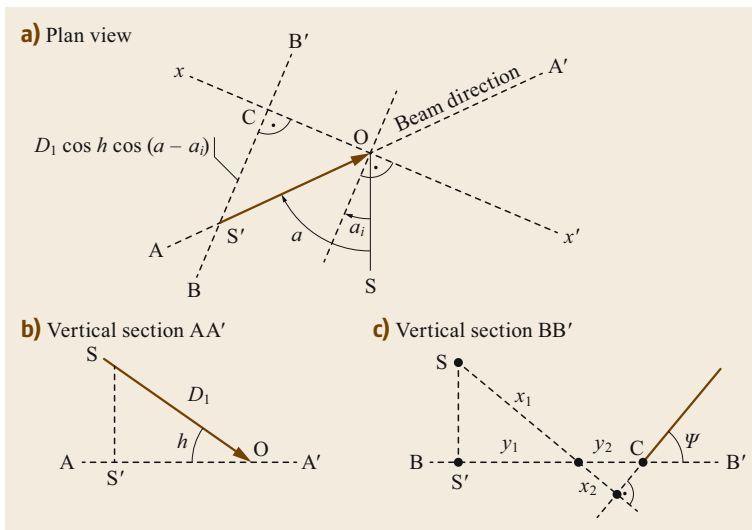
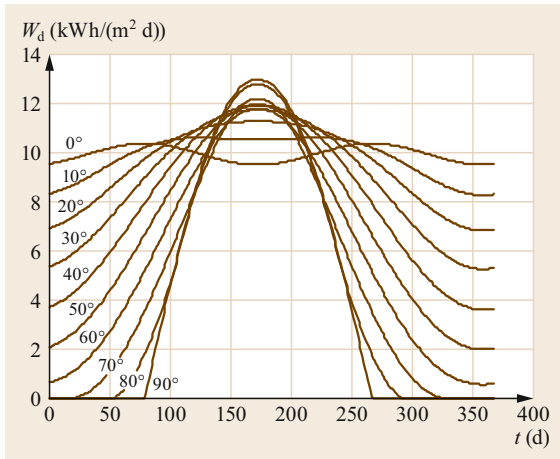
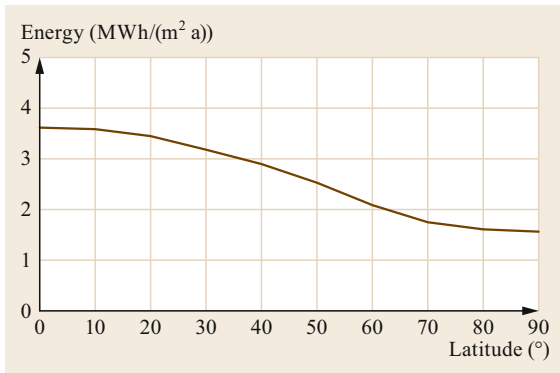


Fig. 2.121a–c Plan view (a) and vertical sections (b,c) for Fig. 2.120; calculation of the vertical component of  $D_1$





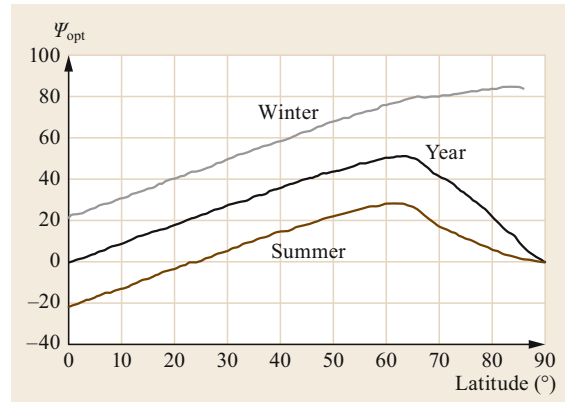
**Fig. 2.122** Annual variation of the daily energy on a horizontal surface for different latitudes (extraterrestrial irradiation  $D_0(\delta) = 1.353 \text{ kW/m}^2$ )



**Fig. 2.123** Annual energy on a horizontal surface without atmosphere as a function of the latitude of the site

Figure 2.122 shows the annual variation of the daily energy for various latitudes and assuming  $D_0(\delta) = \text{const} = 1.353 \text{ kW/m}^2$ . The integral over the year as a function of latitude gives Fig. 2.123.

**Inclined Surface.** If the surface is oriented to the south (northern hemisphere) with slope  $\psi$  (Fig. 2.120), then  $a_i = 0$ , and it is sufficient in (2.226) to replace  $\varphi$  by  $(\varphi - \psi)$ . As a rule, an orientation other than to the south supplies less daily energy. However, there are also cases where this does not apply and another orientation makes sense: the effect of mountain profiles ( $\omega_0$  then does not result from (2.218) for  $h = 0$ , but from  $h_{\min}$ , depending on the mountain profile), regular morning mist, clouds in the afternoon, reflection effects (snow, glaciers, water), diffuse light, etc.



**Fig. 2.124** Optimal slope  $\psi_{\text{opt}}$  as a function of the latitude of the location, without atmosphere (during the year, summer or winter with unchanged slope)

Integration of (2.226) gives the general result

$$W_d = \frac{24}{\pi} D_0 [(\cos \psi \sin \varphi - \sin \psi \cos \varphi) \sin \delta \omega_0 + (\cos \psi \cos \varphi + \sin \psi \sin \varphi) \cos \delta \sin \omega_0]. \tag{2.227}$$

If the slope and orientation of the surface are not changed over a certain period of time (month, season, year), the summation

$$W = \sum_{n_d} W_d(\delta(n_d)), \tag{2.228}$$

gives an expression of the form

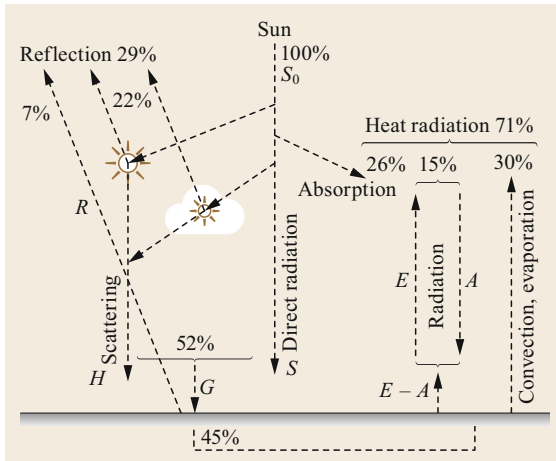
$$W = A \cos \psi + B \sin \psi, \tag{2.229}$$

$$\text{with } \begin{cases} A = \frac{24}{\pi} D_0 \times (\sin \varphi \sum_{n_d} \sin \delta \omega_0 + \cos \varphi \sum_{n_d} \cos \delta \sin \omega_0) \\ B = \frac{24}{\pi} D_0 \times (-\cos \varphi \sum_{n_d} \sin \delta \omega_0 + \sin \varphi \sum_{n_d} \cos \delta \sin \omega_0) \\ \times \cos a_i. \end{cases}$$

The energy of the period is maximized for  $dW/d\psi = 0$ , from which the optimal inclination is

$$\tan \psi_{\text{opt}} = \frac{B}{A} \tag{2.230}$$

that is shown in Fig. 2.124 as a function of the latitude of the location with orientation to the south (northern hemisphere). It increases up to the Arctic Circle,



**Fig. 2.125** Separation of incident solar radiation by reflection, scattering and absorption, and also heat radiation (numbers correspond to the world average)

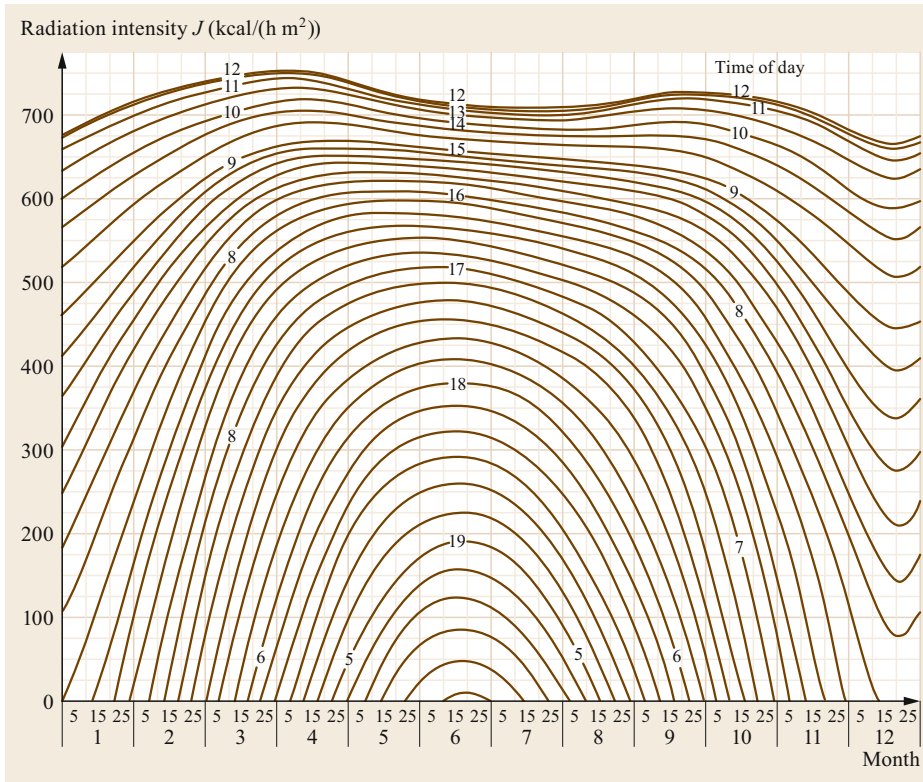
then decreases again. With an atmosphere, the optimum slope is somewhat smaller because the horizontal position gives the best result for the diffuse-light component.

### Effect of the Atmosphere

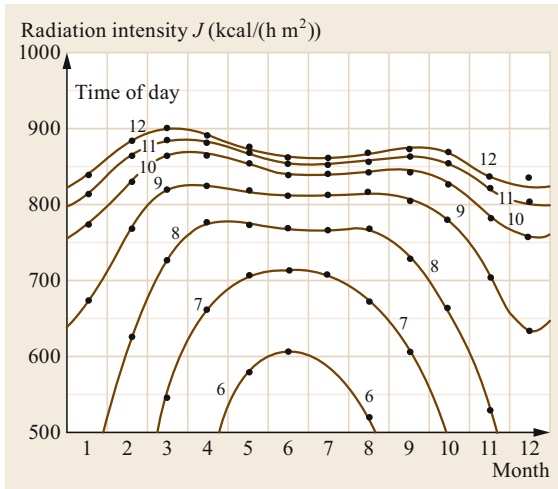
If the previous calculations are applied to geostationary satellites, they deliver exact results (the elevation angle at SA and SU is not zero, but slightly negative and depends on the satellite altitude).

For installations on Earth, the effect of the atmosphere must be taken into account, that can only be determined empirically. The atmosphere causes reflection, scattering and absorption of solar radiation. Above all, absorption at 20–30 km altitude by ozone and in the lower layers by H<sub>2</sub>O and CO<sub>2</sub> causes not only a decrease of the radiation intensity, but also a change of the spectrum (see also Fig. 2.104). The distribution of solar radiation in the atmosphere can be explained in more detail using the diagram in Fig. 2.125.

The incoming short-wave radiation  $S_0$  is partly absorbed by the atmosphere and converted into long-wave heat radiation. A further part is reflected or scattered directly into space by air and clouds. What remains meets the earth as *direct radiation*  $S$ . The scattered radiation also reaches the earth as *sky radiation*  $H$ . The *diffuse radiation* measured on the ground can also contain some of the reflective radiation from the environment, in addition to the sky radiation. The sum of direct radiation and



**Fig. 2.126** Daily and seasonal distribution of direct solar radiation on normal surface for the Swiss Midlands at 400 m above sea level, with a clear sky,  $1 \text{ kcal}/(\text{h m}^2) = 1.163 \text{ W}/\text{m}^2$  (Meteo Schweiz, Zurich)



**Fig. 2.127** Seasonal variation of direct radiation for various hours of the day at 2000 m.a.s.l., with clear sky,  $1 \text{ kcal}/(\text{h m}^2) = 1.163 \text{ W}/\text{m}^2$  (courtesy Battelle Institute)

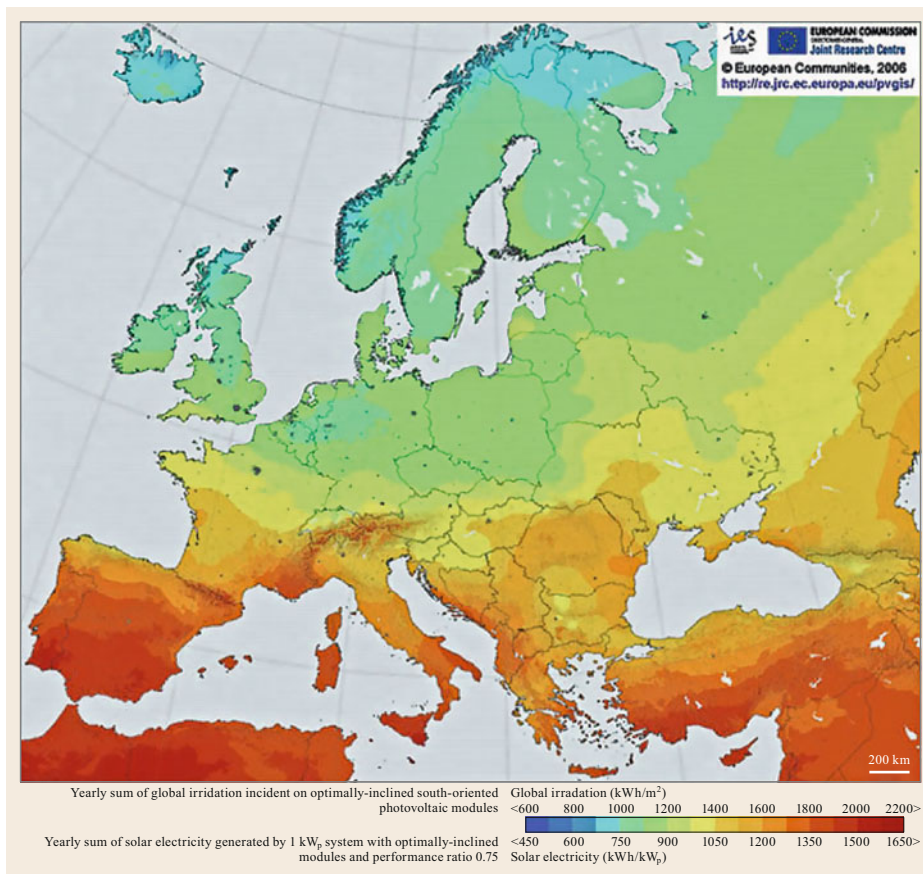
sky radiation (or diffuse radiation) is called the *global radiation*  $G$ .

After subtracting the radiation  $R$  reflected from the Earth, the rest is the radiation absorbed by the Earth, which is converted into heat. Since the Earth is in thermal equilibrium, this heat must be emitted again, about  $2/3$  by convection and evaporation and  $1/3$  by thermal radiation ( $E - A$ ) into the atmosphere. The atmosphere as a whole radiates approximately  $71\%$  of the solar radiation as heat into space.

#### Radiation Intensity with the Atmosphere

The radiation intensity can be measured by measuring global radiation and direct radiation [2.30]. For Switzerland, measurements of direct radiation are available for a clear sky and different altitudes (Figs. 2.126 and 2.127) and of global radiation for individual stations.

At maximum radiation intensity (TS = 12:00, Sect. 2.9.4), the indicative values in Table 2.7 (on a surface area normal to the radiation) apply to direct radiation.



**Fig. 2.128** Annual energy yield in kWh/kW<sub>p</sub> with optimum alignment of the PV system. (Photovoltaic geographical information system (PVGIS) European Communities)

The maximum global radiation in the Swiss Midlands has a typical value of  $1000 \text{ W/m}^2$  under a cloudless sky, of which about 10% is diffuse under a clear blue sky. On a hazy summer afternoon, the diffuse component is up to 50%. On a cloudy winter day, the global radiation can only be  $50\text{--}100 \text{ W/m}^2$  (100% diffuse).

Figure 2.128 gives an estimate of the possible energy yield in  $\text{kWh/kW}_p$  in Europe with photovoltaic (PV) systems, with optimal orientation of the solar generators.

**Table 2.7** Direct radiation in Switzerland (around 12:00 LT, in  $\text{W/m}^2$ ) as a function of altitude (in m) for different times of year

Altitude	End of March/ start of April	June	December
Extraterrestrial	1350	1320	1390
4000	1158	1139	1086
3000	1115	1086	1037
2500	1086	1051	1001
2000	1047	1012	954
1500	1000	870	900
400	870	830	770

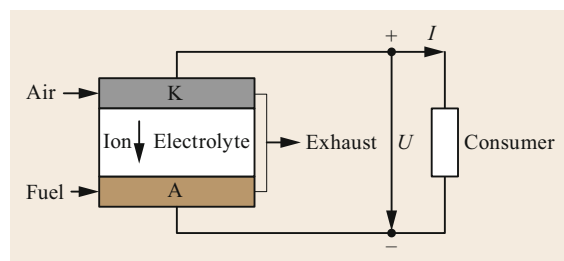
## 2.10 Fuel Cells

Fuel cells can be used to directly convert hydrogen as well as natural gas or biogas, and other hydrocarbons (e.g., petrol, methanol) electrochemically into electrical energy. Compared to thermal machines, which make a detour via mechanical energy, this results in higher efficiencies and this is without rotating parts and the associated noise emissions. Efficiencies of 50–60% can be achieved, even for small outputs, that is only possible with conventional technology with combined systems in the 10–100 MW range. The environmental impact of using natural gas is lower than with conventional thermal power plants due to the higher efficiency and different combustion methods (no soot, no nitrogen oxides, no unburned hydrocarbons).  $\text{CO}_2$  emissions can be further reduced by increasing the hydrogen content.

The technology is evolving but it has not yet reached the economic viability threshold except in special applications, such as spaceships or submarines. However, it is predictable that in the course of the next decades it will open up a wide range of applications for *mobile* and *stationary* applications.

### 2.10.1 Structure and Fuel Cell Types

Figure 2.129 shows the basic structure of a fuel cell. It consists of an *anode*, *cathode*, and *electrolyte*, like



**Fig. 2.129** Structure of a fuel cell

a battery. Fuel gas ( $\text{H}_2$ ,  $\text{CO}$ ,  $\text{CH}_4$ ) flows through or around the anode and air through or around the cathode. The electrolyte is *gas-tight* and therefore does not allow a direct contact between fuel and oxygen. Ions transport the electrons from cathode K to anode A, the type of ion being dependent on the electrolyte used.

Five fuel cell families are known and under development. They differ primarily in the *electrolyte* used. Sorted in descending order of cell temperature, these are the following:

1. **SOFC: solid oxide fuel cell**,  $\approx 800^\circ\text{C}$ : A ceramic layer of zirconium oxide is used as the electrolyte. The atmospheric oxygen is ionized on the cathode side to  $\text{O}^{2-}$  by taking up two electrons. It can thus penetrate the electrolyte as an ion, is neutralized again on the anode side by electron release and initiates the oxidation reaction. The cell can also be operated directly with natural gas, propane or biogas.
2. **MCFC: molten carbonate fuel cell**,  $650^\circ\text{C}$ : A molten carbonate (mostly lithium and potassium carbonate) is used as the electrolyte. The carbonate ion serves as the ion. The air is enriched with  $\text{CO}_2$  to form new carbonate ions. On the anode side it dissociates into  $\text{CO}_2$  and oxygen, that oxidizes the fuel. Hydrogen and CO can be used as fuels.
3. **PAFC: phosphoric acid fuel cell**,  $200^\circ\text{C}$ : Diluted phosphoric acid is used as the electrolyte. The fuel is hydrogen, that gives off its electron on the anode side and crosses the electrolyte as a hydrogen ion  $\text{H}^+$ . It takes up an electron again on the cathode side and is oxidized by atmospheric oxygen. The air must contain little or no CO.
4. **PEFC: polymer electrolyte fuel cell**,  $80^\circ\text{C}$ : The electrolyte is a plastic film that behaves like an acid.

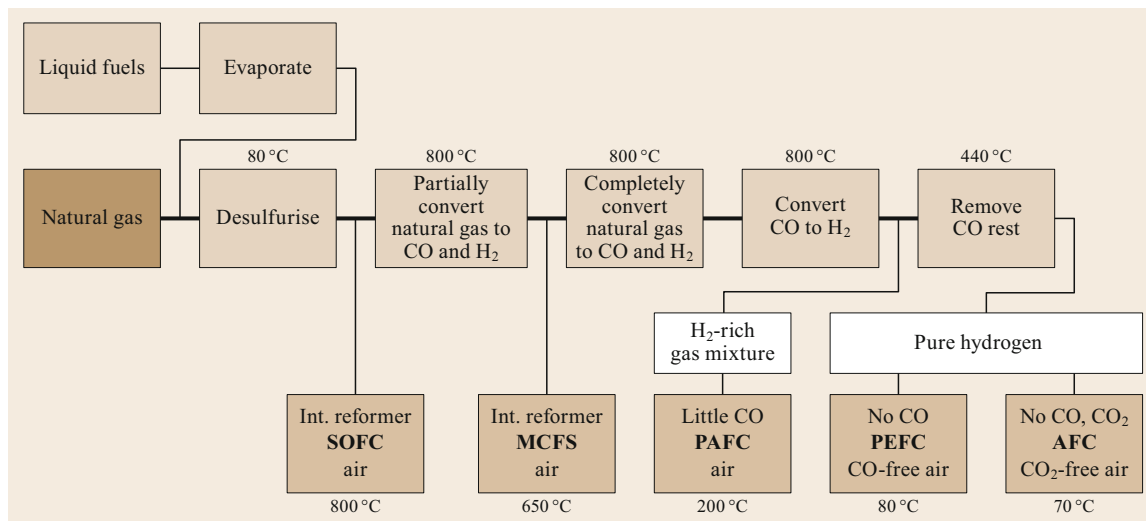


Fig. 2.130 Processing of natural gas for the five fuel cell types (adapted from [2.47])

Also in PEFCs, the hydrogen ion  $H^+$  (processes as in PAFC) serves as the ion.

5. *AFC: alkaline fuel cell, 70°C*: Diluted potassium hydroxide solution is used as the electrolyte. The hydroxyl ions  $OH^-$  formed from the reaction  $H_2O + O = 2OH^-$  take over the electron transport. The oxidation reaction takes place on the anode side with pure hydrogen. The air must not contain  $CO_2$ .

All five types of fuel cell can operate with natural gas, and all fuel cell types except SOFC and MCFC must first convert natural gas into hydrogen or hydrogen + CO. This conversion is very costly (also in terms of space requirements, up to 60% of the construction volume). Figure 2.130 provides an overview.

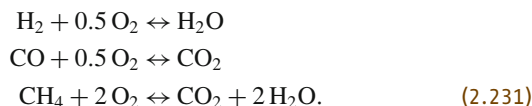
Today, the AFC families are expected to have only limited future prospects [2.47]. The PEFC is of interest for mobile applications and is being further developed primarily by the automotive industry. In addition to the five families mentioned, the direct methanol fuel cell DMFC should also be mentioned. It can be operated directly (without reformer) with methanol (working temperature similar to PEFC). Its prospects are still not clear.

PAFC, MCFC and SOFC are predestined for stationary energy applications. The phosphoric acid fuel cell is the most highly developed and already commercially available. It is economically viable for certain applications. The ceramic fuel cell is still under development, but has great potential. Section 2.10.3 shows these two fuel cells in more detail.

## 2.10.2 Principles and Modeling

### Electrochemical Fundamentals

The most important chemical reactions for energy conversion are the following



The associated specific enthalpy change  $\Delta h$  is 120 MJ/kg at normal pressure for  $H_2$ , 10 MJ/kg for CO and 50 MJ/kg for  $CH_4$ . The temperature has only a minor effect on these values (slight increase for  $H_2$ , for more details see [2.48]), standard enthalpy change). At a mass flow of  $m$  (kg/s), the available chemical power is

$$P_{ch} = m\Delta h \quad \left( \frac{\text{kg}}{\text{s}} \frac{\text{J}}{\text{kg}} = \text{W} \right). \quad (2.232)$$

From the enthalpy  $\Delta h$  only the *free enthalpy*  $\Delta h_f$  (Gibbs potential) can be converted into electrical energy [2.49, 50]. This is defined by

$$\Delta h_f = \Delta h - T\Delta s \quad (\text{Ws/kg}), \quad (2.233)$$

where  $\Delta s$  denotes the specific entropy change [2.9, Annex A.1]. The corresponding maximum electrical energy is  $w_{e0} = \eta_e \Delta h_f$ , where

$$\begin{aligned} w_{e0} &= QE = n \frac{F}{M} E \quad \left( \frac{\text{As}}{\text{kg}} \text{V} \right), \\ P_{e0} &= mw_{e0} = nm \frac{F}{M} E = IE \quad (\text{W}), \end{aligned} \quad (2.234)$$

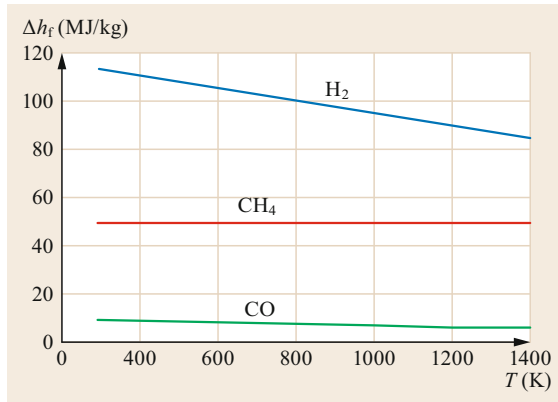


Fig. 2.131 Free enthalpy  $\Delta h_f$  as a function of temperature

where:

- $F$  Faraday's constant ( $9.6485 \times 10^4$  A s/mol)
- $M$  molar mass (kg/kmol)
- $n$  number of exchanged electrons (valence)
- $E$  EMF (open circuit voltage, V)
- $m$  mass flow (kg/s).

The efficiency  $\eta_e$  takes into account that, especially at low temperatures, the reaction induced by the catalytic converter proceeds through several steps, of which only the first contributes to voltage formation. The open-circuit voltage therefore does not correspond to the Gibbs potential (at low temperatures, e.g., PEFC cell,  $\eta_e \approx 0.8$ ).

$P_{e0} = EI$  represents the *internal electrical power* of the cell. The free enthalpy for the three most important reactions (2.231) is shown in Fig. 2.131 (calculated from [2.48]). The EMF  $E$  can be determined from (2.234)

$$E = \frac{w_{e0} M}{n F} \quad (2.235)$$

with  $n = 2$  for  $H_2$  and  $CO$  and  $n = 8$  for  $CH_4$ . Then, for the methane reaction, for example, at  $25^\circ C$ ,  $E = 1.06\eta_e$  (V), for the  $H_2$  reaction  $E = 1.23\eta_e$  (V). By connecting fuel cells in series to form a *fuel cell stack*, the open-circuit voltage required for practical applications can be achieved.

The voltage  $U$  effectively available at the electrodes is lower than the EMF when the cell is loaded due to the internal voltage drop. As a result, the effectively obtained electrical power is further reduced

$$\begin{aligned} P_e &= P_{e0} \frac{U}{E} = P_{ch}, \\ \eta_e \frac{\Delta h_f}{\Delta h} \frac{U}{E} &= P_{ch} \eta_e \eta_0 \eta_u, \end{aligned} \quad (2.236)$$

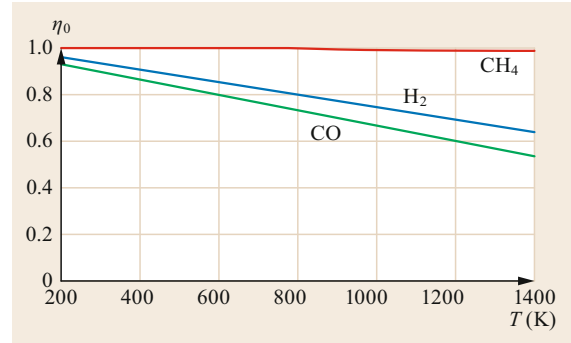


Fig. 2.132 Theoretical efficiency  $\eta_0$  as a function of temperature

where  $\eta_0$  denotes the theoretical no-load efficiency, and  $\eta_u$  is the voltage efficiency. Figure 2.132 shows the theoretical no-load efficiency as a function of the cell temperature for the three reactions of (2.231) [2.48]. The good efficiency of the methane reaction is striking, if we take into account that the fuel is not used 100%, i.e., that the effectively converted chemical power  $P_{ch} = u_f P_b$  is smaller than the delivered chemical gross power  $P_b$ , where  $u_f$  is the fuel utilization factor  $< 1$ , we have

$$P_e = \eta_e \eta_0 \eta_u u_f P_b = \eta P_b. \quad (2.237)$$

#### Linear Model

If we assume as a first approximation that the internal resistance of the cell is independent of the current, the following applies

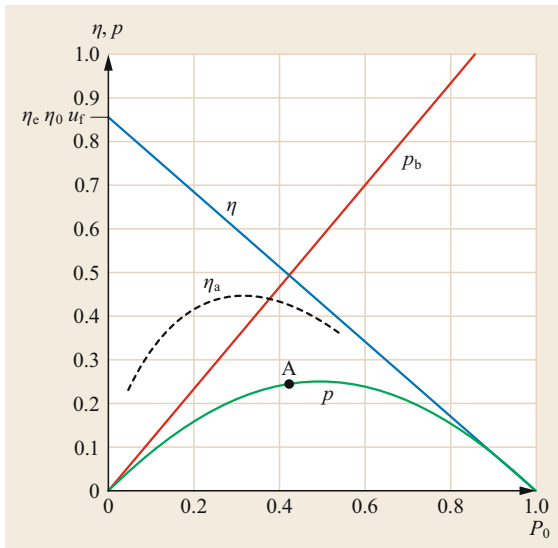
$$\eta_u = \frac{E - RI}{E} = 1 - \frac{RI}{E}. \quad (2.238)$$

If the current is replaced by the power, the voltage efficiency follows from (2.234), (2.235), and (2.236) and,

$$\begin{aligned} \eta_u &= 1 - \frac{R \eta_e \eta_0 u_f P_b}{E^2} = 1 - \frac{P_{e0}}{P_k} = 1 - p_0 \\ \text{with } P_{e0} &= \eta_e \eta_0 u_f P_b, \quad P_k = \frac{E^2}{R} = EI_k, \end{aligned} \quad (2.239)$$

where  $p_0$  is the internal electrical power related to the short-circuit power. The *short-circuit power*  $P_k$  was defined as the product of the short-circuit current and open-circuit voltage, as is usual in power supply technology. If all powers are related to the short-circuit power, the overall efficiency  $\eta$  of the fuel cell stack and the electrical output power  $p$  then

$$\begin{aligned} \eta &= \eta_e \eta_0 u_f (1 - p_0), \\ p &= \frac{P_e}{P_k} = P_0 (1 - p_0). \end{aligned} \quad (2.240)$$



**Fig. 2.133** Typical graph of power and efficiency of fuel cells:  $p_0 = P_{e0}/P_k$  = internal power,  $p_b = P_b/P_k$  = gross power (chemical),  $p = P_e/P_k$  = electrical output power,  $\eta$  = efficiency of the fuel cell stack,  $\eta_a$  = plant efficiency, A = design point (example:  $\eta \approx 50\%$ ,  $\eta_a \approx 45\%$ )

Figure 2.133 shows these two quantities as a function of the internal electrical power  $p_0$ . The maximum output power is obtained when  $P_{e0} = 0.5P_k$  and  $P_e = 0.5P_{e0} = 0.25P_k$ . At this maximum power, however, the efficiency of the fuel cell stack is only  $\eta = 0.5\eta_e\eta_0\eta_f$ . The economic optimization of the system usually leads to a design point corresponding to a power  $P_{e0} < 0.5P_k$ , and the stack efficiency will be 50% or more.

For smaller loads, the efficiency of the fuel cell theoretically increases, i.e., the fuel cell has a generally good part-load behavior. If the load becomes too

small, however, the energy requirement of the auxiliary equipment, such as pumps, fans, controls, etc., which is practically independent of the load, has an unfavorable effect, as shown by the expected plant efficiency  $\eta_a$ , indicated in Fig. 2.133.

### 2.10.3 Fuel Cells for Stationary Applications (German Original by Prof. Michael Höckel, see [2.9])

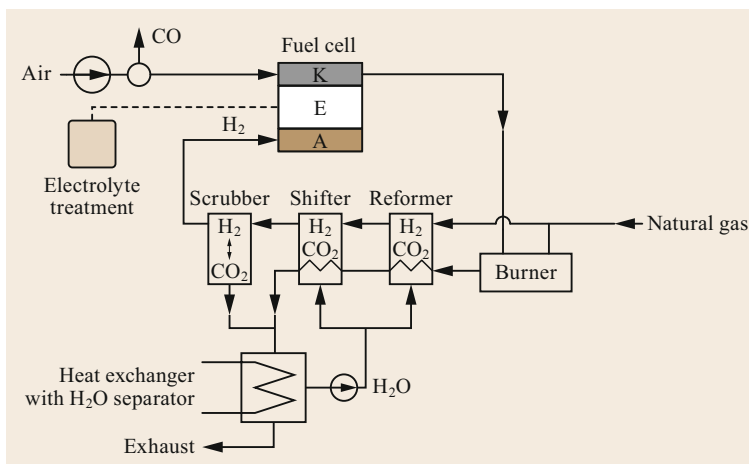
#### Phosphoric Acid Fuel Cell (PAFC)

Figure 2.134 shows the basic structure of a PAFC plant. Since this cell requires a gas mixture rich in  $H_2$  (without CO), it must be extracted from natural gas in the reformer using steam. The reform reaction produces  $H_2$  and CO. In two subsequent stages, the CO is oxidized to  $CO_2$  and the  $CO_2$  is partially rejected. The hydrogen is ionized at the anode and passes through the electrolyte as an  $H^+$  ion before being oxidized to water at the cathode. The exhaust gas is water vapor and  $CO_2$ .

The cell temperature is  $200^\circ C$ . The power density achievable today is  $1.3 \text{ kW/m}^2$  and should be able to be increased to about  $2 \text{ kW/m}^2$ . The PAFC fuel cell technology is the most advanced and tested. Plants from 1 kW and greater are commercially available. The largest plant built to date has an output of 11 MW (Japan). Hydrogen is used as the fuel for small plants, as the complex conversion of natural gas becomes economical only for outputs above 100 kW. The investment for a 200 kW plant is around 3300 €/kW, but the business calculation looks favorable thanks to the long service life of more than 8000 h/a.

#### Molten Carbonate Fuel Cell (MCFC)

The MCFC uses the alkaline carbonates lithium, potassium and sodium as electrolytes. For sufficient ionic



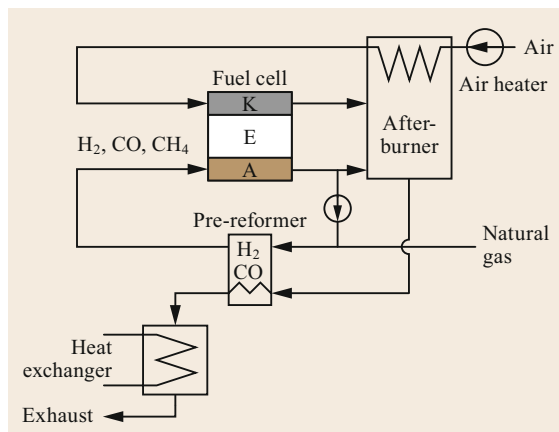
**Fig. 2.134** Basic system of a PAFC plant (adapted from [2.47])

conduction, the mixture must be in molten form, that requires an optimum operating temperature of 600 °C. The mixed melt is retained in a matrix. Special catalysts are not necessary and nickel can be used as electrode material. The MCFC is therefore relatively inexpensive from the point of view of the materials, but the achievable power densities are relatively low and for a long service life it is necessary to operate as consistently as possible and to regenerate the electrolyte. Consequently, the MCFC is suitable for stationary applications with waste heat recovery.

MTU Friedrichshafen developed its *HotModule* over a longer period of time until it was ready for series production. The MCFC is operated directly with natural gas, that is internally reformed using part of the waste heat and achieves an electrical efficiency of almost 50%. The *HotModule* was offered in plant sizes of 250 kW<sub>el</sub> and 345 kW<sub>el</sub> and a total of 10 plants were produced. Due to the poor sales forecasts, the planned series production was not started by the Tognum fuel cell division, which emerged from the former MTU, and the activities were discontinued in 2010.

### Solid Oxide Fuel Cell (SOFC)

The SOFC is the simplest concept in terms of structure (Fig. 2.135). Thanks to the high operating temperature of 800 °C, the natural gas (or other hydrocarbons) can be converted directly at the anode into hydrogen and carbon monoxide. Since carbon precipitation at the anode leads to problems, the natural gas is partially processed in the pre-reformer after desalination in order to accelerate the reactions. The proportion of carbon in the fuel gas is reduced and a hydrogen-rich gas is produced. The oxygen O<sup>2-</sup> ionized on the cathode side penetrates the electrolyte consisting of



**Fig. 2.135** Basic system of a SOFC plant (adapted from [2.47])

zirconium oxide and oxidizes the fuels on the anode side.

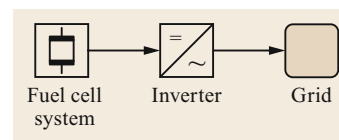
The operating temperature of the SOFC can be easily controlled by the excess air, and the high temperature of the exhaust gases allows heat to be extracted for a wide variety of applications or for the plant to be operated as a block-type thermal power station. The SOFC fuel cell is still under development, and only prototypes up to 100 kW are currently in operation. Although many technological problems still have to be solved and the economic threshold has not yet been reached, it should have a promising future due to its simplicity and high power density (today approximately 6 kW/m<sup>2</sup>, proven in the laboratory up to 19 kW/m<sup>2</sup>) as well as its high efficiency (plant efficiency over 50%).

Sulzer AG started the development of a fuel cell heater based on SOFC technology under the project name *Hexis* in 1991. In 2006 the development team of the product founded a company of the same name with the aim of continuing the development. In 2011, the third generation of the fuel cell heater *Galileo 1000 N* was presented. The system is designed for an output of 1 kW<sub>el</sub> and 1.8 kW<sub>th</sub>. With additional burners, the thermal output can be increased up to 20 kW. The device can be connected directly to the natural gas grid and can also be operated with biogas. In the meantime, more than 200 devices have already been manufactured, that provide practical operating experience within the framework of funding programs.

### System Technology

Fuel cell systems generate a direct current similar to photovoltaic systems, that is used directly for small applications and converted into alternating current by means of inverters for larger applications in stand-alone operation or grid connection (Fig. 2.136). The inverter, having problems similar to those of photovoltaics (Sect. 2.8.5), has the possibility of regulating the reactive power output or consumption within certain limits.

In addition to the application of the SOFC cell as a block-type thermal power station, as already mentioned, which can have fuel efficiency rates of 80%, the combination with microturbine technology is also of interest. The hot exhaust gases of the fuel cell are used at pressures of 3–4 bar for the operation of a downstream gas turbine (Fig. 2.137). Pilot plants up to 1 MW are planned.



**Fig. 2.136** Basic design of a grid-connected fuel cell system



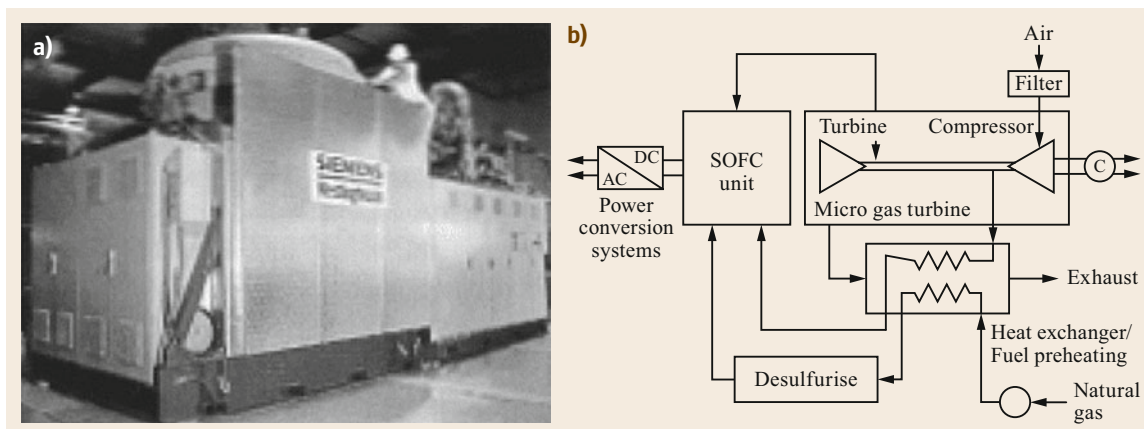


Fig. 2.137a,b Hybrid system SOFC micro gas turbine (courtesy Siemens Westinghouse, [2.51])

## References

- 2.1 V. Crastan: *Energiewirksame Kennzahlen I*, 2nd edn. (Springer Vieweg, Wiesbaden 2018)
- 2.2 V. Crastan: *Energiewirksame Kennzahlen II*, 2nd edn. (Springer Vieweg, Wiesbaden 2019)
- 2.3 V. Crastan, D. Westermann: *Elektrische Energieversorgung*, Vol. 3 (Springer Vieweg, Wiesbaden 2018)
- 2.4 H. Happoldt, D. Oeding: *Elektrische Kraftwerke und Netze* (Springer, Berlin, Heidelberg 1978)
- 2.5 J. Giesecke, E. Mosonyi: *Wasserkraftanlagen* (Springer, Berlin, Heidelberg 1998)
- 2.6 INFEL: *Strom aus Wasser* (INFEL, Zurich 1987)
- 2.7 INFEL: *Strom aus unseren Kraftwerken* (INFEL, Zurich 2001)
- 2.8 F. Dietzel: *Turbinen, Pumpen und Verdichter* (Vogel, Würzburg 1980)
- 2.9 V. Crastan: *Elektrische Energieversorgung 2* (Springer Vieweg, Wiesbaden 2018)
- 2.10 W. Bohl: *Turbomaschinen 2* (Vogel, Würzburg 1995)
- 2.11 W. Bohl: *Turbomaschinen 1* (Vogel, Würzburg 1990)
- 2.12 L. Borel: *Stabilité de réglage des installations hydroélectriques* (Payot/Dunod, Paris 1960)
- 2.13 PACER: *Kleinwasserkraftwerke, Wasserturbinen* (EDMZ, Berne 1995)
- 2.14 A. Gardel: *Chambres d'équilibre* (F. Rouge, Lausanne 1956)
- 2.15 L. Allievi: *Théorie générale du mouvement varié de l'eau dans les tuyaux de conduite* (Dunod, Paris 1904)
- 2.16 E. Truckenbrodt: *Strömungsmechanik* (Springer, Berlin, Heidelberg, New York 1968)
- 2.17 V. Crastan: *Elektrische Energieversorgung 1* (Springer Vieweg, Wiesbaden 2015)
- 2.18 H. Weber: *Dynamische Netzreduktion zur Modalanalyse von Frequenz- und Leistungspendelungen in ausgedehnten elektr. Energieübertragungsnetzen*, Ph.D. Thesis (University of Stuttgart, Stuttgart 1990)
- 2.19 H.U. Fruttschi: Das Kombikraftwerk – Schlüssel zur thermischen Stromerzeugung aus Erdgas, ABB-Tech. 3, 12–18 (1999)
- 2.20 T. Bohn (Ed.): *Konzeption und Aufbau von Dampfkraftwerken*, Handbuchreihe Energie, Vol. 5/6 (Resch/TüV Rheinland, Köln 1985)
- 2.21 K. Kugeler, P.W. Phlippen: *Energiertechnik* (Springer, Berlin, Heidelberg 1993)
- 2.22 K. Strauss: *Kraftwerkstechnik* (Springer, Berlin, Heidelberg, New York 1998)
- 2.23 G. Klefenz: *Die Regelung von Dampfkraftwerken* (Bl, Mannheim, Vienna, Zurich 1991)
- 2.24 INFEL: *Strom aus unseren Kraftwerken* (INFEL, Zurich 2001)
- 2.25 W.-D. Krebs, D. Schneider, W. Bretschuh: New approaches to the development of conventional fission reactors, Bulletin SEV 21, 19–23 (2000)
- 2.26 M.A. Schultz, M. Marxen: *Steuerung und Regelung von Kernreaktoren und Kernkraftwerken* (Berliner Union, Stuttgart 1965)
- 2.27 NAGRA: *Nukleare Entsorgung Schweiz, Konzept und Realisierungsplan* (NAGRA, Wettingen 1992)
- 2.28 M. Volkmer: *Kernenergie, Radioaktivität und Strahlenschutz* (IKK, Bonn 1991)
- 2.29 M. Volkmer: *Kernenergie, Basiswissen* (IKK, Bonn 1993)
- 2.30 M. Kleemann, M. Meliss: *Regenerative Energiequellen* (Springer, Berlin, Heidelberg, New York 1988)
- 2.31 J.P. Molly: *Windenergie* (C.F. Müller, Karlsruhe 1990)
- 2.32 E. Hau: *Windkraftanlagen* (Springer, Berlin, Heidelberg, New York 1988)
- 2.33 F. von König: *Wie man Windräder baut* (Udo Pfriemer, Munich 1984)
- 2.34 Windpower Monthly (2001) October
- 2.35 S. Kunz, J. Remund, D. Wittwer, H. Buser: *Planung von Windenergieanlagen* (SFOE, Berne 1999)
- 2.36 M. Kaltschmitt, A. Wiese: *Erneuerbare Energien* (Springer, Berlin, Heidelberg, New York 1995)
- 2.37 L.H. Hansen, P.H. Madsen, F. Blaabjerg, H.C. Christensen, U. Lindhard, K. Eskildsen: Generators and power electronics technology for wind turbines.

- In: *IECON'01. 27th Annu. Conf. IEEE Ind. Electron. Soc., Denver* (2001), <https://doi.org/10.1109/IECON.2001.975598>
- 2.38 J.D. Chatelain: *Dispositifs à semiconducteur, Traité d'Électricité*, Vol. VII (EPFL, Georgi, Lausanne 1979)
- 2.39 H.J. Lewerenz, H. Jungblut: *Photovoltaik* (Springer, Berlin, Heidelberg, New York 1995)
- 2.40 A. Goetzberger, B. Voss, J. Knobloch: *Sonnenenergie: Photovoltaik* (Teubner, Stuttgart 1997)
- 2.41 H. Häberlin: *Photovoltaik* (AZ/VDE, Aarau 2007)
- 2.42 V.U. Hoffmann: *Photovoltaik – Strom aus Licht* (Teubner/vdf, Leipzig, Zürich 1996)
- 2.43 M.A. Green, P.A. Basore, N. Chang, D. Clugston, R. Egan, R. Evans, D. Hogg, S. Jarnason, M. Keevers, P. Lasswell, J. O'Sullivan, U. Schubert, A. Turner, S.R. Wenham, T. Young: Crystalline silicon on glass (CSG) thin-film solar modules, *Sol. Energy* **77**(6), 857–863 (2004)
- 2.44 A.V. Shah: *IMT 2000–2002: Technologische Weiterentwicklung der mikromorphen Solarzellen* (IMT, Neuchâtel 2002)
- 2.45 A.V. Shah, H. Schade, M. Vanecek, J. Meier, E. Vallat-Sauvain, N. Wyrsh, U. Kroll, C. Droz, J. Bailat: Thin-film silicon solar cell technology, *Progress Photovolt.* **12**, 113–142 (2004)
- 2.46 H.K. Köthe: *Praxis solar- und windelektrischer Energieversorgung* (VDI, Düsseldorf 1982)
- 2.47 U. Bossel (1998) Brennstoffzellen, Bedeutung für die Schweiz. Bericht des Brennstoffzellen-Förderkreises
- 2.48 U. Bossel, L. Dubal: *Facts and Figures, an International Energy Agency SOFC Task Report* (SOFC, Bern 1992)
- 2.49 G. Mierdel: *Elektrophysik* (Hüthig, Heidelberg 1972)
- 2.50 E. Philippow: *Taschenbuch Elektrotechnik*, Vol. 6 (Hanser, München, Wien 1982)
- 2.51 H.R. Joost: Die Hochtemperaturzelle auf dem Weg zur Marktreife, *Bulletin SEV/VSE* **92**(21), 29–34 (2001)

### Valentin Crastan

Evilard, Switzerland  
[valentin.crastan@bluewin.ch](mailto:valentin.crastan@bluewin.ch)



Dr-Ing Valentin Crastan is professor emeritus. After practical and managerial work in energy technology companies (Brown Boveri/ABB, Baden, Swiss electricity and transport company (Suisselectra), Basel), he has been appointed professor of energy systems and control engineering at the Bern University of Applied Sciences, Engineering and Computer Science, Biel. He also served as the Dean of the Department of Electrical Engineering/Communications for nine years.

# High Voltage

## 3. High Voltage Engineering

Ernst Gockenbach

High-voltage engineering is knowledge about power transmission at high voltages and about stress on equipment used in high-voltage transmission systems. The basis for the design of high-voltage equipment is stress on the insulation by the electric field, whereby the stress magnitude depends on the voltage type. The electric field distribution is given by relative permittivity for alternating current (AC) and by conductivity for direct current (DC) and homogeneity of the electrode arrangement. Evaluation of the electric strength requires statistical and adjusted test methods. Basic knowledge about the breakdown behavior in gases is the basis for understanding the breakdown in fluids and solids. The breakdown of fluids is influenced by moisture, impurities, and stressed volume. Solids suffer from the same parameters, but thermal and erosion breakdowns and residual life time are of interest. Different kinds of insulation gases, fluids and solids, inorganic and organic, as well as impregnated solids are used in high-voltage insulation, and each of them has its own characteristics, which requires a careful selection depending on the equipment and the expected electric stress. Generation of test voltages requires specialized voltage and current generators for AC, DC, and impulse voltages. The measurement of different voltage types also requires specialized measuring circuits, including partial discharge and dielectric characteristics measurement.

Additional information and supplementary exercises for this chapter are available online.

3.1	<b>Why High-Voltage Engineering?</b> .....	131
3.2	<b>Lightning</b> .....	135
3.2.1	Generation of a Lightning Stroke .....	135
3.2.2	Lightning Protection .....	137
3.3	<b>Electric Field</b> .....	137
3.3.1	Basics .....	137
3.3.2	Homogenous Electric Field .....	138
3.3.3	Layered Dielectrics .....	138
3.3.4	Inhomogeneous Electric Field .....	140
3.4	<b>Electric Strength</b> .....	142
3.4.1	Basics of Statistical Analysis .....	143
3.4.2	Distribution Functions .....	143
3.4.3	Breakdown in Gases .....	144
3.4.4	Breakdown in Fluids .....	150
3.4.5	Breakdown in Solids .....	152
3.5	<b>Insulating Materials</b> .....	156
3.5.1	Gases .....	157
3.5.2	Fluids .....	157
3.5.3	Solids .....	158
3.5.4	Impregnated Solids .....	162
3.6	<b>Test Techniques</b> .....	163
3.6.1	AC Voltage .....	163
3.6.2	DC Voltage .....	165
3.6.3	Impulse Voltage and Current .....	167
3.7	<b>Measuring Techniques</b> .....	171
3.7.1	Voltage Measurement .....	172
3.7.2	Current Measurement .....	175
3.7.3	Partial Discharge Measurement .....	176
3.7.4	Measurement of Dielectric Characteristics .....	179
	<b>References</b> .....	181

### 3.1 Why High-Voltage Engineering?

Someone may ask why high voltage and high-voltage engineering? With the invention of the dynamo-electric principle by Werner von Siemens in 1866, the use of electric power started its worldwide triumph due to the fact that power transmission with electricity was much easier than mechanical transmission by belts or gears. The transmission of electric power can be easily car-

ried out with overhead lines, cables, or gas-insulated lines. The fundamental requirements on the transmission systems are the cross section of the conductor, depending on the required current and the material of the conductor, copper or aluminum, and the strength of the insulation between the conductor and ground, because a potential difference between the conductor

and ground, generally expressed as voltage, is necessary to drive a current through the conductor. There are some further requirements on electric power transmission, like the thermal behavior of cable insulation or the allowed sag of an overhead line, but they very often depend on the local situation and, therefore, will not be described here in detail.

An actual electric system consists of generation stations with conventional energy sources like coal, gas, or oil, or with nuclear or regenerative sources like water, wind, sun, biomass, or geothermal ones. Transmission systems are necessary to bring electric power to the consumer, and these days these systems are usually divided into transmission systems for large distances and distribution systems for local distribution of the electric power.

Electric power is given by the voltage multiplied with the current

$$P = UI. \quad (3.1)$$

The values for  $U$  and  $I$  are peak values for DC voltage of the root mean square (rms) value for AC voltages, where the phase angle between voltage and current should also be taken into account. The simple equation (3.1) will be used to explain the reason why different voltage levels are used in the entire transmission system and, therefore, no details concerning active or reactive power are considered. There are two parameters in (3.1), and for a given power  $P$ , the optimum of the combination of the two parameters is important for an economic transmission system of electric power. Electric power transmission will have some losses, and these losses  $P_{\text{los}}$  are mainly given by the resistance of the conductor and the square of the current

$$P_{\text{los}} = RI^2. \quad (3.2)$$

This means that the losses increase with the square of the current, and the reduction of the losses requires a larger cross section of the conductor. On the other hand, the increase of the voltage  $U$  requires a higher insulation performance, and this can be reached depending on the insulation material, for example, with thicker insulation for cables or larger distances for air insulation of overhead lines. For a given transmission length and power, the total costs, investment, and losses have a minimum at a certain voltage level, because the investment costs increase with the voltage level, and the losses decrease with the voltage level. Figure 3.1 schematically shows the total costs for an electric power transmission system.

Following this general rule according to Fig. 3.1 would lead to a large number of voltage levels depending on the length and power of the transmission system.

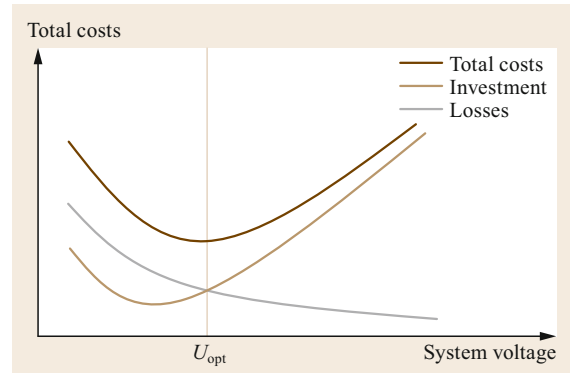
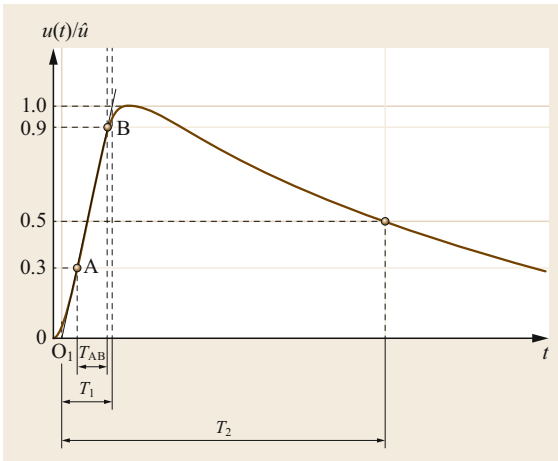


Fig. 3.1 Typical total costs for an electric power transmission system as function of the system voltage

This is economically not reasonable and, therefore, the International Electrotechnical Commission (IEC) and its relevant Technical Committees in cooperation with the scientific organization Conseil International des Grands Réseaux Électriques (CIGRE) have fixed a number of voltage levels, as given in [3.1]. The tables in [3.1] divide the voltage levels into two ranges, range I from 3.6 kV as the highest voltage for equipment  $U_m$  up to 245 kV, and range II from 300 kV as the highest voltage for equipment  $U_m$  up to 1200 kV. These voltage ranges for high-voltage equipment are related to different test procedures, with AC voltage at a power frequency between 48 and 62 Hz and to withstand tests with switching- and lightning-impulse voltages. The main reason for the coordination of the kind and value of the different test voltages is that the selected withstanding voltages should be associated with the highest voltage for equipment  $U_m$  for insulation coordination purposes only. Further advantages of fixed voltage levels are standardization of the equipment and simplified requirements for the equipment manufacturer.

The number of voltage levels has led to some expressions in the high-voltage range that are not fixed as well-defined voltage levels. Up to 1 kV, the voltage level is named low voltage, above 1 kV there exist expressions like medium voltage in the range up to about 60 kV, very often termed the distribution system voltage level, high voltage up to 400 kV, extra high voltage up to 800 kV, and ultra-high voltage (UHV) above 800 kV. These terms are not standardized and may be used differently in various countries.

For reliable insulation coordination, standardized test voltages in frequency, amplitude, and shape are defined by the IEC recommendation IEC 60060-1 [3.2]. An AC test voltage should be in the frequency range from 48 to 62 Hz with a small deviation from the sinusoid shape, which is defined as that the ratio of peak to rms values equals  $\sqrt{2}$  within  $\pm 5\%$ . The tests



**Fig. 3.2** Standard lightning-impulse voltage according IEC 60060-1 (adapted from [3.2])

with impulse voltages should represent the voltage stress caused by switching operations by a standardized switching-impulse voltage and the stress caused by atmospheric overvoltage by a standardized lightning-impulse voltage. Both impulse voltages can generally be described as a sum of two exponential functions, like

$$u(t) = KU_0[\exp(-t/\tau_1) - \exp(-t/\tau_2)], \quad (3.3)$$

where  $K$  is a constant depending on the parameters of the impulse voltage generator,  $U_0$  is the DC charging voltage of the impulse generator, and  $\tau_1$  and  $\tau_2$  are time constants that also depend on the impulse generator.

A standard lightning impulse according IEC [3.2] is shown in Fig. 3.2.

The time  $T_1$  is the front time, defined as 1.67 times the time  $T_{AB}$ , which is the measured time between

points A (30%) and B (90%) of the maximum value of test voltage  $\hat{u}$ . The front time of a standard lightning impulse is  $1.2 \mu\text{s} \pm 30\%$ . The time  $T_2$  is the time to half value, which means the difference between the two 50% points of the voltage curve. The time to the half value of a standard lightning impulse is  $50 \mu\text{s} \pm 20\%$ . The virtual origin  $O_1$  is the intersection with the time axis of a straight line drawn through the reference points A and B on the front assuming a linear time scale, which is usually the case for lightning impulse measurements.

There are two other standard impulse voltages in [3.2], where the impulse is chopped in the front of the impulse or in the tail of the impulse. Figure 3.3 shows the two chopped impulses.

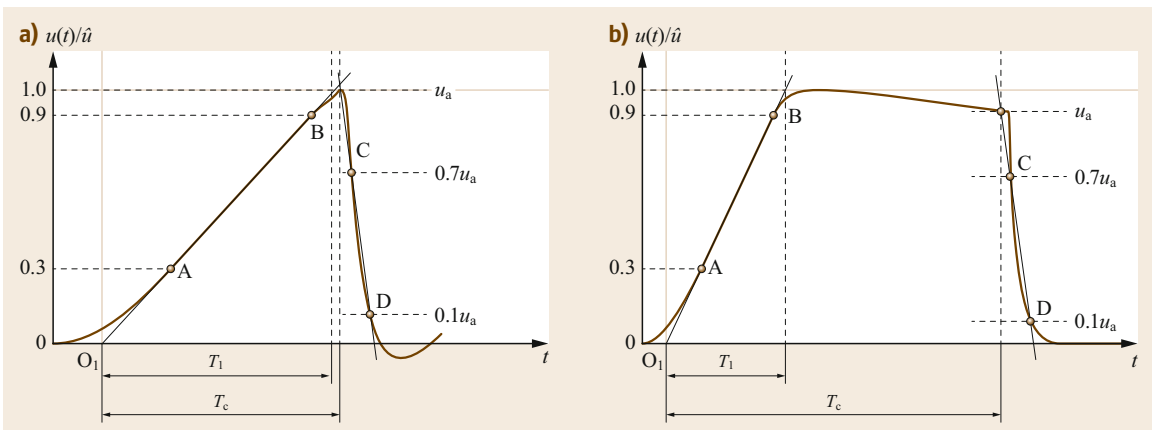
Additional parameters like chopping time  $T_c$  and the chopping steepness, based on the time interval between points C and D in Fig. 3.3 are introduced, whereby the values are defined by the relevant technical committees and also depend on the chopping device used.

The stress of the equipment during switching operations is simulated by the standard switching impulse shown in Fig. 3.4.

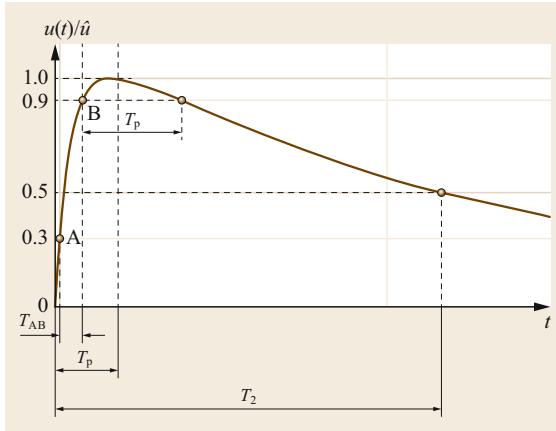
The time  $T_{AB}$  is the measured time between point A (30%) and B (90%) of the maximum value of test voltage  $\hat{u}$ . The time to peak  $T_p$  is then calculated according to

$$T_p = KT_{AB} \quad \text{with } K = 2.42 - 3.08 \times 10^{-3} T_{AB} + 1.51 \times 10^{-4} T_2, \quad (3.4)$$

which is valid for the standard switching impulse with a time to peak of  $250 \mu\text{s} \pm 20\%$  and a time to the half value of  $2500 \mu\text{s} \pm 60\%$  and where  $T_{AB}$  and  $T_2$



**Fig. 3.3a,b** Chopped lightning-impulse voltages (a) front-chopped (b) tail-chopped according to IEC 60060-1 (adapted from [3.2])



**Fig. 3.4** Switching impulse according to IEC 60060-1 (adapted from [3.2])

are given in microseconds. A simpler definition of  $T_p$  is given in IEC 60060-3 for on-site tests with

$$T_p = 2.4T_{AB} \quad (3.5)$$

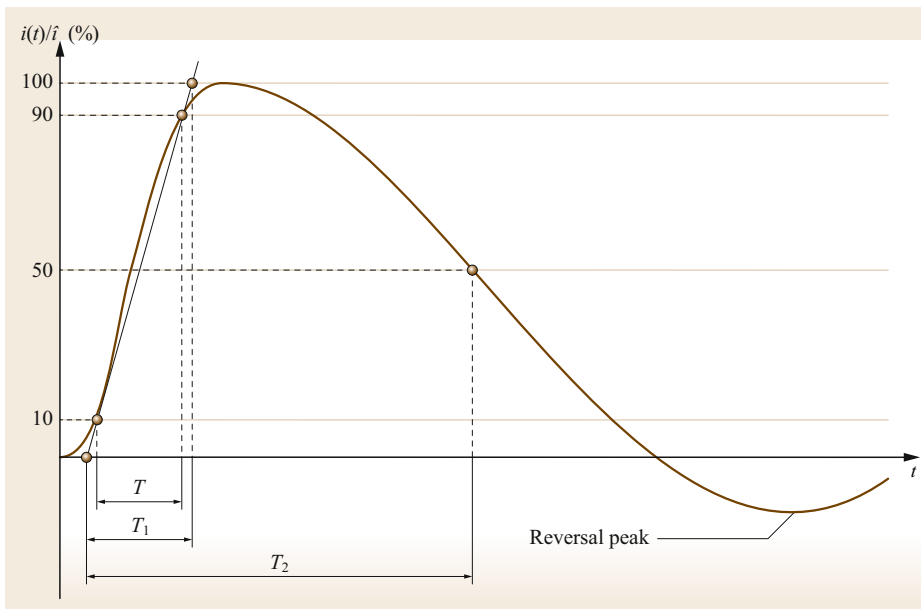
Some further voltage shapes representing overvoltage with different frequencies and voltage amplitudes are also described in IEC 60071-1 [3.1]. In the low-frequency range, temporary overvoltage exists within a frequency range from 10 to 500 Hz, which may be caused by changes in the electric power system. The duration of the temporary overvoltage ranges between ms and up to 1 h. The transient overvoltage can be divided into three parts: slow-front transient overvoltage with a time to peak  $T_p$  in the range from 20 to

5000  $\mu$ s and a duration up to 20 ms, fast-front transient overvoltage with a front time between 0.1 and 20  $\mu$ s with a duration of less than 300  $\mu$ s, and very-fast-front transient overvoltage with a raise time of less than 100 ns and superimposed high-frequency oscillations in the range of 300 kHz up to 100 MHz on lower frequencies in the range of 30 up to 300 kHz.

Besides the standardized impulse voltages, current impulses are also defined and described in IEC 62475 [3.3]. An example of an impulse current is shown in Fig. 3.5.

The definition of the front time  $T_1$  is different to that of the impulse voltage, and it is 1.25 times the measured time  $T$  between 10 and 90% of the maximum value of the test current  $\hat{i}$ . The time to half value  $T_2$  is defined analogously to the lightning-impulse voltage as the time difference between the two 50% values. Depending on the test objects, the front time  $T_1$  varies between 1 and 10  $\mu$ s, and the time to half value  $T_2$  between 20 and 350  $\mu$ s, whereby the tolerances for the front time are in the range from 10 to 30% and for the time to half value 20%.

In recent years, the DC voltage for transmission systems has become increasingly important. The DC voltage is usually generated by rectification of an AC voltage, supported by a capacitor, and, therefore, the amplitude of the DC voltage is not smooth. The deviation from the mean value is named ripple, and the allowed value for a standard DC voltage is  $\pm 3\%$  of the mean value, whereby the ripple is defined as half of the difference between the maximum and minimum values of the applied voltage.



**Fig. 3.5** Typical shape of an impulse current according to IEC 62475 (adapted from [3.3])

The task of high-voltage engineering is to design high-voltage equipment that is safe and economical with respect to operation and insulation systems. Transmission systems are necessary because generation and consumption of electric power usually do not occur at the same place, even if recently a decentralization of electric power generation has been demanded. Due to the losses of electric power transmission and also to an increase in

insulation costs with increasing voltage level, a compromise is required to obtain the optimum parameters of an electric power transmission system. As a general rule, it can be stated that the voltage level in kV should be similar to the distance in km, whereby also exceptions exist. Finally, high-voltage applications also exist, e.g., in the medical sector, electromagnetic interference tests, x-ray technology, and lightning protection.

## 3.2 Lightning

Lightning is the effect of thunderstorms. Most lightning occurs between clouds, and these are not of interest for high-voltage engineering, except the possible magnetic field that may be caused by lightning discharge. Some lightning strokes touch the ground or objects on the ground, and the most favored objects are those that tower above their surroundings, like high buildings, church towers, or overhead line towers. Therefore, lightning protection is one parameter regarding insulation coordination, and the risk of lightning can be defined by the frequency of lightning strokes and the ground flash density, which is given as the average number of strokes per unit area and per unit time at a particular location. Another parameter is the keraunic level, which gives the average number of thunderstorm days for a given locality. For most regions, maps are available for ground flash density and keraunic level. For high-voltage engineering, the possible voltages that may occur on overhead lines or outdoor substations belong to the group of external overvoltage, and it should be noted that the voltage level of a lightning stroke in an electric power system is independent of the system voltage.

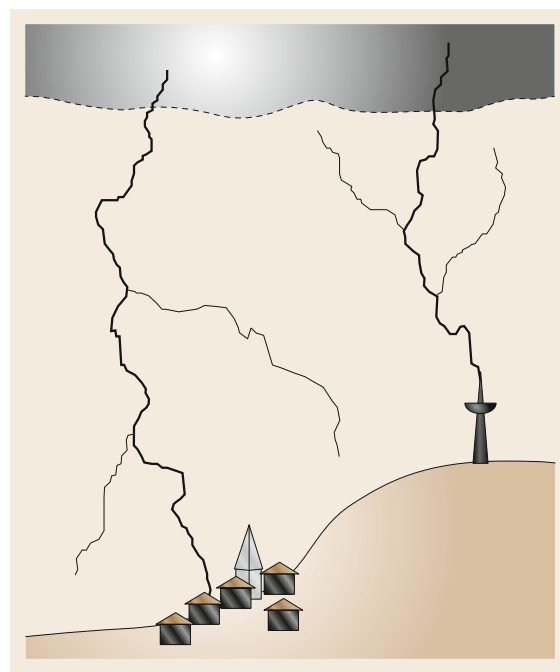
### 3.2.1 Generation of a Lightning Stroke

The basis for a lightning stroke is a thunderstorm cloud. This requires strong up winds and wet air. Within the thunderstorm cloud a separation of positive and negative charges occurs due to upwards-moving condensed water droplets and downwards-moving ice crystals, and freezing rain. The typical distribution of charges within a thunderstorm cloud is positive ice crystals in a high area of about 8–10 km, a main area below with negative charges at a level of about 5 km, and, sometimes, a limited area with positive charge below the main negative charge area. The discharge then occurs between the cloud and the ground, and in most cases, a negative charge will be transferred from the cloud to the ground. The direction of the discharge is downwards in most

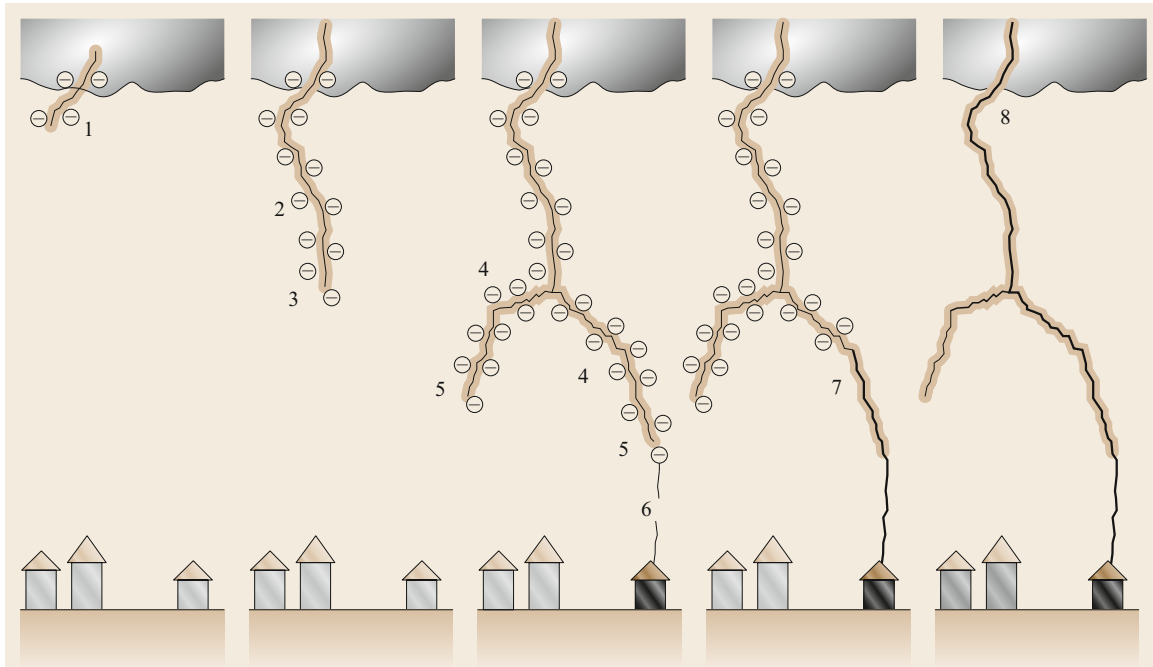
cases, and in a few cases of discharge upwards if tall structures like a tower exist. Figure 3.6 shows the final situation with a still image of downwards lightning (left part) and upwards lightning (right part) starting from a high tower.

The development of lightning can be divided into several parts: the leader discharge, starting from the cloud, the downwards and upwards leader, the main discharge channel, and a number of possible subsequent strokes. Figure 3.7 shows schematically the development of a negative cloud into ground lightning.

A leader starts from the cloud (1 in Fig. 3.7) but due to missing charges, the leader stops and only continues if enough charges flow in the channel again. Then, the



**Fig. 3.6** Downwards (*left*) and upwards (*right*) lightning (adapted from [3.4])



**Fig. 3.7** Chronological development of a negative lightning stroke (adapted from [3.4])

leader grows further in steps of about 50 m (2 and 3 in Fig. 3.7), but the direction depends on the conditions in the neighborhood. The leader now jumps in the direction towards the ground (4 and 5 in Fig. 3.7), and it may happen that a higher building will be bypassed, because the leader path is not influenced by the structure on the ground. If the leader approaches the ground, discharge channels start from the tip of the leader (negative, downwards leader) and at the same time from the protection device or air (6 in Fig. 3.7) (positive, upwards leader) due to the high electric field. Then, the main discharge occurs (7 in Fig. 3.7) with possible subsequent so called return strokes (8 in Fig. 3.7). Limited downwards and upwards leader lengths (6 in Fig. 3.7) are the cause of lightning strokes being possible alongside higher structures like buildings or towers. Therefore, air terminations have a limited protection area. The individual shapes of lightning strokes may differ significantly, but a standardized lightning impulse test voltage is defined with  $1.2 \mu\text{s}$  front time and  $50 \mu\text{s}$  time to half value in order to simulate the reproducible effect of a lightning stroke.

The effect of a lightning stroke can be divided into direct and indirect effects. Direct effects are overvoltage, traveling waves on overhead lines, and mechanical forces between conductors. Furthermore, heat generation can damage conductors in the path of the lightning current. Indirect effects can cause voltage drops across impedances with transient potential differences

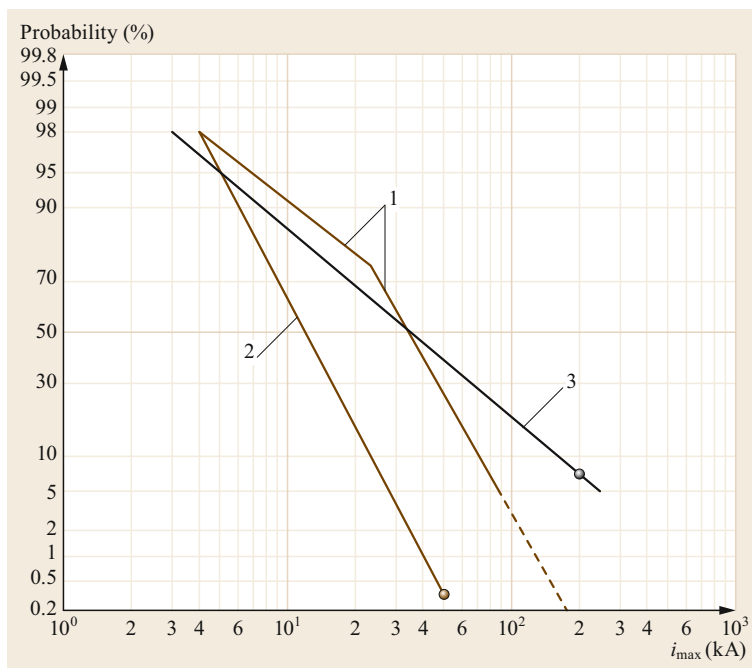
between grounded parts and can cause so-called *back flashovers* from grounded conductors into active lines of electric systems. The strong and varying magnetic field of a lightning stroke current may induce high voltages in loops.

Lightning can be characterized by its current parameter. The peak value is responsible for the voltage drop over earthing resistances for overvoltage and traveling waves. The rate of current rise  $di/dt$  allows the calculation of voltage drops at inductances and induced voltages in nearby conductor loops. The charge of the lightning stroke is the integral of the current over the time and is responsible for the heat energy, which may cause fusing of the conductors. The integral of the squared current over time is related to the ohmic losses in the conductors and the mechanical impulse.

The range of the current of a lightning stroke is a few kA up to 200 kA, according to Fig. 3.8.

The dots in Fig. 3.8 are values that are used for the evaluation of lightning protection level I. Lightning protection levels are divided into four levels; level I has the strongest requirements. The maximum value for a positive lightning is 200 kA at a probability of about 7%. At a glance this seems to be a relatively high value, but it should be taken into account that the number of positive lightning strokes is about 10% of the total number of lightning strokes, which results in a probability of 0.7% for a positive lightning stroke. The probability of a first negative lightning with an amplitude of 200 kA





**Fig. 3.8** Probability of lightning stroke current (1 – first negative lightning, 2 – subsequent negative lightning, 3 – positive lightning) (adapted from [3.5])

is, according Fig. 3.8, so low that the probability of all lightning strokes reaching 200 kA is in the range of 1%, and this was the reason to fix 200 kA as the basis for lightning protection level I.

### 3.2.2 Lightning Protection

A general concept of lightning protection is given in IEC 62305-1:2010 [3.6]. There are several methods to evaluate the necessary protection devices, and the most common methods are classical empirical curve design using a fixed protection angle, electrogeometric model known as the rolling sphere method and the collection volume method. The first method is not recommended for high-voltage substations, particularly for substations at higher system voltages. The second method contains an imaginary sphere of a fixed radius, representing the lightning stroke distance and the stroke current; the sphere is rolled over the structure, and no part of the equipment intersects with the sphere. However, the

method assumes a fixed striking distance, regardless of the height of a structure. The third method is based on Eriksson's Attractive Radius Model and takes into account the physical features of the structure. Based on this and the intensification of the electric field created by different points of the structure, the method provides recommendations for the optimum placement of lightning rods or air terminals. General statements for high-voltage engineering regarding lightning protection are the following. Lightning strokes cannot be prevented because they are natural events. Lightning protection devices should attract the lightning stroke so that the discharge takes place at a defined point. The protection of high-voltage apparatus should then be ensured by proper insulation coordination with the help of surge arresters or with a controlled discharge by an adapted conductive lead between the lightning protection device and the ground. In most cases, the interception unit is a metallic rod, which is reasonably higher than the environment and is well known as the Franklin rod.

## 3.3 Electric Field

### 3.3.1 Basics

In most cases, the high-voltage engineer is dealing with an electric field and mostly with an electrostatic electric field. Due to the low power frequency of 50 or 60 Hz,

the coupling between the electric and magnetic fields is very small and can be neglected. In consequence, the Maxwell equations can be simplified, because all the terms with a time derivative become zero. If the conductivity  $\kappa$  is negligible or theoretically zero, the electric

and magnetic fields are totally decoupled. The electric field  $\mathbf{E}$  can be expressed as

$$\oint_s \mathbf{E} ds = 0, \quad (3.6)$$

which means that the integral of the electric field for a closed loop is zero. Another equation describes the displacement density  $\mathbf{D}$ , which is related to the electric field  $\mathbf{E}$  and the product of the permittivity of vacuum  $\varepsilon_0$  and relative permittivity of the relevant material  $\varepsilon_r$ ,

$$\mathbf{D} = \varepsilon_0 \varepsilon_r \mathbf{E}. \quad (3.7)$$

With (3.7) the charge  $Q$ , which is enclosed by a closed area  $A$ , can be calculated

$$\oint_A \mathbf{D} d\mathbf{A} = Q. \quad (3.8)$$

These equations are the result of the simplified Maxwell equations, and (3.8) is often named the basic law of the electric field.

The electric field can also be described by a scalar potential, which is sometimes clearer. The electric field is then given by gradient of the potential

$$\mathbf{E} = -\text{grad } \varphi. \quad (3.9)$$

The minus sign comes from the definition of the direction of the electric field; the electric field vector is positively directed in the direction of the decreasing potential, which gives a negative gradient, and with the minus sign a positive direction of the electric field [3.4, 7].

### 3.3.2 Homogenous Electric Field

The typical electrode arrangement for a homogenous electric field is a capacitor under disregard of the edges of the electrodes, as shown in Fig. 3.9.

The potential of the upper electrode is  $U$ , and the potential of the lower electrode is 0. The equipotential lines are linearly distributed, and only the lines for  $3/4 U$ ,  $1/2 U$  and  $1/4 U$  are plotted. The electric field lines go from potential  $U$  to potential 0, and this also gives the orientation of the field vector of the electric field, as well as the vector of the displacement density. The vectors  $\mathbf{D}$  and  $d\mathbf{A}$  are parallel oriented and, therefore, the vectors can be replaced by the magnitudes. The electric field stress can be calculated as

$$E(x) = \frac{Q}{\varepsilon_0 \varepsilon_r A} = E_0 = \text{const.} \quad (3.10)$$

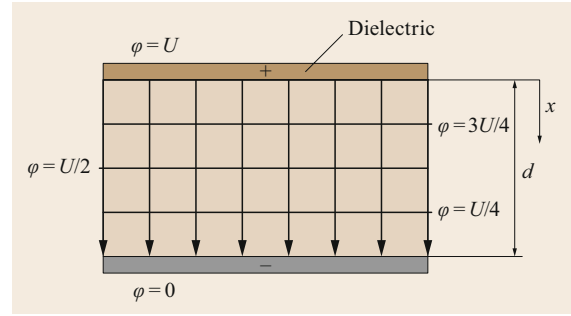


Fig. 3.9 Capacitor with a homogeneous dielectric

The parameter charge  $Q$ , permittivity of the vacuum  $\varepsilon_0$ , and relative permittivity of the related material  $\varepsilon_r$  (homogeneous material), and the area  $A$  are all independent of the variable  $x$  or on the location within the capacitor and, therefore, the electric field is constant in the entire volume of the capacitor. The electric field is the main parameter of the performance of a dielectric; however, in high-voltage engineering the main parameter is the applied voltage during service or during tests. Therefore, the relation between the electric field stress and applied voltage is important. From (3.9), the voltage can be calculated by the following steps

$$\begin{aligned} E &= -\text{grad } \varphi \Rightarrow E = -\frac{d\varphi}{dx} \\ \Rightarrow \int_0^d E dx &= - \int_{\varphi=U}^{\varphi=0} d\varphi \Rightarrow Ed = U. \end{aligned} \quad (3.11)$$

The charge  $Q$  and the capacitance of the capacitor can then be expressed by

$$Q = \varepsilon_0 \varepsilon_r A \frac{U}{d} \quad \text{and with} \quad C = \frac{Q}{U} \Rightarrow C = \varepsilon_0 \varepsilon_r \frac{A}{d}. \quad (3.12)$$

### 3.3.3 Layered Dielectrics

In high-voltage components, layered dielectrics very often exist, and, therefore, the distribution of the electric field within the complete insulation system and in the individual sections is important. This situation can be described by three simplified models with only two different materials. The first example is the arrangement where the boundary is transverse to the vector of the electric field; the second example is the arrangement where the boundary is parallel to the vector of the electric field, and the third example is the arrangement where the boundary has a random angle to the vector of the electric field.

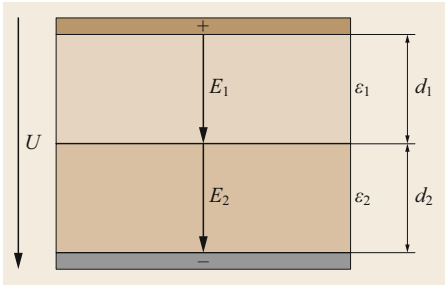


Fig. 3.10 Electric field with transverse boundary

#### Arrangement with Transverse Boundary

Figure 3.10 shows a schematic sketch of the first example.

The permittivity of materials is given by  $\varepsilon_1$  and  $\varepsilon_2$ , which is the abbreviation for the product of the permittivity of the vacuum  $\varepsilon_0$  and the relative permittivity for the material  $\varepsilon_r$ .

The applied voltage is  $U$  and the electric field stress  $E_1$  and  $E_2$  should be evaluated. According to (3.7), the vector of the electric field  $\mathbf{E}$  has the same direction as the vector of the displacement density  $\mathbf{D}$ . These vectors can generally be separated in a component rectangular to the boundary, named with index n, and a component parallel to the boundary, named with index t. For the displacement density it applies that the normal component  $D_n$  is equal in both materials, and this leads to

$$D_{1n} = D_{2n} . \quad (3.13)$$

This results in the different electric fields in the two materials according to

$$\varepsilon_1 E_{1n} = \varepsilon_2 E_{2n} \Rightarrow \frac{E_{1n}}{E_{2n}} = \frac{\varepsilon_2}{\varepsilon_1} \Rightarrow E_{1n} = E_{2n} \frac{\varepsilon_2}{\varepsilon_1} . \quad (3.14)$$

The material with the lower relative permittivity will be more stressed due to the higher electric field, and the increase is reversed proportional to the relative permittivity; this consequence is very important for the evaluation of the electric stress in insulation systems with different materials and different permittivities.

#### Arrangement with Parallel Boundary

Figure 3.11 shows a schematic sketch of the second example with the same nomination as for Fig. 3.10.

In this case, the tangential components of the electric field vectors are the same in both materials, and no normal components exist. This can be expressed as

$$E_{1t} = E_{2t} . \quad (3.15)$$

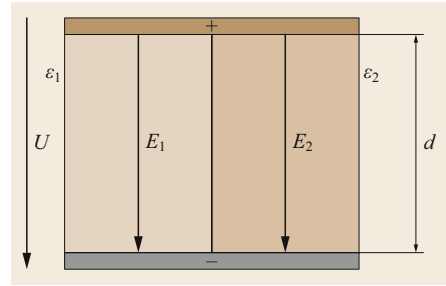


Fig. 3.11 Electric field with parallel boundary

This results in the displacement density in the two materials according to

$$\frac{D_{1t}}{\varepsilon_1} = \frac{D_{2t}}{\varepsilon_2} \Rightarrow \frac{D_{1t}}{D_{2t}} = \frac{\varepsilon_1}{\varepsilon_2} \Rightarrow D_{1t} = D_{2t} \frac{\varepsilon_1}{\varepsilon_2} . \quad (3.16)$$

The displacement density is proportional to the relative permittivity.

The equations (3.13)–(3.16) are only valid for AC and impulse voltage, where the conduction current is negligible. However, for DC voltage, the same fundamental equations can be used if the permittivity  $\varepsilon$  is replaced by the related conductivity  $\kappa$  under the assumption that the displacement current can be neglected.

#### Arrangement with Random Boundary

Figure 3.12 shows an example of the situation where the electric field or the displacement density vector have a certain angle to the boundary.

For the evaluation of the different displacement densities in the two insulation materials, the following equations can be used, and then it is clear that only the two special cases, shown in Figs. 3.10 and 3.11, and their relevant equations (3.14) and (3.16) are required,

$$\frac{D_{1t}}{D_{2t}} = \frac{\varepsilon_1}{\varepsilon_2} \quad \text{and} \quad \frac{E_{1n}}{E_{2n}} = \frac{\varepsilon_2}{\varepsilon_1} \quad \varepsilon_2 > \varepsilon_1 . \quad (3.17)$$

Due to these conditions, the angle  $\alpha$  will be changed from the insulation material to the other one. The same applies for the electric field vector.

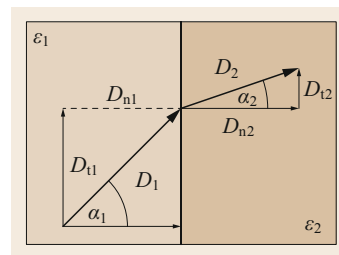


Fig. 3.12 Displacement density with random boundary

### 3.3.4 Inhomogeneous Electric Field

The magnitude of the electric field is one of the main parameters for insulation materials with respect to its strength and breakdown behavior. A homogeneous electric field in a plate–plate capacitor can be reached for material investigations in a laboratory, but in real electrode arrangements in high-voltage equipment, the electric field is not completely homogenous. The arrangements with inhomogeneous electric fields can be divided into weak inhomogeneous or strong inhomogeneous fields, but there is no clear definition for the differentiation. Very often, the maximum value of the electric field in an insulation system is the source for the beginning of a breakdown process and, therefore, to know this value is very important. The degree of inhomogeneity was already evaluated a long time ago, and the calculation of the electric field was very difficult and time consuming. In [3.8], a method is described that gives a relation between the actual electric field configuration and the electric field in an arrangement with the same electrode distance but a homogeneous electric field, and this relation is named after the inventor the *Schwaiger utilization factor*  $\eta$ . Depending on the value of this factor, also a separation of the inhomogeneous electric fields can be made. Nowadays, this factor is still very convenient for estimating the maximum electric field in an arrangement, even if the field calculation with the different methods uses the charge simulation method, the finite differences methods, and the finite element method, as numerical field calculation methods deliver more precise values. The factor is defined as

$$\eta = \frac{E_0}{E_{\max}} \quad \text{with} \quad E_0 = \frac{U}{d}, \quad (3.18)$$

with the maximum electric field  $E_{\max}$  and the average field  $E_0$  given by the applied voltage  $U$  divided by the electrode distance  $d$  of the electrode arrangement, simulating a homogeneous electric field. A further method for calculation of the electric field is the conformal map based on the theory of complex variables; however, nowadays it is only available in textbooks on high-voltage engineering.

A typical electrode arrangement in high-voltage equipment is the coaxial electrode arrangement shown in Fig. 3.13, which can be found in a high-voltage cable, a high-voltage gas insulated system, or in gas-insulated switchgears (GIS) or gas-insulated transmission lines (GIL).

The inner electrode is a cylinder with the radius  $r_1$ , and the outer electrode a cylinder with the radius  $r_0$ . The electric field vector  $\mathbf{E}$ , as well as the displacement

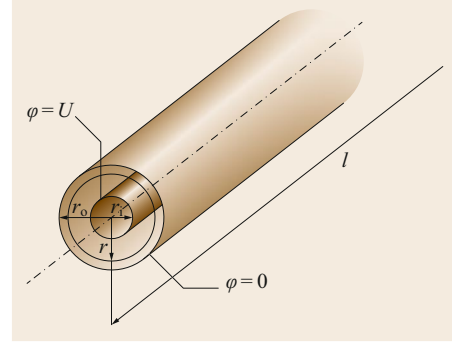


Fig. 3.13 Coaxial electrode arrangement

density vector  $\mathbf{D}$ , are perpendicular to the surface of the inner and outer electrodes. With (3.8), the charge  $Q$  can be applied to calculate the electric field. The area  $A$  of the inner electrode is given by the surface of the inner electrode (conductor), neglecting the area of the surface of the two ends of the conductor, because the length  $l$  is much larger than  $\pi r_1^2$ . The electric field at the position  $r$  is given by (3.19), whereby  $r_1 \leq r \leq r_0$ ,

$$\oint_A \mathbf{D} dA = Q \Rightarrow Q = DA = \varepsilon_0 \varepsilon_r E_r 2\pi r l$$

$$\Rightarrow E_r = \frac{Q}{\varepsilon_0 \varepsilon_r 2\pi r l}. \quad (3.19)$$

The electric field is only dependent on the radius  $r$ , and with (3.11) the electric field can be expressed as a function of the derivative of the potential  $\varphi$ ,

$$E_r = \frac{Q}{\varepsilon_0 \varepsilon_r 2\pi r l} = -\frac{d\varphi}{dr}. \quad (3.20)$$

An integration of (3.20) from  $r_1$  to  $r_0$  is equivalent to the integration of the potential  $\varphi$  from  $U$  to zero or ground

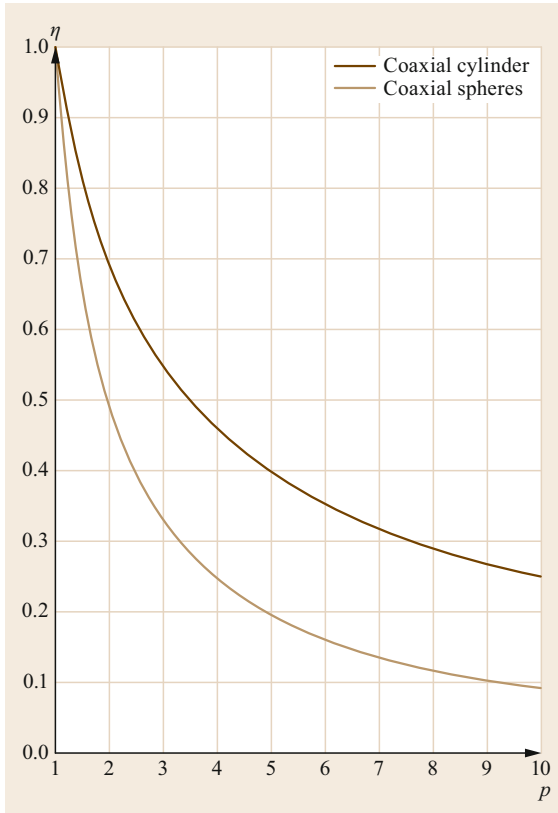
$$\int_{\varphi=0}^{\varphi=U} d\varphi = -\frac{Q}{\varepsilon_0 \varepsilon_r 2\pi l} \int_{r_0}^{r_1} \frac{1}{r} dr$$

$$\Rightarrow U = -\frac{Q}{\varepsilon_0 \varepsilon_r 2\pi l} (\ln r_1 - \ln r_0), \quad (3.21)$$

and this leads to the final equation concerning the dependence of the electric field on the radius  $r$

$$E_r = \frac{U}{r \left( \ln \frac{r_0}{r_1} \right)}. \quad (3.22)$$

The electric field of a simple electrode arrangement can be manually calculated, and from (3.22) it can be de-



**Fig. 3.14** Schwaiger utilization factor as function of electrode geometry (adapted from [3.4])

pictured that the electric field has its maximum at  $r = r_i$ , which means on the surface of the inner electrode.

For such an electrode arrangement, but also for other configurations, the Schwaiger utilization factor can be found in the literature [3.4] and [3.9]. The coaxial cylinder and the coaxial spheres are listed as the same electrode configuration due to the same cross section defined with the variable  $p$ , depending on the electrode distance and the radius of the inner electrode

$$p = \frac{r_i + (r_o - r_i)}{r_i} . \quad (3.23)$$

For the value of the Schwaiger utilization factor, it should be differentiated between the plane electric field, coaxial cylinder, and the rotational symmetry electric field and coaxial spheres, as shown in Fig. 3.14.

As an example, the electric field in a gas-insulated line (GIL) should be calculated using (3.22) and the Schwaiger utilization factor according Fig. 3.14.

The dimensions of the GIL should be  $r_o = 250$  mm and  $r_i = 75$  mm. According to (3.22), the electric field

at the inner electrode is

$$E_r = \frac{318 \text{ kV}}{75 \text{ mm} \left( \ln \frac{250 \text{ mm}}{75 \text{ mm}} \right)} = 3.52 \frac{\text{kV}}{\text{mm}} . \quad (3.24)$$

With these data, the parameter  $p$  is given as

$$\begin{aligned} p &= \frac{r_i(r_o - r_i)}{r_i} \\ &= \frac{75 \text{ mm} + (250 \text{ mm} - 75 \text{ mm})}{75 \text{ mm}} = 3.33 , \end{aligned} \quad (3.25)$$

and according to Fig. 3.14,  $\eta$  is 0.52 for a coaxial cylinder. With (3.18), the maximum electric field can be calculated or estimated to

$$\begin{aligned} E_{\max} &= \frac{E_0}{\eta} = \frac{1.82 \frac{\text{kV}}{\text{mm}}}{0.52} = 3.5 \frac{\text{kV}}{\text{mm}} \\ \text{with } E_0 &= \frac{U}{d} = \frac{318 \text{ kV}}{175 \text{ mm}} = 1.82 \frac{\text{kV}}{\text{mm}} . \end{aligned} \quad (3.26)$$

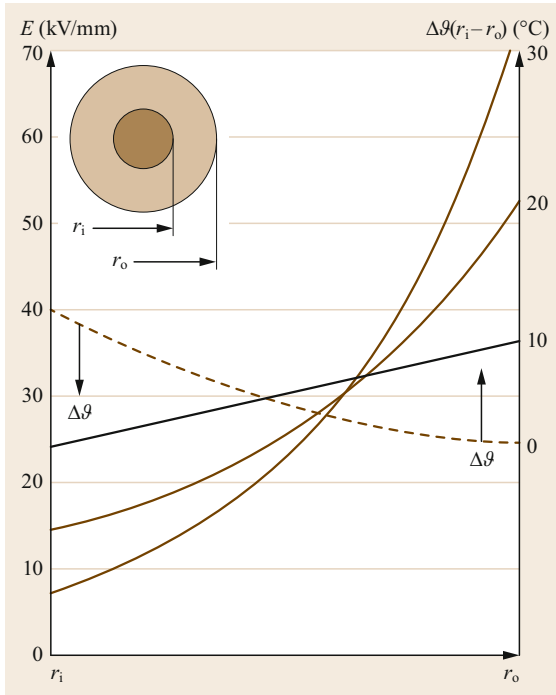
The difference between both values for the maximum electric field is very small, only about 0.6%, and this confirms the helpful use of the Schwaiger utilization factor for the estimation of the maximum electric field in an inhomogeneous electric field arrangement.

As a general statement concerning electrode arrangements for homogeneous and inhomogeneous electric field it can be stated that the best configuration is a plane-plane electrode with a homogeneous electric field, assuming a perfectly smooth electrode surface. The coaxial cylinder arrangements usually have a weak inhomogeneous electric field, which is shown in Fig. 3.14 by the higher values of  $\eta$  at the same value of  $p$ . The stronger inhomogeneous electric field has coaxial sphere arrangements, but these usually do not exist in high-voltage equipment.

### High-Voltage Cables as an Example of the Inhomogeneous Electric Field

Figure 3.13 shows a cross section of a typical coaxial cylinder. The insulation is a polymeric material, e.g., crosslinked polyethylene (XLPE) with inner and outer conductive layers as electrodes with a smooth surface. The task of a high-voltage engineer could be to optimize the design of the cable, so that the maximum electric field at the conductor reaches a minimum at a given radius of the outer electrode. The solution can be found by the partial derivative of (3.22) with respect to the radius of the inner electrode  $r_i$

$$\frac{\partial E_r}{\partial r_i} = U \frac{\partial}{\partial r_i} \frac{1}{r_i \ln \left( \frac{r_o}{r_i} \right)} \Rightarrow \frac{r_o}{r_i} = e , \quad (3.27)$$



**Fig. 3.15** Electric field distribution in a DC cable depending on temperature ( $E$  – field strength,  $\Delta\vartheta(r_i - r_o)$  – temperature difference) (adapted from [3.10])

### 3.4 Electric Strength

The performance of high-voltage equipment is mainly based on the performance of the insulation system and its electric strength, which means the ability to withstand an electrical breakdown. The evaluation of the performance is based on an empirically determined withstand voltage, where different types of voltages are applied, such as the system voltage AC with 50 or 60 Hz, the system voltage DC, and the relevant impulse voltages. In [3.1], the amplitudes for the voltages for withstand tests are listed as depending on the system voltage and sometimes depending on the local insulation coordination. These test voltages are related to high-voltage equipment like transformers, switchgears, insulators, surge arresters, etc. For insulation materials, the manufacturer usually describes the electric performance in addition to some other important parameters, depending on the type of material – gaseous, fluid, or solid, with the breakdown voltage. For an insulating fluid based on mineral oil, the breakdown voltage  $V_b$  at power frequency is given in kV, based on an IEC recommendation IEC 60156 [3.11] in which the determination of the breakdown voltage is defined with a special

without a detailed derivation of the mathematical steps. The interpretation of (3.27) means that  $\ln(r_o/r_i)$  is equal to 1 to minimize the maximum electric field on the inner electrode. However, for a real high-voltage cable maybe other parameters, like the manufacturing process, limitation of the insulation thickness, etc., will determine the final cable design, which will then lead to a slightly inhomogeneous electric field. A special case are high-voltage DC cables with polymeric insulation, which are coming increasingly into operation also at voltage levels above 500 kV. The electric field distribution is related to the conductivity  $\kappa$  and not to the relative permittivity  $\epsilon$ . Figure 3.15 shows the change of the electric field with an increasing temperature difference between the inner conductor ( $r_i$ ) and the outer conductor ( $r_o$ ).

The reason that the electric field can be higher at the outer electrode than on the inner electrode is the strong dependency of the conductivity on the temperature. The conductivity  $\kappa$  changes in the temperature range from 25 to 80 °C depending on the material, by about two orders of magnitude. The change of the permittivity  $\epsilon$  is, in contrast, in the range of some 10% [3.10].

electrode arrangement. The two partially spherical electrodes have a distance of 2.5 mm and a radius of 25 mm. The ratio between the average electric field and the maximum electric field on the surface of the electrodes is 0.97 [3.7], and this means that the electric field is nearly homogeneous. The breakdown voltage is given as a rms value in kV as the average value of six consecutive breakdowns. Furthermore, the voltage is increased continuously with  $2 \text{ kV/s} \pm 0.2 \text{ kV/s}$ , and the temperature is  $20 \text{ }^\circ\text{C} \pm 5 \text{ K}$ .

The determination of the electric strength of an insulating material requires breakdown tests and an evaluation of the results, because the breakdown voltages differ. In [3.11], the procedure and test parameters are described, and in the case of mineral oil, the average breakdown voltage is the mean value of six breakdown tests; furthermore, the standard deviation and the coefficient of variation, which is the ratio between the standard deviation and the mean breakdown voltage, should be calculated. It is also mentioned that the reproducibility in measuring individual dielectric breakdowns has shown a range of  $\pm 30\%$ . Such tests are different from

the withstand voltage tests for high-voltage equipment, where the performance should be checked with different types of voltages, power frequency AC or DC, and impulse voltages, with voltage levels according to the table of the insulation coordination given in [3.1].

### 3.4.1 Basics of Statistical Analysis

A fundamental requirement in high-voltage technology is to ensure that the electric stress is lower than the electric strength of the insulation under all expected conditions. This requires knowledge of the electric stress as well as of the electric strength of the insulation. The electric strength, however, has a random behavior and, therefore, statistical evaluation procedures are necessary to determine the electric strength. The failure of an insulation system is generally a breakdown, and this can happen due to high electric stress, for example at a voltage test. Furthermore, the decrease of the electric performance may be caused by partial discharges (PD), an electric discharge that only partially bridges the insulation between conductors, which later lead to a breakdown of the insulation, or by ageing of the insulation system caused by several effects like electrical, mechanical, thermal, or chemical stress. In conclusion, the electric strength depends on many parameters, which require a statistical evaluation, because a breakdown is a random event. Depending on the insulation material, the test procedure can be different, for example the breakdown voltage of gas insulation can be determined by several voltage tests with a breakdown, assuming that the performance of the gas is not be changed by previous breakdowns. However, the breakdown voltage of solid insulation can be determined using a new test sample for each breakdown test, and

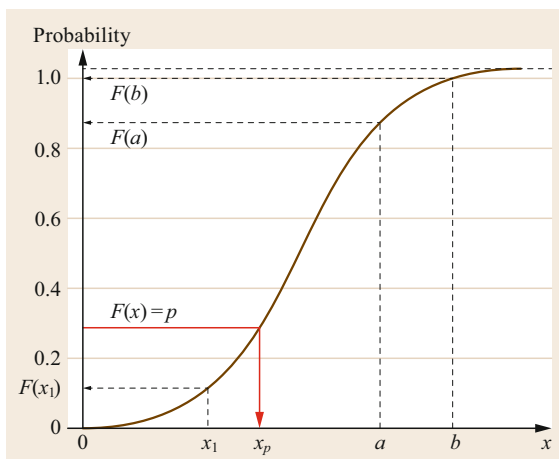


Fig. 3.16 Gaussian or normal probability function (adapted from [3.12])

besides the normal scattering of the breakdown voltage, this contributes additionally to the scattering. A very large number (infinitely large) of tests would allow us to determine the withstand voltage with a probability of breakdown of 0%, a probability of breakdown of 50%, and a breakdown probability of 100%, but in reality, the number of tests is limited for several reasons, like costs, time, the number of test samples, etc. Therefore, the parameter for the discharge or breakdown must be estimated from a limited number of test results, and the estimation is more precise the more results that are available. With the same procedure, further parameters, like time to breakdown or breakdown as a function of the stress time, can be determined.

### 3.4.2 Distribution Functions

The breakdown voltage of the sphere gap in air can be determined by a progressive stress test. The evaluation follows the typical treatment for random variables, where all independent variables, randomly distributed, contribute to an insignificant amount to the sum. Figure 3.16 shows the distribution function, where the parameter  $x$  can be the breakdown voltage of a progressive stress test [3.12].

The type of distribution is very often used to determine the 50% value, because the distribution is characterized by its 50% value (arithmetic value) and the standard deviation  $\sigma$  estimated by the difference of the values of  $x$  at the probabilities 84 and 50 or 50 and 16%, according to

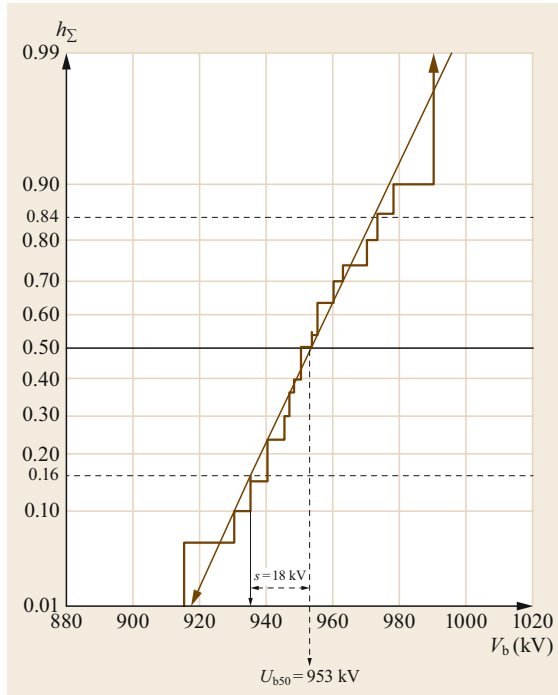
$$\sigma = (x_{84} - x_{50}) = (x_{50} - x_{16}) . \quad (3.28)$$

This Gaussian distribution is useful for random events and, therefore, also for breakdown tests. In addition to some other probability functions, the Weibull function is very often used to describe extreme values, but it should be used with care due to the possible adaption of the structure. The definition is given in (3.29) and is characterized by three parameters: its 63% value ( $x_{63}$ ), the Weibull exponent  $\delta$  as a measure of the dispersion, and the initial value  $x_0$

$$F(x; \eta; \delta; x_0) = 1 - \exp \left[ - \left( \frac{x - x_0}{\eta} \right)^\delta \right] \\ \text{with } x > x_0 . \quad (3.29)$$

The value of  $F$  is zero for  $x \leq x_0$  and  $\delta = 1.2898 / \log(x_{63}/x_{05})$  [3.12].

For the investigations of time to breakdown, the Weibull function is ideal, setting  $x_0 = 0$ . However, for breakdown voltage investigations, the function should be handled carefully due to the fact that for  $x = x_0$ ,



**Fig. 3.17** Cumulative breakdown frequency  $h_\Sigma$  function in a Gaussian distribution scale (adapted from [3.12])

the value of  $F$  is 0, and this means a breakdown probability of  $p = 0$ , which represents the ideal withstand voltage. For the estimation of the withstand voltage, the proper selection of a theoretical distribution function is very important, and confidence estimation should be performed, where different methods for the estimation of the mean value and the standard deviation are used [3.13].

In high-voltage tests, the empirical distribution function is usually determined from a limited number of experimental test results. The results are ordered according to an increasing magnitude between the lowest and highest value and the cumulative breakdown frequency  $h_\Sigma$ , which is equivalent to the probability, as is shown in Fig. 3.17.

The interpretation of Fig. 3.17 is the following. Impulse voltage tests at a voltage level of 940 kV leads to breakdown probability of 25%, at a voltage level of 960 kV to breakdown probability of 70%. It is clear the evaluation of the breakdown percentage is more precise as more impulses at the same voltage and more different voltage levels are applied. If the approximation of the test results gives a straight line the used distribution function is acceptable and the 50% value can be determined as 953 kV. With the so called maximum likelihood method which is an efficient estimation of parameters including confidence levels the estimated

value can be judged. In Fig. 3.17 the standard deviation  $\sigma$  can also be evaluated according to (3.28) and is 18 kV which is about 2%.

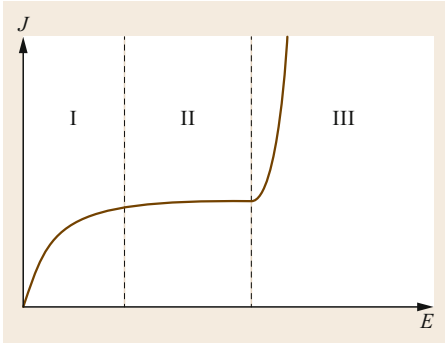
### Test Methods

The simplest method to determine the breakdown voltage is the voltage rise test, which can be applied with self-restoring insulation material. The voltage is increased with a given speed until breakdown happens, and this value is then recorded. The test is repeated several times, and then the average value will be the breakdown voltage. With impulse voltage, two methods can be used. The first one is the up and down method. The test starts with a voltage value at which it is certain that no breakdown occurs. Then the voltage value is increased by fixed steps until the first breakdown occurs. Then the voltage value is reduced by the same step until no breakdown occurs. The voltage value is again increased by the same step until, again, a breakdown occurs. Then the reduction of the voltage value is repeated. After a certain number of impulses, the voltage varies around the 50% value, which has to be estimated. The second method is the application of a given number of impulses at a voltage value where at least one breakdown is expected. For example, with ten impulses and one breakdown, the estimation of the breakdown probability is 10%. If lower values are required, the number of applied impulses should be increased, which increases the test time and the costs. Then the applied voltage value is increased, and the percentage of breakdowns is again calculated. The tests are stopped if a probability of 90% is reached, because no information is available if all impulse tests at the chosen value lead to a breakdown. At the end, probabilities between 10 and 90% are available, and if these values fit in a straight line in a distribution function grid, the 50% value can be estimated. Depending on the kind of insulation, further test methods for the characterization of the material performance should be used, but these methods are described in sections on the breakdown of insulating materials (Sect. 3.4.4 and 3.4.5).

### 3.4.3 Breakdown in Gases

Breakdown in gases depends on the electric field stress and, therefore, the applied voltage, which for a given distance and the arrangement of the electrodes is responsible for the electric field, is less meaningful. A simple example should confirm this. In a homogeneous electrode arrangement, with a plate–plate arrangement of 1 cm distance, the breakdown in air under reference conditions such as air pressure 1013 mbar and temperature 20 °C, occurs at 30 kV, which is an electric field of 3 kV/mm. In an integrated circuit, the distance





**Fig. 3.18** Current density  $J$  as function of the electric field  $E$

between conductors is in the range of some nm or some 10 nm, which at a voltage of 3 V leads to an electric field of  $3\text{ V}/10\text{ nm} = 300\text{ kV}/\text{mm}$ , which is much higher than the electric field in air.

Air is a fundamental gaseous insulation material because it is available everywhere but not always under the same conditions, because pressure, temperature, and humidity can be different, and these parameters influence the general breakdown behavior. At low electric fields gases are very good insulation material due to their low conductivity  $\kappa$  and nearly frequency-independent constant relative permittivity  $\varepsilon \approx 1$ . The current through an air gap is proportional to the applied voltage at low electric fields, and the free charge carriers, like electrons and positive or negative ions, move to the relevant electrodes, the negative charge carrier to the anode and the positive one to the cathode. This behavior is shown in Fig. 3.18, area I, where the current density increases and then passes to a stable value. With increasing electric field, the current density remains constant, where all free charge carriers, generated by different sources like photo-ionization or thermal ionization, are adsorbed by the electrodes before any recombination happens, as is shown in Fig. 3.18 area II. A further increase of the electric field leads to possible impact ionization if the free charge carrier gets enough energy by the acceleration due to the force of the electric field. At this voltage, free-charge carriers are generated by the applied voltage itself, and this process is called the self-sustaining discharge, as is shown in Fig. 3.18, area III. Depending on the character of the electric field and the impedance of the test circuit, this voltage is called the breakdown voltage for a homogeneous electric field and a low impedance test circuit or inception voltage for partial discharges, or glow or corona discharge for an inhomogeneous electric field and high impedance test circuit.

### Homogeneous Electric Field

The breakdown behavior of gases in a homogeneous electric field can be described by the generation of avalanches, also known as generation or the Townsend mechanism or the streamer mechanism. The basis for ionization and generation of an avalanche is the mobility of the free-charge carrier, the electric field, and the ambient gas condition, like gas pressure and temperature, and less gas humidity. The mobility of the electrons and ions is very different. The mobility values  $b$  for the different types of free-charge carriers are given in [3.7] with some simplifications:

- Mobility  $b$  for electrons  $\approx 500\text{ cm}^2/(\text{Vs})$
- Mobility  $b$  for ions (positive or negative)  $\approx 1\text{--}2\text{ cm}^2/(\text{Vs})$ .

This leads to a drift velocity of electrons of  $150\text{ mm}/\mu\text{s}$  and for ions of  $0.3\text{--}0.6\text{ mm}/\mu\text{s}$  for an electric field in air of  $30\text{ kV}/\text{cm}$  and, therefore, only the electrons are taken into account for the breakdown development in gases. The ionization of neutral molecules requires certain energy, and this energy should be equal to or higher than the ionization energy of the used gas, for example the ionization energy  $W_1$  for  $\text{N}_2$  is  $15.6\text{ eV}$  and for  $\text{O}_2$   $12.1\text{ eV}$  [3.7]. Assuming a mean free path  $\lambda$  of an electron in a gas, depending on the gas pressure and the gas temperature, the energy  $W$  is given by the charge of the electron  $q$  and the integral of the electric field  $E$  over the mean free path length

$$W = q \int_0^{\lambda} E(x) dx. \quad (3.30)$$

In a homogeneous electric field, the electric field stress is independent of the position  $x$ , and, therefore, (3.30) can be simplified to become

$$W = qE\lambda \quad (3.31)$$

and can be used to calculate the required ionization voltage  $U_1 = E\lambda$  or the required electric field  $E$ .

In a plate–plate arrangement in air, the breakdown will occur according to the generation or Townsend mechanism [3.14]. Figure 3.19 shows the idealized process.

The electric field is homogeneous, and, therefore, the electrons will get the same energy independently of their location. The number of electrons at the beginning of the discharge process is  $n_0$ , and this already demonstrates one of the conditions of a breakdown: that at least one electron should be available. The best condition for a breakdown is the start of the first electron

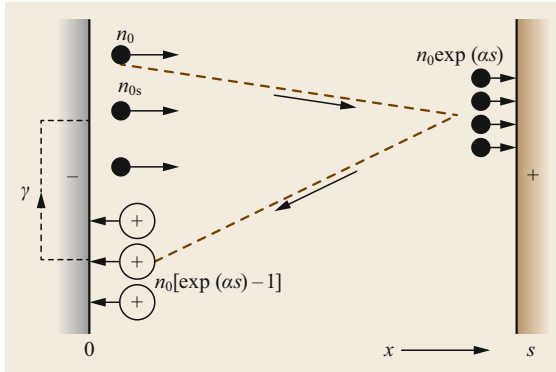


Fig. 3.19 Townsend breakdown mechanism

from the cathode. On its way to the anode, the electron may ionize some neutral molecules, and the number of ionization processes is given by the so-called Townsend ionization coefficient  $\alpha$ . This coefficient is defined as the number of ionization processes of one electron per path length, usually in cm, in the direction of the electric field. The last condition is necessary, because the path of an electron after a collision is not always parallel to the electric field direction. The increase of the number of electrons on the way from the cathode to the anode is given by

$$dn = \alpha(x)n(x)dx, \quad (3.32)$$

where  $\alpha$  is independent of  $x$ , and, therefore, the solution of the differential equation is

$$n = n_0 \exp(\alpha x) \quad (3.33)$$

for the distance between the plate  $s$  and the number of electrons  $n_0$  in the position  $x = 0$  in air. In some gases, the atomic structure allows to catch an electron, and this behavior will be characterized by the attachment coefficient  $\eta$ . For example, the gas sulfur hexafluoride ( $\text{SF}_6$ ), which is actually often used in high-voltage equipment but will in future be replaced by more environmentally friendly alternative gases, has a strong affinity to catch an electron due to the fact that the six fluor atoms endeavor to catch an electron to get the so-called inert gas configuration. For gases with an electron affinity, the ionization coefficient  $\alpha$  is reduced by the attachment coefficient  $\eta$ , and this leads to an effective ionization coefficient of  $(\alpha - \eta)$ . The number of electrons reaching the anode is given by (3.33), and it can be clearly seen that the increase follows an exponential function with  $\alpha$  or  $(\alpha - \eta)$  in the exponent. The number of positive ions reaching the cathode is

$$n = n_0 \{ \exp[(\alpha - \eta)s] - 1 \}. \quad (3.34)$$

These positive ions generate electrons at the impact on the cathode, depending on the cathode material, the gas and the gas pressure, and the number of electrons is given by the so-called second Townsend ionization coefficient  $\gamma$ . These electrons are the starting electrons for the next generation of ionization processes and are named in Fig. 3.19,  $n_{0s}$ . The electrons again move to the anode and generate further electrons and positive ions. Then two conditions exist, first, the number of the electrons in the second generation is smaller than the number of the starting electrons, and then the discharge process stops due to the lack of starting electrons. Second, the number of the electrons in the second generation is higher than the number of starting electrons, and then the total number of electrons increases with the number of generations, which leads to a breakdown. The theoretical condition for a breakdown in air ( $\eta \approx 0$ ) is given if the number of electrons of the second generation  $n_{0s}$  is equal to the number of starting electrons  $n_0$ , as is shown in (3.35)

$$\begin{aligned} n_{0s} &= \gamma n_0 [\exp(\alpha s) - 1] = n_0 \\ &\Rightarrow \gamma [\exp(\alpha s) - 1] = 1 \\ &\Rightarrow \exp(\alpha s) = \frac{1}{\gamma} + 1, \end{aligned} \quad (3.35)$$

$$\alpha s = \ln \left( \frac{1}{\gamma} + 1 \right) = k. \quad (3.36)$$

In [3.7], a value of  $\gamma = 10^{-5}$  is given that leads to a value of  $k = 9.2$ , but there are also values between 11 and 3 [3.4]. For air, a value of  $k = \alpha s = 20$  is also possible, which leads to a number of electrons in the range of  $10^8$ . The validity of the theory of this breakdown mechanism is limited to small gap distances and low pressure, with a low value of the Townsend ionization coefficient  $\alpha$ .

With an increase in the gap distance, the gas pressure, and the applied voltage, the theory of the generation mechanism could not explain the experimental results. An initial electron generates an avalanche, where the electrons are concentrated at the head of the avalanche, and the larger and less mobile ions are distributed within the tail of the avalanche. Figure 3.20 shows schematically the development of such a discharge process, which is named streamer breakdown.

The electric field of the avalanche is superimposed on the electric field generated by the applied voltage, and the increase of the electric field at the head and the tail of the avalanche generates radiation emission and photons. The photons are responsible for the generation of further avalanches, and they move with the speed of light. The numerous avalanches will finally bridge the whole gap in a time that is much shorter than the time

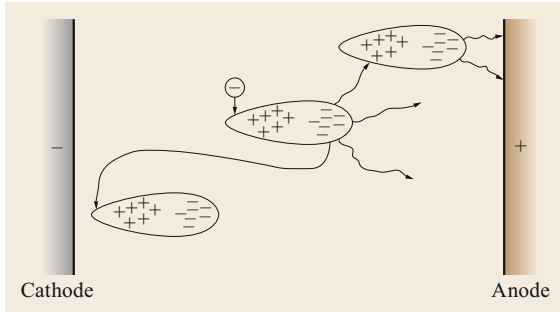


Fig. 3.20 Streamer breakdown

necessary for a breakdown after the generation mechanism. The criterion for a streamer breakdown is that the electric field around the avalanche be more or less equal to the electric field generated by the applied voltage. Assuming that all charges of the electrons in an avalanche are concentrated in the center of the head of the avalanche and with constant electron mobility, the critical number of electrons in the avalanche head is about  $10^8$ . This leads to (3.37), if at least one starting electron  $n_0 = 1$  is available

$$\begin{aligned} n &= n_0 \exp(\alpha - \eta)s = 10^8 \\ \Rightarrow (\alpha - \eta)s &= \ln(10^8) = 20.7. \end{aligned} \quad (3.37)$$

The criteria of the generation mechanism and the streamer mechanism are very similar, and, therefore, the main parameter for the breakdown in gases is the difference between the ionization and attachment coefficient called the effective ionization coefficient  $(\alpha - \eta)$ .

Paschen showed with his experiments that the breakdown voltage in a homogeneous electric field with a gap distance  $s$  and pressure  $p$  depends on the product of  $ps$  [3.15]. Figure 3.21 shows the Paschen curves for air and  $\text{SF}_6$ .

The breakdown criterion according to (3.36) and (3.37) is reached if the product of the effective ionization coefficient  $(\alpha - \eta)$  and the gap distance  $s$  is about 20, which represents  $10^8$  electrons generated by either the generation or the streamer mechanism. The strong increase of the current density, shown in Fig. 3.18, as a function of the electric field occurs at different electric field values depending on the kind of gas. The values for air and  $\text{SF}_6$  are  $24.4 \text{ kV}/(\text{cm bar})$  and  $87.7 \text{ kV}/(\text{cm bar})$  [3.7], and are called the limit electric field stress with respect to the breakdown behavior of the gas. For the calculation of the effective ionization coefficient, the following equations can be used

$$(\alpha - \eta)s = k \Rightarrow \frac{(\alpha - \eta)}{p} = \frac{k}{ps} = f\left(\frac{E}{p}\right). \quad (3.38)$$

The dependence of the effective ionization coefficient from the electric field can be described with a linear equation for  $\text{SF}_6$  or with a quadratic equation for air,

$$\begin{aligned} \frac{(\alpha - \eta)}{p} &= K \left( \frac{E}{p} - 87.7 \frac{\text{kV}}{\text{cm bar}} \right) \\ \text{with } K &= 28 \frac{1}{\text{kV}}, \end{aligned} \quad (3.39)$$

for the electric field in  $\text{SF}_6$  between  $60 \text{ kV}/(\text{cm bar})$  and  $120 \text{ kV}/(\text{cm bar})$  and

$$\begin{aligned} \frac{(\alpha - \eta)}{p} &= K \left( \frac{E}{p} - 24.4 \frac{\text{kV}}{\text{cm bar}} \right)^2 \\ \text{with } K &= 0.22 \frac{\text{cm bar}}{(\text{kV})^2}, \end{aligned} \quad (3.40)$$

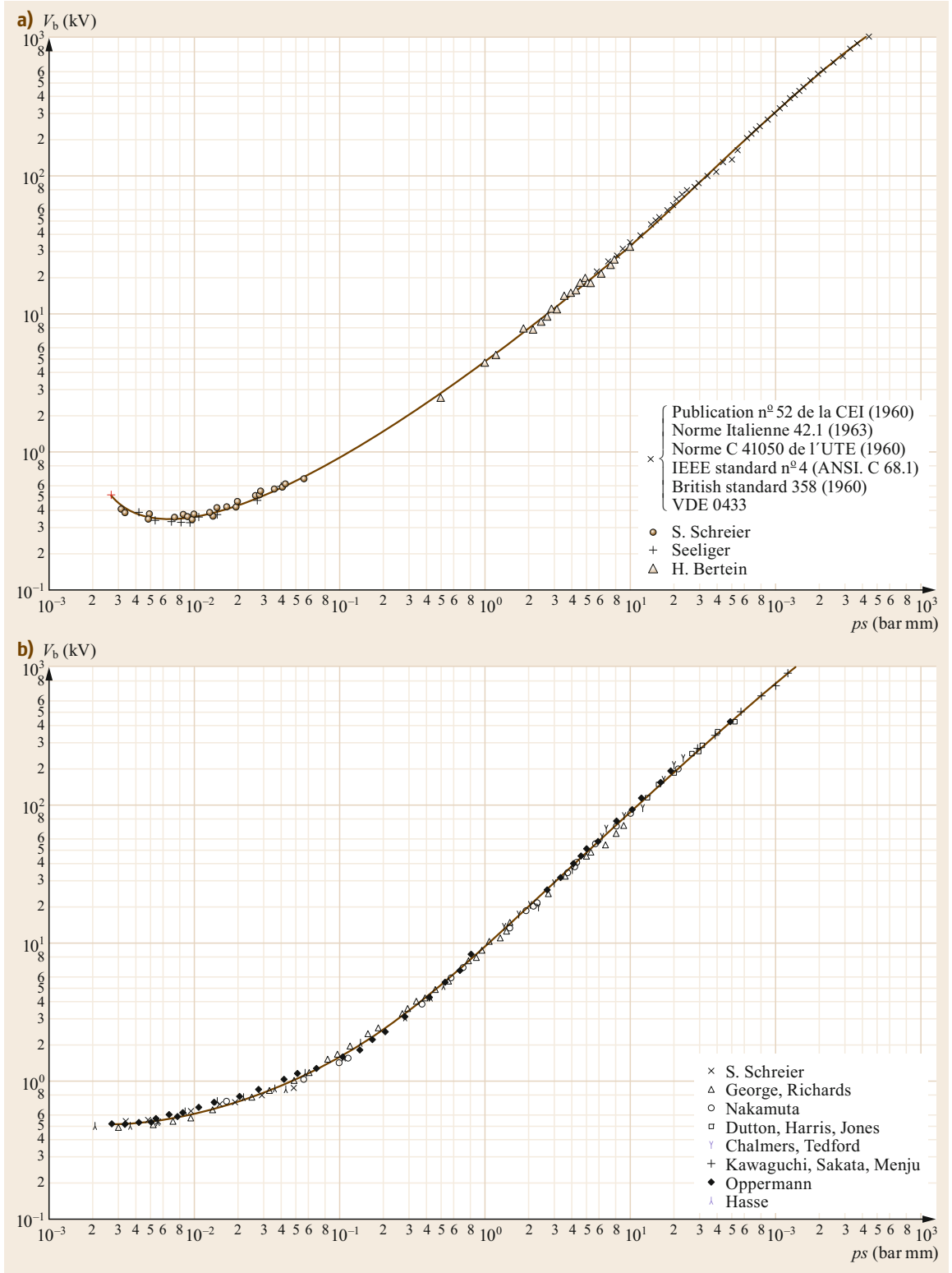
for the electric field in air between  $24.4 \text{ kV}/(\text{cm bar})$  and  $60 \text{ kV}/(\text{cm bar})$ .

From (3.39), it can be seen that in a homogeneous electric field, the breakdown of  $\text{SF}_6$  happens if the actual electric field at a pressure of 1 bar is slightly above the limit of the electric field strength of  $87.8 \text{ kV}/(\text{cm bar})$ . If the applied electric field is  $88.4 \text{ kV}/(\text{cm bar})$  at 1 bar and a 1 cm gap distance  $s$ , the value of  $(\alpha - \eta)$  is about 20, which, according to (3.37), is the criterion for breakdown. The difference between the applied electric field and the limit electric field is only 0.8%, which is within the uncertainty of the voltage measurement from which the electric field is calculated by the applied voltage divided by distance of the electrode. Furthermore, it should be taken into account that the difference in the electric field becomes much smaller for higher pressure, for example, only  $0.24 \text{ kV}/(\text{cm bar})$  at a pressure of 5 bar and a 1 cm gap distance.

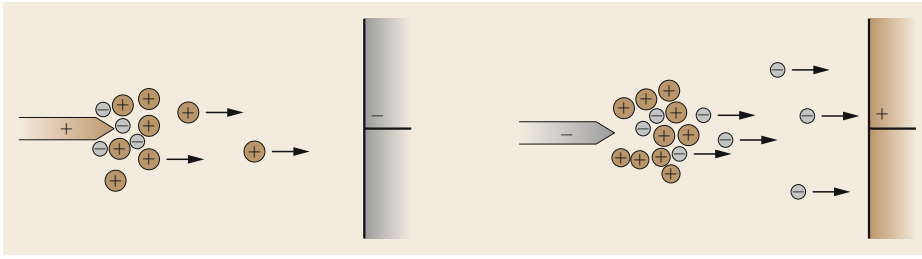
For air the breakdown criterion of  $(\alpha - \eta)s \approx 10$  is fulfilled if the applied electric field is in the range of  $31 \text{ kV}/(\text{cm bar})$ , which is about 27% above the limit electric field. The reason for this behavior is the low increase of the effective ionization coefficient with increasing electric field, represented by the low value of factor  $K$  compared to  $\text{SF}_6$ .

### Inhomogeneous Electric Field

The breakdown criteria for an homogeneous electric field can also be used for an inhomogeneous electric field, but then the dependence of the effective ionization coefficient on the electric field, and, thereby, on the location within the gap should be taken into account. Furthermore, the criteria only describe the start of stable pre-discharges, and the following development of a complete breakdown takes place with streamer and leader discharges. Also space charges influence the breakdown



**Fig. 3.21a,b** Paschen curves for air (a) and SF<sub>6</sub> (b) (air temperatures: 20 °C) (adapted from [3.15], where all details of the measurements are given)



**Fig. 3.22** Space charges in rod–plane electrode arrangements

behavior, and a typical electrode arrangement is the rod–plane. Here, the polarity of the rod is important for the electric field distribution and the breakdown value. Figure 3.22 shows the space charge distribution of rod–plane air gaps with different polarity of the rod.

The electric field is high near the rod in both arrangements, and, therefore, discharge processes start at the rod. In the case of negative polarity of the rod, the provision of electrons is supported by the electrode material, whereas with positive polarity of the rod, the electrons are only provided by the free electrons in the gas. Therefore, predischarges occur at a lower voltage if the rod has negative polarity. Further development of the discharges is shown in Fig. 3.22. For a positive rod, the ionization takes place in front of the rod, and the slow ions are placed around the rod and reduce the electric field there but enhance the electric field in the rest of the gap. For a negative rod, the slow ions are also placed around the rod, but there they increase the electric field and reduce it in the rest of the gap. Therefore, the breakdown voltage of a positive rod is lower than that of a negative rod.

For an inhomogeneous electric field in  $\text{SF}_6$ , (3.37) and (3.39) should be modified, because the effective ionization coefficient depends on the location, and the integral over the path from the electrode with the highest electric field to the other electrode in the direction of the electric field should be calculated there,

$$\int_0^{x_{\text{cr}}} (\alpha - \eta) dx = \int_0^{x_{\text{cr}}} p \frac{28}{\text{kV}} \left( \frac{E}{p} - 87.7 \frac{\text{kV}}{\text{cm bar}} \right) dx \approx 20. \quad (3.41)$$

The interpretation of (3.41) is that from the electrode with the highest electric field up to the point  $x_{\text{cr}}$ , the value of the integral should be around 20, because no ionization takes place between  $x_{\text{cr}}$  and the electrode with a lower electric field due to the fact that the value of the attachment coefficient  $\eta$  is higher than that of the ionization coefficient  $\alpha$ .

### Breakdown Parameters

In the previous sections on breakdown in gases, the conditions were more or less ideal. In reality, the breakdown is influenced by some more parameters. One influencing factor is the roughness of the electrode surface. As was already mentioned, the pressure is also important; the breakdown electric field strength, therefore, depends on the product of the surface roughness and the pressure, and this should be taken into account with increasing pressure.

For impulse voltage, the breakdown depends on the availability of a starting electron, the time to develop a first avalanche and the time to the final breakdown. The surge characteristic of a gas insulation is given by the so-called voltage–time area, which means that for higher voltage amplitudes, a shorter time is necessary, and for lower voltages, a longer time, but the product voltage times time is always constant [3.16].

As air is the most used insulation gas, the breakdown behavior will be described here in more detail. The breakdown depends on air pressure, air temperature, and air humidity. In [3.2], the relevant details concerning the influencing factors are given. The influence of humidity on the breakdown of air has been under discussion for a long time, and, actually, a revision of [3.2] will probably deliver more information. The influence of air pressure and air temperature is handled in [3.1], where it is called the altitude correction factor, and in [3.2], where it is called the atmospheric correction factor. The altitude correction factor is a kind of average value of the atmospheric correction factor used for the design of high-voltage equipment and takes the air density depending on the height above sea level into account. The atmospheric correction factor is for the correction of test voltage depending on the actual situation during the withstand test. In [3.2], the air density correction factor is

$$k_1 = \delta^m, \quad (3.42)$$

where the exponent  $m$  depends on the type of pre-discharge, but very often  $m$  is 1. Then, the air density

correction factor  $k_1$  can be calculated

$$\delta = \frac{p}{p_0} \frac{273 + t_0}{273 + t} = k_1, \quad (3.43)$$

where the temperatures  $t$  and  $t_0$  are expressed in  $^{\circ}\text{C}$ , and the atmospheric pressures  $p$  and  $p_0$  are expressed in the same units. Usually, the reference temperature  $t_0$  is  $20^{\circ}\text{C}$ , and the reference pressure  $p_0$  1013 mbar. The test voltage should then be corrected according to (3.43), and the applied voltage should be increased, if the air pressure is above the reference value or decreased, if the temperature is above the reference temperature. Another use of (3.43) is the evaluation of the test voltage, if a withstand voltage test should be done at, for example, a high-voltage laboratory at sea level, but the equipment under test should be installed at 2000 m above sea level. Assuming a withstand voltage of 1050 kV, according to the insulation coordination [3.1] and a place of operation at 2000 m above sea level, the test voltage in a high-voltage laboratory at sea level and an ambient temperature of  $25^{\circ}\text{C}$  should be

$$\begin{aligned} U_{\text{test}} &= \frac{1050 \text{ kV}}{\delta} \quad \text{with } \delta = \frac{794}{1013} \times \frac{273 + 20}{273 + 25} \\ &= \frac{1050 \text{ kV}}{0.77} = 1362 \text{ kV}. \end{aligned} \quad (3.44)$$

### 3.4.4 Breakdown in Fluids

Discharges in fluid cannot be described by a comprehensive theory like it was possible for gases. Fluids include a number of substances with different physical and chemical behavior, and these characteristics may change due to manufacturing conditions, impurities, or ageing processes, which lead to a large spread and deviation in the electrical performance. Therefore, the difference in electric strength under ideal conditions and service conditions can be within one order of magnitude. Generally the discharge processes in fluids are hindered by an increased density of the fluids compared to gases and the shorter free-path length, and, therefore, ionization processes are rarer, which leads to a higher electric strength.

The advantages of fluids are the high electric strength, the high thermal conductivity, and the impregnation properties. Typical application areas of fluid insulating materials are transformers, capacitors, bushings, and in the past, cables. However, the use of fluids requires a tight container. Due to the high density of fluids, the formation of electron avalanches by ionization is nearly impossible, and, therefore, a theory was developed, called masked gas discharge, assuming that micro bubbles exist in the fluid, and the breakdown happens in these micro bubbles, similarly to breakdown in

gas. Another theory is that the breakdown is caused by percolation, whereby the structure of the molecules of the fluid generates channels with a higher current density. Local heating produces evaporation of the fluid and a lower density, which allows the generation of streamer. The breakdown behavior in an inhomogeneous electric field shows a clear polarity effect. In a rod–plane gap there exists a higher breakdown voltage for a rod with positive polarity compared with a rod with negative polarity. Such breakdown behavior occurs at short-time voltage stress.

For longer stress times, another theory may explain the breakdown behavior of fluids. If fluids are used in combination with paper as an insulating material fibrous impurities exist, and they are adjusted according to the applied electric field due to electrostatic forces. These impurities may contain humidity due to the largely hygroscopic behavior of paper, and their conductivity is much higher than the ambient fluid. Then a conductive path will be created, which becomes overheated and finally leads to a breakdown. This type of breakdown is called a fiber bridge breakdown.

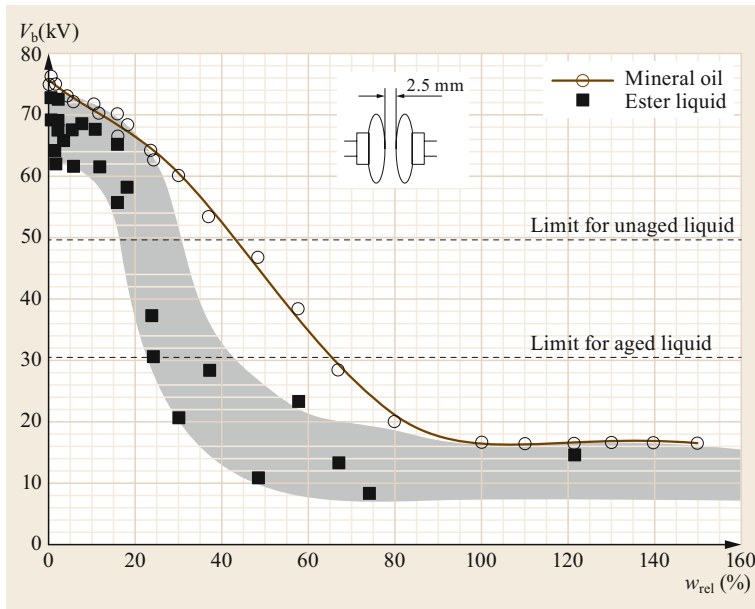
The breakdown of fluids depends on humidity, temperature, volume, and electrode coating. With an increase of the electrode distance, the probability of generating a fiber bridge increases, and an empiric function for the breakdown field strength at AC voltage  $E_d$  for transformer design was developed in [3.17],

$$E_d = E_0 \left( \frac{d}{\text{mm}} \right)^{-a}, \quad (3.45)$$

where  $E_0$  is a reference for different kinds of fluids, ranging for coated electrodes from 21 kV/mm for dry and degassed mineral oil up to 17.8 kV/mm for gas saturated mineral oil, and for blank electrodes from 17.8 kV/mm for dry and degassed mineral oil up to 13.5 kV/mm for gas saturated mineral oil [3.4];  $d$  is the distance of the electrode in mm, and the parameter  $a$  depends on the type of electrode and the quality of the fluid and ranges between 0.364 and 0.375.

Besides the ageing of fluids and the generation of impurities and gases, the humidity has the most influence on the breakdown of fluids and, particularly, on mineral oil, which is still the most used fluid in high-voltage equipment. Figure 3.23 shows the breakdown behavior of two kinds of fluids, mineral oil and ester, as a function of the relative water content  $w_{\text{rel}}$ .

The breakdown voltage was determined with a standard sphere–sphere electrode arrangement with a curvature radius of 25 mm and a gap distance of 2.5 mm, following the procedure given in [3.11]. The dependency of the breakdown voltage on the temperature is not directly visible in Fig. 3.23, but the relative water



**Fig. 3.23** Breakdown voltages  $V_b$  of oil and ester as a function of the relative water content  $w_{rel}$  (adapted from [3.7])

content is defined as the percentage of the actual water content  $w_{act}$  in relation to the water saturation content  $w_{sol}$  at the relevant temperature,

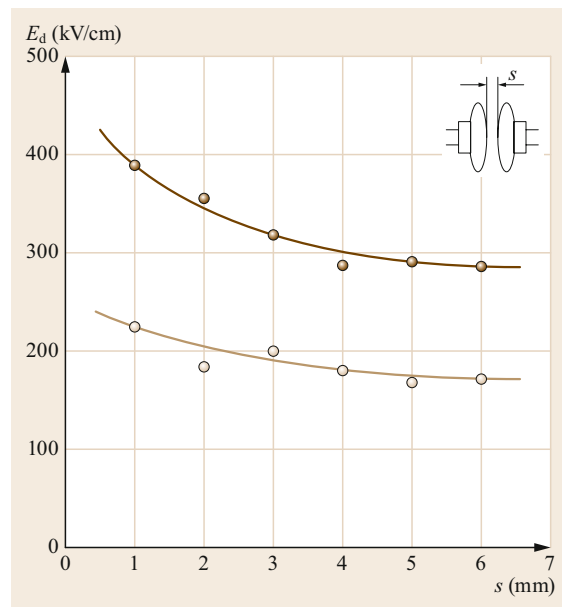
$$w_{rel} = \frac{w_{act}}{w_{sol}(\vartheta)} 100\% . \quad (3.46)$$

Figure 3.23 also shows that for mineral oil, a defined function exists between the breakdown voltage and the relative water content, but for ester only a certain range exists. The large difference between these two fluids regarding the influence of humidity or water content is the difference in the performance of the water solution. For an absolute water content of 20 ppm at 20 °C, the relative water content is 40% at a water saturation content of 50 ppm at 20 °C for mineral oil, but only 1% for a water saturation content of 2000 ppm at 20 °C for ester fluid.

The stressed fluid volume also has an effect on the electric strength. Figure 3.24 shows the influence of the gap distance and stressed volume on the electric breakdown field  $E_d$  for two different temperatures [3.7].

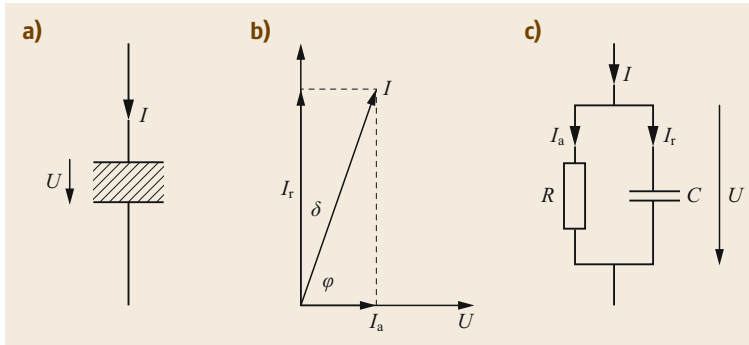
It can be seen that the electric field strength decreases with increasing stressed volume.

In a real electrode arrangement, the field configuration is not ideally homogeneous but slightly or strongly inhomogeneous. In this case, the estimation of the breakdown voltage for a homogeneous electrode arrangement can be used to evaluate the inception voltage for partial discharges. Partial discharges are discharges in a limited area and will not lead directly to a complete breakdown of the arrangement. It may happen that



**Fig. 3.24** Breakdown electric field strength  $E_d$  for mineral oil as function of gap distance  $s$  for a fluid temperature of 20 °C (light brown curve), and 100 °C (dark brown curve) (adapted from [3.7])

a limited number of partial discharges takes place for a long time, sometimes longer than the service time of the equipment. However, partial discharge measurements are a very good tool to detect a weak point within an insulation system, and, therefore, many recommendations for high-voltage equipment require a limit of



**Fig. 3.25a–c** Definition of the loss factor (also named dissipation factor). (a) Symbol of a solid test sample, (b) pointer diagram, (c) equivalent circuit diagram

partial discharges at a certain voltage. In addition, the measurement of the partial discharge inception voltage at a defined point–plane electrode arrangement with a fixed radius of the point electrode and a fixed electrode distance can be used to qualify the insulating fluid under test for use in high-voltage equipment [3.18]. The partial discharge inception voltage (PDIV) is defined as the lowest peak value of the test voltage at which the charge becomes greater than the specified discharge magnitude when the test voltage is increased above a low value for which no discharge occurs [3.19].

### 3.4.5 Breakdown in Solids

The breakdown mechanisms in solid insulation systems are, in general, similar to the mechanism in gas and fluids. A specific feature for solids is the reduced heat transfer, which may lead to an overheating of the insulation and damage. Therefore, the loss factor of a solid is important, and this factor usually has three components: the losses due to conduction processes, polarization, and ionization.

The conduction processes are temperature and electric field-dependent, similarly to the processes in gas shown in Fig. 3.18. This means that the losses are constant up to a critical electric field and then increase exponentially. The sources for the conduction process are impurities in the solid insulation or in the solid insulation itself by dissociation of ions. In principle, the polarization losses are based on deformation of the molecule, on orientation of the dipoles in the solid, and on boundary polarization. For power frequencies of 50 or 60 Hz, only the boundary surface polarization is important for the loss factor. Boundaries can be grain boundaries within the solid or boundaries between two different materials, like in solid–fluid insulation systems. The ionization losses are partial discharges in voids in the solid, and they occur if the voltage across the void is higher than the partial discharge inception voltage. This means that partial discharges start at a discrete voltage level, but it should be taken into account

that voids in a solid may have different geometric dimensions and, therefore, different inception voltages. The ionization losses are fixed, which means that the discharges always take place at the same location, and this may finally lead to a breakdown of the complete solid insulation system.

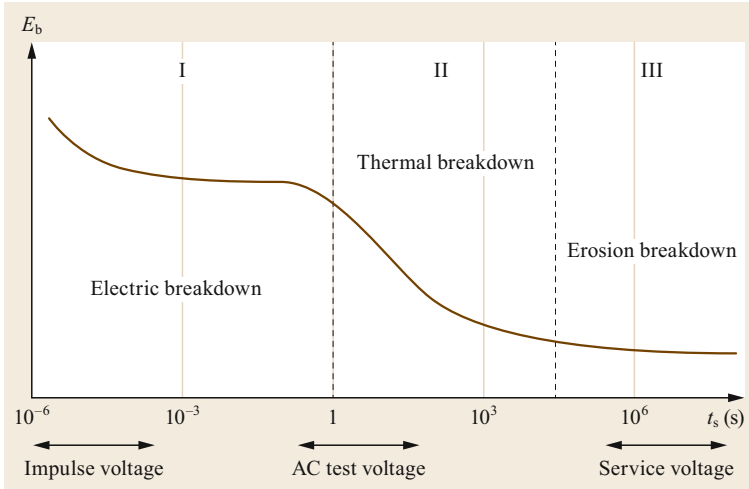
A general characterization of a solid is the loss factor, which is very often denoted as  $\tan \delta$ , which represents the ratio of the reactive current to the active current. Figure 3.25 shows a simplified schematic diagram of a solid and the related voltage and currents.

Figure 3.25a shows a solid insulation system with applied voltage  $U$  and current  $I$ . Voltage and current are complex variables, and in Fig. 3.25b these variables are shown as pointers. An ideal solid is an ideal capacitor without any losses. A real solid can be characterized by a resistor and capacitor in parallel, as shown in Fig. 3.25c. The electric loss factor of a solid can be described by the  $\tan$  of the loss angle  $\delta$ , which represents the deviation of the solid from an ideal capacitor. The complex phasor of the current  $I$  can be divided into a pointer of the active current  $I_a$  parallel to the pointer of the applied voltage  $U$  and a pointer of the reactive current  $I_r$  rectangular to the pointer of the applied voltage  $U$ . Then the following equations can be derived

$$\tan \delta = \frac{I_a}{I_r} = \frac{U/R}{U\omega C} = \frac{1}{\omega RC}. \quad (3.47)$$

Measurements of the loss factor showed that the losses depend on the temperature and the frequency, but this means that the equivalent circuit diagram in Fig. 3.25c cannot describe all effects in a solid. The losses are represented by the resistor  $R$ , which is not frequency dependent, and the impedance of the capacitive path is certainly frequency dependent but without losses. The use of a complex relative permittivity  $\epsilon_r$  can improve the equivalent circuit diagram in Fig. 3.25c by replacing the capacitor  $C$  by a complex capacitor  $C_c$ . The complex capacitor  $C_c$  is given by the complex relative permittivity  $\epsilon_r$  and the related capacitor with vacuum





**Fig. 3.26** Breakdown field strength  $E_b$  as function of stress time  $t_s$

$C_0$ . For a parallel plate capacitor as reference, the following equations will be used to describe the loss factor more correctly

$$C_0 = \varepsilon_0 \frac{A}{d}, \quad (3.48)$$

where  $\varepsilon_0$  is the permittivity of the vacuum,  $A$  the area of the parallel plate capacitor, and  $d$  the distance between the two plates. Then the complex capacitor  $C_c$  is

$$C_c = \varepsilon_r C_0 = (\varepsilon'_r - j\varepsilon''_r) C_0. \quad (3.49)$$

The current  $I$  can then be described by

$$I = \frac{U}{R} + j\omega C_c U = \frac{U}{R} + j\omega(\varepsilon'_r - j\varepsilon''_r) C_0 U, \quad (3.50)$$

and separated into the active and reactive parts

$$I_a = \frac{U}{R} + j\omega\varepsilon''_r C_0 U = \left( \frac{1}{R} + \omega\varepsilon''_r C_0 \right) U \quad \text{and} \\ I_r = \omega\varepsilon'_r C_0 U. \quad (3.51)$$

The dielectric loss factor is then

$$\tan \delta = \frac{I_a}{I_r} = \frac{\left( \frac{1}{R} + \omega\varepsilon''_r C_0 \right)}{\omega\varepsilon'_r C_0} = \frac{1}{R\omega\varepsilon'_r C_0} + \frac{\varepsilon''_r}{\varepsilon'_r}, \quad (3.52)$$

where the first part represents the conduction processes and the second part the polarization effects.

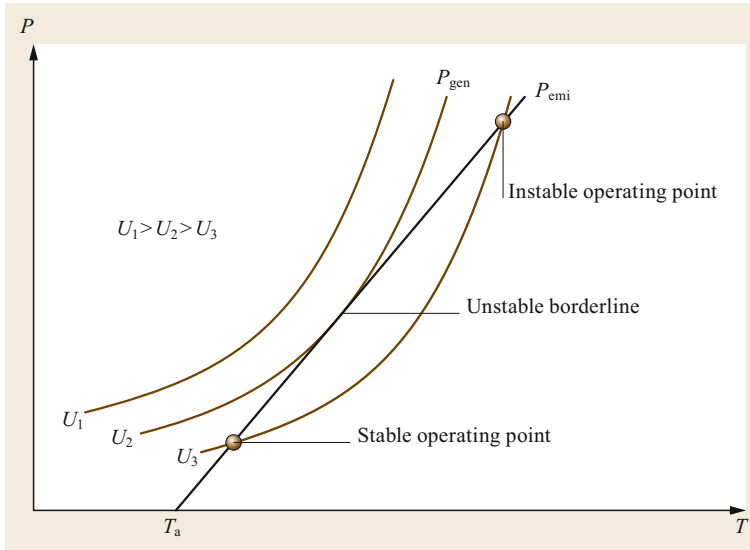
The breakdown in solids has two further characteristics: the dependency on the duration of the voltage stress or relevant electric field stress and on the stressed volume. Figure 3.26 shows the electric field strength as a function of the stress duration. The longer the

stress duration, the lower the electric breakdown field strength. In the range of the impulse voltage stress, the electric strength of solids is high, but with increasing stress time, the thermal behavior becomes more important, and the electric strength decreases, which is a typical disadvantage of solid insulation systems. For longer stress times, the effect of the erosion usually triggered by partial discharge in small voids within the solid determines the electric strength. The behavior in this area depends on several factors, like the quality of the solid, temperature, electric field stress, and the duration of the electric field stress.

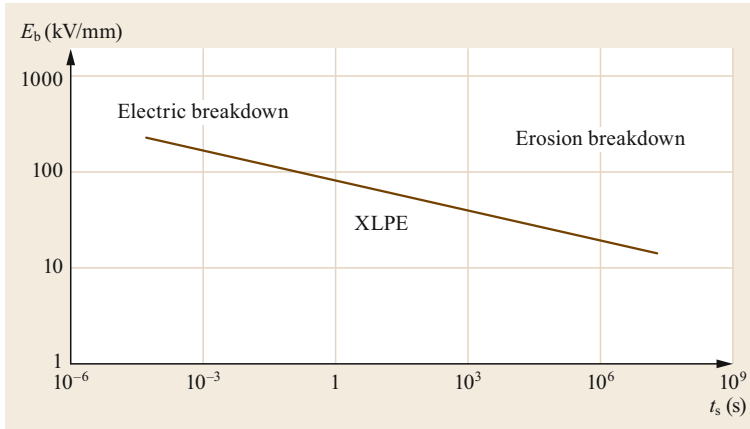
The behavior shown in Fig. 3.26 is typical for a solid with a high loss factor. Two parameters are of importance here: the duration of the stress and the thermal conditions. For a plate–plate electrode arrangement with a constant electrode distance and location-independent temperature, the generated power in the solid  $P_{\text{gen}}$  due to losses depends on the applied voltage and the difference of the temperatures between the electrodes and the inside of the solid,

$$P_{\text{gen}} \approx U^2 \exp[\beta(T - T_a)], \quad (3.53)$$

where  $\beta$  is a parameter depending on the geometry of the test sample,  $T$  the inside temperature,  $T_a$  the ambient temperature, and  $U$  the applied voltage. The losses for DC applications depend on  $U^2/R$  and for AC applications on  $U^2\omega C \tan \delta$ , but for both cases, the losses follow an exponential function as shown in (3.53), and the generated power  $P_{\text{gen}}$  increases exponentially with the increase of the inside temperature. Figure 3.27 shows the generated and emitted power assuming that the heat can be emitted only via electrode surfaces. The emitted power  $P_{\text{emi}}$  increases linearly with the temperature difference  $T - T_a$ .



**Fig. 3.27** Generated power  $P_{gen}$  and emitted power  $P_{emt}$  as functions of temperature  $T$



**Fig. 3.28** Breakdown field strength  $E_b$  as a function of stress time  $t_s$  for XLPE

A safe and reliable service can only be achieved if the emitted power is equal to the generated power. For the voltage level,  $U_1$  this condition does not exist. For the lower voltage level  $U_2$ , the condition is fulfilled, but the straight line of  $P_{emt}$  is only a tangent on the curve  $P_{gen}$  for the voltage level  $U_2$ , and the relevant point is called an unstable borderline. A simple check shows that if the temperature  $T$  changes, the generated power is higher than the emitted power. A further reduction of the voltage level with  $U_3$  delivers two points where the generated power and the emitted power are equal. However, only one point is called a stable operating point, because an additional requirement should be fulfilled,

$$\frac{dP_{gen}}{dT} < \frac{dP_{emt}}{dT}, \tag{3.54}$$

which is not true for an instable operating point.

With increasing AC-system voltages, the importance of the loss factor increases due to the fact that the losses increase with the square of the system voltage, frequency is fixed, and capacitance can be only influenced within narrow limits. Therefore, solids with low or very low loss factor are preferred for the application in high-voltage equipment, because no thermal breakdown occurs. A typical material is crosslinked polyethylene (XLPE) for high-voltage cables, because cables are apparatus where the performance depends strongly on the thermal behavior. Figure 3.28 shows the electric field strength of XLPE as a function of the stress time.

The area of thermal breakdown has disappeared, and there is a transition from the electric breakdown to the erosion breakdown. Due to the logarithmic scale of the y-axis, in contrast to Fig. 3.26, the function is not exponential but linear. This can be expressed with (3.55)

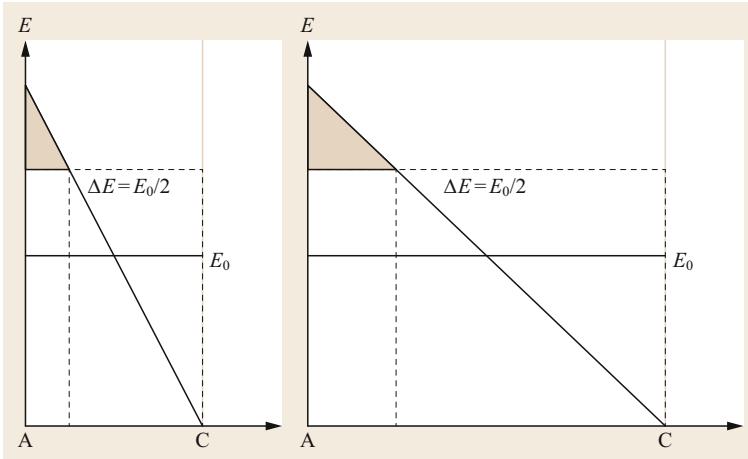


Fig. 3.29 Physical volume effect in solids

and is called the life law,

$$E^N t = \text{const.} \Rightarrow \log E = \text{const.} - \left(\frac{1}{N}\right) \log t, \quad (3.55)$$

where  $E$  is the electric field strength and  $t$  the expected life time. The parameter  $N$  depends on the material and represents the gradient of the straight line. For technical applications with solids, the value of  $N$  is between 10 and 15 [3.7].

The performance of solids is usually checked with small test samples. Therefore, the extrapolation of larger volumes of solids should be done carefully considering the so-called volume effect. This effect has two components: the statistical volume effect and the physical volume effect. The statistical volume effect is based on the assumption that with a larger volume also the number of defects in the solid increases. The theoretical evaluation of the breakdown probability can originate from two extreme cases. The first one is that all defects exist in parallel, which means that the breakdown of one of the defects leads to the breakdown of the test sample. The second one is that all defects are connected in series, and that a breakdown of one defect will increase the stress of the rest of the defects at the following stresses, whereby the increase of breakdown probability depends on the number of defects in the series, and the breakdown probability of the test sample should be calculated step by step. The first case is the most critical and should, therefore, be handled in more detail. Assuming similar defects, the breakdown probability for such a single defect can be determined and denoted by  $F$  as function of the applied voltage. The withstand probability  $W$  of one defect can then be expressed as

$$W(u) = [1 - F(u)]. \quad (3.56)$$

If the number of defects in parallel in the test sample is  $n$ , the withstand probability of the complete test sample  $W_n$  can be calculated by the multiplication of the probability of each of  $n$  defects,

$$W_n = [1 - F(u)]^n. \quad (3.57)$$

From (3.57), it can be seen that the withstand probability decreases exponentially with the increase of the number of defects.

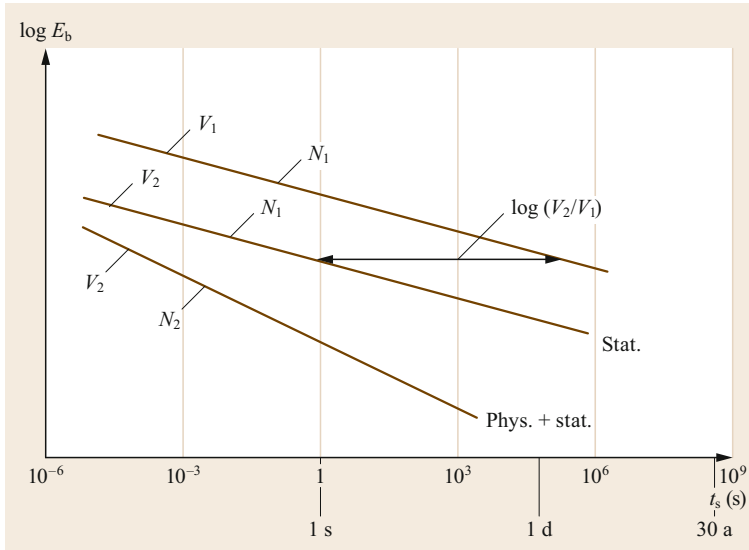
The second volume effect is based on the increase of the stressed volume. Figure 3.29 shows the electric field in a solid with space charges. The average electric field is  $E_0$ , but due to space charges in the solid, the maximum electric field at the actual anode (A) can be  $2E_0$ . The reference value should be, for example,  $\Delta E = E_0/2$ . In the left part of Fig. 3.29 the applied voltage should be  $U$  and in the right part  $2U$ , doubling the electrode distance and resulting in the same electric field.

From Fig. 3.29, it can be seen that the highly stressed volume (dashed area) in front of the anode with an electric field of  $E \geq E_0 + \Delta E$  has been increased due to the increase of the electrode's distance, which is equivalent to the increase of the volume.

Both volume effects can be taken into account for the evaluation of the life time of a solid. Figure 3.30 shows the life law for two different volumes  $V_1$  and  $V_2$  (statistical effect) and also for the consideration of the physical volume effect.

For a given material with life time exponent  $N_1$  and a volume  $V_1$ , the life law can be calculated according to (3.55),

$$E^{N_1} t = \text{const.} \Rightarrow \log E = \text{const.} - \left(\frac{1}{N_1}\right) \log t. \quad (3.58)$$



**Fig. 3.30** Influence of statistical and physical volume effects on the life law (adapted from [3.7])

The influence of the volume can be considered by a volume factor  $v$ , because the statistic volume effect complies with the statistic behavior. Then (3.55) will be changed to

$$vE^N t = \text{const.} \Rightarrow \log E = \text{const} - \left(\frac{1}{N}\right) \log(vt), \quad (3.59)$$

with  $v = V_2/V_1$  and  $V_2 > V_1$ .

In Fig. 3.30 it can be seen that an increase of the volume will result in a shift of the life time line to a lower electric field, but the gradient is unchanged. If the phys-

ical effect is added, the life-time line is again shifted to a lower electric field, but in this case, with an increase of the gradient, which means a reduction of the life time for the required electric field strength.

The determination of the characteristics of solids is similar to that of gases and fluids, but only the determination of the breakdown of the electric field or voltage is governed by a larger spread of test results due to the fact that for each breakdown test, a new sample is required, and this already contributes to scatter. Furthermore, the defects within the solid are responsible for the breakdown, and these defects are randomly distributed.

### 3.5 Insulating Materials

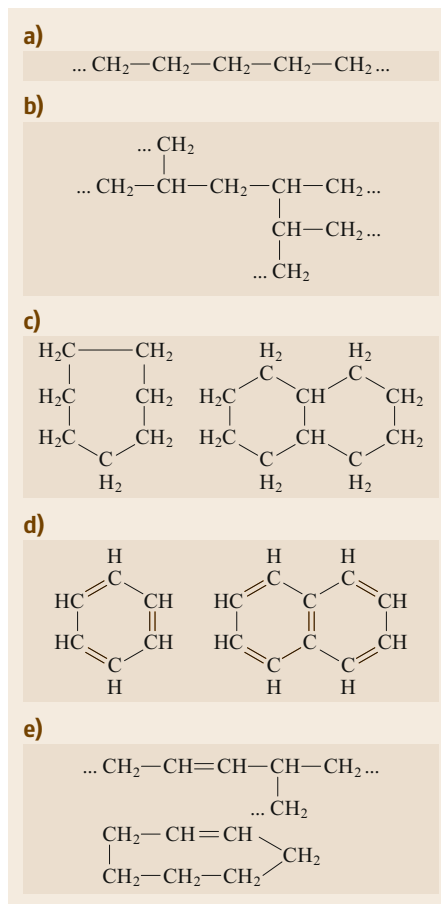
Insulating materials have different functions, which determine the choice of the material. The basic purpose is the separation of elements with different potential. Air and gas insulation is unlimitedly available and free of charge, but the electric performance depends on the ambient conditions, which are uncontrollable. Other gases, like nitrogen  $N_2$ , sulfur hexafluoride  $SF_6$ , carbon dioxide  $CO_2$ , or new synthetic gases require a shell. The electric performance can be controlled by the gas pressure within a certain limit, and is partly independent of the ambient conditions. It should be taken into account that gases may have a dew point that is above the lowest service temperature, and then the liquefaction will reduce the remaining partial gas pressure. In any case, fluids require a shell and, besides the electric performance, fluids can be used for

impregnation, typically in combination with paper or, more correctly, with cellulose, and for cooling purposes. Furthermore, the choice of a specific fluid may depend on the fire behavior and environmental compatibility. A typical example is the replacement of a fluid based on mineral oil by a fluid based on ester, synthetic or natural. The combination of a fluid with cellulose has big advantages, because the holes in the cellulose can be filled with the fluid, preventing partial discharges there, and at the same time, the fluid can carry the heat generated, which makes this system particularly suitable for the insulation of transformers. Finally, solids are necessary to take over the mechanical tasks combined with good electric performance but with limited thermal performance. The limitation of the power transmission of a high-voltage cable with solid insula-

tion, e.g., XLPE, is given by the heat transfer of the solid.

### 3.5.1 Gases

Air is an insulation gas that is available anywhere, free of charge, and for many applications has a sufficient electric performance. The breakdown electric field strength in a homogeneous electrode arrangement is about 30 kV/cm, which is little bit higher than the breakdown electric field for nitrogen, due to the fact that air is a combination of nitrogen (about 80%) and oxygen (about 20%), and oxygen belongs to gases with electron affinity. These gases have the characteristic that they attract electrons and detract these from the discharge process. A further gas that has a stronger electron affinity than oxygen is sulfur hexafluoride (SF<sub>6</sub>). Due to its molecular structure, the six fluor atoms are eager to catch an electron to get a so-called inert gas configuration. Therefore, SF<sub>6</sub> is used in gas-insulated substations, and the size of the substations may in some cases be reduced up to a factor of 10. The breakdown electric field strength of SF<sub>6</sub> at a pressure of 1 bar is about 90 kV/cm, which is three times higher than air. With increasing pressure, the electric field strength could be enhanced and, therefore, the dimensions of the SF<sub>6</sub>-insulated substations could be limited even for very high system voltages up to 1200 kV. Furthermore, SF<sub>6</sub> may also be used in circuit breakers due its good performance as a medium for arc quenching. However, the disadvantage of SF<sub>6</sub> is the high greenhouse effect, which is about 23 000 times higher than the effect of CO<sub>2</sub>. Therefore, research was conducted to reduce the amount of SF<sub>6</sub> while retaining the good electric performance of this gas. A technical and economical solution was a mixture of 80% N<sub>2</sub> and 20% SF<sub>6</sub> as the insulation gas for gas-insulated lines [3.20]. With such a mixture, an electric strength of about 80% of pure SF<sub>6</sub> can be reached. With the intention to eliminate SF<sub>6</sub> as the insulating gas in high-voltage equipment, further investigations were carried out and so-called fluoroketones and fluoronitrile with low greenhouse potential were found to replace SF<sub>6</sub> [3.21–23]. However, high boiling points of the given fluoro-organic gas types require a mixture with other gases, like N<sub>2</sub> or CO<sub>2</sub>, in order to keep the partial pressure of the fluorinated component under a certain limit. The chemical formula for the fluoroketone is (CF<sub>3</sub>)<sub>2</sub>CFC(O)CF<sub>3</sub> or the shorter C<sub>5</sub>-FK, and for the fluoronitrile (CF<sub>3</sub>)<sub>2</sub>CFCN or the shorter C<sub>4</sub>-FN. The electric performance of the two fluoro-organic gas types is equal or sometimes better than the mixture of 80% N<sub>2</sub> and 20% SF<sub>6</sub>, but the boiling point should be taken into account.



**Fig. 3.31a–e** Structures of hydrocarbons of mineral oil. (a) Paraffin, (b) iso-paraffin, (c) naphthene, (d) aromatics, (e) olefin (adapted from [3.7])

### 3.5.2 Fluids

The fluid most used in high-voltage apparatus is oil based on mineral oil. The purpose of this fluid is governing the required insulation, impregnation, and heat transfer from the inner part of the apparatus to the walls or the cooling system. Mineral oil is a combination of different kinds of hydrocarbons with different chemical bonds. Figure 3.31 shows the kinds of hydrocarbons [3.7].

Figure 3.31a shows the molecular structure of paraffin with a linear combination of the molecules CH<sub>2</sub>. Figure 3.31b shows the so-called isoparaffin with some branches in the structure, and Fig. 3.31c shows a naphthenic structure sometimes called cycloparaffin. None of the hydrocarbons have a double bond, which results in high stability but less potential to react with other molecules. Figure 3.31d shows the structure of aromatics with double bonds in a cyclic arrangement, and Fig. 3.31e olefin, again with double bonds but in a more linear structure. These two kinds of hydrocarbon with double bonds are less stable but have a higher potential to react with other molecules. In a standard mineral

oil, the content of all kinds of paraffin is about 80–90%, the content of aromatics is in the range of a few percent to 20%, and the content of olefin is only in the range of 1%. The breakdown electric field varies between 200 and 350 kV/cm, which is about ten times higher than air and about three times higher than SF<sub>6</sub> at 1 bar. One of the disadvantages of mineral oil is ageing, supported by oxygen, humidity, high temperature, and catalysts such as copper or other metals. Also, the missing environmental compatibility counts as a disadvantage of mineral oil, even if in any case a protection against environmental contamination for high-voltage apparatus exists. Another disadvantage of mineral oil is the high flammability and, therefore, another kind of fluid generated interest in the 1930s for the insulation of transformers, and this was polychlorinated biphenyl. The advantages were the flame-resistant behavior and a similar relative permittivity to paper. However, the disadvantage of polychlorinated biphenyl is the generation of high toxic components like dioxins, and, therefore, production was stopped in the 1980s.

A replacement for mineral oil, as well as for polychlorinated biphenyl, is an ester fluid, which exists in two types, synthetic ester and natural ester. Besides the advantages of low flammability and environmental compatibility, the water solubility of ester is much higher compared to mineral oil, and, therefore, the influence of moisture in the fluid on the electric breakdown performance is less important. Much research was carried out concerning the behavior of new fluids as a replacement for mineral oil with respect to electric and ageing characteristics. In some cases, further fluids like silicon oil, castor oil, rape seed oil, coconut oil, sunflower oil, or palm oil, were included in the investigations [3.23–26]. In recent years, synthetic ester fluids were used more and more, and also natural esters from different manufacturers are now in service as insulation fluids for high-voltage power transformers [3.27]. Ester fluids are environmentally friendly fluids and belong to the class of fluids that are *slightly hazardous to water*. The increasing use of ester fluids delivers more experience and also more information concerning diagnosis methods, which are well developed for mineral oil and can be probably transferred to ester fluids.

The increase of the requirements on a fluid in a transformer regarding ageing behavior, higher electric stress, the influence of sulfur, and higher system voltages (up to 1200 kV AC and 1100 kV DC) has resulted in a synthetic fluid based on gas-to-liquid technology. The fluid has the structure of an isoparaffin without any defects compared to a natural isoparaffin, and, therefore, the performance is in many characteristics better, such as the higher flashpoint, the low loss factor, and a very low sulfur content [3.28].

### 3.5.3 Solids

Similarly to fluids, solids have several tasks in high-voltage apparatus. The main part is the use as a design element with strong mechanical characteristics. Other tasks are the separation of different fluids or gases and use as dielectric medium with a high relative permittivity. There are various types of solids, and it is not possible to cover them all in this chapter. Therefore, a selection of solids will be handled with particular importance for high-voltage engineering and further information concerning chemical, thermal, and mechanical characteristics is available in the relevant literature, which covers about 100 years of research on solids [3.29, 30].

#### Inorganic Solids

The group of inorganic solids includes porcelain, glass, and mica. All these are characterized by a high temperature resistance and insensitivity to chemical influences, climatic influences, irradiation, and partial discharges. Furthermore, some of these solids have a very high mechanical strength. Porcelain is the main solid for air-insulated systems like overhead lines, substations, surge arrestors, or post insulators. However, in future porcelain will become increasingly replaced by so-called composite insulators. The characteristic of porcelain with respect to thermal strength, electrical strength, or mechanical strength can be modified to a certain limit by a mixture of the three components feldspar, responsible for electrical strength, quartz, responsible for mechanical strength, and kaolin, responsible for thermal strength. Regarding mechanical strength, porcelain has a strong mechanical strength for pressure but a much lower one for bending, and the ratio is about 1/7. For some specific applications, it should be noted that porcelain is sensitive to fast temperature changes. Glass, where the main component is quartz (SiO<sub>2</sub>), can replace porcelain in some applications, for example, as overhead insulators, but for high-voltage applications, glass should have a very low content of alkali, and it should contain boron oxide to reduce the melting point of the mixture. Glass can also be used in the form of fibers to enhance the mechanical strength of polymers. Mica is a natural mineral and is used as mica lamination on tapes or in polymers for the insulation of the windings of rotating machines due to its high resistance to partial discharges, and high mechanical and thermal strength.

#### Polymers

Polymers for high-voltage applications contain a large number of molecules, where the connections of the molecules can be in a line like a thread, in two dimen-

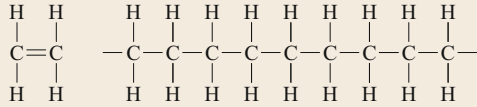


Fig. 3.32 Ethylene (left) and polyethylene (right)

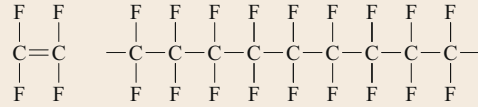


Fig. 3.34 Structure of tetrafluoroethylene (left) and polytetrafluoroethylene (right)

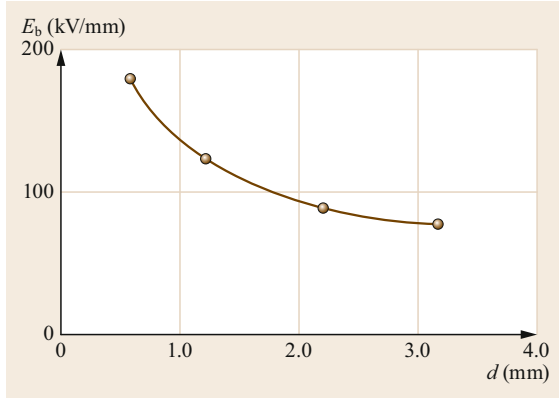


Fig. 3.33 Electric breakdown field strength  $E_b$  as function of thickness  $d$  of polyethylene (adapted from [3.7])

sions like an area, or in three dimensions like a cube. The characteristics are different, and the materials can be grouped into thermoplastics, elastomers, and duroplastics. The preparation of polymers is a poly reaction, where polymerization, polycondensation, and polyaddition are possible. Thermoplastics can be melted and formed again, while duroplastics cannot be melted, and above the glass transition temperature the material remains elastic, and a further increase in temperature leads to thermal destruction. Polyethylene was used at the beginning of the replacement of fluid-impregnated paper insulation for high-voltage cables. Figure 3.32 shows the molecule structure of ethylene and polyethylene.

The connection between the chains of polyethylene leads to so-called cross-linked polyethylene, which has a better thermal performance than polyethylene and is nowadays the standard polymer insulation material for high-voltage cables. Belonging to the same family of polymers, polypropylene in combination with paper and fluid was developed for high-voltage cables for DC transmission in the voltage range up to 700 kV. The electric breakdown field of polymers depends strongly on the thickness of the test sample. As an example Fig. 3.33 shows the electric breakdown field  $E_b$  as function of the thickness of polyethylene.

The manufacturing procedure of polyethylene differs with respect to the low-pressure procedure, which results in a high-density polyethylene (HDPE), and the high-pressure procedure, which results in a low-density

polyethylene. The very high electric performance of polyethylene can be seen in Fig. 3.33, where the electric field strength for 2 mm thickness is about 100 kV/mm or 1000 kV/cm, which is about three to four times higher than mineral oil and about ten times higher than SF<sub>6</sub> at 1 bar. At the beginnings of the application of polyethylene a problem arose, which was called *water treeing*. Conductive structures were built under the influence of the electric field and in combination with diffused humidity, and they looked like a tree. These water trees resulted in so-called *electrical trees*, and finally in a breakdown of polymer insulation. This problem is now solved by a watertight design of high-voltage cables, through the use of very clean polyethylene material and a manufacturing process with threefold extrusion of the inner and outer conductive layers and insulation material.

Polyvinyl chloride (PVC) is another polymer that has been for high-voltage cables up to 30 kV, but it is nowadays mainly used for low voltage cables. PVC requires some addition of a plasticizer to be flexible and tensile, but in combination with Cl molecules the loss factor increases and excludes PVC as an insulating material for high-voltage cables above 30 kV. PVC is still used for cable sheaths. One critical characteristic of PVC is the diffusion of the plasticizer with time.

Polymers with fluorine molecules form another group of polymers. Figure 3.34 shows the polymer polytetrafluoroethylene (PTFE) as an example.

This polymer has a good thermal performance and a very low loss factor, but it is very sensitive to partial discharge, which is of consequence in the low electric field strength for stress endurance. A combination of fluorine containing polymer forms two further so-called copolymers. The copolymer tetrafluoroethylene-hexafluoropropylene (FEP) is a mixture of tetrafluoroethylene (10–50%) and hexafluoropropylene (90–10%) where the characteristics can be modified by the mixture ratio. The copolymer perfluoroalkoxy (PFA) is a combination of tetrafluoroethylene and perfluoropropylvinylether and has the same characteristics as PTFE.

Polymers with only C–H as chemical bonds are limited in their thermal performance, because the continuous service temperature should not be significantly higher than 100 °C. Polymers with benzene rings, oxy-

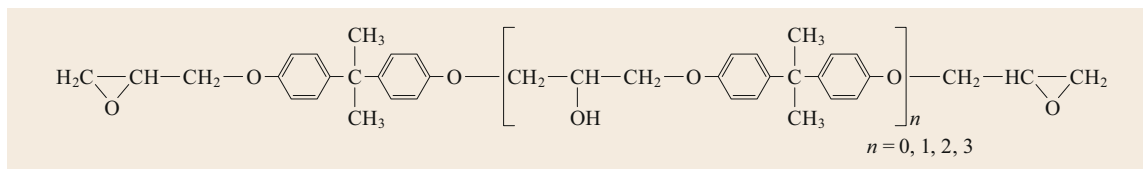


Fig. 3.35 Chemical structure of bisphenol A-based epoxy resin

gen, nitrogen, and sulfur allow much higher continuous service temperatures. Polyimides (PI) belong to this group of polymers, with a continuous service temperature of 250 °C; polyamides (PA) show a strong mechanical performance with respect to the tensile strength and toughness and abrasion resistance, and their applications are electrical and mechanical stress components in high-voltage apparatus. The different kinds of polyamides are characterized by the length of the carbon strings, for example PA 6 or PA 12.

Polymer compounds of silicone are exceptional elastic, flexible, and nondeformable. Depending on the temperature at the crosslink, two types of silicone exist: RTV silicone with crosslinking at room temperature and HTV with crosslinking at higher temperatures. Silicones are inflammable and resistant against chemicals, climatic influences, and ageing, but swell up and lose their mechanical strength in combination with some kinds of mineral oils. With fillers like titanium oxide or with soot, the characteristics of silicone can be modified, and typical applications are prefabricated cable joints of silicone with an in-built electric field grading by conductive silicone cones. An outstanding characteristic of silicone is its hydrophobicity, which qualifies silicone as insulation material for outside insulators, often in combination with reinforced glass fiber epoxy resin rods to cover both the mechanical and the electric strength. The hydrophobicity characteristic keeps for a long time, and even pollution will not influence this performance.

A polymer with similar characteristics to silicone is the copolymer ethylene propylene (EPR), often modified with diene and known as EPDM. The advantage of this polymer is the resistance to water and electrical treeing [3.31].

In the group of polymer resins, epoxy resin is the dominant material. In general, epoxy resins contain resin and hardener as the main components, but also catalysts, fillers, pigments, and flexibilizers. Therefore, a large number of epoxy resins exist with tailored characteristics for the relevant applications. The combination of bisphenol A and epichlorohydrin is the most-used epoxy resin in high-voltage applications. The chemical structure is shown in Fig. 3.35.

Dicarboxylic anhydrides are often used as hardener in combination with flexibilizers in order to compensate

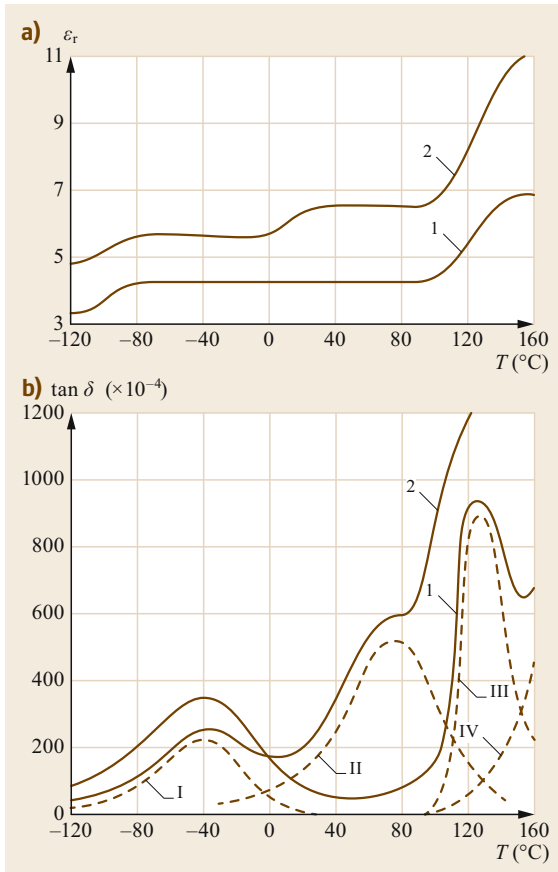
or at least reduce the mechanical tension for a material combination metal epoxy resin with different expansion coefficients. Examples of dicarboxylic anhydrides are phthalic anhydride (PSA), hexahydrophthalic anhydride (HHPSA), and methylhexahydrophthalic anhydride (MHHPA), and for flexibilizers, polyols and glycidyl ester. For all combinations it should be taken into account that flexibilizers compromise electric performance and heat distortion. Fillers have the task to improve the mechanical characteristics, to reduce the exothermic processes during the manufacture of epoxy resin insulators with a large volume, and to reduce the price. Quartz powder ( $\text{SiO}_2$ ) is a common filler, but in  $\text{SF}_6$ -insulated apparatus aluminum oxide ( $\text{Al}_2\text{O}_3$ ) or dolomite are used, because in the case of discharges in the gas-insulated system, partial discharges, or arcs, the filler will not be attacked by a decomposition product of  $\text{SF}_6$ .

The manufacture of epoxy resin entails a chemical reaction between resin and hardener, and later a processing of the mixed material. Due to the sensitivity of voids within a polymer, the preparation of the material and manufacturing procedure should be done under vacuum. Different technologies exist, like casting, pressure gelation or an injection molding process, or impregnation, whereby the choice of the technology depends on the manufacturing time, the type of object, and the requirements.

The characteristics of epoxy resin concerning the mechanical, thermal, and electrical performance depend on the kind of epoxy resin and the manufacturing processes, for example weathering and UV (ultraviolet) radiation lead to a reduction of the mechanical performance and tracking resistance for bisphenol A-based epoxy resin. Furthermore, the loss factor and the relative permittivity of epoxy resin depend on the glass transformation temperature, and as well as on the service temperature. Figure 3.36 shows the relative permittivity and the loss factor of two types of epoxy resin as a function of the temperature.

It can be seen that a maximum of the polarization mechanism leads to an increase of the relative permittivity, and that with addition of a filler, here quartz powder, a further maximum, area II, appears. The measurement of the loss factor over the temperature allows the determination of polarization mechanism; however,



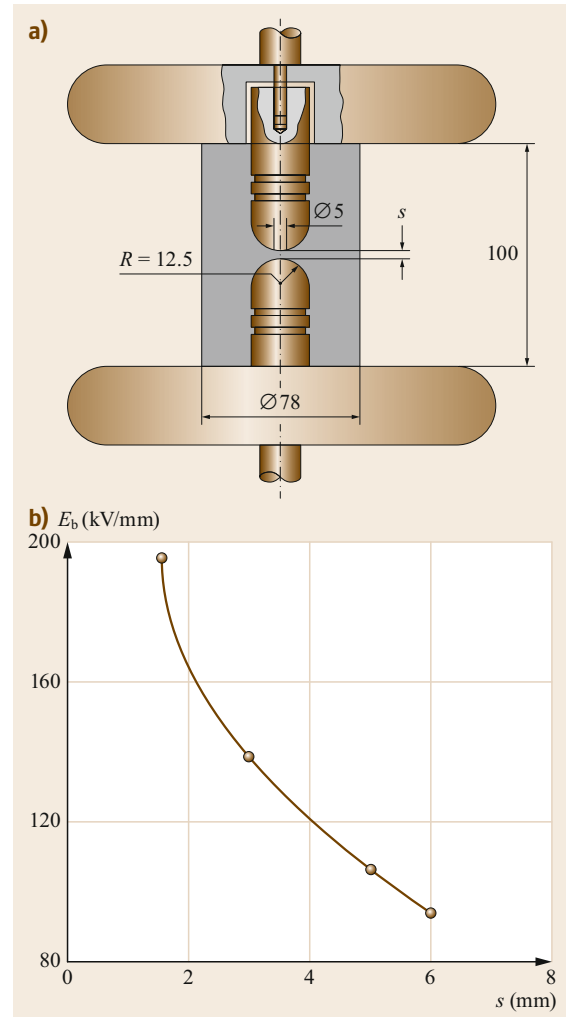


**Fig. 3.36a,b** Relative permittivity  $\epsilon_r$  and loss factor  $\tan \delta$  as functions of the temperature  $T$  (1 – pure epoxy resin, 2 – filled epoxy, I – area of small polar chain segments, II – area of boundary polarization, III – area of larger polar chain segments, IV – area of ion conduction) (adapted from [3.7])

the maxima are not always detectable. Therefore, the measurement of the relative permittivity gives a clearer picture of the polarization effects. The electric field strength also influences the loss factor and the relative permittivity. With an increase of the electric field, the loss factor and the relative permittivity also increase, and the increase is stronger the higher the temperature.

The conductivity of epoxy resin under DC stress is constant up to a certain electric field strength and increases with temperature and the addition of filler. With increasing electric field strength the conductivity increases exponentially, and this effect starts at a lower electric field strength with increasing temperature.

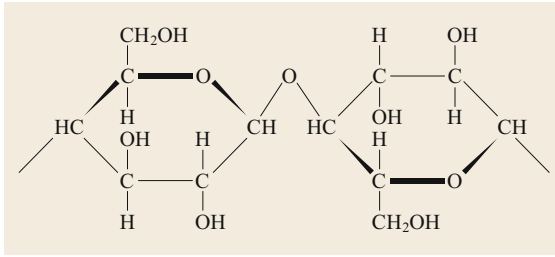
Similarly to the breakdown behavior of fluids, the volume of the tested samples influences the breakdown voltage. Figure 3.37 shows the short time breakdown electric field of a sphere–sphere electrode arrangement



**Fig. 3.37a,b** Breakdown electric field strength  $s$  at 50 Hz AC for a sphere–sphere gap with unfilled epoxy resin as a function of the gap distance  $s$  and gap volume: (a) electrode arrangement, (b) breakdown electric field strength (adapted from [3.7])

as a function of the gap distance and volume under stress, with a pure unfilled epoxy resin. This arrangement represents a more or less uniform electric field distribution. The voltage rise was 3 kV/s to prevent a thermal breakdown.

Unlike a void in a fluid, where the void can possibly move by fluid flow, a void in a solid is locally fixed, and if partial discharges occur in the void, the possible deterioration is always at the same place. The deterioration may erode the solid and finally lead to a total breakdown of the solid. The time for this process may vary from several minutes up to several years, and this effect is called erosion breakdown, as shown in



**Fig. 3.38** Structure of cellulose

Fig. 3.26. Another effect that may influence the interpretation of partial discharge measurements is the fact that in a closed void in solids, partial discharges increase the gas pressure. Then, according to Paschen's law, see Fig. 3.21, the inception voltage for partial discharges increases. As a consequence, partial discharges disappear, assuming that the applied voltage is constant, until the gas pressure in the void is reduced by diffusion, and then partial discharges appear again.

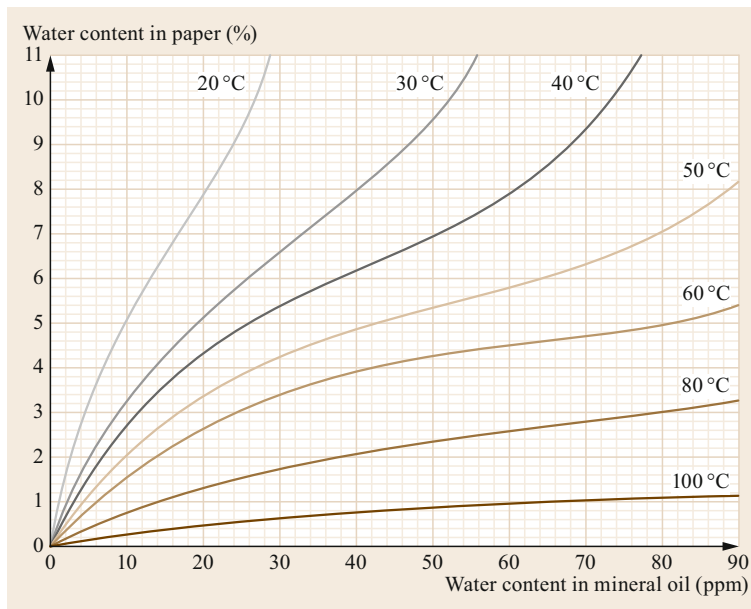
Another group of solids are polyurethanes (PU), which are mainly used in low or medium-voltage applications. The electric performance is lower compared to epoxy resin, but leakage current resistance is high, and viscosity and elasticity are very good. The rheological behavior is also good, and, therefore, polyurethanes are often used for void-free impregnation.

### 3.5.4 Impregnated Solids

Polymers exhibit a high electric performance, and this characteristic can be used if the polymers are thin foils

and impregnated with a gas or fluid. The most-used impregnated solid is paper in combination with a fluid, mineral oil, or ester fluid. Paper is based on cellulose, which is a molecule with a number of elements connected as a string. Figure 3.38 shows the chemical structure of a cellulose molecule.

Cellulose molecules are connected via an oxygen atom. If paper strings are cut, the free oxygen atoms build up together with two hydrogen atoms water molecules  $H_2O$ , and according Fig. 3.23, this may influence the breakdown voltage of the impregnation fluid. The length of the paper string is also a measure of the mechanical strength. New paper for the insulation of power transformers has a string length of about 1200 molecules. The end-of-life for such paper is reached at a string length of about 200. The relative permittivity of cellulose is 6.1, and, therefore, it should be taken into account that the electric field distribution in a paper-fluid combination is given by the relative permittivity of the different materials, and the electric field stress is higher for the fluid than for the paper. As an example, in a cellulose-mineral oil combination, the electric field stress in oil is higher than in paper ( $\epsilon_{r,oil} = 2.2$ ,  $\epsilon_{r,cell} = 6.1$ ). Humidity is a main factor affecting the electrical and mechanical performance of fluid and paper, and, therefore, both paper and fluid should be dry. After generation of cellulose from the raw material wood, for example spruce or pine, the cellulose is cut and macerated. Undesired constituents are removed by washing with water. Afterwards, a careful drying of the cellulose and very often a compression are performed to manufacture paper foils and pressboard elements. The drying



**Fig. 3.39** Water concentration in paper as a function of the water concentration in mineral oil [3.32]

process, as well as the impregnation process, should be done under vacuum in order to remove as much as possible of the remaining humidity and to fill up all voids with impregnation fluid. It is recommended to use more than a layer of paper as an insulation system, because imperfections are unavoidable in paper foils, and these represent weak points in the insulation.

The combination of mineral oil and paper is the dominant insulation system for power transformers, and with respect to the humidity, it is very important to know the humidity concentration in the two components. Figure 3.39 shows the water concentration in the paper as function of the water concentration in the mineral oil with the equilibrium temperature as a parameter.

The water content in paper is in the range of %, but the water in mineral oil is in the range of ppm. Furthermore, it can be seen that water moves from paper to mineral oil if the temperature increases, and vice versa if the temperature decreases. The curves in Fig. 3.39 are only valid for an equilibrium of the temperature, and depending on the size of the transformer, this requires a long time at a constant temperature. However, it is important to realize that in a transformer at 100 °C, water moves from the paper to the mineral oil. If the

transformer is switched off and cools down, the water will move to the paper, but this requires time, and in the meantime the relative water content in the mineral oil is high, and a breakdown may occur if the transformer is switched on again.

Another impregnated solid, mainly used for transformers but also for indoor substations, is resin-bonded paper (RBP). Several layers of paper are bonded with resin, typically phenol or cresol, nowadays also epoxy resin (void-free resin-impregnated paper (RIP)), and manufactured as a preproduct for plates, tubes, and differently shaped pieces. A similar material combination is known as a transformer board. A large number of paper layers are bonded in a hot-pressing procedure. The product is pure cellulose, which can be used and impregnated with fluids. The shaped piece combines the high electrical performance of soft paper with the high mechanical performance of RBP. A further advantage of transformer boards is that also complex elements like angular rings and pipe elbows can be directly manufactured.

A new group of impregnated solids is the combination of aramid fiber with a fluid. Aramid fibers are synthetic and have a lower mechanical performance than paper but can be used at higher temperatures.

## 3.6 Test Techniques

High-voltage equipment is tested at different stages of development and manufacturing. The first step is the test at the design stage, usually on a prototype. Then follows a so-called design test on regularly manufactured equipment in order to check all design criteria and compliance with the relevant standards, national or international. Furthermore, the test results are used to have a record of performance for the relevant equipment. There are many tests for nonelectrical parameters, but only electrical tests will be described in the following chapters. Routine tests are carried out on every piece or, depending on the evaluated quality of manufacturing, on a random or fixed selection of the manufactured pieces. Finally, after transportation and assembly, an on-site test is done in order to detect damage during transportation or failure during assembly. This test is usually called the acceptance test, but the routine test can also be a kind of acceptance test. The test voltages are AC, DC, or impulse voltage, and are in some cases combined with measurements of some parameters that may contain some information about the status of the insulation. The performance of the test voltage sources can be different for factory or on-site tests, depending on the requirement and availability [3.33].

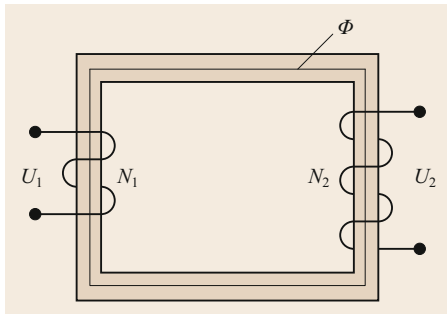
The IEC standard [3.2] defines a test voltage by its amplitude, frequency, and/or shape within specified tolerances. It also describes preferred test voltages, but it may sometimes be necessary to modify the frequency or shape of the test voltage in order to enable testing of the test object.

### 3.6.1 AC Voltage

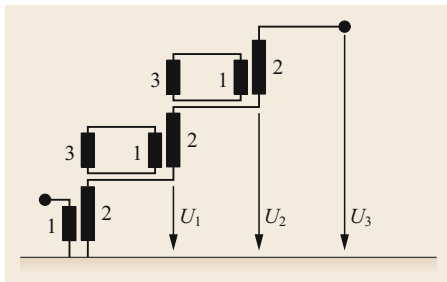
Alternating voltage is defined by its rms value and/or by its peak value, depending on the purpose. For a pure sinusoidal wave form, the relation between the peak value  $\hat{U}$  and the rms value  $U$  is given by the square root of 2. This relation is also used in the recommendations [3.2] to define the tolerance of the sinusoidal wave shape by the following equation

$$\frac{\hat{U}}{U} = \sqrt{2} \pm 5\% . \quad (3.60)$$

For short time stress, the flashover or breakdown behavior of insulating material depends on the peak value of the voltage supplied. At a longer stress time or under service stress, the rms value is very often the most im-



**Fig. 3.40** A voltage transformer ( $\Phi$  – magnetic flux,  $N$  – number of windings)



**Fig. 3.41** Equivalent diagram of a three-stage transformer cascade (1 – primary winding, 2 – secondary winding, 3 – tertiary winding)

portant parameter for the breakdown. This depends on the thermal behavior of the insulating material and the loss characteristics.

The ratio of the basic frequency and the harmonics of different order define the wave form of AC voltage. For the measurement, the harmonics should be taken into account, particularly because some measurement systems use the peak value in order to evaluate the rms value. This is becoming increasingly important due to the increase of power electronics, which generates a higher harmonic content. AC voltage can be generated by a very simple circuit. Figure 3.40 shows a simplified equivalent diagram of a voltage transformer.

The ratio of the number of windings defines the ratio of the two voltages  $U_1$  and  $U_2$ , and, therefore, theoretically every voltage ratio can be reached by a single-stage transformer. The nonlinear behavior of the insulation performance leads to the generation of high AC voltage by means of a transformer cascade, reducing the cost of the insulating material, and for using a flexible combination of a number of single transformer units. Figure 3.41 shows a typical three-stage cascade arrangement with identical units. Each unit needs only the insulation for a single-stage transformer.

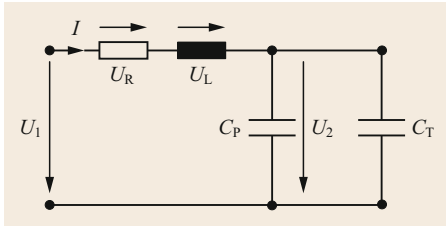
The short-circuit impedance and the harmonic content as functions of the load are the important param-



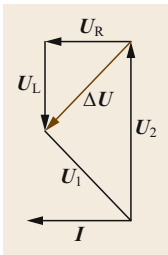
**Fig. 3.42** AC transformer cascade for 1000 kV with a voltage divider (courtesy of BTU Cottbus-Senftenberg)

eters for an AC voltage generator. The short-circuit impedance, given in percent, represents the voltage drop under full load conditions. It is assumed that the resistive part is negligible in comparison to the inductive part. For a cascade, the short-circuit impedance is higher than the sum of the short-circuit impedances and increases more than linearly with the number of stages.

The combination shown in Fig. 3.41 can also be used with two transformers at the bottom stage and one transformer at the second stage. Thus, giving a higher output current, but at a lower output voltage. The use of each unit as a single transformer or the combination of the units offers a number of possibilities. Concerning the power distribution within a cascade, it is important that the primary winding of the first stage should be designed to carry the full output power of the cas-



**Fig. 3.43** Equivalent diagram of a transformer with capacitive load ( $U_1$  – input voltage, referred to the high-voltage side,  $U_2$  – output voltage, across the capacitive load,  $I$  – transformer current,  $C_T$  – capacitor, representing the transformer capacitance,  $C_P$  – capacitor, representing the load capacitance)



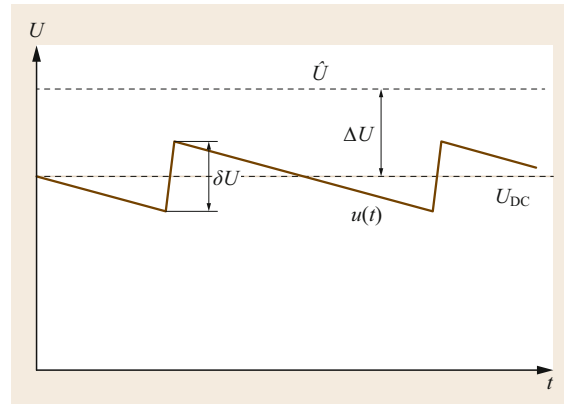
**Fig. 3.44** Vector diagram of a transformer with capacitive load

cade. In all stages, the secondary windings are loaded with the same power. They are calculated by the output power divided by the number of stages, assuming that all transformers are identical. The tertiary winding of the first stage is loaded with two-thirds of the output power. In all other stages, the windings are loaded with the relevant load distribution within the transformer. Figure 3.42 shows an AC transformer cascade with a voltage divider for 1000 kV.

For AC voltage generation by a transformer, another factor is the voltage increase due to the capacitive load. This is usually the case for AC test objects. The vector diagram for a simplified transformer circuit is shown in Fig. 3.43, where all elements are referred to the high-voltage side.

The output voltage  $U_2$  can normally be calculated using the ratio of the windings, but the voltage  $U_2$  is higher than calculated. This is demonstrated by the vector diagram shown in Fig. 3.44.

An increase of the output voltage due to the capacitive load is normally undesirable. Nevertheless, for AC tests, the increasing voltage can be used to reduce the input voltage or the size of the test equipment. If the capacitance of the load including the transformer capacitance and the inductance of the transformer including the circuit inductance are equal, the circuit is in resonance, and the output could theoretically increase up to infinity. Because of the resistance in the circuit, the voltage will be limited. The ratio between the input voltage



**Fig. 3.45** Parameters of DC voltage

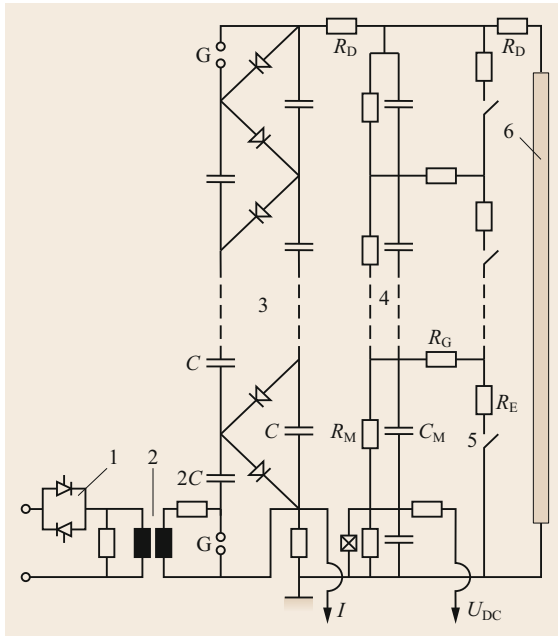
and the output voltage can be very high, up to 100, and the necessary active power is very low.

The resonance conditions can be used for voltage tests by changing the inductance of the circuit, which results in resonance conditions at constant frequency. Alternatively, changing the frequency results in resonance conditions at different frequencies. With this type of test equipment, test objects with very high capacitance can be tested with a reasonable size and power of the test equipment. In all cases, the regulation of the test system should be adapted very carefully to the required voltage level to avoid overshooting of the test voltage.

### 3.6.2 DC Voltage

A direct voltage is defined as the mean value between the highest and lowest levels within a time period. The duration of the period depends on the generating system. Figure 3.45 shows a typical example of DC voltage generated by rectification of AC voltage.

The DC voltage  $U_{DC}$  is the arithmetic mean value of the voltage  $u(t)$ . The voltage drop  $\Delta U$  is the difference between the peak voltage of the AC power supply and the DC voltage. This is given by the so-called *internal impedance* of a multiple stage rectifier. The ripple  $\delta U$  is the difference between the highest and lowest values of  $u(t)$ . It represents the charging of the capacitors by an AC source during the conductive period of the diodes and the discharging of the capacitors by the load during the nonconductive period of the diodes. It should be taken into account for the design of the diodes that the charging time is much shorter than the discharging time, and the charging current is much higher than the discharge current. According to [3.2], the value of the ripple  $\delta U$  should be less than 3% of  $U_{DC}$ . The main parameters influencing the ripple are the frequency of the AC supply voltage, the value of the smoothing capaci-



**Fig. 3.46** Equivalent diagram of a multiple-stage rectifier (1 – thyristor controlled voltage regulation, 2 – high-voltage transformer, 3 – rectifier with diodes, charging and smoothing capacitors, 4 – resistive voltage divider with grading capacitors, 5 – discharging and grounding device, 6 – test object,  $C$  – charging or smoothing capacitor,  $C_M$  – grading capacitor of the measuring resistor,  $R_M$  – measuring resistor,  $R_D$  – damping resistor,  $R_E$  – earthing resistor,  $R_G$  – grading resistor of the earthing switch)

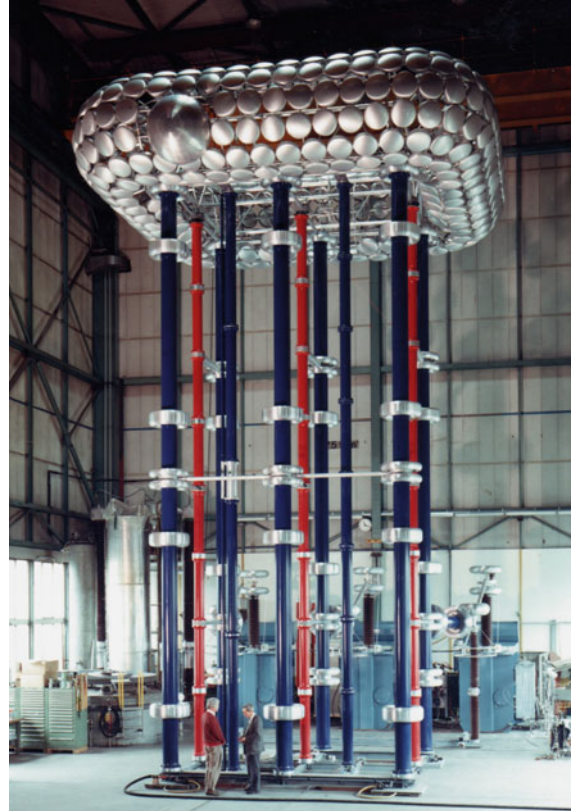
tance, and the load current. For small load currents, the ripple can be estimated by

$$\delta U \approx \frac{I}{fC} \frac{N}{4} (N + 1), \quad (3.61)$$

where  $I$  is the load current,  $f$  the frequency of the AC power supply,  $C$  the smoothing capacitance, and  $N$  the number of stages of a multiple-stage rectifier. Equation (3.61) depicts that the ripple increases linearly with the load current and quadratically with the number of stages. It decreases with increasing frequency and smoothing capacitance. The voltage drop  $\Delta U$  influences only the mean value  $U_{DC}$  of a DC generator and also depends on the design of the generator. For a multiple stage generator, the voltage drop can be estimated according to

$$\Delta U \approx \frac{I}{fC} \frac{N}{3} (2N^2 + 1), \quad (3.62)$$

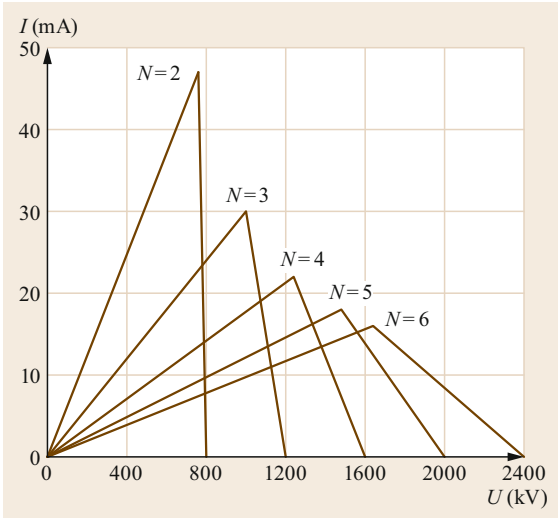
with the same parameters as in (3.61).



**Fig. 3.47** DC generator for 1200 kV and 2 A (courtesy of Haefely Test AG)

Equation (3.62) shows that the increase of the voltage drop  $\Delta U$  is by the cube power of the number of stages  $N$ . This can be accounted for by choosing the adequate no-load voltage of the generator and a fast voltage-regulating system. Therefore, the highest requirements are made in DC pollution tests, where the load current can change very rapidly from some mA up to some A. Thus, the voltage should be kept stable within given limits requiring a strong AC power source, a large smoothing capacitance, and a fast regulation system. A multiple-stage rectifier and its main components are shown in Fig. 3.46. Some measures to reduce the ripple  $\delta U$  can be gained from (3.61). Normally, the voltage drop  $\Delta U$  is no problem for the test generator, because it can be adjusted by proper design and the no-load output voltage. Figure 3.47 shows a DC generator with a three-phase AC supply for 1200 kV DC and a current of 2 A for pollution tests with DC.

During DC voltage tests, the voltage drop on polluted insulators may influence the test results due to the fast change of load. Therefore, the transient behavior of the voltage regulator should be controlled in case of high load current. The energy supply has to be regulated



**Fig. 3.48** Output current  $I$  as a function of the output voltage  $U$  at 3% ripple;  $N$  = number of stages (400 kV rated voltage)

very fast by feeding the current from the smoothing capacitor, from the main power supply, or from both. The dependence of the number of stages, the maximum load current, and the output voltage for a standard multiple-stage rectifier is shown in Fig. 3.48. It has a no-load voltage of 400 kV per stage.

### 3.6.3 Impulse Voltage and Current

The peak value and its time parameter define an impulse voltage or current. For reproducible results in impulse voltage tests, the wave shapes are defined in general recommendations [3.2] or device-related descriptions are given in [3.34, 35]. The generation of an impulse voltage or current as in Fig. 3.2 or Fig. 3.5 is generally accomplished by the charging and discharging of capacitors through resistors. This gives an impulse, which can be described by two exponential functions.

Figure 3.49a shows a simplified equivalent circuit for impulse voltage generation without any inductance.

Figure 3.49b shows a similar circuit but with a different arrangement of the resistors, which is commonly used.

In both circuits, a wave shape that represents the sum of two exponential functions is generated. The ratio of the output voltage or the voltage across the load capacitor  $C_1$  and the input charging voltage  $U_0$  is different. In a circuit of type A, Fig. 3.49a, the voltage across the load capacitor can be calculated with (3.63), neglecting the influence of the inductance of the circuit and the discharge through the resistor  $R_e$  during the charging time of  $C_1$

$$u(t) = U_0 \frac{C_s}{C_s + C_1} \frac{R_e}{R_d + R_e} \quad (3.63)$$

The output voltage is not only given by the ratio of the capacitor but also by the ratio of the resistors. In circuit type B Fig. 3.49b, the output voltage is only determined by the capacitors and is, therefore, higher than in circuit A according to

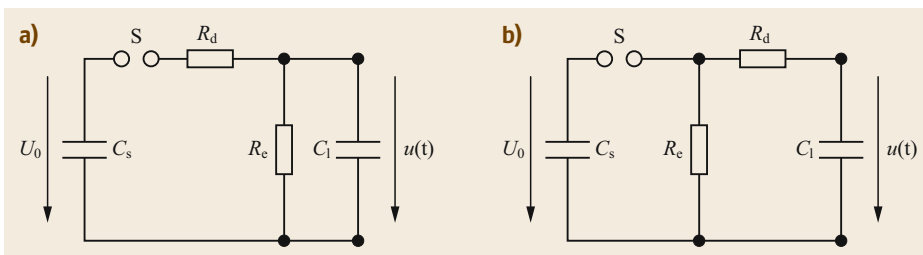
$$u(t) = U_0 \frac{C_s}{C_s + C_1} \quad (3.64)$$

An empirically-based estimation of the real output voltage  $u(t)$  of the circuit type B) is given by

$$u(t) = U_0 \frac{C_s}{C_s + C_1} 0.95, \quad (3.65)$$

which also uses the damping effect of the resistors.

For a given capacitance of  $C_1$ , the front time is determined by the load capacitance and the damping resistance. The front time can be adjusted by variation of the damping resistance, assuming that the load cannot be changed. The time to half-value is mainly determined by the earthing resistance and the impulse capacitance, assuming that the impulse capacitance is



**Fig. 3.49a,b** Simplified equivalent circuit of an impulse-generating circuit type A (a) and B (b). ( $C_s$  – charging or impulse capacitor ( $C_s \gg C_1$ ),  $R_d$  – damping resistor,  $R_e$  – earthing resistor ( $R_e \gg R_d$ ),  $C_1$  – load capacitor (test object, divider, etc.),  $S$  – spark gap)

much higher than the load capacitance. Then, a reasonably high output voltage is reached. For tests with a standard lightning impulse, the value of the resistance should be calculated depending on the test object and the generator to be used. The mathematical description of the circuit leads to a differential equation whereby the solution of the differential equation is not consistent, and, therefore, assumptions for the time constant  $T_f$  (front time) and the time constant for the tail  $T_t$  (time to half value) are given in the following equations

$$T_f \approx R_d \frac{C_s C_1}{C_s + C_1}, \quad (3.66)$$

$$T_t \approx R_e (C_s + C_1). \quad (3.67)$$

The relations of the time constants  $T_f$  and  $T_t$  to the relevant time parameter for the front time  $T_1$  and the time to half-value  $T_2$  (Fig. 3.2) for a standard lightning impulse  $1.2/50 \mu\text{s}$  are

$$T_1 = 2.96 T_f, \quad (3.68)$$

$$T_2 = 0.73 T_t. \quad (3.69)$$

For a standard switching-impulse voltage  $250/2500 \mu\text{s}$  (Fig. 3.4), the relations to the time to peak  $T_p$  and the time to half value  $T_2$  are

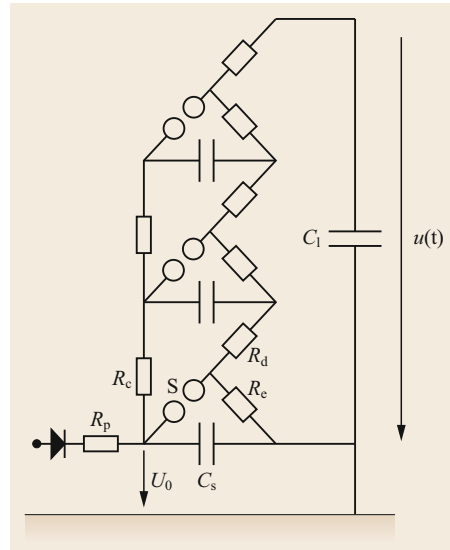
$$T_1 \approx 2.41 T_f, \quad (3.70)$$

$$T_2 = 0.87 T_t. \quad (3.71)$$

Impulse voltages with high amplitude are normally generated with a multistage impulse generator, called the Marx generator after the inventor. The generator's principle is the parallel charging of a number of impulse capacitors followed by discharging of these capacitors in series. The equivalent simplified circuit, again for the type B circuit, is shown in Fig. 3.50.

The most important part for high reproducibility of the impulse shape and amplitude is the behavior of the spark gap S. The breakdown process and time of a spark gap depend on the uniformity of the electrical field. Therefore, sphere gaps are generally used. With an electrode material of tungsten for reduction of surface damage by the arc, it is also necessary that the breakdown of the spark occurs at the same charging voltage to generate impulses with identical amplitude and time parameters. Triggering the spark gap is the method of choice.

Two methods may be used: triggering at a constant distance of the spark gap or triggering at a constant voltage. For the first method, the spark gap should have a distance that is larger than the breakdown distance at the desired voltage. The impulse capacitors are



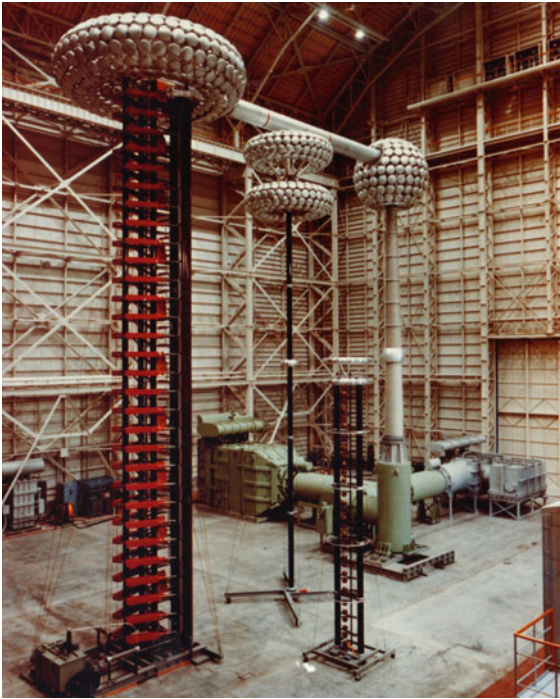
**Fig. 3.50** Simplified equivalent circuit of a multistage impulse generator ( $C_s$  – charging or impulse capacitor per stage ( $C_s \gg C_1$ ),  $R_d$  – damping resistor per stage,  $R_e$  – earthing resistor per stage ( $R_e \gg R_d$ ), S – spark gap per stage,  $C_1$  – load capacitor (test object, divider, etc.),  $R_p$  – protection resistor)

charged in parallel up to the required charging voltage and reach the full charging voltage at different times, which should be taken into account. When all capacitors are fully charged, the gap is reduced, and the breakdown takes place at the flashover distance, which is constant for a given charging voltage. Then all capacitors are connected in series through the spark gaps and the damping resistors  $R_d$ , and they charge the load capacitor  $C_1$  and generate the impulse by discharging later on through the earthing resistors  $R_e$ .

The second method is more frequently used and is based on a triggering device within the bottom spark gap. The spark gap distance is slightly longer than the required breakdown distance. Then the impulse capacitors are charged up to the preselected voltage and kept constant. A trigger impulse at the bottom spark gap generates a breakdown of the bottom spark gap, and due to natural overvoltage in the other stages, all spark gaps flash over. This method has a high reproducibility and reliability, in particular for transformer impulse tests, where a comparison between impulses at different charging voltages is required.

For the evaluation of the required charging voltage of an impulse generator, the so-called efficiency factor is helpful, which is defined as the ratio of the output voltage to the total charging voltage of the generator. In (3.65), the common efficiency factor for lightning





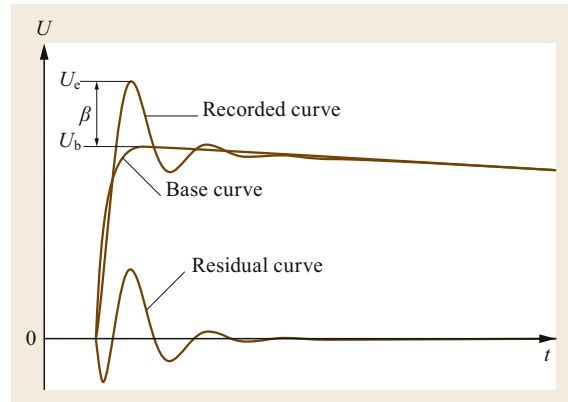
**Fig. 3.51** 6 MV impulse generator (courtesy of Mitsubishi Electric Corporation)

impulses is about 0.95, whereas this factor can go down up to 0.5 for switching impulses. Figure 3.51 shows an impulse generator with 6 MV charging voltage together with an impulse divider and a chopping device.

Furthermore, the total inductance of the test circuit is also important for lightning impulses. For an aperiodically damped impulse consisting of two exponential functions for the front and the tail, a minimum value of the resistance can be calculated according to

$$R_d = 2 \sqrt{L \frac{\frac{C_s}{n} + C_l}{\frac{C_s}{n} C_l}}, \quad (3.72)$$

with  $L$  as the inductance of the complete circuit,  $C_s$  the charging capacitance per stage,  $n$  number of stages, and  $C_l$  the total load capacitance. With the given impulse and the load capacitor, the damping resistor for an aperiodically damped impulse is determined by the inductance. At a given front time, the required damping resistor may be lower than for an aperiodically damped shape. Then the impulse may show some oscillations if the inductance cannot be reduced due to the size of the test circuit and the inner inductance of the capacitors.



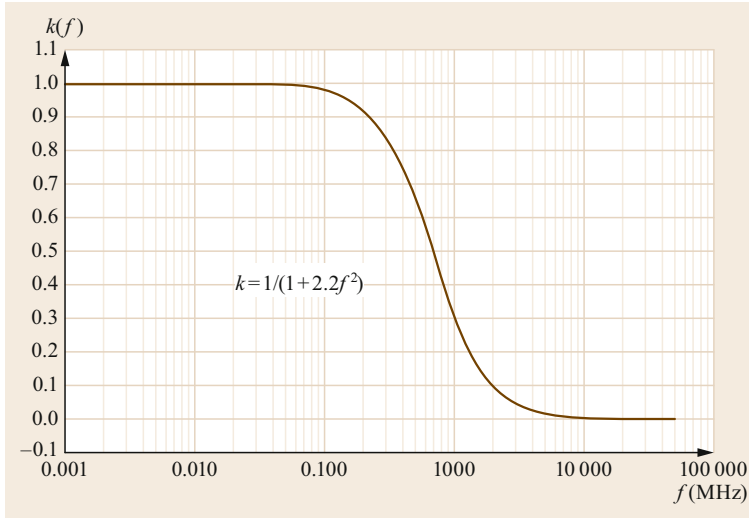
**Fig. 3.52** Example of a lightning impulse with overshoot (adapted from [3.2])

In [3.2], the time parameters and the allowed oscillations or overshoot for lightning-impulse voltages are defined, and an evaluation procedure is also described. As an example, Fig. 3.52 shows a lightning-impulse voltage, where the resistance is lower than for the aperiodically damped case, and an overshoot occurs in the peak area. In order to increase the reproducibility of the evaluation of the test voltage, a so-called test voltage factor  $k$  was introduced to prevent the discontinuity in a former version of [3.2].

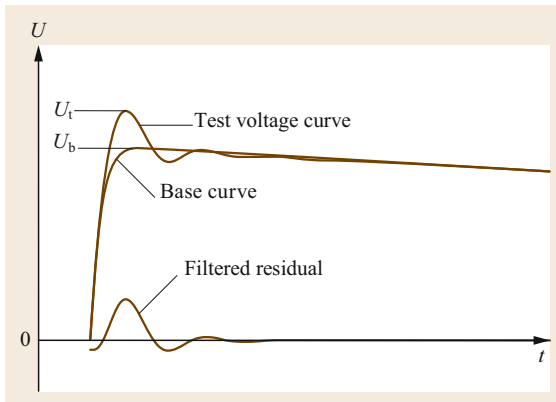
The recorded curve has an extreme value  $U_e$  and an overshoot  $\beta$  above the base curve, calculated as the difference between  $U_e$  and  $U_b$ . The allowed relative overshoot magnitude is 10% of the extreme value  $U_e$ . The evaluation of the base curve is given in [3.2] based on the assumption that the impulse voltage is composed of two exponential functions, and that the recorded curve is available in digital form. The difference between the recorded curve and the base curve is shown as a residual curve. Investigations on the breakdown behavior of materials have demonstrated that the frequency content of the oscillation should be taken into account, and from these investigations, the  $k$  factor was developed [3.36, 37]. Figure 3.53 shows the  $k$  factor as a function of the frequency of the overshoot or oscillation and the approximate function.

The  $k$  factor represents a mean value of the influence of overshoot on the breakdown behavior of air, SF<sub>6</sub>, mineral oil, and polyethylene. The filtering of the residual curve with the  $k$  factor function is shown in Fig. 3.54 together with the ascertained test voltage curve, which is the sum of the base curve and the filtered residual curve. The test voltage  $U_t$  is, then, the highest magnitude of the test voltage curve.

The limits for a standard lightning impulse with the tolerances given in [3.2] are physically given by the in-



**Fig. 3.53** The  $k$  factor as a function of the frequency  $f$  of overshoot or oscillation (adapted from [3.2])



**Fig. 3.54** Determination of the test voltage curve (adapted from [3.2])

ductance and the capacitance of the test object and can be approximated as

$$R_d = 2 \sqrt{L \frac{\frac{C_s}{n} + C_1}{\frac{C_s}{n} C_1}} \approx 2 \sqrt{\frac{L}{C_1}} \quad \text{for } \frac{C_s}{n} \gg C_1. \quad (3.73)$$

Usually, the capacitance of the load  $C_1$  varies, and, therefore, the resistance  $R_d$  should be adapted. Large impulse generators may have 20–30 stages, and this also requires 20–30 resistor elements. Therefore, a customized selection of resistors and a clever design of the interconnec-

tion of the resistors within one stage can optimize the impulse generator. For example, with two resistor elements and the possibility of parallel and serial connections, four magnitudes of resistances are possible.

Impulse currents are generated similarly to an impulse voltage [3.38], the main difference being that the capacitors are all connected in parallel, thus increasing the capacitance and reducing the inductance of the circuit. Since the steepness of the current impulse depends on the derivative of the current as shown in (3.74),

$$\frac{di}{dt} = \frac{U}{L}, \quad (3.74)$$

current impulses with short front times need special arrangements of the capacitors. Here,  $U$  is the charging voltage and  $L$  the inductance of the complete test circuit. Although a lower inductance leads to a higher steepness of the current, in many cases, the inductance is fixed, and the steepness can only be adapted by increasing the charging voltage, which should be realized by a sophisticated design of the current generator [3.39].

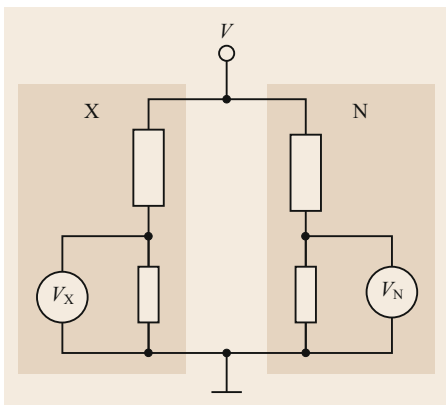
From the many activities within CIGRE and IEC, the most important ones from the point of view of test techniques for ultra-high-voltage (UHV) equipment are the requirements on the overshoot and front time due to large test circuits, wet tests, the time-to-peak of the switching-impulse voltage due to the breakdown voltage minimum as a function of the time-to-peak for large air-gap distances and the atmospheric and altitude correction factors.

## 3.7 Measuring Techniques

Because the amplitudes are high, and they cannot be measured directly with conventional measuring and recording systems, the measurements of voltage and current in high-voltage tests are difficult to obtain. Furthermore, not only the peak value but also the shape of the signal should be measured and evaluated. This requires an adequate recording system. Generally, a high-voltage or high-current measuring system consists of converting, transmission, and recording devices. A measuring system is as good as the weakest part of the system, and, therefore, it is not necessary to ask for exceptional performance of one of the components. The amplitude of the signal to be measured should be reduced by the converting device to a value suitable for transmission and recording. The output signal of the converting device must be an exact replica of the input signal with respect to the wave shape and time parameters. This requirement is very strong in many cases, and, in addition, measurement uncertainty should be estimated and evaluated carefully.

The converting device is usually the critical component due to its transfer behavior and physical size. The preferred calibration method is by comparison with an approved measuring system under normal operating conditions shown in Fig. 3.55.

The comparison with an approved measuring system results in an uncertainty with respect to the evaluation and output of the system to be calibrated. The calibration should reach at least at 20% of the rated operating voltage of the converting device. For example, a reference measuring divider for impulse voltage with a rated voltage of 500 kV can be used to calibrate a converting device up to 2500 kV. However, the linearity of the converting device between the calibration



**Fig. 3.55** Arrangement for comparison measurements ( $V$  = applied voltage; system  $N$  = reference system; system  $X$  = system to be calibrated) (adapted from [3.40])

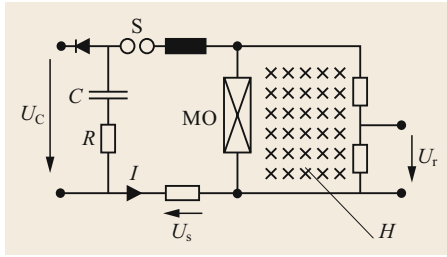
voltage level and the rated voltage of the converting device must be checked. This is even more important for the testing of UHV equipment, where lightning-impulse voltages up to 2700 kV and switching-impulse voltages up to 1950 kV are used [3.1].

Stability within the specified range of operating conditions, keeping the scale factor of the measuring system constant over long periods, is a further important requirement for converting, transmission, and recording devices. The dynamic behavior of a converting device should preferably be evaluated by an amplitude/frequency response measurement or by a unit step response measurement.

The performance of an approved measuring system is given by its uncertainty budget [3.40]. The individual uncertainty of the scale factor measurement, the linearity check, the dynamic check, the short and long-time behavior, the ambient temperature effect, and the proximity effect compose the uncertainty budget. If software is used for the evaluation of the parameters, then also the uncertainty of the software should be taken into account. Depending on the voltage shape, the uncertainties may contribute differently to the total uncertainty budget. Therefore, in [3.40], the evaluation procedure for the uncertainty budget of the different types of voltages like DC, AC, and impulse voltage is described.

The transmission device is generally a coaxial cable, which should not influence the amplitude. In special cases, it does influence the transfer behavior of the complete measuring system. The recording device is very often equipped with an additional converting device on its input. Again, this is to reduce the amplitude, but this converting device is small and normally has sufficiently good transfer behavior. The transformation characteristics are normally not critical, but they should be checked and included in the evaluation of the entire system.

Particularly at high voltage or high current, an important problem for all measuring systems, is the sensitivity to electromagnetic interferences. The most critical tests are impulse tests, where the impulse generation is at the same time a radiation source of an electromagnetic wave. This wave penetrates the whole system – the converter, the transmission, and the recording device – and not all components can be properly shielded. Thus, reducing the amplitude of the radiation and increasing the signal level in order to get a very high signal-to-noise ratio is mandatory. Nowadays, recording devices are analog–digital converters instead of analog devices. A careful selection should be made for moving coil instruments (mean average value) or moving iron instruments (RMS value).



**Fig. 3.56** Metal oxide residual voltage measuring circuit ( $U_C$  – charging voltage of capacitor  $C$ ,  $C$  – charging capacitor,  $R$  – damping resistor,  $S$  – spark gap,  $MO$  – metal oxide surge arrester,  $U_r$  – representing the residual voltage across the surge arrester,  $U_s$  – voltage across the shunt, representing the current  $I$ ,  $I$  – current through the surge arrester,  $H$  – magnetic field in the residual voltage measuring loop)

Another source of electromagnetic interference are voltages and currents floating within the test object and measuring cables, because they can induce voltages by capacitive or inductive coupling or by loops of the measuring cable. Proper shielding, or in special cases, double shielding of the measuring and control cables, prevention of loops by a star connection of all measuring and control cables and compensation of unwanted effects like magnetic fields can reduce the electromagnetic interference. The residual voltage measurement of a metal oxide arrester is a typical example. In this case, the high magnetic field induces a voltage in the loop, which is superimposed on the residual voltage. Figure 3.56 shows the schematic diagram.

If the earth connection of the divider cannot be changed for some reason, a suitable connection of the voltage divider is necessary, because the magnetic field  $H$  induces a reasonable voltage in the residual voltage measuring loop. A simple check is the replacement of the surge arrester by a metallic tube with the same geometry and the application of a current impulse. In this case, the measured residual voltage across the metallic tube should be close to zero.

Variations of the scale factor or of a parameter of a measuring device, due to proximity effects, should be considered and can be determined by measurements performed for different distances of the device from earthed walls or energized structures.

The simplest device for voltage measurement are standard air gaps [3.3], but they have some disadvantages. First of all, the information about the magnitude of the voltage can only be reached if a breakdown of the air gap occurs. Furthermore, at impulse voltages only the peak value can be evaluated but not the time parameter. In [3.3], tables showing the breakdown voltage as a function of the gap distance and in the case of spheres

as electrodes of the sphere radius. For DC, a rod–rod electrode arrangement is a requirement, for all other voltage forms a sphere–sphere arrangement. With the tables and a tape measure, the applied voltage can be evaluated and with certain care, an uncertainty of 3% can be reached, if the atmospheric correction factors are carefully used.

### 3.7.1 Voltage Measurement

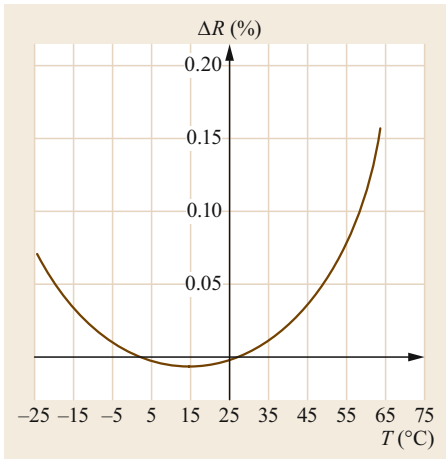
#### DC Voltage

The main parameter of a DC voltage is the amplitude, but often the deviation from the ideal DC voltage, defined as ripple, is important (Fig. 3.45). The uncertainty for the amplitude measurement is 3%, for the ripple less than 10% of the ripple amplitude or 1% of the arithmetic mean value of the DC voltage, whichever is larger.

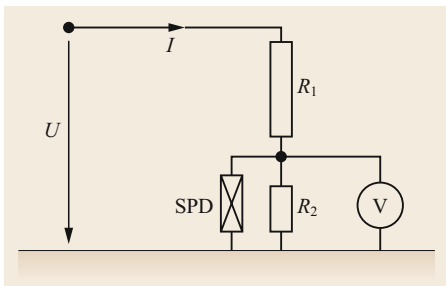
A simple measuring device is a high ohmic resistor and a current measuring device in series. The current through the resistor is proportional to the applied voltage, and it is recommended that the current be as high as 0.5 mA at the rated voltage to ensure that the influence of leakage current is negligible. For safety reasons, it is necessary to have a surge protective device in parallel to the measuring device, because in the case of disconnection of the measuring cable or flashover of the high-voltage resistor, the full voltage will be applied to the measuring device. A high-voltage resistor normally consists of many elements that are connected in series. The resistance of each element has a voltage and temperature coefficient, and both influence the magnitude of the resistance and, therefore, the uncertainty of the measurement. Under normal conditions, the voltage and temperature coefficients do not play an important role. However, for very small measuring uncertainties, the temperature coefficient must be taken into account, because it has a greater influence than the voltage coefficient. Figure 3.57 shows the relative change of the resistance as function of the temperature for a carefully selected number of resistor elements. The relative change of the total resistance is less than 0.05% in the temperature range between  $-20^\circ\text{C}$  and  $+50^\circ\text{C}$ , but each resistor element may have a larger coefficient than that allowed for the complete chain.

Another way for compensation of the effect of the voltage and temperature is by the use of voltage dividers. Since the elements in the high-voltage and low-voltage part are subject to the same voltage and temperature stress, this type of measuring device is commonly used as a high-voltage DC measuring technique. Figure 3.58 shows the simplified equivalent circuit diagram.

In the case of fast transient voltages, the distribution is important because even in DC test systems



**Fig. 3.57** Relative resistance change as a function of temperature



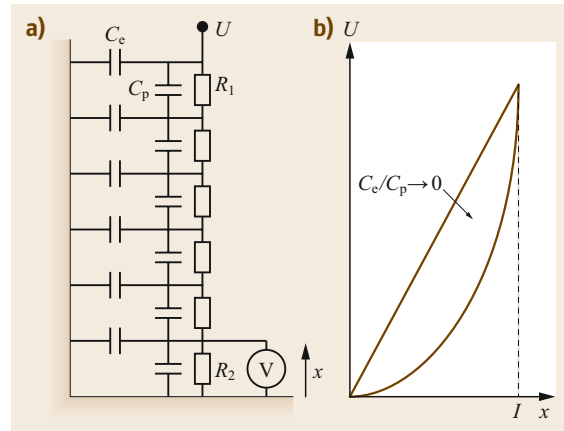
**Fig. 3.58** DC voltage divider ( $U$  – DC voltage,  $I$  – DC current,  $R_1$  – high-voltage arm resistor,  $R_2$  – low voltage arm resistor, SPD – surge protective device,  $V$  – voltage measuring device with very high resistance)

a breakdown with a very fast voltage change may occur. A resistive divider as shown in Fig. 3.59 has a linear voltage distribution as long as the frequency is near zero for DC or AC at very low frequency. When the stray capacitances  $C_e$  start influencing the voltage distribution, e.g., in the case of higher frequency content in the voltage, the voltage distribution is no longer linear.

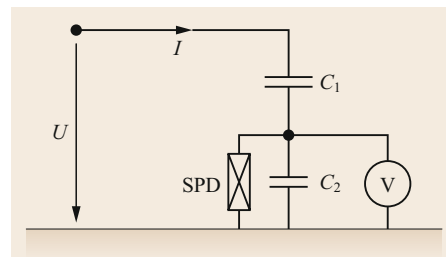
The voltage distribution is strongly influenced by the ratio of the stray capacitances. The voltage distribution becomes more and more nonlinear, if the parallel stray capacitance decreases, or the earth stray capacitance increases. When designing a pure resistive voltage divider, this phenomenon should be taken into account. Adding capacitors in parallel to the resistors can keep the ratio  $C_p/C_e$  high is one of the measures.

### AC Voltage

The main parameter of AC voltage is amplitude, but here also the rms value is often used, particularly for the evaluation of energy and thermal aspects. In some



**Fig. 3.59a,b** Resistive divider with stray capacitances (**a**) and shape of voltage distribution (**b**) ( $U$  – DC voltage,  $R_1$  – high-voltage resistor,  $R_2$  – low voltage arm resistor,  $C_p$  – parallel stray capacitance,  $C_e$  – earth stray capacitance,  $V$  – voltage measuring device with very high resistance,  $x$  – distance from ground potential)



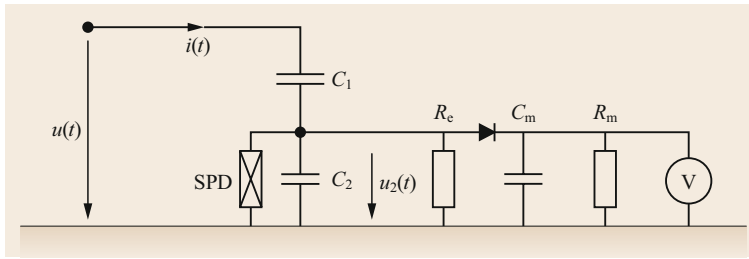
**Fig. 3.60** AC voltage divider ( $U$  – AC voltage,  $I$  – AC current,  $C_1$  – high-voltage arm capacitor,  $C_2$  – low voltage arm capacitor,  $V$  – voltage measuring device with very high impedance, SPD – surge protective device)

cases, the frequency should be taken into account, but for electric energy systems, 50 or 60 Hz are the common frequencies. If the voltage shape is purely sinusoidal, the relation between the peak value and the rms value is given by

$$\frac{\hat{U}}{U} = \sqrt{2}. \tag{3.75}$$

This ratio can be changed if the AC voltage contains higher frequencies than the operating frequency, and the allowed deviation is 5%. The uncertainty for AC voltage measurement is 3%.

A capacitive voltage divider, which is not influenced by the temperature and voltage coefficient of the capacitors, will normally be used for AC measurements. Figure 3.60 shows the simplified equivalent circuit diagram.



**Fig. 3.61** AC peak value measuring circuit with a capacitive divider ( $u(t)$  – AC voltage,  $i(t)$  – AC current,  $C_1$  – high-voltage arm capacitor,  $C_2$  – low-voltage arm capacitor,  $R_e$  – earthing resistor,  $R_m$  – measuring resistor,  $C_m$  – measuring capacitor,  $u_2(t)$  – measured voltage, V – voltage measuring device with very high impedance, SPD – surge protective device)

The divider output voltage is given by the ratio of the capacitors according to

$$V = U_2 = U \frac{C_1}{C_1 + C_2 + C_i}, \quad (3.76)$$

with  $C_i$  the capacitance of the measuring instrument.

The measured voltage is the rms value. In some cases, the peak value is of interest, or the rms value is evaluated from the peak value measurement according to (3.75), which is only correct if the applied voltage is sinusoidal. In any case, an additional uncertainty should then be accepted. The peak value of a voltage can also be measured with a capacitive voltage divider similar to what is depicted in Fig. 3.60 and with a supplement shown in Fig. 3.61.

The measuring instrument shows the peak value of the voltage when the measuring capacitor  $C_m$  is charged up to the peak value of  $u_2(t)$ . This is only a part of the high voltage  $u(t)$  given by the divider ratio. It is desirable that the series resistance of the diode is small and, thus, gives a negligible voltage drop across the diode. Mainly three parameters influence the uncertainty of measuring the peak voltage measuring circuit. The transformation ratio is influenced by resistor  $R_e$ , the resistor  $R_m$  discharges the measuring capacitance  $C_m$ , and during the charging time, the capacitor  $C_m$  is in parallel with the capacitor  $C_2$  and changes the capacitive transformation ratio. The latter two factors are, additionally, frequency dependent. Fortunately, for all these influences, compensation measures exist.

Nowadays, the measurement of the peak value is only carried out by an analog digital converter as the recording device. The integrated computer can make more calculations, e.g., fast Fourier transformation (FFT) and can evaluate the amplitudes of the relevant harmonics. With the 12-bit resolution of a commercially available digital recorder, the measurement uncertainty of the recording device is negligible compared

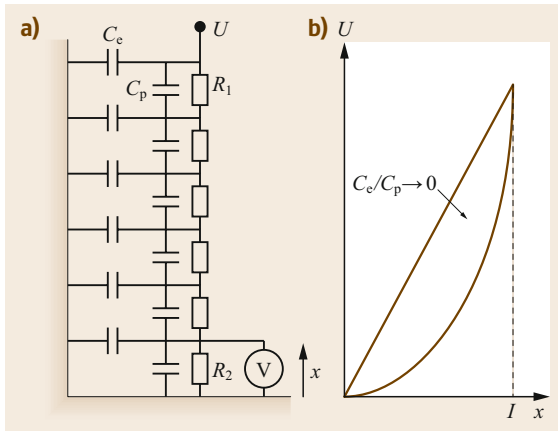
with the other components of the measuring system. IEC recommendations for DC and AC measurements with digital recorders are under preparation [3.3].

### Impulse Voltage

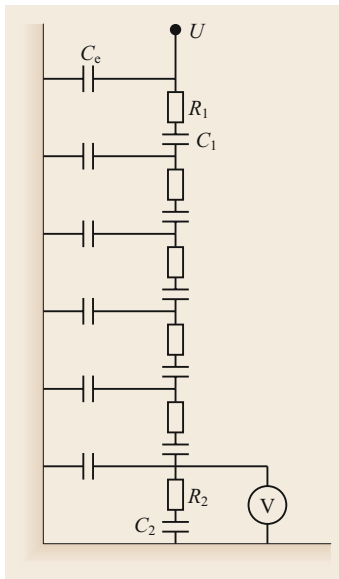
Impulse voltages require a measurement system having a known scale factor and an adequate dynamic behavior. This is because not only the peak value but also the wave shape should be recorded and evaluated. Under certain conditions for impulse measurements, resistive dividers can be used. If the resistance is low enough, the transfer behavior is not influenced by the stray capacitance. A good estimation of the time constant  $T$  of the unit step response characterizing the transfer behavior is given by  $T = (RC_e)/6$ , where  $C_e$  is the stray capacitance and  $R$  the resistance of the divider. The stray capacitance and the resistance should be as small as possible. Because of the low resistance of the measuring system with resistive dividers, the wave shape of the impulse may be changed so that no switching impulses can be measured. Therefore, resistive–capacitive dividers are the common divider type for the measurement of impulse voltages. Figure 3.62 shows the schematic, which is the same as for DC measurements (Fig. 3.59) regarding fast voltage changes.

If the time constants in the high-voltage  $R_1 C_p$  and the low-voltage arm  $R_2 C_p$  are identical, the divider is frequency independent. Nevertheless, the inductance caused by the high-voltage lead, and the capacitance of the divider built up of a series resonance circuit may cause oscillations. A combination of resistors and capacitors in series, in particular for high-voltage dividers with large dimensions, is a solution that is used very often. Figure 3.63 shows a so-called damped capacitive divider.

It is obvious that the divider is frequency independent if the time constants  $R_1 C_1$  and  $R_2 C_2$  are equal. Two types of damped capacitive dividers exist, the optimum damped divider and the slightly damped divider. For an



**Fig. 3.62a,b** Resistive–capacitive voltage divider (a) and voltage distribution (b) ( $U$  – impulse voltage,  $R_1$  – high-voltage resistor,  $R_2$  – low-voltage arm resistor,  $C_p$  – parallel stray capacitance;  $C_e$  – earth stray capacitance,  $V$  – voltage measuring device with very high impedance,  $x$  – distance from earthed floor)



**Fig. 3.63** Damped capacitive voltage divider ( $U$  – impulse voltage,  $R_1$  – high-voltage resistor of the  $n$ -element,  $R_2$  – low-voltage arm resistor,  $C_1$  – high-voltage capacitor of the  $n$ -element,  $C_2$  – low-voltage arm capacitor,  $C_e$  – earth stray capacitance,  $V$  – voltage measuring device with very high impedance)

optimum damped divider, the total resistance  $R$  can be estimated by

$$R \approx 0.2 \sqrt{\frac{L}{\frac{C_1}{n}}} \quad (3.77)$$

and leads to a resistance of 60–100  $\Omega$  for a divider in the MV range.

If the damped capacitive voltage divider is completed by a parallel column of resistors with the same

voltage distribution as the capacitive–resistive column, then this divider will be called a *universal* voltage divider because it can DC, AC, and impulse voltage measure.

For impulse voltage measurements, the measuring cable must match with its characteristic impedance. Recording devices such as oscilloscopes or analog digital converters show very high input impedance if the cable is directly connected to the deflecting system or the input divider. Then the characteristic impedance of the standard transmission system is at the beginning of the measuring cable. The equivalent circuit diagram for the low-voltage side of a capacitive divider is shown in Fig. 3.64, together with a compensated measuring circuit for a constant ratio at high and low frequencies [3.41, 42]. For a correct measurement, the requirement is given by

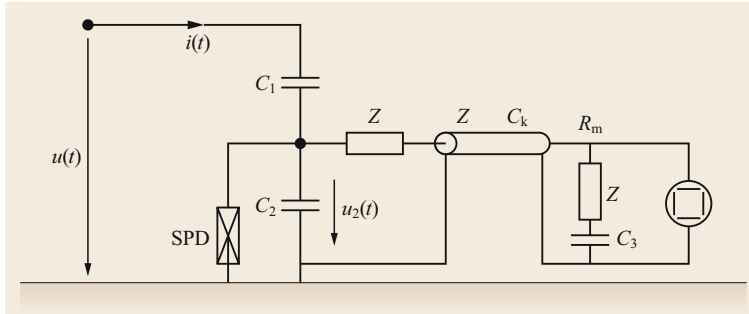
$$C_1 + C_2 = C_k + C_3 . \quad (3.78)$$

An oscilloscope, a peak voltmeter, or a digital recorder can be used for the evaluation or measurement of the peak value. The determination of the mean curve through oscillations according to the relevant recommendations is best accomplished by an oscillogram or digital record evaluation. In many cases, the highest amplitude recorded by a peak voltmeter is not sufficient, and the wave shape must be checked by an oscilloscope or a digital recorder. With an analog digital converter as the recording device, the full data set, amplitude, front time, and time to half-value can be evaluated, stored, and treated, depending on the need of the test.

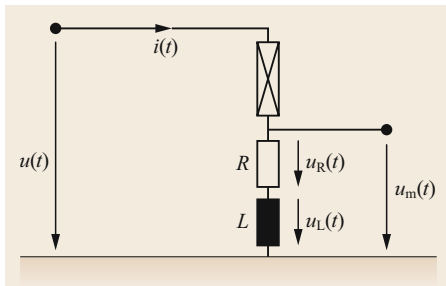
An indirect voltage measurement is the use of sensors like electro-optical sensors based on the so-called Pockels or Kerr effect. The sensitivity of these sensors is based on the polarization effect on light by the applied electric field. A further sensor is the capacitive electric field sensor, which can be three-dimensional in order to measure the electric field in space. If such a sensor is connected via fiber optics with the recording device, it can be placed anywhere in the high-voltage laboratory. The disadvantage of this sensor is the requirement to calibrate the sensor with another voltage measuring device at the precise and fixed position of the sensor, because any position change will change the relation between the measured electric field and the applied voltage.

### 3.7.2 Current Measurement

When the influence of the high magnetic field is considered, the measurement of an impulse current can be accomplished by measuring the voltage across a de-



**Fig. 3.64** Equivalent circuit of a capacitive divider with compensation of a long measuring cable ( $u(t)$  – impulse voltage,  $i(t)$  – impulse current,  $u_2(t)$  – impulse voltage across the low voltage capacitor,  $C_1$  – high-voltage arm capacitor,  $C_2$  – low-voltage arm capacitor,  $C_3$  – compensation capacitor,  $C_k$  – measuring cable capacitance,  $Z$  – characteristic impedance, SPD – surge protective device)



**Fig. 3.65** Impulse current measurement with a shunt ( $u(t)$  – impulse voltage;  $i(t)$  – impulse current;  $R$  – shunt resistor;  $L$  – shunt inductor;  $u_m(t)$  – measured impulse voltage representing the impulse current;  $u_R(t)$  – resistive part of the measured impulse voltage;  $u_L(t)$  – inductive part of the measured impulse voltage)

finer resistor. Current testing and measurements are described in [3.3]. Figure 3.65 shows a simplified measuring arrangement of the voltage drop across a resistor or shunt and considering the voltage induced by the magnetic field of the current flowing through the shunt.

The measured voltage  $u_m(t)$  consists of  $u_R(t)$  and  $u_L(t)$ . The part  $u_R(t)$  is proportional to the current  $i(t)$  but the part  $u_L(t)$  is proportional to the derivative of the current  $i(t)$  over time  $t$ . This should be compensated by the design of the shunt or by other means. The loss power and the mechanical forces, on the other hand, must be coped with by the proper design of a high impulse current shunt.

The so-called Rogowski coil is another technique for impulse current measurement. The measuring method is rather simple and is based on the induction of a voltage in a winding through changing magnetic field. The voltage is proportional to the change of the current. This needs integration, and it is necessary to obtain the current that can be gained by an RC circuit.

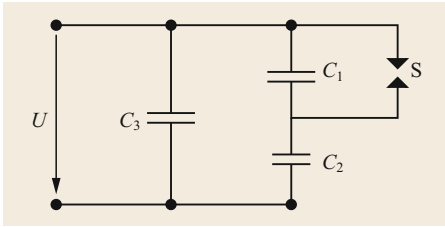
The advantage of the Rogowski coil is the potential-free measurement of the current [3.43].

An indirect current measurement is the use of sensors like Hall-probe or magneto-optical devices. The measurand is the magnetic field generated by a current and with calibration, these devices can be also used for current measurement.

### 3.7.3 Partial Discharge Measurement

A localized electrical discharge is called a partial discharge (PD). It bridges the insulation between conductors, which may or may not occur adjacent to a conductor [3.44]. Partial discharges are, in general, a consequence of local electric stress in the insulation or on the surface of the insulation. Usually, the discharges appear as pulses with durations of less than 1  $\mu$ s. Partial discharges are a sensitive measure of local electric stress, and, therefore, the measurement is very often used as quality check of the insulation. Before a complete discharge between conductors occurs, the inception of partial discharges gives information about the limit of the electric strength of the insulating material. Therefore, the insulating material can be tested without damaging or reducing its performance. Partial discharge measurements also imply that every stress of the insulation will influence the life expectancy of the material. A reasonable compromise between stress during measurement and the influence on lifetime should be found and fixed in the relevant standards for particular equipment, such as transformers, cables, switchgears, etc. As a typical nondestructive test, the partial discharge measurement can be used to examine the insulation's performance at the beginning of its service time. This includes the reduction of the performance during the service time by ageing, depending on numerous parameters such as electrical, thermal, and





**Fig. 3.66** Equivalent circuit for partial discharges ( $U$  = applied voltage at power frequency,  $C_1$  = capacitor representing the cavity,  $C_2$  = capacitor representing the insulating material around the cavity,  $C_3$  = capacitor representing the remaining insulating material,  $S$  = spark gap representing the discharge of the capacitor  $C_1$ )

mechanical stress. Different kinds of insulating material have different limits for the allowed partial discharge value at a given stress level. They are defined in the relevant recommendations. Particularly for solid insulators, where a complete breakdown damages the test object seriously, PD measurement is a tool for quality assessment.

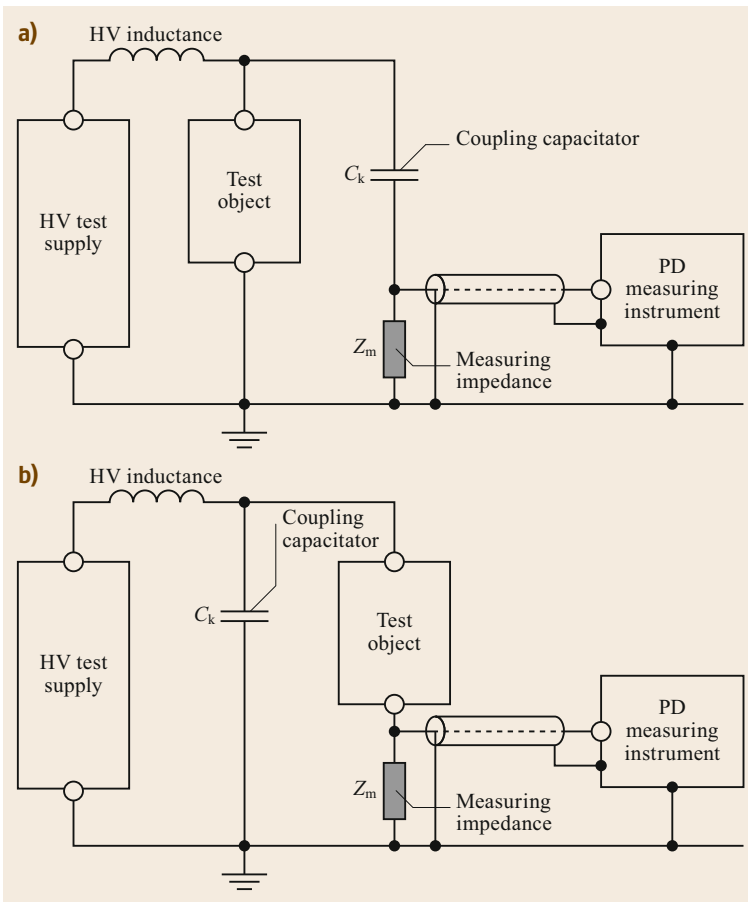
It is assumed that small cavities exist in the insulating material where discharges take place, which are the basis for the detection and measurement of PDs. This discharge causes a charge transfer in the whole circuit by an impulse-shaped current, which can be detected and measured. The relation of the discharge event and the phase angle of the applied voltage at power frequency are also important for the measurement. A simplified equivalent circuit for the PD is shown in Fig. 3.66.

The voltage across the capacitor  $C_1$  is given by

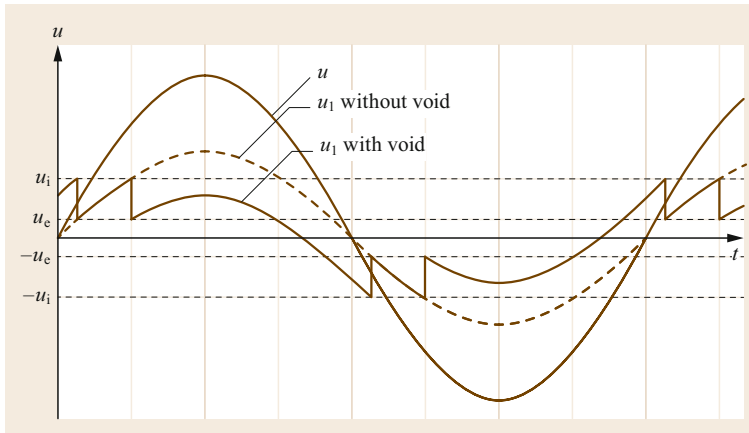
$$u_1 = U \frac{C_2}{C_1 + C_2}. \quad (3.79)$$

The capacitor  $C_3$  represents the part of the test object where no partial discharge occurs. In a real test setup, the capacitances of  $C_1$  up to  $C_3$  are within the test object, and a coupling capacitor  $C_k$  is added, as shown in Fig. 3.67.

The discharge of the spark gap  $S$  in Fig. 3.66 represents partial discharge, and this takes place when the



**Fig. 3.67a,b** Basic partial discharge measurement circuits: (a) measuring impedance  $Z_m$  in series with coupling capacitor  $C_k$ , common circuit; (b) measuring impedance  $Z_m$  in series with test object, not always possible (adapted from [3.45])



**Fig. 3.68** Voltage behavior of a void in a solid insulation system ( $u_i$  – inception voltage,  $u_e$  – extinction voltage)

voltage  $u_1$  has reached the so-called inception voltage. Under ideal conditions, the discharge process of the spark gap  $S$  needs no time, but for real arrangements, the discharge process is still very fast but can be neglected with regard to the timescale of the applied voltage. Due to the discharge of the capacitor  $C_1$ , the capacitor  $C_2$  is now stressed with the applied voltage  $U$ , and this causes a change of the charges. According to Figs. 3.66 and 3.67 there are three sources for the allocation of charges. The first source is the high-voltage test supply, but the inductance prevents the fast delivery of charges. The second source is the capacitor  $C_3$  in Fig. 3.66, but the capacitance and, therefore, the amount of charges which can be delivered is unknown. The third source is the coupling capacitor  $C_k$ , which is well known, and the delivered charges can be measured via the measuring impedance  $Z_m$ . It should be mentioned that the applied AC test voltage also charges the coupling capacitor  $C_k$ , but this happens with power frequency. The partial discharge effects are, however, in the range of ns or  $\mu$ s, and the separation from the power frequency occurs in the measuring impedance  $Z_m$ . In order to measure the charge of the partial discharge correctly, as much as possible, the charges delivered from the coupling capacitor should be much larger than the charges delivered from the voltage supply and the internal capacitor  $C_3$ , the capacitance of the coupling capacitor should in this respect be as high as possible. However, on the other hand, the coupling capacitor is a capacitive load of the high-voltage test supply, and this limits the magnitude of the capacitance.

Figure 3.68 shows the voltage behavior for the simplified capacitive equivalent circuit and a void in a solid insulation system.

Assuming that the applied voltage  $u$  is sinusoidal, the inception voltage for partial discharges  $u_i$  and the extinction voltage  $u_e$  are the same for positive polarity and negative polarity. According to (3.79), the voltage

$u_1$  across the capacitor  $C_1$  depends on the capacitance of  $C_1$  and  $C_2$ , which are both unknown. If there is no void, the voltage  $u_1$  follows the voltage  $u$ , but with a lower amplitude. If there is a void, and the voltage  $u_1$  is above the inception voltage  $u_i$ , then a discharge occurs, and the voltage drops to the extinction voltage  $u_e$ . After that, the voltage  $u_1$  increases again with the shape of the applied voltage  $u$ , until the inception voltage  $u_i$  is reached again. Finally, it can be seen in Fig. 3.67 that the discharges occur around the zero crossing of the applied voltage  $u$ , and this is a typical behavior of partial discharges in a void of solids. The simple capacitive model of a void in a solid is replaced by the so-called dipole model, which is described in detail in [3.45], with a view to explaining, for example, partial discharges in crosslinked polyethylene cables more precisely.

The electrical partial discharge measurement described is based on the assumption that the frequency content of partial discharges is high at much higher frequencies compared to the power frequency of 50 or 60 Hz. The PD measuring instrument in Fig. 3.67 should be able to record the high frequencies, and there is a differentiation between so-called narrow-band and wide-band partial discharge measuring systems. For a narrow-band system, the recommended middle frequency is between 50 kHz and 1 MHz, depending on the noise frequencies. The bandwidth is in the range of 9–30 kHz. For wide-band recording devices, the lower frequency limit is between 30 and 100 kHz, the upper limit between 130 kHz and 1 MHz, and the bandwidth in the range from 100 to 970 kHz [3.45]. These frequency ranges should be taken into account if a calibration of the test circuit is to be done. An impulse with a known charge is injected at the point where the partial discharge measuring circuit is connected with the test object. The frequency content of such an impulse should cover the frequency range of the recording de-

vice. The readout of the measuring instrument is then equivalent to the injected charge, and this has a relation to the signal that appears on the same accessible place of the test object and is called the apparent charge. The apparent charge is a charge generated by partial discharge within the test object and appears on the accessible points for measurement but may be influenced in amplitude and shape by traveling from the point of generation to the point of measurement.

The analog measuring devices for partial discharge usually delivers a mean value of the periodically appearing signals; and all the requirements in the actual recommendations are based on this performance and also on the experience. For example, an apparent charge of 10 pC for crosslinked cables at a voltage of  $1.5U_0$ , whereby  $U_0$  is the voltage between conductor and ground, is a convention based on scientific researches and on practical experience of the operators of cable systems [3.46]. With an analog digital recorder for partial discharge measurements, modifications of the existing recommendations are necessary due to the fact that now every partial discharge signal is recorded, and the question is how to handle this information. Partial discharge measurements generally suffer from noise and random noise signals, but their influence on the indication disappears when only the average is shown, which is reasonable from the test point of view. Furthermore, a digital record of partial discharges allows many more evaluations, which supply additional information [3.44].

Besides the detection of partial discharges, very often the location of the partial discharge source is also important. With acoustic or ultra-high-frequency sensors, the location of a partial discharge source, for example in a transformer, is possible by triangulation [3.47]. Another method is the calculation of the partial discharge signal behavior on the way from the source to the measuring point via a transfer function. With the measurement of the same partial discharge signal on bushing and the neutral point of a transformer, locating of the partial discharge source is possible [3.48]. For extensive equipment like cables, the partial discharge location can be found by evaluation of the traveling time, because a partial discharge signal travels from the source to the measuring point and to the end of the cable. Then the reflected signal also travels to the measuring point but with a delay depending on the length of the cable and the traveling speed within the cable. The partial discharge location can be calculated from the time difference.

There are also other technologies for partial discharge measurement or detection, like acoustic methods, ultra-high-frequency (UHF) measurements, optical measurements, and chemical analysis, for example dissolved gas analysis (DGA) measurements whose ap-

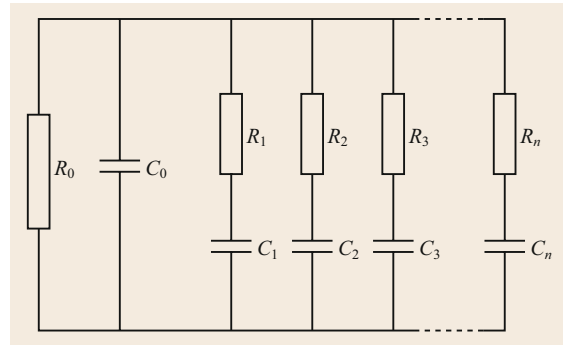


Fig. 3.69 Equivalent circuit for a solid

plications depend on the test object and the design. General information about acoustic and UHF methods for partial discharge measurements are available in [3.49].

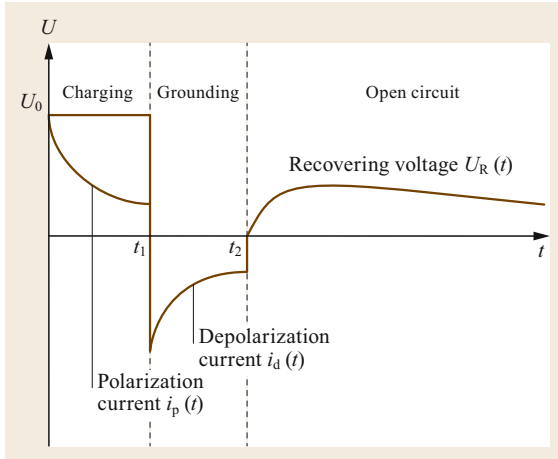
### 3.7.4 Measurement of Dielectric Characteristics

In contrast to partial discharge measurement and detection, which reveal local defects, the measurement of dielectric characteristics gives information about the integral characteristic of the insulation. This is, in general, less important for gas insulation but more important for fluids and solids, and the expectation from these measurements is the evaluation of ageing and rest-of-life time, whereby the test voltage and frequency can differ from the service conditions.

#### Response Measurements

A solid insulation can be described by a number of R-C combinations, representing the different kinds of polarization effects. If such a solid is stressed by a DC voltage, dipoles are oriented, and the resulting current is now caused by the conductivity of the material and the polarization effects. Figure 3.69 shows the equivalent circuit of a solid.

The procedure for the response measurement is to charge the test sample with DC for a certain time, then the DC source is disconnected, and the test sample short-circuited to discharge the main capacitor  $C_0$ . Afterwards, the voltage, called return or recovery voltage, can be measured as a consequence of the relaxation of the dipoles, oriented by the former DC voltage. The shape, the peak value, and the peak time can be used to evaluate the condition of the solid, for example the moisture of oil-impregnated paper insulation, by comparison with former measurements, but it is not possible to determine the absolute moisture content from only one measurement. Figure 3.70 shows the procedure and the relevant parameters.



**Fig. 3.70** General procedure for recovery voltage measurements

Instead of the recovery voltage, the so-called relaxation current can be measured, which also delivers some information about the condition of the solid, but also here a comparison with former measurements is necessary, and the temperature should be taken into account for both procedures.

**Loss Factor and Capacitance**

The loss factor has already been described in Sect. 3.4.5, and, therefore, only the measurement of the loss factor and the capacitance of a solid will be listed here. Figure 3.71 shows the classic Schering bridge, which is commonly applied for such measurements.

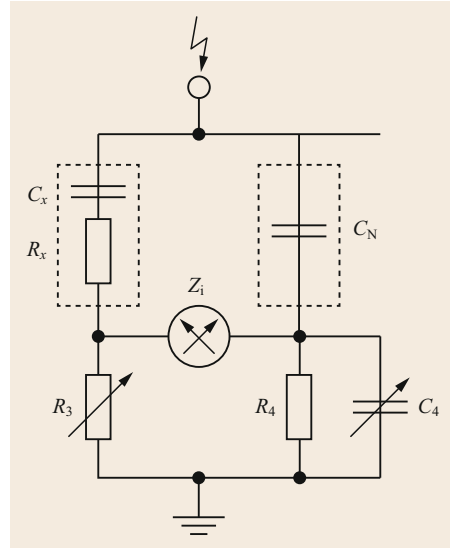
The equivalent circuit for the solid is the series connection of capacitor  $C_x$  and resistor  $R_x$ . The capacitor  $C_N$  is a reference capacitor that is very often called a standard capacitor, which should have a very low/negligible loss factor, usually a gas-filled capacitor. The elements in the dotted area are at high potential, whereas the others are at low potential, and this allows an operator to adjust the resistor  $R_3$  and the capacitor  $C_4$ . Protection devices against high voltage in the case of a breakdown of the test sample are not shown in Fig. 3.71.

If the zero indicators shows zero, then the left and right branches are in balance, and this can be expressed by the ratio of the impedances

$$\frac{Z_x}{Z_3} = \frac{Z_N}{Z_4} \quad \text{with} \quad Z_x = R_x + \frac{1}{j\omega C_x}$$

$$Z_N = \frac{1}{j\omega C_N}, Z_3 = R_3, \quad (3.80)$$

$$Z_4 = \frac{R_4 + \frac{1}{j\omega C_4}}{\frac{R_4}{j\omega C_4}}.$$



**Fig. 3.71** Schering bridge ( $R_x$  – unknown resistor of solid;  $C_x$  – unknown capacitor of solid,  $C_N$  – reference capacitor,  $R_3$  – variable resistor,  $R_4$  – fixed resistor,  $C_4$  – variable capacitor,  $Z_1$  – zero indicator) (adapted from [3.50])

After some calculations and a comparison of real and imaginary parts, the loss factor can be expressed as

$$\tan \delta = \omega C_4 R_4. \quad (3.81)$$

With a fixed resistance of 318.3  $\Omega$  for the resistor  $R_4$ , the loss factor  $\tan \delta$  can be expressed at an applied test frequency of 50 Hz as

$$\tan \delta = \frac{C_4}{10 \mu\text{F}}. \quad (3.82)$$

Some precautions are necessary if the current through the test object is high and may damage the resistor  $R_3$ . A defined resistor parallel to  $R_3$  may solve this problem.

For test objects with a very low loss factor, for example crosslinked polyethylene cables, further measures like an auxiliary branch are required. Nowadays, automatic Schering bridges are available, which adjust the bridge without the help of an operator, and digital signal processing allows the use a Schering bridge without an exact balance.

**Additional Information and Exercises**

Additional information and supplementary exercises relating to this chapter can be found at

[https://go.sn.pub/SHb\\_PowerSystems\\_Gockenbach\\_HighVoltageEngineering](https://go.sn.pub/SHb_PowerSystems_Gockenbach_HighVoltageEngineering).

## References

- 3.1 IEC 60071-1: *Insulation co-ordination – Part 1: Definitions, principles and rules*, Edition 9.0 (IEC, Geneva 2019)
- 3.2 IEC 60060-1: *High-voltage test techniques – Part 1: General definitions and test requirements*, Edition 3.0 (IEC, Geneva 2010)
- 3.3 IEC 62475: *High-current test techniques – Definitions and requirements for test currents and measuring systems*, Edition 1.0 (IEC, Geneva 2010)
- 3.4 A. KÜchler: *High Voltage Engineering – Fundamentals – Technology – Applications* (Springer, Berlin, Heidelberg 2018)
- 3.5 K. Berger, R.B. Anderson, H. Kröninger: Parameters of lightning flashes, *Electra* **41**(1), 23–37 (1975)
- 3.6 IEC 62305-1: *Protection against lightning – Part 1: General principles* (IEC, Geneva 2010)
- 3.7 M. Beyer, W. Boeck, K. Möller, W. Zaengl: *Hochspannungstechnik – Theoretische und praktische Grundlagen* (Springer, Berlin, Heidelberg 1986)
- 3.8 A. Schwaiger: *Elektrische Festigkeitslehre* (Springer, Berlin, Heidelberg 1925)
- 3.9 H. Prinz: *Hochspannungsfelder* (Oldenbourg, München 1969)
- 3.10 E. Peschke, R. von Olshausen: *Cable Systems for High and Extra-High Voltage* (Publicis, Erlangen 1999)
- 3.11 IEC 60156: *Insulating liquids – Determination of the breakdown voltage at power frequency – Test method*, Edition 3 (IEC, Geneva 2018)
- 3.12 W. Hauschild, E. Lemke: *High-Voltage Test and Measuring Techniques* (Springer, Berlin, Heidelberg 2014)
- 3.13 W. Hauschild, W. Mosch: *Statistical Techniques for High Voltage Engineering* (Verlag Technik, Berlin 1984)
- 3.14 J.S. Townsend: *Electricity in Gases* (Oxford Univ. Press, Oxford 1915)
- 3.15 T.W. Dakin, G. Luxa, G. Oppermann, J. Vigreux, G. Wind, H. Winkelkemper: Breakdown of gases in uniform fields. Paschen curves for nitrogen, air and sulfur hexafluoride, *Electra* **32**, 61–82 (1974)
- 3.16 D. Kind: *Die Aufbaufläche bei Stoßspannungsbeanspruchung von technischen Elektrodenanordnungen in Luft*, Dissertation (TH München, München 1957)
- 3.17 H.P. Moser: *Transformerboard* (H. Weidmann AG, Rapperswil 1979)
- 3.18 IEC TR 61294: *Insulating liquids – Determination of the partial discharge inception voltage (PDIV) – Test procedure* (IEC, Geneva 1993)
- 3.19 IEC 60050: *International electrotechnical vocabulary* (IEC, Geneva 2019)
- 3.20 H. Koch: *GI: Gas-Insulated Transmission Lines* (Wiley, Hoboken 2012)
- 3.21 H. Koch, F. Goll, T. Magier, K. Juhre: Technical aspects of gas insulated transmission lines and application of new insulating gases, *IEEE Trans. Dielectr. Electr. Insul.* **25**(4), 1448–1453 (2018)
- 3.22 M. Claessens, F. Schober, M. Ahl, T. Berth, M. Klemm, P. Körbel, D. Lana: Insulation performance of environmentally friendly, fluoroketone based insulation gas mixtures. In: *Proc. 21th Int. Symp. High Volt. Eng.*, Vol. 2, ed. by B. Nemeth (Springer Nature, Cham 2020) pp. 377–386
- 3.23 M. Hyrenbach, S. Zache: Alternative insulation gas for medium-voltage switchgear. In: *Pet. Chem. Ind. Conf. Eur. (PCIC Europe)* (2016), <https://doi.org/10.1109/PCICEurope.2016.7604648>
- 3.24 K. Dumke, H. Borsi, E. Gockenbach: Fundamental investigations on the influence of temperature and water content on the electrical behaviour of fluid impregnated insulating papers. In: *IEEE Int. Symp. Electr. Insul.*, Vol. 2 (1996) pp. 542–545
- 3.25 S. Tenbohlen, M. Koch: Aging performance and moisture solubility of vegetable oils for power transformers, *IEEE Trans. Power Deliv.* **25**(2), 825–830 (2010)
- 3.26 S. Azeehan Azli, M.H.F. Rahiman, Z.M. Yusoff, N.F. Razali, S.S. Abd Wahid, M.S. Ramli: A review on alternative oils as dielectric insulating fluids on power transformer. In: *IEEE 15th Int. Colloq. Signal Process. Appl. (CSPA 2019)* (2019) pp. 198–201
- 3.27 Siemens: 420-kV Transformator mit natürlicher Ester-Isolierung, <http://www.siemens.com/energy/transformatoren> (2015)
- 3.28 S.Y. Matharage, Q. Liu, Z.D. Wang, P.W.R. Smith, P. Mavrommatis, P. Dyer: Ageing assessment of a gas to liquid hydrocarbon transformer oil compared with an inhibited mineral oil. In: *19th Int. Symp. High Volt. Eng.* (2015)
- 3.29 H. Schering: *Die Isolierstoffe der Elektrotechnik* (Springer, Berlin 1924)
- 3.30 M. Kahle: *Elektrische Isoliertechnik* (Springer, Berlin, Heidelberg 1989)
- 3.31 R.M. Eichhorn: A critical comparison of XLPE and EPR for use as electrical insulation on underground power cables, *IEEE Trans. Dielectr. Electr. Insul.* **16**, 469–482 (1981)
- 3.32 Y. Du, M. Zahn, B.C. Lesieutre, A.V. Mamishev, S.R. Lindgren: Moisture equilibrium in transformer paper-oil systems, *IEEE Electr. Insul. Mag.* **15**(1), 11–20 (1999)
- 3.33 H.M. Ryan (Ed.): *High Voltage Engineering and Testing*, IET Power and Energy Series, Vol. 66, 3rd edn. (IET, London 2013)
- 3.34 IEC 60076: *Power transformers – Part 3: Insulation levels, dielectric tests and external clearances in air* (IEC, Geneva 2018)
- 3.35 IEC 60076: *Power transformers – Part 4: Guide to the lightning impulse and switching impulse testing – Power transformers and reactors* (IEC, Geneva 2002)
- 3.36 J. Hällström, S. Berlijn, M. Gamlin, F. Garnacho, E. Gockenbach, T. Kato, Y. Li, J. Rungis: Applicability of different implementation of K-factor filtering schemes for the revision of IEC 60060-1 and -2. In: *14th Int. Symp. High Volt. Eng.* (2005), Paper B-32
- 3.37 P. Simon, F. Garnacho, S.M. Berlijn, E. Gockenbach: Determining the test voltage factor function for the evaluation of lightning impulses with oscillations and/or an overshoot, *IEEE Trans. Power Deliv.* **21**(2), 560–566 (2006)

- 3.38 IEC 62475: *High-current test techniques: Definitions and requirements for test currents and measuring systems* (IEC, Geneva 2010)
- 3.39 M. Modrusan: Realisation of the prescribed exponential currents for kinds of test samples. In: *2nd Int. Symp. High Volt. Eng.*, Vol. 1 (1975) pp. 155–160
- 3.40 IEC 60060-2: *High-voltage test techniques – Part 2: Measuring systems*, Edition 3.0 (IEC, Geneva 2010)
- 3.41 F.G. Burch: On potential dividers for cathode oscillographs, *Philos. Mag.* **13**, 760–774 (1932)
- 3.42 W. Zaengl: Ein Beitrag zur Schrittantwort kapazitiver Spannungsteiler mit langen Messkabeln, *Elektrotechn. Z. A* **98**, 792–795 (1977)
- 3.43 K. Schon: *Stoßspannungs- und Stoßstrommesstechnik: Grundlagen – Messgeräte – Messverfahren* (Springer, Berlin, Heidelberg 2010)
- 3.44 IEC 60270: *High-voltage test techniques – Partial discharge measurements* (IEC, Geneva 2015)
- 3.45 W. Hauschild, E. Lemke: *High-Voltage Test and Measuring Techniques* (Springer, Berlin, Heidelberg 2014)
- 3.46 IEC 62067: *Power cables with extruded insulation and their accessories for rated voltages above 150 kV ( $U_m = 170$  kV) up to 500 kV ( $U_m = 550$  kV) – Test methods and requirements* (IEC, Geneva 2011)
- 3.47 S. Tenbohlen, A. Pfeffer, S. Coenen: On-site experiences with multi-terminal IEC PD measurements, UHF PD measurements and acoustic PD localisation. In: *IEEE Int. Symp. Electr. Insul.* (2010)
- 3.48 A. Akbari, P. Werle, H. Borsi, E. Gockenbach: Transfer function-based partial discharge localization in power transformers: A feasibility study, *IEEE Electr. Insul. Mag.* **18**(5), 22–32 (2002)
- 3.49 IEC TS 62478: *High voltage test techniques – Measurement of partial discharges by electromagnetic and acoustic methods* (IEC, Geneva 2016)
- 3.50 H. Schering: Brücke für Verlustmessungen, *Z. Instrumentenk.* **40**, 124 (1920)

### Ernst Gockenbach

Schering Institute  
Leibniz University of Hannover  
Hannover, Germany  
[ernst.gockenbach@ifes.uni-hannover.de](mailto:ernst.gockenbach@ifes.uni-hannover.de)



Ernst Gockenbach has 40 years of experience in high-voltage engineering, including several years as Chief Engineer for high-voltage test and measuring equipment in Switzerland and 24 years in teaching high-voltage engineering and insulation systems at university level. He was Chair of the CIGRE Study Committee D1 on Materials and Emerging Test Techniques and Chairman of IEC TC 42 High-Voltage and High Current Test Techniques.

# 4. High Currents and Contact Technology

Steffen Großmann

Section 4.1

Electrical power systems and transport systems are subject to profound changes all around the world. This is accompanied by higher requirements for the components of stationary or mobile equipment of electrical power engineering. Especially a compact design, a higher current load under normal operating conditions, and in the case of a fault, disparate environmental conditions and the demand for higher availability, reliability, and safety are great challenges for designers, manufacturers, constructors, and operators.

This chapter gives an overview of current-conducting arrangements (conducting systems) whose load is caused by electric current and ambient conditions, the resulting thermal and mechanical stress, and the long-term and reliably necessary strength of the conducting components.

Fundamentals on the thermal behavior of equipment and analytical approaches to the calculation of temperatures at relevant spots are presented that have proven themselves over decades in practice. If necessary, they can be supplemented by numerical methods, which will not be explicitly discussed here. Regarding the mechanical-dynamical behavior of current-conducting arrangements exposed to short-circuit currents or thermal elongation due to current load, methods for determining the strain and the necessary strength are presented with regard to the material properties in the elastic range and the

plastic range. Stationary electrical contacts and connections have been the subject of scientific research at TU Dresden for more than four decades and will be discussed here in an overview in terms of design, operating, and long-term behavior.

All results presented in this chapter are, to a great extent, results of scientific research at TU Dresden and have been taken from the course material presented to the students.

<b>4.1</b>	<b>Current-Conducting Arrangements (Conducting Systems)</b> .....	183
4.1.1	Concerning Conductor Material .....	184
4.1.2	Concerning the Structure of the Conductor .....	184
4.1.3	Concerning Conductor Connections.....	185
4.1.4	Concerning Insulation Arrangement and Insulation Material.....	188
4.1.5	Concerning Mechanical Properties .....	189
<b>4.2</b>	<b>Current-Carrying Capacity</b> .....	190
4.2.1	Load .....	190
4.2.2	Stresses.....	190
4.2.3	Strength.....	192
<b>4.3</b>	<b>Design Principles</b> .....	194
4.3.1	Thermal Design.....	194
4.3.2	Mechanical Dimensioning.....	219
4.3.3	Connections in Current Paths .....	238
	<b>References</b> .....	271

## 4.1 Current-Conducting Arrangements (Conducting Systems)

During the conversion, transport, and distribution of electrical energy, *current-carrying configurations* consisting of the *electrical conductor*, its contacts, its *electrical insulation*, and its *external mounting* in a wide variety of designs form the core of the electrical power system [4.1–3]. Driven by a voltage  $U$ , carriers  $Q$  move in a conductor with a resistance  $R$  and, thus, form a current  $I$ . This current leads, depending on the conductor cross section  $A$ , to a current density  $J$ , which

causes thermal losses  $P_{\text{vth}}$  in the conductor and, thus, will increase the conductor temperature by  $\Delta\vartheta$ . In addition, each current-carrying conductor is subjected to a magnetic field  $H$  that is responsible for eddy-current and hysteresis losses,  $P_{\text{vW}}$ ,  $P_{\text{vH}}$  (Sect. 4.2) and also has a mechanical-force effect  $F$  (Sect. 4.3.2). Particularly at very high voltages, dielectric losses  $P_{\text{D}}$  can lead to heating of the current-conduction arrangement. However, the mechanical and electrical properties of

**Table 4.1** Conductor materials (small selection with approximates, the exact values depend on the specific alloy and the posttreatment, as well as on the temperature of the conductor materials)

Material	Trade name	EN	Density ( $\text{g cm}^{-3}$ )	Electrical conductivity at 20 °C ( $\text{MS m}^{-1}$ )	Thermal conductivity at 20–200 °C ( $\text{W m}^{-1}\text{K}^{-1}$ )	Specific heat at 20–200 °C ( $\text{J kg}^{-1}\text{K}^{-1}$ )	Coefficient of thermal expansion at 20–100 °C ( $\times 10^{-6}\text{K}^{-1}$ )	Modulus of elasticity (GPa)
Cu99.9	Cu_ETP	CW004A	8.94	$\geq 58$	$> 390$	385	17.7	127
CuNi2Si	Copper DIN 20855	CW111C	8.88	18	200	377	17.0	130
G-CuSn5Zn1Pb	Red brass Rg5 DIN 1705	CC491K	8.70	8	71	380–400	18.2	65–105
CuZn37	Brass Ms63 DIN 1709	CW508L	8.44	15	120	404	18.5	78–132
Al99.5	DIN 573-3	AW1050	2.70	34.5	232	897	23.5	70
AlMgSi	Aluminum alloy	AW6082	2.70	24–32	174	1060	24	70
G-AISI7	Sand casting	AC42100	2.70	21–32	169	963	22	73

a current-conducting device are largely determined by its temperature. Temperatures must be maintained within a limited range to ensure long-term reliable and economical operation of electrical power systems.

Conductor arrangements must be designed so that the requirements for reliability and availability, as well as plant and personal safety, are guaranteed for all loads possible in the respective case.

Depending on the technical requirements and the operating conditions, conductor arrangements can be divided into the following:

#### 4.1.1 Concerning Conductor Material

In electrical power engineering, copper and aluminum are the preferred conductor materials due to their good electrical conductivity, adequate mechanical properties, machinability, availability, and acceptable price. An improvement in mechanical properties can be achieved by copper or aluminum alloys, but this always leads to a reduction in conductivity (Table 4.1).

Due to its low price and low specific weight, and despite its lower electrical conductivity, aluminum is becoming increasingly important for selected applications (Fig. 4.1). In addition to traditional power cables and overhead-line and switchgear construction, aluminum is now also used successfully as a conductor material in the automotive and aviation industries, in transformer construction and in the equipment industry. However, the different electrical and mechanical properties, as well as the different technologies for installing and connecting aluminum conductors, must be taken into account when designing and dimensioning (Sect. 4.3.3) equipment or systems.

Composite materials or material systems are used, e.g., copper-coated aluminum conductors, Al-Cu sheets, aluminum-steel cables, or high-temperature overhead-line conductors made of aluminum alloys with a mechanically supporting carbon-fiber core. Moveable conductor arrangements, e.g., in rotating electrical machines (collectors, slip rings) or in the overhead contact lines of electrical railways and cranes, are usually implemented with carbon-copper (alloy) systems.

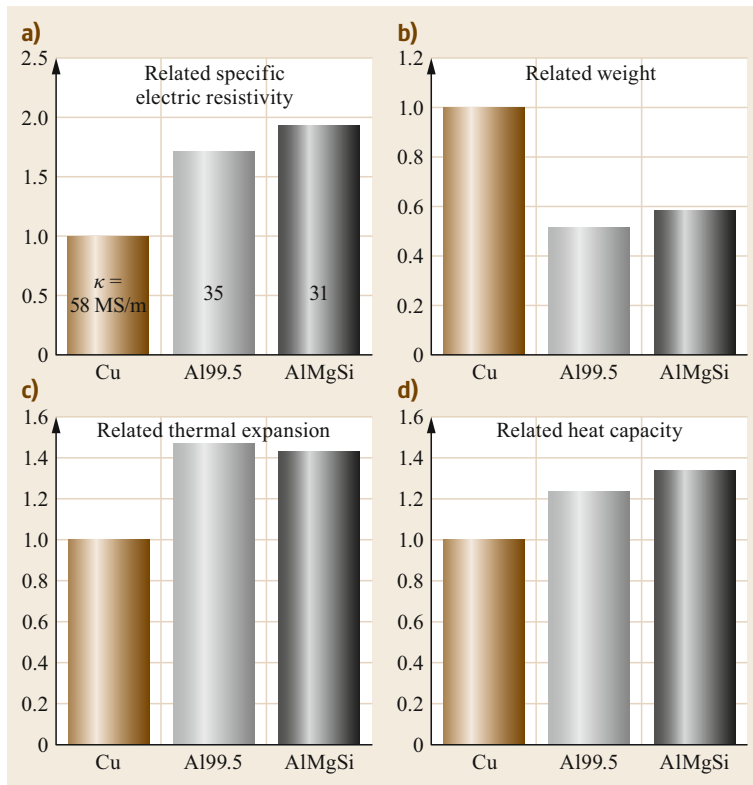
#### 4.1.2 Concerning the Structure of the Conductor

The level of the operating and short-circuit current to be conducted, the required mechanical strength and the necessary flexibility and mobility, fastening and support conditions, as well as application-related requirements, determine the appropriate design of the electrical conductors (Table 4.2).



**Table 4.2** Structure of electric conductors

Rigid Solid, massive	Tubular	Moveable Stranded, laminated	Flexible Thin-wire
Characteristics: Low volume	High flexural rigidity and high short circuit currents Low skin effect Large heat-emitting surface	Bendable Compensation of thermal expansion	High flexibility Compensation of mechanical vibration
Examples: Bus bars	Bus bars	Overhead line conductors Power cable Expansion clamps	Flexible line



**Fig. 4.1a-d** Relations between conductors from aluminum and copper for equal electric resistance. (a) Cross section of aluminum related to copper for equal resistance, (b) aluminum has half weight of copper for equal resistance, (c) larger thermal extension of aluminum has to be taken in account for bus bar length and for sag of overhead lines, (d) larger heat capacity of aluminum is an advantage in case of short circuits

### 4.1.3 Concerning Conductor Connections

In an electrical system, conductors made of different conductor materials and with different conductor structures must be joined together for the purpose of:

- Conductor connections
- Equipment connections
- Branching points or tap-offs.

Depending on the function of the connection, they can be designed as permanent, nondetachable closed, detachable, or as movable or pluggable connections.

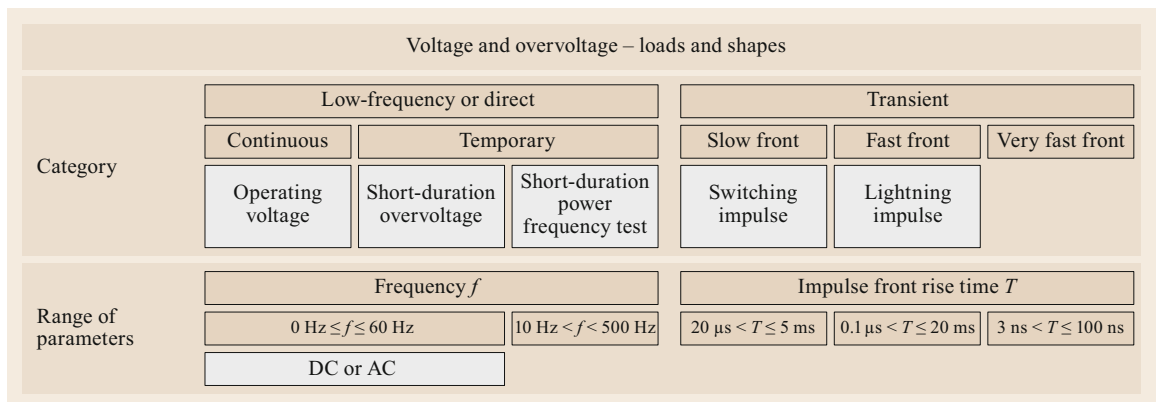
Electrical connections are exposed to a multitude of loads (Table 4.3) that stress the connection and, thus, lead to aging of the connection over time (Sect. 4.3.3). The load-dependent aging of the connection must, therefore, already be known during installation in order to ensure a reliable connection over the projected

**Table 4.3** Criteria for connections in conductor systems

Connecting current paths		
Load caused by load		Strength attainable by strengths
<i>Electrical load</i> Operating current, causes long-term heating of the current path Short-time current, causes short-term heating Short-circuit current, causes electrodynamic forces Operating voltage, may cause partial discharges <i>Ambient conditions</i> Temperature Humidity Chemical agents in the environment Service conditions External mechanical loads Vibrations Plug-in operations, plug-in forces Thermomechanical forces due to elongation <i>Operational requirements</i> Service and maintenance Flexibility Modularity Safety of personnel and plant	⇒	⇒
	<b>Loading with stresses</b>  <i>Temperature rise</i> Limit temperatures must not be exceeded Operating temperature of the connection significantly determines its aging <i>Mechanical stresses</i> Tensile Bending Torsional <i>Mechanical vibrations</i> Twice power frequency ( $2 \times 50$ Hz) Wind-induced <i>Swing/galloping</i> Natural mechanical frequency is system specific <i>Chemical reaction with the environment (pollution layers)</i> Electrochemical corrosion Oxidation of the contact surfaces Reaction of the contact surfaces with admixtures, e.g., salt, sulfur, etc. Intermetallic diffusion <i>Fretting</i> Plug-in connectors Moving connections <i>Electric field strength</i> Partial discharge initiation	<b>Strength attainable by strengths</b>  <i>Ampacity</i> Conductor material Dimensioning Shape Joining methods <i>Aging resistance</i> Conductor material Surface treatment (Limit) temperature Shape <i>Mechanical strength</i> Conductor material Shape Dimensioning Energy accumulators, springs, connecting elements <i>Abrasion resistance</i> Contact materials Lubricants <i>Dielectric strength</i> Electrode geometry

**Table 4.4** Criteria for insulation conductor systems

Insulation of current paths		
External loads		Strengths
<i>Electrical load</i> Operating voltage, power frequency, continuous or intermittent Transient switching or lightning overvoltages (Fig. 4.2) <i>Ambient conditions</i> Temperature Humidity Air pressure	⇒	⇒
	<b>Stresses</b>  <i>Electric field strength</i> Partial discharges Puncture through an insulating material Flashover on the insulation surface	<b>Strengths</b>  <i>Dielectric strength</i> Shape of the electrode geometry of the insulation system Insulating materials



**Fig. 4.2** Categories and types of voltage and overvoltage loads

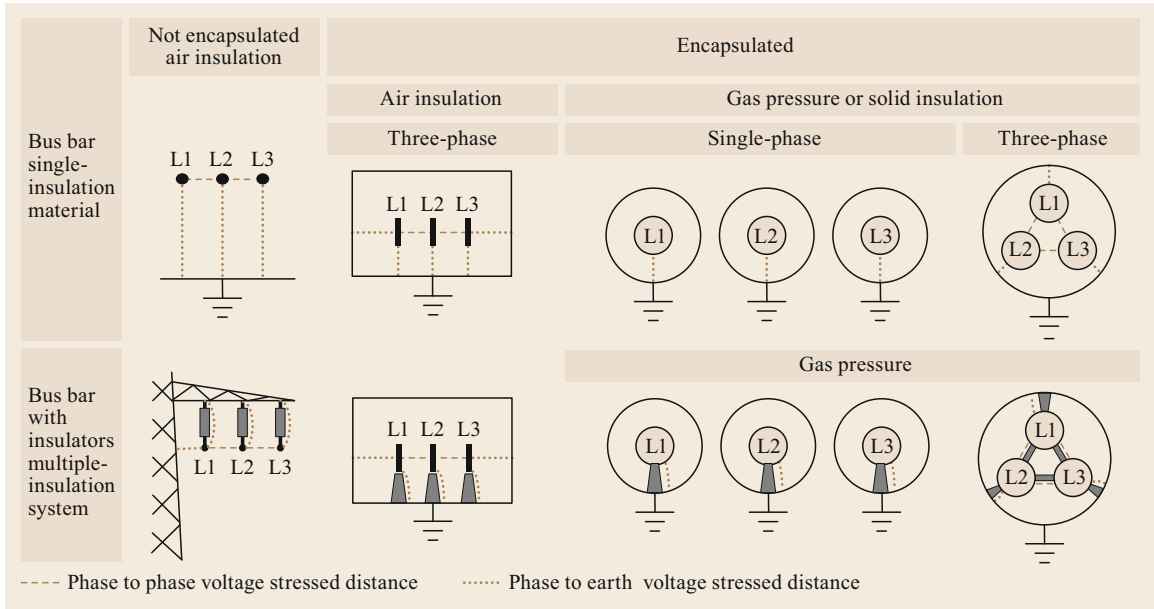


Fig. 4.3 Dielectric insulation arrangements for conductors

Gaseous insulation		Liquid insulation	Solid insulation
Air insulation	Gas pressure insulation		
<b>Characteristics:</b> Air is available anywhere Restrengthenable after breakdown	Very high dielectric strength SF <sub>6</sub> or alternative gases Restrengthenable after breakdown	Very high dielectric strength Mineral or silicon oil Semi-restrengthenable after breakdown	Very high dielectric strength Anorganic, organic or elastomeric materials Irreparable after failure
<b>Examples:</b> High-voltage overhead transmission lines and substations Rail contact lines Air-insulated switchgears (AIS for low and medium voltage)	Gas-insulated switchgears (GIS) and lines (GIL)	Electrodes of tap changer in power transformers	Cables Solid insulated bus bars
↓			
Combined dielectric insulation systems			
Air/solid	Pressured gas/solid	Solid/liquid	
<b>Characteristics:</b> Typical for mechanical fastening the bus bar conductor Along, transverse or a slant interface course change of dielectric strength field or displacement electric flow Effects of sedimentation, pollution and space-charge on insulators surfaces		Very high dielectric strength Semi-restrengthenable after breakdown	
<b>Examples:</b> Insulators in high-voltage overhead transmission lines and substations Insulators and bushings in air-insulated switchgears	Insulators in gas-insulated switchgears (GIS) and lines (GIL)	Oil-paper insulation of windings in power transformers	

Fig. 4.4 Dielectric insulation material for conductor

**Table 4.5** Criteria for fastening of current-carrying systems

Fastenings for power tracks	
External loads	Stresses
<i>Dead weight</i> of the current path	⇒ <i>Mechanical stress</i>
Conductors	Tensile
Insulation	Bending
Fittings (clamps, spacers)	Torsional
Accessories (joints, terminations)	Buckling
<i>Ambient conditions</i>	<i>Mechanical oscillations</i>
Temperature	Twice power frequency ( $2 \times 50$ Hz)
Wind	Wind induced
Ice load	Swing galloping
Tremor	Mechanical natural frequency is system specific
Topographical location in the terrain	<i>Electric-field strength</i>
Geological conditions	Partial discharge initiation
<i>Service conditions</i>	<i>Temperature rise</i>
Tensile forces	Heat in the conductor
Bending forces	Additional losses in enclosure and fittings
Torsion forces	
Compressive forces	
Vibrations	
<i>Operational needs</i>	
Servicing and maintenance	
Versatility	
Modularity	
Personnel and plant safety	
Visual quality	
<i>Electrical load</i>	
Operating voltage, determined design of the mounting with regard to partial discharge resistance	
Operating current, causes heating and linear expansion or sag	
Short-time current, causes heating and linear expansion	
Shock short-circuit current, causes electrodynamic forces	
	⇒ <i>Strengths</i>
	<i>Internal mechanical strength</i> of the current path (stiffness) against
	Tension
	Bending
	Torsion
	Buckling
	Vibration
	<i>Supporting</i> under tensile stress (Fig. 4.4)
	Anchoring points
	Supporting points
	e.g., bare and insulated overhead lines, traction lines, overvoltages in substations
	<i>Erection</i>
	Underground (earth, concrete, etc.)
	On the ground with or without defined fixing points (cable trays, cable racks etc.)
	In pipes or cable blocks
	e.g., cables and wires
	<i>Storing</i> on bases
	Stiff conductors (insulated or bare) on moving and fixed supports, e.g., substations (Fig. 4.4)
	Flexible conductors on cable consoles, clamps, e.g., cables and wires

service life of the system through suitable joining of the conductors. Occasionally, little attention is paid to electrical connections in the planning, design, and installation of systems, which can lead to considerable long-term problems with reliability and related very high costs.

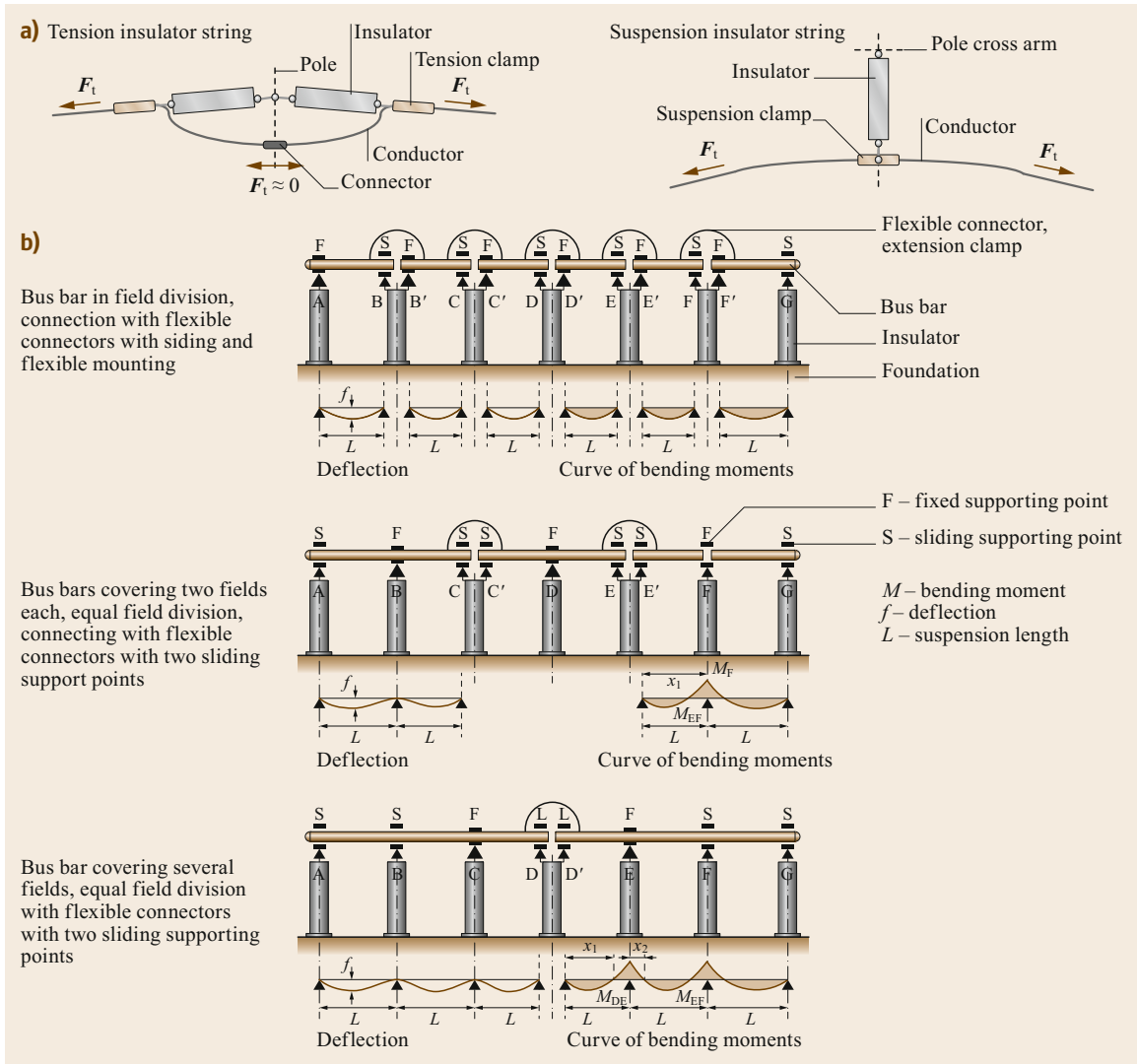
#### 4.1.4 Concerning Insulation Arrangement and Insulation Material

The conductor arrangement must reliably separate the electrical potentials between the conductors and between the conductor and earth. The insulation is exposed to various loads, which lead to permanent and

transient stresses on the insulation arrangement (Table 4.4, Fig. 4.2 [4.4]).

Whether electrical conductors are used bare (i.e., insulated with air) or insulated with a suitable solid or liquid insulating material to each other, to ground and against touch contact depends on the specific application, the operating voltage, the space requirements, the ambient conditions, the costs, etc. A distinction is made between the type of insulation arrangement and the insulation material (Figs. 4.2 and 4.3).

The type of insulation closely interacts with the current-carrying capacity, design, installation, and flexibility of the system during operation, maintenance, and system losses.



**Fig. 4.5a,b** Fastening of electric conducting systems. (a) Conductor with mechanical tensile stress, (b) conductor without mechanical tensile stress

**4.1.5 Concerning Mechanical Properties**

Conductor arrangements must be designed in such a way that the requirements for reliability and availability, as well as plant and personal safety, are guaranteed for all possible loads. This includes the fittings, the insulators, and the supports.

The type of mechanical fastening to be selected depends on the operating current and the resulting lon-

gitudinal expansion of the conductor arrangement, as well as the short-circuit forces acting on the conductor, the insulators, and the support. The criterion here is that neither conductors, insulation, nor fastening may be permanently distorted and that the striking distance of insulation sections must not fall below the values specified to avoid puncture or flash-over (Table 4.5, Figs. 4.4 and 4.5).

## 4.2 Current-Carrying Capacity

Conductor arrangements must be able to reliably and safely carry operating and fault currents over the entire projected service life, usually several decades [4.1, 2, 5]. This means that the functions of conducting current, insulating electrical potentials, connecting, branching, and fixing conductors must be guaranteed for a long time under all operating conditions. The temperature of the current path plays a central role. In the event of a fault, electrodynamic forces and power arcs must also be withstood. With the associated physical processes, the operating states, namely:

- Normal operation: continuous and alternating load (Table 4.6a)
- Short circuit: outside (Table 4.6b) and inside (Table 4.6c) of the network considered

pose different challenges and technical objectives (Table 4.6), which must be equally taken into account in the design of power-distribution systems.

### 4.2.1 Load

Conductor arrangements with their components (conductors, insulations, connections, fasteners) are loaded by *external effects*, the current flow, and the ambient conditions:

Thermal loads caused by power-heat losses are:

- Continuous current load
- Intermittent current load
- Short-circuit current load.

Mechanical loads are caused by:

- Bending moments and line loads on conductors and forces on support and fastening points in the event of a short circuit.  
Examples: bus bars, conductors, insulators, fittings, parallel single-core cables.
- Deflection of nonrigid conductors due to the effect of the wind. Examples: overhead lines with single or bundled conductors, field spacers, separators.

Loads due to ambient conditions are caused by:

- Ambient temperature
- Heat generation through solar and sky radiation
- Humidity and air pollutants
- Snow and ice loads as additional weight loads
- Wind inducing conductor vibrations and constituting an additional mechanical load.

The relevant standards contain the design-relevant ambient conditions. On the other hand, it is not feasible to incorporate in the standards all climatic conditions for all regions of the globe, which might differ substantially. Thus, for extreme ambient conditions, specific long-time tests, e.g., for connections and contacts, are required [4.6].

### 4.2.2 Stresses

The external loads of a conductor arrangement lead to *internal stresses* of the same arrangement. The interaction of different, mostly temperature-dependent loads leads to the aging of the components of a conductor arrangement, which, depending on the strength of the construction, may lead to partial or complete failure after a period.

Examples (Table 4.6):

1. The dielectric strength of various insulations decreases over time. Higher temperatures can accelerate this process. In particular, transient overvoltages can become critical.
2. The long-term behavior of electrical contacts and connections reacts very sensitively to elevated temperatures, since most aging mechanisms follow Arrhenius' law (4.1),

$$k = ae^{-\frac{E}{RT}}, \quad (4.1)$$

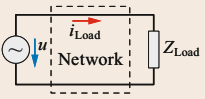
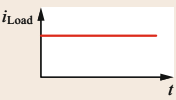
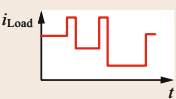
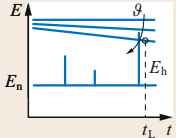
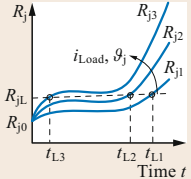

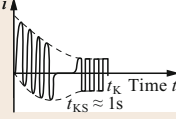
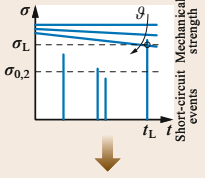
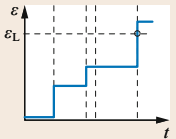

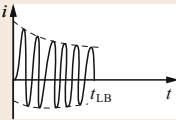
where  $k$  = aging rate,  $a$  = factor of proportionality,  $E$  = activation energy,  $R$  = universal gas constant, and  $T$  = absolute temperature.

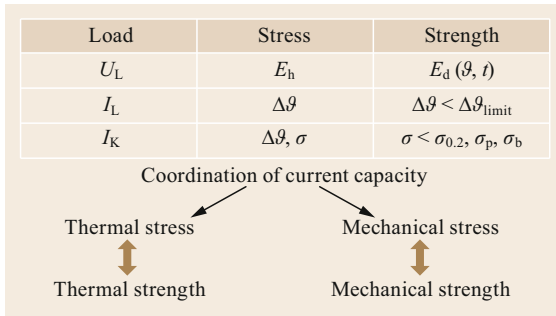
The higher the initial resistance of a connection  $R_{J0}$ , the faster it ages at higher temperatures, and thus the sooner it will fail. Higher current loads and higher ambient temperatures, therefore, have an accelerating effect on the aging of electrical connections (Sect. 4.3.3).

3. The mechanical strength of many materials decreases over time, which is accelerated by increased temperatures (Arrhenius' law). Especially under short-circuit currents, high electromagnetic forces occur, which will cause higher permanent plastic deformations, which accumulate with each short-circuit event (Sect. 4.3.2).

The permissible thermal stress of the conductor arrangements is, therefore, limited and is specified in standards as the *limit temperatures* for various materials and applications. A distinction is made between normal operation (continuous or alternating current) and short-circuit

**Table 4.6** Current-carrying capacity

	Physical effects Thermal	Mechanical	Technical requirements Behavior	Purpose
<b>a) Normal operation</b>				
<p>Typical circuit</p>  <p>Continuous current load</p>  <p>Varying current load</p> 	<p><math>\Delta\vartheta \leq \Delta\vartheta_L</math>  <math>\Delta\vartheta</math> – heating  <math>\Delta\vartheta_L</math> – limit of heating                      Criteria:                      Power lost <math>P_V</math></p> <p><math>P_{input} = P_{output}</math>  <math>P_{input} = P_V = ki_{load}R(\vartheta)</math>  <math>P_{output} = P_L + P_S + P_K</math>  <math>P_L</math> – heat conduction  <math>P_S</math> – heat radiation  <math>P_K</math> – heat convection</p> <p><math>P_{input} = P_{output} + \frac{dQ}{dt}</math>  <math>dQ_c = mc\Delta\vartheta</math>  <math>Q_c</math> – heat storage capacity</p>	<p><math>\sigma &lt; \sigma_L</math>  <math>\sigma</math> – mechanical stress  <math>\sigma_L</math> – limit of mechanical stress                      Criteria:                      Uniform load <math>q</math> in between bus bars  <math>q = i_{Load}B</math>  <math>B</math> – electromagnetic flux density                      In the case of normal operation, <math>q</math> is not significant</p>	<p>Dielectric strength depending on temperature</p>  <p>Lifetime of joints depending on loads</p> 	<p>No failure during 40–60 yr operation time.                      Load &lt; Limit ≤ Strength                      Dielectric: no breakdown or flashover                      Mechanical: no break, no deformation                      Thermal: no overheating                      Contact: Limited joint resistant</p>
<b>b) Short-circuit failure outside the relevant network</b>				
<p>Typical circuit</p>  <p>Short-circuit current</p> 	<p><math>\Delta\vartheta \leq \Delta\vartheta_{LKS}</math>                      Criteria:                      Energy lost <math>Q_V</math></p> <p><math>Q_{input} = \int_0^{t_{KS}} ki_{KS}^2 R d t_{KS}</math></p> <p><math>Q_{output} = Q_C + Q_L</math>  <math>dQ_c = mc\Delta\vartheta</math>                      KS – Short circuit  <math>k</math> – current displacement factor  <math>i_{KS}</math> – short-circuit current  <math>R(\vartheta)</math> – temperature depending resistance  <math>t_{KS}</math> – short-circuit duration  <math>Q_C</math> – heat storage capacity  <math>Q_L</math> – heat conduction</p>	<p><math>\sigma &lt; \sigma_L</math>                      Criteria:                      Equilibrium of forces <math>F</math>  <math>F_{el\ mag} = F_{el\ plast} + F_{inertia}</math>  <math>F_{el\ mag}</math> – electromagnetic force  <math>F_{el\ plast}</math> – elastoplastic force  <math>F_{inertia}</math> – inertial (mass) force</p>	<p>Mechanical stress <math>\sigma</math></p>  <p>Deformation <math>\epsilon</math></p> 	<p>Load &lt; limit ≤ strength</p> <p><math>\epsilon &lt; \epsilon_L</math>  <math>\epsilon</math> – deformation  <math>\epsilon_L</math> – limit of deformation</p>
<b>c) Short-circuit failure inside the relevant network</b>				
<p>Typical circuit</p>  <p>Short-circuit current</p> 	<p>Extreme high temperature in plasma (6000 K approximately)</p> <p><math>\Delta P = K \int_0^{t_{KS}} u_B i_{KS} dt_{KS}</math></p> <p><math>K = k_p \frac{R}{V c_v}</math></p> <p><math>\Delta P</math> – additional arc power input  <math>k_p</math> – factor for convective heat  <math>u_B</math> – arc voltage  <math>c_v</math> – specific heat at constant volume  <math>R</math> – gas constant  <math>V</math> – Volume</p>	<p>Extreme high pressure, especially in encapsulated devices.                      Impulse at housing:  <math>\int_A \int_0^{t_{LB}} p dA dt = m v</math></p> <p><math>p(t, x, y, z)</math> – pressure  <math>A</math> – surface  <math>m</math> – mass of volume  <math>v</math> – speed</p>	<p>Localization on the area of origin, no damage of complete installation                      Control of electric arc                      No danger to persons                      Fast detection by sensors (optical, pressure, current characteristic)                      Extreme fast shorting bar (10–100 ms)</p>	



**Fig. 4.6** Electrical load, stress, and strength of conducting systems

operation (Sect. 4.3.1). Electrical power equipment constitutes capital goods that are designed for a service life of several decades and must, therefore, be dimensioned not only for new conditions but also taking aging into account. This is often difficult in practice, because the loads can change during operation, and their patterns are not always known. There is still a need for research in this area, since suitable diagnostic methods are not available for all stresses and are also not always practical and economical. Rather, comparatively simple technical systems, such as power conductor arrangements, should be so robustly dimensioned and designed that a diagnosis is only necessary in special cases.

For mechanical stress (Sect. 4.3.2), the permissible limits are not to be defined trivially with general limit values. Rather, suitable calculations based on models or corresponding experiments are required. The technical criterion is the *permanent deformation*, which should not exceed values that have been agreed upon and are based on design and material properties. This affects bending, tensile, compressive, and torsional stresses in the electrical conductor, in connections and fasteners, as well as in technical insulations that are in the glass state (e.g., porcelain, insulating resins) or in the elastic state (e.g., silicone rubber, PVC, PE, VPE).

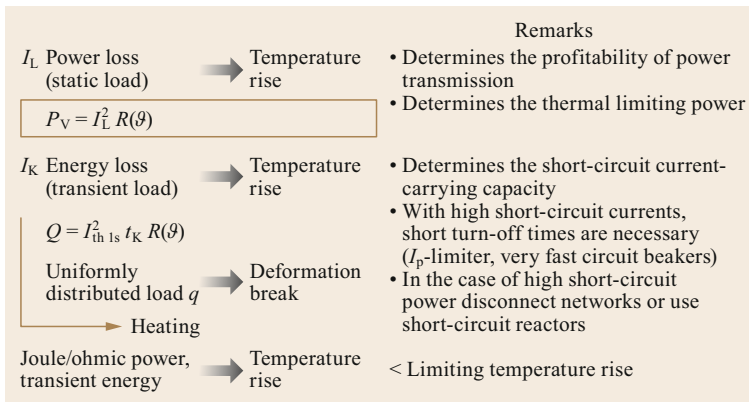
### 4.2.3 Strength

The strength of a current-conducting device is the ability to withstand the electrical, mechanical and environmental stresses to such an extent that its function is ensured under all possible external and internal loads (Figs. 4.6 and 4.7). Aspects of technical requirements, reliability, personnel and plant safety, economic efficiency, and occasionally also the quality of appearance must be taken into account.

In order to guarantee the required thermal strength, the limit temperatures specified in standards must be observed. This makes sense from a technical point of view, as they ideally take into account the new condition of the equipment, its aging, its normal and extraordinary (e.g., under fault) operation, as well as the expected environmental loads. Compliance with the limit temperatures is provided by tests or analytical calculations, insofar as this is accepted by the user. For practical application, it is essential to question whether the boundary conditions specified in the standards for the verification of the limit temperatures also correspond to those to be expected in the respective application.

Example: low-voltage switchgear is tested according to uniform, easily comparable criteria. However, this test arrangement does not roughly correspond to the many installation cases of low-voltage switchgear and control-gear assemblies [4.7], which can be found in practice. Due to the much shorter connecting cables and the significantly worse conditions for heat dissipation, significantly higher temperatures occur in practice than in the standard test, or the current-carrying capacity in the actual application will generally be significantly lower than indicated on the nameplate of the switching device. In this case, it is the responsibility of the system manufacturer to prove compliance with the limit temperatures.

The temperature of the current path is the essential criterion for the current-carrying capacity. Compliance



**Fig. 4.7** Influence of power loss, energy loss, and mechanical load on current-carrying capacity and heating



**Table 4.7** Temperature-rise limit (at ambient temperature  $\leq 40\text{ }^{\circ}\text{C}$ ) for low and for high-voltage switchgears and control gears, a selection (adapted from [4.7–12])

Nature of the part	Stock	Temperature-rise limit (K)	Ambient temperature	
<b>Low-voltage switchgear and control gear: IEC 60947-1 [4.8], DIN EN 60947-1 [4.9]</b>				
Terminals	Bare copper	60	Limit under normal service conditions: 35 °C (24 h), 40 °C max., During test: 10–40 °C, Shall not vary more than 10 K	
	Bare brass	65		
	Tin-plated copper	65		
	Silver or nickel-plated copper	70		
Accessible parts, manual operating means	Metallic	15		
	Nonmetallic	25		
Accessible parts, intended to be touched but not hand-held	Metallic	30		
	Nonmetallic	40		
<b>Low-voltage switchgear and control-gear assemblies: IEC 61439-1 [4.7], DIN EN 61439-1 [4.10]</b>				
Bus bar	Copper	105	35 °C	
<b>High-voltage switchgear and control gear: IEC 62271-1 [4.11], DIN EN 62271-1 [4.12]</b>				
Contacts (Plug-in connectors)	Bare copper or copper alloy		Limit under normal service conditions: 35 °C (24 h), 40 °C max., During test: 10–40 °C,	
	• in air			
	• in SF <sub>6</sub>			
	• in oil			
	Tin or nickel-coated			
	• in air			
	• in SF <sub>6</sub>			
	• in oil			
	Silver or nickel-coated			
	• in air			
	• in SF <sub>6</sub>			
	• in oil			
	Connections, bolted, or the equivalent			Bare copper or copper alloy
				• in air
• in SF <sub>6</sub>				
• in oil				
Tin or nickel-coated				
• in air				
• in SF <sub>6</sub>				
• in oil				
Silver or nickel-coated				
• in air				
• in SF <sub>6</sub>				
• in oil				
Accessible parts, expected to be touched in normal operation		30		
Accessible parts, which need not to be touched in normal operation		40		

with limit temperatures must be proven in standardized heating tests. Temperature is decisive for mechanical strength and aging. It serves as an indirect but measurable criterion for meeting the technical objectives with regard to electrical, dielectric, thermal mechanical, and safety-related tasks.

The level of the permissible limit temperature depends on the materials of the conductors, the insulation, the connections and the fasteners, as well as on the time variation of the load current, and is determined on the basis of practical experience and systematic aging

tests. If these limit temperatures are maintained during a temperature-rise test, a service life of several decades can very probably be expected for mature equipment from the point of view of current-carrying capacity.

Examples:

1. ACSR conductors for overhead lines are designed for a maximum conductor temperature of 80 °C. This is based on an ambient temperature of 35 °C, a wind speed of 0.6 m s<sup>-1</sup>, and solar radiation of 1000 W m<sup>-2</sup>. In the case of deviating ambient con-

ditions, the current load can be temporarily adapted while maintaining the specified limit temperature. It should be noted that accelerated aging of the connections must be taken into account when the current load is increased, although the limit temperature of the conductor is not exceeded [4.13, 14].

2. High-temperature, low-sag (HTLS) conductors may be operated at temperatures up to 210°C. This results in temperatures at the connectors of 120–150°C [4.15, 16].
3. Selected examples of limit temperatures in low and high-voltage switchgear (Table 4.7).

It should be noted that the boundary conditions for heating tests are not always uniformly specified in the various standards. Therefore, the limit temperatures and their boundary conditions for individual components and for the entire system must always be taken as a basis for the design of conductor arrangements.

Most of the limit temperatures specified in the standards are based on knowledge of physical laws, electrical, thermal, and mechanical material properties, and operating experience over several decades and have generally proven themselves as accepted technical certainties. The increasing need to allow for higher limit temperatures for certain new applications compared to those which have been proven over a long period of time requires special care and responsibility in their usage and is often associated with additional preliminary long-term investigations (Sect. 4.3.3).

## 4.3 Design Principles

### 4.3.1 Thermal Design

Current-conducting arrangements must be dimensioned in such a way that the limit temperatures for the conductor, the insulation, the contact and connecting elements and the fasteners, and for the operator are maintained under the expected loads in normal operation and in the event of a fault (short circuit). Permissible limit temperatures are specified in standards or must be determined experimentally or analytically for special applications (Sect. 4.2). In order to meet this requirement, design principles are required that have been successfully applied for decades. In addition, modern calculation methods (e.g., the finite element method (FEM), etc.) are useful, with the help of which partial solutions can be determined even more precisely and displayed clearly where this is necessary [4.1, 2, 5, 19].

Examples:

1. Investigations on the long-term behavior of bolted connections with copper bus bars in low-voltage switchgear and control-gear assemblies up to 140°C [4.17]
2. Investigations on the electrical contact and long-term behavior of compression connectors with HTLS conductors up to 210°C [4.18]

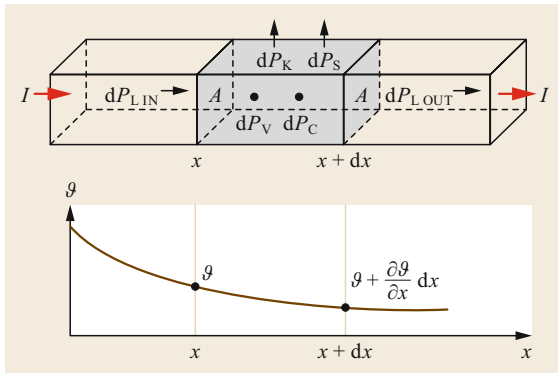
In the near future, it will be a challenge to additionally investigate the influence of nonsinusoidal currents or currents with higher frequencies on the heating of current paths and the aging of connections and to describe them in test standards. The increasing integration of renewable energy sources (wind-energy plants, photovoltaic plants) and the associated ever-broader use of the advantages of power electronics are major motivations for this.

The proof of the mechanical strength against the effect of the electrodynamic forces in the event of a short circuit outside the equipment under consideration (Table 4.6b) must be provided in a short-circuit test in an electrical power test field or by suitable calculations.

The proof of the strength against the thermal and pressure effects in the case of an arc fault in the equipment under consideration (Table 4.6c) must be performed in an arc-fault test in a high-performance test field or by suitable calculations.

### Thermal Balance Equation for a Current Path

During the transport of electrical energy, part of the power to be transmitted in the current paths of the equipment is converted into heat losses,  $P_v$ . This leads to an increased temperature of the current path itself and other components (insulation, connections, contacts, fasteners) in the equipment. This creates a thermal stress for the current-conducting arrangement (Sect. 4.2). Between heat losses  $P_v$ , heat dissipation along the electrical conductor by heat conduction  $P_L$ , heat dissipation radially outwards by convection  $P_K$ , heat radiation  $P_S$ , and the heat stored in the current path  $P_C$ , thermal equilibrium is reached. For a differentially small-volume elements in a homogeneous, long conductor inside (Fig. 4.8), the *heat balance equation* can be given as a second-order differential equation, with spatial and temporal depen-



**Fig. 4.8** Balance of thermal power in a homogeneous, straight conductor ( $dP_V$  joule, ohmic power loss,  $dP_C$  stored thermal power,  $dP_{L,IN}$  heat conduction in the element,  $dP_{L,OUT}$  heat conduction out of the element,  $dP_K$  radially dissipated heat power by convection,  $dP_S$  radially dissipated heat power by radiation)

dence

$$dP_V - dP_C - dP_L - dP_K - dP_S = 0. \quad (4.2)$$

For example, for a bus bar, these terms can be described as follows:

- Heat dissipation generated in the volume element  $dP_V$

$$\begin{aligned} dP_V &= kI^2 \frac{\rho(\vartheta) dx}{A} \\ &= kI^2 \frac{\rho_{20}}{A} dx [1 + \alpha T(\vartheta_L - 20^\circ\text{C})], \end{aligned} \quad (4.3)$$

where  $k$  = current displacement factor,  $\rho$  = resistivity,  $\rho_{20}$  = specific electrical resistance at  $20^\circ\text{C}$ ,

$A$  = conductor cross section,  $\alpha_T$  = temperature coefficient of electrical resistance, and  $\vartheta_L$  = conductor temperature.

- Heat stored in the volume element

$$dP_C = Ac\delta \frac{\partial \vartheta}{\partial t} dx \quad (4.4)$$

with  $c$  = specific thermal capacity of the conductor material (Table 4.8), and  $\delta$  = density of the conductor material.

- Heat entering the volume element at position  $x$  and exiting at position  $x + dx$  conducted out heat conduction (heat flow rate)

$$dP_L = \underbrace{\left(-\lambda A \frac{\partial \vartheta}{\partial x}\right)}_{\text{In}} + \underbrace{\left[-\lambda A \frac{\partial \vartheta}{\partial x} \left(\vartheta + \frac{\partial \vartheta}{\partial x} dx\right)\right]}_{\text{Out}}, \quad (4.5)$$

where  $\lambda$  = thermal conductivity of the conductor material.

- Heat dissipated radially over the surface of the volume element by convection

$$dP_K = \alpha_K(\vartheta) U_K(\vartheta_L - \vartheta_0) dx, \quad (4.6)$$

where  $\alpha_K$  = heat transfer coefficient for convection.  $U_K$  = convective heat-emitting circumference of the conductor over the length  $dx$ ,  $\vartheta_L$  = conductor temperature, and  $\vartheta_0$  = ambient temperature.

- Heat dissipation radially over the surface of the volume element by thermal radiation

$$dP_S = \alpha_S(\vartheta) U_S(\vartheta_L - \vartheta_0) dx \quad (4.7)$$

where  $\alpha_S$  = thermal transfer coefficient for radiation, and  $U_S$  = heat-emitting circumference of the conductor over the length  $dx$ .

**Table 4.8** Thermal characteristic of selected materials: specific electric resistance (at  $20^\circ\text{C}$ ), temperature coefficient electric resistance, density at  $20^\circ\text{C}$ , specific thermal capacity, and thermal conductivity

Material	$\rho_{20}$ ( $\Omega \text{ mm}^2/\text{m}^{-1}$ )	$\alpha_T$ ( $\times 10^{-3} \text{ K}^{-1}$ )	$\delta_{20}$ ( $\text{g cm}^{-3}$ )	$c$ ( $\text{Ws g}^{-1} \text{ K}^{-1}$ )	$\lambda$ ( $\text{W m}^{-1} \text{ K}^{-1}$ )
Copper	0.0175	3.92	8.92	0.385	385
Aluminum	0.0278	4.08	2.7	0.896	223
Brass	0.056	2.4	8.4	0.39	81–116
Silver	0.0163	4.1	10.5	0.24	423
Lead	0.21	3.9	11.3	0.13	36
Epoxy <sup>a</sup>	–	–	1.2–1.9	0.8–1.2	0.2–0.9
Pressed-paper	–	–	1.2	2.4	0.24
Polyethylene	–	–	1.4	1.0–1.25	0.15–0.17
Transformer oil	–	–	0.84–0.87	1.9–2.1	0.12

<sup>a</sup> 0–300% quartz flour

**Table 4.9** Demand depending current load and thermal behavior;  $I_r$  – rated current load,  $I_L$  – current load,  $I_{th\ 1s}$  – thermal equivalent 1-second short circuit current,  $\vartheta_0$  – ambient temperature,  $\vartheta_L$  – conductor temperature,  $\Theta$  – overtemperature,  $\vartheta_{Gr}$  – limiting temperature, and  $\vartheta_a$  – origin temperature in normal operation (adapted from [4.5])

	Permanent current load	Flexible current load	Short-term current load Short-circuit current
Current and thermal behavior			
Equivalent thermal network			
Thermal power losses	$P_{IN} = P_{OUT} = P_K + P_S + P_L$ $P_V = I_L^2 R_{el}(\vartheta)$	$P_{IN} = P_{OUT} + \frac{dQ}{dt}$	$P_{IN} = \frac{dQ}{dt}$ $Q = \int_0^{t_K} P_{IN}(\vartheta) dt = mc \Delta \vartheta$ $= \int k I_{th\ 1s}^2 R_{el}(\vartheta) dt$

If the circumference transmitting heat through radiation and convection  $U$  is the same, the following applies in simplified form

$$dP_K + dP_S = [\alpha_K(\vartheta) + \alpha_S(\vartheta)]U(\vartheta_L - \vartheta_0)dx$$

$$= \alpha(\vartheta)U(\vartheta_L - \vartheta_0)dx, \quad (4.8)$$

with

$$\alpha = \alpha_K + \alpha_S. \quad (4.9)$$

Inserting (4.3)–(4.9) into (4.2) results in

$$\frac{kI^2 \rho(\vartheta)}{A} - Ac\delta \frac{\partial \vartheta}{\partial t} + \lambda A \frac{\partial^2 \vartheta}{\partial x^2} - \alpha(\vartheta)U(\vartheta_L - \vartheta_0) = 0. \quad (4.10)$$

This differential equation for the heat balance of the homogeneous, long conductor is solved for four special cases:

1. Stationary heating – continuous load (Table 4.9, left column)

A constant current flows, which causes the heat losses  $P_V$ . Those increase the conductor temperature to  $\vartheta_L$  (4.3). Since the current  $I$  is assumed to be constant with time, there is no storage of heat (4.4). In addition, it is assumed that there is no axial heat

transfer in the conduct. Thus, the following boundary conditions apply:

- $dP_C = 0$  no heat storage
- $dP_{LIN} = dP_{LOUT}$  no heat flow along the conductor.

Because of this all heat losses,  $P_V$  have to be radially transmitted to the surroundings via radiation  $P_S$  and convection  $P_K$

$$dP_V = dP_K + dP_S. \quad (4.11)$$

With (4.9) and (4.10), it follows that

$$\frac{kI^2 \rho(\vartheta)}{A} = \alpha(\vartheta)U(\vartheta_L - \vartheta_0). \quad (4.12)$$

The permissible continuous current  $I_r$ , at which the conductor temperature  $\vartheta_L$  is less than or equal to the permissible limit temperature of the conductor  $\vartheta_{Gr}$  is given by (4.12) to be

$$I_r = \sqrt{\frac{\alpha(\vartheta)UA(\vartheta_L - \vartheta_0)}{k\rho_{20}[1 + \alpha_T(\vartheta_L - 20^\circ\text{C})]}}. \quad (4.13)$$

Thereby, the current  $I_L$ , which depends on the conductor temperature  $\vartheta_L$  and the ambient temperature  $\vartheta_0$ , should not exceed the permissible continuous current  $I_r$ , so that the limit temperature  $\vartheta_{Gr}$  of the conductor will be observed.

2. Transient heating – short-term load (Table 4.9, right column)

During a short-term current flow up to 1 s, there is practically no heat conduction or convection and radiation, because these are relative slow physical processes. Thus, the following boundary conditions apply:

- $dP_K = dP_S = 0$ , i.e., no convection and no radiation
- $dP_{LIN} = dP_{LOUT}$  no heat flow along the conductor.

The total power losses  $P_V$  in the conductor must, therefore, be stored in the conductor itself during the duration of the current (adiabatic heating)

$$dP_V = dP_C. \quad (4.14)$$

From (4.14), the following differential equation is obtained

$$\frac{kI^2\rho(\vartheta)}{A} = Ac\delta \frac{\partial\vartheta}{\partial t}. \quad (4.15)$$

Its solution is the thermally permissible short-term current  $I_{th}$  for a time duration  $t_K$  in (4.15),

$$I_{th} = \sqrt{\frac{c\delta A^2}{k\rho_{20}\alpha_T t_K} \ln \left[ \frac{1 + \alpha_T(\vartheta_{Gr} - 20^\circ\text{C})}{1 + \alpha_T(\vartheta_a - 20^\circ\text{C})} \right]}. \quad (4.16)$$

Here, the current  $I_{th}$  depends on the time duration  $t_K$ , the temperature of the conductor  $\vartheta_a$  before the onset the short-term load, and the permissible limit temperature of the conductor  $\vartheta_{Gr}$  for the short-term load. Usually, this limit value is higher than for a continuous current load and is specified in the standards.

When the short-term thermal current  $I_{th}$  or the short-term current density  $J_{th}$  are known, the conductor temperature can be calculated  $\vartheta_L$  as a function of the time duration  $t_K$  of the short-term current

$$\vartheta_L = \frac{1}{\alpha_T} \left\{ [1 + \alpha_T(\vartheta_a - 20^\circ\text{C})] \exp \frac{kJ^2\rho_{20}\alpha_T}{c\delta} t_K - 1 \right\} + 20^\circ\text{C}, \quad (4.17)$$

where  $J$  = current density

3. Variable heating – variable load (Table 4.9, middle column)

The most frequent load case is probably a variable load for which both the ambient temperature and

the current load change over time. Because of the heat-storage capacity of the conductor, the conductor temperature  $\vartheta_L$  always lags behind the current  $I_L(t)$ . Assuming that there is no heat transfer along the conductor, the following boundary condition applies

$$dP_{LIN} = dP_{LOUT}$$

(no heat flow along the conductor), where the radial heat transfer by convection  $P_K$  and by radiation  $P_S$ , as well as the heat storage  $P_C$ , enter the heat balance equation

$$dP_V - dP_C - dP_K - dP_S = 0. \quad (4.18)$$

With (4.9) and (4.10), one obtains

$$\frac{kI^2\rho(\vartheta)}{A} - Ac\delta \frac{\partial\vartheta}{\partial t} - \alpha(\vartheta)U(\vartheta - \vartheta_0) = 0. \quad (4.19)$$

For a transient situation and for a lower ambient temperatures  $\vartheta_0$ , a temporary overcurrent,  $I_L$ , higher than the rated current  $I_r$  can be sustained without the limit temperature of the current path being exceeded. Knowledge of the thermal time constants of all related components is indispensable for the practical use of this effect.

The time dependence of the temperature (heating) of a conductor  $\vartheta_L(t)$  [4.20] after switching a current  $I_L(t)$  on (Fig. 4.9a) is obtained by solving (4.19)

$$\vartheta(t) = \Delta\vartheta_{\text{end}} \left( 1 - e^{-\frac{t}{\tau}} \right) + \vartheta_0, \quad (4.20)$$

where

$$\tau = \frac{c\delta A}{\alpha(\vartheta)U}, \quad (4.21)$$

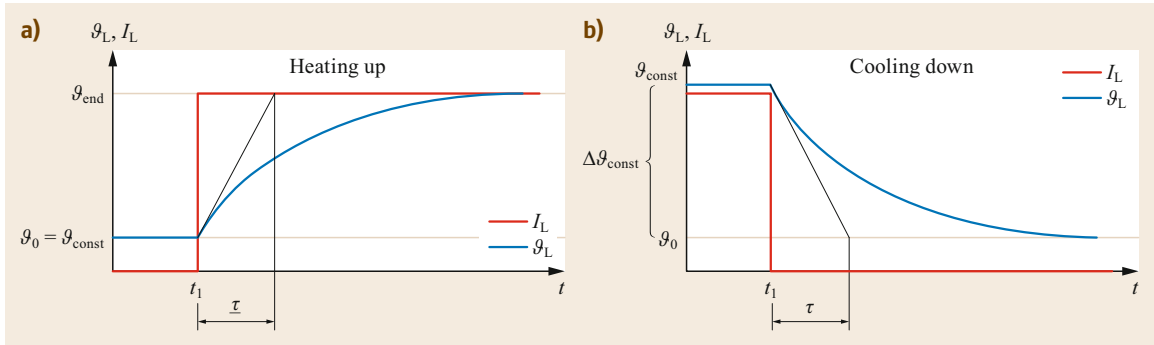
and  $\tau$  = thermal time constant, and  $\Delta\vartheta_{\text{end}}$  = final temperature value in the stationary state after heating.

Cooling a conductor after switching a current  $I_L(t)$  off (Fig. 4.9b) follows as

$$\vartheta(t) = \Delta\vartheta_{\text{const}} e^{-\frac{t}{\tau}} + \vartheta_0. \quad (4.22)$$

Examples: the thermal time constant  $\tau$  amounts to:

- 15–25 min with air-cooled copper conductors
- 2–3 min for oil-cooled conductors
- 1 min for water-cooled conductors
- 10 min for aluminum overhead-line conductors.



**Fig. 4.9a,b** Conductor temperature  $\vartheta_L(t)$  after switching on and off a current  $I_L$ . After  $3\tau$  the temperatures deviate only by 5% of the final value  $\vartheta_{end}$ . **(a)** Temperature rise after switching on, **(b)** temperature fall after switching off

4. Heating of a long, linear conductor with additional temperature distribution along the conductor from a heat source (Fig. 4.10).

When there are points along a conductor with additional power losses  $P_V$ , these result in hot spots with a temperature of  $\vartheta_V$ . The heat conduction  $P_L$  along the conductor, though, reduces such local temperature rises  $\Delta\vartheta_V$  until their effect is no longer noticeable, i.e., until  $\vartheta_{endL}$ .

Examples:

- Damaged or highly-aged connections with a high resistance (Sect. 4.3.3); these impose a hot spot.
- Local reduction of the conductor cross section.

- Additional losses in components with hysteresis and eddy current losses (old type dead-end clamps from malleable cast iron in overhead lines, steel bushings, and fasteners).

From the heat balance equation (4.9), one obtains under the boundary condition that there is no heat storage, as this process is time invariant, i.e.,  $dP_C = 0$ ,

$$dP_V - dP_L - dP_K - dP_S = 0, \tag{4.23}$$

which leads to

$$\frac{kI^2\rho(\vartheta)}{A} + \lambda A \frac{\partial^2\vartheta}{\partial x^2} - \alpha(\vartheta)U(\vartheta - \vartheta_0) = 0, \tag{4.24}$$

or

$$\frac{d^2\vartheta}{dx^2} - \frac{\alpha(\vartheta)U}{\lambda A}\vartheta + \frac{\alpha(\vartheta)U}{\lambda A}\vartheta_0 + \frac{kI^2\rho(\vartheta)}{\lambda A} = 0, \tag{4.25}$$

with the homogeneous part

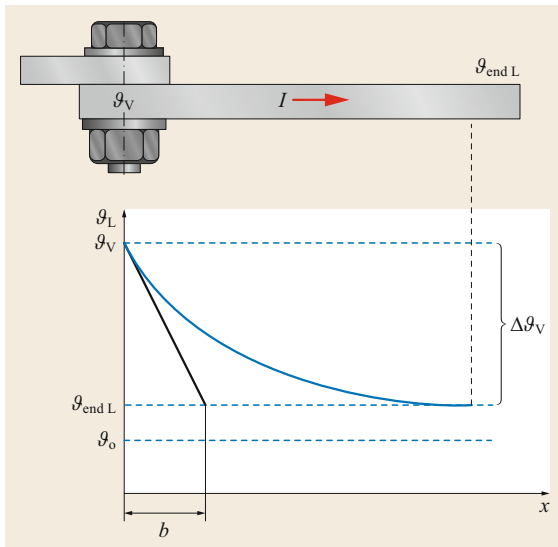
$$\frac{d^2\vartheta(x)}{dx^2} - \frac{1}{b^2}\vartheta(x) = 0. \tag{4.26}$$

Assuming

$$\vartheta(x) = e^{ax}, \quad \ddot{\vartheta}(x) = a^2e^{ax}, \tag{4.27}$$

and inserting in (4.26), one obtains

$$a^2e^{ax} - \frac{1}{b^2}e^{ax} = 0,$$



**Fig. 4.10** Distribution of the conductor temperature  $\vartheta_L(x)$  with unequal dissipation of power loss along the conductor. After  $3b$  the temperatures deviate only by 5% of the final value  $\vartheta_{end}$

with the solution

$$a^2 - \frac{1}{b^2} = 0, \quad a^2 = \frac{1}{b^2}, \quad a = \sqrt{\frac{1}{b^2}} = \pm \frac{1}{b}. \tag{4.28}$$

Thus, the temperature distribution along the conductor becomes (Fig. 4.10)

$$\vartheta(x) = \Delta\vartheta_{\text{ve}} e^{-\frac{x}{b}} + \vartheta_{\text{endL}}, \tag{4.29}$$

where  $b$  is the thermal local constant

$$b = \sqrt{\frac{\lambda A}{\alpha(\vartheta)U}}. \tag{4.30}$$

This means that the temperature difference  $\Delta\vartheta$  (higher or lower) along a conductor subsides after a distance of three times the thermal local constant  $b$  to about 5% of its original value.

Examples: the thermal local constant  $b$  is approximately:

- 30–35 cm for a copper bus bar 100 mm × 10 mm
- 20–25 cm for an aluminum bus bar 40 mm × 10 mm
- 22 cm for an aluminum overhead conductor 240 mm<sup>2</sup>.

### Calculation of Temperature Distribution

In order to calculate the spatial temperature distribution of a device, knowledge of the relevant heat sources, i.e., the heat conduction along the current path, is required according to the thermal balance equation;  $P_L$  the heat dissipation by convection  $P_K$ , the radiation  $P_S$  radially to the current path and with dynamic processes and also the heat capacities  $P_C$  are required. The necessary information on the design, dimensions, and materials must be known. Even if these often have to be procured laboriously or determined experimentally, they are indispensable.

Heat sources in electrical equipment can usually be the following (Fig. 4.11):

- Electrical heat losses  $P_V$  in the conductor,  $P_{VL}$  and in the electrical contacts and connections  $P_{Vj}$ ,

$$P_{VL} = kI_L^2 R_{\sim}(\vartheta) = kI_L^2 \frac{\rho_{20}l}{A_L} [1 + \alpha_{T20}(\vartheta_L - 20^\circ\text{C})], \tag{4.31}$$

where

$$k = \frac{P_{\sim}}{P_{=}} = \frac{R_{\sim}}{R_{=}}, \tag{4.32}$$

and  $P_{\sim}$  = alternating current (AC) power,  $R_{\sim}$  = AC resistance of the conductor,  $P_{=}$  = direct current (DC) power, and  $R_{=}$  = DC resistance of the conductor.

The skin effect factor  $k$  is a measure of the higher resistance for alternating current (AC) (skin effect for single conductors, proximity effect for the mutual influence of parallel conductors) than for direct current, for common current paths and can be taken as an example for rectangular conductors from Table 4.10 (Fig. 4.12). For common rectangular, round, tubular, and profile conductors, these factors are already taken into account when specifying the current-carrying capacity [4.19, 21, 22].

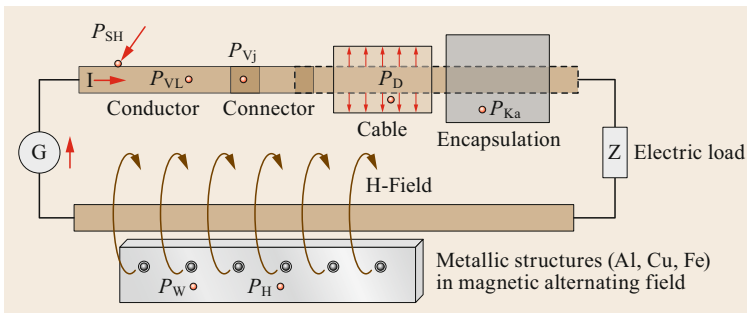
The current heat losses in electrical connections  $P_{Vj}$  result in

$$P_{Vj} = I^2 R_j(\vartheta, t), \tag{4.33}$$

and

$$R_j(\vartheta, t) = R_m(\vartheta) + R_c(t) + R_f(t), \tag{4.34}$$

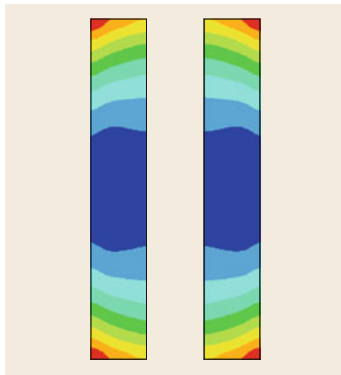
where  $P_{Vj}$  = heat or dissipation in one connection,  $I$  = current flowing in the connection,  $R_j(t)$  = joint



**Fig. 4.11** Thermal power losses in an electric power circuit;  $P_{VL}$  = electric heat losses in conductors,  $P_{Vj}$  = electric heat losses in connectors,  $P_D$  = dielectric losses (in cables  $\geq 200$  kV),  $P_{Ka}$  = losses in encapsulation and concentric external conductor,  $P_W$  = eddy-current losses,  $P_H$  = hysteresis losses, and  $P_{SH}$  = thermal power from solar and sky radiation

**Table 4.10** Current displacement factor  $k$  for rectangular flat bus bars ( $k = R_{\sim}/R_{=}$  for rectangular flat bus bars with subconductors;  $f = 50\text{ Hz}$ ;  $\vartheta_L = 70^\circ\text{C}$ ; space between subconductors = 10 mm)

Dimensions		1 bus bar		2 subconductors		3 subconductors		4 subconductors	
(mm <sup>2</sup> )	$b : h$	Cu	Al	Cu	Al	Cu	Al	Cu	Al
40 × 10	1 : 4	1.03	1.01	1.07	1.03	1.06	1.07	1.22	1.12
50 × 10	1 : 5	1.05	1.02	1.12	1.05	1.25	1.12	1.33	1.18
60 × 10	1 : 6	1.07	1.03	1.17	1.08	1.34	1.17	1.45	1.25
80 × 10	1 : 8	1.11	1.05	1.27	1.13	1.49	1.26	1.66	1.38
100 × 10	1 : 10	1.15	1.08	1.34	1.19	1.61	1.35	1.82	1.51
120 × 10	1 : 12	1.18	1.10	1.40	1.23	1.70	1.45	1.94	1.62
160 × 10	1 : 16	1.23	1.14	1.48	1.31	1.84	1.54	2.14	1.78
200 × 10	1 : 20	1.27	1.17	1.54	1.36	1.96	1.63	2.29	1.90


**Fig. 4.12** Related current density distribution  $J$  in a  $2 \times (60 \times 10)\text{ mm}^2$  rectangular flat bus bar (schematically)

resistance (time-dependent quantity  $\rightarrow$  aging),  $R_m =$  metallic lead resistance/self-resistance,  $R_c(t) =$  constriction resistance (time-dependent variable  $\rightarrow$  aging), and  $R_f(t) =$  impurity film resistance (time-dependent variable  $\rightarrow$  aging).

Just like the losses in the conductor, the losses in the joints also depend on the current load  $I_L$  and, thus, the temperature of the conductor. In addition, in this case, the time variation of the joint resistance  $R_v(t)$  by aging processes (Sect. 4.3.3) has to be considered:

- Dielectric losses  $P_D$  have to be considered in high-voltage cables with operating voltages  $\geq 220\text{ kV}$  and are calculated as

$$P_D = U_B^2 \omega C_B \tan \delta, \quad (4.35)$$

where  $U_B =$  operating voltage,  $\omega =$  angular frequency,  $C_B =$  electrical capacity of the equipment, and  $\tan \delta =$  loss factor.

- Eddy current losses  $P_W$  occur when alternating magnetic fields penetrate components made of non-ferromagnetic materials

$$P_W = \frac{1}{24} \kappa \omega^2 d^2 \hat{B}_m^2 V F(x), \quad (4.36)$$

with

$$F(x) = \frac{3 \sinh x \sin x}{x \cosh x \cos x}, \quad (4.37)$$

$$x = \beta d, \quad (4.38)$$

$$\beta = \sqrt{\pi f \kappa \mu}, \quad (4.39)$$

where  $\kappa =$  conductance,  $\omega =$  angular frequency,  $f =$  power frequency,  $\mu =$  permeability,  $d =$  thickness of the sheet,  $\hat{B}_m =$  peak value of the mean magnetic induction, and  $V =$  volume.

- If components made of ferromagnetic materials, e.g., steel parts, are penetrated by alternating magnetic fields, hysteresis losses  $P_H$  occur

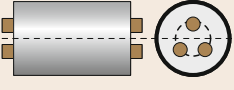
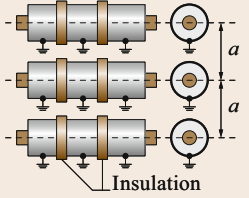
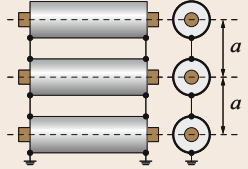
$$P_H = \frac{8}{3} \nu f \hat{H}_m^3 V, \quad (4.40)$$

where  $\nu =$  material constant, determined by the hysteresis of the material,  $f =$  power frequency,  $\hat{H}_m =$  peak value of the mean magnetic field strength, and  $V =$  volume.

- Losses  $P_{Ka}$  in the enclosure of modern switchgear and in concentric outer conductors of cables are generated by induction or eddy currents. The driving voltage required for this is induced by the alternating magnetic field of the conductor currents in the enclosure. The smaller the distance between the conductor and the concentric outer conductor and the larger the conductor current, the greater these losses become. In three-phase systems, a distinction must be made between single-pole and three-pole enclosure. In single-pole insulated systems, the arrangement *side-by-side* must also be distinguished from the *triangular* arrangement, since the magnetic fields of the three conductors in the three-phase system compensate each other in different ways, which affects the losses (Table 4.11). Thereby the individual segments of the enclosure



**Table 4.11** Typical configurations for encapsulated bus bars or cables

Three-phase encapsulation	Single-phase encapsulation	
Triangular ( $3 \times 120^\circ$ )	Side-by-side	Triangular ( $3 \times 120^\circ$ )
	Not electrically connected	Electrically connected through
		

can be electrically connected through or insulated from each other (not connected for  $l < 10\text{ m}$ ) and individually/each one earthed [4.2].

– Single-pole encapsulation

In a symmetrical three-phase system with single-pole insulated current paths, the mean enclosure losses of a concentric outer conductor are calculated as

$$P_{Ka} = mKI_L^2 \frac{\rho_{20}}{A_K} l [1 + \alpha_T (\vartheta_{Ka} - 20^\circ\text{C})], \tag{4.41}$$

where  $A_K$  = conductor cross section of the enclosure,  $a$  = conductor spacing,  $d_{Ka}$  = enclosure diameter,  $I_{Ka}$  = capsule current,  $I_L$  = conductor current,  $K$  = enclosure power-loss factor (Fig. 4.14a),  $k'$  = enclosure factor (Fig. 4.14a),  $l$  = length of the enclosure,  $m$  = correction factor (0.9–1.04) (Fig. 4.14b), and  $R_{Ka}$  = enclosure resistance, which are dependent from the temperature, and where the enclosure power-loss factor  $K$  represents the ratio of the actually generated heat output to the output that arises when the enclosure current  $I_{Ka}$  is equal to the phase current  $I_L$  (Fig. 4.16).

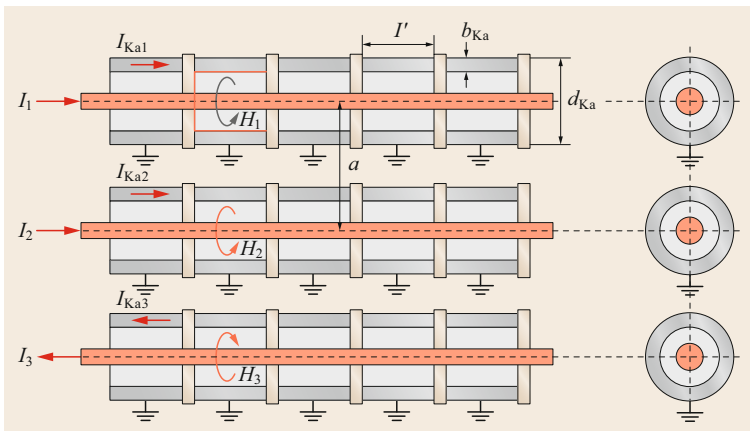
If the individual segments of the current path are not connected (Table 4.11, column 2, Fig. 4.13), the enclosure power-dissipation factor becomes  $K < 1$  for nonferromagnetic materials and for a ratio of the enclosure diameter to the conductor distance  $d_{Ka}/a < 0.82$ . For  $0.82 < d_{Ka}/a < 0.9$   $K$  becomes 1.5 (Fig. 4.14a). This diagram applies for an enclosure factor  $k' = 20$  according to the relationship (4.42) is calculated to

$$k' = \omega \kappa \mu_0 b_{Ka} r_{Ka}, \tag{4.42}$$

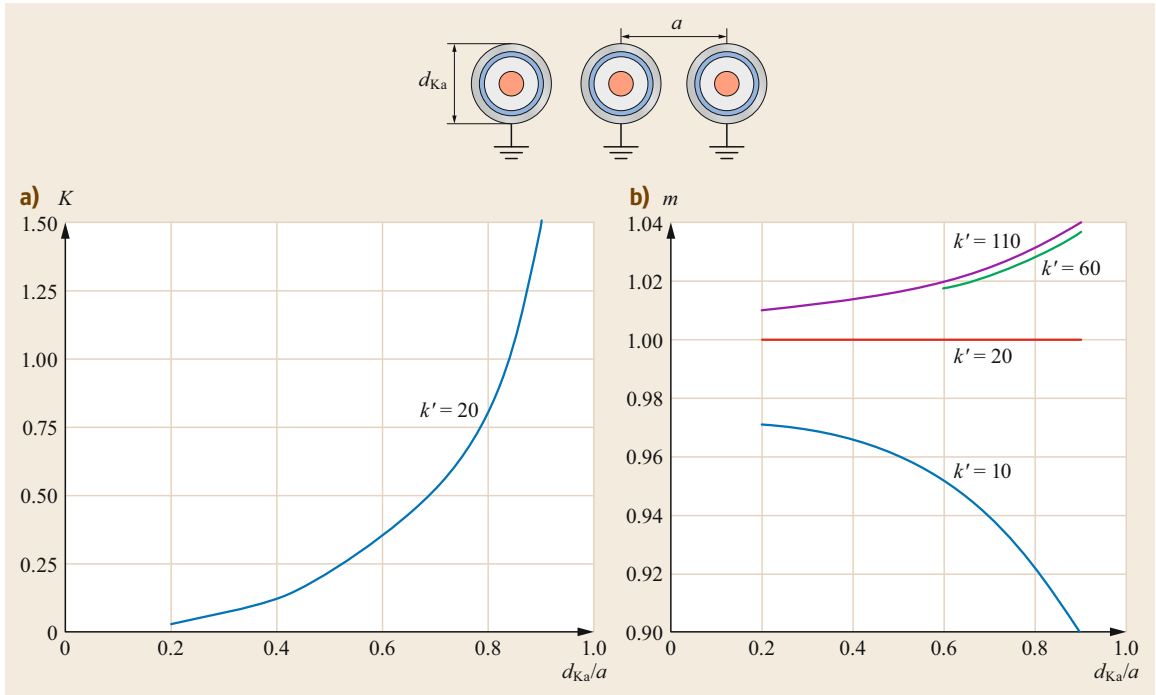
with  $b_{Ka}$  = thickness of enclosure,  $r_{Ka}$  = enclosure diameter,  $\omega$  = angular frequency of the network, and  $\kappa$  = electrical conductivity of the enclosure material.

For enclosure factors deviating from  $k' = 20$ , correction factors  $m$  must be taken into account, which use the geometric and electrical conditions in accordance with (4.42) (Fig. 4.14b).

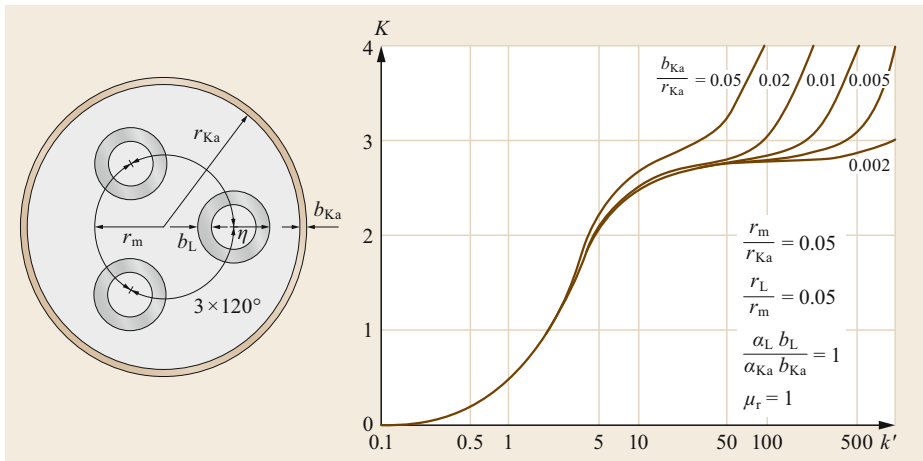
With a smaller conductor distance  $a$  and more compact design, the enclosure power-loss factor  $K$  and, thus, the losses  $P_{Ka}$ , are larger. The enclosure losses of the concentric outer conductor also increase with poorer conductivity of the enclosure material.



**Fig. 4.13** Power losses  $P_{Ka}$  in encapsulated bus bars and a concentric external conductor, GIL with a single pole, not connected encapsulation, side-by-side, length of segments  $l < 10\text{ m}$ , symmetrical current load in three phases (adapted from [4.2])



**Fig. 4.14** (a) Encapsulation power factor  $K$  for calculation of power losses in all three capsules in the case of symmetric current load (single-pole, unconnected encapsulation) (b) correcting factor  $m$  for encapsulation factor  $k'$  if  $k' \neq 20$  (adapted from [4.2])



**Fig. 4.15** Encapsulation power-loss factor  $K$  with three-pole cylindrical encapsulation (adapted from [4.2])

If the individual segments of an enclosure are electrically connected along the current path ( $l > 10$  m) (Table 4.11, columns 3 and 4), then for practically relevant applications, the conductor ( $I_L$ )- and the enclosure currents ( $I_{Ka}$ ) have about the same magnitude, i.e.,

$$K = \left( \frac{I_{Ka}}{I_L} \right)^2 \approx 1, \tag{4.43}$$

thus, the enclosure losses  $P_{Ka}$  can be computed as

$$P_{Ka} = I_{Ka}^2 R_{Ka}(\vartheta). \tag{4.44}$$

- Three-pole enclosure If the three conductors of a symmetrical three-phase system are arranged together in an equilateral triangle in a cylindrical enclosure of nonferromagnetic material (Ta-

ble 4.11 column 1), the mean enclosure losses can be calculated with (4.41) with  $m = 1$ . The enclosure power factor  $K$  depends on the enclosure factor  $k'$  and the ratio of wall thickness  $b_{Ka}$  of the encapsulation to the mean radius of the three conductors  $r_m$  (Fig. 4.15).

- Heating capacities  $P_{SH}$  by *solar and celestial radiation*, to be taken into account in outdoor installations, especially in countries with intensive solar radiation. The maximum daily output is

$$P_{SH} = ik'\alpha'P_{SH}^*(h) \sin \gamma A \quad (4.45)$$

$$h = (90^\circ + \delta) - \phi, \quad (4.46)$$

where  $i$  = pollution factor (Fig. 4.16c),  $k'$  = correction factor for height above sea level (Fig. 4.16d),  $\alpha'$  = absorption coefficient,  $\gamma$  = inclination of the surface to the incidence of the Sun,  $A$  = illuminated surface,  $h$  = sun elevation (Fig. 4.16a),  $\phi$  = latitude, and  $\delta$  = declination of the Sun (Fig. 4.16b)

For the time variation of the heat output caused by solar and celestial radiation, the day and year movement of the Sun must be taken into account (Fig. 4.16e)

$$P_{SH} = ik'\alpha'P_{SH}^*(h) \sin \gamma A \cos \alpha, \quad (4.47)$$

where  $A$  = azimuth,  $h$  = solar elevation,  $t$  = hour angle,  $WOZ$  = true local time,  $\alpha$  = angle between the position of the surface in relation to the azimuth and the position of the Sun, and  $\beta$  = surface azimuth.

Example: the daily variation of the directly and diffusely irradiated heat  $P_{SH}$  on an equipment enclosure with the dimensions length  $\times$  width  $\times$  height = 1 m  $\times$  1 m  $\times$  1 m on 21 June at a location  $51^\circ$  N latitude, at sea level  $NN = 0$  depending on true local time must be determined.

The maximum Sun elevation is calculated taking into account the declination  $\delta = 23.5^\circ$  on 21 June, the day with the highest position of the Sun

$$h_{\max}(90^\circ + 23.5^\circ) - 51^\circ = 62.5^\circ. \quad (4.48)$$

This allows the maximum possible solar power of approximately  $980 \text{ W m}^{-2}$  to be absorbed (Fig. 4.17). At this solar elevation, the pollution factor  $i$  is 0.8 (Fig. 4.16c).

The altitude of the Sun  $h(t)$  changes during the day with

$$h(t) = 90^\circ - [\arccos(\sin \delta \sin \phi \cos \delta \cos \phi \cos t)], \quad (4.49)$$

where the hour angle  $t$  results from

$$t = -(12 \text{ h} - WOZ)\omega, \quad (4.50)$$

with

$$\omega = \frac{2\pi}{d} = \frac{360^\circ}{24 \text{ h}} = 15 \frac{\text{deg}}{\text{h}}. \quad (4.51)$$

The azimuth  $a$  is calculated by

$$a = \arctan \frac{\cos \delta \sin t}{\sin \phi \cos \delta \cos t - \cos \phi \sin \delta}. \quad (4.52)$$

The angle  $\alpha$  is the difference between the position of the surface in relation to the direction  $\beta$  and the Sun's azimuth  $a$

$$\alpha = (\beta - a). \quad (4.53)$$

The result of this calculation (Fig. 4.17) shows the temporally and spatially uneven thermal load of the individual surfaces on the north, east, south, and west locations as caused by solar and celestial radiation. The normal surface experiences the largest heat load. Such calculations can be helpful in optimizing the thermal design, construction, and installation of thermally highly loaded equipment [4.2, 23].

### Thermal Storage

For dynamic thermal processes, the *heat energy*  $Q_C$  stored in the conductor, in the insulation and in the connectors must be taken into account during dimensioning

$$Q_C = mc\Delta\delta = mc(\vartheta - \vartheta_0) = C_{th}(\vartheta - \vartheta_0), \quad (4.54)$$

where  $Q_C$  = stored heat energy,  $m$  = mass of the heat-storing volume,  $c$  = specific heat (Table 4.8),  $\Delta\vartheta$  = temperature difference,  $\vartheta$  = temperature of the volume to be heated,  $\delta_0$  = initial temperature before heating, and  $C_{th}$  = thermal capacity.

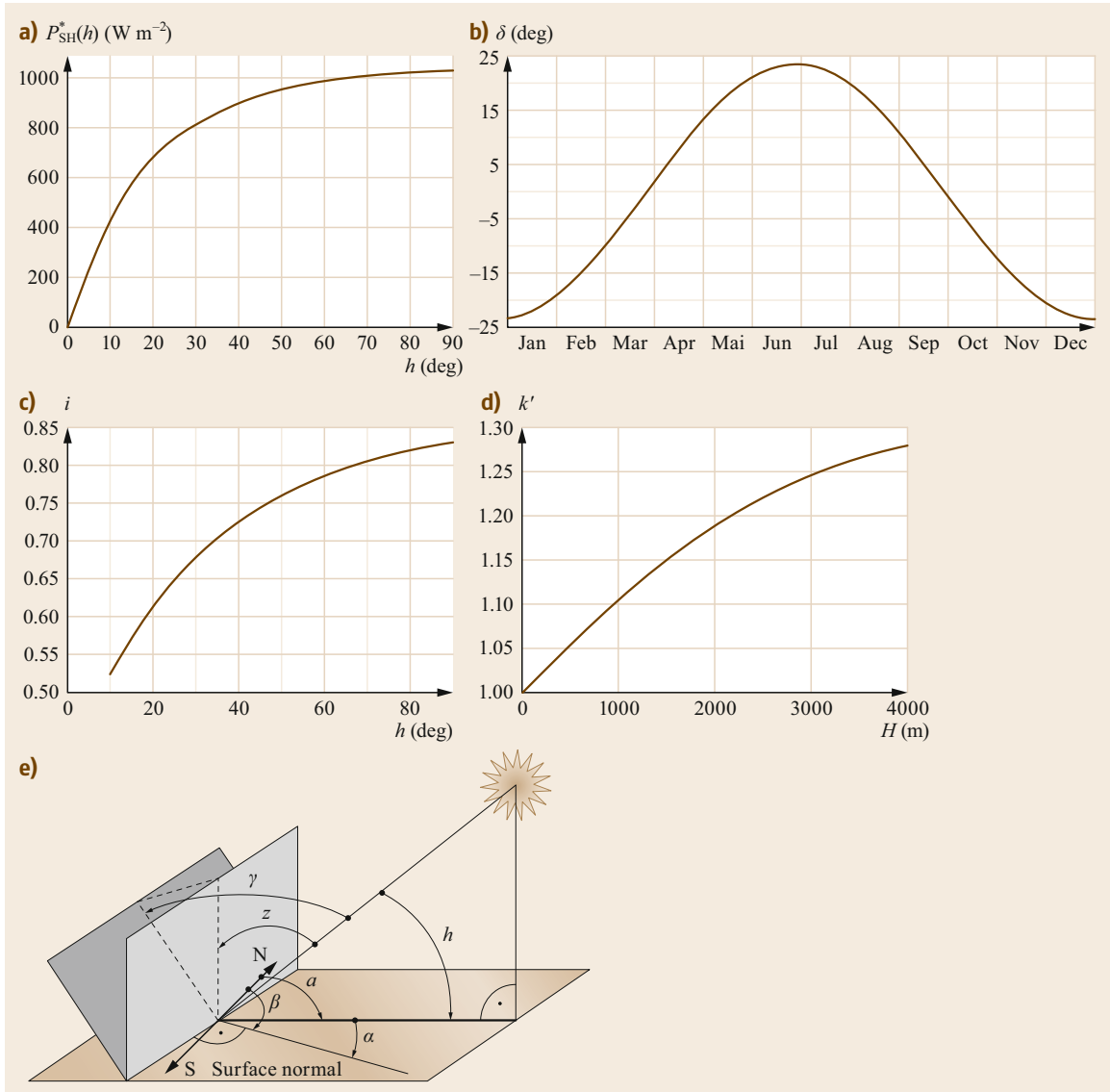
### Heat Transfer

Heat is transferred from high-temperature to low-temperature regions by means of different physical processes, which depend on the materials involved.

*Heat conduction*  $P_L$ :

- In solids: by lattice vibrations, electron movement
- In liquids: by lattice vibrations, diffusion
- In gases: by diffusion.

Heat flow flows through a body during heat conduction  $P_L$ . According to the Fourier law of heat conduction, this can be calculated as (stationary heat



**Fig. 4.16a–e** Heat output from solar and sky radiation. (a) Power consumption of a normal area ( $1 m^2$ ) at NN due to global radiation as a function of the solar altitude  $h$  in clean air ( $a' = 1$ ), (b) declination  $d$  of the Sun depending on the course of a year ( $50^\circ N$  latitude), (c) pollution factor  $i$  of a normal area ( $a' = 1$ ) at NN due to global radiation as a function of the altitude of the Sun, (d) correction factor  $k'$  depending on  $H$ , the altitude above sea level NN, (e) the influence of the position of the Sun on the power curve

conduction)

$$P_L = -\lambda A \frac{d\vartheta}{dx}, \tag{4.55}$$

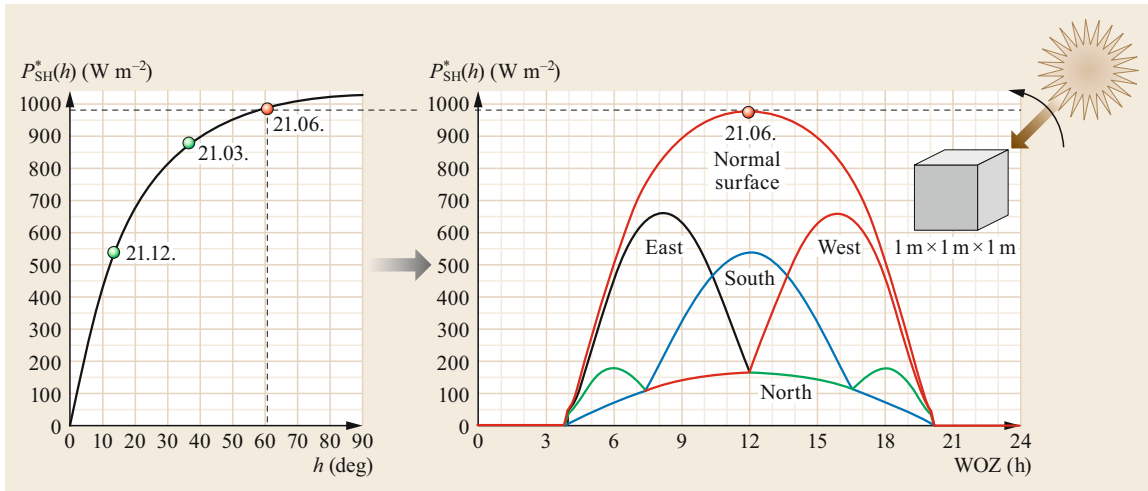
where  $\lambda$  = specific thermal conductivity (Table 4.8),  $A$  = surface perpendicular to heat flow, and  $d\vartheta/dx$  = thermal gradient.

The negative sign considers that heat flow takes place from the higher to the lower temperature.

Examples:

1. Stationary heat conduction through a flat wall (one-dimensional) (Fig. 4.18a)  
 From (4.55) it follows that

$$-\int_{\vartheta_i}^{\vartheta_a} d\vartheta = P_L \int_0^d \frac{dx}{\lambda A}, \tag{4.56}$$



**Fig. 4.17** Example of thermal power absorbed by solar and celestial radiation. Power consumption by direct and diffuse radiation on the side surfaces of a cube (1 m × 1 m × 1 m) on 21 June, 50° N latitude depending on the true local time (WOZ) [4.2, 23]

with the solution

$$\vartheta_i - \vartheta_a = \Delta\vartheta = P_L \frac{d}{\lambda A}, \tag{4.57}$$

which can also be written as

$$\Delta\vartheta = P_L R_{th,w}, \tag{4.58}$$

or in analogy to electrical engineering as *Ohm's law* of thermal fluid mechanics

$$R_{th,w} = \frac{d}{\lambda A}, \tag{4.59}$$

where  $\vartheta_i, \vartheta_a$  = temperature on the inside or outside of the flat wall,  $d$  = wall thickness, and  $R_{th,w}$  = thermal resistance of a flat wall.

2. Stationary heat conduction through a coaxial cylinder (one-dimensional) (Fig. 4.18b)

From (4.55), it follows that

$$-\int_{\vartheta_i}^{\vartheta_a} d\vartheta = P_L \int_{r_i}^{r_a} \frac{dr}{\lambda 2\pi r l}, \tag{4.60}$$

with the solution

$$\vartheta_i - \vartheta_a = \Delta\vartheta = P_L \frac{1}{\lambda 2\pi l} \ln\left(\frac{r_a}{r_i}\right), \tag{4.61}$$

which can also be written as

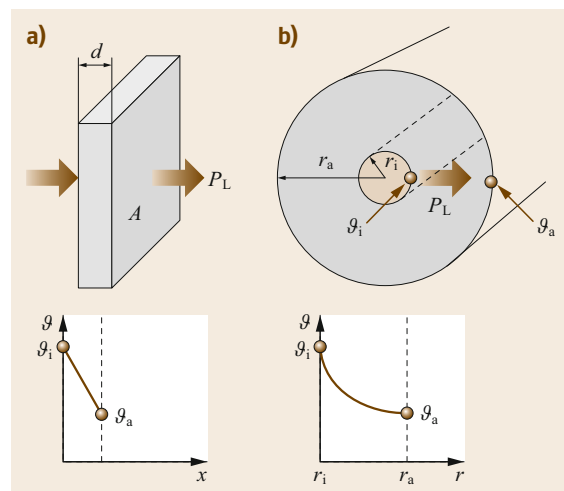
$$\Delta\vartheta = P_L R_{th,koax}, \tag{4.62}$$

or in analogy to electrical engineering as *Ohm's law* of thermal fluid mechanics

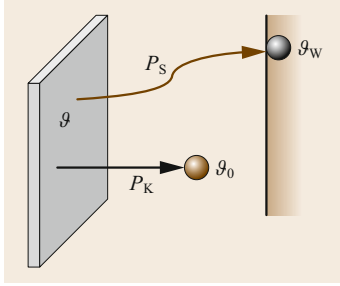
$$R_{th,koax} = \frac{1}{2\pi\lambda l} \ln\left(\frac{r_a}{r_i}\right), \tag{4.63}$$

where  $l$  = length of coaxial cylinder,  $r_a, r_i$  = outer and/or inner radius of the coaxial heat flow field, and  $R_{th,koax}$  = thermal resistance of the coaxial cylinder.

Heat transfer after Newton comprises convective heat transfer  $P_K$  and heat radiation  $P_S$  by electromagnetic waves from a solid through the surrounding gas



**Fig. 4.18a,b** Stationary heat conduction: (a) through a plane wall, (b) through a coaxial cylinder



**Fig. 4.19** Heat transfer from a warm surface with temperature  $\vartheta$  to the cooler environment by radiation and convection according to Newton

or liquid (Fig. 4.19), where  $\vartheta_0$  = ambient temperature,  $\vartheta_W$  = temperature of opposite wall,  $P_S$  = heat transfer by radiation, and  $P_K$  = heat transfer by convection.

$$P_U = \alpha O \Delta \vartheta, \quad (4.64)$$

whereby

$$\alpha = \alpha_S + \alpha_K, \quad (4.65)$$

and, therefore,

$$P_U = P_S + P_K = \alpha_S O_S (\vartheta - \vartheta_W) + \alpha_K O_K (\vartheta - \vartheta_0), \quad (4.66)$$

with the thermal radiation resistances

$$R_S = \frac{1}{\alpha_S O_S} \quad (4.67)$$

and the thermal convection resistance

$$R_K = \frac{1}{\alpha_K O_K}, \quad (4.68)$$

where  $P_U$  = heat transfer by radiation and convection,  $\alpha$  = heat-transfer coefficient,  $\alpha_S$  = heat-transfer coefficient for radiation,  $\alpha_K$  = heat-transfer coefficient for convection,  $O_S$  = surface for heat radiation,  $O_K$  = surface for heat convection,  $\vartheta_0$  = temperature of the surrounding medium (for convection),  $\vartheta_W$  = temperature of the opposite wall (for radiation),  $R_S$  = thermal radiation resistance, and  $R_K$  = thermal convection resistance.

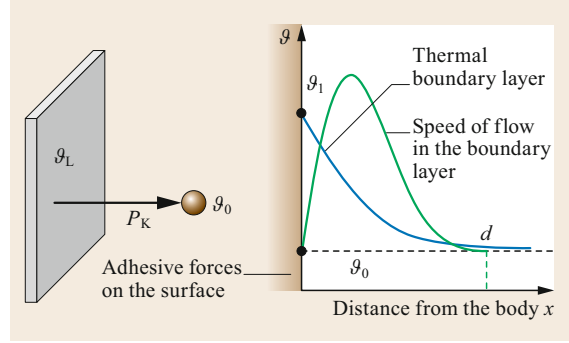
*Heat radiation*  $P_S$  takes place between the surfaces of solid bodies with different temperatures by electromagnetic waves in vacuum or in transparent materials (e.g., air) with wavelengths  $\lambda$ :

- At  $100^\circ\text{C} \Rightarrow \lambda = 7.76 \text{ mm}$  (infrared)
- At  $6000 \text{ K} \Rightarrow \lambda = 0.48 \text{ mm}$  (visible).

According to Wiens's law, the following applies

$$\lambda_{\max} T = 2896 \text{ mm K}, \quad (4.69)$$

where  $\lambda$  = wavelength of the electromagnetic wave, and  $T$  = absolute temperature.



**Fig. 4.20** Heat transfer by convection

The radiated power is calculated according to the Stefan–Boltzmann law

$$P_S = \varepsilon_{1,2} C_S O_S [(T_S)^4 - (T_W)^4], \quad (4.70)$$

with  $T_S$  = absolute temperature of the surface emitting heat through radiation  $O_S$ , and  $T_W$  = absolute temperature of the wall absorbing heat through radiation  $O_W$ .

The resulting emission number  $\varepsilon_{1,2}$  is based on the ratio of the radiating and the receiving surfaces, i.e.

- Parallel surfaces

$$\varepsilon_{1,2} = \frac{1}{\frac{1}{\varepsilon_1} + \frac{1}{\varepsilon_2} - 1}. \quad (4.71)$$

- Surrounding bodies with the surfaces  $O_{S1}$  and  $O_{S2}$

$$\varepsilon_{1,2} = \frac{1}{\frac{1}{\varepsilon_1} + \frac{O_{S1}}{O_{S2}} \left( \frac{1}{\varepsilon_2} - 1 \right)}, \quad (4.72)$$

where  $C_S = 5.67 \times 10^{-8} \text{ W m}^{-2} \text{ K}^{-4}$  = radiation coefficient of an ideal black body,  $\varepsilon_1, \varepsilon_2$  = emission number of areas 1 and 2, and  $O_{S1}, O_{S2}$  = size of the mutually emitting surfaces 1 and 2.

*Thermal convection*  $P_K$  is a mass transport taking place in liquids and gases along the surface of a solid body at a higher temperature  $\vartheta$  than the ambient temperature  $\vartheta_0$  (Fig. 4.20).

*Convection:*

- Heat transfer between solid body and fluid (gas/liquid)
- Bound to a motile medium
- Transfer of heat output in the boundary layers by heat conduction
- Transfer of heat output outside the boundary layers by mass transport.

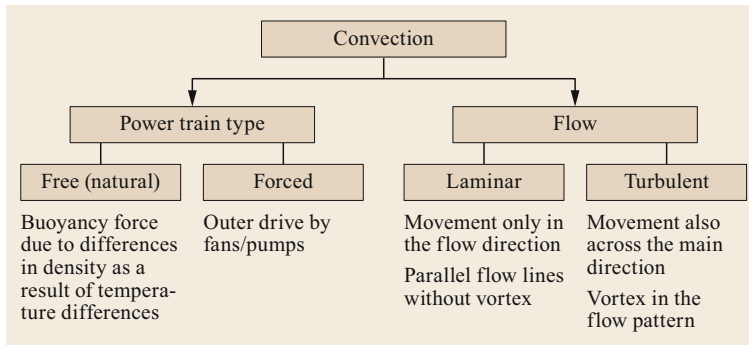


Fig. 4.21 Types of convection

Depending on the type of mass transport and the type of flow, different convection types can be distinguished (Fig. 4.21), which is reflected in the different heat-transfer coefficients  $\alpha_K$  (4.65) and (4.66). Because of the complexity of the physical processes involved, an analytical description is generally not available.

Nevertheless, according to *similarity theory*, it becomes possible to use *similarity criteria* to determine the relationship between the physical parameters involved, i.e.:

- Temperature  $\vartheta$ , position and dimensions of the heat-emitting surface  $O_K$
- The physical properties of the ambient cooling medium, e.g., its thermal conductivity  $\lambda$ , density  $\delta$ , specific heat capacity  $c$ , kinematic viscosity  $\nu$
- The type of convection (laminar or turbulent flow) (Fig. 4.21)

on the basis of experimental investigations of typical arrangements and to generalize this to similar arrangements within a range of validity (Tables 4.12–4.14).

For free convection

$$\text{Nu} = f(\text{GrPr}) = c_1 (\text{GrPr})^{n_1} \quad (4.73)$$

For forced convection

$$\text{Nu} = f(\text{Re}' \text{Pr}) = c_2 (\text{Re}')^{n_2} \quad (4.74)$$

$\text{Re}'$  takes into account the superposition of free and forced convection, e.g., in outdoor substations with low wind speed  $v \leq 1.0 \text{ m s}^{-1}$ . It is calculated from the superposition of forced flow with  $\text{Re}^*$  and free flow with  $\text{Re}$  to

$$\text{Re}' = \sqrt{\text{Re}^2 + \text{Re}^{*2}}, \quad (4.75)$$

where  $\text{Re}^*$  results from

$$\text{Re}^* = c^3 (\text{GrPr})^{n_3}, \quad (4.76)$$

with

$$c_3 = \left( \frac{c_1}{c_2} \right)^{\frac{1}{n_2}}, \quad (4.77)$$

and

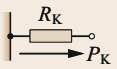
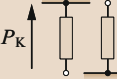
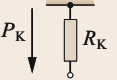

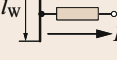
$$n_3 = \frac{n_1}{n_2} \quad (4.78)$$

**Table 4.12** Similarity criteria (characteristic values) for convective heat transfer

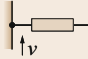
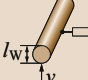
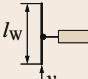
Nusselt number Nu	Determination of the heat-transfer coefficient for convection	$\text{Nu} = \frac{\alpha_K}{\lambda_{\text{med}}} l_w$ (Nusselt criterion) $\alpha_K = \text{Nu} \frac{\lambda_{\text{med}}}{l_w}$
Grashof number Gr	Free convection	$\text{Gr} = \frac{g \beta l_w^3}{\nu^2} (\vartheta - \vartheta_0)$
Reynolds number Re	Forced convection	$\text{Re} = \frac{v}{\nu} l_w$
Prandtl number Pr	Free convection	$\text{Pr} = \frac{\nu}{\alpha}; \alpha = \frac{\lambda_{\text{med}}}{c \delta}$

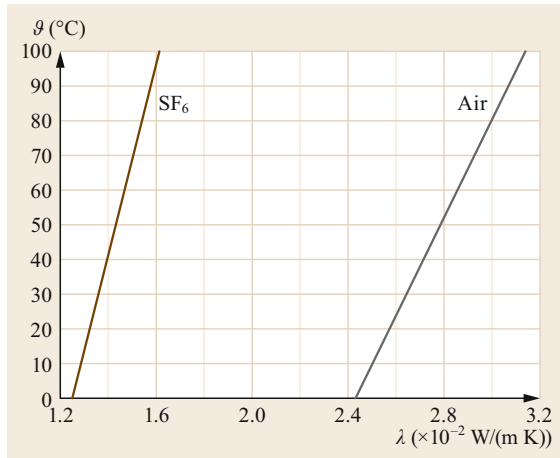
$\alpha_K$  = heat transfer coefficient for convection,  $\alpha$  = thermal diffusivity,  $l_w$  = characteristic length (Tables 4.13 and 4.14),  $\lambda_{\text{med}}$  = thermal conductivity of the medium (Fig. 4.22),  $g$  = gravity,  $\beta$  = coefficient of expansion of the medium,  $\nu$  = kinematic viscosity (Fig. 4.23),  $v$  = flow velocity.

**Table 4.13** Similarity functions to free convection,  $Nu = c_1(GrPr)^{n_1}$

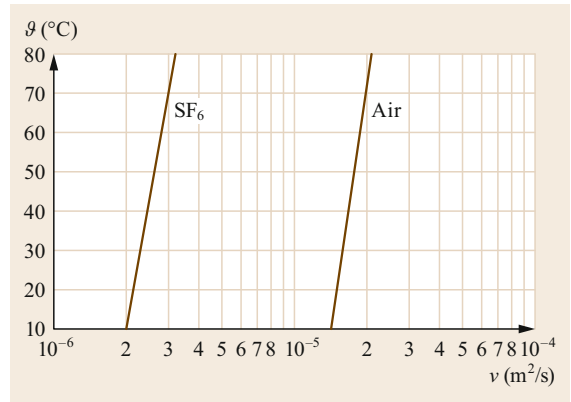
Arrangement	Application (example)	Schema	$c_1$	$n_1$	Range of validity
Vertical plate	Vertical wall of switchgear housing		0.15	0.33	$1.7 \times 10^7 < GrPr < 2 \times 10^{10}$
Horizontal plate (convection upside)	Roof of switchgear housing, inside and outside		0.17	0.33	$2.3 \times 10^8 < GrPr < 2.1 \times 10^9$
Horizontal plate (convection downside)	Channel bottom		0.095	0.33	$1.7 \times 10^8 < GrPr < 1.2 \times 10^9$
Horizontal cylinder	Cable, round conductor		0.56	0.25	$5 \times 10^2 < GrPr < 2 \times 10^7$
Bus bar, rectangular, single, twin, triple placed upright	Space between subconductors is equal to thickness of bus bar, free in air		0.60	0.25	$9 \times 10^4 < GrPr < 4.6 \times 10^6$

**Table 4.14** Similarity functions to forced convection in air,  $Nu = c_2(Re)^{n_2}$

Arrangement	Application (example)	Schema	$c_2$	$n_2$	Range of validity
Vertical plate, flowed along	Vertical wall of switchgear housing, forced cooled		0.16	0.66	$Re < 10^5$
Horizontal cylinder, flowed across	Forced cooled cable or round conductor		0.170	0.62	$10^3 < Re < 10^4$
Bus bar, rectangular, placed upright, flowed across	Forced cooled bus bar		0.400	0.60	$1.5 \times 10^3 < Re < 4.2 \times 10^4$

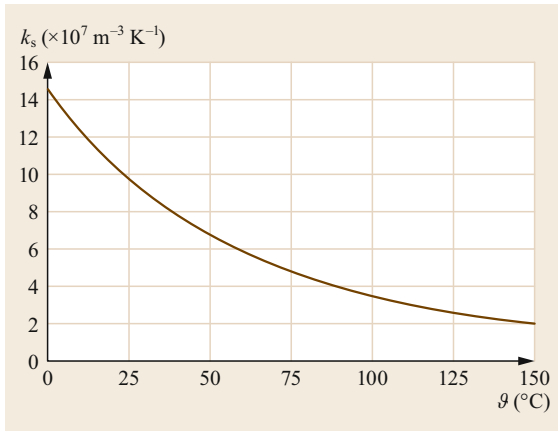


**Fig. 4.22** Thermal conductivity  $\lambda$  of gases at normal pressure



**Fig. 4.23** Kinematic viscosity  $\nu$  of gases





**Fig. 4.24** Coefficient of material value  $k_s$  for air at normal pressure (adapted from [4.5])

For this calculation, the physical properties of the cooling medium (Figs. 4.22 and 4.23) are adequately combined, taking into account their temperature dependence, in a material value coefficient  $k_s$  [4.2, 5] (Fig. 4.24).

$$k_s(\vartheta_m) = \frac{g\beta}{v^2} \text{Pr} = \frac{g\beta c\delta}{v\lambda_{\text{med}}}, \quad (4.79)$$

where  $k_s(\vartheta_m)$  = temperature-dependent material value coefficient, and  $\vartheta_m$  = average temperature.

Thereby the relevant temperature is the average temperature  $\vartheta_m$  between the heat-emitting surface  $O_K$  with temperature  $\vartheta$  and the temperature of the cooling medium  $\vartheta_0$

$$\vartheta_m = \frac{\vartheta + \vartheta_0}{2}. \quad (4.80)$$

Therefore,

$$(\text{GrPr}) = k_s l_w^3 (\vartheta - \vartheta_0),$$

where the heat-transfer coefficient  $\alpha_K$  can be calculated using the equations in Table 4.12 and (4.73)–(4.74). The values for  $c_1, c_2, c_3$  or  $n_1, n_2, n_3$  in (4.73), (4.74), and (4.76) must be determined experimentally. For typical arrangements, these values and their ranges of validity are available (Tables 4.13 and 4.14) [4.2].

Example: heat emission of a vertical surface 1.0  $\times$  1.0 m at a temperature of  $\vartheta = 70^\circ\text{C}$  and ambient air with  $\vartheta_0 = 30^\circ\text{C}$  by radiation (surface bare or coated) and by free or forced convection (Fig. 4.19, Table 4.15).

Results, depending on the combination of possible heat emission by radiation and convection are shown in Table 4.16.

The example shows the great influence of the surface treatment of the heat-emitting surface as well as of

**Table 4.15** Example calculation for the heat emission of a vertical surface  $O_S = O_K = 1 \text{ m}^2$ ,  $\vartheta = 70^\circ\text{C}$  ( $T_S = 273.15 \text{ K} + 70^\circ\text{C} = 343.15 \text{ K}$ ) to the ambient air at  $\vartheta = 30^\circ\text{C}$  and the surrounding walls with  $\vartheta_W = 30^\circ\text{C}$  ( $T_W = 273.15 \text{ K} + 30^\circ\text{C} = 303.15 \text{ K}$ )

Radiation		Convection	
Blank $\epsilon_1 = 0.25$	Painted $\epsilon_1 = 0.9$	Free $v = 0 \text{ m s}^{-1}$	Forced $v = 3 \text{ m s}^{-1}$
$\alpha_S = \frac{\epsilon_{1,2} C_S (T_S^4 - T_W^4)}{\vartheta_L - \vartheta_W}$		$\alpha_K = \frac{\lambda}{l_W} c_1 [\text{GrPr}]^{n_1}$	
$\epsilon_{1,2} = \frac{1}{\frac{1}{\epsilon_1} + \frac{O_{S1}}{O_{S2}} \left(\frac{1}{\epsilon_2} - 1\right)}$		$= \frac{\lambda}{l_W} c_1 [k_s(\vartheta_m) l_W^3 (\vartheta - \vartheta_0)]^{n_1}$	
$\epsilon_{1,2} = 0.25$ since $O_{S1} \ll O_{S2}$	$\epsilon_{1,2} = 0.9$ since $O_{S1} \ll O_{S2}$		
Radiation capacity of an ideal black body $C_S = 5.67 \times 10^{-8} \text{ W m}^{-2} \text{ K}^{-4}$		Characteristic length $l_W = 1.0 \text{ m}$	Characteristic length $l_W = 1.0 \text{ m}$
		Constant $c_1 = 0.15 \quad (\text{GrPr}) > 2 \times 10^7$	Constant $c_2 = 0.032 \quad (\text{Re}) > 1.667 \times 10^5$
		Exponent $n_1 = 1/3$	Exponent $n_2 = 0.8$
		Material coefficient $k_s = 6.7 \times 10^7 \text{ K}^{-1} \text{ m}^{-3}$	Kinematic viscosity $\nu = 18 \times 10^{-6} \text{ m}^2 \text{ s}^{-1}$
			Thermal conductivity of air $\lambda_{\text{med}} = 2.8 \times 10^{-2} \text{ W m}^{-1} \text{ K}^{-1}$
$\alpha_S = 1.92 \text{ W m}^{-2} \text{ K}^{-1}$	$\alpha_S = 6.9 \text{ W m}^{-2} \text{ K}^{-1}$	$\alpha_K = 5.83 \text{ W m}^{-2} \text{ K}^{-1}$	$\alpha_K = 13.48 \text{ W m}^{-2} \text{ K}^{-1}$
$P_S = \alpha_S O_S (\vartheta - \vartheta_0)$		$P_K = \alpha_K O_K (\vartheta - \vartheta_0)$	
$P_S = 76.8 \text{ W m}^{-2}$	$P_S = 276 \text{ W m}^{-2}$	$P_K = 233.2 \text{ W m}^{-2}$	$P_K = 539 \text{ W m}^{-2}$

**Table 4.16** Example calculation for total heat emission  $P$  by radiation and convection according to Table 4.15

Surface	$\varepsilon_1$ and $v$	$\alpha$ ( $\text{W m}^{-2} \text{K}^{-1}$ )		$P$ ( $\text{W m}^{-2}$ )	
Blank surface with free convection	$\varepsilon_1 = 0.25$ $v = 0 \text{ m s}^{-1}$	$\alpha_S$	1.92	$P_S$	76.8
		$\alpha_K$	+5.83	$P_K$	+233.2
		$\alpha$	7.75	$P$	310.0
Coated surface with free convection	$\varepsilon_1 = 0.9$ $v = 3 \text{ m s}^{-1}$	$\alpha_S$	6.90	$P_S$	276.0
		$\alpha_K$	+5.83	$P_K$	+233.2
		$\alpha$	12.73	$P$	509.2
Bare surface with forced convection	$\varepsilon_1 = 0.25$ $v = 0 \text{ m s}^{-1}$	$\alpha_S$	1.92	$P_S$	76.8
		$\alpha_K$	+13.48	$P_K$	+539.0
		$\alpha$	15.40	$P$	615.8
Coated surface with forced convection	$\varepsilon_1 = 0.9$ $v = 3 \text{ m s}^{-1}$	$\alpha_S$	6.90	$P_S$	276.0
		$\alpha_K$	+13.48	$P_K$	+539.0
		$\alpha$	20.38	$P$	815.0

forced air flow, e.g., by fans on the heat emission of the same surface.

Heat transfer by a *coolant flow*  $P_{\dot{V}}$  is the heat transport in enclosed systems by convection from the current path via a fluid (air, insulating gas) directly to the enclosure, such as in *ventilated current conducting arrangements* (air flow rate). The heat emitted from the heated components results in

$$P_{\dot{V}} = c\delta\dot{V}(\vartheta_a - \vartheta_e). \quad (4.81)$$

The air flow rate depends on the temperature-dependent pressure difference  $\Delta p$  and the sum of all flow resistances  $S$

$$\dot{V} = \sqrt{\frac{\Delta p}{S}}, \quad (4.82)$$

where the driving pressure difference depends on the mean temperature  $\vartheta_m$  between inlet and outlet openings and on the coefficient of expansion  $\beta$  of air

$$\vartheta_m = \frac{\vartheta_e + \vartheta_a}{2}, \quad (4.83)$$

$$\Delta p = gh\delta \left( \frac{1}{1 + \beta\vartheta_0} + \frac{1}{1 + \beta\vartheta_m} \right), \quad (4.84)$$

where  $P_{\dot{V}}$  = heat flow through the coolant,  $\dot{V}$  = volume flow rate between inlet and outlet,  $c$  = heat capacity of air,  $\delta$  = specific mass of air,  $\vartheta_e$  = temperature of air at the inlet,  $\vartheta_a$  = temperature of air at the outlet,  $\Delta p$  = pressure difference, and  $S$  = flow resistance.

This means that heat can only be transferred through a coolant flow if there are both air inlet and air outlet openings, and these are at different heights.

The flow resistance  $S$  is determined by the air inlet and outlet openings, as well as by cross-sectional narrowings

$$S = S_e + S_a + S_q. \quad (4.85)$$

Flow resistance at the air inlet opening  $S_e$

$$S_e = \frac{\delta(1 + \beta\vartheta_e)}{2A_e^2} \left[ \zeta_e + \left( 1 - \frac{A_e}{A_{Ka}} \right)^2 \right]. \quad (4.86)$$

Flow resistance at the air outlet opening  $S_a$

$$S_a = \frac{\delta(1 + \beta\vartheta_a)}{2A_a^2} (\zeta_a + 1). \quad (4.87)$$

Flow resistance at a cross-sectional narrowing  $S_q$

$$S_q = \frac{\delta_0(1 + \beta\vartheta_q)}{2A_q^2} \zeta_q, \quad (4.88)$$

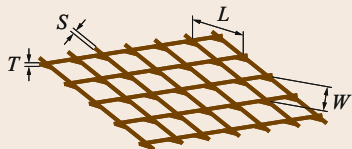
where  $A_{Ka}$  = cross section of the flow channel,  $A_e$  = cross section of the air inlet opening,  $A_a$  = cross section of the air outlet opening,  $A_q$  = cross section of the cross section's narrowing,  $\zeta_a$  = coefficient of resistance of the air flow at the inlet opening,  $\zeta_e$  = coefficient of resistance of the air flow at the outlet opening,  $\zeta_q$  = coefficient of resistance of the air flow at the cross section's narrowing, and  $\delta_0$  = specific mass of air at  $0^\circ\text{C}$ .

The resistance coefficients of the air flow  $\xi$  must be determined experimentally. Selected typical values are given in Tables 4.17–4.23.

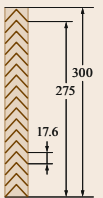

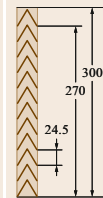


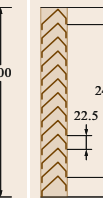
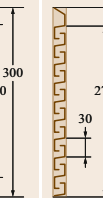
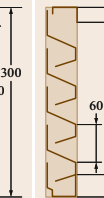
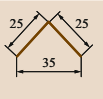
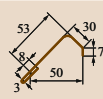
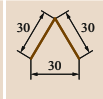
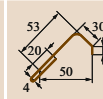
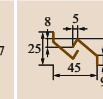
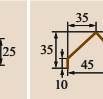
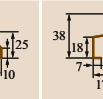
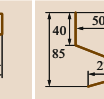
#### Thermal-Network Method

For the thermal calculation of simple, but extensive and complex arrangements, the heat-network method has proven to be very effective. The increased efforts for a necessary manual creation of the network are compensated by very short calculation times and a simple variation of the input parameters for comparative studies. The accuracy of the calculation depends on the correct selection of the design and material input parameters and the appropriately selected structure of the thermally simulated plant components and, generally, fully satisfies engineering requirements [4.2, 5, 23].

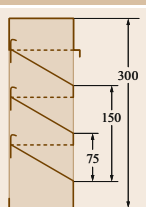
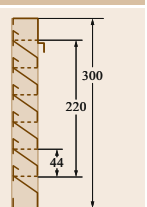
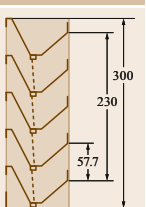
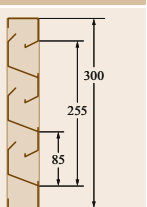
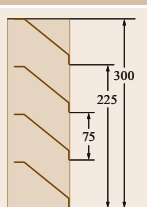
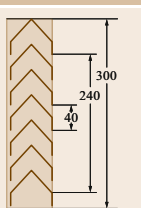
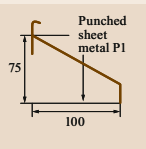
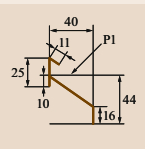
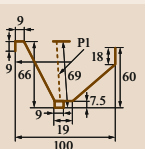
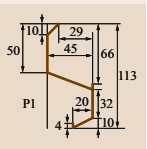
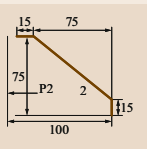
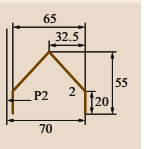
**Table 4.17** Experimentally determined resistance coefficients  $\zeta$  for ventilation openings and cross-section changes, air vent, free ventilation slot and with expanded metal (all dimensions in mm) (adapted from [4.5, 23])

	Free slot	E1	E2	E3
Expanded metal				
Details	Free ventilating slot			
Width of mesh $W$		2.7	16.0	40.0
Length of mesh $L$		6.3	6.3	12.5
Width of stud $S$		1.0	1.6	2.5
Thickness of stud $T$		0.5	1.0	1.5
Coefficient of aerodynamic drag $\zeta$ ( $v = 0.2 \text{ m s}^{-1}$ )	0.7	2.7	2.2	1.1
Coefficient of aerodynamic drag $\zeta$ ( $v = 0.6 \text{ m s}^{-1}$ )	0.9	4.5	3.6	1.3

**Table 4.18** Experimentally determined resistance coefficients  $\zeta$  for ventilation openings and cross-section changes, air vent with lattices without additional meshes or grids (all dimensions in mm) (adapted from [4.5, 23])

Lattice								
Detail								
Effective lattice width	300	300	300	300	300	300	300	300
Effective lattice height	275	290	270	300	280	240	270	240
Coefficient of aerodynamic drag $\zeta$	9.7	10.3	30.8	39.7	47.1	49.4	73.2	76.8

**Table 4.19** Experimentally determined resistance coefficients  $\zeta$  for ventilation openings and cross-section changes, air vent with lattices and punched sheet metals (all dimensions in mm) (adapted from [4.5, 23])

	P1	P1	P1	P1	P2	P2
Lattice with punched sheet metal						
Detail						
Effective lattice width	300	300	300	300	300	300
Effective lattice height	150	220	230	255	255	240
Coefficient of aerodynamic drag $\zeta$	17.1	36.0	48.0	171.7	74.1	120.1

**Table 4.20** Experimentally determined resistance coefficients  $\zeta$  for ventilation openings and cross-section changes, air vent with lattices and expanded metal (all dimensions in mm) (adapted from [4.5, 23])

	E1	E1
Lattice with expanded metal – Width of mesh = 2.7 mm – Length of mesh = 6.3 mm – Width of stud = 1.0 mm – Thickness of stud = 0.5 mm		
Effective lattice width	300	300
Effective lattice height	275	255
Coefficient of aerodynamic drag $\zeta$	40.2	40.7

**Table 4.21** Experimentally determined resistance coefficients  $\zeta$  for ventilation openings and cross-section changes, air vent with lattices and meshed wire (all dimensions in mm) (adapted from [4.5, 23])

	M1
Lattice with expanded metal Diameter of wire = 1 mm Mesh = 10 mm	
Effective lattice width	300
Effective lattice height	230
Coefficient of aerodynamic drag $\zeta$	24.7

**Table 4.22** Experimentally determined resistance coefficients  $\zeta$  for ventilation openings and cross-section changes, ventilation slots covering plate with ventilation slots (all dimensions in mm)

Covering plate with ventilation slots	
Coefficient of aerodynamic drag $\zeta$ ( $v = 0.3 \text{ m s}^{-1}$ )	0.7
Coefficient of aerodynamic drag $\zeta$ ( $v = 0.8 \text{ m s}^{-1}$ )	1.0

The heat-network method is based on the analogy (Table 4.24) between the electric and the thermal field and uses known solution algorithms in freely available software for network calculations in electrical engineering.

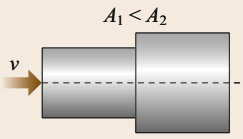
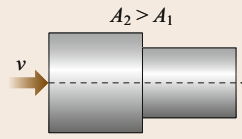
This makes it possible to display the thermal behavior of a device, which is a heat network, in an analog electrical network and to calculate its behavior for both stationary and transient operation (for examples, see Figs. 4.25–4.29), where  $P_V$  = power losses in the bus bar,  $P_{ca}$  = power losses in the capsule,  $C_{bar}$  = thermal capacity of bus bar,  $C_{ca}$  = thermal capacity of capsule,  $\vartheta_i$  = air temperature inside capsule, and  $\vartheta_{ca}$  = temperature of capsule.

For larger devices and systems, it makes sense to combine the different heat networks into modules for recurrent components, store them in a library, and then, depending on the respective application, only connect the finished modules.

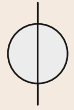
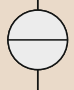


### Heating Test

During the heating test, it is necessary to assure that the limits of permissible excessive temperature  $\vartheta_{0,max}$  for the electrical conductors, the connections and the insulation, as well as the fastening and control elements at *continuous current load* or at the short-circuit current load are observed. In the short-circuit thermal test, a distinction must be made whether the short-circuit current is applied to the test object at no-load or when it has reached its operating temperature at normal load. These limit temperatures are specified in national and international standards (Sect. 4.2). The temperature-rise test is an energy test (4.2), which makes it clear that the temperature of the test object depends on several parameters:

**Table 4.23** Experimentally determined resistance coefficients  $\zeta$  for ventilation openings and cross-section changes, cross-section variations in flow channel (all dimensions in mm) (adapted from [4.5, 23])

Cross-section variation			
$\zeta (A_1/A_2)$	0.1	0.81	0.44
$\zeta (A_1/A_2)$	0.2	0.66	0.42
$\zeta (A_1/A_2)$	0.4	0.38	0.35
$\zeta (A_1/A_2)$	0.6	0.17	0.26
$\zeta (A_1/A_2)$	0.8	0.05	0.14

**Table 4.24** Analogies between electric and thermal fields

Parameter	Icon	Electric field	Thermal field
Drive		Potential difference, Voltage source	Temperature difference
		$\Delta\varphi = U \text{ (V)}$	$\Delta\vartheta \text{ (K)}$
Flow		Electrical current, current source	Heat flow, heat source
		$I \text{ (A)}$	$P \text{ (W)}$
Obstruction		Electrical resistance	Heat resistance for – Heat conduction – Convection – Emission – Coolant flow
		$R \text{ (V A}^{-1}\text{)}$	$R_{th} \text{ (C W}^{-1}\text{)}$
Energy storage		Electrical capacity	Heat capacity
		$C \text{ (As V}^{-1}\text{)}$	$C_{th} \text{ (Ws K}^{-1}\text{)}$
Time delay		Electrical time constant	Thermal time constant
		$\tau = RC$ $\tau \text{ (s)}$	$\tau = R_{th}C_{th}$ $\tau \text{ (s)}$
Energy		Electrical energy	Thermal energy
		$W \text{ (Ws)}$	$E_{th} \text{ (Ws) or (J), (1 Ws = 1 J)}$

- Ambient conditions (temperature, air flow)
- Adjacent walls (temperature, distance to the test object, emission behavior)
- Power supply to the test object (cross section, conductance, length)
- Arrangement of the test object (free, on test table, close to other test objects)
- Mounting (heat transfer or heat conduction on mounting)
- Temperature measurement (measuring method, measuring point, time variation).

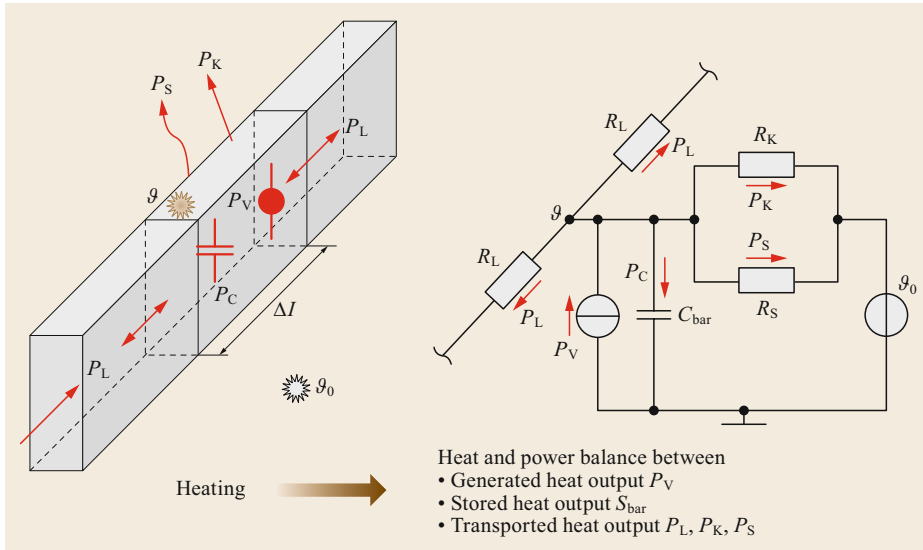
In order to make the test results comparable, standards for individual equipment groups define the ambient conditions and their permissible deviations. How-

ever, it should be noted that these conditions are not identical in different standards (Table 4.25).

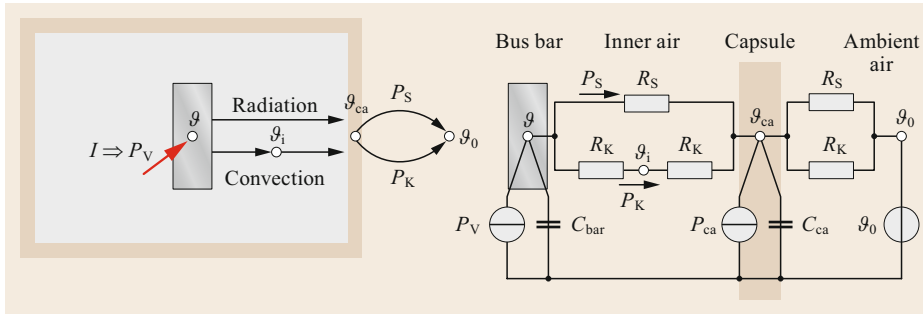
The ambient conditions of the test chamber influence the test result, e.g., as follows.

- The ambient temperature  $\vartheta_0$  determines the heat transfer from the test object to the environment by convection.
- The temperature of the wall or lacquered steel doors  $\vartheta_w$  determines the heat transfer from the test object to the wall by radiation.

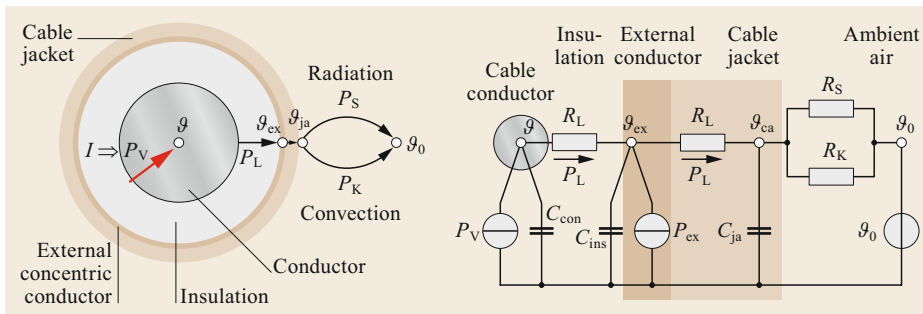
For  $\vartheta_0 \neq \vartheta_w$ , heat can be emitted uncontrollably by radiation to the wall. In this way, cold walls can influence the test result towards lower temperatures or apparently



**Fig. 4.25** Thermal network of a current-carrying bus conductor



**Fig. 4.26** Thermal network of a current-carrying encapsulated bus bar



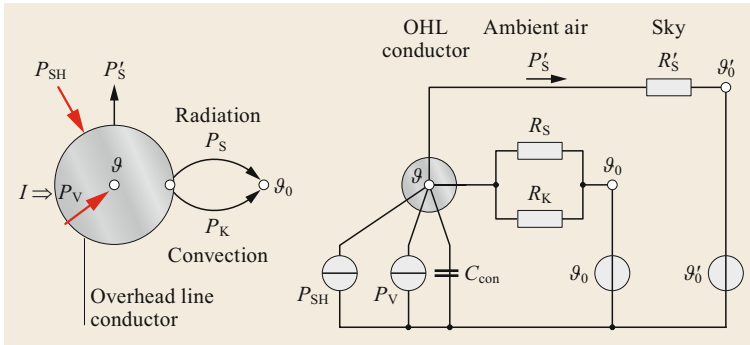
**Fig. 4.27** Thermal network of an air-installed cable;  $P_V$  = power losses in the bus bar,  $P_{\text{ex}}$  = power losses in the external concentric conductor,  $C_{\text{con}}$  = thermal capacity of cable conductor,  $C_{\text{ins}}$  = thermal capacity of cable insulation,  $C_{\text{ja}}$  = thermal capacity of cable jacket,  $\vartheta_{\text{ex}}$  = temperature of the external concentric conductor, and  $\vartheta_{\text{ja}}$  = temperature of cable jacket

higher current-carrying capacity of the test object (Table 4.26). This is possible despite observing the ambient air temperature through more intensive heat radiation, depending on the emission behavior of the test object.

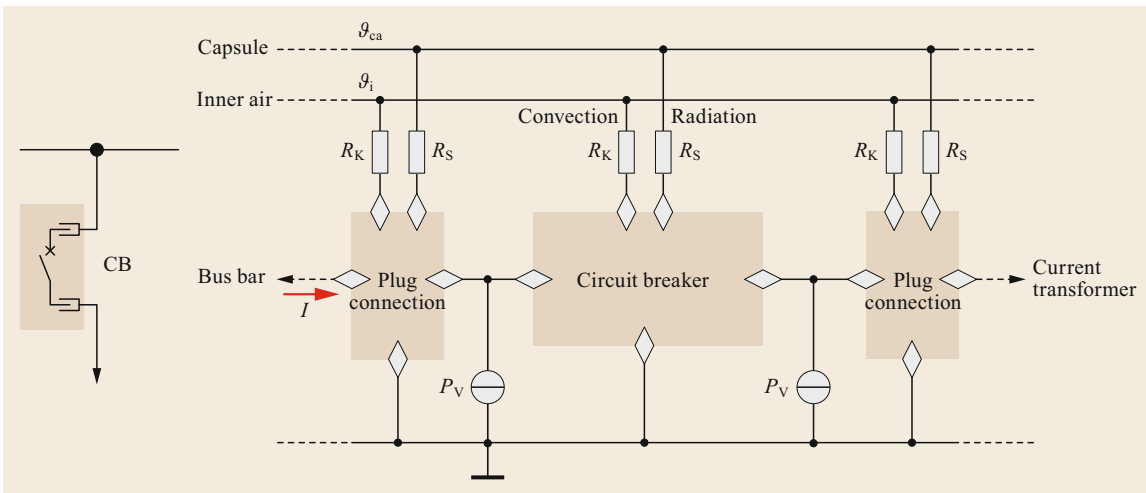
The permissible current-carrying capacity  $I$  of a test object becomes particularly clear for free, i.e., without enclosure, test arrangements, even at very low flow ve-

locities, influenced by the air flow in the test chamber (Fig. 4.30 and (4.78)).

It is particularly important to ensure that the temperature of the test object has reached its stationary final value when all thermal capacities are saturated, which can take many hours, especially in enclosed systems, such as equipment with insulating oil or solid insulation



**Fig. 4.28** Thermal network of an overhead line conductor;  $P_V$  = power losses in the OHL conductor,  $P_{SH}$  = power input from solar radiation,  $P'_S$  = heat transfer by radiation to sky,  $C_{con}$  = thermal capacity of OHL conductor, and  $\vartheta'_0$  = air temperature in the sky



**Fig. 4.29** Thermal network modules for components, removable circuit breaker in an encapsulated, air-insulated switchgear

**Table 4.25** Heat test, influence of ambient conditions on temperature of test samples, examples for requirements in DIN EN-standards (adapted from [4.9, 10, 12])

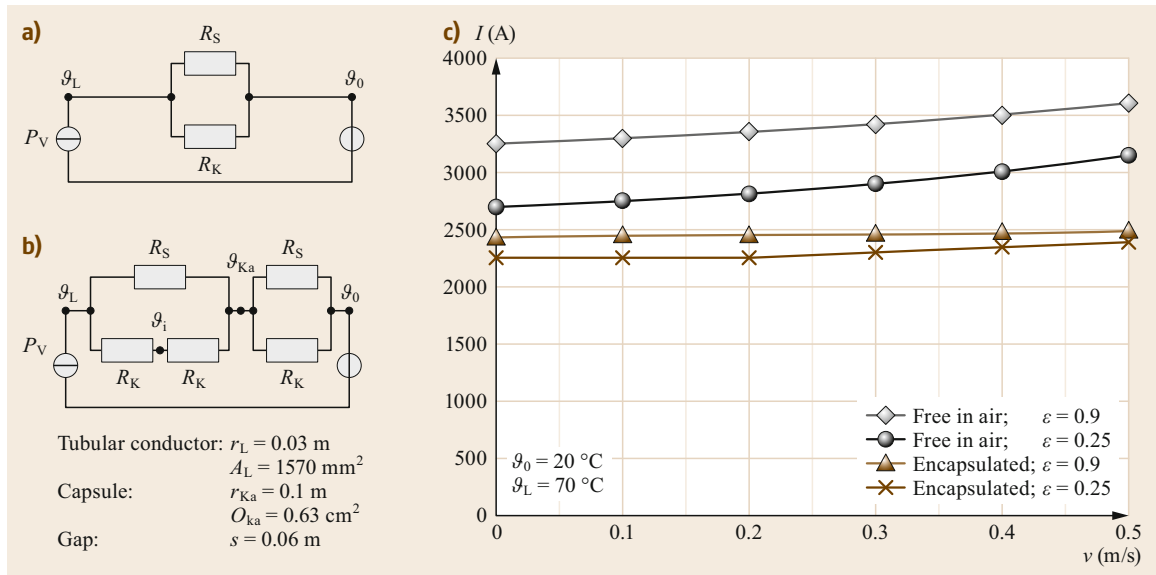
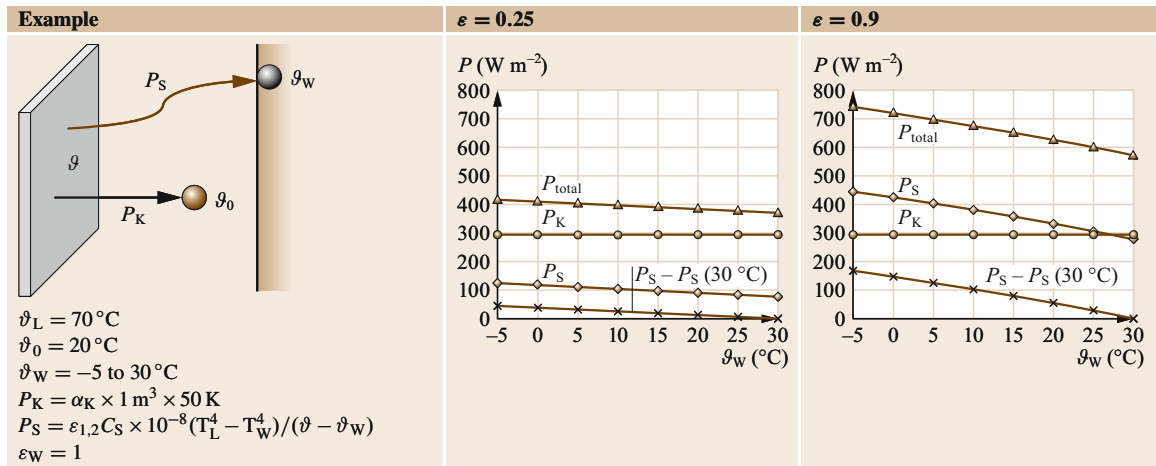
	DIN EN 61439-1 [4.10] (Low voltage)	DIN EN 60947-1 [4.9] (Low voltage)	DIN EN 62271-1 [4.12] (High voltage)
Reference temperature (°C)	35	35	40
Ambient temperature $\Delta\vartheta_0$ (°C)	$10 \leq \vartheta_0 \leq 40$ the last 1/4 $\sum t_{test}$ : $\Delta\vartheta_0 \leq 1 \text{ K h}^{-1}$	$10 \leq \vartheta_0 \leq 40$ $\sum t_{test}$ : $\Delta\vartheta_0 \leq 0 \text{ K}$ if $\Delta\vartheta_0 > 3 \text{ K}$ use correction factors	$10 \leq \vartheta_0 \leq 40$ the last 1/4 $\sum t_{test}$ : $\Delta\vartheta_0 \leq 1 \text{ K h}^{-1}$
Measuring points for ambient temperature	Min. 2 × measurements halfway up the test sample in 1 m distance	Min. 2 × measurements halfway up the test sample in 1 m distance	Min. 3 × measurements in the high of current-carrying conductors, 1 m distance
Air flow in the test room ( $\text{m s}^{-1}$ )	–	–	$v_{air} \leq 0.5$
Wall temperatures in test room	No information in the standard		

((4.21) and Fig. 4.31). Standards usually accept that the stationary final value is reached when the temperature rise  $\Delta\vartheta < 1 \text{ K h}^{-1}$  [4.9, 10, 12].

The type of power supply, its cross section, conductance, and length are responsible for whether power is supplied or dissipated to the test object by heat conduc-

tion, which can strongly influence the temperature of the test object. The aim is to select the supply line in such a way that neither significant heat input nor output can occur. However, this is not always stipulated, especially in the standards for low-voltage switchgear. An oversized power supply cable draws far more heat

**Table 4.26** Heat test, influence of wall-temperature  $\vartheta_w$  on heat transfer  $P$



**Fig. 4.30a–c** Heat test, operating current of a free (a) and an encapsulated conductor (b) depending on air flow velocity  $v$  in the test chamber (c)

from the device under test than in practical use in a low-voltage switchgear and control gear. This means that, in practice, depending on the installation conditions, a low-voltage device may only be subjected to considerably less load than the value indicated on its rating plate (Figs. 4.32 and 4.33)

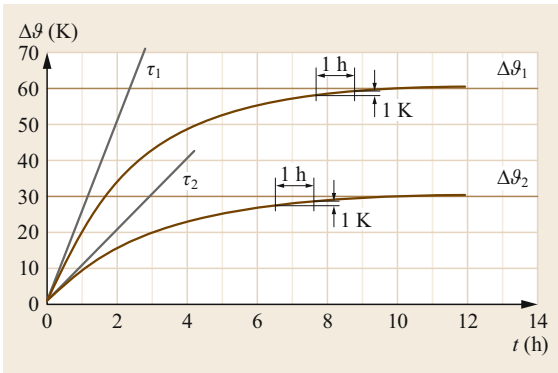
$$|P_L| = \frac{\lambda A}{d} \Delta\vartheta = \frac{\lambda A}{b} \Delta\vartheta, \tag{4.89}$$

$$b = \sqrt{\frac{\lambda A}{\alpha(\vartheta)U}}, \tag{4.90}$$

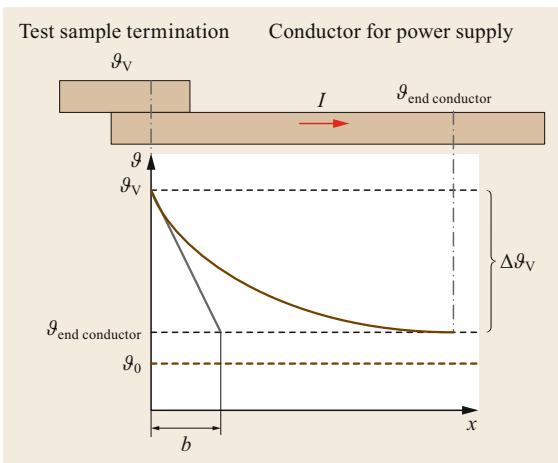
with Al:  $b \approx 0.3 \text{ m}$  and Cu:  $b \approx 0.4 \text{ m}$ .

Example: determine the influence of the power supply line on the thermal power dissipated from a 1000 A switchgear during the heating test. The temperature gradient along the feed line can vary significantly, i.e., from  $\Delta\vartheta = 70 \text{ K}$  at the connections of the test object to  $\Delta\vartheta = 50 \text{ K}$  at the power supply line (Fig. 4.34a); this depends on the cross section of the copper bus bars (here,  $2 \times (60 \times 5) \text{ mm}^2$ ). Assuming a permissible excess temperature at the connections of  $\Delta\vartheta = 70 \text{ K}$ , the power dissipated by heat conduction in the power supply line results in  $P_L = 70 \text{ W}$  with a load current of  $I = 1000 \text{ A}$  (Fig. 4.34b). While in this example painted bus bars ( $\epsilon = 0.9$ ) are used, a bare bus bar would only have a thermal

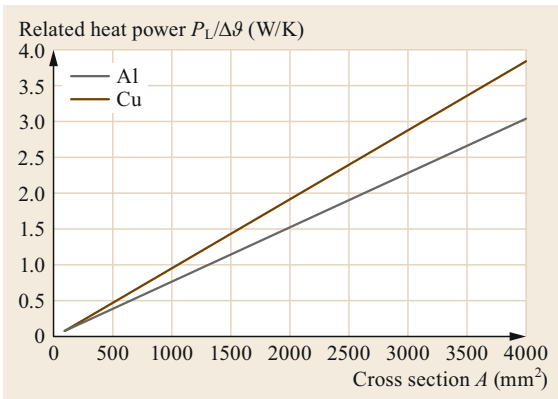




**Fig. 4.31** Heat test, heating curve dependent on the time constant  $\tau$  ( $\tau = C_{th}R_{th} = c\delta VR_{th}$ )

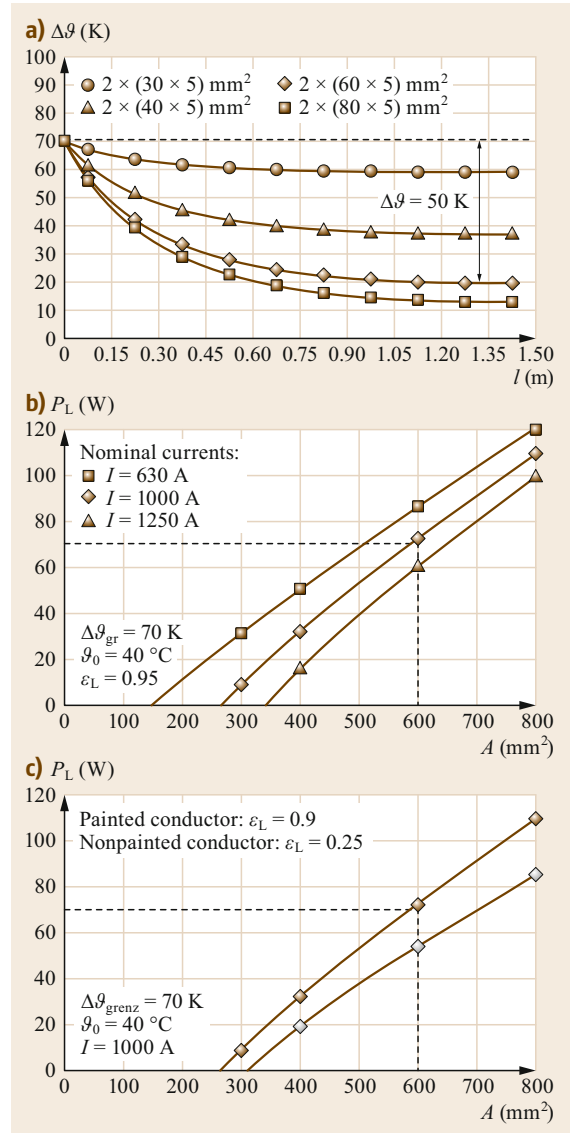


**Fig. 4.32** Heat dissipation from the test object by heat conduction in the power supply line



**Fig. 4.33** Dissipated heat output through heat conduction in the power supply conductors

output of  $P_L = 56$  W (Fig. 4.34c). Here, it becomes clear what influence the choice of the current-supply line has on the temperature of the test object.

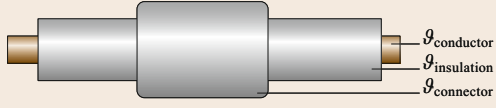


**Fig. 4.34a-c** Example: influence of the power supply conductor on the heat output dissipated from a switching device for  $I_n = 1000$  A. (a) Temperature distribution along the power supply conductor for different conductor cross sections ( $\Delta\vartheta =$  overtemperature), (b) dissipated heat output for each power supply conductor, (c) influence of the emission factor  $\varepsilon$  of the power supply conductor

### On the Temporary Current Overload Ability of Power Control Systems and Installations

Occasionally, it is intended to load existing bus bar arrangements and equipment with higher current than stationarily permissible, without exceeding the limit temperature.

**Table 4.27** Electric devices as a dynamic system

General	Input ( $x_{IN}(t)$ ) $\Rightarrow$	Dynamic system weighting function $\Rightarrow$	Output ( $x_{OUT}(t)$ )
Electrotechnical system	Current square $P_V \propto I^2$	Electric device	Temperatures at critical points $\vartheta_1$ $\vdots$ $\vartheta_n$
Example: solid insulated bus bar	$I^2$		$\vartheta_{\text{conductor}}$ $\vartheta_{\text{insulation}}$ $\vartheta_{\text{connector}}$

For *electrical equipment and drives*, ten corresponding operating modes – S1–S10 – for periodically recurring load cycles and short-term loads are defined in standards and are taken into account in the design and operation of the equipment by utilizing its heat capacity [4.24].

For *equipment and systems*, two possibilities can be used for current overload capability:

- The temperature signal follows the current signal with a time lag (Table 4.9, middle column).
- The ambient conditions (temperature, wind speed, solar radiation) determine the temperature of the equipment with their magnitude and time dependence.

For example, a low ambient temperature makes it possible to take advantage of the higher temperature difference up to the limit temperature. Also at higher wind speeds, forced convection results in better heat dissipation, which also permits a higher current load. Since the current load of conductors and equipment, as well as the heat output due to radiation and convection and the heat storage (input variables), vary over time, knowledge of the past is always required in order to determine the current load (output variable) permitted in the next time interval (Table 4.27). For not necessarily periodic, pulse-shaped input variables [4.14, 20],  $x_{IN}$  is the weight function,  $g(\tau)$  is a measure of how strong the input variables at the time  $t$  and at the period before ( $t - \tau$ ) influence the output variables  $x_{IN}$ ; this is expressed by the convolution integral

$$x_{OUT} = \int_0^t g(\tau)x_{IN}(t - \tau)d\tau. \quad (4.91)$$

Since the weight function  $g(\tau)$  is constant over a time interval  $\Delta T$ , the convolution integral for a time  $k$  can be

expressed as

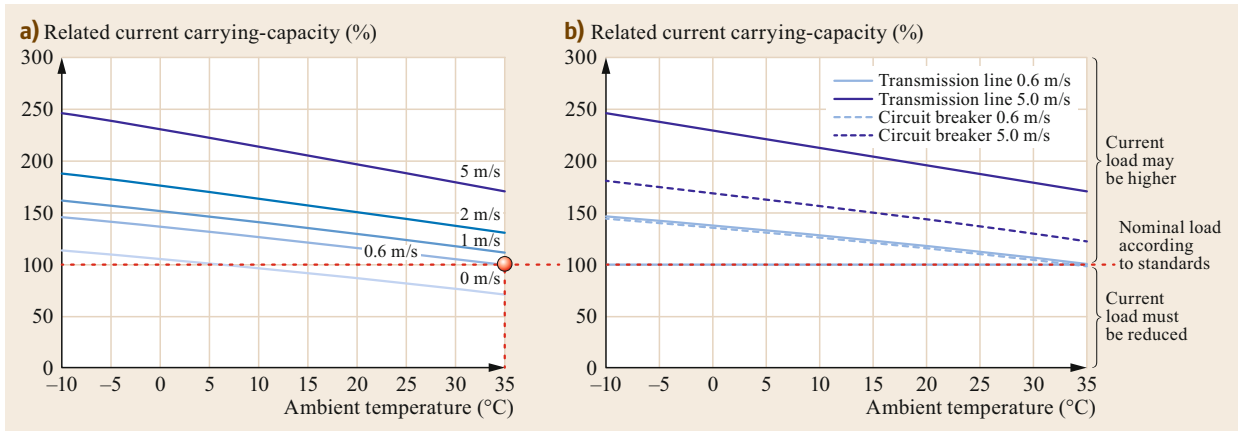
$$x_{OUT}(k\Delta T) = \Delta T \sum_{l=0}^n g(l\Delta T)x_{IN}[(k-l)\Delta T] + x_{OUT0}, \quad (4.92)$$

where  $x_{IN}$  = input variable, e.g., current load, wind velocity,  $x_{OUT}$  = output variable, e.g., temperature at a critical location,  $g$  = weight function,  $t$  = time variable,  $\tau$  = runtime in convolution integral,  $\Delta T$  = time interval,  $k$  = time after measurement of the output variable during memory time,  $l$  = time difference +  $(l\Delta T)$  from time  $k$ , and  $x_{OUT0}$  = value of the output variable at the operating point  $x_{IN} = 0$ .

The weight functions  $g$  for the memory time of the conductor, the insulation, and the connection in Table 4.27 can be determined experimentally or by means of the heat-network method and, thus, serve to predict the temperature to be expected in the future depending on the future load current and the load history of the equipment. This way, in the next time interval  $(k + 1)\Delta T$ , the permissible current that does not violate the limit temperature  $\vartheta_{Gr}$  can also be calculated [4.20].

If one considers, initially in stationary operation, the influence of the ambient conditions, e.g., air temperature, wind velocity, etc., a significant influence on the temperature of the device can be determined. Using the example of an ACSR 380/50 overhead-line conductor (382-AL1/49-ST1A, outer diameter 27.0 mm) with the standardized boundary conditions [4.25], i.e.:

- Ambient temperature:  $\vartheta_0 = 35^\circ\text{C}$
- Wind velocity perpendicular to the line:  $v = 0.6\text{ m s}^{-1}$
- Permissible maximum conductor temperature:  $\vartheta_{Gr} = 80^\circ\text{C}$ .
- Permissible continuous current:  $I = 840\text{ A}$



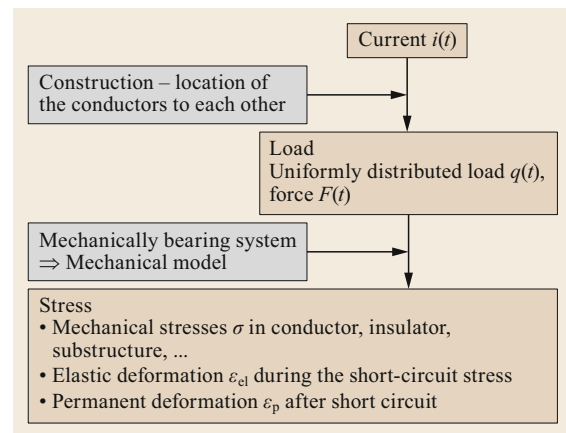
**Fig. 4.35a,b** Current-carrying capacity of a transmission-line conductor and of a high-voltage circuit breaker depending on ambient temperature and wind velocity (global radiation  $P_{SH} = 1000 \text{ W m}^{-2}$ , transverse flow with  $v = 0$  to  $5 \text{ m s}^{-1}$ , and ambient temperature  $\vartheta_0 = -10$  to  $+40^\circ\text{C}$ ). (a) Current-carrying capacity of a transmission-line conductor at a limiting temperature  $\vartheta_{Gr} = 80^\circ\text{C}$ , (b) current-carrying capacity of a high-voltage circuit breaker at a limiting temperature on contact elements  $\vartheta_{Gr} = 105^\circ\text{C}$  in comparison to the overhead line in (a)

its thermal rating can be determined by means of the heat-network method or by experiments in the wind tunnel (Fig. 4.35a). It should be noted that, for the rather unlikely case of wind velocities  $v < 0.6 \text{ m s}^{-1}$ , the thermal rating will decrease, while for wind velocities  $v > 0.6 \text{ m s}^{-1}$  and at ambient temperatures  $\vartheta_0 < 35^\circ\text{C}$  a higher thermal rating of the conductor is theoretically possible in the case the same ambient conditions apply along the line, and the limit conductor operating temperature  $\vartheta_{Gr} = 80^\circ\text{C}$  is not exceeded, and, therefore, the admissible sag limits are not violated [4.14]. However, these apparent reserves are reduced to a temporary *overload capacity of the conductor* by accelerated aging of connectors and clamps at higher temperatures (Sect. 4.3.3).

Furthermore, the thermal behavior of all other equipment in the current path must also be considered, which can differ considerably from that of the overhead conductor. For example, the influence of the wind on a high-voltage circuit breaker is comparatively much less than on an overhead-line conductor, so that the reserve calculated above can only be used to a limited extent (Fig. 4.35b); nevertheless, a certain temporary overload capacity may exist, taking into account the actual ambient temperature.

### 4.3.2 Mechanical Dimensioning

Current-conducting arrangements are stressed by the electric current  $i(t)$  not only thermally, but also mechanically, depending on the design and position of the conductors relative to each other. External mechanical loads may cause line loads  $q(t)$  and forces

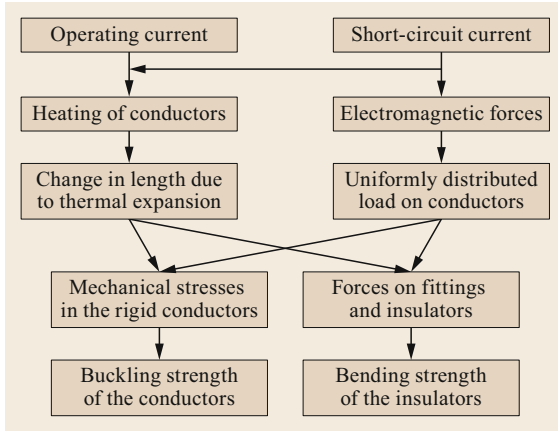


**Fig. 4.36** Emergence of mechanical stress

$F(t)$ , which lead to mechanical stresses in the conductors themselves and their support points, such as clamps, tap-offs, and insulators (Figs. 4.36 and 4.37). It goes without saying that these mechanical loads must not exceed the damage and deformation limits of the components of the electrical equipment [4.1, 26–33].

#### Load: Forces Due to Thermal Expansion

Forces due to thermal expansion result from a constrained expansion due to the heating of a current-carrying conductor and its insulation, especially under a short-term load. These forces can occur longitudinally and radially and be of static nature. They act so slowly that inertial forces caused by moving masses do not have to be taken into account.



**Fig. 4.37** Effects of electrical load on mechanical stress

The longitudinal expansion of a pinned but, flexurally stiff conductor (Fig. 4.38b) is

$$\Delta l = l \alpha_{th} \Delta \vartheta \Rightarrow \varepsilon_{th} = \alpha_{th} \Delta \vartheta, \quad (4.93)$$

where  $l$  = conductor length,  $\Delta l$  = thermal linear expansion,  $\alpha_{th}$  = coefficient of linear expansion (Table 4.28),  $\Delta \vartheta$  = heating of the conductor in relation to the initial state at  $\vartheta_0$ , where the conductor temperature is  $\vartheta > \vartheta_0$  at operating current, and  $\vartheta \gg \vartheta_0$  at short circuit current, and  $\varepsilon_{th}$  = relative elongation of the conductor ( $\Delta l/l$ ) by thermal expansion.

With a fixed conductor (Fig. 4.38c), a mechanical stress occurs in the conductor.

$$\sigma_{th} = E \alpha_{th} \Delta \vartheta = \varepsilon_{th} E = \frac{F_{th}}{A}, \quad (4.94)$$

where  $\sigma_{th}$  = mechanical stress in the conductor,  $E$  = modulus of elasticity (Table 4.28),  $F_{th}$  = compressive force in the conductor, and  $A$  = conductor cross section.

**Table 4.28** Modulus of elasticity  $E$ , coefficient of linear thermal expansion  $\alpha_{th}$ , and the limit elastic stress  $\sigma_{0.2}$  of selected conductor materials

Material	$E$ (kN mm <sup>-2</sup> )	$\alpha_{th}$ ( $\times 10^{-6}$ K <sup>-1</sup> )	$\sigma_{0.2}$ (N mm <sup>-2</sup> )
Aluminum (Al) F7	60–65	23.8	34
Aluminum (Al) F9			62
Copper (Cu)	110	16.5	> 220
Brass (Ms)	85	20.2	60–100
Steel (St)	210	11.5	200–400

This will cause a compression load on the conductor and a corresponding bending load  $F_{th}$  on the insulator at the support.

$$F_{th} = AE \alpha_{th} \Delta \vartheta. \quad (4.95)$$

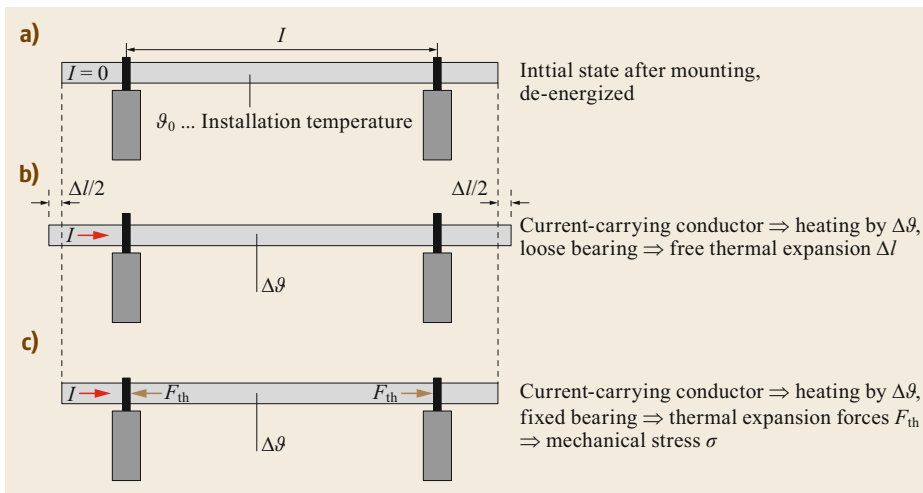
Example: fixed bus bar made from aluminum alloy (AlMgSi)  $A$  (40 × 10) mm<sup>2</sup>;  $\Delta \vartheta = 70$  K;  $E = 69$  kN/mm<sup>2</sup>, and  $\alpha_{th} = 23.4 \times 10^{-6}$  K<sup>-1</sup>,

$$\begin{aligned} \sigma_{th} &= E \alpha_{th} \Delta \vartheta = 69 \frac{\text{kN}}{\text{mm}^2} \cdot 23.4 \times 10^{-6} \frac{1}{\text{K}} \cdot 70 \text{ K} \\ &= 113 \frac{\text{N}}{\text{mm}^2}, \end{aligned} \quad (4.96)$$

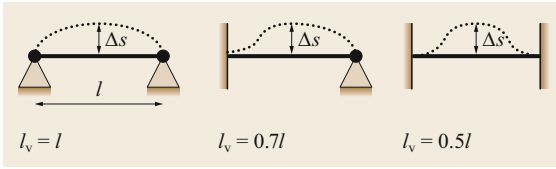
$$\begin{aligned} F_{th} &= AE \alpha_{th} \Delta \vartheta = 400 \text{ mm}^2 \cdot 113 \frac{\text{N}}{\text{mm}^2} \\ &= 45.21 \text{ kN}. \end{aligned} \quad (4.97)$$

The top of the support insulator is subjected to an upheaval bending force of  $F_{th} = 45.21$  kN.

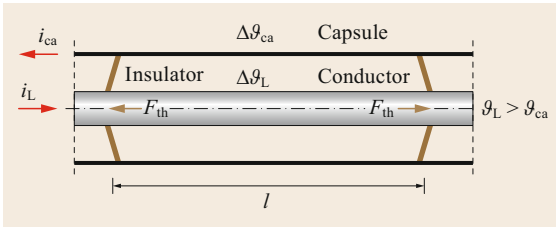
With straight, flexurally stiff conductors, such as tubular bus bars, the compressive force leads to buckling  $\Delta s$  of the conductor, depending on the type of clamping at the support (Fig. 4.39). If the elastic limit



**Fig. 4.38a,b** Thermal expansion forces on a rigid conductor



**Fig. 4.39** Bending  $\Delta s$  of conductors and reduction of the effective length  $l_v$  depending on the type of clamping/fixing



**Fig. 4.40** Thermal expansion forces in encapsulated bus bar systems (GIL, GIS)

of the conductor material is exceeded, the maximum buckling load depends on the reduced length  $l_v$  of the conductor, the slenderness ratio  $s_r$ , and the radius of inertia  $i$ , and if exceeded will cause excessive plastic deformation by abrupt buckling.

$$s_r = \frac{l_v}{i}, \tag{4.98}$$

$$i = \sqrt{\frac{I}{A}}, \tag{4.99}$$

$$\sigma_{Gr} = \pi \sqrt{\frac{E}{\sigma_{0.2}}} \tag{4.100}$$

$$\Delta s_p = \sqrt{\frac{3}{8}} l_v \Delta I_o, \tag{4.101}$$

where  $S_r$  = slenderness ratio,  $l_v$  = reduced length according to type of clamping (Fig. 4.39),  $i$  = radius of gyration,  $I$  = moment of inertia of the cross section (Table 4.29),  $A$  = area of the cross section,  $\sigma_{GR}$  = limit buckling stress, and  $\Delta s_p$  = buckling (plastic deformation).

Comparable loads result from thermal expansion in encapsulated gas-insulated switchgear (GIS) and lines (GIL). In this case, the different temperature increases of the conductor and the enclosure ( $\Delta\theta_L > \Delta\theta_{ca}$ ) and, thus, their differing elongations have to be considered (Fig. 4.40).

In order to reduce such mechanical loads on the conductors and support points, sliding bearings, expansion bands, or expansion clamps are used in practice (Figs. 4.5 and 4.41).

**Table 4.29** Moments of inertia and resistance of different conductor cross sections in the direction of uniformly distributed load  $q$

Cross section	Moment of inertia	Moment of resistance
	$I = \frac{bh^3}{12}$	$W = \frac{bh^3}{6}$
	$I = \frac{BH^3 - bh^3}{12}$	$W = \frac{BH^3 - bh^3}{6H}$
	$I = \frac{\pi d^4}{64}$	$W = \frac{\pi d^3}{32}$
	$I = \frac{\pi(D^4 - d^4)}{64}$	$W = \frac{\pi(D^4 - d^4)}{32D}$

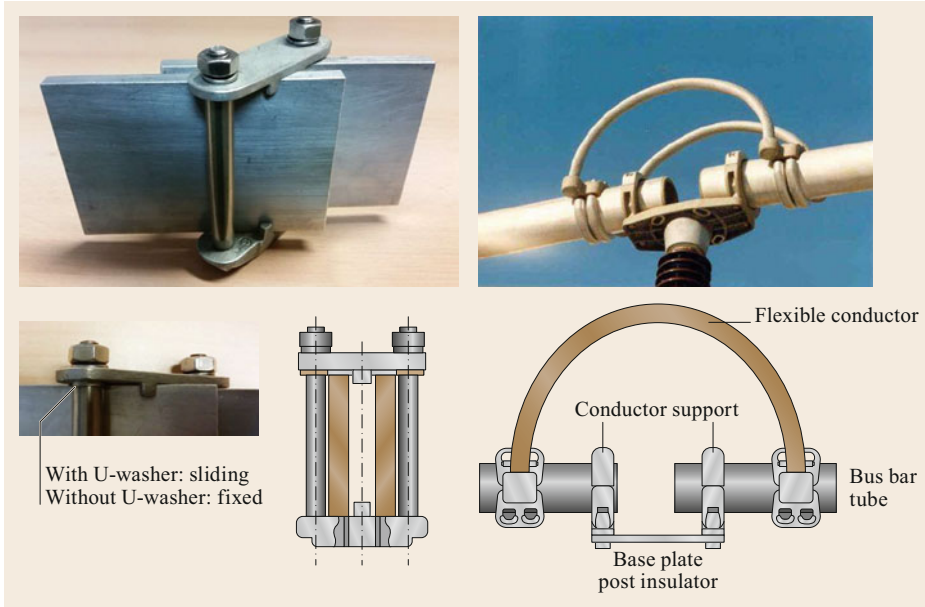
**Table 4.30** Comparison of coefficients of linear thermal expansion  $\alpha_{th}$  for conductor and insulation materials

Conductor material	$\alpha_{th}$ ( $\times 10^{-6} K^{-1}$ )	Insulation material	$\alpha_{th}$ ( $\times 10^{-6} K^{-1}$ )
Aluminum	23.8	Epoxy resin	30
Copper	16.5	Quartz	0.5
Brass	11.5	Glass	4–10
Steel	10.5	Porcelain	3.8–7
Cast iron	18.4	Polyethylene	$\approx 200$

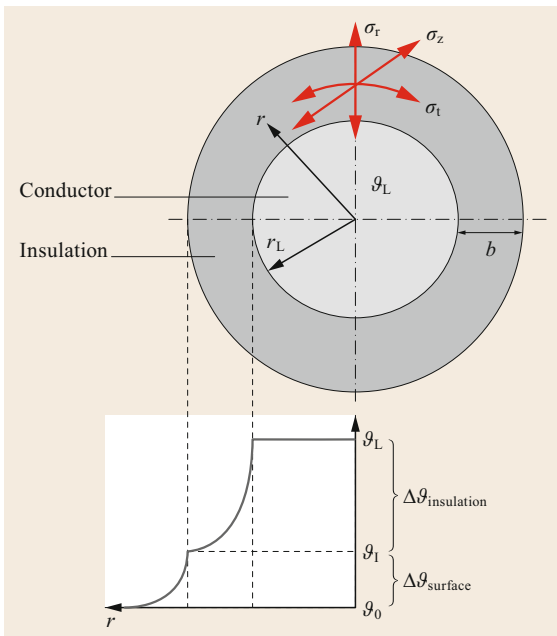
Thermomechanical stresses in current-conducting arrangements also occur when conductor and insulation materials with different coefficients of thermal linear expansion  $\alpha_{th}$  are used and are firmly connected (cast-resin insulation, cables) (Table 4.30).

For solid insulated conductors, especially for insulation made of filled epoxy resin (insulating material in the *glass state*, and, thus, not elastic), the *radial thermal compressive stresses*  $\sigma_r$  can cause considerable hoop stresses  $\sigma_t$  at the circumference of the insulation which, in turn, can cause the insulation to burst and, thus, fail (Fig. 4.42) [4.27].

In low and medium voltage systems at *uninterrupted operation*, it is critical to consider that the supporting and clamping components also heat up and expand, thus, the differences in extension shall be used for the calculation. In the *case of a short circuit*, adiabatic heating of the conductor can be assumed, which is considered particularly critical for high short-circuit-currents and long short-circuit periods.



**Fig. 4.41** Examples for bus bar supports and expansion clamps



**Fig. 4.42** Radial pressure, tangential, and tensile stresses in a heated solid-insulated conductor;  $\sigma_r$  = radial compressive stress,  $\sigma_t$  = tangential tensile stress,  $\sigma_z$  = axial tensile stress,  $\vartheta_L$  = temperature of conductor,  $\vartheta_1$  = temperature of insulation depends on radius  $r$ ,  $r$  = radius, and  $\vartheta_0$  = ambient temperature

#### Loads Due to Electromagnetic Forces on Conductors – Individual and Distributed Forces on Conductors and Supports

Conductors through which current flows are surrounded by a magnetic field  $\mathbf{B}$ , whereby a force  $\mathbf{F}$  or a line load  $q$  is created on adjacent, parallel conductors that are also current-carrying (effect). Depending on whether the currents of the parallel conductors flow in the opposite or in the same direction, the conductors will repel or attract each other (Fig. 4.43 and Table 4.31).

The differential force  $d\mathbf{F}$  depends on the current  $i$ , the effective length  $dx$  of the conductor, and the magnetic induction  $\mathbf{B}$  at this location (Fig. 4.44).

$$d\mathbf{F} = i(dx \times \mathbf{B}) . \tag{4.102}$$

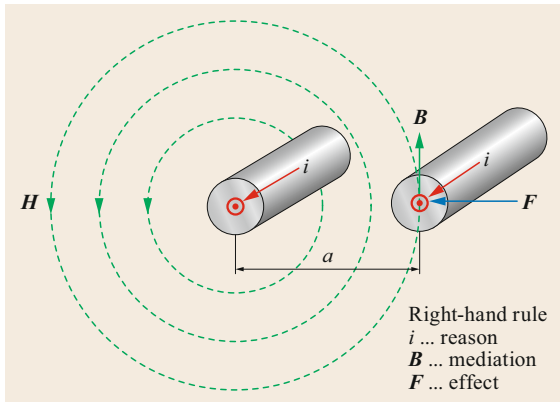
In the case where  $dx$  and  $d\mathbf{B}$  are orthogonal to each other, which is true for many applications, this relationship is simplified to

$$dF = iBdx . \tag{4.103}$$

Dividing the force  $d\mathbf{F}$  by the length  $dx$  one obtains the related line load  $q$

$$q = \frac{dF}{dx} = iB . \tag{4.104}$$

The Biot–Savart law enables the calculation of the magnetic field strength  $dH_{21}$  caused by current  $i_1$  in one



**Fig. 4.43** Electromagnetic forces on current-carrying, parallel conductors – right-hand rule. Carrying conductors arise between current-electromagnetic forces that have a static and/or dynamic stress result

conductor at a distance  $r$  of conductor point P on the adjacent conductor 2 (Figs. 4.44 and 4.45)

$$dH_{21} = \frac{i_1}{4\pi} \frac{r \times dy}{r^3} \tag{4.105}$$

With

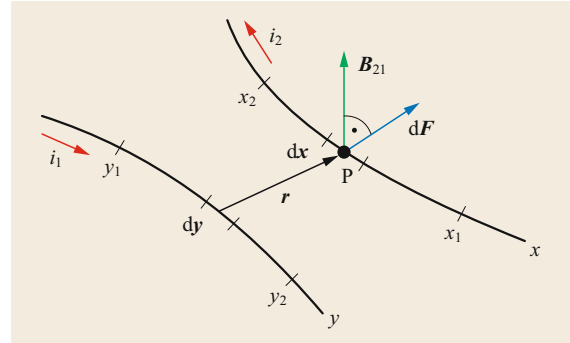
$$dy \times r = r dy \sin \delta \quad \text{and} \quad B = \mu H \tag{4.106}$$

one obtains

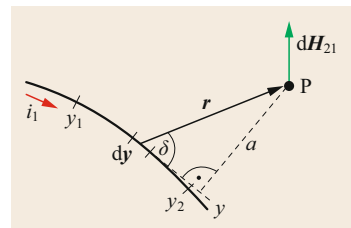
$$dB_{21} = i_1 \frac{\mu_0}{4\pi} \frac{\sin \delta}{r^2} dy, \tag{4.107}$$

and by integration over  $dy$

$$B_{21} = i_1 \frac{\mu_0}{4\pi} \int_{y_1}^{y_2} \frac{\sin \delta}{r^2} dy, \tag{4.108}$$



**Fig. 4.44** Electromagnetic forces on current-carrying conductors;  $i$  = reason,  $B$  = mediation,  $F$  = effect



**Fig. 4.45** Magnetic field strength  $H_{21}$  in conductor point P at distance  $r$  from conductor 1. The following parameters must be taken into account: time curve of the currents  $i_1$  and  $i_2$ , geometry of the arrangement, characterized by  $y_1, y_2, r$ , and  $\delta$  (or  $a$ )

and with (4.104) the line load  $q$  can be calculated as

$$q = \frac{dF}{dx} = i_1 i_2 \frac{\mu_0}{4\pi} \int_{y_1}^{y_2} \frac{\sin \delta}{r^2} dy. \tag{4.109}$$

The load  $F$ , which acts on the supports of a current path, becomes

$$F = i_1 i_2 \frac{\mu_0}{4\pi} \int_{y_1}^{y_2} \frac{\sin \delta}{r^2} dy dx, \tag{4.110}$$

**Table 4.31** Electromagnetic forces on current-carrying parallel conductors

Application of the right-hand rule (R-M-E rule)		
	Opposite currents $+I_1; -I_2$	Parallel currents $+I_1; +I_2$
Reason R		
Mediation M	Overlay of the magnetic fields $H_1$ and $H_2$ ⇒ Field enhancement between the conductors	Overlay of the magnetic fields $H_1$ and $H_2$ ⇒ Compensation of the magnetic fields between conductors ⇒ Fields outside the conductors determine the effect of $F$
Effect E	Effect of forces ⇒ conductors repel	Effect of forces ⇒ conductors attract/approach

where  $y$  or  $dy =$  conductor, from which  $B_{21}$  is generated,  $x$  or  $dx =$  conductor on which the line load acts, and  $\mu_0 = 4\pi \times 10^{-7} \text{Vs/Am}$  – magnetic permeability.

For the time dependence of the line load  $q(t)$  between parallel conductors and the force  $F(t)$ , the type of short circuit and the time dependence of the short-circuit current  $i(t)$  must be observed.

*Steady-state short-circuit current.*

$$i = \hat{I}_K \sin \omega t, \tag{4.111}$$

and

$$\hat{I}_K = \sqrt{2}I_K \tag{4.112}$$

gives a line load  $q(t)$  of

$$q(t) = \frac{\mu_0}{2\pi a} \hat{I}_K^2 \sin 2\omega t.$$

Which, with

$$\sin 2x = \frac{1}{2}(1 - \cos 2x) \tag{4.113}$$

becomes

$$q(t) = \frac{\mu_0}{2\pi a} \left(\sqrt{2}I_K\right)^2 \frac{1}{2}(1 - \cos 2\omega t), \tag{4.114}$$

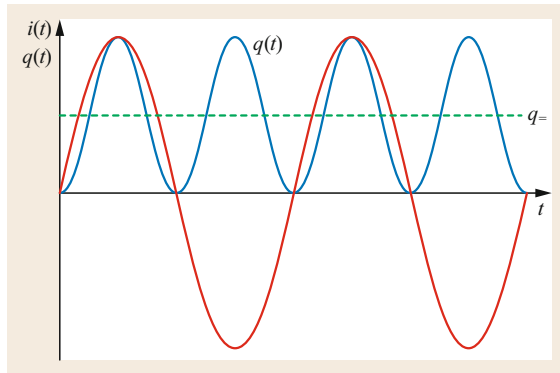
$$q(t) = \frac{\mu_0}{2\pi a} I_K^2 (1 - \cos 2\omega t) \tag{4.115}$$

with a DC and a AC component (Fig. 4.46)

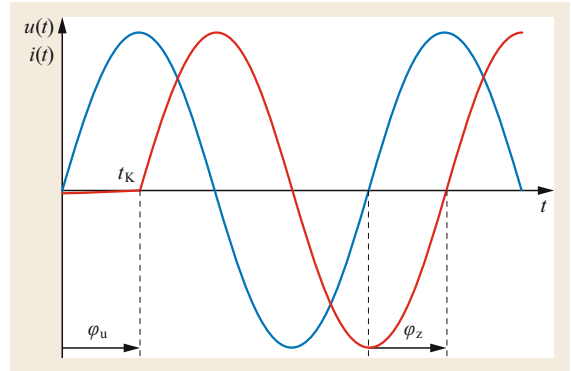
$$q_+(t) = \frac{\mu_0}{2\pi a} I_K^2, \tag{4.116}$$

$$q_-(t) = -\frac{\mu_0}{2\pi a} I_K^2 \cos 2\omega t. \tag{4.117}$$

*Remote generator short circuit with decaying DC component and symmetrically driving voltage without tran-*



**Fig. 4.46** Uniformly distributed load  $q(t)$  between parallel conductors at a continuous short-circuit current  $i(t)$



**Fig. 4.47** Short circuit remote from generator, time course of short-circuit current  $i(t)$  and voltage  $u(t)$  with impedance angle  $\varphi_z$  (phase displacement  $u$  and  $i$  at stationary short-circuit current  $\varphi_z = \arctan(X/R)$ ) and phase angle of voltage at the time of short-circuit  $\varphi_u$

sient component due to decay processes in the generator ( $I''_K = I_K$ ) (Fig. 4.47)

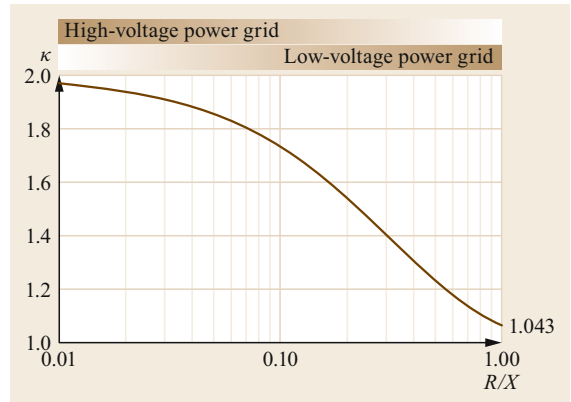
$$i = \sqrt{2}I''_K \left[ \underbrace{e^{-\frac{R}{X}\omega t} \sin \alpha + \sin(\omega t - \alpha)}_{\text{for crest factor } \kappa \text{ see Fig. 4.48}} \right], \tag{4.118}$$

with  $R/X =$  ratio of resistance to reactance of the short-circuit current path, where

$$\alpha = \varphi_z - \varphi_u. \tag{4.119}$$

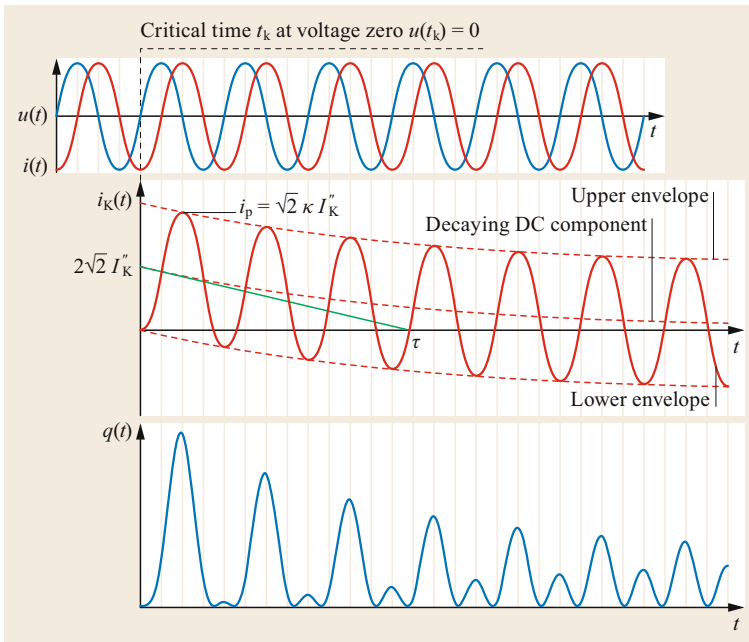
The maximum current (Fig. 4.49) takes place at:

- Phase angle  $\varphi_u = 0$  (short circuit in voltage zero crossing)
- Impedance angle at short-circuit entry  $\varphi_z \approx 90^\circ$  ( $R/X \rightarrow 0$ ).



**Fig. 4.48** Crest factor  $\kappa$  for a remote short-circuit depending on the  $R/X$  ratio of the upstream network





**Fig. 4.49** Short-circuit remote from generator, short-circuit current  $i(t)$ , voltage  $u(t)$ , and uniformly distributed load  $q(t)$  with phase angle  $\varphi_u = 0$  and  $R/X = 0.05$

The maximum current over time takes place at

$$t - \varphi_Z \approx \frac{\pi}{2} \rightarrow \omega t = \frac{\pi}{2} + \varphi_Z = \pi, \quad (4.120)$$

which, at a mains frequency of  $f = 50$  Hz, corresponds to a time of

$$t = \frac{\pi}{2\pi f} = \frac{1}{2f} = \frac{1}{100} = 10 \text{ ms}. \quad (4.121)$$

For a real high-voltage network with  $R/X = 0.05$  and, thus,  $\varphi_Z = 87.1$ , and, therefore  $\sin \alpha \approx 1$  a decaying DC component as per (4.118) with:

- $R/X = 0.05 \rightarrow X/R = 20$
- $e^{-t/\tau}$  with a time constant,

$$\tau = \frac{L}{R} = \frac{X}{\omega R} = \frac{20 \text{ s}}{2\pi 50} = 64 \text{ ms}. \quad (4.122)$$

Thus, the maximum current over time at  $t = 10$  ms, the value of the decaying exponential function becomes

$$e^{-\frac{10 \text{ ms}}{64 \text{ ms}}} = 0.855, \quad (4.123)$$

which means that, at this point in time, the DC component has dropped to a value of 85.5% due to the damping. With the crest factor  $\kappa$ , the peak short-circuit current  $i_p$  can be calculated as

$$i_p = \sqrt{2} \kappa I_K'', \quad (4.124)$$

where (with (4.123))

$$\kappa = 0.855 + 1 = 1.855. \quad (4.125)$$

The crest factor cannot, theoretically, exceed the value  $\kappa = 2$ ; in practical cases it is usually  $\kappa \leq 1.8$ .

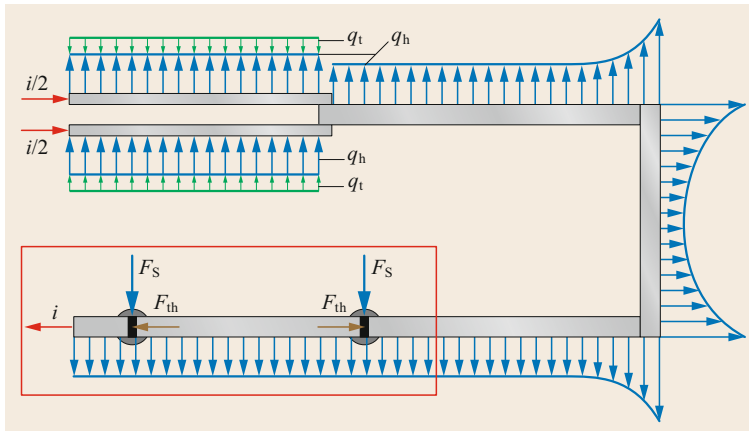
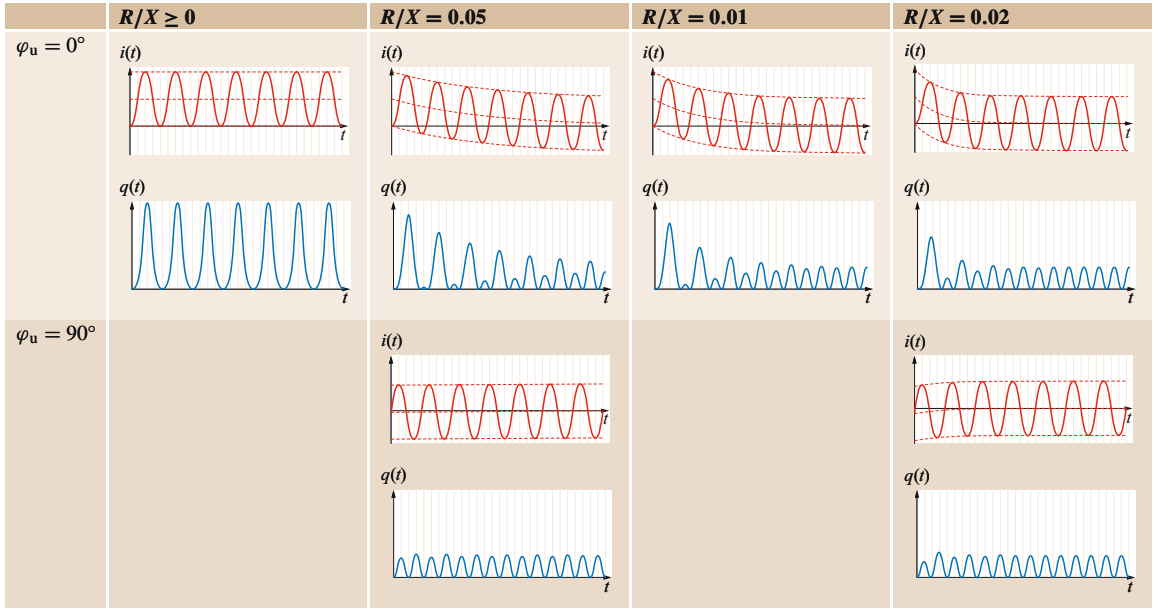
The peak short-circuit current  $i_p$  is the maximum amplitude occurring immediately after the short circuit and is decisive for the design of the mechanical strength of the current-conducting arrangement. The stress over time curve due to the line load  $q(t)$  depends on the  $R/X$  ratio of the feeding network and, thus, on the time function of the short-circuit current  $i(t)$  (Table 4.32) as well as the phase angle of the voltage  $\varphi_u$  at the instant the short-circuit occurs (Fig. 4.47).

Selected practical examples of electromagnetic forces  $F$  on support points (insulators) and line loads  $q$  on conductors in electrical installations (Figs. 4.50 and 4.51) or on contacts in electrical connections and on switching contacts can be calculated with the equations in Table 4.33 (maximum values) [4.1, 26].

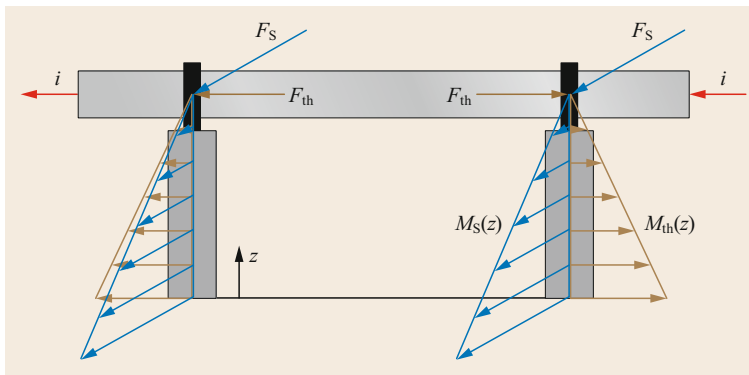
For conductors with rectangular cross section, a mechanically effective main conductor spacing of  $a_m$  is considered, which depends on the conductor height  $d$ , its width  $b$ , and the geometric center distance  $a$  (Fig. 4.52)

$$\frac{1}{a_m} = \frac{1}{b} \left[ \varphi \left( \frac{b}{a} \right) + \frac{d^2}{a^2} \eta \left( \frac{b}{a} \right) \right], \quad (4.126)$$

**Table 4.32** Short-circuit remote from generator, short-circuit current  $i(t)$  and uniformly distributed load  $q(t)$ , and examples for several  $R/X$ -ratios



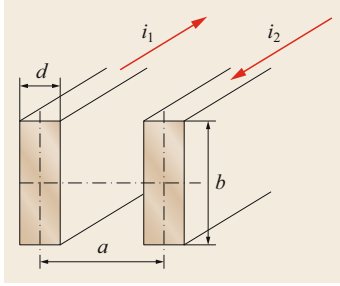
**Fig. 4.50** Electromagnetic forces  $F$  and uniformly distributed load  $q(t)$ . (Top view).  $q_h$ : uniformly distributed load between main conductors;  $q_t$ : uniformly distributed load between subconductors;  $F_S$ : electromagnetic force at fittings and insulators;  $F_{th}$ : thermal expansion force



**Fig. 4.51** Electromagnetic and thermal expansion force on supports (fittings and insulators), side view.  $F_S$ : electromagnetic force on fittings and insulator;  $F_{th}$ : thermal expansion force;  $M_S(z)$ : moments at insulator caused by electromagnetic force;  $M_{th}(z)$ : moments at insulator caused by thermal expansion force

**Table 4.33** Uniformly distributed load and force for selected arrangements

Arrangement and application	Schema	Uniformly distributed load or force
Parallel, endless long conductors e.g., overheadline conductors, substation bus bar (opposing currents, conductors repel each other)		$q = \frac{i_1 i_2 \mu}{2\pi a}$
Bundled conductors, subconductors in bus bars (parallel conductor, conductors attract)		
Conducting arrangement with 90°-angles e.g., bus bar derivation, cross connection of parallel conductors		$q = \frac{i^2 \mu}{4\pi x}$
Circular ring e.g., winding of a coil (radial forces to the outside)		$q_r = \frac{i_2 \mu}{2\pi R} \left( \ln \frac{8R}{r} - 0.75 \right)$ applies for: $R \gg r$
Circles next to each other e.g., uniformly distributed load between windings of a coil (conductors repel each other)		$q = \frac{i_1 i_2 \mu}{2\pi a}$ $F = i_1 i_2 \mu \frac{R}{a}$ applies for: $\frac{R}{a} > 2$
Conducting arrangement with several corners e.g., MV-insulator, MV-circuit breaker with trolley, NH-fuse links (forces try to open the current path)		At both corners each $q = \frac{i^2 \mu}{4\pi x}$
Contact point in a connection e.g., plug-in connectors, switching contacts (lift-off force)		$F \approx \frac{i^2 \mu}{4\pi} \ln \frac{r_2}{r_1}$



**Fig. 4.52** Parallel main conductors with rectangular cross section

whereby

$$\varphi\left(\frac{b}{a}\right) = 2 \arctan\left(\frac{b}{a}\right) - \frac{a}{b} \ln\left[1 + \left(\frac{b}{a}\right)^2\right], \quad (4.127)$$

$$\eta\left(\frac{b}{a}\right) = \frac{bd^2}{6a(a^2 + b^2)}. \quad (4.128)$$

For bus bars with several subconductors ( $a_s < b$ ) (Fig. 4.53), the line load is calculated as

$$q_s = \left(\frac{\hat{i}}{2}\right)^2 \frac{\mu_0}{2\pi a_s}, \quad (4.129)$$

where

$$\frac{1}{a_s} = \frac{1}{b} \left[ \varphi\left(\frac{b}{a_t}\right) + \left(\frac{d}{a_t}\right)^2 \eta\left(\frac{d}{a_t}\right) \right]. \quad (4.130)$$

In symmetrical three-phase systems, different currents flow in the three conductors when a three-pole short circuit occurs:  $i_{L1}$ ,  $i_{L2}$ , and  $i_{L3}$ , whose mechanical load effects overlap. Two typical cases in the praxis are the arrangement of the three conductors in one plane with a distance  $a$  and the arrangement of the conductors in an equilateral triangle.

*Conductors in one plane.* Line currents  $i_L$  (Fig. 4.54)

$$i_{L1} = \sqrt{2I''_{K(3)}} \left[ e^{-\frac{R}{X}\omega t} \sin \alpha + \sin(\omega t - \alpha) \right], \quad (4.131)$$

$$i_{L2} = \sqrt{2I''_{K(3)}} \left\{ e^{-\frac{R}{X}\omega t} \sin\left(\alpha + \frac{2\pi}{3}\right) + \sin\left[\omega t - \left(\alpha + \frac{2\pi}{3}\right)\right] \right\}, \quad (4.132)$$

$$i_{L3} = \sqrt{2I''_{K(3)}} \left\{ e^{-\frac{R}{X}\omega t} \sin\left(\alpha + \frac{4\pi}{3}\right) + \sin\left[\omega t - \left(\alpha + \frac{4\pi}{3}\right)\right] \right\}. \quad (4.133)$$

Static line loads  $q_{pe}$

$$q_{L1(3)} = \frac{\mu_0}{2\pi a} \left( i_{L1}i_{L2} + \frac{i_{L1}i_{L3}}{2} \right), \quad (4.134)$$

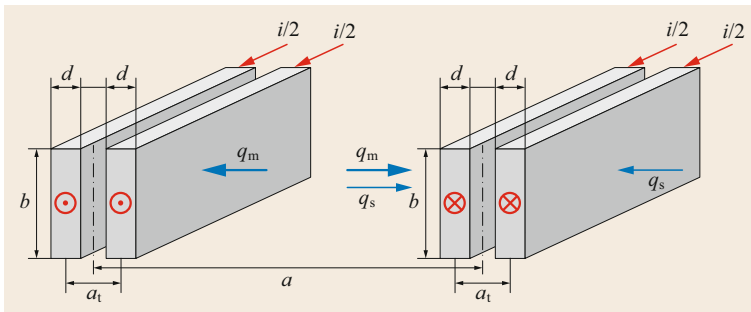
$$q_{L2(3)} = \frac{\mu_0}{2\pi a} (i_{L2}i_{L1} - i_{L2}i_{L3}), \quad (4.135)$$

$$q_{L3(3)} = \frac{\mu_0}{2\pi a} \left( -i_{L2}i_{L3} - \frac{i_{L1}i_{L3}}{2} \right). \quad (4.136)$$

This results in:

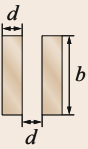
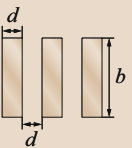
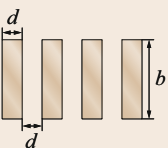
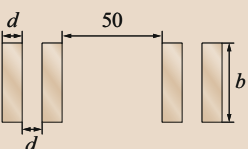
- Phase conductors L1 and L3 moving outwards by the resulting line load.
- The resulting line load on phase conductor L2 is zero.
- The sum of all line loads is zero at all times.

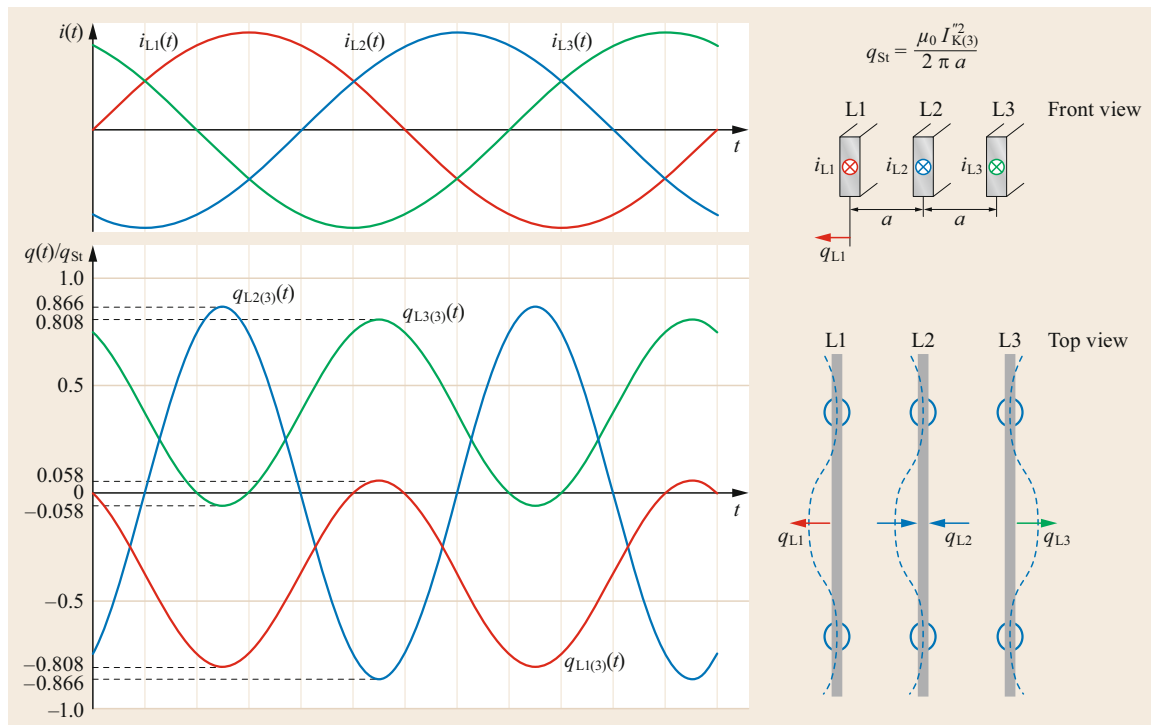
*Conductors in an equilateral triangle.* The vectors of the forces act in different directions (attracting and repulsive) depending on time, and they have to be added for every time instant  $t$  vectorially, resulting in a lo-



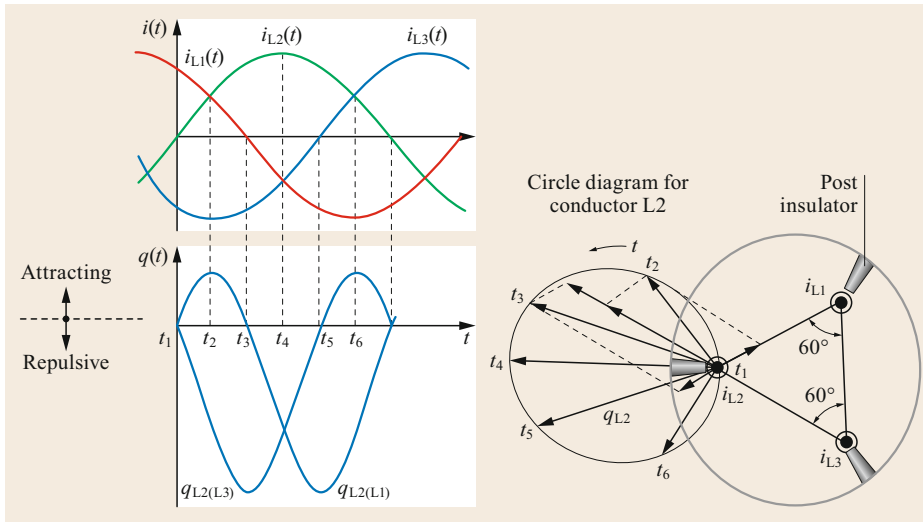
**Fig. 4.53** Uniformly distributed load at main and subconductor arrangements ( $a$  = geometric center-to-center distance of the main conductors,  $a_t$  = geometric center-to-center distance of the subconductors,  $a_m$  = effective main conductor spacing,  $a_s$  = effective subconductor spacing (Table 4.34),  $b$  = width of the rectangular conductor,  $d$  = height of the rectangular conductor,  $i/2$  = current per subconductor (with two subconductors),  $q_m$  = line load due caused by the main conductors,  $q_s$  = line load by the subconductors)

**Table 4.34** Effective subconductor spacing  $a_s$  for a rectangular cross section (all dimensions given in mm)

Rectangular profile	$d$	$b = 40$	$b = 50$	$b = 60$	$b = 80$	$b = 100$	$b = 120$	$b = 160$	$b = 200$
	5 10	20 28	24 31	27 34	33 41	40 47	– 54	– 67	– 80
	5 10	– 17	13 19	15 20	18 23	22 27	– 30	– 37	– 43
	5 10	– 14	– 15	– 16	– 18	– 20	– 22	– 26	– 31
	5 10	– 17	14 18	15 20	18 22	20 25	– 27	– 32	– –



**Fig. 4.54** Short-circuit current – uniformly distributed load profiles with three-pole short circuit – one-level arrangement



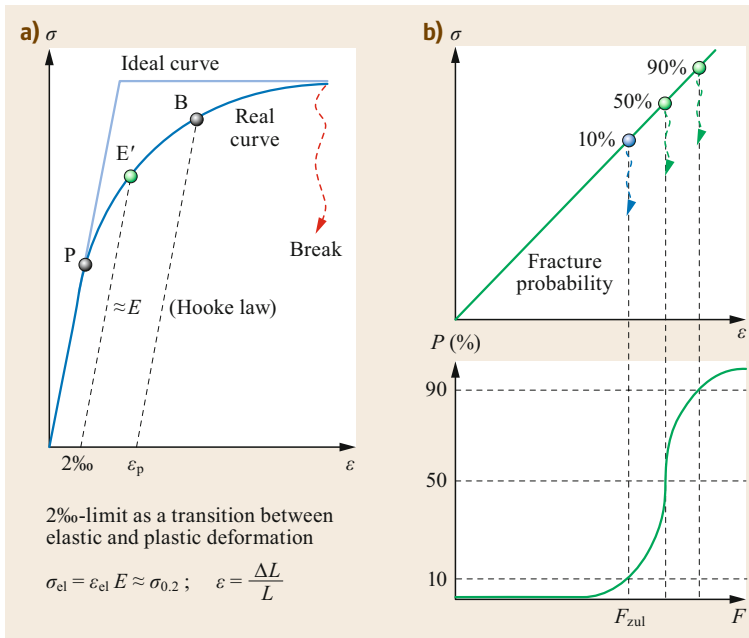
**Fig. 4.55** Short circuit current – uniformly distributed load profiles with three-pole short circuit – arrangement in triangle

cus curve that is run through once in each half-wave of the current. The resulting forces always act outwards, so that the support insulators should ideally be arranged in such a way that they are subjected to compression. The sum of all line loads is zero at all times (Fig. 4.55).

**Mechanical Stress**

*Elastic and plastic deformation of current paths under short-circuit current load.* The load of current-conducting arrangements by short-circuit currents leads to mechanical stresses  $\sigma$  on the conductors

(L), the insulators (I), and the structural substructure (U). With metals (conductor, substructure), this leads to elastic deformation ( $\sigma < \sigma_{el} \approx \sigma_{0.2} \Rightarrow \epsilon < \epsilon_{el}$ ) or, for larger stresses, to permanent plastic deformation ( $\sigma = \sigma_p > \sigma_{0.2} \Rightarrow \epsilon = \epsilon_p > \epsilon_{el}$ ). When the material strength is exceeded ( $\sigma_b$ ), the metal will fail (Fig. 4.56a). In the case of brittle insulating materials in the glass state, the failure occurs directly after the slightly elastic state without prior permanent deformation (Fig. 4.56b). Depending on the material structure, its strength is subject to  $\sigma_b$  scatters and is described by a distribution function for the probability of failure.



**Fig. 4.56a,b** Behavior of materials under mechanical stress. (a) Conductors/metals, (b) insulating materials in vitreous state

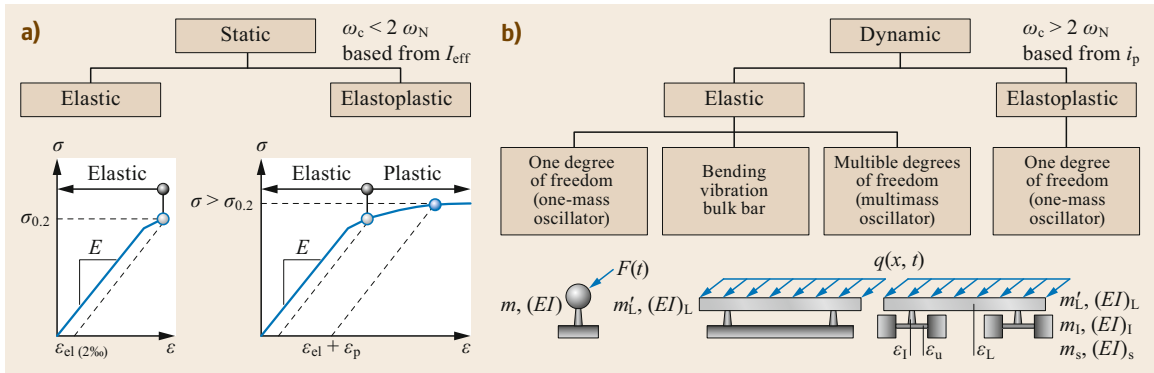


Fig. 4.57 (a) Static and (b) dynamic models for mechanical stress due to short-circuit currents

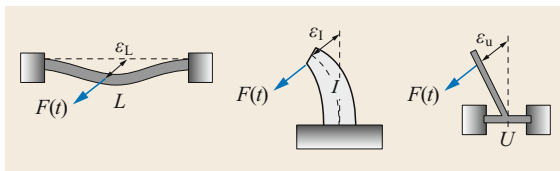


Fig. 4.58 Models for mechanical stress due to short-circuit currents, flexibility of conducting systems

If the mechanical natural frequencies  $f_c$  – which is caused by the line load  $q(t)$  or the force  $F(t)$  – of the stressed conductors – insulators and the substructure are considerably lower than twice the electrical mains frequency  $f_n$  (based on the current peak load  $\hat{I}_{max}$ ), said components cannot follow the line load time curve  $q(t)$ , which oscillates with a frequency of  $2 f_n$  (Fig. 4.46), and thus a static model can be used for the calculation of the mechanical stresses (spatial problem). If, on the other hand, the natural frequencies are significantly greater than twice the mains frequency, a dynamic stress (spatio-temporal problem) must be assumed (Fig. 4.57), whereby, taking into account the flexibility (elasticity) (Fig. 4.58), a distinction must be made between single-mass oscillators, mass-covered beams, and multimass oscillators, which are to be treated differently.

That *elastostatic model* (Fig. 4.57) can be used under the following conditions:

- The arrangement can follow the load without delay  $\rightarrow f_c \gg 2f_n$  (very high bending stiffness of the supporting elements or insulators  $(EI)_I$  and torsional stiffness of the substructure  $(GI)_U$ ).
- Step-like load changes are not considered.
- Application of mechanical equivalents (Fig. 4.59):
  - Beam fixed on both sides (central field of a bus bar)
  - Beam fixed on one side and pinned on the other (edge field of a bus bar)
  - Beam fixed on one side (support insulator).

For an elastically deformable beam with transverse oscillations, this partial differential equation applies

$$\frac{\partial^2}{\partial x^2} \left( EI \frac{\partial^2 v}{\partial x^2} \right) + \frac{\partial}{\partial x} \left( m \frac{\partial^2 v}{\partial t^2} \right) + \frac{\partial}{\partial x} \left( 2\delta m \frac{\partial v}{\partial t} \right) = q(t, x), \quad (4.137)$$

where  $m$  = mass, and  $\delta$  = density,  $v$  = deflection.

Under the conditions of a constant mass per unit of length, a constant bending stiffness  $(EI)$  and a constant line load  $q$ , (4.54) is simplified to

$$EI \frac{\partial^4 v}{\partial x^4} + m \frac{\partial^2 v}{\partial t^2} + 2\delta m \frac{\partial v}{\partial t} = q(t). \quad (4.138)$$

For the static case ( $\partial/\partial t = 0$ ), the differential equation of elastic bending (Table 4.35) results.

The constants  $C_1$  to  $C_4$  result from the boundary conditions for the static model (clamping conditions) (Table 4.36).

Table 4.35 Differential equation of elastic bending

Mechanical quantity	Differential equation
Line load	$EI \frac{\partial^4 v}{\partial x^4} = q$
Shear force	$EI \frac{\partial^3 v}{\partial x^3} = FQ(x) = qx + C_1$
Bending moment	$EI \frac{\partial^2 v}{\partial x^2} = M(x) = q \frac{x^2}{2} + C_1 x + C_2$
Bending angle	$EI \frac{\partial v}{\partial x} = EI v'(x) = q \frac{x^3}{6} + C_1 \frac{x^2}{2} + C_2 x + C_3$
Deflection	$EI v = EI v(x) = q \frac{x^4}{24} + C_1 \frac{x^3}{6} + C_2 \frac{x^2}{2} + C_3 x + C_4$

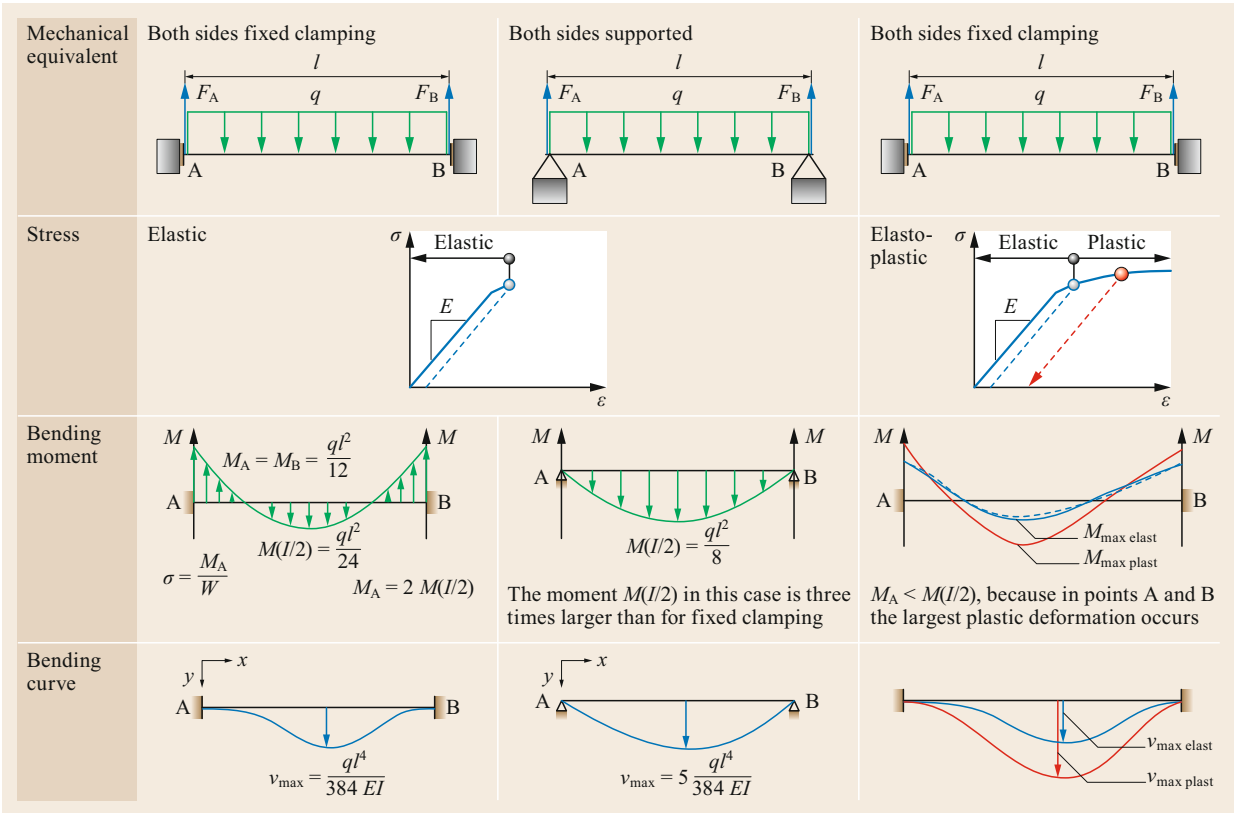


Fig. 4.59 Reactions of a conductor rail to the static load

Table 4.36 Clamping conditions in the static models

Clamping conditions	Seriousness	Stipulation	Constant
Fixed	No deflection	$v = 0$	$C_3 = 0$
	No deflection angle	$\frac{dv}{dx} = 0$	$C_4 = 0$
Pinned	No deflection	$v = 0$	$C_2 = 0$
	No bending moment	$\frac{d^2v}{dx^2} = 0$	$C_4 = 0$
Free	No bending moment	$\frac{d^2v}{dx^2} = 0$	$C_1 = 0$
	Zero shear force	$\frac{d^3v}{dx^3} = 0$	$C_2 = 0$

The *elastoplastic model* (Fig. 4.57) can be applied under the following conditions:

- The application is similar to the elastostatic model, however, the plastic properties of the conductor materials are also taken into account.
- The model describes the behavior of the flexurally stiff conductors in the overall system.

- Common materials for support insulators (e.g., porcelain, epoxy resin) are practically not plastically deformable. From this it follows that they will fail at the end of their elastic range (Fig. 4.56b).

The following ideas are behind the elastoplastic model:

- Materials can be subjected to higher loads, in which the limit loads are derived from their plastic behavior and the permanent deformation.
- Permanent deformation must not inadmissibly reduce the functionality of the device and/or the breakdown voltage between deflected conductors.
- The calculation of the maximum permanent deflection depends on the load.
- Edge stresses of the bending beam are smaller, and edge strains are higher than calculated for the elastic case.
- The permanent deformation is calculated numerically as a function of the line load using experimentally determined stress-strain curves.



Dynamic models (Fig. 4.57) apply under the following conditions:

- After displacement from the equilibrium position following a damped oscillation with eigenfrequency, the mechanical stresses return to zero.
- Preferred application when a large mass is supported by an elastically deformable element, and a time-varying force acts on the mass (e.g., elastic support insulator  $I$  fixed on one side and carrying a conductor  $L$ ).
- System elements behave elastically:
  - Applies in good approximation to support insulators up to failure.
  - Applies to metals (conductors, substructure), as they can deform plastically.
  - Only qualitative comparison between elastostatic and elastodynamic models are possible.
- Eigenfrequency  $\omega_c$  and damping constant  $\delta$  can be determined experimentally (decay test) or analytically (dynamic model with several degrees of freedom).

**Typical application case 1 – Stresses on support insulators.** The mechanical equivalent is a spring-mass oscillator as a first-degree oscillating element with the mechanical eigenfrequency  $\omega_c$  and the damping constant  $\delta$  with a transfer function  $G(s)$

$$G(s) = \frac{\omega_0^2}{\omega_0^2 + 2\delta\omega_0s + s^2}, \tag{4.139}$$

where

$$\omega_0^2 = \sqrt{\omega_c^2 + \delta^2}, \tag{4.140}$$

where  $G$  = transfer function,  $s$  = Laplace operator,  $\delta$  = damping constant, and  $\omega_c$  = eigenfrequency of the mechanical oscillating system.

With this model, it is possible to calculate the mechanical stress depending on the load. The input

variable for the model is the time-dependent force  $F(t)$ , which acts at the head of the support insulator and emerges from the line load  $q(t)$  or the quadratic current curve  $i^2(t)$ . The output variable can, for example, be the deflection  $y(t)$ , the edge strain  $\varepsilon(t)$ , or other mechanical quantities, which can then be compared with the permissible strength values of the respective material. The solution of the transfer function  $G(s)$  takes place in the Laplace domain and is then transformed backwards into the time domain.

Example: the behavior of a support insulator  $I$  on rigid ground  $U$  under load with a 50 Hz short-circuit current and the resulting line load curve at the top of the insulator  $q(t)$  is illustrated in Fig. 4.60 for four different mechanical eigenfrequencies ( $f_c = 25, 50, 100,$  and  $150$  Hz) and discussed with regard to its DC and AC components. The dominant loads for the individual natural frequencies are marked with an arrow.

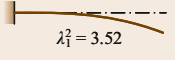
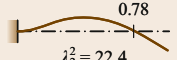
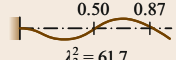
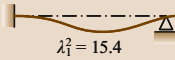
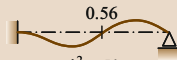
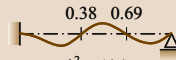
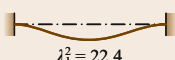
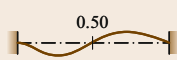
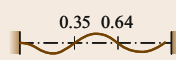
**Typical application 2 – Vibrations of electrical conductors.** The mechanical equivalent are bending vibrations of mass-covered beams with rigid subsoil under the following conditions:

- Mass, bending stiffness, and elasticity along a conductor or insulator are continuously distributed.
- The profile of the cross section is double-symmetrical (e.g., rectangle, circle) (Table 4.29).
- The oscillating beam is fixed or pinned on one or both sides. This means that the conductors oscillate independently of the overall system (Fig. 4.61 and Table 4.37).

The mechanical natural frequency  $f_c$  of the oscillating conductor is mainly determined by its length  $l$  between the clamping points

$$f_c = \frac{22.4}{2\pi l^2} \sqrt{\frac{EI}{\delta A}}, \tag{4.141}$$

**Table 4.37** Bending waves of mass-compounded beam, types of natural oscillations (adapted from [4.1])

Fixed/supported	$k = 1$	$k = 2$	$k = 3$	$\lambda_k$ in Table 4.35
One side fixed	 $\lambda_1^2 = 3.52$	 $\lambda_2^2 = 22.4$	 $\lambda_3^2 = 61.7$	$\lambda_k^2 = \left(k - \frac{1}{2}\right)^2 \pi^2$
Fixed/supported	 $\lambda_1^2 = 15.4$	 $\lambda_2^2 = 50$	 $\lambda_3^2 = 104$	$\lambda_k^2 = \left(k + \frac{1}{4}\right)^2 \pi^2$
Both sides fixed	 $\lambda_1^2 = 22.4$	 $\lambda_2^2 = 61.7$	 $\lambda_3^2 = 121$	$\lambda_k^2 = \left(k + \frac{1}{2}\right)^2 \pi^2$

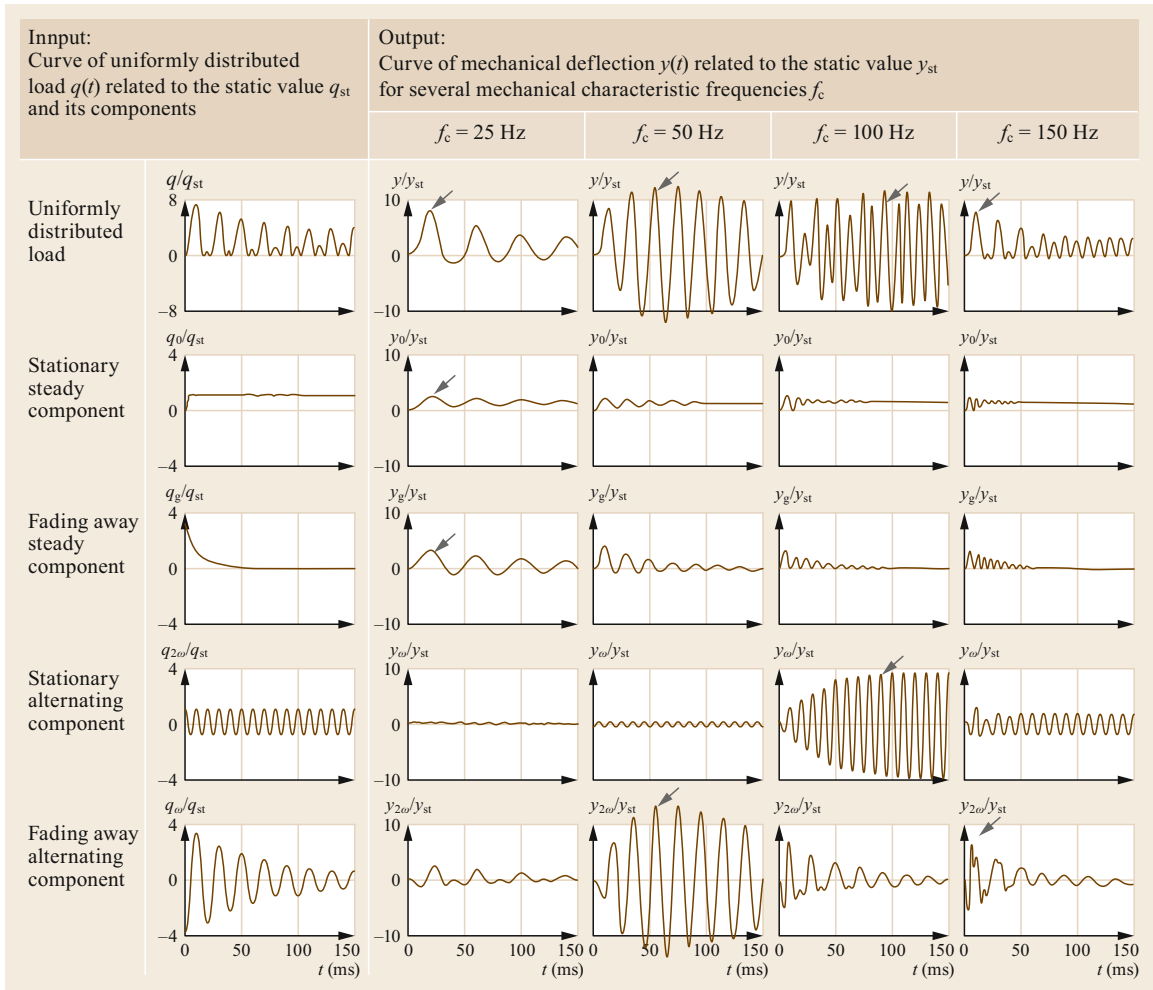


Fig. 4.60 Typical oscillation behavior of a spring-mass system, e.g., elastic post insulator ( $I$ ) in a rigid system

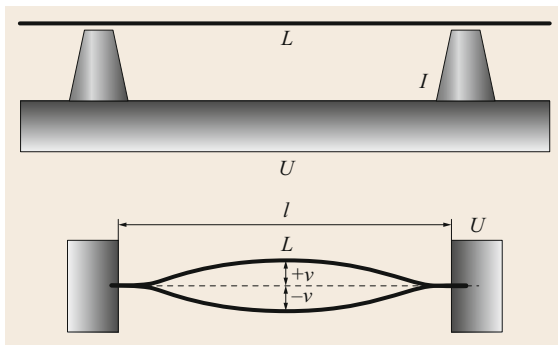


Fig. 4.61 Oscillation of an electric conductor ( $L$ ) with rigid substructure ( $U$ ) and insulator ( $I$ )

where  $E$  = modulus of elasticity,  $I$  = moment of inertia (Table 4.29),  $\delta$  = specific mass,  $A$  = conductor cross section,  $l$  = length between clamping points, and

$22.4 = \lambda^2$ -factor for first natural frequency with fixed clamping (Table 4.37,  $k = 1$  bottom).

For the elastically deformed beam with lateral oscillations, the partial differential equation for the line load applies

$$\frac{\partial^2}{\partial x^2} \left( EI \frac{\partial^2 v}{\partial x^2} \right) + \frac{\partial}{\partial x} \left( m \frac{\partial^2 v}{\partial t^2} \right) + \frac{\partial}{\partial x} \left( 2\delta m \frac{\partial v}{\partial t} \right) = q(t, x) \quad (4.142)$$

With the assumptions of constant mass  $m$ , constant bending stiffness  $EI$ , and no damping ( $\delta = 0$ ), and without line load ( $q = 0$  results) in the differential equation for the free oscillation

$$EI \frac{\partial^4 v}{\partial x^4} + m \frac{\partial^2 v}{\partial t^2} = 0 \quad (4.143)$$

The solution for the deflection  $v(x,t)$  becomes

$$v(x,t) = \sum_{k=1}^{\infty} a_k v_k(x) \sin(\omega_k t + \beta_k), \quad (4.144)$$

with the integration constants  $\alpha_k$  and  $\beta_k$ . The deflection  $v(x,t)$  is a superposition of oscillations with a multitude of natural frequencies  $\omega_k$  (Table 4.37)

$$\omega_k = \lambda_k^2 \sqrt{\frac{EI}{\delta A l^4}}. \quad (4.145)$$

Special cases:

- The mechanical natural frequency  $f_c$  is significantly greater than twice the mains frequency  $f_n$  ( $f_c \gg 100$  Hz). The conductor follows the load without delay, and the stresses on the conductor can be determined as with a statically loaded conductor. This means that the highest line load that occurs leads to maximum mechanical stress  $\sigma_{\max}$ .
- The mechanical natural frequency  $f_c$  is twice the mains frequency  $f_n$  ( $f_c = 100$  Hz). The system resonates in the elastic range; at higher loads, plastic deformation occurs, and the resonance frequency is detuned, i.e., the system *heals* itself.
- The mechanical natural frequency  $f_c$  is significantly smaller than twice the mains frequency  $f_n$  ( $f_c \ll 100$  Hz); the electrical conductor cannot follow the load due to its inertia (elastostatic load case).

**Typical application 3 – Electrical conductor with elastic substructure.** The dynamic model with several degrees of freedom (multimass oscillator) (Fig. 4.57) serves as the mechanical equivalent. In real switchgear systems, the short-circuit current load on the conductor also causes the insulating support points and the supporting substructure to deform. The lowest natural frequencies (fundamental frequency) of the overall system is smaller than, for example, the natural frequencies of a rigidly fixed conductor bus bar (flexibility). High and short-term loads due to surge currents can cause smaller loads in the system than can be expected from static models. Prerequisites and objectives for calculations with this model are:

- It must be possible to derive a multimass model with known distribution of masses and bending stiffness from the design in order to be able to calculate the characteristic dynamic properties (fundamental frequency).
- The system is assumed to be linear, i.e., no plastic deformations are taken into account. Damping plays a subordinate role or is completely neglected.

- The system load can be estimated for periodic loads (continuous short-circuit current) and short-term loads (surge short-circuit current).

The vibration of the system, i.e., conductor (L), support insulator (I), and substructure (U), depends on the displacement of the bus bar  $d_L$  and of the insulator  $d_I$ , as well as the elasticity (property of a body loaded with a force to give way by deformation, elasticity) of the substructure  $d_U$ . The maximum occurring forces  $F_{\max}$  during this process are calculated: for three-pole short circuit; conductors are in a plane arrangement

$$F_{\max} = V_F \frac{\mu_0 \sqrt{3} l}{4\pi a_m} \left( \kappa \sqrt{2} I''_{K(3)} \right)^2. \quad (4.146)$$

for a bipolar short circuit ( $I''_{K(2)} = 0.866 I''_{K(3)}$ )

$$F_{\max} = V_F \frac{\mu_0 l}{2\pi a_m} \left( \kappa \sqrt{2} I''_{K(2)} \right)^2, \quad (4.147)$$

where  $V_F$  = factor for comparing dynamic to static force ( $F_{\text{dyn}}/F_{\text{stat}}$ ) (Fig. 4.62),  $l$  = length between clamping points,  $a_m$  = effective conductor spacing, and  $\kappa$  = crest factor.

In the practical case where the flexibility of the conductor  $d_L$  and the support insulator  $d_I$  clearly distinguish ( $d_L/d_I$ ), the model can be simplified as a vibrating conductor with the mass  $m_L$  and an oscillating support insulator with a top mass  $m_I$  (dual-mass model). The frequency of the system related to the frequency of the clamped conductor ( $f_{\text{sys}}/f_L$ ) results from the ratio of the vibrating masses ( $m_I/m_L$ ) and the related deflections ( $d_L/d_I$ ) (Fig. 4.63).

The maximum possible load current  $\hat{i}_{\max}$  for a conductor fixed at both ends of length  $l$  and distance  $a$  to the adjacent conductor is the current at which the permissible mechanical stress remains in the elastic range of the conductor material, i.e.,  $\sigma_{\text{zul}} = \sigma_{0.2}$  is not exceeded. This stress is calculated as

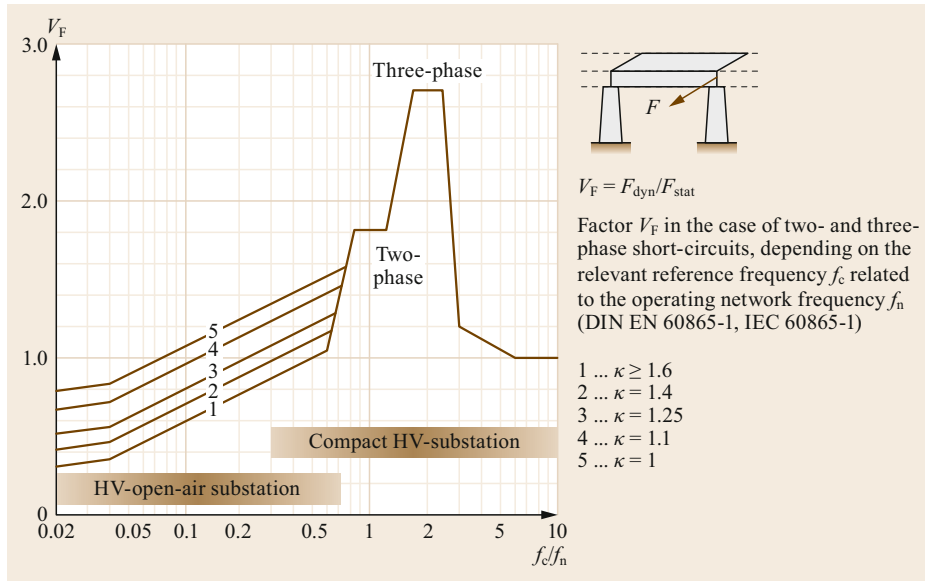
$$\sigma_{0.2} = \frac{M}{W} V_{\sigma}, \quad (4.148)$$

where with  $i_1 = i_2$  in (4.111) and

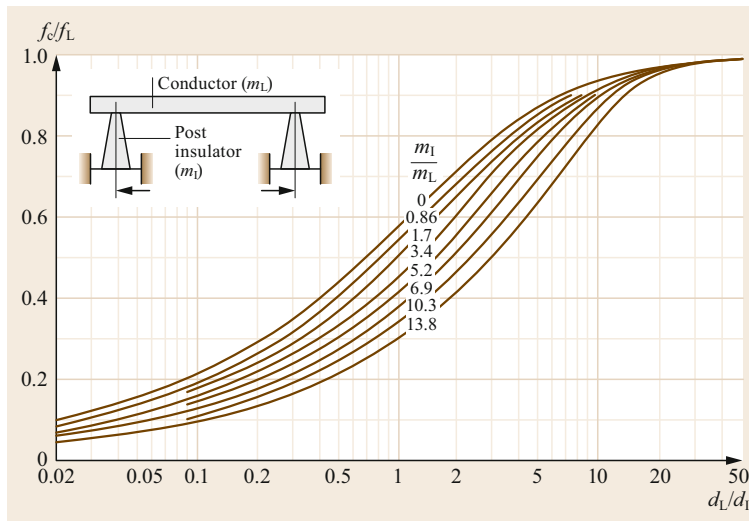
$$M = \frac{q l^2}{12} \quad (4.149)$$

insertion into (4.148) results in

$$\sigma_{0.2} = \frac{\mu_0 l^2 \hat{i}_{\max}}{2\mu q a 12 W} V_{\sigma}. \quad (4.150)$$



**Fig. 4.62** Ratio of dynamic force to static force on the support (adapted from [4.28])



**Fig. 4.63** Dynamic model – diagram-related natural frequencies for a two-mass model (adapted from [4.28])

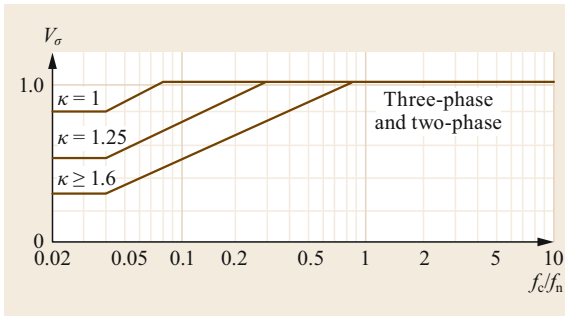
With this equation, one obtains the maximum permissible current as

$$\hat{i}_{\text{max}} = \sqrt{\frac{4\pi abh^2\sigma_{0.2}}{\mu_0 l^2 V_\sigma}}, \quad (4.151)$$

where  $a$  = center distance of the conductors,  $b$  = conductor width (Table 4.30), and  $h$  = conductor height (Table 4.30),  $V_\sigma$  = factor for comparing the dynamic to static conductor bending stress ( $\sigma_{\text{dyn}}/\sigma_{\text{stat}}$ ) (Fig. 4.64).

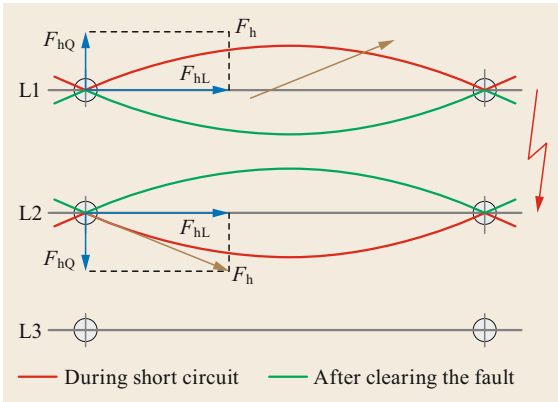
**Flexible conductors.** For example, overhead line conductors, can move relatively freely in contrast to flexurally stiff conductors. The mechanical natural frequency

of a sagging conductor is approximately  $f_c \approx 0.3$  Hz, compared to the force of the short-circuit current, which oscillates with double mains frequency  $2f_n = 100$  Hz; thus, the issue becomes a quasi elastostatic problem. In the case of a two-pole short circuit (Fig. 4.65), the affected conductors are repelled during the short circuit (currents in the opposite direction). In the case of a three-pole short circuit (Fig. 4.66), this affects the two outer conductors, while the middle conductor remains mechanically neutral. In both cases, the peak short-circuit current (acting like an impulse relative to the natural frequency of the rope) stimulates the conductors to oscillate slowly, causing them to move towards each other. Due to the very large distances between the main conductors, es-

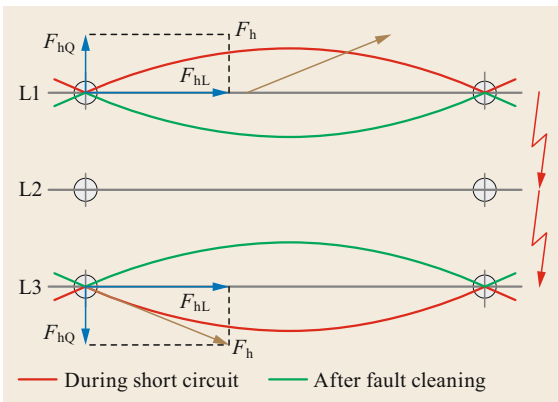


Factor  $V_\sigma$  for two- and three-pole short circuits, depending on the relevant reference frequency  $f_c$  related to the operating network frequency  $f_n$  (DIN EN 60865-1, IEC 60865-1)

**Fig. 4.64** Factor  $V_\sigma$  to determine the conductor



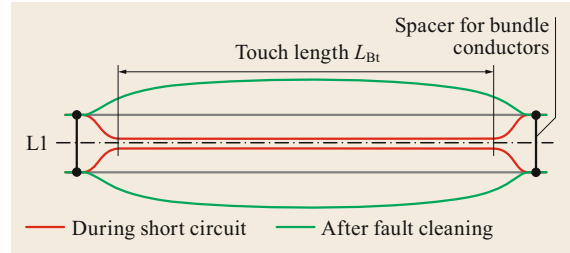
**Fig. 4.65** Mechanical stress on stranded overhead line conductors (main conductor) in the phase-to-phase fault



**Fig. 4.66** Mechanical stress on stranded overhead line conductors (main conductor) in the three-phase fault

pecially with high-voltage overhead lines, the line loads on the main conductors are usually negligibly small.

These issues are significantly different for bundled conductors (Fig. 4.68) in which the short-circuit current is divided between two, three, four, or more subconductors of a bundle, which are, however, only a few decimeters apart. This leads to a strong contraction of

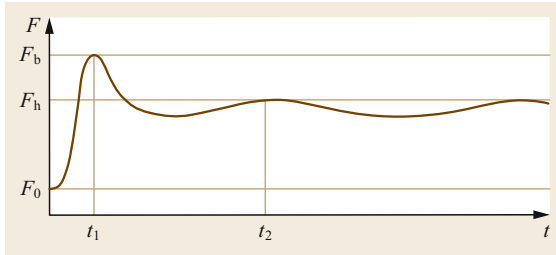


**Fig. 4.67** Mechanical stress on stranded overhead line conductors (bundled conductors) during and after short circuit



**Fig. 4.68** Quad-bundled conductors with spacer dampers

the bundle between spacer locations along the bundle (Fig. 4.67) and subsequent expansion. This can lead to clashing of the conductors at the instant of the short-circuit, as well as to high compressive and tensile forces at the spacers. The resistance of the spacers to short circuits must, thus, be verified. Only very short distances



**Fig. 4.69** Curve of tensile force in a span with bundled conductors. Maximum force  $F_b$  after short-circuit entry due to contraction of the bundle conductors, depending on the short-circuit current  $i_p$  and the rope elongation; force effect between the main conductors is built up, due to the large inertia of a span (natural frequency  $f_c < 1$  Hz), comparatively slow ( $F_h$  depending on the rms value of the short-circuit current); initial force  $F_0$  before short-circuit

between the spacer frames (5–10 m) could prevent the conductors from clashing even with high short-circuit currents, which is at best possible in open air substations. Furthermore, the high bending stress at the spacer clamps can lead to plastic deformation of the individual wires in the outer conductor layer (birdcaging, which will cause disturbing acoustic emissions).

The contraction of the bundle conductors after the short circuit occurs (at  $t_1$ ) results in a large increase in the conductor tensile force  $F_b$  (depending on the peak short-circuit current  $i_p$  and the rope elongation) (Figs. 4.67 and 4.69). Moreover, this force is partially reduced by decreasing the sag and, possibly, by a time-dependent plastic elongation of the conductors. After that (at  $t_2$ ), a force is comparatively slowly applied between the main conductors (because of the high inertia of the span with a natural frequency  $f_c \approx 0.3$  Hz). ( $F_h$  depends on the rms value of the short-circuit current.)

### 4.3.3 Connections in Current Paths

*Electrical connections* are used to connect, terminate, and branch electrical conductors. *Electrical connectors* are hardware components, which are suitable for making such connections in current paths [4.3, 17, 18, 34–42]. The *electrical contact* is a physical state in which two or more electrical conductors are joined together in such a way that a current can be conducted from one to the other. Electrical contacts are the physically necessary prerequisite for the function of electrical connections.,

#### Theory of Electrical Connections and Contacts

When connecting electrical conductors, within the apparent contact area  $A_a$  there exist either single or multiple contact points that can be of a point or a linear

shape. In these contact points, the electric current flow is constricted to microscopically small metallic surfaces  $A_m$  (*metallic contact area*). This results in an additional electrical *constriction resistance*  $R_c$ . Since there is always an impurity layer (usually an oxide layer) with a higher specific electrical resistance on every metallic surface, the resulting *impurity film resistance*  $R_f$  must be taken into account. Constriction and impurity film resistance result in the *contact resistance*  $R_k$ , which, in addition to the metallic lead resistance  $R_m$  of the conductive path, represents an additional heat source. Contact and material resistance can be determined analytically and experimentally as *joint resistance*  $R_j$  (Figs. 4.70 and 4.72) [4.43]:

- Contact resistance

$$R_k(t) = R_c(t) + R_f(t), \quad (4.152)$$

- Joint resistance

$$R_j(t) = R_k(t) + R_m = R_c(t) + R_f(t) + R_m. \quad (4.153)$$

In the case of plastic deformation due to high contact forces, the size of the metallic contact surface  $A_m$  and the resulting constriction resistance  $R_c$  are dependent on the effective contact force  $F_j$  and the material properties, i.e., hardness  $H_k$  and specific electrical resistance  $\rho$  of the contact partners to be connected, and can be based on the *Holm* contact model (4.154) to (4.156), (Fig. 4.71). The contact hardness is determined experimentally (Table 4.38 [4.34, 44]).

$$A_m = \frac{F_j}{H_k}, \quad (4.154)$$

$$r_m = \sqrt{\frac{A_m}{\pi}}, \quad (4.155)$$

$$R_c = \frac{\rho}{2} \sqrt{\pi \frac{H_k}{F_j}}, \quad (4.156)$$

where  $F_j$  = joint force,  $r_m$  = radius of metallic, load bearing area,  $A_m$  = metallic, load bearing area,  $H_k$  = contact hardness, and  $\rho$  = specific electric resistance of contact material.

**Table 4.38** Contact hardness

Metal	$H_k$ ( $\times 10^8 \text{ N m}^{-2}$ )
Cu	4–7
Al	1.8–4
Ag	3–7
Ni	7–20
W	12–14

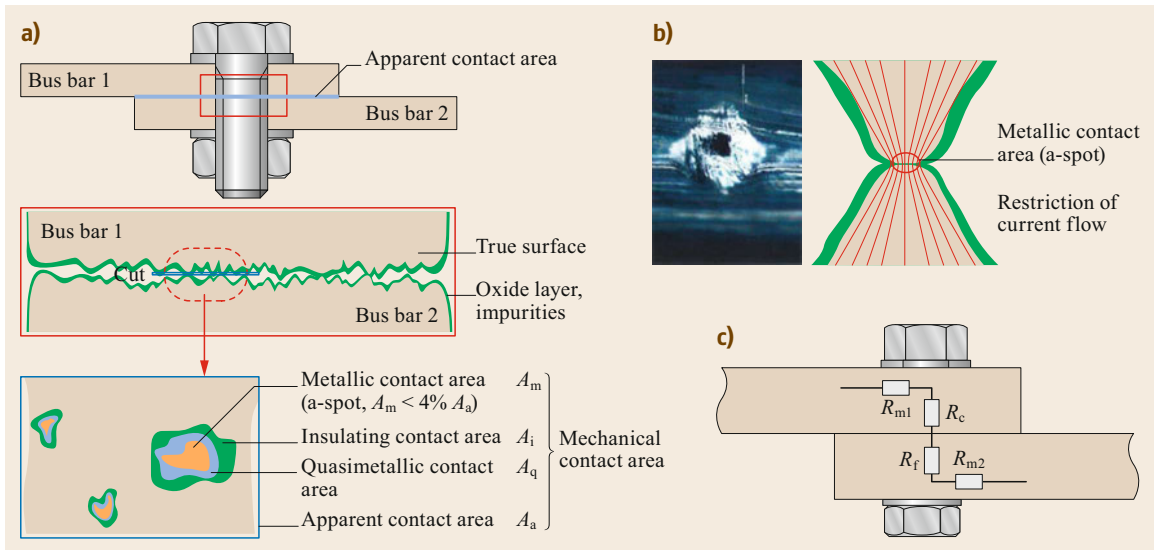


Fig. 4.70a-c Bolted connection of two bus bars. (a) Contact areas, (b) a-spot in detail, (c) joint and contact resistance

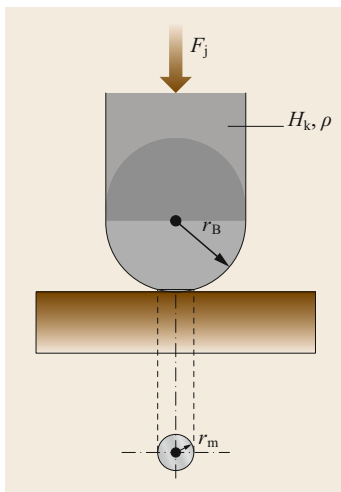


Fig. 4.71 Contact surface and constriction resistance depending on material and force – plastic deformation

With high contact forces, as is usual in most electrical power engineering connections, several parallel contact points are created. Assuming a power-law relationship (with an exponent  $m$ ) between the number  $n$  of the parallel contact points  $A_{mn}$  and the contact force  $F_c$ , one obtains, after Babikow [4.45], constriction resistance  $R_c$  of

$$R_c = \frac{10^{-3} C \rho}{(0.1 F_c / N)^m} \quad [\Omega] \quad (4.157)$$

with empirically determined values for  $C$  and  $m$  (Tables 4.39 and 4.40).

The connection resistance  $R_j$  can be evaluated independently of the dimensions and contact material of

Table 4.39 Coefficient  $C\rho$  for clean surfaces in (4.157)

Contact material	$C\rho$
Copper-copper	0.08–0.14
Copper-tinned copper	0.01–0.07
Tinned copper-tinned copper	0.01
Aluminum-aluminum	3–6.7
Aluminum-brass	1.9
Aluminum-copper	0.98
Aluminum-steel	4.4
Brass-brass	0.67
Brass-copper	0.38
Steel-steel	7.6
Steel-brass	3.04
Steel-copper	3.1
Steel-silver	0.06

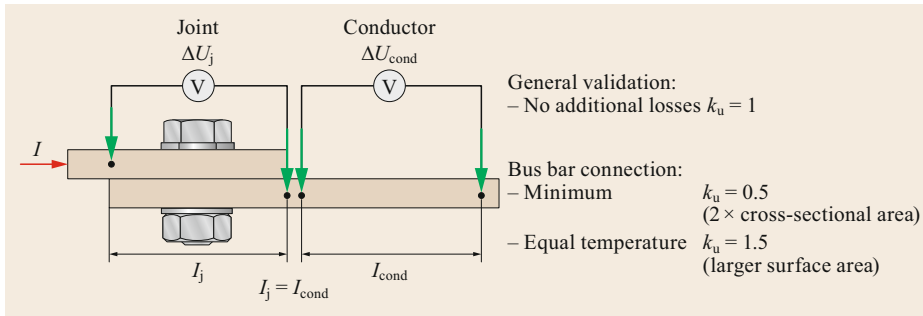
Table 4.40 Exponent  $m$  for different surface types in (4.157)

Surface type	$m$
Flat-flat	1
Point-flat	0.5
Ball-flat	0.5
Ball-ball	0.5
Bus bar connection	0.5–0.7

a linearly shaped connection, consisting of identical conductors, with the help of the quality factor  $k_u$

$$k_u = \frac{\Delta U_j}{\Delta U_{\text{cond}}} = \frac{R_j}{R_{\text{cond}}} = \frac{P_j}{P_{\text{cond}}}, \quad (4.158)$$

where  $k_u$  = quality factor,  $\Delta U_j$ ,  $\Delta U_{\text{cond}}$  = voltage drop across the connection or over a conductor of equal



**Fig. 4.72** Characteristic criteria for connections: performance factor  $k_u$

length,  $R_j$ ,  $R_{cond}$  = resistance of the connection or a conductor of equal length,  $P_j$ , and  $P_{cond}$  = power loss in the connection or in a conductor of equal length.

The quality factor of a bolted bus bar connection amounts to:

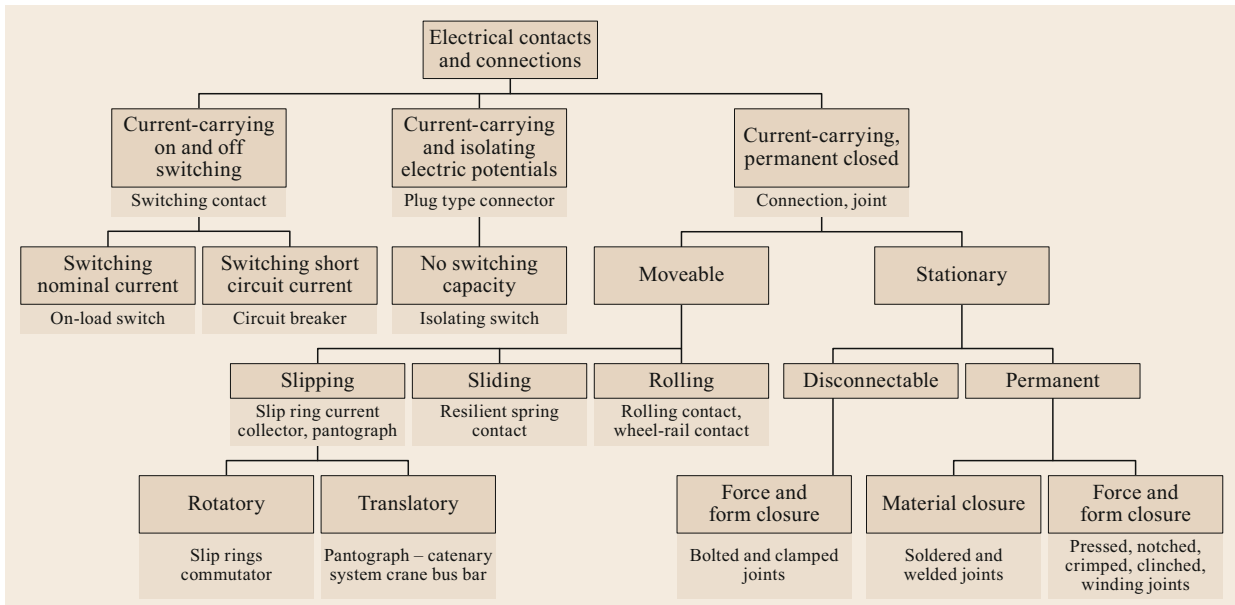
- $k_u = 1$  for the same losses in the connection as in the conductor of equal length, i.e., no additional losses through the connection.
- $k_u = 0.5$  for the theoretical, smallest possible value, since the conductor cross section in the area of the connection is twice as large as in the bus bar.
- $k_u = 1.5$  for approximately the same temperature in the connection and in the conductor due to the larger, heat-emitting surface.

A good electrical bolted connection ( $k_u < 1.5$ ), thus, always has a lower temperature than the connected conductors. Only poor connections ( $k_u > 1.5$ ) become hot

spots. This applies analogously to most other types of connections. The heat dissipation in the joint causing a temperature rise can be calculated with (4.33) in Sect. 4.3.1. The local temperature distribution along a conductor around a connection (Fig. 4.10) results from (4.29).

### Electrical Connections and Their Properties

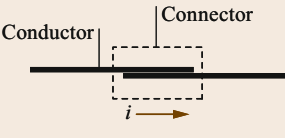
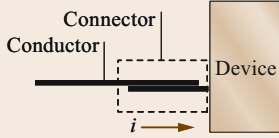
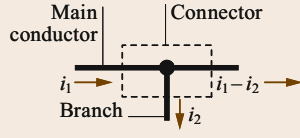
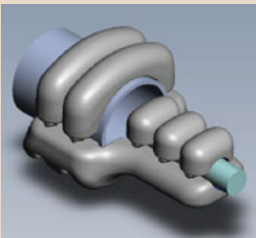
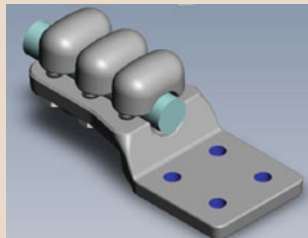
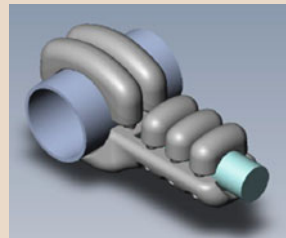
According to their function, electrical contacts and connections can be divided into those that are closed during operation and which can be opened to separate electrical potentials (isolating sections), and those that are suitable for interrupting (switching off) or establishing (switching on) the current flow (Fig. 4.73). According to design requirements, a distinction is made between connecting of conductors, connecting of conductors to equipment, and branching off conductors for the purpose of current distribution (Table 4.41).



**Fig. 4.73** Overview of electrical connections



**Table 4.41** Examples of electrical connection functions

Connection	Terminal	Derivation
		
		
Straight connector	Straight flat terminal connector	T-connector

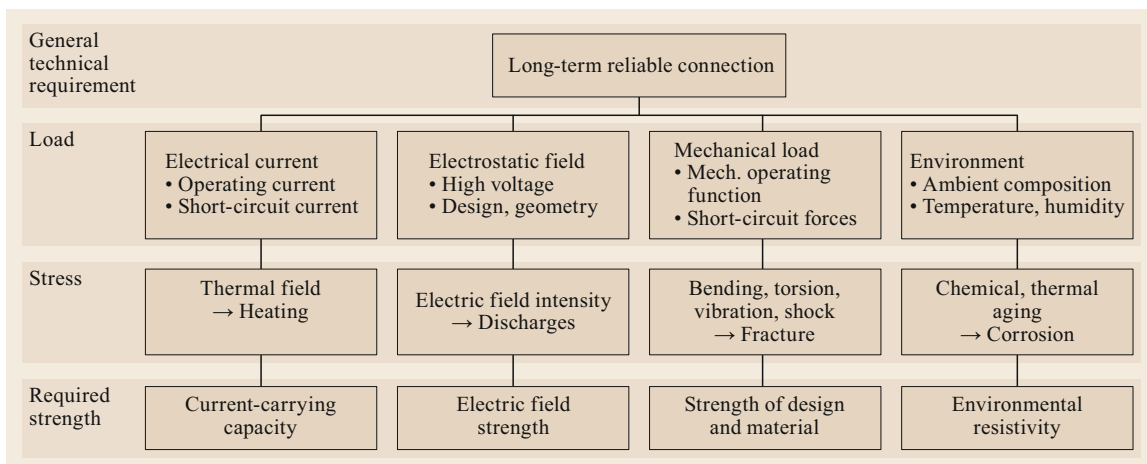
In *stationary electrical connections*, the contact points created during the joining of the contact pieces remain in first approximation during the current flow and do not change their position. In the case of thermal load cycles or aging, changes in the contact points can also be expected. Depending on the joining process, these can be *separable* (terminal and bolted connections, plug-in connections, disconnection points for plug-in connectors or disconnectors), or *fixed* (rivet, solder, weld connections) (Table 4.42).

For *moving electrical connections*, the contact pieces can move relative to each other during the current flow. These include, for example, slip rings on rotating electrical machines, crane conductor lines, and current collectors for electrical trains on the contact wire. While the contact pieces move towards each other, new electrical contacts must be permanently formed to maintain the current flow (Table 4.43).

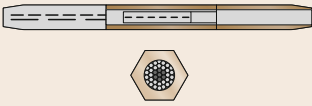
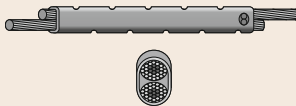

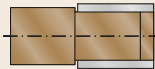
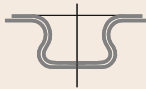
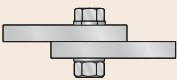
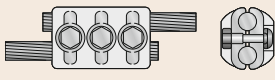



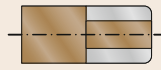
Depending on the joining process, the electrical contact is established within connections through:

- Adhesion (e.g., bolted connections)
- Form-fit and force-fit connection (e.g., plug connection)
- Material-fit (e.g., soldered, friction and welded connections).







Electrical connections must meet the *requirements* by all electrical, thermal, mechanical, and environmental stresses (Fig. 4.74). This should be verified by suitable, mostly standardized tests and additional long-term investigations. With regard to the load duration, recommended long-term tests go far beyond the requirements of standardized tests not only to prove compliance with minimum requirements, but also to confirm part of the planned service life under practical conditions.

**Fig. 4.74** Electrical connection requirements

**Table 4.42** Examples of joining processes for static electrical connections

<b>Conjugate and frictional, functional integration between current-carrying and joint-forcing elements</b>			
Type	Compressed 	Notched 	Helically formed rod fittings 
Application	Full-tension and nontensioned, hexagon press connector cable lugs	Full-tension notch-type connectors	Line splices for stranded conductors
Type	Shrinking 	Clinching 	
Application	Cylindrical bus bar connections	Connection of current-carrying metal sheets	
<b>Conjugate and frictional, with separate force storage</b>			
Type	Bolted 	Clamped 	Cone or wedge-type 
Application	Bolted bus bar connection	Nontensioned connecting clamps Substation clamps	Full-tension connectors Wedge-/cone tension clamps
<b>Cohesively</b>			
Type	Welded, soldered 	Glued 	Metal spraying 
Application	Special applications in substations Flexible and thermal linear expansion tapes	Connection between metallic sponge and solid conductors in special apparatus	Local connecting areas on bus bars

**Table 4.43** Examples of moving electrical connections

Type	Plug-in	Multicontact plug	Blade V-type connector	Disconnecter	Slipping connectors	Sliding connector
						
Application	Tulip-type eight parallel connecting fingers	Straight multiparallel lam connector	Fuse and socket	Rotary disconnecter	Slip collecting ring of a rotating machine	Pantograph with overhead line of a tramway

Standards for testing electrical connections (Table 4.44) usually take into account the many years of experience of the respective users and represent the state-of-the-art in the related industry. These standards are not consistent in all cases with regard to their technical contact requirements. From the point of view of contact physics, long-term safe and reliable current-carrying capacity is independent of the voltage level in which the connection is used.

Connections must be designed in such a way that their joint resistance will only increase, under consideration of all loads during the planned service life, to such

an extent that thermal damage or destruction of the connection itself, the current path, and adjacent insulations and fittings – under-rated and short-circuit currents – is ruled out. The effects of the mechanical loads, e.g., by tensile force in overhead lines, mechanical vibrations in moving equipment components, thermal expansion and friction between the contact pieces, on the long-term behavior must also be investigated. Special ambient conditions, e.g., high ambient temperatures, aggressive pollutants, high SO<sub>2</sub>-content or salinity of the air, extreme climates, etc., can also increase the connection resistance in the long term. In addition, connections

**Table 4.44** Overview of selected standards for testing electrical connections

Norm	DIN EN 61284: 1998	DIN EN 61238-1: 2004	DIN EN 60999: 2000
Application	Overhead lines – requirements and tests for fittings > 45 kV	Compression and mechanical connectors for power cables for rated voltages up to 36 kV	Connecting devices – electrical copper conductors; safety requirements for screw-type and screwless-type clamping units up to 1 kV (AC)/1.5 kV (DC)
Number of test samples	4	6	10
Number of cycles $n$	1000/500/100 additionally $I_k$	1000 additionally $I_k$	196
Arrangement	Distance between samples > $3b$ , free convection	Free arrangement, no retroactive effects from floor, ceiling, and walls to the test circuit	No movement of samples during test
$\Delta\vartheta$ or $\vartheta$ (partial reference conductor)	70 K/100 K/130 K < 180 °C (short term)	120–140 °C < 250–270 °C (short term)	Heat cabinet with test current
$\vartheta_0$ (°C)	15–30	15–30	Heat cabinet 20–40
Plateau phase	30 min (VL)	10 min median connector	Heat cabinet, thermal stability 10 min, $\Delta\vartheta$ max. 5 K
Measuring of resistance	DC, max. 10% $I_p$	DC, max. 10% $I_p$	DC or AC $I_p$
Criteria for resistance	$R_{j0}$ (30% Str.) $R_{j<0.1n} < 0.75R_{j,VL}$ $R_{j>0.5n} < 1.5R_{j0}$	$k_{u0}$ (30% Str.) $k_{u,1000} < 2k_{u0}$	Voltage drop ( $I_p$ ) < 22.5 mV or $1.5R_{j,n=24}$

$I_k$  short-term current,  $R_j$  joint resistance,  $k_u$  performance factor,  $I_p$  test current,  $b$  local constant,  $n$  number of cycles, VL reference conductor.

in high-voltage installations must be designed in such a way that the electric field in the vicinity of the connection does not adversely affect the insulation, e.g., through partial discharges (avoiding small radii and sharp edges, providing shielding).

**Design and Dimensioning.** During the *design and dimensioning* of the current path equal power losses in the connection and the current path outside the connection (quality factor  $k = 1$ ) should be targeted. This means that the connection will not reach a higher temperature than the rest of the current path and, therefore, does not represent a hot spot. This is achieved by the following:

- Suitable *conductor materials* (copper, aluminum and their alloys), *surface coating* with selected contact materials (silver, nickel, tin), as well as the design and dimensions of the contact pieces, the joining process and the assembly technology.

For pressed, notched, and clinched connections, the forming of the conductors and the fittings must be coordinated with the assembly tools to ensure an optimum balance between the mechanical and electrical requirements, even in long-term behavior. Compression connectors for high-temperature conductors (operating temperatures up to 240 °C) in high-voltage overhead lines and switchgear for which conventional compression

connectors are not stable over the long-term deserve special attention.

Bolted and clamped connections must be dimensioned so that at least the required conductor cross section is also available within the connection and the heat-emitting surface of the connection is larger than in the conductor itself in order to dissipate the additional heat losses occurring in the contact points. The mechanical connecting elements (screws, washers, nuts, pressure plates, springs) for high-current connections, particularly for highly-loaded connections, should consist of nonferromagnetic material to reduce additional hysteresis and eddy-current losses (Fig. 4.75) [4.38]:

- *Parallel contact points* distribute the total current  $i$  at  $n$  parallel current paths.

In the case of bolted or clamped connections, this can be achieved, for example, by grooving the contact surfaces in the connection. The connection resistance or the quality factor of such multipoint contacts can, thus, be significantly reduced (Fig. 4.76) [4.46].

Thus, the power dissipation of  $n$  parallel, similar contact points with a resistance ( $R/n$ ), related to the power dissipation  $P$  of a single contact with the connection resistance  $R$ , in simplified form is

$$\frac{\sum P_n}{P} = \frac{n[(i/n)^2(R/n)]}{i^2R} = \frac{1}{n^2} \quad (4.159)$$

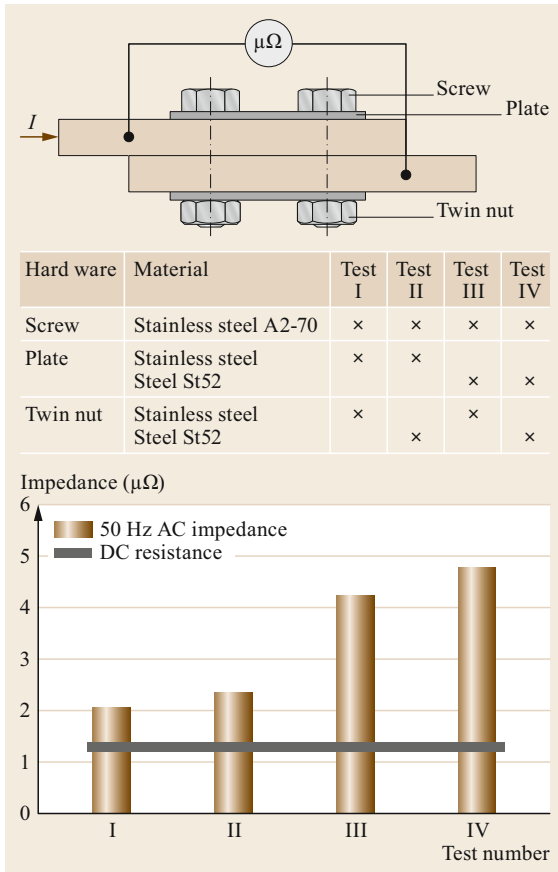


Fig. 4.75 Influence of ferromagnetic design elements on the resistance of highly-stressed connections

For plug connections with parallel contact fingers or multilamella contacts (Table 4.43), the total connection force is limited due to friction in order to still be able to move the plug [4.3]. The connection force is distributed almost evenly among the  $n$  parallel contact points. The ratio total connection resistance  $R_n$  to a single-point

connection resistance  $R_1$  (Fig. 4.77), becomes, under consideration of (4.157) a constant connection force

$$\frac{R_n}{R_1} = \frac{C\rho/(n(F/n)^m)}{C\rho/F^m} = n^{(m-1)}. \tag{4.160}$$

The losses in the plug connection with  $n$  parallel contact points are reduced to

$$\frac{\sum P_n}{P_1} = n^{(m-2)}. \tag{4.161}$$

Since it is generally not possible to assume that the parallel partial resistances will be of equal size, further individual investigations, in particular into the aging mechanisms, are required for specific arrangements [4.3].

- In addition to the *design of the connection*, a basic prerequisite for their long-term reliable operation (Fig. 4.78) is the professional and careful *assembly* of the connection.

It is essential to ensure that only suitable conductors and connectors are joined using the prescribed assembly tools and technologies. Prior to assembly, the contact surfaces of the conductors and connectors must be thoroughly cleaned and any oxide layers removed. Dirt and grease are removed with a chemically neutral solvent. For decades, clean, sharp wire brushes have proven their utility on aluminum surfaces of conductors, bus bars, and equipment connections. These remove the hard, insulating aluminum oxide layer with about 30 brush strokes and simultaneously roughen the conductor surface in such a way that a large number of parallel contact points are formed as a microstructure. Once cleaned, contact surfaces must not be touched again with a dirty hand and should be installed as soon as possible (Fig. 4.79) [4.47]. Surfaces of copper conductors can be easily cleaned of foreign layers with

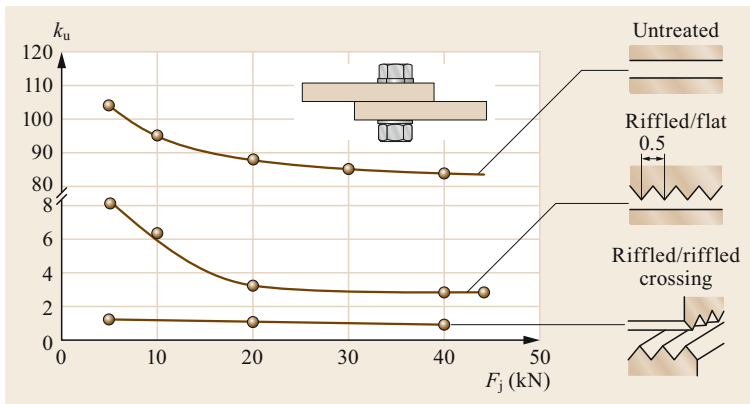
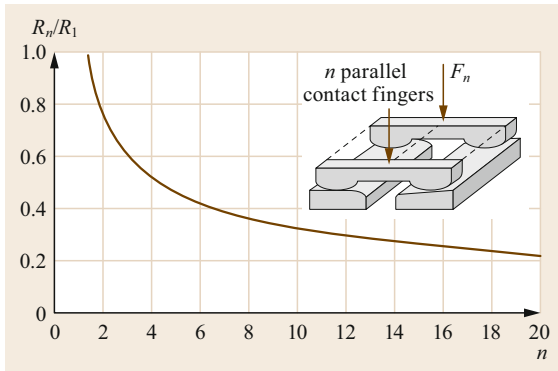


Fig. 4.76 Influence of the surface structure on the quality factor of aluminum connection surfaces (adapted from [4.46])



**Fig. 4.77** Relative resistance of a connector depending on the number of parallel contact fingers;  $F = nF_n = \text{const.}$ ,  $R_n/R_1 = n^{(m-1)}$ , with  $R_n$  = joint resistance of  $n$  parallel fingers,  $R_1$  = joint resistance of on finger, and  $m = 0.5$ , (Table 4.40 point-to-flat contact) [4.3]

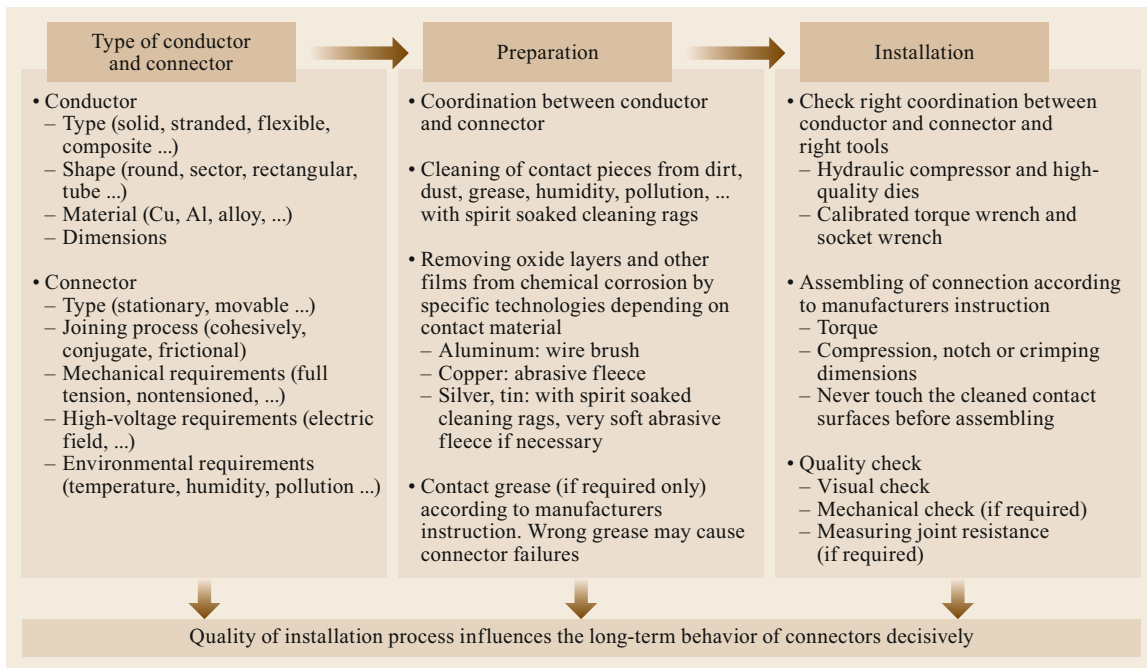
abrasive fleece to minimize the connection resistance (Fig. 4.80) [4.38]. For silver-plated, tinned, or nickel-plated surfaces, cleaning with a clean rag and spirit is usually sufficient. Heavily soiled or oxidized surfaces can also be gently cleaned with a soft abrasive fleece. The initial quality factor  $k_{uo}$  resulting from the quality of the installation is decisive for the long-term behavior of a connection in operation.

Contact pastes may only be used for the applications specified by the manufacturer; otherwise, e.g., particles

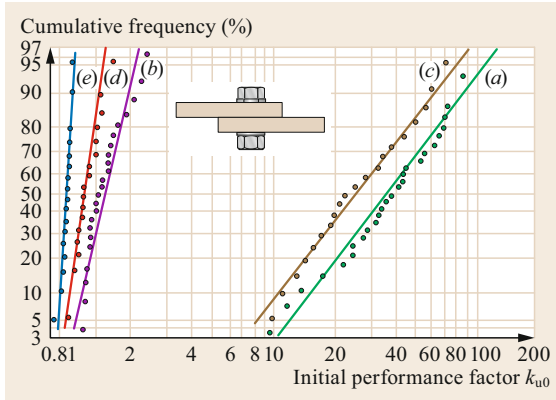
mixed into contact pastes for press connections, if used for bolted connections, can lead to catastrophically poor connection resistances due to the lower degree of deformation of the latter. The connection resistance of a frictional connection is determined by the number and size of the true contact points within the apparent contact surface and depends on the surface condition and the connection force (4.157).

The bolt force (or the bolt tightening torque) essentially determine the connection resistance (quality factor) of a force-fit *bolted joint* (Fig. 4.81) or a *clamp connection*. The connection force should be selected so large that the stable range of the connection is reached. The resistance-force-hysteresis behavior guarantees a low connection resistance even during force degradation (see the subsequent section on the *aging and long-term behavior of electrical connections*), especially with aluminum connections. However, a minimum force (approximately 5 kN) must not be reduced in order to prevent the contacts from breaking open under mechanical loads (short-circuit forces, vibrations, or shock). If an aged joint is to be refurbished, simply retightening the bolts is usually not sufficient, as thicker oxide layers have formed around the contact points, which are often not broken open during retightening. In this case, the connection must be opened and the contact surfaces cleaned and reassembled.

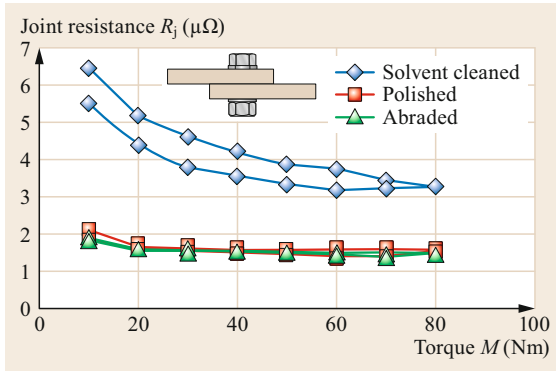
To connect or to terminate multiwire underground cables, insulated wires, or overhead line conductors,



**Fig. 4.78** Installation process for electric connectors



**Fig. 4.79** Initial performance factor  $k_{u0}$  of bolted aluminum bus bar connections depending on surface treatment. (a) Untreated, (b) brushed (30×), (c) brushed and touched by hand, (d) treated with DESOX (anti-oxidizing contact paste), (e) ruffled surface

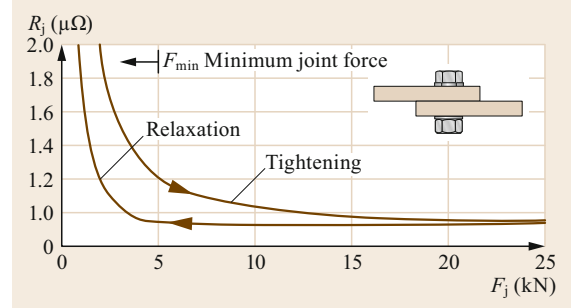


**Fig. 4.80** Influence of surface preparation on the joint resistance and hysteresis of bolted copper bus bar joints (adapted from [4.38])

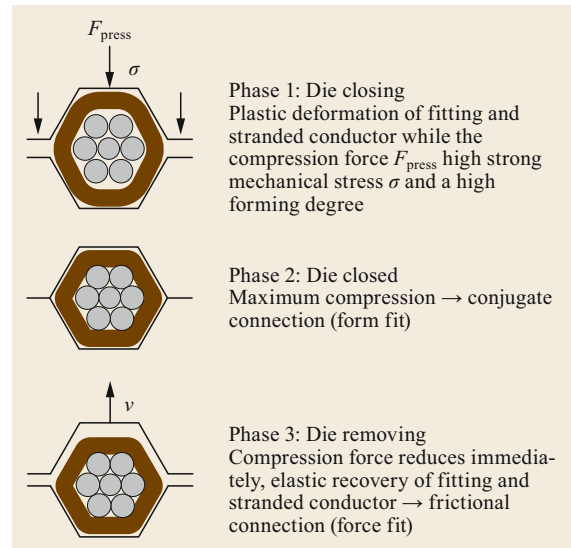
the *circumferential compression* (often with hexagonal presses) (Fig. 4.82, left column) in special fittings (compression cable lugs, compression sleeves) has been established as the preferred joining method for both nontension-proof and tension-proof connections (Fig. 4.82, first row, left column). The electrical and mechanical behavior of a compression fitting is determined by the proper material selection, the dimensioning, and the assembly. The high degree of deformation produced during compression causes impurity layers to be ruptured. The contact force (Fig. 4.82) remaining after the assembly process ensures the integrity of the large contact areas [4.18].

From the geometric conditions (Fig. 4.83), the space factor  $f$  of the conductor is calculated as

$$f = \frac{A_{Al} + A_K}{\frac{\pi}{4} d_L^2}, \quad (4.162)$$



**Fig. 4.81** Hysteresis behavior of aluminum screw connections



**Fig. 4.82** Principle phases of the joining process of hexagonal compression connections (adapted from [4.18])

where  $A_{Al}$  = total cross-section aluminum,  $A_K$  = total cross-section core,  $d_L$  = total diameter of a stranded conductor, and  $f$  = space factor.

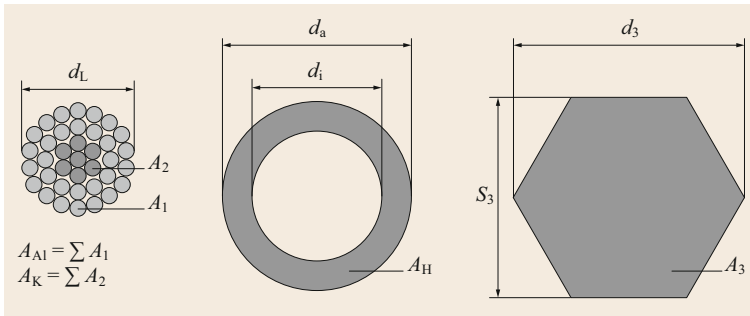
The fit factor  $p$  of a compression fitting is the ratio of the nominal outside diameter  $d_L$  to the inner diameter of the press sleeve  $d_i$

$$p = \frac{d_L}{d_i}. \quad (4.163)$$

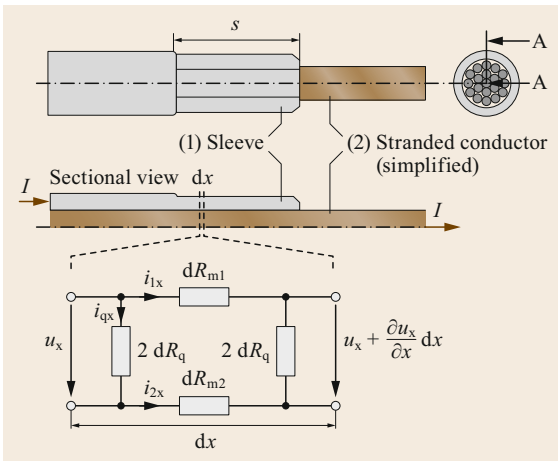
The compression factor  $K_F$  describes the compaction of the aluminum cross sections  $A_{Al}$  and  $A_H$  in the cross section of the hexagon  $A_3$ , assuming that the core  $A_K$  is incompressible

$$K_F = \frac{A_{Al} + A_H}{A_3 - A_K}. \quad (4.164)$$

In analogy to the quality factor  $k_u$  for bolted connections (4.158), a resistance ratio  $k'$  between the real and



**Fig. 4.83** Dimensions of stranded conductor (overhead-line conductor), compression sleeve, and compression hexagon;  $A_1$  = single-aluminum-wire cross section,  $A_2$  = single-core-wire cross section,  $A_3$  = cross section of the hexagonal compression,  $A_H$  = total cross section of the aluminum compression sleeve,  $A_K$  = total cross-section core,  $d_a$  = outer diameter of the compression sleeve,  $d_i$  = inner diameter of the compression sleeve,  $d_3$  = corner distance of a regular hexagon, and  $S_3$  = edge distance of a regular hexagon (adapted from [4.18])



**Fig. 4.84** Equivalent network for a differential part of a compression joint (adapted from [4.18])

the ideal connection resistance is used for evaluating the electrical properties of compression connections. From this and with the help of the specific transverse resistance  $R'_q$ , a generally-valid electrical model for compression connections is derived, which uses the differential resistance per unit length in order to analyze the connection (Fig. 4.84).

Assuming that the material resistances do not change along the compression and that the microcontact points are equally large and equidistantly distributed over the apparent contact surface, a differential equation can be solved from the mesh equation of the model, from which the connection resistance  $R_j$  can be calculated

$$R_j = \frac{R'_{m1}}{R'_{m1} + R'_{m2}} \left[ R'_{m2}s + \frac{R'_{m1} - R'_{m2}}{\alpha} \tanh\left(\frac{s\alpha}{2}\right) \right] + \frac{R'_{m1} + R'_{m2} \cosh(s\alpha)}{\alpha \sinh(s\alpha)}, \quad (4.165)$$

and

$$\alpha = \sqrt{\frac{R'_{m1} + R'_{m2}}{R'_q}}, \quad (4.166)$$

where  $R_j$  = joint resistance of compression type connector,  $R'_{m1}$ ,  $R'_{m2}$  = metallic lead (material) resistance of conductor 1 and 2, per unit length,  $R'_q$  = joint cross (link) resistance, related to the length, and  $s$  = compression length.

The ideal connection resistance  $R_{j\text{ideal}}$ , which would theoretically be the smallest possible resistance without contact resistance, is calculated as follows

$$R_{j\text{ideal}} = \frac{R'_{m1}R'_{m2}}{R'_{m1} + R'_{m2}} K_F s. \quad (4.167)$$

This enables the real connection resistance to be compared with the ideal connection resistance

$$k' = \frac{R_j - R_{j\text{ideal}}}{R_{j\text{ideal}}}. \quad (4.168)$$

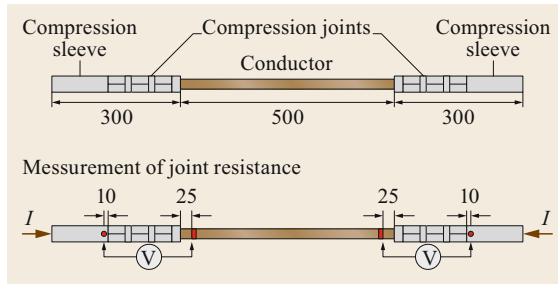
The current distribution along the compression joint depends mainly on the material resistances  $R_{m1}$  and  $R_{m2}$ . If the current transfer between the two contact partners mainly takes place at the two ends of the compression, while the cross current in the middle of the connection is low, the specific cross resistance is calculated as

$$R'_q = \left(\frac{c}{a} k'\right)^2, \quad (4.169)$$

and

$$a = \frac{R'_{m1}}{R'_{m2}} + \frac{R'_{m2}}{R'_{m1}}, \quad (4.170)$$

$$c = s\sqrt{K_F (R'_{m1} + R'_{m2})}. \quad (4.171)$$



**Fig. 4.85** Test arrangement and measurement of joint resistance (adapted from [4.18])

Experimental investigations of compression joints made of two different materials such as ACSR and HTLS conductors for overhead lines (Fig. 4.85) show the effect of different design parameters on the specific transverse resistance (Fig. 4.86).

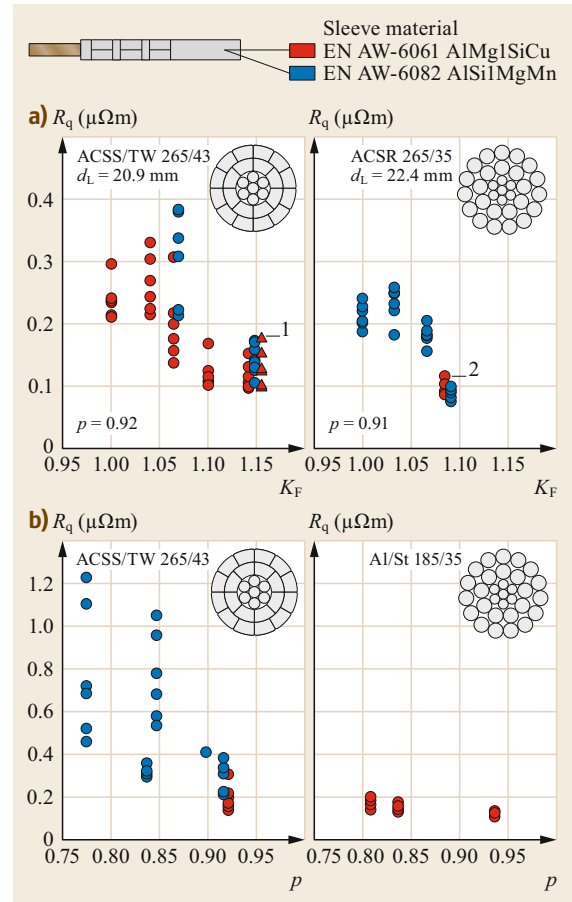
This demonstrates the general relationship between design and electrical operating behavior of compression joints (Fig. 4.87).

Figure 4.88 schematically shows the effect of the compression force  $F_{\text{press}}$  when mounting the connection on the apparent contact area  $A_s$  for conductors with trapezoidal individual wires and the on-load-bearing, mechanical contact area  $A_m$  for conductors with round wires, as well as on the constriction resistance  $R_c$  and the film resistance  $R_f$ .

For compression connections subject to high electrical loads, in particular for full-tension compression joints and dead end clamps on high-temperature overhead line conductors, the long-term electrical behavior can be significantly influenced already during the design stage of the fitting and also during installation. Nevertheless, long-term experiments that clearly exceed the duration of a standard-type test are indispensable for proving a stable connection resistance even under high current loads.

*Plug-in-type connectors* (Table 4.43) [4.3, 36, 41] are used in electrical power applications:

- For operational disconnection of electrical potentials (disconnection points).
- For connecting of factory-made, exchangeable modules on site (e.g., in low-voltage switchgear equipment, transformer plugs).
- For connecting movable components (e.g., railway wagons).
- For extending or connecting cables.
- To compensate for thermal expansions of conductors and encapsulations (e.g., modules in GIS and GIL). The mobility of the contact partners relative to each other means that new microcontacts will

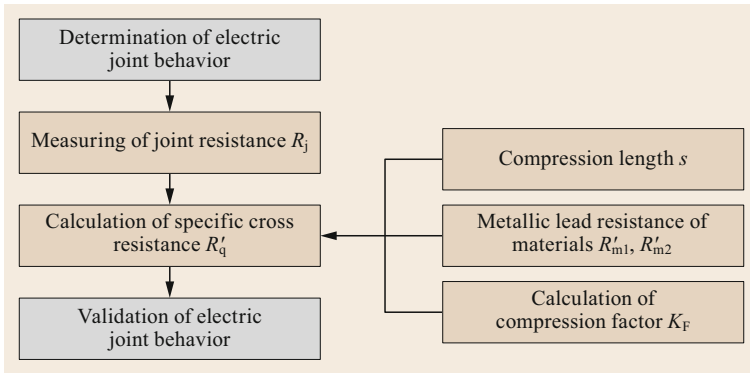


**Fig. 4.86a,b** Specific cross resistance  $R_q$  of compression joints at ACSR and ACSR conductors, experimentally determined. (a) Depending on compression factor  $K_F$ , (b) depending on fit factor  $p$  (adapted from [4.18])

carry the current and, thus, after each movement, the contact resistance will vary.

To close a plug connection (e.g., a disconnection point or during assembly) and to move the contact pieces of a connection in the closed state, axially-acting plug forces  $F_S$  are required, which are sometimes, depending on the application, limited, so that the connection can still be plugged in. Depending on the effective static and sliding friction  $F_R$  between the contact pieces, also the radially acting connection forces  $F_j$  and, thus, the contact forces  $F_c$  on the individual contact points are limited. The design of the contact pieces has a significant influence on the required insertion forces, while the tensile unplug forces  $F_Z$  when opening a plug connection are usually subordinate for the dimensioning of a connection (Fig. 4.89).





**Fig. 4.87** Principal influence of compression joint design on electric contact behavior (adapted from [4.18])

To compensate for smaller contact forces, compared to bolted, clamped, or compression joints, many parallel contacts are arranged in plug connections, e.g., as contact pins, coil springs, or multilamellae, onto which the current is to be distributed as evenly as possible. Under this assumption, the current-density distribution, the current heat losses, and the temperature distribution, based on the Wiedemann–Franz law, can be calculated for known contact geometries and material properties. The analogy between electrical conductivity and thermal conductivity is taken into account, since both the heat flow and the electrical current are transported in the metal as a function of temperature [4.34, 41, 48]

$$\frac{\lambda}{\kappa} \approx LT = L(\vartheta + 273 \text{ K}), \quad (4.172)$$

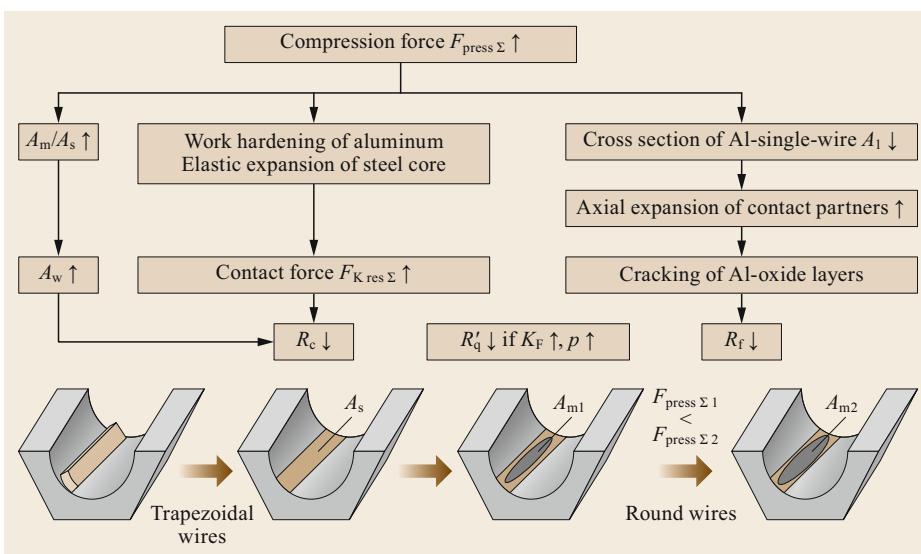
where  $L$  = Lorenz-number =  $2.44 \times 10^{-8} \text{ V}^2/\text{K}^2$ ,  $T$  = absolute temperature,  $\vartheta$  = temperature,  $\kappa$  = specific electric conductivity, and  $\lambda$  = specific thermal conductivity.

For thermally symmetrical contact arrangements, the following relationship between the electrical voltage drop  $u$  across the contact point, the temperature in the contact  $\vartheta$  and the material parameters  $\kappa$  and  $\lambda$  applies (Fig. 4.90)

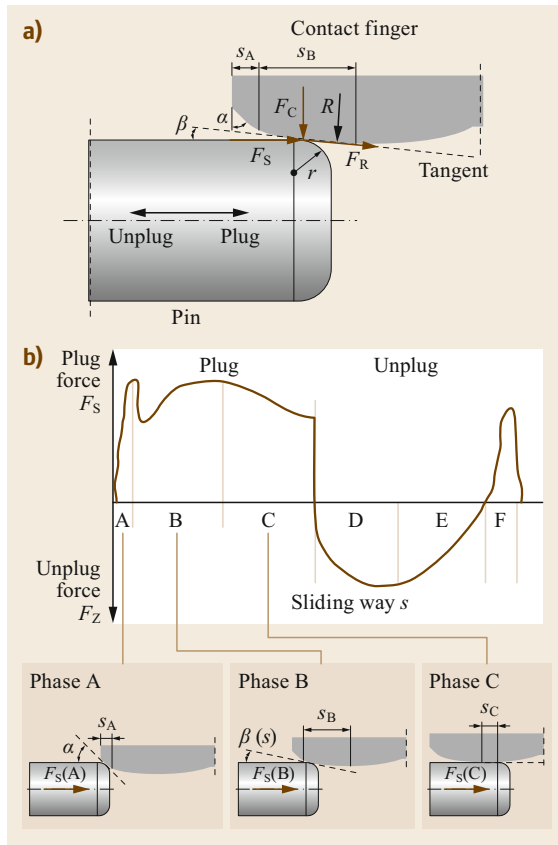
$$u^2 = 8 \int_{\vartheta_1}^{\vartheta_{\max}} \frac{\lambda}{\kappa} d\vartheta, \quad (4.173)$$

where  $u$  = contact voltage drop,  $\vartheta_1$  = temperature of contact pieces 1 and 2 (if symmetrically), and  $\vartheta_{\max}$  = maximum temperature.

For electrically and thermally highly-loaded plug-in connectors with many small parallel contact pieces, the temperature dependence of the specific electrical and thermal conductivity due to the higher internal heating in the contact point must be taken into account. This model enables, based on the actually measured connection resistance  $R_j$ , calculation of the contact voltage



**Fig. 4.88** Influence of the compression force on the electric contact behavior (adapted from [4.18])



**Fig. 4.89a,b** Plug-in-type finger connector, axial plug force – principal behavior. **(a)** Arrangement of plug (contact finger) and pin, **(b)** behavior of axial plug force;  $F_C$  = contact force,  $F_R$  = friction force,  $F_S$  = axial plug force,  $F_Z$  = axial unplug force,  $s_A$  = friction distance in phase A (positioning of contact partners),  $s_B$  = friction distance in phase B (spreading of contact fingers),  $s_C$  = friction distance in phase C (sliding of plug and pin),  $\alpha$  and  $\beta$  = tangent angles between pin and finger, depending on positions A, B, and C (adapted from [4.3])

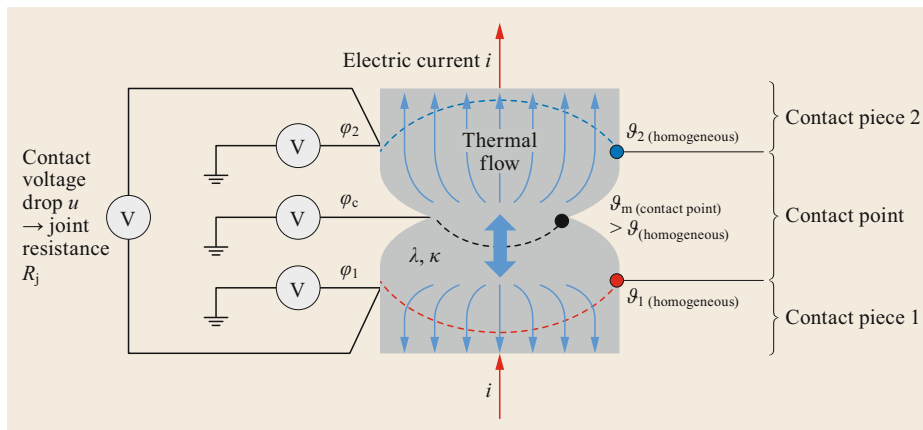
$u$  also of the temperature distribution in the contact for stationary and transient operation using the material properties. This is particularly necessary for the design of high-current connectors with lamellae, coil springs, or other slender contact elements [4.41].

In addition to the thermal load of the parallel contact points of a plug connection, the electrodynamic lift-off forces in the event of a short circuit must be taken into account for dimensioning (Table 4.33, bottom), as these counteract the comparatively small contact force in the case of an impulse current. In the event of a lift-off, arcs may form, and the contact pieces may subsequently be welded together. This means that the plug connection is no longer movable (Fig. 4.91)

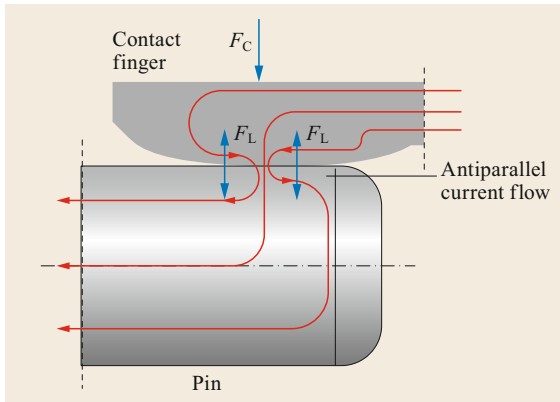
**Quality Assurance Tests.** *Quality assurance tests* are indispensable in the manufacture and assembly of connections. Proof that the design and dimensioning of live electrical connections meet the relevant requirements in long-term stationary operation and in the event of a short circuit must be verified in type tests and is required in most cases. In addition, measurements of the resistance of highly-loaded connections after assembly in the factory or on the construction site are strongly recommended as a routine or random test for quality assurance (see the subsequent section on measuring electrical connections). For bolted connections with long-term stability, output quality factors of  $k_{u0} \leq 1.5$  are required. In order to gain knowledge about the long-term behavior of electrical connections, long-term investigations (possibly during their field operation) with significantly longer test duration than provided for in the type tests are indispensable.

#### Aging and Long-Term Behavior of Electrical Connections

The *aging and long-term behavior of electrical connections* are dependent on the design, dimensioning, and installation of the connection itself and on the in-



**Fig. 4.90** Thermal-electrical model of a contact point (adapted from [4.41])



**Fig. 4.91** Electrodynamic short-circuit forces between contact pieces

teraction of the various loads (electrical, thermal, and environmental) to which the connection is exposed during operation. Accordingly, various aging processes are effective, which superimpose each other and determine the time curve of the connection resistance or of the quality factor (Fig. 4.92). All aging processes (except fretting) are temperature-dependent and can generally be described with Arrhenius' law.

$$k_u = Ce^{Q_a/(R'T)}, \tag{4.174}$$

where  $C$  = factor,  $Q_a$  = activation energy,  $R'$  = gas constant ( $8314 \text{ J K}^{-1} \text{ mol}^{-1}$ ), and  $T$  = absolute temperature.

This shows that for all aging mechanisms, a higher temperature will generally lead to a rise of the connection resistance or of the quality.

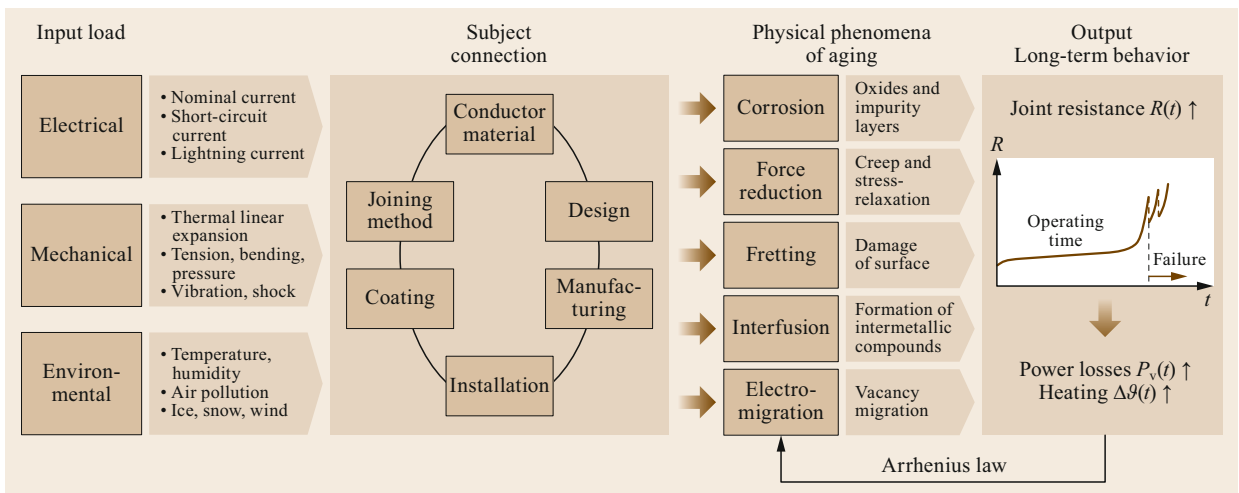
The basic time development of the quality factor  $k_u(t)$  (Fig. 4.93) can be described with the four phases [4.35]:

- *Formation phase*, depending on the contact materials (takes days to weeks).
- *Relative stability phase*, the actual operating time (should take several decades).
- *Accelerated aging*: an increased temperature at contact points causes a clearly faster reaction in one or more aging processes, thus increasing quality factor, power dissipation, and heating in the contact points (upward spiral) up to the melting point. Then, at the latest, the service-life limit of the connection is reached.
- *Intermittent failure*: newly-welded contact points repeatedly lead to a decrease of the performance factor (intermittent). However, these melting points do not have the required current-carrying capacity and burn out until the entire connection is destroyed.

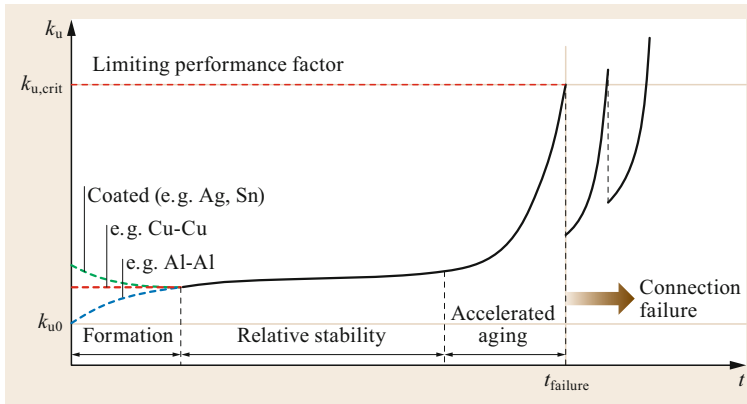
From the aforesaid, a mathematical model can be derived that can describe the long-term behavior of a specific connection type, based on experiments. This makes it possible to estimate an extrapolation beyond the duration of the test [4.3, 35, 49, 50]

$$k_u(t + \Delta t) = k_u(t) + \frac{[k_u(t) - k_{ui}]de^{-[b/(R'T_E)+1/2]}}{t_0(t/t_0)^m} \Delta t, \tag{4.175}$$

where  $k_u$  = measured performance factor at time  $t$ ,  $k_{ui}$  = ideal performance factor ( $R_k = 0$ ),  $T_E$  = absolute temperature at constriction point,  $t_0$  = reference time (e.g., 1 h),  $m$  = exponent, empirically determined from the experiments,  $d$  = factor, empirically determined from the experiments, and  $b$  = factor, empirically determined from the experiments.



**Fig. 4.92** Complexity of contact and long-term behavior of electric connections under superposition of several load conditions and aging phenomena



**Fig. 4.93** Time dependency of performance factor  $k_u$  (schematic).  $k_{u0}$  = initial performance factor directly after construction ( $t = 0$ ),  $k_{u,crit}$  = critical (limiting) performance factor ( $t = t_{failure}$ )

**Table 4.45** Empirically determined parameters  $b$ ,  $d$ , and  $m$  from the experiments (preparation before installation: cleaning with spirit and wire brush) with bolted bus bar connections (example) (adapted from [4.35])

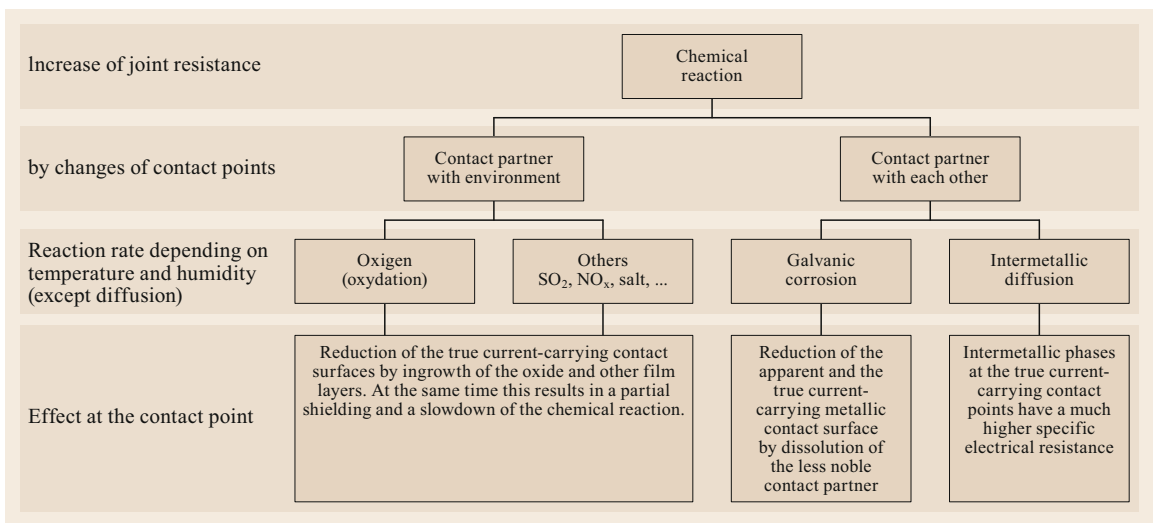
Material	$\vartheta$ (°C)	$m$	$b$ (J mol <sup>-1</sup> )	$d$
Al99.5F7	90–150	0.478	9709	0.1
Al99.5-Cu-ETP	90	0.616	14432	5

In this approach, the effects of all aging processes are superimposed without one being able to consider them separately. It is further assumed that the physical aging processes do not change during the period under consideration.

The parameters  $b$ ,  $d$ , and  $m$  must be determined experimentally for specific arrangements and operating conditions in long-term tests (duration of at least 1 year, but better 3 years). As an example, Table 4.45 shows the values for two bus bar bolted connections [4.35].

**Aging Due to Chemical Corrosion.** Aging due to chemical corrosion can be based on various processes that cause different effects at the contact location [4.42, 49] (Fig. 4.94).

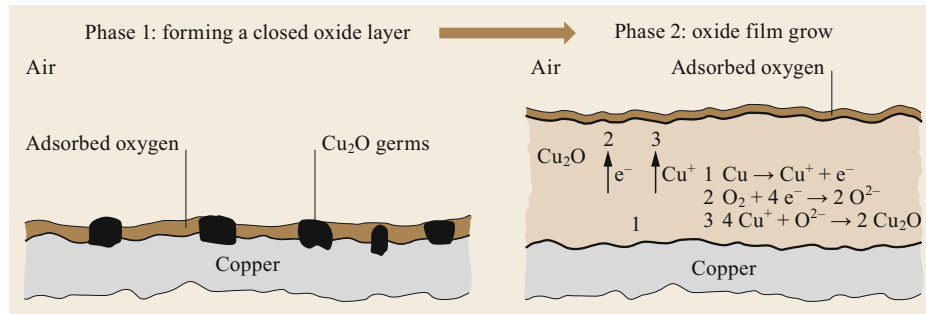
Oxidation of the contact materials produces an oxide layer. Its specific electrical resistance is several orders of magnitude greater than that of the contact materials and, therefore, causes a film resistance  $R_f$ , which increases the connection resistance  $R_j$  considerably and, thus, the power dissipation in the connection. It is, therefore, essential that the related oxide layer be removed before assembly, particularly in the case of connections subject to high electrical loads. While the metallic contact points should be almost free of oxide layers, an oxide layer will form again after assembly in the joints between the contact partners as oxygen is adsorbed on the surface. If sufficient oxygen is available, oxide nuclei are formed, from which a closed, protective oxide layer grows. This, in turn, hinders the access



**Fig. 4.94** Overview on influences of chemical reactions on the aging of electric connections

**Table 4.46** Physical properties of aluminum and copper and their oxides (adapted from [4.42, 51, 52])

Property	Cu-ETP CW004A	Al99.5 EN AW-1350A	Cu <sub>2</sub> O	Al <sub>2</sub> O <sub>3</sub>
Performance	R250	H112	–	–
Melting temperature $\vartheta_s$ (°C)	1083	660	1242	2050
Density $\delta$ (g cm <sup>-3</sup> )	8.93	2.71	5.8–6.11	3.97
Electrical conductivity $\kappa$ (m/Ω mm <sup>2</sup> )	Min. 57	34–36	$1.82 \times 10^{-11}$	$10^{-12}$ – $10^{-14}$
Hardness HV	90	21–48	109–189	1730–2060
Thermal elongation $\alpha_L$ ( $\times 10^{-6}$ K <sup>-1</sup> ) (at 20–200 °C)	17.7	23.8	–	6.2
Thermal conductivity $\lambda$ (W m <sup>-1</sup> K <sup>-1</sup> )	394	215–235	6.3–8	40

**Fig. 4.95** Chemical reactions in the oxidation of copper. 1 Oxidation of copper, 2 adsorption and reduction of oxygen, 3 diffusion of copper ions and electrons through the oxide layer (adapted from [4.42])

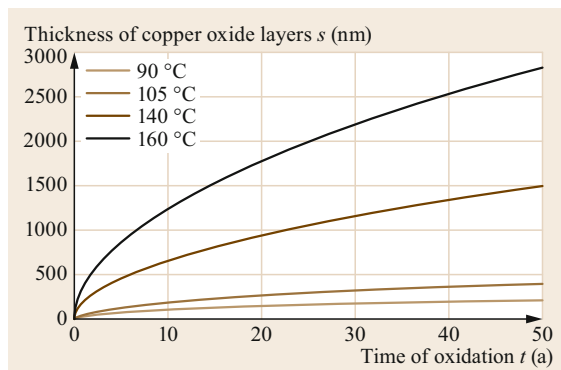
of further oxygen and, thus, slows down the reaction. However, higher temperatures accelerate the growth of thicker oxide layers (Figs. 4.95–4.98).

Mechanical stresses, e.g., due to the different coefficients of thermal expansion from the metal to the oxide layer or due to mechanical stresses perpendicular to the contact area within a joint can tear open the oxide layer, and further oxygen or moisture can infiltrate into the cracks.

The physical properties of copper(I) oxide Cu<sub>2</sub>O and aluminum oxide Al<sub>2</sub>O<sub>3</sub> are, in particular, their specific electrical conductivities  $\kappa$ , which are by a factor of tens smaller, and their much greater hardness  $H$  compared to the related metals leads over time to an in-

crease in the film resistance  $R_f$  (Table 4.46, Figs. 4.98–4.100) [4.35, 36, 42, 54].

**Dependence on time and temperature.** For bimetallic connections with a large difference in the standard potentials within the electrochemical voltage series (e.g., Al (–1.66 V)/Ag (+0.80 V) or Al (–1.66 V)/Cu (+0.34 V)) (Table 4.47) and the presence of moisture, electrochemical corrosion occurs in which electrons of the less noble metal migrate to the more noble metal at the contact points. The result is that the less noble metal is gradually deteriorated and the contact points are destroyed (Fig. 4.101). At temperatures slightly below 100 °C and at very low humidity (dry interior), the electrolyte is hardly present, and the chemical reactions become slower. In contrast, moist, high-salinity atmosphere (near the sea, industrial atmosphere, roads) significantly accelerates electrochemical corrosion.

**Fig. 4.96** Influence of temperature and time on the growth of oxide layers Cu<sub>2</sub>O on copper (adapted from [4.17])**Table 4.47** Electro-potential series of selected contact materials with ion layer in front of the electrode surface at 25 °C (adapted from [4.41])

Material	Normal potential (V)	Material	Normal potential (V)
Al/Al <sup>3+</sup>	–1.66	Fe/Fe <sup>3+</sup>	–0.04
Fe/Fe <sup>2+</sup>	–0.44	Cu/Cu <sup>2+</sup>	+0.34
Ni/Ni <sup>2+</sup>	–0.25	Cu/Cu <sup>+</sup>	+0.52
Sn/Sn <sup>2+</sup>	–0.14	Ag/Ag <sup>+</sup>	+0.80
Pb/Pb <sup>2+</sup>	–0.13	Au/Au <sup>+</sup>	+1.70

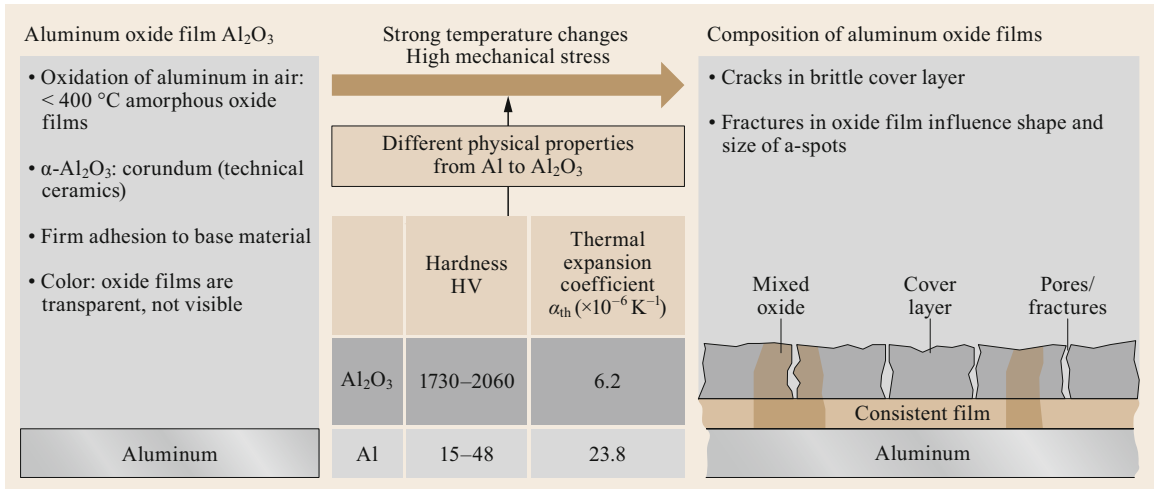


Fig. 4.97 Chemical reactions in the oxidation of aluminum

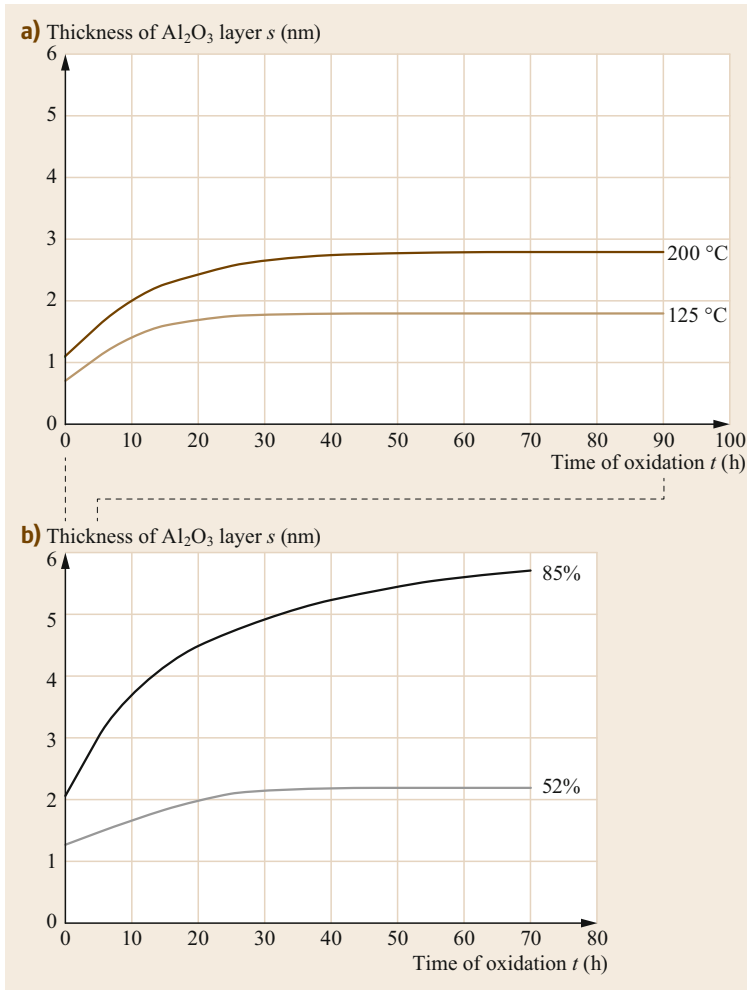
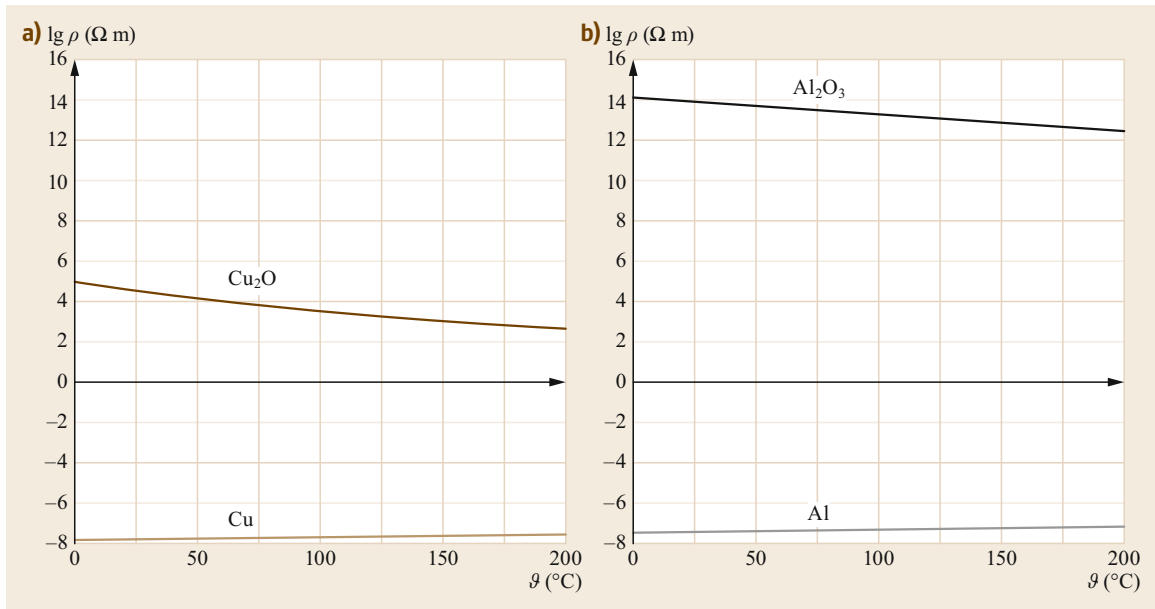
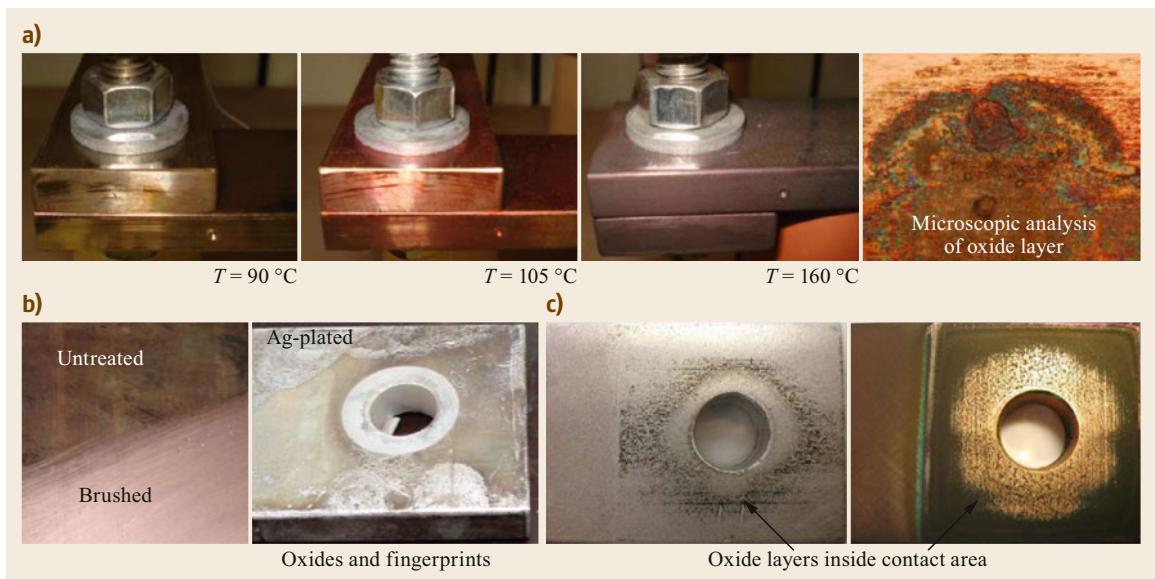


Fig. 4.98a,b Influence of temperature and humidity on the growth of  $Al_2O_3$  layers on aluminum (schematic). (a) Influence of temperature, (b) influence of humidity



**Fig. 4.99a,b** Specific electrical resistivity of oxide layers from (a) copper and (b) aluminum (y-axis in decades) depending on temperature



**Fig. 4.100a,b** Chemical reactions on Cu bus bars depending on temperature. (a) Cu-Cu bus bar connection:  $Cu_2O$ . (b) Cu-bus bar. (c) Al-Cu bus bar joint (7800 h/ $90^{\circ}C$ )

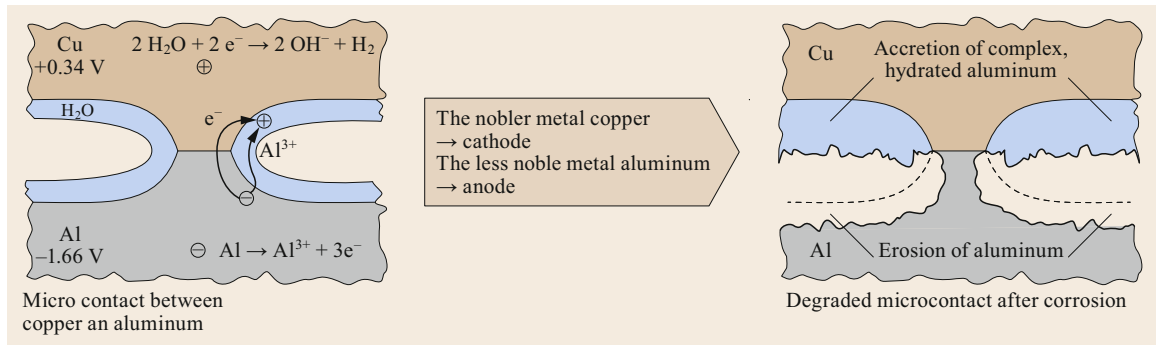


Fig. 4.101 Bimetallic, galvanic corrosion between copper and aluminum (adapted from [4.42])

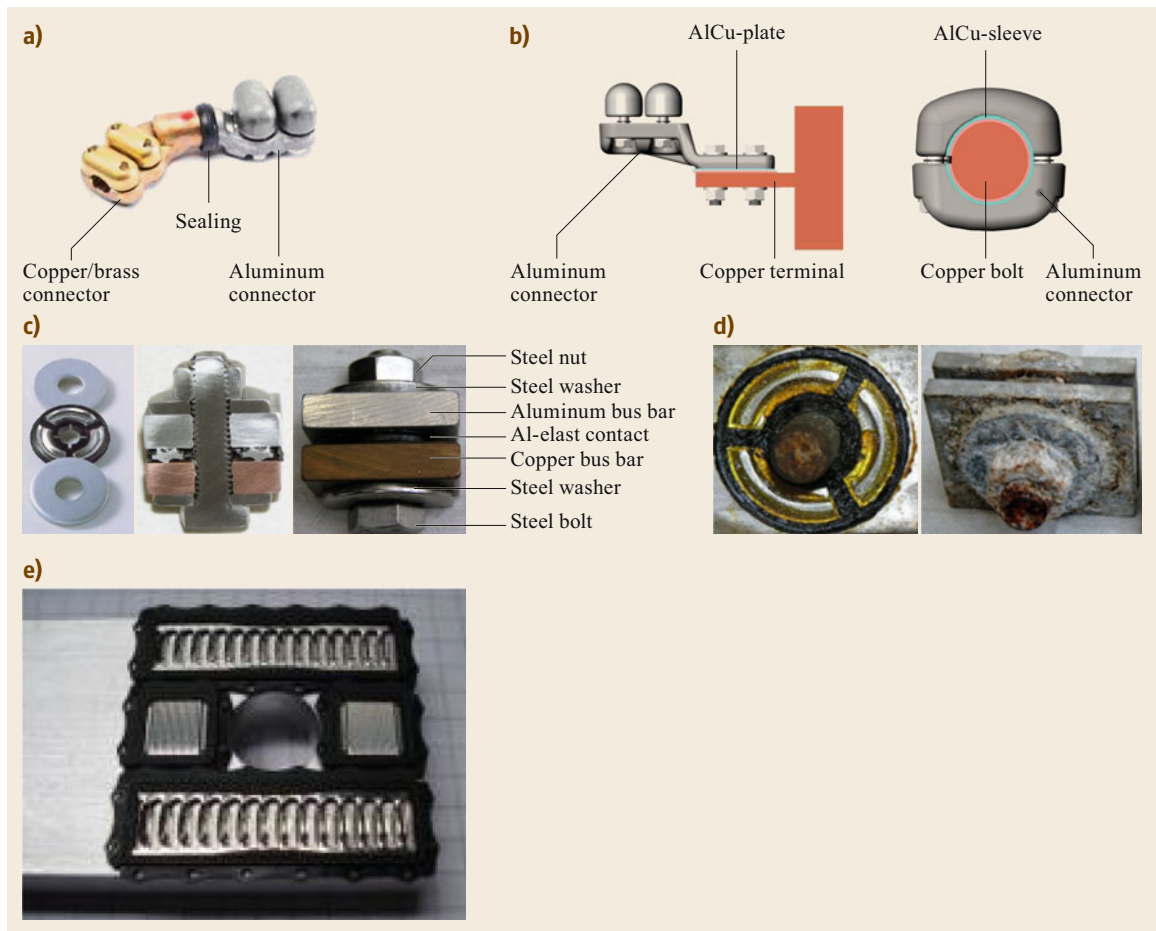


Fig. 4.102a–e Bimetallic connections in practical applications. (a) Copper-aluminum connector, (b) connectors with bimetallic AlCu-plate and sleeve, (c) special washers for bolted aluminum-copper connections, (d) same as (c) after 30 years, (e) special multilam elements for bolted aluminum-copper connections (adapted from [4.42, 51–53])



**Table 4.48** Physical properties of coating materials and their film layers (adapted from [4.42, 52])

Property	Ag	Ag <sub>2</sub> O <sup>a</sup>	Ag <sub>2</sub> S <sup>b</sup>	Sn	SnO <sup>c</sup>	SnO <sub>2</sub> <sup>d</sup>	Ni	NiO <sup>e</sup>
Melting temperature $\vartheta_s$ (°C)	962	230	836	222	1042		1453	1957
Density $\delta$ (g/cm <sup>3</sup> )	10.49	7.2	7.3	7.30			8.90	7.47
Electrical conductivity $\kappa$ (m/( $\Omega$ mm <sup>2</sup> ))	62.9		0.28	9.09	10 <sup>-2</sup>		14.60	10 <sup>-11</sup>
Thermal coefficient of electrical resistance $\alpha$ ( $\times 10^{-3}$ K <sup>-1</sup> )	4.3			4.60			6.80	
Hardness $H$ (HV)	30–90		30–60	5	36–60			536
Thermal elongation $\alpha_L$ ( $\times 10^{-6}$ K <sup>-1</sup> ) (at 20–200 °C)	19.5		14	26.70			13	
Thermal conductivity $\lambda$ (W m <sup>-1</sup> K <sup>-1</sup> )	429			66.60			90.70	12.3
Typical thickness of galvanized layer $d$ ( $\mu$ m)	0.5–10 (40)			1–25			0.5–4	
Grow of oxide layers after 10 <sup>5</sup> h at 100 °C $t$ (nm)					36		34	

Performance

<sup>a</sup> Nearly black color, very soft oxide with only weak adhesive properties, easy to remove, not critical for electrical connections.

<sup>b</sup> Gray to black color.

<sup>c</sup> Blue to black color, soft material but harder than Sn.

<sup>d</sup> Transparent, harder than Sn and SnO.

<sup>e</sup> Light yellow, gray green, black color, very hard, highly resistive.

**Table 4.49** Physical properties of intermetallic phases in aluminum systems up to 200 °C (adapted from [4.40])

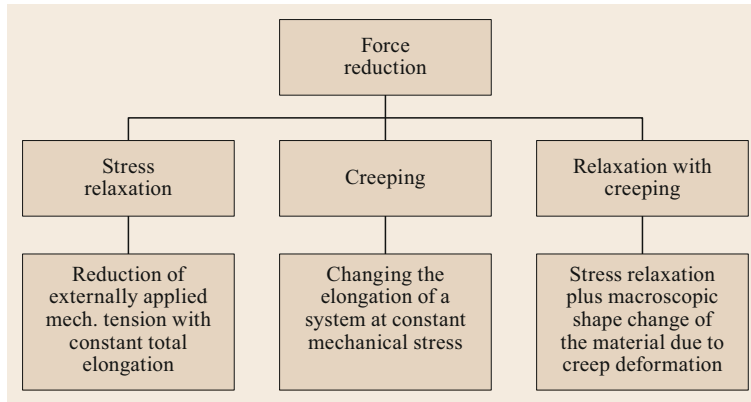
Phase	Al-Cu system			Al-Ag system	
	$\vartheta$ Al <sub>2</sub> Cu	$\eta_2$ AlCu	$\gamma_2$ Al <sub>4</sub> Cu <sub>9</sub>	$\delta$ Ag <sub>2</sub> Al	$\mu$ Ag <sub>3</sub> Al
Melting temperature $\vartheta_s$ (°C)	550	591	1030	–	–
Density $\delta$ (g/cm <sup>3</sup> )	4.36	2.70	6.85	8.12	8.70
Electrical conductivity $\kappa$ (m/( $\Omega$ mm <sup>2</sup> ))	11.2–15	7.6–13.3	2.8–5.3	2.9–3.1	1.7–1.9
Hardness HV	632	794	636	291–303	437–488
Thermal elongation $\alpha_L$ ( $\times 10^{-6}$ K <sup>-1</sup> ) (at 20–200 °C)	16.1	11.9	17.6	–	–
Thermal coefficient of electrical resistance $\alpha$ ( $\times 10^{-3}$ K <sup>-1</sup> )	3.5–3.8	2.7–3.3	0.8–1.7	0.93–0.9	0.55–0.6

**Table 4.50** Physical properties of intermetallic phases in copper systems up to 200 °C (adapted from [4.17, 49])

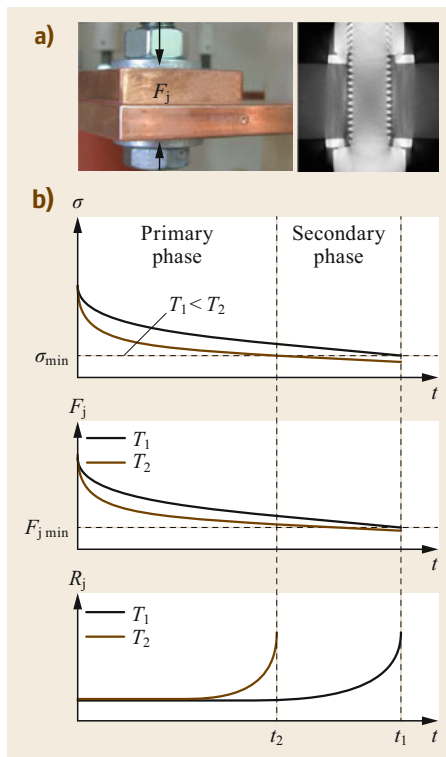
Phase	Cu-Sn system	
	$\eta'$ Cu <sub>6</sub> Sn <sub>5</sub>	$\varepsilon$ Cu <sub>3</sub> Sn
Melting temperature $\vartheta_s$ (°C)	415	676
Density $\delta$ in g cm <sup>-3</sup>	8.28	8.9
Electrical conductivity $\kappa$ (m/( $\Omega$ mm <sup>2</sup> ))	8.2	4.9
Hardness HV	539	472
Thermal elongation $\alpha_L$ ( $\times 10^{-6}$ K <sup>-1</sup> ) (at 20–200 °C)	16.3	19
Thermal coefficient of electrical resistance $\alpha$ ( $\times 10^{-3}$ K <sup>-1</sup> )	0.45	0.2

For this reason, preventive measures must be taken. Long-term stable bimetallic connectors can be produced by suitable, usually material-locking connection technologies and subsequent sealing of the connection point against moisture. Alternatively, AlCu sheets, sleeves, and washers (thickness ratio Al/Cu: 70/30) have also proven themselves suitable for some applications. These rolled AlCu bimetallic sheets with a large surface and a material-locking aluminum-copper connection are placed between the aluminum and copper contact pieces to be joined. This way, electrochemical corrosion only occurs in the peripheral areas. For this

reason, these AlCu sheets and sleeves are always dimensioned a few millimeters larger than the apparent contact surface, and thus the material loss at the edge is taken into account (Fig. 4.102a,b). Special washers based on the described effects: – defined contact lines (real metallic contacts) instead of big apparent contact areas and – using designs creating elasticity, are an additional solution for e.g., Al-Cu connections. This solution, plastic housing in combination with contact protection grease, has been used successfully over the last 40 years in millions of applications worldwide (Fig. 4.102c,d).



**Fig. 4.103** Force reduction by various mechanisms (adapted from [4.17])



**Fig. 4.104a,b** Force reduction in bolted connection: (a) test sample and distribution of mechanical tension, (b) time dependence of mechanical tension  $\sigma$ , joint force reduction  $F_j$  and increasing joint resistance  $R_j$  for two different temperatures, where  $T_1 < T_2$  (adapted from [4.17, 49])

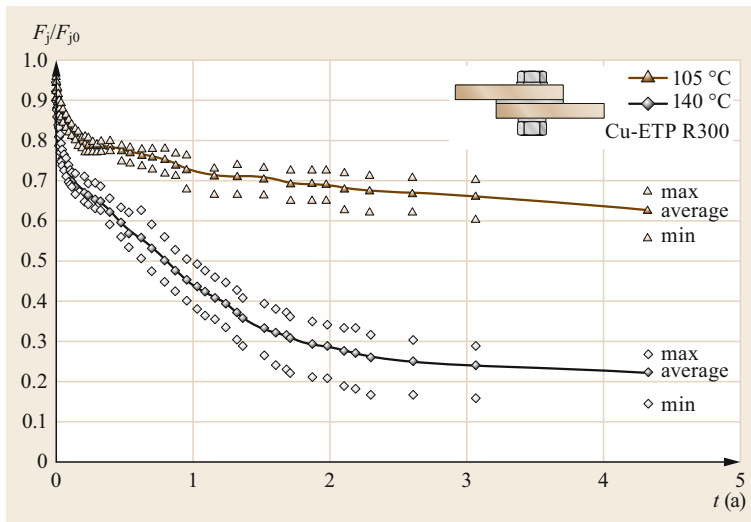
In addition, the surfaces of contact pieces made of copper, aluminum, or their alloys are coated with silver, nickel, or tin, especially for moving joints, because the oxides of these materials have a higher electrical conductivity and a lower hardness than the oxides of copper and aluminum (Tables 4.46 and 4.48). This allows the oxide layer to be destroyed and a current-carrying contact to be established with every relative movement of

the contact pieces. However, the electrochemical series (Table 4.47) must also be considered when selecting the material pairings.

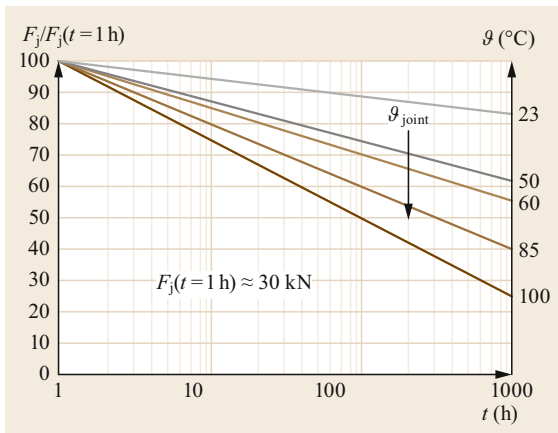
**Intermetallic Diffusion.** Another aging process to be considered in electrical contacts is the *intermetallic diffusion* during joining of different metals. Due to differences in the atomic density of the metals, a particle transportation to free locations of the atomic lattice takes place at the interface layer. This process is accelerated by increasing temperature. The intermetallic phases (IMP) thus created show a significant higher conductivity than the initial materials (Tables 4.49 and 4.50).

**Reduction of the Mechanical Connection Force.** Besides the chemical reactions, the *reduction of the mechanical connection forces* has a significant influence on the long-term behavior of a joint (Fig. 4.92). The contact force  $F_j$  has a great influence on the contact resistance  $R_k$  and, thus, on the connection resistance  $R_j$  (4.156) and (4.157), Figs. 4.80 and 4.81). The connection force applied during joining is reduced over time by setting (leveling surface roughness of mechanically supporting contact surfaces by plastic deformation) and by stress relaxation in the primary area (dynamic primary recrystallization) and in the secondary area (secondary recrystallization with grain coarsening) (Figs. 4.103 and 4.104).

This process is considerably accelerated at higher temperatures. Due to the hysteresis behavior of copper and, especially, of aluminum (Figs. 4.80 and 4.81), the loss of contact force, which only occurs when it falls below a critical value  $F_{min}$  causes a rapid increase in connection resistance  $R_j$ . Tests for force reduction on bolted connections with copper bus bars at 105 and 140 °C (Fig. 4.105) and for clamps on high-temperature aluminum conductors at 23–100 °C clamp temperature (Fig. 4.106) clearly show the temperature dependence of setting and stress relaxation and the associated force reduction.



**Fig. 4.105** Related force reduction of bolted copper bus bar connections (adapted from [4.49])



**Fig. 4.106** Related force reduction of bolted connectors with stranded aluminum conductors TAL 550/70 (adapted from [4.55])

Since the microcontact points, which have been reduced or augmented by the force reduction, have over time oxidized in their environment at high temperatures, and pollution layers have been formed, retightening of bolted connections is often not very successful. If there is a risk that the connection force will reach the critical value  $F_{\min}$ , which is indicated, for example, by an increased temperature of the connection, it is advisable to completely open the connection, clean the contact surfaces, and remove the pollution layers before reassembling the connection and tightening it to the specified torque or the necessary contact force. A measurement of the resistance of the bolted or clamped connection after reassembly proves that the inspection was successful.

**Aging Due to Friction.** With electrical connections whose contact pieces move relative to each other (plug-type connectors, insulators, moveable connections), friction wear can lead to a further aging mechanism by removal of coatings or destruction of the surface of contact pieces. Mechanical load can be caused, for example, by oscillating movements with a frequency of 100 Hz (in high-current systems with 50 Hz alternating current); gradual, periodically recurring thermal linear expansion of the current path; switching operations; or mechanical vibrations or shocks acting from outside. The stress of the contact pieces during sliding or rolling friction is dependent on structural and environmental influences and can lead to various impermissible changes in the shape, size, and material properties of the contact pieces and their coating (Fig. 4.107) and, thus, adversely affect the connection resistance and the required plug-in force.

The simultaneous interaction of the many influencing variables makes a mathematical model for the description of aging very difficult to create, so that the experiment is recommended for concrete applications. Examples are shown in Figs. 4.108 and 4.109.

In the following, some experiments on the long-term behavior of electrical connections are presented, in which the various aging mechanisms act simultaneously (Table 4.51).

**Experiments – A Small Selection.** Experiments with bolted connections of aluminum, aluminum alloy, and copper show that reliable connections can be produced over decades even under high thermal loads and harsh climatic conditions (Figs. 4.110 and 4.111a). Aluminum-copper connections already show a signif-

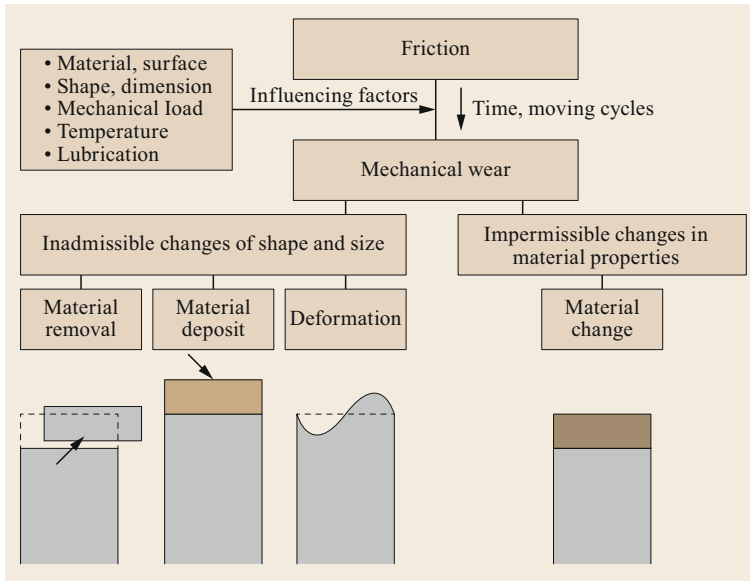


Fig. 4.107 Abrasion influences and states of wear (adapted from [4.3])

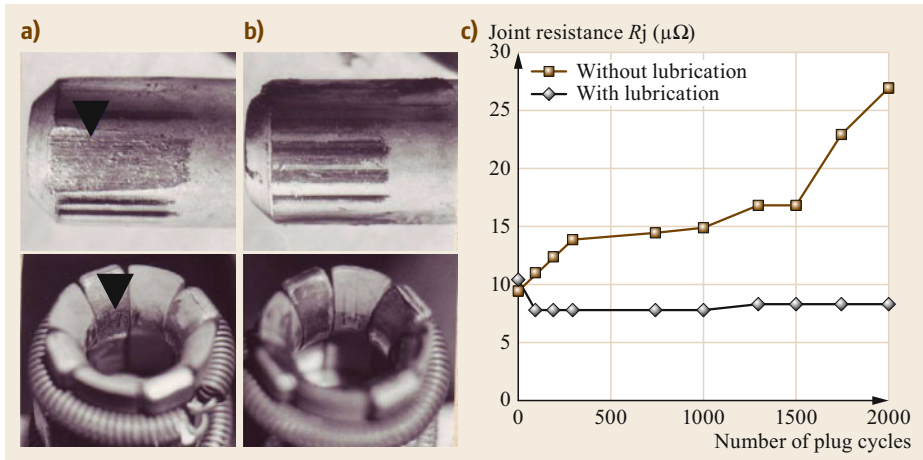
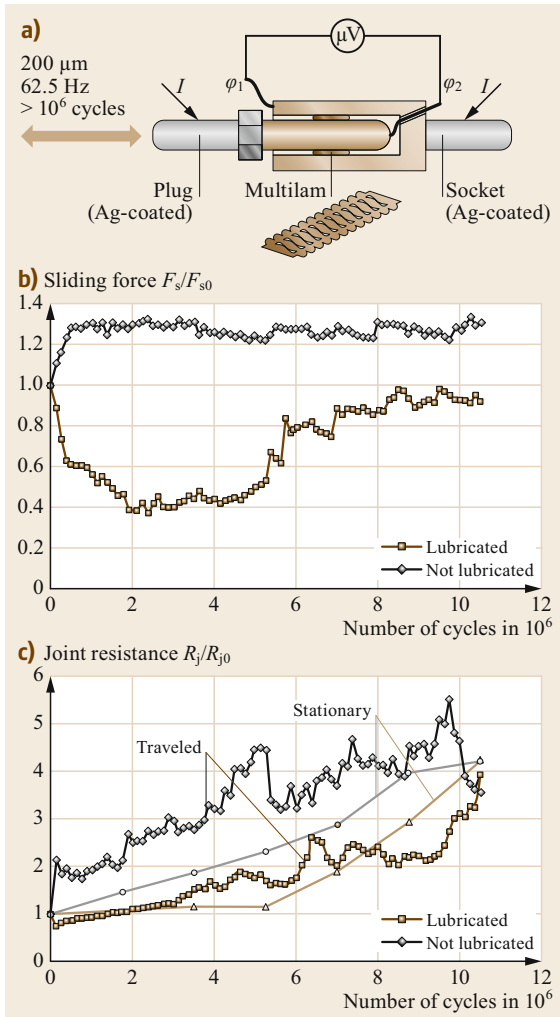


Fig. 4.108a–c Abrasion on tulip connectors with Ag coating. (a) Coating without and (b) with lubrication (vaseline), (c) connecting resistance (adapted from [4.3])

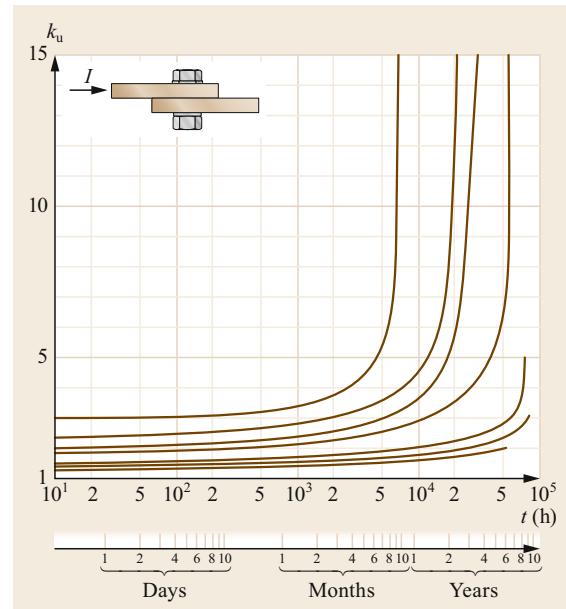
Table 4.51 Experimental investigations on the long-term behavior of connections (examples)

Connection	Ambient condition	Material	Temperature (°C)	Important influence	Figure
Bolted bus bar	Laboratory, indoor	Al 99.5	100–160	Initial performance factor $k_{u0}$	4.110
Bolted bus bar	Tropical	Al 99.5		Harsh environmental ambient conditions	4.111a
	Subtropical	CU			
	Subarctic	AlMgSi-Cu			4.111b
	Tropical	AlMgSi-AlCu-sheet-Cu			
Subarctic	AlMgSi-AlCu-sheet-Cu				
Subtropical	AlMgSi-AlCu-sheet-Cu				
Connector for stranded conductors	Laboratory, indoor	Al, Al-alloy	< 80	Initial performance factor $k_{u0}$ , current load	4.112
Plug-type connector	SO <sub>2</sub> /air atmosphere	Cu, Cu with Ag coating	-10 to 25	Ambient conditions, material	4.113
	Industry, indoor		15–25		



**Fig. 4.109a–c** Multilam plug-type connectors, silver coated under sinusoidal oscillations 200  $\mu\text{m}$ . **(a)** Test arrangement, **(b)** changes in the related sliding force  $F_s/F_{s0}$  with and without lubricant (adapted from [4.39])

icant increase in the quality factor after a few months, especially at high humidity. AlCu sheets can slow down the rapid aging process considerably, but cannot completely prevent it (Fig. 4.111b). The quality of the connection after assembly has a very significant influence on the long-term behavior of highly-stressed bolted connections (initial quality factor  $k_{u0}$ ). Especially with aluminum and aluminum alloys, it is essential to thoroughly remove the hard, electrically insulating aluminum-oxide layer before assembly (Fig. 4.79, Table 4.46). The time dependency of the quality factor  $k_u(t)$  reacts extremely sensitively to the quality of the assembly (target:  $k_{u0} < 1.5$  by proper assembly). For connections that had a quality factor  $k_{u0} = 1.2$  just af-

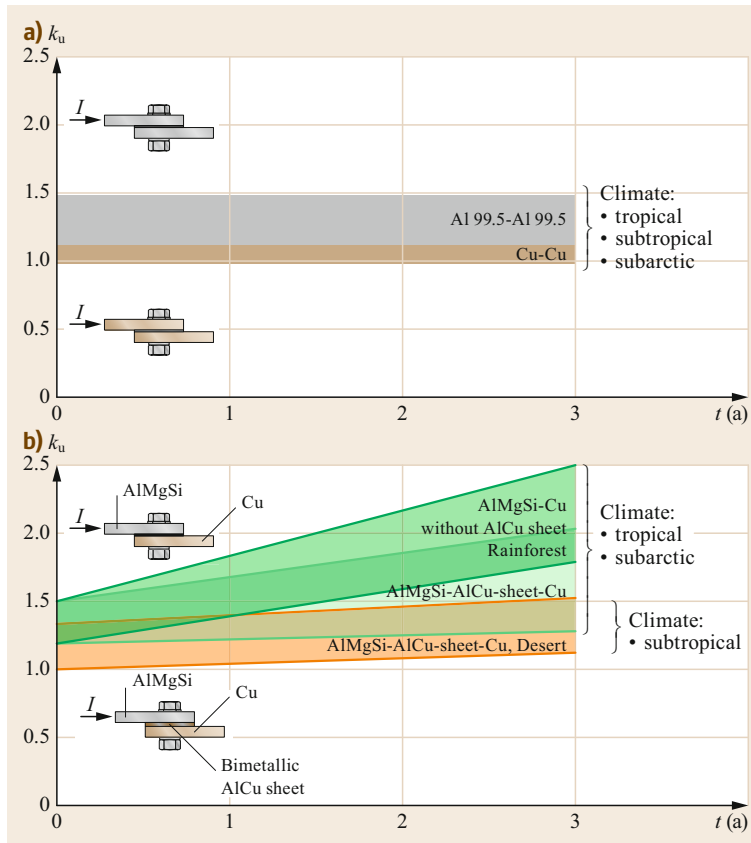


**Fig. 4.110** Long-term behavior of bolted connections under indoor laboratory conditions, experimental results; influence of the initial performance factor  $k_{u0}$  ( $1.2 < k_{u0} < 2.7$ ) on the long-term behavior of current-carrying bolted aluminum bus bar connections (bolts M12, 8.8, joint force after installation  $F_j$  16–30 kN, initial joint temperature  $\vartheta_{j0}$  100–160  $^{\circ}\text{C}$ ), experiments over 8.2 yr,  $k_{u0} = 1.2$  (ca. 100  $^{\circ}\text{C}$ )  $\rightarrow$  1.7 after 20 000 h,  $k_{u0} = 2.1$  (160  $^{\circ}\text{C}$ )  $\rightarrow$  12 after 20 000 h (adapted from [4.56])

ter assembly, after 20 000 h the quality factor rose to  $k_u$  (20 000 h) = 1.7. Already with a quality factor of  $k_{u0} = 2$ –3, a failure is to be expected after about 1 yr of continuous high-current loading of the connections. For uncleaned connections (Fig. 4.79,  $k_{u0} \geq 10$ ), operation with high current loads is not possible.

The long-term behavior of connections with stranded-aluminum conductors, e.g., overhead line conductors, is also very much dependent on the thorough pretreatment of the conductors and the associated initial quality factor (in the example,  $k_{u0} = 0.76$ –1.40) (Fig. 4.112). The long-term experiments carried out over several years with continuous-current loads also clearly show the influence of the current load (in the example 60, 100, and 130% of the rated current of the overhead-line conductor). While properly manufactured and installed connections in overhead lines function for decades at lower than rated loads, which corresponds to practical experience, a continuous high load or overload drastically reduces the service life.

Plug-in-type connectors are influenced significantly by the environment because of their predominantly single-point contacts. Their chemically induced aging



**Fig. 4.111a,b** Long-term behavior of bolted connections under harsh environmental conditions, experimental results. **(a)** Aluminum and Copper. **(b)** Bimetallic aluminum-copper connections with and without AlCu-sheets (adapted from [4.42, 49])

can be considerably reduced by suitable coatings with low chemical reaction potential with the environment or with low-resistivity coatings (e.g., silver plated), (Fig. 4.113). Lubricants reduce the static and rolling friction during contact movement and can, thus, reduce the undesirable abrasion process. However, when the coating has been worn down or when it does not even exist, the lubricant alone cannot prevent the aging process (Fig. 4.114).

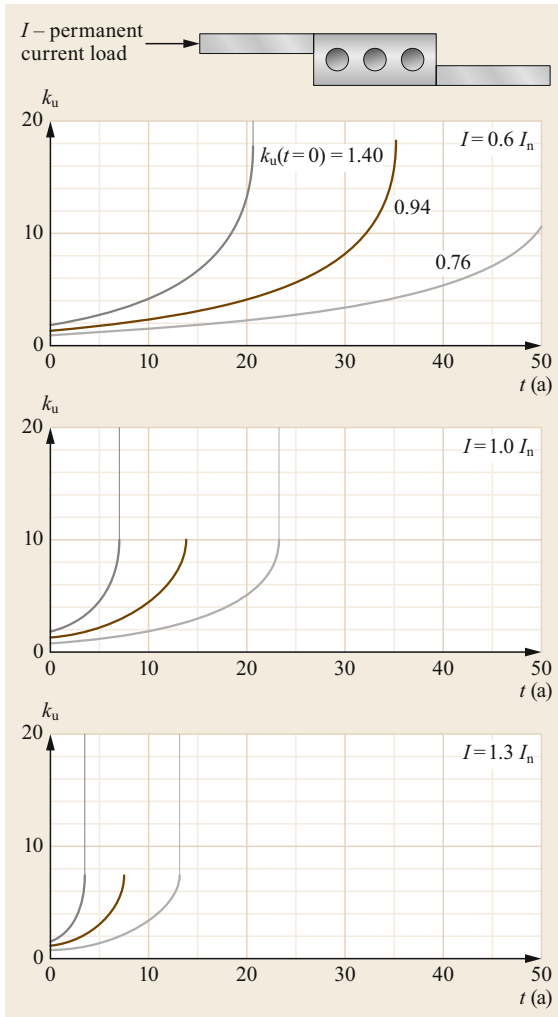
#### Measurement and Evaluation of Connection Resistances

Measuring the connection resistance is essential for developing and testing, as well as for quality control and condition assessment of electrical connections. Connections in electrical power engineering usually have connection resistances in the range of less than  $1 \mu\Omega$ . This means that special attention must be paid to measuring this quantity by means of four-point measurement (current-voltage measurement). The following basic options are available:

- Measurement with high alternating current (AC), e.g., the rated current. For voltage measurement,

a sensitive voltmeter is sufficient. However, the values in the measuring circuit must be determined by the magnetic field in and around the current-carrying conductor-induced voltages compensated (see the subsequent section on AC measurements, voltage compensation, Fig. 4.121). The conductor and the connection heats up during operation at high current. The connection temperature and the connection resistance must be measured, and the latter converted to  $20^\circ\text{C}$ .

- Measuring with high direct current (DC) is the simplest method, but DC high-current sources with low ripple of the current are usually not available or are not transportable, and, therefore, are only suitable for special applications. As with AC, the heating of the conductors must be considered.
- Measuring with low DC current (20–100 A DC) is possible with consideration of the previously mentioned disadvantages and is the most frequently used method. Here, however, the values of the voltage drop measured are in the microvolt range. Systematic measurement errors due to thermoelectric or other external voltages must be compensated. Microohmmeters with small DC measuring currents usu-



**Fig. 4.112** Long-term behavior of connectors for stranded-Al conductors under indoor laboratory conditions; influence of initial performance factor and permanent current load; 3 yr experiment and estimated lifetime according to (4.175). Initial performance factor  $k_u$  after installation (conductor AL/St 185/30): min.: 0.76, average: 0.94, max.: 1.40 (adapted from [4.57])

ally show the measured and corrected resistance value and, because of their mobility, are suitable for a wide variety of applications in practice.

For all measurement methods, the choice of the current-injection and the voltage-drop locations has to ensure a current flow as homogeneous as possible (Fig. 4.114).

**Measuring with Small DC Currents.** When measuring with small DC currents  $I_m$ , e.g., with a  $\mu\Omega$ -meter,

**Table 4.52** Thermoelectric voltage (excerpt) (adapted from [4.58])

Material	Thermal constant $K_{ptM}$ ( $\mu\text{V K}^{-1}$ ) at 0 °C (relative to platinum)
Copper	7.2–7.7
Aluminum	3.5
Silver	6.5
Nickel	−19.4 to −12
Palladium	−2.8
Constantan	−34.7 to −30.4
Silicium	448
Nickel chrome	22
Iron	18.7–18.9
Platinum <sup>a</sup>	0

<sup>a</sup> Reference material.

(Fig. 4.115a), thermoelectric voltages  $U_{th}$  are generated in the voltage-measuring circuit when different conductor materials (test object, connecting leads, electronic processing of the measured variable) and different temperatures occur within the measuring arrangement. These can be of the same order of magnitude as the actual measured value  $U_j$  and are superimposed on it (Fig. 4.115b).

The magnitude of the thermoelectric voltages results from the thermal constants  $K_{ptM}$  (Table 4.52) and the absolute temperature  $T$  at the point of contact of two metallic conductors M1 and M2

$$U_{th} = K_{ptM1M2} \Delta T, \tag{4.176}$$

with

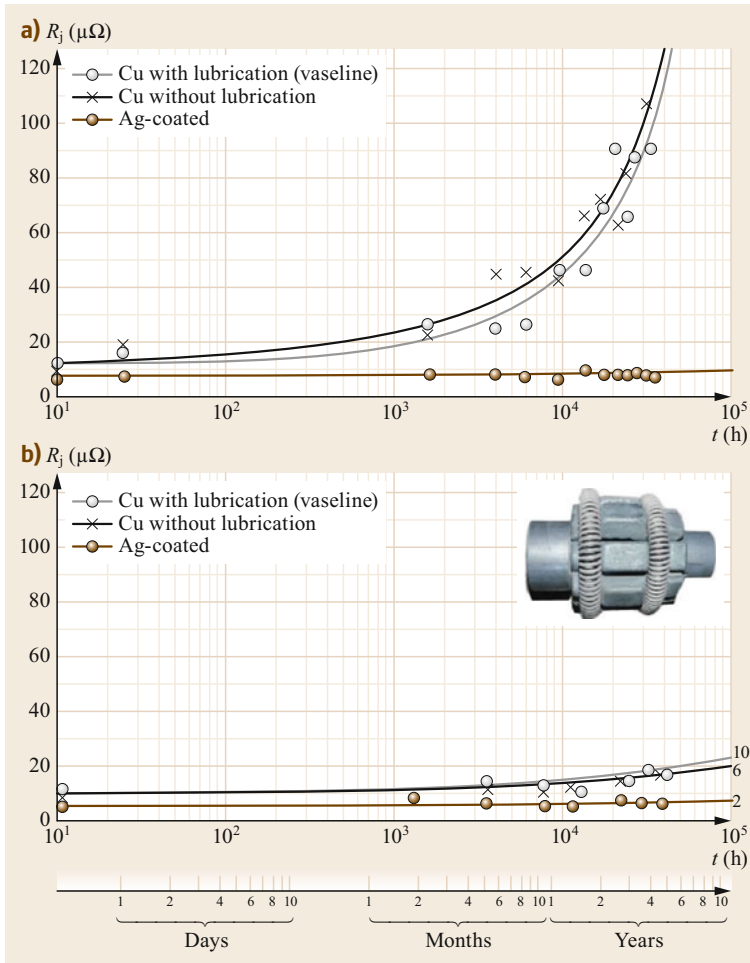
$$K_{ptM1M2} = K_{ptM1} - K_{ptM2}, \tag{4.177}$$

where  $U_{th}$  = thermoelectric voltage,  $K_{ptM}$  = thermal constant with reference to platina, M1 and M2 = metallic conductors 1 and 2, and  $\Delta T$  = absolute temperature difference.

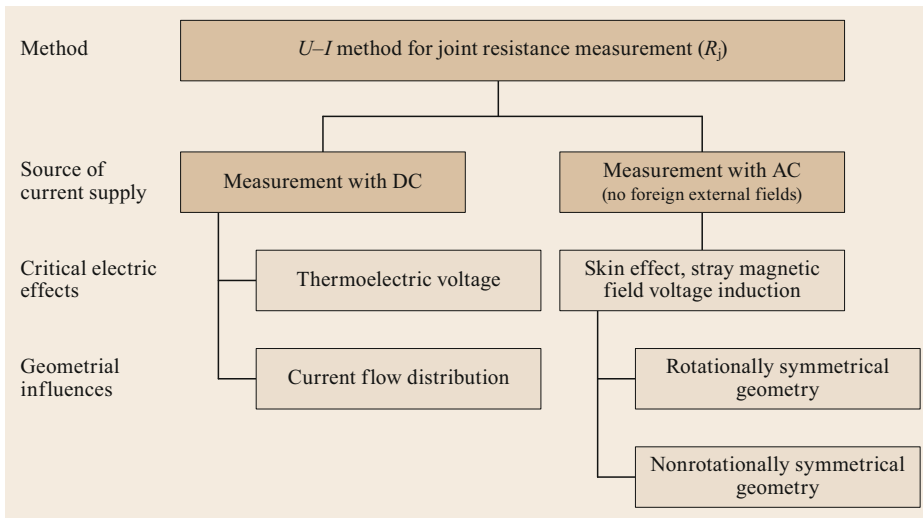
With  $n$  bimetallic contact points in a measuring circuit, the individual thermoelectric voltages add up to the total voltage  $U_{th\text{total}}$ .

$$U_{th\text{total}} = \sum_1^n U_{th\ n}. \tag{4.178}$$

The compensation of these thermoelectric voltages  $U_j$  can be achieved by measuring the voltage drop across the connection, i.e., in two steps with reversal of the current direction and subsequent averaging (Fig. 4.116a). In an alternative method, the voltage drop across the connection without external current flow ( $I_m = 0$ ) is caused by the sum of the thermoelectric voltages  $U_{th}$  in the measuring circuit. Only in a second step of the measuring process is the measuring current  $I_m$  switched on,



**Fig. 4.113a,b** Long-term behavior of plug-in-type connectors (tulip-type); experimental results; influence of the atmosphere (indoor switchgear compared to  $\text{SO}_2$  outdoor switchgear) on the joint resistance  $R_j$  with a silver-plated and plain copper surface. **(a)**  $\text{SO}_2$ -air atmosphere ( $0.75 \text{ mg/m}^3$ , wet) and **(b)** switchgear room (indoor). Average of the joint resistance from experimental results (measuring points of six samples each) and estimation of the long-term behavior according to (4.175) (lines). Test without current load ( $I = 0$ ) (adapted from [4.3])



**Fig. 4.114** Methods of joint-resistance measurement



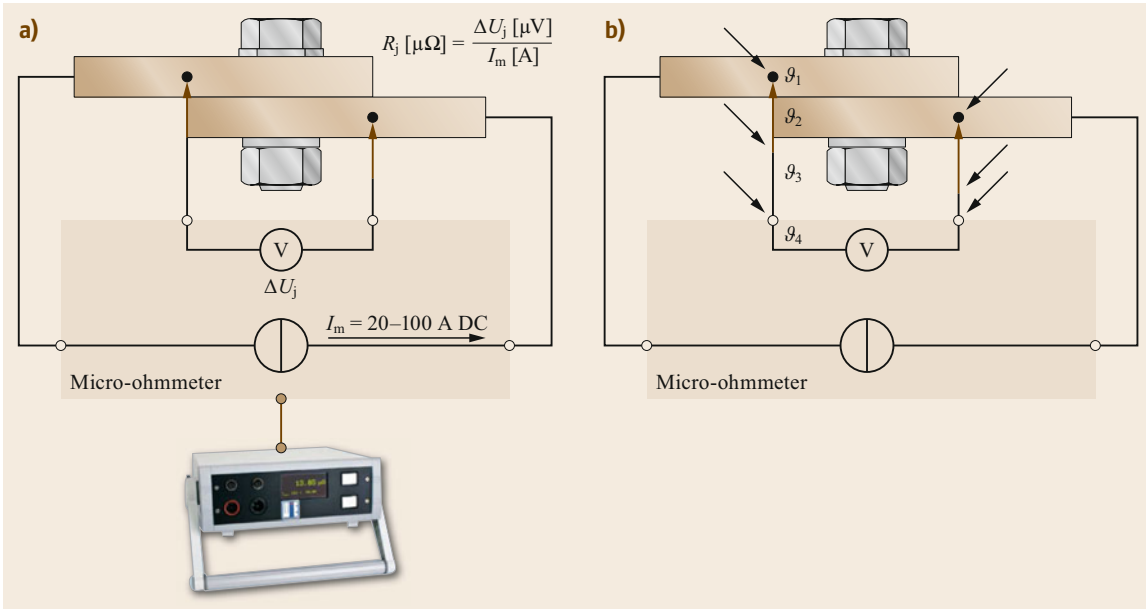


Fig. 4.115a,b DC measurement of joint resistance. (a) Measuring circuit, (b) thermoelectric voltages

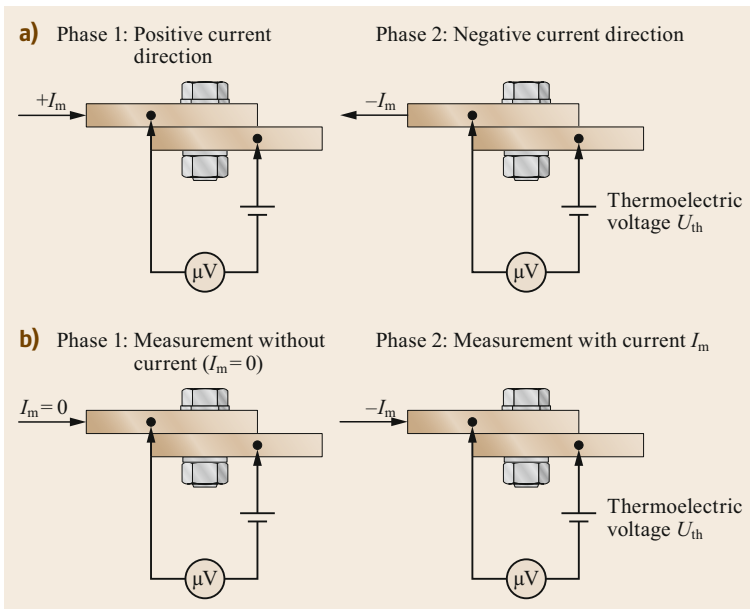
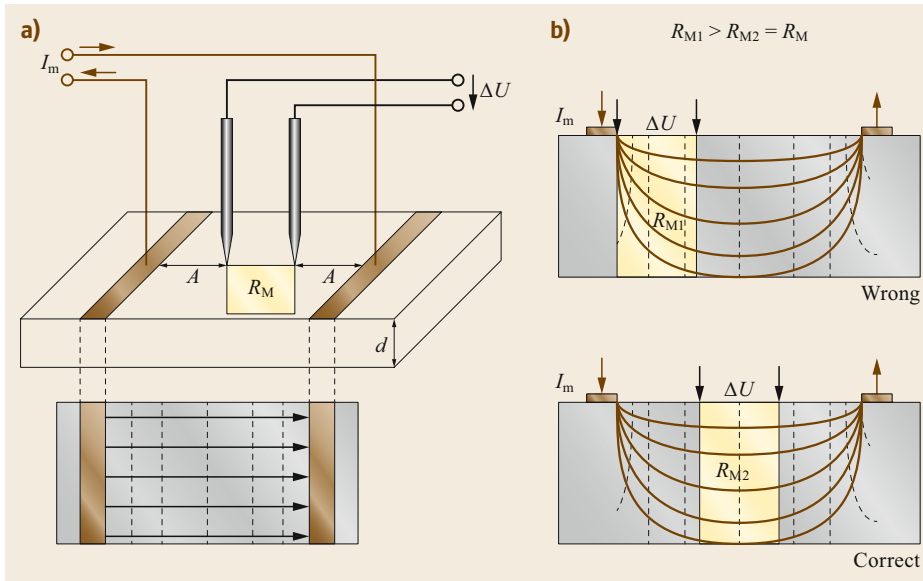
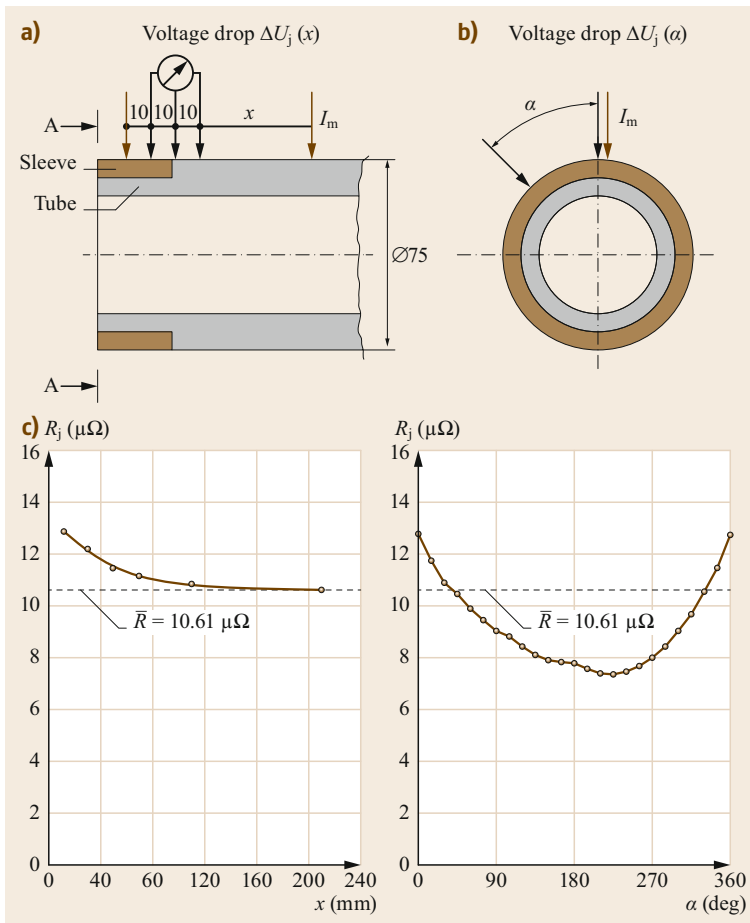


Fig. 4.116a,b Compensation of thermoelectric voltages in two steps. (a) Reversible direction of measuring current. (b) Separation of thermoelectric voltages



**Fig. 4.117a,b** DC measurement of micro-ohmic resistances  $R_M$ , geometric influence of measuring current flow distribution. **(a)** Top view, **(b)** sectional view



**Fig. 4.118a-c** Connector **(a)** Longitudinal section, **(b)** sectional view A-A, **(c)** DC measurement of joint resistance  $R_j$  (between sleeve and tube), geometric influence of measuring ( $x$  = distance between current supply and measuring point), current flow distribution in a tubular connection with contact sleeve (example)

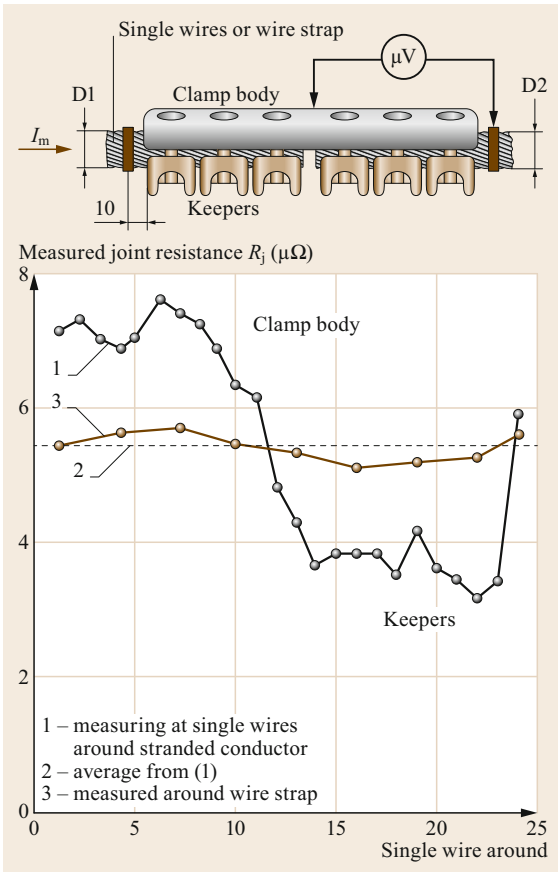


Fig. 4.119 DC measurement of joint resistance at stranded conductors around the wires

and from the difference between the two measurements, one can determine the true value of the connection resistance  $R_j$  (Fig. 4.116b). Reversible direction of measuring current

$$R_j = \frac{\Delta U_j}{I_m} = \frac{\overbrace{(\Delta U_j + U_{th})}^{\text{phase 1}} - \overbrace{(-\Delta U_j + U_{th})}^{\text{phase 2}}}{2I_m}, \quad (4.179)$$

and separation of thermoelectric voltages

$$R_j = \frac{\Delta U_j}{I_m} = \frac{\overbrace{U_{th}}^{\text{phase 1}} - \overbrace{(-\Delta U_j + U_{th})}^{\text{phase 2}}}{I_m}. \quad (4.180)$$

Resistance measurements in the  $\mu\Omega$ -range by carrying out a current–voltage measurement and applying Ohm’s law assume that the current flow fields in the proximity of the voltage-drop location is as homogeneous as possible. This is reasonable for long, slender conductors with their connections. For bulky test objects though (Fig. 4.117), such as connectors with high lateral dimensions compared to their length or to the length of the related conductor (Fig. 4.118) [4.59], an inhomogeneous current flow field has to be taken into account. In this case, the current-injection and the voltage-drop measurement point have to be carefully selected so that measurement occurs in a mostly homogenous region of the flow field. Possibly multiple measurements at the circumference of the connector and subsequent averaging can deliver a useful result.

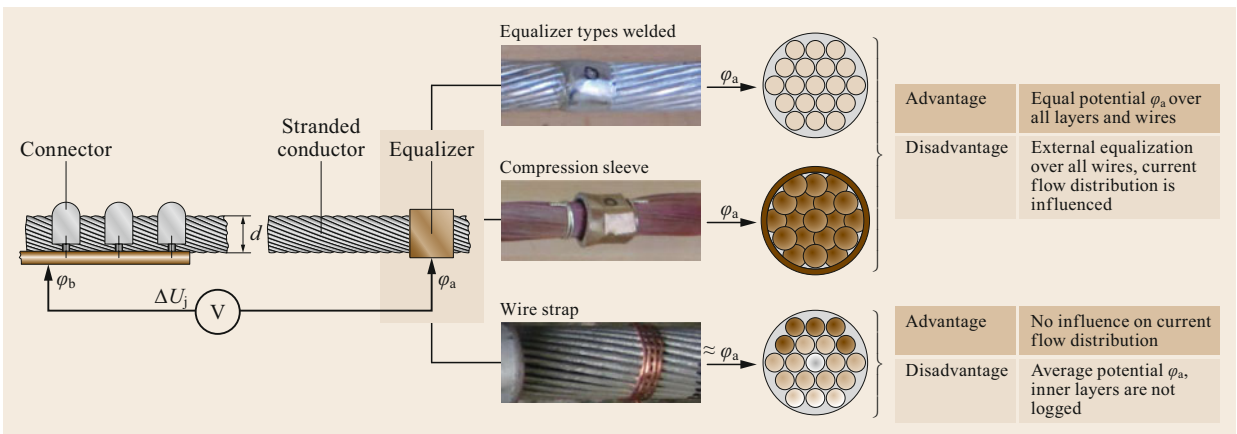
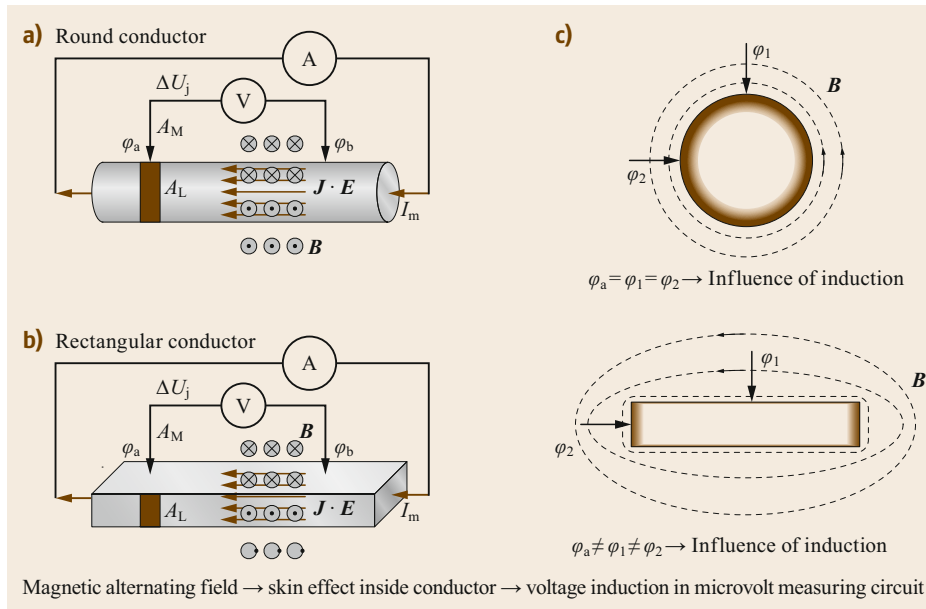


Fig. 4.120 DC measurement of joint resistance at stranded conductors, potential tap



**Fig. 4.121a–c** AC measurement of joint resistance, influence of magnetic field and geometry. (a) Rotationally symmetrical geometry, (b) non-rotationally symmetrical geometry, (c) influence of current density distribution and connector geometry on measured voltage drop  $\Delta U_j = \varphi_a - \varphi_b$  in section  $A_L$

When measuring connection resistances on stranded conductors, it must be assumed that depending on the contact arrangement, not all individual wires conduct the same partial current and have different potentials in the area of the voltage tap (Fig. 4.119). Equalizers in the form of welded joints, ferrules, or wire coils can largely solve this problem (Fig. 4.120). However, with welded and pressed equalizers, an idealized current distribution is forced, which does not correspond to the distribution in the connector in practice.

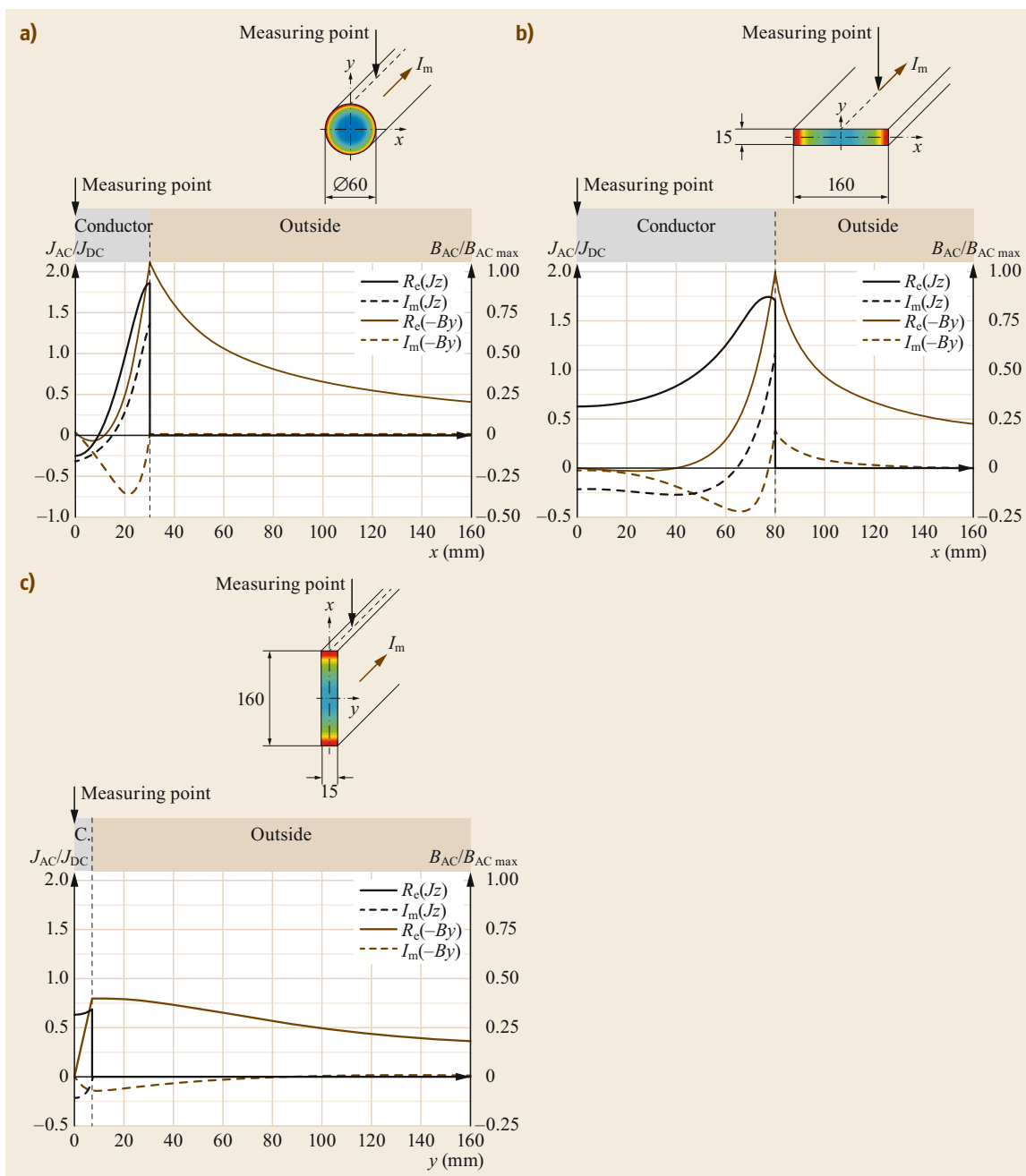
**Measuring with AC Current.** If the connection resistance must be measured with AC, the effect of the electromagnetic field depending on the conductor geometry must be taken into account (Fig. 4.114). While the skin effect of rotationally symmetrical, round conductors is evenly distributed over the circumference of the conductor, the current density  $J$  in rectangular conductors, and, thus, the measured potential, depends on the measuring point (Fig. 4.121).

In addition, in the measuring loop, to determine the voltage drop  $\Delta U_j$ , a surface  $A_L$  in the conductor and a surface  $A_M$  outside the conductor are created, which are permeated by the alternating internal and external magnetic field  $B$ . An electromagnetic voltage is induced and is superimposed on the measured variable. While the outer surface can be reduced to a minimum by clever arrangement and twisting of the measuring conductors, the inner surface with the highest magnetic flux density  $B$  remains, namely, at the boundary layer between conductor and environment in the measuring circuit (Fig. 4.122). Through an *outcrossing* measuring loop

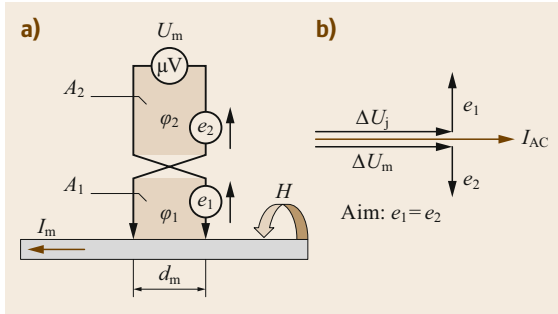
two surfaces  $A_1$  and  $A_2$  of different sizes (Fig. 4.123a) are created, in which the magnetic flow is in opposite directions. The induced voltages, therefore, result in  $e_1$  and  $e_2$ , which are opposite and ideally complement each other to zero, if the two surfaces are matched to the minimum of the voltage to be measured (by trial and error). In this case, the induced voltages are compensated, and the measured variable  $\Delta U_m$  corresponds to the true value of the real proportion of the voltage drop  $\Delta U_j$  over the connection (Fig. 4.123b).

Another way to evaluate live electrical connections is to measure the connection temperature using infrared thermography. Here, the measured temperature is a mediating variable for the connection resistance. Prerequisites for correct measurement of the connection temperature include:

- A sufficiently high, constant current load before and during the measurement.
- The power dissipation generated by the connection and the resulting excess energy.
- The temperature of the connection depends on the square of the current (4.33). For example, if only half the rated current flows, then only about a quarter of the heating can be expected. This can lead to critical misjudgments of the condition of a connection.
- The current distribution within the equipment and on parallel current paths must be known and taken into account.
- The emission coefficient  $\varepsilon$  of the surface under consideration must be known and must be considered (4.70).



**Fig. 4.122a–c** Examples for AC measurement of resistances, finite element simulation of current density inside the conductor  $J_{AC}/J_{DC}$ , and magnetic flux density inside and outside conductor  $B_{AC}/B_{AC\ max}$ , influence of geometry ( $x$  and  $y$ : distance from measuring point). **(a)** Rotationally symmetrical geometry, round conductor; **(b)** nonrotationally symmetrical geometry for rectangular conductor, flat, and **(c)** rectangular conductor, edgewise



**Fig. 4.123a,b** AC measurement of joint resistances, elimination of magnetic induced voltages in the measuring circuit. (a) Arrangement of measuring circuit with crossed measuring leads to compensate induced voltages in area  $A_1$  (conductor inside and outside) by area  $A_2$  (larger loop outside), (b) phasor diagram for ideal compensated induced voltage

- Knowledge and consideration of all ambient conditions, particularly outdoors (ambient temperature, precipitation, air speed, solar and sky radiation). This way, conspicuous connections can be identified and hot spots can be detected quickly.

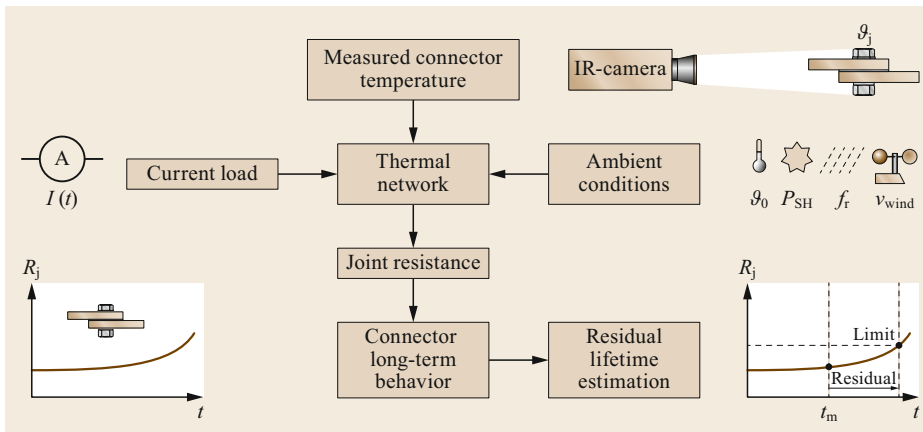
It is possible to estimate the remaining service life of connectors in operation if the fundamental long-term behavior of such connectors is known from experiments. With the help of a thermal network and using the already measured temperature rise and the known test parameters (current environment) (Sect. 4.3.1) the connection resistance of the connector can be calculated and compared with the known long-term performance of this type of connector. Taking into account past and future current loads the remaining life-time of the connector can then

be estimated (Fig. 4.124). This way, inspections can be planned long in advance, and urgent maintenance actions can be initiated without delay [4.60].

**IR Measurement.** Using IR measurement can result in more precise analysis doing a so-called fingerprint measurement.

After installation of a new line or a substation there are used hundreds of same connections. For example, 1 year after starting operation a first measurement on a group of samples is made. The above-mentioned influencing parameters like current, ambient temperature, . . . , should be recorded. After some period of operation e.g., 5 years, the IR measurement is repeated with parameters similar to the initial ones. The evaluation of this recording compared to the starting values allows a statement concerning the state of quality of the connection.

**Acknowledgments.** The author would like to thank the current and former staff of the Institute for Electrical Power Supply and High Voltage Technology at Dresden University of Technology for their kind support while he was working on this chapter; in particular, special thanks go to PD Dr.-Ing. habil. Helmut Löbl, Dr.-Ing. Stephan Schlegel, Dr.-Ing. Robert Adam, and Dr.-Ing. Christian Hildmann for providing related documents and reviewing this material. Thanks also go to the companies RIBE SubCon GmbH, Austria, Pfisterer Kontaktsysteme, Germany, and Werner Industrielle Elektronik Kreischa, Germany for providing illustrations. This chapter could not have been published in English if it had not been for the editor of the book, Prof. Konstantin O. Papailiou, whom I also would like very much to thank.



**Fig. 4.124** Infrared diagnosis principle to estimate residual lifetime

## References

- 4.1 H. Böhme: *Mittelspannungstechnik – Schaltanlagen berechnen und entwerfen* (Huss-Medien, Berlin 2005)
- 4.2 H. Löbl: *Zur Dauerstrombelastbarkeit und Lebensdauer der Geräte der Elektroenergieübertragung*, Habilitationsschrift (TU Dresden, Dresden 1985)
- 4.3 S. Großmann: *Zur Gestaltung und zum Betriebsverhalten von Steckverbindungen der Elektroenergie-etechnik*, Ph.D. Thesis (TU Dresden, Dresden 1988)
- 4.4 IEC 60071-1: *Insulation Co-ordination – Part 1: Definitions, Principles and Rules* (IEC, Geneva 2006)
- 4.5 H. Löbl, H.-J. Stoye: *Beitrag zur Optimierung elektrotechnischer Schalt- und Verteileranlagen hinsichtlich ihrer thermischen Dauerstrombelastbarkeit*, Ph.D. Thesis (TU Dresden, Dresden 1972)
- 4.6 S. Threesome, G. Moustafa, D. Santos Guimarães dos, B. Ramati Pereira da Rocha: Long-term behavior of stationary electrical connections in areas with harsh natural environmental conditions, *Cigre Sci. Eng.* **3**, 40–54 (2015)
- 4.7 IEC 61439-1: *Low-Voltage Switchgear and Controlgear Assemblies, General Rules* (IEC, Geneva 2014)
- 4.8 IEC 60947-1: *Low-Voltage Switchgear and Controlgear, General Rules* (IEC, Geneva 2004)
- 4.9 DIN EN 60947-1: *Niederspannungsschaltgeräte – Teil 1: Allgemeine Festlegungen/Low-Voltage Switchgear and Controlgear – Part 1: General Rules* (Beuth, Berlin 2015)
- 4.10 DIN EN 61439-1: *Niederspannungs-Schaltgeräte-Kombinationen – Teil 1: Allgemeine Festlegungen/Low-Voltage Switchgear and Controlgear Assemblies* (Beuth, Berlin 2011)
- 4.11 IEC 62271-1: *High-Voltage Switchgear and Controlgear, Common Specifications* (IEC, Geneva 2007)
- 4.12 DIN EN 62271-1: *Hochspannungs-Schaltgeräte und –Schaltanlagen – Teil 1: Allgemeine Bestimmungen/High-Voltage Switchgear and Controlgear – Part 1: Common Specifications* (Beuth, Berlin 2009)
- 4.13 DIN VDE 0101: *Power Installations with Rated AC Voltage Above 1 kV* (VDE, Berlin 2011)
- 4.14 I. Berg: *Untersuchungen zur Strombelastbarkeit der Geräte der Elektroenergieübertragung unter Freiluftatmosphäre* (Shaker, Aachen 2011)
- 4.15 C. Hildmann, S. Schlegel, S. Großmann, M. Murr, S. Lippmann: Influence of force and form-fit component on the electrical contact behavior of press-fit connections. In: *Proc. 23rd Albert-Keil-Kontaktsemin., Karlsruhe* (2015) pp. 136–145
- 4.16 C. Hildmann, C. Schlegel, S. Großmann, T. Dockhorn: Investigations on the long-term-behavior of current carrying fittings for high temperature low sag conductors. In: *Proc. 23rd Int. Conf. Electr. Distrib., Lyon* (2015)
- 4.17 S. Schlegel: *Langzeitverhalten von Schraubenverbindungen mit Stromschienen aus Reinkupfer in der Elektroenergieetechnik unter besonderer Berücksichtigung der Temperatur*, Ph.D. Thesis (TU Dresden, Dresden 2011)
- 4.18 C. Hildmann: *Zum elektrischen Kontakt- und Langzeitverhalten von Pressverbindungen mit konventionellen und Hochtemperatur-Leiteseilen mit geringem Durchhang*, Ph.D. Thesis (TU Dresden, Dresden 2017)
- 4.19 S. Kämpfer, G. Kopatsch (Eds.): *Schaltanlagen-Handbuch der ABB AG Deutschland*, 12th edn. (Cornelsen, Berlin 2011)
- 4.20 H. Böhme, S. Großmann, M. Aliche: Zur Stromüberlastbarkeit elektrotechnischer Betriebsmittel, *Elektrie* **85**(10), 377–380 (1985)
- 4.21 G. Winkler (Ed.): *VEM-Handbuch Hochstromtechnik: Grundlagen, Dimensionierung und Ausführung von Hochstromanlagen* (Verlag Technik, Berlin 1987), Chaps. 2.1–2.3
- 4.22 R. Adam: *Beitrag zur thermischen Dimensionierung von Niederspannungs-Schaltgerätekombinationen*, Ph.D. Thesis (TU Dresden, Dresden 2018)
- 4.23 M. Schenk: *Thermische Bemessung von Netzstationen* (VWEW Energieverlag, Frankfurt a. M. 2002)
- 4.24 IEC 60034-1: *Rotating Electrical Machines – Part 1: Rating and Performance* (IEC, Geneva 1997)
- 4.25 DIN EN 50182: *Leiter für Freileitungen – Leiter aus konzentrisch verseilten runden Drähten* (Beuth, Berlin 2001)
- 4.26 W. Schufft (Ed.): *Taschenbuch der elektrischen Energietechnik* (Hanser, München 2007) p. 200
- 4.27 V. Kobisch: *Zur elektrischen Alterung von Epoxidharzisolierungen unter besonderer Berücksichtigung der durch den Stromfluß entstehenden thermischen und mechanischen Beanspruchungen*, Ph.D. Thesis (TU Dresden, Dresden 1982)
- 4.28 G. Stauch: *Zur mechanisch-dynamischen Beanspruchung kompakter Schaltanlagen bei Kurzschlussstrombelastung*, Ph.D. Thesis (TU Dresden, Dresden 1984)
- 4.29 F. Golletz: *Zur Erschließung von Reserven der mechanischen Belastbarkeit von Stromleitanordnungen bei Kurzschlussstrombelastung*, Ph.D. Thesis (TU Dresden, Dresden 1989)
- 4.30 IEC60865-1: *Short-Circuit Currents – Calculation of Effects – Part 1: Definitions and Calculation Methods* (IEC, Geneva 2011)
- 4.31 F. Kießling, P. Nefzger, U. Kaintzyk: *Freileitungen – Planung, Berechnung, Ausführung* (Springer, Berlin, Heidelberg 2011)
- 4.32 L. Möcks: *Berechnung der elektromagnetischen Kurzschlussstromkräfte an den Feldabstandhaltern im Bündelleiter einer Hochspannungs-Freileitung*, Ph.D. Thesis (TU Dresden, Dresden 2000)
- 4.33 B. Wartmann: *Beitrag zum dynamischen Verhalten von Stützern in Schaltanlagen bis 36 kV bei Kurzschlußstrombelastung*, Ph.D. Thesis (TU Dresden, Dresden 1981)
- 4.34 R. Holm: *Electric Contacts – Theory and Applications* (Springer, Berlin, Heidelberg, New York 2000)
- 4.35 R. Bergmann: *Zum Langzeitverhalten des Widerstands elektrischer Stromschienenverbindungen*, Ph.D. Thesis (TU Dresden, Dresden 1996), Fortschritt-Berichte VDI: Reihe 21, Elektrotechnik, Ausgabe 195

- 4.36 F. Blumenroth: *Zum Langzeitverhalten von Steckverbindungen mit Schraubenfedern in Anlagen der Elektroenergie-technik*, Ph.D. Thesis TU Dresden (Shaker, Aachen 2010)
- 4.37 R. Schneider: *Langzeitverhalten geschraubter Stromschienenverbindungen in der Elektroenergie-technik*, Ph.D. Thesis (TU Dresden, Dresden 2012)
- 4.38 G. Moustafa: *Experimental Investigations on the Behavior of Connectors in High Current Systems*, Ph.D. Thesis (Port Said University, Port Said 2010)
- 4.39 N. Lücke: *Das Langzeitverhalten elektrischer Steckverbindungen mit Kupfer-Beryllium-Kontakt-lamellen*, Ph.D. Thesis (TUDpress, Dresden 2014)
- 4.40 S. Pfeifer: *Einfluss intermetallischer Phasen der Systeme Al-Cu und Al-Ag auf den Widerstand stromtragender Verbindungen im Temperaturbereich von 90 °C bis 200 °C*, Ph.D. Thesis (TU Dresden, Dresden 2015)
- 4.41 M. Gatzsche: *Elektrisch-thermisches Betriebs- und Langzeitverhalten hochstromtragfähiger Kontaktelemente*, Ph.D. Thesis TU Dresden (Shaker, Aachen 2016)
- 4.42 S. Dreier: *The Impact of Films on the Long-Term Behavior of Stationary Electrical Connections and Contacts in Electric Power Systems*, Ph.D. Thesis (TUDpress, Dresden 2016)
- 4.43 S. Schoft: *Langzeitverhalten elektrotechnischer Verbindungen unter Berücksichtigung des Kriechens der Leitermaterialien*, Ph.D. Thesis (VDI, Düsseldorf 2008)
- 4.44 E. Philippow: Elemente und Baugruppen der Elektroenergie-technik. In: *Taschenbuch Elektrotechnik*, Vol. 5, ed. by E. Philippow (Verlag Technik, Berlin 1980) p. 599
- 4.45 M. Babikow: *Wichtige Bauteile elektrischer Apparate* (Verlag Technik, Berlin 1954)
- 4.46 D. Mücksch: *Kontaktwiderstand von Schraubenverbindungen bei Stromschienen*, Diploma Thesis (TU Dresden, Dresden 1981)
- 4.47 H. Böhme, S. Großmann, H. Löbl: Zum Langzeitverhalten von Kontaktverbindungen der elektrischen Energie-technik, *Wiss. Z. Tech. Univ. Dresd.* **22**(4), 153–159 (1988)
- 4.48 M. Gatzsche, N. Lücke, S. Großmann, T. Kufner, G. Freudiger: Evaluation of electric-thermal performance of high-power contact systems with the voltage-temperature relation. In: *Proc. IEEE Trans. Compon. Packag. Manuf. Technol.*, Vol. 7 (2017) pp. 317–328
- 4.49 S. Schlegel: *Stromführende Verbindungen und Leiterwerkstoffe der Elektroenergie-technik, Gestaltungskriterien und Langzeitverhalten von Schraubenverbindungen mit Flächenkontakten*, Habilitationsschrift (TU Dresden, Dresden 2019)
- 4.50 H. Böhme, H. Löbl: Zur Theorie des Langzeitverhaltens von Aluminium-Schraubverbindungen, *Elektrie* **41**(5), 179–183 (1987)
- 4.51 E. Vinaricky, G. Horn, V. Behrens: *Datenbuch der elektrischen Kontakte* (DODUCO, Pforzheim 2012)
- 4.52 E. Vinaricky: *Elektrische Kontakte, Werkstoffe und Anwendungen – Grundlagen, Technologien, Prüfverfahren* (Springer Vieweg, Berlin, Heidelberg 2016)
- 4.53 T. Fuhrmann, S. Schlegel, S. Großmann, M. Hoidis: Comparison between nickel and silver as coating materials of conductors made of copper or aluminum used in electric power engineering. In: *Proc. 27th Int. Conf. Electr. Contacts (ICEC)*, Dresden (2014) pp. 478–483
- 4.54 P.G. Slade: *Electrical Contacts – Principles and Applications*, 2nd edn. (CRC Press, Boca Raton 2014)
- 4.55 H. Löbl, S. Großmann, K.-H. Friebe: Zum Langzeitverhalten von Verbindungen der Elektroenergie-technik mit Hochtemperatur-Leiterseilen – TAL, *Elektrizitätswirtschaft* **99**(10), 27–34 (2000)
- 4.56 S. Grossmann, H. Löbl, H. Böhme: Contact lifetime of connections in electrical power systems. In: *Proc. 16th Int. Conf. Electr. Contacts* (1992) pp. 129–134
- 4.57 S. Großmann, H. Löbl, D. Böhlke, U. Schäfer: Erhöhung der Strombelastbarkeit von Freileitungen und Schaltanlagen – Möglichkeiten und Risiken. In: *Proc. 11. Symp. Energieinnov., Graz* (2010)
- 4.58 W. Schmusch: *Elektronische Messtechnik: Prinzipien, Verfahren, Schaltungen*, 5th edn. (Vogel, Würzburg 2001)
- 4.59 H. Böhme, S. Großmann, H. Löbl: Messung des Verbindungswiderstandes, *Elektrotech. Z.* **114**(4), 264–269 (1993)
- 4.60 R.-D. Rogler: *Infrarotdiagnose an Verbindungen der energetischen Elektrotechnik*, Ph.D. Thesis TU Dresden (VDI, Düsseldorf 1999)

### Steffen Großmann

Institute of Electrical Power and High Voltage Engineering  
Technische Universität Dresden  
Dresden, Germany  
[steffen.grossmann@tu-dresden.de](mailto:steffen.grossmann@tu-dresden.de)



Steffen Großmann (VDE, CIGRE) received the Dr.-Ing. degree in Electrical Engineering from the Technische Universität Dresden, Germany (1988). In 1990, he started working at RIBE-Richard Bergner GmbH, dealing with the electrical and mechanical behavior of fittings for substations and overhead lines. In 1997 he became Product Team Manager for substations and low-voltage materials. He is Full Professor at the institute for Electrical Power Systems and High-Voltage Engineering at TU Dresden.



# Basics of Power Systems Analysis

Carlo Alberto Nucci , Alberto Borghetti , Fabio Napolitano , Fabio Tossani 

This chapter provides the background required to understand the main aspects of power systems analysis and operation under steady-state and transient or dynamic conditions. It is intended for senior undergraduate or graduate students of electrical engineering as well as practitioners, so readers are assumed to have a solid background knowledge of electrical engineering.

The main technical issues associated with power systems analysis are addressed, focusing in particular on alternating current (AC) transmission lines, networks, load-flow and short-circuit calculations, stability analysis, frequency control, and electromagnetic transient appraisal. The chapter also references the most important and popular model frameworks and calculation/modeling tools that have been developed by researchers and engineers working within the electric power systems area in the last few decades. It is emphasized in this chapter that an understanding of the issues dealt with here is required to comprehend other chapters of this handbook devoted to distributed generation and smart grids, and this knowledge will also be needed to be able to operate upcoming power systems.

The chapter is divided into sections focusing on the following topics:

1. Power systems evolution, from the origins to the traditional structure
2. Transmission lines in steady state, transmitted active and reactive power
3. Power flow analysis (load-flow equations and resolution methods)
4. Short-circuit calculations for unbalanced faults (symmetrical components, fault equations, and sequence networks)
5. Stability (states of operation, classification, P-delta curves, rotor angle stability, equal area criterion, multi-machine stability and voltage stability)
6. Generators reserve and dynamics, frequency dependence of the load, control structure for frequency control

7. Traveling waves in a lossless line, reflection and transmission coefficients, multiple reflections in a line of finite length; electromagnetic transients (classification of transients, EMTP)
8. Power systems in the future (why we need a smart(er) grid, microgrids and energy communities)

Additional information and supplementary exercises for this chapter are available online.

<b>5.1</b>	<b>Electric Power System Evolution</b> .....	274
5.1.1	The Dawn of Electric Power Systems.....	274
5.1.2	From the War of the Currents to the Twenty-First Century .....	275
<b>5.2</b>	<b>Mission and Traditional Structure</b> .....	276
<b>5.3</b>	<b>Transmission Line Equations in the Steady State</b> .....	279
5.3.1	The Telegrapher's Equations .....	279
5.3.2	The Line as a Two-Port Network.....	283
5.3.3	Transmitted Active and Reactive Power Expressions .....	284
<b>5.4</b>	<b>Load Flow</b> .....	285
5.4.1	From the Real Network to the Admittance Matrix.....	285
5.4.2	The Equations .....	290
5.4.3	Capability Curves .....	292
5.4.4	Solution Methods.....	293
5.4.5	Approximations for Calculating the Load Flow.....	295
5.4.6	Concluding Remarks.....	298
<b>5.5</b>	<b>Unsymmetrical Fault Analysis</b> .....	300
5.5.1	Types of Faults in Electric Power Systems	300
5.5.2	Protection Measures Against Faults.....	301
5.5.3	Unbalanced Faults: Short-Circuit Calculation .....	301
5.5.4	Direct, Inverse, and Homopolar Sequence Impedances.....	307
5.5.5	Fault at Any Point in the Network .....	309
5.5.6	Three-Phase Short Circuit at a Synchronous Generator's Terminals	311
<b>5.6</b>	<b>Stability</b> .....	319
5.6.1	Transient Phenomena .....	319

5.6.2	Definition of Stability .....	320	5.8.2	Reflection and Transmission Coefficients	348
5.6.3	States of Operation .....	320	5.8.3	Multiple Reflections in a Line of Finite Length .....	352
5.6.4	Classification of Power System Stability	320	5.9	<b>Electric Power Systems of the Future: Smart Grids</b> .....	360
5.6.5	$P$ - $\delta$ Curves of Synchronous Machines.....	321	5.9.1	Evolution of Power Systems Towards Increased Deployment of Renewable Energy Resources .....	360
5.6.6	Rotor Angle Stability .....	327	5.9.2	Power System Structure: Why We Need Smart(er) Grids .....	361
5.6.7	Voltage Stability .....	333	5.9.3	The Definition of a Smart Grid.....	362
5.7	<b>Power System Control</b> .....	336	5.9.4	Growth in the Utilization of ICT in Power Systems.....	362
5.7.1	Generation Reserve .....	336	5.9.5	Microgrids .....	363
5.7.2	Dynamics of the Generators .....	337	5.9.6	Energy Communities .....	363
5.7.3	Frequency Dependence of the Load .....	338	<b>References</b> .....		364
5.7.4	Dynamic Response of an Uncontrolled Power System .....	338			
5.7.5	Control Structure for Frequency Control	339			
5.8	<b>Propagation of Electromagnetic Transients Along Transmission Lines</b> ....	345			
5.8.1	Traveling Waves in a Lossless Line.....	345			

In this chapter, we present a succinct summary of the fundamentals of power systems analysis and operation under steady-state, dynamic, and transient conditions. We consider the main technical issues that are relevant to the transmission of electric energy, focusing mainly on AC transmission lines and networks and addressing load-flow and short-circuit calculations, stability, frequency control, voltage control, and electromagnetic transient appraisal. However, it should be noted that there are a number of excellent books that cover these subjects in a far more comprehensive manner than possible in this chapter (e.g., [5.1–32]).

In the context of this handbook, an understanding of the subjects covered by this chapter is useful for comprehending Chap. 15 on distributed generation and smart grids, and thus how modern power systems work, given that renewables are increasingly being con-

nected to networks through power electronic converters. It should, however, be noted that HVDC (high-voltage direct current) and DC (direct current) applications, modeling, analysis, and operation are deliberately overlooked in this chapter, as these topics are covered in Chap. 12.

This chapter is intended for use by senior undergraduate or graduate electrical engineering students and practitioners who are familiar with the theory of electrical circuits and of electrical machines. We therefore assume that the reader has a solid background knowledge of electrical engineering, along with an understanding of the per unit method.

After some sections or paragraphs, there are web-links to files that contain illustrative examples, exercises, or even animations, which are generally accompanied by the input file of the relevant program codes.

## 5.1 Electric Power System Evolution

### 5.1.1 The Dawn of Electric Power Systems

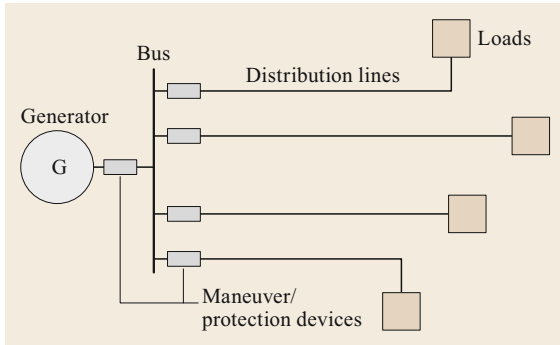
In its simplest form, an electric power system consists of an electric power generator, a distribution system consisting of one or more distribution lines connecting the generator to users, and some protection/maneuver devices (see Fig. 5.1). Nowadays, this simple configuration is used for off-grid power systems or microgrids operating under islanded conditions, but it is also the configuration that was employed for the first power systems built at the end of the nineteenth century to provide lighting in New York City [5.33].

The history of electric power systems is commonly considered to have begun in the year 1882, when a power station on Pearl Street in New York was inau-

gurated by Thomas Alva Edison (Fig. 5.2). This plant, which generated DC power using 175 HP high-speed steam engines, was designed to supply electrical energy to 400 lamps belonging to 82 customers in the business district of Wall Street.

The construction of the first power station was hugely important: although Volta had invented the first primary cell a century earlier, and more efficient primary cells had been constructed since then (such as the one devised by George Leclanché in 1865), these modest electrochemical power sources were not able to provide the amount of energy needed to power a whole district.

Immediately after the discovery of electromagnetic induction by Faraday in 1831, a variety of generators



**Fig. 5.1** The simplest configuration of an electric power system

were proposed. In 1869, not only was the first DC dynamo revealed in Vienna by Gramme and Pacinotti, but its working principle was also discovered to be reversible, resulting in the creation of the motor.

Furthermore, following the invention of the arc lamp by Foucault in 1841, it was subsequently improved by others until a satisfactory design was devised by Jablochkov in 1876. While the resulting lamp was suitable for generating the large luminous intensities required for public lighting (indeed, it was used along the Avenue de l'Opéra in Paris from 1879 to 1881), it was too bright for private use. Edison's lamp, consisting of a filament housed in a glass vacuum bulb, was far more appropriate for this purpose.

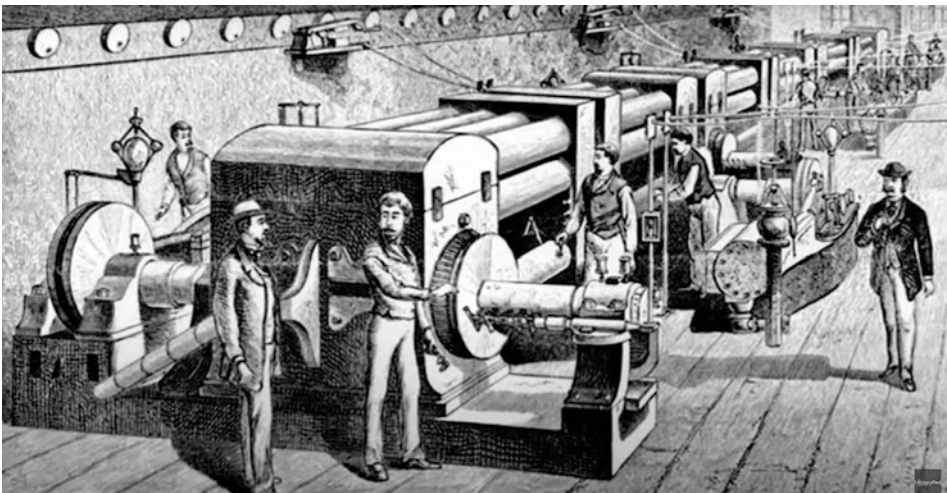
Thus, in summary, two types of light sources and two types of power sources (direct current and alternating current) were available in 1882, but the transformer was yet to be invented.

Table 5.1 summarizes the advances discussed above as well as subsequent developments that are discussed in the next section.

## 5.1.2 From the War of the Currents to the Twenty-First Century

There is no general consensus concerning the year in which the transformer was invented, although it seems fair to ascribe its invention to the Hungarian engineers Zipernowski, Blàthi, and Dèri in 1984. However, there is little doubt that the introduction of transformers was the factor that ultimately caused AC power systems to become more convenient and therefore popular than DC power systems, even though Edison was a passionate supporter of the use of DC (which is as convenient as AC for powering filament lamps, and more convenient than AC for powering arc lamps).

We now consider some of the main steps that shaped the evolution of power systems towards those that are used today. In 1889, René Thury developed the first commercial HVDC transmission system in Europe. This system used hydroturbines on the Gorzente River to supply Genoa in Italy. The generators were connected in series to attain the high transmission voltages needed. When loads were added to the system, more generators were added to maintain the voltage at the load. The first long-distance transmission of DC electricity in the US occurred in 1889 at Willamette Falls Station in Oregon. A flood destroyed this station in 1890, but it was quickly rebuilt, and the Falls Electric Company replaced the DC generators with experimental AC generators from Westinghouse in the same year. In 1896, the construction of the first AC generation and transmission system was completed at Niagara Falls using Westinghouse equipment. Nikola Tesla's work, such as his invention of the induction motor in 1888, helped to make AC power systems increasingly attractive. But the event that marked the success of alternating current was a few years before 1896: The Frankfurt ex-



**Fig. 5.2** Thomas Edison's power station on Pearl Street (adapted from [5.34])

**Table 5.1** Key scientific advances and events (including dates and relevant scientists) that facilitated the development of power systems engineering

Primary cells	Generators
1800 – Volta (pile)	1831 – Faraday (electromagnetic (EM) induction)
1830 – Grove (Zn-Pt)	1832 – Pixii (rudimentary alternator)
1841 – Bunsen (Zn-C)	1856 – Siemens & Alliance
1877 – Leclanché (Zn-Mn)	1860 – Pacinotti (dynamo)
1881 – Thiebaut and Gassner	1869 – Gramme (dynamo)
Light sources (lamps)	Transformers, AC, and three-phase
1841 – Foucault (first arc lamp)	1884 – Zipernowski, Blàthi, and Dèri (transformer)
1876 – Jablochkov (arc lamp)	1888 – Ferraris (AC rotating field)
1878 – Edison (1879 Menlo Park)	1888 – Tesla (induction motor)
	1889 – Blàthi (induction meter)
	1891 – Dobrowolski (three-phase systems)

hibition in August 1891: three-phase transmission line (42 Hz) at 25 000 V, which started from the hydroelectric plant built for a cement factory in Lauffen, on the Neckar river and with a distance of 175 km reached Frankfurt. Promoted by industrialists such as George Westinghouse, the major advantages of AC electric utility services soon became obvious, so DC systems declined in popularity towards the end of the nineteenth century. The advent of the transformer, three-phase circuits, and the induction motor all helped to drive the adoption of AC electric systems as the global standard [5.35].

There are objective advantages of operating electric power systems using AC rather than DC. First, only AC systems can make use of transformers, which allow the same power to be transported at higher voltages and lower current amplitudes—thus minimizing power losses and voltage drops along power lines—and different voltage levels to be used for generation, transmission, distribution, and utilization. With AC, it is possible to implement three-phase networks, allowing smooth, nonpulsating power flows and easy interruption of current in high-voltage equipment. Also, induction motors—which are inexpensive, rugged, and can serve most of the needs of industrial and residential users—can be employed with AC power systems. Further, the advent of steam turbines (which work best at high speeds) made AC generators highly advantageous, as

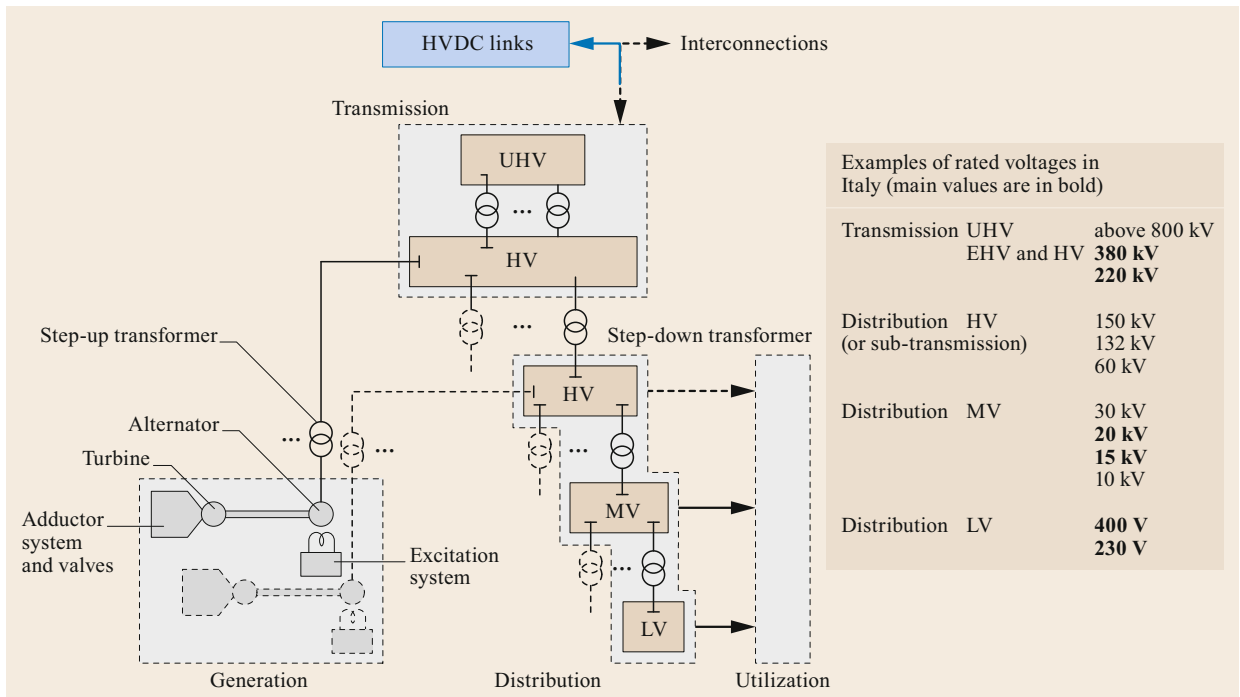
the commutators of DC motors and generators impose limitations on the voltage, size, and especially the speed of those machines.

Inventors such as Galileo Ferraris, Nicola Tesla, William Stanley, Michael von Dolivo-Dobrowolsky, Elihu Thomson, Lucien Gaulard, John Gibbs, and others working in Europe and North America all contributed to advances in AC technology. Much has been written about the so-called *War of the Currents* in the late 1880s, but it was more of a media fight; it was not a significant factor in the subsequent dominance of AC power systems [5.35]. The final decision on the type of system to be applied in a particular scenario has always been made based largely on technical aspects, and AC systems offered more advantages than DC systems given the system requirements and the technology available at that time. It should be noted, however, that although AC power systems have dominated around the world since the late nineteenth century, some DC distribution systems are still used in electric traction systems (trolley bus, railways, or subways). Also, some cities continued to use DC well into the twentieth century: Helsinki had a DC network until the late 1940s, Stockholm lost its dwindling DC network as late as the 1970s, London had some DC loads until 1981, and certain locations in Boston still used 110 V DC in the 1960s. The last DC circuit—a vestige of the nineteenth-century DC system of New York City—was shut down in 2007 [5.35].

## 5.2 Mission and Traditional Structure

The traditional mission of a power system is to provide electricity at the rated frequency and the rated voltage to customers. While the frequency is the same in all parts of the system, the rated voltage can differ depending on the part of the network of interest. The rated voltages of alternators located at power stations typically

range between 15 and 25 kV. Such voltages need to be substantially increased to 66–1000 kV or more by the step-up transformers that connect power stations to high-voltage (HV) and extra-high voltage (EHV) transmission networks (which are relatively well meshed) if the power is to be transmitted with minimal line losses



**Fig. 5.3** Basic elements of an electric power system in its traditional form (EHV, HV, MV, and LV refer to extra-high, high, medium, and low voltage, respectively; adapted from [5.9])

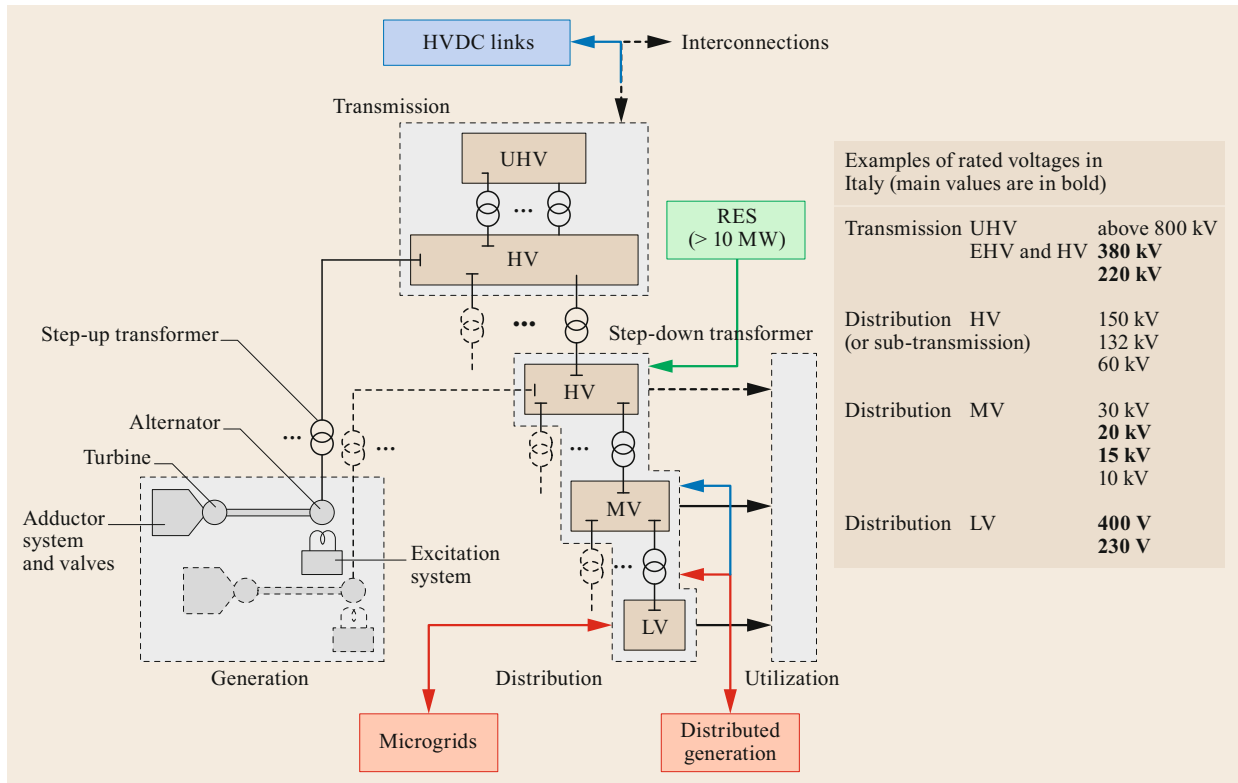
and voltage drops. A single generic HV or EHV line of the transmission network carries hundreds or even thousands of megawatts, possibly in both directions, depending on its operating conditions. Very large power systems (e.g., those of neighboring countries) are generally interlinked through their transmission networks. In some cases, HVDC links are employed to interconnect systems that are not synchronized with each other, to transmit power over very long distances, and for long underground/submarine links. The high-voltage part of the network is then connected to the *high-voltage distribution network*, which is frequently referred to as the *subtransmission network*, to carry power towards a load area. The geographical extent of the subtransmission network depends on the user density in the load area (the power typically ranges from a few megawatts to tens of megawatts for each HV distribution line). Electric power is then carried to each user via *medium-voltage (MV) distribution networks*, where each line can carry around a megawatt of power, and by *low-voltage (LV) distribution networks*. Such a structure is depicted in Fig. 5.3, which also shows possible interconnections with other networks.

We now consider the power system scenario in Italy, which is representative of the situation in quite a few

other countries. The aim of the power system in Italy is to meet the demand for electricity 24 h a day, 365 days a year. This demand arises from:

- 700 HV users (20%)
- 100 000 MV users (35%)
- 35 000 000 LV users (20% domestic, 25% others).

Up to the end of the twentieth century, this aim was accomplished using a number of thermal power plants equipped with steam turbines driven by traditional fuels (coal, oil, gas, etc.) or with gas turbines and/or hydroelectric plants (with a reservoir or basin, or the fluent-water type). Over the last couple of decades, however, the increasing popularity of so-called *distributed generation*, which often utilizes renewable energy sources, has led to some significant changes to the traditional power system structure. In Italy, as well as in many other countries, a considerable amount of power has been connected to the distribution network (LV and MV). To realize large power values (e.g., larger than 10 MW), renewable energy sources (RESs) must be connected directly to the HV network, which is in turn interconnected to the synchronous grid of continental Europe. This structure is depicted in Fig. 5.4; note the presence of *microgrids*—small networks of electricity



**Fig. 5.4** Basic elements of a modern electric power system; note the inclusion of distributed generation, which is connected to the MV and LV distribution networks, as well as the presence of microgrids and a massive amount of renewable energy sources (RES) that is connected to the HV network (adapted from [5.9])

users with a local source—that are usually attached to the centralized national grid but are also able to function independently. The relatively complex operation of modern networks such as this will be briefly addressed in Sect. 5.9.

In Italy, there are over 560 000 power plants (including thermal, hydro, and RES plants), one transmission system operator – Terna (<https://www.terna.it>), which is part of the European Network of Transmission System Operators for Electricity, ENTSO-E –, and 150 entities that are involved in distribution.

If an electric power system is to accomplish its mission, a number of classical issues must be addressed:

- Planning
- Unit commitment and economic dispatch (according to market constraints)
- Power flow
- Fault analysis and protection system design
- Frequency control and voltage control
- Stability
- Insulation coordination and protection against the effects of lightning and overvoltages
- Power quality.

Due to its introductory nature, this chapter will ignore all aspects relating to the planning of power systems and those concerning the generation of power (i.e., traditional power station or RES generating plant design, operation and control, unit commitment, and economic dispatch). Nor are power system relays, insulation coordination, protection against overvoltages, and power quality covered here; most of these topics are dealt with in other chapters of this handbook.

In what follows, we shall focus on the fundamentals of transmission line theory in both the steady-state and transient regimes, on power flow and fault analysis, on stability assessment, and on frequency (and voltage) control, in order to impart the technical background required to understand and develop modern power systems as well as upcoming power systems (the topic covered in the last section of the chapter).

### 5.3 Transmission Line Equations in the Steady State

#### 5.3.1 The Telegrapher's Equations

Let us consider a symmetrical, balanced, three-phase line in a sinusoidal steady state. By making these assumptions, we can refer to the positive-sequence single-phase equivalent model of the line. The relevant distributed parameter circuit is represented in Fig. 5.5. The infinitesimal element  $dx$  is located a distance  $x$  from the origin of the line. Therefore, the reference frame is oriented in the positive direction from the start of the line—where we can imagine a power source to be located (indicated by the subscript p)—to the end of the line, where the power arrives (indicated by the subscript a).

In Fig. 5.5,  $r$  and  $l$  are the resistance and inductance of the line per unit length, while  $c$  and  $g$  are the capacitance and conductance per unit length.

We define the primary parameters of the line as follows:

- Longitudinal impedance per unit length

$$\bar{z} = r + j\omega l \quad [\Omega \text{ m}^{-1}] \quad (5.1)$$

- Transverse admittance per unit length

$$\bar{y} = g + j\omega c \quad [\text{S m}^{-1}]. \quad (5.2)$$

#### Derivation and Integration of the Equations

Utilizing Steinmetz's symbolic notation and setting  $e(x, j\omega) = \bar{E}_x$  and  $i(x, j\omega) = \bar{I}_x$ , the line equations can be derived by applying Kirchhoff's voltage law to the positive-oriented loop in Fig. 5.5, thus obtaining (5.3) below, and Kirchhoff's current law to the bus, thus obtaining (5.4). In these equations, higher-order infinitesimals are neglected.

$$\frac{d\bar{E}_x}{dx} + \bar{z}\bar{I}_x = 0 \quad (5.3)$$

$$\frac{d\bar{I}_x}{dx} + \bar{y}\bar{E}_x = 0. \quad (5.4)$$

Differentiating (5.3) and (5.4) with respect to  $x$  yields the differential equations

$$\frac{d^2\bar{E}_x}{dx^2} + \bar{z}\frac{d\bar{I}_x}{dx} = 0 \quad (5.5)$$

$$\frac{d^2\bar{I}_x}{dx^2} + \bar{y}\frac{d\bar{E}_x}{dx} = 0. \quad (5.6)$$

Upon combining (5.5) with (5.4) and (5.6) with (5.3), we obtain

$$\frac{d^2\bar{E}_x}{dx^2} - \bar{z}\bar{y}\bar{E}_x = 0 \quad (5.7)$$

$$\frac{d^2\bar{I}_x}{dx^2} - \bar{z}\bar{y}\bar{I}_x = 0. \quad (5.8)$$

We define the following secondary parameters of the line:

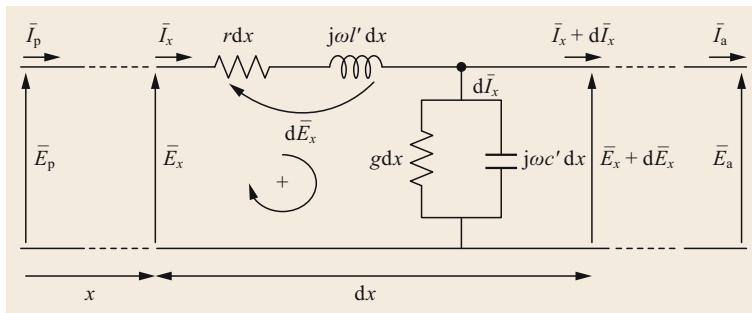
- Propagation constant

$$\bar{\gamma} = \sqrt{\bar{z}\bar{y}} = \alpha + j\beta = \sqrt{(r + j\omega l)(g + j\omega c)} \quad [\text{m}^{-1}] \quad (5.9)$$

- Characteristic impedance

$$\bar{Z}_0 = \sqrt{\frac{\bar{z}}{\bar{y}}} = \sqrt{\frac{r + j\omega l}{g + j\omega c}} \quad [\Omega]. \quad (5.10)$$

The real and imaginary parts of the characteristic impedance are the *attenuation constant*  $\alpha$  and the *phase or distortion constant*  $\beta$ , which are given by the expres-



**Fig. 5.5** Single-phase representation of a three-phase line in a symmetrical, balanced, sinusoidal steady state

sions

$$\alpha = \sqrt{\frac{1}{2} \left[ \sqrt{(r^2 + \omega^2 l^2)(g^2 + \omega^2 c^2)} + rg - \omega^2 lc \right]} \quad (5.11)$$

$$\beta = \sqrt{\frac{1}{2} \left[ \sqrt{(r^2 + \omega^2 l^2)(g^2 + \omega^2 c^2)} - rg + \omega^2 lc \right]} \quad (5.12)$$

It is worth noting that  $\alpha = 0$  and  $\beta = \omega \sqrt{lc}$  for a lossless line.

Under steady-state conditions and at a frequency of 50 Hz, typical values for the phase constant are as follows:

- Overhead line:  $\beta = 1 \times 10^{-6} \text{ rad m}^{-1}$
- Cable line:  $\beta = (3-5) \times 10^{-6} \text{ rad m}^{-1}$ .

When there are losses, typical values for the attenuation constant are as follows:

- Overhead line:  $\alpha = (0.05-0.5) \times 10^{-6} \text{ m}^{-1}$
- Cable line:  $\alpha = (0.2-2) \times 10^{-6} \text{ m}^{-1}$ .

If the primary line parameters are constant, the general integrals of (5.7) and (5.8) are

$$\bar{E}_x = \bar{K}_1 e^{\bar{\gamma}x} + \bar{K}_2 e^{-\bar{\gamma}x} \quad (5.13)$$

$$\bar{I}_x = \frac{1}{\bar{Z}_0} (-\bar{K}_1 e^{\bar{\gamma}x} + \bar{K}_2 e^{-\bar{\gamma}x}). \quad (5.14)$$

Alternatively, using hyperbolic functions, the solutions to (5.7) and (5.8) can be expressed as

$$\bar{E}_x = (\bar{C}_1 \cosh \bar{\gamma}x + \bar{C}_2 \sinh \bar{\gamma}x) \quad (5.15)$$

$$\bar{I}_x = \frac{1}{\bar{Z}_0} (-\bar{C}_1 \sinh \bar{\gamma}x - \bar{C}_2 \cosh \bar{\gamma}x). \quad (5.16)$$

The constants in (5.13)–(5.16) can be determined by setting appropriate boundary conditions; for instance, by fixing the conditions at the left termination of the line ( $\bar{E}_x|_{x=0} = \bar{E}_p$  and  $\bar{I}_x|_{x=0} = \bar{I}_p$ ).

If we impose these conditions and introduce (5.13) and (5.14), we obtain the system

$$\bar{E}_p = \bar{K}_1 + \bar{K}_2 \quad (5.17)$$

$$\bar{I}_p = \frac{1}{\bar{Z}_0} (-\bar{K}_1 + \bar{K}_2), \quad (5.18)$$

which yield

$$\bar{E}_x = \frac{1}{2} (\bar{E}_p - \bar{Z}_0 \bar{I}_p) e^{\bar{\gamma}x} + \frac{1}{2} (\bar{E}_p + \bar{Z}_0 \bar{I}_p) e^{-\bar{\gamma}x} \quad (5.19)$$

$$\bar{I}_x = \frac{1}{2} \left( \bar{I}_p - \frac{\bar{E}_p}{\bar{Z}_0} \right) e^{\bar{\gamma}x} + \frac{1}{2} \left( \bar{I}_p + \frac{\bar{E}_p}{\bar{Z}_0} \right) e^{-\bar{\gamma}x}. \quad (5.20)$$

On the other hand, if we use (5.15) and (5.16), we obtain

$$\bar{E}_p = \bar{C}_1 \quad (5.21)$$

$$\bar{I}_p = \frac{1}{\bar{Z}_0} (-\bar{C}_2), \quad (5.22)$$

which give

$$\bar{E}_x = \bar{E}_p \cosh \bar{\gamma}x - \bar{Z}_0 \bar{I}_p \sinh \bar{\gamma}x \quad (5.23)$$

$$\bar{I}_x = \bar{I}_p \cosh \bar{\gamma}x - \frac{\bar{E}_p}{\bar{Z}_0} \sinh \bar{\gamma}x. \quad (5.24)$$

It is worth noting that (5.19) and (5.20) are equivalent to (5.23) and (5.24), respectively.

Choosing a reference frame oriented in the opposite direction (i.e., with  $x$  increasing from the right terminal of the line to the left), the solutions to the line equations can be expressed by introducing a change of variable of the type  $\tilde{x} = -x$  into (5.19) and (5.20). Moreover, the boundary conditions for the left-hand side of the line ( $x = 0$ ) become  $\bar{E}_x|_{x=0} = \bar{E}_a$  and  $\bar{I}_x|_{x=0} = \bar{I}_a$ , leading to the equations

$$\bar{E}_x = \frac{1}{2} (\bar{E}_a + \bar{Z}_0 \bar{I}_a) e^{\bar{\gamma}x} + \frac{1}{2} (\bar{E}_a - \bar{Z}_0 \bar{I}_a) e^{-\bar{\gamma}x} \quad (5.25)$$

$$\bar{I}_x = \frac{1}{2} \left( \bar{I}_a + \frac{\bar{E}_a}{\bar{Z}_0} \right) e^{\bar{\gamma}x} + \frac{1}{2} \left( \bar{I}_a - \frac{\bar{E}_a}{\bar{Z}_0} \right) e^{-\bar{\gamma}x}. \quad (5.26)$$

Using hyperbolic functions, the expressions become

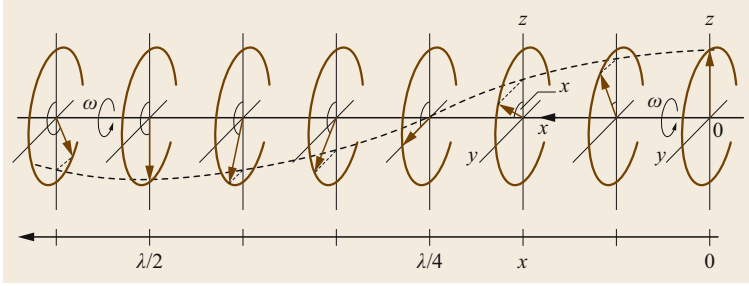
$$\bar{E}_x = \bar{E}_a \cosh \bar{\gamma}x + \bar{Z}_0 \bar{I}_a \sinh \bar{\gamma}x \quad (5.27)$$

$$\bar{I}_x = \bar{I}_a \cosh \bar{\gamma}x + \frac{\bar{E}_a}{\bar{Z}_0} \sinh \bar{\gamma}x. \quad (5.28)$$

### Direct and Inverse Waves

Let us consider the solutions to the line equations (5.25) and (5.26), where the positive  $x$  direction is oriented from the load to the generator (from right to the left). These equations show that either the voltage distribution or the current distribution can be considered the





**Fig. 5.6** Voltage distribution along an infinitely long lossless line in the steady state and at 50 Hz (adapted from [5.36])

result of two components. The first component, proportional to  $e^{\bar{\gamma}x}$ , is called the *direct wave*, which increases in the positive  $x$  direction. The second component, proportional to  $e^{-\bar{\gamma}x}$ , is called the *inverse wave* and decreases in the positive  $x$  direction. Similar considerations are valid for (5.27) and (5.28), where the positive  $x$  direction is oriented from the generator to the load.

With reference to (5.25), we set

$$\bar{E}_d = \frac{\bar{E}_a + \bar{Z}_0 \bar{I}_a}{2} \quad (5.29)$$

$$\bar{E}_r = \frac{\bar{E}_a - \bar{Z}_0 \bar{I}_a}{2}, \quad (5.30)$$

where the symbols have obvious meanings. The voltage at a generic point  $x$  along the line can then be expressed as

$$\bar{E}_x = \bar{E}_d e^{\bar{\gamma}x} + \bar{E}_r e^{-\bar{\gamma}x}. \quad (5.31)$$

The superposition of the direct and inverse waves determines the line operation and consequently the voltage and current distributions along the whole line.

Intuitively, all of these considerations for the voltage can also be applied to the current, which leads us to

$$\bar{I}_x = \frac{\bar{E}_d}{\bar{Z}_0} e^{\bar{\gamma}x} - \frac{\bar{E}_r}{\bar{Z}_0} e^{-\bar{\gamma}x}. \quad (5.32)$$

Finally, it should be noted that the inverse wave (i.e., the second terms of (5.19) and (5.20) or (5.25) and (5.26)) is equal to zero in the case of an infinitely long line.

### Propagation Wavelength and Propagation Speed

Let us consider the voltage distribution along a lossless line of infinite length under steady-state conditions and a frequency of 50 Hz. The propagation wavelength is defined as the distance  $\lambda$  such that

$$\lambda\beta = 2\pi \Rightarrow \lambda = \frac{2\pi}{\beta} \quad [\text{m}], \quad (5.33)$$

i.e., such that two measured voltage phasors separated by a distance of  $\lambda$  are in phase (i.e., the distance between two consecutive maxima in Fig. 5.6).

In the additional material for this chapter, there is an animation that demonstrates the voltage and current propagation (sinusoidal waveforms at the utility frequency) for a matched line and for a line terminated at a resistance that differs from the characteristic impedance.

The wave propagation speed as a function of the frequency  $f$  is

$$v = \lambda f = \frac{2\pi f}{\beta} = \frac{\omega}{\beta} \quad [\text{m s}^{-1}]. \quad (5.34)$$

For a lossless overhead line, the propagation speed is

$$v_a = \frac{\omega}{\beta} = \frac{1}{\sqrt{LC}} = \frac{1}{\sqrt{\mu_0 \epsilon_0}} = 3 \times 10^8 \quad [\text{m s}^{-1}]. \quad (5.35)$$

Therefore, the propagation speed is equal to the speed of light in vacuum and is not dependent on the line geometry. If losses cannot be ignored, the speed will be slightly lower.

The wavelength is inversely proportional to the frequency, so

$$\text{At 50 Hz: } \lambda_a = \frac{v}{f} = \frac{3 \times 10^8}{50} = 6 \times 10^6 \text{ m}$$

$$\text{At 60 Hz: } \lambda_a = \frac{v}{f} = \frac{3 \times 10^8}{60} = 5 \times 10^6 \text{ m}.$$

If losses are considered, these values will be slightly lower.

For a lossless cable line with a relative permittivity  $\epsilon_r = 3.5$ , the propagation speed and wavelength are calculated as

$$v_c = \frac{1}{\sqrt{3.5\mu_0\epsilon_0}} = 1.6 \times 10^8 \quad [\text{m s}^{-1}] \quad (5.36)$$

$$\lambda_c = \frac{v_c}{f} = \frac{1.6 \times 10^8}{50} = 3.2 \times 10^6 \quad [\text{m}]. \quad (5.37)$$

Let us consider a voltage wave with a generic profile for a generic angular frequency  $\omega$ . If the Heaviside condition  $r/g = l/c$  is respected, then  $\alpha = \sqrt{rg}$  and  $\beta = \omega\sqrt{lc}$ , therefore  $v = 1/\sqrt{lc}$ , which means that both  $\alpha$  and  $v$  are independent of  $\omega$ ; the transmitted voltage waveform along the line is not distorted, only attenuated. Although this fact is not relevant for power transmission lines at the utility frequency, it is important for telecommunication lines.

### Line Terminated with its Characteristic Impedance

Let us now consider a line with a load equal to the characteristic impedance  $\bar{Z}_0$ , such that

$$\bar{Z}_2 = \frac{\bar{E}_a}{\bar{I}_a} = \bar{Z}_0. \quad (5.38)$$

In this case, we obtain the important relationships

$$\begin{cases} \bar{E}_x = \bar{E}_a e^{\bar{y}x} \\ \bar{I}_x = \bar{I}_a e^{\bar{y}x} \\ \frac{\bar{E}_x}{\bar{I}_x} = \frac{\bar{E}_a}{\bar{I}_a} = \bar{Z}_0. \end{cases} \quad (5.39)$$

The propagation of voltage and current waves along a line that terminates on its characteristic impedance is equivalent to the case in which the line is infinitely long, since the ratio of the voltage to the current is the same at every point along the line. As a consequence, voltage and current waves that are directed to the load are not affected by any reflection.

For a lossless line, the characteristic impedance is a real quantity, and its value is expressed as

$$\bar{Z}_0 = \sqrt{\frac{l}{c}}. \quad (5.40)$$

In this particular case, the characteristic impedance is called the *surge impedance*.

Figures 5.7 and 5.8 show the value of the surge impedance in some practical cases.

### Natural Power

The complex power at the termination in the case where the line terminates on its characteristic impedance is given by

$$\begin{aligned} \bar{S}_{0a} &= P_{0a} + jQ_{0a} = 3\bar{E}_a\bar{I}_a^* = 3\bar{E}_a\frac{\bar{E}_a^*}{\bar{Z}_a} \\ &= \frac{V_a^2}{Z_0(\cos\psi - j\sin\psi)} = \frac{V_a^2}{Z_0}(\cos\psi + j\sin\psi). \end{aligned} \quad (5.41)$$

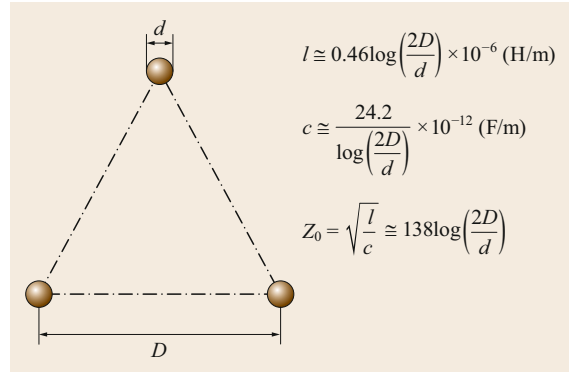


Fig. 5.7 Formulas for the positive sequence line parameters of lossless overhead transmission lines

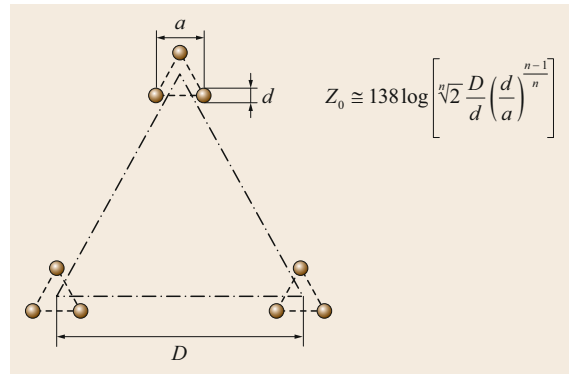


Fig. 5.8 Formulas for the positive sequence line parameters of lossless overhead transmission lines with bundle conductors

For a lossless line, we obtain

$$P_0 = \frac{V_a^2}{Z_0}, \quad (5.42)$$

which is called the *natural power*.

Under these conditions, the line transmits active power to the load without absorbing reactive power (the power factor is equal to 1), i.e.,

$$Z_0^2 = \frac{E_x^2}{I_x^2} = \frac{\omega dx}{\omega c dx}. \quad (5.43)$$

For each infinitesimal element of the line, we can observe that

$$\omega dx I_x^2 = \omega c dx E_x^2. \quad (5.44)$$

This equation gives perfect compensation between the electromagnetic energy and the electrostatic energy of the line (i.e., the line is compensated regarding the reactive power). Therefore, the voltage magnitude is

**Table 5.2** Typical surge impedance and characteristic power values for overhead lines

Voltage (kV)	Overhead line	
	$Z_0$ (P)	$P_0$ (MW)
20	400	1
50	400	6
132	400	44
220	390	124
380	260	560
700	240	2000
1000	240	≈ 4000

constant along the line. This represents ideal operating conditions for an overhead line (not for a cable line, as surge impedances are one order of magnitude lower in that case, so current values would be too high). Table 5.2 shows typical values of the surge impedance and characteristic power for overhead lines.

### 5.3.2 The Line as a Two-Port Network

A single conductor line in steady state can be represented as two port passive network as shown in Fig. 5.9, therefore voltage and currents at one port can be expressed as

$$\begin{aligned} \bar{E}_p &= \bar{A}\bar{E}_a + \bar{B}\bar{I}_a \\ \bar{I}_p &= \bar{C}\bar{E}_a + \bar{D}\bar{I}_a \end{aligned} \tag{5.45}$$

The system considered has two degrees of freedom, which are characterized by two independent relationships between four quantities (voltages and currents) that identify the electric states of the two pairs of terminals.

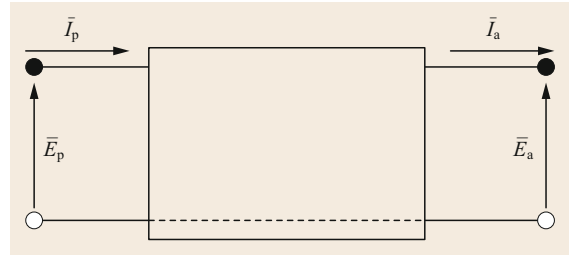
Using hyperbolic functions, the constants  $\bar{A}$ ,  $\bar{B}$ ,  $\bar{C}$ , and  $\bar{D}$  can be expressed as

$$\begin{cases} \bar{A} = \bar{D} = \cosh \bar{\gamma}L \\ \bar{B} = \bar{Z}_0 \sinh \bar{\gamma}L \\ \bar{C} = \frac{1}{\bar{Z}_0} \sinh \bar{\gamma}L \end{cases} \tag{5.46}$$

The constants  $\bar{A}$ ,  $\bar{B}$ ,  $\bar{C}$ , and  $\bar{D}$  are called *chain matrix parameters*. It is easy to verify that the two-port network is symmetric ( $\bar{A} = \bar{D}$ ) and reciprocal ( $\bar{A}\bar{D} - \bar{B}\bar{C} = 1$ ).

The chain matrix parameters have the following characteristics:

- Constant  $\bar{A}$ : the ratio between the input and output voltages of the open line or between the input and output currents of the short-circuited line. This constant is a pure number and can be expressed via



**Fig. 5.9** Two-port network representation of a transmission line

the Cartesian coordinates  $a_1 + ja_2$  ( $a_1 < 1; a_2 \ll 1$ ) or the polar coordinates  $Ae^{j\alpha_A}$ .

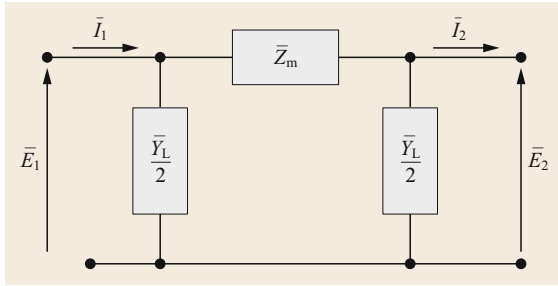
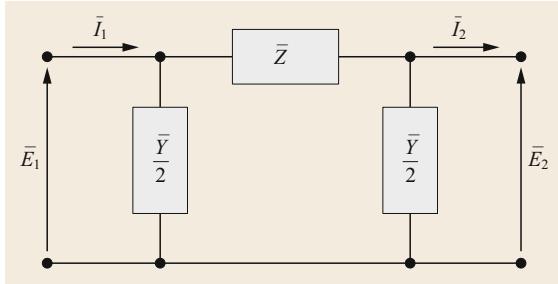
- Constant  $\bar{B}$ : the ratio of the input voltage to the output current of the short-circuited line. This ratio has the dimensions of an impedance and can be expressed via the Cartesian coordinates  $b_1 + jb_2$  ( $b_1 \approx rL = R; b_2 \approx xL = X$ ) or the polar coordinates  $B e^{j\beta_B}$  ( $\bar{B} \approx \bar{Z}$ , the total longitudinal impedance of the line).
- Constant  $\bar{C}$ : the ratio between the input current and the output voltage of the open line. It has the dimensions of an admittance and can be expressed via the Cartesian coordinates  $c_1 + jc_2$  ( $c_1$  is really small and usually negative when the line is really long, and  $c_2 \approx B$  is the susceptance of admittance  $Y$ ) or the polar coordinates  $C e^{j\gamma_C}$  ( $\bar{C} \approx \bar{Y}$ , the total transverse admittance of the line). A passive reciprocal two-port network can always be represented by three impedances or admittances that are connected to form a  $\Pi$  circuit, as represented in Fig. 5.10, or a T circuit. The equations relevant to the equivalent  $\pi$  circuit of a generic line are

$$\begin{aligned} \bar{Y}_L &= \bar{Y} \frac{\tanh(\bar{\gamma}L/2)}{\bar{\gamma}L/2} \\ \bar{Z}_m &= \bar{Z} \frac{\sinh \bar{\gamma}L}{\bar{\gamma}L} \end{aligned} \tag{5.47}$$

For lines with typical lengths (i.e.,  $50 \text{ km} < L < 200 \text{ km}$ ) in the steady state, we can assume that  $\sinh \bar{\gamma}L \approx \bar{\gamma}L$  and  $\tanh(\bar{\gamma}L/2) \approx \bar{\gamma}L/2$ , which in turn yield

$$\begin{aligned} \bar{Y}_a &= \bar{Y}_b = \bar{Y} \\ \bar{Z}_m &= \bar{Z} \end{aligned} \tag{5.48}$$

In this case the calculation of the parameters of the equivalent circuit is simplified, as shown in Fig. 5.11.

Fig. 5.10 Equivalent  $\pi$  circuit of a transmission lineFig. 5.11 Equivalent  $\pi$  circuit of a short transmission line

### 5.3.3 Transmitted Active and Reactive Power Expressions

Let us consider the equations

$$\begin{aligned}\bar{E}_p &= \bar{A}\bar{E}_a + \bar{B}\bar{I}_a \\ \bar{I}_p &= \bar{C}\bar{E}_a + \bar{D}\bar{I}_a\end{aligned}\quad (5.49)$$

which are relevant to the phasor diagram of Fig. 5.12. This phasor diagram is known as a Perrine–Baum diagram.

When the line is open, we can see that  $E_p < E_a$  (known as the Ferranti effect).

The voltage drop along the line varies with the load; e.g.,

$$\begin{aligned}P_a + jQ_a(R) &\rightarrow \text{voltage drop} = 21\% \\ P_a(R') &\rightarrow \text{voltage drop} = 6\%.\end{aligned}$$

In order to compensate for the voltage drop by keeping the absorbed active power  $P_a$  constant, it is necessary to ensure that the end of phasor  $E_p$  coincides with  $R''$ . In this configuration, the load has to be capacitive. We should therefore generate the reactive power  $Q = RR''$  at the end of the line. The fraction  $RR'$  is absorbed by the load, while the fraction  $R'R''$  is necessary to compensate for the reactive power absorbed by the line.

### Some Remarks on the Transmitted Active and Reactive Power

The absolute value of the complex power at the end of the line is (superscript \* for phasors denotes their conjugate)

$$\bar{S}_a = P_a + jQ_a = 3\bar{E}_a\bar{I}_a^* \quad (5.50)$$

Observing that

$$\begin{aligned}\bar{E}_p &= \bar{A}\bar{E}_a + \bar{B}\bar{I}_a \Rightarrow \bar{I}_a = \frac{\bar{E}_p - \bar{A}\bar{E}_a}{\bar{B}} \\ \Rightarrow \bar{S}_a &= 3\bar{E}_a \left( \frac{\bar{E}_p - \bar{A}\bar{E}_a}{\bar{B}^*} \right),\end{aligned}\quad (5.51)$$

assuming that  $\bar{E}_a$  is real, and introducing  $\theta$  as the phase difference between  $\bar{E}_p$  and  $\bar{E}_a$ , we obtain

$$\begin{aligned}\bar{S}_a &= P_a + jQ_a = 3 \frac{\bar{E}_a \bar{E}_p^*}{\bar{B}^*} - 3 \frac{\bar{E}_a \bar{E}_a \bar{A}^*}{\bar{B}^*} \\ &= 3 \frac{E_a E_p}{B} \frac{e^{-j\theta}}{e^{-j\beta_B}} - 3 \frac{E_a^2 A}{B} \frac{e^{-j\alpha_A}}{e^{-j\beta_B}} \\ &= 3 \frac{E_a E_p}{B} e^{j(\beta_B - \theta)} - 3 E_a^2 \frac{A}{B} e^{j(\beta_B - \alpha_A)} \\ &= \frac{3E_a E_p}{B} \cos(\beta_B - \theta) - 3E_a^2 \frac{A}{B} \cos(\beta_B - \alpha_A) \\ &\quad + j \left[ \frac{3E_a E_p}{B} \sin(\beta_B - \theta) - 3E_a^2 \frac{A}{B} \sin(\beta_B - \alpha_A) \right].\end{aligned}\quad (5.52)$$

Therefore,

$$P_a = \frac{3E_a E_p}{B} \cos(\beta_B - \theta) - 3E_a^2 \frac{A}{B} \cos(\beta_B - \alpha_A) \quad (5.53)$$

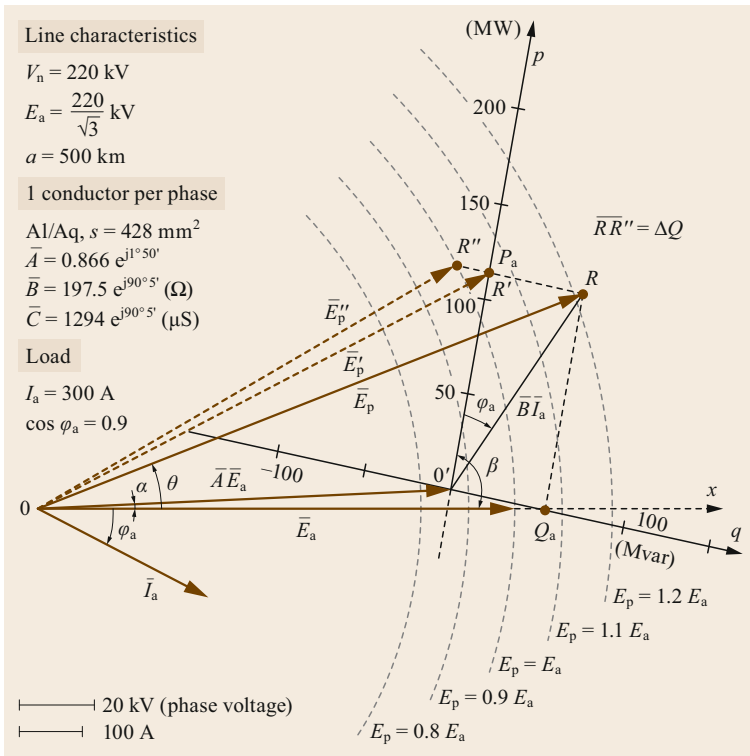
$$Q_a = \frac{3E_a E_p}{B} \sin(\beta_B - \theta) - 3E_a^2 \frac{A}{B} \sin(\beta_B - \alpha_A) \quad (5.54)$$

$$P_p = -\frac{3E_a E_p}{B} \cos(\beta_B + \theta) + 3E_p^2 \frac{A}{B} \cos(\beta_B - \alpha_A) \quad (5.55)$$

$$Q_p = -\frac{3E_a E_p}{B} \sin(\beta_B + \theta) + 3E_p^2 \frac{A}{B} \sin(\beta_B - \alpha_A). \quad (5.56)$$

If the line is lossless and transverse capacities are neglected ( $\alpha_A = 0$ ,  $A = 1$ ,  $\beta_B = \pi/2$ , and  $B = X$ ), the expressions assume the simplified forms

$$P_p = P_a = \frac{3E_p E_a}{X} \sin \theta \quad (5.57)$$



**Fig. 5.12** Perrine–Baum diagram (adapted from [5.3])

$$P_p = P_a = \frac{3E_p E_a}{X} \sin \theta \tag{5.58}$$

$$Q_a = \frac{3E_a}{X} (E_p \cos \theta - E_a) \tag{5.59}$$

$$Q_p = \frac{3E_p}{X} (E_p - E_a \cos \theta), \tag{5.60}$$

which leads us to conclude that:

- The active power flow  $P$  is proportional to the sine of the phase shift  $\theta$  (i.e., the difference between the voltage phases of the line terminals).
- The reactive power flow  $Q$  is proportional to the difference between the magnitudes of the voltages at the line terminals, and the sign of  $Q$  also depends on that difference. Note that the function  $\cos \theta$  does not vary much for small values of the argument (typically,  $\theta = 10\text{--}25^\circ$ ).

## 5.4 Load Flow

### 5.4.1 From the Real Network to the Admittance Matrix

A classical transmission network essentially comprises:

- *Buses*, which may be divided into *generation buses* (corresponding to the terminals of the alternators or, in general, the electric power sources), *reactive compensation buses* (corresponding to synchronous and static compensator terminals), *interconnection buses* (where many lines are connected to each other), and *load buses* (which supply the equivalent loads seen by the high-voltage network)
- *Capacitor banks*
- *Transformers*

- *Reactors*
- *Lines*; either overhead lines or cable lines that connect the various buses.

The study can be simplified by focusing only on the high-voltage part of the network and assuming that the parts at lower voltages, namely the distribution network, can be represented by their equivalent concentrated loads. Even so, the network is remarkably complex; for example, the Italian 380–220 kV network shown in Figs. 5.13 and 5.14 contains hundreds of buses, while the inclusion of the 132 kV network boosts this up to a thousand buses.

For the load flow study (also commonly denoted as power flow study) a number of assumptions are made.



**Fig. 5.13** Italian 380 kV network on 31.12.2018 (<https://www.terna.it>)

The three-phase symmetric and balanced network is in its steady state; the parameters and the configuration of the system as well as the load power request are considered to be constant. We also assume all the electric components are linear. All voltages, power flows, and impedances will be represented by their per-unit values. The active power injected by the generators at the buses is known.

Based on these assumptions, the load flow problem consists of determining the real and reactive power flowing in various components of the network (lines and transformers) under steady-state conditions. As the structure of the system and the values of the admittances of the network are known, the real and reactive power flow on each branch as well as the reactive power output of the generators can be determined analytically once the bus voltages are known. For this reason, the goal of a load-flow study is to determine voltage phase and magnitude values for each bus of a power system.

There are several reasons we need load-flow studies:

(a) To determine—on a daily basis, or more precisely every quarter of an hour—the network operating

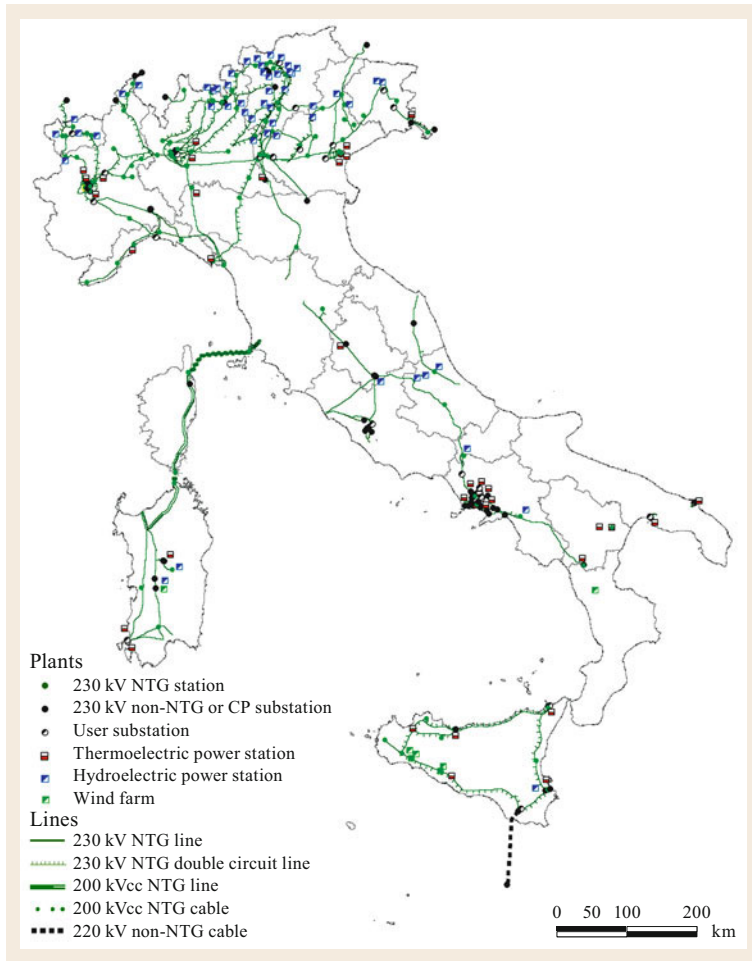
conditions that best satisfy the required load under secure conditions and with the minimum operational cost

- (b) To plan the expansion of a power system (either *long- or medium-term planning*, in which plans are made for 5–15 years into the future, or *short-term planning*, in which the plans are made for 1–3 years ahead)
- (c) To monitor and control the network in *real time*.

### Nodal Analysis of the Network

Nodal analysis of the network involves determining the voltages at the various nodes (buses) of the network in terms of the branch currents. It is important to bear in mind that each component of the network can be replaced by its  $n$ -port representation, as shown in Fig. 5.15.

Using the assumptions mentioned above, let us consider a generic bus of a network containing  $n + 1$  buses, including  $g$  generation buses and  $u$  load buses, as shown in Fig. 5.16. Conductor  $n + 1$  is the reference bus or *neutral*. Note that buses that are neither generation nor load buses (interconnection buses) can be seen as either



**Fig. 5.14** Italian 230 kV network on 31.12.2018 (<https://www.terna.it>)

generation or load buses with zero active and reactive power injected or absorbed, respectively. The total number of buses in the network,  $n + 1$ , is not necessarily equal to  $g + u + 1$ , as we need to have at least one bus that is not a generation or load bus. The network consists of  $m$  branches, each of which is characterized by a single linear admittance.

For the generic bus, or node  $i$ , we shall make use of the following notation:

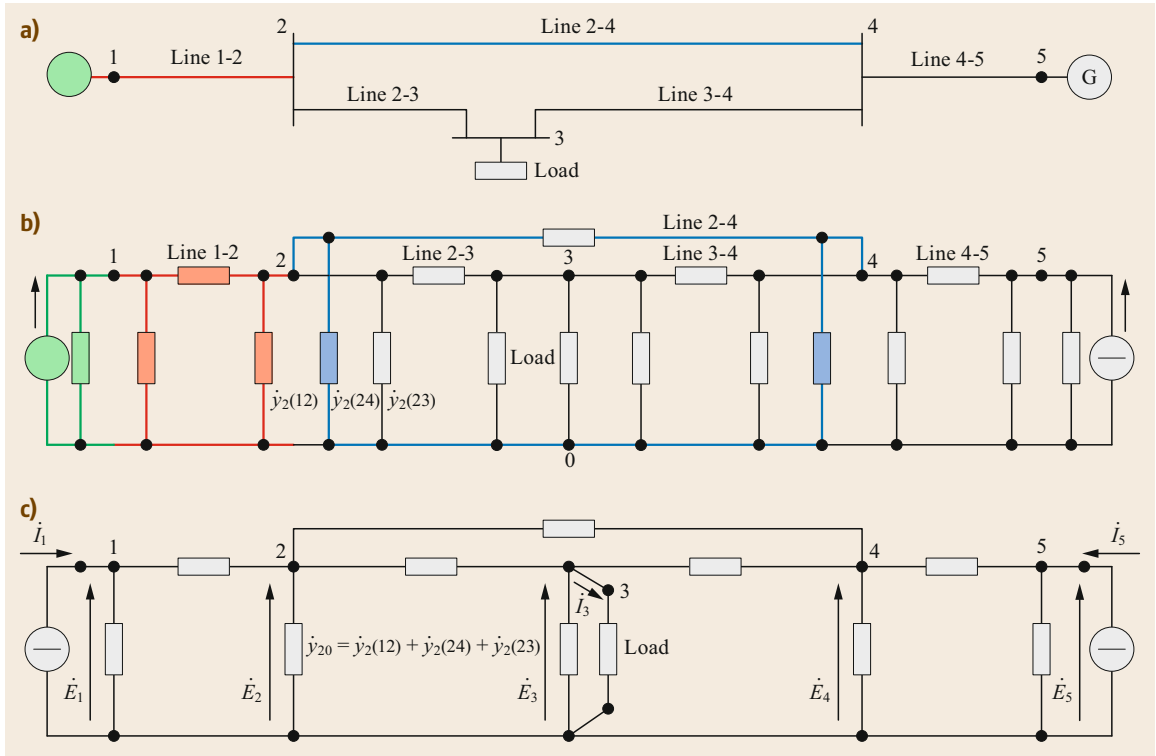
- $E_i$  is the bus voltage
- $I_i$  is the nodal current (i.e., the current supplied by the generator or absorbed by the load connected to the bus)
- $I_{ij}$  is the current flowing in the branch that connects node  $i$  to node  $j$
- $y_{ij}$  is the admittance between nodes  $i$  and  $j$
- $y_{i0}$  is the sum of all the admittances between the  $i$ th node and the neutral.

For the currents flowing in the branches connected to node  $i$ , we get

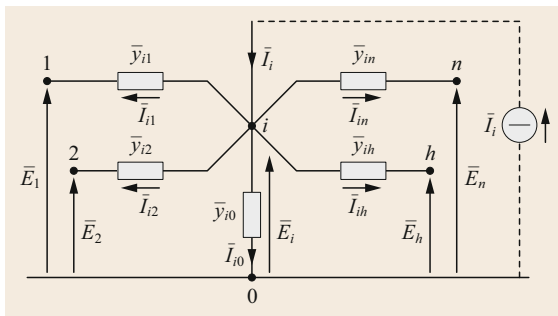
$$\begin{cases} \bar{I}_{i0} = \bar{y}_{i0} \bar{E}_i \\ \bar{I}_{i1} = \bar{y}_{i1} (\bar{E}_i - \bar{E}_1) \\ \vdots \\ \bar{I}_{in} = \bar{y}_{in} (\bar{E}_i - \bar{E}_n), \end{cases} \quad (5.61)$$

and by using the Kirchoff law, we obtain

$$\begin{aligned} \bar{I}_i &= \bar{y}_{i0} \bar{E}_i + \bar{y}_{i1} (\bar{E}_i - \bar{E}_1) + \cdots + \bar{y}_{in} (\bar{E}_i - \bar{E}_n) \\ &= (\bar{y}_{i0} + \bar{y}_{i1} + \cdots + \bar{y}_{in}) \bar{E}_i - \bar{y}_{i1} \bar{E}_1 - \cdots - \bar{y}_{in} \bar{E}_n \\ &= (\bar{y}_{i0} + \bar{y}_{i1} + \cdots + \bar{y}_{in}) \bar{E}_i - \sum_{\substack{h=1 \\ h \neq i}}^n \bar{y}_{ih} \bar{E}_h. \end{aligned} \quad (5.62)$$



**Fig. 5.15** (a) One-line diagram of a three-bus power network (buses 3, 4, and 5) with two generators (connected at buses 1 and 5) that supply one equivalent load impedance (connected at bus 3). (b) Relevant circuit representation where each generator is represented by its Norton equivalent one-port circuit and each line is represented by its two-port p equivalent circuit, and (c) simplified version of this circuit in which line admittances connected to the same bus have been added to each other. Voltage, current, and admittance symbols with dots are complex quantities (adapted from [5.2])



**Fig. 5.16** Network presentation used for nodal analysis

Setting

$$\begin{aligned} \bar{Y}_{ii} &= \bar{y}_{i0} + \bar{y}_{i1} + \dots + \bar{y}_{in} = \sum_{h=0}^n \bar{y}_{ih} \\ \bar{Y}_{i1} &= -\bar{y}_{i1} \\ &\vdots \\ \bar{Y}_{in} &= -\bar{y}_{in}, \end{aligned} \tag{5.63}$$

we get

$$\begin{aligned} \bar{I}_i &= \bar{Y}_{i1}\bar{E}_1 + \bar{Y}_{i2}\bar{E}_2 + \dots + \bar{Y}_{ii}\bar{E}_i + \dots + \bar{Y}_{in}\bar{E}_n \\ &= \sum_{h=1}^n \bar{Y}_{ih}\bar{E}_h \end{aligned} \tag{5.64}$$

and, analogously for the other buses,

$$\begin{cases} \bar{I}_1 = \bar{Y}_{11}\bar{E}_1 + \dots + \bar{Y}_{1h}\bar{E}_h + \dots + \bar{Y}_{1n}\bar{E}_n \\ \vdots \\ \bar{I}_h = \bar{Y}_{h1}\bar{E}_1 + \dots + \bar{Y}_{hh}\bar{E}_h + \dots + \bar{Y}_{hn}\bar{E}_n \\ \vdots \\ \bar{I}_n = \bar{Y}_{n1}\bar{E}_1 + \dots + \bar{Y}_{nh}\bar{E}_h + \dots + \bar{Y}_{nn}\bar{E}_n. \end{cases} \tag{5.65}$$



These equations can be conveniently written in matrix form as

$$\begin{bmatrix} \bar{I}_1 \\ \vdots \\ \bar{I}_h \\ \vdots \\ \bar{I}_n \end{bmatrix} = \begin{bmatrix} \bar{Y}_{11} & \dots & \bar{Y}_{1h} & \dots & \bar{Y}_{1n} \\ \vdots & \vdots & \vdots & \vdots & \vdots \\ \bar{Y}_{h1} & \dots & \bar{Y}_{hh} & \dots & \bar{Y}_{hn} \\ \vdots & \vdots & \vdots & \vdots & \vdots \\ \bar{Y}_{n1} & \dots & \bar{Y}_{nh} & \dots & \bar{Y}_{nn} \end{bmatrix} \cdot \begin{bmatrix} \bar{E}_1 \\ \vdots \\ \bar{E}_h \\ \vdots \\ \bar{E}_n \end{bmatrix}. \quad (5.66)$$

Using a compact notation, we get

$$[\mathbf{I}] = [\mathbf{Y}] [\mathbf{E}], \quad (5.67)$$

where  $\bar{\mathbf{Y}}$  is the *admittance matrix* of the network.

The elements of  $\bar{\mathbf{Y}}$  satisfy a number of conditions (see also (5.63)), as follows.

The off-diagonal elements  $\bar{Y}_{ij}$  are called *mutual admittances* of the buses, and each equals the negative of the sum of all admittances connected directly between the buses  $i$  and  $j$ , i.e.,

$$\bar{Y}_{ij} = -\bar{y}_{ij} = \bar{I}_i \Big|_{\substack{\bar{E}_j=1 \\ \bar{E}_h=0 \ \forall h \neq j}}. \quad (5.68)$$

The diagonal elements  $\bar{Y}_{ii}$  are called *self-admittances* of the buses, and each equals the sum of all the admittances connected to the buses identified by double subscripts, i.e.,

$$\bar{Y}_{ii} = \bar{y}_{i0} + \sum \bar{y}_{ij} = \bar{I}_i \Big|_{\substack{\bar{E}_i=1 \\ \bar{E}_j=0 \ \forall j \neq i}}. \quad (5.69)$$

The calculation of the admittance matrix is demonstrated as an exercise in the supplementary material for this chapter.

### Admittance Matrix Update

The previous equations provide the relationship between the bus impedance and the admittance matrix. However, it is possible for the topology of the power system to change due to the connection or disconnection of a line, a transformer, etc. Below, we show that it is not necessary to redetermine the admittance matrix from scratch in this case. Before doing so, however, we examine the three basic changes that can occur to an  $n$ -bus network:

1. *The addition of bus  $n+1$ , which is connected to the generic bus  $k$  with an admittance  $\bar{y}_{n+1,k}$ .*

The updated matrix order is now  $n+1$ .

Bus  $k$  is the only bus adjacent to the new bus. Therefore, the only change in the matrix is the  $k$ th self-admittance.

By denoting the parameters of the updated matrix with a prime symbol, we get

$$\begin{aligned} \bar{Y}'_{k,k} &= \bar{Y}_{k,k} + \bar{y}_{n+1,k} \\ \bar{Y}'_{n+1,n+1} &= \bar{y}_{n+1,k} \\ \bar{Y}'_{n+1,k} &= \bar{Y}'_{k,n+1} = -\bar{y}_{n+1,k}. \end{aligned} \quad (5.70)$$

All the other elements of the  $(n+1)$ th row and column of matrix  $[\bar{\mathbf{Y}}']$  are equal to zero.

2. *The addition of an admittance  $\bar{y}^*_{k,0}$  from an existing bus  $k$  to the reference bus.*

In this case, the matrix order does not change. The only term that must be updated is the self-admittance of bus  $k$ , i.e.,

$$\bar{Y}'_{k,k} = \bar{Y}_{k,k} + \bar{y}^*_{k,0}. \quad (5.71)$$

3. *The addition of an admittance  $\bar{y}^*_{k,i}$  between two generic buses  $k$  and  $i$ .*

Again, the matrix order does not change; the only terms that need to be updated are the self-admittances of buses  $k$  and  $i$  and their relative mutual admittances such that

$$\begin{aligned} \bar{Y}'_{k,k} &= \bar{Y}_{k,k} + \bar{y}^*_{k,i} \\ \bar{Y}'_{i,i} &= \bar{Y}_{i,i} + \bar{y}^*_{k,i} \\ \bar{Y}'_{k,i} &= \bar{Y}'_{i,k} = \bar{Y}_{i,k} - \bar{y}^*_{k,i}. \end{aligned} \quad (5.72)$$

When appropriately combined and repeated, the three basic operations described above allow the admittance matrix to be updated for any physical modification of the network configuration.

Let us now consider a few typical cases:

- A line (represented by its  $\pi$ -equivalent two-port circuit) is added between two existing buses  $k$  and  $i$ . In this case, operation (2) is applied twice and operation (3) once.
- A new line (represented by its  $\pi$ -equivalent two-port circuit) is added that connects an existing bus  $k$  in the network with a new bus  $(n+1)$ . Here, operation (1) is applied once and operation (2) twice.
- A line between two buses is disconnected. Removing a branch is equivalent to adding admittances with opposite values to the admittances that are already present in the network. Hence, this case is analogous to the first one, but with opposite admittance values.

### 5.4.2 The Equations

In an  $n$ -bus system, the  $n$  voltages and the  $n$  complex currents are related by  $n$  equations with complex variables and coefficients. These relationships comprise the *internal or network constraints*. The  $2n$  complex voltages and currents are equivalent to  $4n$  real variables. On the other hand, the  $n$  equations with complex variables and coefficients are equivalent to  $2n$  linear equations with real variables and coefficients that can be obtained by separating the real and imaginary parts (or magnitudes and arguments). Thus, among the  $4n$  real variables,  $2n$  can be set arbitrarily, and the remaining  $2n$  can be calculated by solving the system of network equations.

When the solution to the system of equations has been evaluated and the bus voltages and currents have been determined, the active and reactive power absorbed and injected in the buses along with the power and current flows along the lines and the active and reactive power losses can be determined relatively simply. If the operating conditions of the network can be effectively represented by imposing only RMS values and phases of bus voltages and currents as external constraints, it follows from the above discussion that the power flows can be calculated by solving a system of linear equations.

In practice, the operating conditions imposed on the networks—the *external constraints*—are expressed by setting other quantities. This implies that the system of equations to be solved becomes nonlinear, as will be clarified shortly.

In particular:

- For *load buses*, the quantities that are generally set are the active and reactive power required at the buses:  $P_i^*$  and  $Q_i^*$ . It is worth noting that the use of constant admittances to represent loads is not generally appropriate. Consider, for instance, asynchronous motors, which absorb active power almost independently of the voltage (for voltage variations of  $\pm 10\%$ ), thus conflicting with the quadratic law that applies to impedances. Moreover, the dependence on the voltage is expressed by the general relations

$$P = P_0 \left( \frac{V}{V_0} \right)^{\alpha_p} \quad (5.73)$$

$$Q = Q_0 \left( \frac{V}{V_0} \right)^{\alpha_q}, \quad (5.74)$$

where the values of the exponentials depend on the nature of the load (they vary between 0 and 2).

- For *generation buses*, it is convenient to set the generated active power  $P_i^*$  and the RMS value of the voltage at their terminals  $E_i^*$ . The power  $P_i^*$  is assumed to be equal to the power that each generation unit must provide in accordance with the optimal repartition plan of the total grid demand among all production plants (namely the result of the *dispatching problem*, which will be briefly summarized at the end of this section). Setting the voltage  $E_i^*$  instead of the reactive power  $Q_i^*$  is convenient for various reasons. First, fixing the voltage value (at a value between  $E_n$  and  $1.1E_n$ , depending on the distance between the generation bus and the loads) leads to rapid convergence of the numerical procedure that is used to solve the nonlinear system of equations. Second, the reactive power of each generator can be varied by acting on the excitation system. Clearly, it will then be necessary to check that the upper and lower limits on  $Q$  imposed by the capability curves of each generator are not exceeded, and—more generally—that the maximum active and reactive power loadings can be supplied without exceeding the heating limits of each generator.

It is important to realize that it is not possible to fix the active power at an arbitrary value for each and every generation and load bus simultaneously. This would be equivalent to arbitrarily fixing the power losses of the network, which actually depend on the solution we are seeking. It is therefore possible to fix a maximum of  $(n-1)$  active power values. It is useful to fix the magnitude and the phase of the voltage for the  $n$ th bus, which is commonly termed the *slack bus*. The real power at this bus will be equal and opposite to the sum of all real load powers, all of the network losses, and all the real powers of the other generators. The slack bus is commonly considered to be a generation bus with a high capability for real power generation, and it is also the phase-reference bus ( $\arg(\bar{E}) = 0$ ).

Table 5.3 summarizes the types of buses that we have defined so far.

Because the operating conditions of the grids (external constraints) are expressed mainly by setting power

**Table 5.3** Types of buses used in a power network, and relevant electric quantities to be imposed and determined

Type of bus	Fixed quantities ( $2n$ )		Quantities to be determined ( $2n$ )	
Generation buses	$P_G$	$E_G$	$Q_G$	$\arg(E_G)$
Load buses	$P_L$	$Q_L$	$E_L$	$\arg(E_L)$
Slack bus	$E_n$	$\arg(E_n) = 0$	$P_n$	$Q_n$

values rather than currents, we can conclude from the above considerations that the equation system to be solved becomes nonlinear, as further clarified below.

### Cartesian Coordinates

The following notation will be used for the equations in Cartesian coordinates

$$\begin{aligned}\bar{E}_i &= E'_i + jE''_i && \text{voltage at bus } i \\ \bar{E}_h &= E'_h + jE''_h && \text{voltage at bus } h \\ \bar{Y}_{ih} &= G_{ih} + jB_{ih} && \text{element } ih \text{ of admittance matrix } [\bar{\mathbf{Y}}],\end{aligned}\quad (5.75)$$

where the meanings of the symbols are obvious.

The complex power injected or absorbed at each bus is

$$\bar{S}_i = P_i + jQ_i = \bar{E}_i \bar{I}_i. \quad (5.76)$$

Given that

$$\bar{I}_i = \sum_{h=1}^n \bar{Y}_{ih} \bar{E}_h \Rightarrow \bar{I}_i = \sum_{h=1}^n \underline{Y}_{ih} \underline{E}_h, \quad (5.77)$$

(5.76) becomes

$$\begin{aligned}\bar{S}_i &= \bar{E}_i \sum_{h=1}^n \underline{Y}_{ih} \underline{E}_h \\ &= (E'_i + jE''_i) \sum_{h=1}^n (G_{ih} - jB_{ih})(E'_h - jE''_h).\end{aligned}\quad (5.78)$$

The active and reactive powers of the  $i$ th node will therefore be expressed as

$$\begin{cases} P_i = E'_i \sum_{h=1}^n (G_{ih} E'_h - B_{ih} E''_h) \\ \quad + E''_i \sum_{h=1}^n (B_{ih} E'_h + G_{ih} E''_h) \\ Q_i = -E'_i \sum_{h=1}^n (B_{ih} E'_h + G_{ih} E''_h) \\ \quad + E''_i \sum_{h=1}^n (G_{ih} E'_h - B_{ih} E''_h). \end{cases}\quad (5.79)$$

Recall that  $g$  and  $u$  are used to indicate the number of generator nodes and users (loads), respectively. Since we also need to account for one slack bus, it follows that  $g + u = n - 1$ .

In Cartesian coordinates, the entire system of equations takes the form

$$\begin{cases} E''_i = 0 \\ i = n \text{ for slack bus only} \\ E_i^{*2} = E_i'^2 + E_i''^2 \\ i = 1, 2, \dots, g + i = n \text{ for } g \text{ generation buses} \\ \quad + \text{slack bus} \\ P_i^* = E'_i \sum_{h=1}^n (G_{ih} E'_h - B_{ih} E''_h) \\ \quad + E''_i \sum_{h=1}^n (B_{ih} E'_h + G_{ih} E''_h) \\ i = 1, 2, \dots, g + u \text{ for generation buses} \\ \quad + u \text{ load buses} \\ Q_i^* = -E'_i \sum_{h=1}^n (B_{ih} E'_h + G_{ih} E''_h) \\ \quad + E''_i \sum_{h=1}^n (G_{ih} E'_h - B_{ih} E''_h) \\ i = g + 1, \dots, g + u \text{ for load buses,} \end{cases}\quad (5.80)$$

where an asterisk indicates a quantity that is set (i.e., imposed by the transmission system operator). Thus, we eventually obtain  $1 + (g + 1) + (g + u) + u = 2(g + u + 1) = 2n$  equations.

### Polar Coordinates

The following notation will be used for the equations in polar coordinates, where  $\varphi_i$  and  $\theta_i$  are the arguments of the current and the voltage of the  $i$ th bus, respectively, and  $\gamma_{ih}$  is the argument of the admittance  $\bar{Y}_{ih}$ :

- $\bar{E}_i = E_i e^{j\theta_i}$  is the voltage of the  $i$ th bus
- $\bar{I}_i = I_i e^{j\varphi_i}$  is the current of the  $i$ th bus
- $\bar{Y}_{ih} = Y_{ih} e^{j\gamma_{ih}}$  is element  $ih$  of the admittance matrix.

The complex power injected or absorbed at each bus is

$$\bar{S}_i = P_i + jQ_i = \bar{E}_i \bar{I}_i. \quad (5.81)$$

Thus, using (5.67) for the current, we get

$$\begin{aligned}\bar{S}_i &= \bar{E}_i \sum_{h=1}^n \underline{Y}_{ih} \underline{E}_h = \sum_{h=1}^n \bar{E}_i \underline{Y}_{ih} \underline{E}_h \\ &= \sum_{h=1}^n E_i E_h Y_{ih} e^{j(\theta_i - \theta_h - \gamma_{ih})}.\end{aligned}\quad (5.82)$$

The real and reactive power at the  $i$ th bus are therefore

$$\begin{cases} P_i = \sum_{h=1}^n E_i E_h Y_{ih} \cos(\theta_i - \theta_h - \gamma_{ih}) \\ Q_i = \sum_{h=1}^n E_i E_h Y_{ih} \sin(\theta_i - \theta_h - \gamma_{ih}) \end{cases} \quad (5.83)$$

The entire system of equations in polar coordinates takes the form

$$\begin{cases} 0 = \theta_i \\ i = n \text{ for the slack bus only} \\ E_i^* = E_i \\ i = 1, 2, \dots, g \text{ and } i = n \\ \text{for the slack bus and the generation buses} \\ P_i^* = E_i \sum_{h=1}^n E_h Y_{ih} \cos(\theta_{ih} - \gamma_{ih}) \\ i = 1, 2, \dots, g + u \text{ for load and generation buses} \\ Q_i^* = E_i \sum_{h=1}^n E_h Y_{ih} \sin(\theta_{ih} - \gamma_{ih}) \\ i = g + 1, \dots, g + u \text{ for } u \text{ load buses,} \end{cases} \quad (5.84)$$

where, as before, an asterisk indicates a quantity that is set (imposed by the transmission system operator). Also, we again ultimately obtain  $1 + (g + 1) + (g + u) + u = 2n$  equations, of which  $g + 2$  are identities.

#### Power Flow

The power flowing from bus  $i$  to bus  $h$  is given by

$$\bar{S}_{ih} = P_{ih} + jQ_{ih} = \bar{E}_i (\underline{E}_i - \underline{E}_h) y_{ih} + E_i^2 y_{i(ih)} \quad (5.85)$$

In polar coordinates,

$$\begin{aligned} \bar{S}_{ih} &= \bar{E}_i (\underline{E}_i - \underline{E}_h) y_{ih} + E_i^2 y_{i(ih)} \\ &= E_i e^{j\theta_i} (E_i e^{-j\theta_i} - E_h e^{-j\theta_h}) y_{ih} e^{-j\gamma_{ih}} + E_i^2 y_{i(ih)} e^{-j\gamma_i} \\ &= E_i^2 y_{ih} e^{-j\gamma_{ih}} - E_i E_h y_{ih} e^{j(\theta_i - \theta_h - \gamma_{ih})} + E_i^2 y_{i(ih)} e^{-j\gamma_i}, \end{aligned} \quad (5.86)$$

where  $\gamma_i$  is the argument of the admittance  $y_{i(ih)}$ .

In Cartesian coordinates,

$$\begin{aligned} P_{ih} &= (g_{ih} + g_{i(ih)}) (E_i'^2 + E_h''^2) - g_{ih} (E_i' E_h' + E_i'' E_h'') \\ &\quad + b_{ih} (E_i' E_h'' - E_h' E_i'') \\ Q_{ih} &= -(b_{ih} + b_{i(ih)}) (E_i'^2 + E_h''^2) + g_{ih} (E_i' E_h'' - E_h' E_i'') \\ &\quad + b_{ih} (E_i' E_h' + E_i'' E_h''). \end{aligned} \quad (5.87)$$

Expressing the voltages in polar coordinates and the admittances in Cartesian coordinates, we obtain the useful relationship

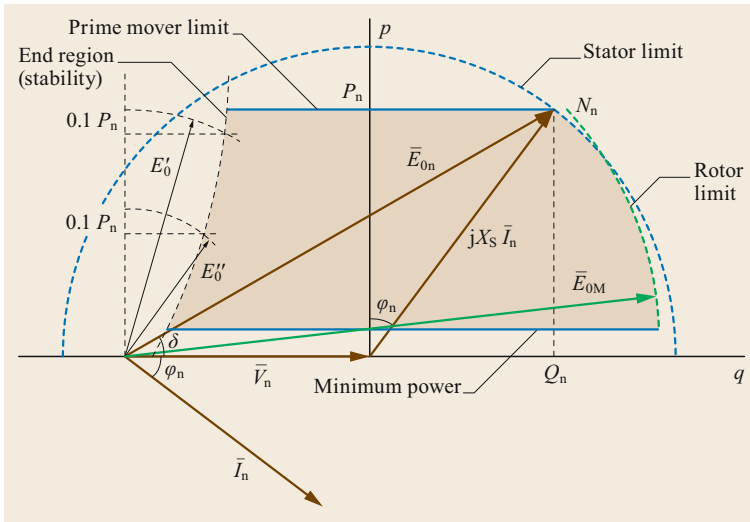
$$P_{ih} = E_i^2 (g_{ih} + g_{i(ih)}) - E_i E_h (g_{ih} \cos \theta_{ih} + b_{ih} \sin \theta_{ih}) \quad (5.88)$$

$$Q_{ih} = -E_i^2 (b_{ih} + b_{i(ih)}) - E_i E_h (g_{ih} \sin \theta_{ih} - b_{ih} \cos \theta_{ih}). \quad (5.89)$$

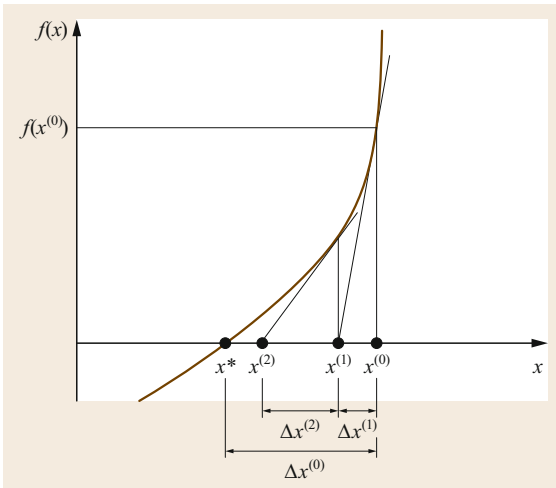
### 5.4.3 Capability Curves

In this section, we briefly review the concept of generator capability curves. The generator must be able to meet the active and reactive power demands within the limits of appropriate generator operation under both steady-state and transient conditions. Let us consider a round-rotor synchronous generator with a linear magnetic circuit. We can define the following operational limits, which are known as *capability limits* (see also Fig. 5.18):

- The *armature current limit*. The maximum allowable heating of the stator windings sets the maximum value of the phase current  $I_n$  for the machine. This is equivalent to setting the maximum apparent power of the generator.
- The *field current limit*. The maximum allowable heating of the rotor excitation windings sets the maximum field current  $I_F$  of the machine. This is equivalent to setting the maximum no-load emf  $E_{0M}$  for the machine. Note that  $E_{0M}$  is larger than  $E_{0n}$ .
- The *stability limit*. During underexcitation, the power angle must not exceed a certain value in order to maintain steady-state stability  $\delta < \delta_{\max}$ , therefore, the supplied active power should not exceed a certain threshold. A particular safety margin, e.g., 10% of the rated active power  $P_n$  power should be maintained for stability reasons.
- The *end region*. During underexcitation, the current leads the voltage by almost  $90^\circ$  and leakage flux is directed along the direct axis—a condition which can produce some local heating in the end regions of some machines.
- The *prime mover limit*. Limits on the mechanical input power from the prime mover impose constraints on the active power generated. The maximum and minimum active power generated ( $P_{\max}$  and  $P_{\min}$ , respectively) are determined directly from the characteristics of the prime mover. This is shown in Fig. 5.17.



**Fig. 5.17** Capability curve showing the mechanical, rotor, and stator limits



**Fig. 5.18** Graphical interpretation of Newton–Raphson’s method

### 5.4.4 Solution Methods

#### Newton–Raphson’s Method

Let us first briefly recall the basis for Newton–Raphson’s method for solving nonlinear equations and systems of nonlinear equations. Given a generic function  $f(x)$  that is derivable and nonlinear, we want to determine the value  $x^*$  of the unknown  $x$  such that  $f(x)$  assumes a fixed value  $y^*$ ; in other words,

$$f(x^*) = y^* . \tag{5.90}$$

Since  $x^{(0)}$  is close to  $x^*$ , we can define

$$\Delta x^{(0)} = x^* - x^{(0)} . \tag{5.91}$$

We now consider the Taylor expansion of  $f(x)$  in the neighborhood of  $x^{(0)}$ ,

$$\begin{aligned} f(x^*) &= f(x^{(0)} + \Delta x^{(0)}) \\ &= f(x^{(0)}) + \left(\frac{df}{dx}\right)^{(0)} \Delta x^{(0)} \\ &\quad + \left(\frac{d^2f}{dx^2}\right)^{(0)} \frac{(\Delta x^{(0)})^2}{2!} + \dots \end{aligned} \tag{5.92}$$

Provided that  $x^{(0)}$  is close enough to  $x^*$ , we can linearize and write

$$f(x^*) \cong f(x^{(0)}) + \left(\frac{df}{dx}\right)^{(0)} \Delta x^{(0)} . \tag{5.93}$$

Equation (5.90) can be rewritten as

$$f(x^{(0)}) + \left(\frac{df}{dx}\right)^{(0)} \Delta x^{(0)} = y^* . \tag{5.94}$$

Using (5.94), we can infer a value of  $\Delta x$  that will generally differ from that expressed by (5.91) because of the above approximation (the truncation of the Taylor expansion after the first term). We shall therefore denote this value  $\Delta x^{(1)}$ , where

$$\Delta x^{(1)} = \frac{y^* - f(x^{(0)})}{\left(\frac{df}{dx}\right)^{(0)}} = \frac{\Delta y^{(0)}}{\left(\frac{df}{dx}\right)^{(0)}} \tag{5.95}$$

and

$$\Delta y^{(0)} = y^* - f(x^{(0)}) . \tag{5.96}$$

If we now add the value of  $\Delta x^{(1)}$  to the value of the initial guess  $x^{(0)}$ , we get a new value of  $x$  that is closer to the initial solution. We shall call this new value  $x^{(1)}$ , and

$$x^{(1)} = x^{(0)} + \Delta x^{(1)} = \begin{cases} x^{(0)} + \frac{\Delta y^{(0)}}{\left(\frac{df}{dx}\right)^{(0)}} & \text{if } y^* \neq 0 \\ x^{(0)} - \frac{f(x^{(0)})}{\left(\frac{df}{dx}\right)^{(0)}} & \text{if } y^* = 0. \end{cases} \quad (5.97)$$

Generalizing, the  $(v + 1)$ th iteration yields

$$x^{(v+1)} = x^{(v)} + \Delta x^{(v+1)} = \begin{cases} x^{(v)} + \frac{\Delta y^{(v)}}{\left(\frac{df}{dx}\right)^{(v)}} & \text{if } y^* \neq 0 \\ x^{(v)} - \frac{f(x^{(v)})}{\left(\frac{df}{dx}\right)^{(v)}} & \text{if } y^* = 0, \end{cases} \quad (5.98)$$

where

$$\begin{aligned} \Delta x^{(v+1)} &= x^{(v+1)} - x^{(v)} \\ \Delta y^{(v)} &= y^* - f(x^{(v)}), \end{aligned}$$

so we obtain

$$\left(\frac{df}{dx}\right)^{(v)} \Delta x^{(v+1)} = \begin{cases} \Delta y^{(v)} & \text{if } y^* \neq 0 \\ -f(x^{(v)}) & \text{if } y^* = 0, \end{cases} \quad (5.99)$$

which is Newton–Raphson’s iterative formula. A graphical interpretation of this method is given in Fig. 5.18.

The iterative process performed in Newton–Raphson’s method stops when either

$$\Delta x^{(v+1)} < \varepsilon \quad (5.100)$$

or

$$\begin{cases} \Delta y^{(v+1)} < \varepsilon & \text{if } y^* \neq 0 \\ f(x^{(v+1)}) < \varepsilon & \text{if } y^* = 0, \end{cases} \quad (5.101)$$

where  $\varepsilon$  is defined as the *tolerance* and  $f(x^{(v+1)})$  or  $\Delta y^{(v+1)}$  is the *residual*.

If the function exhibits smooth behavior around  $x^{(0)}$  (i.e., its derivative does not change sign or vary too much), convergence can be attained after a reasonable (i.e., not excessive) number of iterations, even without recalculating the derivative at each iteration.

When there are  $n$  equations with  $n$  unknowns, the system

$$\begin{cases} f_1(x_1, x_2, \dots, x_n) = y_1^* \\ f_2(x_1, x_2, \dots, x_n) = y_2^* \\ \vdots \\ f_n(x_1, x_2, \dots, x_n) = y_n^* \end{cases} \quad (5.102)$$

is considered. Using a procedure similar to that followed for a single-variable function, the  $(v + 1)$ th iteration yields

$$\begin{bmatrix} \frac{\partial f_1}{\partial x_1} & \frac{\partial f_1}{\partial x_2} & \dots & \frac{\partial f_1}{\partial x_n} \\ \frac{\partial f_2}{\partial x_1} & \frac{\partial f_2}{\partial x_2} & \dots & \frac{\partial f_2}{\partial x_n} \\ \vdots & \vdots & \ddots & \vdots \\ \frac{\partial f_n}{\partial x_1} & \frac{\partial f_n}{\partial x_2} & \dots & \frac{\partial f_n}{\partial x_n} \end{bmatrix}^{(v)} \times \begin{bmatrix} \Delta x_1 \\ \Delta x_2 \\ \vdots \\ \Delta x_n \end{bmatrix}^{(v+1)} = \begin{bmatrix} \Delta y_1 \\ \Delta y_2 \\ \vdots \\ \Delta y_n \end{bmatrix}^{(v)}, \quad (5.103)$$

which can be written in compact form as

$$[\mathbf{J}]^{(v)} \times [\Delta \mathbf{x}]^{(v+1)} = [\Delta \mathbf{y}]^{(v)}, \quad (5.104)$$

where

$$[\mathbf{J}]^{(v)} = \begin{bmatrix} \frac{\partial f_1}{\partial x_1} & \frac{\partial f_1}{\partial x_2} & \dots & \frac{\partial f_1}{\partial x_n} \\ \frac{\partial f_2}{\partial x_1} & \frac{\partial f_2}{\partial x_2} & \dots & \frac{\partial f_2}{\partial x_n} \\ \vdots & \vdots & \ddots & \vdots \\ \frac{\partial f_n}{\partial x_1} & \frac{\partial f_n}{\partial x_2} & \dots & \frac{\partial f_n}{\partial x_n} \end{bmatrix}^{(v)} \quad (5.105)$$

$$\Delta x_i^{(v+1)} = x_i^{(v+1)} - x_i^{(v)} \quad (5.106)$$

and

$$\Delta y_i^{(v)} = y_i^* - f_i(x_1^{(v)}, x_2^{(v)}, \dots, x_n^{(v)}). \quad (5.107)$$

The solution is given by

$$\begin{bmatrix} x_1 \\ x_2 \\ \vdots \\ x_n \end{bmatrix}^{(v+1)} = \begin{bmatrix} x_1 \\ x_2 \\ \vdots \\ x_n \end{bmatrix}^{(v)} + \begin{bmatrix} \Delta x_1 \\ \Delta x_2 \\ \vdots \\ \Delta x_n \end{bmatrix}^{(v+1)}, \quad (5.108)$$

where

$$\begin{bmatrix} \Delta x_1 \\ \Delta x_2 \\ \vdots \\ \Delta x_n \end{bmatrix}^{(v+1)} = \left( \begin{bmatrix} \frac{\partial f_1}{\partial x_1} & \frac{\partial f_1}{\partial x_2} & \dots & \frac{\partial f_1}{\partial x_n} \\ \frac{\partial f_2}{\partial x_1} & \frac{\partial f_2}{\partial x_2} & \dots & \frac{\partial f_2}{\partial x_n} \\ \vdots & \vdots & \ddots & \vdots \\ \frac{\partial f_n}{\partial x_1} & \frac{\partial f_n}{\partial x_2} & \dots & \frac{\partial f_n}{\partial x_n} \end{bmatrix}^{(v)} \right)^{-1} \times \begin{bmatrix} \Delta y_1 \\ \Delta y_2 \\ \vdots \\ \Delta y_n \end{bmatrix}^{(v)}. \quad (5.109)$$

In compact form,

$$[\mathbf{x}]^{(v+1)} = [\mathbf{x}]^{(v)} + [\Delta \mathbf{x}]^{(v+1)} \quad (5.110)$$

$$[\Delta \mathbf{x}]^{(v+1)} = ([\mathbf{J}]^{(v)})^{-1} \times [\Delta \mathbf{y}]^{(v)}. \quad (5.111)$$

To solve the system represented by (5.102), we make an initial guess of  $(x_1^{(0)}, x_2^{(0)}, \dots, x_n^{(0)})$  and then calculate  $\Delta y_i^{(0)} = y_i^* - f_i(x_1^{(0)}, x_2^{(0)}, \dots, x_n^{(0)})$ . It is reasonable to assume that  $\Delta y_i^{(1)}$  will not satisfy the condition  $\Delta y_i^{(1)} < \varepsilon_i$  at the first iteration, so we need to calculate the elements of the Jacobian using  $(x_1^{(0)}, x_2^{(0)}, \dots, x_n^{(0)})$  in order to obtain all terms  $\Delta x_i^{(1)}$ , which are then used to derive the values of  $x_i(1)$ . This process is repeated until the  $(n+1)$ th iteration, when condition  $\Delta y_i^{(n+1)} \leq \varepsilon_i$  or condition  $\Delta x_i^{(n+1)} \leq \varepsilon_i$  is satisfied.

Let us now apply this method to the load-flow problem [5.37–39].

For the  $u$  load buses, we have

$$\begin{bmatrix} \frac{\partial P}{\partial E} & \frac{\partial P}{\partial \vartheta} \\ \frac{\partial Q}{\partial E} & \frac{\partial Q}{\partial \vartheta} \end{bmatrix}^{(v)} \times \begin{bmatrix} \Delta E \\ \Delta \vartheta \end{bmatrix}^{(v+1)} = \begin{bmatrix} \Delta P \\ \Delta Q \end{bmatrix}^{(v)}. \quad (5.112)$$

For the  $g$  generation buses, we have

$$\begin{bmatrix} \frac{\partial P}{\partial E} & \frac{\partial P}{\partial \vartheta} \end{bmatrix}^{(v)} \times \begin{bmatrix} \Delta E \\ \Delta \vartheta \end{bmatrix}^{(v+1)} = \begin{bmatrix} \Delta P \end{bmatrix}^{(v)}. \quad (5.113)$$

Note that we have a total of  $g$  equations rather than the  $2g$  equations that would be obtained with the Cartesian formulation. This is because the remaining  $g$  ones, which correspond to the amplitudes of the voltages of the generator buses, are known quantities.

The overall compact formulation of the problem is

$$\begin{bmatrix} J_{PE} & J_{P\vartheta} \\ J_{QE} & J_{Q\vartheta} \end{bmatrix}^{(v)} \times \begin{bmatrix} \Delta E \\ \Delta \vartheta \end{bmatrix}^{(v+1)} = \begin{bmatrix} \Delta P \\ \Delta Q \end{bmatrix}^{(v)}, \quad (5.114)$$

in which the elements of the Jacobian are expressed as

$$\begin{cases} \frac{\partial P_i}{\partial E_i} = Y_{ih} E_i \cos(\vartheta_i - \vartheta_h - \gamma_{ih}) \\ \frac{\partial P_i}{\partial E_i} = 2Y_{ii} E_i \cos \gamma_{ii} + \sum_{h=1, h \neq i}^n Y_{ih} E_h \cos(\vartheta_i - \vartheta_h - \gamma_{ih}) \\ \frac{\partial P_i}{\partial \vartheta_h} = Y_{ih} E_i E_h \sin(\vartheta_i - \vartheta_h - \gamma_{ih}) \\ \frac{\partial P_i}{\partial \vartheta_i} = -E_i \sum_{h=1, h \neq i}^n Y_{ih} E_h \sin(\vartheta_i - \vartheta_h - \gamma_{ih}) \end{cases} \quad (5.115)$$

and

$$\begin{cases} \frac{\partial Q_i}{\partial E_h} = Y_{ih} E_i \sin(\vartheta_i - \vartheta_h - \gamma_{ih}) \\ \frac{\partial Q_i}{\partial E_i} = -2Y_{ii} E_i \sin \gamma_{ii} + \sum_{h=1, h \neq i}^n Y_{ih} E_h \sin(\vartheta_i - \vartheta_h - \gamma_{ih}) \\ \frac{\partial Q_i}{\partial \vartheta_h} = -Y_{ih} E_i E_h \cos(\vartheta_i - \vartheta_h - \gamma_{ih}) \\ \frac{\partial Q_i}{\partial \vartheta_i} = E_i \sum_{h=1, h \neq i}^n Y_{ih} E_h \cos(\vartheta_i - \vartheta_h - \gamma_{ih}) \end{cases} \quad (5.116)$$

A load-flow calculation that uses the Newton–Raphson method and is performed with the EMTP-RV (electromagnetic transient program) code is included in the supplementary material for this chapter.

## 5.4.5 Approximations for Calculating the Load Flow

### Carpentier's Approximation

Before we dive any further into this section, it is important to note that the word *approximation* is not used in this section to describe the nature of the results (which are always approximate given that we utilize iterative solution methods), but to refer to the nature of the equations used to compute the load flow.

The first approximation that we introduce is Carpentier's approximation [5.40], which makes the assumption that the active powers injected in the nodes depend only on the phases of the voltages, whereas the reactive powers depend only on the magnitudes of the voltages. This allows us to decouple system (5.114). In other words, the elements of the submatrix  $[\partial P / \partial \vartheta]$  are normally much larger than those of the submatrix  $[\partial P / \partial E]$ , and the elements of  $[\partial Q / \partial E]$  are much larger than those of  $[\partial Q / \partial \vartheta]$ .

The new system of equations becomes

$$\begin{aligned} & \begin{bmatrix} \frac{\partial P}{\partial E} & \frac{\partial P}{\partial \vartheta} \\ \frac{\partial Q}{\partial E} & \frac{\partial Q}{\partial \vartheta} \end{bmatrix}^{(v)} \times \begin{bmatrix} \Delta E \\ \Delta \vartheta \end{bmatrix}^{(v+1)} = \begin{bmatrix} \Delta P \\ \Delta Q \end{bmatrix}^{(v)} \\ \Rightarrow & \begin{bmatrix} 0 & \frac{\partial P}{\partial \vartheta} \\ \frac{\partial Q}{\partial E} & 0 \end{bmatrix}^{(v)} \times \begin{bmatrix} \Delta E \\ \Delta \vartheta \end{bmatrix}^{(v+1)} = \begin{bmatrix} \Delta P \\ \Delta Q \end{bmatrix}^{(v)}, \end{aligned} \quad (5.117)$$

which corresponds to the two subsystems

$$\begin{bmatrix} \frac{\partial P}{\partial \vartheta} \end{bmatrix}^{(v)} \times \begin{bmatrix} \Delta \vartheta \end{bmatrix}^{(v+1)} = \begin{bmatrix} \Delta P \end{bmatrix}^{(v)} \quad (5.118)$$

$$\begin{bmatrix} \frac{\partial Q}{\partial E} \end{bmatrix}^{(v)} \times \begin{bmatrix} \Delta E \end{bmatrix}^{(v+1)} = \begin{bmatrix} \Delta Q \end{bmatrix}^{(v)}. \quad (5.119)$$

What we have achieved here is known as *active and reactive power decoupling*.

It is useful to recall that, for a very short line (i.e., a line in which transversal admittance can be neglected), the expressions for the active and reactive power in absolute values (i.e., not in pu) at the terminations are

$$P_1 = P_2 = \frac{3E_1 E_2}{X} \sin \vartheta \quad (5.120)$$

$$Q_1 = \frac{3E_1}{X} (E_1 - E_2 \cos \vartheta) \quad (5.121)$$

$$Q_2 = \frac{3E_2}{X} (E_1 \cos \vartheta - E_2). \quad (5.122)$$

In general, especially when the line is short and not overloaded,  $\vartheta$  is a small angle. As a first approximation,

we can therefore state that the active power depends on the phase shift between the two voltages, while the reactive power depends on the voltage magnitudes.

The statements made above regarding a very short line are normally also valid for longer lines, and generally extend to the grids. Recall the equations for power transmission along a generic transmission line,

$$\begin{cases} P_{ih} = E_i^2(g_{ih} + g_{i(ih)}) - E_i E_h [g_{ih} \cos(\vartheta_i - \vartheta_h) \\ \quad + b_{ih} \sin(\vartheta_i - \vartheta_h)] \\ Q_{ih} = -E_i^2(b_{ih} + b_{i(ih)}) - E_i E_h [g_{ih} \sin(\vartheta_i - \vartheta_h) \\ \quad - b_{ih} \cos(\vartheta_i - \vartheta_h)]. \end{cases} \quad (5.123)$$

Differentiating with respect to the magnitudes and phases of the voltages, we obtain the real power derivatives

$$\begin{cases} \frac{\partial P_{ih}}{\partial E_i} = 2E_i(g_{ih} + g_{i(ih)}) \\ \quad - E_h [g_{ih} \cos(\vartheta_i - \vartheta_h) + b_{ih} \sin(\vartheta_i - \vartheta_h)] \\ \frac{\partial P_{ih}}{\partial E_h} = -E_i [g_{ih} \sin(\vartheta_i - \vartheta_h) + b_{ih} \cos(\vartheta_i - \vartheta_h)] \end{cases} \quad (5.124)$$

$$\begin{cases} \frac{\partial P_{ih}}{\partial \vartheta_i} = E_i E_h [g_{ih} \sin(\vartheta_i - \vartheta_h) - b_{ih} \cos(\vartheta_i - \vartheta_h)] \\ \frac{\partial P_{ih}}{\partial \vartheta_h} = -\frac{\partial P_{ih}}{\partial \vartheta_i} \end{cases} \quad (5.125)$$

and the reactive power derivatives

$$\begin{cases} \frac{\partial Q_{ih}}{\partial E_i} = -2E_i(b_{ih} + b_{i(ih)}) \\ \quad - E_h [g_{ih} \sin(\vartheta_i - \vartheta_h) - b_{ih} \cos(\vartheta_i - \vartheta_h)] \\ \frac{\partial Q_{ih}}{\partial E_h} = -E_i [g_{ih} \sin(\vartheta_i - \vartheta_h) - b_{ih} \cos(\vartheta_i - \vartheta_h)] \end{cases} \quad (5.126)$$

$$\begin{cases} \frac{\partial Q_{ih}}{\partial \vartheta_i} = -E_i E_h [g_{ih} \cos(\vartheta_i - \vartheta_h) + b_{ih} \sin(\vartheta_i - \vartheta_h)] \\ \frac{\partial Q_{ih}}{\partial \vartheta_h} = -\frac{\partial Q_{ih}}{\partial \vartheta_i} \end{cases} \quad (5.127)$$

The conductance  $g_{ij}$  and the angle  $\vartheta_{ih} = \vartheta_i - \vartheta_h$  are generally small. As a consequence, we can state that

$$\frac{\partial P_{ih}}{\partial E_i} \ll \frac{\partial P_{ih}}{\partial \vartheta_i}, \quad \frac{\partial Q_{ih}}{\partial \vartheta_i} \ll \frac{\partial Q_{ih}}{\partial E_i}. \quad (5.128)$$

As a result, small variations in the voltage magnitudes do not appreciably affect the active power transmission and, analogously, small phase variations do not substantially alter the reactive power flow. It follows that the active power transmission mainly depends on the voltage phase shifts, while the reactive power flow is mainly influenced by the difference in the voltage magnitudes at the line terminations.

### Stott's Approximation

This approximation is also known as fast decoupled load flow [5.41, 42]. As discussed earlier, the power injection at bus  $i$  can be written as

$$\bar{S}_i = \bar{E}_i \sum_{h=1}^n \underline{Y}_{ih} \bar{E}_h = \sum_{h=1}^n \bar{E}_i \underline{Y}_{ih} \bar{E}_h. \quad (5.129)$$

We know that

$$\begin{cases} \bar{E}_i = E_i e^{j\vartheta_i} = E_i (\cos \vartheta_i + j \sin \vartheta_i) \\ \bar{E}_h = E_h e^{-j\vartheta_h} = E_h [\cos(-\vartheta_h) + j \sin(-\vartheta_h)] \\ \underline{Y}_{ih} = G_{ih} - jB_{ih}, \end{cases} \quad (5.130)$$

so we can substitute (5.130) into (5.129), which yields

$$\begin{aligned} \bar{S}_i &= E_i \sum_{h=1}^n E_h (G_{ih} - jB_{ih}) [\cos(\vartheta_i - \vartheta_h) + j \sin(\vartheta_i - \vartheta_h)] \\ &= E_i \sum_{h=1}^n E_h (G_{ih} - jB_{ih}) [\cos \vartheta_{ih} + j \sin \vartheta_{ih}]. \end{aligned} \quad (5.131)$$

Using (5.131), it is possible to obtain the expressions for  $P$  and  $Q$  presented in the previous section, i.e.,

$$\begin{cases} P_i = E_i \sum_{h=1}^n E_h (G_{ih} \cos \vartheta_{ih} + B_{ih} \sin \vartheta_{ih}) \\ Q_i = E_i \sum_{h=1}^n E_h (G_{ih} \sin \vartheta_{ih} - B_{ih} \cos \vartheta_{ih}). \end{cases} \quad (5.132)$$

Extracting the term relevant to node  $i$  from the summation, we have

$$\begin{cases} P_i = G_{ii} E_i^2 + E_i \sum_{h \neq i}^n E_h (G_{ih} \cos \vartheta_{ih} + B_{ih} \sin \vartheta_{ih}) \\ Q_i = -B_{ii} E_i^2 + E_i \sum_{h \neq i}^n E_h (G_{ih} \sin \vartheta_{ih} - B_{ih} \cos \vartheta_{ih}). \end{cases} \quad (5.133)$$

Differentiating the active power with respect to  $\vartheta_i$  and the reactive power with respect to  $E_i$  leads to

$$\begin{aligned} \frac{\partial P_i}{\partial \vartheta_i} &= -E_i \sum_{\substack{h=1 \\ h \neq i}}^n E_h (G_{ih} \sin \vartheta_{ih} - B_{ih} \cos \vartheta_{ih}) \\ &= -B_{ii} E_i^2 - Q_i \\ \frac{\partial Q_i}{\partial E_i} &= -2B_{ii} E_i + \sum_{\substack{h=1 \\ h \neq i}}^n E_h (G_{ih} \sin \vartheta_{ih} - B_{ih} \cos \vartheta_{ih}) \\ &= -2B_{ii} E_i + \frac{Q_i + B_{ii} E_i^2}{E_i} = \frac{Q_i}{E_i} - B_{ii} E_i. \end{aligned} \quad (5.134)$$



We can make the following assumptions (known as Stott's assumptions) based on (5.134) [5.41]:

- $B_{ih} \cos \vartheta_{ih} \cong B_{ih}$ , given that the displacements  $\vartheta_{ih}$  at the ends of a single link are small (i.e.,  $Q_i \ll B_{ii}E_i^2$ )
- $G_{ih} \sin \vartheta_{ih} \ll B_{ih}$  as both the conductances and  $\vartheta_{ih}$  are small
- $Q_i \ll B_{ii}E_i^2$ , which is explained below.

Let us consider a generation node connected to the high-voltage grid by means of the corresponding elevator transformer, which has a reactance  $x$  of 0.1 pu (referred to its own rated power  $A_n$ ). Taking  $E_i$  to be equal to 1 pu, we obtain  $B_{ii}E_i^2 = 10$  pu. It is reasonable to assume that the reactive power produced or absorbed by a generator under normal operating conditions is 0.6–0.7 pu; furthermore, as the rated power of the elevator transformer is approximately equal to that of the generator, we can conclude that the assumption is acceptable ( $B_{ii}E_i^2 = 10 \gg Q_i \cong 0.7$ ).

Similar statements can be made for the load nodes. It can be observed that the longitudinal reactance of a line (in pu of the characteristic power) is about 0.1 pu for a 100 km overhead line. The reactive power absorbed by the loads is usually very small compared to the active one ( $\cos \varphi \cong 0.8$ – $0.9$ ), and two lines converge in every load bus on average.

In view of the discussion above, introducing Stott's assumptions into (5.134) leads us to

$$\begin{cases} \frac{\partial P_i}{\partial \vartheta_h} = -E_i E_h B_{ih} \\ \frac{\partial P_i}{\partial \vartheta_i} = -E_i^2 B_{ii} \end{cases} \quad h \neq i \Rightarrow \frac{\partial P_i}{\partial \vartheta_h} = -E_i E_h B_{ih} \quad \forall h \quad (5.135)$$

$$\begin{cases} \frac{\partial Q_i}{\partial E_h} = -E_i B_{ih} \\ \frac{\partial Q_i}{\partial E_i} = -E_i B_{ii} \end{cases} \quad h \neq i \Rightarrow \frac{\partial Q_i}{\partial E_h} = -E_i B_{ih} \quad \forall h. \quad (5.136)$$

Like Carpentier's method, Stott's method is based on the approximation that the active power and reactive power are related to the voltage angles and magnitudes, respectively, i.e., it is also based on active/reactive decoupling. If we consider the load-flow equations obtained using Carpentier's approximation,

$$\begin{cases} \Delta P_i^{(v)} = \sum_{h=1}^n \frac{\partial P_i^{(v)}}{\partial \vartheta_h} \Delta \vartheta_h^{(v+1)} \\ \Delta Q_i^{(v)} = \sum_{h=1}^n \frac{\partial Q_i^{(v)}}{\partial E_h} \Delta E_h^{(v+1)}, \end{cases} \quad (5.137)$$

replacing the partial derivatives with expressions (5.135) and (5.136) yields

$$\begin{cases} \frac{\Delta P_i^{(v)}}{E_i} = \sum_{h=1}^n -B_{ih} E_h^{(v)} \Delta \vartheta_h^{(v+1)} \\ \frac{\Delta Q_i^{(v)}}{E_i} = \sum_{h=1}^n -B_{ih} \Delta E_h^{(v+1)}. \end{cases} \quad (5.138)$$

The great advantage of Stott's method is that the partial derivatives of the Jacobian matrix are replaced with simple susceptances, so there is no need to update the Jacobian at each iteration.

### DC Approximation

The load-flow solution methods shown so far have been *AC methods* in the sense that the unknowns to be determined are the voltages (magnitude and phase) that affect the distributions of active and reactive power in the various branches of the network.

Considerable time is needed to perform these methods when dealing with large networks. On the other hand, in some situations it is sufficient to estimate only the active power flows in the various lines, which leads to a marked reduction in computational time. Such situations include the initial planning stage of a transmission network, short-term operational planning (daily and weekly programs implemented *off-line*), and even the *on-line* control of a transmission system that checks for the consequences of a possible sudden loss of a critical component (such as a line or large generator) every few minutes.

The *direct current* load-flow solution method [5.42] is based on the following simplifications:

- The conductor resistances are generally negligible compared to the series reactances of the lines and transformers. The ratio between the reactance and the resistance is about 10 for a distribution line, but can reach 50 for large interconnecting lines. Therefore, losses are neglected in this method.
- The transversal admittances of power components are neglected. The line capacitances generate reactive power that does not significantly affect the active power flow.
- The transversal conductances are neglected.
- Based on similar considerations, the shunt reactances and bank of capacitors can also be neglected.

Let us now consider a branch of the network characterized by a longitudinal reactance  $x_{ih}$ .  $\bar{E}_i$  and  $\bar{E}_h$  are the voltages at the ends of the line, with a phase shift  $\vartheta_{ih}$  between them.

The active power flow in the branch is

$$P_{ih} = \frac{3E_i E_h}{x_{ih}} \sin \vartheta_{ih}. \quad (5.139)$$

Let us also assume that the voltages are close to their nominal values, i.e.,

$$\bar{E}_i \cong \bar{E}_h. \quad (5.140)$$

Also, noting that the angle  $\vartheta_{ih} = \vartheta_i - \vartheta_h$  is generally small, the pu expression of (5.139) becomes

$$p_{ih} = \frac{1}{x_{ih}} \vartheta_{ih}. \quad (5.141)$$

This relationship is analogous to Ohm's law in a DC circuit with a current  $p_{ih}$  flowing through a resistor of value  $x_{ih}$ , causing a voltage drop  $\vartheta_{ih}$  across it.

As a consequence of this expression, the active power injection in the generic node  $i$  (in pu) is

$$p_i = \sum_{\substack{h=1 \\ h \neq i}}^n p_{ih} = \frac{\vartheta_{i1}}{x_{i1}} + \frac{\vartheta_{i2}}{x_{i2}} + \dots + \frac{\vartheta_{in}}{x_{in}}$$

$$\stackrel{\vartheta_{ih} = \vartheta_i - \vartheta_h}{\Rightarrow} \left( \frac{1}{x_{i1}} + \frac{1}{x_{i2}} + \dots + \frac{1}{x_{in}} \right) \vartheta_i - \sum_{\substack{h=1 \\ h \neq i}}^n \frac{1}{x_{ih}} \vartheta_h. \quad (5.142)$$

The terms in parentheses can be interpreted as self-admittances, while the terms in the summation can be considered transadmittances. Therefore, we define that

$$\sum_{\substack{h=1 \\ h \neq i}}^n \frac{1}{x_{ih}} = \frac{1}{X_{ii}} \quad ; \quad \frac{1}{x_{ih}} = \frac{1}{-X_{ih}}, \quad (5.143)$$

and the active power injection becomes

$$p_i = \sum_{h=1}^n \frac{1}{X_{ih}} \vartheta_h \Rightarrow p_i = \sum_{h=1}^n B_{ih} \vartheta_h. \quad (5.144)$$

Thus, the linear matrix equation

$$[\mathbf{p}] = [\mathbf{B}] \times [\boldsymbol{\vartheta}] \quad (5.145)$$

is obtained for the whole network, where  $[\mathbf{B}]$  is the susceptance matrix of the entire transmission network in pu. The diagonal terms  $B_{ii}$  of this matrix are the sum of the susceptances of all the lines that converge at the  $i$ th node, and are positive since the susceptances are inductive. The other terms are all negative and satisfy the condition  $B_{hk} = B_{kh} = -b_{hk} = -b_{kh}$ .

An exercise to calculate the load flow of a simple three-bus network using the current approximation is included in the supplementary material.

### 5.4.6 Concluding Remarks

The methods examined so far do not consider any constraints. In real applications, however, there can be many types of constraints:

- The voltages in the various nodes must not be too different from the nominal ones

- In the generation nodes, the reactive power injection resulting from the calculation must be compatible with the capability curves of the generators
- When the slack bus—which is also a generation node—is assumed to be concentrated in one bus and not distributed, it must have an active and reactive power output compatible with the above production of the generators.

The limits are therefore of the type

$$\begin{cases} Q_{i,\min} \leq Q_i \leq Q_{i,\max} \\ i = 1, 2, \dots, g \end{cases} \quad (5.146)$$

$$\begin{cases} E_{i,\min} \leq E_i \leq E_{i,\max} \\ i = 1, 2, \dots, g + u \end{cases} \quad (5.147)$$

$$P_{n,\min} \leq P_n \leq P_{n,\max}. \quad (5.148)$$

Load-flow calculations with constrained variables must be performed to account for these issues ([5.43], from which the following discussion is adapted).

Now suppose that constraints (5.146) are violated; in other words, the computation yields reactive powers that exceed the limit in some generation buses and are lower than the limit in others. In order to obtain a load-flow solution that is technically feasible, it is necessary to change the voltages in the various buses. These buses, originally of  $(P, E)$  type, can therefore be converted into  $(P, Q)$  ones by fixing their reactive power production (i.e.,  $Q_i \cong Q_{i,\max}$  or  $Q_i \cong Q_{i,\min}$ ), so the voltage magnitude  $E_i$  becomes unknown. Note that the effect of forcing a generator to decrease its reactive power production is that the reactive power generation of the other groups must increase, because the loads do not change.

If the violated constraints are of the type represented by (5.148) for the active power, it will be necessary to vary the power distribution among the other generators of the network. If, for instance, the upper limit is violated (i.e., if the active power to be produced in the slack bus is larger than the maximum allowed), it is necessary to increase the production of the other groups. This does not guarantee a priori that the constraints will be respected, as changing the active power production changes the phases of the voltages and therefore the currents in the branches. Consequently, the transmission losses change too. In other words, it will be necessary to verify that the new calculated active power respects constraints (5.148).

Modern computer software can automatically consider:

- The effects of generator speed control and shifting transformers, in order to determine their optimal set-ups
- The dependence of the loads on the voltage

- Primary and secondary frequency control and the frequency dependence of the loads
- Secondary voltage regulation.

These topics are discussed in the optimal load flow, more commonly known as optimal power flow, (OPF) chapters of several books [5.13, 43]. OPF is closely related to economic dispatch and unit commitment, and any attempt to realize OLF will need to take electricity market rules and constraints into consideration (see Chap. 18). We do not address these topics in this chapter, but we do delve into the essential elements of economic dispatching below.

### Some Basic Elements of Economic Dispatching

For simplicity's sake, suppose that we have a system, as depicted in Fig. 5.19, consisting of:

- $g$  thermal power stations
- one network
- $u$  users.

In a vertically integrated system, we wish to determine the power that the generators (the power plants) must provide in order to meet the power requirements of the users at minimum cost. Any technical constraints on the groups are disregarded for simplicity.

The plot presented in Fig. 5.20 shows the hourly cost curve of a power plant: the efficiency is constant regardless of the power produced. The curved line, on the other hand, shows a more realistic trend for the hourly

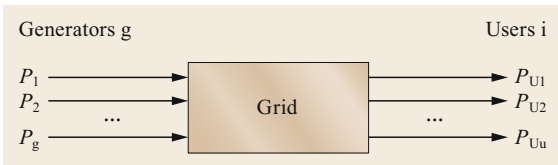


Fig. 5.19 Single-bus power system

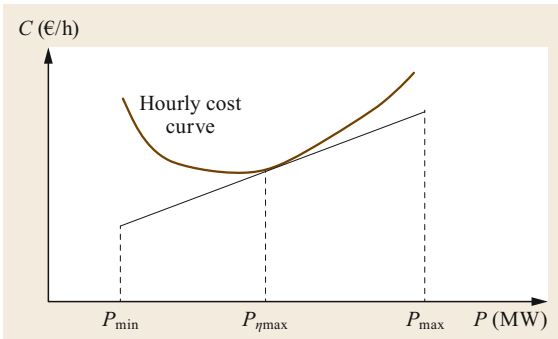


Fig. 5.20 Hourly cost curve for a thermal power plant as a function of the power produced

cost—there is a point on the curve at which the cost is minimized, and we would like to operate the plant at the power corresponding to this point.

Defining  $C$  as the overall cost, the function to be minimized is

$$C = C_1(P_1) + C_2(P_2) + \cdots + C_g(P_g). \quad (5.149)$$

In accordance with the constraint,

$$P_1 + P_2 + \cdots + P_g - (P_{U1} + P_{U2} + \cdots + P_{Uu}) - p = 0, \quad (5.150)$$

where  $p$  represents the losses of the system. It is worth noting that

$$p = p(P_1, P_2, \dots, P_g); \quad (5.151)$$

in other words, the losses are linked to the power produced, as expected.

To solve the problem, it is necessary to use the method of Lagrange multipliers. We define the Lagrangian as

$$\begin{aligned} L &= (\text{condition to be minimized}) - \lambda(\text{constraint}) \\ &= C(P_1, P_2, \dots, P_g) - \lambda \left( \sum_{i=1}^g P_i - \sum_{i=1}^u P_{Ui} - p \right). \end{aligned} \quad (5.152)$$

In order to solve it, we must calculate

$$\begin{cases} \frac{\partial L}{\partial P_i} = 0 \\ \frac{\partial L}{\partial \lambda} = 0 \end{cases} \Rightarrow P_1, P_2, \dots, P_g, \lambda, \quad (5.153)$$

which means that

$$\begin{cases} \frac{\partial C_1}{\partial P_1} - \lambda \left( 1 - \frac{\partial p}{\partial P_1} \right) = 0 \\ \frac{\partial C_2}{\partial P_2} - \lambda \left( 1 - \frac{\partial p}{\partial P_2} \right) = 0 \\ \vdots \\ \frac{\partial C_g}{\partial P_g} - \lambda \left( 1 - \frac{\partial p}{\partial P_g} \right) = 0 \\ P_1 + P_2 + \cdots + P_g \\ = P_{U1} + P_{U2} + \cdots + P_{Uu} + p \end{cases} \Rightarrow P_1, P_2, \dots, P_g, \lambda. \quad (5.154)$$

If the system losses  $p$  are negligible, it follows that  $p = 0$ . This is equivalent to neglecting the power losses along the lines, i.e.,

$$\frac{\partial p}{\partial P_1}, \frac{\partial p}{\partial P_2}, \dots, \frac{\partial p}{\partial P_g}, p = 0. \quad (5.155)$$

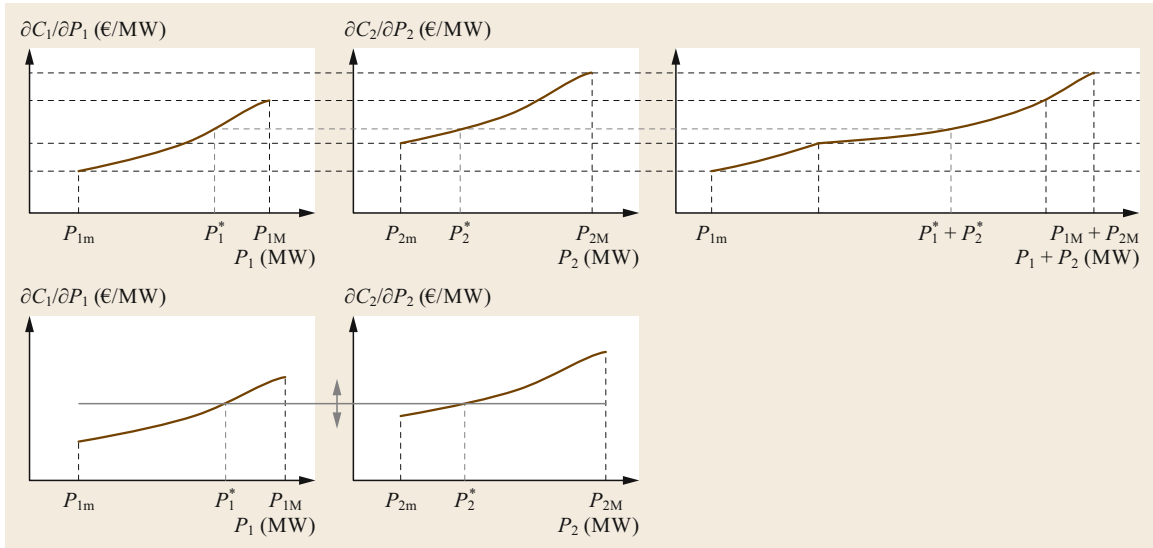


Fig. 5.21 Dispatched Power for two Power Stations 1 and 2 (adapted from [5.36])

In this case, the system is called a *single-bar system*, and the equations reduce to

$$\frac{\partial C_1}{\partial P_1} = \frac{\partial C_2}{\partial P_2} = \dots = \frac{\partial C_g}{\partial P_g} \quad (5.156)$$

Rewriting the partial derivatives as total derivatives yields

$$\frac{dC_1}{dP_1} = \frac{dC_2}{dP_2} = \dots = \frac{dC_g}{dP_g} = \lambda \quad (5.157)$$

Equality of marginal hourly costs is therefore the minimum condition sought.

The simplified assumptions of this section permit the problem to be solved in a simple way graphically using the known hourly cost curves for two power stations, as shown in Fig. 5.21. The incremental hourly cost is obtained by deriving the hourly costs with respect to the power variable. To determine the operating point, it is sufficient to draw a horizontal line that intercepts both curves such that the sum of the power on the first graph ( $P_1^*$ ) and that on the second graph ( $P_2^*$ ) equals the power required by the load.

## 5.5 Unsymmetrical Fault Analysis

A short circuit is the term given to the unintended flow of current along a low-impedance connection between two points at different potentials in an electric circuit (phase-to-phase or phase-to-ground) rather than along the intended path. The most common types of faults in power systems are single line-to-ground (or phase-to-ground), three-phase, line-to-line (or phase-to-phase), and double line-to-ground. Faults can occur for various reasons, such as insulation breakdown (due to overvoltage or aging) or direct contact with bare conductors.

### 5.5.1 Types of Faults in Electric Power Systems

The following fault phenomena can occur in electric power systems:

- (a) A sudden increase in conductor temperature  $\theta$  due to the Joule effect, as calculated via

$$\Delta\theta = KI^2\Delta t \quad (5.158)$$

As the temperature  $\theta$  increases, the extra heat alters the dielectric properties of the insulating materials. Heating also alters the mechanical properties of the conductor, and the disconnecter contacts deteriorate. For faults of this nature, it is clear that reducing the duration of the fault is of paramount importance.

- (b) Electrodynamical forces that are proportional to the square of the peak current amplitude, i.e.,

$$F = KI_p^2 \quad (5.159)$$

which deform or even disrupt conductors and insulation materials.

There are a range of relevant effects, including:

- Damage caused by an electric arc at the location of the fault is common, and often leads to fusion or erosion of the relevant parts (conductors, electrical machines, ferromagnetic plates), representing a fire risk.
- Voltage dips at the faulty bus and in the adjacent network portion, causing malfunctions, trips (of, e.g., synchronous motors and mercury-vapor lamps), disturbing users that are sensitive to voltage drops, and possibly leading to a loss of system stability.
- Dangerous step and touch voltages caused by the large short-circuit currents
- Electromotive force (EMF) induction in telecommunication circuits that are located parallel to power lines
- When present, homopolar sequence current circulation through cable sheaths, pipelines, or other underground structures leads to heating or electric arcs and metal fusion, pipeline punctures, and the potential for fire.

### 5.5.2 Protection Measures Against Faults

Although electric power systems are well designed, faults are relatively frequent phenomena in such systems, so relevant countermeasures must be taken, including:

- i. Installing circuit breakers and fuses with adequate short-circuit breaking capacities to withstand/open the short-circuit current
- ii. Ensuring that components are designed/selected to withstand thermal and electrodynamic stresses without incurring damage
- iii. Designing appropriate grounding systems that keep touch and step voltages within standard limits
- iv. Appropriate calibration/setting of protection relays. Note that setting these devices to open the maximum short-circuit current may result in the failure of the devices to open the lowest fault currents.

To realize the above measures, it is necessary to perform fault current calculations for the various types of possible faults at each network bus. Indeed, as already mentioned, ignoring the calculation of a modest fault current (corresponding to the minimum load operation of the network with different units out of service) during the calibration and validation of protection relays can be critical.

To determine the breaking capacity, it is convenient to calculate short circuits with null fault impedance ( $Z_g = 0$ ). Since this type of fault is rare, for complete-

ness, we shall extend the discussion to the more general case of a nonzero  $Z_g$ .

In fault analysis, the network is generally unbalanced, as most short circuits have this characteristic (e.g., single-line to ground, line-to-line, double line-to-ground).

### 5.5.3 Unbalanced Faults: Short-Circuit Calculation

To simplify the analysis of fault currents in networks, we follow the approach given in [5.3] and make the following simplifications:

- Transmission lines are represented by their series reactance
- Transformers are represented by their short-circuit reactance
- Synchronous machines are modeled as a Thévenin equivalent network consisting of an ideal generator and the direct-axis transient (or subtransient) reactance
- Induction motors are ignored or treated as synchronous machines
- Other (nonspinning) loads are ignored
- The voltage level of the neutral conductor is common to all the voltage levels of the network (i.e., there are no voltage levels with an isolated neutral).

We shall denote the phase voltages and currents by  $\bar{E}_a, \bar{E}_b, \bar{E}_c, \bar{I}_a, \bar{I}_b,$  and  $\bar{I}_c$ , respectively, and the direct (or positive), inverse (or negative), and homopolar (or zero) sequence symmetrical components of the voltages and currents by  $\bar{E}_d, \bar{E}_i, \bar{E}_0, \bar{I}_d, \bar{I}_i,$  and  $\bar{I}_0$ , respectively. Fortescue theory provides various phase voltage and current transformations,

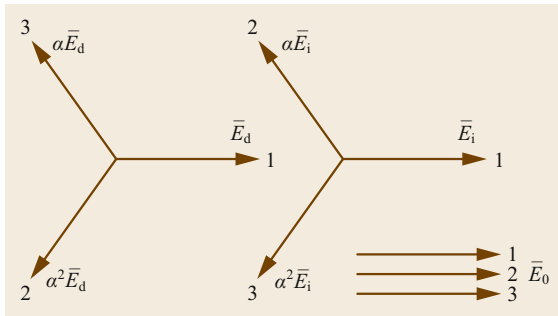
$$\begin{cases} \bar{E}_d = \frac{1}{3}(\bar{E}_a + \alpha\bar{E}_b + \alpha^2\bar{E}_c) \\ \bar{E}_i = \frac{1}{3}(\bar{E}_a + \alpha^2\bar{E}_b + \alpha\bar{E}_c) \\ \bar{E}_0 = \frac{1}{3}(\bar{E}_a + \bar{E}_b + \bar{E}_c) \end{cases} \quad (5.160)$$

$$\begin{cases} \bar{I}_d = \frac{1}{3}(\bar{I}_a + \alpha\bar{I}_b + \alpha^2\bar{I}_c) \\ \bar{I}_i = \frac{1}{3}(\bar{I}_a + \alpha^2\bar{I}_b + \alpha\bar{I}_c) \\ \bar{I}_0 = \frac{1}{3}(\bar{I}_a + \bar{I}_b + \bar{I}_c) \end{cases} \quad (5.161)$$

$$\begin{cases} \bar{E}_a = \bar{E}_d + \bar{E}_i + \bar{E}_0 \\ \bar{E}_b = \alpha^2\bar{E}_d + \alpha\bar{E}_i + \bar{E}_0 \\ \bar{E}_c = \alpha\bar{E}_d + \alpha^2\bar{E}_i + \bar{E}_0 \end{cases} \quad (5.162)$$

$$\begin{cases} \bar{I}_a = \bar{I}_d + \bar{I}_i + \bar{I}_0 \\ \bar{I}_b = \alpha^2\bar{I}_d + \alpha\bar{I}_i + \bar{I}_0 \\ \bar{I}_c = \alpha\bar{I}_d + \alpha^2\bar{I}_i + \bar{I}_0, \end{cases} \quad (5.163)$$

where  $\alpha = e^{j2\pi/3}$ . Note that for simplicity  $\alpha$  has not been overlined.



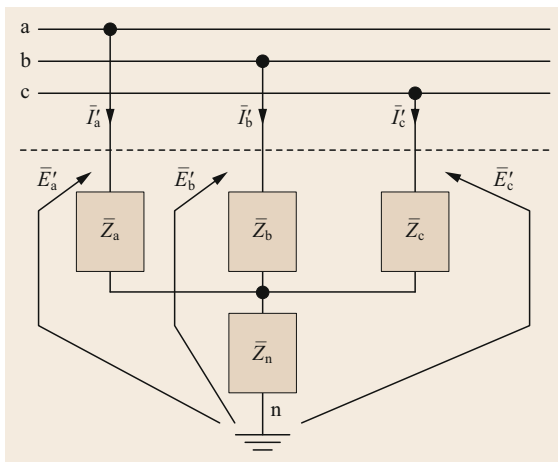
**Fig. 5.22** Direct, inverse, and homopolar sequence components of the phase voltages. The amplitudes of  $E_d$ ,  $E_i$ , and  $E_0$  are not necessarily equal

A phasor diagram of the direct, inverse, and homopolar sequence components of the phase voltages is reported in Fig. 5.22.

Let us connect a system of nonsymmetrical (unbalanced) impedances to a point in the symmetrical three-phase network, as shown in Fig. 5.23.

After the relevant transient, the voltages  $\bar{E}'_a$ ,  $\bar{E}'_b$ , and  $\bar{E}'_c$  and the currents  $\bar{I}'_a$ ,  $\bar{I}'_b$ , and  $\bar{I}'_c$  are obtained (note that the relevant quantities are denoted by an apex). It is clear that these values depend on the impedances  $\bar{Z}_a$ ,  $\bar{Z}_b$ ,  $\bar{Z}_c$ , and  $\bar{Z}_n$  shown in Fig. 5.23, as well as the network parameters. In the postfault steady state, the system in Fig. 5.23 is equivalent to both of those presented in Fig. 5.24.

Note that if we connect the three voltage sources  $\bar{E}'_a$ ,  $\bar{E}'_b$ , and  $\bar{E}'_c$  at the fault point (Fig. 5.24a), the three currents in the considered section will actually be equal to the three currents  $\bar{I}'_a$ ,  $\bar{I}'_b$ , and  $\bar{I}'_c$  injected at the fault point by the three current sources shown in Fig. 5.24b.



**Fig. 5.23** Connection of unsymmetrical (unbalanced) impedances

Let us suppose that  $\bar{E}'_a$ ,  $\bar{E}'_b$ , and  $\bar{E}'_c$  are known quantities. According to the superposition principle and the Fortescue theorem, each of the three voltage sources can be decomposed into three series generators (as shown in Fig. 5.24b), and further decomposed into three different circuits (as presented in Fig. 5.26).

The asymmetrical network of Fig. 5.25 has now been decomposed into three symmetrical three-phase ones (Fig. 5.26). In the first network, only the positive (direct) sequence set of sources  $\bar{E}'_d$  is present, in addition to those impressed by the generators of the network. The second network only has the negative (inverse) sequence source  $\bar{E}'_i$ , whereas the third only has the zero (homopolar) sequence source  $\bar{E}'_0$ . It is worth noting that, because it is symmetrical, the starting network only has direct-sequence internal emfs.

The three networks of Fig. 5.26 are symmetrical (balanced), so they can be studied by means of three equivalent single-phase circuits, as shown in Fig. 5.27. Once all the quantities in the sequence networks have been determined, the starting network voltages and currents can be calculated using (5.162) and (5.163).

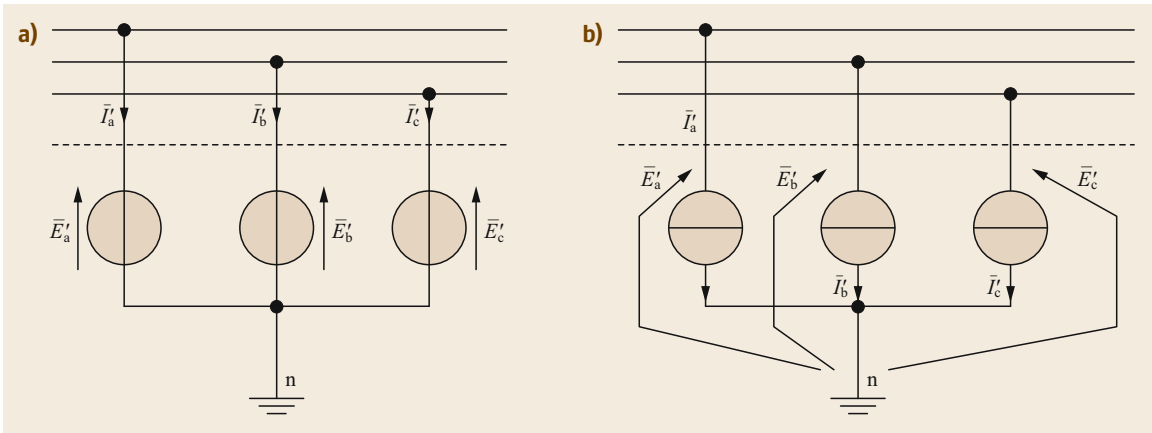
Note that the three sequence networks only differ from each other and the given network in the following ways:

- The set of three emfs that simulate the set of impedances  $\bar{Z}_a$ ,  $\bar{Z}_b$ ,  $\bar{Z}_c$ , and  $\bar{Z}_n$  differ for each of the three networks and differ from the emfs of the starting network
- In inverse and homopolar networks, there is no internal EMF (power system generators only provide direct emf).

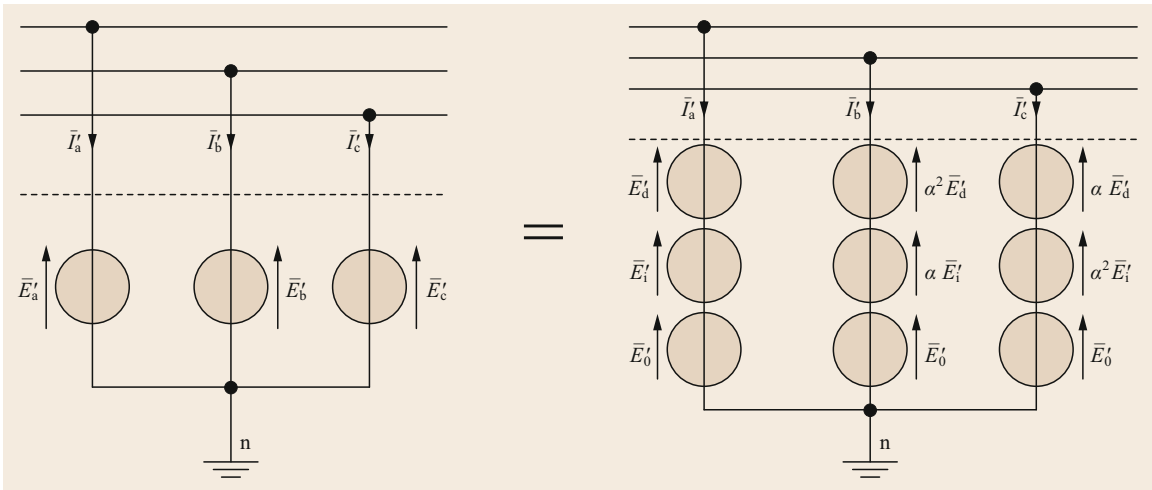
In view of the above, we can now transform the three networks of Fig. 5.27 into their Thévenin equivalent networks, as represented in Fig. 5.28.

The parameters in these single-phase Thévenin equivalent networks are as follows:  $\bar{E}$  is the voltage present before nonsymmetrical impedance insertion (i.e., the prefault voltage) at the fault position;  $\bar{Z}_d$ ,  $\bar{Z}_i$ , and  $\bar{Z}_0$  are the equivalent sequence impedances of the network measured at the faulty bus. Voltage  $\bar{E}$  is known from the load-flow calculation. In the absence of further information, it can be assumed to be equal to the rated voltage  $E_n$ , or, conservatively, to the maximum permissible operating voltage, which is often  $1.1E_n$ . It is evident that this assumption leads to the largest short-circuit current values.

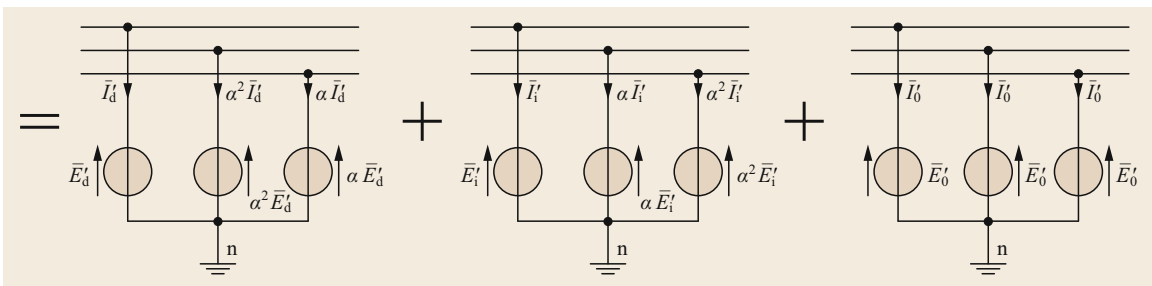
The six quantities  $\bar{E}'_d$ ,  $\bar{E}'_i$ ,  $\bar{E}'_0$ ,  $\bar{I}'_d$ ,  $\bar{I}'_i$ , and  $\bar{I}'_0$  can be determined once  $\bar{Z}_a$ ,  $\bar{Z}_b$ ,  $\bar{Z}_c$ , and  $\bar{Z}_n$  are known. Three vector equations are therefore needed (six scalars), in addition to the three expressed by the Thévenin circuits



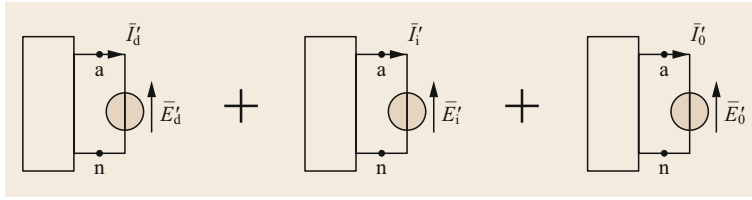
**Fig. 5.24a,b** Equivalent circuits of the system shown in Fig. 5.23 after the fault in terms of equivalent ideal voltage sources (a) and ideal current sources (b)



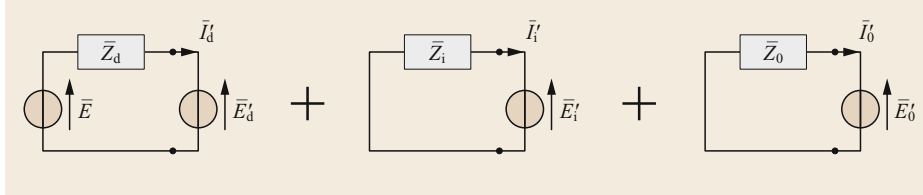
**Fig. 5.25** Representation of the Fortescue transformation



**Fig. 5.26** Representation of the Fortescue transformation: superposition of the three different circuits



**Fig. 5.27** Single-phase equivalent networks of the systems represented in Fig. 5.26



**Fig. 5.28** Single-phase Thévenin equivalent networks

$(\bar{E} = \bar{Z}_d \bar{I}_d + \bar{E}_d; 0 = \bar{Z}_i \bar{I}_i + \bar{E}_i; 0 = \bar{Z}_0 \bar{I}_0 + \bar{E}_0)$ , which depend on the particular nature of the fault.

Note that different emf systems are applied in the three networks: direct, inverse, and homopolar, respectively. Therefore, the reduction to single-phase circuits described above leads to different parameters for the equivalent circuits of the various elements of the network.

### Three-Phase Fault

Let us consider the general case depicted in Fig. 5.29a. The system shown in Fig. 5.29a is obtained from Fig. 5.20 by setting  $\bar{Z}_a = \bar{Z}_b = \bar{Z}_c = \bar{Z}_a$ . Due to the symmetrical configuration of the system,  $\bar{E}'_n$  is equal to zero regardless of the value of  $\bar{Z}_n$ , so the circuits presented in Fig. 5.29a and b are equivalent.

In this symmetrical configuration, the only nonzero current is the positive-sequence one. In phase a, the cur-

rent is

$$\bar{I}'_a = \bar{I}'_d = \frac{\bar{E}'_d}{\bar{Z}} \quad (5.164)$$

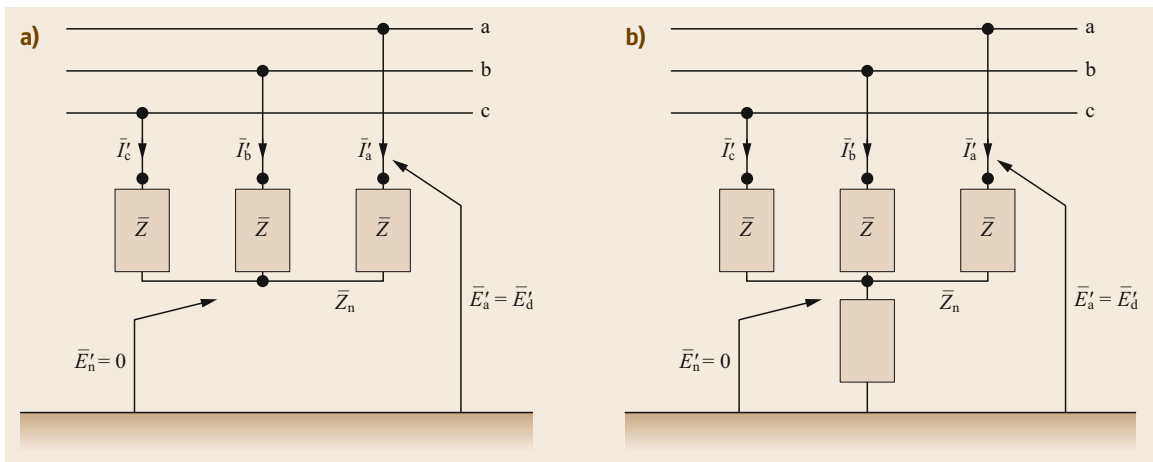
The equivalent circuit for the three-phase fault is provided in Fig. 5.30, and consists of the positive-sequence Thévenin equivalent network for Fig. 5.25.

The fault current is therefore

$$\bar{I}'_a = \bar{I}'_d = \frac{\bar{E}}{\bar{Z}_d + \bar{Z}} \quad (5.165)$$

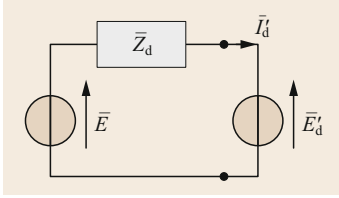
In the case of a bolted fault, this becomes

$$\bar{I}'_a = \bar{I}'_d = \frac{\bar{E}}{\bar{Z}_d} \quad (5.166)$$



**Fig. 5.29a,b** Three-phase balanced fault





**Fig. 5.30** Equivalent circuit at the positive sequence of a three-phase fault

$$\bar{E}'_d - \bar{E}'_i = 2\bar{Z}\bar{I}'_d, \text{ so}$$

$$\begin{cases} \bar{I}'_0 = 0 \\ \bar{I}'_1 = -\bar{I}'_d \\ \bar{E}'_d - \bar{E}'_i = -2\bar{Z}\bar{I}'_d \end{cases} \quad (5.168)$$

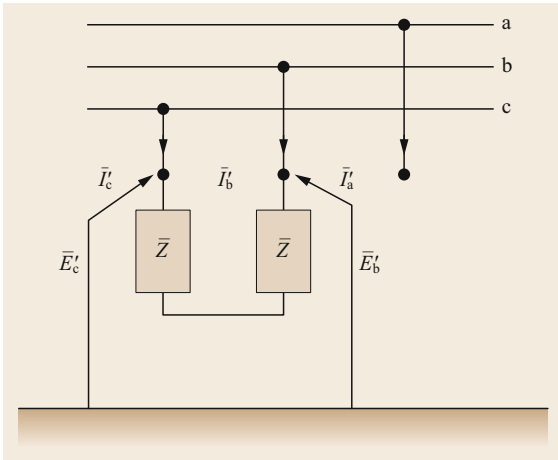
**Line-to-Line Fault**

Now consider the circuit presented in Fig. 5.31. In this case,  $\bar{Z}_a = \infty, \bar{Z}_b = \bar{Z}_c = \bar{Z}, \bar{Z}_n = \infty$ .

The system of equations

$$\begin{cases} \bar{I}'_a = 0 \\ \bar{I}'_b + \bar{I}'_c = 0 \\ \bar{E}'_b - \bar{Z}\bar{I}'_c = \bar{E}'_c - \bar{Z}\bar{I}'_b \end{cases} \quad (5.167)$$

are obtained from Fig. 5.31. Upon applying Fortescue's current transformations (5.161), we find that  $\bar{I}'_d = -\bar{I}'_i$  and  $\bar{I}'_0 = 0$ . Then, utilizing the second and third equations of (5.162) and (5.163), respectively, we obtain



**Fig. 5.31** Line-to-line fault

Using (5.168), it is possible to infer the equivalent circuit of the system, which is shown in Fig. 5.32. The zero sequence is not involved in the fault.

Employing the circuit shown in Fig. 5.32, we can derive the expressions

$$\begin{cases} \bar{E}'_0 = 0 \\ \bar{I}'_d = \frac{\bar{E}}{\bar{Z}_d + \bar{Z}_i + 2\bar{Z}} = -\bar{I}'_i \\ \bar{E}'_i = \frac{\bar{E}\bar{Z}_i}{\bar{Z}_d + \bar{Z}_i + 2\bar{Z}} \\ \bar{E}'_d = \frac{\bar{E}(\bar{Z}_i + 2\bar{Z})}{\bar{Z}_d + \bar{Z}_i + 2\bar{Z}} \end{cases} \quad (5.169)$$

Finally, by applying Fortescue's transformations, the line-to-line fault current is obtained as

$$\bar{I}'_b = \frac{-j\sqrt{3}\bar{E}}{\bar{Z}_d + \bar{Z}_i + 2\bar{Z}} \quad (5.170)$$

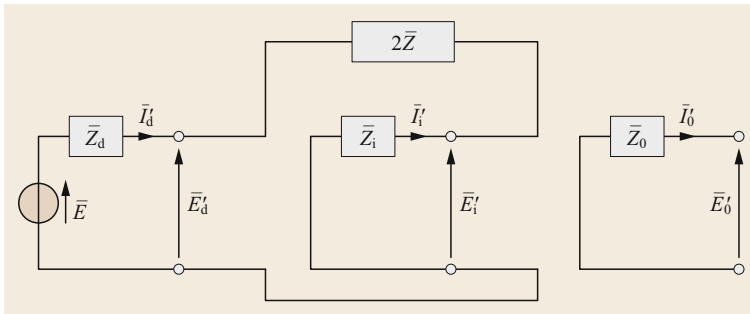
**Double Line-to-Ground Fault**

The circuit of interest here is that reported in Fig. 5.33, with  $\bar{Z}_a = \infty, \bar{Z}_b = \bar{Z}_c = 0, \bar{Z}_n = \bar{Z}$ .

From Fig. 5.33, we can infer that

$$\begin{cases} \bar{I}'_a = 0 \\ \bar{E}'_b = \bar{E}'_c \\ \bar{E}'_b = \bar{Z}(\bar{I}'_c + \bar{I}'_b) \end{cases} \quad (5.171)$$

If we employ the same procedure we adopted for the line-to-line fault, i.e., we apply Fortescue's transforma-



**Fig. 5.32** Equivalent circuit of the line-to-line fault

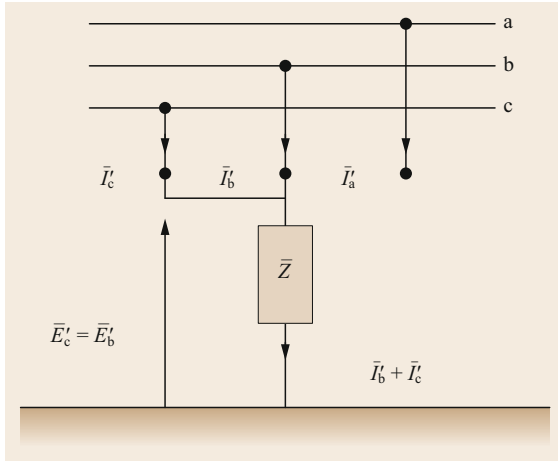


Fig. 5.33 Double line-to-ground fault

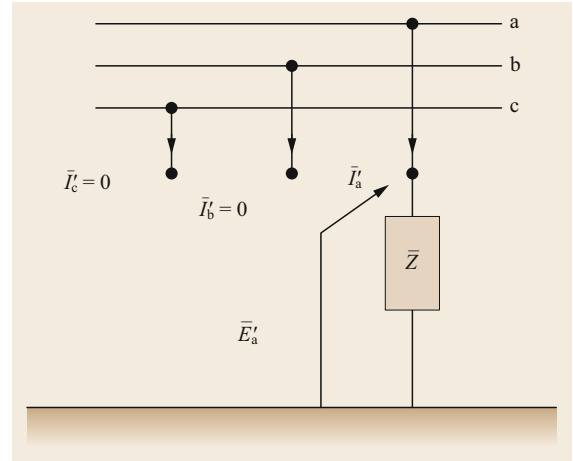


Fig. 5.35 Line-to-ground fault

tions to (5.171), we obtain the system

$$\begin{cases} \bar{I}'_d + \bar{I}'_i + \bar{I}'_0 = 0 \\ \bar{E}'_i = \bar{E}'_d \\ \bar{E}'_0 = \bar{E}'_d + 3\bar{Z}\bar{I}'_0 \end{cases} \quad (5.172)$$

Figure 5.34 presents the equivalent circuit resulting from (5.172); this equivalent circuit leads to the expressions

$$\begin{cases} \bar{I}'_d = \frac{\bar{E}}{\bar{Z}_d + [(\bar{Z}_0 + 3\bar{Z})\bar{Z}_i] / (\bar{Z}_i + \bar{Z}_0 + 3\bar{Z})} \\ \bar{I}'_i = -\bar{I}'_d \frac{\bar{Z}_0 + 3\bar{Z}}{\bar{Z}_i + \bar{Z}_0 + 3\bar{Z}} \\ \bar{E}'_d = \bar{E} - \bar{Z}_d \bar{I}'_d = \bar{E}'_i \\ \bar{E}'_0 = -\bar{Z}_0 \bar{I}'_0 \end{cases} \quad (5.173)$$

After some mathematical manipulation, we get

$$\bar{I}'_b = -j\sqrt{3}\bar{E} \frac{\bar{Z}_0 - \alpha\bar{Z}_i}{\bar{Z}_d\bar{Z}_i + \bar{Z}_d\bar{Z}_0 + \bar{Z}_i\bar{Z}_0} \quad (5.174)$$

for a bolted fault.

### Line-to-Ground Fault

We now investigate the circuit depicted in Fig. 5.35, with  $\bar{Z}_a = \bar{Z}$ ,  $\bar{Z}_b = \bar{Z}_c = \infty$ ,  $\bar{Z}_n = 0$ .

Figure 5.35 leads to the expressions

$$\begin{cases} \bar{E}'_a = \bar{Z}\bar{I}'_a \\ \bar{I}'_b = 0 \\ \bar{I}'_c = 0 \end{cases} \quad (5.175)$$

Applying Fortescue's transformations to (5.175) yields

$$\begin{cases} \bar{I}'_d = \bar{I}'_i = \bar{I}'_0 \\ \bar{E}'_d + \bar{E}'_i + \bar{E}'_0 = 3\bar{Z}\bar{I}'_0 \end{cases} \quad (5.176)$$

The equivalent circuit resulting from system (5.176) is shown in Fig. 5.36. Note that the impedance  $3\bar{Z}$  is in series with the direct, inverse, and homopolar circuit.

The expressions

$$\begin{cases} \bar{I}'_d = \bar{I}'_i = \bar{I}'_0 = \frac{\bar{E}}{\bar{Z}_d + \bar{Z}_i + \bar{Z}_0 + 3\bar{Z}} \\ \bar{E}'_d = \bar{E} - \bar{Z}_d \bar{I}'_d \\ \bar{E}'_i = -\bar{Z}_i \bar{I}'_i \\ \bar{E}'_0 = -\bar{Z}_0 \bar{I}'_0 \end{cases} \quad (5.177)$$

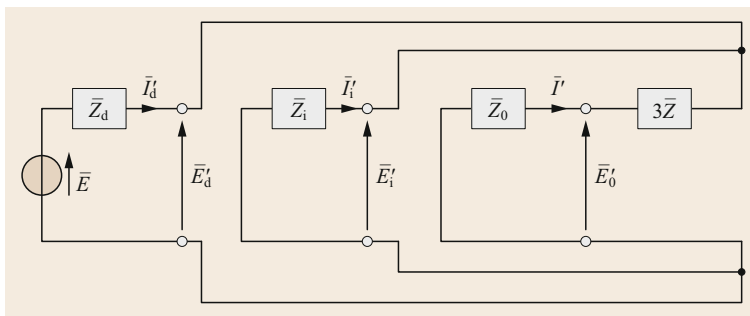
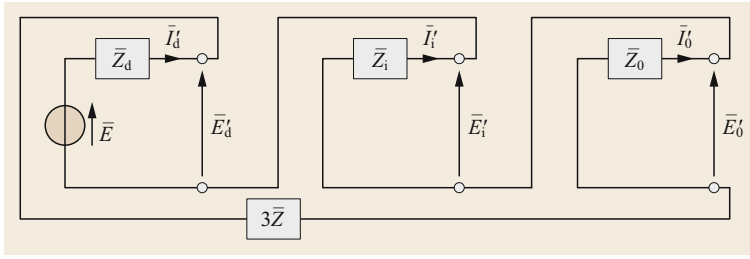


Fig. 5.34 Equivalent circuit of the double line-to-ground fault



**Fig. 5.36** Equivalent circuit of the line-to-ground fault

are readily obtained from the circuit shown in Fig. 5.36. Finally, the fault current for the line-to-ground fault is

$$\bar{I}'_a = \frac{3\bar{E}}{\bar{Z}_d + \bar{Z}_i + \bar{Z}_o + 3\bar{Z}} \quad (5.178)$$

### 5.5.4 Direct, Inverse, and Homopolar Sequence Impedances

This section provides the main guidelines for determining the direct, inverse, and homopolar sequence impedances of the main power system elements. The following simplifying assumptions are made:

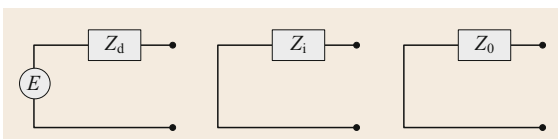
- Transversal parameters are negligible
- The equations are written using the per unit (pu) method.

The pu values of the component parameters (e.g., the reactance  $\dot{x}$  of a generator or transformer, etc.), which are provided by the manufacturer based on the rated voltage  $V_b$  and the rated apparent power of the equipment  $S_b$ , need to be converted to suitable base values of power, voltage  $V'_b$ , and apparent power  $S'_b$  for the various parts of the system according to

$$\dot{x}' = \dot{x} \left( \frac{V_b}{V'_b} \right)^2 \frac{S'_b}{S_b} \quad (5.179)$$

For *generators*, the equivalent circuits for direct, inverse, and homopolar sequences are shown in Fig. 5.37. Note that:

- To a good approximation,  $z_d$  can be represented by  $x''_d$ , the direct-axis subtransient reactance (which is



**Fig. 5.37** Equivalent circuit of a generator: direct, inverse, and homopolar sequences

provided by the manufacturer and is typically in the range 0.1–0.3 pu).

- The inverse sequence  $z_i \approx x''_d$  does not produce an effective armature reaction.
- $z_0$  is given by the manufacturer. Any impedance that is connected between the neutral point and the earth is multiplied by 3 and inserted into the equivalent circuit in series with  $Z_0$ .

For *power transformers*, the inverse sequence is equal to the direct sequence and—as shown in Fig. 5.38—can be assumed to be equal to the short-circuit impedance in pu, i.e.,

$$z_{cc} = 0.01 v_{cc}\% \quad (5.180)$$

In the case of a three-winding transformer, the impedance of a particular winding can be calculated on the basis of the short-circuit test measurements

$$z_1 + z_2 = v_{cc,p-s}\% \times 0.01 \quad (5.181)$$

$$z_1 + z_3 = v_{cc,p-t}\% \times 0.01 \quad (5.182)$$

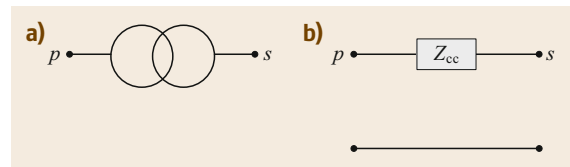
$$z_2 + z_3 = v_{cc,s-t}\% \times 0.01 \quad (5.183)$$

$$z_1 = 0.5(v_{cc,p-s}\% + v_{cc,p-t}\% - v_{cc,s-t}\%) \times 0.01 \quad (5.184)$$

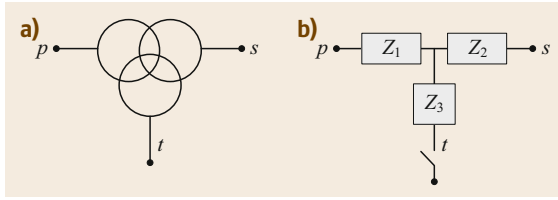
$$z_2 = 0.5(v_{cc,p-s}\% + v_{cc,s-t}\% - v_{cc,p-t}\%) \times 0.01 \quad (5.185)$$

$$z_3 = 0.5(v_{cc,s-t}\% + v_{cc,p-t}\% - v_{cc,p-s}\%) \times 0.01 \quad (5.186)$$

where  $v_{cc,p-s}\%$ ,  $v_{cc,s-t}\%$ , and  $v_{cc,p-t}\%$  are the short-circuit impedances measured in three cases: when winding 1 is supplied, 2 is short-circuited, and 3 is open; when winding 2 is supplied, 3 is short-circuited, and 1 is open; and



**Fig. 5.38a,b** Equivalent circuit of a transformer at the direct (a) and inverse sequences (b)



**Fig. 5.39** Equivalent circuit of a three-winding transformer at the direct (a) and inverse sequences (b)

when 2 is supplied, 3 is short-circuited, and 1 is open, respectively. The equivalent circuit of a three-winding transformer at the direct and inverse sequences is represented in Fig. 5.39b.

Finally, Figs. 5.40 and 5.41 show the homopolar sequence impedances of the transformer and the three-winding transformer for different groups and connections of windings.

Any impedance connected between the neutral point and the earth is multiplied by 3 and introduced into the equivalent circuit in series to  $Z_0$  (or, for the three-winding transformer, in series to  $Z_p$  or  $Z_s$ ).

The equivalent circuits of a *transmission line* can be approximated as shown in Fig. 5.42. The positive and negative-sequence impedances  $Z_d$  and  $Z_i$  are equal. The

zero-sequence impedance  $Z_0$  is typically 3 to 4 times larger than  $Z_d$ .

For three-phase and single-phase faults in a *generic network with given short-circuit power* (Fig. 5.43), the equivalent impedances are given by

$$z_d = \frac{E_{nom}}{I_{cc,3}} \tag{5.187}$$

$$z_d = z_i \tag{5.188}$$

$$z_0 = 3 \frac{E_{nom}}{I_{cc,1}} - 2z_d, \tag{5.189}$$

where  $I_{cc,3}$  and  $I_{cc,1}$  are the values for balanced and line-to-ground faults, respectively.

The short-circuit power for a three-phase fault is calculated via

$$P_{cc,3f} = E_{nom} I_{cc,3f}, \tag{5.190}$$

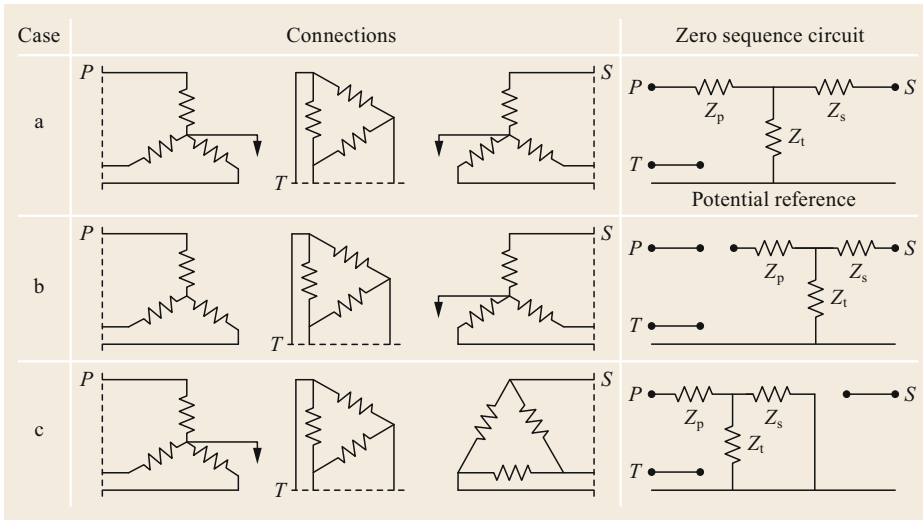
while the short-circuit power for a single-phase fault is obtained using

$$P_{cc,1f} = E_{nom} I_{cc,1f}. \tag{5.191}$$

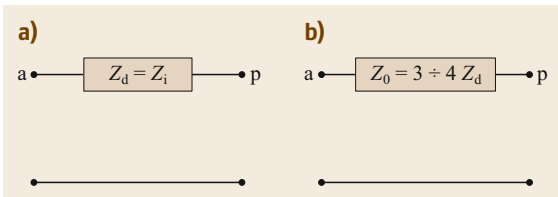
An *infinite power bus* can be assumed to be equivalent to the bus of a network with infinite short-circuit cur-

Case	Connections	Zero sequence circuit
a		
b		
c		
d		
e		

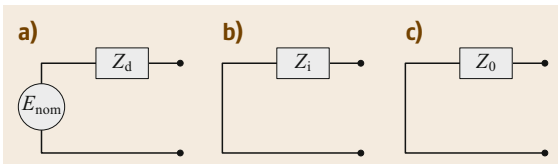
**Fig. 5.40** Equivalent circuit of a transformer at the homopolar sequence (adapted from [5.6, 44])



**Fig. 5.41** Equivalent circuit of a three-phase transformer at the homopolar sequence (adapted from [5.6, 44])



**Fig. 5.42a,b** Equivalent circuits of a transmission line: (a) positive sequence = negative sequence, (b) zero sequence



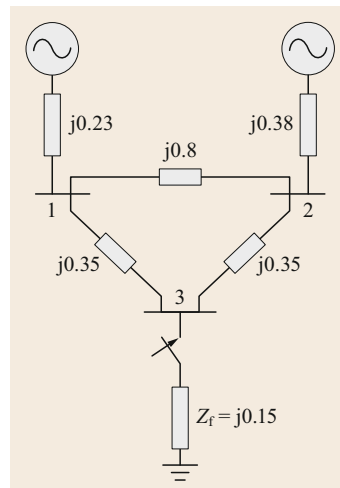
**Fig. 5.43a-c** Generic network with given short-circuit power: (a) positive sequence, (b) negative sequence, and (c) zero sequence

rent (for single-phase and three-phase faults). Also, we can assume that a bus without generators is equivalent to the bus of a network with null short-circuit current (for single-phase and three-phase faults). Loads, unless otherwise indicated, are neglected in the calculations.

### 5.5.5 Fault at Any Point in the Network

Consider the network depicted in Fig. 5.44. A symmetrical fault occurs at bus 3. We shall refer to the equivalent single-phase network, neglecting the presence of loads (no current is absorbed).

According to Thévenin’s theorem, the linear part of the network can be replaced with an ideal indepen-



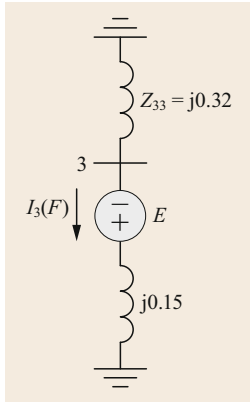
**Fig. 5.44** The network considered; there is a fault at bus 3 (adapted from [5.12])

dent generator with an emf  $E$  (*no-load* emf) and an impedance  $Z_{th}$  (the equivalent impedance with all emfs short-circuited) in series, as shown in Fig. 5.45.

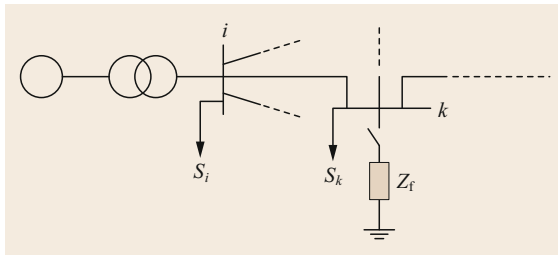
In the presence of loads, the voltage prior to the fault is given by the steady-state solution. Otherwise, it is approximated by the maximum permissible operating voltage of the transmission network, 1.1 pu.

By neglecting the loads and the transversal parameters of the network components,  $Z_{th}$  can be obtained by calculating the equivalent series and parallel impedances and by star-delta transformations ( $Z_{33}$  in Fig. 5.45, which is equal to  $j0.34$ , was obtained in this way).

The equivalent impedance  $Z_{th}$  can also be determined by inverting the nodal admittance matrix of the network to obtain the impedance matrix;  $Z_{th}$  is the element of the main diagonal of the impedance matrix that corresponds to the fault node.



**Fig. 5.45** The network following the application of Thévenin's theorem; there is a fault at bus 3 (adapted from [5.12])



**Fig. 5.46** Power system consisting of  $n$  buses; there is a fault at bus  $k$  (adapted from [5.12])

Let us consider the bus of a power system consisting of  $n$  buses, as shown in Fig. 5.46.

We now assume a symmetrical fault at bus  $k$  such that the fault impedance is  $Z_f$ .

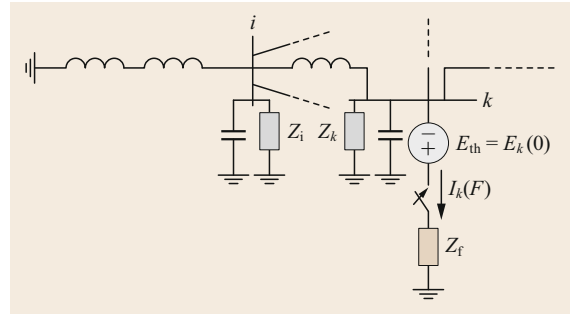
The nodal voltages before the fault can be obtained by calculating the load flow, and are represented by the vector

$$\mathbf{E}(0) = \begin{bmatrix} E_1(0) \\ \vdots \\ E_k(0) \\ \vdots \\ E_n(0) \end{bmatrix}. \quad (5.192)$$

The voltage variations caused by the fault with impedance  $Z_f$  are equivalent to those caused by the voltage  $E_k(0)$  when all the other generators are short-circuited.

The Thévenin equivalent circuit, as shown in Fig. 5.47, can be obtained by short-circuiting all of the generators and representing all of the loads and network components by their respective impedances.

Although we have ignored loads so far (since the steady-state currents are much lower than the short-circuit ones), the loads at the various buses can be accounted for by introducing a constant impedance. The



**Fig. 5.47** Thévenin equivalent network of a power system consisting of  $n$  buses; there is a fault at bus  $k$  (adapted from [5.12])

value of this impedance can be obtained by

$$Z_{iL} = \frac{|E_i(0)|^2}{S_L}, \quad (5.193)$$

$S_L$  being the power absorbed by the load before the fault. Let us denote the fault-induced nodal voltage variations by the vector

$$\Delta \mathbf{E} = \begin{bmatrix} \Delta E_1 \\ \vdots \\ \Delta E_k \\ \vdots \\ \Delta E_n \end{bmatrix}. \quad (5.194)$$

The nodal voltages during the fault are therefore given by the sum of the voltages before the fault and the variations due to the fault current, i.e.,

$$\begin{bmatrix} E_1(F) \\ \vdots \\ E_k(F) \\ \vdots \\ E_n(F) \end{bmatrix} = \begin{bmatrix} E_1(0) \\ \vdots \\ E_k(0) \\ \vdots \\ E_n(0) \end{bmatrix} + \begin{bmatrix} \Delta E_1 \\ \vdots \\ \Delta E_k \\ \vdots \\ \Delta E_n \end{bmatrix}. \quad (5.195)$$

In compact form,

$$\mathbf{E}(F) = \mathbf{E}(0) + \Delta \mathbf{E}. \quad (5.196)$$

The voltages at the nodes are related to the current by the expression

$$\mathbf{I} = \mathbf{Y} \cdot \mathbf{E}. \quad (5.197)$$

In the Thévenin circuit shown in Fig. 5.47, the incoming current at each node is zero except at node  $k$ , where it is

considered positive if injected (so we consider it to be negative).

Therefore, we get

$$\begin{bmatrix} 0 \\ \vdots \\ -I_k(F) \\ \vdots \\ 0 \end{bmatrix} = \begin{bmatrix} Y_{11} & \dots & Y_{1k} & \dots & Y_{1n} \\ \vdots & \vdots & \vdots & \vdots & \vdots \\ Y_{k1} & \dots & Y_{kk} & \dots & Y_{kn} \\ \vdots & \vdots & \vdots & \vdots & \vdots \\ Y_{n1} & \dots & Y_{nk} & \dots & Y_{nn} \end{bmatrix} \begin{bmatrix} \Delta E_1 \\ \vdots \\ \Delta E_k \\ \vdots \\ \Delta E_n \end{bmatrix}, \quad (5.198)$$

which can be rewritten in compact form as

$$\mathbf{I}(F) = \mathbf{Y} \cdot \Delta \mathbf{E}, \quad (5.199)$$

leading to

$$\Delta \mathbf{E} = \mathbf{Z} \cdot \mathbf{I}(F), \quad (5.200)$$

where

$$\mathbf{Z} = \mathbf{Y}^{-1}, \quad (5.201)$$

which is known as the impedance matrix.

Therefore, from (5.196),

$$\mathbf{E}(F) = \mathbf{E}(0) + \mathbf{Z} \cdot \mathbf{I}(F). \quad (5.202)$$

In matrix form,

$$\begin{bmatrix} E_1(F) \\ \vdots \\ E_k(F) \\ \vdots \\ E_n(F) \end{bmatrix} = \begin{bmatrix} E_1(0) \\ \vdots \\ E_k(0) \\ \vdots \\ E(0)_n \end{bmatrix} + \begin{bmatrix} Z_{11} & \dots & Z_{1k} & \dots & Z_{1n} \\ \vdots & \vdots & \vdots & \vdots & \vdots \\ Z_{k1} & \dots & Z_{kk} & \dots & Z_{kn} \\ \vdots & \vdots & \vdots & \vdots & \vdots \\ Z_{n1} & \dots & Z_{nk} & \dots & Z_{nn} \end{bmatrix} \begin{bmatrix} 0 \\ \vdots \\ -I_k(F) \\ \vdots \\ 0 \end{bmatrix}. \quad (5.203)$$

This leads to

$$E_k(F) = E_k(0) - Z_{kk} I_k(F). \quad (5.204)$$

We also know from Fig. 5.47 that

$$E_k(F) = Z_f I_k(F), \quad (5.205)$$

and that  $E_k(F) = 0$  for a solid balanced fault (i.e.,  $Z_f = 0$ ). Therefore,

$$I_k(F) = \frac{E_k(0)}{Z_{kk} + Z_f}. \quad (5.206)$$

Hence, for a fault at bus  $k$ , we only need the element  $Z_{kk}$ , which is the Thévenin equivalent impedance of the network viewed from the fault location.

We also have that

$$E_k(F) = Z_f I_k(F). \quad (5.207)$$

Substituting the previous expression for  $I_k$  into this equation yields

$$E_i(F) = E_i(0) - \frac{Z_{ik}}{Z_{kk} + Z_f} E_k(0). \quad (5.208)$$

The knowledge of the nodal voltages during the fault allows the fault current to be calculated for all of the lines. The short-circuit current in the line that connects buses  $i$  and  $j$  (where the current is defined to be positive in the  $i \rightarrow j$  direction) through impedance  $z_{ij}$  is given by

$$I_{ij}(F) = \frac{E_i(F) - E_j(F)}{z_{ij}}. \quad (5.209)$$

Note that the knowledge of the impedance matrix allows the fault current and the node voltage during the fault to be readily evaluated for every node of the network.

This method is simple and practical: all the calculations relevant to a specific fault are formulated with respect to the fault bus using the impedance matrix  $\mathbf{Z}$  which can be calculated by inverting  $\mathbf{Y}$ , although this inversion is computationally prohibitive for large power systems with many nodes. A more efficient method of determining  $\mathbf{Z}$  is to construct it by adding one element of the network at a time.

### 5.5.6 Three-Phase Short Circuit at a Synchronous Generator's Terminals

A synchronous machine operating as a generator can be studied by considering it as an active two-port network. It is also linear when the working conditions are far from saturation, as is usual during faults. The following considerations are made for a round rotor machine, but they can easily be extended to the case of a salient pole machine.

The equivalent two-port equation of the alternator is

$$\bar{E} - \bar{Z}_s \bar{I} = \bar{V}, \quad (5.210)$$

where:

- $\bar{E}$  is the emf generated in the alternator by the excitation current  $I_f$  (the voltage measured at the machine's terminal under no-load conditions)
- $\bar{V}$  is the voltage measured at the machine's terminal when the machine supplies current  $\bar{I}$
- $\bar{Z}_s$  is the internal impedance of the machine, commonly termed the synchronous impedance, which is the sum of two components: (i) the impedance of the stator's windings and (ii) the armature's reaction.

For a given value of the excitation current and a given current  $\bar{I}$  flowing in the stator's windings, the voltage  $\bar{V}$  at the machine's terminals is different from the no-load emf  $\bar{E}$ . The difference

$$\bar{Z}_s \bar{I} = \bar{E} - \bar{V} \quad (5.211)$$

is the voltage drop due to the current  $\bar{I}$  and its shift with respect to  $\bar{V}$ . This voltage drop is given by the two components mentioned above:

- The drop in the impedance of the stator's windings  $(R_1 + jX_1)\bar{I}$ , where  $R_1$  and  $X_1$  are the resistance of the stator's windings and the leakage reactance, respectively
- The armature's reaction, which is equal to  $jX_r\bar{I}$  for a round rotor machine.

Therefore, it holds that

$$\bar{Z}_s = R_1 + j(X_1 + X_r) \quad (5.212)$$

The quantity

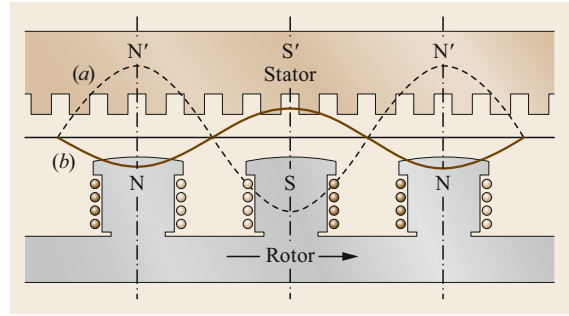
$$X_s = X_1 + X_r \quad (5.213)$$

is the synchronous reactance of the machine.

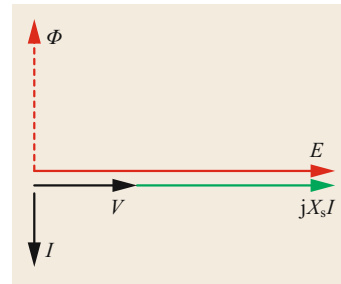
Let us assume that a synchronous generator is supplying an inductive load. In this case, we assume that  $I$  lags  $E$  and  $V$  by  $90^\circ$  (ignoring the circuit resistance): the flux produced by the stator (the armature flux) has the opposite polarity to the main flux  $\Phi$ , thus reducing the main flux. Consequently, the total emf induced in the stator decreases. This phenomenon is called the demagnetizing effect and it is represented in Figs. 5.48 and 5.49.

Let us assume that the synchronous generator is supplying a capacitive load. In this case, we assume that  $I$  leads  $E$  and  $V$  by  $90^\circ$  (the excitation current is kept the same as in the previous case): the flux produced by the stator (armature flux) is in phase with the main flux  $\Phi$ , thus increasing the main flux. Consequently, the total emf induced in the stator increases. This phenomenon is known as the magnetizing effect and it is represented in Figs. 5.50 and 5.51.

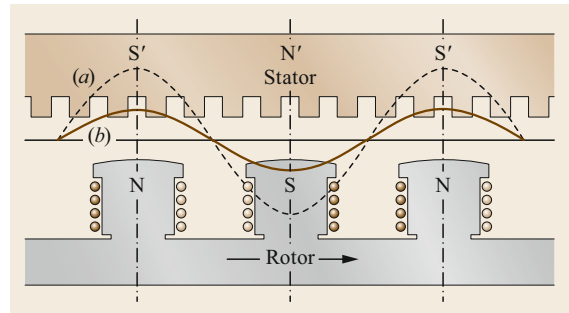
In order to simulate the alternator under transient conditions, we make use of the EMTP-RV model pre-



**Fig. 5.48** Armature reaction: the current  $I$  lags the voltage by  $90^\circ$ . Waveform (a) shows the main flux  $\Phi$ , while waveform (b) shows the armature flux (adapted from [5.1])



**Fig. 5.49** Phasor diagram of the alternator for an inductive load



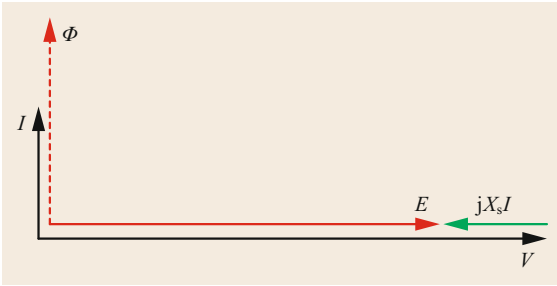
**Fig. 5.50a,b** Armature reaction: current  $I$  leads the voltage by  $90^\circ$ . Waveform (a) shows the main flux  $\Phi$ , while waveform (b) shows the armature flux (adapted from [5.1])

sented in [5.8, 45]. Park's transformation is initially used with saturation neglected to obtain linear relations and apply superposition.

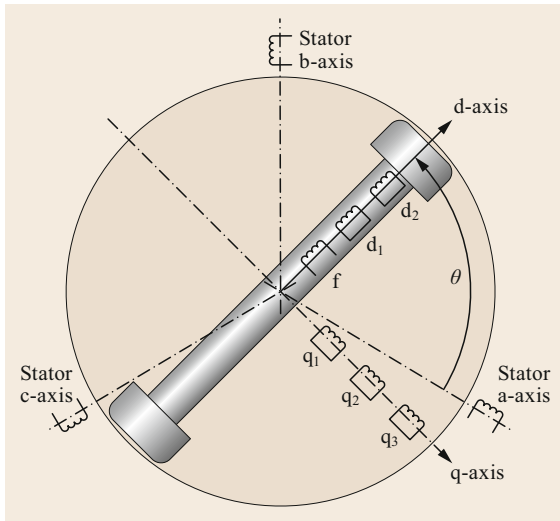
The magnetic circuits of the rotor windings are assumed to be symmetric with respect to the direct axis, which is the axis of the field created by the rotor. The quadrature axis lags the direct one by  $90^\circ$ .

A current in any winding produces a sinusoidal magnetic field in the air gap. This field can be decomposed along the direct and quadrature axes. The effects of harmonics in the field distribution are negligible for a correctly dimensioned machine. The effects of hysteresis are neglected. Eddy currents are negli-





**Fig. 5.51** Phasor diagram of the alternator for a capacitive load



**Fig. 5.52** Schematic representation of the machine showing the d-axis and q-axis (adapted from EMTP-RV help)

ble, except in the case of a solid rotor (cylindrical rotor) machine, where they can be represented by a q-axis winding.

The synchronous machine model consists of nine windings:

- Three for the stator (one for each phase); these are denoted by the indices a, b, and c, respectively.
- Six for the rotor. Along the axis of the rotor field (the direct axis), we have the excitation winding  $f$  and a maximum of two damper windings:  $d_1$  and  $d_2$ . There are also a maximum of three damper windings, denoted  $q_1$ ,  $q_2$ , and  $q_3$ , along the quadrature axis.

This machine is represented in Fig. 5.52.

### Short-Circuit Currents with the Generator Initially at No Load

Let us consider a three-phase synchronous generator with the following parameters:

- Rated power: 1000 MVA
- Nominal frequency: 50 Hz
- Rated voltage (RMSLL (RMS line-to-line)): 20 kV
- Winding (armature) resistance: 0.002 pu
- Armature leakage reactance: 0.188 pu
- Direct-axis synchronous reactance:  $x_d = 2$  pu
- Quadrature-axis synchronous reactance:  $x_q = 2$  pu
- Direct-axis transient reactance:  $x'_d = 0.4$  pu
- Quadrature-axis transient reactance:  $x'_q = 0.4$  pu
- Direct-axis short-circuit transient constant:  $T'_d = 1$  s
- Quadrature-axis short-circuit transient constant:  $T'_q = 1$  s.

It is initially assumed that the d-axis and q-axis sub-transient reactances are negligible. As a consequence, if we refer to the equivalent model in Fig. 5.52, only the field winding is relevant along the d-axis, while only one damper is considered along the q-axis (winding  $q_1$ ).

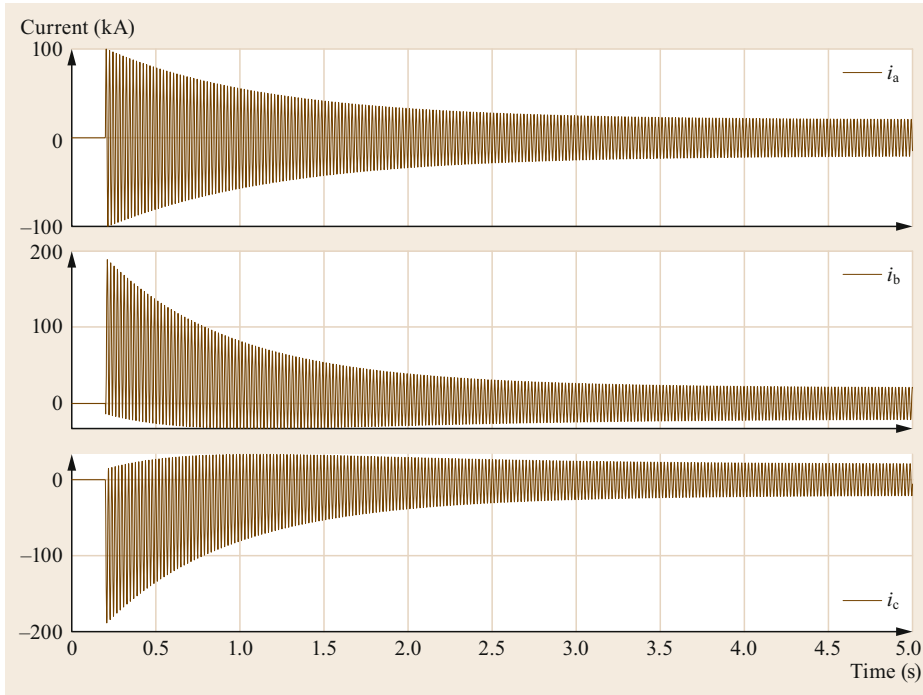
Let us assume that no-load steady-state conditions apply. A three-phase short circuit occurs at the machine's terminals at  $t = 200$  ms. At  $t_{\text{fault}} = 200$  ms, a three-phase bolted short circuit occurs at the machine's terminals. Figure 5.53 shows the currents in the three stator windings during the fault. The subtransient reactance is neglected. If the winding resistances are neglected, the stator current lags the voltage by  $90^\circ$ , as the machine's reactances are equivalent to a purely inductive load. Therefore, at the instant that the short circuit occurs, the current in phase a is at its natural zero crossing, so this current has no unidirectional component—only the symmetrical component. Initially, the current reaches a peak value of approximately 100 kA, before decreasing exponentially to reach its steady-state value. The current in phase b reaches its maximum and the current in phase c reaches its minimum at the instant that the short circuit occurs, meaning that those currents have unidirectional components, as shown in Fig. 5.53.

The envelope for the current in phase a is shown in Fig. 5.54, and is given by

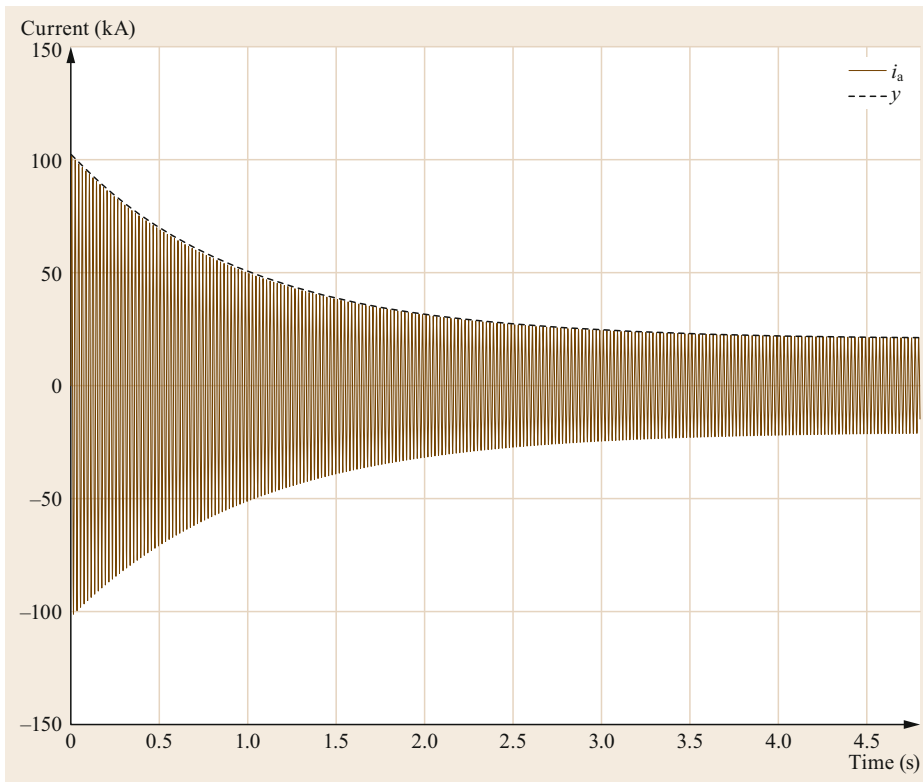
$$y(t) = \sqrt{2} \left[ \left( \frac{1}{x'_d} - \frac{1}{x_d} \right) e^{-\frac{t}{T'_d}} + \frac{1}{x_d} \right] I_{\text{base}}, \quad (5.214)$$

where

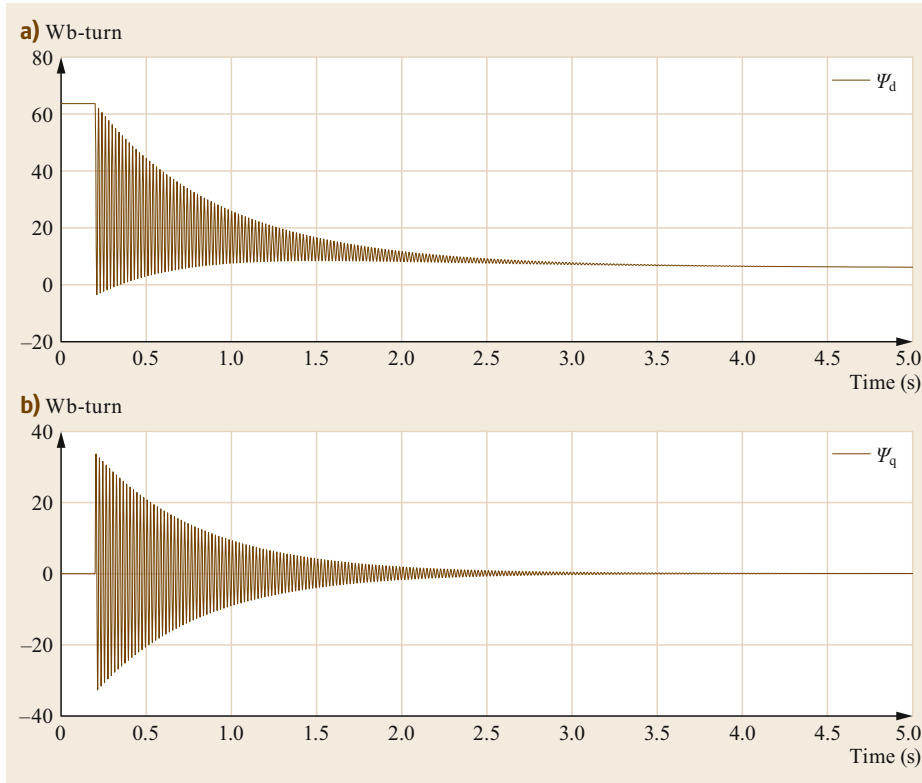
$$I_{\text{base}} = \frac{A_n}{\sqrt{3}V_n} = 28.9 \text{ kA}. \quad (5.215)$$



**Fig. 5.53** Phase currents: three-phase fault at 200 ms (subtransient state neglected)



**Fig. 5.54** The current and the current envelope in phase a (subtransient state neglected); 200 ms time shift



**Fig. 5.55a,b** Flux linkages along (a) the d-axis and (b) the q-axis (subtransient state neglected)

The envelope of the symmetrical component of the short circuit current  $y(t)$ , in pu, is initially equal to

$$y(t = t_{\text{fault}}) = \frac{1}{x'_d} \quad (5.216)$$

In the first few moments, the armature reaction is weakened by the rapid variation of the total flux linkage. At the beginning of the electromagnetic transient, therefore, the armature reactance is not equal to the synchronous reactance of the machine but to the transient one (ignoring the subtransient state).

The steady-state value of the symmetrical component (in pu) is given by

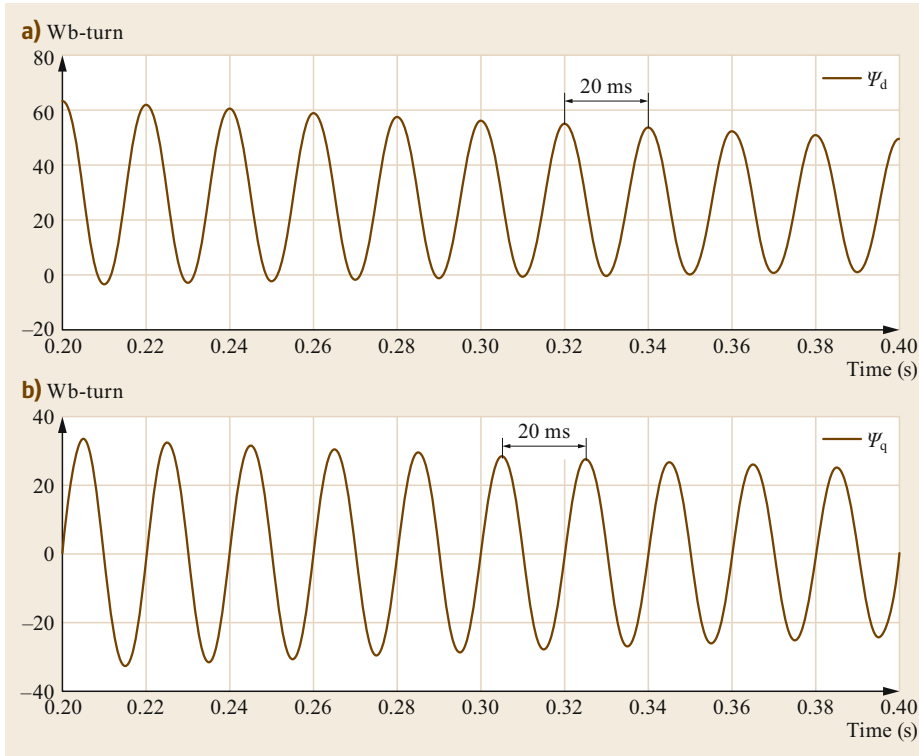
$$y(t \rightarrow \infty) = \frac{1}{x_d} \quad (5.217)$$

Upon substituting the values of the reactances into (5.214), it becomes apparent that the peak value of  $y(t)$  for the configuration of interest is initially equal to 102 kA, and it reaches 20.4 kA in the steady state.

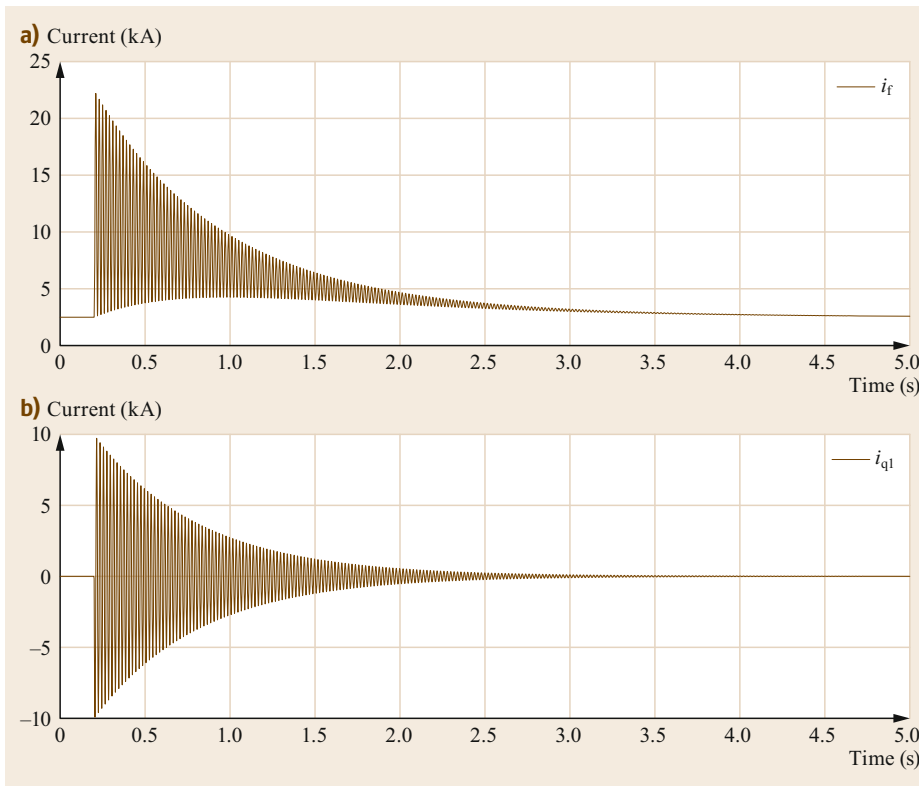
The flux linkages along the d-axis and the q-axis are shown in Fig. 5.55. Prior to short-circuit inception, the flux along the d-axis is at a constant value dictated by

the excitation winding current. During the transient, it decreases exponentially until it attains a low constant value in the steady state. This is due to the demagnetizing effect of the short-circuit current, in agreement with the phasor diagram of Fig. 5.49. Since the machine operates under no-load conditions before the fault, the total flux is equal to the d-axis flux, while the flux linkage along the q-axis is null. The sudden variation in the armature current leads to rapid variation of the q-axis flux, which quickly reaches its peak value before decreasing exponentially to zero again.

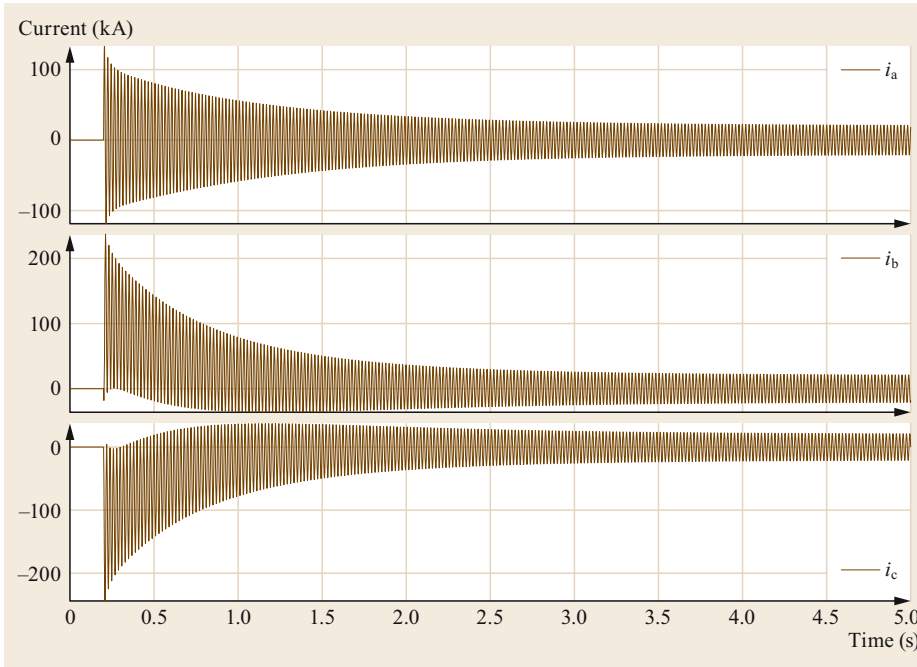
It is worth noting that, besides the exponential decay, the flux along each axis shows an oscillatory component. This component oscillates at a frequency of 50 Hz with respect to the d-q frame because it is induced by the unidirectional components of the currents in phases b and c. These components generate a magnetic field that is stationary with respect to the stator but appears to be a magnetic field rotating at 50 Hz in the d-q frame. This is confirmed by the detail shown in Fig. 5.56. The amplitude of the oscillatory component along the q-axis decays with the same time constant as the unidirectional component of the stator winding current. Similar considerations apply for the current flowing in the q-axis damper winding  $i_{q1}$ , as shown in



**Fig. 5.56a,b** Flux linkages along (a) the d-axis and (b) the q-axis shown in detail (the subtransient state is neglected)



**Fig. 5.57a,b** Currents in the field winding (a) and the first q-axis damper winding (b)



**Fig. 5.58** Phase currents with the subtransient state considered

Fig. 5.57. According to the Faraday–Neumann–Lenz law, the magnetic field generated by the current flowing in the damper windings during the transient opposes the initial changing magnetic field. The current  $i_f$  that flows in the rotor field winding is also reported in Fig. 5.57. Before the fault,  $i_f$  is set to 2494 A. The sudden variation in the current in the stator windings induces an emf in the rotor field winding, which causes an increase of the currents in both the field and damper windings, as shown in Fig. 5.57. Just as for the damper windings, the magnetic field created by the current induced in the field winding opposes the initial changing magnetic field. Similar to the flux linkage and  $i_{q1}$ , the oscillatory component of  $i_f$  is generated by the unidirectional component of the stator winding current. In the steady state, as the flux linkage is constant with respect to the rotor frame of reference, the value of the rotor current  $i_f$  returns to its previous value, 2494 A.

Let us now consider the effects of the damper windings on the direct axis and a second damper on the q-axis. The d-axis and q-axis subtransient reactances are  $x_d'' = x_q'' = 0.3$  pu, and the short-circuit subtransient constant is  $T_d'' = 0.03$  s.

Figure 5.58 shows the currents in the three stator windings during the fault. The current waveforms in the three stator windings are similar to those in the previous case in which the subtransient state was neglected, but the initial current peaks are larger.

The envelope of the current in phase a is shown in Fig. 5.59 and is given by the expression

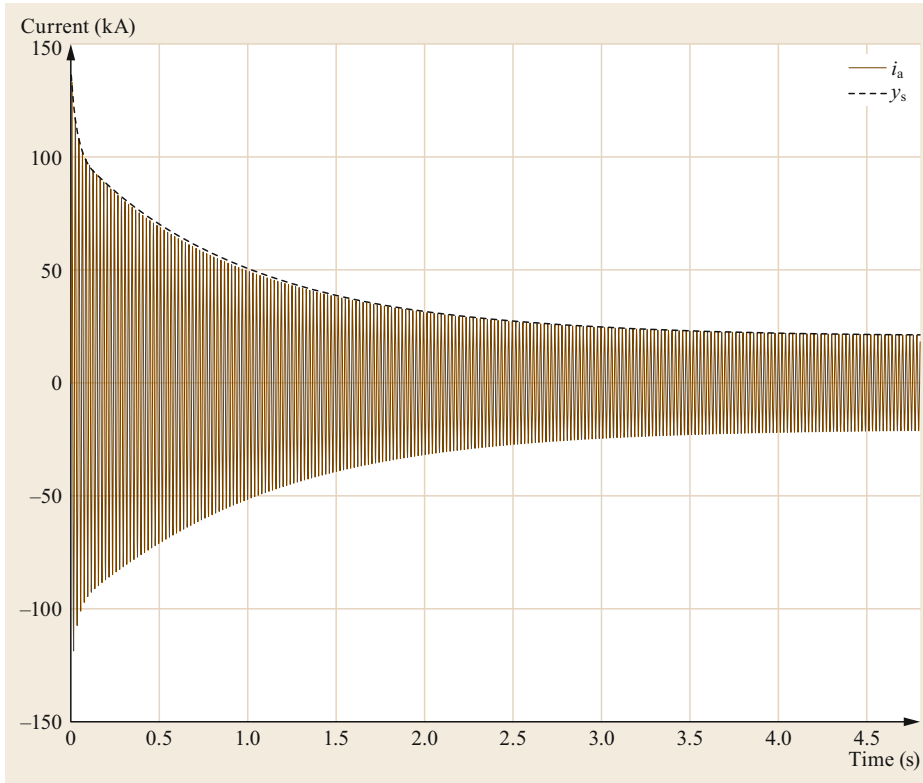
$$y_s(t) = \sqrt{2} \left[ \left( \frac{1}{x_d''} - \frac{1}{x_d'} \right) e^{-\frac{t}{T_d''}} + \left( \frac{1}{x_d'} - \frac{1}{x_d} \right) e^{-\frac{t}{T_d}} + \frac{1}{x_d} \right] I_{\text{base}} \quad (5.218)$$

The armature reaction during the subtransient state is lower than those in the transient and steady states. As a consequence, the initial value of the current is higher than that given by (5.214).

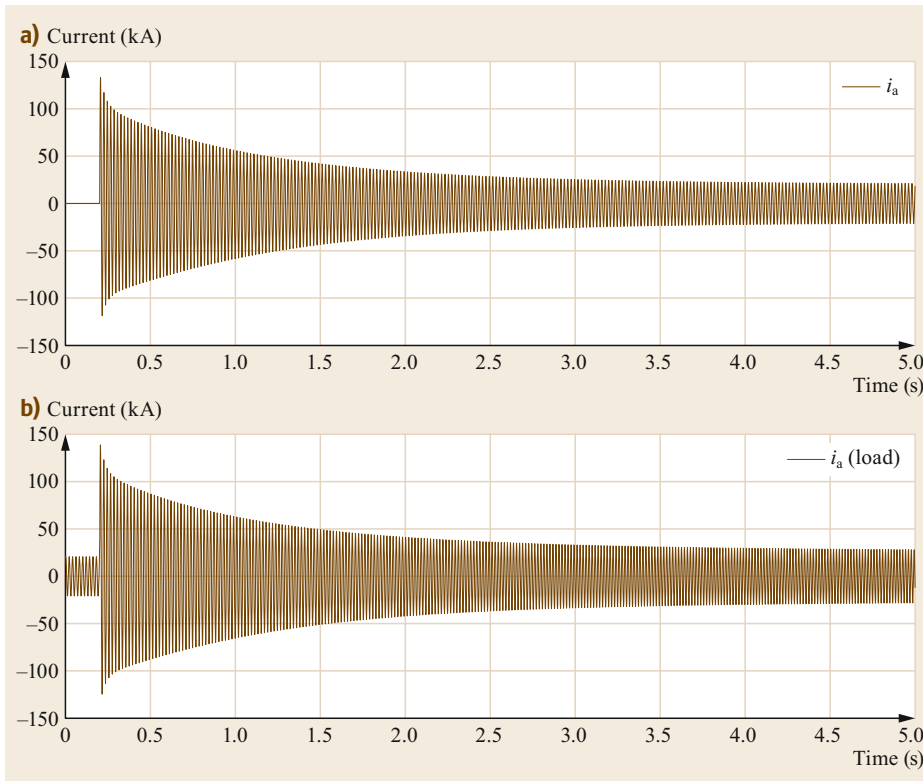
#### Short-Circuit Currents in the Loaded Generator

In this final comparison, we consider the case in which the generator is supplying a load before the fault occurs. Figure 5.60 shows the current in phase a when the machine is under no-load and on-load conditions. In the latter case, the current is not null before the fault. The peak value is similar to that calculated for the machine under no-load conditions, but the final steady-state current amplitude is slightly larger.

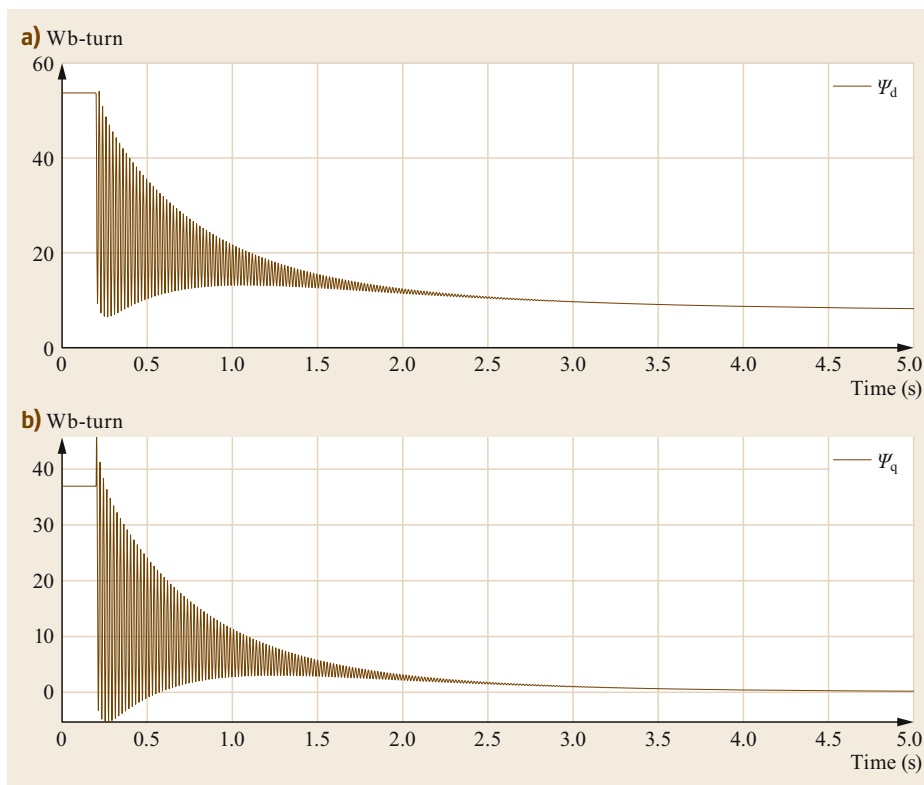
It is interesting to observe the variation in the flux linkage—particularly that along the q-axis (see Fig. 5.61)—during the transient. Unlike the case shown in Fig. 5.55, the flux is not null before fault inception, but the steady-state value after the fault is zero due to the demagnetizing effect of the short-circuit current.



**Fig. 5.59** The current and the current envelope in phase a with the subtransient state considered; 200 ms time shift



**Fig. 5.60a,b** Current in phase a under (a) no-load and (b) on-load conditions



**Fig. 5.61a,b** Flux linkages along (a) the d-axis and (b) the q-axis under on-load conditions

## 5.6 Stability

A wide variety of dynamic phenomena occur in electric power systems. These phenomena are often called transients. Transients have various physical origins and timescales. Ignoring small variations in the operating conditions (which are always present), a transient corresponds to a significant perturbation of the steady state of a system. During the transient, several other perturbations may occur due to control and protective actions.

### 5.6.1 Transient Phenomena

Listed in order of the fastest to the slowest, transients in power systems are usually categorized into:

- Propagating electromagnetic transients that affect lines, transformers, and other connected components. These transients are caused by lightning or switching maneuvers, and have typical time horizons of between  $10^{-7}$  and  $10^{-3}$  s (corresponding to frequencies ranging from 10 MHz to kHz).
- Electromagnetic transients in rotating machine windings that are caused by disturbances, switch-

ing maneuvers, or interactions between machines (time horizon:  $10^{-3}$ – $10^{-1}$  s; frequency: a few kHz to 10 Hz).

- Electromechanical transients, namely rotor swings in synchronous machines and motors. These originate in the same way as for the two types of transients defined above, as well as from voltage and frequency control (0.1–10 s; 10–0.1 Hz).
- Non-electrodynamic transients, including mechanical phenomena, thermodynamic phenomena, and their interactions with the control systems of power plants ( $10$ – $10^4$  s, 0.1 Hz–0.1 mHz).

Obviously, real events can be very complex and often involve dynamics associated with all four groups listed above. For example, when lightning strikes a power line, it produces traveling surges that propagate along the line. The overvoltage may cause a fault, which may cause transients in the synchronous machines, leading to interventions by relays. Also, protective operations can cause frequency transients that may require interventions from power-plant governors and control systems.

### 5.6.2 Definition of Stability

For given operating conditions, the power system stability is the ability of the system to regain the state of operating equilibrium after being subjected to a disturbance, with most system variables bounded such that practically the entire system remains intact. As a power system is a nonlinear system, its behavior after any disturbance depends on the type and magnitude of the disturbance, its consequences, and the initial operating point. Even though the system does not reach the same steady-state operating equilibrium as that prior to the disturbance, the system is considered stable if the final operating equilibrium after the perturbation is an acceptable steady state, meaning that further intervention through protective or control actions can be avoided.

To introduce this analysis, it is useful to first provide a brief overview of the different operating states of power systems as well as a classification of power-system stability studies.

### 5.6.3 States of Operation

There are typically considered to be five possible states of operation, as shown in Fig. 5.62.

This classification refers to three sets of equations that describe the dynamic phenomena: one differential and two algebraic (generally nonlinear) equations corresponding to equality constraints, which represent the balance between the generation and the load demand; and inequality constraints, which represent the operating limits.

The normal secure state is a system operating condition that is able to satisfy both the equality and inequality constraints with adequate reserve margins for both transmission and generation taking into account the reasonable stresses to which the system may be sub-

jected. For example, the N-1 security criterion implies that a system in its normal state can withstand a single contingency (i.e., the loss of a line, a transformer, or a generator) and that the new steady state still satisfies all the equality and inequality constraints.

The alert state characterizes a system operating condition that satisfies both the equality and inequality constraints but the security level is considered to be insufficient. This implies that the system is vulnerable; in other words, some of the inequality constraints will be violated in the event of some reasonable contingencies. To bring the system to a normal state, some preventive control actions should be taken.

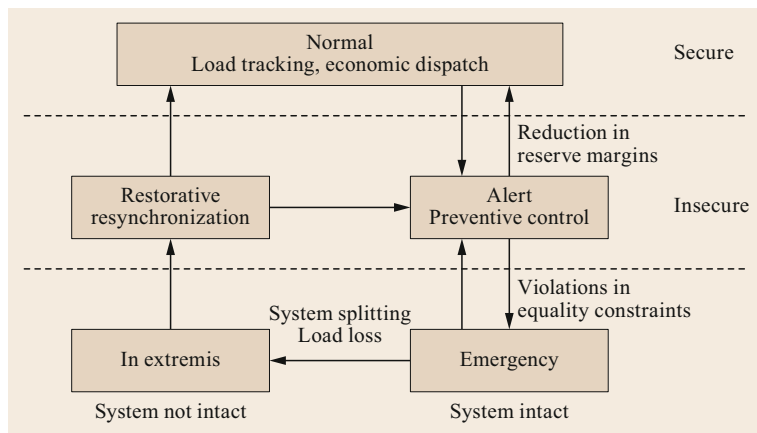
The emergency state characterizes a system operating condition in which at least one of the inequality constraints is violated but the system is still intact (i.e., all the equality constraints are met). Emergency corrective actions should be initiated to restore the system to the alert state. If these measures are not taken in time or are ineffective, the system will break down and reach the in extremis state in which both equality and inequality constraints are violated. The in extremis state corresponds to a system failure characterized by a loss of system integrity involving uncontrolled islanding and the uncontrolled loss of large blocks of loads.

The restorative state describes a system that is separated into areas that may or may not be energized, and in which restorative actions are carried out to bring the system to either an alert or a normal state.

### 5.6.4 Classification of Power System Stability

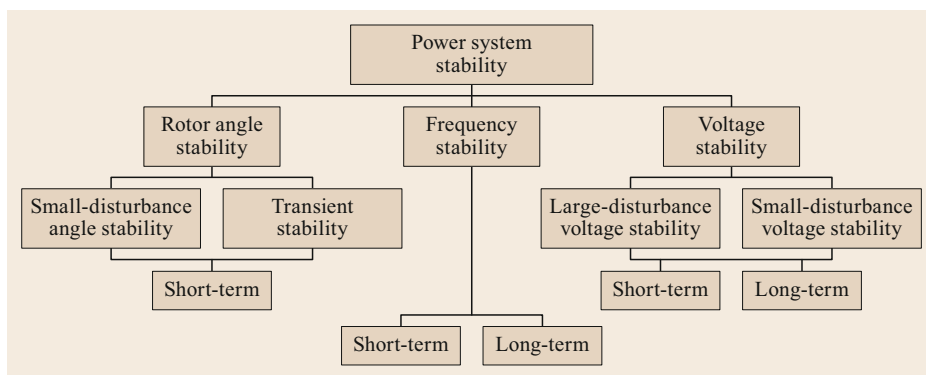
The traditional classification of power system stability is summarized in Fig. 5.63.

A common cause of instability phenomena is an excessive imbalance of active and reactive power in the system, either locally or globally.



**Fig. 5.62** Classification of power system states (adapted from [5.46, 47])





**Fig. 5.63**  
Classification of power system stability (adapted from [5.48])

### Rotor Angle Stability

Rotor angle stability refers to the balance of the torques in the rotors of the synchronous generators. This balance is achieved when the mechanical power provided by the prime mover (e.g., the hydro and steam turbines) meets the load fed by the alternator. If there is an imbalance, the rotors of the generators will act as an energy buffer and the kinetic energy stored in them will decrease or increase. Rotor angle stability refers to the ability of a synchronous machine in the power system to maintain synchronism after a disturbance and regain a steady-state condition characterized by a constant speed without long-lasting oscillations. If the disturbance is local and substantial, such as a fault in a line close to a generator, the generator can fall out of step, as it is accelerated during the fault. A protection will promptly trip the generator in order to avoid machine damage. This kind of dynamic phenomenon is called transient instability, and typically develops within a couple of seconds. On the other hand, small-disturbance (or small-signal) stability instead refers to the ability of the power system to maintain synchronism and regain a steady-state condition after disturbances so small that linearization of the system equations is acceptable for the analysis. Transient instability is associated with insufficient synchronizing torque, whilst small-disturbance problems are associated with insufficient damping of oscillations.

### Frequency Stability

Frequency stability issues are associated with global power imbalances due to the difference between the total power fed into the system by the prime movers and the power consumed by the loads, including losses. The imbalance is compensated for by the kinetic energy stored in the rotors of the machines, resulting in a frequency deviation. If the imbalance is limited, the frequency is controlled by the governors of the prime movers. If the imbalance is too large, the amplitude of the frequency deviation can prompt interventions from

protections that disconnect loads and generators. The time horizon of frequency stability issues ranges from a few seconds (short-term instability) up to several minutes (long-term instability).

### Voltage Stability

Voltage stability refers to the ability of a power system to maintain steady voltages at all buses after a small or large disturbance. Voltage problems are often local and caused by the dynamic responses of loads to disturbance. They are called voltage instabilities, voltage collapses, and load instabilities. Depending on the timescale, voltage stability issues are classified as either short-term (a couple of seconds) or long-term (tens of seconds to minutes). Short-term phenomena are associated with the dynamic responses of fast-acting components (such as induction motors, electronically controlled loads, and HVDC converters) to perturbations. Long-term phenomena are due to the actions of slow-acting equipment, such as step-changing transformers, thermostatically controlled loads, and generator current limiters. As explained above, generators (i.e., synchronous machines) are strongly linked to angular instabilities, and it is sometimes said that they are the driving force for this instability.

### 5.6.5 $P$ - $\delta$ Curves of Synchronous Machines

Before discussing how to study rotor angle stability, we first recall some concepts relating to the operation of a synchronous machine under steady-state and transient conditions.

#### Selection of the Machine Model

Let us ignore the presence of automatic voltage regulators (AVRs). When the stator current varies for any reason (e.g., a sudden load variation or short circuit), the excitation and damper circuits tend to oppose the consequent variation in the flux. Specifically, some currents start to circulate in these circuits, producing a flux

**Table 5.4** Typical parameter values for large generators (adapted from [5.11])

Parameter	Round rotor			Salient pole rotor	
	200 MVA	600 MVA	1500 MVA	150 MVA	230 MVA
$X_d$	1.65	2.00	2.20	0.91	0.93
$X_q$	1.59	1.85	2.10	0.66	0.69
$X'_d$	0.23	0.39	0.44	0.3	0.3
$X'_q$	0.38	0.52	0.64	–	–
$X''_d$	0.17	0.28	0.28	0.24	0.25
$X''_q$	0.17	0.32	0.32	0.27	0.27
$T'_d$	0.83	0.85	1.21	1.10	3.30
$T'_q$	0.42	0.58	0.47	–	–
$T''_d$	0.023	0.028	0.030	0.05	0.02
$T''_q$	0.023	0.058	0.049	0.06	0.02

that instantaneously opposes the mentioned flux variation. It is possible to distinguish two different states: the subtransient state, which persists until all of the currents in the damper windings have been extinguished, and the subsequent transient state, which ends when the current in the excitation circuit eventually vanishes. The durations of these subtransient and transient states are related to the time constants of the damper and excitation windings, respectively. Accordingly, it is possible to identify the subtransient and transient reactances as they are the reactances of the machine during these two different states. Although the detailed illustration of the synchronous machine model provided by Park is beyond the scope of this chapter, it is worth mentioning that each of these two reactances—subtransient and transient—can be split into two components along the d-axis and the q-axis.

A comparison of typical values of the time constants of alternators (Table 5.4) with the period of the oscillations (0.5–1 s) suggests that the transient model of a synchronous machine should be assumed (the flux is kept constant by the currents induced in the rotor circuits—mainly in the excitation winding—since the currents induced in the damping circuits cease in the subtransient state).

At this point, we feel that it would be helpful to remind the reader of several important points.

In the steady state:

- In a salient pole generator, the large air gap along the q-axis causes the q-axis reactance  $X_q$  to be lower than the d-axis reactance  $X_d$ ; i.e.,  $X_q < X_d$
- In a round-rotor generator,  $X_q \approx X_d$ .

During a transient state:

- In a salient pole generator, once the subtransient state has ended, there are no induced currents along the q-axis. Thus, the flux adopts its rated value, so the transient q-axis reactance  $X'_q = X_q$ . Also,  $X'_q =$

$X_q$  is larger than the transient d-axis reactance  $X'_d$ ; i.e.,  $X_q > X'_d$ .

- In a round-rotor generator (where currents can be induced in the rotor's iron as well as in the damping circuits during transients), once the subtransient state has ended, the currents induced in the excitation circuit along the d-axis have an appreciable effect, meaning that  $X'_q > X'_d$ .

#### Salient Pole Synchronous Machines: Vector Diagram and $P$ - $\delta$ Curves in Steady-State and Transient Conditions

The vector diagrams of a salient pole synchronous machine in steady-state and transient conditions are presented in Table 5.5, which also lists the relevant equations for convenience. These equations can be used to infer the expressions for the  $P$ - $\delta$  curves. It follows from the vector diagrams and the equations reported in Table 5.5 that the expression for the active power as a function of the rotor electrical angle for a three-phase machine in the steady state is

$$P = 3VI \cos \varphi = 3 \frac{EV}{X_d} \sin \delta + \frac{3}{2} \frac{X_d - X_q}{X_d X_q} V^2 \sin 2\delta, \quad (5.219)$$

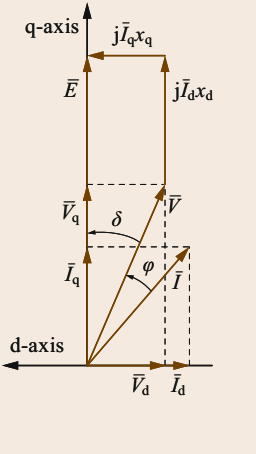
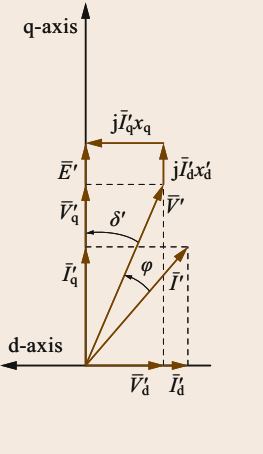
while the expression for a salient rotor machine in a transient state is

$$P' = 3V'I' \cos \varphi' = 3 \frac{E'V'}{X'_d} \sin \delta' + \frac{3}{2} \frac{X'_d - X_q}{X'_d X_q} V'^2 \sin 2\delta'. \quad (5.220)$$

To reinforce these ideas, we now present a quantitative example of a round-rotor synchronous generator that is characterized by the following reactance values:

- $x_d = 1.2$  pu
- $x'_d = 0.25$  pu
- $x'_q = x_q = 0.7$  pu.

**Table 5.5** Vector diagrams of a salient pole synchronous machine in steady-state and transient conditions (adapted from [5.11])

Steady state		Transient	
	$x_q < x_d$ $\frac{V}{\sqrt{3}} + jX_d \bar{I}_d + jX_q \bar{I}_q = \bar{E}$ $\text{Re}(\bar{V} \bar{I}) = V_d I_d + V_q I_q$ $X_q I_q = V_d = V \sin \delta$ $X_d I_d = E - V_q = E - V \cos \delta$ $VI \cos \varphi = V_d I_d + V_q I_q$ $= V \sin \delta \frac{E - V \cos \delta}{X_d} + V \cos \delta \frac{V \sin \delta}{X_q}$ $= \frac{EV}{X_d} \sin \delta + V^2 \left( \frac{1}{X_q} - \frac{1}{X_d} \right) \sin \delta \cos \delta$ $= \frac{EV}{X_d} \sin \delta + \frac{V^2}{2} \frac{X_d - X_q}{X_d X_q} \sin 2\delta$		$x_q > x'_d$ $\frac{V'}{\sqrt{3}} + jX'_d \bar{I}'_d + jX'_q \bar{I}'_q = \bar{E}'$
<p>For a three-phase machine, we have</p> $P = 3VI \cos \varphi = 3 \frac{EV}{X_d} \sin \delta + \frac{3}{2} \frac{X_d - X_q}{X_d X_q} V^2 \sin 2\delta$		<p>For a three-phase machine, we have</p> $P' = 3V'I' \cos \varphi = 3 \frac{E'V'}{X'_d} \sin \delta' + \frac{3}{2} \frac{X'_d - X'_q}{X'_d X'_q} V'^2 \sin 2\delta'$	

Let us assume that the generator is connected to an infinite power bus with a voltage  $v = 1$  pu, and that it is supplying an active power  $p = 0.8$  pu and a reactive power  $q = 0.2$  pu through an external reactance of  $x = 0.2$  pu.

$$p = \frac{ev}{x_d + x} \sin \delta + \frac{(x_d + x) - (x_q + x)}{2(x_d + x)(x_q + x)} v^2 \sin 2\delta$$

$$= 1.2 \sin \delta + 0.2 \sin 2\delta$$

$$p' = \frac{e'v}{x_d + x} \sin \delta + \frac{(x'_d + x) - (x_q + x)}{2(x'_d + x)(x_q + x)} v^2 \sin 2\delta$$

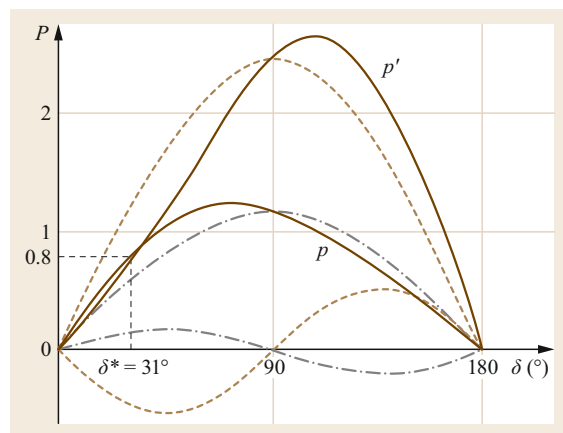
$$= 2.5 \sin \delta - 0.55 \sin 2\delta$$

The two curves are shown in Fig. 5.64. Changing the active and reactive power initially supplied to the infinite power bus from the values  $p = 0.8$  pu and  $q = 0.2$  pu, respectively, results in the same steady-state  $P$ - $\delta$  curve as that shown in the figure but a different transient  $P$ - $\delta$  curve. We shall come back to this observation later.

**Round-Rotor Synchronous Machines: Vector Diagram and  $P$ - $\delta$  Curves in Steady-State and Transient Conditions**

The vector diagrams for a round-rotor synchronous machine in steady-state and transient conditions are presented in Table 5.6, along with the relevant equations for convenience. These equations can be used to infer the expressions for the  $P$ - $\delta$  curves.

It follows from the vector diagrams and the equations reported in Table 5.5 that the expression for the



**Fig. 5.64**  $P$ - $\delta$  curves for a salient pole synchronous machine in steady-state and transient conditions (adapted from [5.11])

active power as a function of the rotor electrical angle for a three-phase round-rotor machine in the steady state is

$$P = 3 \frac{EV}{X} \sin \delta, \tag{5.221}$$

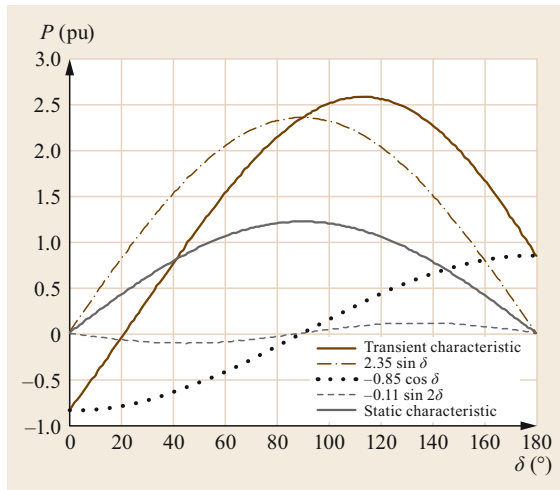
while the expression for a round-rotor machine in the transient state is

$$P' = 3 \frac{E'_q V'}{X'_d} \sin \delta - 3 \frac{E'_d V'}{X'_d} \cos \delta + \frac{3}{2} \frac{X'_d - X'_q}{X'_d X'_q} V'^2 \sin 2\delta. \tag{5.222}$$

**Table 5.6** Vector diagrams of round-rotor synchronous machines in steady-state and transient conditions (adapted from [5.11])

Steady state	Transient
$\frac{x_q \approx x_d}{\bar{V} + jX\bar{I} = \bar{E}}$	$\begin{aligned} \frac{x'_q > x'_d}{\bar{V}' + jX'_d \bar{I}'_d + jX'_q \bar{I}'_q = \bar{E}'} \\ X'_q I'_q = V'_d - E'_d = V' \sin \delta - E'_d \\ X'_d I'_d = E'_q - V'_q = E'_q - V' \cos \delta \\ X'_q = X_q \rightarrow E'_d = 0 \\ V' I' \cos \varphi = V'_d I'_d + V'_q I'_q \\ = V' \sin \delta \frac{E'_q - V' \cos \delta}{X'_d} + \\ V' \cos \delta \frac{V' \sin \delta - E'_d}{X'_q} \\ = \frac{E'_q V'}{X'_d} \sin \delta - \frac{E'_d V'}{X'_q} \cos \delta + \\ V^2 \left( \frac{1}{X'_q} - \frac{1}{X'_d} \right) \sin \delta \cos \delta \end{aligned}$
<p>For a three-phase machine, we have</p> $P = 3 \frac{EV}{X} \sin \delta$	<p>For a three-phase machine, we have</p> $P' = 3 \frac{E'_q V'}{X'_d} \sin \delta - 3 \frac{E'_d V'}{X'_q} \cos \delta + \frac{3}{2} \frac{X'_d - X'_q}{X'_d X'_q} V'^2 \sin 2\delta$

Section 5.6



**Fig. 5.65**  $P$ - $\delta$  curves for a round-rotor synchronous machine in steady-state and transient conditions

To demonstrate these ideas, we now present a quantitative example of a round-rotor synchronous generator that is characterized by the following reactance values:

- $x_d = x_q = 1.2$  pu
- $x'_d = 0.25$  pu
- $x'_q = 0.3$  pu.

Also, let us assume that the generator is connected to an infinite power bus with a voltage  $v = 1$  pu, and that it supplies an active power  $p = 0.8$  pu and a reactive power  $q = 0.2$  pu through an external reactance of

$x = 0.2$  pu. The transient and static characteristics, illustrated in Fig. 5.65, are

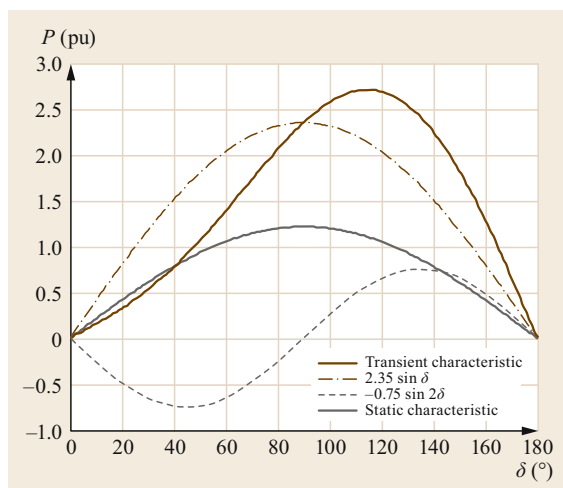
$$\begin{aligned} p &= \frac{ev}{x_d + x} \sin \delta = 1.2 \sin \delta \\ p' &= \frac{e'_q v}{x_d + x} \sin \delta - \frac{e'_d v}{x_d + x} \cos \delta \\ &\quad + \frac{(x'_d + x) - (x'_q + x)}{2(x'_d + x)(x'_q + x)} v^2 \sin 2\delta \\ &= 2.35 \sin \delta - 0.85 \cos \delta - 0.11 \sin 2\delta . \end{aligned}$$

We can get various curves for this machine depending on the assumptions made. For instance, if we assume that  $x'_q = x_q$ , the transient characteristics becomes (Fig. 5.66)

$$\begin{aligned} p' &= \frac{e'_q v}{x_d + x} \sin \delta + \frac{(x'_d + x) - (x_q + x)}{2(x'_d + x)(x_q + x)} v^2 \sin 2\delta \\ &= 2.35 \sin \delta - 0.75 \sin 2\delta . \end{aligned}$$

On the other hand, if we assume that  $x'_q = x'_d$  (i.e., isotropy), the transient characteristics becomes (Fig. 5.67)

$$\begin{aligned} p' &= \frac{e'_q v'}{x'_d} \sin \delta - \frac{e'_d v'}{x'_d} \cos \delta \\ e'_d &= e' \cos \alpha \\ e'_q &= e' \sin \alpha \\ p' &= \frac{e' v'}{x'_d} \sin(\delta - \alpha) \\ p' &= 2.35 \sin \delta - \cos \delta = 2.6 \sin(\delta - 22.9^\circ) . \end{aligned}$$



**Fig. 5.66**  $P$ - $\delta$  curves for a round-rotor synchronous machine in steady-state and transient conditions assuming  $x'_q = x_q$

For illustrative purposes, Fig. 5.68 presents the three  $P$ - $\delta$  curves obtained in transient conditions based on the assumptions specified above.

Note that all of the  $P$ - $\delta$  characteristics presented in this section were obtained using a MATLAB file that can be found in the chapter's supplementary material.

#### Salient Pole Synchronous Machines: Effect of Varying the Initial Steady-State Operating Conditions on the ( $P$ - $\delta$ ) Curves Obtained in Steady-State and Transient Conditions

Let us consider a generator with the following reactances:

- $x_d = 1.2$  pu
- $x'_d = 0.25$  pu
- $x_q = x'_q = 0.7$  pu.

The generator has a no-load excitation emf  $e = 1.7$  pu that is connected to an infinite power bus with a voltage  $v = 1$  pu through a reactance  $x = 0.2$  pu.

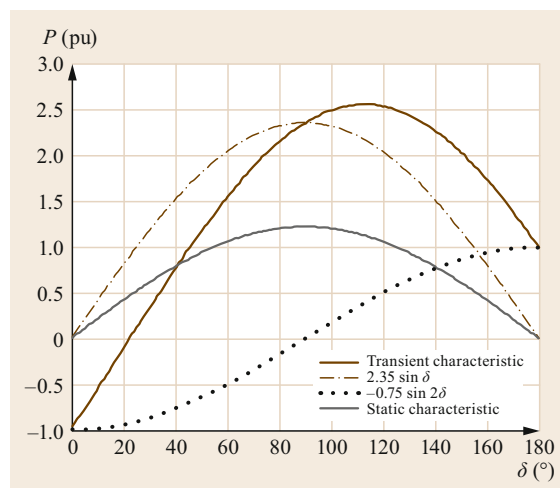
Let us consider three initial conditions:

- $\delta = 20^\circ \rightarrow p = 0.5, q = 0.4$
- $\delta = 40^\circ \rightarrow p = 1.0, q = 0.1$
- $\delta = 60^\circ \rightarrow p = 1.2, q = -0.4$ .

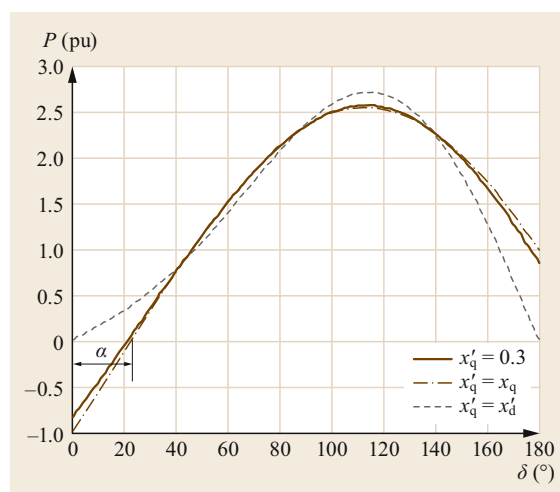
In pu, the expressions for active and reactive power are

$$p = \frac{ev}{x_d + x} \sin \delta + \frac{v^2}{2} \frac{x_d - x_q}{x_d + x_d + 2x} \sin 2\delta$$

$$q = \frac{ev}{x_d + x} \cos \delta - v^2 \left( \frac{\sin^2 \delta}{x_q + x} + \frac{\cos^2 \delta}{x_d + x} \right).$$

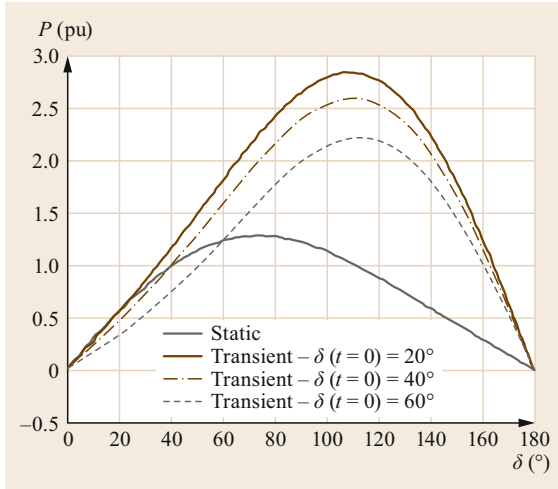


**Fig. 5.67**  $P$ - $\delta$  curves obtained in steady-state and transient conditions for a round-rotor synchronous machine assuming  $x'_q = x'_d$  (i.e., isotropy)

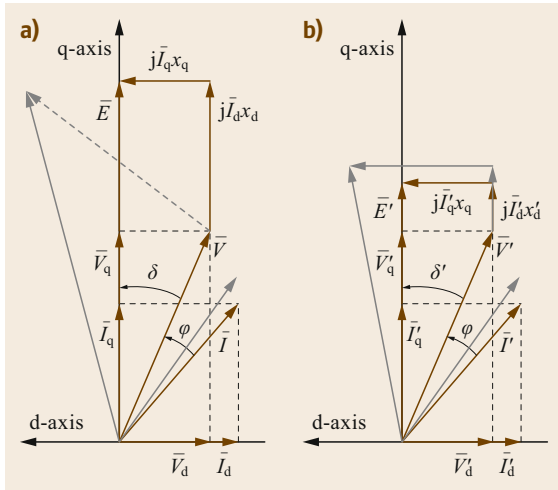


**Fig. 5.68** Comparison of the  $P$ - $\delta$  curves obtained in transient conditions for a round-rotor synchronous machine assuming that  $x'_q = 0.3$ ,  $x'_q = x_q$ , or  $x'_q = x'_d$  (i.e., isotropy)

In the steady state, the magnitude of  $E$  remains constant, as do  $V$  and all of the reactances. Therefore, applying a different initial active power  $P$ , and thus a different  $\delta$ , does not change the steady-state  $P$ - $\delta$  curve. Apart from  $\delta$ , the quantities that differ in the new initial state are the current and its power factor; however, changes to these quantities do not alter the steady-state curve. However, the vector diagram does change if we start from new steady-state operating conditions, as  $\delta$ ,  $I$ , and  $E$  (which simply rotates) change.



**Fig. 5.69**  $P$ - $\delta$  curves obtained in steady-state and transient conditions for a salient pole synchronous machine with three different initial steady-state operating conditions



**Fig. 5.70** (a) Steady-state and (b) transient vector diagrams for different initial operating conditions, marked in gray (adapted from [5.11])

In the transient state, changing the initial values of the current and the power factor alters the voltage drops at the transient reactances and changes the transient emf, meaning that the  $P$ - $\delta$  characteristic in the transient state varies depending on the initial operating conditions. Thus, three different initial steady-state operating conditions yield three different transient curves, as shown in Fig. 5.69. The relevant vector diagrams are shown in Fig. 5.70.

### Round-Rotor Synchronous Machines: Effect of Varying the Initial Steady-State Operating Conditions on the ( $P$ - $\delta$ ) Curves Obtained in Steady-State and Transient Conditions

Let us consider a generator with the following reactances:

- $x_d = 1.2$  pu
- $x'_d = x'_q = 0.25$  pu.

This generator has a no-load excitation emf  $e = 1.7$  pu, which is connected to an infinite power bus with a voltage  $v = 1$  through a reactance  $x = 0.2$  pu.

Let us consider three initial conditions:

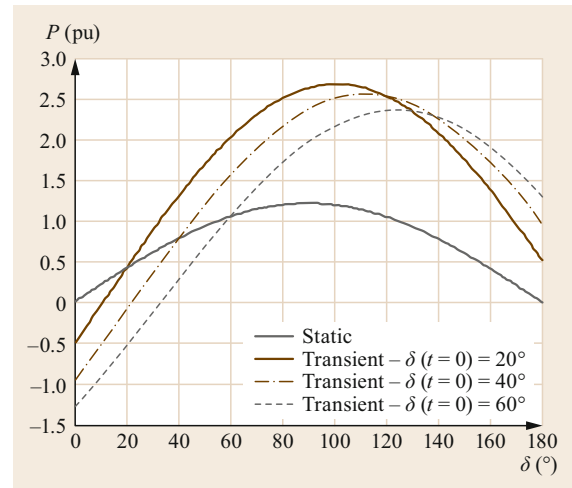
- $\delta = 20^\circ \rightarrow p = 0.5$  pu,  $q = 0.4$  pu
- $\delta = 40^\circ \rightarrow p = 1.0$  pu,  $q = 0.1$  pu
- $\delta = 60^\circ \rightarrow p = 1.2$  pu,  $q = -0.4$  pu.

In pu, the expressions for the active and reactive power are

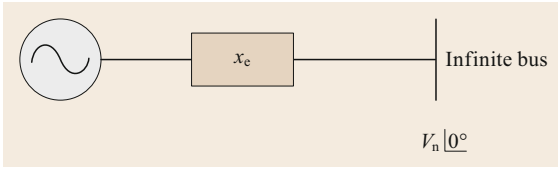
$$p = \frac{ev}{x_d + x} \sin \delta$$

$$q = \frac{ev}{x_d + x} \cos \delta - \frac{v^2}{x_d + x} .$$

The same considerations that were relevant to the salient pole machine also apply to a round-rotor machine, so again three different initial steady-state operating conditions yield just one steady-state curve but three different transient curves, as shown in Fig. 5.71.



**Fig. 5.71**  $P$ - $\delta$  curves obtained in steady-state and transient conditions for a round-rotor synchronous machine with three different initial steady-state operating conditions



**Fig. 5.72** Synchronous machine connected to an infinite power bus

## 5.6.6 Rotor Angle Stability

### Classical Methods

We now review the classical method of analyzing a simple system consisting of a synchronous machine connected to an infinite power bus, as shown in Fig. 5.72.

The following simplifications are made [5.49]:

- The synchronous machine is modeled as a constant emf  $\vec{E}$  behind the transient reactance  $x'$ , and the angle  $\delta$  of the emf is assumed to coincide with the difference between the rotor electrical angle and  $\omega_0 t$  as illustrated in Fig. 5.73
- The resistances of lines, transformers, and the synchronous machine are ignored
- Voltage and currents are assumed to be symmetrical (i.e., positive sequence)
- The angular velocity is close to nominal
- Static models are used for lines
- The mechanical power  $P_m$  (the power from the prime mover) is constant during the transient studied.

### Swing Equation

In the following, a subscript m denotes a mechanical quantity while a subscript e denotes an electrical quantity.

The differential equation that describes the rotor dynamics is

$$J \frac{d^2 \theta_m}{dt^2} = T_m - T_e, \quad (5.223)$$

where:

- $J$  = total moment of inertia (kg m<sup>2</sup>)
- $\theta_m$  = mechanical angle of the rotor (rad)
- $T_m$  = mechanical torque from turbine (N m)
- $T_e$  = electrical torque on the rotor (N m).

Multiplying (5.223) by the mechanical angular speed  $\omega_m$  yields

$$J \omega_m \frac{d^2 \theta_m}{dt^2} = P_m - P_e, \quad (5.224)$$

where:

$$P_m = T_m \omega_m = \text{mechanical power acting on the rotor (W)}$$

$$P_e = T_e \omega_m = \text{electrical power acting on the rotor (W)}.$$

We can express the angular acceleration via the electrical angle instead by inserting  $\theta_m = (\theta_e)/p - \theta_{e0}/p$  (where  $p$  is the number of pairs of poles on the machine) into (5.224), which gives

$$\frac{1}{p} \omega_m J \frac{d^2 \theta_e}{dt^2} = P_m - P_e. \quad (5.225)$$

It is now convenient to introduce the inertia constant  $H$  (in s), defined as

$$H = \frac{\frac{1}{2} J \omega_{m0}^2}{S}, \quad (5.226)$$

where  $\omega_{m0}$  is the rated mechanical angular speed and  $S$  is the MVA rating of the machine.

Using (5.226), and noting that  $d^2 \theta_e / dt^2 = d^2 \delta / dt^2$  (where  $\delta = \theta_e - \omega_0 t - \theta_{e0}$ ), (5.225) becomes

$$\frac{2H}{\omega_0} \frac{d^2 \delta}{dt^2} = P_m^{\text{pu}} - P_e^{\text{pu}}, \quad (5.227)$$

where  $\omega_0$  indicates the rated electrical angular speed ( $\omega_0 = p \omega_{m0}$ )<sup>2</sup>, and a superscript pu indicates that the electrical power and mechanical power are expressed in pu with respect to the rating of the synchronous machine. In the case of a synchronous machine connected to an infinite power bus, we can write (omitting the superscript pu for simplicity)

$$P_e = P_e(\delta, \dot{\delta}) = P_s(\delta) + P_d(\dot{\delta}), \quad (5.228)$$

where  $P_s$  is the synchronizing power, i.e., making reference to Fig. 5.74,

$$P_s(\delta) = \frac{E' V_n}{x' + x_e} \sin(\delta), \quad (5.229)$$

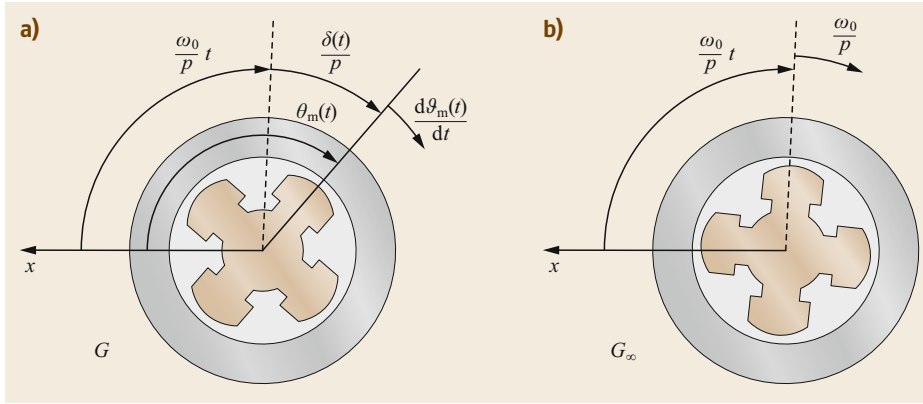
and  $P_d$  is the damping power, with

$$P_d(\dot{\delta}) = D \dot{\delta}. \quad (5.230)$$

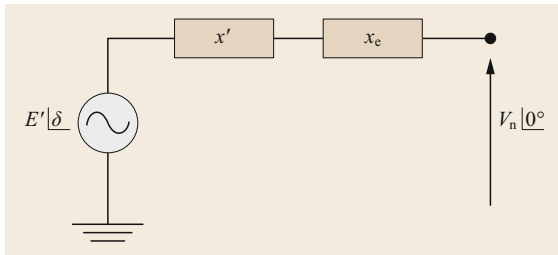
$P_d$  is due to the currents in the rotor circuits, and tends to damp out the oscillations.

Taking  $x_1 = \delta$  and  $x_2 = d\delta/dt$  to be the state variables, (5.227) can be expressed in the state form as

$$\begin{cases} \dot{x}_1 = x_2 \\ \dot{x}_2 = \frac{\omega_0}{2H} (P_m^{\text{pu}} - P_e^{\text{pu}}) \end{cases} \quad (5.231)$$



**Fig. 5.73a,b** Definitions of the quantities used to derive the swing equations. The alternator of interest is shown in (a), while the infinite power machine is depicted in (b)



**Fig. 5.74** Simple circuit representation of a generator in the transient state

The vector  $x = [x_1, x_2]^T$  is the state vector of the system; the equilibrium points (EPs) for the system of equations are given by  $\dot{x} = 0$ , i.e.,

$$\begin{aligned} x_1 &= \arcsin\left(\frac{P_m}{P_{\max}}\right) \\ x_2 &= 0, \end{aligned} \tag{5.232}$$

where  $P_{\max} = E' V_n / (x' + x_c)$ .

For the power angle curve shown in Fig. 5.75, there are two values of  $\delta$  for each value of  $P_m$  (when  $P_m < P_{\max}$ ), i.e., two EPs:  $\delta_s$  and  $\delta_u$ .

After linearizing (5.231) and introducing a small deviation ( $\Delta x_1, \Delta x_2$ ) from an EP, we can write

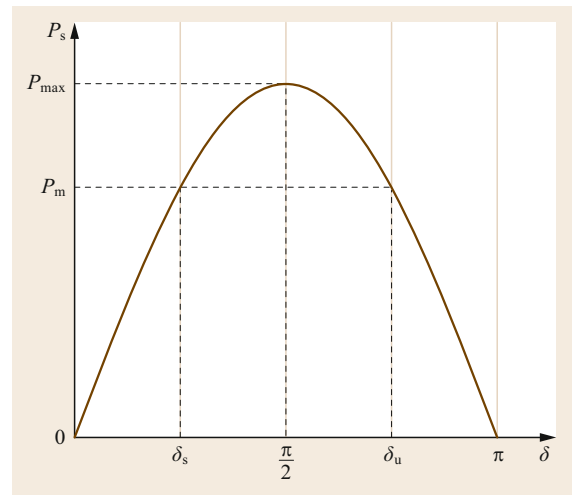
$$\begin{bmatrix} \Delta \dot{x}_1 \\ \Delta \dot{x}_2 \end{bmatrix} = \begin{bmatrix} 0 & 1 \\ -\frac{\omega_0}{H} k & -\frac{\omega_0}{H} D \end{bmatrix} \cdot \begin{bmatrix} \Delta x_1 \\ \Delta x_2 \end{bmatrix}, \tag{5.233}$$

where  $k = P_{\max} \cos(\delta_e)$  and  $\delta_e$  is the angle at equilibrium ( $\delta_s$  or  $\delta_u$ ).

The eigenvalues of the linearized system are given by

$$\lambda = -\frac{1}{2} \frac{\omega_0}{2H} D \pm \sqrt{\frac{\omega_0^2 D^2}{16H^2} - \frac{\omega_0}{2H} k}. \tag{5.234}$$

If  $k$  is positive, both eigenvalues have negative real parts. If  $k$  is negative, one of the eigenvalues is positive



**Fig. 5.75** Power angle curve; note that there are two values of  $\delta$  for each value of  $P_m$

real. Therefore,  $\delta_s$  is a stable EP and  $\delta_u$  is an unstable EP. The criterion for stability is algebraic and given by

$$\frac{dP_s}{d\delta} > 0. \tag{5.235}$$

If  $D$  is small and  $k > 0$ , the eigenvalues are complex and are obtained via

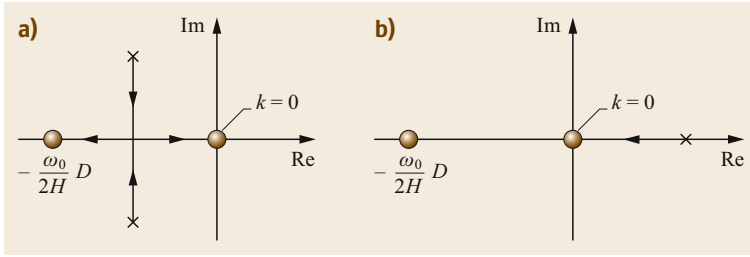
$$\lambda = -\sigma \pm j\omega_p, \tag{5.236}$$

where

$$\sigma = \frac{1}{2} \frac{\omega_0}{2H} \times D \quad \text{and} \quad \omega_p = \sqrt{\frac{\omega_0}{2H} \times k - \frac{\omega_0^2 D^2}{16H^2}}.$$

The two EPs ( $\delta_s$  and  $\delta_u$ ) become closer to each other as  $P_m$  increases. The maximum power supplied by the generator is equal to  $P_{\max}$  and occurs at  $\delta^* = \pi/2$ .





**Fig. 5.76a,b** Loci of eigenvalues in the  $s$  plane (a) at the SEP and (b) at the UEP

The condition for stability can also be stated as

$$\delta_s < \delta^* . \quad (5.237)$$

The loci of eigenvalues in the  $s$  plane as  $P_m$  is varied are shown in Fig. 5.76.

At the SEP (state equilibrium point), the eigenvalues are initially complex and split into two real values. One of them reaches origin as  $P_m$  is increased to  $P_{\max}$  (when  $k = 0$ ), while the other eigenvalue approaches  $-D\omega_0/(2H)$ .

At the UEP (unstable equilibrium point), both eigenvalues are real. As  $P_m$  increases, both move towards the origin. At  $P_m = P_{\max}$ , one of the values is 0 while the other is  $-D\omega_0/(2H)$ .

There is no equilibrium when  $P_m > P_{\max}$ .

### Equal Area Criterion

Quite often, we are not interested in the exact behavior of the solution to (5.227), only whether the system is stable after a given contingency. By applying the equal area criterion described below, it is possible to investigate the stability of the system in Fig. 5.76 following various disturbances using simple calculations. As our interest is focused on the dynamics during the first swing, the damping can be neglected, i.e.,  $D = 0$ . A necessary but not sufficient condition for stability is that there is a moment in time  $t_m$  during this swing when  $\dot{\delta}(t_m) = 0$ . The corresponding angle is  $\delta_m$ .

The stability criterion is obtained by manipulating (5.227) and applying the condition  $\dot{\delta}(t_m) = 0$ . Multiplying (5.227) by  $\dot{\delta}$  on both sides yields

$$\dot{\delta} \frac{d^2\delta}{dt^2} = \frac{\omega_0}{2H} P_a \dot{\delta} , \quad (5.238)$$

which can be written as

$$\delta \frac{1}{2} \frac{d}{dt} \left( \frac{d\delta}{dt} \right)^2 = \frac{d}{dt} \left( \frac{\omega_0}{2H} \int_{\delta_i}^{\delta} P_a d\delta \right) , \quad (5.239)$$

where  $P_a = P_m - P_e$ .

Equation (5.239) can be integrated to give

$$\frac{d\delta}{dt} = \sqrt{\frac{\omega_0}{H} \int_{\delta_i}^{\delta} P_a d\delta + c} , \quad (5.240)$$

where  $c$  is an integration constant with a value of 0 since  $\dot{\delta} = 0$  when  $\delta = \delta_i$  ( $\delta_i$  is the pre-disturbance rotor angle).

Thus, a necessary condition for stability is that there is an angle  $\delta_m$  such that

$$\int_{\delta_i}^{\delta} P_a d\delta = 0 , \quad (5.241)$$

i.e., there is an angle  $\delta_m$  such that the area below the accelerating power  $P_a$  in the  $\delta$ - $P$  diagram between  $\delta_i$  and  $\delta_m$  vanishes. In other words,

$$\int_{\delta_0}^{\delta^*} P_a d\delta = \int_{\delta_0}^{\delta^*} (P_m - P_e) d\delta = 0 . \quad (5.242)$$

A graphical interpretation of this formula is shown in Fig. 5.77. This is the *equal area criterion*. The two areas represent the *fictitious* kinetic energies absorbed/released and then released/absorbed by the rotor.

### Heffron–Phillips Model of a Generator Connected to an Infinite Power Bus

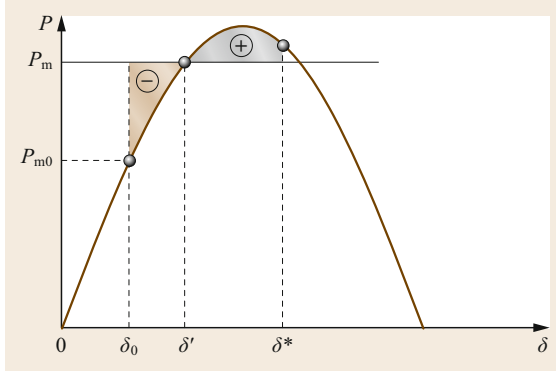
The Heffron–Phillips model is a linear model that takes into account the actions of the voltage control and the exciter [5.50]. This model justifies and illustrates the use of power system stabilizers (PSS).

The rotor angle dynamics in pu can be written as

$$\frac{d\delta}{dt} = \omega_0(\omega_{pu} - 1) \quad (5.243)$$

$$2H \frac{d\omega_{pu}}{dt} = T_m - T_s - D\omega_{pu} , \quad (5.244)$$

where  $\omega_{pu} = \omega/\omega_0$ ,  $D$  is the damping coefficient, and  $T_m$  and  $T_s$  are the mechanical and the synchronizing



**Fig. 5.77** Graphical interpretation of the equal area criterion

torques, respectively. Assuming that  $\omega_{pu} \approx 1$  pu, we can write

$$T_s = \frac{|E'| |V_\infty|}{x' + x_e} \sin \delta, \quad (5.245)$$

where  $E'$  is the transient internal voltage,  $V_\infty$  is the voltage at the infinite power bus (the bus of the network to which many generators are connected),  $x'$  is the transient reactance of the alternator, and  $x_e$  is the reactance of the link between the alternator and the infinite power bus. For small variations, the linearized approximation of (5.245) is

$$\Delta T_s = k_1 \Delta \delta + k_2 \Delta |E'|, \quad (5.246)$$

where

$$k_1 = \left( \frac{\partial T_s}{\partial \delta} \right)_0 = \frac{|E'_0| |V_\infty|}{x' + x_e} \cos \delta_0 \quad (5.247)$$

$$k_2 = \left( \frac{\partial T_s}{\partial |E'|} \right)_0 = \frac{|V_\infty|}{x' + x_e} \sin \delta_0. \quad (5.248)$$

In order to account for the variation of  $|E'|$  with respect to both  $\Delta E_f$  (which is proportional to the variation of the excitation voltage) and to  $\Delta \delta$ , the equation relevant to the flux decay of the excitation winding is included as

$$v_f = r_f i_f + \frac{d\lambda_f}{dt}, \quad (5.249)$$

where  $v_f$  is the excitation voltage,  $i_f$  is the excitation current, and  $\lambda_f$  is the flux linkage. Equation (5.249) can be written at the stator side as

$$|E_f| = |E| + T'_0 \frac{d|E'|}{dt}. \quad (5.250)$$

Here,  $T'_0 = L_f / r_f$ , where  $r_f$  is the resistance and  $L_f$  is the self-inductance of the excitation winding.

As a first approximation, we can write

$$\frac{|E| - |V_\infty| \cos \delta}{|E'| - |V_\infty| \cos \delta} \approx \frac{\tilde{x}}{\tilde{x}'}, \quad (5.251)$$

where  $\tilde{x}' = x' + x_e$  and  $\tilde{x} = x_s + x_e$  ( $x_s$  is the synchronous reactance).

From (5.251),

$$|E| = \frac{1}{k_3} |E'| + \left( 1 - \frac{1}{k_3} \right) |V_\infty| \cos \delta, \quad (5.252)$$

where

$$k_3 = \frac{\tilde{x}'}{\tilde{x}}. \quad (5.253)$$

Inserting (5.252) into (5.250) gives

$$k_3 T'_0 \frac{d|E'|}{dt} + |E'| = k_3 |E_f| + (1 - k_3) |V_\infty| \cos \delta. \quad (5.254)$$

Introducing the Laplace transform for small variations leads to

$$(sk_3 T'_0 + 1) \Delta |E'| = k_3 \Delta |E_f| - k_4 k_3 \Delta \delta, \quad (5.255)$$

where

$$k_4 = \left( \frac{1}{k_3} - 1 \right) |V_\infty| \sin \delta. \quad (5.256)$$

The relevant block diagram is shown in Fig. 5.78.

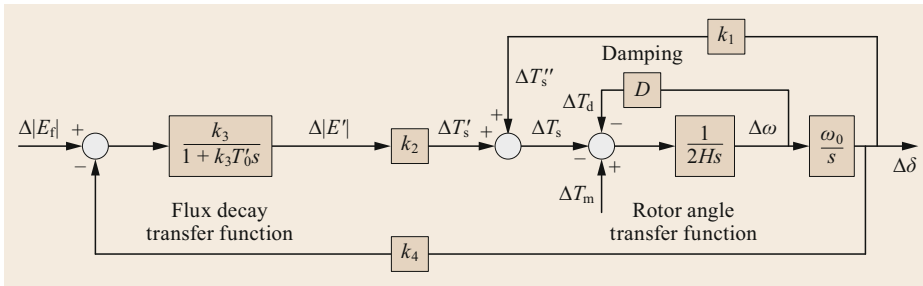
As shown in Fig. 5.78, the feedback loop arises because of the link between  $\Delta |E'|$  and  $\Delta \delta$ . When the exciter and voltage regulator are included,  $\Delta |E_f|$  depends on the output voltage at the generator terminals  $|V_t|$  through the excitation system.

When the excitation voltage is constant ( $\Delta |E_f| = 0$ ), the field flux variations  $\Delta |E'|$  are only caused by the feedback of  $\Delta \delta$  through the coefficient  $k_4$ . This represents the demagnetizing effect of the armature reaction.

The change in air-gap torque due to the field flux variations caused by rotor angle changes (indicated as  $\Delta T'_s$  in the block diagram) is given by

$$\left. \frac{\Delta T'_s}{\Delta \delta} \right|_{\Delta |E_f|=0} = \frac{k_2 k_3 k_4}{1 + sk_3 T'_0}, \quad (5.257)$$

where the constants  $k_2$ ,  $k_3$ , and  $k_4$  are usually positive. The contributions of  $\Delta |E'|$  to the synchronizing torque  $\Delta T'_s$  and the damping torque  $\Delta T_d$  depend on the oscillating frequency as follows:



**Fig. 5.78** Block diagram of an alternator with damping and flux decay accounted for

- (1) In the steady state and at very low oscillating frequencies (i.e.,  $s = j\omega \rightarrow 0$ ),

$$\Delta T'_s = -k_2 k_3 k_4 \Delta \delta. \tag{5.258}$$

The variation in the field flux due to  $\Delta \delta$  feedback introduces a negative synchronizing torque component. The system becomes monotonically unstable when this exceeds  $k_1 \Delta \delta$  (i.e.,  $T'_s$ ). The steady-state stability limit is reached when

$$k_2 k_3 k_4 = k_1. \tag{5.259}$$

- (2) At oscillating frequencies  $\gg 1/(k_3 T'_0)$ ,

$$\Delta T'_s = \frac{-k_2 k_3 k_4 \Delta \delta}{j\omega k_3 T'_0}. \tag{5.260}$$

Equation (5.260) can be written as

$$\Delta T'_s = j \frac{k_2 k_4 \Delta \delta}{\omega T'_0}. \tag{5.261}$$

Thus, the component of the air-gap torque due to  $\Delta |E'|$  leads  $\Delta \delta$  by  $90^\circ$ , or is in phase with  $\Delta \omega$ . Hence,  $\Delta |E'|$  results in a positive damping component that is added to  $\Delta T_d$ .

- (3) At a typical machine oscillating frequency of about 1 Hz,  $\Delta |E'|$  results in a positive damping torque component and a negative synchronizing torque component. The net effect is to slightly reduce the synchronizing torque component and increase the damping torque component.

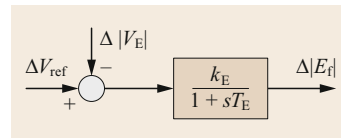
$k_4$  is generally positive, although there are a few cases in which it may be negative, such as for a hydraulic generator without damper windings that is operating with a light load and is connected by a line with a relatively high resistance to reactance ratio to a larger system.

A simple model of the voltage control system and exciter is shown in Fig. 5.79.

For small variations, we can write

$$\Delta |V_t| = k_s \Delta \delta + k_6 \Delta |E'|, \tag{5.262}$$

where  $k_s = |\partial |V_t| / \partial \delta|_0$  and  $k_6 = |\partial |V_t| / \partial |E'|_0$ .



**Fig. 5.79** Simple model of the voltage control system and exciter

$k_6$  is positive whereas  $k_5$  can be positive or negative (it is negative under heavy loading conditions and with high external impedance).

The block scheme of Fig. 5.80 is obtained by including the block scheme of Fig. 5.79 in that of Fig. 5.78.

The stability criterion is given by

$$k_5 k_E + k_4 > 0, \tag{5.263}$$

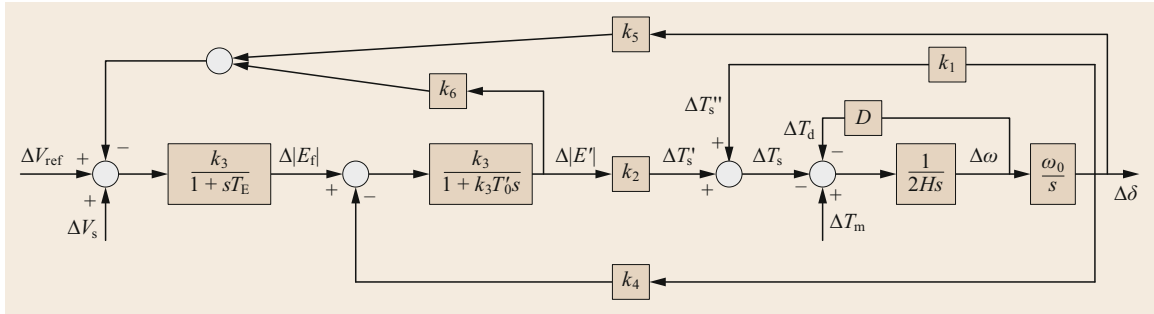
so when  $k_5 < 0$ , (5.263) limits the value of  $k_E$ . In order to maintain a high value of  $k_E$  in the steady state, a PSS is adopted.

A simple PSS scheme is shown in Fig. 5.81.

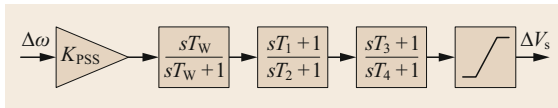
### Multi-Machine Stability Studies

The equal area criterion cannot be used directly in systems with three or more machines. When a multi-machine system operates under electromechanical transient conditions, machine oscillations occur in the transmission system connecting the machines. In this case, we introduce the following assumptions to formulate the so-called classical model:

1. The mechanical power input of each machine remains constant throughout the swing computation
2. The damping power is negligible
3. Each machine can be represented by a constant transient reactance in series with a constant transient internal voltage
4. The mechanical rotor angle of each machine coincides with  $\delta$ , the electrical phase angle of the internal voltage
5. All loads can be considered shunt impedances to ground, with values that are governed by the prevailing conditions immediately prior to the transient condition.



**Fig. 5.80** Block diagram of an alternator with the damping, flux decay, voltage control system, and exciter considered



**Fig. 5.81** Simple PSS scheme, where  $K_{PSS}$  is the gain,  $T_w$  is the washout time constant, and the other time constants ( $T_1$ ,  $T_2$ ,  $T_3$ , and  $T_4$ ) are those of the two stage lead-lag block for phase compensation

The system conditions before the fault and the network configuration both during and after the fault must be known in any transient stability study. Consequently, in the multi-machine case, two preliminary steps are performed:

- The steady-state pre-fault conditions for the system are calculated using a power flow code
- The pre-fault network representation is determined and then modified to account for the fault and post-fault conditions.

We know the active power, reactive power, and voltage values at each generator terminal and load bus for the preliminary steps. The transient internal voltage of each generator is then calculated using

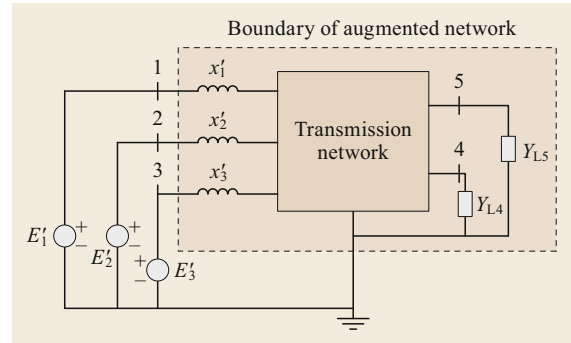
$$\vec{E}' = \vec{V}_t + jx'\vec{I}, \tag{5.264}$$

where  $\vec{V}_t$  is the corresponding terminal voltage and  $\vec{I}$  is the output current. Each load is converted into a constant admittance to ground and its bus using

$$Y_L = \frac{P_L - jQ_L}{V_L^2}, \tag{5.265}$$

where  $P_L + jQ_L$  is the load and  $\vec{V}_L$  is the magnitude of the corresponding bus voltage.

The bus admittance matrix used for the pre-fault power flow calculation is now augmented to include the transient reactance of each generator and the shunt admittance of each load, as illustrated in Fig. 5.82.



**Fig. 5.82** Model of augmented network nodal analysis

The injected currents are zero at all buses except for the internal buses of the generators. In the second preliminary step, the bus admittance matrix is modified to correspond to the faulted and post-fault conditions. Since only the internal buses of the generator have injections, all other buses can be eliminated by Kron reduction. The power injected into the network from each generator is calculated using the corresponding power angle equation. For example, in Fig. 5.82, the power supplied by generator 1 is given by

$$P_{1l} = E_1'^2 G_{11} + E_1' E_2' Y_{12} \cos(\delta_{12} - \vartheta_{12}) + E_1' E_3' Y_{13} \cos(\delta_{13} - \vartheta_{13}), \tag{5.266}$$

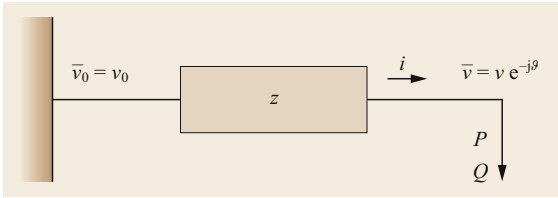
where  $\delta_{12} = \delta_1 - \delta_2$ ,  $\bar{Y}_{12} = Y_{12} e^{j\vartheta_{12}}$ , and  $\bar{Y}_{13} = Y_{13} e^{j\vartheta_{13}}$ .

Similar equations can be written for  $P_{l2}$  and  $P_{l3}$  using the  $Y_{ij}$  elements of the  $3 \times 3$  bus admittance matrix.

The  $P_{li}$  expressions are used in the swing equations

$$\frac{2H_i}{\omega_0} \frac{\partial^2 \delta_i}{\partial t^2} = P_{mi} - P_{ei} \quad i = 1, 2, 3, \tag{5.267}$$

which represent the motion of each rotor during and after the fault. The solution depends on the location and the duration of the fault and the  $Y_{bus}$  that results from the removal of the faulted line.



**Fig. 5.83** Scheme of a load connected to an infinite bus through a line

### 5.6.7 Voltage Stability

Just as the single machine to infinite bus system is used to describe some basic properties of angular stability, some fundamental aspects of voltage stability can be described by referring to the simple system shown in Fig. 5.83, where a load with active power  $P$  and reactive power  $Q$  is supplied through a line with longitudinal impedance  $z$  (shunt capacitance is neglected) from a bus with constant voltage  $v_0$  (infinite bus).

In steady-state and balanced conditions, this simple system is expressed by

$$\bar{i} = \frac{\bar{v}_0 - \bar{v}}{\bar{z}} \quad (5.268)$$

$$P - jQ = \bar{v}^* \bar{i}, \quad (5.269)$$

where  $\bar{v}^*$  indicates the conjugate of the voltage phasor.

Replacing  $i$  in (5.269) with (5.268) yields the equation

$$P - jQ = \frac{v^* v_0 - v^2}{z}, \quad (5.270)$$

which can be rearranged by introducing the line resistance  $r$ , the reactance  $x$ , and the angle  $\theta$  (the difference between the angles of  $v_0$  and  $v$ ),

$$(r + jx)(P - jQ) + v^2 = vv_0(\cos \vartheta + j \sin \vartheta). \quad (5.271)$$

Equating the real and imaginary parts leads to

$$\begin{aligned} rP + xQ + v^2 &= vv_0 \cos \vartheta \\ xP - rQ &= vv_0 \sin \vartheta. \end{aligned} \quad (5.272)$$

The angle  $\theta$  can be eliminated by squaring both sides and adding the two equations, to give

$$v^4 + (r^2 + x^2)(P^2 + Q^2) + 2(rP + xQ)v^2 = v^2 v_0^2. \quad (5.273)$$

Dividing by  $|v|^2$  results in the typical equation used in the Distflow method [5.51] to calculate the steady-state operating conditions in a radial distribution network,

$$v^2 = v_0^2 - (r^2 + x^2)i^2 - 2(rP + xQ). \quad (5.274)$$

By neglecting the effects of voltage variations on both  $P$  and  $Q$ , (5.273) can be written as a quadratic equation in the variable  $u = v^2$ ,

$$u^2 - [v_0^2 - 2(rP + xQ)u + (r^2 + x^2)(P^2 + Q^2)] = 0. \quad (5.275)$$

Equation (5.275) only has feasible solutions (i.e., solutions that are real numbers) if the discriminant is larger than or equal to 0, i.e.,

$$v_0^4 - 4(rP + xQ)v_0^2 - 4(xP - rQ)^2 \geq 0, \quad (5.276)$$

which can also be used as a stability index.

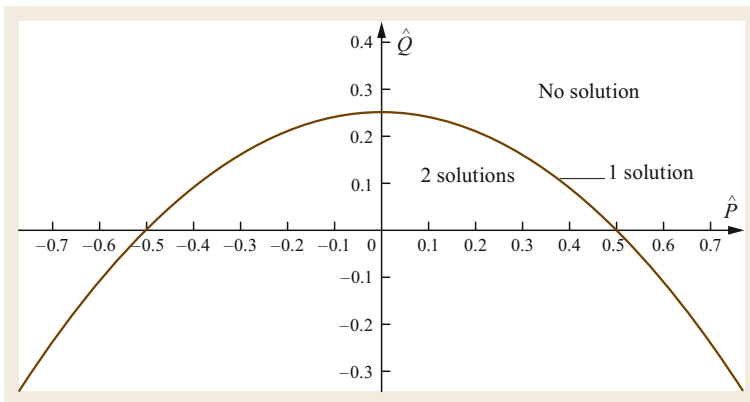
If  $r$  can be ignored, (5.275) can be rewritten as

$$\hat{u}^2 + (2\hat{Q} - 1)\hat{u} + \hat{P}^2 + \hat{Q}^2 = 0, \quad (5.277)$$

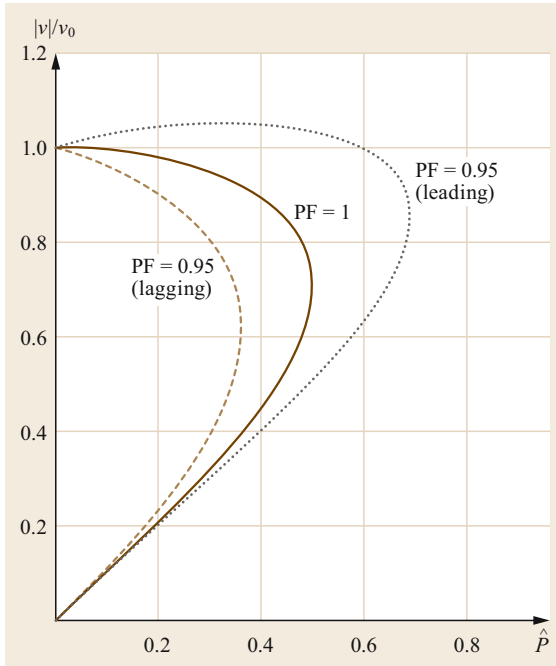
where  $\hat{u} = u/v_0^2$ ,  $\hat{P} = xP/v_0^2$ , and  $\hat{Q} = xQ/v_0^2$ .

The solutions to (5.277) are

$$\hat{u} = \frac{1}{2} - \hat{Q} \pm \sqrt{\left(\frac{1}{2} - \hat{Q}\right)^2 - \hat{P}^2 - \hat{Q}^2}, \quad (5.278)$$



**Fig. 5.84** Feasibility condition when the resistance is ignored



**Fig. 5.85** Nose curves for different values of the power factor PF

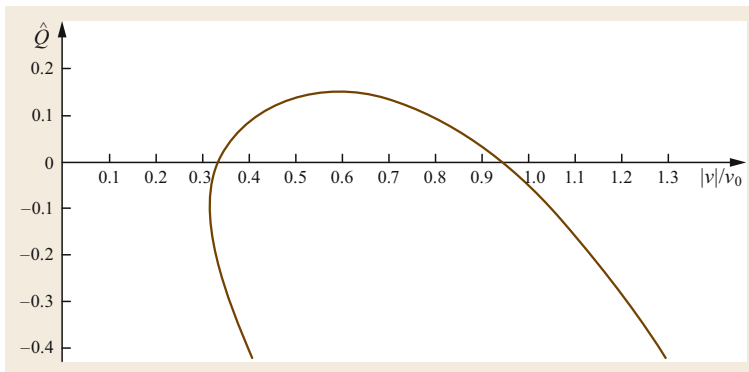
with the feasibility condition

$$\hat{P}^2 + \hat{Q} \leq \frac{1}{4}. \quad (5.279)$$

The feasibility condition is depicted in Fig. 5.84. Below the curve there are two real solutions; on the curve there is a single solution; and above the curve there are no real solutions.

In the case of a constant power factor (i.e.,  $\hat{Q} = \hat{P} \tan \varphi$  with  $\tan \varphi$  constant), the feasibility condition (5.279) becomes

$$\hat{P}^2 + \hat{P} \tan \varphi - \frac{1}{4} \leq 0. \quad (5.280)$$



**Fig. 5.86** QV curve for  $\hat{P} = 0.1$

When  $\hat{P} \geq 0$  (load consumption), the critical conditions are  $\hat{P}_{\max} = \cos \varphi / [2(1 + \sin \varphi)]$ ,  $\hat{Q}_{\max} = \sin \varphi / [2(1 + \sin \varphi)]$ , and  $\hat{u}_{\text{cr}} = 1 / [2(1 + \sin \varphi)]$ .

For constant power factor values, the curves presented in Fig. 5.85 are obtained. These show the variation of  $v/v_0$  as a function of  $\hat{P} \geq 0$  based on (5.278). Such curves are often called nose curves or power voltage (PV) curves. Just as for the case considered in Fig. 5.84, three cases can be distinguished regarding the number of possible operating points: (a) there are two solutions when  $\hat{P}$  is less than the tip of the nose; (b) there is one solution at the tip of the nose; and (c) there are no solutions for larger values of  $\hat{P}$ .

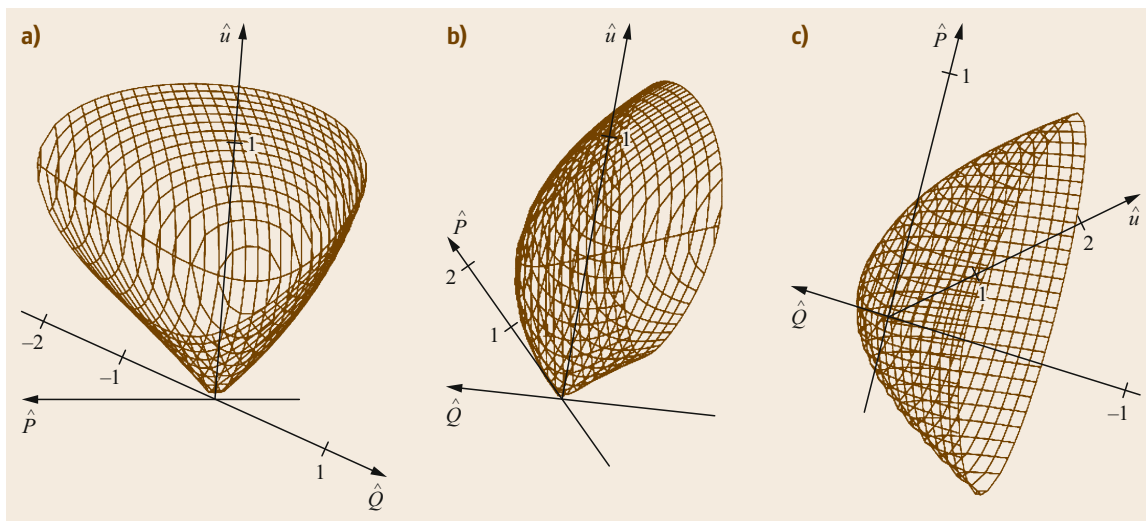
In case (a), the upper solution corresponds to high voltage and low current while the lower one corresponds to low voltage and high current. The upper solution is obviously of particular interest since it reduces the power loss.

The power factor has a significant influence on the nose curve (as shown in Fig. 5.85), and therefore on the voltage stability limit.  $\hat{P}_{\max}$  decreases as the reactive power drawn by the load increases.

If  $\hat{P}$  is assumed to be constant, applying (5.277) yields the QV curve, which shows the amount of reactive power that must be provided to the network with a given load to obtain a predefined voltage level. Figure 5.86 shows this curve for  $\hat{P} = 0.1$ . The voltage sensitivity factor  $dv/dQ$  can be used as a stability criterion. Since we usually expect the voltage to increase when the adsorption of reactive power from the bus decreases, stability is obtained when  $dv/dQ$  is negative. This condition is met for voltages higher than 0.6 pu in Fig. 5.86.

In three dimensions, (5.277) defines an infinite paraboloid, as illustrated by Fig. 5.87.

The relationship between the load power and voltage variations depends on the timescale considered. At short timescales of a few seconds, the physical processes associated with the load device determine the characteristics, whereas various control actions must be considered at longer timescales.



**Fig. 5.87a–c** Surfaces illustrating the relationship between voltage, active power, and reactive power; (a) and (b) show lateral views whereas (c) depicts the top view

One generic model often used for short timescales is the exponential

$$P_L = P_{L0} \left( \frac{V}{V_0} \right)^{k_p}, \quad (5.281)$$

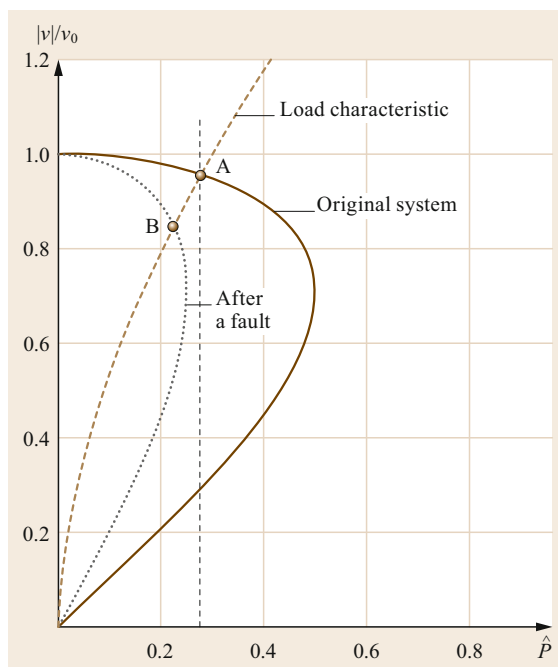
where  $P_{L0}$  is the active power absorbed when the voltage is equal to the rated value  $V_0$ . A similar expression, albeit usually with a different exponent value, can be used for the reactive power.

At longer timescales, the control actions that are applied to keep the load power constant are typically those of the thermostatically controlled load and those of the variable tap changers of distribution transformers.

Figure 5.88 shows the load characteristic (with  $k_p = 1.75$ ) plotted together with two different nose curves. The solid one is the unity power factor curve of Fig. 5.85; the dotted nose curve refers to the case in which the reactance doubles due to a fault.

Load control is achieved by increasing the load admittance in order to increase the load power. Indeed, one of the definitions of voltage stability is that an increase in load admittance results in an increase in load power.

At point A in Fig. 5.88, an increase in load admittance shifts the load curve to the right and then increases the load power. Thus, the system is voltage stable according to the definition above. If a disturbance occurs, the equivalent network impedance increases dramatically and the nose curve shifts to the dotted one. The new operating point will be point B. The load controller will try to restore the load power to the previous value



**Fig. 5.88** The load characteristic crosses the nose curve at point A before and at point B after a network fault that doubles the equivalent reactance

represented by crossing point A. The controller will increase the load admittance, decreasing the voltage and shifting the operating point to the tip of the nose. The power cannot be restored to the original value since the tip of the nose curve is to the left of the vertical curve.

With the operating point at the tip of the nose, increasing the load admittance further causes a decrease in power because the voltage drop is larger than the in-

crease in current. This situation is clearly unstable and the system will collapse. Note that this description does not consider the actions of undervoltage protections.

## 5.7 Power System Control

In this section, we largely focus on frequency control. We will refer to the basic scheme shown in Fig. 5.89, which comprises a generating unit equipped with a turbine-alternator group connected to the grid. However, this scheme is becoming less common in real power systems due to the increasing utilization of renewable energy from solar (mainly photovoltaics) and wind technologies, as these types of generators are usually connected to the network and make use of inverters.

Frequency control is performed due to power quality considerations and requirements (some loads and components of power plants such as induction motors, steam, gas, and hydro turbines may be significantly affected by frequency deviations of a few Hz) and to maintain the global equilibrium in the network between the power produced by the power stations and the power consumed by the loads. The disconnection of a generating unit, a line trip, or an increased load decrease the frequency, while the disconnection of a load or a sudden increase in the power produced increases the frequency. Within this context, each mismatch is initially compensated for mainly by the kinetic energy stored in the rotors of the synchronous generators and induction motors. However, this kinetic energy is limited, so frequency deviations need to be promptly compensated through appropriate frequency control actions.

In the scheme shown in Fig. 5.89, a load increase (decrease) corresponds to a decrease (increase) in the alternator angular velocity that needs to be compensated for through appropriate action of the speed governor (Reg), which opens (closes) the turbine valve. The speed governor control system may require some other input signals (b) in addition to the angular velocity.

The frequency regulation and the available reserve of a system are designed such that the frequency does not shift outside predefined limits even when the largest

disturbances that can be reasonably expected occur (e.g., the largest generator in the system trips).

### 5.7.1 Generation Reserve

As the energy stored in the rotating masses is fairly small, a power reserve must always be available to ensure that the balance between the power provided by the turbines and the power requested by the electrical system is maintained. In this respect, during the system planning stage, it is useful to distinguish between *normal operation* and a *disturbance* as reasons for utilizing the reserve. Power imbalances due to incorrect load forecasts and random load variations are both compensated for using the normal operation reserve. On the other hand, typical disturbances are plant outages or line trips.

The reserves are categorized according to the time needed to activate them:

- The *spinning reserve* is provided by the margins between the current power output and the maximum and minimum limits of a generating unit. This reserve can be activated in a few seconds, and is used during primary frequency control.
- The *supplementary reserve* is employed to restore the spinning reserve when it has been used in the event of a large perturbation, and it is often activated by automatic generation control (AGC) after tens of seconds. Thus, it is significantly slower to activate than primary frequency control; indeed, it is designed not to interact with it. This phase is known as secondary frequency control.
- The *back-up reserve* is a slow reserve that can be activated within a couple of hours to restore a faster reserve when it has been used. This phase is known as tertiary frequency control.

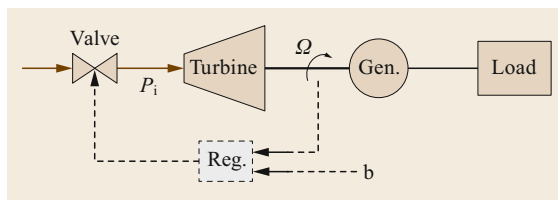
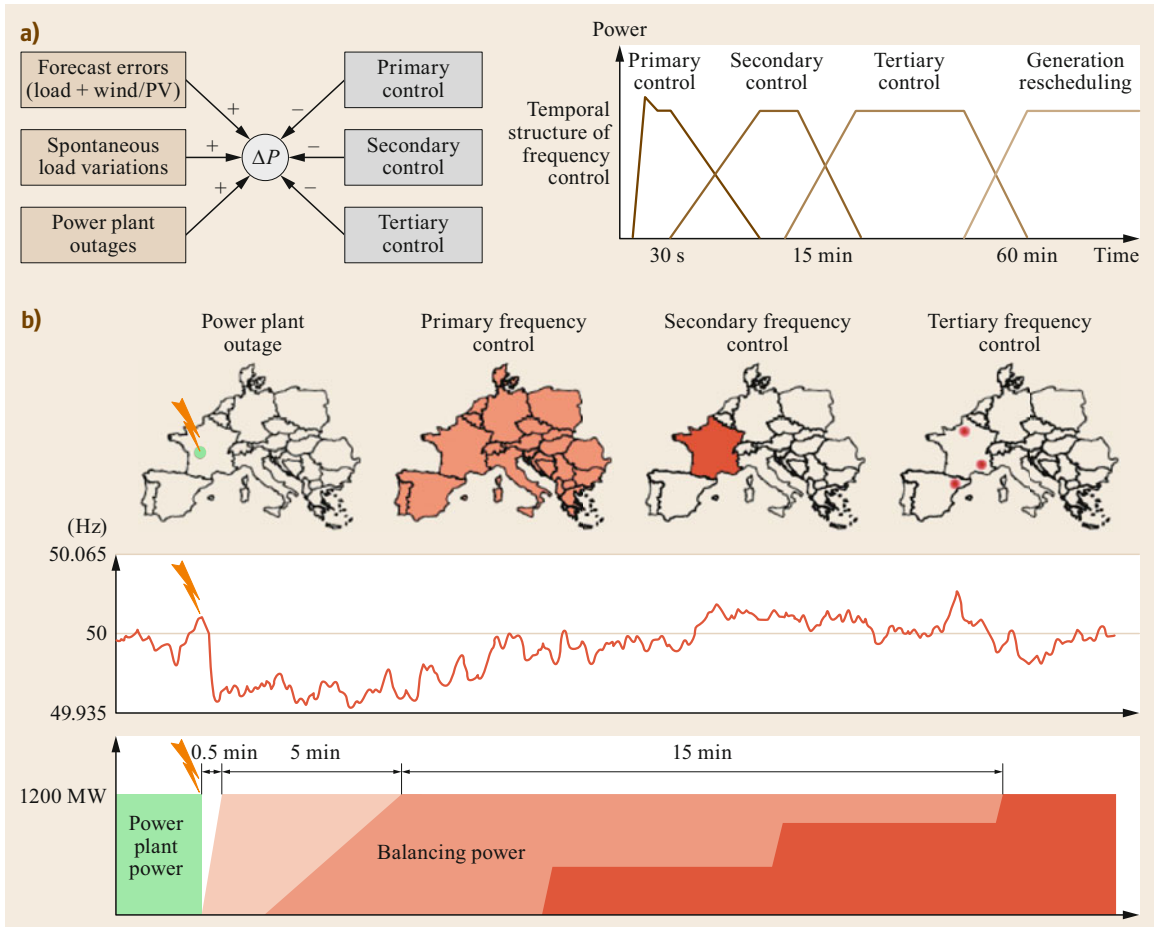


Fig. 5.89 Basic scheme of a speed governor

Figure 5.90 illustrates the concepts of primary, secondary, and tertiary frequency control using an example of a large perturbation in the network of continental Europe. The entire system is involved during primary control; secondary control action is expected to be limited to the affected area only; whilst the rescheduling associated with tertiary control is applied to just a few power stations.





**Fig. 5.90a,b** Primary, secondary, and tertiary frequency control: (a) general scheme and (b) example showing the activation of each control phase after a large perturbation in the European network [5.52]

### 5.7.2 Dynamics of the Generators

After a disturbance in a large power system, the frequency varies across the system. For typical disturbances, however, the frequencies of the different machines can be regarded as being close to an average *system frequency* defined by a *center of inertia* (COI). A model that is valid for reasonable frequency deviations is described below.

We start with the swing equation (torque version) in pu,

$$\dot{\omega}_i = \frac{1}{2H_i}(T_{mi} - T_{ei}) \tag{5.282}$$

The initial condition for (5.282) is the pre-disturbance frequency, which is assumed equal to the rated frequency  $\omega_i(t_0) = \omega_0$ . The angular frequency deviation

$\Delta\omega_i$  is given by

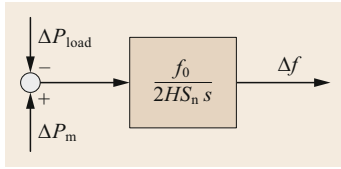
$$\Delta\omega_i = \omega_i - \omega_0, \tag{5.283}$$

which, in SI units, yields

$$\frac{2H_i S_{ni}}{\omega_0} \Delta\dot{\omega}_i = \frac{\omega_0}{\omega_i} (P_{mi} - P_{ei}), \tag{5.284}$$

where, for each unit  $i$ ,  $S_n$  is the rated power,  $H$  is the constant of inertia, and  $P_m$  and  $P_e$  are the mechanical and electrical power, respectively. If we assume that it is a highly meshed system, all generating units can be assumed to be connected to the same bus. The COI frequency can be defined as

$$\omega = \frac{\sum_i H_i S_{ni} \omega_i}{\sum_i H_i S_{ni}} \tag{5.285}$$



**Fig. 5.91** Block diagram representing the inertia of the system

All generating units can be considered to be aggregated into a single unit

$$\Delta \dot{\omega} = \frac{\omega_0^2}{2HS_n} (P_m - P_e), \quad (5.286)$$

where:

$S_n = \sum_i S_{ni}$  is the total rating, i.e., the sum of the power ratings of the generators

$H = \sum_i H_i S_{ni} / \sum_i S_{ni}$  is the total constant of inertia

$P_m = \sum_i P_{mi}$  is the total mechanical power

$P_e = \sum_i P_{ei}$  is the total electrical power.

By assuming that  $\omega = \omega_0$  on the right-hand side, a linear approximation of (5.286),

$$\Delta \dot{\omega} = \frac{\omega_0}{2HS_n} (P_m - P_e), \quad (5.287)$$

can be obtained. Equation (5.284) can also be expressed in terms of frequency as

$$\Delta \dot{f} = \frac{f_0}{2HS_n} (P_m - P_e). \quad (5.288)$$

After a disturbance, we can write

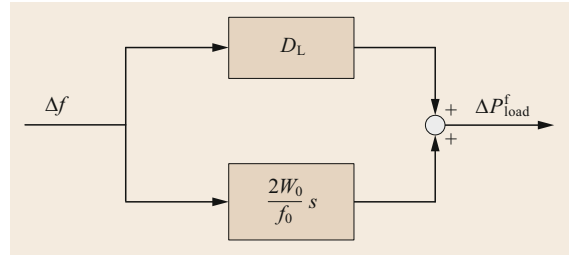
$$\Delta \dot{f} = \frac{f_0}{2HS_n} (\Delta P_m - \Delta P_{load}), \quad (5.289)$$

where  $\Delta P_m$  and  $\Delta P_{load}$  denote the variations in the total mechanical and electrical power outputs (taking into account the variations in the system power losses) with respect to the respective steady-state values before the perturbation.

Equation (5.289) can be represented by the block diagram shown in Fig. 5.91, where  $s$  is the Laplace variable.

### 5.7.3 Frequency Dependence of the Load

The aggregated system load is clearly frequency dependent. This has a stabilizing effect on the system frequency  $f$ . In addition to a component that depends on  $f$ , large rotating motors provide a contribution that depends on the time derivative  $\dot{f}$  (known as the rate of change of the frequency, ROCOF) due to the change in



**Fig. 5.92** Model used for the frequency-dependent behavior of the aggregated load

the kinetic energy stored in the rotating masses of the motor. Both of these frequency dependences are incorporated into the load model

$$\Delta P_{load}^f = D_L \Delta f + g(\Delta \dot{f}). \quad (5.290)$$

The function  $g(\Delta \dot{f})$  can be derived by observing that the kinetic energy of rotating masses can be expressed by

$$W(f) = \frac{1}{2} J (2\pi f)^2 \quad (5.291)$$

and that  $\Delta W$  can be approximated by

$$\Delta W = \frac{2W_0}{f_0} \Delta f, \quad (5.292)$$

where  $W_0 = J/2(2\pi f_0)^2$ . Hence,

$$g(\Delta \dot{f}) = \frac{2W_0}{f_0} \Delta \dot{f}. \quad (5.293)$$

The values of  $W_0$  and  $D_L$  are highly dependent on the composition of the load and can vary over time. Typical values of the constant  $D_L$  are such that the load variation is between 0 and 2% of the frequency variation.

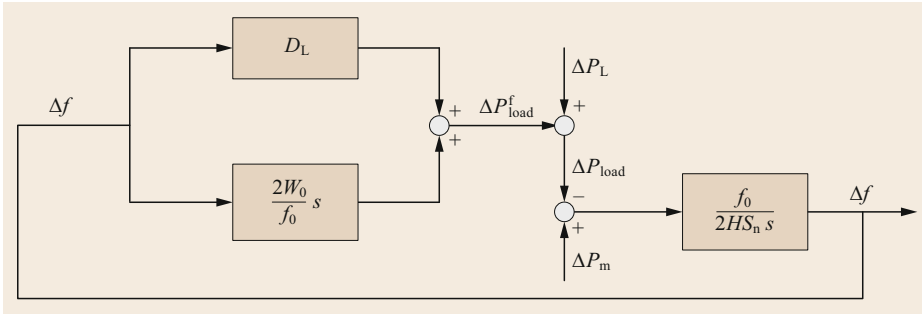
A model of the loads is provided in Fig. 5.92.

### 5.7.4 Dynamic Response of an Uncontrolled Power System

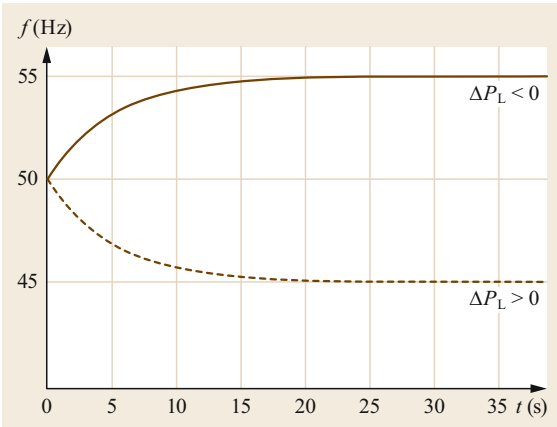
The model generated by combining the models used for the system inertia and the load is shown in Fig. 5.93.

Figure 5.94 shows the typical stable response of the frequency over time following an increasing or decreasing disturbance  $\Delta P_L$ .

The stabilizing effect of the frequency dependence of the load is generally too small to maintain the frequency within reasonable bounds.



**Fig. 5.93** Model of an uncontrolled system



**Fig. 5.94** Typical behavior of the frequency in the system shown in Fig. 5.93 after a perturbation

frequency control, the goal is to quickly return the frequency to acceptable values. However, even after primary control has acted, some of the frequency error will remain. Moreover, all of the generators must contribute to primary control, irrespective of the location of the disturbance.

In secondary frequency control (also called AGC or load frequency control), the power set points of the generators are adjusted in order to compensate for the frequency error remaining after the primary control has acted. Moreover, for large systems consisting of several control areas, the secondary control returns the power flows in the tie lines between the areas to the scheduled value.

Underfrequency load shedding is a form of system protection that acts on timescales of less than a second. As this scheme is only applicable when there is a loss of load across entire regions, it must only be activated when necessary to save the system from a blackout.

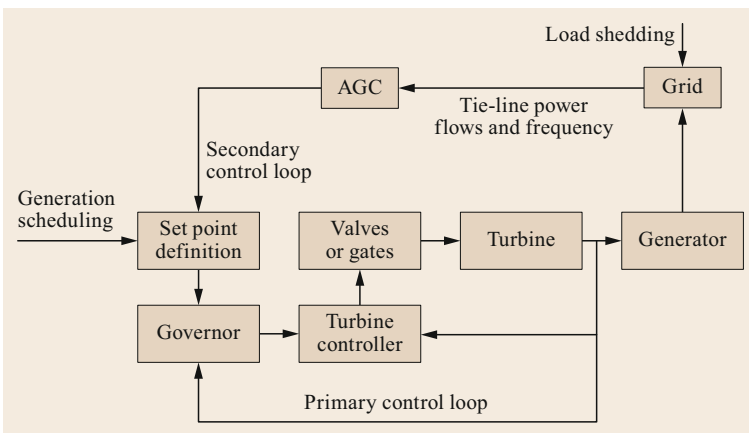
### 5.7.5 Control Structure for Frequency Control

The automatic control system consists of two main parts: primary control and secondary control, as shown in Fig. 5.95. Primary control refers to control actions that are performed locally (at the power plant) based on the set points for frequency and power. In primary

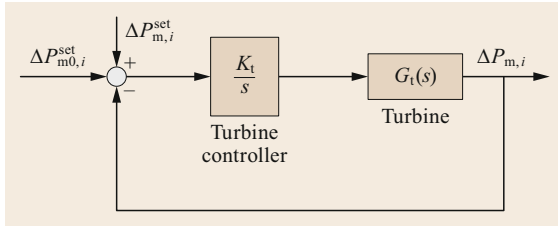
#### Dynamic Characteristics of Primary Control

The action of the governor for the generic unit  $i$  can be described by

$$(f_0 - f) \frac{1}{R_i} + (P_{m0,i}^{\text{set}} - P_{m,i}^{\text{set}}) = 0, \quad (5.294)$$



**Fig. 5.95** Structure of the frequency control system



**Fig. 5.96** Scheme of the turbine control loop

where  $R_i$  is the speed droop (in Hz/MW), which typically ranges from 4% to 8%.

Assuming an integral turbine power controller, we obtain the scheme depicted in Fig. 5.96.

If the dynamics of the turbine are neglected, we get

$$\Delta P_{m,i}(s) = \frac{1}{1 + T_i s} [\Delta P_{m0,i}^{set}(s) + \Delta P_{m,i}^{set}(s)], \quad (5.295)$$

where the time constant  $T_i = 1/K_i$  is small compared to the frequency dynamics of the system.

By defining

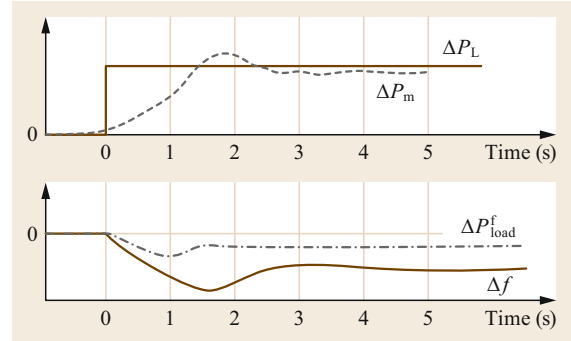
$$\frac{1}{R} = \sum_i \frac{1}{R_i}, \quad (5.296)$$

we get

$$\Delta P_{m,i}^{set} = -\frac{1}{R} \Delta f, \quad (5.297)$$

where  $\Delta P_m^{set} = \sum_i \Delta P_{m,i}^{set}$  and  $\Delta f$  is the frequency variation of the COI.

The models for the turbine control and the governor can be inserted into the model derived in the previous section, as shown in Fig. 5.97.



**Fig. 5.98** Typical response of the system with primary control

We now analyze the effect of a disturbance in the system above. Both a loss of generation and a loss of load can be simulated by imposing a positive or negative step input on the variable  $\Delta P_L$ . For obvious reasons, a change in the set value of the system frequency  $f_0$  is not considered here.

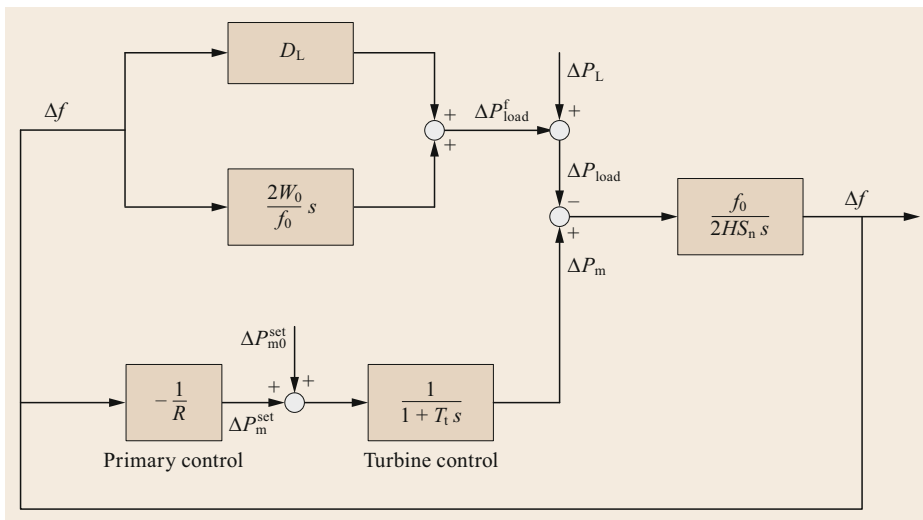
From the block diagram shown in Fig. 5.100, the transfer function between  $\Delta P_L$  and  $\Delta f$  ( $\Delta P_m^{set} = 0$ ) is

$$\Delta f(s) = -\frac{1 + sT_t}{\left[ \frac{1}{R} + D_L(1 + sT_t) + \left( \frac{2W_0}{S_n} + 2H \right) \frac{S_n}{f_0} s(1 + sT_t) \right]} \Delta P_L(s). \quad (5.298)$$

The step response for  $\Delta P_L(s) = \Delta P_L/s$  is illustrated in Fig. 5.98.

The frequency deviation in the steady state is

$$\Delta f_\infty = \lim_{s \rightarrow 0} (s \Delta f_s) = -\frac{\Delta P_L}{\frac{1}{R} + D_L}. \quad (5.299)$$



**Fig. 5.97** Model of the system with primary control

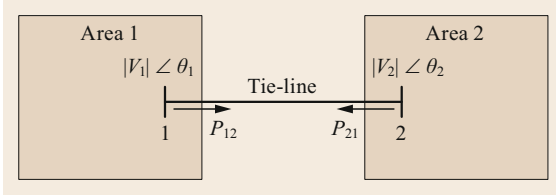


Fig. 5.99 Scheme for a two-area system

In real systems, the turbine controller time constant  $T_t$  is much smaller than the time constant of the frequency dynamics  $T_M$  presented in Fig. 5.94, so

$$T_M = \frac{2W_0}{S_n} + 2H. \quad (5.300)$$

Transfer function (5.298) can be approximated as

$$\Delta f(s) = -\frac{1}{1 + \frac{S_n}{f_0} T_M \frac{1}{R + D_L} s} \frac{\Delta P_{L,1}(s)}{\frac{1}{R} + D_L}. \quad (5.301)$$

The equivalent time constant for a step response is

$$T_{eq} = T_M \frac{S_n}{f_0} \frac{1}{\frac{1}{R} + D_L}. \quad (5.302)$$

#### Dynamic Model of a Two-Area System

In practice, a large interconnected power system is always divided into various control blocks or areas. For a simplified analysis, a system with two areas can be represented by two single bus systems with a tie-line between them, as shown in Fig. 5.99.

If we assume that  $|V_1|$  and  $|V_2|$  are constant and ignore the power loss in the tie-line, the power exchange  $P_{12}$  over the tie-line is

$$P_{12} = \frac{|V_1||V_2|}{x} \sin(\theta_1 - \theta_2), \quad (5.303)$$

where  $x$  is the equivalent reactance of the tie line and  $\theta_1$  and  $\theta_2$  are the voltage angles.

For small deviations, we obtain

$$\begin{aligned} \Delta P_{12} &= \left. \frac{\partial P_{12}}{\partial \theta_1} \right|_0 \Delta \theta_1 + \left. \frac{\partial P_{12}}{\partial \theta_2} \right|_0 \Delta \theta_2 \\ &= \frac{|V_1||V_2|}{x} \cos(\theta_1^0 - \theta_2^0) (\Delta \theta_1 - \Delta \theta_2) \end{aligned} \quad (5.304)$$

or

$$\Delta P_{12} = P_T (\Delta \theta_1 - \Delta \theta_2) \quad (5.305)$$

with

$$P_T = \frac{|V_1||V_2|}{x} \cos(\theta_1^0 - \theta_2^0). \quad (5.306)$$

Using this model, the block diagram of the power system can be extended as shown in Fig. 5.100.

We now study the behavior after a load change in area 1, where area 1 is considered to be much smaller than area 2, which can be regarded as an infinite bus. As  $\Delta f_2 = 0$ ,  $\Delta \theta_2 = 0$ , so

$$\Delta P_{12} = 2\pi P_T \int \Delta f_1 dt. \quad (5.307)$$

Without any generator setpoint changes (i.e.,  $\Delta P_{m0,1}^{\text{set}} = 0$ ), the transfer functions for a change of  $\Delta P_{L,1}(s)$  are

$$\Delta f_1(s) = -\frac{s}{\left[ 2\pi P_T + \left( D_{L1} \frac{1}{R_1(1+sT_{t1})} \right) s + \left( \frac{T_{M1} S_{n1}}{f_0} \right) s^2 \right]} \Delta P_{L,1}(s) \quad (5.308)$$

$$\Delta T_{12} = \frac{2\pi P_T}{s} \Delta f_1(s) \quad (5.309)$$

$$\Delta T_{12}(s) = -\frac{2\pi P_T}{\left[ 2\pi P_T + \left( D_{L1} \frac{1}{R_1(1+sT_{t1})} \right) s + \left( \frac{T_{M1} S_{n1}}{f_0} \right) s^2 \right]} \Delta P_{L,2}(s). \quad (5.310)$$

The step response for  $\Delta P_{L,1}(s) = \Delta P_{L,1}/s$  is shown in Fig. 5.101.

The steady-state frequency deviation is

$$\Delta f_\infty = \lim_{s \rightarrow 0} s \Delta f_1(s) = 0, \quad (5.311)$$

and the steady-state deviation of the tie-line power is

$$\Delta P_{12\infty} = \lim_{s \rightarrow 0} s \Delta P_{12}(s) = \Delta P_{L,1}. \quad (5.312)$$

The infinite bus brings the frequency deviation  $\Delta f_1$  back to 0. This is achieved by increasing  $P_{21}$  such that the load variation  $\Delta P_{L,1}$  is fully compensated for.

While this is beneficial for the system frequency in area 1, unscheduled and persistent energy exchange has arisen between the two areas.

#### Automatic Generation Control

Following the application of primary frequency control after a disturbance, a static frequency error will generally persist unless additional control actions are taken.

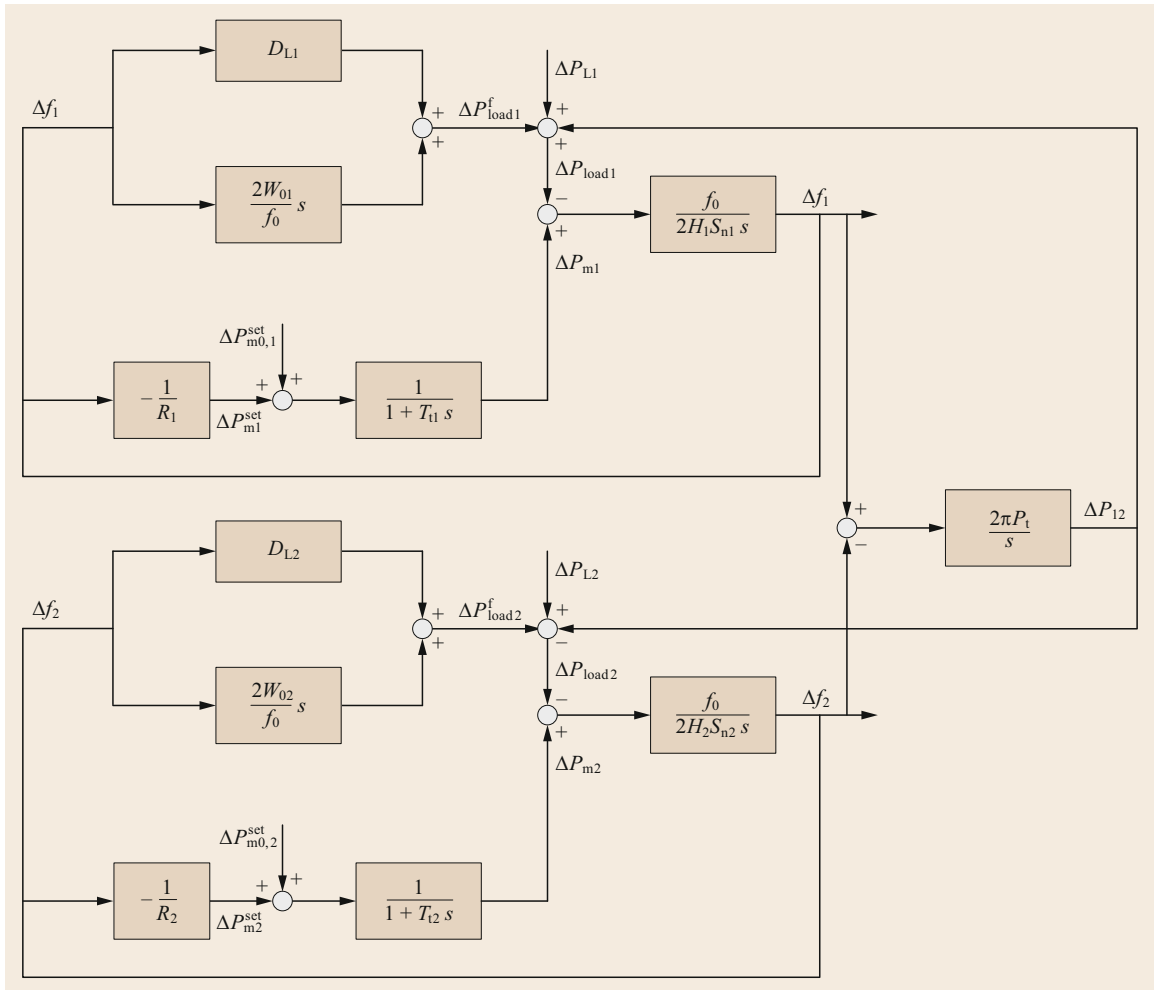


Fig. 5.100 Dynamic model of a two-area system

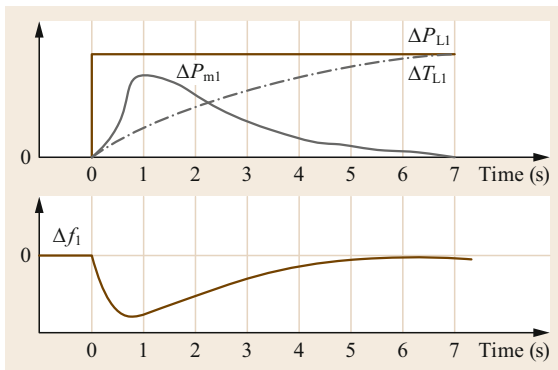


Fig. 5.101 Step response of the two-area system model

Furthermore, primary frequency control may change the scheduled interchanges between different areas in an interconnected system. The restoration of both the

frequency and the power interchanges to their pre-disturbance values is accomplished through the AGC.

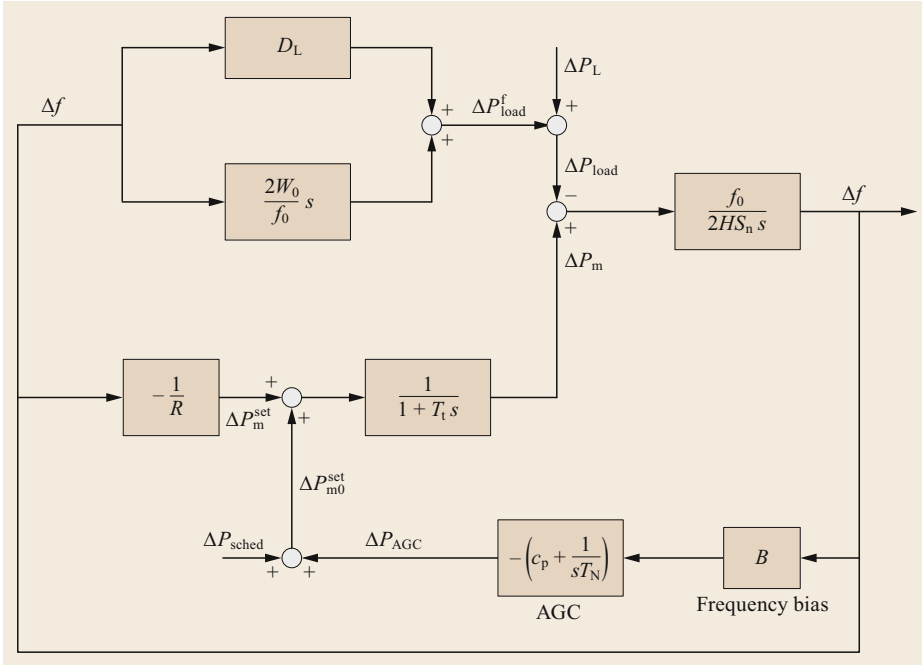
In an  $N$ -area system, there are  $N$   $AGC_i$  controllers, one for each area  $i$ . Each implements a proportional-integral (PI) controller, i.e.,

$$\Delta P_{AGC_i} = - \left( C_{P_i} + \frac{1}{s T_{N_i}} \right) \Delta e_i, \quad (5.313)$$

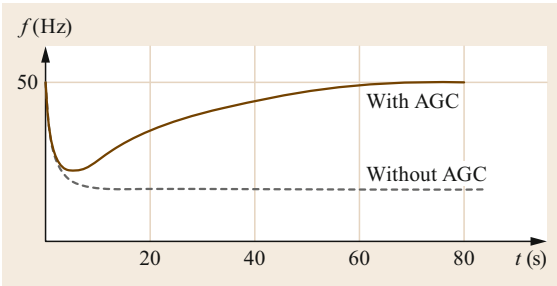
with  $C_{P_i}$  typically ranging between 0.1 and 1 and  $T_{N_i}$  between 30 and 200 s, implying that AGC reacts much more slowly than primary frequency control.

The error  $\Delta e_i$  is termed the area control error (ACE) for area  $i$ , and

$$ACE_i = \sum_{j \in \Omega_i} (P_{ij} - P_{ij}^0) + B_i (f_i - f_0), \quad (5.314)$$



**Fig. 5.102** Model of a single-area system with AGC



**Fig. 5.103** Step response of a single-area system with AGC

where  $P_{ij}$  is the power transfer from area  $i$  to area  $j$  and  $P_{ij}^0$  is the corresponding scheduled value. Defining

$$\Delta P_i = \sum_{j \in \Omega_i} (P_{ij} - P_{ij}^0), \tag{5.315}$$

where the summation includes all of the areas  $j$  directly connected to area  $i$ ,  $ACE_i$  can be written as

$$ACE_i = \Delta P_i + B_i(f_i - f_0). \tag{5.316}$$

The constant  $B_i$  is called the frequency bias factor (MW/Hz). It is assumed that the frequency references are the same in all areas. The goal is to bring all  $ACE_i$  values to 0.

The variables are thus  $\Delta P_i$  and  $f$ , i.e., there are  $N + 1$  variables in total, which are uniquely defined by  $N$

linear equations ( $ACE_i = 0$ ) and

$$\sum_i \Delta P_i = 0. \tag{5.317}$$

### Selection of Frequency Bias Factors

Let us consider a two-area system. The load is increased by  $\Delta P_L$  in area 2. If the power in the tie-line is to be kept constant, the generation in area 2 must be increased by  $\Delta P_L$  after the AGC has reacted. Before the AGC has reacted, we have a frequency deviation of  $\Delta f$  in both areas, which means that for area 1,

$$\Delta f = -R_1 \Delta P_{12}, \tag{5.318}$$

and for area 2,

$$\Delta f = -R_2(\Delta P_L - \Delta P_{12}), \tag{5.319}$$

and  $\Delta P_{12} = \Delta P_{21}$ . The two ACEs can now be written as

$$\begin{aligned} ACE_1 &= \Delta P_{12} + B_1 \Delta f = \Delta P_{12} + B_1(-R_1 \Delta T_{12}) \\ &= \Delta P_{12}(1 - B_1 R_1) \end{aligned} \tag{5.320}$$

and

$$\begin{aligned} ACE_2 &= \Delta P_{21} + B_2 \Delta f \\ &= \Delta P_{21} + B_2[-R_2(\Delta P_L - \Delta P_{12})] \\ &= \Delta P_{12}(1 - B_2 R_2) - B_2 R_2 \Delta P_L \end{aligned} \tag{5.321}$$

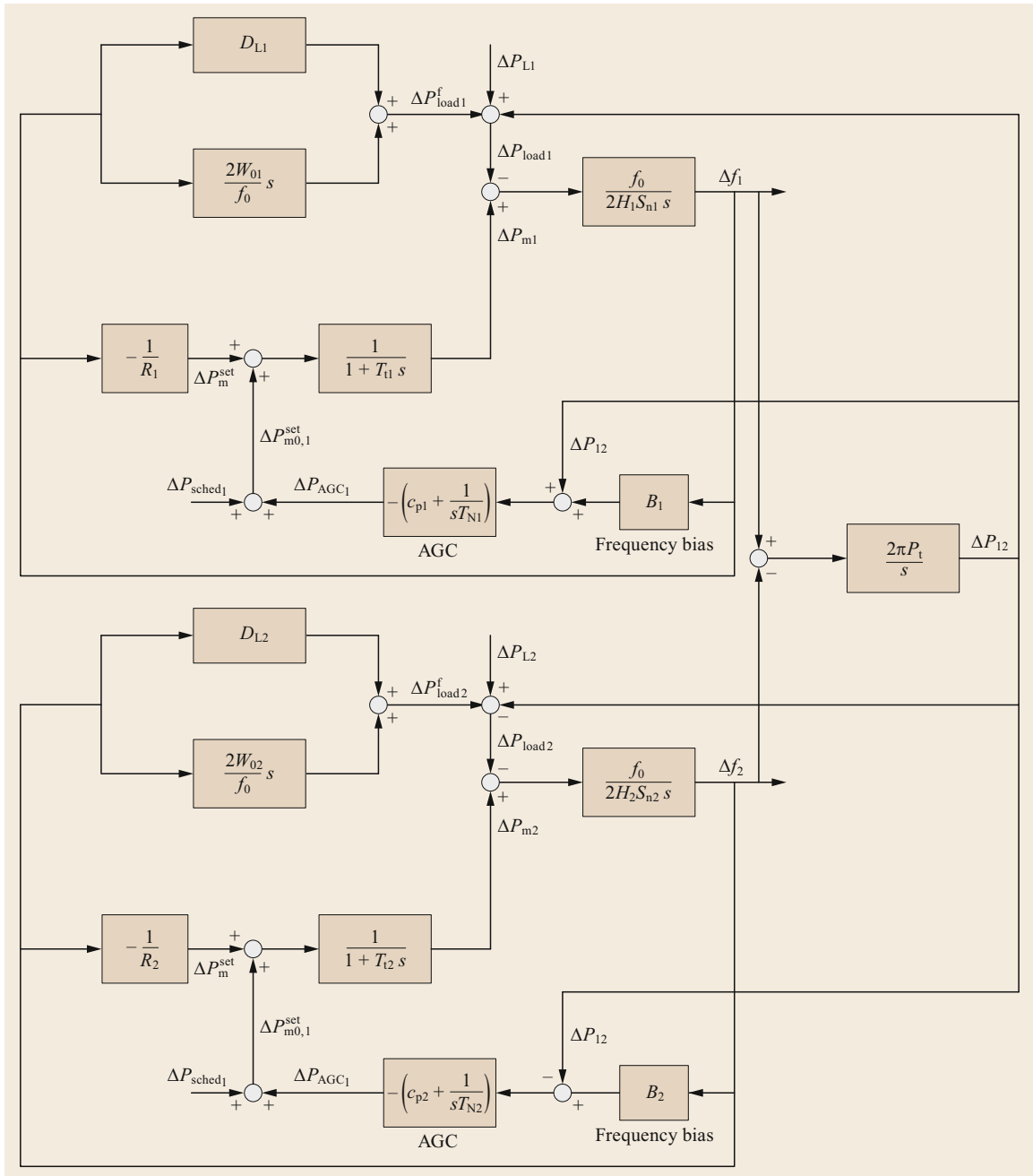


Fig. 5.104 Model of a two-area system with AGC

In this case, it is desirable that the AGC controller for area 1 should not react. If we set  $B_1 = 1/R_1$ , we can see from (5.320) that  $ACE_1 = 0$ . If  $B_2 = 1/R_2$  is chosen, the ACE in area 2 becomes

$$ACE_2 = -\Delta P_L. \tag{5.322}$$

This means that only controller 2 reacts to a load perturbation  $\Delta P_L$  in the same area.

In the multi-area case, this corresponds to selecting  $B_i = 1/R_i$  for all areas, which is known as noninteractive control. However, for the controller described by (5.313), all positive values of  $B_i$  will guarantee that all



**Fig. 5.105** Step response of a two-area system model with AGC ▶

the  $ACE_i$  tend to 0. The application of noninteractive control results in reduced control effort and costs.

#### Dynamic Characteristics of AGC

We now include the AGC control in both the single-area and two-area models.

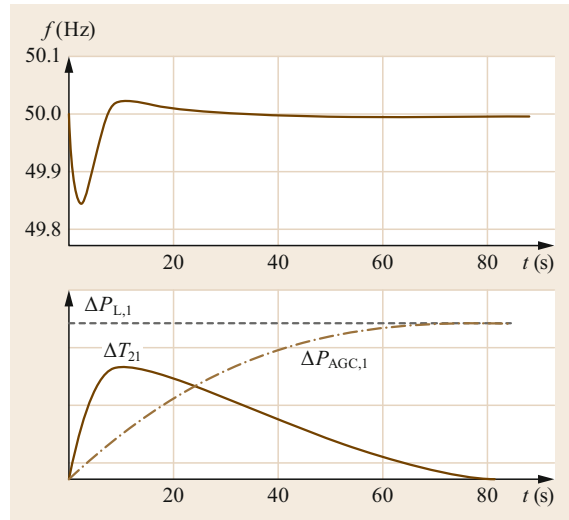
#### Single-Area System

AGC only acts to restore the nominal system frequency, as illustrated in Fig. 5.102, where  $P_{\text{sched}}$  indicates the scheduled value of the power output of the generators. Figure 5.103 shows how the system frequency response is brought back to the rated value after a load increase.

#### Two-Area System

A model of a two-area system with AGC is shown in Fig. 5.104.

If area 1 is assumed to be much smaller than area 2, the step response of the system for a load increase



of  $\Delta P_{L,1}$  is shown in Fig. 5.105. Due to the action of AGC, the perturbation in area 1 is fully compensated for by the generators in the same area (area 1) after the transients have decayed.

## 5.8 Propagation of Electromagnetic Transients Along Transmission Lines

In *steady-state* operating conditions, the wavelength of the sinusoidal currents and voltages is large compared with the physical dimensions of the network. Therefore, for steady-state analysis, a *lumped* element representation of transmission lines is generally adequate. However, for transient analysis, this is no longer the case, and the travel time of the electromagnetic waves must be taken into account.

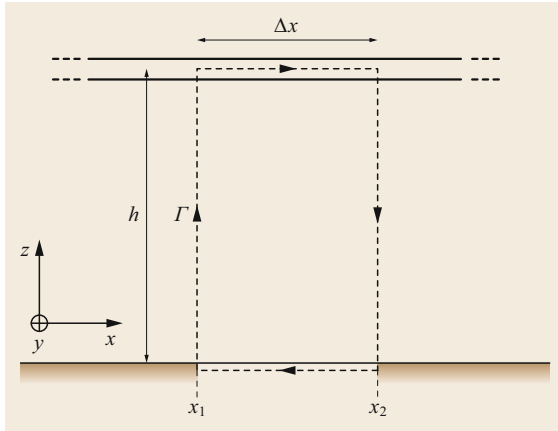
For example, in the case of insulation coordination analysis against overvoltages (particularly those due to lightning), we need to account for the fact that voltages and currents induced by lightning strikes have non-negligible frequency contents above 1 MHz. If the travel time of the electromagnetic field within the boundaries of the region of interest cannot be neglected with respect to the period over which electromagnetic quantities vary, then the lumped element model must be replaced in order to accurately represent electromagnetic field propagation along the line. Although the electric field cannot be expressed as the gradient of a scalar potential in our analysis of the electromagnetic field along lossless transmission lines, we can assume a transverse electromagnetic mode (TEM) of propagation (i.e., no component of the electric field or the magnetic field in the direction of propagation), so the rotor of the electric field is null in each plane orthog-

onal to the direction of propagation. This means that the integrals of the electric field in these planes can be expressed as potential differences. For lossy lines, and assuming a quasi-transverse electromagnetic mode of propagation, we can still apply the useful concepts of phase-to-ground and line-to-line voltages. In the quasi-TEM approximation, it is assumed that the electric and magnetic field components along the line are non-null but small enough to make the rotor of the electric field practically null in the plane orthogonal to the line.

Research into electromagnetic transients along transmission lines and relevant phenomena has developed impressively since the introduction of the Electromagnetic Transients Program [5.8] developed by *Herman Dommel* in the 1970s, and there have been various textbooks devoted to this subject [5.27, 28, 53, 54]. In this section, we limit our discussion to a brief summary of the basic concepts.

### 5.8.1 Traveling Waves in a Lossless Line

In order to introduce the equations describing the response of a transmission line to a transient, we consider a single line conductor that has ground return and is at a constant height above the ground (Fig. 5.106). The developments that follow are somewhat inspired



**Fig. 5.106** A single line-conductor section and the path of integration of the electric field that passes through the line

by [5.55], except that we consider a voltage source at one of the line terminations rather than an overhead line excited by an external electromagnetic field. The following approach can also be applied to a line consisting of two straight conductors that are parallel to each other.

Let us assume a triplet of Cartesian orthogonal axes  $x$ ,  $y$ , and  $z$ , where the  $x$ -axis is parallel to the axis of the line conductor that lies in the  $x$ - $z$  plane. The line height is  $z = h$ . The current in the line conductor is assumed to be positive if it is directed along the positive  $x$ -axis. Let us consider a closed path  $\Gamma$  that passes through the line and the ground (which lies in the  $x$ - $y$  plane), with vertical sections perpendicular to the ground. Let the path  $\Gamma$  be oriented according to the  $y$ -axis and the right-hand rule. The integral of the electric field along  $\Gamma$  is given by

$$\oint_{\Gamma} \bar{E} d\bar{l} = \int_0^h E_z(x_1, 0, z, t) dz + \int_{x_1}^{x_2} E_x(x, 0, h, t) dx - \int_0^h E_z(x_2, 0, z, t) dz - \int_{x_1}^{x_2} E_x(x, 0, 0, t) dx \quad (5.323)$$

If the conductors are ideal (i.e., both the line and the ground have infinite conductivity), the electric field components along  $x$  are null, so

$$\oint_{\Gamma} \bar{E} d\bar{l} = \int_0^h E_z(x_1, 0, z, t) dz - \int_0^h E_z(x_2, 0, z, t) dz \quad (5.324)$$

Assuming TEM propagation, the integrals of the electric field in the  $y$ - $z$  plane can be expressed as differences in scalar potentials. Therefore, assuming that the potential is zero at the ground, the integral of  $E$  along  $\Gamma$  can

be written as

$$\oint_{\Gamma} \bar{E} d\bar{l} = u(x_2, t) - u(x_1, t) \quad (5.325)$$

The law of electromagnetic induction

$$\oint_{\Gamma} \bar{E} d\bar{l} = -\frac{\partial}{\partial t} \int_{S_{\Gamma}} \bar{B} d\bar{S} \quad (5.326)$$

where  $B$  is the magnetic flux density and  $S_{\Gamma}$  is any surface with  $\Gamma$  as a contour, gives

$$u(x_2, t) - u(x_1, t) = -\frac{\partial}{\partial t} \int_{x_1}^{x_2} \int_0^h B_y(x, 0, z, t) dx dz \quad (5.327)$$

By taking  $x_2 = x_1 + \Delta x$ , where  $\Delta x$  is small, we can write

$$\int_{x_1}^{x_2} \int_0^h B_y(x, 0, z, t) dx dz = \int_0^h B_y(x_1, 0, z, t) dz \Delta x \quad (5.328)$$

where

$$\int_0^h B_y(x_1, 0, z, t) dz = L' i(x_1, t) \quad (5.329)$$

in which  $L'$  is the line inductance pu length.

We can then write

$$u(x_1 + \Delta x, t) - u(x_1, t) = -\frac{\partial}{\partial t} [L' i(x_1, t) \Delta x] \quad (5.330)$$

Dividing by  $\Delta x$  and assuming that the line is nondeformable, we get

$$\frac{u(x_1 + \Delta x, t) - u(x_1, t)}{\Delta x} = -L' \frac{\partial i(x_1, t)}{\partial t} \quad (5.331)$$

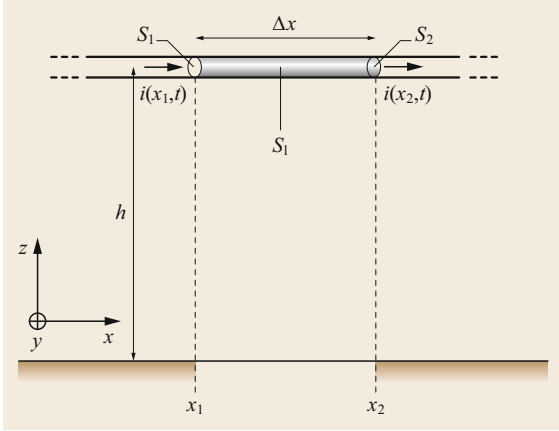
By taking the limit as  $\Delta x$  approaches zero, we obtain the first telegrapher's equation,

$$\frac{\partial u(x_1, t)}{\partial x} = -L' \frac{\partial i(x_1, t)}{\partial t} \quad (5.332)$$

Let us now consider a cylindrical surface surrounding the  $\Delta x$  section of the line conductor (Fig. 5.107). We denote the base surfaces orthogonal to the plane  $y$ - $z$  at  $x_1$  and  $x_2$  as  $S_1$  and  $S_2$ , respectively, and label the lateral surface as  $S_l$ .

The flux of the current density through the cylindrical surface has three components, i.e.,

$$\oint \bar{J} d\bar{S} = -\int_{S_1} J_x dS + \int_{S_l} \bar{J} d\bar{S} + \int_{S_2} J_x dS \quad (5.333)$$



**Fig. 5.107** A single line-conductor section and the surface of integration of the current density

If the insulating medium surrounding the conductor is ideal (i.e., it has null conductivity), the radial component of the current density is null, so

$$\oint \bar{J} d\bar{S} = - \int_{S_1} J_x dS + \int_{S_2} J_x dS. \quad (5.334)$$

The fluxes of the current density through  $S_1$  and  $S_2$  are the line currents at  $x_1$  and  $x_2$ ; therefore,

$$\oint \bar{J} d\bar{S} = i(x_2, t) - i(x_1, t). \quad (5.335)$$

The law of charge conservation

$$\oint_S \bar{J} d\bar{S} = - \frac{\partial}{\partial t} \int_{\tau_S} \rho d\tau, \quad (5.336)$$

where  $\rho$  is the charge density and  $\tau_S$  is the volume with  $S$  as a boundary, gives

$$i(x_2, t) - i(x_1, t) = - \frac{\partial}{\partial t} [C' u(x_1, t) \Delta x], \quad (5.337)$$

where  $C'$  is the line capacitance pu length. By taking  $x_2 = x_1 + \Delta x$ , where  $\Delta x$  is small, we can write

$$\frac{i(x_1 + \Delta x, t) - i(x_1, t)}{\Delta x} = -C' \frac{\partial u(x_1, t)}{\partial t}. \quad (5.338)$$

Taking the limit as  $\Delta x$  approaches zero, we obtain the second telegrapher's equation

$$\frac{\partial i(x_1, t)}{\partial x} = -C' \frac{\partial u(x_1, t)}{\partial t}. \quad (5.339)$$

Rewriting the two telegrapher's equations with reference to a generic abscissa  $x$  yields

$$\frac{\partial u(x, t)}{\partial x} + L' \frac{\partial i(x, t)}{\partial t} = 0 \quad (5.340)$$

$$\frac{\partial i(x, t)}{\partial x} + C' \frac{\partial u(x, t)}{\partial t} = 0. \quad (5.341)$$

By differentiating the first wave equation with respect to  $x$  and the second with respect to  $t$  and using substitution, we obtain

$$\frac{\partial^2 u(x, t)}{\partial x^2} = L' C' \frac{\partial^2 i(x, t)}{\partial t^2}. \quad (5.342)$$

Differentiating the first wave equation with respect to  $t$  and the second with respect to  $x$  and using substitution, we get an analogous equation for the current,

$$\frac{\partial^2 i(x, t)}{\partial x^2} = L' C' \frac{\partial^2 u(x, t)}{\partial t^2}. \quad (5.343)$$

Both of these equations have the form of the 1-D (one-dimensional) wave equation

$$\frac{\partial^2 f(x, t)}{\partial x^2} = \frac{1}{v^2} \frac{\partial^2 f(x, t)}{\partial t^2}, \quad (5.344)$$

where  $v$  is the speed of the wave in the direction of propagation.

Therefore, the telegrapher's equations describe the propagation of the voltage and the current along a transmission line. It is worth noting that the propagation speed, given by

$$v = \frac{1}{\sqrt{L' C'}}, \quad (5.345)$$

for a lossless line is practically equal to the speed of light. In fact, for a single line conductor of radius  $R$  and height  $h$  above the perfectly conducting ground,

$$L' = \frac{\mu_0}{2\pi} \ln \left( \frac{2h}{R} \right) \quad (5.346)$$

$$C' \approx \frac{2\pi\epsilon_0}{\ln(2h/R)}. \quad (5.347)$$

Inserting this into (5.345) gives

$$v = \frac{1}{\sqrt{\mu_0 \epsilon_0}}. \quad (5.348)$$

According to D'Alembert, the solution to the 1-D wave equation is

$$f(x, t) = f_1(x - vt) + f_2(x + vt), \quad (5.349)$$

where  $f_1$  is a forward-traveling wave (i.e., a wave traveling in the positive  $x$  direction) while  $f_2$  is a backward-traveling wave (i.e., a wave traveling in the negative  $x$  direction).

It is easy to verify that (5.349) is a solution of (5.344) by observing that

$$\begin{aligned}\frac{\partial f_1(x-vt)}{\partial t} &= -v \frac{\partial f_1(x-vt)}{\partial x} \\ \frac{\partial f_2(x+vt)}{\partial t} &= v \frac{\partial f_2(x+vt)}{\partial x}.\end{aligned}\quad (5.350)$$

We then find that the solution of the wave equation for the voltage takes the form

$$u(x, t) = u_1(x - vt) + u_2(x + vt), \quad (5.351)$$

and that there is an analogous equation for the current,

$$i(x, t) = i_1(x - vt) + i_2(x + vt). \quad (5.352)$$

These two solutions are not independent; in fact, the relationship between forward and backward voltage and current waves can be shown (via substitution and differentiation) to be

$$\begin{aligned}i_1(x) &= \frac{u_1(x)}{Z_0} \\ i_2(x) &= -\frac{u_2(x)}{Z_0},\end{aligned}\quad (5.353)$$

where  $Z_0$  is the surge impedance of the line, given by

$$Z_0 = \sqrt{\frac{L'}{C'}}. \quad (5.354)$$

Substituting (5.346) and (5.347) into (5.354) yields

$$Z_0 = 60 \ln \left( \frac{2h}{R} \right) \quad (5.355)$$

for a single lossless line conductor.

It is worth noting that  $u_1(\xi)$  with  $\xi = x - vt$  represents a forward-traveling wave, because  $\xi$  assumes the same value at  $x_0$  and time  $t_0$  as it does at  $x_0 + v\Delta t$  and time  $t_0 + \Delta t$ , and that an observer traveling forward at speed  $v$  would see the same voltage value.

A forward-traveling voltage wave is shown schematically in Fig. 5.108.

The same approach can be adopted for backward-traveling waves.

Note that it is changes in charge density that travel at the propagation speed  $v$ , not the charges themselves.

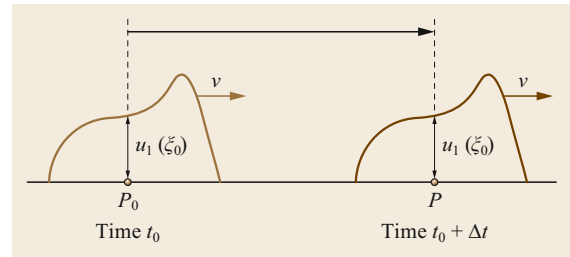


Fig. 5.108 Schematic of a forward-traveling voltage wave (adapted from [5.36])

In the absence of an external electromagnetic field coupled with the transmission lines, the traveling voltage and current waves depend on the boundary conditions at the line terminations (i.e., energizations, surge impedance discontinuities, loads, etc.).

Figure 5.109 presents four simple cases involving traveling waves: forward-traveling waves at the top and backward-traveling waves at the bottom with different polarities. According to (5.353), forward-traveling voltage and current waves have the same polarity, while backward-traveling voltage and current waves have opposite polarities.

## 5.8.2 Reflection and Transmission Coefficients

We now consider a discontinuity in the surge impedance of the line. Such a discontinuity may occur where there is a change in geometric size or a junction of a cable line with an overhead line that has bare conductors, or where there is a busbar with several lines connected, or where lumped devices are connected (e.g., a load or a transformer or a surge-protection device). When the traveling waves reach such a discontinuity, reflection and transmission (or refraction) processes occur due to the principle of energy conservation, and new voltage and current waves start to travel away from that point.

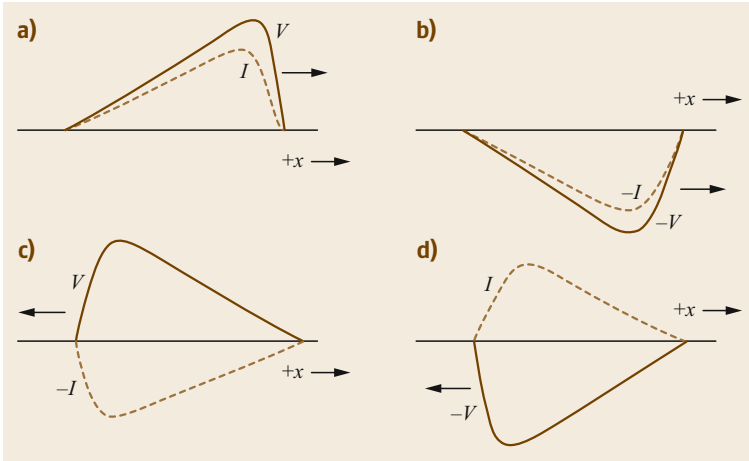
If the point of discontinuity  $M$  connects two lines  $L_1$  and  $L_2$  with different surge impedances  $Z_1$  and  $Z_2$ , a pair of incident voltage and current waves  $v_i$  and  $i_i$  from  $L_1$  give rise to a pair of transmitted waves  $v_t$  and  $i_t$  that travel forward along  $L_2$  as well as a pair of reflected waves  $v_r$  and  $i_r$  that travel backward along  $L_1$ .

The voltage and the current at the point of discontinuity must obey the equations (see also Fig. 5.110)

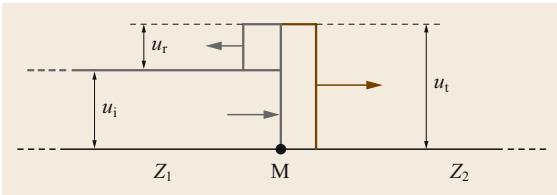
$$u_i + u_r = u_t \quad (5.356)$$

$$i_i + i_r = i_t. \quad (5.357)$$

If we define the transmission coefficient  $\tau_v$  as the ratio of  $v_t$  to  $v_i$  and the reflection coefficient  $\rho_v$  as the



**Fig. 5.109a-d** Schematic of four combinations of forward- and backward-traveling voltage and current waves: (a) positive forward-traveling waves, (b) negative forward-traveling waves, (c) negative backward-traveling current wave, (d) positive backward-traveling current wave (adapted from [5.28])



**Fig. 5.110** Voltage waves reflected and transmitted at a point of discontinuity in the surge impedance (adapted from [5.36])

ratio of  $v_r$  to  $v_i$ , (5.356) yields

$$1 + \rho_v = \tau_v \tag{5.358}$$

Analogously, we can define the transmission coefficient  $\tau_i$  as the ratio of  $i_t$  to  $i_i$  and the reflection coefficient  $\rho_i$  as the ratio of  $i_r$  to  $i_i$ .

Inserting (5.353) into (5.357) gives

$$\frac{u_i}{Z_1} - \frac{u_r}{Z_1} = \frac{u_t}{Z_2} \tag{5.359}$$

By adding and subtracting each member of (5.356) and (5.359), we obtain

$$u_t = \frac{2Z_2}{Z_1 + Z_2} u_i \tag{5.360}$$

$$u_r = \frac{Z_2 - Z_1}{Z_2 + Z_1} u_i \tag{5.361}$$

Therefore, the transmission coefficient  $\tau_v$  is

$$\tau_v = \frac{2Z_2}{Z_1 + Z_2} \tag{5.362}$$

while the reflection coefficient  $\rho_v$  is

$$\rho_v = \frac{Z_2 - Z_1}{Z_1 + Z_2} \tag{5.363}$$

Analogously, the transmission coefficient  $\tau_i$  is

$$\tau_i = \frac{2Z_1}{Z_1 + Z_2} \tag{5.364}$$

and the reflection coefficient  $\rho_i$  is

$$\rho_i = \frac{Z_1 - Z_2}{Z_2 + Z_1} \tag{5.365}$$

Line terminations are line discontinuities that give rise to surge wave reflections. For an ideal lossless line that is terminated on a resistive lumped device, these reflections can easily be explained using reflection and transmission coefficients, as they are constant and scalar in this case. The reflections at a short-circuited end and at an open end can be considered a particular case of resistive termination, as illustrated below.

The surge response at a generic line termination can be calculated via Thévenin's theorem so long as reflections at the far termination of a line of finite length do not influence phenomena at the termination of interest within the considered observation time.

The system corresponding to (5.356), (5.357), and (5.353), i.e.,

$$\begin{cases} u_i + u_r = u_t \\ i_i + i_r = i_t \\ u_t = Z_2 i_t \\ u_r = -Z_1 i_r \end{cases} \tag{5.366}$$

yields

$$2v_i - Z_1 i_t = u_t \tag{5.367}$$

which is the equation of a Thévenin equivalent circuit with a no-load voltage of  $2v_i$  and an equivalent impedance of  $Z_1$ .

Analogously, system (5.366) can also be solved for the incident current,

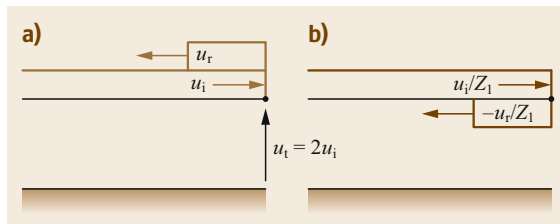
$$2i_i - \frac{u_t}{Z_1} = i_t. \tag{5.368}$$

This corresponds to a Norton equivalent circuit with a short-circuit current of  $2i_i$  and an equivalent conductance of  $1/Z_1$ .

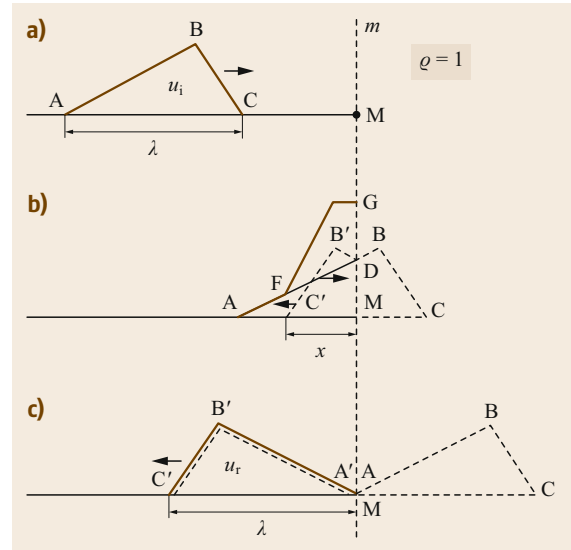
### Reflections at an Open Termination

An incident voltage wave undergoes complete reflection at an open termination. Superposition of the incident wave on a reflected wave of the same amplitude and polarity produces voltage doubling at the line termination. On the other hand, the incident current wave is canceled out by a reflected wave of equal and opposite amplitude, thereby resulting in a null current overall at the open end. The amplitudes and polarities of the reflected voltage and current waves can be deduced by considering the boundary conditions and the energy balance at the line termination. Voltage doubling can be viewed as a consequence of the increase in electric energy associated with the cancellation of the current at the line termination, as well as the associated magnetic energy. The same results can be deduced by noting that an open end can be considered a termination on a device with a very large equivalent resistance. The surge impedance seen by the surge waves is therefore very large. By taking the limits of (5.361) and (5.365) as  $Z_2$  approaches infinity, we obtain  $\rho_v = 1$  and  $\rho_i = -1$ . Ultimately, we have  $v_t = 2v_i$ ,  $v_r = v_i$ ,  $i_t = 0$ , and  $i_r = -i_i$  at an open end. The effect of incident and reflected wave superposition at an open line end in the case of stepwise incident voltage and current waves is presented schematically in Fig. 5.111.

For a surge waveform of limited duration, superposition of the incident and reflected voltage waves only occurs close to the open end, and the ultimate effect of the reflection is a voltage with a mirrored waveform that propagates in the opposite direction. The case of a tri-



**Fig. 5.111a,b** Incident and reflected voltage waves (a) and current waves (b) at the open end of a transmission line (adapted from [5.36])

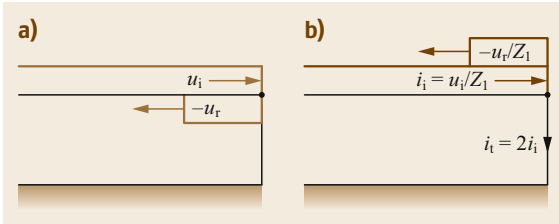


**Fig. 5.112a-c** A triangular voltage (a) before, (b) during, and (c) after reflection at the open end of a line (adapted from [5.36])

angular wave is presented in Fig. 5.112, which shows the diagram of the incident wave (ABC, propagating to the right) in Fig. 5.112a, the superposition of the diagram of the incident wave (ADM) on the wave  $C'B'DM$  (the mirror image of the wave  $CBDM$  with respect to the straight line  $m$ ), which gives rise to wave  $AFG$  in Fig. 5.112b, and the mirrored wave  $C'B'A'$  propagating to the left in Fig. 5.112c.

### Reflections at a Short-Circuited End

Another extreme case is a short-circuited end. An identical approach to that used for an open end can be applied for a short-circuited end, but with the behavior of the voltage and current waves swapped. An incident voltage wave undergoes complete but negative reflection, resulting in a null voltage overall at the short-circuited end, while the current amplitude doubles. The amplitudes and polarities of the reflected voltage and current waves can be deduced by considering the boundary conditions and the energy balance at the line termination, as well as by noting that a short-circuited end can be considered a termination on a device with very low resistance. Thus, by taking the limits of (5.361) and (5.365) as  $Z_2$  approaches zero, we obtain  $\rho_v = -1$  and  $\rho_i = 1$ . Ultimately, we have  $v_t = 0$ ,  $v_r = -v_i$ ,  $i_t = 2i_i$ , and  $i_r = 0$  at the short-circuited end. The effect of superposing the incident and reflected waves at a short-circuited line end in the case of stepwise incident voltage and current waves is presented schematically in Fig. 5.113.



**Fig. 5.113a,b** Incident and reflected voltage waves (a) and current waves (b) at the short-circuited end of a transmission line (adapted from [5.36])

**Reflections at an Inductive Termination**

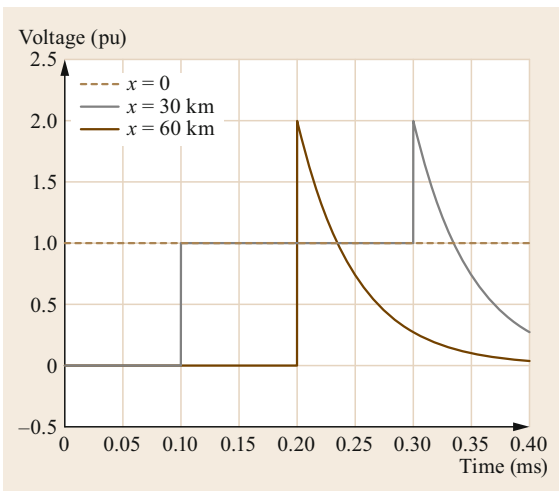
Reflection at an inductive termination is similar to that at an open circuit immediately after the arrival of the incident wave, but ultimately resembles reflection at a short circuit. The voltages (in pu with respect to the amplitude of the voltage source) at three points along a 60 km line with a step voltage source at  $x = 0$  and a 25 mH inductance at  $x = 60$  km are depicted in Fig. 5.114. Figure 5.115 reports the voltage profiles along the line at three different times. The results presented in this and subsequent sections are obtained using a finite-difference time-domain solution of the telegrapher’s equations, and using Bergeron’s lines to solve the boundary conditions.

The waveform of the inductive terminal voltage can be justified by substituting the Laplace transform of the inductor constitutive equation

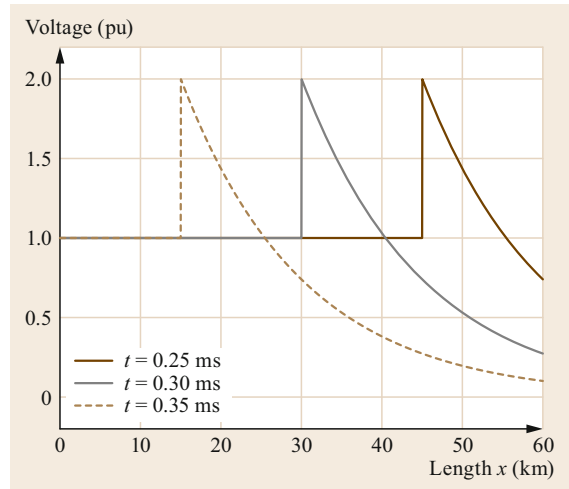
$$u_t(s) = Ls i_t(s) \tag{5.369}$$

into the Laplace transformation of (5.367), with

$$u(s) = \frac{E}{s} \tag{5.370}$$



**Fig. 5.114** Voltage waveforms along a 60 km line in the case of an inductive termination



**Fig. 5.115** Voltage profiles along a 60 km line at different times in the case of an inductive termination

This leads to

$$u_t(s) = E \frac{2T}{1 + Ts} \tag{5.371}$$

$$i_t(s) = \frac{E}{Z_1} \frac{2}{s(1 + Ts)} \tag{5.372}$$

where

$$T = \frac{L}{Z_1} \tag{5.373}$$

which correspond to

$$u_t(t) = 2Ee^{-\frac{t}{T}} \tag{5.374}$$

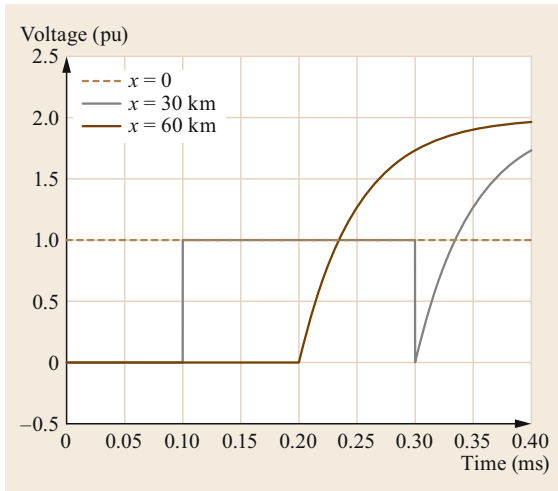
$$i_t(t) = \frac{2E}{Z_1} (1 - e^{-\frac{t}{T}}) \tag{5.375}$$

**Reflections at a Capacitive Termination**

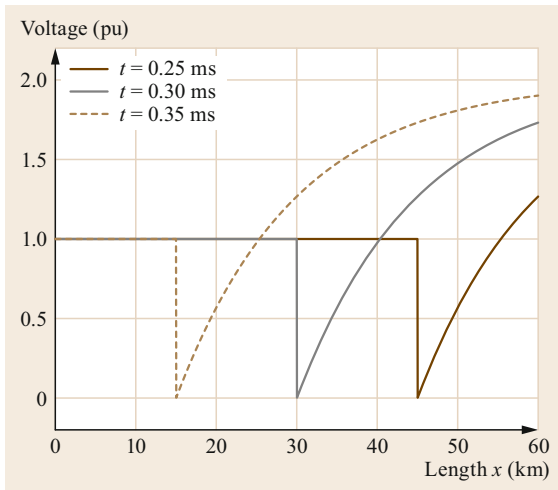
Reflection at a capacitive termination is similar to that at a short circuit immediately after the arrival of the incident wave, but ultimately resembles reflection at an open circuit. The voltages (in pu with respect to the amplitude of the voltage source) at three points along a 60 km line with a step voltage source at  $x = 0$  and a 100 nF capacitance at  $x = 60$  km are presented in Fig. 5.116. Figure 5.117 shows the voltage profiles along the line at three different times.

The waveform of the capacitive terminal voltage can be justified by substituting the Laplace transform of the capacitor constitutive equation

$$u_t(s) = \frac{1}{Cs} i_t(s) \tag{5.376}$$



**Fig. 5.116** Voltage profiles along a 60 km line at different times in the case of a capacitive termination



**Fig. 5.117** Voltage waveforms along a 60 km line in the case of a capacitive termination

into the Laplace transformation of (5.367) and using (5.370), thus obtaining

$$u_t(s) = E \frac{2}{s(1 + Ts)} \tag{5.377}$$

$$i_t(s) = E \frac{2C}{1 + Ts} \tag{5.378}$$

where

$$T = CZ_1 \tag{5.379}$$

Finally, antitransforming these equations yields

$$u_t(t) = 2E \left( 1 - e^{-\frac{t}{T}} \right) \tag{5.380}$$

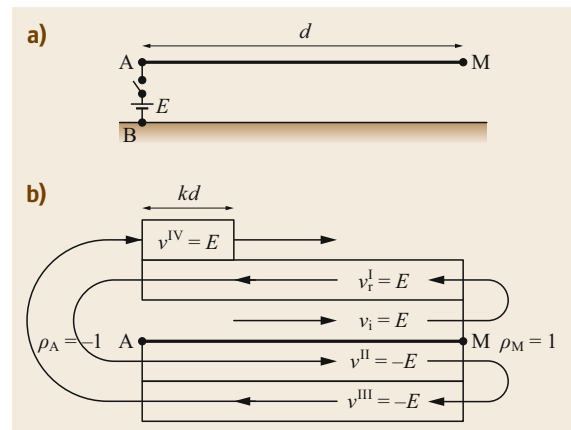
$$i_t(t) = \frac{2E}{T} e^{-\frac{t}{T}} \tag{5.381}$$

### 5.8.3 Multiple Reflections in a Line of Finite Length

In a line of finite length, the voltage and the current at a point along the line are obtained by superposing the waves traveling in both directions—the incident wave and the waves that have been reflected at the line ends. If one of the terminations is connected to an ideal voltage source, the voltage at that terminal will always be equal to the voltage impressed by the generator, meaning that any reflected wave that moves backward from the opposite end will be canceled out by the new reflection at the generator. In other words, the reflection coefficient at the generator side is equal to  $-1$ . In this section, we consider multiple reflections along the line in the extreme cases of open and short-circuited ends, as well as two cases of multiple reflection along a line with a resistive termination.

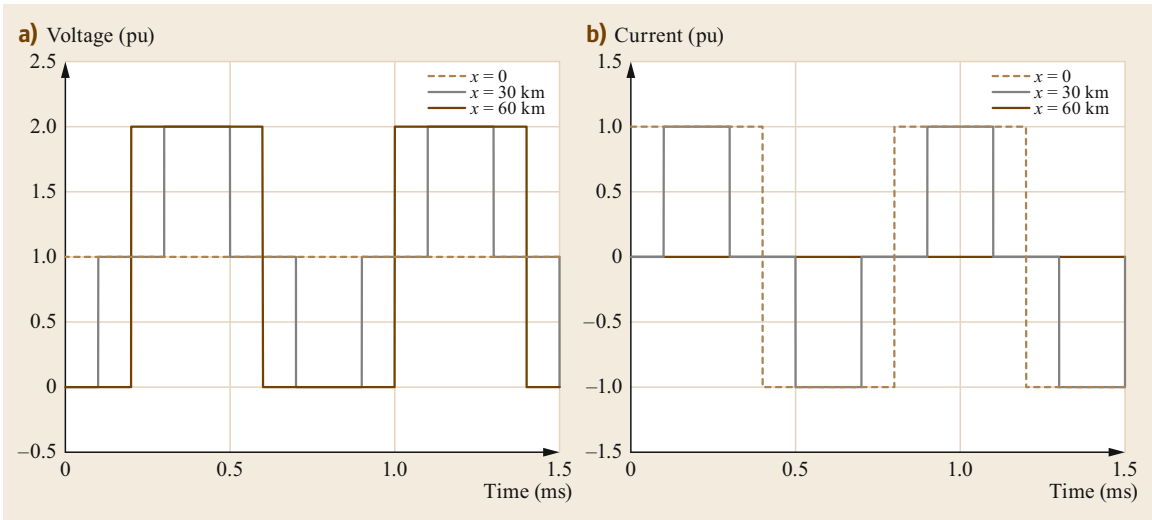
#### Open End

Figure 5.118 presents the case of a single conductor line of finite length  $d$  with one termination (A) connected to a DC voltage source and the other termination (M) kept open. The voltage reflection coefficients are 1 at A and  $-1$  at M. Therefore, the voltage is doubled at the open end and restored to the impressed voltage value  $E$  at the source. Due to the backward voltage wave reflected by the open end, the voltage along the line is  $2E$  so long as the doubling effect is canceled out by the



**Fig. 5.118** (a) The schematic depicts a single line conductor of finite length  $d$  with a DC voltage source at the left end (A) and an open right end (M), while the schematic in (b) shows the effect of multiple reflections on the voltage at the point a distance  $kd$  along the line from the powered end (adapted from [5.36])





**Fig. 5.119** (a) Voltages and (b) currents at different points along a 60 km line with a step voltage source at  $x = 0$  and an open end at  $x = 60$  km. Voltage/current values are in pu with respect to the incident voltage/current wave amplitude

forward voltage wave from the source, as illustrated in Fig. 5.119 for the terminal ends and the middle point of a 60 km line. The figure also shows the currents at the same points along the line; the waveform can be justified by observing that the current reflection coefficients are  $-1$  at the open end and  $1$  at the receiving end. The voltage and current waveforms along the line present oscillatory components that persist due to the assumed absence of dissipative elements along the line and at the line ends.

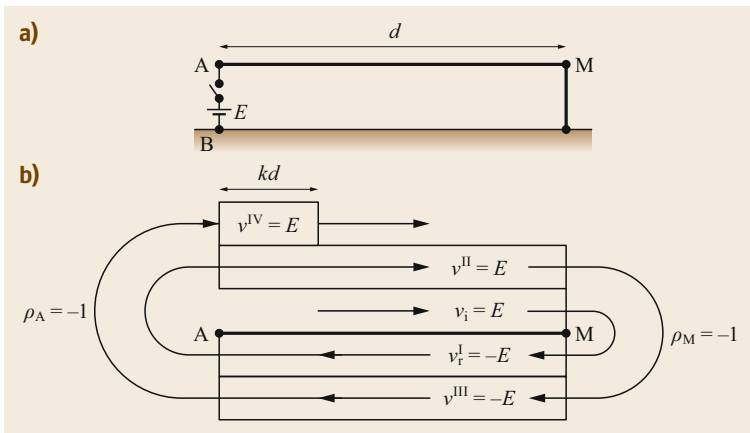
**Short-Circuited End**

Figure 5.120 presents the case of a single line conductor of finite length  $d$  with one termination (A) connected to a DC voltage source and the other termination (M) short-circuited. The voltage reflection coefficients are  $-1$  at both ends. Therefore, the voltage is canceled at

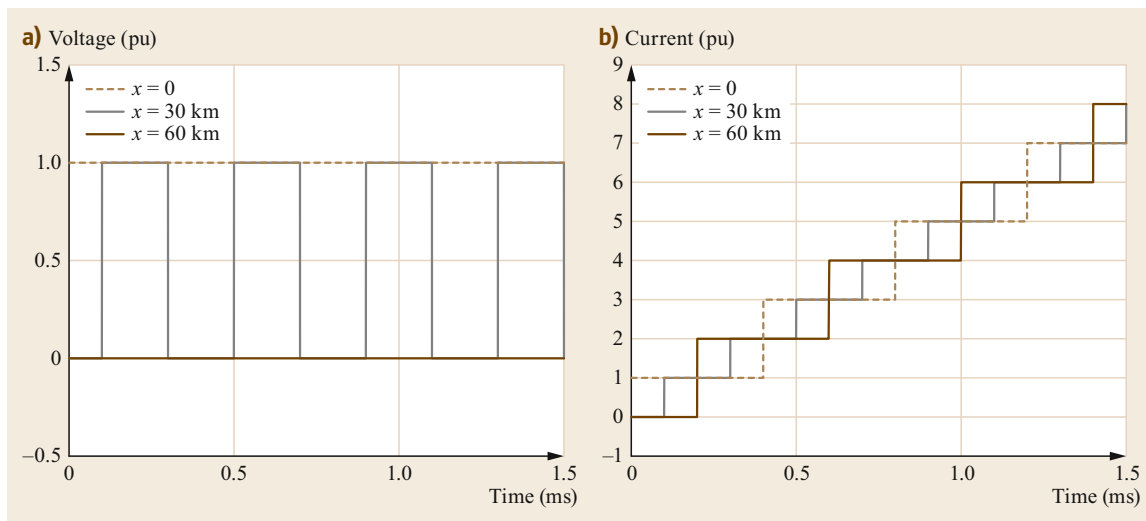
the short-circuited end and restored to the impressed voltage value  $E$  at the source. The voltage along the line is  $E$  so long as it is not canceled out by the backward voltage wave reflected at the short-circuited end, as illustrated in Fig. 5.121 for the terminal ends and the middle point of a 60 km line. The figure also shows the current at the same points; the waveform can be justified by observing that the current reflection coefficient is  $1$  at both ends.

**Resistive End**

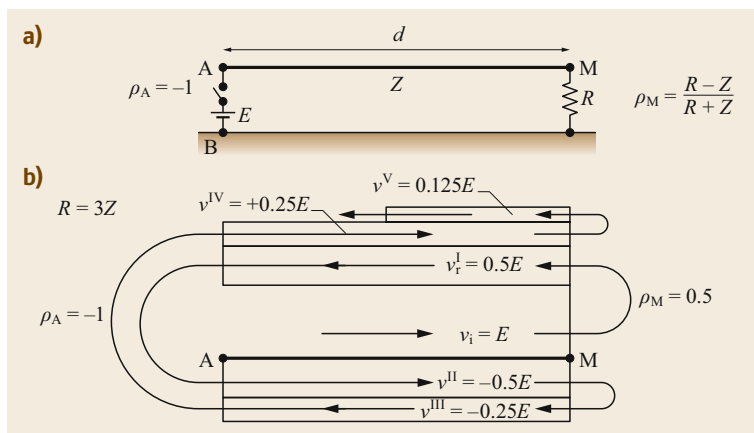
Figure 5.122 presents the case of a single line conductor with one termination (A) connected to a DC voltage source and the other termination (M) feeding a resistance  $R$ . The diagram showing the reflected voltage waves refers to the case where  $R$  is equal to  $3Z$  ( $Z$  is the surge impedance of the line), which—according



**Fig. 5.120** (a) The schematic depicts a single line conductor of finite length  $d$  with a DC voltage source at the left end (A) and a short-circuited right end (M), while the schematic in (b) shows the effect of multiple reflections on the voltage at a point a distance  $kd$  along the line from the powered end (adapted from [5.36])



**Fig. 5.121** (a) Voltages and (b) currents at different points along a 60 km line with a step voltage source at  $x = 0$  and a short-circuited end at  $x = 60$  km. Voltage/current values are in pu with respect to the incident voltage/current wave amplitude



**Fig. 5.122** (a) The schematic depicts a single line conductor of finite length  $d$  with a DC voltage source at the left end (A) and a resistance  $R$  (which is three times larger than the surge impedance of the line,  $Z$ ) at the right end (M), while the schematic in (b) shows the effect of multiple reflections of the voltage at a point along the line (adapted from [5.36])

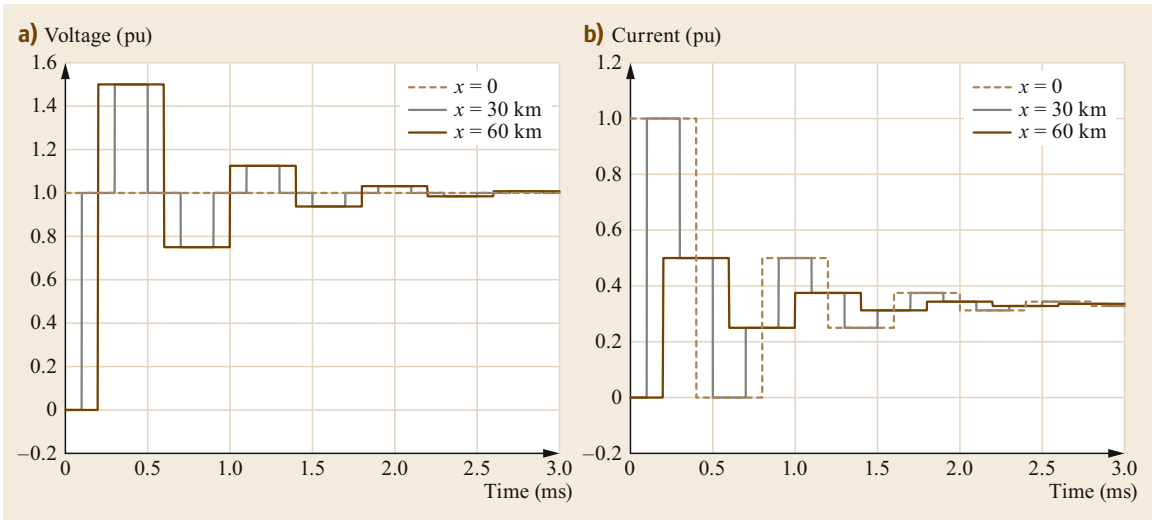
to (5.363)—gives a voltage reflection coefficient of 0.5 at M. The voltage coefficient is  $-1$  at A, just as in the previous cases. The backward-traveling voltage waves increase the voltages along the line, whereas the forward-traveling ones reflected by the source reduce them. The voltages along the line, and in particular the voltage at M (see Fig. 5.123), show an oscillatory trend with an overshoot with respect to the steady-state value. It is worth noting that the oscillations are not persistent as they are damped by the energy dissipation in  $R$ .

Figure 5.124 presents a case study that is similar to the previous one but with  $R$  equal to one-third of the surge impedance of the line  $Z$ , which gives—according to (5.363)—a voltage reflection coefficient of  $-0.5$  at M. In this case, the backward-traveling voltage

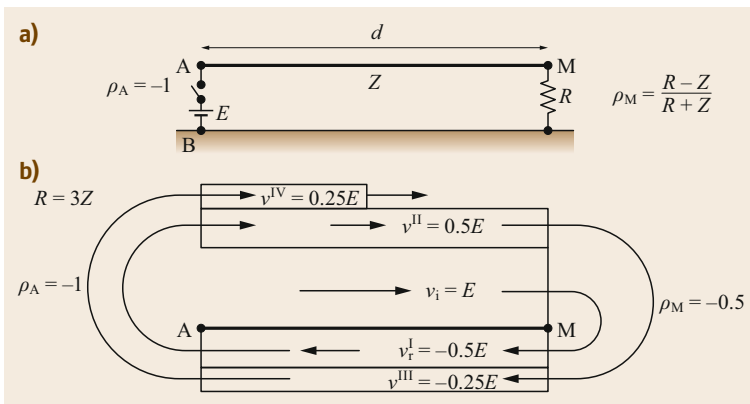
waves reduce the voltages along the line, whereas the forward-traveling ones reflected by the source increase them (due to the voltage reflection coefficient of  $-1$  at A). The voltages along the line, and in particular the voltage at M (see Fig. 5.125), show an increasing aperiodic trend towards the steady-state value.

### Sinusoidal Source

We now consider the case of a transmission line energized by an ideal 50 Hz sinusoidal voltage source. The voltages in the figures presented in this section are expressed in pu with respect to the amplitude of the voltage source, while the currents are given with respect to the amplitude of the incident current wave (i.e., the ratio of the voltage source amplitude to the surge impedance of the line).



**Fig. 5.123** (a) Voltages and (b) currents at different points along a 60 km line with a step voltage source at  $x = 0$  and a resistance that is three times the surge impedance at  $x = 60$  km. Voltage/current values are in pu with respect to the incident voltage/current wave amplitude



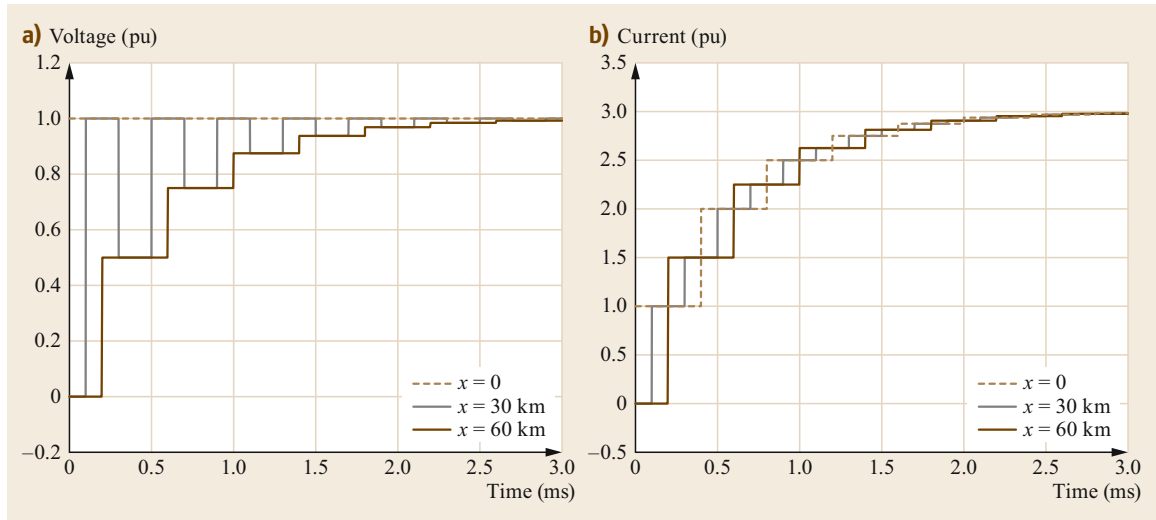
**Fig. 5.124** (a) The schematic depicts a single line conductor of finite length  $d$  with a DC voltage source at the left end (A) and a resistance  $R$  that is one-third the surge impedance of the line ( $Z$ ) at the right end (M), while the schematic in (b) shows the effect of multiple reflections of the voltage at a point along the line (adapted from [5.36])

Figures 5.126 and 5.127 present the voltage profiles along a 6000 km transmission line 1 ms before and 1 ms after the incident voltage wave reaches the non-energized termination. Different resistive terminations are considered; in particular, the receiving end is assumed to be connected to a resistance  $R$  that is equal to the surge impedance  $Z_0$ , three times  $Z_0$ , or one-third of  $Z_0$ . The voltage profiles before the arrival of the wave at the receiving end are the same, but they differ after the wave has been reflected. It is worth noting that the incident voltage amplitude varies sinusoidally along the line length with a period of 6000 km, which is the wavelength of a signal at 50 Hz traveling at the speed of light.

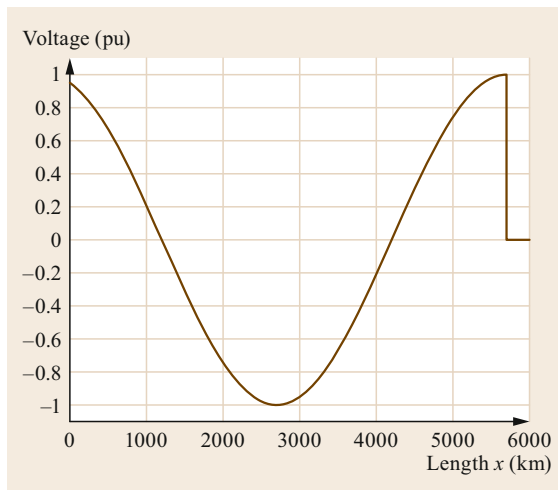
Figures 5.128 and 5.129 show the same comparison as Fig. 5.127, but they present the results obtained for

lines 600 and 60 km long, respectively. Note that the incident voltage wave amplitude still varies sinusoidally in these two figures, but that the variation is less prominent.

Figure 5.130 compares the above three cases with different line lengths in terms of the voltage and current waveforms obtained at the two ends of the line. The resistive termination is assumed to have a resistance equal to the surge impedance of the line. Under these conditions, neither voltage nor current reflection takes place, and the line is often said to be *matched*. The voltage and current waves (in pu) coincide. When the line length is equal to the wavelength, the voltage waveforms at the line ends coincide, except for the delay with which the receiving end is energized. For shorter lines, a displacement between the waveforms can be observed.



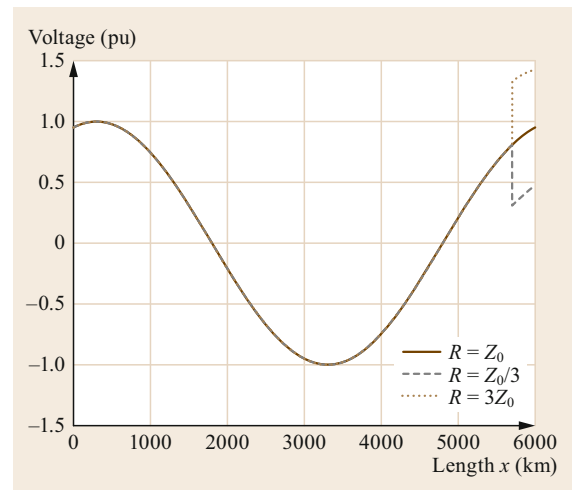
**Fig. 5.125** (a) Voltages and (b) currents at different points along a 60 km line with a step voltage source at  $x = 0$  and a resistance that is one-third of the surge impedance at  $x = 60$  km. Voltage/current values are in pu with respect to the incident voltage/current wave amplitude



**Fig. 5.126** Voltage profile along a 6000 km line 19 ms after energization by a 50 Hz sinusoidal voltage source connected at  $x = 0$ . Voltage values are given in pu with respect to the source voltage amplitude

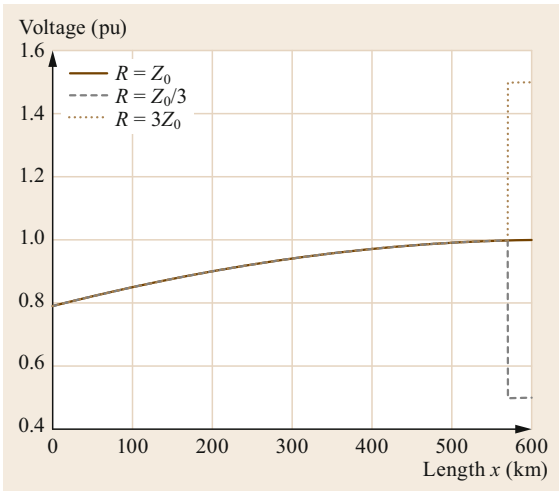
A comparison between the voltage waveforms obtained at the receiving end when different resistive terminations are present is provided in Fig. 5.131. It can be observed that the speed of the transition between the transient and the steady-state responses of the line increases as the line shortens and the termination resistance increases.

Comparisons between the current waveforms obtained at the sending and receiving line terminations when different resistive terminations are present are re-

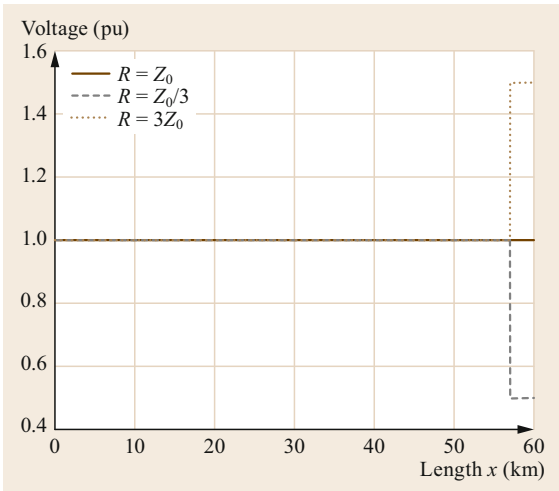


**Fig. 5.127** Voltage profile along a 6000 km line 21 ms after energization by a 50 Hz sinusoidal voltage source connected at  $x = 0$ . The other termination at  $x = 6000$  km is resistive; cases where this resistance  $R$  is equal to, larger than, or lower than the surge impedance  $Z_0$  of the line are considered. Voltage values are given in pu with respect to the source voltage amplitude

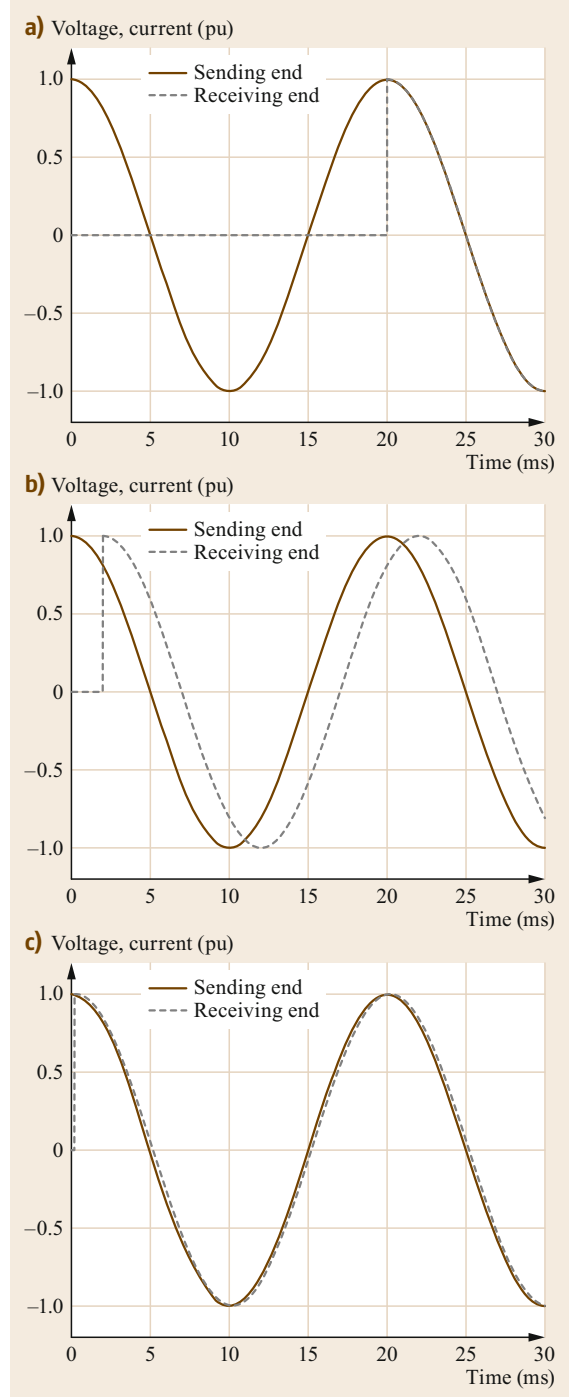
ported in Figs. 5.132 and 5.133, respectively. In contrast to the voltage waveform, which only changes at the receiving end depending on the resistance of the resistive termination, it should be noted that the current at the sending end can vary too. In particular, for line lengths of 600 and 60 km, the current waveform is modified by the backward-reflected current waves.



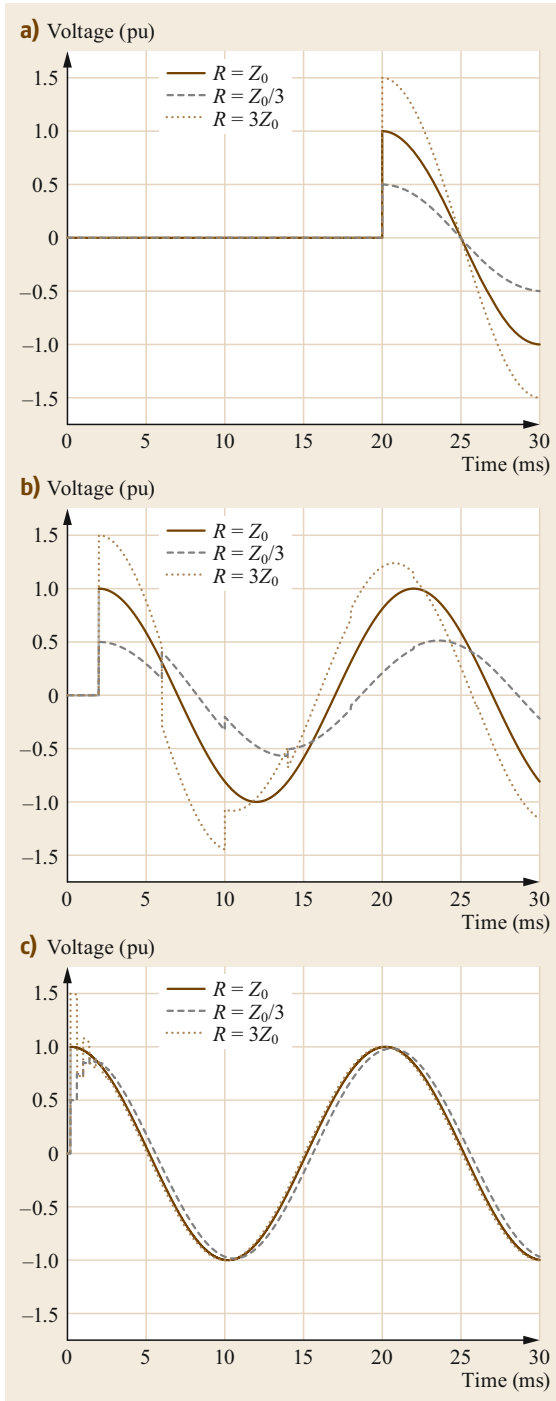
**Fig. 5.128** Voltage profile along a 600 km line 2.1 ms after energization by a 50 Hz sinusoidal voltage source connected at  $x = 0$ . The other termination at  $x = 600$  km is resistive; cases where this resistance  $R$  is equal to, larger than, or lower than the surge impedance  $Z_0$  of the line are considered. Voltage values are given in pu with respect to the source voltage amplitude



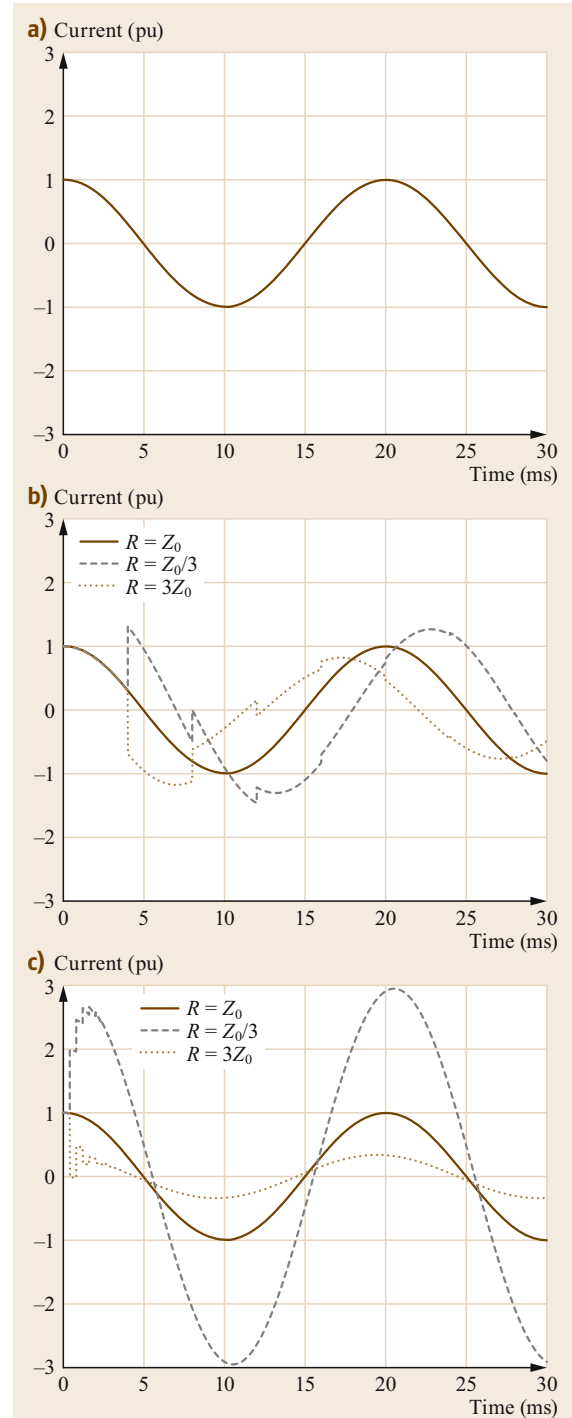
**Fig. 5.129** Voltage profile along a 60 km line 0.21 ms after energization by a 50 Hz sinusoidal voltage source connected at  $x = 0$ . The other termination at  $x = 60$  km is resistive; cases where this resistance  $R$  is equal to, larger than, or lower than the surge impedance  $Z_0$  of the line are considered. Voltage values are given in pu with respect to the source voltage amplitude



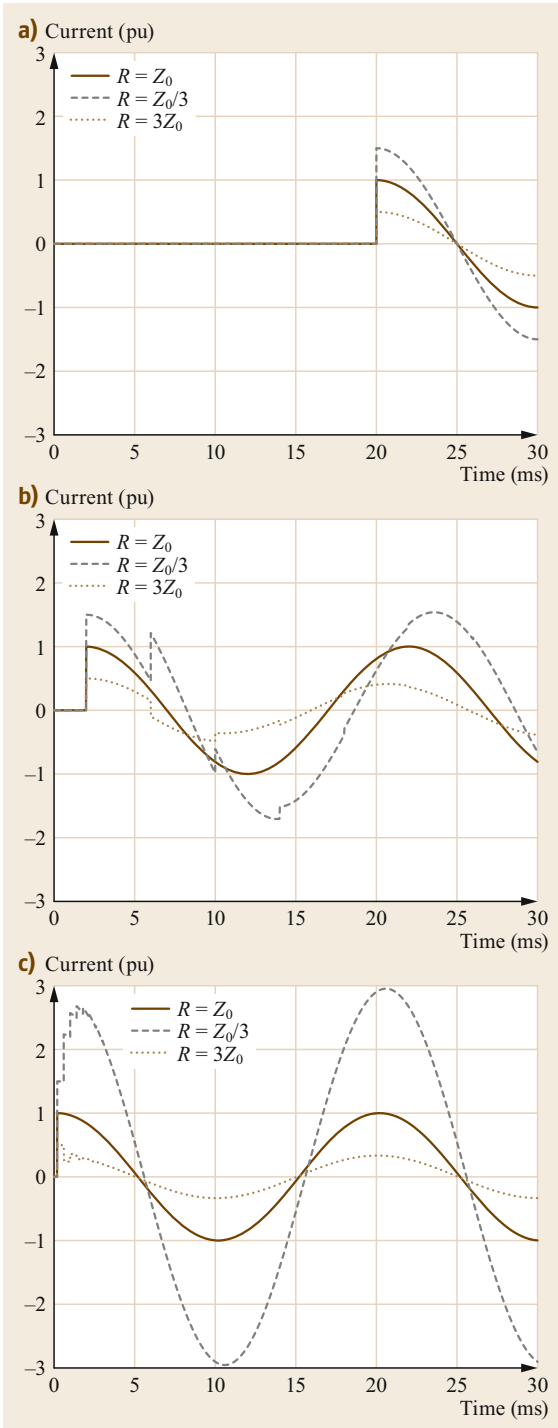
**Fig. 5.130a–c** Voltage and current waveforms at the sending and receiving ends of a transmission line, where the sending end is connected to a 50 Hz sinusoidal voltage source and the receiving end is connected to a resistance  $R$  that is equal to the surge impedance  $Z_0$  of the line. Values are given in pu with respect to the source voltage amplitude  $E$  and  $E/Z_0$ . Line lengths: (a) 6000 km, (b) 600 km, (c) 60 km



**Fig. 5.131a–c** Voltage waveforms at the receiving end of a transmission line, where the sending end is connected to a 50 Hz sinusoidal voltage source and the receiving end is connected to a resistance  $R$  that is equal to, larger than, or lower than the surge impedance  $Z_0$  of the line. Values are given in pu with respect to the source voltage amplitude. Line lengths: (a) 6000 km, (b) 600 km, and (c) 60 km



**Fig. 5.132a–c** Current waveforms at the sending end of a transmission line, where the sending end is connected to a 50 Hz sinusoidal voltage source and the receiving end is connected to a resistance  $R$  that is equal to, larger than, or lower than the surge impedance  $Z_0$  of the line. Values are in pu with respect to the amplitude of the incident current wave. Line length: (a) 6000 km, (b) 600 km, and (c) 60 km



**Fig. 5.133a–c** Current waveforms at the receiving end of a transmission line, where the sending end is connected to a 50 Hz sinusoidal voltage source and the receiving end is connected to a resistance  $R$  that is equal to, larger than, or lower than the surge impedance  $Z_0$  of the line. Values are in pu with respect to the amplitude of the incident current wave. Line length: (a) 6000 km, (b) 600 km, and (c) 60 km

## 5.9 Electric Power Systems of the Future: Smart Grids

Electric power systems are continually evolving. Drivers of this evolution over the last few decades include the liberalization and development of competitive electricity markets, the increasingly widespread use of HVDC links to improve transmission capabilities and enhance interconnection, the growth in renewable energy sources (RESs), and the integration of distributed generation (DG). In the future, the expected large-scale adoption of electric vehicles and electric transportation technologies will lead to further power system development. Such development may include the implementation of a global power grid [5.56].

### 5.9.1 Evolution of Power Systems Towards Increased Deployment of Renewable Energy Resources

In this section, we focus on DG. There are many reasons for using DG in power systems, but the two main motivations are the introduction of the open electricity market and environmental requirements [5.57].

In Italy, the amount of power generated by RESs has increased considerably since the mid-2000s. Figure 5.134 shows how the power produced by each type of electric power plant has evolved in Italy since 1963. This graph is largely representative of those of many other countries in Europe too. From 2004 to 2013, the share of the total power generated in Italy that is contributed by RES plants increased from 26% to 39%, and this share reached 45% in 2017 (Fig. 5.135).

Since many RES technologies (photovoltaic units and several types of wind turbines in particular) are used in conjunction with power electronic convert-

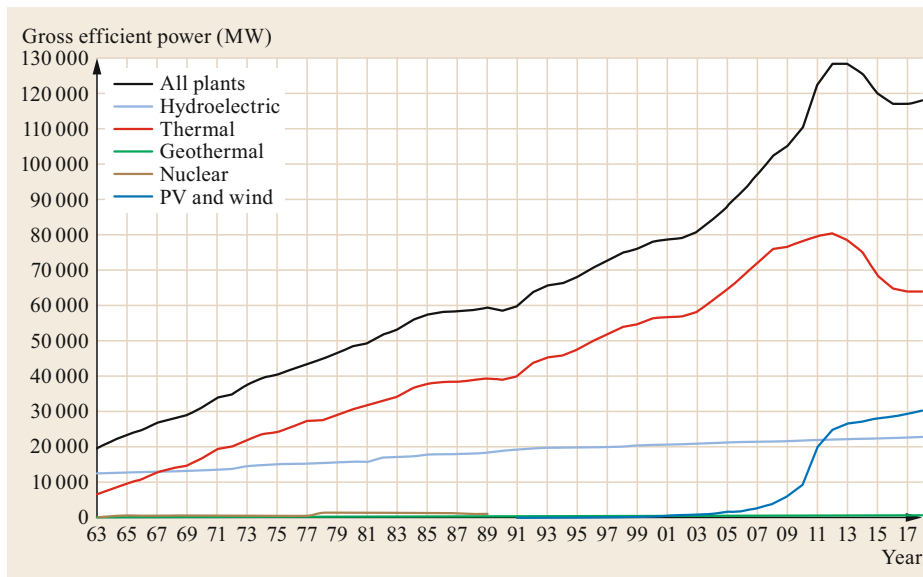
ers [5.58, 59], the characteristics and fast dynamics of these devices tend to modify the behavior of the power system, especially during large perturbances.

The trends expected for Italy over the next decade are also expected to occur for Europe in general. Figure 5.136 shows the European targets for 2030 in relation to the transition to a zero-carbon economy, as well as the ambitions for 2050. This framework was adopted by the European Council in October 2014, and the targets for renewables and energy efficiency were revised in 2018.

The key targets for 2030 are:

- Cuts of at least 40% in greenhouse gas emissions with respect to 1990 levels
- A renewable energy share of at least 32%
- An improvement in energy efficiency of at least 32.5%.

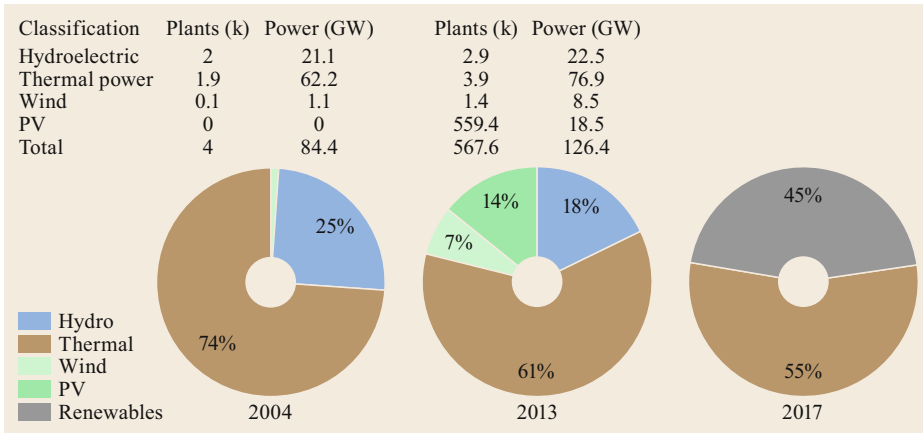
The compositions of power systems in the future will also be influenced by the actions of transmission system operators (TSOs). Both Terna and ENTSO-E (the Italian TSO and the European network of TSOs, respectively) have set out possible future scenarios for the evolution of power systems up to 2040 [5.52, 61]. ENTSO-E forecasts that by 2040, between 65% and 81% of the electricity demand in the European Union (EU) will be met by renewable energy sources. Ensuring that this scenario is feasible and guaranteeing the economic sustainability and reliability of the electricity supply will require the implementation of technical solutions for storage system development and the strengthening of interconnections between states. Such measures should make it possible to exploit up to



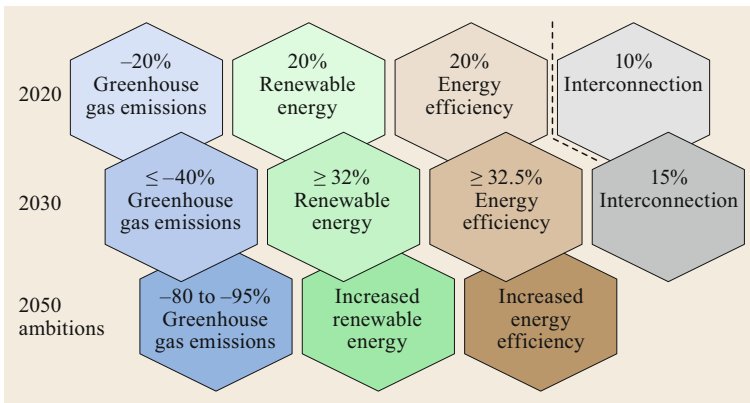
**Fig. 5.134**

Evolution of the contributions of various types of electric power plants to the total power produced in Italy since 1963 (from [www.terna.it](http://www.terna.it))





**Fig. 5.135** Italian power generation mix in 2004, 2013, and 2017. The pie charts and tables for 2004 and 2013 provide data on the power generation mix in Italy, including the types of power plants that contribute power, the number of plants of each type, the power contributed by each type, and the percentage contribution of each type to the total power generated in Italy. The pie chart for 2017 only presents the percentage contributions of renewables and thermal plants to the total power (from [www.terna.it](http://www.terna.it))



**Fig. 5.136** European targets for 2030 in relation to the transition to a zero-carbon economy (adapted from [5.60])

150 TWh of energy produced from nonprogrammable sources that would otherwise remain unused. In this regard, the EU has announced a thousand billion euro investment plan that aims to convert all conventional generation units to renewables ones by 2050 [5.62]. Unity across borders will be crucial to achieving clean energy production [5.63]. The European electric grid is the largest synchronous grid in the world, and the level of interconnectivity among European countries is expected to grow significantly over the next few decades in order to improve cross-border energy exchange.

The intermittent nature of the output from renewable energy sources (e.g., wind and solar) necessitates sufficient backup generation to meet the demand for electricity [5.64]. This is even more important if wind and solar generate 100% of the required energy on average. The need for backup generation can, however, be reduced through the utilization of storage systems and/or grid extensions. Interconnections can improve grid stability

and reduce energy prices, so huge investments aimed at strengthening transmission line capabilities in order to create a European supergrid are expected. The EU has set an interconnection target of at least 10% by 2020 in order to encourage EU countries to link their installed electricity production capacities [5.63]. This means that each nation should have sufficient transmission lines to allow at least 10% of the electricity produced by its power plants to be transported across its borders to neighboring countries at any time. The level of interconnection is also expected to rise to 15% by 2030 [5.65].

### 5.9.2 Power System Structure: Why We Need Smart(er) Grids

We discussed the structure of a power system in Sect. 5.1. Historically, generators were connected directly at the transmission level, and power flows were unidirectional from the transmission level towards the

loads connected at lower voltage levels. However, power systems have changed in structure over the last few decades to allow the deployment of a large number of RESs. The increasing penetration of RESs and DG into power systems has totally changed the power flows in these systems, as many generating units are now connected directly at the subtransmission and distribution levels, meaning that distribution grids have been transformed from passive to active networks.

The impact of renewable generation on electric power systems presents a challenge to transmission and distribution systems operators [5.66], and has resulted in a need for *smarter* grids for the reasons listed below.

#### High Variability in the Amount of Power Produced by RESs

This characteristic of RESs requires:

- Smarter management of the grid
- Extensive information and communications technology (ICT) deployment (e.g., metering, cosimulation tools, . . .)
- Deployment of storage systems.

#### Penetration of RESs

The increasingly widespread adoption of RESs poses problems:

- Generators are often used in conjunction with power electronic converters, which degrades system stability due to a lack of inertia
- Power quality issues arise.

#### Integration of Electric Vehicles

The expected increase in electric vehicle utilization implies that:

- Network transformers must be upgraded in terms of size and capability
- The possibility of supporting the network with vehicle-to-grid (V2G) applications should be explored.

#### Inverted Power Flows

The inverted power flows that result from the inclusion of RESs in power systems are problematic because:

- The lines were not designed for bidirectional flows
- Voltage profiles along the distribution feeders are altered
- Protection failures may occur.

### 5.9.3 The Definition of a Smart Grid

The reasons mentioned above have led to the introduction of the concept of a *smart grid*. There are various definitions of a smart grid; we report a few of them below:

1. *European Technology Platform on SmartGrids*: “A SmartGrid is an electricity network that can intelligently integrate the actions of all users connected to it—generators, consumers and those that do both—in order to efficiently deliver sustainable, economic and secure electricity supplies.”
2. *US Department of Energy*: “A smart grid uses digital technology to improve reliability, security, and efficiency (both economic and energy) of the electric system from large generation, through the delivery systems to electricity consumers and a growing number of distributed-generation and storage resources.”
3. *Department of Energy and Climate Change, UK*: “A smart grid uses sensing, embedded processing and digital communications to enable the electricity grid to be observable (able to be measured and visualized), controllable (able to be manipulated and optimized), automated (able to adapt and self-heal), fully integrated (fully interoperable with existing systems and with the capacity to incorporate a diverse set of energy sources).”
4. *Electric Power Research Institute, USA*. This institute is developing the IntelliGrid<sup>SM</sup> initiative, which is laying the technical foundations for smart grids. According to the Electric Power Research Institute, a smart grid is a “power system made up of numerous automated transmission and distribution systems, all operating in a coordinated, efficient and reliable manner;” “a power system that handles emergency conditions with *self-healing* actions and is responsive to energy-market and utility business-enterprise needs;” and “a power system that serves millions of customers and has an intelligent communications infrastructure enabling the timely, secure and adaptable information flow needed to provide reliable and economic power to the evolving digital economy.”
5. *Eurelectric*: “A smart grid is an electricity network that can intelligently integrate the behavior and actions of all users connected to it—generators, consumers and those that do both—in order to efficiently ensure sustainable, economic and secure electricity supply. As such, a smart grid, involving a combination of software and hardware allowing more efficient power routing and enabling consumers to manage their demand, is an important part of the solution for the future.”

### 5.9.4 Growth in the Utilization of ICT in Power Systems

The increasing use of ICT is an important characteristic of the development of power systems, as illustrated in Fig. 5.137. In transmission and distribution networks, the adoption of DG, together with electricity market procedures and the expected sudden growth in elec-

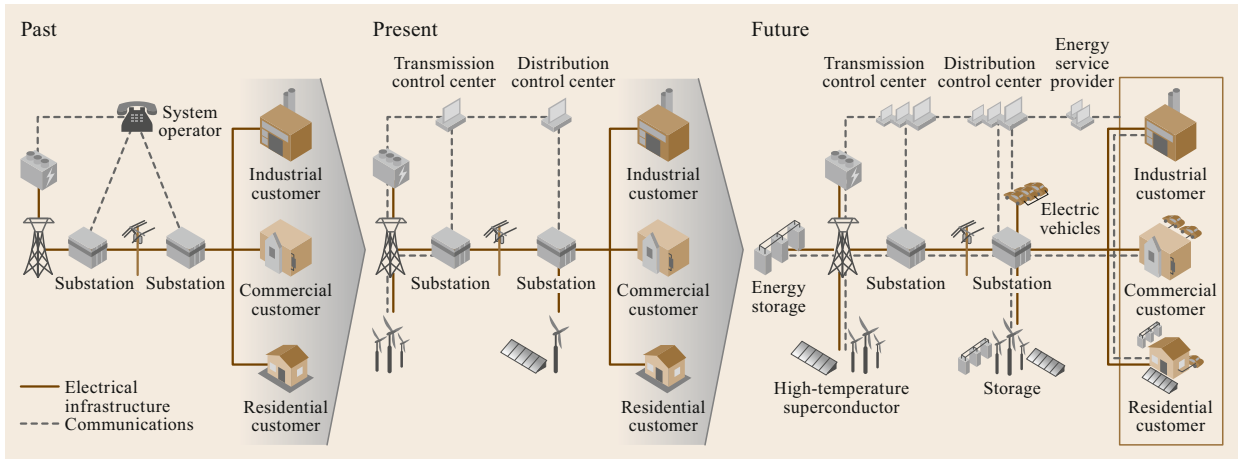


Fig. 5.137 Evolution of the utilization of ICT in power systems (from IEA, International Energy Agency)

tric vehicle deployment, is leading or will lead to more complex interactions among system components. Thus, in the future, it will be necessary to apply the most advanced ICT solutions to power system operation to ensure that reliability and performance targets are met. Enhancing MV and LV distribution network observability using both direct (smart metering) and indirect (state estimation [5.67], pseudomeasures [5.68], and load and production forecasts) methods can lay the groundwork for the development of new services and value-added functionalities [5.69].

The development of new tools that can be used to model the dynamic behavior of power systems and communications networks should facilitate the increased application of new ICT-based monitoring, control, and protection approaches in electric power grids [5.70, 71]. The expected key requirements of a ITC–power system cosimulation platform are easy configuration, good operating system compatibility, an ability to interconnect with external third-party programs/systems, a hardware-in-the-loop (HIL) capability, time synchronization, the ability to adjust the level of detail of the model (in both power and communications modeling), the interoperability needed to import models, and scalability.

### 5.9.5 Microgrids

The implementation of active distribution network technologies is leading to the formulation of new system concepts. The microgrid paradigm is perhaps the most promising novel network type [5.64]. A microgrid consists of a group of interconnected distributed energy resources such as microturbines, fuel cells, and photovoltaic arrays together with storage devices (i.e., flywheels, energy capacitors, and batteries) and controllable loads. Such systems offer considerable scope

for control and autonomous operation. They are interconnected to the distribution network but have the ability to voluntarily perform connection and disconnection maneuvers, meaning that they can smoothly and reliably switch between grid-connected and island modes (Fig. 5.138).

### 5.9.6 Energy Communities

Mechanisms enabling energy transactions between neighbors are becoming feasible in several countries. These mechanisms provide an incentive to install DG units (especially those based on RESs), which will encourage power generation that exceeds the local load, thus allowing the power demands of users connected nearby to the same distribution network to be exploited. As an example, on December 2018, the European Union approved the first part of a comprehensive legislative package entitled *Clean Energy for All Europeans* (CEP) [5.74]. This EU directive establishes appropriate legal frameworks for energy communities. A local energy community (LEC) can be defined as a set of end-users with local generation and storage units that cooperate to achieve common goals, in particular the minimum energy procurement costs and the efficient use of renewable resources [5.75].

Figure 5.139 illustrates the concepts of self-consumption, collective self-consumption, and the LEC [5.73]. Collective self-consumption, which builds on the well-established idea of self-consumption, involves cooperation between renewable energy self-consumers located in the same building or apartment block. In the figure, the LEC consists of a set of residential or small industrial sites, each acting as a prosumer, and it generally includes generation and battery energy storage units as well as loads. The LEC operates on an internal LV distribution network connected to the

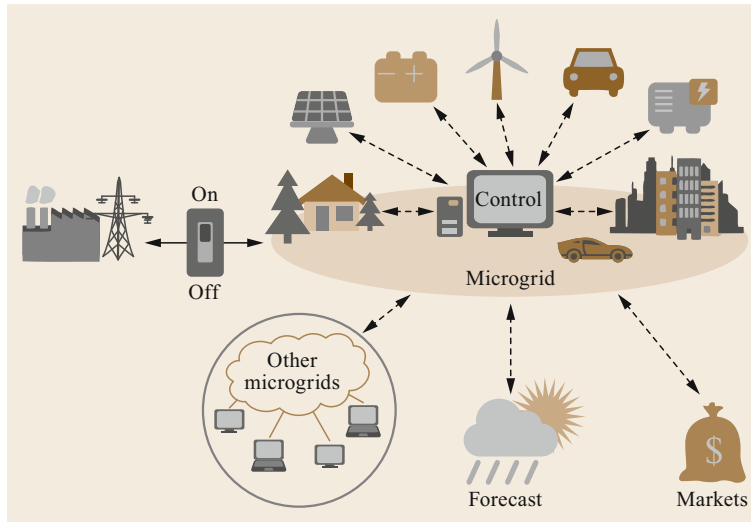


Fig. 5.138 Schematic of a microgrid (adapted from [5.72])

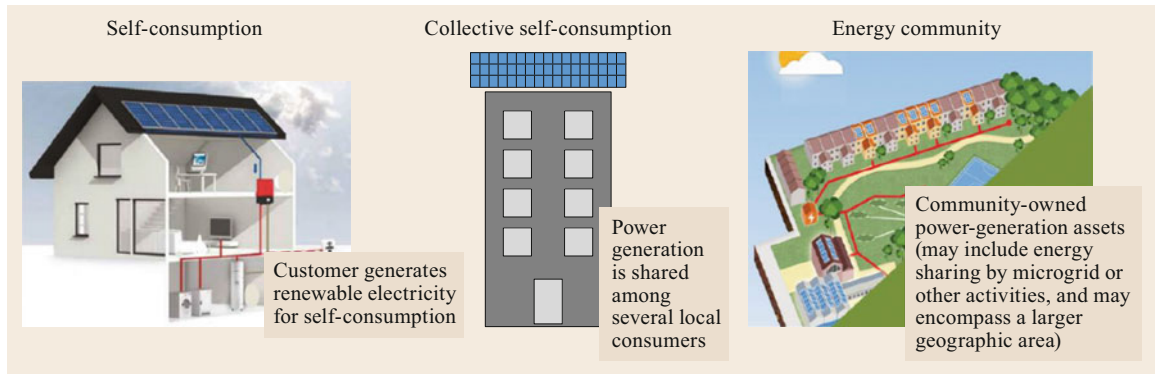


Fig. 5.139 From self-consumption to LEC (adapted from [5.73])

external utility grid, and the prosumers use the available energy resources cooperatively. Specific scheduling procedures are generally needed to fully exploit the available resources and the flexibility of the system (see, for example, [5.76] and references therein). Technologies such as demand response appear to be more easily applicable in LECs than by the utility. Local en-

ergy communities may also incorporate aggregators for electric vehicles [5.77].

#### Additional Information and Exercises

Additional information and supplementary exercises relating to this chapter can be found at [https://go.sn.pub/SHb\\_PowerSystems\\_Nucci\\_PowerSystemsAnalysis](https://go.sn.pub/SHb_PowerSystems_Nucci_PowerSystemsAnalysis).

#### References

- 5.1 E.W. Kimbark: *Synchronous Machines*, Power System Stability, Vol. 3 (Wiley, New York 1956)
- 5.2 D. Zanobetti, M. Pezzi: *Lezioni di impianti elettrici* (Clueb, Bologna 1981)
- 5.3 F. Iliceto: *Impianti elettrici* (Pàtron, Bologna 1984)
- 5.4 R. Marin, M. Valtorta: *Trasmissione e interconnessione* (CEDAM, Padova 1973)
- 5.5 P. Kundur: *Power System Stability and Control* (McGraw-Hill, New York 1994)
- 5.6 J. Grainger, W. Stevenson: *Power System Analysis* (McGraw-Hill, New York 1994)
- 5.7 J.P. Barret, P. Bornard, B. Meyer: *Power System Simulation* (Springer, Berlin, Heidelberg 1996)
- 5.8 H.W. Dommel: *EMTP Theory Book*, 2nd edn. ((Microtran Power System Analysis Corporation, Vancouver 1996)
- 5.9 F. Saccomanno: *Electric Power Systems Analysis and Control* (Wiley, New York 2003)
- 5.10 R. Marconato: *Steady State Behavior Controls, Short Circuits and Protection Systems*, Vols. 1 and 2 (CEI, Milano 2004)
- 5.11 J. Machowski, J.W. Bialek, J.R. Bumby: *Power System Dynamics: Stability and Control* (Wiley, New York 2008)
- 5.12 H. Saadat: *Power System Analysis*, 3rd edn. (McGraw-Hill, New York 2010)

- 5.13 A.J. Wood, B.F. Wollenberg, G.B. Sheblé: *Power Generation, Operation, and Control*, 3rd edn. (Wiley, Hoboken 2013)
- 5.14 J.D. Glover, M.S. Sarma, T.J. Overbye: *Power System Analysis and Design* (Cengage Learning, London 2012)
- 5.15 A. Gómez Expósito, A.J. Conejo, C. Cañizares: *Electric Energy Systems: Analysis and Operation*, 2nd edn. (CRC, Boca Raton 2018)
- 5.16 B.J. Cory, N. Jenkins, J. Ekanayake, G. Strbac, B.M. Weedy: *Electric Power Systems* (Wiley, Hoboken 2013)
- 5.17 F. Milano: *Power System Modelling and Scripting* (Springer, Heidelberg, Berlin 2013)
- 5.18 N. Mohan: *Electric Power Systems: A First Course* (Wiley, Hoboken 2012)
- 5.19 L.L. Grigsby: *The Electric Power Engineering Handbook* (CRC, Boca Raton 2012)
- 5.20 D.P. Kothari, I.J. Nagrath: *Modern Power System Analysis* (Tata McGraw-Hill, New Delhi 2011)
- 5.21 M.D. Ilic, J. Zaborszky: *Dynamics and Control of Large Electric Power Systems* (Wiley, New York 2000)
- 5.22 A.K. Singh, B.C. Pal: *Dynamic Estimation and Control of Power Systems* (Elsevier, Amsterdam 2018)
- 5.23 P.M. Anderson: *Power System Protection* (McGraw-Hill, New York 1999)
- 5.24 V. Vittal, J.D. McCalley, P.M. Anderson, A.A. Fouad: *Power System Control and Stability*, 3rd edn. (Wiley-IEEE, Hoboken 2020)
- 5.25 P.W. Sauer, M.A. Pai, J.H. Chow: *Power System Dynamics and Stability: With Synchrophasor Measurement and Power System Toolbox*, 2nd edn. (Wiley-IEEE, Hoboken 2018)
- 5.26 M. Eremia, M. Shahidehpour: *Handbook of Electrical Power System Dynamics: Modeling, Stability, and Control* (Wiley, Hoboken 2013)
- 5.27 A. Ametani, N. Nagaoka, Y. Baba, T. Ohno, K. Yamabuki: *Power System Transients: Theory and Applications*, 2nd edn. (CRC, Boca Raton 2016)
- 5.28 A. Greenwood: *Electrical Transients in Power Systems*, 2nd edn. (Wiley, New Delhi 1991)
- 5.29 M. Ceraolo, D. Poli: *Fundamentals of Electric Power Engineering: From Electromagnetics to Power Systems* (Wiley, Hoboken 2014)
- 5.30 J.C. Das: *Power System Analysis: Short-Circuit Load Flow and Harmonics*, 2nd edn. (CRC, Boca Raton 2012)
- 5.31 M.L. Crow: *Computational Methods for Electric Power Systems*, 3rd edn. (CRC, Boca Raton 2015)
- 5.32 A.A. Sallam, O.P. Malik: *Power System Stability: Modelling, Analysis and Control* (IET, London 2015)
- 5.33 C. Sulzberger: Pearl Street in miniature: Models of the electric generating station, *IEEE Power Energy Mag.* **11**(2), 76–85 (2013)
- 5.34 The Edison Electric Lighting Station, *Sci. Am.* **47**(9), 127–130 (1882)
- 5.35 L. de Andrade, T.P. de Leao: A brief history of direct current in electrical power systems. In: *Third IEEE Hist. Electro-Technol. Conf. (HISTELCON)* (2012) pp. 1–6
- 5.36 A. Paolucci: *Lezioni di trasmissione dell'energia elettrica* (Cleup, Padova 1990)
- 5.37 J.B. Ward, H.W. Hale: Digital computer solution of power-flow problems, *Trans. Am. Inst. Electr. Eng.* **75**(3), 398–404 (1956)
- 5.38 J.E. Van Ness: Iteration methods for digital load flow studies, *Trans. Am. Inst. Electr. Eng.* **78**(3), 583–586 (1959)
- 5.39 H.W. Hale, R.W. Goodrich: Digital computation of power flow – Some new aspects, *Trans. Am. Inst. Electr. Eng.* **78**(3), 919–923 (1959)
- 5.40 J. Carpentier: Optimal power flows, *Int. J. Electr. Power Energy Syst.* **1**(1), 3–15 (1979)
- 5.41 B. Stott: Decoupled Newton load flow, *IEEE Trans. Power Appar. Syst.* **91**(5), 1955–1959 (1972)
- 5.42 B. Stott, O. Alsac: Fast decoupled load flow, *IEEE Trans. Power Appar. Syst.* **93**(3), 859–869 (1974)
- 5.43 R. Marconato: *Steady State Behavior Controls, Short Circuits and Protection Systems*, *Electric Power Systems*, Vol. 2 (CEI, Milano 2004)
- 5.44 V. Cataliotti: *Impianti Elettrici*, Vol. 1 (Flaccovio, Palermo 2008)
- 5.45 J. Mahseredjian, S. Denettière, L. Dubé, B. Khodabakhchian, L. Gérin-Lajoie: On a new approach for the simulation of transients in power systems, *Electr. Power Syst. Res.* **77**(11), 1514–1520 (2007)
- 5.46 L.H. Fink, K. Carlsen: Operating under stress and strain, *IEEE Spectrum* **15**(3), 48–53 (1978)
- 5.47 T.E.D. Liacco: Systems security: The computer's role, *IEEE Spectrum* **15**(6), 43–50 (1978)
- 5.48 P. Kundur, J. Paserba, V. Ajjarapu, G. Andersson, A. Bose, C. Canizares, N. Hatziaargyriou, D. Hill, A. Stankovic, C. Taylor, T. Van Cutsem, V. Vittal, IEEE/CIGRE Joint Task Force on Stability Terms and Definitions: Definition and classification of power system stability, *IEEE Trans. Power Syst.* **19**(3), 1387–1401 (2004)
- 5.49 G. Andersson: *Power System Analysis* (ITET ETH, Zurich 2012), Lecture 227–0526–00
- 5.50 D. Mondal, A. Chakrabarti, A. Sengupta: *Power System Small Signal Stability Analysis and Control* (Academic Press, New York 2020)
- 5.51 M.E. Baran, F.F. Wu: Network reconfiguration in distribution systems for loss reduction and load balancing, *IEEE Trans. Power Deliv.* **9**(4), 101–102 (1989)
- 5.52 L. Schmitt: *Connecting Europe: Electricity*, ENTSO-E Reports (ENTSO-E AISBL, Brussels 2018)
- 5.53 N.R. Watson, J. Arrillaga: *Power Systems Electromagnetic Transients Simulation* (IET, London 2003)
- 5.54 J.A. Martínez-Velasco: *Transient Analysis of Power Systems: A Practical Approach* (Wiley, New York 2020)
- 5.55 C.A. Nucci, F. Rachidi, M. Rubinstein: Derivation of telegrapher's equations and field-to-transmission line interaction. In: *Electromagnetic Field Interaction with Transmission Lines* (WIT Press, Boston 2008)
- 5.56 P. Deane, M. Brinkerink: Connecting the continents – A global power grid, *IEEE Power Energy Mag.* **18**(2), 121–127 (2020)
- 5.57 M. Bollen, H. Fainan: *Integration of Distributed Generation in the Power System*, IEEE Press Series on Power Engineering (Wiley-Blackwell, New York 2011)
- 5.58 V. Perelmutter: *Renewable Energy Systems: Simulation with Simulink and SimPowerSystems* (CRC, Boca Raton 2016)
- 5.59 F. Blaabjerg, D.M. Ionel: *Renewable Energy Devices and Systems with Simulations in MATLAB and ANSYS* (CRC, Boca Raton 2017)

- 5.60 A. Ali, W. Li, R. Hussain, X. He, B.W. Williams, A.H. Memon: Overview of current microgrid policies, incentives and barriers in the European Union, United States and China, *Sustainability* **9**(7), 1146 (2017)
- 5.61 Terna: *Documento di descrizione degli scenari* (Terna, Rome 2018)
- 5.62 European Commission: *Financing the Green Transition: The European Green Deal Investment Plan and Just Transition Mechanism* (EC, Brussels 2020)
- 5.63 Commission Expert Group: *Electricity Interconnections with Neighbouring Countries. Second Report of the Commission Expert Group on Electricity Interconnection Targets* (EC, Brussels 2019)
- 5.64 D. Connolly, H. Lund, B.V. Mathiesen: Smart Energy Europe: The technical and economic impact of one potential 100% renewable energy scenario for the European Union, *Renew. Sustain. Energy Rev.* **60**, 1634–1653 (2016)
- 5.65 European Commission: *Communication on Strengthening Europe's Energy Networks* (EC, Brussels 2017)
- 5.66 M. Bollen: *The Smart Grid: Adapting the Power System to New Challenges*, Synt. Lect. Power Electron. (Morgan, London 2011) p. 2013
- 5.67 A. Abur, A.G. Expósito: *Power System State Estimation* (CRC, Boca Raton 2004)
- 5.68 S. Sarri, L. Zanni, M. Popovic, J.Y. Le Boudec, M. Paolone: Performance assessment of linear state estimators using synchrophasor measurements, *IEEE Trans. Instrum. Meas.* **65**(3), 535–548 (2016)
- 5.69 F. Conte, S. Massucco, M. Saviozzi, F. Silvestro: A stochastic optimization method for planning and real-time control of integrated PV-storage systems: Design and experimental validation, *IEEE Trans. Sustain. Energy* **30**(29)(LV), 1–10 (2017)
- 5.70 R. Bottura, A. Borghetti: Simulation of the volt/var control in distribution feeders by means of a networked multiagent system, *IEEE Trans. Ind. Inform.* **10**(4), 2340–2353 (2014)
- 5.71 A. Borghetti, R. Bottura, M. Barbiroli, C.A. Nucci: Synchrophasors-based distributed secondary voltage/VAR control via cellular network, *IEEE Trans. Smart Grid* **8**(1), 262–274 (2017)
- 5.72 M. Stadler, A. Naslé: Planning and implementation of bankable microgrids, *Electr. J.* **32**(5), 24–29 (2019)
- 5.73 Council of European Energy Regulators: *Regulatory Aspects of Self-Consumption and Energy Communities* (CEER, Brussels 2019)
- 5.74 European Commission: Clean energy for all Europeans, *Euroheat Power* **14**(2), 3–4 (2019)
- 5.75 Council of European Energy Regulators: Renewable Self-Consumers and Energy Communities. CEER White Paper Series, paper # VIII (CEER, Brussels 2017)
- 5.76 S. Lilla, C. Orozco, A. Borghetti, F. Napolitano, F. Tossani: Day-ahead scheduling of a local energy community: An alternating direction method of multipliers approach, *IEEE Trans. Power Syst.* **35**(2), 1132–1142 (2020)
- 5.77 E.L. Karfopoulos, K.A. Panourgias, N.D. Hatziargyriou: Distributed coordination of electric vehicles providing V2G regulation services, *IEEE Trans. Power Syst.* **31**(4), 2834–2846 (2016)

### Carlo Alberto Nucci

Department of Electrical, Electronic and Information Engineering  
University of Bologna  
Bologna, Italy  
carloalberto.nucci@unibo.it



Carlo Alberto Nucci graduated in Electrical Engineering in 1982 from the University of Bologna, where he is Professor of Electrical Power Systems since 2000. He has received fellowships from IEEE and CIGRÉ, an HC degree from University Politecnica di Bucharest, the CIGRE TC award, and the ICLP SC Golde Award. He is Editor-in-Chief of the journal *Electric Power Systems Research* and a Member of the Academy of Science of the Institute of Bologna.

### Alberto Borghetti

Department of Electrical, Electronic and Information Engineering  
University of Bologna  
Bologna, Italy  
alberto.borghetti@unibo.it



Alberto Borghetti (IEEE M'97–SM'03–F'15) graduated in electrical engineering from the University of Bologna in 1992, and is now Professor of Electrical Power Systems at the same institution. He received ICLP SC and CIGRÉ TC awards in 2016 and 2018, respectively. He is currently serving as an Editor on the journal *IEEE Transactions on Power Systems* and as Editor-in-Chief of the journal *Electrical Engineering*.

### Fabio Napolitano



Department of Electrical, Electronic and Information Engineering  
University of Bologna  
Bologna, Italy  
fabio.napolitano@unibo.it

Fabio Napolitano received his MS and PhD (Hons.) in electrical engineering from the University of Bologna in 2003 and 2009, respectively. He subsequently became an Assistant Professor (in 2010) and an Associate Professor (in 2020). His research interests include power system transients—particularly those due to indirect lightning strikes—and lightning protection systems.

### Fabio Tossani



Department of Electrical, Electronic and Information Engineering  
University of Bologna  
Bologna, Italy  
fabio.tossani@unibo.it

Fabio Tossani received his BS (Hons.), MS (Hons.), and PhD in electrical engineering from the University of Bologna in 2010, 2012, and 2016, respectively. He is currently a junior Assistant Professor in the Power Systems Laboratory of the Department of Electrical, Electronic and Information Engineering “Guglielmo Marconi,” University of Bologna.

# Rotating Elec

## 6. Rotating Electrical Machines

Erli F. Figueiredo

One of the most striking features in the development of rotating electrical machines has been the steady increase in their output. This marked increase was made possible by a combination of several factors, of which the most important include improvements in the magnetic properties of the sheet steel used for core material, as well as the development of insulating materials capable of withstanding relatively high temperatures, and better provision for cooling. This chapter is divided into two parts: Synchronous Machines and Induction Motors. For both types of machines considerations about insulating materials, cooling and construction are presented with a focus on the main aspects involved, as well as about their performance under different conditions of operation. Special emphasis was given to international standards. The effect of machine dimensions on the rating of synchronous and induction machines is included, as well as other design parameters. The application of variable frequency drives on induction motor speed control is highlighted. Some advanced technologies in synchronous generators and motors such as: superconducting generators and motors; permanent magnet motors; switched reluctance motors and line start permanent magnet motors, as well as those related to die cast copper and linear induction motors are presented.

6.1	<b>Synchronous Machines</b> .....	368
6.1.1	Construction Features.....	368
6.1.2	Cooling and Insulation.....	370
6.1.3	Armature Windings.....	373
6.1.4	Basic Concepts.....	376
6.1.5	Armature Reaction and Phasor Diagrams .....	382
6.1.6	Open and Short-Circuit Characteristics .	386
6.1.7	Efficiency .....	388
6.1.8	Reactances and Time Constants .....	389
6.1.9	Power Angle Characteristic of Synchronous Machines .....	393
6.1.10	Parallel Operation of Synchronous Generators .....	395
6.1.11	Synchronization of a Generator.....	396
6.1.12	Generator Excitation for Constant Terminal Voltage: Compounding Curve.	398
6.1.13	Generator Load Characteristic .....	398
6.1.14	Generator Capability Chart.....	398
6.1.15	Synchronous Motor: V Curves .....	401
6.1.16	Voltage-Frequency Limits.....	402
6.1.17	Excitation Systems .....	403
6.1.18	Synchronous Generators During a Short-Circuit.....	406
6.1.19	The Electromechanical Equation .....	409
6.1.20	Design Considerations.....	410
6.1.21	Advanced Technologies .....	413
6.2	<b>Induction Machines</b> .....	415
6.2.1	Construction .....	416
6.2.2	Insulation and Cooling.....	417
6.2.3	Operating Principles.....	418
6.2.4	Equivalent Circuit of an Induction Motor.....	420
6.2.5	Power and Torque Relations of an Induction Motor.....	421
6.2.6	Operation as a Brake and Generator....	422
6.2.7	Determining of Induction Machine Parameters .....	423
6.2.8	Effects of Rotor Resistance .....	425
6.2.9	Motor Applications .....	427
6.2.10	Energy Efficient Motors.....	428
6.2.11	Speed Control.....	429
6.2.12	Variable Speed Drives (VSDs) .....	434
6.2.13	Power Quality.....	437
6.2.14	Advanced Motor Technologies.....	439
	<b>References</b> .....	440

## 6.1 Synchronous Machines

A synchronous machine may be constructed with a stationary armature and a rotating field, or a rotating armature and a stationary field. The former has been widely used because the armature winding is more complex than the field winding, and it is constructed more easily in a fixed structure. Besides that, the armature winding handles the load power of the machine, while the field winding consumes a small percentage (0.5–2%) of the rated load power. Thus, if the synchronous machine was constructed with a rotating armature, it would require slip rings and brushes to deliver energy to the load. This would cause a fast wear of the brushes and sparking on the slip rings, that could cause short-circuits. This type of construction may be found in small machines.

### 6.1.1 Construction Features

When synchronous generators are driven by steam/gas turbines they are referred to as a turbogenerator, and when they are driven by water turbines as a hydro-generator. Steam/gas turbines are high-speed units and these turbogenerators are built as cylindrical-rotor (also called round-rotor or nonsalient-pole rotor or turbine generators) machines. On the other hand, hydrogenerators are salient-pole machines, since hydraulic turbines run at low/medium speeds. When synchronous motors are required for high-speed operation, they are designed, similar to turbogenerators, as nonsalient-pole machines.

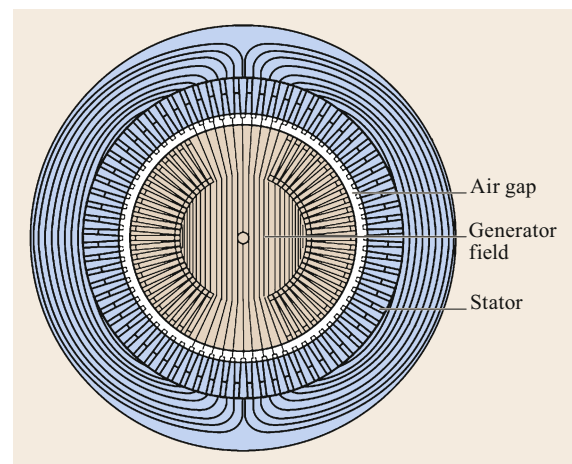
The armature core of both cylindrical-rotor and salient-pole machines is made of insulated steel laminations, in order to minimize eddy current and hysteresis losses. The core is mounted onto the frame through spring bars. The core is slotted and the coils/bars making the winding are placed in the slots around the periphery of the stator to provide better heat dissipation. The chief characteristics of the AC windings are defined by such features as: the number of circuits in parallel per phase, which may be one or more; the connections between phases, usually in star formation for generators and in delta formation for motors; the number of coil layers per slot, that may be either one or two, but with the two-layer type predominating; the angular spread of conductors belonging to a given phase belt; the pitch factor of the coils comprising the winding and the arrangement of the end connections. For the field winding a series connection is regularly used.

The field winding is arranged to produce as many pairs of poles as may be needed. The number of poles will depend upon the speed at which the machine should operate, which in turn depends upon the driven

machine or prime mover, and the desired frequency of the system to be supplied, in the case of generators. The field winding is fed by direct current by an exciter through a pair of brushes and slip-rings, except for the case of turbogenerators, that usually have a brushless exciter, i.e., an exciter without brushes and slip-rings.

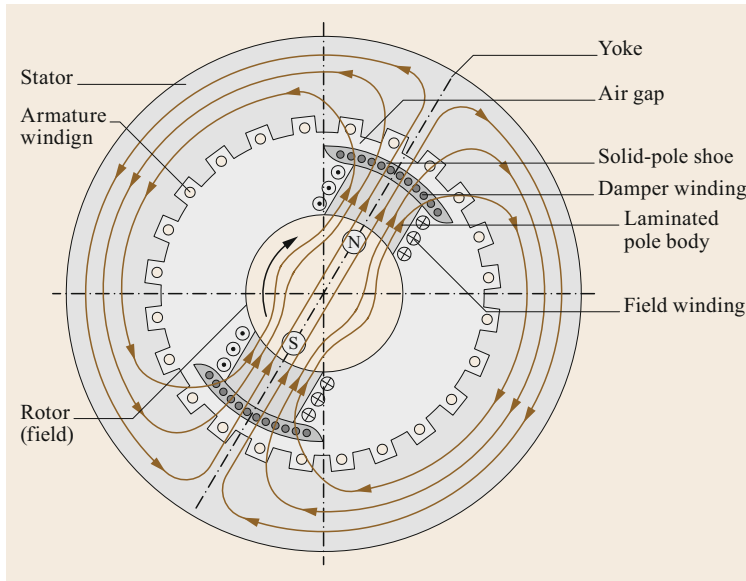
When the number of poles is small, such as two, four, or sometimes six, as in the case of cylindrical-rotor machines, the generator is typically driven by steam or gas-turbine prime movers. The field winding is distributed in slots cut in the round surface of the rotor and retained, against large centrifugal forces, in the slots by wedges and in the end connections by retaining rings. Normally two thirds of the rotor periphery is slotted to accommodate the field winding and the remaining one third unslotted portion acts as poles. Rotors of cylindrical machines are constructed of solid steel forgings or of thick steel disks suitably bolted together. Figure 6.1 shows the rotor magnetic flux linking rotor and stator across the airgap of the cylindrical-rotor machine.

When the number of poles is larger, each pole is separate and distinct, forming a salient-pole structure, attached to the rotor. The winding on each pole is a concentrated coil wound closely around the pole. The field winding is then made up of a number of concentrated coils. The flux distribution is controlled by shaping the face of the pole, so that the airgap is a minimum at the pole center and increases toward the tips, thus helping to produce the desired sinusoidal flux distribution. Successive poles are wound in opposite directions so that the poles are alternately magnetically north and south. The terminals of the field winding are brought to



**Fig. 6.1** Cylindrical machine: Rotor magnetic flux linking the rotor and stator





**Fig. 6.2** Cross-sectional view of a salient-pole synchronous machine

two collector rings attached to, but insulated from the shaft.

The rotor of salient-pole machines consists of a steel spider to which poles of laminated steel, carrying the field winding, are keyed or bolted. Generally rectangular or round pole constructions are used for such type of alternators. Generators driven by water wheel turbines are of either horizontal or vertical shaft type. Generators of lower power ratings with fairly higher speeds are built with a horizontal shaft and the generators of higher power ratings and lower speeds are built with a vertical shaft design. Three types of construction are used for vertical shaft generators:

- (i) Umbrella type where the thrust bearing and a single guide bearing are mounted below the rotor.
- (ii) Semi-Umbrella type, similar to the Umbrella type, but with an additional guide bearing mounted above the rotor.
- (iii) Suspended type with a thrust and one guide bearing mounted above the rotor and another guide bearing mounted below the rotor.

Most salient-pole machines have an additional winding in the rotor, called the damper-winding (also known as an amortisseur), made of copper bars embedded in the head of the pole, and short-circuited at both ends by short-circuiting rings similar to end rings as in the case of squirrel cage rotors. In case of synchronous motors and compensators its purpose is to start the motor or compensator as an induction motor, and take it unloaded to almost synchronous speed, when the rotor is pulled in synchronism by the synchronous torque.

This structure, usually, includes all synchronous hydrogenerators. A cross-sectional view of a salient-pole machine is shown in Fig. 6.2.

Bearings are used to prevent friction between parts during relative movement. They fall into two primary categories: anti-friction or rolling element bearings and hydrodynamic journal (fluid film) bearings. There are applications where rolling bearings are the best choice. Smaller generators and motors commonly use rolling bearings.

In the case of large rotating machines the machine's shaft is most commonly isolated from the stationary equipment through the use of journal bearings, that are filled with lubricant in order to maintain low friction and as a consequence minimize wear of the surfaces. To inspect the journal bearings, that are generally split, rotor removal is not required. Journal bearing fatigue damage is usually visible at an early stage and allows for better diagnostics of failure modes so that corrective action can be taken to prevent recurrence. For these reasons, special care must be taken when selecting and implementing a lubrication system and special vibration monitoring techniques must be applied. The most important aspects of the health and longevity of a journal bearing are proper selection, proper installation, proper lubrication, and the alternating hydrodynamic loads imposed on the bearing surface by relative shaft-to-bearing vibration. While split rolling element bearings are also available they are costly and not common in large machines.

The proper alignment of turbo-units and hydro-units is critical to trouble free operation. A misalignment cannot only cause the premature failure of bearings, but

through excessive vibration, can cause wear and stress on other machine components as well. Unscheduled outages caused by misalignment can be avoided if the machinery is initially aligned correctly.

## 6.1.2 Cooling and Insulation

### Cooling

Losses in electrical machines appear in the form of heat. Heat is transferred from one machine part to another and to the surrounding medium by conduction, radiation and convection. Since the losses are produced mainly in the active parts of the machine, i.e., in the iron that carries the flux and in the conductors which carry the currents, the heat appears mainly in these machine parts. The result is an increase in temperature of the iron and copper above that of the surroundings. Cooling of the machine is necessary in order to keep the temperature rises of the iron and copper within the prescribed limits (Table 6.1).

The cooling system may be of two types: indirect and direct. In the indirect cooling system the windings are not in direct contact with the cooling medium, that is blown along the airgap, through ducts in the core and over the surface of the windings. In the direct cooling system the coolant in a closed circuit passes directly in contact with the windings. IEC and National Electrical Manufacturers Association standards describe the cooling systems in detail [6.1, 2].

### a) Cylindrical (Round)–Rotor Machines.

**a.1) Indirect Cooling.** The indirect cooling system may be of two types: open-circuit and closed-circuit. In an open-circuit cooling system a machine is cooled by the in-take of cold air, which passes through the machine and is expelled into the atmosphere. To prevent clogging of the machine with dust, that the air always contains, a filter is mounted at the air in-take. The closed-circuit cooling system is one in which the air or hydrogen passes through the machine becomes heated, then it passes through a cooler returning to the machine. In the indirect cooling system the windings are not in direct contact with the cooling medium (air or hydrogen), which is, usually, fed into the generator by fans at both sides of the rotor, i.e., the windings are cooled by flowing air or hydrogen over their surfaces and through the core.

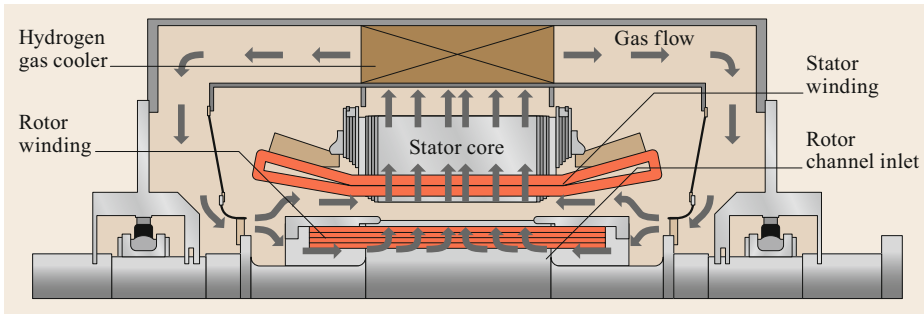
The output equation of a generator in MVA (apparent power) is  $S = CD^2Ln$  (Sect. 6.1.20, *Apparent Nominal Power: Output Equation*), where  $C$  is the output coefficient in MVA s/m<sup>3</sup>;  $D$  is the inner stator diameter in meters;  $L$  is the axial length of the core in meters and  $n$  is the speed in rps (rotation per second). In

the case of cylindrical-rotor machines the effect of the high speed  $n$  is to reduce the amount of active material, i.e., the generator size ( $D^2L$ ), much below that required in a slow speed machine of the same capacity, thereby greatly reducing the area available for direct radiation.

If the rotating speed  $n$  is constant, an increase of generator capacity can be attained by increasing the output coefficient  $C$  or the generator size or both. A larger stator and consequently rotor diameter, and active length greatly increase the windage losses. For instance, the surface friction loss, that represents a significant portion of the windage losses, rises as the fourth power of the diameter, and linearly with an increasing active length. Thus to reduce windage losses the most important parameter to consider is a reduction in the rotor diameter. Besides that, the diameter must be kept as small enough as possible to keep the peripheral speed  $v$  of the rotor within safe limits ( $v = \pi D_r n$ ), where  $D_r$  is the rotor diameter in meters,  $n$  is the rotating speed in rps, and  $v$  is in m/s, so that for large capacity machines the axial length must be considerable. This adds to the difficulty of cooling the central portion of the core with air, that is too far from the end of the rotor where fans are installed. Indirect air-cooled generators have been built up to 400 MVA.

All of these considerations point to the necessity of completely enclosing the machine in order to permit the use of hydrogen instead of air to carry away the heat, for larger size machines than those which use air cooling. The hydrogen density is about 1/14 that of air, for the same pressure and temperature, thus reducing windage loss and noise; its heat conductivity is around 6.7 times greater than that of air, that implies in a heat transfer coefficient of 1.5 times that of air, so more readily taking up and giving up heat. The hydrogen is maintained at a pressure above atmospheric in order to avoid the penetration of air and forming an explosive mixture inside the machine, which is totally closed. At 3.45 kPa its rating can be increased by about 30% above its air-cooled rating. An additional pressure increase from 3.45 to 103.5 kPa and a further increase to 207 kPa allows the machine rating to be increased additionally by 15 and 25% for the same temperature rise, respectively. The gas coolers are located inside the generator casing. Indirect hydrogen-cooled generators (Fig. 6.3) have been built up to 600 MVA.

**a.2) Direct Cooling.** To further increase the capacity of cylindrical-rotor machines, in relation to those obtained using indirect hydrogen-cooling, it is necessary to use an effective direct winding cooling system in which the stator and rotors windings are designed with internal ducts for the circulation of the coolant directly in contact with the windings. Direct cooling permits a specific electric load (Sect. 6.1.20, *Apparent Nominal Power:*

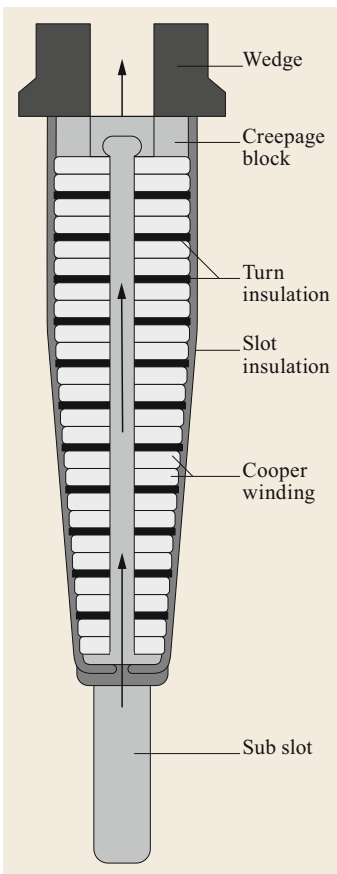


**Fig. 6.3**  
Simplified section  
of an indirect  
hydrogen-cooled  
generator [6.3]

*Output Equation*), i.e., and the armature current to be increased, while maintaining the limits of temperature rise. Hydrogen has been used, by some manufacturers, for rotor and stator winding cooling.

Figure 6.4 shows the cross-section of a rotor slot in a direct cooled cylindrical-rotor machine, where hydrogen enters the subslot in an axial direction, bringing it in direct contact with the copper conductors, thus reducing the thermal drop through the insulation.

However, for machines larger than 800 MW, in general, the volume of hydrogen required to cool the



**Fig. 6.4** Rotor slot  
in a direct hydrogen  
cooled cylindrical  
machine

machine may be so large that its use results in a great increase in machine cost. Thus, due to its excellent heat conductivity being about 60 times that of air and 40 times of that of hydrogen for the same pressure, highly purified water has been used for direct stator winding cooling, allowing a further increase in machine capacity, and lower costs when compared with direct stator hydrogen-cooled machines. Besides that, the duct area for water is smaller than for hydrogen, allowing more space for the conductors in the slot, giving a greater conductor cross section and as consequence a decrease in its resistance and lower losses, for the same armature current. Water may also be used for cooling the rotor winding, instead of hydrogen, to increase the output available from the same frame size. In this latter case the water-pipes have to be designed to support the centrifugal force and the internal pressure.

To take advantage of the good performance of water and hydrogen as a cooling medium, a 1350 MW round-rotor generator was constructed with the stator and rotor windings cooled by water and the steel sheet core cooled by hydrogen.

**b) Salient-Pole Machines.** These are characterized by low speed, large diameter and small axial length compared to cylindrical-rotor machines. In addition to the large areas available for direct radiation, there is the fanning action of the rotor. Even so, it is still necessary to subdivide the core by providing ventilating ducts to allow the flow of cooling radially through the core. In general, hydrogenerators are air-cooled where the air circulates through a heat exchanger in a closed circuit. Direct water cooling of hydrogenerators stator windings, where water is passed through the stator conductors has been applied to machines larger than 500 MW, while the rotor may be cooled by air.

#### Insulation

Electrical insulation is a combination of materials designed to perform the functions needed in electric equipment. They can be divided into two main categories: groundwall and conductor insulation [6.4].

**Table 6.1** Thermal classes of insulating materials

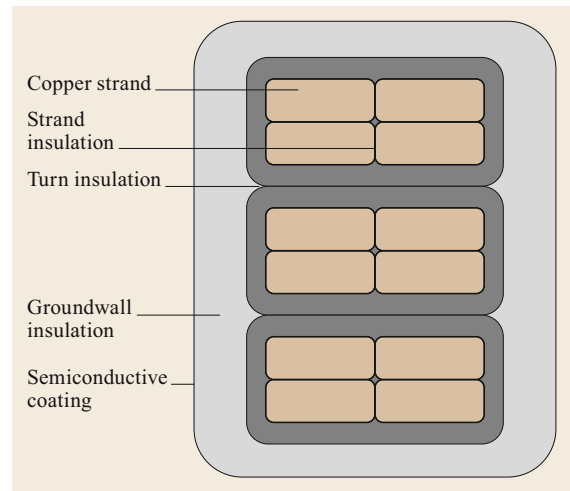
Numerical classification (°C)	Previous designation (class)	Hottest spot permitted (°C)	Permitted average winding temperature <sup>a</sup> (°C)
90	Y	90	NA
105	A	105	NA
130	B	130	120
155	F	155	140
180	H	180	165

<sup>a</sup> Temperature determined by resistance measurement (NA = not available)

A groundwall insulation separates those components that may not be in contact with each other, i.e., separation of the coil from the grounded stator core of the machine. Conductor insulation separates the wires and turns of a coil. Organizations like ANSI/IEEE (American National Standards Institute/Institute of Electrical and Electronic Engineers) and IEC have produced thermal classifications of materials for rotating electrical machines. A table adapted from IEC 60034-1 [6.5] and IEC 60085 [6.6] is shown in Table 6.1. A brief description of materials for each insulating class is presented in Table 6.2.

**Table 6.2** Description of material for each insulating class

Numerical classification (°C)	Material description
90	Materials or combinations of materials such as cotton, silk, paper, cellulose, and similar materials when neither impregnated nor immersed in a liquid electrical insulating material
105	Materials or combinations of materials such as cotton, silk, paper, and similar materials when either impregnated or coated or when immersed in a liquid electrical insulating material
130	Materials or combinations of materials such as mica, asbestos, fiberglass, used as suitable binding substances
155	Materials or combinations of materials such as mica, asbestos, fiberglass, and similar inorganic materials suitably bonded with organic (varnishes or resins) or synthetic inorganic thermo-setting resins of two types: epoxy mica and polyester mica
180	Materials or combinations of materials such as mica, asbestos, fiberglass, and similar inorganic materials in built-up form with binding substances composed of silicone resins, or materials with equivalent properties

**Fig. 6.5** Cross section showing the stator winding insulation components

*a) Stator Winding Insulation.* The basic stator winding insulation components are shown in Fig. 6.5, with:

- Strand insulation—to reduce the skin effect of copper strands
- Turn insulation—to prevent electrical shorts between turns
- Groundwall insulation—to prevent ground faults from high potential and
- Semiconductive coating—to prevent partial discharge of the coil or bar surface.

These insulation components together ensure that an electrical short does not occur, that the heat from the conductor losses are transmitted to a heat sink, and that the conductor does not vibrate in spite of the magnetic force.

Besides the insulation components above, on the coil or bar surface there is a special coat made of silicon carbide having a voltage dependent resistance. This coat is applied to the parts of the coil or bar that come out from the slots. In such a way, a uniform spread of electric potential is obtained thus avoiding partial discharges at exits from the slots.

*b) Rotor Winding Insulation.* Turn insulation (in both cylindrical-rotor and salient-pole machines) and groundwall insulation (in cylindrical-rotor machines) in a rotor can be relatively thin since the voltage in a rotor is much lower than in a stator.

For salient-pole machines rated at less than a few megawatts a magnetic wire, instead of a copper wire, is wrapped around the pole. A magnet wire is technically just an insulated copper wire which is coated

with an enamel insulation. This feature makes it ideal for winding coils where every millimeter is considered important. Thin insulated material helps to make more turns in a small area in machines. Common copper wire is insulated with thicker material which can require more area for more turns. Insulating washers and strips are placed between the magnetic wire and the field pole laminations to act as the ground insulation.

*c) Life Expectancy of Electric Equipment.* Apart from accidental electrical and mechanical failures, the life expectancy of an electrical apparatus is limited by the temperature of its insulation: The higher the temperature, the shorter its life. A rule of thumb (based upon the Arrhenius equation of chemical reaction time versus temperature) adapted to approximate the relationship between insulation life and operating temperature states that if the operating temperature is raised by  $10^{\circ}\text{C}$ , the thermal life expectancy of the insulation system is reduced by one half, and conversely if the operating temperature is reduced by  $10^{\circ}\text{C}$ , the thermal life of the insulation system is approximately doubled. Thus if a machine has a normal life expectancy of thirty years at a constant temperature of  $105^{\circ}\text{C}$ , it will have a service life of only seven and a half years at  $125^{\circ}\text{C}$ . This explains why sometimes a machine is specified for class F insulation, but operates as class B.

The factors that contribute most to the deterioration of insulators are (1) heat, (2) humidity, (3) vibration, (4) acidity, (5) oxidation, and (6) time. Because of these factors, the state of the insulation changes gradually; it slowly begins to crystallize and the transformation takes place more rapidly as the temperature rises.

In crystallizing, organic insulators become hard and brittle. Eventually, the slightest shock or mechanical vibration will cause them to break. Under normal conditions of operation, most organic insulators have a life expectancy of 8–10 years provided that their temperature does not exceed  $100^{\circ}\text{C}$ . On the other hand, some synthetic polymers can withstand temperatures as high as  $200^{\circ}\text{C}$  for the same length of time.

Low temperatures are just as harmful as high temperatures are, because the insulation tends to freeze and crack. Special synthetic organic insulators have been developed, which retain their flexibility at temperatures as low as  $-60^{\circ}\text{C}$ .

### 6.1.3 Armature Windings

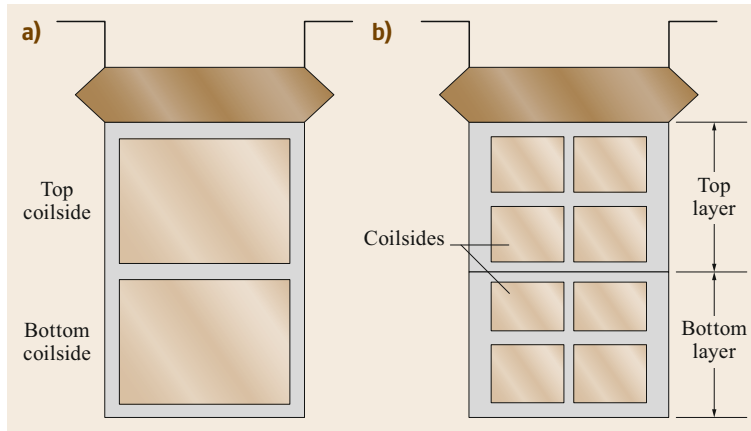
This section summarizes single and double-layer, as well as integral and fractional slot armature windings. More extensive information can be found in references [6.4, 7, 8].

Armature windings comprise a set of coils/bars embedded in slots, uniformly spaced round the armature periphery. The main characteristics of alternating current windings are: the types of coils; the number of phases; the connections between phases; the number of coil layers per slot; the pitch of the individual coils comprising the winding; the number of circuits in parallel; and the arrangement of the end connections.

The types of stator coils include random-wound coils, form-wound coils and form-wound bars (called Roebel bars):

- a) Random-wound coils consist of round, insulated copper conductors that are wound continuously through slots in the stator core to form a coil. A cross-section of the coil shows that turns are randomly distributed and can be in close proximity to a number of other turns. Throughout the axial length of the coil, wires can migrate during manufacturing and take new positions with respect to other coils. Random windings are typically used for machines less than 1500 kW, where the size of the stator and the minimum wire thickness usually do not allow form-wound coils.
- b) Form-wound multiterm coils are preformed coils consisting of a continuous loop of magnetic wire shaped into a coil. Individual turns are arranged in precise locations with respect to each other. That is, turn one is always next to turn two, turn two is always next to turn three, and so on. The coils are shaped in a forming machine to the final configuration that they will occupy in the stator. They are used in generators rated up to 50–100 MVA and in most large motors.
- c) Form-wound Roebel bars are used in large generators as the form-wound multiterm coil is large enough so that there are difficulties in inserting both legs of the coil in the narrow slots in the stator core without risking mechanical damage to the coil during the insertion process. Thus, most large generators are not made from multi-turn coils, but rather from half-turn coils, often referred to as Roebel bars. With a Roebel bar construction, only one half of a coil is inserted into the slot at a time, which is considerably easier than inserting two sides of a coil in two slots simultaneously.

The EMFs are induced in armature coils/bars due to relative motion between them and the flux density wave in the airgap established by the field windings. In a three-phase AC machine the armature coils/bars are symmetrically connected to form a set of three balanced phases (equal EMF magnitudes with a relative phase



**Fig. 6.6a,b** Double-layer winding: (a) two coil sides per slot (b) eight coil sides per slot

displacement of  $2\pi/3$  rad). When the armature winding carries current, it establishes the same number of alternating (north-south) poles for which it is wound.

The active coil-side length in which the EMF is induced equals the armature length (over which the flux density is established). The pitch of a coil is the space angle (electrical) between its two sides and must equal an integral number of slots. The coil pitch may be full (equal to one pole pitch or  $180^\circ$  E) or short-pitch (chorded) coils may be used. The pitch of a coil could be expressed in terms of its angular span or in terms of slots. The slots/pole must be an integral number for a full-pitch coil.

Practically there are two types of windings, viz. single-layer and two-layer (or double-layer). In a single-layer winding each coil side of a coil occupies the whole slot, thus the number of coils is half the number of slots. In a double-layer winding one coil side of a coil occupies the upper position in one slot and the second coil side occupies the lower position in a slot displaced from the first coil-side by the coil-span. In a double-layer winding each slot is occupied by two coil-sides, one placed on top of the other, referred to as top and bottom coil sides. The number of coils is equal to the number of slots.

(Nomenclature:  $m$  = number of phases;  $p$  = number of poles;  $Q$  = number of slots (must be divisible by 3 in a three-phase AC machine);  $Q/p$  = slots per pole, i.e., pole pitch in terms of slots (is noninteger for fractional-slot winding);  $\gamma = (180p)/Q$  ° E = angle between midpoint of adjacent slots or slot pitch;  $q = Q/(mp)$  = number of slots per phase and pole and  $\sigma = q\gamma$  = phase belt or phase spread angle in ° E.)

### Single-layer Windings

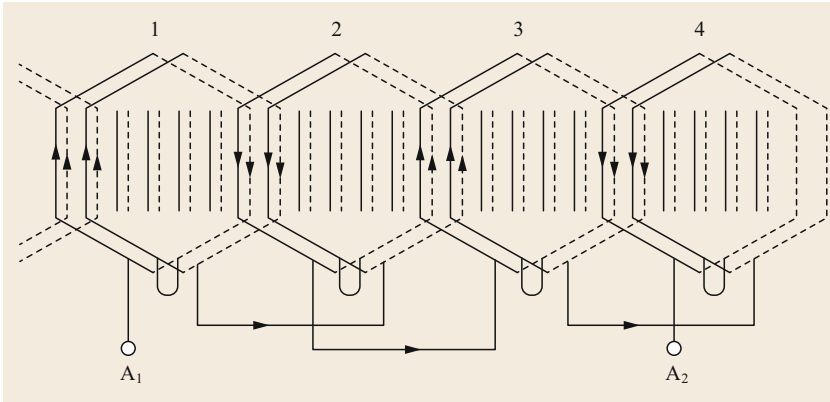
Single-layer windings for a three-phase machine requires an overhang designated to allow the end connections to be placed in separate plans. They may be

classified into two main categories, i.e., unbifurcated (or half-coiled) and bifurcated (whole-coiled). In the former type the coils comprising a phase group in adjacent pole pitches are concentric. The individual coils may have a span greater or less than a pole pitch but the average coil-span equals one pole-pitch. This kind of arrangement is provided to avoid crossing of two coils under one phase-group. In a bifurcated winding, each coil group is split into two sets of concentric coils and the return coil-sides are shared with those of another group. This kind of arrangement is only possible when  $q$  is even.

For accommodating the windings for all the three-phases, the overhang must be arranged in two or three planes. The jointing of individual conductors to form the finished coil is usually done by electrical resistance welding and each turn must after joining be suitably insulated over the butt joint. This procedure is expensive which accounts for the decline in the use of single-layer in favour of double-layer windings. Single-layer windings are, therefore, rarely used in modern machine practice except in small sizes. Machines are of course still found in use with single-layer windings.

### Double-layer Windings

Double-layer windings usually lead to simpler end connections and to a machine which is more economical to manufacture and are found in all machines except small motors below 10 hp in size. The number of coils is the same as the number of slots. They fall into two main classes depending upon the value of  $q$ : integral slot winding when  $q$  is an integer and fractional-slot winding, when  $q$  is a fractional number. To meet the requirement of symmetry among phases, the number of slots/phase ( $Q/m$ ) must be a whole number. In Fig. 6.6a there are two coil sides per slot while in Fig. 6.6b there are eight coil sides per slot. For placing double-layer windings, usually open slots are used.



**Fig. 6.7** Detailed double-layer lap winding diagram for phase A for 3-phase armature having 24 slots, 4 poles, phase spread  $60^\circ$

**a) Integral-Slot Winding.** Here  $q$  is an integer. The winding arrangement is further illustrated through an example. Let  $q = 2$ ,  $p = 4$ ,  $Q/p = 6$ ,  $\sigma = 60^\circ$  E, full-pitch coils, double-layer, lap winding.

The winding diagram for one phase is shown in Fig. 6.7. The first set of phase-group coils (coil-group 1) lying under one pole-pair NS (North and South) are connected in series (finish end of the first coil is connected to the start of the next coil lying to the right of the first). The second coil-group of the phase lies under S-N poles and must therefore be connected in reverse to the first coil-group for additive EMF. Note that alternate coil-groups are reverse connected and that the winding appears like a bifurcated one. Observe that coil-sides lying in any given slots pertain to the same phase. All the coil-groups of the phase could be connected in series or in series-parallel.

In practice, however, it is common to use chorded or short-pitched coils. This type of arrangement offers certain inherent advantages such as reduction in the amount of copper needed for end connections. Furthermore, certain harmonics present in the EMF wave are greatly suppressed. The effect of coil chording on the EMF generated is shown in Sect. 6.1.4.

**b) Fractional-Slot Winding.** These windings have fractional values for the slots per pole ( $Q/p$ ) and number of slots per phase and pole ( $q$ ). Advantages of fractional-slot windings when compared with integral slot windings are:

- Great freedom of choice with respect to the number of slots.
- Possibility to reach a suitable magnetic flux density with the given dimensions.
- Multiple alternatives for short-pitching.
- If the number of slots is predetermined, the fractional-slot winding can be applied to a wider

range of numbers of poles than the integral slot winding.

- The segment structures of large machines are better controlled by using fractional-slot windings.
- Reduction of high-frequency slot harmonics, and as consequence this winding reduces the high-frequency harmonics in the EMF and MMF waveforms.

Fractional-slotting is practicable only with double-layer windings. While  $q$  is a noninteger in a fractional-slot winding,  $mQ'$ , i.e., the total number of slots, must be divisible by 3, i.e., the total slots per phase must be an integer in order to obtain a symmetrical 3-phase winding. The pole pitch,  $mQ'/p$ , is also fractional, so that the coil-span cannot be of full-pitch. The coil-span chosen is less than the full-pitch because of the inherent advantages of chording.

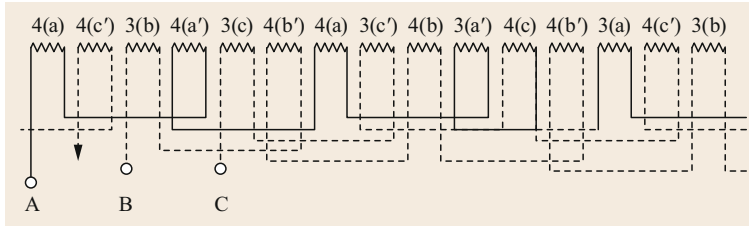
A winding constituting a basic unit under a pole-pair (N and S) is repeated for any number of pole pairs when  $q$  is integral. In order to obtain the *basic unit* for fractional-slot winding,  $q = Q/(mp)$  is reduced to the irreducible fraction, as shown

$$q = \frac{Q}{mp} = \frac{Q'}{p'} = a + \frac{b}{p'}. \quad (6.1)$$

For a fractional-slot winding:

- The basic unit of the winding has  $p'$  poles.
- Each phase has within  $p'$  poles  $Q' = qp'$  slots.
- All phases have within  $p'$  poles,  $mQ'$  slots.
- Each phase has within  $p'$  poles  $p' - b$  coil groups with  $a$  coils and  $b$  coil groups with  $a + 1$  coils.
- The maximum possible number of parallel circuits is  $p/p'$ .

In a double-layer winding, the phase-grouping of coil-sides for the top layer is repeated in the bottom layer



**Fig. 6.8** Layout of three-phase double-layer fractional-slot winding

with corresponding coil-sides being located one coil-span away. Therefore, all that is needed is to establish the phase-grouping of the top layer of coil-sides. An example of a fractional-slot winding for a three-phase, 10 pole machine with 108 slots is as follows

$$q = \frac{108}{3 \times 10} = \frac{18}{5} = 3 + \frac{3}{5}.$$

Then,  $p' = 5$  makes the basic unit of this winding. Each phase has in the 5 poles  $Q' = 18$  slots. All three-phases have in the 5 poles  $mQ' = 3 \times 18 = 54$  slots. Each phase has in the 5 poles  $p' - b = 5 - 3 = 2$  coil groups with  $a = 3$  coils and  $b = 3$  coil groups with  $a + 1 = 4$  coils. The groupings could be 4,4,3,4,3 coils and the basic unit would cover 5 pole-pitches. This allows one circuit with both units in series or two parallel circuits only.

The angle between two consecutive slots of the stator is

$$\gamma = \frac{180 \times 10}{108} \circ \text{E} = 16 \frac{2}{3} \circ \text{E}.$$

Figure 6.8 shows the layout of the winding for the basic unit of five poles (note that this need not be even). The sequence of slot groups (4,4,3,4,3) is determined to give the greatest symmetry in the winding.

Though the fractional-slot winding may appear to be somewhat complicated, it can be easily manufactured. The number of armature slots chosen is not an integral multiple of the number of poles. Consequently one may choose a particular number of slots for which the notching gear is available. This results in savings on machine tools. This flexibility can be effectively used where the number of poles (machine speed) varies over a wide range as in the case of synchronous machines.

As already said the high-frequency harmonics caused by slotting are considerably reduced by the use of fractional-slot winding. As the poles move past a slotted armature, the flux/pole fluctuates (does not move) as the slot-teeth pattern facing a pole repeats. This causes induction (static) of EMF harmonics of high frequency. If  $Q/p$  (slots per pole) is integral, the disposition of armature slots relative to pole simultaneously repeats (in time phase) at every pole so that the harmonics in phase-groups of a given phase are in

phase. Nonintegral  $Q/p$  causes the harmonics in phase-group to become out-of-phase thereby reducing their strength in the phase voltage.

### 6.1.4 Basic Concepts

The frequency  $f$  can be expressed in terms of revolutions per minute of the rotor and the number of poles.

#### Frequency, Speed and Angle Relations

In one complete revolution of the rotor, the EMF induced in the coil has one complete cycle. If the rotor rotates at  $n$  revolutions per minute, the EMF frequency in cycles per second will be  $f = n/60$ , that is the number of revolutions per second. This applies to a 2 pole machine. If the number of poles is  $p$  instead of 2, it still holds that the EMF goes through a complete cycle when the coil passes two poles of the machine and therefore the frequency is

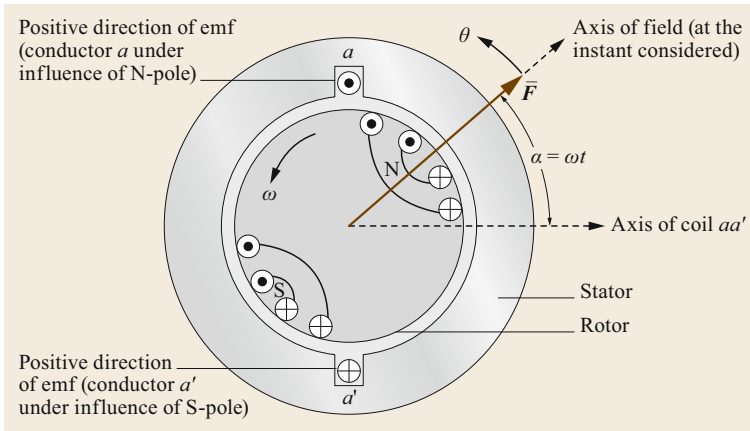
$$f = \frac{p}{2} \frac{n}{60} = \frac{pn}{120} \text{ Hz}. \quad (6.2)$$

Hydraulic turbines operate at a relatively low speed and a great number of poles are necessary for obtaining a frequency of 50 or 60 Hz. Therefore, hydrogenerators have salient-poles. On the other hand, gas, oil, and nuclear turbines operate at high speeds and it is only necessary to have 2 or 4 poles for obtaining a frequency of 50 or 60 Hz. Therefore, these machines have nonsalient-poles. Multiplying  $f$  by  $2\pi$ ,

$$\omega = 2\pi f = \frac{p}{2} 2\pi \frac{n}{60} = \frac{p}{2} \omega_m. \quad (6.3)$$

Where  $\omega$  specifies angular velocity in terms of frequency, and this velocity is called the electrical angular speed, while  $\omega_m$  is the mechanical angular velocity. When a machine has more than two poles it is convenient to focus the analysis of the machine on a unique pair of poles because the electric, magnetic and mechanic conditions associated with another pair of poles are repetitions of those that occur on the pair of poles under consideration. For this reason it is convenient to express angles in electrical degrees (or radians electri-





**Fig. 6.9** Cylindrical-rotor synchronous machine

cal) instead of using mechanical units. Thus,

$$\theta_c = \frac{p}{2} \theta_m, \quad (6.4)$$

where  $\theta_c$  is the angle in electrical units and  $\theta_m$  is the angle in mechanical units.

#### Electromotive Force of a Concentrated Full-Pitch Armature Coil

The cross-sectional view of a 2 pole cylindrical-rotor AC synchronous machine is shown in Fig. 6.9.

The distribution of the field MMF and flux density in the airgap of Fig. 6.9, for nonsalient and salient-pole machines, is not sinusoidal, but is periodic, symmetrical in successive half loops. Single-value functions that do not include infinite discontinuities, in accordance with Fourier's theorem, can be resolved into a fundamental sine wave and a series of odd harmonics.

The field winding on the rotor is assumed, for the time being, to produce a sinusoidal space wave of flux density  $B_f$  at the stator surface, given by

$$B_f = B_p \sin \theta, \quad (6.5)$$

where  $B_p$  is peak flux density at the rotor pole center and  $\theta$  is measured in electrical radians from the rotor pole axis. The airgap field flux per pole is the integral of the field flux density over the pole area, where  $L$  is the active coil-side length (axial stator length) and  $r$  is the inner radius of the armature at the airgap; thus for a two pole machine

$$\phi_f = \int_{\alpha}^{\pi+\alpha} B_p \sin \theta L r d\theta = 2B_p L r \cos \alpha. \quad (6.6)$$

Because the pole area is  $2/P$  times that of a two pole machine of the same length and diameter, for a  $P$  pole

machine

$$\phi_f = \frac{2}{p} 2B_p L r \cos \alpha = \Phi_f \cos \omega t. \quad (6.7)$$

As the pole pitch is  $\tau = \pi D/P$ , where  $D$  is the inner stator diameter, the amplitude of the flux is given by

$$\Phi_f = \frac{2}{\pi} \tau L B_p \quad (6.8)$$

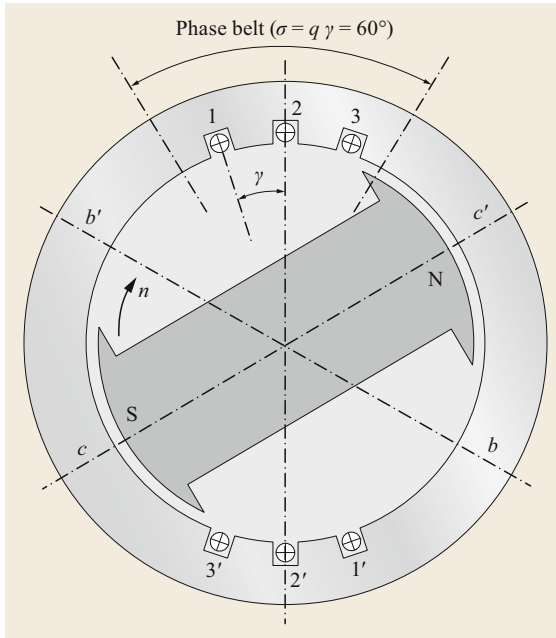
and the instantaneous EMF induced in the coil  $aa'$  of  $N$  turns is given by Faraday's law,

$$e = -\frac{d\lambda}{dt} = \omega N \Phi_f \sin \omega t - N \frac{d\Phi_f}{dt} \cos \omega t. \quad (6.9)$$

In steady state conditions the value of  $\Phi_f$  is constant, and the second term is zero. Thus, the only EMF induced in the coil is due to the first term, called the speed voltage.

#### Electromotive Force of a Full-Pitch Distributed Armature Winding

The winding of phase a in the machine of Fig. 6.10 has three coils ( $11'$ ,  $22'$  and  $33'$ ), that are placed in three slot-pairs distributed in space with an angular separation of  $\gamma$  electrical degree. The phase belt or phase band may be defined as the group of adjacent slots belonging to one phase under one pole, and the angle  $\sigma = q\gamma$  ( $^\circ$  E) occupied by each phase winding along the armature periphery per pole is the phase belt angle and  $q$  is the number of slots per pole and per phase, i.e.,  $q = Q/(mp)$  (Sect. 6.1.3). Such a winding is referred to as a distributed winding. As the machine is always wound with identical coils, the rms (root mean square) value ( $E$ ) of the sinusoidal EMFs induced in coils  $11'$ ,  $22'$  and  $33'$  are equal, but the EMFs have a progressive time phase difference  $\gamma$  because the coils are uniformly distributed in space.



**Fig. 6.10** Synchronous machine with distributed winding

The coils, in Fig. 6.10, are series connected to yield the resultant phase voltage  $E_a$ , which is the phasor sum of the coil EMFs. The number of EMF phasors  $n$  is equal to the number of slots where the coils of one phase are distributed divided by two, i.e., equal to  $q$ . Because of distribution, the rms resultant phase voltage is less than the arithmetic sum of the rms coil voltages. This reduction ratio called the distribution factor (also breadth factor), where the index 1 is for the fundamental frequency, and is given by

$$k_{d1} = \frac{\sin \frac{q\gamma}{2}}{q \sin \frac{\gamma}{2}} \quad (6.10)$$

The rms value  $E$  of the armature fundamental EMF induced per phase with  $N$  turns in series per phase of a three-phase winding is given by

$$E_1 = 4.44fNk_{d1}\Phi_{f1} \text{ V} \quad (6.11)$$

The amplitude of the fundamental flux per pole is

$$\Phi_{f1} = \frac{2}{\pi} B_1 \tau L \quad (6.12)$$

The windings of each phase are a combination of coils connected in series, forming a number of coil groups, that are distributed in parallel paths. For instance, if there are four coil groups connected in series, where  $N_c$  is the number of turns of each coil, the total number

of turns in (6.11) is  $N = 4N_c$ , but if the four coil groups are connected in two parallel paths  $N = 2N_c$ .

The distribution of the field MMF and field flux density in the airgap are not sinusoidal, being in the case of cylindrical-rotor machines represented approximately by a single trapezoidal section, in which the field MMF has a constant maximum value in the central region of the pole and decreases linearly in the slotted region at each side to zero at the position  $+\pi/2$  and  $-\pi/2$  electrical radians, while in the case of salient-pole machines the MMF distribution is rectangular. Because of symmetry the MMF and flux density waves, in both machines, are symmetrical about the direct-axis. As these waves are periodic, symmetrical in successive half loops, single-value functions that do not include infinite discontinuities and in accordance with Fourier's theorem, they can be resolved into a fundamental sine wave and a series of odd harmonics. The angle of displacement between two adjacent slots for a field harmonic of the  $h$  order is equal to  $h\gamma$ , and the distribution factor for the  $h$ -th harmonic becomes

$$k_{dh} = \frac{\sin \frac{qh\gamma}{2}}{q \sin \frac{h\gamma}{2}} \quad (6.13)$$

For the  $h$ -th harmonic, the rms value  $E_h$  for the EMF is

$$E_h = 4.44hfNk_{dh}\Phi_h \text{ V} \quad (6.14)$$

and the amplitude of the flux per pole for the  $h$ -th harmonic is

$$\Phi_h = \frac{2}{\pi} B_h \frac{\tau}{h} L \quad (6.15)$$

### Electromotive Force of a Short-Pitch Armature Winding

The assumption that the coil pitch is equal to the pole pitch ( $180^\circ$  E) is seldom true for an AC winding. Normally the coil pitch is smaller than the pole pitch, i.e., normally AC windings, besides being distributed over the surface of the machine, are short-pitched or chorded. If the coil pitch is called  $\rho$ , the coil is referred to as fractional-pitched. In this coil, there will be a phase difference between induced EMFs in two coil-sides of less than  $180^\circ$ . Hence, the resultant terminal voltage of the coil is the phasor sum of these two EMFs and it is less than that of a full-pitched coil of a distributed winding. Pitch factor is a measure of the resultant EMF ( $E_R$ ) of a short-pitched coil in comparison with resultant EMF of a full-pitched coil ( $2E$ ) and is given by

$$\begin{aligned} k_{p1} &= \frac{\text{EMF induced in a short pitch coil}}{\text{EMF induced in a full pitch coil}} \\ &= \frac{2E \cos \frac{\pi-\rho}{2}}{2E} = \cos \frac{\pi-\rho}{2} \end{aligned} \quad (6.16)$$

The fundamental frequency EMF of a phase consisting of  $n$  coils, in which the number of turns in series is  $N$ , can be written as

$$E_1 = 4.44fNk_{p1}\Phi_{f1} \text{ V.} \quad (6.17)$$

It should be noted that the coil span is rarely made less than  $2/3$  pole pitch =  $120^\circ$  E, because additional turns become necessary that offset the saving of overhang copper.

A  $h$ -th harmonic component of the flux wave may be imagined as being produced by  $h$  fictitious poles as compared to one pole for the fundamental component. Thus, the angle of displacement between two adjacent slots for a field harmonic of the  $h$  order is equal to  $h$  times the chording angle for the fundamental component and the pitch factor for the  $h$ -th harmonic is given by,

$$k_{ph} = \cos h \left( \frac{180 - \rho}{2} \right). \quad (6.18)$$

For the  $h$ -th harmonic, the rms value  $E_h$  for the EMF is

$$E_h = 4.44hfNk_{ph}\Phi_{fh} \text{ V.} \quad (6.19)$$

With an appropriated choice of the pitch factor an elimination of certain harmonics of the EMF is possible, by making  $h(180 - \rho)/2$  equal to  $90^\circ$  E, i.e., if the pole pitch  $\rho = 120^\circ$  E, that is equivalent to a coil (winding) pitch of  $120/180 = 2/3$ ; the 3rd harmonic of per phase EMF and the odd harmonics multiples of the 3rd, i.e., 9th, 15th, 21st, 27th, etc. . . . , are also eliminated. However, there will be a reduction in the fundamental component of the EMF as its pitch factor will be  $k_{p1} = 0.866$ .

### Winding Factor

Both distribution and pitch factors apply for a phase winding of  $N$  turns in series. Their product ( $k_d k_p$ ) is the winding factor  $k_w$ . Thus, for the fundamental and the  $h$ -th harmonic the expressions for the per phase EMFs are for the fundamental frequency,

$$E_1 = 4.44fNk_{w1}\Phi_{f1} \text{ V,} \quad (6.20)$$

for the  $h$ -th harmonic,

$$E_h = 4.44hfNk_{wh}\Phi_{fh} \text{ V,} \quad (6.21)$$

where

$$k_{wh} = k_{dh}k_{ph}, \quad \text{for the } h\text{-th harmonic.} \quad (6.22)$$

The quantity  $Nk_w$  can be considered as the number of effective turns per phase. It is smaller than the actual number of turns per phase  $N$ , owing to the distribution of the winding over several slots under each pole and to the chording of the coils.

In studying electrical machines the windings of each phase are represented by a full-pitch coil, taking into account the fact that in an actual machine the windings are distributed and have fractional-pitches by means of the winding factor that multiplies the resultant EMFs and MMFs.

### General Expression for the Electromotive Force of AC Machines Armature Windings Including Harmonics

The instantaneous value for the EMF of phase a can be written as

$$\begin{aligned} e_a &= \sqrt{2} \sum_{h=1,3,5,\text{etc.}} E_{fh} \sin h\omega t \\ &= \sqrt{2} (E_{f1} \sin \omega t + E_{f3} \sin 3\omega t \\ &\quad + E_{f5} \sin 5\omega t + \dots) \end{aligned} \quad (6.23)$$

and the rms EMF per phase will be

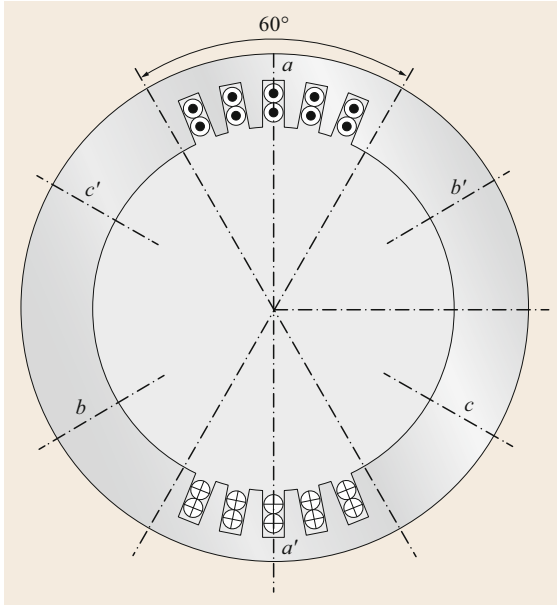
$$E_r = \sqrt{E_{f1}^2 + E_{f3}^2 + E_{f5}^2 + E_{f7}^2 + \dots} \quad (6.24)$$

The triple harmonic voltage components do not appear in the line to line terminal voltages, whether the machine is connected as star or delta. However, this should not be taken to mean that unbalanced triple harmonics voltages resulting from unbalanced loads or other causes may not occur.

### The Magnetomotive Force (MMF) of a Distributed and Short-Pitch One-Phase Armature Winding

Consider a basic 2-pole structure with a round rotor, with  $q = 5$  slots/pole/phase and a two-layer winding as shown, for phase a, in Fig. 6.11. Note that  $q$  is also equal to the number of full-pitch coils. The two-layer winding simplifies the geometrical problem of getting the end turns of the individual coils past each other. The corresponding developed diagram is shown in Fig. 6.12 along with the MMF diagram that is a stepped wave—much closer to a sine wave than the rectangular MMF wave of a single coil. At each slot the MMF wave has a step jump of  $2Ni$  ampere-turns, where  $N =$  coil turns and  $i =$  coil current. The resultant field produced by the armature MMF has the same of poles as that produced by the field MMF [6.9].

The fundamental frequency MMF of a full pitch coil of  $N$  turns at each airgap, for a two pole machine, by



**Fig. 6.11** A two-layer winding (phase a) of a 3-phase round rotor machine

Fourier's series, is

$$F_1 = \frac{4 Ni}{\pi} \tag{6.25}$$

and for the  $h$ -th harmonic

$$F_h = \frac{4}{\pi} \frac{1}{h} \frac{Ni}{2} \tag{6.26}$$

In the case of  $q$  full-pitch coils with  $N$  turns per coil in a single layer winding there are  $q$  MMFs, when all

the coils are connected in series. Thus in each airgap the MMF due to  $q$  coils is equal to  $qF_1$ . In the case of a distributed and short-pitch double layer winding, the instantaneous amplitude of the fundamental MMF of all coils (in a phase)  $F_{\text{phase1}}$  is

$$F_{\text{phase1}} = 2qF_1 k_{d1} k_{p1} = 2qF_1 k_{w1} \tag{6.27}$$

where the distribution and short-pitch factors are given by the same equations derived for the expression of an EMF (see Sects. 6.1.4, *Electromotive Force of a Full-Pitch Distributed Armature Winding* and *Electromotive Force of a Short-Pitch Armature Winding*).

Using (6.25) in (6.27),

$$F_{\text{phase1}} = 2q \frac{4}{\pi} \frac{Ni}{2} k_{w1} = \frac{4}{\pi} qNk_{w1}i \tag{6.28}$$

Similarly, for the  $h$ -th harmonic

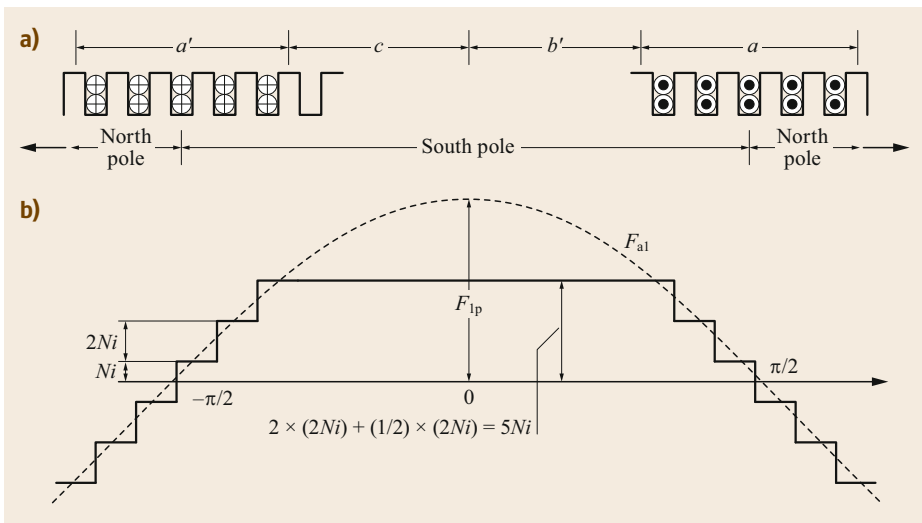
$$F_{\text{phase } h} = \frac{4}{\pi} \frac{1}{h} qNk_{wh}i, \quad \text{where } k_{wh} = k_{dh}k_{ph} \tag{6.29}$$

A machine with 2 poles was considered above. With more than 2 poles and an integral number of slots per pole and phase, the MMF will be similar to that in the above machine over each pole pair arc. When all the coil groups of the double layer winding are connected in series the number of turns per phase will be

$$N_{\text{ph}} = qNp, \quad \text{where } p = \text{number of poles} \tag{6.30}$$

and the coil current

$$i = \sqrt{2}I \sin \omega t \tag{6.31}$$



**Fig. 6.12** (a) Developed diagram and (b) MMF wave of Fig. 6.11

Upon introducing these relations into (6.28) and (6.29), the MMFs amplitudes are

$$F_{\text{phase } 1} = \frac{4\sqrt{2} N_{\text{ph}}}{\pi p} k_{w1} I, \quad (6.32)$$

$$F_{\text{phase } h} = \frac{4\sqrt{2} 1}{\pi h} \frac{N_{\text{ph}}}{p} k_{wh} I. \quad (6.33)$$

The expressions (6.32) and (6.33) are also valid for a winding (phase) with parallel branches if  $N_{\text{ph}}$  is the number of series connected turns per path and  $I$  is the total winding (one phase) current. The expression for the total MMF of the winding (one phase) can be written as

$$F_t = F_{\text{phase } 1} \sin \omega t \cos \theta + F_{\text{phase } 3} \sin \omega t \cos 3\theta + \dots + F_{\text{phase } h} \sin \omega t \cos h\theta, \quad (6.34)$$

where the angle  $\theta$  is counted from the winding (phase) axis.

### The Magnetomotive Force of a Distributed and Short-Pitch Three-Phase Armature Winding

In a three-phase machine the armature windings are  $120^\circ$  E apart and the expressions for the currents in phases a, b and c are

$$i_a = \sqrt{2} I \sin \omega t, \quad (6.35)$$

$$i_b = \sqrt{2} I \sin \left( \omega t - \frac{2\pi}{3} \right), \quad (6.36)$$

$$i_c = \sqrt{2} I \sin \left( \omega t - \frac{4\pi}{3} \right) \quad (6.37)$$

where  $\omega = 2\pi f_1$  is the synchronous angular frequency.

For a certain time instant the three-phases contribute for the armature MMF at a point on the armature surface represented by the angle  $\theta$ . The equations for the MMFs of each phase are

$$F_a = [F_{\text{phase } 1} \cos \theta + F_{\text{phase } 3} \cos 3\theta + \dots + F_{\text{phase } h} \cos h\theta] \sin \omega t,$$

$$F_b = \left[ F_{\text{phase } 1} \cos \left( \theta - \frac{2\pi}{3} \right) + F_{\text{phase } 3} \cos 3 \left( \theta - \frac{2\pi}{3} \right) + \dots + F_{\text{phase } h} \cos h \left( \theta - \frac{2\pi}{3} \right) \right] \sin \left( \omega t - \frac{2\pi}{3} \right),$$

$$F_c = \left[ F_{\text{phase } 1} \cos \left( \theta - \frac{4\pi}{3} \right) + F_{\text{phase } 3} \cos 3 \left( \theta - \frac{4\pi}{3} \right) + \dots + F_{\text{phase } h} \cos h \left( \theta - \frac{4\pi}{3} \right) \right] \sin \left( \omega t - \frac{4\pi}{3} \right). \quad (6.38)$$

The fundamental space component the resultant MMF of the three-phase winding is

$$\begin{aligned} F_1 &= \frac{3}{2} F_{\text{phase } 1} \sin(\omega t - \theta) \\ &= \frac{6\sqrt{2} N_{\text{ph}}}{\pi p} K_{w1} I \sin(\omega t - \theta) \\ &= 2.7 \frac{N_{\text{ph}}}{p} K_{w1} I \sin(\omega t - \theta) = A_1 \sin(\omega t - \theta). \end{aligned} \quad (6.39)$$

Hence it follows that the fundamental space harmonic of the resultant MMF in a three-phase machine is no longer a wave pulsating in space as in a single phase winding, but a wave traveling to the right around the stator periphery.

For the  $h$ -th harmonic, the MMF is

$$F_{h1} = 2.7 \frac{N_{\text{ph}}}{\text{HP}} K_{wh} I \sin(\omega t \pm h\theta) = A_h \sin(\omega t \pm h\theta), \quad (6.40)$$

where for phases b and c,  $\theta = \theta - 120^\circ$  and  $\theta = \theta - 240^\circ$ , respectively.

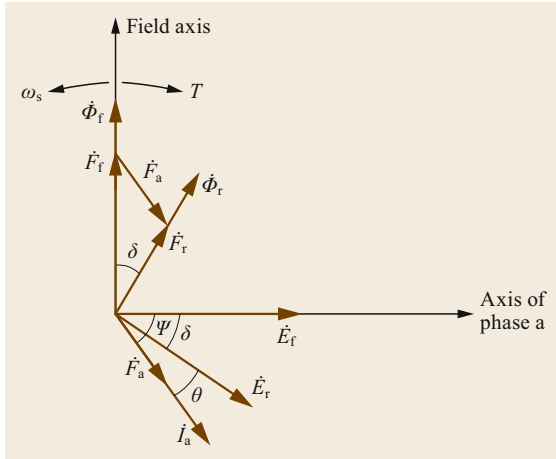
The resultant MMF  $F_r$  of all three-phases including harmonics is

$$\begin{aligned} F_r &= A_1 \sin(\omega t - \theta) + A_5 \sin(\omega t + 5\theta) \\ &\quad + A_7 \sin(\omega t - 7\theta) + \dots + A_h \sin(\omega t \pm h\theta). \end{aligned} \quad (6.41)$$

The resultant MMF is the sum of the MMFs due to:

- Harmonics of order  $h = 6k + 1$ , i.e.,  $h = 1, 7, 13, \dots$ , that produce a magnetic field rotating to the right, in the same direction of the fundamental MMF field and rotor, with a speed equal to  $\omega/h$ .
- Harmonics of order  $h = 6k - 1$ , i.e.,  $h = 5, 11, 17, \dots$ , that produce a magnetic field rotating to the left, opposite to the direction of the fundamental MMF field and the rotor, with a speed equal to  $\omega/h$ .
- The harmonics of order  $h = 3k$ , multiples of 3, i.e., 3, 6, 9,  $\dots$ , do not produce MMFs at the airgap.

The fifth and seventh harmonics create in the rotor a frequency of  $6f_1$ , the 11th and the 13th a frequency of  $12f_1$ , and so on, where  $f_1$  is the synchronous frequency of the armature currents. The fluxes due to these MMFs harmonics give rise not only to eddy currents losses in the rotor, which reduce the efficiency of the machine, but also to pulsating torques in the shaft at the frequencies  $6f_1, 12f_1$ , etc.  $\dots$



**Fig. 6.13** Synchronous generator supplying an inductive load

### 6.1.5 Armature Reaction and Phasor Diagrams

#### Cylindrical (Round) Rotor Machines

The winding of phase a is represented by a single concentrated coil  $aa'$ . The armature MMF, called the armature-reaction MMF  $F_a$ , depends on the amplitude of armature current  $I_a$  and its effect over the field MMF  $F_f$  depends on the type of load that is connected to a generator or motor, which establishes the angle  $\psi$  between the voltage  $E_f$  induced in the armature by the field magnetic flux  $F_f$  and the armature current  $I_a$ . The following conditions are considered.

**a) Operation as a Generator.** 1) When the generator supplies an inductive load,  $0 < \psi \leq -90^\circ$ . In this case  $I_a$  lags  $E_f$  by an angle  $\psi$ , the positive current maximum in coil  $aa'$  will occur at an angle  $\psi^\circ$  later;  $F_f$  lies  $(90^\circ + \psi)$  ahead of  $F_a$  as shown in the phasor diagram of Fig. 6.13. The output apparent power is

$$S = E_r I_a \exp(j(\theta)) = P + jQ, \quad (6.42)$$

where it can be concluded that the generator will supply reactive power to the load, when the power factor is inductive.

From Fig. 6.13 it is observed that the component  $F_a \sin \psi$  of  $F_a$  is directly opposite to the field MMF. Thus, when the current in a phase lags its excitation voltage a demagnetizing effect appears on the field axis, which will decrease the resulting EMF  $E_r$ , unless the DC field current increases, increasing  $F_f$  and maintaining  $E_r$  constant.

2) When the generator supplies a capacitive load ( $0 < \psi \leq 90^\circ$ ). In this case the armature current  $I_a$  is

ahead of EMF  $E_f$  and a magnetizing effect appears and to keep the resulting EMF constant  $E_r$  the DC field current must decrease. The output apparent power is

$$S = E_r I_a \exp(j(-\theta)) = P - jQ, \quad (6.43)$$

where it can be concluded that the generator will absorb reactive power when the power factor is capacitive.

3) When the generator supplies a resistive load  $\psi = 0$ . In this case the armature current  $I_a$  is in phase with EMF  $E_f$ , and neglecting saturation there will be no effect of MMF  $F_a$  over the field MMF  $F_f$ . The output apparent power is

$$S = E_r I_a \exp(j(0)) = P + j0, \quad (6.44)$$

where it can be concluded that the generator will supply no reactive power to a resistive load.

The effects of  $F_a$  on the field MMF  $F_f$  are called the direct-axis armature reaction for generating action.

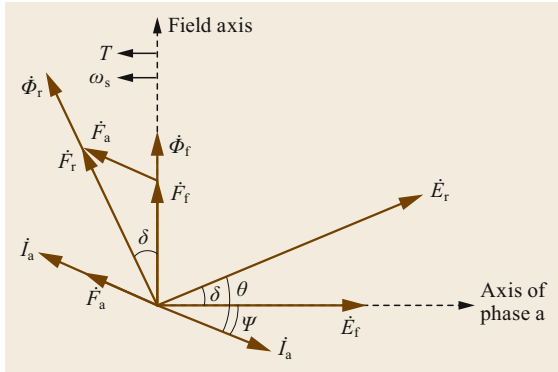
**a.1) Additional Considerations.** It is seen from Fig. 6.13 that the field poles lie an angle  $\delta$  ahead of the resultant MMF (or resultant flux) wave. The electromagnetic torque developed in the machine tries to align the field poles with the resultant field and is, therefore, opposite to the mechanical torque of the turbine, i.e., against rotation, and this is true for every other operating condition of the generator. The magnitude of the torque in a cylindrical (round) rotor synchronous machine is given by

$$T = \frac{\pi}{2} \left( \frac{P}{2} \right)^2 \Phi_r F_f \sin \delta = KE_r E_f \sin \delta. \quad (6.45)$$

When  $\Phi_r$  and  $F_f$  are held constant in magnitude, the machine meets the changing requirements of the load by adjustment of the angle  $\delta$ , which is known as the torque (power) angle.

**b) Operation as a Motor.** In motoring action two conventions can be used for the armature current. The first considers the current flowing in the same sense as that of a generator, i.e., out of the machine, and the second considers the current with an opposite sense as that of a generator, i.e., current into the machine. In the latter one, the current is considered negative in the equations to be derived.

Figure 6.14 shows a phasor diagram with both conventions when a motor is connected to an inductive source, where it can be seen that there is a component of  $F_a$ , which acts over the field excitation, and is called the magnetizing component of the armature-reaction MMF. This component will increase the resulting EMF



**Fig. 6.14** Synchronous motor connected to an inductive source

$E_r$ , unless the DC field current decreases  $F_f$  in order to maintain the resultant EMF  $E_r$  constant. The motor input apparent power is given by

$$\begin{aligned} S &= E_r I_a \exp(j(\theta - 180)) = -E_r I_a \exp(j(\theta)) \\ &= -P - jQ, \end{aligned} \quad (6.46)$$

where it can be concluded that the motor receives active and reactive power from the source.

#### Phasor Diagrams and Equations for Cylindrical (Round) Rotor Machines

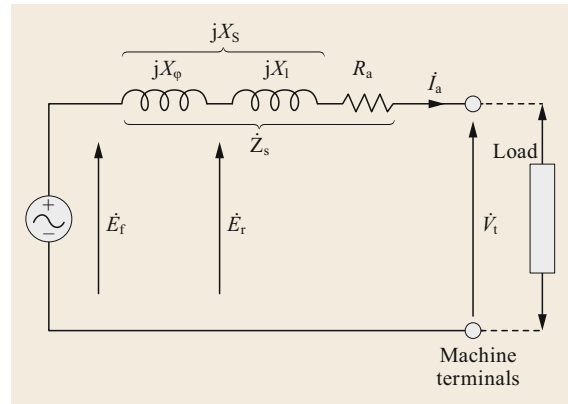
**a) Operation as a Generator.** The resultant flux is the phasor sum of the fluxes generated by the field and armature MMFs. These fluxes induce the EMFs  $\dot{E}_f$  and  $\dot{E}_a$  in the armature, respectively. The resultant EMF is

$$\dot{E}_r = \dot{E}_f + \dot{E}_a. \quad (6.47)$$

The EMF  $E_a$  is proportional to the armature current  $I_a$  and lags it by  $90^\circ$  as the EMF induced in an inductive reactance, so the effect of armature reaction is exactly as if the stator had a reactance  $X_\varphi$ , called the magnetizing or armature reaction reactance, thus

$$\dot{E}_a = -j\dot{I}_a X_\varphi \quad \text{and} \quad \dot{E}_r = \dot{E}_f - j\dot{I}_a X_\varphi. \quad (6.48)$$

The flux produced by the armature currents consists of two parts, the mutual flux that links the field winding (whose effect is represented by the EMF  $E_a$ ) and the leakage flux that only links the armature windings. The leakage flux includes the flux across the armature slots linking part or all of the coils in the slots, the end flux at the ends of the armature that links the loops or *end turns* of the armature coils where they emerge from the slots to cross over and complete the paths of the coils from slot to slot, and the tooth-top flux which is the flux between the tooth tops in the airgap without going through



**Fig. 6.15** Equivalent circuit for a cylindrical-rotor generator

the iron of the armature. The effect of the leakage flux is represented by a voltage drop in an armature leakage reactance  $X_l$  due to armature current.

The EMF resultant differs from the terminal voltage by the voltage drops in the armature resistance  $R_a$  and leakage reactance  $X_\lambda$  due to armature current  $I_a$ . Thus

$$\begin{aligned} \dot{V}_t &= \dot{E}_r = \dot{I}_a (R_a + jX_l) \\ \Rightarrow \dot{V}_t &= \dot{E}_f - j\dot{I}_a X_\varphi - (\dot{I}_a R_a + jX_l \dot{I}_a) \\ \Rightarrow \dot{E}_f &= \dot{V}_t + j\dot{I}_a (X_\varphi + X_\lambda) + \dot{I}_a R_a \\ \Rightarrow \dot{E}_f &= \dot{V}_t + \dot{I}_a R_a + j\dot{I}_a X_s, \end{aligned} \quad (6.49)$$

where  $X_s = X_\varphi + X_\lambda$  is the synchronous reactance and considers the effect of all the fluxes due to armature current  $I_a$ , while the excitation EMF  $E_f$  considers the flux due to the DC field current.

The synchronous impedance is denoted by

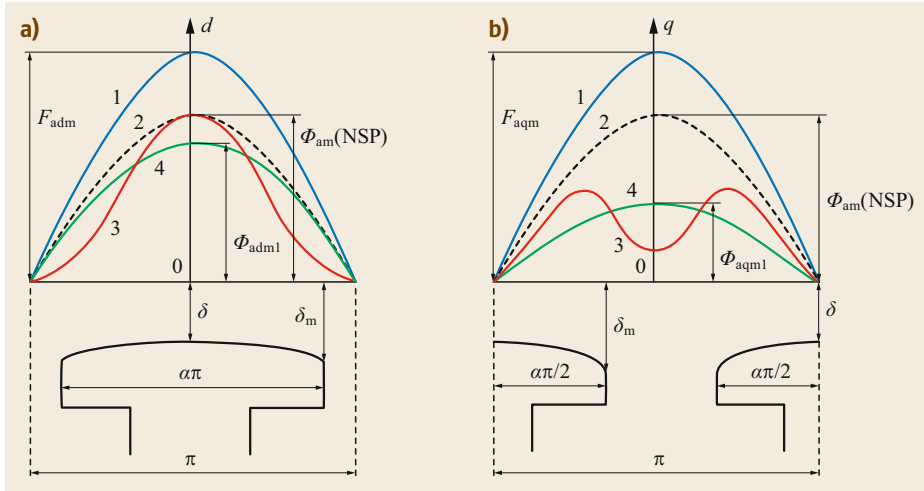
$$Z_s = R_a + jX_s. \quad (6.50)$$

According with (6.48)–(6.50) the equivalent circuit of a cylindrical generator can be represented by Fig. 6.15.

Typical values of resistance, leakage reactance and synchronous reactance for large machines, in per-unit, are

$$R_a = 0.01 \text{ p.u.}; \quad X_l = 0.15 \text{ p.u.}; \quad X_s = 1.10 \text{ p.u.}$$

In large machines the armature resistance is usually neglected except insofar as its effect on losses and heating is concerned. The per-unit armature resistance increases and the synchronous reactance decreases with decreasing size of the machine. In very small machines the armature resistance may be in the vicinity of 0.05 p.u. and the synchronous reactance in the vicinity of 0.5 p.u.



**Fig. 6.16a,b** Armature MMF and flux waves components in the (a) direct and (b) quadrature-axis. The index  $m$  means maximum values and  $\alpha\pi$  is the pole arc

**b) Operation as a Motor.** If in the equations for synchronous cylindrical generators the armature current is considered with a negative signal, i.e., current with an opposite sense as that of a generator, i.e., current into the machine, the equations for a synchronous motor are obtained, as

$$\dot{E}_t = \dot{E}_f + j\dot{I}_a X_\varphi \quad \text{and} \quad \dot{V}_t = \dot{E}_f + j\dot{I}_a X_s + \dot{I}_a R_a. \quad (6.51)$$

#### Armature Reaction in Salient-Pole Rotor Machines

**a) Operation as a Generator.** In the case of salient-pole machines the airgap reluctance varies from a low value when the armature MMF axis coincides with the direct (field) axis—which is the case when  $\psi = \pm 90^\circ$ —up to a high value when the armature MMF axis coincides with the quadrature-axis, which is the case when  $\psi = 0^\circ$ . It is relatively simple to determine the effect of the armature MMF reaction for these positions because the direct and quadrature-axis are both axis of symmetry for the rotor, but it is not so easy to determine the effect which the armature MMF has in intermediate positions. This difficulty was overcome by the use of Blondé's two-reaction theory.

This theory consists essentially of the replacement of the sinusoidal armature MMF of amplitude  $F_a$  by two sinusoidal waves, one of which has its amplitude coinciding with the direct-axis, and the other has its amplitude coinciding with the quadrature-axis. Thus the fundamental components amplitudes of armature MMF are

$$F_{ad} = F_a \sin \psi = 1.35 \frac{N_{ph}}{p} K_{w1} I_d, \quad \text{where} \quad I_d = I_a \sin \psi, \quad (6.52)$$

$$F_{aq} = F_a \cos \psi = 1.35 \frac{N_{ph}}{p} K_{w1} I_q, \quad \text{where} \quad I_q = I_a \cos \psi, \quad (6.53)$$

where

$$F_a = 1.35 \frac{N_{ph}}{p} K_{w1} I_a, \quad I_a = \text{rms armature current}. \quad (6.54)$$

In Fig. 6.16 the direct and quadrature-axis components of the armature MMF  $F_a$  are shown. Curves 1 represent the fundamental frequency components of direct ( $F_{ad}$ ) and quadrature-axis ( $F_{aq}$ ) armature MMFs; curves 2 show, just for comparison, the fundamental frequency component of armature flux for cylindrical machines, considering a uniform airgap (NSP = nonsalient-pole); curves 3 represent the actual armature fluxes in the direct ( $\phi_{ad}$ ) and quadrature-axis ( $\phi_{aq}$ ) for salient-pole machines, and curves 4 depict the fundamental frequency components of armature fluxes in the direct ( $\phi_{adm}$ ) and quadrature-axis ( $\phi_{aqm}$ ) for salient-pole machines. The slots and teeth effects were neglected.

**a.1) The Generator Supplies a Resistive Load ( $\psi = 0$ ).** Considering the current in phase a with its maximum value, the currents in phases b and c will have half of their maximum values. The current in phase a is in phase with the generated EMF  $E_f$  ( $\psi = 0$ ), there is no armature reaction demagnetizing or magnetizing effect, because the armature MMF has its symmetry axis coincident with the quadrature (interpolar)-axis and the resultant magnetic flux is distorted. The field flux has an increase under the trailing pole tips and a decrease, by the same amount (neglecting the effect of saturation), under the leading pole tips. This is called the cross-



magnetizing effect as the armature flux crosses the field flux perpendicularly. However, due to magnetic saturation the resultant flux decreases and the resultant EMF  $E_r$  is less than the excitation voltage  $E_f$ .

a.2) **The Generator Supplies a Pure Inductive/Capacitive Load ( $\psi = \pm 90^\circ$ ).** In this case the current differs in phase from  $E_f$  by  $\psi = \pm 90^\circ$ , the cross-magnetizing effect vanishes, and the entire armature MMF is demagnetizing if  $\psi$  is an angle of lag, i.e., the armature flux weakens the field flux and has only a direct-axis component; or the entire armature MMF is magnetizing if  $\psi$  is an angle of lead, i.e., the armature flux reinforces the field flux and has also a direct-axis component.

b) **Operation as a Motor.** In motoring action, for salient-pole motors the same conclusions as seen in the case of cylindrical-rotor synchronous motors apply for salient-pole rotor synchronous motors, i.e., when the current in a phase lags its excitation voltage a magnetizing effect appears on the field axis, which will increase the resulting voltage, unless the DC field current decreases, decreasing  $F_f$  and maintaining  $\bar{E}_r$  constant. Reciprocally, when the current in a phase is ahead of  $\bar{E}_r$  a demagnetizing effect appears and to maintain constant  $\bar{E}_r$  the DC field current must decrease. These effects are called the direct-axis armature reaction for motoring action. In both of these situations there will be a component of the armature MMF  $F_a$  that is perpendicular to the field axis MMF  $F_f$  and causes distortion and reduction (because of saturation effect) in the resultant magnetic field. This is called the cross-magnetizing effect of the armature reaction. However, if the angle between the armature current and the excitation voltage  $\psi = \pm 90^\circ$  there will be no cross-magnetizing effect of the armature reaction.

#### Phasor Diagrams and Equations for Salient-Pole Rotor Machines

a) **Operation as a Generator.** A method for obtaining the phasor diagram of a salient-pole machine was developed from the Blondel diagram by Doherty and Nickle, and consists of representing, in the same diagram, the EMFs due to each flux in the machine, as shown in Fig. 6.17.

With respect to Fig. 6.17 the following equations can be written

$$\begin{aligned} \dot{E}_f + \dot{E}_{aq} + E_{ad} - \dot{E}_r &= 0 \Rightarrow \dot{E}_{aq} = -j\dot{I}_q X_{\varphi q} \\ \Rightarrow \dot{E}_{ad} &= -j\dot{I}_d X_{\varphi d}, \end{aligned} \quad (6.55)$$

where  $X_{\varphi q}$  and  $X_{\varphi d}$  are called the direct and quadrature-axis magnetizing or armature reaction reactance's, re-

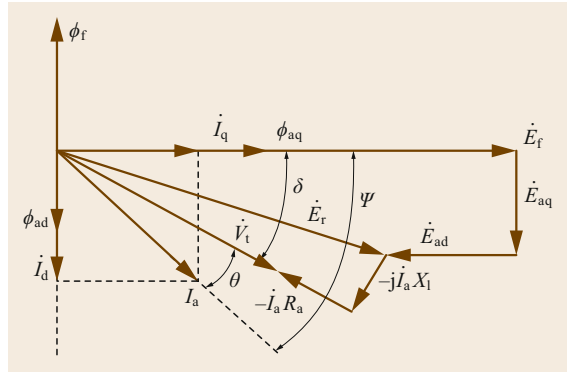


Fig. 6.17 Modified phasor diagram showing fluxes and EMFs of a salient-pole generator supplying an inductive load

spectively. They take into account the inductive effects of the direct ( $\phi_{ad}$ ) and quadrature-axis ( $\phi_{aq}$ ) fluxes. Thus

$$\begin{aligned} \dot{E}_f &= \dot{E}_r + j\dot{I}_q X_{\varphi q} + j\dot{I}_d X_{\varphi d} \\ \text{and } \dot{E}_r &= R_a \dot{I}_a + jX_1 \dot{I}_a + \dot{V}_t. \end{aligned} \quad (6.56)$$

As

$$\begin{aligned} \dot{I}_a &= \dot{I}_d + \dot{I}_q \\ \Rightarrow \dot{E}_f &= \dot{V}_t + \dot{I}_a R_a + j\dot{I}_d (X_{\varphi d} + X_1) + j\dot{I}_q (X_{\varphi q} + X_1). \end{aligned} \quad (6.57)$$

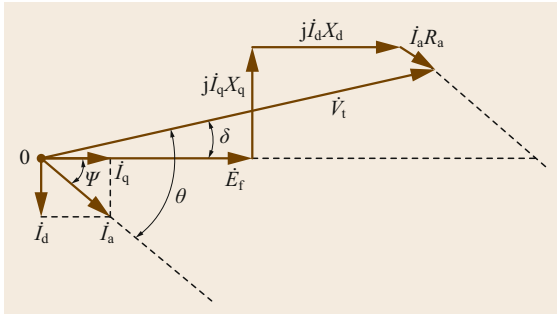
Defining:

$X_d = X_{\varphi d} + X_\lambda$  (direct-axis synchronous reactance)  
 $X_q = X_{\varphi q} + X_\lambda$  (quadrature-axis synchronous reactance),

$$\dot{E}_f = \dot{V}_t + \dot{I}_a R_a + j\dot{I}_d X_d + j\dot{I}_q X_q. \quad (6.58)$$

In machines larger than 100–200 kW, the resistance is usually small enough to be neglected. In salient-pole machines the reactance  $X_q$  is less than the reactance  $X_d$  because of the greater reluctance of the airgap in the quadrature-axis. Usually  $X_q = 0.6\text{--}0.7$  of  $X_d$ .

In turbogenerators a small salient-pole effect is present, even though they are cylindrical-rotor machines, because of the effect of the rotor slots in the quadrature-axis reluctance, which causes a slightly longer average airgap in this axis than in the direct-axis, and as a consequence the permeance in the quadrature-axis will be lower than in the direct-axis, and  $X_q$  is slightly smaller than  $X_d$ . However, in most problems involving cylindrical-rotor machines,  $X_d$  and  $X_q$  may be assumed equal with negligible error.



**Fig. 6.18** Phasor diagram of a salient-pole synchronous motor—lagging current

**b) Operation as a Motor.** For a motor the procedure is similar to obtaining the phasor diagram for a generator, but adopting the convention of an armature current entering into the machine. Thus, in the equations for the operation as a generator the armature current must be considered negative. In this case the excitation voltage is given by

$$\dot{E}_f = \dot{V}_t - \dot{I}_a R_a - j\dot{I}_d X_d - j\dot{I}_q X_q. \quad (6.59)$$

The phasor diagram for a lagging current is shown in Fig. 6.18, where it can be noted that  $V_t$  is ahead of  $E_f$  and the angle  $\delta$  is negative.

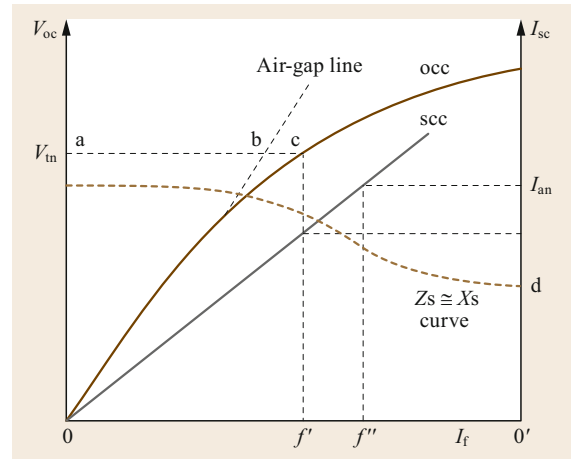
### 6.1.6 Open and Short-Circuit Characteristics

The synchronous impedance/direct-axis reactance's, for cylindrical-rotor and salient-pole rotor machines, can be obtained by the open and short-circuit characteristics. In addition, machine losses are obtained, that makes it possible to calculate its efficiency.

#### Open-Circuit Characteristic and No-Load Rotational Losses

The open-circuit characteristic (OCC) is obtained, with the machine rotating at synchronous speed, and with the armature terminals open, by reading the values of the terminal armature voltage as ordinate, and the field current as abscissa. The general shape of the OCC is the same in all synchronous machines, but the slope of the air-gap line and the rate at which the OCC bends over will differ in machines of different design. The air-gap line is the extended straight line part of the OCC. This characteristic is shown in Fig. 6.19, together with the short-circuit characteristic and the synchronous impedance reactance curve.

At low values of field excitation the OCC is a straight line because the MMF required for the iron parts of the magnetic path is negligible in comparison with the MMF needed to maintain the flux in the airgap



**Fig. 6.19** Open and short-circuit characteristics, with air-gap line and the synchronous impedance curve

between the rotor and stator. The field excitation necessary to induce rated (nominal) terminal voltage  $V_{tn}$  in the stator winding is equal to ac. The ab part corresponds to the excitation MMF necessary to drive the flux through the airgap, and the bc part is necessary to drive the flux through the iron parts of the magnetic path.

If the mechanical power is measured during the open-circuit test [6.10], the open-circuit or no-load rotational losses ( $P_{rot}$ ) can be determined. No-load rotational losses comprise the sum of the no-load core losses ( $P_c$ ) with the mechanical losses.

The no-load core losses consist of hysteresis and eddy current losses due to excitation flux, which induces in the armature the open-circuit voltage, and are confined largely to the armature iron, although the flux pulsations arising from slot openings will cause losses on the pole surfaces, as well as on an iron surface in salient-pole machines and on the surface of the solid rotor in cylindrical-rotor machines.

Mechanical losses are the sum of losses due to friction in the bearings and brushes ( $P_a$ ), with the loss due to windage ( $P_w$ ), i.e., the machine loss due to the resistance offered by air (salient-pole machines) or hydrogen (cylindrical-rotor machines) to the rotation of the shaft. The losses due to friction and windage are constant at synchronous speed. Bearing friction losses depend on the first power of shaft speed, bearing type, properties of the lubricant and the load on the bearing. Windage losses depend on the density of the coolant (air/hydrogen) surrounding the rotor, machine geometry, surface roughness, torque coefficient, and increases with the cube of rotor speed. Due to the cubic relationship with speed, windage is an important loss to manage in the design of high speed machines. The use

of hydrogen instead of air as a cooling medium reduces the windage losses to about 10% of those which appear with air. Thus

$$P_{\text{rot}} = P_a + P_w + P_c. \quad (6.60)$$

With zero excitation,  $P_c = 0$  and the no-load rotational losses are the sum of  $P_a$  and  $P_w$ . With nonzero excitation the  $P_c$  can be obtained from the difference between the mechanical power and the sum of  $P_a$  and  $P_w$ . The no-load core loss  $P_c$  may be plotted as a function of armature voltage.

### Short-Circuit Characteristic and Short-Circuit Load Losses

If the armature terminals of a synchronous machine that is operating as a synchronous speed generator are short-circuited and armature current  $I_a$  and excitation current  $I_f$  readings are obtained, the losses caused by the armature current are obtained.

The mechanical power ( $P_m$ ) supplied by the machine during the short-circuit test is equal to the sum of the losses due to friction in the bearings and brushes ( $P_a$ ), the losses due to windage ( $P_w$ ) and the losses caused by the armature current ( $P_{\text{la}}$ ) (also referred to as short-circuit load losses). Thus

$$P_{\text{la}} = P_m - (P_a + P_w). \quad (6.61)$$

The short-circuit load losses due to  $I_a$  are in turn the sum of the losses in the copper in the armature windings considering the value of the DC armature resistance and the additional losses, also called stray-load losses.

The stray-load losses are equal to the sum of the losses in the core of the armature due to the leakage flux, the losses in the core of the armature and rotor due to the resulting flux and the increase of the losses in the copper due to nonuniform distribution of the current in the conductors, i.e., the difference between the copper losses of the armature due to alternating current and direct current. As seen in short-circuit the resulting flux is very small and the losses in the core due to it are usually neglected.

Copper losses of the armature due to direct current (DC) resistance can be calculated if this resistance is known for a certain temperature  $t$  by measuring the average winding temperature of the armature  $T$  during the test by the formula

$$\frac{R_T}{R_t} = \frac{K + T}{K + t}, \quad (6.62)$$

where  $K = 234.5^\circ\text{C}$  for copper conductors.

Thus, by subtracting from the short-circuit losses, the losses in the DC resistance of the armature, we obtain the stray-load losses due to  $I_a$  ( $P_{\text{ad}}$ ). As in any equipment, the effective resistance of the armature is equal to the losses attributed to the current of the armature divided by the square of the current. Generally, the rated value is used for  $I_a$ , and

$$R_a(\text{effective}) = \frac{\text{short-circuit load loss}}{I_a^2}. \quad (6.63)$$

### Determination of Synchronous Impedance/Reactances and Short-Circuit Relation

*a) Determination of Synchronous Impedance/Reactances.* For a cylindrical-rotor machine on short-circuit the excitation voltage is  $\dot{E}_f = (R_a + jX_s)\dot{I}_a$ , where  $\dot{I}_a$  is the armature current. Its amplitude is  $|\dot{E}_f| = Z_s |\dot{I}_a|$ , where  $Z_s = \sqrt{R_a^2 + X_s^2}$  is the synchronous impedance.

For a salient-pole machine on short-circuit, also from Sect. 6.1.6,

$$\begin{aligned} \dot{E}_f &= \dot{I}_a R_a + j\dot{I}_d X_d + j\dot{I}_q X_q \\ &= \dot{I}_a R_a + j\dot{I}_a X_d \quad \text{as } \dot{I}_q = 0. \end{aligned}$$

$$\text{Then, } \dot{I}_d = \dot{I}_a. \quad (6.64)$$

If the value of the voltage from the no-load characteristic is divided by the value of the current obtained from the short-circuit characteristic for the same value of field excitation, the synchronous impedance  $Z_s$  is obtained. Considering other points for the field excitation, and assuming the same open-circuit characteristic for a cylindrical-rotor and a salient-pole machine, the synchronous impedance curve may be found, where

$$Z_s = \sqrt{R_a^2 + X_s^2}$$

for a cylindrical-rotor machine

$$\text{and } Z_s = \sqrt{R_a^2 + X_d^2}$$

for a salient-pole machine. (6.65)

The  $Z_s$  curve is constant only in the unsaturated part of the open-circuit characteristic, and decreases with increasing excitation.

Considering  $R_a$  neglected in relation to synchronous reactance

$$X_s \quad \text{or} \quad X_d = \frac{|\dot{E}_f|}{|\dot{I}_a|}. \quad (6.66)$$

Thus, the saturated values of the synchronous reactance  $X_s$  for cylindrical-rotor machines and of the direct-axis

synchronous reactance  $X_d$  for salient-pole machines are obtained. To find the unsaturated values for these reactances, the voltage on open-circuit, before the short-circuit, should be taken from the airgap line, instead of the open-circuit characteristic. The unsaturated values for these reactances are always greater than their saturated values.

**b) Determination of Short-Circuit Ratio (SCR).** The SCR of a synchronous generator is defined in the IEC 60034-4 [6.11] standard as “The ratio of the field current for rated armature voltage on open-circuit (OC) to the field current for rated armature current on sustained symmetrical short-circuit, both with the machine running at rated speed”. The short-circuit ratio is the inverse of the saturated value of the synchronous reactance in p.u. From Fig. 6.20

$$\text{SCR} = \frac{\text{OF}_O}{\text{OF}_S} = \frac{\text{CF}_O}{\text{BF}_S} = \text{CF}_O \quad \text{in p.u.}, \quad (6.67)$$

where:

$\text{OF}_O$  = p.u. field current required to develop rated voltage on the open-circuit characteristic (OCC)

$\text{OF}_S$  = p.u. field current required to develop rated current on the short-circuit characteristic (SCC)

$\text{CF}_O$  = p.u. sc armature current, also herein designated as  $I'_a$

$\text{BF}_S$  = p.u. rated armature voltage on open-circuit (OC).

The armature resistance is very small when compared with the synchronous reactance, so for a short-circuit at the machine terminal the short-circuit current may be considered totally inductive and the impedance seen by the machine is  $X_s$  for a nonsalient-pole machine

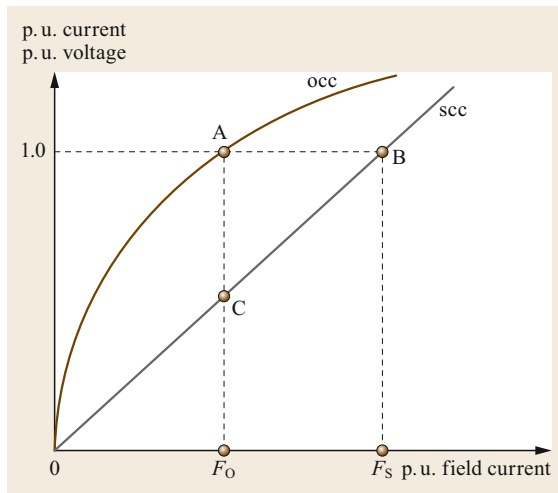


Fig. 6.20 Determination of short-circuit ratio (SCR)

(NSPM – round rotor) or  $X_d$  for a salient-pole machine (SPM).

For operation near or at the rated voltage the machine may be considered as equivalent to a nonsaturated machine whose magnetizing curve is a straight line passing through the points O and A. According to this approximation and supposing the same graphic for nonsalient and salient-pole machines,

$$\begin{aligned} X_s \text{ (p.u.)} &= X_d \text{ (p.u.)} = (V_{tn}/V_{tn})/(I'_a/I_{an}) = I_{an}/I'_a \\ &= I'_a \text{ in p.u.}, \end{aligned}$$

where  $I'_a$  in p.u. =  $\text{CF}_O$  in p.u. Therefore, the SCR is equal to the inverse of the synchronous reactance in p.u.

$$\begin{aligned} \text{SCR} &= \frac{1}{X_s \text{ p.u. (sat)}} \quad (\text{NSPM}) \\ &= \frac{1}{X_d \text{ p.u. (sat)}} \quad (\text{SPM}). \end{aligned} \quad (6.68)$$

Note that these values of reactances are saturated values.

### 6.1.7 Efficiency

The efficiency is equal to the ratio of output power to machine-supplied power. In small machines, such as those used in laboratories, these powers are obtained by measurement. On larger machines where mechanical power cannot be measured accurately, the efficiency is calculated on the basis of the losses obtained in the tests performed to obtain the characteristics of open-circuit and of short-circuit. The following losses are considered:

- Friction and windage loss
- Core losses due to the resulting (voltage) flux
- Stray-load loss
- Joule losses of armature winding, using the direct current resistance
- Resistive losses of field winding
- Ventilation and cooling losses.

It should be noted that only losses in the field winding are computed. The rheostat loss (if the excitation is provided by a rotary exciter) and the thyristor bridge loss (if the excitation is provided by a static exciter), that controls the field current, and all losses in external sources that supply excitation to the machine are not considered in the determination of machine efficiency. These losses are charged against the plant.

The values of  $I_a$  and  $I_f$  to be used in calculating copper losses are those for the operating conditions of the

machines in which it is desired to calculate their efficiency, in general, for the nominal operating condition. If the temperature values of field windings and armature are not obtained, a conventional value of 75 °C should be used.

For a synchronous machine the efficiency  $\eta$ , in percentage, is calculated by the expression

$$\eta(\%) = \left( 1 - \frac{\sum \text{losses}}{\text{output power} + \sum \text{losses}} \right) \times 100. \quad (6.69)$$

The core loss is obtained from the loss curve with the machine on open-circuit (Sect. 6.1.6), using the resulting voltage in the armature due to the resulting flux, for the operating conditions of the machine on which the efficiency is to be calculated. For generators,

$$\dot{E}_r = \dot{V}_t + \dot{I}_a R_a + j\dot{I}_a X_l. \quad (6.70)$$

As the stray-load loss already takes into account the core loss due to the leakage flux, the term  $j\dot{I}_a X_l$  is neglected in (6.70), therefore the voltage  $\dot{E}_r = \dot{V}_t + \dot{I}_a R_a$  is used to calculate the core loss. For the case of motors the resulting voltage to be considered in the core loss calculation is

$$\dot{E}_r = \dot{V}_t - \dot{I}_a R_a. \quad (6.71)$$

The ventilating and cooling loss includes any power required to circulate the cooling medium through the machine (if used) by fans or pumps that are driven by external means (such as a separate motor), so that their power requirements are not included in the friction and windage loss.

## 6.1.8 Reactances and Time Constants

### Reactances

The choice of base field current as the current required to produce rated voltage at rated speed on the airgap line is convenient for constructing phasor diagrams, but not for including the effects of currents in rotor circuits additional to the field circuit. This can best be done by defining base currents for each rotor winding so that the mutual inductances in per-unit between stator and rotor in the direct-axis are equal and the mutual inductances in per-unit between stator and quadrature-axis are also equal.

For the stator the base quantities are maintained, i.e., rated apparent power, rated voltage and rated frequency, from which other base quantities like impedance, current and flux linkage are derived. For a comprehensive

treatment of the per-unit system and equivalent circuits of synchronous machines see [6.12–14].

Unbalanced operation and faults conditions are usually analyzed by the method of symmetrical components by defining expressions for the reactances according to each sequence component of the method, which are presented hereafter.

**a) Positive-Sequence Reactances.** If positive-sequence currents of rated frequency are applied to the armature, a fundamental space wave of magnetomotive force (MMF) is produced that rotates forward in synchronism with the rotor. The airgap permeance offered to this MMF wave depends upon its position relative to the poles and whether the armature currents are suddenly applied or are sustained, and, if suddenly applied, whether the machine has a damper winding.

**a.1) Direct-Axis Synchronous Reactance  $X_d$  and Quadrature-Axis Synchronous Reactance  $X_q$ .** Designating the magnetizing reactance in the direct-axis  $X_{qd} = X_{ad}$  and the magnetizing reactance in the quadrature-axis  $X_{qq} = X_{aq}$  (Sect. 6.1.5),

$$X_d = X_{ad} + X_l \quad \text{and} \quad X_q = X_{aq} + X_l. \quad (6.72)$$

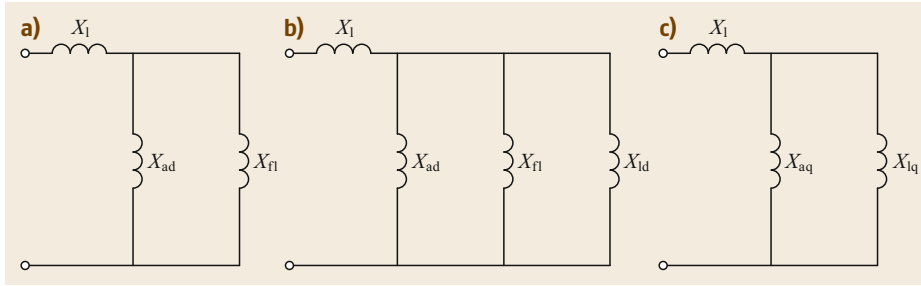
These two-reactances take into account the inductive effects of the fluxes due to the armature current.

**a.2) Direct-Axis Transient Reactance  $X'_d$  and Subtransient Reactance  $X''_d$ .** If field currents are expressed in the reciprocal per-unit system,  $X'_d$  may be determined from the per-unit reciprocal equivalent circuit of Fig. 6.21a, where  $X_{fl}$  is the field leakage reactance,  $X_{ff}$  is the total field reactance,  $X_l$  is the armature leakage reactance, and  $X_{ad}$  is the mutual reactance between armature and field. Direct-axis transient reactance  $X'_d$ , which is a reactance viewed from the armature terminals is given by

$$\begin{aligned} X'_d &= X_l + \frac{X_{ad} X_{fl}}{X_{ad} + X_{fl}} = X_l + \frac{X_{ad} (X_{ff} - X_{ad})}{X_{ff}} \\ &= X_d - \frac{X_{ad}^2}{X_{ff}}. \end{aligned} \quad (6.73)$$

It should be noted that direct-axis synchronous reactance  $X_d$  is obtained by opening the field leakage reactance branch  $X_{fl}$  of Fig. 6.21a.

Direct-axis subtransient reactance  $X''_d$  may be determined from the equivalent circuit of Fig. 6.21b, in which the damper winding in the direct-axis is represented as an equivalent single winding having a leakage reactance  $X_{1d}$ . This circuit, based on the assumption that the mutual reactances between armature and field, between armature and damper, and between damper and



**Fig. 6.21 (a-c)** Reciprocal per-unit equivalent circuits for armature and rotor circuits for determining  $X'_d$ ,  $X''_d$  and  $X'_q$ , respectively

field are all equal to  $X_{ad}$ . The direct-axis subtransient reactance  $X''_d$  is given by

$$X''_d = X_l + \frac{X_{ad}X_{fl}X_{ld}}{X_{ad}X_{fl} + X_{ad}X_{ld}X_{fl}X_{ld}} \quad (6.74)$$

**a.3) Quadrature-Axis Transient Reactance  $X'_q$  and Subtransient Reactance  $X''_q$ .** Consider a salient-pole machine without a damper winding. With the rotor rotated at synchronous speed, let the positive-sequence quadrature-axis currents of rated frequency be suddenly applied. The voltages induced in one-half of the field winding balance those induced in the other half, so that no currents are induced in the rotor circuit. The flux paths under this condition are the same as those for sustained conditions, i.e., there will be no linkage with the field winding. Thus, the quadrature-axis subtransient, transient and synchronous reactances are equal, i.e.,

$$X'_q = X''_q = X_q = X_l + X_{aq} \quad (6.75)$$

where  $X_l$  is the leakage reactance and  $X_{aq}$  is the quadrature-axis magnetizing or quadrature-axis armature reaction reactance.

In the case of a salient-pole machine with a damper winding, quadrature-axis subtransient reactance  $X''_q$  may be determined from the equivalent circuit of Fig. 6.21c, in which the  $X_{aq}$  is the mutual reactance between the armature and rotor circuit in the quadrature-axis and  $X_{lq}$  represents the leakage reactance of the damper winding of a salient-pole machine or the analogous effect in a cylindrical-rotor machine. Viewed from the armature terminals,

$$X''_q = X_l + \frac{X_{aq}X_{lq}}{X_{aq} + X_{lq}} \quad (6.76)$$

In a salient-pole-machine a representation with one damper winding on each axis has been considered satisfactory.

For cylindrical-rotor (turbogenerator) machines the eddy current paths in the iron can be considered as a squirrel cage having an infinite number of bars, and

require an infinite number of damper coils for their representation. Thus, the representation of Fig. 6.21c is an approximation. However, if data is available, a second damper winding with reactance  $X_{2q}$  in parallel to  $X_{lq}$  can be represented in Fig. 6.21c, so that transient and subtransient effects can be both considered. In this case  $X'_q > X''_q$ .

**b) Negative-Sequence Reactance.** The rotating space wave of MMF produced by rated-frequency armature currents of negative-sequence order differ from those due to positive-sequence phase order in their direction of rotation, i.e., it rotates backward at twice the synchronous speed with respect to the rotor. As this MMF wave passes rapidly over each axis of the poles, the permeance presented varies rapidly from that in the direct and quadrature-axis, the reactance corresponding alternately to direct and quadrature-axis subtransient reactances. Thus, the negative-sequence reactance  $X_2$  is given by

$$X_2 = \frac{X''_d + X''_q}{2} \quad (6.77)$$

**c) Zero-Sequence Reactance.** If zero-sequence currents of fundamental frequency are applied to a three-phase machine, the MMF waves in all phases pulsate in phase and produce a stationary field that alternates at the fundamental frequency. When the equations for each phase are added the fundamental and all harmonic space MMF waves, that pulsate at the fundamental frequency disappear, except the third harmonic MMF and multiples of the third. At other than full pitch, the coil sides in some of the slots carry currents in opposite directions and the slot, airgap, and end-leakage fluxes are all small. The zero-sequence reactance may vary greatly, depending upon the coil pitch, but it is never greater than positive-sequence armature leakage reactance and may be less than half of it.

**d) Effect of Saturation on Machine Reactances.** Both the saturated synchronous reactance  $X_s$  of a cylindrical-rotor machine and the saturated direct-axis syn-

chronous reactance  $X_d$  of a salient-pole machine may be obtained according to Sect. 6.1.6, as well their unsaturated reactances. Concerning the quadrature-axis synchronous reactance  $X_q$  the usual assumption is that it is not affected by saturation. This assumption is suitable especially where external impedance is associated with the machine. Nevertheless, its saturated value may be obtained by testing.

The direct-axis transient and subtransient reactances  $X'_d$  and  $X''_d$  are predominantly determined by armature leakage and field or damper-winding leakage, although magnetizing or mutual reactances also enter. They are therefore influenced by saturation to a lesser extent than is  $X_d$ . Usually two values of each reactance are available. One, called the rated-voltage, or saturated value, is determined from short-circuit tests in which the field current is adjusted to give a pre-fault terminal voltage at or near the rated machine voltage. The other, called the rated-current value or unsaturated value is also found from short-circuit tests in which the field current is reduced so that the initial symmetrical transient or subtransient current is equal to the rated current. The rated-voltage value of these reactances is usually 10–15% lower than the rated-current value. The choice between them depends on the specific application. For studies involving circuit-interruption duties, protective relay settings, and short-circuit stresses, the rated-voltage value ordinarily is used. For stability studies, the rated-current value is usually employed because it leads to conservative synchronizing powers and torques.

The saturated value and unsaturated value of  $X'_q$  may be obtained by test, while specifically for cylindrical-rotor machines the saturated value of  $X'_q$  is around 87% of its unsaturated value.

### Time Constants

In a synchronous machine, because the coupling between armature and rotor circuits differ in the direct and quadrature-axis, there are direct-axis and quadrature-axis time constants. Subtransient time constants apply to rapidly decreasing components and transient time constants to slowly decreasing components of current or voltage. There is also the time constant of the armature winding which applies to DC armature current and to the alternating current induced in the field winding. It should be noted that when defining time constants, resistances are added in Fig. 6.21, in series with the respective leakage winding reactances, as:  $R_f$ , in series with  $X_{fl}$ ,  $R_{1d}$  in series with  $X_{1d}$  and  $R_{1q}$  in series with  $X_{1q}$ , being  $\omega = 2\pi f$  and armature resistance neglected, except when determining the armature time constant.

### a) Open-Circuit Time Constants.

a.1) Direct-Axis Transient Open-Circuit Time Constant  $T'_{d0}$ . The change of field current in response to sudden application, removal, or change of EMF in the field circuit, with the armature open-circuit, is governed by the field open-circuit time constant, or direct-axis transient open-circuit time constant, given by

$$T'_{d0} = \frac{X_{ff}}{\omega R_f} . \quad (6.78)$$

a.2) Direct-Axis Subtransient Open-Circuit Time Constant  $T''_{d0}$ . This determines the decrement curve of the rapidly decreasing component of the quadrature-axis fundamental frequency armature voltage, after the sudden removal of a three-phase short-circuit, with the machine running at synchronous speed. It is given by

$$T''_{d0} = \frac{X_{1d} + X_{fl}X_{ad}/(X_{fl} + X_{ad})}{\omega R_{1d}} . \quad (6.79)$$

a.3) Quadrature-Axis Transient and Subtransient Open-Circuit Time Constants  $T'_{q0}$  and  $T''_{q0}$ . These time constants are analogous to  $T'_{d0}$  and  $T''_{d0}$  the difference being that they are defined in terms of components of voltage in the direct-axis instead of in the quadrature-axis. The quadrature-axis transient open-circuit time constant  $T'_{q0}$  has no significance in a salient-pole machine, as there is no low resistance winding in the quadrature-axis which corresponds to the field winding in the direct-axis. In the case of a cylindrical-rotor machine represented as two damper windings in the quadrature-axis, both constants  $T'_{q0}$  and  $T''_{q0}$  may be defined, however with the consideration of just one damper winding in the quadrature-axis the induced currents are of a subtransient nature, and the subtransient time constant  $T''_{q0}$  is

$$T''_{q0} = \frac{X_{1q} + X_{aq}}{\omega R_{1q}} . \quad (6.80)$$

### b) Short-Circuit Time Constants.

b.1) Direct-Axis Transient and Subtransient. The time constant  $T'_d$  governs the slowly decreasing component of the AC armature current under a suddenly applied symmetrical three-phase short-circuit at the armature terminals, while the time constant  $T''_d$  applies to the rapidly decreasing component. They are given by

$$T'_d = \frac{X_{fl} + X_l X_{ad}/(X_l + X_{ad})}{\omega R_f} = T'_{d0} \frac{X'_d}{X_d} , \quad (6.81)$$

$$T_d'' = \frac{X_{1d} + X_l X_{fl} X_{ad} / (X_{ad} X_l + X_{ad} X_{fl} + X_l X_{fl})}{\omega R_{1d}}$$

$$= T_{d0}'' \frac{X_d''}{X_d'} \quad (6.82)$$

### b.2) Quadrature-Axis Transient and Subtransient.

If a synchronous machine is operated under load, there will be flux mutual to the armature and rotor current in the quadrature-axis; therefore, if a three-phase short-circuit is suddenly applied under load there will be quadrature-axis AC components of current which decrease rapidly in accordance with the quadrature-axis subtransient short-circuit time constant  $T_q''$ , and then less rapidly in accordance with the quadrature-axis transient short-circuit time constant  $T_q'$ .  $T_q'$  and  $T_q''$  are analogous to  $T_d'$  and  $T_d''$ , respectively, except that they apply to components of current in the quadrature-axis of the AC component of armature current.  $T_q'$  is applied only for a cylindrical-rotor machine with two damper circuits represented. For the representation of Fig. 6.21c, then

$$T_q'' = \frac{X_{1q} + X_{aq} X_l / (X_{aq} + X_l)}{\omega R_{1q}} = T_{q0}'' \frac{X_q''}{X_q'} \quad (6.83)$$

c) *Armature Short-Circuit Time Constant  $T_a$ .* The time constant  $T_d'$  governs the decay of the DC armature current and the alternating currents induced by it in the field and damper windings, under a suddenly applied symmetrical three-phase short-circuit at the armature terminals. It depends on the DC armature resistance and the inductive coupling between armature, field and damper circuits. As the rotor revolves the DC stationary MMF created by the armature currents passes by the direct and quadrature-axis rotor circuits, so that the equivalent reactance seen by the MMF wave, on an intuitive basis, may be considered as an arithmetic mean of  $X_d''$  and  $X_q''$ . Thus,

$$T_a = \frac{X_d'' + X_q''}{2\omega R_a} \quad (6.84)$$

d) *Relations Between Time Constants.* From the previous values of time constants the followings relations can be derived

$$T_d' = T_{d0}' \frac{X_d'}{X_d}, \quad T_d'' = T_{d0}'' \frac{X_d''}{X_d'}, \quad T_q'' = T_{q0}'' \frac{X_q''}{X_q'} \quad (6.85)$$

### Poitier Reactance

The armature leakage reactance can not be obtained by testing. It is determined from geometric and physical details usually only available to the designer, while

the manufacture can provide its value. However, from the Poitier diagram it is possible to obtain a reactance called Poitier reactance, that is an approximate value for the leakage reactance. For this it is necessary to have the open-circuit (OCC) and the zero-power factor characteristics (ZPFC). This latter characteristic may be obtained from testing with the generator connected to a reactor whose reactance may be varied or to an idle synchronous motor, so that the current in the machine is maintained constant and equal to the rated value  $I_{an}$ , while the field current is adjusted to give various values of terminal voltage, including nominal voltage  $V_{tn}$ . In the case of a large machine tested in a power station, the desired test to obtain the Poitier diagram, may be done with its active power loading close to zero, by redistribution of its reactive power loading among other machines on the same bus or system, without removing them from service. The armature MMF under nominal current can be obtained from this test.

### Additional Considerations

Testing for reactances and time constants is performed by applying a three-phase fault on the machine terminals with the machine unloaded and on open-circuit. Values obtained from such tests are direct-axis values. Quadrature-axis transient and subtransient values can be calculated, but can not be tested by tests from open-circuit pre-fault conditions. IEC 60034-4 [6.11] describes unconfirmed tests for determining transient and subtransient quadrature-axis synchronous machine characteristic values.

In recent years standstill frequency response testing based on impedance measurements has been developed to obtain parameter values for the elements of the direct and quadrature-axis equivalent circuits. These tests are made with the rotor held stationary and by appropriate alignment of the rotor, the armature is excited with variable frequency currents ranging from as low as 0.001 to around 100 Hz, and the corresponding impedance is measured. These impedances correspond to the input impedances of direct and quadrature-axis equivalents such as those of Fig. 6.21. Experience has shown that for certain types of analysis, models based on frequency measurements may exhibit increased accuracy over analysis based on parameters obtained by the traditional methods. Difficulties with such tests include the fact that measurements are made at low excitation levels and the fact that contact resistances of the rotor elements such as slot wedges and retaining rings are different when the rotor is stationary from when the rotor is rotating and centrifugal forces are acting on them. Many discussions of modeling are found in the growing literature on synchronous machines.



**Table 6.3** Synchronous machine reactances and resistances in per unit based on rating

Reactance/resistance	Turbogenerators		Salient-pole generators (with dampers)	
	Nonsaturated	Saturated	Nonsaturated	Saturated
$X_d$	1.49–1.87	1.35–1.65	0.70–1.50	0.60–0.95
$X_q$	1.45–1.83	1.32–1.60	0.52–1.00	0.45–0.85
$X_l$	0.11–0.20		0.11–0.20	
$X'_d$	0.19–0.30	0.17–0.27	0.20–0.40	0.16–0.34
$X'_q$	0.19–0.30	0.17–0.27	0.25–0.80	0.20–0.65
$X''_d$	0.11–0.25	0.10–0.22	0.16–0.35	0.13–0.30
$X''_q$	0.12–0.26	0.11–0.23	0.25–0.45	0.20–0.38
$X_2$	0.11–0.25	0.10–0.22	0.20–0.40	0.17–0.34
$X_0$	0.01–0.15	0.01–0.13	0.05–0.18	0.04–0.15
$R_a$ (ca)	0.0030–0.0070		0.0035–0.0160	
$R_a$ (dc)	0.0020–0.0070		0.0030–0.0180	
$R_2$	0.0280–0.0430		0.0100–0.1800	

**Table 6.4** Synchronous machine time constants

Time constant	$T'_{d0}$	$T''_{d0}$	$T'_d$	$T''_d$	$T''_{q0}$	$T''_q$	$T_a$
Turbogenerators	4–12	0.02–0.06	1–2	0.02–0.05	0.02–0.06	0.02–0.05	0.04–0.36
Salient-pole generators (with dampers)	3–8	0.01–0.06	1.5–3	0.01–0.05	0.01–0.09	0.01–0.05	0.03–0.25

Tables 6.3 and 6.4 show the range of typical values of reactances, resistances and time constants. It is to be noted that these values indicate usual values of parameters, although exceptions may be found depending on individual machine design.

For salient-pole machines without damper windings  $X''_q = X'_q = X_q$  and  $X_2 = (X'_d + X_q)/2$ .

### 6.1.9 Power Angle Characteristic of Synchronous Machines

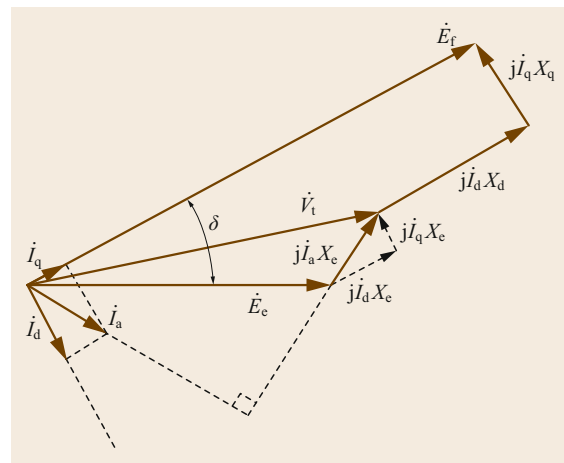
The expressions for the active and reactive power supplied by a salient-pole generator at an infinite bus through an external reactance will be derived. It will be assumed that the generator is connected to the infinite bus by an external reactance  $X_e$ . From these expressions the equations for a nonsalient-pole (round rotor) machine are derived. The expressions including the armature and external resistances will be presented.

#### Operation as a Salient-Pole Generator (SPG)

Figure 6.22 shows the phasor diagram for a salient-pole generator supplying an inductive load, and connected to an infinite bus by an external reactance  $X_e$ .

The active power, in p.u., supplied to the infinite bus, neglecting resistances, is

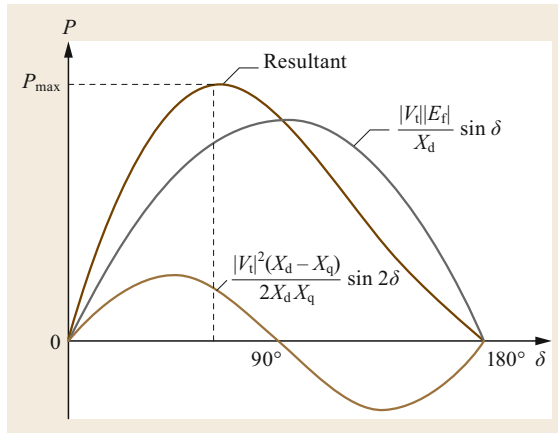
$$\begin{aligned}
 P &= P_f + P_r = \frac{E_f E_c}{X_D} \sin \delta + E_c^2 \frac{X_D - X_Q}{2X_D X_Q} \sin 2\delta \\
 &= P_{f\max} \sin \delta + P_{r\max} \sin 2\delta, \quad (6.86)
 \end{aligned}$$

**Fig. 6.22** Phasor diagram for lagging power factor

where  $X_D = X_d + X_e$  and  $X_Q = X_q + X_e$  and the angle  $\delta$  is called the power angle, torque angle or load angle.

The resultant active power  $P$  at the infinite bus has two terms. The first  $P_f$  is the power due to the field excitation, designated as excitation power and the second  $P_r$  is the power due to the differences in direct-axis and quadrature-axis reluctances, designated as the reluctance power. Figure 6.23 shows these two terms and the resultant power for a salient-pole generator.

The electromagnetic power or internal active power  $P_e$ , i.e., the power that is converted from mechanical to electrical, is the power at the infinite bus plus the losses in the armature resistance  $R_a$  and external resistance  $R_e$ ,



**Fig. 6.23** Power-angle curve of a salient-pole generator including the operation as a motor with resistances neglected

when considered

$$P_c = P + I_a^2 (R_a^2 + R_c^2). \quad (6.87)$$

The expression for reactive power is

$$Q = \frac{E_c (E_f - E_c \cos \delta) \cos \delta}{X_D} - \frac{E_c^2 \sin^2 \delta}{X_Q}. \quad (6.88)$$

Taken into consideration the armature and external resistances

$$P = \frac{E_f E_c (R_E \cos \delta + X_Q \sin \delta) + E_c^2 \frac{X_D - X_Q}{2} \sin 2\delta - E_c^2 R_E}{R_E^2 + X_D X_Q}, \quad (6.89)$$

$$Q = \frac{E_f E_c (X_Q \cos \delta - R_E \sin \delta) - E_c^2 (X_D \sin^2 \delta + X_Q \cos^2 \delta)}{R_E^2 + X_D X_Q}, \quad (6.90)$$

where  $R_E = R_a + R_c$ .

Note that the salient-pole generator can supply active power without excitation ( $E_f = 0$ ). In this case,  $P_f = 0$  and the power is due to  $P_r$ , that is, to the reluctance power that is very small when compared to the excitation power. Under this condition, the machine will absorb capacitive power irrespective of the angle  $\delta$ . In this case the machine would have transient instability when the excitation is lost.

#### Operation as a Non-Salient-Pole Generator (NSPG)

In the case of a nonsalient-pole generator where  $X_D \cong X_q \Rightarrow X_D \cong X_Q$  and with resistances neglected, the active power is

$$P = \frac{E_f E_c \sin \delta}{X_D} \quad (6.91)$$

and the term  $E_c^2 (X_D - X_Q) \sin 2\delta / (2X_D X_Q)$  due to reluctance power is null. The reactive power is

$$Q = \frac{E_f E_c \cos \delta}{X_D} - \frac{E_c^2}{X_D}. \quad (6.92)$$

Considering the resistances

$$P = \frac{E_f E_c (R_E \cos \delta + X_D \sin \delta) - E_c^2 R_E}{R_E^2 + X_D^2}, \quad (6.93)$$

$$Q = \frac{E_f E_c (X_D \cos \delta - R_E \sin \delta) - E_c^2 X_D}{R_E^2 + X_D^2}. \quad (6.94)$$

When  $E_f$  goes to zero this time, the round-rotor machine cannot supply any real power to the system. Under this condition, however, the machine will still absorb a large amount of capacitive power irrespective of the angle  $\delta$  and it would have transient instability.

#### Maximum Power

For maximum power  $\Rightarrow dP/d\delta = 0$  and  $d^2P/d\delta^2 < 0$ . For a salient-pole generator

$$\begin{aligned} \frac{dP}{d\delta} &= \frac{d}{d\delta} (P_{f\max} \sin \delta + P_{r\max} \sin 2\delta) = 0 \Rightarrow \\ \cos \delta &= -\frac{E_f X_Q}{4E_c (X_D - X_Q)} \\ &\pm \sqrt{\left[ \frac{E_f X_Q}{4E_c (X_D - X_Q)} \right]^2 + \frac{1}{2}}. \end{aligned} \quad (6.95)$$

Only positive values of the radical, giving  $\delta < 90^\circ$ , will correspond to maximum power, the other root being greater than 1.0 is not considered. The maximum active power is obtained by replacing  $\delta$  in expression (6.86).

#### Additional Remarks

The maximum power of a salient-pole generator (SPG) occurs at a power angle below  $90^\circ$ , while for a round rotor generator (NSPG) the maximum power occurs when the power angle is  $90^\circ$ . The influence of the resistances in these power angles are practically none.

The rise of power with power angle, the so called synchronizing power coefficient— $dP/d\delta$ —used to be an indication of stability or instability in steady state conditions, which is associated with small variations in the operating point, but without the action of automatic controls, such as excitation systems and speed governors.

To assure stability the synchronizing power coefficient must have a positive value. In the case of

a salient-pole generator  $dP/d\delta$ , for the same angle  $\delta$ , is greater than for a round rotor generator making the machine stiffer.

A general study of power-system stability is outside the scope of this book. If complete system equations are investigated, the power limit found may be either greater or smaller depending on circumstances; and, on the other hand, if the system is said to be stable after the determination of a positive value of  $dP/d\delta$ , it is assumed that the system introduces no other torques, such as negative damping torques arising from terms depending on rotor speed than rotor angle, which might produce instability.

The phasor diagram shown in Fig. 6.22, for a salient-pole machine, brings out the dependence of the power-angle on the cross-armature reaction effect  $I_q X_q$  on which the torque depends; while the excitation required for given working conditions—that is, the length of  $E_f$ —is largely settled by the direct-armature reaction  $I_d X_d$ .

### 6.1.10 Parallel Operation of Synchronous Generators

Considering two equal round-rotor generators in parallel, supplying the same active power to a load or system, with constant terminal voltage  $V_t$ . In the general case if they are supplying different armature currents  $I_{a1}$  and  $I_{a2}$ , being  $Z_L$  the load impedance. This situation is depicted in Fig. 6.24, where  $I_c$  is the circulating current, which will be later discussed. The following equations in per-unit or per phase may be written  $\dot{E}_{f1} = \dot{V}_t + j\dot{I}_{a1}X_s$ ,  $\dot{E}_{f2} = \dot{V}_t + j\dot{I}_{a2}X_s$ . Thus

$$\dot{E}_{f1} + \dot{E}_{f2} = 2\dot{V}_t + jX_s (\dot{I}_{a1} + \dot{I}_{a2}), \quad (6.96)$$

$$\dot{I}_{a1} + \dot{I}_{a2} = I_L = \frac{\dot{V}_t}{Z_L}, \quad (6.97)$$

$$\dot{E}_{f1} + \dot{E}_{f2} = 2\dot{V}_t + jX_s \frac{\dot{V}_t}{Z_L}. \quad (6.98)$$

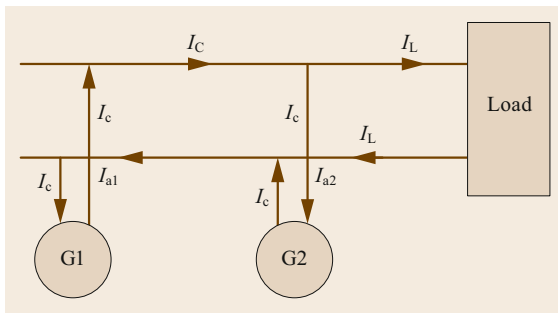


Fig. 6.24 Two generators in parallel

From (6.98), if the excitation of machine 1  $E_{f1}$  increases or decreases, the excitation of machine 2 must decrease or increase  $E_{f2}$ , respectively, to maintain an unaltered terminal voltage  $V_t$ .

As the generators are supplying the same active power and considering that initially they are supplying the same reactive power to the load, their power factors ( $\cos \theta$ ) are the same, if  $I_a$  is the armature current of each generator, the load current  $I_L = 2I_a$ . Noting also that  $OA = V_t$ ,  $AB = jI_a X_s \Rightarrow OB = E_f$ , the excitation EMF of each generator. The phasor diagram of Fig. 6.25 shows this situation.

The active power per phase or in per-unit for each generator can be expressed by

$$P = \frac{E_f V_t}{X_s} \sin \delta = \text{const.}$$

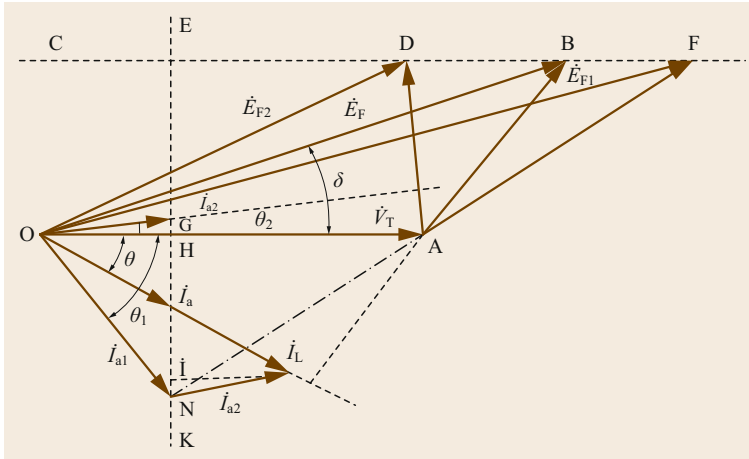
$$\text{or } P = V_t I_a \cos \theta = \text{const.} \quad (6.99)$$

As  $V_t$  and  $X_s$  are constants, it follows that  $E_f \sin \delta$  and  $I_a \cos \theta$  are constants for each generator. Thus, the ends of phasor  $E_f$  are located on a horizontal line (CF) parallel to  $V_t$  and at a distance from it equal to  $E_f \sin \delta$ . Also, the active component of the armature currents are located on the vertical line (KE), that is perpendicular to  $V_t$  and a distance from point O equal to  $OH = I_a \cos \theta$ . These considerations are valid for whatever variations may occur in the excitation of the generators.

Supposing that the excitation EMF of generator 1 increases from  $E_f$  to  $E_{f1}$  (point F). It is seen that  $AF = jI_{a1} X_s$  is greater than  $AB = jI_a X_s$ , that means that there was an increase in the armature current ( $I_{a1} > I_a$ ), the generator 1 power factor angle was increased from  $\theta$  to  $\theta_1$  and consequently its inductive reactive current ( $I_{a1} \sin \theta_1$ ) also has increased, increasing its inductive reactive power to the load.

To find  $I_{a2}$ , a parallel from phasor  $I_{a1}$  is drawn at the end of  $I_L$ . At the point of intersection G with line KE,  $I_{a2}$  is obtained. Note that  $I_{a2}$  is a leading current and its reactive component is given by the distance GH. The reactive component of  $I_{a1}$  (HN) is greater than the reactive component of the load current (HI) by  $IN = GH$ , and this additional reactive current goes from generator 1 to generator 2. It does not appear in the external circuit, i.e., in the load circuit. This circulating or internal current ( $I_c$ ) flows in the armature windings of both generators, causing additional losses. Figure 6.24 shows the path of this current. To avoid this current, the field excitation of generator 1 should decrease, until current  $I_{a2}$  is inductive.

In conclusion, the distribution of reactive power among generators is realized by means of their excitation systems.



**Fig. 6.25** Effect of changing the excitation on two generators in parallel

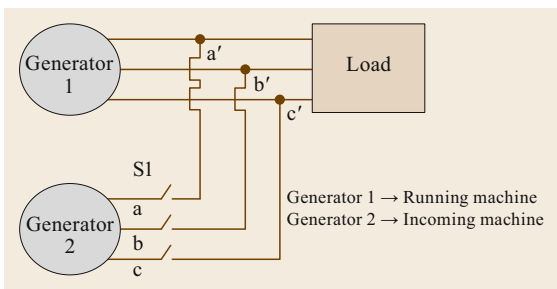
### 6.1.11 Synchronization of a Generator

Figure 6.26 illustrates a synchronous generator G1 supplying power to a load with another generator G2 that is about to be paralleled with G1 by closing the switch S1, which represents a circuit breaker. If the switch is closed at some arbitrary moment, the generators could be severely damaged and the load may lose power. If the voltages are different in the phases being tied together, there will be very large current flow when the switch is closed.

In order to be synchronized, an oncoming generator must meet the following conditions:

1. The generator voltage amplitude must be the same as the amplitude of the system voltage.
2. The phase sequence of the generator must be the same as that of the system.
3. The generator voltage must be in phase with the system voltage.
4. The generator frequency must be equal to the system frequency.

These conditions can be summarized in only one statement: At the instant of synchronization the instanta-



**Fig. 6.26** Synchronization

neous values of the potential differences among the generator terminals and those correspondents of the system, should be identical. Thus, with regard to Fig. 6.26

$$v_{ab} = v_{a'b'} , \quad v_{bc} = v_{b'c'} , \quad v_{ca} = v_{c'a'} , \quad (6.100)$$

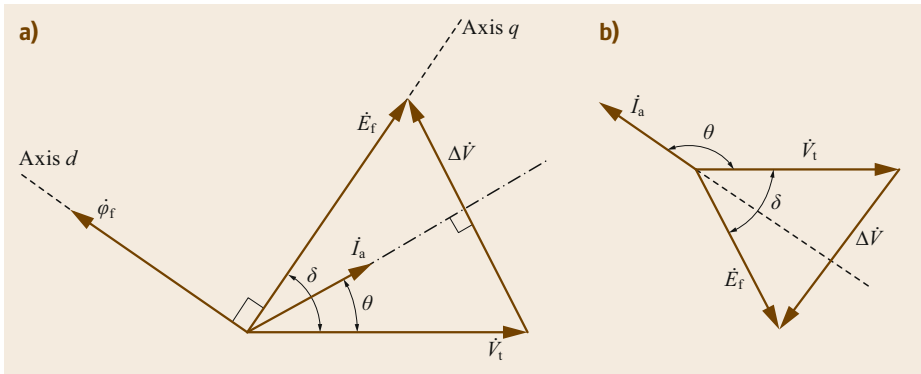
where

$$\begin{aligned} v_{ab} &= V_m \cos(\omega t + \theta) , \\ v_{bc} &= V_m \cos(\omega t + \theta - 120) , \\ v_{ca} &= V_m \cos(\omega t + \theta - 240) \end{aligned} \quad (6.101)$$

$$\begin{aligned} v_{a'b'} &= V'_m \cos(\omega' t + \theta') , \\ v_{b'c'} &= V'_m \cos(\omega' t + \theta' - 120) , \\ v_{c'a'} &= V'_m \cos(\omega' t + \theta' - 240) . \end{aligned} \quad (6.102)$$

In (6.101) and (6.102), the phase sequence of the generator was considered as equal to that of the system. To synchronize a generator the following steps should be taken:

1. The field current should be adjusted so that the generator excitation voltage  $E_f$  is equal to the system voltage, i.e., equal to the generator terminal voltage  $V_t$ .
2. The phase sequence of the generator should be checked by means of a phase sequence indicator, that is connected to its terminals. For more details of indicators, see IEEE Std 115<sup>TM</sup> – 2009 [6.10]. If the phase sequence of the generator is not equal to that of the system, it can be corrected by swapping the connections on any two of the three-phases of the oncoming generator.
3. The speed regulator of the turbine should be adjusted so that the generator frequency is close to the system frequency, as it is very difficult to obtain equal frequencies. This means that the phase



**Fig. 6.27a,b** Synchronization with an angular difference. **(a)** The generator frequency is higher than that of the system. **(b)** The generator frequency is lower than that of the system

angle of the oncoming generator will change slowly relative to the phase angle of the running system.

- Use a synchroscope to verify the phase angle between  $E_f$  and  $V_t$ . This instrument has a pointer that continually indicates the phase angle between these two voltages. Although the degrees are not shown, the dial has a zero mark, at the top, to indicate when the voltages are in phase, and when they are  $180^\circ$  out of phase the pointer is at the bottom.
- If the generator frequency is slightly higher than the system frequency, the pointer rotates clockwise. Conversely, if the generator frequency is slightly lower, the pointer rotates counterclockwise. Then, at the moment the pointer crosses the zero mark, the circuit breaker is closed, connecting it to the system.

In most power stations, synchronization is done automatically.

The frequency of the oncoming generator is adjusted to a slightly higher frequency to ensure that when it is connected, it will come on-line supplying power as a generator, instead of consuming it as a motor.

### The Synchronization Power

If the magnitude of the generator EMF  $E_f$  is the same as that of the system  $V_t$ , but its frequency is higher, the phasor  $E_f$  will be ahead of the phasor  $V_t$ , and a difference of potential  $\Delta V$  will appear across the switch. An armature current  $I_a$  lagging  $90^\circ$  behind  $\Delta V$  will flow, as shown in Fig. 6.27a. Neglecting the armature resistance,

$$I_a \exp(j\theta) = -j \left[ \frac{E_f \exp(j\delta) - V_t \exp(j0)}{X_s} \right], \quad (6.103)$$

where  $E_f = V_t$ ,  $\theta = \delta/2$  and  $X_s I_a = 2V_t \sin(\delta/2)$ .

As the angle  $\delta$  is positive the generator will supply power to the system. If  $P_a$  is the accelerating power,  $P_m$  is the mechanical power supplied by the turbine just before synchronization, which is equal to the rotational losses, and  $P_e$  is the electrical power supplied by

the generator (neglecting power losses),  $P_a = P_m - P_e$ , where in per-unit or per phase, for a round-rotor generator  $P_e = E_f V_t / X_s \sin \delta = V_t^2 / X_s \sin \delta$ . As  $P_m$  is constant (the speed governor did not have time yet to increase  $P_m$ ),  $P_a$  is negative and the generator slows down until, after some small damped oscillations around  $V_t$ , the phasors  $E_f$  and  $V_t$  will be in phase, and  $I_a$  and  $\delta$  will be null.

If, instead the generator frequency is lower, the phasor  $E_f$  will be behind the phasor  $V_t$ , and a difference of potential  $\Delta V$  will appear across the switch. An armature current  $I_a$  will flow, as shown in Fig. 6.27b. The angle  $\delta$  is negative and the generator will receive power from the system. As a consequence, the generator speeds up until, after some small damped oscillations around  $V_t$ , the phasors  $E_f$  and  $V_t$  will be in phase, and  $I_a$  and  $\delta$  will be null.

The synchronization power, in p.u.,  $P_e = V_t^2 / X_s \sin \delta$ , is the power supplied or received when the generator is turning faster or slower with respect to the system, and it will be slowed down or accelerates, respectively, to match its frequency with that of the system. If the synchronization is done with the generator completely out of phase with the system voltage, the angle  $\delta$  will be  $180^\circ$ , and the current in the armature will be  $I_a = 2V_t / X_s$ . This is twice the three-phase short-circuit current of the incoming generator. The stresses in the windings can cause severe damage to the generator.

It is to be noted that in the expressions above the synchronous reactance in the steady state was considered, for simplicity of drawing the phasor diagrams. In reality, with a damper winding the subtransient reactance  $X_d''$  must be used. If the machine does not have a damper winding the transient reactance  $X_d'$  is the one to be used.

According to IEEE Std C50.12-2005 [6.15] for salient-pole and IEEE Std C50.13-2014 [6.16] for cylindrical-rotor synchronous generators the following limits, shown in Table 6.5, should not be exceeded.

**Table 6.5** Synchronizing limits [6.15, 16]

Breaker closing angle	$\pm 10^\circ$
Generator side voltage difference relative to system	0 to +5%
Frequency difference	$\pm 0.067$ Hz

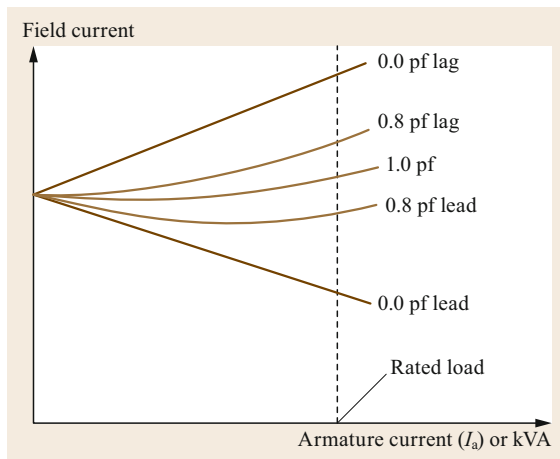
The synchronization is helped by the damping windings, in which induced currents are due to the speed difference between the rotating armature and field magnetic fields. When the generator is connected to the system the speed of the armature field is determined by the system frequency; if the rotor turns at a speed lower than that of the armature field, the currents induced in the damping windings produce a torque that tends to accelerate the rotor. Conversely, if the rotor field turns at a speed greater than that of the system, the torque tends to slow down the rotor.

After synchronization, the generator active power should be adjusted by the speed governor of the turbine and its reactive power (power factor) by the excitation system.

### 6.1.12 Generator Excitation for Constant Terminal Voltage: Compounding Curve

The curves of Fig. 6.28 show how the field excitation of a synchronous machine should be varied to maintain constant terminal voltage (in general rated voltage) and constant power factor as the load is varied. These curves are called compounding curves.

It is known that for a round-rotor machine  $\dot{E}_f = \dot{V}_t + j\dot{I}_a X_s$ , neglecting  $R_a$ . If the power factor angle is  $\theta$ , the terminal voltage  $V_t$ , the excitation EMF  $E_f$  and



**Fig. 6.28** Generator excitation for constant terminal voltage and power factor

the armature current  $I_a$ , the following relation can be written

$$E_f = \sqrt{(V_t \pm I_a X_s \sin \theta)^2 + (I_a X_s \cos \theta)^2}, \quad (6.104)$$

where the plus sign is for an inductive load and the minus sign for a capacitive load.

From (6.104) the following conclusions can be drawn:

In an open-circuit,  $I_a = 0$  and  $E_f = V_t$  for whatever power factor. When the power factor is zero capacitive  $E_f = V_t - I_a X_s$ . Thus, when the load  $I_a$  increases the excitation must decrease to maintain  $V_t$  constant. In this case the armature reaction MMF is totally magnetizing, and the machine receives reactive power from the system. When the power factor is zero inductive,  $E_f = V_t + I_a X_s$ . Thus, when the load  $I_a$  increases the excitation must increase to compensate the voltage drop in the armature impedance and to maintain  $V_t$  constant. In this case the armature reaction MMF is totally demagnetizing, and the machine supplies reactive power to the system. Intermediate load power factors produce voltage/current characteristics shown in Fig. 6.28.

### 6.1.13 Generator Load Characteristic

This characteristic shows the behavior of the terminal voltage of a generator when the load changes, with constant excitation and load power factor. From (6.104) of Sect. 6.1.12 the following analysis can be done.

In an open-circuit,  $I_a = 0$  and  $V_t = E_f$  and all the curves in Fig. 6.29 begin at point 1 on the vertical axis, no matter the power factor. In short-circuit  $V_t = 0$ ,  $\theta = \pm 90^\circ$ , with the plus sign for an inductive load and the minus sign for a capacitive load, thus,  $I_a = E_f/X_s$ . When the load is pure inductive the power factor is equal to zero and  $\theta = -90^\circ$ . In this case  $V_t = E_f - I_a X_s$ , which is a straight line with the armature MMF demagnetizing the field MMF, and the terminal voltage decreases with the load increase. For a leading load of zero power factor  $V_t = E_f + I_a X_s$  and the armature MMF is totally magnetizing, increasing the field MMF, and the terminal voltage increases with the load increase. In this case very high terminal voltages can be produced, especially when the machine is radially connected to high voltage transmission lines, and the lines are disconnected at their far ends, a situation known as load rejection. Intermediate load power factors produce voltage/current characteristics shown in Fig. 6.29.

### 6.1.14 Generator Capability Chart

This chart shows the active and reactive power limits that generators can be safely operated, since the condi-

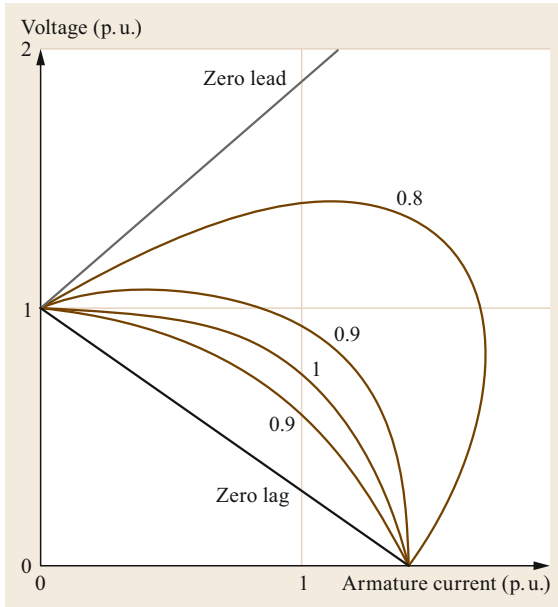


Fig. 6.29 Generator load characteristic

tion of zero inductive power factor up to zero capacitive power factor.

Synchronous generators are specified in function of the maximum apparent power in MVA that they can supply continuously without overheating for a given rated voltage (with a variation of  $\pm 5\%$ ), rated current and power factor. The field and armature currents for this condition are the maximum currents allowed in the field and armature windings, respectively. MW (active power) loading cannot exceed the turbine rating.

The chart is drawn in per-unit for rated terminal voltage, armature current and power factor, with resistance neglected, considering nonsaturated values for the reactances, in order to be conservative. The consideration of saturated values for the reactances will enlarge, a little bit, some of the limits presented.

### Cylindrical-Rotor Generator

To draw the capability curve of the synchronous generator, its voltage phasor diagram multiplied by  $jV_t/X_s$  is redrawn in Fig. 6.30. It is recognized that OMN is the complex power triangle, wherein OM is the nominal apparent power,  $P$  and  $Q$  are the nominal active and inductive reactive power, respectively, and  $\phi$  is the rated power factor. The segment  $O'O$  is the capacitive reactive power and a machine design with a high short-circuit relation (SCR) will increase the capacity of the machine in absorbing reactive power from the system, providing a better voltage control. The segment  $O'M$  corresponds to the maximum excitation power, that is

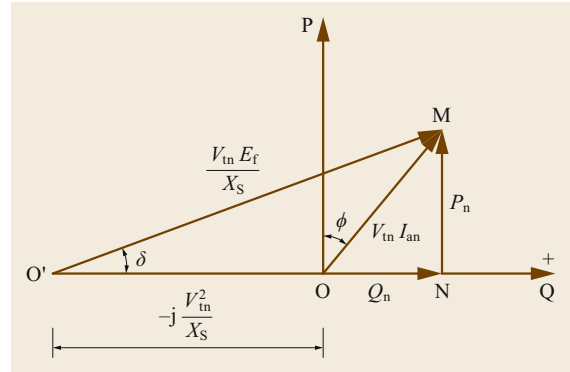


Fig. 6.30 Diagram showing the apparent, active, reactive and excitation power of a cylindrical-rotor generator

obtained for an excitation voltage equal to the rated excitation voltage  $E_f$ .

The steps in the construction of the capability chart are:

- With a center at  $O$  and radius  $OM$  a circle is drawn, that represents the limit of armature winding heating.
- With a center at  $O'$  and radius  $O'M$  a circle is drawn, that represents the limit of field winding heating.
- From point  $M$  drawing a straight line perpendicular to the active power axis  $P$ , the limit of maximum power of the turbine is obtained.
- The theoretical stability limit in the steady-state is obtained when  $\delta = 90^\circ$ , and the expression for the apparent power of the generator is given by

$$S_n = \frac{V_{tn} E_f}{X_s} - j \frac{V_{tn}^2}{X_s} = P_n - j Q_n \quad (6.105)$$

indicating that the theoretical stability limit in steady-state is given by a straight line ( $O'WUTS$ ) from point  $O'$ , perpendicular to the horizontal axis. It is not desirable to operate a generator at its steady-state theoretical stability limit because there will be no margin for an oscillation that may increase the angle  $\delta$ , causing the machine to lose stability. Thus, a margin of 10% (TU) in the active power with constant excitation  $E_f$  is considered and various circles with excitation constant are traced, determining the steady-state practical stability limit ( $O'VR$ ), as shown in Fig. 6.31.

If the excitation current goes to zero, the active power will be zero and excitation voltage induced in the armature  $E_f$  also will be zero and in this case,

$$\dot{E}_f = 0 = \dot{V}_{tn} + j \dot{I}_{an} X_s \Rightarrow \dot{I}_{an} = j \frac{\dot{V}_{tn}}{X_s} \quad (6.106)$$

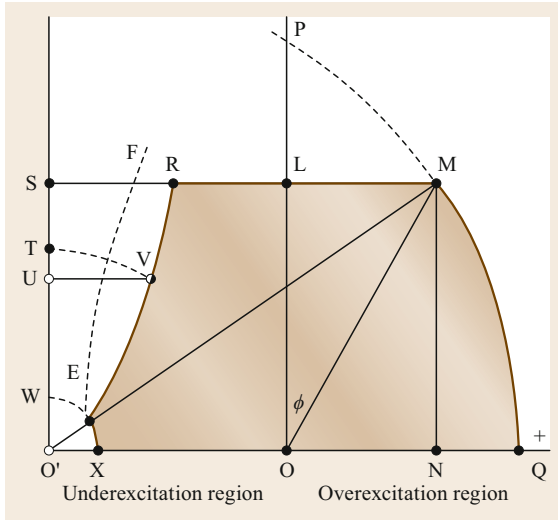


Fig. 6.31 Capability chart of a cylindrical-rotor generator

Thus the armature current will be capacitive indicating that the generator receives reactive power from the system, and as its electrical power is zero and the mechanical power is constant (at least in the following few seconds), the rotor will be accelerated and the machine starts to function as an induction generator until it is disconnected from the system by the loss-of excitation protection. Therefore, excitation current on the chart is normally limited to a value of 5–10% of its rated value (circle WX).

When the generator operates as overexcited, the field current is high and the retaining ring becomes saturated, so that the effects of the flux in the end region of the armature is small. However, in the underexcited region the field current is low and the retaining ring is not saturated, allowing an increase in armature end leakage flux, which adds to the flux produced by the field current, occasioning heating in the end core packets and clamping plates, that may severely limit the generator output, particularly in the case of a round rotor machine. Thus a limit is put on the amount of reactive power that can be absorbed, which is given by line EF [6.17]

**Salient-Pole Generator**

If in the voltage diagram of a salient-pole generator a parallel line to AB is drawn from point C, point F is determined on the horizontal axis, as shown in Fig. 6.32, where  $HC = AB = E_f$ ,  $BC = I_q(X_d - X_q)$  and  $FA = [V_{tn}(X_d - X_q)]/X_q$ .

If the diagram of Fig. 6.32 is multiplied by  $-jV_{tn}/X_d$ , a chart showing only powers quantities is obtained, as shown in Fig. 6.33.

Along the semi-circle FHA the excitation voltage is equal to zero. The field winding heating limit  $CC'K$

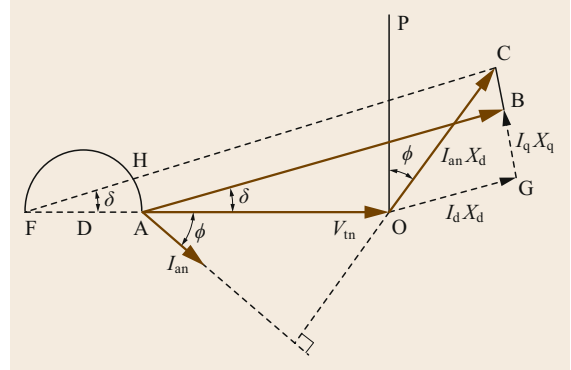


Fig. 6.32 Voltage diagram of a salient-pole generator

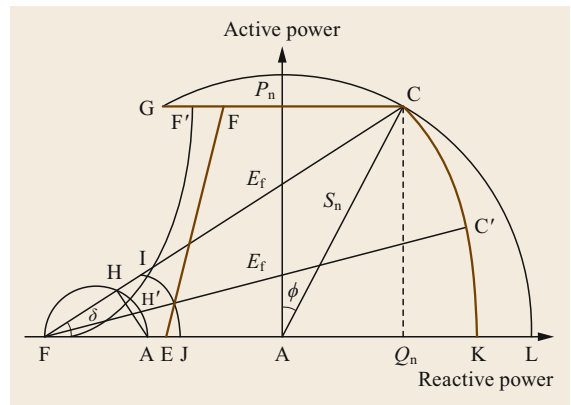


Fig. 6.33 Capability chart of a salient-pole generator

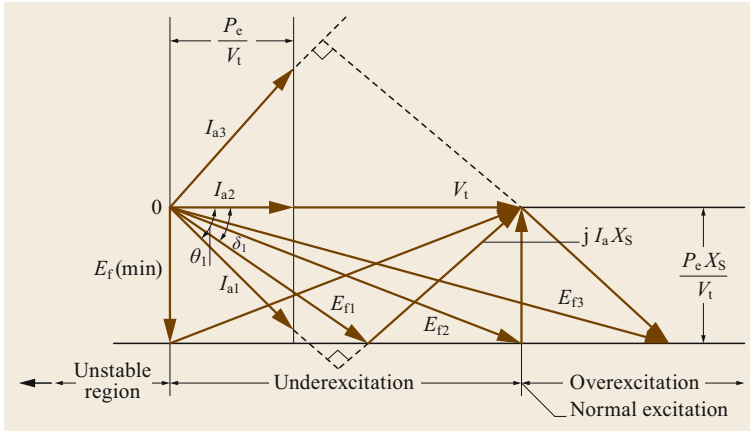
is obtained by drawing several lines from point F and marking distances  $H'C' = HC = E_f$  starting at the semi-circle. The limit of armature winding heating (curve GCL) and the limit of maximum power of the turbine (CG) are obtained following the same procedure as used in the case of cylindrical-rotor generator. When the excitation is zero the active and reactive power of the generator are

$$P = \frac{V_{tn}^2}{2} \left( \frac{1}{X_q} - \frac{1}{X_d} \right) \sin 2\delta, \tag{6.107}$$

$$Q = \frac{V_{tn}^2}{2} \left( \frac{1}{X_q} - \frac{1}{X_d} \right) \cos 2\delta - \frac{V_{tn}^2}{2} \left( \frac{1}{X_q} + \frac{1}{X_d} \right). \tag{6.108}$$

The generator can supply a certain active power. The locus of the points where the excitation voltage is equal to zero is given by the semi-circle FHA. In the chart, following the same observation for the case of a cylindrical-rotor generator, in order to avoid operation with zero excitation, the minimum excitation was considered equal to a value of 5–10% of rated excitation, obtaining the circle IJ.





**Fig. 6.34** Synchronous motor operation at constant load and variable excitation

At point A,  $\delta = 0$  and the reactive power is capacitive and equal to  $V_{in}^2/X_d$ . At point F, where  $\delta = 90^\circ$  the reactive power is also capacitive and equal to  $V_{in}^2/X_q$ , however, operation at this latter point is not allowed because in the case of a salient-pole machine the steady-state stability limit occurs for an angle  $\delta$  less than  $90^\circ$ . Besides that, operation inside the semi-circle of zero excitation would be only possible if the excitation system is designed for negative excitation current. The theoretical steady-state stability limit may be obtained by the following expression.

$$P = -\frac{\left(Q + \frac{V_{in}^2}{X_q}\right)^2}{Q + \frac{V_{in}^2}{X_d}} \tag{6.109}$$

In the chart the practical steady-state stability limit is given by curve FF', where a safety margin of around 10% was given from the theoretical steady-state stability limit, with constant excitation. The EF curve represents the heating limit of the frontal stator sheet packs.

### 6.1.15 Synchronous Motor: V Curves

When a synchronous motor delivers constant mechanical power while energized from a source of constant voltage and constant frequency, the armature current is a function of the field excitation. Considering the armature resistance and mechanical losses neglected and the theory of cylindrical-rotor applied, when the armature current is plotted against field excitation, the result is the so-called V curves, due to the shape of the curves. The following equations, in per-unit or per phase, apply

$$\begin{aligned} \dot{V}_t &= \dot{E}_f + \dot{I}_a(R_a + jX_s), \quad \text{with } R_a \text{ neglected} \\ \Rightarrow \dot{V}_t &= \dot{E}_f + j\dot{I}_a X_s, \end{aligned} \tag{6.110}$$

$$P_e = \frac{E_f V_t}{X_s} \sin \delta \text{ or } P_e = V_t I_a \cos \theta. \tag{6.111}$$

As  $P_e$  and  $V_t$  are constants

$$E_f \sin \delta = \text{const.} \tag{6.112}$$

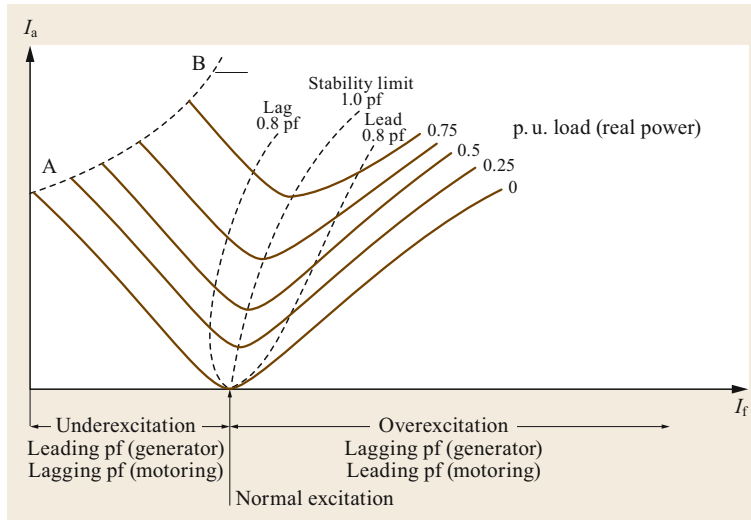
Likewise,

$$\frac{P_e}{V_t} = I_a \cos \theta \Rightarrow I_a \cos \theta = \text{const.} \tag{6.113}$$

The expressions (6.112) and (6.113) are valid for any power factor value. Neglecting losses the mechanical power load is equal to the electrical power supplied to the motor from its terminal. The machine behaviour is described by means of the phasor diagram of Fig. 6.34. When the excitation EMF  $E_f$  increases from the condition of unity power factor, i.e., from the normal excitation  $E_{f2}$  to  $E_{f3}$ , the power angle  $\delta$  decreases so that the product  $E_f \sin \delta = P_e X_s / V_t$  is maintained constant and the phasor  $E_f$  moves along a line parallel to  $V_t$ . Also, the phasor  $I_a$  is located along a line perpendicular to  $V_t$  at a distance  $I_a \cos \theta = P_e / V_t$  from the origin. The minimum armature current occurs when the motor operates at a unity power factor.

The following conclusions can be obtained from Fig. 6.34:

- The machine as a motor operates over-excited and supplies reactive power to the grid when the power factor is capacitive, i.e., when the armature current leads the terminal voltage. If the machine was a generator it would receive reactive power when the power factor was capacitive, i.e., the armature current leads the terminal voltage.
- The machine as a motor operates under-excited and receives reactive power from the grid when the power factor is inductive, i.e., when the armature current lags the terminal voltage. If the machine was a generator it would supply reactive power when the



**Fig. 6.35** V curves of a synchronous motor indicating also the operation as a generator

power factor was inductive, i.e., the armature current lags the terminal voltage.

The nature of  $I_a$  versus excitation ( $I_f$ ) plot for various values of active power load is shown in Fig. 6.35. These are known as V-curves of a synchronous machine by virtue of their shape. Though the figure is drawn for motoring operation, an indication of operation as a generator is given as the V-curves for a generator are similar, but inverted.

#### Minimum Excitation and Stability Limit

From (6.109), the angle  $\delta$  continuously increases when the excitation is reduced. The minimum permissible excitation,  $E_f$  (min), for a specific value of constant active power occurs for  $\delta = 90^\circ$ . Thus

$$E_f(\text{min}) = \frac{PX_s}{V_t} \quad (6.114)$$

Minimum field current and the corresponding armature current for a given pu load at the limit of stability is indicated, in Fig. 6.35, by the dashed curve AB. At the stability limit the motor power factor is inductive, while in a generator the stability limit occurs for a capacitive power factor. In both cases, for motor and generator, the stability limit occurs in a region of minimum field excitation.

#### Synchronous Compensator

A synchronous compensator is a synchronous machine, usually of the salient-pole type, that has neither a prime mover nor a mechanical load; it is in effect a synchronous motor running idle. The V curve for zero mechanical power in Fig. 6.35 approximately represents

synchronous compensator operation. When rotational losses and armature resistance are neglected, the real power of a synchronous compensator is zero, and consequently the torque angle  $\delta = 0$ . The reactive power in per-unit or per phase is given by

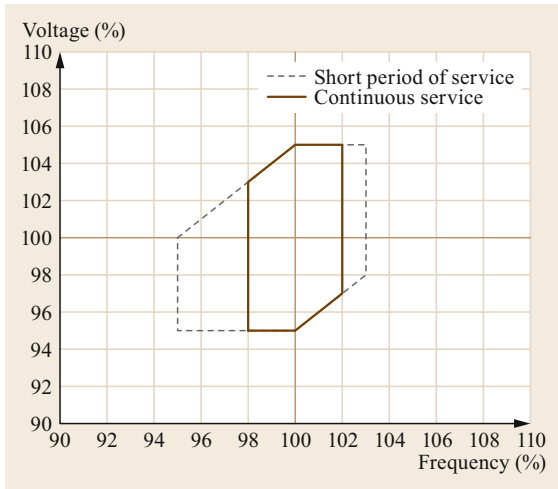
$$Q = \frac{V_t E_f - V_t^2}{X_s} \quad (6.115)$$

By controlling excitation  $E_f$ , it can supply or absorb reactive power and maintain the terminal voltage  $V_t$  constant.

**Observation.** In a synchronous machine the active electrical power exchanged with the bus-bars is controlled by the mechanical shaft power, by means of the speed governor, irrespective of excitation. The excitation system, on the other hand, controls only the power factor of the machine without affecting the real power flow. For example, if a generator needs to supply more active power into the bus-bars, the throttle (gates) must be opened admitting more steam (water) into the turbine (coupled to the generator) thereby supplying more mechanical power into the shaft. As a consequence the power angle  $\delta$  increases and so does the electrical power output. However, if it is desired to adjust the machine power factor, its excitation should be varied.

#### 6.1.16 Voltage–Frequency Limits

The voltage and frequency limits, as per IEEE C50.12 [6.15] and IEEE C50.13 [6.16] standards, must be in accordance with the values shown in Fig. 6.36. That is, the generators shall be thermally capable of continuous operation within the confines of their ca-



**Fig. 6.36** Continuous and short-time limits of voltage–frequency variations, according to IEEE C50.12 and IEEE C50.13 [6.15, 16]

pability curves over the range of  $\pm 5\%$  in voltage and  $\pm 2\%$  in frequency, as defined by the brown area.

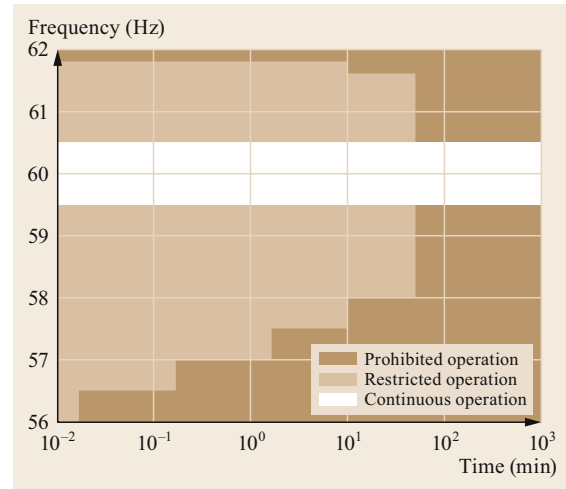
To minimize the reduction of the generator’s life-time due to the effects of temperature, operation outside the brown area and within the gray line should be limited in extent, duration and frequency of occurrence.

IEEE C37.106-2003 standard [6.18] addresses abnormal frequency protection for power generating plants. It recognizes that the generator’s prime mover is more susceptible to damage from off-frequency operation than the generator itself. Specifically turbine blade fatigue is the main concern. The length of the blades and its design dictates their resonant frequencies. Turbine blades are designed to have their natural frequencies displaced sufficiently from rated speed and multiples of rated speed. Operation at frequencies other than rated or near-rated speed is time-restricted to the limits shown for the frequency bands provided by the manufacturer. Figure 6.37 shows the frequency limits of a typical steam turbine.

### 6.1.17 Excitation Systems

The excitation system fulfills two main functions:

- It produces DC voltage (and power) to force current to flow in the field windings of the generator.
- It provides a means for regulating the terminal voltage of the generator to match a desired set point, as well as providing damping for power system oscillations and through its fast response, contributes to improving system transient stability.



**Fig. 6.37** Frequency limits of a typical steam turbine [6.19]

Prior to the 1960s, generators were generally provided with rotating exciters that fed the generator field through a slip ring arrangement, a rotating pilot exciter feeding the main exciter field.

Since the 1970s, the most common arrangement for hydrogenerators is a static excitation system where the main field excitation is regulated by a controlled rectifier. One of these static excitation systems, shown in Fig. 6.38 is the *potential source controlled rectifier high initial response exciter*, known as the *bus-fed static exciter*, where excitation power is supplied through a transformer from the main generator terminals and a six-pulse thyristor bridge controls the main field excitation. Field flashing equipment is provided to build up generator terminal voltage during starting. Power for field flashing is provided either from the station battery or alternating current (AC) station service.

During system conditions that leads to self-excitation of the generator, causing abnormal voltages on machine terminals and possible damage to stator windings, a second thyristor bridge in antiparallel to the one shown in Fig. 6.38, can be used so that the machine inverts its field current and delay the self-excitation. As this second bridge is used for transient conditions it may be specified for a short time operation, for example 10 s. Also, negative field current can be used in a salient-pole synchronous machine, operating as a condenser, to increase the reactive power absorption. This can be useful for near high-voltage direct current (HVDC) stations or long transmission lines where extra reactive power absorption is required. Due to firing angle margin requirements of the thyristors, the magnitude of the negative ceiling voltage is normally less than the positive ceiling voltage, usually around 70% of the positive ceil-

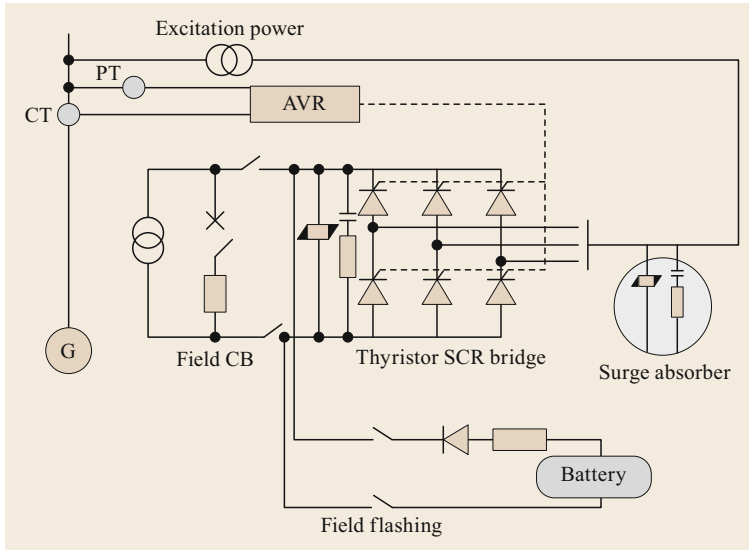


Fig. 6.38 Potential-source controlled-rectifier excitation system

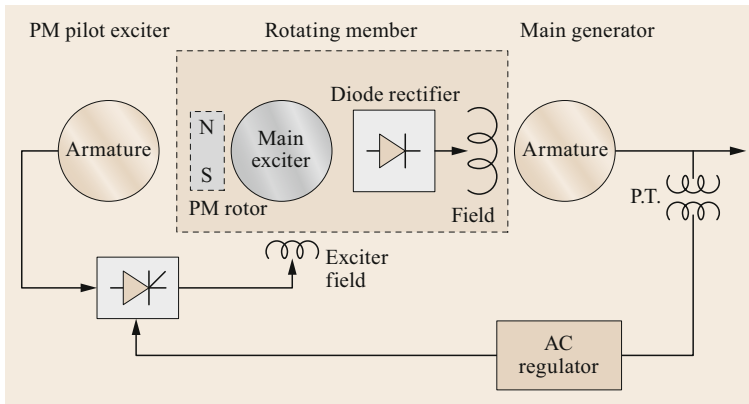


Fig. 6.39 Brushless excitation system

ing voltage, and in cases where it is used for transient conditions it may be specified for a short time operation, for example 10 s. Ceiling voltages of 3–5 p.u. where one per-unit voltage is defined as the generator field voltage required to produce one per-unit terminal (stator) voltage on the open-circuit airgap line at a specified field winding temperature, are considered usual for static exciters and brushless exciters. Values outside this range imply an increased excitation system cost.

Another system, a rotating exciter system, used for turbogenerators is the brushless exciter, i.e., an excitation system without carbon brushes and slip-rings. In turbogenerators the number of field winding turns is much less than in hydrogenerators requiring a large field current, which may cause a fast wear of brushes and sparking on slip rings, if used. Figure 6.39 presents a brushless excitation system. The brushless excitation

system consists of two major parts: pilot exciter and main exciter. The pilot exciter is a PMG (permanent magnet generator) whose field winding is mounted on the rotor shaft. Armature winding of the PMG is the stationary part mounted on a stator and supplying a thyristor bridge. The thyristor bridge/voltage regulator controls the field current to the main exciter due to which its AC output is also controlled and directly feeds the diode bridge rectifier whose output feeds the field winding of the turbogenerator. In this way the field current input to the field winding of the turbogenerator is controlled. The PMG is used because its AC output has a high frequency, for instance, if a PMG has 16 poles its AC output frequency will be 400 Hz ( $f = np/120$ ,  $n = 3000$  rpm) and as a consequence the ripple in the rectified DC output will be low. The time delays in the response to a controlling signal are short when compared with the time constant of the generator field.

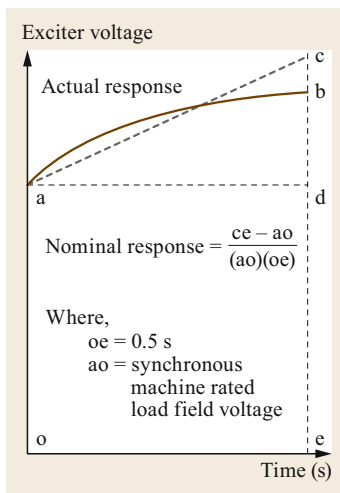
### Excitation Limiters

The excitation system is provided with limiting control functions that prevent certain quantities from exceeding set limits, protecting both the excitation system and the synchronous machine. These limiting functions generally have no effect on the excitation output during normal operating conditions, but protect the exciter and machine during severe unit or power system disturbances in which the excitation system is pushed near or beyond defined operating limits. Typical excitation limiters include overvoltage (OV), volts/hertz (V/Hz), instantaneous and timed overexcitation limiter (OEL), underexcitation limiter (UEL), and stator overcurrent limiters (SCL). The effects of excitation limiters are described in IEEE Std 421.2 [6.20].

### Performance of Excitation Systems During Large Disturbances (Transient Stability)

A figure of merit for comparison among older nonhigh initial response rotating excitation systems is the excitation system nominal response, that is related to the ability of the excitation system to respond to large disturbances. The nominal response describes the rate of increase of the excitation system output voltage and is determined from the excitation system voltage response curve, shown in Fig. 6.40. This parameter has nowadays little practical significance as the modern static exciters or brushless can reach the ceiling voltage in less than 0.1 s.

Modern exciters have the advantage of providing extremely fast response times and high field ceiling voltages for forcing rapid changes in the generator terminal voltage during system faults. This is necessary to overcome the inherently large time constant in the response between terminal voltage and field voltage ( $T'_{d0}$ ,



**Fig. 6.40** Definition of excitation system nominal response

typically in the range of 4–10 s). Rapid terminal voltage forcing and higher ceiling voltages are necessary to improve transient stability of the power system during and immediately after system faults.

A large difference between the ceiling voltage and the rated field voltage indicates a large field forcing capability. Some excitation systems will have both positive and negative values of ceiling voltage. Positive ceiling voltage provides an indication of the voltage available to force the field current from rated field current toward ceiling current, while negative ceiling voltage provides an indication of the voltage available to force the field current to zero. Thus, large negative ceiling voltage aids in rapidly demagnetizing the synchronous machine.

### Performance of Excitation Systems During Small Disturbances (Small-Signal Stability)

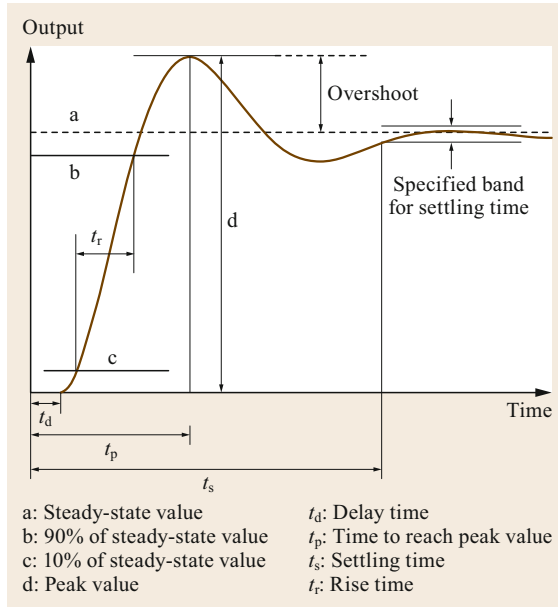
The ceiling voltage and exciter nominal response criteria are useful for comparing the performance of different systems and they are valuable as design criteria that can be used to verify that the manufacturer fulfilled specification requirements. However, these single values criteria do not provide sufficient information in all instances for model parameter selection or verification. A match of these values can be achieved using models with different combinations of model parameters. Comparing model results with dynamic responses can reduce this ambiguity. Thus, dynamic response, also associated with small signal analysis, is a useful tool for large signal performance evaluation, especially for applications involving the refinement or validation of computer models. Small signal analysis provides a means of evaluating the response of the closed-loop excitation control system to incremental changes in system conditions. It is a convenient means for determining or verifying the performance of excitation systems. A typical dynamic response to a step input of a feedback control system is shown in Fig. 6.41. The principal characteristics of interest are the 10–90% rise time, overshoot, peak time, and settling time as indicated.

Performance indexes for small signal dynamic analysis of excitation systems are presented in Table 6.6.

The performance indexes in Table 6.6 are applicable to any feedback control system having a single major

**Table 6.6** Performance indexes for small signal dynamic analysis of excitation systems

Performance index	Range of expected values
Overshoot	0–60%
Rise time	0.025–2.5 s
Settling time	0.2–10 s
Damping ratio	0.25–1



**Fig. 6.41** Typical dynamic response of a feedback control system to a step change in input [6.20]

feedback loop, that is, a single ultimately controlled variable. As such, they are applicable to an excitation control system with the synchronous machine open-circuited or feeding an isolated load.

However, when a synchronous machine is connected to a power system, its operating level, and the parameters of the external system greatly influence performance. A complex multiloop, multivariable, high order control system is formed with a power system connection. The determination of eigenvalues by means of a state space technique gives a direct indication of system stability for the linearized system and is an effective method for the determination of the parameters that have most influence on system performance. In the case of undamped oscillations, power system stabilizers are applied to static or brushless excitation systems for damping the dynamic oscillations, using an input signal that could be derived from generator speed or electric power or accelerating power or frequency deviations. After, the system performance must be tested for large disturbances, and some further adjustments may be required on the controls of the system to assure stability [6.21, 22].

### 6.1.18 Synchronous Generators During a Short-Circuit

The short-circuit currents may cause mechanical and thermal damages in electrical machines if not cleared quickly. Their calculation is also important to ascertain

the rating of the protective switchgear, that must be able to deal with the worst possible conditions. Also, short-circuit currents create a large torque on the machine. Of particular importance is the initial shock torque on the stator housing, since the foundations must be designed to withstand it.

#### The Armature Current

From the instant when a three-phase fault occurs at the terminals of an unloaded generator the following stages may be distinguished:

- There is an increase in the armature currents and as a consequence, an increase in the alternating armature magnetic field, which in the absence of resistances, is located in the direct-axis and tends to demagnetize the magnetic field of the rotor. The theorem of the constant flux linkages says that: In an inductive circuit of negligible resistance that is closed on itself, with no external voltages in the circuit, the total flux linkage must remain constant. Thus currents are induced in the field and damping windings to keep the flux linkages constant.
- These armature currents not been sustained by an electromotive force (EMF) begin to decrease and the same happens with the field and damping windings currents until the steady state regime is reached.

The amplitude of the a phase short-circuit current for a three-phase fault, under open-circuit conditions neglecting armature resistance is given by the following expression

$$\begin{aligned}
 i_a = & \sqrt{2}E_{f0} \left[ \frac{1}{X_d} + \left( \frac{1}{X'_d} - \frac{1}{X_d} \right) e^{-t/T'_d} \right. \\
 & \left. + \left( \frac{1}{X''_d} - \frac{1}{X'_d} \right) e^{-t/T''_d} \right] \cos(\omega t + \theta_0) \\
 & - \sqrt{2}E_{f0} e^{-t/T_a} \left( \frac{X''_d + X''_q}{2X''_d X''_q} \right) \cos \theta_0 \\
 & - \sqrt{2}E_{f0} e^{-t/T_a} \left( \frac{X''_q - X''_d}{2X''_d X''_q} \right) \cos(2\omega t + \theta_0),
 \end{aligned} \tag{6.116}$$

where:

$E_{f0}$  is the rms phase to neutral EMF induced in the armature by the excitation field on open-circuit. It is equal to the rms phase to neutral generator terminal voltage  $V_t$  on open-circuit

- $\theta_0$  is the angle between the direct-axis of the rotor and the magnetic axis of phase a when the short-circuit occurs, that is, at  $t = 0$
- $\omega$  is the synchronous speed in electrical radians per second and
- $\theta = \omega t + \theta_0$  is the angle between the direct-axis of the rotor and the magnetic axis of phase a for  $t > 0$ .

The currents in phases b and c are obtained by replacing  $\theta_0$  in the expression for  $i_a$  by  $\theta_0 - 120^\circ$  and  $\theta_0 - 240^\circ$ , respectively.

In the expression for  $i_a$  there are the following terms:

- A symmetrical alternating current of fundamental frequency consisting of:
  - A steady-state undamped component of amplitude  $\sqrt{2}E_{f0}/X_d$
  - A transient component with initial amplitude  $\sqrt{2}E_{f0}(1/X'_d - 1/X_d)$ , damped with time constant  $T'_d$
  - A subtransient component with initial amplitude  $\sqrt{2}E_{f0}(1/X''_d - 1/X'_d)$ , damped with time constant  $T''_d$
- A unidirectional or asymmetrical current with initial amplitude  $\sqrt{2}E_{f0}(X'_d + X''_q/2X'_dX''_q) \cos \theta_0$ , damped with time constant  $T_a$ . This component is usually called the direct current (DC) component.
- A second-harmonic current with initial amplitude  $\sqrt{2}E_{f0}(X''_q - X''_d/2X'_dX''_q)$ , damped with time constant  $T_a$ .

The value of the current in all three-phases, when the short-circuit occurs ( $t = 0$ ), is equal to zero as the machine is in open-circuit. The initial amplitude of the alternating current of fundamental frequency occurs at the instant of the short-circuit and is equal to  $\sqrt{2}E_{f0}/X''_d$ . Its subtransient component has a fast decay as the time constant  $T''_d$  is very small. The transient component presents a slow decay due to the time constant  $T'_d$ . The steady state component is the permanent short-circuit current.

The unidirectional or continuous short-circuit current, designated by  $i_{dc}$ , in phase a, does not exist at the instant  $t = 0$ , when the short-circuit occurs at angle  $\theta_0 = \pm 90^\circ$ . However, these currents are not zero in phases b and c because of the  $120^\circ$  displacement among the phases. These components decay with time constant  $T_a$ .

The second-harmonic current is very small as it depends on the difference between the two subtransient reactances and is usually neglected.

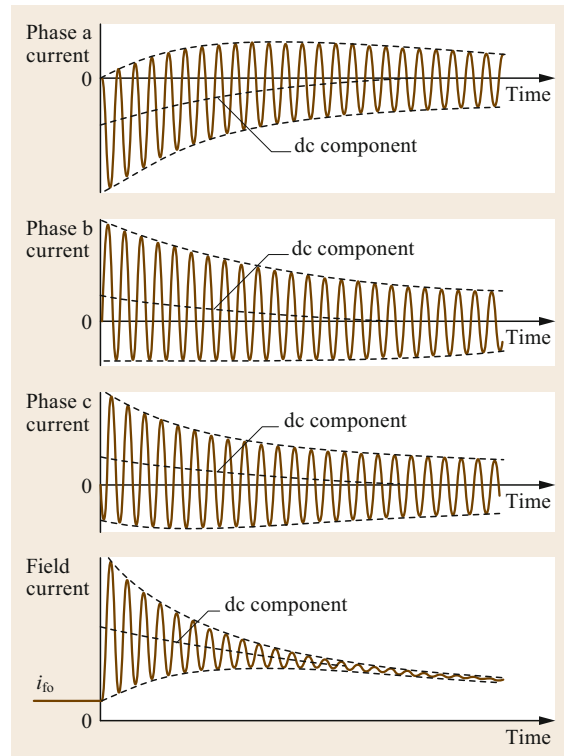
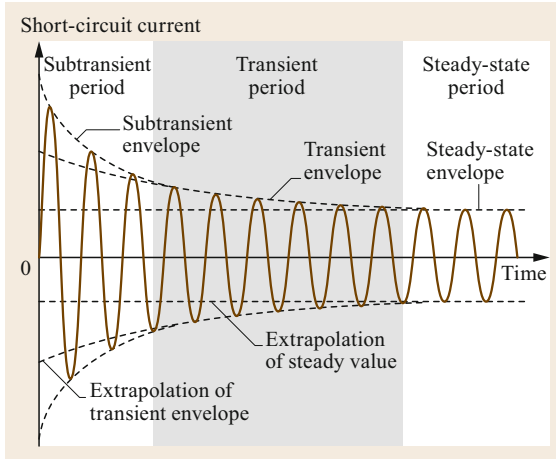


Fig. 6.42 Oscillograms of the armature and field currents after a short-circuit on an initially unloaded generator

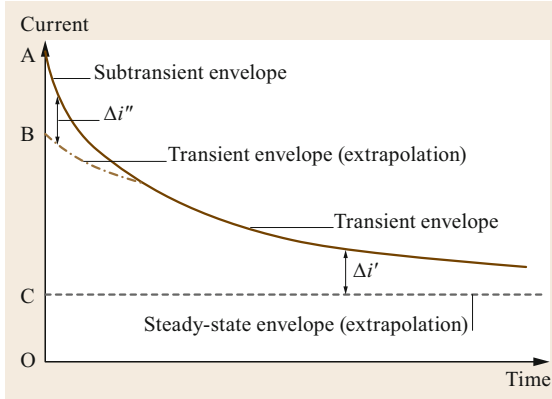
Figure 6.42 shows the curves of armature current after a short-circuit and the corresponding field current. Envelope lines are drawn through the peaks of the alternating current waves and dotted lines are drawn half-way between the envelope curves. Thus the current can be divided into a unidirectional component represented by the dotted lines, and an alternating component of supply frequency. Both components start with a certain initial value that reduces as time proceeds. The initial values of the alternating components are determined by tracing the envelope curves back to zero time. The field current is addressed in a separate article [6.23].

The unidirectional currents correspond to the fourth term in (6.116) and by the fourth terms of the corresponding expressions for the currents in phases b and c. The initial values of these currents are different in the three-phases b, and c, being proportional to  $\cos \theta_0$ ,  $\cos(\theta_0 - 120^\circ)$ , and  $\cos(\theta_0 - 240^\circ)$  respectively, but all three currents die away to zero with the same time constant  $T_a$ .

As said before if the short-circuit occurs in phase a at  $\theta_0 = \pm 90^\circ$  there will be no unidirectional or asymmetrical component and the short-circuit current will



**Fig. 6.43** Symmetrical alternating component of the three-phase fault current for phase a



**Fig. 6.44** Envelope of the symmetrical alternating component of the fault current for phase a

only have the alternating component of fundamental frequency in this phase and it will be symmetrical in relation to the horizontal axis, as shown by the Fig. 6.43.

The envelope of the symmetrical alternating component of the fault current is shown in the Fig. 6.44.

The subtransient current envelope is

$$\Delta i'' = i_d'' - i_d' = \sqrt{2} (I_d'' - I_d') e^{-t/T_d''} \quad (6.117)$$

and the transient current envelope is

$$\Delta i' = i_d' - i_d = \sqrt{2} (I_d' - I_d) e^{-t/T_d'} \quad (6.118)$$

$I_d''$ ,  $I_d'$ , and  $I_d$  are the rms values of the respective currents.

The expression for the envelope of the symmetrical alternating current is

$$I_a = \sqrt{2} E_{f0} \left[ \frac{1}{X_d} + \left( \frac{1}{X_d'} - \frac{1}{X_d} \right) e^{-t/T_d'} + \left( \frac{1}{X_d''} - \frac{1}{X_d'} \right) e^{-t/T_d''} \right] \quad (6.119)$$

or in terms of currents the equation for the envelope can be written as

$$I_a = \sqrt{2} \left[ I_d + (I_d' - I_d) e^{-t/T_d'} + (I_d'' - I_d') e^{-t/T_d''} \right]. \quad (6.120)$$

The subtransient component of fault current is superimposed on the transient and steady-state components. From the envelopes of the symmetrical alternating currents, the currents and the direct-axis reactances can be calculated.

The initial rms value of the subtransient short-circuit current may be calculated from Fig. 6.44 for a specific phase, and is given by

$$I_d'' = \frac{OA}{\sqrt{2}} = \frac{E_{f0}}{X_d''} \quad (6.121)$$

This value is obtained by extending the envelope of the subtransient short-circuit current to the vertical axis.

For each phase the values of the difference between the envelope of the subtransient current and the envelope of the transient current should be plotted on a semilogarithmic scale on the vertical axis, with time on the horizontal axis, thus obtaining the subtransient component of fault current  $\Delta i''$ . The result is expected to be very nearly a straight line. Extending this line back to zero time gives the initial value of the subtransient component of fault current. The sum of this component  $\Delta i''$ , the initial transient component  $\Delta i'$ , and the sustained component, for each phase, gives the corresponding maximum initial value of subtransient current, whose rms value is  $I_d''$ . The values of  $I_d''$  determined in this way are more accurate than those obtained by extrapolating the envelopes back to the beginning of the short-circuit. The three values are averaged to obtain the final value of  $I_d''$  and the subtransient reactance is calculated by

$$X_d'' = \frac{E_{f0}}{I_d''} \quad (6.122)$$

The direct-axis short-circuit subtransient time constant  $T_d''$  can be determined from the semilogarithmic graph of the subtransient alternating component of the short-circuit current.



The transient component of fault current is superimposed on the steady-state component. The initial rms value of the transient short-circuit current for a specific phase may be calculated from Fig. 6.44, and is given by

$$I'_d = \frac{OB}{\sqrt{2}}. \quad (6.123)$$

Two other values of the rms value of the transient current are calculated for the other two phases. These values are averaged and a final rms value for  $I'_d$  is obtained. The transient reactance is

$$X'_d = \frac{E_{f0}}{I'_d}. \quad (6.124)$$

The direct-axis short-circuit transient time constant  $T''_d$  can be determined from one of the graphs of the transient alternating component of the short-circuit current.

The rms value of the steady-state short-circuit current from Fig. 6.44 is given by

$$I_d = \frac{OC}{\sqrt{2}} = \frac{E_{f0}}{X_d} \quad (6.125)$$

and the synchronous reactance is

$$X_d = \frac{E_{f0}}{I_d}. \quad (6.126)$$

Note that  $X_d > X'_d > X''_d$ . The time constants  $T''_d$ ,  $T'_d$ , and  $T_a$  may all be found from the oscillograms of the armature currents shown in Fig. 6.43 and 6.44, and the technique for doing this is explained in detail in [6.24] and will not be repeated here.

### The Field Current

The field current is given by

$$i_f = i_{f0} + i_{f0} \left( \frac{X_d - X'_d}{X'_d} \right) \left[ e^{-t/T'_d} - \left( 1 - \frac{T_{kd}}{T''_d} \right) e^{-t/T''_d} - \frac{T_{kd}}{T''_d} e^{-t/T_a} \cos \omega t \right]. \quad (6.127)$$

In the oscillogram of the field current from Fig. 6.42 the total current consists of a unidirectional or asymmetrical component given by the dotted line and an alternating component. The alternating component corresponds to the last term of (6.127). It is of fundamental frequency and dies away with time constant  $T_a$ . The unidirectional or asymmetrical component starts with the steady value  $i_{f0}$  and rises suddenly at the instant of the short-circuit and follows the dotted line until it finally returns to the steady value [6.23].  $T_{kd}$  is the direct-axis damper leakage time constant. Its value varies from

0.01 to 0.05 s for salient-pole machines and from 0.01 to 0.03 s for cylindrical-rotor machines.

Note that there is a correspondence between the field current (6.127) and the armature currents (6.116). The theorem of the constant flux linkages says that: In an inductive circuit of negligible resistance that is closed on itself, with no external voltages in the circuit, the total flux linkage must remain constant.

Thus, the unidirectional armature currents appear to maintain the flux linkage constant in each phase of the armature and not being sustained by a voltage in the armature will decrease with the time constant  $T_a$ . These unidirectional armature currents establish a stationary pulsating field in the airgap that induces a voltage and current of fundamental frequency in the field circuit which is rotating at synchronous speed.

### The Electromagnetic Torque

For a three-phase short-circuit, the electromagnetic torque is given by

$$T_e = E_{f0}^2 \left[ \frac{1}{X_d} + \left( \frac{1}{X'_d} - \frac{1}{X_d} \right) e^{-t/T'_d} + \left( \frac{1}{X'_d} - \frac{1}{X_d} \right) e^{-t/T'_d} \right] e^{-t/T_a} \sin(\omega t) + \frac{E_{f0}^2}{2} \left( \frac{X'_d - X''_d}{X'_d X''_d} \right) e^{-2t/T_a} \sin(2\omega t). \quad (6.128)$$

The principal component of the electromagnetic torque oscillates at normal frequency and has an initial amplitude  $E_{f0}^2/X_d$ . The double frequency torque represented by the second term of (6.128) is very small.

### 6.1.19 The Electromechanical Equation

If  $J$  is the moment of inertia of the generator, including the turbine, in  $\text{kg m}^2$ ,  $\alpha$  is the rotor angular acceleration in mechanical radians/ $\text{s}^2$  and  $T_a$  is the net torque on the rotor in N m, which includes the shaft (mechanical) torque  $T_m$ , corrected for torque due to rotational losses (friction and windage), and  $T_e$  is the electromagnetic torque due to the process of electromechanical energy conversion, then

$$T_a = J\alpha = T_m - T_e. \quad (6.129)$$

In steady-state operation  $T_m = T_e$  and there is no acceleration. However, during disturbances  $T_a$  is different from zero, and with  $\omega_r$  as the rotor angular speed in mechanical radians/s, where  $\omega_r = d\theta_r/dt$ , where  $\theta_r$  is the rotor angle in mechanical radians and  $t$  the time in seconds,

$$J \frac{d\omega_r}{dt} = T_a = T_m - T_e = J \frac{d^2\theta_r}{dt^2} = T_m - T_e. \quad (6.130)$$

The angular position of the rotor  $\theta_c$  (electrical radians) in relation to a fixed reference axis, can be expressed by the equation, where  $\delta$  is the angle between the phasors  $E_f$  and  $V_t$  rotating at synchronous speed  $\omega_0$  (electrical radians per second)

$$\theta_c = \frac{\pi}{2} + \delta + \omega_0 t \Rightarrow \frac{d^2\theta_c}{dt^2} = \frac{d^2\delta}{dt^2} = \frac{p}{2} \frac{d^2\theta_r}{dt^2}. \quad (6.131)$$

The angle  $\delta$ , in rad E/s, measures the angular position of the rotor in relation to an axis that is rotating at synchronous speed (axis of phasor  $V_t$ ). The factor  $p/2$  converts angle in mechanical radians, into angle in electrical radians. By substitution of (6.131) into (6.130),

$$J \frac{2}{p} \frac{d^2\delta}{dt^2} = T_m - T_c. \quad (6.132)$$

Equation (6.132) can be written in terms of the inertia constant  $H$ , that is defined as the kinetic energy stored at rated speed in megajoule (MJ) divided by the rated apparent power  $S$  of the machine in MVA, i.e.,

$$H = \frac{1}{2} \frac{J\omega_0^2}{S} \text{ (MJ/MVA)}. \quad (6.133)$$

By substituting (6.133) into (6.129) and adding a term corresponding to the damping torque due to the damper winding, where  $D$  is the damping coefficient, the resultant equation, known as the electromechanical equation or swing equation is,

$$\left( \frac{2H}{\omega_0} \right) \frac{d^2\delta}{dt^2} = \bar{T}_m - \bar{T}_c - \left( \frac{D}{\omega_0} \right) \frac{d\delta}{dt}, \quad (6.134)$$

where  $\delta$  is in electrical radians and  $\bar{T}_m$  and  $\bar{T}_c$  are in per-unit.

For turbogenerators around 30 up to 60% of the total inertia is due to the turbine, while in hydrogenerators 4 up to 15% is due to the turbine, the greater percentiles increase with the size of the machine. For turbogenerators the value for  $H$  varies from 3 up to 10 s, while for hydrogenerators it varies from 2 up to 5 s.

### 6.1.20 Design Considerations

#### Apparent Nominal Power: Output Equation

There is a well-defined relation between the principal dimensions of a rotating machine and its volt-ampère or horsepower rating, in terms of quantities that define the specific utilization of the materials of its magnetic and electric circuits. This relation, called the output

equation, is given for a 3-phase generator, by the expression

$$S = 1.11 K_w \pi^2 B_{av} A D^2 L n \times 10^{-6} \text{ (MVA)}, \quad (6.135)$$

where  $S$  = three-phase output power (MVA),  $K_w$  = winding factor,  $B_{av}$  = specific magnetic loading (T),  $A$  = specific electric loading (A/m),  $D$  = inner stator diameter (m),  $L$  = axial length of the core (m), and  $n$  = speed in rps.

Thus, the rating of the machine is proportional to the average gap density  $B_{av}$ , the armature surface current density  $A$ , the volume of the rotating member (represented by the  $D^2L$  product), and the speed of rotation.

For convenience in design, the following specific loadings are defined, where  $\Phi$  is the flux per pole (Wb),  $p$  the number of poles,  $N$  is the number of turns in series per phase and  $I$  is the effective value of stator current (A):

a) Specific magnetic loading,

$$B_{av} = \frac{\Phi p}{\pi D L} \text{ (T)}. \quad (6.136)$$

b) Specific electric loading, i.e., the number of ampere-conductors per meter length of stator surface circumference or the peripheral current density,

$$A = \frac{2mNI}{\pi D} \left( \frac{A}{m} \right), \quad m = 3 = \text{number of phases}. \quad (6.137)$$

Calling  $C$  the output coefficient,

$$C = 1.11 K_w \pi^2 B_{av} A \times 10^{-6} \text{ (MVA)}. \quad (6.138)$$

The output equation may be written as

$$S = C D^2 L n \text{ (MVA)}. \quad (6.139)$$

$S$  is the output power for a generator or the input power for motors. In terms of mechanical output for motors in horsepower (HP),

$$S = \frac{\text{HP} \times 745.7 \times 10^{-6}}{\eta \cos \theta} \text{ (MVA)}, \quad (6.140)$$

where  $\eta$  and  $\cos \theta$  are the efficiency and power factor of the motor, respectively.

Turbogenerators are normally designed with two/four poles with a speed of 3000/1500 rpm for a frequency of 50 Hz, or with a speed of 3600/1800 rpm for a frequency of 60 Hz. Hence, the peripheral speed  $v = \pi D_r n$ , where  $D_r$  is the rotor diameter, is very high and increases with diameter. The centrifugal forces in

the rotor cause an increase in the mechanical forces in the teeth, windings and end-bells. Thus, for a given volume since the diameter of turbo generators has to be kept small, their axial length must be large.

However, in the case of hydrogenerators the speed is low and a large number of poles are necessary. This will increase the diameter of the machine and for a given volume the length of the machine reduces. Hence, hydro generators have a large diameter and small axial length in contrast to turbo generators.

For the same rating, due to the higher speed of turbo generators than for hydro generators, the volume of turbo generators are lower than the volume of hydro generators.

**Additional Considerations.** To increase the output of a machine for a given speed the following alternatives may be possible:

- a) Altering the dimensions enables a notable increase in output to be achieved. For example, increasing both the stator diameter (and consequently the rotor diameter) and the active length by 10% raises the output by approximately 33%. Using a 300 MVA rating as reference, this would allow an increase to about 400 MVA.  
However, a larger stator diameter rotor and active length greatly increase the windage losses. For instance, the surface friction loss, which represents a significant portion of the windage and therefore the total losses rises as the fourth power of the stator diameter and linearly with an increasing active length.
- b) Increase in the specific magnetic loading  $B_{av}$ . However,  $B_{av}$  is limited by saturation in parts of the magnetic circuit. Also, an increase in  $B_{av}$  leads to higher flux in the iron parts of the machine, that results in increased iron losses and reduced efficiency.
- c) Increase in the specific electric loading  $A$  by increasing the armature current, that determines to a large extent the  $I^2R$  loss leading to a high temperature rise, and subsequent need for improvements in the cooling system. The stray-load losses will increase with current too.  $I^2R$  loss can be decreased by decreasing the resistance. This means conductors of larger cross section, that in turn calls for increased slot dimensions; wider slots imply narrower teeth and correspondingly higher flux densities; and deeper slots imply greater leakage reactance.
- d) It is evident that the physical dimensions and the quantitative characteristics of the magnetic and electric circuits are all interrelated, and that the problem for the designer is to adjust their magni-

tudes so that they are not only mutually consistent, but also to ensure that the resultant machine will meet specifications and standards.

#### Short-Circuit Relation (SCR)

As defined previously, the SCR for cylindrical-rotor machines, also called nonsalient-pole (NSPL) and salient-pole machines (SPM) is given by

$$\begin{aligned} \text{SCR} &= \frac{1}{X_s \text{ p.u. (sat)}} \quad (\text{NSPM}) \\ &= \frac{1}{X_d \text{ p.u. (sat)}} \quad (\text{SPM}) . \end{aligned} \quad (6.141)$$

The effects of the SCR on the machine performance and design are as follows:

- a) When the SCR is high (low synchronous reactance):
  - The transient stability limit is improved.
  - The machine has a better voltage regulation.
  - The synchronous, transient and subtransient reactances are also lower. So, the short-circuit currents from the machine increases, implying more costly switchgear in the generation station, as well as an increase in the forces and stresses on the machine end windings under sudden short-circuits.
  - The machine has a larger airgap, and as a consequence a large volume and an increase in losses.
  - The influence of the demagnetizing armature reaction flux on the field winding flux decreases, improving the performance of the excitation system in these conditions.
  - The machine can absorb more reactive power from the transmission system, specially when it operates as synchronous compensator.
  - The cost of the machine increases.
- b) When the SCR is low (high synchronous reactance):
  - The voltage regulation is impaired.
  - The transient stability limit decreases likely resulting in more onerous excitation system requirements, for example higher ceiling voltages and/or faster rise times.
  - The parallel operation becomes somewhat difficult due to low synchronizing power.
  - The short-circuit current decreases.
  - There is the possibility of self excitation when the generator feeds long transmission lines, as this would lead to a large terminal voltage on load rejection due to line charging.

With fast-acting excitation systems the voltage regulation and stability limits are enhanced and the influence of the SCR on the machine stability performance dimin-

ishes. Increasing a nonsalient-pole generator SCR from 0.4 to 0.5 may result in an increase in total volume of about 5–10%.

In salient-pole generators, depending on their sizes and construction, the SCR varies from 0.80 up to 1.20 p.u., while in nonsalient-poles machines the SCR may lie between 0.35–0.60 p.u., these being the lower values for larger machines.

IEEE C50.12 [6.15] also states that the short-circuit ratio of salient-pole generators should be fixed by agreement. If not specified by the purchaser it should be no less than 0.80 p.u.

IEEE C50.13 [6.16]. states that the short-circuit ratio should be fixed by agreement and if not specified by the purchaser it should be no less than 0.35 p.u.

### Length of the Air-Gap

The air-gap in a synchronous machine affects the value of the SCR and hence it influences many other parameters. The choice of airgap length is very critical in the case of synchronous machines. The following are the advantages and disadvantages of a larger airgap and as a consequence lower synchronous reactances and higher SCR.

Advantages:

- Stability: Higher value of stability limit
- Regulation: Smaller value of inherent regulation
- Synchronizing power: Higher value of synchronizing power
- Cooling: Better cooling
- Noise: Reduction in noise
- Magnetic pull: Smaller value of unbalanced magnetic pull

Disadvantages:

- Field MMF: A larger value of field MMF is required
- Size: Larger diameter and hence larger size
- Magnetic leakage: Increased magnetic leakage
- Weight of copper: Higher weight of copper in the field winding
- Cost: Increase in the overall cost.

The airgap length should be designed while considering the above factors.

### Effects of a Reduction in the Number of Stator Series Turns per Phase ( $N_{ph}$ )

The reduction in  $N_{ph}$  will lead to a decrease in armature excitation voltage  $E_f$  and as a consequence in terminal voltage  $V_m$ . To avoid that, the excitation flux per pole  $\Phi_f$  must be increased. As the flux density  $B_f$  should be, in general, at its value at the knee of the magne-

tization curve in order to avoid excessive generation of odd harmonics, and not to increase the iron losses, which would lead to a high temperature rise in the core, the airgap area per pole  $A_g$  must be increased. That is,  $A_g \cong \pi DL/p$ , where  $D$  = stator diameter;  $L$  = stator length;  $p$  = number of poles. Then, an increase in the airgap area involves an increase in the rotor and stator diameters without modifying the airgap length and/or an increase in  $L$ .

### Direct-Axis Transient and Subtransient Synchronous Reactances

A reduction in  $X_d$ , i.e., an increase in SCR also reduces the direct-axis transient and subtransient synchronous reactances. With lower values for these reactances the generator will supply more power during the subtransient and transient periods, which is beneficial to transient stability. On the other hand the short-circuit current will increase and the manufacturer should be consulted to verify if the generator can be submitted to the stresses resulting from this increase in the SCR.

### Damper Windings Ratio: $X'_q/X''_d$ (Salient-Pole Machines)

During normal operation, the generator is operating at synchronous speed. The damper windings also move at the same speed. Thus, they are inactive.

During a transient, the generator speed changes. The damper windings are now moving at a different speed than the synchronous speed. The currents induced in the damper windings generate an opposing torque to the relative motion. This action helps return the rotor to its normal speed.

Some considerations about damper windings:

- The damper torque is always a braking torque. Therefore it has the same effect on the angular motion of the rotor as a decrease of mechanical input torque. Stability of the machine is improved.
- In general, where beneficial effects can be obtained with the use of damper windings, the benefits are greater for a continuous damper than for non-continuous dampers. The non-continuous damper winding lends itself somewhat easier to the removal of a pole but not to a sufficient extent to be a consideration in the choice of type to install.
- When the generators are submitted to high over-speeds, it is desirable for mechanical reasons to have only flexible connections among the poles.
- The lowest overvoltage on the unfaulty phase and the greatest torque and damper power occur with the continuous damper.
- The reduction in overvoltage when continuous dampers are used is an important factor in the

reliable operation of lightning arresters and other equipment in the power station, that, otherwise, could be damaged during load rejection.

- A ratio  $X_q''/X_d''$  as low as 1.35 can be obtained with non-continuous and below width continuous dampers.

Damper windings are to a lesser extent used in turbogenerators as the steel rotor cores of such machines provide paths for eddy currents and thus produce similar effects as dampers.

### Power Factor (pf)

When the voltages, speed, temperatures and the active power from the turbine are maintained constant, if the pf decreases the armature reaction increases and the field current must increase to maintain the airgap flux. Both the field and armature amperes-turns increase. For instance, a reduction in pf from 0.95 to 0.90, increases armature current from  $1/0.95 = 1.052$  p.u. to  $1/0.90 = 1.111$  p.u., i.e., an increase of 5.6%. This may require more conductors in the field and armature to control the increase in temperature for the same insulation and cooling systems. The apparent power of the machine also increases due to the greater reactive power capacity of the generator when the pf decreases. Thus, the cost of the machine increases. As an estimate, the design of a generator for a pf of 0.90 would imply an increase in cost between 2.5–5.5% when compared with a pf of 0.95.

If generators are located a great distance from load centers, a pf of 0.95 may be suitable, while if they are located near load centers a lower power factor may be desirable to control the system voltage, that might reduce or eliminate other methods of voltage control.

### Terminal Voltage

The expression below gives the rms phase to phase terminal voltage  $V_t$  of a machine with windings connected in star formation

$$V_t = \frac{3.85q_s n_s f k_w \Phi_f}{mC}, \quad (6.142)$$

where  $q_s$  = total slots in the stator,  $n_s$  = number of conductors in each slot,  $f$  = frequency,  $k_w$  = winding factor,  $\Phi_f$  = field flux per pole,  $m$  = number of phases and  $C$  = number of parallel paths in the armature.

From (6.142), we can conclude:

- Increasing the field flux per pole may be allowed up to a certain limit due to saturation in parts of the magnetic circuit. A high flux implies an increase in iron losses and reducing efficiency.

- If the number of slots increase the voltage increases, but the machine cost increases.
- If the number of parallel paths increases the terminal voltage decreases.

### Inertia Constant

The minimum inertia requirements are usually determined from hydraulic system considerations, since inertia affects the maximum rate of closure of turbine gates and the corresponding pressure transients, as well as the stability of the hydraulic system. The inertia constant is a function of the apparent nominal power of the generator and of the moment of inertia  $J$  of the rotating parts (turbine + generator), multiplied by the square of the radius of gyration. It is given by

$$H = 5.48 \times 10^{-9} J \frac{(\text{rpm})^2}{\text{MVA}_{\text{rating}}} \quad (\text{s}). \quad (6.143)$$

The speed is tied with the specific speed  $N_s$ , that is a characteristic of each design of a turbine runner and varies with the head and type of turbine. The speed can be determined by

$$\text{rpm} = \frac{N_s h^{5/4}}{\sqrt{P}}, \quad (6.144)$$

where  $P$  is the power developed by the turbine and  $h$  is the net head.

A greater value of  $H$  has influence on the behavior of the machine during transient conditions of operation, improving the stability of the generator. Once the rated voltage and current are set up, the MVA is fixed. Then, to increase  $H$  it will be necessary to increase the rotor diameter. This will increase the size of the machine and may require reinforcement of the foundations of the power house. The efficiency of the generator will decrease due to the increase in mechanical losses.

## 6.1.21 Advanced Technologies

Some advanced technologies in synchronous generators and motors such as: superconducting generators and motors; permanent magnet motors; switched reluctance motors and line start permanent magnet motors, are presented.

### Superconductor Synchronous Generator (SSG) and Compensator

A SSG is expected to have about 1/3 of the overall volume of an equivalent conventional generator, so that a power station can accommodate more generators for the same space. They are the promising alternative for increasing generation efficiency, reducing weight and

improving power system stability, in comparison with conventional generators. As HTS (high-temperature superconductor) tapes are sensitive to AC fields and AC currents, their use in electrical machines is economically attractive in DC windings, as in rotor field windings of synchronous machines [6.25]. Advanced heat and electric insulation along with cryogenic refrigeration technology is required by the superconducting generators to maintain the low temperature requirement and the functionality of the superconducting coil. The stator windings carry alternating currents. However, the cooling system has greater cost, size and weight when compared with conventional generators, and the motor bearings and lubrication oil need to be able to withstand cold temperatures or need to be insulated from the cold rotor.

A major benefit of HTS generators is lowered armature reactances. The value of synchronous reactance may be from 1/5 to 1/4 lower than that of a conventional generator, consequently in normal operation the load angle is much lower, resulting in larger margins against loss of stability. The reactive power absorption increases substantially. The efficiency of the generator, usually in the range of 98.0–99.0%, can be increased by 0.3–0.5%, depending on the design of the cooling system.

A marine superconducting generator, rated 4 MVA, 60 Hz, and 3600 rpm, was manufactured in 2002. The rotor winding is made of HTS conductors. The armature winding is fixed to the stator core by nonmagnetic fibre plastic elements [6.26]. This generator is now operating as a synchronous compensator in a 20 kV distribution network, after undertaking a long test program.

### Superconductor Synchronous Compensator (SSC)

An 8 MVAR, 13.8 kV high-temperature superconductor synchronous compensator (SSC) was developed and has been in operation since the end of 2004. The stator winding is of the conventional type while the rotor is made of superconducting coils. In a normal field winding of a synchronous machine, the coils expand and contract when there is load variation due to an increase or decrease in the temperature of the conductors. This results in insulation fatigue that can lead to premature failure of the field winding. In the case of the use of superconductive coils this is not verified because the conductors operate at a constant temperature and have practically no resistance, leading to a longer life expectancy of the winding. This can be explained by means of Fig. 6.45, which presents the V-curves for conventional synchronous compensators and SSC, where it can be noted that the field current of a conventional machine to generate its rated power should be

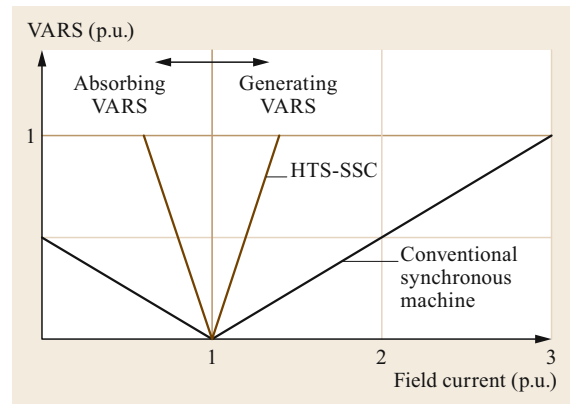


Fig. 6.45 V-curves for conventional and high-temperature superconductor synchronous compensator (SSC) machines

increased by about three times its value at no-load. As a consequence there is an increase in the resistive losses in the field winding by a factor of nine, causing heating in the coils. In the case of the SSC this is practically nonexistent, with the field current being increased, to generate its nominal power, less than 1.5 times its no-load value [6.27].

A static var compensator (SVC) and a static synchronous compensator (STATCOM) vary their reactive power with the square of the voltage and directly with the voltage, respectively, while in SSCs their reactive power is independent of the system voltage and can reach several times its nominal power with a static excitation system, and may avoid the occurrence of a voltage collapse in the system, presenting a performance superior to that obtained with an SVC or a STATCOM.

In addition, SSCs do not produce harmonics such as SVCs and STATCOMs, and do not require filters. Although to date the SSCs have been manufactured for relatively small nominal power, with economies of scale due to increasing use, their cost will be reduced and their use is particularly advantageous in systems that present problems of voltage collapse or abrupt voltage variations.

### Superconducting Motors

In superconducting motors, like superconducting generators, HTS nonresistance coils replace the conventional copper field winding, leading to a sharp reduction of electrical losses in the rotor. The HTS field winding can carry larger currents producing stronger magnetic fields in comparison with a conventional copper winding motor, resulting in increased power density and a smaller size for the motor, reducing its dimensions and weight, while the motor efficiency increases and the operating costs reduce.

They will find application in ratings above 1000 HP, especially in large industries such as chemical, oil and gas refining, steel milling, pulp and paper processing, and other heavy-duty applications. An important application for HTS motors will be in transportation systems, particularly naval and commercial ship propulsion, because of their small size and less weight savings, that are an important benefit where limited space is a key requirement.

A HTS ship propulsion motor of 36.5 MW has been successfully tested. This motor has less than half the size of a conventional motor, reduces the ship weight and frees up space. This development raises the possibility of building an HTS wind generator, particularly those for offshore farms [6.28].

### Permanent Magnet Motors

Permanent magnet (PM) synchronous motors largely used in servo motor applications, are being increasingly used in industrial motor drive systems. The traditional aluminum rotor cage of an induction motor is replaced by a powerful ceramic or rare earth neodymium iron boron (NdFeB) magnets attached to the surface of the rotor or to the rotor interior to establish a permanent magnetic field. The joule losses in the rotor are significantly reduced. As the PM motor is designed for variable speed operation, it must be controlled by a variable speed drive (VSD). PM motors have been demonstrated to exceed proposed super premium efficiency levels (IE4), even when controller losses are included. They have a high power factor [6.29].

PM motors due to their high torque, light weight, and low inertia, are often specified for regenerative elevator drives and electric vehicle hub motor drives. Industrial applications suitable for PM motors include: Adjustable speed pumps, winders, crane and hoist systems, fans and compressors, conveyors, plus extruders, and printing presses.

### Switched Reluctance Motors

The rotor of a switched reluctance (SR) motor does not have magnets (unlike the PM motor), bars, or windings. It is essentially a piece of shaped iron and exploits the fact that forces from a magnetic field on the rotor

iron can be many times greater than those on the current carrying conductors. A SR drive system requires, like a PM motor, an electronic power converter to control the torque and speed. The controller eliminates low speed cogging by switching motor phases on and off in relation to the rotor position. They allow repeated starting under full-load. The rotor produces no heat at stall, so prolonged operation at stall is also possible. Switching losses for the SR motor controller are also reduced to about half of those for an AC motor inverter [6.30].

They may be used in low-speed, high-torque applications, such as: refrigerant compressors, extruders and conveyors, centrifuges, weaving looms, and pumps for reverse osmosis systems, as well as with blowers and high-speed pumps. Like the PM motors, the SR motors are available in NEMA and IEC frames. SR motors with drives are available in the 30–335 HP size range with base speeds from 200 to 10 000 rpm or more depending upon application requirements.

### Line Start Permanent Magnet Motors (LSPMs)

A LSPM has a conventional three-phase distributed winding in the stator (identical to conventional induction motors), but its rotor has an aluminum cage and internal permanent magnets. It operates at a fixed, synchronous speed regardless of the load. It can start and accelerates directly connected to the line, without the need for a controller. There are no resistance losses in the aluminum rotor cage, as it turns at synchronous speed, so that LSPM motors have higher efficiency than premium efficiency motors (IE3) and can achieve super premium efficiency levels (IE4). They operate with the same current and power factor as premium efficiency induction motors. Similar to PM motors, due to the high strength rotor magnets, care must be taken when removing or inserting the motor rotor.

LSPM motors are available in NEMA Design A ratings from 1 to 10 HP at a synchronous speed of 1800 rpm and from 1 to 5 HP at 1200 rpm. While the price of a LSPM motor is currently about double that of a high efficiency (IE2) class motor, attractive simple payback periods for the additional investment in a LSPM motor may be available for applications that operate for more than 6000 h per year [6.31].

## 6.2 Induction Machines

The three-phase induction motor is mostly used in industrial drives. It is also called an asynchronous motor because it does not run at a synchronous speed. It consists of two basic components: the stator or pri-

mary winding, and the rotor or secondary winding. The former supporting windings which receive energy from the supply circuit, the latter carrying windings in which current is induced. The stator of the motor con-

sists of two main parts: the stator frame and the stator core.

### 6.2.1 Construction

The stator frame of the motor is the outer most part of the motor, and with the associated end shields, transmit the torque to the base of the frame and supports the stator core and winding. It takes various forms depending upon the operating conditions to which the motor is to be subjected, such as: open, open drip-proof (ODP), guarded, splash-proof, totally-enclosed, totally-enclosed nonventilated (TENV), totally-enclosed fan-cooled (TEFC), weather protected (Type I), weather protected (Type II), encapsulated, explosion-proof and inverter duty. As these stator frames are related to cooling of the motor, they will be described in details in Sect. 6.2.2, *Cooling*.

The stator core carries three-phase windings and produces a rotating magnetic field. A terminal box connects the six terminals of the windings (two of each phase). Depending on the speed, the stator is wound for a definite number of poles. Normally the motor operates with a delta connected stator. The stator core is laminated to reduce eddy current losses. This laminated structure is made up of steel stampings that are about 0.3–0.6 mm thick and are isolated from each other. The stampings are slotted to receive the windings and are fixed to the stator frame. The slots are punched on the inner side of the stampings as shown in the Fig. 6.46. To reduce hysteresis losses the stampings are generally made up of high-grade silicon steel.

Depending on the rotor winding construction there are two types of three-phase induction motor.

#### (a) Squirrel-Cage Three-Phase Induction Motor

The rotor of the squirrel-cage three-phase induction motor consists of a cylinder of electrical steel laminations with slots on its periphery. The bearings that support the rotor shaft are either sleeve or ball bearings. Copper or aluminum bars are placed in the slots on the periphery of the rotor and are permanently short-circuited by copper or aluminum rings called end-rings, that do not add any external resistance in series with the rotor circuit for starting purposes. Since the voltage developed in the squirrel cage winding is very low, no intentional insulation layer is present between the bars and the rotor steel. In order to provide mechanical strength these rotor bars are welded or electrically braced or even bolted, to the end rings forming a complete closed circuit resembling a cage-like shape and hence the name, squirrel-cage induction motor. The rotor conducting bars are usually not parallel to the shaft,

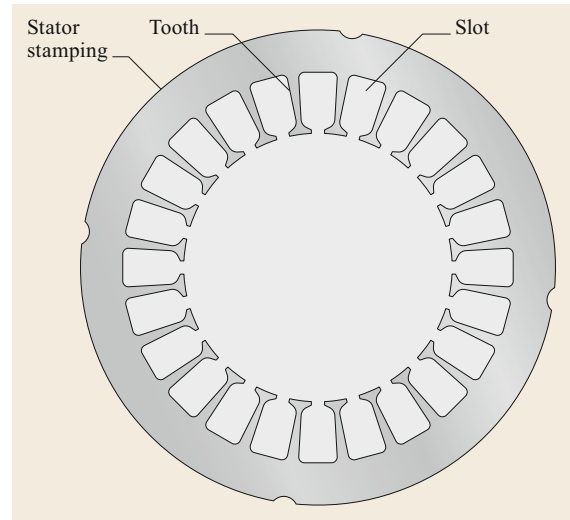


Fig. 6.46 Stator construction of an induction motor

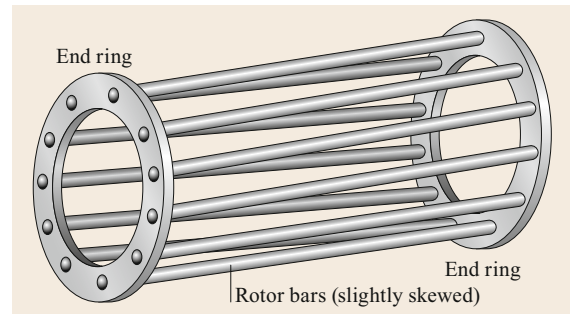


Fig. 6.47 Rotor bars of a squirrel-cage motor

but are purposely given a slight skew as the skewing helps in reduction of magnetic hum, thus keeping the motor quiet, and helping to avoid *cogging*, i.e., the locking tendency of the rotor teeth to remain under the stator teeth due to the direct magnetic attraction between the two.

As the bars are permanently short-circuited by end rings, the rotor resistance is very small. The absence of commutator or slip ring and brushes make the construction of squirrel-cage three-phase induction motor very simple, reliable and robust and hence widely used in industry. These motors have the advantage of adapting any number of pole pairs. A squirrel-cage induction rotor is shown in Fig. 6.47.

The advantages of the squirrel-cage motor are:

- The cage rotor is cheaper, and the construction is robust.
- The absence of brushes reduces the risk of sparking.
- It requires less maintenance.



**Table 6.7** Maximum temperatures of some insulation classes

Insulation class	A	B	F	H
Maximum temperature (°C)	105	130	155	180

### (b) Wound-Rotor or Slip-Ring Three-Phase Induction Motor

Wound-rotor induction machines have a three-phase winding on the rotor, similar to the stator winding. The rotor winding is usually wye-connected with the terminals of the three phases connected to slip-rings, which are mounted on the end of the shaft, and where external circuits can be connected to the rotor, allowing external control of the machine. Wound-rotor motors can be started with low inrush current and with a high torque, by inserting high resistance into the rotor circuit. In normal operation, the windings at the slip-rings are short-circuited. Compared to a squirrel-cage rotor, the rotor of the slip-ring motor has more winding turns, the induced voltage is then higher, and the current lower. Wound-rotor induction machines are usually significantly more expensive than cage rotor machines. They are particularly attractive in some applications, such as:

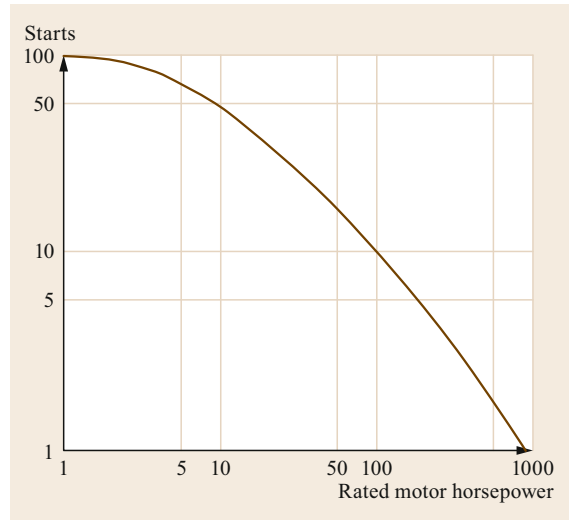
- Speed control of very large machines
- Doubly-fed induction generation (used in wind turbines)
- To gradually bring up to speed high-inertia loads
- To drive loads that require high starting torque and low starting current (cranes, hoists, etc.).

## 6.2.2 Insulation and Cooling

### Insulation

The insulation system must ensure that short-circuits do not occur, that the conductors do not vibrate in spite of the magnetic forces, and that the heat developed in windings due to joule losses is transmitted to a heat sink. Insulation life is a function of the length of time it is exposed to temperature. The most common insulation classes are presented in Table 6.7, excerpted from NEMA standards [6.32].

Motors are designed with an allowable increase in temperature above ambient during operation. This is referred to as temperature rise (Table 6.8). The maximum allowable temperature rise during operation for a motor varies with respect to insulation class, altitude, and the motor service factor. The service factor is essentially a safety margin and refers to the motor's ability to deliver horsepower beyond its nameplate rating under specified conditions. Most three-phase motors are rated with a 1.0 or 1.15 service factor. If the ambi-



**Fig. 6.48** Allowable number of starts per hour for a class B motor driving a low inertia load

ent temperature exceeds 40°C or at elevations above 3300 feet, the motor service factor must be reduced or a higher horsepower rated motor should be specified. As an oversized motor will be under-loaded, the operating temperature rise is less and overheating is reduced [6.30].

During starting high energy flows into the motor, that may cause thermal-aging of the winding insulation. This is a fatigue phenomenon. Repeated exposure to excessive temperature, whether sustained over long periods or in often-repeated short cycles, will eventually break down the insulation material leading to a winding failure, and depending on the insulation system, that breakdown may begin between turns in a coil, or within the ground wall insulation layers. In the rotor of squirrel-cage motors the individual bars and end rings can undergo expansion because some parts reach higher temperatures than others. Bars can bend, lift out of their slots, or break loose from attachment to the rings. Repeated bending back and forth, even at a fairly low stress level, eventually can cause breakage. Thus, the number of starts per hour should be limited. Figure 6.48 shows for a class B motor driving a low inertia load at rated voltage and frequency, the number of starts allowed per hour. The stress on the motor can be reduced by means of a *soft start* mechanism (autotransformer, part-winding, electronic soft-start, etc.), increasing the number of starts per hour.

### Cooling

All rotating electrical machines dissipate heat as a result of joule losses, iron losses, stray losses and mechanical losses. These losses are higher during the process

**Table 6.8** Allowable rise and operating temperature limits for some insulation classes considering the service factor

Service factor	Enclosure	Insulation temperature	Class A (°C/°F)	Class B (°C/°F)	Class F (°C/°F)	Class H (°C/°F)
1.0/1.15	All	Ambient	40/104			
1.0	All	Allowable rise	60/140	80/176	105/221	125/257
1.0	All	Operating limit	100/212	120/248	145/293	165/329
1.15	All	Allowable rise	65/149	90/194	115/239	140/284
1.15	All	Operating limit	105/221	130/266	155/311	180/356

of starting the motor and dynamic braking, and increase with the size of the motor. Thus, insulation that can withstand higher temperatures and cooling to remove the heat from the windings, core and bearings, must be provided as the motor size increases. Fractional horsepower motors, generally, do not require forced cooling, while larger integral motors, usually incorporate a built in cooling fan to force air through the machine [6.33].

According to its enclosure type and cooling, motors can be classified in several categories. The most important are:

- a) *Open*. It has ventilating openings that allow external air to pass over and around the motor windings to provide cooling. This design is seldom used.
- b) *Open drip-proof (ODP)*. An open motor in which ventilation openings prevent liquids and solids, that fall from above at angles up to 15° from the vertical, from entering the interior of the motor and causing damage. When the motor is not in the horizontal position, such as when it is mounted on a wall, a special cover might be necessary to protect it. This type of enclose can be specified when the environment is free from contaminants and where wind-driven rain is not a consideration. Suitable for most indoor or protected areas.
- c) *Totally enclosed fan-cooled (TEFC)*. A totally enclosed motor with an external fan that blows air over the frame to dissipate heat more quickly. With this arrangement no outside air enters the interior of the motor. They can be used in dirty, moist, or mildly corrosive atmospheres, or where wind-driven rain is anticipated.
- d) *Totally enclosed nonventilated (TENV)*. Similar to TEFC but the motor is designed with a low enough temperature rise so that an external fan is not required for cooling, or duty is limited so the motor does not overheat. Not for use where combustible vapors are present.
- e) *Guarded*. An open motor in which all ventilation openings are limited to specified size and shape. This protects the intrusion of fingers or foreign objects into the motor.

- f) *Weather protected (Type I)*: Similar to an ODP motor with the addition of screens to prevent rain, snow and large particles from entering the motor. Suitable for most indoor or protected areas that have relatively clean environments.
- g) *Weather protected (Type II)*: In this type air is forced to change direction by 90° by means of baffles placed at the inlet of the motor, preventing water from entering the motor. It is suitable for outdoor applications with up to 100 mph winds driving rain at the motor.
- h) *Splash proof*. An open motor designed with ventilation openings that prevent liquid or solids particles from entering the motor at any angle less than 100° from the vertical.
- i) *Encapsulated*. The windings are covered with a heavy coating of material to provide protection from moisture, dirt, and abrasion.
- j) *Explosion proof*. Similar in appearance to a TEFC motor and designed to withstand an internal explosion and to prevent ignition of specified gases or vapors surrounding the motors. It is suitable for safe operation of the motor in hazardous environments.

Motors and modern generators rated less than about 100 MVA are almost always cooled by air flowing over the rotor and stator. IEC and NEMA standards describe the various types of cooling methods in detail.

### 6.2.3 Operating Principles

When an induction motor is connected to a three-phase power supply the stator currents create a rotating magnetic field that travels at synchronous speed in relation to the stator and rotor. Electromotive forces are induced in the stator and rotor windings, and currents circulate in the rotor windings, like currents in the secondary of a transformer. These rotor currents, when the rotor is at standstill, have the same frequency as the stator, however, when the rotor rotates the frequency of these currents are lower than the synchronous frequency of the stator currents. Thus the rotor magnetic field produced by the rotor currents, in relation to the rotor, travel at a speed lower than synchronous speed and

equal to the difference between the synchronous speed and the speed of the rotor, but at synchronous speed with respect to the stator. The two magnetic fields are then stationary and a constant torque is produced, that accelerates the rotor in the direction of the rotating stator magnetic field.

The stator is connected to a circuit with a voltage  $V_1$ . As mentioned, the three-phase currents enters the stator windings and creates a rotating magnetic field, called the main flux,  $\Phi_m$ , within the airgap, rotating at a speed  $n_1 = [(120f_1)/p]$  (rpm), linking both stator and rotor. This flux induces, in the stator and rotor, the EMFs  $E_1$  and  $E_2$ , respectively. With the rotor open-circuit and stationary, the current in the stator  $I_1$  is practically equal to the exciting current  $I_0$ , i.e.,  $I_1 = I_0$ , where  $I_0 = I_m + I_c$ , being  $I_{mc}$  the magnetizing component of  $I_0$ , that produces the main flux  $\Phi_m$  and  $I_c$  is the core-loss component of  $I_0$ , which supply hysteresis and eddy-current losses in the stator and rotor due to the main flux. In the case of the induction motor as compared to a transformer the exciting current  $I_0$  is considerably larger. In a transformer the excitation current varies from 2 to 5% of the rated current, whereas in an induction motor, due to the airgap, the excitation current is about 25–50% of the rated current, depending upon the size of the motor.

When currents flow in the rotor windings, a MMF wave is produced, and this MMF wave, i.e., the armature reaction, reacts upon the stator MMF wave, such that it opposes the stator MMF and tends to reduce the main flux and  $E_1$ . Then the stator is forced to draw more current ( $I_2'$ ) from the lines, thus compensating the armature reaction and sustaining the main flux, i.e.,  $E_1$ . As a consequence, the stator current  $I_1 = I_0 + I_2'$ . The primary and secondary leakage fluxes induces, in the windings, the leakage EMFs  $jI_1X_1$  and  $jI_2X_2$ , respectively. Considering the stator and rotor resistances  $R_1$  and  $R_2$ , the following equations, per phase, can be written for both types of rotors, noting that the stator voltage  $V_1$  has to counter balance the self induced EMF  $E_1$  and has to supply voltage drops  $I_1R_1$  and  $I_1X_1$ . The rotor induced EMF  $E_2$  has to supply the drop across rotor impedance.

$$\dot{V}_1 = -\dot{E}_1 + (R_1 + jX_1)\dot{I}_1 \quad \text{and} \quad \dot{E}_2 = (R_2 + jX_2)\dot{I}_2 \quad (6.145)$$

From (6.145) the phasor diagram of an induction motor on load can be obtained (Fig. 6.49). This diagram is very similar to the diagram of a loaded power transformer. The differences are that in the case of an induction motor the rotor (secondary) supplies a rotating mechanical load, while the transformer secondary supplies an electrical load. Note that  $\theta_1$  is the angle be-

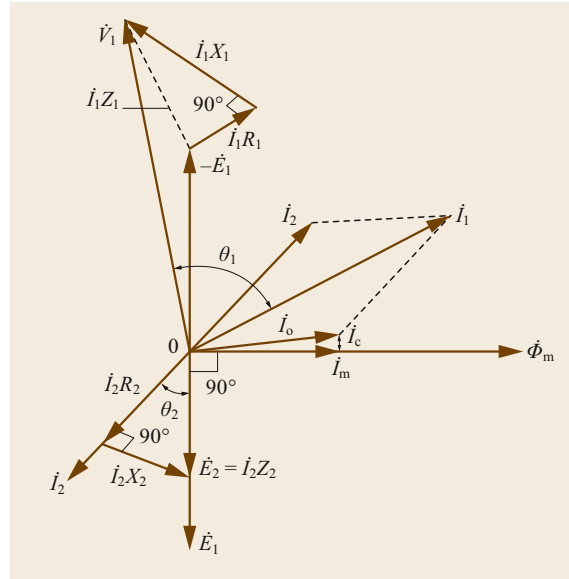


Fig. 6.49 Phasor diagram of an induction motor

tween  $V_1$  and  $I_1$  and  $\cos \theta_1$  gives the power factor of the induction motor, while  $\cos \theta_2$  is the load power factor.

The EMFs induced in the stator  $E_1$  and rotor  $E_2$ , are given by

$$E_1 = 4.44f_1N_1k_{w1}\Phi_m \quad \text{and} \quad E_2 = 4.44f_2N_2k_{w2}\Phi_m, \quad (6.146)$$

where  $f$  = frequency,  $N$  = turns,  $k_w$  = winding factor and  $\Phi_m$  = main or resultant field. Stator quantities are designated by the index 1 and rotor quantities are designated by the index 2. The stator frequency is the synchronous frequency, thus  $f_1 = f_s$ .

The main or resultant field  $\Phi_m$  turns at synchronous speed ( $n_s$ ) and the rotor turns at a speed  $n$ . Then,  $\Phi_m$  cuts the rotor windings at a speed  $n_s - n$ . The rotor frequency  $f_2$  is

$$f_2 = \left( \frac{n_s - n}{n_s} \right) \left( \frac{p}{2} \frac{n_s}{60} \right) = sf_s, \quad (6.147)$$

where  $s$  is the rotor slip with relation to the stator, i.e.,

$$s = \left( \frac{n_s - n}{n_s} \right) \quad (6.148)$$

and

$$f_s = \left( \frac{p}{2} \frac{n_s}{60} \right), \quad (6.149)$$

where  $p$  is the number of poles and  $f_s$  is the synchronous frequency.

Two situations will be analyzed:

a) When the motor operates at rated speed or close to it.

In this case the slip is very low, and the rotor reactance  $X_2 = 2\pi f_2 L_{12} \cong 0$ , where  $L_{12}$  is the secondary leakage inductance.  $E_2$  is practically in phase with  $I_2$ . The load power factor is close to unity. The rotor current  $I_2$  is

$$I_2 = \frac{E_2}{R_2} = ks, \quad \text{i.e., directly proportional to the slip.}$$

b) When the motor operates with nonneglected slip (during acceleration).

In this case  $X_2 = 2\pi f_2 L_{12} = 2\pi s f_s L_{12}$  can not be neglected and the actual rotor current is

$$I_2 = \frac{E_2}{Z_2} = \frac{E_2}{\sqrt{R_2^2 + X_2^2}} = \frac{k_1}{\sqrt{(R_2/s)^2 + (2\pi f_s L_{12})^2}}. \quad (6.150)$$

The rotor current is no longer directly proportional to the slip. At starting  $s = 1, f_2 = f_s$  and the current has its maximum value.

### 6.2.4 Equivalent Circuit of an Induction Motor

Based on (6.145)–(6.150) and the phasor diagram, the equivalent circuit of a three-phase induction motor can be drawn, as shown in Fig. 6.50, where the circuits for the stator and rotor were represented separately, and according with (6.145)  $R_1$  and  $jX_1$  are the stator winding resistance and reactance, respectively;  $R_c$  is the core loss component,  $X_m$  is the magnetizing reactance;  $R_2$  and  $X_2$  are the rotor winding resistance and reactance, respectively. The effect of developed mechanical power and rotor copper loss is represented by the resistance  $R_2/s$ .

The equivalent circuit with the rotor (secondary) quantities referred to the stator (primary) is shown in Fig. 6.51, where  $R_2'$  is the rotor winding resistance referred to the stator winding and  $X_2'$  is the rotor winding inductance referred to the stator winding.

Some simplification results, without any significant error, when the core loss resistance  $R_c$  of the parallel branch is removed and the associated core loss is subtracted from the internal mechanical power  $P$ , i.e., the core loss is added to the rotational losses and stray-load losses. Such a procedure has the advantage of not needing to separate the core loss from the rotational losses during motor testing. The error introduced is very small and the circuit equivalent becomes that of Fig. 6.52 [6.34].

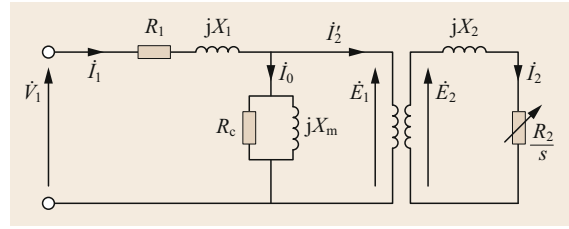


Fig. 6.50 Equivalent circuit of an induction motor with stator and rotor windings separately

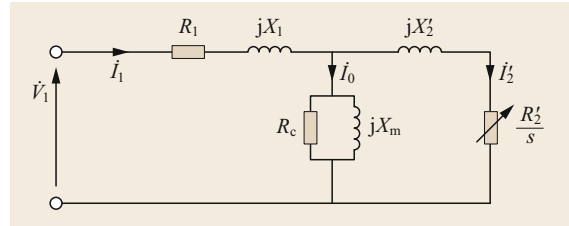


Fig. 6.51 Equivalent circuit of an induction motor with the rotor winding referred to the stator

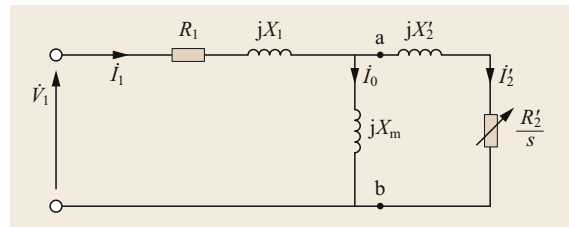


Fig. 6.52 Simplified equivalent circuit of an induction motor

For transferring quantities from the secondary to the primary, the secondary quantities should be multiplied by the factors:

- For voltage:  $(N_1 k_{w1}) / (N_2 k_{w2})$
- For current:  $(m_2 N_2 k_{w2}) / (m_1 N_1 k_{w1})$
- For resistance and reactance:  $m_1 (N_1 k_{w1})^2 / [m_2 (N_2 k_{w2})^2]$ .

The squirrel-cage induction motor produces the same number of poles as that of the stator. It is seen as a polyphase winding with  $m_2 = 2Q_2/p$  phases, where  $Q_2$  is the number of rotor bars, and the number of turns per phase  $N_2 = 1/2$ , because each phase consists of one conductor. The distribution and pitch factors are equal to 1.  $R_2$  and  $X_2$  are the values per bar. Considering the rotor skew,  $N_2$  in the previous equations has to be multiplied by the skew factor  $k_s$ , that is given by

$$k_s = \frac{\sin(\theta_s/2)}{\theta_s/2}, \quad (6.151)$$

where  $\theta_s$  is the skew angle in electrical radians.

### 6.2.5 Power and Torque Relations of an Induction Motor

#### Power Relations

The three-phase active power transferred from the stator to the rotor through the airgap is  $P_{sr} = 3(I_2')^2 R_2'/s$ , and the active power loss in the copper of the rotor is  $P_{copr} = 3(I_2')^2 R_2'$ . Thus the developed internal mechanical power  $P$  is

$$P = P_{sr} - P_{copr} = (1-s)P_{sr} = 3(I_2')^2 R_2' \frac{1-s}{s}. \quad (6.152)$$

Thus, the part  $(1-s)$  of the power transferred to the rotor by the stator is converted to mechanical power  $P$ . So, if an induction motor has a high slip it will have a low efficiency. Also, as  $R_2'/s = R_2' + R_2'(1-s)/s$ , the equivalent circuit of Fig. 6.52 could be redrawn by separating the resistance  $(R_2'/s)$  into two components, obtaining the copper loss in the rotor  $P_{copr} = 3(I_2')^2 R_2' = sP_{sr}$ , and the power that is converted to developed mechanical power  $P = [3(I_2')^2 R_2'(1-s)/s]$ .

The core losses  $P_{core}$  occur in normal operation basically in the stator, because the frequency of flux density variation in the rotor core of the induction machine is very low ( $f_2 = sf_1$ , where  $f_1$  is the stator synchronous frequency) under normal operating conditions so that the rotor has negligible core-losses.

The useful mechanical power or load power  $P_L$ , i.e., the mechanical power delivered at the shaft to a load is less than the developed internal mechanical power  $P$  by the rotational losses  $P_{rot}$  (the sum of bearing friction losses, brush friction losses in the case of wound rotors, windage losses) and by the stray-load losses or additional losses  $P_{add}$ . Stray-load losses are iron losses in the teeth and on the surface of rotor and stator caused by a ripple on the flux density wave due to the slot-openings of the stator and rotor, and also include the copper losses created by harmonic currents induced in the rotor windings by high-order stator MMF harmonics. It is assumed that stray-load losses may be subtracted directly from  $P$  like the rotational losses, thus they may be added to the rotational losses.

$$P = P_L + P_{rot} + P_{add}. \quad (6.153)$$

The heat developed by the losses increases the temperature of the machine and directly affects the specification of the insulation system, the thickness of the laminations and the material of the core, the type of bearings and the ventilation system. Some measures can be taken to reduce windage losses, such as: cast copper rotors lower rotor resistance losses; thinner laminations decrease the eddy current losses; premium grade steel

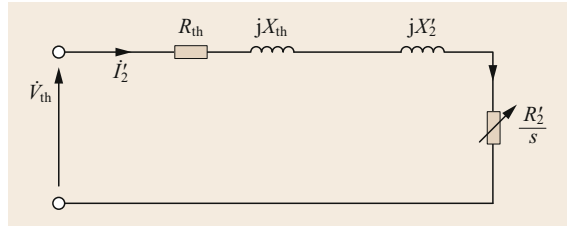


Fig. 6.53 Approximate equivalent circuit of an induction motor by Thévenin's theorem

sheets reduce the hysteresis losses; and making the rotor and stator surfaces as smooth as possible, and keeping the rotor-stator gap as large as practical without compromising electrical efficiency.

Applying Thévenin's theorem between points a and b of Fig. 6.52 the equivalent circuit is reduced to that shown in Fig. 6.53 and the voltage and impedance resultant are

$$V_{th} = V_1 \frac{X_m}{\sqrt{R_1^2 + (X_1 + X_m)^2}}, \quad (6.154)$$

$$Z_{th} = R_{th} + jX_{th} = \frac{jX_m(R_1 + jX_1)}{R_1 + j(X_1 + X_m)}. \quad (6.155)$$

The amplitude of the rotor current referred to the stator is

$$I_2' = \frac{V_{th}}{\sqrt{(R_{th} + R_2'/s)^2 + (X_{th} + X_2')^2}}. \quad (6.156)$$

The airgap three-phase power is given as  $P_{sr} = 3(I_2')^2 R_2'/s$ , and the developed internal mechanical power  $P = (1-s)P_{sr}$  may be written as

$$P = \frac{3(1-s)R_2'V_{th}^2}{s \left[ \left( R_{th} + \frac{R_2'}{s} \right)^2 + (X_{th} + X_2')^2 \right]}. \quad (6.157)$$

#### Torque Relations

The developed mechanical torque or internal or electromagnetic torque  $T$  on the rotor has to overcome the load (useful) torque  $T_L$  and the torque associated with the rotational and additional losses  $T_0$ . Dividing equation (6.154) by the rotor angular mechanical speed  $\omega_r$ ,

$$T = T_L + \frac{P_m + P_{add}}{\omega_r} = T_L + T_0, \quad (6.158)$$

where

$$\omega_r = (1-s)\omega_s \quad \text{and} \quad \omega_s = \frac{4\pi f}{p} \quad (\text{radians mec./s}). \quad (6.159)$$

Considering (6.157) the developed mechanical torque is

$$T = \frac{3 \frac{R'_2}{s} V_{th}^2}{\omega_s \left[ \left( R_{th} + \frac{R'_2}{s} \right)^2 + (X_{th} + X'_2)^2 \right]} \quad (6.160)$$

The maximum torque developed by the motor is determined by  $dT/ds = 0$ , and the corresponding slip is given by

$$s_{\max T} = \frac{R'_2}{\sqrt{R_{th}^2 + (X_{th} + X'_2)^2}} \quad (6.161)$$

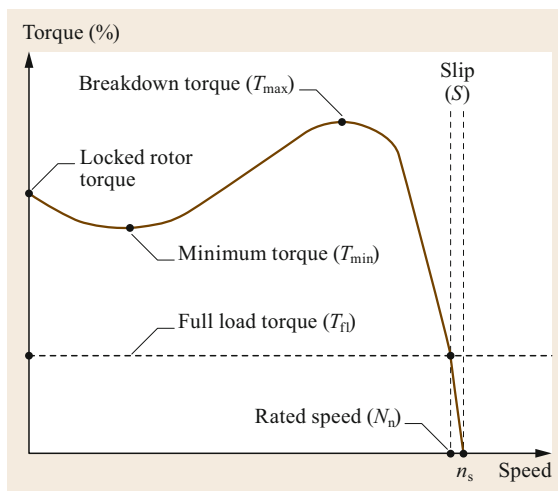
Substituting (6.161) in (6.160) the maximum (breakdown) torque developed by the motor is

$$T_{\max} = \frac{3V_{th}^2}{2\omega_s \left[ R_{th} + \sqrt{R_{th}^2 + (X_{th} + X'_2)^2} \right]} \quad (6.162)$$

At starting  $s = 1$  ( $\omega_r = 0$ ) and  $T = T_p$  (starting torque, also designates as locked torque) and if theoretically  $s = 0$  ( $\omega_r = \omega_s$ ) the  $T = 0$ .

The operating torques of an electric motor (Fig. 6.54) are defined as:

- Full load torque: Is the torque necessary to produce its rated horsepower at full-load speed.
- Locked rotor or starting torque: Is the torque that it will develop at rest with rated voltage applied at rated frequency.
- Minimum (pull-up) torque: Is the minimum torque the motor develops while accelerating from standstill to the rated speed. If the load applied to the



**Fig. 6.54** Typical torque  $\times$  speed characteristic of NEMA class B induction motors

motor shaft exceeds the pull-up torque, but not the locked rotor torque, the motor will turn, but will never accelerate to the rated speed. Not all motors have a pull-up torque rating. Design D (high slip) motors, for example, do not.

- Breakdown (pull-out) torque: Is the maximum torque that it will develop with rated voltage applied at rated frequency.

### Effect of Harmonics on the Torque

According to Sect. 6.1.4 of the synchronous machines the MMF harmonics create flux harmonics that induce harmonic currents in the rotor. Besides the fundamental frequency harmonic, the effect of the fifth and seventh harmonics, which have greater influence on the performance of the machine, will be considered.

The slips for the first ( $s_1$ ), fifth ( $s_5$ ) and seventh ( $s_7$ ) harmonics are

$$s_1 = \frac{n_s - n}{n_s}, \quad s_5 = \frac{-(n_s/5) - n}{-n_s/5} = \frac{n_s + 5n}{n_s},$$

$$s_7 = \frac{(n_s/7) - n}{n_s/7} = \frac{n_s - 7n}{n_s}, \quad (6.163)$$

where  $n_s$  is the synchronous speed and  $n$  is the rotor speed.

When  $n$  varies from 0 (zero) up to  $n_s$ ,  $s_1$  varies from 1 to 0,  $s_5$  from 1 to 6 and  $s_7$  from 1 to  $-6$ . The torque due to fifth harmonic, that creates a flux on the stator in the opposite direction of the rotor direction (the direction of the fundamental frequency torque) is always negative. The torque due to the seventh harmonic, that creates a flux on the stator in the same direction of the rotor direction is positive for  $1 > s_1 > 6/7$  and null for  $s_1 = 6/7$ , and then becomes negative.

When the torques created by the fifth and seventh harmonic are added to the fundamental torque, the resultant torque, around the region where  $s_1$  is slightly greater than  $6/7$ , may be inferior to the load torque and the motor will stop.

### 6.2.6 Operation as a Brake and Generator

#### Operation as a Brake

Braking in induction motors refers to quickly bringing the speed of the motor to zero by a method called plugging. Plugging involves reversing the supply in two of the phases. This leads to a torque being developed in the opposite direction to the rotation of the motor,  $s > 1$ , the power  $P = (1 - s)P_{sr}$  developed by the motor will be negative, the motor speed starts to decrease, as the mechanical power delivered to the load is supplied by the kinetic energy of the motor and the motor comes to a stop. Once the motor stops, the reverse supply is cut

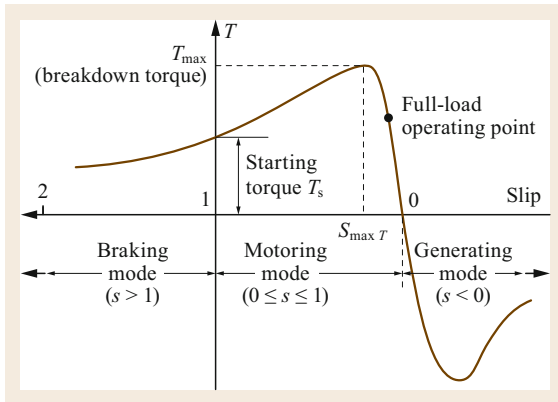


Fig. 6.55 Induction machine torque–slip curves

off to prevent the motor from running in the opposite direction. The rotor is secured by a mechanical brake.

### Operation as a Generator

For this operation an other machine drives the shaft so that the rotor speed is greater than synchronous speed, i.e.,  $\omega_r > \omega_s$ , i.e.,  $s < 0$ . The torque and power will be negative and the machine operates as an induction generator.

As the slip is negative the active component of the stator current changes its sign while the reactive component maintains the same sign as for motor operation. Then the machine delivers active power and receives reactive power. This supply of reactive power must come from the grid to which the machine is connected, preferentially by means of a shunt capacitor bank connected to the generator terminals, so as to relieve the power system from the supply. Induction generators are particularly suitable for wind generating stations as in this case speed is always a variable factor. Unlike synchronous generators, induction generators cannot be used for grid voltage control. Thus, the generator voltage must be maintained by the external power system to which the induction generator is connected.

The induction machine torque–slip curves for motor, brake and generator regions are shown in Fig. 6.55.

## 6.2.7 Determining of Induction Machine Parameters

Three tests are needed to determine the parameters in an induction machine model. Detailed testing is quite involved and is specified in IEEE Standard 112 [6.35].

### Direct Current Resistance Test

The stator resistance can be found by applying a DC voltage across two terminals of the motor and measuring the stator current. There will be no induced

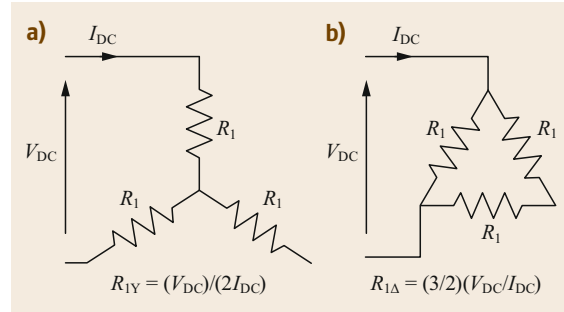


Fig. 6.56a,b Determination of DC stator resistance. (a) Stator connected in star, (b) stator connected in delta

voltage on the rotor and no potential difference across the inductances and the parameters of the motor will be reduced to the stator winding resistance. Values may be obtained for a delta or wye stator connection. The values of the stator resistance for both connections are obtained, as shown in Fig. 6.56a,b.

### No-Load Test

The no-load test of an induction machine enables the core loss resistance  $R_c$ , magnetizing reactance  $X_m$ , and rotational losses  $P_{rot}$  (friction + windage losses) to be obtained. The following measurements are taken: the stator voltage  $V_1$ , the stator current  $I_1$  and the three-phase power  $P_{NL}$ .

During the no-load test, rated voltage and frequency are applied, the machine runs close to synchronous speed, the slip approaches zero causing the rotor current to fall to a very small value, and as a consequence the rotor copper losses can be neglected. Differently from the continuous magnetic core of a transformer, where at no-load the primary current is very small and the joule losses  $3RI^2$  can be neglected, the magnetizing path of an induction motor includes the airgap and its exciting current is around 25–50% of its rated current, implying that the joule losses in the stator cannot be neglected. The magnetizing branch is shunted by a very high impedance rotor branch and the resultant parallel impedance very nearly approaches that of the magnetizing branch, as shown in Fig. 6.57, where the stator current  $I_1$  is equal to the excitation current  $I_0$ .

The measured three-phase input active power is the total losses in the motor at no-load  $P_{NL}$ . These losses consist of the stator losses  $3I_1^2R_1$ , core losses  $P_{core} = 3E^2/R_c$  (hysteresis + eddy current losses) and rotational losses  $P_{rot}$ . The value of the per phase stator DC resistance  $R_1$ , should be corrected for the winding temperature during the test. The skin effect in the value of stator resistance, although the stator frequency is always equal to the line frequency, is small, being about 5–15% of the joule losses in the stator resistance, for

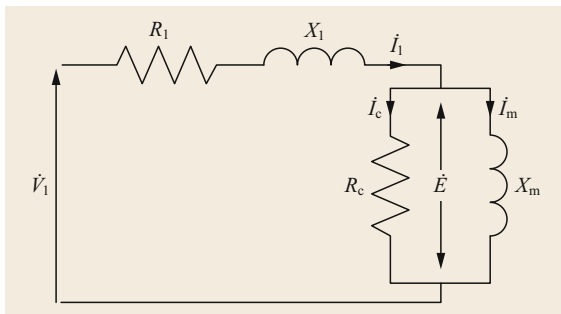


Fig. 6.57 Circuit with parameters for the no-load test

medium-size and large motors, and is usually neglected, and the stator resistance is considered as its DC value. Being  $E$  the EMF induced by the rotating flux in the stator winding at no-load, which is approximately equal to  $E \simeq V_1 - I_1 X_1$ , i.e., the voltage across the parallel branch, the equations for the input active power  $P_{NL}$  and reactive power  $Q_{NL}$  at no-load are

$$\begin{aligned} P_{NL} &= 3I_1^2 R_1 + 3 \frac{E^2}{R_c} + P_{\text{rot}} \quad \text{and} \\ Q_{NL} &= 3I_1^2 X_1 + 3 \frac{E^2}{X_m}. \end{aligned} \quad (6.164)$$

The friction and windage losses (rotational losses) can be determined, for example, by another test in which the rotor of the induction motor is driven by another machine at a speed equal to the no-load speed of the induction motor. The friction and windage losses (rotational losses) are supplied by the driving machine and are equal to its output power.

The friction and windage loss may also be determined by performing a linear regression analysis using three or more lower points of the power versus voltage squared curve. To determine the friction and windage loss, subtract the stator resistance loss (at the temperature of the test) from the total losses  $P_{NL}$  (i.e., input power) at each of the test voltage points and plot the resulting power curve versus voltage, extending the curve to zero voltage. The intercept with the zero voltage axis is the friction and windage loss. This intercept may be determined more accurately if the input power minus stator resistance loss is plotted against the voltage squared for values in the lower voltage range (IEEE standard 112 [6.35]).

Using the value of  $X_1$  from the locked rotor test, the EMF  $E \simeq V_1 - I_1 X_1$  is obtained and the core loss  $P_{\text{core}}$  at rated voltage may be calculated as

$$P_{\text{core}} = P_{NL} - 3I_1^2 R_1 - P_{\text{rot}} = 3 \frac{E^2}{R_c}. \quad (6.165)$$

Thus, the core loss resistance  $R_c$  is

$$R_c = 3 \frac{E^2}{P_{\text{core}}}. \quad (6.166)$$

As per Sect. 6.2.4 some simplification results, without any significant difference in the results, when the core loss is added to the rotational losses. Such a procedure is equivalent to represent the T branch of the equivalent circuit by the magnetizing reactance  $X_m$  only. In this case the no-load reactance is

$$X_{NL} = X_1 + X_m. \quad (6.167)$$

As the three-phase apparent power is  $S_{NL} = 3V_1 I_1$ , the no-load reactive power can be calculated as

$$Q_{NL} = \sqrt{S_{NL}^2 - P_{NL}^2} \quad (6.168)$$

and the no-load reactance is given by

$$X_{NL} = \frac{Q_{NL}}{3I_1^2}. \quad (6.169)$$

#### Locked-Rotor Test

The parameters  $R_2'$ ,  $X_2'$ , and  $X_1$  can be determined by this test. The following measurements are taken: stator terminal voltage  $V_1$ , stator current  $I_1$  and the three-phase power input  $P_{LR}$ . In the locked-rotor test, the rotor of the machine is prevented from rotating and the supply voltage is increased until a current of approximately rated value is obtained. If rated line voltage  $V_1$  is applied the current becomes high, about four to eight times the rated current, and the windings will be overheated. When the rotor is stationary (locked), the slip  $s = 1$ , and only a small exciting current flows in the exciting branch, resulting in small flux and core losses. At standstill there are no mechanical (rotational) losses. Therefore, the power input at standstill  $P_{LR}$  is mainly consumed by the copper losses of the stator and rotor windings, with the core losses neglected.

Accurate prediction of machine characteristics in the normal operating range will depend primarily upon the closeness by which  $R_2'$  represents the actual rotor resistance to currents of low frequency and, secondarily, upon the closeness by which  $X_2'$  represents the actual rotor leakage reactance to currents of low frequency. Typically, this test is done at 1/4 rated (nominal) frequency, i.e., at 15 Hz in a 60 Hz system, and then the reactances must be scaled to find the correct value at rated frequency. Thus, the reactance  $X_m$  will be preserved in the equivalent circuit for the determination of the parameters  $R_2'$ ,  $X_2'$ , and  $X_1$ , as shown in Fig. 6.52.



The three-phase reactive power input  $Q_{LR}$  with the rotor locked can be calculated as

$$Q_{LR} = \sqrt{S_{LR}^2 - P_{LR}^2}, \quad (6.170)$$

where the three-phase apparent power is

$$S_{LR} = 3V_1 I_1. \quad (6.171)$$

The resistance  $R_{LR}$  and the reactance  $X_{LR}$  with the rotor locked, corrected for the rated, can be determined by

$$R_{LR} = \frac{P_{LR}}{3I_1^2} \quad \text{and} \quad X_{LR} = \frac{f_n}{f_{LR}} \frac{Q_{LR}}{3I_1^2}. \quad (6.172)$$

The impedance of the equivalent circuit  $Z_{LR}$ , with  $s = 1$  and with the reactances at the rated frequency is given by

$$Z_{LR} = R_1 + jX_1 + (R'_2 + jX'_2) \quad \text{in parallel with } X_m. \quad (6.173)$$

As  $X_m \gg R'_2$  the rotor resistance and reactance at the rated frequency, are

$$R'_2 = (R_{LR} - R_1) \left( \frac{X'_2 + X_m}{X_m} \right)^2 \quad (6.174)$$

and

$$X'_2 = (X_{LR} - X_1) \left( \frac{X_m}{X_1 + X_m - X_{LR}} \right). \quad (6.175)$$

At this point, only the total leakage reactance is known. The relative values of stator and rotor leakage must be found from experience and are summarized in the Table 6.9.

Replacing in (6.175)  $X_m = X_{NL} - X_1$  from the no-load test (6.167) and using the relations in Table 6.9 for the appropriated motor type, the reactances  $X_1$  and

**Table 6.9** Relations of stator and rotor leakage reactances (Source: Standard IEEE 112 [6.35])

Motor type	$X_1/X'_2$
Wound rotor	1.00
Class A	1.00
Class B	0.67
Class C	0.43
Class D	1.00

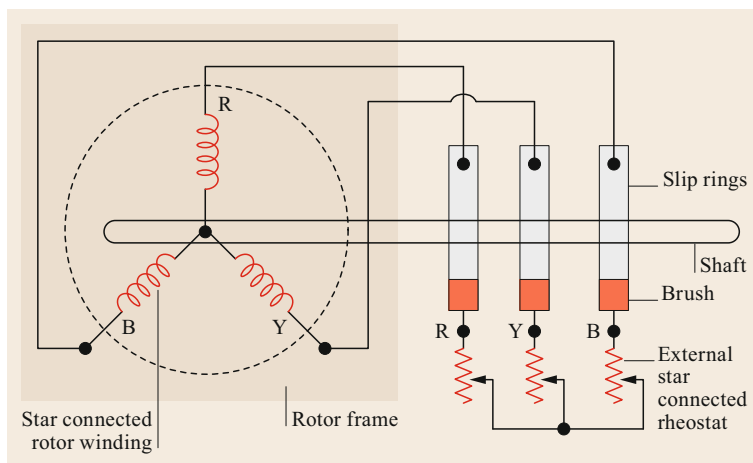
$X'_2$  can be determined. With  $X_1$  the magnetizing reactance  $X_m$  can be obtained and from (6.174), the rotor resistance is found. For motors of less than the 20 kW rating, the effects of the frequency are negligible, and the locked-rotor test can be performed directly at the rated frequency.

## 6.2.8 Effects of Rotor Resistance

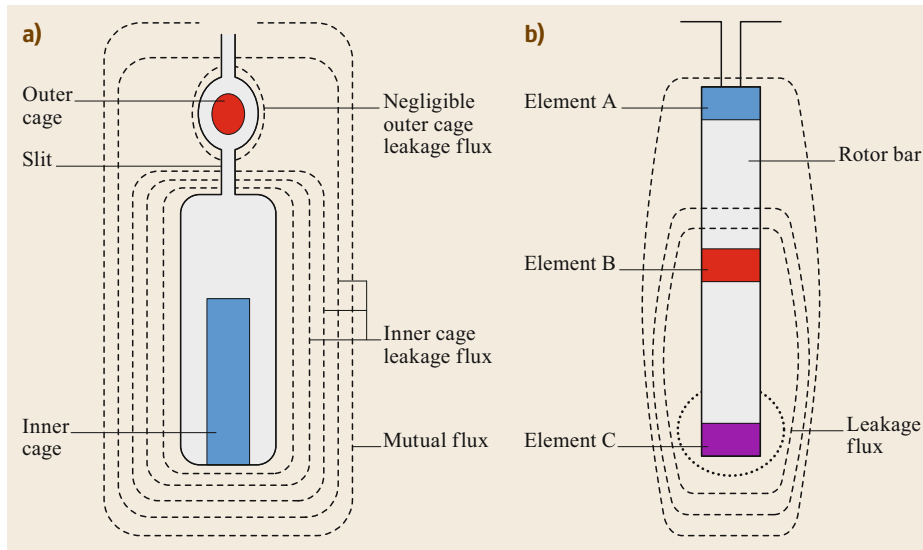
### Wound Rotor Motors

By inserting resistances in series with the rotor windings (Fig. 6.58), the resistance of the rotor circuit is increased, the starting torque and power factor are increased, while the starting current is decreased [6.36]. Also, by resistance control, the speed can be varied.

The resistances are connected to the terminal ends of the rotor windings by means of slip rings and brushes. The resistances are assembled as branches of a resistor bank unit. These resistance branches can be externally switched on and off in the resistor bank at different intervals, thus providing multiple stages of speed levels and torque capacity. The resistor bank may consist, for instance, of three resistances per phase making up a total of nine resistances in the entire resistor bank network. Thus, there are correspondingly three branches of resistances in the resistor bank. Each stage of the resistor branch is provided with its own individ-



**Fig. 6.58** Wound rotor three-phase induction motor



**Fig. 6.59a,b**  
Rotors of squirrel-cage motors.  
**(a)** Double-cage rotor. **(b)** Deep-bar rotor

ual magnetic contactor switches. Each of these resistor branches are shorted individually according to an order of operational sequence relative to the efficient running of the wound rotor motor. By suitable choice of the external resistances the maximum torque can occur at standstill. For normal running the rotor winding is short-circuited directly at the brushes, so that the efficiency of the motor is increased by removing the external resistances.

Modern wound-rotor controllers use solid-state devices in place of magnetic contactors to obtain stepless control, thus allowing smooth acceleration up to running speed.

The wound rotor main advantage over the squirrel-cage motor is that it offers greater flexibility for starting and speed control. They are used where the load requirements are high starting torque and variable speed, or where the motor is to be started under heavy load. Typical applications of these motors are crane and hoist control. Wound rotor motors are always started with full voltage as the starting current can be controlled by the resistance external to the rotor.

### Squirrel-Cage Motors

By use of suitable shapes and arrangements for rotor bars, squirrel-cage motors can be designed so that their rotor effective resistance at starting (60 Hz) is several times their resistance at rated conditions (2–4 Hz). The arrangements use the inductive effect of the slot leakage flux on the current distribution in the rotor bars. High starting torque and good running performance are achieved by incorporating two squirrel cages in the rotor, as illustrated in Fig. 6.59a or by the use of deep-bar rotors, as shown in Fig. 6.59b [6.37].

The double-cage induction motor consists of two layers of bars short-circuited by end rings. The outer cage bars are made of high resistivity material like aluminum, brass, bronze, etc. . . . , while the inner cage is made of copper that has a lower resistivity as compared to the materials used in the outer cage. The cross-sectional area of the outer bars is smaller than that of the inner bars. Thus the resistance of the outer cage is much higher than that of the inner cage. The slot-leakage flux is higher at the inner bars, so that the inductance of the inner bars is much higher than that of the outer bars.

At starting with  $s = 1$ ,  $f_2 = f_1$ , and due to the higher reactance and lower resistance of the inner cage in relation to the outer cage, the current in the inner cage is much smaller than that of the outer cage, and is approximately  $90^\circ$  out-of-phase with the induced voltage, resulting in a low starting torque, while the current in the outer cage is much higher and is practically in-phase with the induced voltage, resulting in a much higher starting torque. The outer cage is called the starting cage.

When the motor accelerates the rotor frequency  $f_2$  decreases, the inner cage reactance decreases, its current increases and as a consequence its torque increases. When the rated speed is reached, the rotor frequency  $f_2$  is very low, the reactances of the two cages are negligible, and the rotor current is divided between the two cages inversely proportional to their resistances. As the resistance of the outer cage is around 5–6 times the resistance of the inner cage, the current in the outer cage is much smaller than that of the inner cage, and the torque is basically due to the inner cage called the operating cage.

The current distribution in a deep-bar rotor undergoes a similar change from starting to running, producing high rotor resistance on starting and low resistance at normal speed.

For loads that require a large starting torque a double-cage or deep-bar motor is used, while for low starting loads a normal induction motor is usually used. Wound rotor motors are used to start large loads, that require a high starting torque and large starting periods.

## 6.2.9 Motor Applications

### Wound Rotor Motors

The applications of wound rotor motors are:

- To drive loads requiring high starting torque and where a lower starting current is required. Depending on the value of the external resistance the starting current may be less than 150% of the rated value.
- To drive high inertia loads.
- To drive loads that require a smooth acceleration.
- To drive loads that require speed control.
- The full load slip may be as low as 3% and the maximum torque above 200% of the full load value. The efficiency is about 90%.
- Are used in large pumps, conveyors, compressors, cranes, hoists, elevators, etc.

Their range of application is, generally, from 5 to 30 000 kW.

### Squirrel-Cage Motors

The national electrical manufacturers association (NEMA) has specified different design classes of three-phase squirrel-cage induction motors, based on their torque characteristics in relation to the speed and starting current. Typical torque speed curves for the most common design classes A–D are shown in Fig. 6.60.

The main features of these design classes are listed here:

- Class A motors have normal starting torque, high break down torque, high starting current of five to ten times the rated current, and less than 5% slip. The design has low resistance single cage rotor. The efficiency of the motor is high at full load. Because of the high starting current, a reduced voltage starter by means of an autotransformer, resistor/reactor or Y– $\Delta$  connection is required. Applications of Class A motors are fans, blowers, centrifugal pumps, etc. Range of application: 5–150 kW.
- Class B motors, known as *general purpose* motors, have about the same starting torque as Class A with

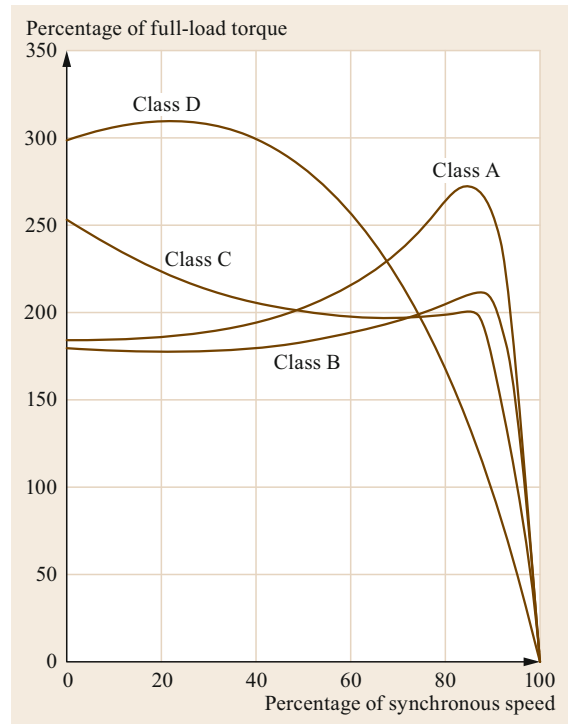


Fig. 6.60 Typical speed/torque characteristics of NEMA design classes A–D induction motors

starting current of five to six times the rated current and the efficiency and slip are comparable with the Class A. The starting torque and lower starting current are maintained by use of a double-cage or deep-bar rotor. They have a medium breakdown torque and full voltage starting, generally, can be used. The applications are same as that of Class A motors, i.e., in the range from 5 to 150 kW.

- Class C motors have high starting torque (around 250% of rated torque), low breakdown torque (190–200% of rated torque) and medium starting current (three to five times rated current). Such motors are of the double-cage bar, but with a higher rotor resistance than Class B motors in order to ensure that the maximum torque occurs at starting. Due to its high starting torque it has a fast acceleration. The loads are compressors, conveyors, reciprocating pumps and crushers. Range of application: 15–150 kW.
- Class D motors have a single-cage with high resistance bars, assuring a very high starting torque (higher than all the NEMA motor types), and low starting current. The rotor bars are made of high resistivity material such as brass instead of copper and the bars have a small cross-sectional area. The slip at maximum torque is, generally, above 50% and the

**Table 6.10** Summary of the performance of the motor design classes (Source: [6.38] with modifications)

	<b>Class A</b>	<b>Class B</b>	<b>Class C</b>	<b>Class D</b>
Type	Normal starting torque	General purpose	High starting torque	Very high starting torque
Starting torque	100% rated for larger motors, 200% rated, smaller motors	100% rated for larger motors, 200% rated, smaller motors	Approx. 250% rated	> 275% rated
Starting current	500–1000% rated	500–600% rated	300–500% rated	300–500% rated
Pullout torque	200–300% rated	≥ 200% rated	Slightly lower than Class B	Usually same as starting torque
Rated slip	< 0.05, lower than similar sized Class B	must be < 0.05, usually < 0.03	< 0.05, higher than Class B	High, typically 0.07–0.11, can be up to 0.17
Applications	Fans, blowers, pumps, machine tools	As for Class A	Compressors, pumps, conveyors	Punch presses, shears, elevators, extractors, winches, hoists
Notes	High starting inrush current causes power system problems, it can cause the supply voltage to sag and requires special starting techniques. More efficient than same sized Class B	Replacement for Class A due to lower starting current. The standard off-the shelf commodity motor	Applications that require high starting torques. Note that the pull up and pull-out torque can both be lower than the starting torque. Less efficient than Class B	Applications that require high starting torques. Are used to drive intermittent and high-impact loads. The efficiency at full-load is low

slip at rated speed is between 7 and 11%, as a consequence the rated efficiency is low. Are used to drive intermittent loads requiring rapid acceleration and high-impact loads as: punch presses, shears, elevators, extractors, winches, hoists, oil-well pumps and wiredrawing machines. When driving high-impact loads, as punch presses, they are provided with a flywheel to give energy to the load during the working stroke, smoothing out the peaks in the supply grid. Range of application: 15–150 kW

- Class E motors have low starting torques (but not inferior to 50% full load torque), normal starting current and low slip at rated load. For motors above 5 kW rating, starting current may be high, so they may require a starter, like Class A. The rotor has low resistance and correspondingly high efficiency. They are usually high-speed motors directly connected to loads that require low starting torques, such as fans and centrifugal pumps. Range of application: 30–150 kW.
- Class F motors have low starting torques like Class E, low starting current, that allows them to start at full voltage. The rotor is designed so that it gives high reactance at starting. The blocked rotor current and full load slip, with full applied voltage, is similar to that of Class B or C. The field of application is the same to that of Class E. Range of application: 30–150 kW.

A summary of the performance of the motor classes A–D is provided in Table 6.10.

### 6.2.10 Energy Efficient Motors

With ever-increasing energy cost the life-time operating cost of an induction motor can be traded against a high efficiency and high capital cost induction motors. With rising demand for high efficiency, energy efficient induction motors designers and manufacturers are stepping up their production of such motors. Some of the important techniques, that are employed to construct a high efficiency induction motor compared to the standard design, are listed here:

- Modification of stator slot design to allow a larger diameter wire resulting in reduced current density and reduced copper losses
- Increase of the stator and rotor core length to improve heat transfer out of the motor, thus reduction of the operating temperature
- Use of thinner laminations and of premium-grade core steel, with consequent reduction in eddy-current and hysteresis losses
- Rotor fans are designed with refined aerodynamic fin shapes to reduce windage loss
- Improved bearings.

When compared to standard efficient motors, high efficient motors have fewer losses and better cooling, resulting in less heat generated and a temperature decrease, on average, of 10 degrees centigrade in relation to standard motors. This has as an additional benefit an increase in insulation life. They have, generally, 30%

more lamination steel and 20% more copper than standard motors. Overall, energy efficient motors are better motors.

There is always a trade-off involved. A machine of more efficient design normally requires more material and therefore is bigger and costlier. In general, energy efficient motors can cost as much as 15% more than standard efficient motors. Users normally select the *lowest-cost* solution to a given requirement. However, it would be prudent to choose an energy-efficient motor as normally the increased capital cost would be offset by energy savings over the expected lifetime of the machine.

The full-load efficiency for motors in the range 0.75 to 0.75–375 kW varies from about 83 to 97%. The efficiency typically increases with the size of the motor. Motor losses being broken down roughly as:

- Friction and windage, 5–10%
- Iron or core losses, 20–25%
- Stator losses, 30–50%
- Rotor losses, 20–25%
- Stray load losses, 5–15%.

Various regulatory authorities in many countries have introduced and implemented legislation to encourage the manufacturing and use of higher efficiency electric motors.

### Energy Efficiency Standards

The international electrotechnical commission (IEC) has introduced standards relating to three-phase energy efficient motors. IEC 60034-30 [6.39] defines efficiency classes for a wide range of electric motors. IEC 60034-30-1 [6.40] (that became valid in 2014) takes a step further in widening the scope of motors subject to efficiency classes and introduces the IE4 class and IEC 60034-2-1 [6.41] specifies rules concerning efficiency testing methods. Motors rated 1 MW and above have a full-load efficiency between 95 and 98% and are of secondary importance when assigning efficiency classes.

In the IEC 60034-30-1 the following efficiency classes are defined for induction motors, where IE stands for international efficiency:

- IE1 (Standard Efficiency)
- IE2 (High Efficiency)
- IE3 (Premium Efficiency)
- IE4 (Super Premium Efficiency)

Figure 6.61 shows the correlation between required efficiency and output for the four efficiency classes. The efficiency values increase from IE1 to IE4.

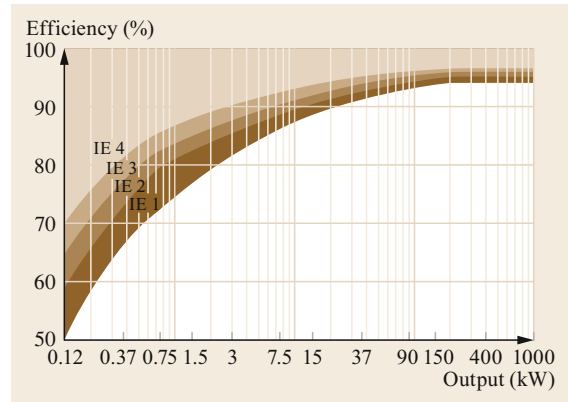


Fig. 6.61 Efficiency and output for the four efficiency classes at 50 Hz

The scope of IEC 60034-30-1 standard is wider than that of IEC 60034-30, covering motors up to eight poles, rated voltage up to 1000 V, with a power range from 0.12 to 1000 kW, any ambient temperature within the range of  $-20$  to  $+60^{\circ}\text{C}$  and marked with an altitude up to 4000 m above sea level. Excluded are, among a few other exceptions, motors completely integrated into a machine (for example, pump, fan or compressor) that cannot be tested separately from the machine.

The efficiency levels defined in IEC 60034-30-1 are based on the low uncertainty test methods specified in IEC 60034-2-1 *Standard methods for determining losses and efficiency from tests*, which recognizes several methods for determining motor efficiency, each of which has certain advantages as to the accuracy, cost, and ease of testing, depending primarily on motor rating. Some of the methods in IEC 60034-2-1 are harmonized with national standards such as IEEE 112 Part B and CSA (Canadian Standards Association) C390.

An IE5 level, with the goal of further reducing losses by around 20% relative to IE4, is envisaged for a future edition of IEC standards.

### 6.2.11 Speed Control

The speed control of induction motors can be obtained by the following methods:

- a) Changing the terminal voltage
- b) Changing the number of pair of poles (part-winding)
- c) Changing the resistance in the rotor circuit
- d) By static slip power recovery
- e) By constant stator voltage frequency ratio (V/Hz)
- f) By vector control
- g) By double feeding.

### a) Changing the Terminal Voltage

The speed can be varied by reducing the voltage of constant frequency applied to the stator. This method is limited to certain drives, because the developed torque for a given speed is directly proportional to the square of the applied voltage, and in the case of constant load torque the current must increase with decreasing voltage, since the flux is proportional to the voltage. However, this method finds considerable application where the load torque decreases with a reduction of speed, as in the case of fans and pumps.

The stator voltage may be varied by means of variable impedance in series with the motor, but the use of thyristors between the line and the motor seems to offer the most economical and effective operation.

### b) Changing the Number of Pair of Poles

The stator winding can be designed so that by simple changes in coil connections the number of poles can be changed in the ratio 2 to 1, thus obtaining two synchronous speeds. With two independent sets of stator windings, each arranged for pole changing, as many as four synchronous speeds can be obtained: 600, 900, 1200 and 1800 rpm. The motor is invariably of the squirrel-cage type as the cage winding always reacts by producing a rotor field having the same number of poles as the inducing stator field. If a wound rotor motor is used additional complications are introduced because the rotor winding must also be rearranged for pole changing. In this method the speed can be changed in discrete steps and the elaborate stator winding makes the motor expensive.

### c) Changing the Resistance in the Rotor Circuit

With external resistors  $R_{ext}$  in the rotor circuit the slip for the maximum torque is,

$$s_{max T} = \frac{R'_2 + R_{ext}}{\sqrt{(R_1)^2 + (X_1 + X'_2)^2}} \quad (6.176)$$

From Fig. 6.62 it may be seen that the speed of operation can be varied by controlling the external resistance. If the value of  $R_{ext}$  is increased the slip for maximum torque increases and the maximum torque can occur at starting. This method is similar to the speed control of direct-current shunt motors by resistance in series with the armature. The steady-state speed is given by the intersection of the load and motor torque-speed curves as in all motor drives.

While by this method a high starting torque can be obtained, it causes the motor to develop excessive slip and high rotor losses at rated torque, that results in poor efficiency and poor speed regulation. This method may be applied to loads that have high static torque and loads

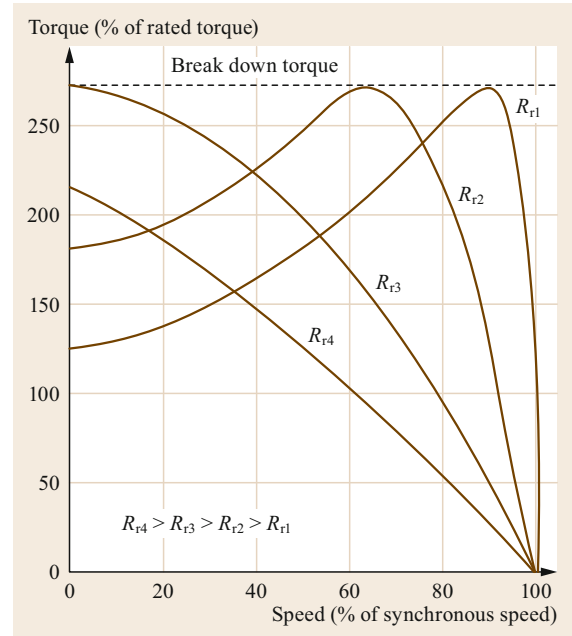


Fig. 6.62 Speed control by external resistances

having high inertia, like conveyors. In this type of speed control, the external resistances generate huge losses, and as a consequence large heat in the system, so it requires more maintenance [6.42].

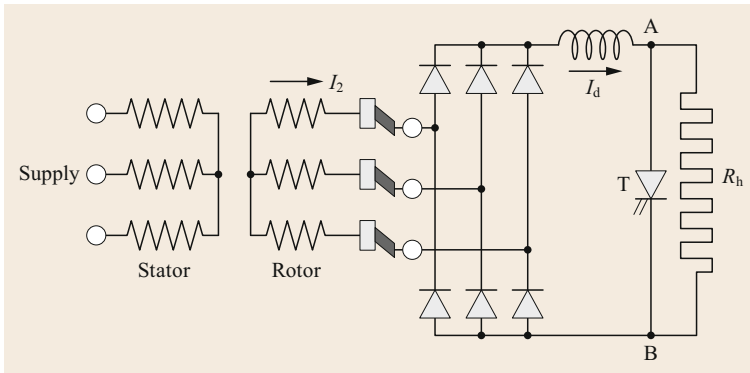
However, the speed control can be obtained without mechanical switching of resistances by means of modern controllers using controllable switches, as shown in Fig. 6.63. The AC output voltage of the rotor is rectified by a diode bridge and fed to a parallel combination of fixed resistor  $R_h$  and a semiconductor switching device T. The DC supply is switched on and off at high frequency (typically 10 kHz or more) using electronic switching devices such as MOSFETs (metal-oxide-semiconductor field effect transistors), IGBTs (insulated gate bipolar transistors) or GTOs (gate turn-off thyristors) to provide a pulsed DC wave form. The average level of the output voltage can be controlled by varying the duty cycle of the semiconductor power device T. The effective resistance  $R_e$  between points A and B is

$$R_e = (1 - k)R_h \quad (6.177)$$

where  $k$  is the duty cycle of the controllable switch.

The rms value of current in each secondary phase is  $I_2 = I_d \sqrt{2/3}$ . The additional resistance of each secondary phase  $R_{2h}$ , is such that  $3R_{2h}I_2^2 = (1 - k)R_h I_d^2$ . Thus,

$$R_{2h} = (1 - k) \frac{R_h}{2} \quad (6.178)$$



**Fig. 6.63** Speed control by a controllable switch

#### d) By Static Slip Power Recovery

Neglecting joule losses in the resistance of the rotor windings the slip power ( $sP_{sr}$ ) in the rotor circuit may be returned to the system by means of a rectifier and an inverter operating with a delay angle between  $90^\circ$  and  $150^\circ$  approximately. The feedback power converter is connected to the power system, usually through a transformer that matches the output voltage of the converter to the power system, as shown in Fig. 6.64. If  $E_{20}$  is the value of the induced rotor EMF in each rotor phase when the rotor is at standstill, when the rotor rotates at a speed  $\omega_r = (1-s)\omega_s$  (rad/s) the value of the rotor EMF is  $E_2 = sE_{20}$  and the rotor frequency is  $f_r = sf_s$ . The average value of the voltage at the output of the rectifier is

$$V_{dr} = k_1 s E_{20}. \quad (6.179)$$

The AC voltage at the inverter terminals must be equal to the system voltage  $V_1 = (V_{LL}/\sqrt{3})$ . Thus, the DC voltage at the inverter is  $V_{di} = k_1 V_1 |\cos \alpha|$ , where  $\alpha$  is the delay angle and as the converter is operating as an inverter  $180^\circ > \alpha > 90^\circ$ . The smoothing inductor prevents the ripple in the voltage  $V_{dr}$  from causing excessive ripple in the DC current. As the resistance of the

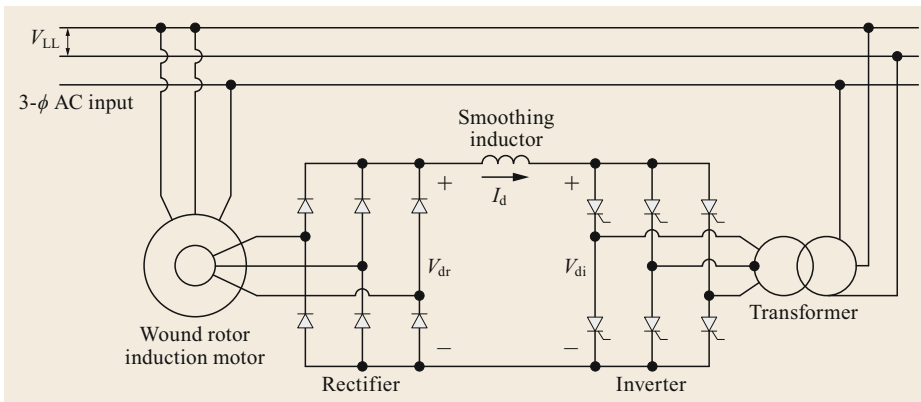
inductor is very small it is possible to equalize the voltages at the rectifier ( $V_{dr}$ ) and inverter ( $V_{di}$ ) terminals, obtaining

$$s = \frac{V_1}{E_{20}} |\cos \alpha|. \quad (6.180)$$

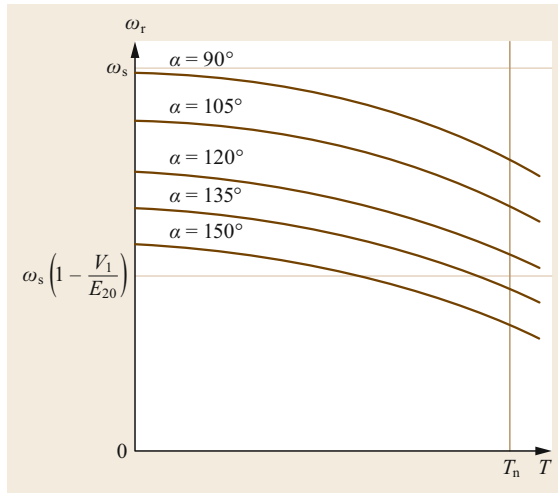
If  $|\cos \alpha|$  is varied from a value near to zero up to a value near to 1, the slip  $s$  will vary from a value near to zero up to a value near to  $s = V_1/E_{20}$  and the rotor speed will vary, approximately, from  $\omega_r = \omega_s$  to  $\omega_r = \omega_s(1 - V_1/E_{20})$ , respectively.

Figure 6.65 shows the characteristic torque-speed for several values of  $\alpha$ . The drop of the curves is due to the voltage drops in the motor and in the other parts of the scheme. The slip increases with the torque.

This scheme requires a wound rotor motor with slip rings and is known as a static Kramer scheme. It is used in applications such as pumps and blowers of great power, where the speed needs to be controlled only in a small range around its nominal value, because a small speed range results in a smaller rating of the converters, thus making this scheme competitive. Due to the harmonics generated by the converters filters are necessary at the DC and AC sides. For larger motors the energy



**Fig. 6.64** System for recovering the rotor slip power



**Fig. 6.65** Torque-speed control by a static slip power recovery

that is lost in the scheme with external resistors is now saved and returned to the grid, that amounts to significant cost savings.

#### e) By Constant Stator Voltage Frequency Ratio (V/Hz)

When the voltage drop in the impedance of the stator winding is neglected, the main or resultant magnetization flux  $\Phi_m$  is

$$\Phi_m \simeq \frac{V_1}{4.44f_1N_1k_{\omega 1}} \quad (6.181)$$

If the stator voltage  $V_1$  and frequency  $f_1$  are equal to their rated values, the flux will be equal to its rated value, but if the frequency is reduced below its rated value of 60 or 50 Hz maintaining the voltage  $V_1$  constant, the flux will increase beyond its rated value and it may cause saturation of the core and high losses in the motor. Thus to maintain the flux constant at its rated value the voltage  $V_1$  must increase in a linear proportion to  $f_1$ . For small values of slip, i.e., in normal operation, the rotor resistance is much greater than the rotor reactance, the load power factor will be high, and for a constant flux the developed torque is

$$T = k_1 (\omega_s - \omega_r) = k_1 \omega_{sl} \quad (6.182)$$

where  $\omega_{sl}$  is the slip speed and the corresponding slip frequency is given by

$$f_{sl} = f_s - f_r \quad (6.183)$$

Such a characteristic is shown in Fig. 6.66a for a synchronous frequency  $f_{s1} = 60$  Hz with a corresponding

slip speed  $\omega_{s1}$ , with three other values for the synchronous frequency:  $f_{s2}$ ,  $f_{s3}$  and  $f_{s4}$ , being  $f_{s1} > f_{s2} > f_{s3} > f_{s4}$ . The torque-speed characteristics shift horizontally in parallel for the four different values of synchronous frequency.

Considering that equal load torque is to be delivered at synchronous frequencies, for instance,  $f_1$  and  $f_2$ , the synchronous speeds are, respectively,  $\omega_{s1}$  and  $\omega_{s2}$ . From (6.182)  $\Rightarrow \omega_{s11} = \omega_{s12}$ , and the respective slip frequencies are also constant. The slip increases as the synchronous frequency decreases ( $s_1 = f_{s11}/f_1$  and  $s_2 = f_{s12}/f_2$ ). The rotor resistance losses increase as the synchronous speed decreases to reduce speed. However, in many loads such as centrifugal pumps, compressors and fans, the load torque varies by the square of the speed, and  $f_{sl}$  as well as the slip declines with decreasing frequency, as shown in Fig. 6.66b and the rotor losses remain small [6.43].

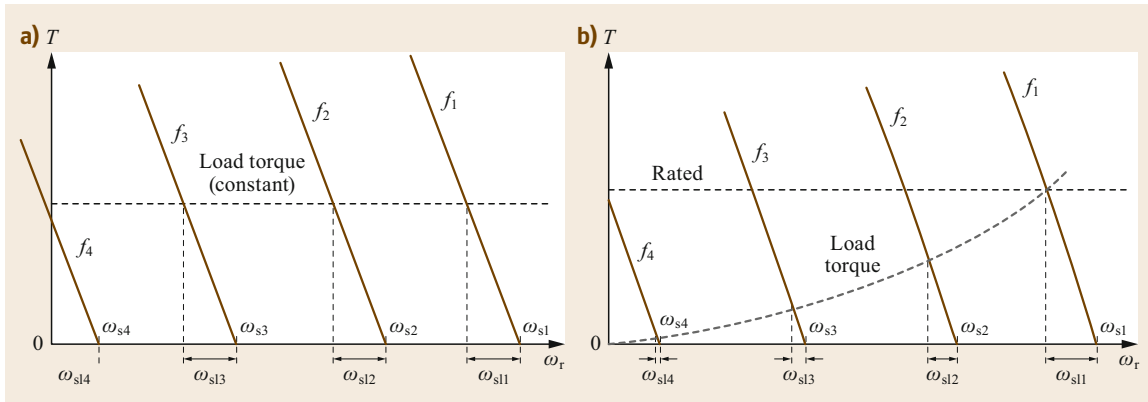
#### f) By Vector Control

All the previous methods of speed control are termed scalar speed controls. With the ever increasing use of electronic switches for speed control the vector control of induction motors is used when accurate torque and speed control is desired. Before introducing vector control some additional considerations are made with respect to scalar control of speed by voltage/frequency ratio.

The stator voltage/frequency ratio control method, as seen in the previous item, is the most scalar technique used to control the speed of the motor where the magnetizing flux of the motor is kept unchanged. The torque developed in the motor depends on the slip speed, and only speed feedback is required, simplifying the control system. It is generally applied when there is no need for a fast response or high precision of the control system, which is the case for most applications. Another scalar control method uses the torque control technique, in which the magnitude and frequency of the stator currents are adjusted so that the steady-state torque is controlled, while the magnetic field is again maintained constant. In this case, the speed feedback has to be supplemented by a current feedback that makes this method somewhat more complicated than that of the voltage/frequency ratio control method.

By scalar speed control the response of induction motors to changes in speed, due to load variations is relatively slow because the motor current cannot change instantaneously following the applied voltage, due to the delay caused by the inductance of the motor windings. However, fast responses and high precision speed control of the motor are possible by means of vector control, where the vector components of the stator current, i.e., its magnetizing current that produces the airgap flux and the in-phase current that produces the





**Fig. 6.66a,b** Torque-speed characteristics at small slip with constant flux: **(a)** constant load torque, **(b)** load torque varies as speed squared

torque are separately controlled. The necessity of controlling the magnetizing current is to keep the airgap flux constant at its optimum level, while the torque needed is controlled by the in-phase stator current. Vector control is a more complex technique than scalar control, the evolution of which was inevitable, because its superior dynamic performance, as compared with scalar control. It is also known as field-oriented control, because in the course of implementation the identification of the field flux of the motor is required. Before the introduction of vector control fast dynamic torque responses were only possible by the use of separately excited DC motors, where the magnetic fields created by the armature and field currents allow independent control of torque and flux in the motor [6.44].

The vector control gives fast transient response including fast acceleration and deceleration, precise control of torque, speed and position compared to scalar control. The vector control can be realized by closed loop (feedback) control or open loop (sensorless) control, also called, direct and indirect control, respectively. In direct control there is

**Closed Loop (Feedback) Control or Direct Torque Control.** Direct torque control (DTC) is one of the best control strategies of torque control, and thus speed control, of an induction motor. The aim is to effectively control the torque, as well as the flux. The method allows accurate, fast control and high dynamic speed response. It uses the adaptive motor model that is based on the mathematical expressions of the motor theory. The method requires the basic parameters of the motor such as stator resistance, self inductance, etc. to calculate the flux and torque, that are given to a two level comparator of the flux and torque. The outputs of the flux and torque comparators are given to a switch selection table, wherein the selected switch position is applied to an inverter without any modulation. With

the joint progress of power electronics and numerical electronics, it is possible to deal with the speed control with great accuracy, even at very low speeds. With these technological projections, various command approaches have been developed to master, in real time, the flux and the torque of the motor. Hence the name direct torque control (DTC), as the motor torque and flux become direct controlled variables.

#### *Open Loop (Sensorless) Control or Indirect Control.*

The currents in the three-phases of the stator are measured and initially converted to the  $\alpha, \beta$  two-phase system of coordinates, from which the rotor angle and velocity are estimated. These signals are then compared with reference values and controlled by using proportional integral (PI) controllers. Thus, in the sensorless speed control method there is no need to use a speed sensor as in the direct control method. The  $\alpha, \beta$  currents are converted to direct and quadrature-axis components,  $i_d$  and  $i_q$  by means of a Park transformation. The direct-axis current  $i_d$  controls the magnetic flux and the quadrature-axis current  $i_q$  controls the torque.

The output of the flux and torque controllers are  $d$  and  $q$  voltage components, that are transformed from the  $d, q$  coordinate system back to the  $\alpha, \beta$  coordinate system, and by means of an inverse Park transformation the  $a, b, c$  voltage components. Thus, using the space vector modulation technique, the corresponding inverter switching is pulse width modulated. There are different types of vector control techniques, such as: stator flux oriented control, rotor flux oriented control and magnetizing flux oriented control. The sensorless vector control is shown in Fig. 6.67. Sensorless control of AC drives is attractive for cost and reliability considerations. The speed sensor of the direct method is replaced by mathematical techniques. The sensorless control method can be used to control motor speed almost down to zero.

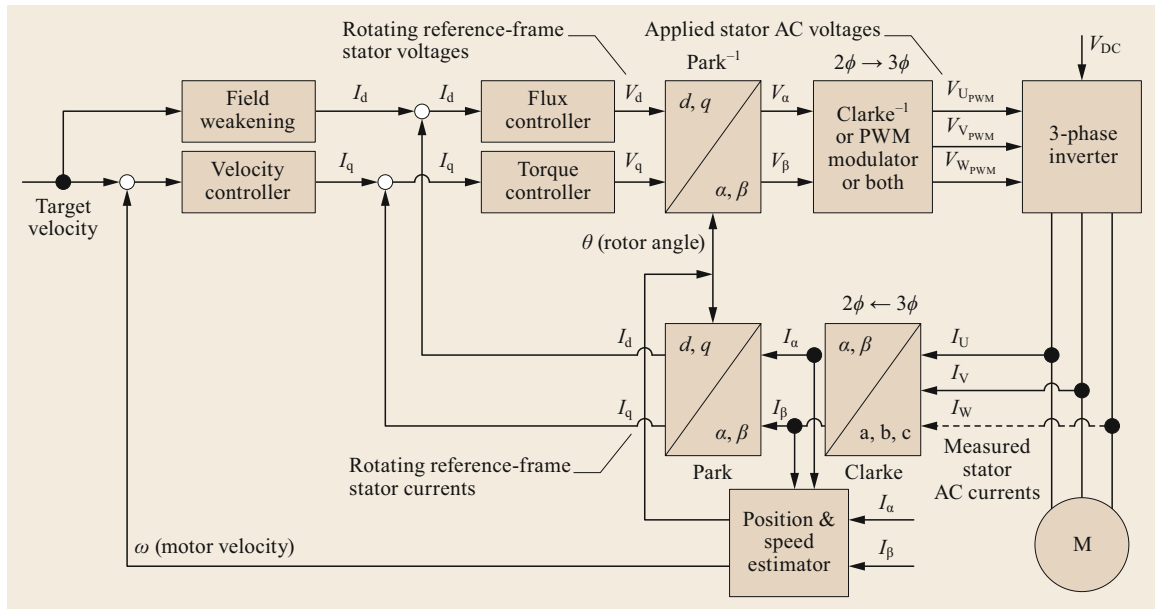


Fig. 6.67 Sensorless vector control of induction motors

**Servo Systems.** Many of the techniques involved in vector control are applicable to servo systems and consequently vector controlled systems are replacing some of the traditional servo systems.

### g) Speed Control by Double Feeding

In this method the stator windings are supplied with three-phase power at a synchronous frequency  $f_1$ , as usual, and the rotor windings are also fed with three-phase power at a variable frequency  $f_2$  by means of a PWM (pulse width modulation) converter. The speed of the stator MMF with respect to the stator is  $n_{s1} = (120f_1)/p$  and the speed of the rotor MMF with respect to the rotor is  $n_{s2} = (120f_2)/p$ . If the rotor is fed so that its MMF rotates in the same direction as the stator MMF, the rotor speed is  $n = n_{s1} - n_{s2}$ , but if the rotor is fed so that its MMF rotates in opposite direction to the stator MMF, then the rotor speed is  $n = n_{s1} + n_{s2}$ . Thus, the motor speed  $n$  may be adjusted below or above the synchronous speed by adjusting the rotor excitation frequency  $f_2$ , as

$$n = \frac{120(f_1 \pm f_2)}{p} \quad (6.184)$$

If  $f_2$  is zero, i.e., the rotor is supplied from a DC source, the motor speed  $n$  will be equal to the synchronous speed and the motor is a synchronous motor.

**Additional Considerations.** Before the development of semiconductor power electronics, it was difficult to

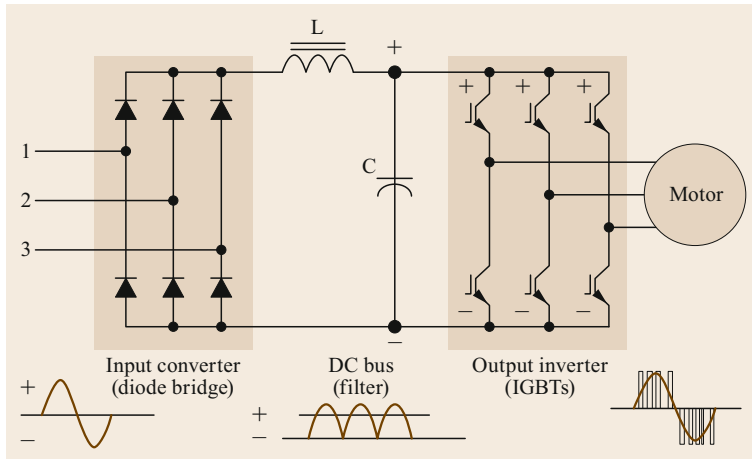
vary the frequency, and cage induction motors were mainly used in fixed speed applications. Pole changing finds its application when two or four speeds are required, thus it is a limited method for speed control. Changing the terminal voltage is restricted to certain drives, because the developed torque is reduced directly proportional to the square of the applied voltage. Variable external resistance control for wound rotor motors, allows speed control in a broad range, however the method suffers from low efficiency at reduced speeds and poor speed regulation with respect to a change in load. The advent of power electronics allows speed control by other methods with better efficiency, such as: static slip power recovery (for large wound rotor drives), stator voltage frequency ratio (V/Hz) and vector control. Due to its simplicity and compactness variable frequency driven squirrel-cage induction motors are displacing DC and wound rotor motors drives in many industrial variable speed applications.

### 6.2.12 Variable Speed Drives (VSDs)

This section summarizes the applications, benefits, technologies, problems and solutions when VSDs are used for controlling the torque and speed of induction motors. More extensive information can be found in references [6.45–48].

#### Applications and Benefits

A variable speed drive (VSD) is an adjustable-speed control used in electromechanical drive systems to con-



**Fig. 6.68** Pulse width modulated voltage source inverter (PWM-VSI)

control AC motor torque and speed by varying motor input voltage and frequency. It consists of an AC/DC rectifier, a DC link and a DC/AC inverter, mostly based on pulse width modulation (PWM).

VSDs are suitable to control the motor torque and speed to drive loads where the torque varies approximately with the square of the speed, such as centrifugal pumps, fans, blowers and similar applications, by supplying only the correct amount of energy that is needed. For these types of loads the energy-efficiency benefits of a VSD are high, eliminating control valves, dampers, throttles, bypasses, gears, transmissions and clutches, etc., and reducing cost and losses in partial load.

Loads where the change of power varies linearly with speed (constant torque loads) such as: air compressors, conveyors, escalators, positive-displacement pumps, hoists, cranes and similar applications also benefit from VSDs, that can continuously adjust the speed from almost standstill to full speed without steps, thus minimizing the required power, although the benefits are not so high because the required input power only varies linearly with speed.

Some loads such as: machine tools and traction applications, behave as constant power loads and they can benefit by the use of VSDs, that allow soft starting and stopping and less wear of the machinery involved. The cost and energy-efficiency benefits are small when compared with other types of loads.

As the total energy consumption by the electric motor systems in all sectors (industrial, commercial, residential, agriculture and transport) is about 45% of the total world electrical energy consumption, it can be foreseen that an appreciable amount of energy can be saved by the combination of VSDs and high-efficiency motors.

#### Technologies for VSDs

The different technologies for VSDs are listed here.

*a) Pulse Width Modulated Voltage Source Inverter (PWM-VSI).* Typically for motors of up to 3000 hp, but each manufacturer may list larger sizes. An uncontrolled rectifier (diode) transforms supply AC voltage to DC voltage to the inverter. Switches in the inverter are IGBTs, in general (Fig. 6.68). The inverter controls the magnitude and frequency of the AC output voltage by PWM of the inverter switches.

*b) Square-Wave Voltage Source Inverter (Square-Wave VSI).* Ranges available are typically up to 500 hp but can be up to 1000 hp. the converter rectifier switches are diodes with a DC chopper. The DC input voltage to the inverter must be controlled to control the magnitude of the inverter output voltage, that has a form similar to a square-wave. The inverter controls only the frequency of the AC output voltage.

*c) Current Source Inverter (CSI).* The rectifier and inverter use thyristors. The DC link uses large inductors to regulate current ripple, that makes the input to the inverter appears as a current source. Torque pulsations or cogging is common with the CSI design. Torque pulsations are the result of a high harmonic content in the output current of the drive. Torque pulsations result in stress to motor shafts and pumps, fans, conveyor (belts), or any ultimate driven load, requiring the installation of filters. For HVDC transmission systems basically SCRs are used due to their greater voltage and current capabilities.

*d) High Voltage Insulated Gate Bipolar Transistor (HVIGBT).* The HVIGBT consists of several IGBTs placed in series to develop a high voltage level, having the advantage of low stress on the motor insulation and low current harmonic content in the supply to the high voltage motor with no need of a filter. IGBTs are used due to the low energy necessary to switch them on, this

allows fast turn-on and turn-off times on the order of 1  $\mu$ s, a small on-state voltage, small snubberless switching, small conduction losses. Combined with zero or slightly negative gate drive current makes them a good choice for moderate speed, high voltage applications. Like lower voltage devices, the HVIGBT module includes a reverse connected fast/soft recovery free wheel.

*e) Integrated Gate Commuted Thyristors (IGCT).* An IGCT is a special type of thyristor similar to a gate turn-off thyristor (GTO). They can be turned-on and off by a gate signal, have lower conduction losses as compared to a GTO, and withstand higher rates of voltage rise ( $dv/dr$ ), such that no snubber is required for most applications. The IGCT faster turn-off times compared to that of a GTO allows it to operate at higher frequencies, up to several kHz for very short periods of time. However, because of high switching losses, the typical operating frequency is up to 500 Hz. An IGCT enables performance improvements of PWM converters for industrial and traction applications. IGCTs are the mature devices for high voltage drives today. They are available as multiple level voltage source inverters. With a series connection of elements its power range can be higher than 100 MW.

#### Problems and Solutions with the Application of VSDs

a) Problems that may arise with the application of VSDs are:

A VSD with faster rise time and higher switching frequencies above 5 kHz, can produce high voltage overshoots and voltage spikes, that can damage motor windings. This problem also happens when the cable length between the VSD and the motor is longer (above 50–100 feet, in general), resulting in a motor impedance greater than the impedance of the cable, thus reflecting the voltage wave and causing voltage overshoot and spikes at the motor terminals.

VSDs produce high frequency harmonic voltages and currents. These harmonics increase the hysteresis losses that are proportional to frequency, as well as eddy current losses that are proportional to the frequency squared, leading to additional core losses, and as a consequence a temperature increase of the core and windings surrounding the core. The harmonics also increase the joule and stray-load losses. Besides these effects there is the possibility of an interaction between the positive and negative sequence harmonic magnetic fields causing torsional oscillations of the motor shaft, that in turn, lead to shaft vibrations that may be amplified if the frequency of the oscillations coincides with the natural mechanical frequency of the shaft, resulting in severe damage to the motor shaft.

Even when overvoltage is not high enough to cause voltage spikes, the fast rise time pulses from a VSD may cause the appearance of currents flowing through the bearings. This current is due to a voltage called the shaft voltage that may appear due to a voltage imbalance at the motor terminals because the voltage output of a VSD is made up of a series of square waves.

b) To avoid eventual problems with VSDs the following possible solutions should be implemented as required.

To avoid overshoots:

- Use an inverter fed motor with a voltage of 230 V or less when possible.
- Use the lowest carrier frequency that satisfies the motor requirements. A lower switching frequency results in less overshoots per second.
- The control of multiple motors in parallel by the same VSD should be avoided. The use of multiple motors with a single control can result in a higher probability of having problems with repetitive high voltage overshoots at the terminals of the motor.
- If the peak voltage is over the recommended limit, a filter or reactor between the VSD and the motor must be used.
- Avoid long lead lengths. The maximum recommended cable distance between VSD and motor is about 50–100 feet or less, depends on the impedances of the cable and the motor. If a short cable is not possible and if the peak voltage is over the recommended limit, use a filter or reactor between the control and the motor.
- Use premium varnish conductors to reduce partial discharges.

To avoid excessive overheating:

- Oversize the motor and control
- Provide an independent cooling system (external ventilation) when the load is of the constant torque type, and the motor runs at low speed
- Install a drive filter.

To avoid shaft currents:

- Use an inverter fed motor with a voltage of 230 V or less when possible.
- Use the lowest carrier frequency that satisfies the motor requirements.
- Add a shaft grounding device to the motor. Some devices have a brush that rides on the motor shaft. Current does not go through the bearing but is instead conducted directly to ground through the brush. These brushes are especially selected to tol-

erate misalignment and maintain rotating contact throughout the brush's life when properly maintained.

- Use a motor with both bearings insulated. This approach will avoid damage to the motor's bearings.
- Use nonconductive couplings for restricted and loads or which may be damaged by bearing currents.
- Ensure that the control and motor are grounded per the manufacturers' instructions.

### 6.2.13 Power Quality

#### General Considerations About Power Quality

Power quality may be defined as the control of a power system, in order to assure the reliable operation of the entire system, including generation, transmission and ultimately electric power distribution, during steady-state and transient/dynamic conditions. The complexity of the system to move electric energy from the point of production to the point of consumption combined with variations in weather, generation, demand and other factors provide many opportunities for the quality of supply to be compromised. The quality of the electrical power may be described as a set of conditions and values for some parameters, whose deviations must be within prescribed limits so that they do not affect consumers and system performance. The following conditions and parameters must be observed and controlled in order to assure the power quality supply:

- Variations in voltage magnitude
- Harmonic content in the AC waveforms
- Variations in frequency
- Low power factor.

**Variations in Voltage Magnitude.** Undervoltage may occur, for instance, when there is the disconnection of a capacitor bank or an increase of the apparent power in lines and equipments over their nominal ratings, due to the loss of one element of the system, causing an overload in the power supply. The undervoltage is characterized by a decrease in voltage, typically to 80–90% of the nominal for more than 1 min. A voltage sag, a type of undervoltage, happens when the voltage decreases between 10 and 90% of nominal voltage with a duration varying from 3 s to 1 min, when a severe condition like a short-circuit happens. Overvoltage occurs when the voltage rises above 110% of the nominal for more than 1 min, for instance, due to a load disconnection. A swell is a momentary voltage increase in the range from 1.10 to 1.80 per unit of nominal voltage, with a duration varying from 0.5 cycles to 1 min, and it may be caused by a single line to ground fault and when

large capacitor banks are switched-on, for example. Abrupt, very brief increases in voltage, called *spikes*, *impulses*, or *surges*, are caused by nonlinear loads, such as VFDs operation or more severely by lightning. Another cause of problems is the voltage imbalance when the phase voltages are unequal. The primary source of voltage imbalances are single-phase loads on a three-phase circuit.

**Harmonic Content in the AC Waveforms.** One of the sources of voltages and currents departure from the ideal sinusoidal, is due to nonlinear drives, such as VSDs, where the harmonics cause distortions in the sinusoidal waveforms. The relative contribution of harmonics to the distortion of the ideal waveform is called total harmonic distortion (THD). Low harmonic content in a waveform is desirable because harmonics can cause many problems. Harmonics, arising within the customer's own installation if propagated onto the network may affect other customers and system operation. High voltage DC transmission systems with their associated rectifiers and inverters, and transformers due to saturation of their magnetic core also produce harmonics. Harmonic problems can be dealt with by a combination of good design practice and well proven harmonic reduction equipment.

**Variations in Frequency and Low Power Factor.** Frequency variations occur when the dynamic balance between load and generation is severely disturbed. The main cause of frequency variations that may affect the reliable performance of a power system and loads are due to short-circuits with the disconnection of more than one high-voltage transmission line and equipments on the bulk-power transmission system, and also by a large power plant going off-line or by the disconnection of a large block of load. On modern interconnected power systems, significant frequency variations are rare. Low power factors are due to the consumption of reactive power by the loads. They increase the losses in equipment, feeds, distribution and transmission lines, most of time requiring the addition of capacitors.

#### Power Quality Problems in Induction Motors

Electric motors are everywhere in modern society. In industry they comprise about 80% of the electrical load and their failure or disconnection cause loss of production and consequently economic losses. Motors are a prime example of the ways electrical equipment can be both a source and a victim of power quality disruptions in an industrial facility. Large motors can cause voltage sags in local and adjacent areas when they are started, individually or in groups. Induction motors can have a negative impact on a power factor, due to their

need for reactive energy. However, motors can also be negatively affected by disturbances in a number of ways, with results that can include decreased efficiency, reduced lifespan and even complete failure. Generally the factors mentioned above are the cause of several types of power quality problems commonly seen in induction motors, described as follows.

Overvoltage may cause, depending on the design of the motor, saturation of the core iron, leading to generation of harmonics and motor overheating. The induction motor torque may be increased significantly over the load torque and the motor may reach an undesirable overspeed. On the other hand an undervoltage decreases the torque and the current increases in order to supply the load torque. The decrease in torque may be enough as to not start the load or the motor may stall due to insufficient running torque. The increase in current results in greater joule losses in the rotor and stator, that may lead to overheating. A voltage imbalance may cause overheating of one or two phase windings, as well as shaft vibrations. Imbalance should be less than 1% in order to properly supply the load and the motor should not operate if the voltage imbalance exceeds 5%. The aforementioned situations result in a decrease in motor efficiency and shortens its life. A voltage sag usually leads to a motor disconnection from the supply by the protection system. Voltage transients stress motor-winding insulation, causing degradation over time, or even complete failure. All the voltage problems described can lead to a load disconnection impairing the power quality of the consumers supplied by the motors.

A major effect of harmonic voltages and currents in induction motors is increased heating, as already mentioned, due to iron and copper losses at the harmonic frequencies, especially due to the harmonics of low orders, that have larger magnitudes. The harmonic components thus affect the machine efficiency, and can also affect the torque developed. Harmonic currents in a motor can give rise to a higher audible noise emission as compared with sinusoidal excitation. The harmonics also produce a resultant flux distribution in the airgap, that can cause or enhance phenomena called cogging (refusal to start smoothly) or crawling (very high slip) in induction motors.

Each harmonic voltage, the fifth, seventh, eleventh, etc., will induce a corresponding harmonic current in the stator of the machine. Each of these harmonics is a positive or negative sequence symmetrical component of the total current. These currents will induce additional heating in the stator windings, thus adding to the temperature rise caused by the fundamental current.

Another generally greater concern is the flow of harmonic currents in the rotor. The flow of each current in the stator will produce a magnetomotive force in the

airgap that will induce current flow in the rotor of the machine. Just as each characteristic harmonic can be defined as being a positive or negative sequence, the rotation of that harmonic will be either forward or backward with respect to rotor rotation. The fifth harmonic will rotate in a backward direction (negative sequence), so a harmonic current will be induced in the rotor with a frequency corresponding to the net rotational difference between the fundamental airgap frequency and the fifth, i.e., the fifth plus one, or the sixth harmonic. Since the seventh harmonic will rotate in a forward direction (positive sequence), a harmonic current will be induced in the rotor with a frequency corresponding to the net rotational difference between the seventh and the fundamental airgap frequency, i.e., the seventh minus one, or the sixth harmonic. Thus, from a rotor heating standpoint, the fifth and the seventh harmonics in the stator combine to produce a sixth harmonic current in the rotor. The 11th and the 13th harmonics act in the same manner to produce the 12th harmonic current in the rotor, and so on with higher order harmonic pairs. There are two major concerns with these rotor harmonics:

- Resultant rotor heating
- Pulsating or reduced torques.

The amount of rotor heating that can be tolerated, as well as the amount that is incurred in a given case, depends on the type of rotor involved. Wound-rotor machinery is more likely to be more seriously affected than squirrel-cage rotor machinery, and deep bar squirrel-cage rotors are more affected than ordinary squirrel cages. Winding losses generally are of more concern than iron losses. The sum effect of the harmonics is a reduction in the efficiency and life of the machinery. Neither reduction is pronounced for normally encountered harmonic content, but the harmonic heating typically reduces performance to 90–95% of that which would be experienced with pure fundamental sine waves applied.

As noted before, the harmonics can also cause a pulsating torque output. This can affect product quality where motor loads are sensitive to such variations, e.g., in some synthetic fiber spinning or some metal working applications. In cases in which substantial inertia is coupled to the rotor shaft, e.g., in a motor-generator or engine-generator, the electrical harmonics can excite a mechanical resonance. The resulting mechanical oscillations can cause shaft fatigue and accelerated aging of the shaft and connected mechanical parts.

In an induction motor due to the airgap a large magnetizing current is needed to produce the required flux in the motor. At zero-load the active component of the current is very low while the magnetizing current is

high, and as a consequence the power factor is very low, between 10 and 20%. When the motor is loaded, the power factor increases because the active component of current increases while the magnetizing component remains about the same, and the power factor is between 85 and 90% at full load. A low power factor demands more current from the supply than a load with a high power factor. The higher currents increase the energy lost in the distribution and transmission systems and require larger wires and sometimes the installation of new equipment, such as power transformers, circuit-breakers, current transformers, etc. Because of the costs of larger equipment and the wasted energy, electrical utilities will usually charge a higher cost to industrial or commercial customers where there is a low power factor.

### 6.2.14 Advanced Motor Technologies

Advanced technologies such as the squirrel-cage AC induction motors that use die cast copper rotors and linear induction motors are briefly presented.

#### Die Cast Copper Rotor Motors

Until recently, die cast motor rotors were universally produced using aluminum because rotor fabrication by aluminum pressure die-casting was an established practice, and copper pressure die-casting was not. When die-casting copper rotors using conventional die-casting techniques, the short die life results from the large temperature difference between the pouring temperature of the liquid copper (melting temperature is 1083 °C) and the temperature of the die (typically 100–200 °C), while for aluminum the melting temperature is 660 °C. When the hot copper contacts the die, the resultant thermal expansion of the die surface results in the generation of extremely large plastic strains following each shot. However, this problem has been surpassed when the die is pre-heated and operating temperatures are increased to about 600 °C, so that the surface strain can be reduced into the elastic range, greatly reducing heat checking and so extending die life [6.49, 50].

Although the cost of die-casting a copper rotor is higher than that of die-casting an aluminum rotor, the overall cost of the motor utilizing the copper rotor can be lower. General purpose die cast copper rotor motor costs are about 11–17% higher than conventional premium efficiency motors (IE3 class), but the overall loss reductions may be around 25%. As the reduction in losses implies a lower temperature in the motor, the use of a small fan is possible, that in turn causes a reduction in friction and windage losses. Running the motor cooler is known to extend motor life. An empirical law suggests that a 10 °C reduction in operating

temperature will extend the motor life by a factor of two. Low losses implies less energy consumption, reducing the stress on the environment as a result of low CO<sub>2</sub> emissions. Copper rotor motors generally exceed the premium minimum full-load efficiency motors (IE3 class), by 0.6–2 percentage points. High efficiency implies reduced electrical energy consumption year after year due to significantly lower losses, with attractive payback and return on capital investment. Due to the higher efficiency of the copper rotor, the overall length of the rotor (and motor) can be decreased. Shortening the motor eliminates some of the rotor and stator laminations, decreases the amount of stator windings, and reduces the length of the shaft, reducing cost in each case. The increased cost of die-cast copper rotors is more than off-set by the cost savings elsewhere in the motor.

Copper rotor motors are being manufactured in small sizes where permanent magnet synchronous motors are also a choice for higher energy efficiency, although the latter are generally more expensive. Thus, die cast copper rotor motors, because of their higher efficiencies appear to be the appropriate advancement for the general industrial motor population. As the size of the motor increases the efficiency gains of the die cast copper rotor motors are expected to decrease, as over 200 HP other motor technologies will provide better efficiency improvement opportunities. However, for the majority of industrial motors, in the range 1–200 HP, die cast copper rotor motors are the newest technology for lowering motor operating costs, especially in the lower horsepower ranges. Die cast rotor motors come in NEMA and IEC frames, so they can be drop-in replacements for conventional motors [6.51].

#### Linear Induction Motor

In a linear induction motor (LIM) both the primary and secondary are laid out flat. The primary consists of a three-phase coil assembly, equivalent to the stator of a rotary motor. The secondary, known as a rotor in a traditional rotary induction motor is a plate, made of aluminum or copper. In fact the basic difference with respect to a conventional induction motor is the substitution of the angular movement by a linear movement. Thus, the properties of a linear induction motor are almost identical to those of a conventional induction motor. Thus, the slip is

$$s = \frac{v_s - v}{v_s}, \quad (6.185)$$

where  $v_s$  = synchronous linear speed and  $v$  = rotor speed.

When three-phase AC power is applied to the primary, a traveling flux wave with a wavelength of  $\lambda$

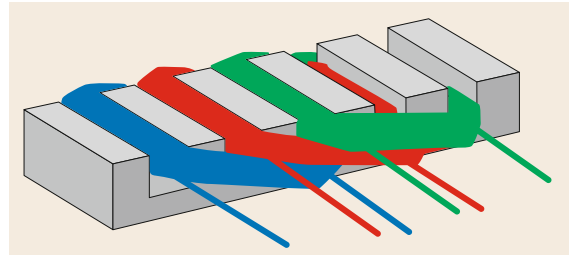
and linear velocity  $v_s = \lambda f$ , where  $f$  is the supply frequency, induces an electric current in the secondary plate. The induced electric current interacts with the magnetic flux to produce a linear force or thrust that moves the secondary plate in the direction of the traveling flux wave

$$F = \frac{P}{v_s}, \quad (6.186)$$

where  $F$  is the force or thrust and  $P$  is the power transferred from the stator to the rotor.

In general, the rotor has a single plate, while two flat stators are usually mounted, face to face, on opposite sides of the rotor to increase the power and to reduce the reluctance of the magnetic path. The direction of the motor can be reversed by interchanging any two stator leads. The speed of the motor can be varied by changing the input frequency using an adjustable frequency drive.

A typical three-phase linear induction motor is shown in Fig. 6.69. The primary core has grooves, and the windings are laid into them on top of each other. An aluminum plate above (not shown) serves as



**Fig. 6.69** Typical three-phase linear induction motor (from Wikipedia)

the secondary and will move relative to the primary if a three-phase AC is applied.

LIMs have been built in fractional-horse-power ratings up to several thousand horsepower. The main application of the LIM is in transportation and in electric traction systems. The primary is mounted on the train and the secondary is laid on the track. It is also used in: metallic conveyor belts, material handling in cranes, pumping of liquid metals, freight cars in yards, reciprocating motion for machine tools and actuators for the movement of doors.

## References

- 6.1 IEC 60034: *Rotating Electric Machines—Part 6, Methods of Cooling* (IEC, Geneva 1991)
- 6.2 National Electrical Manufacturers Association: *Motors and Generators*, NEMA MG 1 (NEMA, Rosslyn 2011)
- 6.3 H. Sako, K. Koga, H. Maeda, M. Onoda, K. Tanaka, Y. Nakamura: Development of larger output indirectly hydrogen-cooled turbine generator with high heat transfer main insulation. In: *Proc. CIGRE Bienn. Conf.* (2016), Rap. A1-116
- 6.4 G.C. Stone, E.A. Boulter, I. Culbert, H. Dhirna: *Electrical insulation for rotating machines—design, evaluation, aging, testing, and repair* (Wiley, New York 2004)
- 6.5 IEC 60034-1: *Rotating Electrical Machines—Part 1: Rating and Performance* (IEC, Geneva 2010)
- 6.6 IEC 60085: *Electrical Insulation—Thermal Evaluation and Designation* (IEC, Geneva 2007)
- 6.7 J. Pyrhönen, T. Jokinen, V. Hrabovcová: *Design of Rotating Electrical Machines* (Wiley, Chichester 2014)
- 6.8 M.L. Garik, C.C. Whipple: *Alternating-Current Machines* (Van Nostrand, Princeton 1966)
- 6.9 EEEGUIDE.com: MMF of distributed AC windings, <https://www.eeeguide.com/mmf-of-ac-distributed-winding/> (2016)
- 6.10 IEEE Std 115: *IEEE Guide for Test Procedures for Synchronous Machines* (IEEE, New York 2009)
- 6.11 IEC 60034-4: *Rotating electrical machines—Part 4: Methods for determining synchronous machine quantities from tests* (IEC, Geneva 2008)
- 6.12 A.W. Rankin: Per-unit impedances of synchronous machines part I, *AIEE Transactions* **64**, 569–573 (1945)
- 6.13 A.W. Rankin: Per-unit impedances of synchronous machines part II, *AIEE Transactions* **64**, 839–841 (1945)
- 6.14 A.W. Rankin: The direct- and quadrature-axis equivalent circuits of the synchronous machine, *AIEE Transactions* **64**, 861–869 (1945)
- 6.15 IEEE Std C50.12: *IEEE Standard for Salient-Pole 50 Hz and 60 Hz Synchronous Generators and Generator/Motors for Hydraulic Turbine Applications Rated 5 MVA and Above* (IEEE, New York 2005)
- 6.16 IEEE Std C50.13: *Cylindrical-Rotor 50 Hz and 60 Hz Synchronous Generators Rated 10 MVA and Above* (IEEE, New York 2014)
- 6.17 CIGRE W.G. A1.38: *Generator On-Line Over and Under Excitation Issues* (CIGRE, Paris 2014)
- 6.18 IEEE Std. C37.106: *Guide for Abnormal Frequency Protection of Power Generating Plants* (IEEE, New York 2003)
- 6.19 CIGRE WG A1.29: *Guide on New Generator-Grid Interaction Requirements* (CIGRE, Paris 2016)
- 6.20 IEEE Std. 421.2: *Guide for Identification, Testing, and Evaluation of the Dynamic Performance of Excitation Control Systems (Revision of IEEE Std 421.2-1990)* (IEEE, New York 2014)
- 6.21 IEEE Std 421.4: *Guide for the Preparation of Excitation System Specifications* (IEEE, New York 2014)
- 6.22 IEEE Std. 421-5: *Recommended Practice for Excitation System Models for Power System Stability Studies* (IEEE, New York 2006)
- 6.23 B. Adkins: *The General Theory of AC Machines* (Chapman Hall, London 1964)



- 6.24 E.W. Kimbark: *Power System Stability: Synchronous Machines* (Dover, London 1968)
- 6.25 W. McCown: Advances in the development of synchronous machines with high-temperature superconducting field winding at Siemens AG. In: *IEEE Power Eng. Soc. General Meet. N. Y.* (IEEE, New York 2006)
- 6.26 J. Frauenhofer, J. Grundmann, G. Klaus, W. Nick: Basic concepts, status, opportunities, and challenges of electrical machines utilizing high-temperature superconducting (HTS) windings, *J. Phys. Conf. Ser.* **97**, 012189 (2008)
- 6.27 S. Kalsi, D. Madura, M. Ingram: Superconductor synchronous condenser for reactive power support in an electric grid, *IEEE Trans. Appl. Supercond.* **15**(2), 2146–2149 (2005)
- 6.28 D.U. Gubser: *Superconducting motors and generators for naval applications* (Elsevier, Amsterdam 2003)
- 6.29 A.T. de Almeida, F.J.T.E. Ferreira, J.A.C. Fong: Standards for super-premium efficiency class for electric motors. In: *2009 IEEE Ind. Commer. Power Syst. Tech. Conf. Calgary* (2009) pp. 1–8, <https://doi.org/10.1109/ICPS.2009.5463983>
- 6.30 U.S. Department of Energy (DOE): *Premium Efficiency Motor Selection and Application Guide—a Handbook for Industry* (DOE, Washington 2012)
- 6.31 A. de Almeida: Beyond induction motors. In: *Motor Summit 2012, Zurich* (2012)
- 6.32 National Electrical Manufacturers Association: *Motors and Generators, NEMA MG 1* (NEMA, Rosslyn 2011)
- 6.33 G.C. Stone, E.A. Boulter, I. Culbert, H. Dhirna: *Electrical Insulation for Rotating Machines—Design, Evaluation, Aging, Testing, and Repair* (Wiley, New York 2004)
- 6.34 A.E. Fitzgerald, C. Kingsley, S.D. Umans: *Electric Machinery*, 6th edn. (McGraw-Hill, New York 2003)
- 6.35 IEEE Std 112: *Test Procedure for Polyphase Induction Motors and Generators (Rev. IEEE Std 112-1996)* (IEEE, New York 2004)
- 6.36 Electrical4U: Construction of three phase induction motor, <https://www.electrical4u.com/construction-of-three-phase-induction-motor/> (2019)
- 6.37 Circuit Globe: Double cage rotor of an induction motor, <https://circuitglobe.com/double-cage-rotor-of-an-induction-motor.html> (2017)
- 6.38 J. Nelson: Torque characteristics of NEMA A, B, C, D, & E Motors, <https://info.panelshop.com/blog/torque-characteristics-of-nema-a-b-c-d-e-motors> (2019)
- 6.39 IEC 60034-30: *Rotating Electrical Machines—Part 30: Efficiency Classes of Single-Speed, Three-Phase, Cage-Induction Motors* (IEC, Geneva 2008)
- 6.40 IEC 60034-30-1: *Rotating Electrical Machines—Part 30-1: Efficiency Classes off Line Operated AC Motors* (IEC, Geneva 2014)
- 6.41 IEC 60034-2-1: *Rotating Electrical Machines—Part 2-1: Standard for Determining Losses and Efficiency from Tests (Excluding Machines for Traction Vehicles)*, 2nd edn. (IEC, Geneva 2014)
- 6.42 M.H. Rashid: *Power Electronics—Circuits, Devices, and Applications* (Prentice-Hall, Upper Saddle River 1993)
- 6.43 N. Mohan, T.M. Undeland, W.P. Robbins: *Power Electronics*, 2nd edn. (Wiley, New York 1995)
- 6.44 G. Kohlruz, D. Fodor: Comparison of scalar and vector control strategy off induction motors, *J. Ind. Chem.* **39**(2), 265–270 (2011)
- 6.45 National Electrical Manufacturers Association: *Application Guide for AC Adjustable Speed Drive Systems* (NEMA, Rosslyn 2001), Standards Publication
- 6.46 IEC 60034-31: *Selection of Energy-Efficient Motors Including Variable Speed Applications* (IEC, Geneva 2010)
- 6.47 A.T. De Almeida, P. Angers, C.U. Brunner, M. Doppelbauer: Motors with adjustable speed drives: testing protocol and efficiency standard. In: *Proc. EEMODS'09, 14–17 September, Nantes* (2009)
- 6.48 P. Waide, C.U. Brunner: *Energy-efficiency policy for electric motor-driven systems* (International Energy Agency, Paris 2011)
- 6.49 Copper Development Association: Tests show mass-produced copper-rotor motors more efficient than nameplate claims, *Copper Motor Rotor* **6**(3) (2006)
- 6.50 F. Parasiliti, M. Villani, C. Paris, O. Walti, G. Songini, A. Novello, T. Rossi: Three phase induction motor efficiency improvements with die-cast copper rotor cage and premium steel. In: *Proc. SPEEDAM Symp., Capri* (2004) pp. 338–343
- 6.51 Copper Development Association: Copper motor rotor commercialized, Update, *Copper Motor Rotor* **3**(3) (2003)

### Erli F. Figueiredo

Electrical Engineering Department  
Rio de Janeiro State University  
Rio de Janeiro, Brazil  
[erliff@uol.com.br](mailto:erliff@uol.com.br)



Erli F. Figueiredo received his masters degree from the Rensselaer Polytechnic Institute (RPI), Troy, New York, and his doctorate degree from Rio de Janeiro Federal University. He was the head of the electrical system department at Rio de Janeiro State University, from 1998 to 2000 and from 2006 to 2008. From 2008 to 2014 he was chairman of the CIGRE study committee on “Rotating Electrical Machines” (SC A1). He was a distinguished member of CIGRE in 2012 and an honorary member of CIGRE in 2014. He has authored/co-authored numerous papers, CIGRE technical brochures and reports.

# Transformers

## 7. Transformers

Peter Werle , Hartmut Brendel 

All industrialized countries depend on functioning and flawless power transmission and distribution at various voltage levels, which is achieved through the use of power transformers. This implies that power transformers are among the most important (and expensive) devices used in power transmission and distribution systems. Indeed, transformers are indispensable, as they are used to transition between voltage levels at the junctions of energy supply systems. A transformer failure can therefore cause an interruption in the power supply, which can have terrible consequences. However, many transformers remain in service for many decades without showing any notable malfunctions, and these devices are generally considered to be reliable and efficient.

In this chapter, the fundamental design and functional principles of a power transformer are described in detail, differentiating between its active and passive parts. Power transformer testing is also discussed, referencing various international standards. Finally, various types of transformers are briefly introduced. Thus, the chapter provides a comprehensive overview of all the basic technical aspects of power transformers, although the servicing, maintenance, and asset management of transformers are only outlined here, as a more detailed discussion of these important topics would require an additional chapter.

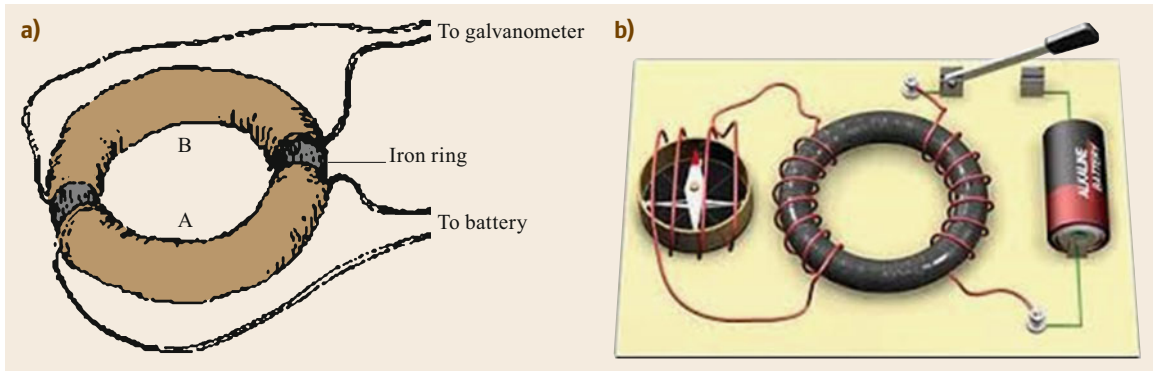
7.1	<b>Fundamentals</b> .....	443
7.1.1	History .....	443
7.1.2	Functional Principle and Basic Design ..	445
7.1.3	Single-Phase Considerations .....	449
7.1.4	Three-Phase Operation .....	455
7.2	<b>Active Part</b> .....	460
7.2.1	Core .....	460
7.2.2	Windings .....	465
7.2.3	Tap Changers .....	478
7.2.4	Bushings and Lead Exits .....	480
7.2.5	Cooling Types and Insulating Fluids .....	482
7.2.6	Tank and Protection System .....	484
7.3	<b>Testing Power Transformers</b> .....	484
7.3.1	Types of Tests .....	486
7.3.2	High-Voltage Test Equipment .....	494
7.4	<b>Types of Transformers</b> .....	497
7.4.1	GSU Transformers .....	498
7.4.2	Substation Transformers .....	498
7.4.3	Autotransformers .....	499
7.4.4	Distribution Transformers .....	500
7.4.5	Phase Shifters .....	500
7.4.6	HVDC Transformer .....	501
7.4.7	Arc-Furnace Transformer .....	501
7.4.8	Rectifier and Converter Transformers ...	502
7.4.9	Traction Transformers .....	503
7.4.10	Test Transformers .....	504
7.4.11	Variable Differential Transformers .....	504
7.4.12	Other Types of Transformers .....	505
	<b>References</b> .....	507

## 7.1 Fundamentals

### 7.1.1 History

As is often the case for important inventions, the transformer was not devised by just one person. The design of this invaluable device is the cumulative result of a whole series of groundbreaking discoveries and inventions. In 1831, *Michael Faraday* discovered the principle of induction using a device that presented all of the characteristics of a transformer [7.1], as shown in Fig. 7.1a.

Faraday applied two windings of copper wires that were insulated from each other using fibers and calico on a soft-iron ring. As shown in Fig. 7.1b, he placed one winding around a magnetic needle and connected the other winding to a battery. By switching the battery supply on and off, Faraday generated an alternating current and was able to demonstrate magnetic induction in the second coil because the magnetic needle started to move. This arrangement of two separate windings that are magnetically coupled by a soft-iron ring fulfills



**Fig. 7.1** (a) Sketch of Faraday's experiment [7.1]. (b) Modern version of the experiment [7.2]

the principles of a transformer, but it took more than 50 years for Faraday to develop a practical use for this system [7.3].

In 1856, Cromwell Fleetwood Varley obtained an English patent (3059/1856) for the first apparatus with a closed magnetic circuit in the form of a shell-type transformer. However, a practical use for this circuit remained elusive during that period.

In 1882, Lucien Gaulard and John Gibbs invented a transformer with disc windings on an iron core (English patent 4362), as shown in Fig. 7.2. They called their transformer a *secondary generator*, which subsequently led to the classification of the transformer as an electrical machine – a classification that is still used today. At the same time, they also patented an energy distribution system based on alternating currents with transformers connected in parallel in a circular network several kilometers long. Light bulbs were connected to the secondary sides of the transformers; this represented the first commercial application of transformers.

In 1885, George Westinghouse purchased the transformer patents of Gaulard and Gibbs. In the same year, the Hungarians Károly Zipernowsky, Miksa Déri, and Ottó Bláthy received a patent (Deutsches Reichspatent, DRP 40414) for the parallel connection of generators, transformers, and consumers, and used the term *transformer* for the first time [7.4]. They developed a kind of shell-type transformer, as illustrated in Fig. 7.3, with a core made from soft magnetic wires wrapped around the coils. This represented the first example of a transformer with a closed iron core. It was subsequently manufactured by the company Ganz & Cie in Budapest and commercialized around the globe.

All of these breakthroughs relate to single-phase systems. Further development was achieved through the work of Westinghouse, based on Nikola Tesla's invention of two-phase alternating current, and this development allowed the alternating current promoted by Westinghouse and Tesla to prevail against the direct cur-



**Fig. 7.2** Model in the Museo Galileo (Florence, Italy) of the transformer constructed by Gaulard and Gibbs [7.4]

rent championed by Thomas Edison in the so-called battle of currents.

The three-phase system was essentially developed by Mikhail Dolivo-Dobrovolsky while he was working for the Berlin-based company Allgemeine Elektrizitäts-Gesellschaft (AEG), where he later took on managerial positions. He introduced the term *Drehstrom* (rotary current) for German-speaking countries; in other



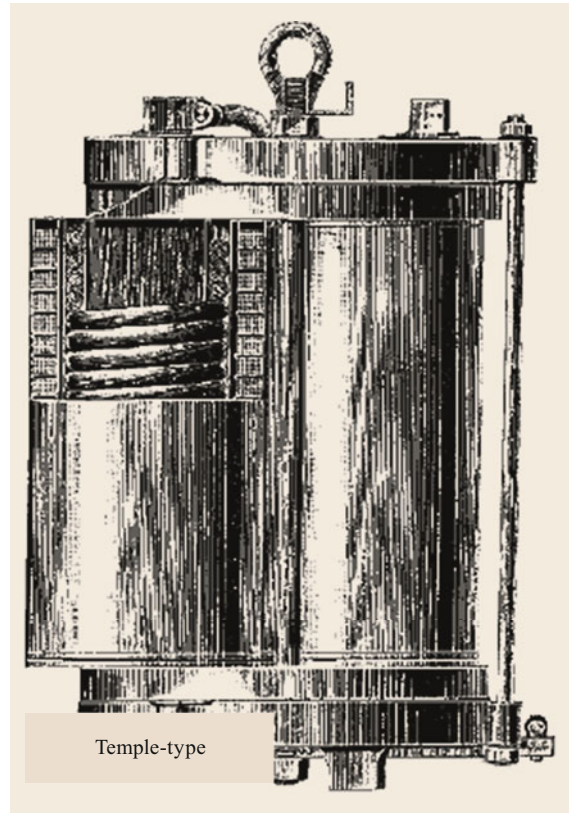
**Fig. 7.3** The transformer manufactured by Ganz & Cie [7.4]

territories, the term *three-phase (alternating) current* is used. Energy transmission using a 15 kV three-phase system occurred for the first time in a successful experiment to transmit energy over the considerable distance (175 km) from the hydroelectric power plant in Lauffen (on the Neckar River in Germany) to the international electrotechnical exhibition of 1891 in Frankfurt [7.5]. Figure 7.4 shows the oil-insulated transformers that were used in this experiment. These transformers, made by AEG, were based on a design known as *temple core*. The basic principle of this oil-insulated transformer design resulting from the pioneering work of Dolivo-Dobrovolsky at AEG in the 1920s is still employed today.

After that, power transformer development continued in a discontinuous manner: phases of new inventions were repeatedly interrupted by new advances based on new materials and technologies. After 1945, there were particularly notable advances in oil-insulated power transformer reliability and service life. Among the most important innovations were the transitions from hot-rolled core sheets to cold-rolled textured sheets and from soft paper insulation to molded parts made from pressboard. These innovations, which were incorporated into transformer construction over a period of just a few years, had a major impact on the quality and longevity of transformers.

As already mentioned, the definition of a transformer as an electrical machine can be traced back to Gaulard and Gibbs, who defined the transformer as a *secondary generator*. Note that, in principle, all electrical machines can be considered *electromagnetic energy converters*.

According to the European Machinery Directive, a machine should contain at least one moving part [7.6]. This requirement is met by all rotating electrical machines. However, all of the components of a transformer



**Fig. 7.4** Three-phase oil-insulated transformer with a temple core, as constructed by the company AEG in 1891 [7.5]

are rigidly connected to each other. Thus, a transformer can be categorized as a stationary electrical machine that electromagnetically transfers electrical energy from one system with particular current and voltage values to another system with different current and voltage values at the same frequency [7.7].

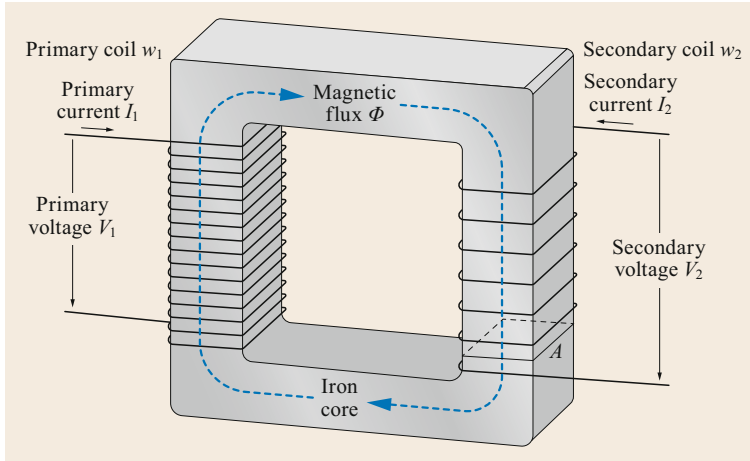
It should be noted that the device referred to as a transformer in this chapter is actually known by various names, depending on the area of electrical engineering considered:

- In power engineering  $\Rightarrow$  power transformer
- In information technology  $\Rightarrow$  transducer
- In measurement technology  $\Rightarrow$  instrument transformer.

In the following, only transformers in the area of power electrical engineering are considered.

## 7.1.2 Functional Principle and Basic Design

In a transformer, two separate windings are coupled via a magnetic circuit in the form of an iron core, as depicted in Fig. 7.5.



**Fig. 7.5** Principal components of a transformer [7.2]

A magnetic field is generated in a transformer according to the following general principle:

*A moving electric charge generates a magnetic field of intensity  $H$ .*

The moving electric charge can be a current flowing in an electrical conductor with current density  $J$  or a time-varying displacement current density  $D$  caused by a temporally changing electrical field. Both types of moving charge are generalized as a flux  $\Theta$ . Mathematically, this is formulated as *Ampère's law*, the fourth of *Maxwell's equations*, which states that the ring integral around the closed curve  $x$  is equal to the sum of the current densities through the surface  $A$ , i.e., [7.7]

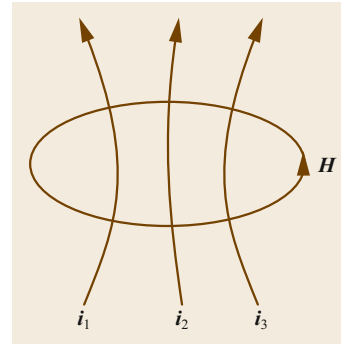
$$\oint_x \mathbf{H} dx = \iint_A \left( \mathbf{J} + \frac{\partial \mathbf{D}}{\partial t} \right) d\mathbf{A} = \Theta . \quad (7.1)$$

Transformers operate with quite slowly changing fields that are termed quasi-stationary fields. The displacement current in the highly conductive materials used in a transformer is negligible compared to the conduction current. Therefore, (7.1) can be simplified to

$$\oint_x \mathbf{H} dx = \iint_A \mathbf{J} d\mathbf{A} = \sum I = \Theta . \quad (7.2)$$

This equation directly links the magnetic field strength  $H$  to the current.

The closed loop integral of the magnetic field strength is equal to the current in the loop. From Fig. 7.6,  $\oint_x \mathbf{H} dx$  is  $i_1 + i_2 + i_3$ , which is equal to  $wi$ , where  $w$  is the number of turns of the winding in Fig. 7.7 and  $i$  is the current through the winding. The magnetic field strength  $H$  (in A/m) is independent of the surrounding medium. The magnetic flux density  $B$  (in  $V\,s/m^2 = T$ ) is a function of the magnetic field strength



**Fig. 7.6** Ring integral of the magnetic field strength

and the permeability  $\mu$  of the surrounding medium (as a proportionality factor). Thus, the expression

$$\mathbf{B} = \mu \mathbf{H} \quad (7.3)$$

is valid.

The permeability is the product of the vacuum permeability or magnetic constant  $\mu_0$  and the relative permeability  $\mu_r$ , i.e.,

$$\mu = \mu_0 \mu_r . \quad (7.4)$$

The value of the magnetic constant  $\mu_0$  is given by

$$\mu_0 = 4\pi \times 10^{-7} \frac{V\,s}{A\,m} = 1.257 \times 10^{-6} \frac{V\,s}{A\,m} . \quad (7.5)$$

The materials used for transformer cores are ferromagnetic ( $\mu_r \gg 1$ ); meaning that they can bundle a magnetic flux  $\Phi$  and conduct it along a specified path. The magnetic flux  $\Phi$  [V s] is given by the area integral of the magnetic flux density

$$\Phi = \iint_A \mathbf{B} d\mathbf{A} . \quad (7.6)$$

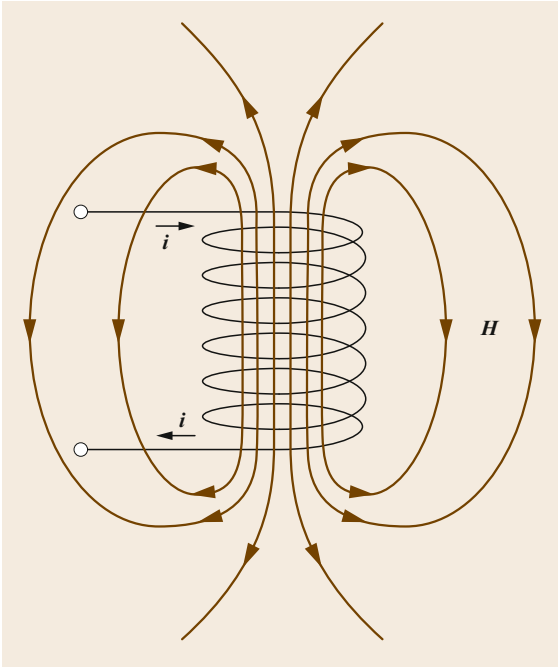


Fig. 7.7 Cylindrical winding with  $w$  turns

When the flux density over a surface  $A$  is constant, the flux  $\Phi$  is equal to the product of the flux density  $B$  and the surface area  $A$ , i.e.,

$$\Phi = B \cdot A. \quad (7.7)$$

If the primary voltage  $V_1$  in Fig. 7.5 is a direct current (DC) voltage and therefore  $I_1$  is a DC current, an electrical flow is generated and a constant magnetic flux  $\Phi$  builds up in the core, but no permanent voltage is induced in the secondary winding.

Only when  $V_1$  is an alternating voltage, and therefore  $I_1$  is an alternating current, an alternating voltage ( $V_2$ ) is induced in the secondary winding. This happens due to the alternating magnetic flux  $\Phi$  generated in the magnetic circuit by the presence of  $I_1$ , thus an electrical field  $E$  is induced according to the second of Maxwell's equations. This equation is called Faraday's law of induction, and can be written in an integral form as [7.8]

$$\oint_x E dx = -\frac{\partial}{\partial t} \iint_A B dA. \quad (7.8)$$

The voltage along the edge of the surface is the time derivative of the magnetic flux  $\Phi$  through the surface  $A$ . If the edge of this surface is a conductor loop (e.g., a winding turn of the secondary winding in Fig. 7.5), a voltage  $V_i$  is induced, as shown in Fig. 7.8.

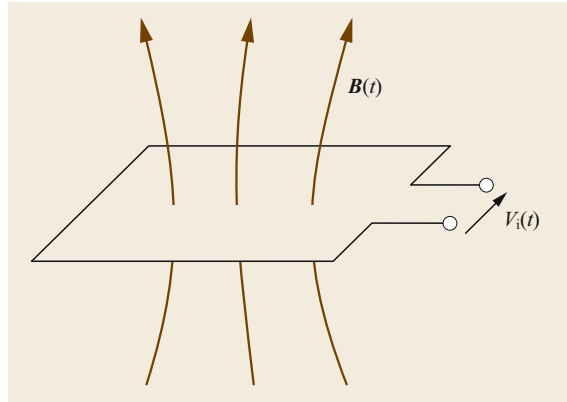


Fig. 7.8 Voltage  $V_i(t)$  induced in a time-varying magnetic field  $B(t)$

Assuming a varying flux  $\Phi$  through area  $A$ , the winding turn voltage  $V_i(t)$  of the conductor loop of area  $A$  is calculated according to Fig. 7.8 as

$$V_i(t) = -\frac{d\Phi(t)}{dt} = -A \cdot \frac{dB(t)}{dt}. \quad (7.9)$$

The negative sign in (7.9) indicates that the induced voltage is in the opposite direction to the magnetic field that creates it (Lenz's law). A voltage  $V_2$  is induced across all of the turns  $w_2$  of the secondary winding in Fig. 7.5.

$$V_2(t) = -w_2 \frac{d\Phi(t)}{dt} = -w_2 A \cdot \frac{dB(t)}{dt}. \quad (7.10)$$

This form of induction is called *mutual induction*.

If the magnetic flux is sinusoidal, the change in flux is zero at the maximum value of the flux, whereas the change in flux is greatest at the zero crossing of the sinusoidal function. Therefore, the induced voltage  $V_i(t)$  is phase shifted by a  $90^\circ$  lag with respect to the magnetic flux  $\Phi(t)$ . The maximum induced sinusoidal voltage can be calculated via

$$V_{\max} = w \left( \frac{d\Phi}{dt} \right)_{\max} = wA \cdot \left( \frac{dB}{dt} \right)_{\max}. \quad (7.11)$$

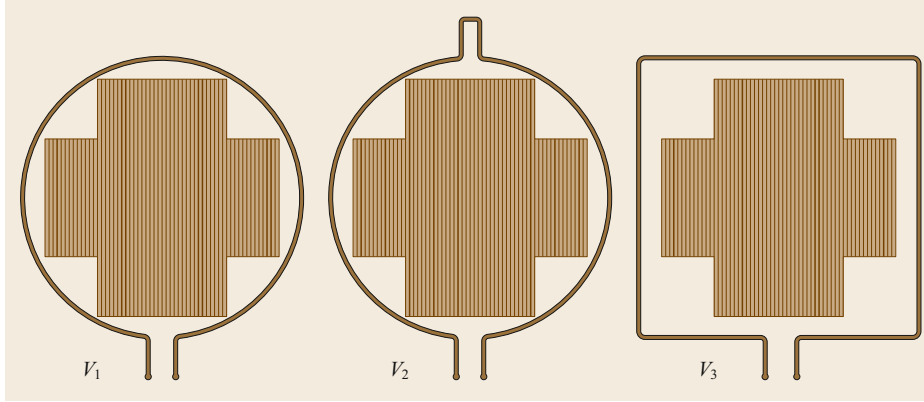
For sinusoidal functions such as  $\sin(\omega t)$  with a circular frequency  $\omega$  of

$$\omega = 2\pi f, \quad (7.12)$$

this results in

$$V_{\max} = w2\pi f \Phi_{\max} = w2\pi f A \cdot B_{\max}. \quad (7.13)$$

Since the root mean square (RMS) value of the induc-



**Fig. 7.9** Different conductor loops around a core with  $\mu_r = \infty$

tion voltage is  $V = V_{\max}/\sqrt{2}$ , the RMS value of the induced voltage can be obtained as

$$V_{1(\text{RMS})} = \frac{2\pi f}{\sqrt{2}} w \Phi_{\max} = \frac{2\pi f}{\sqrt{2}} w A \cdot B_{\max}. \quad (7.14)$$

This is known as the *transformer equation*. It shows that, for a transformer operating at a constant frequency  $f$ , the magnitude of the induced voltage is determined by the magnitude of the magnetic flux  $\Phi_{\max}$  [7.9].

According to Ampère's law, *no winding voltage is induced in incomplete windings*.

The iron core of the simple transformer shown in Fig. 7.5 has a particularly high magnetic conductivity and encloses the magnetic flux. Although it is not infinite, the relative permeability of the core material is so high that it can be assumed that all magnetic field lines pass through the iron core. Such a transformer with no leakage of magnetic flux is said to be *ideal*.

Therefore, the closed loop integrals of the areas enclosed by the conductors in the arrangements shown in Fig. 7.9 are identical, meaning that the induced voltages  $V_1$ ,  $V_2$ , and  $V_3$  are also identical, irrespective of the path shape. Thus, only the effective cross-sectional area of the core column  $A_{\text{Fe}}$  in Fig. 7.5 is relevant to the induction. For the secondary winding of the transformer shown in Fig. 7.5, the RMS of the induced voltage  $V_2$  can be determined via the transformer equation as

$$V_2 = \frac{2\pi f}{\sqrt{2}} w_2 \Phi_{\max} = \frac{2\pi f}{\sqrt{2}} w_2 A_{\text{Fe}} \cdot B_{\max}. \quad (7.15)$$

For a constant frequency, the magnitude of the induced voltage depends on the number of turns  $w$  and the effective core cross-section  $A_{\text{Fe}}$ . For power transformers, the primary voltage is usually specified by the network. However, the primary winding also encloses the core and therefore the magnetic flux, so a voltage is induced, which is known as the self-induction voltage

$V_1$ . This voltage is calculated as

$$V_1 = \frac{2\pi f}{\sqrt{2}} w_1 \Phi_{\max} = \frac{2\pi f}{\sqrt{2}} w_1 A_{\text{Fe}} \cdot B_{\max}. \quad (7.16)$$

For an ideal transformer, the primary voltage  $V_1$  applied determines the magnitude of the magnetic flux  $\Phi_{\max}$ . If the flux distribution in the core cross-section  $A_{\text{Fe}}$  is uniform, the resulting flux density  $B_{\max}$  determines the secondary induced voltage  $V_2$  [7.8]. Therefore, using (7.15) and (7.16), the voltage ratio for an ideal transformer can be determined as

$$\frac{V_1}{V_2} = \frac{\frac{2\pi f}{\sqrt{2}} w_1 \Phi_{\max}}{\frac{2\pi f}{\sqrt{2}} w_2 \Phi_{\max}} = \frac{w_1}{w_2}, \quad (7.17)$$

which results in

$$\frac{V_1}{V_2} = \frac{w_1}{w_2} = n. \quad (7.18)$$

According to the law of conservation of energy for an ideal lossless transformer, the equation

$$V_1 I_1 = V_2 I_2 \quad (7.19)$$

is valid, which yields the current ratio

$$\frac{I_1}{I_2} = \frac{V_2}{V_1} = \frac{w_2}{w_1} = \frac{1}{n}. \quad (7.20)$$

Given that the impedance  $Z = V/I$ , the impedance ratio can be determined as

$$\frac{Z_1}{Z_2} = \frac{V_1}{I_1} \cdot \frac{I_2}{V_2} = \frac{V_1 I_2}{V_2 I_1} = \left(\frac{w_1}{w_2}\right)^2 = n^2. \quad (7.21)$$

It is clear from the ratio equations that a transformer can be used for different purposes: voltage transformation is used to generate the high voltages needed to facilitate low-loss electrical energy transmission; current transformation is employed to produce the high currents needed by various industries (e.g., for melting processes); and impedance transformation is performed in transducers utilized in information technology applications.

### Technical Design

Any transformer can be divided into two parts: the active and passive parts (see Fig. 7.10).

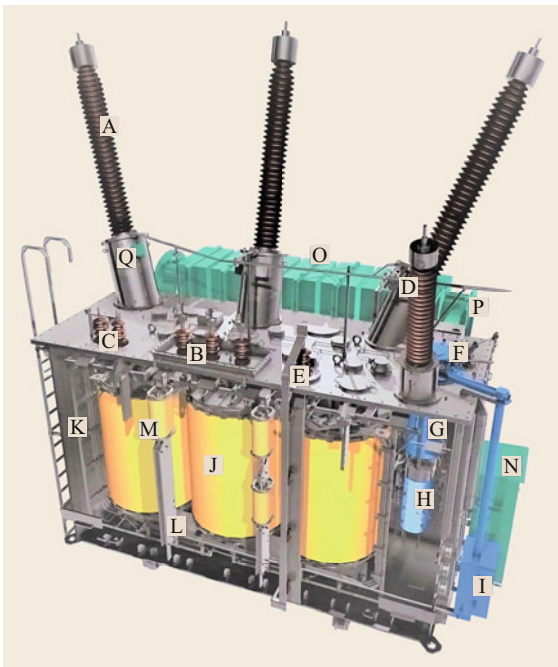
*Components in the active part* (shown in yellow in Fig. 7.10):

- The magnetic circuit, consisting of the core with limbs, reflux limbs, and yokes
- Electrical circuits along with the windings and tap changers.

*Components in the passive part:*

- Supporting and pressing elements
- Bushings
- Containers, such as a tank, cover, or housing and the cooling system
- Protection, measuring, and control equipment, including their power supplies.

Sometimes the active part is considered to comprise all of the components that can be lifted out of the tank.



**Fig. 7.10** Components of a liquid-filled power transformer [7.10]. A: high voltage bushing, B: low voltage bushings, C: tertiary winding bushings, D: HV neutral bushing, E: LV neutral bushing – rigidly grounded, F: top of on-load tap changer (OLTC), G: diverter switch with separate compartment, H: selector, I: OLTC motor drive, J: winding block, K: part of the lead system, L: core, M: voltage dependent resistor, N: control cabinet, O: cooling radiators, P: cooling fans, Q: connection to current transformer

Depending on the transformer design, such a definition is only partially correct, because supporting elements and tank parts (such as the cover) are sometimes lifted out along with the main active components.

The components of a transformer are explained in more detail in the next section.

### 7.1.3 Single-Phase Considerations

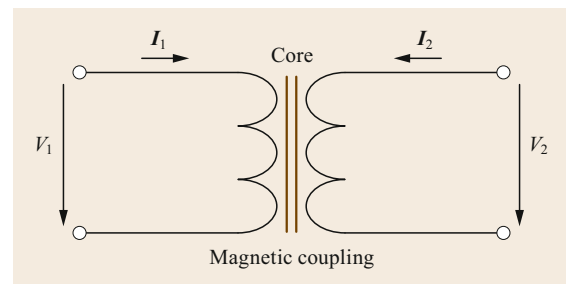
According to the induction law, a single-phase transformer can only be operated in an alternating current (AC) network. This network usually has various consumers, so the transformer interacts with these consumers. This operational interaction is discussed in more detail in the following.

#### Equivalent Circuit

In order to investigate the interaction mentioned above, the transformer is simplified by representing it as an equivalent circuit with ideal components. For sinusoidal processes, the relationships between electrical parameters are presented using phasor diagrams. However, the transmission ratio for a real transformer is usually  $\gg 1$ , meaning that the voltage and current phasors have different lengths on the primary and secondary sides, which causes problems. Therefore, either the phasor scale must be adjusted or a transformation ratio of  $n = 1$  must be assumed. The latter is a simpler approach and is used below.

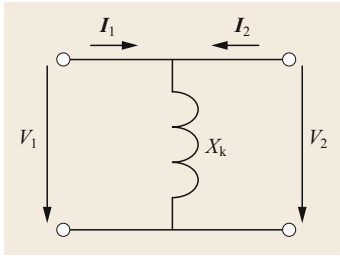
A circuit diagram of a single-phase transformer is shown in Fig. 7.11. The primary and secondary sides are each represented by a coil, so a secondary voltage  $V_2$  is induced through the coupling based on the primary voltage  $V_1$ .

It is clear from the circuit diagram shown in Fig. 7.11 that a single-phase transformer is a two-port network. If the coils or windings have the same number of turns (i.e., if  $n = 1$ ), the equivalent circuit can be simplified by using an inductive reactance  $X_k$ , as depicted in Fig. 7.12.

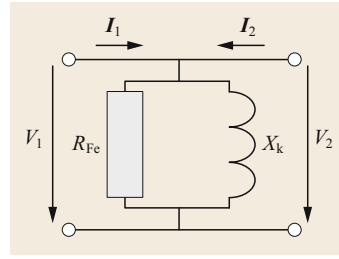


**Fig. 7.11** Circuit diagram of a single-phase transformer with primary and secondary windings





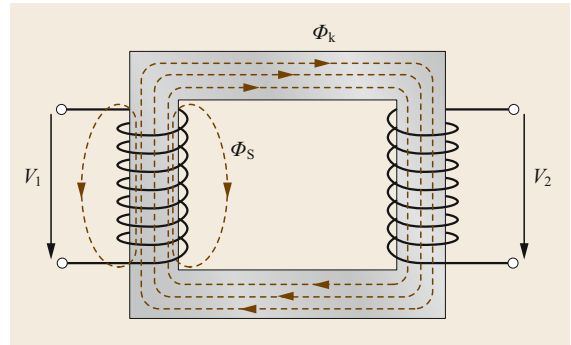
**Fig. 7.12** Single-phase transformer with windings represented by an inductive reactance  $X_k$



**Fig. 7.13** Accounting for core losses through  $R_{Fe}$

In order to determine the operational behavior of a real transformer, it is necessary to consider the following deviations from ideality and incorporate them into the equivalent circuit scheme:

1. The relative permeability of the iron core is not infinite ( $\mu_{Fe} \neq \infty$ ). The relationship between  $\mathbf{B}$  and  $\mathbf{H}$  is given by the hysteresis loop as the nonlinear dependence  $\mathbf{B} = f(\mathbf{H})$  (see the next section). Losses occur in the core material due to the change in direction of the magnetic flux in the iron core. These are called hysteresis losses.
2. The resistance of the core material is not infinite. According to the law of induction, eddy currents can also form within the core material, causing ohmic losses. Accordingly, when  $n = 1$ , the sum of the primary and secondary currents is not equal to zero in Fig. 7.12 ( $I_1 + I_2 \neq 0$ ). The hysteresis and eddy current losses in the transformer core are incorporated into the equivalent circuit diagram by including a resistor  $R_{Fe}$  connected in parallel, as shown in Fig. 7.13.
3. The relative permeability of the material surrounding the core and the windings (air, insulating fluid) is  $\mu_{air,fluid} \neq 1$ . This, together with the fact that the relative permeability of the iron core is not infinite ( $\mu_{Fe} \neq \infty$ ), implies that a small portion of the magnetic flux flows not only through the core but also through the surrounding materials. This part of the magnetic flux is called the leakage flux. The flux through the primary winding is larger than the flux through the secondary winding, as shown in Fig. 7.14.
4. The resistance of the conductor used in the windings is not zero. The current flowing through the primary and secondary windings generates ohmic losses. According to the law of induction, leakage fluxes can also prompt the formation of eddy currents within the winding material, which leads to further ohmic losses. The winding losses therefore consist of the ohmic losses of the winding conductors and the eddy current losses in them as a function of the leakage flux. In the equivalent circuit of the transformer, the primary and secondary



**Fig. 7.14** Main flux  $\Phi_k$  and leakage flux  $\Phi_S$

leakage fluxes are represented by leakage or stray inductances  $X_{S1}$  and  $X_{S2}$ , and the sums of the ohmic and eddy losses in the windings are denoted by the ohmic winding resistances  $R_1$  and  $R_2$ , as illustrated in Fig. 7.15.

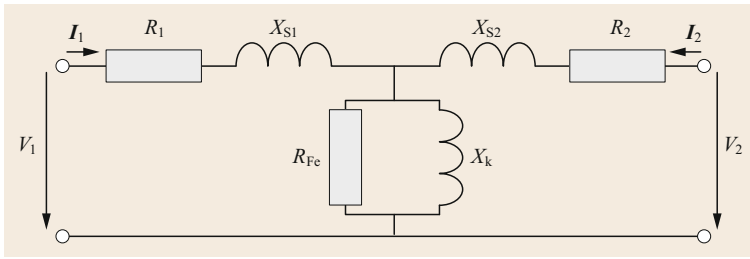
Due to the voltage drops at the winding resistances and reactances, the primary and secondary voltages are not equal ( $V_1 \neq V_2$ ).

### No-Load Operation

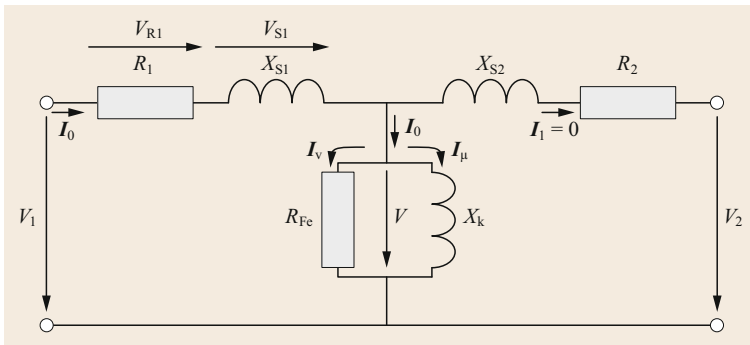
No-load operation is the operating state of the transformer in which a voltage  $V_1$  is applied on the primary side with no load (consumer) on the secondary side, as illustrated in Fig. 7.16.

The applied voltage  $V_1$  produces the no-load current  $I_0$ . The no-load current consists of the iron leakage current  $I_v$  (a pure active current) and the magnetizing current  $I_\mu$  (a pure reactive current) to build up the magnetic flux. The no-load current  $I_0$  generates the alternating magnetic flux  $\Phi$  in the core, which induces the voltage  $V_2$  in the secondary winding and the self-induction voltage  $V$  in the primary winding. The small difference between the voltages  $V_1$  and  $V$  drives the tiny current  $I_0$ , which is delayed compared to  $V_1$ . In modern transformers, the no-load current is on the order of just 1–2% of the rated current on the primary side [7.11].

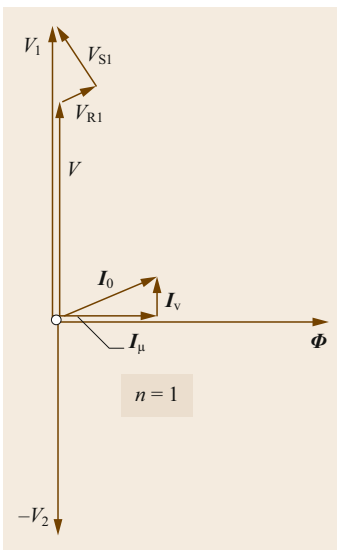
The phasor diagram for no-load operation is illustrated in Fig. 7.17. This diagram shows the no-load situation qualitatively, whereas the voltages  $V_{R1}$  and  $V_{S1}$



**Fig. 7.15** Equivalent circuit of a single-phase transformer



**Fig. 7.16** Equivalent circuit for no-load operation



**Fig. 7.17** Phasor diagram for no-load operation according to the equivalent circuit shown in Fig. 7.16

decreases sinusoidally, the magnetic flux increases sinusoidally, and no unusual stresses occur. However, if the transformer is energized at the zero crossing of the primary voltage  $V_1$ , the magnetic flux  $\Phi$  should be at its maximum value, which causes a high inrush magnetizing current to flow in order to establish the maximum magnetic flux so that the normal situation between  $V_1$  and  $\Phi$  is attained. Due to the high magnetization current, the core can be driven to saturation because the magnetization current can be up to 50 times higher than the normal magnetizing current in unfavorable circumstances [7.12]. Due to the ohmic resistance  $R_1$  and the leakage inductance  $X_{S1}$  of the primary winding, the inrush magnetization current is strongly attenuated and therefore decays rapidly. The inrush current can be limited in power networks by reducing the supply voltage as far as possible before energization. Another way to limit the inrush current is to use compensation inductances in the network.

can be neglected in reality, meaning that the voltages  $V_1$ ,  $V$ , and  $V_2$  are almost equal.

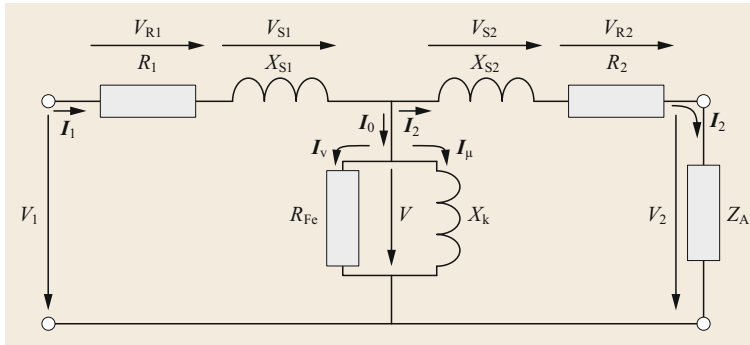
The magnitude of the no-load current  $I_0$  can be influenced by the construction of the transformer; in particular the design of the transformer core.

**Inrush Current.** When transformers are energized, current impulses with high amplitudes can occur. As shown in Fig. 7.16, the primary voltage  $V_1$  is shifted with respect to the magnetic flux  $\Phi$  by  $90^\circ$ . If the transformer is connected to the network at maximum voltage, the magnetic flux  $\Phi$  is zero. As the voltage

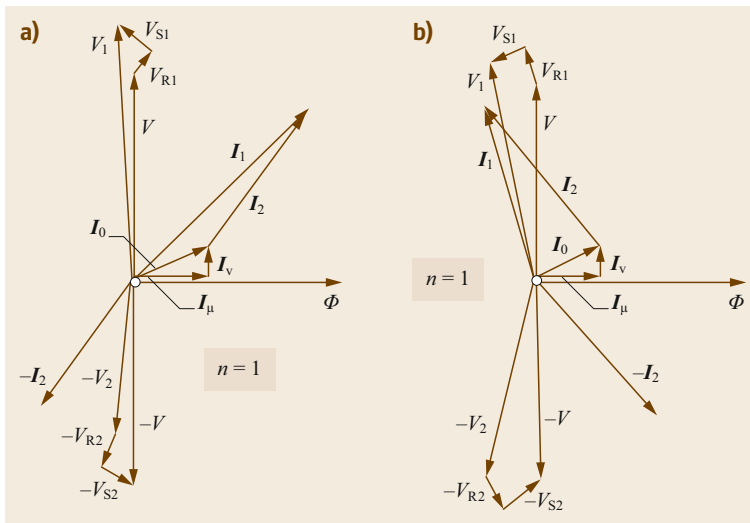
### Operation Under Load

When the transformer is loaded, a voltage  $V_1$  is applied on the primary side and a load  $Z_A$  is connected to the secondary side, as shown in Fig. 7.18. Hence, the current  $I_2$  flows through the secondary winding and the load. The primary current  $I_1$  flows through the primary winding and, despite the galvanic isolation between the primary and secondary circuits, load changes on the secondary side affect the current on the primary side.

The applied voltage  $V_1$  establishes the primary current  $I_1$ , which consists of the no-load current  $I_0$  and the current  $I_2$  corresponding to the secondary load.  $I_1$



**Fig. 7.18** Equivalent circuit for operation under load



**Fig. 7.19** (a) Phasor diagram for ohmic-inductive load. (b) Phasor diagram for ohmic-capacitive load

generates the primary voltage drops on  $R_1$  and  $X_{S1}$  and creates the magnetic flux  $\Phi$ , whereas the secondary current  $I_2$  generates voltage drops on  $R_2$  and  $X_{S2}$  and influences the magnetic flux  $\Phi$ .

The pointer diagrams for operation with an ohmic-inductive load and an ohmic-capacitive load are shown in Fig. 7.19a,b, respectively. The phasor diagrams are again presented for a transmission ratio  $n = 1$ , and some voltage drops and the no-load current are shown larger than in reality to highlight the qualitative correlations.

When the transformer is subjected to a more capacitive load, as assumed in Fig. 7.19b, the secondary winding and the capacitive load form an oscillating circuit, so the voltage  $V_2$  can be greater than  $V$ . This is called a capacitive voltage increase.

In reality, the phasor diagrams can be simplified by neglecting the no-load current  $I_0$  (which is much smaller than the rated current) so that the currents  $I_1$  and  $I_2$  coincide. If the voltage drops on the winding resistances  $V_{R1}$  and  $V_{R2}$  are combined to give  $V_R$  and the voltage drops  $V_{S1}$  and  $V_{S2}$  are combined to give  $V_S$ , the

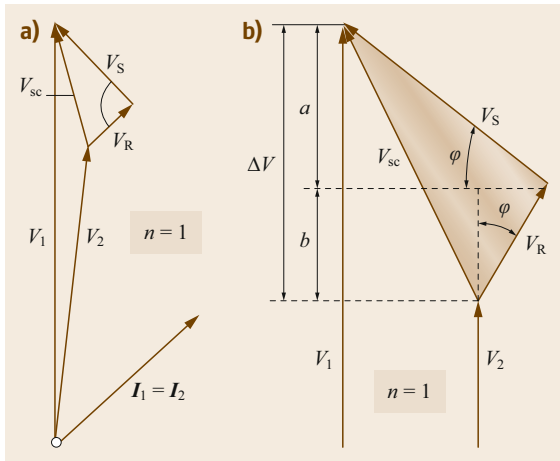
phasor diagram shown in Fig. 7.20a is obtained. The triangle created by the voltages  $V_R$ ,  $V_S$ , and  $V_{sc}$  (short-circuit voltage) is called the Kapp triangle after its developer Gisbert Johann Eduard Kapp [7.13].

The Kapp triangle as shown in Fig. 7.20b describes the load-dependent longitudinal voltage drop of a transformer. This consists of an ohmic component and an inductive component.

If a transformer is short-circuited on the secondary side and the primary voltage  $V_1$  is increased until the rated current flows on the primary side, the primary voltage at this point is called the short-circuit voltage  $V_{sc}$ . Based on Fig. 7.20a, this voltage can be calculated as the sum of  $V_R$  and  $V_S$ . The voltage  $V_{sc}$  can be determined by splitting the voltages  $V_R$  and  $V_S$  back into the voltages  $V_{R1}$ ,  $V_{R2}$ ,  $V_{S1}$ , and  $V_{S2}$  and by considering the transformer ratio  $n$  and therefore the current  $I_2 = nI_1$ ; in other words,

$$V_{sc} = (V_{R1} + nV_{R2}) + (V_{S1} + nV_{S2}),$$

$$|V_{sc}| = \sqrt{(V_{R1} + nV_{R2})^2 + (V_{S1} + nV_{S2})^2}. \quad (7.22)$$



**Fig. 7.20** (a) Simplified phasor diagram (ohmic-inductive load). (b) Kapp triangle (shaded area)

Therefore, the short-circuit voltage  $V_{sc}$  of a transformer is the geometric sum of its internal voltage drops at nominal load.

A transformer can increase or decrease voltages, so it has two different transmission ratios and two different short-circuit voltages. However, normalizing the absolute short-circuit voltage to the primary nominal voltage via

$$v_{sc} = \frac{V_{sc}}{V_1} \times 100\% \quad (7.23)$$

gives a percentage value that is identical for both cases. The relative short-circuit voltage  $v_{sc}$  has the advantage that it is valid for both the primary and the secondary sides. At the same time, it allows different transformers to be compared. Analogous results can be achieved for the ohmic and inductive voltage drops, as shown below.

$$v_R = \frac{V_R}{V_1} \times 100, \quad (7.24)$$

$$v_S = \frac{V_S}{V_1} \times 100, \quad (7.25)$$

$$v_{sc} = \sqrt{v_R^2 + v_S^2}. \quad (7.26)$$

The short-circuit voltage influences:

- The magnitudes of the secondary voltage and the load-dependent voltage changes
- The magnitudes of the surge and continuous short-circuit currents
- The load distribution for transformers operating in parallel.

The short-circuit voltage  $V_{sc}$  is influenced by the design of the transformer and – in particular – the design of the windings.

From the vector diagrams shown in Figs. 7.19 and 7.20, it is clear that the magnitude of the secondary clamping voltage  $V_2$  depends on the load  $Z_A$  connected to the transformer. For resistive or inductive loads, the secondary voltage  $V_2$  decreases with increasing load. For capacitive loads, this voltage increases with increasing load. The influence of the type of load on the secondary voltage can be illustrated in a simplified form by an extended Kapp diagram. This assumes that the applied primary voltage  $V_1$  is constant for an ideal transformer with a transmission ratio  $n = 1$ , which is sufficiently accurate if a power network is connected to the primary side of the transformer. The extended Kapp diagram depicted in Fig. 7.21 can be drawn based on the equivalent circuit shown in Fig. 7.18. At its base point A, the Kapp triangle is drawn with  $V_{sc}$ ,  $V_R$ , and  $V_S$ . Semicircles with radii corresponding to the applied voltage  $V_1$  are drawn around A and B. Semicircle I with A at its center represents the locus curve for  $V_1$ , whereas semicircle II with B at its center is the locus curve for the secondary voltage  $V_2$ .

The diagram in Fig. 7.21 illustrates the decrease in  $V_2$  for an inductive load and the increase in voltage for a capacitive load.

**Efficiency.** The efficiency  $\eta$  of an electrical machine is defined as the ratio of the active output power  $P_{out}$  to the active input power  $P_{in}$ , i.e.,

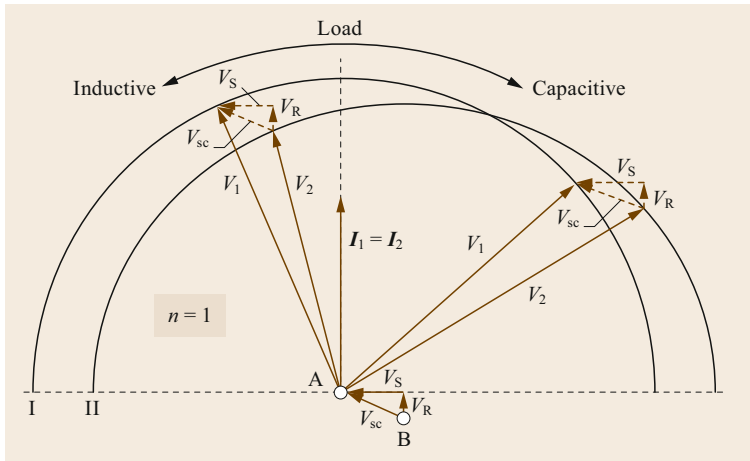
$$\eta = \frac{P_{out}}{P_{in}}. \quad (7.27)$$

The difference between these power terms corresponds to the total losses  $P_{loss}$ ; in other words,

$$P_{loss} = P_{in} - P_{out}. \quad (7.28)$$

Transformer losses can be divided into *no-load losses*  $P_0$  and *short-circuit losses*  $P_{sc}$ . The no-load losses (also known as iron losses) include hysteresis losses (re-magnetization losses) and the eddy current losses in the core. The short-circuit losses arise mainly from ohmic losses and the eddy current losses in the windings, meaning that these losses depend on the current. If a transformer is only partially loaded, the losses decrease quadratically according to  $P_{sc} = I^2 R$ , which means that the short-circuit losses drop to 36% ( $= L_f^2 P_{sc}$ ) of the load losses  $P_{sc}$  when the load is 60% (load factor  $L_f = 0.6$ ). Therefore, the total losses  $P_{loss}$  can be calculated via

$$P_{loss} = P_0 + L_f^2 P_{sc}. \quad (7.29)$$



**Fig. 7.21** Extended Kapp diagram illustrating the effect of load type

The efficiency is then determined as

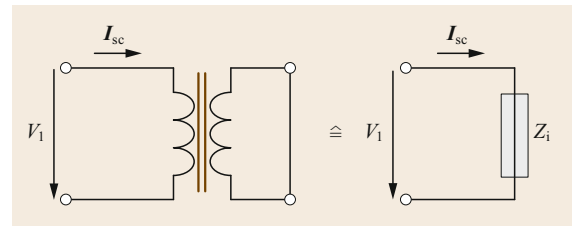
$$\eta = \frac{P_{out}}{P_{loss} + P_{out}} \quad (7.30)$$

Today, the efficiency of a modern power transformer at rated power is usually above 98%. As an example, a modern generator step-up transformer with a power level of a few hundred MVA has a typical efficiency exceeding 99.5%.

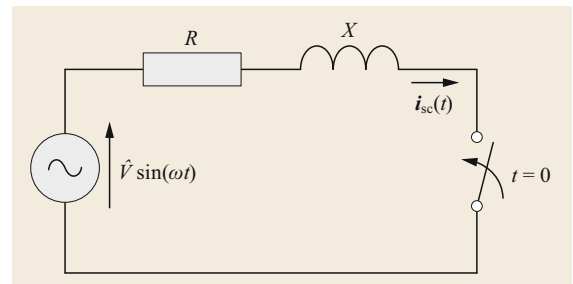
### Short-Circuit Behavior

During operation, power transformers can be exposed to short circuits in the electrical network. The closer the short circuit to the transformer, the greater its impact on the transformer. The worst-case scenario is a terminal short circuit on the secondary side. Every power transformer must be able to withstand a secondary terminal short circuit for a short period of time (typically only a few seconds, e.g., 2 s). Since the current often exceeds the rated current when there is a short circuit, the no-load current can be ignored in an equivalent circuit. With the collapse of the secondary voltage, the magnetic flux in the transformer core is also drastically reduced, and the short-circuit current is only limited by the internal resistances of the transformer. The circuit diagram of a transformer for short-circuit operation with the short-circuit current  $I_{sc}$  is shown in Fig. 7.22.

The complex impedance  $Z_i$  in the network includes the internal impedances  $R$  and  $X$  of the transformer and the impedances of the network transposed with the transmission ratio  $n$ . The latter depend on the location of the transformer and are therefore not taken into account when designing the transformer. This means that, in reality, the short-circuit current  $I_{sc}$  that occurs upon



**Fig. 7.22** Simplified equivalent circuit of a transformer for short-circuit operation

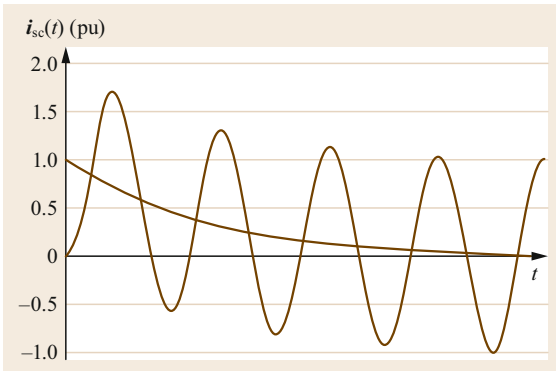


**Fig. 7.23** Equivalent circuit for a short circuit

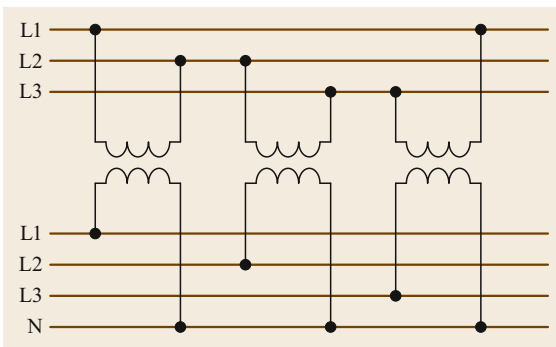
a secondary-side terminal short circuit is always smaller than that considered in the design.

In the following considerations, only the complex internal resistance  $Z_i$  of the transformer is taken into account. During a short circuit, a balancing process that brings the transformer to stationary short-circuit conditions occurs. The simplified circuit shown in Fig. 7.23, in which the internal resistances  $R$  and  $X$  of the transformer are connected to an AC source, is used.

If the switch in Fig. 7.23 is closed, the current  $i_{sc}(t)$  is time dependent, as illustrated in Fig. 7.24. As can be seen, the current initially has a higher amplitude than the stationary short-circuit current.



**Fig. 7.24** Variation in the short-circuit current over time [7.9]



**Fig. 7.25** Three-phase bank using three single-phase transformers

For  $X = L$  (inductance), the time-dependent function  $i_{sc}(t)$  in Fig. 7.25 can be approximated by

$$i_{sc}(t) = \hat{I} \left[ \sin \left( \omega t - \frac{\pi}{2} \right) + e^{-\frac{R}{L}t} \right], \quad (7.31)$$

where  $\hat{I}$  is the peak current. The maximal value of the current is obtained for  $\omega t = \pi$  as

$$\hat{I}_{sc \max} = I_{sc} \sqrt{2} k, \quad (7.32)$$

where  $k$  is the correction factor determined via

$$k = 1 + e^{-\frac{\pi R}{X}} = 1 + e^{-\frac{\pi}{\tau}}. \quad (7.33)$$

For the typical ratio  $R/X = 1/8$ , the calculated correction factor  $k$  is 1.675, which results in a surge short-circuit current of  $\hat{I}_{sc \max} = 2.37 I_{sc}$ .

This surge short-circuit current dictates the forces that occur in the windings during a short circuit. The continuous or stationary short-circuit current  $I_{sc} = V_1/Z_i = V_{sc}/Z_i$  according to Fig. 7.22, and can be obtained from the relative short-circuit voltage using

$$I_{sc} = I_1 \frac{100}{v_{sc}}. \quad (7.34)$$

The relative short-circuit voltage  $v_{sc}$  for power transformers is typically between 3% and 12.5%, depending on the size of the transformer. According to (7.34), this results in continuous short-circuit currents that are 8 times higher for large transformers and 33 times higher for network transformers. Knowledge of the continuous short-circuit current is important when defining the permitted short-circuit duration and designing current transformers and circuit breakers.

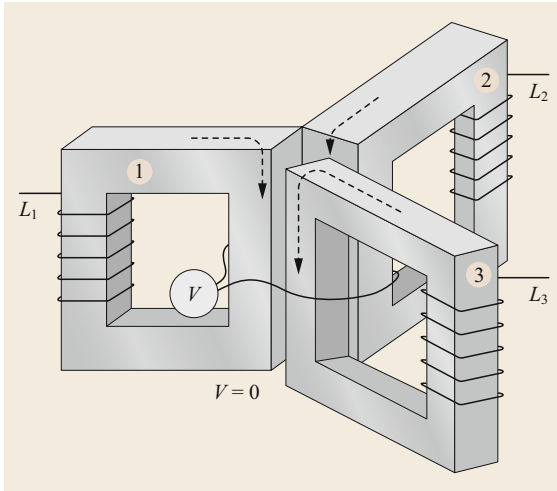
### 7.1.4 Three-Phase Operation

Concatenating three  $120^\circ$  phase-shifted alternating voltages leads to the creation of a three-phase system that allows effective energy transmission. This is the system used in conventional electrical power transmission networks. It can be realized by combining three single-phase transformers to form a transformer bank, as shown in Fig. 7.25. Single-phase transformers are still used in modern networks with voltages of 750 kV or more, since three-phase units for such networks would be too large and heavy to transport. Indeed, single-phase transformers may even be installed in networks with lower voltages, as only one unit needs to be put out of operation when there is a single-phase failure, and a spare unit is often stored on-site, meaning that power interruption can be minimized. Thus, although this setup is much more expensive than using one three-phase transformer, this extra expense may be acceptable given that it should lead to increased reliability of the power supply.

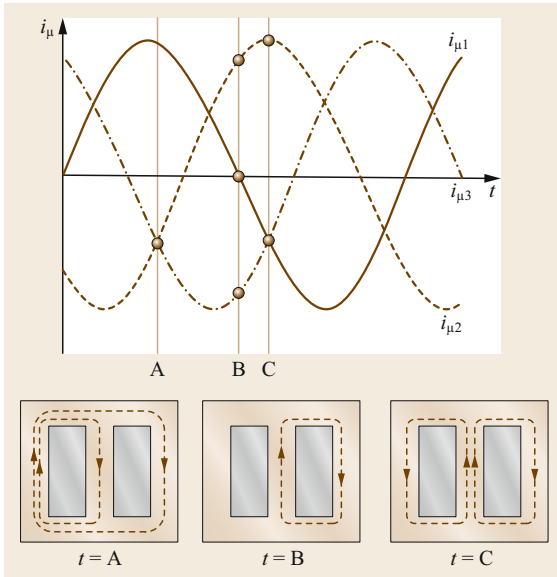
Transformers become highly effective when they include three or five limb cores. This approach was first adopted in 1891 with the utilization of the so-called temple core, as shown in Fig. 7.4. Ensuring that the voltages in the *symmetrical* three-phase network and thus the magnetic fluxes in the core legs of the transformers are zero saves materials and costs.

If the windings of three single-phase transformers are wound on only one leg, the cores can be assembled at an angle of  $120^\circ$  so that the unwound cores touch each other, as illustrated in Fig. 7.26.

When a symmetrical three-phase voltage is applied, the cores are magnetized. The voltages are phase shifted by  $120^\circ$ , so their geometric sum is zero. Therefore, the unwound core limb in the center can be eliminated and the wound limbs can either be joined together in a temple configuration or, as developed by Dolivo-Dobrovolsky for AEG, they can be joined together in one plane [7.14]. This is demonstrated in Fig. 7.27. It is assumed that the magnetic flux  $\Phi$  flows from the bottom to the top for a positive magnetizing current. Therefore, various magnetic fluxes  $\Phi(t)$  result in the core at times A, B, and C.



**Fig. 7.26** The magnetic fluxes in three single-phase cores add up to zero at the center [7.8]



**Fig. 7.27** Magnetic flux distribution in a three-leg core with a symmetrical load [7.8]

Figure 7.27 clearly shows that the center limb in Fig. 7.26 can be removed, so a core with three limbs is typically used for a three-phase system. Windings are mounted on each limb, and they can be connected separately on the low- and high-voltage sides (e.g., using a star or delta connection).

### Vector Groups

The connection possibilities for the three low-voltage or high-voltage windings on the three core limbs are shown in Fig. 7.28a–c. The zigzag connection represents a special case.

**Table 7.1** Abbreviations used for terminals and connections [7.10]

Winding		HV	LV
Terminals	Start	A B C	a b c
	End	X Y Z	x y z
Connections	Delta	D	d
	Star (wye)	Y	y
	Zigzag		z
	Open	I I I	i i i

For the delta connection, the phase-to-phase voltage (e.g.,  $V_{AB}$ ) is equal to the line voltage  $V_{AX} = V_A$ , whereas the line current  $I_{AX}$  is equal to the phase current  $I_A$  divided by  $\sqrt{3}$ . The delta connection is therefore not suitable for very high voltages because the full voltage is always applied to each winding. Consequently, the delta connection is more suitable for low-voltage (LV) windings, and it has the additional advantage that the current through the windings  $I_{AX}$  is smaller than the phase current  $I_A$ . The opposite is true of the star connection: the phase and line currents are equal but the line voltage  $V_A = V_{AX}$  is equal to the phase voltage  $V_{AB}$  divided by  $\sqrt{3}$ , which makes the star connection more suitable for high-voltage (HV) windings. The complicated zigzag circuit is a combination of the star and delta connections. It is particularly useful for compensating for unbalanced loads in the network, but it is only used for a small number of transformers because the winding production process is more complicated and the number of turns in the windings is 15% higher than in the star connection [7.15].

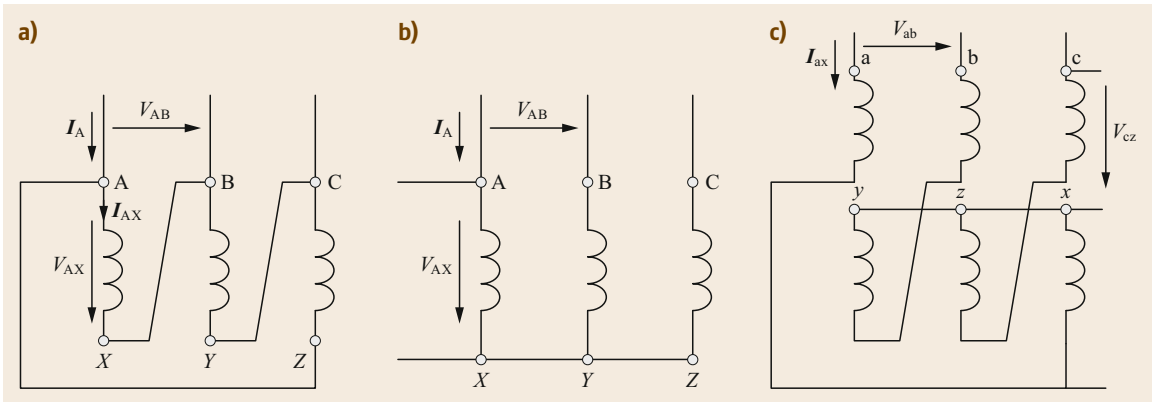
The connections Yy, Yd, Yz, Dy, Dd, and Dz (see the list of abbreviations used for various types of HV and LV connections in Table 7.1) are possible and are used in practice, whereas Zy, Zd, and Zz are theoretically possible but are not used.

The abbreviation Yy means that both the HV and LV windings are connected in a star, but, as illustrated in Fig. 7.29, there are various possible configurations for a Yy connection.

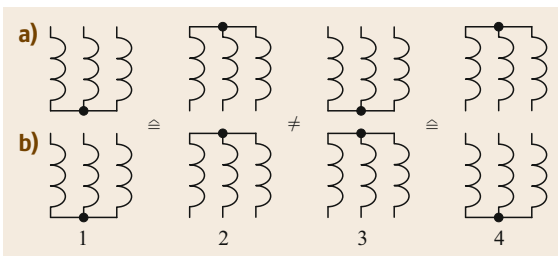
If the neutral winding is accessible from outside (a separate bushing on the tank), an N (for the HV side) or n (for the LV side) is added after the code letter for the type of connection. As an example, the *vector group* YNd5, which is typically used for generator step-up transformers, implies that:

- A star connection is used for the HV windings, and the star is accessible
- The LV windings are connected in a delta
- The high voltage is  $5 \times 30^\circ = 150^\circ$  ahead of the low voltage.

It can be shown that phase shifts of multiples of  $30^\circ$  between the HV and LV sides can be generated by



**Fig. 7.28** (a) Delta connection. (b) Star connection. (c) Zigzag connection



**Fig. 7.29a,b** Possible configurations for a Yy connection: (a) high-voltage windings; (b) low-voltage windings [7.8]

applying particular star, delta, and zigzag interconnections [7.16]. This is indicated by the number or phase-shift index at the end of each vector group, which corresponds to a multiple of  $30^\circ$ . The vector diagram for the vector group Yd5 is shown in Fig. 7.30.

Among the 42 possible vector groups, there are 12 that are particularly important. These are listed in Table 7.2. The vector groups Yy0, Yd5, Yd11, and Dy5 are the most popular.

**Operation Under Unsymmetrical Load**

As shown in Figs. 7.26 and 7.27, the number of core limbs can be reduced to three for a symmetrical load. In three-phase networks, however, asymmetrical loads can occur, with only one phase supplying a load in the

worst case. Therefore, in the following, a single-phase loaded transformer is considered.

Based on (7.3) and (7.7), the magnetic flux  $\Phi$  can be calculated for a core cross-section of  $A$  via

$$\Phi = B \cdot A = A \cdot \mu H . \tag{7.35}$$

According to Ampère’s law for a quasi-stationary field,

$$\oint_x H dx = \sum I = w i , \tag{7.36}$$

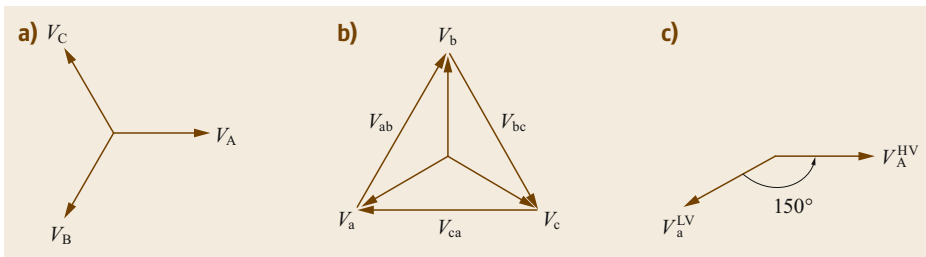
the magnetic field strength  $H$  is strongly dependent on the number of turns  $w$  in the winding and the current  $i$  through the winding. The closed loop integral can be simplified to

$$\oint_x H dx = H \Delta x = H L_{Fe} , \tag{7.37}$$

where  $L_{Fe}$  is the average core length through which the flux  $\Phi$  flows. This leads to

$$\Phi = A \cdot \mu H = \frac{A \cdot \mu w i}{L_{Fe}} \propto (w i) , \tag{7.38}$$

which implies that the magnetic flux in a core limb is directly proportional to the product of the number of turns  $w$  of the winding around the core limb and the magnetizing current  $i$  flowing through this winding.

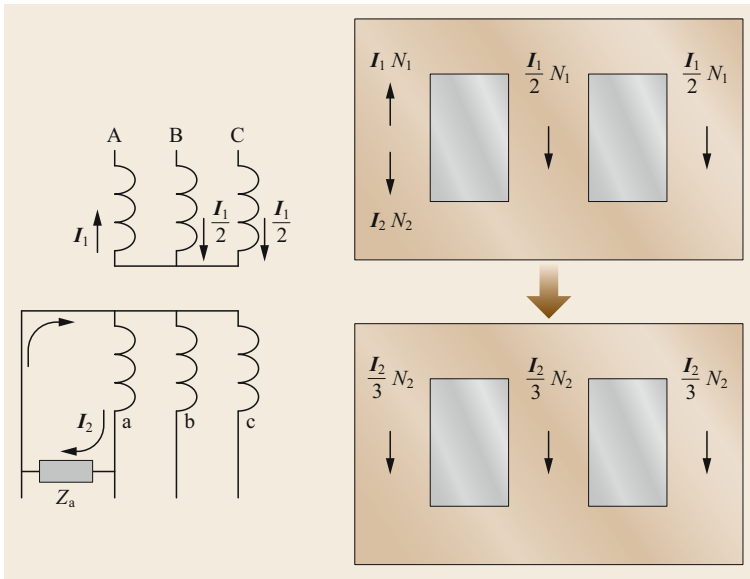


**Fig. 7.30a–c** Vector diagram for the vector group Yd5: (a) HV windings (star connection), (b) LV windings (delta connection), and (c) phase shift between the HV and LV sides [7.13]



**Table 7.2** Phasor and connection diagrams for a selection of vector groups, as defined by the International Electrotechnical Commission (IEC) 60076 [7.17]

Index	Vector multicolumn	Phasor diagram		Connection diagram	
		HV	LV	HV	LV
0	D d 0				
	Y y 0				
	D z 0				
5	D y 5				
	Y d 5				
	Y z 5				
6	D d 6				
	Y y 6				
	D z 6				
11	D y 11				
	Y d 11				
	Y z 11				

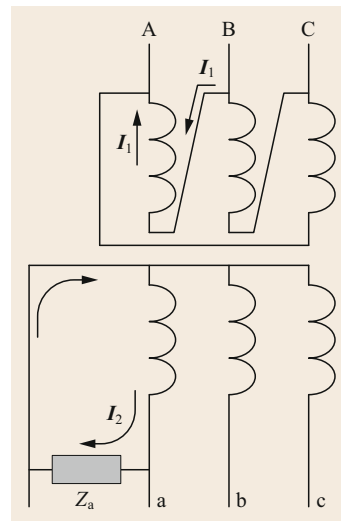


**Fig. 7.31** Single-phase loading of a Yy6 transformer

These considerations result in the scenario presented in Fig. 7.31. This figure shows the magnetic flux for a Yy6 transformer in which only one phase has a load ( $Z_a$ ).

As shown in Fig. 7.31, a magnetic flux is generated in each of the three core limbs, and all of these fluxes are oriented in the same direction, so the sum of the fluxes in the core yokes does not equal zero. As a consequence, core saturation is exceeded and the flux searches for another path, resulting in stray flux that passes through the tank walls for instance. Consequently, high losses caused by eddy currents and hysteresis losses lead to overheating in some areas, which can result in transformer failure in the worst case. These stray fluxes also induce voltages in the windings that significantly shift the potential of the star point. This leads to a voltage drop in the loaded phase, whereas the voltages of the unloaded phases increase. To avoid such a scenario, the star points of Yy transformers are permitted to be loaded with up to 10% of the rated current so long as there is no additionally installed compensation winding (e.g., a tertiary winding system in a delta connection). This is an important restriction on the use of Yy transformers in three-phase networks.

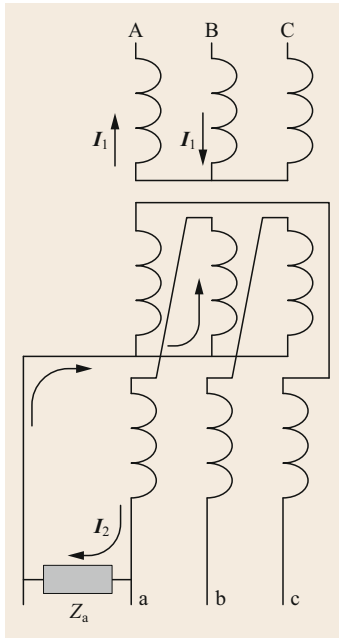
However, if a Yy transformer is equipped with an additional (tertiary) winding system in a delta connection, the tertiary windings compensate for an unbalanced load situation. In the case of a single-phase load, a current flows in the tertiary winding on the loaded phase and conditionally through the tertiary windings on the other two core limbs. These currents create counterfluxes that compensate for the uniformly oriented magnetic fluxes depicted in Fig. 7.31. For complete compensation, the tertiary windings must be dimensioned for one-third of the rated power of the transformer [7.18].



**Fig. 7.32** Single-phase loaded Dy5 transformer

Figure 7.32 shows a Dy5 transformer with only one phase connected to a load  $Z_a$ . In this case, it can be deduced that the current  $I_1$  flows directly through the network and not via the two unloaded phases when the transformer is single-phase loaded. It is therefore possible to fully load the star point of this vector group because the delta winding has a compensating effect.

For a LV-side zigzag connection, an asymmetrical load is distributed over two phases, as shown in Fig. 7.33. The voltages induced in the HV windings and the currents flowing through them generate magnetic fluxes that compensate for the magnetic fluxes generated on the LV side. The disadvantages of a zigzag connection are that a higher number of turns are needed for the windings, which are also more complicated to



**Fig. 7.33** Single-phase loaded Yz5 transformer

produce. Therefore, this vector group is rarely used for transformers with reduced power.

In summary, for transformers with a pure star connection, the star point can only be loaded up to 10% of the rated current. For all transformers with a delta-connected winding designed for at least one-third of the rated power, the star point can be fully loaded for as long as permitted by the design and the rating plate.

### Parallel Operation

According to the equivalent circuit diagram, transformers connected in parallel represent voltage sources connected in parallel, and must therefore fulfill certain conditions [7.19]:

1. *Parallel-connected transformers must have the same transformation ratios.*

If the transformation ratio deviates slightly, a compensation current  $I_A$  flows on the secondary side of the transformer. If the internal resistance of the transformer (see Sect. 7.1.3, *Short-Circuit Behavior*) is replaced with the quotient of the relative short-circuit voltage  $v_{sc}$  and the voltage deviation

$\Delta$  in percent, this compensation current can be calculated with sufficient accuracy via [7.8]

$$I_A = \frac{\Delta}{\frac{v_{sc1}}{I_1} + \frac{v_{sc2}}{I_2}} \quad (7.39)$$

If  $v_{sc1} = v_{sc2} = v_{sc}$  and  $I_1 = I_2 = I$ , then

$$I_A = \frac{\Delta}{2v_{sc}} I \quad (7.40)$$

Note that a small deviation of the transformation ratio can cause a significant current to flow continuously, even during no-load operation. This needs to be considered appropriately.

2. *The short-circuit voltages must be approximately the same (the maximum difference in short-circuit voltage should not exceed  $\pm 10\%$ ).*

Since the short-circuit voltages represent the internal resistances of the transformers, deviations lead to different load levels. The transformer with the lowest short-circuit voltage will be overloaded, while the transformer with the highest short-circuit voltage will not be fully utilized.

3. *The ratio of the rated powers should not be greater than 3 : 1.*

The ratio of the ohmic voltage drop to the leakage voltage drop changes as the rated power is increased. For larger transformers, the relative ohmic voltage drop decreases. As a result, the currents have different phase angles. The busbars of the parallel circuit are loaded with the geometric sum of the currents, which is smaller than the arithmetic sum of the currents. This limits the maximum power at the busbars and reduces the utilization factor of the system.

4. *The LV sides of the transformers connected in parallel must be in phase.*

Both the effective and the instantaneous values of the rated voltages must be the same. Therefore, no phase shift between the LV sides of the parallel-connected transformers is allowed. For example, connecting vector groups with phase-shift indices of 0 and 6 in parallel would result in a short circuit.

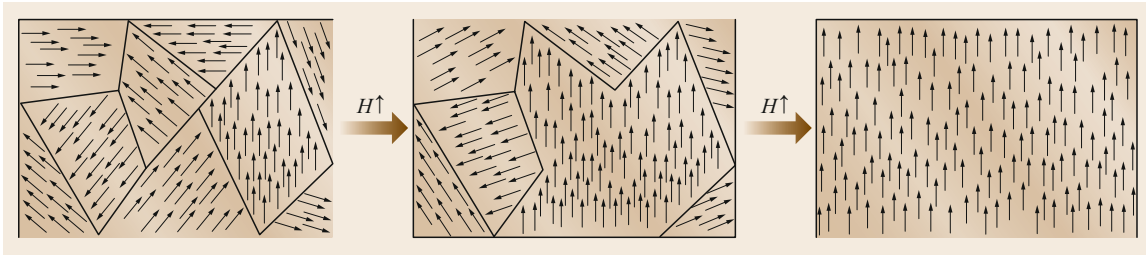
Transformers can be operated effectively in parallel as long as these operational conditions are consistently adhered to.

## 7.2 Active Part

### 7.2.1 Core

It was noted earlier that one way in which a real transformer deviates from an ideal one is that the relative permeability of the iron core is not infinite ( $\mu_{Fe} \neq \infty$ ).

In ferromagnetic materials, the magnetic moments of the atoms are aligned in parallel. The French physicist Pierre Ernest Weiss discovered that, in ferromagnetic materials, the process of magnetic alignment occurs in large regions (known as Weiss regions) that are



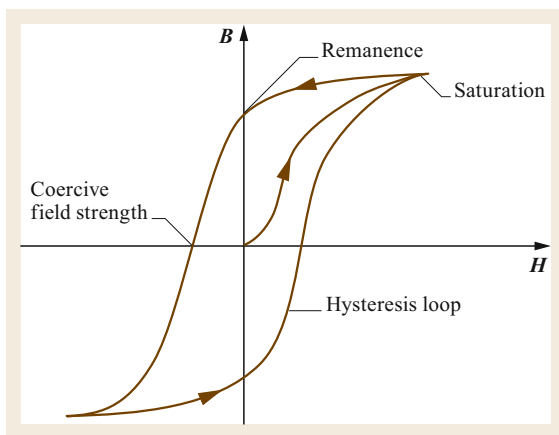
**Fig. 7.34** Schematic depicting the enlargement of Weiss regions

approximately 10–1000  $\mu\text{m}$  in size. The direction of magnetization is determined by the crystal lattice of the material. Boundaries between Weiss areas are called Bloch walls. Upon the application of a magnetic field that increases in strength over time, the Bloch walls shift to favor the creation of areas that are oriented towards the external field [7.20]. More and more areas change their polarities until saturation is reached, as shown in Fig. 7.34.

### Losses

The relationship between  $\mathbf{B}$  and  $\mathbf{H}$  is given by a nonlinear function  $\mathbf{B} = f(\mathbf{H})$  representing the hysteresis loop. The magnetic flux density  $\mathbf{B}$  is determined by the surrounding magnetic field strength  $\mathbf{H}$ . If  $\mathbf{H}$  increases above a certain threshold,  $\mathbf{B}$  increases only very slightly due to saturation. When the magnetic field decreases, the flux density decreases too, but a residual magnetism known as the *remanence* remains due to the aligned Weiss regions. This remanence only disappears when an opposite field with a coercive field strength is activated. The resulting curve (shown in Fig. 7.35) is called the hysteresis curve.

The nonlinear hysteresis curve makes the transformer into a nonlinear two-port. A sinusoidal primary voltage produces a sinusoidal primary current but



**Fig. 7.35** Hysteresis curve

a nonsinusoidal secondary voltage. For quasi-stationary fields, the effective flux in the transformer winding is the product of the current strength and the number of turns. As shown in Fig. 7.36, a nonlinear flow can be generated pointwise by mirroring the hysteresis curve [7.21].

The hysteresis curve cannot be represented as a cohesive mathematical function. This causes some problems when constructing transformers and attempting to perform calculations for them. In particular, the switch-on behavior and possible resonances in the network are influenced by the nonlinearity. Today, this can be calculated and simulated very precisely using numerical methods, but the effort involved is still significant because the nonlinearity generates unwanted harmonics in the network.

Remagnetization of the Weiss regions generates losses known as hysteresis losses  $P_{L\text{Hysteresis}}$ . These are proportional to the area of the hysteresis curve and are a component of the iron losses  $P_{L\text{Fe}}$ . However, the alternating magnetic flux induces a voltage in not only the surrounding windings but also the iron core itself. This voltage induced in the core drives eddy currents in the core perpendicular to the magnetic flux, resulting in eddy current losses  $P_{L\text{Eddy Currents}}$ . Thus,

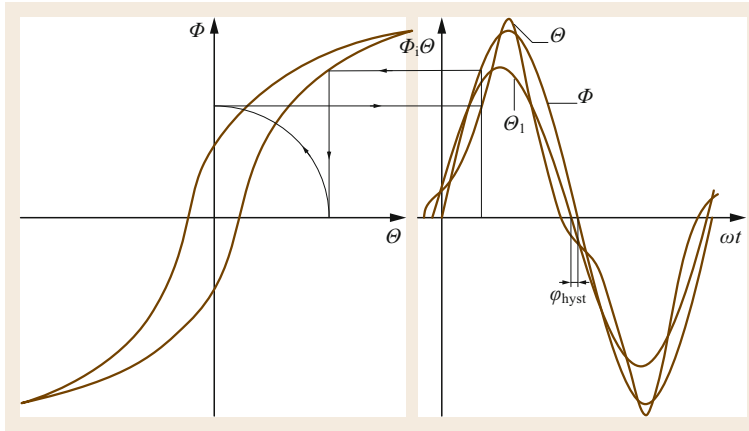
$$P_{L\text{Fe}} = P_{L\text{Hysteresis}} + P_{L\text{Eddy Currents}} \quad (7.41)$$

The eddy current losses heat up the iron core. As these eddy currents flow perpendicular to the magnetic flux, they can be effectively reduced by laminating the core, as illustrated in Fig. 7.37.

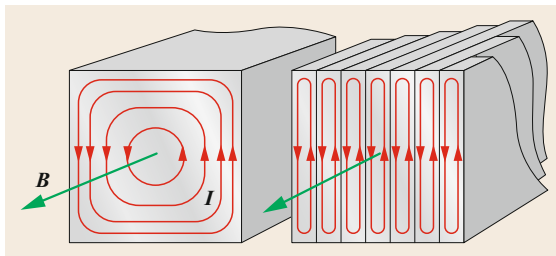
Another effective way of reducing eddy currents in the iron core is to increase the ohmic resistance of the core material.

### Acoustic Noise

The transformer core produces noise due to magnetostriction. As already discussed, the Weiss regions align themselves when an alternating magnetic field is applied. As the dipoles rotate, the length of the material changes in the direction of the field. Depending on the material, this change in length can be as much as 2 mm/m [7.22]. Since the operating frequency for



**Fig. 7.36** Pointwise construction of the nonlinear flow due to hysteresis



**Fig. 7.37** Eddy currents in the iron core (*left*) and the use of core lamination to reduce these currents (*right*)

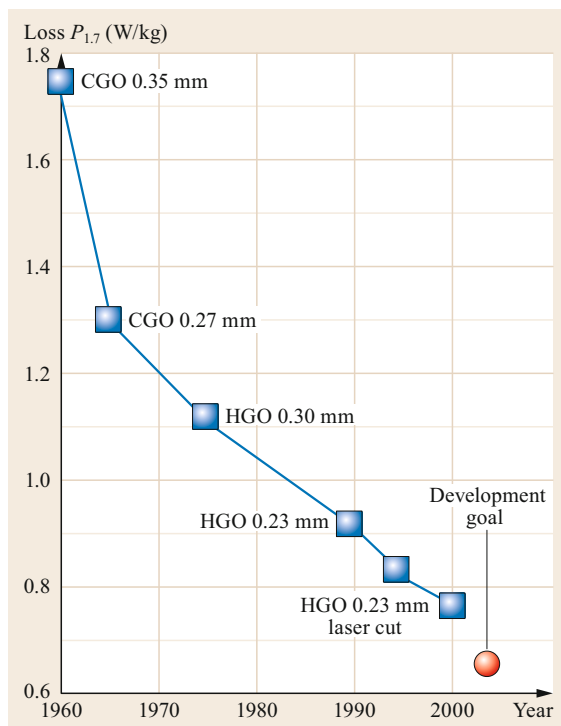
transformers and reactors in Europe is 50 Hz, noise with double this frequency (100 Hz) is typically generated. The noise generated in this way is directly dependent on the induction in the transformer. Since acoustic noise is an important type of noise pollution in urban centers, the noise from transformers must be limited. Noise development can be effectively reduced by lowering the induction from the normal range of 1.7–1.85 T to approximately 1.2 T. However, lowering the induction leads to a larger and more expensive transformer. Transformer noise can also be reduced by improving the clamping of the core, as this suppresses the transmission of the core noise via the tank walls to the surroundings of the transformer.

### Materials

Until the start of the 1960s, transformer cores were manufactured with hot-rolled core sheets. Core sheets with a thickness of 0.5–0.35 mm were first hot-rolled and then insulated with a layer of varnish. Due to their magnetic properties, these sheets allowed a maximum induction of  $\approx 1.55$  T based on the isotropic properties caused by the melt and the resulting hysteresis. In order to guarantee the strength of the limbs, both the core limbs and the upper and lower yokes were held together by insulated, nonmagnetic steel bolts that passed

through holes punched in the core sheets. These bolts braced nonmagnetic core clamping elements on both sides of the core, thus tightening the whole core. A further advantage of applying the varnish insulation to the core sheets was that the edges of the punched holes could be reinsulated with insulating lacquer. Unfortunately, the insulating lacquer was found to detach itself after several years of operation. The original insulating lacquer, which was made of water glass and named after its inventor, Drengenburg, formed an ochre-brown sludge after several years. Also, synthetic resin lacquers used subsequently were not permanently resistant to oil and high temperatures, which led to a reduction in the service life of the transformer due to repeated core burns. Rapidly increasing energy demands in the 1950s resulted in increasingly powerful and large transformers with high no-load losses, but this increase was ultimately limited by the low induction in the hot-rolled sheets, especially with regard to transportability. For this reason, new processes were developed in the USA in the mid-1950s in which transformer core sheets were alternately cold rolled as strips and then annealed again, yielding anisotropic grain orientation (texture) in the magnetic regions. During annealing, a very thin layer (2–5  $\mu\text{m}$ ; similar to an enamel layer) of inorganic material (phosphate) was applied as insulation to the very thin glass surface of the metal sheet. This new insulation proved to be long lasting and efficient even at extreme temperatures (several hundred  $^{\circ}\text{C}$ ).

Along with using a higher silicon content to increase the ohmic resistance, the core sheet quality was drastically improved. The packing density of the core sheets was increased, the sheet thickness was reduced to 0.23 mm, and the working induction in the cores was increased to over 1.8 T. Due to the higher silicon content and the application of selected alloys, magnetic aging of the sheets was prevented. This breakthrough, in conjunction with the development of indestructible



**Fig. 7.38** Evolution of losses in the core material over the last half-century according to Thyssen Krupp Electrical Steel [7.23]

core insulation, permitted the creation of transformer cores that age extremely slowly.

Hysteresis losses were effectively reduced by increasing the orientation of the grains, and eddy current losses were decreased by making the sheet thinner and by using a higher silicon content to increase the resistance of the sheet material. However, this approach also has its limits, because the number of sheets required for the core increases as the sheet is made thinner, resulting in the need for greater manufacturing effort and increasing costs.

The development of so-called Hi-B sheets with even stronger grain orientation and a special surface coating led to a further reduction in losses and decreased magnetostriction, suppressing acoustic noise. Current developmental work in the field of transformers includes attempts to reduce the size of the magnetic domain walls, thus reducing eddy current losses, by laser treatment of the sheet surfaces. Also, research aimed at refining the domain structure by optimizing the coating and eliminating near-surface crystal defects appears promising. Figure 7.38 illustrates the progress made in reducing specific sheet losses in recent years.

Recently, cores made of amorphous material have been produced for smaller transformers. The lack of

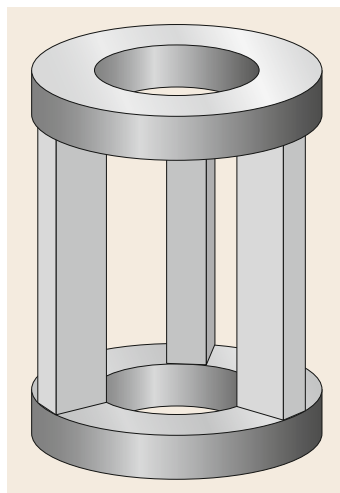
grain orientation eliminates hysteresis losses. The application of new core designs such as strip or tape-wound cores that have technological advantages also enables cost savings. However, amorphous material is yet to become established as a core material for larger power transformers. Since the core losses from the transformer occur during no-load operation, reducing these losses also saves a considerable amount of energy, aiding efforts to protect the environment and climate. In recent years, substantial loss reductions have been achieved with new metal sheets.

### Construction Types

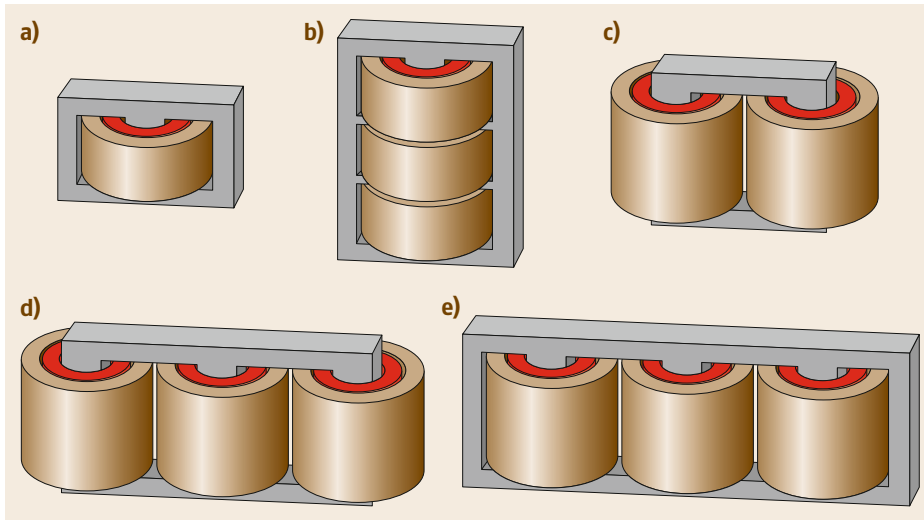
The first three-phase transformers (employed along the previously mentioned Lauffen–Frankfurt test track in 1891) used a temple-type core construction, as shown in Fig. 7.39. This core type is still used today for three-phase reactors.

Later, core types diversified in two directions. In the USA, shell-type cores became popular, whereas the flat core types introduced by Dolino-Dobrowolski became established in Europe. Figure 7.40 shows various designs of the active parts of single- and three-phase transformers. The windings are colored red (LV side) or yellow (HV side).

Because they are vertically orientated, shell-type cores require little floor space but considerable height clearance during transportation. They are more complicated to produce, but represent the only option for power plants with little floor space. Flat-core types (so-called limb cores) require more floor space but a much lower height clearance during transportation. Due to the generally low height clearance available when transporting transformers by rail, flat-core types have established themselves in Europe. The five-limb core was developed for extremely large power trans-



**Fig. 7.39** Three-phase temple-type core



**Fig. 7.40a–e** Various designs of the active parts of single- and three-phase transformers. (a) Single-phase transformer with a shell-type core. (b) Three-phase transformer with a shell-type core [7.10]. (c) Single-phase transformer with a flat two-limb core. (d) Three-phase transformer with a flat three-limb core. (e) Three-phase transformer with a flat five-limb core

formers. Since some of the magnetic flux flows through the outer return flow limbs, which have half of the core's cross-section, the yokes can also be flatter in flat-core types, so that even three-phase transformers with a power range exceeding 1000 MVA can be built for rail transportation. There is also a design with two additional outer return limbs on the single-phase transformer, resulting in a four-limb core.

Since there is no insulation at the cut edges of the core laminations, transitions from the core limb to the yoke are designed to have one protruding lamination (achieved using bevel cuts). This means that each cut edge without sheet insulation is always opposite a larger sheet with insulation. This is known as step-lap construction. The sheets of limbs and yokes are cut at an angle such that the ends of the legs look like roofs (they are said to be roof cut).

#### Core Clamping and Grounding Systems

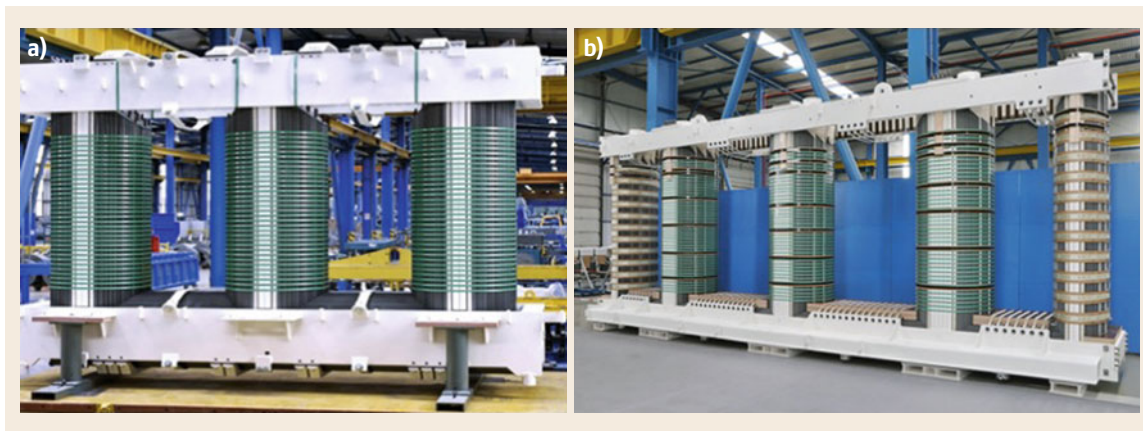
To press the core sheets together, core clamps made of wood or steel are used at the top and bottom. The core clamps on the two sides of the core are connected via bolts or straps. In order to absorb the short-circuit forces and the forces of the own transportation weights, the upper and lower core clamps are then connected to tie rods on each side of the core. Each transformer manufacturer has developed its own system of tie rods. Originally, four external tie rods were used on each side of a three-limb core. This configuration is still frequently used today for smaller and medium-sized



**Fig. 7.41** Transformer cores with step-lap and outer tie rods [7.24]

transformers. Figure 7.41 shows transformer cores with roof-cut, step-lap, and outer tie rods.

Internal tie rods that also act as vertical core clamps are used in large transformers. The tie rods are installed below the core clamps on the upper and lower yokes. Originally, hot-rolled cores were bolted through holes in the core sheets so that the core clamps on both sides of the core could be connected, but this type of construction cannot be used for cold-rolled cores. Punching holes through cold-rolled core sheets destroys the sheet insulation, and it is not possible to reliably reinsulate the punched holes with paint. Therefore, cold-rolled cores



**Fig. 7.42a,b** Modern three-limb (a) and five-limb (b) cores with inner tie rods [7.25]

are usually braced using circumferential strips of non-magnetic steel or fiberglass tape (see Fig. 7.42). The core clamps are still connected via bolts, but these are placed above and below the yokes, as can be seen in Fig. 7.42b. This approach also maintains the effective core cross-section, unlike passing bolts through holes in hot-rolled core sheets, which reduces the effective core cross-section.

Connecting the tie rods directly to the yokes would create short-circuit windings, so they are insulated from each other. The different parts of the clamping system as well as the core are connected to ground via cables, and the ends of these cables are sometimes accessible via small bushings on the tank cover. The core itself is grounded using a core sword, which is a metallic nonmagnetic sheet placed in between the core sheets. This creates a capacitive grounding impedance. If this grounding system is accessible via small bushings, it is possible to perform measurements during servicing to check that the core is still isolated from the clamping structure. This type of grounding is called CC/CL, which refers to core clamping and core lamination.

## 7.2.2 Windings

In a transformer, high voltages and large currents are concentrated into a small space, meaning that large electric and magnetic fields and high temperatures and forces are generated. This is due to the compact nature of the active parts of the transformer (mainly the windings and core).

### Calculation and Construction

In the following, the most important steps of the winding calculation are described. The basis of all transformer calculations, even when performing computer-

aided optimization, is the transformer equation (see Sect. 7.1)

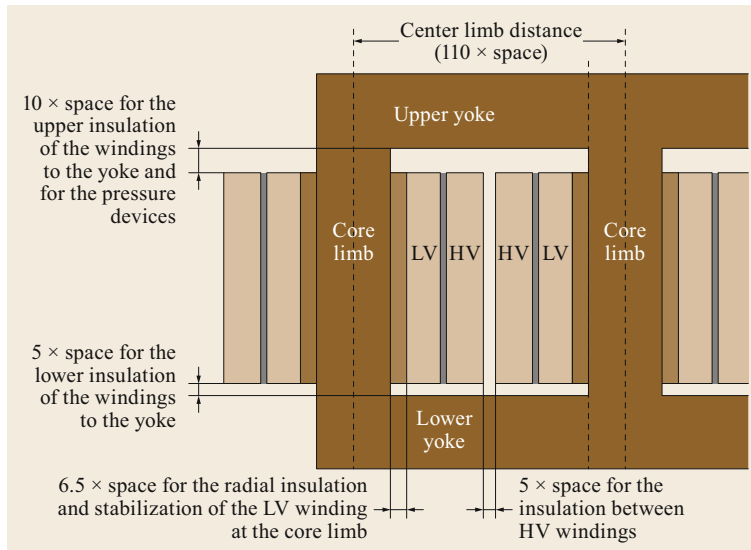
$$V = \frac{2\pi f}{\sqrt{2}} w A_{\text{Fe}} \cdot B_{\text{max}} \quad (7.42)$$

Assuming that the primary voltage  $V$  and the frequency  $f$  are defined by the network and the maximum induction  $B_{\text{max}}$  is limited by the core material,  $B_{\text{max}}$  depends on the number of winding turns  $w$  and the effective core cross-section  $A_{\text{Fe}}$  via

$$B_{\text{max}} = \frac{V}{\frac{2\pi f}{\sqrt{2}} w A_{\text{Fe}}} \propto \frac{1}{w A_{\text{Fe}}} \quad (7.43)$$

This equation enables a certain degree of flexibility in transformer construction. For instance, the designer can choose a large core cross-section  $A_{\text{Fe}}$  and a smaller number of winding turns, leading to a reduced need for conductor material at the expense of requiring more core iron. On the other hand, the designer can increase the number of winding turns  $w$  to reduce the amount of core material needed. In order to find the optimal solution based on many additional boundary conditions, the calculation is performed iteratively until a certain optimization criterion is reached. This is done because various parameters are strongly dependent on each other, so if one of them is modified, many others will also be affected. Modern numerical calculation programs used by transformer manufacturers perform optimization based on not only technical parameters but also economic ones. If, for example, the global market price of the core lamination is low compared to the price of copper, transformers with larger core cross-sections  $A_{\text{Fe}}$  and fewer winding turns  $w$  are designed. If the conductor material used in the windings (preferably





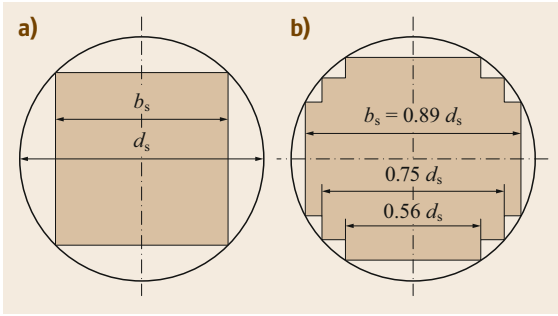
**Fig. 7.43** Simplified axial cut through the active parts of a three-phase transformer with a flat core

copper) is inexpensive but the core material is expensive, smaller core cross-sections and a larger number of winding turns are preferred. Therefore, it is possible that a transformer that was calculated and built a few years ago has identical technical data to a transformer that has just been calculated using a completely different active part design.

However, the design flexibility for transformers is limited by numerous boundary conditions. For large power transformers, the permissible transport height limits the leg length, and the distance between the legs cannot be increased infinitely, since the winding diameter is limited by the transport width. In addition to the specified technical data such as nominal voltage, test voltage, nominal power, vector group, maximum no-load and short-circuit losses, short-circuit impedance, temperatures, noise, and maximum dimensions and masses, there are also a large number of additional boundary conditions in the design, such as specified connection dimensions. Due to the variety of variables, optimization based on certain objective characteristics such as costs, losses, maximum performance, or other parameters is only possible if restrictive boundary conditions are assumed, even when using the latest calculation software. Since each modified calculation involves considerable design work, two different methods of dimensioning are used. For small and medium-sized transformers, a modular principle is often used; in other words, for the same core series, the windings are provided according to the specified voltage and vector group. This saves design costs and expenses associated with technological preparation, which are often markedly higher than the possible savings from opti-

mization (e.g., in terms of material prices). However, large power transformers are always recalculated and redesigned. The repetition rate for these designs is usually on average about 2–3 objects per calculation for manufacturers. In the following, the essential steps involved in the design and calculation of a transformer and its windings are addressed.

The dependencies of a simple design are shown in Fig. 7.43, which illustrates parts of a section through a three-phase core transformer with just one LV winding and one HV winding. The radial space available for the windings in the so-called core window (half the space between the core limbs) is reduced internally by the insulation distance of the windings from the core (a space that also serves to support the windings on the core limb). On the outside half, the insulation distance between the windings of the different phases must be subtracted. This distance must be correspondingly large and well designed in terms of insulation because the full phase voltage is applied between the adjacent windings on different limbs. The available winding space is reduced axially at the top and bottom by the insulation distances to the partially sharp-edged corners of the core yokes. Furthermore, the structures used for the short-circuit-proof axial bracing of the windings must also be accommodated within this distance. The sizes of the mentioned distances that reduce the winding space depend to a large extent on their type and design, and therefore vary from manufacturer to manufacturer. However, regardless of the manufacturer, the following simplified procedure for transformer design along with winding calculations and winding construction can be described, based on the simple design shown in Fig. 7.43:



**Fig. 7.44a,b** Simplified representation of the transition from the square leg cross-section (a) to the usual core grading (b)

1. *Initial data.*

The (phase-to-phase and phase-to-ground) voltages, currents, and the rated power within the transformer are calculated according to the specified data and (in particular) the specified vector group.

2. *Number of turns on the LV winding.*

The integer number of turns  $w_{LV}$  for the LV winding is calculated using (7.43), assuming typical maximum induction  $B_{max}$  and effective core cross-section  $A_{Fe}$  values for the specified rated power.

3. *Core sheet material, geometry, and dimensions.*

This includes specifying the core lamination material and lamination thickness, determining the geometric core cross-section through back calculation from the effective core cross-section (with the packing density of the core lamination considered to be a design-dependent empirical value from the respective manufacturer), determining the leg geometry along with the number of core leg steps and their size, and deriving the core leg diameter.

Circular windings are produced because this shape has the best ability to withstand short-circuit forces, so the lamination distribution must be adapted to the core diameter  $d_s$  by grading the lamination stacks, as shown in Fig. 7.44. The optimal lamination width  $b_s$  and the corresponding core steps are determined using mathematical optimization programs.

The core diameter  $d_s$  determined in this way serves as the starting point for the radial winding design.

4. *LV winding type, conductor cross-sections, parallel wires, number of layers, and length and width.*

This involves selecting the LV winding type, determining the required conductor cross-section based on empirical values, and initial geometrical dimensioning of the winding according to the parallel wires, number of layers, and the length and width.

5. *Number of turns for the HV winding.*

The number of turns for the HV winding  $w_{HV}$  is calculated based on the specified voltage ratio, taking the vector group into account.

6. *HV winding type, conductor cross-sections, parallel wires, number of layers, and length and width.*

This includes selecting the HV winding type, determining the required conductor cross-section based on empirical values, and initial geometrical dimensioning of the winding according to the parallel wires, number of layers, and the length and width.

7. *Stray voltage.*

The stray voltage  $V_s$  is determined as it provides the basis for determining the short-circuit voltage. Since the stray voltage is the main contributor by far to the short-circuit voltage in normal transformers, it is important to correctly dimension this parameter. In the event of a short circuit, the induction in the transformer core largely collapses. Therefore, the stationary short-circuit current  $I_k$  is essentially limited by the inductance  $X$  (see Sect. 7.1) that is formed by the stray field in and between the windings. The idealized distribution of the leakage flux for the two-winding transformer with just one stray duct mentioned above is shown in Fig. 7.45.

From the above representation, the percentage stray voltage drop  $v_s$  can be derived starting from

$$X = 2\pi f \mu_0 w^2 \frac{U}{h_w} \left( t_{12} + \frac{t_1 + t_2}{3} \right) \quad (\Omega) . \quad (7.44)$$

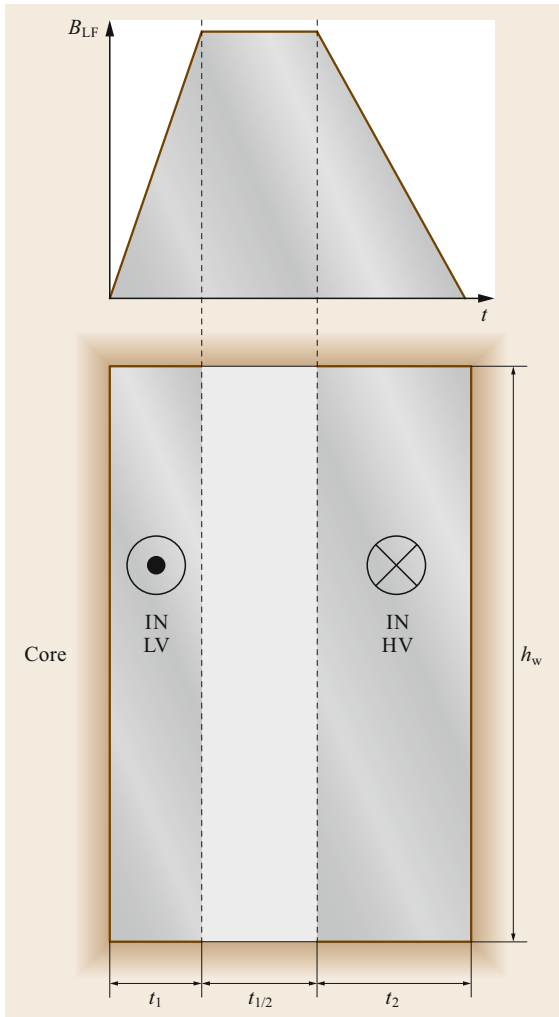
Here,  $U$  is the mean circumference of the stray gap. Using  $\mu_0 = 4\pi \times 10^{-7} \text{ N/A}^2$  and  $XI = V_s$ , we obtain

$$V_s = I 8\pi^2 f w^2 \frac{U}{h_w} \left( t_{12} + \frac{t_1 + t_2}{3} \right) \times 10^{-7} \quad (\text{V}) \quad (7.45)$$

if all dimensions are in meters. Upon introducing the relative stray voltage  $v_s = V_s/V \times 100$  as well as the winding turn voltage  $V_w$  with  $V = V_w w$ , normalizing the frequency to 50 Hz, and dividing the mean stray gap circumference  $U$  by the mean of the inner and outer coil circumferences  $(U_1 + U_2)/2$ , the following is achieved

$$v_s = 8\pi^2 50 \frac{f}{50} \frac{I}{V_w} w \times \frac{(U_1 + U_2)}{2h_w} \left( t_{12} + \frac{t_1 + t_2}{3} \right) \times 10^{-5} \quad (\%) . \quad (7.46)$$

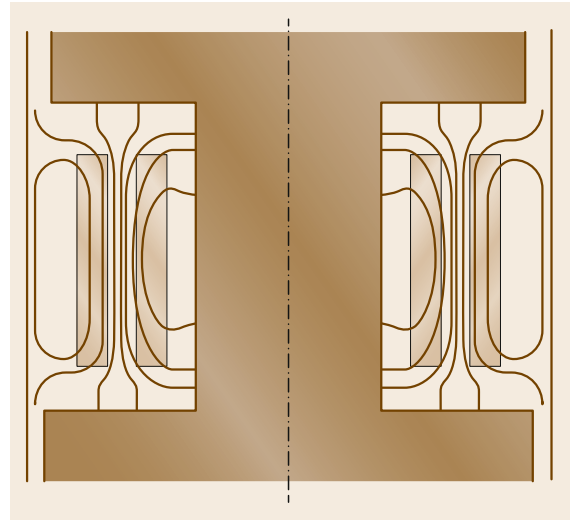
The leakage flux distribution shown in Fig. 7.45 is idealized and based on various assumptions; for example, that the windings are completely surrounded



**Fig. 7.45** Idealized leakage flux in the leakage channel and in the windings

at the end sides by core laminations with infinite permeability. This is not the case in reality, so Fig. 7.46 shows the magnetic leakage field through the windings and the leakage field duct determined numerically with a 2-D model.

It can be seen that the magnetic stray field at the upper and lower ends of the winding deviates from the idealized field distribution. As it is still not possible – even with modern simulation tools – to calculate the leakage flux numerically in three dimensions because a complete 3-D model of all windings along with each individual conductor (including junctions, insulating parts, and leads) is required, a correction factor is used. This factor was developed by Walter Rogowski in Germany at the beginning of the last century. The Rogowski factor



**Fig. 7.46** Simulation of leakage flux using a 2-D model [7.10]

$k_R$  accurately determines the deviations of the actual field curve shown in Fig. 7.46 from the original assumed curve depicted in Fig. 7.45, and is calculated via

$$k_R = 1 - \frac{t_1 + t_{12} + t_2}{\pi h_w} \left( 1 - e^{-\frac{\pi h_w}{t_1 + t_{12} + t_2}} \right). \quad (7.47)$$

This leads to an equation for calculating the percentage stray voltage drop,

$$v_S = 8\pi^2 50 \frac{f}{50 V_w} \frac{\mathbf{I}}{w} \times 0.5 \frac{(U_1 + U_2)}{h_w} \times \left( t_{12} + \frac{t_1 + t_2}{3} \right) k_R \times 10^{-5} \quad (\%), \quad (7.48)$$

which can be simplified to

$$v_S \approx 2 \frac{f}{50 V_w} \frac{\mathbf{I}}{w} \frac{(U_1 + U_2)}{h_w} \times \left( t_{12} + \frac{t_1 + t_2}{3} \right) k_R \times 10^{-2} \quad (\%). \quad (7.49)$$

Today, various correction factors that allow precise calculations are available, even for complicated winding arrangements. For very large transformers where there is a risk of heating in the core clamping elements and tank walls due to eddy currents caused by the leakage flux, the maximum leakage flux in these components is determined via 2-D field calculations for simplified winding models. These results are then converted to be applicable in three-dimensional reality using correction factors based on empirical values.

If the determined stray voltage is not within the required range, the situation must be modified. Increasing the radial winding dimensions and the width of the stray channel causes an increase in the stray voltage, whereas increasing the winding length and thus the stray gap length reduces the stray voltage. Due to the eddy current losses explained below and the dependence of the ohmic winding losses on the winding circumference, the radial winding width must be kept as small as possible, which limits the flexibility of the electrical designer accordingly.

8. *Winding losses or short-circuit losses.*

The preliminary specifications of the winding dimensions, the stray channel width, and the stray channel length provide the fundamentals required to calculate the short-circuit losses. The ohmic resistance of each winding is the specific resistance of the winding material multiplied by the average turn circumference and the number of turns. The conductor losses are determined as the product of the squared current and the resistance. As the windings are not evenly penetrated by the stray field, even in the simplified diagram shown in Fig. 7.45, current displacement occurs, leading to increased resistance, which is accounted for in the calculations by introducing correction factors. Eddy currents and associated eddy current losses also occur in the windings, analogous to the core laminations. The alternating magnetic flux induces a voltage not only in the windings but also in the winding wire itself. This voltage drives eddy currents in the conductor perpendicular to the magnetic flux lines, which additionally heat up the windings and contribute to the total losses from the windings. According to the idealized stray flux distribution in the windings shown in Fig. 7.45, the conductors that are closest to the stray channel are subjected to the highest stress and therefore become the hottest. In this case, subdividing the conductor width can provide effective compensation. Because the stray field decreases with distance from the stray channel, there are different induced voltages in parallel conductors, leading to additional compensation currents. In order to avoid these balancing currents that also increase the temperature and the losses, the conductors are twisted parallel to the stray channel. These conductors are called transposed conductors. The percentage voltage drop  $v_R$  can be then determined from the sum of the ohmic losses and eddy current losses. At the same time, it is important to check that the heat caused by the losses in the windings can be effectively dissipated. This can be roughly

estimated by considering both the losses and the available cooling surfaces of the windings.

9. *Determining the short-circuit voltage.*

As discussed in the last section, the percentage short-circuit voltage can be calculated via

$$v_{sc} = \sqrt{v_R^2 + v_S^2}. \quad (7.50)$$

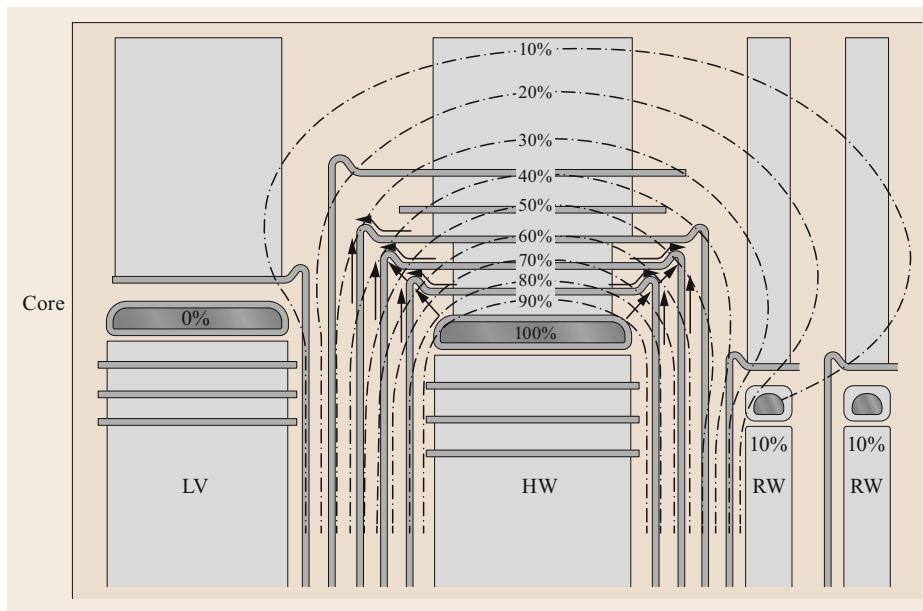
Thus, the calculated voltages  $v_R$  and  $v_S$  must be adjusted until the specified short-circuit voltage is achieved.

10. *Core design and determining the no-load losses.*

Provided the winding height and the diameter of the outer winding have been specified, the dimensions of various aspects of the core, such as the leg diameter, the center limb distance between the legs, and the leg length can be determined by adding the empirical values for the distances in Fig. 7.43 to the respective dimensions. It is then possible to calculate the core losses. These are determined from the respective inductions  $B_{max}$  for the core limbs and the yokes, which should be as equal as possible, and by multiplying by the respective sheet masses, taking into account material parameters and design correction factors. If parameters specified by the customer or standard specifications are not achieved, the calculation process is restarted. If the calculated core losses are too low, the transformer may be too large and heavy and thus too expensive. If the no-load losses are too high, either the number of winding turns or the leg cross-section  $A_{Fe}$  must be increased, see (7.43). Both of these actions cause the induction and therefore the no-load losses to decrease. However, the effect of decreasing the induction by increasing the effective cross-sectional area of the core limb is limited, just like the effect of lengthening the core limb to increase the number of winding turns, because both procedures increase the core mass and therefore the no-load losses.

11. *Determining the voltage stress in windings and leads.*

Winding insulation is dimensioned according to the test voltages, which are defined in national and international standards. For example, a modern 400 kV power transformer is usually tested by applying a voltage of 630 kV for 1 min, a switching impulse voltage of 1175 kV, and a lightning impulse voltage of 1425 kV, based on the IEC standards. It must be able to withstand these overvoltages without showing any defects that could lead to partial discharges (PDs). Normally, the insulation structure of the windings would have to be calculated and dimensioned axially towards the yokes and radially



**Fig. 7.47** Windings with soft paper insulation and so-called goosenecks, which are formed under axial winding pressure

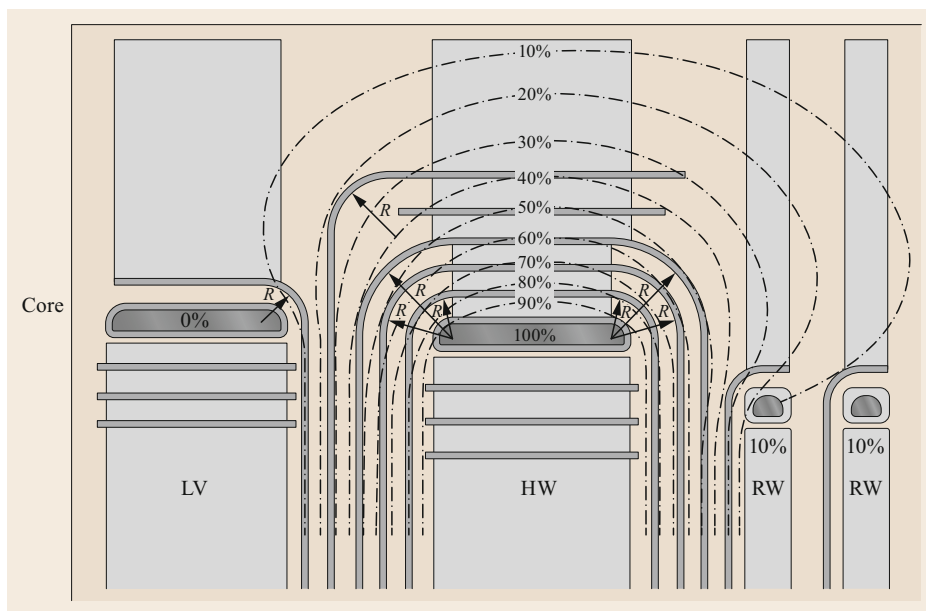
towards the core leg and the adjacent winding for complicated insulation arrangements such as that illustrated in Fig. 7.47. Design engineers account for the fact that insulation can withstand much higher electrical field strengths if the field is active for a very short time (lightning and switching impulses) than if the field is active for a much longer period (e.g., 1 min in the applied voltage test). Therefore conversion factors (which vary slightly from manufacturer to manufacturer) are used to make the various short-term and long-term voltage stresses comparable. If the test voltage is multiplied by a correction factor, a uniform comparison value for different voltage stresses can be derived: the so-called design insulation level (DIL), which represents the maximum voltage stress permitted for the insulation. For normal power transformers, the 1 min applied voltage test is usually assigned a correction factor of 1. High DIL values for the switching or lightning impulse tests are only obtained using the conversion factors when the switching or lightning impulse stresses are particularly high. This process has led to standardized insulation design.

Paper impregnated with mineral oil has proven to be the ideal insulator for high voltages, whereas insulation systems based on epoxy resin or gas can be used up to medium voltage levels. Therefore, transformers can be split into three categories: liquid-filled transformers, gas-insulated transformers, and dry-type transformers. Mineral-oil-filled transform-

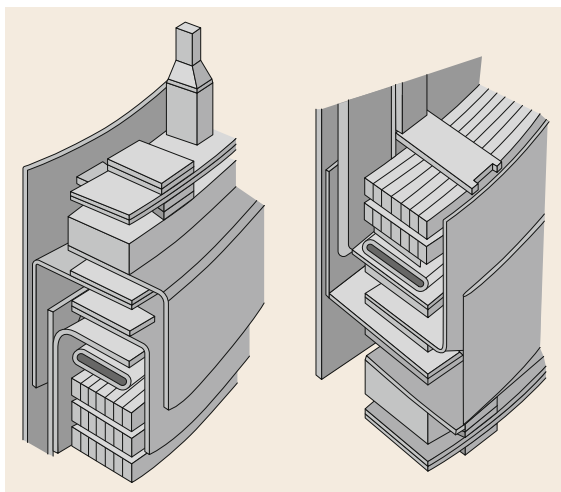
ers are very complex to manufacture, and when the windings are pressed so-called goosenecks can be formed, with fatal consequences (reduced cooling, PD generation), as shown in Fig. 7.47. However, the development of molded parts made from pressboard by the Swiss company *Weidmann AG* in the 1960s led to the creation of a much more technologically stable manufacturing process and better insulation [7.26, 27].

Insulation schemes have developed and improved over time. Insulation of winding ends is now carried out radially using pressboard barriers and axially with angle ring segments made from pressboard moldings and pressboard rings, as shown in Fig. 7.48. High field strengths at the corners of windings are reduced by shielding rings with conductive foils that are connected to the potential of the winding exit, as shown in Fig. 7.49.

To accelerate and thus optimize the winding assembly process, the components of the insulation are increasingly being preassembled by suppliers [7.28]. Electric field strengths and creepage distances are taken into account when designing an insulating arrangement. In the past, this was often a very difficult task, but engineers now have access to powerful workstations that can perform 2-D and 3-D calculations; the latter became available at the beginning of this century. Since most of the insulation arrangements used today were actually developed in the 1960s when computers were not available, there is still room to improve these insulation arrangements.



**Fig. 7.48** Upper edge field insulation made with molded pressboard parts, which eliminates goosenecks. The components of the insulation follow the electrical field better than the arrangement shown in Fig. 7.47



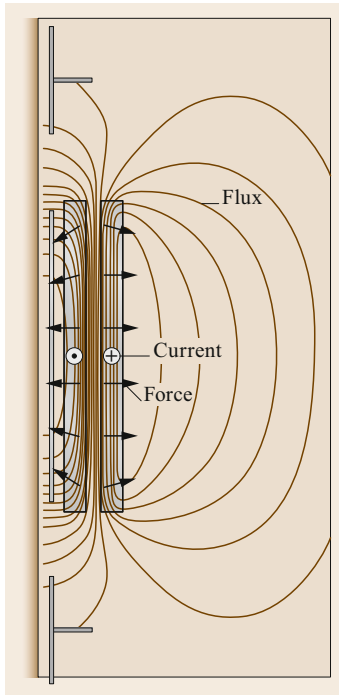
**Fig. 7.49** Upper and lower edge field insulation with shield rings and yoke collars (angle-shaped barriers) made of pressboard segments. High-voltage windings are enclosed by angle-shaped barriers towards the yokes and shield rings at the winding ends for dielectric control

Switching and lightning voltages are not sinusoidal and include higher frequencies due to their shapes. Therefore, it is rather complicated to calculate the propagation of these surge waves in the windings. Calculations of detailed equivalent circuits have, however, led to improvements in winding design, such as the development of interleaved disc windings.

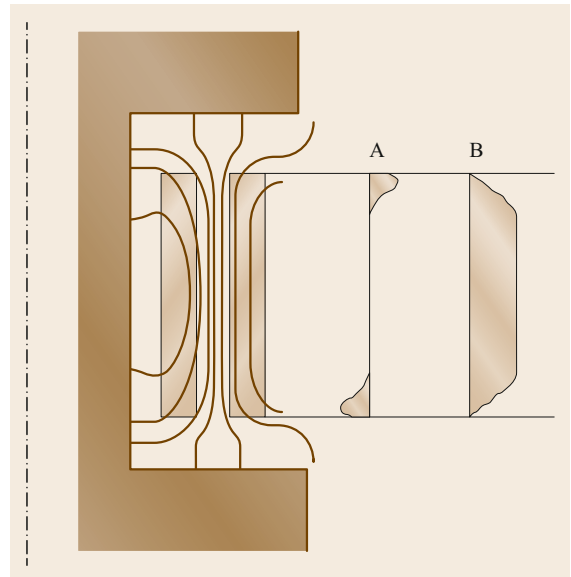
- Following the calculations of the winding insulation, the short-circuit strength must be verified.
12. *Determining short-circuit forces and calculating the winding pressure and compaction.*

According to the Lorentz force law, a force is exerted on each current-carrying conductor in a magnetic field. This force is always perpendicular to the field lines of the magnetic field and the direction of the current. Assuming the ideal stray field distribution shown in Fig. 7.45, the conductors of the windings are only stressed by radial forces. The forces on the inner winding are directed toward the inside, and those on the outer winding are directed towards the outside, as shown in Fig. 7.50. This figure also shows that the force has an axial component as well as a radial one at the ends of the windings, as also indicated by Fig. 7.51. The axial forces result in axial pressures in the windings, as shown in Fig. 7.52 [7.29].

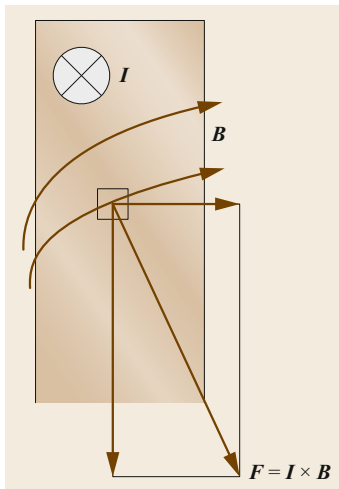
Winding wires are usually insulated with paper and the winding supports are made of pressboard. These insulating materials deform plastically under high pressure, which reduces the winding tension. This can destroy the winding because the reduced winding tension cause the winding to vibrate more, which leads to a grinding of the insulation until the winding is destroyed. Thus, after the production and drying processes, the windings are axially prepressed under forces and pressures that are at least as large as those that occur during a short circuit. This allows the effect of a short circuit to be simu-



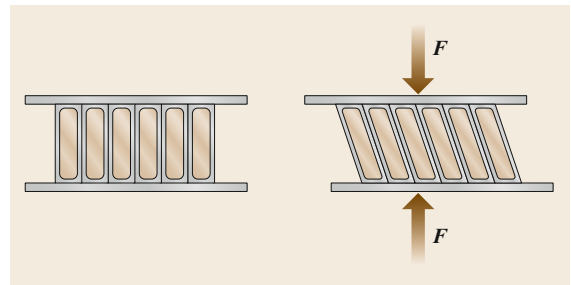
**Fig. 7.50** Stray field distribution and short-circuit forces in windings



**Fig. 7.52** Axial forces and pressure in the windings (A axial current forces, B resulting axial pressure)



**Fig. 7.51** Short-circuit forces on the top of a winding



**Fig. 7.53** Conductor tilting under high axial stress

lated in advance, and ensures that further loosening of the windings cannot occur in an extreme case. In addition, the axial forces can tilt the conductors as shown in Fig. 7.53 if the geometric conductor dimensions are unfavorable (i.e., if the width is too small in the radial direction and the axial length exceeds the maximum value). This must be considered during the design process too. As a rule of thumb, the finished windings are actually prepressed by applying forces and pressures that are almost up to the tilting limit, markedly beyond those associated

with axial short-circuit forces. If calculations indicate that the wires are already tilting away when the axial force applied is equivalent to that encountered during a short circuit, the designer must redesign the windings, even though many other calculations will have already been carried out. This is necessary because selecting other winding wires changes almost all of the other parameters.

However, short-circuit stress causes not only radial and axial forces in the winding wires but also tangential tensile forces, as shown in Fig. 7.54 [7.30]. If the tangential pressure stress on the windings is too high, *buckling* occurs during the short circuit, as illustrated in Fig. 7.55.

Every power transformer must be able to withstand an external short circuit for a short time (usually 2 s). For calculation purposes, the short circuit is assumed to occur directly at the transformer terminals. However, if a short circuit occurs within the trans-

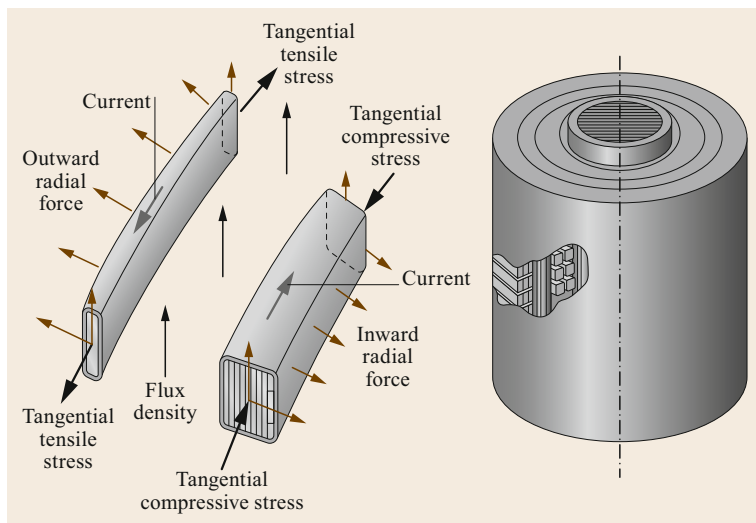


Fig. 7.54 Tangential tensile forces

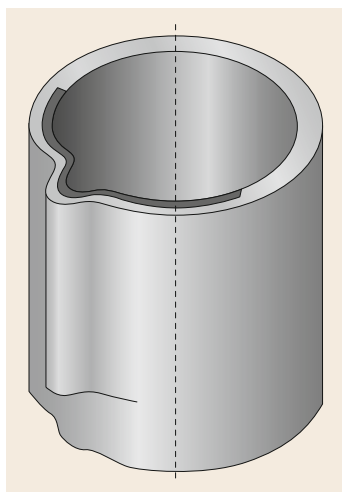


Fig. 7.55 Buckling due to high short-circuit forces

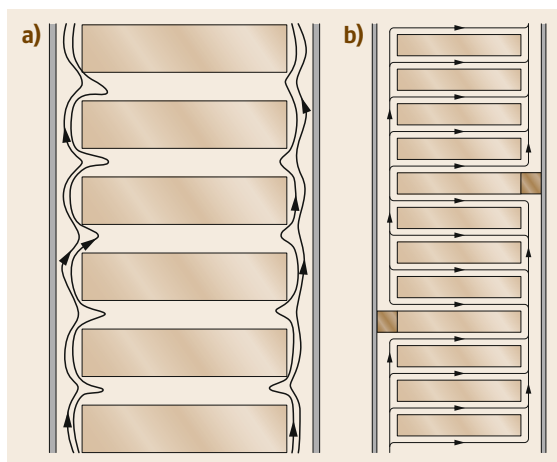


Fig. 7.56a,b Cooling without (a) and with (b) guided oil flows

former, the situation is completely different, and the consequence is often the catastrophic destruction of the transformer.

### 13. Calculating the cooling of the windings and winding hot spots.

Once the winding dimensions have been determined, the cooling of the windings and winding hot spots must be calculated. Cooling liquids such as mineral oils are incompressible, meaning that heat flow calculations are simpler for oil-cooled than for air-cooled transformers. However, the viscosity of the insulating liquid is temperature dependent.

In the past, windings were usually cooled exclusively by the thermosiphon effect, which is based on the difference in density between hot and cold insulating fluid. In this approach, the heated oil

risks in the insulation channels of the windings, which hinders the cooling process, especially for disk windings. Increasing power ratings led to increased heat generation in the windings, making improvements necessary.

One of these improvements was the transition to guided oil flows, as shown in Fig. 7.56. In this process, barriers that take the form of oil control segments around the winding in the axial cooling channels force oil to flow over the entire surface of each disc coil. For even better cooling performance, pressure chambers are built into the winding blocks at the lower end of the windings. These chambers are filled with oil under pressure, which is then forced into the oil channels of the windings.



The insulation is usually made of cellulose, which is subject to thermal aging. For this reason, maintaining an appropriate temperature range is crucial to achieving a long transformer service life. The hot spot temperature in the upper area of the winding is the most important factor to consider. In addition, the temperature jump between the oil inlet and outlet for the winding must be maintained precisely to ensure the stability of the entire cooling system. The whole temperature distribution is usually calculated through analogy: by simulating the temperature transitions as thermal resistances based on precise measurements and calculating the overall effect linearly in the form of a thermal resistance network.

If any problems are encountered during the temperature calculations, the calculations are usually performed again until all of the requirements are fulfilled. This process depends on the software used and the experience of the designer. Modern computer programs carry out the calculations several hundred times to optimize the system.

Once the designer has finally successfully dimensioned the windings using the procedure described above, and assigned values to all of the specified parameters, the mechanical designers begin their work. They prepare production and assembly drawings according to the specified winding data. Since engineering hours are expensive, the proportion of the transformer manufacturing process that is devoted to electrical and mechanical design is a decisive cost factor.

### Conductors and Insulating Materials

Today, the conductors used in windings are generally made of high-purity copper. In the past, winding conductors were also made out of aluminum due to a lack of affordable copper. Although aluminum is lighter than copper, it also has a higher specific resistance, resulting in larger windings that also require larger cores. However, changes in the prices of these two materials in the

global market have caused aluminum windings to be virtually phased out.

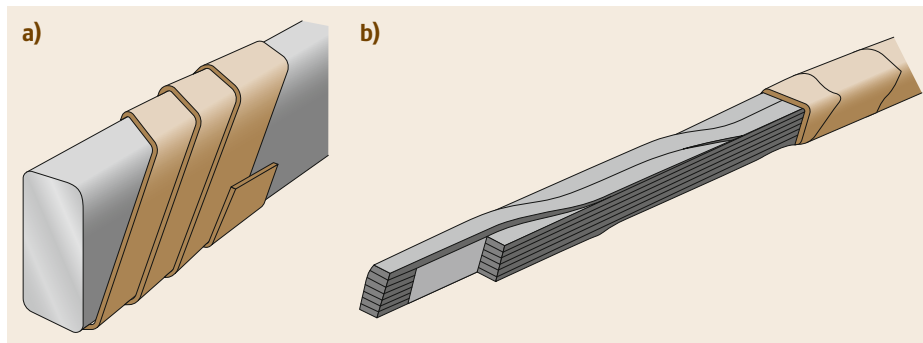
Winding conductors usually have rectangular cross-sections with slightly rounded corners to suppress the generation of excessive electric field strengths. Smaller transformers with round conductors that are usually insulated with enamel lacquer are also manufactured. To enhance the packing density, these round conductors are flattened on both sides. In dry-type transformers, the conductors are often cast directly with resin, or special resin-impregnated fiberglass insulation is used. Rectangular copper conductors are used in fluid-insulated transformers. These are usually insulated with overlapping layers of thin paper up to the required thickness, as shown in Fig. 7.57a.

Transposed conductors, as shown in Fig. 7.57b, were developed to reduce eddy current losses and have largely replaced so-called twisted winding, which is a special form of single-layer winding containing several parallel conductors that are twisted at intervals, as shown in Fig. 7.58. Today, twisted winding is usually only used in smaller transformers or in high-current windings, where either the geometry or the price prohibits the use of transposed conductors.

Especially when the windings are highly thermally stressed, for example in industrial transformers or traction transformers, the paper insulation is replaced with thermally upgraded paper or (even better, but much more expensive) aramid paper. The decisive factor when selecting the insulation material is the thermal class, as shown in Table 7.3.

Dry-type transformers designed for thermal classes E–H require special insulation materials. The insulation materials previously used for class H contained asbestos, which is carcinogenic, so it is no longer allowed.

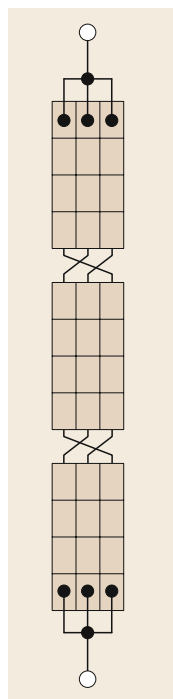
Conductors used in windings can also take the form of a foil made of copper or aluminum. The utilization of foils drastically reduces eddy current losses while offering a high current-carrying capacity. They are mainly used as LV windings in distribution transformers.



**Fig. 7.57**  
 (a) Conductor strand with paper insulation.  
 (b) Continuously transposed conductors

**Table 7.3** Thermal classes for transformers according to the relevant IEC standard [7.31, 32]

	Transformer part	Thermal resistance class				
		A	E	B	F	H
Dry-type transformer	Windings (K)	60	75	80	100	125
Oil transformer	Windings (K)	65	Normal			
		70	Forced cooling			
	Oil in upper layer (°C)	60	Normal case (conservator)			
		55	Without conservator and airtight closure			
	Iron core and other parts	Excessive temperatures must not damage neighboring parts				

**Fig. 7.58** Twisted winding

hand, from the perspective of manufacturing technology, disc winding is a cylindrical winding made of disc coils. In the following, the most important windings are categorized according to manufacturing technology.

**Layer Winding.** Layer winding, as shown in Fig. 7.59a, is the simplest type of cylindrical winding. It is manufactured on horizontally rotating winding machines and is mainly used for small and medium-sized transformers. Its advantage is its low manufacturing cost, but its disadvantage is its relatively low withstand capability to incoming voltage peaks. This can be increased by reinforcing the insulation of the wires at the edge of the winding and by using edge collars.

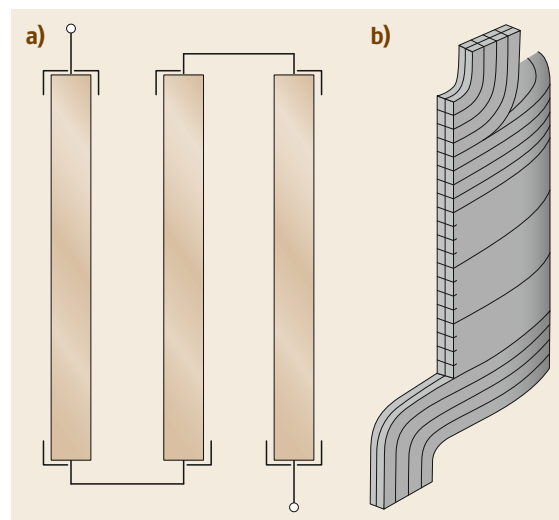
In the regulating windings shown in Fig. 7.59b, the individual regulating steps are wound as individual loop-layer windings. This is the most frequently used winding type for regulating windings. The loops that are wound into each other are connected or disconnected depending on the voltage regulation, resulting in an even axial distribution of the magnetic field and eliminating large transverse fields, thus reducing the short-circuit strength of the transformer.

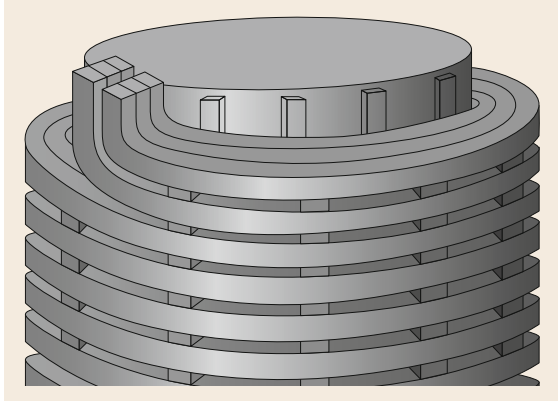
### Winding Types

The long history of transformer development has resulted in the creation of many different types of windings. The most important of these can be categorized based on the following characteristics:

1. Geometric shape (e.g., foil, cylindrical, and disc windings)
2. Function in the transformer (e.g., LV, HV, tertiary voltage (TV), regulating windings (RW))
3. Manufacturing technology (e.g., layer, helical, and disc windings).

Note that the disc winding referred to in geometric categorization is a special form of winding in which the LV and HV disc coils alternate. Therefore, the stray channels are parallel to each other, leading to extremely low stray voltages. This design is therefore used only for special high-current and test transformers. On the other

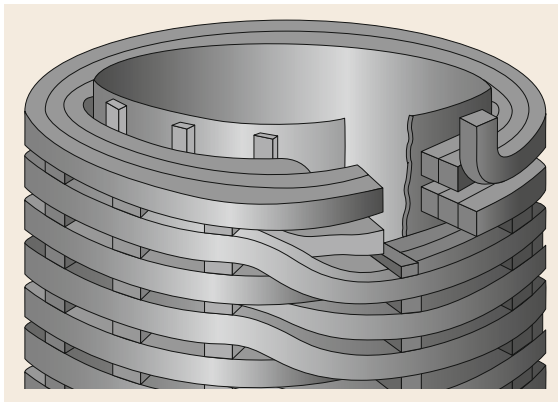
**Fig. 7.59** (a) Layer winding with edge collar. (b) Single-layer winding used as a regulating winding



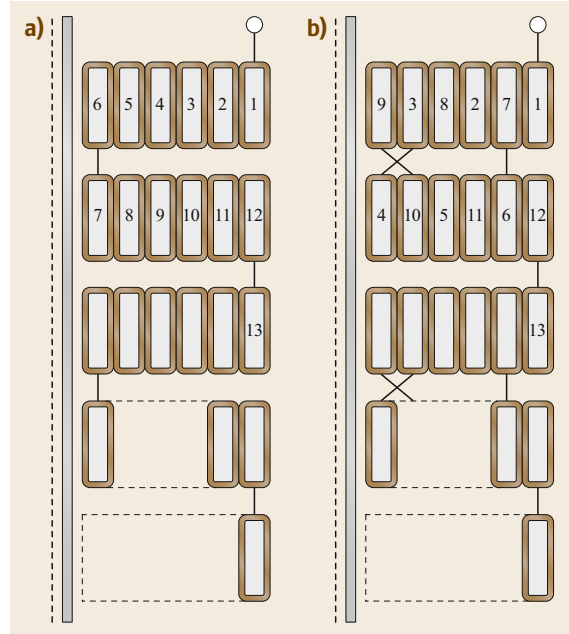
**Fig. 7.60** Single-layer helical winding

**Helical Winding.** This winding type using transposed conductors was developed for windings with particularly high currents and combines the advantages of layer and disc winding. Several conductors are wound in parallel in the form of a helical coil as shown in Fig. 7.60, whereby the individual winding turns are kept apart by spacers. This type of winding is available in single and double layers; in the latter case, the conductors are twisted in the layer transition.

**Disc Winding.** Disc winding (see Fig. 7.61) is usually employed instead of layer winding when the winding has a large number of turns (as required for high voltages), as disc winding can better withstand transient overvoltages due to an improved capacitive behavior. To avoid the need to reconnect the conductors between the discs after each coil, the second disc is wound in stock and then rewound such that no solder joints are created. Although disc winding is better suited than layer winding to fast transient voltages, these voltages drop in a very nonlinear manner over a few turns, especially at the beginning of the winding in the middle or at the top



**Fig. 7.61** Disc winding



**Fig. 7.62a,b** Comparison of conventional disc winding (a) with interleaved disc winding (b)

of the disc. Inadmissibly high field strengths can arise between the conductors and also between the discs. By interleaving the conductors (i.e., returning the conductors as shown in Fig. 7.62), the capacities between them are artificially increased. This achieves a linear distribution of the transient voltages that penetrates further along the winding. In this way, high local field strengths at the top of the winding can be avoided.

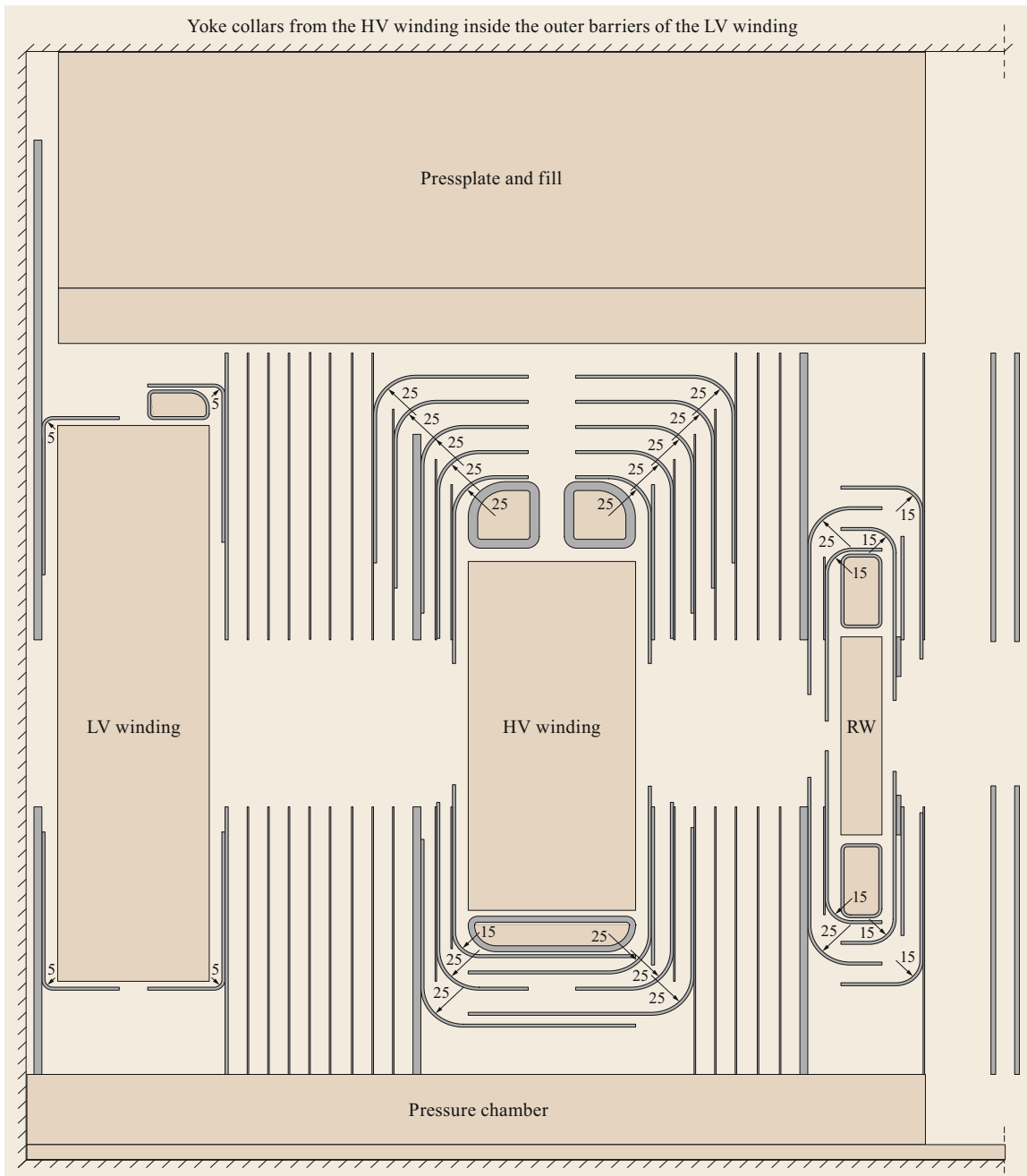
Interleaved windings for large transformers (such as that shown in Fig. 7.62) are usually manufactured on vertically rotating, height-adjustable winding benches.

#### Drying, Compression, and Winding Block Assembly

A winding block consists of all the windings together with their radial and axial supports and press structures. This block is mounted concentrically around one core leg.

**Drying.** In liquid-insulated transformers that mainly use cellulose-based insulating materials such as paper, pressboard, or press wood, the insulation can absorb moisture from the air, reducing the insulating performance. The windings must therefore be dried immediately after manufacturing using thermo-vacuum drying processes.

**Compression.** Subsequent to drying, the windings are compressed axially and then tensioned under low pres-



**Fig. 7.63** Block layout of a 400 kV power transformer with oil-directed cooling via a pressure chamber [7.32]

sure. Two winding pressing processes can be distinguished:

- Hydraulic soft pressing in a vacuum drying oven during drying is a complex (and therefore expensive) but gentle process with high compression efficiency.

- Conventional mechanical winding pressing after drying is less complex and therefore less expensive.

**Winding Block Assembly.** The windings must be assembled concentrically from the inside to the outside while being radially insulated from each other with barriers and oil ducts. The axial end insulations consist

of yoke collars comprising overlapping segments with axial spacer rings between them. Two technological approaches to winding assembly are available:

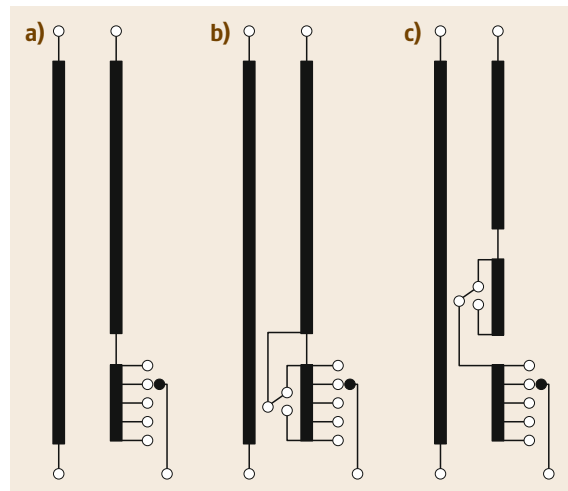
1. The windings are assembled one after the other directly on the transformer core leg, from the inside to the outside. The winding insulations are completed in the upper area after assembly on the core leg, and the windings are dried and braced together with the active part of the transformer. This approach to assembly takes longer and risks axial elongation of the individual windings due to moisture absorption from the air.
2. A winding block is built separately outside the active part. The windings are preassembled in a block, dried, compressed again, and then mounted in one piece on the core leg. This is much faster and avoids the disadvantages of the first method, but is more complex technologically and in terms of preparation. In this process, hydraulic soft pressing can be used effectively for all windings on the entire winding block.

The main insulation diagram for the winding block of a 400 kV power transformer with three windings (LV, HV, and RWs from inside to outside) shown in Fig. 7.63 represents the classic winding distribution of an oil-immersed power transformer.

### 7.2.3 Tap Changers

Aside from applying magnetic current regulation using the saturation properties of magnetic materials (e.g., using transductors), which is only employed in very special transformers, the most effective way of regulating a transformer in the grid is to change its ratio by modifying the number of windings on one side. For historical reasons, regulation is implemented on the LV side in North America, whereas the rest of the world regulates the voltage by changing the number of turns on the HV side, usually at the neutral point. There are three basic schemes for this type of voltage regulation, as shown in Fig. 7.64. In this figure, the left bar always represents the LV winding and the right bar represents the HV winding, which can be divided into a main and a regulation winding. The regulation winding can consist of a fine winding only or a fine winding and a coarse winding. The neutral point is connected to the regulating winding such that the number of active winding turns can be changed, meaning that the voltage can be adjusted.

Voltage regulation requires a switch that can connect the neutral to different taps on the winding in order to increase or decrease the number of effective turns.



**Fig. 7.64a–c** Voltage regulation schemes: (a) linear, (b) plus-minus, and (c) coarse and fine

This switch is called an on-load tap changer if the voltage can be regulated during operation or an off-load tap changer if it cannot. Depending on the number of voltage steps or taps involved, a lot of conductors (leads) for each phase are needed between the winding blocks and the tap changer, which is usually located on the front side of the active part. Even if the regulation is done on the HV side, several hundred amperes of current can flow through these lead conductors, so their weight is not negligible. Furthermore, forces are applied to these leads during a short circuit, so the whole lead system must be mechanically supported.

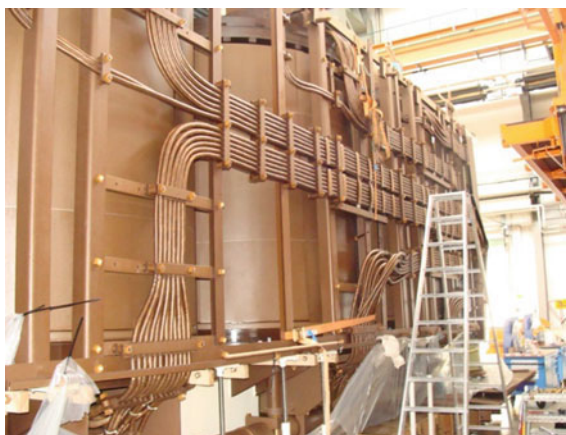
#### Lead Support System

The design of the lead support system depends on the manufacturer. Some manufacturers use solid and thickly insulated round copper conductors for the leads because they are very strong. This results in high insulation costs and a lack of mounting flexibility, and requires a complex connection technology. Other manufacturers use industrially insulated round copper stranded wires, allowing greater mounting flexibility at the expense of lower mechanical strength. In principle, all lead support systems have a similar design, which is shown in Fig. 7.65 [7.33].

Patented U-shaped pressboard channels that can enhance the mechanical stability, creepage path strength, and installation are available under a registered trademark [7.34], as shown in Fig. 7.66a,b.

#### Off-Load Tap Changers

Off-load tap changers (see Fig. 7.67) are relatively simple devices that can only be operated without voltage. Modern off-load tap changers have 2–11 positions and

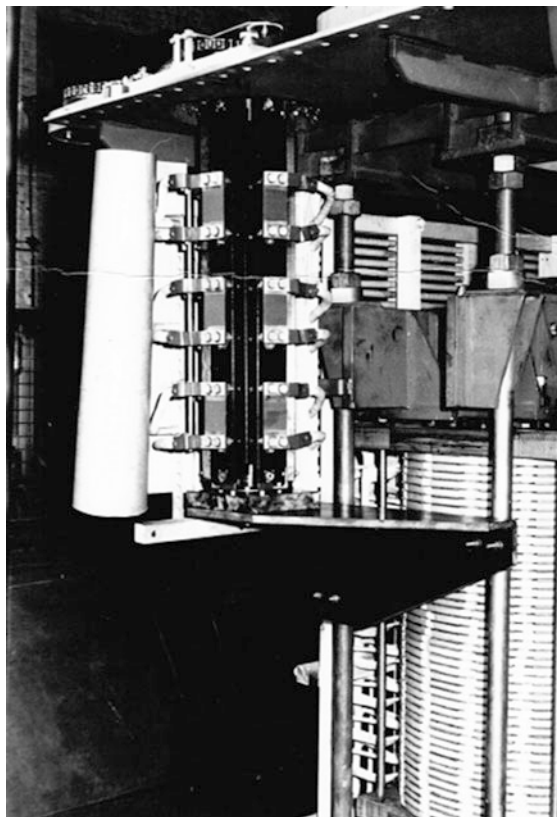


**Fig. 7.65** Leads and lead support system

can handle voltages across the whole tap-changer system of up to 60 kV and maximum currents of 1250 A. Off-load tap changers are widely used in smaller distribution transformers, but are often not operated for years. In such cases, chemical processes in the oil can lead to the formation of deposits, increasing the resistance at the contact surface and generating hot spots on the corroded contact during operation. For this reason, off-load tap changers must be cleaned regularly.

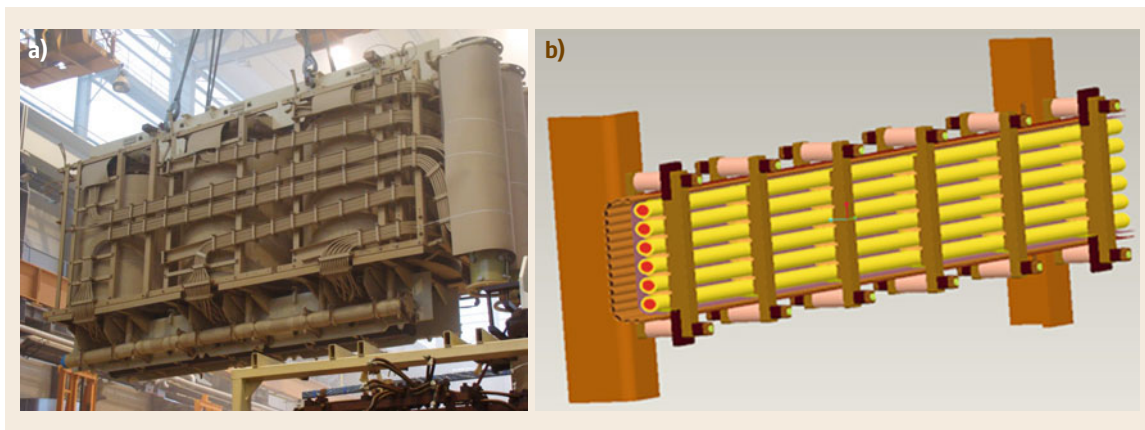
#### On-Load Tap Changers

The main challenge when switching the ratio of a transformer under load is to avoid interruptions in the current flow, because the transformer will then act like an ignition transformer in a vehicle and will probably be damaged. Modern on-load tap changers (OLTC) operate according to the *Jantzen principle*, named after its inventor, in which the switching process is rapid and is performed by contacts operated by energy-

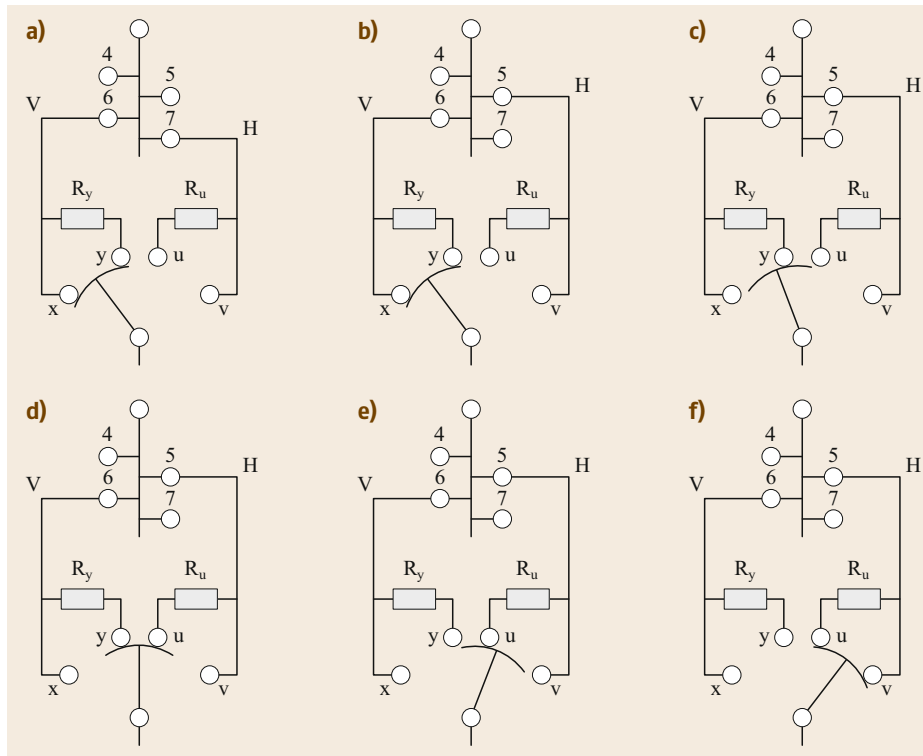


**Fig. 7.67** Off-load tap changers used for voltage adjustment in a high-current test transformer [7.36]

storage devices and switchover resistors without interrupting the current flow. The process used is illustrated by Fig. 7.68. Here, the starting position is tap 6 (Fig. 7.68a), which needs to be switched to tap 5. Therefore, the selector H must move from position 7 to



**Fig. 7.66** (a) Lead support system with special channels for the leads [7.35]. (b) Diagram showing the lead support system in more detail [7.34]



**Fig. 7.68a,b** The Jantzen principle for tap changers [7.37]

position 5 (Fig. 7.68b), after which the diverter switch is operated (Fig. 7.68c–f). In Fig. 7.68d, the switch short-circuits taps 5 and 6 through resistors, which are dimensioned such that the current through the short-circuit loop is in the range of the rated current. In the next step, the connection to tap 6 is interrupted and the connection to tap 5 is established, first via a resistor and then (in the final step) via a direct connection, thus bypassing the resistor. The switch from tap 6 to tap 5 is then complete.

When the contacts open during the changeover process, arcs occur that are only extinguished when the current passes the zero crossing. This results in strong discharges in oil, which is why the tap changer is located in a separate sealed compartment containing oil and is not integrated into the transformer tank. The relevant stages are preselected by the selector, which is located below the diverter switch compartment and installed inside the transformer tank (see Fig. 7.69). When using plus–minus or coarse–fine regulation (see Fig. 7.64), the selector must be equipped with a separate additional changeover switch.

If the tap changer is not working properly, serious damage can be caused to not only the tap changer itself but also the transformer windings – especially regulating windings. Due to the arcing, which leads to burnt contacts and degraded oil, on-load tap changers need

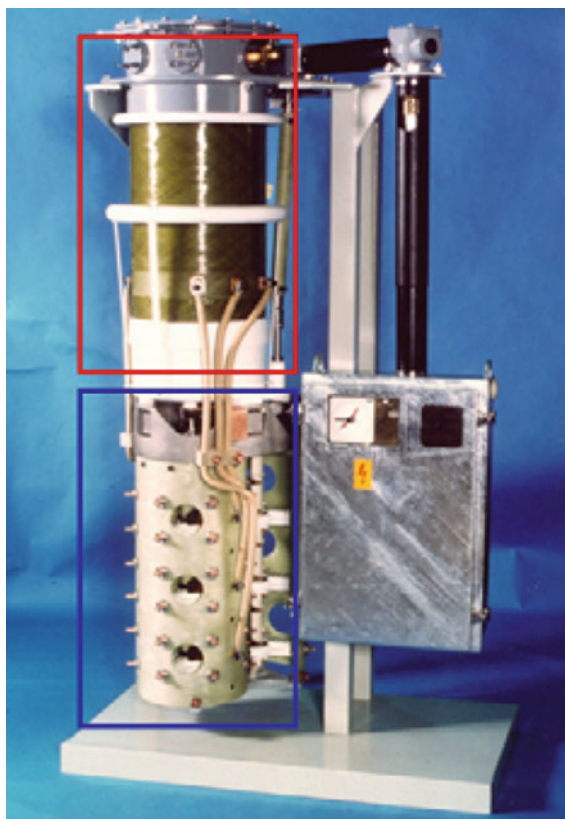
to be periodically serviced. In recent years, improved OLTCs in which the contacts work in vacuum have been developed. This can prolong the service life of the device, but there are also some disadvantages of a vacuum on-load tap changer that make it necessary to check the types of transformers that it can be used with. Figure 7.69 shows a conventional on-load tap changer [7.38].

## 7.2.4 Bushings and Lead Exits

### Structure and Types of Bushings

While unencapsulated dry-type transformers can be connected directly to the network, transformers that use tanks require components that conduct the current through the metallic tank and insulate the high potential of the conductor from the ground potential of the tank. This is achieved through the use of bushings – typically oil-air bushings (i.e., one part of the bushing is in oil, the other part is in air), which can be divided into LV bushings, high-current LV bushings, and HV bushings.

**Low-Voltage Bushings.** For nominal voltages of up to  $\approx 36$  kV, simple, standardized bushings are sufficient, as shown in Fig. 7.70. These consist of an insulator with an inner conductor and are sealed on the cover of the transformer by flat seals or round rubber

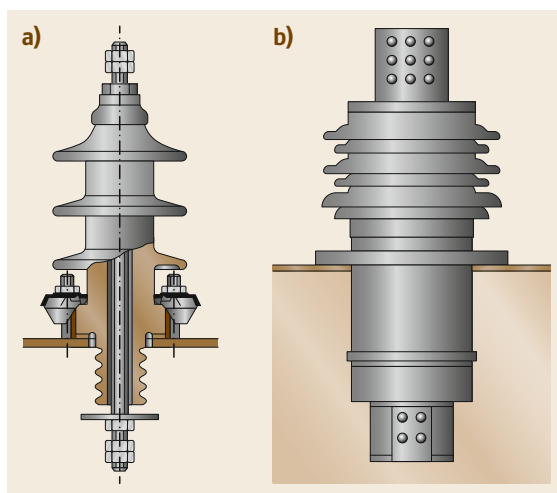


**Fig. 7.69** On-load tap changer with a diverter (red frame), selector (blue frame), and motor drive (silver cabinet)

seals. Due to their low voltages and the resulting low field strengths between the conductor potential and the edge of the feedthrough hole in the tank cover, the electric field does not need to be controlled.

**High-Current Bushings.** A high-current bushing is a special type of LV bushing, as shown in Fig. 7.70 [7.39]. Although high-current bushings do not differ fundamentally from LV bushings, they can conduct currents of up to 30 kA. These high currents generate large magnetic fields around the conductor, which can cause enormous eddy currents in the tank cover (which is up to 30 mm thick), and these eddy currents can cause the tank cover to glow if constructive countermeasures are not taken. Therefore, nonmagnetic steel is used around the high-current bushing holes in the tank cover.

**High-Voltage Bushings.** For higher voltages, so-called condenser bushings are used, which are equipped with metal foils radially and are graded axially towards their ends, as shown in Fig. 7.71. The metal foils have equipotential surfaces, so the electrical field



**Fig. 7.70a,b** Low-voltage (a) and high-current (b) bushings

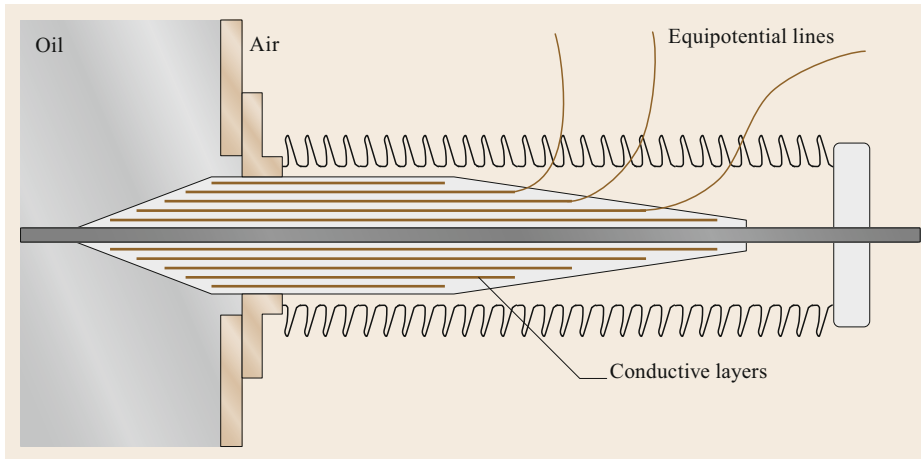
is controlled and homogenized. The foils also act as capacitors, so the voltage and PDs can be evaluated at an integrated measurement tap at the flange of the bushing. The bushing is connected to one of the outer metal layers, forming a capacitive divider.

As can be seen in Fig. 7.71, a HV bushing consists of a solid conductor around which insulating material is wrapped, together with conductive layers at certain distances from the central conductor. An insulator made of porcelain or silicone rubber is used on the outside of the bushing, and the central conductor of the condenser body extends into the liquid-filled transformer tank without any additional insulation. Various types of bushings can be distinguished based on the insulation material used:

- OIP (oil-impregnated paper)
- RBP (resin-bonded paper)
- RIP (resin-impregnated paper)
- RIS (resin-impregnated synthetics).

Although OIP bushings are the oldest type of bushing, they are still used today, in contrast to RBP bushings, which can create a lot of problems when they age. RIP bushings are state of the art, although they may be replaced in the future by the newest technology: RIS bushings. In the latter, the paper used in RIP bushings is replaced with a synthetic material that absorbs less moisture and is more resistant to aging. It should be noted that the lifetime of a transformer usually exceeds the lifetime of a HV bushing, so HV bushings need to be replaced after few decades [7.40]. A bushing failure will often lead to the catastrophic failure of the whole transformer, and the resulting damage will be much more





**Fig. 7.71**  
High-voltage  
bushing [7.7]

expensive than the cost of a new bushing. Thankfully, there are various diagnostic techniques for assessing the condition of a HV bushing.

#### Lead Exits

The components of the transformer that connect the windings directly to the bushings are called lead exits or line leads.

**LV Lead Exits.** The lead exits on the low-voltage side have a similar construction to the leads of the regulation winding shown in Fig. 7.65. Either parallel round conductors or bars made of copper (or, in rare cases, aluminum) are used when there are high currents. It is important to fix the bars in the transformer so that they are protected against short-circuit forces. When there are high currents, the magnetic field generated by the conductors must be included in the stray voltage calculation.

**HV Lead Exits.** For rated voltages of up to 220 kV, the lead exits consist of thick, round conductors that are insulated with thick crepe paper and fixed like the standard lead exits. The field strengths must be observed, and creepage distance stresses on the holders must be limited. For rated voltages above 220 kV, and especially those above 400 kV, the field strength approaches the critical region, so special connections must be used. In this case, the lead exits pass through insulated shielding tubes made out of metal that are connected to the lead exit potential. These thin-walled shielding tubes made from aluminum or copper reduce and homogenize the electrical field strength. The diameter of the tube used increases with the nominal voltage (e.g., a diameter of at least 80 mm is used for a nominal voltage of 400 kV). The insulation on the screen tubes, which is also made thicker for higher voltages, has two negative effects:

1. In thick insulation, dielectric losses can cause heating, which eventually leads to thermal breakdown.
2. In the presence of various dielectric materials, the field strengths are distributed according to the inverse ratio of their permittivities. The permittivities of crepe paper and pressboard are in the range of 3.5–3.8, while the permittivity of insulating oil is 2.2. This means that field stress is higher in the oil, which has a lower dielectric strength than paper and pressboard.

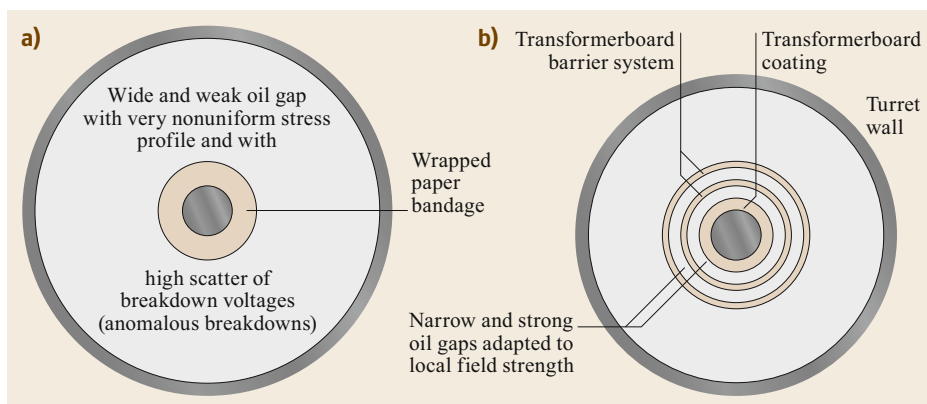
This problem was solved through the development of lead exits with barrier insulation [7.41]. The theoretical basis for this approach (see Fig. 7.72) was developed by a team of researchers and presented in 1998 [7.42].

Instead of pressboard barriers, another approach uses barriers that are made from calendered special crepe paper over flexible strips, which makes the barriers more resistant to breakdown. This approach allows any number of bends to be realized in the lead exit with minimal effort [7.43–45]. Figure 7.73 shows a model and a real-world example of a flexible lead exit system.

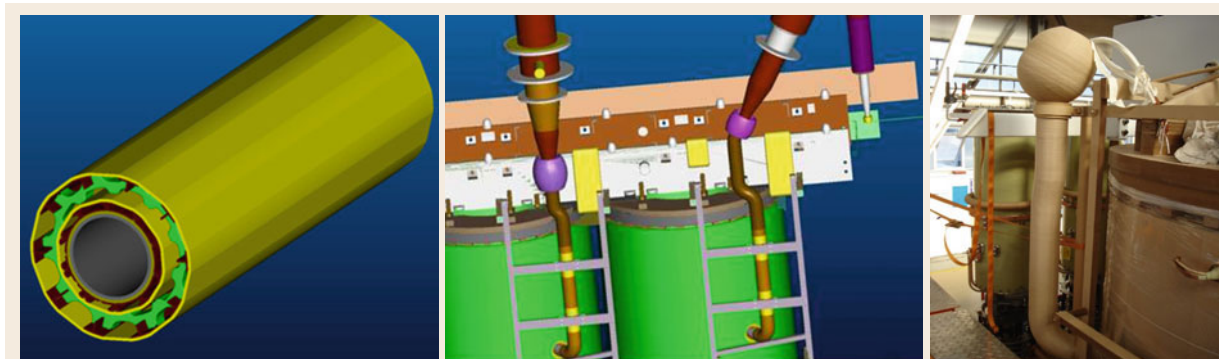
### 7.2.5 Cooling Types and Insulating Fluids

The cooling systems used in transformers are internationally standardized and categorized. Each type of cooling system is assigned a two- or four-character code, as described below:

- First character: type of coolant inside the transformer.
- O: Mineral oil or similar with a flash point below 300 °C
  - A: Air (for dry-type transformers)
  - K: Alternative liquid with a flash point above 300 °C



**Fig. 7.72a,b** Comparison between (a) conventional and (b) barrier lead exits. The dielectric strength of the barrier insulation is high, whereas the field enhancement in the oil gaps and the insulation volume (and thus the related costs) are minimal [7.42]



**Fig. 7.73** 3-D model of a flexible lead exit system, and a real-world example of a lead exit with three bends (right)

Second character: method used to circulate the internal coolant.

N: Natural

F: Forced

D: Directed (directly pumped through the windings from the bottom)

Third character: type of external coolant.

A: Air

W: Water

Fourth character: method used to circulate the external coolant.

N: Natural

F: Forced.

The cooling types AN or AF are used for dry-type transformers; additional fans are installed at the transformer if the air is forced. More effort is required for liquid-filled transformers, which usually have higher power ratings, so a medium-sized power transformer below 50 MVA will often use ONAN, whereas such a transformer below 100 MVA will often use ONAF. Water-cooled OFWF systems in which there is forced oil flow driven by pumps are used for industrial or

large power transformers. The best cooling that can be achieved is ODWF (oil/directed/water/forced), which is, however, also the most expensive cooling method.

### Insulating and Cooling Fluids

The most popular transformer coolants are now discussed.

**Mineral Oil.** The transformers used in the experiment in Frankfurt in 1891 were filled with oil. Since then, there have been notable advances in the use of mineral oil in transformers, as well as setbacks. The first oils were not stable over the long term. In the 1950s and 1960s, oils that formed black, soot-like deposits on the active parts were used. Later, it was discovered that certain types of oils were contaminated with toxic polychlorinated biphenyls (PCBs). In the 1990s, certain types of oils were found to release corrosive sulfur, leading to partial discharges and ultimately to breakdowns. Modern transformer oils may be refined from crude oil or produced synthetically from natural gas. Inhibitors can be added to delay the aging of the oil. Thus, today, inhibited mineral oil and inhibited gas-to-liquid (GtL) oil are the most cutting-edge oils that are

used in transformers. Considering the total volume of each type of liquid used in transformers worldwide, oil is by far the most important, representing over 95% of the total volume of all liquids used in transformers.

**Other Insulating Fluids.** Other insulating fluids are usually more expensive than mineral oil, but they can have the advantage of being more environmentally friendly or having higher flash points. Their dielectric properties are usually different from those of oil. Thus, given their different permittivities and electrical field strengths, it is not possible to swap from mineral oil to another insulating fluid in a transformer design without performing appropriate verification. Due to the fact that oil has a market share among all transformer insulation fluids of more than 95%, the most important alternatives to mineral oil are mentioned only briefly below:

- Silicone liquids (still seldom used)
- Synthetic esters
- Natural esters.

There are only a few companies in the world that produce synthetic and natural esters, but the market share is slowly increasing (especially in the distribution and wind-energy sectors), albeit from a low level. Natural esters cannot be used in free-breathing transformers (i.e., transformers that have a conservator – an oil expansion vessel – with no membrane) because the natural ester would be in direct contact with ambient air in such transformer, leading to highly accelerated aging of the liquid.

## 7.2.6 Tank and Protection System

### Dry-Type Transformers

Dry-type transformers cannot be operated outside because the resin does not exhibit long-term UV stability. Furthermore, these transformers are not usually designed to operate under ambient conditions such as rain

and snow, so dry-type transformers are installed inside. Given that dry-type transformers of up to 145 kV are available [7.46], some larger units can have a special housing, but these cases are rare.

Dry-type transformers are usually equipped with a temperature monitoring system that prevents overtemperatures and can detect abnormal hot spots.

### Liquid-Filled Transformers

Small distribution transformers are usually manufactured with finned vessels, and it is becoming increasingly common for them to be hermetically sealed. Medium-sized power transformers are usually built with housings that are equipped with radiators onto which additional fans can be mounted. Hermetic arrangements are possible up to approximately 100 MVA, but are difficult for higher power ratings than this. Power transformers are either built with a tank and a cover or with a bell-type tank with a bell-shaped cover. When this cover is removed, the active part, which stands in a kind of tub that forms the rest of the housing, is freely accessible. As demonstrated by the examples shown in Fig. 7.74, it is easy to distinguish between a free-breathing transformer equipped with a conservator and a hermetically sealed transformer without an oil expansion vessel on the top of the tank. In recent years, a membrane has often been integrated into the conservator to reduce the absorption of oxygen and moisture from the ambient air and thus suppress insulating fluid aging.

The most important protection system for power transformers is the *Buchholz relay*, as shown in Fig. 7.75. This relay was developed in 1921 and named after its inventor Max Buchholz. It is installed in the pipe from the tank to the expansion vessel, collects gas, and monitors the oil flow speed in the pipe. It is equipped with at least one float that triggers a warning in the event of slow gas development or an oil loss. Furthermore, a damper detects the rapid oil or gas flow caused by a sudden fault, thus the transformer is tripped.

## 7.3 Testing Power Transformers

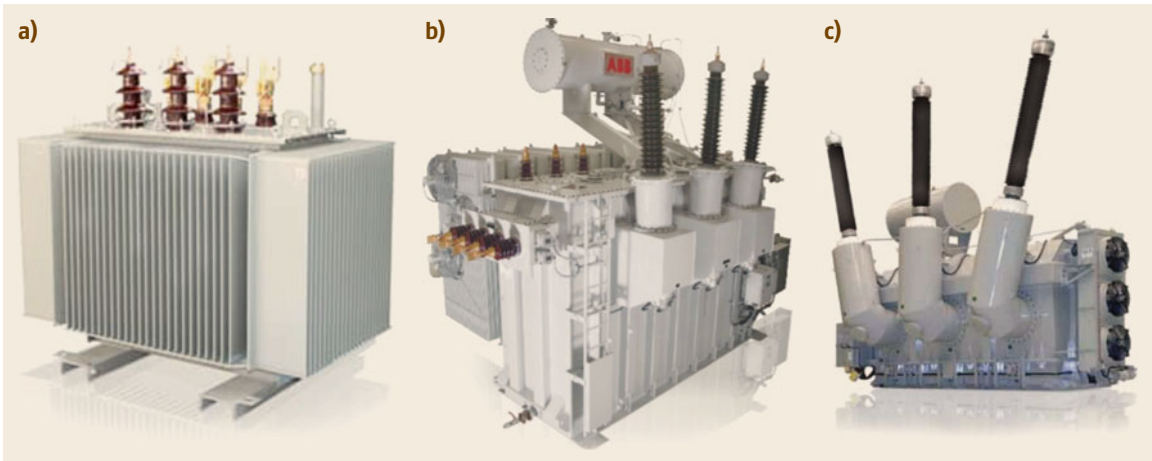
There are various reasons for testing a transformer, but three are particularly common:

- The final acceptance test (FAT) of a new transformer after it has been manufactured
- The acceptance test of a repaired transformer
- Diagnostic/service tests.

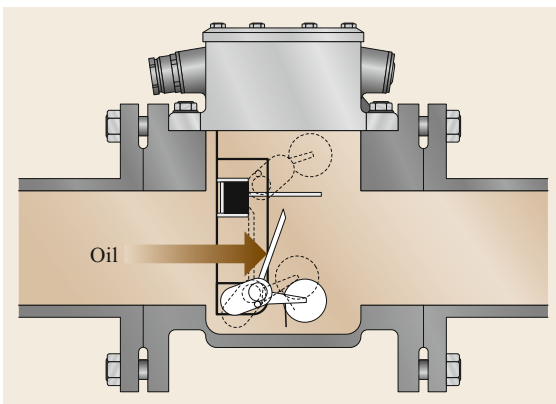
The scope of the tests performed as well as the sequence of tests and the equipment used vary depending on the type of testing performed.

The final acceptance test is performed on a new transformer after it has been manufactured, in order to verify that the transformer fulfills the contractual specification as well as the requirements of applicable standards. In addition, the FAT is part of the internal quality assurance or management system of the manufacturer. Thus, the results of this final quality check should be used to gauge whether the transformer can be put into service.

Sometimes a transformer is produced and tested in a workshop but is then completely disassembled and



**Fig. 7.74a–c** Examples of (a) small, (b) medium-sized, and (c) large (400 MVA, three-phase) power transformers [7.47]



**Fig. 7.75** Scheme of a Buchholz relay [7.48]

transported to the site, where it is reassembled again. In this context, completely disassembled means that the whole active part is disassembled; it is not the case that only bushings or the conservator are/is removed, which is the usual approach for transformer transportation. This very special case can occur if it is not possible to transport the assembled unit to the site due to several restrictions (e.g., when the transformer is to be installed underground). In such cases, the customer and the manufacturer must agree upon the tests that should be repeated (and passed) before the transformer is put into operation. CIGRE Working Group WG A2.59 deals with these questions and provides some recommendations regarding this matter [7.49].

The second category is similar to the first because tests must be performed after a repair to check the specification and quality of the repair. However, since some components of the transformer may be reused, and depending on how long the asset has been in operation,

the voltage tests performed after a repair are carried out at a lower voltage level than used in the FAT, which is in accordance with the standards. Due to the fact that the number of repairs performed on-site is increasing [7.50], the number of on-site tests is also rising, which has led to the development of special equipment for on-site tests over the last decades. The scope of these tests after a repair is similar to the scope of the tests performed during the FAT, as long as the tests are performed in a high-voltage test field. If the tests are performed on-site, the scope of the tests is usually reduced due to the higher complexity involved, increased costs, and problems with the availability of the test equipment to be used.

For diagnostic tests, the scope of the tests is usually significantly reduced compared to the scope of the tests performed during a FAT, because only tests that are useful for detecting a possible failure are carried out. One example is when an induced voltage test with partial discharge (PD) measurement is performed because DGA (dissolved gas analysis) has indicated PD activity. Therefore, only certain tests are performed, but often with additional special equipment. Thus, for the PD example, aside from the electrical PD measurement (which is implemented in the same way as during the FAT), acoustic or UHF (ultra high frequency) PD detection techniques are applied to localize the source of the PD, which is required before the risk of failure can be quantified. Therefore, most of the tests performed during the FAT can also be used to assess the condition of the transformer, which enables efficient asset management [7.51] because each test probes the likelihood of a different type of failure. This why many of these tests are also carried out during maintenance or a service [7.52].

### 7.3.1 Types of Tests

Compared to other components of the HV transmission systems, power transformer testing is far more complicated. This is simply because so many more tests are available and necessary for power transformers. Furthermore, most HV assets only require single-phase HV tests, whereas single- and three-phase dielectric tests are necessary for a three-phase transformer. Each test that is available for a power transformer can be categorized as one or more of the following:

- A routine test (RT)
- A type test (TT)
- A special test (ST)
- A diagnostic test (DT).

All transformers must undergo routine tests as part of the FAT, whereas type tests are performed on just one representative transformer among a group of transformers that are identical in construction. Special tests do not belong in the previously mentioned categories and are usually agreed upon by the customer and the manufacturer. Diagnostic tests include all tests that may aid the identification of the cause of a failure, so such tests are mainly performed on transformers that are in service or on a transformer that did not pass the acceptance test and requires further failure analysis. All routine tests and diagnostic tests can be performed on-site, so these tests are also used during a service and during maintenance to assess the condition of the transformer. Of course, some of these tests are quite complex and therefore expensive, so they are only carried out if there are certain indications or problems.

Due to the fact that transformers are often unique and specially designed components, the scope of the testing is usually defined by the customer or agreed upon by the customer and manufacturer. Table 7.4 provides an overview of the most important tests and their categories as well as the corresponding IEC and IEEE (Institute of Electrical and Electronics Engineers) standards. The tests listed in the table increase in measurement complexity and the stress exerted on the transformer from top to bottom.

Table 7.4 shows that tests on power transformers are multifarious and extensive, so not all of the tests mentioned in the table are discussed in detail below. More information or detail can be obtained from the corresponding IEC and IEEE standards mentioned in the table, or from relevant literature [7.77, 78] (there are books that focus entirely on the testing of power transformers).

In the following, short descriptions of the tests together with some remarks about them are presented [7.77].

#### Tests of the Liquid Insulation

The liquid that is used in power transformers can be subjected to different physicochemical and electrical tests. The standard oil test (SOT) affords information on the condition of the liquid insulation. Thus, the main parameters are tested, such as the breakdown voltage, dielectric dissipation factor, moisture content, acidity, interfacial tension, inhibitor content, and the purity of the oil. It is necessary to perform the SOT before any HV test and before the transformer is put into operation because the dielectric strength of the liquid must fulfill the requirements defined in the standards mentioned above. If, for example, the breakdown voltage of the liquid is not appropriate considering the voltage level of the transformer, the transformer can neither be tested nor be put into service. The SOT is also performed regularly during the whole lifetime of the transformer because the measured parameters provide insight into the performance and aging of the whole insulation system. If the liquid no longer fulfills the requirements, a special cleaning procedure (e.g., a regeneration) must be performed [7.79].

Another test that must be carried out regularly is a dissolved gas analysis (DGA), which is among the most well-established diagnostic methods for liquid-immersed power transformers. When there is a defect, specific gases are generated that dissolve in the liquid. For example, partial discharges produce predominantly hydrogen and methane. Based on the concentrations and the ratio of these fault gases, a DGA can provide information on the nature of the fault [7.80]. In addition, the rate of increase of the fault gas concentration within a certain time interval delivers information about the severity of the fault. There are a number of interpretation guidelines for the data acquired via DGA measurements; examples include [7.81, 82]. The IEC standard 60599 enables faults to be assessed and evaluated by distinguishing between types of electrical faults (PD, D1, and D2: partial discharges, low-energy discharges, and high-energy discharges, respectively) and thermal faults (by dividing them into three temperature ranges: T1, T2, and T3), and by gauging the degree of paper aging (via the CO<sub>2</sub>/CO ratio). In addition, a low oxygen concentration indicates oxidation processes for free-breathing transformers. Furthermore, when there is a severe failure, a huge amount of gas can be produced that cannot rapidly dissolve fully in the oil, meaning that gas bubbles rise to the top and can be collected in the Buchholz relay (for instance). These free gases can also be analyzed and compared to the results of a DGA, allowing additional conclusions about the failure to be drawn.

Regarding HV tests, it is recommended that a DGA should be performed both before and after the tests in order to check whether there are any small weak points

**Table 7.4** Test types for transformers

Test	Standards	RT	TT	ST	DT
Standard oil test (SOT)	IEC 60422 [7.53] IEEE Std. C57.106-2015 [7.54]	o			o
Dissolved gas analysis (DGA)	IEC 60599 [7.55] IEEE Std. C57.104-2019 [7.56]	o <sup>a</sup>			o
Functional test of tap changer and auxiliary equipment	IEC 60076-1 [7.17] IEC 60076-3 [7.57] IEEE Std. C57.12.00-2015 [7.58]	o			o
Measurement of voltage ratio and vector group	IEC 60076-1 [7.17] IEC 60076-11 [7.32] IEEE Std. C57.12.90-2015 [7.59]	o			o
Frequency-response analysis (FRA) Frequency-domain spectroscopy (FDS)	IEC 60076-18 [7.60] IEEE Std. C57.149-2012 [7.61] IEEE Std. C57.161-2018 [7.62]			o	o
Measurement of dielectric dissipation factor and capacitances	IEC 60076-1 IEEE Std. C57.12.90-2015	o		o	o
Measurement of winding resistances	IEC 60076-1 IEC 60076-11 IEEE Std. C57.12.90-2015	o			o
Measurement of insulation resistance	IEC 60076-1 IEEE Std. C57.12.90-2015	o			o
Determination of no-load losses	IEC 60076-1 IEC 60076-8 [7.63] IEC 60076-11 IEEE Std. C57.12.90-2015	o			o <sup>a</sup>
Measurements of the harmonics of the no-load current	IEC 60076-1 IEC 60076-11			o	
Sound level measurement	IEC 60076-10 [7.64] IEEE Std. C57.12.90-2015			o	
Measurement of short-circuit voltage	IEC 60076-1 IEC 60076-11 IEEE Std. C57.12.90-2015	o			o
Determination of load losses	IEC 60076-1 IEC 60076-11 IEC 60076-8 IEEE Std. C57.12.90-2015	o			o <sup>a</sup>
Temperature rise test	IEC 60076-2 [7.65] IEC 60076-7 [7.66] IEC 60354 [7.67] IEEE Std. C57.12.00-2015 IEEE Std. C57.12.90-2015		o		
Zero-sequence measurement	IEC 60076-1 IEEE Std. C57.12.90-2015			o	
Impulse tests	IEC 60060-1 [7.68] IEC 60060-2 [7.69] IEC 60076-1 IEC 60076-3 [7.57] IEC 60076-4 [7.70] IEC 60076-11 IEEE Std. C57.12.00-2015 IEEE Std. C57.98-2011 [7.71]	o			
Applied voltage test	IEC 60076-1 IEC 60076-3 IEC 60076-11 IEEE Std. C57.12.00-2015 IEEE Std. C57.12.90-2015	o			o

Table 7.4 (continued)

Test	Standards	RT	TT	ST	DT
Induced voltage test, including PD measurement	IEC 60076-1 IEC 60076-3 IEC 60076-11 IEC 60270 [7.72] IEEE Std. C57.12.00-2015 IEEE Std. C57.12.90-2015	o			o
Acoustic and UHF PD measurements	IEC 60270 IEC TS 62478 [7.73] IEEE Std. C57.12.90-2015 IEEE Std. C57.113-2010 [7.74] IEEE Std. C57.127-2018 [7.75]				o
Short-circuit withstand test	IEC 60076-5 [7.76] IEEE Std. C57.12.00-2015 IEEE Std. C57.12.90-2015			o	

<sup>a</sup> Sometimes/depending on the size of the transformer

in the active part. A temperature rise test is usually accompanied by several DGA measurements in order to verify whether hot spots are present inside the active part, and to determine if the fault gases have exceeded certain limits.

#### Functional Tests

All auxiliary equipment must be subjected to functional testing. For example, the fans or pumps of the cooling system and all of the control equipment must be tested to check that it is operating appropriately. In addition, all of the auxiliary wiring must pass a 60 s dielectric AC separate-source test to prove that the insulation system is suitable.

If the transformer is equipped with a tap changer, this system must also be tested. If this is an on-load tap changer, various switching operations must be carried out with the transformer energized and deenergized.

#### Voltage Ratio and Vector Group

The transmission or voltage ratio must be evaluated for all tap positions by directly measuring the voltages on the primary and secondary sides using voltmeters, or by using ratio-measuring bridges. For three-phase transformers, this measurement is usually conducted for one phase at a time. The maximum error in the relative ratio or the deviation of the measured from the nominal ratio in percent should be within  $\pm 0.5\%$  or less than than 0.1 times the actual short-circuit voltage (whichever is lower) according to IEC 60076-1.

Furthermore, it is essential to check the vector group of the transformer and the phase displacement between the LV and HV side for each phase. This is especially important when the transformers are operated in parallel.

Several compact systems are on the market that integrate voltage ratio, vector group, and winding resistance measurements into one system. Such devices are usually fitted to a small trolley, which makes it easier to position the measuring system at appropriate points close to transformers of differing sizes.

#### Frequency Response

Some additional tests have become increasingly popular over the last decades. These are used as diagnostic tests for transformers that are in service and to obtain a *fingerprint* during the FAT of a new transformer. They are based on systems theory, which states that if a system is changed, the system response must also change. Therefore, the system response (the fingerprint) is measured and compared with a previous response (the reference fingerprint) of the same system. If a reference fingerprint is not available, the result is compared with either the response of a similar system or a simulated reference. In the following, two methods that are increasingly being used in transformer testing and servicing are described. Both methods examine a system response: one probes the dielectric system response (FDS), whereas the other examines the electric system response (FRA).

Frequency-domain spectroscopy (FDS) involves the measurement of the dielectric dissipation factor over the frequency range of 1 mHz to 1 kHz. The response is then compared to a reference that depends on the insulation system of the transformer – in particular concerning the relation of the amount of liquid to solid insulation – and this comparison allows the average moisture content in the solid insulation to be gauged [7.83].

In frequency-response analysis (FRA), an electrical transfer function (typically a voltage–voltage transfer function) is measured for each phase of the LV and HV sides over a typical frequency range of 1 kHz to 1 MHz. Afterwards, the measured transfer function is compared with a corresponding measurement performed during the FAT or (more commonly, since FRA measurements were not performed during the FAT for older transformers) with the measured transfer function of another phase. Differences between the transfer functions can indicate winding deformations or core problems, although the precise interpretation of these differences is still being researched [7.84].

Small portable devices that can perform these methods are available. These devices are often connected to a computer such as a laptop, as this allows the measurements to be controlled and the resulting data to be evaluated and visualized graphically using a software package.

#### Dielectric Dissipation Factor and Capacitance

The dielectric dissipation factor ( $\tan \delta$ ) of an insulation system is defined in the relevant IEC standard as the relation between the active and the reactive power when a sinusoidal voltage is applied to the insulation. The power factor PF is defined in the relevant IEEE standard as the relation between the active and the apparent power. The relation between the dielectric dissipation factor and the power factor is

$$\text{PF} = \frac{\tan \delta}{\sqrt{1 + \tan^2 \delta}}. \quad (7.51)$$

The value of the dissipation factor is usually small, and it is clear from the equation that the difference between the dielectric dissipation factor and the power factor is often negligible for small values of the dissipation factor. The dielectric dissipation factor or the power factor as well as the capacitance of the insulation system can be measured using the famous Schering bridge [7.85]. The dissipation factor can be used to assess the condition of the insulation, although this factor depends on many parameters such as the temperature, frequency, and electrical field strength. Compact systems of a similar size to the voltage ratio measurement devices mentioned above are available to measure the dissipation factor.

#### Winding Resistance

The winding resistance is defined as the temperature-dependent ohmic DC resistance of a winding. It is measured at room temperature and then converted to the winding resistance at the standard temperature of 75 °C.

The winding resistance is used to extrapolate the copper losses ( $I^2R$ ) of the transformer, as well as for diagnostic purposes. Measuring the winding resistance allows the path of the electrical current to be probed: it can highlight contact problems at the tap changer or between windings and bushings, interruptions within the windings, and even significant interturn short circuits. For transformers with tap changers, the winding resistances of all phases are measured at all tap changer positions. In this case, to avoid unacceptable heating, the direct current supplied may not exceed 10% of the nominal winding current according to IEEE Std. C57.12.90-2015, but it must also be at least 1.2 times the value of the no-load current to ensure core saturation.

Different approaches are used to measure the resistance. A simple method involves injecting a current into the winding and measuring the corresponding voltage drop across it. Ohm's law can then be used to calculate the winding resistance. Another method is to utilize a bridge to measure the resistance by balancing the two arms of the bridge circuit. Thus, a comparison is performed, with a known resistance to determine the exact value of an unknown resistor.

#### Insulation Resistance

The insulation resistance between winding systems or between windings to ground is measured. To do this, an applied voltage test is performed: one winding system is short-circuited and connected to a voltage source, while the other winding systems are short-circuited and connected to ground. A DC voltage of a few kV is then applied and the insulation resistance is measured in M $\Omega$  using a typically small and portable device.

The insulation resistance depends on various parameters; aside from the design of the transformer, external influences such as humidity and dirt on the bushings significantly affect the insulation resistance. It also depends on the duration of application of the voltage because of dielectric effects in the insulating medium, so the resistance is often measured after 15, 60, or 600 s. The ratio of the resistance after 60 s of voltage stress to that after 15 s of voltage stress ( $R_{60}/R_{15}$ ) is often in the range 1.3–3, and its value is linked to the quality of the insulating medium. Furthermore, values of the polarization index (PI; i.e., the ratio  $R_{600}/R_{60}$ ) that are above 2 are indicative of good insulation, while values of less than 1 indicate unsatisfactory insulation.

As a rule of thumb, the insulation resistance should be at least 1 M $\Omega$  per kV of nominal voltage, so an insulation resistance of at least 110 M $\Omega$  is required for a 110 kV transformer. The insulation resistance of a new transformer is usually more than ten times higher



than this rule of thumb, and is therefore in the  $G\Omega$  range [7.86].

#### No-Load Losses and Harmonics of the No-Load Current

The no-load losses are guaranteed by the manufacturer because they are an important influence on the operational economics, given that they occur whenever the transformer is energized. The setup for measuring the no-load losses is rather simple: one winding system is energized with the nominal voltage at the nominal frequency, while none of the other winding systems are connected to a load. It is necessary to energize the transformer with an appropriate voltage waveform and the exact nominal frequency since the no-load losses strongly depend on the waveform of the voltage as well as the frequency. In the tests, the voltage is usually decreased from 115 to 110, 100, 90, and 80%, because overexcitation at the beginning reduces any effects on the remanence (caused by DC winding resistance measurements for example). The active power must be remeasured with a calibrated power analyzer, and the measured value is corrected to the no-load losses using a factor that considers the harmonics in the voltage waveform.

The no-load losses can also be used to diagnose the condition of the core of an old transformer, so they are usually measured before an old transformer undergoes a repair or an overhaul.

As a special additional test, the harmonics of the no-load current can also be measured. In the past, or for older transformers, information on the harmonic content of the no-load current was used to adjust the transformer protection relays, especially when electromechanical systems were used. However, such measurements have become less important for modern power transformers because their no-load currents are below 1% of the nominal current.

#### Sound Level Measurements

The measurement of the sound level is a special test that is becoming increasingly important because transformers are being installed closer and closer to populated areas, where there are various rules and regulations concerning sound emissions. In order to check that a transformer is operating within specified noise limits or the noise range guaranteed by the manufacturer, sound level measurements can be performed in various configurations: no-load/load, cooling on/off, and pumps on/off.

Aside from the cooling system, the sound generated by an operational transformer is a combination of core noise (no-load sound) and winding noise (load sound). The no-load noise arises from magnetostriction (small

elastic variations in the length of a magnetic material) of the core, whereas the load noise is a result of vibrations of the windings and the tank due to magnetic forces caused by the load current. For modern low-induction transformers, the load noise is usually louder than the no-load noise. The sound level measurement procedure is quite complicated because a lot of sound level measurement points need to be recorded and evaluated given the sizable dimensions of large power transformers.

A simple sound measurement can also be used to make a rough estimation of the condition of the core or core clamping, but this is a seldom-used procedure and is usually only performed under no-load conditions.

#### Short-Circuit Voltage and Load Losses

By definition, the short-circuit voltage is the AC voltage that must be applied to the primary terminals of a transformer that is short-circuited on the secondary side so that nominal currents flow on the primary side, in which case the absorbed active power of the transformer corresponds to the load losses. Both the short-circuit voltage and the load losses are guaranteed by the manufacturer and must therefore be measured precisely using calibrated power analyzers. For transformers with tap changers, the short-circuit voltage must be determined for the two extremes as well as for the main tap position, because the short-circuit voltage is important when operating two or more transformers in parallel.

The difference between the measured and calculated load losses provides insight into the eddy losses caused by the leakage fluxes in metal mechanical parts of the transformer (e.g., the tank walls).

Depending on the size of the transformer and the test equipment available, capacitive compensation is usually needed to perform the test. Therefore, capacitor banks are connected in parallel to the transformer, increasing the effort required for the test. In order to measure the short-circuit voltage on-site, usually low voltage is applied to the primary side while the secondary side is short-circuited. The current and voltage on the primary side are then measured, and the measured voltage is multiplied by the ratio of the rated current to the measured current to obtain the short-circuit voltage. The reason for determining the short-circuit voltage on-site is that this measurement can be also used as a diagnostic procedure, because the short-circuit voltage is very sensitive to changes in the winding structure, meaning that it can be used to detect winding deformations.

#### Temperature-Rise Test

When a transformer is operating, heat is produced, which increases the temperature of the internal struc-

ture of the transformer. Since temperature is one of the main influences on the overload capability and life expectancy of a transformer, the temperature-rise test is of great importance to both manufacturers and operators. The temperature-rise test uses the same setup as employed to determine the short-circuit voltage and load losses, and is performed to check that the temperature rises for the windings and the oil are compliant with the values guaranteed by the manufacturer. A two-step approach is performed:

- The rise in top-oil temperature when the total losses are injected is determined
- The average winding temperature rise for rated currents is evaluated.

In step 1, the voltage is regulated such that the total losses are the sum of the load losses and the no-load losses. During this test, the current is slightly above the rated current, and the test ends when the top-oil temperature reaches a steady state. The rise in the top-oil temperature can then be determined as the difference between the top-oil temperature and the temperature of the external cooling medium (the ambient temperature for air-cooled systems or the water inlet temperature for water-cooled transformers).

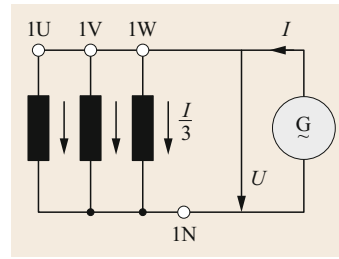
After the top-oil temperature rise has been determined, the test immediately moves on to the second step, in which the current is reduced to the rated current for a 1 h period. After that, the winding resistances must be measured to determine the average temperature of the windings and therefore the average winding temperature rise as defined in the standards.

Sometimes fiber-optic temperature sensors are installed in the windings or the active part of the transformer. These are used to determine the temperature distribution across the active part as well as the hot-spot temperature during the temperature rise test. The sensors are installed during production and subsequently (when the transformer is operational) integrated into a monitoring system to produce a thermal image of the transformer [7.87] that is used to optimize the cooling efficiency or calculate the aging factor due to thermal stress.

As mentioned before, the temperature-rise test is often accompanied by DGA tests because an analysis of the gases dissolved in the oil can be used to detect possible local overheating that does not show up as an unusual temperature rise during the test.

### Zero-Sequence Measurement

Asymmetrically loaded three-phase systems can be calculated using the method of symmetrical components. In this method, an asymmetrically loaded three-phase



**Fig. 7.76**  
Zero-sequence  
impedance for a star  
winding

system is divided into three superimposed subsystems: the positive-sequence phase system, the negative-sequence phase system, and the zero-sequence phase system. Each of these three systems comprises corresponding symmetrical voltage, current, and impedance components. For transformers, the positive-sequence impedance is usually equal to the negative-sequence impedance, whereas the zero-sequence impedance can significantly differ from the other two impedances.

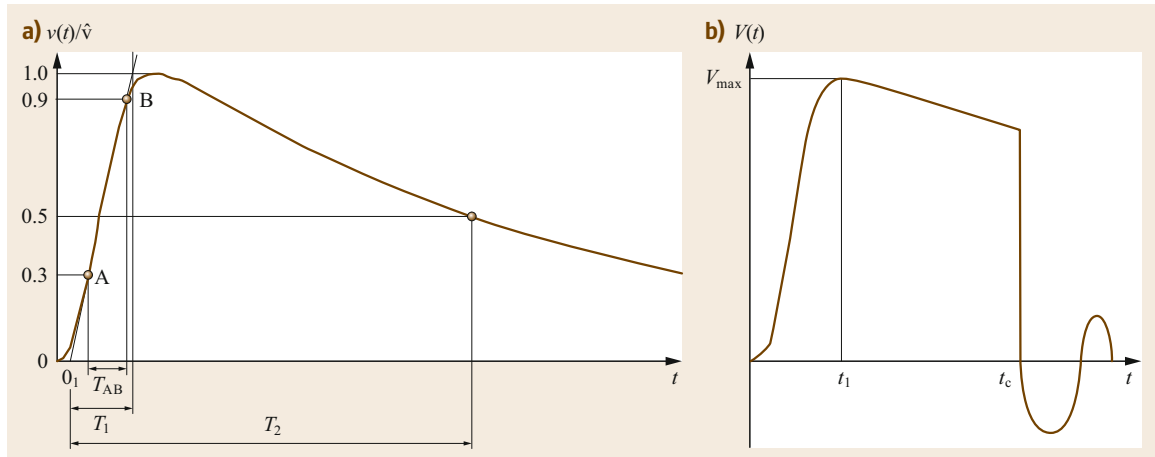
The zero-sequence impedance can only be determined for star or zigzag winding connections, and is measured at the rated frequency between the interconnected terminals of the winding system and its neutral point.

If the voltage  $V$  is applied between the interconnected winding terminals and the neutral, as shown in Fig. 7.76, the zero-sequence impedance  $Z_0$  can be calculated as

$$Z_0 = \frac{V}{I} = 3 \frac{V}{I}. \quad (7.52)$$

For the setup shown in Fig. 7.76, it is important to note that the current at the neutral point must not exceed the maximum permissible value. Also, the zero-sequence magnetic flux should be considered for different transformer designs. For example, for an YNyn transformer with a three-limb core, if the voltage  $V$  is applied between Y and N while the LV side yn is open, the flux – which is  $\Phi/3$  in each limb – needs to close over the tank walls, cover, clamping construction, etc. This may generate excessive heat in these metallic parts, so the measured current should be drastically reduced compared to the rated current. If the YNyn transformer has a five-limb core, the situation is completely different because the two outer limbs are available to close the flux, and because a YNyn transformer with a five-limb core usually has a delta tertiary winding that will generate an appropriate compensation current [7.88].

This example shows that the zero-sequence impedance depends strongly on the design (i.e., the vector group and core construction) of the transformer, meaning that various test circuits are used to measure



**Fig. 7.77a,b** Lightning impulse voltage: (a) full waveform with front time  $T_1$  and time to half-value period  $T_2$  and (b) chopped at the tail ( $t_1$  is the front time and  $t_c$  is the time until chopping is performed)

the zero-sequence impedances of transformers with various high and low winding connections. Therefore, in some cases, the test circuit to be used will need to be agreed upon between the manufacturer and the operator.

#### Dielectric Tests

Dielectric tests include the most important transformer tests – those that verify the integrity of the transformer under operational and also abnormal stresses. This requires the application of voltage levels that are significantly above the nominal voltage stress. Therefore, unsurprisingly, transformers that do not pass the final acceptance test have often failed one of the following dielectric tests:

- Impulse tests
- Applied voltage test
- Induced voltage test with PD measurement.

The levels used in these dielectric tests are defined in the standards and depend on the voltage  $V_m$ , which is the highest rms phase-to-phase voltage in a three-phase system for which a transformer winding is designed in respect to its insulation according to IEC 60076-3.

**Impulse Tests.** Transformers must be subjected to impulse tests to verify the integrity of their insulation during transient overvoltages, which may appear due to atmospheric lightning or switching operations in the network. There are therefore two different impulse tests: the lightning impulse (LI) test and the switching impulse (SI) test. The LI test can be subdivided into a full voltage wave test and a test where the voltage wave is chopped at either the front or the tail, as shown

in Fig. 7.77. Impulse tests are routinely performed for transformers that are designed to operate above a certain voltage level, but the voltage limit is different for full LI tests, chopped LI tests, and SI tests. In addition, these limits are slightly different in the IEC and IEEE standards.

According to Fig. 7.77, the typical 1.2/50  $\mu\text{s}$  full lightning impulse waveform can be characterized by three values:

- The peak voltage (the test voltage with a tolerance of  $\pm 3\%$ )
- The front time  $T_1 = 1.2 \mu\text{s} \pm 30\%$
- The time to half value  $T_2 = 50 \mu\text{s} \pm 20\%$ .

For a chopped LI, instead of the time to half value, the waveform is characterized by the time until chopping is performed,  $T_c$ . A SI has a similar waveform to a LI, so both impulses can be generated with the same system but with different setups of the Marx generator (designed in 1923 by Erwin Marx in Braunschweig, Germany).

However, the SI is longer than the LI. Therefore, according to the IEC standards, the time to peak  $T_p$  of a SI must be at least  $100 \mu\text{s}$ , the time  $T_d$  spent above 90% of the specified amplitude must be at least  $200 \mu\text{s}$ , and the time to zero  $T_z$  must have a minimum value of 1 ms. Due to the longer voltage stress on the SI, its test level is lower than that of the LI, whereas the test level of the chopped LI is usually 110% of the full LI. The LI and SI tests are usually carried out with negative polarity in order to avoid external flashovers, and both tests start with a reduced voltage level as a calibration impulse. Afterwards, three full waveforms are typically applied. This test sequence must be performed on all

phases. The tap-changer positions change for each of the three phases of a three-phase transformer during the LI tests, so the two extreme tap positions as well as the main tap position are used once. For SI tests, it is often necessary to apply a number of reduced impulses with opposite polarities prior to each test impulse in order to avoid core saturation and therefore reduced impedance, which will influence the SI waveform.

Generally, the transformer passes these tests if there is no voltage breakdown during the tests and when the calibration and full impulses for the recorded LI waveforms are almost identical.

**Applied Voltage Test.** During the separate-source AC withstand test or the so-called applied voltage test, the integrity of the main insulation is examined, meaning that the insulation between the windings themselves, between the windings and the ground, and between all connections to ground and to each other is tested. The setup is rather simple and is also used for insulation resistance measurements: all winding systems (HV, LV, TV) are interconnected or short-circuited (all terminals of a winding system as well as the neutral, if applicable, are connected to each other), the winding system that is being tested is connected to the test voltage, and all other windings and parts are grounded. This procedure is repeated until all of the winding systems have been tested. The applied voltage test is usually performed at the rated frequency, and the test voltage is applied for 60 s, as specified by the IEC. The test is passed if the voltage does not collapse and there are no other fault indications, such as a sudden increase in the test current.

For large power transformers, the neutral often has a reduced level of insulation compared to the phase exits. Thus, for such nonuniform windings, the test level must be determined according to the test level specified for the neutral.

**Induced Voltage Test with PD Measurement.** The induced voltage test is one of the most conclusive tests of the quality of the transformer insulation system. During this test, the insulation between turns, discs, windings, and terminals at different phases is evaluated by applying electrical stress from a voltage that is around 1.5 times higher than the rated voltage to all of them simultaneously. Any deficiencies in the design, insulation dimensioning, or manufacturing process will cause weaknesses in the insulation system of the transformer, leading to PD activity during the induced voltage test. These weak points can be detected by simultaneously performing electrical PD measurements according to IEC 60270. Since the test voltage is

higher than the rated voltage, the test frequency is usually increased to at least twice the rated frequency in order to avoid core saturation.

The relevant IEC and IEEE standards exhibit some important differences for the induced voltage test. In fact, these differences between the standards are more significant than for any other test mentioned so far, and include dissimilar voltage limits for the PD measurement as well as differences in the procedure itself, the test setups, and the test duration. In general, the induced voltage is increased stepwise until the HV test level is reached, and this voltage is maintained for a rather short time (around a minute, depending on the voltage frequency). The voltage is then reduced stepwise. Both standards state that the first step down after the highest test voltage should be held for up to 1 h (this time mainly depends on the voltage  $V_m$  of the transformer). The test is passed if there is no collapse of the voltage, the PD levels do not reach certain limits, and the PD activity does not show any increasing trend.

The PD measurements performed during the induced voltage test are usually electrical PD measurements, as they can be calibrated and can be used to detect various failures that generate PD activity. If the transformer does not pass the test due to PD activity, additional PD measurement techniques such as acoustic or UHF methods can be used to determine the location of the PD fault. However, for the following main reasons, these techniques should not be used during the induced voltage test to judge whether the system has acceptable levels of PD activity [7.89, 90]:

- Neither acoustic nor UHF PD techniques can be calibrated. Thus, the apparent charge associated with the PD cannot be measured and compared with the PD acceptance criteria. This means that these techniques do not comply with the standards.
- Neither acoustic nor UHF PD methods can reliably detect an increasing trend in PD activity.
- Neither acoustic nor UHF PD measurements are able to detect all defect types, since their sensitivity depends on the location of the sensor.

For these reasons, the recommended PD measurement is an electrical measurement according to IEC 60270.

PD measurement is the most sensitive method of detecting weak points in the insulation system, so the induced voltage test with PD measurement is usually the last test that the transformer is subjected to. If a defect developed during previous tests but was not detected in those tests, it will most likely be detected during the PD measurement, so carrying out this test ensures that even small defects will be discovered.

### Short-Circuit Withstand Test

A short-circuit withstand test cannot usually be performed in the high-voltage test lab of the manufacturer because a high-voltage and high-power laboratory is needed, and there are only a few such labs around the world. Therefore, this is a special test, and one that requires agreement between the manufacturer and the purchaser regarding the setup to be used. In general, this expensive test checks the overall performance of the insulation system of a transformer in the case of a severe short circuit that produces strong mechanical forces. This test should be implemented on a new transformer that has just passed the FAT. In the test, the fully assembled transformer is subjected to a number of short circuits within a period that is usually shorter than 1 s (and often between 0.25 and 0.5 s). Either of the following actions may be performed:

- A breaker is closed in order to apply a short circuit to the energized transformer (post-established failure)
- A breaker between the power supply and the primary side of the transformer which is short-circuited on the secondary side is closed (pre-established failure).

Post-established failure is closer to reality, so this test is often preferred. However, due to the great expense of this test as well as the fact that a transformer failure usually leads to catastrophic damage and extremely high costs, so-called mock-up tests are becoming increasingly popular as an alternative to testing new complete transformers. During a mock-up test, a special model of the transformer or a certain part of the transformer is tested in order to prove the general integrity and mechanical stability of the design [7.91].

### Test Sequence

The international standards IEC 60076-1/60076-3 and IEEE Std. C57.12.90-2015 both provide some general advice and remarks regarding the test sequence. They recommend performing the tests in a way that ensures that the stress experienced by the transformer increases gradually rather than rapidly. Regarding the overall sequence of all the tests mentioned above, the standards provide recommendations but also state that an agreement between the manufacturer and the purchaser regarding the sequence is still allowed. On the other hand, more obligatory instructions are given regarding the sequence that should be used for the dielectric tests. In general, the following sequence seems to comply with the standards [7.77]:

- Basic tests without power (oil, ratio, vector group, FDS, FRA, etc.)

- No-load test (followed by a sound level test if required)
- Short-circuit voltage and load losses
- Zero-sequence impedance (if specified)
- Dielectric tests:
  - Switching impulse tests (if required)
  - Lightning impulse tests (if required)
  - Applied voltage test
  - Induced voltage test with PD measurement.

Depending on the size of the transformer and the number of tests specified, a period of some days up to 2 weeks in the high-voltage laboratory are typically needed to perform the FAT.

### 7.3.2 High-Voltage Test Equipment

High-voltage tests are usually performed in the high-voltage laboratory of the manufacturer, which should contain the following devices:

- A Marx generator for impulse tests
- A single-phase transformer for the applied voltage test
- A motor-generator set connected to a three-phase adaption transformer for the induced voltage test (including filters that enable sensitive PD measurement)
- Capacitor bank for the compensation required during load loss tests.

However, there is an increasing trend for performing high-voltage tests on power transformers on-site; for instance, after a repair on-site, after the complex transportation of a new transformer, or for diagnostic purposes. Therefore, in the following, state-of-the-art techniques for performing high-voltage tests on-site are presented.

#### High-Voltage Tests On-Site

Aside from the electrical and economic parameters, the requirements for high-voltage test systems that are used to test transformers on-site are mainly a compact design for simpler transportation, mechanical stability, fast installation, and operability with only a few personnel. The newest technologies allow this, so there are systems on the market that can be used to perform complete dielectric tests, even on the largest transformers. These systems are usually installed in containers, guaranteeing efficient transportation around the world.

Motor-generator sets were often used in the past for high-voltage AC tests on-site. However, these are usually quite heavy and therefore difficult to transport, and so modern techniques are superseding these old

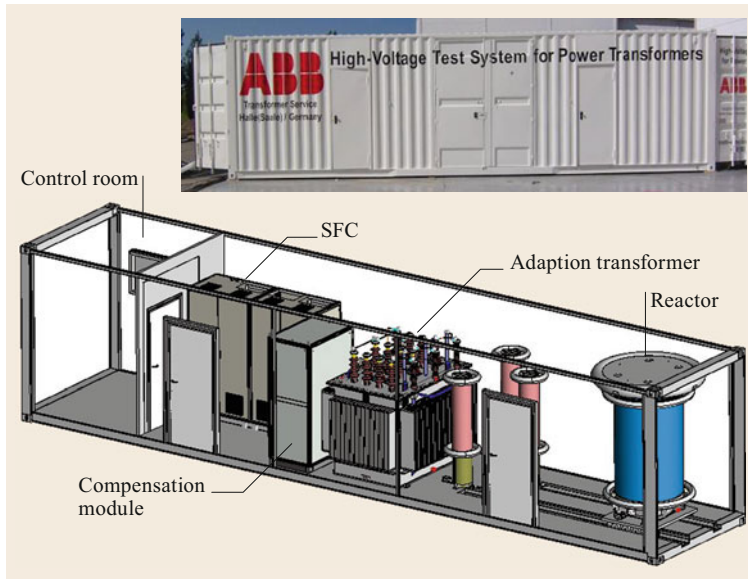


Fig. 7.78 HV-AC mobile test system

systems. The example shown in Fig. 7.78 focuses on a state-of-the-art three-phase AC test system installed in a 40 ft container. This system essentially consists of the following four devices [7.92]:

- Control and measurement system
- Static frequency converter (SFC)
- Adaption transformer
- Reactor for the single-phase applied voltage test.

The heart of the system, as shown in Fig. 7.78, is the static frequency converter, in which an external three-phase supply voltage is first rectified, so the direct voltage is buffered by a capacitor bank. The DC voltage then feeds an inverter module, which consists of insulated-gate bipolar transistors (IGBTs) and is driven by a microcontroller, thus generating sinusoidal modulated voltage pulses of adjustable frequency and amplitude. A controlled power sine-wave filter connected to the converter output is used to filter the fundamental wave, which finally feeds a step-up transformer [7.93]. This SFC system is integrated into two cabinets, each with dimensions of approximately 2 m (height)  $\times$  1 m (width)  $\times$  0.5 m (depth).

The adaption transformer has various bushings on its cover, allowing various voltage ratios and various vector groups to be realized in order to adjust the adaption transformer to the transformer being tested as well as possible. In the case of an induced voltage test, the adaption transformer is then connected to the transformer being tested using special HV cables and superior filters (see Fig. 7.79) that reduce the noise from the voltage source, permitting sensitive PD measurements.

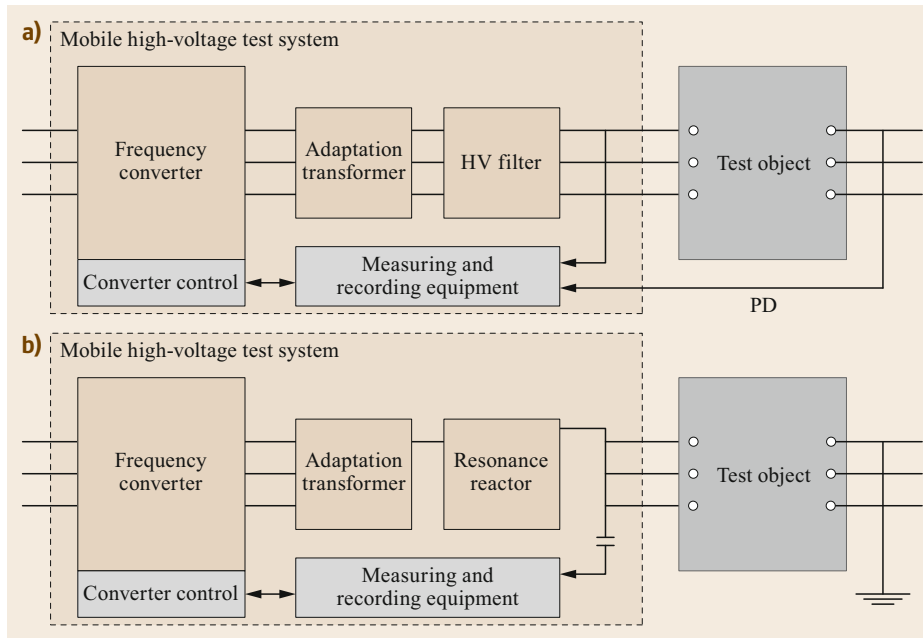
In an applied voltage test, the transformer being tested is connected to a reactor, supplied by one phase of the adaption transformer, as illustrated by Fig. 7.79. The frequency converter is then automatically tuned to the resonant frequency of the reactor in series with the tested transformer, which represents a capacitor in an equivalent circuit. The ability to tune the frequency in the region between 15 and 200 Hz in 0.1 Hz steps is one of the advantages of modern converters. A high-voltage divider that is parallel with the transformer being tested and is directly connected to the reactor is used to measure the applied voltage.

All tests are controlled from the control room using a compact device tower that contains the control system to which a power analyzer and the PD measurement apparatus are connected.

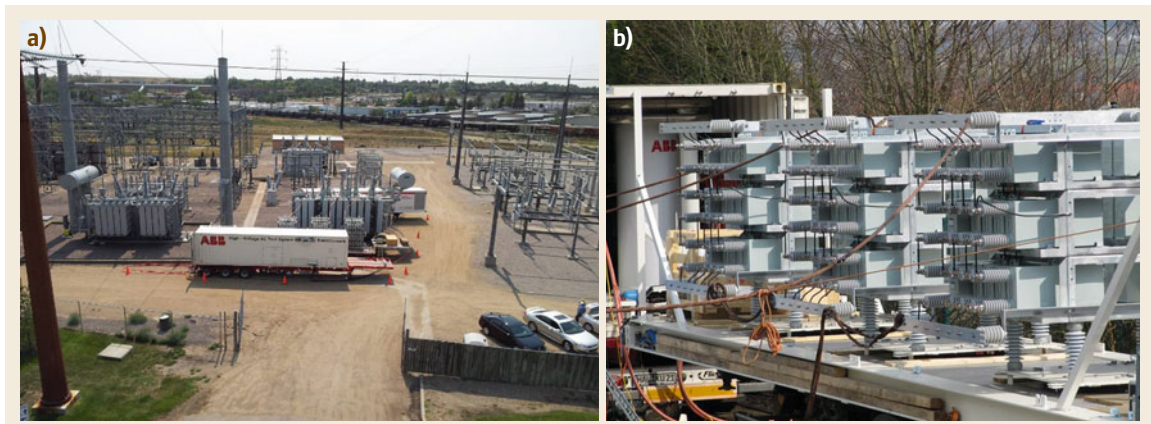
This system can have a converter power of up to 1350 kW and a 2 MVA adaption transformer with an output of 90 kV, so induced voltage tests can be performed up to 90 kV with a total harmonic distortion that is typically below 2% [7.94]. Applied voltage tests of up to 500 kV are possible with a reactor, which is usually enough for even the largest transformers because nonuniform winding systems are used at high voltage levels.

The power from an adaption transformer is somewhat higher than that from a frequency converter because a compensation module (also installed in a cabinet) can be connected on the low-voltage side of the transformer, as shown in Fig. 7.78. More information on this can be found in [7.95].

Electrical PD measurements usually utilize the measuring taps at the HV bushings of the tested transformer (see Fig. 7.79), or – rarely – separate capacitive coupling



**Fig. 7.79a,b** Setups used for induced (a) and applied (b) voltage tests



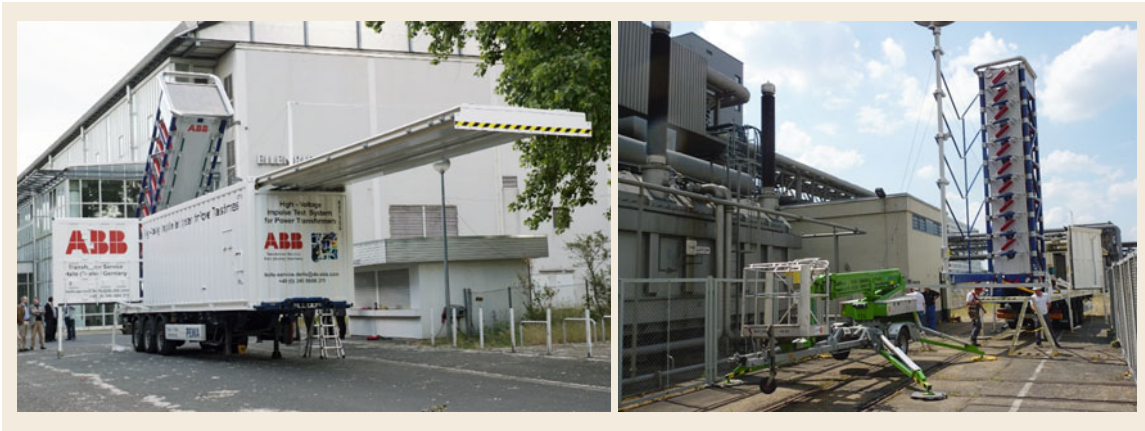
**Fig. 7.80a,b** Heat run tests (a) with a connected capacitive compensation module (b)

capacitors. The noise level on-site obviously depends on the environmental conditions and on the filters integrated into the PD measuring equipment, so noise levels of between 50 and 100 pC are typically achieved, although 10 pC is possible under favorable conditions [7.96].

If the power of the mobile test system described above is insufficient, it is theoretically possible to run up to eight systems in parallel, although this will not be economically efficient. Thus, a maximum of two parallel operating systems are used in rare cases. For heat run tests, additional capacitive compensation can be used. This can also be installed into a 40 ft container, as shown in Fig. 7.80. In other words, all HV AC tests can now be performed on-site [7.97].

It should be mentioned that the SFC technique used in mobile AC test systems is also increasingly being used in stationary HV test laboratories instead of old motor-generator sets. In such cases, the previously mentioned SFC modules are generally used, but several of these modules are connected in parallel to increase the power. Using this approach, HV-SFC systems with active powers of more than 8 MW have been built, and much higher power levels are undoubtedly possible [7.98].

Aside from AC voltage tests, it is sometimes necessary to perform impulse voltage tests on-site, and systems are available to achieve this. Figure 7.81 shows a mobile impulse generator system with a charging volt-



**Fig. 7.81** A mobile impulse test system

age of 2 MV and an energy of 300 kJ [7.99]. Lightning impulse tests up to 1800 kV and switching impulse tests up to 1300 kV can be performed using this system, which is installed in a 40 ft container. The ten-stage Marx generator in the container is transported horizontally. The roof of the container must be opened before the impulse generator is erected automatically using a hydraulic system. This procedure takes less than 1 h and requires no manpower [7.100].

The voltage divider needed for the test (see Fig. 7.81) is stored together with the generator. A special telescopic system is used to ensure the appropriate distance from the divider, so neither a crane nor special tools are needed to erect the system, which can of course be used to test other HV equipment [7.101].

These examples demonstrate that it is possible to perform HV tests of power transformers on-site, even for the largest units that are located far from labs.

## 7.4 Types of Transformers

Transformers can be categorized into types based on their main applications in the electrical network or in industry. Power transformers can be divided into dry-type transformers and liquid-filled transformers. Dry-type transformers have insulation made from epoxy resin, enamelled wires, or gas, whereas liquid-filled transformers – also called oil-immersed transformers – use an insulating fluid in combination with paper insulation around the wires. Insulating liquids are usually based on mineral oil. However, synthetic or natural esters and silicone liquids are becoming more popular because they are more environmentally friendly and have higher flashpoints than mineral oil. Transformers that are filled with a gas such as SF<sub>6</sub> have a market share of less than 1%, but are useful in special applications, such as underground installations with special fire safety requirements [7.102]. Dry-type transformers are now available up to a voltage level of 100 kV and a power level of around 60 MVA [7.103]. However, only a few dry-type transformers with such high voltage and power levels have become available, so typical applications of dry-type transformers involve the medium voltage

level, with a power rating of less than 10 MVA. In contrast, liquid-filled transformers are available up to the highest voltage levels – e.g., 1200 kV in India [7.104] – and the highest power levels, so three-phase power transformers with more than 1 GVA have been installed. Due to the enhanced cooling characteristics and superior dielectric properties of liquid-paper insulation, there are almost no restrictions on the voltage and power levels of transformers that use such insulation, but there is a limit on the weight of the components; the main restriction is therefore the transportability of the transformers [7.105]. A huge generator step-up (GSU) transformer with a power level of around 1 GVA can have a total weight of more than 500 t, so it would normally be transported without oil, which reduces the weight transported by around 100 t.

Below, different types of transformers used for various applications are briefly introduced, and typical differences in design are discussed. However, it should be noted that large transformers in particular are tailor-made, so it is not possible to provide universal design rules for them.



### 7.4.1 GSU Transformers

The traditional generator step-up (GSU) transformer is located in a large power-generation plant. These oil-filled transformers often use kraft paper or thermally upgraded paper on the HV side, whereas a special varnish coating that provides enhanced mechanical stability after it has undergone the oven process may be used on the LV side. They are typically built as core-type units, and a five-limb core is often used for power levels above several 100 MVA. GSUs may also be built as shell-type units, although the estimated market share of such units is less than 20%. The main function of GSU transformers is to elevate the voltage from the generator, which is normally less than 30 kV, to the transmission network voltage, which normally exceeds several 100 kV. This is why GSU transformers typically have a voltage transformation ratio above 1:10, which is higher than those for some other types of transformers. Step-up transformers usually use a star-delta (Yd) vector group, have an on-load tap changer (OLTC), and can be implemented as either a three-phase unit or three single-phase units. The cooling systems of large GSUs are often oil-forced (OF) or oil-directed (OD) in combination with air-forced (AF) or even water-forced (WF), so a service lifetime of approximately 30 years and a risk of failure of around 1% per year have been estimated for these GSUs by a CIGRE working group [7.106]. As shown in Fig. 7.82, large GSUs have a conservator, which may be unsealed (as a free-breathing transformer) or sealed with a membrane, which is the state of the art.

Due to the global demand for more renewable energy, more and more wind and solar parks are being installed. The transformers used in these power generation systems are also generator step-up transformers, but with power levels that are often below 10 MVA and



**Fig. 7.82** 1100 MVA step-up transformer with a nominal voltage of 19 kV/345 kV [7.10]

voltage levels on the HV side of a few tens of kV. Therefore, sealed liquid-filled or dry-type transformers that usually contain epoxy-resin insulation are used. They are equipped with an off-load tap changer, not an on-load tap changer. Under typical conditions, conventional large GSU transformers operate with a high constant load, whereas wind-park GSUs are subjected to drastic changes in the load. Furthermore, in many cases, the transformers are installed inside the wind power station, so the size of the transformer must be minimized. Thus, instead of mineral oil, a synthetic or natural ester is used in combination with aramid paper, as this allows the transformer to be operated at higher temperatures during strong wind periods. In addition, these liquids are more environmentally friendly and therefore facilitate a green energy strategy. In such cases, the cooling system is usually KNAN, because the transformers should be as maintenance-free as possible, but AF is also applied in some cases.

### 7.4.2 Substation Transformers

Substation transformers serve as interconnections between different points of the network and act as step-down and regulating units. They are installed across the transmission network at voltage levels of 100 kV and higher and operate at a wide range of voltages. The transmission ratios of these transformers are typically less than 1:5. Substation transformers, as depicted in Fig. 7.83, are usually filled with mineral oil, have an on-load tap changer, and are mainly designed as core-type units, although shell-type units are occasionally produced (their market share is less than 5%).

The cooling systems of such transformers vary according to the design requirements. Normal configurations are oil-natural (ON) or oil-forced (OF) and air-natural (AN) or air-forced (AF). For higher power levels, free-breathing systems are widely used, but the conservators are increasingly being equipped with membranes. Sealed units with a gas cushion are also constructed, and expansion radiators can be used up to power levels of approximately 150 MVA [7.107].

If the HV and LV sides of a substation transformer have voltage levels above the 100 kV level, a star-star (Yy) vector group is normally used, and a tertiary system with a voltage of a few tens of kV is added to the active part of the transformer to facilitate induced voltage tests. In HV tests, typical voltages ranging up to almost 100 kV can be generated for the induced voltage tests, so the device under test (DUT) should have a winding system with a nominal voltage of a few tens of kV that can be used for excitation during the FAT.

The service life of a substation transformer can exceed 40 years, as they (usually) do not operate contin-



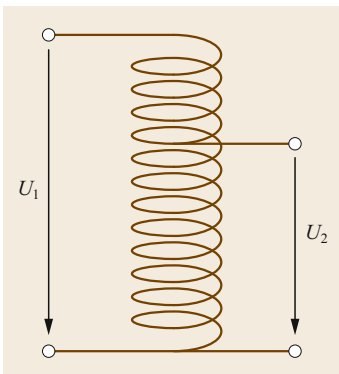
**Fig. 7.83** Transformer in a substation [7.10]

uously under high load, which also explains the reduced failure risk of approximately 0.5% per year for a substation transformer as compared to a GSU transformer, based on the CIGRE statistic mentioned above [7.106].

### 7.4.3 Autotransformers

Autotransformers have a special design in which the same winding system is used for the HV and LV sides, as shown in Fig. 7.84. This construction is only reasonable for relatively small transmission ratios that usually do not exceed 1:5, so autotransformers can be used as substation transformers at all voltage levels and power rates. Therefore, the other design characteristics (the preferred insulation, core, and cooling) of autotransformers are similar to those of substation transformers. Construction as either a three-phase unit (as shown in Fig. 7.85) or a single-phase unit is possible, but each phase of a three-phase unit will typically have a separate on-load tap changer.

Especially for low transmission ratios, the compact construction of an autotransformer means that less material is used during construction, so cost, weight, and volume savings become possible. That said, there are,



**Fig. 7.84** The functional principle of an autotransformer



**Fig. 7.85** 220/110/10 kV and 250 MVA autotransformer [7.38]

of course, certain disadvantages of autotransformers. For instance, due to the galvanic connection between the HV and LV sides, there is the possibility that the HV will be on the common winding and therefore on the LV side of the transformer during a failure. In order to avoid such a breakdown on the LV side, it is necessary to design the LV part to withstand higher voltages. Furthermore, the main leakage flux between the primary and secondary windings is relatively small, resulting in a low impedance. Thus, high short-circuit currents may occur if there is a fault. The main disadvantage of the galvanic connection between the voltage systems is that the zero-sequence currents generated by line-to-earth failures (the most common short circuits in the network) are transferred from one voltage system to the other. All of the equipment and protection for both voltage systems must be designed for those short-circuit currents.

However, the expected lifetime and failure rate of autotransformers are comparable to those of substation transformers.

As can be seen in Fig. 7.85, a tertiary system (in this case with a nominal voltage of 10 kV) is also necessary when performing an induced voltage test on an autotransformer.

#### 7.4.4 Distribution Transformers

These transformers operate at the medium-voltage level and distribute the energy to the low-voltage network, to which the end users are connected. Due to the low voltages and the typical power levels of these transformers (below 10 MVA), they can be liquid-filled transformers or dry-type transformers with epoxy-resin insulation (Fig. 7.86). These transformers have a core-type design and tend to have an ONAN cooling system. They are equipped with an off-load tap changer, but due to the drive to switch to renewable energy sources, so-called RONT (adjustable local network transformer; *regelbarer Ortsnetztransformator* in German) systems that have an on-load tap changer are increasingly being installed [7.108]. For liquid-filled transformers, sealed systems are preferred, but free-breathing transformers (without conservator membrane) are also available.

The service life of this type of transformer, which often uses a delta-star (Dy) vector group, generally exceeds 50 years due to its low utilization rate.

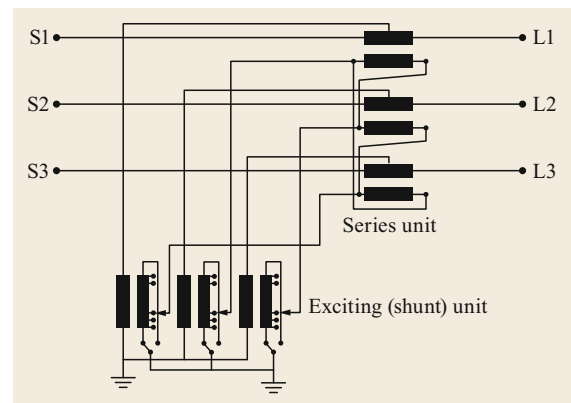


**Fig. 7.86** 2 MVA 36/0.4 kV dry-type distribution transformer [7.109]

#### 7.4.5 Phase Shifters

Phase-shifting transformers, sometimes called phase-angle regulators (PAR) or quadrature/quad boosters, are the largest and most expensive transformer units. They are used to regulate the power flow between electrical networks, so they are often located, for example, at transnational interconnections with nominal voltages of 400 kV or more. They work by adding a voltage that is usually shifted from the line voltage by  $90^\circ$ , thus changing the phase angle of the line voltage and allowing the load flow to be controlled. Sometimes a voltage that is phase shifted by only  $60^\circ$  compared to the line voltage is added to the line voltage. Phase shifters usually consist of two active parts – a series unit and an exciter unit (often called a shunt unit). The output of the exciter unit supplies the series unit, the secondary winding of which is connected to the line (as shown in the schematic presented in Fig. 7.87), although many different connection schemes are possible. Usually (in more than 90% of all phase shifters), the exciter unit is connected in YNyn while the series unit is connected in III<sub>d</sub>, and the terminals on the *source* side are generally named S1, S2, and S3 whereas the *load*-side terminals are called L1, L2, and L3.

As depicted in Fig. 7.87, the shunt unit consists of windings that are connected across the phases to generate an output voltage that is shifted by  $90^\circ$  in comparison to the input or supply voltage. By using this voltage as the input voltage to the series unit, the output voltage will be the sum of two voltage vectors: the supply voltage and the  $90^\circ$  quadrature voltage. This yields an output voltage that is shifted by a certain degree or angle compared to the supply voltage, and this angle can be adjusted using an OLTC inside the shunt unit in



**Fig. 7.87** Schematic representation of a phase-shifting transformer



**Fig. 7.88** Phase-shifting transformer [7.110]

order to vary the magnitude of the  $90^\circ$  quadrature component.

As illustrated in Fig. 7.88, large phase-shifter transformers with power ratings of up to the 1500 MVA level are installed in two tanks, resulting in a total weight that can exceed 1000t. The two tanks are therefore transported separately and connected on-site. Typical phase shifters have a core-type design, are filled with mineral oil and use a forced-forced cooling system, employ a conservator with an integrated membrane, and have a transmission ratio of 1:1. For nominal voltages above 110kV, tertiary windings are often necessary for induced voltage tests, similar to substation transformers or autotransformers. Another property that they share with autotransformers is the fact that each phase usually has a separate OLTC, which is necessary to change the phase angle of the line voltage.

The typical lifetime and failure rate of a phase shifter are estimated to lie between those of a GSU and a substation transformer.

#### 7.4.6 HVDC Transformer

High-voltage direct-current (HVDC) power transmission is usually quite expensive, but it has some advantages over high-voltage alternating-current (HVAC) power transmission. For instance, HVDC does not generate any reactive power, so there is no need for compensation. For very long distances, or when the capacitance of the transmission line would be too high (e.g., if an offshore wind park is connected through a 100km long undersea cable to an onshore station), HVDC connections are preferred. HVDC systems up to a voltage level of 1100kV are currently in use, meaning that HVDC transformers stand alongside phase shifters as the largest and most expensive types of transformers.

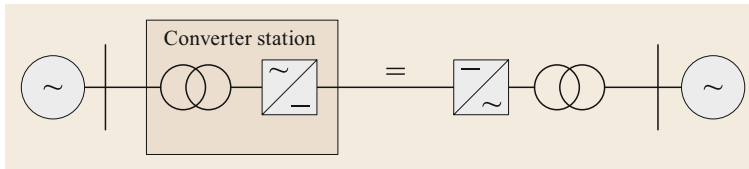
A simplified scheme of a basic HVDC transmission system is presented in Fig. 7.89, from which it is obvious that two converter stations are necessary for the whole transmission line. Each station consists of a HVDC transformer and a valve system, which makes HVDC transmission expensive. Figure 7.90 shows a 12-pulse rectifier, which is typically used in such systems, fed by a HVDC transformer, which usually has a star and a delta valve winding. However, for large voltages and high power levels, the symbol of the HVDC transformer shown in Fig. 7.90 actually corresponds to several single-phase transformers. Thus, HVDC transformers are normally single-phase transformers. Sometimes the core of a HVDC transformer will consist of two main limbs and two return limbs, with one valve winding placed on each main limb, whereas the primary winding is split into equal parts on the two main limbs. In that case, the valve windings are connected outside the transformer to a star and delta system, each feeding a six-pulse converter. Another configuration uses only one main limb and two return limbs, so primary and valve windings are placed on the main limb.

Figure 7.91 shows a large HVDC transformer with the primary bushing on the top and the two valve bushings on the front of the tank. HVDC transformers are also equipped with an OLTC that usually has a wide tapping range in order to control the service voltage adequately. HVDC transformers commonly use an oil-immersed paper insulation system, forced cooling, and a conservator with an integrated membrane. It is thought that the lifetime and failure risk of a large HVDC transformer is similar to that of a large GSU transformer.

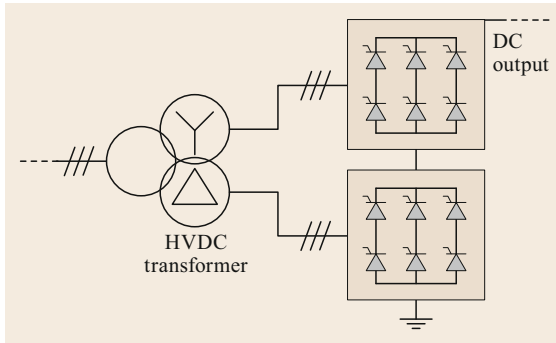
HVDC transformers are subjected to additional tests during the FAT. A separate-source DC voltage withstand test as well as a polarity reversal test are performed according to IEC 61378-2 [7.112] on the valve windings. From a design perspective, it is necessary to account for the fact that currents flowing through the windings of HVDC transformers contain certain harmonics that influence the losses of the transformer.

#### 7.4.7 Arc-Furnace Transformer

Arc-furnace transformers are used in the metallurgical industry for smelting purposes. When they are connected to the electrical network, they reduce the voltage to levels that are often around 1 kV or less in order to obtain high currents that are used in the melting process. Their mode of operation resembles short-circuit operation and requires special design considerations that are atypical for other types of transformers. The most unusual characteristic is the position of the LV winding, which is not the innermost winding close to the core (as is usually the



**Fig. 7.89** AC-DC-AC connection scheme



**Fig. 7.90** Converter station with a 12-pulse converter



**Fig. 7.91** 800 kV HVDC transformer [7.111]

case) but the outermost winding because of the high currents that need to be transferred to the outside of the tank. This is often achieved not through the use of traditional bushings but with a special bus bar system integrated into the tank wall, as shown in Fig. 7.92.

Usually, arc-furnace transformers are filled with mineral oil and employ thermally upgraded or aramid paper. However, because aramid paper is expensive, mixed insulation is sometimes used. In this mixed insulation scheme, only certain LV winding parts are insulated with aramid paper; the other parts use thermally upgraded paper to reduce the costs. On the HV side, voltages of 100 kV or more are possible, while on the LV side, only a few kV will be generated, with power rates reaching approximately 200 MVA, meaning that extremely large systems can be produced. Normally a core-type design is used, and three- or single-phase systems are available, typically with the Diii or Ii vector group. Each phase in the three-phase system usually



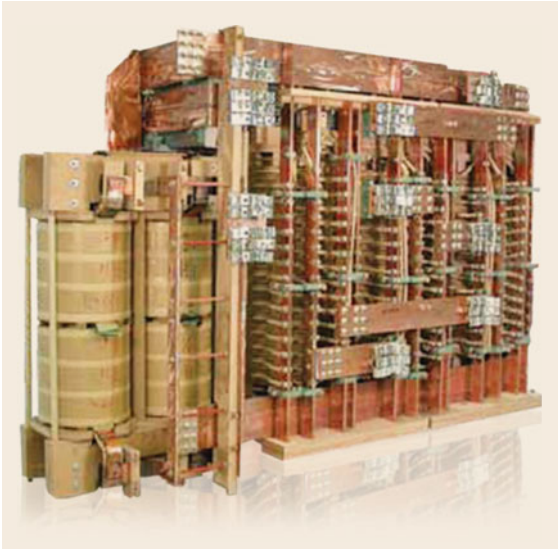
**Fig. 7.92** Arc-furnace transformer [7.10]

has its own OLTC, which is operated much more often than in any other transformer. Therefore, systems for purifying the oil in the OLTC compartment are also often installed. Large arc-furnace transformers are free-breathing transformers or have a membrane inside the conservator. An enhanced cooling system is commonly installed, so a forced-forced cooling system is typically used, often with water as the coolant.

The mode of operation of an arc-furnace transformer is close to the continuous full-load regime, typically combined with overloading situations that have a negative impact on the lifetime (estimated at 20–30 years).

#### 7.4.8 Rectifier and Converter Transformers

Rectifier transformers are typically used in the metallurgical and chemical industries and therefore exhibit some similarities with arc-furnace transformers,



**Fig. 7.93** Active part of a rectifier transformer [7.113]

whereas converter transformers are used for variable-speed drives in different areas.

In a normal 12-pulse rectifier unit, two output winding systems are installed in a double-tier design – one system in a delta and one in a star connection. Due to the high currents (which can exceed 100 kA) at the output windings, large copper bus bars are needed to form the star or delta connection, so these low-voltage windings are the outermost windings (see Fig. 7.93), just as in arc-furnace transformers. Another way in which they resemble arc-furnace transformers is that a special bus bar system is integrated into a tank wall to transfer the high currents to an external valve unit.

Due to the direct connection between the transformer and the converter, the load currents contain higher harmonics (just as in HVDC transformers), leading to increased losses. Regulating transformers are commonly used between the supplying network and the rectifier transformer in order to adapt the voltage for the rectifier transformer. A regulating transformer usually has a lower current harmonic content than a rectifier transformer because the harmonics of the combined 12-pulse system are lower than those for the individual 6-pulse system. Often, an additional filter is installed to further reduce the harmonics transferred to the network and to compensate the high reactive power generated by the rectifier. On occasion, the regulating transformer and the rectifier transformer are installed in the same tank, resulting in a compact but heavy arrangement.

These transformers are usually filled with oil and use thermally upgraded paper, sometimes in combination with aramid paper. Such transformers tend to employ a core-type design and a conservator equipped

with a membrane. With a forced cooling system, power ratings of up to around 200 MVA are achievable.

The lifetime of such a transformer is assumed to be similar to that of an arc-furnace transformer. However, dry-type rectifier and especially converter transformers with epoxy-resin insulation have also been constructed; these have power levels of up to a few 10 MVA.

### 7.4.9 Traction Transformers

Traction transformers are used in railway vehicles and therefore have some special characteristics such as compactness, mechanical robustness, reduced downtime and maintenance, and high reliability. There is also a particular focus on their safety and environmental behavior. They have special load profiles with supply frequencies ranging from 16.7 to 60 Hz, depending on the country. A typical traction transformer is a single-phase transformer with an input voltage of up to 25 kV at 50 Hz or up to 15 kV at 16.7 Hz and a rated power of up to around 10 MVA for liquid-filled systems. The input voltage is stepped down to a voltage in the kV range, which is often used to feed a rectifier that is employed to run DC traction motors. Nevertheless, some systems use a DC input voltage, in which case the traction transformer unit has an internal converter.

An important design goal is to increase the efficiency of traction systems, which is influenced by the transformer losses and the short-circuit impedance (this impedance has a significant effect on the converter efficiency). Further design aims are to reduce the volume and weight of a traction transformer without decreasing its mechanical stability. This can be achieved by reducing the amount of material used in its construction, although this leads to increased temperatures. Therefore, insulation systems that can withstand higher temperatures are preferred; instead of paper, glass-fiber insulation and aramid-paper insulation are often used in combination with high-temperature liquids instead of mineral oil in a free-breathing system. Nowadays, dry-type traction transformers are also available up to a power level of  $\approx 4$  MVA. These are insulated with epoxy resin, as shown in Fig. 7.94.

Both types typically use a core type with two limbs, employ a forced cooling system, and have many bushings (oil type) or output connections (dry type) to feed systems such as the motor, a heating and cooling system, and the internal supply. In contrast to most other transformer types, traction transformers are similar to distribution transformers in that they are mass-produced, so large quantities of these transformers are manufactured. Furthermore, these transformers must pass special mechanical and safety tests because they are mounted on rolling stock systems.

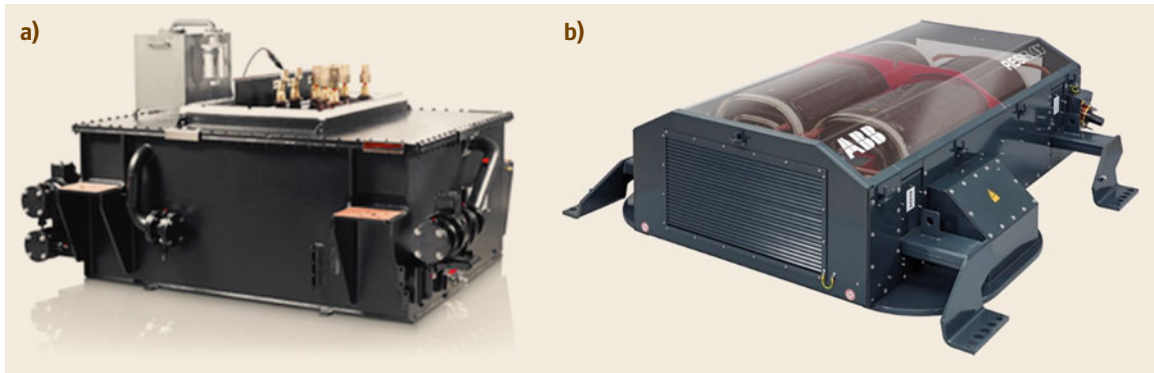


Fig. 7.94 (a) Liquid-filled and (b) dry-type traction transformers [7.114]

### 7.4.10 Test Transformers

High-voltage quality-control tests of newly manufactured HV components are mandatory. These tests are usually applied voltage tests, so a single-phase test transformer is needed to apply the test voltage. The main exception is the induced voltage test, which is usually performed as a three-phase test for a three-phase transformer. In such cases, the voltage is typically generated by a motor-generator set connected to an adaption transformer with a wide tapping range that can deliver the required test voltage at the higher frequencies (e.g., 150 or 200 Hz) provided by the motor-generator set. These adaption transformers are single-piece units produced according to the specific requirements of the test field operator. They are usually designed as sealed or open liquid-filled core-type transformers with three limbs and normal cooling, and with voltages on the HV side that are typically below 100 kV and power ratings of a few 10 MVA.

However, for the applied voltage test, single-phase transformers with voltages of 1 MV or more are needed, depending on the device to be tested. This is realized in practice through the use of a cascade of identical single-phase test transformers, as shown in Fig. 7.95. As can be seen, the second transformer operates on the HV level of the first transformer, and the third transformer operates on the output voltage level of the second transformer. Therefore, the total output voltage of the cascade is equal to  $n$  times of the output voltage of each single-phase transformer, where  $n$  is the number of stages in the cascade.

These single-phase transformers use oil-paper insulation and a tank made out of insulating material, as shown in Fig. 7.96, so they can be stacked on top of each other to form a cascade. Another possibility is to use a normal tank design made out of steel, as shown in Fig. 7.95, where the transformers representing the second and higher stages of the cascade need to be placed

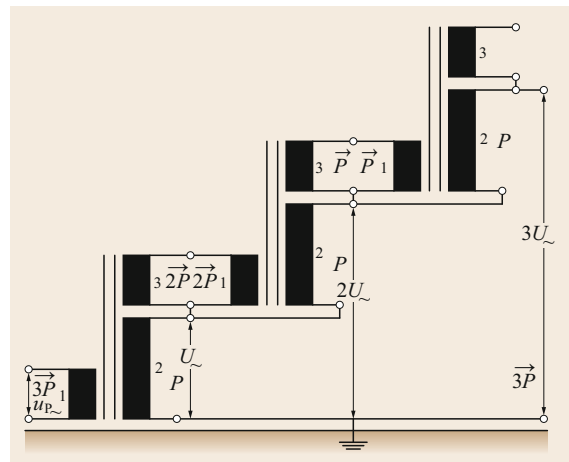


Fig. 7.95 Three-stage Fischer cascade showing the voltage ( $U$ ) and power ( $P$ ) distributions [7.115]

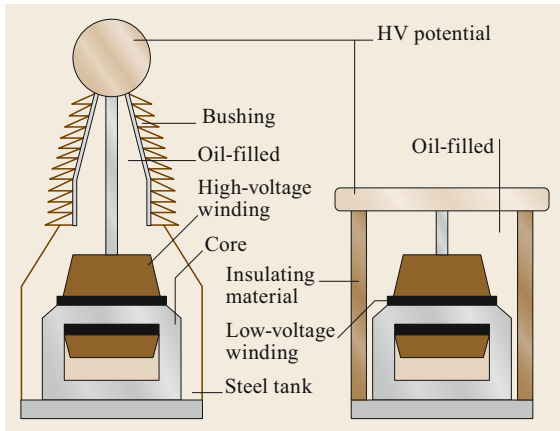
on insulators. A disadvantage of cascading is the resulting imbalanced temperature distribution of the stacked single-phase transformers: the initial stages have higher temperatures because they deliver higher power than the subsequent stages, as shown in Fig. 7.95.

Among all transformer types, these single-phase transformers have the highest transmission ratios (approximate range: 1:100 to 1:1000), so a substantial distance between the LV and HV sides is needed, resulting in increased stray flux and thus higher short-circuit impedance. As a consequence, the short-circuit current is limited and the short-circuit stability is increased.

The lifetime of a test transformer is usually quite high – often exceeding 50 or 60 years – because they are only utilized sporadically.

### 7.4.11 Variable Differential Transformers

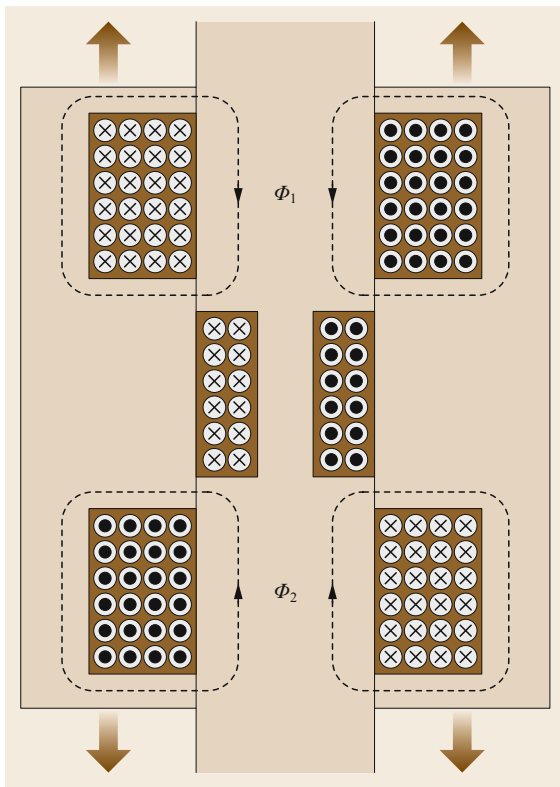
A variable differential transformer allows stepless regulation of the output voltage based on the relative



**Fig. 7.96** Schematic design of a single-phase test transformer

displacement between a secondary coil, which is placed in slots on one core limb, and two identical primary coils, which are connected in parallel and placed on a movable yoke. Figure 7.97 shows a schematic of the working principle of such a transformer.

The primary coils are positioned such that they create magnetic flows in opposite directions. The voltage



**Fig. 7.97** Schematic of the functional principle of a variable differential transformer

induced in the secondary coil depends on the position of the movable primary coils. Figure 7.98 shows three possible positions of the movable yoke [7.116]. At position 1 (Fig. 7.98a), the magnetic flux  $\Phi_1$  closes the magnetic circuit through the secondary coil and induces a voltage  $V = V_{\max}$ . At position 2 (Fig. 7.98b), the magnetic flux through the secondary coil is zero and so the induced voltage  $V = 0$ . Finally, at position 3 (Fig. 7.98c), the voltage induced in the secondary coil is  $V = -V_{\max}$ .

Since intermediate positions are also accessible, continuous regulation of the voltage induced in the secondary coil between  $V_{\max}$  and  $-V_{\max}$  is possible. However, the mechanical complexity of these transformers significantly limits their practical use in high-power applications, although they are sometimes used for testing.

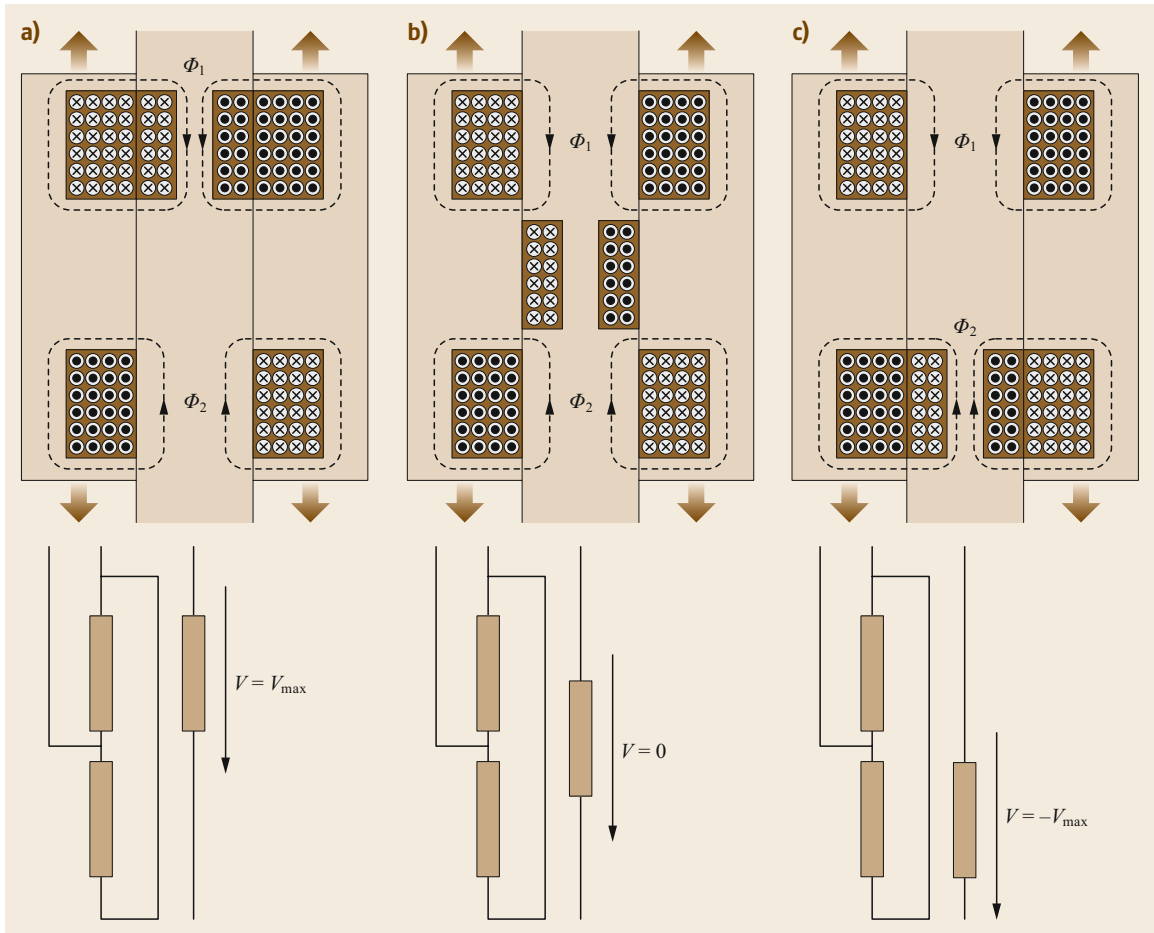
### 7.4.12 Other Types of Transformers

There are also many other special types of transformers, because power transformers are often tailor-made to specific customer requirements, and a wide range of such requirements are now technically feasible. Additional transformer types include instrument transformers, isolation transformers, welding transformers, and many different kinds that are used with low voltages and in electronics but are not considered in this chapter because they are not power transformers. However, it should be mentioned that reactors, which are also important components of the electrical energy transmission and distribution network, bear some similarities to power transformers in their design and construction. Large reactors are single- or three-phase systems that contain similar components to power transformers, such as windings, a core, bushings, a tank, a conservator, and oil-immersed paper insulation. The main difference is the structure of the reactor core, which has nonmagnetic gaps in the core limbs. However, there are other differences too, such as in the tightening of the active part and the high-voltage testing of reactors, which often requires special equipment. Reactors can be divided into the following categories [7.10]:

- Shunt reactors
- Current-limiting reactors
- Neutral grounding reactors
- Capacitor damping reactors
- Tuning or filter reactors
- Arc-suppression reactors
- Smoothing reactors.

Among these, shunt reactors are of particular importance up to the highest voltage levels, since they are used to compensate reactive power in transmission networks. Figure 7.99 illustrates a three-phase shunt re-





**Fig. 7.98a–c** Schematic showing how the voltage induced in the secondary coil of a variable differential transformer depends on the position of the movable coils. Cases (a) and (c) illustrate the maximum positive (a)/negative (c) induced output voltage. Between these extreme values all output voltage are possible, thus in case (b) the output voltage is adjusted to 0 V

actor, which looks like a transformer at first glance, but can be identified as a reactor by noting the absence of LV bushings.

**Acknowledgments.** The authors would like to thank Mohammad Akbari Azirani, M.Sc. and Javier Torres, M.Sc. (both from the Schering-Institute of High Voltage Engineering and Asset Management of the Leibniz University Hannover, Germany) for their support.

Furthermore, we express our deep gratitude to ABB Power Grids and ENPAY A.S. for permitting us to use various pictures.



**Fig. 7.99** Example of a three-phase shunt reactor [7.117]

## References

- 7.1 M. Faraday: Electro-magnetic current, *Q. J. Sci.* **19**, 338 (1825)
- 7.2 LEIFI-Physik: *Elektro-Magnetische Induktion, Aufbau, Durchführung und Beobachtung des ersten gelungenen Versuchs von Faraday zur Induktion* (Joachim Herz Stiftung, Hamburg 2020)
- 7.3 Model of a transformer of Gaulard and Gibbs; Museo Galileo Florence, Room XVI
- 7.4 H.R. Johannsen: *Eine Chronologie der Entdeckungen und Erfindungen vom Bernstein zum Mikroprozessor*, Vol. 3 (VDE, Berlin 1987)
- 7.5 G. Neidhöfer: *Michael Dolivo-Dobrowolsky und der Drehstrom, Anfänge der modernen Antriebstechnik und Stromversorgung*, Geschichte der Elektrotechnik, Vol. 19, 2nd edn. (VDE, Berlin 2008)
- 7.6 Europäische Maschinenrichtlinie; 2006/42/EG Artikel 2 Abs. a.
- 7.7 A. Küchler: *Hochspannungstechnik*, 3rd edn. (Springer, Berlin, Heidelberg 2009)
- 7.8 H. Spanneberg: *Ruhende elektrische Maschinen* (VEB Technik, Berlin 1982)
- 7.9 ABB: *Aufbau eines Transformators*, ABB Review (ABB, Zurich 2010)
- 7.10 ABB: *Transformer Handbook*, 3rd edn. (ABB, Zurich 2007)
- 7.11 IEC 60076-4: *Power Transformers – Part 4: Guide to the Lightning and Switching Impulse Testing – Power Transformers and Reactors* (IEC, Geneva 2002)
- 7.12 W. Höger: *Elektrische Maschinen und Antriebe* (FH München, Munich 2002), Skript
- 7.13 B.R. Oswald: *Transformatoren* (Leibniz Univ. Hannover, Institut für Energieversorgung und Hochspannungstechnik, Hannover 2000)
- 7.14 G. Müller: *Elektrische Maschinen, Grundlagen, Aufbau und Wirkungsweise*, 3rd edn. (VEB Verlag Technik, Berlin 1970)
- 7.15 M. Vidmar: *Der Transformator im Betrieb* (Springer, Berlin 1927)
- 7.16 E. Arnold, J.L. la Cour: *Die Wechselstromtechnik – Die Transformatoren*, 2nd edn. (Springer, Berlin, Heidelberg 1920)
- 7.17 IEC 60076-1: *Power Transformers – Part 1; General* (IEC, Geneva 2011)
- 7.18 H.-P. Beck: *Elektrische Energietechnik: Eine Einführung in die Energieumwandlung, Transformatoren* (TU Clausthal/IEE, Clausthal 1998)
- 7.19 R. Küchler: *Die Transformatoren, Grundlagen für ihre Berechnung und Konstruktion*, 2nd edn. (Springer, Berlin, Heidelberg 1966)
- 7.20 H. Fischer: *Werkstoffe der Elektrotechnik*, 2nd edn. (Hauser, München, Wien 1982)
- 7.21 G. Müller, B. Ponick: *Grundlagen elektrischer Maschinen*, 9th edn. (Wiley-VCH, Weinheim 2006)
- 7.22 W. Fuller Brown Jr.: *Magnetoelastic Interaction* (Springer, Berlin, Heidelberg 1966)
- 7.23 S. Tenbohlen: Leistungstransformatoren – Neue Trends bei Design, Produktion und Betriebüberwachung. In: *Micafil Symp., Stuttgart* (2004)
- 7.24 ENPAY A.S.: *ENPAY – Power and Distribution Transformer Cores* (ENPAY Broch, Kullar 2020)
- 7.25 ENPAY A.S.: ENPAY transformer components, <http://www.enpay.com/icerik/power-transformer.cores> (2020)
- 7.26 H.P. Moser (Ed.): *Transformerboard; Die Verwendung von Transformerboard in Grossleistungstransformatoren* (Birkhäuser, Basel 1979)
- 7.27 H.P. Moser (Ed.): *Transformerboard II; Eigenschaften und Anwendung von Transformerboard aus verschiedenen Fasern* (Weidmann, Rapperswil 1987)
- 7.28 PUCARO: *Documentation Insulation KITs* (PUCARO, Roigheim 2020), <https://www.pucaro.com/en/en-kits>
- 7.29 G. Bertagnolli: *Short-circuit Duty of Power Transformers*, 3rd edn. (ABB, Zurich 2008)
- 7.30 J.C. Mendes: *High Voltage Power Transformers: Short-Circuit-Stress, Strength, Design, Testing, Advanced technologies and Recommendations* (ABB Brazil Power Products Division, Sao Paulo 2020), [www04.abb.com/seitp/seitp202nsf3.+Jose+Carlos+Mendes.pdf](http://www04.abb.com/seitp/seitp202nsf3.+Jose+Carlos+Mendes.pdf)
- 7.31 IEC 60085: *Electrical Insulation – Thermal Evaluation and Designation* (IEC, Geneva 2007)
- 7.32 IEC 60076-11: *Power Transformers – Part 11: Dry-type Transformers* (IEC, Geneva 2018)
- 7.33 H. Brendel: *Advanced Retrofit – die Verbesserung von Öltransformatoren bei der Instandsetzung mit innovativen Konstruktionslösungen*. In: *TLM 2014, Transformer-Life-Manag. Conf., Neuss* (2014)
- 7.34 H. Brendel, M. Starke, M. Hübner, R. Büchner, K. Herkert, I. Li Pira: *Oil transformer switching frame (HaPuchannel)*, European Patent No. EP 2 816 575 B1 (2015)
- 7.35 PUCARO: *HaPuchannel* (Pucaro, Poigheim 2020), Brochures
- 7.36 H. Brendel: *Off Load Tap Changer Assembled in a High Current Test Transformer* (VEB Transformatorenreparaturwerk Halle, Halle 1978)
- 7.37 B. Jansen: *Einrichtung zum Umschalten zweier Anzapfungen eines Stufentransformators während des Betriebes durch gegenläufig bewegte Leistungsschalter mit Vorkontakten*, Patentschrift Deutsches Reich, Nr. 474613, Klasse 21 d2 – Gruppe 53 (1929)
- 7.38 ABB: *Service Handbook for Transformer*, 3rd edn. (ABB, Zurich 2007)
- 7.39 IEC 600137: *Insulated Bushings for Alternating Voltages Above 1000V* (IEC, Geneva 2017)
- 7.40 CIGRE Working Group WG A2.43, TB 755: *Transformer Bushing Reliability* (CIGRE, Paris 2019)
- 7.41 B. Heinrich, C. Krause, K. Wick: *Electrical Insulation Tests on the Modular 400 kV/AC Lead Exit System for Power Transformers*. In: *20th Int. Power Syst. Conf., PSC, Iran* (2005) p. 46–E-TRN-325
- 7.42 V. Dahinden, K. Schultz, A. Küchler: *Function of Solid Insulation in Transformers* (H. Weidmann, Munich 1998)
- 7.43 H. Brendel: *Ausleitungsrohr (HaPuflex550-Rohr)*, European Patent Office No. EP 2 287 864 B1 (2012)
- 7.44 H. Brendel, R. Büchner, J. Braatz, K. Herkert: *Durchführung für Hochspannungsausleitungen in Trans-*

- formatoren (HaPuflex-Kalotte 1), European Patent Office No. EP 2 442 319 B1 (2012)
- 7.45 H. Brendel, R. Büchner, J. Braatz, K. Herkert: Durchführung für Hochspannungsausleitungen in Transformatoren (HaPuflex-Kalotte 2), European Patent Office No. EP 2 442 321 B1 (2012)
- 7.46 ABB: *HiDry: Dry-type Power Transformers for Sub-transmission (up to 145 kV/63 MVA)* (ABB, Zurich 2017)
- 7.47 ABB: *ABB Product Brochures* (ABB, Zurich 2020)
- 7.48 Crushtymks: Öltransformator mit Buchholzrelais schützen, <https://crushtymks.com/protection/1397-protecting-oil-type-transformer-with-buchholzrelay.html> (2020)
- 7.49 CIGRE WG A2.59 TB: *On-Site Assembly, On-Site Rebuild, and On-Site High Voltage Testing of Power Transformers* (CIGRE, Paris 2021)
- 7.50 P. Werle: On-site tests of power transformers. In: *HIGHVOLT Colloq.*, Dresden (2007)
- 7.51 CIGRE Working Group WG A2.49, TB 761: *Condition Assessment of Power Transformers* (CIGRE, Paris 2019)
- 7.52 CIGRE Working Group WG A2.34, TB 445: *Guide for Transformer Maintenance* (CIGRE, Paris 2011)
- 7.53 IEC 60422: *Mineral Insulating Oils in Electrical Equipment – Supervision and Maintenance Guidance* (IEC, Geneva 2013)
- 7.54 IEEE Std. C57.106–2015: *IEEE Guide for Acceptance and Maintenance of Insulating Mineral Oil in Electrical Equipment* (IEEE, New York 2015)
- 7.55 IEC 60599: *Mineral Oil-filled Electrical Equipment in Service – Guidance on the Interpretation of Dissolved and Free Gases Analysis* (IEC, Geneva 2015)
- 7.56 IEEE Std. C57.104–2019: *IEEE Guide for the Interpretation of Gases Generated in Mineral Oil-Immersed Transformers* (IEEE, New York 2019)
- 7.57 IEC 60076–3: *Power Transformers – Part 3: Insulation Levels, Dielectric Tests and External Clearances in Air* (IEC, Geneva 2018)
- 7.58 IEEE Std. C57.12.00–2015: *IEEE Standard for General Requirements for Liquid-Immersed Distribution, Power, and Regulating Transformers* (IEEE, New York 2015)
- 7.59 IEEE Std. C57.12.90–2015: *IEEE Standard Test Code for Liquid-Immersed Distribution, Power, and Regulating Transformers* (IEEE, New York 2015)
- 7.60 IEC 60076–18: *Power Transformers – Part 18: General* (IEC, Geneva 2007)
- 7.61 IEEE Std. C57.149–2012: *IEEE Guide for the Application and Interpretation of Frequency Response Analysis for Oil-Immersed Transformers* (IEEE, New York 2012)
- 7.62 IEEE Std. C57.161–2018: *IEEE Guide for Dielectric Frequency Response Test* (IEEE, New York 2018)
- 7.63 IEC 60076–8: *Power Transformers – Part 8: Application Guide* (IEC, Geneva 1997)
- 7.64 IEC 60076–10: *Power Transformers – Part 10: Determination of Sound Levels* (IEC, Geneva 2016)
- 7.65 IEC 60076–2: *Power Transformers – Part 2: Temperature Rise for Liquid-immersed Transformers* (IEC, Geneva 2011)
- 7.66 IEC 60076–7: *Power Transformers – Part 7: Loading Guide for Mineral-oil-immersed Power Transformers* (IEC, Geneva 2018)
- 7.67 IEC 60354: *Loading Guide for Oil-immersed Power Transformers* (IEC, Geneva 1991)
- 7.68 IEC 60060–1: *High-voltage Test Techniques – Part 1: General Definitions and Test Requirements* (IEC, Geneva 2010)
- 7.69 IEC 60060–2: *High-voltage Test Techniques – Part 2: Measuring Systems* (IEC, Geneva 2010)
- 7.70 IEC 60076–4: *Power Transformers – Part 4: Guide to the Lightning Impulse and Switching Impulse Testing – Power Transformers and Reactors* (IEC, Geneva 2002)
- 7.71 IEEE Std. C57.98–2011: *IEEE Guide for Transformer Impulse Tests* (IEEE, New York 2011)
- 7.72 IEC 60270: *High-voltage Test Techniques – Partial Discharge Measurements* (IEC, Geneva 2000)
- 7.73 IEC TS 62478: *High Voltage Test Techniques – Measurement of Partial Discharges by Electromagnetic and Acoustic Methods* (IEC, Geneva 2000)
- 7.74 IEEE Std. C57.113–2010: *IEEE Recommended Practice for Partial Discharge Measurement in Liquid-Filled Power Transformers and Shunt Reactors* (IEEE, New York 2010)
- 7.75 IEEE Std. C57.127–2018: *IEEE Guide for the Detection, Location and Interpretation of Sources of Acoustic Emissions from Electrical Discharges in Power Transformers and Power Reactors* (IEEE, New York 2018)
- 7.76 IEC 60076–5: *Power Transformers – Part 5: Ability to Withstand Short Circuit* (IEC, Geneva 2006)
- 7.77 A. Carlson, J. Fuhr, G. Schemel, F. Wegscheider: *Testing of Power Transformers, Routine Tests, Types Tests and Special Tests* (ABB, Zurich 2003)
- 7.78 W. Hauschild, E. Lemke: *High-Voltage Test and Measuring Techniques*, 2nd edn. (Springer Nature, Cham 2019)
- 7.79 L. Eklund, P. Lorin, P. Werle, P. Köstinger, M. Oktem: Increase transformer reliability and availability. In: *Power-Gen Conf. Middle East, Manama* (2007)
- 7.80 CIGRE Working Group JWG D1/A2.47, TB 771: *Advances in DGA Interpretation* (CIGRE, Paris 2019)
- 7.81 R. Müller, H. Schliesing, K. Soldner: Prüfung und Überwachung von Transformatoren durch Analyse der im Öl gelösten Gase, *Elektrizitätswirtschaft* **23**, 683–691 (1974)
- 7.82 M. Duval: Dissolved gas analysis: it can save your transformer, *IEEE Electr. Insul. Mag.* **5**(6), 22–27 (1989)
- 7.83 P. Werle: Practical aspects of different new diagnostic methods for the condition assessment of power transformers. In: *17th Int. Symp. High Volt. Eng. (ISH), Hannover* (2011)
- 7.84 N. Abeywickrama, D. Bormann, J.L. Bermudez, O. Kouzmine, P. Werle: Sensitivity of FRA in detecting transformer faults: results of a measurement campaign. In: *CIGRE SC A2 & D1 Jt. Colloq.*, Kyoto (2011)
- 7.85 H. Schering: Brücke zur Verlustmessung, *Z. Instrum.* **40**, 24 (1920)
- 7.86 P. Lorin, L. Eklund, P. Werle, E. Zeitz: Increase transformer reliability and availability: from condition assessment to site repair. In: *TechCon Asia-Pacific, Sydney* (2009)

- 7.87 CIGRE Working Group WG A2.38, TB 659: *Transformer Thermal Modelling* (CIGRE, Paris 2016)
- 7.88 K. Schlosser: Die Nullimpedanzen des Voll- und Spartransformators, BBC-Mitteilungen **44**(2), 78–83 (1962)
- 7.89 H. Jahangir, A. Akbari, P. Werle, J. Szczechowski: Possibility of PD calibration on power transformers using UHF probes, IEEE Trans. Dielectr. Electr. Insul. **24**(5), 2968–2976 (2017)
- 7.90 H. Jahangir, A. Akbari, P. Werle, J. Szczechowski: UHF PD measurements on power transformers—advantages and limitations, IEEE Trans. Dielectr. Electr. Insul. **24**(6), 3933–3940 (2017)
- 7.91 G. Leber, H. Passath, M. Ryadi, P. Hurlet: Short circuit verification for a 570 MVA, 420 kV single-phase GSU-transformer by SC-withstand tests on a mock-up unit, e & i Elektrotech. Informationstech. **8**, 340–348 (2014)
- 7.92 P. Werle: On-site tests of power transformers. In: *20th Nordic Insul. Symp. (NORD-IS)*, Lyngby (2007)
- 7.93 P. Werle: TrafoSiteTesting. In: *OMICRON DMPT, Diagn. Meas. Power Transf., Feldkirch* (2008)
- 7.94 P. Werle, P. Lorin, L. Eklund: Innovative asset management using MTMP and TrafoSiteTesting. In: *10th Int. Electr. Gas Netw. Conf., Energy 21C, Melbourne* (2009)
- 7.95 J. Szczechowski, P. Werle: Experiences with on-site testing of power transformers – TrafoSiteTesting. In: *16th Int. Symp. High Volt. Eng. (ISH)*, Cape Town (2009)
- 7.96 J. Szczechowski, P. Werle: High voltage testing on transformers on-site. In: *2nd Int. Transf. Life Manag. Conf., Dubai* (2014)
- 7.97 J. Szczechowski, P. Werle: Enhanced methods of high voltage testing on power transformers on-site. In: *Int. Conf. Condition Monit. Diagn. (CMD)*, Tokyo (2010)
- 7.98 P. Werle, J. Szczechowski, T. Asshauer: HV-testing of power transformers with electronic power sources. In: *ITCE Int. Transf. Conf., Tehran* (2016)
- 7.99 J. Szczechowski, P. Werle, O. Kouzmine: Experience and benefit with on-site testing of power transformers using mobile high voltage impulse and AC test systems. In: *CIGRE SC A2 & D1 Jt. Colloq., Kyoto* (2011)
- 7.100 P. Werle: TrafoSiteTesting™. In: *Int. Transf. Life Manag. Conf., Guangzhou* (2014)
- 7.101 P. Werle: Trends in der Hochspannungsprüftechnik. In: *Transf. Life Manag. Tag. (TLM), Halle* (2012)
- 7.102 C.W. Reed, W.N. Kennedy, H.M. Schneider: Compressed SF<sub>6</sub> gas insulation technology development for advanced concepts in gas-insulated power transformers. In: *CIGRE, Session 1984, Paris* (1984)
- 7.103 D.C.M. Yuen, V. Choi, L.Z. Gao, J. Han: The first 110 kV/35 kV –31.5 MVA cast resin transformer. In: *Conference Record 2004 IEEE Ind. Appl. Conf., 39th IAS Annu. Meeting, Seattle* (2004)
- 7.104 M.G. Unde, B.E. Kushare: Analysis of electromagnetic fields of 1200kV UHV-AC transmission lines. In: *CICN 2013, 5th Int. Conf. Comput. Intell. Commun. Netw., Mathura* (2013)
- 7.105 CIGRE Working Group WG A2.42, TB 673: *Guide on Transformer Transportation* (CIGRE, Paris 2016)
- 7.106 CIGRE Working Group WG A2.37, TB 642: *Transformer Reliability Survey* (CIGRE, Paris 2015)
- 7.107 T. Stirl, M. Saravolac, J. Harthun: The new hermetic power transformer generation – hermetic 2.0. In: *13th Int. Electr. Insul. Conf. (INSUCON 2017)*, Birmingham (2017)
- 7.108 FNN (Forum Netztechnik/Netzbetrieb): *Voltage Regulating Distribution Transformer (VRDT); Use in Grid Planning and Operation* (FNN, VDE, Berlin 2016)
- 7.109 ABB: *Dry-Type Transformers – RESIBLOC; Transformer Technology Reducing Environmental Impact* (ABB, Brilon 2018)
- 7.110 ABB: *Phase Shifting Transformers; Reliable and Efficient Power Flow Control* (ABB, Zurich 2011)
- 7.111 ABB: *ABB Review* (ABB, Mannheim 2017)
- 7.112 IEC 61378–2: *Converter Transformers – Part 2: Transformers for HVDC Applications* (IEC, Geneva 2001)
- 7.113 ABB: *Special Transformers; Furnace and Rectifier Transformers* (ABB Oy, Vaasa 2013)
- 7.114 ABB: *RESIBLOC Rail; Breakthrough Oil-free Traction Transformer* (ABB, Brilon 2018)
- 7.115 M. Beyer, W. Boeck, K. Möller, W. Zaengl: *Hochspannungstechnik* (Springer, Berlin 1986)
- 7.116 I. Baciu: Contributions concerning the short-circuited mobile coil transformers. *Corpus ID: 55298841* (2010)
- 7.117 ABB: *Shunt Reactors; Proven History for Future Success* (ABB, Zurich 2018)

### Peter Werle

High Voltage Engineering and Asset Management (Schering-Institute)  
Leibniz Universität Hannover (LUH)  
Hannover, Germany  
[peter.werle@ifes.uni-hannover.de](mailto:peter.werle@ifes.uni-hannover.de)



Peter Werle received his PhD in electrical engineering from the University of Hannover. Before becoming Director of the Schering Institute in 2014, he was General Manager of the ABB Transformer Service in Germany. He is active in the VDE, DKE, IEC, and CIGRÉ, the inventor of more than 20 patents, and has authored/coauthored more than 300 publications in the fields of high-voltage engineering and asset management.

### Hartmut Brendel

Retired Head of Technical Development,  
ABB Transformer Service  
Consultant for Transformers and HV  
Applications  
Halle, Germany



Hartmut Brendel studied electrical engineering at the Technical University of Ilmenau. He worked for more than thirty years as an electrical and mechanical designer in the transformer business. Before his retirement, he was Head of Technical Development at the Engineering Solutions division of ABB in Halle (Saale), Germany. He has been a technical consultant on transformers and high-voltage applications since 2014.

# High Voltage

## 8. High Voltage Equipment

Hiroki Ito

This chapter focuses on substation equipment, which is used in power systems to transport and distribute the electric energy from power-generation plants to households, offices, and factories efficiently. In transmission and distribution networks, switching equipment such as circuit breakers and disconnecting switches is required to open and close circuits in power systems. When a fault occurs, circuit breakers are needed to clear the fault quickly to ensure system stability. Circuit breakers must also be able to carry a load current without excessive heating and withstand the system voltage during normal and abnormal conditions.

Measuring equipment such as instrument transformers and overvoltage protection units such as surge arresters are also used in power systems. Surge arresters are installed at different locations in power systems to limit lightning-induced and switching-induced overvoltages to a specified protection level below the withstand voltage of the equipment.

It is also mainly devoted to technical description of switching equipment used in both high-voltage alternating current (HVAC) and high-voltage direct current (HVDC) power systems. Fundamental interrupting and switching phenomena for different switching equipment are discussed.

Readers should note that more detailed and specific information on switching equipment can be found in many technical brochures and documents published by CIGRE, including the CIGRE Green Book on switching equipment.

8.1	<b>High-Voltage Equipment in Power Systems</b> .....	512
8.1.1	Substation Equipment .....	513
8.1.2	Surge Arresters .....	515
8.1.3	Instrument Transformers .....	517
8.1.4	Series Capacitor, Shunt Capacitor, and Shunt Reactor Compensation .....	522
8.1.5	Substation Post Insulators .....	525
8.1.6	Technical Requirements and Design Parameters .....	527
8.2	<b>History and Principles of High-Voltage Circuit Breakers</b> .....	528
8.2.1	History of Circuit Breaker Development .....	528
8.2.2	Interrupting Phenomena for Oil and Air Circuit Breakers .....	531
8.2.3	Interrupting Phenomena for Gas Circuit Breakers .....	532
8.2.4	Interrupting Phenomena for Vacuum Circuit Breakers .....	539
8.2.5	Comparison of the Dielectric Withstands of Various Interrupting Media .....	542
8.2.6	Summary .....	542
8.3	<b>Switching Phenomena in Power Systems</b> .....	542
8.3.1	Fundamental Switching Phenomena .....	543
8.3.2	Bus Terminal Fault Interruption .....	543
8.3.3	Short Line Fault Interruption .....	547
8.3.4	Capacitive Current Switching .....	552
8.3.5	Small Inductive Current Switching .....	555
8.3.6	Transformer Limited Fault Clearing .....	557
8.3.7	Out-of-Phase Current Switching .....	560
8.3.8	Mechanical Model of Power System Stability .....	564
8.3.9	Comparison of the Switching Phenomena Obtained at 50 and 60 Hz .....	566
8.3.10	Switching Requirements for UHV Transmission .....	568
8.3.11	Summary .....	576
8.4	<b>Controlled Switching</b> .....	576
8.4.1	Principle of Controlled Switching .....	577
8.4.2	Capacitor Switching Applications .....	579
8.4.3	Reactor Switching Applications .....	581
8.4.4	Transformer Energization .....	582
8.4.5	Line Switching Applications .....	587
8.4.6	Summary .....	590
8.5	<b>DC Circuit Breakers</b> .....	591
8.5.1	HVDC Networks .....	591
8.5.2	Current Zero Creation Schemes for DC Circuit Breakers .....	591
8.5.3	DC Current Interruption .....	592
8.5.4	MV and LVDC Circuit Breakers .....	594

8.5.5 Behavior When Using the Passive Current Creation Scheme ...	596	8.5.8 Hybrid Mechanical and Power Electronic Switch.....	602
8.5.6 Field Experience of MRTB.....	598	8.5.9 HVDC Disconnecting Switches.....	606
8.5.7 Application of the Active Resonant Current Injection Scheme in HVDC Circuit Breakers.....	600	8.5.10 Summary.....	608
		<b>References</b> .....	608

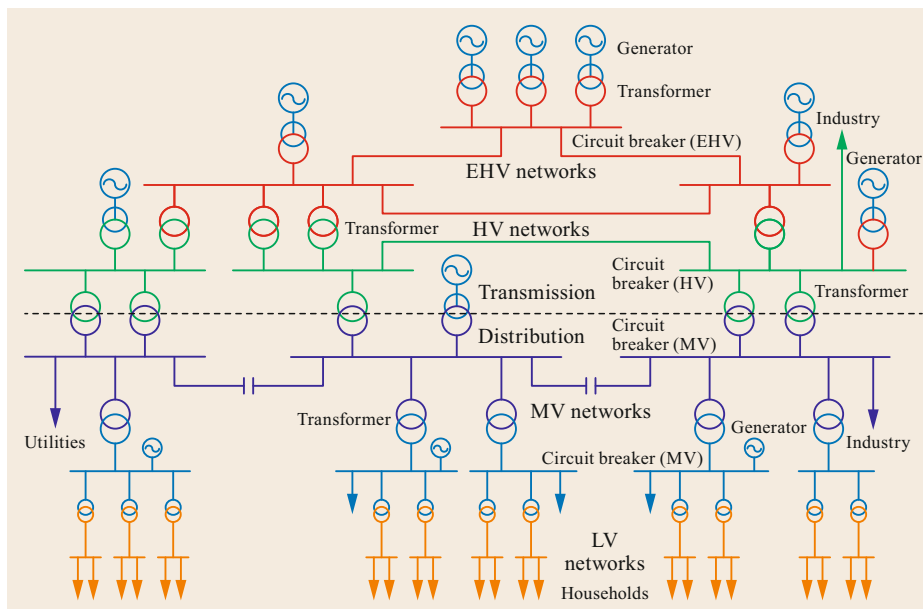
## 8.1 High-Voltage Equipment in Power Systems

Power systems with various types of substation equipment efficiently transport and distribute the electric energy from power-generation plants to households, offices, and factories. Alternating current (AC) power systems are generally used for energy transportation because the voltage can easily be stepped up and down to reduce energy losses during transportation, but direct current (DC) power systems have recently increased in popularity. The number of applications of DC power systems have recently increased due to rapid development of power electronics technology and the need for a long distance connection of offshore or remote wind farms and/or large hydro power generators. HVDC transmission has several benefits such as lower transmission losses, fewer lines required for the same power transmission, and less system stability problems in comparison with HVAC transmission.

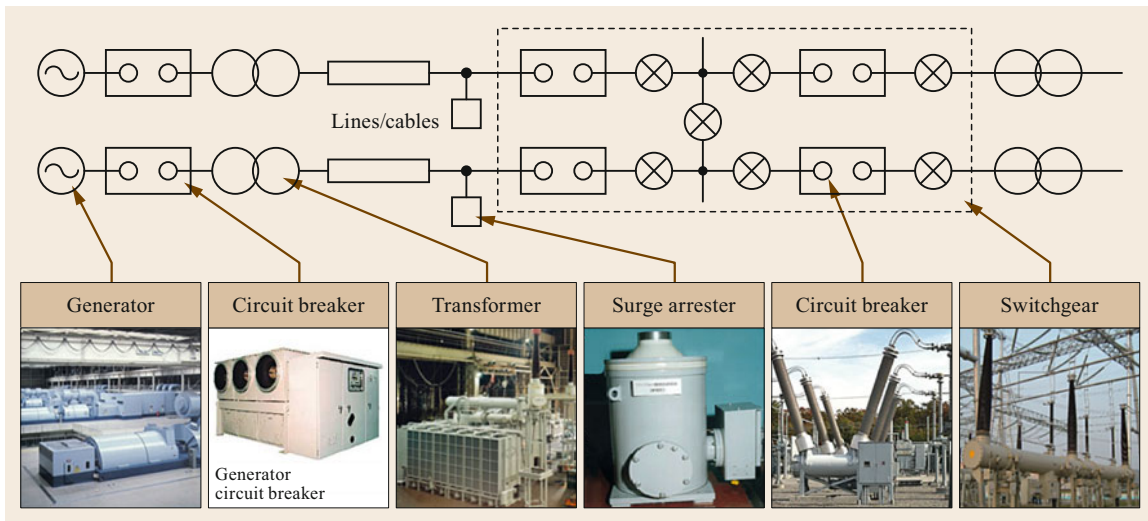
When power systems were first invented, there was what is now known as the *war of the currents*. Thomas Edison developed the first DC-based electric power transmission system in 1882, which was then used to

provide 110 V DC current to some households in the US. However, from the early 1880s on, with the development of power transformers in Europe and in the US, respectively, that enabled the voltage to be easily stepped up and down, AC-based power distribution systems began to grow in popularity compared to DC-based systems because it was possible to transmit electricity over much longer distances and through cheaper wires using AC. Therefore, by the early 1890s, AC power systems dominated the market, ending the war of the currents in 1892. The first circuit breaker was developed in the early twentieth century, which enabled to disseminate electricity networks, because circuit breakers can quickly disconnect a faulted circuit and allow continuous transmission and distribution in the healthy networks.

Figure 8.1 shows a typical AC power system from power generation to energy transportation and distribution. Power generators convert mechanical energy into electric energy, while aluminum and copper conductors in overhead lines and underground cables transport the



**Fig. 8.1** Typical AC power system



**Fig. 8.2** Typical AC substation equipment

electric energy to where it is needed. In substations, power transformers step up the voltage at the source side and step it down at the load side. Along with measuring equipment and overvoltage protection units such as surge arresters, switching equipment is used to close a circuit or interrupt a nominal or fault current.

Depending on the system voltage used, transmission networks are generally classified into ultrahigh voltage (UHV), extra-high-voltage (EHV), and high-voltage (HV) networks, whereas distribution networks are classified into medium-voltage (MV) and low-voltage (LV) networks. MV generally refers to voltages up to and including 52 kV, and HV to voltages higher than 52 kV. Some countries do not have a MV classification; in those countries, all voltages higher than 1 kV are generally considered to be HV. EHV usually refers to a voltage range of around 230 kV (this value can vary from country to country) to 800 kV. UHV generally refers to voltages exceeding 800 kV.

Power systems are required to efficiently transport the electricity from the generator to the load site, while maintaining the voltage and frequency within the specified levels. For this purpose, switching equipment is required to perform the following operations:

- Energizing and deenergizing cables, overhead lines, and power transformers
- Connecting and disconnecting to shunt capacitors or shunt reactors
- Transferring the current from one circuit to another
- Interrupting a fault current and isolating a faulty part of the system
- Isolating particular substation equipment for maintenance or to allow it to be replaced.

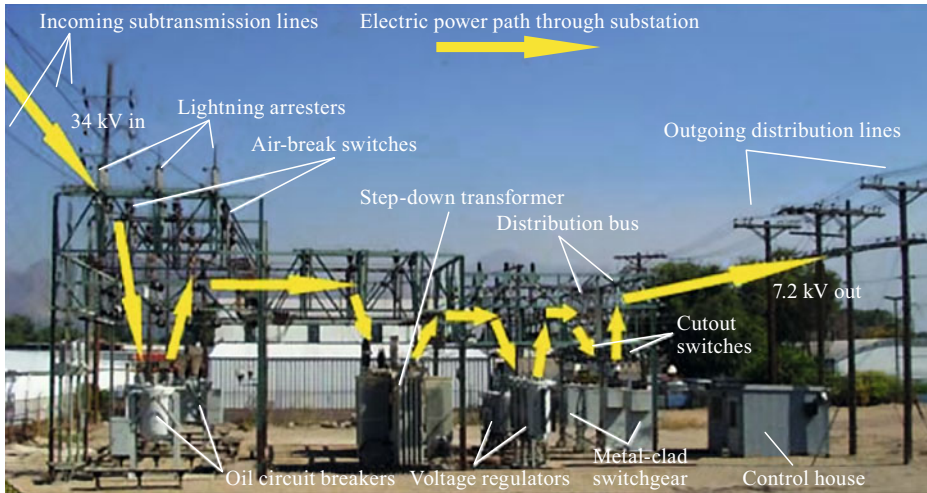
In the next section, we introduce various types of substation equipment such as circuit breakers, disconnecting switches, earthing switches, surge arresters, and instrument transformers.

### 8.1.1 Substation Equipment

Figure 8.2 shows a one-line diagram of a typical substation, including the main substation equipment. The substation serves several functions: it transforms voltage from low to high and vice versa and it switches circuits off and on. To achieve these functions, the substation has power transformers, circuit breakers, and metal oxide surge arresters that protect the system and equipment from excessive overvoltages. Figure 8.3 shows a photograph of a typical MV substation, including power transformers, circuit breakers (circuit switches), and surge arresters. The voltage received from the incoming overhead line (34 kV) is changed to an appropriate level (7.2 kV) before the electricity is directed into the outgoing distribution line at the substation.

The main switching equipment in the substation is a circuit breaker, which is used to quickly clear a fault and ensure system stability. The circuit breaker must be able to carry the load current without excessive heating and withstand the system voltage during normal and abnormal conditions. Unlike a fuse, a circuit breaker can be reclosed either manually or automatically to resume normal operation.

A circuit breaker with interrupters inside a tank insulated from earth potential is termed a live-tank circuit breaker (Fig. 8.4). The tank is normally composed of porcelain or a composite of insulators. The conductor



**Fig. 8.3** Photograph of a typical substation. (From the website of Occupational Safety & Health Administration, United States Department of Labor; <https://www.osha.gov>)

can be connected directly to the live part of the breaker terminals.

In contrast, a circuit breaker with interrupters inside an earthed metal enclosure is termed a dead-tank circuit breaker (Fig. 8.5). The conductor carrying the system voltage from the interrupters is fed outside through bushings.

A disconnecting switch is a type of switching equipment capable of opening and closing a circuit where only a negligible current is flowing through the electrodes, without significantly changing the voltage across the terminals of each pole of the disconnecting switch. It is capable of carrying currents under normal circuit conditions as well as currents under abnormal circuit conditions (e.g., a short circuit) for a specified time. Disconnecting switches are employed to interrupt small currents of 1 A or less, since they are operated under live conditions.

There are various types of air-break disconnecting switches: vertical break, center side break, double side

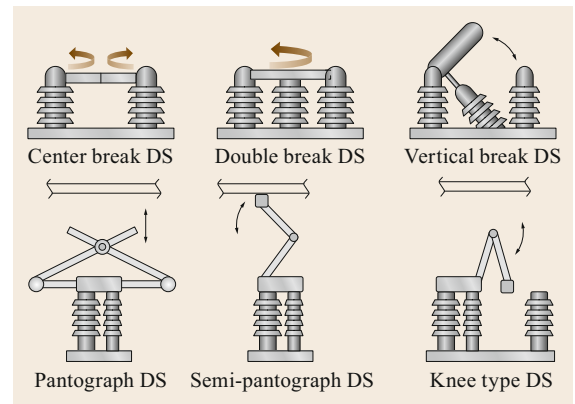
break, knee, and pantograph, as shown in Fig. 8.6. Vertical break disconnecting switches are usually mounted horizontally, but some are vertically mounted. Center side break disconnecting switches require wider phase spacing. Knee-type disconnecting switches are favored



**Fig. 8.5** Photograph of a 550 kV AC dead-tank circuit breaker. (Courtesy of Chugoku Electric Power)



**Fig. 8.4** Photograph of a 550 kV live-tank SF<sub>6</sub> gas circuit breaker. (Courtesy of Dominion Energy)



**Fig. 8.6** Typical disconnecting switches





**Fig. 8.7** Photograph of 77 kV composite-type MOSAs in a substation. (Courtesy of Chubu Electric Power)

when the clearance above the switch is restricted. The pantograph type is the most compact design for installation.

An earthing switch is manually or automatically closed for earthing/grounding and insulating a circuit before working on that circuit. It is open during normal power transmission operation.

An instrument transformer is a measuring device that uses the secondary current or voltage, which is essentially proportional to the primary current or voltage.

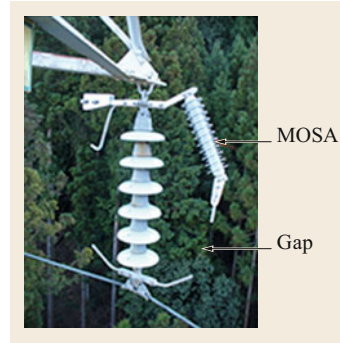
A surge arrester can limit the duration and (frequently) the amplitude of the voltage, and is therefore used to protect the system and equipment from excessive overvoltages due to lightning strikes or switching operations. One important role of a surge arrester is to maintain the reliability of the power system and equipment, as described in more detail below.

All types of substation equipment are assigned a rated voltage by the manufacturer of the equipment. The manufacturer-specified performance of the equipment in a power system corresponds to the performance achieved at the rated voltage.

### 8.1.2 Surge Arresters

There are two different types of overvoltages in a power system: those generated by lightning strokes and those produced by switching operations. Substation equipment must be able to withstand these overvoltages up to the specified overvoltage withstand level. Surge arresters [8.1] perform an important role in suppressing excessive overvoltages in substations (Fig. 8.7) and in transmission lines (Fig. 8.8).

Surge arresters are installed at different locations in substations to limit lightning-induced and switching-induced overvoltages to a specified protection level, which should (in principle) be below the withstand voltage of the equipment. An ideal surge arrester would

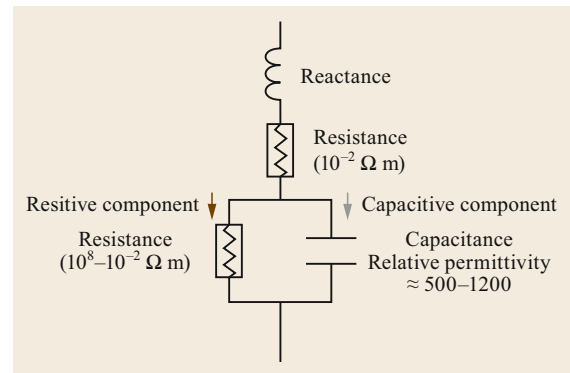


**Fig. 8.8** Photograph of a MOSA with a gap used in a transmission line. (Courtesy of Chubu Electric Power)

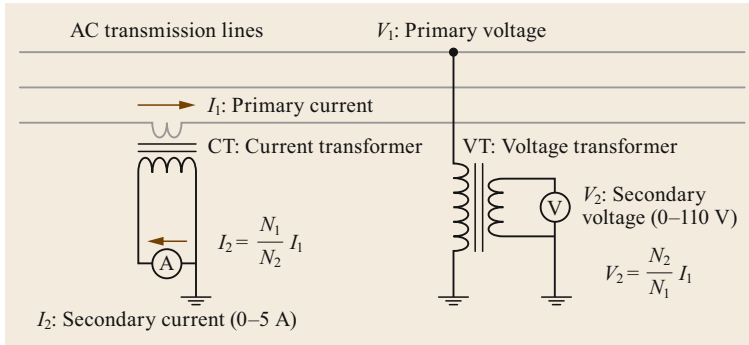
convert from an insulating state to a conducting one at a specified voltage in order to maintain the voltage level and avoid an excessive overvoltage, and would shift from a conducting state to an insulating one as soon as the voltage across the surge arrester drops below the specified voltage level. Therefore, a surge arrester only has to absorb the energy associated with the overvoltage.

Figure 8.9 shows the equivalent circuit of a metal-oxide surge arrester (MOSA) element. The current-voltage characteristic of the MOSA presents a degree of nonlinearity, which results in a low protection level (due to the dispersion of the resistive current-voltage characteristic at high current) and low power dissipation at the operating voltage of the system. A MOSA can be connected to the system without the need for a series of spark gaps that disconnect the varistors from the operating voltage. However, this is only possible if the current-voltage characteristic of the MOSA remains stable over time and if the correct MOSA has been selected for use given the voltage stresses that occur in service. Surge arresters must also be thermally stable. The current through the metal-oxide varistor block at the operating voltage has to stay well within the current-voltage characteristic.

When the residual current flows through the metal-oxide varistor, it remains capacitive and the voltage



**Fig. 8.9** Equivalent circuit of a MOSA disk element



**Fig. 8.10** Principles of conventional instrument transformers (CT and VT)

across the varistor elements is determined by their capacitance and thus influenced by stray capacitances. Stray capacitances to earth cause a deviation from the linear axial voltage distribution, because of higher voltage stress imposed on the upper elements in the arresters. This deviation is influenced by physical parameters of the arrester such as its height, number, and length of arrester elements and its grading rings.

With increasing varistor temperature during operation, the ohmic current component of the varistor increases the linearity of the voltage distribution in the arrester. Grading rings are often inserted as a passive and effective measure to improve the voltage distribution.

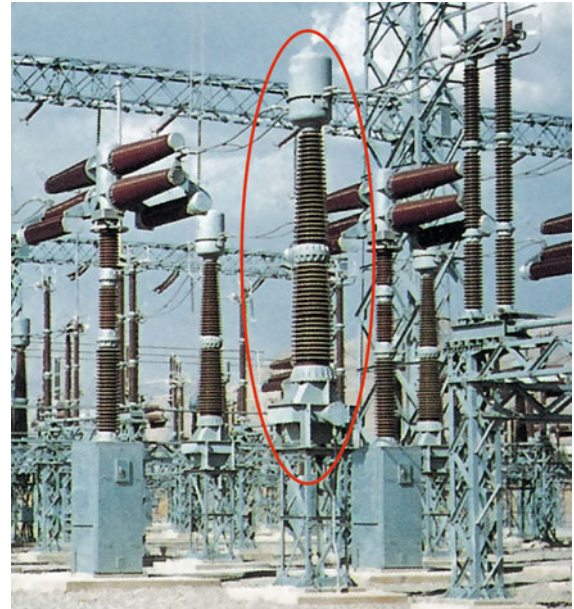
The design and operation of surge arresters has changed radically over the last thirty years from valve-type or spark-gap-type silicon carbide (SiC) surge arresters to gapless metal-oxide (MO) or zinc-oxide (ZnO) surge arresters.

A MOSA essentially consists of billions of microscopic junctions of metal-oxide grains that turn on and off in microseconds to create a current path from the top terminal to the earth terminal of the arrester. Therefore, it can be regarded as a very fast-acting electronic switch that is open to operating voltages. The current-voltage characteristic of the metal-oxide material offers the nonlinearity necessary to fulfill the contradictory requirements of an adequate protection level at overvoltages and low energy dissipation at the system operating voltage. MOSAs are suitable for protection against switching overvoltages at all operating voltages.

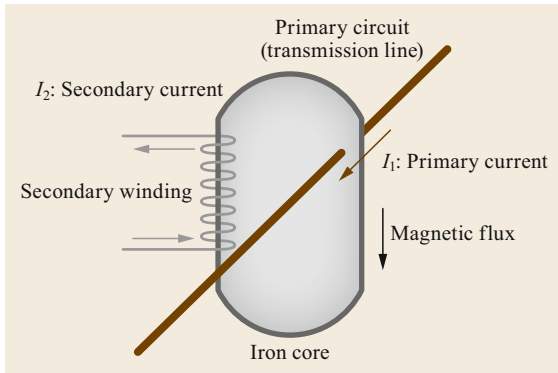
Traditionally, metal-oxide surge arresters were housed in porcelain. For satisfactory performance, it is important that the units are hermetically sealed for the lifetime of the arrester discs. The sealing arrangement at each end of a porcelain-housed arrester consists of a stainless-steel plate with a rubber gasket. A rapid increase in the internal arc pressure due to a failure may cause the sealing plate to open and the gases to flow

out through venting ducts. Since these ducts are oriented towards each other, this results in an external arc, relieving the internal pressure and preventing the insulator from being violently shattered.

The benefits of a leak-tight design employing the polymers highlighted in Fig. 8.7 are now generally accepted, which has resulted in a shift from porcelain to polymer (composite-type) housing. The bonding of the silicone rubber with the active parts in polymer-housed arresters is very reliable, so gaskets or sealing rings are not required. When failure occurs, the arc easily burns through the soft silicone material, permitting the rapid release of the resultant gases. Hence, the special pressure-relief vents incorporated into porcelain housing to avoid explosions are not required with composite-type housing.



**Fig. 8.11** Photograph of a conventional 550 kV electromagnetic-type current transformer



**Fig. 8.12** Basic configuration of a conventional current transformer (CT)

### 8.1.3 Instrument Transformers

Instrument transformers are electrical devices that are used to probe the voltage and current in an AC power system and to generate an information signal that can be sent to measuring instruments, meters, and protective or control systems. The fundamental function of instrument transformers is to step down the high voltage and current present in transmission and distribution systems to low voltage (110–120 V) and current (5 A) levels. The term *instrument transformer* encompasses both current transformers and voltage transformers [8.2].

Current transformers (CTs) and voltage transformers (VTs) convert the primary current and voltage to the secondary current and voltage, respectively. The secondary current and voltage are essentially proportional to the primary current and voltage, respectively, and differ from them by a phase angle that is approximately zero for an appropriate connection. The windings of CTs or VTs connected to the primary side are isolated from those of the secondary side, and there is usually a meter or relay in the secondary circuit. Due to the low

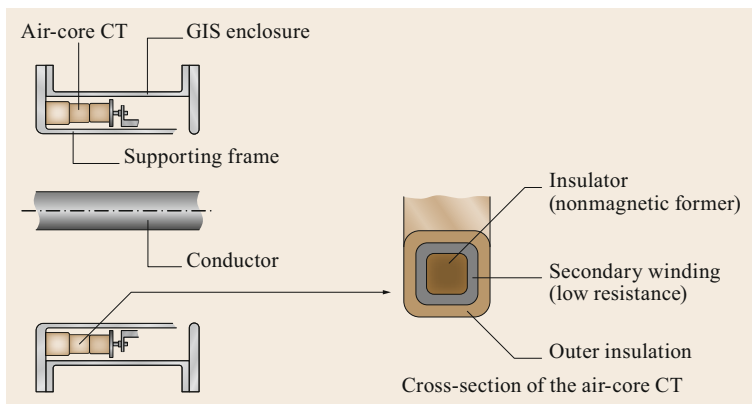
voltage and current levels in the secondary circuit, the power consumption of instrument transformers and protective circuits is advantageously low.

CTs and VTs are used to step down the primary current and voltage of power systems to lower levels so that they can be measured by an ammeter or voltmeter with a small rating (e.g., 5 A or 110 V). Figure 8.10 shows a conventional CT and VT arrangement on transmission lines, where the secondary circuit is isolated from the primary circuit with a transformer. Figure 8.11 shows a conventional 550 kV electromagnetic-type current transformer.

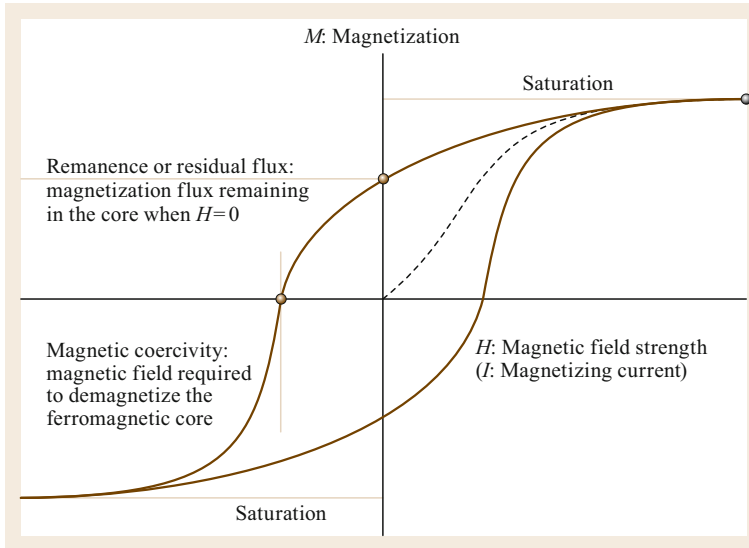
The winding of a conventional CT at the primary side has only a few turns or, more commonly, consists of a primary conductor (bar) with just one turn. On the other hand, the winding of a CT on the secondary side normally has a large number of turns (Fig. 8.12). The secondary winding is directly connected to an ammeter. As the ammeter has a stray impedance, the secondary circuit of a CT usually operates under short-circuit conditions. One terminal of the secondary circuit is earthed to avoid overvoltage.

Conventional CTs with an iron core have long been widely applied for current measurements in AC power systems. However, nonconventional CTs such as a CT with an air core, an electronic CT (ECT) with a Rogowski coil, and an optical CT have recently found increasing application in this context due to some technical advantages: nonsaturation, a wide dynamic range, a compact design, and a low weight. Conventional CTs used in EHV and UHV power systems require a heavy iron core with a large diameter to avoid core saturation, especially for gas-insulated switchgear (GIS) applications, as shown in Fig. 8.13.

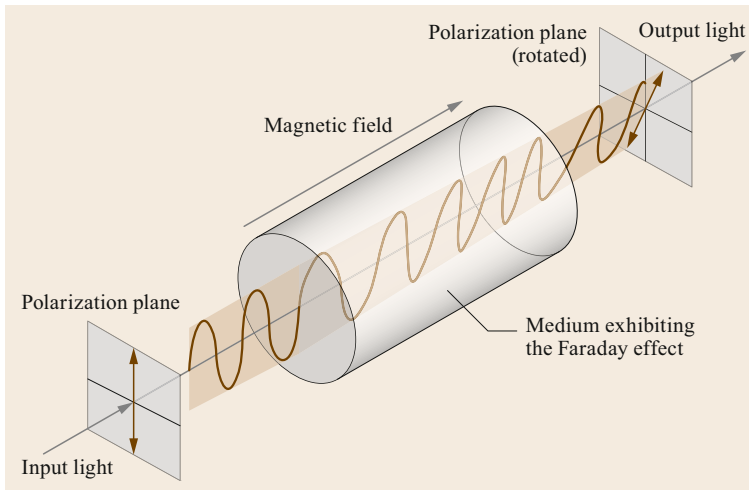
The magnetization ( $M$ ) of a magnetic core normally increases with the external magnetic field ( $H$ ) or the magnetizing current through the core (caused by the magnetic field). However, the magnetization eventu-



**Fig. 8.13** Configuration of an air-core CT for EHV-class GIS



**Fig. 8.14** Hysteresis loop (MH-characteristic) of an air-core CT for EHV-class GIS



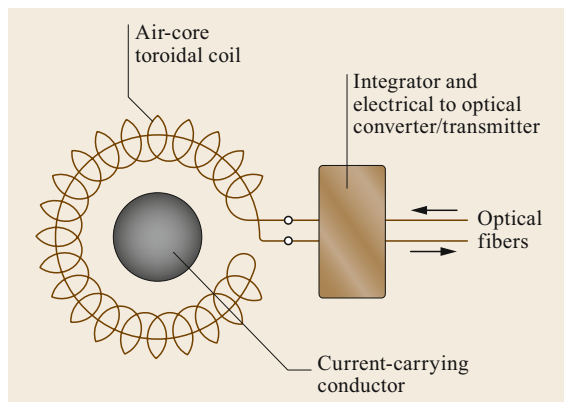
**Fig. 8.15** Use of the Faraday effect in an optical CT

ally saturates when the external magnetic field reaches a certain threshold value where the magnetic field cannot increase the magnetization of the core further. This threshold value depends on the ferromagnetic material involved. Above the saturation level, an instrument transformer does not respond linearly with magnetic flux to increases in current in the primary circuit, meaning that the secondary current is no longer proportional to the primary current.

Figure 8.14 shows a schematic of the magnetic hysteresis loop (the  $M$ - $H$  characteristic of the ferromagnetic core). As the magnetic field ( $H$ ) increases, the magnetization ( $M$ ) approaches the saturation value. Above the saturation level, the total magnetic flux density continues to increase with increasing magnetic field, but only very slowly.

When the magnetic field decreases to zero, the magnetization does not become zero because the atoms in the core retain some inherent level of magnetic orientation. This is called the magnetic remanence or the residual flux of the core. The polarity of the magnetic field must be reversed to demagnetize the core.

Air-core CTs and Rogowski coils use a nonmagnetic former instead of an iron core for the secondary winding in order to eliminate core saturation. Unlike conventional CTs, the output signal of a nonconventional CT is a voltage because it detects the voltage induced by the magnetic flux (induced by the primary current) passing through the secondary winding. The output signal from an air-core CT with low impedance in the secondary winding can be connected directly to a protection device. The output signal from a Rogowski



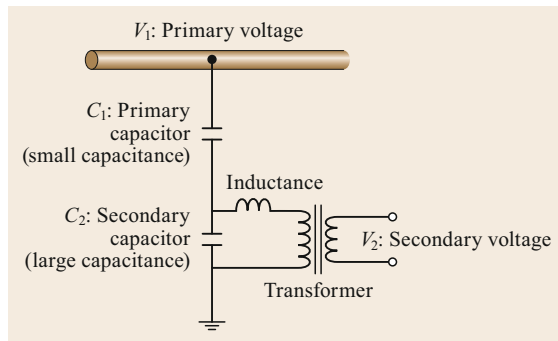
**Fig. 8.16** Use of a Rogowski coil for current measurement

coil for ECT, which has high impedance in the secondary winding, is converted to a digital (optical) output near to substation equipment such as GIS and circuit breakers and then transmitted to a protection device. An optical CT uses the Faraday effect (Faraday rotation) for current measurement. Faraday rotation is a magneto-optical phenomenon resulting from the interaction between light and a magnetic field in a medium. It causes the plane of polarization to rotate to an extent that is linearly proportional to the magnetic field in the direction of propagation, as shown in Fig. 8.15. Table 8.1 summarizes the different principles used by these CTs.

The Rogowski coil is a CT with a very high load impedance but without a ferromagnetic core. The output signal is a function of the first derivative of the current. The secondary winding is wound around a toroid of insulating material. The Rogowski coil is normally connected to measuring or protection equipment through an amplifier. Figure 8.16 shows a schematic of a typical Rogowski coil sensor.

CTs are designed to provide an output of either 1 or 5 A, even when using a modern programmable protection relay, which does not present a problem because the CT ratio can be adjusted to the input received from the CT. Therefore, the output from the CT needs to meet the input requirements of the protection relay. Various ratios (such as 3000/2000/1000/1A) can be supplied by a CT. This allows the lowest current to be measured initially with a ratio of 1000/1A. When the current demand grows, the ratio can be changed to 2000/1A or 3000/1A. CTs with ratios of 2000/1600/1200/800/600/500/400/1A are suitable for measuring a primary current of between 2000 and 400 A. High-voltage CTs are often insulated with mineral oil or SF<sub>6</sub> gas, while medium- and low-voltage CTs are normally insulated with solid epoxy casting resin.

A VT or potential transformer (PT) steps the voltage of the power system down to a lower level. There



**Fig. 8.17** Typical configuration of a capacitor voltage transformer (CVT)

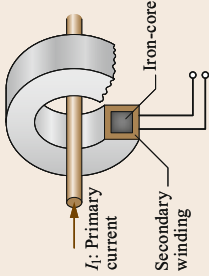
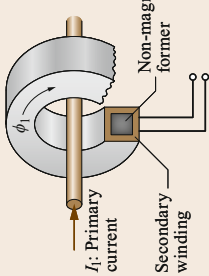
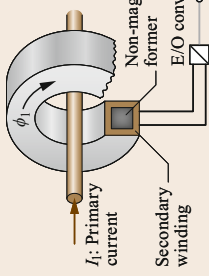
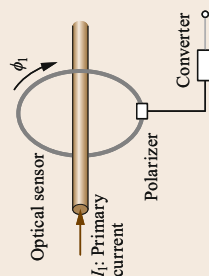
are three major types of VTs or PTs: conventional electromagnetic, capacitor, and optical sensor. A conventional electromagnetic VT uses a transformer with primary and secondary windings. A capacitor voltage transformer (CVT) uses a capacitive potential divider, which provides an economic benefit compared with an electromagnetic VT, especially for higher-voltage applications. The optical voltage transformer exploits the Faraday effect and detects the rotation of polarized light passing through optical materials.

The primary winding of a conventional VT is connected to the line (main circuit) on one side and earthed on the other terminal. The secondary winding of the VT has a few turns that are directly connected to a voltmeter with high impedance and isolated from the primary circuit. The secondary circuit normally operates in the open, with one terminal earthed to ensure safety.

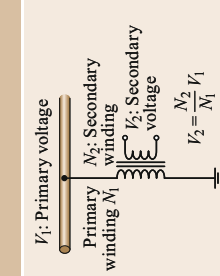
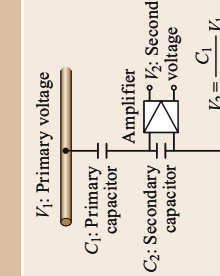
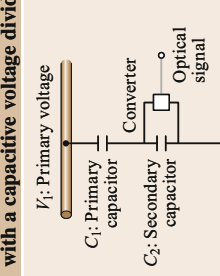
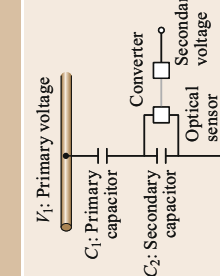
A conventional VT requires a large iron core, especially for EHV and UHV applications. Figure 8.17 shows the typical configuration of a CVT, which provides a low-voltage signal for metering or operating a protective relay. A CVT normally consists of three parts: two dividing capacitors, an inductance to tune the device to the line frequency, and a voltage transformer to isolate the voltage from metering devices or protective relays. Capacitor  $C_1$  is often composed of a stack of smaller capacitors connected in series. This provides a large voltage drop across  $C_1$  and a relatively small voltage drop across  $C_2$ . The dividing capacitors reduce the level of insulation required for the voltage transformer. This makes CVTs more economical than conventional voltage transformers when they are used at transmission levels.

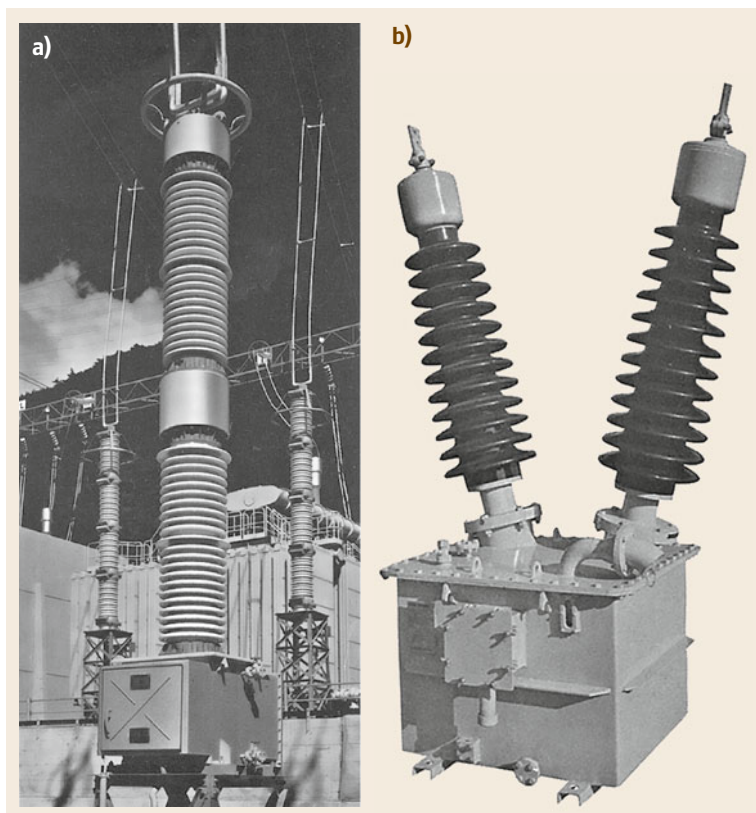
The output voltage of a CVT is converted into a digital signal near equipment and may be transmitted to protection systems. Table 8.2 summarizes the principles of the different types of VTs. Figure 8.18 shows a typical 300kV CVT and a 72kV inductive voltage transformer.

**Table 8.1** Principles of various types of current transformers (CTs)

Conventional electromagnetic CT	Air-core type CT	ECT/Rogowski coil	Optical CT
 <p><math>I_1</math>: Primary current Secondary winding <math>I_2</math>: Secondary current</p>	 <p><math>I_1</math>: Primary current Secondary winding <math>V_2</math>: Secondary voltage</p>	 <p><math>I_1</math>: Primary current Secondary winding <math>V_2</math>: Secondary voltage Optical signal</p>	 <p>Optical sensor <math>I_1</math>: Primary current Polarizer Converter Optical signal or <math>V_2</math>: Secondary voltage</p>
<p>The secondary current is inversely proportional to the ratio of the secondary to the primary winding <math>I_2 = \frac{N_1}{N_2} I_1</math></p>	<p>The secondary voltage is proportional to the magnetic flux (induced by the primary current) through the secondary winding <math>V_2 = \frac{d\phi_1}{dt} = M \frac{dI_1}{dt}</math></p>	<p>The secondary voltage is further converted to a digital (optical) signal; the Rogowski coil is wound around a nonmagnetic former with constant cross-sectional area</p>	<p>The optical fiber (sensor) is arranged around the primary circuit; the magnetic field induced by the primary current rotates the plane of polarization of the light passing through the fiber</p>

**Table 8.2** Principles of various types of voltage transformers (VTs)

Conventional electromagnetic VT	Capacitor VT (CVT) with an amplifier	Electronic voltage transformer (EVT) with a capacitive voltage divider	Optical VT
 <p><math>V_1</math>: Primary voltage Primary winding <math>N_1</math> <math>N_2</math>: Secondary winding <math>V_2</math>: Secondary voltage <math>V_2 = \frac{N_2}{N_1} V_1</math></p>	 <p><math>V_1</math>: Primary voltage <math>C_1</math>: Primary capacitor <math>C_2</math>: Secondary capacitor Amplifier <math>V_2</math>: Secondary voltage <math>V_2 = \frac{C_1}{C_1 + C_2} V_1</math></p>	 <p><math>V_1</math>: Primary voltage <math>C_1</math>: Primary capacitor <math>C_2</math>: Secondary capacitor Converter Optical signal Secondary voltage</p>	 <p><math>V_1</math>: Primary voltage <math>C_1</math>: Primary capacitor <math>C_2</math>: Secondary capacitor Converter Optical sensor Secondary voltage</p>
<p>The secondary voltage is proportional to the ratio of the secondary to the primary winding <math>V_2 = \frac{N_2}{N_1} V_1</math></p>	<p>The secondary voltage is obtained from the voltage divided between a couple of capacitors <math>C_1</math> and <math>C_2</math> connected in series <math>V_2 = \frac{C_1}{C_1 + C_2} V_1</math></p>	<p>The secondary voltage is obtained from the voltage divided between a couple of capacitors; it is converted to a digital signal</p>	<p>The secondary voltage is obtained from the voltage divided between a couple of capacitors; it is converted to a digital signal and converted back to the secondary voltage</p>



**Fig. 8.18** (a) A 300 kV capacitor voltage transformer (CVT). (b) A 72 kV inductive voltage transformer

Oscillations of lower and higher harmonics of the power frequency (known as *ferroresonance*) can be induced by switching operations in power systems due to a resonant interaction between the nonlinear reactance of the electromagnetic voltage transformer (VT) and the capacitances of the network and equipment (e.g., the grading or coupling capacitors of circuit breakers). Ferroresonance can damage electromagnetic VTs through overheating and/or overvoltage stress.

On the other hand, when ferroresonance occurs in CVTs, it normally originates from the interaction of internal components of the VT—specifically the nonlinear inductance—with the stray capacitances of the HV winding. A large amount of magnetic energy is stored in the compensation reactor during a secondary short circuit. This energy is released in the primary winding, which can lead to the saturation of the transformer core when the secondary short-circuit current is interrupted. The high-voltage peaks caused by core saturation can endanger the insulation of the VT and the reactor and may eventually destroy these components. These voltage peaks usually occur at subharmonic frequencies:  $1/5$ ,  $1/4$ ,  $1/3$ , or  $1/2$  of the rated power frequency.

Countermeasures are usually deployed for ferroresonance to prevent faults and the destruction of the voltage transformer. For electromagnetic VTs, ferroresonance is usually suppressed by connecting a damping resistor to the tertiary winding of the VT or to the open delta connection of the tertiary windings of the three VTs in a switching bay. The resistor can either be permanently connected or temporarily inserted by placing a reactor in series with the resistor. The reactor effectively acts as a switch and closes when the voltage peaks occur. Sometimes it is not possible to suppress rated power-frequency ferroresonance by means of a damping resistor, but ferroresonance can be prevented from occurring in such cases by judiciously positioning equipment. For capacitive VTs (CVT), ferroresonance damping devices are an integral part of the IT sensing system. An additional resistor and its switching reactor are included within the electromagnetic unit of the CVT, or the overvoltage peaks are reduced by an active-gap surge arrester or an external arc gap.

Table 8.3 summarizes the major differences between CT and PT.

**Table 8.3** Differences between a CT and a PT

Current transformer (CT)	Potential transformer (PT)
Connected to the main circuit in series	Connected to the main circuit in parallel
Secondary winding is connected to an ammeter	Secondary winding is connected to a voltmeter
Secondary circuit operates under short-circuit conditions	Secondary circuit operates under open-circuit conditions
One terminal of the secondary circuit is earthed to avoid insulation breakdown	One terminal of the secondary circuit is earthed for safety reasons

### 8.1.4 Series Capacitor, Shunt Capacitor, and Shunt Reactor Compensation

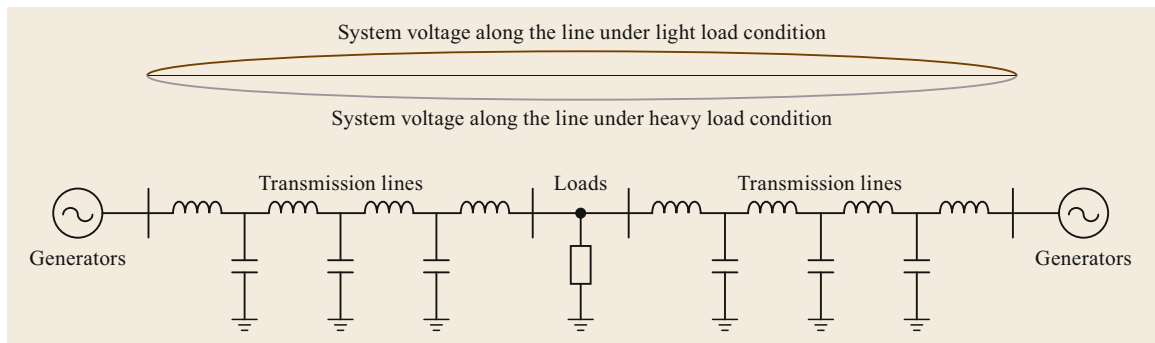
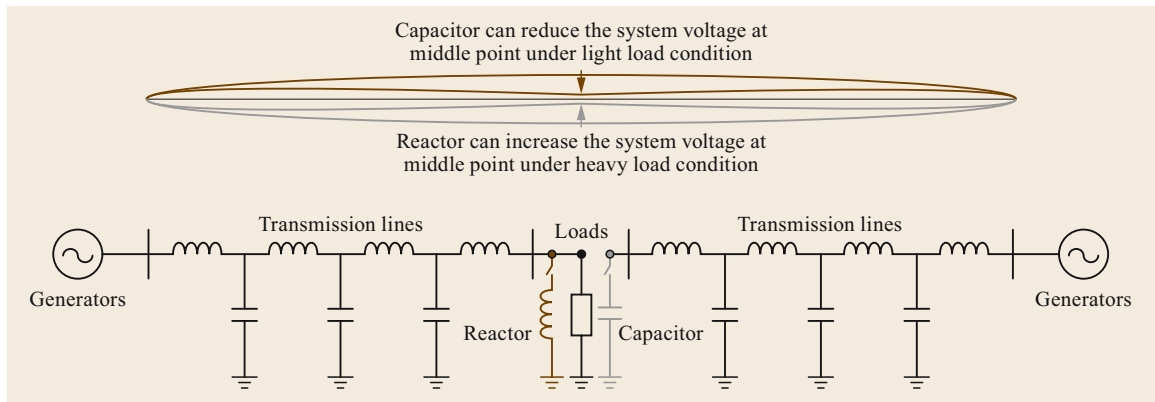
#### Reactive Power Control

Electricity must be supplied with a constant voltage and at a constant power frequency. Since loads are frequently switched on and off, the balance between the amount of electricity supplied (power generation) and the amount of electricity consumed (demand) must be maintained in real time using a demand control system. The utilities normally employ ancillary spinning reserves in addition to bulk base power generators since electricity cannot be effectively stored in large quantities.

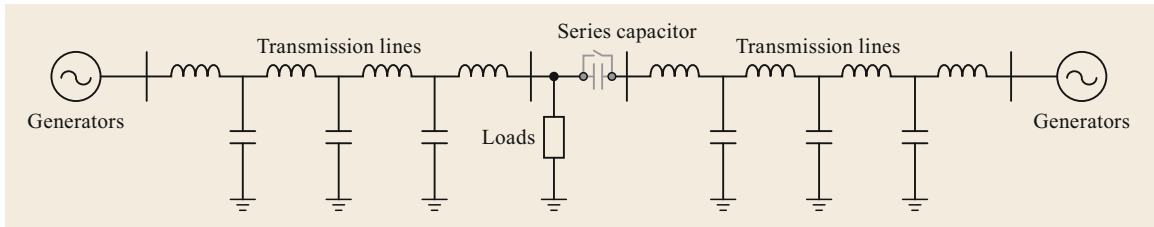
The active power is controlled by this marginal power supply capability. However, if the supply is insufficient (due, perhaps, to a large-scale loss of generators), it may be necessary to reduce the active power consumption by disconnecting some parts of the load. The reactive power can also be controlled by reserve generators as well as by static compensation devices such as capacitors and reactors. Synchronous generators are one of the most important components of the power system for maintaining the active and reactive power balance.

Figure 8.19 shows a schematic of a transmission line connected to generators at both ends. The generators and step-up transformers provide a constant voltage at the bus terminal. However, the system voltage decreases slightly at the midpoint due to reactive power consumption under heavy load conditions. In contrast, the system voltage increases slightly at the midpoint under light load conditions.

In general, static shunt capacitors are applied in transmission lines to inject reactive power into the system, whereas static shunt reactors are applied to consume reactive power, leading to an improved power factor. Figure 8.20 shows that the system voltage is slightly compensated at the middle point by connecting either shunt capacitors under heavy load conditions or shunt

**Fig. 8.19** System voltage distribution along a transmission line under heavy and light load conditions**Fig. 8.20** System voltage distribution along a line when a capacitor or a reactor is connected





**Fig. 8.21** Transmission lines with series capacitors

reactors under normal load conditions. The circuit breakers that are used to switch the static shunt capacitors and reactors on and off frequently operate under reactive power control, which may result in undesirable switching transients. Controlled switching can effectively reduce switching surges by controlling the switching instants of the circuit breakers (Sect. 8.4). More recently, compensators based on power electronic devices—the static VAR compensator (SVC) and the static synchronous compensator (STATCOM)—have also been used to effectively control the reactive power. For example, a STATCOM can control the reactive power by adjusting the amplitude of the supply voltage, which is phase synchronized with the transmission network.

The reactive power in a power system can also be controlled by connecting series compensation equipment to the transmission lines, as shown in Fig. 8.21. Series capacitors are sometimes applied to long transmission lines in order to reduce the line reactance, resulting in increased transmission capacity.

However, great care must be taken when using series capacitors due to potential disadvantages such as subsynchronous resonance of turbine generator shafts and increased transient recovery voltage (TRV) peaks imposed on the terminal of circuit breakers. Standards do not cover the interrupting duties of circuit breakers applied to series-compensated lines.

### Shunt Reactors

Transmission lines or underground cables, particularly those used for voltages of 72.5 kV and above, can produce a large amount of capacitive reactive power that can cause the voltage profile of the transmission network to exceed its maximum level.

Shunt reactors absorb reactive power and influence voltage regulation by reducing the voltage profile. Power transfer from a highly variable renewable-energy source can require the installation of more shunt reactors at the transmission level to control the increase in capacitive reactive power that occurs when the infeed from the energy source is low (when there is no wind at a wind farm, for instance). When they do not carry a large amount of active power, transmission lines exhibit strong line charging due to the Ferranti effect. Shunt reactors keep the voltage within the desired margins.



**Fig. 8.22** Photograph of a 20 kV, 22.5 MVA shunt reactor bank. (Courtesy of J-POWER)

Shunt reactors can be installed as a three-phase unit or as three single-phase units depending on the rated reactive power, the system voltage, or planning and design criteria. The shunt reactor can be permanently connected (a fixed shunt reactor) or switched through a circuit breaker, and it can be installed at the transmission line terminals or connected to the substation busbar. Figure 8.22 shows an example of a 20 kV shunt reactor that has a similar structure to a power transformer with some cooling units.

Variable shunt reactors with a tap changer are applied when precise and slow voltage regulation is required, whereas switched shunt reactors are used for less coarse but flexible voltage regulation. Gapped, oil-immersed shunt reactors with an iron core are employed for large reactive power ratings and high voltage levels in order to minimize losses and reduce audible noise and vibration. For lower voltage levels and smaller reactive power ratings, dry-type shunt reactors are used, sometimes without an iron core to lower the cost.



**Fig. 8.23** Photograph of a 23 kV, 22.5 MVA shunt capacitor bank

### Capacitor Banks

Capacitor banks produce reactive power to compensate for the inductive reactive power that originates from transformers, transmission lines that are loaded above their switching impulse protection level, or inductive loads. The use of capacitor banks increases the transmission capacity, reduces losses due to the improved power factor, and leads to a better voltage profile.

A capacitor bank consists of several capacitors of the same rating that are connected in series or parallel, Fig. 8.23. Capacitor banks can be permanently connected (fixed capacitor bank) or switched through a circuit breaker, and can be installed at the transmission line terminals or at the substation busbar. For voltage ratings of 72.5 kV and higher, each bank has its own circuit breaker. The inrush or outrush currents can be kept under control in an active manner (by controlled switching or with a preinsertion impedance) or in a passive fashion with series reactors.

Series reactors (also called damping reactors) can help to reduce resonance in the network. Power transfer from a highly variable renewable-energy source can require the installation of more capacitor banks at the transmission level to cope with the increase in inductive reactive power that occurs when the infeed from the energy source is high (when there is excessive wind at a wind farm, for instance).

### Series Capacitors

There have recently been some technical advances in the use of series compensation with power electronics. Overvoltage protection schemes have progressed from a sole bypass spark gap to a bypass spark gap with a MOSA or even to fast-acting thyristor-controlled series capacitors (TCSCs) or fast protective devices (FPDs), which can reduce the number of MOSAs needed.

Before the 1980s, when spark gaps were of the self-discharging type, series compensation banks had to be bypassed during (internal or external) line faults, in-

fluencing system availability. MOSAs facilitate series-compensated power transfer in healthy transmission lines by protecting series compensations from power frequency overvoltages [8.3].

Since TCSCs can control the degree of compensation rapidly and flexibly, they can mitigate the risk of subsynchronous resonance (SSR) in power grids and improve power system transient stability by damping low-frequency power oscillations. In thyristor-protected series compensations (TPSCs), the spark gap is replaced by thyristor valves. Since a thyristor valve responds more rapidly and is more accurate than a spark gap, the TRV peak in circuit breakers located on the line side is reduced and energy dissipation from MOSAs is also minimized [8.4].

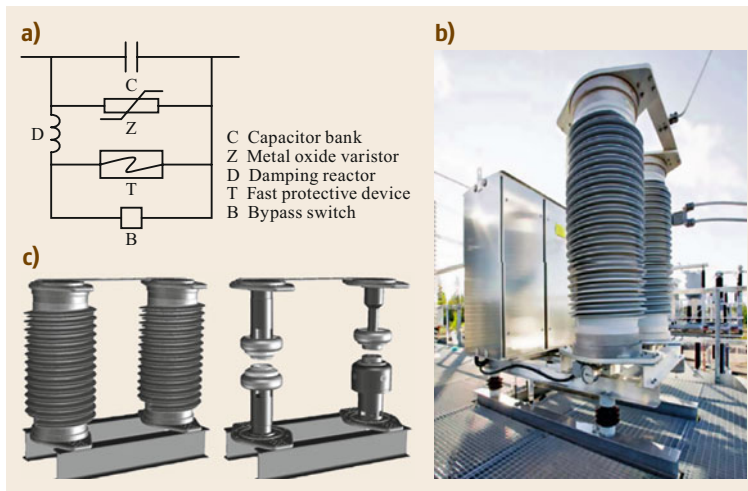
Furthermore, a FPD in which the spark gap is replaced with an immediate bypass on command has been developed and applied to series compensations. This FPD consists of a fast-closing switch in parallel with a sealed plasma triggering gap. FPDs can operate at a very low series-compensation voltage.

Technologies used instead of a triggering gap include a trigatron triggered spark gap, a voltage transformer triggered gap, and a plasma spark gap. These conventional technologies are described in detail in technical brochures. The main gaps for both the trigatron and the voltage transformer triggered spark gap operate in almost the same way. The main gap is required to carry a large power frequency fault current and to maintain a consistent spark-overvoltage characteristic for a long duration in multiple operations.

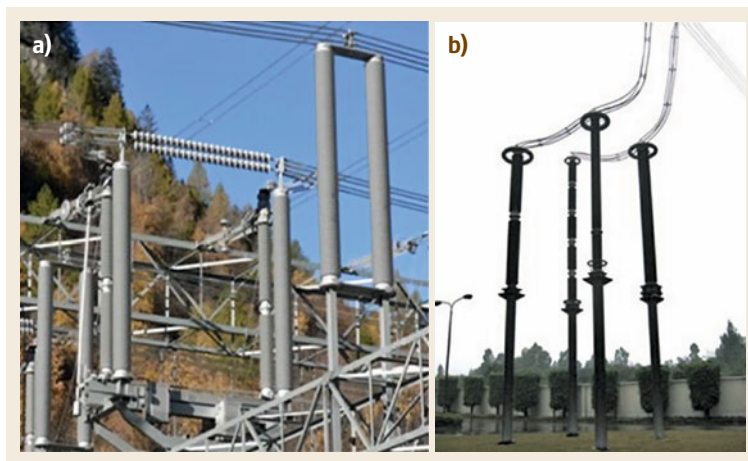
The FPD consists of a hermetically sealed and very fast-acting forced trigger spark gap called an arc plasma injector (API) that is connected in parallel to a mechanical switch termed a fast contact (FC), as shown in Fig. 8.24. The two switches are housed in two composite chambers filled with high-pressure gas. To activate the FPD, a triggering pulse is issued to the API, which can bypass the series-compensation bank. Simultaneously, a command is issued to close the FC within a few ms.

The specification of a MOSA must be able to cope with the worst-case maximum residual voltage. The number of MOSA elements used depends on the energy-dissipating ability of a single MOSA element as well as the current that is divided among the parallel columns. To divide the current equally among the parallel MOSA columns, the residual voltages need to be precisely matched.

Reliability surveys have reported that some MOSAs have failed at energies smaller than indicated by their specifications. This issue was not found to be related to aging problems. In China, UHV bypass switches are normally designed with a T-shaped structure. High-quality WCu material is used for the contacts to stabilize the arc



**Fig. 8.24** (a) Circuit diagram, (b) structure and, (c) a photograph of a fast protective device (FPD) installation



**Fig. 8.25a,b** Photographs of post insulators in a 420 kV AC substation (a) and a 500 kV DC converter station (b) [8.5]

resistance performance. The mass of the insulation rod is reduced and the driving angle and its guide structure are optimized to improve operation performance.

The bypass disconnector must be able to transfer the current to the series compensation and vice versa. Due to the existence of a damping circuit, a voltage will be generated between the contacts of the bypass disconnector during current transfer. A parallel switching branch can be applied at the same time as the main disconnector contact; this parallel switching branch consists of an arcing contact and a 12 kV vacuum breaker connected in series.

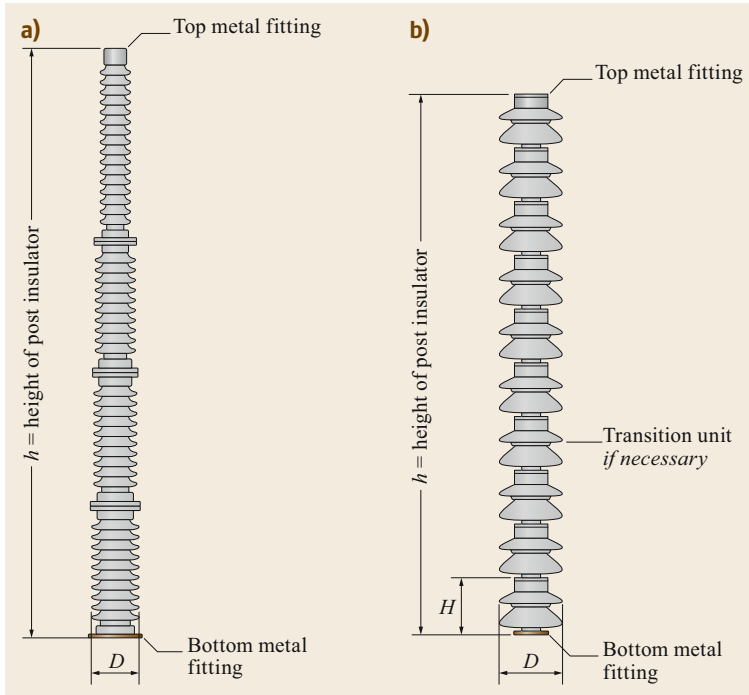
### 8.1.5 Substation Post Insulators

Post insulators provide mechanical support and electrical insulation for high-voltage substation equipment. They are most commonly mounted vertically on a steel

support structure, but may also be mounted horizontally or underhung. A post insulator is an insulator that is intended to give rigid support to a live part that must be insulated from the ground or from another live part, Fig. 8.25.

#### Insulation Material and Type

Post insulators can be classified into two main categories depending on the insulating material used: porcelain and composite. Porcelain is traditionally used in post insulators because this material is very solid, reliable, and well proven. However, composite post insulators have become increasingly popular in recent years because of their design flexibility and relatively light weight, their withstand performance with respect to internal pressure, seismic events, and high contamination, and their ease of handling when they are being manufactured or installed.



**Fig. 8.26a,b** Typical porcelain post insulators. (a) Solid-core cylindrical post insulator. (b) Pedestal post insulator

**(a) Porcelain Post Insulators.** Porcelain post insulators come in two types: solid-core cylindrical and pedestal, which are made up of stacks of single insulator units, as shown in Fig. 8.26. These post insulators are made from wet-processed porcelain machined to the desired specification and are coated with a hard, weatherproof glaze before being kiln dried to give them high electrical and mechanical strength. Galvanized iron or cast aluminum fittings are attached to the insulator ends using Portland cement.

Solid-core cylindrical post insulators consist of solid porcelain with a glazed surface. In some cases, this surface may be coated with silicone rubber for

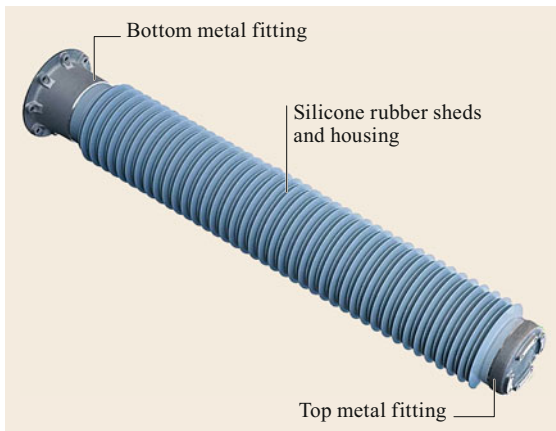
improved pollution performance. For manufacturing reasons, the length of an individual insulator unit is limited. Although the feasible length of an insulator units has increased over time, most post insulators used for higher voltages comprise two or more insulator units that are stacked together in an insulating column to provide the required arcing distance.

Pedestal post insulators have standardized top and bottom fittings between which the insulator stacks are built in order to meet the specification of the post insulator.

**(b) Composite Post Insulators.** Because they are a relatively new technology, composite post insulators (Fig. 8.27) are not as commonly used as porcelain post insulators, but they have found increasing use in recent years. Composite post insulators can have a hollow core or a solid core.

**Solid-core design:** The solid cores used in composite post insulators commonly consist of fiber-glass-reinforced resin rods that provide mechanical strength (similar to line composite insulators). The housing and sheds are made from a polymeric material, most often silicon rubber.

**Hollow-core design:** A hollow core used in a composite post insulator generally consists of a tube that provides mechanical support. In this design, there is also an external insulating part—the housing, including sheds, which provides the necessary creepage distance and protects the tube from the environment (this



**Fig. 8.27** A composite post insulator [8.6]

concept is similar to that used for composite insulators used in other high-voltage equipment, such as circuit breakers and instrument transformers). Composite hollow-core post insulators may be filled with a gaseous, liquid, or solid insulating material (such as urethane foam).

A key advantage of composite post insulators is that the polymeric materials used in them exhibit hydrophobicity, which means that they repel water. Sometimes the polymeric material also repels pollution on the insulator surface, in which case the material is referred to as a hydrophobic transfer material. In theory, this means that a shorter creepage distance may be used in a composite post insulator than in a porcelain post insulator.

### 8.1.6 Technical Requirements and Design Parameters

Post insulator design involves optimizing various parameters to ensure that the post insulator is capable of withstanding specific levels of electrical, mechanical, and environmental stress.

#### (a) Electrical Performance

The main parameters that influence the electrical performance of a post insulator are the arcing distance, creepage distance, and housing profile. Post insulators are designed and tested to withstand specified lightning and switching impulses as well as power frequencies (certain types of post insulators also have a defined minimum puncture voltage). For composite post insulators, the grading of the electric field along the insulator may be another important aspect that impacts the expected life. This grading can be achieved by applying grading rings and adjusting the sizes and shapes of the flanges during the design phase.

#### (b) Mechanical Performance

The length, the core diameter and material, and the design of the end fittings as well as the method used to attach them are regarded as the design parameters that exert the strongest influence on the mechanical performance of a post insulator. The mechanical design of a post insulator must take into account mechanical stresses, such as those arising from short circuits, seismic activity, and external loads. Porcelain post insulators are categorized into mechanical strength classes based on the failing load of the insulator in a bending test. Composite post insulators also undergo a bending test.

#### (c) Environmental Performance

The design phase also involves selecting the shed profile and the number of sheds that will allow good

dielectric withstand at a particular pollution level under wet conditions, thus fulfilling the requirements defined in the standards [8.7–10].

#### Standards and Type Tests

Substation post insulators are covered by a relatively large number of IEC standards:

- IEC 60168:1994 (on tests of indoor and outdoor post insulators made from ceramic or glass for systems with nominal voltages of more than 1000 V)
- IEC 60273:1990 (on characteristics of indoor and outdoor post insulators for systems with nominal voltages of more than 1000 V)
- IEC/TS 60815-2:2008 (on the selection and dimensioning of high-voltage ceramic and glass insulators intended for use in AC systems under polluted conditions) [8.9]
- IEC/TS 60815-3:2008 (on the selection and dimensioning of high-voltage polymeric insulators intended for use in AC systems under polluted conditions) [8.10]
- IEC/TR 61462 (on definitions, test methods, acceptance criteria, and design recommendations for composite hollow-core insulators for use in outdoor and indoor electrical equipment)
- IEC 61462:2007 (on definitions, test methods, acceptance criteria, and design recommendations for pressurized and unpressurized composite hollow-core insulators for use in electrical equipment with rated voltages of more than 1000 V)
- IEC 62217:2012 (on general definitions, test methods, and acceptance criteria for polymeric insulators for indoor and outdoor use in HV systems)
- IEC 62231-1:2015 (on definitions, test methods, and acceptance criteria for composite post insulators for use in substations with AC voltages of 1000 V to 245 kV)
- IEC 62772:2016 (on definitions, test methods, and acceptance criteria for composite hollow-core post insulators for use in substations with AC voltages of more than 1000 V and DC voltages of more than 1500 V).

In general, porcelain post insulators are covered by IEC 60168 and IEC 60273. IEC/TS 60815-2 is applied when it is necessary to dimension for polluted conditions.

IEC 62231-1 covers solid-core but not hollow-core composite insulators. Hollow-core composite insulators are covered by IEC 61462, which does not cover post insulators and is limited to designs with voltages of up to 245 kV. Material-related qualification is covered by IEC 62217, and dimensioning for polluted condi-

tions by IEC/TS 60815-3. IEC 62772 refers to the other relevant standards and creates a system that covers all hollow-core composite insulators.

The following type tests are normally carried out for post insulators in accordance with IEC 60168 and IEC 62231:

- Dry lightning-impulse withstand voltage test
- Wet switching-impulse withstand voltage test (only for insulators in systems with the highest voltages of 300 kV or more)
- Wet power-frequency withstand voltage test
- Mechanical failing load test.

## 8.2 History and Principles of High-Voltage Circuit Breakers

The development of circuit breakers is closely linked to the remarkable growth in the demand for higher-voltage transmission systems with large short-circuit capacities. Since the late 1800s, a wide range of interrupting technologies that use oil, air, vacuum, and SF<sub>6</sub> gas as interrupting media have been developed and have contributed to the construction of large-capacity power transmission systems.

### 8.2.1 History of Circuit Breaker Development

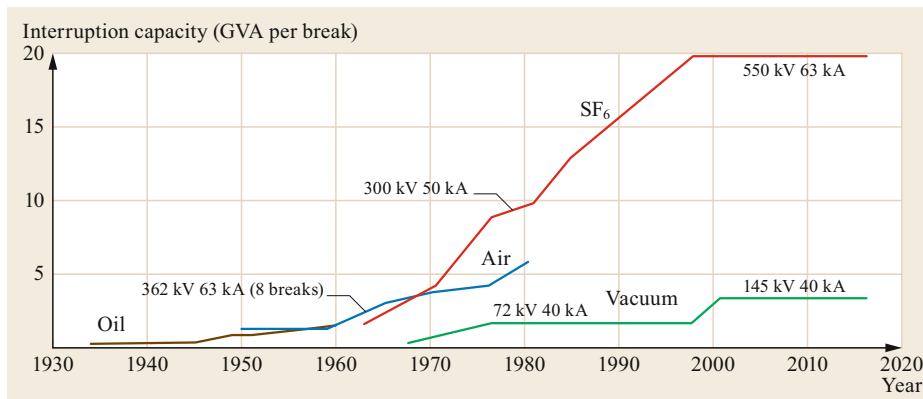
The first circuit breaker, which was of the bulk oil type, was developed by *Kelman* [8.11] in the early 1900s. It consisted of a crude arrangement of switches in separate wooden barrels connected in series and operated simultaneously. Bulk oil circuit breakers evolved over subsequent decades. The main advances were made in the United States by *Slepian* of Westinghouse [8.12] and *Prince* and *Skeats* of General Electric [8.13].

In Europe, bulk oil circuit breakers reigned until the early 1950s, but were then completely supplanted by minimum oil circuit breakers. Bulk oil circuit breakers with eight breaks in series are used in systems with voltages of up to 360 kV, while minimum oil circuit breakers with up to ten breaks in series are used in systems with voltages of up to 420 kV. It should be noted that some utilities are still using these types of oil circuit breakers.

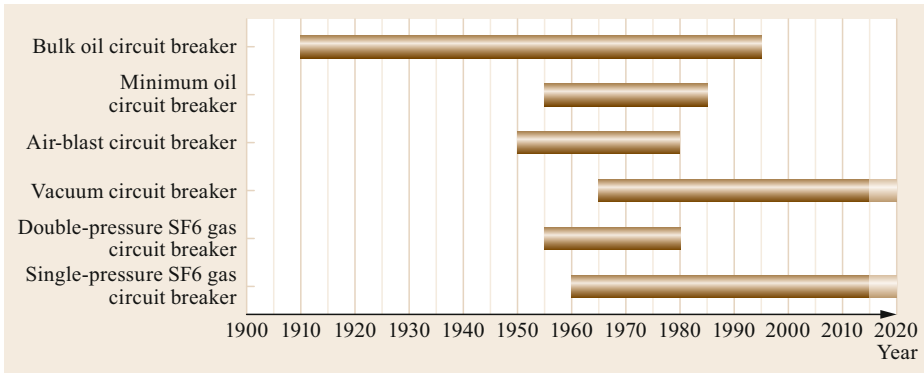
The air-blast circuit breaker was developed in Europe, initially by *Whitney* and *Wedmore* of the British Electrical Research Association [8.14, 15] in 1926 and subsequently in Germany and Switzerland in the 1930s and 1940s. Air-blast circuit breakers became popular in the 1960s and enabled the construction of extra-high-voltage systems of 500 kV and above. This type of circuit breaker was manufactured until the early 1980s, when they were superseded by less expensive and complex SF<sub>6</sub> puffer-type circuit breakers. Air magnetic circuit breakers, a variant of air-blast circuit breakers, were used at medium voltages of up to 52 kV.

SF<sub>6</sub> gas was recognized for its unique dielectric properties in the 1920s, when *Cooper* of General Electric [8.16] applied for a patent on its use in capacitors and gas insulated cables. However, the SF<sub>6</sub> gas circuit breaker did not appear on the market until the mid-to-late 1950s [8.17]. The application of SF<sub>6</sub> gas to current interruption was patented by *Lingal, Browne, and Storm* of Westinghouse in 1956 [8.18]. The first SF<sub>6</sub> gas circuit breakers were designed with dual pressure, based on axial gas blast principles.

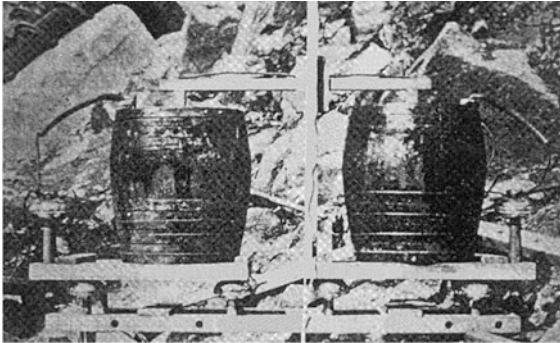
The puffer-type SF<sub>6</sub> circuit breaker, which is often referred to as the single-pressure circuit breaker, was developed in the 1970s based on a principle invented by *Prince* [8.17], who also designed the impulse-type bulk oil circuit breaker [8.12], where the oil flow is produced by a piston driven by the operating mechanism. Further development of SF<sub>6</sub> circuit breakers led to rotating arc



**Fig. 8.28** Evolution of the interruption capacity per break, encompassing different circuit-breaker types



**Fig. 8.29** Approximate manufacturing periods for different circuit-breaker types



**Fig. 8.30** Kelman's oil circuit breaker built in 1901 (40 kV, 300A) [8.19]

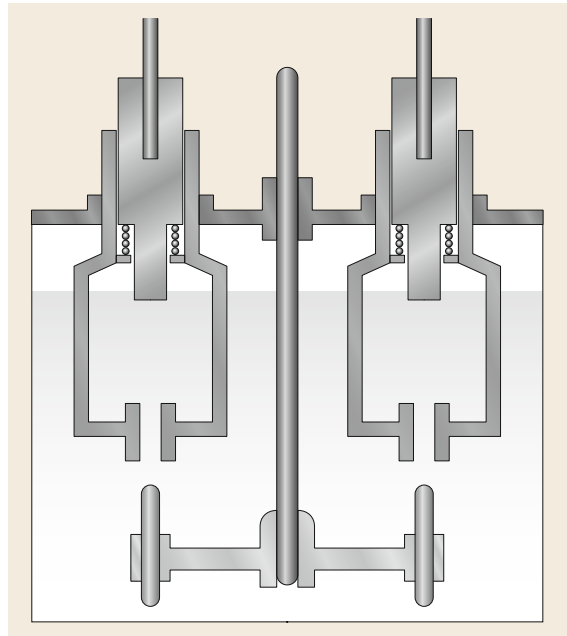
technology for voltages up to 72 kV and self-blast technology for voltages above 72 kV.

Vacuum interrupters were also developed in the 1920s [8.20], but the first commercial vacuum circuit breakers did not appear until the 1960s. The vacuum circuit breaker is still commonly used today at medium voltages and is also available for transmission voltages of up to 170 kV [8.21].

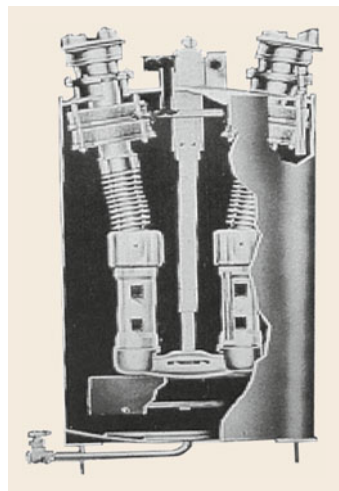
Figure 8.28 provides a historical perspective on the interruption capability per break, encompassing all of the above circuit breaker technologies. It is clear that there have been a couple of technology transitions. The first technical transition—from oil to air—occurred around 1960, which led to the construction of EHV networks; another transition—from air to SF<sub>6</sub>—occurred around 1970, which led to improved high-capacity circuit breakers and enhanced network reliability.

The application time lines for the six major circuit-breaker types are shown in Fig. 8.29. Oil circuit breakers were manufactured from around 1910 until 1990. Air circuit breakers were mainly manufactured from 1950 to 1980. SF<sub>6</sub> circuit breakers have dominated since 1970. Vacuum circuit breakers also have a long history of production.

The first circuit breaker had a switch immersed in a large tank filled with mineral oil, which served as



**Fig. 8.31** An early oil-immersed circuit breaker design



**Fig. 8.32** A cross-sectional drawing of a 145 kV, 63 kA bulk-oil circuit breaker



**Fig. 8.33** Photograph of some 345 kV, 63 kA oil circuit breakers

an extinguishing and insulating medium. Figures 8.30 and 8.31 show a photograph and the design of an early oil-immersed circuit breaker, respectively. Figure 8.32 presents a cross-sectional drawing of a more modern bulk-oil circuit breaker rated at 145 kV and 63 kA. Figure 8.33 shows a photograph of oil circuit breakers rated at 345 kV, which is the highest rated voltage achieved with mineral oil. These circuit breakers were originally designed for an interrupting duty of 40 kA, but were subsequently modified to allow an interrupting duty of 63 kA through the use of internal shields to prevent voltage flashovers to the tank wall during interruption.

During the current interruption process, the arc vaporizes the oil and creates hydrogen gas. The compressed hydrogen gas blasts into the arc, cooling it down. Hydrogen gas has good conductivity, which is a desirable quality for an arc-quenching medium. However, this design presents a significant risk of explosion and fire if an interrupting failure occurs. Later minimum oil circuit breakers were designed to have an effective

and compact cooling enclosure. The contacts and arcing chamber were placed in a porcelain insulator instead of a bulky metal tank. Despite these risks, oil circuit breakers were manufactured until the 1990s.

Air-blast circuit breakers were developed around 1950 and were used in the first 735 kV networks in Canada, which employed a 800 kV multibreak interrupter design. Given that breaking currents are increasing in today's rapidly developing networks, circuit breakers using SF<sub>6</sub> as the interrupting medium are currently favored in high-voltage networks. Figure 8.34 shows an example of the latest generation of 800 kV air-blast circuit breakers.

The first generation of SF<sub>6</sub> gas circuit breakers included high- and low-pressure gas chambers equipped with moving and fixed contacts in an enclosure filled with SF<sub>6</sub>. High-pressure gas was blown into the arc generated between the contacts in the low-pressure chambers. Figure 8.35 shows an example of a double-pressure gas circuit breaker. In current designs, most of the SF<sub>6</sub> gas is in a single pressure chamber, and the SF<sub>6</sub> is compressed in a puffer cylinder under the control



**Fig. 8.34** Photograph of an example of the latest generation of 800 kV air-blast circuit breakers. (Courtesy of GE, produced by Alstom)



**Fig. 8.35** A 240 kV double-pressure gas circuit breaker



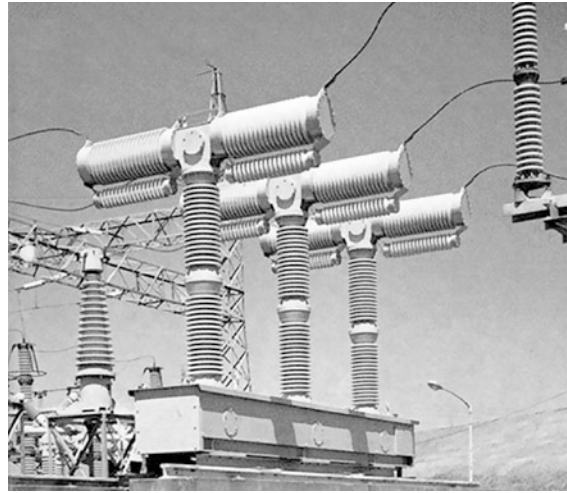


**Fig. 8.36** 245 kV, 50 kA double-break and single-break SF<sub>6</sub> puffer circuit breakers. (Courtesy of ABB, produced by ASEA)

of an operating mechanism and then blasted through a nozzle into the arc. Figure 8.36 shows an example of 245 kV, 50 kA double-break and single-break SF<sub>6</sub> puffer circuit breakers.

In a vacuum circuit breaker, the contacts are operated in a vacuum enclosure. When the vacuum circuit breaker separates the contacts, an arc is generated by the metal ions vaporized from the contact surface. The arc is quickly extinguished because the metallic vapor, electrons, and ions produced during the arc rapidly diffuse and condense on the surfaces of the contacts, resulting in a swift recovery of dielectric strength. Vacuum circuit breakers are commonly used in medium-voltage distribution systems and are available for transmission voltage ratings of up to 170 kV (Fig. 8.37).

The opening and closing operations of mechanical circuit breakers normally generate arc discharge phenomena between the contacts. In the 1940s, *Cassie* [8.22], *Mayr* [8.23], *Cassie and Mason* [8.23, 24], and *Browne* [8.25] showed that interrupting phenomena could be reproduced analytically through the application of dynamic arc equations with a couple of arc parameters in conjunction with circuit equations for power systems [8.26, 27]. Intensive investigations aimed at identifying novel interrupting media with improved properties were performed by the Electric Power Research Institute (EPRI) in the United States [8.28, 29]. Those studies revealed the physical properties of



**Fig. 8.37** Photograph (taken in 1972) of 168 kV, 40 kA vacuum circuit breakers. (Courtesy of Meidensha)

many potential interrupting media. Furthermore, thermofluid dynamics simulation has made it possible to analyze arc interrupting behavior in great detail using more precise arc models [8.30, 31]. The main interrupting phenomena encountered with circuit breakers based on various interrupting media are now described.

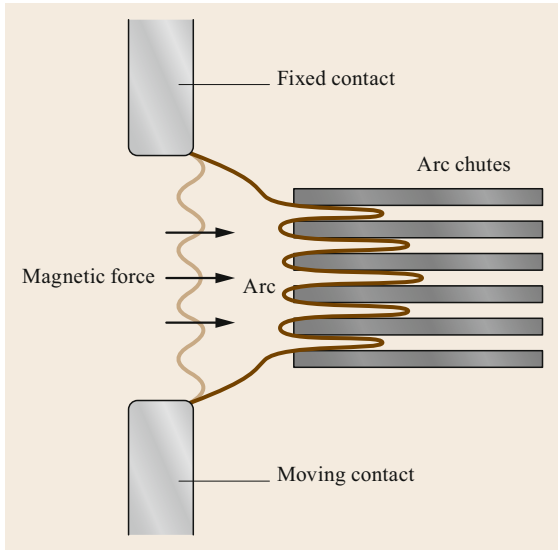
### 8.2.2 Interrupting Phenomena for Oil and Air Circuit Breakers

The interrupting process in a mechanical circuit breaker is normally accompanied by an arc that is generated between the contacts after contact separation. This arc is the main switching element of the mechanical circuit breaker. It is used to transform the circuit breaker from the conducting state to the insulating state economically for all ratings of a power system.

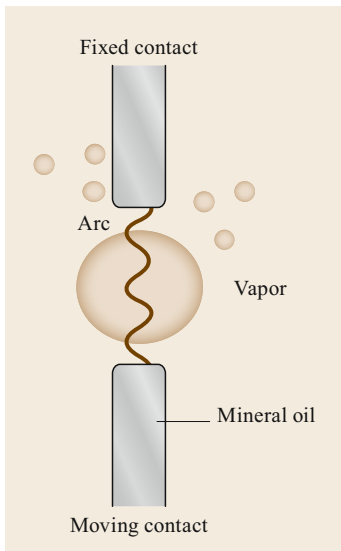
For an AC system, the arc interrupting process normally occurs at one of the periodic current zeros associated with the power frequency. A plasma—an electrically conductive hot ionized gas comprising charged particles such as electrons and positive or negative ions—is generated by the arc, and this can carry a large current though a normally nonconductive interrupting medium such as oil, air, SF<sub>6</sub> gas, or a vacuum with and without metal vapor.

In the hot arc plasma, collisions between moving charged and neutral particles create new charged particles while some of the electrons and positive ions recombine into neutral particles (i.e., deionize).

Low-voltage circuit breakers normally use air to extinguish the arc. Figure 8.38 shows a magnetically driven air circuit breaker equipped with some arc chutes consisting of mutually insulated parallel plates. The arc



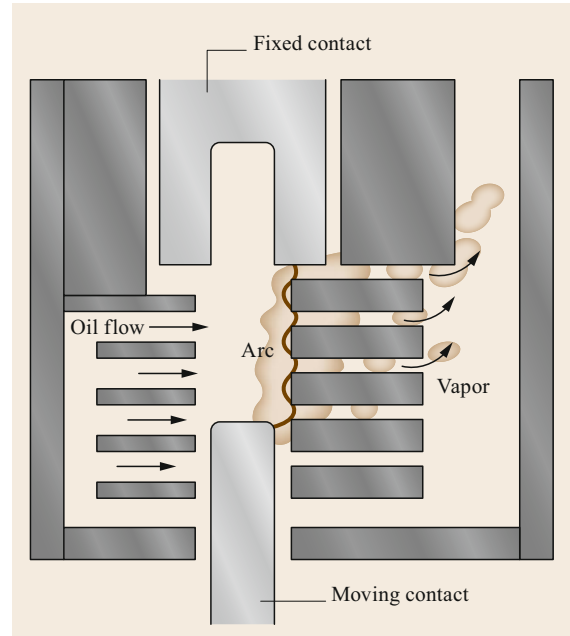
**Fig. 8.38** A magnetically driven air circuit breaker



**Fig. 8.39** Arc interruption in an oil circuit breaker

chutes divide the arc into smaller and extended arc lengths to aid cooling, which increases the arc voltage and thus limits the current through the circuit breaker. The current-carrying parts near the contacts deflect the arc into the arc chutes using the magnetic force from the current path. Magnetic blowout coils or permanent magnets are also used to deflect the arc into the arc chutes.

Oil circuit breakers utilize vaporized mineral oil to extinguish the arc. Mineral oil has better insulating and interrupting properties than air. In an oil circuit breaker, the fixed and moving contacts are immersed in an enclosure filled with oil. When the contacts are separated



**Fig. 8.40** Configuration of a minimum oil circuit breaker

under load-carrying or short-circuit current conditions, an arc is generated, and the oil is heated by the arc and vaporized, whereupon it decomposes into (mostly) hydrogen gas (small amounts of methane, ethylene, and acetylene are also generated). This ultimately leads to a highly compressed hydrogen bubble around the arc. The bubble displaces the oil near to the arc and effectively cools the arc (Fig. 8.39), and it prevents reignition when the power frequency produces the next current zero. Figure 8.40 shows the typical configuration of a minimum oil circuit breaker.

### 8.2.3 Interrupting Phenomena for Gas Circuit Breakers

Gas circuit breakers normally use a gas such as air, sulfur hexafluoride ( $\text{SF}_6$ ), or gas mixtures that include  $\text{SF}_6$  as insulating and interrupting media to extinguish the arc generated between the contacts.  $\text{SF}_6$  has become the dominant insulating and interrupting medium used in circuit breakers today because it has some unique characteristics that make it ideally suited for this purpose. Some of these characteristics are described below.

#### (a) Density of $\text{SF}_6$

The dielectric properties of  $\text{SF}_6$  are strongly dependent on its density. Figures 8.41 and 8.42, respectively, show how the  $\text{SF}_6$  gas density and  $\text{SF}_6$  gas composition depend on the temperature. The density follows the ideal gas equation up to 1600 K, regardless of the

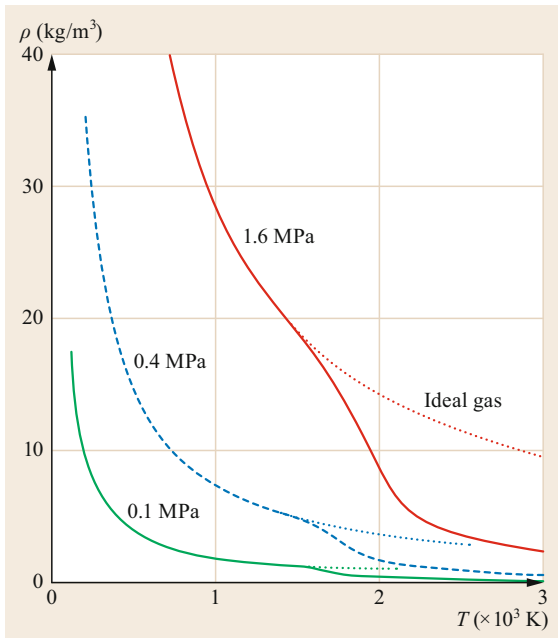


Fig. 8.41 Density of SF<sub>6</sub> gas versus temperature [8.30]

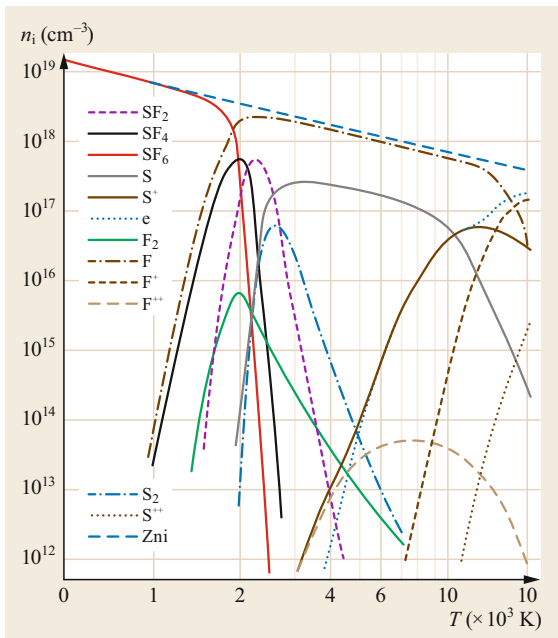


Fig. 8.42 Decomposition of SF<sub>6</sub> versus temperature [8.30]

pressure. When the temperature exceeds 1600 K, the measured SF<sub>6</sub> gas density is found to be lower than that given by the ideal gas equation (Fig. 8.41). This change occurs due to the decomposition of the gas, as shown in Fig. 8.42. Above approximately 2000 K, SF<sub>6</sub> gas decomposition is markedly enhanced, resulting in

the generation of charged species such as S<sup>+</sup>, S<sub>2</sub><sup>+</sup>, F<sup>+</sup>, and electrons. When the temperature exceeds 4000 K, the SF<sub>6</sub> gas is completely decomposed, resulting in the presence of many different particles. Electrons account for about 1% of all the particles present at temperatures between 8000 and 9000 K. The temperature below the boundary of 8000–9000 K band shows the isolating state. In contrast, the temperature above the boundary band shows the conductive state.

### (b) Thermal Conductivity and Electrical Conductivity of SF<sub>6</sub>

The thermal and electrical conductivity of the medium affect the heat loss from the arc plasma with a small diameter arc around current zero, which can strongly affect the arc interruption capabilities of the circuit breaker. You can find an image of an arc with small diameter at the bottom part of Figure 8.49. In particular, SF<sub>6</sub> can make a narrow arc with smaller diameter as compared with other interrupting media. Figure 8.43 shows the thermal conductivity of SF<sub>6</sub> as a function of temperature. Upon increasing the temperature from 300 K, the first peak in the thermal conductivity appears around 1800 K. On the other hand, the electrical conductivity (Fig. 8.44) increases with temperature because the proportion of electrons (with respect to all particles) rises due to increased ionization. The proportion of electrons is 1% and the electrical conductivity increases between 8000 and 9000 K, which is much higher than the temperature (1800 K) at which the thermal conductivity peaks.

The thermal conductivity generally increases with temperature, and presents distinct peaks in the temperature interval corresponding to the decomposition of SF<sub>6</sub> gas (around 1800–2000 K). This means that the arc shows enhanced thermal conductivity but low electrical conductivity, resulting in good cooling performance, when it is close to this temperature region during the low-current period.

### (c) Specific Heat of SF<sub>6</sub>

The specific heat shown in Fig. 8.45 has two distinctive peaks which can be seen at around 2000 and 20 000 K. The heat capacity becomes larger around these temperatures. When considering a contact heat input, the arc will stay at these temperatures since larger energy is required to increase the temperature in the 2000 and 20 000 K regions. In the high-current region, the arc temperature stays around 20 000 K due to the larger specific heat in the high-temperature region. This is why the core temperature of an arc with a large current does not increase much beyond 20 000 K.

In order to understand why SF<sub>6</sub> gas allows effective arc cooling due to adiabatic expansion, the result of

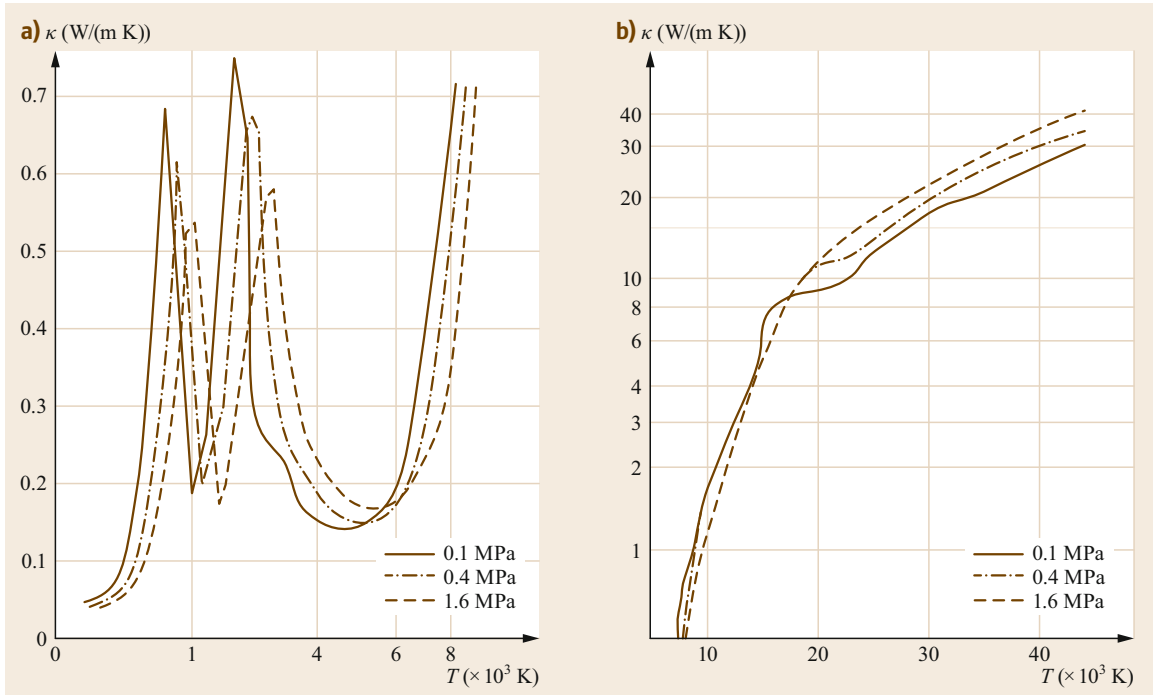


Fig. 8.43a,b Thermal conductivity of SF<sub>6</sub> versus temperature [8.30]

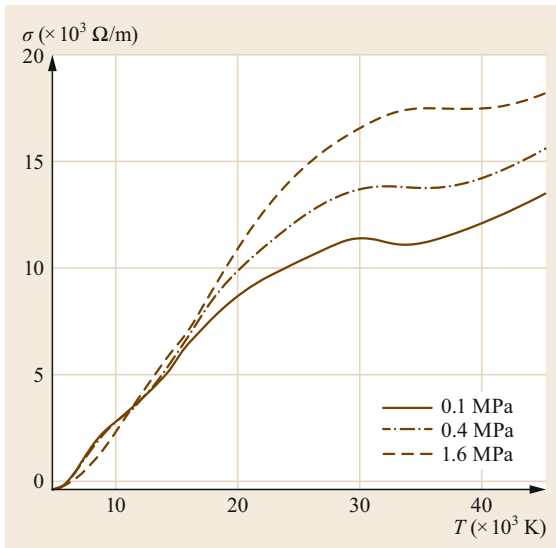


Fig. 8.44 Electrical conductivity of SF<sub>6</sub> versus temperature [8.30]

mixing two gas volumes—a large-volume ( $V_0 = 1$ ) arc at 20 000 K (corresponding to a large-current state) and a small-volume ( $V_d = 0.1$ ) arc at 1700 K (corresponding to a current of almost zero) at 0.6 MPa—in an isentropic cooling process can be investigated (Fig. 8.47). After mixing the gases, the temperature is found to be

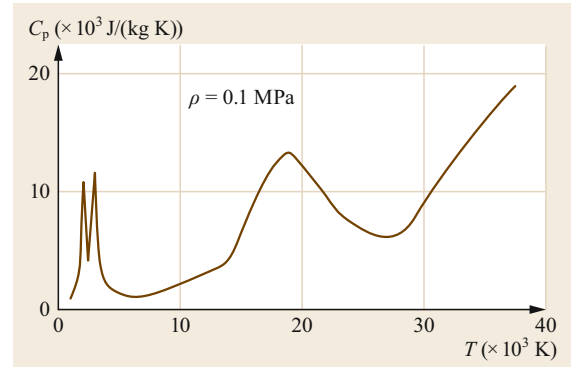


Fig. 8.45 Dependence of the specific heat on the temperature at 0.1 MPa

2600 K (the pressure is 0.35 MPa), which is within the temperature interval corresponding to particularly high heat conduction, leading to enhanced cooling.

The specific heat ratio ( $C_p/C_v$ ) of SF<sub>6</sub> is 1.08, which is considerably lower than those of air and hydrogen (around 1.4). A hot gas with a relatively low specific heat rate, such as SF<sub>6</sub>, requires the removal of less heat to cool it to the dielectric level during an isentropic cooling process involving a volume change.

In a SF<sub>6</sub> gas circuit breaker, the arc is usually generated in a cylindrical insulating nozzle, as this allows the arc to be cooled effectively by controlling the SF<sub>6</sub>

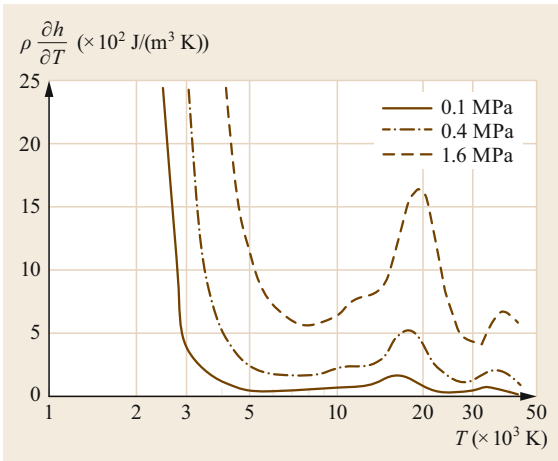


Fig. 8.46 Thermal capacity of SF<sub>6</sub> gas [8.30]

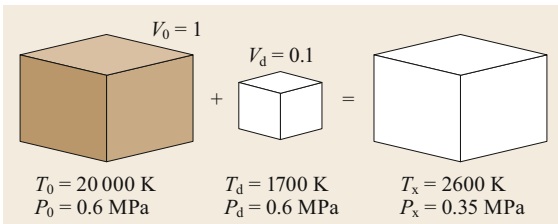


Fig. 8.47 Mixing two volumes of SF<sub>6</sub> gas with different temperatures

gas blowing into the arc. The hot gas generated by the arc is then exhausted from the open contact of the interrupter chamber. The insulating nozzles are generally made from polytetrafluoroethylene (PTFE), which can control and restrict arc movement inside the nozzle.

In an interrupter that uses SF<sub>6</sub> gas as the interrupting medium, a gas flow is induced to flow over the arc, which results in thermal exchange between the arc and the medium, ultimately extinguishing the arc. Various possible arc-quenching configurations are shown in Fig. 8.48.

Figure 8.48a illustrates a plain break. In this case, there is no preconfigured gas flow; instead, the temperature (or density) gradient caused by the arc and gravity induces a gas flow that in turn affects the temperature distribution and extinguishes the arc. Another example, shown in Fig. 8.48b, makes use of the pressure built up by the arc. The resulting pressure gradient causes a gas flow that cools the interrupted arc. In the structure shown in Fig. 8.48c, a high-pressure SF<sub>6</sub> gas flow is generated by a gas compressor for example. This flow is passed over the arc, thus extinguishing it. Figure 8.48d shows an arrangement in which the gas pressure needed to induce a gas flow is generated by the mechanical motion of a cylinder passing over a piston. The resulting gas flow is then directed over the arc. This arc-quenching approach leads to a so-called puffer-type

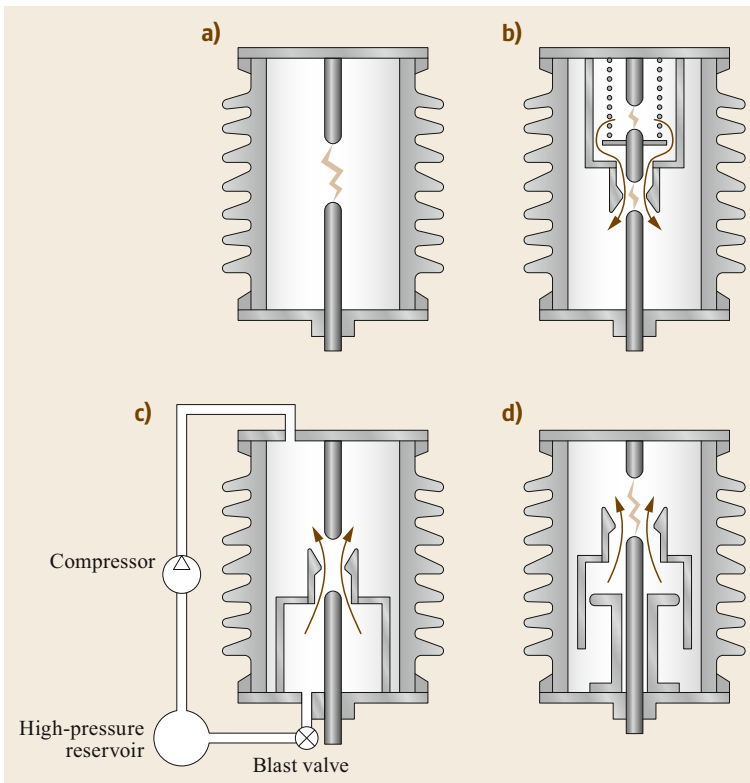
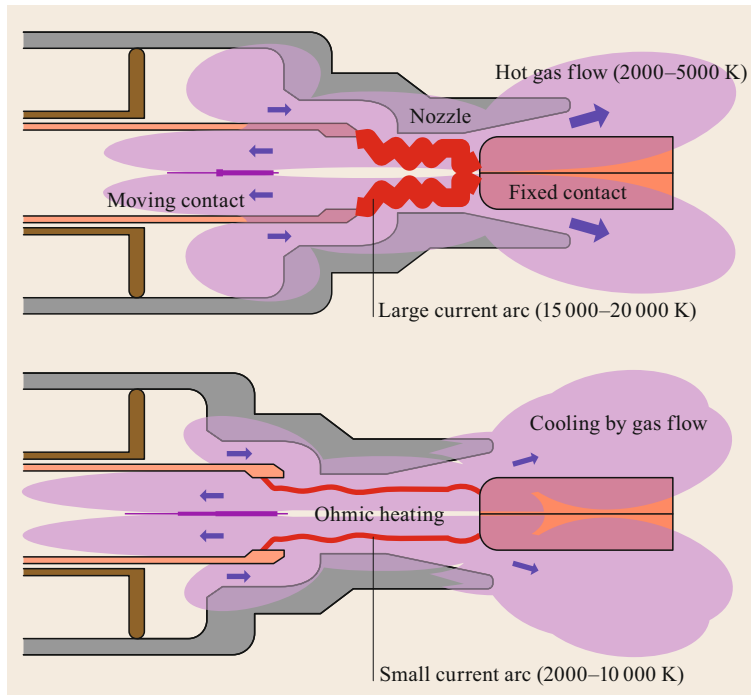


Fig. 8.48 Various arc-quenching arrangements for SF<sub>6</sub> blasting. (a) Plain break, (b) self-blast, (c) double-pressure blast, (d) puffer blast



**Fig. 8.49** Arc quenching process with a gas circuit breaker

circuit breaker. Modern circuit breakers use this basic concept in some form.

The pressure buildup in the puffer chamber and the energy exchange with the arc are the most important concepts in arc interruption. The mechanical motion of the arcing contact, especially in the puffer chamber, is affected by the existence of the arc because of the interaction of the pressure buildup in the puffer chamber with the arc current.

The SF<sub>6</sub> arc plasma generated between the contacts of a gas circuit breaker is a conductor due to the presence of charged particles such as ions and electrons. These charged particles originate from decomposed SF<sub>6</sub> gas as well as contact material that is ionized through arc current heating. Radiative heat transfer from the arc to the surrounding materials, the evaporation of nozzle materials (loss due to latent heat), along with convection from the turbulent gas flow and conduction all contribute to arc cooling, which changes the characteristics of the arc. The thermodynamic characteristics of SF<sub>6</sub> gas are largely responsible for its excellent arc cooling mechanism (switching function) and its interrupting and dielectric withstand capabilities.

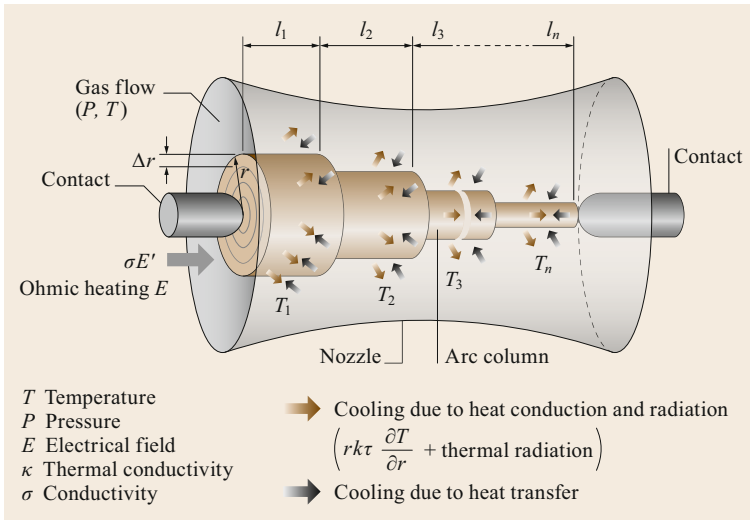
In particular, a gas circuit breaker with SF<sub>6</sub> loses most of its electrical conductivity when the temperature of the vanishing arc drops below 2000 K.

Figure 8.49 shows a schematic of arc currents generated across the contacts of a single-pressure-type SF<sub>6</sub>

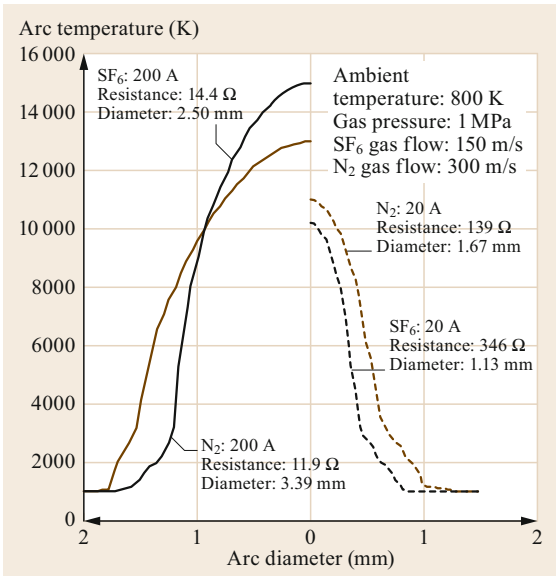
gas circuit breaker. The temperature of an arc with a large current (several tens of kA) is 15 000–20 000 K, resulting in a high-density conductive plasma with a low arc voltage. The temperature of an arc carrying a small current (almost zero) is 2000–5000 K. The arc voltage shows a suppression peak before a current zero.

Every time the current passes through zero after contact separation, the circuit breaker has an opportunity to extinguish the arc. When the arc current reaches zero, the conductivity ( $g$ ) of the vanishing arc across the contacts is still nonnegligible, so the arc maintains a very small current due to the presence of charged particles where there used to be an arc column. This current is called the residual or post-arc current ( $I$ ). The residual current contributes to the energy input due to ohmic heating ( $I^2/g$ ) by the electric field across the contacts, which can raise the temperature and conductivity, while the cooling induced by a gas flow contributes to energy loss and tends to reduce the conductivity.

Figure 8.50 shows an example of a physical model for the arc interrupting process near to a current zero in the case of a gas circuit breaker. The arc is heated by ohmic heating and cooled by heat transfer due to a gas flow, heat conduction to the ambient temperature, and radiation [8.33]. The balance between the energy input and the cooling will determine the success or failure of the interruption.



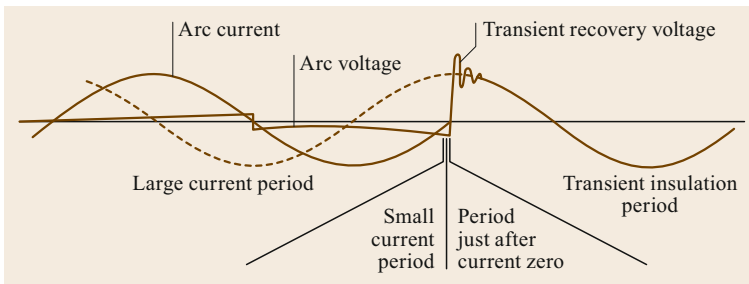
**Fig. 8.50** Arc interrupting process in a gas circuit breaker [8.32]



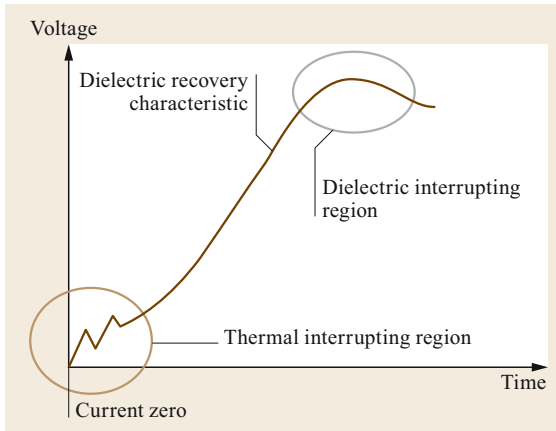
**Fig. 8.51** Temperature profiles of SF<sub>6</sub> and N<sub>2</sub> arcs at currents of 20 A and 200 A

Figure 8.51 shows calculated temperature profiles for SF<sub>6</sub> and N<sub>2</sub> arcs at stable currents of 20 and 200 A. Compared with the profile for a N<sub>2</sub> arc, that for a SF<sub>6</sub> arc shows a smaller arc diameter, implying a larger temperature gradient and increased heat conduction. The SF<sub>6</sub> arc diameter increases with the temperature at the center of the arc for larger currents. However, the maximum diameter occurs at around 20 000 K because the thermal capacity is highest around this temperature, as described before.

During the large arc current period, the arc shows high conductivity and a temperature of 15 000–20 000 K. The arc conductivity gradually decreases with decreasing current during the small arc current period. The arc is extinguished when the cooling due to the gas flow exceeds the ohmic heating due to the residual current generated by the electrical field during the short period (up to a few milliseconds) of post-arc current. Then the dielectric recovery between the contacts competes with the TRV during the transient recovery period. When the dielectric recovery surpasses the TRV at all times, the interruption has been successfully completed.



**Fig. 8.52** The four periods of a current interruption process



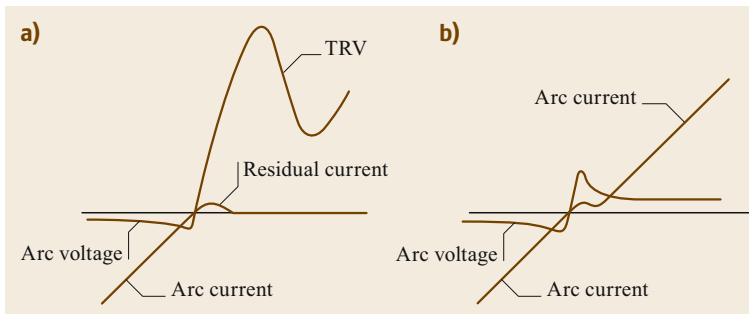
**Fig. 8.53** Critical instants that determine interruption success or failure

Figure 8.52 shows the four periods of the current interruption process. There are two notable regions for interruption: the thermal interrupting region during the post-arc current period just after current interruption, and the dielectric interrupting region during the transient recovery voltage period.

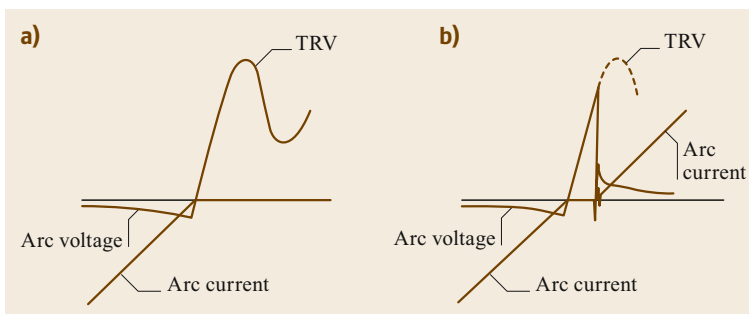
Figure 8.53 shows the two critical regions that determine the success or failure of interruption: the thermal interrupting region and the dielectric interrupting (recovery) region. A circuit breaker must meet the interrupting requirements during these two interrupting regions under various network conditions.

After a current zero, there is a residual current that increases the energy of the vanishing arc by ohmic heating. When a circuit breaker cannot provide sufficient cooling, thermal reignition may occur. Figure 8.54 gives an example of the current and voltage variations that occur in the thermal interrupting region during a successful and a failed current interruption. When thermal reignition occurs, the residual current through the vanishing arc will increase the temperature and an arc current will be reestablished. When a restriking occurs at a current zero, a circuit breaker will have one of two possibilities for interrupting the current at subsequent current zeros. The recovery voltage during the thermal interrupting region is very small, so reignition does not generate harmful transients to the system and the equipment in the power system.

After the thermal interrupting region, the TRV is applied between the contacts, and the moving contact continues to operate until it reaches the fully open position. The dielectric strength across the contacts generally increases with the contact gaps. When the TRV exceeds the dielectric strength across the contacts during the dielectric interrupting region, a dielectric breakdown called a restrike occurs. Figure 8.55 compares the current and voltage variations that occur during successful and failed current interruptions in the dielectric interrupting region. When a restrike happens, the arc is immediately restored and the current is reestablished. The restrike may generate transients that could be harmful to the system and the equipment in the power system.

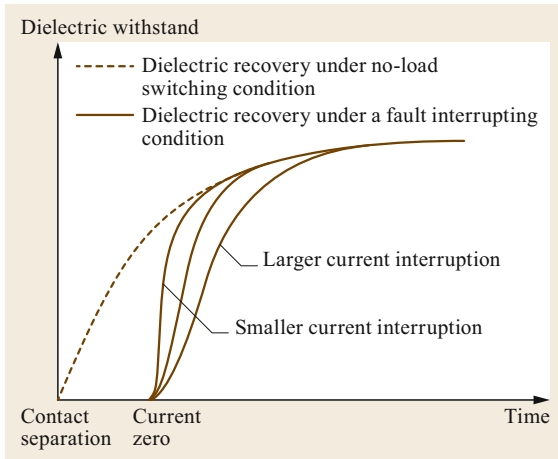


**Fig. 8.54** (a) Success and (b) failure (reignition) during thermal interrupting process

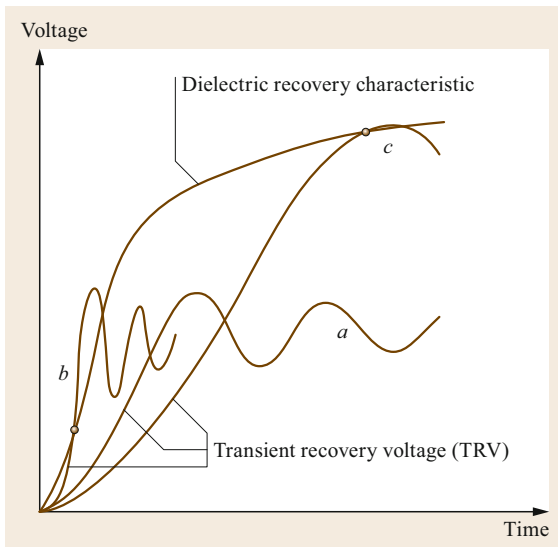


**Fig. 8.55** (a) Success and (b) failure (restrike: voltage breakdown) during the dielectric interrupting process





**Fig. 8.56** Dielectric recovery characteristics between the contacts of a circuit breaker for various scenarios



**Fig. 8.57** Comparison of the dielectric recovery characteristics obtained with various transient recovery voltages (labels *a*, *b*, and *c* are explained in the text)

Figure 8.56 shows the dielectric recovery characteristics between the contacts of a circuit breaker during no-load switching, a small fault current interruption, and a large fault current interruption. When a gas circuit breaker interrupts a low current, the dielectric recovery withstand voltage starts to increase rapidly after current interruption at current zero as the distance between the contacts increases. When a circuit breaker interrupts a large fault current, the dielectric recovery withstand voltage tends to recover slowly compared to when a small current interruption occurs.

Figure 8.57 schematically shows a comparison of the dielectric recovery characteristics obtained with three transient recovery voltages for different switching duties. For successful dielectric interruption, the dielectric recovery withstand voltage between the contacts of a circuit breaker must exceed the transient recovery voltage after current interruption at all times (case *a* in Fig. 8.57).

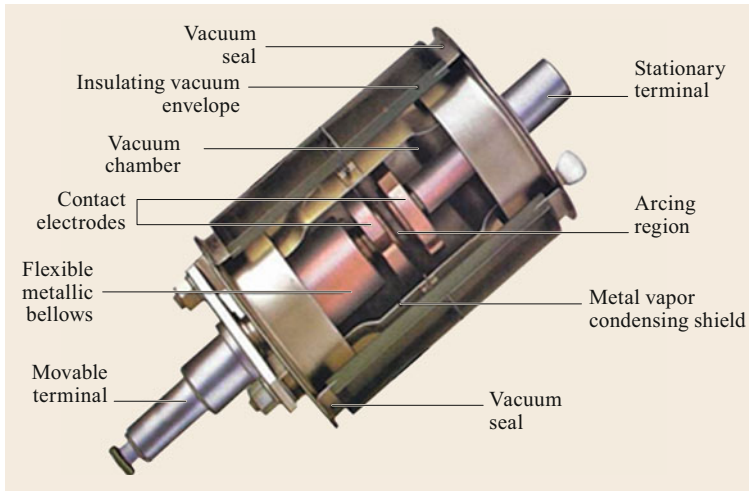
A high rate of rise in recovery voltage (RRRV) leads to a dielectric restrike (case *b* in Fig. 8.57). Such TRVs are typically obtained during transformer limited faults and series reactor faults. When the RRRV exceeds the rate of rise of the dielectric recovery characteristic, a dielectric interrupting failure will occur. On the other hand, a fault interruption in a long transmission line may generate a high TRV peak. A dielectric interrupting failure will also occur if the TRV peak exceeds the dielectric recovery characteristic (case *c* in Fig. 8.57).

The whole interruption process is successfully completed when both the thermal interrupting and dielectric interrupting regions have been successfully cleared. Many interrupting tests are required to clarify the thermal and dielectric interrupting capabilities of a circuit breaker under the various switching duties expected in a power system. When performing type tests in a high-power laboratory, given that the initial part of the TRV can influence current interruption, it is important to check that the time delay for the recovery voltage after a current zero does not exceed standard values under network conditions.

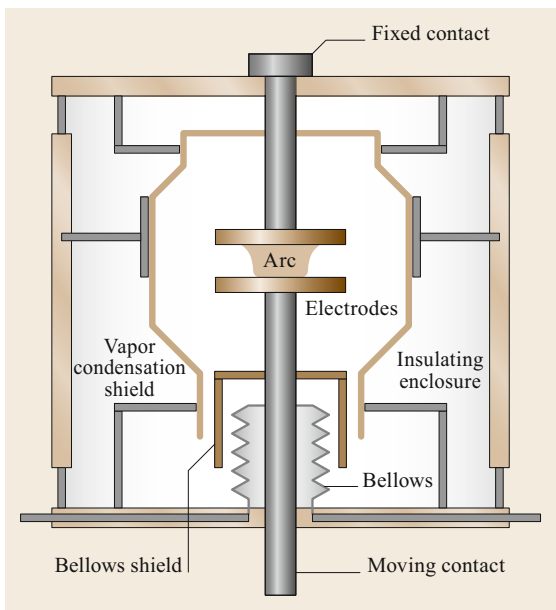
#### 8.2.4 Interrupting Phenomena for Vacuum Circuit Breakers

In vacuum circuit breakers [8.34], there are a couple of disk-shaped electrodes in the vacuum enclosure (vacuum tube) that are separated by a small gap (possibly less than 2–4 mm) and are employed to extinguish the arc. Figures 8.58 and 8.59 show a cutaway and schematic, respectively, of the configuration of a typical vacuum interrupter.

While gas circuit breakers use an interrupting medium to carry the current, vacuum circuit breakers do not contain any material to sustain the plasma except for the metal vapor emitted from the cathode and anode contact surfaces (which are also termed the cathode and anode spots). The vacuum pressure inside a vacuum interrupter is normally maintained at  $10^{-6}$  Pa. The dielectric withstand is excellent with a small contact gap. The vaporized contact material (typically a Cu-Cr alloy) plays an important role in the switching function (between current carrying and current interruption) of a vacuum circuit breaker.



**Fig. 8.58** Cutaway showing the configuration of a typical modern vacuum interrupter



**Fig. 8.59** Schematic of the typical configuration of a vacuum interrupter

The vacuum arc occurs at the cathode spots and carries a current with high-density plasma. The cathode spots supply the metal vapor and emit electrons that are accelerated in the arc plasma and ionize the other metal atoms through bombardment. The newly created ions move toward the cathode and collide with metal atoms. During the large current period, the vacuum arc also initiates from the anode spots, which are much larger than the cathode spots.

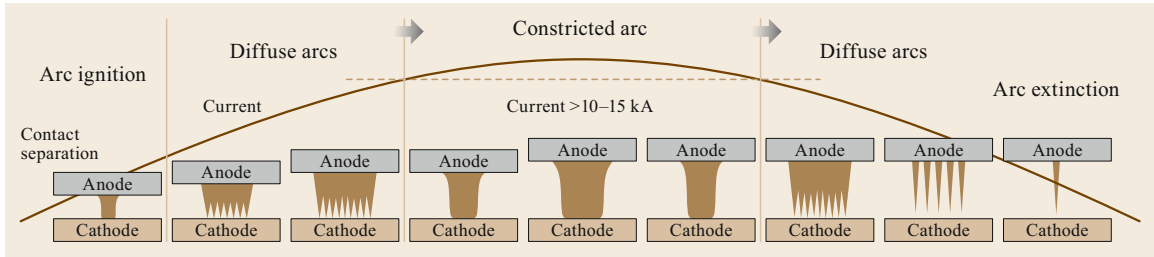
There are two vacuum arc modes: diffuse and constricted arcs (Fig. 8.60). A constricted arc is a single thick arc similar to a gaseous arc with a large current (typically larger than 10–15 kA) and high plasma den-

sity. It has a high atmospheric pressure due to excessive metal vapor (implying that the voltage of a constricted arc is higher than that of a diffuse arc).

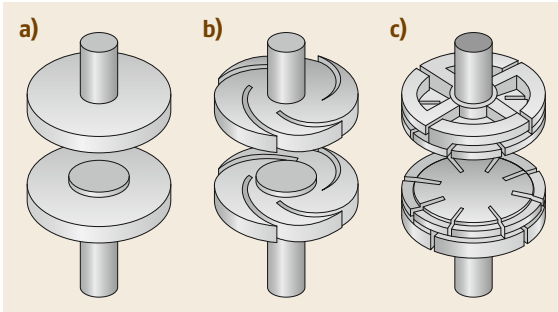
As the current decreases, a constricted arc transforms into a diffuse arc, which consists of many arc columns with plasma cones directed from the small cathode spots to the anode during the small current period. These arc columns can move very quickly on the contact surface. The arc voltage across the contacts becomes very small (compared with that in gas circuit breakers)—about 20 V (irrespective of the electrode spacing)—before the current interruption, and does not present a prominent extinction peak (this is because the existence of fast-moving charged ions and electrons results in high conductivity).

Several measures have been applied to improve the interrupting performance of a vacuum interrupter by suppressing the creation of constricted arcs at higher current levels, which is also desirable because constricted arcs cause severe electrode erosion. One of the most well known of these measures involves moving the anode spots continuously by applying a transverse magnetic field (TMF) to the arc in order to reduce local electrode melting. Another method is to reduce the bombardment of the anode spots by the plasma by spreading the arc across the whole of the electrode while applying an axial magnetic field (AMF) between the electrodes.

Figure 8.61 shows some examples of the electrode configurations used in vacuum interrupters. A plane electrode is used for a vacuum interrupter with small interrupting currents. A spiral electrode has several spiral grooves, leading to a radially directed arc magnetic field. The magnetic field pushes the arc to the edge of the spiral fin, thus avoiding excessive local erosion due to the arc. An axial magnetic field electrode consists of several coils that can generate an axial arc magnetic



**Fig. 8.60** Interrupting process in a vacuum



**Fig. 8.61a–c** Electrode configurations for a vacuum interrupter. (a) Plane electrode, (b) spiral electrode, (c) axial magnetic field electrode

field. These specially designed contacts along with the radial and axial magnetic fields force the arc to keep moving on the electrode under the influence of its own magnetic field, which minimizes contact erosion and spreads it uniformly across the electrode.

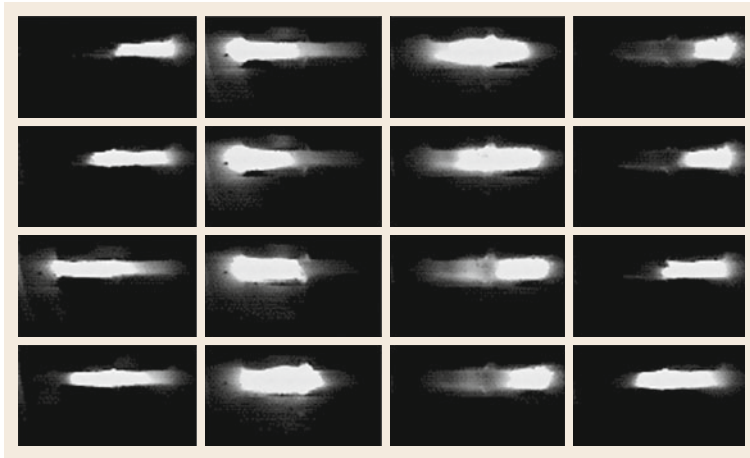
Figure 8.62 shows a series of photographs showing the behavior of a traveling arc between the contacts, as driven by a transverse magnetic field.

A vacuum circuit breaker interrupts the current at current zero by establishing the dielectric strength between the contacts. It is very difficult for the arc plasma

to reestablish itself after current zero (after complete depletion of charged metal particles and electrons) because of the excellent dielectric strength of vacuum. Thermal interrupting failures are seldom observed. Since there is a very small amount of charged particles between the electrodes at current zero, a residual arc current flows when a recovery voltage is applied between the electrodes because the charged ions and electrons are removed by the small electric field after current zero. Even though the residual current tends to be larger than that in SF<sub>6</sub> gas circuit breakers, the presence of a large residual current after current interruption in a vacuum interrupter will not affect its thermal interrupting performance.

The interruption has been successfully completed when the dielectric strength across the contacts always surpasses the recovery voltage after current interruption. Some dielectric breakdown of a statistical nature may be observed, as the dielectric strength in a vacuum is strongly affected by the contact surface conditions and small metal particles can considerably modify the electrical field across the contacts.

The dielectric recovery characteristic during the dielectric recovering region is an important determinant of the success or failure of a circuit breaker, especially for low-current interruptions such as line-charging current switching and capacitor bank current switching.



**Fig. 8.62** Traveling arc behavior between the contacts, as driven by a transverse magnetic field

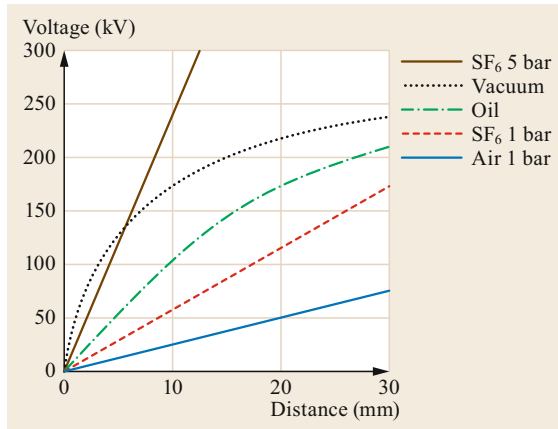


Fig. 8.63 Dielectric performance in a vacuum [8.21]

### 8.2.5 Comparison of the Dielectric Withstands of Various Interrupting Media

Figure 8.63 shows the dielectric recovery characteristics for various interrupting media with no load. The dielectric recovery characteristic is mainly determined

by the distance between the contacts, the density of the insulating medium if it is a gas, the opening speed, and the configuration of the electrodes. The dielectric strength increases linearly with the contact gap in a gaseous medium. In a vacuum, good dielectric strength is observed with a small gap but it gradually saturates as the gap increases.

On the other hand, the density of  $\text{SF}_6$  gas drops in some regions of the enclosure of an interrupter after a large current interruption due to the transfer of thermal energy from the arc plasma into the enclosure during the interruption process. This leads to the degradation of the dielectric recovery characteristic to some extent compared to that observed at no load and under small current switching conditions.

### 8.2.6 Summary

This section has described the interrupting phenomena encountered with different interrupting media. Circuit breakers play an important role in securing other substation equipment in power systems and have been a key component in the development of high-voltage and large-capacity transmission networks.

## 8.3 Switching Phenomena in Power Systems

A circuit breaker should be capable of making, carrying, and interrupting the current under both normal and abnormal conditions, especially in the case of a short circuit or fault. Various short-circuit conditions including single-phase grounded, three-phase grounded, and phase-to-phase ungrounded faults are expected to occur in power systems [8.35, 36]. When a circuit breaker interrupts a short-circuit current, different switching phenomena are observed depending on the conditions [8.37].

The short-circuit current is greatest for a three-phase grounded fault in most power systems. However, the short-circuit current for a single-phase grounded fault is larger than that of a three-phase grounded fault in a solidly earthed system where the zero sequence impedance ( $X_0$ ) is less than the positive sequence impedance ( $X_1$ ). The current ratio of a single-phase grounded fault to a three-phase grounded fault is given by  $3/(2 + X_0/X_1)$ , so the single-phase fault current is lower than the three-phase fault current when  $X_0 > X_1$ .

The short-circuit current after a fault occurrence comprises a decaying DC component superimposed on a symmetric AC current that also decays over time, as shown in Fig. 8.64. The decay of the AC component depends strongly on the reactance in the short circuit, including the generator reactance. The DC component

decays rapidly with the time constant of the power system ( $L/R$ ). The circuit breaker must withstand the electrical and mechanical stresses imposed by the short-circuit current.

A transient voltage is imposed between the contacts (the electrodes) of a circuit breaker when it interrupts a current. The TRV that appears immediately after interruption shows a damping oscillation around the prospective system voltage. After that, it approaches the system voltage (albeit with a slight shift caused

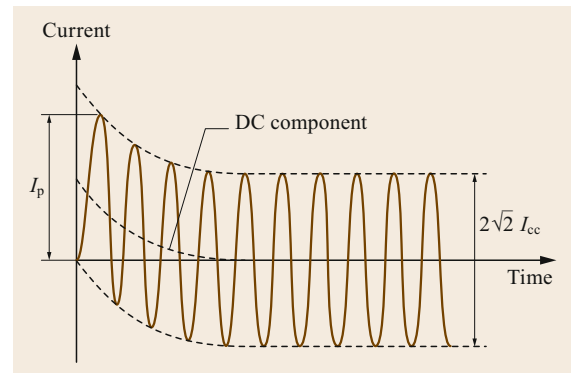


Fig. 8.64 DC component of a short-circuit current

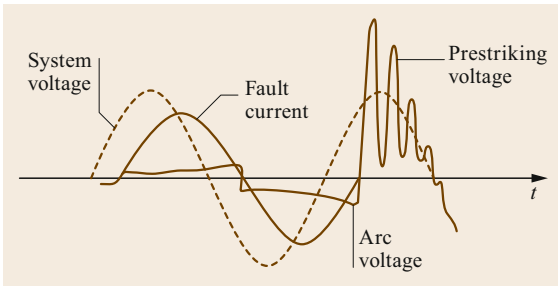


Fig. 8.65 TRV and RV waveforms

by an imbalance in the short-circuit currents among the phases), which oscillates with the power frequency, as shown in Fig. 8.65. The TRV significantly affects the interrupting performance of the circuit breaker. The severity of the TRV strongly depends on the prospective system voltage, which varies with the system and the fault conditions, including the neutral connection. For example, the first-pole-to-clear factor is 1.3 for an effectively earthed neutral system and 1.5 for an isolated neutral system. The amplitude of the TRV also changes with the system and equipment conditions.

This section explores how the main switching phenomena of circuit breakers vary depending on the conditions and the fault location in power systems.

### 8.3.1 Fundamental Switching Phenomena

A circuit breaker is required to clear any faults that occur in a power system or to interrupt the currents stipulated in international standards such as IEC 62271-100 [8.38], even though, in order to ensure that circuit breakers are economical, the standards generally cover

Table 8.4 Switching duties in a power system

Switching duties	Fault location	Circuit breaker responsible
Bus terminal fault interruption	F1	CB1
Short line fault interruption	F2	CB2
Long line fault interruption	F3	CB2
Transformer limited fault interruption	F4	CB3
No-load line switching	–	CB4
Small capacitive current switching	–	CB5
Small inductive current switching	–	CB5

only 90% of the switching duties expected in existing power systems.

Figure 8.66 shows and Table 8.4 summarizes various switching duties imposed on a circuit breaker.

### 8.3.2 Bus Terminal Fault Interruption

A circuit breaker is normally located at both terminals of a transmission line. When a circuit breaker is required to clear a bus terminal fault that has occurred in the vicinity of a circuit breaker, another circuit breaker, located at the other end of the connected line, is required to clear a long line fault covered in the standards by terminal fault test duties T10 or T30.

The fault current and the TRV imposed on the circuit breaker after fault clearing vary depending on the location of the fault in the power system. The fault current increases with the amount of current flowing from the transmission lines and power transformers connected to power generators into a fault point.

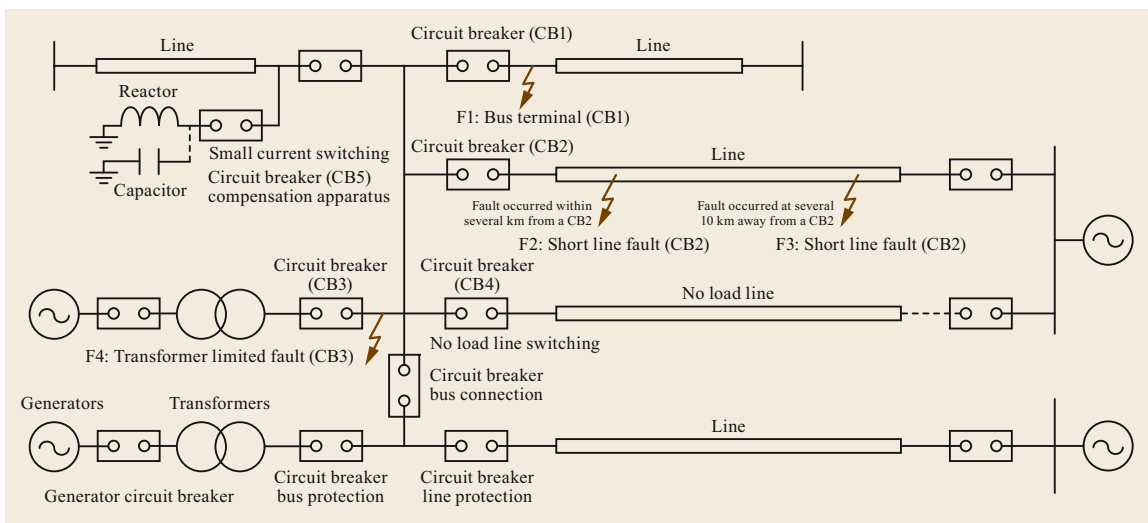


Fig. 8.66 Different switching duties depending on fault location in a power system

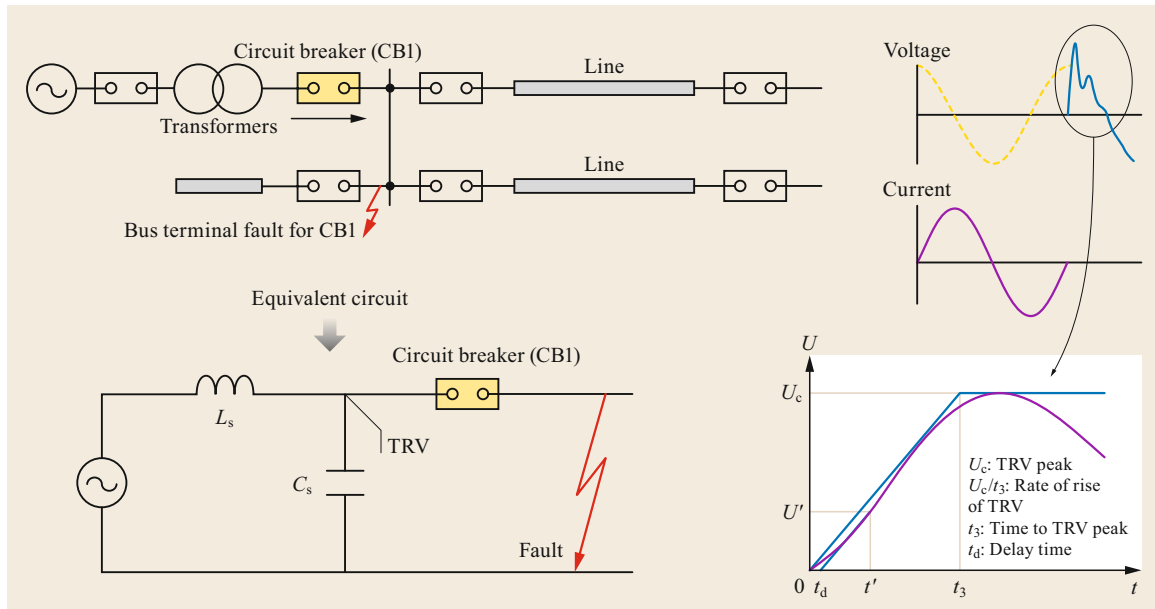


Fig. 8.67 TRV waveform of bus terminal fault corresponding to test duty T10

When only one current source (such as a load transmission line or a power transformer) supplies the current to a fault point, as shown in Fig. 8.67, the fault current is relatively small—normally less than 10% of the rated interrupting current (corresponding to test duty T10). The associated TRV generally shows a single frequency with a high TRV peak value that is determined by the amplitude factor in the related circuit. The TRV amplitude factor tends to be large due to the single frequency contributed by a single current source.

In particular, if a fault is generated immediately after a power transformer and there is no appreciable capacitance between the transformer and the circuit breaker, a severe TRV with a high TRV frequency may occur, which could exceed the standard RRRV values for test duty T10. This duty is often termed transformer limited fault interruption.

Even though a circuit breaker must be able to remove the arc energy generated in the interrupter during the arcing time after contact separation, the circuit breaker does not need to exhibit very strong interrupting performance during the thermal interrupting region because the rate of rise of the TRV (RRRV) is smaller than that for a short line fault (SLF) interruption. Therefore, the dielectric recovery capability of the circuit breaker, which must surpass the TRV at all times, is one of the main concerns if the circuit breaker is to clear a fault at test duty T10. The TRV presents a single frequency that is specified using a two-parameter reference line and a delay time in the standard when most of the current is supplied by a single power generator.

When several current sources from load transmission lines or power transformers supply the current to a fault point, as shown in Fig. 8.68, the fault current is relatively large—up to about 60% of the rated interrupting current (corresponding to test duty T60). The associated TRV shows multiple frequencies due to the different circuits for the various current sources. TRVs with multiple frequencies and different times to the peak due to the presence of multiple current sources tend to show reduced amplitude factors, resulting in lower TRV peaks for higher interrupting currents.

Figure 8.69 summarizes different bus terminal fault conditions for a power system configuration with several transmission lines, power transformers, and power generators. This figure shows that the amplitudes of the fault current and TRV waveforms depend on the fault location. When a fault is generated at F1, the circuit breaker (CB1) is required to clear a fault current that is about 10% of the rated interrupting current of CB1 and is mainly fed by one power transformer (the fault current flow is shown by a red arrow). After clearing the fault at F1, the TRV presents a high peak and a damping oscillation with a simple frequency determined by the circuit conditions of the single current source.

When a fault is generated at F2, the circuit breaker (CB2) is required to clear a fault current that is 30–60% of the rated interrupting current of the CB2 and is fed by several current sources through transmission lines and power transformers (the fault current flow is shown by a green arrow). After clearing the fault at F2, the TRV presents a lower peak than at F1 as well as multiple

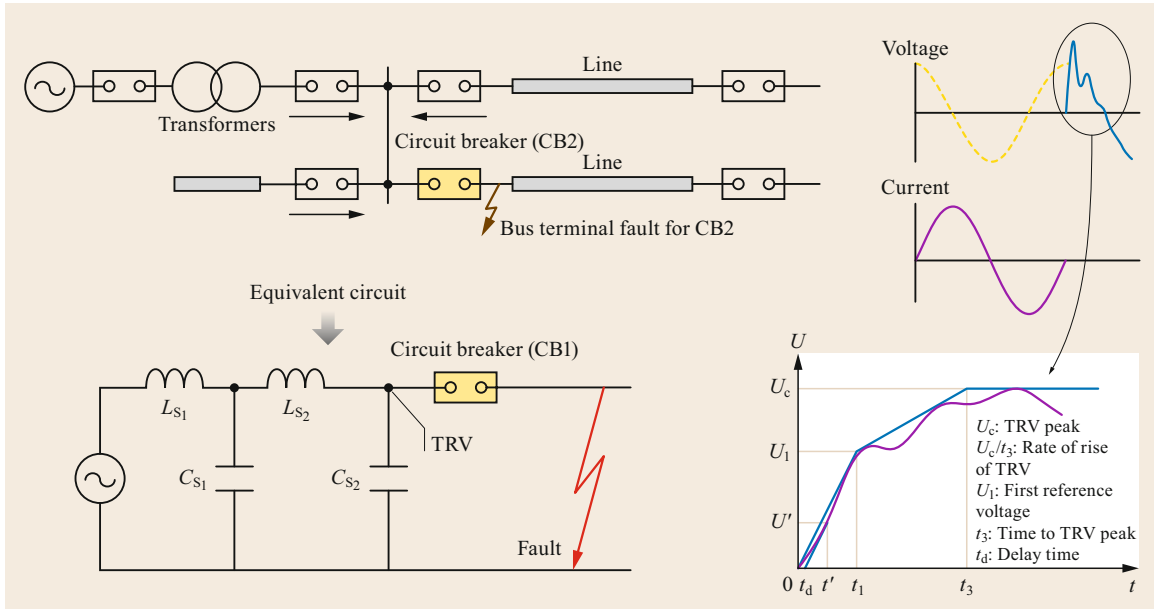


Fig. 8.68 TRV waveform of a bus terminal fault corresponding to test duty T60

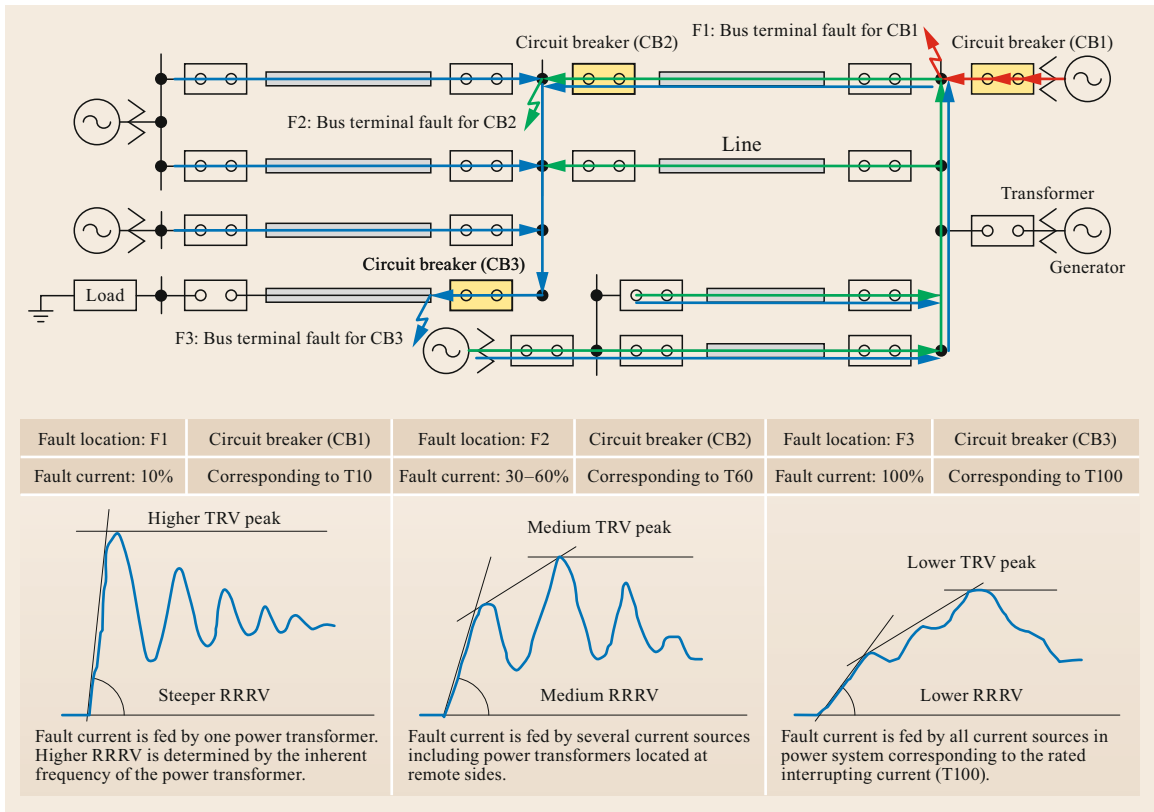
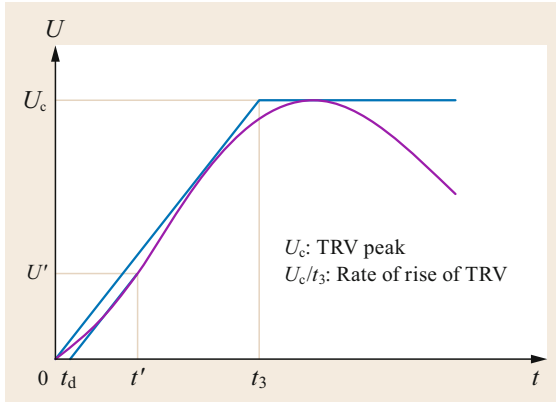
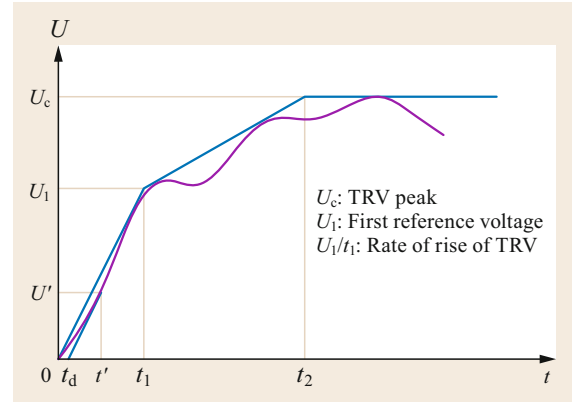


Fig. 8.69 Dependence of the TRV waveform of a bus terminal fault on the fault location



**Fig. 8.70** Specifying the TRV using a two-parameter reference line and a delay line



**Fig. 8.71** Specifying the TRV using a four-parameter reference line and a delay line

frequencies determined by the circuit conditions of the multiple current sources.

In the most severe case, when a fault is generated at F3 and all the transmission lines are loaded, the circuit breaker (CB3) is required to clear the fault current with the rated interrupting current of CB3, which is fed by all the current sources in the power system (the fault current flow is shown as a blue arrow). After clearing the fault at F3, the TRV presents a low peak as well as complex frequencies determined by the circuit conditions of all the current sources.

For bus terminal fault interruptions, the standard requires that the circuit breaker will interrupt symmetrical currents that are 10%, 30%, 60%, and 100% of the rated interrupting current as well as 100% of the current with the standard values of DC component (in asymmetrical current) with the corresponding TRV peaks and RRRVs shown in the standards, respectively. These test requirements correspond to test duties T10, T30, T60, T100s, and T100a.

For rated voltages equal to or higher than 100 kV, the TRV for terminal fault test duties is described by the two parameters shown in Fig. 8.70 for test duties T10 and T30 or the four parameters shown in Fig. 8.71 in the case of multiple TRV frequencies for test duties T60 and T100.

The peak value of the TRV ( $U_c$ ) applied to a circuit breaker during bus-terminal interruption is given by

$$U_c = U_r \sqrt{\frac{2}{3}} k_{pp} k_{af},$$

where:

$U_c$  is the TRV peak

$U_r$  is the rated voltage

$k_{pp}$  is the first-pole-to-clear factor

$k_{af}$  is the amplitude factor.

For a given rated voltage, both the first-pole-to-clear factor and the amplitude factor must be defined to determine the peak value of TRV. The power frequency recovery voltage ( $U$ ) is a function of the rated voltage and the first-pole-to-clear factor

$$U = \frac{U_r k_{pp}}{\sqrt{3}}.$$

IEC 62271-100 specifies a first-pole-to-clear factor of 1.3 for effectively earthed neutral systems at rated voltages of up to 800 kV. This value of  $k_{pp}$  is calculated from the zero-sequence reactance  $X_0$  and the positive-sequence reactance  $X_1$  using

$$k_{pp} = \frac{3}{2 + \frac{X_1}{X_0}}.$$

In a network with long transmission lines, the first-pole-to-clear factor tends to increase, because the ratio  $X_1/X_0$  of the lines decreases. On the other hand, in a network connected to large power transformers (a star connection with an earthed neutral or a delta connection), the first-pole-to-clear factor decreases and is occasionally less than 1.2 because the ratio  $X_1/X_0$  is equal to or larger than 0.5 ( $2X_1 > X_0$ ). In cases where most of the short-circuit currents are fed through large-capacity power transformers, the first-pole-to-clear factors are small because the zero-sequence impedance is reduced due to the delta connection of large-capacity power transformers ( $X_1/X_0$  approaches unity, or  $X_0$  approaches  $X_1$ ).

The impedance of overhead (OH) lines is almost inversely proportional to the square of the system operating voltage, so the ratio of the line impedance to the total transmission system impedance tends to be smaller for a system with higher voltages. This tendency reduces the zero-sequence impedance in UHV systems



**Table 8.5** Amplitude factors for terminal fault test duties

Test duty	Amplitude factor
T10	$1.7 \times 0.9(1.76)^a$
T30	1.54
T60	1.50
T100	1.40

<sup>a</sup> For UHV, the first-pole-to-clear factor of 1.2 is recommended instead of 1.3 for lower voltage ratings based on the large influence of a large capacity power transformer. The amplitude factor of 1.76 ( $1.7 \times 0.9 \times 1.5/1.3$ ) is stipulated for T10 duty to cover the TRV peak of long-line fault (LLF) interruption.

(at rated voltages of 1100 and 1200kV) due to the increasing influence of large-capacity power transformers, which have a smaller zero-sequence impedance  $X_0$  than transmission lines. Accordingly, the first-pole-to-clear factor in UHV systems is defined as 1.2 [8.37].

The amplitude factor of the TRV tends to decrease with the interrupting current because the superimposition of the TRVs (with multiple frequencies and different times to the TRV peak) originating from the various current sources (power generators) that contribute to the bus terminal fault reduces the amplitude factor.

Table 8.5 gives the amplitude factors in IEC 62271-100 for terminal fault interruption by circuit breakers with a rated voltage of 100kV and above. The amplitude factor is  $1.7 \times 0.9 = 1.53$  for test duty T10 at rated voltages of up to 800kV based on a first-pole-to-clear factor of 1.5 with a voltage reduction of 0.9 across the transformer. Note that the amplitude factor of the TRV tends to increase in UHV systems due to smaller losses from power transformers and transmission lines as well as reduced damping of traveling waves. It is therefore defined as 1.76 for UHV systems, keeping the same magnitude of the first-pole-to-clear factor times

**Table 8.6** RRRV values for terminal fault test duties

Test duty	RRRV (kV/ $\mu$ s)
T10	7
T30	5
T60	3
T100	2

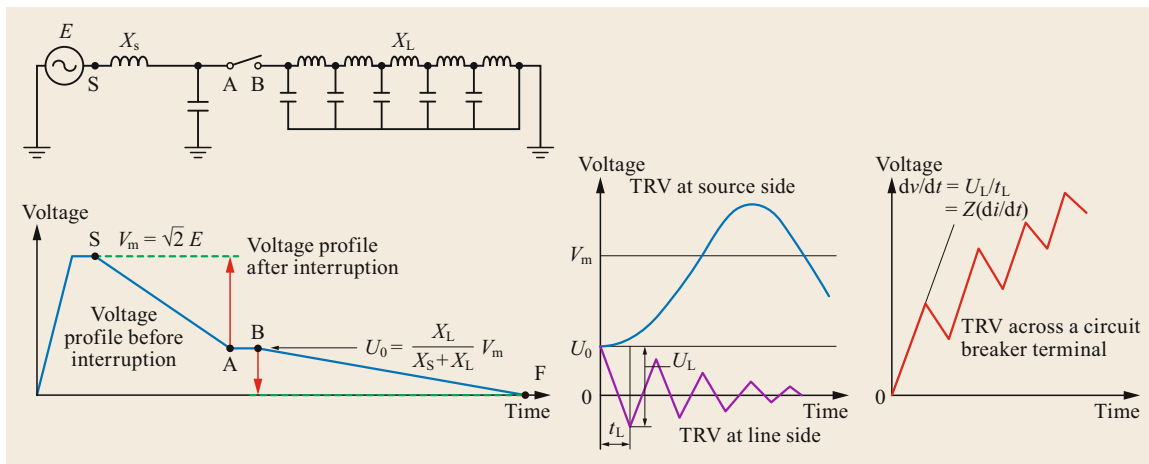
the amplitude factor based on the first-pole-to-clear factor of 1.3 stipulated for lower voltages.

Table 8.6 gives the rate of rise of TRV (RRRV) values in IEC 62271-100 for terminal fault interruption by circuit breakers with rated voltages of 100kV and above. Similarly, the RRRV tends to decrease with the interrupting current because the superimposition of the TRVs (with multiple frequencies and different times to the TRV peak) originating from the various current sources that contribute to the bus terminal fault reduces the RRRV.

### 8.3.3 Short Line Fault Interruption

When a fault occurs in a transmission line at a distance ranging from 100 m to a few kilometers down the line, a circuit breaker is required to clear this short line fault (SLF). When a circuit breaker clears the SLF generated on the line, a steeply rising TRV with a waveform similar to a sawtooth waveform is observed due to high-frequency oscillations generated by waves propagating along the line and reflecting between the circuit breaker terminal and the fault point.

Figure 8.72 shows an equivalent circuit and the associated voltage distribution when a SLF is generated on the line. The circuit breaker is connected to the generator through a power transformer at the source side and is connected to the transmission line at the line side, all of which can be modeled using a multiple lattice cir-



**Fig. 8.72** Equivalent circuit and TRV waveforms obtained under short line fault (SLF) conditions

circuit comprising a reactor and a capacitor, as shown in Fig. 8.72.

When the circuit breaker interrupts the fault current under SLF conditions, the voltage of the circuit breaker terminal at the source side is back to the system voltage at the transformer terminal, which causes an oscillation with a frequency corresponding to the power frequency in the source circuit. The source-side circuit can be approximated by a lumped circuit with constant concentrated parameters. The amplitude factor of the TRV is similar to that in the case of a terminal fault.

On the other side, the voltage of the circuit breaker terminal at the line side is dropped to the ground level, which creates another oscillation with a sawtooth (triangular) shape due to the propagation and reflection of waves along the line. The line-side circuit can be approximated by a small attenuated circuit with distributed parameters.

Figure 8.73 shows the TRV propagation at the line side without considering any attenuation of the traveling waves. After SLF interruption, the transients travel along the line in both directions. One propagates from the breaker terminal to the fault point and the other propagates from the fault point to the breaker terminal with a contact propagating velocity of  $c$ , which is about  $300 \text{ m}/\mu\text{s}$  through a transmission line.

The transient initiated from the breaker terminal (which has a voltage of  $U_0$  immediately after interruption) decreases with time and arrives at the fault point (where the voltage is always at the ground level) at  $t = L/c$ , where  $L$  is the line length. The transient is reflected at the fault point (discontinuity), travels back along the line, and returns to the breaker terminal at  $t = 2L/c$  with a voltage of  $-U_0$  (negative polarity), which corresponds to the first TRV peak ( $U_L$ ).

The transient continues to travel along the line in both directions at a constant velocity and reflects at the breaker terminal and the fault point, leading to the formation of a saw-tooth (triangular) waveform.

The waveform of the TRV across the circuit breaker terminals is a superimposition of those at both the source and the line sides, and the initial rate of rise of the TRV is given by  $dv/dt = Z(di/dt)$ , where  $Z$  is the line surge impedance. The TRV on the line side increases with increasing distance to the fault point, while the TRV on the source side decreases.

When a circuit breaker interrupts the SLF, the thermal interrupting performance is the main determinant of interruption success or failure given the severe energy input that occurs immediately after current interruption due to the high RRRV. When a circuit breaker cannot provide sufficient coolability for the energy

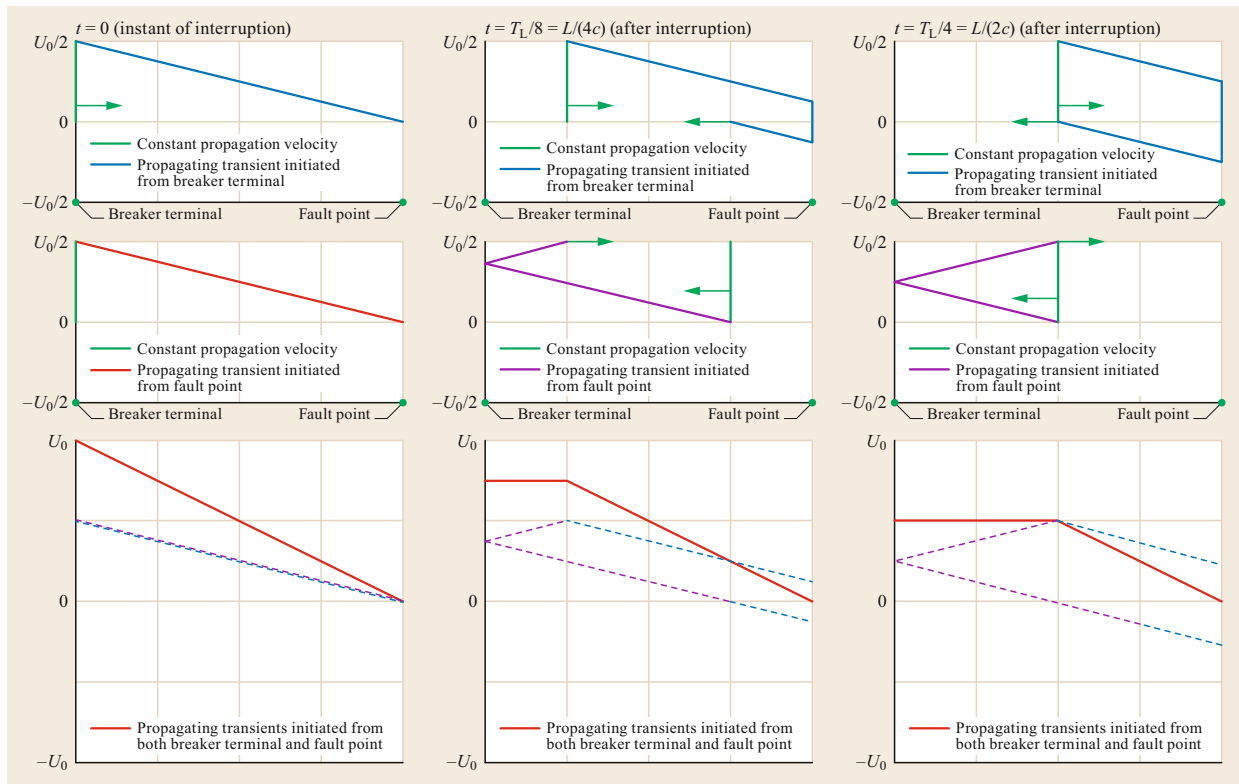
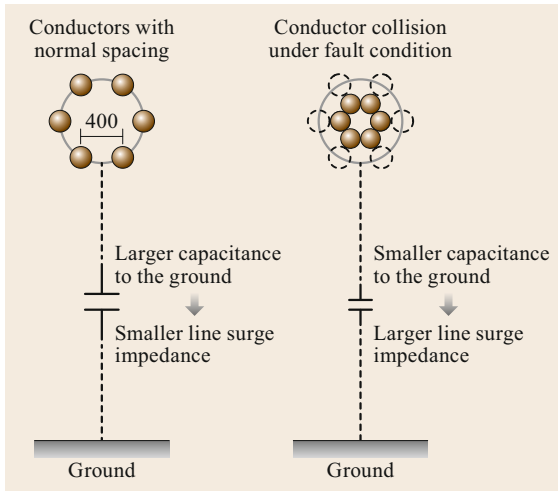


Fig. 8.73 TRV propagation under short line fault (SLF) conditions at the line side



Fig. 8.73 (continued)



**Fig. 8.74** Multibundle conductors under normal conditions and bundle collisions that occur under fault conditions

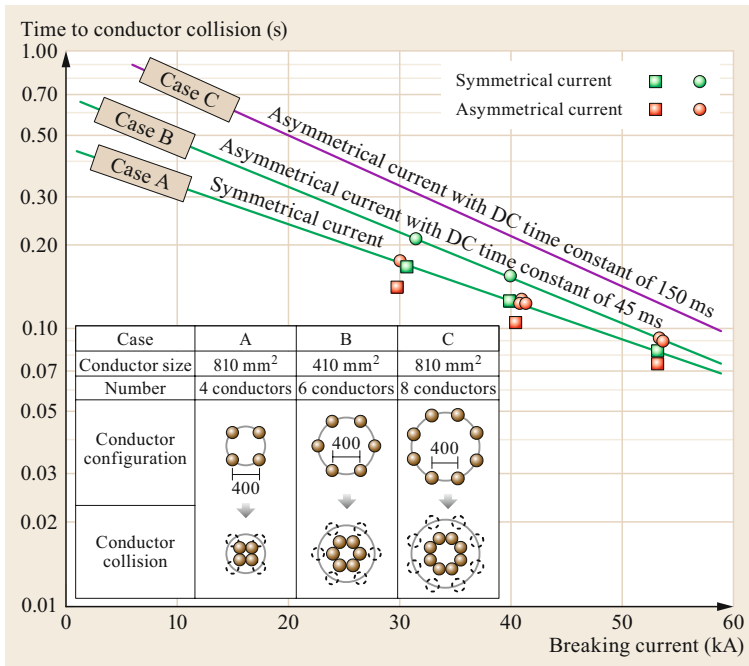
input during the thermal interrupting period, thermal reignition may happen.

The standardized value of  $Z$  in IEC 62271-100 and IEEE C37.04 is  $450 \Omega$ , which roughly corresponds to the surge impedance of a single conductor. In EHV and UHV systems, multibundle conductors are used, which give lower line surge impedances of  $250\text{--}400 \Omega$  under normal current carrying conditions, which can be found using  $\sqrt{L/C}$  with a large capacitance to ground. Here,  $L$  is the reactance of the line. The capacitance

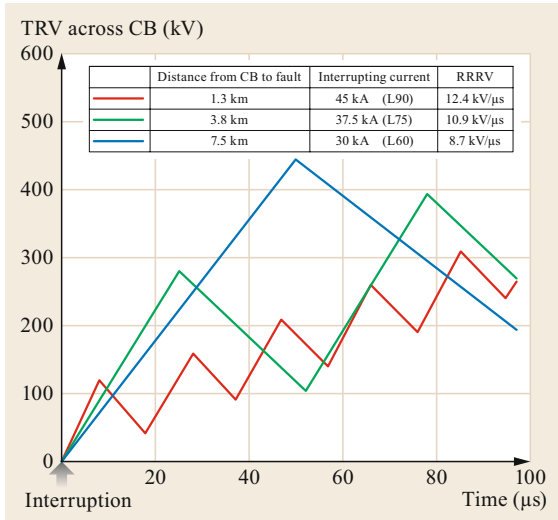
of multi-bundle conductors to the ground is larger than that of a single conductor due to its higher equivalent cross-section to the ground. When a SLF is generated, the conductors in the multibundle conductors attract each other due to Lorentz forces that push the conductors together. Figure 8.74 shows a schematic of multibundle conductors under normal conditions and the bundle collision that occurs under fault conditions.

Besides the fault current, the line surge impedance depends on the multibundle conductor design (materials, cross-sections, span, and spacer size) and the mechanical tension applied to the conductors in the lines. Several studies, including those of CIGRE WG 13.01, have examined and reported the time required for a bundle collision. For example, twin conductors that were  $686 \text{ mm}^2$  in cross-section and carried  $40 \text{ kA}$  collided  $50 \text{ ms}$  after a fault occurrence, and quadruple conductors that were  $810 \text{ mm}^2$  in cross-section and carried  $30\text{--}50 \text{ kA}$  collided  $100\text{--}200 \text{ ms}$  after a fault occurrence, as shown in Fig. 8.75. A longer time to bundle contraction is expected for UHV lines, as they use more conductors and each conductor has a relatively large cross-section. A value of  $330 \Omega$  is standardized for the surge impedance of lines in UHV systems.

The severity of a SLF test duty depends mainly on the rate of rise of the recovery voltage, which is determined by the line surge impedance and slope of the fault current. The equivalent line surge impedance ( $Z$ ) for each pole-to-clear is given by the following equa-



**Fig. 8.75** Collision times of multi-bundle conductors



**Fig. 8.76** Comparison of the TRV waveforms obtained for interrupting currents corresponding to L90, L75, and L60

tions, where  $Z_0$  is the zero-sequence surge impedance and  $Z_1$  is the positive-sequence surge impedance

$$Z_{\text{first pole}} = \frac{3Z_1Z_0}{Z_1 + 2Z_0}, \quad (8.1)$$

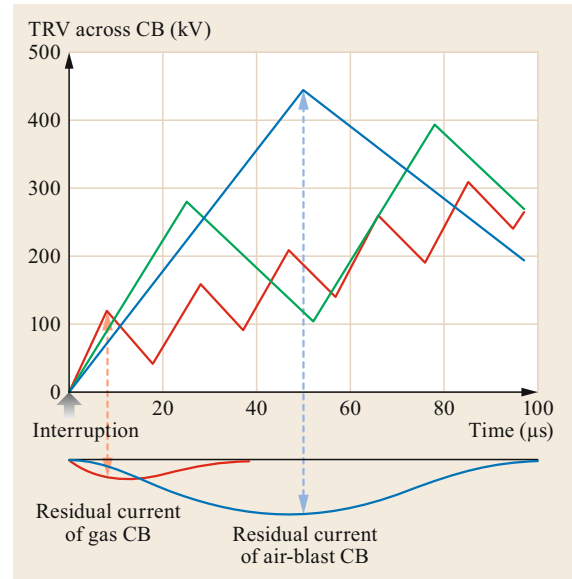
$$Z_{\text{second pole}} = \frac{Z_1(Z_1 + 2Z_0)}{2Z_1 + Z_0}, \quad (8.2)$$

$$Z_{\text{third pole}} = \frac{2Z_1 + Z_0}{3}. \quad (8.3)$$

In an actual substation, a circuit breaker is connected to the bus terminal using a short line. The surge impedance of the short line is  $260 \Omega$  due to high capacitance to the ground because the short line is normally closer to the ground and is often connected to a capacitor voltage transformer. The surge impedance of the transmission line is  $450 \Omega$ . The short length of this line creates a similar triangular waveform with a high frequency and low amplitude that is termed the initial TRV (ITRV). The ITRV may exert severe thermal stress on the circuit breaker, depending on the conditions.

In the standards IEC 62271-100 and IEEE C37.04, L90 and L75 are the type test duties for short line fault (SLF) conditions. The fault current is equal to 90%, 75%, and 60% of the rated short-circuit breaking current, respectively. The requirements for a SLF at different current levels originated from the thermal interrupting capability of an air-blast circuit breaker, which generates a higher residual current after current interruption than a gas circuit breaker does.

Figure 8.76 shows TRV waveforms calculated for different current levels corresponding to L90, L75, and L60, assuming a 550 kV transmission line with

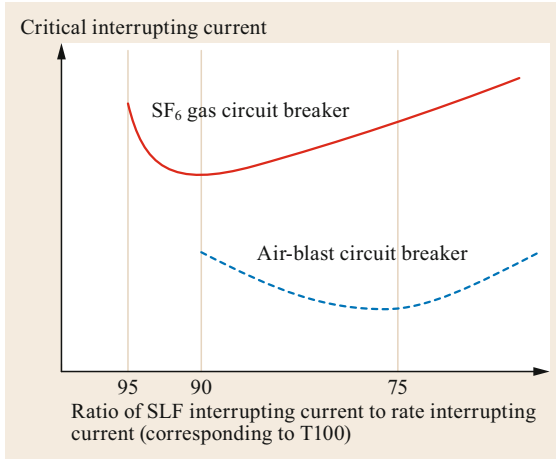


**Fig. 8.77** Comparison of the residual currents and TRVs obtained with an air-blast circuit breaker and a gas circuit breaker (the TRV curves are color-coded as in Fig. 8.76)

a rated interrupting current of 50 kA and a power frequency of 60 Hz. The line surge impedance is  $450 \Omega$ . The TRV presents a high RRRV, low TRV peak, and high TRV frequency at an interrupting current of 45 kA (L90, where a fault occurs 1.3 km from the circuit breaker). The RRRV gradually decreases, the TRV peak increases, and the TRV frequency decreases as the interrupting current is decreased from L75 (a fault occurs 3.8 km from the CB) to L60 (a fault occurs 7.5 km from the CB).

Figure 8.77 shows a comparison of the residual current and TRV waveforms obtained for different interrupting currents with an air-blast CB and a  $\text{SF}_6$  gas CB. The air-blast CB tends to conduct larger residual currents after current zero than the  $\text{SF}_6$  gas CB, and the peak residual current roughly corresponds to the TRV peak for test duty L60. In contrast, the smaller peak residual current obtained with the  $\text{SF}_6$  gas CB roughly corresponds to the TRV peak for test duty L90. Therefore, the energy input is highest for the TRV corresponding to L90 in the case of the  $\text{SF}_6$  gas CB, and for the TRV corresponding to L60 or L75 in the case of the air-blast CB. Accordingly, the thermal interruption duties represented by L60 or L75 may be more severe for an air-blast CB than the L90 duty.

Figure 8.78 shows the critical interrupting capabilities of an air-blast CB and a  $\text{SF}_6$  gas CB, respectively. Whereas L90 appears to be the most severe interrupting duty for the  $\text{SF}_6$  gas CB, L75 and L60 seem to be the most severe for the air-blast CB.

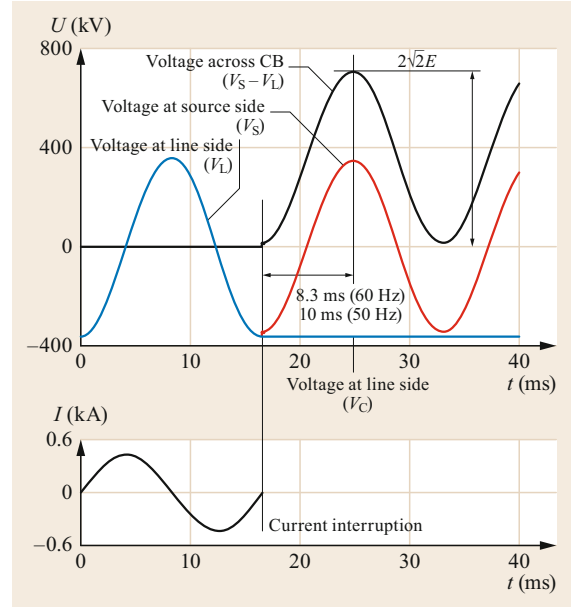


**Fig. 8.78** Thermal interrupting capabilities of an air-blast circuit breaker and gas circuit breaker for different currents

### 8.3.4 Capacitive Current Switching

When a circuit breaker connects or disconnects no-load transmission lines, no-load cables, and shunt capacitor banks (as shown in Fig. 8.79), it switches small capacitive currents of several tens to several hundreds of amperes that are 90° in advance of the voltage phase. After current interruption at the voltage peak of the load side with  $-E$  level (red line), the recovery voltage at the source side (black line) shows a  $1 - \cos$  waveform and is raised from  $-E$  to  $E$  level, while the voltage at the load side is kept as  $-E$  level. Therefore the voltage across CB is  $2E$  at maximum. The first reignition occurs at the voltage peak, the voltage at the load side is raised up to the voltage at the source side from  $-E$  to  $E$  level (the voltage across CB is dropped to zero), but it passes through  $E$  level and further up to  $3E$  level without attenuation. Thus, the voltage at the load side remains at  $3E$  level. Figure 8.80 shows the waveforms for the TRV across a circuit breaker, the TRV at the source side, and the TRV at the line side.

If a circuit breaker interrupts the current at this voltage peak ( $-5E$ ), again the recovery voltage at the source side shows an  $(1 - \cos)$  waveform and is raised from the  $-E$  to  $E$  level, while the voltage at the load side is kept as  $3E$  level. Therefore, the voltage across CB is

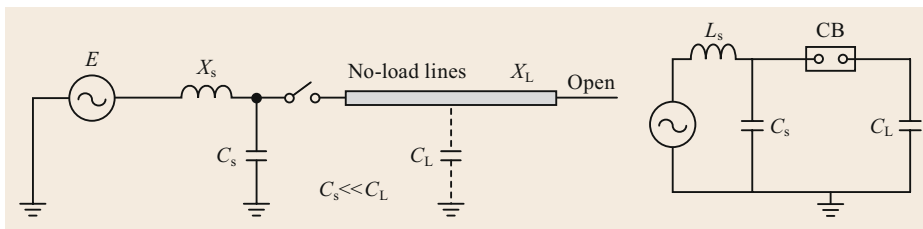


**Fig. 8.80** Recovery voltage (RV) waveforms after disconnecting a no-load line

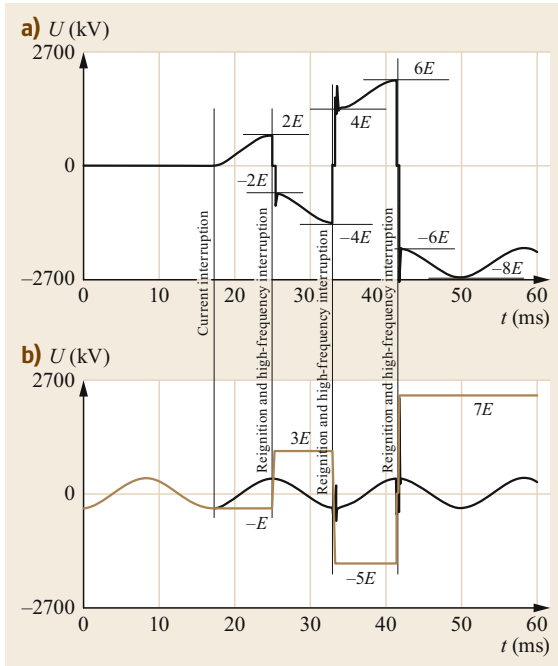
$6E$  at maximum. The third reignition occurs at the voltage peak, the voltage at the load side is raised up to the voltage at the source side from the  $-5E$  to the  $E$  level (the voltage across CB is dropped to zero), but it passes through  $E$  level and further up to  $7E$  level without attenuation. Thus, the voltage at the load side attains  $7E$  level at this moment.

If a circuit breaker interrupts the current at this voltage peak ( $7E$ ), again the recovery voltage at the source side shows an  $(1 - \cos)$  waveform and is decreased from  $E$  to  $-E$  level, while the voltage at the load side is kept at  $7E$  level. Therefore, the voltage across CB is  $8E$  at maximum. The fourth reignition occurs at the voltage peak, the voltage at the load side is decreased to the voltage at the source side from  $7E$  to  $-E$  level (the voltage across CB is dropped to zero), but it passes the  $-E$  level and further down to the  $-9E$  level without attenuation. Thus, the voltage at the load side attains the  $-9E$  level at this moment, as shown in Fig. 8.81.

Since a circuit breaker can easily interrupt a small capacitive current, the dielectric interrupting performance



**Fig. 8.79** No-load transmission line switching

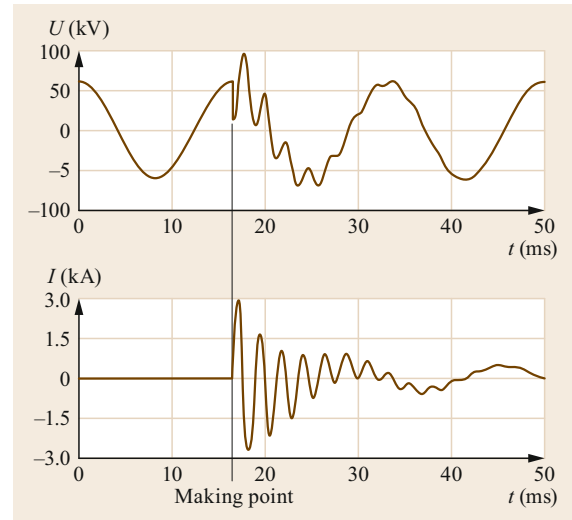


**Fig. 8.81a,b** Voltage escalation across CB caused by multiple reignitions, (a) voltage across CB, (b) voltage at line side

is the dominant influence on whether an interruption is successful for small capacitive current switching. The interruption is successfully completed when the dielectric strength across the contacts always surpasses the recovery voltage after current interruption.

When the TRV exceeds the dielectric recovery performance across the circuit breaker terminals, dielectric breakdown occurs. Dielectric breakdowns are categorized into reignitions and restrikes depending on when they occur. If the dielectric breakdown happens within an interval of less than a quarter cycle of the power frequency after an interruption at current zero, it is a restrike, which will not generate a severe overvoltage. However, if it happens with an interval of a quarter cycle of the power frequency or longer after an interruption at current zero, it is a reignition, which may generate a severe overvoltage.

Reignition at peak voltage with a load-side voltage (at the line side) of  $-E$  and a voltage across the circuit breaker of  $2E$  causes the load-side voltage to jump to  $3E$  (i.e.,  $E$  from the reverse polarity of the remaining DC plus  $2E$  from the TRV peak), as shown in Fig. 8.81. If the circuit breaker can interrupt the high-frequency current immediately after reignition, the load-side DC voltage at the line side remains  $3E$ . The recovery voltage across the circuit breaker presents a  $\cos - 1$  waveform that starts at  $-2E$  and reaches  $-4E$ . However, reignition

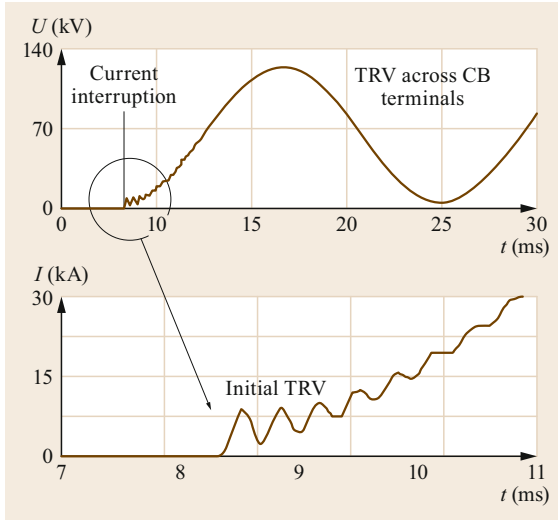


**Fig. 8.82** The severe inrush current and associated overvoltage generated when a circuit breaker makes the voltage peak during no-load line energization

at peak voltage with a load-side voltage (at the line side) of  $3E$  and a voltage across the circuit breaker of  $-4E$  causes the load-side voltage to jump to  $5E$  (i.e.,  $3E$  from the reverse polarity of the remaining DC plus  $2E$  from the TRV peak). In this case, if the circuit breaker can interrupt the high-frequency current immediately after reignition, the load-side DC voltage at the line side remains  $-5E$ . The recovery voltage across the circuit breaker presents a  $1 - \cos$  waveform that starts at  $4E$  and reaches  $6E$ . Finally, reignition at peak voltage with a load-side voltage (at the line side) of  $-5E$  and a voltage across the circuit breaker of  $6E$  causes the load-side voltage to jump to  $7E$  (i.e.,  $5E$  from the reverse polarity of the remaining DC plus  $2E$  from the TRV peak). The voltage escalation due to multiple high-frequency interruptions immediately after reignitions can impose serious stress on the equipment in the power system.

Energization of a no-load transmission line or a shunt capacitor bank may generate high inrush currents and associated overvoltages depending on the making instants of the voltage across a circuit breaker. Figure 8.82 shows the inrush current and associated overvoltage generated when a circuit breaker makes the voltage peak during no-load line energization, which may exert excessive mechanical and electrical stresses on the capacitor bank and other equipment in the power system and erode the circuit-breaker contact. Controlled switching can effectively reduce switching surges during no-load transmission line or shunt capacitor bank energization.

In a real substation, a circuit breaker is connected to the bus terminal using a short line. The short length

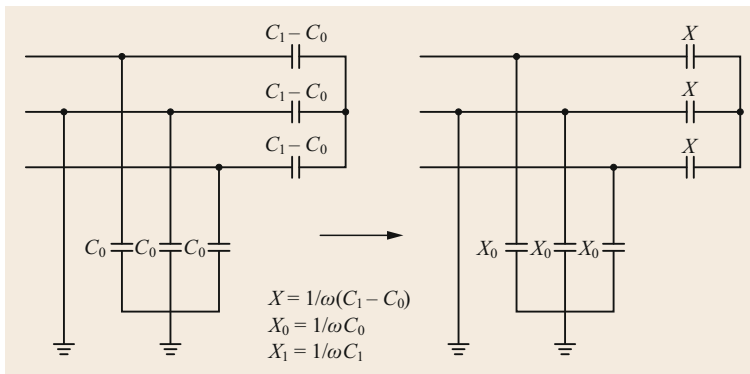


**Fig. 8.83** TRV and ITRV waveforms for no-load line disconnection

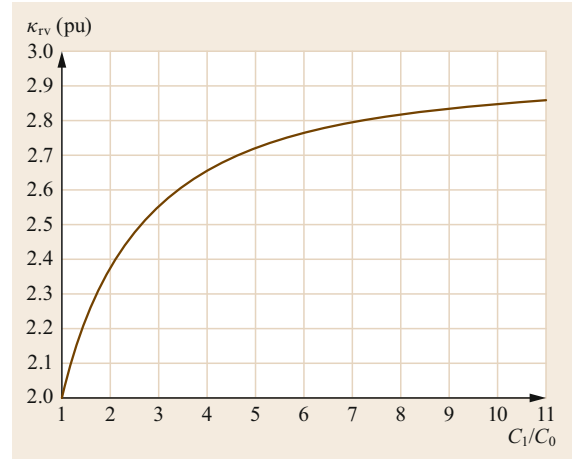
of this line creates an ITRV waveform with a high frequency and low amplitude. This waveform is called an ITRV, just as for SLF interruption. Figure 8.83 shows the TRV waveform that occurs when a circuit breaker disconnects a no-load transmission line.

The three-phase switching of no-load transmission lines and no-load cables is slightly more complex than that for shunt capacitor banks because the capacitance is distributed along the line rather than lumped and both line-to-earth and line-to-line capacitances are involved.

Figure 8.84 shows equivalent circuits of no-load transmission lines and cables characterized by a positive capacitance  $C_1$  and a negative capacitance  $C_0$ . Here  $C_1 = C_0$  corresponds to shunt capacitor bank switching with an earthed neutral. TRV will present a  $1 - \cos$  waveform similar to that for capacitor bank switching but with a different peak TRV that depends on the ratio  $C_0$  to  $C_1$ .



**Fig. 8.84** Equivalent circuits of no-load lines and cables



**Fig. 8.85** Peak TRV of the first-pole-to-clear for no-load line switching

When the load impedance  $X_L$  is  $1/\omega C_1$  for capacitor bank switching with an earthed neutral (where  $C_1 = C_0$ ), the peak TRV is  $2E$  (where  $E$  is the peak system voltage). The line impedance  $X_L$  for no-load transmission is given by

$$X_L = \frac{1.5X_0X}{1.5X + X_0}$$

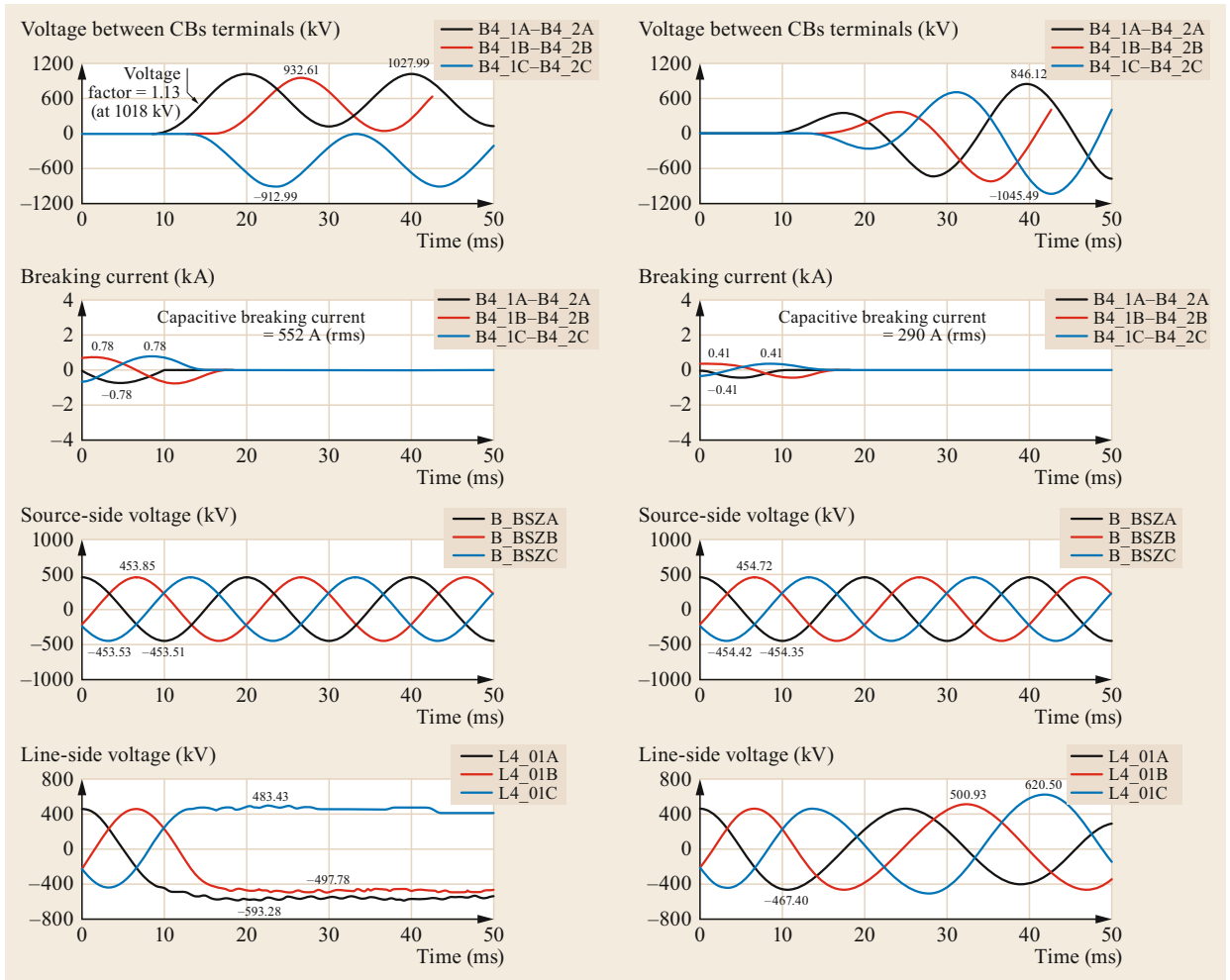
where  $X$  is  $1/\omega(C_1 - C_0)$  and  $X_0$  is  $1/\omega C_0$ . The peak TRV is given by

$$\text{Peak TRV} = \frac{6C_1/C_0}{1 + C_1/C_0}$$

Figure 8.85 shows the peak TRV as a function of  $C_1/C_0$ ; the peak TRV approaches a value of 3 with increasing  $C_1/C_0$ .

The peak TRV is  $2.4E$  when switching a no-load overhead transmission line (OHL), where  $C_1 = 2C_0$ , and it is  $3E$  when switching a no-load cable with an isolated neutral, where  $C_0 \approx 0$ .





**Fig. 8.86** Influence of a shunt reactor on the TRV for no-load line breaking in a 550 kV double-circuit network model with the system and equipment parameters employed in Thailand

In some cases the transmission line is equipped with shunt-reactor compensation, in order to absorb reactive power and keep the voltages along the line with desired margin by preventing from excessive voltage increase due to Ferranti effect under light load conditions or excessive renewable power generations. In case of a compensated line, the degree of line compensation (reactance) has a significant effect on the voltage at line side. The voltage across CB has a prominent beat especially in case of a high degree of compensation, because the line oscillation (TRV frequency) falls in the range of 30–50 Hz.

The influence of shunt reactors on the TRV during the switching of a 360 km no-load line was calculated for a 550 kV double-circuit transmission line. Figure 8.86 shows TRV waveforms obtained for no-load line switching with and without shunt reactors. The

TRV frequency is several tens of Hz and depends on the inductance of the reactor and the capacitance of the line, and the peak TRV in the network can be reduced considerably when a large shunt reactor is connected. For example, the peak TRV when a fault occurs at a remote distance of 360 km under line charging conditions in a 550 kV network is 1018 kV without a shunt reactor but less than 400 kV when a shunt reactor is connected. Therefore, shunt reactors can significantly reduce the first TRV peak obtained when disconnecting under no-load line charging conditions.

### 8.3.5 Small Inductive Current Switching

When a circuit breaker opens and closes a shunt reactor bank or unloaded power transformer, it switches small inductive currents of several tens of amperes with

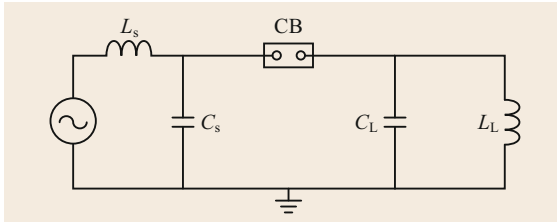


Fig. 8.87 Equivalent circuit for small inductive switching

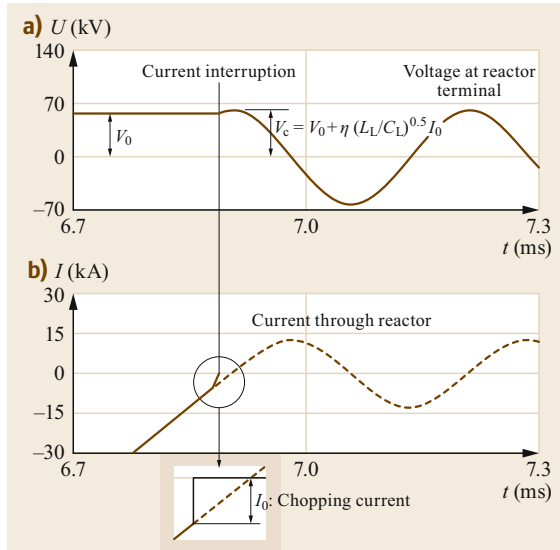


Fig. 8.88 (a) Voltage and (b) current behavior when current chopping occurs upon small inductive current interruption

a  $90^\circ$  lag with respect to the voltage phase. Figure 8.87 shows an equivalent circuit for small inductive current switching. Small inductive switching is generally not a significant test duty for a circuit breaker. However, a circuit breaker that presents high thermal interrupting performance may interrupt a small inductive current before an inherent current zero (current chopping), generating chopping overvoltage, which tends to increase with increasing chopping current.

Figure 8.88 shows the typical voltage and current behavior observed when current chopping occurs upon small inductive current interruption. The current chopping is sometimes accompanied by an expanding high-frequency current oscillation that leads to a sudden current zero. This is an arc instability phenomenon caused by the characteristics of the arc and the circuit conditions. The chopping current of a modern  $\text{SF}_6$  gas circuit breaker is no higher than 10 A, which does not generally lead to a severe chopping overvoltage.

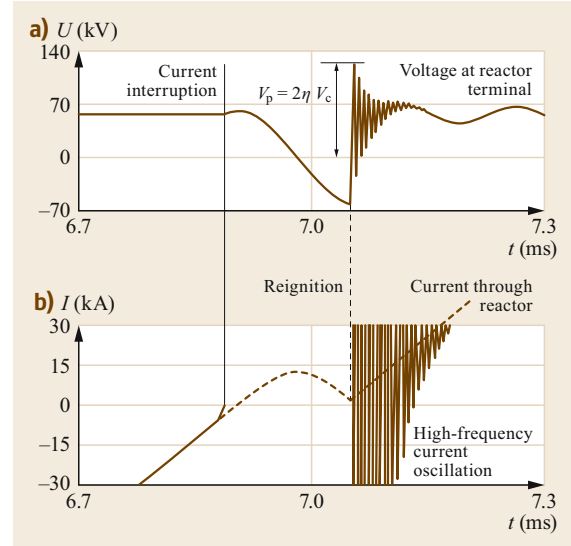
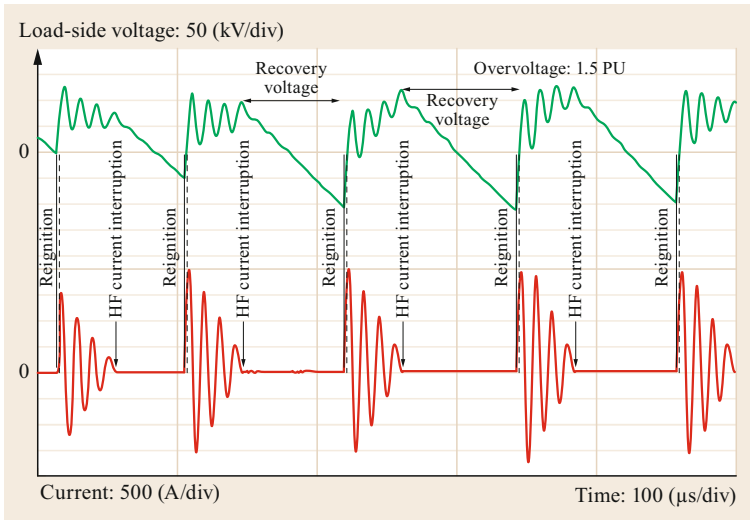


Fig. 8.89 (a) Voltage and (b) current behavior when reignition occurs upon small inductive current interruption

Another prominent phenomenon that is observed after small inductive current interruption is reignition. A circuit breaker can easily interrupt a small inductive current, even if the arcing time and contact gap are small. The dielectric withstand strength of a circuit breaker increases with the contact gap, so a small contact gap tends to generate voltage breakdown during the period when the TRV exceeds the dielectric withstand across the contact gap. Reignition provokes high-frequency current oscillations and associated overvoltages, as shown in Fig. 8.89. These reignition overvoltages may damage the nozzle and the contacts of the circuit breaker as well as the reactor insulation. Controlled switching is often applied to avoid reignitions during small inductive switching by increasing the arcing time.

Multiple reignitions and associated voltage disturbances may be observed, especially for vacuum interrupters (due to their excellent thermal interrupting capabilities), as shown in Fig. 8.90. If a high-frequency (HF) current generated after a reignition cannot be interrupted, the current will be interrupted at the next current zero in the power frequency. However, the high-frequency current may be interrupted immediately after a reignition if the circuit breaker has excellent thermal interrupting capabilities. Repeated reignition may occur if the dielectric strength is insufficient for the TRV withstand imposed immediately after current interruption. The overvoltage gradually increases in amplitude with multiple reignitions, and this overvoltage is repeatedly applied to substation equipment at the load side.



**Fig. 8.90** Multiple reignitions and high-frequency current interruptions

### 8.3.6 Transformer Limited Fault Clearing

One of the most severe fault current interruption duties of a circuit breaker is the clearing of a transformer limited fault (TLF). In Fig. 8.91 the two topology conditions of a TLF are given: the transformer-fed fault (TFF) and the transformer secondary fault (TSF). In both cases, the characteristics of the transformer are the dominant influences on the short-circuit current, its AC and DC components, the power frequency recovery voltage (the first-, second-, and third-pole-to-clear factors given by the neutral treatment of the system; the voltage drop), and the high-frequency TRV.

Due to the dominance of the transformer impedance, the TRV is largely dictated by the power-frequency voltage drop across the transformer. The higher the TLF current, the lower the voltage drop. A fault current of 6.3 kA will cause a voltage drop of roughly 90%, while a fault current of 12.5 kA will yield a voltage drop of around 70%. In practice, 12.5 kA corresponds to approximately 30% of the rated short-circuit current of the circuit breaker.

The ratio  $X_0/X_1$  varies considerably depending on the neutral treatment of the network and the transformer involved. However, for effectively earthed networks and transformers with an earthed neutral,  $X_0/X_1$  will be smaller than 1.0, leading to a reducing effect on the

first-pole-to-clear factor ( $k_{pp}$ ). However, under other conditions where transformer neutrals are not (always) connected to earth,  $k_{pp}$  may reach 1.5, although this is the exception rather than the rule, and it can be stated that at the transformer side, connected to networks of 100 kV and above, the first pole-to-clear factor for TLF will generally be close to 1.0 or even lower. The first-pole-to-clear factors as specified in the IEC standard for circuit breakers (1.2 for UHV and 1.3 for EHV) are therefore undoubtedly larger than those observed under service conditions. In cases where transformer neutrals are isolated from earth or connected by Petersen coils (resonance earthing),  $k_{pp}$  must be specified as 1.5.

Neglecting the contribution from the supply, which is at a much lower frequency, the peak TRV for a TLF is given by:

$$U_c = k_p k_{af} k_{vd} \frac{U_r \sqrt{2}}{\sqrt{3}}, \quad (8.4)$$

where:

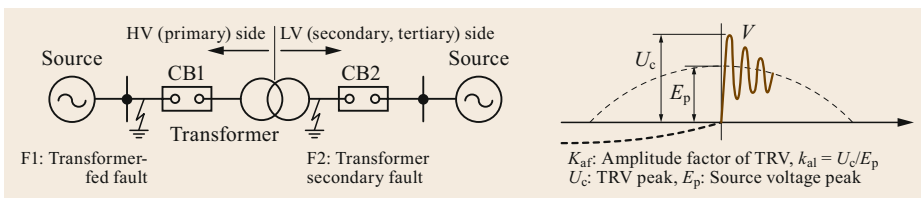
$U_c$  is the TRV peak

$k_p$  is the pole-to-clear factor ( $k_{pp}$  for the first-pole-to-clear)

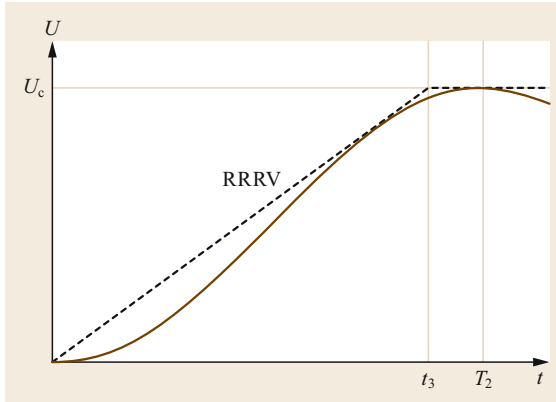
$k_{af}$  is the amplitude factor

$k_{vd}$  is the voltage drop factor

$U_r$  is the rated voltage.



**Fig. 8.91** The transient recovery voltage (TRV) for transformer limited faults (TLFs)



**Fig. 8.92** Two-parameter TRV envelope for TLF conditions

When the capacitance to earth of the connection between the circuit breaker and transformer is large enough, the frequency response at the moment of fault current interruption (i.e., the TRV as a function of the frequency) will be dominated by this capacitance in parallel with the transformer short-circuit inductance. The TRV as a function of time will appear to be a rather simple single-frequency response: a damped  $1 - \cos$  function described by a two-parameter envelope, as defined in the IEC standard for high-voltage circuit breakers [8.38].

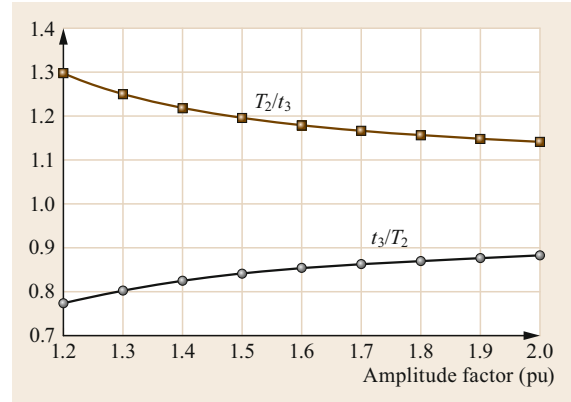
Figure 8.92 illustrates the TRV envelope for TLF conditions, which is covered by terminal fault test duties T10 and T30, corresponding to short-circuit currents of 10% and 30%, respectively, of the rated short-circuit current of the circuit breaker. The peak value  $U_c$  occurs at time  $T_2$  and  $t_3$  is the time taken for the line segments constituting the envelope to intersect. Figure 8.92 shows the steepness of the TRV expressed as the RRRV (rate of rise of TRV), which is immediately imposed after interruption as it is an important dielectric stress factor for the contact gap. Figure 8.93 presents the ratio of  $T_2$  to  $t_3$  as a function of the damping, which is expressed as the amplitude factor ( $k_{af}$ ). A factor of 2.0 means no damping, and an amplitude factor of 1.7 covers most real cases [8.39].

The corresponding RRRV can be then calculated from the peak TRV  $U_c$  and  $t_3$  as shown in Fig. 8.92 and below

$$\text{RRRV} = \frac{U_c}{t_3}, \quad (8.5)$$

where  $t_3$  can be derived from  $T_2$ , the time to peak TRV, as a function of the amplitude factor, as shown in Fig. 8.93.

When there is no external capacitance, the TRV is determined by a complicated transformer model. Several models that describe the transient behavior of



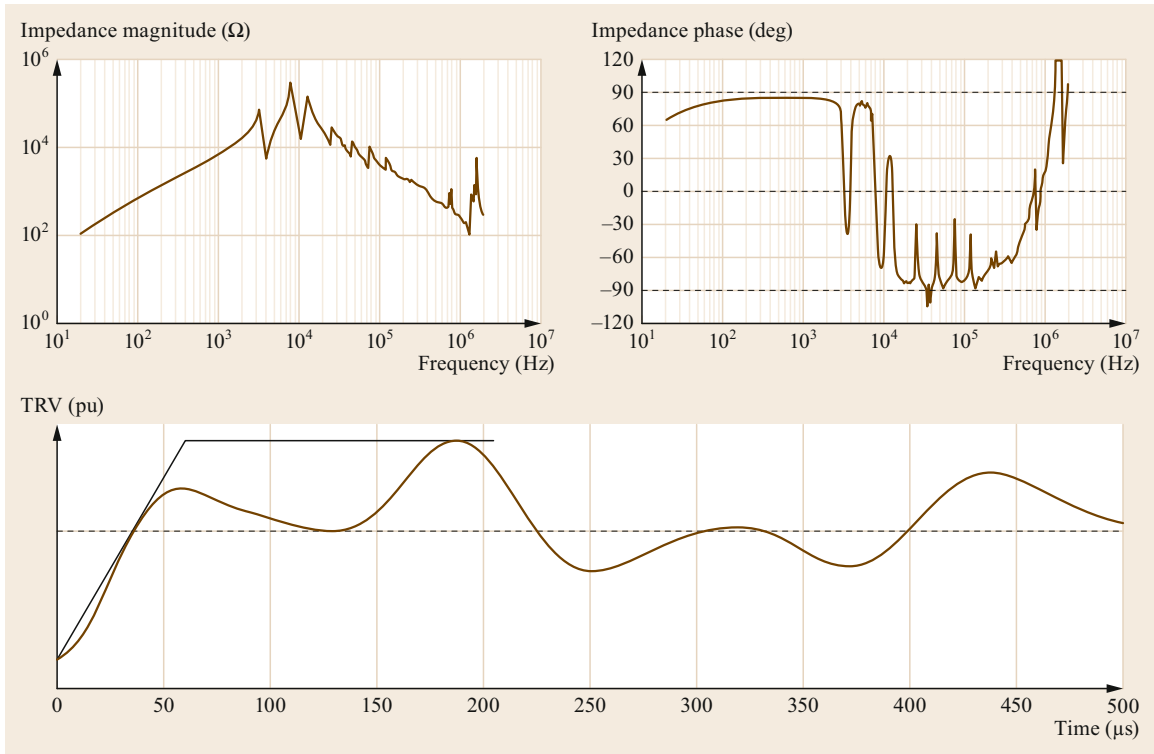
**Fig. 8.93** The ratios  $T_2/t_3$  and  $t_3/T_2$  as functions of  $k_{af}$

a transformer are available. However, it should be noted that the relevant range of frequencies for estimating the TRV waveform is between about 10 and 100 kHz. This range is much lower than most transient transformer models refer to, since they address the frequencies (up to tens of MHz) that accompany the internal stresses in the transformer's windings. Frequency response analysis (FRA) measurements are applied to study very-high-frequency models, but they are also useful for the low-frequency range and for determining the TRV waveform. They are used to obtain the frequency-dependent ratio of the output voltage to the input voltage in various configurations of shorted LV windings and excited HV phases of a power transformer.

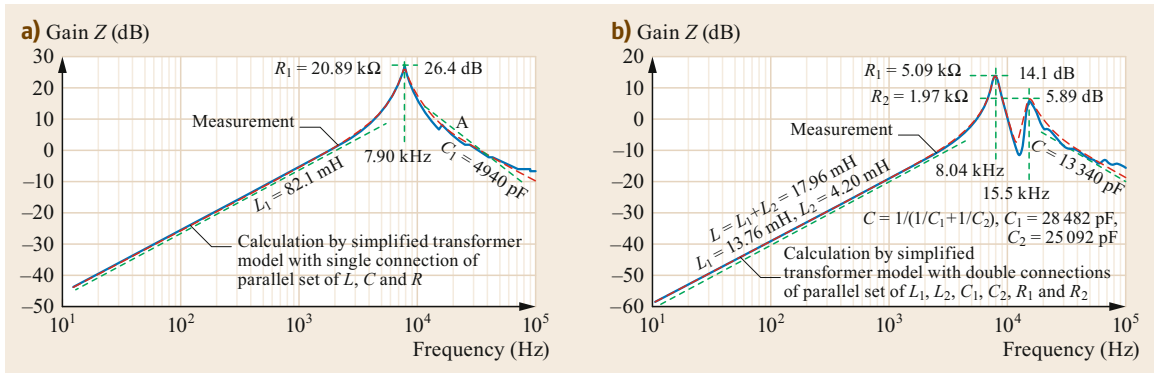
The impedance can also be measured directly using adequate measuring equipment. Figure 8.94 shows the magnitude and the argument (the phase angle shift) of the frequency-dependent transformer impedance.

FRA measurements indicate the transformer response in the frequency domain. Multiplying the transformer impedance in the frequency domain by the fault current function in the frequency domain gives the TRV in the frequency domain:  $\text{TRV}(\omega) = I_{sc}(\omega)Z(\omega)$ . Reverse Fourier transformation then yields  $\text{TRV}(t)$  in the time domain. Note that the fault current mentioned here is the so-called injected fault current, which has the opposite polarity to the actual fault current, meaning that the superposition of the actual and injected fault currents gives a net effect of zero current, i.e., fault clearing. During the relevant part of the TRV (a few ms), the injected fault current can be regarded as a ramp function:  $I(t) = St$ , or, in the frequency domain,  $I(\omega) = S/\omega^2$ . This reduces the effect of the higher-frequency part of  $Z(\omega)$  on  $\text{TRV}(\omega)$ .

Using the FRA measurements shown in Fig. 8.94, the short-circuit inductance can be obtained by fitting a straight line in the low-frequency range that increases in proportion to the frequency. It is also possible, albeit



**Fig. 8.94** FRA and TRV waveform obtained with a 400 kV, 80 MVA transformer. Transformer characteristics: 1U-1N tap5, 80 MV A, 3 $\Phi$ , HV = 400 kV, LV1 = 11.5 kV, LV2 = 11.5 kV,  $X_k$ @50 Hz = 309.3  $\Omega$ , estimated TRV parameters:  $k_{af} = 1.69$ ,  $t_3 = 61.1 \mu s$



**Fig. 8.95a,b** FRA measurements for a 525 kV, 1500 MVA transformer. (a) Primary side, (b) secondary side

less straightforward, to determine the surge capacitance by fitting a straight line in the upper frequency range that decreases in a manner inversely proportional to the frequency. This allows the surge capacitance to be determined in the relevant range of frequencies (tens of kHz to around 100 kHz).

Thus, a simple single-frequency model can be derived that is based on the short-circuit inductance  $L$  and the surge capacitance  $C$ . The parallel resistance  $R$  can

be estimated from the crest value of  $Z(\omega)$ . The damping of the single-frequency response can be calculated and the peak or amplitude factor  $k_{ap}$  can be derived from  $R/\sqrt{L/C} = R/Z$ . Multiple resonances can also be derived.

Typical responses obtained via FRA measurements with the first-pole-to-clear at the primary and secondary sides of a 1500 MVA shell-type transformer are shown in Fig. 8.95.

The TRV waveform can be reproduced using a simplified transformer model with a series connection of multiple parallel circuits of  $L$ ,  $C$ , and  $R$  based on the FRA measurements. Simplified transformer models for the primary and secondary sides can be obtained from the results of the FRA measurements, as shown in Fig. 8.96. Frequency responses were also calculated using these simplified transformer models, and are plotted in Fig. 8.95. The calculated responses show good agreement with the measured FRA characteristics.

Figure 8.97 shows the TRV waveforms reproduced by the simplified transformer models based on the FRA measurements. These calculated TRV waveforms also show good agreement with the measured TRVs. This confirms that a simplified transformer model that has a series connection of multiple parallel circuits of  $L$ ,  $C$ , and  $R$  and is based on FRA measurements can reproduce the TRV waveform obtained under TLF conditions very precisely [8.40].

The minimum amount of capacitance to earth between a circuit breaker and the power transformer has been investigated. The connection usually occurs through air-insulated conductors along distances ranging from tens of meters up to a hundred meters. Only limited high-voltage equipment is connected, and such equipment (current transformers, surge arresters, disconnectors, and earthing switches) may have a rather low capacitance to earth. Typical examples of the external capacitance of air-insulated substations give a minimum value that seems to be around 500–1000 pF almost independent of the rated voltage.

A substantial capacitance in comparison to the transformer capacitance will change the TRV waveform. When the external capacitance is included in the FRA measurement, it causes a shift in the total impedance to the left, i.e., to lower frequencies. In addition, the peak value of the transformer-frequency-dependent impedance increases, as the quality factor increases. Moreover, while the dominant frequency becomes more prominent, the other natural frequencies tend to diminish. Without external capacitance, the dominant frequencies tend to be between 10 and 20 kHz. When a minimal level of additional capacitance is added, the dominant frequency is around 10 kHz or less.

The given frequencies (around 10 kHz), the higher quality factors (leading to an amplitude factor of about 1.7), the low first-pole-to-clear factor (close to 1.0 but with a considerable margin; reaching up to 1.2 or 1.3), and the voltage drop factor (90% at a relatively low fault current, say 6 kA, and 70% at a relatively high fault current, say 12 kA) provide the basis to define the TRV parameters. Standardization for rated voltages from 100 kV up to and including 800 kV is underway.

### 8.3.7 Out-of-Phase Current Switching

A mandatory test duty for making and breaking out-of-phase currents is specified in the IEC and IEEE standards for high-voltage circuit breakers [8.40, 41]. These out-of-phase switching duties were established many decades ago for both standards. The out-of-phase current and TRV ratings are still based on the original

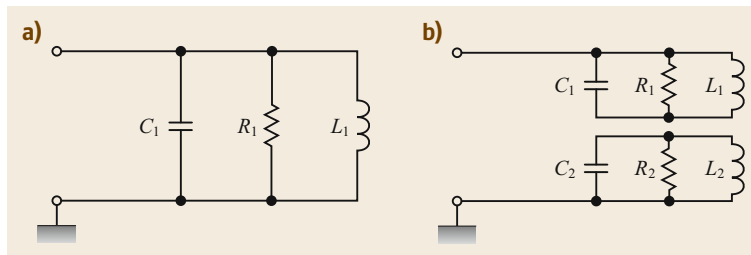


Fig. 8.96a,b Simplified transformer models for (a) the primary and (b) the secondary sides

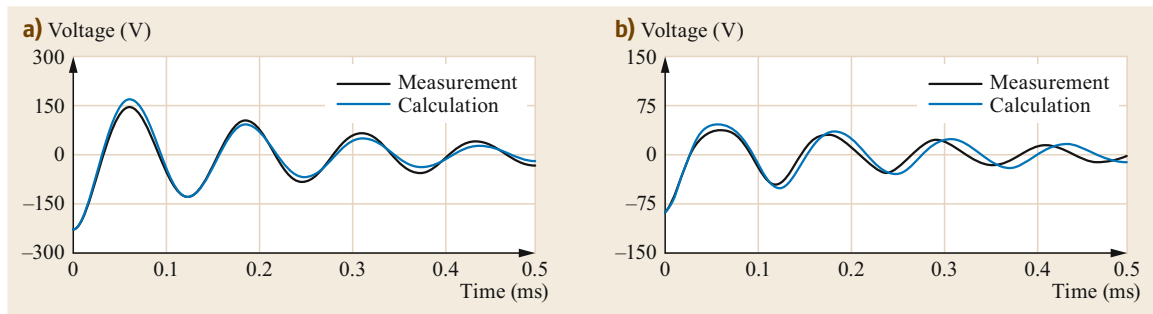


Fig. 8.97a,b TRVs on the (a) primary side and (b) secondary side, as reproduced by simplified transformer models

assumptions made when devising the duties. Although the ratings are still applicable for transmission systems, the background considerations must be adapted, since larger out-of-phase angles may be expected than those deduced from the specifications.

Power swing corresponds to a periodical lowering the amplitude of power frequency or the degradation of power quality, which is evoked by sudden changes like faults or switching operations, which may result in operation of a protective relay, due to the growing load flow in electrical power networks.

Power swing can be detected from 0.1 up to 10 Hz swing frequency, also during open-pole condition and during asymmetrical operation. The coordination of power swing detection, distance protection and out of step protection provides a reliable system protection.

There are always small power swings in a transmission network; these can be caused by small transients and the excitation of inherent oscillation conditions between parts of the power system. The actions of large power-plant controllers (for instance power system stabilizers) and HVDC controllers are typically sufficient to dampen the swings and prevent the escalation of such small power swings. In addition, larger but still stable power swings may occur due to larger excitations (sudden loss of a large power plant, a change in system impedances, a jump in system load). The actions of large power plant controllers (e.g., power system stabilizers) and HVDC controllers are typically sufficient to dampen the swings and prevent these small power swings from escalating. In addition, larger but still stable power swings may occur due to larger excitations (the sudden loss of a large power plant, a change in system impedances, a jump in the system load). When unstable power swings appear, they necessitate a serious intervention by protection and control equipment in the power system. Stable and unstable power swings are caused by an imbalance in active power (frequency instability), an imbalance in reactive power (voltage instability), a short circuit that has not been isolated quickly enough, or excessive power transfer through a generator or a transmission corridor (angular instability) (Fig. 8.98). Frequency, voltage, and angular instabilities often coincide. In this case, out-of-step conditions come into play and the system will be split due to automatic tripping by protective relays or special protection schemes.

Figure 8.98a shows a typical situation, where a fault between a power generation site and a load site leads to a sudden decrease of the voltage, while the power input to the system stays constant. The increase in (rotor) angle  $\delta$  is represented by the angle before up to after the short-circuit. After a fault clearance, the voltage returns to a value between the voltage before and the voltage

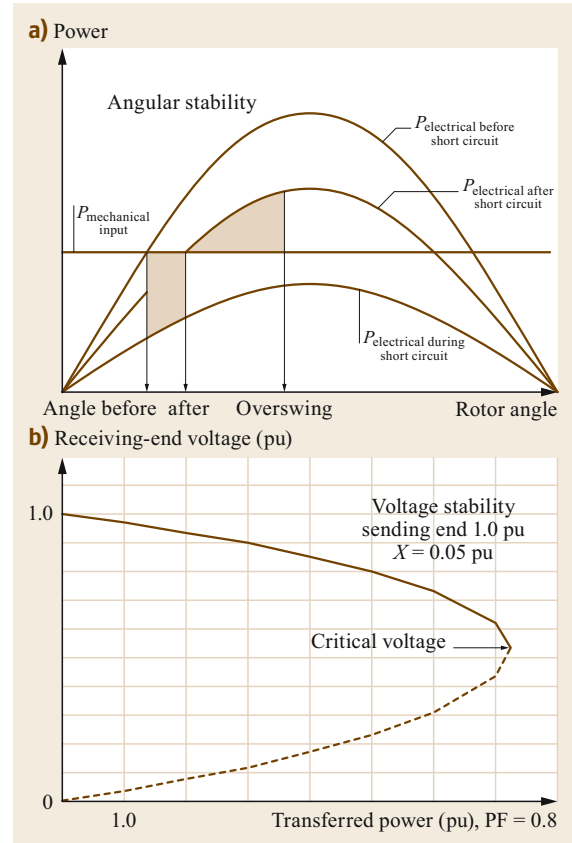


Fig. 8.98 (a) Angular stability and (b)  $P$ - $V$  curve (voltage stability)

during the fault. The power  $P$  that is transferred after short-circuit is larger than the power input and a deceleration takes place so that the angle returns to a new stable operating point. Beyond a certain combination of voltage drop during the fault and duration to clear the fault, it will no longer be possible to prevent a pole slip.

After a pole slip, the generator, the group of generators or the part of the power system may run again synchronously with the remaining part of the power system (this condition is not so common) or it may be separated from the remaining part. Power system instabilities can also be divided into short term phenomena (within seconds for voltage and frequency instability) and long-term phenomena (within tens of seconds to minutes). Rotor angle instability develops within seconds after a large disturbance and within tens of seconds after a small disturbance (leading to inter area oscillations).

A heavily loaded line requires reactive power in order to maintain the operational voltage limits at both line terminals. In addition to the active power to be transmitted, a larger amount of reactive power has to

be transferred as well. Figure 8.98b shows an example of a  $P$ - $V$  curve, which is presented with a transmission line circuit modelled by only a reactance and a resistance. The sending end voltage is kept constant, while the receiving end voltage is given as a function of the active power of the load. The ratio between reactive ( $Q$ ) and active power ( $P$ ) of the load is kept constant by a fixed power factor. Starting from the upper part and increasing the load, the receiving end voltage will drop until the critical point, the point of singularity, is reached and no more active power can be transferred. The critical point gives the voltage stability limit under these conditions.

An out-of-step condition is a power swing that causes a generator or group of generators to experience pole slipping for which some corrective action must be taken [8.42]. The term is synonymous with an unstable power swing [8.42] and a loss-of synchronism [8.43].

An out-of-phase condition is an abnormal circuit condition involving a loss or lack of synchronism between the parts of an electrical system on either side of a circuit breaker. In this condition, at the instant of operation of the circuit breaker, the phase angle between the rotating vectors representing the voltages generated on either side exceeds its normal value [8.42].

System separations and large disturbances occur more often than expected [8.44]. They are experienced in all parts of the world and are not restricted to certain types of networks (e.g., radial networks). Although the probability of system separation is smaller in dense meshed networks, cascading line tripping will change the topology into that of a radial network with identical effects. By definition, out-of-phase switching relates to the last line between the two parts of a power system to be separated. The risk of an out-of-step or out-of-phase condition should not be ignored; it should be taken into account by protection experts as well as circuit-breaker experts.

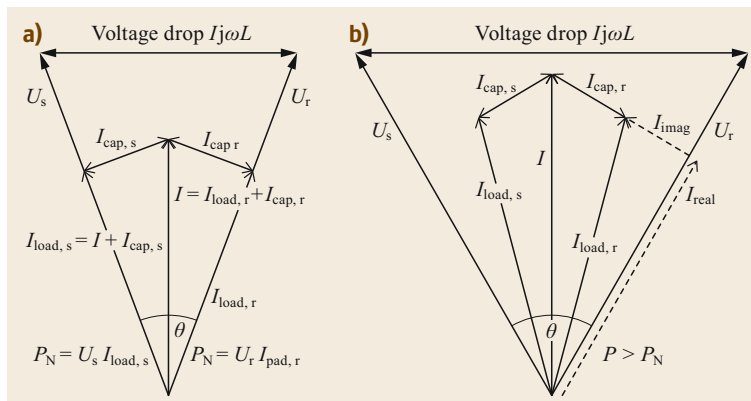
It should be noted that the amplitude of the out-of-phase current is an important stress factor during the

current interruption process, at it directly influences the amount of energy to be absorbed by the arc between the circuit breaker contacts. The larger the amount of energy, the more difficult it is to withstand the transient recovery voltage immediately after current zero. For transmission circuit breakers, an out-of-phase angle of  $180^\circ$  gives a 40% larger out-of-phase current than an out-of-phase angle of  $90^\circ$  and a 40% increase in the steepness of the TRV (RRRV); for generator circuit breakers, an out-of-phase angle of  $180^\circ$  might give a much higher current—up to 80% larger than that which occurs for an out-of-phase angle of  $90^\circ$ . In the standards, the rated (i.e., maximum) out-of-phase current is defined as a percentage of the rated short-circuit current.

System separation proceeds with a cascade of tripping connections, and thus with an increase in the impedance between the representative voltages on both sides of the circuit breaker. Therefore, specified amplitudes of the out-of-phase current as large as 5 and 25% of the rated short-circuit current of the circuit breaker involved are quite reasonable for high-voltage circuit breakers.

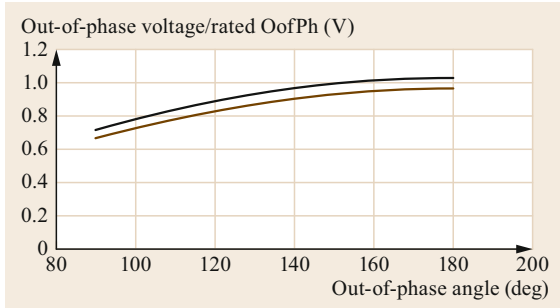
Also, the larger the out-of-phase angle, the larger and the faster the recovery voltage and the transient recovery voltage. The rate of rise of the recovery voltage can be considered to be covered by T30 or by a transformer limited fault test duty when a transformer represents the dominant impedance. However, a high-amplitude  $U_c$  representing the largest of all test duties is typical of out-of-phase TRVs. As such, this also serves as a reference for special cases such as long line fault clearing and the clearing of faults on series-compensated OH-lines.

Shortly before the moment of system separation, both parts of the network are connected by a contracted corridor of just one circuit. This condition is similar to a radial network, and the out-of-phase angle is determined by the power flow and the reactance of the connecting circuit or circuits in series (Fig. 8.99). The



**Fig. 8.99a,b** The out-of-phase angle  $\theta$  can be determined by the power flow, the reactance of the connecting circuit. The larger angle (b) is required to transfer a larger amount of active power and it will be further increased in case of larger impedance of the line





**Fig. 8.100** Out-of-phase recovery voltage at 81.8% of the rated voltage as a function of the out-of-phase angle for  $k_{pp} = 1.3$  (blue) and  $k_{pp} = 1.5$  (brown)

larger the impedance  $\omega L$  and the power flow, the larger the angle along the line.

When detailed information on large disturbances has been published, out-of-phase angles of far greater than  $90^\circ$  have been reported. For instance, during the large disturbances in India on July 30th and 31st, 2012, the angle between the involved regions jumped from  $60^\circ$  to  $260^\circ$  (for system separation at 02:33:15.4 on July 30th) and from  $90^\circ$  to  $190^\circ$  (for system separation at 13:00:18 on July 31st) [8.44, 45].

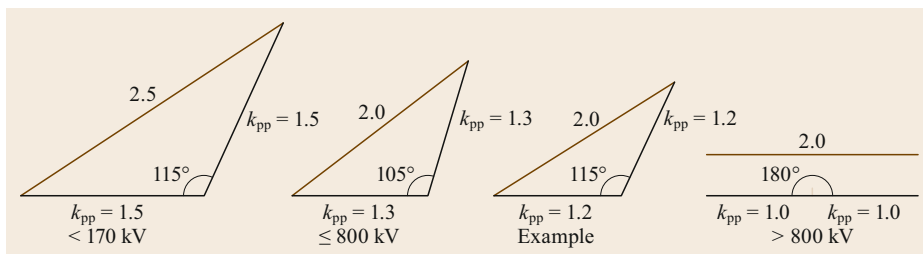
Report [8.45] is one of the few to give detailed information about the development of the difference in angle between two regions to be separated. Obviously, these angles become large and consequently the amplitude of the system voltage near the center of oscillation is low. In addition, large disturbances in the system come with voltage instability problems. Large voltage dips, depressed voltages, and dramatic voltage drops have been reported to occur at the moment of system separation, together with large power flows. For instance, when the Italian grid separated from the European continental grid in 2003 [8.46], the voltage fell below 80% of the nominal value. This phenomenon is also mentioned in [8.47]. The cascading tripping of overhead lines and other components led to a sudden increase in reactive power consumption and consequently to system voltage depression and eventually collapse.

For high-voltage circuit breakers, this means that large out-of-phase angles most probably coincide with voltage levels far lower than the rated voltage of the

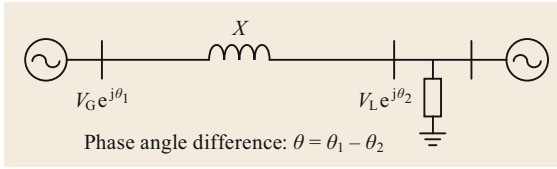
circuit breaker—even below the minimum voltage level acceptable to grid codes, which is normally 20% below the rated value. To be precise, the maximum operating voltage acceptable to grid codes is usually 110% of the nominal voltage, and the minimum voltage is 90% of the nominal voltage (although the minimum voltage under extreme conditions is normally specified to be 85% for a certain amount of time, and an even lower value may be permitted for a very short time). As the rated voltage of the circuit breaker should be at least the maximum operating voltage of the system, the minimum operating voltage is the rated voltage divided by at least 1.1 and multiplied by 0.9 ( $\leq 81.8\%$ ). For the grid codes, the maximum operating voltage is usually 110% of the nominal voltage and the minimum voltage 90% of the nominal voltage (the minimum voltage in extreme conditions is normally specified to be 85% for a certain amount of time and even lower could be indicated for very short time).

As the rated voltage of the circuit breaker should be at least the maximum operating voltage in the system, the minimum operating voltage is the rated voltage divided by at least 1.1 and multiplied by 0.9 ( $> 81.8\%$ ). Figure 8.100 shows the actual out-of-phase recovery voltage at the minimum operating voltage as a function of the out-of-phase angle. It is compared with the out-of-phase recovery voltage stipulated in the standard for high-voltage circuit breakers [8.49] based on the rated voltage and a first-pole-to-clear factor of 1.3 (effectively earthed networks: blue) and a first pole to-clear factor of 1.5 (non-effectively earthed networks: brown). From the standard values, it can be deduced that these correspond to out-of-phase angles of  $105^\circ$  (first-pole-to-clear factor: 1.3) and  $115^\circ$  (first-pole-to-clear factor: 1.5). These angles are explained in Fig. 8.101, together with those for other first-pole-to-clear conditions.

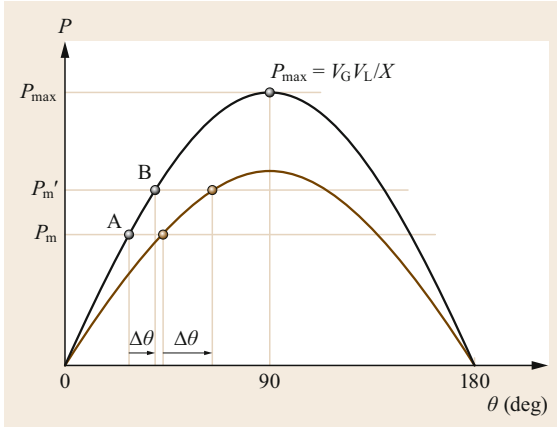
At the minimum operating voltage acceptable to grid codes (which is larger than the system voltages reported during large disturbances), the out-of-phase recovery voltage is found to be (far) less than or equal to the value used for type testing, even for the largest out-of-phase angles. As such, actual cases seem to be covered for smaller out-of-phase angles (up to  $90^\circ$ ) up to the rated voltage and for larger angles and large power flows (up to  $180^\circ$ ) up to the minimum operating voltages [8.44].



**Fig. 8.101** Dependence of the out-of-phase angle on the first-pole-to-clear factor  $k_{pp}$  [8.48]



**Fig. 8.102** AC power transmission with a generator and a load



**Fig. 8.103** AC transmission capacity versus the phase angle (black: normal state, blue: contingency case)

### 8.3.8 Mechanical Model of Power System Stability

Equipment requirements are identified by studying the phenomena in power systems. The engineers involved in equipment design, testing, application, and assessment often need to understand various switching behaviors observed in power systems. The use of a mechanical model as an analogy for a power transmission system is introduced in this section in order to explore system stability during an out-of-phase condition.

Figure 8.102 shows a simple transmission system with a generator and a load, where the voltage at the generator ( $V_G$ ) and the voltage at the load center ( $V_L$ ) are both considered to remain constant. The AC power transmission capacity increases with the system voltage and decreases with the line reactance ( $X$ ). The transmission capacity ( $P$ ) also depends on the difference in voltage phase angle ( $\theta = \theta_1 - \theta_2$ ) between the generator terminal and the transmission line end.

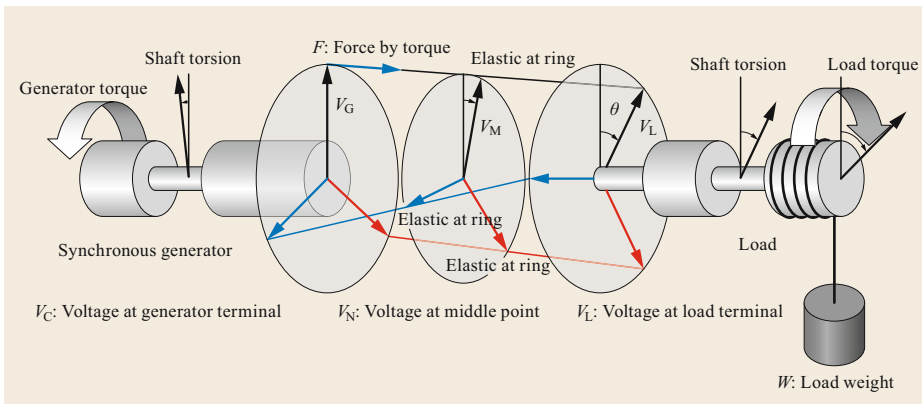
The transmission capacity is given by

$$P = V_G V_L \sin \frac{\theta}{X}, \quad (8.6)$$

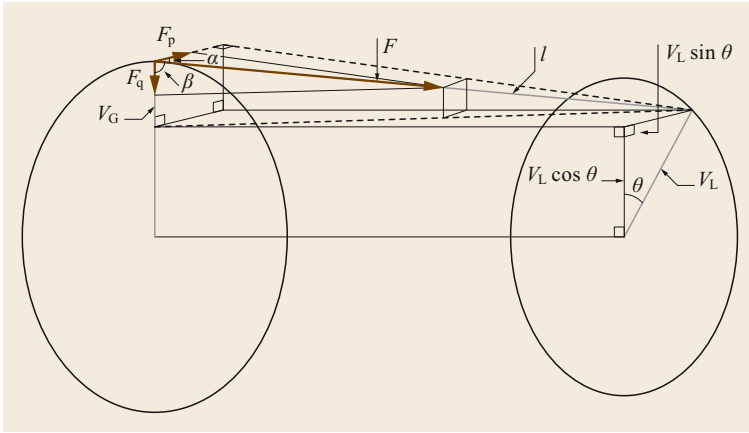
where  $V_G$  and  $\theta_1$  are the voltage and its phase angle at the generator terminal, and  $V_L$  and  $\theta_2$  are the voltage and its phase angle at the line end. The transmission capacity is highest when the difference in voltage phase angle is  $90^\circ$ . Figure 8.103 shows the transmission capacities for different power generation values. A small increase in the phase angle (less than  $90^\circ$ ) can increase the transmission power from  $P_m$  (point A) to  $P'_m$  (point B) in the case of a large power generator.

From Fig. 8.103, it is clear that the power system is more stable when the system is operated in the small phase angle difference region (less than  $90^\circ$ ) because the transmission capacity can increase if demand increases or in a contingency case, such as the loss of a circuit due to a fault (blue line).

Figure 8.104 shows a mechanical analogy for a power transmission system called a Noda model [8.50]. In this model, the generator is represented by a rotary torque handle and the load is shown as a hoist loaded with a weight ( $W$ ). The radii  $V_G$ ,  $V_M$ , and  $V_L$  of the three disks correspond to the system voltages at the generator terminal, the midpoint of the transmission system, and the load terminal, respectively. The three disks are connected by three elastic strings (e.g., rubber wire).



**Fig. 8.104** Mechanical model of power transmission with a generator and a load



**Fig. 8.105** Resolution of the elastic force into circumferential and radial components

The torque power ( $F$ ) generated by turning the handle at the generator side is transmitted through the elastic strings and winds up the weight on the load side.

If  $F$  and  $F_0$  are the tensions of the elastic strings of length  $l$  (the angular difference between the disk at the generator terminal and the disk at the load terminal is  $\theta$ ) and  $l_0$  (the angular difference is zero), respectively, the tension can be expressed as follows, where  $1/X$  is the elastic constant of the string:

$$F - F_0 = \frac{1}{X} (l - l_0), \quad F \cong \frac{l}{X}.$$

If  $F_p$  is the circumferential component of the tension  $F$ , and  $P$  is the angular moment of the force (as shown in Fig. 8.105), the following equation (analogous to the transmission capacity) is obtained

$$F_p = F \cos \alpha = F \frac{V_L \sin \theta}{l} = \frac{V_L \sin \theta}{X},$$

$$P = F_p V_G = \frac{V_G V_L \sin \theta}{X}.$$

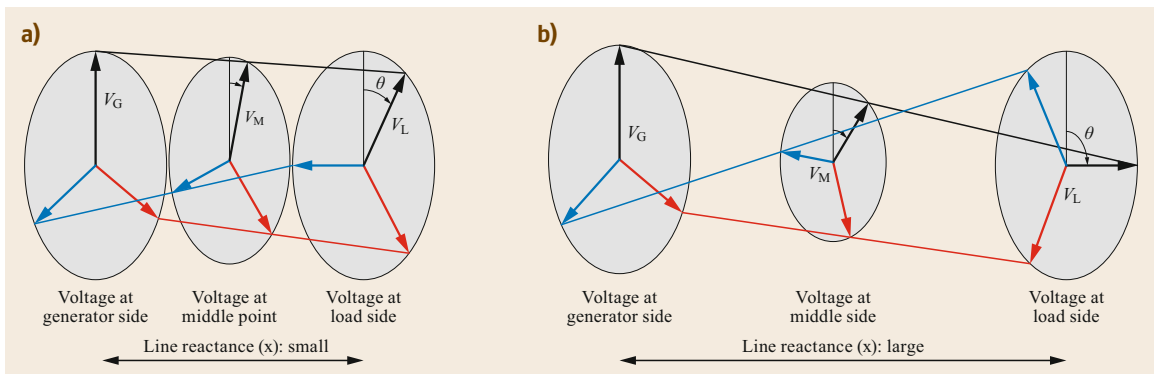
Also, if  $F_q$  is the radial component of the tension  $F$  and  $Q$  is the radial component of the force, the following equation is obtained:

$$F_q = F \cos \beta = F \frac{V_G - V_L \cos \theta}{l} = \frac{V_G - V_L \cos \theta}{X},$$

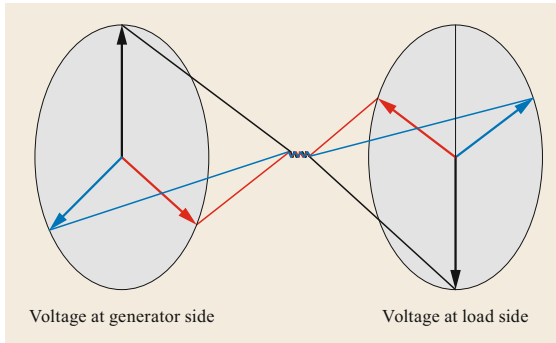
$$Q = F_q V_G = V_G \frac{V_G - V_L \cos \theta}{X}.$$

If the weight (which corresponds to the power load  $P$ ) is increased, the mechanical angular difference ( $\theta$ ) also needs to increase, resulting in the expansion of the three elastic strings and a decrease in the radius (i.e., the voltage) at the midpoint  $V_M$ . The mechanical force ( $Q$ ) compresses the radius  $V_G$  (which corresponds to the reactive power).

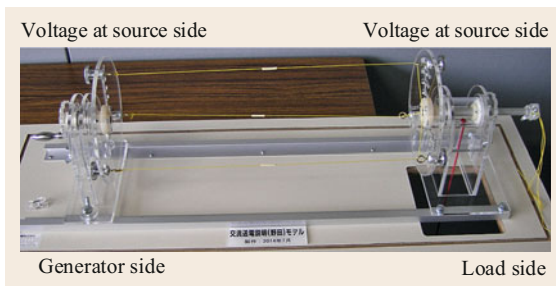
Figure 8.106 shows a schematic of three disks and the elastic strings connected to these disks, which correspond to small and large line reactances. The system stability is enhanced when the voltage is high and the line reactance is small, which results in the operation of the power system at a small phase angle difference.



**Fig. 8.106a,b** Two schematics of three disks: (a) small line reactance and phase angle; (b) large line reactance and phase angle



**Fig. 8.107** Twisted elastic strings corresponding to power system breakdown due to a large phase angle difference (out-of-phase condition)



**Fig. 8.108** Photograph of a Noda model

When the phase angle exceeds the critical condition, the elastic strings are eventually twisted at the midpoint (as shown in Fig. 8.107), which corresponds to an out-of-phase condition or breakdown at the midpoint of the power system.

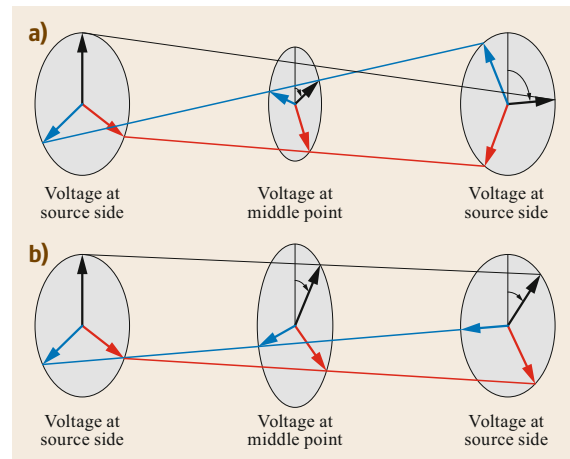
Figure 8.108 shows an actual demonstration model proposed by Noda.

Flexible alternating current transmission systems (FACTSs) and series capacitor compensation are often used for reactive power compensation in a long transmission line. The relevant Noda model can explain the impact of positioning these compensation devices in the middle of the transmission line by increasing the voltage at the midpoint. This results in more stable power transmission and a larger transmission capacity, as shown in Fig. 8.109.

### 8.3.9 Comparison of the Switching Phenomena Obtained at 50 and 60 Hz

#### (A) Power Frequency

Even though power systems are operated at 50 Hz in most countries, some countries and regions, such as the United States and west Japan, use a power frequency of 60 Hz, as shown in Fig. 8.110. Both frequencies coexist



**Fig. 8.109a,b** Noda model illustrating reactive power compensation. Voltage at middle point: (a) low, (b) reactive power compensation; out-of-phase angle  $\theta$ : (c) large, (d) small

and there is presently no push for worldwide standardization in this regard.

Some electric appliances may not operate efficiently or even safely if used on anything other than the intended power frequency. However, most substation equipment, especially circuit breakers, can be operated at both power frequencies (50 and 60 Hz).

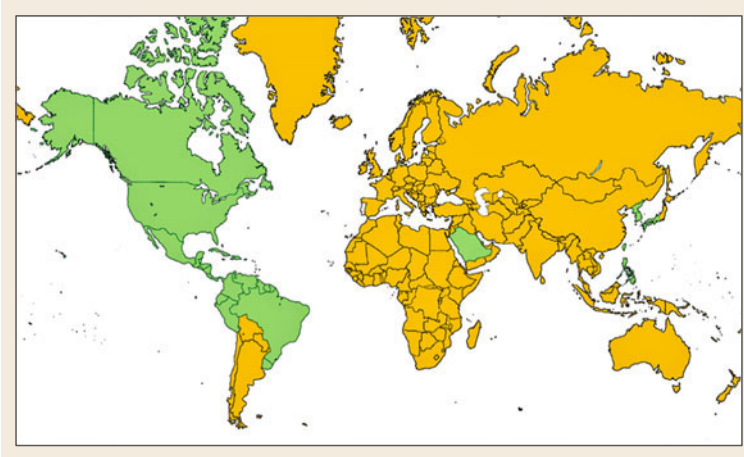
Strictly speaking, changing the power frequency will affect the performance of substation equipment. For instance, if we consider a power transformer with a particular capacity, a more compact transformer can be used with a higher power frequency than with a lower power frequency. The effects of the power frequency on the interrupting performance for various switching duties are given below.

#### (B) Thermal Interrupting Capability

When a circuit breaker interrupts the same current under SLF conditions, better cooling performance (higher thermal interrupting) is needed when the power frequency is 60 Hz as shown in Fig. 8.111, because the current and voltage slopes ( $di/dt$ ,  $dv/dt$ ) at current zero are 1.2 times higher than those obtained when the power frequency is 50 Hz, resulting in higher ohmic heat input around the current zero. Some circuit breaker designs employ a larger grading capacitor for 60 Hz than for 50 Hz because it enhances the thermal interrupting capability by reducing the current slope at the current zero.

#### (C) Dielectric Interrupting Capability

A circuit breaker is required to interrupt the short-circuit current under bus terminal fault (BTF) conditions

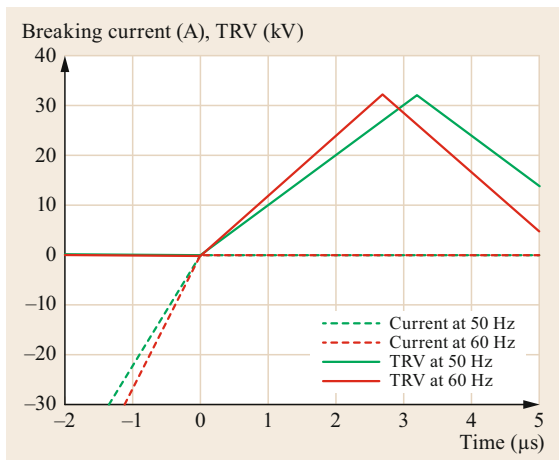


**Fig. 8.110** World map showing the use of different power frequencies (50 Hz in yellow and 60 Hz in green) in different regions and countries

at any current zero when the minimum arcing time after the contact separation has elapsed. This means that the circuit breaker should have an interrupting window a half-cycle wide at minimum (for symmetrical current). The intervals between current zeros are 10 ms at 50 Hz and 8.3 ms at 60 Hz as shown in Fig. 8.112. Therefore, the circuit breaker must have a longer interrupting window, resulting in a longer effective gas flow period, if 50 Hz is used.

#### (D) Capacitive Switching Capability

TRV peaks appear half a cycle after interrupting the current under capacitive switching conditions, which corresponds to 10 and 8.3 ms from current interruption at 50 and 60 Hz, respectively, Fig. 8.113. Therefore, the circuit breaker must have a better dielectric withstand strength recovery between the contacts in case of 60 Hz,

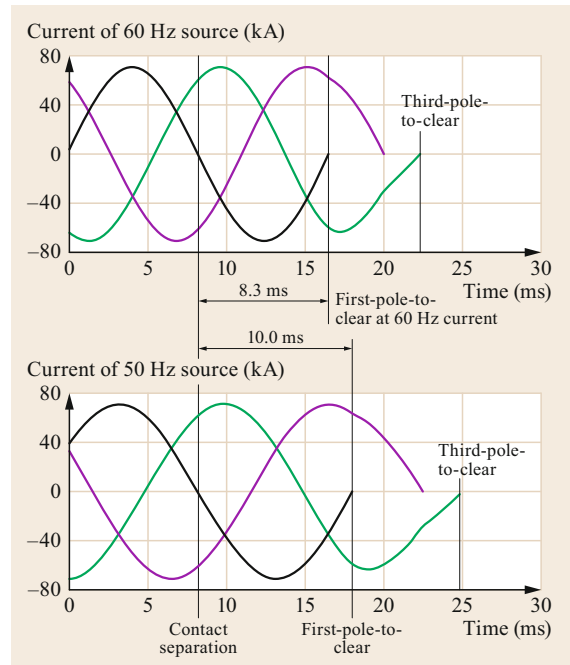


**Fig. 8.111** Comparison of  $(di/dt)$  at current zero and TRV obtained for power frequencies of 50 and 60 Hz

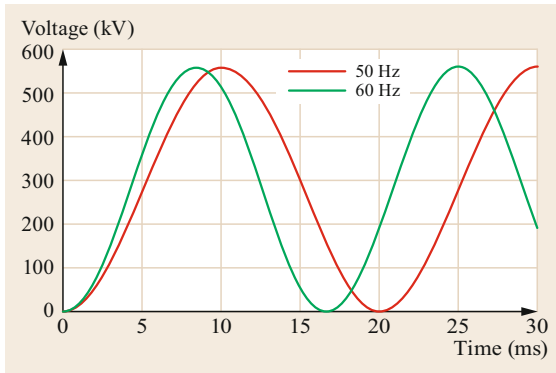
which is normally attained by increasing the contact opening speed.

#### (E) Inductive Switching Capability

There is no significant difference in switching performance between 50 and 60 Hz under inductive switching conditions because the TRV is determined by the circuit conditions at the load side (not the power-frequency source side). In addition, the amplitude and the fre-



**Fig. 8.112** Comparison of the interval between current zeros in a three-phase current for power frequencies of 50 and 60 Hz



**Fig. 8.113** Recovery voltage after capacitive current interruption for power frequencies of 50 and 60 Hz

quency of high-frequency current oscillations and associated overvoltages associated with reignitions do not show any dependence on whether the power frequency is 50 or 60 Hz. Therefore, the standard IEC 62271-100 permits inductive switching tests to be performed at either 50 or 60 Hz.

#### (F) Current-Carrying Capability

The short time current withstand test can also be performed at either 50 or 60 Hz, because the energy and mechanical stresses imposed on an interrupter do not vary significantly depending on whether the power frequency is 50 or 60 Hz considering the current-carrying duration of 1 s, even though the current at the first peak is 2.5 times and 2.6 times the root-mean square of the current for 50 and 60 Hz, respectively. Therefore, the standard IEC 62271-100 allows the short time current withstand test to be performed at either 50 or 60 Hz.

In general, manufacturers provide circuit breakers that are applicable for use with both power frequencies (50 and 60 Hz) even though the power frequency impacts the switching performance.

#### (G) Continuous Current-Carrying Capability

IEC 62271-1 states that the performance of switching devices of the open type with no ferrous components adjacent to the current-carrying parts at 60 Hz can be deemed to be the same as their performance in tests carried out at 50 Hz provided that the temperature rise recorded during the test at 50 Hz does not exceed 95% of the maximum permissible value. This recognizes the fact that the temperature rise is generally slightly higher when carrying a continuous current at 60 Hz.

### 8.3.10 Switching Requirements for UHV Transmission

The first commercial UHV transmission system with a rated voltage of 1100 kV AC commenced operation

on January 6th, 2009 following on-site commissioning tests during December 2008 in China. Since then, UHV AC (up to 1200 kV) and UHV DC (up to 1000 kV) networks have steadily expanded in some countries such as China and India.

In October 2006, CIGRE SC A3 published WG A3.22 on the technical requirements for substation equipment exceeding 800 kV as well as some technical documents summarizing the specifications for substation equipment ( $\geq 800$  kV) based on investigations performed for various UHV and EHV projects [8.49, 51–53].

In order to minimize the costs and visual impact of UHV transmission lines and substations, advanced technological solutions and analytical optimization techniques were introduced. Furthermore, the results of studies relating to reduced insulation coordination requirements and the requirements for some system transients (e.g., TRVs, ITRVs, very fast transient overvoltages (VFTOs)) at UHV levels have an impact on the insulation coordination requirements (distances, dimensions, insulation thickness) for EHV voltages (800, 550, 420 kV).

In the 1970s and 1980s, some utilities around the world started pilot schemes for AC power systems with voltages above 1000 kV. The former USSR (Union of Soviet Socialist Republics) performed long-term testing of a plant with a rated voltage of 1200 kV, while in the USA, Bonneville Power Administration (BPA) and American Electric Power (AEP) ran pilot schemes that operated at 1200 and 1500 kV, respectively. During the 1980s, the former USSR even had a pilot plant with a rated voltage of 1800 kV, and they operated a commercial 1200 kV transmission system that included 1900 km of OH lines (although only half of that network was actually operated at 1200 kV) from 1985 until 1991. In the 1990s, a 1050 kV pilot plant was operated in Italy for two years. Also, in Japan, a 1100 kV pilot scheme has been in operation since 1996, together with 430 km of UHV OH lines (which are operated at 550 kV) [8.51].

Table 8.7 shows various issues specifically associated with UHV AC power systems that could have a considerable impact on substation equipment. In particular, the use of multibundle conductors with large-diameter, large-capacity power transformers leads to distinctive phenomena for UHV power systems. In addition, the application of high-performance surge arresters (MOSAs) with low protection voltages to effectively limit overvoltages is integral to the design of some UHV systems. The impact of this design approach and its influence on specifications are briefly described in this section.

The technical and economic consequences of insulation levels are becoming increasingly important, especially for UHV systems. Optimal insulation coordination can be achieved using high-performance

**Table 8.7** Issues specifically associated with UHV AC power systems

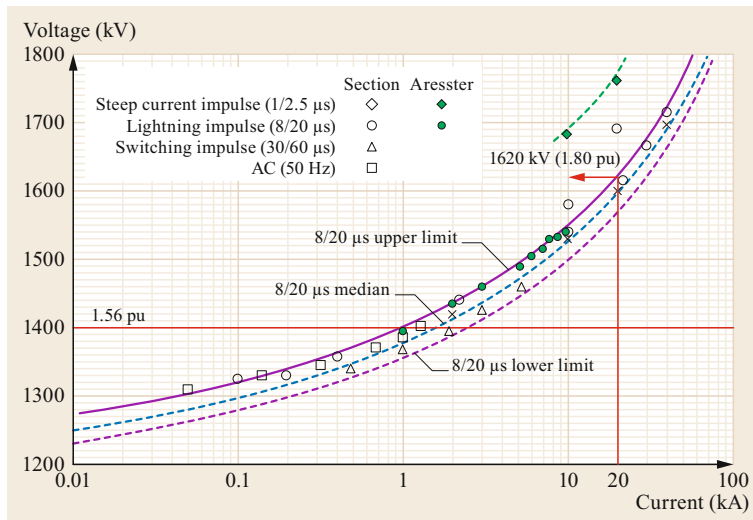
Equipment	Phenomena specific to UHV systems	CIGRE investigations
Substation equipment	Increased insulation levels (reduced LIWV/LIPL)	Various mitigation schemes are applied to suppress the SIWV levels as much as possible
Four-legged reactor HSGS	Prolonged secondary arc extinction time due to higher coupled voltage and induced current	Four-legged shunt reactor can facilitate successful autoreclosing under the 1LG condition for a single circuit
Surge arrester shunt reactor	Prominent Ferranti effect and TOV due to high capacitance of overhead lines	Severe voltage factor and breaking current are not seen for capacitive current switching
Circuit breaker GIS, transformer	Severe VFTO due to geometry and topology of UHV substation	Resistor-fitted DS can effectively suppress VFTO for GIS substation
Circuit breaker	Large time constant of DC component in fault current due to low losses from transformers and lines	Time constants in UHV systems are 100 ms for India, 120 ms for China, and 150 ms for Japan
Circuit breaker	Reduced first-pole-to-clear factor due to small zero-sequence impedance in UHV systems	First-pole-to-clear factors are 1.1 for Japan, 1.2 for India, and 1.0–1.23 for China
Circuit breaker surge arrester	High amplitude factor in TRVs due to low losses from power transformers and transmission lines	RRRV for TLF exceeds the existing standard value; MOSA can suppress the TRV peak for terminal faults
Circuit breaker surge arrester	High TRV peak value corresponding to out-of-phase duty due to low damping of traveling waves	Further investigations are expected to provide some solutions for out-of-phase phenomena
Circuit breaker	Reduced line surge impedances due to multibundle conductors with large diameters	Line surge impedance is suggested to be 330 Ω for 8-bundle conductors designed for UHV OH lines
Line substation (AIS)	Possibility of a reduced corona onset voltage with increased corona losses and audible noise	UHV lines employ 8 conductors with a cross-sectional area of 400–810 mm <sup>2</sup> depending on the allowable level of corona noise

MOSAs [8.54] with the *I*–*V* characteristic shown in Fig. 8.114.

Studies of the insulation coordination using accurate computer-aided simulations are common in such projects. Another important aspect of insulation coordination is the utility’s policy regarding withstand margins for severe lightning impulse or switching impulse conditions with a very low probability of occurrence.

As lightning overvoltages dominate the nonself-restoring internal insulation design of substation equip-

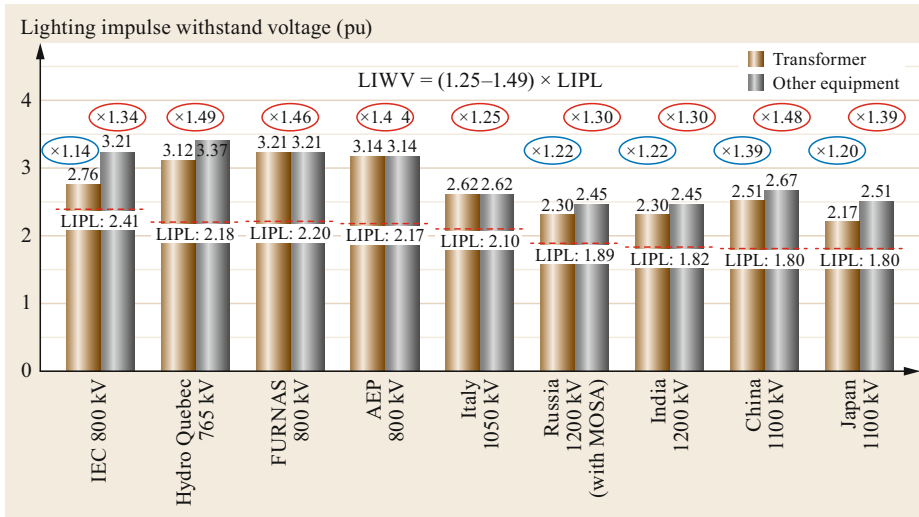
ment, it is important to rationalize lightning overvoltages by positioning a sufficient number of MOSAs at appropriate locations, such as at line entrances, busbars, and transformers. Table 8.8 lists examples of several MOSA arrangements along with the corresponding costs and lightning impulse withstand voltages (LIWVs) at UHV substation equipment. The arrangement that includes two surge arresters per circuit at the line entrance, two per quarter bus, and one per transformer bank is one of the most favored for UHV transmission in Japan.



**Fig. 8.114** Typical *I*–*V* characteristic of a high-performance MOSA

Layout of surge arrester						
Transformer overvoltage LIWV (kV)	1950	1943	1895	1943	1938	1896
GIS overvoltage LIWV (kV)	2898	2854	2730	2628	2506	2208
Cost (%)	102	105	109	103	103	100

**Table 8.8**  
Relationship between LIWVs and MOSA layouts



**Fig. 8.115** LIWV specifications for transformers and substation equipment

VFTO levels are reduced to 1.3 pu or below through the application of a resistor-fitted disconnecting switch with a 500 Ω resistor [8.55, 56]. This scheme also effectively suppresses electromagnetic interference in the secondary circuits of CTs, VTs, and protection and control equipment.

Utilities generally use both analytical and simplified IEC approaches to evaluate LIWV levels. The specified LIWVs of UHV switchgear for 1050, 1100, and 1200 kV systems range from 1.25 to 1.49 times the lightning impulse protection level (LIPL) value, as shown in Fig. 8.115.

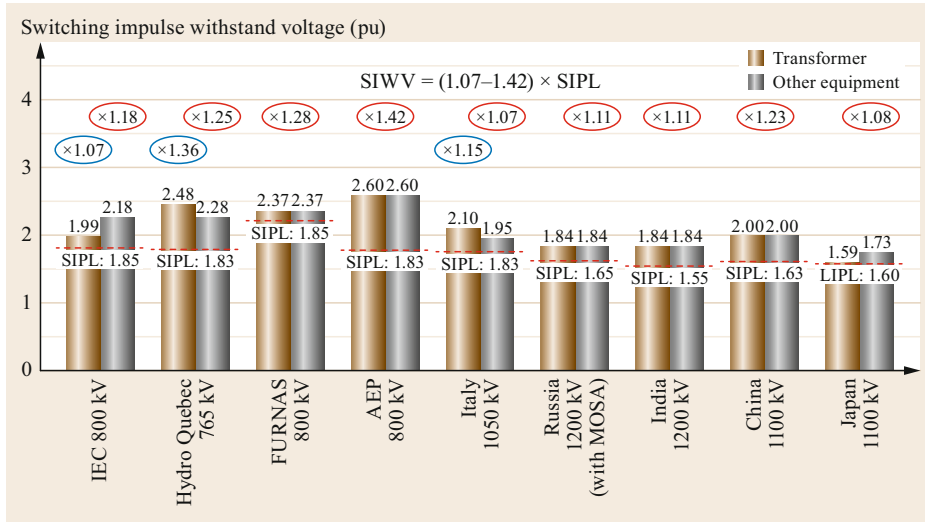
In addition, it is important to suppress switching overvoltages as much as possible because it allows air clearances to insulation to be reduced, which in turn allows the heights of transmission towers and the dimensions of open-air parts in substations to be suppressed. Therefore, as well as MOSAs, switching equipment

equipped with preinsertion closing/opening resistors are applied to limit switching overvoltages. Additional MOSAs along OH lines and controlled switching are other options that can be employed to reduce switching overvoltages even further. The application of mitigation schemes can markedly change the switching impulse withstand voltage (SIWV) level, so simulations are useful to evaluate their effects. Figure 8.116 shows that the UHV system in Japan takes full advantage of these schemes.

Tables 8.9 and 8.10 show examples of the processes used to determine the LIWV and SIWV in China and Korea. Note that the calculated maximum overvoltage is found to be similar to the switching impulse protection level (SIPL) for each system.

The short-circuit current observed in an UHV system also shows some remarkable features. The use of large-capacity power generators and large-capacity





**Fig. 8.116** SIWV specifications for transformers and substation equipment

**Table 8.9** Examples of processes used to determine the LIWV

Country	Korea 800 kV	China 1100 kV (pilot)
LIPL	1310 kV (2.00 pu) at 20 kA	1620 kV (1.80 pu) at 20 kA
MOSA layout	1 unit for line entrance 1 unit for busbar 1 unit for transformer	1 unit for line entrance 2 units for busbar 1 unit for transformer
Maximum LIWV analysis		1796 kV for transformer 2040 kV for GIS
Acceptable failure rate	0.4 faults/100 km-year-line	0.112 faults/100 km-year-line
Safety factor	-	1.15 for internal insulation
LIWV for transformer	2050 kV (3.14 pu)	2400 kV (2.67 pu)
LIWV for other equipment	2250 kV (3.44 pu)	2250 kV (2.51 pu)
LIWV/LIPL	1.72	1.48

**Table 8.10** Examples of processes used to determine the SIWV

Country	Korea 800 kV	China 1100 kV (pilot)
SIPL	1200 kV (1.85 pu) at 2 kA	1460 kV (1.63 pu) at 2 kA
Resistance for GCB	1000 Ω for closing	600 Ω for closing
Maximum overvoltages	1124 kV for grounding fault 999 kV for closing 1186 kV for opening	1472 kV for opening
Maximum line length	160 km	420 km (tentative)
Flashover probability	0.1%/1 flashover per 1000 operations	0.1%/1 flashover per 1000 operations
Safety factor	-	1.15 for internal insulation
SIWV for transformer	1500 kV (2.30 pu)	1800 kV (2.0 pu)
SIWV for other equipment	1425 kV (2.18 pu)	1800 kV (2.0 pu)

power transformers result in a high  $X/R$  ratio, which leads to an increased DC time constant in fault currents. EHV and UHV transmission lines employ multibundle conductors with large diameters in order to reduce corona noise as well as to increase the transmission capacity.

Table 8.11 summarizes the analytical results for DC time constants calculated based on various tower

designs and multibundle conductors used in different projects. In IEC62271-100, a special case time constant of 75 ms for rated voltages of 550 kV and above, which corresponds to the medium value of the constants surveyed for 800 kV lines, is indicated. Since the DC time constant in an UHV system must be larger than this, a standard time constant of 120 ms is stipulated for UHV.

**Table 8.11** Conductor sizes and DC time constants of short-circuit currents in EHV and UHV transmission lines

Maximum voltage	Conductor size (mm <sup>2</sup> )	Bundle	DC time constant (ms)
765 kV (Canada)	686	4	75
800 kV (USA)	572	6	89
800 kV (South Africa)	428	6	67
800 kV (Brazil)	603	4	88
800 kV (China)	400	6	75
1200 kV (Russia)	400	8	91
1050 kV (Italy)	520	8	100
1100 kV (Japan)	810	8	150
1100 kV (China)	500	8	120

TRVs with high amplitude factors are expected in UHV systems due to the use of low-loss UHV power transformers and UHV transmission lines. An important parameter to consider when defining the TRV envelope of UHV circuit breakers is the first-pole-to-clear factor, which is specified to be 1.3 for lower-voltage systems with an effectively earthed neutral in IEC standard 62271-100. The first-pole-to-clear factor depends on the ratio  $X_0/X_1$  of the system at the location of the circuit breaker. OH lines give a  $X_0/X_1$  of around 3, while large transformers tend to have a ratio of less than or close to 1. In UHV substations, the short-circuit current will be determined to a large extent

by the contribution from the transformers rather than the contribution from the OH lines, so the first-pole-to-clear factor tends to be lower than 1.3. The standard value for UHV systems is stipulated to be 1.2.

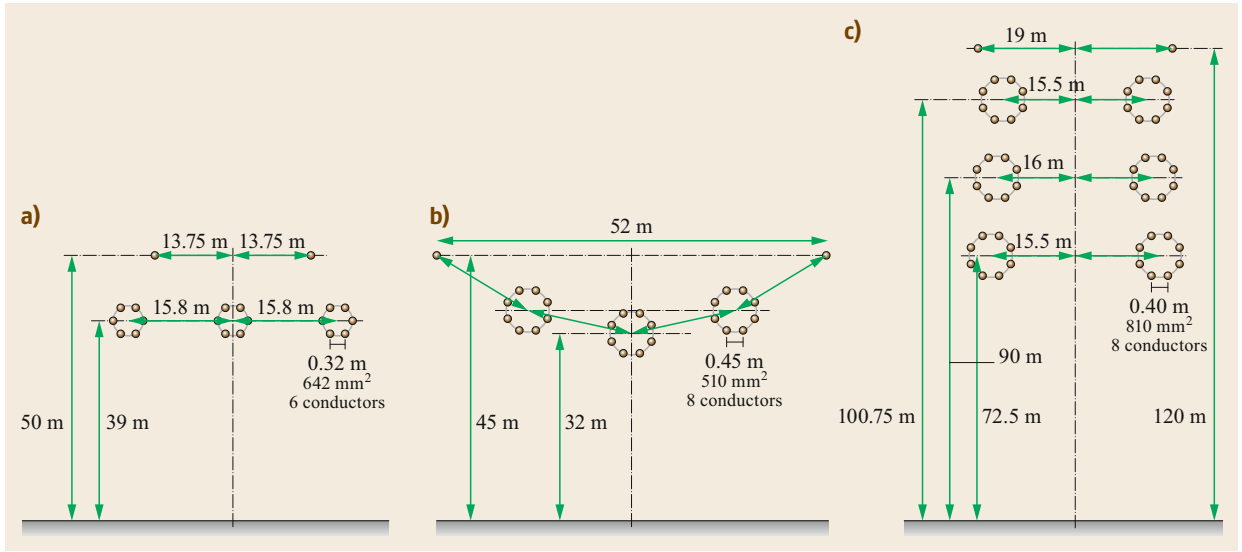
Another characteristic that should not be overlooked is the equivalent surge impedance of the OH lines, which is especially important for short line faults. The standards cover the interruption of a single fault to earth and therefore require the equivalent surge impedance of the last clearing pole. The interruption of short line faults is associated with frequencies in the kHz range, and large eight-bundle conductors will not contract completely during the first 100–200 ms. Under these conditions, the equivalent surge impedance will be much lower than 450  $\Omega$ , as shown in Table 8.12 and Fig. 8.117. Therefore, the equivalent surge impedance of UHV OH lines is reduced from 450 to 330  $\Omega$ .

Equivalent surge impedances also play a role when clearing long line faults (LLF) and out-of-phase (OP) currents. MOSAs can reduce peak TRV values to a certain extent, but MOSAs have a much greater effect during breaker terminal faults (test duties T100 and T60) and the interruption of transformer limited faults (TLFs: test duty T10).

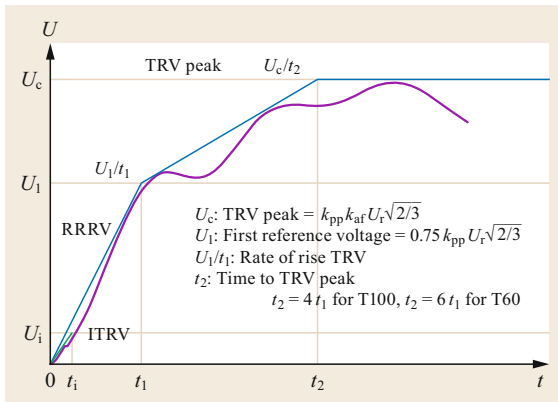
Figure 8.118 shows how the TRV waveform can be expressed using four parameters—an approach that is used for test duties T60 and T100 (60% and 100% of the rated interrupting current of a circuit breaker). The curve for the four-parameter TRV consists of three parts: an interval where the voltage rises at the rate  $U_1/t_1$  until the first reference voltage ( $U_1$ ) is attained, another interval where the voltage rises at the rate  $U_c/t_2$  until peak TRV ( $U_c$ ) is reached, and then the period after peak TRV.

**Table 8.12** Surge impedance of transmission lines

Highest voltage (kV)	Conductor size (mm <sup>2</sup> )	Number of conductor	Conditions (TRV frequency)	$Z_0$ ( $\Omega$ )	$Z_1$ ( $\Omega$ )	Equivalent surge impedance ( $\Omega$ )		
						1st pole	2nd pole	3rd pole
550 (Japan)	410	6	Normal conduction (60 kHz)	444	226	270	281	299
			Bundle contraction (60 kHz)	580	355	408	417	430
800 (South Africa)	428	6	Normal conduction (27.5 kHz)	403	254	290	296	304
			Bundle contraction (27.5 kHz)	509	359	398	403	409
1050 (Italy)	520	8	Normal conduction (26.2 kHz)	406	210	250	260	275
			Bundle contraction (26.2 kHz)	532	343	389	396	406
1100 (Japan)	810	8	Normal conduction (25 kHz)	476	228	276	289	311
			Bundle contraction (25 kHz)	595	339	396	407	424



**Fig. 8.117a–c** UHV line configurations used in different countries (see also Table 8.12): (a) South Africa (800 kV), (b) Italy (1050 kV), (c) Japan (1100 kV)



**Fig. 8.118** Plot showing the TRV waveform expressed using four parameters

Table 8.13 summarizes the standard TRV values for an UHV circuit breaker and compares them with the corresponding values for lower voltages, including EHV (up to 800 kV). The values for UHV systems may be considered also for the requirements of EHV systems.

Using the proposed impedance of  $330 \Omega$  and information available on the minimum equivalent surge impedance in an UHV substation, it was concluded that the RRRV,  $U_1$ ,  $t_d$ , and  $t_{dL}$  for UHV can be kept the same as those specified for the test duties T100, T60, T30, T10, and SLF at lower rated voltages. For the ITRV, the value for the busbar surge impedance is proposed to be the same as that for 800 kV ( $325 \Omega$  instead of  $260 \Omega$  for the lower rated voltages), but the time  $t_i$  is proposed to be  $1.5 \mu\text{s}$ , as the dimensions of UHV air insulated

switchgear (AIS) are considerably larger than those of the AIS for lower rated voltages. However, the conditions under which such a long  $t_i$  may occur may also be applicable to 800 kV.

Based on the information collected so far, it has been proposed that the same amplitude factors should be used as those employed for lower voltages, with the exception of  $k_{af}$  for T100, where it is recommended that this factor should be increased from 1.4 to 1.5. The reasons for doing so are, on the one hand, the results of system studies, mainly for the proposed UHV system in Japan, and on the other hand, the fact that  $(k_{pp}k_{af})$  gives the same peak value with both the existing IEC parameters and the proposed values. This peak value for T100 and T60 happens to be about 5% above the MOSA clipping level; the margin of 5% above SIPL accounts for differences in design.

From simulations, it is clear that MOSAs have a reducing effect on the peak TRV, as can be seen in Fig. 8.119.

Based on the equivalent surge impedance seen by the circuit breaker's clearing pole and the number of MOSAs connected at the source side of the circuit breaker (present at the substation), it is possible to determine the intersection point with the  $I-V$  characteristic(s) of the surge arrester, which gives the clipping level (Fig. 8.120).

The ratings for disconnecting switches and earthing switches applied in UHV systems are higher than those applied at lower voltages. The specified currents and related voltages for bus transfer duty and bus charging current switching duty are relatively high. Figure 8.121

**Table 8.13** TRV parameters of UHV circuit breakers

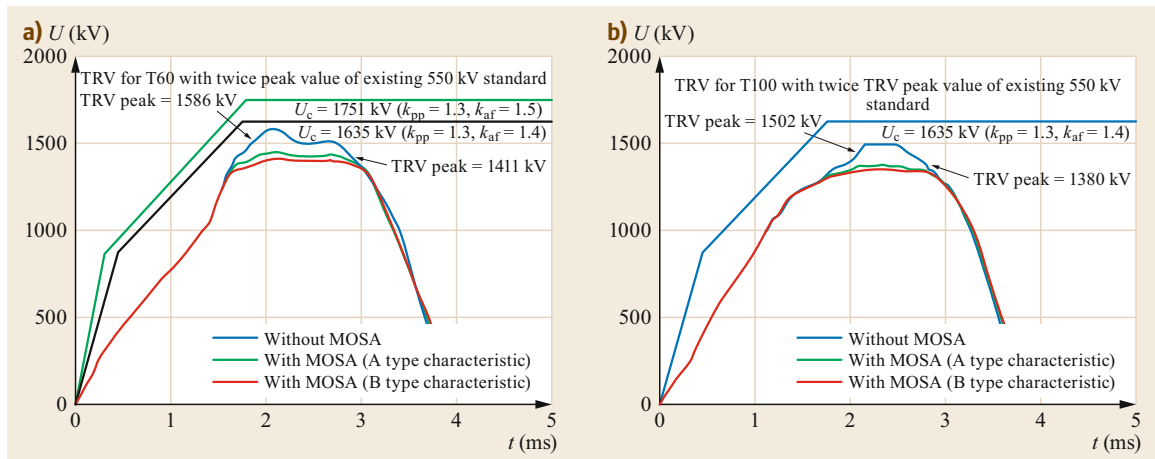
UHV	First-pole-to-clear factor	Amplitude factor	1100 kV	1200 kV	Rate of rise of TRV	Time to TRV peak	Time to TRV peak
Duty	$k_{pp}$	$k_{af}$	TRV peak (kV)	TRV peak (kV)	RRRV (kV/ $\mu$ s)	$t_2$	$t_3$
T100	1.2 (1.3)	1.5 (1.4)	1617	1764	2	3.0 $t_1$ (4 $t_1$ )	
T60	1.2 (1.3)	1.5	1617	1764	3	4.5 $t_1$ (6 $t_1$ )	
T30	1.2 (1.3)	1.54	1660	1811	5		$t_3$ ( $t_3$ )
T10	1.2 (1.3)	1.76	1897	2076	7		$t_3$ ( $t_3$ )
TLF	1.2 (1.5)	0.9*1.7	1649	1799	( <sup>a</sup> )		( <sup>a</sup> )
Out-of-phase	2.0	1.25	2245	2450		1.38 $t_1$ (2 $t_1$ )	

Values in parentheses are standards for systems with voltages of 800 kV and below.

$t_1$  and  $t_3$  are based on  $k_{pp} = 1.2$

(<sup>a</sup>) RRRV =  $U_c/t_3$  with  $t_3 = 6U_T/I^{0.21}$ , as shown in ANSI C37.06.1-2000 for transformers up to 550 kV.

For UHV transformers, RRRV and  $t_3$  are determined by the transformer impedance and its equivalent surge capacitance (specified as 9 nF)



**Fig. 8.119a,b** Effect of a MOSA on the TRV waveform [8.57]: (a) T60, breaking current 26.2 kA; (b) T100, breaking current 33.8 kA

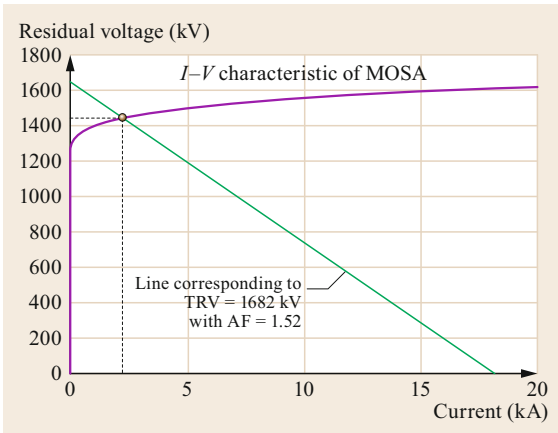
shows the load capacitance and equivalent length of the GIS for different voltage levels and bus charging currents. The bus charging currents evaluated for several existing UHV substation layouts can reach 0.4 A. Schemes for future UHV substations with maximum busbar lengths of up to 200 m suggest that a bus charging current of 2 A should also be sufficient for future applications [8.57].

Bus transfer currents must be defined according to the actual current rating, the type of substation involved, and the maximum loop length. As Fig. 8.122 shows, for the GIS, bus transfer voltages of 80 and 300 V correspond to currents of 1600 and 8000 A, respectively, while for AIS and MTS (mixed technology switchgear),

a bus transfer voltage of 400 V corresponds to 1600 A as well as 4000 A, respectively [8.59].

In Annex C of IEC 62271-102 [8.60], electromagnetically and electrostatically induced currents and voltages are standardized for 550 and 800 kV earthing switches, which are designated for use in circuits with relatively long lines or high coupling to an adjacent energized circuit (class B earthing switches).

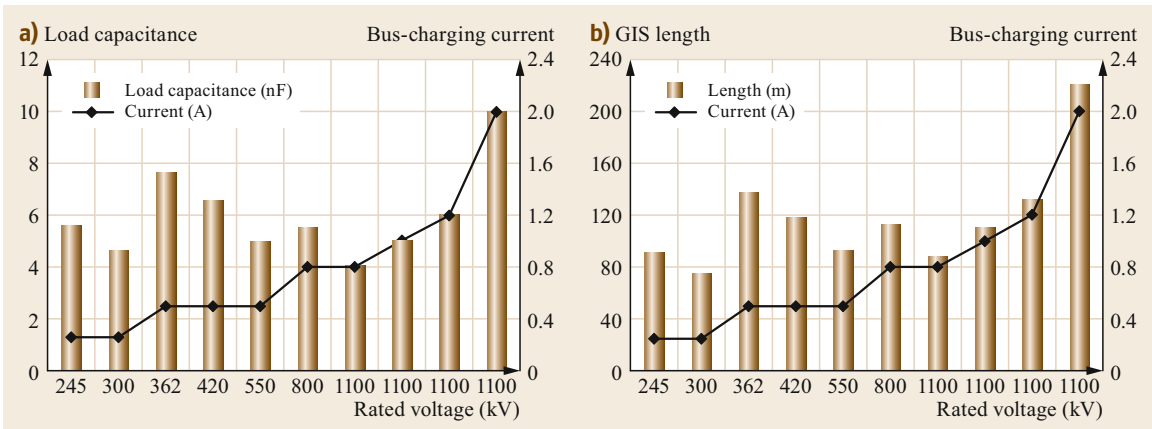
One special topic in this context is the occurrence of VFTO due to the charging and discharging of busbar sections by disconnecting switches in GIS. Such switching causes a large number of restrikes and pre-strikes with high-frequency responses of the traveling waves in the GIS. These high-frequency voltages may



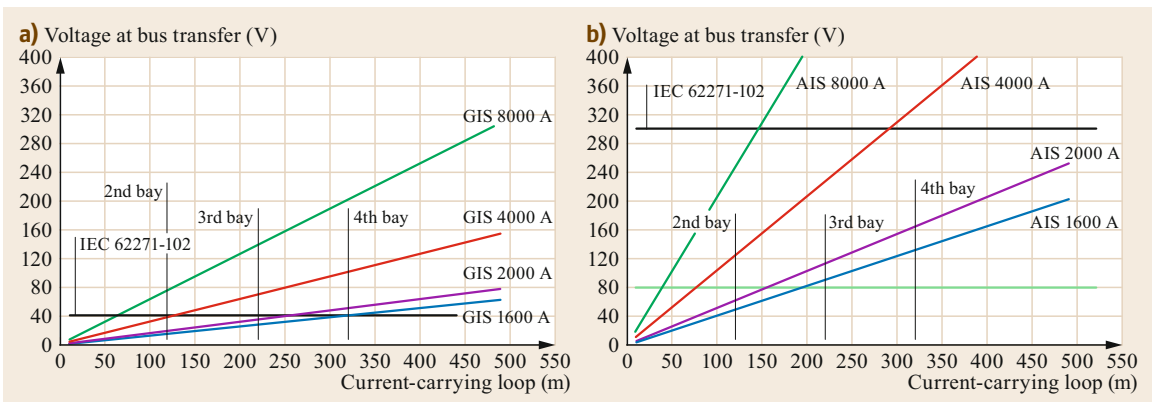
**Fig. 8.120** Intersection of the system response line with the  $I-V$  characteristic of the MOSA

reach amplitudes that could endanger the insulation of the GIS equipment as well as directly connected equipment, such as transformers and shunt reactors. As shown in Fig. 8.123, this phenomenon is a more serious problem at UHV than at 800 kV. When necessary, one countermeasure is to apply a preinsertion resistor to disconnecting switches [8.57, 59].

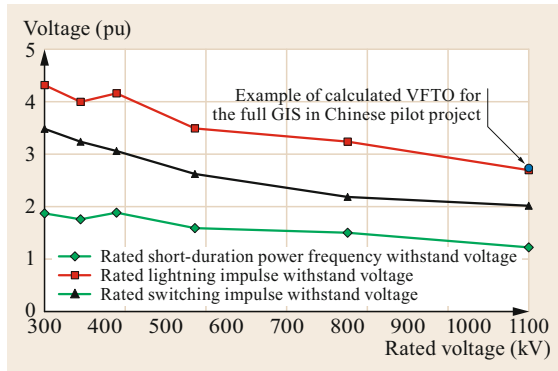
Other dedicated switching equipment in EHV and UHV systems is used to stimulate secondary arc extinction. When an arc grounding fault occurs in one phase, a circuit breaker separates the faulty phase to clear this single phase fault; the secondary arc is induced by electrostatic and electromagnetic induction by healthy or non-faulted lines with the system voltage. It does not disappear at the same instant of fault interruption but will continue a certain time until insulation recovery where the grounding fault was generated.



**Fig. 8.121a,b** Rated voltage dependence of the (a) bus charging current and load capacitance and (b) bus charging current and equivalent busbar length, as per IEC 62271-203 [8.58]



**Fig. 8.122a,b** Bus transfer voltage as a function of the length of (a) the current-carrying loop with GIS and (b) the current-carrying loop with AIS (including MTS)



**Fig. 8.123** Dependence of VFTO and LIWL of the GIS on the rated voltage [8.59]

Since a single-phase or multi-phase auto reclosing can be completed successfully the arc (fault) extinction, it is important to comprehend a typical time of secondary arc extinction in UHV and EHV systems.

When single phase auto reclosure (SPAR) is used, most utilities apply four-leg shunt reactors to limit the secondary arc current, so that it will extinguish within a reasonably short time (mostly within 1 s), but some utilities apply a special scheme to switch off the shunt reactor(s) of a healthy phase [8.59] or apply three-phase high-speed reclosure TPHSR or apply high speed grounding switch (HSGS) to bypass the secondary arc by a short duration (typically 0.5 s) short-circuit, in order to extinguish it. Such solutions are used for UHV, 800 kV and lower rated voltages. Specifications for the HSGS are now within IEC in the process of standardization. Switchgear for the special switching scheme of a healthy phase shunt reactor is yet to be addressed.

HSGSs have been applied to both ends of 550 kV transmission lines in the United States and have shown the ability to successful extinguish secondary arcs in the field. This corresponds to inductive current switching with 700 A for the first switch to open and capacitive current switching with 120 A for the second switch [8.61, 62].

## 8.4 Controlled Switching

Controlled switching systems (CSSs) have become an economical way to reduce switching surges in various switching applications [8.64–67]. Recent developments in transformer switching that account for the residual flux can provide an effective means of mitigating severe inrush currents and temporary overvoltages that could lead to the inappropriate operation of protective relays and power quality degradation [8.68–70]. The

**Table 8.14** HSGS requirements

	USA	Korea	Japan	Japan <sup>a</sup>
Highest voltage (kV)	550	800	1100	1100
Interrupting current (kA)	700	8000	7000	7830
TRV peak (kV)	260	700	900	570
RRRV (kV/ $\mu$ s)	0.1	1.3	1.15	0.46

<sup>a</sup> Duty for delayed current zero interruption with an arcing time of 80 ms + minimum arcing time

In Korea, HSGSs are installed at both ends of 800 kV double-circuit transmission lines with line lengths exceeding 80 km, and they implemented 22 successful high-speed multiphase reclosures with HSGS in the period 2003–2007.

UHV systems in Japan with vertically configured double-circuit OH lines decided to employ HSGSs to achieve high-speed single-phase and multiphase reclosing for all fault modes (e.g., 1LG, 2LG, 3LG, and 4LG).

Table 8.14 summarizes the technical requirements for HSGSs intended for the UHV and EHV systems in the US, Korea, and Japan.

### 8.3.11 Summary

Various switching phenomena are observed in power systems. Generally speaking, a circuit breaker must be able to cope with all switching duties expected for a power system, in accordance with the standards.

There is a well-known rule that, to avoid imposing excessively severe requirements, the standards cover 90% of current network conditions, implying that there are special requirements are not covered by the existing standards. For example, a circuit breaker may not comply with some of the excessive interrupting requirements for transformer limited faults, some reactor switching requirements, and some excessive TRV requirements for series-capacitor bank switching. Special care must be taken when applying circuit breakers for those requirements.

use of CSSs applied to lines of combination with metal oxide surge arresters can reduce undesirable overvoltages caused by the energization of a long transmission line in order to comply with the insulation coordination [8.71, 72]. Real-world examples of the application of line switching are limited, which may be due to initial difficulties resulting from insufficient consideration of technical aspects, including idle time compensation.

**Table 8.15** Testing requirements for the components of a CSS and an integrated CSS system [8.63]

Components and system	Test items	Characteristics/remarks
Type test for circuit breakers	Electrical performance	Rate of rise of dielectric strength (RRDS) Rate of decrease of dielectric strength (RDDS) Maximum making voltage for voltage zero target Minimum arcing time to avoid a reignition or restrike
	Mechanical performance	Scatter in the operating time Variation in the operating time under operational conditions Delay in the operating time after idle time
Type tests for controllers and sensors	Functional test	Scatter in the timing of open/close commands All compensation functions Self-check function, etc.
	Electromagnetic, mechanical, environmental	Dielectric withstand, EMI Vibration, shock, seismic activity Cold, dry heat, temperature/humidity, etc.
Commissioning tests for the integrated system	Controlled switching test	Distribution of switching instants Distribution of making voltage Verification of restrike-free or reignition-free interruptions

The CIGRE guide emphasizes the importance of compensating for variations in the operating time because a CSS requires high operational consistency during the circuit breaker lifetime. Compensation for operating time variations due to external variables such as the ambient temperature, control voltage, and mechanical energy of the drives can be performed by the controller based on the dependence of the variations on the variables, evaluated according to the testing requirements listed in Table 8.15 [8.63].

### 8.4.1 Principle of Controlled Switching

Controlled switching is a term that is commonly used to describe the application of electronic control equipment (a controller) to facilitate the operation of the contacts of a switching device at a predetermined point in relation to an electrical reference signal in order to reduce switching surges.

The components used in CSSs are normally tested in the factory during routine and type tests. For circuit breakers, factory tests include electrical performance tests of, say, dielectric characteristics such as the rate of decrease of dielectric strength (RDDS), the rate of rise of dielectric strength (RRDS), and the minimum arcing time to avoid a reignition, as well as mechanical performance tests of variations in the operating time due to operating conditions and the delay in the operating time after idle time. The controller and the related sensors are tested to verify their functions and their electromagnetic, seismic, and environmental compatibilities. Finally, the controlled switching performance of the integrated system is assessed [8.63].

The term *controlled opening* (deenergization) refers to the technique of adjusting the contact separation of

each pole of a circuit breaker with respect to the phase angle of the current and thereby controlling the arcing time in order to minimize stresses on the components of the power system.

Figure 8.124 shows typical timing sequences for controlled opening or deenergization.

To achieve controlled opening, the current through the circuit breaker or a reference voltage is monitored; for example, the controller often detects periodic current zeros for the reference signal. The arcing time for each pole is controlled by setting the instant of contact separation with respect to the current waveform.

The initial opening command is issued randomly with respect to the reference signal. This command is delayed in order to separate the contact of each phase independently when the circuit breaker can secure an optimum arcing time. This can substantially reduce the restrike probability during consecutive capacitor deenergization or avoid reignition in the case of reactor deenergization.

Similarly, the term *controlled closing* (energization) refers to the technique of controlling the instant of making (current initiation) with respect to the system voltage waveform (phase angle). Typical timing sequences for controlled closing (energization) at voltage zero are given in Fig. 8.125.

In controlled closing, the source voltage is monitored by the controller. Again, the closing command is issued randomly with respect to the reference signal. The command is delayed in order to achieve the optimum phase angle of each voltage independently. This example relates to a capacitive load, where the optimum making instant is the voltage zero, which can be attained with an ideal circuit breaker with infinite RDDS and no mechanical scatter. Pre-arcing before the con-

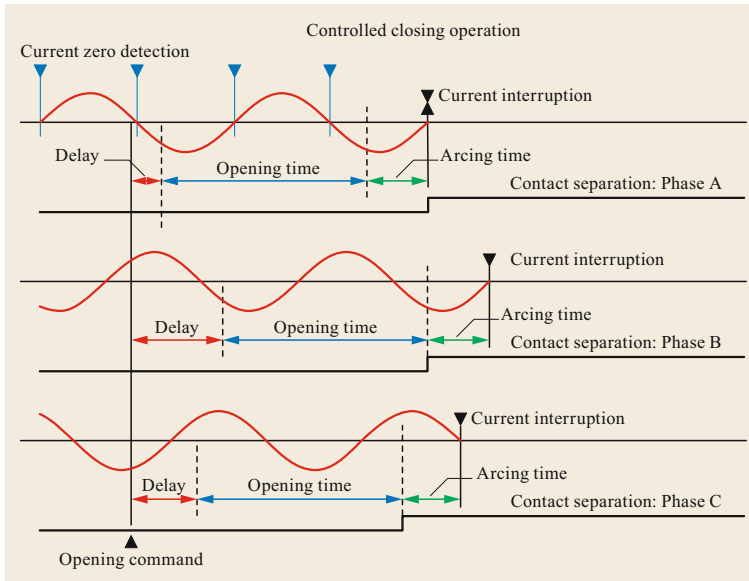


Fig. 8.124 Controlled deenergization

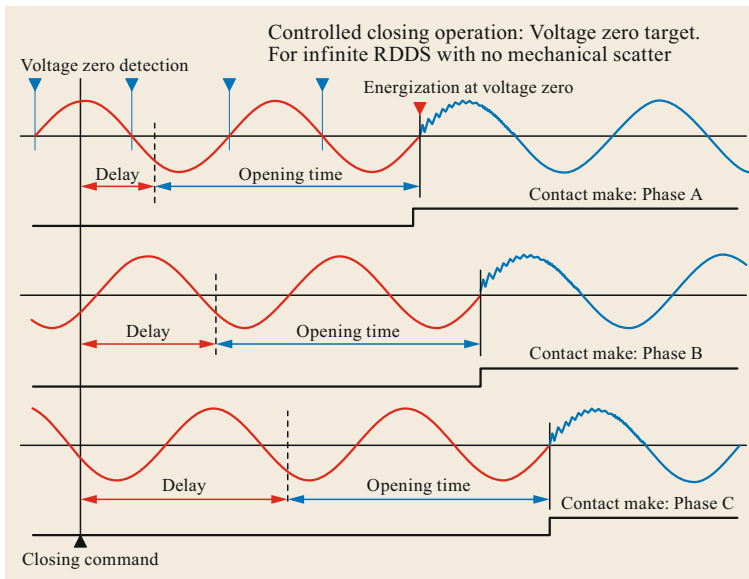


Fig. 8.125 Controlled energization at voltage zero

tacts touch is not considered. A practical case in which voltage zero is targeted is described in the next section.

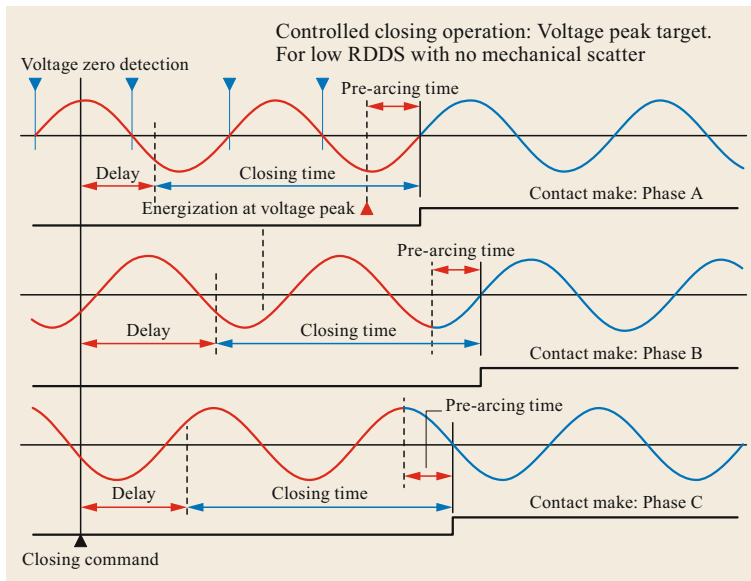
In the case of an inductive load, the optimum making instant is the voltage peak, as shown in Fig. 8.126, where the pre-arcing time between prestrike and the instant at which the contacts touch is assumed to be a quarter of a cycle. The dependence of the opening time on the operating conditions and the prestrike behavior is particular to each type of circuit breaker.

The optimum targets for different applications are summarized in Table 8.16.

The voltage peak energization strategy is suitable for a transformer with a large parallel capacitance, as it will result in a significant reduction in the residual flux after deenergization. The optimum making instant for a practical transformer is when the prospective normal core flux at energization is identical to the residual flux (see Sect. 8.4.4).

Modern SF<sub>6</sub> circuit breakers generally present very low restriking probabilities for capacitive current interruption, meaning that restriking-induced problems are rare. Nevertheless, the restriking probability can be fur-





**Fig. 8.126** Controlled energization at peak voltage

ther reduced via controlled switching, which is employed to ensure long arcing times and hence larger contact gaps at current interruption.

When controlled switching is applied to reactor deenergization, the optimum opening instant is often selected so as to achieve the maximum arcing time. Even though the use of controlled switching may increase chopping overvoltages due to an increased prearcing time, reignition overvoltages are normally more severe than chopping overvoltages (especially for a modern SF<sub>6</sub> circuit breakers).

All circuit breakers exhibit a high probability of reignition for arcing times of less than the minimum arcing time, and reignition may damage the nozzle and contacts of the circuit breaker. In contrast, depending on the number of series-connected breaking units (the interrupting performance) and the capacitance across the circuit breaker, chopping overvoltages may be prominent when the arcing time is maximized, especially for air-blast circuit breakers. Thus, the approach adopted should depend upon the relative importance of reignition versus current chopping. However, users must

decide upon the relative importance of reignition versus current chopping.

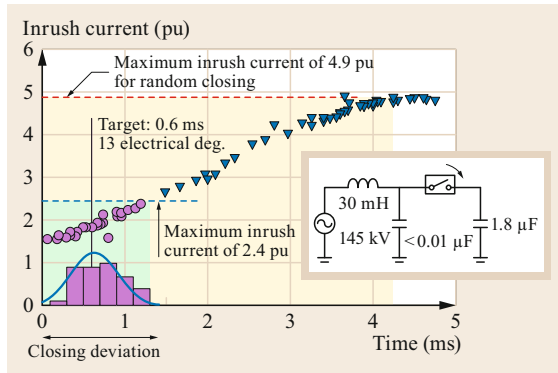
#### 8.4.2 Capacitor Switching Applications

Controlled switching of shunt capacitor banks is used to minimize stresses on the power system and its components. Controlled closing reduces the magnitudes of inrush currents and the associated overvoltages and provides an alternative to the use of fixed inductors. Controlled opening leads to a further reduction in the restrike probability for the circuit breaker. Single capacitor bank switching leads to higher local and remote overvoltages, whereas back-to-back switching generates large inrush currents.

Shunt capacitor bank energization causes local effects in the substation and remote effects at the receiving ends of transmission lines connected to the substation. Local effects include inrush currents and overvoltages, mechanical and dielectric stresses in the capacitor bank and other equipment in the substation, erosion of the circuit breaker contacts, transient po-

**Table 8.16** Optimum instants for controlled switching [8.64]

Switching application	Optimum instant for controlled switching	Benefits
No-load transformer energization	Voltage peak with no residual flux or prospective core flux identical to the residual flux	Reduction of inrush current and associated overvoltage
No-load line energization	Voltage zero across the circuit breaker	Reduction of overvoltage and elimination of need for closing resistor
Shunt capacitor energization	Voltage zero across the circuit breaker	Voltage zero across the circuit breaker
Shunt capacitor deenergization	Maximum arcing time	Minimization of restrike probability
Shunt reactor deenergization	Maximum arcing time (to avoid reignition)	Reduction of overvoltage and elimination of reignition



**Fig. 8.127** Example of the analysis of inrush currents obtained when energizing 145 kV capacitor banks

tential rises in the substation earthing mesh, and the coupling of transient surges to control and protection wiring. Remote effects include overvoltages at the far ends of radially connected transmission lines as well as overvoltages in MV and LV networks connected to the secondary side of transformers at the end of these lines. The optimum making instant for wye-connected, earthed-neutral shunt capacitor banks should be a voltage zero across the circuit breaker in each phase.

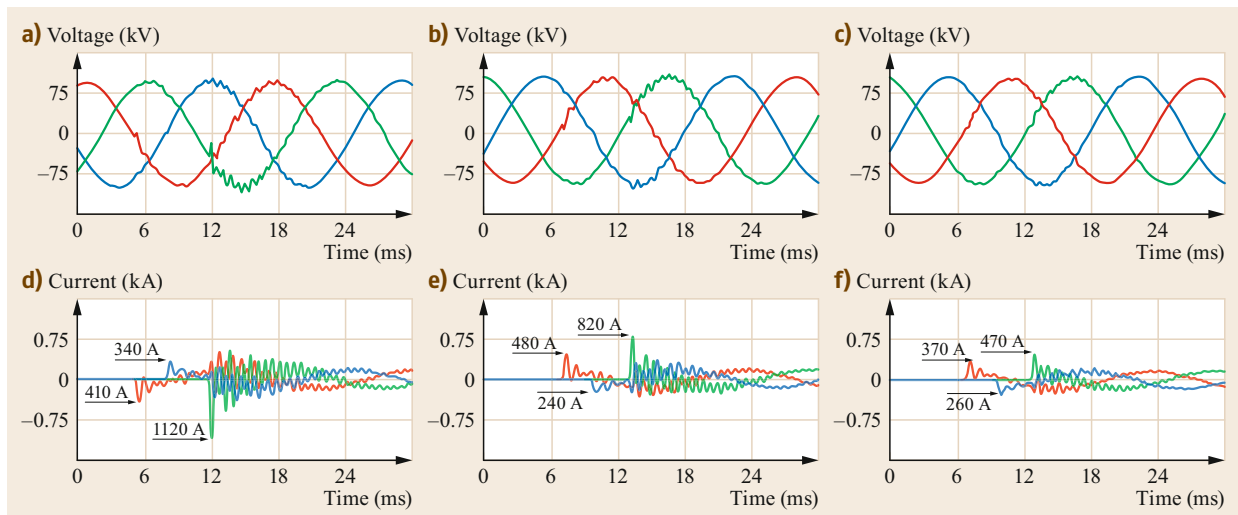
Figure 8.127 shows an example of the analysis of inrush currents obtained when energizing 145 kV capacitor banks. The maximum inrush current is 4.9 pu of the nominal current. This can be suppressed to less than 2.4 pu with a CSS. The energization target is set to make a  $13^\circ$  electrical angle with the voltage waveform.

After calibration on site, controlled switching tests were performed at the system voltage of 121 kV using a target for the closing operation of 8 electrical degrees, as determined by the RDDS and mechanical scatter plus a slight safety factor. The target for the opening operation was set to give the maximum arcing time before the current zero.

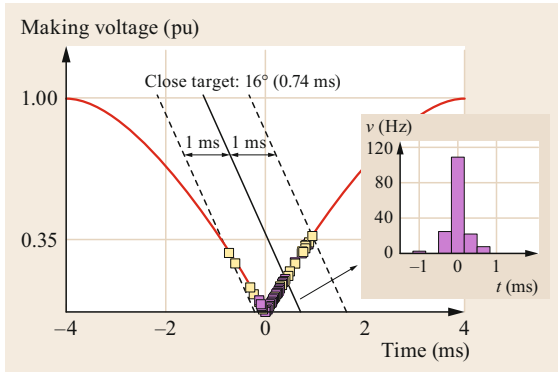
Figure 8.128 shows the voltage and current waveforms obtained during the second, third, and sixth of ten controlled energization tests conducted during the commissioning tests. For the first making test, the making instant of the third phase shows a slight delay, even though the inrush current of 1290 A is within the permissible tolerance. This delay is probably caused by a difference of the actual RDDS due to design tolerances of the interrupter dimensions or closing velocity scatter because of individual properties of the components. The controller applied to this circuit breaker can compensate for this difference through adaptive control.

A circuit breaker with a normalized RDDS of less than 1 can be applied for capacitor switching because the inrush current can be sufficiently suppressed if the making voltage is less than half of the maximum pre-strike voltage. Idle time compensation is recommended for drives with operating times that have an idle time dependence. Adaptive control is also required to compensate for any operating time drift that persists over a number of consecutive operations.

Controlled switching tests were performed at a system voltage of 145 kV using a target closing instant of 16 electrical degrees, as determined by the measured RDDS and mechanical scatter. The circuit breaker



**Fig. 8.128a-f** Voltage waveforms obtained in the second (a), third (b), and sixth (c) energization tests and current waveforms obtained in the second (d), third (e), and sixth (f) energization tests performed using a 121 kV CSS in the field (ten tests were performed in total)



**Fig. 8.129** Making-voltage distribution and closing-instant distribution

has been operated daily in the field since the commissioning tests. Figure 8.129 shows the distribution of closing instants measured by the controller along with the distribution of making voltages calculated from the data. The closing instants present a normal distribution around the closing target of 16 electrical degrees, with a small standard deviation of less than 0.3 ms, which corresponds to the maximum making voltage of 0.35 pu.

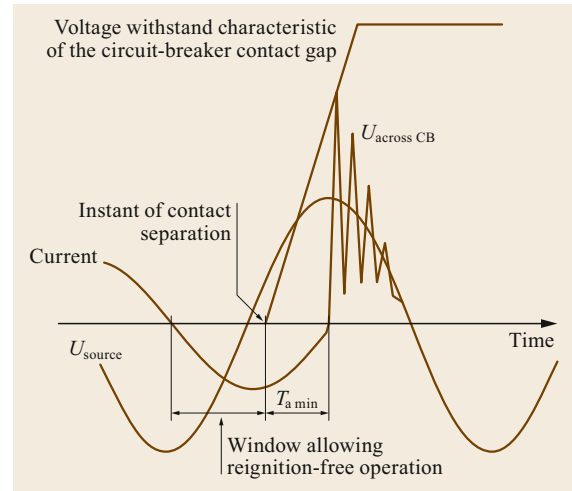
### 8.4.3 Reactor Switching Applications

Shunt reactor switching is a known source of current and voltage transients. Overvoltages due to current chopping and reignition can damage any high-voltage equipment. High asymmetrical inrush currents may be generated by performing shunt reactor energization at an unfavorable instant. These inrush currents can provoke electromechanical stress or a high-magnitude zero-sequence current of an extended duration. Controlled switching can be applied in both cases to reduce the expected transients.

During shunt reactor deenergization, overvoltages can be generated in two ways: by current chopping and by reignition.

Chopping overvoltages are a consequence of the forced interruption of the inductive current before its natural zero. They mainly depend on the number of series-connected breaking units present, the chopping number of the circuit breaker, the capacity (in MVA) of the reactor, the capacitance in parallel with the circuit breaker, and (in certain cases) the arcing time. For modern SF<sub>6</sub> circuit breakers, chopping overvoltages are not very high (they typically reach up to 1.5 pu), but they increase with arcing time.

Reignition overvoltages are generated by reignitions following the initial interruption. Reignitions are provoked when the voltage between the contacts ex-

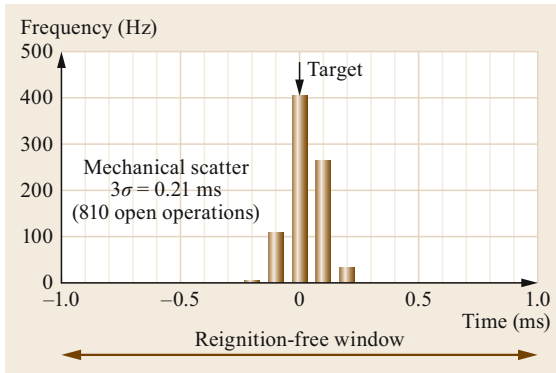


**Fig. 8.130** Definition of the minimum arcing time for reactor deenergization

ceeds the dielectric withstand of the contact gap. The rate of rise of voltage during a reignition ranges between lightning and fast-front transients, depending on the length of the busbar between circuit breaker and reactor, while chopping overvoltages are similar to slow-front transients (switching surges). Reignition may affect circuit breaker elements such as the nozzle and contacts and the reactor insulation. For example, perforation of an insulating nozzle, signs of arcs occurring away from the arcing contacts, and metal particles in the interrupter have been reported. The CIGRE international reliability survey for the years 2004–2007 shows that the major failure frequencies for circuit breakers operating on shunt reactors are around an order of magnitude higher than those for line and transformer breakers. Even though not all types of circuit breakers are damaged in the same way, it is desirable to eliminate reignitions.

All circuit breakers exhibit a high probability of reignition for arcing times that are less than the minimum arcing time ( $T_{a\min}$ ). Figure 8.130 shows a schematic of the voltage withstand characteristic of a circuit breaker along with the transient recovery voltage across the circuit breaker for reactor deenergization. Since the main criterion for eliminating reignition is to avoid the reignition window, the optimum instant for contact separation is when the expected arcing time exceeds  $T_{a\min}$ . When promoting increased arcing times in this way, it should also be noted that chopping overvoltages can increase with arcing time.

Since reignition overvoltages are normally more severe than chopping overvoltages, controlled switching is commonly used to increase the arcing time. It is important to determine the relative importance of reig-



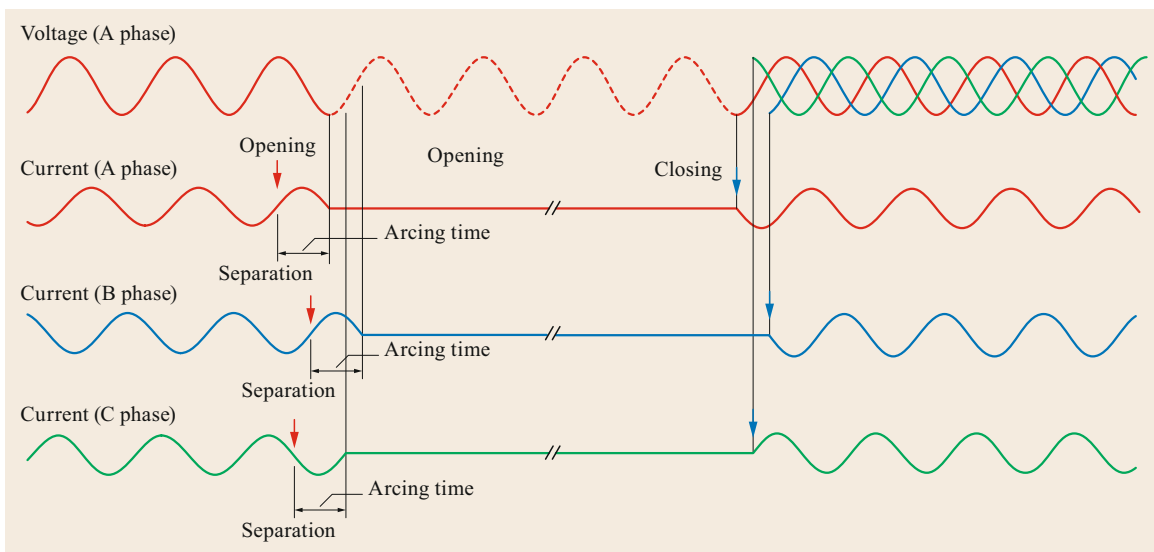
**Fig. 8.131** Distribution of opening instants during controlled reactor opening

nition and current chopping according to the circuit breaker design.

In this section, we have extolled the benefits of controlled opening. However, there are certain cases where controlled opening provides little or no advantage. For example, tests in which controlled reactor opening was applied to a minimum oil circuit breaker were not successful due to the occurrence of reignitions regardless of the arcing time. In this case, controlled switching cannot avoid reignitions.

Figure 8.131 shows an excellent reignition-free performance with CSS demonstrating the deviation of de-energization instants within only 0.21 ms.

Figure 8.132 shows voltage and current oscillograms for the deenergization and energization of a 245 kV controlled shunt reactor in the field. The maximum inrush current of 1270 A observed upon random closing was suppressed to below 50 A.



**Fig. 8.132** Voltage and current behavior during controlled shunt reactor switching

#### 8.4.4 Transformer Energization

The energization of an unloaded transformer can generate high-amplitude inrush currents, which stress the windings and can cause maloperation of protection relays and prolonged temporary harmonic voltages, which can in turn degrade the quality of the electricity supply. High inrush currents also impose severe mechanical stresses on the transformer windings and may reduce the life expectancy of a transformer exposed to frequent energization. For example, step-up transformers in hydroelectric power plants are frequently switched to adapt to daily load variations. These risks can be ameliorated through the use of a closing resistor (or by controlling the making instant of simultaneously operated three-phase circuit breakers).

The interruption of no-load transformer currents is similar in nature to the interruption of shunt reactor currents. However, the natural frequencies are much lower and the damping is very high, meaning that the overvoltages generated at deenergization have extremely low amplitudes. Breaking instant control is similar to that applied for shunt reactors when the residual flux in the transformer cores is negligible.

The magnetic circuits of transformers have magnetization curves with a pronounced bend from the nonsaturation region to the saturation region. For economic reasons, power transformers are designed to have an operational peak flux value as close as possible to the saturation value. The flux in a transformer energized by a steady-state alternating voltage varies from a negative peak value to an equivalent positive value during one half cycle of the voltage waveform. The change in flux of twice the maximum flux value is proportional to the

time integral of the voltage waveform between two successive zero points. If the circuit breaker is closed at a voltage zero, the full change in flux is required during the first half cycle. When the flux is initially at zero, the maximum flux developed will be twice the normal operational peak value. Since the operational peak flux is already close to the saturation value, an increase in flux to double this value corresponds to extreme core saturation. Consequently, the inductance drops and the current rapidly rises to a very high value.

At the making instant, residual flux from the previous opening may be present in the transformer. If this residual flux is of the same polarity as the change in flux, the combination of the change in flux with the residual flux will lead to even greater saturation of the magnetization circuit.

The processes that occur when a three-phase transformer is energized are more complex because the three phases are linked both magnetically and galvanically. The structure of the winding connection and the neutral point treatment influence the value of the inrush current.

It is possible to propose a general principle for reducing inrush currents during controlled closing by adopting the hypothesis that there is no residual flux and that the flux in all cores is nil prior to closing. Closing must first be performed on either one phase (if the neutral of the primary winding is earthed) or two phases (if the primary winding is isolated). The making target

is the maximum line-to-earth voltage (earthed neutral) or the maximum phase-to-phase voltage (isolated neutral) so that fluxes are generated without transients. The making instant of the remaining phase(s) must be chosen such that the flux that circulates in the corresponding cores following the initial closing is the same as the flux that circulates in these cores under steady-state conditions. This stops flux transients from being created in the cores [8.68].

Figure 8.133 shows the energization strategy for a three-core transformer with a wye (star) connection and an isolated neutral. Energizing a single phase has no effect, since there is no flow path for magnetizing current due to the isolated neutral point. The phase-to-phase voltage  $U_{13}$  is switched on when its maximum value occurs at time  $t_1$ . The corresponding stationary core fluxes  $\phi(F)_1$  and  $\phi(F)_3$  have instantaneous values of zero at that instant ( $t_1$ ). They attain their maximum values 90 electrical degrees later, at time  $t_2$ , when the fluxes are identical to the steady-state core flux values. This means that voltage  $U_2$  can be switched without any transient reaction at time  $t_2$ .

On the other hand, Fig. 8.134 shows the energization strategy for a three-core transformer with a wye (star) connection and a solidly earthed neutral. Phase  $L_2$  is energized when the phase voltage  $U_2$  is at its peak at time  $t_1$ . The magnetizing current  $J_2$  is able to flow through the earthed neutral point. The magnetizing

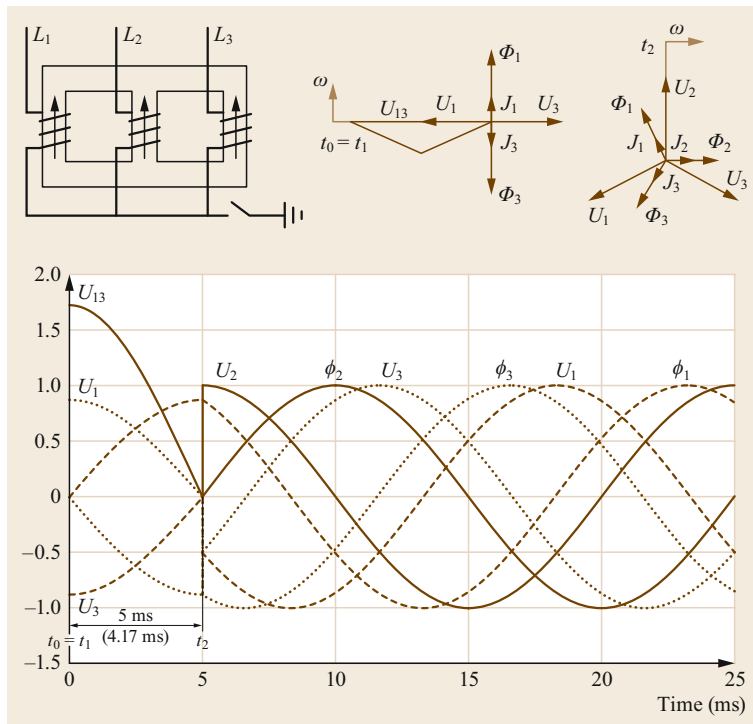
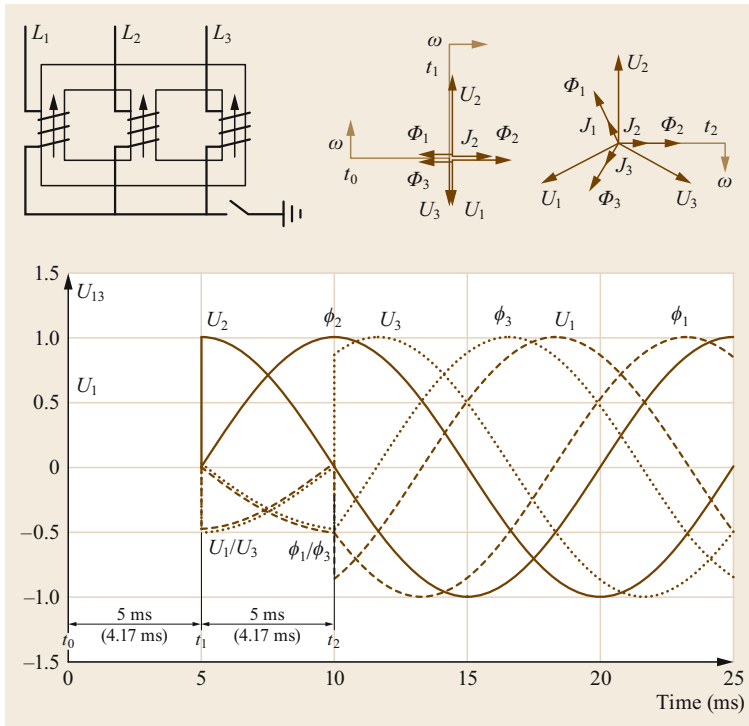


Fig. 8.133 Closing strategy for an isolated neutral transformer



**Fig. 8.134** Closing strategy for a solidly earthed transformer

field  $\phi(F)_2$  begins without any transient. The associated magnetizing current  $J_2$  must also allow for the excitation of the other two phases, each of which has half the flux during this stage. Consequently, this current is 1.5 times its three-phase steady-state value.

By  $t_2$ , the fluxes  $\phi_1$  and  $\phi_3$  have reached levels corresponding to their three-phase steady-state values. Phases  $L_1$  and  $L_3$  may therefore be energized without transients at time  $t_2$ .

The optimal making instants for the different phases to minimize the inrush current (based on the hypothesis that there is no residual flux in the cores) are summarized in Table 8.17. Phase  $L_2$  is wound around the middle core in three- or five-leg (core) power transformers. The voltages of the different phases can be written as

$$U_1 = U \sin\left(\frac{\omega t + 2\pi}{3}\right),$$

$$U_2 = U \sin(\omega t),$$

$$U_3 = U \sin\left(\frac{\omega t - 2\pi}{3}\right).$$

The making instant is given in relation to the zero-voltage instant of  $U_2$ ; see Figs. 8.133 and 8.134.

For any practical application of a CSS to transformer energization, the residual fluxes in the transformer cores should be considered when determining

the optimal energization instants, especially when the capacitance between the windings and the ground is small. Therefore, the inrush currents will depend on the following characteristics:

- The magnetic characteristics of the transformer cores
- The making instants of the circuit breaker
- The electrical connections of the power transformer
- The residual flux
- The electrical characteristics of the source system [8.68–70].

Figure 8.135 shows the dynamic magnetic flux and the current behavior observed when a transformer is energized. Energization of a transformer with no residual flux in its cores at peak voltage will not lead to transients. However, the level of saturation of the magnetizing current caused by the change in flux after energization depends on the residual flux and the energization instant. Therefore, the targets should be adjusted taking into account the residual flux. The inrush current can be only minimized by energization when the prospective normal core flux is identical to the residual flux.

An innovative and field-proven approach to residual flux measurement has been developed. It can evaluate the residual flux by integrating transformer deenergization and also compensating the flux value caused by a

**Table 8.17** Ideal making instants for different power transformers with no residual flux in their cores

Primary winding connection	Secondary of tertiary coupling	Magnetic circuit	Making instant voltage for phase 2	Making instant voltage for phase 1	Making instant voltage for phase 3
Wye (star) Connection with isolated neutral $Y$	Wye (star) or delta	3- or 5-core transformers Transformer banks	5 ms (50 Hz) 4.17 ms (60 Hz) (90°) $1.5 U$	0 ms (50 Hz) 0 ms (60 Hz) (240°) $U\sqrt{\frac{3}{2}}$	0 ms (50 Hz) 0 ms (60 Hz) (120°) $U\sqrt{\frac{3}{2}}$
Wye (star) Connection with earthed neutral $Y_n$	Wye (star) or delta	3- or 5-core transformers	5 ms (50 Hz) 4.17 ms (60 Hz) (90°) $1.5 U$	10 ms (50 Hz) 8.33 ms (60 Hz) (60°) $U\sqrt{\frac{3}{2}}$	10 ms (50 Hz) 8.33 ms (60 Hz) (300°) $U\sqrt{\frac{3}{2}}$
Wye (star) Connection with earthed neutral $Y_n$	Delta $\Delta$	Transformer banks	5 ms (50 Hz) 4.17 ms (60 Hz) (90°) $1.5 U$	10 ms (50 Hz) 8.33 ms (60 Hz) (60°) $U\sqrt{\frac{3}{2}}$	10 ms (50 Hz) 8.33 ms (60 Hz) (300°) $U\sqrt{\frac{3}{2}}$
Wye (star) Connection with earthed neutral $Y_n$	Wye (star) $Y$ or $Y_n$	Transformer banks	5 ms (50 Hz) 4.17 ms (60 Hz) (90°) $1.5 U$	1.67 ms (50 Hz) 1.39 ms (60 Hz) (270°) $U\sqrt{\frac{3}{2}}$	10 ms (50 Hz) 8.33 ms (60 Hz) (270°) $U\sqrt{\frac{3}{2}}$
Delta $\Delta$	Wye (star) or delta	3- or 5-core transformers Transformer banks	5 ms (50 Hz) 4.17 ms (60 Hz) (90°) $1.5 U$	0 ms (50 Hz) 0 ms (60 Hz) (240°) $U\sqrt{\frac{3}{2}}$	0 ms (50 Hz) 0 ms (60 Hz) (120°) $U\sqrt{\frac{3}{2}}$

small voltage change induced by a remote fault clearing. In 2001, Canada installed two prototype systems which ensure that high-voltage step-up transformers are energized at the ideal instant. Each system consists of a CSS with a new residual magnetic flux measurement system [8.69] that uses the following relation between the magnetic flux  $\Phi$  of a coil with  $N$  turns and the applied voltage  $E$ :  $\Phi = \int E/N + \Phi_r$ , where  $\Phi_r$  is the residual magnetic flux.

The algorithm for evaluating the residual flux generally consists of the following four steps (see also Fig. 8.136):

- (1) The zero level (or offset level) of the dynamic flux must be calibrated precisely. The zero level for the integration of the voltage signal is determined by monitoring several cycles of voltage waves before current interruption.
- (2) The time duration for voltage integration is defined as the time before the voltage amplitude becomes smaller than a specified value where the flux draws a microhysteresis loop.
- (3) Voltage integration is performed over the time determined in the second step.
- (4) The difference between the value obtained in the third step and the zero level evaluated in the first step gives the residual flux.

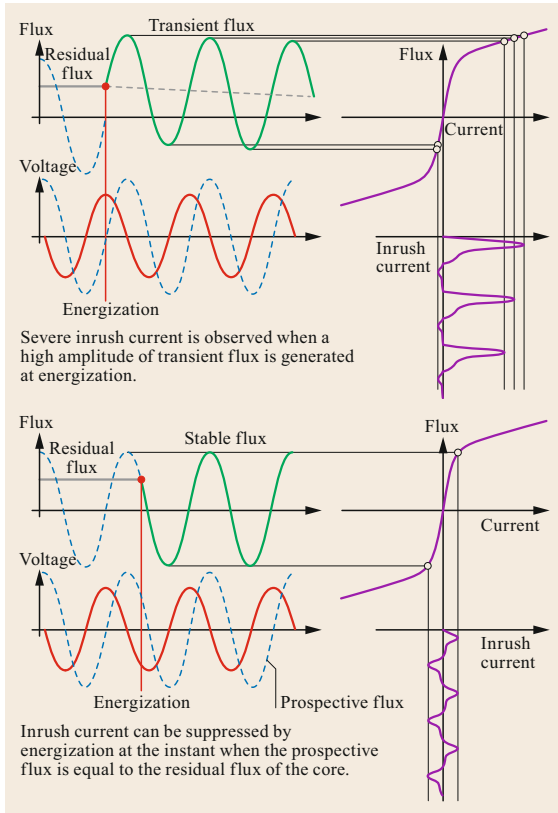
A novel built-in transformer voltage sensor was developed to measure each phase voltage of the transformer shown in Fig. 8.137 [8.69].

Figure 8.138 shows a typical record of the residual fluxes for three phases measured at transformer deenergization. This was used to determine the optimal energization instant for each phase.

Figure 8.139 shows an example of the dependence of the residual flux patterns on the opening phase angle at random (de)energization in the field. Three patterns were observed in the field measurements (note that the residual fluxes of the three phases sum to zero):

- In pattern I ( $X, -X, 0$ ), two phases have large fluxes with the same amplitude but different polarities. The remaining phase has minimum flux.
- In pattern II ( $X + Y, -X, -Y$ ), all three phases have significantly different fluxes, and one of the phase fluxes has a different polarity from the other two phase fluxes.
- In pattern III ( $2X, -X, -X$ ), one phase has a large flux with a different polarity to the other two phase fluxes, both of which are roughly half the value of the phase with a large flux.

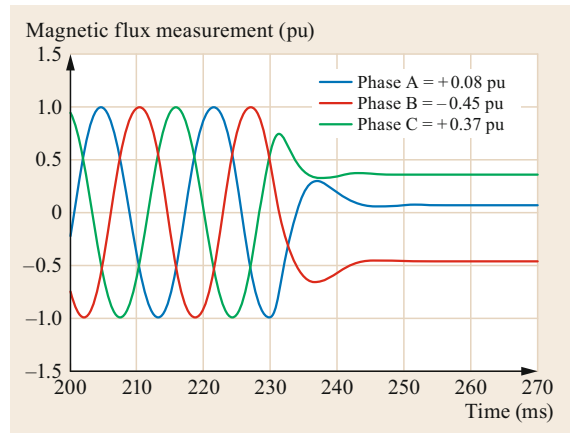
Pattern III is clearly advantageous for the control strategy because the residual fluxes in the second and the third phases are similar to the flux obtained after ener-



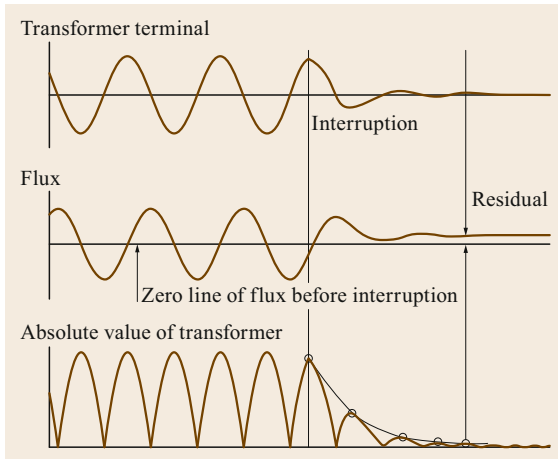
**Fig. 8.135** Magnetizing flux in a transformer core and the corresponding magnetizing current



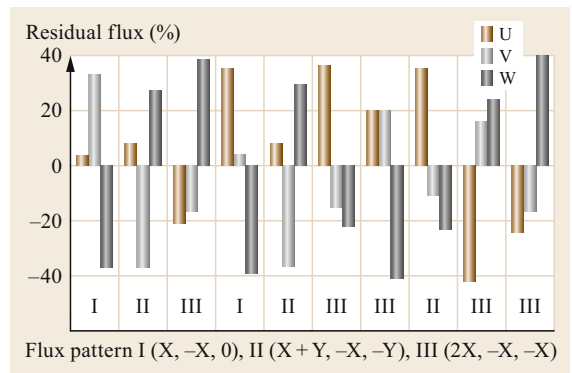
**Fig. 8.137** Transformer bushing voltage sensor for application in a CSS. (Courtesy of Hydro Québec)



**Fig. 8.138** Typical record of residual fluxes for three phases measured at transformer deenergization

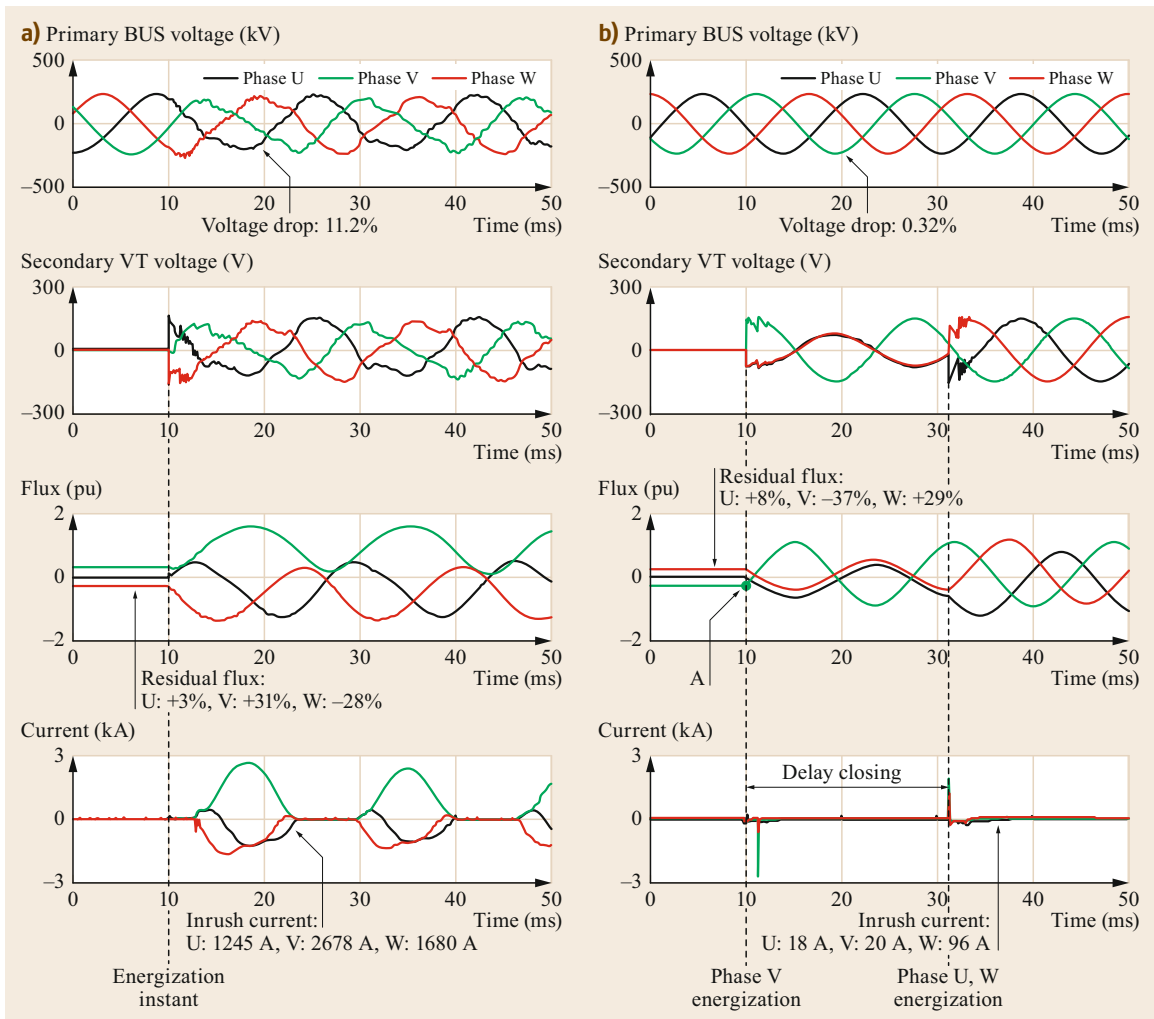


**Fig. 8.136** Residual flux evaluation based on the integration of voltage measurements



**Fig. 8.139** Example of the dependence of the residual flux patterns on the deenergization phase angle





**Fig. 8.140** (a) Simultaneous three-phase energization, (b) controlled energization that takes the individual residual phase fluxes into account

gization of the first phase. This pattern will give flux conditions in the second-phase and third-phase cores that are close to ideal, with a limited closing delay.

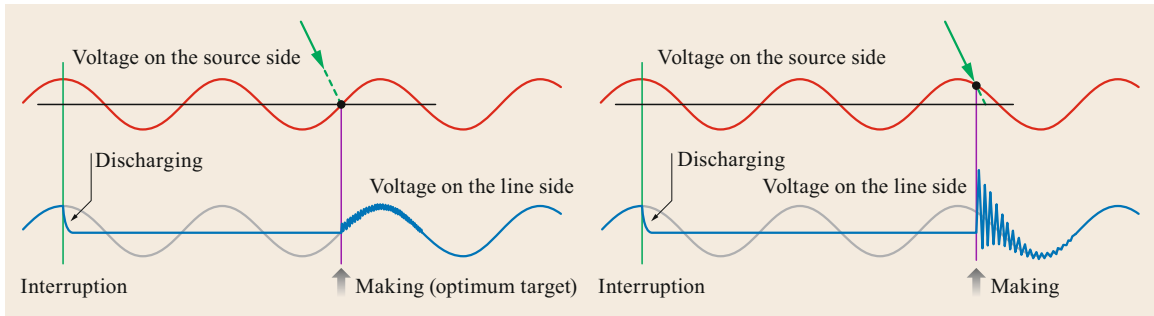
This suggests that controlled transformer switching can be further improved through the application of controlled deenergization. In other words, the circuit breaker can deenergize the current at a specific phase angle corresponding to the phase with the largest residual flux at one phase or two phases.

Figure 8.140a shows typical core voltages, currents, and fluxes calculated for simultaneous three-phase energization. High inrush currents ranging from 1245 to 2678 A are obtained due to magnetic saturation in the cores, which causes the voltage to drop by up to 11.2% at the primary bus terminal. On the other hand, Fig. 8.140b shows a typical example of controlled trans-

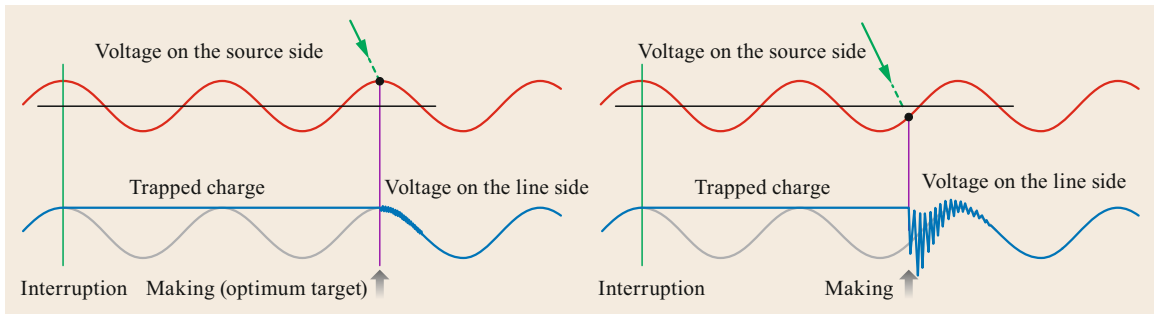
former energization. The controller chooses to close the phase with the largest residual flux (phase V) first. The first phase is closed at the instant when the prospective normal core flux is identical to the residual flux. The second and third (U and W) phases are closed 1.5 cycles later, at a voltage peak for the first phase. The inrush currents are therefore reduced to below 100 A and the voltage disturbance is effectively suppressed by choosing to deenergize the phase with the largest residual flux first, greatly reducing mechanical and electrical stresses on the transformer [8.70].

### 8.4.5 Line Switching Applications

Energization and autoreclosing of long transmission lines can cause undesirable overvoltages in the trans-



**Fig. 8.141** Optimum target for an uncompensated line equipped with an inductive potential transformer. Making should be performed at a zero crossing of the source-side voltage for lines that are rapidly discharged, such as those equipped with an inductive potential transformer (RC is typically  $< 100$  ms)



**Fig. 8.142** Optimum target for an uncompensated line equipped with a capacitive potential transformer. Making should be performed at a source voltage peak of the same polarity as the trapped charge for lines with no leakage path for the trapped charge, such as those equipped with a capacitive potential transformer. The controller should detect the line voltage polarity at the instant of line charging current interruption

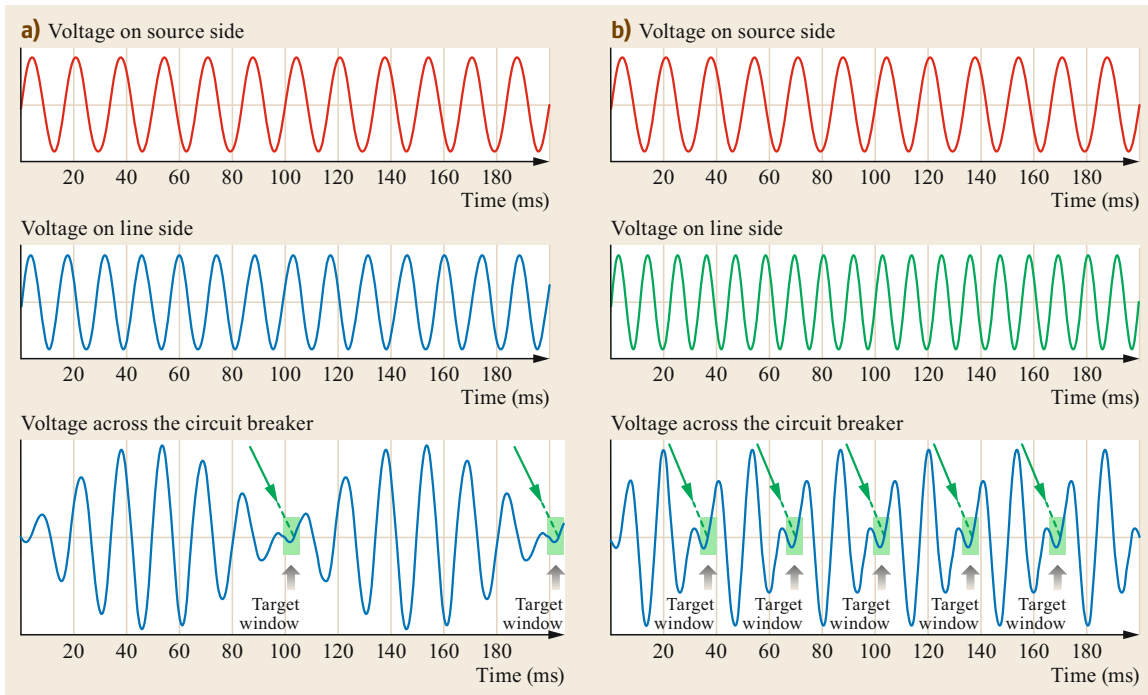
mission network, so special measures for mitigating these overvoltages are employed to meet the insulation coordination. Most commonly, these measures correspond to the application of a MOSA, often in combination with a closing resistor to improve reliability, but this approach is relatively expensive. There is also a growing need to use shunt reactors to mitigate the phase-to-ground transient overvoltages caused by line switching, especially high-speed autoreclosing. The highest phase-to-ground transient overvoltages tend to appear in the middle of the line because they are limited at the ends of the line by the presence of shunt reactors, MOSAs, and CSSs. These overvoltages can be reduced by positioning a MOSA in the middle of the line.

A CSS can potentially reduce reclosing transients and suppress restrikes. It can also provide economic benefits such as eliminating the need for closing resistors and reducing the insulation levels needed for surge arresters and transmission towers. For line applications, a circuit breaker with a high RDDS is generally preferable, although the operating scenario and targeting strategies should be studied thoroughly. Idle-time

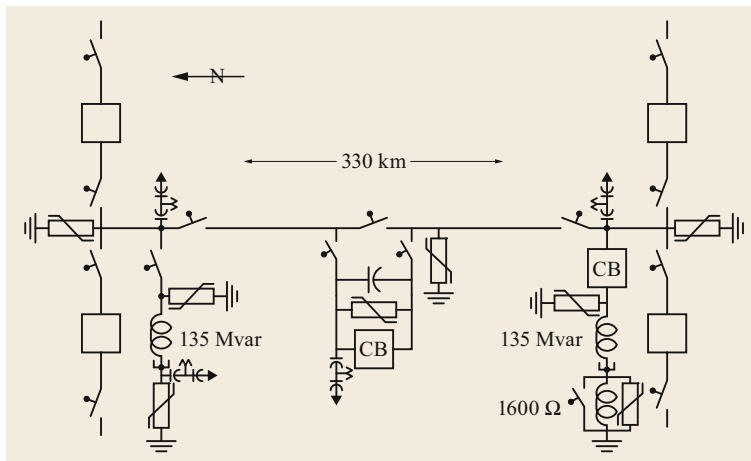
compensation is essential for drives with operating times that depend on the idle time [8.63, 71].

The physical phenomenon that governs line-switching overvoltages is the propagation of electromagnetic waves along the line; these are generally called traveling waves. The wave propagation is initiated by the making operation of the circuit breaker, and the initial voltage amplitude is the circuit breaker pre-arc voltage, i.e., the instantaneous value of the voltage across the circuit breaker pole at the instant of line charging current making. One consequence of the propagation of traveling waves is that the optimum making instant for the controlled switching of unload transmission lines is a voltage minimum across the circuit breaker pole. The strategies for different line configurations are as follows:

- (a) For an uncompensated line with an inductive potential transformer, the controller can effectively suppress the surge (to less than 1 pu) by performing controlled closing at voltage zero on the source side. This is because the trapped DC charge is discharged rapidly, typically within 100 ms (Fig. 8.141).



**Fig. 8.143a,b** Optimum making targets for compensated line switching. (a) The voltage across the circuit breaker has a pronounced beat for high degrees of compensation. (b) For lower degrees of compensation, the voltage across the circuit breaker exhibits a complex voltage waveshape with a less pronounced beat pattern

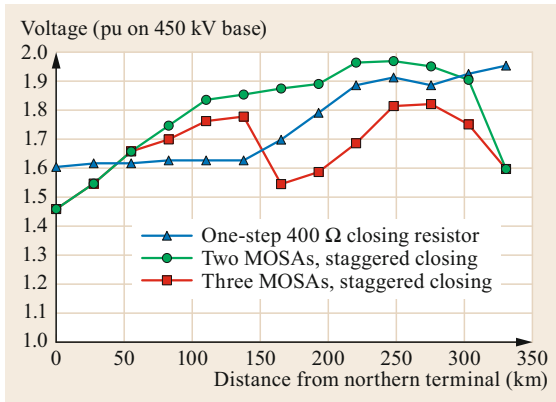


**Fig. 8.144** Arrangement for a series capacitor compensated 550 kV transmission line

- (b) For an uncompensated line with a capacitive potential transformer, there is no leakage path for the trapped charge. The optimum target is a source-side voltage peak of the same polarity as the trapped charge (Fig. 8.142).
- (c) For a compensated line, the degree of compensation significantly influences the line-side voltage. The voltage across the breaker presents a prominent beat (especially for a high degree of com-

pensation) because the line oscillation frequency is typically within the range 30–50 Hz. The optimal instant is a voltage minimum across the CB; preferably during the minimum of the voltage beat [8.72], as shown in Fig. 8.143.

Figure 8.144 presents an example (from Canada) of a series capacitor compensated 550 kV transmission line with a length of 300 km. This system is equipped



**Fig. 8.145** Voltage profiles obtained with a closing resistor or with two or three MOSAs [8.72]

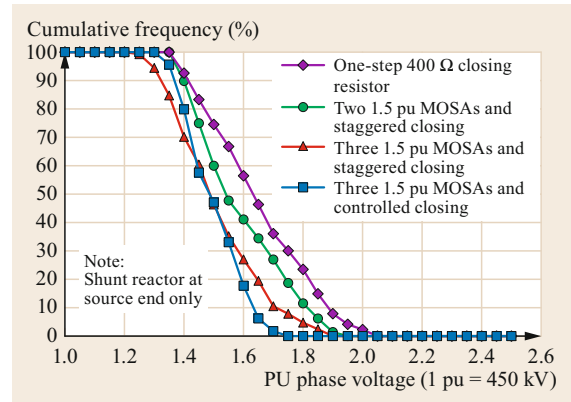
with mid-line series capacitors that provide 50% compensation. Economics resulted in the decision to assign the bypass protection of this bank to a MOSA rated at 2.2 pu, 89 MJ with no self-triggered or triggered gap. The line is equipped with 135 MVA/525 kV three-phase shunt reactors at each end of the line; the reactor at the receiving end is switchable.

The line will be operated with single pole reclosing, so the shunt reactor at the southern end is equipped with a neutral reactor rated at 1600  $\Omega$  for secondary arc damping. The reactor at the northern end is grounded through a surge arrester to achieve a high grounding impedance and therefore optimize the secondary arc control [8.72].

Figure 8.145 compares the voltage profile along a line with a conventional closing resistor to the use of two and three MOSAs with staggered closing. The effectiveness of overvoltage control using a closing resistor decreases when the line length becomes longer than 150 km. It is evident that with three MOSAs, only a small portion of the line experiences voltages over the design target, even with the nonoptimal times inherent to staggered closing.

Figure 8.146 indicates the improvement that can be obtained using a line-connected MOSA. Two alternatives are considered: a MOSA at each terminal of the line or three MOSAs with the third connected mid-line. Note that the objective, to reduce the overvoltage to less than 1.7 pu, can only be achieved using three MOSAs plus controlled closing.

According to the results, the general performance of the CSS is similar to that of the closing resistor in terms of controlling phase-to-ground and phase-to-phase switching transient overvoltages at both receiving ends and mid-line. It is clear that the CSS can substantially mitigate switching overvoltages in the middle of the line. Of course, it should be noted that there is the potential for phase-to-phase TOV mitigation.



**Fig. 8.146** Comparison of various methods of mitigating three-phase reclosing overvoltages

The use of a more compact UHV OH line design significantly lowers the capital costs of the line itself due to the resulting reductions in the dimensions and weights of mechanical structures. Employing both MOSAs and CSSs can potentially allow transmitting large amounts of powers considering the increased economic and environmental constraints of recent years.

#### 8.4.6 Summary

The rapid increase in the use of CSSs can be ascribed to several factors, such as the successful deployment of systems with an effective compensation algorithm in the field, the CIGRE proposal for type-testing recommendations, and versatile operations and controls of transmission systems due to changes in the electrical industry globally. Since CSSs provide significant technical and economic benefits, including enhanced power quality and operational flexibility, they may be incorporated into circuit breaker control systems as standard in the near future [8.73].

CSSs provide many economic benefits when they are applied to shunt reactor banks and transformer energization in power systems. When making at the voltage minimum, a RDDS of at least 186 kV/ms at 60 Hz (155 kV/ms at 50 Hz) is required for 550 kV single-break and 1100 kV two-break GCBs, which corresponds to RDDS = 1.

Step-up power transformers in hydroelectric power plants are frequently switched to cope with daily load variations. Controlled transformer switching that takes into account the residual flux is one scheme that can be employed to effectively reduce the overvoltage caused by transformer energization. Since the effectiveness of a closing resistor at reducing the overvoltage decreases for very long lines (typically longer than 200 km), combined CSS and MOSA use could be one of the solutions used for long UHV and EHV transmission lines.

In the case of transformer energization, inrush currents can be reduced to satisfactory levels through the simultaneous application of a CSS with a gang-operated circuit breaker.

The potential to achieve more compact transmission towers and lines through the associated shunt reactors in addition to MOSAs for TOV mitigation, requires thorough investigation during the planning or engineering design phases of power systems.

## 8.5 DC Circuit Breakers

HVDC transmission has increased in popularity in recent years due to rapid progress in power electronics technology driven by the need to connect increasing numbers of offshore or remote wind farms and/or large hydropower generators. HVDC brings several technical benefits in this context, such as fewer system stability problems compared with AC transmission and lower energy losses during long-distance transmission. In the near future, multiterminal HVDC transmission networks connected to offshore wind farms will be constructed [8.74].

### 8.5.1 HVDC Networks

Two different converter technologies are available for HVDC transmission: line commutated converter (LCC) and voltage source converter (VSC) technology. For LCC HVDC,  $\pm 800$  kV HVDC transmission systems for up to 8 GW have been implemented in China and in India using converters based on thyristors, and  $\pm 1100$  kV UHV DC transmission is under investigation in China. For VSC HVDC, a  $\pm 320$  kV HVDC transmission system for up to 1000 MW using converters based on insulated-gate bipolar transistor (IGBT) devices was brought on-line in 2015.

Multiterminal HVDC networks must continuously operate healthy transmission lines even when a fault occurs at the remote end of the HVDC network. Rapid fault clearing is a prerequisite for a DC circuit breaker because a voltage collapse will spread across the network due to the lower impedance in a HVDC system than in an AC system. The fault clearing time varies depending on the system conditions, including:

1. The DC transmission system configuration
2. The VSC design
3. The transmission capacity
4. Whether a DCL reactor is connected in series with the line/cable
5. The impedance of the line/cable.

As information technology develops, it may become possible to use CSS for fault current interruption, the uprating of modern and aged circuit breakers, and compensated line autoreclosure with a reduced number of surge arresters in the future. Furthermore, data from the monitoring of circuit breakers by the controller could be used for remote diagnostics and condition-based maintenance to further improve equipment reliability and optimize maintenance practice.

Applications of DC circuit breakers in multiterminal HVDC networks are still limited, but available information on DC circuit breakers intended for future HVDC applications is described below [8.75].

### 8.5.2 Current Zero Creation Schemes for DC Circuit Breakers

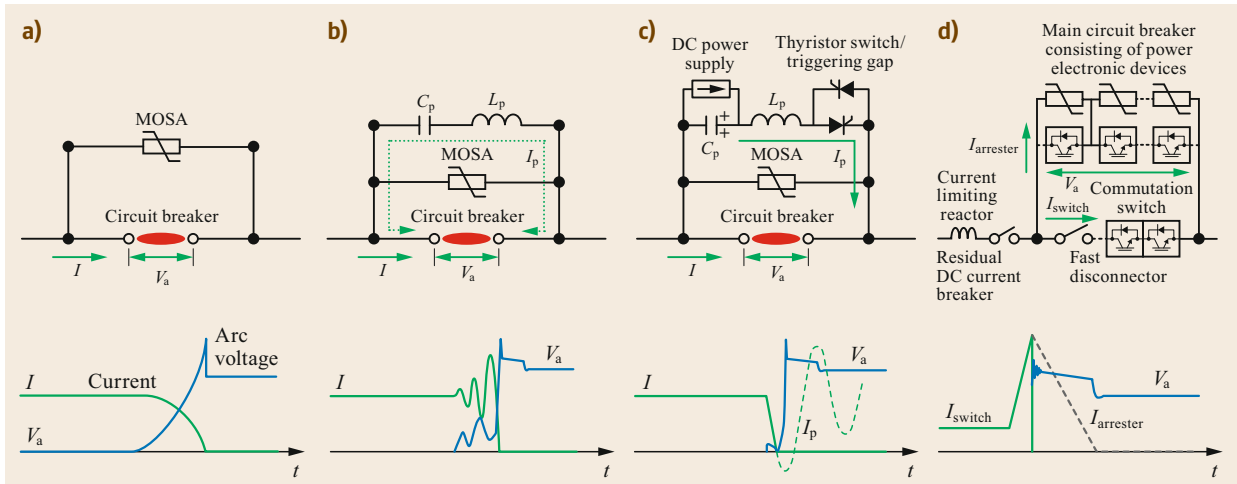
Any DC circuit breaker requires a current zero creation scheme to interrupt the DC fault current because DC current does not have periodic current zeros, in contrast to AC current. Figure 8.147 shows typical current zero creation schemes that can force the creation of a zero current crossing.

#### (a) Arc Voltage Current Limiting Scheme

Here, the DC current is limited to current zero by increasing the arc voltage induced between the contacts of a circuit breaker. The circuit breaker is required to induce an arc voltage that is higher than the system voltage in order to create the current zero. This scheme is often applied to a low-voltage-class DC no-fuse breaker (NFB). For example, a 2 kV air-blast type high-speed switch is used for industrial and railway power systems. Even though a DC circuit breaker that uses this scheme can interrupt a large current of up to 100 kA, it can be difficult to design HV DC circuit breakers that use this scheme because the arc voltage induced by air or SF<sub>6</sub> across the contacts of the circuit breaker is limited to several kV at maximum. This scheme is also applied to most DC disconnecting switches and DC earthing switches used in HVDC LCC and VSC networks.

#### (b) Passive Resonant Current Zero Creation Scheme

In this scheme, a small oscillatory perturbation in the DC current caused by contact separation continues to grow in amplitude until it eventually produces a current zero. The interaction between the arc and the parallel



**Fig. 8.147a–d** DC circuit breakers with different current zero creation schemes. (a) Arc voltage current limiting scheme, (b) passive resonant current zero creation scheme, (c) active resonant current zero creation scheme with current injection, (d) hybrid mechanical and power electronic switch

capacitor and reactor connected across the DC circuit breaker generates an expanding current oscillation with a frequency range of 1–3 kHz. A circuit breaker that can generate a high arc voltage across the contacts (e.g., air) is advantageous when attempting to create a rapidly growing oscillation. A larger capacitance can also facilitate a rapidly expanding oscillation, and there is an optimal reactance to achieve this too. This scheme is often applied to metallic return transfer breakers (MRTBs), which clear faults generated on the neutral return line due to a lightning stroke and commute currents of up to a few thousand amperes to the neutral line in the HVDC transmission line after fault clearing. This scheme generally requires 20–40 ms to create a current zero for a fault interruption of a few thousand amperes.

#### (c) Active Resonant Current Zero Creation Scheme (Active Current Injection Scheme)

This scheme utilizes an external voltage source that can inject a high-frequency reverse current with respect to the DC current, immediately creating a current zero. The external voltage source consists of a precharged capacitor with a reactor and a high-speed switch (e.g., a thyristor switch, a triggering gap, or a mechanical switch) imposes a high-frequency (several kHz) inverse current on the interrupting fault and nominal DC current. This scheme is potentially applicable to the interruption of HV DC fault currents in multiterminal HVDC networks, even though a large capacitor is required in accordance with the DC system voltage. A prototype HV DC circuit breaker that uses this scheme with a HV AC vacuum interrupter has been shown to interrupt faults in up to 16 kA DC within 8–10 ms.

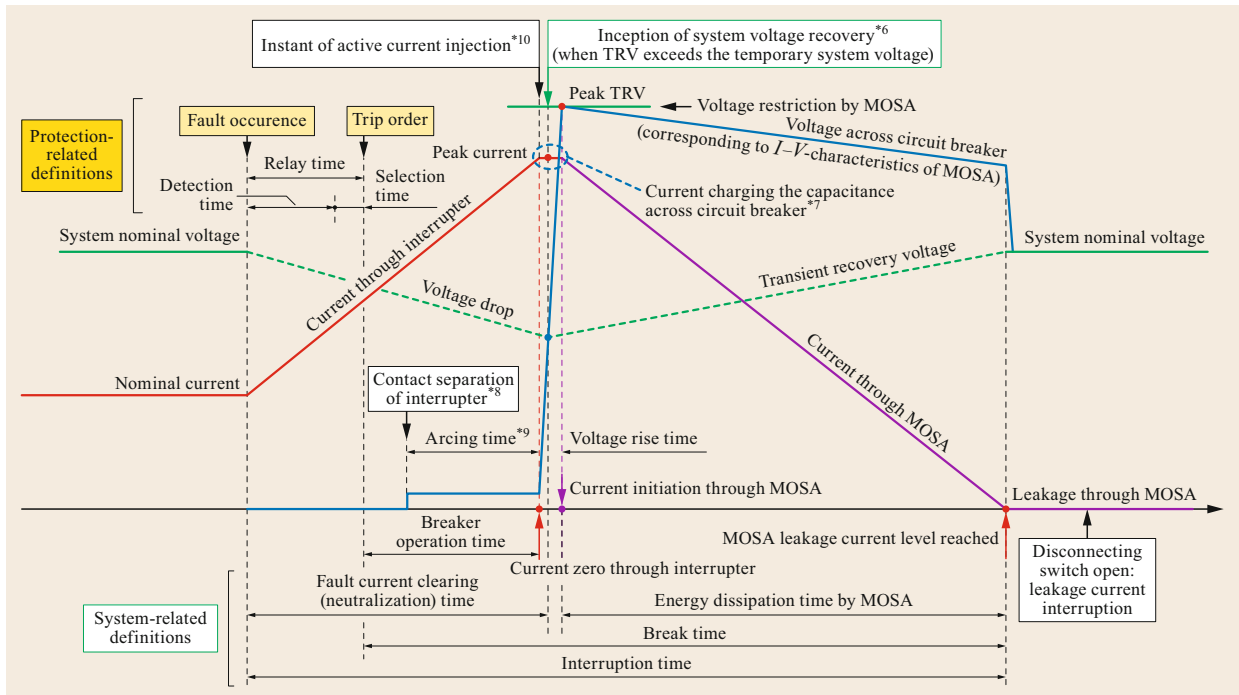
#### (d) Hybrid Mechanical and Power Electronic Switch

This breaker is composed of both mechanical switches and power electronic (semiconductor) devices. The DC circuit breaker commutates the DC fault current from the main circuit, consisting of a high-speed mechanical switch and a commutating power electronic device, to series- and parallel-connected power electronic (IGBT) devices that can block the current within a few ms. A prototype 230 kV DC circuit breaker that was placed in service in multiterminal HVDC networks in China and a 500 kV DC circuit breaker were shown to interrupt 25 kA DC in less than 3 ms. Due to the rapid progress in high-voltage, large-capacity, and low-loss power electronic device technology, this scheme may be applied to AC circuit breakers in the future.

### 8.5.3 DC Current Interruption

Figure 8.148 shows the typical voltage and current behavior during a DC fault current interruption using a mechanical DC circuit breaker with active current injection.

When a fault occurs in a DC system, the fault current through the interrupter unit increases and the system voltage starts to drop. After fault detection, a trip command is issued to the DC circuit breaker and an interrupting unit (typically a vacuum interrupter) starts to open the electrodes. As soon as the vacuum interrupter has secured a sufficient contact gap, the active resonant current injection circuit imposes a high-frequency current with a reversed polarity on the DC current and immediately creates a current zero. When



**Fig. 8.148** Voltage and current behavior during DC current interruption using a mechanical DC circuit breaker with an active current injection scheme. Notes: \*<sup>6</sup> The voltage recovery is initiated when the voltage across the breaker (TRV) exceeds the temporary system voltage. The current through the MOSA is initiated when the TRV is clipped at the restriction voltage by the MOSA. \*<sup>7</sup> The time taken to charge the capacitance across the DC circuit breaker. The capacitance required for active current injection by a mechanical DC circuit breaker is on the order of microfarads. \*<sup>8</sup> The specially designed mechanical DC breaker requires a few milliseconds to open the electrodes (or separate the contacts) after receiving a trip order. \*<sup>9</sup> The arc voltage across the vacuum interrupter is almost constant after contact separation regardless of the contact gap. \*<sup>10</sup> The fault current through the vacuum interrupter is forced to make a current zero at the instant of active current injection, and the vacuum interrupter can immediately interrupt this high-frequency current

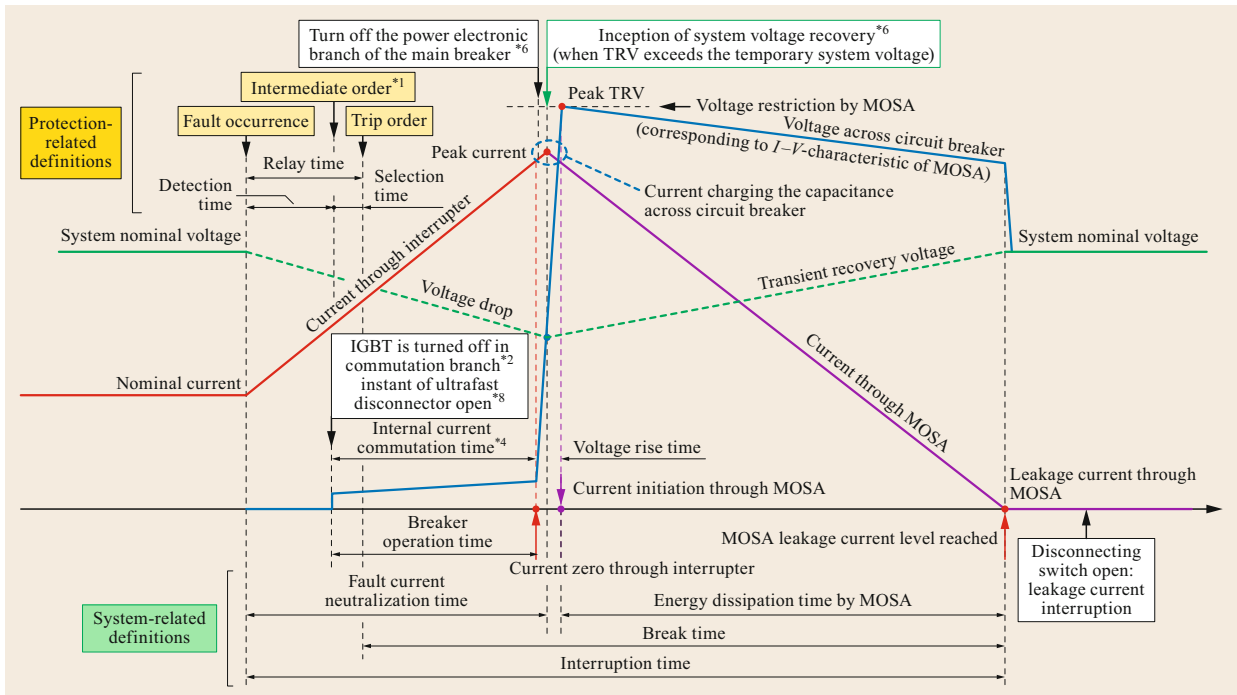
the vacuum interrupter can interrupt the high-frequency current, the voltage across the DC circuit breaker suddenly increases and exceeds the system voltage. It is then clipped (limited) by the MOSA restriction voltage (which is typically 1.5 times higher than the system voltage). The transient system voltage begins to recover to the nominal voltage and the MOSA dissipates the energy stored by the inductance in the DC system.

In contrast, Fig. 8.149 shows the typical voltage and current behavior during a DC fault current interruption using a hybrid mechanical and power electronic DC circuit breaker with IGBT devices.

In this case, when a fault occurs in a DC system, the fault current through the interrupter unit increases and the system voltage starts to drop as described before. After fault detection, an intermediate order is issued to turn off the load-commutating IGBT devices in order to commutate the current to the power electronic branch (power electronic interrupter unit, which consists of many IGBT devices connected in series and parallel), and an ultra-

fast disconnecting switch connected to the main circuit opens the commutation branch. When the current starts to commutate to the power electronic branch, the voltage across the hybrid DC circuit breaker increases with the current due to the resistance of the power electronic devices. When a trip command is issued after the current has been fully commutated, the power electronic branch turns off all of the IGBT devices and blocks the current. After the current has been blocked, the voltage across the DC circuit breaker suddenly increases and exceeds the system voltage. Then the voltage across the DC circuit breaker is clipped at the restriction voltage by the MOSA. The transient system voltage begins to recover to the nominal voltage and the MOSA dissipates the energy stored by the inductance in the system.

Figure 8.150 shows a magnified plot of the voltage and current behavior from the instant that there is a current zero through the interrupter branch until the instant that the voltage across the DC circuit breaker is clipped by the MOSA. The capacitance (stray capacitance when



**Fig. 8.149** Voltage and current behavior during DC current interruption using a hybrid mechanical and power electronic DC circuit breaker. Notes: <sup>\*1</sup> Any order before the order to start the interruption process (such as operations referred to in notes <sup>\*2</sup> and <sup>\*3</sup>). <sup>\*2</sup> The instant at which the load-commutating IGBT devices are turned off immediately after fault detection. The voltage across the hybrid DC breaker increases with the current. <sup>\*3</sup> The instant at which the ultrafast disconnecter in the commutation branch (main circuit) is opened. <sup>\*4</sup> The time required to commutate the fault current from the commutation branch using the load-commutating IGBT devices to the power electronic branch of the main breaker. <sup>\*5</sup> The instant at which the power electronic branch in the main breakers is turned off, which immediately blocks and interrupts the current after a time delay to secure the voltage withstand of the ultrafast disconnecter. <sup>\*6</sup> The voltage recovery is initiated when the voltage across the breaker (TRV) exceeds the temporary system voltage. Current flow through the MOSA is initiated when the TRV is clipped at the restriction voltage by the MOSA. <sup>\*7</sup> The stray capacitance across the DC circuit breaker is charged during the period of rising voltage. <sup>\*8</sup> The specially designed mechanical DC breaker requires a few milliseconds to open the electrodes (or separate the contacts) after receiving a trip order

using the hybrid DC circuit breaker) across the DC circuit breaker begins charging when the current is forced to the current zero by either current injection or current blocking.

During the charging of the capacitor, the current that charges the capacitance is almost constant and the voltage starts to recover. When the recovery voltage attains the restriction voltage imposed by the MOSA, the charging current to the capacitance stops, and the current through the MOSA is initiated and then gradually decreases in accordance with the  $I-V$  characteristic of the MOSA unit.

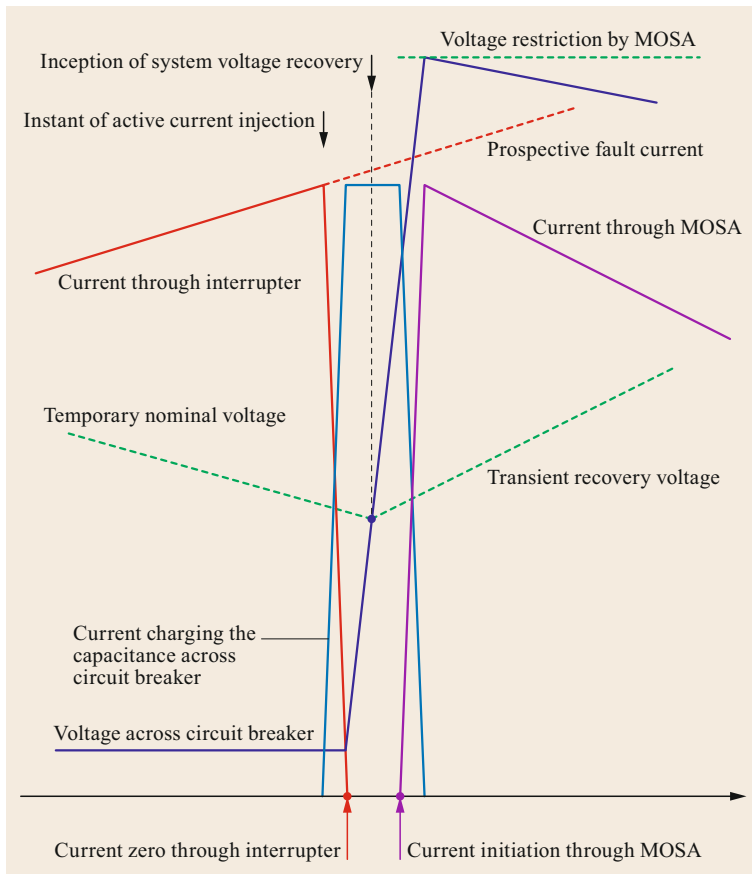
#### 8.5.4 MV and LVDC Circuit Breakers

Figure 8.151 shows a 480 V, 10 kA DC circuit breaker (a molded case circuit breaker, MCCB) that employs

the arc voltage current limiting scheme and is used in industrial applications. When the arc voltage between the electrodes of the MCCB is higher than the system voltage, it limits the current and rapidly creates a current zero for about 5 ms. Figure 8.152 shows an example of the current behavior during DC current interruption (where  $t_1$  is the time to the MCCB trip current level,  $t_2$  is the contact separating time,  $t_3$  is the time from contact parting to peak current,  $t_4$  is the arcing time,  $t_T$  is the total interruption time, and  $q$  is the rate of rise of the current).

Figure 8.153 shows a 1500 V DC circuit breaker used in track power systems that employs the active resonant current zero creation scheme and has an interrupting capability of up to 100 kA. It is equipped with a thyristor switch to impose a reverse current from an external DC power source onto the DC fault cur-





**Fig. 8.150** Voltage and current behavior from the instant at which there is a current zero through the interrupter until MOSA activation

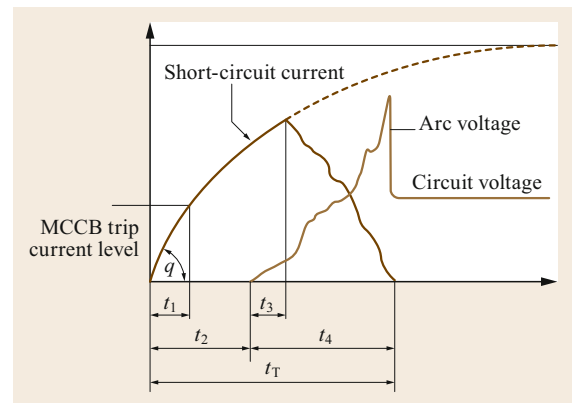
rent and immediately create a current zero. Figure 8.154 shows typical oscillograms obtained when the DC circuit breaker interrupts the fault current within a few milliseconds. After the vacuum interrupter has interrupted a high-frequency current at the current zero, the

voltage recovers to the system voltage and the MO surge arrester dissipates the energy in the circuit.

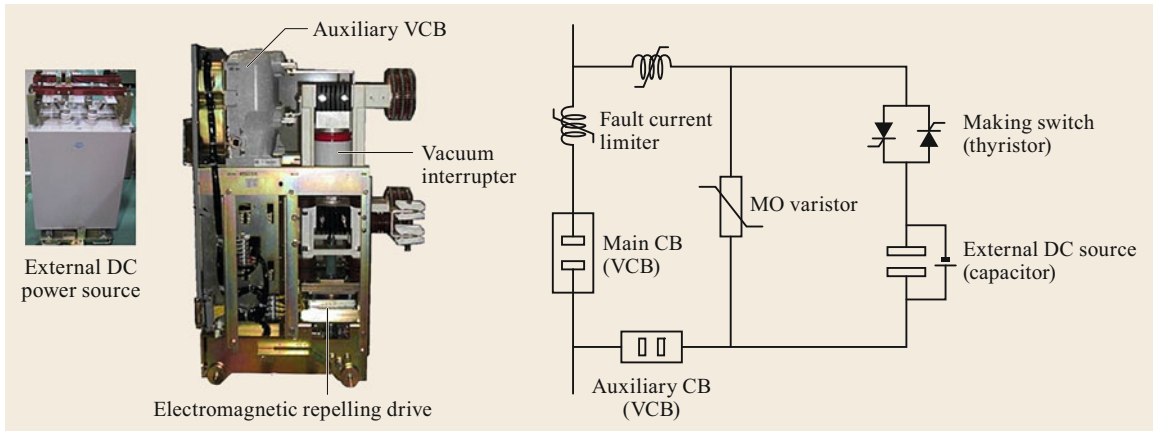
Figure 8.155 shows a 550 kV, 2200 A DC circuit breaker that uses the passive resonant current scheme (often termed MRTB; this breaker is used in the Pacific



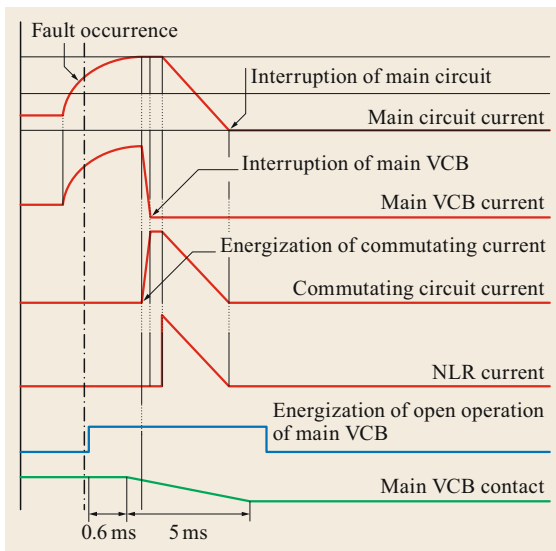
**Fig. 8.151** LV DC circuit breakers that use the arc voltage current limiting scheme. (Courtesy of Mitsubishi Electric)



**Fig. 8.152** Oscillograms showing the behavior of the current during an interruption performed by a LV DC circuit breaker using the arc voltage current limiting scheme



**Fig. 8.153** MV DC circuit breakers that use the active resonant current zero creation scheme, along with the relevant circuit diagram



**Fig. 8.154** Oscillograms showing the behavior of the current during an interruption performed by a MV DC circuit breaker using the active resonant current zero creation scheme

DC Intertie in the United States) [8.76]. This breaker can clear a DC fault generated in a neutral line by performing a closing operation and commutating the current back to the neutral line after fault clearing. Figure 8.156 presents oscillograms showing typical current and voltage behavior during the expansion of the current oscillation that is used to create the current zero.

### 8.5.5 Behavior When Using the Passive Current Creation Scheme

When using the passive resonant current zero scheme, a DC current interruption is initiated by separating the

arcing contacts. A change in the state of the arc during interruption (e.g., a local extension or short circuit of the arc caused by the gas flow) manifests as small perturbations of the arc voltage and arc current, which continue to grow when the circuit conditions are unstable and eventually lead to a current zero.

The influence of small perturbations of the arc voltage and arc current on current oscillation can be evaluated through a combined analysis of the interruption circuit and a mathematical model of the arc. An example of an investigation of the expanding current oscillation phenomenon in case of the passive resonant current zero creation scheme, and the optimization of the inductance and capacitance connected in parallel with the circuit breaker can be evaluated by the simulation with a mathematical arc model.

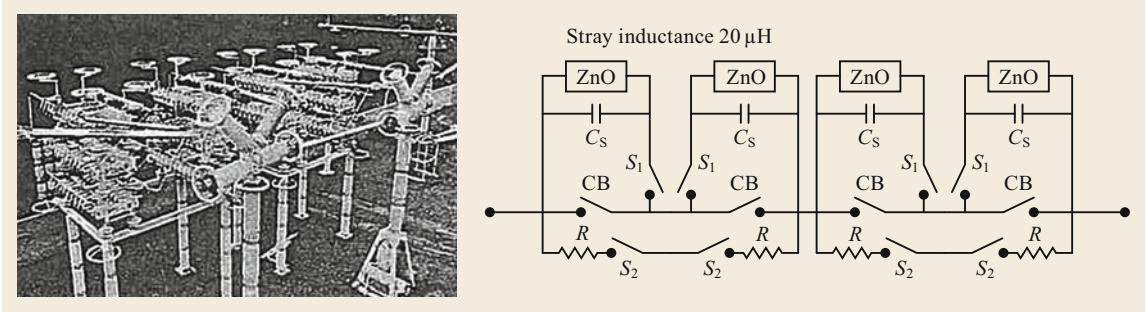
The Mayr arc model has two parameters (the time constant of the arc  $\theta$  and the arc power loss  $n$ ) that express the exchanging sensitivity (energy balance of the arc) of thermal energy between the arc and the gas around it (see Eq. (8.7) below). In addition, using the circuit shown in Fig. 8.157 for a DC circuit breaker that utilizes the passive resonant current zero scheme, the behavior of the arc voltage ( $v_a$ ) and the arc current ( $i_a$ ) in the DC circuit breaker can be expressed as in (8.7–8.10), and their behavior in the circuit can be expressed via (8.8–8.10)

$$\frac{dr_a}{dt} = \frac{r_a}{\theta} \left( 1 - \frac{v_a i_a}{n} \right), \quad (8.7)$$

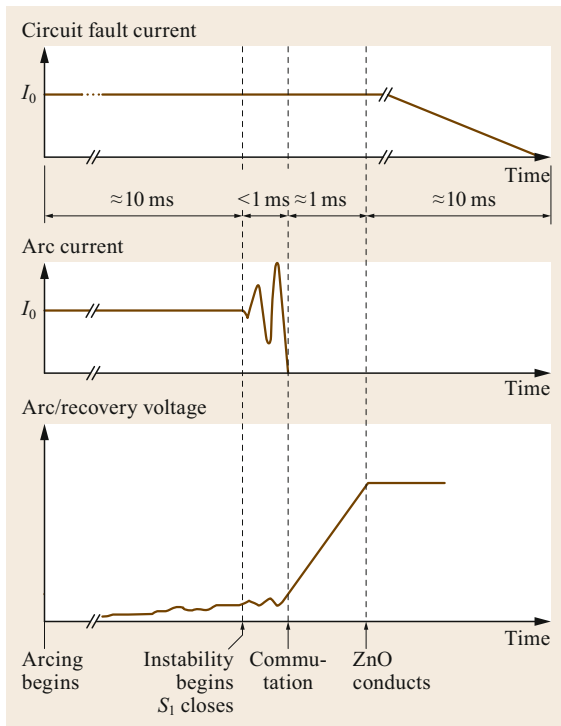
$$\frac{dv_e}{dt} = \frac{i_0 - i_a}{C_e}, \quad (8.8)$$

$$L_e \frac{d(i_0 - i_a)}{dt} = v_a - v_e - r_e (i_0 - i_a), \quad (8.9)$$

$$v_a = r_a i_a. \quad (8.10)$$



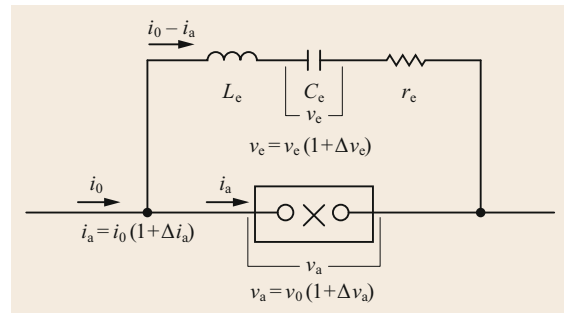
**Fig. 8.155** Photograph of HV DC circuit breakers that use the passive resonant current zero creation scheme, and the relevant circuit diagram [8.76]



**Fig. 8.156** Oscillograms showing the behavior of the current during an interruption performed by a HV DC circuit breaker using the passive resonant current zero creation scheme [8.76]

In these equations,  $i_a$ ,  $r_a$ ,  $L_c$ ,  $C_c$ , and  $r_c$  represent the interruption current, arc resistance, parallel reactance, parallel capacitance, and stray resistance, respectively.  $v_c$  is the voltage across the capacitor. When the arc current  $i_a = i_0$  and the arc voltage  $v_a = n/i_0$ , (8.7) is balanced and the arc current and arc voltage remain constant.

The response to a small perturbation of the arc current  $\Delta i_a$  can be obtained via (8.7) to (8.10) using the



**Fig. 8.157** Circuit configuration for a DC circuit breaker that uses the passive resonant current zero scheme [8.77]

perturbation method, which yields

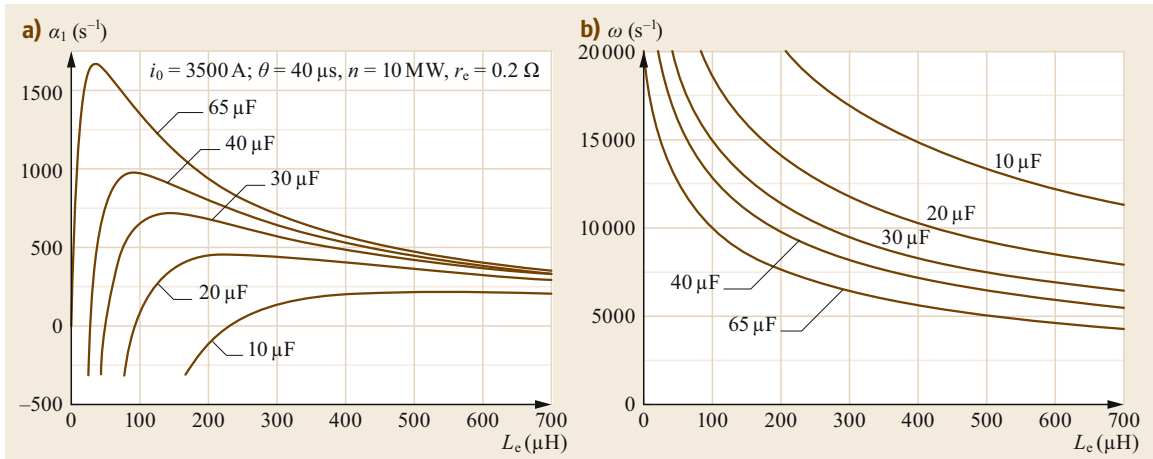
$$L_c \frac{d^3 \Delta i_a}{dt^3} + \left( \frac{L_c}{\theta} + r_c + \frac{n}{i_a^2} \right) \frac{d^2 \Delta i_a}{dt^2} + \left( \frac{r_c}{\theta} + \frac{1}{C_c} - \frac{n}{\theta i_a^2} \right) \frac{d \Delta i_a}{dt} + \frac{1}{\theta C_c} \Delta i_a = 0. \quad (8.11)$$

This differential equation has either three real solutions or one real and two complex solutions. When the differential equation has two complex solutions,  $\Delta i_a$  is an oscillatory mode. When the real part of the complex solution is positive, the solution  $\Delta i_a$  is unstable and the perturbation grows with continuing oscillation. When the differential equation has only real solutions,  $\Delta i_a$  is a nonoscillatory mode (it increases monotonically when at least one real solution is positive, and it decreases monotonically when all real solutions are negative).

An oscillatory mode is required for a DCCB that uses the passive resonant scheme. Assuming that differential (8.11) can be factorized as in (8.12) below, the general solution of (8.12) for an oscillatory mode is (8.13)

$$(p - \alpha_0)(p - \alpha_1 - j\omega)(p - \alpha_1 + j\omega) = 0, \quad (8.12)$$

$$\Delta i_a = \Delta_0 e^{\alpha_0 t} + \Delta_1 e^{\alpha_1 t} (\sin \omega t + \varphi). \quad (8.13)$$



**Fig. 8.158a,b** Calculated effects of the parallel inductor (reactor) and parallel capacitor on the amplification coefficient (a) and the angular frequency (b) of current oscillation

It can be shown that the amplification coefficient  $\alpha_1$  and the angular frequency  $\omega$  can be expressed as the function with six parameters ( $C_c$ ,  $L_c$ ,  $r_c$ ,  $n$ ,  $\theta$ , and  $i_0$ ). When the arc parameters  $n$  and  $\theta$ , the interruption current  $i_0$ , and the stray resistance  $r_c$  are constant, the relationships of the amplification coefficient  $\alpha_1$  and the angular frequency  $\omega$  to the passive resonant circuit parameters  $C_c$  and  $L_c$  can be obtained.

Figure 8.158 shows the calculated effects of varying the parallel reactance and parallel capacitor on the amplification coefficient and the angular frequency of the current oscillation under specified circuit conditions (interruption current  $i_0 = 3500$  A, stray resistance  $r_c = 0.2 \Omega$ , arc time constant  $\theta = 40 \mu\text{s}$ , and arc power loss  $n = 10$  MW). This figure indicates that, for a given capacitance, there is an optimum reactance at which the amplification coefficient is maximized. Also, the angular frequency  $\omega$  decreases as the circuit parameters  $C_c$  and  $L_c$  increase.

To ensure that the current oscillation grows and eventually produces a current zero,  $C_c$  and  $L_c$  must be selected such that the amplification coefficient becomes positive. For example, when the capacitance is  $30 \mu\text{F}$ , more than  $50 \mu\text{H}$  of parallel reactance is required, although increasing the parallel reactance also increases the time until current zero.

A circuit breaker has a limited arc time (less than about 30 ms) to enable interruption, which does not depend on the interruption scheme used (double-pressure type or single-pressure type). Therefore, it necessary to find a combination of parallel reactance and capacitance that causes the oscillation to produce a current zero within the limited arc time to facilitate interruption.

Figure 8.159a shows the arc voltage and arc current waveforms obtained during an interruption test of

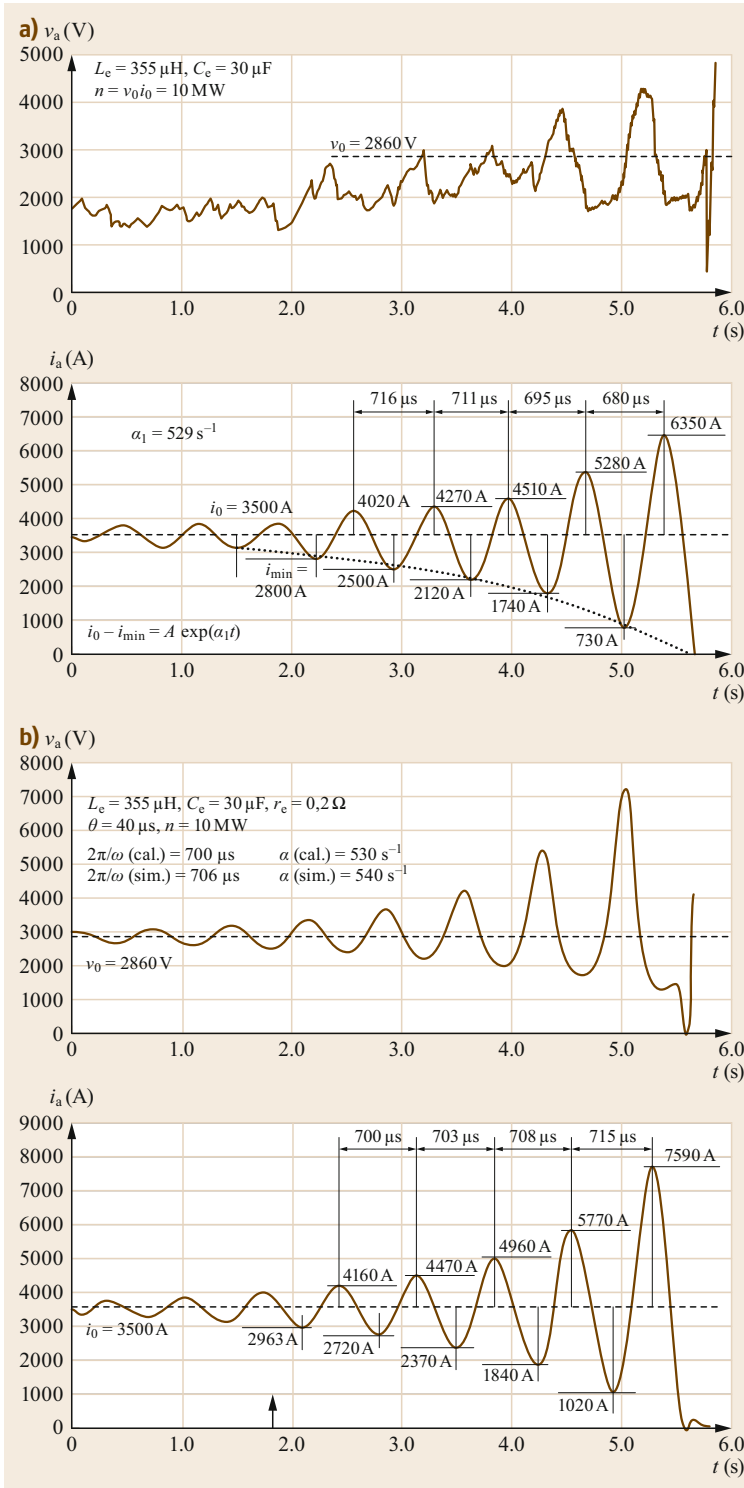
a DC current generation circuit consisting of a three-phase rectifier circuit and a smooth reactor. In this case, the interruption current was 3500 A, and the parallel reactance  $L_c$  and capacitance  $C_c$  were  $350 \mu\text{H}$  and  $30 \mu\text{F}$ , respectively. The stray resistance was  $0.2 \Omega$ . The model breaker was a puffer-type  $\text{SF}_6$  gas circuit breaker. The arc power loss from the arc voltage and interruption current was 10 MW, and the arc constant  $\theta$  estimated from the amplification coefficient and angular frequency was  $40 \mu\text{s}$ . Figure 8.159b shows the calculated waveform, which accurately reproduces the observed waveform shown in Fig. 8.159a. It can be seen that the calculated result reproduces both the amplification coefficient and the angular frequency of the test waveform well.

### 8.5.6 Field Experience of MRTB

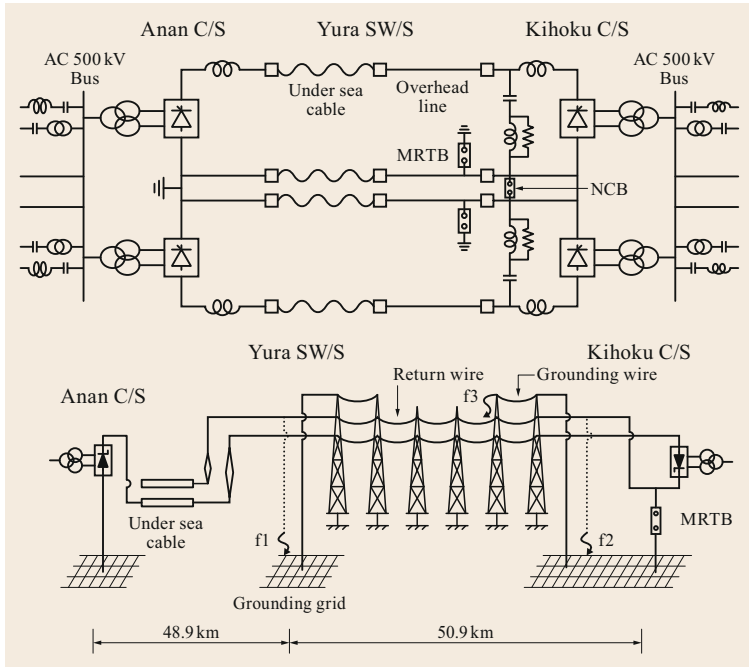
When a DC fault occurs at one pole of a bipolar HVDC system, the operational mode should be shifted from bipolar operation to monopolar operation. In some applications, monopolar operation also requires a switch from ground return to metallic return using the faulted transmission line.

The MRTB connected to the neutral metallic return line is used to clear a DC grounding fault by performing a closing operation. The return current is split into two paths: the ground return and the ground wire. Since the MRTB is directly earthed to the grounding mesh, connection to the MRTB reduces the voltage between the fault point on the neutral line to the ground. Accordingly, an arc generated due to a lightning strike cannot maintain its voltage and the current is rapidly reduced to current zero.

After clearing the DC fault, the MRTB is opened to commutate the current to the neutral metallic re-



**Fig. 8.159a,b** Comparison of the experimental (a) and simulated (b) current and voltage behavior of a MRTB



**Fig. 8.160** Bipolar HVDC system with neutral metallic return lines [8.78]

turn line and thus return to healthy bipolar operation. Figure 8.160 illustrates the system configuration of a real-world bipolar HVDC system with two neutral metallic return lines. Each pole can be operated independently to ensure continued power transmission during maintenance work on one pole or a fault occurrence in one of the metallic transmission lines.

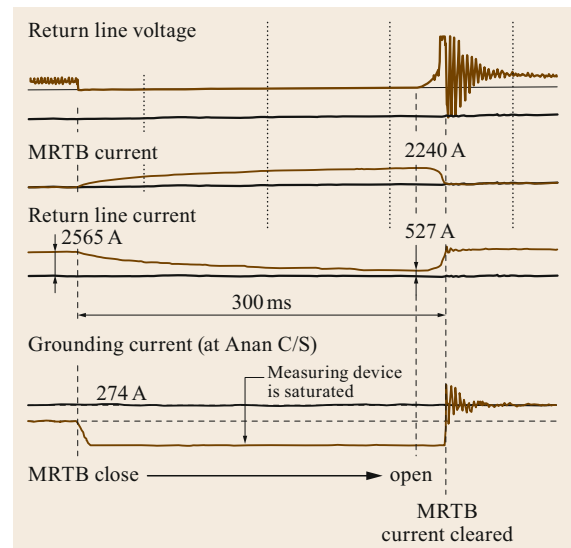
Since the MRTB was first installed in 2000, it has been operated more than 300 times, successfully clearing faults in the neutral line. Figure 8.161 shows an oscillogram obtained when a lightning fault occurred at a transmission tower about 18 km from C/S (converter station). It can be seen that the return line current drops and is commuted to the MRTB. Furthermore, the MRTB interrupts the commuted current 300 ms after closing, and then the return line voltage recovers and the system returns to a healthy condition.

### 8.5.7 Application of the Active Resonant Current Injection Scheme in HVDC Circuit Breakers

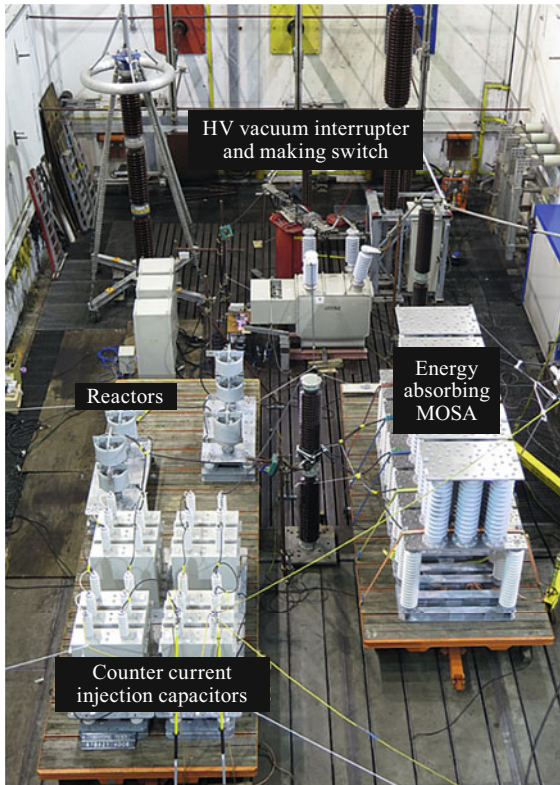
A mechanical DC circuit breaker consisting of a HV vacuum interrupter with a rapidly operating mechanism was tested with currents of up to 16 kA [8.80]. In this circuit breaker, the active resonant current zero creation scheme superimposes the high-frequency current with the reverse polarity (as compared with the polarity of DC current) on the DC current to create a zero current on the DC fault current, which was achieved by dis-

charging a precharged capacitor connected in parallel with the interrupter. The MOSA unit of the DC circuit breaker was designed to dissipate up to 4 MJ of energy after current interruption.

Figure 8.162 shows the HVDC circuit breaker test conducted at the KEMA laboratory as a part of the research and innovation program known as the Horizon 2020 project, funded by the European Union under



**Fig. 8.161** MRTB operation during a lightning fault at a transmission tower



**Fig. 8.162** Photograph of the setup for a HVDC circuit breaker test conducted at the DNV GL/KEMA laboratories [8.79]

grant agreement no. 691714 [8.79]. Figure 8.163 shows a schematic of the test circuit of the DC circuit breaker.

The active resonant circuit consisted of a capacitor ( $C_p$ ) as well as a reactor ( $L_p$ ), a spark gap, and a MOSA that were connected in parallel to  $C_p$ . For the DC circuit breaker interruption tests, the discharge time of the precharged  $C_p$  (kept at a constant applied voltage) had a delay of only a few ms following con-

tact separation of the vacuum interrupter. The active resonant discharge created a current zero by superimposing a high-frequency inverse current injected by the series-connected capacitance  $C_p$  and reactance  $L_p$ . The interrupting current was supplied by an AC current source that provided an equivalent DC current when the DC circuit breaker interrupted a peak current from a power-frequency short circuit.

Test conditions were determined in accordance with the dielectric requirements for a high-voltage AC circuit breaker, and the DC interrupting currents ranged from 0.5 kA (corresponding to the nominal current) up to 16 kA.

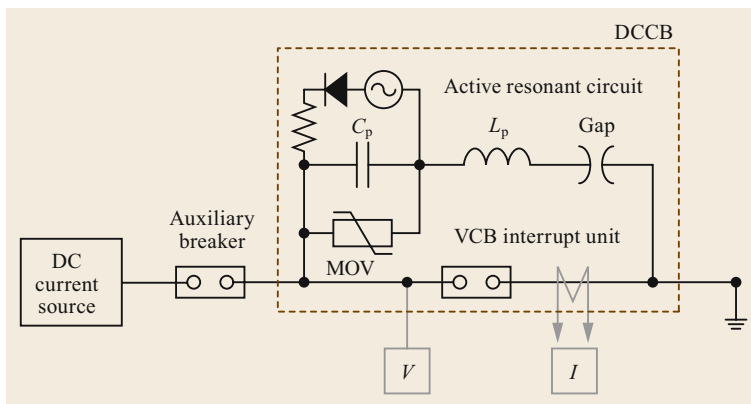
Figure 8.164 shows the full test-sequence waveforms and magnifications of those waveforms recorded during interruption tests on the DC circuit breaker using interrupting currents of 16 and 5 kA. Tests showed that the DCCB successfully interrupted the first current zero created by an injected current when it was used to interrupt currents of 16 and 5 kA.

The rate of rise of the recovery voltage (given by  $L_p di/dt$ ) becomes steeper as the interrupting current decreases. The overvoltage generated after interruption is determined as

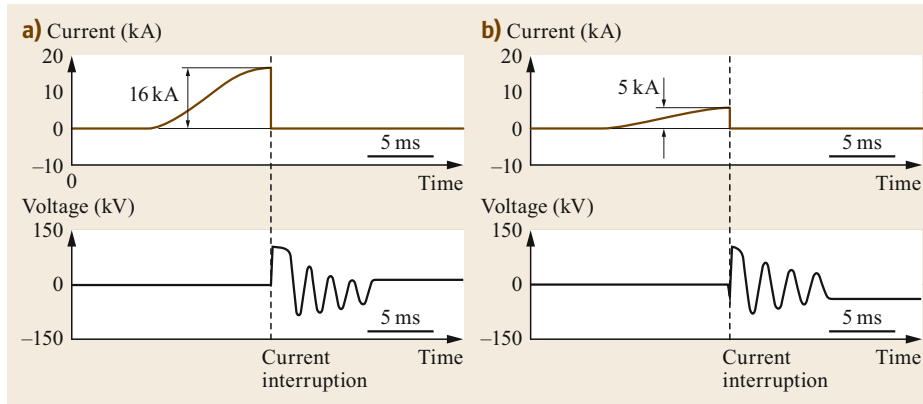
$$V_p = k \sqrt{\frac{L_s}{C_p}} I, \quad (8.14)$$

where  $L_s$  is the inductance of the source circuit,  $C_p$  is the capacitor connected in parallel with the interrupter unit,  $I$  is the breaking current, and  $k$  ( $< 1$ ) is a damping factor caused by stray resistance of each component of the circuit. Therefore, the overvoltage ( $V_p$ ) increases with increasing breaking current  $I$ , but it is limited by the restriction voltage of the MOSA connected in parallel to  $C_p$ .

During a CIGRE session in 2018, China reported the application of a 160 kV, 9 kA mechanical DC circuit breaker with active resonant current injection to



**Fig. 8.163** Test circuit for a DC circuit breaker utilizing the active resonant current zero creation scheme



**Fig. 8.164a,b** Voltage and current behavior of DC CB with current injection scheme tested at interrupting currents of DC 16 and 5 kA



**Fig. 8.165** Photograph of a 160 kV, 9 kA mechanical DC circuit breaker with current injection [8.81]

three terminal HVDC grids (Fig. 8.165). They also conducted an artificial grounding test and confirmed that the DC circuit breaker was able to clear a 1.4 kA DC fault within 3.5 ms.

### 8.5.8 Hybrid Mechanical and Power Electronic Switch

The configuration of a hybrid mechanical and power electronic switch is shown in Fig. 8.166 [8.82]. This type of DC circuit breaker consists of a load com-

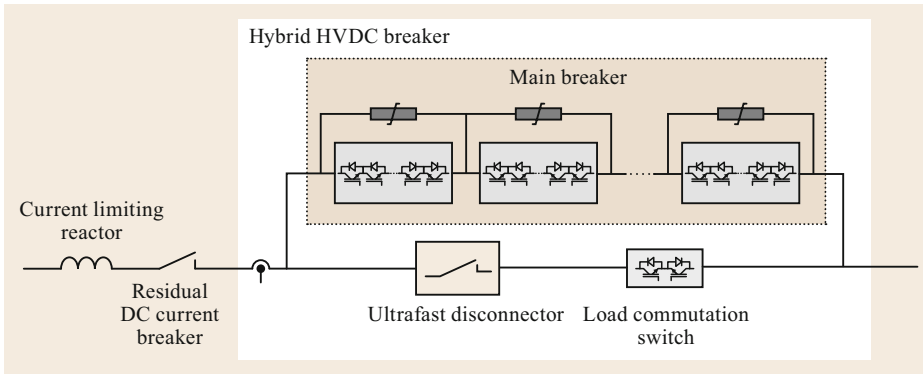
mutation switch, an ultrafast disconnecter, and a main breaker branch. The load commutation switch has a few power electronic devices. This switch can rapidly commute the DC current to the main breaker branch after receiving a trip command. The ultrafast disconnecter is a fast-opening mechanical switch that isolates the load commutation switch from the main breaker during interruption. The main breaker consists of a large number of power electronic devices (IGBTs) connected in series and in parallel. MOSAs are connected in parallel across the main breaker branch to limit the overvoltage after the main breaker interruption.

Figure 8.167 shows the sequence of operations for this type of DC circuit breaker. During normal operation, the load current flows through the load commutation switch and ultrafast disconnecter (Fig. 8.167a). Since the few power electronic devices in the load commutation switch are small and the ultrafast disconnecter is a mechanical switch, the on-state loss from this current path is relatively low.

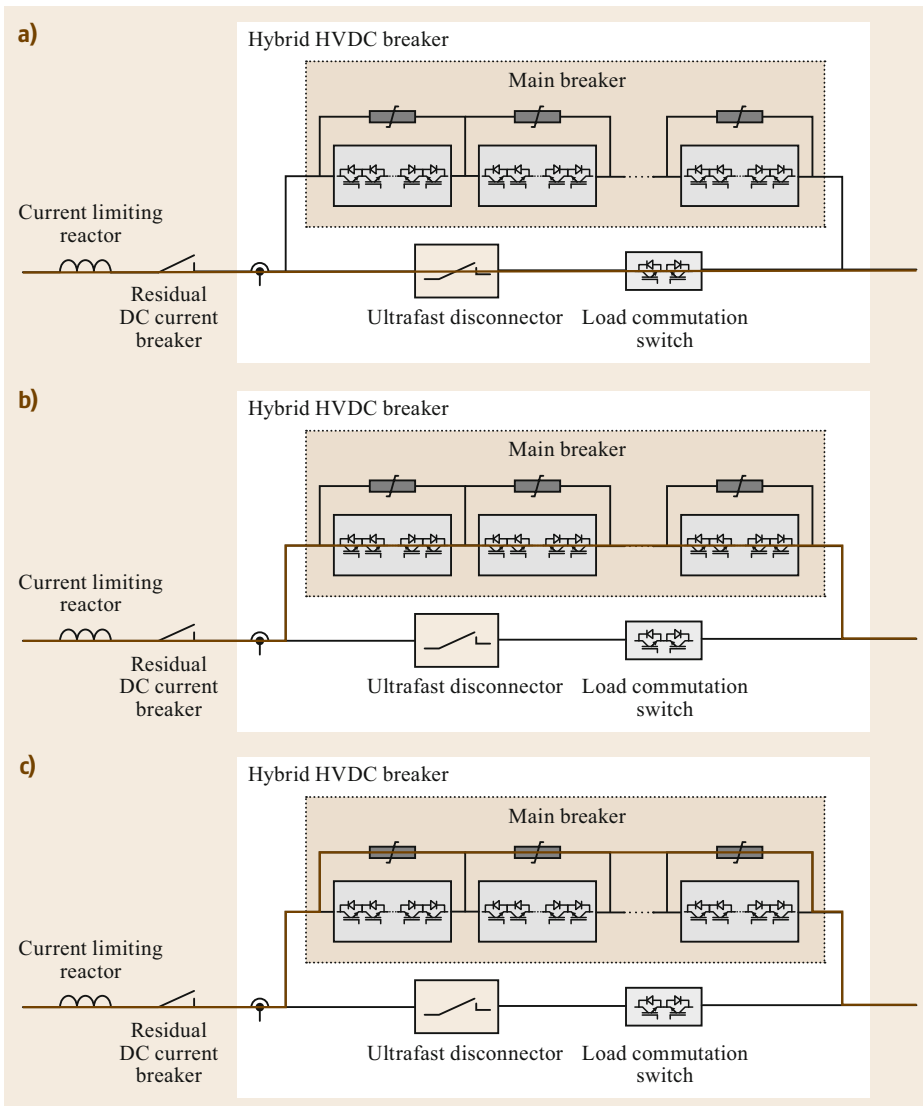
When the DC circuit breaker receives a trip command, the load commutation switch turns off, which commutates current into the main breaker branch (Fig. 8.167b). After current commutation, the ultrafast disconnecter opens. The power electronic devices in the main breaker branch are turned off after a time delay determined by the time needed for the ultrafast disconnecter to achieve the required voltage withstand. Upon turning the main breaker off, the current commutates to the MOSA and the MOSA dissipates energy (Fig. 8.167c). When the current reaches zero, the residual DC current breaker outside the DC breaker opens and interruption is completed.

Figure 8.168 shows test results for an 80 kV hybrid mechanical and power electronic switch. In this test, the DC circuit breaker interrupted a fault current of about 9 kA.





**Fig. 8.166**  
Configuration of a hybrid mechanical and power electronic switch [8.82]



**Fig. 8.167a–c**  
Operation of a hybrid mechanical and power electronic DC circuit breaker. (a) Current through the commutation branch, (b) current through the main breaker branch, (c) current through the MOSA

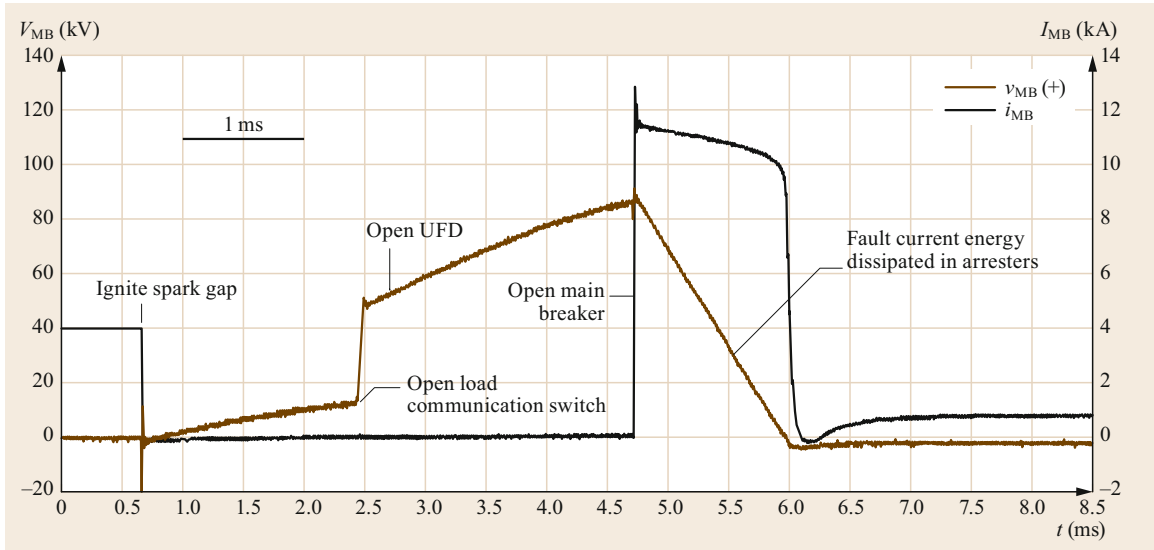


Fig. 8.168 Test results for a hybrid mechanical and power electronic DC circuit breaker [8.82]

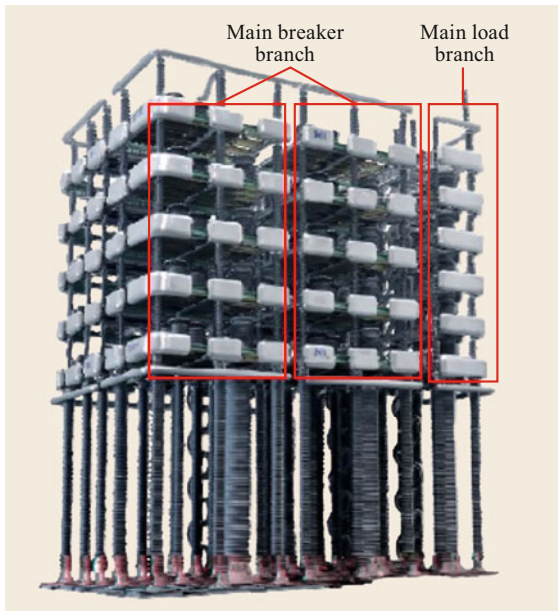


Fig. 8.169 Photograph of a 535 kV, 26 kA DC circuit breaker (a hybrid mechanical and power electronic switch). (Courtesy of NR Electric, State Grid Corporation of China)

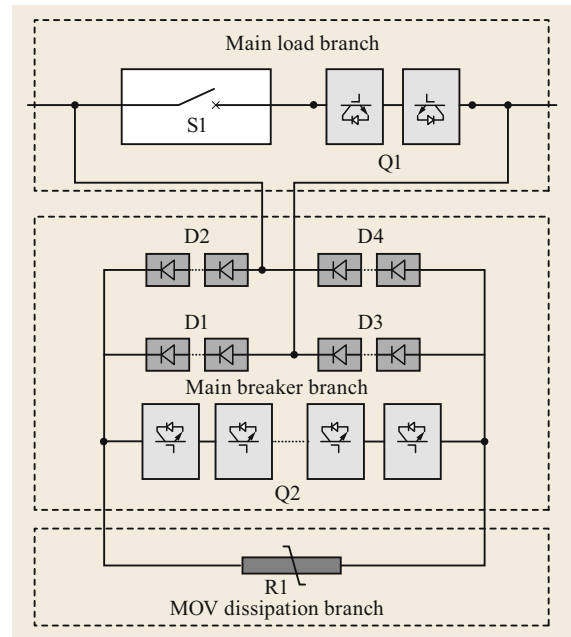
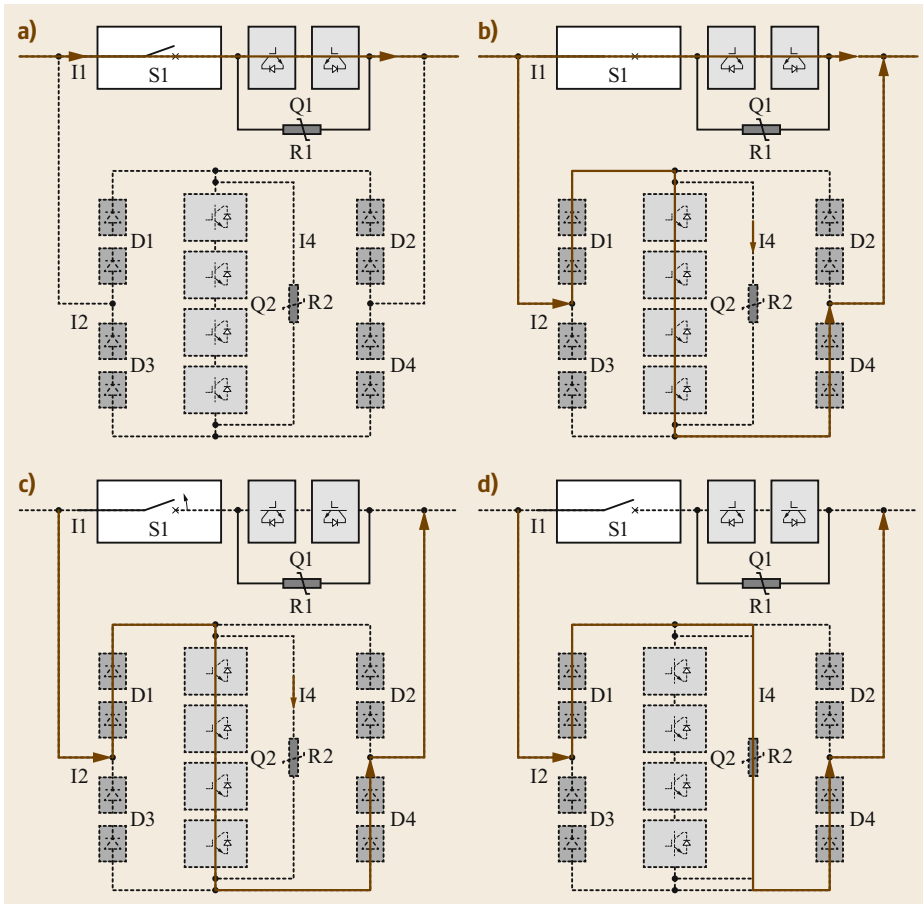


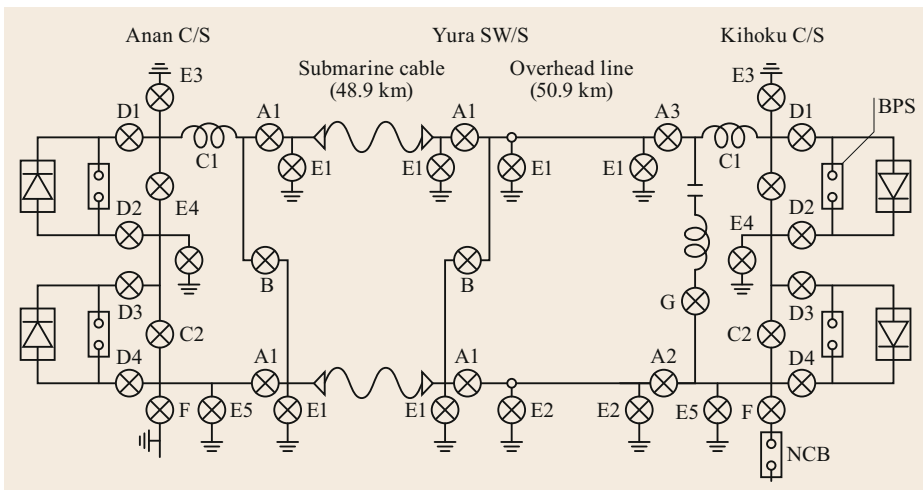
Fig. 8.170 Configuration of the hybrid 500 kV DC circuit breaker

Figure 8.169 shows a photograph of a prototype 535 kV, 26 kA hybrid mechanical and power electronic DC circuit breaker [8.83], and Fig. 8.170 shows its configuration. The hybrid HVDC circuit breaker consists of a main load branch and a main breaker branch. The main load branch includes a fast mechanical switch and an IGBT commutation module. The main breaker

branch consists of series-connected IGBT modules with several diodes and an energy-dissipating MOSA connected in parallel. Figure 8.171 shows the DC current interruption process for the 535 kV DC circuit breaker. A prototype 220 kV hybrid mechanical and power electronic DC circuit breaker of this design has already been installed in a multiterminal HVDC grid in China [8.84].



**Fig. 8.171a–d** DC current interruption process for the 500 kV DC circuit breaker [8.70]. (a) Nominal current carrying (load) condition, (b) current is commutated from the load branch to the breaker branch, (c) current commutation to the breaker branch is completed, (d) the current is blocked by IGBT modules and energy is dissipated by the MOSA. (Courtesy of NR Electric, State Grid Corporation of China)



**Fig. 8.172** Example of a single-pole diagram of a HVDC disconnecting switch in a bipolar HVDC system. A: line switching DS, B: cable switching DS, C: valve bypass DS, D: valve switching DS, E: earthing switch, F: pole switching DS, G: filter switching DS

**Table 8.18** Main switching duties of disconnecting switches (DSs) used in bipolar HVDC systems

Switching duty	DS group in Fig. 8.172	Switching duty	Specification
Line discharging current switching	A1, A2, A3	Interrupt the line discharging current that flows through a snubber circuit in the converter resulting from charge remaining in the lines after the converter has been stopped.	HVDC 0.1 A
No-load line transfer current switching	B	Switch a circuit connected between a no-load positive line and a negative line when a phase-to-ground fault has occurred along the lines. The system is stopped prior to DS operation.	HVDC 0.1 A
Loop current switching	C1, C2	Transfer the loop current through a disconnecting switch (DS) to a bypass switch (BPS) connected in parallel with a converter unit by opening the DS when the converter stops operating. Closing duty is also required when a converter unit starts operating.	LVDC 2800 A
Converter charging current switching	D1, D2	Interrupt the charging current through a converter unit when the converter stops operating. The current present during converter operation includes a ripple current. When the converter unit starts operating, a closing surge is generated by DS operation.	HV DC 1 A

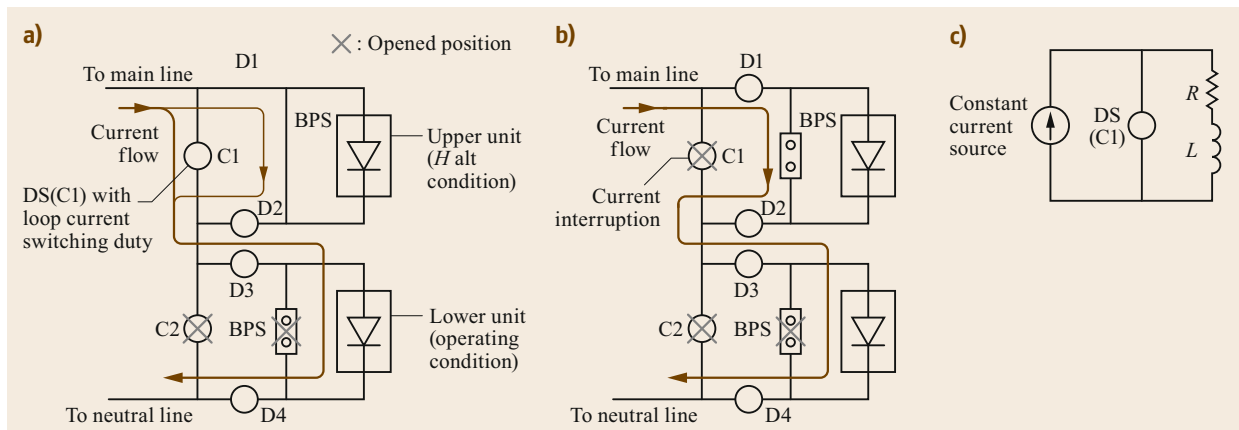
### 8.5.9 HVDC Disconnecting Switches

HVDC disconnecting switches (DSs) are used to disconnect various circuits in HVDC transmission networks. For example, HVDC DSs are used for switching duties such as line or cable charging current switching and no-load line or cable transfer switching, and for disconnecting equipment such as a converter bank (thyristor valve), filter bank, and grounding line. HVDC DSs are also used in DC switchgear to terminate the residual or leakage current through an interrupter after a fault current has been cleared.

Figure 8.172 shows an example of a single-pole diagram of the relevant switching equipment (except for MRTBs) in a bipolar HVDC transmission system in Japan. In general, the requirements for HVDC DSs and earthing switches (ESs) in the HVDC system are similar to those for HVAC DSs and ESs used in the AC system,

but there are additional requirements for some equipment, depending on their applications. Table 8.18 lists the major switching duties imposed on these HVDC DSs [8.66].

- Group A:** Here, the DS is required to interrupt the line discharging current resulting from residual charge in a submarine cable with a relatively large capacitance (approximately  $20 \mu\text{F}$ ). The residual voltage induced in the line after a converter halt is discharged through a snubber circuit in a converter bank at both C/Ss (Anan C/S and Kihoku C/S) to ground. The discharge time constant is about 40 s, which corresponds to a discharging time of 3 min. The discharge current was set to 0.1 A based on the value calculated from the residual voltage of 125 kV and the resistance of the snubber circuit in the thyristor valve.



**Fig. 8.173a–c** Current transfer process for a group C DS. (a) DS closed, (b) DS open, (c) equivalent circuit of the DS ( $R$ ,  $L$ : resistance and induction of loop circuit)

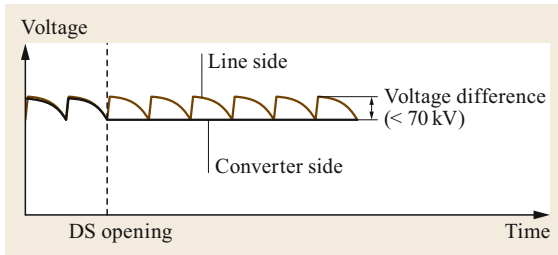


Fig. 8.174 Voltage difference between the DS contacts

- **Group B:** In this case, the DS is normally used to switch a faulted transmission line to a healthy neutral line that is temporarily or permanently used for transmission after the system has been completely stopped. This requires the same specifications as those for group A DSs.
- **Group C:** These DSs are required to transfer the nominal load current from the DS to a bypass switch (BPS) connected in parallel with a converter bank in order to restart the bank unit. The specification of the transfer current is 2800 A in this project.

Figure 8.173 illustrates the nominal current transfer process from the DS to the BPS. First, the upper converter bank unit is stopped and the lower converter bank unit is operated. In order to operate the upper bank unit from a halted condition, DS C1 is then opened to commutate the nominal current into the BPS. The requirements

for group C DSs are based on an analysis of the equivalent circuit for the current transfer process (shown in Fig. 8.173c) and a voltage of 1 V DC at a nominal current of 2800 A. The voltage was calculated for a resistance and inductance per unit length corresponding to the current transfer length including the DC-GIS.

- **Group D:** In this case, the DS is required to interrupt a converter bank charging current when the converter bank unit is stopped. Even if the thyristor valve is halted, a ripple current flows due to the stray capacitance of the converter bank. Analytical results show that the ripple current is very likely to be chopped to less than 1 A, and that the recovery voltage due to the difference between the residual DC voltage on the converter side and the DC voltage on the line side (which includes ripple components) is less than 70 kV, as shown in Fig. 8.174.

Furthermore, the DS is equipped with a closing resistor of 1 k $\Omega$  to suppress switching surges caused by the operation of the DS. Figure 8.175 shows a schematic of the DS with the closing resistor, as well as the closing sequence. Although this resistor is used to suppress the closing surge, the resistor is also included during the opening sequence due to the design of the DS.

The switching performance of HVDC DSs (all groups) is based on that of AC DSs, and HVDC DS performance is established in factory tests performed

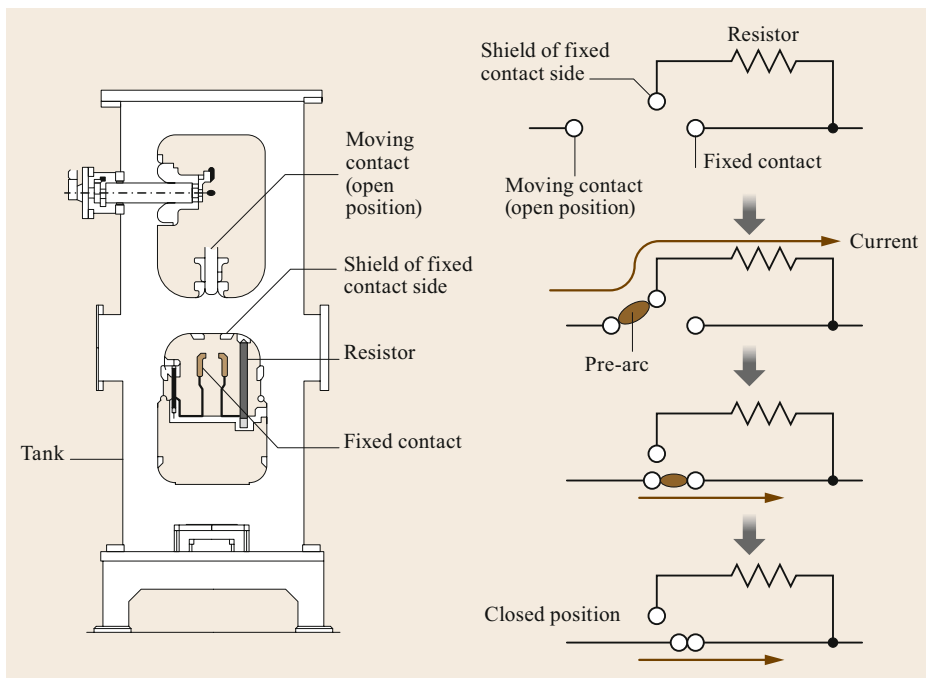
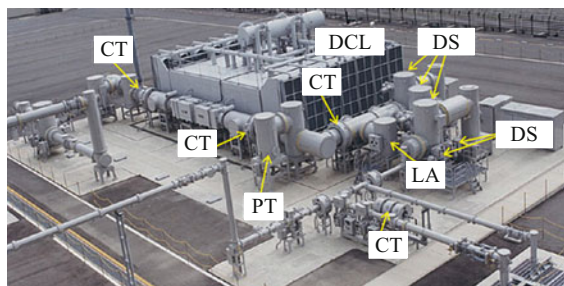


Fig. 8.175 DC 500 kV DS with a closing resistor and the closing sequence used



**Fig. 8.176** DC DSs, ESs, CTs, VT, and a MOSA (labeled LA in the photograph) used in the 500 kV DC GIS

under the conditions shown in Table 8.18. There are no significant design differences between HVAC DSs and HVDC DSs except for the creepage distance, which is about 20% longer for HVDC applications.

DC gas-insulated switchgear (DC-GIS) consisting of several HVDC DSs and ESs are also applied in HVDC networks close to a coastline. Figure 8.176 shows an example of DC-GIS (including DC DSs and ESs) that was installed at a converter station in a bipolar HVDC system commissioned in 2000.

### 8.5.10 Summary

DC circuit breakers with different current zero creation schemes have been applied in many industrial applications. MRTBs are commonly applied in bipolar HVDC systems. However, field demonstrations of HVDC circuit breakers in multiterminal HVDC networks are still awaited. CIGRE provides continuous updates on the development of and progress in HV circuit breaker technologies that are applicable to future multiterminal HVDC networks.

DC circuit breakers with active current injection and hybrid DC circuit breakers with IGBT devices have been developed for use up to the 80 kV, 16 kA and 500 kV, 25 kA levels, respectively.

Air- and gas-insulated HVDC disconnecting switches (DSs) have been applied in many bipolar HVDC systems. There are no significant design differences between HVAC DSs and HVDC DSs except for the creeping distance, which is about 120% longer for HVDC applications.

**Acknowledgments.** This chapter focuses on the basics of power-system switching equipment for the benefit of students as well as young engineers who are starting out in their careers and are involved in research into and/or the development, design, production, deployment, and operation of switching equipment used in HVAC and HVDC power systems. The information provided here is based on long-term investigations that were mainly conducted by CIGRE Study Committees 13 and A3. This chapter explains the basics of switching equipment used in power systems, including the interrupting principles of circuit breakers with different technologies, switching phenomena observed in power systems, and the history of circuit breakers, including oil circuit breakers, air-blast circuit breakers, vacuum interrupters, and gas circuit breakers. It also describes some important substation equipment such as surge arresters, instrument transformers, and substation post insulators. This book represents a useful aid to understanding CIGRE publications such as technical brochures, which include state-of-the-art information on emerging subjects but are often targeted at experts.

The author wishes to express his appreciation to all of the switching experts involved in CIGRE activities past and present. In particular, the author is grateful for the kind advice and encouragement given by the main editor of the book, Dr. Konstantin Papailiou. The author is also very grateful for the devoted efforts of many SC A3 experts, and to Dr. Harley Wilson for supporting a review of the technical documents during the publication process.

### References

- 8.1 CIGRE TB 696: *MO Varistors and Surge Arresters for Emerging System Conditions* (CIGRE, Paris 2017)
- 8.2 CIGRE TB 394: *State of the Art of Instrument Transformers* (CIGRE, Paris 2009)
- 8.3 CIGRE TB 336: *Changing Network Conditions and system requirements Part 2* (CIGRE, Paris 2007)
- 8.4 CIGRE TB 693: *Experience with equipment for Series/Shunt Compensation* (CIGRE, Paris 2017)
- 8.5 CIGRE TB 455: *Aspects for the Application of Composite Insulators to High Voltage Apparatus* (CIGRE, Paris 2011)
- 8.6 CIGRE TB 725: *Ageing high voltage substation equipment and possible mitigation techniques* (CIGRE, Paris 2018)
- 8.7 IEC 60060-1: *High-voltage test techniques – Part 1, General definitions and test requirements* (IEC, Geneva 2011)
- 8.8 IEC 60815-1: *Selection and dimensioning of high-voltage insulators intended for use in polluted conditions – Part 1, Definitions, information and general principles* (IEC, Geneva 2016)
- 8.9 IEC 60815-2: *Selection and dimensioning of high-voltage insulators intended for use in polluted con-*

- ditions – Part 2, Ceramic and glass insulators for a.c. systems (IEC, Geneva 2016)
- 8.10 IEC 60815-3: Selection and dimensioning of high-voltage insulators intended for use in polluted conditions – Part 3, Polymer insulators for a.c. systems (IEC, Geneva 2016)
- 8.11 J. N. Kleman: US Patent 874601 (1907)
- 8.12 J. Slepian: Theory of the de-ion circuit breaker, Trans. AIEE **48**, 523–553 (1929)
- 8.13 D.C. Prince, W.F. Skeats: Oil blast circuit breaker, Trans. AIEE **81**, 629–639 (1931)
- 8.14 W. B. Whitney, E. B. Wedmore: British Patent 278764 (1926)
- 8.15 W. B. Whitney, E. B. Wedmore: British Patent 366998 (1930)
- 8.16 F. S. Cooper: US Patent 2221671 (1940)
- 8.17 H.J. Lingal, T.E. Browne, A.P. Storm: An investigation of the arc quenching behavior of sulphur Hexafluoride, Trans. AIEE **72**, 242–246 (1953)
- 8.18 H. J. Lingal, T. E. Browne, A. P. Storm: US Patent 2757261 (1956)
- 8.19 R. Wilkins, E.A. Cretin: *High Voltage Oil Circuit Breakers* (McGraw-Hill, New York 1930)
- 8.20 R.W. Sorensen, H.E. Mendenhall: Vacuum switching equipment at California Institute of Technology, Trans. ALL **45**, 1102–1105 (1926)
- 8.21 CIGRE TB 589: *Vacuum Switchgears at transmission voltages* (CIGRE, Paris 2014)
- 8.22 A.M. Cassie: *Arc Rupture and Circuit Severity, A New Theory*, CIGRE Session Report, Vol. 102 (CIGRE, Paris 1939)
- 8.23 O. Mayr: Beitrage zur Theorie des statischen und des dynamischen Lichtbogens, Arch. Electrotech. **37**(12), 566–608 (1943)
- 8.24 A.M. Cassie, F.O. Mason: *Post-arc Conductivity in Gas Blast Circuit Breakers*, CIGRE Session Report, Vol. 103 (CIGRE, Paris 1956)
- 8.25 T.E. Browne: *Circuit Interruption, Theory and Technique* (Marcel Dekker, New York 1984)
- 8.26 CIGRE WG 13.01: Applications of black box modeling to circuit breakers, *Electra* **118**, 65–79 (1988)
- 8.27 CIGRE WG 13.01: Applications of black box modeling to circuit breakers, *Electra* **149**, 41–71 (1993)
- 8.28 EPRI report EL-284: *Fundamental Investigation of Arc Interruption in Gas Flows* (EPRI, Palo Alto 1977)
- 8.29 EPRI report EL-1455: *Fundamental Investigation of Arc Interruption in Gas Flows* (EPRI, Palo Alto 1980)
- 8.30 L.S. Frost, R.W. Liebermann: Composition and transport properties of SF<sub>6</sub> and their use in a simplified enthalpy flow arc model, Proc. IEEE **59**(4), 474–485 (1971)
- 8.31 A.D. Stokes, et al.: *Circuit Interruption Prediction Using a Current Dependent Arc Model*, CIGRE Session Report, Vol. 13-02 (CIGRE, Paris 1984)
- 8.32 H. Kuwahara, T. Tanabe, K. Ibuki, M. Sakai, S. Sakuma: New approach to analysis of arc interruption capability by simulation employed in the development of SF<sub>6</sub> GCB series with high capacity interrupter, IEEE Trans. Power Apparatus Syst. **PAS-102**(7), 2262–2268 (1983)
- 8.33 T. Tanabe, K. Ibuki, S. Sakuma, T. Yonezawa: Simulation of the SF<sub>6</sub> arc behavior by a cylindrical arc model, IEEE Trans. Power Apparatus Syst. **PAS-104**(7), 1903–1909 (1985)
- 8.34 J.M. Lafferty (Ed.): *Vacuum Arcs Theory and Application* (Wiley, New York 1980) pp. 152–160
- 8.35 CIGRE TB 304: *Guide for application of IEC 62271-100 and IEC 60694. Part 1* (CIGRE, Paris 2006)
- 8.36 CIGRE TB 305: *Guide for application of IEC 62271-100 and IEC 60694. Part 2* (CIGRE, Paris 2006)
- 8.37 CIGRE TB 570: *Switching Phenomena for EHV and UHV Equipment* (CIGRE, Paris 2014)
- 8.38 IEC62271-100: *High-voltage switchgear and controlgear – Part 100, Alternating current circuit-breakers* (IEC, Geneva 2008)
- 8.39 A. Janssen, D. Dufournet, H. Ito: *Transient recovery voltage at transformer limited fault clearing*, CIGRE Science & Engineering, Vol. CSE004 (CIGRE, Paris 2016)
- 8.40 IEC Std. IEC 62271-100 ed. 2.1: *High-voltage switchgear and controlgear – Part 100, High-voltage alternating current circuit breakers* (IEC, Geneva 2012)
- 8.41 IEEE Std. C37.09 – 1999, Cor 1–2007: IEEE Standard Test Procedure for AC High-Voltage Circuit Breakers Rated on a Symmetrical Current Basis – Corrigendum 1
- 8.42 IEEE PSRC WG D6: *Report to the Power System Relaying Committee of the IEEE Power Engineering Society, Power Swing and Out-of-Step Considerations on Transmission Lines* (IEEE, New York 2005)
- 8.43 IEC 60050-448-14-35: Chap. 448, Power system protection. In: *International Electrotechnical Vocabulary* (IEC, Geneva 1995)
- 8.44 CIGRE TB 716: *System Conditions for and Probability of Out-of-phase, Background, Recommendations, Developments of Instable Power Systems* (CIGRE, Paris 2018)
- 8.45 CERC: *Final report on the grid disturbance on 30th July 2012 and grid disturbance on 31st July 2012* (2012). <http://www.cercind.gov>
- 8.46 UCTE: *Final Report of the Investigating Committee on the 28 September 2003 Blackout in Italy* (UCTE, Paris 2004)
- 8.47 D.Z. Meng: *Maintaining System Integrity to Prevent Cascading Blackout, CIGRE SC B5 Session 2006, B5-207* ((CIGRE, Paris 2006)
- 8.48 IEC Guide IEC 62271-306: *High-voltage switchgear and controlgear – Part 306, Guide to IEC 62271-100, IEC 62271-1 and other IEC standards related to alternating current circuit breakers* (IEC, Geneva 2012)
- 8.49 H. Ito, et al.: *Technical requirements for substation equipment exceeding 800 kV, 2007 IEC-CIGRE UHV Symposium, Report 2-4-1* (CIGRE, Paris 2007), on behalf of CIGRE WG A3.22
- 8.50 Y. Hase: *Handbook of Power System Engineering*, 2nd edn. (Wiley, New York 2007)
- 8.51 CIGRE TB 362: *Technical requirements for substation equipment exceeding 800 kV AC, GRE WG A3.22* (CIGRE, Paris 2008)
- 8.52 CIGRE TB 462: *Background of Technical Specifications for UHV Substation Equipment, CIGRE WG A3.22* (CIGRE, Paris 2011)
- 8.53 CIGRE TB 570: *Switching Phenomena for EHV and UHV Equipment, CIGRE WG A3.28* (CIGRE, Paris 2014)

- 8.54 E. Zaima, et al.: *System Aspects of 1100 kV AC Transmission Technologies in Japan, Solutions for Network Problems Specific to UHV AC Transmission System and Insulation Coordination*, IEC-CIGRE UHV Symposium 2007, Report 2-1-2 (CIGRE, Paris 2009)
- 8.55 T. Kobayashi, et al.: *Basic design and specifications of GIS for UHV AC and its verification test at site*, IEC-CIGRE UHV Symposium 2007, Report 2-3-3 (CIGRE, Paris 2009)
- 8.56 Y. Yamagata, et al.: *Development of 1100 kV gas circuit breakers and their verification tests*, IEC-CIGRE UHV Symposium 2007, Report 2-4-3 (CIGRE, Paris 2009)
- 8.57 H. Ito, et al.: *Technical requirements for UHV substation equipment*, CIGRE Session Paper, Report A3-211 (CIGRE, Paris 2008), on behalf of CIGRE WG A3.22
- 8.58 IEC Int. Standard 62271-203: *High-voltage switchgear and controlgear. Part 203: Gas-insulated metal-enclosed switchgear for rated voltages above 52 kV*, 1.0 edn. (IEC, Geneva 2003)
- 8.59 A.L.J. Janssen, et al.: *UHV Equipment Requirements, State of the Art and Prospects for Equipment*, 2nd IEC-CIGRE UHV Symposium, New Delhi (CIGRE, Paris 2009), on behalf of CIGRE WG A3.22
- 8.60 IEC Int. Standard 62271-102: *High-voltage Switchgear and Controlgear, Part 102, Alternating Current Disconnecting Switches and Earthing Switches*, 1.0 edn. (IEC, Geneva 2001)
- 8.61 A.J. Keri, et al.: Single phase switching tests on the AEP 765 kV system – extinction time for large secondary arc currents, IEEE Trans. Power Apparatus Syst. **8** (1983)
- 8.62 G.E. Agafonov, et al.: *High Speed Grounding Switch for Extra-high voltage Lines*, CIGRE Session Paper, Report, Vol. A3-308 (CIGRE, Paris 2004)
- 8.63 CIGRE TB264: *Planning, Specifications and Testing of controlled switching systems*, WG A3.07 (CIGRE, Paris 2004)
- 8.64 CIGRE WG13.07: Controlled switching of HVAC circuit breakers, guide for application, part 1, ELECTRA **183**, 43-73 (1999)
- 8.65 CIGRE WG13.07: Controlled switching of HVAC circuit breakers, guide for application, part 2, ELECTRA **185**, 37-57 (1999)
- 8.66 CIGRE WG13.07: Controlled switching of HVAC circuit breakers, planning, specification and testing of controlled switching systems, ELECTRA **197**, 23-733 (2001)
- 8.67 CIGRE TB 262: *Benefits and Economic Aspects*, WG A3.07 (CIGRE, Paris 2004)
- 8.68 CIGRE TB 263: *Guidance for further applications including unloaded transformer switching, load and fault interruption and circuit-breaker uprating*, WG A3.07 (CIGRE, Paris 2004)
- 8.69 A. Mercier, et al.: *CIGRE 2002 Session 13-201, Transformer Controlled Switching Taking into Account the Residual Flux* (CIGRE, Paris 2002)
- 8.70 H. Kohyama, K. Kamei, H. Ito: *CIGRE SC A3 and B3 2005 Colloquium-209, Application of Controlled Switching System for Transformer Energization taking into account a Residual Flux in Transformer Core* (CIGRE, Paris 2005)
- 8.71 K. Fröhlich, et al.: Controlled closing on shunt reactor compensated transmission lines, IEEE Trans. Power Deliv. **12**, 734-740 (1997)
- 8.72 B.L. Avent, et al.: *CIGRE 2002 Session 13-107, Application of 500 kV Circuit Breakers on Transmission Line with MOV Protected Series Capacitor Bank* (CIGRE, Paris 2002)
- 8.73 A. Mercier, H. Kohyama, et al.: *CIGRE 2015 Nagoya Colloquium A3 and B3-107, Special Considerations with Controlled Switching Projects* (CIGRE, Paris 2015)
- 8.74 CIGRE TB 533: *HVDC grid feasibility study, Appendix H, Switching DC in an HVDC system* (CIGRE, Paris 2013)
- 8.75 CIGRE TB 683: *Technical Requirements and Specifications of State-of-the-art HVDC Switching Equipment* (CIGRE, Paris 2017)
- 8.76 A. Lee, et al.: The development of a HVDC SF<sub>6</sub> breaker, IEEE Trans. Power Apparatus Syst. **104**(10), 2721-2729 (1985)
- 8.77 H. Ito, et al.: Instability of DC Arc in SF<sub>6</sub> circuit breaker, IEEE Trans. Power Deliv. **12**(4), 1508-1513 (1997)
- 8.78 S. Hara, et al.: Fault protection of metallic return circuit of Kii channel HVDC system, IEE GD **95**, 132-137 (1995)
- 8.79 S. Tokoyoda, R.P.P. Smeets, R. Nijman, N.A. Belda, K. Tahata, F. Page, H. Ito, C. Spallarossa: *Full Power Short-circuit Tests of HVDC Circuit Breakers using AC generator operated with reduced power Frequency*, CIGRE Session report, A3-115 (CIGRE, Paris 2018)
- 8.80 K. Tahata, et al.: *HVDC circuit breakers for HVDC grid applications*, CIGRE A0RC Technical meeting 2014, Report No. 1120 (CIGRE, Paris 2014)
- 8.81 S. Xu: *160 kV Mechanical HVDC Circuit Breaker Development and Application*, CIGRE SC A3 and B4 Workshop on HVDC Circuit Breakers (CIGRE, Paris 2018)
- 8.82 R. Derakhshanfar, et al.: *Hybrid HVDC Breaker – A Solution for Future HVDC System*, CIGRE Session Report B4-304 (CIGRE, Paris 2014)
- 8.83 B. Yang, D. Dao, W. Shi, W. Lv, W. Wang, B. Liu: *A Novel Commutation-based Hybrid HVDC Circuit Breaker*, 2017 CIGRE Winnipeg SC A3/B5/D1 Colloquium, A3/B4-15 (CIGRE, Paris 2017)
- 8.84 A. Ting: *HVDC Breaker Experience in China*, CIGRE SC A3 and B4 Workshop on HVDC Circuit Breakers (CIGRE, Paris 2018)

**Hiroki Ito**

Energy & Industrial Systems Group  
Mitsubishi Electric Corporation  
Tokyo, Japan  
ito.hiroki@aj.mitsubishielectric.co.jp



Hiroki Ito is involved in high-voltage DC and AC circuit breaker research and development. He received his PhD from Tokyo Institute of Technology. He was the technical director of Mitsubishi Electric High Voltage and High Power Testing Laboratories from 2005 to 2012. He was chairman of CIGRE Study Committee A3: *High Voltage Equipment* (now *Transmission and Distribution Equipment*) from 2012 to 2018.



# Overhead Lin

## 9. Overhead Lines

Konstantin O. Papailiou

Overhead transmission lines have formed the backbone of electric power systems over their history of more than 125 years, being at the same time the largest man-made artifacts on Earth. Another peculiarity of overhead lines is that their study encompasses quite a few engineering disciplines, such as electrical, mechanical, civil, and environmental. As system operation issues of lines are covered in Chap. 5, this chapter concentrates on line components. It starts by explaining the design philosophy of lines, with an emphasis on the calculation of typical line loads, mainly coming from wind and ice, and includes the latest findings on electromagnetic fields (EMF) and health. It continues by treating the individual line components, from material selection, manufacturing processes, stress calculations, to special applications. For instance, for conductors, the most costly and important component of a line, emphasis is placed on different types of conductor, their material properties, and what is called their internal mechanics, including sag-tension calculations. However, sufficient space is also dedicated to the ever-important issue of conductor vibrations, thermal rating and monitoring, bundle conductors, as well as new types of conductor. Similarly for insulators, after an in-depth presentation of pollution issues, the focus is on three different types of insulator, i.e., porcelain, glass, and composite. Conductor fittings are addressed next, covering, beside the different types of clamps and joints, also conductor hardware for vibration control, such as Stockbridge and spacer dampers. Line supports, being the most visible component of a line, have seen a significant shift in recent years towards esthetic structures and compactness, while their foundations have benefited from improved designs and new site investigation techniques. The final sections cover construction and maintenance, including new technologies such as robotics, and line uprating and upgrading, the latter reflecting the increasing trend towards augmenting the power transfer capacity of existing lines, as it is not always easy to build new lines. The goal of this chapter is

thus to provide the reader with all the basic information required to understand how an overhead line is designed, constructed, and maintained and help in taking the right decisions regarding material selection, the calculation of external loads and internal stresses, and the choice of appropriate standards and testing procedures. Some 300 references facilitate these tasks.

Additional information and supplementary exercises for this chapter are available online.

9.1	<b>History and Present Challenges</b> .....	612
9.1.1	First Steps .....	612
9.1.2	Important Milestones .....	614
9.1.3	Present Challenges .....	614
9.2	<b>Planning</b> .....	615
9.2.1	Planning Process .....	615
9.2.2	Line Optimization .....	617
9.2.3	Costs .....	619
9.2.4	Asset Management .....	621
9.3	<b>Line Design</b> .....	625
9.3.1	Design Methods .....	625
9.3.2	Line Loads .....	627
9.3.3	Electrical Clearances .....	632
9.3.4	Environmental Issues .....	634
9.3.5	Approval Procedure .....	638
9.4	<b>Conductors</b> .....	640
9.4.1	Types and Basic Properties of Conductors .....	640
9.4.2	Conductor Manufacture .....	643
9.4.3	Tests .....	643
9.4.4	Mechanical Properties .....	646
9.4.5	Thermal Rating .....	652
9.4.6	Corona .....	653
9.4.7	Bundle Conductors .....	655
9.4.8	Earth Wires .....	656
9.4.9	High-Temperature Conductors .....	656
9.4.10	Real-Time Monitoring .....	659
9.4.11	Conductor Vibrations .....	660
9.5	<b>Insulators</b> .....	671
9.5.1	Classification .....	671

9.5.2	Pollution .....	674	9.8	<b>Construction</b> .....	733
9.5.3	Porcelain Insulators .....	680	9.8.1	Survey and Tower Spotting .....	734
9.5.4	Glass Insulators .....	681	9.8.2	Transportation and Site Clearance .....	734
9.5.5	Composite Insulators .....	682	9.8.3	Foundations .....	735
9.5.6	Insulator Tests and Standards .....	694	9.8.4	Supports .....	735
9.6	<b>Fittings</b> .....	697	9.8.5	Conductor Stringing .....	737
9.6.1	Conductor Fittings .....	698	9.8.6	Installation of Conductor Hardware ...	739
9.6.2	Fittings for Insulator Strings .....	704	9.9	<b>Maintenance</b> .....	740
9.6.3	Vibration Dampers .....	707	9.9.1	Maintenance Activities and Strategies	740
9.6.4	Tests .....	713	9.9.2	Common Defects and Condition	
9.7	<b>Supports and Foundations</b> .....	715		Assessment of Line Components .....	741
9.7.1	Wood Poles .....	716	9.9.3	Live Line Work .....	743
9.7.2	Concrete Poles .....	717	9.9.4	Transmission Line Robotics .....	744
9.7.3	Metallic Poles .....	718	9.10	<b>Upgrading and Upgrading</b> .....	745
9.7.4	Composite Poles .....	719	9.10.1	Upgrading .....	745
9.7.5	Steel Lattice Towers .....	720	9.10.2	Upgrading .....	747
9.7.6	Esthetic or Landscape Supports .....	727	9.11	<b>Conclusions and Further Reading</b> .....	751
9.7.7	Earthing .....	727	9.11.1	Additional Information and Exercises.	751
9.7.8	Lightning Protection .....	728	<b>References</b> .....		751
9.7.9	Foundations .....	729			

## 9.1 History and Present Challenges

Since their first installation in 1891, overhead transmission lines have formed the backbone of electric power systems, with more than a million kilometers now in service worldwide. In Europe alone, more than 200 000 km (system length) at 380 kV and more than 100 000 km at 220 kV are in operation. Lines at lower voltages, often called subtransmission or distribution lines, reach millions of kilometers.

Despite some acceptance problems faced mainly by high-voltage lines in recent years, their future seems bright, as they are considered indispensable for the transmission of bulk electric power over long distances.

This trend is enhanced by the following facts:

- Approximately 20% of the world's population has no access to electrical power.
- Demand for electrical power will more than double by 2035.

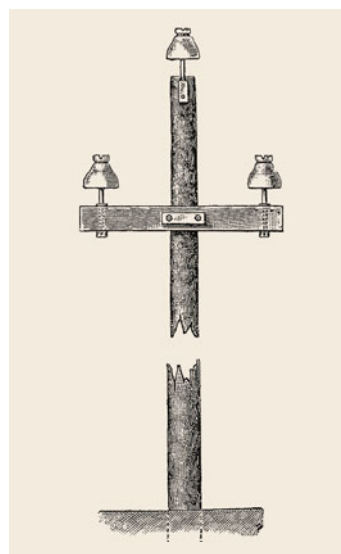
Because of this, worldwide investment in electrical networks of approximately USD 20 billion will be required up to this date, 40% of which will go on transmission and distribution networks.

In addition, because of the megatrend in recent years in many countries towards renewables and in particular wind farms, which are often located in remote areas, there is an increasing demand for new overhead lines. As an example, in Germany, a pioneer in the use

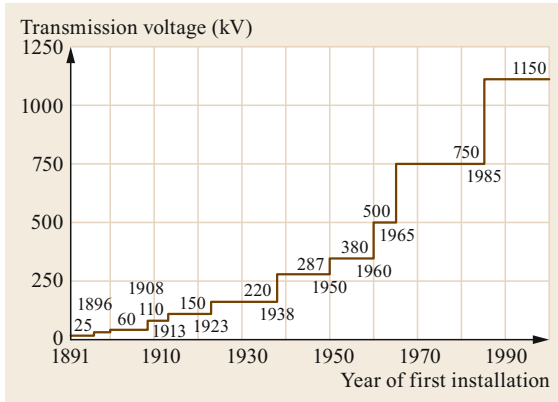
of renewable generation, the demand for new 380-kV lines has been estimated to be about 4000 km.

### 9.1.1 First Steps

The first *high-voltage* alternating-current (AC) overhead line was built in Germany in 1891, from Lauffen am Neckar (a small city in Southern Germany) to Frankfurt am Main (Fig. 9.1). The italics indicate that



**Fig. 9.1** First HV AC overhead line



**Fig. 9.2** Development of overhead line (OHL) voltages

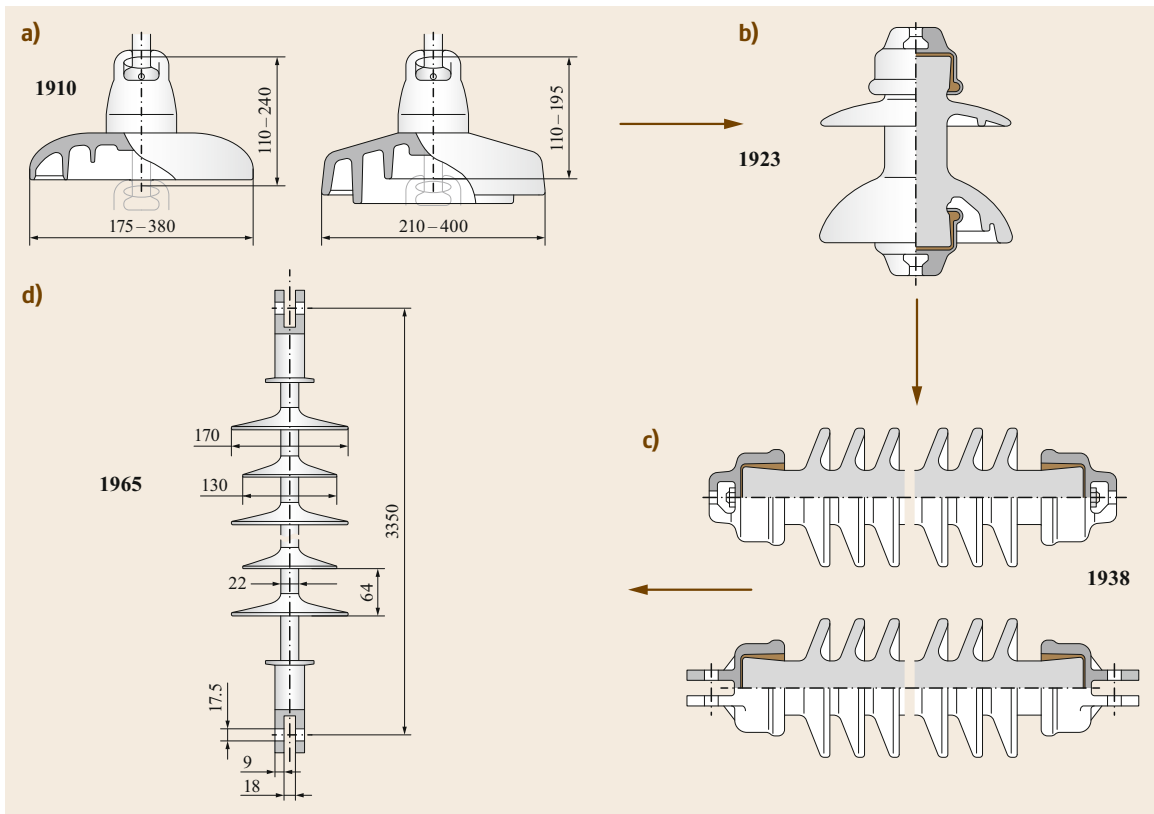
high voltage in those days was only 15 kV (although the line was later operated at 25 kV). It is interesting to note that, although industrial-scale transmission of electrical power was developed in direct current (DC) for long-distance transmission for railways between Vizille and Grenoble in France as early as 1883 by Marcel Deprez,

preference was given to AC over DC because the use of the transformer gave AC an essential advantage.

The line had a length of 175 km and was used to provide electrical power to 1000 lamps and an AC motor for an artificial waterfall installed at the premises of the Frankfurt Fair. Based on the technology of telegraph lines at that time, 3200 wooden poles were used to carry the 12.6-mm<sup>2</sup> copper conductors, supported by oil-filled porcelain insulators. No wonder the losses were about 25%.

The father of the transmission project for the Frankfurt Fair was Oskar von Miller from Munich, who later established the Deutsches Museum there. The designers of the electrical equipment were Charles Brown and Walter Boveri from Switzerland, who established the Brown-Boveri Company (BBC) soon thereafter. The designer of the overhead line as well as the electrical pump was Michail Ossipowitsch Doliwo-Dobrowolski from Allgemeine Electricitäts-Gesellschaft (AEG).

What started as a single, point-to-point connection for a rather fancy application became in subsequent



**Fig. 9.3a-d** Milestones of OHL insulators (source Pfisterer Lapp): (a) cap-and-pin porcelain insulators, (b) motor insulator, (c) porcelain longrods, (d) silicone rubber composite insulators



**Fig. 9.4** 1200 kV AC line at a test station in Bina, India (photo: A. Pigini)

years probably the most complex *machine* mankind has ever conceived, the power grid.

### 9.1.2 Important Milestones

It was soon recognized by early overhead line engineers that, to transmit large amounts of electrical power, the current and voltage had to be increased. This spurred intense development of conductors for higher currents and insulators for higher voltages.

As the copper wires originally used were heavy and expensive, aluminum wires were soon introduced, and a seven-strand aluminum conductor was put in service in 1897 in Connecticut. An important milestone was the introduction of bimetallic conductors, namely aluminum conductor steel-reinforced (ACSR) conductors, in 1907. Today's conductors with diameters of 50 mm or more can carry up to 1500 A, and modern high-temperature low-sag (HTLS) conductors (Sect. 9.4.9) even more.



**Fig. 9.5** Study *Walking giants* (photo: Landsnet, Iceland)

The necessity for higher voltages (Fig. 9.2 [9.1]) could only be addressed by the parallel development of suitable insulators (Fig. 9.3). From the invention of cap-and-pin porcelain (or glass) insulators (Fig. 9.3a), which enabled, by simply adding more units, long insulator strings and thus higher voltages, to the so-called motor insulator (Fig. 9.3b) to porcelain long-rods (Fig. 9.3c) to today's silicone rubber composite insulators (Fig. 9.3d), insulators have proven to be an extremely innovative—and reliable—component of overhead lines.

With the introduction of higher voltages and larger conductors, the appropriate support technology had to keep pace. This is visually evident in the development of the towers, the most visible elements of an overhead line: from the wooden poles of the early days (Fig. 9.1), to the impressive structures of 1200-kV AC lines of the present (Fig. 9.4).

In recent years, the esthetics of overhead lines have attracted considerable attention from the public, fostering the development of compact lines and so-called esthetic or design towers [9.2] (Fig. 9.5).

### 9.1.3 Present Challenges

Overhead lines are and will be for a long time the prime medium for transmitting bulk electrical power, despite serious objections from the public in many countries and recent advances in HV underground cable technology. While always an interesting subject, OHL have over the years tended to become *business as usual*, also suffering from the liberalization of electricity markets and the partly negative effects on utility investments. This situation has changed dramatically—and positively for OHL—in recent years with the worldwide megatrend—led by Germany—toward renewables. The result of this development is the requirement for a considerable number of new power transmission corridors. Overhead

lines are thus becoming, not only in Europe, *big business*.

Technically, there is broad agreement that these lines are badly needed to maintain system stability and reliability, with even traditionally critical organizations such as Greenpeace seeming to agree and project financing not representing a barrier. The big issue with system expansion is the strong opposition from the public to new lines, faithful to the well-known not in my backyard (NIMBY) principle. This has resulted in approval processes that last—if they are ever successful—between 10 and 20 years, with endless discussions and mainly emotional arguments from opponents, with the media doing their best to keep the fire burning.

In this context, the Conseil International des Grands Réseaux Électriques (CIGRE; International Council on Large Electric Systems, <http://www.cigre.org>), the largest and most important nongovernmental, nonprofit organization in the field of electrical power networks, and in particular its Study Committee on Overhead Lines (SC B2), which covers all aspects of the design, construction, and maintenance of overhead power lines, play a key role and help all involved stakeholders by providing unbiased information through international

conferences and broadly accepted publications such as technical brochures, major reference works (Green Books), etc.

Related to this, it is interesting to consider which issues are of particular importance to the OHL community worldwide, as determined in a quite recent survey by the Customer Advisory Group (CAG) of SC B2. They are:

- Increase capacity of existing lines
- New materials for use with OHL
- Public acceptance of OHL.

Other issues of interest identified by this survey are:

- Condition assessment and estimated remaining asset life
- Methods to optimize design
- Best construction and maintenance techniques and procedures
- Foundations for difficult soil conditions.

All these are covered extensively in the following sections of this chapter.

## 9.2 Planning

An overhead line is, in a sense, a unique device. Electrically, they are wave guides carrying electromagnetic waves at high power, in most cases over long distances. Mechanically, and because of the long distance issue, they sustain a spectrum of external, mainly climatic loads (e.g., wind and ice) but also temperature variations. The foundations for their supporting structures face a wide variety of soil conditions, from normal soil to hard rock, which call for different foundation techniques. All this, in combination with the potential hazards of high voltages and high currents, requires meticulous planning, design, construction, and maintenance of a transmission line project, while bearing in mind that the most important physical parameter is cost.

### 9.2.1 Planning Process

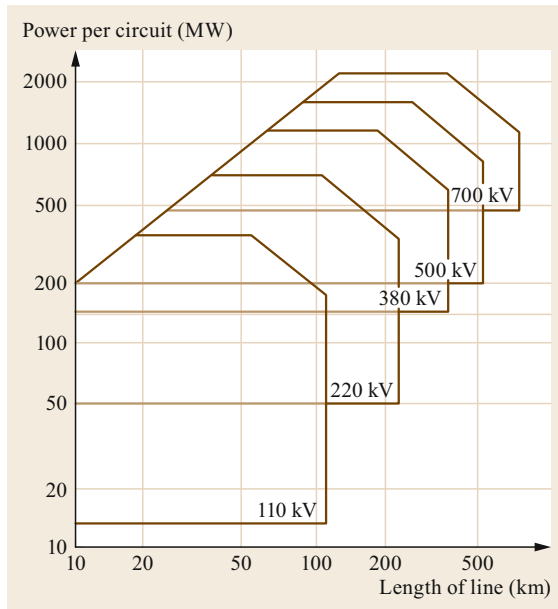
As in many human activities, the focus of power grids has changed over the years. While at the beginning of electrification capital was not a major issue, investors in grids soon became more price conscious, until current times, where environmental issues have become predominant.

In this sense, and in line with the rapid increase in the awareness and participation of the public, the

initiation and most importantly completion of a transmission line project has become a difficult puzzle, as an appropriate balance must be found between security of supply, safety, sustainability, and as far as possible cost-efficiency, in order to be acceptable to the public and thus politically viable.

New transmission line projects are always initiated by system planners, who have the best overview of present and future system requirements regarding load growth. The system planner should cooperate closely with line designers at an early stage of the project, as their input can significantly influence the design of the line and provide the following information to the line designers [9.3]:

- The profile of the proposed line load on a yearly and daily basis, which is essential for the designer to determine the templating temperature of the line
- The load growth, which is necessary to determine the optimum aluminum area of conductors
- The characteristic impedance (Chap. 5), which is necessary to determine the optimum bundle and phase configuration (for AC lines)
- The voltage of the line, which is often fixed based on the well-accepted rule of thumb for



**Fig. 9.6** Optimum transmission voltage (adapted from [9.4])

the optimum transmission voltage of 1 kV/km (Fig. 9.6).

Because of the latter, the design *window* in the planning stage of new lines is often limited mainly to the choice of the conductor and insulator, and for voltages above 220 kV to the decision on the bundle configuration. Important parameters for this selection process are:

- Line losses
- Corona
- Thermal rating
- Mechanical loads
- EMF limits.

The choice of the insulators depends mainly on the past experience of the utility, the pollution level, and the insulation coordination of the network.

Overhead line supports are often standardized for a utility, so the freedom of choice may be rather limited. On the other hand, because of increased public awareness—and often objections—to new lines, so-called esthetic supports (Sect. 9.7.6) are considered as alternatives.

The next and very important step in the planning process is line route selection and related property acquisitions to establish the necessary right of way (ROW). As this requires negotiations with land owners, which by nature can become emotional, this takes quite a long time to accomplish. CIGRE TB 147 [9.5]

covers the requirements for route selection, consultation models, and property acquisition. After completion, the detailed design stage can begin.

The detailed design phase precedes the execution phase. The output of this phase is a detailed design and costing, which is then presented to management for execution approval, as shown exemplarily here [9.6]:

- Planning information:
  - Reason for the line, including extract from the planning proposal documentation
  - Information from network planners on line requirements, including time and cost constraints
- Survey and environmental:
  - Possible routes with cost options
  - Environmental impact assessment (EIA)
  - Route and profile
- Initial tower, conductor, and foundation combinations:
  - Options selected for analysis
  - Appropriate technology index (ATI) analysis and results
  - Design options for further analysis
- Towers:
  - Tower design chosen
  - Tower schedule summary
- Conductor and earth wire:
  - Final conductor or conductor bundle chosen
  - Final earth wire chosen
- Foundations:
  - Geotechnical survey results
  - Foundation designs for each soil category and tower type
  - Schedule summary of foundation types
- Hardware:
  - Outline of suspension and strain assemblies
  - Damping system used
  - Clamps and fittings
- Insulators:
  - Analysis of pollution and other requirements
  - Insulator options that could be used
  - Final insulator selection
- Performance assessment:
  - Performance analysis of other lines in the vicinity
  - Lightning performance studies
  - Environmental impact studies such as bird pollution/interaction with the line, forest, grass, or cane fires.

The importance of the planning stage and the great attention it deserves are well documented in Fig. 9.7, showing a quite optimistic time schedule for a transmission line project, as nowadays line route acquisition

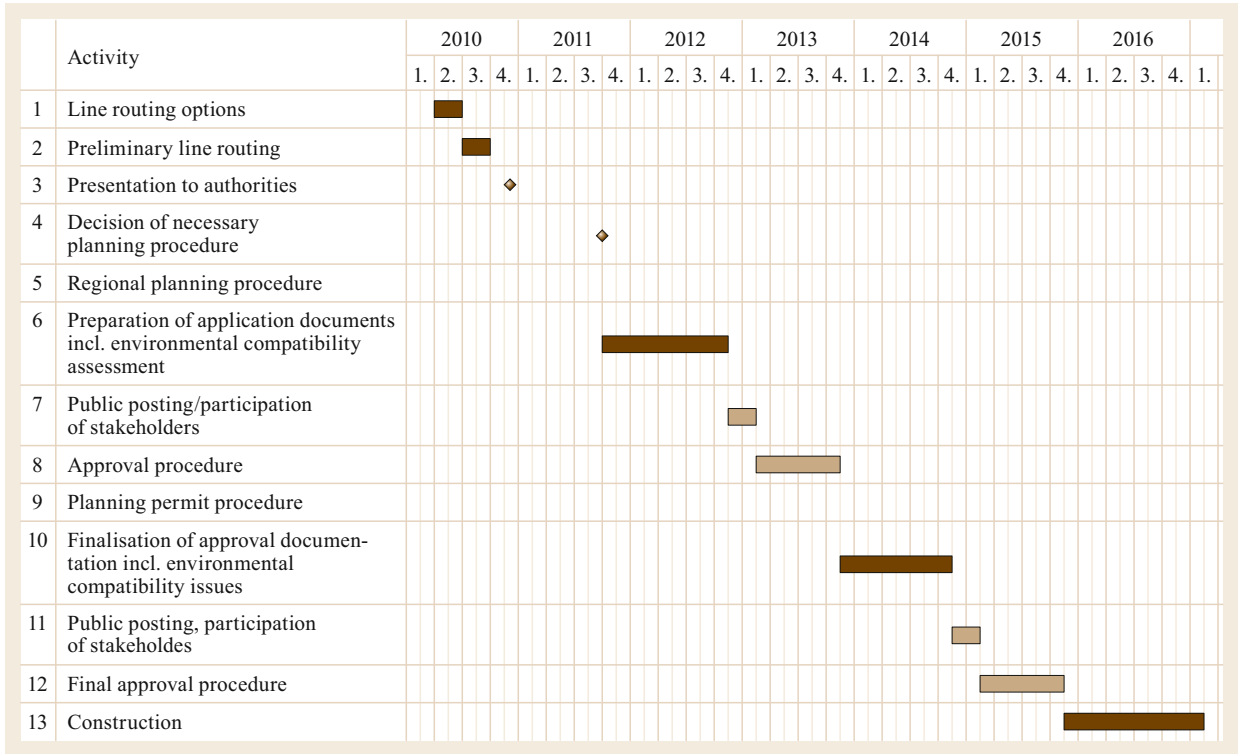


Fig. 9.7 Time schedule of a transmission line project in Germany

alone may sometimes take up to 20 years. Thus, the planning process consumes more than 80% of the project execution time.

### 9.2.2 Line Optimization

As mentioned above, the design options for a new line are in most cases de facto limited. In particular in industrialized countries, where the power grid is already well developed, many line components are standardized by the utilities due to logistics, storekeeping, and maintenance issues. Also, alternative line routes are difficult to find in densely populated areas. There are exceptions though: Presently in Germany new cross-country transmission corridors are planned for the better diffusion of renewable power to the grid; these new lines, which will have to be partially undergrounded, will be executed in DC with all design options open.

This is also the case in developing countries, where often long distances in lightly populated areas have to be covered and where financial constraints demand the most cost-efficient solution. Good examples in recent years for such projects are the 1000-kV AC and 800-kV DC lines in China, the 1200-kV AC lines in India, and the very long 600-kV DC and 765-kV AC lines in Brazil and South Africa, respectively.

In such cases, it is important to apply an objective optimization procedure, such as the one described in [9.6].

For AC lines, the line parameters that affect the ability of the line to transmit power over long distances are primarily the resistance, inductance, and capacitance values. The thermal rating can be affected by the height above ground as well as the conductor choice, which affects the sag–temperature relationship of the conductor. An optimal line should have low inductance, high capacitance, and low resistance. To achieve this, it is also important to observe constraints regarding corona and mechanical loading.

Table 9.1 presents the relationship between the surge impedance loading (SIL), corona, mechanical loading, and thermal rating.

For DC transmission lines, the corona limitation related to losses, the corona inception voltage for the conductor  $E_c$ , and  $E_{max}$  are the important parameters. The bundle design and the positive and negative pole separation as well as the voltage chosen for the optimal power flow are critical for the optimization of high-voltage direct-current (HVDC) lines.

Table 9.2 [9.6] summarizes the options relating to conductor and bundle selection for HVDC lines. Note that the SIL mentioned in the AC section is not valid for

**Table 9.1** Relationship between actions taken in AC line design and effect on SIL, corona, mechanical loading, and thermal rating

	SIL	Corona	Mechanical loading	Thermal rating
Phase spacing decrease	Good	Bad	Good (minor effect)	Neutral
Large Al area/cond. (less conductors)	Bad	Bad	Good	Bad
Diameter bundle increase	Good	Bad	Bad (minor effect)	Neutral
High steel content	Neutral	Neutral	Bad	Good

HVDC. Hence, this column is replaced with the voltage drop. In Tables 9.1 and 9.2:

- *Bad* implies that the option chosen will require in-depth study of this parameter and mitigating actions to be taken.
- *Good* indicates that the parameter will be favorably influenced by the action (e.g., the voltage drop will be lower along conductors with large Al area).
- *Neutral* means that the parameter chosen will not be affected by the choice of action.
- *Minor effect* means that the effect is secondary but must be taken into account in the design.

To determine the best set of design options among a number of alternatives, an indicator called the appropriate technology indicator (ATI) has been proposed, utilizing [9.6] the *bang for your buck* concept, the *bang* being in this case the surge impedance loading and the thermal rating of the line and the *buck* being the initial cost, with the life cycle cost also being included to avoid focus on the initial cost only; thus, the higher the ATI, the better the design option.

The following indicators have been proposed:  
For AC lines,

$$ATI_{AC} = w_1 LCC + w_2 \frac{IC}{MVA_{sil}} + w_3 \frac{IC}{MVA_{th}}, \quad (9.1)$$

where the life cycle cost (LCC) includes system losses, maintenance, and the initial cost (IC) of the line,  $MVA_{sil}$  is the surge impedance loading,  $MVA_{th}$  is the thermal limit under contingency conditions, and  $w_i$  are the weights for each term.

For DC lines,

$$ATI_{DC} = w_1 LCC + w_2 P_{cor loss} + w_3 \frac{IC}{MVA_{th}}, \quad (9.2)$$

where LCC is the life cycle cost including system losses, maintenance, and the initial cost,  $P_{cor loss}$  is the power loss due to corona, IC is the initial cost, and  $MVA_{th}$  is the thermal rating of the line.

The terms in (9.1) and (9.2) are normalized to a score out of 10 to enable their addition.

The weights  $w_i$  are determined by the network planners, who determine the importance of each component in relation to the needs of the line in the network; for example, the LCC would be given a high rating if the cost of capital is relatively low but the marginal cost of generation is high. It is recommended that the weights be varied and the option with the highest ranking, representing the most robust design, be adopted.

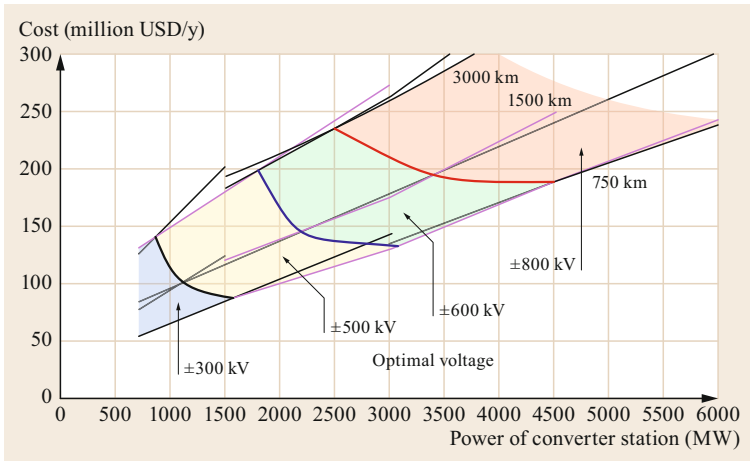
It is worth noting that, for DC lines, pioneering work was reported in [9.7], where a detailed analysis of a range of line configurations, voltages, and terminal station options was evaluated. Based on this report and in particular on Fig. 9.8 therefrom, the voltage level of a new DC line can be determined for a given power transfer and line length requirement. In this case, the optimization process will be as follows [9.8]:

- Determine the voltage level using the method proposed in [9.7].
- Determine the conductor/bundle configurations that meet the corona level limits for the selected voltage level.
- Determine the range of tower, conductor, and foundation combinations using an objective indicator.
- Once the group of line design options has been finalized, revisit the voltage, converter, and line design options to confirm that the options chosen are indeed valid. If not, the process needs to be restarted.
- Finalize the system design.

**Table 9.2** Relationship between actions taken in DC line design and effect on voltage drop, corona, mechanical loading, and thermal rating

Action	Voltage drop	Corona	Mechanical loading	Thermal rating
+ and – pole spacing decrease	Neutral	Bad	Good	Neutral
Large Al area/cond. (less conductors)	Good	Bad	Good (minor effect)	Bad
Diameter bundle increase	Neutral	Bad	Bad (minor effect)	Neutral
High steel content	Neutral	Neutral	Bad	Good





**Fig. 9.8** Optimal DC voltage as a function of converter station power and line length. Yearly cost: line investment and losses as well as station cost (station losses not included, equal for same station power and different voltage). (Adapted from [9.7])

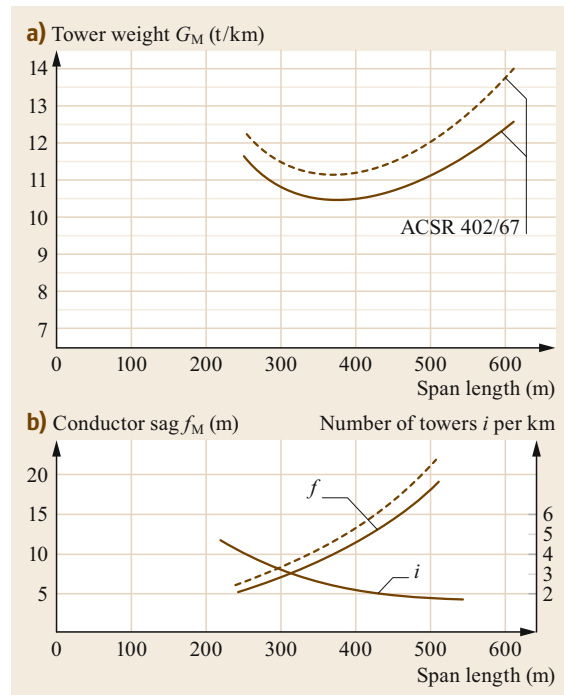
### 9.2.3 Costs

Reliable cost estimation at an early stage of the planning process is advantageous for the utility, in order to forecast and set aside necessary investments. This is not always easy, as the cost interactions of the various line components are rather complex. This situation was well explained in an early, remarkable paper [9.9].

Figure 9.9 presents in a nutshell quite valuable information for the optimum span length of a 220-kV double circuit line using ACSR 402/67 conductors (402-mm<sup>2</sup> aluminum, 67-mm<sup>2</sup> steel), i.e., the often used aluminum-to-steel ratio of 6 : 1, for two different conductor everyday stresses (EDS) at 10 °C. The higher this stress, the heavier the towers and the larger the foundations of the line. On the other hand, in this case, the conductor sag  $f$  and thus the number of towers  $i$  per km will decrease, leading to an optimum span length between 360 and 375 m. The span length with minimum investment costs is normally 10% higher, i.e., around 400 m, because other costs such as insulators, fittings, and earthing are directly proportional to the number of towers.

Interestingly enough, in recent years, there has been a trend in areas with low ice loads towards conductors with higher aluminum content, i.e., aluminum-to-steel ratios of up to 11 : 1 or even all aluminum conductors (AAC). These cost less than ACSR cables with the same aluminum cross-section, and although their lower tension increases the sag, at the same time, because of their smaller weight and diameter, they impose lower mechanical loads, leading to less expensive towers and foundations.

In 2013, CIGRE WG B2.51 carried out a worldwide survey on overhead line costs and published them in [9.6], from which Fig. 9.10 is reproduced, showing the total line cost per route kilometer for a number of



**Fig. 9.9** (a) Tower weight per km  $G_M$  and (b) sag  $f$  (at 40 °C) over the span length for a 380-kV line to determine the optimal span length. *Dashed lines:*  $G_{EDS} = 55 \text{ N/mm}^2 = 17\%$  of  $G_{RTS}$ ; *solid lines:*  $G_{EDS} = 65 \text{ N/mm}^2 = 20\%$  of  $G_{RTS}$  [9.9]

lines in various parts of the world, which partly explains the wide spread of costs.

Table 9.3 from the same source presents a comparison of line component costs between 1991 [9.10, 11] and 2013 [9.6].

Because the sample of answers to the survey in 2013 was considerably smaller than the more than 200 par-

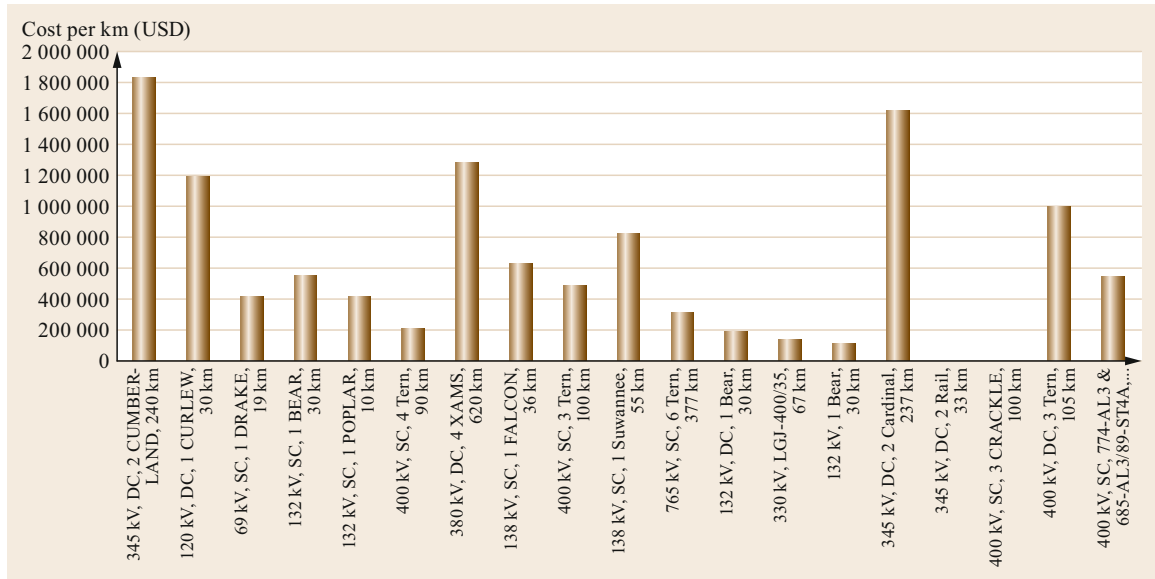


Fig. 9.10 Line costs in US dollars (USD) per route kilometer (adapted from [9.6])

Table 9.3 Comparison of line component costs between 1991 and 2013 (adapted from [9.6])

	Year	Material costs	Construction costs	Cond.	Shield wire	Insul.	Towers	FNDN
For all lines and voltages	1991	63.7	36.3	32.7	3.8	8.1	36.2	19.2
	2013	42.4	57.6	31.8	2.7	7.6	46.3	11.6
For all lines up to 150 kV	1991	64.3	35.7	31.6	4.1	8.8	36.0	19.5
	2013	46.4	53.6	28.6	2.0	7.9	49.6	11.9
For all lines over 300 kV	1991	62.6	37.4	34.1	3.9	6.9	36.4	18.7
	2013	46.8	53.2	35.7	3.0	7.2	42.7	11.4
All single-circuit lines	1991	63.6	36.4	33.1	4.2	8.2	35.6	18.8
	2013	42.8	57.2	33.4	2.8	6.9	43.7	13.3
All double-circuit lines	1991	63.8	36.2	32.0	3.3	7.9	37.1	19.7
	2013	31.0	69.0	24.7	2.3	10.6	58.1	4.3
Guyed-structure lines	1991	59.6	40.4	32.8	3.2	8.3	36.0	19.8
	2013	55.0	45.0	36.5	3.2	6.3	41.3	12.7
Lines with one conductor/phases	1991	64.4	35.6	32.2	4.2	8.5	36.3	18.8
	2013	38.7	61.3	28.3	2.0	7.8	45.1	16.9
Lines with two conductors/phases	1991	64.6	35.4	32.3	4.0	8.1	36.2	19.4
	2013	38.0	62.0	32.3	2.3	10.6	48.4	6.3
Lines with three conductors/phases	1991	60.8	39.2	35.1	3.7	7.0	40.3	13.8
	2013	41.5	58.5	36.6	4.6	6.6	42.6	9.6
Lines with four conductors/phases	1991	61.4	38.6	33.4	2.7	7.6	33.5	22.9
	2013	56.5	43.5	34.2	3.4	7.9	37.9	16.7

Participants in 1991, care should be taken when drawing conclusions. Nevertheless, analysis of the figures reveals certain trends:

- The cost per kilometer of lines increased from 1991 to 2013 in real terms mainly due to cost of labor and environmental issues.
- Design costs average around 20% of the line cost, which includes landowner and environmental considerations.
- Material costs have significantly reduced compared with construction costs.
- There were small changes in the relative shares of conductors, insulators, and fittings in the total line

**Table 9.4** Design parameters and cost breakdown for HV AC OHL

Design parameters	Nominal voltage (kV)				
	110	220	380	500	750
Thermal rating (MVA)	10–350	300–1000	1400–2700	1800–3000	3000–5000
Optimal rating (MVA)	20–100	120–350	500–1200	700–1500	2000–3000
Right of way (ROW) (m)	40–50	55–60	60–70	60–70	80–120
Tower weight (t/km)	15–25	25–35	45–65	20–40	28–50
Concrete for foundations (m <sup>3</sup> /km)	100–200	120–250	150–300	120–250	150–300
Total line costs (k€/km)	125–200	150–400	650–1200	300–600	400–750
Cost breakdown (%)					
Conductors, insulators, and fittings	35–45	40–50	45–55	45–60	45–60
Towers	35–45	35–45	35–45	30–45	30–45
Foundations	15–25	10–20	7–15	7–15	7–15
Planning	5	4	3	3	3

costs, with conductors accounting for about 20% of the total line cost.

- The percentage of costs spent on towers seems to be higher than in 1991. This increase in tower costs as a percentage may be a result of an increased number of angle and strain structures due to environmental pressures resulting in certain line routes which are not conducive to low-cost tower designs.
- Foundations costs have increased at a lower rate than other components.

In addition, Table 9.4 contains valuable information on overhead line parameters and costs, mainly from Europe. The partly lower costs at 500 and 750 kV can be explained by the fact that these are single-circuit lines compared with double-circuit 380-kV lines.

### 9.2.4 Asset Management

Asset management applies to the full life cycle, including planning, design, construction, commissioning, operation, maintenance, and decommissioning. In this sense, asset management is described in [9.12] as “coordinated activity of an organization to realize value from assets.” In addition, as many line faults remain *unknown*—which leads to incomplete analysis and action—another important task of the asset owner should be to reduce the number of unknown faults to a minimum.

The electric utility industry is in a transient condition brought on by privatization, deregulation, and competition. It is becoming increasingly difficult to obtain the required permits and/or funding to acquire new rights of way and build new lines, thus utilities are seeking ways to get the most from their existing OHL assets. In this context, owners and asset managers of overhead lines increasingly have to ask themselves the following questions [9.13]:

- Can investments in the overhead transmission system be justified?
- Can the probability of the next overhead line failure event be reasonably predicted?
- Are the right data in case of a failure event being collected and managed effectively?
- Is the present capability of the overhead line components adequately known?

In the past, such questions were answered using qualitative data and mostly based on personal experience. However, in the future, related decisions will need to be supported by quantitative information and databases which were not previously available. Using these data, risk management techniques can be applied to support management decisions. In the following, some guidelines which should be helpful to answer the questions posed above and take the right decisions are presented [9.14].

#### Investments

The goal of a management decision regarding an investment is to minimize the net present value (NPV) of the annual expenditures over a predetermined investment period. To obtain comparable results, future costs must be discounted to the present [9.14, 15], which can be calculated as follows

$$\text{NPV} = \sum_{i=0}^{i=n} \frac{C_i}{(1+r)^i}, \quad (9.3)$$

where NPV is the net present value of the annual expenditures,  $n$  is the period taken into consideration,  $r$  is the discount rate, and  $C_i$  is the annual expenditures in year  $i$ , with

$$C_i = E_i + R_i, \quad (9.4)$$

**Table 9.5** Annual expenditures related to different levels (adapted for [9.14])

Expenditures connected mainly to	Annual expenditures Planned expenditures	Risk of failure
Company level	Investments	Injury or death Serious damage to the built environment Bad publicity, loss of customers, even more difficulties finding new ROW Cascade <i>failures</i> with electrical system breakdown
System operation level	Energy and <i>capacity</i> losses	Additional energy and <i>capacity</i> losses More expensive power generation Loss of profit due to nondelivered energy Penalties by the regulator
OHL operation level	Operation and maintenance (including landowner compensation for damage to vegetation) Overhead costs for information collection and maintenance of a database	Regular inspections and patrols for checking the condition of OHL Painting, tree trimming, and smaller interventions that are performed regularly Repairs as necessary

where  $E_i$  is the deterministic costs, or planned expenditures, in year  $i$ , and,  $R_i$  is the probabilistic costs associated with a risk of failure in year  $i$ .

These components are discussed below.

### Expenditures

Planned expenditures include the cost of investments and of normal operations. These costs are related to different levels within the company, i.e., the company as a whole, the system operation division—also called electricity commerce—and the overhead lines division. Typical values for such costs are presented in Table 9.5 [9.14].

### Failures

Defects and failures in OHL occur in practice due to:

- Unforeseen external causes such as faults in an adjoining grid, extreme weather conditions, sabotage
- Internal causes such as wear, aging, deformation, poor construction, or material failure
- Operational aspects such as electrical overload, switching faults, and improper functioning of protection and control.

Failures often involve the subsequent effects:

- Fluctuations in the voltage level, leading to disturbances of operational processes of the customer
- Reconfiguration of the system, resulting in increased losses and/or higher generation costs
- Disruption to planned maintenance programs
- Restoration costs
- Financial claims arising from unavailability of the transmission line.

The risk of failure of an OHL is defined based on the probability of failure times the sum of the resulting consequences and whether the event causing failure can be predicted or not.

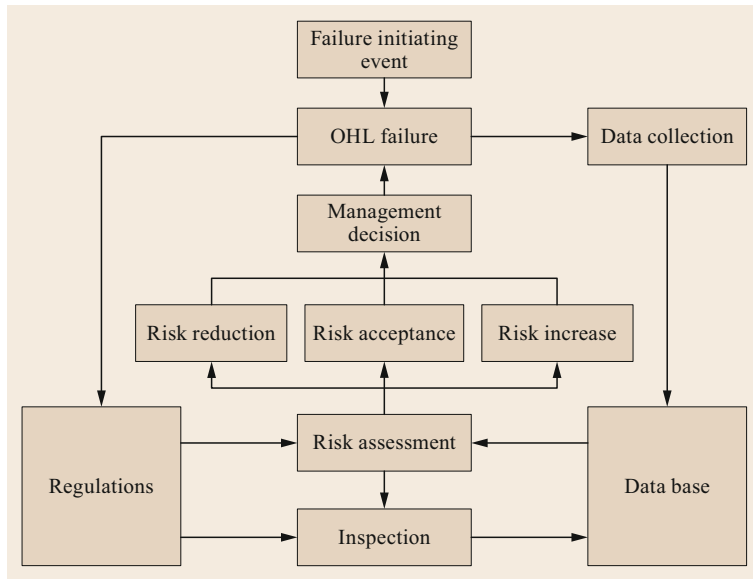
**Predictable Events.** The components of a line are subjected to many types of deterioration, such as wear, fatigue, corrosion, deformation, and elongation. Since they are made from different materials with different properties in different environments, it is likely that some of these components will deteriorate faster than others. The current capabilities including residual electrical and mechanical strength of all OHL components can be determined using appropriate inspection/assessment technology (Sect. 9.9). In addition, if a database of past component capabilities exists, then their future capabilities can be extrapolated. The weakest link, i.e., the OHL component with the highest probability to fail first, can then be determined. This is accomplished by sequentially applying to the line the relevant loading conditions and increasing the related actions stepwise, such as the magnitude of the wind velocity at different angular directions, weight of accreted ice, or combined wind and ice, until the loading on a component reaches its present capability. That represents the critical loading condition for that component, and the probability of occurrence of that loading condition (Sect. 9.3) indicates the reliability level of that component.

Failures due to predictable events can thus be managed using proactive measures, due to their predictability.

**Unpredictable Events.** Unpredictable events can only be managed by reactive measures, since their probabil-

**Table 9.6** Properties of predictable and unpredictable events (adapted from [9.14])

Properties	Failure due to Predictable events	Unpredictable events
The probability of failure is	Relatively high	Relatively low
An economic way to avoid failure	Does exist	Does not exist
<i>Proactive</i> action	Can be taken economically	Cannot be taken economically
In case of proper action, the OHTL	Will survive the <i>event</i>	Will not survive the <i>event</i>
<i>Reactive</i> actions are	Possible depending on economic evaluation	The only opportunities to reduce the <i>risk</i> economically



**Fig. 9.11** Flowchart for OHL asset management (adapted from [9.14])

ity of occurrence cannot be economically reduced using proactive measures. These include, in particular, natural disasters such as hurricanes, cyclones or typhoons, tornadoes, massive ice storms, floods, earthquakes, and earthslides, which fortunately occur infrequently. When they do, these disasters can cause total failure. Intuition, judgment, experience, and information available from a database must be used to assign the probability of failure due to unpredictable events, thus the assignment of such probabilities in situations of uncertainty proceeds on a subjective rather than objective basis (Table 9.6 [9.14]).

**Asset Management Process**

To determine appropriate options that minimize the net present value of annual expenditures over an investment period, an information system and process must be in place. Figure 9.11 [9.14] shows an idealized process in the form of a flowchart of the activities leading to management decisions for an OHL asset. A key role is played by the collection of data, which will be presented here.

**Data Collection**

To be able to carry out a proper failure or defect analysis, a database should be available, being unambiguous and containing, but not limited to, asset data as built, historical data, and in case of a failure, pre-event, event, post-event, and cost data. The following data are important for any transmission line database and can be tagged with an accuracy level index. Finally, a database should include the costs and duration of actions, as well as the costs of replacement of line segments, components, and elements.

*Asset Data as Built.* The asset data as built should be collected on three successive levels:

- Lines and circuits
- Line components
- Elements of components.

The data stored on the three levels allow one to analyze and compare successively the:

- Performance of lines
- Condition of components
- Condition of elements.

*Historical Data.* Three different kinds of historical data on overhead transmission lines can be distinguished:

- Historical actions such as:
  - Replacement or heightening of a support or a part of a line (for instance due to the construction of a railway), stringing of a second circuit, etc.
  - Maintenance or painting, life extension, refurbishment, uprating, upgrading, etc.
- Historical events such as failures, forced outages, etc.
- Historical observations and measurements on defects of assets registered in periodic inspection reports.

*Pre-event Data.*

- Design criteria and applicable manufacturing and construction standards
- As-built/constructed data including all components, elements, their manufacturer, date of commissioning, and location
- All inspection and maintenance records, including location, date, observation, deterioration, and changes or modification to any component or element
- Any refurbishment, uprating, or upgrading
- Climatic and pollution conditions along the line
- Data from any previous event
- Strategic emergency material and equipment inventory.

*Event Data.*

- Agency recording the event
- Exact time of the beginning of the event
- Distinction between incidents involving manual tripping of the line, automatic tripping, automatic tripping with successful auto-reclose, or automatic tripping with unsuccessful reclose (lockout)
- Description of climatic conditions such as wind, precipitation, and ice accretion as well as pollution influencing the line
- Nominal voltage
- Load current immediately prior to the event and an estimate of the fault current

- Name and code of the circuit involved: arm, suspension, insulator, conductor, earth wire, damper, spacer etc.
- Failure during operation, switching in, switching off, or during works
- Switching off by hand or by protection equipment
- Switching off due to electrical phenomenon, secondary installation, inadequate functioning of protection, error in operating or switching, or cause outside control area
- Cause of electrical phenomenon or defect:
  - Unforeseen external causes such as a fault in an adjoining grid, fault at a user, extreme weather conditions, fire, sabotage, birds, cranes, etc. (if weather related, estimated or measured values of wind and/or ice at the failure site and recorded values from nearby weather stations)
  - Internal causes as wear, aging, deformation, poor construction, material, assembly, manufacturing, and adjustment
  - Operational aspects such as overload, switching or testing errors, poor or insufficient maintenance, and improper operation of protection and control
  - Works in or under the line by or on behalf of the owner
- Any required continued investigation activities involving the failed component or element, or of additional similar components or elements, measurements, outside expert opinions, accident reports, formulation of a repair or replacement plan, and cost analysis
- Exact time to start the repair work
- Exact time to complete the repair work
- Exact time of recommissioning the line.

*Post-event Data.* Obviously, every failure or defect causing the line to be switched off should be properly analyzed. This analysis is meant to identify the cause and detect possible deficiencies, wear, etc. of the type of component or element involved in order to take action at other points of installation. The results of such an investigation and the measures taken should be recorded unambiguously in a database. At least, the following aspects should be mentioned:

- Reporting agency
- Time of failure
- Name and code of circuit involved
- Failed component
- Failed element

- Manufacturer and type; number of years in operation
- Voltage level
- Comparison of the condition at the time of failure with the original design criteria (i.e., pollution, mechanical loading or electrical loading)
- Material
- Description of the extent of the damage, including photographs
- Description of the manifestation of the damage, including photographs
- Identification of the cause of the damage
- Measures to be taken and action plan.

In addition, the costs incurred because of a specific failure must be recorded, in particular:

- Loss of income due to undelivered energy
- Cost of increased network losses
- Cost of switching operations
- Customer claims or penalties
- Cost of investigation
- Cost of called-in experts
- Total cost of restoration, including manpower, equipment, materials, and outside contracts

**Data Storage.** Today, an electronic database system is the most convenient tool to store, consult, revise, and extract data. Such a database enables statistics on line performance and component and element condition to

be established. To simplify the data collection and storage process, it is recommended to provide checklists so that inspection results can be stored in the database immediately after an inspection. The date of each data record is important for management decisions and thus should be included.

Evidently, the quality of the data cannot be improved by just recording it in a database. Rather, the quality depends mainly on the crew collecting the inspection information and the inspection technique applied. Both must be recorded with the corresponding date to estimate the quality and reliability. It is also important to specify who is responsible for inputting the data and who is in charge of updating them. Another important factor determining the data quality is the inspection technique. The longer the distance between the inspected item and the sensor, the less reliable the data may be.

Experience has shown that, in the past, many databases on overhead transmission lines have failed. The following reasons have been identified: the lack of reliable data for an extensive database, the lack of motivated manpower to collect, store, and maintain the data, non-user-friendly input and output, and especially the lack of a clearly accepted scope or the lack of integration with other databases.

In general, it is relatively easy to store data for a new line, but updating the database is a challenge and can involve a considerable cost. If it is updated, the database must be easy to use for the design of new lines as well as modifications of old ones.

## 9.3 Line Design

Line design is a rather complex process as it encompasses a variety of distinctly differing disciplines, such as electrical, mechanical, chemical, civil, environmental, and meteorological science. In the following, due to unavoidable space limitations, the focus is placed not so much on design details as physically intuitive and understandable explanations—and partly derivations—of the basic concepts.

### 9.3.1 Design Methods

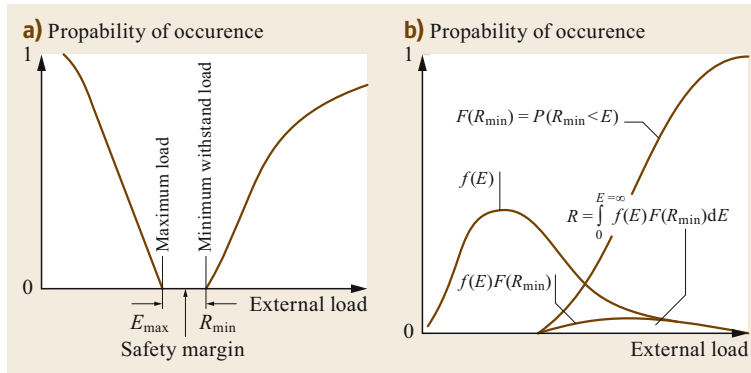
As stipulated in [9.16], an overhead line (OHL) should be designed, erected, and operated in such a way that, during its life expectancy:

- It shall perform its purpose under a defined set of conditions, with acceptable levels of reliability and

in an economic manner. This refers to aspects of reliability requirements.

- It shall be designed to avoid a progressive collapse (cascading) if a failure is triggered in a defined component. This refers to aspects of security requirements.
- It shall be designed to avoid human injuries or loss of life during construction and maintenance. This refers to aspects of safety requirements.

In this sense, all the components of a line should be designed, manufactured, and installed in such a way that, under the prevailing regular climatic conditions, the rated voltage and current, and the expected short-circuit loads, the line will operate without failure. In addition, the impact of atmospheric and switching over-voltages should be adequately considered.



**Fig. 9.12a,b** Principles of deterministic (a) and probabilistic (b) design methods (adapted from [9.1])

These conditions are best met when a line is conceived following a widely accepted national or international standard. In this section, publication [9.16] is exemplarily used, as it is applied extensively throughout Europe.

Natural phenomena, which cause loads to overhead lines, are stochastic; that is, their occurrence and implications cannot be predetermined but must rather be addressed using adequate statistical methods. This is also the case, albeit to a much lesser extent, for the material properties of the line components and in particular their structural response to external loads. Until recently in line design, a conservative approach, the so-called deterministic approach, was almost exclusively applied. In recent years, the more *realistic* but more complex probabilistic method has been standardized and in some cases applied. The concepts of and differences between these two methods are shown schematically in Fig. 9.12 [9.1].

In the deterministic approach (Fig. 9.12a), the maximum load  $E_{\max}$  is determined or estimated, often based on long-time measurements, comparisons, and approximations. For climatic loads, a return period of occurrence of 50 years is usually considered. The maximum load must be lower by a safety margin compared with the minimum strength  $R_{\min}$  of the examined component. This may be a withstand voltage for an insulator or a tensile strength for a tower member.

On the other hand, in the probabilistic method, the load  $Q$  and strength  $R$  are obtained from a statistical evaluation of a multitude of measurements under the assumption of a probability law. For overhead lines, the Gaussian or Gumbel distribution is used. As there will always be an overlap between the load and strength probability density (Fig. 9.12b), a very small probability of failure  $P_f$  remains, expressed as

$$P_f = \int_0^{E=\infty} f(E)F(R)dE. \quad (9.5)$$

This probability of failure  $P_f$  is related to the reliability of the component in question  $P_r$  by

$$P_r = 1 - P_f. \quad (9.6)$$

The required reliability level—related to a certain return period—thus determines the acceptable level of the probability of failure, which can be adjusted via (9.5), for instance by modifying the parameters of the strength function  $F(R)$ .

The focus below is on the deterministic or empirical approach, as it is still widely used and lines designed in this way have proved over the years to be extremely reliable. The deterministic approach is applied here for the mechanical design of the line and its components, while its electrical design, where the probabilistic approach is more often used, such as for insulation coordination issues, is covered in Chap. 3.

External loads or actions on a line  $E_{\max}$ , for example, due to wind or ice, are contested by the structural response, basically the geometry and material properties of the loaded component. In the case of a conductor under a tensile load, e.g., this would be the conductor cross-section and the modulus of elasticity of the conductor material. This leads to mechanical stresses in the component, which should not exceed a related strength  $R_{\min}$ , above which the component will deform permanently or even fail. Both  $E_{\max}$  and  $R_{\min}$  have to be converted considering appropriate safety margins to specified design values  $E_d$  and  $R_d$ , using (9.26) and (9.8). Thus, the basic design formula in the deterministic approach is

$$E_d \leq R_d. \quad (9.7)$$

We have to consider two limits for the external load sustainability of a component, viz. the damage limit and the failure limit, also called the mechanical strength in this context. On one hand, the damage limit



**Table 9.7** Damage and failure limits of components

Component	Loading	Damage limit	Failure limit
Members of lattice steel towers	Tension, compression	Yield strength	Breaking strength buckling
Poles made of			
– Steel	Bending moments	1% nonelastic deformation at the tower top	Collapse by local buckling or bending
– Concrete	Bending moments	Crack opening or 0.5% nonelastic deformation at the tower top	Collapse of the pole
Separate foundations	Uplift	1° rotation of the support	Excessive uplift of 50–100 mm
	Compression	Reduction of 5% in support strength	Excessive settlement of 50–100 mm
Compact foundations	Overtipping moments	1° rotation of the support	Excessive rotation of 5° or more
Conductors	Tension	Approximately 75% of characteristic strength or rated tensile strength (RTS)	Ultimate tensile strength
Insulators	Tension	Approximately 70% of rated strength	Rupture
Interface fittings	Tension	Permanent deformation	Rupture

**Table 9.8** Partial factors for materials  $\gamma_M$ 

Component	Type of stress	Type of loading	$\gamma_M$
Conductors	Tension	Limit load	1.25
Insulators	Tension, bending	Limit load	2.00
Fittings	All types of loading	Minimum failing load	1.90
Lattice towers			
– Members	Tension, compression, buckling, bearing	Limit load	1.10
– Bolted connections	Shearing, bearing	Limit load	1.25
– Welded connections	Shearing	Limit load	1.25
Poles			
– Made of steel	Tension, compression, bending, buckling	Limit load	1.10
– Concrete	Compression	Limit load	1.50
– Reinforcement	Tension	Limit load	1.15
Guyed towers, anchors	Tension	Limit load	1.60
Foundations	Uplift loading	Limit load	National requirements

is the value of the external load or related internal stress that, if exceeded, will cause damage to the component that will impair its functionality. For example, when its damage limit is exceeded, a post composite insulator will exhibit permanent deflection but will not drop the conductor (Sect. 9.5.5). The failure limit, on the other hand, is the load which will cause permanent failure of the component, due to high deformation, loss of stability (buckling), or loss of mechanical integrity (breakage), which will endanger the safety of the related structure.

Table 9.7 presents the damage and failure limits of various line components according to [9.17]. By their nature, these material properties exhibit a certain degree of scatter. Also, the dimensions of the components in question vary slightly due to production processes. This can be taken into account by reducing a material

property  $R_K$  by a suitable safety factor, in [9.16] called the partial factor for materials  $\gamma_M$  (Table 9.8). Thus, the related design value  $R_d$  becomes

$$R_d = \frac{R_K}{\gamma_M} . \quad (9.8)$$

### 9.3.2 Line Loads

A transmission line is subject to a number of different loads, caused by:

- Conductor weight
- Ice weight
- Wind pressure
- Conductor tension
- Conductor vibrations



**Fig. 9.13** Extreme ice accretion on line conductors leading to line outage (photo: Landsnet, Iceland)

- Temperature variations
- Exceptional loads.

These are, with the exception of conductor vibrations, static or quasistatic loads. In addition there are exceptional loads, which occur accidentally, such as during construction and maintenance, short circuits, differential settlement of foundations, or—very seldom—loads from conductor failures (which can cause a tower cascade), avalanches, and earthquakes. The most important loads for line design, besides the weight of the conductors, are the so-called climatic loads, i.e., wind and ice loads, which are examined below.

### Conductor Weight

The conductor weight and ice on conductors cause the main vertical loads on the components of a line. These loads are transferred via the fittings and the insulators to the supports and ultimately to the foundations.

The conductor weight per unit length can be found in manufacturers' tables. Typical values for high-voltage lines are between 10 and 20 N/m. To calculate the related conductor load, one must know the so-called weight span, which is defined as the distance between the low-point sags of one span to the low-point sag of the next. When there is no height difference between the conductor attachment points at the adjacent spans, the weight span is the arithmetic mean of the length of these spans; otherwise, the weight span has to be calculated using the so-called complementary span method [9.4, pp. 541].

### Ice on Conductors

Ice on the conductor increases the conductor weight; ice loads thus act in the vertical direction. In extreme climatic conditions, they can overload the line, causing catastrophic failure and line outage (Fig. 9.13).

Ice accretion on line conductors is a complex physical process, well described in [9.19]. Table 9.9 lists the main characteristics of the different ice types [9.18], and Fig. 9.14 shows common types of ice on conductors.

Ice loads on conductors with a value  $q_i$  per unit length cause vertical loads as well as increased tension in the conductors. The related loads on suspension insulators and supporting structures can be calculated similarly as for the conductor unit weight, i.e., by using the relevant weight span.

Due to the lack of sufficient statistical data on ice, design values for ice loads are mostly based on experience or long-term applications with positive results. Often, these values are related to the conductor diameter  $d$  and vary according to the topography, i.e., height above sea level and differing climatic and atmospheric conditions. A typical value for  $q_i$  for average ice conditions is 20 N/m.

**Table 9.9** Classification of ice types with typical density ranges (adapted from [9.18])

Ice and snow type	Density (kg/m <sup>3</sup> )	Description
Glaze ice	700–900	Pure solid ice, sometimes icicles underneath the wires. The density may vary with the content of air bubbles. Very strong adhesion and difficult to knock off
Hard rime	300–700	Homogeneous structure with inclusion of air bubbles. Pennant shaped against the wind on stiff objects; more or less circular on flexible cables. Strong adhesion and more or less difficult to knock off, even with a hammer
Soft rime	150–300	Granular structure, <i>feather like</i> or <i>cauliflower like</i> . Pennant shaped also on flexible wires. Can be removed by hand
Wet snow	100–850	Various shapes and structures are possible, mainly dependent on the wind speed and torsional stiffness of the conductor. When the temperature is close to zero, it may have a high content of liquid water, slide to the bottom side of the object and slip off easily. If the temperature drops after accretion, the adhesion strength may be very strong
Dry snow	50–100	Very light pack of regular snow. Various shapes and structures are possible; very easy to remove by shaking of wires
Hoar frost	< 100	Crystal structure (needle like). Low adhesion, can be blown off



**Fig. 9.14a–c** Different types of ice on conductors. (a) Glaze ice (photo: F. Jackl), (b) soft rime, (c) wet snow (photo: Landsnet, Iceland)



**Fig. 9.15** Bora wind causes severe conductor blow-out (photo: F. Jackl)

As an example, the values specified for Germany with respect to altitude are

$$\begin{aligned} q_i &= 5 + 0.1d \text{ N/m} && \text{(below 400 m)} \\ q_i &= 10 + 0.2d \text{ N/m} && \text{(between 400 and 600 m)} \\ q_i &= 15 + 0.3d \text{ N/m} && \text{(between 600 and 750 m)} \\ q_i &= 20 + 0.4d \text{ N/m} && \text{(above 750 m).} \end{aligned}$$

### Wind Loads

Wind can cause severe loads on transmission lines (Fig. 9.15). In particular, wind loads on conductors will cause increased conductor tension, which will not only be transferred via the insulators to the line supports and their foundations, but will also considerably influence the tower top geometry via conductor displacement.

**Wind Action on Line Components.** The value of the force  $Q_{wx}$  caused by a wind blowing horizontally and perpendicular to any element of a line is given by

$$Q_{wx} = q_z G_q G_x C_x A, \quad (9.9)$$

where  $q_z$  is the dynamic wind pressure at height  $z$ ,  $G_q$  is the gust response factor,  $G_x$  is the structural resonance factor for the element considered,  $C_x$  is the drag factor depending on the shape of the element considered, and  $A$  is the area of the element projected onto a plane perpendicular to the wind direction. However, the parameters in (9.9) are defined differently in relevant standards.

The wind pressure  $q_z$  on a surface  $A$  can be calculated from Bernoulli's equation, under the assumption that the kinetic energy at the reference wind velocity  $v_z$  is fully transformed to pressure when the wind is stopped by this surface, i.e.,

$$q_z = \frac{1}{2} \rho v_z^2. \quad (9.10)$$

Use of an air density of  $\rho = 1225 \text{ kg/m}^3$  (15 °C, a.s.l.) yields

$$q_z \approx 0.6 v_z^2 \quad (q_z \text{ in N/m}^2, v_z \text{ in m/s}). \quad (9.11)$$

The reference wind velocity  $v_z$  is obtained from

$$v_z = k v_{\text{mean}}. \quad (9.12)$$

Here,  $v_{\text{mean}}$  is the annual mean of the maximum wind velocity measured in open terrain at a reference height of 10 m above ground and  $k$  is a factor considering the envisaged return period, the number of observation years, and the yearly standard deviation; For example, for a return period of 50 years, a measurement period of 30 years, and a standard deviation of 0.14, one gets  $k = 1.42$ .

The reference wind velocity  $v_z$  increases with height  $h$  above ground due to the boundary effect, since frictional forces reduce  $\rho$  near the ground. It can be calculated from

$$v_z(h) = k_r v_z \ln \left( \frac{h}{z_0} \right), \quad (9.13)$$

**Table 9.10** Terrain categories, roughness length  $z_0$ , and terrain factor  $k_r$ 

Terrain category		$z_0$ (m)	$k_r$
0	Sea or coastal area exposed to open sea	0.003	0.155
I	Lakes of flat and horizontal area with negligible vegetation and without obstacles	0.01	0.169
II	Area with low vegetation such as grass and isolated obstacles (trees, buildings) with separations of at least 20 times obstacle heights	0.05	0.189
III	Area with regular cover of vegetation or buildings or with isolated obstacles with maximum separation of 20 times obstacle heights (such as villages, suburban terrain, permanent forest)	0.3	0.214
IV	Area in which at least 15% of the surface is covered with buildings with average height exceeding 15 m	1	0.233

Note: The terrain categories are illustrated in [9.20].

where  $k_r$  is the terrain factor and  $z_0$  is the roughness length (Table 9.10 [9.16]). The latter can also be used to calculate the turbulence intensity

$$I_v(h) = \frac{1}{c_0 + \ln(h/z_0)}. \quad (9.14)$$

Therein,  $c_0$  is the orography factor, which considers the effects of topography and can be set to  $c_0 = 1$  when the average slope of the upwind terrain is small. Together with  $v_z(h)$  and using

$$q_z = \frac{1}{2} \rho v_z^2, \quad (9.15)$$

one gets the peak wind pressure at a reference height  $h$  above the ground to be used in the calculation of the horizontal wind force on any line component as

$$q_p(h) = [1 + 7I_v(h)]q_z(h). \quad (9.16)$$

The two remaining factors in (9.9), viz. the structural resonance factor  $G_x$  and the drag factor  $C_x$ , differ for different components of the line and are considered in the respective sections.

**Wind Action on Conductors.** For typical conductor sizes, the recommended drag factor is  $C_C = 1.0$ . Also, the structural resonance factor  $G_C$  is called the span factor and considers the spatial effects of the wind on a span, as it is recognized that the wind will not act simultaneously on the whole length of the span. In some standards, this factor drops linearly from 1.0 to 0.7 for spans of 350 to 500 m, respectively. Thus, the wind pressure on the conductors of two adjacent spans will cause the following load on the associated support

$$Q_{WC}(\theta) = q_p(h)G_C C_C d a_W \cos^2(\theta), \quad (9.17)$$

where  $d$  is the conductor diameter,  $a_W$  is the wind span—defined as the arithmetic mean of the spans adjacent to the tower—and  $\theta$  is the angle between the wind direction and the conductor. In the case where the wind

acts perpendicular to the normal conductor,  $\theta = 0^\circ$  and (9.17) becomes

$$Q_{WC}(0^\circ) = q_p(h)G_C C_C d a_W. \quad (9.18)$$

In the case of a conductor bundle, the total wind load is defined as the sum of the wind loads on the individual subconductors, without taking into account any sheltering effects on leeward conductors.

The wind load will cause the conductor to swing; this will affect the distance of the conductor from the other conductors and earthed objects in its neighborhood and has to be adequately considered by respecting the statutory clearances (Sect. 9.3.3). The swing angle  $\varphi_C$  of the conductor follows from

$$\varphi_C = \arctan\left(\frac{q_p(z)G_C C_C d a_W}{m_C g a}\right), \quad (9.19)$$

where  $a_W$  is the wind span and  $m_C$  is the conductor mass per unit length.

**Combination of Wind and Ice Loads.** The wind action on ice-covered conductors must also be considered in the design of line supports, such as an extreme ice load combined with a high-probability wind velocity; in this case, the wind pressure may be reduced by 50%.

The equivalent diameter in m of an ice-covered conductor may be calculated [9.4, p. 185] as

$$D_i = \sqrt{d^2 + \frac{4g_i}{\pi\rho_i}} = \sqrt{d^2 + 0.000170g_i}, \quad (9.20)$$

where  $d$  is the diameter of the conductor [m],  $g_i$  is the characteristic ice load on the conductor [N/m], and  $\rho_i$  is the ice load density [N/m<sup>3</sup>].

The density of the ice  $\rho_i$  may be assumed to be 7500 N/m<sup>3</sup>, and the drag factor to be 1.0.

**Wind Action on Insulators.** Wind forces on insulators result from wind forces on the conductors as well

as from wind pressure on the insulators themselves. The latter is given by the expression

$$Q_{W_{ins}}(h) = q_p(h)G_{ins}C_{ins}A_{ins}, \quad (9.21)$$

where  $q_p(h)$  is the peak wind pressure,  $h$  is the reference height above ground to be used for the insulator set (which is the height of the attachment point on the support),  $G_{ins}$  is the structural factor for the insulator (with a recommended value of 1.0),  $C_{ins}$  is the drag factor for the insulator set (with a recommended value of 1.2), and  $A_{ins}$  is the area of the insulator.

For the design of the insulator itself, the resultant force  $Q_{ins}$  from the weight and the wind load of the suspended conductor has to be considered. This load is important as its direction determines the swing angle  $\varphi_{ins}$  of the insulator and thus the clearance to the line support (Sect. 9.3.3)

$$\varphi_{ins} = \arctan\left(\frac{q_p(z)C_cG_Ld a_W + Q_{W_{ins}}/2}{w_C + w_{ins}/2}\right), \quad (9.22)$$

where  $C_c$  is the drag factor (equal to 1.0 for typical conductors),  $q_p(z)$  is the peak wind pressure,  $G_L$  is the span factor taking into account the effect of the span length,  $d$  is the conductor diameter,  $Q_W$  is the wind span,  $Q_{W_{ins}}$  is the wind load on the insulator set,  $W_C$  is the effective conductor weight taking into account the differences in the level of the conductor attachment points, and  $W_{ins}$  is the dead weight of the insulator set.

**Wind Action on Line Supports.** There are two basic types of line support: The *classical* steel lattice towers and the increasingly used, in particular for compact lines, polygonal or circular poles (steel, concrete, wood, etc.) (Sect. 9.7). For the latter, the calculation of the wind forces is relatively simple, as they have basically a cylindrical shape.

The wind forces on poles can thus be determined by

$$Q_{WP}(h) = q_p(h)G_P C_P A_P, \quad (9.23)$$

where  $q_p(h)$  is the peak wind pressure,  $h$  is the reference height above the ground of the pole,  $G_P$  is the structural factor for the pole (with a recommended value of 1.0),  $C_P$  is the drag factor for the pole (with values between 0.7 for circular and 1.4 for hexagonal cross-section, for wooden poles  $C_P = 0.9$ ), and  $A_P$  is the area (or section) of the pole projected onto a vertical plane perpendicular to the wind direction.

On the other hand, the calculation of the wind forces on steel lattice towers follows basically the same procedure as for other line components as per (9.9), whereby the lattice tower is divided into sections. The related drag factor  $C_T$  depends on the so-called solidity ratio  $\chi$ , defined as the ratio of the effective area  $A_T$  of the tower profile to the circumscribed area of the respective tower section  $h(b_1 + b_2)$  [9.21]

$$\chi = A_T \frac{2}{h(b_1 + b_2)} \quad (9.24)$$

and can be calculated as [9.22]

$$C_T = 3.96(1 - 1.5\chi + \chi^2). \quad (9.25)$$

In case of the usual design with angle sections,  $C_T$  may be assumed to be approximately and uniformly 2.8 [9.22].

**Security Loads.** Security loads as per [9.16] cover one-sided release of static tension in a conductor and conventional unbalanced overloads such as unequal ice loads on adjacent spans, respectively. They cause longitudinal and torsional loads on the line supports and have to be considered accordingly.

**Safety Loads.** Line supports should be able to withstand all construction and maintenance loads that are likely to be imposed on them with an adequate margin of safety, taking into account working procedures, temporary guying, lifting arrangement, etc., as well as loads related to the weight of linesmen, which is assumed not be less than 1.0 kN acting together with the permanent loads.

**Short-Circuit Loads.** Consideration should be given to the effects of the forces imposed on the overhead lines forming part of a transmission system with very high short-circuit characteristics. The main concern during a short circuit is whether uncontrolled swinging of conductors could lead to conductor clashes, resulting in permanent circuit isolation following circuit-breaker operation at that time. The basics of the mechanical effects of short circuits are well explained in [9.23]. Short-circuit conditions may also cause mechanical problems on supports and conductor hardware, such as spacers and spacer dampers. The latter is examined in Sect. 9.6.3.

**Avalanches and Earthquakes.** When routed through mountainous regions, overhead lines may be exposed to avalanches or creeping snow. As such, consideration should be given to the possible additional loads

on the supports, foundations, and possibly conductors. The same applies for lines in seismically active regions, where forces due to earthquakes have to be taken into account, which will depend on the eigenfrequency of the support, the site structure resonance factor—varying with the soil conditions—and the height, weight, and mass distribution of the support. Since the frequency of the support is higher than that of the conductors, the dynamic load from the conductors will not be significant. Conversely, no important effects from the support relative to conductors should be expected.

### Partial Factors for Actions

It is evident from the discussion above that the determination of the different loads is coupled with uncertainties, as most of them are stochastic in nature. Similar to the partial factors for material properties presented in Sect. 9.3.1, partial factors  $\gamma_F$  must also be introduced for actions, which have to be multiplicatively applied to the characteristic value  $E_K$  of a certain action in order to obtain the respective design value  $E_d$ ,

$$E_d = \gamma_F E_K . \quad (9.26)$$

Table 9.11 [9.16] presents recommended values for the partial factor  $\gamma$  and combination factor  $\Psi$  for the actions presented in this section for various reliability levels as per Table 9.12, whereby the reference is level 1.

### 9.3.3 Electrical Clearances

Besides the mechanical issues, line design also has to consider the electrical requirements of a transmission

**Table 9.11** Partial and combination factors for actions (adapted from [9.16])

Action	Sym- bol	Reliability level		
		1	2	3
Variable actions (climate loads):				
Extreme wind load	$\gamma_w$	1.0	1.2	1.4
Nominal wind load	$\Psi_w$	0.4	0.4	0.4
Extreme ice load	$\gamma_i$	1.0	1.25	1.5
Nominal ice load	$\Psi_i$	0.35	0.35	0.35
Permanent actions:				
Self-weight	$\gamma_G$	1.0		
Security loads (accidental actions):				
Torsional loads due to conductor tension	$\gamma_{A1}$	1.0		
Longitudinal loads due to conductor tension	$\gamma_{A2}$	1.0		
Safety loads:				
Construction and maintenance loads	$\gamma_P$	1.5		

**Table 9.12** Reliability levels

Reliability level	Theoretical return period $T$ of climatic actions (years)
1 (reference)	50
2	150
3	500

line, not only from the system perspective (Chap. 5) but also from the reliability and safety point of view. This is basically an issue of insulation coordination (Chap. 3), which leads to certain minimum clearances, which again will influence the support geometry and the necessary right of way (ROW), specifically the distance to objects near the line, such as roads, buildings, crossings with other lines, etc. Nowadays though, in most if not all cases, the ROW will be determined by the imposed electromagnetic field (EMF) limits presented in Sect. 9.3.4.

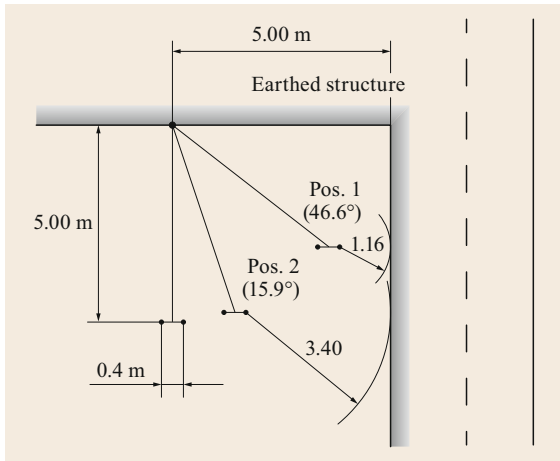
### Internal Clearances

The geometry of the top of the line supports must be designed so as to ensure that the so-called internal clearances between live parts and supporting earthed structures as well as between conductors within the span, especially in mid-span, are respected. Thereby and because of economic considerations, a very small number of interphase flashovers is considered acceptable, as these will not affect the safety of the public.

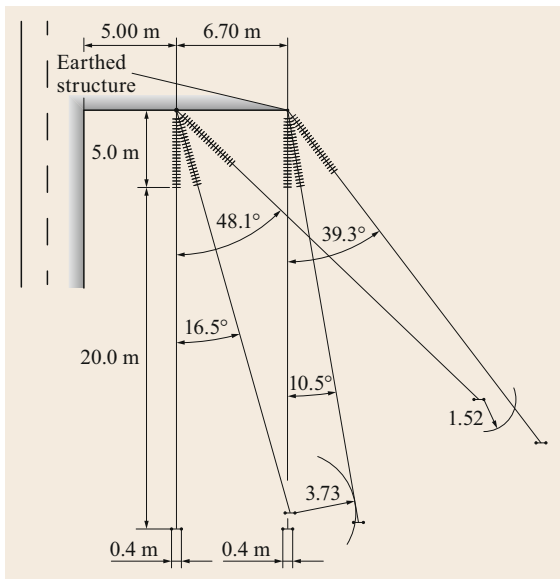
In a first step, the conductor and insulator positions due to the action of wind have to be determined. Methods to calculate the conductor and insulator displacement are detailed in [9.24] (Fig. 9.16) for the clearances between live conductors and earthed structures, such as the supports, while [9.25] (Fig. 9.17) gives guidance on the calculation of these displacements for the clearances between conductors within the span. In the case of long spans, differential swing angles may occur between horizontal phase conductors, thus one phase conductor may swing more than an adjacent one, causing reduced clearances. This situation has been designated more recently as *asynchronous swing*, resulting in a tower top geometry design based upon statistical considerations.

In [9.25], valuable information was gathered from quite a large number of countries and completed with information from standards. The related review resulted in a proposal to consider two situations when designing the tower top geometry and mid-span clearances in view of conductor and insulator swing under the action of wind load:

- In *still air* or under moderate winds, there should be adequate clearance to withstand lightning or switch-



**Fig. 9.16** Clearance between insulator set and earthed structure (400 kV, twin-bundle ACSR Finch (ACSR 564/72), 5 min wind velocity, 400 m wind span) (adapted from [9.24])



**Fig. 9.17** Clearances between adjacent conductors in mid-span (400 kV, twin-bundle ACSR Finch (ACSR 564/72), 5 min wind velocity, 400 m wind span) (adapted from [9.25])

ing surge impulse voltages with a probability of more than 90%. Still-air conditions apply to conductor positions occurring during at least 99% of the operation period.

- Under *high wind*, the clearances should be adequate to withstand the power frequency voltage only. The probability of flashovers depends on the probability

**Table 9.13** Type of internal clearance per load case

Type	Electrical stress of the air gap	Load case
1	Lightning/switching impulse voltage	Still-air conditions with maximum conductor temperature or ice load
2	Reduced impulse voltage	Reduced wind load ( $T = 3$ years)
3	Power frequency voltage	Extreme wind load ( $T = 50$ years)

of occurrence of the corresponding wind velocity. For a wind velocity having a return period of 50 years, the probability of flashover will be 1% per year at maximum.

In [9.16], three load cases for the internal clearances are considered. They are summarized in Table 9.13, where  $T$  is the return period of the wind load.

Certain countries consider additional load cases such as galloping (Sect. 9.4.11) and different wind or ice loads on adjacent conductors.

In a second step, the clearances necessary to withstand given electrical stresses have to be determined. These are derived from the electrical characteristics of the transmission system, in particular from its insulation level as per [9.26]. This standard prescribes that, for lines up to 245 kV, lightning (fast front) impulses determine the insulation level, while for lines above 245 kV, switching (slow front) impulses do.

Finally, coordination between the conductor positions and electrical stresses has to be established. For this purpose, [9.25] proposes to consider at least two cases when designing the tower top geometry and mid-span clearance (Table 9.14).

Case 1 is described by the conductor and insulator positions which would occur under the action of the design wind velocities having a return period  $T$  of 50 years. These positions are combined with the clearances required to withstand power frequency voltages. The probability of flashovers depends on the probability of occurrence of the corresponding design wind velocity. For a wind velocity having a return period of 50 years, the probability of flashover will be 1% per year at maximum.

Case 2 is described by the conductor and insulator positions which are assumed not to be exceeded during 99% of the time. These positions are combined with the clearances required to withstand the lightning or switching overvoltages with a probability of more than 90%. The flashover probability is that at which the design overvoltage conditions will be exceeded.

**Table 9.14** Coordination of conductor positions and electrical stresses (adapted from [9.25])

Electrical stress of the air gap	Probability	Conductor and still air or moderate wind during 99% of time	Insulator positions High wind velocity with $T = 50$ years
		High	Low
Power frequency voltage	High	Covered by cases 1 and 2	Case 1
Lightning/switching impulse voltage	Low	Case 2	Not considered

**Table 9.15** Required clearances for power frequency voltages

Voltage level		[9.27]		[9.16]	
$U_R$ (kV)	$U_S$ (kV)	$D_{pe\_pf}$ (m)	$D_{pp\_pf}$ (m)	$D_{pe\_pf}$ (m)	$D_{pp\_pf}$ (m)
110	123	0.32	0.42	0.23	0.37
230	245	0.64	0.85	0.43	0.69
400	420	1.16	1.85	0.70	1.17
500	525	1.68	2.20	0.86	1.47

These clearances apply to the following reference conditions for altitudes not exceeding 1000 m:

- Temperature 20 °C
- Air pressure 101.3 hPa (1013 mbar)
- Humidity 11 g/m<sup>3</sup>.

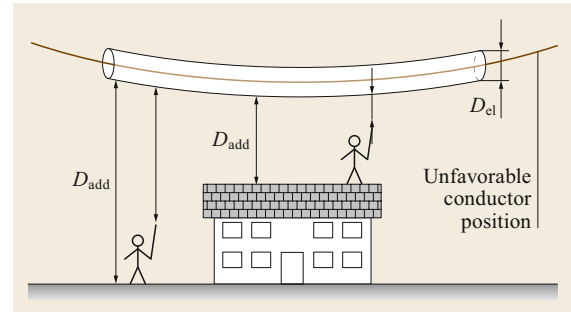
Between live parts of insulator sets or conductors and earthed components, and between conductors and earth wires, minimum phase-to-earth clearances are required, while between live conductors having differing phases, minimum phase-to-phase clearances must be complied with. Tables 9.15 and 9.16 present the clearances under power frequency and impulse voltages, respectively, for the two system voltage categories mentioned above.

### External Clearances

External clearances have to be respected between the live parts of the line and their neighborhood, so that danger from an electrical discharge to the general public and persons working and/or maintaining the power lines can be avoided. The following situations have to be considered:

- Clearances to ground in remote areas
- Clearances to residential and other buildings
- Clearances when crossing lines or adjacent to roads, railways, and navigable waterways
- Clearances when crossing or running parallel to other power lines or overhead telecommunication lines
- Clearances to recreational and sports areas
- Clearances in other specific situations.

These are often vertical clearances, where the maximum conductor temperature is of paramount impor-

**Fig. 9.18** Definition of external clearances (adapted from [9.4])

tance, as this will result in the maximum conductor sag. Sag calculations (Sect. 9.4.4) should be based on the maximum continuous service temperature of the conductor.

External clearances consist of the necessary electrical distance  $D_{el}$  and an additional safety distance  $D_{add}$  so that neither persons nor objects come dangerously close to the live line (Fig. 9.18 [9.4, p. 59] and Table 9.17 [9.16]).

### 9.3.4 Environmental Issues

The first 380-kV—in practice 400-kV—overhead line worldwide was constructed and put into operation in 1952 in Sweden. Many other similar lines followed in order to keep pace with the enormous demand for electricity necessary to resurrection the economy after World War II. In those days, overhead lines were neither ugly nor beautiful and were not considered harmful to health. On the contrary, it was a privilege to be connected to the electrical grid, which by the way is still the case in many developing countries.

However, things have changed. Since then, the ecological conscience of the public in industrialized countries—and elsewhere—has been awakened, and transmission lines are often criticized and their construction strongly objected to, on one hand due to their visual impact and on the other due to the purported harmful impact of their electromagnetic fields (EMF) on health. This attitude of the public—and some journalists and politicians—has caused in many cases serious delays to the approval and construction of new



**Table 9.16** Required clearances for impulse voltages

Voltage level		Impulse voltages			[9.28]	[9.27]	[9.16]		
$U_R$ (kV)	$U_S$ (kV)	$U_{90\%_{ff}}$ (kV)	$U_{50\%_{ff}}$ (kV)	$U_{max_{sf}}$ (kV)	$D_{pe}$ (m)	$D_{pe}$ (m)	$D_{pp}$ (m)	$D_{pe}$ (m)	$D_{pp}$ (m)
110	123	450	490	–	0.9	0.94	0.96	0.89	1.00
		550	590	–	1.1	1.13	1.17	1.07	1.20
230	245	850	920	–	1.7	1.76	1.83	1.67	1.86
		950	1030	–	1.9	1.97	2.05	1.87	2.07
		1050	1140	–	2.4	2.18	2.26	2.05	2.29
400	420	1175	1270	850	2.4	2.40	2.70	2.25	2.67
		1300	1410	950	2.9	2.80	3.20	2.64	3.15
		1425	1540	1050	3.4	3.25	3.73	3.02	3.68
500	525	1300	1410	950	2.9	2.80	3.20	2.64	3.15
		1425	1540	1050	3.4	3.25	3.73	3.02	3.68
		1550	1680	1175	4.1	3.90	4.48	3.60	4.40

$U_R$  nominal voltage;  $U_S$  highest system voltage for equipment;  $U_{ff}$  fast front (lightning impulse) withstand voltage;  $U_{max_{sf}}$  maximum slow front (switching impulse) withstand voltage;  $D_{pe}$  minimum phase-to-earth clearance;  $D_{pp}$  minimum phase-to-phase clearance

**Table 9.17** Distances  $D_{add}$  (m) to obstacles in addition to  $D_{el}$  (adapted from [9.16])

Crossed obstacle	Maximum conductor temperature; ice load; average wind load	Local ice load
Ground in open countryside		
– Normal ground profile, used by agriculture	5.0	a
– Steep slopes	2.0	a
Trees		
– Impossible to climb	0.0	a
– Possible to climb	1.5	a
Buildings with fire-resistant roofs		
– Slope greater than 15°	2.0 <sup>b</sup>	2.0 <sup>b</sup>
– Slope less than 15°	4.0 <sup>c</sup>	4.0 <sup>c</sup>
Non-fire-resistant roofs	10.0	10.0
Antennas, street lamps, flag poles, and similar structures	2.0	2.0
Roads	6.0	6.0
Electric overhead contact lines	2.0	2.0
Ropeways	2.0	2.0
Towers of ropeways	4.0	4.0
Gauge of navigable waterways	2.0	2.0
Power lines and telecommunication lines	$D_{pp}^d$	$D_{pp}^d$
Recreational areas		
– General	7.0	7.0
– Swimming pools	8.0	8.0
– Permanently installed facilities	3.0	3.0

<sup>a</sup> Verification of clearances is not required for local ice loads <sup>b</sup> Required minimum clearance distance 3 m <sup>c</sup> Required minimum clearance distance 5 m <sup>d</sup> Required minimum clearance distance 1 m

lines, many of which are badly needed for the integration of the increasing number of renewable energy sources (RES). The industry has reacted and introduced a plethora of measures not only to inform the public but also to comply with the related laws and regulations; the latter will evidently influence line design. In addition, line components have to be selected and de-

signed with consideration of the life cycle assessment (so-called LCA) of the line. In this sense, this section covers:

- Calculation of EMFs
- Impact of EMFs on health
- Other environmental issues

- Consultation models
- LCA.

### Calculation of EMFs

Overhead lines create both electric and magnetic fields with a low frequency of 50 or 60 Hz. Electric fields in general influence electric charges, also on the surface of the human body, affecting the current flow within the body, while magnetic fields induce currents in it, which depend on the dimensions as well as the conductivity of the different parts of the human body. A first necessary step is thus to calculate the electric and magnetic fields in the vicinity of a line.

Nowadays, such calculations are done using computer simulations based on approaches such as the finite element method (FEM) or boundary element method (BEM). The problem can be simplified to a good approximation to be only two dimensional, whereby the conductors are considered to be of infinite length.

**Electric Field.** The electric field resulting from a high-voltage line depends on the voltage, the form of the tower, and the configuration of the conductors. It is easily calculated from Maxwell's equations if the charges on the conductors and the ground are known. In the two-dimensional approximation, a charge  $q$  gives rise to a field strength  $E(R)$

$$E(R) = \frac{q}{2\pi\epsilon_0 R}, \quad (9.27)$$

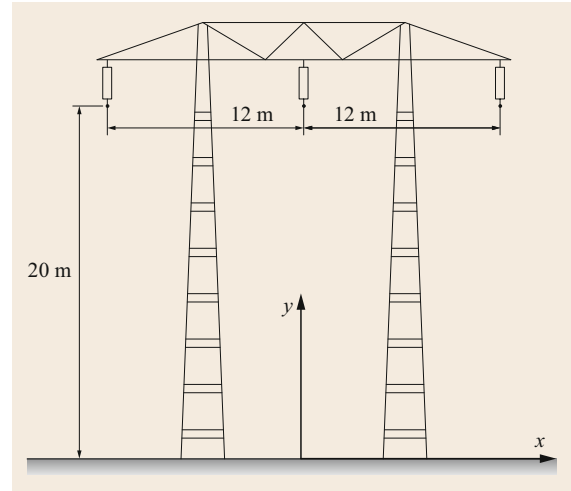
where  $R$  is the distance to the charge and  $\epsilon_0$  is the dielectric constant of vacuum.

For this calculation, the charges on the conductors and ground first have to be calculated by solving Poisson's equation. This can be done, for example, by means of the capacity matrix. A typical plot is shown in Fig. 9.20 for the conductor arrangement in Fig. 9.19 [9.29]. The maximum root-mean-square (rms) values of the electric field shown there are obtained at the time instants when the voltage of the middle conductor is at its maximal value or passes through zero, i.e., when the voltage values of the left and right conductors are equal.

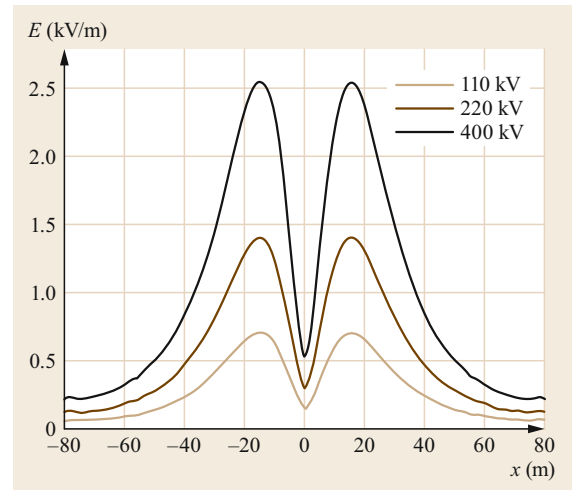
**Magnetic Field.** The value of the magnetic field  $B(R)$  due to a current  $I$  at a radial distance  $R$  from the conductor is given in the two-dimensional (2-D) approximation considered here by the simple expression

$$B(R) = \frac{I}{2\pi\mu_0 R}, \quad (9.28)$$

where  $\mu_0$  is the permeability of vacuum.

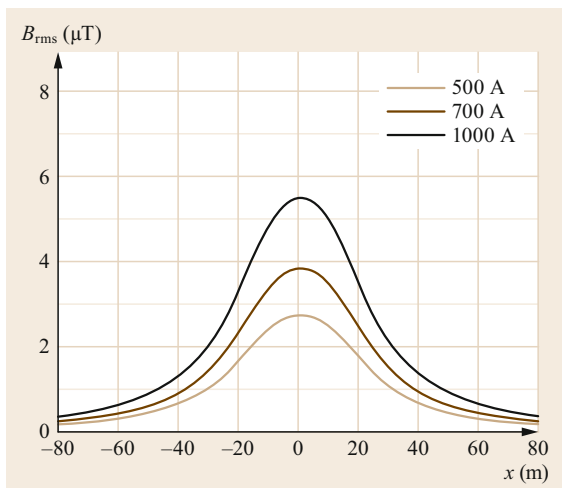


**Fig. 9.19** Schematic of a high-voltage line for EMF calculations (earth wires neglected) (adapted from [9.29])



**Fig. 9.20** Lateral distribution of maximum (rms) electric field  $E$  of the line in Fig. 9.19 at 2 m above the ground with a conductor 20 m above the ground (adapted from [9.29])

The direction of the magnetic field vector is always tangential to concentric circles around the conductor, following the so-called right-hand rule. As in the case of the electric field above,  $B(R)$  is the value of the total magnetic field strength, i.e., the value of the vector sum of the magnetic field strengths of the three phases. Figure 9.21 [9.29] shows the related rms value for the line configuration in Fig. 9.19, and Fig. 9.22 shows a schematic of the three-dimensional (3-D) magnetic field distribution for a line with so-called Danube-type towers. Evidently, the highest field values occur in the center of the span (greatest sag) and fall off rapidly.



**Fig. 9.21** Lateral distribution of maximum magnetic field (rms) of the line in Fig. 9.19 at 2 m above the ground with a conductor at 20 m above the ground

The electric and magnetic field values depend strongly on the line design and in particular on the support geometry and conductor arrangement (Table 9.18 [9.30]). Therein, the influence of these parameters on the radio interference (RI) and acoustic noise (AN), both arising from the so-called corona effect (Sect. 9.4.7), is also shown.

Specifically:

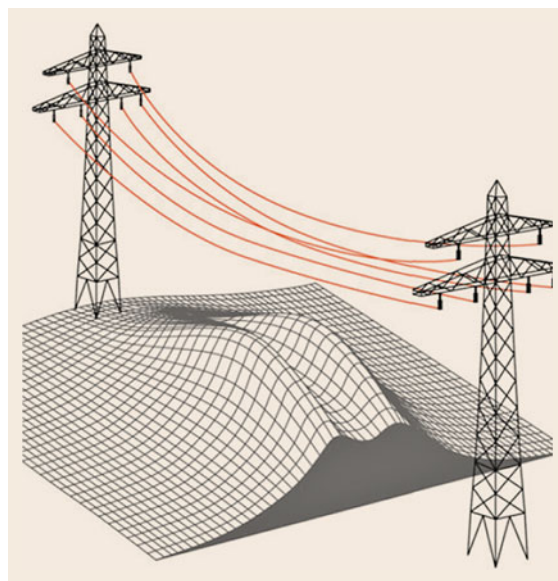
- Compaction is the best way to reduce the EF at ground level.
- Compaction is the best way and increasing the height of the conductor the easiest way to reduce the MF at ground level [9.31].
- Compaction increases the AN and RI levels, as the related EF increases on the conductor surface of the phase conductors.
- The best way to reduce the RI and AN levels is to increase the number of subconductors.

In addition, transposition of the conductors can reduce the EMF considerably [9.32].

**Table 9.18** Influence of line parameters on electrical line design

Parameter	EF	MF	RI	AN
Phase-to-phase distance ↑	↑	↑	↘	↓
Conductor height above the ground ↑	↓	↓	↘	↘
Number of subconductors (for given total cross-section) ↑	↓	=	↓	↓
Subconductor spacing ↑	↗	=	↗	↗
Total conductor cross-section ↑	↗	=	↘	↘

↑ Strong increase, ↓ Strong decrease, ↗ Slight increase, ↘ Slight decrease, = no significant effect, EF: electric field, MF: magnetic field, RI: radio interference, AN: acoustic noise



**Fig. 9.22** 3-D distribution of the magnetic field of a double-circuit line

### Impact of EMFs on Health

In the 1970s, a new issue emerged, namely the purported negative effects that lines might have on public health. In line with the megatrend of the growing environmental awareness of the public, this has become a major concern for the industry, beside line esthetics (Sect. 9.7.6). For many years, this health issue has been closely monitored by a special-purpose, permanent CIGRE working group, WG C3.01, which recently published two state-of-the-art reports, from which the following information is extracted [9.33, 34].

It all started with a study carried out in Denver, Colorado in 1979 [9.35]. The authors were looking for possible environmental factors around the homes of children who had leukemia. The magnetic field produced in houses by the current flowing in the wires was estimated to be about  $0.2 \mu\text{T}$ , and the authors suggested that it might be the reason for this association. The design of the original Denver study was exploratory in nature and subject to many possi-

ble sources of error. Despite the skepticism, the study was given very serious consideration by the authorities, academia, and the industry and led to a vast international research effort. Practically all studies showed that an association between the presence of power lines and childhood leukemia almost certainly could not be attributed to magnetic fields generated by power lines. One of the largest studies carried out among a collection of over than 225 000 electrical utility workers looked at past exposure to magnetic and electric fields in 4154 cases of cancer [9.36]. The cancer risk for all types of cancer among the highest exposed group was not different from the lowest exposed group.

Many of these studies were carried out among exposed workers, where average fields are up to 20 times, with short periods of exposure at up to 1000 times the residential exposure level. Those studies also failed to show an increased risk of cancer. Results consistently showed cancer mortality rates 20–30% lower among workers, compared with the general public, an observation known as the *healthy worker effect*.

Another portion of such studies has examined carcinogenicity in animals: human beings are mammals, and their respective physiology is very similar. Thus, it is no surprise that, among the hundred or so human carcinogens confirmed so far, all of them, with no exception, have been shown to be carcinogenic to animals. For this reason, magnetic field carcinogenicity has been extensively tested on animals. Results are highly consistent: overall, no evidence of an increase in the incidence of benign or malignant tumors including leukemia was reported.

A few experimental studies have been carried out on human volunteers at high field levels up to 3000  $\mu\text{T}$ . The subjects were not able to perceive the presence of the fields, nor were adverse effects or signs of toxicity reported. Thus, the absence of any toxicity at levels up to 30 000 times the average field in homes (0.1  $\mu\text{T}$ ) makes a carcinogenic effect extremely unlikely.

In conclusion, it can today safely be assumed that the hypothesis raised by the Denver study in 1979 is very likely to be a false alarm. The exceptional amount of data accumulated over the last 35 years confirms that fields below the above-mentioned recommended power-frequency magnetic field levels are much too weak to influence human biology.

Despite the fact that no consistent adverse findings have been identified and no particular health effect reported, the International Commission on Non-Ionizing Radiation Protection (ICNIRP) as a precautionary measure has recommended exposure limits of 200  $\mu\text{T}$  for the public and 1000  $\mu\text{T}$  for workers; quite a few countries have implemented even lower values. These values

**Table 9.19** Typical electric and magnetic field value of lines

Line voltage (kV)	Electric field at ground level (1 m height) (kV/m)	Magnetic field at ground level (1 m height) ( $\mu\text{T}$ )
765	8–13	28–32
525	5–9	25–30
420	4–8	22–28
245	2–3.5	20–25
123	1–2	12–15
70	1–1.5	2–2.5

are much lower than typical field values from lines (Table 9.19) but often also from magnetic fields from household appliances.

Electric fields are in general not considered carcinogenic, but they induce electric charges on the body surface that affect the current flow within the body. These currents, depending on their magnitude, may cause eye flickering, stimulation of muscles and nerves, and in extrema the often lethal heat fibrillation. A widely accepted limit is 5 kV/m.

### 9.3.5 Approval Procedure

The approval process for building a new, but also for modifying a line is an important part of the design process, as it takes quite a long time, much more than the time needed to technically plan and build the line (Fig. 9.7). In addition, and as the line has to fulfill increasing and not always easily understandable environmental constraints, the line design often has to be modified during the approval procedure; For example, suspension insulators may have to be replaced with insulated cross-arms (Fig. 9.66) to avoid conductor swing, the height of the tower may have to be increased to reduce the EMFs at ground level, or even parts of the line have to be partially undergrounded, which will require special terminal structures.

A CIGRE inquiry in 1999 [9.5] revealed the top five problems that utilities face when planning an OHL project. These are valid, even more, nowadays:

- EMF health concerns
- Visual impact
- Landowner negotiations and access
- Community opposition
- Property values.

In drawing up proposals for new overhead transmission lines, undertaking environmental impact assessments (EIAs), and seeking rights, permits, and consents to construct, transmission companies are increasingly,

whether legally required or voluntarily, undertaking more stakeholder consultation. Community involvement can be key to the success of often-controversial new transmission infrastructure proposals, requiring the use of innovative and *best-practice* approaches. Public hearings are a key feature of most processes [9.37].

Best practices for consultation models and stakeholder engagement strategies in sustainable development for OHL projects have been summarized in [9.38, 39].

### Consultation Models

Most companies undertake much more consultation than legislation requires. Mandatory consultation requirements often only exist in environmental assessment legislation. Whilst consultation takes time, it also helps identify likely concerns and possible points of objection and helps refine proposals, address concerns, and smooth the eventual permitting process. Companies should establish a consistent approach to mapping stakeholders and understanding their viewpoints, needs, and expectations. Use of independent specialists when considering options, preparing consultation information, and assisting at advisory meetings increases the credibility of the information presented and helps secure understanding and cooperation from stakeholders.

Presenting as much information as possible, trying to get the balance right, and tailoring information to suit the audience, as well as communicating via the best methods available (e.g., company website, detailed publications or brochures, periodic newsletters, advertorials in local newspapers, etc.) and conducting open and engaging consultation with a broad range of representative and interested groups are often used as methods to accelerate the approval procedure.

### Stakeholder Engagement Strategies

Stakeholder engagement should be appropriate for the purpose and the target audience and should be proactive and meaningful. Stakeholders should generally be involved at project stages where they are able to influence an outcome or decision.

The following checklist may prove useful for successful stakeholder engagement:

- Consistent approach
- Project scoping
- Stakeholder identification
- Early engagement
- Targeted mix of consultation/engagement methods
- Open and transparent process
- Feedback to stakeholders.

### Life Cycle Assessment

Life cycle assessment (LCA) is a very valuable tool for overhead lines engineers, planners, and utilities to assist in the evaluation of the impact or interaction of overhead lines and the environment. It can be used and developed across a range of applications from environmental reporting to product improvement and comparison. However, it should be noted that its use has some restrictions.

CIGRE WG B2.15 was set up in 2000 to examine LCA issues as applied to overhead lines and to study aspects of overhead lines relating to environmental concerns. Based on the work across the range of LCA issues investigated and informed by the studies undertaken within the working group and elsewhere, conclusions are presented in [9.40].

The results of actual LCA studies carried out on some of the principal overhead line components lead to the following recommendations:

To reduce the environmental impact, especially in terms of resource exhaustion, it is strongly recommended that lattice steel towers be recycled. This could reduce the amount of iron as well as zinc reserve consumption.

In addition, related to gas emissions as well as resource exhaustion, it is strongly recommended that conductors be recycled. It is commonly known that the energy required to recycle aluminum is about 3% of that needed for original aluminum production. The electrolysis process applied to extract alumina from bauxite for original aluminum production requires a large amount of electricity, while the aluminum recycling process basically consists of melting and molding processes, which need less energy than the electrolysis process.

Another way to reduce the environmental impact is to reduce transmission losses. In this respect, the development of low-resistance conductors seems to represent an effective approach that could be recommended. Upgrading to a higher-voltage may also seem to be effective; however, a more comprehensive analysis of the whole power system would be needed to draw this conclusion.

With regard to insulators, only a small percentage of removed insulators are experimentally recycled as construction materials, and a porcelain insulator recycling system is not fully established. Given that more energy is consumed in the manufacturing processes of insulators than in the raw material manufacturing processes, the establishment of the reuse of removed insulators as value-added materials is desirable.

Another approach to reduce environmental impacts might be to extend the function of insulators as long as possible. In this respect, the development of efficient

and reliable diagnostic methods as well as life span extension technologies is recommended.

Last but not least, efforts should be made to keep the duration of overhead line construction to a minimum, as significant environmental impacts can arise at this stage. It is recommended that environmental manage-

ment plans should be developed and used. If required by the authority or landowner, access roads should be removed and the related material recycled. Maintenance activities should be organized and scheduled to eliminate or minimize the environmental impact, particularly painting of towers.

## 9.4 Conductors

The phase conductors of an overhead power line are considered to be the most important component of the line, since they are required to transmit electric power, and their cost contribution toward the total cost of the line is significant. Conductor costs (material and installation) associated with the capital investment of a new overhead power line can contribute up to 40% of the total capital costs of the line. In addition, the longitudinal (tension), transverse (wind), and vertical loads produced by the conductor system, and the maximum sag at high current levels, largely determine the cost of the towers and their foundations. Consequently, much attention has always been given to proper selection of the conductor to meet present and predicted future load requirements [9.41].

With regard to environmental effects, the conductor system largely determines the corona noise and audible noise levels produced by the line and the electrical resistance, as well as the energy losses over the life of the line.

A relatively recent focus on line uprating (Sect. 9.10) has led to the development of new conductor options and applications and in particular of so-called high-temperature low-sag (HTLS) conductors. This section covers, besides the basic mechanical and electrical properties of conductors, their behavior under wind-induced oscillations, conductor hardware, conductor monitoring, and HTLS conductors.

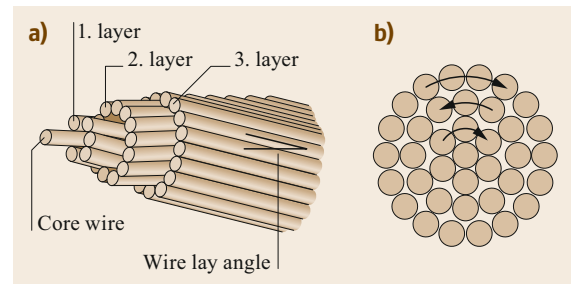
### 9.4.1 Types and Basic Properties of Conductors

The most widely used form of bare overhead conductors are concentrically stranded, with the outer, current-carrying layers consisting of aluminum wires, helically wrapped around a core consisting of steel wires, whose purpose is to provide mechanical strength. Such conductors are called aluminum conductor steel-reinforced (ACSR). The number of aluminum layers varies from one to four or more in very large-diameter conductors, while the steel core normally consists of 7–37 wires depending on the strength required. In areas with mild

ice and wind loads, the steel core may be replaced with aluminum or aluminum alloy. In lines designed or uprated to maximum design temperatures over 100°C, the steel core may be replaced with special core materials consisting for example of embedded carbon or ceramic fibers. Stranding improves conductor flexibility compared with a solid rod, and thereby its ease of handling and reeling. Stranding also enables the manufacture of considerable lengths of conductors without the need for joining.

All standard overhead conductors are reverse lay; i.e., the direction of rotation of each layer is opposite to that of the layer below (Fig. 9.23). Use of reverse lay reduces the torque that is created in conductors when they are tensioned and which can cause problems during stringing. Reverse lay in addition improves the electrical characteristics, in particular the self-inductance and AC resistance. For phase conductors, the usual convention is to wrap the outer layer with a right-hand lay, as opposed to the shield, also called earth or ground wires, which have a left-hand lay in their outer layer. For conductor layers with equal-diameter wires, each layer has six wires more than the layer beneath it, which provides a good fit between the conductor wires. This and other important information on conductor design and fabrication are covered extensively in [9.42].

An important property of the conductor geometry is the lay length  $\ell_L$  or *pitch*. This is defined as the



**Fig. 9.23a,b** Conductor characteristics. (a) Conductor geometry, (b) direction of lay (adapted from [9.42])

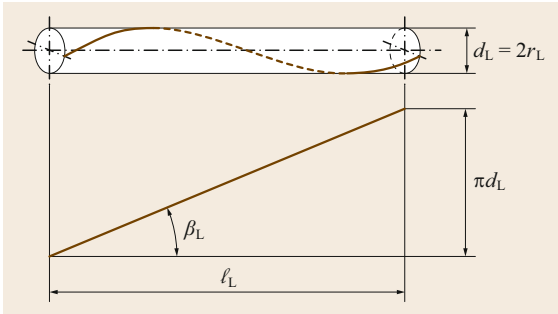


Fig. 9.24 Conductor geometry

axial length of a complete turn of the helix formed by an individual wire in a stranded conductor. The respective lay angle  $\beta_L$  is the angle of the wire axis to the conductor axis.

These properties are best illustrated in terms of a wire that has been *unrolled* from its helix onto a plane (Fig. 9.24). If the diameter of the cylinder defined by the helical axis of the wires in a layer is  $d_L$ , then its circumference is  $\pi d_L$ , and the lay angle  $\beta_L$  is obtained as

$$\beta_L = \arctan\left(\frac{\pi d_L}{\ell_L}\right). \quad (9.29)$$

Lay angles are usually in the region of  $10\text{--}15^\circ$  if the so-called lay ratio, defined as the ratio of the lay length  $\ell_L$  to the mean diameter  $d_L$  of the helix of a wire layer, lies within the values permitted in the respective standards, i.e., between 10 and 17—preferably around 13—for aluminum layers and between 12 and 30—preferably 20–25—for steel layers. These values result in satisfactory layer fill and good handling characteristics of the finished conductor. It should be noted that, the smaller the lay ratio, the more turns the wire makes in a given length and the more flexible the stranded conductor becomes [9.43].

Very early on, i.e., at the end of the 19th century, aluminum-based conductors began to replace the copper conductors that had originally been used. Modern aluminum wires are produced in a rolling/casting process and are called Properzi blanks [9.43]. Some overhead conductors are constructed only from pure aluminum and are referred to as all aluminum conductors (AAC). Because of their relatively low strength-to-weight ratio, these types of conductor are suitable for short spans in distribution networks and for areas where ice and wind loads are limited, as well as for flexible busbars in substations. For added strength, various aluminum alloys with inclusion of magnesium and silicon have been developed, referred to as all aluminum alloy conductors (AAAC), also called Almelec or Al-

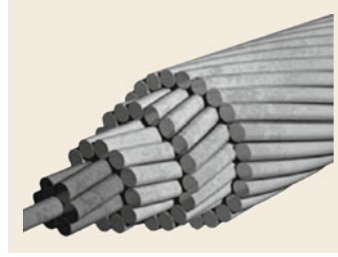


Fig. 9.25 ACSR conductor (steel wires are dark shaded)

drey conductors. Their excellent corrosion resistance has made AAACs the conductors of choice for use in coastal areas.

When a higher strength-to-weight ratio is desired, a strength member has to be added to the conductor. This is usually done by including a core of steel wires, leading to the aluminum conductor steel-reinforced (ACSR) configuration (Fig. 9.25) that has been the most commonly used type of conductor worldwide since the beginning of the 20th century, estimated to account for about 80% of the total. ACSR cables are available with a wide range of steel content—from 7% by weight for 36/1 stranding to 40% for 30/7 stranding (Table 9.20) [9.44, Table F.19]. Early designs of ACSR such as 6/1, 30/7, 30/19, 54/19, and 54/7 strandings featured high steel content of 26–40%, with an emphasis on strength perhaps due to fears of vibration fatigue problems (Sect. 9.4.11). Today, the most widely used strandings are 18/1, 45/7, 72/7, and 84/19, with a range of steel content of 11–18%. The high-strength ACSR 8/1, 12/7, and 16/19 strandings are used mostly for overhead ground wires, extralong spans, river crossings, etc.

The steel core wires used in most ACSR overhead conductors are made of medium-strength zinc-coated (galvanized) steel containing 0.50–0.85 wt% carbon with a nominal tensile strength of 1400 MPa, or more seldom aluminum-coated (aluminized) or aluminum-clad steel, in which the aluminum cladding accounts for 25% of the area of the wire, with a minimum coating thickness of 10% of the overall radius.

The multiple-layer aluminum envelope of composite conductors permanently protects the zinc-coated steel wires against corrosion, when the steel cores are greased. However, especially in regions with a hot climate, grease of an inappropriate type could melt and drop from the conductor, thus producing corona discharges. Therefore, attention should be paid to a sufficiently high drop point of the grease (above  $80^\circ\text{C}$ ) and a high viscosity. Standard [9.45] applies to greases.

In homogeneous conductors, i.e., conductors employing only a single material (AAC and AAAC), all the wires have the same diameter; this is also the case

**Table 9.20** Characteristic data of ACSR conductors

Designation	Former code	Cross section total (mm <sup>2</sup> )	Number of strands		Conductor diam. (mm)	Mass per unit length (kg/km)	Rated strength (kN)	DC resistance (Ω/km)	Current-carrying capacity (A)
	ACSR		Al	St					
15-AL1/3-ST1A	16/2.5	17.8	6	1	5.40	61.6	5.80	1.8769	105
24-AL1/4-ST1A	25/4	27.8	6	1	6.75	96.3	8.95	1.2012	140
34-AL1/6-ST1A	35/6	40.1	6	1	8.10	138.7	12.37	0.8342	170
44-AL1/32-ST1A	44/32	75.6	14	7	11.2	369.3	44.24	0.6574	200
48-AL1/8-ST1A	50/8	56.3	6	1	9.60	194.8	16.81	0.5939	210
51-AL1/30-ST1A	50/30	81.0	12	7	11.7	374.7	42.98	0.5644	230
70-AL1/11-ST1A	70/12	81.3	26	7	11.7	282.2	26.27	0.4132	290
94-AL1/15-ST1A	95/15	109.7	26	7	13.6	380.6	35.93	0.3060	350
97-AL1/56-ST1A	95/55	152.8	12	7	16.0	706.8	77.85	0.2992	370
106-AL1/76-ST1A	105/75	181.2	14	19	17.5	885.3	105.82	0.2742	400
122-AL1/20-ST1A	120/20	141.4	26	7	15.5	491.0	44.50	0.2376	410
122-AL1/71-ST1A	120/70	193.4	12	7	18.0	894.5	97.92	0.2364	415
128-AL1/30-ST1A	125/30	157.8	30	7	16.3	587.0	56.41	0.2260	425
149-AL1/24-ST1A	150/25	173.1	26	7	17.1	600.8	53.67	0.1940	470
172-AL1/40-ST1A	170/40	211.8	30	7	18.9	788.2	74.89	0.1683	520
184-AL1/30-ST1A	185/30	213.6	26	7	19.0	741.0	65.27	0.1571	535
209-AL1/34-ST1A	210/35	243.2	26	7	20.3	844.1	73.36	0.1381	590
212-AL1/49-ST1A	210/50	261.5	30	7	21.0	973.1	92.46	0.1363	620
231-AL1/30-ST1A	230/30	260.8	24	7	21.0	870.9	72.13	0.1250	630
243-AL1/39-ST1A	240/40	282.5	26	7	21.8	980.1	85.12	0.1188	645
264-AL1/34-ST1A	265/35	297.7	24	7	22.4	994.4	81.04	0.1095	680
304-AL1/49-ST1A	300/50	353.7	26	7	24.4	1227.3	105.09	0.0949	740
305-AL1/39-ST1A	305/40	344.1	54	7	24.1	1151.2	96.80	0.0949	740
339-AL1/30-ST1A	340/30	369.1	48	7	25.0	1171.2	91.71	0.0852	790
382-AL1/49-ST1A	380/50	431.2	54	7	27.0	1442.5	121.30	0.0758	840
389-AL1/34-ST1A	385/35	420.1	48	7	26.7	1333.6	102.56	0.0749	850
434-AL1/56-ST1A	435/55	490.6	54	7	28.8	1641.3	133.59	0.0666	900
449-AL1/39-ST1A	450/40	488.2	48	7	28.7	1549.1	119.05	0.0644	920
490-AL1/64-ST1A	490/65	553.8	54	7	30.6	1852.9	150.61	0.0590	960
494-AL1/34-ST1A	495/35	528.4	45	7	29.9	1632.6	117.96	0.0584	985
511-AL1/45-ST1A	510/45	585.8	48	7	30.7	1765.3	133.31	0.0566	995
550-AL1/71-ST1A	550/70	620.9	54	7	32.4	2077.2	166.32	0.0526	1020
562-AL1/49-ST1A	560/50	611.2	48	7	32.2	1939.5	146.28	0.0515	1040
571-AL1/39-ST1A	570/40	610.6	45	7	32.3	1887.1	136.40	0.0506	1050
653-AL1/45-ST1A	650/45	698.8	45	7	34.4	2159.9	156.18	0.0442	1120
679-AL1/86-ST1A	680/85	764.5	54	19	36.0	2549.7	206.56	0.0426	1150
1046-AL1/45-ST1A	1045/45	1090.9	72	7	43.0	3249.2	218.92	0.0277	1580

in some ACSR conductors. However, in the majority of the latter, all the aluminum wires have the same diameter while all the steel wires have another, different diameter. Wire diameters in overhead line conductors range between 2 and 5 mm.

Apart from the *standard* conductor designs, there are also a number of special designs, such as conductors with high steel content for very long spans such as river crossings, smooth-body conductors, and expanded conductors. One way to improve and tailor conductors for special situations is to form the

aluminum wires in a trapezoidal or z-shape. These conductors make better use of their space compared with round-wire conductors and are, therefore, called *compact* (Fig. 9.26).

The proper designation of conductors is an interesting issue. In Central Europe, the conductor name contains the abbreviation of the conductor material(s) and the respective cross-section(s) in mm<sup>2</sup>. For example, a commonly used ACSR conductor with an aluminum cross section of 243 mm<sup>2</sup> and a steel cross-section of 39 mm<sup>2</sup>, in the old days simply called Al/St





**Fig. 9.26** Compact ACSR conductor

240/40 [9.46], is nowadays denoted as 243-AL1/39-ST1A. In other parts of the world, the North American practice is often followed, whereby conductors carry names of flowers, cities, and birds, e.g., Tulip, Rose, and Magnolia for AAC, Akron, Montreal, and Halifax for AAAC, and Pelican, Hawk, and Drake for ACSR.

### 9.4.2 Conductor Manufacture

Conductor manufacture is a complex process and a crucial one as the manufacturing method employed determines the stress regime in the conductor strands, which, in turn, significantly influences the behavior of the conductor under mechanical loads in service.

This is best explained by describing the operation of a so-called orbital strander (Fig. 9.27 [9.47]), which is mainly used for manufacturing smaller conductors with up to 19 strands as well as steel cores of up to 19 strands for ACSR.

In this type of strander, spools of wire are mounted in *heads* which rotate about the conductor axis, with each head supplying the strands for one layer. A *closing die*, usually made of fiber material or wood, forces the strands snugly into their final position. Just before reaching the closing die, the wires pass through so-called *preformers* (Fig. 9.28 [9.47]), which have the task of forming the strands to approximately the shape that they will adopt in the finished conductor. In this way, the built-in stresses and moments in the strands are reduced, as well as their tendency to spring back after cutting. The handling characteristics of these con-

ductors are greatly enhanced by this process. Finally, the capstan supplies the pulling force to draw the layer wires from their spools and also the core wire from its reel. The capstan speed is synchronized to the rotational speeds of the strander heads by gearing, to achieve the desired pitch of the strand helices.

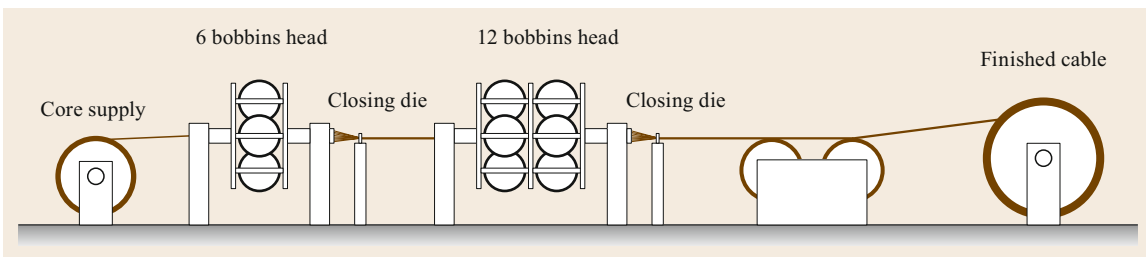
The influence of the manufacturing process has been thoroughly investigated and presented in [9.48] using a 3-D FEM model and verified by extensive full-size tests. In particular it has been shown that the path of the individual wires from their round shape on the bobbin to their helical shape when embedded in the conductor is of paramount importance for the residual stresses in the conductor wires. In Fig. 9.29, the two extreme conditions are shown schematically, together with the FEM simulation results for the axial stresses in the conductor. As can be seen, due to room-temperature viscoplastic effects, stress relaxation occurs during storage, reducing the magnitude of the residual stresses.

### 9.4.3 Tests

#### Wire Tests

Tests of the individual conductor wires are prescribed in a number of national and international standards. Usually, sample tests are carried out on every 10% of the wire length ready for stranding:

- *Wire diameter*: Accuracy two decimal places; max. deviation from value in the standard:  $\pm 0.003$  mm for diameters up to 3 mm,  $\pm 1\%$  above.
- *Wire surface*: Smooth, free from cracks, fissures, and other damage, no inclusion of copper particles in the aluminum wires.
- *Tensile strength*: Tested on a wire sample of 250 mm length; should meet the prescribed value.
- *Wrapping test*: An aluminum sample wire is coiled eight times around a mandrel of the same diameter, then six turns are uncoiled and coiled again; the test is passed if the wire does not break.
- *Galvanizing*: The zinc mass of galvanized steel wire is determined by removing the zinc coat-



**Fig. 9.27** Schematic of orbital strander (adapted from [9.26])

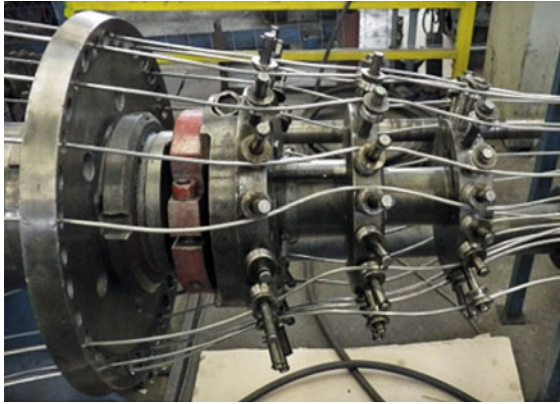


Fig. 9.28 Preforming head (adapted from [9.47])

ing using hydrochloric acid, while the uniformity of the coating is tested by applying the zinc dip test.

- **Resistivity:** In this test, the wire resistance is first measured at a temperature of 10–30°C and then adjusted to the reference temperature of 20°C using

the well-known formula

$$R_{20} = \frac{R_T}{1 + \alpha(T - 20)}, \tag{9.30}$$

where  $T$  is the measurement temperature,  $R_T$  and  $R_{20}$  are the resistance at temperature  $T$  and 20°C, respectively, and  $\alpha$  is the temperature coefficient of resistance.

In this regard,  $\alpha = 23 \times 10^{-6}$  for aluminum and  $\alpha = 11.5 \times 10^{-6}$  for steel; i.e., the ratio is 2 : 1, a value to be remembered for later.

- **Welding:** When aluminum wires are broken during stranding, they can be joined again by welding under the following prerequisites:
  - The number of joints is limited.
  - The minimum distance between two joints in the same wire or any other wire is 15 m.
  - The joints should be rendered smoothly.
  - The joints should withstand a minimum tensile stress of 75 N/mm<sup>2</sup>.

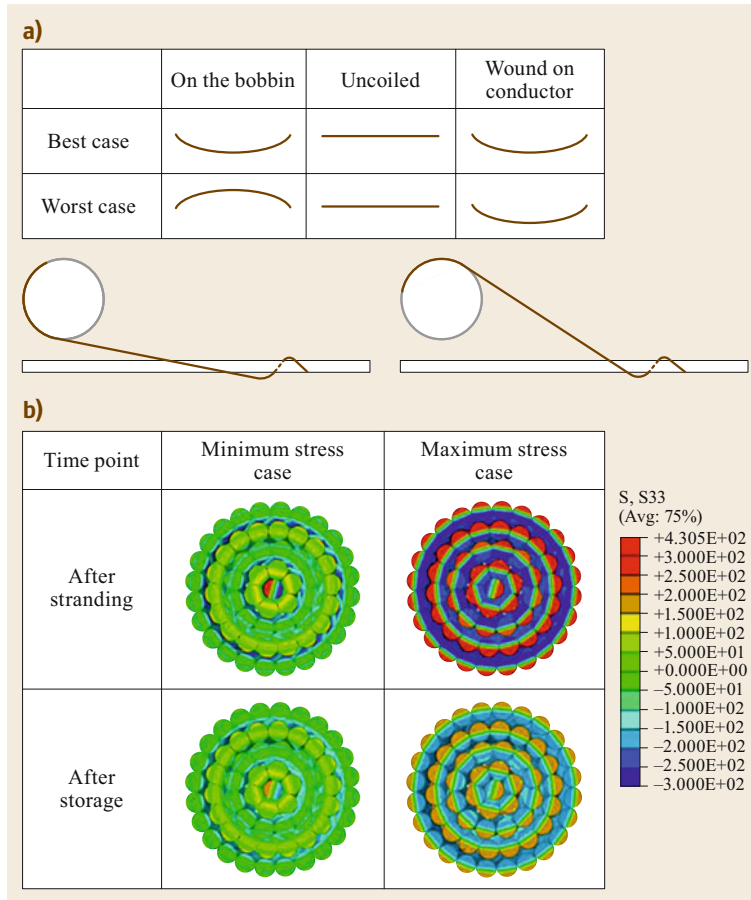


Fig. 9.29a,b Minimum and maximum stress case in the conductor. (a) Schematic of the wire stranding process; (b) residual axial stresses in the conductor wires in N/mm<sup>2</sup>

**Table 9.21** Type and sample tests for conductors (adapted from [9.44])

Conductor	Type test	Sample test
– Surface condition	×	×
– Diameter	×	×
– Inertness	×	×
– Lay ratio and direction of lay	×	×
– Number and type of wires	×	×
– Mass per unit length	×	×
– Stress–strain curve	<sup>a</sup>	–
– Tensile breaking strength	<sup>a</sup>	–
– Stringing test	<sup>a</sup>	–
– Creep test <sup>b</sup>	<sup>a</sup>	–
<b>Grease</b>		
– Mass per unit length	×	×
– Drop point	×	×

<sup>a</sup> According to agreement between manufacturer and purchaser  
<sup>b</sup> According to [9.49]

It is good practice to mark by tape the welding locations on the wires of the outer layer.

### Conductor Tests

For the finished conductors, the tests listed in Table 9.21 [9.44] are required.

These tests are of particular importance as they provide the necessary input for the mechanical behavior of a conductor in service.

**Stress–Strain Test.** This test describes the behavior of the conductor under mechanical load and is carried out on a conductor sample of at least 400 times the conductor diameter but not less than 10 m. The *test loads* should be applied on the conductor using the follow-

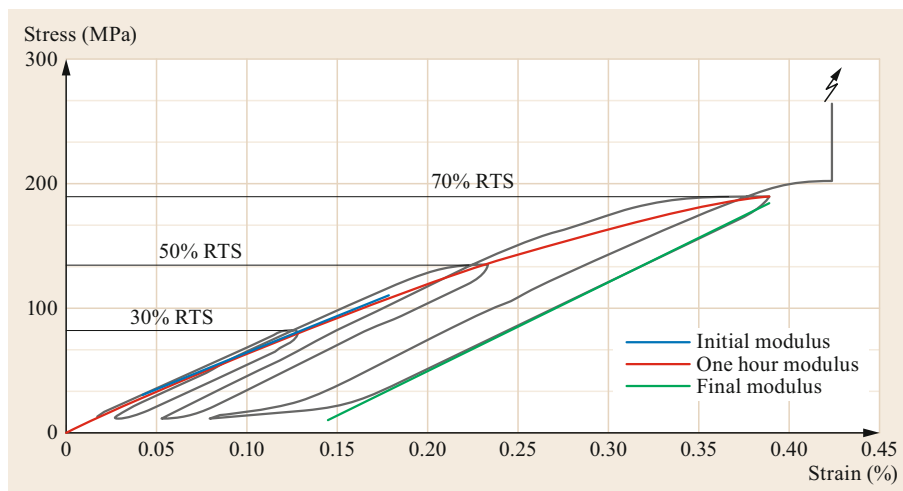
ing steps, where the load should be completely released after each step:

- Initial load of 5% of the *rated tensile strength* (RTS) to straighten the conductor
- Load with 30% RTS and holding the load for 0.5 h
- Reload to 50% RTS and holding for 1 h
- Reload to 70% RTS and holding for 1 h
- Reload to 85% RTS and holding for 1 h
- After the fourth application of load, the conductor is loaded again by increasing the tensile force steadily until the actual breaking strength is reached.

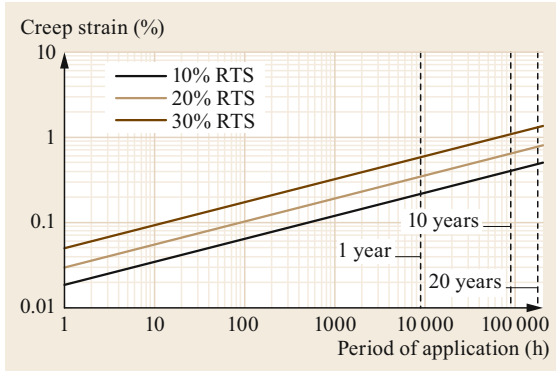
The initial stress–strain diagram is obtained by drawing a smoothed line through the strain point after 0.5 h at 30% RTS and the strain points after 1 h at 50%, 70%, and 85% RTS. The curve should be adjusted to pass through the zero point. The initial stress–strain diagram is represented by the blue line marked *initial modulus* in Fig. 9.30. The characteristic final stress–strain diagram may be determined from the unloading part (from 50%, 70%, or 85% RTS) of the graph, as agreed upon between the manufacturer and client. Figure 9.30 shows an example stress–strain diagram [9.50].

The rated tensile strength (RTS) of bimetallic conductors is determined in accordance with [9.44, Sect. 5.9]. For  $AL_x/ST_{yz}$  and  $AL_z/y_zSA$  conductors, it is equal to the minimum tensile strength  $\sigma_{BAl}$  of the aluminum wires before the stranding process, multiplied by their nominal cross section  $A_{Al}$  plus the tensile stress  $\sigma_{1\%Fe}$  of the steel or aluminum-clad steel wires at 1% elongation on a 250-mm gauge length before stranding, multiplied by their nominal cross section  $A_{Fe}$ .

$$RTS = \sigma_{BAl}A_{Al} + \sigma_{1\%Fe}A_{Fe} \quad (9.31)$$



**Fig. 9.30** Typical stress–strain curve of a conductor (adapted from [9.50])



**Fig. 9.31** Creep curves for ACSR Cardinal (483-AL1/63-ST1A) (adapted from [9.4])

The requirements on the RTS of a conductor are considered to be met by a test when failing of individual wires occurs only after 95% of its rated strength has been reached.

**Creep Test.** Creep is another expression for plastic elongation and is explained in [9.51]. Aluminum strands, and, to a much lesser extent, steel strands used in bare overhead conductors, undergo plastic (i.e., permanent) elongation as the result of tension applied over time. Initial plastic conductor elongation includes the *strand settlement and deformation* which occurs during stringing and sagging (initial *plastic elongation*), plastic elongation which occurs during relatively brief, high-tensile-load events, and long-time *metallurgical creep elongation*, which occurs at everyday tension levels over the life of the line. Metallurgical creep of aluminum is accelerated at sustained high temperatures (above 20 °C). This effect has been extensively studied recently and presented in [9.47].

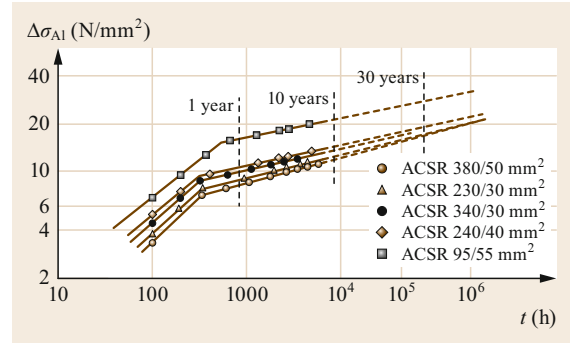
The creep strain  $e$  of the conductor is described according to [9.52] by

$$e = e_{1h} t^n, \quad (9.32)$$

where  $t$  is the time in hours and  $e_{1h}$  and  $n$  are parameters which depend on the conductor type and load condition.

These values are measured by means of the tests described in [9.53], which are performed on a sample which is at least as long as 100 times the conductor diameter, clamped in a test bench, which keeps the load constant during the test, with an accuracy of  $\pm 1\%$  or  $\pm 120$  N. The measuring intervals are selected on a logarithmic scale, and the results of the tests are then presented on a double logarithmic scale corresponding to the equation

$$\log e = \log e_{1h} + n \log t. \quad (9.33)$$



**Fig. 9.32** Tensile stress decrease  $\Delta\sigma_{Al}$  due to creep in the aluminum wires of different ACSR with a load of 25% RTS at 20 °C (adapted from [9.54])

In this way, the creep strain  $e$  in the ideal case forms a straight line where  $e_{1h}$  is the intersection with the ordinate for  $t = 1$  h and  $n$  is the slope of the straight line. Figure 9.31 [9.4] shows such a creep diagram, presenting a mean straight line through the measuring points on a double logarithmic scale. The creep strain can then be extrapolated out to 100 000 h (approximately 10 years). Indicative data for  $e_{1h}$  and  $n$  can be found in [9.53].

The creep of steel wires is much less significant and is normally neglected. Due to this fact, the creep in the aluminum wires of a bimetallic conductor reduces their tensile load by  $\Delta\sigma_{Al}$  but increases the load in the steel core wires. This load shift also depends on the ratio of aluminum to steel (Fig. 9.32 [9.54]).

#### 9.4.4 Mechanical Properties

Conductors have to sustain a plethora of electrical, mechanical, and environmental loads. Moreover, it is expected that, during the projected lifetime of a line, i.e., 40 years or more, and under all foreseeable conditions, they must not break under high tension, nor fail under fatigue caused by wind-induced oscillations, nor sag such that minimum electrical clearances are compromised. This can be ensured by understanding the behavior of the conductor under such loads and applying appropriate calculation methods [9.51].

##### Tensile Behavior

In a straight piece of conductor loaded in tension, the load  $H$  is distributed in the individual conductor wires following the basic rules of engineering mechanics. In the determination of the tensile forces in the individual wires, it is assumed that the conductor cross-section remains plane and all wires are in the linear elastic region, i.e., that Hooke's law is applicable. The changes in the lay angle and the transverse contraction (Poisson effect) of the wire cross-sections amount to around 2% of the

total tensile stress in the wire and are usually neglected. In a homogeneous conductor such as AAC and AAAC with  $n$  wires of the same diameter  $d$  and with modulus of elasticity  $E$ , the stress  $\sigma$  in a single wire is given by

$$\sigma = \frac{H}{n\pi d^2/4}. \quad (9.34)$$

This is related to the corresponding wire strain  $\varepsilon$  by

$$\sigma = E\varepsilon. \quad (9.35)$$

The situation becomes more complex for a bimetallic conductor, notably ACSR. In this case, the wires of the conductor *stick* to each other, because the tensile load creates radial compression (Fig. 9.51); they are also held firmly together by the conductor hardware, mainly the dead-end clamps (Fig. 9.108). Consequently, the wire strains  $\varepsilon_{Al}$  and  $\varepsilon_{St}$  for the aluminum and steel wires are equal

$$\varepsilon_{Al} = \varepsilon_{St}. \quad (9.36)$$

And since

$$\sigma_{Al} = E_{Al}\varepsilon_{Al} \quad \text{resp.} \quad \sigma_{St} = E_{St}\varepsilon_{St}, \quad (9.37)$$

it follows that

$$\sigma_{St} = \frac{E_{St}}{E_{Al}}\sigma_{Al}. \quad (9.38)$$

From (9.38) and considering typical values of  $E_{St} = 190$  GPa and  $E_{Al} = 55$  GPa as indicated in [9.55] for stranded steel and aluminum wires, respectively, it can be concluded that the tensile stresses in the steel wires of an ACSR are more than three times higher than the corresponding stresses in its aluminum wires.

The value of the stresses themselves can then be calculated as

$$\sigma_{Al} = H \frac{E_{Al}}{AE_C} \quad (9.39)$$

and

$$\sigma_{St} = H \frac{E_{St}}{AE_C}, \quad (9.40)$$

where  $E_C$  is the so-called composite modulus of elasticity of the conductor, given by

$$E_C = E_{Al} \frac{A_{Al}}{A} + E_{St} \frac{A_{St}}{A}, \quad (9.41)$$

and  $A$  is the total conductor area. Calculations using (9.39)–(9.41) show that even modest steel areas (e.g., 11% of the total area) greatly *stiffen* ACSR conductors, increasing the composite modulus from 55 to 70 GPa, i.e., by approximately 25%.

### Thermal Behavior

Conductors do not only elongate when under tension, but also change their length by a fraction  $\Delta L$  under the influence of temperature. For individual conductor wires with original length  $L$ , the following well-known relationship applies

$$\frac{\Delta L}{L} = \alpha \Delta T, \quad (9.42)$$

where  $\alpha$  is the coefficient of linear expansion and  $\Delta T$  is the temperature difference. For the two most common conductor materials, i.e., aluminum and its alloys and steel, the coefficients of linear expansion exhibit a ratio of 2. Specifically, the coefficient of linear expansion of aluminum ( $\alpha_{Al} = 23 \times 10^{-6} \text{ }^\circ\text{C}^{-1}$ ) is twice that of steel ( $\alpha_{St} = 11.5 \times 10^{-6} \text{ }^\circ\text{C}^{-1}$ ). This fact has important consequences in the calculation of conductor sag in a span.

Based on a reasoning similar to that applied for the tensile behavior of a bimetallic conductor above, the composite coefficient of linear expansion can be calculated as

$$\alpha_C = \alpha_{Al} \frac{E_{Al}}{E} \frac{A_{Al}}{A} + \alpha_{St} \frac{E_{St}}{E} \frac{A_{St}}{A}. \quad (9.43)$$

Since the thermal expansion coefficients of steel and aluminum are different, a load shift takes place between aluminum and steel depending on the change of temperature. For a temperature increase, the load shifts from aluminum to steel, whereas the opposite is true for a temperature decrease. In this case, the aluminum strands of the conductor have to carry a greater mechanical load [9.56], which can be critical in the winter period, when this unfavorable characteristic coincides with the highest tension in the conductor. This issue is also important for vibration assessment (Sect. 9.4.11).

### The Catenary

The shape of a conductor suspended from two points at equal height above the ground having between them a distance  $S$  (the span) and loaded by a weight  $w$  (which can be its own weight plus an additional weight, e.g., from ice) and a tensile load  $H$  is a curve called a *catenary* (Fig. 9.33), because it is the curve that an idealized chain assumes (from the Latin *catena* for chain). Its mathematical function can be derived by applying the three conditions of static equilibrium in a plane on the differential elements of the curve as shown schematically on the right-hand side of Fig. 9.33 [9.4]; this leads to the differential equation

$$\frac{d^2 y}{dx^2} = \frac{w}{H} \sqrt{1 + \left(\frac{dy}{dx}\right)^2}. \quad (9.44)$$

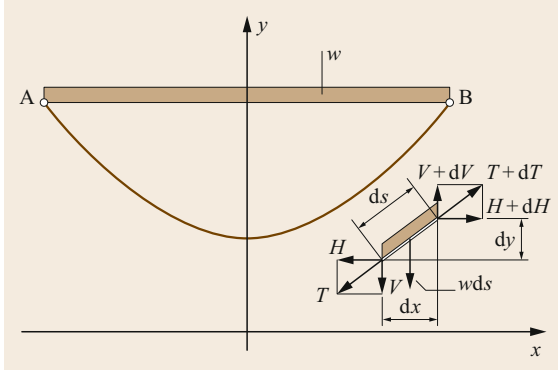


Fig. 9.33 The catenary (adapted from [9.4])

Its solution delivers the mathematical expression for the catenary

$$y(x) = \frac{H}{w} \left[ \cosh \left( \frac{wx}{H} \right) - 1 \right], \quad (9.45)$$

which can be simplified to the equation of a parabola

$$y(x) = \frac{wx^2}{2H}. \quad (9.46)$$

The maximum deflection, which occurs at the center of the span  $S$  and is called the sag  $D$ , can be obtained by inserting  $x = S/2$  into (9.45), thus

$$D = \frac{H}{w} \left[ \cosh \left( \frac{wS}{2H} \right) - 1 \right], \quad (9.47)$$

which can be simplified to

$$D = \frac{wS^2}{8H}. \quad (9.48)$$

Equation (9.48) for the sag follows intuition, as evidently the sag will increase with the conductor weight and span length but decrease with the conductor tension. The sag is further proportional to the square of the span length; i.e., when the span length is doubled, the sag will increase four times, which is an important issue for long spans.

These approximations for the catenary curve and the sag are valid when

$$\frac{w^2 S^2}{48H^2} \ll 1, \quad (9.49)$$

which applies for the majority of overhead lines, with the exception of long, steep, or deep spans such as may be found in river, lake, or fjord crossings.

For a typical 380-kV line with a horizontal span length  $S$  of 300 m, equipped with a Drake conductor (ACSR 403-A1/S1A, 26/7) with a weight per unit length  $w$  of 16 N/m and a tension  $H$  of 28 kN, corresponding to 20% of its RTS of 140 kN, the sag  $D$  becomes 6420 mm with the exact solution (9.47) and 6417 mm with the approximation (9.48), i.e., a difference of only 3 mm, evidently well below the practical accuracy of sag measurements in the field. In this context, it is instructive to verify that the condition (9.49) is met

$$\frac{16^2 \times 300^2}{48 \times 28000^2} = 0.0006 \ll 1.$$

The length of the catenary  $L$  between the supports A and B (Fig. 9.33) can be calculated from the line integral of the catenary curve differential  $ds$

$$\begin{aligned} L &= \int_A^B ds = \int_A^B \sqrt{dx^2 + dy^2} \\ &= \int_A^B 1 + \sqrt{1 + \left( \frac{dy}{dx} \right)^2} dx. \end{aligned} \quad (9.50)$$

Inserting (9.45) and under the assumption of (9.49), we obtain a very good approximation for the length of the catenary of

$$L \cong S + \frac{8D^2}{3S}, \quad (9.51)$$

and for the so-called *slack*, i.e., the difference between the catenary length  $L$  and the span length  $S$ , we obtain

$$L - S \cong \frac{8D^2}{3S}. \quad (9.52)$$

For the example, we get  $L = 300.366$  m and  $L - S = 0.366$  m, which is only about 0.1% of the span length  $S$ .

Another interesting observation is that the difference between the total tension  $T$  and the horizontal tension  $H$  in the conductor is normally very small, in this case amounting to just over 100 N.

The ratio  $H/w$  (with dimension m), which appears in the preceding equations, is commonly referred to as the catenary constant. An increase in the catenary constant causes the catenary curve to become shallower and the sag to decrease. The catenary constant typically has a value in the range of 500–2000 m for most transmission line catenaries under most conditions, and it also plays an important role in the assessment of conductor vibration severity (Sect. 9.4.11).

**Sag–Tension Calculations.** As explained above, the shape of the catenary changes with the conductor temperature, ice and wind loading, and time (creep). To ensure adequate vertical and horizontal clearance under all weather and electrical loadings, and to ensure that the breaking strength of the conductor is not exceeded, the shape of the conductor catenary under all conditions must be determined. This is done through calculations commonly referred to as sag–tension calculations; these are extensively described in [9.51].

The basic idea behind sag–tension calculations is to relate mathematically two physically distinct conductor states. The first state—designated in the following by a subscript “1”—is defined by the conductor temperature  $T$ , tension  $H$ , and load  $w$  and related to a second conductor state (indicated by a subscript “2”) through a change of the conductor length  $L$ , as the latter depends on the mentioned parameters. The basic conductor state corresponds to the time of installation, when the conductor sag and the related tension with the conductor unloaded and at a known temperature are measured and fixed in such a way that the limiting conductor parameters (Fig. 9.36) are not exceeded. Specifically

$$L_2 = L_1 [1 + \alpha (T_2 - T_1)] \left( 1 + \frac{H_2 - H_1}{EA} \right), \quad (9.53)$$

where  $\alpha$  is the coefficient of linear expansion,  $E$  is the modulus of elasticity, and  $A$  is the area of the cross-section of the conductor in question. Inserting for  $L$  (9.51) into (9.53) with  $D$  from (9.48), we arrive at what is often called in literature the conductor state-change equation

$$\begin{aligned} H_2^2 (H_2 - H_1) + \frac{EA (w_1 S)^2}{24H_1^2} + EA\alpha (T_2 - T_1) \\ = \frac{EA (w_2 S)^2}{24H_2^2}, \end{aligned} \quad (9.54)$$

or in the more convenient stress form

$$\begin{aligned} \sigma_2^2 (\sigma_2 - \sigma_1) + \frac{E (w_1 S)^2}{24A^2 \sigma_1^2} + E\alpha (T_2 - T_1) \\ = \frac{E (w_2 S)^2}{24A^2}. \end{aligned} \quad (9.55)$$

In (9.55) it has been assumed that the conductor behaves linear elastically, with a single elastic modulus and a single coefficient of thermal elongation, which is a reasonably good approximation for many overhead lines, in particular for conductors with a maximum operating temperature up to 60°C. Consequently, it is

called the linear elastic (LE) model. The above cubic equation (9.55) can be solved easily, even analytically.

However, overhead conductors are not purely elastic. They elongate with tension, but when the tension is reduced to zero, they do not return to their initial length; that is, conductors are plastic, and their stress–strain curves are nonlinear (Fig. 9.30). Such curves can be obtained in laboratory tests and then introduced into dedicated software, which can carry out all the necessary calculations using more sophisticated conductor models such as the simplified plastic elongation (SPE) and experimental plastic elongation (EPE) models described in [9.51]. Specifically:

- The LE model ignores the settlement and strand elongation as well as the long-time or high-tension plastic elongation, although these may be allowed for by the use of adequate clearance buffers.
- The SPE model ignores the settlement and strand elongation that occur during initial tensioning of the conductor but accounts for long-time or high-tension creep plastic elongation by considering an equivalent increase in temperature

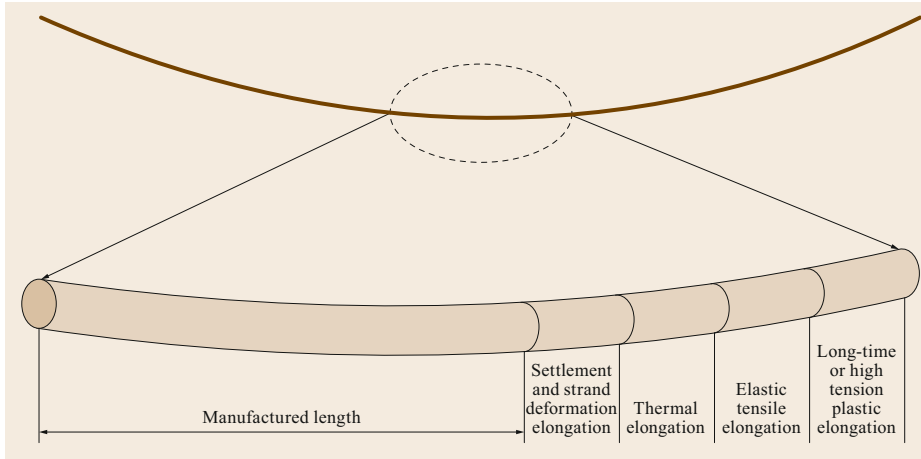
$$\Delta T_{\text{creep}} = \frac{\epsilon_{\text{creep}}}{\alpha}. \quad (9.56)$$

- The EPE elongation model enables the calculation of both settlement and strand elongation as well as long-time or high-tension plastic elongation based on laboratory conductor test results and an assumed line design and load sequence.

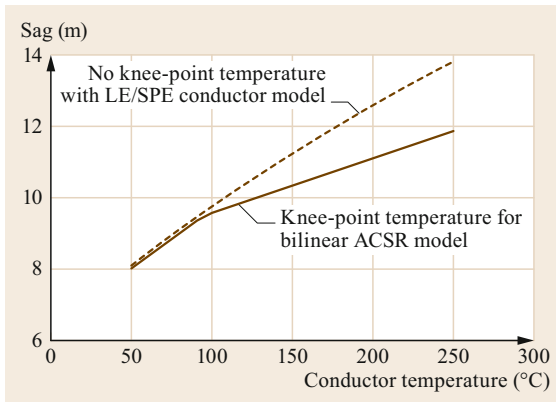
Conductor test data for use in the SPE and EPE models can be found in [9.55].

The various contributions to the conductor elongation are shown schematically in Fig. 9.34 [9.51].

However, the situation becomes more complicated when ACSR are operated at elevated temperatures [9.57]. Such conductors, being composed of two metal components with different thermal expansion rates, show a more complex sag–tension characteristic at elevated temperature. As the temperature increases, the tension carried by the aluminum shell shifts to the steel core as its expansion rate is twice the rate of the steel core. Hence, in steel-reinforced conductors, the percentage of the load supported by the steel core increases as the conductor temperature increases. Above a particular conductor temperature, called the *knee-point temperature* (KPT), the mechanical load carried by the aluminum wires is completely off-loaded to the steel core and hence add to the core’s tensile loading, although there is an understanding that the inner, constricted aluminum wires can sustain a small amount of compression [9.58]. There are



**Fig. 9.34** Contributions to conductor elongation (adapted from [9.51])



**Fig. 9.35** Sag versus temperature of a 300-m span for ACSR Cardinal (54/7) using the LE/SPE and EPE conductor models (adapted from [9.60])

also indications that the KPT is influenced by the manufacturing process [9.59]. High-temperature sags of multiple-layer ACSR conductors may thus be smaller than those predicted by simpler sag–tension models (Fig. 9.35 [9.60]).

Another important issue to be considered in sag–tension calculations is the fact that, in a typical overhead line and depending on the utility design philosophy and the terrain, the suspension spans between dead-end strain structures can vary in length, although normally not over a wide range. If all of the suspension spans were of the same length and reasonably level, and all were subject to the same ice and wind loads, then the sag and tension change with ice and wind and conductor temperature would be the same for all the spans. This is evidently not the case, as changes in conductor temperature or load will yield different tensions in each span. Small movements of the suspension points, however, will equalize the tension between spans.

Although exact sag–tension calculations for multiple, mechanically coupled suspension spans are now carried out using customized software, it is instructive, in order to better understand the physical background of the situation, to carry out the sag–tension calculation for a single *ruling*, also called *equivalent*, span [9.61, 62]. The ruling span is defined by

$$S_R = \sqrt{\frac{S_1^3 + S_2^3 + \dots + S_n^3}{S_1 + S_2 + \dots + S_n}}, \quad (9.57)$$

where  $S_R$  is the ruling span for a line section containing  $n$  suspension spans,  $S_1$  is the span length of the first suspension span,  $S_2$  is the span length of the second suspension span, and  $S_n$  is the span length of the  $n$ -th suspension span.

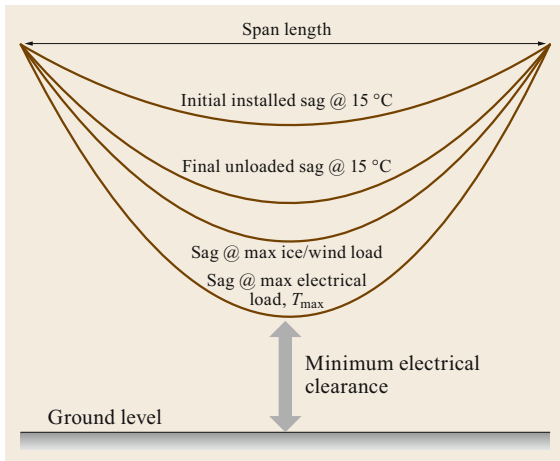
Since the numerator in (9.57) depends on the cube of the span length, the value of the ruling span is greatly influenced by the longest spans. And, since the tension in all the suspension spans in the line section is assumed to be reasonably equal, once the sag  $D_R$  for the ruling span has been calculated, the sag  $D_i$  in any of the related suspension spans can be calculated as

$$D_i = D_R \left( \frac{S_i}{S_R} \right)^2. \quad (9.58)$$

Using sag–tension calculations, the sagging condition, i.e., the tension in the conductor during installation, can be determined. For this purpose, firstly the limit stresses at the critical conductor conditions (Fig. 9.36 [9.51]) are calculated and the prevailing condition is selected.

These conditions vary depending on the environment, the utility practice, and the standards to be followed; For example, in Germany [9.63], the maximum conductor stresses are calculated for:





**Fig. 9.36** Sag variation with conductor temperature, ice and wind loads, and time after installation calculated from the initial sag during stringing (adapted from [9.51])

- $-20^{\circ}\text{C}$  without ice loads or
- $-5^{\circ}\text{C}$  and ice load according to 4.5.2/DE.1 or
- $-5^{\circ}\text{C}$  and ice load combined with wind load according to 4.6.6.1/DE.1 or
- $+5^{\circ}\text{C}$  with wind load according to 4.4.1/DE.1.

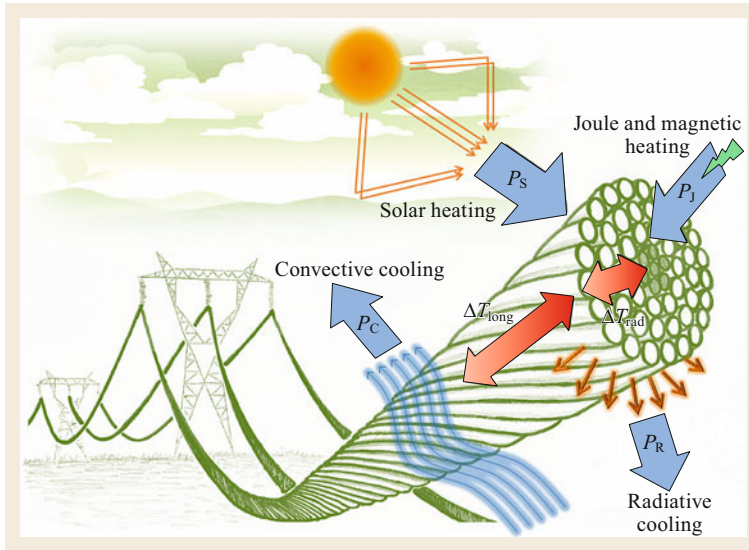
Thereby, the tensile stress at the fixing point of the conductor multiplied by the partial factor  $\gamma_C = 1.35$  should not exceed the value obtained as 95% of the rated tensile strength of the conductor divided by the material partial factor  $\gamma_M = 1.25$ . RTS values of ACSR are listed in Table 9.20.

In addition and at the annual mean temperature, which can be assumed to be  $+10^{\circ}\text{C}$ , the horizontal component of the conductor tensile stress without wind load should not exceed the everyday stress (EDS). Depending on the design of the suspension assemblies and the efficiency of the vibration protection, the horizontal component of the conductor tensile stress may exceed the specified values by up to 25%. Table 9.22 [9.64] lists these values for typical ACSR.

The maximum conductor and structure tensile loads increase with increasing initial installed tension, while the sag decreases. To avoid conductor tensile failure, but also, unless constrained by design, failure of supporting structures plus splices and dead-end fittings under high ice and wind loads, the conductor tension under maximum ice and wind is usually limited to 50–60% of the RTS [9.66]. For this purpose, the conductor’s initial unloaded tension at the time of construction or reconductoring is limited to a rather modest

**Table 9.22** Mechanical characteristics and permissible everyday stress for standard conductors (adapted from [9.64])

Conductor type and reference standard	Cross-sectional ratio	Number of strands	Coefficient of thermal expansion $\alpha$ ( $\times 10^{-6} \text{ K}^{-1}$ )	Effective modulus of elasticity $E$ ( $\text{kN/mm}^2$ )	Everyday stress ( $\text{N/mm}^2$ )	
					AL1/ST1A	AL3/ST1A
AL1/ST1A and AL3/ST1A	1.4 : 1	14/7	15.0	110	90	104
		14/19				
	1.7 : 1	12/7	15.3	107	84	102
		30/7	17.8	82	57	69
	6.0 : 1	6/1	19.2	81	56	67
		26/7	18.9	77		
		24/7	19.6	74	52	63
		54/7	19.3	70		
7.7 : 1	54/19	19.4	68			
	48/7	20.5	62	44	53	
	45/7	20.9	61	40	50	
23.1 : 1	72/7	21.7	60	35	–	
AL1	/	7	23.0	60	30	
		19		57		
		37				
		61		55		
		91				
AL3 (E-ALMgSi)	/	7	23.0	60	44	
		19		57		
		37				
		61		55		
		91				



**Fig. 9.37** Factors affecting the thermal equilibrium of an OHL conductor (adapted from [9.65])

value, i.e., 15–25% of the RTS. In addition, limiting the initial and final unloaded tensions to certain percentage ranges of the RTS is common as a means of vibration control, while recent work by CIGRE [9.67] suggests that limiting the so-called catenary constant  $H/w$  for the coldest month is better. This is discussed in Sect. 9.4.11.

### 9.4.5 Thermal Rating

The *purpose* of an overhead line conductor is to carry electrical current safely and efficiently under normal and emergency operating conditions, under all weather conditions, through the whole life expectancy of the line. To avoid overheating and damage to the phase conductors, the line's *thermal rating* is calculated as described extensively in [9.65]. This important document covers static and dynamic thermal rating calculations for both AC and DC operation, particularly at high temperatures and current densities, which are common nowadays because of the increased power flows in the grid.

Figure 9.37 [9.65] shows schematically the various contributions to the thermal state of the conductor and indicates that the resulting temperature distribution in the conductor is not necessarily constant, varying along the line with weather conditions (particularly wind) and at current densities above  $2 \text{ A/mm}^2$  often increasing towards the core by more than  $5^\circ\text{C}$  [9.68].

We concentrate here on the static steady-state condition of the conductor under the reasonable assumption that the conductor will have reached thermal equilibrium, i.e., that its temperature will not change significantly over time. Thereby, conservation of energy must

be observed

$$P_J + P_S = P_C + P_R . \quad (9.59)$$

The different contributing factors are addressed briefly below.

#### Joule Losses

The Joule losses per unit length  $P_J$  in a conductor are mainly caused by the resistance that the conductor material poses to electrons moving within it. This resistance increases with the average temperature of the conductor  $T_{av}$ , which can be explained intuitively by the fact that, as the temperature increases, the amplitude of the vibration of atoms in the metal lattice of the conductor also increases, thus impeding the passage of electrons. The increase in the DC resistance with temperature amounts to approximately 4% for every  $10^\circ\text{C}$  change in the conductor temperature.

$$\begin{aligned} P_J &= R_{DC} I^2 = \frac{\rho_{DC}}{A} I^2 \\ &= \rho_{DC} [1 + \alpha_{20} (T_{av} - 20)] \frac{I^2}{A} , \end{aligned} \quad (9.60)$$

where  $A$  is the cross-sectional area of the conductor.

Additional effects which increase the conductor resistance in the case of AC are the skin effect and magnetic losses [9.69]. Their combined contribution is accounted for in (9.61) by the factor  $k_J$ , which has, with very few exceptions, a value of less than 1.1; i.e., it causes an increase of  $R_{AC}$  with respect to  $R_{DC}$  by a maximum of 10%

$$R_{AC} = k_J R_{DC} . \quad (9.61)$$

Evidently, the main contributor to the Joule, also often called ohmic, losses is the square of the current magnitude  $I$ . For ACSR Drake with a diameter of 28 mm and a resistivity of  $0.073 \Omega/\text{km}$ , they amount to  $6.8 \text{ W/m}$  at 300 A and  $75 \text{ W/m}$  at 1000 A.

### Solar Heating

The solar heat gain per unit length by a conductor  $P_S$  is directly proportional to the conductor diameter  $D$ , the absorptivity  $\alpha_S$  of the conductor surface, and the global radiation intensity  $I_R$  [9.70]

$$P_S = \alpha_S I_R D. \quad (9.62)$$

The value of  $\alpha_S$  varies from around 0.2 for a bright new conductor to near 1.0 for a weathered conductor in an industrial environment after one or more years. As it is not easy to measure the absorptivity accurately, a default minimum value of 0.8 is often used.

The global radiation intensity  $I_R$  is a combination of the direct solar radiation on a surface normal to the sun's beam, the diffuse sky radiation onto a horizontal surface, and the incident radiation reflected from the ground, the so-called albedo. Transmission lines are often rated with a value of  $I_R = 900 \text{ W/m}^2$ .

### Convective Cooling

Convection is the transfer of heat in the direction of a temperature gradient due to bulk movement of molecules within fluids such as gases. The heat transfer from an overhead conductor to the surrounding atmosphere is quantified by the convective cooling  $P_C$ , which depends on the thermal conductivity of the air  $\lambda_f$ , the dimensionless Nusselt number  $\text{Nu}$ , and the difference between the temperatures of the conductor surface  $T_s$  and surrounding air  $T_a$

$$P_C = \pi \lambda_f (T_s - T_a) \text{Nu}. \quad (9.63)$$

There are two types of convection. Natural convection occurs when motion of air molecules is caused by buoyancy forces that result from density variations in the air. Forced convection occurs when a stream of air molecules flows over the conductor surface and transfers heat away from the *hot* conductor to the *cold* surrounding air. Already at quite low perpendicular wind speeds, even less than 0.5 m/s, forced convection dominates and natural convection can be ignored. At very low wind speeds though, natural convection may have a significant effect, becoming the dominant convection mechanism at 0.3 m/s and below; For example, for a Drake conductor at  $100^\circ\text{C}$  in air at ambient temperature of  $40^\circ\text{C}$ , natural convection contributes  $42 \text{ W/m}$  to its cooling while forced convection contributes 82

and  $115 \text{ W/m}$  at a wind velocity perpendicular to the conductor of 0.6 and 1.2 m/s, respectively. The total convection at low wind speeds can be found by adding the natural and forced convection vectorially.

### Radiative Cooling

Radiation is the result of the random movements of atoms and molecules in matter, which takes place at any temperature above absolute zero. Since these atoms and molecules are composed of charged particles (protons and electrons), their movement results in the emission of electromagnetic radiation in the form of photons, which carry energy away from the surface of the object in question, here the conductor. The radiative heat transfer, specifically the radiative cooling  $P_R$  of a conductor, is given by the Stefan–Boltzmann law

$$P_R = \pi D \sigma_B \varepsilon_S \left[ (T_s + 273)^4 - (T_a + 273)^4 \right], \quad (9.64)$$

where  $D$  is the conductor diameter,  $\sigma_B$  is the Stefan–Boltzmann constant,  $\varepsilon_S$  is the emissivity of the conductor surface, and  $T_s$  and  $T_a$  are the temperature of the conductor surface and the ambient, respectively. For bare overhead conductors, radiative cooling is generally much weaker than convective cooling. For a Drake conductor at  $75^\circ\text{C}$  with a suitably conservative wind speed of 0.6 m/s, the convective cooling is approximately three times the radiative cooling per unit length. Inserting (9.60)–(9.64) into (9.59), we get the relationship between the thermal rating, i.e., the maximum current  $I_{AC}$  that the conductor can carry at thermal equilibrium for an ambient conductor temperature  $T_a$

$$I_{AC} = \sqrt{\frac{P_C + P_R - P_S}{k_J \rho_{DC} [1 + \alpha_{20} (T_{av} - 20)] / A}}. \quad (9.65)$$

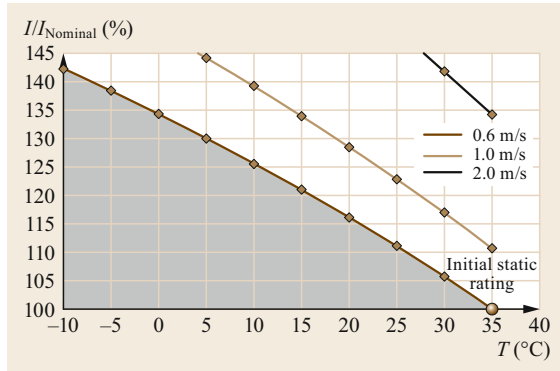
Table 9.23 presents an example calculation, and Fig. 9.38 [9.71] the strong dependence of the thermal rating on the wind velocity and ambient temperature. The maximum permissible conductor temperature is usually set at  $80^\circ\text{C}$  (Sect. 9.4.9).

### 9.4.6 Corona

Corona is an ionization process caused by the acceleration of electrons in an inhomogeneous electric field. If the field strength is high enough, electrons will acquire enough energy to ionize neutral molecules in the ambient air [9.72]. Thus, new free electrons are created, which, subjected to the same field, likewise ionize

**Table 9.23** Thermal rating of ACSR 265/35 for solar radiation of 900 W/m<sup>2</sup> with wind perpendicular to the line (adapted from [9.71])

Conductor	ACSR 265/35	ACSR 265/35
Wind velocity (m/s)	0.6	2
Ambient temperature (°C)	35	20
Max. conductor temperature (°C)	80	80
Thermal rating (A)	688	1055



**Fig. 9.38** Thermal rating of ACSR 265/35 over ambient temperature with wind velocity as parameter (adapted from [9.71])

molecules, leading through progressive multiplication to partial discharges in the air.

Depending on the voltage polarity, there are two types of such discharge:

- Negative corona or glow, which is characterized by blue light with lower intensity and low audible noise.
- Positive corona or streamers, which is characterized by sparkles with white light and high audible noise, thus being an important design issue for AC and DC lines; for the latter, corona effects get more complicated because of accumulation and wind dispersion of space charges.

The onset field intensity  $E_c$  for corona discharge of conductors can be reasonably well predicted using Peek's formula [9.73], which has been defined based on corona cage experiments

$$E_c = mE_0\delta \left( 1 + \frac{K}{\sqrt{\delta r}} \right). \tag{9.66}$$

For AC voltages,  $E_c$  is the peak value of the field intensity in kV/cm,  $r$  is the radius of the conductor in cm, and  $\delta$  is the relative air density.

**Table 9.24** Typical three-phase corona losses in W/m

Line voltage (kV)	Fair weather	Fog	Rain	Rime
110	0.001	–	–	1.0
220	0.3	2.9	8.0	30.0
380	0.6	4.3	12.0	50.0

Furthermore,  $E_0 = 31$  kV/cm is the breakdown voltage of air in a quasihomogeneous field and  $K = 0.308$  is an empirical factor. These values are also valid for DC voltages with a negative polarity, while for DC voltages with positive polarity  $E_0 = 32.7$  kV/cm and  $K = 0.241$  [9.74]. Peek's formula was developed for smooth cylindrical bodies and not for stranded conductors, whose circumference is by definition not round. In addition, local surface irregularities are produced during conductor manufacture and stringing, which cause local concentrations of the electric field and consequently decrease the corona onset voltage. This is taken into account in (9.66) by including a surface state coefficient  $m$ .

A typical value of  $m$  caused by stranding alone is 0.9; rain may reduce it to 0.6 or even lower.

In practice, it is recommended that the conductor surface gradient of overhead conductors should be limited to about 17 kV<sub>rms</sub>/cm [9.4].

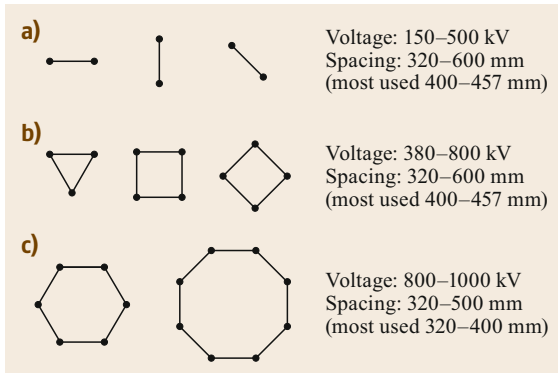
Corona can cause:

- Ozone (O<sub>3</sub>)
- UV radiation
- Corona loss (CL)
- Audible noise (AN)
- Electromagnetic interference (EMI)
- Radio interference (RI)
- Television interference (TVI).

In particular, as shown in Table 9.24, under adverse weather conditions, corona losses can reach values close to those of the Joule losses of the line.

For AC lines, design levels of 70 dB for radio interference and 60 dBA for AN at the edge of the right of way are often used. With the increased sensitivity of the public in respect to OHLs, audible noise caused by corona, in particular in poor weather, has motivated considerable research on understanding the physics of the problem as well as suitable mitigation methods in recent years [9.75].

Another important investigation [9.76] revealed the dependence of the electric field gradient (EF), AN, and RI on various key design parameters of the line, as presented in Table 9.18, and provided recommendations on how to reduce unacceptably high levels of RI and AN, both related to corona discharges.



**Fig. 9.39a–c** Typical conductor bundles and dimensions (adapted from [9.81]). (a) Twin bundles, (b) triple and quad bundles, (c) six and eight conductor bundles

### 9.4.7 Bundle Conductors

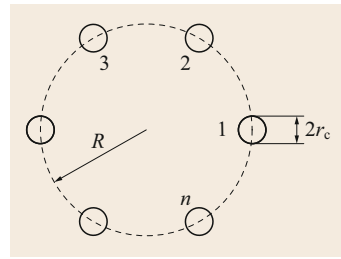
For voltages above 220 kV, the conductor diameter required to ensure that the limit of the field intensity at the conductor surface is not exceeded becomes prohibitive, leading to conductor sizes which are difficult to manufacture and to handle in the field; For example, if single conductors were to be used, they would have a diameter of 4.7, 8.5, and 13.8 cm for 400, 735, and 1100 kV AC, respectively [9.77]. This, together with the necessity to maximize the surge impedance load (SIL) of the line, has led to the development of so-called bundle conductors [9.78–80]. Typical bundle configurations are twin bundles for 220 kV, triple and quad bundles for 380 kV, six bundles for 765 kV, and eight bundles for 1000 kV (Fig. 9.39 [9.81]). Incidentally, the first field installation of bundle conductors took place in 1952 for a 380-kV line in Sweden equipped with quad bundles.

As per [9.82] for a balanced three-phase system voltage  $V_{\text{smax}}$ , the average electric field gradient on the surface of the conductor bundle  $E_{\text{avg}}$  (kV<sub>rms</sub>/cm), can be estimated using

$$E_{\text{avg}} = \frac{0.354\sqrt{3}V_{\text{smax}}}{nr_c \ln(D_{\text{eq}}/R_b)}, \quad (9.67)$$

where  $V_{\text{smax}}$  is the maximum system voltage, usually with a 5–10% margin above the nominal system (phase to phase) rms voltage,  $n$  is the number of conductors in the bundle,  $r_c$  (cm) is the outside radius of the subconductors,  $D_{\text{eq}}$  is the equivalent phase conductor spacing with  $D_{ij}$  (cm) being the center-to-center distances among phases, and  $R_b$  (cm) is the geometric mean radius of the bundle (9.68). It is normal to use a 5% margin above the nominal system voltage in corona calculations

$$D_{\text{eq}} = \sqrt[3]{D_{ab}D_{ac}D_{bc}}. \quad (9.68)$$



**Fig. 9.40** Geometry of an  $n$ -conductor bundle (adapted from [9.83])

The maximum field intensity  $E_{\text{max}}$  (kV<sub>rms</sub>/cm) is related to the average field  $E_{\text{avg}}$  by

$$\frac{E_{\text{max}}}{E_{\text{avg}}} = 1 + \frac{2r_c}{D_{\text{min}}}(n-1) \sin\left(\frac{\pi}{n}\right), \quad (9.69)$$

where  $D_{\text{min}}$  is the minimum distance among the  $n$  conductors in the bundle with typical values for a quad bundle of 400 mm in Europe and 457 mm in North America and elsewhere. Thereby the *geometric mean radius*  $R_b$  of a bundle of  $n$  conductors, each with outside radius  $r_c$  (cm), is given by

$$R_b = R \sqrt[n]{n \frac{R}{r_c}}, \quad (9.70)$$

where  $R$  is the radius of the cycle of the locus of the subconductors (Fig. 9.40). Physically, a single conductor of radius  $R_b$  has the same capacitance as the bundle with  $n$  subconductors. Figure 9.41 finally shows the field plots and the reduction factors of the maximum field intensity for different bundle arrangements [9.83].

The second big advantage of bundle conductors is that, while they reduce the series inductance, at the same time they increase the shunt capacitance, and consequently reduce the characteristic impedance of the line. At the same time, the surge impedance load (SIL), which is the limiting factor for the maximum power transfer along long lines, will increase [9.84]. Increasing the number and reducing the spacing of the subconductors as well as decreasing the distance between the phases of the line are favorable for a higher SIL (Table 9.1); For example, in a recent project in Brazil for a more than 600-km-long 500-kV AC line, by introducing expanded six-conductor bundles with 2580-mm spacing in lieu of the usual quad bundles of 457 mm, the SIL of the line was increased considerably from the standard 1000 to 1640 MW [9.6], i.e., by more than 60%, although this is partly counterbalanced by higher costs due to the use of more subconductors, difficulties encountered during the stringing of the bundle, and also problems during maintenance because of the large size and reduced rigidity of the related fittings.

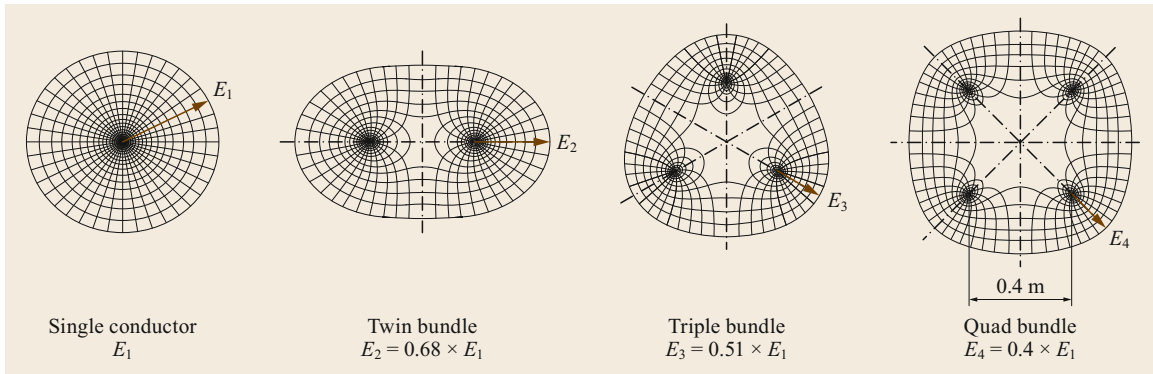


Fig. 9.41 Field plots and reduction factors of different bundle arrangements (adapted from [9.83])

### 9.4.8 Earth Wires

Most overhead transmission lines operating at voltages of 110 kV or above are provided with earth wires, which are also called shield or ground wires. In this context, the term *earth wire* is used for all types of conductors at earth potential. The main purpose of earth wires is to protect the conductors against the direct incidence of lightning strokes, which can cause line outages. Because of this, earth wires are earthed at each tower and have to carry, during the normal operation of the line, only small currents due to electromagnetic induction or electrostatic effects, resulting in negligible losses.

However, when a phase-to-earth short circuit occurs, a short-circuit current, often with significant magnitude, will flow through the earth wire and heat it up adiabatically, meaning that, because of its short duration, there will be no heat transfer to the environment. Earth wires thus have to be selected so that they should not exceed the maximum permissible temperature as per their material properties. This temperature is often indicated in the range of 160–220 °C. The design of earth wires under short-circuit conditions can be carried out according to [9.85]. Table 9.25 [9.4] lists technical data and maximum short-circuit currents of some typical steel earth wires.

In addition, the tensile stresses and sags of earth wires and the relevant stringing conditions need to be established so that the separation between earth wires and conductors at mid-span is wider than their separation at the towers. It should also be demonstrated that long-term vibrations with large amplitudes that could cause unacceptable damage do not occur. Thus, attention should be given to their proper vibration protection. It is usual to set the earth wire sag as 90–95% of the conductor sag at the average yearly temperature (everyday condition), for instance 10 °C in Europe, then to

ensure that the earth wire sag never exceeds the conductor sag.

In the past, earth wires having low conductivity, such as steel strands or AL1/STyz (ACSR) conductors with low aluminum content, were mostly employed, and they are still used in several countries. However today, most utilities, especially in Europe, have changed to the use of larger AL1/STyz (ACSR) conductors.

In some developing countries, the use of earth wires has been extended to the transmission of small amounts of energy at lower voltages, thus enabling rural electrification schemes [9.86]. Also the utilization of earth wires to carry telecommunication signals on integrated glass fibers has become very popular. Such earth wires are called optical ground wires (OPGW), and they are available in various designs:

- Self-supporting optical ground wires (OPGW)
- All dielectric self-supporting cables (ADSS)
- Optical fiber cables attached to earth or messenger wires.

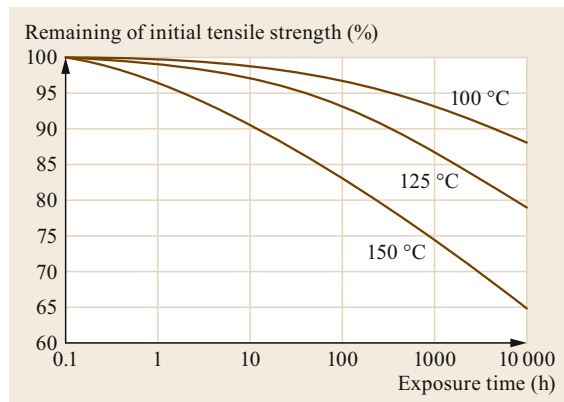
Optical fiber cables and their design, installation, and maintenance are aptly described in [9.87]. Because the inclusion of optical fibers results in sensitivity to mechanical damage, particular attention must be given to the proper selection of their fittings. This issue is covered in detail in [9.88–90].

### 9.4.9 High-Temperature Conductors

One of the most successful methods to increase the power transfer capacity of an existing line without extensive reconstruction is to increase the current it can safely carry by reconductoring it with so-called high-temperature low-sag (HTLS) conductors. The term *safely* has two aspects here: Firstly, as an increase in current will also increase the temperature of the con-

**Table 9.25** Technical data of steel earth wires

Shield wire type	Cross-sectional area $A$ (mm <sup>2</sup> )	Specific heat $c$ (W s/(kg K))	Resistivity $\rho$ ( $\Omega$ mm <sup>2</sup> /m)	Specific mass $\gamma$ (kg/(m mm <sup>2</sup> ))	Short-circuit duration		
					0.2 s (kA)	0.5 s (kA)	1.0 s (kA)
49-ST1A	49.5	481	0.192	0.00778	4.9	3.3	2.4
66-ST1A	65.8	481	0.192	0.00778	6.6	4.4	3.2
93-ST1A	93.3	481	0.192	0.00778	9.2	6.2	4.5
117-ST1A	117.0	481	0.192	0.00778	11.6	7.8	5.6

**Fig. 9.42** Loss of strength (annealing) of hard-drawn aluminum wire (adapted from [9.92])

ductor, it has to be considered that conventional hard-drawn aluminum [9.91] recrystallizes at temperatures above 100 °C and loses its mechanical strength over time (Fig. 9.42 [9.92]). This applies to aluminum-magnesium-silicon alloys [9.93] as well and is called *annealing*. Annealing occurs via the diffusion of atoms within a solid material, here aluminum, so that the material progresses towards its equilibrium state. Heat increases the rate of diffusion by providing the energy needed to break bonds. The movement of atoms has the effect of redistributing and eradicating dislocations and allows the metal to deform more easily, increasing its ductility. Temperatures below 300 °C do not affect the tensile strength of steel strands, but extended operation above 200 °C can damage the galvanization on steel wires. Aluminum conductors having a steel core (ACSR) also experience a loss of their total strength if operated above 100 °C, but since the strength of the steel core is unaffected, the reduction in the tensile strength of the aluminum strands is of less concern than for conductors made entirely of aluminum or aluminum alloy.

Secondly, the elevated temperature will cause greater conductor sag, which may violate the required clearances along the line. In this regard, it is worth mentioning that the conductor sag at elevated temperatures is influenced by some additional factors, which will increase it unfavorably. This is evident from Ta-

ble 9.26 [9.92], where the influence of these factors is quantified.

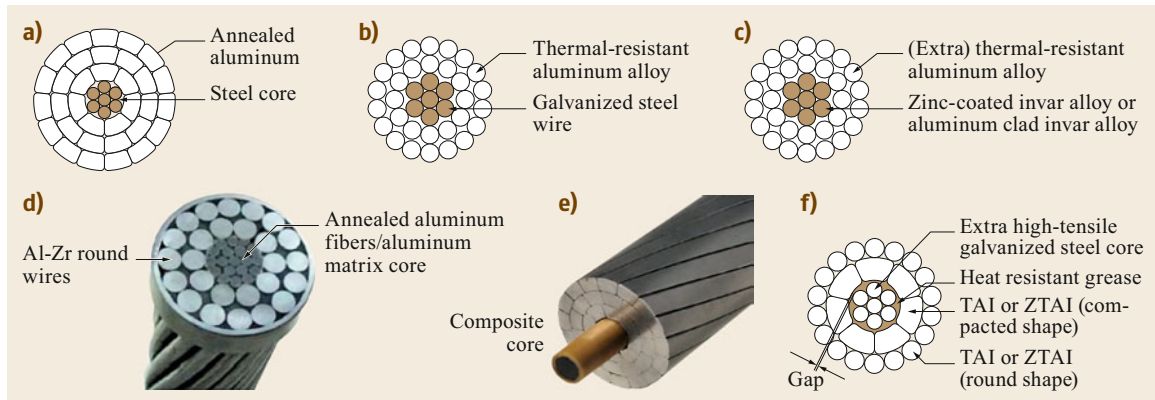
To address these issues, in the last years, HTLS conductors have been developed [9.92, 94]. They are capable of operating continuously at temperatures of at least 150 °C and as high as 250 °C during emergencies. For HTLS conductors with zirconium-aluminum wires [9.95], it is generally agreed that the emergency temperature should not apply for more than 10 hours per year. The main types of HTLS conductors are described below.

An ACSS (aluminium conductor steel-supported) consists of a steel core with one or more layers of aluminum, showing no difference in appearance or geometry from ACSR, including the possibility of being compacted. They can operate continuously up to 250 °C, because, since the aluminum wires have been annealed in the factory before stranding, there is no concern that the conductor will lose strength at high temperatures. When an ACSS is heated up in service, the aluminum wires elongate and quickly shift their load onto the steel core. From this point onwards, the conductor essentially behaves as a steel conductor, that is, its thermal elongation and modulus of elasticity are those of the steel core. In addition, and since the elongation at failure of annealed aluminum wires is approximately 20%, compared with that of the steel core, which is limited at 1%, the conductor can utilize the steel core at its full strength. Moreover, the high elongation of the aluminum means that the creep properties of the conductor are ruled by the steel core, which usually exhibits very low creep. For further increase of the conductor ampacity, trapezoidal wires (TW), as shown in Fig. 9.43a, are used.

(Z)TACSR (Fig. 9.43b) has the same construction as conventional ACSR, with galvanized steel wires for the core and (Z)TAL, i.e., thermally resistant zirconium-aluminum alloy wires, which do not anneal at temperatures up to 210 °C. On the other hand, it has the same thermal elongation behavior as ACSR, which will affect clearances. Thus, such conductors are mainly installed in new lines expecting high power transfer and for which high sags can be considered in the design stage.

**Table 9.26** Typical error magnitudes in high-temperature sag calculations (adapted from [9.92])

	ACSR Drake	ACSR Condor	ACSR Tem
Aluminum area (strands) (mm <sup>2</sup> )	403 (26)	403 (54)	403 (45)
Steel area (strands) (mm <sup>2</sup> )	66 (7)	53 (7)	28 (7)
Final tension at 20 °C (N)	25 800	23 150	19 100
Equivalent span length (m)	250	250	250
Sag at 20 °C (m)	4.84	5.06	5.36
<b>Effects of calculation methods on final 120 °C sag (m)</b>			
Calculation assuming constant modulus	7.76	7.78	8.53
Graphical method with no AI compression	7.00	7.53	8.53
Graphical method with typical 20 MPa maximum compression	7.32	7.73	8.53
<b>Additional sag errors at 120 °C (m)</b>			
Temperature difference core/surface	+0.03	+0.05	+0.06
Change of elastic modulus versus temperature	+0.15	+0.11	+0.06
High-temperature creep	0	0	+0.50
Multiple span effects	+0.6 to -1.0	+0.5 to -0.9	+0.5 to -0.8
Effect of core magnetization losses	0	+0.07	+0.05
Effect of manufacturing temperature	±0.14	±0.12	0

**Fig. 9.43a–f** HTLS conductors: (a) ACSS/TW, (b) (Z)TACSR, (c) (Z)TACIR, (d) ACCR, (e) ACCC, (f) G(Z)TACSR (adapted from [9.94])

The increased sag issue can be addressed by using (Z)TACIR (Fig. 9.43c), which has galvanized or aluminum-clad Invar alloy steel wires in lieu of the steel strands of (Z)TACSR. Invar is an iron-nickel alloy with a coefficient of thermal expansion of around one-third that of galvanized or aluminum-clad steel wire. These conductors can operate continuously up to 210 °C with relatively low sag.

G(Z)TACSR or gap-type conductors have a small gap between the steel core and innermost shaped aluminum layer, to allow the conductor to be tensioned on the steel core only, thereby allowing the low-sag properties of the steel core to be exploited over a greater temperature range. The gap is filled with heat-resistant grease, to reduce friction between the steel core and aluminum layer and prevent water penetration.

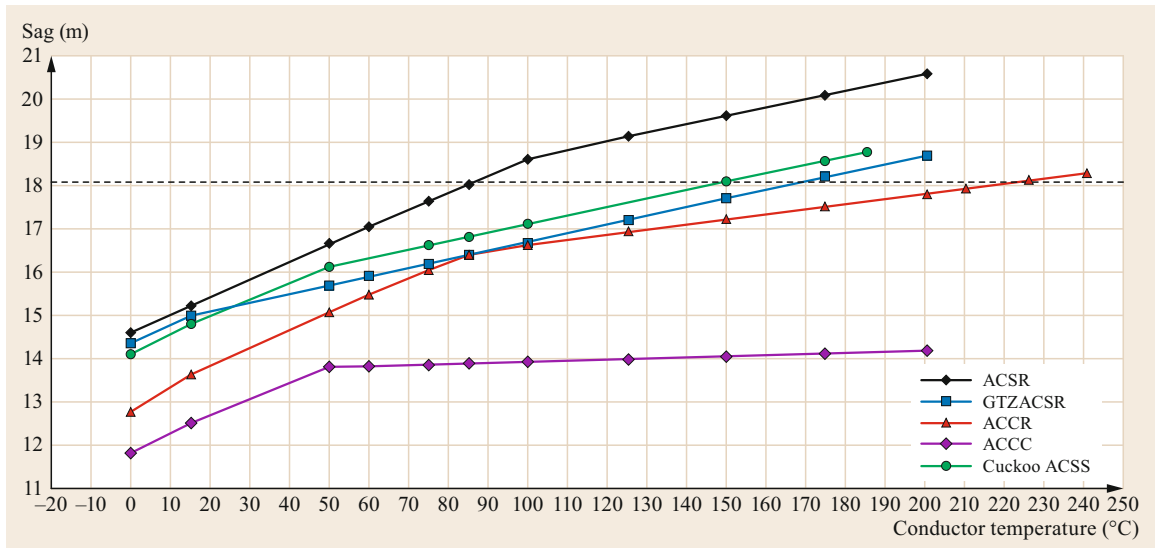
Aluminum conductor composite reinforced (ACCR) (Fig. 9.43d) is an HTLS conductor consisting of zirco-

nium-aluminum alloy strands over a reinforcing core of ceramic fibers in an aluminum matrix. The high elastic modulus of the aluminum composite core and its low thermal elongation rate (half that of steel) makes this conductor particularly useful for existing lines with heavy ice loads and minimum high-temperature sag clearances.

Finally, aluminum conductor composite core (ACCC) is a HTLS conductor with a single-strand carbon-reinforced high-temperature thermoset resin core and trapezoidal annealed aluminum wires. The core has a very low thermal elongation rate, making this conductor very effective for limiting sag at high temperatures, while because of the thermoset resin, the manufacturer recommends a maximum continuous operating temperature of 180 °C.

Figure 9.43 [9.94] portrays all these conductors, while Fig. 9.44 [9.92] compares their sag variation with





**Fig. 9.44** Sag versus temperature for different HTLS conductors; *dashed horizontal line* depicts maximum sag of an equivalent ACSR Drake for 420-m span (adapted from [9.92])

conductor temperature for ACSR Drake in a 420-m-long span.

However, it should be remembered that, for high currents  $I$  such as those in HTLS conductors, the ohmic losses, which vary with  $I^2$ , become prohibitive for line lengths above approximately 80–100 km, thus the benefits of installing such conductors may be limited. Further, the application of some types of HTLS conductors is still a developing technology, requiring better calculation tools and additional laboratory and field test data.

### 9.4.10 Real-Time Monitoring

As an alternative or sometimes in addition to HTLS conductors, real-time monitoring (RTM) systems can be employed to determine the rating of the line in real time. They consist of devices that measure directly or indirectly the temperature and sag of the conductor. From these measurements, the actual thermal rating or ampacity of the conductor can be calculated. The main objectives of an RTM system are therefore to:

- Determine the actual sag in critical spans and corresponding mean conductor temperature
- Compare the actual sag with the maximum allowable sag or maximum permissible temperature in each of these spans.

Using this information, *safe buffers* for the critical spans based on the known actual load can be determined

and converted into electrical loads for each critical span.

Such thermal rating methods can be direct or indirect. Direct methods involve measuring at least one physical parameter of the line, such as tension, temperature, vibration frequency, or ground clearance, which is then used to derive parameters such as sag, temperature, and tension where not directly measured. With indirect methods, weather parameters are first measured and then used in conjunction with conductor electrical load data to calculate the temperature and subsequently the sag and/or tension of the conductor. These are described in [9.96], from which the following information is extracted.

#### Donut Devices

So-called donut devices were probably the earliest RTM systems to be conceived and used. They employ temperature sensors and are clamped directly onto the conductor (Fig. 9.45). They can measure simultaneously, besides the conductor surface temperature, the line-to-ground voltage and the actual current, and transmit these data to a base station or the next control room for evaluation. They are cheap and easy to apply, but their relatively high mass acts as a heat sink and can negatively influence the vibration behavior of the conductor.

#### Tension Monitoring

Tension monitoring systems are probably the most often used. They measure the conductor tension using



**Fig. 9.45** Power donut (adapted from [9.96])



**Fig. 9.47** Monitoring through vibration analysis (adapted from [9.96])



**Fig. 9.46** Load cells (red) for tension monitoring (adapted from [9.96])

a load cell installed on the earth side of a dead-end insulator string (Fig. 9.46) and transmit this information wirelessly to the line operator. There, the tension can be expertly converted to a conductor temperature and sag, thereby enabling calculation of the actual conductor current and possible reserves in the thermal rating of the line. Tension monitoring systems are well developed, robust, and proved in numerous installations worldwide, but their installation is rather complicated.

#### Monitoring Through Vibration Analysis

In a relatively recent development, the conductor tension and sag—and *backwards* therefrom the conductor temperature—can be derived by detecting the fundamental frequency of the span due to aeolian vibrations (Sect. 9.4.11) using a so-called smart monitor (Fig. 9.47), which can be applied anywhere along the span. Such monitors are light, easy to install, self-sustaining (by harvesting energy from the conductor), and capable of data transmission, although operating experience remains limited.

### 9.4.11 Conductor Vibrations

Conductor vibrations are quite a common phenomenon and, if not properly damped, can cause serious damage not only to the conductors themselves but also to other line components. Such vibrations are part of a broad class of external line loads, the so-called dynamic or cyclic loads, such as loads caused by conductor rupture, short circuits, ice shedding, and rarely seismic loads. We will concentrate here on so-called wind-induced vibrations, as they are by far the most common.

Wind-induced vibrations started to plague overhead lines with the wide introduction of aluminum-based conductors early in the 20th century, due to their greater susceptibility, mainly due to their low weight compared with the copper conductors previously used. In addition, because of its metallographic structure, aluminum is quite sensitive to fatigue. To understand this better, consider the various mechanisms of vibration excitation by wind as well as their consequences for the fatigue strength of the conductor involved.

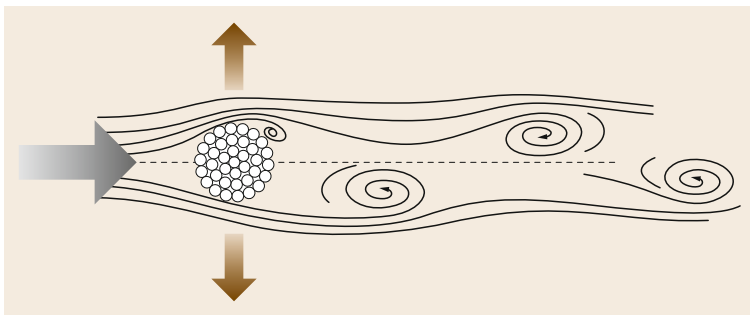
Three main types of wind-induced vibrations are recognized: aeolian vibrations, wake-induced or sub-span oscillations, and galloping. Their main properties are summarized in Table 9.27 [9.97]. Anecdotally, for 1 case of galloping, there are 10 cases of subspan oscillations and 1000 cases of aeolian vibration.

#### Aeolian Vibrations

**Wind Excitation and Strouhal Frequency.** The most common type of wind-induced conductor motions are the so-called *aeolian vibrations*, named after Aeolus, the keeper of the winds in Greek mythology. They are excited by moderate, laminar winds, and their peak-to-peak amplitude seldom exceeds one conductor diameter. Physically, the flow of a fluid, here air, interacting with a cylindrical shape, here the conductor, has been observed to generate so-called von Kármán vortices, which are shed in a downstream wake (Fig. 9.48). The pressure fluctuation due to such vortex shedding is responsible for up- and downlift forces on the conductor with a prevailing frequency equal to the Strouhal fre-

**Table 9.27** Comparison of types of cyclic conductor motion (adapted from [9.97])

	<b>Aeolian vibration</b>	<b>Conductor galloping</b>	<b>Wake-induced oscillation</b>
Types of overhead lines affected	All	All	Lines with bundled conductors
Approximate frequency range (Hz)	3–150	0.08–3	0.15–10
Approximate range of vibration amplitudes (peak-to-peak) (expressed in conductor diameters)	0.01–1	5–300	Rigid-body mode: 0.5–80 Subspan mode: 0.5–20
Weather conditions favoring conductor motion – Wind character – Wind velocity (m/s)	Steady 1–7 (3.5–25 km/h)	Steady 7–18 (25–65 km/h)	Steady 4–18 (15–65 km/h)
Conductor surface	Bare or uniformly iced (i.e., hoarfrost)	Asymmetrical ice deposit on conductor	Bare, dry
Design conditions affecting conductor motion	Line tension, conductor self-damping, use of dampers, armor rods	Ration of vertical natural frequency to torsional natural frequency: sag ratio and support conditions	Subconductor separation, tilt of bundle, subconductor arrangement, subspan staggering
<b>Damage</b>			
Approximate time required for severe damage to develop	3 months to 20+ years	1–48 h	1 month to 8+ years
Direct causes of damage	Metal fatigue due to cyclic bending	High dynamic loads	Conductor clashing, accelerate wear in hardware
Line components most affected by damage	Conductor and shield wire strands	Conductor, all hardware, insulators, structures	Suspension hardware, spacers, dampers, conductor strands

**Fig. 9.48** Aeolian vibration initiated by vortex shedding (gray arrow: wind velocity, brown arrows: up- and downlift forces)

quency  $f_s$  (in Hz)

$$f_s \approx 0.2 \frac{v_w}{d_c} \quad (9.71)$$

In this expression,  $v_w$  is the wind velocity perpendicular to the conductor in m/s,  $d_c$  is the conductor diameter in m, and  $S$  is the so-called Strouhal number, which for aeolian vibrations has a (dimensionless) value in the range of 0.2. Consequently and as explained later, when the velocity of the wind is such that the Strouhal frequency of the vortices approaches a modal frequency of the conductor, the latter will start moving transverse

to the wind direction. In reality, aeolian vibrations occur over a range of wind velocities, and once the conductor starts to vibrate, a lock-in effect takes place and the vortex-shedding frequency is controlled by the vibration, even if the wind velocity varies in the range of 90–130% of the initial wind velocity.

**Wave Equation and Natural Frequencies.** The conductor movements propagate as traveling waves to the span extremities, where they are fully or partly reflected and superpose to form standing waves along the span. In this case, the conductor can be modeled as a taut

string with negligible flexural rigidity, obeying the well-known wave equation [9.98–101]

$$T \frac{\partial y^2}{\partial x^2} = m \frac{\partial y^2}{\partial t^2}, \quad (9.72)$$

from which the shape of the conductor can be obtained as a harmonic oscillation in space and time

$$y(x, t) = y_{\max} \sin\left(n\pi \frac{x}{L}\right) \sin(\omega t), \quad (9.73)$$

with a propagation velocity of

$$v = \sqrt{\frac{T}{m}} \quad (9.74)$$

and a wave impedance of

$$Z_c = \sqrt{mT}, \quad (9.75)$$

where  $T$  is the conductor tension,  $m$  is its mass per unit length,  $y_{\max}$  is the maximum vibration amplitude,  $L$  is the span length, and  $n$  is the order of the vibration mode. Considering that

$$n \frac{\lambda}{2} = L \quad (9.76)$$

and the definition

$$v = f\lambda, \quad (9.77)$$

combination of (9.74) and (9.76) with (9.77) yields the spatial frequency of the  $n$ -th vibration mode as

$$f_n = \frac{n}{2L} \sqrt{\frac{T}{m}}. \quad (9.78)$$

This mode can only be excited if its characteristic frequency  $f_n$  coincides with the Strouhal frequency  $f_s$ , i.e., by equating (9.78) with (9.71) and solving for  $n$

$$n = 2Lf_s \sqrt{\frac{m}{T}} = 0.4 \frac{v_w L}{d_c} \sqrt{\frac{m}{T}}. \quad (9.79)$$

For example, for a Drake conductor (ACSR 400/70 mm<sup>2</sup>, (26×4.44 Al + 7×3.47 St) with 28 mm diameter and a mass of 1.63 kg/m), tensioned at 28 000 N in a 400 m span, the 43rd mode is excited at a wind velocity of 1 m/s and the 215th mode at a wind velocity of 5 m/s, the corresponding wavelengths  $\lambda = 2L/n$  being 18.6 and 3.7 m, respectively.

The situation is different in the vicinity of the suspension clamp, where the conductor is considered to be fixed, i.e., the tangent to its deflection is horizontal. At this location, the bending stiffness of the conductor cannot be neglected and plays an important role in determining the stress regime within the conductor [9.102, 103].

**Table 9.28** Terrain categories and characteristics for aeolian vibration assessment (adapted from [9.67])

Terrain category	Terrain characteristics
1	Open, flat, no trees, no obstruction, with snow cover, or near/across large bodies of water; flat desert
2	Open, flat, no obstruction, no snow; e.g., farmland without any obstruction, summer time
3	Open, flat or undulating with very few obstacle; e.g., open grass or farmland with few trees, hedgerows and other barriers; prairie, tundra
4	Built-up with some trees and buildings, e.g., residential suburbs; small towns; woodlands and shrubs. Small fields with bushes, trees, and hedges

**Energy Balance Principle.** When a conductor starts to vibrate, the energy imparted to it by the wind  $P_w$  will feed the vibration and continuously increase its amplitude. The relative wind power input  $P_w/S$  (where  $S$  is the span length) depends on the maximum vibration amplitude  $y_{\max}$ , also called the antinode or the free loop amplitude, the excitation Strouhal frequency  $f_s$ , and the conductor diameter  $d_c$  and can be approximated as

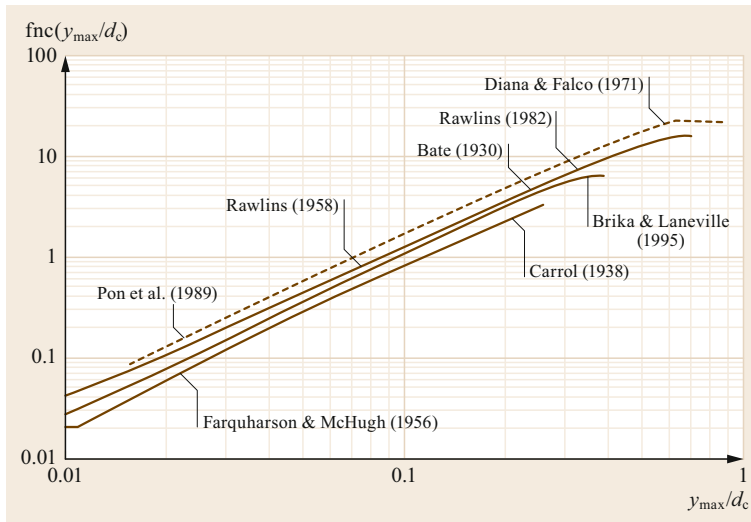
$$\frac{P_w}{S} = f_s^3 d_c^4 \text{fnc} \left( \frac{y_{\max}}{d_c} \right), \quad (9.80)$$

where the function is usually determined by measurements in wind tunnels and given by [9.104]

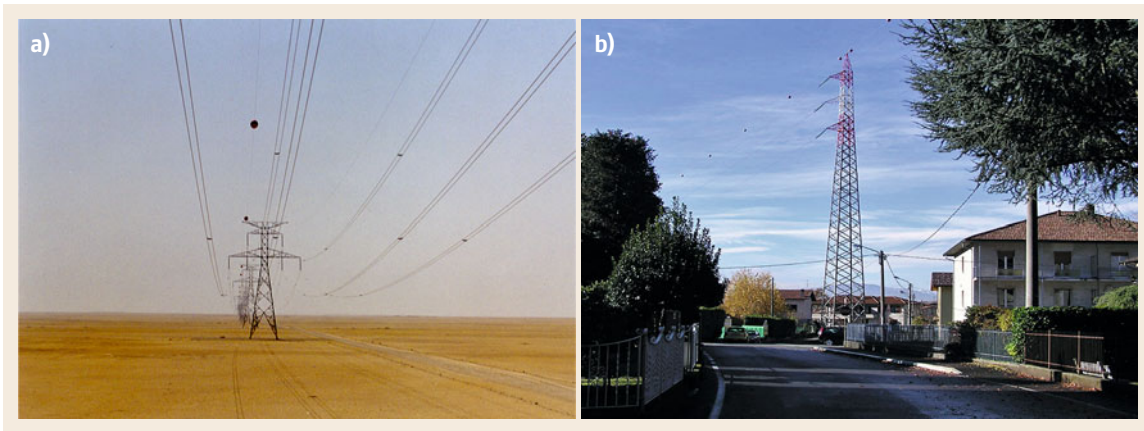
$$\begin{aligned} \text{fnc} \left( \frac{y_{\max}}{d_c} \right) &= 0.2256 + 0.1677 \left( \frac{y_{\max}}{d_c} \right) \\ &+ 101.62 \left( \frac{y_{\max}}{d_c} \right)^2 \\ &- 99.73 \left( \frac{y_{\max}}{d_c} \right)^3. \end{aligned} \quad (9.81)$$

Typical curves for this function are shown in Fig. 9.49 [9.105].

It has been recognized and is easily understood that terrain is the single most important factor for the excitation of aeolian vibrations. This has to do with the amount of turbulence created by the terrain and particularly by the ground cover; For example, wind blowing over a desert area (Fig. 9.50a) or a water body, such as a lake, will be more laminar in nature and thus more favorable for conductor vibrations than the same wind blowing over a built-up area with trees and buildings (Fig. 9.50b). To facilitate vibration assessment, four terrain categories with growing turbulence intensity have been introduced [9.67] (Table 9.28).



**Fig. 9.49** Maximum wind power input coefficient  $fnc(y_{\max}/d_c)$  per unit length for a single conductor as obtained by different researchers (adapted from [9.105])

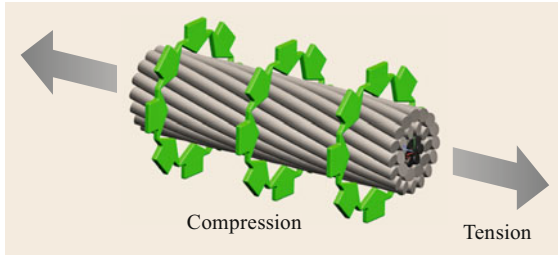


**Fig. 9.50** (a) Terrain category 1 per Table 9.28, (b) Terrain category 4 per Table 9.28

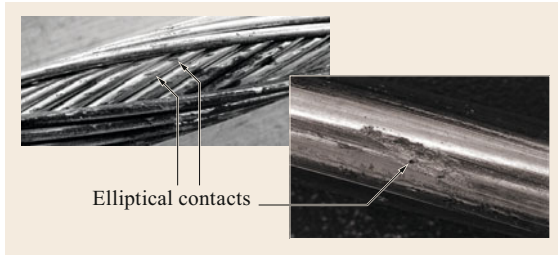
Fortunately, in addition to the resistance that the surrounding air poses to the conductor movement (aerodynamic damping) and the intrinsic damping of the conductor material (Coulomb damping), the conductor itself contributes the greatest amount to its so-called self-damping. To understand this issue, consider that, when the conductor is tensioned, the radii of the helices of the conductor wires are reduced, imposing a lateral pressure on the crossing points with the underlying wires (Fig. 9.51 [9.106]). In reality, these point-to-point contacts have an elliptical shape (Fig. 9.52) with a size that depends on the material properties of the wires and the tension level; i.e., the *softer* the material and the higher the tension, the larger the contact area. When the conductor starts to vibrate, it actually bends and, at low amplitudes, the friction between the wires is high enough to prevent sliding; i.e., the wires *stick* together. However, above a certain vibration amplitude,

this interwire friction is overcome and the wires start to slip over one another [9.102, 103], firstly only at the edges of the contact ellipses, which is called *microslip*, and then via rigid-body motion, i.e., *full slip*. Evidently, during this process, energy is dissipated at each wire contact, and the sum of the energy dissipated over all contacts within the conductor results in the *self-damping* of the conductor. Intuitively, self-damping decreases with increasing conductor tension, as the onset of the wire slip is then retarded, and increases with the vibration frequency and amplitude, as these will increase the bending of the vibration loops and thus facilitate wire slip. Figure 9.53 [9.1] confirms these observations.

Conductor self-damping is usually measured in the laboratory using dedicated test spans [9.107], forming the basis for [9.108], which describes the current methodologies, including apparatus, procedures,



**Fig. 9.51** Tension-induced compression in a conductor (adapted from [9.106])



**Fig. 9.52** Elliptical contacts at the surface of conductor aluminum wires (photo: U. Cosmai)

and accuracies for such measurements and data handling. Publication [9.109] provides details of various self-damping measurements of several conductors and OPGWs originating from five different laboratories. Data measured on laboratory spans are generally expressed empirically using a power law [9.110]

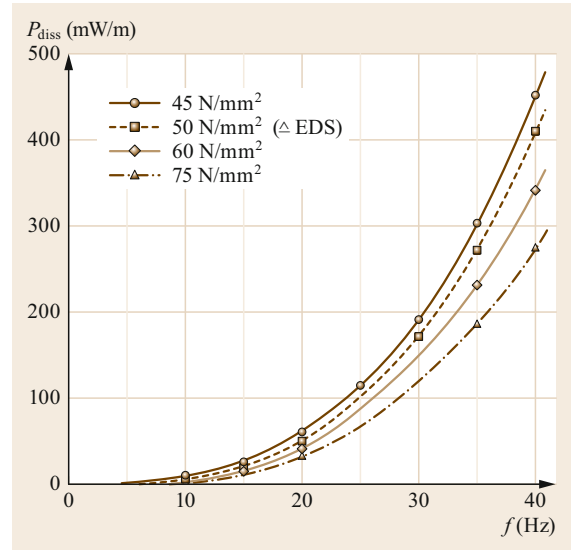
$$P_{\text{diss}} = \frac{P}{L} = \frac{kA^l f^m}{T^n}, \tag{9.82}$$

where  $P/L$  is the power per unit length dissipated by the conductor,  $A$  is the antinode displacement of the vibration, and  $f$  is the frequency of the vibration, while  $l$ ,  $m$ , and  $n$  are the amplitude, frequency, and tension exponents, respectively. The so-called conductor factor  $k$  combines the conductor diameter  $D$  (mm), its rated strength  $RS$  (kN), and its mass per unit length  $m$  (kg/m) [9.97]

$$k = \frac{D}{\sqrt{RSm}}. \tag{9.83}$$

Using the empirical rule (9.83), the self-damping determined using short laboratory spans can be extrapolated to actual, much longer spans.

Self-damping data have always been difficult to measure and obtain. In case no experimental data are available, an alternative is to use the so-called similarity laws [9.111]. These laws are derived from the assumption that self-damping should be the same for all



**Fig. 9.53** Self-damping of ACSR 560/60 ( $d_c = 32$  mm) over vibration frequency  $f$  at a free-field bending angle of  $20^\circ$  with EDS as parameter (adapted from [9.1])

conductors of the same construction. Noiseux’s findings can be expressed in the form

$$\frac{P}{L} = D^4 \sigma_{\text{Al}}^{-2.76} A^{2.44} f^{5.63}, \tag{9.84}$$

where  $D$  is the overall conductor diameter (mm) and  $\sigma_{\text{Al}}$  is the stress in the aluminum wires in  $\text{N/m}^2$ .

If the wind power input and the power dissipated through self-damping are now plotted on the same diagram versus the dimensionless amplitude  $y_{\text{max}}/D$  (Fig. 9.54), the prevailing amplitude of vibration can be determined from the point of intersection of these two curves; at this point, energy equilibrium occurs. This is the idea of the energy balance principle (EBP) [9.110]

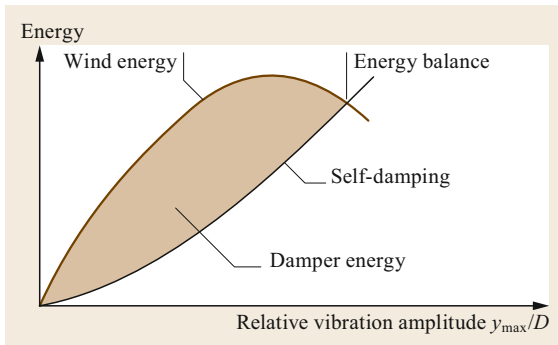
$$E_W = E_C, \tag{9.85}$$

where  $E_W$  is the energy imparted to the conductor by the wind and  $E_C$  is the energy dissipated by the vibrating conductor.

In most cases, the conductor self-damping mechanism is insufficient to control the levels of vibration within limits which do not produce high accumulation of damaging fatigue cycles. Therefore, often additional, external damping has to be considered, and the EBP equation becomes

$$E_W = E_C + E_D, \tag{9.86}$$

where  $E_D$  is the minimum energy dissipated by the dampers (Sect. 9.6.3), indicated by the dashed area in Fig. 9.54.



**Fig. 9.54** EBP explained schematically (source U. Cosmai)

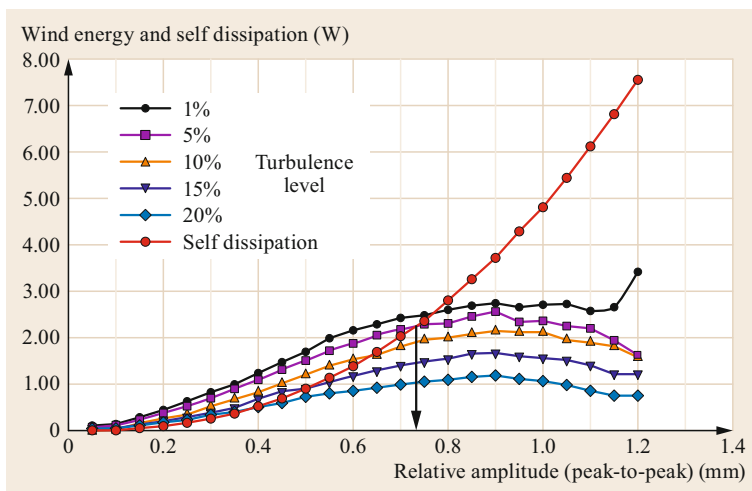
The EBP acts in the frequency domain; i.e., one mode of vibration at a time is considered, and the steady-state solutions corresponding to the maximum vibration amplitude which could be excited on that conductor at that frequency are computed; this is considered to be acceptable for most engineering applications, as it is on the safe side.

On the other hand, Fig. 9.55 shows the calculation results for a real case, where the arrow marks the *balanced* amplitude for a wind input with 5% turbulence and the self-damping curve of the conductor for a given frequency.

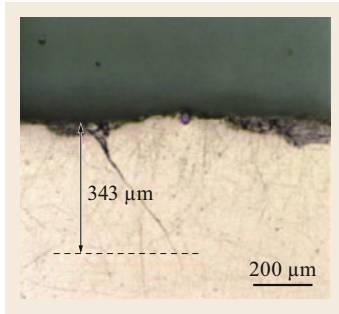
**Fatigue.** The wire movement in the conductor is, on one hand, beneficial towards vibration control, as it is by far the major contributor to the conductor self-damping. However, on the other hand, it is also the main factor causing internal conductor damage, via a phenomenon called *fretting fatigue* [9.112]. This occurs at locations where the conductor is fixed by hardware and mainly at suspension clamps (Fig. 9.105).

There, conductor bending but also lateral contact forces which influence the wire slip are the highest within the span. When the wires start moving, surface material is abraded, i.e., for aluminum wires, aluminum oxide, a hard, powder-like substance with black color, which acts as an abrasive. In combination with the high local stresses in the contact areas, but also the high bending stresses in the bulk of the wire, cracks can be initiated at local surface imperfections (Fig. 9.56) due to irregularities in the wire material properties or caused during manufacturing. These cracks start propagating across the wire until it fails (Fig. 9.57a). As the remaining sound wires will then have to carry a higher mechanical load, if the vibration continues, further wire failures will take place until the full conductor fails (Fig. 9.57b), with detrimental consequences. It is worth noting that wire failures will often occur in the inner layers of the conductor and be concentrated in the lower part of the conductor close to the clamp mouth, making it difficult to detect them during visual inspections.

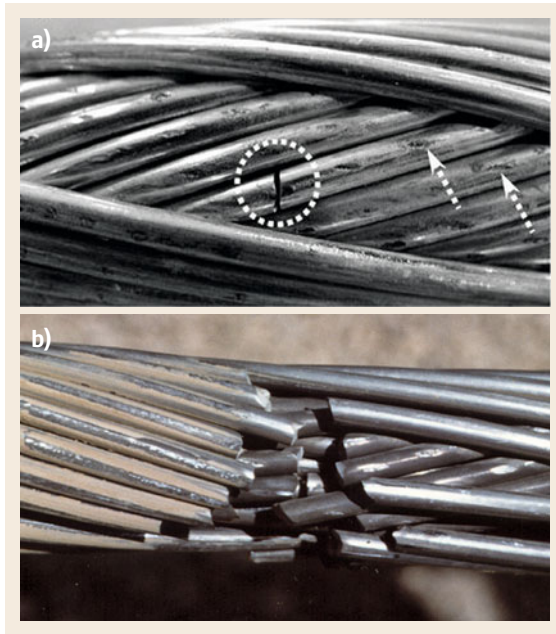
**Laboratory Fatigue Tests.** In these tests, the conductor is forced to vibrate at various amplitudes until a predetermined number of wires fail. In this way, the so-called *S/N* or Wöhler curve of the conductor is determined [9.113]. It was recognized early on that the conductor endurance capability depends largely on the associated hardware, namely the suspension clamp [9.114], and it is thus recommended to carry out such tests using the same conductor clamp combination as used in the field [9.115]. As these tests are time consuming and rather expensive, a generic *S/N* curve has been proposed [9.54], viz. the so-called safe-border line, which can be used to determine the conductor endurance limit. This can be either a dynamic bending stress/strain or the so-called bending amplitude. The



**Fig. 9.55** EBP in a real case (source J.L. Lilien)



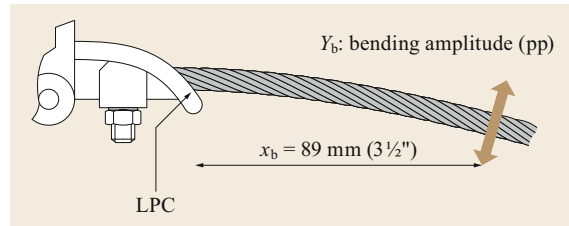
**Fig. 9.56** Crack initiation in a wire (picture L. Cloutier)



**Fig. 9.57a,b** Wire failure (a) leading to conductor rupture (b) (photos U. Cosmai)

latter is the dynamic peak-to-peak bending amplitude measured at a distance of 89 mm (equal to 3.5 in) from the last point of contact (LPC) of the conductor with the clamp (Fig. 9.58 [9.81]).

**Field Measurements.** Vibrating conductors are complex mechanical systems for which field measurements are indispensable in order to determine their vibration activity and also to check related theoretical predictions. For quite a few years now, the state of the art has been to monitor conductor vibrations in the field under real-life conditions using modern vibration recorders [9.116]. The majority of these recorders measure the bending amplitude  $Y_b$  versus the vibration frequency and the corresponding number of cycles. Modern recorders (Fig. 9.59) work autonomously for many months and store and transmit the measured data to a base station; such mea-



**Fig. 9.58** Definition of bending amplitude (adapted from [9.81])



**Fig. 9.59** Modern vibration recorder in the field (photo: Pfisterer Sefag)

surements and the associated data evaluation procedures are described in [9.117, 118].

**Vibration Safe Design.** To control aeolian vibrations to acceptable levels, a methodology had to be developed to establish limits beyond which vibration will not harm the conductor.

One way to do this, predominantly in the design stage, i.e., before the line has been built, is to limit the conductor tension or a parameter related to it. For many years and still nowadays, the recommendations of the so-called CIGRE EDS panel were followed [9.119]. These prescribed the so-called everyday stress (EDS), i.e., the stress in the conductor at the average yearly ambient temperature, and the related tensile load, as a percentage of the RTS of the conductor, with a value of 20% often being used (Table 9.29 [9.67]).

However, this has proved to cause problems in certain cases of ACSR and also to be rather on the high side for monometallic conductors such as AAAC. For this purpose, the subject has been reassessed and new recommendations have been issued [9.67]. They are based on  $H/w$ , the ratio between the tensile load  $H$  (N) of the conductor and its weight per unit length  $w$  (N/m).



**Table 9.29** EDS panel recommendations for safe design tensions as a percentage of RTS (adapted from [9.67])

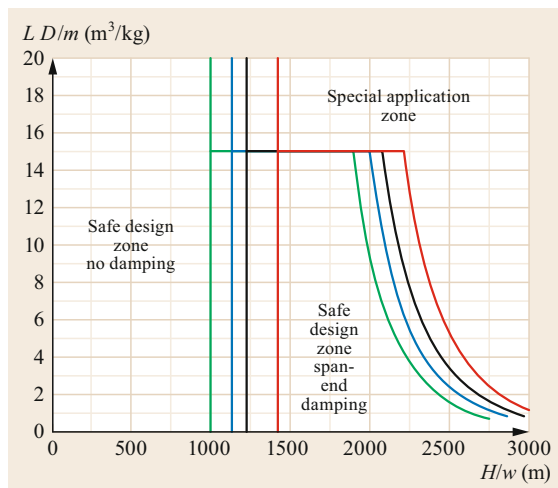
	Unprotected lines	Line equipped with		
		A armor rods	Dampers	Both
Copper	26			
ACSR	18	22	24	24
Aluminum conductors	17			
Aldrey conductors	18		26	
Steel conductors				
– Rigid clamps	11			
– Oscillating clamps	13			

**Table 9.30** Recommended admissible conductor safe design tension at the average temperature of the coldest month as a function of terrain category, valid for homogeneous aluminum and aluminum alloy conductors Ax (AAC and AAAC), bimetallic aluminum conductors Ax/Ay (ACAR, aluminum conductor alloy reinforced), and steel-reinforced aluminum conductors A1/Syz (ACSR) (adapted from [9.67])

Terrain category	Terrain characteristics	(H/w) <sub>adm</sub> (m)
1	Open, flat, no trees, no obstruction, with snow cover, or near/ across large bodies of water; flat desert	1000
2	Open, flat, no obstruction, no snow; e.g., farmland without any obstruction, summer time	1125
3	Open, flat or undulating with very few obstacle; e.g., open grass or farmland with few trees, hedgerows and other barriers; prairie, tundra	1225
4	Built-up with some trees and buildings, e.g., residential suburbs; small towns; woodlands and shrubs. Small fields with bushes, trees, and hedges	1425

Here,  $H$  is the initial horizontal tension before any significant wind and ice loading and before creep at the average temperature of the coldest month at the site of the line. For single conductors, this parameter depends mainly on the terrain (Table 9.30).

On the other hand, adding dampers in a span is expensive and may allow higher conductor tensions resulting in significant cost savings during line construction. For this reason, based upon extensive theoretical studies and in-depth evaluation of field experience, additional recommendations for single conductors which consider the effect of Stockbridge dampers (Sect. 9.6.3)

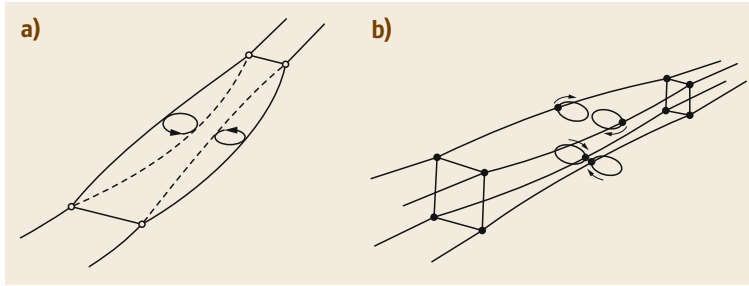


**Fig. 9.60** Recommended safe design tension for single conductor lines ( $H$ : initial horizontal tension;  $w$ : conductor weight per unit length;  $L$ : actual span length;  $D$ : conductor diameter and  $m$ : conductor mass per unit length). Terrain categories: green line: open, flat, no trees, no obstruction, with snow cover, or near/across large bodies of water or flat desert; blue line: open, flat no obstruction, no snow, e.g., farmland without any obstruction, summer time; black line: open, flat, or undulating with very few obstacles, e.g., open grass of farmland with few trees, hedgerows and other barriers, prairie, tundra; red line: built-up with some trees and buildings, e.g., residential suburbs, small towns, woodlands and shrubs, small fields with bushes, trees, and hedges (adapted from [9.67])

when added at both ends of a span have been prepared [9.67]. This practice is summarized in Fig. 9.60, where the *safe design zone – no damping* applies to undamped and unarmored single conductors, the *safe design zone – span end damping* constitutes a zone where full protection of single conductors against aeolian vibrations is assuredly feasible by means of one or more Stockbridge-type dampers set at the span extremities, and finally in the *special application zone*, aeolian vibrations, it is recommended that line designers determine the availability of adequate protection before finalizing the design.

For bundle conductors, which are not so sensitive to aeolian vibrations due to the interaction of the sub-conductors, the safe  $H/w$  value is recommended as a matter of prudence to be limited to 2500 m in any terrain category and irrespective of whether they are equipped with spacer dampers (Sect. 9.6.3), although there is evidence that quite a few bundle lines have operated for many years safely at higher  $H/w$  values [9.67].

A second approach to vibration safe design is to limit the conductor stresses/strains that occur during vi-



**Fig. 9.61a,b** Schematic of a subspan oscillation of a twin (a) and quad (b) bundle (adapted from [9.81])

bration. This happens in the design stage of the line through the application of dedicated simulation software [9.104]. Most such programs first calculate the displacements at the antinode as well as in the vicinity of critical locations, mainly at the suspension clamps; these are then converted to stresses or equivalent strains in the conductor, which can be compared with their corresponding limit values obtained from tests in the laboratory or the field.

**Internal Conductor Mechanics.** An important issue that has kept researchers busy for decades is how to properly estimate conductor stresses. The simplest way to do this is to assume that the vibrating conductor bends as a rigid cylindrical body under tension, whereby all its individual wires act independently. This approach provided the basis for the famous Poffenberger–Swart formula (9.87) [9.120], which is widely used in the industry for converting the bending amplitude  $Y_b$  at a distance  $x_b$  from the last point of contact of the conductor with the suspension clamp (Fig. 9.58) to the wire stress  $\sigma_a$  at the top of the conductor at the suspension clamp

$$\sigma_a = \frac{d_a E_a p^2 / 4}{e^{-px_b} - 1 + px_b}, \quad (9.87)$$

where  $E_a$  is the modulus of elasticity of the wire material, normally aluminum,  $d_a$  is the wire diameter,  $EI$  is the minimum bending stiffness of the conductor

$$EI = n_{Al} E_{Al} \frac{\pi d_{Al}^4}{64} + n_S E_S \frac{\pi d_S^4}{64}, \quad (9.88)$$

and

$$p = \sqrt{\frac{H}{EI}}. \quad (9.89)$$

This formula assumes that, during vibration bending, the wires act individually; i.e., they bend around their own axis. However, for low amplitudes, the conductor acts more like a solid body with all its wires sticking together; this will considerably increase the bending stiffness of the vibrating conductor, which will vary

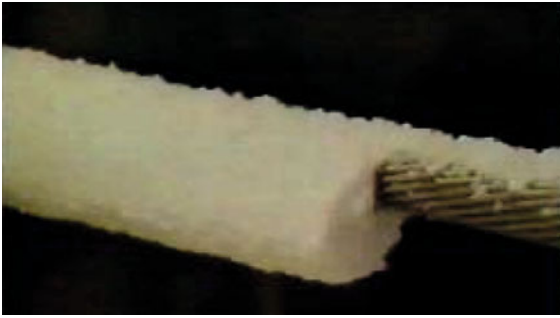
during a vibration cycle, as the curvature of the conductor then changes continuously. This concept was presented for the first time in [9.102, 103, 121] and has formed the basis for further developments of this issue since then [9.122]. In recent years, powerful simulation software has also been extensively used for such calculations [9.106].

For vibration safe design, the following *limit values* are widely used:

**IEEE Maximum Allowable Bending Strain.** In 1966, the Institute of Electrical and Electronics Engineers (IEEE) provided an evaluation criterion for aluminum-based conductors based on a maximum allowable bending strain [9.123]. A value of 150  $\mu\text{inch}/\text{inch}$  (microstrain  $\mu\epsilon$ ) peak to peak was given as a conservative value, and it was suggested that maximum strains on the order of 200  $\mu\epsilon$  peak to peak may well prove to be safe. With accumulating experience, these limits were found to be rather conservative, and values up to 300  $\mu\epsilon$  peak to peak have been adopted by many utility specifications. Subsequently and in order to reduce the severity of the method, some concessions have been granted [9.118]:

- The bending amplitude may exceed the endurance limit for no more than 5% of total cycles.
- No more than 1% of the cycles may exceed 1.5 times the endurance limit.
- No cycles may exceed 2 times the endurance limit.

**EPRI Endurance Limits.** In 2009, the Electric Power Research Institute (EPRI) suggested a bending stress endurance limit of 8.5 MPa for multilayer ACSR conductors, which corresponds to a bending strain of 247  $\mu\epsilon$  peak to peak. For multilayer AAAC conductors, a more conservative limit of 5.7 MPa, which corresponds to a bending strain of 165  $\mu\epsilon$  peak to peak, was introduced [9.97]. It is worth noting that, comparable values for ACSR, i.e., 9.09 MPa and 264  $\mu\epsilon$  peak to peak, can be deducted from the CIGRE Safe Border Line [9.54], which is considered asymptotic at  $5 \times 10^8$  cycles, the upper limit for laboratory tests.



**Fig. 9.62** Typical ice shape as observed on a line conductor, which may cause galloping (adapted from [9.81])

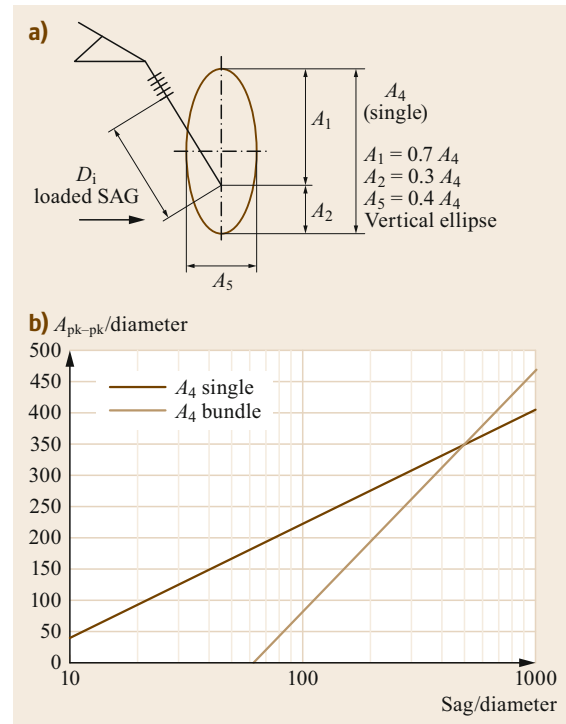
**CIGRE Life Expectancy Estimation.** As early as 1979, the CIGRE developed a method to estimate the life expectancy of a vibrating conductor [9.54]. This method is quite common in the automotive and aircraft industries for structures undergoing fatigue and is based on the assumption that fatigue damage is accumulated linearly in the structure material, independently of the sequence of loads causing it; this is expressed by the so-called Miner rule [9.124]. The method is useful mainly for quantitative comparison of similar setups, i.e., the same conductors in the same vibration environment, but with different clamps or different dampers. Details of related measurements and their evaluation are described in [9.117].

### Subspan Oscillations

Subspan oscillations are wake-induced oscillations. They occur only on conductor bundles and are caused by the wake produced by the windward conductors of the bundle on the leeward ones. The mechanism of subspan oscillation takes the form of one or two loops between adjacent spacers in a span, with nodes at or near the spacers. The trajectories of individual subconductors are elliptical, and windward–leeward pairs of subconductors often move approximately in phase opposition (Fig. 9.61 [9.81, 97]).

The frequencies of subspan oscillations lie in the range of a few hertz. They occur at wind speeds in the range of 8–20 m/s, and their amplitudes may be high enough to cause subconductors to clash, produce damaging strains on the wires at spacer clamp locations, and lead to excessive forces on the spacer arms that may lead to subconductor wire damage and spacer clamp loosening.

Typical values for the ratio  $a/d$ , i.e., the ratio of the bundle separation  $a$  to the conductor diameter  $d$ , usually lie in the range of 10–17, with ratios of 12 or below being considered critical. Analytical simulations and measurements lead to a limit on the maximum subspan length depending on the wind [9.125]; For in-



**Fig. 9.63a,b** Ellipse for clearance design against galloping (a) and curves for galloping maximum peak-to-peak amplitude  $A_{pk-pk}$  over sag (b), both related to conductor diameter (adapted from [9.81])

stance, for a site characterized by high wind speeds ( $>20$ – $25$  m/s), this value should be around 65 m. In nonsevere conditions, maximum subspan lengths of around 80 m have been used without problems. Short end subspans (25–45 m) prevent subspan oscillations at span extremities, which can damage insulators and hardware. Also the use of unequal (staggered) subspan lengths in conjunction with spacers or spacer dampers has proved to be effective against subspan oscillations, with a subspan ratio, i.e., ratio of the lengths of two adjacent subspans, of around 0.85–0.9 being the optimum solution [9.126].

### Gallopings

Of all the wind-induced motions of overhead transmission line conductors, galloping is the most noticeable and spectacular. The resulting damage can be equally dramatic and very costly, with broken conductors and fittings, damaged tower components, and even whole towers collapsing. Galloping is the oscillation of single or bundle conductors due to wind action caused by, in most cases asymmetrical, accretion of ice or wet snow on the conductors (Fig. 9.62 [9.81]), although instances of non-ice-related galloping have also been recorded.

**Table 9.31** Overview of antigalloping devices (adapted from [9.81])

No.	Device name	Applic.	Weather condition		Line construction			Comments
			Glaze	Wet snow	Distribution	Single transmission	Bundle	
1	Rigid interphase spacer	Widely used	Yes	Yes	Yes	Yes	Yes	Prevents flashovers, reduced galloping motions
2	Flexible interphase spacer	Widely used	Yes	Yes	Yes	Yes	Yes	Prevents flashovers, reduced galloping motions
3	Air flow spoiler	Widely used	Yes		Yes	Yes	Yes	Covers 25% of span limited by voltage extensive field evaluation
4	Eccentric weights and rotating clamp spacers	Used in Japan	No	Yes	No	Yes	Yes	Three per single span, one per spacer per subconductor
5	AR twister	Used in USA	Yes		Yes	Yes	Yes	Two per span
6	AR winddamper	Used in USA	Yes		Yes	Yes	Yes	Two per span
7	Aerodynamic galloping controller (AGC)				Yes	Yes	Yes	Number based on analysis
8	Torsional control device (TCD)	Used in Japan		Yes	No	No	Yes	Two per span
9	Galloping control device (GCD)	Used in Japan		Yes	No	No	Yes	Two to four per span Uses armor rods if tension is high. Most extensive field evaluations
10	Detuning pendulum	Widely used	Yes		Yes	Yes	Yes	Few cases have been reported where detuning pendulums increased galloping amplitude
11	Torsional damper and detuner (TDD)	Experimental	Yes	Yes	No	No	Yes	Two or three per span

Galloping can be characterized by:

- Frequencies from 0.08 to 3 Hz
- Maximum galloping amplitude of ten, exceeding the conductor sag
- Minimum wind velocity of approximately 25 km/h.

Galloping is a complex aerodynamic/aeroelastic instability, which on the one hand has caused serious operational problems on transmission lines since their inception and on the other hand attracted quite early interest from many scientists, who have tried to describe it [9.127, 128]. Galloping theory is beyond the scope of this book; we will concentrate here on some practical recommendations.

A detailed analysis of a great number of observed and recorded cases of galloping [9.129] has resulted in the suggestion of an elliptical form for the locus of a galloping conductor (Fig. 9.63a) and its magnitude

(Fig. 9.63b). This should be considered in the clearance design of a line known to exhibit or suspected of experiencing galloping.

There are three main classes of countermeasures against galloping:

- Making lines tolerant to galloping by robust design, provision of increased phase clearances, or controlling the mode of galloping with interphase spacers (Sect. 9.5.5)
- Interfering with the galloping mechanisms to prevent galloping from building up or from attaining high amplitudes
- Removal of ice or preventing its formation on conductors [9.130].

A list of antigalloping devices is presented in Table 9.31 [9.81].

## 9.5 Insulators

According to [9.131], an insulator is a “device intended for electrical insulation and mechanical fixing of equipment or conductors which are subject to electric potential differences”. In this sense, insulators in an overhead line have the primary responsibility of separating the system potential present at the conductor from the earth potential present at the support. It is interesting to note that their name comes from the Latin word *insula*, island—which comes from the Greek word *νήσος* (read *níssos*)—i.e., a piece of land separated by water from the mainland. In addition to fulfilling their electrical duty not only under the system voltage but also under over-voltages from lightning and switching operations, they have to transfer safely the mechanical loads acting on the conductor to the support and achieve this under all, partly very adverse, environmental conditions. A power flashover can occur in all three voltage scenarios. To ensure safe behavior in such a situation, insulators are often equipped with so-called insulator protection fittings (Sect. 9.6.2). The atmospheric pollution ultimately determines the shape of the insulator, i.e., its shed profile, which exists mainly to combat the leakage current due to surface contamination of the insulator, which applies to hydrophilic insulators, while hydrophobic insulators have water repellency as their primary leakage current suppression mechanism. Whereas a 3-m-long column of air provides sufficient insulation for a 400-kV AC conductor, a surface liable to outdoor contamination must provide at least three times that path length [9.132] or the required creepage distance in accordance to the in-situ conditions. In addition, the mechanical integrity of the insulator is of paramount importance for the proper functioning of a line, as its loss will most probably lead to loss of power with all its detrimental consequences and may also cause serious damage and injuries.

Insulators have their origin in 1849, with the introduction of the so-called Siemens insulator for the telegraph line from Frankfurt a. M. to Berlin, followed by the insulators designed by Brown for a 8-km-long, 2-kV DC line from Kriegstetten to Solothurn in Switzerland and in 1891 for the 15-kV AC (later 25-kV AC), 175-km-long line from Lauffen on the Neckar to Frankfurt am Main in Germany (Fig. 9.1).

### 9.5.1 Classification

Several criteria exist for the classification of insulators depending on their:

- Material
- Shape
- Function.

#### Material

Nowadays, three materials are used for insulators:

- Ceramic
- Glass
- Polymer.

Ceramic (mainly porcelain) insulators were the first to be used, followed a few decades later by glass, with polymer or composite insulators, also called nonceramic insulators (NCI), coming many years later (in the 1960s) but now dominating the greatest market share worldwide.

#### Shape

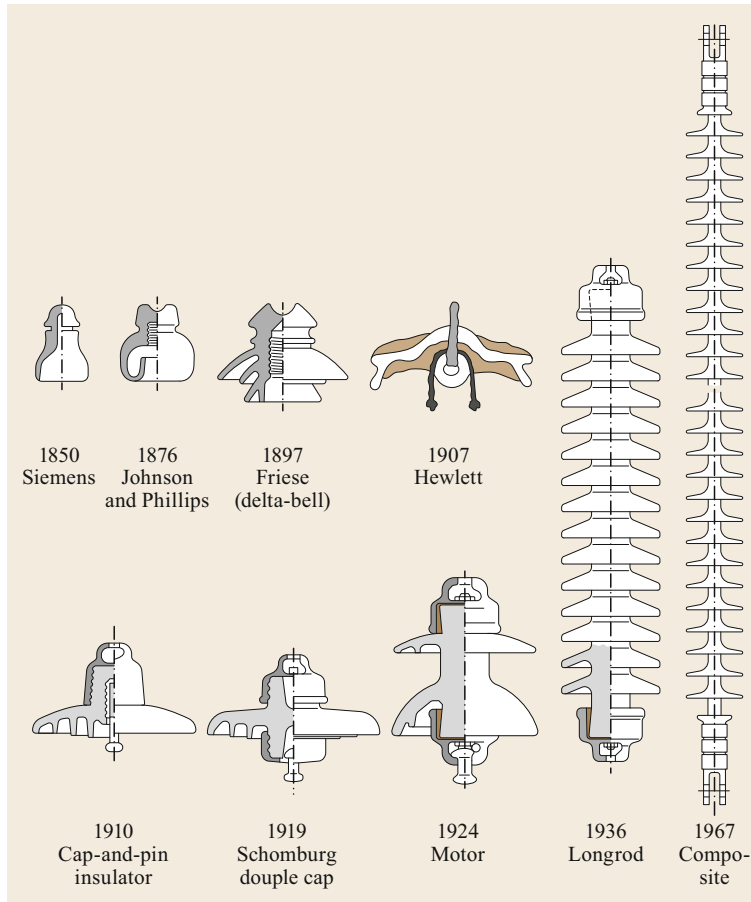
Over the years, three basic insulator shapes have evolved:

- Bell
- Cap and pin
- Longrod.

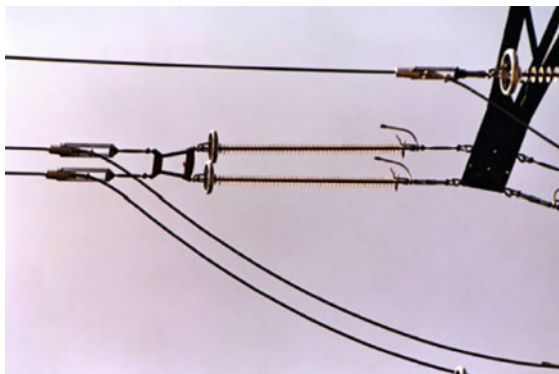
Although bell-type porcelain insulators were the first to be used, they were mechanically too weak to support the larger conductors over longer spans necessary for increased power transmission and the required higher voltages. For this purpose, cap-and-pin insulators were developed at the beginning of the 20th century in porcelain and from the 1920s in glass. Bell-type insulators, also called pin insulators, are still used as support insulators for low voltage (LV) and medium-voltage (MV) lines.

According to [9.133, 134], overhead line insulators can be classified into two types, type A and type B. Type A insulators are characterized by the fact that the length of the shortest puncture path through the insulating body is at least half of the flashover path on the insulator surface. This applies to longrod insulators. Such insulators are considered to be puncture proof. Insulators in which the length of the shortest puncture path through the body is less than half of the flashover path are classified as type B insulators, for instance cap-and-pin insulators. They are considered to be not puncture proof.

The understandable wish of many users to install puncture-proof (type A) insulators on their HV lines could be fulfilled by advances in the manufacturing technology of porcelain longrod insulators (as puncture-proof solid-core insulators cannot be manufactured from glass) and in particular the possibility of manufacturing large bodies of porcelain without air pockets, leading in around 1936 in



**Fig. 9.64** Historical development of overhead line insulators (source Pfisterer Lapp)



**Fig. 9.65** Double tension string (adapted from [9.112])

Germany to the development of the porcelain longrod, a logical development of the first double-shed solid-core and thus puncture-proof insulator, the so-called motor insulator developed in 1917/19 in Switzerland. Finally, the introduction of polymer materials, mainly silicone rubber for HV insulation, led in the

1960s to the concept of composite longrod insulators.

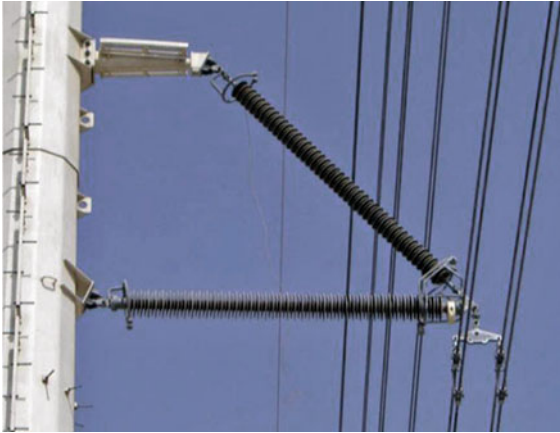
On rare occasions, hollow-core composite insulators have also been used for transmission lines, e.g., as insulated cross arms in compact lines [9.135], with their main application being as housings of HV equipment in substations [9.136].

Figure 9.64 summarizes the historical development of overhead line insulators.

### Function

The function of an insulator on a line primarily determines the mechanical loads it must sustain. As shown in Figs. 9.65–9.67 [9.112], one can distinguish between:

- Ties, such as suspension or dead-end insulators, which are loaded in tension (Fig. 9.65)
- Struts, such as posts in insulating cross-arms, which are loaded in compression (Fig. 9.66)
- Beams, such as vertical and horizontal posts, which are loaded in bending (Fig. 9.67).



**Fig. 9.66** Horizontal strut in an insulating cross-arm (adapted from [9.112])



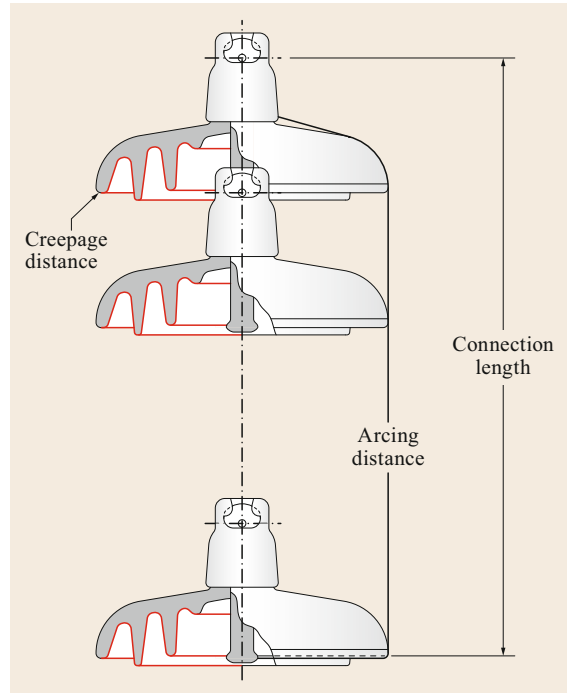
**Fig. 9.67** Vertical post insulators in the so-called trident configuration (adapted from [9.112])

### Geometry

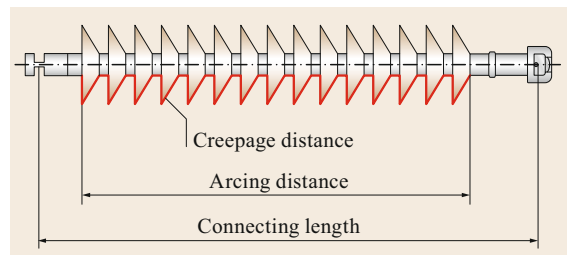
Common to all insulator types are the following geometric properties.

**Connection length:** Shortest distance in air between the two end fittings. This dimension is important for the necessary clearances and thus the tower width and height.

**Arcing distance:** Shortest path in air between the two insulator end fittings. This dimension determines the flashover properties of the insulator when not polluted and is thus important for the insulator coordination of the power system.



**Fig. 9.68** Dimensional properties of cap-and-pin insulators (porcelain/glass) (adapted from [9.137])



**Fig. 9.69** Dimensional properties of longrod insulators (porcelain/composite) (adapted from [9.138])

**Creepage or leakage distance:** Path along the insulator surface between the end fittings. This dimension determines the pollution performance of the insulator (Sect. 9.5.2).

Figure 9.68 [9.137] shows schematically these properties for a cap-and-pin and Fig. 9.69 [9.138] for a composite longrod insulator.

The electrical characteristics of a nonpolluted insulator, i.e., the lightning, switching, and power frequency withstand and flashover voltages, whether wet or dry, depend mainly on its arcing distance (Fig. 9.70). However, in polluted conditions, the creepage distance formed by the insulator shed profile is the key, as explained in Sect. 9.5.2.

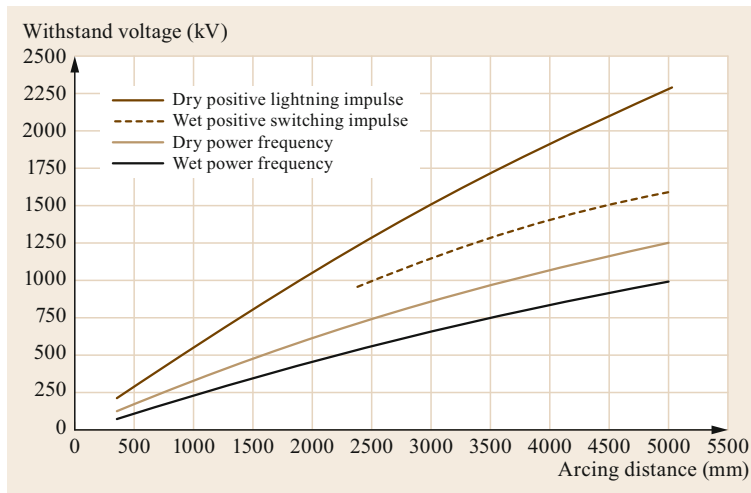


Fig. 9.70 Withstand voltages versus arcing distance

## 9.5.2 Pollution

The corrugated shape of the insulator surface, independent of the insulating material used, is necessary to ensure its performance under pollution. For the proper selection of insulators and the determination of their relevant dimensions to be used in high-voltage systems with respect to pollution, an IEC standard [9.139–142] forms the basis from which the following information is extracted. CIGRE publications [9.143–145] are a useful complement for those wishing to study the performance of insulators under pollution in greater depth.

### Pollution Flashover

The prerequisite for good insulator design with respect to pollution is a basic understanding of pollution flashover. This is described in [9.139]. For the so-called predeposit pollution (type A), we distinguish the following phases:

- *Phase 1:* The insulator becomes coated with a layer of pollution.
- *Phase 2:* The surface of the polluted insulator becomes wetted. The wetting of an insulator can occur by moisture absorption, condensation, and precipitation. Precipitation by heavy rain may wash away the electrolytic components of part or the entire pollution layer without initiating other phases in the breakdown process, or it may promote flashover by bridging the gaps between sheds. Moisture absorption occurs during periods of high relative humidity (> 75%) when the temperature of the insulator and ambient air are the same. Moisture can also gain access to the pollution layer at lower relative humidity if the pollution is hygroscopic. Condensation usually occurs at sunrise or just before, when moisture in the air condenses on the insulator surface, whose temperature is lower than the dew point.
- *Phase 3:* Once an energized insulator is covered with a conducting pollution layer, surface leakage currents flow and their heating effect starts (within a few power-frequency cycles) to dry out parts of the pollution layer. Under the modeled assumption of a uniform pollution layer, this occurs where the current density is highest, i.e., where the insulator is at its narrowest. These result in the formation of what are known as dry bands.
- *Phase 4:* The pollution layer never dries uniformly, and in places the conducting path becomes broken by dry bands which interrupt the flow of leakage current.
- *Phase 5:* The line-to-earth voltage appearing across multiple dry bands (which may be only a few millimeters wide) causes air breakdown, and the dry bands are bridged by arcs which are electrically in series with the resistance of the still wet and conductive portion of the pollution layer. This causes a surge of the leakage current each time the dry bands on the insulator spark over.
- *Phase 6:* If the resistance of the still wet and conductive part of the pollution layer is low enough, the arcs bridging the dry bands are sustained and may finally continue to extend along the insulator, bridging more and more of its surface. This in turn decreases the resistance in series with the arcs, increasing the current and permitting them to bridge even more of the insulator surface. As a rule of thumb, flashover becomes very likely after bridging 2/3 of the creepage distance. Ultimately, it is completely bridged and a line-to-earth fault (flashover) is established.



**Table 9.32** Typical environments (adapted from [9.139])

Example	Description of typical environments
E1	> 50 km <sup>a</sup> from any sea, desert, or open dry land > 10 km from man-made pollution sources <sup>b</sup> At a shorter distance from pollution sources than mentioned, but <ul style="list-style-type: none"> <li>• prevailing wind not directly from these pollution sources</li> <li>• and/or with regular monthly rain washing</li> </ul>
E2	10–50 km <sup>a</sup> from the sea, a desert, or open dry land 5–10 km from man-made pollution sources <sup>b</sup> Within a shorter distance than E1 from pollution sources, but <ul style="list-style-type: none"> <li>• prevailing wind not directly from these pollution sources</li> <li>• and/or with regular monthly rain washing</li> </ul>
E3	3–10 km <sup>c</sup> from the sea, a desert, or open dry land 1–5 km from man-made pollution sources <sup>b</sup> Within a shorter distance from pollution sources than mentioned above, but <ul style="list-style-type: none"> <li>• prevailing wind not directly from these pollution sources</li> <li>• and/or with regular monthly rain washing</li> </ul>
E4	Further away from pollution sources than mentioned in E3, but <ul style="list-style-type: none"> <li>• dense fog (or drizzle) often occurs after a long (several weeks or months) dry pollution accumulation season</li> <li>• and/or heavy, high-conductivity rain occurs</li> <li>• and/or there is a high nonsoluble deposit density (NSDD) level, between 5 and 10 times the equivalent salt deposit density (ESDD)</li> </ul>
E5	Within 3 km <sup>c</sup> of the sea, a desert, or open dry land Within 1 km of man-made pollution sources <sup>b</sup>
E6	At a greater distance from pollution sources than mentioned in E5, but <ul style="list-style-type: none"> <li>• dense fog (or drizzle) often occurs after a long (several weeks or months) dry pollution accumulation season</li> <li>• and/or there is a high NSDD level, between 5 and 10 times the ESDD</li> </ul>
E7	Within the same distance of pollution sources as specified for <i>heavy</i> areas and <ul style="list-style-type: none"> <li>• directly subjected to sea spray or dense saline fog</li> <li>• or directly subjected to contaminants with high conductivity, or cement-type dust with high density, and with frequent wetting by fog or drizzle</li> <li>• desert areas with fast accumulation of sand and salt, and regular condensation</li> </ul>
<sup>a</sup> During a storm, the ESDD level at such a distance from the sea may reach a much higher level	
<sup>b</sup> The presence of a major city will have an influence over a longer distance, i.e., the distance specified for seas, desert, and dry land	
<sup>c</sup> Depending on the topography of the coastal area and the wind intensity	

For so-called instantaneous pollution (type B), such as salt spray, salt fog, or industrial acid fog, which can occur in areas located close to the coast or near chemical plants, the flashover process starts at phase 3 and can progress rapidly to phase 6. A particular case of type B pollution is a bird streamer. This is a type of bird excrement, which, on release, forms a continuous, highly conductive (20–40 kΩ/m) stream of such length that the air gap is sufficiently reduced to cause flashover. In this case, the insulator geometry and characteristics play little or no role and the best solution may be to fit bird-dissuasive devices appropriate to the local fauna and structure design.

#### Insulator Design for Pollution

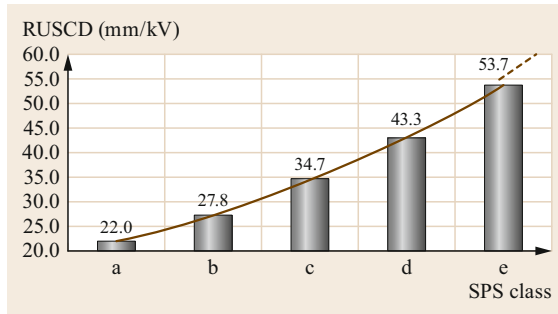
Standard [9.139] describes the three basic approaches to insulator selection and dimensioning for pollution, i.e.:

1. Use past experience
2. Measure and test
3. Measure and design.

For the purposes of standardization, five classes of site pollution severity (SPS) are qualitatively defined in [9.139], from very light pollution to very heavy pollution as follows:

- a Very light
- b Light
- c Medium
- d Heavy
- e Very heavy.

Typical pollution environments are indicated in Table 9.32 [9.139], where E2 corresponds to light, E3 to medium, E5 to heavy, and E7 to very heavy pollution.



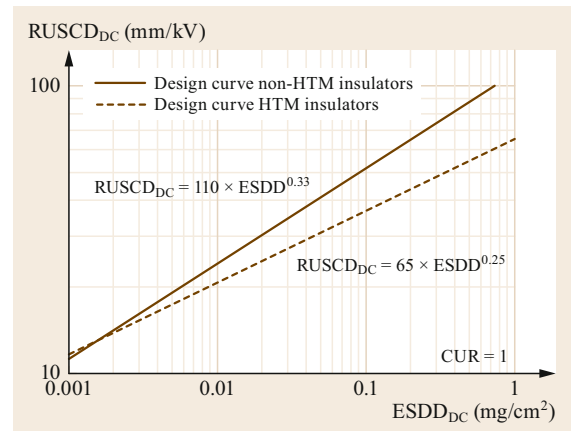
**Fig. 9.71** RUSCD as a function of SPS class for AC

**Creepage Distance.** The SPS class is used to determine the reference unified specific creepage distance (RUSCD) for AC voltages (Fig. 9.71 [9.139–142]), i.e., the creepage distance of an insulator divided by the rms value of the highest operating voltage  $U_m$  across the insulator. This definition differs from that of the specific creepage distance, where the line-to-earth value of the highest voltage for the equipment is used (for AC systems usually  $U_m/\sqrt{3}$ ). For line-to-line insulation, this will result in a value that is  $\sqrt{3}$  times that given by the definition of the specific creepage distance in [9.146], now replaced by [9.139–142]. In Fig. 9.71, the bars are preferred values representative of a minimum requirement for each class. If exact SPS measurements are available, it is recommended to take a RUSCD which corresponds to the position of the SPS measurements within the class by following the curve shown.

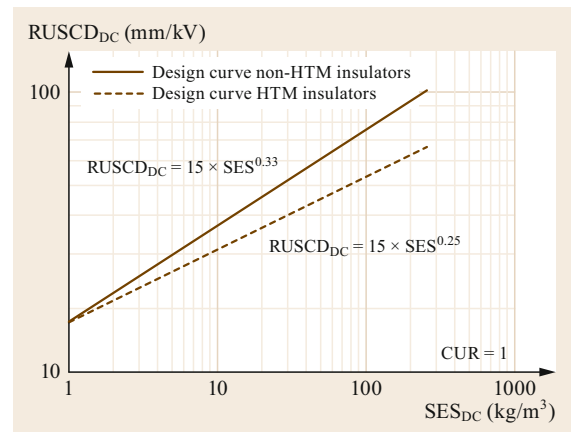
It is worth noting that there is no difference in the RUSCD between insulators made from different materials, specifically the well-documented advantages of polymer insulators under pollution [9.2], which can result in a reduction of RUSCD by up to 30% if their hydrophobicity is not lost.

**DC Applications.** For DC voltages, the design process is complicated by several factors [9.140], as DC insulators exhibit a greatly different pollution behavior compared with those operating at AC. This is mainly due to electrostatic effects because of:

- The influence of wind, particle size, etc. on the accumulation of pollution
- The composition of the pollution (low-solubility or slow-dissolving salts)
- The effect of the amount of nonsoluble deposit
- The contamination uniformity ratio (CUR)
- The effect of diameter on pollution accumulation
- The nonuniformity of the pollution layer along or around the insulator
- The effect of diameter on pollution performance



**Fig. 9.72** RUSCD for DC and type A pollution ( $ESDD_{DC}$  at  $NSDD = 0.1 \text{ mg/cm}^2$ )



**Fig. 9.73** RUSCD for DC and type A pollution (SES: site equivalent salinity)

- The effect of insulator material on pollution performance.

Due to these, some early applications of nonceramic insulators were for HVDC lines, where the superior behavior of polymer material is indisputable [9.147]. This is recognized in [9.140], where polymer materials, which exhibit hydrophobicity but also have the capability to transfer hydrophobicity to the pollution layer, are referred to as hydrophobicity transfer materials (HTM). They require less RUSCD (in mm/kV) as shown in Figs. 9.72 and 9.73 [9.140]. These figures also indicate that, for the proper design of DC insulators under pollution, site severity measurements are necessary as indicated in the parameters on the abscissa ( $ESDD_{DC}$ ,  $NSDD$ ,  $SES_{DC}$ ). Details are given in [9.140].

SPS Class	Deviations for CF	
a	None	3.5 Minor, 4.25 Major
b	None	3.625 Minor, 4.4 Major
c	None	3.75 Minor, 4.55 Major
d	None	3.875 Minor, 4.7 Major
e	None	4.0 Minor, 4.85 Major

CF 2.5 3.0 3.5 4.0 4.5 5.0 5.5

**Table 9.33**  
CF values for ceramic and glass AC insulators

SPS Class	Deviations for CF	
a	None	
b	None	
c	None	Minor, Major
d	None	
e	None	

CF 2.5 3.0 3.5 4.0 4.5 5.0 5.5

**Table 9.34**  
CF values for polymer AC insulators

**Table 9.35** CF values for DC insulators

Glass and porcelain insulators	Composite and hybrid insulators, non-HTM	Composite and hybrid insulators, HTM
Cap and pin typically below 3.4 Rarely greater than 3.75	Line insulators typically below 4.5 Rarely greater than 4.8	Typically below 4.5 Rarely greater than 4.8
Posts, long rods and hollow cores typically below 3.5 Rarely greater than 4.0	Posts and hollow cores typically below 4.4 Rarely greater than 4.6	

The final step is to determine the  $USCD_{req}$  of the insulator in question, i.e.,

$$USCD_{req} = RUSCDC_d C_a, \quad (9.90)$$

where  $C_d$  is the diameter correction factor, which considers the effect of diameter on the pollution withstand performance of the candidate insulator and applies only to insulators with diameters above 250 mm, i.e.,  $C_d = 1$  for line insulators, and  $C_a$  is the altitude correction factor given in [9.148] as

$$C_a = e^{n \frac{H}{8150}}, \quad (9.91)$$

where  $H$  is the height above sea level in meters. The current design practice in industry is to use  $H - 1000$  instead of  $H$  in (9.91) and to only apply the correction above 1000 m. Until further information is available, a value of 0.35 is suggested for  $n$ .

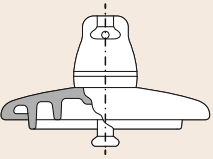
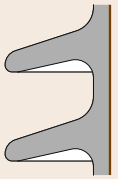
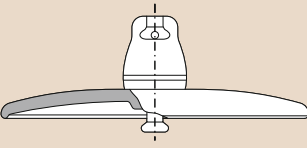

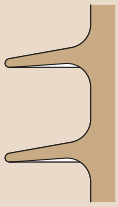
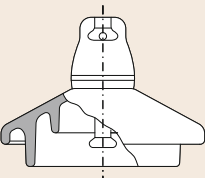
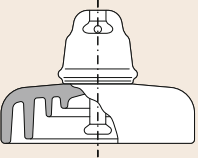
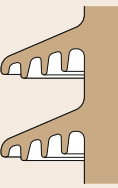

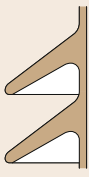
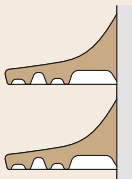
**Creepage Factor.** The creepage factor (CF) is equal to  $l/s$ , where  $l$  is the total creepage distance and  $s$  is the arcing distance of the insulator unit (Figs. 9.68 and 9.69); it is used as a global check of the overall density of the creepage distance. For cap-and-pin insulators, the CF is determined for a string of five insulators or more. CF values encountered in DC applications are often higher than those used for AC because, in general, a higher creepage distance is needed for given insulator length in DC. It is important to bear in mind that greatly increasing the CF can have no or even a negative effect on the performance. Tables 9.33 to 9.35 [9.140–142] contain recommendations for the CF of AC and DC insulators.

**Shed Profiles.** In order to obtain the required creepage distance as explained above, but also in order to keep a certain portion of it dry and more resistant to accumulation of pollutants, various insulator shapes and profiles have been developed over the years. In addition, variations in the nature of the pollutant may make some shapes of insulator more effective than others. It should be borne in mind that the minimum or maximum overall length of the insulation is an important imposed parameter, e.g., for insulation coordination or tower height. Table 9.36 summarizes the main characteristics of each type of profile. More advice on profiles is given in the relevant parts of [9.139–142].

**Corrosion.** Another issue arising from pollution is the corrosion of the insulator fittings and in particular of the connection pins of cap-and-pin insulators.

When the surface of the insulator becomes contaminated and wet, a biased leakage current starts to flow,

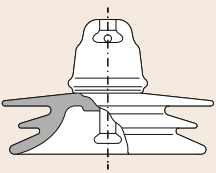

**Table 9.36** Typical profiles and their main characteristics (adapted from [9.139–142])

<p><b>Standard profiles</b> Standard profiles are effective for use in <i>very light</i> to <i>medium</i> polluted areas where a long creepage distance or an aerodynamically effective profile is not required</p>	 <p>Cap and pin standard discs insulators</p>	 <p>Porcelain standard profile, long rod insulators, post insulators, hollow insulators</p>
<p><b>Aerodynamic or open profiles</b> Aerodynamic or open profiles prove to be beneficial in areas where the pollution is deposited onto the insulator by wind, such as deserts, heavily polluted industrial areas or coastal areas which are not directly exposed to salt spray. This type of profile is especially effective in areas that are characterized by extended dry periods. Open profiles have good self-cleaning properties and are also more easily cleaned under maintenance</p>	 <p>Aerodynamic disc insulators</p>  <p>Porcelain long rod insulators, post insulators, hollow insulators</p>	 <p>Polymeric long rod insulators, post insulators, hollow insulators</p>
<p><b>Anti fog profiles</b> The use of anti fog profiles with steep sheds or deep under-ribs is beneficial in areas exposed to a salt water fog or spray, or to other pollutants in the dissolved state. These profiles may also be effective in areas with a particulate pollution precipitation containing slow dissolving salts. They can also be effective in areas with low NSDD and slow dissolving salts</p>	 <p>Steep anti-fog disc insulators</p>  <p>Deep under-ribs disc insulators</p>  <p>Deep under-ribs on porcelain long rod insulators, post insulators, hollow insulators</p>	 <p>Steep porcelain long rod insulators, post insulators, hollow insulators</p>  <p>Steep polymeric long rod insulators, post insulators, hollow insulators</p>  <p>Under-ribs on polymeric long rod insulators, hollow insulators, post insulators</p>

causing electrolytic corrosion of the pins. Even under AC voltages, corrosion takes place, and is enhanced when the leakage current has a DC component. The corrosion is much more harmful for DC voltages be-

cause the current is unidirectional but also because, as explained above, the deposition and formation of pollution are enhanced via electrostatic phenomena related to DC. Corrosion will, on one hand, reduce the diameter

**Table 9.36** (Continued)

<p><b>Alternating shed profiles</b> Alternating shed arrangements are in general feasible for all profiles, although steep sheds are less beneficial. They offer increased creepage distance per unit length without penalizing performance in heavy rain or icing. Similar benefits to open profiles are also provided by simple alternating profiles</p>	 <p>Alternating shed disc insulators</p>	 <p>Porcelain long-rod insulators, post insulators, hollow insulators</p> <p>Polymeric long rod insulators, post insulators, hollow insulators</p>
----------------------------------------------------------------------------------------------------------------------------------------------------------------------------------------------------------------------------------------------------------------------------------------------------------------------------------------------------------------	---------------------------------------------------------------------------------------------------------------------------	--------------------------------------------------------------------------------------------------------------------------------------------------------------------------------------------------------------------------------------



**Fig. 9.74** Corroded pin of a glass cap-and-pin insulator; note the reduced diameter of the pin and the rust products at the boundary with the dielectric

of the pin and thus the mechanical strength of the insulator, while on the other, the related rust products may cause cracks through expansion and subsequent failure of the dielectric (Fig. 9.74).

The corrosion resistance of insulators can be improved on the one hand by using reinforced galvanized fittings, i.e., by increasing the average coating zinc mass specified in [9.133, 134] of  $600 \text{ g/m}^2$ , corresponding to  $85 \mu\text{m}$ , up to  $140 \mu\text{m}$  for very high-corrosion areas such as coastal areas, and on the other by using a so-called sacrificial zinc sleeve (Fig. 9.75a), a must for HVDC insulators made of glass or porcelain. The cast iron cap itself can also suffer from corrosion. However, the time required for significant corrosion of the cap is longer than for the pins, and the corrosion effects are not so dramatic. As a remedy, a zinc collar is often used (Fig. 9.75b).

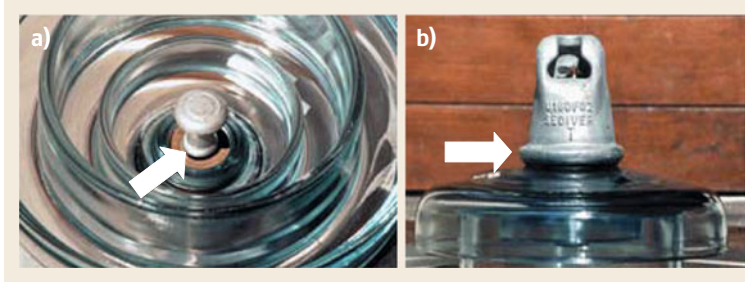
The zinc sleeve has a large electrochemical potential difference to iron and thus acts as a sacrificial electrode at the cement boundary where the current flows. Because of this, the boundary remains free from accumulation of corrosive products, which, as men-

tioned above, could become detrimental for the insulating body. The standard [9.150] specifies the minimum requirements for the zinc sleeve.

**Mitigating Measures.** There are various ways to improve the pollution performance of insulators. This can become necessary in case of a poor original design of the insulator or when a new industry, such as a cement plant, is built close to the line and at the same time insulator replacement is prohibitive because of costs or clearance violations. The definitive solution is to install composite (polymer) insulators (Sect. 9.5.5), which exhibit excellent pollution performance. Alternatives include [9.151]:

- Booster shed
- Shed extender
- Shed protector
- Coating
- Semiconducting glaze
- Washing.

Among these techniques, washing is still quite often used in areas of extreme (in particular desert-type) pollution, in the great majority of cases being undertaken with the line energized, which is referred to as *live* or *hot line washing* [9.143]. In addition, coatings have gained a certain popularity, in particular for substation insulators where replacement with composite insulators is not always feasible. The good service record of silicone rubber insulators for outdoor applications has stimulated the development of room-temperature vulcanized (RTV) silicone rubber coatings [9.152], service experience of which has shown that the useful life of



**Fig. 9.75a,b** Zinc sleeve on pin (a) and zinc collar on cap (b) (source [9.149])

a RTV coating can vary from less than a year to many years.

### 9.5.3 Porcelain Insulators

Porcelain insulators have the longest history, well above 100 years, and an excellent service record. Due to historical developments, two types have emerged: the cap-and-pin type and longrod type (Fig. 9.76).

While cap-and-pin insulators are used worldwide, longrod insulators are mainly installed in Central Europe, as well as some Middle East and other countries with serious desert pollution because of the excellent aerodynamic properties of their sheds, which hinder the accumulation of pollutants. For both types, the arcing distance and creepage distance can easily be adjusted to specified flashover values and the pollution regime, respectively, by simply adding more units.

Cap-and-pin insulators retain their integrity when a cap shatters (which is not the case for longrods), and because of their inherent flexibility, they are much less sensitive to bending loads such as those caused by load transposition in double strings, which, if not adequately addressed by special hardware, can cause a problem for longrods [9.153].

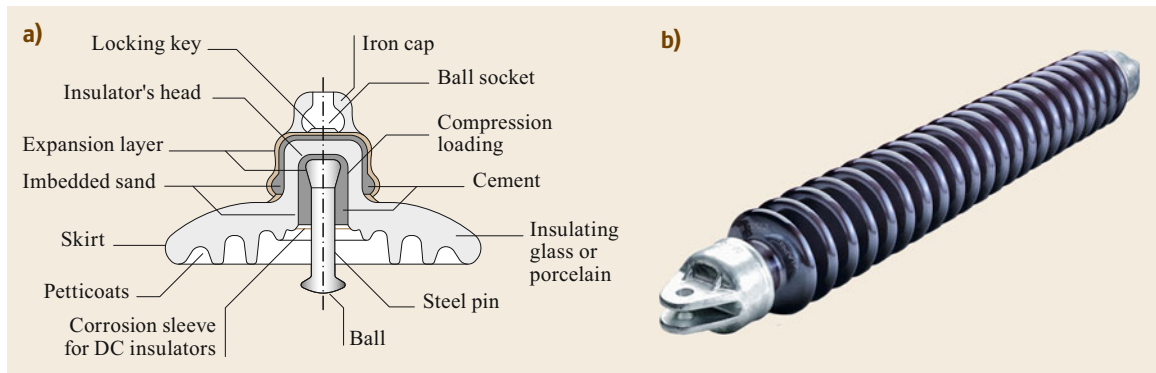
On the other hand, porcelain longrods offer certain advantages over (porcelain or glass) cap-and-pin insulators: They are puncture proof and can be easily

protected against power arcs. They also show excellent performance, in particular when heavily contaminated, and, because of their fewer intermediate fittings compared with cap-and-pin strings, they are not prone to cascade flashovers and have very low radio interference values. They are standardized in [9.154].

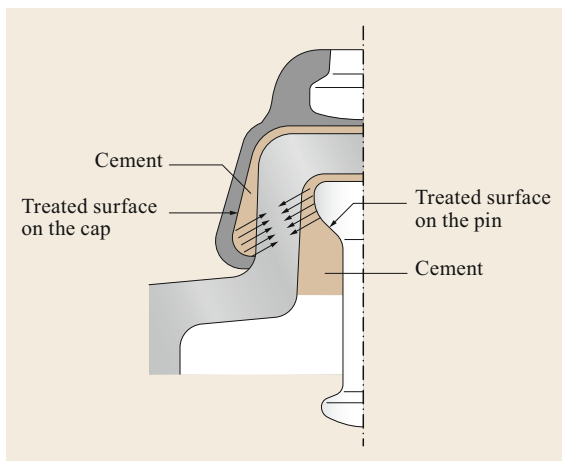
Porcelain insulators are made from quartz porcelain C-110 for low-strength insulators or C-120 or C-130 aluminum oxide porcelain for high-strength insulators, all according to [9.155]. Their main material properties are specified in [9.156].

Porcelain insulators are manufactured using a wet process, so called because a considerable amount of water is added to the raw materials, i.e., ca. 50% clay as the base material, ca. 25% quartz or alumina as the filler, and ca. 25% feldspar as the flux, with the aim of wetting the other ingredients and facilitating their dissolution in the melt.

These are quite complex processes that have been continuously developed over long time. They are based on extensive manufacturer-specific knowhow and require stringent quality control at all stages in order to obtain a low-porosity and thus mechanically strong porcelain body. Also, the glazing process is of paramount importance, as the glaze not only forms a smooth and easily washable surface, but also seals it and thus practically eliminates crack initiation from surface imperfections. In addition, as it has a lower ther-



**Fig. 9.76a,b** Porcelain cap-and-pin (a) longrod with clevis caps, overall length 1270 mm (b) (source Pfisterer Lapp)



**Fig. 9.77** Compressive stresses in the porcelain shell caused by tensile load (adapted from [9.137])

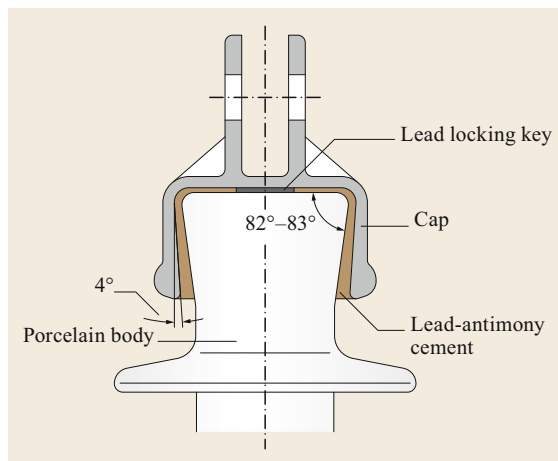
mal expansion coefficient compared with the porcelain bulk material, it induces beneficial compressive stresses upon the insulator surface.

Last but not least, the porosity of the porcelain depends strongly on the maximum firing temperature and its duration, the optimum being  $1150 \pm 15^\circ\text{C}$ .

#### End Fittings

End fittings are used to transfer the mechanical loads acting on the conductor, such as wind and/or ice loads, to the porcelain dielectric (Sect. 9.3.2) and from there to the line support. The main materials in use are malleable or ductile iron, forged steel, and rarely, for distribution insulators, aluminum. Ferrous fitting materials are hot-dip galvanized with a minimum of  $600\text{ g/cm}^2$  zinc, resulting in a minimum zinc thickness of  $85\ \mu\text{m}$ , and are attached to the porcelain using Portland cement for cap-and-pin insulators or lead-antimony alloy for longrods. There is also an important difference in the mechanical action of the fittings. Cap-and-pin fittings, on one hand, when loaded in tension, impose compressive stresses upon the porcelain body (Fig. 9.77 [9.137]). Longrod fittings, on the other hand, transfer the external tensile loads via their conical shape and the resulting shear stresses at the metal–porcelain interface, resulting in axial tensile stresses in the porcelain body of the insulator (Fig. 9.78).

End fittings are well standardized [9.157, 158] in order to enable easy replacement and exchange with other insulator types, including those made of glass or composite. For cap-and-pin insulators, ball-and-socket connections prevail. These are secured by W-clips or split pins, the latter providing a more reliable coupling in a string, as the cross-section area of a split-pin is twice that of a W-clip.



**Fig. 9.78** End fitting of a longrod porcelain insulator (source Pfisterer Lapp)

#### 9.5.4 Glass Insulators

Although the first LV overhead lines built in the 1880s used glass insulators, adapted from counterparts used in telegraph lines, the glass quality in those days could not cope with the higher loads which came with increasing voltages and the need for heavier conductors and longer spans. This changed with the introduction of the glass toughening process around 1930, since when glass insulators have been used extensively worldwide in overhead lines up to the highest voltages. They are shaped with few exceptions, e.g., glass pin insulators for distribution, as cap-and-pin insulators (Fig. 9.79). As in the case of porcelain cap-and-pin insulators, their arcing and creepage distances can be adjusted by simply adding more units. Similarly, because of their inherent flexibility, they are not sensitive to bending loads and they also retain their integrity when a cap shatters, this being on the one hand an advantage for easy spotting during inspections, while on the other attracting shooting enthusiasts, who enjoy the explosion-like shattering of the toughened glass shell. While they require fewer production steps and their shell is thinner than porcelain—because glass is a more homogeneous material and thus a better dielectric—their manufacturing process is very energy intensive and there is considerable variation amongst the few available renowned manufacturers in terms of raw material quality, composition, and processing, in particular toughening, which is a knowhow-intensive procedure.

The raw materials for the glass dielectric consist of ca. 57% silica (silicon dioxide found in nature as quartz), ca. 9% limestone, ca. 14% soda ash, ca. 4% feldspar, ca. 11% dolomite, and ca. 6% other mineral salts. About 1/3 of the mass is cullet, i.e., glass



**Fig. 9.79** Glass insulator (source MacLean Power Systems)

which has shattered during the production process or been rejected during inspection, as well as unused gobs of glass from mold changeovers. Cullet contributes to the stability and consistency of the manufacturing process [9.159]. The raw materials are crushed and mixed, then delivered to the furnace for melting, which is a critical step in the production sequence, as on the one hand it has to ensure very high homogeneity of the molten mass and on the other it has to be designed in such a way that it can run for years at temperatures up to 1400 °C without shutdowns, e.g., for maintenance. The glass exits the furnace in the form of a calibrated molten glass gob and is delivered to a preheated cast iron mold for pressing into shape at a temperature just over 1000 °C. Spinning after removal from the mold allows the internal screw shape to form inside the glass shell. This is followed by the decisive and critical toughening process, whereby the surface of the shells is cooled using jets of cold air, while their body remains molten. As the body contracts at a faster rate than the surface, this results in tensile stresses in the body and compressive stresses at the surface, leading to higher tensile strength, improved fatigue characteristics, higher puncture voltage, and higher impact resistance of the glass insulator. Subsequently the shells are immersed in cold water for thermal shock treatment, during which the great majority of defective shells can be recognized and eliminated. Finally, the assembly of the metal fittings, i.e., the cap and pin, takes place; these are fastened to the glass shell normally by using alumina cement. The process ends with testing. It is advisable to store the finished glass insulators before packing, as the considerable stress redistribution that occurs in the glass shell during this period will lead to self-shattering of some insulators, which can then be removed from delivery.

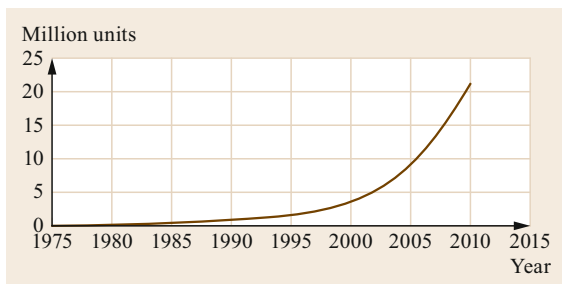
### End Fittings

The end fittings of glass insulators are very similar to those of porcelain cap-and-pin insulators. The pins are normally steel forgings, as they have to exhibit greater uniformity and higher strength than can be achieved by casting. The latter is used to make the caps from malleable iron. Both the caps and pins are hot-dip galvanized for corrosion protection then covered with a bituminous paint wherever they will come into contact with the alumina cement. As mentioned above, when deemed necessary for DC applications or use in highly polluted areas, a zinc sleeve is pressed around the pin to form a sacrificial electrode and protect it from corrosion.

### 9.5.5 Composite Insulators

The development of composite or nonceramic insulators basically started in the 1940s, when organic materials, namely epoxy resins, started being used for indoor high-voltage insulators, being advantageously lightweight and impact resistant, and also enabling large complex parts [9.160]. Unfortunately, field trials outdoors with such structural insulators led to many failures, so cycloaliphatic epoxy resins are now only used on a small scale for some distribution and railway insulators. Progress developed instead towards composite insulators, i.e., insulators where the various duties of the insulator, such as mechanical, electrical, and environmental, are shared between its different components. Composite insulators for overhead lines were developed as early as 1964 in Germany [9.161], where the first units for field testing were provided in 1967. In the late 1960s and early 1970s, manufacturers from Germany, France, the UK, the USA, and Switzerland introduced the first generation of commercial composite transmission line insulators. They came into general use in the 1980s and today account for (together with polymer distribution and hollow core apparatus insulators) approximately 40% of the insulator market worldwide. In fact, the number of units of composite insulators installed has grown exponentially, reaching more than 20 million units for AC lines today (Fig. 9.80 [9.162]). In addition there are more than 100 000 units installed on HVDC lines, confirming the advantages of composite insulators for HVDC applications as recognized early on [9.147], mainly because of their superior performance in comparison with ceramic insulators under the more intense and concentrated pollution in the DC field, which makes them considerably shorter than porcelain or glass strings. This is decisive for the tower silhouette and the ROW width, and thus the costs of DC overhead lines.





**Fig. 9.80** Estimated growth in composite insulator ( $\geq 69$  kV) use in AC transmission lines

This extraordinary and for many unexpected development has been enabled by the following factors:

Advantageous properties:

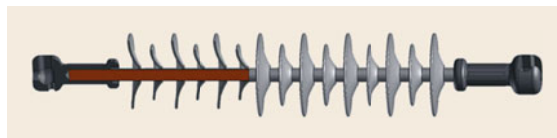
- The connection length and dry arc distance can be easily and precisely adjusted to grid and site requirements.
- The creepage distance can be similarly adjusted by proper choice of the size, shape, and number of sheds.
- They are not prone to vandalism (gunshots).
- They offer high bending strength and are flexible, thus not being endangered by load transposition.
- They show excellent pollution performance because of their surface hydrophobicity and hydrophobicity transfer to the pollution layer.
- They have low weight (e.g., for 400 kV, 10% of an equivalent ceramic insulator string).

Positive service experience:

- The continuous research by a few dedicated manufacturers has eliminated the flaws in the early generations of composite insulators.
- The creation of numerous international standards has enabled unbiased comparison and selection of insulators.
- More than 40 years of positive field experience worldwide, also and in particular in high pollution environments (marine, desert, and industrial).
- CIGRE and other surveys have consistently shown very low failure rates, comparable to those of porcelain and glass [9.162–165].

New applications:

- With the introduction of high-power transfer over long distances with line voltages up to 1200 kV AC and 1000 kV DC, composite insulators with single lengths of 10 m and above and mechanical ratings



**Fig. 9.81** Structure and elements of a silicone rubber composite insulator

up to 1000 kN offer significant cost savings because they are much lighter and considerably shorter than ceramic insulators.

- Because of the shift towards renewables—*green energy*—in many countries, a voltage upgrade or a voltage conversion from AC to DC of existing transmission lines is often the preferred approach to comply with the related significant variations in power transfer. This is feasible only with the use of composite insulators [9.166].
- Increasing environmental concerns by the public regarding the construction of new lines can often be addressed by proposing compact lines (Fig. 9.151), which are more slender and optically less obtrusive. Such lines have become practically feasible only through the use of composite insulators [9.167].

Competitive prices:

- The dissemination of knowhow by the few suppliers of raw materials, e.g., silicone, and production machinery companies led to a large number of new manufacturers, mainly in developing countries, and thus significantly lower production costs.
- At the same time, due to economies of scale and automated industrial production, the prices of the few experienced, renowned manufacturers have also declined dramatically in the last years, while at the same time the quality of their products has continuously improved.

The structure of composite insulators has basically remained unchanged over the years (Fig. 9.81 [9.2]). They consist of:

- A fiber-reinforced plastic (FRP), also known as glass-reinforced plastic (GRP), rod with high mechanical strength to take up the external loads and provide the internal insulation
- Metal fittings at both ends of the rod for transmission of mechanical loads
- A polymer housing with sheds surrounding the rod, designed to provide the necessary creepage distance and to achieve the best performance under pollution.

**Table 9.37** Elastic properties and mechanical strengths of FRP rods (adapted from [9.168])

Elastic property (GPa)		Mechanical strength (MPa)	
$E_1$	44	$\sigma_{11+}$	1038
$E_2, E_3$	10.3	$\sigma_{11-}$	-794
$G_{23}$	4.3	$\sigma_{22+}, \sigma_{33+}$	32
$G_{31}, G_{12}$	5.1	$\sigma_{22-}, \sigma_{33-}$	-141
$\nu_{23}$	0.5 [-]	$\tau_{12}, \tau_{13}$	54
$\nu_{31}, \nu_{21}$	0.32 [-]	$\tau_{23}$	$\approx 30$

### FRP Rod

The heart of any composite insulator is the FRP rod. It is made of thousands of glass fibers ( $\varnothing 10\text{--}30\ \mu\text{m}$ ) embedded in an epoxy resin matrix (Fig. 9.82 [9.168]). A glass content of 60–70 wt% enables a high axial tensile strength of the rod of around  $1000\ \text{N}/\text{mm}^2$ . On the other hand, the FRP rod, being a so-called orthotropic material, is mechanically weak in the transverse direction, i.e., perpendicular to the fibers. This has to be adequately considered in the design and the method of application of the end fittings—which are isotropic—to the rod. Table 9.37 [9.168] presents the elastic and strength properties of a typical FRP rod. Typical rod sizes range from 12 mm for distribution insulators up to 250 mm for heavy-duty post insulators or insulated cross-arms.

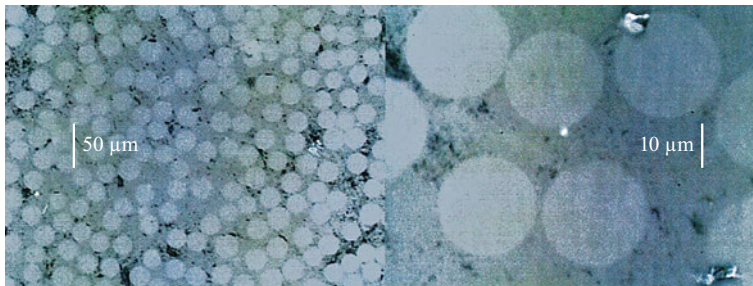
Nowadays, FRP rods are manufactured using the pultrusion process (Fig. 9.83 [9.2]), with diameters of up to 250 mm and lengths up to 15–20 m or even higher if needed. Various methods are used to control the quality of pultruded rods. These include determination of the density and the modulus of elasticity and measurement of the glass-transition temperature  $T_g$ . In addition, a dye penetration test [9.169] is used as a design and, due to its simplicity, also as a routine test, in order to detect fine cracks, seeds, and pores in the rod, which can become detrimental during service.

**Glass Fibers.** The glass fibers are manufactured by pulling from a glass melt and are wound directly in parallel, without twisting, onto bobbins. This is known as *direct roving*. Rovings used in rod manufacture can be differentiated by the fiber diameter, the sizing (coatings

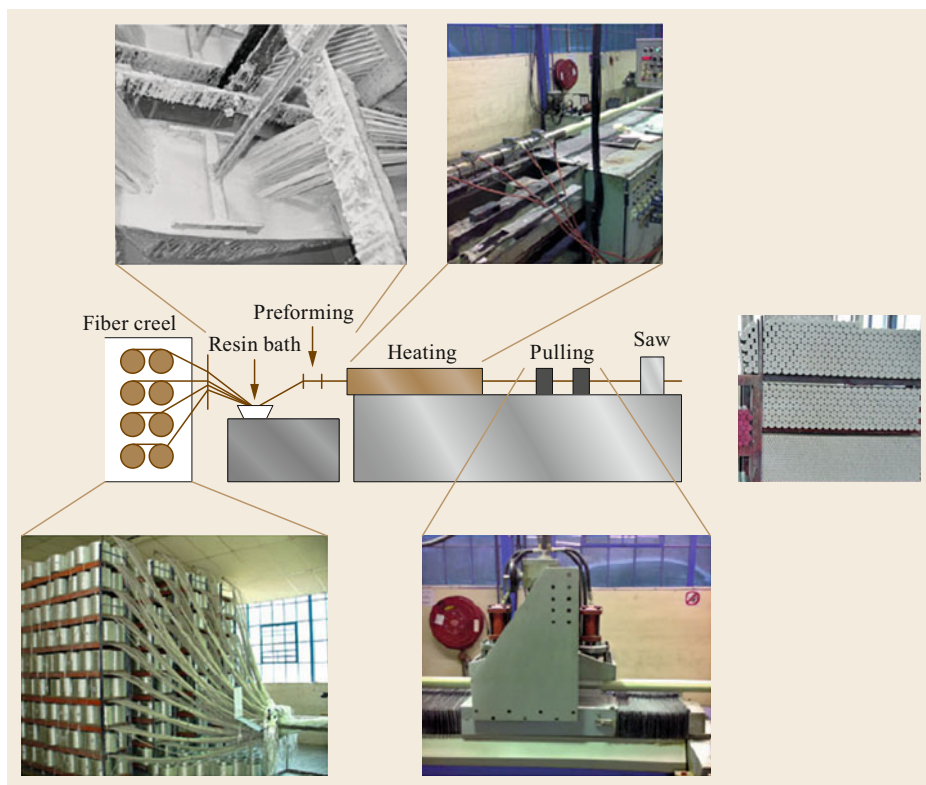
with protective layers, or combined protective layers with adhesive agents), the tex number (tex numbers between 4400 and 9600 are common for rod pultrusion, meaning rovings with a weight of 4.4 and 9.6 g/m, respectively), and the level of corrosion resistance, as explained below.

Glass fibers used in the FRP rods of modern insulators—in particular insulators loaded in tension—are in most cases made from E-CR glass. This is an acid-resistant glass, which does not contain boron and which in recent years has in most cases replaced the E-glass previously in use, in order to avoid so-called brittle fractures [9.170]. These are *clear-cut*, planar fractures of the FRP rod followed by a broomstick-type fracture (Fig. 9.84 [9.171]), which occasionally plagued early composite insulators. They take place under relative low (15–20% of the failing load) tensile loading conditions and are mainly attributed to acidic moisture ingress, whether from external corona or internal partial discharges, at the connection of the rod to the end fitting. Their occurrence in the field and their failure mode chemistry have been extensively investigated and are presented in [9.172, 173]. The influence of the resin as a possible cause of the susceptibility of FRP rods to brittle fracture is also explained therein. An acid withstand test to determine the glass quality of the FRP rod of an insulator is prescribed in [9.174–176].

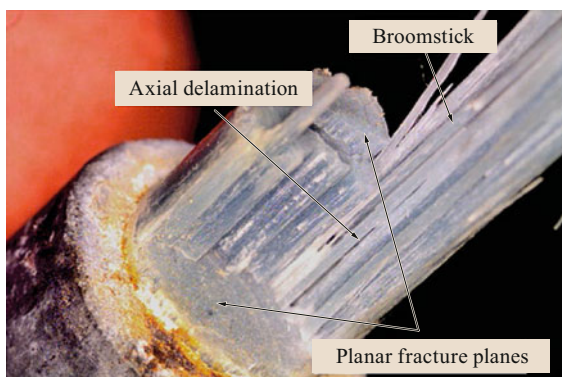
**Epoxy Resin.** For the impregnation of the glass fibers, various thermosetting plastics, such as epoxy resin, vinyl ester resin, unsaturated polyester resin, or blends thereof, have been used. High-quality insulators primarily use epoxy resins as it safeguards important properties of the FRP rod such as the breaking strain and glass-transition temperature  $T_g$ ; For example, if the failing strain of the epoxy resin is lower than that of the glass fiber, the composite material will behave similarly to the pure resin and fail prematurely, as the tensile strength of the glass fiber is not fully utilized. On the other hand,  $T_g$  specifies the temperature above which the rod softens [9.174–176]. A  $T_g$  range of 110–160 °C is advantageous for composite insulator rods because of the processing of the insulator hous-



**Fig. 9.82** Cross-section of a FRP rod at two different magnifications, showing the glass fibers and epoxy matrix



**Fig. 9.83** FRP rod pultrusion process



**Fig. 9.84** Brittle fracture of the FRP rod of a composite insulator

ing. When high-temperature vulcanized elastomers are used, a high  $T_g$  will prevent rod deformation in the injection mold, which would result in rod eccentricity and an undesirable asymmetric thickness of the polymer housing.

#### End Fittings

Steel fittings are typically used for composite solid-core insulators. Depending on the application and load, these are either steel castings (EN-GJS 400) or steel forgings

(CK 45). Forged steel is the material of choice for insulators which are subjected to tensile loads greater than 70 kN. It is characterized by a modulus of elasticity of  $E = 200\,000\text{ N/mm}^2$ , Poisson's ratio of  $\nu = 0.29$ , tensile strength of  $\sigma^- = 1000\text{ N/mm}^2$ , and compressive strength of  $\sigma^+ = 800\text{ N/mm}^2$ .

**End Fittings for Composite Longrods.** Because of the need for substitution compatibility with porcelain and glass insulators, the connection dimensions for composite longrod insulators are based on the standards for conventional insulators [9.157, 158], being standardized in [9.178] up to 550 kN. Typical end fittings are shown in Fig. 9.85 [9.138]. Their dimensions have been standardized in such a way that composite insulators are fully interchangeable with porcelain or glass insulators. End fittings are hot-dip galvanized with a zinc layer thickness of  $85\ \mu\text{m}$  in accordance with standard industry practices and [9.133, 134]. When greater layer thicknesses of up to  $150\ \mu\text{m}$  are required for highly corrosive operating conditions such as deserts and coastal routes or DC applications, it is important to ensure that delamination resulting from partial splintering of the zinc layer does not occur during the crimping of the end fitting to the rod. DC applications may further require an additional sac-

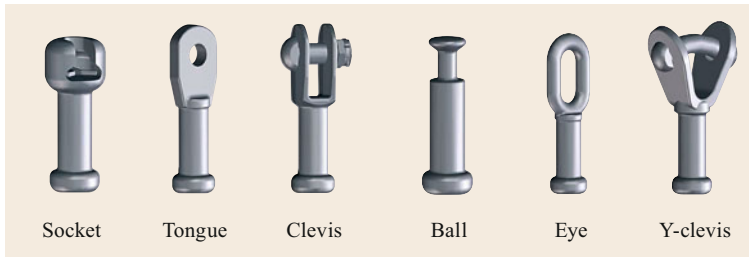


Fig. 9.85 Types of end fittings for composite longrod insulators

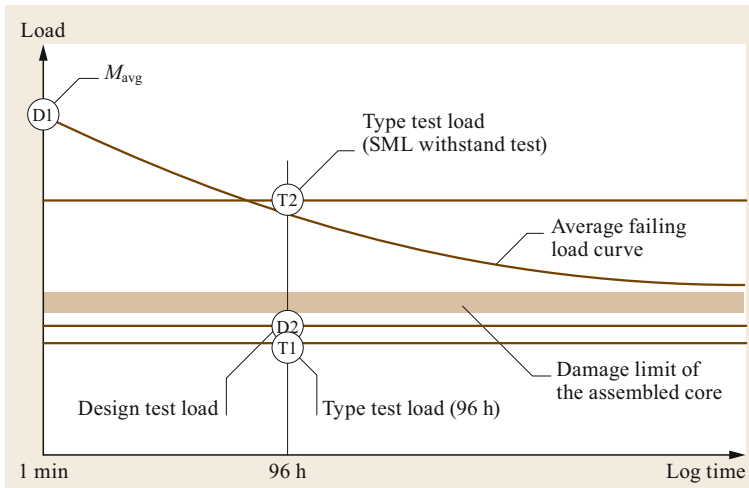


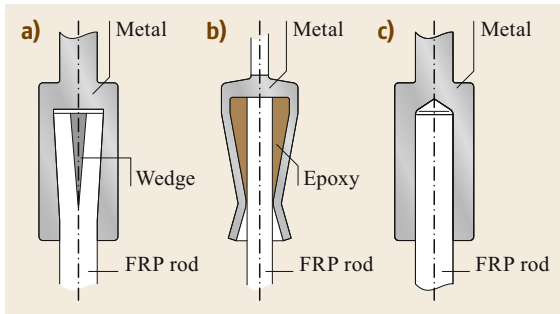
Fig. 9.86 Load-time curve of a composite insulator (adapted from [9.177])

rificial zinc collar on the outer contour of the end fitting, similar to the one used for glass insulators (Sect. 9.5.4).

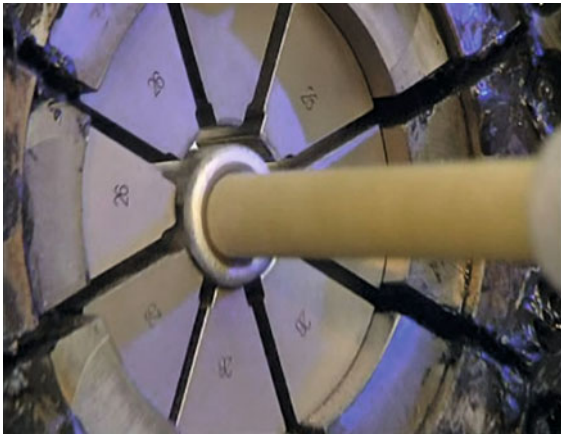
**Relation of Loads.** The majority of composite insulators for overhead lines, whether used as suspension insulators or as dead ends, are loaded in tension and are sometimes called composite longrods, having typical rod diameters between 16 and 32 mm. Their key mechanical parameter is the *specified mechanical load* (SML), defined as the load that the insulator must withstand in a 1-min tensile test after a 96-h test at 70% of its value; it is determined in a type test. In addition, each composite longrod has to pass a routine test at the so-called *routine mechanical load* (RML), which corresponds to 50% of the SML. A third important mechanical parameter is the *damage limit load* (DLL). This is the threshold tensile load below which hardly any fibers will fail, even if the load is applied to the insulator for an *infinite* period of time. The DLL of high-quality insulators can be assumed to be up to 60% of the *average failing load*  $M_{avg}$ . These loads and the load-time behavior of a composite insulator are shown schematically in Fig. 9.86 [9.177]. The related physical background is well explained in [9.179, 180].

**Crimping.** One of the most critical procedures in the manufacturing process of a composite insulator is the application of the metallic end fitting to the FRP rod. This is understandable, as the two materials have distinctly different elastic and strength properties (Table 9.37). Historically, the first composite insulators used conical or wedge-type fittings to be followed by polygonal compressed, crimped fittings (Fig. 9.87). The latter have been proven to show by far the best long-term performance under static and dynamic loads [9.181, 182] and thus are today the state of the art for most composite insulator manufacturers.

The crimping process is accomplished using hydraulic presses with octagonal tools, depending on the outer diameter of the end fitting (Fig. 9.88). This is mechanically complex, as during the compression stage, the steel of the end fitting will deform plastically while the rod will deform elastically. After the maximum crimping pressure has been reached and released, the metal fitting springs back, i.e., it is partly relieved of its elastic deformation, while its remaining, permanent plastic deformation continues to apply a radial pressure to the circumference of the FRP rod. Consequently, the stresses in the FRP rod are then approximately 30% lower than during crimping. The rod stresses caused by crimping are even higher than the stresses occurring at



**Fig. 9.87a–c** Development of end fittings for composite insulators: (a) conical, (b) wedge, (c) crimped



**Fig. 9.88** Crimping tools

the ultimate tensile load of the insulator, i.e., at failure. For this reason, high-quality manufacturers have introduced the acoustic emission technique, which enables continuous monitoring and safeguarding of the quality of the crimp during manufacturing [9.183].

The mechanical behavior of crimped end fittings has been thoroughly investigated in [9.168]. An important result therefrom is that the fitting–rod interface, and thus the composite insulator, when properly crimped, will fail in traction when the shear strength of the FRP rod, typically  $50 \text{ N/mm}^2$ , has been exceeded. This will become evident by a *clean* pull-out of the rod from the end fitting (Fig. 9.89a). When a *broom-type* failure occurs (Fig. 9.89b), this is a sign of sharp edges within the fitting which have predamaged the FRP rod. In this case, the insulator will most probably not reach its rated tensile strength. More critical is a *lateral* failure of the rod (Fig. 9.89c), as in this case the insulator has been overcompressed and the rod has been partly fractured during the crimping process. Although such an insulator will probably pass the routine RML test (50% of the SML), *hidden* rod fractures may well lead to insulator failure in service.

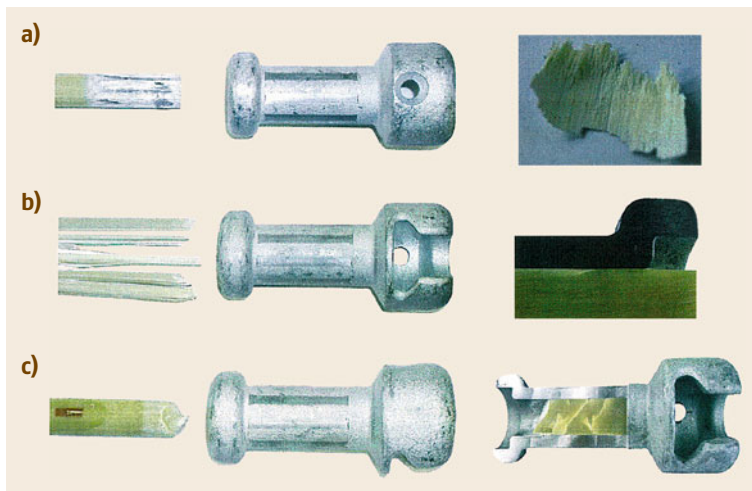
Based on the discussion above, the following simple formula can be derived for the ultimate tensile load  $F_{\max}$  of a composite longrod insulator

$$F_{\max} = 2\pi r l \tau_{\max} \quad (9.92)$$

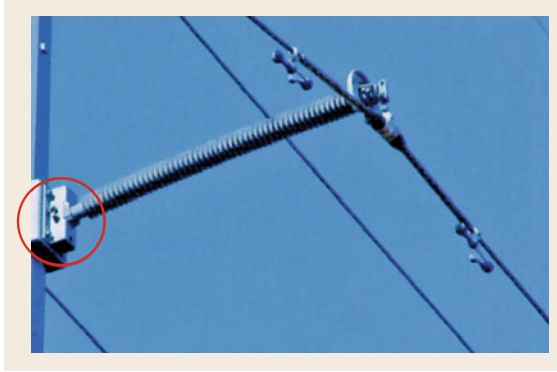
where  $r$  is the rod diameter,  $l$  is the crimping length, and  $\tau_{\max}$  is the ultimate shear stress of the rod, generally around  $50 \text{ N/mm}^2$ .

For example, for a typical insulator with  $r = 9.285 \text{ mm}$ ,  $l = 50 \text{ mm}$ , and  $\tau_{\max} = 50 \text{ N/mm}^2$ , this yields a maximum tensile load  $F_{\max}$  of  $155 \text{ kN}$ , which compares well with the measured value of  $148 \text{ kN}$ .

**End Fittings for Composite Post Insulators.** A common application of composite insulators is horizontal posts (Fig. 9.90). In this case, the insulator is predominantly loaded perpendicular to its axis, i.e., in bending.



**Fig. 9.89a–c** Failure modes of crimped composite longrod insulators: (a) correctly compressed, (b) rod predamaged, (c) overcompressed (adapted from [9.168])



**Fig. 9.90** Composite post insulator for 245 kV; red circle: the so-called gain base (source: Insulator News and Market Report, INMR)

The resulting nonuniform stress distribution over the FRP rod cross-section requires higher-diameter rods than for longrods. Typical rod diameters for posts are 44, 51, 63, 76, and 88 mm and nowadays can go up to 250 mm.

Typical end fittings of composite posts are shown in Fig. 9.91. These are mainly steel castings which are fastened by bolts at the base fitting, which in turn attaches to the supporting structure. One can distinguish between a bendable base made from formed steel and a fixed base made from cast iron (Fig. 9.92), which mates with the quite common 5" bolt circle, 4 bolts end fitting of the insulator. Whereas the bendable designs allow for some articulation of the insulator, the fixed base does not. Both bases come in flat and gain designs, i.e., with 0 and 12° upsweep angles, respectively, the latter marked by a red circle in Fig. 9.90, and also with alternative attachment options for a flat or round pole surface. The end fittings are attached to the rod mostly using a similar compression technique, as described above for longrods, but also using epoxy glue or temperature shrinking as alternatives.

**Relation of Loads for Line Posts.** The following loads characterize the bending performance of a composite line post [9.184]:

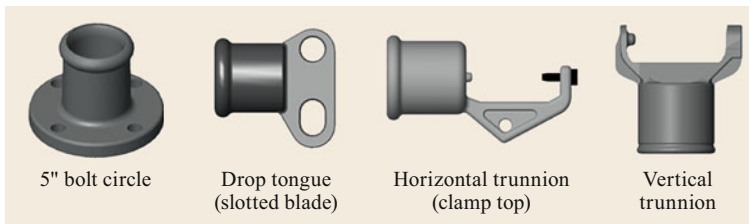
- The *specified cantilever load* (SCL) is the bending load which an insulator can withstand at the conductor side during testing.
- The *cantilever failing load* (CFL) is the maximum load which is achieved during testing of the insulator; it should be higher than the SCL.
- The *maximum design cantilever load* (MDCL) is the limit for the loads occurring during operation; it should be at least 25% below the DLL.

Another important load is the *damage limit load* (DLL), which is the load above which damage to the core is initiated. A relatively simple test to determine the DLL (and thus the MDCL) is to measure the load–deflection curve of the post in a short-time test. Such a curve is shown in Fig. 9.93 [9.168]. The load at which the slope of the curve starts to change is the DLL of the insulator, above which cracks will start forming in the inside of the rod, being practically invisible from the outside. This fast-track test is very practical compared with the MDCL test prescribed in [9.184], which is a tedious 96-h test and thus often *overlooked* during the inspection and acceptance process.

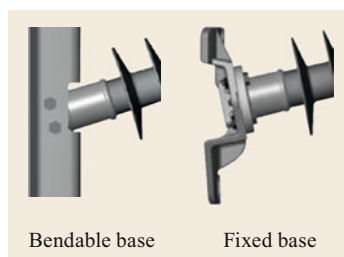
An important feature of composite post insulators is that, because of the high flexibility of the FRP rod, there is no physical separation of the insulating body in the event of mechanical failure of the insulator, as is the case with brittle porcelain insulators. Thus, there is no risk of a catastrophic dropping of the conductor. The term *safe failure mode* is introduced in [9.185] to describe this. For example, a composite post typically used for voltages from 36 to 52 kV and having an SCL of 10 kN, after sustaining prior damage as a result of the CFL test, was subjected to a 96-h test at 5 kN in accordance with the MDCL test procedure of [9.184] and passed this test successfully without any visible external damage to the FRP rod, let alone physical separation thereof.

The bending behavior of composite posts has been thoroughly studied and is presented in [9.168, 186], where the following simple analytical formula for the cantilever failing load (CFL) is derived

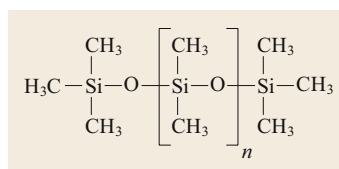
$$\text{CFL} = \frac{\pi r^3 \sigma^-}{4(L-l)}, \quad (9.93)$$



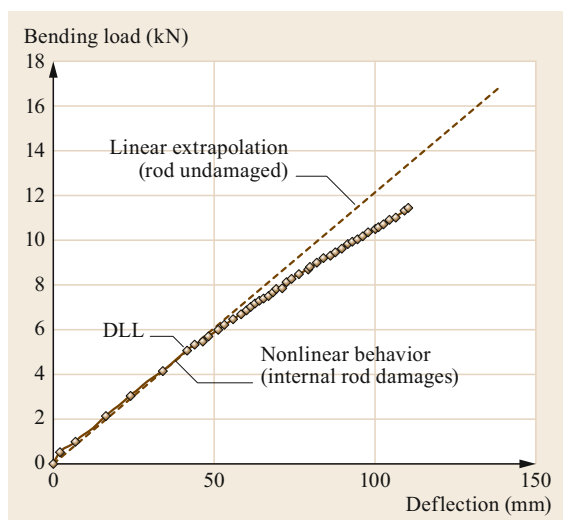
**Fig. 9.91** Typical end fittings for composite posts (source MacLean Power Systems)



**Fig. 9.92** Bendable and fixed bases as gain bases with upsweep angle of  $12^\circ$  (source MacLean Power Systems)



**Fig. 9.94** Chemical structure of polydimethylsiloxane (PDMS), with  $n$  being the number of repeating monomer units (adapted from [9.187])



**Fig. 9.93** Load–deflection curve of a 38-mm composite post insulator (adapted from [9.168])

where  $r$  is the rod diameter,  $\sigma^-$  is the compression strength of the rod,  $L$  is the insulator length, and  $l$  is the attachment length of the end fitting to the rod. If  $L = 760$  or  $1030$  mm,  $l = 70$  or  $90$  mm,  $r = 25.5$  or  $31.7$  mm, and  $\sigma^- = 800$  MPa then  $CFL = 15$  and  $20.7$  kN, respectively, for the two insulators tested in [9.168] with diameter of 51 and 63 mm, respectively. These values are consistent with the values obtained by testing, i.e., 15.6 and 21.7 kN.

### Silicone Rubber (SR) Housing

The polymer housing of a composite insulator has the double duty of protecting the FRP rod, which, if left unprotected in particular against ultraviolet (UV) radiation and pollution, will become brittle and degrade, but also providing the necessary creepage distance in order to avoid pollution flashovers. This is the reason why polymer insulator housings and in particular their sheds mimic the well-known shape of the sheds of ceramic insulators.

Concerning overhead line insulators, for many years, various polymers such as ethylene propylene di-

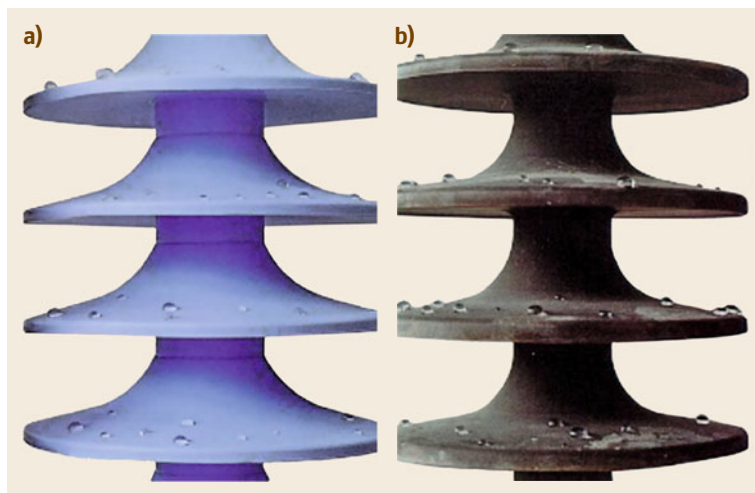
ene monomer (EPDM), ethylene propylene monomer (EPM), liquid silicone rubber (LSR), room-temperature vulcanized (RTV) and high-temperature vulcanized (HTV) silicone rubber (SR), but also polytetrafluoroethylene (PTFE, often called Teflon), have fought for this application. Nowadays, the material of choice for polymer insulators is doubtless HTV SR, because of its superior properties and performance in the field.

**Properties of Silicone Rubber.** The main components of silicone rubber are:

- Base polymer
- Fillers (pyrogenic or precipitated silica, quartz powder, and others)
- Vulcanizers (peroxides, H-siloxane)
- Catalysts (platinum compounds, tin compounds, and others)
- Additives (adhesive agents, softening agents, pigments, and others)
- Carbon blacks (pigment types, conductivity types, and special types)
- Aluminum trihydrate (ATH), i.e.,  $Al_2O_3$  (aluminum hydroxide).

Normally, the base polymer is a three-dimensionally cross-linked polydimethylsiloxane (PDMS). Silica, having a specific surface area between 100 and  $400\text{ m}^2/\text{g}$ , is incorporated to improve the mechanical properties. The tracking and erosion properties can be usefully improved by adding, e.g.,  $Al_2O_3$ , aluminum trihydrate (ATH). For a rubber to be considered a silicone rubber, it must consist of a polymer having an inorganic main backbone chain of Si–O bonds, where each silicone atom is bonded to two methyl groups (Fig. 9.94 [9.187]).

This structure explains some of the remarkable chemical and physical properties of this elastomer. Its high flexibility even at low temperatures is a result of the low intermolecular bonding forces; i.e., the cause of the flexibility is inherent in the silicone polymer itself and is not achieved by the addition of softeners. Thus, even at high temperatures, no sweating out of



**Fig. 9.95a,b** Hydrophobic surface behavior of a SR insulator when new (a) and polluted (b) (source Pfisterer Lapp)

softeners with the resulting unpleasant effects of contamination of the environment and no embrittlement of the polymer material can occur. Silicone rubber exhibits good thermal stability and excellent resistance to ozone, corona discharge, and moisture. As silicone dioxide also possesses good insulating properties, concentrated electrical discharges (e.g., flashovers, which at their bow can reach temperatures of up to 1300 °C) do not result in the formation of conducting tracks in silicone rubber, unlike the case of other elastomers, and also no corrosive or directly toxic products are formed; silicone rubber is completely free of halogens. Silicone rubber is classified as slow burning and should pass the [9.188] vertical burning test in class FV 0. When exposed to flame, the main combustion products formed are water vapor and carbon dioxide, leaving silicone dioxide as a solid residue. The main Si–O-bonded backbone of silicones has a high dissociation energy (100–120 kcal/mol) compared with the lower dissociation energies of hydrocarbons of 85.5 kcal/mol for C–O and 82.6 kcal/mol for C–C. In turn, this results in silicone rubber having good UV radiation resistance. Additionally, PDMS has a very low surface free energy and a very flexible backbone. This flexibility of the backbone allows PDMS to rearrange itself, resulting in quick regeneration of the surface characteristics of the silicone rubber. In particular, the low surface tension makes the surface very hydrophobic (Fig. 9.95a) and allows the diffusion of low-molecular-weight (LMW) content to pollution layers, encapsulating them and rendering also these hydrophobic via so-called hydrophobicity transfer (Fig. 9.95b). This is not the case for porcelain and glass, which are hydrophilic. A guide for the measurement of the hydrophobicity of insulator surfaces has recently been updated [9.189].

As mentioned above, HTV silicone rubber is the preferred material for OHL insulators. This is mainly because it exhibits superior tracking and erosion performance under the local surface discharges that can occur when pollution is heavy and hydrophobicity is temporarily lost. To achieve this, an amount of > 50% by weight of ATH filler is required. An easy way to determine whether the silicone rubber used for an insulator is indeed of HTV grade is to measure the Shore hardness of the sheds, which should be between 65 and 75 Shore A, but also to determine the specific weight of a piece of rubber cut from the shed, which should be above 1.5 g/mm<sup>3</sup>. LSR, which is sometimes sold as HTV, has a Shore A hardness below 60 and a specific weight of around 1.2 g/mm<sup>3</sup> [9.190]. The reason is that LSR, which is fluid with a viscosity of 10 000–30 000 mPa s, is much easier to process than HTV, which is solid with a viscosity of 5–20 × 10<sup>6</sup> mPa s. However, it is worth noting that solely adding a certain quantity of ATH is not per se sufficient. Rather, the entire system (polymer, fillers, treatment of fillers, etc.) needs to be optimized in a balanced manner [9.191]. In addition, recent research has examined the possibility of improving the electrical and mechanical properties of silicone rubber by the addition of nanoparticles [9.192].

**Manufacturing of SR Housings.** The traditional methods applied to process silicone rubber for insulator housings are compression molding, transfer molding, and injection molding. The latter is the most well-developed method and is used by the majority of established manufacturers of composite insulators. However, this process is demanding and requires, besides considerable investment in production machinery and molding



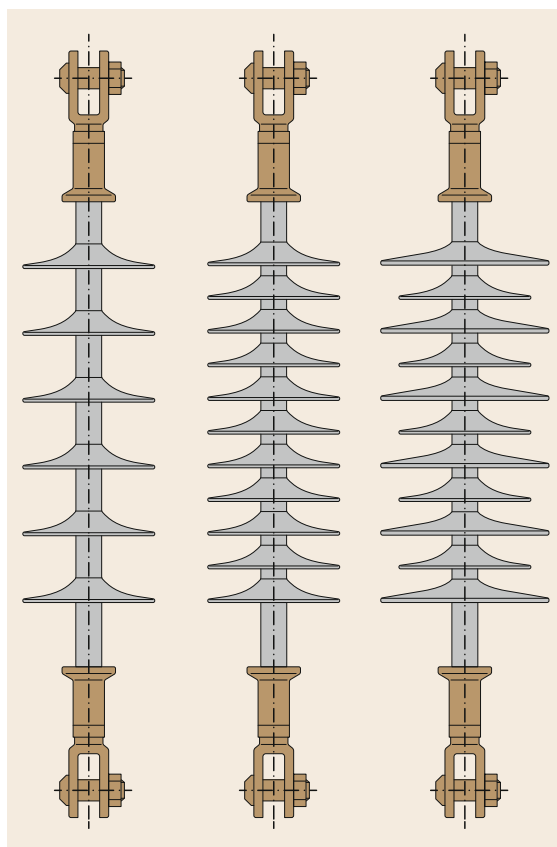


**Fig. 9.96** Injection molding of a 420-kV SR composite insulator using the stepping technology (source Pfisterer Sefag)

technology, high-level process knowhow. Specifically, with pressure levels of up to 1500 bar and temperatures up to 200 °C, there are a quite a few challenges to obtaining a void-free housing regarding the following process parameters:

- Mold temperature
- Injection unit temperature
- Plasticizing profile and dynamic pressure
- Injection velocity and pressure
- Filling of cavity
- Postfilling pressure
- Preheating in the injection piston
- Vulcanization time
- Process time for injection unit
- Velocity profile at the clamping unit
- Mold clamp force.

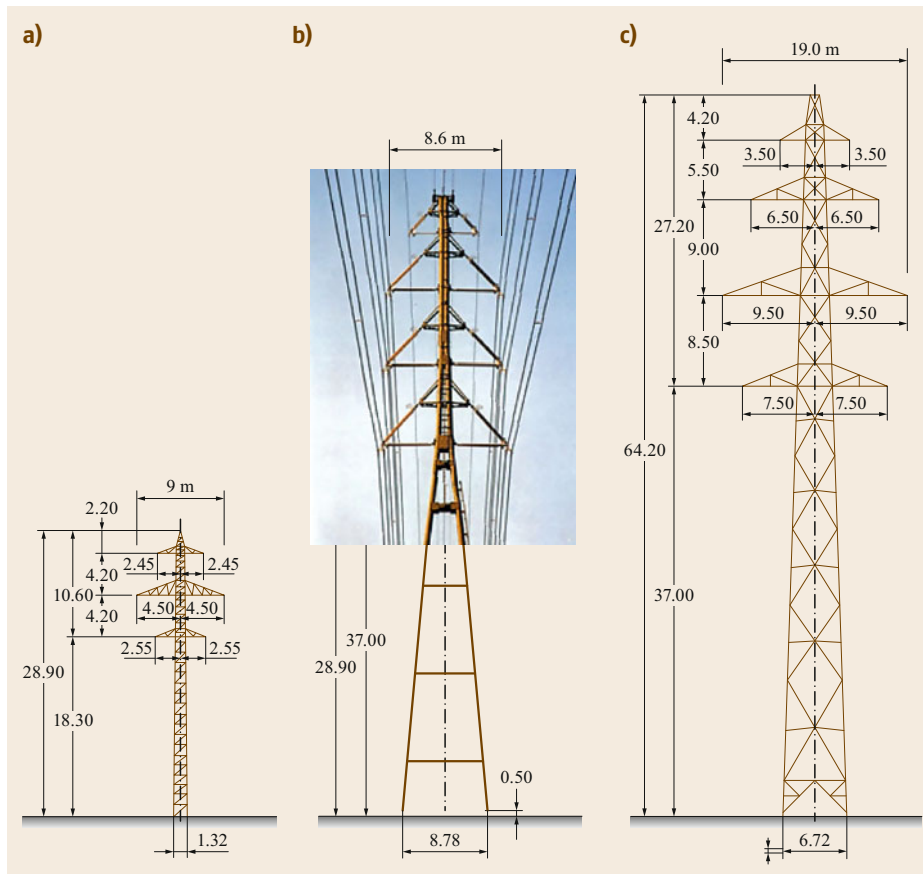
In addition, HTV stepping, viz. the injection of SR on the FRP rod while the preceding section of the insulator housing is being vulcanized in the mold, has been successfully used for longrod insulators since the 1990s and enables the manufacturing of composite insulators with no length restriction (Fig. 9.96). In this regard, due to the high vulcanizing temperature and the process pressure that arises, special attention should be paid to centering the rod.



**Fig. 9.97** Flexibility of modular process (adapted from [9.2])

Indeed, depending on the length of the mold, even rods with a diameter of 88 mm may be deformed when using an asymmetrical injection nozzle system, thus jeopardizing the minimum requirement of a uniform 3 mm thickness for the SR sheath around the rod. HTV stepping is also suitable for a high degree of automation, thus minimizing human error, such as in the ACIM (automated continuous injection molding) method [9.2].

A viable, well-developed alternative is the modular manufacturing process. In this approach, the rod is first covered with a uniform HTV SR sheath with minimum 3 mm thickness, by using an extrusion process, while the individual HTV SR sheds, which are produced separately by compression molding, are subsequently applied to the SR sheath of the rod by radial expansion and vulcanized thereon with the aid of a special RTV-based silicone adhesive. This modular process offers a high degree of flexibility regarding creepage for a given connection length (Fig. 9.97 [9.2]), at the cost of an additional interface between the sheds and the sheath of the rod, which, if not manufactured properly, may create problems during service.



**Fig. 9.98a–c** Steel lattice tower of existing 125-kV line (a) and Swiss compact line (bipod) for 400 kV/132 kV (b) and standard design (lattice) (c) (source INMR)

An important feature common to both of these methods, i.e., HTV injection molding and the modular process, is the interface between the SR and the rod. This must be absolutely tight, as any ingress of moisture via air pockets at the interface will cause partial discharges and ultimately catastrophic failure of the insulator through a so-called *flashunder*. High-quality manufacturers use automated spraying and detection techniques based on a suitable, visually easily detectable primer on the rod, which will ensure seamless and durable application of the SR onto the rod.

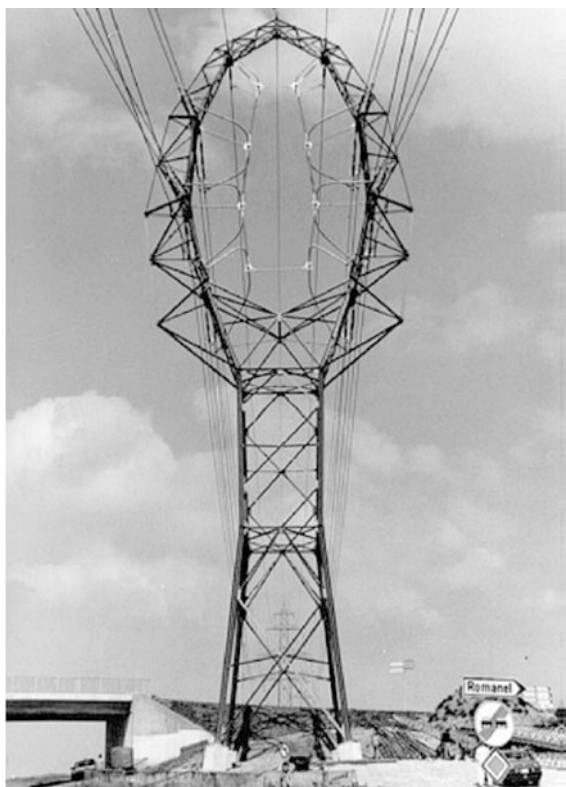
#### Unique Applications of Composite Insulators

In recent years, composite insulators have come to play an increasing role in new, innovative solutions for the realization of so-called esthetic line supports and also in the uprating of existing overhead lines, i.e., lines to carry substantially higher electrical power than they were originally designed for. Both issues are related, on one hand, to the increased demand worldwide either for new lines, often because of the massive expansion of renewable energy sources (RES), but also because the first generation of HV OHL is reaching the end of its

expected useful life (the first 400-kV OHL was put in operation in 1952 in Sweden), and on the other hand, the increased public opposition to new lines because of their purported health hazards (Sect. 9.3.4). For both issues, the massive development of composite insulators in recent decades has been decisive, as documented by the following two application examples.

**Compact Lines.** Compact lines were first developed in the 1970s but only started to become more popular with the widespread introduction of composite insulators, because the insulated cross-arms that are indispensable for the design of compact lines are loaded primarily in compression and are subject to relatively large deformations, which can be better sustained by composite than conventional insulating materials (porcelain and glass). More specifically, the following properties of composite insulators are advantageous for use in insulated cross-arms:

- High bending strength
- Elastic limit in the region of ultimate strength
- High ultimate strain
- Nonbrittle.



**Fig. 9.99** The 400-kV tennis racket tower in Western Switzerland (adapted from [9.193])

A good example is the world's first 400-kV compact line using composite insulators, which was installed in Switzerland in 1998 [9.135]. The line became necessary as the existing 125-kV line (Fig. 9.98a) was no longer sufficient to carry the increased power demand in the region of Lake Geneva and had to be replaced by a 400-kV line. The conventional steel lattice towers that are normally used for this type of line (Fig. 9.98c) require a considerable right of way (ROW), which was not available at certain locations where the route had to pass very close to inhabited buildings. The solution was to design very slender two-dimensional (2-D) towers and use insulated cross-arms with composite insulators for the 400-kV circuits and also for the two single-phase 132-kV circuits for the feeder lines of the Swiss Railways, SBB (Schweizerische Bundesbahnen) (Fig. 9.98b). It is worth noting that, because at that time, available FRP rod sizes were restricted to 76 mm, which could not take the compressive loads, hollow-core composite insulators had to be used. Interestingly, at another location along this line, a so-called landscape tower, so called because it lies in a specific landscape (in this case the local tennis club), was installed, becoming well known as a unique, tennis racket tower



**Fig. 9.100** 400-kV interphase spacer in the transmission line at the Vorab Glacier in Switzerland (adapted from [9.194])

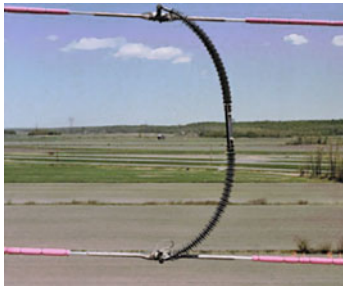
(Fig. 9.99 [9.193]). Its delicate, spider-like phase arrangement could only be realized using lightweight and optically nondisturbing composite longrod insulators.

**Interphase Spacers.** Line compaction is primarily based on the principle of minimizing interphase spacing. As a result, there is greater risk of interphase flashovers, i.e., when two phase conductors are moved close to one another as a result of wind, ice shedding, or short circuit. This can be avoided by the use of interphase spacers (IPS). Although some applications of porcelain IPSs are known, the increased use of IPSs in recent years has been enabled only by the introduction of composite insulators, mainly because of their low weight and high flexibility; For example, Fig. 9.100 shows such an IPS in a critical span of a 400-kV line at altitude of 3000 m at the Vorab Glacier in Switzerland. At this location, serious damage often occurred during winter, when sudden ice shedding caused the conductors to jump by up to 20 m and detrimentally clash with each other [9.194]. The individual IPSs between two phases are between 10 and 12 m long and weigh approximately 100 kg, including their special fittings which allow fully articulated coupling to the phase conductors, thus preventing damage in the event of sudden movements. Each IPS consists of four to five silicone composite insulators having a rod diameter of 76 mm. Such IPSs have been used with success since 1995; that is to say, there have been no outages caused by ice shedding since their installation.

Another interesting application, this time for MV lines, is shown in Fig. 9.101. In this case, a second 12-kV circuit could be installed on an existing 50-/12-kV line on concrete poles with the help of silicone compos-



**Fig. 9.101** IPSs enable the addition of a second 12-kV circuit on an existing 50/12-kV line in Switzerland



**Fig. 9.102** IPS under heavy compressive load

ite IPSs, which were installed around every 40 m along the span, helping to maintain the required midspan clearances. In the meantime, thousands of such IPSs have been operating successfully for many years in Switzerland.

**Mechanical Design of IPSs.** Interphase spacers predominantly have to sustain compressive loads and are designed using the well-known Euler formalism. Because of their high flexibility (Fig. 9.102), an exact calculation using third-order bending theory [9.195] reveals an additional compressive load reserve of approximately 30% compared with the critical Euler load

$$P_{\text{Euler}} = \frac{\pi^2 EI}{L^2}. \quad (9.94)$$

This condition is met when the diameter  $d$  of the IPS is related to its length  $L$  by

$$d > \frac{L}{100}. \quad (9.95)$$

## 9.5.6 Insulator Tests and Standards

The paper [9.196] provides a good overview of the development of standards for insulators and their relation to the evolution of insulator technology. Tests for all types of insulators are well established and described in numerous standards. Table 9.38 [9.16] summarizes standard electrical test requirements, while Table 9.39 [9.4] is a good check-list for the required insulator tests.

A comprehensive list of standards for composite insulators can be found in the “Standards” chapter of [9.2]. In addition though, for composite insulators, the following issues are of particular importance:

### Intensified Testing

While there are numerous stringent design tests for composite insulators, bulk volume orders of the same have to pass only relatively *easy* routine tests. It cannot therefore be excluded that some inferior-quality samples will also *pass*, which subsequently may cause problems during service. To avoid this, certain meaningful and at the same time simple tests were proposed in [9.190] under the philosophy of *intensified inspection and acceptance tests*. These comprise:

#### Visual Inspection.

- Overall appearance of the insulators
- Voids in the housing
- Sealing area.

#### Tensile-Loaded Insulators.

- 96-h acid test of rod
- Tensile load up to failure, control of failure mode (Fig. 9.89).

#### Bending-Loaded Insulators.

- Simplified verification of MDCL (Fig. 9.93).

#### Material.

- Adhesion test before and after boiling.
- Verification of physical housing properties, in particular specific weight and Shore hardness.
- Tracking and erosion test as per [9.197] with housing sample from a finished insulator (Fig. 9.103).

As an example from this list, the adhesion test is briefly explained here, as it is not only easy to perform, but is also of extreme importance for the service performance of the insulator, because if there is no proper

**Table 9.38** Standard electrical test requirements for insulators at two different voltage ranges (adapted from [9.16])

Insulator type	1 kV < $U_s$ ≤ 245 kV Insulator sets				$U_s$ > 245 kV Insulator sets		
	Cap and pin <sup>a</sup>	Longrod <sup>a</sup>	Composite <sup>b</sup>	Line post <sup>a</sup>	Cap and pin <sup>a</sup>	Longrod <sup>a</sup>	Composite <sup>b</sup>
Wet power frequency withstand voltage	×	×	×	×	–	–	–
Dry lightning impulse withstand voltage	×	×	×	×	×	×	×
Wet switching impulse withstand voltage	–	–	–	–	×	×	×
Puncture withstand voltage (single unit)	×	–	–	×	× <sup>c</sup>	–	–

<sup>a</sup> Tests carried out to [9.133, 134]  
<sup>b</sup> Tests carried out to [9.177] (applicable to composite insulator units only) and [9.184] as appropriate  
<sup>c</sup> For those line post insulators which are not puncture proof

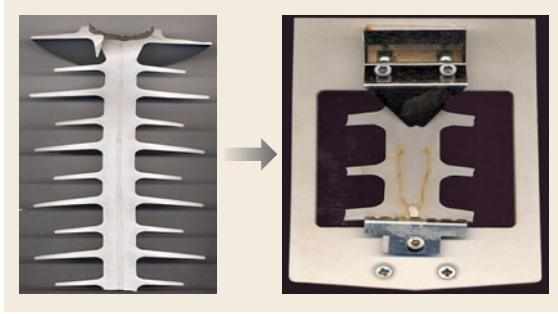
**Table 9.39** Tests on overhead line insulators (adapted from [9.4])

Standard type tests	String insulator units		
	Longrod	Cap and pin	Line post insulators
Verification of dimensions	×	×	×
Wet power frequency withstand voltage test	×	×	×
Dry lightning impulse withstand voltage test	×	×	×
Thermal mechanical performance test	×	×	–
Mechanical or electromechanical failing load test	×	×	×
<b>Optional type tests</b>			
Impulse withstand puncture test	–	×	–
Zinc sleeve test	–	×	–
Residual strength test	–	×	–
<b>Sample tests</b>			
Verification of dimensions	×	×	×
Verification of locking system and displacements	×	×	–
Temperature cycle test	×	×	×
Mechanical or electromechanical failing load test	×	×	×
Thermal shock test (toughened glass insulators only)	–	×	×
Puncture voltage withstand test	–	×	–
Porosity test (porcelain insulators only)	×	×	×
Galvanizing test	×	×	×
<b>Optional sample test</b>			
Radio interference voltage (RIV) test	–	×	–
Impulse voltage puncture test	–	×	–
Zinc sleeve test	–	×	–
<b>Routine tests</b>			
Visual inspection	×	×	×
Mechanical test	×	×	×
Electric test	–	× <sup>a</sup>	–
<b>Optional routine tests</b>			
Ultrasonic examination	×	–	–

<sup>a</sup> Applicable only to insulators made of ceramic materials [9.133, 134]

adhesion between the housing and the rod, ingress of moisture and subsequent partial discharges (PD) can destroy the insulator.

Firstly, squares are cut on the surface of the housing, penetrating to the rod (Fig. 9.104a). A pair of pliers is then used to grip and pull the squares of sili-



**Fig. 9.103** Modified tracking and erosion test [9.197]; only little erosion of reference material after 6 h at 4.5 kV; poor materials will fail much sooner, i.e., in 40–70 min

cone vertically from the rod surface (Fig. 9.104b). This easy test is performed on the housing preferably twice, firstly without any pretreatment and secondly after boiling. The boiling process as per [9.177] is used, i.e., the specimens are immersed in a vessel of boiling solution consisting of deionized water with 0.1 wt% NaCl for 42 h.

Good adhesion to the rod should result in a cohesive failure of the rubber (Fig. 9.104c), rather than an adhesive failure between the rubber and the rod (Fig. 9.104d). The aim of this test is to ascertain the quality of the bonding between the housing and the core. If insulator designs with overmolded end fittings are used, the bonding between the end fitting and housing can be evaluated in the same way.

#### Tests for Composite Insulators Withdrawn from Service

Composite insulators are still a relatively new technology, and it is thus understandable that their users, mainly electrical utilities, are keen to evaluate an insulator population in order to enable one or more of the following:

- Provide an indication of population health/life expectancy and therefore determine whether to leave

the population or individual units in service or to take any countermeasures such as removal of the units

- Determine the inspection/assessment frequency
- Modify design philosophies, e.g., new pollution maps, *E*-field grading, and need for power arc protection.

This is best done by testing insulators which have been in service as described in [9.198], which is based on similar work presented in [9.199] for conventional insulators. The start of such tests is always a thorough visual inspection. This requires considerable knowhow and experience but is indispensable to determine the status and/or aging mode of the insulator and subsequently define the test philosophy and procedure. Such tests can include:

#### Mechanical Investigation.

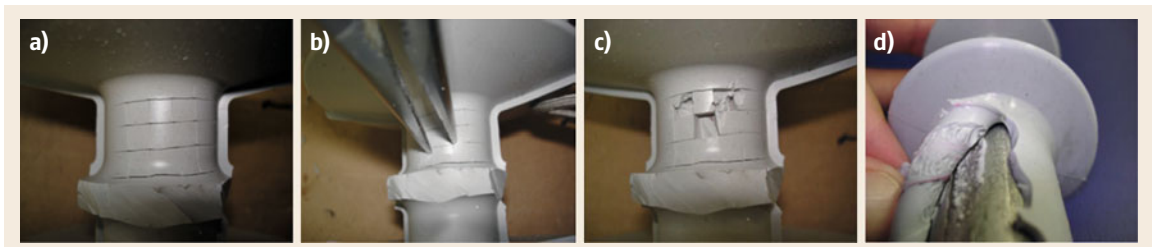
- Verification of SML
- 96-h load-time test.

#### Electrical Investigation.

- Dry power frequency withstand voltage test (PF dry)
- Wet power frequency withstand voltage test (PF wet)
- Dry lightning impulse withstand voltage test (BIL)
- Wet switching impulse withstand voltage test (if applicable,  $U_m > 245$  kV) (BSL)
- Quick salt fog
- Rapid clean fog
- Modified clean fog.

#### Material Analysis. Housing materials:

- High-voltage water diffusion test [9.177]
- High-voltage low-current discharge resistance test [9.200]
- Modified tracking and erosion test [9.197]



**Fig. 9.104a–d** Simple adhesion test. (a) Cutting the surface, (b) pulling the housing with pliers, (c) good bonding to the rod, (d) poor bonding to the rod (adapted from [9.177])

- Thermogravimetric analysis (TGA)/differential scanning calorimetry (DSC) for determination of filler content and material fingerprinting
- Fourier-transform infrared (FTIR) analysis for determination of chemical nature and material fingerprinting
- X-ray fluorescence (XRF)/X-ray diffraction (XRD) analyses for material identification
- Gravimetric analysis for determination of filler content
- Flammability test [9.177]
- Hardness test [9.201], preferably carried out before and after prestressing by boiling
- Measurement of surface roughness (ISO 4287)
- Test on interfaces and connection of end fittings [9.177] (*design test*)
- Tightness of the interface between the insulating body and metal end fittings, sealing verification test in accordance with [9.177] (*sample test*)
- Tests of the housing [9.202]: 1000h, wheel test, 5000h test in order to assess the tracking and erosion performance of service-aged housing materials and housing designs.

Core materials:

- High-voltage water diffusion test [9.177]
- TGA/DSC for determination of filler/fiber content and material fingerprinting
- FTIR analysis for determination of chemical nature and material fingerprinting
- XRF/XRD analysis for material identification
- Dye penetration test [9.169].

## 9.6 Fittings

Overhead line fittings, sometimes also called line hardware or line accessories, serve for the mechanical attachment, electric connection, and protection of conductors and insulators. In relevant standards, fittings are frequently designated as accessories which may consist of elements or assemblies.

Fittings for conductors serve to terminate, suspend, or join the conductors and are directly connected to the conductors. Suspension and dead-end clamps, connectors, branch-off clamps, vibration protection fittings, as well as bundle spacers lie within this category. According to their function, they may form an assembly consisting of several elements, e.g., suspension and dead-end clamps including the required connecting links.

Fittings for insulator sets and other attachments serve to connect the tension or suspension insulators with the attachment points at the supports. In case of

End fittings:

- Thickness of galvanizing coating in accordance with [9.133, 134]
- Structural analysis of the metal material by means of raster electron microscopy (REM) analysis (ground and polished material samples).

### Surface Layer Analysis.

- Pollution accumulation (mainly ESDD, NSDD, and surface conductivity)
- Surface changes (e.g., chalking, discoloration, surface cracking, etc.)
- Wettability class [9.189]
- Grade of hydrophobicity transfer mechanism (HTM) [9.203]
- Hydrophobicity transfer (HT) [9.204]
- Chemical analysis of the pollution layer by means of FTIR or atomic absorption spectrometry (AAS)
- XRF and XRD analyses.

The results of these tests can be compared with those carried out on samples in storage, e.g., insulators from warehouse stock, if available. Major deviations may be suggestive of aging. CIGRE publication [9.198] contains a number of very interesting case studies on real applications of the said.

### In-Service Diagnostic Methods

CIGRE has published two documents on this topic [9.171, 205]. A brief summary of the relevant diagnostic methods is given in Sect. 9.9.

insulator strings, components to connect insulators with each other also lie within this category, while the insulators themselves are excluded. These fittings comprise all the components arranged between the assembly of the dead-end or suspension clamps and the first detachable element at the support, e.g., the jointing pin or U-bolt. Yoke plates, corona protection fittings, and grading rings are also included.

Most fittings look like simple pieces of metal. However, they must sustain all kinds of mechanical, electrical, chemical, and environmental loads. Therefore, it is important to understand their function and underlying design principles.

Fittings should be designed so as to:

- Avoid damaging the conductor under service conditions

- Withstand the mechanical loads relevant to installation, maintenance, and service, the designed service current, including short-circuit current, the service temperatures, and environmental circumstances
- Ensure that individual components are secured against becoming loose during service
- Exhibit limited corona effects, better than the performance of the conductor on which they are installed.

Fittings for live-line maintenance should be suitably designed for safe and easy handling with current hot line techniques.

The surfaces of compression fittings in contact with the conductor or earth wire should be protected from becoming contaminated before installation, and brittleness of the finished parts should be avoided by adopting suitable materials and manufacturing processes.

Nonmetallic materials such as elastomers, if employed, should exhibit good resistance to aging and be capable of withstanding service temperatures, without detrimental changes in their properties. These materials should show adequate resistance to the effects of ozone, ultraviolet radiation, and air pollution over the whole range of service temperature. They should not induce corrosion in materials which are in contact with them [9.206].

### 9.6.1 Conductor Fittings

Conductor fittings are those line accessories which are in direct contact with the conductor or earth wire, such as:

- Suspension clamps (top clamps, helical ties, distribution fittings)
- Tension or dead-end clamps
- Connectors or joints
- Branch-off or T-clamps
- Aerial markers
- Vibration dampers
- Spacers and spacer dampers.

#### Suspension Clamps

Suspension clamps are used to suspend the conductor from a suspension or straight-line support (Fig. 9.105) and have to fulfill a number of important duties:

- Withstand the mechanical loads imposed by the conductor
- Avoid damage to the conductor in the clamp area
- Prevent/reduce strand failures because of vibration
- Offer high corrosion resistance



Fig. 9.105 Suspension clamp

- Provide a sufficient corona inception voltage
- Withstand short circuits and have low contact resistance and low electrical losses
- Allow simple and safe installation.

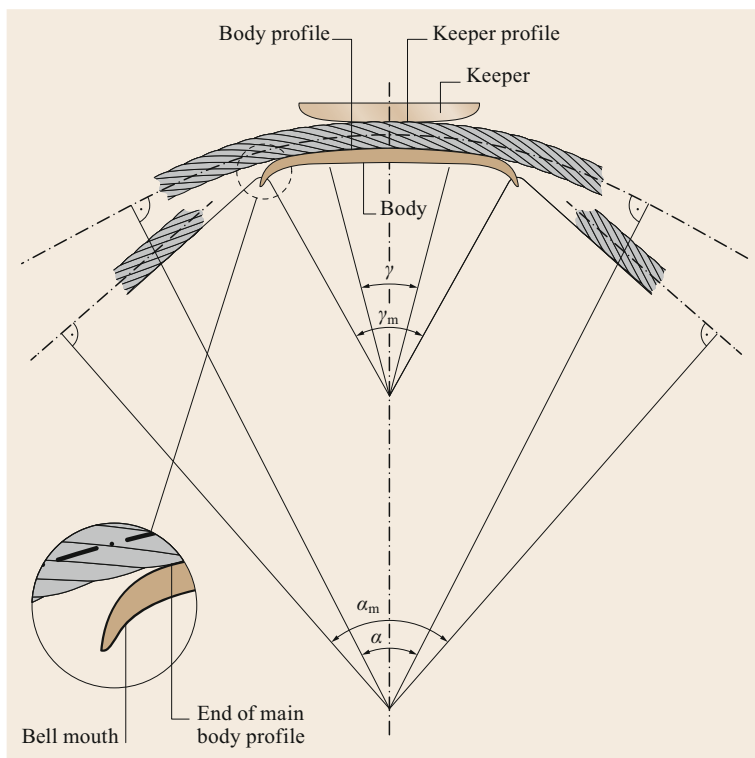
Because practically 99% of conductor vibration failures occur very near to or at the suspension clamp location, its design is of great importance for the mechanical integrity of the conductor and thus the operational safety of a line. The Task Force on Suspension Clamps of CIGRE SC 22, WG 01 prepared, in 1989, a guide for good clamp design, which is summarized below with reference to Fig. 9.106 [9.207].

**Body and Keeper Profile.** The profile of the clamp body should follow the curvature of the conductor and thereby not reduce its failing load, whereby an optimum profile design of the body and keeper must be found for different load assumptions and contact length of the suspension clamp. The profile of the body must be rounded and curved into a bell mouth at the ends to avoid damage to the conductor during the variation of the exit angle due to conductor tension variations. This consideration should also apply to the keeper design when conductor uplift is assumed. To prevent damage to the conductor surface, all parts of the clamp that are in contact with the conductor should be smooth.

**Turning Angle.** The profile of a suspension clamp should accommodate the various required turning angles, for example:

- Low-tensioned conductor with a high turning angle: assumption of high temperature
- High-tensioned conductor with a small turning angle: assumption of low temperature
- High-tensioned conductor with a high turning angle: assumption of ice or wet snow load.





**Fig. 9.106** Technical terms related to suspension clamps ( $\gamma$ : exit angle;  $\gamma_m$ : maximum exit angle,  $\alpha$ : turning angle,  $\alpha_m$ : maximum turning angle) (adapted from [9.207])

As is often the case, the proper selection of the turning angle is ultimately a compromise. With turning angles of the conductor at the clamp end normally lying in the range of  $\alpha = 10\text{--}20^\circ$ , the majority of suspension clamps are designed with a maximum turning angle of  $\alpha_m = 30^\circ$ .

**Mobility.** A suspension clamp should be able to rotate in a longitudinal vertical plane in order to accommodate asymmetrical loads and different spans on each side of the clamp, whereby the axis of rotation should not be placed more than a few conductor diameters from the conductor axis, in order to reduce additional bending stresses upon the conductor. In this context, keeping the clamp mass low and thus reducing its rotational inertia is an advantage. *Metacentric* suspension clamps (Fig. 9.105) present the minimum moment of inertia, i.e., the maximum mobility.

**Sliding.** The suspension clamp should, on one hand, keep the conductor locked in place, but on the other, slip at a known sliding force to avoid tension overloads and consequential damage to the conductor. This is achieved mainly by applying a specified pressure on the conductor via the clamp keeper and related fastening elements, typically U-bolts. With a high torque on the clamp bolts, the yield point of the strands can be

exceeded on a bare conductor. Even under armor rods, strains on the order of 500–1000 microstrain have been measured on aluminum strands.

Some utilities install *controlled sliding clamps* as a mechanical fuse at selected locations, to avoid line cascade. The conductor must slide within such clamps as a result of either conductor rupture or an exceptional, unbalanced ice load. The load that will cause the conductor to slide through the clamp is nowadays based on controlled tightening of the clamp bolts; these clamps are called *controlled tightening clamps*. Details on such clamps and load control devices (LCD) in general can be found in [9.208].

**Common Clamps.** Different types of suspension clamps are used in transmission construction:

- Bolted suspension clamps on bare conductor
- Bolted suspension clamps over armor rods
- Helically attached elastomeric suspension clamps (HAES)
- Elastomeric suspension clamps without helical rods (ES).

*Bolted clamps on bare conductor* (Fig. 9.105) are the most commonly used, on some 50% of all installations.



**Fig. 9.107** Helically attached elastomeric suspension (adapted from [9.209])

They come in various shapes and are simple to install, competitive in price, and when properly designed and manufactured, offer adequate support and protection to the conductor.

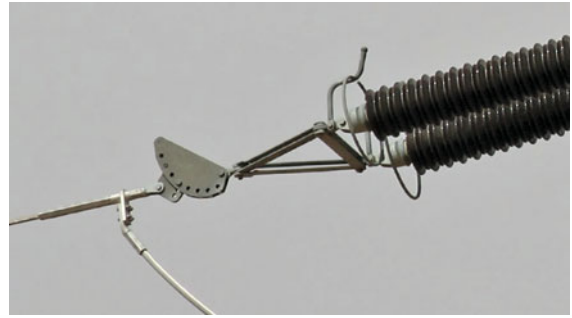
*Bolted clamps over armor rods* are used in around 25% of suspension clamp applications. They consist of helically formed wires which are wrapped around the conductor, effectively stiffening it at the suspension location. A larger-size clamp body is then placed over the armor rods.

*Helically attached elastomeric suspension (HAES)*, also known by its commercial name *Armor-Grip Suspension (AGS)* (Fig. 9.107), utilizes elastomeric inserts and helical attachment rods, which have proved to be beneficial in situations with severe conductor motions. This approach is probably used in around 10% of suspension applications, predominantly on OPGW and ADSS. On the other hand, it costs more than metal-to-metal clamps, and its installation is longer and more complicated due to several loose components, especially for hot-line installations. CIGRE recently published recommendations for safe design tensions with such clamps [9.209], establishing an allowable increase of 10–25% in  $H/w$  (Sect. 9.4.11) for the HAES.

*Elastomeric suspension (ES)* clamps, which utilize an elastomeric insert—but no helical rods—in the metallic clamp body, are becoming more popular. These clamps are lighter and cheaper than the HAES, and it takes less time to install them. In addition, fatigue tests have shown that the fatigue performance of conductors is improved with ES compared with standard clamps.

### Tension Clamps

Tension or dead-end clamps hold the conductor at support locations where the full mechanical tension of the conductor has to be sustained, such as at terminal towers, anticascading towers, and heavy angle towers. There are four main types of tension clamps:

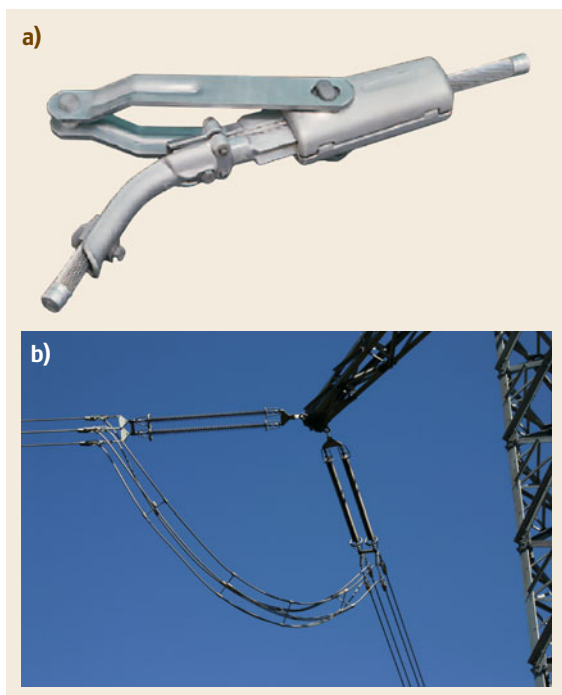


**Fig. 9.108** Compression-type tension clamp with sag adjusting plates

- Compression clamps
- Wedge clamps
- Helical terminations
- Bolted clamps.

*Compression clamps* (Fig. 9.108) are the most commonly used clamps worldwide. They are composed of two main parts: an aluminum or aluminum alloy tube, compressed over the conductor, and a steel terminal inserted into the aluminum tube and joined by compression to attach the clamp to the insulator string. In ACSR, the steel core is inserted into this terminal and also compressed. Compression takes place using hydraulic tools, whereby different dies are required for conductors of different sizes. This compression process is of great importance, as it is crucial for the long-term performance of the clamp. Evidently, readjusting the conductor or shifting the clamp after installation is not possible. Using compressed dead-end clamps, conductor sag adjustment can be performed by using turnbuckles or adjustable extension links or plates (Fig. 9.108).

*Wedge-type clamps* (Fig. 9.109) do not require special tools for installation and are relatively simply to fit. Correction of conductor sag can be achieved by shifting the clamp, so that sag adjusting plates or links are not necessary. Wedge-type clamps are in particular suited to monometallic conductors and to bimetallic conductors with more than one aluminum or aluminum alloy layer and low steel content. They consist of a wedge system tailored and fixed to the conductor and of a one- or two-piece clamp body with pins to which the terminal straps of the insulator set are attached. According to the design principle of the wedge-type clamp, the wedge system slides within the wedge body when the conductor tensile force increases. As a consequence, there is a progressive rise of the transverse force on the conductor, which will increase the holding force of the clamp accordingly. In case of bimetallic conductors, the steel core participates adequately and sufficiently at the to-

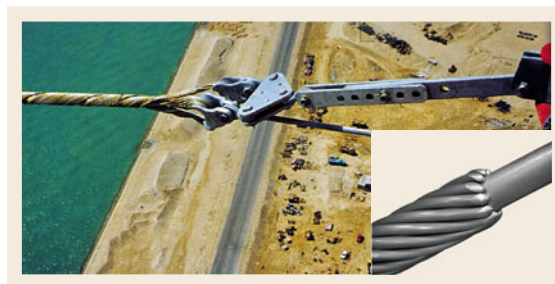


**Fig. 9.109a,b** Wedge-type clamp (a) and in service (b) at an angle tower with jumper (source Pfisterer Sefag)

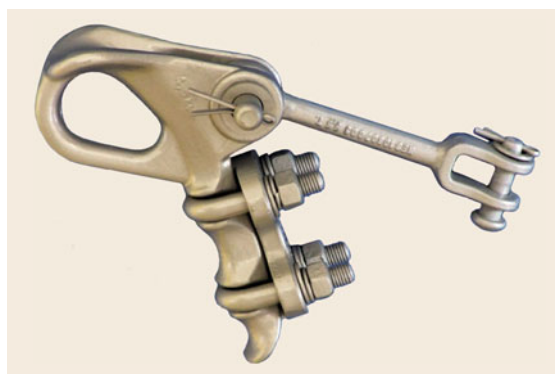
tal holding force due to frictional interlocking with the aluminum layers of the conductor. The greasing of the steel core may impair the extent of interlocking [9.210].

**Helical Terminations.** *Preformed dead-end rods* distribute the radial compression forces required for the friction locking over a longer section than dead-end clamps and, therefore, are in particular suitable for terminating metallic ground wires with optical fibers (OPGW), dielectric cables with optical fibers (ADSS), and other aerial cables. They are also often used in distribution lines.

Preformed dead-end rods also meet all the requirements on conductor terminations (Fig. 9.110). They can be simply installed by bare hand without tools and are widely used worldwide. They consist of several helically formed circular metal rods, the inner diameter being somewhat smaller than the outer diameter of the conductor to be terminated. The tensile forces are transferred onto the conductor through the helices by means of friction generated by radial pressure. The length and shape of the preformed dead-end rods keep the radial pressure at a low level and thus avoid any damage to the conductor. This inner surface of the preformed dead-end rods is sand-covered to increase the ultimate terminating forces. To meet the corona and RIV requirements and for safe handling, the rod extremities are



**Fig. 9.110** Helical termination with adjustable extension links at the Suez crossing; *inset*: rod ends with parrot bill shape



**Fig. 9.111** Bolted dead-end clamp (*pistol grip*)

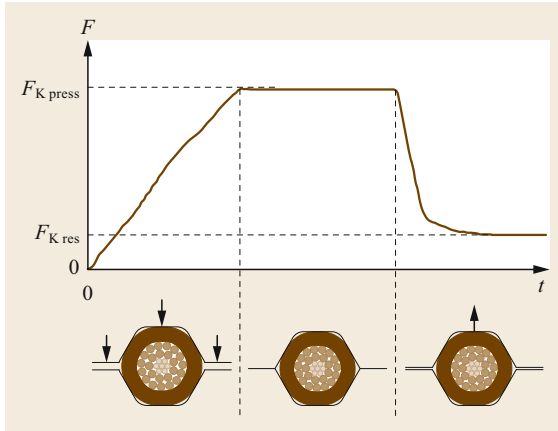
rounded, which is known as *ball-ending*. However, for most HV applications, the rod extremities assume a *parrot bill* shape to enhance the electrical performance of the inlet (Fig. 9.110).

Bolted dead-ends (Fig. 9.111) are occasionally used to terminate conductors for lower-voltage transmission and distribution lines. In such fittings, the conductor passes through this clamp without being cut. The bolt torque and the length of the clamp are calibrated to prevent slipping of the conductor and avoid any damage to its outermost layer. Correction of conductor sag can be achieved by shifting the clamp, so that, as for wedge-type clamps, sag adjusting plates or links are not necessary.

### Connectors

Connectors, also called joints or splices, are fittings that connect two pieces of the same phase conductor or the same earth wire or enable a branch-off or tap. There are two main types of connectors: full-tension and nontension.

Full-tension joints—and dead-end clamps—being tensile loaded, must sustain the conductor with 1.55 times the tensile forces in case of maximum load, or by 0.85 times 95% of its rated tensile force; the lower value



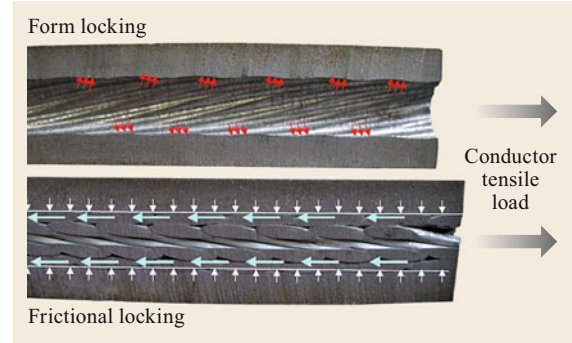
**Fig. 9.112** Compression force variation during the compression process (adapted from [9.211])

is decisive [9.63]. In addition, connectors intended to carry the rated current of the conductor should not, when subjected to the maximum continuous current in the conductor or to short-circuit currents, exhibit corresponding temperature rises greater than those of the associated conductor. Further, the voltage drop across current-carrying conductor fittings should not be greater than the voltage drop across an equivalent length of conductor.

Full-tension joints for high-voltage lines are in their great majority of compression type. These consist of an aluminum or aluminum alloy sleeve for monometallic conductors. Joints for ACSR conductors also have an additional steel sleeve for joining the steel cores. As described for dead-end clamps, the compression is applied using hydraulic tools with generally hexagonal dies.

The compression process in general, i.e., for all types of compression hardware, might look simple, but is in reality a complex problem in elastoplasticity, as during the compression process the joint and conductor experience high plastic deformations. The external compression force  $F_{K,press}$ , generated in most cases by hydraulic tools, is applied to the often hexagonal steel die and transferred via the tubular aluminum joint body to the conductor. In this way, the conductor and joint are plastically deformed and thus form-locked. When the external compressive load is removed, the conductor and joint spring back, whereby the elastic springback of the conductor is limited by the lateral rigidity of the joint. Thus, as the permanent compression force  $F_{K,res}$  between the conductor and joint is about 20% of the original compression force  $F_{K,press}$  (Fig. 9.112 [9.211]), also frictional locking opposes external tensile loads (Fig. 9.113 [9.212]).

However, experience has shown that the failure of a joint is usually the result of an increased electrical



**Fig. 9.113** Joint resistance to traction via form and frictional locking (adapted from [9.212])

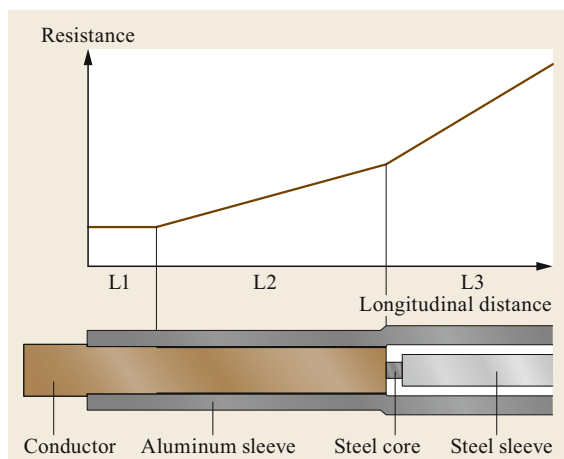
resistance due to corrosion, leading to an unacceptable increase in temperature and unstable mechanical conditions. Very few joints have been reported to display failure resulting purely from mechanical loads. The reported events involving mechanical failures have occurred on joints that have been asymmetrically installed, i.e., where the intrusion of the aluminum layers of an ACSR at one end of the joint has been less than 2.5 times the conductor diameter [9.213]. The most important qualification factor for the proper function of a joint is his electrical resistance. This can be calculated based on an empirical model (Fig. 9.114) [9.214]

$$R_s = \frac{1}{\frac{1}{R_c 2(L_1+x)} + \frac{1}{R_{asc} 2L_1}} + \frac{R_{con}}{D} 2L_2 + \frac{1}{\frac{1}{R_c 2L_2} + \frac{1}{1.08 + R_{asc} + 2L_2}} + R_{as} 2L_3, \quad (9.96)$$

where  $R_s$  is the joint resistance ( $\mu\Omega$ ),  $D$  is the conductor diameter (m),  $L_1$  is the length of the entrance (m),  $L_2$  is the length of the contact area (m),  $L_3$  is the length of the uncompressed part (m),  $x$  is the length of conductor outside the joint (m),  $R_c$  is the conductor resistance ( $\mu\Omega/m$ ),  $R_{as}$  is the aluminum sleeve resistance when uncompressed ( $\mu\Omega/m$ ),  $R_{asc}$  is the aluminum sleeve resistance when compressed ( $\mu\Omega/m$ ), and  $R_{con}$  is the contact resistance ( $\mu\Omega$ ).

For example, a new joint with dimensions  $D = 0.0286$  m,  $L_1 = 0.075$  m,  $L_2 = 0.155$  m, and  $x = 0.005$  m and partial resistances  $R_c = 67.4 \mu\Omega/m$ ,  $R_{as} = 19.5 \mu\Omega/m$ ,  $R_{asc} = 21.4 \mu\Omega/m$ , and  $R_{con} = 60$  n $\Omega$  has a resistance  $R_s = 13.76 \mu\Omega$ , which amounts to just 28% of the resistance of the same length of conductor, here an ACSR Zebra, with  $R_c = 49.54 \mu\Omega$ .

Publication [9.213] proposes the following acceptance criteria for joints on old transmission lines, which should trigger replacement of the joints:



**Fig. 9.114** Distribution of electrical resistance in a joint for ACSR (adapted from [9.214])

- For joints where a failure and a drop of the conductor have a high influence and endanger the reliability of the line:  $R_{\text{joint}} < 70\%$  of  $R_{j,T_j=T_c}$ , i.e. the—measured—joint resistance should be less than 70 % of the calculated resistance value at which the joint and the conductor would be at the same temperature
- For joints where a failure and a drop of the conductor have an influence and jeopardize the reliability of the line:  $R_{\text{joint}} < R_{j,T_j=T_c}$
- For joints where a failure and a drop of the conductor have a low influence on the reliability of the line:  $R_{\text{joint}} < R_{j,T_j=T_c+10\text{K}}$ ,

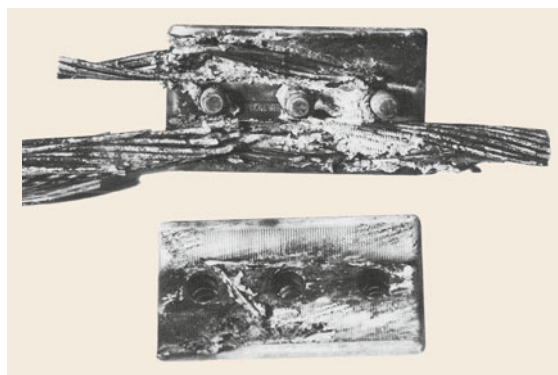
where  $R$  is resistance,  $T$  temperature,  $j$  joint and  $c$  conductor.

Recently, and with the increasing tendency of transmission line owners to operate their lines with conventional conductors at higher temperatures, even above  $100^\circ\text{C}$  [9.57], better understanding of the design and operation of the related joints has become necessary. In this regard, extensive research has revealed, based upon long-term tests with duration of up to 3.5 years [9.211], that properly designed and installed joints show stable long-term performance up to temperatures of about  $150^\circ\text{C}$ .

For nontension connections, such as in the jumpers at heavy angle, anticascading, or strain towers, so-called parallel groove clamps are often applied (Fig. 9.115). For such devices, a good and stable contact



**Fig. 9.115** Parallel groove clamp



**Fig. 9.116** Conductor failure in a parallel groove clamp due to faulty installation (source: Richard Bergner Holding GmbH & Co. KG, RIBE)

between the conductor and the clamp body is essential, and quite a few disastrous outages (Fig. 9.116) have been caused because of poor contact, fading contact force, and/or not properly cleaned conductor and clamp surfaces just before the installation.

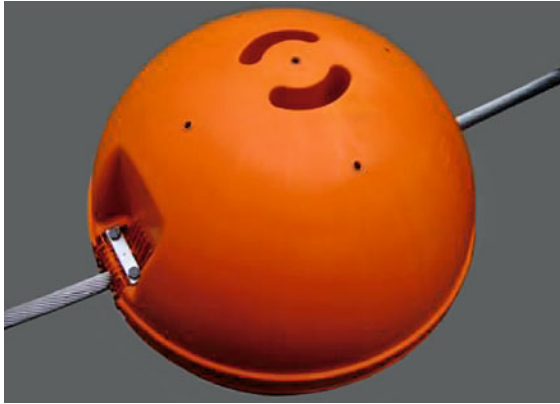
**Repair Sleeves.** When only a few elementary wires of the conductor outer layer are broken, repair sleeves can be used to restore 100% of the mechanical strength and the electrical resistance of the damaged conductor. Repair sleeves generally consist of two interlocking semi-circular elements that are installed by compression. Repair sleeves made from short armor rod sets are also used.

#### Fittings for HTLS Conductors

With the increased use of HTLS conductors (Sect. 9.4.9), best practices for their fittings become of importance. For this purpose, a worldwide survey has been launched and its results presented in [9.215]. The main findings therefrom are summarized here, although it must be considered that, since at the time of the survey the majority of HTLS conductors were in operation in Japan (things are different nowadays), the responses may overweight Japanese practices.

**Suspensions.** The most common type of suspension reported was a bolted clamp over armor rods, being used in over 70% of the responses. Bolted clamps were used in 19% of the responses, while elastomer cushioned clamps were used in 11% of the responses. The elastomers must be able to perform satisfactorily and not degrade over time at these high conductor temperatures.

**Dead-Ends.** The most common type of dead-end reported was a compression dead-end, being used in 62% of the responses. The balance of the responses used a wedge-type or bolted dead-end.



**Fig. 9.117** Warning sphere (note the intrusions on the top for easy handling) (source Pfisterer Sefag)

**Spacers.** The most common type of spacer reported was rigid (59%), followed by flexible spacers (30%). Articulated and spacer dampers made up the balance.

The use of rigid spacers on bundled spans is a typical Japanese practice: in other countries this practice is opposed in favor of spacer dampers with flexible and articulated spacers.

**Splices.** The two-piece compression splice was by far the most reported type, being used in 82% of the responses. Single-piece compression splices made up the balance.

**Dampers.** Stockbridge-type dampers were used in 32% of the responses. In some applications, a short set of armor rods was placed on the conductor before installing the clamp of the damper. Double torsional dampers were used in 54% of the cases (all from Japan). No dampers were reported in 7% of the responses. In some cases, helical dampers or festoon dampers were reported.

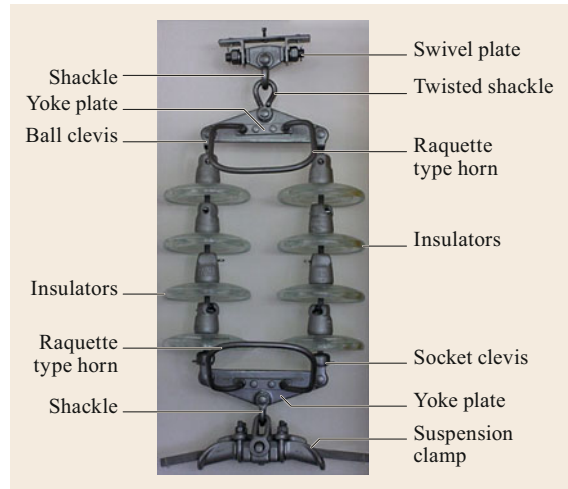
#### Aircraft Warning Markers

Aircraft warning markers (AWM) are highly visible indicators in daylight, used on power lines to warn low-flying airplanes and helicopters of the obstruction. The most common AWM is the warning sphere shown in Fig. 9.117. AWMs are covered in [9.216].

Night warning devices using lamps energized by the line voltage or current are also available and in use in many countries.

#### Fittings for Distribution Lines

Distribution lines [9.217] are in this context LV and MV lines with voltages up to and including 33 kV, where of-



**Fig. 9.118** Suspension string with string fittings (source U. Cosmai)

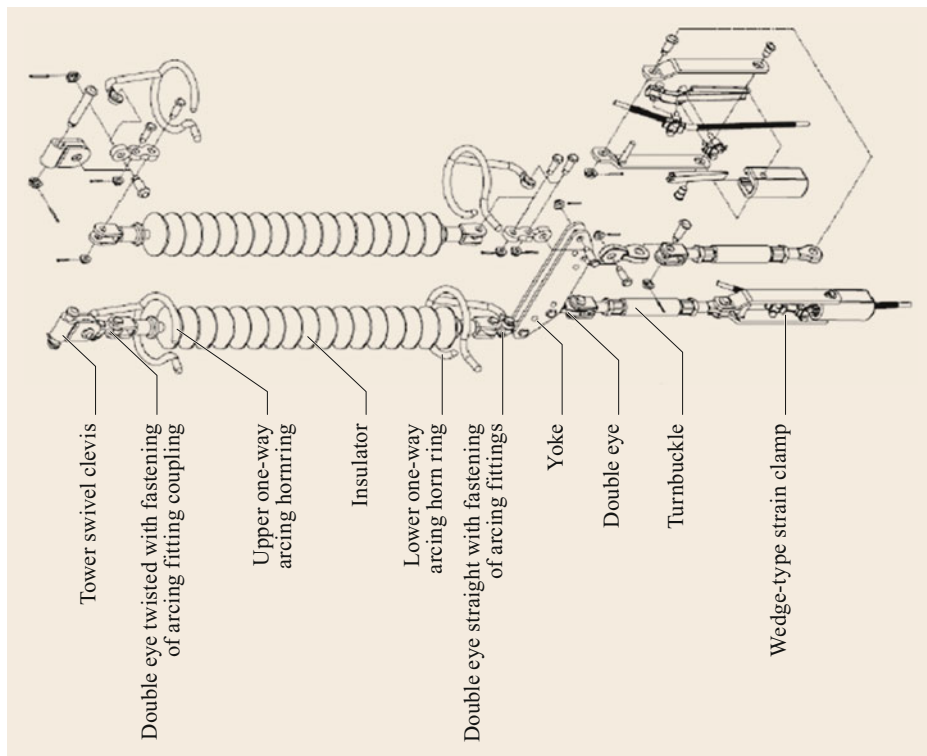
ten shackle (LV) and post (MV) insulators are used. In this case, the conductors are fastened to the insulators by either a soft wire binding or a so-called stirrup-type binding. With ACSR, it is customary to wrap the conductor with soft aluminum tape before fitting the stirrups. At straight line positions, the conductor is bound in the top groove of the insulator; at angle positions, this is done in the side groove so that the insulator and not the binder takes the conductor lateral pull. As an alternative, preform wire wraps are often used for securing the conductor to insulators for MV and LV lines.

#### 9.6.2 Fittings for Insulator Strings

String fittings connect the conductor fittings to the insulators and the insulators to the support. A subcategory are the insulator protection fittings. Figures 9.118 and 9.119 show a suspension and a tension string, respectively, where the different types of fittings are indicated.

String fittings are mainly produced from structural steel (straps, yoke plates), forged steel (ball fittings), and iron castings (sockets, clevises) and are then practically always hot-dip galvanized in accordance, for example, with [9.218] with a recommended minimum zinc thickness of 40–50  $\mu\text{m}$ .

These fittings must be able to withstand the specified mechanical loads as well as the electrical short current loads caused by power arcs and short-circuit conditions. Figure 9.120 shows the different types of couplings in use. The general requirements are specified in [9.206], while the standards for their dimensions are listed in Table 9.40.



**Fig. 9.119** 110-kV double tension string for twin bundle and the related string fittings (source Pfisterer Lapp)



**Fig. 9.120** Couplings for string fittings

**Table 9.40** Standards for dimensions of string fitting couplings

Fitting type	Applicable standard
Eye–clevis	IEC 60471 and DIN 48074: Eyes and clevises; connecting dimensions
Ball–socket	IEC 60120: Dimensions of ball and socket couplings of string insulator units ANSI C 29.2/52-3 for Ball 16, /52-5 for Ball 18, /52-8 for Ball 22 IEC 60372: Locking devices for ball and socket couplings of string insulator units – Dimensions and tests

Last but not least, string fittings must withstand short circuits, and the related temperature increase should not influence their mechanical functionality or

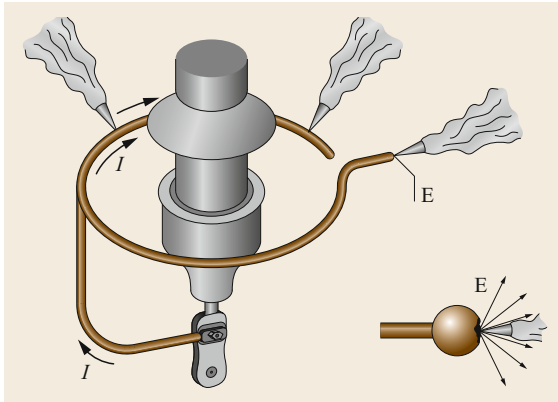
damage their protective zinc coating. For this purpose, their short-circuit current density should be limited to  $70 \text{ A/mm}^2$  (1 s) for fittings loaded in tension, and to  $80 \text{ A/mm}^2$  (1 s) for unloaded fittings, such as, for example, power arc protection fittings.

#### Insulator Protection Fittings

Insulator protection fittings, such as arcing horns and arcing rings, are indispensable components of insulator strings, in particular for high voltages. The voltage limit is almost a *philosophical* matter: The tendency in Europe is to use protection fittings for 50 kV and above, while in the Americas this often happens from 145 kV or even 220 kV upwards.

In any case, such fittings are installed in order to control power arcs due to:

- Overvoltages from lightning strokes and switching maneuvers
- Pollution flashovers
- Bridging of the air gap, i.e., by animals or so-called bird-streamers (feces of birds, released while flying off from the top of an insulator)
- Insulator failure in case of composite insulators because of *flashunder*
- Reduced clearances because of strong winds, ice shedding, or galloping



**Fig. 9.121** Schematic movement of the power arc (current  $I$ ) to the foot point by the fitting and correct shape of its extremity E (sacrificial sphere)

- Reduction of the insulation strength of the air gap, e.g., because of *sugar cane fires* below the line.

Power arcs can reach temperatures above 5000 K, thus the main duty of arc protection fittings is to speedily take over the arc and move it away from the insulator, so that it will not be thermally overstressed, with porcelain and glass being far more sensitive than composite insulators in this regard. This is done by offering the arc a conductive path and a suitable burning point in the form of a sphere, i.e., with enough sacrificial material (Fig. 9.121 [9.219]). The material loss at the end burning point can be calculated for steel with  $0.4 \text{ cm}^3/(\text{kA s})$  and for aluminum with  $1.4 \text{ cm}^3/(\text{kA s})$ ; For example, for 420 kV, a sphere diameter of 80 mm is required for a RIV level of 40 dB. This diameter far exceeds the above-mentioned requirements for the material loss caused by the power arc.

Steel is the preferred material versus aluminum for insulator protection fittings, for the following reasons:

- The speed of arc root movement is higher for steel by—empirically determined—50%. This reduces the thermal effect of the power arc on the protection fitting, while for aluminum, there is an unfavorable combination of lower speed and lower melting point.
- The combustion heat of aluminum is five times higher than that of steel. This correlates with a higher heat radiation intensity of burning aluminum as well. This increases the risk of insulator damage, as evaporated aluminum can precipitate onto the insulator surface and lead to reduced insulation performance.
- The higher thermal conductivity of aluminum would lead to a faster heat transfer into the struc-



**Fig. 9.122** C-ring for combined power arc and corona protection (source Pfisterer)

ture of the bulk material, and due to its low melting point, the aluminum profile can be deformed.

Consequently, an aluminum arc protection device equivalent to a steel design would require more material, which would negate the weight advantage of aluminum.

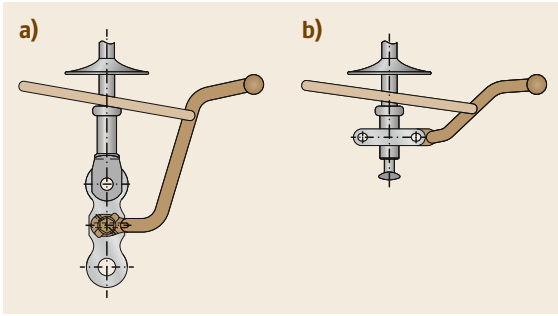
Power arc protection fittings should preferably have an orientation so that the forces during a power arc event support the movement of the power arc away from the insulator. Also, if possible, the end burning point should not face towards the conductor, which will prevent the power arc from moving onto the conductor or its damage by flying molten steel particles from the fitting.

For higher operating voltages, the field gradient at the insulator extremities, and primarily at the hot end, reaches values above the corona inception voltage. This is more critical for composite insulators, because of the small diameter of their core compared for example with porcelain longrods. Consequently, their grading rings should reduce the field gradient on the polymeric material of the insulator below the recommended maximum of  $4.5 \text{ kV/cm}$  [9.220].

Arc protection fitting designs are also available for addressing both tasks, i.e., power arc and corona field control, such as the so-called C-ring (Fig. 9.122).

The best practice for composite insulators is to not attach the power arc protection fittings directly to the insulator end fitting (Fig. 9.123a), as if this is not the case (Fig. 9.123b), the full short-circuit current will pass through it and possibly overheat and radially expand it to the extent that the core will slip out and the insulator will lose its mechanical integrity. Also, the glass-transition temperature of the rod may be ex-





**Fig. 9.123a,b** Best practice for positioning an arc protection fitting on a composite insulator end fitting. **(a)** Configuration for high-current power arc, **(b)** configuration for low-current power arc

ceeded. The trade-off is a longer insulator string, which can become problematic in some cases, such as when replacing conventional insulators by composites, because of clearance issues. Recommendations on the use of power arc protection fittings for composite insulators have been published in [9.221, 222].

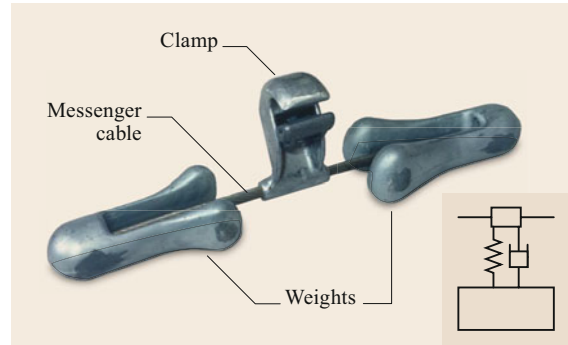
### 9.6.3 Vibration Dampers

Since the early days of high-voltage overhead transmission, wind-induced vibrations (Sect. 9.4.11) have been a major cause of concern to line engineers, as, if not controlled, they can cause wire and in extreme cases conductor failures due to fatigue. An early requirement in the industry was thus to develop suitable vibration dampers.

#### Stockbridge Dampers

The most widely used damper is the Stockbridge damper, so named for its inventor [9.223]. The Stockbridge damper was invented in the 1920s by George H. Stockbridge, who was an engineer for Southern California Edison. Stockbridge obtained US patent 1675391 on 3 July 1928 for a *vibration damper*. His patent described three means of damping vibrations on lines: a sack of metal punchings tied to the line, a short length of cable clamped parallel to the main cable, and a short length of stranded cable called a *messenger* with a concrete mass fixed at each end. It would be this last device that developed into the widely used Stockbridge damper (Fig. 9.124).

**Basic Theory.** The Stockbridge damper is a so-called tuned mass damper (TMD), i.e., a device that suppresses the vibration of a primary structure, here the conductor, by transferring its energy to a secondary mass. In a first approximation, the Stockbridge damper can be modeled as a spring–mass–damper system,



**Fig. 9.124** Stockbridge damper as a mass–spring system

where the counterweight is the mass, and the messenger wire the spring (Fig. 9.124). The energy dissipated by friction at the interlayer contact points of the messenger wires in the form of heat is represented in the schematic inset in Fig. 9.124 with a viscous damping dashpot. The Stockbridge damper strongly influences the vibration at its point of attachment to the conductor through the application of an interface force and an interface bending moment, causing a local distortion of the deflection shape of the conductor.

Neglecting the mass of the messenger cable and of the attachment clamp and assuming the messenger wire to be linear elastic with a constant bending stiffness and no self-damping, the eigenfrequencies of one half of the Stockbridge damper can be calculated as [9.101]

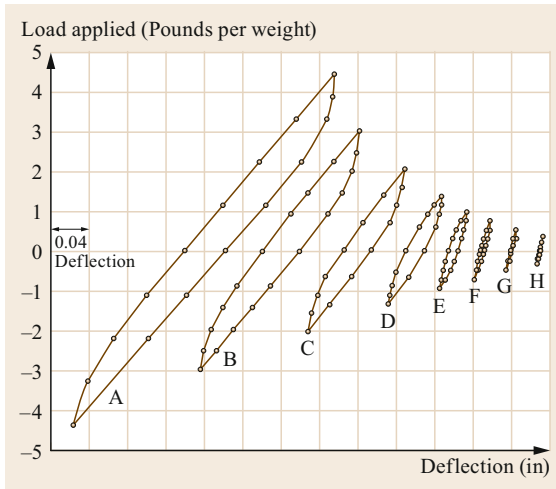
$$\omega_{1,2}^2 = 2k \frac{\frac{1}{3}L^2M + J_a - LGM}{MJ_a - M^2G^2} \mp \frac{\sqrt{(\frac{1}{3}L^2M + J_a - LGM)^2 - \frac{1}{3}L^2(MJ_a - G^2M^2)}}{MJ_a - M^2G^2}, \quad (9.97)$$

and the spring constant  $k$  of the messenger cable as

$$k = \frac{3E_m J_m}{L^3}. \quad (9.98)$$

$O$  is the center of gravity of the counterweight,  $O'$  is the attachment point of the cable to the counterweight,  $G$  is the distance between  $O$  and  $O'$ ,  $M$  is the counterweight mass,  $J_a$  is the moment of inertia of the counterweight about the point  $O'$ ,  $L$  is the length of the messenger cable,  $E_m$  is the Young's modulus of the cable, and  $J_m$  is the moment of inertia of the cross section of the messenger cable (considered as a homogeneous beam).

In reality, the bending behavior of the messenger cable obeys a similar bending process as explained



**Fig. 9.125** Load–deflection curves obtained from bending tests on a Stockbridge damper

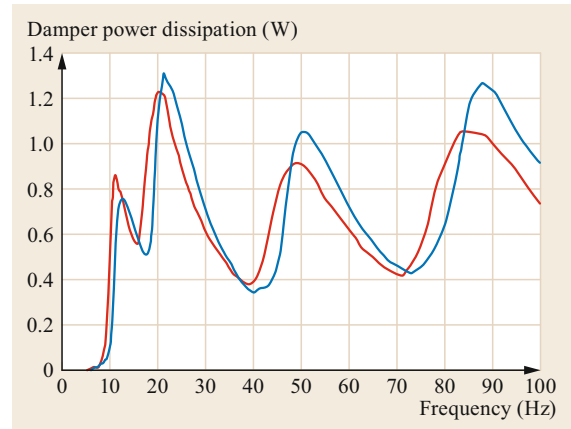
in [9.102, 103] for conductors; i.e., the messenger bending stiffness is nonlinear, specifically it decreases, because of the wire slippage, with increasing curvature or deflection [9.224]. In other words, if we consider the messenger wire as a spring, it becomes *softer*, which is evident in Fig. 9.125 [9.98, 99] from the decreased slope of the bisectors of the hysteresis curves. Because of this, the resonance frequencies of the damper will move toward lower values. This will beneficially increase the damper response and reduce the vibration amplitude as, at the same time, the energy dissipated by the damper, equivalent to the area of the hysteresis in Fig. 9.125, will considerably increase. Thus, the effect of nonlinearity is to make the damper self-tuning.

Equation (9.99) defines and Fig. 9.126 presents  $P_d$ , the power dissipated by the damper over a complete cycle, and the resonance frequencies of a Stockbridge damper when new and after a fatigue test as prescribed in [9.225]

$$P_d = \frac{1}{2} F_c v_c \cos \varphi, \quad (9.99)$$

where  $F_c$  is the force at the damper clamp,  $v_c$  is the clamp velocity, and  $\varphi$  is the phase angle between the force and velocity.

Another important characteristic of a Stockbridge damper is its mechanical impedance  $Z_d(\omega)$ , i.e., the relationship between the driving force  $F_c$  at the damper clamp, the clamp velocity  $v_c$ , and the phase angle  $\varphi$  between said force and velocity. The damper impedance is frequency but also clamp velocity dependent



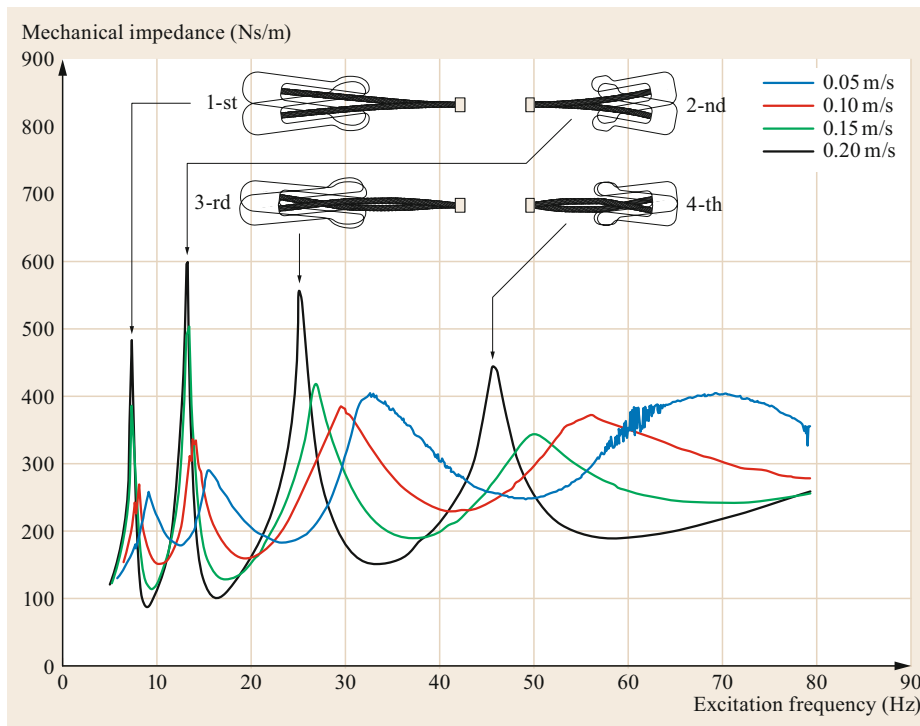
**Fig. 9.126** Power dissipated by a Stockbridge damper before (blue) and after (red) fatigue test (source RIBE)

dent (Fig. 9.127 [9.226])

$$Z_d(\omega) = \frac{F_c}{v_c} e^{j\varphi}. \quad (9.100)$$

The peaks in this figure correspond to the eigenmodes of the damper, also shown schematically on top, which can be reasonably excited in the aeolian vibration regime: At the first and second (lower) eigenfrequencies, the outer ends of the two weights are the points of maximum motion, whereas at the second and fourth (upper) eigenfrequency, the motion of the weights is a rotation about their own center of gravity. For a given vibration amplitude of the damper clamp, e.g., when tested on a shaker, the greatest dissipation occurs at these resonant frequencies. However, they may not be the frequencies providing greatest dissipation when the damper is attached to a span, because if the force resonances have sharp peaks, the damper clamp will be hard to drive since it then presents high mechanical impedance to the vibrating conductor. On the other hand, reduced damper performance also occurs when the damper is too easily driven by the conductor and does not produce sufficient energy dissipation. This may happen at frequencies between and outside the resonances.

**Damper Design.** A good damper design has thus to consider the proper choice of damper weight, shape, and moment of inertia in such a way that it should not resist too *softly* between resonances neither too *stiffly* at resonances, as well as the sharpness and spacing of the resonances. For the latter, two approaches are currently used. One is to employ closely spaced resonances, so that at least one is partly excited. The other is to use a special messenger cable with a high loss factor and



**Fig. 9.127**  
Impedance of  
a four-resonance  
(4-R) Stockbridge  
damper at different  
clamp velocities

thus produce broad, low resonance peaks in the overall damper response.

An interesting approach is to design dampers by taking advantage of the electromechanical analogy, i.e., the fact that the mechanical relationships for a vibrating conductor and the electrical relationships for a long transmission line are equivalent [9.227, 228]. Specifically and in a first approximation, the damper impedance (9.100) should be in the range of the wave impedance of the conductor (9.75) in order to provide optimum damping. However, the former varies with frequency and the second with changes in unit mass and tension (e.g., by ice loads), thus perfect matching is only possible for a specific vibration frequency. Nevertheless, a properly designed vibration damper can provide effective damping when the damper impedance is in the range of 0.5–3 times the characteristic impedance of the conductor [9.229].

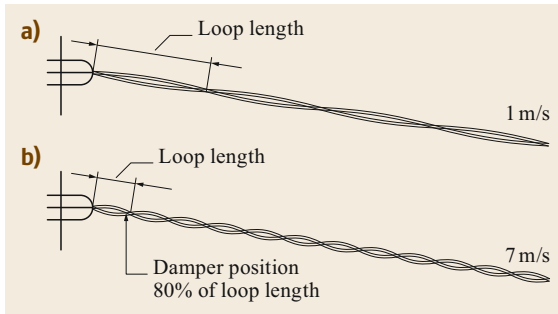
**Damper Placement.** Even the best damper will malfunction if not placed properly on the conductor. For this, there are two approaches: In the first, dedicated software is applied to calculate the damper location on the conductor using adequate modeling of the conductor and damper [9.104]. This approach is particularly useful in critical cases, such as long spans with high conductor tension. The second approach, applicable in *standard* situations, is more practical and is

based upon experience and a good understanding of the physics involved. Specifically, regardless of how effective a damper is, it cannot be expected to reduce the amplitude of vibration to zero, as a small amount of vibration will always be necessary to actuate the damper. In addition and as explained above, the damper is not equally effective at all the vibration frequencies that the conductor will encounter. In this sense, it is generally accepted that, if the damper is placed at a distance  $S_d$  from the clamp equal to 80% of the shorter vibration loop, i.e., at the highest vibration frequency occurring at the highest wind velocity  $v_{w_{\max}}$  causing aeolian vibrations, normally 7 m/s (Sect. 9.4.11), it should provide sufficient damping in the relevant wind velocity range of 1–7 m/s (Fig. 9.128). Combining (9.76) and (9.79) yields

$$S_d = \frac{2d_c}{v_{w_{\max}}} \sqrt{\frac{T}{m}}. \quad (9.101)$$

An average value for  $S_d$  is 2 m.

If a second damper is deemed necessary, e.g., for span lengths above 400 m, then it should be placed approximately at the same distance from the first damper towards the span. In spans to be equipped with two dampers, the best solution is to apply one damper per span end, positioned at the same distance from each end. For tension–suspension spans, when using one



**Fig. 9.128a,b** Recommendations for Stockbridge damper placement: vibration profile under low winds (a) and high winds (b)

damper, the damper should be placed near the suspension clamp. Since tension clamps are vibrationwise less critical than suspension clamps, the installation of a vibration damper at a tension clamp as well as near other fittings such as warning spheres can be based on the recommendations above for suspension clamps. Table 9.41 summarizes recommendations for the necessary number of dampers by a well-known utility [9.230].

**Damper Materials and Construction.** For the *messenger cable*, so called because Stockbridge's original model used the type of cable employed, at that time, in overhead telephone lines, galvanized steel is most common, although the 7-strand messenger cables originally employed have now been replaced by 19-strand cables because of their superior damping capacity (more interwire contact points). Messenger cables made of stainless steel are used in polluted areas.

*Damper clamps* must be as light as possible, and care must be exercised in selecting the clamp materials, especially those that are in contact with the conductors, to avoid any corrosion problems. For the clamps, primary aluminum alloys are used for aluminum- and steel-based conductors, with only a few cases of steel clamps for steel shield wire. Clamps are either cast directly onto the messenger cable or cast separately and then assembled onto the messenger cable by compression. They are designed in a cantilever hook shape that



**Fig. 9.129** Cantilever hook clamp of a Stockbridge damper (source Pfisterer Sefag)

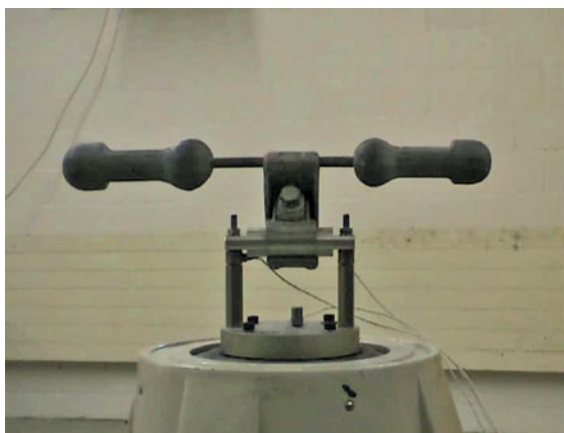
allows the damper to be easily attached onto the conductor during installation (Fig. 9.129). Also, in case of clamp loosening, the damper may slip toward the center of the span, but the hook clamp prevents the damper from falling to the ground. Damper clamps contain a single bolt of galvanized steel, with a plain washer and a split washer or a *Belleville washer*, and must be designed to avoid losses of clamp pressure and to prevent loosening.

The first *damper weights* were bell-shaped masses of galvanized cast iron, installed on the messenger cable by means of tapered aluminum sleeves. Later, an assembly technique based on pouring zinc alloy or aluminum between the messenger cable and the hole in the mass was developed. Alternatively, zinc-aluminum alloys with density similar to cast iron have been used for the masses, being cast directly on the messenger cable. Also, forged steel masses, or extruded steel rods or tubes bent upwards, have been used; these masses are compressed onto the messenger cable.

**Other Types of Dampers.** Over the years, other types of dampers have also been developed, such as the Elgra damper, the Haro damper, the festoon damper, the tor-

**Table 9.41** Number of dampers depending on span length and terrain (adapted from [9.230])

Terrain	Vegetation	Span length (m)			
		< 150	150–350	350–550	> 550
Hilly or valleys parallel with the line	Other type of vegetation from dense forest on one side to flat terrain with no obstacles	0	1	2	2
Flat or valleys perpendicular to the line	Other type of vegetation from dense forest on one side to flat terrain with no obstacles	1	1	2	4
Lakes or water courses		1	2	2	4



**Fig. 9.130** Shaker test of a Stockbridge damper (source Pfisterer Sefag)

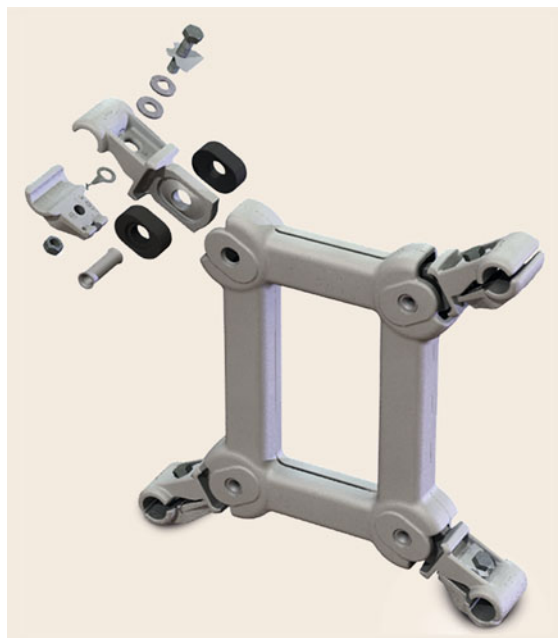
sional damper, dampers with elastomeric articulations, spiral impact dampers, and Bretelle dampers [9.214]. However, none of these could really compete with or replace the Stockbridge damper, and their use has been restricted to certain countries and/or special applications, like the festoon damper for long fjord crossings in Norway and the Bretelle damper in France.

**Damper Tests.** Dynamic testing of dampers takes place according to [9.225]. Therein the following test methods are described:

- Inverse standing wave ratio (ISWR) test
- Power test
- Decay test
- Forced response (shaker) test (Fig. 9.130).

The latter is quite popular, as it allows the dynamic characteristics of the damper to be established and is at the same time easier to accomplish in comparison with the other tests, which require the damper to be tested when attached to the conductor in a laboratory test span. However, the drawback of the shaker test is that only the vertical motion of the damper can be considered, whereas in reality the damper also rotates slightly, thereby providing an additional contribution to the energy dissipation, especially when the damper is close to a vibration node of the conductor.

The shaker test is also important in order to establish the fatigue performance of the damper. A sign of fatigue in the messenger cable of Stockbridge dampers is the drooping or sagging of the masses. Such damage may be caused by excessive vibration levels, an inadequate damping system, or poor quality of the damper. It may also be caused by gallop-



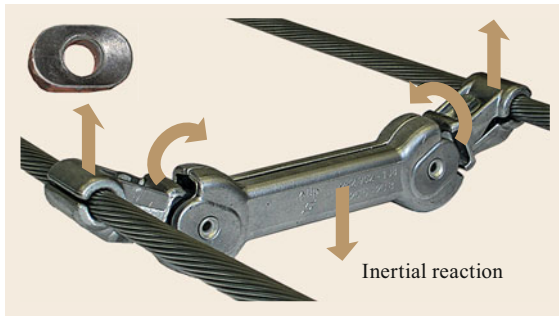
**Fig. 9.131** Typical spacer damper for quad bundles (source Pfisterer Sefag)

ing or ice-shedding events. In corrosive environments, e.g., near the sea, corrosion of the messenger cable may be a failure mechanism. In these environments, stainless-steel messenger cables can be advantageously used.

From the two alternative methods proposed in [9.225] for the damper fatigue test, the most commonly used is the one which excites vibration with constant amplitude of 0.5 mm (zero peak) at the higher resonant frequency of the damper and accumulates 10 million cycles.

### Spacers and Spacer Dampers

Early in the 20th century, when, in order to transmit more power, line voltages started to increase dramatically, limits because of corona and surge impedance soon became prominent, the solution to both issues being the introduction of bundle conductors [9.78–80] (Sect. 9.4.7), and with them, a new type of fittings, i.e., spacers and spacer dampers. Their main duty is to maintain the design geometry of the bundle and at the same time avoid clashing of the bundle subconductors because of wake-induced oscillations (Sect. 9.4.11), gusts, or short circuits as well as twisting of the bundle because of unequal ice loads. At a later stage and in a clever design move, damping properties were also integrated into the spacers to suppress disturbing aeolian vibrations of the subconductors; they became spacer dampers. A spacer damper is a device which keeps the



**Fig. 9.132** Working principle of spacer dampers, shown for a twin spacer damper. *Inset*: elastomer bushing (source Pfisterer Sefag/U. Cosmai)

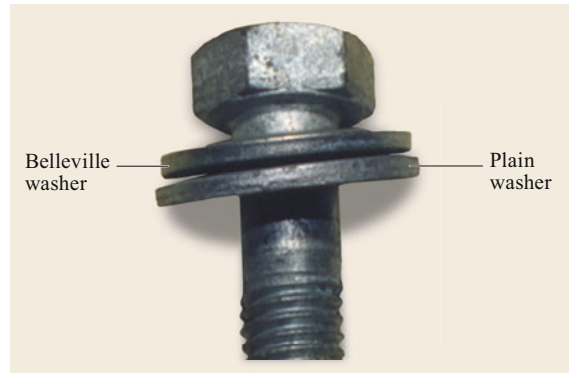
subconductors of a bundle apart in a given geometrical configuration and at the same time can reduce aeolian vibrations and subsan oscillations of the subconductors.

Nowadays, the vast majority of bundle fittings are spacer dampers, with the possible exception of twin bundles. For these, flexible, articulated, or semirigid spacers are often combined with Stockbridge dampers placed on each subconductor. An exploded drawing of a typical spacer damper for quad bundles is shown in Fig. 9.131.

In general, spacers and spacer dampers must withstand the mechanical, electrical, and environmental loads imposed during installation, operation, and maintenance, without failures and without damaging the conductors.

A good reference on various designs, materials, and service experience of spacers and spacer dampers can be found in [9.125]. For reasons of brevity, we present therefrom two important features, viz. the properties of the elastomer material used for vibration damping and the proper clamp design, as the latter has been in many cases a cause of concern and serious damage to the related conductors.

**Elastomer Bushing and Clamp Lining.** The working principle of spacer dampers, shown exemplarily in Fig. 9.132 for a twin spacer damper, is that, during aeolian vibration of the attached subconductors, the inertial forces of the the spacer damper frame initiate rotation of the spacer damper clamps, which leads to dissipation of energy as the related articulations contain damping elements, generally made of elastomer (Fig. 9.132, inset). The most widely used elastomers are chloroprene (neoprene) rubber, EPDM rubber, NBR (nitrile butadiene rubber), silicone rubber, and special compounds. These elastomers should be semiconductive, because nonconductive elastomers are liable to experience electrical discharges as a result of the pollutants



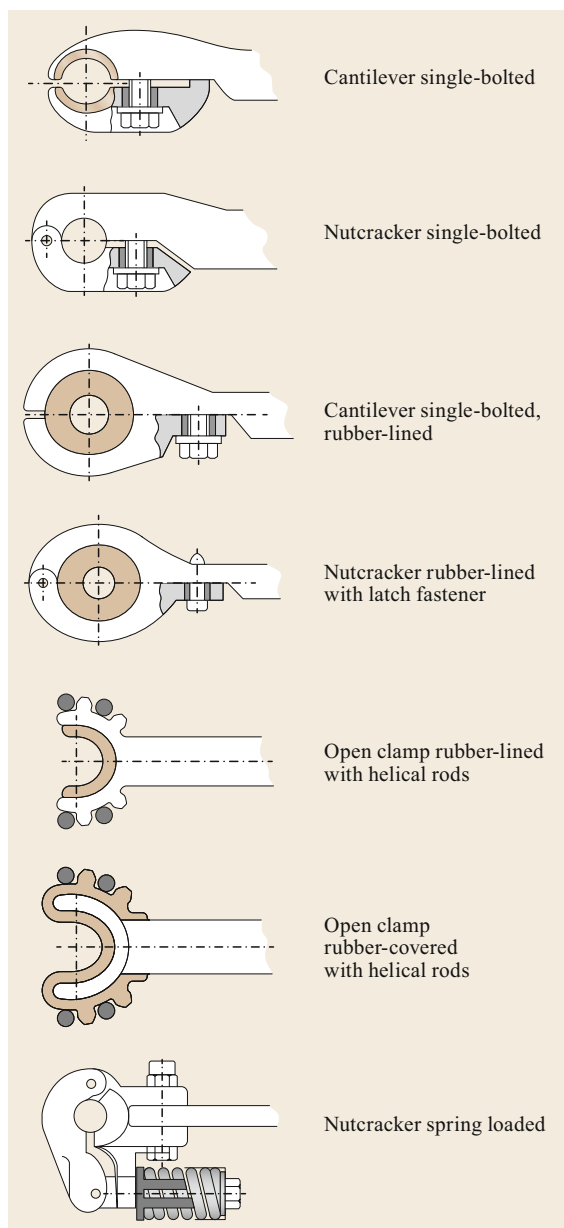
**Fig. 9.133** Spacer damper clamp bolt with Belleville and plain washer (source U. Cosmai)

coating their surface. Such discharges encourage further growth of carbon deposits, leading to escalation of the tracking situation and generating radio interference and audible noise. Elastomers with too high a carbon content and, therefore, too high a conductivity, are subjected to overtemperatures that can cause accelerated aging and galvanic corrosion between the elastomer and spacer components, as well as the conductor strands in case of elastomer-lined clamps. Elastomers for spacers have to withstand contact with the oils and greases used in conductors and stringing machinery. In addition, the elastomers should not absorb water. Damping elastomers used in spacer damper articulations should exhibit high hysteresis losses, appropriate stiffness, and good fatigue resistance over the entire range of service temperature. Last but not least, they should be suitably protected, as corona activity on conductors and fittings increases the presence of ozone, which rapidly deteriorates organic materials; these materials also need to be protected from ultraviolet radiation.

The dynamic behavior of spacers as related to wind-induced vibrations is a complex matter and lies beyond the scope of this book. Different methodologies are available and are well described in [9.81, 104].

**Clamp Design.** Spacer and spacer damper clamps should be designed in order to:

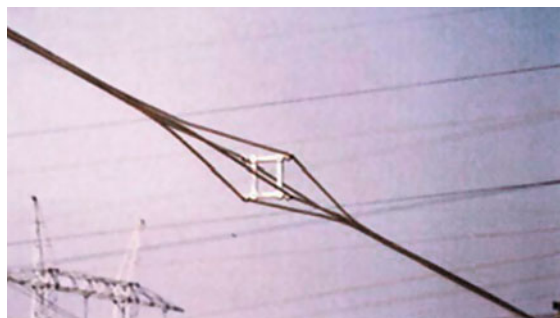
- Avoid high, localized clamping stresses; this is a function of clamp length, clamping force (bolt torque), and clamp geometry.
- Avoid damage to the conductor due to clamping surface irregularities; the conductor contact surfaces must be smooth.
- Minimize the possibility of incorrect installation.
- Ensure that, if feasible, all components are captive; bolts may be peened or, if in a blind tapped hole, secured by an O-ring to the clamp keeper, which



**Fig. 9.134** Different designs of spacer damper clamps (source U. Cosmai)

itself may be secured to the body of the clamp by a tie or captive hinge.

- Incorporate a stored energy mechanism, like a Belleville washer, to prevent clamp loosening due to temperature cycling and conductor creep. This is a conical spring washer and should be supported by a plain washer (Fig. 9.133).
- Exert an adequate, nondamaging long-term axial and torsional grip on the conductor.



**Fig. 9.135** Subconductor clashing during short-circuit test

- Be manufactured from a material that is compatible with the conductor and generally avoids corrosion.
- Be profiled to minimize the possibility of corona and RI discharge at specified line voltages.
- Be easily installed on the conductor, possibly also using hot line/helicopter techniques.
- Facilitate ground-level inspection to verify correct installation.

These requirements have led to various designs of space damper clamps, as shown in Fig. 9.134.

One important design load on spacers and spacer dampers is caused by electromagnetic forces arising from short-circuit currents in the subconductors of the bundle. Short-circuit currents cause strong attractive forces between the subconductors, which induce large deflections and even clashing of the subconductors (Fig. 9.135 [9.81]), consequently considerably increasing the subconductor tension. The latter results in significant compressive loads on the clamp arms of the spacer, which can reach up to 15 kN and above for short-circuit currents in the region of 50 kA, which are not uncommon nowadays. These forces are usually calculated by the method proposed in [9.231], although this underestimates their magnitude by about 25–30% for short subspans, e.g., in jumper locations, and high short-circuit currents, e.g., at towers close to a substation. In such cases, it is recommended to apply more sophisticated methods [9.232] that consider the subspan length. This is important because, the shorter the subspan, the greater the pinch force  $F_{pi}$  and the greater the compressive load  $F_c$  on the spacer or spacer damper.

#### 9.6.4 Tests

Conductor and insulator fittings should be tested in accordance with the requirements of [9.206] or equivalent standards. Specific tests for vibration dampers and spacers can be found in [9.225] and [9.234], respectively. Tests relevant for new conductor and insulator fittings are listed in Table 9.42 [9.206].

**Table 9.42** Tests on new fittings (adapted from [9.206])

	Type of test	Visual examination	Verification of dimensions and material	Hot-dip galvanizing	Non-destructive testing	Damage and failure load test	Slip test	Clamp bolt tightening test	Tensile test	Test of attachment point	Magnetic loss test	Heart cycle test	Corona and RIV test
Insulator and earth wire fitting	T	X	X	X <sup>a</sup>	X <sup>a</sup>	X	-	-	-	X	-	-	X <sup>a,b</sup>
	S	X <sup>c</sup>	X	X	X <sup>a</sup>	X	-	-	-	X <sup>a</sup>	-	-	-
	R	X <sup>a</sup>	X <sup>a</sup>	-	X <sup>a</sup>	X <sup>a,d</sup>	-	-	-	-	-	-	-
Suspension clamps	T	X	X	X <sup>a</sup>	X <sup>a</sup>	X	X	X	-	-	X <sup>a</sup>	-	X <sup>a,b</sup>
	S	X <sup>c</sup>	X	X	X <sup>a</sup>	X	X	X <sup>c</sup>	-	-	-	-	-
	R	X <sup>a</sup>	X <sup>a</sup>	-	X <sup>a</sup>	X <sup>a,d</sup>	-	-	-	-	-	-	-
Tension-proof joints and clamps	T	X	X	X <sup>a</sup>	X <sup>a</sup>	X	-	X	X	X	X <sup>a</sup>	X <sup>e</sup>	X <sup>a</sup>
	S	X <sup>c</sup>	X	X	X <sup>a</sup>	X <sup>a</sup>	-	X <sup>c</sup>	X	X <sup>a</sup>	-	-	-
	R	X <sup>a</sup>	X <sup>a</sup>	-	X <sup>a</sup>	-	-	-	-	X <sup>a,d</sup>	-	-	-
Partial tension-proof fittings	T	X	X	X <sup>a</sup>	X <sup>a</sup>	-	-	-	X	-	-	X <sup>e</sup>	X <sup>a</sup>
	S	X <sup>c</sup>	X	X	X <sup>a</sup>	-	-	-	-	-	-	-	-
	R	X <sup>a</sup>	X <sup>a</sup>	-	-	-	-	-	-	-	-	-	-
Repair sleeves	T	X	X	X <sup>a</sup>	-	-	-	-	X	-	-	-	X <sup>a</sup>
	S	X <sup>c</sup>	X	X	-	-	-	-	X	-	-	-	-
	R	X <sup>a</sup>	X <sup>a</sup>	-	-	-	-	-	-	-	-	-	-
Insulator protective fittings <sup>f</sup>	T	X	X	X <sup>a</sup>	X <sup>a</sup>	X <sup>a</sup>	-	-	-	-	-	-	X <sup>a,b</sup>
	S	X <sup>c</sup>	X	X	X <sup>a</sup>	X <sup>a</sup>	-	-	-	-	-	-	-
	R	X <sup>a</sup>	X <sup>a</sup>	-	X <sup>a</sup>	X <sup>a</sup>	-	-	-	-	-	-	-

T: type tests; S: sample tests; R: routine tests

<sup>a</sup> By agreement between purchaser and supplier

<sup>b</sup> Only in connection with complete insulator set <sup>c</sup> Inspection by attributes only

<sup>d</sup> Only as regards damage load test

<sup>e</sup> Only for current-carrying joints

<sup>f</sup> Including field grading fittings



**Table 9.43** Tests on aged fittings (adapted from [9.233])

Type of test	Activity	Which fittings	Measurement or observation	Standard
Visual inspection	General condition of surface	All	0–25/25–50/50–75/ 75–100% Cracks, abrasion, indication of rocking Punctures, welding points	
	Percentile of corroded surface (%)	All		
	Mechanical damage	All		
	Electrical damage	All		
	Wear of holes	All		
Dimensional inspection	Welding of string components (due to short circuit) such as shackles to eye fittings	Shackles, bolts, plates, and eyes		
	Diameter of bolt	Bolts	Wear on diameter of bolt and remaining area Wear on diameter of bolt and remaining area	
	Diameter of pin	Pin fittings		
Diameter (ovality) of holes	All holes			
Corrosion protection	Thickness of remaining zinc layer	All steel parts		ISO 1461
Nondestructive tests	Penetration tests to detect tiny cracks	All parts		
Mechanical tests	Tensile test to discover: Fracture surface	All where appropriate to take samples		Samples according to DIN 50125 Calculation and setup: EN 10002/1
	Brittleness	All where appropriate to take samples		
	Elongation	All where appropriate to take samples		
	Yield strength	All where appropriate to take samples		IEC 61284
	Breaking strength	All where appropriate to take samples		EN 10045
Alternative: Metallurgical investigation	Impact test (Charpy)	All where appropriate to take samples		
	Metallographic examination	All		
	Spectral analysis to investigate the carbon and nitrogen content			

In addition, and as in many parts of the world lines are about to exceed or have already exceeded their projected design life of say 40–50 years, testing on aged fittings, i.e., fittings which have been in service for more than

30 years, are also of importance, as the failure of a fitting can have catastrophic consequences. Recommendations for such tests, based on international best practices, can be found in [9.233] and are listed in Table 9.43.

## 9.7 Supports and Foundations

Overhead line supports are definitely the most impressive components of an overhead line. They are also, together with the conductors, the most expensive line components. Over the years, their shape and materials have undergone a great development. In recent decades, so-called esthetic supports have come to play an ever-

increasing role in line design, as they are a serious option to address the public sensitivity to environmental issues. Since supports are earthed, they have to safely sustain and conduct lightning strokes to ground, thus their proper earthing is very important. However, above all, line supports carry (in the full sense of the word)

a great responsibility for the reliability and safety of the line, as their failure can have catastrophic consequences. On the other hand, to properly support the line conductors, supports require solid foundations into the ground. The operational safety of the supports is thus irrevocably connected with the stability of their foundations. In addition, foundation movements can cause severe and unexpected loads on the supports and thus have to be understood and controlled.

In this regard, this section covers:

- Support types (poles, steel lattice towers, new materials)
- Design
- Esthetic supports
- Prototype tests
- Foundations
- Grounding
- Earthing.

### 9.7.1 Wood Poles

Wood was the first material to be used in the supports of overhead lines (Fig. 9.1). Today, with few exceptions, wood poles are mainly used for low-voltage (LV) and medium-voltage (MV) lines, say up to 50/69 kV (Fig. 9.136 [9.235]). They are classified as light, medium, and stout. An often used wood for poles comes from the Scots pine (*Pinus silvestris*), generally referred to as redwood [9.236]. An important issue for wood poles is that they have to be adequately protected against decomposition by fungi (rot). To avoid this, impregnation is necessary, but care is required in the selection of proper chemicals, as some of them can cause health hazards and pollute the environment. The characteristics of wood poles for overhead lines are covered in [9.237].

In cases of increased transverse loads at angle or terminal positions, double, guyed, or so-called A-frame poles are used. In some countries, wood poles in the form of H-frames have also been used for higher voltages up to 345 kV.

#### Design

The design of a self-standing wood pole (Fig. 9.137 [9.4]) is straightforward. The pole is basically a cantilever beam loaded in transverse direction. The maximum bending moment at ground level becomes

$$M = Ph + Q_w \frac{L}{2}, \quad (9.102)$$

where  $P$  is the transverse load at the top of the pole due to the wind action on the conductors and  $Q_w$  is the wind



**Fig. 9.136** Wood pole (adapted from [9.235])

load on the pole itself. This bending moment causes tensile and compressive stresses in the pole cross-section, given by

$$\sigma = \frac{N}{A} \pm \frac{M}{W}, \quad (9.103)$$

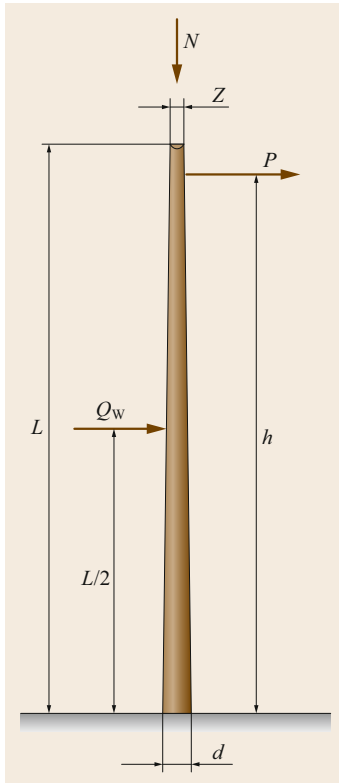
where  $N$  is the force from axial loads such as the weight of the conductors, the dead weight of the pole, and the vertical component of the stay load in case of guyed poles,  $d$  is the diameter,  $A = \pi d^2/4$  is the area, and  $W = \pi d^3/32$  is the section modulus of the pole cross-section at the ground.

As wood is a relatively flexible material, it is important to consider the maximum pole deflection at the top, which can be calculated as [9.4]

$$f_d = \left( \frac{P}{3} + \frac{Q_w}{8} \right) \frac{h^3}{EI}, \quad (9.104)$$

where the modulus of elasticity  $E$  can be assumed to be 10 000 N/mm<sup>2</sup>,  $I$  is the moment of inertia at ground level given by  $I = \pi d^4/64$ , and  $d$  is the pole diameter. Considering the resilience of the upper soil layers, the length  $h$  and diameter  $d$  in (9.104) should be related to a cross section approximately 0.5 m below the ground surface level. According to [9.16], it is recommended that the deformation be limited to a maximum of 10% of the pole length under the relevant external load.

Wood poles are normally inserted directly into the ground. The subsurface length of the pole should be, as



**Fig. 9.137**  
Schematic for  
the calculation of  
a wood pole



**Fig. 9.138** Line with concrete poles (adapted from [9.238])

a good practice, one-sixth of its total length, but a minimum of 1.6 m. In case of soft soils, a crushed stone ring is placed around the base of the pole to provide sufficient grip of the pole in the ground.

### 9.7.2 Concrete Poles

Concrete poles are often used for lines in the voltage range of 60–150 kV (Fig. 9.138 [9.238]) and very rarely up to 400 kV. Their main advantage is that they practically do not require maintenance. Other advantages are their slim shape and narrow base as compared with lattice towers. On the other hand, they are quite bulky and heavy, so their transport over long distances becomes arduous, an issue which has encouraged local production, mainly in developing countries. Often, site accessibility is a critical issue for the use of concrete poles as OHL supports.

According to how they are manufactured, they can be divided into the following two categories.

#### Spun Concrete Poles

These poles are manufactured by spinning of two-piece horizontal molds which are rotated quickly around their longitudinal axis. This leads to centrifugal accelerations of 10–30g and thus to very dense, high-strength con-

crete. The steel reinforcement can be either slack or prestressed and is placed in the mold before the start of the spinning process. An innovative alternative is the use of carbide fibers instead of steel for prestressing, thus reducing the concrete thickness and pole weight as well as avoiding possible steel corrosion by water ingress [9.239].

#### Vibrated Concrete Poles

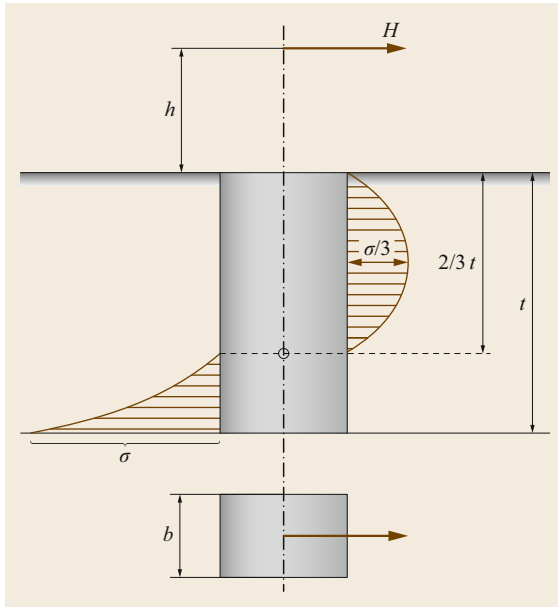
These mostly have a square but sometimes H cross-section, and they are produced locally. The steel reinforcement is placed in metallic molds with suitable cross-sections, then the concrete is poured in and compacted using vibrators attached to the outer surface of the molds every 1.5–2.0 m along the length of the pole. The vibration frequency lies between 3000 and 15 000 Hz.

#### Design

Concrete poles can be dimensioned using standard design methods for reinforced and prestressed concrete.

#### Foundations

The majority of concrete poles use so-called block concrete foundations (Fig. 9.139 [9.4]). For small-size poles, up to a total length of approximately 15 m and



**Fig. 9.139** Design of monoblock foundations for concrete poles (adapted from [9.4])

for prismatic foundation bodies, with a height  $t$  greater than their width  $b$ , the load is predominantly transferred by lateral embedment. The design will be conservative if the contribution of the foundation base is—as often—neglected. Assuming the pivoting axis of the foundation body at two-thirds of its depth, and further a parabolic distribution of the bearing lateral pressure between the foundation body and the soil, the maximum bearing pressure  $\sigma_e$  occurs at the foundation lower edge

$$\sigma_e = 12M \frac{h + (2/3)t}{bht^2}. \quad (9.105)$$

The significance of  $h$ ,  $b$ , and  $t$  can be seen in Fig. 9.139 [9.4]. The virtual height of the load attack  $h$  results from the ultimate moment  $M$  and the sum of the transverse

loads  $H$  according to

$$h = \frac{M}{H}. \quad (9.106)$$

The permissible or ultimate moment is obtained from

$$M_u = \frac{\sigma_u t^2 b}{\gamma_M 12(h + (2/3)t)}, \quad (9.107)$$

where  $\gamma_M$  is the partial safety factor and amounts to 1.0 for characteristic values with a minimum of 1.2 for ultimate values.

A good review of foundation design methods is given in [9.240].

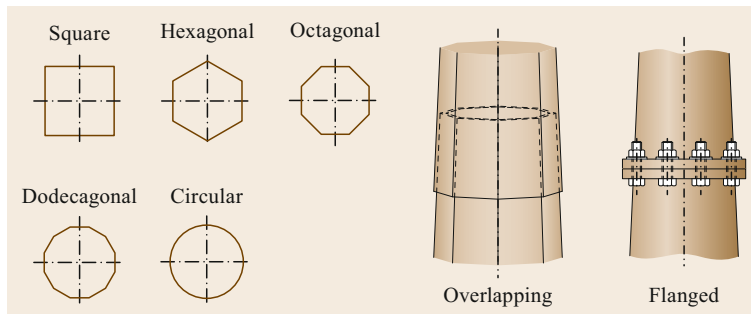
### 9.7.3 Metallic Poles

Metallic poles are currently made of carbon steel, mainly from high-strength low-alloy material, although aluminum has also been used sometimes.

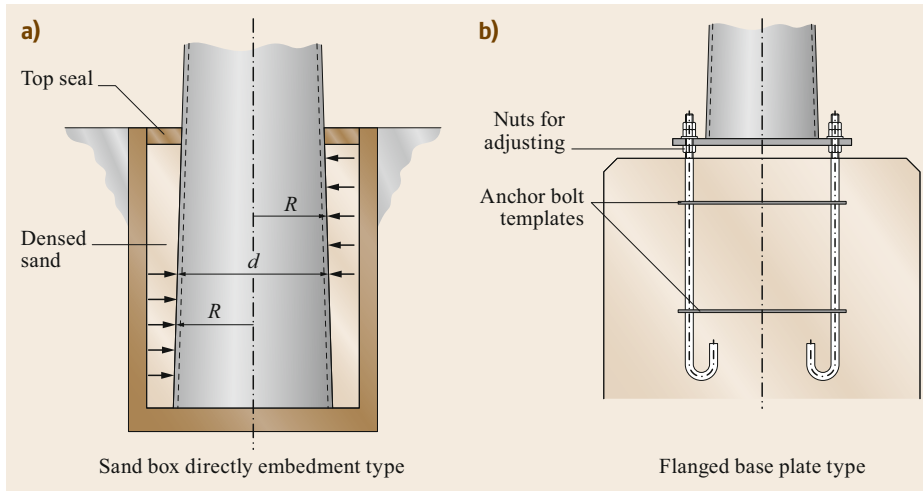
Solid-wall *steel poles* with various designs are used for low-, medium-, and high-voltage lines. *Polygonal conical poles* usually have 8-, 12-, or 16-sided shapes, whereby the plates are bent and finally welded in longitudinal direction. The steel grades S235 and S355 are mainly used for these poles. The lengths of the poles sections or their parts are limited to approximately 9–15 m by the weights/lengths for transportation and galvanization capabilities. The joints required for taller pole lengths can be designed as *slip joints* (overlapping) or *flange joints* with prestressed high-tensile bolts (Fig. 9.140 [9.4]).

Bolted flange joints are necessary for poles used for higher loads, for which prestressed high-strength bolts, e.g., with strength grade 8.8 or 10.9, are used. The flange joints can be arranged outside or inside the pole shaft. In case of an inside arrangement, the dimensions of the pole must be sufficiently wide to enable arrangements of cut-outs and ladders inside the pole.

Regarding their finishing, steel poles should preferably be hot-dip galvanized. Sometimes, painting sys-



**Fig. 9.140** Typical pole cross-sections and joints of steel poles (adapted from [9.4])



**Fig. 9.141a,b** Steel pole foundations: (a) sand box direct embedment type; (b) flanged base plate type

tems are also required for esthetic purposes, since hot-dip galvanizing surfaces do not have a uniform color appearance.

Steel pole design follows the basic rules of engineering mechanics. Special care should be taken when openings are required in the pole shaft, e.g., for small access doors, as the design must take them into account, as the cross-section will become an open section profile at such locations, where warping torsion has to be considered.

The top deflection of steel poles should be limited, since those poles are quite flexible. The following limits are recommended:

- At EDS condition: maximum top deflection equal to or less than 1.5–2% of the pole height
- At ultimate load: 4–5% of the pole height.

Steel poles often use monoblock concrete foundations, or more seldom piles for soft soil conditions. They are either directly embedded in the concrete or placed in a dense sand concrete box, or even connected on the top surface of the foundation body by means of flange and anchor bolts (Fig. 9.141 [9.4]). The design of these foundations follows the same principles and procedures as for concrete poles (Sect. 9.7.2).

#### 9.7.4 Composite Poles

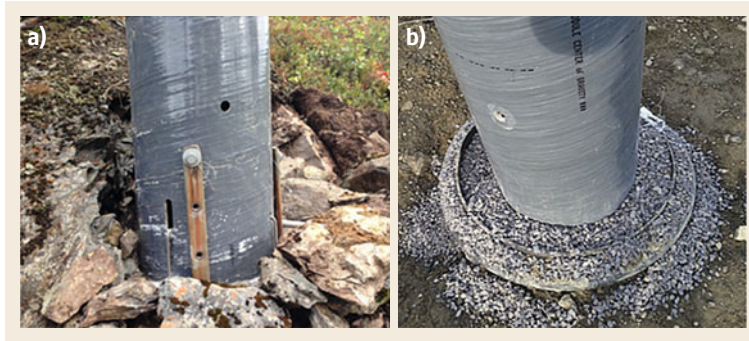
A rather new development is the use of composite poles made of fiber-reinforced polymer (FRP) (Fig. 9.142). To this end, CIGRE very recently published an extensive document [9.241], from which the following information is extracted.

FRP poles consist of E-glass embedded in a resin matrix. Commonly used resins are epoxy, polyester,

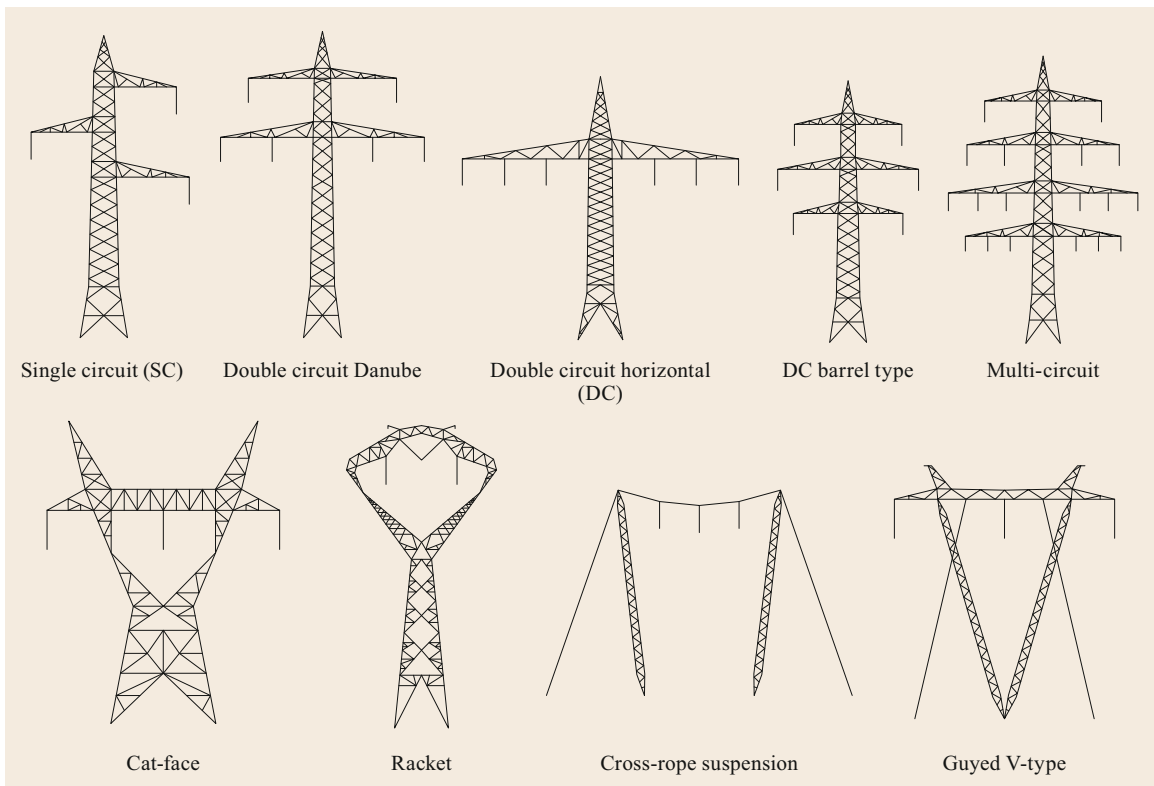


**Fig. 9.142** FRP cross-braced H-frame

vinyl ester, and polyurethane. Additives are used to improve some of the properties of FRP, such as its UV protection, fire resistance, flow improvement, abrasion resistance, etc., while fillers are applied to reduce the weight. Although their material costs are higher than for traditional materials, their low weight enables lower installation costs. Also, due to their long service life and low maintenance requirements, life cycle costs can be lower with FRP components. Their foundations follow the same practices as other pole-type supports (Fig. 9.143).



**Fig. 9.143a,b** Typical foundations for FRP poles: (a) crushed stones around the pole shaft in rock; (b) barrel with backfill in normal soil



**Fig. 9.144** Common tower types

### 9.7.5 Steel Lattice Towers

For higher voltages, e.g., normally above 110 kV, steel lattice towers are still the choice of preference, the main reason being that, when properly designed, they can achieve relatively long spans economically. In addition, when orderly maintained, they have a long service life, and as they are modular, they are easy to transport from the manufacturing plant to the site. Their modular concept is also advantageous when modifications in case of uprating (Sect. 9.10) or repairs of individual tower members become necessary. They also provide easy

adaptation to the terrain by means of an adaptable system of body and leg extensions.

Over the years and depending on system planning, the number of circuits to be supported, experience, topography, etc., a plethora of tower shapes have been installed. They can basically be grouped into self-supported and guyed towers. Figure 9.144 shows various common tower shapes [9.242].

#### Materials and Layout

Publication [9.243] gives a good overview of industry practices for lattice tower design and detailing. The

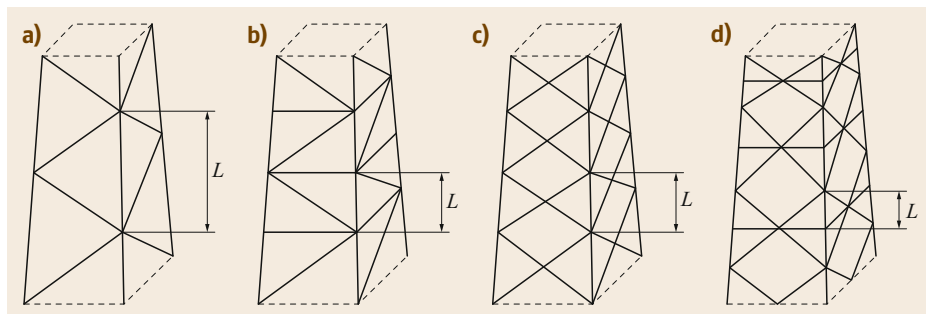
**Table 9.44** Yield and ultimate tensile strength of tower steel profiles and bolts (adapted from [9.4])

Steel grade	Bolt grade	Yield strength $f_y$ (N/mm <sup>2</sup> )	Ultimate strength $f_u$ (N/mm <sup>2</sup> )
S235		235	360
S355		355	510
	4.6	240	400
	5.6	300	500
	8.8	640	800
	10.9	900	1000

materials used in the fabrication of line supports should comply with the requirements of [9.244, 245] or equivalent standards. In general, high-strength steel of grade S355 and mild steel of grade S235 are used. Members are practically always connected with bolts compliant with [9.246] or equivalent. The relevant properties of tower steel profiles and related bolts are listed in Table 9.44 [9.4]. Low-tensile bolts of grades 4.6 and 5.6 are often preferred, as they exhibit, because of their relative high ductility, benign deformation behavior at failure.

In most cases, lattice towers have a square cross-section, although there are some cases with a rectangular cross-section. Their absolute width on the upper part and their width gain are selected by optimizing the strength and length of the steel profiles; these should be selectable from the available standard sizes. Gain values of 40–50 mm/m for suspension towers and 60 mm/m for angle towers have proven useful. Often the lowest part of the tower is designed with even higher width gains, as this enlarges the cross-section at ground level, reducing the forces on the tower legs and consequently the size of the foundations. An interesting early publication focused on the influence of such tower geometry parameters on the economic design of steel lattice towers [9.247].

Figure 9.145 [9.4] shows typical brace arrangements for leg members with their related *effective buckling length*  $L$ . The distance between the brace connections should be reduced as much as possible in order to avoid secondary bending of the leg sections in between.



**Fig. 9.145a–d** Brace arrangements of steel lattice towers for (a) light, (b) moderate, (c) high, and (d) very high loads (adapted from [9.4])

Single angle sections are the most widely used and economic design profile; they are manufactured from 40×3 mm up to a size of 250×28 mm. For towers supporting multicircuit lines and, particularly, for very tall towers, member designs with higher strength may be necessary. In these cases, cruciform sections made up of two, three, or four angle sections are used for leg members.

While formerly rivets were used for lattice steel towers, bolted connections predominate by far today. This connection element is adequate for the hot-dip galvanization process. The individual members and bolts can be galvanized separately and bolted together afterwards.

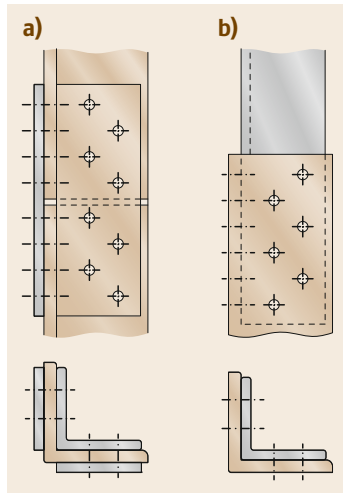
For leg members, either butt joints or lap joints are used (Fig. 9.146 [9.4]). Butt joints can be designed with two shear planes and are preferred in case of towers with higher strengths to facilitate the erection. Lap joints save material but are not frequently used anymore because of their inherent eccentricity and relatively higher erection costs.

All nuts should be secured against loosening. Frequently, *spring washers* are used for this purpose, or a strong adhesive. Alternatively, the nuts can be punched on three points spaced at 120° and protected with anticorrosive dyes.

To ensure a long service life, adequate protection against rust is of great importance. Whenever possible, hot-dip galvanizing should be applied, while, already in the tower design stage, the length of the galvanizing facilities (length of the zinc bathtub) has to be taken into consideration. Lengths up to 9 m for member sections are common [9.243]. The best corrosion protection is achieved by the so-called in-factory duplex system, i.e., by coating the steel members after their galvanization.

### Tower Types

Steel lattice towers, as with all other types of line support, can be distinguished based on their function in the transmission line, i.e., suspension, angle, terminal towers, etc. A typical classification is based on the line route deviation angle:



**Fig. 9.146a,b** Leg member joints: (a) butt joint, (b) lap joint (adapted from [9.4])

- *Suspension or tangent towers (S)* support the conductors in a straight line and up to small line angles up to say  $3^\circ$ ; they are equipped with suspension insulators.
- *Light angle towers (LA)* support the conductors up to line angles of  $10^\circ$ , seldom up to  $20^\circ$ ; they are equipped with suspension insulators.
- *Angle towers (A)* must be designed to sustain the resultant component of the conductor tensions when the line changes direction; they are equipped with tension insulators.
- *Tension or strain (T) towers* have to sustain the full conductor—and ground wire—tensions in the line direction but also for relatively large line angles up to  $60^\circ$ . They serve as rigid points of the line and are equipped with tension insulators.
- *Dead-end or terminal towers* are used to terminate the line, e.g., at a substation or an overhead to underground change-over station, and are equipped with tension insulators.
- *Tie-off towers* are used where a branch-off of the line is required; such a design is the so-called *Mercedes tower*.

### Structural Design

As with every lattice structure, tower design proceeds via the following steps:

- Assess external loads
- Group into load cases
- Calculate forces in tower members (legs, braces, cross-arms)
- Calculate stresses in tower members
- Verification of members and connections.

**Loads and Load Cases.** External loads basically arising from conductors and insulators, i.e., self-weight, ice

**Table 9.45** Standard load cases (adapted from [9.16])

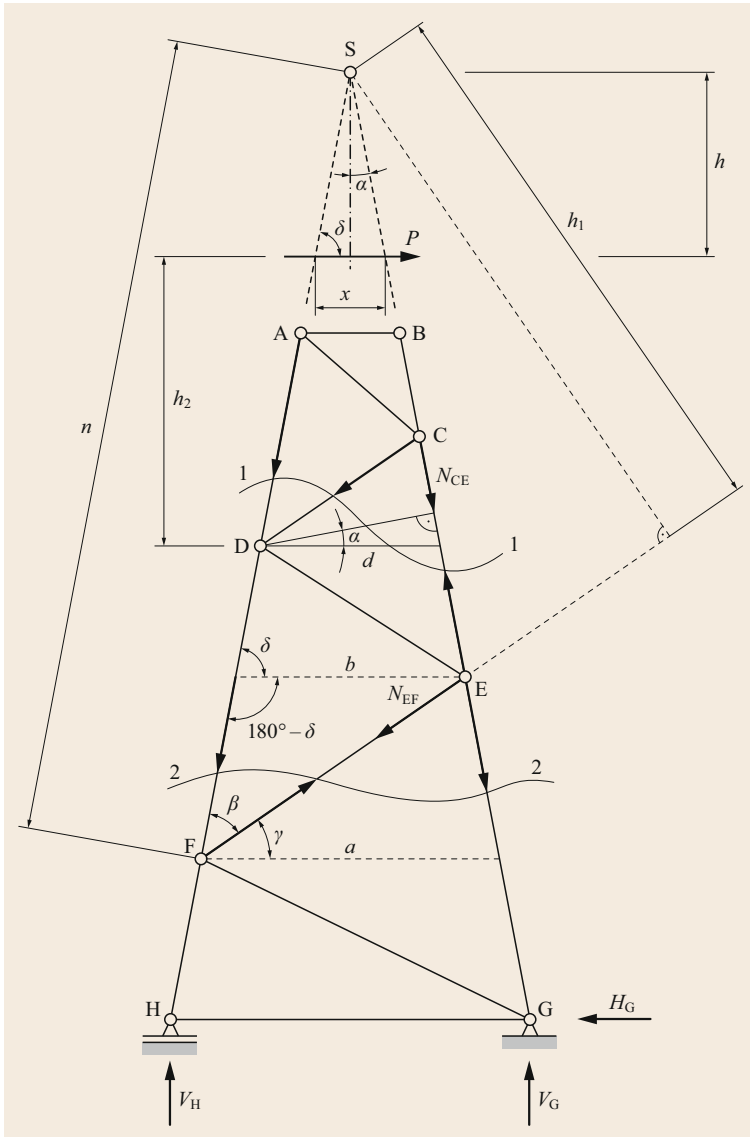
Load case	Conditions
1a	Wind loads (transverse, longitudinal, inclined)
2a	Uniform ice loads on all spans
2b	Uniform ice loads, transversal bending
2c	Unbalanced ice loads, longitudinal bending
2d	Unbalanced ice loads, torsional bending
3	Combined wind and ice loads
4	Minimum temperature with/without wind loads
5a	Security loads, torsional loads
5b	Security loads, longitudinal loads
6a	Safety loads, construction and maintenance loads
6b	Safety loads, loads due to the weight of linesmen

and wind loads, and conductor tensions, have been adequately dealt with in Sects. 9.3 and 9.4. The next step is to group loads together into so-called *load cases*, which take into account probable scenarios of load combinations. From the relevant standards, for example [9.16], the load cases are prescribed in Table 9.45. In all load cases, the vertical component of the so-called permanent actions, i.e., self-weight of supports, insulator sets and other fixed equipment, as well as the weight of conductors from the adjacent spans, should be included. It is common and helpful to display the forces for every load case schematically in the form of so-called load-ing trees.

It is worth mentioning that the so-called security loads (load cases 5a and 5b in Table 9.45), which arise from one-sided release of conductor tension, for instance when a conductor breaks, are intended to prevent cascading or uncontrollable failures and are by nature dynamic. What is normally done, though, is to load the supports with the related residual static load (RSL), applying a dynamic impact factor to compensate the peak dynamic effect [9.248]. An option against the detrimental effects of a broken conductor is to install controlled sliding clamps (Sect. 9.6.1) [9.208].

**Structural Analysis.** The core of any structural design is the calculation of the forces and subsequently of the *stresses* acting in the components of the structure, here in the case of steel lattice towers, the legs, the braces, and the cross-arms. The method of analysis for transmission line towers has advanced quite a lot since the first towers were designed. In the beginning, transmission line engineers often had to use graphical analysis methods such as the so-called *Cremona plan* to determine the member forces. However, with the introduction of computers, simulations using the finite element method (FEM) were developed, mostly based on a linear elastic 3-D truss model. Thereby members are assumed to be axially loaded and having pinned connections. For more deformable structures, such as guyed towers or poles, nonlinear





**Fig. 9.147** Schematic for the calculation of the tower member forces

analysis is required. A good overview of computer programs available for line support calculations is given in [9.238].

Nevertheless, it is quite educative to present here some simplified calculations, which can be performed *by hand* and which give quite satisfactory results. For this purpose, when the tower body has, as is often the case, a square cross-section, the external loads acting on the tower are split and deemed to act equally on the two related parallel tower faces, thus the factor 2 in (9.110) and (9.123). In this case, the tower faces can be treated as plane trusses and simple analytical methods can then be applied to determine the member forces.

**Calculation of Tower Member Forces.** The equivalent static system is shown in Fig. 9.147. The easiest approach is to use the method of sections, viz. the so-called *Ritter method*, i.e., to divide the truss into two sections—which evidently have to be in equilibrium with themselves—in such a way that only three members are cut (slices 1–1 and 2–2). Applying, after cutting along 1–1, the equilibrium of moments at node D and assuming that this node is in static equilibrium, it is possible to calculate the load on main member CE as

$$2N_{CE}d \cos \alpha - Ph_2 = 0 . \tag{9.108}$$

Thus,

$$N_{CE} = + \frac{Ph_2}{2d \cos \alpha} . \quad (9.109)$$

Establishing a generic equation with all external loads for calculation of any main member ( $m$ ) we get

$$N_m = \pm \frac{\sum_i M_i}{2d \cos \alpha} , \quad (9.110)$$

where  $N_m$  is the force for any main member ( $m$ ) in tension or compression,  $\sum_i M_i$  is the sum of the moments due to all external loads  $P_i$  above the panel of the main member ( $m$ ) at the node (O) opposite to the considered main member ( $m$ ),  $d$  is the width of the truss in the main member ( $m$ ) or panel, and  $\alpha$  is the inclination angle of the main member in relation to the vertical direction.

Again, looking at Fig. 9.147 and *cutting* along 2–2, it is possible to calculate the load on the diagonal EF by applying the equilibrium equation of moments at point S as

$$-Ph + N_{EF}xh_1 = 0 . \quad (9.111)$$

Thus,

$$N_{EF} = + \frac{Ph}{h_1} . \quad (9.112)$$

But

$$h = \frac{x}{2} \tan \delta , \quad (9.113)$$

$$h_1 = n \sin \beta , \quad (9.114)$$

and with

$$n = \frac{a/2}{\cos \delta} , \quad (9.115)$$

it follows that

$$h_1 = \frac{a}{2 \cos \delta} \sin \beta . \quad (9.116)$$

Taking

$$\frac{b}{\sin \beta} = \frac{l_{EF}}{\sin \delta} , \quad (9.117)$$

one gets

$$\frac{\sin \delta}{\sin \beta} = \frac{l_{EF}}{b} . \quad (9.118)$$

Therefore,

$$N_{EF} = \frac{Px \sin \delta}{2 \cos \delta} \frac{2 \cos \delta}{a \sin \beta} , \quad (9.119)$$

or

$$N_{EF} = \frac{Px \sin \delta}{a \sin \beta} = \frac{Px l_{EF}}{a b} . \quad (9.120)$$

Rearranging leads to

$$N_{EF} = \frac{Px}{ab/l_{EF}} . \quad (9.121)$$

Or, considering two parallel panels as mentioned above,

$$N_{EF} = \frac{Px}{2ab/l_{EF}} . \quad (9.122)$$

Thus, for a generic external load system, the force  $N_d$  on the generic diagonal ( $d$ ) becomes

$$N_d = \pm \frac{\sum_i P_i x_i}{2ab/l_d} , \quad (9.123)$$

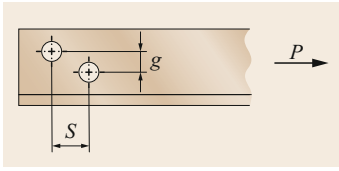
where  $N_d$  is the force for any diagonal ( $d$ ) in tension or compression, depending on the direction of that diagonal,  $P_i$  are the external loads applied on the structure above the panel where the diagonal ( $d$ ) is located,  $x_i$  is the truss width at level  $i$  where the load  $P_i$  is applied (i.e.,  $x_1$  at  $P_1$ ,  $x_2$  at  $P_2$ , etc.),  $a$  is the lower truss width in the panel of the diagonal ( $d$ ),  $b$  is the upper truss width in the panel of the diagonal ( $d$ ), and  $l_d$  is the length of the diagonal ( $d$ ).

However, considering that there are often two crossing diagonals per truss panel (a so-called *tension/compression* structural system or just *composed truss*) (Fig. 9.145 cases (c) and (d)), then the generic equation to calculate the member forces on diagonals becomes

$$N_d = \pm \frac{\sum_i P_i x_i}{2 \times 2ab/l_d} , \quad (9.124)$$

where one diagonal is always in tension (+ sign) and the other in compression (– sign).

The maximum leg forces can be obtained by superposition of the individual leg forces coming from the horizontal loads (transverse or longitudinal) on the tower, in  $x$ - and  $y$ -direction, and—in a minor part—by the vertical loads (conductor, tower, and insulator self-weights and ice loads); these are considered to be equally distributed between the four legs. However, note that, as horizontal loads caused by the wind must also be considered in the opposite direction, the same leg will have to be designed for the maximum tension and compression forces.



**Fig. 9.148** Tower member loaded in tension—*net cross section* (adapted from [9.238])

**Selection of Member Size.** The verification and selection of member size to adequately resist the member forces follows the classical, strength of materials approach; For example, a member loaded in tension will have a cross-section large enough to sustain the related tensile material stresses, whereby the derating effect of boreholes needed for the connection elements (bolts) has to be considered, resulting in a *net cross section resistant area* (Fig. 9.148 [9.238]).

According to [9.243, 249], the tensile stress on a tension member can be calculated as

$$f_t = \frac{P}{A_n} \leq f_y, \tag{9.125}$$

with

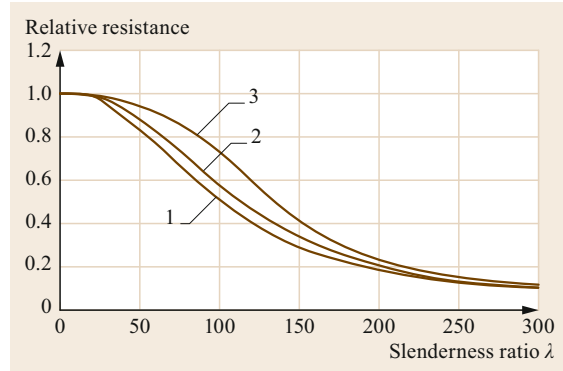
$$A_n = A_g - nd_0t + t \sum \left( \frac{s^2}{4g} \right), \tag{9.126}$$

where  $f_t$  is the tensile stress on the net area,  $f_y$  the yield strength of the material,  $P$  the axial force acting on the bolt,  $s$  the distance between holes in the direction parallel to the axial force,  $g$  the distance between holes in the direction perpendicular to the axial force,  $A_n$  the net cross section area,  $A_g$  the gross cross section area,  $n$  the number of holes,  $t$  the plate (angle) thickness, and  $d_0$  the hole diameter.

When the load is eccentric, i.e., when the profile is connected on only one side, the cross-section has to be reduced by 10%, thus the effective cross section  $A_e$  becomes

$$A_e = 0.9A_n. \tag{9.127}$$

In the critical case of compression, members experience and ultimately fail in buckling, an instability issue. Thereby, the limit load depends not only on the material properties but also on the geometry of the loaded element. It can reasonably be assumed here that the slender members of steel lattice towers can be considered to be straight and compressed only axially, i.e., neglecting lateral loads on the member, which would cause bending moments. The resistance of a member to compressive loads is determined from buckling curves. Figure 9.149 [9.4] shows such curves from two of the most widely used standards. Therein,  $\lambda$  is the so-called



**Fig. 9.149** Buckling curves as per [9.16] (1, 2) and [9.249] (3) (adapted from [9.4])

**Table 9.46** Slenderness ratio limits

Leg members and chords	$L/i \leq 150$
Primary bracing members	$L/i \leq 200$
Redundant members	$L/i \leq 250$
Tension-hanger members	$L/i \leq 375$
Tension-only members	$300 \leq L/i \leq 500$
Web member—multiple lattices	Not specified
Horizontal edge members	Not specified

slenderness ratio, defined by

$$\lambda = \frac{L}{i}, \tag{9.128}$$

$$i = \sqrt{I/A},$$

where  $L$  is the unsupported buckling length, which depends on the type of bracing (Fig. 9.145), and  $i$  is the radius of gyration around the profile axis perpendicular to the assumed direction of buckling ( $I$  is the second moment of area and  $A$  is the cross-sectional area of the profile).

As per [9.243, 249], the slenderness ratio  $\lambda$  should be limited to the values in Table 9.46.

All members which can be used as steps to climb the tower during erection and maintenance works should be designed to support the related bending loads (due to personnel, equipment, etc.). These are deemed to act in the center of the steel member in question and amount according to [9.16] to 1.0 kN with a partial factor of  $\gamma_p = 1.5$ . For this load case, calculations are performed for a beam hinged at both ends, delivering the maximum allowable member length  $L_{max}$  for commonly used profiles (Table 9.47 [9.4]).

### Connections

The design of the connections follows standard methods from machine elements. Specifically for bolted connections, which are almost exclusively used in steel lattice

**Table 9.47** Maximum length for tower members loaded with 1.0 kN in bending (adapted from [9.4, Sect. 12.5.12])

Section	$L_{\max}$ (m)	
	S235 steel	S355 steel
35 × 4	0.57	0.85
35 × 5	0.68	1.02
40 × 4	0.75	1.12
40 × 5	0.90	1.35
45 × 4	0.95	1.43
45 × 5	1.16	1.74
50 × 4	1.19	1.78
50 × 5	1.46	2.19
50 × 6	1.69	2.54
55 × 4	1.45	2.17
55 × 5	1.77	2.67
55 × 6	2.10	3.15
60 × 5	2.13	3.19
60 × 6	2.52	3.77

towers, the following two loading situations should be considered:

**Shearing of the Bolt.** The cross-section of the bolt is subjected to shear. The related shear stress should not exceed the limit shear stress of the bolt, as presented in Table 9.44 for *single shear* connections (Fig. 9.150a)

$$f_v = \frac{N}{nA_g} \leq F_u, \quad (9.129)$$

or, for *double shear* (Fig. 9.150b),

$$f_v = \frac{N}{2nA_g} \leq F_u, \quad (9.130)$$

where  $f_v$  is the shear stress acting on the bolt,  $N$  is the force acting on the joint,  $n$  is the number of bolts in the joint,  $A_g = \pi D^2/4$  is the cross section of the bolt with  $D$  being the bolt diameter, and  $F_u$  is the ultimate shear stress of the bolt.

**Bearing Pressure.** The shearing forces are introduced to the bolt shank through the bearing pressure on the

bore face of the profile (Fig. 9.150c). This can be calculated for *single shear* connections as

$$f_p = \frac{N}{nDt} \leq F_p \quad (9.131)$$

and for *double shear* connections as

$$f_p = \frac{N}{2nDt} \leq F_p, \quad (9.132)$$

where  $f_p$  is the bearing stress acting on the bore hole,  $N$  is the force acting on the joint,  $n$  is the number of bolts in the joint,  $D$  is the nominal bolt diameter,  $t$  is the plate thickness, and  $F_p$  is the ultimate bearing stress.

It should not exceed the ultimate tensile strength of the related profile (Table 9.44).

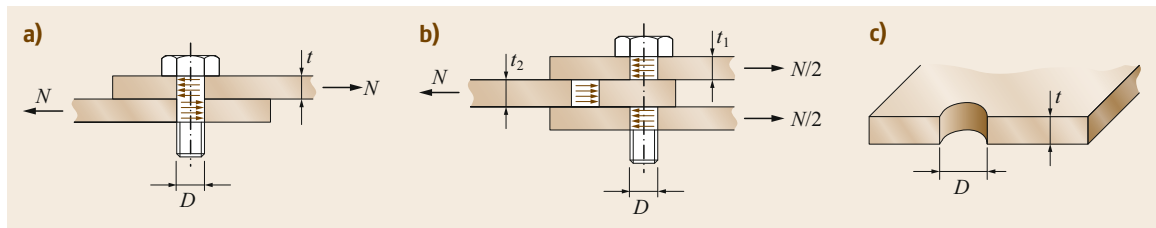
### Prototype Tests

It is current practice for new OHL support designs to be validated by full-scale prototype tests [9.250]. Clients, designers, and tower manufacturers meet in a test facility area at a so-called *test station*, for simulation of all the extreme operational conditions to be supported by the structure during its expected lifetime. IEC standard [9.251] provides the basis for the performance of all such full-scale prototype tests around the world.

Full-scale tests are carried out on tower prototypes to verify the design method and related assumptions, the detailing process, as well as the quality of the materials and fabrication procedures. In this sense, full-scale tests are performed in the following circumstances:

- To verify the compliance of the support design with the specifications, known as *type tests*
- To validate the fabrication process
- As part of the research and development of an innovative support.

The tests to be performed can be of *normal* or *destructive* type. They are considered to be *normal tests* when they are carried only up to 100% of the specified design loadings. As a general rule, all loading cases that are critical for any support member should be simulated during the normal tests. On the other hand, *destructive*



**Fig. 9.150a–c** Schematic of single (a) or double shear (b) and bearing pressure on bolted connections (c)



**Fig. 9.151** Visual side-by-side comparison of conventional and compact 420-kV lines with the same power transfer capacity (adapted from [9.252])

tests are carried out to provide information on the actual versus predicted behavior or, in case of suspension towers, to determine the real failure load and then judge whether the result is acceptable in terms of security and cost.

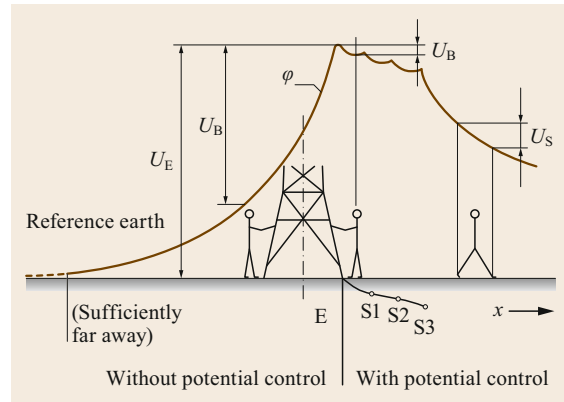
### 9.7.6 Esthetic or Landscape Supports

As mentioned above, in recent decades, there has been considerable resistance from the public against new—and even existing—overhead lines, the suggested alternative being underground cables (Chap. 10). One concern is often the purported health hazards related to EMF (Sect. 9.3.4), the other being the supposedly disturbing visibility of overhead lines in the landscape. Evidently, the visual impact of a line is mainly caused by the shape and appearance of its supports, thus it is no surprise that network owners and line designers started addressing these concerns early on, leading to the development of so-called *esthetic* or *landscape* supports, which are briefly presented below.

For this type of supports, CIGRE prepared a seminal publication [9.235], which includes practically all available information on esthetic supports. Their development has followed basic ideas to:

- Compact the lines and the supports as much as possible
- Reduce the number of structural elements on the towers
- Make them invisible or camouflaged in the landscape.

The next step was to design esthetic solutions for unique places, for a single line, or to develop standard esthetic solutions. A good example of a unique support



**Fig. 9.152** Voltage distribution close to the support in case of a fault ( $U_E$  earthing voltage,  $U_B$  touch potential,  $U_S$  step voltage,  $\phi$  surface potential,  $S_1, S_2, S_3$  ring electrodes connected to the earth electrode E for earth potential control,  $x$  distance to the earth electrode E) (adapted from [9.4])

is the *pylône raquette* (tennis racket tower) in Switzerland (Fig. 9.99), which helped the approval of a badly needed new 400-kV line [9.135].

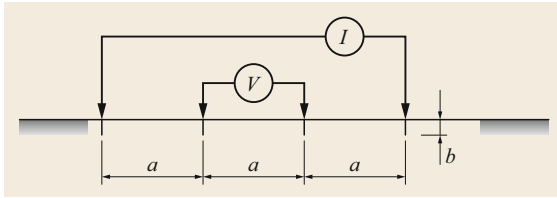
Recently, and with the general acceptance by utilities of composite insulators, the so-called compact lines with improved esthetics are gaining ground (Sect. 9.5.5 [9.253]). They are becoming the choice of preference in many countries, to facilitate the construction of new lines, also in cases with limited space (Fig. 9.151 [9.252]).

### 9.7.7 Earthing

Earthing or grounding systems are installed in the structures of a transmission line with the following primary objectives [9.254]:

- To provide a preferential path to earth for currents generated by faults in the line
- To provide a grounding system with a resistance low enough to enable the overcurrent protection to detect a ground fault in the line
- To provide a preferential path to earth for lightning discharge currents
- In urban areas, to control the step and touch voltages generated during ground faults on the line
- To reduce the rise in the ground potential of the structure during a lightning discharge and thereby the probability of occurrence of *back-flashover*.

When a phase-to-ground fault occurs on an overhead line, one of the most probable paths of the current flow is to or from earth. This results in a potential rise on the grounded support and voltage gradients



**Fig. 9.153** Schematic of the Wenner four-point method (adapted from [9.255])

on the surface of the ground surrounding the support (Fig. 9.152 [9.4]). Requirements to protect the public in the vicinity of grounded line supports from the hazard of electrical shock caused by power frequency faults were presented in a recent CIGRE publication [9.255], whereby the related methods can also be applied in the case of faults caused by lightning and related overvoltages (Chap. 3). The earthing resistance of the electrode for a given current discharge is the ratio of the potential difference between the electrode and a distant point on the earth, in volts, and the current discharge in amperes. It consists of three parts:

1. Resistance of the electrode itself and its connections
2. Contact resistance between the electrode and the adjacent soil
3. Resistance of the surrounding earth.

A low value of the tower earthing resistance, with  $10\ \Omega$  often being recommended, is a prerequisite to reduce the possibility of back-flashovers: When lightning strikes a tower (or the overhead ground wires), the current on the tower in combination with the earthing resistance causes a rise of the tower voltage, which becomes much larger than the phase conductor voltages. If this voltage difference exceeds a critical value, a flashover occurs, called *back-flashover*. The term *back* refers to the fact that the highest voltage is on a part of the power system normally at ground potential, i.e., the tower or the shielding wires.

To design a grounding system, the soil resistivity must be known. Typical values are indicated in Table 9.48 [9.16]. For more accurate results, the soil resistivity should be measured in situ. This is commonly done by the *Wenner four-point method* (Fig. 9.153 [9.255]). As the probe penetration depth  $b$  is practically always much smaller than the distance  $a$  between the electrodes, the soil resistivity  $\rho_E$  can be determined accurately enough by

$$\rho_E = 2\pi aR, \quad (9.133)$$

where  $R$  is the measured resistance ( $R = V/I$ ).

**Table 9.48** Typical soil resistivities (adapted from [9.16])

Type of soil	Soil resistivity $\rho_E$ ( $\Omega\text{m}$ )
Marshy soil	5–40
Loam, clay, humus	20–200
Sand	200–2500
Gravel	2000–3000
Weathered rock	Mostly below 1000
Sandstone	2000–3000
Granite	Up to 50 000
Moraine	Up to 30 000

Details of earthing calculations can be found in [9.4, 16, 254, 255].

The worldwide practice regarding overhead lines is to solidly earth the earth wires at each tower as well as solidly earth the tower to the ground. For the latter, the following methods are widely used (often in combination):

- Connection of reinforcing of foundation to tower steel
- Counterpoise conductor laid in a horizontal trench
- Earthing rods driven at the base of the tower.

The dimensions of the earth electrodes and earthing conductors should be rated such that the permissible temperature of  $300\ ^\circ\text{C}$  for copper and steel or of  $200\ ^\circ\text{C}$  for aluminum will not be exceeded.

Mechanical strength and *corrosion resistance* determine the minimum dimensions of electrodes and earthing or bonding conductors. In this sense, the minimum cross section for earthing conductors is  $16\ \text{mm}^2$  for copper,  $35\ \text{mm}^2$  for aluminum, and  $50\ \text{mm}^2$  for steel. Electrodes having direct contact to earth should withstand mechanical or biological attack, oxidation, formation of an electrolytic couple, and electrolysis. The dimensions listed in Table 9.49 [9.16] comply with these requirements.

### 9.7.8 Lightning Protection

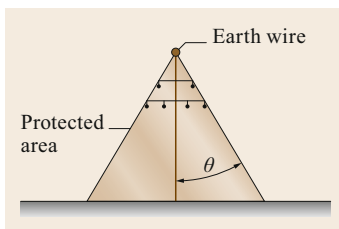
Lightning discharges (Chap. 3) constitute the main cause of most nonprogrammed outages of electric systems. International statistics show that about 65% of *line outages* originate from lightning strokes that hit the overhead transmission lines [9.256]. However, it is possible to reduce the number of line outages to an acceptable level by using a convenient protection scheme, with adequate installation of earth wires and appropriate earthing of the towers.

While protection issues as a whole are covered in Chap. 13, earthing issues were discussed in the previous section, and lightning protection by earth wires is briefly treated below. An excellent overview of the lightning

**Table 9.49** Minimum dimensions of earth electrode materials ensuring mechanical strength and corrosion resistance (adapted from [9.16])

Material	Steel	Type of earth electrode	Minimum size			Coating/sheath		
			Core Diameter (mm)	Cross section (mm <sup>2</sup> )	Thickness (mm)	Single value (μm)	Average values (μm)	
Steel	Hot-galvanized	Strip <sup>a</sup>	–	90	3	63	70	
		Profile (inc. plates)	–	90	3	63	70	
		Pipe	25	–	2	47	55	
		Round bar for earth rod	16	–	–	63	70	
		Round bar for surface earth electrode	10	–	–	–	50	
		With lead sheath <sup>b</sup>	Round wire for surface earth	8	–	–	1000	–
	With extruded copper sheath	Round bar for earth rod	15	–	–	2000	–	
	With electrolytic copper sheath	Round bar for earth rod	14.2	–	–	90	100	
	Copper	Bare	Strip	–	50	2	–	–
			Round wire for surface earth	–	25 <sup>c</sup>	–	–	–
Stranded cable			1.8 <sup>d</sup>	25 <sup>c</sup>	–	–	–	
Pipe			20	–	2	–	–	
Tinned		Stranded cable	1.8 <sup>d</sup>	25 <sup>c</sup>	–	1	5	
Galvanized		Strip <sup>a</sup>	–	50	2	20	40	
With lead sheath <sup>b</sup>		Stranded cable	1.8 <sup>d</sup>	25 <sup>c</sup>	–	1000	–	
		Round wire	–	25 <sup>c</sup>	–	1000	–	

<sup>a</sup> Strip, rolled, or cut with rounded edges, <sup>b</sup> not suitable for direct embedding in concrete, <sup>c</sup> in conditions where experience shows that the risk of corrosion and mechanical damage is extremely low, 16 mm<sup>2</sup> may be used, <sup>d</sup> diameter of single wire



**Fig. 9.154** Shielding angle  $\theta$  and protected area of an earth wire for a Danube-type tower (adapted from [9.258])

performance of overhead transmission and distribution lines is given in [9.257]. In regions with high or even medium *keranic* levels, it is standard practice to equip transmission lines with earth wires to shield them against lightning discharges, as these can cause, if the *lightning stroke* hits the conductors directly, considerable damage and even conductor failures.

Earth wires are installed with shielding angles  $\theta$  that usually vary between  $10^\circ$  and  $35^\circ$ , depending on the importance of the line and the *keranic* level (Fig. 9.154 [9.258]).

## 9.7.9 Foundations

Foundations are the last part in the chain of load transfer from the external loads on an OHL to the ground; their role and consequently their proper design are crucial to the reliability and safety of the line. Foundation design faces considerable challenges, as it is closely related to the properties of the soil, which are not always easy to determine, while the soil conditions may also vary considerably along the route of the line. For this reason, serious consideration should be given to site investigations, and it is good and current practice to adopt an additional safety coefficient for foundation design of 1.10–1.20 (depending on the tower type) in comparison with normal tower design.

### Site Investigations

Evaluation using various in situ tests together with an indication of geotechnical information that may be derived from in situ test results (Table 9.50 [9.259]) and

**Table 9.50** Comparison of ground investigation methods (adapted from [9.259])

Method	Advantages	Disadvantages
Trial pit	Allows detailed examination of ground conditions Easy to obtain discrete and bulk samples Rapid and relatively inexpensive	Limited by machine size Not suitable for sampling below water or excavation in rock Greater potential for disruption/damage to site than boreholes or probe holes Depth restricted to 4.5 m below ground level Width and height restrictions of equipment
Cable percussion	Allows greater sampling depth than with trial pits, window sampler, or probing Can penetrate most soils Allows collection of undisturbed samples Enables installation of permanent sampling/monitoring wells	Not suitable for investigation in rock Smaller sample volumes than for trial pits More costly and time-consuming than trial pits Width and height restrictions of equipment
Rotary boring	Allows greater sampling depth than with trial pits, window sampler, or probing Can penetrate all soils and rocks Allows collection of undisturbed samples Enables installation of permanent sampling/monitoring wells	Smaller sample volumes than for trial pits More costly and time-consuming than trial pits Width and height restrictions of equipment
Window sampler	Allows greater sampling depth than with trial pits Undisturbed samples of the complete soil profile can be recovered A variety of measuring devices can be installed once a hole is formed Substantially faster than cable percussion Portable, so can be used in areas with poor or limited access	Not suitable for investigation in rock and cannot penetrate obstructions Depth restricted to 8 m under favorable circumstances Smaller sample volumes than for trial pits Poor sample recovery in noncohesive granular soils Width and height restrictions of equipment
Cone penetration test (CPT)	Allows greater sampling depth than with trial pits Substantially faster than cable percussion	Not suitable for investigation in rock and cannot penetrate obstructions No sample recovery Ground water level not recorded Width and height restrictions of equipment
Dynamic probing	Essentially a profiling tool Portable, so can be used in areas with poor or limited access Very quick and inexpensive	Not suitable for investigation in rock and cannot penetrate obstructions No sample recovery Ground water level not recorded

laboratory tests for determining specific geotechnical design parameters (Table 9.51 [9.260]) are also often used to complement the field observations.

### Foundation Types

Foundations can be categorized as follows:

- Compact foundations:
  - Monoblocks
  - Direct embedment
- Separate foundations
- Spread footings
- Drilled shaft foundations
- Piles
- Anchors
- Raft foundations
- Grillage foundations.

There are also various subcategories. For example, anchor foundations can be divided into various types as shown schematically in Fig. 9.155 [9.259].

### Foundation Design

Basically, all foundation designs should comply with the following main stability conditions:

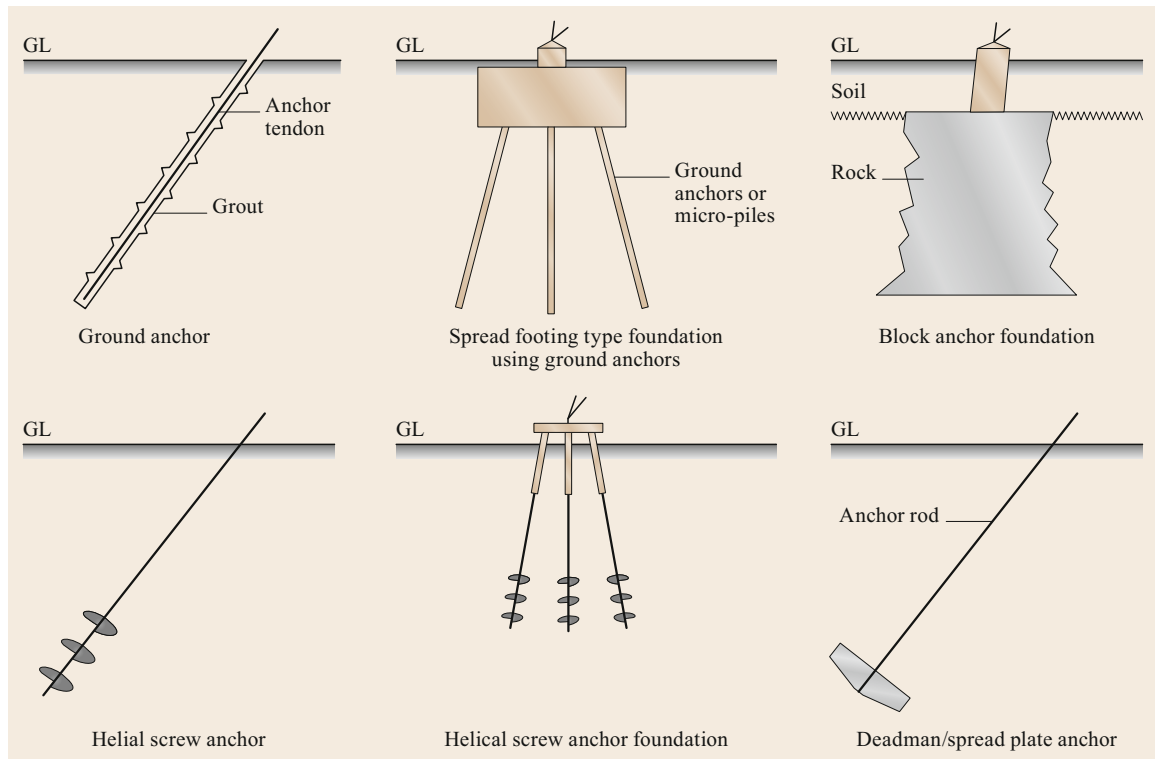
- The capacity to support the loads coming from the towers
- The ability to distribute them in a manner compatible with the soil capacity in terms of compression, uplift resistance, and shear stresses.

The design of concrete monoblock foundations for poles was briefly presented in Sect. 9.7.2. Hereunder, the focus is on the basic design of typical foundations



**Table 9.51** Laboratory tests—geotechnical design parameters (adapted from [9.260])

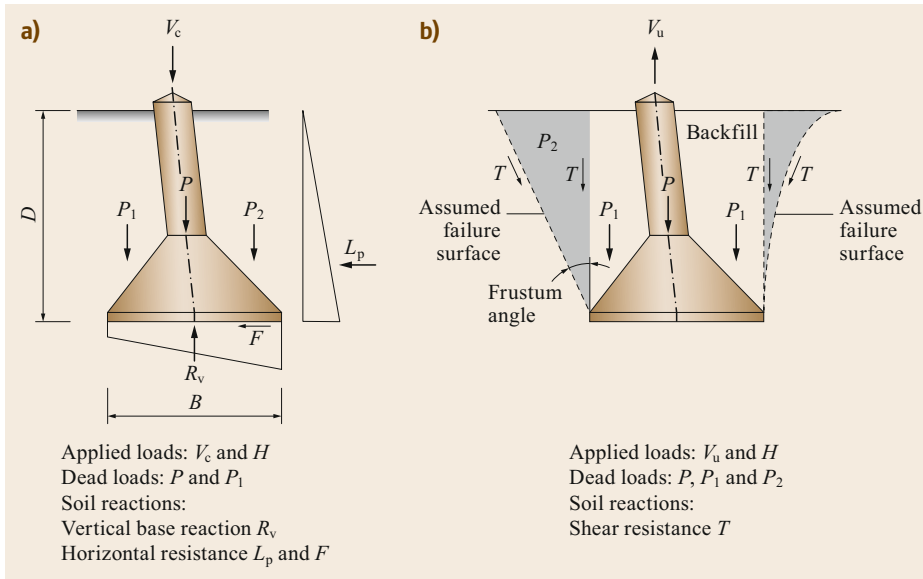
Category of test	Name of test or parameter measured	Remarks
Classification	Moisture content	Used in conjunction with liquid and plastic limits, it gives an indication of undrained strength
	Liquid and plastic limits (Atterberg limits)	To classify fine-grained soil and fine fraction of mixed soil
	Particle size distribution	Identification of soil type
	Mass density	
Soil strength	Triaxial compression	Both undrained and drained tests or undrained tests with measurement of pore pressure and required
	Unconfined compression	Alternative to undrained triaxial test for saturated nonfissured fine-grained soil
	Laboratory vane shear	Alternative to undrained triaxial test or unconfined compression test for soft clays
	Direct shear box	Alternative to the triaxial test for coarse-grained soils
Soil deformation	One-dimensional compression and consolidation tests	Compressibility indices for the in situ soil
Rock strength	Uniaxial compression and point load test	
Chemical	Mass loss in ignition	Measures the organic content in soils, particularly peat

**Fig. 9.155** Different types of anchor foundations (adapted from [9.259])

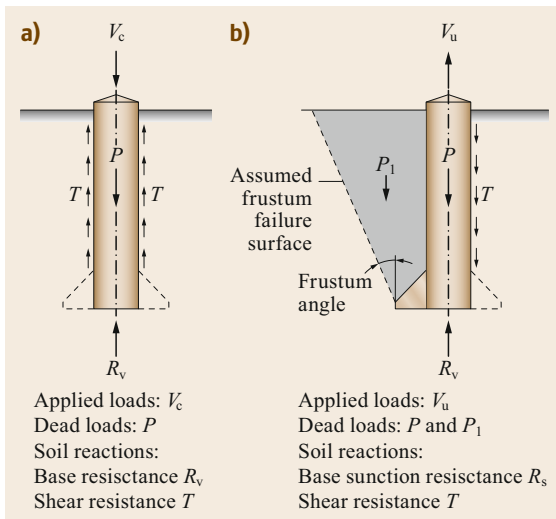
for steel lattice towers, and in particular of separate foundations for each tower leg, these being the most common type for high-voltage lines.

Each leg of a steel lattice tower and subsequently the related foundation must be able to sustain both

compression and uplift loads, as both wind directions perpendicular to the line axis have to be considered. Table 9.52 [9.261] provides an indication of the magnitude of the loads on the foundation for different voltage levels and tower types.



**Fig. 9.156a,b** Free body diagram of spread foundations: (a) compression, (b) uplift (adapted from [9.259])



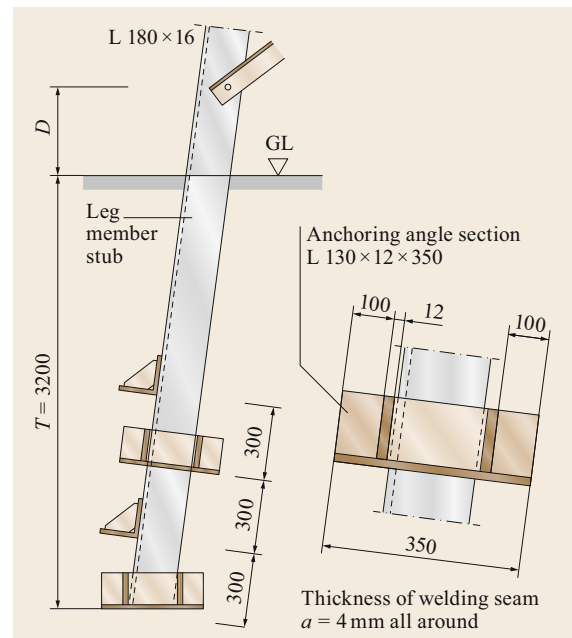
**Fig. 9.157a,b** Free body diagram of drilled shaft foundations: (a) compression, (b) uplift (adapted from [9.259])

**Table 9.53** Soil parameters

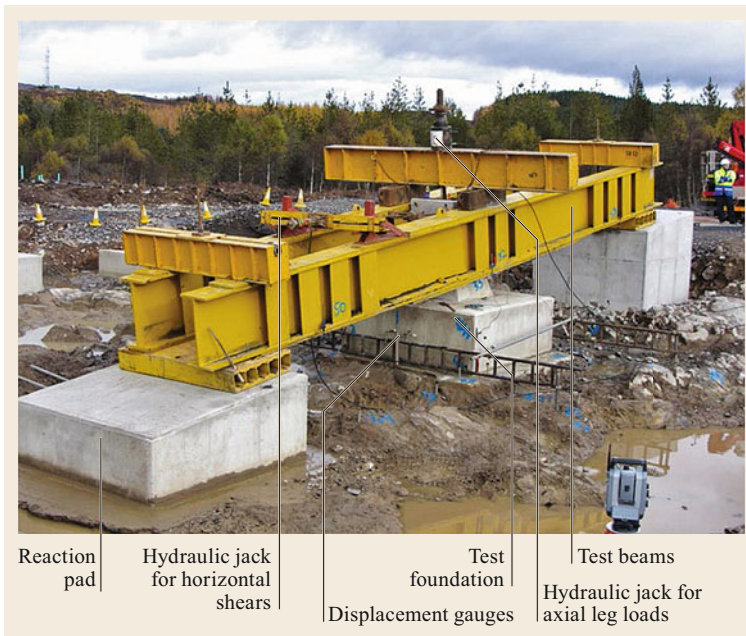
Parameter	Sand	Clay
Frustum angle ( $^\circ$ )	30–35	10–20
Shear resistance (N/mm $^2$ )	0	20–40

**Table 9.52** Forces on legs of steel lattice towers (adapted from [9.261])

Tower type	Voltage (kV)	Uplift (kN)	Compression (kN)
Suspension	110	10–25	12–30
	220	20–40	25–50
	380	30–150	40–180
Tension	110	30–60	35–80
	220	40–100	80–120
	380	80–200	100–350
Special (e.g., river crossing)		$\leq 400$	$\leq 450$



**Fig. 9.158** Anchoring of steel leg members in the concrete foundation (adapted from [9.4])



**Fig. 9.159** Full-scale test arrangements for a rock anchor foundation (adapted from [9.259])

The compressive loads are mainly resisted by the allowable soil pressure at the bottom of the foundation, and the uplift loads by the weight of the soil contained within an assumed failure surface. In some cases, also the shear forces acting at the surface of the foundation body in contact with the soil are taken into account. This concept is shown schematically in Figs. 9.156 and 9.157 for spread and drilled shaft foundations, respectively [9.259].

According to this design concept, the soil parameters are crucial; they can be determined from soil investigations and laboratory tests as explained above, but also from previous experience. For an initial assessment, the values in Table 9.53 are often used.

## 9.8 Construction

The construction of a high-voltage overhead line is a complex undertaking, being unique due to the fact that very few if any construction sites are so extended as a transmission line site. This requires high logistical skills but also considerable geotechnical expertise, as the soil and thus foundation type can and in most cases will change drastically along the line route. In addition, line construction encompasses the stringing of long lengths of conductors, which is a very special and demanding process not required in other construction works. In this sense, line construction has to

*Anchoring of leg members (stubs) into the concrete can be carried out either using additional cleats or by bonding between the leg member stubs and the concrete alone (Fig. 9.158 [9.4]). Usually, a connection just above ground level, between the lower main member and the stub itself, is provided to enable physical separation between the tower and the respective foundation. This practice is important for tower erection, but also facilitates the installation of a new tower over the existing foundation in case of tower failure.*

For system-critical lines and/or extreme soil conditions, full-scale foundation tests—primarily for uplift—are recommended, being by nature complex and costly, as is evident from Fig. 9.159 [9.259]. Thereby, the load on and displacement of the foundation are recorded.

follow highly demanding quality standards, also because the life expectancy of lines is set quite high by the asset owners, with values of 40–70+ years not uncommon, and some lines over 100 years old still being in service. In this sense, line construction considerably influences line maintenance, as it may initiate the application of suitable maintenance practices, including hot line techniques and robotics, as in most cases lines cannot be easily disconnected from the network for maintenance and/or repair purposes. Other challenges worth mentioning are difficulties with access and the

need to work in parallel on many fronts with many crews.

### 9.8.1 Survey and Tower Spotting

The on-site activities start with the transfer of the selected route to the terrain, in particular by fixing the angle points. The line axis is designed as a straight connection of the line angle points. Along the line axis, center-line beacons are installed to identify and secure the line. This step is called line alignment. A survey of the longitudinal profile follows, whereby the terrain and all objects within the right of way are surveyed, such as roads, stretches of water, buildings, and trees. The pegging of the support sites, characterized by their centers, and the survey of diagonal profiles at tower sites in inclined terrain, complete the survey activities on site.

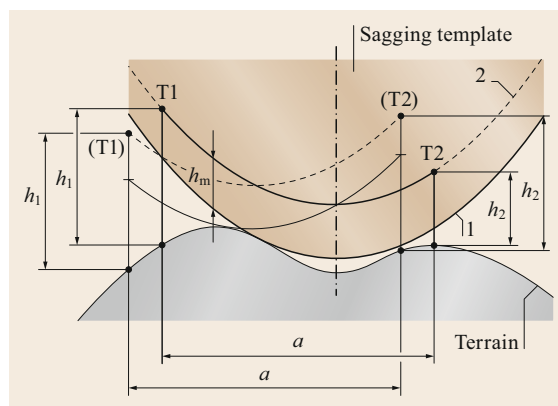
As in other fields, survey procedures have profited greatly from digitalization and automation. While in the past surveys were carried out using classical topography methods, i.e., using tachymeters, nowadays the process is accelerated and simplified and its accuracy improved, either by the use of so-called total stations, i.e., automatically recording theodolites, or with the help of real-time global positioning system (GPS) systems. Both approaches enable the measurement, correction, and immediate evaluation directly on site with a mean precision of profile points below 10 mm over distances up to 3 km [9.4, Sect. 15.3].

So-called indirect survey systems are also often used to record the route corridor, either based on photographs (*aerial photogrammetry*) or using signals obtained by scanning.

The more recently developed light detection and ranging (lidar) method adopts rotating lasers installed on an airplane or helicopter to scan the Earth's surface and existing installations such as overhead lines.

Using GPS, the position of the helicopter can be controlled to provide a continuous three-dimensional determination of the laser positions. The helicopter flies at approximately 100 m above the ground at around 50 km/h. The laser scanning method enables one to survey the position of any objects in three dimensions. It is possible to scan 200 km of lines per day, whereby digital profiles are obtained with the relevant information on the terrain, infrastructure, and existing lines.

As a result of the terrain survey, a longitudinal profile of the line route with all information relevant for the detailed line design such as type of terrain and utilization, crossed traffic roads, waters, and railways is available. In the next step, the support locations have to be defined and the support types and heights determined; this is known as tower spotting, which in the past was done manually by the design engineer. Although nowa-



**Fig. 9.160** Manual tower spotting with the aid of a sagging template (1: ground clearance curve; 2: conductor catenary curve; T1: suspension tower 1; T2: suspension tower 2;  $h_1$ : height of T1;  $h_2$ : height of T2;  $h_m$ : minimum ground clearance;  $a$  span length) (adapted from [9.4])

days this process is carried out by specialized computer programs, it is instructive to understand its basic principles (Fig. 9.160 [9.4]). The route profile drawing and a template showing the catenary to the same scale as the profile drawings were used, and a so-called sagging template was produced based on the sags related to the expected equivalent span (ruling span, Sect. 9.4.4) and maximum conductor temperature. In parallel to the ground curve, which is represented by the edge of the template, the conductor catenary is shown at a distance according to the stipulated ground clearance. If the template touches the terrain, this parallel curve represents the conductor position and enables the conductor attachment points to be determined and the clearances to crossed objects to be checked.

### 9.8.2 Transportation and Site Clearance

Line construction is basically a serious logistics issue, as heavy material has to be transported and correctly deposited at construction sites—the tower locations—which are a few hundred meters apart and often span from the beginning to the end of the line over distances of many—sometimes hundreds—of kilometers. This activity is combined with the construction of access roads required to bring in materials and construction equipment to the individual tower sites and also for the clearing of the ROW of the line from vegetation, as this, if left to grow, can cause—and has caused—serious operational problems, such as persisting earth faults. Clearing techniques range from the use of shear blades to remove most of the vegetation to the use of chain saws to remove individual trees as well as manual methods in sensitive, selective clearing areas.

### 9.8.3 Foundations

Foundations provide stability to the supported structures and protection from extensive deformation or failure; if not constructed properly, the consequences for the overall transmission line system can be catastrophic. Publication [9.262] provides a comprehensive overview of various foundation options and also contains an installation guide, a review of health and safety concerns, as well as an assessment of the environmental impacts and various mitigation measures. On the other hand, [9.263] deals with the installation of the micropiles and ground anchors that are often used for terrain with poor soil conditions or difficult access. An additional source of good information on foundation installation is the standard [9.264].

#### Excavation

The foundation installation process starts with excavation. To start with, a trial pit is excavated at a structure site to identify the soil conditions. Hydraulic excavators are often used for the excavation in normal soils such as clay. Excavations with unshielded walls may only be performed in unsaturated soils and while maintaining safe wall inclination. In rock, hydraulic hammers or explosives may be required. Other construction equipment used in excavations include trucks, energy generators, vibration plates, jumping jacks, vibration hammers, levelers, etc. During excavation, water should be prevented from entering the foundation excavation; when required, an appropriate drainage system is used. During foundation works, increasingly extensive—and costly—measures are required to minimize the negative impact on the environment and surroundings.

#### Concrete and Reinforcement Works

In a first step, the tower stub angles are positioned in the excavation prior to insertion of the steel reinforcement. Proper alignment of the steel stub angles is achieved by the use of rigid steel templates. The reinforcement bars/rods should be joined by means of tie wire or welding. To ensure proper setbacks, plastic distance holders providing a minimum distance between the reinforcement and formwork are used.

The concrete used in foundation works may be mixed directly at or delivered to the site from a concrete mixing plant. While pouring the concrete in the foundation pit, the free drop height of the concrete mix should be made as small as possible, i.e., should not exceed 100 cm. After pouring, the most widespread method of concrete consolidation is vibration. In practice, vibrations are applied to the mix for 10–30 s using internal or external vibrators. Proper concrete curing is essential to achieve the desired mechanical parameters. The concrete, particu-

larly in the summer time, requires proper humidity to be maintained. Unrestricted water evaporation can lead to undesired concrete shrinking. Therefore, the concrete must be protected from water loss due to extensive wind and temperature, using a special curing compound, covering with foil, or pouring with water.

#### Backfilling

Backfilling is crucial to achieve the desired uplift resistance; i.e., the main target of proper backfilling is to achieve soil characteristics close to those of natural soil, the most popular method being the compacting of the backfill. For this purpose, noncohesive backfill should be placed in layers of 20–25 cm and compacted using vibration plates, jumping jacks, or vibration hammers. Compaction can be improved by dampening the filling with water. Another method for increasing the load-bearing capacity is stabilization with cement. Cohesive soils should be condensed in layers every 20–25 cm, using nonhammering methods, e.g., tamping rollers or vibration plates. Dampening the filling soil with water is in this case a gross mistake.

### 9.8.4 Supports

Essential for the efficient erection of steel lattice towers, the most common type of line supports in all parts of the world, is good logistical planning, as multiple resources are active simultaneously on site and also large quantities of steel angles, nuts and bolts, and gusset plates have to be delivered from a marshaling yard called the *cemetery* at the different tower locations bundled by *component*.

#### Tower Erection

This is amongst the activities posing the highest safety risks to the construction crews, and therefore it requires special individual and collective protection and strict compliance with safety rules. As a general safety rule, every piece of equipment, tools, ropes, pulleys, hooks, safety clamps, etc. must be inspected, calibrated, and have their nominal capacity tested and certified, prior to release to sites and being put into service. There are four main methods of erection of steel lattice transmission towers, as described below.

**Manual Method.** This method consists of building the tower, member by member, from the bottom upwards. The tower members are laid down serially on the ground according to their sequence and as close as possible to their erection position, to avoid delays. While this approach is still used extensively in many parts of the world, it is a labor-intensive and low-productivity method and is only suitable if the use of heavy equip-

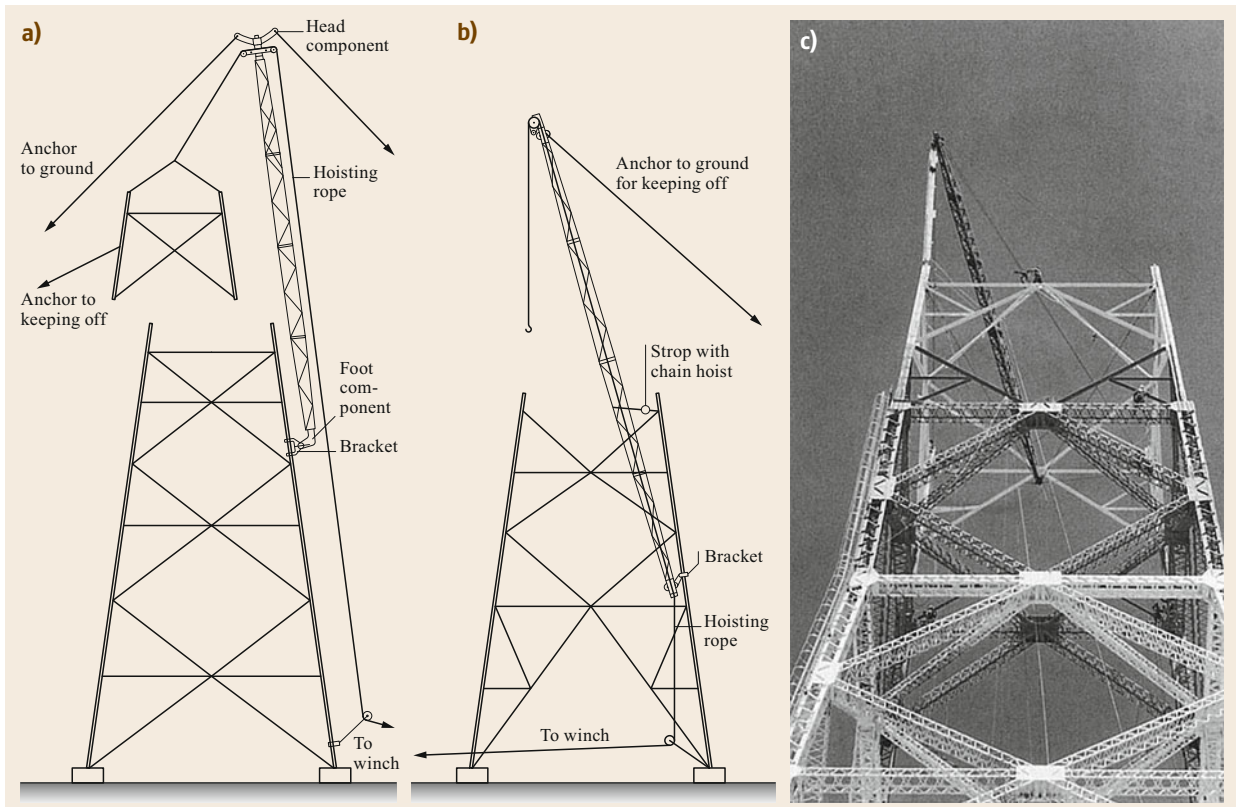


Fig. 9.161a–c Erection with a gin pole outside (a), inside (b), and at the center (c) of the tower body (adapted from [9.4])

ment, such as a crane or helicopter, is not feasible and there is qualified and cheap labor available, and/or access to the tower location is difficult.

**Section Method.** This method consists of preassembling the major sections of the tower on the ground and then rigging and lifting them using a gin pole. The gin pole used consists of a steel or aluminum truss-type beam, approximately 10 m long and held in place by means of guys. We distinguish between an *outside* and an *inside* gin pole (Fig. 9.161a,b), and a gin pole at the center of the tower (Fig. 9.161c); the picture shows the erection of the tower for the Suez Canal crossing, the latter being especially suited for towers with large width and/or at tower locations with limited space, as no anchors to the ground are necessary.

**Tilting Method.** This method consists of assembling the whole tower or part of it on the ground and then lifting it as a complete unit using a mobile crane (Fig. 9.162). This is the most productive method for the erection of self-supporting towers, particularly in flat terrain with good access conditions.



Fig. 9.162 Lifting of the upper part of a 400 kV Danube type tower (photo Eduard Steiner AG/CH)



**Fig. 9.163** Tower erection using a helicopter (photo Edward Steiner AG/CH)

**Helicopter Method.** The use of helicopters may be advantageous when towers have to be erected within very short periods of time, lines are converted, or access is difficult, e.g., in mountainous terrain. The use of helicopters, however, is expensive and connected with stress for the erection staff, and to a great extent weather dependent. To achieve an economic advantage, the components of the tower are preassembled on the ground surface corresponding to the capacity of the helicopter used (Fig. 9.163). It may be worth mentioning that helicopters have weight-lifting limitations of up to 8000 kg.

Wood, concrete, and steel poles are often erected by manual tilting, with the use of cranes, or in difficult terrain by helicopters.

**Installation of Bolts.** After erection, the bolts (and nuts), which have been placed but not fully tightened in order to give the structure some flexibility to sus-

tain erection loads, have to be fixed (a torque wrench is mandatory), observing the prescribed torques as per Table 9.54 [9.4].

### 9.8.5 Conductor Stringing

Installation of overhead conductors is unique, as its theater of activities is a long, narrow corridor of a few kilometers in length, being considered by many to be the most challenging task in transmission line erection. Careful planning and a thorough understanding of pull requirements and stringing procedures are needed to prevent damage to the conductor during stringing operations. The selection of stringing sheaves, tensioning methods, and measurement techniques are critical factors in obtaining the desired sagging results. Conductor stringing, sagging equipment, and techniques are discussed in detail in [9.265]. There are three stringing methods: the tension method, the slack method, and the helicopter method. These are briefly described below.

#### Tension Method

By far the most common method used for conductor stringing is the tension method. In this method, the conductor reel is mounted on a payoff that is capable of applying a braking force to the reel to maintain tension on the conductor. The conductor is then strung (or *reeved*) through a multigroove bull-wheel tensioner so that the conductor is under tension during pulling and is not allowed to contact the ground (Fig. 9.164 [9.4]). At the other end of the line section to be strung, i.e., between two strain towers, sits the nowadays hydraulically driven, *twin bull-wheel puller*, in order to haul the conductor, but also the pilot and/or the pulling rope.

It is important to coordinate the bull-wheel speed with the puller speed to prevent excessive sagging or dynamic loading (*jerking*) of the conductor during the pull. In a typical tension stringing operation, blocks, also known as *travelers* or *sheaves*, are attached to each structure or the end of an insulator string. For new constructions, a pilot line is pulled through the blocks and used to pull in a heavier pulling line, which is then used to pull the conductor through the blocks, while for re-conductoring applications, the existing conductor can be transferred to the blocks at each tower, then connected to the new conductor and used to pull in the new conductor as it is removed.

**Table 9.54** Typical torques for bolt tightening (adapted from [9.4])

Bolt type	M12	M16	M20	M22	M24	M27
Bolt diameter (mm)	12	16	20	22	24	27
Torque (N m)	40–60	80–120	130–180	190–230	300–340	475–610

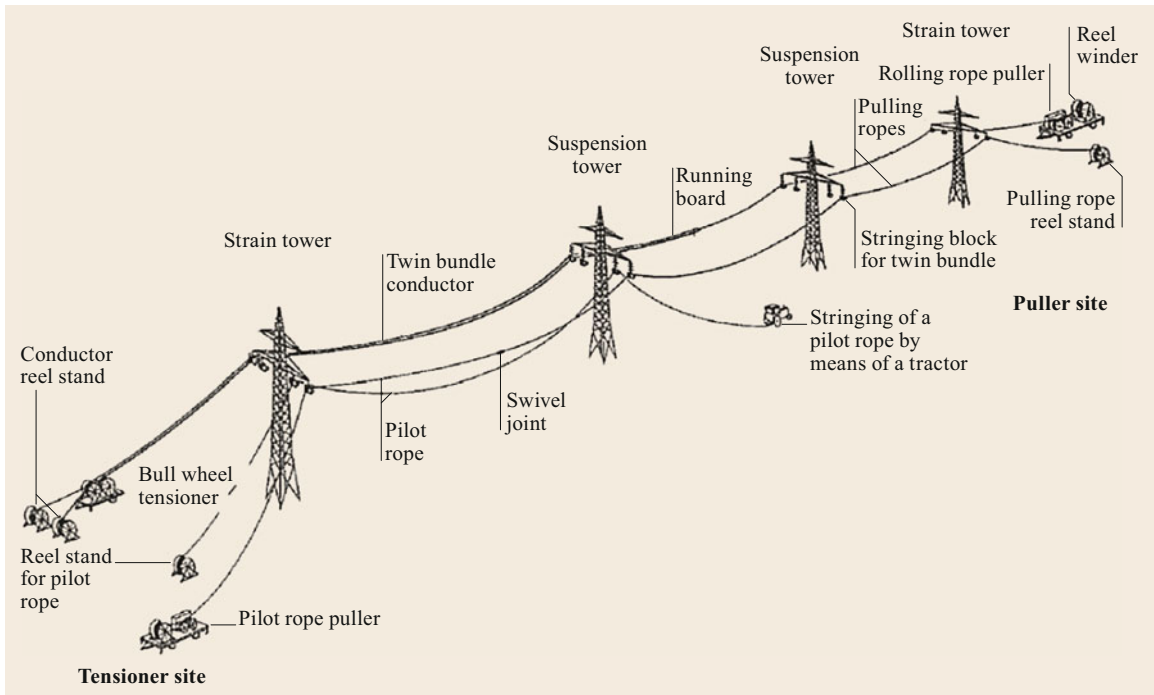


Fig. 9.164 Stringing of a twin bundle conductor (adapted from [9.4])

#### Slack or Layout Method

Slack stringing of a conductor is limited to lower-voltage distribution lines and smaller conductors, where some surface damage is tolerable. The conductor reel(s) are placed on reel stands (*jack stands*) at the beginning of the stringing location. The conductor is unreeled from the shipping reel and dragged along the ground by means of a vehicle or pulling device. This method requires heavy traffic in the ROW and is not recommended for transmission applications.

#### Helicopter Method

Helicopters are engaged in stringing operations in case of terrain with difficult relief and poor accessibility to the support locations and at the same time reduce construction time considerably. The main tasks are as follows:

- Linemen are transferred via helicopter to each structure, where they climb the towers. They then hang the stringing wheels on each conductor suspension point, i.e., at the line end of the insulator string.
- Synthetic rope is hooked onto the helicopter and pulled through the stringing wheels.
- Wire rope is connected and pulled back the opposite way through the stringing wheels.

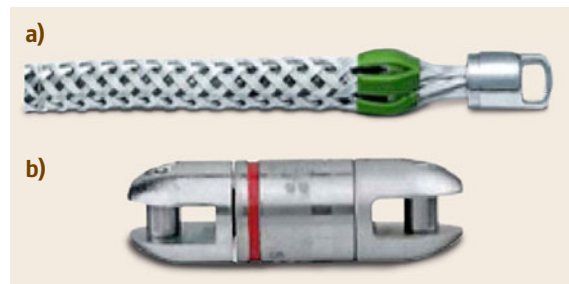


Fig. 9.165a,b Basket grip (a) and swivel (b) (adapted from [9.266])

- The conductor is connected and pulled back through the stringing wheels using a puller located on the ground, as in most cases it is too heavy to be pulled by the helicopter.
- The stringing wheels are removed from each suspension point.

#### Ancillary Equipment

During stringing, it is necessary to use the proper tool to grip the conductor strands evenly to avoid damaging the outer layer of wires. The preferred grip type is often referred to as a *basket grip* (Fig. 9.165a). It is often used because its flexibility and small size make it



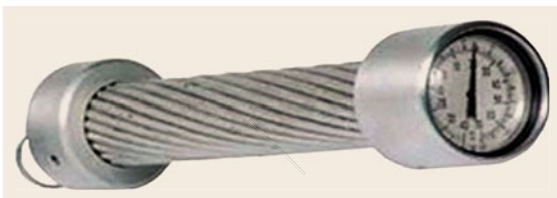


**Fig. 9.166** Single lined block (adapted from [9.266])

easily pulled through blocks during the stringing operation. A *swivel* should be installed between the pulling grip and pulling line, or between grips when double-socked, to allow free rotation of both the conductor and the pulling line (Fig. 9.165b) [9.266].

Also crucial to the success of stringing is the use of proper stringing blocks (Fig. 9.166 [9.266]). These consist of one or more sheaves or pulley wheels enclosed in a frame to allow their suspension from insulator strings and with a latching mechanism for insertion and removal of the conductor during the stringing operation. Blocks are designed for a maximum safe working load, which must not be exceeded during pulling or sagging.

Sheaves are often lined with neoprene or urethane to prevent scratching of the conductor, while the block diameters (at least 20 times the conductor diameter) and groove design must be properly sized for the conductor being used. Proper maintenance is essential, since high longitudinal tensile loads can develop on transmission structures if a block should *freeze* during tension string-



**Fig. 9.167** Sagging thermometer (adapted from [9.266])

ing, possibly causing conductor and/or structure damage and posing a safety risk to the construction crews.

Since most sagging information is given relative to the conductor temperature, a sagging thermometer (Fig. 9.167 [9.266]) should be used to accurately determine the temperature of the conductor. This handy equipment contains a bimetal thermometer mounted on a short piece of a conductor mock-up, allowing the user to accurately determine the temperature of the conductor being sagged and not just the ambient temperature.

### Sagging

Once the conductor has been pulled in and is lying in the blocks, the conductor can be pulled up to the design or *sagging* tension, as determined in Sect. 9.4.4. For this purpose, a grip is applied to the free end of the conductor and the grip is attached to a ratcheting tensioning device, like a come-along, to pull the conductor up to sag.

There are three different methods available for sagging lines, using a transit, a stopwatch, and a dynamometer. Publication [9.265] lists three methods of sagging conductors with a transit: *calculated angle of sight*, *calculated target method*, and *horizontal line of sight*. In the stopwatch method, by initiating a pulse on a tensioned conductor and measuring the time required for the pulse to move to the nearest termination and back, the tension and sag of the conductor can be determined. Sagging with a *dynamometer* is sometimes used for small conductors over one or two spans.

Last but not least, sagging must consider the unavoidable conductor creep described in Sect. 9.4.3. To provide for creep, the conductor sag should be calculated not for the ambient temperature during sagging but for a lower temperature; the temperature difference  $\Delta T$  can be calculated from

$$\Delta T = \frac{e}{\alpha}, \quad (9.134)$$

where  $e$  is the creep strain (Sect. 9.4.3) and  $\alpha$  is the coefficient of thermal expansion of the conductor (Sect. 9.4.4).

Often, crews wait some days or even weeks before fixing the conductor in the clamps in order for the conductor creep to have settled.

OPGW stringing is similar, but typically involves fiber splicing, a specialized activity.

### 9.8.6 Installation of Conductor Hardware

For installation but also inspection and maintenance, it is common to work in-span on the conductors, shield wires, and perhaps optical ground wires (OPGW). This



**Fig. 9.168** Spacer installation on a horizontal twin bundle with the help of a cart [9.267] ◀

is often done by using carts or man-baskets, although sometimes the work is done without any apparatus at all to support and transport the person(s) on the wires. Working in-span on conductors is common, especially when accessibility using alternative methods such as the use of bucket trucks, cranes, or helicopters is problematic or restricted. Carts are wheeled rigs that ride along single and bundle conductors, ground wires, and OPGW. Typical examples of their use are for installation of spacers, dampers, or aircraft warning markers (Fig. 9.168 [9.267]).

## 9.9 Maintenance

### 9.9.1 Maintenance Activities and Strategies

Due to difficulties encountered in building new and even upgrading existing lines, and since many lines worldwide are approaching their design life or beyond, a good maintenance strategy is important to ensure their integrity and reliable operation. Defects and failures of overhead lines occur in practice due to:

- External causes such as lightning, earth faults in the grid, extreme weather conditions, and very seldom sabotage, as well as mechanical impacts (i.e., vehicular collisions)
- Internal causes such as wear, aging, deformation, corrosion, and poor construction or materials
- Operational aspects such as electrical overload, switching overvoltages, and improper functioning of protection and control
- Approaching the projected end of life of the line.

*Maintenance activities* can be divided into three basic categories:

- Periodic normal maintenance
- Preventive maintenance or component repair
- Emergency restoration or repair.

Periodic normal maintenance consists of activities such as:

- Vegetation management
- Tower painting
- Insulator washing.

The optimum time intervals between these activities can be determined based on risk assessment and cost evaluation [9.268, 269].

Preventive maintenance or component repair consists of activities such as:

- Damaged insulator replacement
- Conductor repair
- Joint replacement
- Spacer and spacer damper replacement
- Repair of structural tower members or foundation repair
- Correcting electrical clearance problems, as these may have been affected by conductor creep, new buildings near the line, etc.

Finally, *emergency restoration* is usually a result of component failure and therefore line failure, or the result of major storm damage, sabotage, or delayed maintenance [9.270]. The key to the development of an adequate emergency response plan is for the asset owner and senior management to commit to a proactive long-term plan for responding to anticipated emergency situations, and the formulation of a corporate policy on how the utility will respond to emergencies.

Formulating a successful transmission line *maintenance strategy* is dependent on the transmission line asset owner's drivers and constraints. The maintenance strategy will depend on the asset owner's particular environment, the existing condition of assets, and perhaps most importantly, how critical a line is to the operation of the network. However, no matter what the maintenance activities are, they all share similar requirements that must be considered when developing a successful maintenance strategy. These include:

- Prioritizing the transmission lines
- Periodic inspection of the lines
- Database management

- Consideration of in-house or outsourcing of maintenance work
- Performing live work or deenergized work
- Planning for people, equipment, and training
- Finding outside resources
- Condition assessment
- Benchmarking and continual improvement.

### 9.9.2 Common Defects and Condition Assessment of Line Components

In the following, common defects found in different line components are presented, together with the techniques currently employed for their detection in situ.

#### Conductors and Associated Hardware

**Corrosion.** Steel corrosion of conductors is principally caused by industrial and salt pollution in the environment in the presence of moisture. The state of conductor corrosion is often checked using a so-called overhead line corrosion detector (OHLCD). It introduces eddy currents into the conductor from a coil that clips around the conductor and measures with a second coil the irregularity in the induced magnetic field in regions where the galvanization of the steel core has been attacked. The OHLCD can also be used on ground wires made of galvanized steel by adding to the sensing head a plastic shell with an adequate number of aluminum wires fit in it to simulate an ACSR conductor.

Aluminum corrosion of conductors by sulfurous pollutants deposited on the outer surface of the conductor causes pitting of the surface. Normally, this type of corrosion is evenly spread on the outside of the conductor and does not reduce its strength to the same extent as internal corrosion; it can be detected by visual inspection of conductor bulging due to the corrosion products from the discoloration of the aluminum strands.

**Damage from Wind-Induced Vibration.** As explained in Sect. 9.4.11, overhead lines are often affected by wind-induced vibrations; these can initiate the following forms of damage:

- Drooping/missing/slipped vibration dampers (Fig. 9.169)
- Missing nuts from suspension clamps or hardware
- Split pins missing or displaced
- Corona rings or insulator strings displaced
- Broken conductor strands (Fig. 9.57)
- Aircraft warning markers moved or missing
- Loose or broken tower members
- Severe wear of suspension hardware (Fig. 9.170) [9.271].



Fig. 9.169 Drooping vibration dampers (20 past 8 o'clock look)

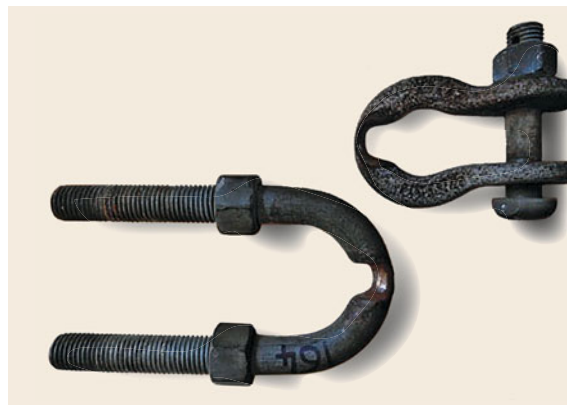


Fig. 9.170 Wear of string hardware

Inspection techniques include visual inspection from the ground or a helicopter, use of a stabilized video camera (helicopter), and corona measurements. The latter help to detect broken strands as their sharp edges lead to high field gradients that cause high-frequency corona discharges (Sect. 9.4.6). Quite recently, an innovative equipment which can detect broken strands, also inside the conductor, using x-ray technology was presented [9.272].

**Conductor Joints.** Most joints used on ACSR are of the compression type, although bolted joints are often used in jumpers. Inadequate compression due to poor joint design or problems during installation, such as use of the wrong dies, can lead to aluminum oxide formation within the joint, a related resistance increase, and excess current flowing in the steel core of the conductor, which can then overheat and ultimately rupture. Consequently, the electrical resistance of a joint is the main factor used to assess its condition (Sect. 9.6.1). Measurement of joint temperature using infrared photography—normally with resolution of



**Fig. 9.171** Thermographic joint inspection performed from the ground (adapted from [9.271])

1 °C—from the ground (Fig. 9.171 [9.271]), and comparison with the detected temperatures at the conductor, can be a time-saving method that enables a utility to get a good indication of the condition of the joints along a line. A recommendation for the evaluation of such measurements is proposed in [9.273].

The absolute temperature difference method can be described as follows:

- a. Detection principle: The highest temperature of conductors or line fittings 1 m from the measured object, operating normally, acts as the reference temperature. The temperature of the measured object is  $t$ , then there is  $\Delta t = t - t_a$ , and  $\Delta t$  is used to judge the thermal defect. It is regarded as a minor fault when  $\Delta t$  is below 10 °C; it is regarded as a general fault when  $\Delta t$  is between 10 and 20 °C; and it is regarded as a serious fault when  $\Delta t$  exceeds 20 °C.
- b. Detection characteristics: The absolute temperature difference method is able to eliminate the effects of an additional temperature rise caused by solar radiation. At the same time, because of the inaccuracies of parameters such as similar orientation, detection distance, environmental temperature, humidity, and wind speed, the errors decrease correspondingly.

Further details are described in [9.213] as well as other measurement methods such as:

- Electric resistance test
- Magnetic resistance test

- Radiography (x-ray) test
- Boroscope test.

**Aged Fittings.** Nowadays, as the erection of new lines faces problems in many countries, it is of paramount importance to develop reliable testing techniques for the evaluation of aged string and conductor fittings and to decide whether it is safe for them to remain in service or if they have to be replaced. This issue is covered extensively in [9.233]. Therein, aged fittings are defined as those installed for over 30 years. It is also recommended to cut out a representative number of fitting samples with a sufficient length of conductor without opening the fittings.

**Carts for In-Span Work.** As line components age, concerns arise regarding the safety of in-span work insofar as it increases the mechanical tension in the conductor, which may be weakened. Publication [9.267] identifies the factors that affect the structural integrity of aged conductors and the risks associated when carts are used, and provides guidelines for inspection and assessment of safe conditions as well as alternative methods for dealing with presumed unsafe conditions. These include lowering the damaged conductor to the ground or to the level of another undamaged conductor, using a bucket truck or a crane, a helicopter, or applying robotics (Sect. 9.9.4).

### Insulators

**Porcelain Insulators.** Broken insulator sheds can result from vandalism and defects induced during the manufacturing process. However, the main cause of failure of porcelain cap-and-pin insulators is corrosion of the steel pin in the cap and of the pin assembly, as the expansive corrosion products create a tensile hoop stress, which leads to radial cracks in the porcelain. On the other hand, porcelain longrods have very seldom failed because of unnoticed inferior quality of the raw material.

**Glass Insulators.** With glass insulators, discharges erode the glass and pin, and after fairly minor surface damage, the imbalance in the internal mechanical stresses in the toughened glass causes the shed to shatter completely.

Publication [9.199] provides guidance on how to check the state of insulators and determine the appropriate time for their replacement.

**Composite Insulators.** For composite insulators, which in the meantime have developed as a viable alternative to porcelain and glass, degradation can occur through premature aging or internal manufacturing de-

fects. The latter are the subject of discussion when live line working (Sect. 9.9.3) is an issue, as they cannot be easily detected visually.

**Inspection Techniques.** The inspection techniques listed below can be used for porcelain and glass insulators:

- Visual inspection
- Insulator voltage drop
- Electric field
- Infrared (IR) thermography
- Ultraviolet (UV) detection
- Radiofrequency/microwave emission detector.

In addition, for composite insulators, directional wireless acoustic emission, combined IR–UV measurements (Multicam), and a recently developed high-frequency high-voltage measurement tool, which is directly applied to the insulator using a hot-stick, can be used as fault-detection techniques.

The assessment of aged, old, or failed composite insulators, in order to evaluate their technical condition and reach a conclusion regarding their residual life expectancy with the help of specific laboratory testing, is covered extensively in [9.198].

### Supports

**Steel Towers.** Most supports are constructed using galvanized steel members. Normal maintenance practice is to paint them with protective coatings at regular intervals, typically 10–25 years, depending on the pollution level of the environment. In addition, the support members can be subjected to buckling due to soil movement, loose bolts, or broken members. Excessive wind movements can also cause loose bolts and member failure.

The following inspection techniques may be used to assess the steel structure condition:

- Visual climbing inspection
- Binoculars
- Telescope
- Camera
- Electronic paint and galvanizing thickness measurement
- Cross-hatch cut test.

The latter is the method by which the adhesion values for the paint on the support members as specified in [9.274, 275] can be ascertained.

**Wood Poles.** The main damage to which wood poles are subjected is the degradation of their mechanical

strength due to wear and decay of the wood or the action of insects and woodpeckers. Decay takes place mainly in the ground line zone, where humidity, fungi, bacteria, and pollutants may penetrate inside the pole through natural cracks in the wood or passages created by insects. To protect the pole from these agents, the wood is treated prior to installation. Supplemental in situ treatments may be applied to prolong the life expectancy.

### Concrete Poles

Concrete poles may suffer from cracks in the concrete caused by inappropriate manufacturing (poor mixture or short curing). Water ingress can then corrode the steel bars and even cause catastrophic damage. Remedial approaches include sealing of the cracks by special design and bandaging of the pole by fiber-reinforced tapes at the crack location.

### Foundations

Although for the majority of foundations, when properly constructed, there are no significant modes of degradation, many utilities have to deal with subsurface corrosion. Also, cracks on the upper part of the foundation are relative frequent. Uplift failures can occur if the stub is insufficiently encased in the block or the cleating is inadequate, as well as corrosion of the tower steel when moisture and oxygen are present. These can be detected by using appropriate inspection techniques ranging from the simple (visual) to sophisticated, such as *surface-penetrating radar* and *acoustic pulse echo*. It is also prudent to check the earthing conditions, as this may have deteriorated, e.g., through corrosion of the earthing rods or poor contact of the earthing leads.

## 9.9.3 Live Line Work

Live line work (LLW), i.e., work on energized circuits, has been carried out in different parts of the world for many decades. Live work is the preferred method of maintenance when system integrity, system reliability, and operating revenue are at a premium and removal of the circuit from service is not acceptable. Live work may also be beneficial—and has been used—in construction, upgrading, and uprating.

Most maintenance operations that are performed deenergized can also be performed using live work techniques. To do so requires proper operating procedures that take into account the complexity of the task and technical standards with regards to equipment, procedures, safety, and quality assurance as described in [9.276].

The feedback from utilities performing live work on overhead lines is that the cost is comparable to that in



**Fig. 9.172** Replacement of twin spacers on a live 500-kV line with a helicopter

deenergized conditions. However, there is a minimum additional cost of 1 or 2 more days for preparation of live work plans. The following case study from [9.276] is instructive in order to understand the importance of LLW:

In this case study, a number of spacers which had damaged the conductor had to be replaced live on a 500-kV line with twin ACAR conductors in the USA. Consideration was given to completing the work either deenergized or live. With circuit outage constraint charges of USD 75 000 per hour, the decision was made to complete the work as live work over a 22-day period using a helicopter (Fig. 9.172), which involved changing 6208 spacers with a total cost of under USD 800 000, corresponding to approximately 10 h of outage cost.

#### 9.9.4 Transmission Line Robotics

The expected increase in live line work approaches has stimulated the development and use of robotic devices to minimize the risk to field personnel safety and maintain power system reliability. In the following, an overview and assessment of the future possibilities for transmission line robotics is presented, extracted



**Fig. 9.173** UAV with propeller side protection and camera for visual inspections (adapted from [9.277])

from [9.277]. The following classes of robots are identified:

*Ground-based robots* are designed to remotely capture and control energized conductors and execute tasks that are far beyond human capability from a mechanical and electrical stress perspective and cannot be easily performed with traditional live line tools such as hot-sticks.

*Line-suspended robots* are designed to perform visual inspection of transmission lines in difficult areas, such as large rivers or mountainous terrain. For this purpose, they are equipped with different types of cameras as well as special sensors, e.g., in order to measure the electrical resistance of splices, to record corona-induced audible noise, and to detect corrosion and/or broken conductor strands. One of the first applications of such robots has been conductor deicing [9.278].

*Aerial-based robots* are also designed to perform visual inspections, but in this case unmanned aerial vehicles (UAV) are used. These are normally equipped with GPS, camera, and image transmission equipment and are able to fly on predetermined routes along the power transmission line and wirelessly transmit the images taken to the base station (Fig. 9.173 [9.277]). The inspection costs of this UAV are about half when compared with the costs of a conventional manned helicopter.

Other types of robots have been developed for live line dry cleaning with brushes and live line inspection of insulators by measuring the resistance and the voltage distribution along the insulator, as well as for performing simple repair work such as installation of repair rods.

## 9.10 Uprating and Upgrading

Many countries with major electrical infrastructure are frequently confronted with four coinciding critical issues:

- Much of this infrastructure was constructed in the 1950s and 1960s, which result in the age of the assets being over 50 years.
- The design life of much of the infrastructure is in many cases about 50 years and has matured beyond the engineering serviceability and/or economic life and requires some form of life extension.
- The need to increase the capacity of the existing infrastructure places extraordinary demands on utilities to establish strategies to uprate the existing infrastructure.
- Approvals for the construction of new overhead lines are often difficult to obtain and in many cases result in critical delays to meet network capacity needs.

These issues and how they can be addressed are discussed in detail in [9.279], wherefrom the information presented here is extracted.

Therein, *upgrading* is defined as increasing the original structural strength of an item due to, for example, a requirement for higher meteorological actions or increasing the original electrical performance of an overhead line. Upgrading results in a decrease in the probability of failure but does not change the consequences of failure.

*Uprating* is defined as increasing the electrical characteristics of a line due to, for example, a requirement for higher electrical capacity or larger electrical clearances. Since uprating will mainly increase the electrical capacity of the line, consequently it will potentially increase the consequences of a line failure.

A few years ago, the CIGRE launched a questionnaire to determine international practice on this subject, the response being excellent. The answers and their evaluation are included in [9.279] and can be summarized as follows:

- 43 utilities from 20 countries representing all continents responded.
- 183 lines with voltages ranging from 33 to 765 kV were described.

- In many cases, high-temperature low-sag (HTLS) conductors (Sect. 9.4.9) were used to increase the current plus composite insulators (Sect. 9.5.5) to modify the tower-top geometry in order to increase the voltage.

Table 9.55 presents the share between uprating and uprating applications.

The factors affecting the decision for uprating/upgrading works mentioned in the answers to the questionnaire are ranked below according to preference (total votes 40):

- 68% (27 votes): lower investment of the works
- 58% (23 votes): lower life cycle assessment costs (investments, losses, O&M)
- 35% (14 votes): unacceptable mechanical or electrical reliability
- 18% (7 votes): real return periods lower than design
- 13% (5 votes): political costs of unavailability.

Last but not least, the uprating/upgrading costs were compared with the construction of a new equivalent line, yielding quite a wide range from zero to 100% with a mean of 33% and a median of 20%.

### 9.10.1 Uprating

In recent years, technologies for line uprating have been developed. The basic idea is to use existing line corridors to transfer more power, which can be done by increasing the line current, the line voltage, or both (Table 9.56).

For uprating actions, increasing the current rate is significantly more popular than increasing the voltage level, with 71% or 30 cases for increasing the current rate and 24% or 10 cases for increasing the voltage level. Table 9.57 provides a list of the most common voltage and current uprating mechanisms and the associated techniques, methods, and processes. More details can be found in [9.279].

The following factors should be taken into account before increasing line ampacity:

- Cost of losses: Uprating a line without increasing the aluminum area of the conductors or decreasing

**Table 9.55** Share of uprating and upgrading applications (adapted from [9.279])

Main action	Uprating	Upgrading	Total
No combination	Uprating only 57% (24 cases)	Upgrading only 12% (5 cases)	69% (29 cases)
Combination	Uprating with upgrading 21% (9 cases)	Upgrading with uprating 10% (4 cases)	31% (13 cases)
Total	78% (33 cases)	22% (9 cases)	100% (42 cases)

**Table 9.56** Options for uprating

Increasing	Method	Tool
Current rating	Increasing temperature	Increasing height attachment point Retensioning
	Reconductoring	Compact/smooth conductor High-temperature conductor
	Special engineering methods	Statistical approach Real-time approach
Voltage level	Reinsulation	Adding/substituting insulators, adjusting gaps Cross-arm modification
	Ground clearance	Increasing height attachment point Retensioning
	Phase-phase distance	Conversion of 2 to 1 circuit New tower top

the resistance will result in increased losses. The increased cost of losses, preferably from a system rather than a single line viewpoint, needs to be determined to decide on the best action to take.

- Condition of current-carrying clamps: The clamps need to be in a position to carry an increased current load. This implies that clamps that appear sound at

present loads may fail at the increased load. These connectors therefore need to be checked, preferably by resistance checks to ensure that the resistance of the clamp is lower than that of an equivalent piece of conductor.

- Actual templating or design temperature: The actual as-built templating or design temperature is normally found to be different from that assumed in the determination of the ampacity. This is due to sagging or surveying or location of towers not being as planned. It is therefore critical to determine the present templating or design temperature of the line. This can only be achieved by surveying the line with the temperature of the conductor known.
- Condition of conductor: The conductor could have been damaged by gunshots, lightning strokes, vibration, poor securing of clamps, or other such incidents. The entire conductor therefore has to be checked in detail. Any nicks or damaged strands need to be repaired using repair sleeves or equivalent.

#### Uprating Case Studies

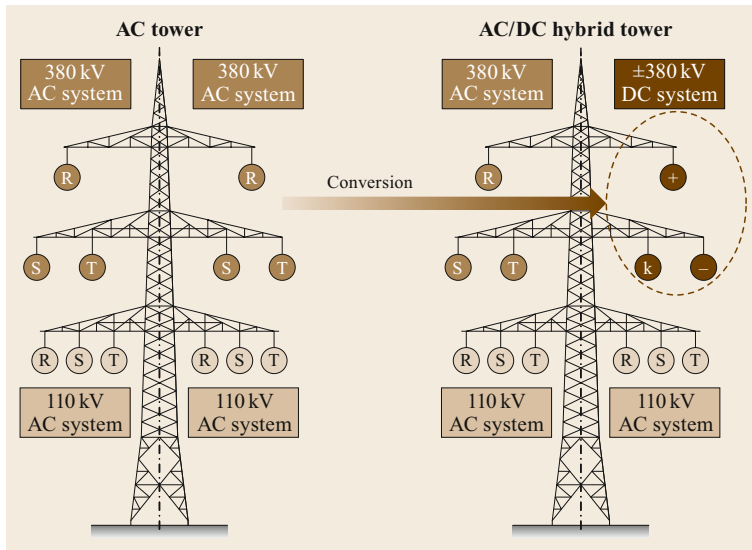
The following case studies are presented exemplarily, being at the time of writing more or less at an experimental stage. More case studies as well as updated information on uprating and upgrading can be found in [9.280].

*400-kV AC/DC Hybrid Line.* Conversion from AC to DC offers certain advantages for long-distance power

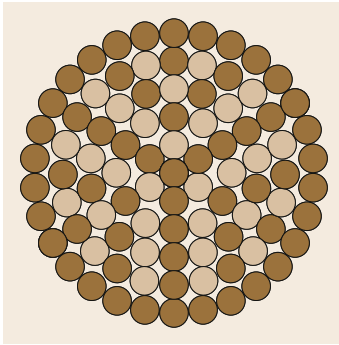
**Table 9.57** Mechanisms for uprating (adapted from [9.279])

Method	Technique and solution	
<b>Increased thermal rating</b>		
Increase conductor rating	Conductor replacement	Increased conductivity area High-temperature conductors Composite conductor systems
	Modify rating criteria	Meteorological study
Increase conductor temperature and maintain ground clearance	Conductor tension	Increase tension Negative sag devices
	Increased conductor attachment height	Structure body extension Insulator cross-arms Interspaced structures
Increased thermal rating by active line rating systems	Line thermal, sag, tension, and/or climatic conditions measurement	Line sag or tension monitors Conductor distributed temperature sensing Weather stations
Probabilistic rating	Actual load profile Modify rating criteria	Temporary increase in rating Probability-based meteorological study
High surge impedance	Conductor bundling and geometry	Physical reconfiguration
<b>Increased voltage rating</b>		
Increased electrical clearances	Insulators Increased conductor attachment height	Insulator body extension Structure body extension Insulator cross-arms Interspaced structures





**Fig. 9.174** Hybrid 380-kV line with conversion from AC to DC (source Amprion)



**Fig. 9.175** Cross-section of the new LWC 604 mm<sup>2</sup>: Aluminum alloy wires in dark brown, hollow elements in light brown (source APG, Austrian Power Grid)

transmission. In particular, in DC, the conductors can be utilized up to their thermal limit, while in AC the surge impedance loading (SIL) often becomes the limiting factor. This interesting subject was covered in an early paper [9.281]. Presently, in a pioneering project in Germany, one of the two circuits of a 380-kV AC line was converted to a  $\pm 380$ -kV DC bi-pole, with the third conductor being used for the metallic earth return (Fig. 9.174). One major prerequisite was to use the same conductors and towers. This was only possible by replacing the existing porcelain strings by composite insulators, as these have proven, significantly better pollution performance in particular under DC, thus their length can be accommodated within the existing tower top geometry. More details about hybrid lines in general can be found in [9.282] and about this project in [9.283].

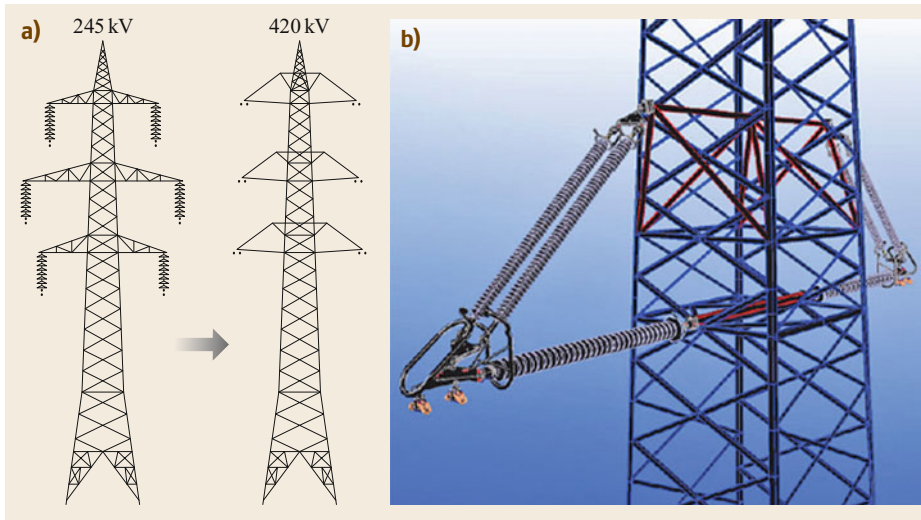
**Conversion of a 245-kV AC Line to a 420-kV AC Line.** A study from Austria was presented in [9.284], where the line uprating was twofold. On one hand, the original

ACSR conductors were replaced by newly designed so-called low-weight conductors (LWC), i.e., conductors with the same amount of aluminum but a higher diameter of 39 mm (Fig. 9.175), which is advantageous to increase their current-carrying capacity and reduce the corona noise. On the other hand, the metallic cross-arms of the steel lattice towers were replaced by insulating cross-arms with composite insulators (Fig. 9.176), enabling the increase of the line voltage from 245 to 420 kV using the same tower body.

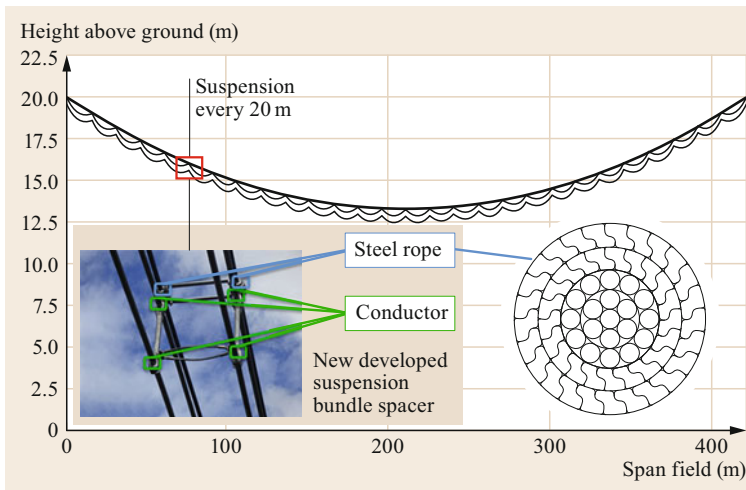
**CompactLine.** This is quite a new concept developed in Germany [9.285]. The idea is to utilize existing 220-kV corridors with a new design of 380-kV low-visibility pylons. In order to do this, the conductor sag has to be limited, which is made possible by suspending the quad bundle conductors from a tightly strung high-strength steel rope (Fig. 9.177) similar to those used in funiculars. In order to keep the support top geometry and the ROW narrow, V-strings with high-strength composite insulators were installed (Fig. 9.178).

## 9.10.2 Upgrading

The main reason for upgrading is to increase the availability of the line. Often, meteorological data collected over many years reveal that there could be higher ice and wind loads on the transmission lines compared with the loads that the lines were originally designed to withstand. Due to this fact, lines need to be upgraded to maintain reliability. New transmission line modeling techniques allow more detailed analyses to assess the adequacy of various transmission line components and thus help to quantify the need for upgrading.



**Fig. 9.176a,b**  
Upgrading of 245 kV AC to 420 kV AC (a) using composite insulating cross-arms (b) (source APG)



**Fig. 9.177** Low-profile pylon of the CompactLine with composite V-strings—last works before commissioning in summer 2018 (source 50hertz)



**Fig. 9.178** Low-profile pylon of the CompactLine with composite V-strings—last works before commissioning in summer 2018 (source 50hertz)

Successful upgrading of transmission lines depends on a number of factors that must be considered. These factors can be classified as:

- Environmental factors
- Operational factors
- Mechanical and electrical degradation factors.

Some examples of various factors are given in Table 9.58 [9.269].

The basic criterion for upgrading a line uses the return period of the limit wind load (or of the limit ice load when applicable), by designing the line for a higher return period (say increasing it from 50 to 80 years). The reliability is a result of the combination of the load

**Table 9.58** Factors affecting life and performance of a transmission line element (adapted from [9.269])

Environmental factors	Operational factors	Mechanical and electrical degradation
<b>Climate:</b> i. Overloading due to ice and/or wind ii. Extreme temperatures iii. Ultraviolet exposure iv. Fungi <b>Pollution:</b> i. Acid rain ii. Salt spay iii. Fertilizer use iv. Industrial gases v. Lightning strikes vi. Fires <b>Other external factors:</b> i. Vandalism (gunshots, theft, abuse) ii. Wildlife (i.e., woodpeckers, rodents, insects) iii. Mechanical impacts (cars, farm equipment, planes)	i. High-temperature operation ii. Increased continuous current iii. Increased fault current iv. Lack of maintenance v. No outage time available for maintenance vi. Installation of telecommunication structures vii. Higher ground clearance viii. Higher voltage level <b>External factors:</b> i. New obstacles in the vicinity of the line (i.e., roads, buildings)	i. Loosening or breakage of connections ii. Fatigue of materials caused by vibrations iii. Corrosion iv. Material wear v. Degradation of insulation

**Table 9.59** Methods and tools for upgrading (adapted from [9.269])

Method	Tool
Reducing impact of climatic loads	Compact/smooth conductor Decreasing ice accretion Decreasing number of sub-conductors Decreasing number of circuits
Increasing characteristic strength	Support: leg members Support: bracings Foundation: uplift Foundation: compression

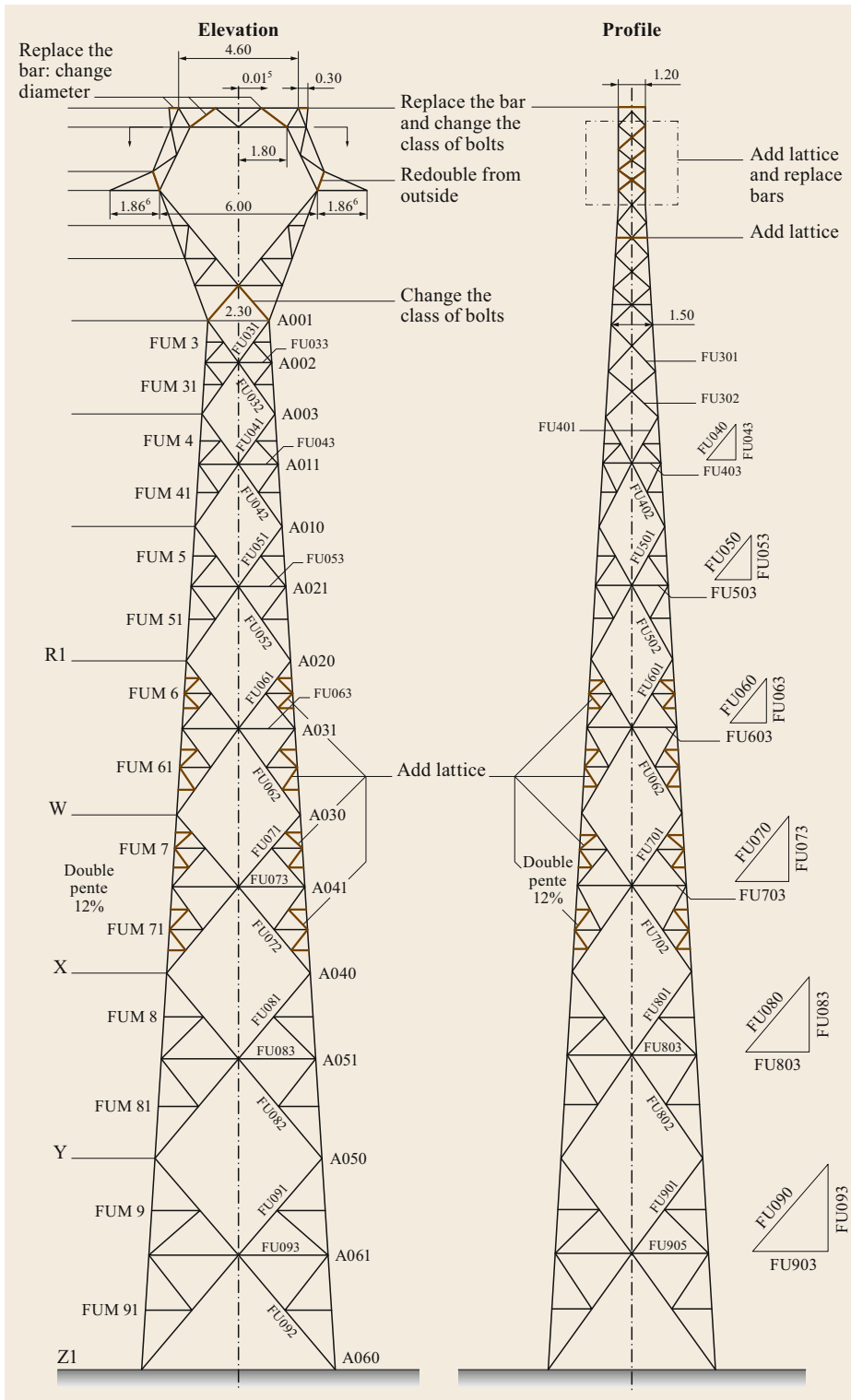
and strength of the overhead line. It is obvious that reliability can be increased by either decreasing the impact of climatic loads or increasing the characteristic strengths (Sect. 9.3). The main methods and tools to upgrade overhead lines summarized in Table 9.59 are from [9.269], where further details can be found.

#### Upgrading Case Studies

**Electrical Upgrading: Replacement of Glass or Ceramic Insulators with Composite Insulators.** In the USA, one utility has replaced both 138-kV, 230-kV, and  $\pm 500$ -kV DC and 500-kV AC ceramic insulators with silicone rubber composite insulators in high-contamination urban areas, with the result of eliminating washing on these lines. Since their installation in 1985 (Fig. 9.179 [9.269]), there have been no reports of insulator flashovers due to contamination (Sect. 9.5.2) on the towers with composite insulators.

**Fig. 9.179** Replacement of ceramic insulators with composite insulators (adapted from [9.269])

**Mechanical Upgrading: Strengthening of Steel Lattice Towers.** In December 1999, storms with wind speeds up to 180–200 km/h caused unprecedented damage to the French electrical network. Implementation of 18 000 (!) *anticascade* towers (Fig. 9.180 [9.269]) was decided to limit the spatial extent of damage to the network in case of exceptional climatic events in the future. One of the goals of this program was to reinforce the mechanical strength of existing towers as well as their foundations and to avoid replacing them, with the objective of controlling costs and limiting the environmental impact of the measure.



**Fig. 9.180** 225-kV anticascade tower showing reinforcement actions

## 9.11 Conclusions and Further Reading

This chapter presents an overview of the history, design, materials, and applications of overhead transmission lines, the backbone of electric power systems from their very early days. Despite the fact that this is a very conservative industry—and rightly so—overhead lines and their components have seen remarkable innovations over recent decades, such as composite insulators, high-temperature conductors, and composite poles, but also new erection and maintenance techniques, notably supported by robotics. Also the ever-present digitalization has reached this industry with GPS-based geoinformation systems plus applications for asset management and such, this being only the beginning. Doubtlessly, overhead lines face acceptance problems in many countries, mainly because of their appearance and the purported health hazards of their electromagnetic fields. Although the industry has reacted with esthetic supports as well as extensive research into said health issues, there is a tendency to partially or even fully place lines underground. As often, there are pros and cons for both technologies, i.e., overhead lines and underground cables. A well-balanced, authoritative but also objective opinion, as provided by CIGRE, on this issue is presented in [9.286, 287]. Nevertheless, because of the huge demand for new transmission corridors, in particular in developing coun-

tries, but also thousands of kilometers of aged lines in Europe and North America, which have to be replaced in the foreseeable future, the great majority of electric power transmission will still be overhead, with a shift to extra high voltage (EHV) and ultra high voltage (UHV) and HVDC. Evidently, this chapter, being part of a handbook which covers the whole power system, cannot go into all the details, but is restricted to basic theory and applications. For further reading, the following *classic* books can be recommended: The books (in German and English) by Kiessling et al. [9.1, 4], which cover the subject extensively and also include quite a few numerical examples, and the more recent CIGRE Green Book on *Overhead Lines* [9.288], which in its more than 1000 pages, not only presents the experience of a plethora of well-known international experts, but also cleverly compiles hundreds of CIGRE publications, which contain the consensual opinion of the worldwide community in this field.

### 9.11.1 Additional Information and Exercises

Additional information and supplementary exercises relating to this chapter can be found at [https://go.sn.pub/SHb\\_PowerSystems\\_Papailiou\\_OverheadLines](https://go.sn.pub/SHb_PowerSystems_Papailiou_OverheadLines).

## References

- 9.1 F. Kiessling, P. Nefzger, U. Kaintzyk: *Freileitungen*, 5th edn. (Springer, Berlin, Heidelberg 2001)
- 9.2 K.O. Papailiou, F. Schmuck: *Silicone Composite Insulators – Materials, Design, Applications* (Springer, Berlin, Heidelberg 2013)
- 9.3 R.G. Stephen: Planning and management concepts. In: *Overhead Lines*, CIGRE Green Book, ed. by K.O. Papailiou (Springer, Cham 2017), Chapter 3
- 9.4 F. Kiessling, P. Nefzger, J.F. Nolasco, U. Kaintzyk: *Overhead Power Lines* (Springer, Berlin, Heidelberg 2003)
- 9.5 CIGRE TB 147: *High Voltage Overhead Lines – Environmental Concerns, Procedures, Impacts and Mitigations* (CIGRE, Paris 1999)
- 9.6 CIGRE TB 638: *Guide to Overall Line Design* (CIGRE, Paris 2015)
- 9.7 CIGRE TB 388: *Impacts of HVDC Lines on the Economics of HVDC Projects* (CIGRE, Paris 2009)
- 9.8 R.G. Stephen: Overall design. In: *Overhead Lines*, CIGRE Green Book, ed. by K.O. Papailiou (Springer, Cham 2017), Chapter 14
- 9.9 W. Bückner: Wirtschaftliche Gestaltung von Hochspannungs-Freileitungen, *SIEMENS Mag.* **10**, 705–714 (1961)
- 9.10 S. Cluts: Parametric studies of overhead transmission cost. In: *Electra*, Vol. 136 (CIGRE, Paris 1991) pp. 31–67
- 9.11 S. Cluts: International survey of component costs of overhead transmission lines. In: *Electra*, Vol. 137 (CIGRE, Paris 1991) pp. 61–79
- 9.12 ISO 55000:2014: *Asset Management – Overview, Principles and Terminology* (ISO, Geneva 2014)
- 9.13 CIGRE TB 175: *Management of Existing Overhead Transmission Lines* (CIGRE, Paris 2000)
- 9.14 J. Doyle: Asset management. In: *Overhead Lines*, CIGRE Green Books, ed. by K.O. Papailiou (Springer, Cham 2017), Chapter 17
- 9.15 CIGRE TB 309: *Asset Management of Transmission Systems and Associated CIGRE Activities* (CIGRE, Paris 2006)
- 9.16 EN 50341-1: *Overhead Electrical Lines Exceeding AC 1 kV – Part 1: General Requirements – Common Specifications* (CEN, Brussels 2012)
- 9.17 CIGRE TB 178: *Probabilistic Design of Overhead Lines* (CIGRE, Paris 2001)
- 9.18 CIGRE TB 179: *Guidelines for Field Measurement of Ice Loadings on Overhead Power Line Conductors* (CIGRE, Paris 2000)
- 9.19 S. Fikke: Overhead lines and weather. In: *Overhead Lines*, CIGRE Green Book, ed. by K.O. Papailiou (Springer, Cham 2017), Chapter 7
- 9.20 EN 1991-1-4:2005+A1: *Actions on Structures – Part 1-4: General Actions – Wind Actions* (CEN, Brussels 2010)

- 9.21 EN 1993-3-1: *Design of Steel Structures – Part 3-1: Towers, Masts and Chimneys – Towers and Masts* (CEN, Brussels 2009)
- 9.22 EN 50341-2-4:2019: *Freileitungen über AC 1 kV – Teil 2-4: Nationale Normative Festlegungen (NNA) für Deutschland (basierend auf EN 50341-1:2012)* (VDE, Berlin 2019)
- 9.23 CIGRE TB 214: *The Mechanical Effects of Short-Circuit Currents in Open Air Substations. Part II. Companion brochure to No. 105* (CIGRE, Paris 2002)
- 9.24 CIGRE TB 48: *Tower Top Geometry* (CIGRE, Paris 1995)
- 9.25 CIGRE TB 348: *Tower Top Geometry and Mid Span Clearances* (CIGRE, Paris 2008)
- 9.26 IEC 60071-1 (RLV): *Insulation Coordination – Part 1: Definitions, Principles and Rules* (IEC, Geneva 2019)
- 9.27 CIGRE TB 72: *Guidelines for the Evaluation of the Dielectric Strength of External Insulation* (CIGRE, Paris 1992)
- 9.28 IEC 60071-2 (RLV): *Insulation Coordination – Part 2: Application Guide* (IEC, Geneva 2018)
- 9.29 G. Andersson, C.M. Franck: *Electric Power Systems*, Lecture notes (ETH Zurich, Zurich 2013)
- 9.30 CIGRE TB 278: *Influence of Line Configuration on Environment Impacts of Electrical Origin* (CIGRE, Paris 2005)
- 9.31 G. Filippopoulos, D. Tsanakas, G. Kouvarakis, J. Voyatzakis, M. Ammann, K.O. Papailiou: Optimum conductor arrangement of compact lines for electric and magnetic field minimization – Calculations and measurements. In: *Mediterranean Power Conf., Athens* (2002)
- 9.32 E.I. Mimos, D.K. Tsanakas, A.E. Tzinevrakis: Electric and magnetic fields produced by 400 kV double circuit overhead lines – Measurements and calculations in real lines and line models, *CIGRE Sci. Eng.* **5**(234), 9 (2016)
- 9.33 M. Plante, J. Lambrozo, M. Souques, D.A. Brown, P. Arnera, J.A. Bulcao, S. Nakasono: 50–60 Hz magnetic fields and cancer, forty years of research: It is time to reassess. In: *Electra*, Vol. 286 (CIGRE, Paris 2016) pp. 38–40
- 9.34 M. Plante, P. Arnera, D.A. Brown, J.A. Bulcao, J. Lambrozo, S. Nakasono, M. Souques, H. Tripp: Living with Electric and Magnetic Fields. In: *Electra*, Vol. 291 (CIGRE, Paris 2017)
- 9.35 N. Wertheimer, E. Leeper: Electrical wiring configurations and childhood cancer, *Am. J. Epidemiol.* **109**(3), 273–284 (1979)
- 9.36 G. Thériault, M. Goldberg, A.B. Miller, B. Armstrong, P. Guénel, J. Deadman, E. Imbernon, T. To, A. Chevalier, D. Cyr, C. Wall: Cancer risks associated with occupational exposure to magnetic fields among electric utility workers in Ontario and Quebec, Canada, and France: 1970–1989, *Am. J. Epidemiol.* **139**(6), 550–572 (1994)
- 9.37 C. Ó Luain, L. Figueroa, P. Penserini: Environmental issues. In: *Overhead Lines*, CIGRE Green Book, ed. by K.O. Papailiou (Springer, Cham 2017), Chapter 6
- 9.38 CIGRE TB 274: *Consultations Models for Overhead Line Projects* (CIGRE, Paris 2001)
- 9.39 CIGRE TB 548: *Stakeholder Engagement Strategies in Sustainable Development – Electricity Industry Overview* (CIGRE, Paris 2013)
- 9.40 CIGRE TB 265: *Life Cycle Assessment for Overhead Lines* (CIGRE, Paris 2005)
- 9.41 C.B. Rawlins: *Analytical Elements of Overhead Conductor Fabrication* (Fultus, Palo Alto 2005)
- 9.42 British Insulated Callender's Cables Limited: *Overhead Conductor Design* (BICC, London 1967)
- 9.43 The Aluminum Association: *Aluminum Electrical Conductor Handbook*, 3rd edn. (Aluminum Association, Washington, D.C. 1989)
- 9.44 EN 50 182: *Conductors for Overhead Lines – Round Wire Concentric-Lay Stranded Conductors* (CEN, Brussels 2001)
- 9.45 EN 50 326: *Conductors for Overhead Lines – Characteristics of Greases* (CEN, Brussels 2001)
- 9.46 VDE 0210:1969-05: *Bestimmungen für den Bau von Starkstrom-Freileitungen über 1 kV* (VDE, Frankfurt a.M. 1969)
- 9.47 M. Frigerio: *Quantifying the Effect of Time and Temperature on the Mechanical Behaviour of Aldrey Overhead Line Conductors*, Ph.D. Thesis 23027 (ETH Zurich, Zurich 2016)
- 9.48 M. Frigerio, P.B. Buehlmann, J. Buchheim, S.R. Holdsworth, S. Dinser, C.M. Franck, K.O. Papailiou, E. Mazza: Analysis of the tensile response of a stranded conductor using a 3D finite element model, *Int. J. Mech. Sci.* **106**, 176–183 (2016)
- 9.49 EN 61 395: *Overhead Electrical Conductors – Creep Test Procedure for Stranded Conductors* (CEN, Brussels 1998)
- 9.50 D. Douglass, M. Lancaster, K. Yonezawa: Conductors. In: *Overhead Lines*, CIGRE Green Book, ed. by K.O. Papailiou (Springer, Cham 2017), Chapter 8
- 9.51 CIGRE TB 324: *Sag-Tension Calculation Methods for Overhead Lines* (CIGRE, Paris 2007)
- 9.52 CIGRE SC22 WG22-04: A practical method of conductor creep determination. In: *Electra*, Vol. 24 (CIGRE, Paris 1974) pp. 105–137
- 9.53 IEC 61395: *Overhead Electrical Conductors – Creep Test Procedure for Stranded Conductors* (IEC, Geneva 1998)
- 9.54 CIGRE WG 22.04: Recommendations for the evaluation of the lifetime of transmission line conductors. In: *Electra*, Vol. 63 (CIGRE, Paris 1979) pp. 103–145
- 9.55 IEC 1597: *Overhead Electrical Conductors – Calculation Methods for Stranded Bare Conductors* (IEC, Geneva 1995)
- 9.56 J. Ziebs: *Über das mechanische Verhalten von Aluminium-Stahl-Freileitungseilen als Beispiel für Verbundseile*, BAM Bericht Nr. 3 (BAM, Berlin 1970)
- 9.57 CIGRE TB 643: *Guide to the Operation of Conventional Conductor Systems Above 100 °C* (CIGRE, Paris 2015)
- 9.58 J.S. Barrett, O. Nigol: Characteristics of Al1/S1A (ACSR) conductors as high temperatures and stresses, *IEEE Trans. Power Appar. Syst.* **PAS-100**(2), 485–493 (1981)
- 9.59 C.B. Rawlins: Some effects of mill practice on the stress strain behavior of ACSR, *IEEE Trans. Power Deliv.* **14**(2), 602–629 (1999)
- 9.60 D.A. Douglass, D. Loudon, R.G. Stephen, G.C. Sibilliant: Calculation accuracy of high-temperature sag for ACSR in existing lines, *CIGRE Sci. Eng.* **7**, 39 (2017)

- 9.61 E.S. Thayer: Computing tensions in transmission lines, *Electr. World Mag.* **84**(2), 72–73 (1924)
- 9.62 E.S. Healy, A.J. Wright: Unbalanced conductor tensions, *Trans. Am. Inst. Electr. Eng.* (1926), <https://doi.org/10.1109/T-AIEE.1926.5061302>
- 9.63 EN 50341-2-4: *National Normative Aspects (NNA) for Germany Based on EN 50341-1:2012* (CEN, Brussels 2019)
- 9.64 EN 50182: *Conductors for Overhead Lines – Round Wire Concentric Lay Stranded Conductors* (CEN, Brussels 2001)
- 9.65 CIGRE TB 601: *Guide for Thermal Rating Calculations of Overhead Lines* (CIGRE, Paris 2014)
- 9.66 IEC 60 826: *Technical Report – Loading and Strength of Overhead Transmission Lines* (IEC, Geneva 1991)
- 9.67 CIGRE TB 273: *Overhead Conductors Safe Design Tension with Respect to Aeolian Vibrations* (CIGRE, Paris 2005)
- 9.68 J.R. Alvarez, C.M. Franck: Radial thermal conductivity of all-aluminum alloy conductors, *IEEE Trans. Power Deliv.* **30**(4), 1983–1990 (2015)
- 9.69 CIGRE TB 345: *Alternating Current (AC) Resistance of Helicly Stranded Conductors* (CIGRE, Paris 2008)
- 9.70 V.T. Morgan: Rating of bare overhead conductors for continuous currents, *Proc. IEE* **114**, 1473–1482 (1967)
- 9.71 R. Puffer: *Freileitungen*, Lecture notes (RWTH Aachen, Aachen 2012)
- 9.72 CIGRE TB 020: *Interferences Produced by Corona Effect of Electric Systems* (CIGRE, Paris 1974)
- 9.73 F.W. Peek: *Dielectric Phenomena in High Voltage Engineering* (McGraw-Hill, New York 1920)
- 9.74 CIGRE TB 61: *Addendum to CIGRE Document No. 20 (1974)* (CIGRE, Paris 2000)
- 9.75 U. Straumann: *Berechnung und Reduktion der tonalen Geräuschemissionen von Hochspannungsfreileitungen*, Dissertation Nr. 17408 (ETH Zurich, Zurich 2007)
- 9.76 CIGRE TB 278: *The Influence of Line Configuration on Environment Impacts of Electrical Origin* (CIGRE, Paris 2005)
- 9.77 L.L. Grigsby (Ed.): *The Electric Power Engineering Handbook* (CRC Press, Boca Raton 2012)
- 9.78 J.B. Whitehead: System of electrical transmission, U.S. Patent No. 1078711 (1910)
- 9.79 G. Markt, B. Mengele: Drehstromübertragung mit Bündelleitern, *Elektrotechn. Maschinenbau* **50**, 293–298 (1932)
- 9.80 G. Markt, B. Mengele: Elektrische Leitung mit Bündelleitern, Österreichisches Patent 121 704 (1930)
- 9.81 U. Cosmai, P. Van Dyke, L. Mazzola, J.L. Lillien: Conductor motions. In: *Overhead Lines*, CIGRE Green Books, ed. by K.O. Papailiou (Springer, Cham 2017), Chapter 10
- 9.82 M. Farzaneh, S. Farokhi, W.A. Chisholm: *Electrical Design of Overhead Power Transmission Lines* (McGraw-Hill, New York 2013)
- 9.83 S. Tenbohlen: *Elektrische Energienetze I*, Lecture notes (University of Stuttgart, Stuttgart 2014)
- 9.84 CIGRE WG B2.38: Evaluation of high surge impedance loading (HSIL) solutions for increased natural capacity of 500 kV overhead lines, *CIGRE Sci. Eng.* **2**, 63 (2015)
- 9.85 EN 60 865-1: *Short-Circuit Currents – Calculation of Effects, Part 1: Definitions and Calculation Methods* (CEN, Brussels 1994)
- 9.86 F. Illiceto, F.M. Gatta, P. Masato, H. Sysoulath: Rural Electrification in developing countries with the shield wire scheme – Applications in Laos. In: *CIGRE Sess., Paris* (2004), Paper C6-301
- 9.87 CIGRE TB 746: *Design, Deployment and Maintenance of Optical Cables Associated to Overhead HV Transmission Lines* (CIGRE, Paris 2018)
- 9.88 CIGRE WG22-11: Guide to fittings for optical cables on transmission lines. Part 1: Selection and use. In: *Electra*, Vol. 176 (CIGRE, Paris 1998) pp. 55–65
- 9.89 CIGRE WG22-11: Guide to fittings for optical cables on transmission lines. Part 2A: Testing procedures for optical ground wire fittings and optical phase conductor fittings. In: *Electra*, Vol. 188 (CIGRE, Paris 2000) pp. 43–53
- 9.90 CIGRE WG22-11: Guide to fittings for optical cables on transmission lines. Part 2B: Testing procedures, all-dielectric self-supporting cable fittings and optical attached cable fittings. In: *Electra*, Vol. 191 (CIGRE, Paris 2000) pp. 63–75
- 9.91 IEC 60889: *Hard-Drawn Aluminium Wire for Overhead Line Conductors* (IEC, Geneva 1987)
- 9.92 CIGRE TB 244: *Conductors for the Uprating of Overhead Lines* (CIGRE, Paris 2004)
- 9.93 IEC 60104: *Aluminium-Magnesium-Silicon Alloy Wire for Overhead Line Conductors* (IEC, Geneva 1987)
- 9.94 CIGRE TB 695: *Experience with the Mechanical Performance of Non-Conventional Conductors* (CIGRE, Paris 2017)
- 9.95 IEC 62004: *Thermal-Resistant Aluminium Alloy Wire for Overhead Line Conductor* (IEC, Geneva 2007)
- 9.96 CIGRE TB 498: *Guide for Application of Direct Real-Time Monitoring Systems* (CIGRE, Paris 2012)
- 9.97 EPRI: *Transmission Line Reference Book: Wind-Induced Conductor Motion*, 2nd edn. (EPRI, Palo Alto 2009)
- 9.98 R.G. Sturm: Vibration of cables and dampers: Part I, *Trans. Am. Inst. Electr. Eng.* **55**(5), 455–465 (1936)
- 9.99 R.G. Sturm: Vibration of cables and dampers: Part II, *Trans. Am. Inst. Electr. Eng.* **55**(6), 673–688 (1936)
- 9.100 R. Helms: *Zur Sicherheit der Hochspannungsfreileitungen bei hoher mechanischer Beanspruchung, BAM-Mitteilung*, VDI Forschungsbericht 506 (VDI, Düsseldorf 1964)
- 9.101 R. Claren, G. Diana: Mathematical analysis of transmission line vibration, *IEEE Trans. Power Appar. Syst.* **PAS-88**(12), 1741–1771 (1969)
- 9.102 K.O. Papailiou: On the bending stiffness of transmission line conductors, *IEEE Trans. Power Deliv.* **12**(4), 1576–1588 (1997)
- 9.103 K.O. Papailiou: On the bending stiffness of transmission line conductors. Discussions and closure by author, *IEEE Trans. Power Deliv.* **15**(4), 1329–1331 (2000)
- 9.104 G. Diana (Ed.): *Modelling of Vibrations of Overhead Line Conductors*, CIGRE Green Books (Springer, Cham 2018)
- 9.105 D. Brika, A. Laneville: A laboratory investigation of the aeolian power imparted to a conductor using

- a flexible circular cylinder, IEEE Trans. Power Deliv. **11**(2), 1145–1152 (1996)
- 9.106 R. Baumann, P. Novak: Efficient computation and experimental validation of ACSR overhead line conductors under tension and bending, CIGRE Sci. Eng. **9**, 5–16 (2017)
- 9.107 CIGRE TB 482: *State of the Art for Testing Self-Damping Characteristics of Conductors for Overhead Lines* (CIGRE, Paris 2011)
- 9.108 IEC 62567: *Overhead Lines – Methods for Testing Self-Damping Characteristics of Conductors, Ed. 1.0* (IEC, Geneva 2013)
- 9.109 F. Tavano: *Conductor Self-Damping*, CIGRE Report SC22–94(WG11)–126 (CIGRE, Paris 1994)
- 9.110 M. Ervik, A. Berg, A. Boelle, R.F. Claren, B. Dalle, A.T. Edwards: Report on aeolian vibration. In: *Electra*, Vol. 124 (CIGRE, Paris 1989) pp. 40–77
- 9.111 D.U. Noiseux, S. Houle, R. Beauchemin: Transformation of wind tunnel data on aeolian vibrations for application to random conductor vibrations in a turbulent wind, IEEE Trans. Power Deliv. **3**(1), 265–271 (1988)
- 9.112 K. Shillai: *Enhanced Fretting Fatigue Resistance of Conductors for High Voltage Overhead Lines*, Dissertation, Vol. 25661 (ETH, Zurich 2019), <https://doi.org/10.3929/ethz-b-000362301>
- 9.113 IEC Standard 62568: *Overhead Lines – Method for Fatigue Testing of Conductors, Ed. 1.0* (IEC, Geneva 2015)
- 9.114 G.E. Ramey, J.S. Townsend: Effects of clamps on fatigue of ACSR conductors, J. Energy Div. **107**(1), 103–110 (1981)
- 9.115 CIGRE TB 429: *Engineering Guideline Relating to Fatigue Endurance Capability of Conductor/Clamp Systems* (CIGRE, Paris 2010)
- 9.116 K.O. Papailiou: *Schwingungsmessungen an Freileitungsseilen*, SEV/ISE Bulletin 23 (Electrosuisse, Fehraltorf 1987)
- 9.117 CIGRE WG B2.11: Guide to vibration measurements on overhead lines. In: *Electra*, Vol. 163 (CIGRE, Paris 1995) pp. 125–137
- 9.118 IEEE Standard 1368: *Guide for Aeolian Vibration Field Measurements of Overhead Conductors* (IEEE, Piscataway 2006)
- 9.119 O.D. Zetterholm: *Bare Conductors and Mechanical Calculation of Overhead Conductors*, CIGRE Report No. 223 (CIGRE, Paris 1960)
- 9.120 J.C. Poffenberger, R.L. Swart: Differential displacement and dynamic conductor strain, IEEE Trans. Power Appar. Syst. **PAS-84**(4), 281–289 (1965), (Discussion pp. 508–513. Errata p.732)
- 9.121 K.O. Papailiou: *Die Seilbiegung mit einer durch die innere Reibung, die Zugkraft und die Seilkrümmung veränderlichen Biegesteifigkeit*, Ph.D. Thesis No. 11057 (ETH Zurich, Zurich 1995), Conductor Bending Considering a Variable Bending Stiffness, which Depends on the Internal Friction, the Tensile Load and the Conductor Curvature
- 9.122 A. Cardou: *Stick-Slip Mechanical Models for Overhead Electrical Conductors in Bending (with Matlab Applications)* (GREMCA, Quebec 2013)
- 9.123 IEEE: Standardization of conductor vibration measurements, IEEE Trans. Power Appar. Syst. **PAS-85**(1), 10–22 (1966)
- 9.124 M.A. Miner: Cumulative damage in fatigue, J. Appl. Mech. **12**, A159–A164 (1945)
- 9.125 CIGRE TB 277: *State of the Art Survey on Spacers and Spacer Dampers* (CIGRE, Paris 2005)
- 9.126 D. Hearnshaw: Spacer damper performance – A function of in-span positioning, IEEE Trans. Power Appar. Syst. **PAS-93**(5), 1298–1309 (1974)
- 9.127 J.P. Den Hartog: Transmission line vibration due to sleet, Trans. Am. Inst. Electr. Eng. **51**(4), 1074–1076 (1932)
- 9.128 CIGRE TB 322: *State of the Art of Conductor Galloping* (CIGRE, Paris 2007)
- 9.129 J.L. Lilien, D. Havard: Galloping data base on single and bundle conductors prediction of maximum amplitudes, IEEE Trans. Power Deliv. **15**(2), 670–674 (2000)
- 9.130 CIGRE TB 438: *Systems for Prediction and Monitoring of Ice Shedding, Anti-Icing and De-Icing for Overhead Power Line Conductors and Ground Wires* (CIGRE, Paris 2010)
- 9.131 IEC 60050–471: *International Electrotechnical Vocabulary (IEV) – Part 471: Insulators* (IEC, Geneva 2007)
- 9.132 J.S.T. Looms: *Insulators for High-Voltages* (Peter Peregrinus, London 1988)
- 9.133 IEC 60383–1: *Insulators for Overhead Lines with a Nominal Voltage Above 1000 V – Part 1: Ceramic or Glass Insulator Units for A.C. Systems – Definitions, Test Methods and Acceptance Criteria* (IEC, Geneva 1993)
- 9.134 IEC 60383–2: *Insulators for Overhead Lines with a Nominal Voltage Above 1000 V – Part 2: Insulator Strings and Insulator Sets for A.C. Systems – Definitions, Test Methods and Acceptance Criteria* (IEC, Geneva 1993)
- 9.135 M. Ammann, K.O. Papailiou, P. Dallèves, M. Leva, S. Villa: A new 400 kV line with compact towers and composite insulated cross-arms. In: *CIGRE Sess., Paris* (1998), Paper 22/33/36–06
- 9.136 CIGRE TB 455: *Aspects for the Application of Composite Insulators for High Voltage (72 kV) Apparatus* (CIGRE, Paris 2011)
- 9.137 R.S. Gorur, E.A. Cherney, J.T. Burnham: *Outdoor Insulators* (Ravi S. Gorur Inc., Phoenix 1999)
- 9.138 S. Bisnath, T. Pillay: *The Planning, Design and Construction of Overhead Power Lines*, Eskom Power Series (Crown, Johannesburg 2005)
- 9.139 IEC TS 60815: *Selection and Dimensioning of High-Voltage Insulators Intended for Use in Polluted Conditions. Part 1: Definitions, Information and General Principles* (IEC, Geneva 2008)
- 9.140 IEC TS 60815: *Selection and Dimensioning of High-Voltage Insulators Intended for Use in Polluted Conditions. Part 4: Insulators for D.C. Systems* (IEC, Geneva 2016)
- 9.141 IEC TS 60815: *Selection and Dimensioning of High-Voltage Insulators Intended for Use in Polluted Conditions. Part 3: Polymer Insulators for A.C. Systems* (IEC, Geneva 2008)



- 9.142 IEC TS 60815: *Selection and Dimensioning of High-Voltage Insulators Intended for Use in Polluted Conditions. Part 2: Ceramic and Glass Insulators For A.C. Systems* (IEC, Geneva 2008)
- 9.143 CIGRE TB 158: *Polluted Insulators – A Review of Current Knowledge* (CIGRE, Paris 2000)
- 9.144 CIGRE TB 361: *Outdoor Insulation in Polluted Conditions – Guidelines for Selection and Dimensioning – Part 1: General Principles and the AC Case* (CIGRE, Paris 2008)
- 9.145 CIGRE C4–101: *Development of Guidelines for the Selection of Insulators with Respect to Pollution for EHV-UHV DC – State of the Art and Research Needs* (CIGRE, Paris 2008)
- 9.146 IEC TR 60815: *Guide for the Selection of Insulators in Respect of Polluted Conditions* (IEC, Geneva 1986)
- 9.147 CIGRE WG 22.03: Service performance of composite insulators used on HVDC lines. In: *Electra*, Vol. 161 (CIGRE, Paris 1995)
- 9.148 IEC 60071–1: *Insulation Co-Ordination – Part 1: Definitions, Principles and Rules* (IEC, Geneva 2019)
- 9.149 J.M. George, Z. Lodi: Design and selection criteria for HVDC overhead transmission lines insulators. In: *CIGRE Canada Conf. Power Syst., Toronto* (2009), Paper No. 189
- 9.150 IEC 61365: *Insulators for Overhead Lines with a Nominal Voltage Above 1000 V – Ceramic or Glass Insulator Units for D.C. Systems – Definitions, Test Methods and Acceptance Criteria* (IEC, Geneva 1995)
- 9.151 D.A. Swift: Insulators for outdoor applications. In: *Advances in High Voltage Engineering*, ed. by A. Haddad, D.F. Warne (IET, London 2004), Chapter 6
- 9.152 IEEE Standard 1523–2018: *IEEE Guide for the Application, Maintenance, and Evaluation of Room-Temperature Vulcanizing (RTV) Silicone Rubber Coatings for Outdoor Ceramic Insulators* (IEEE, New York 2018)
- 9.153 E. Bauer, E. Brandt, R. Brand, H. Klein, L. Möcks, H. Schlotz: *Dynamic Processes During Load Transition in Multiple Sets with Long Rod-Type Insulators*, Session Paper 22–03 (CIGRE, Paris 1982)
- 9.154 IEC 60433: *Insulators for Overhead Lines with a Nominal Voltage Above 1000 V – Ceramic Insulators for A.C. Systems – Characteristics of Insulator Units of the Long Rod Type* (IEC, Geneva 1998)
- 9.155 IEC 60672–1: *Ceramic and Glass Insulating Materials – Part 1: Definitions and Classification* (IEC, Geneva 1995)
- 9.156 IEC 60672–3: *Ceramic and Glass Insulating Materials – Part 3: Specifications for Individual Materials* (IEC, Geneva 1997)
- 9.157 IEC 60120: *Dimensions of Ball and Socket Couplings of String Insulator Units* (IEC, Geneva 1984)
- 9.158 IEC 60471: *Dimensions of Clevis and Tongue Couplings of String Insulator Units* (IEC, Geneva 1977)
- 9.159 C. Baumgartner: Insulator manufacturing processes. In: *INMR Power Engineers Handbook* (INMR, Quebec 2018), Chapter 13
- 9.160 J.F. Hall: History and bibliography of polymeric insulators for outdoor applications, *IEEE Trans. Power Deliv.* **8**(1), 376–385 (1993)
- 9.161 E.A. Bauer, E.H. Miller: *Plastic Composite Insulators to the System Rodurflex*, Presentation to the IEEE Nonceramic/Composite Insulator Working Group in New York (1976)
- 9.162 F. Schmuck, J. Seifert, I. Gutman, A. Pigini: *Assessment of the Condition of Overhead Line Composite Insulators*, Paper B2–214 (CIGRE, Paris 2012)
- 9.163 CIGRE WG 22.03: Worldwide experience with HV composite insulators. In: *Electra*, Vol. 130 (CIGRE, Paris 1990)
- 9.164 CIGRE WG 22.03: Worldwide service experience with HV composite insulators. In: *Electra*, Vol. 191 (CIGRE, Paris 2000)
- 9.165 EPRI: *Survey of Utility Experiences with Composite/Polymer Components in Transmission Class (69–765 kV Class) Substations* (EPRI, Palo Alto 2004)
- 9.166 B. Sander, J. Lundquist, I. Gutman, C. Neumann, B. Rusek, K.–H. Weck: *Conversion of AC Multi-Circuit Lines to AC-DC Hybrid Lines with Respect to the Environmental Impact*, Paper B2–105 (CIGRE, Paris 2014)
- 9.167 K.O. Papailiou: Innovative tower solutions & line upgrading. In: *INMR Power Engineers Handbook* (INMR, Quebec 2019)
- 9.168 A. Prenleloup: *Analyse de l'état de contrainte et de l'endommagement d'assemblages sertis en matériau mixte métal-composite sollicités en traction ou en flexion*, Doctoral Thesis No. 4005 (EPFL, Lausanne 2008)
- 9.169 CIGRE WG B2.21: Investigation of different liquid solutions for dye penetration tests used in standard IEC 62217 for design and routine testing. In: *Electra*, Vol. 251 (CIGRE, Paris 2010)
- 9.170 CIGRE WG 22.03: Guide for the Identification of Brittle Fracture of Composite Insulator FRP Rod. In: *Electra*, Vol. 143 (CIGRE, Paris 1992)
- 9.171 CIGRE TB 545: *Assessment of In-Service Composite Insulators by Using Diagnostic Tools* (CIGRE, Paris 2013)
- 9.172 C. De Tourreil, F. Schmuck: Brittle fractures of composite insulators – Field experience, occurrence and risk assessment. In: *Electra*, Vol. 214 (CIGRE, Paris 2004)
- 9.173 C. De Tourreil, F. Schmuck: Brittle fractures of composite insulators – Failure mode chemistry, influence of resin variations and search for a simple insulator core evaluation test method. In: *Electra*, Vol. 215 (CIGRE, Paris 2004)
- 9.174 CIGRE TB 255: *Material Properties for Non-Ceramic Outdoor Insulation* (CIGRE, Paris 2004)
- 9.175 IEC TR 62662: *Guidance for Production, Testing and Diagnostics of Polymer Insulators with Respect to Brittle Fracture of Core Materials* (IEC, Geneva 2010)
- 9.176 IEC TR 62039: *Selection Guide for Polymeric Materials for Outdoor Use Under HV Stress* (IEC, Geneva 2007)
- 9.177 IEC 61109 Ed. 2: *Composite Suspension and Tension Insulators For A.C. Overhead Lines with a Nominal Voltage Greater than 1000 V–Definitions, Test Methods and Acceptance Criteria* (IEC, Geneva 2008)
- 9.178 IEC 61466–1: *Composite String Insulator Units for Overhead Lines with a Nominal Voltage Greater*

- than 1000 V – Part 1: Standard Strength and End Fittings (IEC, Geneva 2016)
- 9.179 L. Paris, L. Pargamin, D. Dumora, R. Parraud: Rating of composite suspension insulators related to the long-term mechanical strength of rods, *IEEE Trans. Power Deliv.* **9**(4), 2055–2063 (1994)
- 9.180 C. Lumb, K.O. Papailiou: Unterschätzte Dauerkraft der Verbundisolatoren, *SEV/VSE Bull.* **88**(7), 35–38 (1997)
- 9.181 C. De Tourreil, R. Roberge, P. Bourdon: Long-term mechanical properties of high voltage composite insulators, *IEEE Trans. Power Appar. Syst.* **PAS-104**(10), 2918–2921 (1985)
- 9.182 C. De Tourreil: Response of composite insulators to dynamic mechanical loads, *IEEE Trans. Power Deliv.* **5**(1), 379–383 (1990)
- 9.183 A. Preneleloup, T. Gmür, K.O. Papailiou, J. Botsis: Acoustic emission study and strength analysis of crimped steel-composite joints under traction, *Compos. Struct.* **74**, 370–378 (2006)
- 9.184 IEC 61952: *Insulators for Overhead Lines – Composite Line Post Insulators for AC Systems with a Nominal Voltage Greater than 1000 V – Definitions, Test Methods and Acceptance Criteria* (IEC, Geneva 2008)
- 9.185 F. Schmuck, K.O. Papailiou: On the raising application of polymeric post insulators. In: *CIGRE SC 33 Conf., Prague* (2000)
- 9.186 A. Preneleloup, T. Gmür, J. Botsis, K.O. Papailiou, K. Obrist, P. Bonhôte: Acoustic emission inspection and analysis of crimped metal-composite joints subjected to bending. In: *Proc. 4th Int. Conf. NDT, Chania* (2007) pp. 11–14
- 9.187 S. Ansoerge: *Improvement of Silicone Rubber for High Voltage Applications by Addition of Fillers*, Doctoral Thesis (ETH Zurich, Zurich 2015), <https://doi.org/10.3929/ethz-a-010577999>
- 9.188 IEC 60695: *Fire Hazard Testing: Guidance for Assessing the Fire Hazard of Electrotechnical Products* (IEC, Geneva 2016)
- 9.189 IEC TS 62073: *Guidance on the Measurement of Hydrophobicity of Insulator Surfaces* (IEC, Geneva 2016)
- 9.190 F. Schmuck, S. Aitken, K.O. Papailiou: A proposal for intensified inspection and acceptance tests of composite insulators as an addition to the guidelines of IEC 61109 Ed. 2: 2008 and IEC 61952 Ed. 2: 2008, *IEEE Trans. Dielectr. Electr. Insul.* **17**(2), 394–401 (2010)
- 9.191 L.H. Meyer, E.A. Cherney, S.H. Jayaram: The role of inorganic fillers in silicone rubber for outdoor insulation – alumina tri-hydrate or silica, *IEEE Electr. Insul. Mag.* **20**(4), 13–21 (2004)
- 9.192 S. Ansoerge, K.O. Papailiou: Mechanical properties of silicone rubber under high loadings of alumina tri-hydrate filler, *J. Elastom. Plast.* **48**(4), 354–382 (2015)
- 9.193 M. Ammann, P. de Weck, P. Faggiano: Pylone raquette. In: *CIGRE Symp., Leningrad* (1991), Paper 400–04
- 9.194 K.O. Papailiou: Composite insulators are gaining ground – 25 years of Swiss experience. In: *IEEE Transm. Distrib. Conf., New Orleans*, Vol. 2 (1999) pp. 827–833
- 9.195 K.O. Papailiou: *Das mechanische Verhalten von Verbundisolatoren für die elektrische Energietechnik*, Habilitation Thesis (TU Dresden, Dresden 2012)
- 9.196 J. Seifert: Standards & progress in insulator technology, <http://www.inmr.com/standards-progress-insulator-technology/> (2019)
- 9.197 IEC 60587: *Electrical Insulating Materials Used Under Severe Ambient Conditions – Test Methods for Evaluating Resistance to Tracking and Erosion* (IEC, Geneva 2007)
- 9.198 CIGRE TB 481: *Guide for the Assessment of Composite Insulators in the Laboratory After Their Removal from Service* (CIGRE, Paris 2011)
- 9.199 CIGRE TB 306: *Guide for the Assessment of Old Cap and Pin and Longrod Transmission Line Insulators Made of Porcelain or Glass: What to Do and When to Replace* (CIGRE, Paris 2006)
- 9.200 IEC 61621: *Dry, Solid Insulating Materials – Resistance Test to High-Voltage, Low-Current Arc Discharges* (IEC, Geneva 1997)
- 9.201 ISO 868: *Plastics and Ebonite – Determination of Indentation Hardness by Means of a Durometer (Shore Hardness)* (ISO, Geneva 2005)
- 9.202 IEC 62217: *Polymeric HV Insulators for Indoor and Outdoor Use – General Definitions, Test Methods and Acceptance Criteria* (IEC, Geneva 2012)
- 9.203 CIGRE TB 442: *Evaluation of Dynamic Hydrophobicity Properties of Polymeric Materials for Non-Ceramic Outdoor Insulation – Retention and Transfer of Hydrophobicity* (CIGRE, Paris 2010)
- 9.204 I. Gutman, H. Wieck, D. Windmar, L. Stenström, D. Gustavsson: Pollution measurements to access the performance of naturally exposed silicone rubber composite insulators, *IEEJ Trans. Fundam. Mater.* **127**(9), 513–518 (2007)
- 9.205 CIGRE WG 22.03: Review of in-service diagnostic testing of composite insulators. In: *Electra*, Vol. 169 (CIGRE, Paris 1996)
- 9.206 IEC 61284:1997/COR1:1998: *Corrigendum 1 – Overhead Lines – Requirements and Tests for Fittings* (VDE, Berlin 1998)
- 9.207 CIGRE SC22 WG01: Guide on the use of bolted suspension clamps. In: *Electra*, Vol. 123 (CIGRE, Paris 1989) pp. 13–19
- 9.208 CIGRE TB 174: *Load Control Devices on Overhead Transmission Lines* (CIGRE, Paris 2000)
- 9.209 CIGRE TB 653: *Safe Design Tensions for Single Conductors Fitted with Elastomer Cushioned Suspension Units* (CIGRE, Paris 2016)
- 9.210 L. Möcks: *Das Verhalten des Leiterseiles unter dem Einfluss der Armaturen Freileitungen*, *Elektrizitätswirtschaft* **68**, 336–341 (1969)
- 9.211 C. Hildmann: *Zum elektrischen Kontakt- und Langzeitverhalten von Pressverbindungen mit konventionellen und Hochtemperatur-Leiterseilen mit geringem Durchhang*, Doctoral Thesis (TU Dresden, Dresden 2017)
- 9.212 D. Raupp: *Wirkungsweise einer gewalzten Seilendverbindung unter Zug- und Zugschwellbean-*

- spruchung, Doctoral Thesis (University of Stuttgart, Stuttgart 2009)
- 9.213 CIGRE TB 216: *Joints on Transmission Line Conductors – Field Testing and Replacement Criteria* (CIGRE, Paris 2002)
- 9.214 P. Van Dyke, U. Cosmai, C. Freismuth: Fittings. In: *Overhead Lines*, CIGRE Green Books, ed. by K.O. Papailiou (Springer, Cham 2017), Chapter 9
- 9.215 CIGRE TB 341: *Considerations Relating to the Use of High Temperature Conductors* (CIGRE, Paris 2007)
- 9.216 CIGRE TF B2.11.03: State of the Art survey on aircraft warning markers. In: *Electra*, Vol. 224 (CIGRE, Paris 2006) pp. 24–29
- 9.217 J. McCombe, F.R. Haigh: *Overhead Line Practice* (Macdonald, London 1966)
- 9.218 ISO 146: *Hot Dip Galvanized Coatings on Fabricated Iron and Steel Articles – Specifications and Test Methods* (IEC, Geneva 2009)
- 9.219 L. Möcks: *Lichtbogenschutzarmaturen für Isolierstrecken in Freileitungen und Schaltanlagen*, ETZ-Report 16 (VDE, Berlin, Offenbach 1982)
- 9.220 A.J. Phillips, J. Kuffel, A. Baker, J. Burnham, A. Carreira, E. Cherney, W. Chisholm, M. Farzaneh, R. Gemignani, A. Gillespie, T. Grisham, R. Hill, T. Saha, B. Vancia, J. Yu: Electric fields on AC composite transmission line insulators, *IEEE Trans. Power Deliv.* **23**(2), 823–830 (2008)
- 9.221 CIGRE WG 22.03: Use of stress control rings on composite insulators. In: *Electra*, Vol. 143 (CIGRE, Paris 1992)
- 9.222 CIGRE TB 365: *On the Use of Power Arc Protection Devices for Composite Insulators on Transmission Lines* (CIGRE, Paris 2008)
- 9.223 G.H. Stockbridge: Overcoming vibration in transmission lines, *Electr. World* **86**, 1304–1305 (1925)
- 9.224 F. Foti, L. Martinelli: Mechanical modeling of metallic strands subjected to tension, torsion and bending, *Int. J. Solids Struct.* **91**, 1–171 (2016)
- 9.225 IEC 61897: *Overhead Lines – Requirements and Tests for Stockbridge Type Aeolian Vibration Dampers* (IEC, Geneva 1998)
- 9.226 V.G. Guedes, C.F. Matt, E.S.C. Cavalcanti: Experimental investigation of the dynamic behaviour of Stockbridge dampers. In: *18th Int. Congr. Mech. Eng., Ouro Preto* (2005)
- 9.227 J.L. Tompkins, L.L. Merrill, B.L. Jones: Quantitative relationships in conductor vibration damping. In: *AIEE Winter Gen. Meet., New York* (1956), Paper 56–212
- 9.228 H.A. Maier, H. Schlotz, D. Sander, M. Schuster: Ein neues Berechnungsverfahren von Schwingungsdämpfern für Freileitungen, *Elektrizitätswirtschaft* **88**(23), 1616–1623 (1989)
- 9.229 O. Nigol, R.C. Heics, H.J. Houston: Aeolian vibration of single conductors and its control, *IEEE Trans. Power Appar. Syst.* **PAS-104**(11), 3245–3254 (1985)
- 9.230 Swedish National Grid: *Overhead Transmission Lines/Vibration Dampers*, Technical Guideline TR 05–09–1R (SVK, Sundbyberg 2016)
- 9.231 C. Manuzio: An investigation of the forces on bundle conductor spacers under fault conditions, *IEEE Trans. Power Appar. Syst.* **PAS-86**(2), 166–185 (1965)
- 9.232 J.L. Lilien, K.O. Papailiou: Calculation of spacer compression for bundle lines under short-circuit, *IEEE Trans. Power Deliv.* **15**(2), 839–845 (2000)
- 9.233 CIGRE TB 477: *Evaluation of Aged Fittings* (CIGRE, Paris 2011)
- 9.234 IEC 61854: *Overhead Lines – Requirements and Tests for Spacers* (IEC, Geneva 1998)
- 9.235 CIGRE TB 416/416A: Innovative solutions for overhead line supports. In: *Electra*, Vol. 250 (CIGRE, Paris 2010)
- 9.236 B. Wareing: *Wood Pole Overhead Lines*, IEE Power & Energy Series, Vol. 48 (IEE, London 2005)
- 9.237 EN 14229: *Structural Timber – Wood Poles for Overhead Lines* (CEN, Brussels 2010)
- 9.238 J.B.G.F. Silva, A. Fuchs, G. Gheorghita, J.P.M. van Tilburg, R.C.R. Menezes: Supports. In: *Overhead Lines*, CIGRE Green Book, ed. by K.O. Papailiou (Springer, Cham 2017), Chapter 10
- 9.239 F. Schmuck, B. Burkhardt, G. Bättig, K.O. Papailiou, G. Terassi: New solutions with composite insulators and composite structures for compact lines. In: *17th Int. Conf. Electr. Distrib., Barcelona* (2003)
- 9.240 CIGRE TB 206: *The Design of Transmission Support Foundations – An Overview* (CIGRE, Paris 2002)
- 9.241 CIGRE TB xxx: *Transmission Line Structures with Fiber Reinforced Polymer (FRP) Composite* (CIGRE, Paris 2020)
- 9.242 M. Zgrzendek: *Sammlung von Freileitungsmastbildern unterschiedlicher Regionen und Simulation in digitaler Netzberechnung*, Bachelor Thesis (FH Aachen, Jülich 2012)
- 9.243 CIGRE TB 384: Comparison of general industry practices for lattice tower design and detailing. In: *Electra*, Vol. 244 (CIGRE, Paris 2009)
- 9.244 EN 1993–1–1, Eurocode 3: *Design of Steel Structure – Part 1: General Rules for Buildings* (CENELEC, Brussels 2005)
- 9.245 EN 10 025: *Hot-Rolled Products of Non-Alloy Structural Steels, Technical Delivery Conditions* (CENELEC, Brussels 1994)
- 9.246 EN ISO 898–1: *Mechanical Properties of Fasteners Made of Carbon Steel and Alloy Steel, Part 1: Bolts, Screws and Studs* (CENELEC, Brussels 1999)
- 9.247 W. Bückner: Designing OHL structures economically. In: *Siemens Review* (1962) pp. 305–311
- 9.248 CIGRE TB 515: *Mechanical Security of Overhead Lines – Containing Cascading Failures and Mitigating Their Effects* (CIGRE, Paris 2012)
- 9.249 ASCE 10–97: *Design of Lattice Steel Transmission Structures* (ASCE, Reston 2000)
- 9.250 CIGRE TB 399: Improvement on the tower testing methodology. In: *Electra*, Vol. 247 (CIGRE, Paris 2009)
- 9.251 IEC 60652: *Loading Tests on Overhead Line Structures* (IEC, Geneva 2002)
- 9.252 J. George, M. Iqbal, K.O. Papailiou, W. Huiber, F. Schmuck: DEWA's new 420 kV compact line as an example of maximizing capacity of overhead lines in an urban environment. In: *CIGRE/GCC Power Conf., Dubai* (2007)
- 9.253 K.O. Papailiou, F. Schmuck: The past experience and future trends with compact lines to solve

- right-of-way issues. In: *CIGRE Int. Symp., Bologna* (2011)
- 9.254 J.F. Nolasco, J.A. Jardini, E. Ribeiro: Electrical design. In: *Overhead Lines*, CIGRE Green Book, ed. by K.O. Papailiou (Springer, Cham 2017), Chapter 4
- 9.255 CIGRE TB 694: *Ground Potential Rise at Overhead Transmission Line Structures During Power Frequency Faults* (CIGRE, Paris 2017)
- 9.256 W.W. Lewis: *The Protection of Transmission Systems Against Lightning* (Dover, New York 1965)
- 9.257 C.A. Nucci: A survey on CIGRE and IEEE procedures on the estimation of the lightning performance of overhead transmission and distribution lines. In: *X Int. Symp. Light. Prot., Curitiba* (2009)
- 9.258 H. Dorsch: *Überspannungen und Isolationsbemessung bei Drehstrom-Hochspannungsanlagen* (Siemens, Erlangen 1981), [Overvoltages and Insulation Design for Three-Phase High-Voltage Installations]
- 9.259 N.R. Cuer: Foundations. In: *Overhead Lines*, CIGRE Green Book, ed. by K.O. Papailiou (Springer, Cham 2017), Chapter 13
- 9.260 BS 5930: *Code of Practice for Ground Investigations* (BSI, London 2015)
- 9.261 H. Rieger, R. Fischer: *Der Freileitungsbau* (Springer, Berlin, Heidelberg 1975)
- 9.262 CIGRE TB 308: *Foundation Installation – An Overview* (CIGRE, Paris 2006)
- 9.263 CIGRE TB 281: *Design and Installation of Micropiles and Ground Anchors for OHL Support Foundations* (CIGRE, Paris 2005)
- 9.264 IEEE 977-2010: *Guide to Installation of Foundations for Transmission Line Structures* (IEEE, New York 2010)
- 9.265 IEEE 524: *Guide for the Installation of Overhead Transmission Line Conductors* (IEEE, New York 2016)
- 9.266 Z. Kieloch, J.B.G.F. Silva, M.G. Baleeiro, M. Lancaster, M. Tuzim, P. Wojciechowski: Construction. In: *Overhead Lines*, CIGRE Green Book, ed. by K.O. Papailiou (Springer, Cham 2017), Chapter 15
- 9.267 CIGRE TB 471: *Working Safely While Supported on Aged Overhead Conductors* (CIGRE, Paris 2011)
- 9.268 CIGRE TB 175: *Management of Existing Overhead Transmission Lines* (CIGRE, Paris 2000)
- 9.269 CIGRE TB 353: *Guidelines for Increased Utilization of Existing Overhead Transmission Lines* (CIGRE, Paris 2008)
- 9.270 CIGRE WG B2.13: Guidelines for Emergency Resource Planning for Overhead Transmission Line Asset Owners. In: *Electra*, Vol. 222 (CIGRE, Paris 2005)
- 9.271 A. Leblond, K.E. Lindsey: Maintenance. In: *Overhead Lines*, CIGRE Green Book, ed. by K.O. Papailiou (Springer, Cham 2017), Chapter 16
- 9.272 N. Pouliot, G. Rousseau, A. Leblond, S. Montabault: *Portable X-ray System for In Situ Detection of Broken ACSR Strands at Suspension Clamps – Field Results and Introduction onto Line Scout Roboting Technology*, Session Paper B2-106 (CIGRE, Paris 2016)
- 9.273 Y. Hu, K. Liu: *Inspection and Monitoring Technologies of Transmission Lines with Remote Sensing* (Academic Press, New York 2017)
- 9.274 EN ISO 2409: *Paints and Varnishes. Cross-Cut Test* (ISO, Geneva 2013)
- 9.275 ASTM D3359: *Standard Test Methods for Rating Adhesion by Tape Test* (ASTM, West Conshohocken 2017)
- 9.276 CIGRE TB 561: *Live Work – A Management Perspective* (CIGRE, Paris 2013)
- 9.277 CIGRE TB 731: *The Use of Robotics in Assessment and Maintenance of Overhead Lines* (CIGRE, Paris 2018)
- 9.278 CIGRE TB 438: *Systems for Prediction and Monitoring of Ice Shedding, Anti-Icing and De-Icing for Overhead Power Line Conductors and Ground Wires* (CIGRE, Paris 2010)
- 9.279 CIGRE TB 294: *How Overhead Lines Are Redesigned for Uprating/Upgrading – Analysis of the Replies to the Questionnaire* (CIGRE, Paris 2006)
- 9.280 CIGRE TB792: *Compact AC Overhead Lines* (CIGRE, Paris 2020)
- 9.281 P.S. Maruvada, S. Drogi: Field and ion interactions of hybrid AC/DC transmission lines, *IEEE Trans. Power Deliv.* **3**(3), 1165–1172 (1988)
- 9.282 CIGRE TB 583: *Guide to the Conversion of Existing AC Lines to DC Operation* (CIGRE, Paris 2014)
- 9.283 B. Sander, J. Lundquist, I. Gutman, C. Neumann, B. Rusek, K.H. Weck: *Conversion of AC Multi-Circuit Lines to AC-DC Hybrid Lines with Respect to the Environmental Impact*, Session Paper B2-105 (CIGRE, Paris 2014)
- 9.284 U. Schichler, N. Hadinger, W. Troppauer, M. Babuder, S. Vizinin, K. Reich, M. Leonhardsberger, F. Schmuck, E. Hussmann: *Innovation-Section: Test-Run for Uprating a 220 kV OHL to 380 kV Using Insulated Cross-Arms and Coated Conductors*, Session Paper B2-301 (CIGRE, Paris 2016)
- 9.285 S. Behrend: *CompactLine – a New Overhead Transmission Line Concept*, Session Paper B2-307 (CIGRE, Paris 2016)
- 9.286 M. Marelli, P. Argaut, H. Lugschitz, K. Kawakita: *Overhead Transmission Lines, Gas Insulated Lines and Underground Cables*, Reference Paper, ELECTRA No. 307 (CIGRE, Paris 2019)
- 9.287 H. Lugschitz: Overhead lines and underground cables. In: *Overhead Lines*, CIGRE Green Book, ed. by K.O. Papailiou (Springer, Cham 2017), Chapter 19
- 9.288 K.O. Papailiou (Ed.): *Overhead Lines. CIGRE Green Book* (Springer, Cham 2017)

### Konstantin O. Papailiou

Malters, Switzerland  
konstantin@papailiou.ch



Konstantin O. Papailiou has spent his entire career of more than 40 years in Power Systems and in particular Overhead Lines. Until his retirement, he was the CEO of the Pfisterer Group, a company he served for over 25 years. He has held leading positions in various international technical societies and standardization bodies and is also involved in power engineering education. Since 1976 he is strongly involved with CIGRE, and has served as Chairman of its Study Committee “Overhead Lines”. In 2020, he received the CIGRE Medal, the organization’s highest distinction.

# Underground

## 10. Underground Cables

Pierre Argaut

This chapter on insulated cables comprises 13 sections. Section 10.1 is an introduction to this topic that highlights the role of CIGRE in the development of insulated cables, while Sect. 10.2 gives the current state of cable development, describes modern high-voltage (HV) alternating current (AC) systems and the various types of cables used in them, and explores emerging trends in cable design.

Some basics of the theory of insulated conductors are given in Sect. 10.3 to prepare the reader for subsequent sections, including discussions of electrical fields, electrical characteristics of cable systems. In Sect. 10.4, the basic design aspects of insulated cable systems are introduced, such as insulation coordination, ageing mechanisms, special bonding issues, calculation of cable characteristics and rating.

In Sect. 10.5, various applications of insulated cables are described. The main configurations of cable systems in networks are described and the technical issues associated with each configuration are discussed: matching Cable and OHL ratings, Harmonic resonance, Ferranti effect, magnetic field. Offshore generation cables are explored in depth.

Section 10.6 covers cable design and manufacturing. Major steps in the manufacturing processes of lapped and extruded cables are described. Various options for extrusion lines are compared. Submarine cable armoring is discussed. The manufacture of accessory components is also described, including the various molding and casting processes, which depend on the materials used.

Section 10.7 deals with the construction, laying, and installation of cable systems. Traditional techniques are reviewed and innovative techniques are introduced, such as trenchless technologies: mechanical laying, pipe jacking, microtunneling and horizontal drilling. Installation in tunnels or shared structures is detailed. The main installation configurations are illustrated using examples.

In Sect. 10.8, issues relating to testing are addressed. As indicated in the introduction to the

chapter, testing has been a major issue since insulated cables were first invented and used. The introduction of extruded HV and EHV (extra-high voltage) cables would have been impossible without stringent testing procedures.

Various aspects of the operation of insulated cable systems are covered in Sects. 10.4–10.8. Fluid-filled and extruded cable systems operation have been presented. Also briefly described are monitoring techniques that can optimize equipment usage: management of the overload capacity of underground systems, partial discharge (PD) monitoring, and sheath condition monitoring. Strategies for protecting against short circuits are also addressed. To complete this information, Sect. 10.9 is covering the maintenance of land and submarine cable systems and the various diagnostic techniques that are available. Repair and methodologies that are used to limit repair times, such as fault location, are also included in this section. Main failure causes of cable systems are inventoried. Appropriate maintenance strategies are proposed, and tools for asset management are overviewed. Examples of maintenance guidelines, fault-location techniques, and rapid-response repair are also briefly presented.

Appropriate maintenance strategies are proposed, and tools for asset management are overviewed. Examples of maintenance guidelines, fault-location techniques, and rapid-response repair options are given for land and submarine cables.

Section 10.10 introduces the various options for upgrading and uprating existing cable systems. The life expectancy of an underground cable system is usually more than thirty years, which makes it difficult to predict the changes that will occur in the cable environment or how the operating conditions will evolve during the expected lifetime of a cable system. Addressing the need for a cable system to meet a higher demand can be highly problematic. Replacing a power link or installing an additional circuit requires significant financial investment. It may even be impossible for the op-

erator to extend the system in some congested areas. The difficulties involved in obtaining planning permission for new sites also favor extending the lifespans of existing facilities, often with the goal of transmitting higher power with higher reliability in order to minimize the duration of asset unavailability.

Life Cycle Assessment is discussed in Sect. 10.11. A new technology—superconducting cables—offers interesting options for both AC and DC cable systems, as described in Sect. 10.12. Finally, other undergrounding options (gas insulated lines, GILs) are briefly described in Sect. 10.13.

10.1	<b>From the First Electric Telegraph to the Foundation of the CIGRE Study Committee on Insulated Cables</b> .....	761	10.5.9	Magnetic Field .....	802
10.2	<b>Current State of Cable Development</b> .....	763	10.5.10	Life Expectancy .....	803
10.2.1	Basics of Power Transmission .....	763	10.5.11	On-Site Testing .....	804
10.2.2	AC Underground Cables .....	764	10.5.12	Practical Implementation of System Design .....	804
10.2.3	Integration of a New Cable System into a Network .....	768	10.6	<b>Cable Designs</b> .....	806
10.2.4	Reasons for the Growth in the Number of Long Cable Systems .....	770	10.6.1	Mass-Impregnated Cables .....	807
10.2.5	Overall Description of Modern HVAC Systems .....	770	10.6.2	Self-Contained Fluid-Filled Cables ...	807
10.2.6	Cable Design Trends .....	771	10.6.3	Extruded Cables .....	815
10.3	<b>Basics of Cable System Design</b> .....	772	10.6.4	Accessories for Extruded Cables .....	817
10.3.1	Introduction to AC Link Modeling .....	772	10.6.5	Accessory Workmanship .....	821
10.3.2	Cable System Types .....	773	10.6.6	Submarine Extruded Cables .....	822
10.3.3	Step-by-Step Approach to Cable System Design .....	781	10.6.7	New Installation Trends .....	828
10.4	<b>AC Cable Theory in Underground Cable System Design</b> .....	784	10.7	<b>Installation Techniques</b> .....	830
10.4.1	Electric Fields in AC Cables .....	784	10.7.1	Selection of the Best Cable Design According to the Installation Method	831
10.4.2	Electric Fields in DC Cables .....	788	10.7.2	Routes and Rights of Way .....	831
10.4.3	Detailed Calculation of the Electrical Characteristics of Cable Systems .....	789	10.7.3	Route Planning: Traffic Management and Security .....	831
10.4.4	Rating Calculations .....	789	10.7.4	Installation Methods and Definitions	831
10.5	<b>Challenges in Cable System Implementation</b> .....	794	10.8	<b>Testing</b> .....	838
10.5.1	Main Cable Configurations .....	794	10.8.1	Fluid-Filled and Mass-Impregnated Cables .....	838
10.5.2	Connecting to Offshore Generators .....	795	10.8.2	Extruded Cables .....	838
10.5.3	Effect on the Grid .....	797	10.9	<b>Maintenance</b> .....	843
10.5.4	Protection Systems .....	799	10.9.1	Land Cables .....	843
10.5.5	Voltage Effect (Ferranti Effect) .....	801	10.9.2	Submarine Cables .....	846
10.5.6	Zero-Miss Phenomenon .....	801	10.10	<b>Upgrading and Upgrading</b> .....	848
10.5.7	Switching Off Capacitive Currents .....	802	10.10.1	Proposed Methodology .....	849
10.5.8	Harmonic Resonance .....	802	10.11	<b>Life-Cycle Assessment</b> .....	850
			10.12	<b>Superconducting Cables</b> .....	852
			10.12.1	Experience with Superconducting Cables .....	852
			10.12.2	Cryogenic System Issues .....	853
			10.12.3	Future Work .....	853
			10.13	<b>Gas-Insulated Lines</b> .....	854
			10.13.1	Historical Development of GILs .....	857
			10.13.2	Comparison of GILs to Conventional Cables .....	857
			10.A	<b>Appendix</b> .....	858
			10.A.1	Overhead Transmission Lines, Gas Insulated Lines and Underground Cables .....	858
			10.B	<b>Further Reading</b> .....	864
			10.C	<b>CIGRE Technical Brochures to be Published</b> .....	865
			<b>References</b> .....		865

## 10.1 From the First Electric Telegraph to the Foundation of the CIGRE Study Committee on Insulated Cables

As explained in Sect. 9.1 of this book, the first industrial-scale transmission of electrical power was developed on a long distance DC transmission between Vizille and Grenoble in 1883 by Marcel Deprez (1843–1918) for railways, followed by the first installation of AC overhead transmission lines in 1891, in Germany at the voltage of 15 kV and a frequency of 40 Hz. Very soon, the need to increase voltages and currents for higher amounts of electric power transmission was recognized and huge progress was made in the development of overhead line (OHL) voltages as shown in Fig. 9.2.

Parallel to this, the early days of cable industry started by underground distribution of electricity for telegraphy purposes. Buried insulated wires or wires drawn into conduits were tried but very little was done until the advent of the Edison lamp in 1879 and the need to transmit higher power in lighting networks.

As for overhead transmission, the possibility to increase voltage and current for higher power was depending on the development of suitable insulation material.

In underground transmission, cable conductors must be covered by an insulating material along their entire length, and insulated conductors must withstand the full operating voltage of the circuit at any point.

The history of insulated cable is therefore highly linked to the progress of the insulation materials from Gutta-percha (used in telegraphy for the first transatlantic cable in 1868 until about 1930) to paper insulation and later to modern polymeric extruded insulation [10.1].

Gutta-percha was a gum extracted from certain tropical trees, an isomer of rubber becoming supple and malleable at 100 °C and recovering consistency of leather when cold. It could not be used for land cables, owing to the instability of its properties in the air and to its inadequate mechanical characteristics. For the insulation of power cables an evolution of insulation was therefore needed. Two tendencies forced their way in the 1880's:

- The use of vulcanized material: vulcanized natural rubber was known since 1839 but was expensive.
- The use of impregnated material: in 1890, single-core cables at 3000 V, insulated by paraffin and colophony-impregnated jute, were laid in Paris, while similar cables at 2000 V had been already laid in Rome and Milano in 1886.

Later, cable for lighting and power progressively reached the voltages of 5 kV, and 25 kV in 1900 in the US (rubber insulated). At the end of the 19th century, the voltage of 10–11 kV was reached in several countries. In 1911, the first links of high-voltage cables with impregnated paper insulation were commissioned at 60 kV in Germany and 50 kV in Spain. The different steps of this evolutions are well described in several publications listed in Sect. 10.B. It should be noted that one of the earliest technologies called *mass-impregnated cables* developed more than 120 years ago, is still in use, especially for HVDC transmission up to 500 kV and more.

HVAC transmission required some technological advances to increase electrical field and consequently attain higher service voltages and higher transmitted power. One big step forward was achieved when came the idea of the well-known metallic screen placed over each insulated conductor, making possible to realize screened multi-core cables.

Insulated cables were addressed by CIGRE (Conseil Internationale des Grands Réseaux Électriques) from the very beginning, starting with a discussion in the 1921 session under the heading *Construction of Lines* and the sub-heading *Underground and Submarine Lines*. The main subjects considered for discussion (preferential subjects) were:

- Utilization limits of single and multicore cables for AC and DC
- Determination of electric constants
- After laying tests.

A *panoramic* paper on very-high-voltage underground and submarine lines by Couffon, Geoffroy, and Gosselin from France, the first CIGRE paper on insulated cables, was initially presented, and a lively and interesting discussion followed, during which the situations in different countries were compared. At that time, paper-insulated mass impregnated cables for voltages up to about 60 kV were already available. However, design stresses and operating temperatures were limited to avoid early failures caused by ionization and, although there was already a need for higher-voltage cables with the ability to carry more power, it was unclear at that time how this need would be met.

In the 1923 Session, there were seven papers on insulated cables (three from France, two from the Netherlands, one from Italy, and one from the UK), and similar

numbers were put forward in the 1925 Session (five papers) and 1927 Session (seven papers).

It is interesting to note that during the 1923 Session, the Italian delegate Angelo Barbagelata presented a sample of a radically new cable, the basic characteristics of which had been patented by Luigi Emanuelli in 1917. This cable, he argued, was entirely suitable for utilization at 130 kV and completely eliminated the problem of ionization, which had been a subject of intensive discussion at both the 1921 Session and the 1923 Session. He was, of course, referring to the cable which would become known as the self-contained oil-filled (OF) cable. By 1924, a pilot 130 kV installation utilizing this type of cable had been successfully tested in a substation near Milan, as reported in a 1925 Session paper by Luigi Emanuelli himself. This installation, in the words of the official 1925 Session report, “proved the possibility of undergrounding very high voltage overhead lines”.

During the 1927 Session, the General Assembly of CIGRE, having noted the large and growing interest in insulated cables, decided to create a specific Study Committee to deal with this subject. This committee celebrated its 90th anniversary in 2017.

It is particularly interesting to note that 1927, the year in which the Insulated Cables Study Committee was created, also marked the start of the era of modern high-voltage cables, the evolution of which has been and still is one of the main concerns of the Committee. It was during that year, in fact, that the first two long underground OF cable lines operating at 132 kV were put into service in Chicago (29 km of cable) and New York (58 km of cable). The cable voltage barrier, which had up to that point made it practically impossible to reliably deploy cables for voltages higher than 60 kV, had been broken once and for all. Since then, insulated cables have always been able to reliably carry the highest voltages required by electric power systems. So 1927 was a very good year to start a CIGRE Study Committee on high-voltage cables! From the very beginning, this Study Committee has been at the forefront of cable technology, paying close attention to the technical developments arising from the evolution of this technology and, through its work, facilitating the adoption of innovative solutions. Test methods have been agreed and recommended, new solutions have been examined and described, fertile exchanges of views have taken place between users and manufacturers and, par for the course, heated technical discussions have occurred between the manufacturers themselves. The introduction of higher-voltage laminar cable systems (220 kV in the mid-1930s and 400 kV in the 1950s and 1960s),

the evolution towards higher power-carrying capacities, comparisons of different high-voltage cable solutions, the deployment (starting in the 1960s) of extruded cable systems for increasingly high voltages (currently used commercially for up to 550 kV), progress in high-voltage submarine cables (for which the CIGRE test recommendations are still the only internationally recognized de facto standards), the introduction of HVDC cables, and the development of new techniques, systems, and installation methods have all been topics addressed by the Study Committee on Insulated Cables.

A historical perspective on the technical evolution of power cables is presented in a paper prepared for the conference Jicable 1984: *From impregnated paper to polymeric insulating materials in power cables* [10.1].

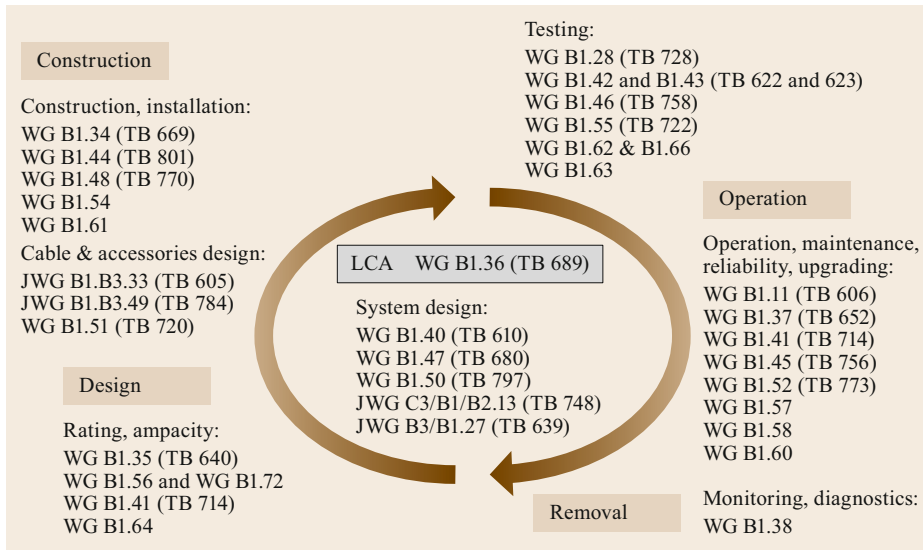
As recalled in the contribution of Study Committee B1 published in *Electra* magazine [10.2] and in the recent Annual Report of SC B1 [10.3], the first Study Committee (SC) on power cables, designated SC 2, was founded in 1927, just a few years after CIGRE itself was founded in 1921. It became SC 21 in 1967 and SC B1 in 2002, and is one of five Study Committees that deal with subsystems (SC B).

During most of its history, SC B1 (formerly SC 21) has focused its activities on technical work and has issued a large number of technical documents, including recommendations used to prepare IEC standardization (e.g., IEC 62067, which was urgently needed by utilities to specify qualification tests for 400 kV cable systems). Since the reorientation of CIGRE to better satisfy the needs of its target groups, SC B1 has extended its work to include economic, environmental, and social aspects of the evolution of the electric power industry.

The field of activity of SC B1 is the development and operation of all types of AC and DC insulated cable systems for land and submarine power transmission. Historically, it has focused mainly on HV, EHV, and (more recently) UHV (ultra-high voltage) [10.4], but MV (medium-voltage) cable applications are receiving increasing attention from SC B1, and Working Groups (WGs) that address specific issues in this area have been launched in recent years.

The scope of the work of SC B1 covers the whole life cycle of insulated cables: the theory, design, applications, manufacture, installation, testing, operation, and maintenance of these cables, as well as diagnostic techniques for them. This scope is illustrated by Fig. 10.1, where most recent and current working bodies are positioned along the life cycle. Information regarding recent working bodies of CIGRE is given in the most recent annual report of SC B1 published in





**Fig. 10.1** Scope of the work of SC B1 (updated in June 2020; courtesy of CIGRE)

April 2020 [10.3]. Future annual reports from SC B1 will update this information.

Subsequent sections of this chapter will cover most of these aspects of the life cycle of insulated cables in power systems.

All the information given in the following sections derives from the most recent technical brochures (TBs) and reports published by SC 21/B1 and by other Study Committees such as SC D1 (on materials and emerging technologies) and SC B4 (on HVDC transmission) in which HVDC cables play an important role.

Reference is made to these documents, allowing the reader to find more detailed, unbiased information on the topic at hand. The reader can also consult many other relevant publications in the bibliography and other documents cited in this chapter. The standards published by the International Electrotechnical Commission (IEC) that are mentioned in this chapter can be found on the official website of the IEC [10.5].

A tutorial presented by SC B1 at the Lund Symposium in 2015 [10.6] is a good example of the exchange of information regarding HVDC cables.

## 10.2 Current State of Cable Development

A considerable amount of highly technical information, including specifications and guides, is currently available on the transmission of bulk electrical power from one area to another. This information can be obtained from bodies such as CIGRE, IEC, national standards, and the Institute of Electrical Technology (IET). There are, however, very few publications that explain the fundamentals of these technologies such that it can be understood by a nontechnical person or a person not involved in this industry on a day-to-day basis.

### 10.2.1 Basics of Power Transmission

Two of the fundamentals of power transmission are the voltage and current levels used to transmit the power from one area to another. Current is the flow of electricity through the conductor. If one thinks of electricity in

terms of water flow, then voltage is equivalent to pressure, i.e., it drives the current through the conductor in the same way that pressure drives water through a pipe. Roughly speaking, the power is the voltage multiplied by the current.

In alternating current (AC), the standard practice internationally is to transmit the power using a three-phase system with three metallic conductors in what is called a circuit to carry the electric current. The size of the conductor governs its ability to carry current: the larger the conductor, the more current it can carry.

Conductors must be insulated from the ground in order to be able to withstand the voltage applied; again, the more insulation they have, the higher the voltage that can be applied.

Three conductors may be combined in an OHL circuit (Chap. 9), an underground cable (UGC) circuit, or a gas-insulated line (GIL) circuit [10.7].

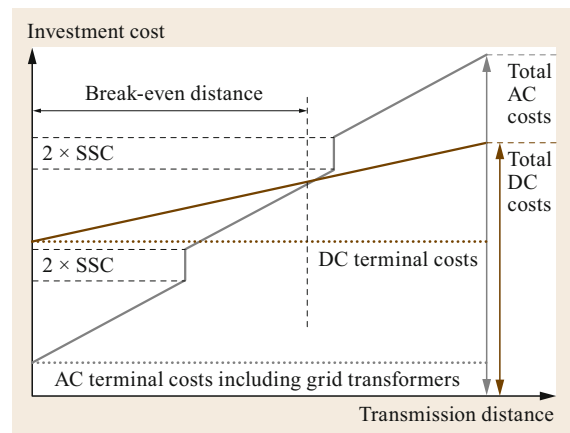
The integration of a HV cable system into a network is covered by TB 250, published by CIGRE WG B1.19 [10.8]. Statistics and service records of UG extruded cables can be found in CIGRE TB 338, published by CIGRE WG B1.07 [10.9], and TB 379, published by CIGRE WG B1.10 [10.10]. WG B1.57 is currently at work updating TB 379 and providing new statistics and recent service records.

Direct current (DC) is the other way to transmit power. As noted in TB 536, published by JWG C4/B4/C1.604 in April 2013 [10.11], HVDC installations date back to the 1950s. This technology exhibits characteristics that have already made it much more attractive than HVAC transmission for specific applications, such as very long distance power transmission, long submarine cable links, and the interconnection of asynchronous systems, as well as bulk energy transport. These characteristics are listed here:

- *Almost no limitation on transmission line length.* In contrast to AC cables, the absence of charging current in DC cables leads to virtually unlimited transmission distances via DC. The environmental advantages of this are mostly related to the transmission medium: since there is no need for reactive compensation, the use of HVDC makes it easier to place cables underground. In the case of overhead lines, the required right-of-way for HVDC transmission is much smaller than that for AC for the same transmitted power. Also, the electromagnetic field emission does not pulsate and can be reduced to a minimum. Ability to offer some advanced control functions within the AC network: optimal power flow control, voltage control, system transient stability improvement, low-frequency damping, the prevention of system cascading failure ... The availability and performance of these features are dependent on the HVDC converter technology, as discussed in TB 536 [10.11].
- *Increased transmission capacity.* For a given conductor cross-section, HVDC transmission can transfer more current than conventional HVAC transmission can. Accordingly, the conversion of a HVAC line into a HVDC line increases its transmission capacity.

For current link lengths of tens of kilometers to a few hundred kilometers, the decision to use AC or DC depends on the costs of both options, including the cost of converter stations.

Converters are designed to transfer large amounts of power over long distances, for instance in sea crossings, where AC cables cannot be used because of their large capacitive currents. The thyristor-based HVDC



**Fig. 10.2** Cost comparison of AC transmission and DC transmission for a given power capability (adapted from [10.11])

system is economical for cables longer than the *break-even distance* (a few hundreds of kilometers), as shown in Fig. 10.2 (in the figure, SSC is short for series and shunt reactive power compensation of AC lines, which is required due to the length of the lines).

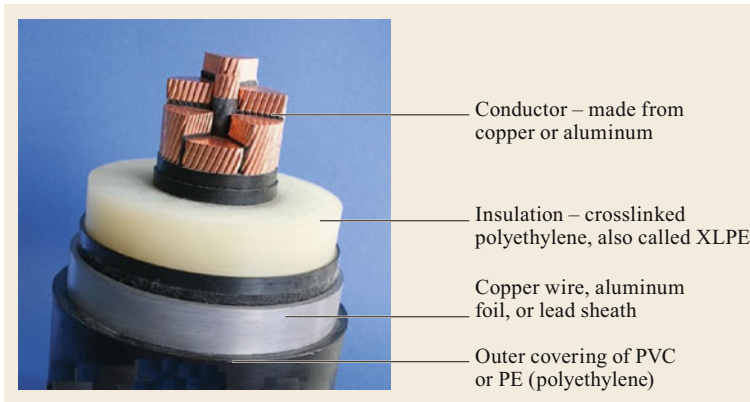
In the following paragraphs, we focus mainly on AC transmission and extruded cables, for which there are a great number of recent relevant CIGRE documents, rather than DC transmission. However, when applicable, differences from DC transmission are pointed out, while related work in progress within CIGRE is mentioned, and reports that are expected to be published in the near future are included in Sect. 10.B.

### 10.2.2 AC Underground Cables

As mentioned above, an AC underground (UG) cable circuit usually consists of three power cables and one communication cable installed in the ground. Increasingly, following the recommendations of CIGRE WG B1.02 in TB 247, a thermal monitoring system is also laid in parallel [10.12]. A typical design of a XLPE (crosslinked polyethylene) power cable is shown in Fig. 10.3, while Fig. 10.4 shows a 400 kV LDPE (low-density polyethylene) cable. Other examples are given in subsequent sections.

Before we proceed any further, it is important to convey a rough idea of the size of a typical modern underground project.

The larger the conductor, the more current it can carry, and the thicker the insulation, the more voltage it can withstand. The cables are manufactured in highly specialized factories, and they are currently delivered in drum lengths of 600–1000 m, as shown in Fig. 10.5 (taken from TB 250 published by



**Fig. 10.3** Typical design of a modern XLPE cable (adapted from [10.7])

WG B1.19 [10.8]). For some applications where transportation limitations are favorable, drum lengths can be 2000 m or more, as explained in TB 680 published by WG B1.47 [10.14].

As an example, for drums containing 1000 m of cable, a circuit 10 km long would require  $10 \times 3$ , i.e., 30 drums in total. Twenty-seven joints would be needed to join the cables together (implying  $27/3 = 9$  joint bays or manholes and associated civil works),

as well as three terminations or sealing ends at each end.

Terminations can be installed in substations or transition compounds (Fig. 10.6), or directly on towers/poles (Fig. 10.7).

The cables are typically installed in one of the following arrangements:



**Fig. 10.4** Typical very-high-voltage LDPE cable used underground for voltages of 170–500 kV (adapted from [10.13])



**Fig. 10.5** Typical cable drums for 400 kV cables (adapted from [10.8])



**Fig. 10.6** EHV transition compound (adapted from [10.8])



**Fig. 10.7** HV terminations installed on a pole (adapted from [10.8])



**Fig. 10.8** Cables installed directly into the ground with native soil backfill (adapted from [10.15])



**Fig. 10.9** Construction swathe for installing cables cross-country; a width of 8 m is typically required for a single trench (adapted from [10.13])

- Directly in the ground (Figs. 10.8 and 10.9)
- In ducts installed in the ground (Fig. 10.10)
- In concrete troughs (Fig. 10.11)



**Fig. 10.10** Cables installed in ducts (adapted from [10.13])

- In a tunnel (Fig. 10.12)
- In a pipe or pipes that are drilled into the ground using drilling equipment and pass under an obstacle or encumbrance (horizontal directional drilling, HDD; see Fig. 10.13)
- On a cable tray attached to a bridge (Fig. 10.14).

Installation in a tunnel or shared structure (such as a bridge) is covered by TB 403 [10.18].

For buried installations, the backfill used to reinstate the trench around a buried cable is a critical engineering component of the cable system, as it (along with the surrounding material) is the means of conducting the heat produced during the operation of the cable to the ground surface, where it is dissipated to the atmosphere. Therefore, the thermal properties of these materials, which are assumed in the design of the cable system, are crucial to the correct operation of the system. As mentioned before, a thermal monitoring system is increasingly installed with such systems [10.12] to optimize the operation of the system. CIGRE WG B1.45 has very recently published TB 756 on this topic [10.19].

Figure 10.11 shows concrete troughs with a lid at ground level. Note that troughs are normally filled with



**Fig. 10.11** Cables installed in troughs (adapted from [10.13])

cement-bound sand to ensure that they are capable of taking traffic or similar loads. In other configurations, troughs are buried at greater depths.

The photograph presented in Fig. 10.12 shows two cable circuits with room for two more circuits in the future. Forced air ventilation may be needed to achieve the required rating for the cables and to ensure the



**Fig. 10.12** Cables installed in a tunnel (adapted from [10.16])

safety of personnel who are carrying out inspections or working in the tunnel. Tunnel design and safety systems is a complex area of design and needs to be considered very carefully to ensure the right balance is achieved.

The photographs in Fig. 10.13 show equipment used for HDD and pipes installed by HDD. More photographs on HDD can be found in later sections of the chapter.

The length that can be drilled depends on the hole size required and the composition of the ground. Drilling lengths exceeding 2000 m are possible.

Depending on the soil and cable rating conditions and the length/profile, it may be possible to put all three cables inside one pipe, or three separate pipes inside a casing pipe may be required.

The design of an underground cable circuit depends on many factors, including:

- *Route availability.* It must be possible to route the underground circuit. The impact of other services that may conflict with the cable route either now or in the future must be considered.
- *Route topography.* If the terrain is very uneven or has lots of hills, it may be difficult to route the circuit.
- *Urbanization.* If the line is to be routed through an urban area, future building or road developments may impact on the circuit.
- *Flooding.* This may undermine the installed cable circuit.
- *Conductor size.* The size of the conductor is dependent on the current to be carried and on the increase in the temperature of the surroundings permitted by regulations. Of course, the size of the conductor also has an impact on the weight and size of the cable drum being delivered; the maximum conductor size currently used is 2500 mm<sup>2</sup>, and drum lengths are typically 600–1000 m long. Jointing of cable



**Fig. 10.13a,b** Drilling machine (a) and pipes (b) for HDD (adapted from [10.17])



**Fig. 10.14** Cables on a cable tray attached to a bridge (adapted from [10.18])

lengths is then required every 600–1000m. The need for jointing bays must be accounted for (e.g., civil works). This explains why there is a strong drive to use longer cable lengths, as it reduces the cost of civil works and jointing. The sizing of the conductor and the overall design of the cable are therefore very important.

- *Soil thermal conductivity.* Heat is created as current flows through the cable when it is delivering power. The conductor size has an impact on the heat losses from the cable. For a cable installed in the ground, this heat must travel through the ground before it is released into the air. The thermal conductivity and temperature of the ground therefore also have an impact on the cable sizing.
- *Cable pulling.* The route and drum lengths and route topography must be such that the cables can be pulled into the selected installation arrangement (trench, duct, tunnel, etc.).

- *Electrostatic effects.* Underground cables have no electrostatic effects initiated by the cable, as the electric field is contained inside the cable.
- *Electromagnetic field.* In this case, the current sets up a magnetic field that must be considered when designing the underground circuit. In some countries there are specific limits—for example, those set by the International Committee on Non-Ionizing Radiation Protection (ICNIRP). It should be noted that underground cables have higher electromagnetic fields than overhead lines close to the cable, but the fields fall off more rapidly with distance from the cable. This topic is addressed in [10.8, 20, 21].

As discussed in TB 250 [10.8], the *Study Area* is the area where the impacts are assessed. It includes the locations of the two ends of the projected underground cable system, and the likely extent of the physical and visual influence of the potential underground cable route corridors between these two points. Since all of the factors listed above can vary along the route of a projected cable link, the Study Area is divided into several sections.

### 10.2.3 Integration of a New Cable System into a Network

Prior to the public unveiling of any new transmission line project (OH or UG), it is important to conduct detailed preparatory studies of the political and social situation in the region affected by the project. It is advantageous to collect information regarding previous large construction projects in the region (especially projects concerning roads, railways, or pipelines). The reactions before, during, and after the completion of these projects may be indicative of the community's involvement in cases affecting the area. Groups of cit-

izens who previously actively protested against other technical construction projects may quickly reemerge to oppose a transmission line project.

Political power relationships should also be studied, such as important politicians or other influential figures who are connected to, are domiciled in, or are elected for the area. Such figures often exert a strong influence on the final design of a transmission line project. It is also important to consider any alliances between local politicians and protest movements.

The results of these preparatory studies may give an idea of the political difficulties that will be encountered during the regulatory process of the project, and how to introduce the project to the public.

The decision to use underground cables in a network or in a section of a transmission line often results from a failure to gain permission to build an overhead line in the area. Therefore, the local community will often consider the decision to use underground cables a success in their fight against new overhead lines and the transmission company in question. The public will then often build up strong political pressure to increase the length of the underground section and thus reduce the lengths of new overhead lines. Consequently, increasingly long underground cable connections are being implemented, as recently reported in [10.14] and discussed in later sections of this chapter.

In many respects, underground cabling is considered to be an environmentally friendly but expensive solution compared to overhead lines. However, when discussing the location of the transition compound (Fig. 10.6) and the length of the underground cable section, the public will probably not display any moderation. This is because increased construction costs for a transmission line project normally do not affect the local community's budget. Many decision-makers have little or no knowledge of underground cable technology, and it is commonly believed that cable projects can be implemented without encountering any problems. There is a great need to supply information to both decision-makers and the public about the sizes of HV underground cable projects. Once the decision has been made to take the underground option, a course of action can be determined.

CIGRE JWG B1/B2/C3.13 has published TB 748 addressing environmental issues associated with high-voltage transmission lines in urban and rural areas [10.22].

The flow chart in Fig. 10.15 (proposed in [10.8]) gives a typical example of a *step-by-step* approach to the planning and design process. However, in practice, iterative actions are often involved. It must be emphasized that the decision on whether or not to build a line

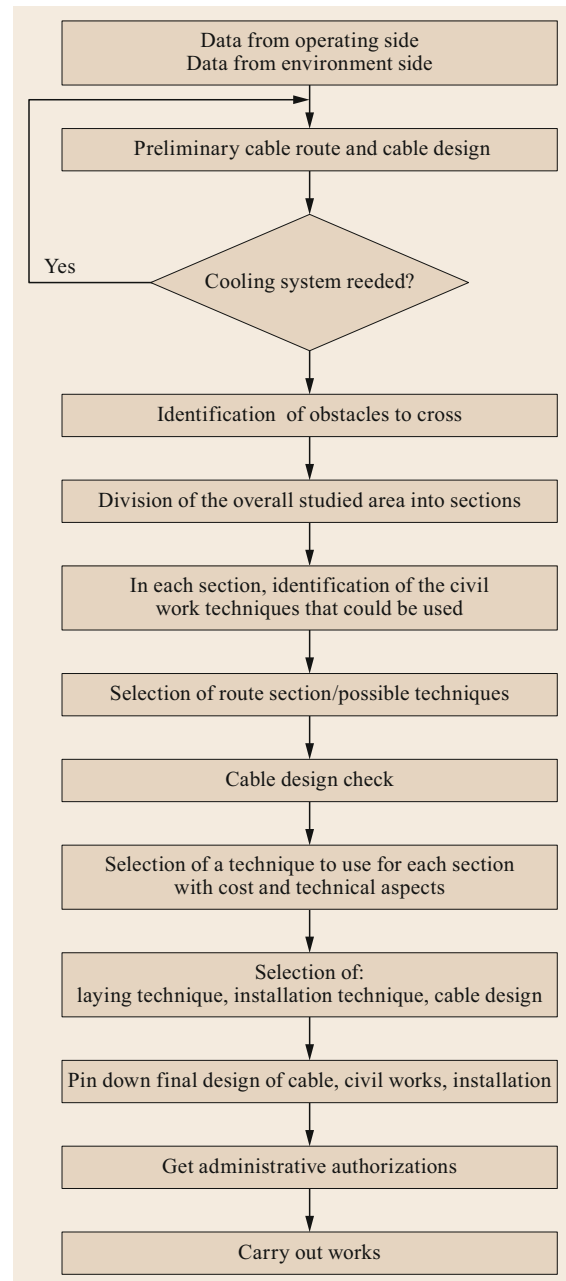


Fig. 10.15 Flow chart for a new cable system (adapted from [10.8])

can depend on different conditions in different countries.

As shown in this diagram, the Study Area is divided into sections depending on the factors listed above. For each of those factors, the UG line is designed taking into account all of the input data for the given section.

Of course, for the overall design of the project, the most important parameters will be those associated with the network, such as system voltage, frequency, basic insulation level (BIL), and some other parameters that are listed in subsequent paragraphs. In addition, each Study Area section is designed through the application of methodologies proposed and detailed later in this chapter.

#### Parameters Dictated by the Network

System planners seek to optimize the parameters that apply to the overall transmission system. They perform network studies that focus mainly on insulation coordination, transient stability, short-circuit levels, and load flow.

#### Main Equipment Parameters

When a utility determines a standardization policy and develops technical requirements, the main characteristics of the primary equipment must be specified by asset managers in close consultation with designers.

The following parameters may be defined:

- The short-circuit current ratings of the equipment, including the supporting structures
- The maximum load currents permissible through the components (which are related to the maximum current-carrying capacities of the lines and underground cables) in normal operation and in overload conditions.

#### Fault Clearance Times

In order to comply with the requirements of the network (system stability) or the specifications of particular utilities, specified fault clearance times must not be exceeded.

Fault clearance times and the reclosing policy may influence the selection of components, the size of the metallic cable screen, and the installation design (depth of burial), as well as the dimensioning of the earthing grid and the mechanical strength of the equipment.

### 10.2.4 Reasons for the Growth in the Number of Long Cable Systems

Typical examples of elements of current UG cable projects were touched upon in previous sections. Insulated cables are now used at the 550 kV level, and tests have indicated that UHVAC extruded cables will soon be available for use at the 800 kV level. In the meantime, self-contained fluid-filled (SCFF) cable systems are already available for higher voltage levels [10.4].

As explained in [10.14, 23], there are several reasons for the strong growth in the use of long HV

and EHV insulated cables operated with AC. Whilst HVAC and EHVAC cables have been available for many years, their use for long-length applications has often been limited by the cable capacitance, dielectric losses, current-carrying capacity, and high installation costs. However, cable performance has greatly improved due to the introduction of cable designs that use new materials, modern processing techniques, and the development of accessories, associated equipment, and installation techniques. At the same time, the cost of supplying and installing underground cables has been significantly lowered.

Until recently, power transmission network designs were principally based on OHLs, mainly because of costs but also for technical reasons: there is no need to compensate for the cable capacitance in OHLs, and there are higher installation costs for undergrounding due to environmental conditions and requirements.

Today, there are often demands to transfer power from renewable energy sources to the grid or to provide electric power to remotely located plants as quickly as possible. In many countries, the process of getting the environmental approvals needed to build an overhead line may take many years, whereas the process of obtaining approval to install underground cables in public areas such as roads and road reserves may be much quicker. The net result is that an AC cable link is often built in a shorter time, leading to a quicker return on the investment, which often justifies the decision to use an AC cable link.

For connections to offshore wind farms, the use of AC cable often provides a lower-cost solution than DC cable when factors such as converter costs, space requirements, and overall system losses are accounted for (Fig. 10.2). At the same time, there is also an interest in reducing transmission losses and gaining community support for improved public safety by providing a supply that is not affected by extreme weather conditions (which appear to be more common these days).

When all of these factors are considered, there can sometimes be a real advantage to adopting an insulated cable transmission solution.

### 10.2.5 Overall Description of Modern HVAC Systems

High-voltage cables form an integral part of any electricity transmission and distribution network. Such a system may consist of different types of cables and a wide range of necessary accessories. For long cable links, it is also necessary to compensate for reactive power generation by installing large reactors at appropriate locations. The design of a high-voltage system is therefore extremely important and requires components



of the highest quality. A high-voltage cable system for a long-distance link must be custom designed to account for power demand and installation conditions. As such, the highest competence is required from system planning through to final testing. As an example, some cables may have an increased insulation thickness to reduce the cable capacitance and therefore the effect of reactive power on the cable system.

A HVAC cable system consists of cables, terminations, joints, link boxes, an earthing system, remote monitoring systems, and compensation reactors. Cables are available in both three- and single-core designs for land and submarine applications, but single-core cables are typically used for long cable lengths on land and three core cables are typically used for long submarine cable lengths. In both cases, optical fiber elements are included in the cable to measure the operating temperature, as conditions may vary along the cable route. Because of transportation restrictions, a land cable is composed of several lengths (each up to 2000 m long), which are installed and jointed together using pre-molded joints. For a submarine system, jointing small lengths together at sea is often not a feasible solution, so the cables are manufactured by jointing together cables up to 10–20 km long in the factory using flexible factory joints *with the same dimensions and properties as the cable*, resulting in cables with very long lengths (over 100 km). The transport capacities of cable installation vessels are in the thousands of tons.

Submarine cables are used for three main reasons:

- To connect two power grids
- To transport power that is generated offshore
- To connect an offshore platform.

Compensation systems take up valuable space on offshore platforms, so compensation is usually carried out at the onshore end of the cable (where practical) when transporting power generated offshore and connecting to offshore platforms.

A submarine cable system is often designed to allow for redundancy because the economic consequences can be very serious if a cable is damaged and out of service. For example, if a cable connecting an offshore wind farm is out of service, the power generated by the wind farm cannot be transferred to land, so the loss of income for the owner is substantial. In addition, the time needed to carry out a repair operation offshore can be quite long. Hence, the solution is often to have two cables installed in parallel. If one cable fails, the other can still be operational for half of the power transfer capacity.

For submarine cables, both ends of the cable are earthed, in strict contrast to land cables, where single-

core cables tend to be more common for long-length and high power transfer requirements. In these land cable systems, special sheath bonding arrangements are required. These so-called cross-bonded systems provide the advantage of an increased rating, but (more expensive) sectionalized joints are required, together with special link boxes that must be installed adjacent to the joint pits/manholes.

The joints used for submarine cables are similar to vulcanized factory joints, and vulcanized or prefabricated joints are used to repair these cables. Typical maximum lengths for HVAC submarine links may be up to 100 km for 400 kV or 200 km for 132 kV. For land cables, longer lengths are made possible through the addition of reactive compensation along the route (Fig. 10.49).

### 10.2.6 Cable Design Trends

As noted in the introduction to this chapter, HV and EHV cables have traditionally been insulated with paper impregnated with oil under pressure. Various designs have been used and significant improvements have been made to increase the operating temperatures and ultimate ratings of such cables, which have an excellent service record. However, as explained later, there are various technical, installation, and service limitations of these designs, such that there are presently very few plants worldwide that produce AC cables based on this technology.

In the last few decades we have seen very rapid development in HV and EHV cable technology that uses crosslinked polyethylene (XLPE) as an insulating medium. As an example, modern XLPE cables have lower dielectric constants and higher operating temperatures than very early paper-insulated, oil-impregnated cables, so they are many times more efficient. Whilst modern pressurized oil-filled cables have higher operating temperatures, XLPE cables are easier to manufacture, which has led to a dramatic increase in the supply and use of these HVAC cables.

There are currently at least ten fully qualified manufacturers of XLPE-insulated AC cable rated at 500 kV worldwide, and the demand for such cables is growing significantly due to the growth of major cities.

Most HVAC submarine cables are three-core cables. Each core contains a conductor: copper or aluminum. Submarine cables often use copper because, although it is more expensive, its electrical resistance is lower, so the cross-section required is smaller than when aluminum is used, meaning that less material is required for the outer layers. Furthermore, it has often been argued that the corrosion resistance of copper is better than that of aluminum, especially in a marine envi-

ronment, but this is actually of little relevance, as a well-designed cable will never allow the conductor to come into contact with seawater.

Hence, aluminum is now becoming more widely accepted because of its lower cost and weight and its better mechanical properties (strength to weight). This is particularly the case for deep installations and dynamic situations.

*For submarine cables*, the insulation system used can be XLPE or SCFF, although—except for very high voltages—most HVAC submarine cables are currently made with XLPE insulation.

The insulation system is protected from the water by a metallic layer, such as lead alloy or a welded metallic sheath, which is also used as electrical screen. A PE layer is extruded to protect this metal sheath. The three phases are laid together and optical fiber elements are often laid in the interstices between the cores, along with some other materials (e.g., PP ropes or PE profiles). The bundle is then protected from mechanical damage by metallic armor made of steel wires. An outer protective covering often made of PP yarns is applied outside the armor.

*For land situations*, different types of cables are available, including LPOF (low-pressure oil-filled), HPGF (high-pressure gas-filled), HPFF (high-pressure fluid-filled), EPR (ethylene propylene rubber), PE (polyethylene), XLPE, GIL-SF<sub>6</sub> (SF<sub>6</sub> gas-insulated lines), and superconducting cables. However, as mentioned above, except in some countries that have considerable experience with fluid-filled cable systems, most new long-length AC cable links are supplied with single-core XLPE cables. Copper conductors are still specified when there are very high current-carrying

capacity requirements, but, due to their lighter weight and the increasing need for longer lengths, aluminum conductor cables are becoming far more common. The trend for long lengths of cable with large conductors means that the mechanical forces exerted due to thermal expansion under load require very careful consideration during system design. This issue is addressed in [10.24].

The insulation thickness of XLPE cables is mainly determined by the withstand voltage. In the case of long-length EHV cables, the insulation thickness will also influence the reactive power produced by the cable.

Reactive compensation is usually achieved by installing shunt reactors (Fig. 10.49). These make the system more complex due to electrical and spatial issues, additional losses, and the need for redundancy. Therefore, it may be desirable to reduce the reactive power produced. This can be done by increasing the insulation thickness or by decreasing the conductor size, although the latter is often impractical.

Thicker insulation results in lower capacitance, which will translate into less reactive power compensation and reduced dielectric loss and charging current. However, increasing the insulation thickness of a XLPE cable has some negative consequences, the most important of which is the maintenance of the quality of the extrusion process when processing very long runs of HV cable. Whilst the insulation thickness may be increased by only a few millimeters, this could lower investment and operational costs for long lengths of EHV cables. Also, some of the additional costs of a cable system with more insulation can be recouped, as less investment in reactive compensation is required and system losses will be lower.

## 10.3 Basics of Cable System Design

As mentioned above, the sections of this chapter largely focus on AC (rather than DC) transmission and extruded cables, as a large number of relevant CIGRE SC B1 documents on these topics have become available in recent years. For specific issues regarding HVDC cables, the reader is advised to read publications from SC D1 [10.11, 25] and the tutorial prepared by SC B1 for the Lund International Symposium [10.6].

### 10.3.1 Introduction to AC Link Modeling

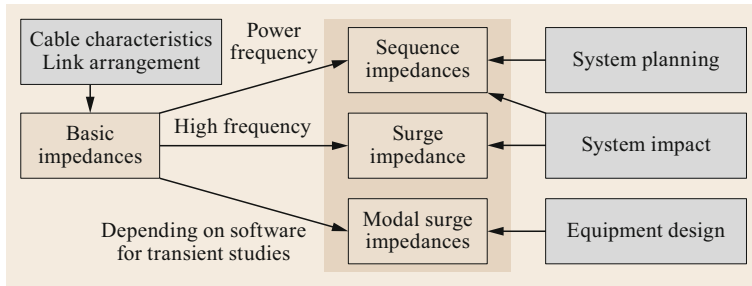
The electrical characteristics of underground transmission cables are significantly different from those of

overhead lines. These differences must be taken into account during system planning, design, implementation, and operation. Modeling is one of the tools used by engineers when designing AC lines and integrating them into HV networks.

Since the very beginning (1927!), one of the most important issues to address during the various stages in the design of UG lines has always been the electrical characteristics of the cables.

In fact, following many years of investigation in this area, it is now clear that successive design phases require different electrical characteristics of the cables.

In this section, various electrical characteristics of cables are defined and introduced, including:



**Fig. 10.16** Electrical characteristics considered in system studies (adapted from [10.26])

- Basic impedances
- Sequence impedances
- Surge impedances.

Relevant formulae are available in the literature. For instance, the formulae used to derive these impedances from common cable and link designs (as identified by the WG; see Appendix A of [10.26]), are given in [10.26]. Critical analysis has been carried out to define the applicability of these formulae; some new formulae are proposed in the technical brochure, which also highlights the need for further studies.

The electrical characteristics considered depend on the study to be carried out. According to [10.27], the models required during system design may be classified into three main categories (Fig. 10.16):

- A *system planning* study determines where new lines are needed as well as the voltage and current ratings, and considers major auxiliary equipment such as shunt compensation.  $N-1$  contingencies are considered at this stage, and overhead versus underground options may be explored. The basic study tool used during system planning is a power flow program, and positive-sequence power frequency models are adequate at this stage.
- A system design or *system impact* study determines the impacts of choosing cable rather than OHLs (and vice versa) on the rest of the power system. The basic project parameters have been determined by this stage. Concerns include harmonic resonance, short-circuit currents, transient stability, voltage stability, and system relaying. The models used vary from positive-sequence to three-phase models, and from power frequency up to a few kHz.
- An *equipment design* study establishes detailed protection and operating procedures for the cable, sheaths, switchgear, shunt compensation, and related equipment. The basic study tool used at this stage is an electromagnetic transients program, which can also handle grounding and bonding connections. Accurate high-frequency models are necessary for many of these studies.

Application to transient studies is not addressed in detail in [10.26], this issue being less a question of cable modeling than the way models are used. More details about transient modeling and transient studies can be found in [10.27].

As a complementary way to get pertinent characteristics, measurement techniques should be considered.

### 10.3.2 Cable System Types

A cable system is as a combination of many different parameters that can influence the electrical characteristics of the cable system. These parameters can be classified into three main categories:

- *Cable design*: all the components of the cable itself
- *Configuration of installation*: all the parameters and dimensions relating to the position of the cables in the surrounding medium
- *Screen bonding*: parameters relating to the electrical connection between the metallic cable screen and the ground, including the possible use of an earth continuity conductor.

Some data on typical cable system design are given in the literature.

#### Land and Sea Cable Types

The evolution of insulated cable development has resulted in three main types of land and sea AC cables: fluid-filled cables (FF), gas-filled cables (GF), and extruded cables.

Figure 10.17 subcategorizes these cable types based on the type of insulation used.

It should be noted that HVAC underground cables with SCFF, XLPE, or EPR insulation usually have a single core, while those that utilize HPFF or HPGF insulation generally comprise three insulated conductors inside a steel pipe.

A typical power cable can consist of four or six main layers: conductor/insulation/metal screen/outer sheath, or conductor/insulation/metal screen/insulation/armor/outer sheath (Fig. 10.18).

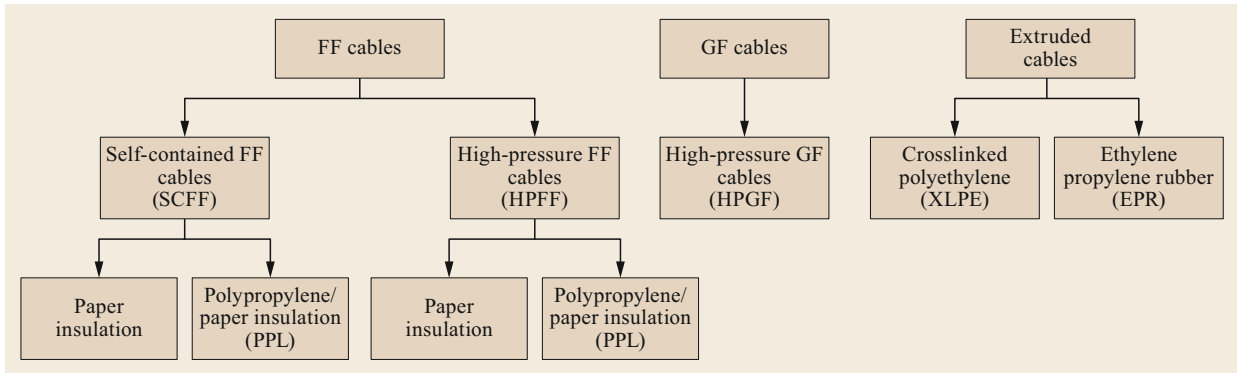


Fig. 10.17 Important types of land and sea cables (adapted from [10.26])

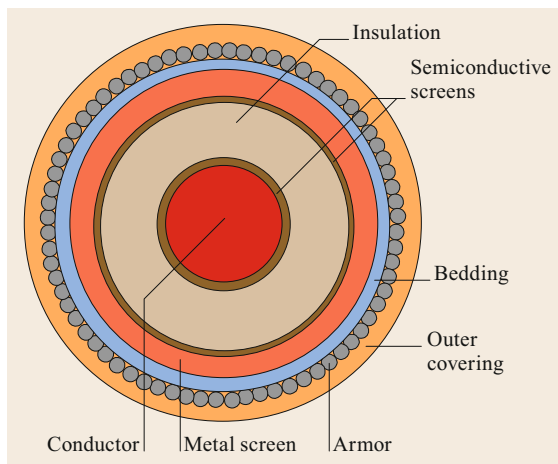


Fig. 10.18 Main components of a single-core cable (adapted from [10.26])

While most HV underground cables have a single core without armor, HV submarine cables have either a single core with armour or—more often—three *four-layer* single-core cables inside a common layer of armor. These cables are referred to as three-core cables.

### Single-Core Cables.

**Conductor.** The purpose of the conductor is to transmit the required current with low losses. Different conductor designs are shown in Fig. 10.19. Hollow conductors usually use oil or water to cool the conductor. Stranded and segmental conductors provide more flexibility and exhibit a reduced skin effect.

The conductor used in HV and EHV cables is either copper (Cu) or aluminum (Al). Compared to Al, Cu has a lower specific resistance, which means that, for the same current capacity, a smaller cross-sectional area of Cu is needed. Ignoring economic considerations, the main advantage of Al over Cu is that it is less dense, so

an Al cable will be much lighter than a Cu cable with the same current rating.

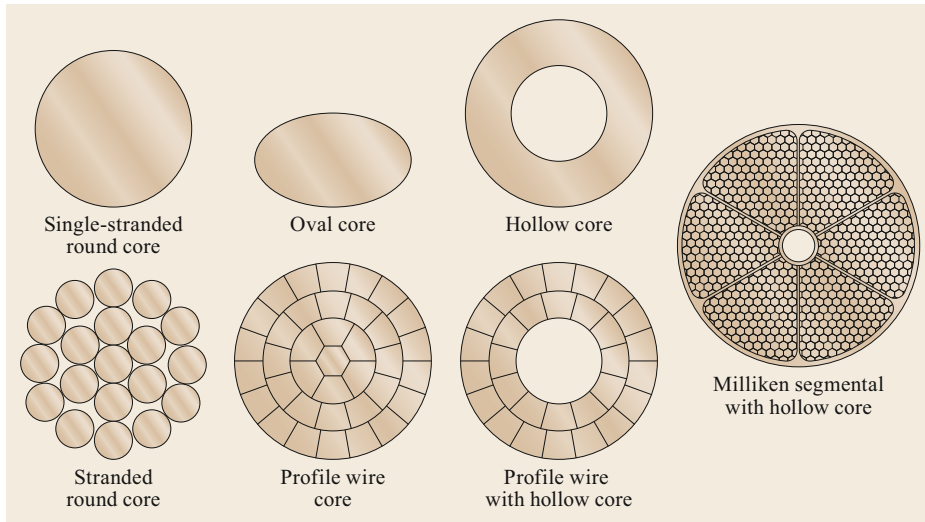
Most conductor materials and designs are referenced in IEC 60287-1-1 (except for oval and aluminum segmental designs). The material and design used affect the DC and AC resistance of the conductor. The methods used to calculate the resistance of the conductor are found in IEC 60287-1-1; the DC and AC resistances at the maximum operating temperature are assigned the symbols  $R'$  and  $R$ , respectively.

The current-carrying capacities of thick stranded conductors can be substantially reduced by skin and proximity effects, which are electromagnetic effects that produce an uneven distribution of current over the cross-section of the conductor and hence effectively increase its resistance.

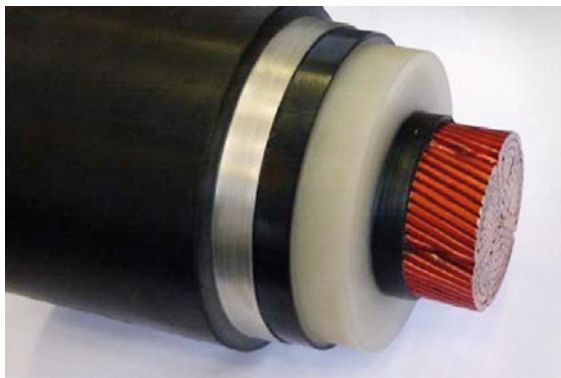
The *skin effect* is the tendency for current to flow predominantly at the periphery of a conductor due to the internal magnetic field in the conductor. The skin effect in a single-core cable is similar to the skin effect in a solid cylindrical conductor with the same DC resistance per unit length.

The *proximity effect* is the tendency for current to flow along one side of a conductor due to the interaction of the magnetic field of the current in the conductor with the currents in adjacent conductors. The proximity effect can be calculated using formulae developed for solid cylindrical conductors provided that the resistance of the conductor is divided by a factor  $k_p$ , which is the ratio of the resistance of the path along the strands to the resistance of the path across the strands. This factor depends on many parameters, such as the surface condition of the strands, the lay of the strands, the impregnation of the core, and the tightness of the insulation on the core.

As noted in [10.28], the AC resistance of a conductor will be greater than the DC resistance of the conductor due to the skin and proximity effects. Solid conductors will be worst affected by these effects.



**Fig. 10.19**  
Conductor designs for HV cables (adapted from [10.26])



**Fig. 10.20** HV cable with an enameled conductor (adapted from [10.7])

The presence of strands in the conductor will disrupt the proximity effect. The skin effect is only reduced in Milliken conductors (Fig. 10.19). Both effects decrease the difference between the AC resistance and the DC resistance. Some manufacturing processes such as extrusion may impact on the stranding (e.g., by compressing the strands together). Milliken conductors are specifically designed to maximize the disruptive effect of strands and optimize the AC resistance of the cable. This disruptive effect of strands can be further enhanced by increasing the electrical resistance between the individual strands using some form of surface treatment (oxidation or enameling, as shown in Fig. 10.20).

The AC resistance can be derived from the DC resistance via two coefficients representing the skin and proximity effects. The methods used to calculate skin and proximity effects for Milliken conductors in extruded cables are given by the IEC.

**Table 10.1** Proposed values for  $k_s$  and  $k_p$  (adapted from [10.29])

Type of conductor	$k_s$ value	$k_p$ value
For enameled copper wires and aluminium wires	0.25	0.15
For oxidized copper wires (value based on a unidirectional study)	0.35	0.20
For interlayer insulated copper	0.50	0.37
For unidirectional stranding of bare copper wires	0.62	0.37
For bidirectional stranding of bare copper wires	0.80	0.37

Reference [10.29] provides extensive guidance on calculating AC resistances for these conductor designs and for conductors with large ( $> 1600 \text{ mm}^2$ ) cross-sections. Given the complexity of these calculations, the publication recommends that the AC resistance should be measured during type tests. When measured values are not available, the publication recommends that the classical IEC 60287 formula should be used, but with the coefficients revised to the values given in Table 10.1.

WG D1.54 is currently establishing guidelines for the basic principles and practical methods to measure the AC and DC resistance of conductors of power cables and overhead lines.

**Insulation.** There are three practical dielectrics for HV and EHV cables: impregnated multilayered paper, oil-filled paper, and an extruded polymer such as XLPE. The purpose of this insulation is to protect the conductor and ensure that there is no connection between the two current-carrying components of the cable: the conductor and the metal screen.



**Fig. 10.21**  
Some screen  
designs (adapted  
from [10.26])

Due to the insulation between the two current-carrying components, HV cables closely resemble very long cylindrical capacitors. AC loads will therefore draw a capacitive charging current per phase (denoted  $I_C$ ) that is proportional to the permittivity  $\epsilon_r$  and the link length.

This charging current is superimposed on the current that is designed to be carried by the conductor. Therefore the length of the cable is limited because of the capacitive load of the cable. The critical length, which is discussed in more depth in other CIGRE documents [10.8, 14, 28], is the length of cable required for the current rating to be completely consumed by the capacitive current, meaning that no active power can flow through the cable. The critical length of the cable decreases as the voltage and the permittivity of the insulation increase.

**Semiconductive Screens.** A field-smoothing or semiconductive layer is placed between the insulation and the conductor and also between the insulation and the sheath.

Semiconductive layers are included in order to:

- Equalize and reduce the electrical stress in the cable dielectric by preventing local field enhancement in nonhomogeneous areas such as the individual wires of the conductor or screen. The semiconductive layers eliminate the effects of the individual wires on the field distribution.
- Prevent the formation of gaps or voids between the voltage-carrying components of the cable (conductor, screen, and metal sheath) and the insulation layer due to mechanical stress, e.g., cable bending or the differential expansions of the various materials under varying thermal stress. A solid and

permanent bond between the semiconductive layers and the insulation prevents the occurrence of partial discharges (this design aspect is very important in polymer-insulated cables, as they have no impregnating medium).

Models do not normally include semiconductive layers. That is, the models include several conductive layers, such as the conductor and metal screen, and insulation materials in between, but no semiconductive layers. Instead, the semiconductive layers are considered part of the insulation, with the thickness and permittivity of the insulation modified accordingly.

**Metal Screen.** The metal screen is a metallic covering of the cable that is used for electrostatic screening and provides a return path for the capacitive charging current. It is also used to conduct the earth fault current when there is a fault in the cable. When a composite metallic screen is used, a sheath is often included to ensure water tightness. Watertight material can be placed on either side of the metal screen. Some examples of screen designs are given in Fig. 10.21.

To minimize sheath overvoltages at the ends of the cable and the current flowing in the metal screen, special screen connection techniques are used. Screen bonding techniques are discussed in more detail in other sections (see also Figs. 10.24–10.26).

**Bedding.** Bedding is used to reduce thermomechanical stresses on the metal screen caused by thermal expansion of the insulation or to fill voids in or around cable, between the metal screen and the armor. Armored cables use a single layer of an insulating bedding compound. Bedding compounds are elastomer based and

consist of a variety of polymer blends or polymers. The exact formulation depends on the cable construction and application.

Bedding compounds make cables round for easier pulling. In addition, by protecting the metal screen from mechanical and/or water damage, bedding compounds can also increase field lifetimes. The bedding layer may act as both an insulating layer between the metal screen and the armor and a water barrier.

**Armor.** Land cables are generally not armored cables, whereas submarine cables are armored to support the cable weight during laying and to provide mechanical protection to the cable during operation.

Depending on the installation depth and the risk of third-party damage, a double layer of armor may be used.

A nonmagnetic material is used for single-conductor cables, whereas galvanized steel wires or strips are preferred for three-core cables.

The armor increases losses and strengthens the electromagnetic screening of the cable, which in turn minimizes the proximity effect from adjacent cables and lowers the stress on the sheath caused by high currents during conditions such as earth faults.

**Outer Covering.** The primary function of the outer covering of the cable is to provide mechanical protection against the surroundings. For land cables, the outer covering is normally a sheath made of high-density polyethylene with a relative permittivity of 2.3. This outer sheath is the final layer of an underground cable and is often covered with a semiconductive compound.

In submarine cables, extruded polymeric sheaths or servings made from wound polyethylene yarn layers may be used.

**Three-Core Cables.** There are many different kinds of three-core cables. In the HV range, they normally consist of three cores inside a common armor or pipe (Fig. 10.22); in this case, each core is similar to a single-core cable without armor (as described above).

Two main types of three-core HV cables can be distinguished. The first are known as *separate-screen cables* (e.g., SL or SA cables, which have separate lead or aluminum sheaths, respectively). In this case, the three cores are assembled together, using fillers to keep the cable round.

The other main type are termed *pipe-type cables*, in which the three cores are pulled simultaneously inside a steel pipe. The pipe is then filled with an insulating medium, either oil or gas (nitrogen) pressurized to about 15 bar.

Skid wires are used to reduce the coefficient of friction between the cores and pipe during installation.

### Configuration of Installation

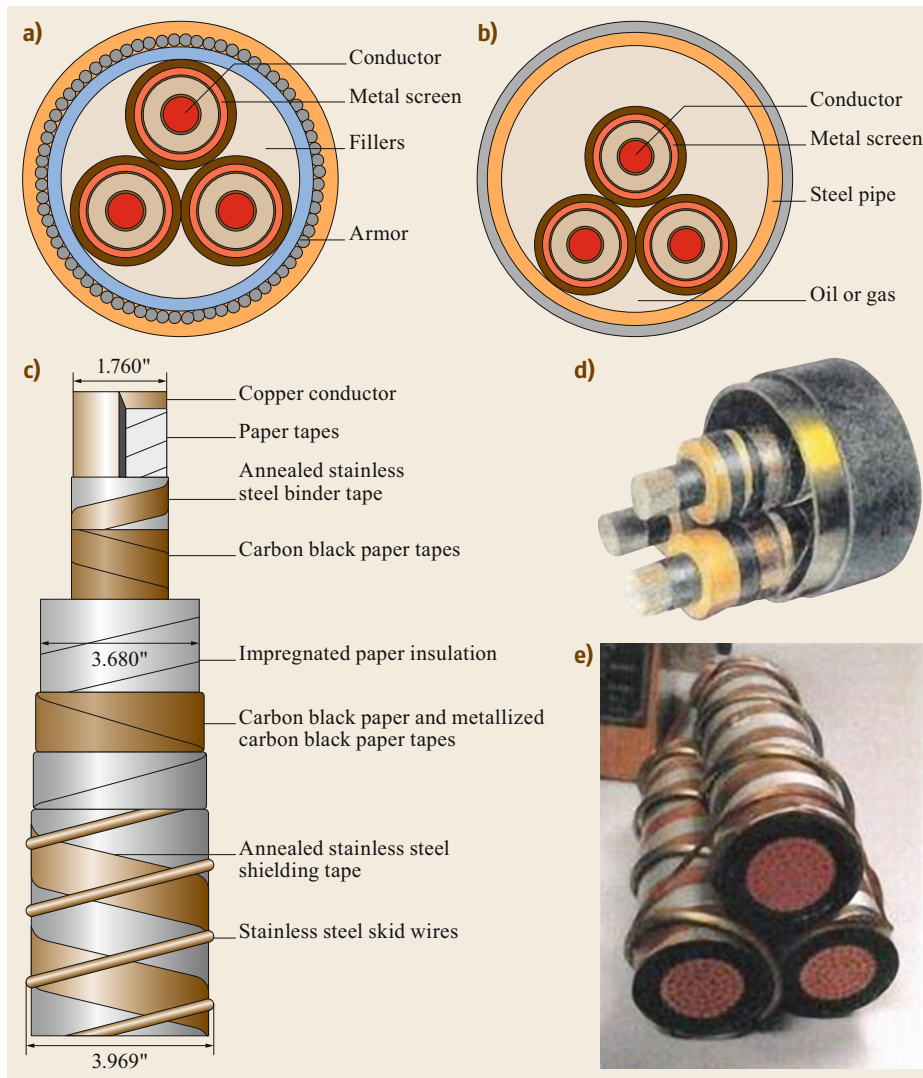
Configurations of installation vary widely according to, for example, the country in which the cable is installed, the construction method used, and the applicable regulations. Some of these configurations have already been briefly described above. More information can be found in subsequent sections of this chapter and in [10.13] (WG B1.60 is currently working to update this document).

In this section, the configuration of the installation is considered to be the set of parameters that can influence the electrical characteristics of the cable system. Very similarly, they can also influence the cable rating (as described in more detail later), since the cable losses can depend on the electrical configuration. The main parameters considered are the relative positions of cables (Fig. 10.23) and the presence of cable transposition.

**Land Cables.** Generally speaking, the construction method used for cable installation will determine most of the parameters of the configuration:

- **Directly buried cables.** Directly buried cables are usually laid in a flat or touching trefoil formation. Some cases also use an open trefoil formation. The spacing between the cables will largely depend on the space available and ampacity considerations. Typical spacings used range between no spacing at all (touching cables) to 4–5 cable diameters. In a double circuit configuration, the spacing between the two circuits can be much larger, up to a few meters.
- **Cables in a trough, filled or unfilled.** This type of installation can use cables in a flat or touching trefoil formation. Due to limited space in the cable trough, the spacing between cables is usually minimal.
- **Cables in a duct.** Cables in a duct tend to be in positioned in a triangular or open trefoil formation. In some cases, flat and/or vertical formations may be used (Fig. 10.8). For this kind of installation, the cable spacing is usually 2–5 cable diameters.
- **Cables in a tunnel.** A wide variety of formations are used for cables in a tunnel as each installation is unique. The spacing between cables is usually large, as these important installations can carry very large loads at very high voltage (Fig. 10.12).

The use of directional drilling may lead to large cable spacing (e.g., 1 m).



**Fig. 10.22a–e**  
Three-core cables:  
(a) separate screens,  
(b) pipe-type cable,  
(c) 345 kV HPFF  
cable, (d) 225 kV  
HPFF cable,  
(e) 69 kV HPFF  
cable (adapted  
from [10.26])

**Cable Transposition.** Cable transposition is used in some countries to reestablish symmetry in a nonsymmetric system. In a three-phase system, each cable (phase) is positioned in each of the three available positions for a third of the length of the system, resulting in a more balanced system. Some countries use cable transposition in a systematic way, transposing cables at each joint location along the links, while other countries do not use cable transposition at all.

**Submarine Cables.** Submarine cables often use a three-core system in which all three cable cores are wound together, resulting in a symmetric system.

For very large cross-sections and higher voltages, single-core cables are generally used. In that case, the spacing between phases is typically very large with re-

spect to the cable diameter (from a few meters up to hundreds of meters or more), much larger than in any land cable installation.

The interactions between the cables—and thus the cable impedances—depend on the arrangement of and the spacing between cables.

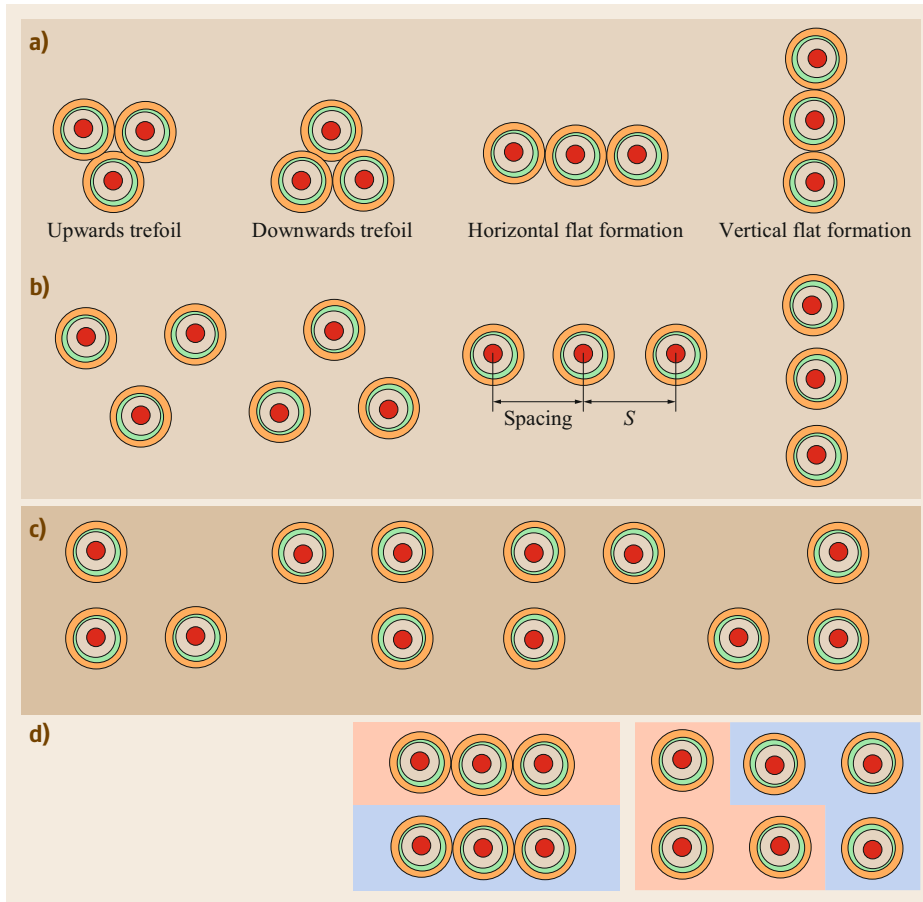
The sequence impedances are only rigidly determined for a trefoil arrangement or a flat formation with transposed cables, as explained in [10.26].

The impact of any magnetic shielding installed at the links is not considered here (for an in-depth discussion of this topic, see [10.21]).

#### Screen Bonding Methods

As mentioned above, special techniques are used to connect the metal screen in order to minimize sheath





**Fig. 10.23a–d**  
Various cable layouts for single-core cable systems: (a) touching cables, (b) nontouching cables, (c) triangle configurations, (d) links involving 2 circuits (adapted from [10.26])

overvoltages at the ends of the cable and the current flowing in the metal screen.

The technique used should comply with the design of the cable and accessories during normal operation and even during a failure.

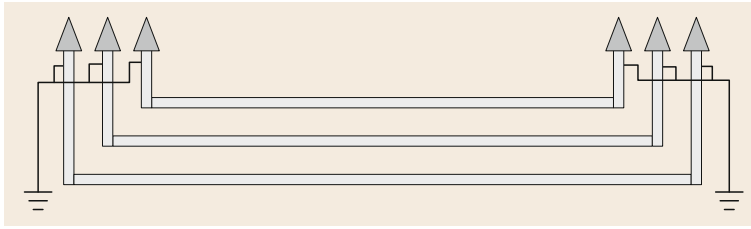
The underground line and the method available for the screen connections is subdued to:

- Electric induction on the sheath during normal operation as well as in the case of a fault.
- Specific rules relating to the maximum voltage that can be induced in the sheath near to any point that someone can touch (wiping bells at the terminations, for example). The voltage allowed varies between 35 and 400 V depending on the country and the regulations applied.
- The resistivity of the ground, which influences the voltage in the sheath.
- The value of the asymmetric factor, which is taken into account during a fault at the power frequency.
- Surge arrester specifications.

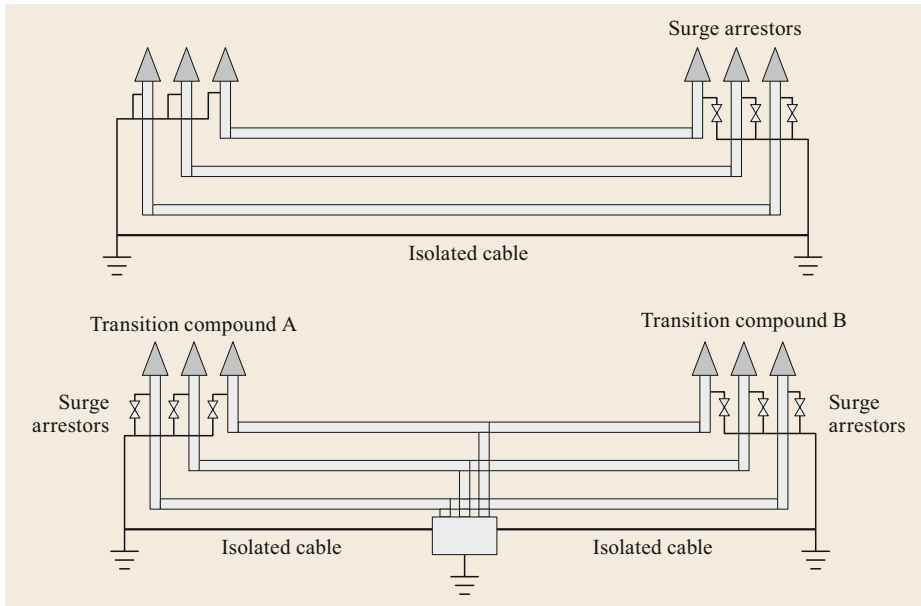
Reference [10.30] includes detailed discussions and calculations relating to modern methods of bonding to a metal screen. Only the most basic design considerations are presented below. Three main types of earthing connections can be distinguished (Figs. 10.24–10.26). In this context, [10.31] is a complementary text that explores *Earth potential rises in specially bonded systems*.

**Solid Bonding Method.** The simplest method of connecting a metal screen is solid bonding (Fig. 10.24), where the metal screen is connected to earth at both ends. This connection method results in large steady-state losses, as induced current is permitted to flow in the metal screen. The voltage level in the sheath is close to zero along the line because it is due only to capacitive currents.

**Single-Point Bonding Method.** This method, illustrated in Fig. 10.25, stops current from flowing in the screen but does not eliminate the potential for problems with sheath overvoltages at the ungrounded end.



**Fig. 10.24** Solid bonding arrangement (adapted from [10.26])



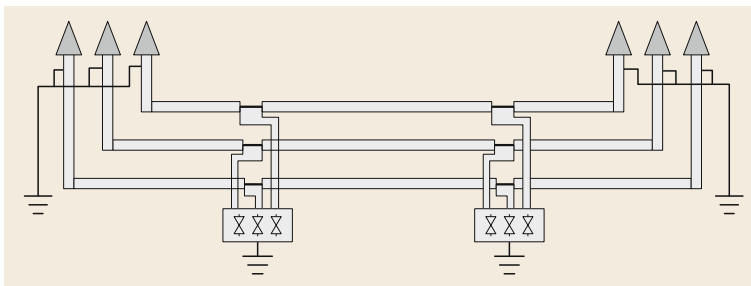
**Fig. 10.25** Single-point bonding arrangements (adapted from [10.26])

Some countries do not use an earth continuity conductor (ecc) along the line; the earth is used to return the fault current during a failure. In other countries, surge arresters are not used.

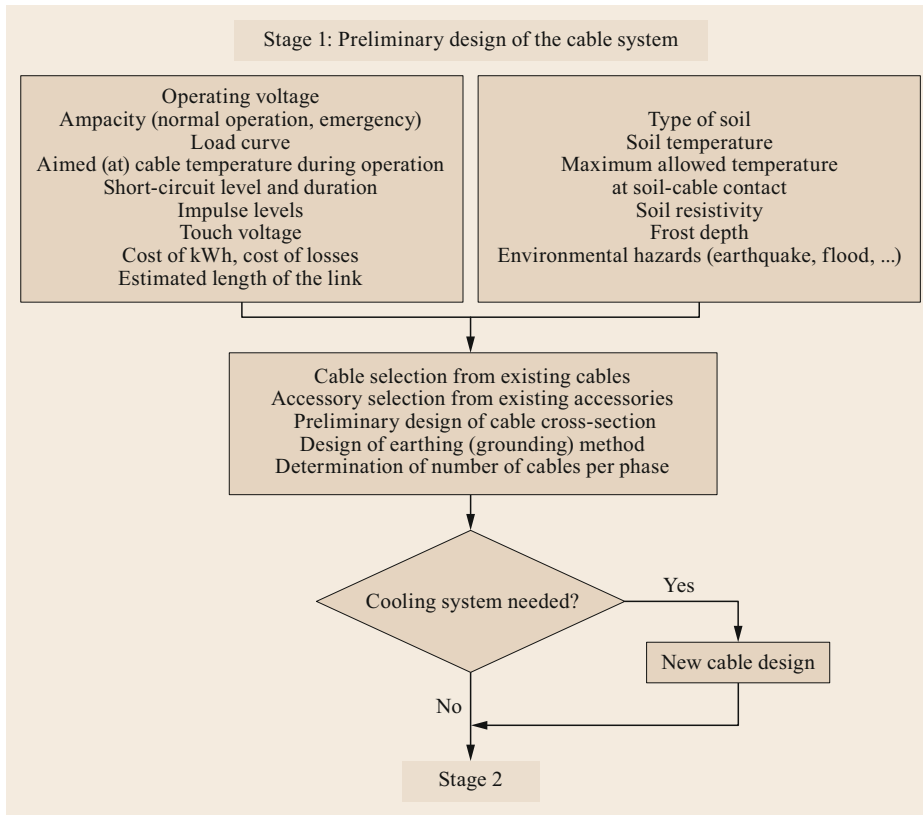
**Cross-Bonding Method.** Long cables usually have cross-bonded sheaths. This grounding method, shown in Fig. 10.26, consists of essentially sectionalizing the sheaths into elementary (minor) sections and cross-connecting in after three consecutive sections (known as major sections). To control possible overvoltages, surge arresters are usually connected to the cross-

bonded points and the sheaths are generally solidly grounded at major section ends.

Induced sheath currents can be canceled out using this method, which results in an improved transmission capacity for an underground cable or a much cheaper cable design for a given transmission capacity; however, permanent and transient voltages can still appear in the sheath and in the metallic parts at the ends of the cable sections. An earth continuity conductor connected to grounding points may be installed to reduce overvoltages that stress the sheath surge arresters during phase-to-earth short circuits.



**Fig. 10.26** Cross-bonding arrangement (adapted from [10.26])



**Fig. 10.27** Stage 1 of the step-by-step approach (adapted from [10.13])

### 10.3.3 Step-by-Step Approach to Cable System Design

Taking into account both operational and environmental data, a preliminary route and a preliminary cable design are selected. After that, as the study progresses, various technical issues will be encountered before the design of the cable and accessories and the laying technique(s) to be used are chosen. The main technical aspects considered during this process are:

- Electrical characteristics
- Thermal dimensioning and rating calculations
- Economic optimization of the conductor area (i.e., *cable sizing*)
- Short-circuit characteristics
- Main insulation coordination
- Grounding technique
- Protection and reclosure issues
- Magnetic fields.

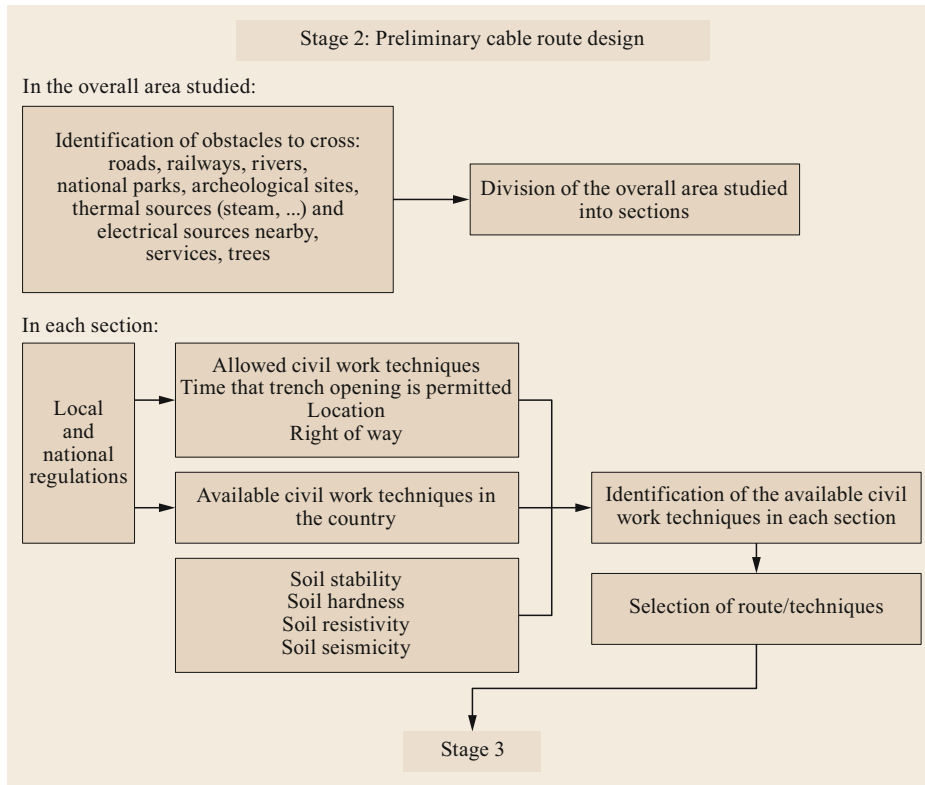
Some elements of the toolbox used to design the cable system are provided in Sect. 10.4.

#### Methodology

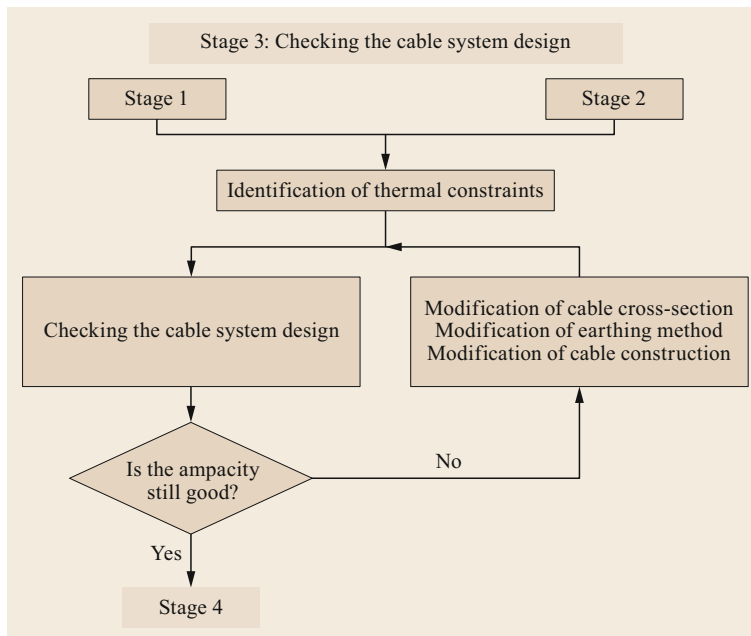
When an engineer is starting a new project, their main consideration is always how the project can be managed to ensure that it is as effective as possible from technical and economic perspectives.

A methodology for a step-by-step approach to cable system project management is proposed by WG B1.17 in [10.13]. The purpose of the chart shown in Figs. 10.27–10.31 (created by WG 21-17 [10.13]) is to help inexperienced engineers to manage their projects. Experts with considerable underground cable system project management experience will bypass some of the proposed steps.

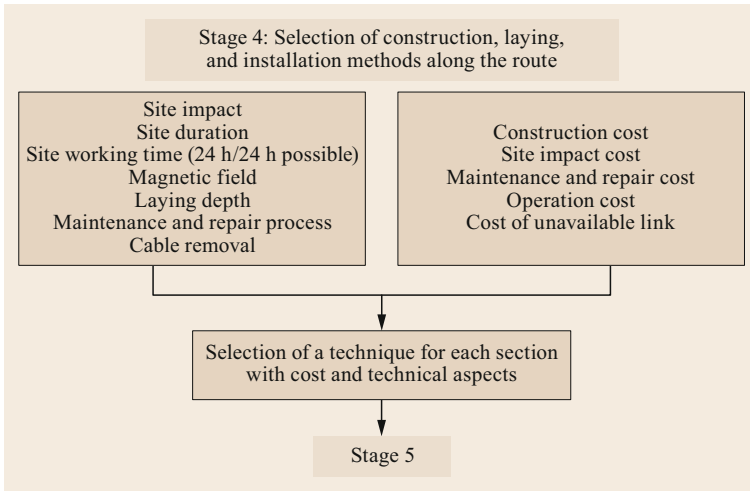
It is clear that this is very much an integrated process: the impacts of the various stages are considered during the process, and steps are taken to modify previous and subsequent stages of the process in order to achieve the optimal end result.



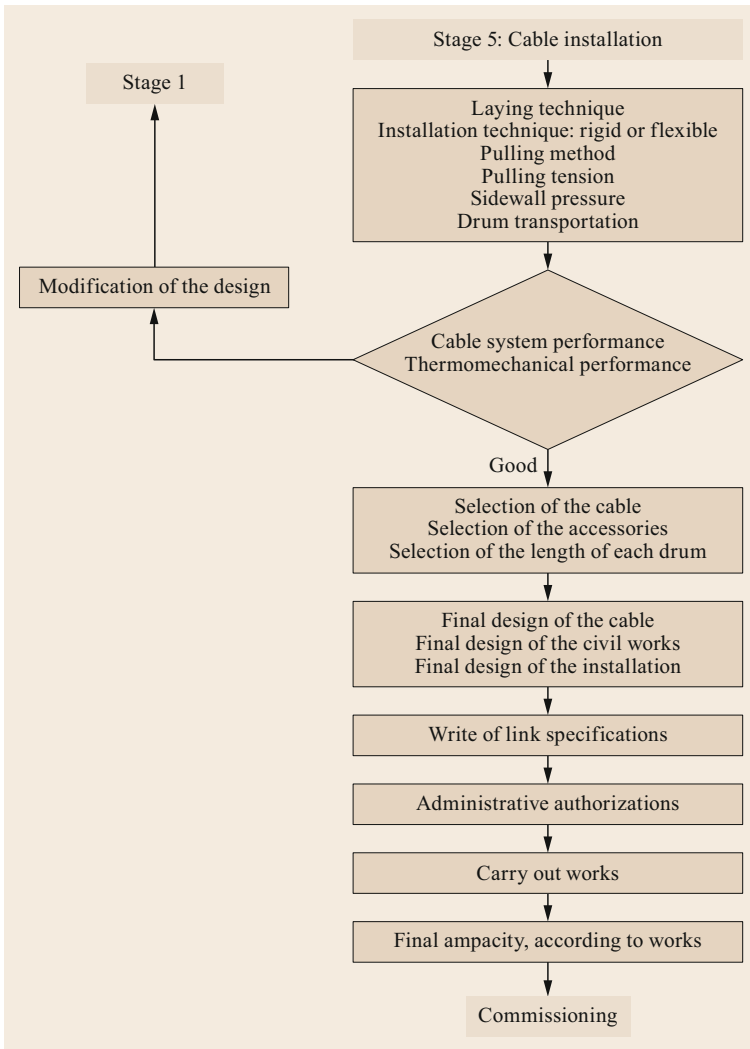
**Fig. 10.28** Stage 2 of the step-by-step approach (adapted from [10.13])



**Fig. 10.29** Stage 3 of the step-by-step approach (adapted from [10.13])



**Fig. 10.30** Stage 4 of the step-by-step approach (adapted from [10.13])



**Fig. 10.31** Stage 5 of the step-by-step approach (adapted from [10.13])

## 10.4 AC Cable Theory in Underground Cable System Design

Two of the fundamentals of power transmission are the voltage and current that are used to transmit the power from one area to another. The current is the flow of electricity through the conductor. As noted above, using the water flow analogy, voltage is equivalent to pressure, i.e., it drives the current through the conductor in the same way that pressure drives water through a pipe. The voltage multiplied by the current is, roughly speaking, equal to the power.

In AC transmission, the standard practice internationally is to transmit the power using a three-phase system with three metallic conductors in a circuit to carry the current. The size of each conductor governs its ability to carry current, i.e., the larger the conductor, the more current it can carry. The conductors must be insulated from the ground in order to be able to withstand the voltage applied; again, the more insulation there is, the higher the voltage that can be applied.

The three conductors may be assembled in an overhead line (OHL) circuit, an underground cable (UGC) circuit, or a gas-insulated line (GIL) circuit.

The basic theory associated with the design of UGCs is described in this section (more detailed information on the topics covered here is available in various publications from CIGRE SC 21/B1 and CIGRE session proceedings). Some of the basics of DC transmission are also described below.

### 10.4.1 Electric Fields in AC Cables

Before we dive more deeply into the theory behind UGC design, it is important to understand what is meant by the electrical stress within the cable insulation and

at the interface between the cable and the accessories (joints and terminations).

For a radial field around a conductor, the equipotential lines are cylindrical and concentric to the conductor, and the electrical stress in kV/mm at a distance  $r$  in mm from the axis is given by

$$E(r) = \frac{U_0}{r \ln \left( \frac{R_e}{R_i} \right)},$$

where  $U_0$  is the phase to ground service voltage in kV,  $R_i$  and  $R_e$  are the internal and external radii of the insulation,  $D = 2R_e$  is the diameter over the insulation, and  $d = 2R_i$  is the diameter over the conductor or the semiconductive layer.

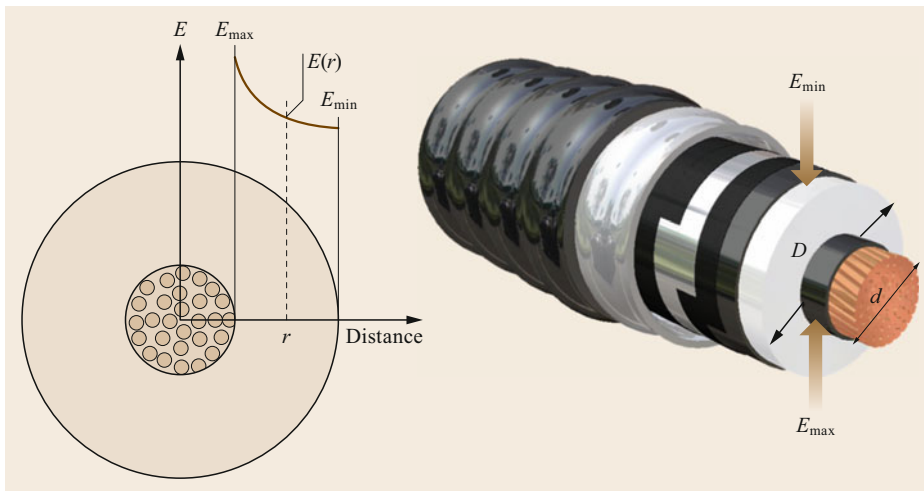
The greatest stress  $E_{\max}$  occurs at  $r = R_i$  on the conductor (or the inner semiconductive layer), and the lowest stress  $E_{\min}$  occurs at  $r = R_e$  on the surface of the insulation layer (Fig. 10.32)

$$E_{\max} = \frac{2U_0}{d \ln \left( \frac{D}{d} \right)}$$

and

$$E_{\min} = \frac{2U_0}{D \ln \left( \frac{D}{d} \right)}.$$

$E_{\max}$  is a crucial influence on the aging of the insulation and the performance of the cable under impulse.  $E_{\min}$  is an important factor in the compatibility of the cable with the associated accessories (joints and terminations), especially for extruded cables.



**Fig. 10.32** Electrical field in an AC cable (adapted from [10.4])

**Cable Insulation Aging: State of the Art**

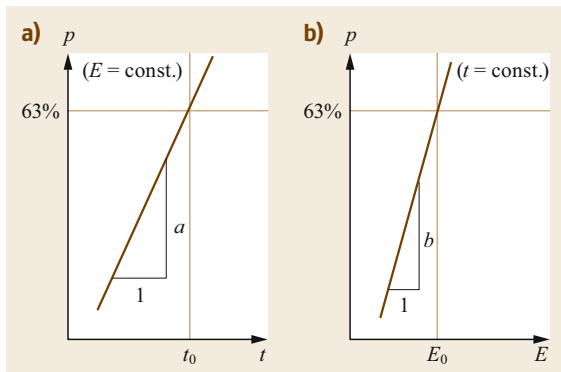
The electrical performance of cable insulation generally decreases over time due to the degradation of the insulating materials. The mechanism of the aging process varies with the physical properties of the materials used for the insulation. These mechanisms are briefly explained in [10.32].

The aging of cables with lapped impregnated insulation is mainly influenced by the operating temperature. Gas production in the insulation due to thermal degradation is the main aging process for this cable type. As long as the gas can be dissolved in the impregnating liquid, the electric withstand stress will remain nearly constant. The applied AC stress does not have a significant influence on the aging provided that it is held below the partial discharge inception stress. *Therefore, the effect of electric aging is negligible in such cables.*

The aging of cables with extruded insulation is significantly influenced by the electrical stress applied. Assuming that the physical process responsible for the aging does not change, the time to breakdown for a given stress as well as the breakdown stress at a particular time are stochastic values that are represented by homogeneous distribution functions. The results of many tests have shown that both values may be approximated by Weibull distributions [10.33] with two parameters (a scale parameter at 63% probability  $t_0$  or  $E_0$  and a Weibull slope  $a$  or  $b$ ; see Fig. 10.33).

According to this mathematical model, the breakdown probability as a function of time for a given cable at constant electrical stress is

$$p(t) = 1 - \exp \left[ - \left( \frac{t}{t_0} \right)^a \right].$$



**Fig. 10.33a,b** Weibull distributions of the breakdown time at constant stress (a) and the stress at a particular time (b) for extruded cable insulation. Both  $x$ -axes use a log scale, while the  $y$ -axes use a double log scale (adapted from [10.32])

For the same cable, the breakdown probability as a function of the electrical stress applied for a given duration can be written as

$$p(E) = 1 - \exp \left[ - \left( \frac{E}{E_0} \right)^b \right].$$

These two distribution functions can be combined such that the complete equation for the breakdown probability of a given cable sample is

$$p(t, E) = 1 - \exp \left[ - \left( \frac{t}{t_0} \right)^a \left( \frac{E}{E_0} \right)^b \right].$$

For a constant breakdown probability, the following relation may be derived from the above

$$\left( \frac{t}{t_0} \right)^a \left( \frac{E}{E_0} \right)^b = \text{const.}$$

We now introduce the lifetime exponent  $n$  as the quotient of the Weibull slopes  $b$  and  $a$

$$n = \frac{b}{a}.$$

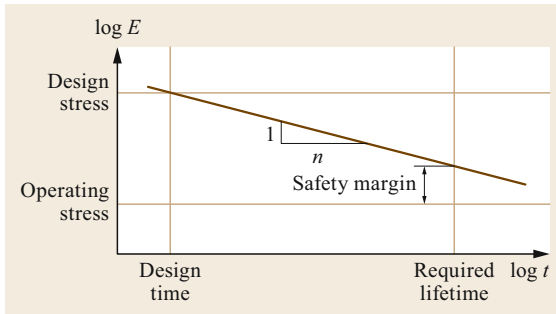
The lifetime law for extruded cable insulation then becomes

$$E^n t = \text{const.}$$

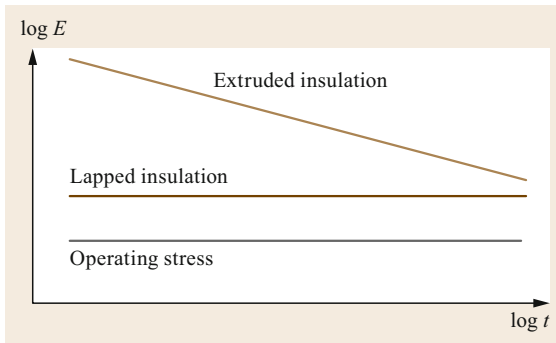
Published values of the lifetime exponent  $n$  for XLPE range from 12 to 20.

According to the lifetime law for extruded cable insulation, applying high electrical stress for a short time causes the same aging as applying low electrical stress for a longer duration, assuming that all other operating conditions remain unchanged. The design philosophy for extruded cables must consider this effect. Basic values of the design stresses are usually derived from short-term tests. Considering the aging effect, it is important to ensure that there is a sufficient safety margin to cover accelerated aging effects due to (for example) temporary overvoltages and surges during the required lifetime.

The different aging behaviors of cables with lapped impregnated insulation and cables with extruded insulation is another reason for the different design and testing philosophies specified in the relevant standards and recommendations for these two types of cables. Typical differences between the lifetime curves for lapped and extruded cable insulation are shown qualitatively in Figs. 10.34 and 10.35.



**Fig. 10.34** Lifetime curve for extruded cable insulation (adapted from [10.32])



**Fig. 10.35** Qualitative lifetime curves for lapped and extruded cables (adapted from [10.32])

#### Design Practices for Insulated AC Cables

The insulation of AC cables consists of a number of thin paper tapes wound around the conductor. The conductor is circular, except in external gas pressure cables, which use oval-shaped conductors. Depending on the type of cable used, the insulation is impregnated with low-viscosity oil or with a nondraining high-viscosity insulating mass.

The surface of the conductor is irregular to some degree due to the interstices between the individual wires. To suppress the creation of pockets of concentrated electrical stress at these irregularities, several layers of semiconductive carbon-black paper tape are applied onto the conductor surface. For high-voltage cables, it is essential to generate an undistorted radial electric field inside the insulation. Therefore, semiconductive carbon-black paper tape is applied over the insulation too, normally in combination with metal-coated paper tape.

**Basic Insulation Designs of High-Voltage AC Cables with Lapped Insulation.** In order to achieve an AC withstand characteristic with a sufficiently long duration, it is necessary to avoid ionization inside the insulation. Ionization can occur in gas-filled voids, which can form in the insulation due to the expansion

and contraction of the cable components at different rates during load cycles. Several cable types that use different mechanisms to overcome the ionization problem have been developed in order to create so-called thermally stable cables.

**Low-Pressure Oil-Filled Cables with Paper Insulation.** The paper insulation of low-pressure oil-filled cables is impregnated with low-viscosity insulating oil. During the heating phase of a load cycle, the expanding oil can flow through longitudinal channels inside the conductor (or in the interstices of three-core cables) to oil expansion vessels, in which the oil is stored under pressure. When the load is reduced and the cable cools down, the vessel forces the oil back into the cable. This mechanism stops voids from occurring in oil-impregnated cables.

The impregnated core is covered by a metallic sheath, which can be an extruded lead sheath with reinforcement or a corrugated aluminum sheath. An anticorrosion layer (compound) is applied over the metallic sheath, and this anticorrosion layer is covered with an extruded oversheath (PE or PVC).

Low-pressure oil-filled cables are used up to a rated voltage of 500 kV. Cables for higher rated voltages have already been developed and successfully tested. The power-frequency withstand stress of this type of cable is about 40 kV/mm, and the maximum stress under operating conditions varies between 10 and 15 kV/mm. The insulation thickness is normally designed on the basis of a maximum permissible lightning impulse stress of 90–95 kV/mm, depending on the conductor design.

**Low-Pressure Oil-Filled Cables with Polypropylene Paper Laminate Insulation.** Low-pressure oil-filled cables with conventional paper insulation are of limited use at extra-high voltages (> 500 kV) due to the resulting dielectric losses, which are proportional to the square of  $U_0$ . Therefore, an alternative tape material called polypropylene paper laminate (PPL) has been developed. The dielectric loss factor of low-pressure oil-filled cables with PPL insulation is about 2.5–3 times lower than that of conventional paper insulation.

The overall cable design in this case is similar to that of conventional low-pressure oil-filled cables. The insulation thickness is again determined by the maximum permissible lightning impulse stress, which is in the range of 100–110 kV/mm due to the enhanced material properties of PPL. The maximum power frequency withstand stress is about 45 kV/mm, and the maximum stress under operating conditions is 17–20 kV/mm.

Cables with paper or PPL insulation were known as low-pressure oil-filled (LPOF) cables until the 1970s,



**Table 10.2** Typical stresses in service for AC lapped cables

Voltage class (kV)	Low-pressure oil-filled (LPOF) or SCFF cables		High-pressure oil-filled (HPOF cables)		High-pressure gas-filled (HPGF) cables	
	$U_m \leq 170$	$U_m > 170$	$U_m \leq 170$	$U_m > 170$	$U_m \leq 170$	$U_m > 170$
AC voltage (kV/mm)	10	15	10	14	8	10
Lightning impulse (design criterion) (kV/mm)	85	95	80	90	60	80
Switching impulse (kV/mm)	75	85	70	80	50	70

when synthetic dielectric liquids began to replace the mineral oils that had previously been used. They are now generally known as self-contained liquid-filled (SCLF) or self-contained fluid-filled (SCFF) cables.

**High-Pressure Oil-Filled Cables.** This type of cable consists of three impregnated-paper-insulated conductors that are drawn into a steel pipe. The steel pipe is subsequently filled with oil maintained at a pressure of approximately 15 bar. Due to this high operating pressure, the insulation remains free of voids during any operational conditions. Regulating equipment consisting of pressure monitors, pumps, and valves control the operating pressure. When the load increases and the cable heats up, the expanding oil flows into a storage container. During a cooling period, the oil is pumped back into the cable. High-pressure oil-filled cables have been constructed for rated voltages of up to 500 kV. This type of cable has only rarely been used in recent installations. Its AC withstand stress is approximately 50 kV/mm and its lightning impulse withstand stress is 100 kV/mm.

**External Gas Pressure Cables.** The paper-insulated cores of external gas pressure cables are impregnated with high-viscosity synthetic oil. Directly over the core, a gastight lead diaphragm sheath is applied, which is exposed to an external gas pressure of about 15 bar. During heating periods, the lead sheath expands due to the internal pressure of the expanding impregnating oil. When the cable cools down, the external gas pressure forces the lead sheath back to its original position. In this way, the insulation remains free of voids. The conductors are oval-shaped to enable this action of the lead diaphragm sheath. External gas pressure cables can be designed as either self-contained cables (earlier installations) or pipe-type cables (more recent installations). Pipe-type cables consist of three cores pulled into a common steel pipe. The steel pipe is filled with compressed nitrogen. External gas pressure cables are used up to rated voltages of 275 kV. Typical lightning impulse design stresses for these cables are in the range

of 85–95 kV/mm; typical operating stresses vary from 8 to 13 kV/mm.

**Internal Gas Pressure Cables.** The insulation of internal gas pressure cables is impregnated with a high-viscosity nondraining insulating compound. Such cables, in contrast to external gas pressure cables, do not have a sheath. Either individual non-laid-up cores, each protected by a gliding wire, or laid-up multicore cables with flat steel wire armor are fed into a steel pipe. The pipe is filled with nitrogen at a pressure of about 15 bar. The gas can penetrate into the insulation and fill any voids that are formed in the insulation due to expansion and contraction during thermal cycles. Due to the high pressure of the gas inside the voids, ionization is suppressed.

The maximum rated voltage for internal gas pressure cables is 110 kV, and typical lightning impulse design stresses vary from 80 to 90 kV/mm. Under operating conditions, the maximum AC stress is usually 8–10 kV/mm (Table 10.2).

**Insulation Design.** The electrical stress that occurs within the extruded insulation of HV and EHV cables was investigated in detail in the 1990s. Important CIGRE publications deal with this topic [10.33–35]. Such insulation consists of an extruded layer of polyethylene (PE), crosslinked polyethylene (XLPE), or ethylene propylene rubber (EPR) around the conductor. The conductor is circular for HV cables.

As mentioned above, the surface of the conductor is irregular to some extent due to the interstices between the individual wires. To stop electrical stress from building up at such irregularities, an extruded layer of semiconductive material is applied onto the conductor surface. For HV cables, it is essential to achieve an undistorted radial electric field inside the insulation, so an extruded semiconductive material is also applied onto the insulation.

In order to achieve an AC withstand characteristic with a sufficiently long duration, it is necessary to stop

**Table 10.3** Typical stresses in service for AC extruded cables

Voltage class (kV)	Polyethylene (PE)			Crosslinked polyethylene (XLPE)		
	$U_m \leq 170$	$170 < U_m \leq 300$	$U_m > 300$	$U_m \leq 170$	$170 < U_m \leq 300$	$U_m > 300$
AC voltage design stress (kV/mm)	7	11–12	16	7	11–12	16
Lightning impulse (kV/mm)	70	80	80	70	80	80
Switching impulse (kV/mm)	60	70	70	60	70	70

ionization (partial discharges, PDs) from occurring in gas-filled voids inside the insulation and at the interfaces between the insulation and the semiconductive layers. This is realized by using appropriately defined process parameters and by bonding the three extruded layers.

An extruded lead sheath, an aluminum sheath, or a wire screen encloses the insulated core. The cable is provided with reinforcement for some applications. There is an extruded oversheath (PE or PVC) over the sheath or screen.

Cables with extruded insulation are now used up to a rated voltage of 500 kV. The power-frequency withstand stress of this type of cable is about 40 kV/mm, and its maximum stress under operating conditions is usually around 16 kV/mm. The thickness of the insulation is normally designed based on the maximum permissible AC voltage stress (Table 10.3).

#### 10.4.2 Basics of Electric Fields in DC Cables

Whilst cables with extruded insulation are generally used for electricity distribution, medium-voltage (MV) cables, and for the transmission of low voltages, extruded materials have recently become the insulation of choice in AC and DC transmission circuits for underground cables used in many utility EHV applications.

Recommended insulation thicknesses for AC cables are tabulated in standards (IEC or national standards and utility specifications). For MV cables, the standards and specifications impose a nominal thickness. For HV cables, however, insulation thicknesses are chosen by the cable manufacturer based on experience and validation via type tests and (where applicable) prequalification tests.

The insulation thickness of a DC cable is chosen by the cable manufacturer taking into account both the capacitive electrical stress (caused by possible transient voltages, e.g., switching and lightning impulses) and the resistive electrical stress (caused by the DC voltage in normal operation). The latter strongly depends on the temperature difference across the insulation, the material used, and the manufacturing process applied.

When applicable, the degassing time and the temperature after extrusion are important parameters for the manufacturer to consider since the level of by-products resulting from the curing process in the insulation can strongly influence its electrical performance.

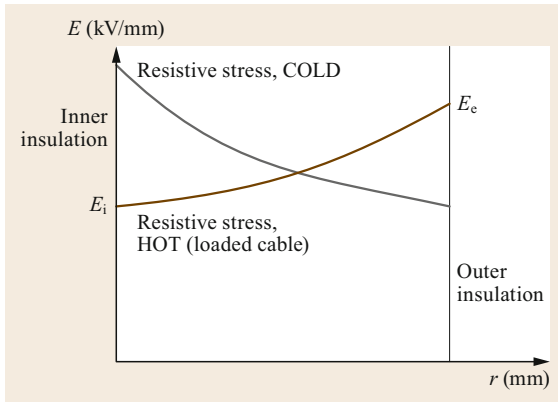
Specific materials have been developed for DC applications, and new materials are currently being developed. Once the most suitable insulation material has been defined, particular attention must be paid to the cleanliness of both the incoming material and the material handling performed in the plant. The required level of cleanliness strongly depends on the rated voltage of the cable.

Extruded submarine HVDC cables are used commercially up to  $\pm 320$  kV. Extruded  $\pm 525$  kV HVDC cables for underground applications are available, and it is expected that they will be made available for submarine use soon. Mass-impregnated (MI) submarine HVDC cables can be used for all voltages, even those over  $\pm 500$  kV. However, mass-impregnated cables cannot be used for HVAC voltages because of ionization in cavities.

The insulation system must be tested in accordance with the relevant standard/recommendation.

In a first approach to analyzing the insulation behavior in DC cables, Fig. 10.36 shows the distribution of the electrical stress inside the insulation of a cold isothermal HVDC cable and the corresponding distribution in the insulation of a loaded HVDC cable. The stress distribution in the insulation is controlled by the ohmic resistance of the insulation layers. In the cold isothermal cable, the specific resistivity of all the insulation layers is almost uniform, and the resulting stress distribution is shown by the gray curve. After running the cable with a load, a thermal gradient will appear in the insulation, causing the specific resistivity of the insulation close to the conductor to be lower than that of the insulation furthest from the conductor. The resulting electrical stress distribution is indicated by the brown curve in Fig. 10.36.

A more detailed analysis of the insulation behavior in DC cables is given in [10.25]. As stated in [10.25], there are a number of formidable challenges associated



**Fig. 10.36** Electric fields in DC cables (adapted from [10.36])

with the process of designing the solid insulation for HVDC equipment that are not (or are less frequently) encountered when designing HVAC equipment.

One fundamental issue is the considerably higher electrical stresses involved, which derive from the compact nature of DC devices/systems. For AC insulation, the electrical design is generally separated from the mechanical and thermal design. In a DC device, however, the electrical design cannot be separated from the mechanical and (in particular) the thermal designs.

A clear example is the strong effect of temperature on insulation conductivity and charging dynamics. TB 520 presents an overview of the key material properties that determine the behavior of solid DC insulation constructions. These properties are important not only for the design process but also for testing. To stress the differences between AC and DC design, properties are identified that play a minor role in AC insulation but a major role in DC insulation. Also, a number of purely AC properties are included, when they are important in connection with DC voltage application and when changing an applied DC field in particular.

Knowledge of the temperature and electric field distributions is of prime importance in the design and testing of an insulation system, as the temperature and electric field are the major sources of stress in the insulation. In an AC design, the electric field distribution is mainly determined by the geometry and permittivity, but it is not as straightforward to determine the field distribution in a DC design. Under steady-state conditions, the DC field distribution is determined mainly by the specific conductivity of the insulation and to a lesser extent by the space charge in the insulation. The specific conductivity is strongly affected by temperature and more weakly by the local electric field. Thus, both the temperature distribution in the insulation and the temperature dependence of the specific conductiv-

ity need to be determined before the electric field can be studied. This is complicated by the fact that the conductivity is also affected by the electric field and that conductive losses from the dielectric affect the temperature distribution. A good example of the major effect of a temperature gradient in an insulation construction is the concept of field inversion in a HVDC cable. Space charge can be generated when charge traps are filled or when there are variations in the conductivity of the insulation, and the effect of this space charge on the electric field distribution must be quantified. To date, this can only be achieved by directly measuring the space charge distribution. It is hoped that in the future it will become possible to adjust the space charge behavior by directly controlling the trap distribution in the dielectric, for instance.

### 10.4.3 Detailed Calculation of the Electrical Characteristics of Cable Systems

As was mentioned earlier, the characteristics of electrical cable systems have been among the main topics addressed by the study committee since it was created; these issues are addressed in [10.26].

All of the formulae reported in the literature were derived based on some assumptions. These assumptions are fulfilled by most of the older cable designs, as those were the main designs used at the time that the formulae were derived. However, the assumptions may or may not be applicable to more modern cable designs. Therefore, studies have been carried out to extend the applicability of the basic formulae.

Simple formulae that may be derived for power frequency considerations are given in [10.26]. They are used to get expressions for the sequence impedance and for the surge impedance, as detailed in Chap. 4 of [10.26].

Further improvements are needed to the formulae. The required improvements are listed in [10.25] for further consideration.

### 10.4.4 Rating Calculations

The cable rating refers to the amount of current a cable system can carry without exceeding the design limitations—particularly the insulation temperature limitations—of the cable system at any position along the circuit. The current rating is highly dependent on the physical construction of the cable, the installation conditions, and expected loading patterns.

It should be noted that system failures due to power cable overloading are rather rare, which is probably explained by the fact that most of the cable systems in use today carry relatively moderate loads. This also means

that if there are significant load (profile) changes in the future, we may approach the limitations of the current ratings of power cable systems much more closely than we are presently. Given the ongoing developments in renewable energy and energy usage, it appears that this topic (the current ratings of power cables) will only increase in importance.

TB 640 [10.28] provides guidance for cable engineers who are attempting to calculate current ratings for new and existing power cables. However, establishing an accurate cable rating for each power cable system regardless of its situation or age is rather difficult, as only a selection of the wide range of existing cable designs and installation and operating situations are covered by the calculations presented in existing standards. For this reason, CIGRE addressed the ratings of insulated AC and DC power cables, including buried, submarine, and in-air installations, as well as the problems associated with establishing the ampacity of the cable circuit for unusual configurations and installation conditions.

TB 640 includes the following:

- A consideration of the starting points—the thermal properties of the cable environment—for cable rating calculations
- A guide to methods of calculating current ratings in situations that are not (fully) covered by existing IEC standards
- A discussion of the tools and techniques available for calculating cable ratings.

#### Calculating the Current Rating of a Power Cable

The first part of [10.28] considers the most important aspects of current rating calculations. Overall issues with rating calculations that must be addressed at a more strategic level before performing the calculations are discussed, such as the grid situation, load factors, time-dependent load flows, and emergency operation. Important considerations include the factors that limit the current ratings of power cables and margin sizes in rating calculations. The following should be noted:

- The accuracies of the starting points, calculation methods, and calculation tools should be relatively evenly balanced. Although a calculation method with an accuracy of a few percent is available for some situations, it is not realistic to expect the same accuracy for the starting points.
- The margins in any rating calculations should be considered during the bidding and design phases of a new cable project, as well as during the operation phase when existing cables are considered.

#### Starting Points for Rating Calculations

TB 640 provides information on the starting points (input information) for rating calculations [10.28]. The results of a worldwide survey elucidate the starting points that are actually used in practice, as well as the starting points that are actually needed to perform rating calculations correctly. Recommendations for improving the setting of starting points are made.

The origin and quality of the data that should be used are defined, and the evaluation of a cable routing in terms of current rating is discussed. Installation conditions and soil parameters are described in detail.

The results of the survey indicate that, in practice, most starting points are assumed or are estimated as conservative values, although there is a growing tendency to perform improved evaluations of such parameters for new installations. This means that there is great potential to better utilize cables by improving the starting points.

#### Calculation Methods and Procedures

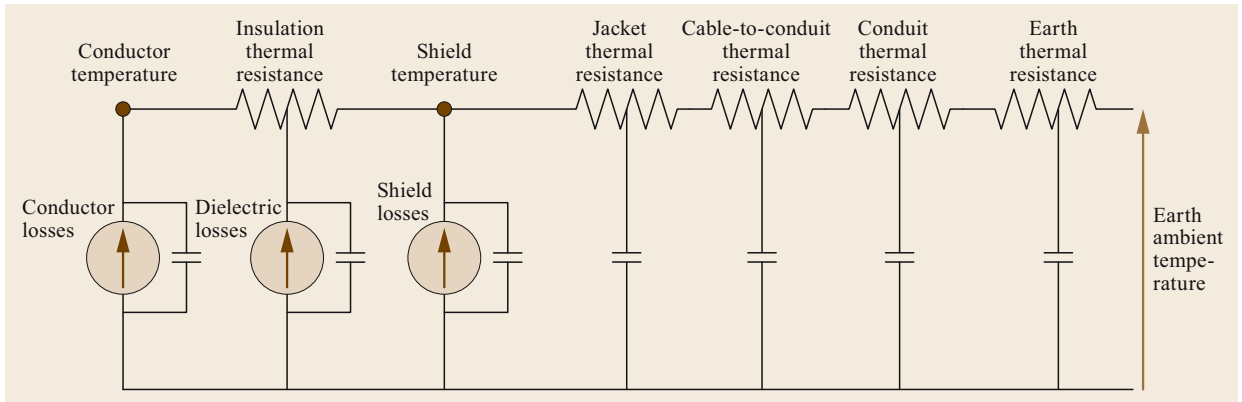
In TB 640, additional guidance for calculating current ratings is given over what is described in the IEC standards for some situations. The specific situation of interest can be found in [10.28] by checking lookup tables, mind maps (e.g., Fig. 10.26), and its chapters and sections.

Guidance on the calculations is given in several ways. The reader is often referred to existing standards, although hints, tips, and descriptions are also given. The WG found that it is very important to give guidance to engineers who need to perform difficult rating calculations.

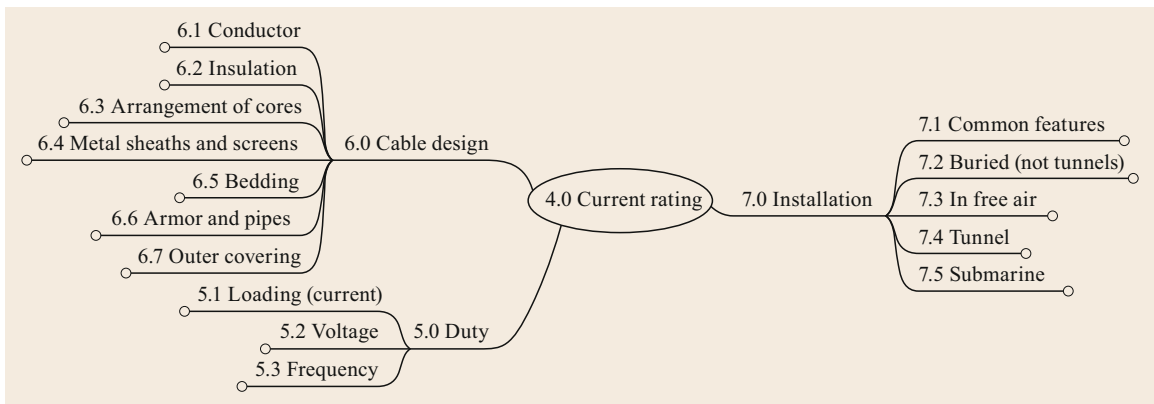
The situations that are discussed comprise:

- *Duty aspects*: cable loading variations (continuous, daily cyclic, emergency, arbitrary, and short-term loading patterns) and the effects of DC and AC at different frequencies
- *Cable aspects*: cable design issues that lead to losses (e.g., skin and proximity effects, dielectric losses, sheath/screen and armor losses) as well as the thermal resistances of cable materials
- *Installation aspects*: installation issues that lead to variations in the heat dissipated from power cables (the TB contains about 50 pages of information on this alone, with discussions of buried cables, in-air cables, cables in different kinds of tunnels, and cables for submarine applications).

Most calculations of underground cable ratings performed using analytical methods make use of the fundamental concept of heat transfer through a solid medium by thermal conduction. The basis for this evaluation



**Fig. 10.37** Equivalent thermal circuit for an extruded or SCFF cable installed in a conduit (adapted from [10.28])



**Fig. 10.38** Overview of the aspects that can affect current ratings (adapted from [10.28])

is an equivalent thermal circuit that is developed to model a specific cable construction. The thermal equivalent is based on the temperature rise resulting from heat flowing through a thermal resistance and capacitance. The thermal capacitance of the various cable layers and surrounding earth introduces a delay in the response of the temperature to changing load conditions that depends on the specific heat characteristics of the cable components and the environment in which the cable system is installed. An example of an equivalent thermal circuit for an extruded or self-contained fluid-filled cable installed in a conduit is shown in Fig. 10.37.

The cable system design parameters that affect current ratings can be divided into three broad categories: duty, cable design, and installation. This is summarized in Fig. 10.38.

In TB 640, each aspect is evaluated in detail, and calculation methods that can accommodate the described situation are recommended. Appendix D of [10.28] gives detailed mind maps for the relevant sections (5/6/7) of the brochure to aid the reader.

As an example, Sect. 7.1 of [10.28] discusses common aspects that can affect many cable installation types (such as the impact of parallel metal conductors), rather than providing the same discussion for each installation. In parts of Sects. 6 and 7, some aspects (e.g., sheath losses) are covered in one section (the metal sheath section) and that discussion is then referenced in other sections (such as in the description of the impact of AC voltages on sheath losses). This avoids any duplication of discussions of calculation methods.

*The most widely used documents for current ratings are the IEC series of standards.* Cable engineers who are experienced in performing current rating calculations will be familiar with the aspects of a cable system described in IEC 60287 (in terms of losses, thermal resistances, and base assumptions). For those experienced cable engineers, Appendix C of [10.28] includes a table that contains a list of calculation methods that are missing from the IEC standards (Table 10.4). The methods in the table are indexed in a similar fashion to IEC 60287 and contain cross-references to the appropriate sections of [10.28].

### Using Calculation Tools and Techniques

TB 640 [10.28] also provides information on available calculation techniques and tools (both static and dynamic, as used for instance in dynamic rating systems, DRSs) as well as the application of distributed fiber optic temperature sensing (DTS) systems. The use of dynamic calculation tools in dynamic rating systems is discussed in detail. The described calculation tools are categorized into analytical (ladder network), empirical, and numerical models, the latter based on finite differences, finite elements, boundary elements, or fluid dynamics.

The results of a global survey of real-world experiences with the various calculation tools and techniques and with DRS and DTS systems is reported in TB 640. For example, experiences of the limitations and problems with DRS and DTS systems are described.

### Recommendations for Future IEC Standardization

TB 640 [10.28] was created to provide clarity on how to perform current rating studies for a wide range of cable

installations. By providing these guidelines, it is hoped that companies worldwide will use similar approaches to deal with similar problems, such that solutions to even the most difficult problems will also become available over time.

It provides results, techniques, and discussions that aid the selection of starting points, as well as calculation methods and tools that can be used to obtain accurate results. Furthermore, it defines areas that require future work by experts and provides recommendations for new work to be performed by CIGRE that are currently being acted upon.

Table 10.4 lists calculation methods that, when [10.28] was published (in December 2015), were missing from IEC Standards or were included in IEC Standards but generated incorrect results. An entry in this table does not necessarily imply that the IEC Standard should be changed, as the omission or error may be negligible, the situation alluded to may be rare in the real world, or the solution may be too complex for inclusion in an IEC Standard.

**Table 10.4** A list of potential improvements to IEC standards (adapted from [10.28])

Section	Description
<b>Losses (conductor)</b>	
6.1	IEC 60287-1-1 Table 2: Skin and proximity effects missing for oval conductors and aluminum sector-shaped
6.3.4	Skin and proximity effects for concentric cables
7.1.3.1	Proximity effects for multiple circuits or multiple cables per phase
<b>Losses (dielectric)</b>	
6.2.2	IEC 60287-1-1 clause 2.2: Calculation of capacitance for sector-shaped or belted cables is not included
<b>Losses (sheath and armour)</b>	
6.4.2	IEC 60287-1-1 clause 2.3 does not cope with copper wire screen and metal sheaths in the same cable
7.1.1	IEC 60287-1-1 clause 2.3.1 to 2.3.6.2: No method for calculation of sheath losses for unequal cable spacings (but method for AC conductor resistance is included) for single core cables. Sheath losses can only be calculated for flat spaced and trefoil formation
6.6.1	IEC 60287-1-1 clause 2.4.2: Armour losses for multi core cables within a common armour are too large when calculated using IEC 60287
7.1.3	IEC 60287-1-1 clause 2.3: The sheath losses of several circuits. The IEC standard considers losses in the three phases of the same circuit without consideration of the effect of neighbouring circuits
7.1.3.4	IEC 60287-1-1 clause 2.4: The electromagnetic effect of several circuits on losses in armours. The IEC standard considers magnetic losses in the three phases of the same circuit without consideration of the effect of neighbouring circuits
5.3.1	IEC 60287-1-1 clauses 2.3 and 2.4: For single phase cables with a separate neutral cable with different construction to the phase cable, the electromagnetic effects of losses in sheaths/armours needs calculation
6.3.4	IEC 60287-1-1 clause 2.3: Sheath loss on concentric cable
5.3.1	IEC 60287-1-1 clause 2.3: Specially bonded two phase single core cables
7.1.11	IEC 60287-1-1 clause 2.3: The effect of an earth continuity conductor on cable rating in a single point bonded system. Additionally other parallel metallic paths may be installed
7.1.6	IEC 60287-1-1, general: The effect of charging current on cable current rating for very long cable routes
7.1.9	IEC 60287-1-1, general: Losses in metalwork near to cable systems, including potentially magnetic materials
6.6	IEC 60287-1-1, general: Cables in magnetic pipes. At the moment, only the pipe type cables in trefoil or cradled configurations are considered in the IEC 60287. This includes the installations in large casings crossing roads, tracks, rivers, etc. This would appear to be an issue for pipe jacking

Table 10.4 (continued)

Section	Description
<b>Thermal resistances of constituent parts of cable</b>	
6.2.1	IEC 60287-2-1 clause 4.1.1: Thermal resistance of layers between conductor and sheath substantially greater than the insulation (e.g., air layers in XLPE cables under corrugated aluminum sheaths) may need to be considered
<b>External thermal resistances for cables installed in air</b>	
7.3.5	BS EN 60287-2-1 general: Cables on riser poles. IEC standard does not recognize this installation
	BS EN 60287-2-1 general: Cables on trays
7.3.2	BS EN 60287-2-1 general: Only limited number of cables in groups are covered in IEC 60287-2-2 for cables installed in air
7.3.3	BS EN 60287-2-1 general: Cables on bridges with the effect of solar radiation and protective panels
<b>External thermal resistances for cables installed buried</b>	
7.2.3.1	IEC 60287-2-1 clause 4.2.6.1: Cables at shallow depths and filled surface troughs Kennelly's hypothesis assumes that the ground/air interface is an isotherm. How to calculate the temperature increase at the earth-air interface above a power cable circuit. This cannot be done using the IEC models as they are based on the Kennelly's hypothesis, although this question is increasingly being raised Additionally IEC 60287-2-1 may not correctly account for solar gain
7.2.3.2	IEC 60287-2-1 clause 4.2.6.2: Cables installed in unventilated unfilled surface troughs IEC 60287 gives an empirical formula
7.2.1.5	IEC 60287-2-1 general: Cables placed underground with more than two soil types. The IEC standard recognizes one backfill/duct bank scenario (see IEC 60287-2-1 clause 4.2.7.4). Note: this can be different backfills or alternatively different layers of soil
7.2.1.9	IEC 60287-2-1 general: Deeply buried cables
7.2.1.4	IEC 60287-2-1 general: Soil dry out with multiple circuits
7.2.2.1	IEC 60287-2-1 clause 4.2.7: Convection in ducts, particularly along the duct
7.2.1.7	IEC 60287-2-1 clause 4.2.3.2: Heat sources such as steam pipes with set temperature rather than set heat output
7.2.1.7	IEC 60287-2-1 general: High water table or water course providing heat sink
7.2.1.3	IEC 60287-3-3 general: Cable crossings with ducts or more than one thermal resistivity
<b>External thermal resistances for cables not installed in IEC considered installation types</b>	
7.2.1.6	Water cooled circuit
7.5.4	Submarine cables installed in J tubes
7.5.2	Submarine cable installed on seabed
7.5.3	Submarine cable installed in free water
7.2.3.2	Cables installed in surface troughs that are unfilled and naturally ventilated
7.2.3.3	Cables installed in surface troughs that are unfilled and force ventilated
7.4.2	Cables in force air ventilated tunnels (not yet published)
7.4.3	Cables in force water cooled tunnels
7.4.1	Cables in naturally ventilated or unventilated tunnels
<b>Additional problems</b>	
7.1.10	Calculation of short lengths with heat flow along the cable
5.3.3	HVDC above 5 kV not covered. DC cables have additional constraints such as temperature dependent stress profiles and void formation
5.3.5	Harmonic currents. This will create extra conductor and sheath losses (note AC conductor resistance will be different to 50 Hz)
7.2.1.2	Ampacity of dissimilar/unequally loaded circuits. The IEC standard gives a formula for the mutual heating effect, but no algorithm for cable rating. Numerical experimentations have shown that the results are different for different approaches (an iterative procedure, maximizing total ampacity, maximizing total power) The effect of measures to reduce magnetic fields. Some papers have been published, but no official method suggested
5.1.2.3	Transients with arbitrary load curves
5.1.2.4	Calculated current ratings may take an unrealistically long time to reach steady state and higher current ratings may be acceptable (e.g., tunnel ratings may take decades)
5.1.3	Current ratings where intermediate (e.g., sheath temperatures) are known. Dynamic ratings
7.1.7	Joints
7.5.1	Method of determining temperature at depth below seabed
6.3.4	Concentric cables not covered
7.2.1.1	What circuit separations are required before a cable circuits are thermally independent?

## 10.5 Challenges in Cable System Implementation

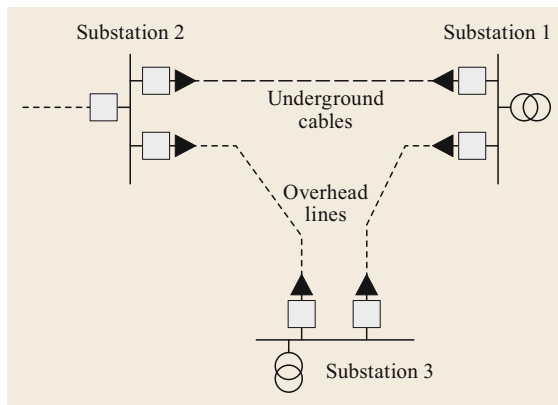
In most countries, transmission grids generally consist of overhead lines for technical and economic reasons. In situations where the use of HV underground cables could not be avoided, the shortest length of cable possible has traditionally been used, except in very densely populated countries such as Singapore and Hong Kong, where underground cable links are an essential part of the grid. However, long HV cables are becoming increasingly common in many countries due to environmental issues and time constraints (it can often take a long time to obtain the permission to construct new overhead lines, and new overhead lines are not permitted at all in some areas).

The incorporation of long HV cables into a grid introduces new technical and environmental challenges. Reasons for this include the different electrical properties of HV cables compared to overhead lines and the different civil construction works (e.g., water crossings, railways, and highways) involved. The effects of electrical capacitance, thermal inertia, impedance, magnetic and electric fields must also be considered, as well as testing methods.

### 10.5.1 Main Cable Configurations

Various configurations are in use, such as single-circuit, double-circuit, and triple-circuit lines with different arrangements of transformer and generator connections.

Many types of connections—including overhead lines, underground cables, or both—are employed. The lengths of transmission lines and cables can vary significantly. In order to provide for high transmission loads, some circuits can consist of more than one cable per phase.



**Fig. 10.39** Underground cable system in a meshed network (adapted from [10.32])

A number of commonly used cable configurations have been identified. The main cable circuit configurations have been identified by JWG 21/11 and are described in TB 189 [10.32] and TB 250 [10.8]. They are given in Figs. 10.39–10.43 and are representative of the most common situations in practice. In any of these figures, each cable could potentially consist of several cable systems.

#### Meshed Underground Network

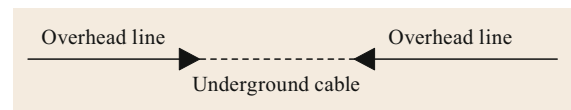
Some parts of a HV network may be entirely underground. This is often the case in large towns, where urbanization limits the construction of overhead lines. Cables connect the busbars in the system, as indicated in Fig. 10.39.

#### Siphon

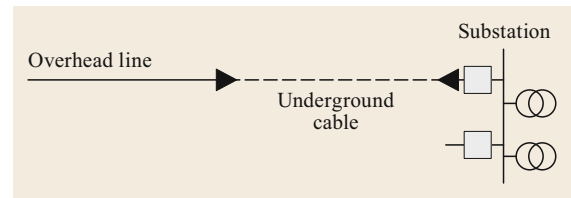
A siphon (Fig. 10.40) is an underground cable that connects two overhead lines. No switching device is located between the lines and the cable. This configuration allows a HV link to pass through areas that are too wide for an overhead line span, such as rivers or small lakes. This configuration also allows a transmission line to pass through or near a protected site or an urbanized area. Transitions between overhead and underground sections are achieved using either simple terminations installed on poles or towers or in a special fenced-off area called a *transition compound*.

#### Substation Entrance

An underground cable is often used as the interface between an overhead line and a substation (Fig. 10.41), especially when it is a gas-insulated substation. This configuration allows more compact stations to be de-

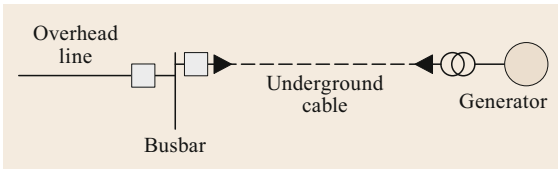


**Fig. 10.40** A siphon—an underground cable connecting two overhead lines (adapted from [10.32])

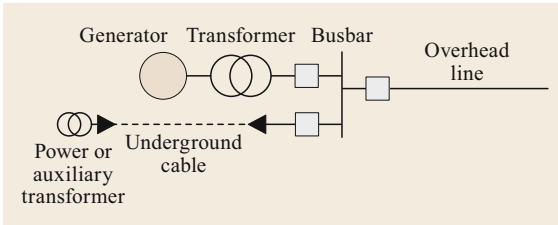


**Fig. 10.41** Underground entry to a substation (adapted from [10.32])





**Fig. 10.42** Power generator output (adapted from [10.32])



**Fig. 10.43** Power or auxiliary transformer supply (adapted from [10.32])

signed, and is particularly useful when there are a large number of incoming overhead lines.

#### Power Generator Output

An underground cable may be used to carry power from an inaccessible generator to a busbar, as shown in Fig. 10.42. In many hydropower stations, the generator is located inside a mountain. In order to save space, the generator is connected directly to the step-up transformer, with no circuit breaker. The secondary side of the transformer is connected to an outdoor substation by a cable that may be several kilometers long. The (air-insulated or gas-insulated) substation is connected to one or more overhead lines.

#### Power or Auxiliary Transformer Supply

In this configuration, a cable is connected between a high-power busbar and the power transformer or the auxiliary transformer of a power unit (Fig. 10.43). The cable is usually short.

### 10.5.2 Connecting to Offshore Generators

The issue of connecting offshore generators to a network has been addressed by WG B1.40 in TB 610 [10.36].

This section discusses the various aspects of system design that should be considered when designing an offshore infrastructure that will be used to collect and transport generated power to an onshore electrical infrastructure.

A detailed examination of the various components of an offshore network is provided in [10.36], as well as examples of existing offshore networks.

The various network topologies given in [10.36] allow the reader to compare the initial capital expenditure (CAPEX) with the long-term operational expenditure (OPEX) for a number of different solutions. The development of an offshore network often impacts the onshore grid as the transmission system must be expanded to accommodate the additional power generated offshore.

In this section, we consider the typical requirements (as specified by the transmission system operator, TSO) when applying for a connection to a transmission system, as well as the key parameters that form part of the grid code. Critical issues that arise when designing a system—such as the impact of reactive compensation, reducing system losses, and determining load profiles—are discussed.

Although the solutions given below are mainly based on offshore wind power generation, the philosophy used is also applicable to all other types of offshore generation. Furthermore, the issues discussed for export cables may also be relevant to the submarine cables generally used in the infrastructure for offshore energy generation. It should also be noted that relevant system aspects (e.g., voltages, frequencies, and protection) are discussed by WG B4.55 in TB 619 [10.37].

#### Connections to Shore: Types and Topologies

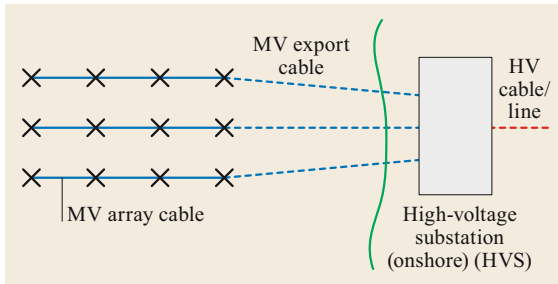
Different solutions for connecting to the shore can be distinguished according to the locations and the number of offshore generation plants considered.

To identify the optimal solution, the following aspects must be taken into account:

- The rated power of the offshore generation plant (or the power supply to the offshore structure)
- The distance to shore, including the onshore connection length
- The CAPEX and OPEX for the each type of connection
- Redundancy, which will have a financial impact
- The losses for the different solutions
- The voltage drop over the AC cables
- Cable derating due to the thermal influence of multiple cables laid in parallel
- The possibility of landing of several cables
- Environmental impacts
- Permits.

The following solutions are mainly used for offshore generation (or power supplies):

- *Medium voltage (MV) solution*: MV cable connecting offshore generators (array cables) and MV



**Fig. 10.44** Example of the connection of a small offshore wind farm to an onshore grid using MV cables (adapted from [10.36])

export cables without an offshore high voltage substation (OHVS).

- **HVAC solution:** MV cable connecting offshore generators (array cables), offshore high voltage substation with transformer and HVAC export cable.
- **HVDC solution:** MV cable connections offshore (array cables), offshore high voltage substation with transformer, HVAC export cable to offshore AC/DC converter station and HVDC export cable to shore.
- **Combined HVAC and HVDC solution:** HVAC connections between more offshore high voltage substations. HVAC connections from each offshore substation to AC/DC offshore converter station. From converter station a HVDC connection to shore.
- **Offshore grid solutions:** Connections to more offshore high voltage substations and/or more onshore grids (interconnectors).

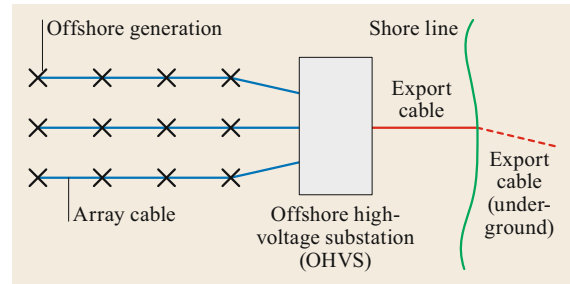
#### MV Solution

Probably the simplest solution is to connect the wind farm to shore via one or more export cables loaded at the  $U_m = 36$  kV level (Fig. 10.44). This solution is useful for smaller wind farms that are relatively close (typically less than 20 km) to shore. The offshore MV cable will be connected to a substation on land. The voltage is usually raised to the required grid voltage by a step-up transformer on land.

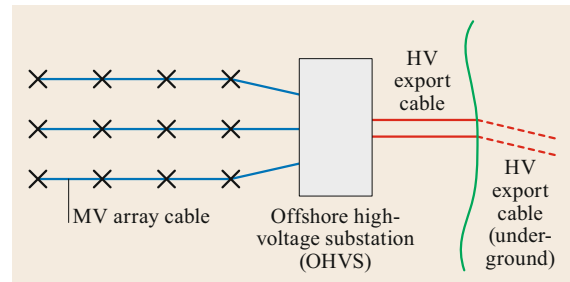
#### HVAC Solution

For offshore generators that are further from shore or have a higher power output, the preferred solution is to use an offshore high-voltage substation (OHVS) to collect all of the power generated at the MV level and then use a HVAC export cable to transport this power to shore.

Figure 10.45 shows an example of the connection of an offshore substation to shore via one export cable circuit. The generated power is transmitted via this ca-



**Fig. 10.45** Using array cables and an export cable to transmit power generated offshore to shore (adapted from [10.36])



**Fig. 10.46** Using array cables and two HV export cables to transmit power generated offshore to shore (adapted from [10.36])

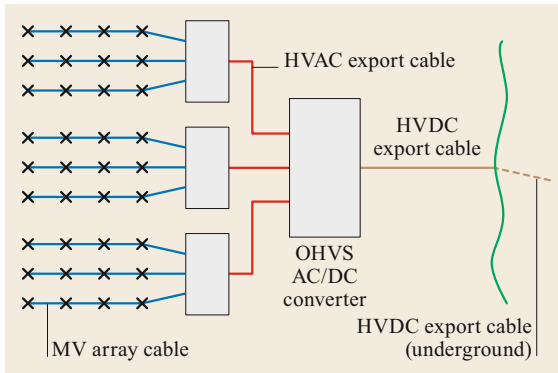
ble to an onshore substation, where it is passed on to the onshore grid. This solution is particularly useful for larger wind farms that are further from shore, typically 20–70 km. In this case, it is recommended that the voltage level of the export cable should be adjusted to the voltage level of the onshore substation; otherwise an extra transformer will be needed on land.

A second export cable circuit can also be installed to increase the availability and reliability of the overall system (Fig. 10.46). In this case, it is also recommended that two or more (depending on the total power generated) transformers should be used at the OHVS.

Instead of using two HV export cable circuits, it may also be possible to use one EHV (e.g., 245 kV) export cable circuit. In this case, there is a choice to be made between using two export cable circuits of lower voltage, which offers redundancy if one of the export cables fails, or using one export cable circuit at a higher voltage with no built-in redundancy if there is a cable failure. Aside from the issue of redundancy, these two solutions have different CAPEXs and OPEXs.

#### HVDC Solution

The HVDC solution is mainly used for offshore generation sites that are far from shore (> 70 km). Several



**Fig. 10.47** Scheme for HVDC connection to three offshore wind farms (adapted from [10.36])

offshore generation plants, each with their own OHVS, will usually be connected to one AC/DC offshore converter station. The generated power is passed from this offshore converter station to shore by means of a HVDC connection. This is because the transmission capacity of a HVDC cable link is higher than that of a HVAC cable link for the same conductor size. This cluster or hub solution has the advantage that the length of cable needed is less than that required in the situation where each offshore wind farm is connected to shore separately. Other advantages are reduced installation costs and fewer landfalls. One of the main disadvantages of this solution is that failure of the main export cable can result in a significant drop in electricity production, which may disturb the balance of the system. Figure 10.47 shows an example in which several offshore generators are connected to an offshore substation, which is in turn connected to shore via one export cable.

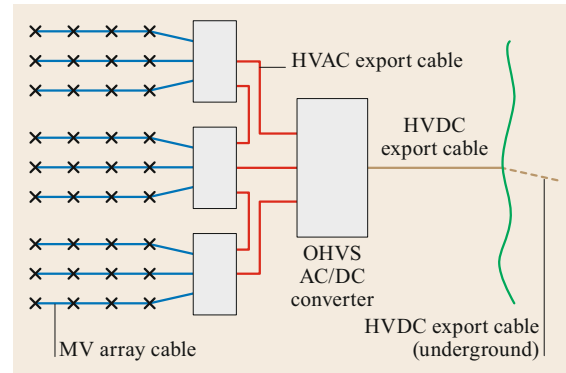
#### Combined HVAC/HVDC Solution

Another solution used to increase the redundancy in the offshore collector grid is to interconnect the different platforms at the HV level (Fig. 10.48).

#### Offshore Grid Solutions

Multiple offshore generation sites are often situated close together. In this case, it can be more prudent to look for a combined solution that can bring the power generated by all of the offshore generators to shore or to different shores.

There are some challenges involved with implementing such a solution. First of all, it is very costly to build and maintain offshore constructions and installations. Secondly, if a HVDC grid is built with multiple terminal converters, it may be necessary to ensure, for example, that a commutation failure will not switch off more than one line, so a HVDC circuit breaker



**Fig. 10.48** Scheme of a combined HVAC AND HVDC solution for collecting the power generated by multiple offshore power generation plants (adapted from [10.36])

must be introduced. The various options for offshore generation connection including offshore grid were the topic of a recent CIGRE Symposium in Aalborg (Denmark) [10.38].

#### 10.5.3 Effect on the Grid

The implementation of AC cables in HV and EHV grids significantly influences the electrical parameters of the grid. For instance, it influences the steady-state voltage due to the production of reactive power. This will be especially noticeable to grid operators when there are low-load conditions in the grid. Generators or dedicated shunt reactors positioned in the grid must absorb this surplus reactive power.

The impedance of a cable connection is far lower than that of an overhead line at the same voltage level. This influences the current distribution between the cable and overhead line when they are operated in parallel, which can cause unbalanced and inefficient use of the overall transmission capacity of the system. This is normally restored by installing series reactors (Fig. 10.49) in the cable circuit. Other alternatives are to insert series capacitors into the overhead line section or to adjust the transmission capacity at the design stage. In the latter case, the transmission capacity of the cable would need to be related to the ratio of impedances. This may require an exceptional cable rating, which is rarely practical.

The application of long HV and EHV cables will significantly change the harmonic impedance of the grid. If a large amount of cable is added, peaks in the impedance curve can strengthen, and the lowest resonance point will slide downwards to the power frequency.

There are two main concerns here: the risk of resonance due to switching actions and the amplification of higher harmonic distortion in the grid. This distortion



**Fig. 10.49** Series reactor in a 380 kV hybrid line (adapted from [10.14])

would already be present or would have been introduced by a customer (for example by a wind farm, or by motors with power electronics).

Switching actions can lead to resonances with substantial voltage rises or overvoltages. Such problems can be particularly severe when switching large transformers and long cable connections. The amplification of higher harmonic voltages causes additional currents that can cause equipment (e.g., transformers, generators, motors, current transformers, and cables) in the transmission grid to overheat. It can also cause issues with grid protection and motor controllers.

Therefore, the reliable application of long AC cable connections necessitates detailed system modeling studies. If the study results show that resonance or unacceptable amplification of higher harmonics can occur, suitable measures must be taken. Naturally, the countermeasures applied depend on the nature of the identified problem and its severity.

Due to different electrical and physical properties of cables and overhead lines, it may be necessary to change existing protection policies and schemes. Most important in this respect are the influence of cables on line-distance relays (impedance relays) and autoreclosure policies for hybrid lines.

The extent to which an AC grid is influenced by the inclusion of an underground cable and the measures that must be taken because of it vary significantly depending on the voltage level, the grid configuration, the short-circuit level, and the reason for using the cable in the power system.

A long AC cable connection feeding a small load (e.g., an oil platform) yields significantly different challenges from those associated with a connection to an offshore wind farm. Partial undergrounding of EHV

overhead line circuits also provides additional challenges. This means that the technical and economic optimization of a long AC cable connection can vary significantly depending on the situation.

### Matching Cable and OHL Ratings

It is much cheaper to achieve a high transmission capacity with an OHL than with an underground cable. The OHL current rating is based on the properties of the conductor and static environmental conditions (temperature, wind speed, and solar radiation). If the same conductor is used for an underground cable, it will have a lower current rating. This is due to the thermal insulation afforded by cable materials and the surrounding ground. The current rating can be increased by making the conductor thicker and more conductive (i.e., using copper instead of aluminum), but this approach is less effective for large conductor sizes due to the skin effect. It can be economically unattractive to match OHL and underground cables based on continuous ratings due to the larger cross-sections or number of cables per phase needed for underground cables.

In many circumstances, the thermal inertia of the underground cable (see the section on rating) needs to be considered when matching a cable to an OHL. This can result in the use of smaller conductor sizes, cheaper conductor materials, and fewer cables per phase, as this will reduce the required installation trench width. The implementation of a smaller installation swath not only reduces civil costs but may also ease right-of-way requirements and allow the cable system to be installed in narrow corridors. Reducing the number of cables per phase also results in less maintenance and, especially for high-voltage cables, less reactive power.

When matching the current rating of a cable system to an overhead line and examining the possibility of using thermal inertia, there are several factors that can be considered. These factors include expected circuit loads and preloads, the dynamics of the load, the cable environment, the laying configuration, and the application in the grid. In particular, the system or circuit operator's requirements for the overall circuit will be a significant driver.

The current rating of an overhead line is determined by either the electrical clearance (allowable sag) or by a thermal limit linked to the preservation of mechanical properties. This continuous or static rating of the overhead line is determined based on the supposed worst-case environmental conditions.

If the grid has an  $n - 1$  safe operation, the current rating during this condition can be set to a lower level in order to reduce cable costs in a hybrid connection.

In the first case, called a pre-fault, the cable in the hybrid connection can be temporarily loaded up to the continuous rating of the overhead line.

In the second case, called a post-fault, if the system operator can guarantee to limit the post-fault rating to a set period of time (for example 24 h) and to not repeat this emergency rating for some agreed time (e.g., until the cable has cooled to its pre-fault rating temperature), then it may be possible to match the post-fault overhead line rating to an emergency cable rating.

In these cases, the continuous current rating of the cable is less than that of the overhead line, allowing the use of a smaller cable. It should, however, be noted that the current-carrying capacity of the overhead line has been compromised. This method is described as emergency ratings in IEC 60853.

If the system operator can guarantee to limit the post-fault rating to a set period (for example 24 h) but may have to repeat the post-fault operation, then it may be possible to match the overhead line rating to a cyclic cable rating. It should be noted that this guarantee to limit the post-fault rating must be given when the transmission network is being planned, and it may be difficult to give such a guarantee because fault durations can be difficult to predict. For example, fixing a cable fault can be a lengthy process (several weeks is not uncommon), causing a considerable delay before the circuit returns to full service. Practical examples are given in [10.14].

### Dynamic Cable Rating

The previous section described how the cable and overhead line ratings can be matched using the thermal inertia of the cable, an assumed preload, and a possible load cycle. This enables the cable system design to be optimized and reduces costs.

Dynamic rating is also economically attractive for wind farm connection, where cables are rated to 70–80% of the full wind-farm rating for example. If periods of high wind strength can be predicted (from observational statistics), then dynamic cable ratings can be applied in a reliable way. Dynamic cable rating is a cost-saving solution and is even more effective when used in combination with distributed temperature sensing (DTS) [10.12]. If this solution is chosen, the operator should monitor the cable connection and may need to constrain the output of the wind farm. This topic was very recently covered by CIGRE WG B1.45 in TB 756 [10.19].

Preload and load-cycle information can also be used for existing cable connections for which only continuous ratings have been calculated (according to IEC 60287) previously. Applying dynamic ratings to existing cable connections allows a potential increase



**Fig. 10.50** 150 kV cables with PT 100 elements at a hot-spot (adapted from [10.14])

in transmission capacity of up to about 30%, depending on the cable type and cable laying configuration as well as the preload and load cycle. It should be noted that higher dynamic ratings can be reached if the actual cable temperature or other system data (such as historic loading levels) can be accessed, or if real-time measurements are available. Dynamic ratings can be higher due to a lower preload rating, as there are often more dynamics in the load cycle and lower environmental temperatures than assumed during the design calculations. The temperature of a cable can be measured with PT elements at the locations with the worst thermal conditions (*hotspots*) (Fig. 10.50). This can be a particularly effective approach for optimizing grid operations by allowing more power to be transmitted than the grid was designed for, or allowing outages that would not normally be considered.

### 10.5.4 Protection Systems

Protection systems used for HV and EHV grids often assume that overhead lines are used. The introduction of cable connections or hybrid connections can therefore lead to a modified protection philosophy. Most issues caused by cables can be mitigated using modern protection devices, which can be digital or numeric and can deal with different types of connections. Additional high-voltage equipment associated with cables such as series and shunt reactors must also be protected. This can be done within the protection zone of the connection or by a separate differential protection system.

Autoreclosure is typically designed for overhead lines, where many faults only occur temporarily. This is not the case with underground cables, where a fault in the insulation cannot heal itself. Autoreclosure is not applicable to full cable connections but should be con-

sidered for hybrid connections. There are a range of policies that can be applied, each of which has its own advantages and disadvantages.

From an insulation coordination perspective, surge arresters are not always needed to protect the cable insulation, although they can still be useful in hybrid lines, where reflections and earth potential rises can occur at transition points [10.30, 31].

#### Power Cable and Hybrid Link Protection

Line distance protection is widely used in HV transmission grids because it does not require telecommunication channels between both ends of the line. Distance protection relays are based on a linear increase in the impedance over the length of the line. If the impedance drops below an adjusted minimum, the fault is within the protection zone, and the line will be switched off.

Distance protection can be used for cables too, but underground cables have different electrical properties. Cable return paths can vary depending on the fault type (core–sheath or core–sheath–earth), the location of the fault (distance to the cross-bonding or grounding point), and the way that the metal sheath is earthed (single point, solid-bonded, cross-bonded, or other). This can lead to a deviation of the linear impedance curve, causing the limits of the protected zone to be determined inaccurately. This is especially true if there is insufficient distinction in the last 20% of the impedance curve, as it is important to determine the setpoint for the first protection zone in this range.

Systems with long cross-bonded cables show smaller deviations of the linear impedance curve due to the decreased relative impedance of each section. Detailed studies are necessary to identify the right setting for the distance relays. Capacitive currents are sometimes neglected for overhead lines but they must be considered for long cable systems.

Differential protection is normally the preferred reliability protection system for cable connections, with line distance protection used as a backup system.

If hybrid links (partial undergrounding, for example a siphon) are present, different impedances are connected in series. On the one hand, this makes it harder to determine the minimum impedance setting for the distance protection, but on the other hand the influence of the cable section on the total impedance decreases as the overall connection increases in length. Modern digital distance relays are a big step forward: they can also deal with multiple cable sections in a hybrid line. If the level of protection provided by line distance relays is unclear, differential protection can always be applied. This is the normal choice for full cable connections, but telecommunication channels are not always available for existing partial undergrounding.

To summarize, cable systems can be protected by distance protection. It is easier to reach an acceptable level of accuracy for longer cable lengths than for (very) short lengths. Differential protection of a full cable connection is preferable, but its dependence on telecommunications must be managed.

#### Autoreclosure and Lockout Systems

Autoreclosure is widely used after faults in overhead lines. The aim of autoreclosure is to optimize the availability of circuits and thus improve the security of supply. For hybrid connections, a range of autoreclosure strategies are available:

- A lockout system for faults in the cable section
- An unchanged autoreclosure system
- No autoreclosure.

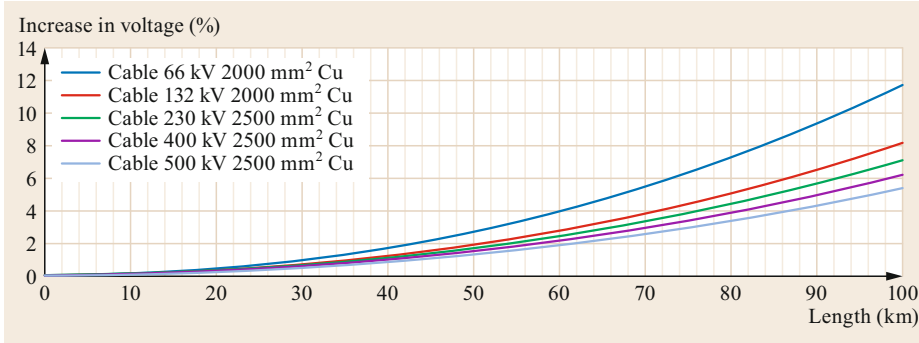
Each of these strategies has its own advantages and disadvantages, and all of them are applied worldwide.

Lockout systems give the best performance, as autoreclosure is still available with these systems but it will not operate when there is a cable failure. There is no additional damage and no further voltage dips with a fault in the cable. However, to detect this fault, measurement and telecommunication channels to the substations are required. A lockout system applies differential protection over the cable section, so current transformers are needed. Such a system is more difficult to implement if there are numerous cable sections in an overhead line.

However, there are considerable financial and space-related disadvantages of using a lockout system. If slip-on current transformers are used at the ends of the cable system, failure of the cable sealing ends will still activate the autoreclosure.

In some circumstances, the use of autoreclosure with hybrid connections is acceptable. The choice of whether to use autoreclosure involves a risk evaluation. A benefit of using autoreclosure is that it keeps the system simple. Issues that need to be considered in this case are the expected number of faults in the cable section (far fewer than in the overhead line section), the additional cable damage, the risk of fire or other injuries, and additional voltage dips.

For hybrid lines with relatively short overhead line sections, the removal of autoreclosure may also be considered. Many factors play a role when deciding whether to remove autoreclosure, such as the failure rate (the protection level against lightning strikes), the amount of redundancy in the meshed grid, and safety aspects (especially in highly urbanized areas). Although removing autoreclosure is not advisable, this approach is used to some extent in the Netherlands for 150 kV



**Fig. 10.51** Relative voltage increases due to the Ferranti effect at different voltage levels and for various conductor cross-sections (adapted from [10.14])

hybrid lines in a highly meshed grid, and has not led to any significant deterioration in the security of supply over a period of more than 15 years.

New technical developments in protection equipment have led to an improved ability to distinguish between an overhead line section and a cable section. This ability means that it is possible to apply autoreclosure only when the fault is in the overhead line section. Autoreclosure can cause overvoltages, especially at transition points where overhead lines are connected to underground cables. Careful examination of this phenomenon is necessary to determine the appropriate cable design, including whether to install any surge arresters in the transition compounds.

### 10.5.5 Voltage Effect (Ferranti Effect)

When the power cable line is operating with an open circuit and the voltage is applied at one side, the voltage increases at the opposite side of the line. This effect is caused by the charging current of the cable capacitance.

This may present an issue after the circuit has been installed and the cables must withstand the HVAC voltage used in a soak test or resonance test. The test voltage  $U_{test}$  is specified by the standards IEC 60840 and IEC 62067. Due to the Ferranti effect, when  $U_{test}$  is applied to one side of the circuit, the test voltage at the remote end will be  $U_{test} + \Delta U$ .

The voltage increases shown in Fig. 10.51 are based on the characteristics given in Table 10.5. The cables are laid in a flat formation 300 mm apart, losses from the metallic screen are 1%, the dielectric loss factor  $-\tan \delta = 0.0005$ , and the the working frequency is 50 Hz.

**Table 10.5** Characteristics of extruded cables (adapted from [10.14])

Phase-to-phase voltage (kV)	66	132	230	400	500
Copper conductor size (mm <sup>2</sup> )	2000	2000	2500	2500	2500
Diameter over conductor (mm)	55	55	64	64	64
AC resistance of conductor ( $\mu\Omega/m$ )	16.13	16.13	14.16	14.16	14.16
Insulation capacitance (nF/km)	375	269	249	219	192

The hyperbolic increase in voltage along the power line must be estimated prior to the HVAC commissioning test of the cable because the test voltage and the no/low-load operation voltage are higher than the nominal voltage  $U_0$ .

### Testing After Installation

The power line owner and the cable contractor must agree on the voltage to be applied on one side of the circuit, given that the voltage will be higher at the remote end. Also, one or multiple shunt reactors located somewhere along the power line are sometimes included in the HVAC test, in which case the voltage rise(s) at the location(s) of the shunt reactor(s) must be calculated beforehand and will influence the selection of the test voltage, which must be agreed upon by the line owner, the cable supplier, and the shunt reactor provider. Additionally, the inclusion of a voltage divider on both sides of the power line is recommended as a means to measure the voltage during the HVAC test.

### Under No or Low Load

The voltage must be no higher than the maximum cable voltage  $U_m$ , which is the reference for cable design and qualification (i.e., 245 and 420 kV, respectively, for 230 and 400 kV cables). Alternatively, a higher  $U_m$  value than that specified by the IEC standards can be defined, especially for cable lengths that will be installed on the side of the circuit where the voltage is higher than  $U_m$ .

### 10.5.6 Zero-Miss Phenomenon

Reactive power compensation by shunt reactors connected directly to the cable will help to reduce the

voltage drop in the grid caused when a long length of cable is energized. If the amount of reactive compensation is more than 50%, the zero-miss effect can occur. This effect can happen in the first few seconds after switching on a cable and connected reactors. Due to the temporary aperiodic current component of the shunt reactors, it takes a few hundreds of milliseconds before the current has its first zero crossing, necessary for opening the circuit breaker without reignition.

There are several ways to solve this problem: the amount of compensation directly connected to the cable can be decreased, point on wave switches can be applied, a preinsertion resistor (closing resistor) can be fitted, or single-phase tripping can be used. As only the healthy phases experience this zero-miss effect, it is possible to postpone the opening time of this phase by a few milliseconds until the effect has passed, which is referred to as automatic sequential switching (first the faulty phase is switched off, then the reactor, and after a few hundred milliseconds the healthy phases are switched off).

For weak grids, one utility in Europe has chosen a solution in which the cable and reactor each have their own circuit breaker. The reactor is connected to the busbar and not to the cable. The breakers work simultaneously to keep the voltage drop within the defined limits and to stop the zero-miss effect from occurring.

### 10.5.7 Switching Off Capacitive Currents

High-voltage cables are highly capacitive by nature. The longer the cable, the higher the capacitive current that must be switched off. Switching capacitive currents can be difficult for a circuit breaker because the voltage is near to maximum when the current becomes zero and restrike can occur. A small capacitive current can be even harder to disconnect than a large one.

Table 10.6 shows that for a long length of high-voltage cable, the no-load capacitive current can exceed the guaranteed capacitive interruption current of the circuit breaker. IEC 62271-100 specifies that a circuit breaker must be able to disconnect a no-load capacitive current of 250 A. Additional testing may be necessary to ensure that the requirements are fulfilled (e.g., 220 kV, 50 km, 1200 mm<sup>2</sup> gives  $50 \times 7.6 = 380$  A of charging current).

**Table 10.6** Indicative values of the charging current for different conductor cross-sections and voltages

Voltage (kV)	220	220	400	400
Cross-section (mm <sup>2</sup> )	1200	2500	1200	2500
Charging current (A/km)	7.6	10.8	13	17.4

### 10.5.8 Harmonic Resonance

The phenomenon of resonance in long AC cables in a grid dominated by overhead lines is a concern, as it can cause unacceptable voltage rises or equipment to overheat due to additional currents. This resonance can occur at the power frequency (50 or 60 Hz) as well as at higher order harmonics of the ground frequency and at interharmonics.

Resonance due to the application of a cable (high capacitance) occurs due to the resulting change in the harmonic impedance of the grid whereby the frequency of a harmonic current or voltage matches that of a peak in the impedance curve. There are two types of resonance in the grid: switching actions or short circuits (damped oscillation) and amplified background higher harmonic voltages (driven oscillation). The latter are fed into the grid by a source. Well-known sources of higher harmonic currents include frequency controllers of motors, HVDC connections, and converters in wind turbines.

Both series and parallel resonances can occur. Series resonance can be generated when energizing a cable. The resonance occurs between the inductance of the grid (the source) and the energized cable when there is a frequency component in the energizing current that corresponds to the resonance frequency of the induction–capacitance (LC) combination.

Parallel resonance can occur during the energization of a transformer. The resonance arises between the inductance and the capacitance of the grid (to which a long cable is connected). The inrush current of a transformer is dominated by a second harmonic component that can be responsible for resonance in the grid at the point of switching.

As more cables are added the resonance frequency of the grid declines.

Switching actions can cause resonance frequency excitation and must be further investigated. Research in the time domain can be performed to detect unacceptable voltage rises (in terms of amplitude and duration). In addition to the short circuit power also the damping by resistance ( $R$ ) of the grid and the load play a role in the degree of over voltages caused by resonance. The extent is often known only approximately and in case of doubt it may be necessary to perform additional measurements.

If a system study indicates an unacceptable transient overvoltage (TOV) due to switching actions, measures must be taken.

### 10.5.9 Magnetic Field

Various requirements must be met when implementing new high-voltage connections. For instance, it is



necessary to fulfill the requirements for electric and magnetic exposure. In this respect, underground cables have some benefits. Due to the presence of the insulation screen and the metallic sheath there is no exposure to electric fields, and there are numerous options to reduce the exposure to magnetic fields.

The main reason for the increased magnetic exposure with high-voltage cables is the suppression of the sheath current by the cross-bonding system and the spacing between the single-phase cables. Both of these steps are taken to optimize the current rating and to lower the costs.

To lower the magnetic exposure levels, the circuit impedance may be changed. For power system planners, it is important to know how the cable system will actually perform in practice. If measures to decrease the magnetic field change the connection impedance, the current distribution in the interconnected power system and short-circuit current levels may also be affected.

Magnetic fields from underground cables can induce voltages in nearby insulated metallic structures such as pipelines if the cables and pipelines are laid in parallel over very long lengths. Safety and corrosion issues can occur in such cases. There are various methods to reduce magnetic field exposure in order to meet requirements at specific locations. The impact of magnetic fields on current ratings is covered by TB 559 [10.21].

### 10.5.10 Life Expectancy

HV and EHV cables are designed to have a typical economic lifetime of 40 years (according to tests and international standards, e.g., those of the IEC). In reality, the technical lifetime of these cables is much longer. Many oil-filled cables that are in use today are over 40 years old, and the operational costs of those cables have not increased significantly over the years.

External damage or incidental internal faults in the cable system are relatively easy to repair, and the repair costs are only a small fraction of the initial investment cost. Thus, repair allows the lifetime of a cable to be extended.

The main reasons for removing a cable from service are a lack of transmission capacity (sometimes combined with the scenario where there is a lack of space to install a new cable with a higher transmission capacity without removing an old cable) and unacceptable oil leakages. In a few cases, end of cable life is caused by degradation of the insulation. Many HV oil-filled cables have been in service for over 60 years, but in many of those cases it has been necessary to replace or recondition the oil-pumping or monitoring systems.

Modern HV XLPE cables have been in operation since the mid-1970s and are continuing to provide excellent performance. They have the same repair options as oil-filled cables, but unlike those cables, XLPE cables cannot leak.

A range of issues must be considered when attempting to maximize cable lifetimes. These issues can be categorized as follows:

- Cable design and manufacturing
- Cable route planning and installation
- In-service maintenance.

#### Cable Design and Manufacturing

There are various cable design considerations. First, the quality of the XLPE insulation must be of the highest possible standard and the most advanced method of applying the insulation should be employed. Second, the selection of an appropriate metal sheath and outer sheath in accordance with the installation method and the environment is crucial. The intended installation technique and the environment of the laid cables will influence the choices that can be made in this regard. When the outer sheath is damaged, an induced voltage causes a current that will flow through this damaged point, degrading the metal sheath and potentially overheating the cable. If the outer sheath is damaged, corrosion can then occur, further damaging the metal sheath (especially if it is aluminum).

A third important aspect is the radial water barrier. When the metal shielding is broken, moisture (water) can penetrate towards the cable insulation and spread itself over a very long length due to capillary action. If this is not addressed in the cable design, it may mean that a substantial length of cable will need to be replaced when failure occurs.

#### Cable Route Planning and Installation

When planning the cable route, and subsequently during operation, the presence of heat sources (other cables, steam pipes, tubes for heating) near to the cable must be avoided or, at the very least, taken into account during engineering. Pulling forces must not be exceeded and damage to the outer sheath must be avoided during cable installation or the service life of the cable will be reduced.

#### In-Service Maintenance

To maximize the service life of the cable, it is important that the outer sheath remains in place over the metallic sheath to avoid water entry. It is also important that link boxes are kept in good condition and that the bonding leads are fully water blocked to stop water from migrat-

ing into the box. Finally, it must be ensured that the cable design temperatures during operation and short circuits are not exceeded. As discussed later, online monitoring of cable temperatures and route conditions is a useful tool for routine maintenance. Well-known threats to the cable that can occur in its environment include depressions in the ground, changes in the groundwater level, trees with deep roots, and any heat sources close to the cable, such as highly loaded cables and heating pipes.

### 10.5.11 On-Site Testing

Testing long AC cables, especially HV and EHV cables, is a challenge due to the amount and size of the test equipment required.

The most important test—the voltage withstand test of XLPE cables—can only be done with an AC voltage. The much easier DC voltage test is not suitable for testing XLPE cables because a DC voltage can leave space charge within the insulation or at interfaces between the cable insulation and the components used in the termination and jointing accessories. These space charges can remain after the DC voltage has been switched off, causing localized high electrical stress in the insulation system when the cable is energized with AC, which would in turn initiate partial discharges and subsequent cable system failure.

In the cable factory, XLPE cables and individual accessories are tested using AC with a typical frequency of 50 or 60 Hz and test equipment with parallel (primary) or series (secondary) reactive compensation.

HV and EHV XLPE cable systems are typically tested on-site using AC with a frequency in the range 10–300 Hz. A mobile resonance test is performed with series reactance (an example of this is given in Fig. 10.102 in Sect. 10.7.1).

To test long AC cables, we need to compensate for the charging current, which is directly related to the frequency and the test voltage as follows

$$I_c = 2f\pi CV,$$

where  $I_c$  is the charging current in A,  $f$  is the test frequency in Hz,  $C$  is the cable capacitance in F, and  $V$  is the test voltage in V.

To compensate for this very high charging current, we need to use high reactive HV compensation (*exciter*) coils, which are very heavy because they contain large amounts of copper and steel. This makes on-site testing very difficult and expensive. One solution is to lower the AC frequency. The standard IEC 62067 prescribes a lowest frequency of 20 Hz, and this has been used for many years to test HV and EHV circuits. A more recent document, CIGRE TB 490 (published by WG B1.27), recommends a minimum of 10 Hz [10.39].

Over the past five years, there has been a dramatic increase in partial discharge testing of new installations around the world, although many utilities still do not perform PD tests. CIGRE TB 728, recently published by WG B1.28 [10.40], provides useful guidance for non-experts in on-site PD measurement. This document collates information on PD testing and presents guidelines and recommendations.

However, testing at this lower frequency is costly due to the equipment required, the space needed for that equipment, and the transport costs involved. Hence, there is currently a global debate on whether to lower the frequency even further, to 0.1 Hz, or whether to adopt the oscillating wave system (OWS) or the damped AC (DAC) system, both of which are currently used to test MV cables. These systems are much smaller, less expensive, and easier to transport. However, there are some important issues that need to be considered for HV and EHV AC systems.

First, research clearly shows that during withstand testing, breakdown is directly related to the energization time at a given frequency, so much longer testing times or higher test voltages will be needed if the 0.1 Hz test is adopted.

This is not a problem for MV cable systems, as they can accept higher test voltage levels, but it could present an issue for HV and EHV systems that are specifically designed for operational and system voltages.

Second, there is concern that space charge could remain in the system if the voltage is not reversed within a very short time interval, meaning that the results of withstand testing with a DAC system could be questionable.

Since this important subject is quite complex, CIGRE WG B1.38 is currently preparing a technical brochure to provide guidance on tests of AC and DC cable systems using new technologies after laying. This document is expected to be completed in early 2021.

### 10.5.12 Practical Implementation of System Design

#### Choosing Between AC and DC Voltage

Given the trend for longer AC and DC cables, it is important to fully understand the benefits and limitations of both systems. The choice of AC or DC is very much dependent on the load transfer requirements and the grid, whether a land or submarine link is needed, and other requirements. Each project needs to be considered on a case-by-case basis, and it should be noted that a DC link is always possible if it is not practical for economic or technical reasons to provide an AC link.

In many situations, an AC solution should be less expensive and lead to lower losses for a radial connection. It is important to carry out an analysis of the power

system losses, total installed capital costs (Fig. 10.2), and operating costs.

Although only two cables are required for DC compared with three for AC, the construction costs, which are often the major factor in the urban environment, may be almost the same for both. The costs for DC conversion are still relatively high, and the losses—albeit substantially lower than they used to be, due to the introduction of modern VSC systems—are still significant. However, if power flows are required in both directions and the route length may need to be increased at a later stage, the selection of modern DC technologies may be justified [10.6, 14].

Having decided that an AC link is the optimum solution, the next step is to consider the transmission voltage, cable design, and general installation method.

### Reactive Compensation

This section provides only a brief overview of system design issues relating to the implementation of reactive compensation on long AC links. For a more complete understanding of the technical issues associated with reactive compensation, the reader is referred to CIGRE TB 556 from WG C4.502 [10.27].

Underground cables produce reactive power according to

$$Q_{\text{cable}} = 2\pi fCV^2,$$

where  $Q_{\text{cable}}$  is the reactive power in var,  $f$  is the power frequency in Hz,  $C$  is the cable capacitance in F, and  $V$  is the line voltage in V.

The reactive power is proportional to the square of the voltage and the cable capacitance. Since the cable capacitance is proportional to the cable length, the reactive power increases linearly with the cable length. Reactive power has two side effects. The first is that it causes the steady-state voltage to rise in the grid and the cable itself. While the grid load and ordinary transformers in the network consume some reactive power, they do not consume enough to compensate for long cable links. The second effect is that it introduces a current into the cable, limiting the transfer of active power. As said above, at a critical cable length, the cable current rating is completely consumed by the capacitive current, meaning that no active power flows through the cable.

To operate the grid and the cable itself within the required limits while also preserving the effectiveness of the cable connection (or to optimize the current rating), it may be necessary to apply reactive power compensation (Figs. 10.49 and 10.52).

Reactive compensation is an optimization process involving many factors such as the voltage level, conductor cross-section, losses, amount of compensation



**Fig. 10.52** Reactive compensator for a 30 km 345 kV PPLP pipe-type cable in the USA (adapted from [10.14])

(partial or full), type of load on the cable (inductive load, generator/wind farm), compensation method (generators, reactors, power electronics), compensation location (effectiveness and available space), level of built-in redundancy, and costs. More detailed information can be found in [10.14].

### Cable Sheath Bonding

Induced sheath voltages must also be considered when designing underground cable links. The induced sheath voltage depends on the cable length, phase current, mean diameter of the metallic sheath, phase spacing, power frequency, and the arrangement of the phases (e.g., trefoil or flat). The aim of sheath bonding is to protect the cable sheath/joint shield break against transient overvoltages. During the transient/subtransient, the surge wave energy resonates along the line at high frequency. These high-frequency overvoltages can cause joint failure and sheath damage.

CIGRE TB 283 [10.30] (published in 2005 and edited by WG B1.18) provides details of current practices around the world concerning the bonding of high-voltage cables and how to calculate the induced voltage/current according to the grounding system used.

Most countries have a national standard that governs the maximum standing voltages allowed at the power frequency, as this is an important safety issue, particularly for maintenance crews. They are typically in the range 50–400 V. If the upper limit of this range (400 V) is acceptable, the number of cable junctions can be reduced, lowering the cost of the project.

Calculations of induced cable sheath voltages (working frequencies and transients) must be performed at the design stage to guide the selection of the appropriate protection/grounding system for the power circuit. Methods of calculating induced voltages are given in [10.30]. A power line model of the electrical circuit can also be

utilized to estimate continuous/transient induced voltages, or special software can be employed.

The standard surge voltage level of the protective jacket/sheath is given by IEC 60229. The cable junction and the concentric bonding lead cable that connect the cable metallic screen to the sheath voltage limiter (SVL) cabinet must also be designed to withstand surge overvoltages.

SVLs are used to protect sheath sectionalizing insulation (a discontinuity electrical node in surge wave propagation) during transient phenomena. SVLs are installed in sealed boxes either underground, in tunnels, or in the air, depending on the locations of the cable joints as well as the terminations. A physical barrier is usually installed in transition compounds linking overhead lines to underground cables to avoid any contact with the SVL. Without the protection provided by the SVL, the occurrence of transient phenomena could lead to failure and damage to the junction/protection sheath. The job of the SVL is to chop peak overvoltages and reduce the number of transient overvoltage signals that occur during transient phenomena. WG B1.50 has recently published a Technical Brochure providing guidance on the design, testing, operation, and monitoring of SVLs [10.41].

As noted in a previous section (see Figs. 10.24–10.26), the following bonding arrangements are generally used in high-voltage cable systems:

- Cross-bonding
- Single-point bonding
- Solid bonding.

## 10.6 Cable Designs

The insulation of lapped cables consists of a number of thin paper tapes wound around the conductor. The conductor is generally circular. Depending on the type of cable, the insulation is impregnated with a nondraining, high-viscosity insulating mass (i.e., mass-impregnated cables) or with low-viscosity oil.

As previously noted, the surface of the conductor is somewhat irregular due to the interstices between the single wires. To stop electrical stress concentrations from forming at such irregularities, several layers of semiconductive carbon black paper tape are applied onto the conductor surface. For high-voltage cables, it is essential to generate an undistorted radial electric field inside the insulation. Therefore, semiconductive carbon black paper tapes are also applied over the insulation, normally in combination with metal-coated paper tapes.

In order to achieve an AC withstand characteristic with a sufficiently long duration, it is necessary to stop

The *cross-bonding system* is the method most commonly used for long onshore/land links. Cross-bonding the metallic cable sheaths causes the induced sheath voltages to cancel out. This reduces circulating currents, resulting in reduced sheath losses and higher cable circuit ratings.

The *single-point bonding system* is generally used in substations when the cable route is relatively short and it is uneconomical to use the cross-bonding method.

*Solid bonding* is the simplest bonding method. It requires the metallic cable sheath/screen to be connected to earth at both ends of the circuit. The solid-bonding method results in higher sheath losses than obtained with other bonding methods due to higher circulating currents in the metallic sheath/screen, resulting in reduced cable circuit ratings. Solid bonding is used in situations where a reduced power-transfer capability is not a major concern. When this arrangement is used, the cable circuit design is simpler, allowing the utility to divert the cable circuit when required without impacting on cable circuit ratings. Solid bonding is generally used for three-core MV cable circuits and for single-core cable circuits where sectionalized joints are not readily available.

For submarine power cable links, the only feasible grounding system is a two-point solid-bonding scheme, which ensures watertight protection of the cables.

The grounding system of a long HVAC power link may consist of a cascading combination of several types of grounding schemes, for instance two-point bonding + cross-bonding + single-point bonding.

ionization from occurring inside the insulation. Ionization can take place in gas-filled voids; such voids can form in the insulation due to the different expansion and contraction rates of the cable components during load cycles.

A solution to this problem was discovered in 1917 by Emanuelli, who proposed a cable containing a hollow conductor that kept the paper insulation under positive pressure regardless of the temperature of the cable by connecting the cable to tanks filled with very fluid mineral oil, which were placed all along the cable route. Although such a *fluid oil cable* had never been installed or tested before, Emanuelli became convinced that it could be used at higher voltages, so he tested it by connecting the fluid oil cable to a 132 kV line. In 1926, he accepted an order for an oil fluid cable that could accommodate this voltage from New York, then another order from Chicago. A year later,

he constructed a 70 kV three-phase cable of this type in Milan.

In 1932, he connected a test cable to the 220 kV network at Cislago in Italy. The results of these tests were highly satisfactory and prompted four French cable manufacturing units to construct the first 220 kV link in Paris 220 kV. This link, commissioned in March 1936, was 18.5 km long.

The maximum voltage gradient in the insulation was 9.5 kV/mm, whereas the field in a mass-impregnated paper cable was about 5 kV/mm. The work of Emanuelli provided the basis for achieving the highest voltage levels used in underground power transmission. Several types of cables that use different mechanisms to overcome the ionization problem and to achieve so-called thermally stable cables have been developed.

### 10.6.1 Mass-Impregnated Cables

The historical perspective given in [10.1] details the evolution of power cables from the birth of the industry to the mid-1980s and the arrival of UHV extruded cables. From the earliest history of power cables, two main types of materials have been used to insulate cables:

- Vulcanized material
- Impregnated material.

Mass-impregnated (MI) paper insulation for 10 kV cables appeared in 1890 and was continuously improved. Over the years, mineral compounds have replaced vegetable-derived substances as the impregnating ma-



**Fig. 10.53** Cross-section of a mass-impregnated cable (adapted from [10.6])

terial, carbon-black paper screens have been adopted for conductors and insulation, and new grades of paper have been introduced, as have thin papers, to increase the impulse strength of the insulation. By 1960, wax-filled compounds were being used in insulation, as they are less fluid and more electrically stable than oil resin compounds.

The fundamentals of the mass-impregnation technique have remained the same, and variants of it have been used in the vast majority of the cables employed by public and private power networks across a wide range of voltages, from low to 60–70 kV and exceptionally 90 kV.

Indeed, mass-impregnated cables were used in HVDC applications as far back as 1906, after which HV and EHV levels were gradually attained for these cables, mostly in submarine links, e.g., to the isle of Gotland in 1954 ( $\pm 100$  kV), from France to England in 1961 ( $\pm 100$  kV), to Vancouver Island in 1969 ( $\pm 300$  kV), and the Skagerrak Strait link in 1976/1977 ( $\pm 250$  kV).

Figure 10.53 shows an example of a mass-impregnated cable used for submarine applications. This type of cable can be used at EHVDC levels.

### 10.6.2 Self-Contained Fluid-Filled Cables

In 2016, CIGRE WG B1.37 published TB 652, which is a guide to operating self-contained fluid-filled (SCFF) cable systems [10.42]. The information given in [10.42] (which is summarized below) can guide the reader towards a better understanding of the differences between SCFF and extruded cable systems.

#### Examples of SCFF Cables

Figures 10.54–10.59 show several examples of SCFF cables with various conductors and shields.



**Fig. 10.54** 500 kV SCFF cable with a compacted circular conductor and a corrugated aluminum sheath (CAS) (adapted from [10.42])



**Fig. 10.55** 400 kV SCFF cable with a Milliken copper conductor and a corrugated aluminum sheath (note the helical duct support) (adapted from [10.42])



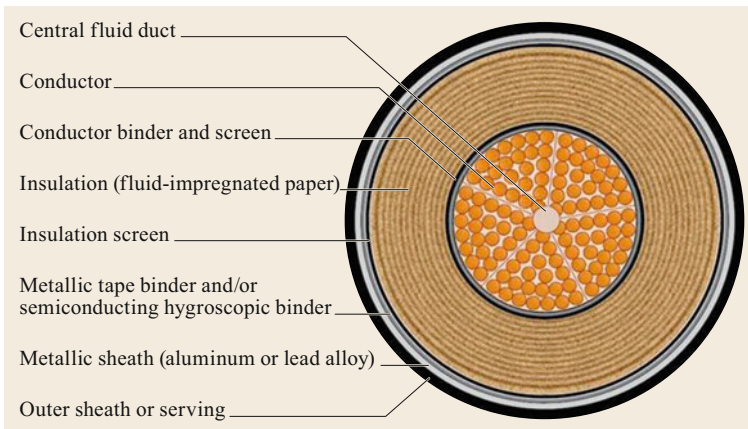
**Fig. 10.57** Example of a 500 kV single-core SCFF submarine cable (adapted from [10.42])



**Fig. 10.56** 500 kV SCFF cable with a 1600 mm<sup>2</sup> copper keystone conductor and a lead sheath (adapted from [10.42])



**Fig. 10.58** Example of a 90 kV three-core SCFF cable; note the heavily coated armor wires that are typical of submarine cables (adapted from [10.42])



**Fig. 10.59** A typical cross-section of a single-core SCFF cable, showing its component parts (adapted from [10.42])

### SCFF Cable Fundamentals

Self-contained fluid-filled cables (SCFF) are cables in which the conductor insulation is composed of multiple layers of paper impregnated with a low-viscosity dielectric fluid encased in a metallic sheath (usually a lead alloy or aluminum). For single-core cables, there is generally a central hollow core that allows the dielectric fluid to move freely along the cable. A three-core SCFF cable usually has a separate helical duct (or ducts) that is bound up in the fillers, with the cores inside its metal sheath. However, some three-core cables are constructed without fillers and the space between the insulated cores allows the fluid to flow freely within the metal sheath.

Heat and vacuum treatment during the manufacturing process removes air and moisture from the papers. The papers are then impregnated with a low-viscosity fluid to prevent the formation of voids and the associated ionization when energized. The fluid is contained at low pressure within a metal sheath in the form of corrugated aluminum or lead alloy (suitably reinforced). An extruded plastic oversheath provides corrosion protection for the sheath. The fluid must be maintained at positive pressure at all times. During operation, the cable fluid expands into sealed storage tanks as the conductor temperature increases and flows back into the cable as the conductor cools.

Three-core SCFF cables are typically limited to voltages of 150 kV or less and conductor cross-sections of 630 mm<sup>2</sup> or less due to manufacturing, cable size, drum handling, and installation limitations.

Submarine cables normally require the application of further mechanical protection in the form of round or flat wire armor that is completely surrounded by synthetic bedding and serving.

Polypropylene paper laminate (PPL), sometimes also referred to as PPP or PPLP, depending on the country of origin, was developed to reduce dielectric losses and increase the impulse strength of the cable insulation. PPL consists of a film of polypropylene coated on both sides with a layer of paper. It is lapped onto the conductor in the same way as for paper-insulated cable. It is similarly hermetically sealed and impregnated with cable fluid maintained at a positive pressure. However, its technical advantages are offset by higher costs, and it is generally only used as an alternative to paper-insulated SCFF cables at extra-high voltages.

Low-pressure cable sheaths are normally made to sustain internal pressures of 5.25 bar with transients of 8 bar. However, pressures of up to 15 bar can also be sustained by some sheaths. For these designs, the accessories must be chosen appropriately, and the cable reinforcement design must be verified. Such high-pressure systems may be used for submarine systems or for high-pressure fluid-filled (HPFF) pipe-type cables.

### Hydraulic Aspects

The appropriate hydraulic design of a SCFF cable system is critical to its reliable operation, and the design used depends largely upon the vertical profile of the cable installation. This is conveniently described graphically by expressing pressure in terms of meters of fluid (Figs. 10.61–10.63). The vertical profile of the cable and the fluid pressure (static or transient) can be depicted on the same diagram, with the pressure at any point in the system given by the difference between the pressure line of interest and the cable profile.

This hydraulic system design takes into account the cable route and elevation (or vertical profile) as well as the thermal expansion and contraction of the cable fluid caused by temperature variations in the cable system. It ensures that any overpressures caused by temperature transients do not cause mechanical damage to any part of the system, including the cable, accessories, and the feeding system. It is normal for longer routes or routes through undulating terrain to be divided into a number of hydraulically separate sections using stop joints that maintain electrical continuity but isolate adjacent hydraulic sections. The design must also ensure that pressures do not fall below well-defined values so that positive pressures are maintained at all times.

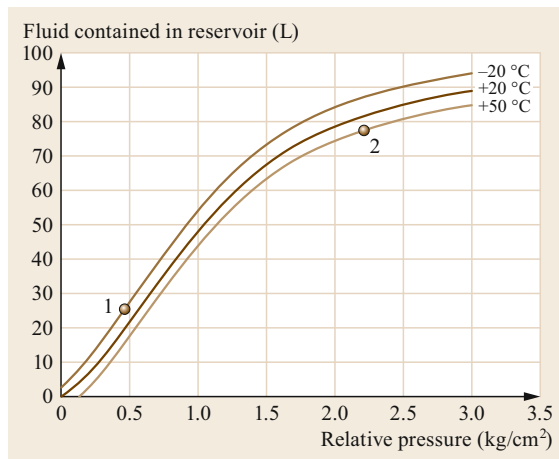
**Fluid Volume Variations.** Temperature variations cause changes in the cable fluid volume. Minimum volume occurs at the minimum temperature (i.e., during winter) with the cable unenergized. Maximum volume occurs at the maximum temperature (usually in summer) under maximum load or during emergency (overload) conditions. Cable fluid reservoirs (usually pressure tanks) positioned at the cable end(s) and possibly at intermediate positions along the cable must accommodate the *static* fluid volume variations. These reservoirs (also known as feeding pressure systems) can be divided into constant-pressure and variable-pressure systems.

**Gravity Fluid Tanks.** Constant-pressure systems are characterized by a feeding system consisting of *gravity tanks*: tanks that do not have internal gas cells and are designed to absorb pressure variations. Since this type of feeding system was the first to come into service, very old SCFF cable systems (in which the original fluid was mineral oil and short cable routes with flat profiles are used) generally belong in this category. Since the tank pressure cannot vary, the tank must be installed such that the tank is at a higher position than the highest system point. The tank must be able to contain all fluid expansion from the cable and the accessories under the hottest conditions and return the fluid to the system by gravity under the coolest conditions whilst

maintaining a positive pressure. Small changes in pressure due to changes in fluid levels in the tank are usually ignored.

**Prepressurized Fluid Tanks.** The SCFF cables in service today are most likely to use prepressurized tanks as their fluid reservoirs. These tanks contain a number of sealed, flexible, expanding cells that contain pressurized gas, usually carbon dioxide or nitrogen. The expansion of the cable fluid is compensated by the compression of these cells. The tank capacity and the pressure setting must be such that the minimum static pressure is higher than the highest system point and the maximum static pressure does not cause unacceptable pressure values for the cable and accessories at the lowest system point. The relationship between the fluid volume and the corresponding pressure of a cable fluid reservoir of a specified type is obtained from either a suitable experimental curve or by performing calculations based on the perfect gas law.

Figure 10.60 shows predicted and experimentally determined pressure–volume curves for a typical 120 L variable-pressure fluid tank. The middle curve is the experimentally determined one, obtained at ambient temperature; the other two curves were derived from the middle curve, via the perfect gas law, for the extreme (seasonal) ambient temperatures expected at the location of the system studied. Positions 1 and 2 in Fig. 10.60 show that a 50 L expansion due to a change in temperature from  $-20$  to  $+50$  °C will result in a static pressure change from  $0.5$  kg/cm<sup>2</sup> (5.8 m of fluid) to  $2.2$  kg/cm<sup>2</sup> (25.3 m of fluid).



**Fig. 10.60** Pressure–volume curves obtained at different ambient temperatures for a typical 120 L variable-pressure tank; the *middle curve* was determined experimentally, whereas the *outer curves* were predicted using the *middle curve* and the perfect gas law (adapted from [10.42])

The variation in cable fluid volume can also be calculated using the perfect gas law according to

$$\Delta V = \left( \frac{T_1}{P_1} - \frac{T_2}{P_2} \right) \frac{P_0 V_0}{T_0},$$

where  $\Delta V$  is the change in fluid volume in L,  $P_1$  and  $P_2$  are the absolute values of the maximum and minimum pressure in kg/cm<sup>2</sup>,  $T_1$  and  $T_2$  are the absolute values of the maximum and minimum ambient temperature in K, and  $P_0$ ,  $V_0$ , and  $T_0$  are the initial pressure, volume, and temperature of the gas inside the cells of the oil tank in kg/cm<sup>2</sup>, L, and K, respectively.

Provided the value of  $P_0 V_0 / T_0$  is known for the type of oil reservoir under consideration, this formula provides a relatively easy way to evaluate the relation between fluid volume, pressure, and temperature.

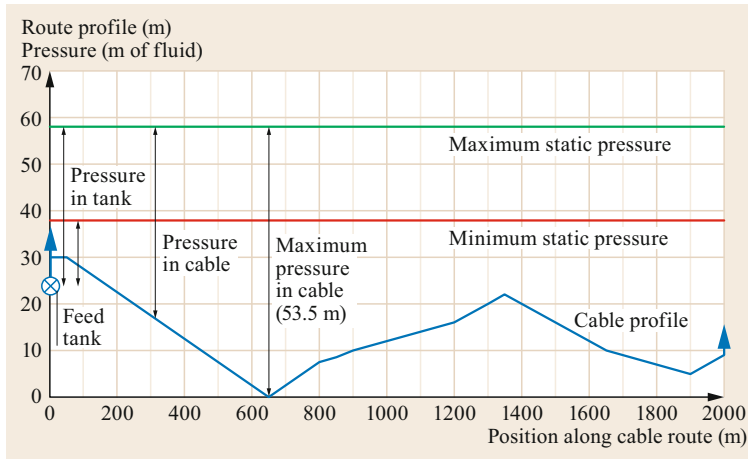
**Static Pressure Considerations.** Gradual variations in temperature result in pressure changes that equalize throughout the cable system. In this case, gravity tanks experience only very small changes in pressure due the volume variations caused by changes in temperature. However, the pressure in prepressurized feed tanks changes significantly with the volume variations caused by temperature changes. The minimum static pressure in such a tank usually occurs in winter with the cable deenergized (no dielectric losses), whereas the maximum static pressure of such a tank tends to occur in summer with the cable under maximum load conditions.

These two extreme static pressure conditions must be considered in conjunction with the route profile to ensure that there is no risk of excessive static pressures or underpressures in the cable, forcing that part of the cable to negative pressure.

Figure 10.61 shows route and pressure profiles for a SCFF cable under static pressure conditions. In this example, the minimum cable pressure occurs at the feeding end termination, while the maximum static pressure occurs 650 m along the cable, where the route profile is at its lowest elevation.

**Transient Pressure Considerations.** Sudden load (and sometimes voltage) variations cause pressure transients in the system. Under extreme operating conditions, the maximum transient pressure must not cause excessive pressures in the cable system whilst the minimum transient pressure must remain positive and above the cable's elevation profile at all points along the circuit route. Longer-length cable routes and those laid in terrain with severe variations in elevation tend to experience higher transient pressures. It should also be noted that lower-viscosity fluids experience lower transient pressures.





**Fig. 10.61** Route and pressure profiles for a SCFF cable under static pressure conditions (adapted from [10.42])

**Heating Transients.** The maximum positive transient pressure occurs in winter, during energization (dielectric losses are added), or when the maximum load is applied suddenly (or in a sufficiently short period of time). Under these conditions, the temperatures of the conductor and other cable layers increase but not as quickly as the temperature of the cable fluid does. The initial temperature rise is the steepest and causes a large transient increase in the volume of the liquid, which then flows through the cable towards the pressure tanks at static pressure. The fluid encounters hydraulic resistance, which is also highest initially, due to the increased viscosity of the fluid at the lower temperature. The cable experiences a pressure transient during this phase.

The general expression for the pressure variation with respect to the static pressure at the feeding end is

$$\Delta p = \left( ABLu - \frac{ABu^2}{2} \right) \times 10^{-4},$$

where  $\Delta p$  is the pressure difference in  $\text{kg}/\text{cm}^2$ ,  $A$  is the volume expansion per unit time and unit length in  $(\text{m}^3/\text{s})/\text{m}$ ,  $\text{m}^3/(\text{s m})$ , or  $\text{m}^2/\text{s}$ ,  $B$  is the friction coefficient of the oil duct per unit length of cable in  $\text{kg s}/\text{m}^6$ ,  $L$  is the length of the hydraulic cable section in m, and  $u$  is the distance along the cable from the feeding end in m.

In particular, the maximum pressure difference between the extremities of a cable fed from only one end is

$$P = \frac{ABL^2}{2} \times 10^{-4}.$$

In other words, halving the feed length by feeding fluid from both ends causes the pressure to drop by three-fourths.

Since the pressure at the tank is set to the static pressure, the pressure at the other end of the line (or at the center of it if the cable is fed from both ends) must inevitably be higher, and is taken into account in the system design.

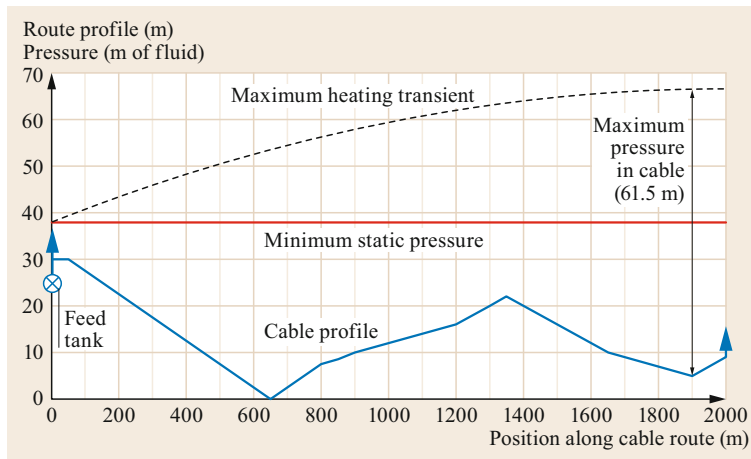
Figure 10.62 shows an example of the maximum positive pressure transient for a hydraulic section fed from one end only. In this example, the maximum pressure (calculated and observed experimentally) occurs at 1900 m.

**Cooling Transients.** Large negative pressure transients can cause some sections of the system to drop below the minimum design pressure or even to enter the negative pressure regime (partial vacuum).

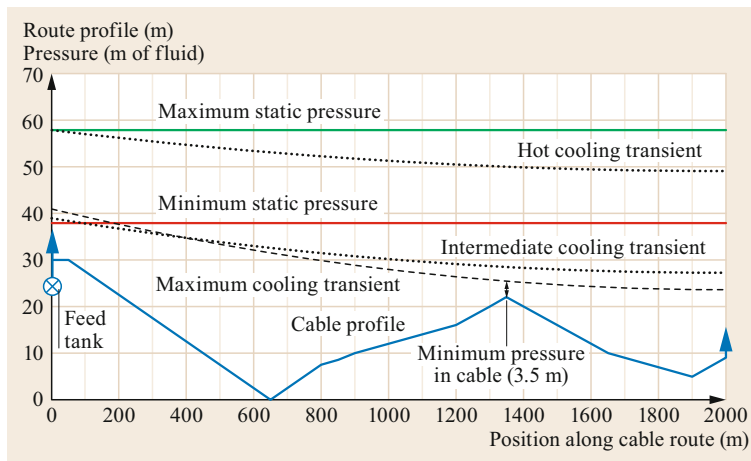
Cooling transients are more complex to evaluate. The most negative cooling transient occurs when the system is energized with maximum load and suddenly deenergized after a particular *critical time* on the order of a few hours.

Figure 10.63 shows pressure profiles for a SCFF cable under various cooling transient conditions. The cooling transient from a hot condition is unlikely to cause an underpressure due to the high initial static pressure in the tank. There is no cooling transient at the minimum static pressure as the cable is already at its coolest. As the cable system starts to transition from cold to hot (when energized with maximum load), the potential cooling transient increases. There comes a critical time when the combination of the increasing potential cooling transient and only a moderate increase in static pressure results in the largest possible negative pressure transient. In this example, minimum pressure occurs 1350 m along the cable.

**Multiple Hydraulic Sections.** When a circuit is long or its elevation varies significantly along the route, stop



**Fig. 10.62** Route and pressure profiles for a SCFF cable under maximum heating transient conditions (adapted from [10.42])



**Fig. 10.63** Route and pressure profiles for a SCFF cable under cooling transient conditions (adapted from [10.42])

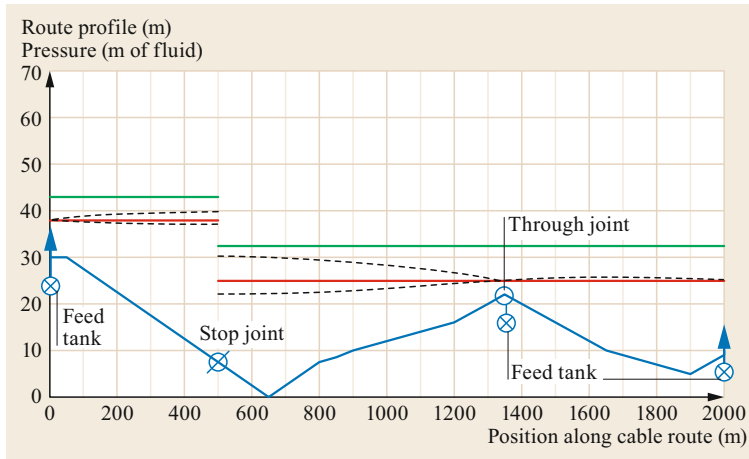
joints are installed that separate the cable route into hydraulic sections while maintaining electrical continuity. This allows the cable system to operate within its design limitations. The stop joints may be connected to tanks that provide feed points to each hydraulic section, or separate feed points can be installed at joints along the hydraulic sections to suit the route profile. This mitigates the risk of excessive static and transient pressures.

Figure 10.64 shows route and pressure profiles of a SCFF cable system with stop and feed joints (the route profile is identical to those in previous figures). The transient pressures are depicted using dashed lines. Detailed annotation has been omitted from the diagram to reduce clutter.

A stop joint has been added (arbitrarily) at 500 m. The feed tank at 0 m caters for fluid volume variations in the section from 0 to 500 m. Since this tank feeds a shorter section, the maximum static pressure of the tank is lower than before. Reducing the section length

also reduces the maximum transient pressure. This pressure difference is 1/16 of the original example. The maximum cable pressure at 500 m is 35.5 m of fluid under maximum static pressure conditions. The transient pressure is less (32.3 m of fluid).

A feed tank has been added at the end of the circuit (at 2000 m), and a feed joint has been added (arbitrarily) at 1350 m. The tanks at these two feed points cater for fluid volume variations in the section from 500 to 2000 m. This also results in a lower maximum tank static pressure than before. The maximum cable pressure at 650 m is 32.5 m of fluid under maximum static pressure conditions. The maximum transient pressure occurs at 550 m (30 m of fluid), but is less than the maximum cable pressure. The minimum cable pressure occurs at 1350 m and equals the minimum tank static pressure. The very low transient pressures in the section from 1350 to 2000 m are due to an effective fluid section length of only 325 m (two end tanks feeding a 650 m section).



**Fig. 10.64** Route and pressure profiles of a SCFF cable system with stop and feed joints installed (adapted from [10.42])

**Submarine Cables.** Submarine cables have a similar design to underground cables from an electrical perspective, but they are specially designed from a mechanical perspective to handle the large axial stresses that occur during installation and the hydraulic challenges encountered by submarine cables.

Both aluminum and copper conductors have been used. Various lead alloys have been used for submarine cable sheaths. Submarine cables have strong longitudinal armor, and different armor designs are applied. The simplest consists of one layer of round steel wires that introduces a torque in the cable when axial tension is applied.

The hydraulic aspects must be considered in a slightly different way to those for land-based cables. Submarine cables often have much longer circuits than those considered for land installations, as the hydraulic circuit cannot be interrupted along the route. This has resulted in single-core cables with large oil ducts, up to 40 mm in diameter, and the use of extra-low-viscosity fluid (3–5 cSt at 20 °C.)

Submarine fluid-filled cables have been in service for more than 60 years. Cables from the 1950s are still in use. Submarine cables were originally used to cross water courses that were too wide to cross with overhead lines.

Cable lengths were originally limited by manufacturing equipment. However, this limitation was overcome with the introduction of factory joints. The need for longer and larger cables also resulted in the construction of submarine cable factories that are close to the sea and have their own loading facilities to minimize problems with transporting very long lengths from the factory to the laying vessel.

Traditionally, cables were laid directly on the sea bottom without additional protection. At shore landings (the splash zone; typically down to water depths

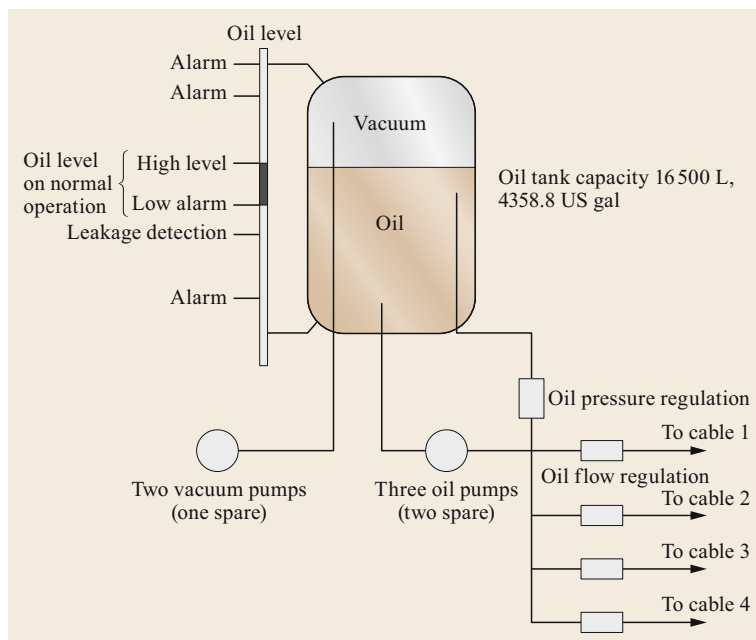
of 10 m), the cables were protected in different ways to minimize or eliminate wear and tear and to suppress corrosion issues, especially with the armor. Types of protection used included trenching where there were trenchable conditions, or the addition of mechanical structures when trenching was not possible. However, since the 1990s it has become increasingly common to protect the entire cable length, preferably by trenching. If trenching is not possible, other protection methods are used, such as rock dumping or mattress coverings of various kinds. More detailed information on this topic and relevant references are given in a later section.

The fluid feeding system for a submarine cable can consist of pressure tanks for short and shallow crossings, similar to land-based cables. Longer and deeper crossings use pumping plants installed at one or both ends of the crossing. Submarine cables carrying voltages up to and including 170 kV are often manufactured as three-core cables, while SCFF cables used for higher voltages always are single-core cables. With the development of conductors with large oil ducts and the use of extra-low-viscosity fluid, cable lengths of up to 60 km between pumping plants have been installed.

Some cable installations have additional corrosion protection systems. This can be a passive system, such as adding anodes to selected parts of the cable. Active systems, such as suppressed current systems, are also added to some cables.

#### Feeding Pressure Systems for Submarine Cables.

Submarine cables normally have circuit lengths that are much longer than those considered for land installations as it is not possible to interrupt the hydraulic circuit along the route. This may require the hydraulic section to be long and deep, necessitating special feeding systems such as pumping plants. Pumping plants for submarine SCFF cables were introduced around 1980,



**Fig. 10.65** Schematic of a typical pumping plant (adapted from [10.42])

when the technology used for HPPF pipe-type cables was adapted to the low-viscosity cable fluids used in SCFF cables. Depending on the feeding pressure required, designs may use a pumping plant installed in one pumping station with a crossover device at the opposite end or pumping stations at both ends.

In terms of transient pressure variations, in addition to the checks performed for land applications, the *apparent profile* of the route must be taken into account due to the difference in the densities of oil and water and applied to the water depth at any point. This generates a further pressure profile, which should not present negative pressures at any point along the route.

The mechanical considerations already discussed for land cable applications are even more important for submarine applications due to the higher system working pressures involved.

A further design requirement for a submarine SCFF cable is to maintain a positive fluid flow out of the cable in order to prevent water ingress until the damage can be sealed and cable repair can be implemented.

Submarine SCFF cables differ from land SCFF systems in which each phase of the circuit is hydraulically separated from the others to avoid fluid loss from the two undamaged phases. In submarine systems, the normal practice is to interconnect the hydraulic circuit of the entire system, which allows to compensate the flow of a leak by pumping fluid through the remaining healthy cables. For a cable system with one pumping station and one crossover device/manifold, when a fault occurs at the cable end close to the crossover device location, the pumping plant feeds the leak from one

end, through the two undamaged cables and through the crossover device at the opposite end.

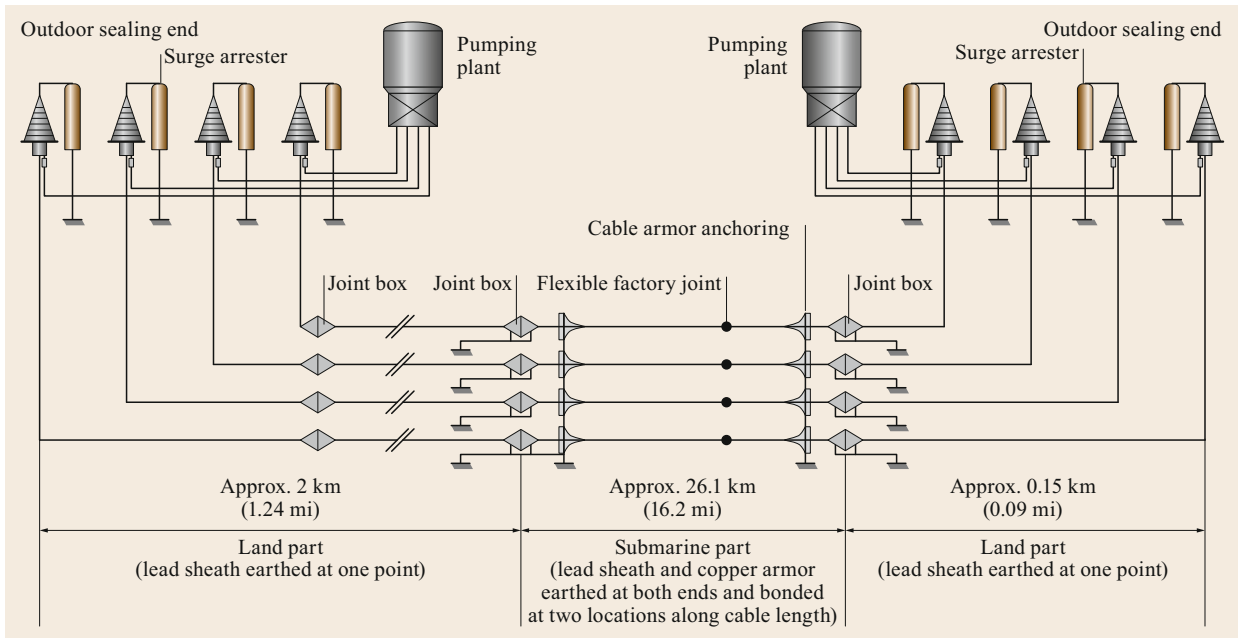
For three-phase cables, it is advisable to have feeds at both ends.

**Submarine Cable Pumping Plants.** A submarine pumping plant consists of a large vacuum-sealed fluid storage tank, vacuum pumps, fluid pumps, valves, and measuring devices. A representative schematic of such a plant (showing project-specific capacities) is depicted in Fig. 10.65. The plant also incorporates a regulation system that maintains the fluid pressure in each cable between preset values based on fluid flow calculations. The system includes alarms that are activated by abnormal conditions; they can be set for values of high or low pressure or a particular fluid level in the tank that indicates the presence of a fluid leak.

A series of flow-limiting valves are installed at the pumping plants and at the crossover devices to limit fluid loss resulting from a cable fault. This system is designed to ensure enough fluid flows out of the cable duct to prevent water ingress at the point farthest from the feed point.

A typical fluid-feeding system design for a submarine cable takes into account the worst feeding conditions, which normally corresponds to a cable cut at the end furthest from a feeding point, considering the oil viscosity and the cable load.

At the maximum operating temperature, a large volume of cable fluid moves from the cable into the pumping plant tanks. When a cable failure occurs, the heating transient ceases and the cooling transient starts.



**Fig. 10.66** Schematic of a typical very long submarine connection (adapted from [10.42])

The cable cools rapidly at low ambient temperatures, causing a large volume of fluid to move from the storage tanks into the cable to compensate for the contraction of the fluid within the cable as well as potential fluid loss from the point of failure. At low ambient temperatures, the tank fluid viscosity is relatively high, so the hydraulic resistance is also high for the cable fluid, which is now forced towards the fault location.

The design of the cable fluid feeding system for a submarine SCFF cable with pumping plants must take the worst-case feeding condition into account. This occurs when the circuit is energized to full load and a failure causing a severe leak occurs at the point on the line furthest from the pumping plant during the heating transient. In this scenario, the fluid initially expands from the cables into the tank(s) during the heating phase (the conductor and fluid are still to reach their maximum operating temperatures) and the fluid exits the cable at the leak location during the cooling phase. Since this fault time is similar to the energization time, the fluid is still cold and consequently its viscosity is high, requiring a sufficiently high pressure to feed the fault location. This condition determines the value of the pressure necessary to feed the cable with a positive pressure with respect to the water pressure at the most remote fault point.

For a cable system with a pumping plant at each end, the worst-case feeding condition will correspond to a severed cable close to one pumping plant. For a cable system with one pumping plant and a crossover device, it will be a severed cable close to the pumping plant

with a fluid feed through one or two healthy cables to the crossover device and returning through the section of cable connected to the crossover.

Figure 10.66 shows a schematic for a typical very long submarine connection with pumping plants at each end of the submarine crossing.

### 10.6.3 Extruded Cables

As mentioned above, increasing operating and maintenance costs for fluid-filled cables prompted the search for other insulating materials. Polyethylene (PE) was tested, but its maximum operating temperature was found to be too low. A much more suitable material was eventually identified: crosslinked polyethylene (XLPE), which is now one of the most common and well-established insulating materials in modern extruded high-voltage cable design. Since the 1970s, fluid-filled cables have gradually been replaced with extruded dielectric cables (Fig. 10.67).

Even today, the popularity of XLPE cables for both land and submarine applications continues to grow rapidly. A major reason for the success of XLPE as an insulating material is its excellent electrical, mechanical, and thermal properties. Its most advantageous features are its low dielectric loss and dissipation factor and its high electrical breakdown strength, modulus of elasticity, and tensile strength. Low operating and maintenance costs combined with good system availability lead to low lifetime costs for XLPE cable systems.



**Fig. 10.67** HV XLPE cable with a corrugated aluminum sheath (adapted from [10.14])

It should be noted that significant technological improvements have been made to the XLPE itself, as well as the methods used to manufacture it, since its introduction in the mid-1960s. The influence of manufacturing quality and raw material purity on the properties of the resulting XLPE was soon discovered, so triple extrusion and dry curing techniques were introduced into XLPE manufacturing. These processes are performed in a sealed environment, ensuring a very high level of cleanliness and therefore quality of the XLPE insulation.

In the triple extrusion process, the inner semiconductive screen, the XLPE insulation, and the insulation screen are all extruded simultaneously. The insulating material is then vulcanized under pure nitrogen. XLPE is a polymeric insulation material based on pure polyethylene (PE). In the vulcanization process, the peroxides in the XLPE form free radicals at elevated temperature and pressure, and these free radicals react with hydrogen in the polyethylene chains. This triggers the chains to react with each other, forming an intricate and complex crosslinked (i.e., crossbonded) network of polyethylene chains.

Although XLPE is derived from PE, PE and XLPE are very different both mechanically and chemically, and the characteristics of XLPE make it far better suited for electrical applications than PE. Indeed, XLPE was developed because of its very useful electrical properties, especially its low loss levels, which are due to its low dielectric constant and negligible dissipation factor.

XLPE is a suitable insulating material for conductor temperatures up to 90 °C, which is the normal maximum operating temperature for XLPE cables. XLPE cables can, however, withstand up to 250 °C under short-circuit conditions. Consequently, these cables have both a high overload potential and a high safety margin.

### New Trends in the Design of Extruded Cables

In the 1980s, power cables generally had a lead sheath or a corrugated aluminum sheath, as described above. However, laminated coverings were beginning to attract interest as a means to obtain lighter and cheaper cables. The first studies of aluminum laminated screens were carried out in the late 1980s. Such screens are now also considered to be advantageous for environmental reasons. TB 446, published by WG B1.25, provides guidelines for the use and testing of advanced laminate designs [10.43].

**New Trends in Laminated Coverings.** A metal laminated covering consists of several layers of plain (not corrugated) metal and plastic materials bonded together to achieve a special set of properties: bending ability, radial water tightness, electrical functions.

It can be used to carry the capacitive current, and the circulating and short-circuit currents. Three main cable designs have been identified:

- Combined design
- Separate design
- Separate semi-conductive design.

**Combined Design.** Laminates combining plastic with copper or another metal are also used. Such a combined design (CD) utilizes the combined properties of these two components. CDs comprise:

- XLPE insulation
- Semiconductive bedding (water swellable if required)
- Thick metal foil, either welded or glued, that is coated and bonded to the outer sheath (usually HDPE) and carries the full short-circuit current.

Additional wires can also be added to match the short-circuit requirement. The metal foil is mainly aluminum; copper can be used as well. However, when copper wires are used in combination with a welded aluminum foil, it is recommended that a nonmetal tape should be placed between them to avoid possible corrosion. A photograph of a CD cable is shown in Fig. 10.68.

**Separate Design.** This design concept was introduced in the 1980s, when the need for a radial moisture barrier in cables with only a wire screen and a PE and PVC jacket became apparent—water trees could form in the insulation of those cables, causing cable faults. The idea of using a laminated moisture barrier was not, however, a new one; this approach was already being used in telecommunication cables.

This separate design (SD) concept utilizes separated mechanical and electrical properties. Bending ability



**Fig. 10.68** 500 kV cable with a combined design (adapted from [10.43])

and water-tightness are mechanical properties ensured by the thin metal foil bonded to the outer sheath. While the wires within ensure the electrical functionality. Such a design includes:

- XLPE insulation
- Copper or aluminum wires
- Water swelling tapes to block the screen area
- Coated laminated metal foil, e.g., 0.2 mm Al with a 0.05 mm coating on one side
- An oversheath (usually MDPE or HDPE).

The metal used is generally aluminum, although copper or other metal laminated foils can also be used. A photograph of a SD cable is shown in Fig. 10.69.

**Separate Semiconductive Design.** The separate semiconductive design (SscD) was introduced in Japan in the 1980s for the same reason as SD was introduced.

In the SscD, electrical and water tightness properties are separated using semiconductive plastic-coated foil. Such a design comprises:



**Fig. 10.69** 400 kV cable with a separate design (adapted from [10.43])



**Fig. 10.70** 275 kV cable using a separate semiconductive design (adapted from [10.43])

- XLPE insulation
- Round copper wire screen with nonswelling semiconductive tape below
- Thin Pb or Al foil (typically 0.05 mm thick) that has glue on one side and is coated with (typically) 0.05 mm thick semiconductive plastic on the other side (the screen side)
- An oversheath (usually PVC).

The first SscD cables used lead laminated foil. Nowadays aluminum laminate is used too. A photograph of a SscD cable is shown in Fig. 10.70.

**Concluding Remarks on Laminated Covering Designs.** Compared to extruded sheaths, the use of laminated coverings (especially aluminum laminated coverings) decreases the weight and diameter of the cable, allows for improved pulling techniques, and permits longer delivery lengths on a drum, which, in turn, decreases the number of joints required in a circuit link. Thus, the use of laminated coverings can significantly reduce the cost of the cable system.

Since the late 1990s, cables with an aluminum laminate screen bonded to a PE oversheath have progressively superseded those with a lead sheath or a PVC oversheath in many countries.

#### 10.6.4 Accessories for Extruded Cables

A CIGRE Green Book dedicated to accessories for HV extruded cables will be published very soon (see Sect. 10.B). The reader is kindly invited to use that book or the following Technical Brochures to obtain more information in this regard:

- CIGRE WG 21.06: TB 89 *Accessories for HV Extruded Cables* [10.44].
- CIGRE WG 21.06: TB 177 *Accessories for HV Cables with Extruded Insulation* [10.45].
- CIGRE WG B1.06: TB 303 *Revision of Qualification Procedures for HV and EHV AC Extruded Underground Cable Systems* [10.46].
- CIGRE WG B1.24: TB 415 *Test Procedures for HV Transition Joints for Rated Voltages 30 kV to 500 kV* [10.47].
- CIGRE WG B1.22: TB 476 *Cable Accessory Workmanship on Extruded High Voltage Cables* [10.48].
- CIGRE WG B1.29: TB 560 *Guidelines for Maintaining the Integrity of XLPE Cable Accessories* [10.49].
- CIGRE JWG B1/B3.33: TB 605 *Feasibility of a Common Dry Type Plug-in Interface for GIS and Power Cables Above 52 kV* [10.50].
- CIGRE WG B1.42: TB 622 *Recommendations for Testing DC Transition Joints for Power Transmission at Rated Voltages Up to 500 kV* [10.51].

Work is also in progress within SC B1 to address issues relating to working under induced voltages or currents. WG B1.44 has very recently published TB 801 to address this issue [10.52].

In TB 758 [10.53], published by WG B1.46, one chapter describes the main cable conductor designs and explains that not all connectors are suitable for all conductor designs. Another chapter provides a short introduction to connection theory. It explains that connectors in accessories may be exposed to significant thermal and mechanical stresses and presents in-depth information on the installation of various connector types as well as proposals for development tests.

All of these topics will be included in the forthcoming CIGRE Green Book on accessories, together with the contents of TB 622 [10.51].

Below, we provide some examples of the items included in TB 89 [10.44] and TB 177 [10.45], published by CIGRE WG 21.06.

### Joints

As noted in TB 89, a joint is the insulated and fully protected connection between two or more cables. It is also termed a *splice*. The following types exist:

- Straight joints
- Transition joints
- Screen interruption joints
- Y branch joints.

In [10.44], and in the CIGRE book [10.54], each of the joint designs is illustrated with a diagram to show the

type of insulation. To aid clarity, other important design details are omitted. The design requirements common to each type of joint are:

- (a) A high-current connection between conductors
- (b) Joint insulation that meets the same performance standard as the cable
- (c) A high-current connection to permit the flow of short-circuit current between the two cable sheaths or screen wires
- (d) A metallic joint shell or screen wire connection that is electrically insulated from the earth potential to match the insulating integrity of the cable oversheath
- (e) Protection of the joint and cable insulation against water ingress
- (f) Protection against corrosion of the joint metal work.

The majority of the HV extruded cables intended for voltages of greater than 60 kV have a single core, so straight joints of the single-core type are illustrated. Three-core joints employ the same types of insulation and are grouped together in one housing.

A straight joint, also termed a *straight splice*, connects two cables of the same type. Such joints include:

- Taped joints
- Prefabricated joints
- Field-molded joints
- Heat-shrink sleeve joints
- Back-to-back joints.

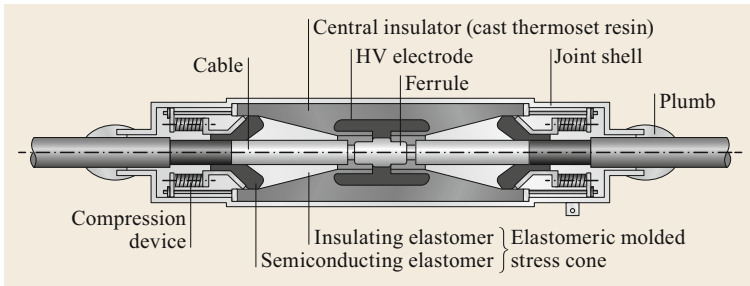
Prefabricated joints are now the most popular type of joint by far. Hundreds of these joints are in service at the highest voltage levels (500 kV AC) worldwide.

Prefabricated straight joints employ insulation that has been preformed and tested in the factory. The molding of elastomeric insulation (e.g., silicone rubber, EPR, EPDM) and the casting of thermoset resin insulation are usually used to manufacture these joints.

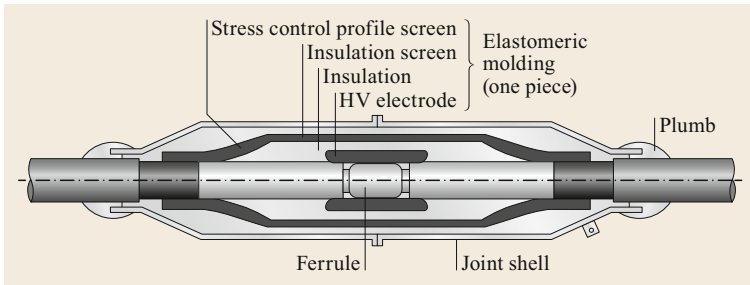
**Composite Type.** In this case, two factory-premolded elastomeric stress cones are inserted into a central insulator of cast thermoset resin, as shown in Fig. 10.71. Pressure is maintained at the stress cone to central insulator interface and at the cable core interface using a compression device that usually consists of metal springs.

**Premolded One-Piece Type.** Here, a single premolded elastomeric sleeve forms the insulation, as shown in Fig. 10.72. This sleeve includes insulation, a connector screen, stress control profile screens, insulation screens, and, where applicable, screen interruption.

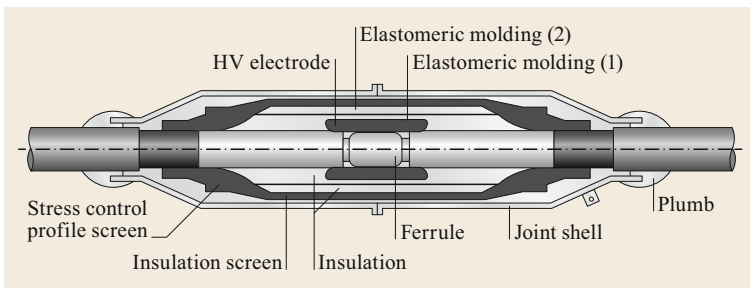




**Fig. 10.71** Prefabricated composite joint (adapted from [10.44])



**Fig. 10.72** Premolded one-piece joint (adapted from [10.44])



**Fig. 10.73** Premolded two-piece joint (adapted from [10.44])

Interfacial pressure at the sleeve to cable core interface is maintained by the elastic memory of the sleeve.

**Premolded Two-Piece Type.** This is a two-piece joint (Fig. 10.73) that is similar to the one-piece type but with elastomeric insulation comprising a large-diameter premolded sleeve that is stretched to fit on top of a smaller-diameter elastomeric adaptor molding.

**Premolded Three-Piece Type.** The three-piece joint has insulation comprising a large-diameter, cylindrical, elastomeric molding that is stretched to fit onto two elastomeric adaptor moldings.

### Terminations

A termination, also termed a *pothead*, is a connection between a cable and other electrical equipment, as described in [10.44]. Types of termination include:

- Indoor terminations
  - Temporary terminations.
- (a) A high-current connection from the cable conductor to an external busbar
  - (b) Insulation to the same performance standard as the cable
  - (c) Provision of support to the cable
  - (d) Ability to withstand cable thermomechanical loads and external forces such as wind, ice, and busbar loading
  - (e) A high-current connection to permit the flow of short-circuit current from the cable metallic sheath or shield wires via a bonding lead to the system earth
  - (f) A connection to the cable metallic sheath or earth wires that is electrically insulated from the earth

potential to match the insulating integrity of the cable oversheath

- (g) Protection for the cable insulation and sheath against the ingress of atmospheric water and the ingress of pressurized dielectric liquid or gas from adjacent metal-clad busbar trunking.

Some termination designs are filled with either a dielectric liquid or pressurized SF<sub>6</sub> gas to provide insulation. Such designs must be able to withstand the effects of the thermal expansion of the insulant. The incompressible nature of a dielectric liquid requires that an expansion volume be provided. The expansion volume can be an air- or gas-filled space that is usually at the high-voltage end of the insulator, or it can be (i) an external header tank, (ii) an external pressurized feed tank, or (iii) a gas-containing internal flexible accumulator that is usually at the low-voltage end of the termination.

When an internal air volume is used, the terminations can only be installed vertically. If they need to

be installed inclined, horizontal, or inverted, it is usual to fill the termination completely with insulating liquid and to provide either external compensation or an internal flexible accumulator containing gas. An expansion volume is not necessary for gaseous insulation because of its compressible nature, but either the termination must be designed to withstand the increased pressure or an external gas cylinder must be connected to limit the pressure to an acceptable level.

As an example, one of the most popular termination types is the dry-type GIS termination.

**Prefabricated Composite Dry Metal-Enclosed GIS Terminations.** For this termination, a premolded elastomeric stress cone is inserted into a cast thermoset insulator (Fig. 10.74). Pressure is maintained at the stress cone to insulator interface and at the stress cone to cable core interface via metal springs. It is not necessary to fill the insulator with either gas or insulating liquid, thereby dispensing with the need to provide pressure monitoring and compensation equipment and/or a thermal expansion reservoir.

JWG B1/B3.33 has published TB 605 regarding the feasibility of a common dry-type plug-in interface for GIS and power cables above 52 kV [10.50]. Following the recommendations of TB 605, JWG B1/B3.49 has published TB 784, which gives a description of a standard termination for a voltage of 145 kV [10.55].

### Transition Joints

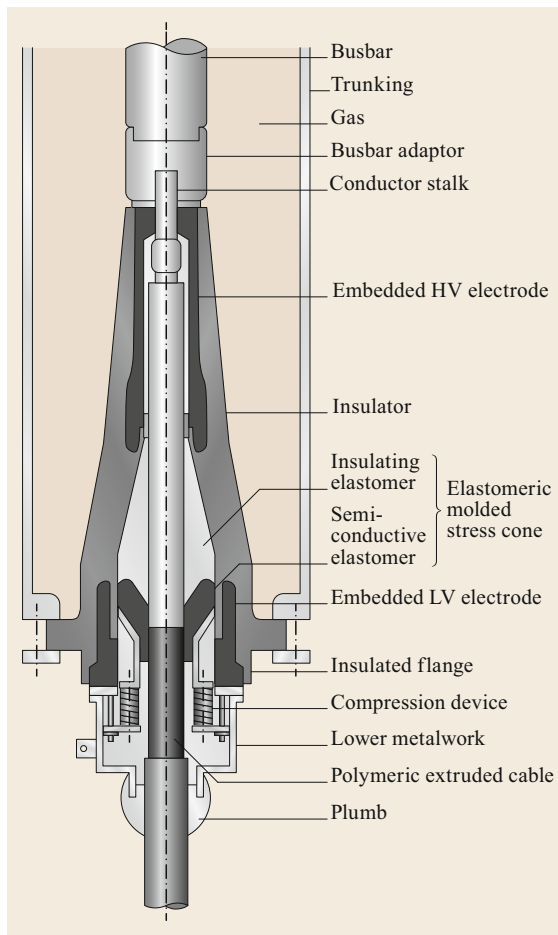
A transition joint connects two cables of different types; for example, a polymeric extruded cable to a self-contained fluid-filled cable. Transition joints are sometimes employed to connect cables of the same type if they have different conductor sizes, in which case they are designed to withstand imbalanced conductor thermomechanical forces. Types of transition joint include:

- Polymeric extruded cable to mass-impregnated cable transition joints
- Polymeric extruded cable to oil-filled paper cable transition joints
- Polymeric extruded cable to gas-pressurized paper cable transition joints.

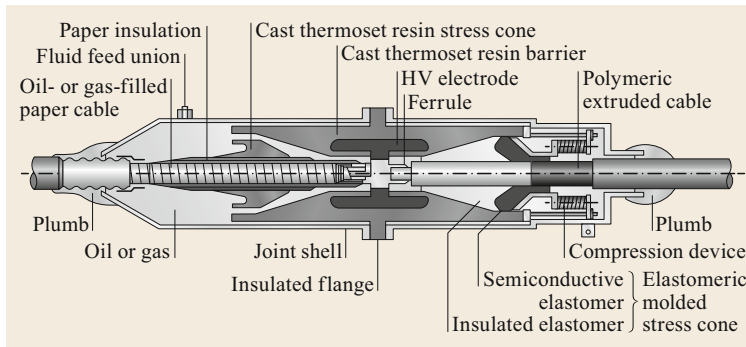
As an example (which can also be found in [10.44]), Fig. 10.75 shows a type of transition joint that can be used at HV/EHV levels.

Recommendations for testing transition joints have been published by:

- CIGRE WG B1.24 in TB 415 for AC cables up to 500 kV [10.47]
- CIGRE WG B1.42 in TB 622 for DC cables up to 500 kV [10.51].



**Fig. 10.74** Prefabricated composite dry metal-enclosed GIS termination (adapted from [10.44])



**Fig. 10.75** A polymeric extruded cable to oil- or gas-filled paper cable transition joint (single-core, fed type) (adapted from [10.44])

### 10.6.5 Accessory Workmanship

CIGRE TB 476 on cable accessory workmanship for extruded high-voltage cables was published in October 2011 [10.48].

TB 476 covers workmanship associated with the jointing and terminating of AC land cables, incorporating extruded dielectrics for the voltage range from 30 kV ( $U_m = 36$  kV) to 500 kV ( $U_m = 550$  kV). This brochure complements TB 177 [10.45]. Although a short chapter in TB 476 covers general risks and skills, the bulk of the document focuses on the specific technical risks and the skills needed to mitigate those risks during each phase of the installation. This TB is not an instruction manual; it provides guidance on the aspects that must be carefully considered when evaluating the execution of the work to be performed. High-voltage cable accessories are manufactured using high-quality materials and very sophisticated production equipment. Recent technical and technological developments in the design, manufacturing, and testing of this equipment have made it possible to obtain premolded joints and stress cones for terminations up to 500 kV and cold shrink joints up to 400 kV. One of the conclusions of TB 476 is that internal failure rates of accessories—particularly for XLPE cables—are higher than those of other components, and are thus of great concern due to the major impact of such a failure. Therefore, the focus on quality control during jointing operations must be maintained.

Many utilities have adopted the *system approach*, in which the cables as well as the major accessories are purchased from the same supplier. Some utilities request that the link should also be installed by the supplier or by a contractor under the supplier's supervision in a *turnkey* fashion. The main advantage of this approach is that the full responsibility for the materials and workmanship is clearly the supplier's. On the other hand, some customers have adopted the *component approach*, in which cables and accessories are purchased from different suppliers and installation is entrusted to a third party. In all cases, the installation must be car-

ried out by qualified jointers who follow the jointing instructions provided by the accessory supplier.

International standards such as those from the IEC and IEEE provide guidelines on the interface between the cables and accessories. However, it is strongly recommended that the compatibility of the different components of the link should be verified by the relevant engineer. It is vitally important for the interface between the cables and the accessories to be managed such that the potential technical risk (e.g., from cables and premolded accessories that have incompatible diameters or other incompatible dimensions or characteristics) is minimized.

One of the international trends in cable technology has been to reduce the cable insulation thickness, which increases the electrical stress. This trend has been driven by greater knowledge and better quality of the insulating material as well as improvements to the extrusion process. Cables and accessory components are made under well-defined factory conditions, and their quality and reliability are assured by adhering to well-defined specifications. However, because the accessories are assembled on-site, even though this job is carried out by skilled and well-trained jointers, it is often performed under more delicate and less strictly controlled conditions than in the factory. This means that correct assembly is even more important, as—given the increased electrical stress caused by the reduced insulation thickness—bad workmanship will sooner or later lead to accessory breakdown.

It should be noted that most of the new HV cable links currently being considered will use XLPE-insulated cables.

TB 476 captures the state of the art in jointing and is considered to define best practices internationally. However, it should be acknowledged that other practices that are not explicitly covered in this brochure are not necessarily bad practices. Great care should be exercised and the approach should be agreed upon in advance when departing from practices recommended in TB 476 [10.48].



**Fig. 10.76** Example of a single-core cable design (adapted from [10.39])

While TB 476 does not directly refer to failures or the consequences of failures, it is a comprehensive document on the assembly of cable accessories. If used properly, it can provide vital advice on how to avoid failures due to bad workmanship.

### 10.6.6 Submarine Extruded Cables

#### Current Technologies for Extruded Submarine Cables

An increasing number of submarine cables are being installed due to the development of offshore wind farms and offshore oil platforms as well as the need to interconnect islands and to bridge power systems across harbors, rivers, lakes, gulfs, seas, and inlets. The CIGRE recommendations for testing HV and EHV submarine cables are published in TB 490 prepared by WG B1.27 [10.39] and completed for mechanical aspects in TB 623 prepared by WG B1.43 [10.56].

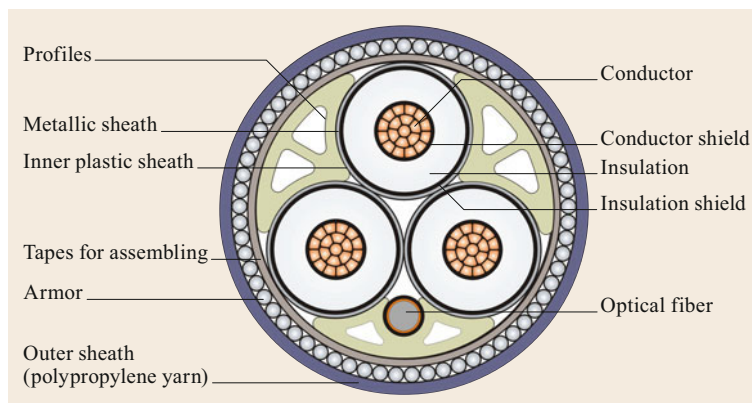
Submarine cables can have either a single core (Fig. 10.76) or three cores (Fig. 10.77). The advantages and disadvantages of each design are listed in Table 10.7.

**Water Tightness.** Submarine cables can have either a wet or a dry design. A wet design allows water to migrate into the cable insulation and the conductor. Dry designs are normally used for the HV and EHV submarine cables considered in this section (as described in TB 490 [10.39]) to achieve the requested service life. Water blocking or water tightness in both the radial and longitudinal directions is crucial. WG B1.55 has recently published TB 722 [10.57], which provides recommendations for additional testing of submarine cables rated from 6 kV ( $U_m = 7.2$  kV) to 60 kV ( $U_m = 72.5$  kV), to address extruded MV and HV AC cables with reduced expected service lives.

Water tightness is the ability of a dry cable design to resist water penetration at the maximum submersion depth of the submarine cable. Water tightness is important for both normal operation and during cable failures, when the physical integrity of the cable is compromised. A weakness in either the conductor or the metallic sheath will reduce the water tightness of the cable.

If a cable fails during its in-service life, water penetration along the cable—either within the conductor or under the metal sheath—must be limited. This will minimize the length of cable that needs to be replaced during repair. Water tightness is improved by selecting the appropriate conductor design, water blocking method used for the conductor, and type of water blocking utilized under the metal sheath.

Water typically penetrates less than 30 m along the cable, although this can vary considerably depending on the design of the cable.



**Fig. 10.77** Example of a three-core cable design (adapted from [10.39])

**Table 10.7** Advantages and disadvantages of single-core and three-core cables

Single-core design	Three-core design
<p><i>Pros</i></p> <ul style="list-style-type: none"> <li>– Lighter weight</li> <li>– Smaller diameter</li> <li>– Longer lengths</li> <li>– Possibly requires fewer joints to be fitted at factory or on-site</li> <li>– Higher current rating</li> <li>– Improved security, can add a fourth cable</li> <li>– Voltage rating can be 500 kV or higher</li> <li>– Reduced repair costs and spares</li> </ul>	<p><i>Pros</i></p> <ul style="list-style-type: none"> <li>– Balanced magnetic field</li> <li>– Minimum sheath circulating currents and voltages</li> <li>– Lower installation costs</li> <li>– One trench on seabed</li> <li>– Lower protection costs</li> <li>– Includes optional FOC (fiber optic cable)</li> </ul>
<p><i>Cons</i></p> <ul style="list-style-type: none"> <li>– Higher magnetic field</li> <li>– Greater installation costs</li> <li>– Individual seabed trenching increases costs</li> <li>– Higher protection costs</li> <li>– Sheath current must be considered</li> </ul>	<p><i>Cons</i></p> <ul style="list-style-type: none"> <li>– Lower current rating</li> <li>– Heavier</li> <li>– Large diameter</li> <li>– Decreased security of cable system</li> <li>– All three phases must be repaired after a fault</li> </ul>

**Conductors.** The design of the conductor influences the water penetration rate or the degree of water blocking of the conductor. Conductor designs can be regular, compressed, compact, solid, or Milliken (also known as type *M*) stranded conductors, or they can be key-stone shaped. A regular stranded conductor consists of circular strands with interstices or spaces between the strands. Compressed conductors have reduced or flattened strands in the outer layer, but the interstices or spaces between the remaining strands remain the same as those for a regular conductor. A compact conductor with reduced spacing between strands is formed by squeezing each conductor layer in a die. A solid conductor will not allow any water penetration, but using such a conductor will lead to a very stiff cable with higher AC losses. For HV and EHV cables, type *M* conductors (Fig. 10.19) are widely used for conductors larger than 800–1200 mm<sup>2</sup> to limit AC losses and achieve more cable flexibility. Semiconducting tapes are normally used between the segments, but there are still interstices unless layer compaction is included in the design. Strand blocking and water-swallowable powders, swellable yarns, or tapes are added to guarantee that the conductor is water blocked. Strand blocking utilizes either a compound that is installed during the stranding or laying-up of the conductor or a pumped compound that is forced into the conductor interstices after the cable has been manufactured. Water-swallowable powders and tapes (with different efficiencies in pure water and salty water) are installed in the conductor during manufacture by adding a powder or applying a fabric tape within the conductor.

**Insulation System.** Most submarine HVAC cables with extruded insulation systems utilize crosslinked polyethylene (XLPE) as insulation. The insulation system consists of an inner conducting screen, an insu-

lation layer, and an outer semiconducting screen. The semiconducting inner and outer screens contain carbon black as an active conducting filler. The properties of the semiconducting screen compounds and the quality of the associated extrusion process are important influences on HV and EHV cable performance. For example, the properties of these compounds are affected by the percentage of carbon added, the carbon particulate size with respect to the base polymer, the dispersion of the carbon through the base polymer, and the extrusion properties of the compounds. In some cases, a volume resistivity stability test may be performed if these properties are a critical influence on cable performance.

The crosslinking of polyethylene (in particular low-density polyethylene, LDPE) is an irreversible process (i.e., the XLPE cannot be remelted) that results in the formation of a three-dimensional network that makes the insulation more thermally stable. This process is implemented after extrusion.

Whilst cables with extruded insulation have found widespread use in electricity distribution systems and for the transmission of lower voltages, extruded materials have only recently become the insulation of choice for underground cables used in EHV transmission circuits. The first submarine cable to use extruded XLPE as an insulation system was introduced in 1973 and used for 84 kV, while the first submarine XLPE cable for 420 kV was installed in 2006.

Another extruded insulation system that may be used is EPR (ethylene propylene rubber), but the applicability of this insulation is mainly limited to systems with  $U_m \leq 150$  kV. EPR differs from XLPE in that it includes fillers to increase mechanical strength and chemical stability. Although EPR is often considered to have better electrical characteristics in the presence of water, its disadvantages are lower electrical design

stress and higher dielectric loss, implying that is mainly useful at lower voltages.

**Metal Screen/Sheath.** The most commonly used metal screen/sheath consists of an extruded lead alloy sheath covered by an extruded anticorrosion polymeric sheath or a semiconducting tape. However, other metal sheath materials are under consideration or being implemented as alternatives to lead alloy sheaths.

The thickness of the metal sheath is dictated by mechanical and electrical criteria.

The metal sheath needs to exhibit a high level of mechanical performance: consistency, bendability during manufacture and installation, and resistance to fatigue during operational thermal cycling.

The suitability of lead alloys sheaths from the perspective of fatigue resistance has been demonstrated by decades of experience with HV and EHV submarine cables containing laminated insulation and, more recently, extruded insulation land cables and HV extruded insulation submarine cables. The CENELEC standard EN 50307-2002 on lead and lead alloy sheaths and sleeves of electric cables highlights the depth of knowledge of and experience gained in the metallurgical control of lead alloy morphology.

Setting practical criteria for calculating the maximum permissible strain on the lead sheath is very difficult because it is complicated to model the behavior of the cable during load cycling. This complexity is due to differences in the fatigue resistance coefficients.

The metal sheath must also have a minimum cross-sectional area to allow for the passage of short-circuit currents without exceeding the maximum permissible temperature at the end of the short circuit (IEC 61443). Additional wires could be used in single-core cables to increase their short-circuit current capabilities. When semiconductive layers are used on each core of a three-core cable, the distribution of the short-circuit current among the three parallel paths must be taken into account.

Continuity of the lead sheath over factory joints is achieved by applying a lead sleeve with a larger diameter over the joint, drawing the sleeve to the underlayer diameter, and then wiping it onto the lead sheath of the cable.

The polymeric anticorrosion oversheath is either insulating or semiconducting in nature and is usually polyolefin based. When an insulating oversheath is used, an overvoltage will occur between the metal sheath and the surrounding metal armor during cable system transients. To avoid dielectric breakdown of the insulating oversheath, a semiconductive oversheath is often used. Alternatively, earthing connections have to be inserted between the metal sheath and the armor at regular distances

along the cable. Particular attention must be paid to the water tightness between the metal sheath and the armor at the earthing connections. Possible corrosion should be taken into account. The cross-sectional area, together with the contact resistances, will direct the flow of capacitive current towards the armor and the sea. Possible overheating by short-circuit currents through these connections is also a sizing parameter.

Radial water tightness is currently provided only by the metal sheath. Longitudinal water tightness is therefore only provided under the metal sheath. This is achieved using semiconductive water-swellaable tapes that are either helically lapped or longitudinally wrapped around the core.

To ensure circularity when laying-up the cores of a three-core cable (onto which the armor will be applied), its outer spaces are filled with non-water-swellaable PP yarns or plastic fillers. A copper tape may be applied as an equalizing counter-helix.

**Armor.** For submarine cable, metal wire armor is normally applied to provide enough tensile strength during the installation. When a cable is installed in the sea, it must withstand the pulling tension  $T = W \cdot d + H$ , where  $W$  is the weight of the cable weight in the water,  $d$  is the depth of the water, and  $H$  is the bottom tension. The tensile strength of a cable is generally verified by mechanical tests performed in accordance with CIGRE recommendations for the mechanical testing of submarine cables [10.56, 58]. For example, the recommendations require the cable to withstand the test condition of  $T = 1.3W \cdot d + H$  for a water depth of < 500 m. Therefore, the armor must be designed to meet this condition.

Copper, steel, or stainless steel wires are normally used as armor. The material chosen depends on various conditions such as the installation method used, operation and cost.

In single-phase submarine cables, the steel armor causes high iron loss, so nonferrous materials such as copper or stainless steel are used, or a return copper conductor is added in conjunction with steel wires to reduce the magnetic flux in the steel wire armor. The reason for this approach is that the magnetic field from the current in the conductor creates eddy currents, leading to heat losses in the armor and other metal parts of the cable under the screen. If the armor was made of a magnetic material such as steel, additional losses due to magnetization would be significant.

For three-core cables, the magnetic field from a symmetrically loaded cable will be significantly lower. The armor, however, is positioned close to the cable cores, where the magnetic field cannot be ignored. Three-core submarine cables typically utilize steel wire

**Table 10.8** Typical values of the permissible tensile stress for various materials used in armor wires

Material	Copper	Steel	Stainless steel
Max. stress (MPa)	60–90	90–600	250–450

armor for cost savings. If the transfer capacity of the cable system must be maximized at a certain voltage level, it is possible to replace the steel armor wires with stainless steel wires. Recent measurements of the steel losses for three-core armored cables have shown that the relevant formulae in IEC 60287 yield higher values than those actually measured. Therefore, the methods used to calculate magnetic losses in the steel armor of three-core cables may need to be reassessed. The magnetic properties of the materials are important when considering losses. From a mechanical perspective, due to its relatively low permissible tensile stress, copper cannot be applied in case the pulling tension due to the very heavy weight of the cable and/or installation in very deep waters is too high. In this case, steel or stainless steel is applied. In more severe cases, a double layer of armor is applied to increase the pulling strength and antitorsion properties of the cable. Typical values of the permissible tensile stress for copper, steel, and stainless steel are shown in Table 10.8.

Figure 10.78 shows schematics of typical cables with a single or double layer of armor wires.

**Outer Protection.** Regardless of whether it has a single-core or three-core design, a submarine cable must have outer protection. Apart from its mechanical function, the outer protection for land-based cables may also have an electrical function. For submarine cables, the outer protection normally has a mechanical function

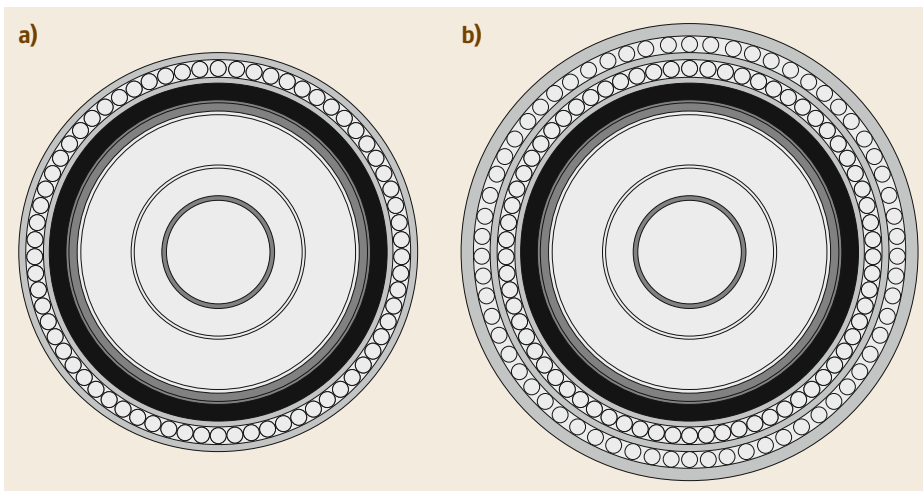
but it is also there to keep the anticorrosion material (e.g., bitumen) in place. The outer protection may consist of either a plastic sheath or, more commonly, one or more layers of yarn over the underlying armor layer(s). One or more threads of yarn may be applied, each with a different color, to make it easier to locate the cable visually after installation. The yarn also stabilizes the armor mechanically so that the risk of birdcaging during cable handling is reduced.

#### Current Technologies.

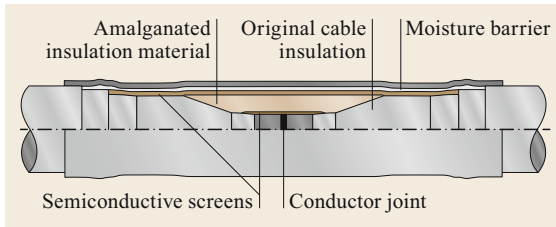
**General Considerations for Factory Joints.** The factory joint is manufactured prior to the armoring operation so that the section of cable containing the joint can be continuously armored without any discontinuity or appreciable distortion of the armor wires in the vicinity of the joint. The main aims of a factory joint are that it should not impose any restrictions on further cable handling or installation operations, and that it should not cause variations in the mechanical and electrical performance of the cable (Fig. 10.79). This generally implies that factory joints need to be fully flexible and to have the same bending radius, pulling force limit, and coiling performance (if applicable) as the original cable.

If the joint imposes some limitations on handling, these limitations must be declared, so that special precautions can be taken during the handling and installation of the joint.

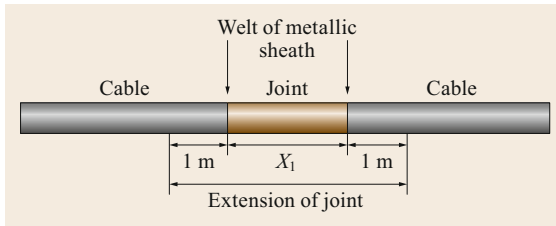
The defined length of a factory joint is the removed length of the metal sheath/outer semiconductive screen ( $X_1$  in Fig. 10.80) plus 1 m at each side of that length (i.e., the defined length of the joint is  $X_1 + 2$  m). For three-core cables, the length of the factory joint is the distance from the beginning of the first core joint to the end of the last core joint plus 1 m at each end of the core joint.



**Fig. 10.78a,b** Schematics of the cross-sections of cables with single (a) and double (b) layers of armor wires (adapted from [10.39])



**Fig. 10.79** Diagram of a factory joint with the same dimensions as the cable (not to scale; adapted from [10.39])



**Fig. 10.80** Defining the length of a factory joint (adapted from [10.39])

Factory joints are required for the following reasons:

- The maximum continuous extrusion length is limited (due to, e.g., filter cleaning and scorch formation).
- There is a limitation on the cable length that can be stored (e.g., on process platforms).
- Limitation of degassing equipment and process incl. size of degassing chamber and the power required to heat the cable.
- Limitation in the laying-up baskets content for three-core cables.
- There is a limitation on the power of the AC testing equipment.
- The cable core could be damaged during handling if factory joints are not used.

In general, the higher the voltage and the larger the cable size, the shorter the individual cable lengths and (therefore) the greater the number of joints that need to be included for a given delivery length.

However, the number of factory joints included in a cable should be limited. Together with improved process compatibility and an advanced testing protocol, this will ensure that the best cable quality is available for the intended application.

In any case, a factory joint should have a robust structure and a highly reliable design and assembly procedure, which should lead to the same design life for the factor joint as for the remaining cable system.

**Typical Procedure for Factory Jointing.** The same procedure applies for single-core or multicore cables, although the joints for the latter are created before laying up the cores.

The two cable ends are suitably prepared.

The conductor is jointed by means of a compression ferrule or by welding. It is better if the conductor joint has the same diameter as the original cable.

The cable core (inner semiconductive layer, insulation, and outer semiconductive layer) is reconstructed using tapes before a curing step is performed. This process can be carried out in separate phases.

Water-swallowable tapes, metal tapes, and/or protective layers are restored.

Lead sheath reconstruction is performed with an extruded lead sleeve that is inserted at one end before the conductors are jointed.

The plastic sheath is reconstructed via taping, heat-shrinkable tubing, or by local extrusion or molding.

Alternative techniques for factory jointing may be developed in the future.

**General Considerations for Repair Joints.** A repair joint is applied to the complete cable, usually onboard a repair vessel or barge. Therefore, the repair vessel or barge should be suitably equipped and have sufficient space to perform the required operation onboard. Repair joints can be divided into three main categories depending on their handling characteristics:

Type A1: Fully flexible joint

Type A2: Flexible joint with some mechanical restrictions

Type B: Rigid joint.

Like a factory joint, a repair joint should have a robust structure and a highly reliable design and assembly procedure that give it the same design life as the rest of the cable system.

It may not be necessary to install the repair joint at the maximum water depth. If the maximum allowable water depth for the repair joint is less than the maximum allowable water depth of the cable, a suitable repair procedure should be performed, including an appropriate length of spare cable to span the deepest point of the route.

Similarly, when the maximum tensile force of the repair joint is lower than the allowable tensile force for the cable, any limitation/restriction that this may represent in terms of repair procedures or environmental conditions (e.g., maximum sea wave height, currents, or wind speed during the repair operation) should be specified.



It should also be noted that it is necessary to have repair joints on hand for most long submarine cable systems. Appropriate storage conditions for these joints should be provided. Requirements for other spare parts such as cable and the shelf lives of joint components should also be taken into account.

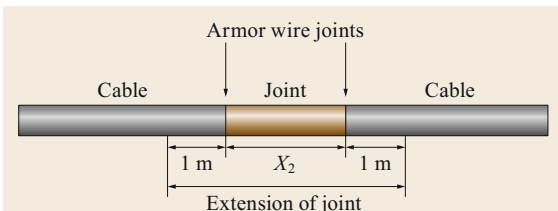
**Typical Procedure for Repair Jointing.** There are a variety of repair jointing procedures for different cable constructions that are based on the manufacturer's or installer's know-how and experience.

Fully flexible repair joints commonly have a similar design to factory joints, especially those used for medium-depth/deep-water applications, while rigid joints often use premolded or preassembled bodies.

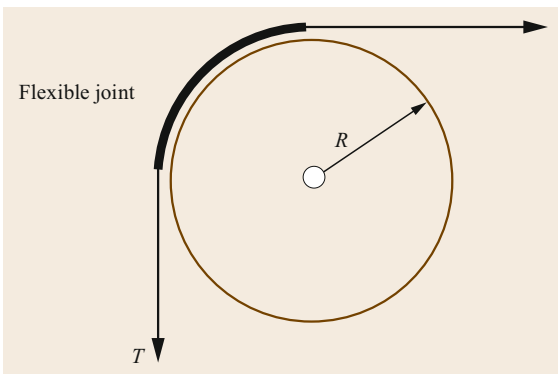
Flexible joints with some mechanical restriction apply to both designs (A1 and A2), though they commonly use premolded or preassembled bodies.

Particular attention should be given to the jointing of the armor to ensure that there is no slack in the armor wires, as this overstresses the inner cores during handling.

The defined length of a repair joint is the length of armor removed ( $X_2$  in Fig. 10.81) plus 1 m at each end of that length (i.e., the defined length of a repair joint is  $X_2 + 2$  m in total).



**Fig. 10.81** Defining the length of a repair joint (adapted from [10.39])



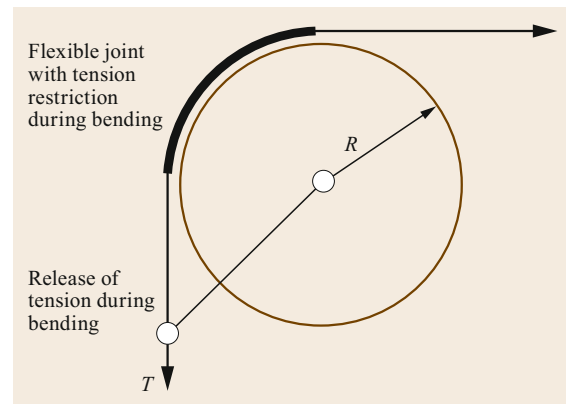
**Fig. 10.82** Fully flexible joint bent over a sheave ( $T$  is the tensile force in N/m and  $R$  is the bending radius in m; figure adapted from [10.39])

*Type A1: Fully flexible joint.* This joint can be bent to a minimum bending radius  $R$  (m) under a tensile force  $T$  (N/m) of the same magnitude as the tensile force that can be applied to the cable itself (Fig. 10.82).

*Type A2: Flexible joint with some mechanical restrictions.* This type of joint can be bent (to the same or a larger bending radius than the minimum bending radius of the cable) over the sheave with low or no tension (minimal tension could mean tens of meters of cable weight); see Fig. 10.83.

After bending, the joint can be pulled with a tensile force  $T$  that is the same as the maximum tensile force that can be applied to the cable itself (Fig. 10.84).

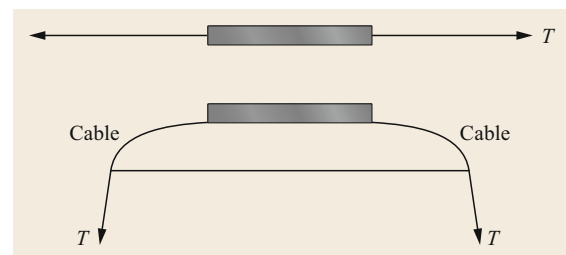
*Type B: Rigid joint.* This cannot be bent or passed through the laying equipment. It must be handled and deployed in a special way, using a crane or similar equipment. In this case, the mechanical stress on the joint/cable depends on the joint design/handling. In any case, the bending radius of the cable should be



**Fig. 10.83** Flexible joint with some mechanical restrictions that is pulled over the sheave by a lower tension than that in the cable (adapted from [10.39])



**Fig. 10.84** Flexible joint after it has been pulled over the sheave (adapted from [10.39])



**Fig. 10.85** Rigid joint lowered by a crane and joint-laying equipment (adapted from [10.39])



**Fig. 10.86**  
Example of a rigid repair joint with bending stiffeners (adapted from [10.39])

above the specified minimum value during joint handling/deployment (Figs. 10.85 and 10.86).

The cable and joint assembly may also be subjected to partial torsion during laying.

**Sea/Land Transition Joints.** A transition joint between a submarine cable and a land cable in a specific project is normally a rigid joint consisting of prefabricated joint bodies, similar to a rigid repair joint for a submarine cable. The testing of a sea/land transition joint should follow the appropriate standard and recommendations for land cables.

The mechanical demands on a sea/land transition joint can differ from case to case. If the submarine cable is jetted into a level seabed and the sea/land joint is placed on the shore, the armor may only need to be terminated, while the situation is different for steep slopes and there may be a need to fix the submarine cable by the armor. This issue needs to be addressed on a project-by-project basis.

If the armor needs to be fixed to hold the weight of the cable, various designs can be considered. One possibility is to terminate the armor in a steel fixture that is rigidly connected to an anchoring block made of concrete. This block or plate may be used as the floor of the joint system.

In any case, the conductor joint needs to have the same mechanical properties as the connecting land cables.

### 10.6.7 New Installation Trends

In the past, when it came to crossing difficult terrain, rivers, roads, and train tracks, overhead lines were the only solution. Today, however, we have directional drilling techniques with the ability to drill for up to 2.5 km. Whilst there has always been the option to use multipurpose tunnels, newer construction techniques that utilize drilling machines or precast assemblies have made such structures more cost-effective. Similarly, where there are open areas, the use of mechanized cable-laying systems (similar to those used to install pipelines) is becoming increasingly practical. Also, the

ability to install submarine cables has advanced considerably during the last 20 years. The net result of all these factors is that the overall cost of long-length AC cable links has dropped, as noted in TB 680 published by WG B1.47 [10.14].

### Associated Equipment

Electric fields in high-voltage terminations and joints must be controlled so that the electrical strength of the insulation of the surrounding material is not put at risk. There are different methods for achieving this (e.g., geometric, refractive, or resistive field control), depending on the voltage level. Geometric field control is generally achieved with premolded stress cones and splicing blocks.

The outer part of a cable termination may consist of a porcelain or composite insulator with sheds, depending on the environment. The internal field control component is normally a premolded stress cone, and the internal space may be dry or filled with insulating oil. There are different types of terminations, such as those for outdoor installations or indoor GIS installations.

There are several different types of joint for land and submarine applications. Many joints have a premolded one-piece body (Fig. 10.72), and joints are available with or without screen interruption depending on the sheath bonding methods used for the system. These prefabricated parts and materials for accessories comprise stress cones for field control, insulators, and housings. The materials used are EPR or EPDM, silicone, epoxy, porcelain, paper and special insulating fluids. These terminations and joints must be installed by very skilled and well-trained personnel.

### Joints and Terminations

Prefabrication lowers the risk of installation-induced failure by making the process of installation easier, leading to better system reliability. The reliability and performance of a HV/EHV cable circuit depends on the quality of the cable and the accessories as well as the quality of the installation of the system components on-site.

The cables are produced in the factory in a controlled process that uses selected clean material of the

highest quality, and are submitted to rigorous routine tests before delivery.

It is important that the same quality standards are applied to all components of the accessories when they are manufactured and (in particular) when they are assembled on-site [10.45, 48].

Modern HV/EHV cable accessories are manufactured using high-quality materials and sophisticated production equipment. Recent technical and technological developments in design, manufacturing, and testing have made it possible to obtain premolded joints and stress cones for terminations rated up to 550 kV, as well as cold shrink joints for voltages up to 420 kV. To ensure that the internal failure rate of accessories for XLPE cables is no higher than that for other system equipment, it is vital to impose strict quality control when manufacturing and assembling HV accessories. It is also very important to manage the interface between the cables and the accessories in order to reduce the technical risk. The HV/EHV cables and accessories used for important HV cable circuits have usually passed a system type test. This is the topic of CIGRE TB 476 [10.48].

**System Approach Versus Component Approach.** As said before, in each of these options, it is strongly recommended that the compatibility of the different components of the link should be verified by appropriate testing and/or calculations.

TB 303 [10.46] proposes some practical tools such as functional analysis to deal with possible changes in components of an approved HV or EHV cable system.

**Main Accessories Needed for a HV/EHV Cable Circuit. Air-Insulated Terminations (Outdoor Terminations).** Air-insulated terminations are generally used outdoors to terminate the HV/EHV cables in air-insulated substations or on poles. They can have porcelain or composite insulators (Fig. 10.87) and can be fluid-filled or unfilled (dry). The design adopted may depend on the local environment with respect to the required BIL, maintenance requirements, pollution, reliability, and altitude. Composite insulators are increasingly used for extra-high voltages. The technical and economic advantages of these insulators are significant and originate from their low weight, ease of handling, safety during explosions, intrinsic hydrophobic characteristics, and reliability during exceptional events such as earthquakes, system faults, and vandalism. WG B1.54 is currently at work studying the behavior of cable systems under large disturbances (earthquakes, storms, floods, fires, landslides, and climate change). WG B1.51 has published TB 720 on fire-related issues for cables installed in air to address this important issue [10.16].



**Fig. 10.87** Typical HV termination with a composite-type insulator (adapted from [10.49])

**GIS and Oil-Immersed Terminations (Transformer Terminations).** EHV and HV cables can also be terminated directly on SF<sub>6</sub>-insulated switchgear (GIS) (Fig. 10.88) and transformers to eliminate air-insulated interfaces.

GIS and oil-immersed terminations (transformer terminations) are constructed very similarly. The electrical stress control for GIS and oil-immersed terminations follows the same approach usually employed for outdoor sealing ends, i.e., it uses a premolded elastomeric stress relief cone.

Proven dry versions of HV/EHV GIS and transformer terminations are available (Fig. 10.74). They have definite advantages compared to fluid-filled types such as no risk of a leak, no need for maintenance, simplified installation (plug-in types), and safety in the case of failure. IEC 62271-209 defines the interface between the HV/EHV cable and the switchgear. As mentioned earlier, CIGRE JWG B1/B3.49 has published TB 784 [10.55], to propose a standard 145 kV GIS Termination as proposed in TB 605 [10.50].



**Fig. 10.88** Typical EHV GIS termination installed in a horizontal position (adapted from [10.49])



**Fig. 10.89** Typical unburied joint installed in a cable chamber/manhole (adapted from [10.49])

**Joints.** Modern HV/EHV voltage joints usually have a premolded elastomeric joint body with an additional covering to protect against moisture and mechanical damage. The additional covering could be a heat shrink tube or metal housing with additional insulation housings/coffins. The joint protection should be chosen according to the type of cable sheath used and, in particular, the location of the joint. Unburied joints may be used in tunnels, on bridges, or in underground chambers or similar enclosures (Fig. 10.89).

The design of the cable joint needs to take the sheath bonding method into account and must be able to withstand sheath voltages under fault conditions. Accessory suppliers offer various types of joints and their associated hardware for various sheath bonding systems, including:

- Shield break or cross-bonding joints
- Earthing joints
- Straight joints.

Accessory suppliers recommend various methods for achieving proper positioning of the premolded or cold shrink joint body and offer special joint installation tools.

## 10.7 Installation Techniques

As noted before, this topic is covered by TB 194, as published by WG 21.17 [10.13]. Methods that can be used to more accurately account for the thermomechanical forces associated with large conductor cross-sections are proposed in TB 669 from WG B1.34 [10.24]. Consequently, it was decided that TB 194 should be updated (by WG B1.61). This update will also consider work published in TB 714 [10.15]

The magnitudes of the forces and motions generated by the cable in the joints (and terminations) must be taken into consideration by the system designer. This includes the civil work aspects of the HV/EHV circuit. The accessories must be positioned and supported. Similarly, the cable must be laid and fixed such that the cable accessories are not exposed to inappropriate mechanical stress [10.13, 24].

**Equipment for Earthing, Bonding, and Screen Disconnection.** Most HV cable accessory suppliers as well as various specialized companies offer equipment that facilitate efficient and reliable earthing, bonding, and disconnection of cable screens, depending on the design of the circuit.

**Surge Arrestors to Protect Cable and Accessories.** Whilst it is important to install surge arrestors at locations where an overhead line enters a substation in order to protect the substation equipment from the effects of lightning, there are differing opinions regarding the need to use surge arrestors to protect cables connected to overhead lines.

When a long cable circuit is directly connected to the substation in an outdoor switchyard, surge arrestors are typically used to protect the substation equipment from a phase-to-earth overvoltage, just as for an overhead line. A similar arrangement is also provided when there is a short section of cable inserted into an overhead line circuit (siphon). It is, however, questionable how effective this will be on a long cable link given that the high impedance of the cable may reduce this transient effect.

**Sheath Voltage Limiters.** Surge protection devices known as sheath voltage limiters (SVLs) are used in link boxes and at termination structures to protect cable sheaths from phase-to-earth faults. When EHV cables are connected to GIS terminations within a substation, special surge protection is provided directly at the GIS.

by WG B1.41 and in TB 770 (on trenchless technologies) [10.59] by WG B1.48.

As explained in TB 714, the backfill used to reinstate the trench around a buried cable is a critical engineering component of the cable system because it (in conjunction with the surrounding material) allows the heat produced during the operation of the cable to be conducted to the ground surface, where it is dissipated

into the atmosphere. Therefore, the thermal properties of these materials, which are assumed during the design of the cable system, are just as important to the correct operation of the system as the selection of the appropriate thermal design. This design is generally derived using detailed calculations that often involve using a computer to perform finite element analysis, as explained in the section of this chapter on rating calculations (Fig. 10.38), whereas the backfill may be installed by manual laborers with no knowledge of the performance requirements of a backfill, other than perhaps the fairly obvious need to support whatever is above (such as a road surface).

Similarly, TB 770 on trenchless technologies [10.59] addresses the factors to be considered when deciding which trenchless technology—HDD, pipe jacking/microtunneling, pipe ramming, or plowing—is best suited to the installation of the circuit of interest. A general summary of the advantages and disadvantages of these four trenchless techniques is provided below. Together with TB 714, TB 770 is an important complement to TB 640 [10.28].

### 10.7.1 Selection of the Best Cable Design According to the Installation Method

It is important to select the cable design and accessories that will provide the best possible service life. For land installations, the use of long lengths of cable is recommended to reduce jointing costs and improve reliability of supply. This will require a robust cable design in order to avoid any damage during installation. It should be noted that while civil costs have been reduced by the introduction of new construction methods, *traffic management costs* can be significant, implying that the use of ducted sections and tunneling in city areas may be the optimal approach.

### 10.7.2 Routes and Rights of Way

When it comes to the installation of OHLs, circuit transmission line designers prefer open fields, whereas those in charge of cable installation prefer roads and railway easements in order to reduce transportation costs and avoid issues with gaining easements on public and private land. Today, even the refurbishment of an OHL with old easements is very expensive and restrictive, as most rural land is subject to environmental protection issues of some kind.

Trenches can be excavated by conventional means with excavators, but trenching machines with rock saws and directional boring techniques are becoming increasingly popular. In some countries, the direct plowing of cables in road reserves and public land is performed.

### 10.7.3 Route Planning: Traffic Management and Security

Traffic management and security requirements should be fully understood and managed during cable installation works. Where there is the potential for cable installation work to disrupt access to private driveways, such disruptions should only be permitted after notifying the occupants of the affected properties. All disruptions should be planned with a clear understanding of, and due regard for, specific requirements of the occupant, and should be kept to an absolute minimum.

There should be minimal impact on pedestrian access. Areas of conflict such as pram crossings at road intersections should be managed with steel plates to cover the trench, and suitable barriers, temporary fencing, and para webbing should be installed to protect and delineate the public and traffic. The security arrangements should remain in place on-site until all cables between joint bays are fully secured or covered by specialized backfill.

### 10.7.4 Installation Methods and Definitions

There are three basic methods of installing cables:

- Rigid constrained
- Semiflexible constrained
- Flexible constrained.

#### Direct Burial and Plowing: Rigid Constrained Installation

For directly buried sections, the cable trench should remain open for the complete section between joint bays until the cable is installed (Fig. 10.90). On completion



**Fig. 10.90** Cables installed in an open cut trench and directly buried (adapted from [10.14])

of the excavation works, the trench should be appropriately shored, dewatered, and cleaned prior to the start of the cable installation works. The base of the trench needs to be inspected to ensure it is firm, relatively smooth, and free of rocks, rubble, or sharp objects. The trench bottom then needs to be filled with approved bedding of suitable thermal resistivity as per the design requirements (see CIGRE TB 714 [10.15] for further information). After the cable has been installed, the trench should be backfilled and then the cables should be tested to ensure that they were not damaged during installation and backfilling before final reinstatement is carried out.

#### Ducts (Conduits and HDD): Semiflexible Constrained Installation

The use of conduits and directional drilling is becoming commonplace in underground cable installations. However, drainage can be an important issue both during and after construction. When an unsealed duct is created (Fig. 10.91), water tends to use the duct for drainage. This is not an issue on flat land, but when the duct is very long, e.g., > 5 km, there is generally a change in elevation or the water table level along the route. Ultimately, the outcome is that the land is flooded, leading to loss of property, property damage, and/or loss of crops. So, when using ducting, special care needs to be taken to ensure that the joints are watertight (fusion



Fig. 10.91 Duct installation (adapted from [10.14])

welds) and that the duct is adequately sealed at both ends.

#### Performing Civil Works.

- First, the trench is dug. Then the bottom and side faces must be trimmed so that the trench presents uniform dimensions. Depending on the soil quality, the side faces of the trench may need to be timbered with wooden props.
- Cable spacers are placed at regular intervals (usually every meter) along with the ducts for the power cables and two smaller ducts at both sides of the trefoil. These smaller ducts are for the earth continuity wire, but they are often placed in cross-bonding connections too.
- A first layer of concrete (Fig. 10.92) is poured on the trench; this must cover the two bottom ducts of each circuit but not the top one.
- This concrete layer must be thoroughly compacted to remove air bubbles, as the presence of air bubbles would lead to higher thermal resistivity of the concrete. This operation can be carried out with a cement vibrating machine.
- The upper duct and the ground continuity wire ducts of each circuit are then installed, as are smaller ducts for communication cables if they are required by the design.
- A second layer of concrete is poured to cover the upper ducts. If ducts for communication cables are required on top of the circuit, a third layer of concrete will be needed after installing them. As with the previous layers, the concrete must be vibrated to eliminate voids and entrapped air (Figs. 10.93 and 10.94).



Fig. 10.92 Double-circuit trench after the first layer of concrete has been poured in (adapted from [10.14])



**Fig. 10.93** Photograph showing the uppermost ducts (red) of two circuits (the other four ducts are under the first layer of concrete) (adapted from [10.14])



**Fig. 10.94** Photograph showing communication cable ducts on top of HV circuits as well as the third (final) layer of concrete (adapted from [10.14])

The last layer of concrete is screened to obtain a flat surface. The joint bays are sometimes made of precast concrete sections, but they are often manufactured on-site. They can be unfilled or filled with sand, but in either case the earthing or cross-bonding box is installed in an unfilled separate chamber for maintenance purposes.

When calculations of the pulling force suggest that it could be difficult to lay the cables at certain points along the line, small sections of the trench are not filled with concrete so that supplementary pulling machines can be used.

Once the concrete is fully hardened, the remaining space in the trench is covered with soil.

Before the cables are pulled into the conduits, a proving mandrel must be pulled through each duct to check its integrity and circularity.

Advantages of this type of installation compared with directly buried cables:

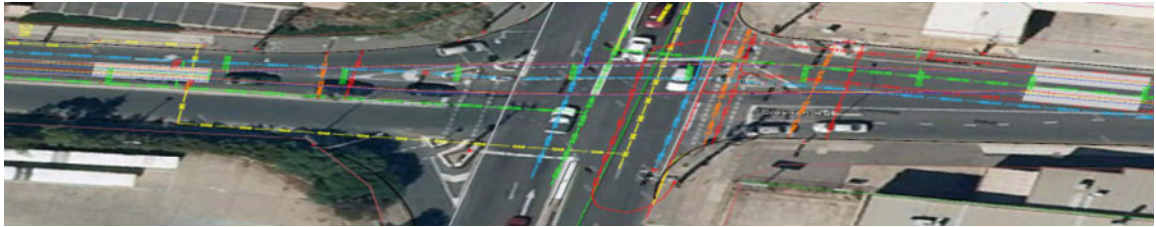
- The civil works do not need to be executed in synchronization with the cable-laying works; they can be done well in advance, at the most convenient time, at each point along the cable route. This is highly convenient for residential and industrial areas, where the digging and trench preparation can be rather disruptive.
- Given the potential for damage due to erroneous digging, the concrete volume around the cables provides strong mechanical protection for the HV line.
- The cables are surrounded by a volume of material with a low thermal resistivity, the value of which is known precisely. Also, concrete is not subject to moisture migration (drying-out effect), which guarantees a higher transmission rating for the line.

Disadvantages of this type of installation compared with directly buried cables:

- The cost of the civil works is higher.
- Fault repairs to the line are more expensive and take longer because it is more difficult to access the damaged part of the cable.
- The minimum bending radius in the cable route is significantly higher, which can be a problem in urban projects. A different type of installation can be used at specific points where the cable route cannot be adapted to the minimum bending radius of the ducts.
- Even with HDPE ducts, pulling forces during cable laying are notably higher than those needed to install directly buried cables with the help of rollers. This adds another layer of difficulty for complex cable routes.

When open cut excavation is not possible for practical reasons (e.g., for deep crossings, river crossings, and busy highways), two types of underbores are widely used for cable installation.

**Horizontal Directional Drilling.** Horizontal directional drilling (HDD) is a steerable trenchless method of installing underground conduits and cables in a shallow arc along a prescribed bore path using a surface-launched drilling rig. This method has minimal impact on the surrounding area and is used when trench-



**Fig. 10.95** Directional bore across an intersection (adapted from [10.14])



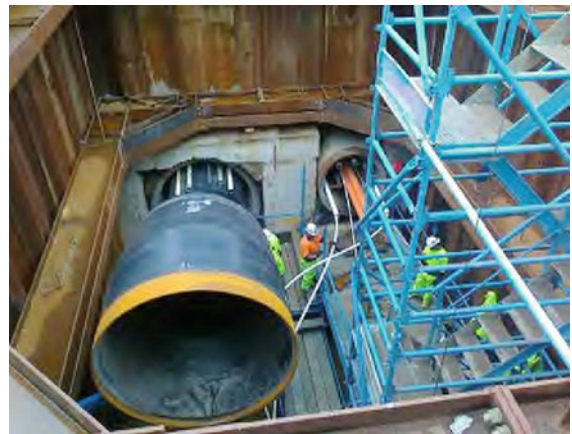
**Fig. 10.96** HDD machine (adapted from [10.14])

ing or excavating is not practical. It is suitable for a variety of soil conditions and jobs including road, landscape, and river crossings, depending on whether the required equipment and experienced contractors are available locally. Different types of heads are used during the pilot-hole process to suit different soil conditions.

The elevations of the bore vary from the shallow open-pit level to the required depth of the crossing and back to ground level at the other end. A directional drilling machine drills the bore, and the cable conduit is drawn back through the bore. The depth of the bore can be monitored and adjusted to the specifications of the bore profile drawing during the drilling process (Figs. 10.95 and 10.96).

**Sleeve Bore/Microtunneling.** Sleeve bore or microtunneling is a technique used to construct small tunnels. In most cases, a remotely operated microtunnel boring machine (MTBM) is used. MTBMs are very similar to tunnel boring machines (TBMs) but smaller (Fig. 10.97).

In most microtunneling operations, the machine is launched through an entry eye and cable conduits are pushed behind the machine—a process that is often called pipe jacking. As the machine advances, more tunnel liner or conduit is pushed from the starting shaft



**Fig. 10.97** Microtunneling (adapted from [10.14])

through the entry eye (Fig. 10.98). Voids between the sleeve and conduits are filled with grout.

The photograph presented in Fig. 10.99 depicts regular HDD with four tubes in one hole. The fourth tube is a spare tube for HV cable.

The photograph in Fig. 10.100 shows HDD for a 380 kV cable circuit with six individual drillings (two cables per phase to reach maximum capacity) that are filled with water and provide water circulation as an option.





**Fig. 10.98** Sleeve bore (adapted from [10.14])



**Fig. 10.100** HDD for a 380 kV cable circuit with six individual drillings (adapted from [10.14])



**Fig. 10.99** Regular HDD with four tubes in one hole (adapted from [10.14])



**Fig. 10.101** Spacer used when installing cables in ducts (adapted from [10.14])

TB 680 [10.14] provides several examples of HV line installation around the world.

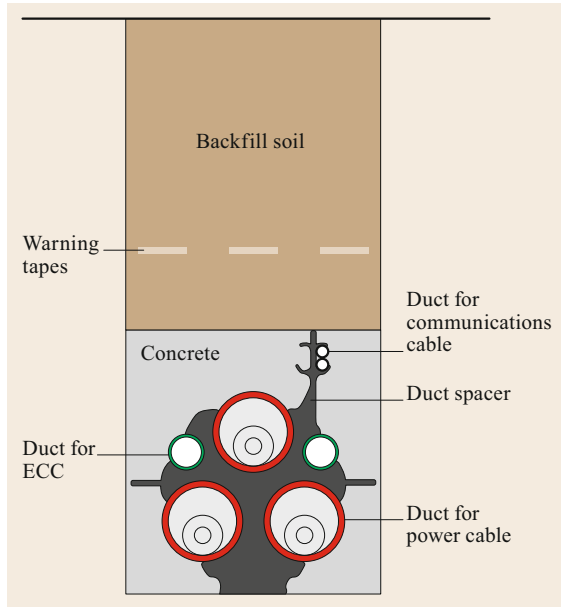
An example (from Spain) of underground high-voltage cable lines installed in ducts embedded in a concrete volume is given in TB 680. These ducts are usually made of high-density polyethylene (HDPE). They have two layers—a corrugated outer layer and a smooth inner layer. HDPE presents good resistance to the chemical agents present in soil and has a lower friction coefficient than polyvinyl chloride (PVC), which facilitates cable laying. Duct spacers are used along the line (Fig. 10.101). These devices have several functions:

- During laying works, they guarantee a safe thickness of concrete between the ducts, thus preventing the steel wire rope used for cable pulling from breaking the duct and entering the adjacent duct in the curved sections of the line.

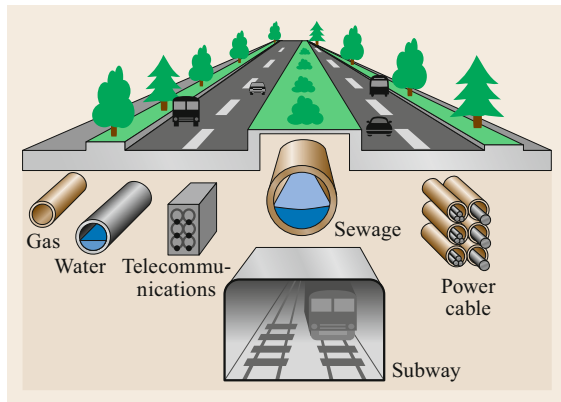
- They separate the cables, which reduces the proximity effect in the conductors and facilitates heat dissipation, thus increasing the capacity of the line.
- They have gauge pins, which are used to ensure that the nominal width and height of the concrete volume are respected.

Figure 10.101 shows that the spacers are usually shaped to accommodate not only the HV cable ducts but also the earth continuity conductor (ECC) ducts and communication cable ducts [10.14]. Figure 10.102 shows a schematic of a typical single-circuit HV cable trench [10.14].

When this type of installation is employed, it is not possible to perform an outer sheath test to check the resistance between the ground and the cable screen. The best solution to this problem is to include a coextruded semiconductive layer over the outer sheath of the ca-



**Fig. 10.102** Schematic of a typical HV cable trench (adapted from [10.14])



**Fig. 10.103** Infrastructural facilities that utility companies are permitted by law to construct under roads in Japan (adapted from [10.14])

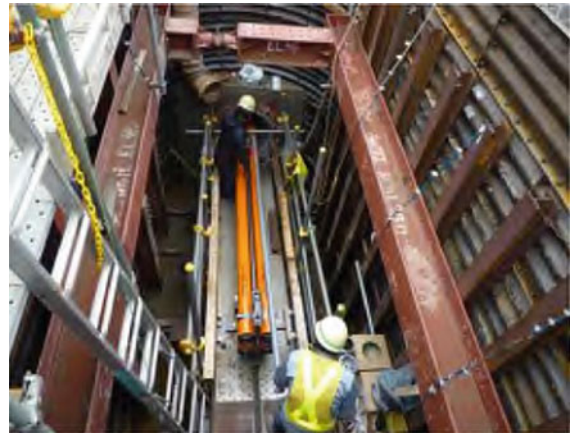
ble. A graphite coating can also be used but is very likely to be wiped away during cable laying (though it can help to reduce the friction quotient during this process).

In another example (from Japan) provided in TB 680, the following practices are reported:

- Utility companies prefer to use the duct method because it is easier to replace the cable if cable breakdown occurs.
- Utility companies have the right to construct infrastructural facilities such as power cables, water and sewage pipes, gas pipes, telecommunication



**Fig. 10.104** Microtunneling in Japan (adapted from [10.14])



**Fig. 10.105** Reinforced concrete sleeve (adapted from [10.14])

lines, and subway lines under roads by law in Japan (Fig. 10.103). Therefore, permission to install underground transmission lines is almost always granted from the road administrator.

- The microtunneling technique is used to cross rivers, railways, and roads with heavy traffic when excavation is difficult or impractical. Microtunneling using a reinforced concrete sleeve is employed to construct small tunnels (Fig. 10.104). After the tunnel has been constructed, pipes are installed in the sleeve (Fig. 10.105).

#### In Air: Flexible Constrained Installation

Underground cables are designed to be *flexible*, as this makes it easier to find an appropriate route via a tunnel or bridge to cross waterways, highways, railways, and other infrastructure (Figs. 10.106, 10.107).

There are two different situations for flexible constrained installation:



**Fig. 10.106**  
Example of flexible constrained, snaked, and cleated cable installation arrangements (adapted from [10.14])

- Dedicated infrastructure is used (this situation is restricted to specific cables)
- Multipurpose infrastructure is used.

In both scenarios the cables are *snaked* (i.e., they meander sinusoidally) and are cleated to the support structures. TB 194 [10.13], the reference document of CIGRE SC B1 on installation techniques, reviews the theory behind the use of two different approaches to the installation of flexible systems in air: the Western approach and the Japanese approach. Both techniques are detailed in TB 194 [10.13] and TB 669 [10.24].

**The Western Approach.** Flexible cable supports are systems that allow the cable to expand in length and to deflect laterally to accommodate this expansion when the cable is heated, as well as to return to the original formation on cooling. In order to control the movement of the cable within predetermined limits, the cable is usually initially installed in an approximately sinusoidal formation with cleats at appropriate intervals such that expansion will lead to an increase in the amplitude of the sine wave.

Because the flexible system accommodates cable expansion, it does not present the high values of thrust that occur in a rigidly restrained system.

There are two possibilities for flexible systems that use the Western approach. The first is a *cleated cable that moves in the vertical plane*. Here, the cable is held in *widely spaced* cleats (Fig. 10.12), and the cable sags between the cleats. This sag increases as the temperature rises.

The other possibility is a *cleated cable that moves in the horizontal plane*. In this type of installation, the cable is arranged in a sinusoidal formation in the horizontal plane, with cleats fixed at the points of flexure along the sinusoidal wave. One option is swivelling cleats that are capable of rotating about a vertical axis



**Fig. 10.107** Example of flexible installation with snaked cables (adapted from [10.14])

as the cable moves, but the use of fixed cleats that are approximately as long as the cable diameter and have a rubber lining 3–5 mm thick is favored. These cleats must be installed at an appropriate angle.

The movement of the cable due to thermal cycling will be strongly influenced by the friction between the outside surface of the cable and the support between the cleats. It is essential to support the cable such that it only moves across a low-friction support in the horizontal plane and to allow adequate air movement around the cable to avoid derating.

**The Japanese Approach.** In the Japanese approach, the design of the snaking applied to the cable is specified. Details are given in TB 194 [10.13] and TB 669 [10.24], and some relevant photographs are provided in TB 403 [10.18].

As explained in TB 403 [10.18], tunnels are very expensive to build and are therefore only used in congested city centers. In this respect, it can be economically attractive to combine an underground cable with other preexisting structures. Such multipurpose tunnels can be attractive, but additional aspects must be considered, such as ventilation, fire protection, division of liability between owners, and security (tunnel access privileges). Laying HV cables in the close proximity of other cables or pipelines can only be done after an intensive survey. Thermal and electrical effects of the cables on each other and safety aspects during normal operation and maintenance must be investigated.

Very few long-length AC cable circuits are installed completely in tunnels due to the high cost of doing so, but this approach is becoming more common in big cities. Many of them are installed in Japan.

In Japan, power cables for underground transmission lines are generally installed in ducts or tunnels.



**Fig. 10.108** Cable installation by motor-driven rollers in a tunnel (adapted from [10.14])

It is therefore necessary to reduce the number of accessories to limit construction costs and construction periods when tunnels are used. This implies that the length of cable between two accessories needs to be as long as possible. As a result, the cable is sometimes transported by sea or river rather than on land. For example, the maximum cable span length was recently increased to approximately 1800 m for 500 kV cables and approximately 2500 m for 275 kV cables.

New methods have been developed to conduct cable installation works efficiently in a tunnel. Synchronized motor-driven rollers that are set up on the floor of the tunnel are used to install the cable (Fig. 10.108). Sensors positioned along the cable installation route can



**Fig. 10.109** Cable installation by a hauling machine (adapted from [10.14])

be used to ensure that the rotating motor-driven rollers are stopped if there is any abnormal behavior during installation. The velocity difference between each roller is controlled to avoid cable buckling and cable sheath damage. Motor-driven rollers are light and easy to install, but many rollers are needed to move the cable because of the small driving force per roller. On the other hand, it is difficult to use motorized rollers when the tunnel is steep, as significant driving force is needed to move the cable.

In this case, hauling machines (Fig. 10.109) are required. The rotation of a caterpillar belt moves the cable. Due to the large gripping force of the caterpillar, the hauling machines must be synchronized.

## 10.8 Testing

### 10.8.1 Fluid-Filled and Mass-Impregnated Cables

The international standards for testing FF and MI cables are well established. Recommended test voltage levels are currently limited to 600 kV for DC applications, although higher voltages are under consideration. WG B1.66, recently launched by SC B1, is currently looking into the possibility of producing recommendations for testing at the 800 kV DC level.

### 10.8.2 Extruded Cables

#### Role of Testing and Condition Monitoring in Extruded Cable Systems

The role of testing and condition monitoring in HV extruded cable systems is outlined by WG B1.29 in TB 569 [10.49].

*Testing.* The role of testing during all stages of system design, set up, and in-service is clearly important to both the supplier and end user, as it can be used to prove that a cable system meets the expectations of the customer. In addition, once a cable system is in service, it may be beneficial to carry out in-service testing to assess the condition of the system and its components. This section examines the types of testing and condition monitoring that may be carried out when assessing a cable system. It is not intended to be an exhaustive account of cable testing but to provide guidance on the areas that should be considered. The level of testing required for a cable system should be decided upon by the customer, based on risk and performance requirements.

International standards for underground cable systems generally define design rules and testing procedures to assess a cable system and ensure it meets the requirements for reliable operation during its de-

sign life. These generally focus on preventing failure rather than actions that can be taken to mitigate the consequences of a fault. Some national standards or individual utility specifications have introduced fault simulation testing and specify requirements for the performance of the system under these conditions (e.g., an internal arc test is carried out by some utilities to evaluate the consequence of an internal fault; this is among the requirements of IEC 62271 for switchgear testing).

It should be noted that a cable system includes the cable, terminations, joints, internal terminations, joint components, filling media, connectors, screen connections, bonding, and so on, so great care must be exercised during testing to ensure that all of the components are properly represented and identified in testing regimes.

**Development Testing.** Development testing is carried out by the cable accessory supplier during the design of a new accessory. The results of these tests may indicate (to the manufacturer, and, where required, the customer) any changes and improvements that can be made to a cable accessory. Examples of development tests include environmental tests such as the salt/fog, rain, and pollution tests carried out on composite insulators, which are not covered by international cable standards. These tests are performed by manufacturers to evaluate the long-term performance of their products and are carried out to test specifications defined in-house. IEC 61462 edition 1.0 covers the test procedures used for composite insulators in AC overhead lines with nominal voltages exceeding 1000 V.

The results of development testing are generally not specified by customers, but they may inform a decision on the suitability of a cable termination or joint for use in a particular application or location; for example, the suitability of terminations for use in areas with high levels of pollution.

Development tests are performed by the manufacturer during the development of a new accessory to check its long-term performance and to assess safety margins. These tests include:

- Analyses of electrical, mechanical, and material compatibility
- Electrical tests to breakdown and mechanical and thermal tests of prototypes
- Wet and pollution tests of outdoor terminations
- Electrical and thermal tests of connectors
- Mechanical tests of premolded components (on the insulators and connectors)
- Fire and disruptive failure performance, including internal power arc testing of terminations.

**Insulators.** IEC 61462 on composite hollow pressurized and unpressurized insulators for use in electrical equipment with rated voltages of greater than 1000 V specifies both design and type test requirements for self-supporting composite insulators. The tests in this IEC standard are designed to provide information on material selection, manufacturing processes, material thickness and adhesion, and end-fitting material selection and attachment.

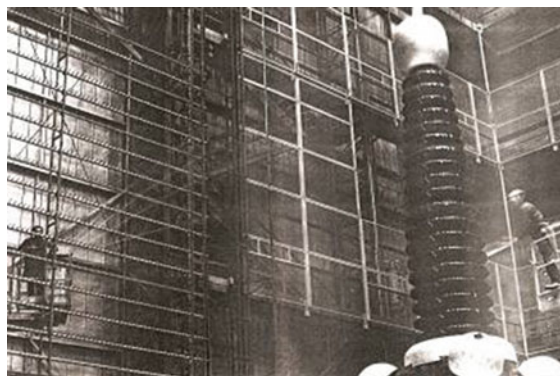
To complete the development of a new accessory, construction drawings should be prepared for all components, and a full-size prototype will need to be manufactured and subjected to tests. If the prototype includes specific components such as premolded parts and composite and epoxy resin insulators, it is necessary to develop the technology to produce these components.

The tests should show the limits on the performance of the accessory and guarantee an appropriate safety margin with respect to the test values stated in the relevant IEC standard.

The tests carried out must ensure that the entire family of accessories are able to withstand the stresses that they may be subjected to during their operational lifetimes.

The termination may be exposed to a saline solution with a concentration that depends on the level of pollution it will experience. It is then subjected to an AC voltage test under these conditions. For composite insulators with a polymeric coating that tends to suffer from surface aging, the pollution test is performed after aging the coating for 1000 h in saline fog (Fig. 10.110) or a multi-stress ageing test of 5000 h (see IEC 62217).

**Connectors.** Development testing of connectors (Fig. 10.111) may also be performed. Thermal cycling of the connectors and contacts used in the accessories is



**Fig. 10.110** Salt-fog test of an insulator (adapted from [10.49])



**Fig. 10.111** Tests of connectors (adapted from [10.49])

carried out at medium voltage according to IEC 61238-1. During the test, the changes in the temperature and electric resistance over time are recorded. Short-circuit current tests are also performed on the connectors. Very recently, WG B1.46 published TB 758 on test regimes for HV and EHV cable connectors [10.53] to address this issue.

**Filling Fluids.** Equipment manufacturers must verify the compatibility of an oil or fluid with a housing material and associated assembly processes and should perform health and safety assessments before the oil or fluid is used within that housing material. This is especially true when new types of fluids or other fillers are considered. Some manufacturers have developed their own qualification procedures, with test conditions specified in terms of temperature, duration, safety, and final acceptance criteria. These are added to the other tests that must be carried out in the development phase.

**Prequalification Tests.** Prequalification tests are long-term tests that are carried out to assess the performance of a cable system and to replicate in-service duty. The test arrangement should be representative of the conditions where the cables are installed (e.g., fixed and flexible sections with both joints and terminations should be tested in order to closely replicate the cable system). These tests are intended to verify the thermomechanical and electrical behavior of the cable and accessories. In some local standards, it is also a requirement to monitor and record the pressure of any insulating media used in order to assess the robustness of any sealing arrangements. After testing, all

accessories are examined to check for any changes or deterioration that might affect their performance.

Prequalification testing is only specified in IEC 62067 and 60840 for cable systems above 150 kV, for systems where the conductor screen stress is designed to be greater than 8 kV/mm, or for systems where the insulation screen stress is designed to be greater than 4 kV/mm.

**Type Tests.** Type tests are carried out on the complete cable system (Fig. 10.112) and are required for all voltages and design stresses. These tests are a minimum requirement to show that specific cables and



**Fig. 10.112** Type-test loop for a 400 kV system (adapted from [10.49])

accessories are fit for a specific purpose. The type tests specified in IEC 60840 and IEC 62067 focus mainly on the short-term voltage withstand performance of the cable system. They consider AC, overvoltage, and lightning transients along with material aging effects. Following the completion of these tests, the cable system must be shown to be free of partial discharges or to only experience discharges that are below a certain specified level. If partial discharges are present (even if they are below the level specified), it may be prudent to identify the cause of this discharge. Once the tests are completed, it is important to disassemble all accessories and closely inspect them for any signs of electrical activity or physical changes that may not have caused an electrical discharge but may still cause mechanical or operational problems. Interpretation of the test results will be based on previous experience with development, prequalification, and other type tests.

**Short-Circuit Tests.** WG B1.29 identified that short-circuit behavior was not addressed by any of the IEC standards relating to HV cable systems. Several utilities have independently taken the step of specifying an additional type test to check the behavior of terminations (especially those containing insulating fluid) when they are subjected to short circuits. Two short-circuit scenarios need to be considered in this context:

- A low-energy external fault. In this case the fault current passes through the conductor. The fault is external to the accessory.
- A high-energy internal fault. In this case the fault is the result of component failure or arcing inside the accessory.

Depending on the design and installation, consideration should be given to whether it is necessary to perform one or both of the above tests to cover the worst-case condition.

**Sample Tests.** Sample test requirements are outlined in IEC 60840 and 62067. These tests are to be carried out on a specified number of components and complete accessories during a production run. When the main insulation of the accessory cannot be routinely tested, IEC 60840 states that a partial discharge test and an AC voltage test should be carried out on the fully assembled accessory. The characteristics of individual components should be verified in accordance with the specifications of the accessory manufacturer through either test reports from the supplier of the component or internal tests. Components should also be inspected against their

drawings, and there should be no deviation outside of the declared tolerances.

**Routine Tests.** Routine tests are carried out on some supplied accessory components. These tests should form part of a robust quality control regime and provide confidence in the quality of the accessory. Among these tests, the main insulation of prefabricated accessory designs is required to undergo AC voltage and partial discharge tests. Finally, each component should be visually inspected for defects.

Insulators filled with oil, gas, or any other material should also undergo a pressure test before delivery.

**Tests of Filling Materials.** Filling materials such as polybutene or synthetic oil are selected based on their material parameters and characteristics and are approved during the development, prequalification, and type tests. Specification IEC 60836 covers silicon oil.

It is recommended that a *fingerprint* of the filling material should be determined after delivery, as this fingerprint might be useful during condition assessment programs or failure analysis.

Well-established material fingerprint techniques include:

- AC electric strength
- Dielectric dissipation factor
- Fourier-transform infrared spectroscopy (FTIR)
- Thermogravimetric analysis (TGA).

**Commissioning Tests.** Commissioning tests are carried out on the assembled cables, joints, terminations, bonding, and earthing once the installation is completed. These final tests performed on the cable system prior to energization provide a final check that the system has been correctly designed and installed. The requirements for commissioning tests vary depending on the type of circuit installed and the consequences of failure.

Very few tests can prove the longevity of cables, joints, and terminations. However, it is recommended that an AC insulation test should be carried out with partial discharge monitoring (if possible) of all joints and terminations. Ideally, this should be implemented using a resonant test voltage generator (Fig. 10.113), as the cable system can then be energized off-line and at low energy, minimizing the risk of a disruptive accessory failure during the test. The tests may provide an early warning of potential failure points before a subsequent breakdown of the complete cable system in service leads to bigger problems. Commissioning tests should be performed according to the relevant IEC standard.



**Fig. 10.113** On-site commissioning test performed with three mobile test sets simultaneously due to the cable length (adapted from [10.49])



**Fig. 10.114** Discharge tracks on the PE outer serving of the cable due to a defect (adapted from [10.49])

It is possible to carry out an AC test by energizing the termination with the system voltage (a soak test) and to use on-line partial discharge monitoring. This is not ideal, as noise from the system can mask discharge activity within the accessory. In addition, if a breakdown does occur it will lead to a disruptive failure of the joint or termination (as the full system short-circuit current is available to flow through the failed accessory), which may lead to an outage and power disruption. Such a failure presents a safety risk on-site and introduces a significant delay into the commissioning of the circuit while the affected components are replaced.

A DC oversheath test should also be carried out to ensure that the cable system and its accessories are insulated from earth. In Fig. 10.114, the discharge tracks are a consequence of fault location pulses.

**Condition Monitoring.** In TB 420, which provides generic guidelines for lifetime condition assessments of HV assets and related knowledge rules, it is recommended that a database of information on each piece of equipment should be established as the equipment ages [10.60]. Useful information on the aging process during the full service life includes loading, maintenance test results, fault history, general ambient and

environmental conditions, and details of any site incidents.

A structured methodology to analyze and prevent in-service failures is recommended in order to effectively manage the aging of HV cable accessories. One suggestion for such a methodology is given in [10.60, clause 4.2]. The final step in this methodology is to gather the outputs from this process into a management strategy that can be used for:

- Preventative maintenance
- Decisions regarding equipment change-out
- Improving the specification, design, or manufacture of new equipment.

Regarding preventative maintenance, there are many possible approaches to monitoring the condition of terminations and unburred joints. These vary from visual inspection to on-line monitoring and regular testing while out of service.

Figure 10.115 gives an example of a condition monitoring technique (X-ray imaging).

The monitoring to be carried out depends on:

- The importance of the circuit
- The history of the circuit and its accessories
- The potential repair time
- The potential cost of the outage
- The potential cost of the damage
- The effect on reputation
- The potential damage from the failure
- The effectiveness of the monitoring system adopted
- The availability of monitoring tools and trained personnel
- The cost of monitoring.



**Fig. 10.115** Example of a condition monitoring technique (X-ray imaging) (adapted from [10.49])



Figure 10.115 shows an X-ray image of a outdoor cable termination used to check any internal displacement of the top connector.

A list of condition monitoring tools is detailed in TB 559 [10.21]. To assist in the selection of a monitoring tool, each tool is described under a number of headings, including:

- *Experience*: each condition monitoring tool is categorized as either a well-established (W) tool or one that is under development (D).
- *Effectiveness*: some diagnostic monitoring tools are considered (based on cost, time required, and results) to be more effective (i.e., useful: U) than others (less useful: L) at finding damage or degradation that will eventually lead to system failure.
- *Level of expertise required*: low or high, depending on whether the tool can be used by a general

operator or only by a trained technician/engineer, respectively.

- *Cost*.

### Testing Extruded Cables for DC Application

The basic principles of DC extruded cable system testing are similar to those discussed above.

In April 2012, CIGRE WG B1.32 published TB 496, which provides recommendations for testing DC extruded cable systems for power transmission at rated voltages up to 500 kV [10.61].

This very important document is the basis for testing of extruded cable systems that have been recently installed or are in the process of installation.

With the huge increase in projects with high system voltages, SC B1 has decided to launch a new Working Group, B1.62, to prepare recommendations for rated voltages up to 800 kV.

## 10.9 Maintenance

This section gives some general guidelines.

Detailed guidelines can be found in TB 279 published by WG B1.04 (all types of cables) [10.62], in TB 358 published by WG B1.09 [10.63], and in TB 652 (fluid-filled cables) published by WG B1.37 [10.42]. SC B1 has directed WG B1.60 to update TB 279, and an update to TB 358 [10.63] is also being considered.

### 10.9.1 Land Cables

#### Maintenance Guidelines

Most HVAC lines should have a specifically designed maintenance program, including periodic tests of the outer sheaths and inspections of the link boxes and SVLs (sheath voltage limiters). These tests and inspections should be scheduled in advance to ensure that all of the necessary permissions and authorizations can be obtained on time and that all of the points in the system that must be visited are accessible.

**Terminations.** The terminations and their structural supports should be examined visually, along with the condition of the clamps that support the cable ends, and appropriate maintenance work should be implemented.

The quality of the *connection contacts* can be checked using an infrared camera that can detect hotspots.

If the arrester has a surge counter, the data from it should be checked regularly as part of the condition reliability maintenance (CRM) program.

**Outer Sheath Test.** An outer sheath test should be performed two years after the system was commissioned and then at least once every five years. However, more frequent testing of systems located where the ground has high levels of humidity or systems in which the outer sheath is made up of PVC may be considered. In this case, the voltage test level needs to be carefully selected to avoid damaging the outer sheath, especially when the system has been in operation for many years. This test should also be performed after any major repair of the cable system.

Access to the link boxes is required to test the outer sheath. It is possible to test one of several major sections of the line in a single operation, depending on the type of equipment and the section length.

To save time, the SVLs can be kept in place during the outer sheath test if desired. In this case, the voltage of the test must be adjusted to a level that the SVLs can withstand. This should be considered during the line design stage when the SVLs are selected. If the link boxes have been filled with epoxy resin (to prevent water ingress and electric arcs), the test will need to be performed with the SVLs fully assembled.

**Link Boxes and Sheath Voltage Limiters.** If the link boxes are not filled with any substance, visual inspection is the simplest way to check their watertightness. Checking the SVLs visually will also help to detect major failures in these components. Inspections of link boxes and their SVLs should be performed on a regu-

lar basis, after any short circuit in the cable system, and after a major system failure.

Additionally, each SVL should either be substituted or tested every ten years to check their condition by analyzing their  $I$ - $V$  characteristic curve. This test can be performed on-site with portable equipment or in a laboratory.

Outdoor link boxes should also be inspected on a regular basis (e.g., every 2–5 years) as they may be exposed to wide temperature fluctuations and sometimes to direct sunlight, leading to significant variations in the internal pressure of the box, which may affect their watertightness. In this case, frequent inspections are advisable.

The use of specific sensors to protect the circuit from vandalism and detect the penetration of water into link boxes should also be considered.

### *Monitoring the Cable Route.*

**Flexible Constrained Systems.** In tunnels or other locations in which cables are installed in the open air, the mechanical fixations of the system should be examined every five years as well as after short circuits or severe climate conditions.

**Underground Systems.** To achieve good reliability, fast repair times, and long service lives, it is necessary to implement monitoring procedures for all of the factors that may harm the cable system. The main issue to check for is any change to the local environmental conditions since the system was commissioned. To minimize risk, routine checks of the state of the system must be performed and complete documentation of these checks must be maintained and available; for example:

- Check if there are changes in the surrounding properties that may have an influence on the cable system.
- Note any change of drainage as this will impact on the current carrying capacity of the cable system
- Nearby building activities may jeopardize the security of the cable.
- Change of ground vegetation, newly build roads or the like may have a long-term impact on the soil parameters resulting in a change of current carrying capacity.
- Check all the signs along the cable route.
- Check if the cable route documentation has been updated by activities that are subject to approval.
- Check spare parts, if any, and in particular those components with limited shelf life.
- Check and update the list of land owners alongside the cable route who must be asked for permission to enter their land in case of a cable failure.
- Communicate to local authorities the persons to be contacted if activities are being undertaken near the cable route.

The cable route cannot be checked from the desktop only. A visual inspection is necessary, supported by clear and coherent documentation. In rural areas, it may be possible to inspect the route with the aid of drones.

If the line incorporates a distributed temperature sensing (DTS) system, any localized temperature rise or hotspot it detects should be investigated. If the installation is not equipped with such a system, routine supervision of the line must be implemented.

The use of internet-based geographic information systems to monitor conditions along the cable route should be approached with caution unless there is clear information about the frequency with which the aerial photographs are updated and the dates that the maps were created.

Close attention must be paid to any alterations along the cable route, such as changes in the ground level due to civil works and significant growth of vegetation (as the roots can dry out the soil).

**Fault Location.** Fault location in AC and DC land and submarine links is addressed in detail by CIGRE WG B1.52 in TB 773 [10.64]. It is important to obtain the necessary permits to get access to the cable system.

**Cable Fault Location Procedure.** The cable fault location should be considered as a procedure covering the following steps:

- Notification of the fault by utility
- Disconnecting and earthing of the cable circuit by utility
- Preliminary discussions to identify the fault by all concerned parties
- Carry out fault location by utility/special contractors
- Identify fault location
- Excavate fault location area to access the cable fault
- Physically locate the fault
- Civil construction works & preparation of the joint bay
- Carry out repair works
- Cable testing and energise.

**Cable Fault Location Methods.** Cable faults are generally located through fault resistance measurements. If there is a low fault resistance or it can be reduced using a high-voltage DC source, the Murray loop bridge method is often adopted. In other circumstances, time-domain reflectometry (TDR) is often used; in this case,

**Table 10.9** Cable fault location methods

Method	Fault characteristics
Impulse reflection method (TDR)	Low-resistance faults, determination of cable end, cable cut, joint location with impedance change
Secondary/multiple impulse method (SIM/MIM, $\approx 80\text{--}90\%$ of all faults)	High-resistance faults, low-resistance faults
Impulse current method (ICM, for long cables)	High-resistance faults, low-resistance faults
Decay method (breakdown voltage higher than 32 kV)	Low-resistance faults
Burn-down techniques, modification of fault characteristics (e.g., influence of water in joints)	High-resistance faults, low-resistance faults
Bridge measurement	Low-resistance faults, cable sheath fault

it is highly desirable to compare the new trace with the latest TDR trace of the healthy system. To precisely locate the cable fault, it is necessary to confirm its position along the cable using further (TDR) measurements, a surge generator and acoustic location (search coils), or any other HV fault location method.

Table 10.9 gives an overview of conventional cable fault location methods.

If there is an integrated optical fiber in the cable damaged by the fault, OTDR can potentially provide an accurate fault location. If the fiber is not damaged, an acoustic method may be feasible.

Surge generator cable fault locators (*thumpers*) provide prelocation and pinpoint cable fault location. The ICM (impulse current method) is preferred for extensive underground cable fault location and for pinpointing cable faults in water-damaged cable joints. A surge generator fault locator (cable thumping) permits very rapid and precise location of cable faults and thus reduces the amount of excavation required. Surge generators have a time-controlled surge output: they periodically produce a discharge in the cable in order to acoustically locate the flashover at the fault using a ground microphone and receiver.

When a high current is used to detect an outer sheath fault, the cable sheath can get damaged in another location. Consequently, after finding and repairing a fault, the outer sheath must be tested again to check its integrity. When a cable is installed in a duct (dry), it may be difficult to pinpoint the fault location due to the insulating properties of the duct.

Currently available technology allows any system fault to be detected with high accuracy. Very often, faults happen in fixed positions (joints, terminations), so if a fault is detected in the vicinity of these accessories, they should be inspected visually first of all.

When an apparently spontaneous fault in the insulation happens, it is often due to the actions of an external or third party, which may be apparent upon arrival at the location of the fault. If the fault is found to be due to external damage, it may be necessary to check the records of the local authorities for previously issued permits.

**Accessory Failures.** Most reported accessory failures are caused by aging or improper installation. Accessory failures are expected to increase with increasing demand for heavier loading operations and high load fault currents, which contribute to aging by imposing thermal stresses.

Accessories undergo either mechanical or thermal failure. Sometimes the accessories have not been installed properly, resulting in mechanical failure. Thermal failure is the result of high resistance heating or individual strands failing, with the same consequences.

These situations can either melt components or cause the joint to lose its connection. Failures generally show evidence of both mechanical and thermal failure. Guidelines in this regard are given in TB 560 from WG B1.29 [10.49].

#### Access to Route Information

It is essential to document the cable route and right of way (ROW) to facilitate monitoring and fault location. The following aspects of the cable route must be documented in detail during cable installation:

- Joints and joint pits
- Terminations
- Cable loops
- Grounding systems, link boxes, and earth cables
- Fiber optic cables
- Laying details such as direct burial, cable ducts, duct laying, and backfill
- Crossings of, e.g., cables, pipes, and roads.

*As-built* cable route drawings are vitally important for long-length HV underground cable systems. These drawings show the finished condition of the work following construction and acceptance, and are a crucial requirement for any HV underground cable project.

#### Typical Durations of Repair Works

When planning the circuit, the utility should consider the total time required for the outages needed to carry out repair works.

The duration of repair works should be specifically defined for each project. The time needed to obtain the necessary authorizations and permits must be considered, which will depend on both the installation type and the local regulations.

The time needed to install high-voltage joints and terminations will depend on the voltage level and the type of insulation used in the cables. Estimates provided by manufacturers are generally based on one jointing team consisting of two jointers and one assistant working 8 h per day. It should be noted that repairs are seldom performed on a 24-h basis, and several teams are often employed to reduce the time taken to get the circuit back in service.

### 10.9.2 Submarine Cables

#### Maintenance Guidelines

Submarine HVAC lines can be surveyed using a remotely operated vehicle (ROV). Equipment for monitoring the laying depth of the cable is available. It is strongly recommended that this operation should be done once a year in areas with high morphological dynamics to prevent the cable from being uncovered. This operation can be performed less frequently in areas with more a stable seabed.

As in any other offshore operation, a ship with appropriate equipment is required, and the operation can only be performed under suitable weather conditions.

Complete geographic information system documentation of the cable route must be provided for every HV submarine line. This is used as a reference to detect any changes to the cable using the data collected by the ROV.

An anchoring map must be provided to any ship operating in the vicinity of a HV submarine cable. This must be a requirement before any vessel (even a recreational boat) is allowed to approach the cable.

#### Origin and Nature of Cable Failures

Repairing submarine cables is an expensive and time-consuming operation as they are very long, remotely located, and difficult to access. Depending on the time taken to locate the fault, the extent of the damage, the time needed to mobilize a suitably equipped ship and crew, and legal discussions about liability, a repair can take weeks, months, or even years. Because of the extensive test program performed on submarine cables when they are manufactured and before they are delivered, internal failures due to issues with the cable itself are rare. Most failures of submarine cables have natural causes; they are often due to human activities. TB 398 published by WG B1.21 deals with third-party damage to underground and submarine cables [10.17]. Furthermore, damage to submarine cables can occur at various times during the lifetime of the cable, i.e., before or after commissioning.

Examples of damage that can occur before commissioning are:

- Overpulling or overbending of the cable due to a loss of the digital position (DP) of the boat installing the cable
- Anchoring damage due to the mooring of the laying barge
- Damage during burial caused by the trenching/burying equipment
- Damage caused when the cable is passed from the transportation vessel to the installation vessel
- Emergency cable cutting due to extreme sea conditions.

After commissioning the cable, natural events that may lead to cable damage include:

- Fatigue at free-hanging sections due to tidal and wave motions
- Abrasion caused by moving material on the seabed
- Underwater landslides or sea-bottom movement induced by seismic events.

However, most of the events that damage cables are due to human maritime activities, including:

- Fishing activities (e.g., trawling and the use of explosives in shallow waters)
- Anchoring
- Dumping of material
- Shipwrecking
- Dredging
- Other submarine installations.

The failure of a submarine cable can have severe consequences both economically and operationally. Thus, a reliable repair should be performed in the shortest possible time. There are no standard cable repair procedures for a submarine cable, although guidelines are available. The owner of the cable system must compile a comprehensive fault location and repair procedure for each cable section according to those guidelines.

Parameters such as the laying depth, cable length, and cable size vary with the cable considered, making each repair operation different from any other. However, a general strategy can be defined. When a cable fault occurs, the following steps should be performed:

- Fault detection and location
- Repair operation planning
- Securing a suitable vessel for the repair, as well as suitable equipment and a qualified crew
- Mobilization of the vessel, equipment, and crew
- Loading the repair joints and spare cable
- Cable recovery or removal of the damaged section of the cable

- Cable repair onboard the vessel
- Relowering the cable/protecting the cable.

### Fault Detection and Location

As already stated above, the issue of fault location in AC and DC land and submarine links is addressed in detail by CIGRE WG B1.52 in TB 773 [10.64].

The fault detection and location steps are important ones in the repair process. The position of the fault along the cable will strongly influence the extent of the repairs required and the means to implement them. It also influences the type of vessel and equipment required. The long length of the line makes it more difficult to pinpoint the exact location of the fault, but it is nonetheless crucial to precisely locate the fault, as cutting the cable at the wrong point can increase both the costs and the duration of the fault repair.

Several methods can be employed to locate the fault, some being more accurate than others. Combining different tests often gives the most accurate results.

For three-core cables, the problem is generally a failure of the insulation on one core, so the first step is to identify the faulty core. Insulation resistance measurements will allow the faulty core to be identified.

Almost all of the submarine three-core cables installed today include at least one fiber-optic element between the power cores. This fiber-optic element is a good indicator of a fault. Indeed, if the armor and possibly the metallic screen of the power cable are damaged, the optical fiber element will probably also be destroyed. Thus, when possible, performing optical time-domain reflectometry (OTDR) from both ends will highlight a discontinuity or a stressed optical fiber and yield the approximate location of the fault.

A failure can also be located by performing time-domain reflectometry (TDR) in the faulty core. This can be done from only one end, but it should be performed from both ends if possible as this will give significantly more accurate measurements. The best results from TDR are obtained for breaks or low-resistance faults. It is very important to get a TDR trace performed upon commissioning and during the regular routine maintenance program.

Another method of locating a fault is to use Murray loop bridge measurements. This can be done if one of the other cores in the cable is not faulty. This method is simple and often allows the fault to be pinpointed to within 1% of the cable length provided that the temperature variation along the route is accounted for.

Even though all of the methods described above give good results, the application of a more accurate method is then recommended in order to identify the

precise location of the fault and thus avoid unnecessary cable wastage. One such location method is to inject a tone current into the faulty core and pass a vessel or ROV equipped with search coils over/along the cable. The search coils will detect the change in magnetic field across the fault. Methods that use emerging technologies such as frequency-domain reflectometry (FDR) are also options.

### Planning the Repair Operation

Once the fault has been located, other information such as the depth or the sea current at the fault location must be obtained before the repair operations can be planned. It is also necessary to assess the condition of the sea bottom at the fault location and perform a survey of that area.

The repair method that should be employed depends on several parameters, such as the water depth, the weather, current, and soil conditions, the type of joint involved, and the results of an unexploded ordnance (UXO) survey. Analysis of this information will lead to the selection of the most suitable vessel, equipment, and crew for the operation. Furthermore, uncertainty over the weather conditions should be considered. It can be challenging to find a suitable window to perform an offshore repair in winter or the storm season.

All aspects and parameters of the operation should be carefully planned to achieve the most efficient operation and avoid expensive mistakes offshore.

The choice of vessel will depend on the location of the fault and the type of repair to be done, but some characteristics of the vessel should be considered. The vessel should be able to remain in a stable position even in rough weather. Thus, the vessel is required to have a good and stable digital positioning system. The deck size of the vessel should be at least 1000 m<sup>2</sup> to be able to install all of the equipment and to allow sufficient area for the jointing. For instance, a flexible joint can be up to 25 m long.

Personnel are needed to maneuver all of the equipment and perform the repair. Representatives of the supplier, the owner of the cable, and the insurance company should also be present during the repair operation. Thus, the vessel should be equipped with sufficient cabins to host all of the people that must be onboard during the repair operation.

Another important aspect of the planning process is the legal discussion between the client and the insurance company. It is very important to define the liability (and its limits) of each party from the beginning. This discussion can take a long time—up to two years in certain cases.

### The Repair Operation

Once the repair has been planned, the vessel, equipment, and the crew will be mobilized. Once it has arrived, the equipment needs to be installed on the vessel and the layout needs to be certified by the appropriate body. This mobilization phase usually takes 10–15 days.

The vessel is then ready to sail to the fault location. Two repair joints and part or all of the spare cable will be used in the repair operation.

### Typical Duration of Repair Work

As mentioned above, repair operations for submarine cables can vary from case to case. The duration of the repair operation is dependent on many parameters, and any estimate of the duration of this operation is generally inaccurate and misleading, so it is important to carefully consider whether such an estimate should be supplied.

Even when a good repair plan is in place in terms of spare parts management and equipment and jointing team availability, the time required for a repair operation is extremely unpredictable due to various factors

including availability of vessels and crew, time of the year, weather, and environmental restrictions.

### Concluding Remarks on the Maintenance of Submarine Cables

Due to the long lengths, remote locations, and difficulties involved in accessing submarine cables, repair operations for such cables are expensive and time-consuming. Depending on the time needed to locate the fault, the extent of the damage, the time taken to mobilize a suitably equipped ship and crew, and the length of legal discussions regarding liability, a repair can take weeks, months, or even years. Because of the extensive test program performed on submarine cables when they are manufactured and before they are delivered, internal failures due to the cable itself are rare. Most failures in submarine cables are caused by third-party damage, a topic that is addressed by WG B1.21 in TB 398 [10.17]. Furthermore, damage can occur to a submarine cable at a different points in its lifetime, i.e., before or after commissioning.

## 10.10 Upgrading and Uprating

The upgrading and uprating of HV cable systems is addressed in TB 606, published by WG B1.11 [10.65].

The life expectancy of an underground cable system is usually more than thirty years. This makes it difficult to predict changes in the cable environment or how the operating conditions will evolve over time. Increases in demand raise major issues. Replacing a power link or installing an additional circuit incurs a significant investment cost. Some congested areas even prevent the operator from carrying out such an extension. The difficulties involved in obtaining planning permission for new sites also favor extending the lifetimes of existing facilities, often with the additional goal of transmitting higher power with higher reliability to minimize the duration of asset unavailability. The challenge is to upgrade the existing cable system with reasonable and relevant solutions.

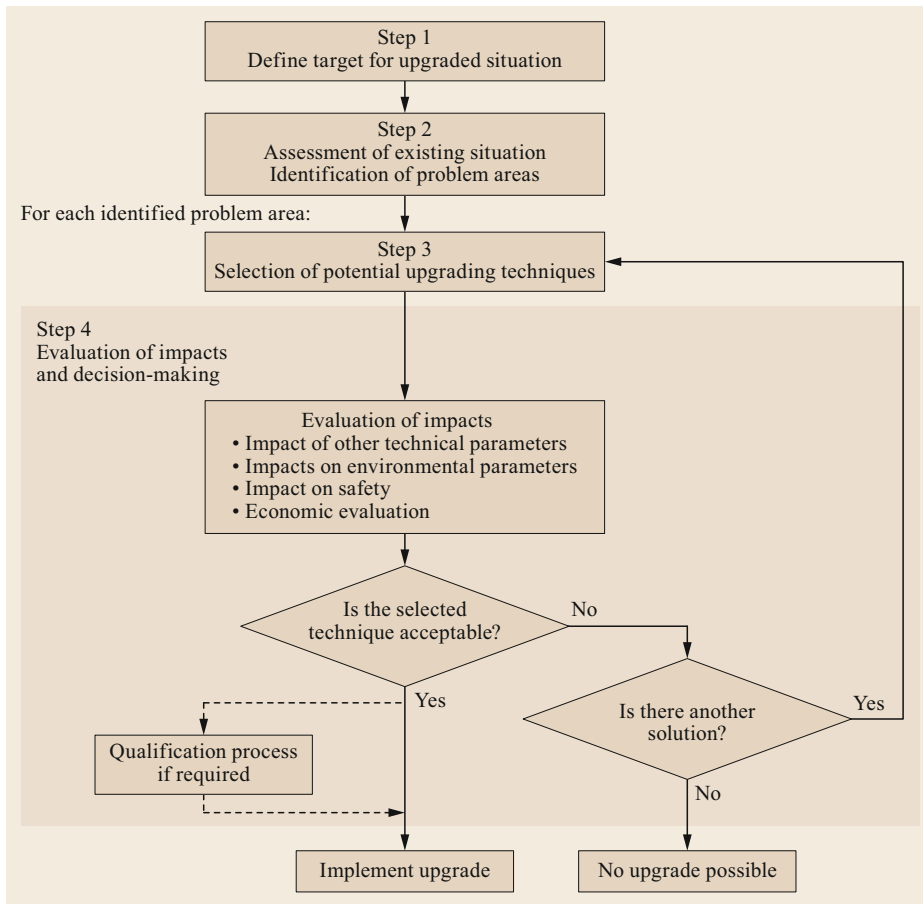
*Upgrading* is generally the process of improving equipment performance by replacing (working) components in order to meet new operating requirements (although other solutions are also discussed in TB 606 [10.65]). This allows the transmitted power, service life, environmental impact, and safety to be improved.

*Uprating* is the process of applying a physical solution that allows the system to be operated at a current level above its rated current, or the process of applying a method or a calculation that allows improved assessment of the performance of the system. In TB 606, uprating is treated as a special type of upgrading [10.65].

A simple step-by-step methodology with flowcharts is proposed in TB 606 to guide the engineer through the upgrading process. The steps involved, from the definition of the target for upgrading to the assessment of the existing situation, the identification of relevant issues, the selection of potential upgrading techniques, the evaluation of their impacts, and the decision-making step, are described.

An assessment of the actual condition and performance of the cable system is the first step in any upgrading process. In a thorough evaluation, a list of the parameters with the greatest influence on the specific aspect of the system to be upgraded (usually the transmitted power) is provided, as well as a list of the many other aspects of the link that could be impacted by the upgrading process.

Increasing the transmitted power is the usual aim of any upgrading process. Possible parameters to ex-



**Fig. 10.116**  
Step-by-step  
methodology  
for upgrading  
a cable (adapted  
from [10.65])

plore include the voltage level, the current rating, and the phase difference between the voltage and the current for AC systems. A fourth possible solution may also be considered: the conversion of the system from AC to DC. A panel of various solutions for increasing the current rating are considered: altering the current capacity (via new overload conditions, new calculation procedures, temperature monitoring), reducing losses, and improving heat transfer (using, e.g., ventilated tunnels, special backfill [10.15], hotspot smoothing, heat pipes, forced cooling, or reconductoring).

Other aspects of the performance of the cable may be upgraded, such as environmental and safety aspects. As an example, transition compounds may require upgrading (in terms of, e.g., audible noise, electromagnetic fields, and fluid leaks). Regarding safety issues, interesting solutions to reduce the risk of fire or an explosion (see also TB 560 published by B1.29 [10.49]) may be implemented. Fault containment should also be

considered in order to limit the consequences of a fault for the environment and people nearby.

Once upgrading solutions have been identified, it is highly recommended that the impact of the upgrade on other system functions should be explored, because changing the existing cable system may interfere with other technical or environmental parameters.

To illustrate possible applications, one chapter of TB 606 provides interesting case studies on upgrading, ranging from a simple reassessment of the current capacity of a link to a more complicated case involving forced cooling and retrofitting of new cable in existing pipes. Other examples can be found in the bibliography of TB 606 [10.65].

### 10.10.1 Proposed Methodology

Engineers design underground cable systems with great care. Since the life expectancy of such a system is often

more than thirty years, the potential evolution of the operating conditions of the power link is accounted for in its specification. The spread of urban areas, the establishment of industrial estates, or changes in the expectations of customers may lead to the need to increase the power transmitted. Some operating rules require circuit redundancy in order to compensate for the loss of a deficient line. In this case, the remaining systems must be able to transmit extra power in an emergency to ensure the reliability and availability of the overall network.

Sometimes the existing power network will become insufficient or inadequate. Replacing a link or installing an additional circuit may involve a substantial investment cost. A reasonable solution may be to improve the existing line or its environment. According to electrical engineering laws, the voltage level and/or the load current must be increased to boost the power transmitted.

It is important to understand that the process of upgrading an existing system involves an assessment of the feasibility of redesigning the cable system that accounts for higher stress levels. This redesign may, for example, include replacing components, modifying the cable environment, or installing monitoring devices.

To identify the most appropriate solution, TB 606 proposes a step-by-step methodology for upgrading

a cable that is illustrated by the chart shown in Fig. 10.116 [10.65].

Techniques for increasing the transmitted power include:

- Increasing the voltage level
- Increasing the current rating by reassessing the current capacity
- Increasing the current rating by assessing lower losses
- Increasing the current rating by improving heat transfer
- Increasing the current rating through forced cooling
- Reconductoring
- Improving the phase difference between the voltage and the current (compensation).

Another solution is to increase the performance by changing from AC to DC with:

- Intrinsic characteristics
- Suitability of the existing cable and its components for DC operation
- Transmittable real power
- Retrofitting of steel pipe when necessary.

## 10.11 Life-Cycle Assessment

WG B1.36 recently published TB 689 [10.66], which discusses the life-cycle assessment (LCA) of underground cables.

Electricity losses have been found to be the most important factor in the life cycle of an underground cable. In order to reduce these losses, the electrical resistance of the cable must be lowered, which can be achieved by increasing the crosssection of the conductor. LCA results can therefore be used in debates about the need to reduce electrical losses.

Based on the conclusions of a LCA, it may also be possible to propose materials and processes that result in a lower environmental impact in manufacturing, installation, and in the end-of-life phase of a cable.

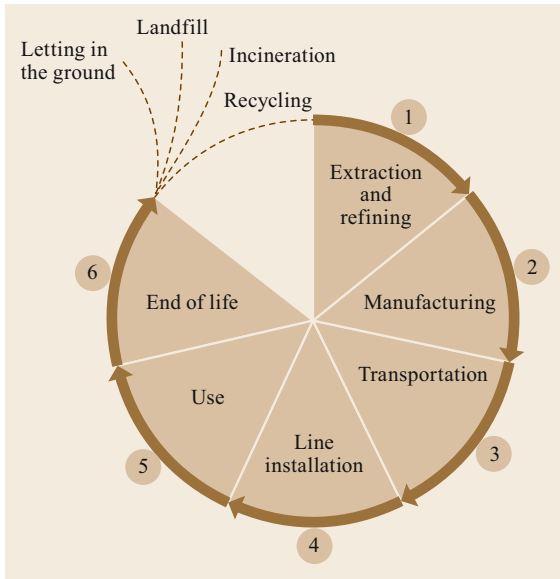
The manufacturing phase may be improved by introducing the use of recycled materials as input materials. This potential improvement should first be evaluated through a sensitivity analysis. For technical reasons that largely relate to recycled material performance, cable manufacturers may only use primary

metals and plastics. However, new technologies that use a thermoplastic insulating material that exhibits similar thermomechanical behavior to crosslinkable materials have recently been developed. Studies to improve the performance of recycled materials should also be carried out. There may be an opportunity to recover cables that have reached the ends of their lives and recycle some of the materials in them to reduce the costs of producing new cables, given that primary materials are becoming increasingly rare and expensive.

The scope of a LCA is from the cradle to the grave. The different steps in the life cycle of a cable that are taken into account are as follows:

- The *extraction, refining, and transportation* of raw materials, including minerals for metals (aluminum and/or copper) and petrochemicals for polymers
- The *manufacture* of intermediate materials, such as plastic granules, wire rods, cables, and accessories





**Fig. 10.117** Stages in the life cycle of an underground cable (adapted from [10.66])

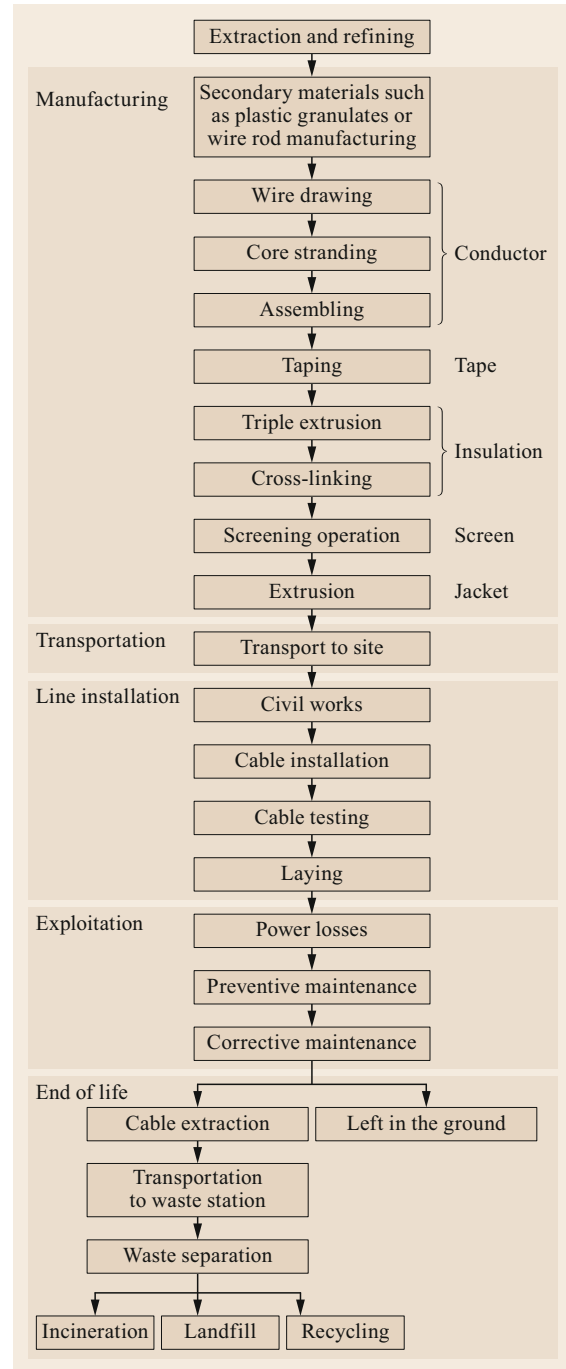
- The *transportation* of the cables and accessories from the construction site to the line installation site
- The *construction and installation* of the line
- The *operation* of the line
- The *end-of-life* phase.

This does not take into account the production, maintenance, and decommissioning processes for facilities and capital goods (such as buildings, machines, and roads) associated with cable manufacture, installation, and operation. This is because these facilities and capital goods are assumed to have a negligible environmental impact.

Figures 10.117 and 10.118 illustrate the life cycle of an underground cable. It is assumed that each cable will be pulled out of the ground after 40 years of operation due to regulatory requirements or for economical motives.

A practical example of a LCA for a 90 kV line is given in TB 689 [10.66].

**Fig. 10.118** Detailed summary of the life cycle of an underground cable (adapted from [10.66]) ▶



## 10.12 Superconducting Cables

Advances in superconducting cable technology [10.67] and in-grid applications of these cables have necessitated the development of an industry testing guideline on the design and performance requirements of superconducting cable systems: TB 538, prepared by WG B1.31 [10.68]. This guideline focuses on the requirements for AC high-temperature superconducting (HTS) cables based on cold dielectric designs. Low-temperature superconducting (LTS) materials, warm dielectric designs, and DC designs are not currently considered in the guideline.

HTS materials and applications of them have attracted considerable interest since the discovery of these materials in 1986. These superconducting materials can be cooled with liquid nitrogen (at  $77\text{ K} = -196^\circ\text{C}$ )—a relatively inexpensive, inert fluid that is easy to manage industrially. Despite this long period of development, HTS cables are still very much a new technology for the power utility industry. The cables covered in TB 538 can be categorized into three general designs:

1. *Single-core designs* (Fig. 10.119). These have one electrical phase per cryogenic envelope. Each phase incorporates a phase conductor, a dielectric, and a concentric neutral conductor. Three single-core cables are required for typical three-phase power system applications. Designs commonly use HTS wires for the concentric neutral layer and may or may not include copper wires to shunt short-circuit currents and protect the HTS wires.
2. *Three-core designs* (Fig. 10.120). These have three single-phase cable cores inside a common cryogenic envelope. This is also called a *triad* design.



**Fig. 10.119**  
Single-core HTS cable (adapted from [10.68])

Each core typically consists of a phase conductor, a dielectric, and a concentric neutral conductor made of HTS wires. The neutral conductor may or may not include copper wires to shunt short-circuit currents and reduce heat generation.

3. *Triaxial designs* (Fig. 10.121). Here, three electrical phases are arranged concentrically around a common core inside a common cryogenic envelope. The dielectric between the phases must withstand the phase-to-phase voltage rather than the typical phase-to-ground voltage. A concentric neutral conductor (HTS or copper) is typically located on the outside of the cable core. This design is used for medium voltages and optimizes the CAPEX (one superconducting screen, one cryostat for the whole system, and one cable to install).

### 10.12.1 Experience with Superconducting Cables

In-grid demonstration projects have shown that superconducting technology works and is technically viable. A list of in-grid demonstrations worldwide is shown in Table 10.10. Other demonstration projects around the world that were installed at test facilities or industrial sites are listed in Table 10.11. Additional development



**Fig. 10.120**  
Three-core HTS cable (adapted from [10.68])



**Fig. 10.121** Triaxial cable (adapted from [10.68])

**Table 10.10** Power grids that include HTS cables (data from 2012)

Country and utility	In-service date	Voltage (kV)	Designed power level (MVA)	Length (m)	Design
Denmark	2001	24	–	30	Warm dielectric, single-core <sup>a</sup>
China, China Southern Power Grid	2004	35	120	33.5	Warm dielectric, single-core <sup>a</sup>
USA, National Grid	2006	34.5	48	350	Three-core
USA, AEP	2006	13.2	69	200	Triaxial
USA, LIPA	2008	138	574	600	Single-core
South Korea, KEPCO	2011	22.9	50	500	Three-core
Japan, TEPCO	2012	66	200	250	Three-core

<sup>a</sup> This design utilizes a conventional extruded dielectric material that is extruded over the cryostat and operated at ambient temperature

**Table 10.11** Laboratory-tested and industrially applied HTS cables (data from 2012)

Country	Date of testing/application	Voltage (kV)	Designed power level (MVA)	Length (m)	Design
Japan, Super-GM	2005	77	133	500	Single-core
US, Carrollton	2000–2006	12.4	27	30	Single-core
South Korea, KEPRI	2007	22	48	100	Three-core
Mexico	2007	23	80	100	Three-core
Germany/Spain	2008	10	17	30	Single-core
Germany/Spain	2010	24	133	30	Single-core
Russia	2010	20	104	200	Single-core
South Korea	2011	154	1000	100	Single-core

and advances are needed in the area of cryogenic refrigeration and in improving the reliability of those systems.

Investments made around the world by various national government agencies and private industry have facilitated rapid advances in HTS cable, accessory, and cooling technologies. This trend is expected to continue, leading to further improvements in performance, efficiency, and ratings in the near future. These advances in HTS cable technology, combined with improvements in the manufacture of materials and components, will enhance the cost-benefit ratio of HTS cable implementation.

The HTS cables in development today are primarily envisioned as a solution to grid constraints in dense urban areas. Following the successful demonstration of the technology and economics needed to support implementation, HTS cables will remain a niche market for the short to mid-term (5–10 years), implying that the number of projects worldwide and the volume of HTS cables installed will remain limited.

### 10.12.2 Cryogenic System Issues

As mentioned earlier, WG B1.31 published TB 538, which gives recommendations for HTS cable testing [10.68]. Annex B of [10.68] provides information on cryogenic system technology that serves as an overview of the technology and the functional parameters associated with HTS cable operation. It also guides the user in key issues for system specifications.

Actual testing requirements and specific performance requirements of cryogenic refrigeration systems are not included.

The specific requirements for the operation and reliability of cryogenic cooling systems vary depending on the overall system design and performance expectations of the HTS cable. For example, the fault-limiting performance depends on different thermal operating parameters of the system. The operational tolerances of parameters such as temperature variation, pressure variation, heat load capacity, and buffer volume (installed to accommodate the expansion of the liquid when warmed above normal operating temperature) can all vary according to the manufacturer's system design philosophy and performance specifications.

TB 538 does briefly address the cryogenic aspects of safety and pressure containment. The piping and cooling system equipment used with HTS cables are commonly classified as high-pressure piping and pressure vessels in the relevant country's laws and specifications. As such, TB 538 does not propose specific requirements for HTS cables, but it does highlight critical issues for the reader.

### 10.12.3 Future Work

There are several key areas that must be addressed in future work on HTS cable testing. These issues represent challenges to the development and commercialization of the technology and will need to be resolved to

achieve the widespread market adoption of HTS cables for a range of applications. For AC cables, these areas of future work include routine/factory testing of completed cable lengths, aging tests of cryostats, and requirements for increased voltage levels.

There is currently no accepted methodology for the factory testing of full lengths of cable after manufacturing. Sample testing is performed at various stages during the manufacturing process and after completion. However, it is impractical to perform high-voltage and high-current tests on a full length of cables. The need to cool the cable to cryogenic temperatures and impregnate the dielectric tapes with the cryogen makes tests on full reels of finished cable impractical. Sometimes the cable reel at the factory does not include the cryostat. In all cases, the thermal contraction of the cable on the reel presents extreme difficulties. Methodologies to enable the factory testing of full lengths of cable in a similar way to conventional cables must be developed to facilitate the widespread adoption of HTS cables by the utility industry.

The cryostat used for HTS cables is typically a double-layer vacuum-jacketed corrugated pipe. Expe-

rience regarding the life expectancy of vacuum-jacketed cryostats is limited, although some cryostats of this type have been used for extended periods in similar applications at scientific and research labs such as CERN.

TB 538 focuses on HTS cables with  $U_m = 170$  kV ( $U = 150$  kV). However, 275 kV AC HTS cables are currently being developed at the time of writing. Testing guidelines will therefore need to be adapted to higher voltage limits in coming years to match research and development efforts around the world.

Some users may request long-term prequalification tests for HTS cable systems, similar to those defined in IEC 62067 or IEC 60840 for XLPE cables, due to the limited experience of HTS cables operating in a grid. The need for a prequalification test and/or its details will need to be discussed, taking into account the opinions of users and manufacturers, by future CIGRE or IEC working groups.

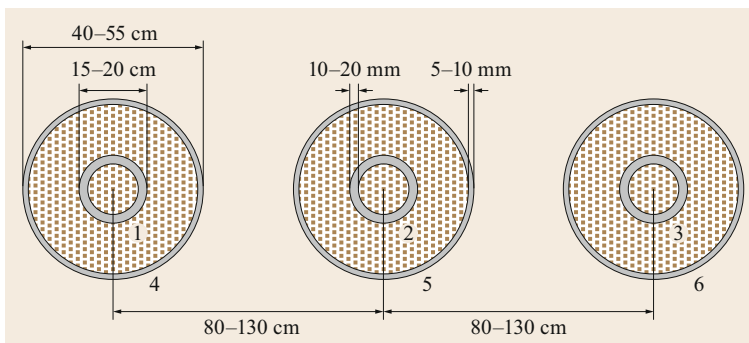
A CD on test methods and requirements for high-temperature superconducting power cables and their accessories with rated voltages from 6 kV ( $U_m = 7.2$  kV) up to 500 kV ( $U_m = 550$  kV), based on TB 538 [10.68], has been prepared by TC 90 and TC 20 of the IEC.

### 10.13 Gas-Insulated Lines

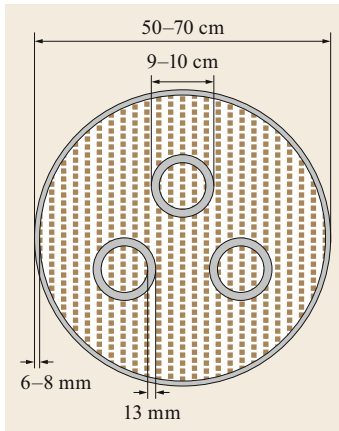
A gas-insulated line is a special type of electric transmission line, i.e., it transmits electric active power (and, in the time domain, electric energy) over a given distance. Gas-insulated lines go by various acronyms. The IEC acronym is GIL, while older acronyms include GITL (gas-insulated transmission line) and CGIC (compressed gas-insulated cable). Regardless of the acronym used, a gas-insulated line consists of a tubular enclosure made of high-conductivity aluminum or aluminum alloy in which each tubular phase conductor (aluminum) is held in a central position by epoxy resin insulators. As described in TB 639 (on factors that impact on the decision to invest in either GILs or cables for AC transmission) [10.7], there are two dif-

ferent kinds of GILs: single-phase (Fig. 10.122) and three-phase (Fig. 10.123) GILs. An example of the internal structure of a GIL is given in Fig. 10.124. The GIL configuration with three conductors in one enclosure suffers from phase-to-phase faults and significant interaction forces between the conductors, so it is generally not used in real-world installations. GILs are not used at the LV and MV levels.

GILs were developed directly from SF<sub>6</sub>-insulated substations (or gas-insulated substations, GISs). However, a GIL differs from a GIS in that the GIL has no switching or breaking functions. In the past, when GILs were called CGICs, they were considered a special type of insulated cable.



**Fig. 10.122** Indicative dimensions of a flat single-phase GIL (rated voltage 420–550 kV); the typical weight of one pipe without gas is 30–60 kg/m and the typical diameter is 400–550 mm (adapted from [10.7])



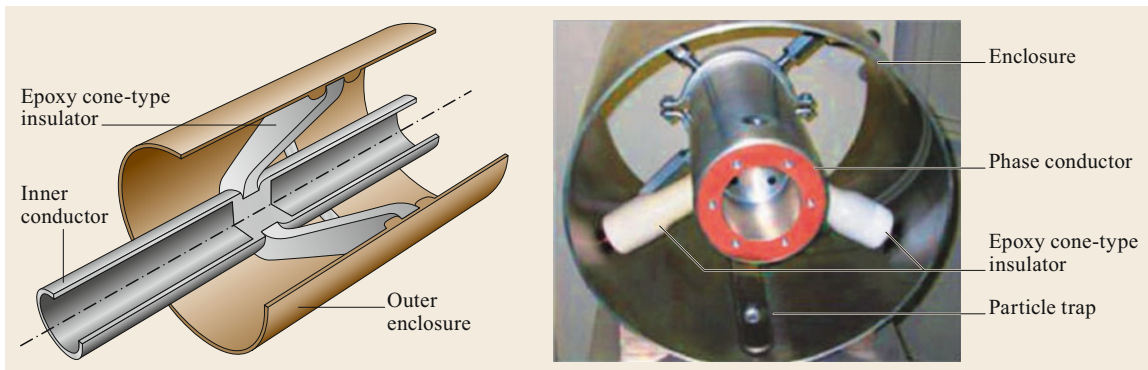
**Fig. 10.123** Three-phase GIL used in GIS at the lower high-voltage range up to 170 kV (adapted from [10.7])

First-generation GILs were built from standard GIS components using pure  $\text{SF}_6$  as the insulating gas and straight enclosures. In the year 2000, a second generation of GILs was introduced that could be used to transmit power over longer distances and had a reduced environmental footprint. These GILs utilize an insulating gas mixture (such as  $\text{SF}_6/\text{N}_2$ ) and a minimum bending radius of enclosures was introduced (typically 400 m).

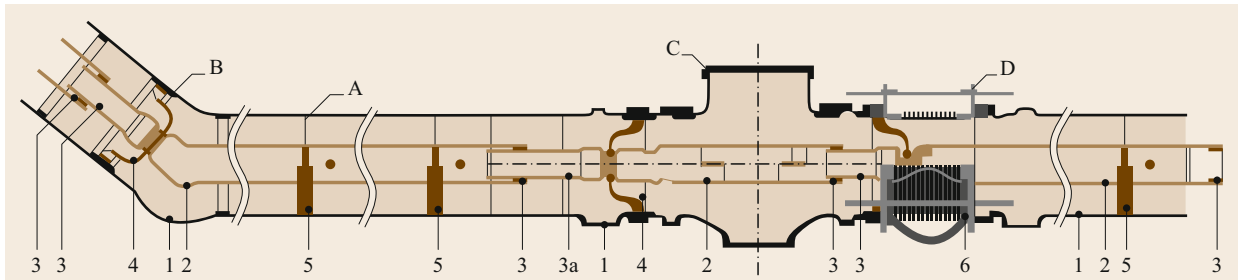
It is well known that isolated phase bus ducts have structures similar to those of GILs, but are often used at MV levels to connect generators to step-up transformers in power plants. These MV isolated phase bus ducts are insulated with air at atmospheric pressure and are manufactured to have the same general structure as GILs but have larger diameters (since the dielectric strength of air is one-third that of the gas most commonly used in GILs,  $\text{SF}_6$ , at a given pressure) and increased spacing. The use of  $\text{SF}_6$  in GILs requires the application of welded joint technology to reduce possible gas losses to a minimum. It is also recommended that  $\text{N}_2/\text{SF}_6$  gas mixtures should be employed on long transmission lines to reduce the amount of  $\text{SF}_6$  used. GILs can be supplied as sections that have been assem-

bled and tested in the factory. The factory-assembled GILs are shipped in sections up to 18 m long and are either bolted together with flanges (sealed with O-rings) or welded together in the field. GILs can also be supplied as elements that need to be assembled on-site. For this solution, conductor and enclosure lengths along with support insulators are transported to the installation site, where they are assembled in situ. Various elements, including a straight unit, an angled unit (such units can be angled by up to  $90^\circ$ ), a compensation unit, and a disconnecting unit, are depicted diagrammatically in Fig. 10.125. The shipping lengths of GIL elements may vary from 6 to 18 m depending on the installation and technology used. The maximum shipping length must be transportable to the installation site.

The assembled sections are joined together via plug-in contacts, and the enclosures are linked by on-site welding or bolted flanges. The quality of the enclosure welds is a crucial influence on line reliability, so a special computer-controlled orbital welding machine is used and every welded part undergoes ultrasonic testing to ensure the highest quality. This welding procedure is known to have a high degree of reliability and quality based on experience of its use in nuclear power plants. For bolted flange technology, tightness is ensured by the use of gaskets or seals. These seals can be different shapes, although O-rings are commonly used. The high degree of tightness is achieved by selecting the appropriate gasket (materials and shape) as well as by using the right installation procedures. The tools, equipment, and skilled labor needed to connect the flange-bolted GILs on-site are simpler than those needed for welded GIL technology. This simpler installation also permits many more bolted sections of GIL than welded GIL sections to be installed per day. In addition, when site maintenance or repairs are performed, the bolted technology is simpler to implement than the welded one. It should be noted that the flange-bolted solution would be very difficult to apply for directly buried GILs, so the welded solution is preferred.



**Fig. 10.124** Internal structure of a GIL (adapted from [10.7])



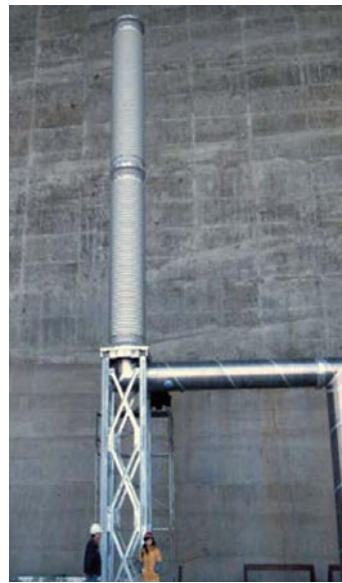
**Fig. 10.125** General overview of the units comprising a GIL: A: straight unit, B: angled unit, C: disconnecting unit, D: compensation unit; also shown are: 1: enclosure, 2: conductor, 3: sliding contact, 4: non-gastight insulator that provides a fixing point for the conductor, 5: sliding post-type insulator, 6: longitudinal thermal expansion compensator (adapted from [10.7])

GIS and GIL manufacturers have made continuous improvements over the last 30 years to ensure that GILs are virtually leak-free. The need for leaktight GIL systems is also driven by environmental concerns. Current standards (from both the IEEE and the IEC) require GIL systems to lose no more than 0.5% (by volume) of their gas per year. Designs for both welded and flange-bolted GIL have both improved to the point where it is straightforward to meet and exceed the required tightness standards. The welded GIL gas tightness easily exceeds these requirements; for instance, the first welded GIL installation, which dates from 1976, is still in service with the original gas fill.

The space between the phase conductor and enclosure is filled with an insulating gas which must withstand the phase-to-earth voltage. This insulating gas can be pure  $\text{SF}_6$  under a pressure of 0.3–0.5 MPa or a more environmentally friendly and less expensive  $\text{SF}_6/\text{N}_2$  mixture (typical ratio: 10–20%) at a higher pressure (up to 1.0 MPa). The insulating gas therefore always contains sulfur hexafluoride ( $\text{SF}_6$ ), an inert, nontoxic, nonflammable gas. More details of the environmental impact of  $\text{SF}_6$  are available in TB 351 [10.69]. The handling of  $\text{SF}_6$  is regulated in IEC 62271-4. The contribution of  $\text{SF}_6$  to global warming is small, and the use of  $\text{SF}_6$  is regulated by several regional directives, chiefly the new EU Regulation No. 517/2014 of 16 April 2014 on fluorinated greenhouse gases.

It is worth noting that the dielectric strength of  $\text{SF}_6$  is approximately three times that of air at a given pressure. This gas is widely used in high-voltage equipment, where its insulating properties permit compact structures. These structures must satisfy the IEC standard 62271-204 (for an insulating gas consisting of pure  $\text{SF}_6$  or a  $\text{SF}_6/\text{N}_2$  mixture under pressure).

With regard to dimensional characteristics, it should be noted that the optimal ratio between the inner diameter of the enclosure and the outer diameter of the conductor to minimize the electric field is 2.72. In prac-



**Fig. 10.126** GIL connection to overhead line via the bushing (800 kV example; adapted from [10.7])

tical applications, however, any ratio between 2.5 and 3 can be adopted since the electric field increases by only 0.5% in this interval.

A GIL enclosure resembles a gas transportation pipeline, which is why GILs are sometimes referred to as *electric pipelines*. So far, all real-world GIL installations have been short runs that were implemented instead of overhead lines or to provide connection points for hydroelectric, thermal, and nuclear power plants. However, the technical features of this electric transmission line indicate that is suitable for long lengths and bulk power transmission, as shown in TB 351 [10.69].

The most widely used laying type for GILs is above the ground inside substations, where they are used to connect overhead lines or transformers with GIS. Steel structures are typically used to hold the GIL above ground. For long-distance transmission, the connection of the GIL to the overhead line is most commonly done via a bushing as shown in Fig. 10.126.

**Table 10.12** Historical development of GILs

1971	First HV installation of a GIL insulated with pure SF <sub>6</sub> (first-generation GIL) in Eastlike, Ohio at a rated voltage of 345 kV (circuit length 122 m)
1972	First directly buried HV installation of a GIL insulated with pure SF <sub>6</sub> (first-generation GIL) at Hudson Switching Station in New Jersey at a rated voltage of 245 kV, 1600 A (circuit length 138 m)
1975	First HV installation of a GIL insulated with pure SF <sub>6</sub> in Ellensburg, Washington at a rated voltage of 550 kV, 3000 A (circuit length 192 m)
1976	First HV European installation of a GIL insulated with pure SF <sub>6</sub> (first-generation GIL) at a hydropump storage plant in Schluchsee, Germany, with a rated voltage of 400 kV (circuit length 670 m)
1981	First HV installation of a GIL insulated with pure SF <sub>6</sub> in Guri Dam, Venezuela at a rated voltage of 800 kV, 1200 A, 1925 kV BIL (total phase length 855 m, 5 circuits)
1997	Longest (phase length) installation (17 010 km) of a GIL insulated with pure SF <sub>6</sub> (first-generation GIL) at PP9, Saudi Arabia, with a rated voltage of 380 kV (circuit length 709 m, 8 circuits, for a total phase length of 17 010 m)
1998	Longest (circuit length) installation (3.3 km) of a GIL insulated with pure SF <sub>6</sub> (first-generation GIL) at Shinmeika-Tokai, Japan, with a rated voltage of 275 kV (circuit length 3300 m, 2 circuits)
2001	First HV installation of a GIL insulated with a SF <sub>6</sub> /N <sub>2</sub> gas mixture (second-generation GIL) in Geneva, Switzerland, with a rated voltage of 220 kV (circuit length 420 m)
2004	First HV installation of a GIL insulated with a SF <sub>6</sub> /N <sub>2</sub> gas mixture (second-generation GIL) in the UK at Hams Hall, with a rated voltage of 400 kV (circuit length 540 m)
2009	First HV installation of a 800 kV, 4000 A GIL (BIL 2100 kV) insulated with pure SF <sub>6</sub> in Laxiwa Dam, China (total phase length 2928 m, 2 circuits)
2012	First directly buried second-generation HV GIL at Kelsterbach substation near Frankfurt, Germany, with a rated voltage of 400 kV (circuit length 880 m)
2013	First installation of a 420 kV GIL with a 80N <sub>2</sub> /20SF <sub>6</sub> gas mixture, a bending radius of 400 m, and all welded joints, which passes under a Bavaria brewery (4 three-phase circuits each 1 km long in one tunnel, each circuit with a rated current of 3150 A)

### 10.13.1 Historical Development of GILs

The historical development of GILs is reported in Table 10.12.

### 10.13.2 Comparison of GILs to Conventional Cables

TB 639, prepared by JWG B3/B1.27 [10.7], was initiated to help clarify if the best solution for a particular transmission line project is extruded cables or a gas-insulated transmission line (GIL). Evaluating the options for a transmission line project is a complex task, and this technical brochure provides the information needed to make solid decisions based on the knowledge of experts in SC B1 (on cables) and SC B3 (on substations).

In TB 639 [10.7]:

- The economic parameters associated with UG cable and GIL installations are identified and the relative cost structures are given.
- Typical transmission solutions for GIL and UG cables are compared.
- Environmental impacts such as health and safety requirements and external electromagnetic fields are taken into account.

Technical definitions of cost factors and drivers are given in TB 639 to permit an informed comparison of solutions. Examples of these cost factors and drivers include

access to and the width of the route, system configuration, rights of way, safety aspects, fire-related aspects, transmission losses, reactive power compensation, aging of equipment, life-cycle costs, service experiences, gas tightness, recycling of the cable/GIL material in the end-of-life phase, CO<sub>2</sub> emissions (during production, installation, lifetime), waste disposal, geographical aspects, construction aspects, O&M, and standards and regulations. Practical applications are shown in TB 639.

The impacts of restoration cost factors in the case of failure and relevant outage durations are also covered in TB 639. Since the publication of TB 639, TB 773 on fault location in land and submarine cable links has also been published [10.64].

It is worth remembering that the aim of TB 639 is not to provide absolute costs but comparative and relative ones. It gives guidelines for case-by-case evaluation. Even though the transmission solutions presented in TB 639 are typical, they are not necessarily representative.

Most of the factors and economic parameters mentioned vary according to local conditions (e.g., civil works) and over time (e.g., the prices of raw materials). As mentioned in the executive summary of TB 639, any relative comparison is inherently insufficient to obtain satisfactory general results.

Section 10.A.1 below is an unbiased Reference Statement from CIGRE regarding AC land power transmission via overhead lines, gas-insulated lines, and

underground cables above 170 kV [10.70]. As noted in the introduction to the Statement, it attempts to explain the fundamentals of these technologies in a manner that can be understood by a nontechnical person or a person

who is not involved in the industry on a day-to-day basis. Of course, more detailed information can be found in previous sections of this chapter or in the chapter dedicated to overhead lines.

## 10.A Appendix

The following CIGRE Reference Paper [10.70], written by M. Marelli, P. Argaut, H. Lugschitz, and K. Kawakita, on behalf of CIGRE Study Committees B1, B2 and B3, is intended to provide unbiased information regarding options for HV and EHV AC transmission lines. The authors and the Technical Council of CIGRE have agreed to include this text in the Chapter 10 of this book, since UG Cables and GIL are covered in this chapter and Overhead Lines are the topic of Chap. 9.

### 10.A.1 Overhead Transmission Lines, Gas Insulated Lines and Underground Cables

There is a considerable amount of highly technical information, specifications and guides available on the transmission of bulk electrical power from one area to another. This information is available from bodies such as CIGRE, IEC (International Electrotechnical Commission), and many National-based organizations. There is, however, very little information that would explain the fundamentals of the technologies in such a manner that it could be understood by a non-technical person or a person not involved on a day-to-day basis in that industry. This paper will attempt to fulfil that need by providing basic information in hopefully a readily understandable manner.

This paper refers to transmission lines exceeding 170 kV alternating current (AC). Direct current (DC) connections and subsea cables are not a part of the scope of this paper (for those, other criteria apply to compare).

#### Technical Basics

Some of the fundamentals of power transmission are the voltage and current levels used to transmit the power from one area to another. Roughly speaking the voltage multiplied by the current is equal to the power. If one thinks of electricity in terms of water flow then voltage is like pressure i.e., it drives the current through the conductor in the same that pressure drives water through a pipe. Current is the flow of electricity through the conductor.

In AC transmission the power is transmitted utilizing a three phase system with three metallic conductors; the size of the conductors govern their thermal capability to carry current i.e., the larger the conductor the more current it can carry. The conductors must be in-

sulated from the ground and from each other in order to be able to withstand the voltage applied; again, the more insulation the higher the voltage that can be used in the transmission circuit.

The three conductors may be assembled in an overhead line circuit (OHL), an underground cable circuit (UGC) or a gas insulated lines (GIL) circuit. Each one will be described below.

One basic technical aspect to be considered is related to routing a transmission line, including:

- *Route availability*: it must be possible to construct the line.
- *Urbanization*: if the line is to be routed through an urban area, then future developments may have an impact on the route and design of the line.
- *Route topography*: if the terrain is very uneven or hilly, the technical challenges and costs increase.

#### Overhead Lines (OHL)

An overhead line circuit is typically composed of lattice steel towers which support the three conductors that make up the circuit. In some lines, tubular poles (pylons) are used instead of lattice structures. The conductors are insulated from the structures by means of insulators, which are made of toughened glass, porcelain or of composite materials.

Typical examples of OHL designs in current use are shown in several CIGRE Technical Brochures and the CIGRE Green Book *Overhead Lines*.





Depending on voltage and terrain, towers are typically 200–500 m apart from each other.

Many OHL designs are fitted with one or several earth wires at the top of the tower. These earth wires have two functions, firstly to protect the conductors from a lightning strike which might cause an outage and secondly in the event of a fault: the fault current will be mainly contained within the conductor/earth wire loop and returned to earth. Earth wires are often fitted with fiber optic elements for communication purpose.

It should be noted that in many cases OHLs have two electric circuits or more on the same tower. Each circuit may have 1–4 conductors in a bundle for each phase (and even more at Ultra High Voltage Lines). These OHLs can carry many times the power of a single circuit line with single conductors.

The design of an OHL depends on many factors including:

- *Conductor size*: the size of the conductor is dependent on the current to be carried. Of course, the size of the conductor also has an impact on the weight the tower must support—currently the standard maximum conductor size used is about 800 mm<sup>2</sup>.
- *Ground clearance*: the conductor must have a safe clearance from the ground and any buildings that may be located underneath it i.e., there must be no possibility of flashover from the conductors to the ground, persons or obstacles.
- *Impact of weather*: very strong winds may exert considerable mechanical loadings on the conductors and the towers; in addition, large ice loadings on conductors can impact on the towers. Of course, the worst loading is the potential combination of wind and ice. The lines are designed for such loadings.
- *Electrostatic/charging effects*: the impacts on metal structures in the proximity of the OHL are eliminated by earthing of such metallic facilities. In some countries, national regulations may apply in addition

to ICNIRP values (International Committee for Non-Ionising Radiation Protection).

- *Magnetic effects*: The current in the conductor produces a magnetic field, and the voltage produces an electric field, both must be considered during the design of the line. There are non-binding, but recommended limit values provided by ICNIRP 1998/2010. The ICNIRP recommendation must be considered taking into account of the costs and benefits and where the time of exposure is significant.

### Underground Cables (UGC)

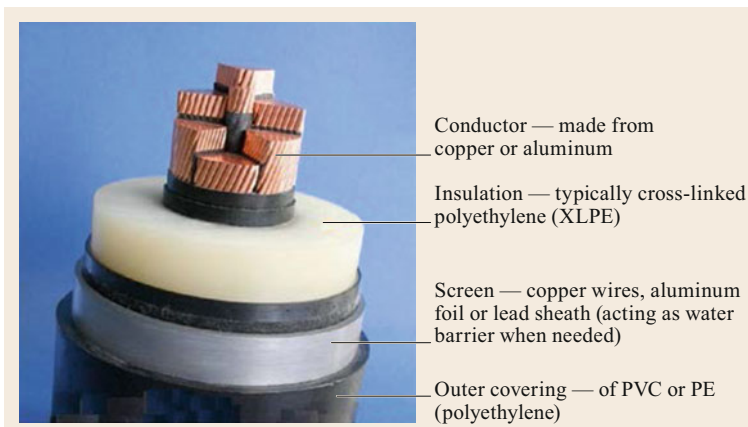
An underground cable circuit is composed of three power cables (three phases) and normally one communication cable installed in the ground to form one electric circuit. A typical design of a power cable is shown in figure below.

If the power to be transmitted is beyond the capability of one circuit, more parallel cable circuits (or more cables per phase) must be installed. The larger the conductor the more current it can carry and the thicker the insulation the more voltage it can withstand. The cables are manufactured in highly specialized factories and they are normally delivered in drum lengths varying from 500–1000 m. In some cases, delivery cuts can be longer (2000 m and above).

Such a circuit of 10 km route length with drums of 1000 m would have 10 × 3 i.e., 30 drums in total. It would require 27 joints to join the cables together and there would be 3 terminations or sealing ends at each end (Substation, Transition Compound or Equipment installed on towers).

The cables are typically installed in one of the following arrangements:

- Directly in the ground (trench)
- In ducts installed in the ground
- In concrete troughs
- In a tunnel



- In a pipe or pipes drilled into the ground to pass under some obstacle or encumbrance
- On a cable tray attached to a bridge.

The design of an underground cable circuit depends on many factors including:

- *Conductor size*: the size of the conductor is dependent on the current to be carried and the increase of temperature (due to the current flowing through the cable) of the surroundings as allowed by regulations. Of course, the size of the conductor also has an impact on the weight and size of the cable drum being delivered – currently the maximum standard conductor size used is 2500 mm<sup>2</sup>.
- *Soil thermal conductivity*: the conductor size has an impact on the ability of the cable to dissipate the heat, which is created by the current flowing through the cable when it is delivering power. In the case of a cable installed in the ground this heat must travel through the soil surrounding the cable. Therefore the ground thermal conductivity and temperature also have an impact on the cable sizing.
- *Presence and possible impact*: of other services in the soil which may conflict with the cable route either now or in the future (e.g., other cables, heating or cooling pipes, water supply and waste water).
- *Urbanization*: if the cable is to be routed through an urban area future building or road developments may impact on the circuit.
- *Possibility of flooding*: flooding may undermine the installed cable circuit.
- *Cable pulling*: the route and drum lengths and route topography must be such that the cables can be pulled into the selected installation arrangement i.e., trench, duct, tunnel, etc.
- *Electrostatic effects*: underground cables have no electrostatic effects initiated by the cable as the electric field is contained inside the cable and shielded by the screen. Electrostatic effect may come from equipment installed above ground (terminations).
- *Magnetic effects*: the current sets up a magnetic field which must be considered during the design of the underground circuit. As for OHL, the ICNIRP recommendation must be considered taking into account of the costs and benefits and where the time of exposure is significant. It should be noted that underground cables have higher magnetic fields than overhead lines at close distance, but the fields fall off more rapidly with distance.

### Gas-Insulated Lines (GIL)

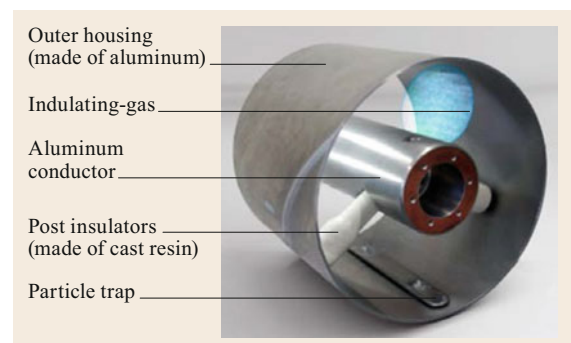
GIL are generally composed of three parallel aluminum tubes for one three phase circuit. The aluminum tubes

are in sections (typically 12–18 m long and 500 mm enclosure diameter). They are bolted together with flanges (sealed with O-rings) or welded together on site to be gas tight (automated welding process including 100% weld quality control by ultra-sonic test). Inside each enclosure pipe a smaller cylindrical aluminum conductor pipe is supported by cast resin post insulators. The GIL enclosure pipe is filled with a gas mixture of 20% sulphur hexafluoride (SF<sub>6</sub>) and 80% nitrogen at 0.8 MPa pressure to reduce the greenhouse impact from SF<sub>6</sub>.

GIL may have approximately the same transmission capacity as an overhead line and about double the capacity of a XLPE cable system, depending on actual situations. GIL systems are mostly used to EHV voltages (> 245 kV) up to 1000 kV. GIL installation is adapted to pipe line laying technologies and is carried out at local assembly and installation on site. All parts are delivered to the construction site and the laying follows a continuing process. The cost efficiency for this on-site laying process increases with the length of the transmission line to be above 1 km. For shorter length the factory orientated laying process may be more cost effective. This on-site laying process has been verified in many projects world-wide and offers a reliable and safe installation of the GIL. When the outer diameter of the enclosure is enlarged to about 750 mm also a clean air solution of GIL can be offered using Nitrogen and Oxygen only with a GWP (Global Warming Potential) of zero.

GIL are typically installed above ground, in tunnels (phases in vertical or horizontal arrangement) or in underground galleries. Direct buried installations are uncommon today, as it requires additional coatings for passive corrosion protection and cathode corrosion. Experiences with GIL worldwide is constantly increasing with ever larger project sizes (10–20 km route length), higher rated voltages (mainly 400, 500 and 1000 kV) and current ratings (3000, 4000 and 5000 A). The longest installation is the Tokai Line of Chubu Electric in Japan with two three phase systems of 275 kV and 5000 A of 3.3 km transmission route length in a tunnel.

The design of a GIL circuit depends on many special factors including:



- *Presence and possible impact:* of other services which may conflict with the GIL route either now or in the future (e.g., cables, heating or cooling pipes, water supply and waste water).
- *Route considerations:* the given bending radius can be a limiting factor for a route.
- *Urbanization:* if the line is to be routed through an urban area, future building or road development may impact on the circuit, that's why separate tunnels for electric transmission lines may be the best solution.
- *Electromagnetic effects:* GIL circuits have negligible electromagnetic effects as the electric field is earthed through the metallic enclosure. The magnetic field is mostly superposed by the induced current into the solid grounded enclosure pipe.

### Advantages and Disadvantages of Various Technologies

It is very difficult to compare the three technologies as each circuit installation is different with respect to location, importance of the circuit, reputational and financial impact if there is an outage, method of installation, operational and maintenance aspects, environmental impact, planning/licensing, etc. In view of this no general conclusions can be drawn, and each installation must be treated on a case by case basis. For the comparison of GIL and UGC see CIGRE TB 639.

In Table 10.13 we endeavor to compare the three technologies under the listed heading.

The operational and environmental aspects are considered in Sects. 10.A.1, *Operational Aspects*, *Environmental Issues* below.

Each of the above factors needs to be considered specifically for the project being investigated taking the potential installation methodologies into account, which is for UGC and GIL e.g., direct burial, ducting, horizontal directional drilling, tunnelling. Lifetime-costs may give other factors than investment costs. They

also depend strongly on the project and must be calculated case by case.

In order to rank the different possibilities, a scoring system could be developed for each of the above factors. Notwithstanding any scoring system experience and mature technology will always be important in any project as the Line owner will not wish to use unproven technology, as that would constitute a high and unacceptable risk.

### Operational Aspects

In the Table 10.14 the various technologies are compared from an operational point of view.

Each of the above factors needs to be considered specifically for the project being investigated taking the potential installation methodologies into account e.g., direct burial, ducting, horizontal directional drilling, tunnelling, etc.

Due to the very different electrical parameters of the UGC, the application of UGC introduces a series of technical challenges that must be addressed during planning, design and operation stages of the UGC system. In AC networks there normally is an offset between the current and voltage. This is due to the different components and loads in the network. The current will fill up the conductor to a certain degree, but only a part of the current can be used as *real power* because of this offset. The rest is *reactive power*. This reactive power shall be compensated to reduce the losses in the network and to control the voltage.

The exchange of reactive power between the UGC and the power system is significantly higher compared to an equivalent OHL. This reactive power must be compensated and therefore a number of additional components are introduced. This adds complexity to the system both in term of operation and maintenance.

Another complication that must be addressed is the shift in system resonance frequencies introduced by

**Table 10.13** Comparison of technologies

	UGC	OHL	GIL
Investment costs	High	Not so high	High
	There are no general rules for the comparison, as the cost of each technology will depend on how that technology deals with the specific factors that apply on each specific project		
Installation difficulty	Yes	No	Yes
Experience	Yes	Yes	Yes
Mature technology	Yes	Yes	Yes, for short lengths above ground
Competitive tendering	Yes	Yes	Yes, some cases with short length
Reliability	Yes	Yes	Yes
Repair time	High <sup>a</sup>	Low	High <sup>a</sup>
Lifetime	> 40 years	> 80 years	> 50 years
Installation time	Depending on local site conditions and requirements	Faster than UGC or GIL	Depending on local site conditions and requirements

<sup>a</sup> Highly dependent on the availability of spare parts and thus on maintenance policy

**Table 10.14** Comparison of operational issues

	UGC	OHL	GIL
Length limitation	Yes (60–100 km depending on voltage)	No	No theoretical technical limitation
Need for electric compensation	Yes, if longer than above	No	No
Extreme weather effects e.g., mechanical overloading due to ice/snow/wind	No	Possible	No
Can be re-energized if temporary fault	No, as faults that occur are not temporary Experience exist of reclosure for combined OHL-UGC lines	Yes	Yes, auto reclosure is possible
Ease of fault finding	No	Yes	Yes
Ease of fault repair	No	Yes	No
High level of expertise required for repair	Yes	No	Yes
Difficult to store repair material	No	No	No
Limited shelf life time of repair material	Yes	No	Yes
Outage time required after fault	Long	Short	Long
Haul road required for access	Yes, if installed in cross country	No	No

the application of UGC. Experience from several countries shows that amplification of background harmonics (electrical noise) occurs due to interaction between the UGC and the power system. Furthermore, the risk of temporary overvoltages is also increased for the same reasons. Both diminished power quality (due to electrical noise) and temporary overvoltages are serious challenges for which mitigation methods are expensive. A further complication is that study and design for the mentioned issues are still comparable immature and little practical experience exist worldwide. Hence, it can be difficult to quantify the risk to the system when a longer UGC is added.

The capacitive load of GIL is much lower (factor 4–5) than for solid insulated cables. Therefore, a phase angle compensation is only needed with GIL transmission length of 100–200 km length. This is depending on the network conditions and needs to be calculated. In principle the GIL can be operated like an OHL including the auto-reclosure function for short time interruption without any danger to the surrounding.

### Environmental Issues

In the Table 10.15 the various technologies are compared from an environmental impact point-of-view.

### Behavior Under Large Disturbances

The Table 10.16 compares the technologies when subject to large disturbances.

### New Technologies

OHL, UGC and GIL continue to evolve with improvements in the manufacturing and in the installation equipment and technologies.

As far as the technology aspect is concerned for OHL, the adoption of composite insulators has been widely adopted. In addition, the use of high temper-

ature conductors and real-time rating applications has become standard use.

For UGC there have been some developments in polymeric materials for insulation other than the currently used XLPE, but it is not yet clear when they will become commercially used. In addition, sensors are often embedded in UGC thus improving the use of real time monitoring and management systems.

There is little further development in the GIL technology, except maybe the routes can become longer. Insulating gases others than  $N_2/SF_6$  gas mixtures are under development for clean air ( $N_2/O_2$ ).

### Better Use of Existing Lines

One of the areas of interest is about the *better use of existing lines* i.e., the possibility to get more power through the existing lines as this might replace or postpone the need for a new development.

In the case of existing OHL it is possible to replace existing conductors with high temperature conductors or to use real time rating applications or to increase the voltage. Existing AC OHL can be converted to DC, if the design of the line allows this. A remarkable increase of transport capacity can be achieved.

In the case of both UGC and GIL the preferred method to increase the power capacity on existing lines consists in the possible use of real time rating applications and the mitigation of hot spots. For buried systems (typically for UGC) this is associated with the longer thermal transients that may allow for cables overloads.

### Conclusions

The fundamentals of UGC, OHL and GIL technologies have been outlined in Sect. 10.A.1, *Technical Basics*. It is very difficult to compare the three technologies as each installation is different with respect to location, importance of the circuit, costs, reputational and financial

**Table 10.15** Comparison of environmental issues

	UGC	OHL	GIL
Landscape and visual	Maybe, if going across open landscape and need construction access roads	Yes	Limited impact, as the construction site for GIL can be kept short (some 100 m)
Electric field effects (voltage)	No	Yes	No
Magnetic field effect (current)	Yes, limited	Yes	No, because of induced return current.
Noise effects	Yes during construction. No during operation	Yes during construction. Can be during operation at certain weather conditions (corona)	Yes during construction. No during operation
Restricted use of land	If UGC going across fields, the area over the cable may be used for ordinary crops but not for trees. No excavation or deep ploughing is allowed. Restrictions depends on local regulations	Limited to tower footing area and possible restrictions regarding trees and buildings under the conductors	If GIL going across fields restrictions similar to those for UGC are expected—dependent on installation method
Geology and soils	Possible impact during construction	Possible limited impact at tower areas	Possible impact during construction
Water resources	Possible impact during construction	Possible limited impact at tower areas	Possible impact during construction
Ecology and nature	Possible impact during construction	Possible limited impact at tower areas	Possible impact during construction
Cultural re-sources	Possible impact on archeological important areas	Possible impact on archeological important areas at tower areas	Possible impact on archeological important areas
Recreation and tourism	Limited impact	Maybe some impact depending on location	Limited impact
Air quality	Possible impact during construction	Possible impact during construction	Possible impact during construction
Traffic and noise	Possible impact during construction	Possible impact during construction	Possible impact during construction
Requirement for dumping material off site	Maybe, during construction	Limited	Maybe during construction
Acceptance by landowners	Yes	Limited acceptance	Yes
Acceptance by public	Yes	Limited acceptance	Yes

**Table 10.16** Comparison of behavior under large disturbances

Heading	UGC	OHL	GIL
Earthquake	Major damage can occur, but flexible mitigation methods can limit damage	Limited damage to structures can occur	Major damage can occur, but flexible designs important
Tsunami	Damage to exposed ends only	Major damage	Damage to exposed ends only
Storms, hurricanes, tornadoes, typhoons etc.	Minimum damage, only to exposed ends	Extensive damage to lines, if not designed for such events. Falling and blown down trees will be an issue	Minimum damage, only to exposed ends
Flood	No damage except in wash-out areas. De-energise circuit for safety reasons	Structures can be taken out in wash-out areas, but otherwise minimum damage	No damage except in wash-out areas. De-energise circuit for safety reasons
Wild fire and bush-fire	Minimum damage to cable route, damage to exposed ends. Burial depth important	Extensive damage during heavy fires	Minimum damage to cable route, damage to exposed ends. Burial depth important
Landslide	Scouring damage only. Otherwise no damage	Damage to concerned structures	Scouring damage only. Otherwise no damage

impact if there is an outage, method of installation, operational and maintenance aspects, environmental impact, planning/licensing, lifetime, etc. In view of this no general conclusions can be drawn and each installation must be treated on a case by case basis using the headings outlined in Sects. 10.A.1, *Overhead Lines (OHL)*, *Underground Cables (UGC)*, *Gas Insulated Lines (GIL)*.

In order to rank the different development possibilities a scoring system could be used for each of the headings. Notwithstanding any scoring system, some headings will always be important in any project as the Project Engineer will not wish to propose an installation that would be unacceptable to the planners or to proceed with a development that may appear too costly or where the technology is not suitable for the proposed end-use.

### Literature

CIGRE published lot of documents and Technical Brochures (TB) that can help to further understand the technologies available for power transmission. Most relevant are:

- TB 194: Construction, laying and installation techniques for extruded and SCFF cable systems
- TB 218: Gas insulated transmission lines (GIL)
- TB 250: Technical and Environmental issues regarding the integration of a new HV underground cable system in the network
- TB 351: Application of long high capacity gas-insulated lines in structures
- TB 498: Guide for application of direct real-time monitoring systems
- TB 583: Guide to the conversion of existing AC lines to DC operation
- TB 601: Guide for thermal rating calculations of overhead lines
- TB 606: Upgrading and uprating of existing cable systems
- TB 639: Factors for investment decision GIL vs cables for AC transmission
- TB 680: Implementation of long AC HV and EHV cable systems
- TB 695: Experience with the mechanical performance of non-conventional conductors
- TB 748: Environmental issues of high voltage transmission lines in urban and rural areas
- TB 756: Thermal monitoring of cable circuits and grid operator's use of dynamic rating systems
- CIGRE Green Book *Overhead Lines*
- CIGRE Green Book *Substations*.

## 10.B Further Reading

- CIGRE Green Book: Accessories, expected end of 2020 (Springer, Cham 2020)
- IEC Standards: <http://webstore.iec.ch/>
- Proceedings of Jicable Conferences: <http://www.jicable.org>
- Annual Reports of SC B1, April issue of Electra, each year since 2012
- Proceedings of CIGRE Sessions including Special Reports and General Reports of the Sessions
- IEEE/PES/ICC Minutes: <https://www.pesicc.org/iccWebSite/>
- R.B. Abernethy: *The New Weibull Handbook*, 5th edition (2006)
- K.C. Agrawal: *Industrial Power Engineering and Applications Handbook* (Newnes, Boston 2001)
- G.J. Anders: *Rating of Electric Power Cables* (IEEE/McGraw-Hill 1997)
- R. Bartnikas, K.D. Srivastiva (Eds): *Power and Communication Cables* (IEEE, New York 2000)
- DNV-RP-J301: *Subsea Power Cables in Shallow Water* (Det Norske Veritas AS, Bærum 2014)
- O. Gilbertson: *Electric Cables for Power and Signal Transmission* (Wiley, New York 2000)
- L. Heinhold (Ed.): *Power Cables and Their Applications* (Siemens AG, Erlangen 1990)
- IEEE Standard 1120: *IEEE Guide for the Planning, Design, Installation and Repair of Submarine Power Cable Systems* (2004, reaffirmed 2010)
- D. McAllister: *Electric Cables Handbook* (Granada Technical Books, St. Albany 1982)
- G.F. Moore: *Electric Cables Handbook*, 3rd edn, BICC Cables (Blackwell Science, Oxford 1998)
- *Offshore Transmission Technology, European Network of Transmission System Operators for Electricity*, 24.11.2011, prepared by the regional group North Sea for NSCOGI (North Seas Countries' Offshore Grid Initiative)
- T. Tanaka, A. Greenwood: *Advanced Power Cable Technology*, Vols I, II (CRC, Boca Raton 1983)
- CIGRE TB 370 *Integration of Large Scale Wind Generation Using HVDC and Power Electronics*
- T. Worzyk: *Submarine Power Cables* (Springer, Berlin, Heidelberg 2009)
- D. Kunze: *Untersuchungen an Grenzflächen zwischen Polymerwerkstoffen unter elektrischer Hochfeldbeanspruchung in der Garniturentechnik VPE-isolierter Hochspannungskabel*, Dissertation (Shaker, Aachen 2000)

## 10.C CIGRE Technical Brochures to be Published

The following Technical Brochures will be published by CIGRE in the near future (note that when a Technical Brochure is published, it is announced at [e-cigre.org/](http://e-cigre.org/)):

- B1.38: *After Laying Tests on AC and DC Cable Systems with New Technologies*
- B1.54: *Behavior of Cable Systems Under Large Disturbances*
- B1.56/B1.72: *Cable Ratings Verifications*
- B1.57: *Update of Service Experience of HV Underground and Submarine Cable Systems*
- B1.58: *Asset Management in MV Cable Networks*
- B1.60: *Maintenance of HV Cable Systems*
- B1.61: *Installation of HV Cable Systems*
- B1.62: *Recommendations for Testing DC Extruded Cable Systems for Power Transmission at a Rated Voltage Up to and Including 800 kV*
- B1.63: *Additional Recommendations for Mechanical Testing of Submarine Cables for Dynamic Applications*
- B1.64: *Evaluation of Losses in Armoured Three Core Power Cables*
- B1.66: *Recommendations for Testing DC Lapped Cable Systems for Power Transmission at a Rated Voltage Up to and Including 800 kV*
- B4/B1/C4.73: *Surge and Extended Overvoltage Testing of HVDC Cable Systems*
- C4/B4/38: *Network Modelling for Harmonic Studies*
- D1.54: *Basic Principles and Practical Methods to Measure, to Establish Recommendations for Measurement of AC and DC Resistance of Conductors of Power Cables and Overhead Lines*

### References

- |                                                                                                                                                                                                                                                                                                                                                                                                                                                                                                                                                                                                                                                                                                                                                                                                                                                                                                                                                                                                                                                                                                                                                                                                                                                                                                                                                                                                                                                                                                                                                                                                                                                                                                                                                                                                                                                                                                                                       |                                                                                                                                                                                                                                                                                                                                                                                                                                                                                                                                                                                                                                                                                                                                                                                                                                                                                                                                                                                                                                                                                                                                                                                                                                                                                                                                                                                                                                                                                                                                                                                                                                                                                                                                                                                                                                                                                                                                                                                                      |
|---------------------------------------------------------------------------------------------------------------------------------------------------------------------------------------------------------------------------------------------------------------------------------------------------------------------------------------------------------------------------------------------------------------------------------------------------------------------------------------------------------------------------------------------------------------------------------------------------------------------------------------------------------------------------------------------------------------------------------------------------------------------------------------------------------------------------------------------------------------------------------------------------------------------------------------------------------------------------------------------------------------------------------------------------------------------------------------------------------------------------------------------------------------------------------------------------------------------------------------------------------------------------------------------------------------------------------------------------------------------------------------------------------------------------------------------------------------------------------------------------------------------------------------------------------------------------------------------------------------------------------------------------------------------------------------------------------------------------------------------------------------------------------------------------------------------------------------------------------------------------------------------------------------------------------------|------------------------------------------------------------------------------------------------------------------------------------------------------------------------------------------------------------------------------------------------------------------------------------------------------------------------------------------------------------------------------------------------------------------------------------------------------------------------------------------------------------------------------------------------------------------------------------------------------------------------------------------------------------------------------------------------------------------------------------------------------------------------------------------------------------------------------------------------------------------------------------------------------------------------------------------------------------------------------------------------------------------------------------------------------------------------------------------------------------------------------------------------------------------------------------------------------------------------------------------------------------------------------------------------------------------------------------------------------------------------------------------------------------------------------------------------------------------------------------------------------------------------------------------------------------------------------------------------------------------------------------------------------------------------------------------------------------------------------------------------------------------------------------------------------------------------------------------------------------------------------------------------------------------------------------------------------------------------------------------------------|
| <p>10.1 R. Arrighi: From Impregnated paper to polymeric insulating materials in power cables, <i>IEEE Trans. Electr. Insul.</i> <b>EI-21</b>(1), 7–18 (1986)</p> <p>10.2 R. Schroth: State, trends and evolutions of HV/EHV power cables systems and contributions of SC B1 to their ongoing progress, <i>Electra</i> <b>229</b>, ELT_229_2 (2006)</p> <p>10.3 M. Marelli: Insulated cables, <i>Electra</i> <b>309</b>, Annual Report SC B1 (2020)</p> <p>10.4 P. Argaut: Insulated cables for energy transmission at UHVAC level. In: <i>CIGRÉ–EIC Colloq., Montreal</i> (2016)</p> <p>10.5 IEC: Standards, <a href="http://webstore.iec.ch/">http://webstore.iec.ch/</a></p> <p>10.6 A. Gustafsson, F. de Wild: Prospects and limitations in respect of future ratings of HVDC cables. In: <i>CIGRÉ Int. Symp. Across Bord. HVDC Syst. Market Integr., Lund</i> (2015)</p> <p>10.7 TB 639: <i>Factors for Investment Decision GIL Versus Cables for AC Transmission</i>, JWG B3/B1.27 (CIGRÉ, Paris 2015)</p> <p>10.8 TB 250: <i>Technical and Environmental Issues Regarding the Integration of a New HV Underground Cable System in the Network</i>, WG B1.19 (CIGRÉ, Paris 2004)</p> <p>10.9 TB 338: <i>Statistics of AC Underground Cables in Power Networks</i>, WG B1.07 (CIGRÉ, Paris 2007)</p> <p>10.10 TB 379: <i>Update of Service Experience of HV Underground and Submarine Cable Systems</i>, WG B1.10 (CIGRÉ, Paris 2009)</p> <p>10.11 TB 536: <i>Influence of Embedded HVDC Transmission on System Security and AC Network Performance</i>, JWG C4.B4/C1 (CIGRÉ, Paris 2013)</p> <p>10.12 TB 247: <i>Optimization of Power Transmission Capability of Underground Cable Systems Using Thermal Monitoring</i>, WG B1.02 (CIGRÉ, Paris 2004)</p> <p>10.13 TB 194: <i>Construction, Laying and Installation Techniques for Extruded and Self-Contained Fluid Filled Cable Systems</i>, WG 21.17 (CIGRÉ, Paris 2001)</p> | <p>10.14 TB 680: <i>Implementation of Long AC HV and EHV Cable Systems</i>, WG B1.47 (CIGRÉ, Paris 2017)</p> <p>10.15 TB 714: <i>Long Term Performance of Soil and Backfill Systems</i>, WG B1.41 (CIGRÉ, Paris 2017)</p> <p>10.16 TB 720: <i>Fire Issues for Insulated Cables in Air</i>, WG B1.51 (CIGRÉ, Paris 2018)</p> <p>10.17 TB 398: <i>Third-Party Damage to Underground and Submarine Cables</i>, WG B1.21 (CIGRÉ, Paris 2009)</p> <p>10.18 TB 403: <i>Cable Systems in Multi-Purpose or Shared Structures</i>, WG B1.08 (CIGRÉ, Paris 2010)</p> <p>10.19 TB 756: <i>Thermal Monitoring of Cable Circuits and Grid Operators' Use of Dynamic Rating Systems</i>, WG B1.45 (CIGRÉ, Paris 2019)</p> <p>10.20 TB 373: <i>Mitigation Techniques of Power-Frequency Magnetic Fields Originated from Electric Power Systems</i>, WG C4.204 (CIGRÉ, Paris 2009)</p> <p>10.21 TB 559: <i>Impact of EMF on Current Ratings and Cable Systems</i>, WG B1.23 (CIGRÉ, Paris 2013)</p> <p>10.22 TB 748: <i>Environmental Issues of High Voltage Transmission Lines in Urban And Rural Areas</i> (CIGRE, Paris 2018)</p> <p>10.23 K.W. Barber: Achievement and experience in service of long length high voltage AC electrical links by insulated power cables. In: <i>AORC Tech. Meet.</i> (2014)</p> <p>10.24 TB 669: <i>Mechanical Forces in Large Cross Section Cable Systems</i>, WG B1.34 (CIGRÉ, Paris 2016)</p> <p>10.25 TB 520: <i>Material Properties of Solid HVDC Insulation Systems</i>, WG D1.12 (CIGRÉ, Paris 2012)</p> <p>10.26 TB 531: <i>Cable Systems Electrical Characteristics</i>, WG B1.30 (CIGRÉ, Paris 2013)</p> <p>10.27 TB 556: <i>Power System Technical Performance Issues Related to Application of Long HVAC Cables</i>, WG C4.502 (CIGRÉ, Paris 2013)</p> <p>10.28 TB 640: <i>A Guide for Rating Calculations of Insulated Cables</i>, WG B1.35 (CIGRÉ, Paris 2015)</p> <p>10.29 TB 272: <i>Large Conductors and Composite Screens</i>, WG B1.03 (CIGRÉ, Paris 2005)</p> |
|---------------------------------------------------------------------------------------------------------------------------------------------------------------------------------------------------------------------------------------------------------------------------------------------------------------------------------------------------------------------------------------------------------------------------------------------------------------------------------------------------------------------------------------------------------------------------------------------------------------------------------------------------------------------------------------------------------------------------------------------------------------------------------------------------------------------------------------------------------------------------------------------------------------------------------------------------------------------------------------------------------------------------------------------------------------------------------------------------------------------------------------------------------------------------------------------------------------------------------------------------------------------------------------------------------------------------------------------------------------------------------------------------------------------------------------------------------------------------------------------------------------------------------------------------------------------------------------------------------------------------------------------------------------------------------------------------------------------------------------------------------------------------------------------------------------------------------------------------------------------------------------------------------------------------------------|------------------------------------------------------------------------------------------------------------------------------------------------------------------------------------------------------------------------------------------------------------------------------------------------------------------------------------------------------------------------------------------------------------------------------------------------------------------------------------------------------------------------------------------------------------------------------------------------------------------------------------------------------------------------------------------------------------------------------------------------------------------------------------------------------------------------------------------------------------------------------------------------------------------------------------------------------------------------------------------------------------------------------------------------------------------------------------------------------------------------------------------------------------------------------------------------------------------------------------------------------------------------------------------------------------------------------------------------------------------------------------------------------------------------------------------------------------------------------------------------------------------------------------------------------------------------------------------------------------------------------------------------------------------------------------------------------------------------------------------------------------------------------------------------------------------------------------------------------------------------------------------------------------------------------------------------------------------------------------------------------|

- 10.30 TB 283: *Special Bonding of High Voltage Power Cables*, WG B1.18 (CIGRÉ, Paris 2005)
- 10.31 TB 347: *Earth Potential Rises in Specially Bonded Screen Systems*, WG B1.26 (CIGRÉ, Paris 2008)
- 10.32 TB 189: *Insulation Co-ordination for HVAC Underground Cable Systems*, JWG 21/33 (CIGRÉ, Paris 2001)
- 10.33 G. Bernard: Application of Weibull distribution to the study of power cable insulation, *Electra* **127**, 77–83 (1989), CIGRÉ WG 21.09
- 10.34 J. Midoz: Working gradients of HV and EHV cables with extruded insulation and its effect, *Electra* **139**, 63–84 (1991), CIGRÉ WG 21.09
- 10.35 CIGRÉ WG 21.04: Criteria for electrical stress design of HV cables, *Electra* **169**, ELT\_169\_5 (1996)
- 10.36 TB 610: *Offshore Generation Cable Connection*, WG B1.40 (CIGRÉ, Paris 2015)
- 10.37 TB 619: *HVDC Connection of Offshore Wind Power Plants*, WG B4.55 (CIGRÉ, Paris 2015)
- 10.38 CIGRÉ International Symposium "Going Offshore. Challenges of the Future Power Grid" Aalborg (Denmark), 4–7th June (2019)
- 10.39 TB 490: *Recommendations for Testing of long Submarine Cables with Extruded Insulation for System Voltage Above 30(36) to 500(550) kV*, WG B1.27 (CIGRÉ, Paris 2012)
- 10.40 TB 728: *On Site Partial Discharge Assessment of HV and EHV Cable Systems*, WG B1.28 (CIGRÉ, Paris 2018)
- 10.41 TB 797: *Sheath Bonding Systems of AC Transmission Cables-Design, Testing and Maintenance*, WG B1.50 (CIGRÉ, Paris 2020)
- 10.42 TB 652: *Guide for Operation of Self Contained Fluid Filled Cable Systems*, WG B1.37 (CIGRÉ, Paris 2016)
- 10.43 TB 446: *Advanced Design of Metal Laminated Coverings: Recommendations for Tests, Guide to Use, Operational Feed Back*, WG B1.25 (CIGRÉ, Paris 2011)
- 10.44 TB 89: *Accessories for HV Extruded Cables*, WG 21.06 (CIGRÉ, Paris 1995)
- 10.45 TB 177: *Accessories for HV Cables with Extruded Insulation*, WG 21.06 (CIGRÉ, Paris 2001)
- 10.46 TB 303: *Revision of Qualification Procedures for HV and EHV AC Extruded Underground Cable Systems*, WG B1.06 (CIGRÉ, Paris 2006)
- 10.47 TB 415: *Test Procedures for HV Transition Joints for Rated Voltages 30 kV to 500 kV*, WG B1.24 (CIGRÉ, Paris 2010)
- 10.48 TB 476: *Cable Accessory Workmanship on Extruded High Voltage Cables*, WG B1.22 (CIGRÉ, Paris 2011)
- 10.49 TB 560: *Guidelines for Maintaining the Integrity of XLPE Cable Accessories*, WG B1.29 (CIGRÉ, Paris 2013)
- 10.50 TB 605: *Feasibility of a Common Dry Type Plug-in Interface for GIS and Power Cables Above 52 kV*, JWG B1/B3.33 (CIGRÉ, Paris 2015)
- 10.51 TB 622: *Recommendations for Testing DC Transition Joints for Power Transmission at Rated Voltage Up to 500 kV*, WG B1.42 (CIGRÉ, Paris 2015)
- 10.52 TB 801: *Guidelines for Safe Work on Cable Systems Under Induced Voltages or Currents*, WG B1.44 (CIGRÉ, Paris 2020)
- 10.53 TB 758: *Test Regimes for HV and EHV Cable Connectors*, WG B1.46 (CIGRÉ, Paris 2019)
- 10.54 P. Argaut (Ed.): *Accessories for HV and EHV Extruded Cables*, CIGRE Green Books (Springer, Cham 2020)
- 10.55 TB 784: *Standard Design of a Common, Dry Type Plug-in Interface for GIS and Power Cables up to 145 kV* JWG B1/B3.49 (CIGRÉ, Paris 2019)
- 10.56 TB 623: *Recommendations for Mechanical Testing of Submarine Cables*, WG B1.43 (CIGRÉ, Paris 2015)
- 10.57 TB 722: *Recommendations for Additional Testing for Submarine Cables from 6 kV up to 60 kV*, WG B1.55 (CIGRÉ, Paris 2018)
- 10.58 CIGRÉ WG 21.02: Recommendations for mechanical tests on submarine cables, *Electra* **171**, ELT\_171\_3 (1997)
- 10.59 TB 770: *Trenchless Technologies*, WG B1.48 (CIGRÉ, Paris 2019)
- 10.60 TB 420: *Generic Guidelines for Life Time Condition Assessment of HV Assets and Related Knowledge Rules*, WG D1.17 (CIGRÉ, Paris 2010)
- 10.61 TB 496: *Recommendations for Testing DC Extruded Cable Systems for Power Transmission at a Rated Voltage up to 500 kV*, WG B1.32 (CIGRÉ, Paris 2012)
- 10.62 TB 279: *Maintenance for HV Cables and Accessories*, WG B1.04 (CIGRÉ, Paris 2005)
- 10.63 TB 358: *Remaining Life Management of Existing Underground Lines*, WG B1.09 (CIGRÉ, Paris 2009)
- 10.64 TB 773: *Fault Location on Land and Submarine Links (AC and DC)*, WG B1.52 (CIGRÉ, Paris 2019)
- 10.65 TB 606: *Upgrading and Uprating of Existing Cable Systems*, WG B1.11 (CIGRÉ, Paris 2015)
- 10.66 TB 689: *Life Cycle Assessment of Underground Cables*, WG B1.36 (CIGRÉ, Paris 2017)
- 10.67 TB 229: *High Temperature Superconducting (HTS) Cable Systems*, WG 21.20 (CIGRÉ, Paris 2003)
- 10.68 TB 538: *Recommendations for Testing of Superconducting Cables*, WG B1.31 (CIGRÉ, Paris 2013)
- 10.69 TB 351: *Application of Long High Capacity Gas-Insulated Lines in Structures*, JWG B3/B1.09 (CIGRÉ, Paris 2008)
- 10.70 M. Marelli, P. Argaut, H. Lugschitz, K. Kawakita: Overhead transmission lines, gas insulated lines and underground cables, *Electra* **307**, RP\_307\_1 (2019)

### Pierre Argaut

Hericy, France  
[pierre.argaut@laposte.net](mailto:pierre.argaut@laposte.net)



Pierre Argaut graduated as an electrical engineer from IEG Grenoble in 1971. He has worked for Delle Alstom (Head of R&D/GIS), for the South European Pipeline (Operation Manager), and for SILEC Cable (Senior VP/R&D). As well as holding various positions within CIGRE, he has received the TC Award (2000) and Distinguished Member Award (2002) from CIGRE, and was appointed CIGRE Honorary Member in 2016.



# Substations

## 11. Substations

Terry Krieg 

This chapter presents an overview of aspects of engineering associated with high-voltage substations, providing the reader with information on the use and application of substations, a description of the various primary, secondary and auxiliary components, and the planning and design of substations through to construction and commissioning. Substations are long-lived assets, and the chapter provides information on the management of substations throughout their life cycle. Information on future trends for substations is also included. Parts of this chapter refer to sections of the Springer Substations Greenbook published in 2018 [11.1].

11.1	<b>Overview and History</b> .....	868	11.3.13	Seismic Considerations .....	904
11.1.1	Function and Purpose of a Substation	868	11.3.14	Fire Control.....	904
11.1.2	Substation Types .....	869	11.3.15	EMF and EMC Design .....	905
11.1.3	Transmission or Distribution		11.3.16	Lighting Design .....	907
	Substations.....	869	11.4	<b>Construction and Commissioning</b> .....	908
11.1.4	Substation Components .....	871	11.4.1	Methods .....	908
11.2	<b>Planning</b> .....	871	11.4.2	Site Logistics .....	908
11.2.1	Network Planning .....	871	11.4.3	Quality Control .....	908
11.2.2	Site Selection .....	872	11.4.4	Documentation .....	908
11.2.3	Primary Equipment Layout.....	874	11.4.5	Commissioning and Testing.....	909
11.2.4	Service Security, Redundancy		11.4.6	Training.....	914
	and Reliability .....	875	11.5	<b>Substation Asset Management</b> .....	914
11.2.5	Typical Substation Layouts.....	876	11.5.1	Asset Management Fundamentals .....	914
11.2.6	Primary Design Layout .....	880	11.5.2	Stakeholders.....	915
11.2.7	Technology Types.....	880	11.5.3	Risk Management.....	915
11.2.8	Specifications and Contracting.....	883	11.5.4	Reliability .....	915
11.3	<b>Design</b> .....	886	11.5.5	Maintenance .....	916
11.3.1	Sustainability.....	886	11.5.6	Strategy and Policy .....	917
11.3.2	Designing for Safety.....	886	11.5.7	Environmental Management .....	917
11.3.3	Substations and the Community .....	888	11.5.8	Whole-of-Life Management.....	917
11.3.4	Key Components .....	889	11.5.9	Condition Monitoring .....	919
11.3.5	Preliminary Design .....	890	11.5.10	Substation Security .....	920
11.3.6	Electrical Clearances .....	890	11.5.11	Spares Management .....	921
11.3.7	Primary Design.....	892	11.6	<b>Secondary Systems</b> .....	921
11.3.8	Insulation Coordination .....	893	11.6.1	Auxiliary Systems .....	921
11.3.9	Earthing and Lightning Protection .....	894	11.6.2	Protection and Control.....	922
11.3.10	Reactive Plant.....	900	11.6.3	Voltage and Reactive Control .....	924
11.3.11	Substations and the Environment.....	900	11.6.4	Metering .....	924
11.3.12	Structural and Civil Design.....	903	11.6.5	Communications .....	925
			11.7	<b>Special-Purpose Substations</b> .....	925
			11.7.1	Mobile Substations.....	925
			11.7.2	Offshore Substations.....	926
			11.7.3	DC Substations .....	927
			11.7.4	Modular Substations.....	927
			11.7.5	UHV Substations .....	928
			11.7.6	Railway Substations .....	929
			11.8	<b>Trends in Substations</b> .....	930
			11.8.1	Digital Substations .....	930
			11.8.2	Novel Materials .....	932
			11.8.3	Alternatives to SF <sub>6</sub> .....	932
			11.8.4	Robotics .....	933
			<b>References</b> .....		933

Substations such as the one shown in Fig. 11.1 from Australia are important parts of the overall power system that includes the generation, transmission and, finally, the distribution of energy to end consumers. Since the first power stations and networks were established across the globe in the 1800s, the sources of generation have changed, the functionality and performance demands of the system have evolved, and customer expectations for reliability have increased, but the important role of substations within the overall power system remains.



**Fig. 11.1** City West Substation, Adelaide, South Australia (Courtesy Electranet)

## 11.1 Overview and History

When substations were first installed, they were considered to be directly associated with a single generating *station*; hence the name *substation* was used, and the name remains to this day.

The first power generators in the 1870s and 1880s were direct current (DC) systems; transmission of electricity over long distances was therefore not feasible, and generation was generally placed within a short distance of the load. In the 1880s, the first alternating current (AC) transmission was installed, and the era of the substation began. Technical development rapidly followed.

In 1884, a single-phase 2000 V, 130 Hz AC line, 34 km long, was built for the International Exhibition of that year in Turin, Italy.

The first three-phase generator and motor is believed to have been built by Mikhail Dolivo-Dobrovolsky in Germany in 1888 [11.2].

The first three-phase AC line was installed in 1891 for the Frankfurt Electro-Technical Exhibition, a 15 kV, 175 km line between Lauffen am Neckar and Frankfurt am Main (Fig. 11.2).

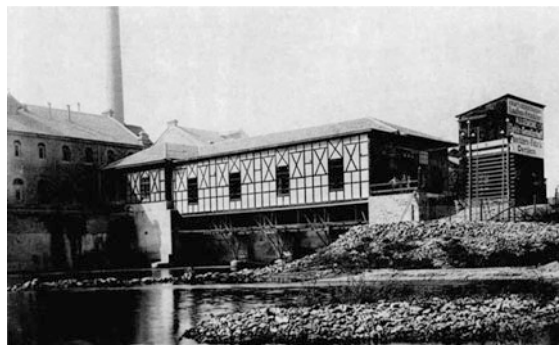
This 40 Hz system is widely considered to be the world's first demonstration of long-distance three-phase AC power, finally proving superiority over Edison's DC and Tesla's two-phase AC systems. Siemens and General Electric began work on three-phase generators the same year as the Frankfurt Exhibition, and General Electric built its first hydroelectric power station in Redlands, California in 1893.

The first large-scale hydroelectric generators were installed in the United States in 1895 at Niagara Falls by Nikola Tesla and George Westinghouse [11.3], pro-

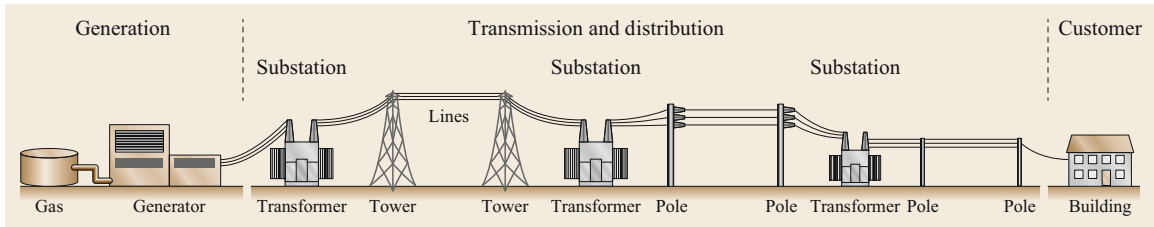
viding electricity to Buffalo, New York via transmission lines and substations built by General Electric. The development and evolution of substations has continued to this day.

### 11.1.1 Function and Purpose of a Substation

The overall function of a substation within a network is to transform voltages from one level to another and also to provide switching functions, providing a connection between the sources of energy and the ultimate consumer, at the same time providing protection and security for the grid and its components. In a power network (Fig. 11.3), substations can be considered as *nodes*, enabling connection between transmission and distribution lines and the safe connection and disconnection of lines, generators and loads to and from one another.



**Fig. 11.2** The Lauffen powerhouse and dam (Courtesy Historisches Museum, Frankfurt)



**Fig. 11.3** Generalized power system

In the modern network, substations play a key role in ensuring network stability and safety by providing sensing and switching functions to detect line faults, and then rapidly isolating these faults to maintain overall network stability, so that for any fault, the actual faulted section (usually the line) is switched out of the network, isolating the faulted section and limiting the impact on the overall grid.

With the rapid expansion of renewable energy sources within the power network, the functions of parts of the network are changing. Where previously energy was supplied from centralized power stations remote from load centers, the increase in renewable, intermittent and dispersed generation means that energy may be produced at any point and in any voltage level within a network. The direction of energy flow in any line may also be different from the top-down (large centralized generators to loads) flows for which the network was originally designed. In the future, power networks will be more dynamic, responding to active and more intelligent loads and smart devices and the changing nature of generation and customer demands.

### 11.1.2 Substation Types

The different types of substations in the power network are generally categorized as:

- Substations attached to power stations
- Interconnection substations providing switching functions
- Step-down substations
- Distribution substations
- Converter substations linking DC transmission lines with AC loads.

Each of these substation types may exist in different combinations, and any substation may perform more than one of these functions. For example, a switching station may include a distribution substation function providing local supply for auxiliaries inside the main station or to nearby customer loads. A step-down sub-

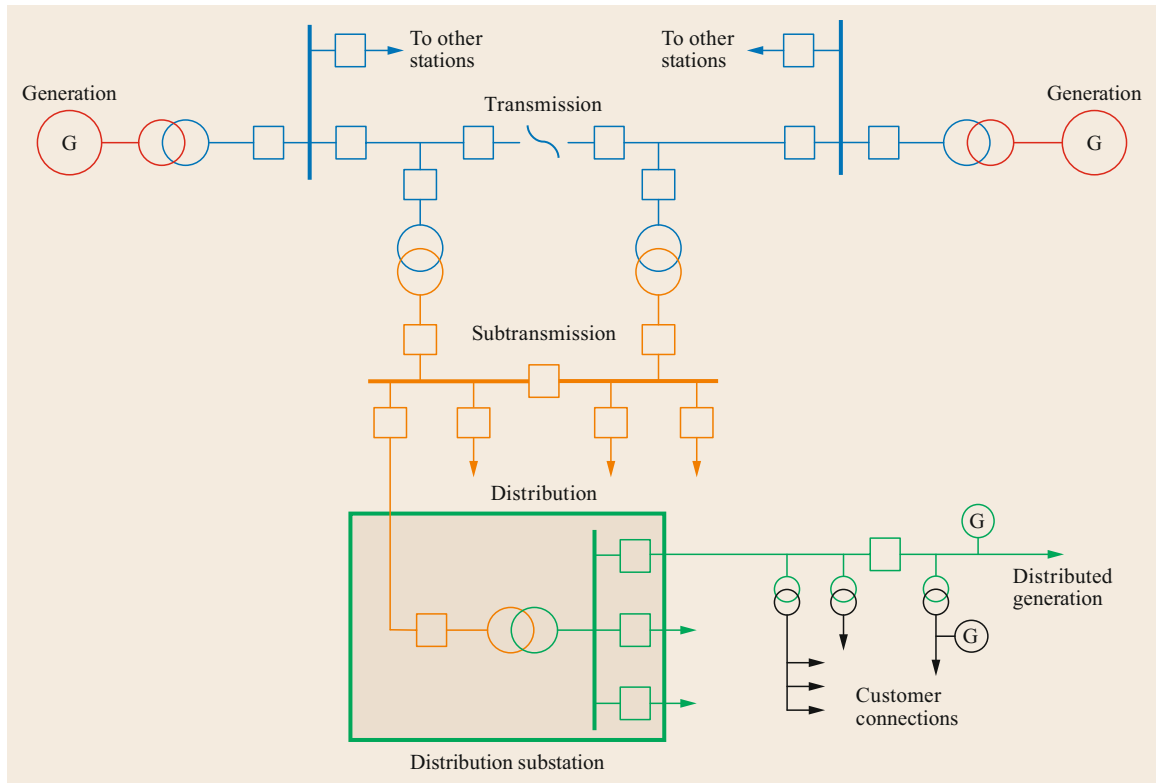


**Fig. 11.4** 1200 kV Bina National Test Substation, Madhya Pradesh, India (Photo: Krieg)

station may incorporate an interim transformation of voltage level, connecting adjacent parts of networks and lines, or the substation may connect to the distribution system providing a final link to the end consumer. However, each of these substation types has a range of common components.

### 11.1.3 Transmission or Distribution Substations

The topic of substations covers a wide range of forms, technologies and voltage levels. Much of the focus in general substation engineering and also in this chapter is on transmission substations with voltage levels typically from 60 up to 1200 kV (Fig. 11.4). Distribution substations are typically designed for the voltage range of 1–60 kV and connect to lines that feed customers directly or to transformers that convert to voltage levels used in industrial and residential premises, usually 110–600 V. A transmission substation can be described as providing interconnection between generation sources, while a distribution substation connects the consumer to the power network. Fig. 11.5 shows the different parts of a typical power network including both transmission and distribution.



**Fig. 11.5** Single-line diagram illustrating major components of the power system



**Fig. 11.6** Typical ground-level suburban 6.6 kV, 100 kV distribution substation in Nagoya, Japan (Courtesy Chubu Electric)

Typically, a distribution substation is physically smaller than a transmission substation (an example is shown in Fig. 11.6), although comprising many of the same basic primary and secondary components.

Distribution substations may also be constructed using pole-mounted equipment such as the example in Fig. 11.7 from Japan.



**Fig. 11.7** Pole-mounted 6.6 kV substation in Nagoya, Japan, comprising switches, surge arresters, and 50 kVA and 75 kVA transformers (Courtesy Chubu Electric)

### 11.1.4 Substation Components

The components of a transmission or a distribution substation include primary equipment such as circuit breakers and switches, busbars, conductors and connections, transformers and measuring devices with associated secondary protection, control, metering, monitoring and

auxiliary systems. All of these components must work together in a safe and effective way to meet the objectives of asset owners and the needs of the overall grid. An important aspect of the substation is the civil engineering associated with its design, the impact of the substation on the environment and local community, and the impact of the environment on the substation itself.

## 11.2 Planning

Substations are important parts of the overall power network and a significant investment for network owners and operators. The need for new or modified substations is usually identified as part of the long-term planning of the power grid. The substation needs to meet the present needs of the grid and, as far as can be determined, the future requirements of the grid, providing sufficient allowance for future expansion.

### 11.2.1 Network Planning

Power networks are designed to transport energy from the sources of generation to loads. The aim is to achieve this transfer of energy safely and efficiently, minimizing losses and with the design of the network providing adequate consideration of redundancy in the event of failures. The power network (a small network model is shown as an example in Fig. 11.8) comprises power stations, substations, transmission and distribution lines, and cables. Substations typically consist of transformers and reactors, capacitors, switching devices, and associated control and protection equipment.

Networks are inherently interconnected on a regional, state, national or international basis. Long-distance transmission allows for generation that may include renewable intermittent sources such as wind and

solar, enabling connection to load centers that might be some distance from the generator.

Historically, long-distance transmission was achieved using three-phase AC systems (50 or 60 Hz), but with the development of power electronics, high-voltage DC (HVDC) lines and networks are increasingly part of the transmission system, enabling asynchronous interconnection and large energy transfer between different parts of the transmission system.

Network planning is required to ensure that networks are able to provide a reliable energy supply to meet all customer load requirements, and planning therefore includes a number of interrelated functions:

- Generation planning, which includes load and capacity forecasting and capacity resource planning
- Transmission planning to ensure that supply loads can be achieved from the most economical sources of generation, allowing flexible operation of generation and overall system reliability and stability
- Distribution system planning including load forecasting, achieving reliability for customer loads and the required connection capacity.

Network (or system) planning is a coordinated process that uses historical data to predict and plan for fu-

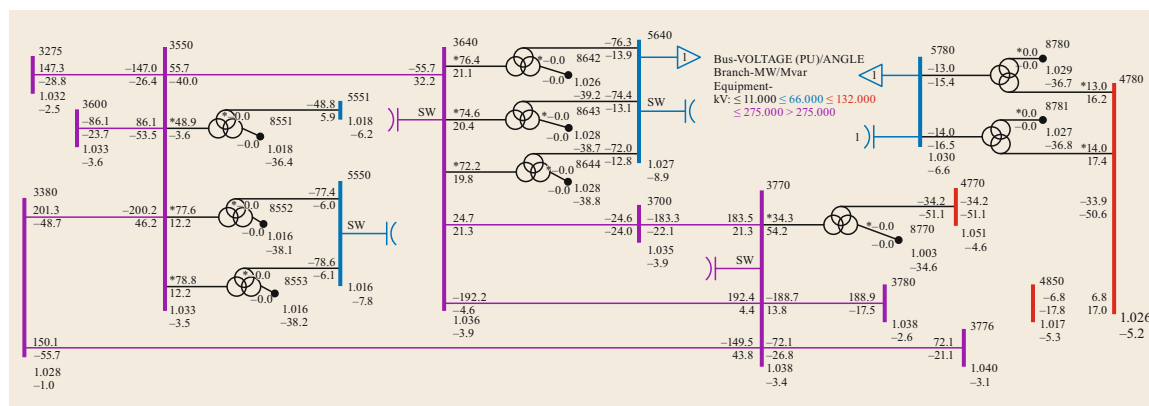
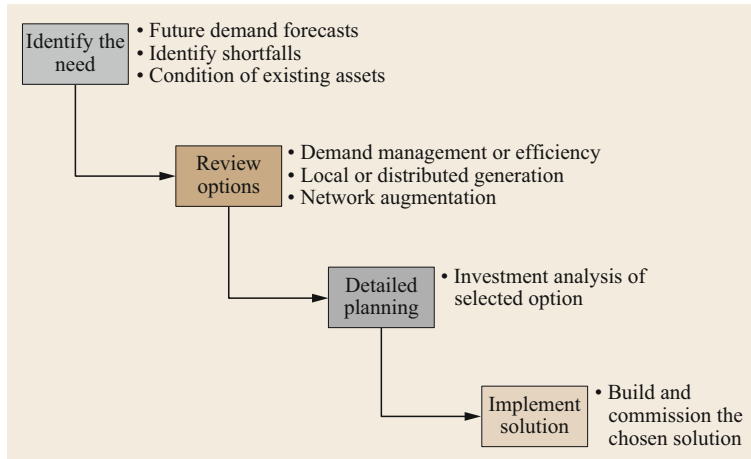


Fig. 11.8 Example of a small network model showing load flows



**Fig. 11.9** Typical transmission utility planning steps

ture requirements. Network planners face considerable challenges in the planning and development of modern power networks due to rapid load growth and changing demand characteristics, changes in the economic and regulatory environments in many countries, climate change, the availability of new technologies and changing customer expectations.

The common stages in network planning for a typical transmission utility are shown in Fig. 11.9.

Substation planning cannot be done in isolation from the requirements of the grid; it is essentially a derivative and an outcome of the overall network planning functions. System studies are carried out regularly by network planners to ensure that the network is capable of satisfactorily fulfilling the above functions, and these studies will indicate when the network needs to be augmented and whether this augmentation requires the construction of a new substation, a capacity increase or the extension of existing ones. Planning may also indicate that a substation needs to be adapted to meet changing requirements, downgraded or bypassed, and this may also be a driver for substation modification such as removing feeders or line exits, reducing site size or decommissioning of a substation. Once the need for a new substation, capacity increase, or modification or extension of an existing substation has been established and the range of requirements and key attributes are determined, then the more detailed planning of the substation can commence.

Typical broad requirements for substation planning may include:

- General physical location within the network
- Required maximum capacity (the loading) for both the present and future
- The fault clearance time required to maintain network stability

- Fault current levels at the proposed point of connection
- The type and characteristics of the earthing system to be employed to suit the proposed section of the network
- Number and type of lines or cables to be connected
- Primary circuit availability, redundancy and security requirements that will affect the choice of substation bus configuration
- General control and protection requirements such as the method of control and the degree of automation, whether manned or unmanned, and the degree of secondary system redundancy required
- Type and availability of communications
- General requirements such as the type of site (urban or rural), local requirements such as aesthetics and environmental controls required
- Design life required (50 years is typical, but shorter design times are also feasible for specific applications).

Some of these factors will be governed by overall network planning criteria, local standards and regulatory requirements; in other cases, consideration of all factors will be required.

### 11.2.2 Site Selection

One of the first decisions in the detailed planning of a new substation will be the physical site location. Broadly speaking, the location will be influenced by the planning carried out at the network level and the presence or absence of existing generation, transmission or distribution infrastructure. A switching station, for example, may be built at a site where multiple lines intersect. A generator substation will obviously be located near or adjacent to the actual generator, although

there may be situations where a site is chosen so that the substation is located away from sources of pollution such as dust or sea spray that might be adjacent to a power station and detrimental to future substation performance.

Site selection is important and needs to balance future risks and substation objectives to determine a suitable site location in the required general area defined in planning.

The substation site should be in a *protected* location to minimize hazards and risks, and should be capable of providing a stable surface for the construction of a substation to meet the requirements detailed below, including during and after the specified disaster incidents.

The location of the substation site should not expose the future substation or workers to hazards (worker safety). In particular, the following locations should be avoided:

- Sites located close to the outside of a bend in a road—risk of vehicle impact
- Sites located close to the ocean, forests, agricultural fields or heavy industries, where there may be a risk of salt spray, fire or windblown debris and contamination from pollutants
- Sites located close to hazardous industries such as petrol service stations or chemical plants, due to the risk of explosion, fire and contamination from pollutants.

In addition to worker safety needs, the chosen site should not expose the substation infrastructure to high levels of risk during service life. The following locations should be avoided in order to minimize risk:

- Sites located close to waterways, dams or wells—risk of pollution of drinking water sources from the substation in the event of a spill
- Sites located in close proximity to underground services and to residential and commercial buildings—risk of transferred potential electrocuting humans or animals
- Sites located close to schools, parks or playgrounds—sensitive areas, risk to children and from vandalism and unauthorized entry
- Sites close to heavily populated areas—prudent avoidance of electromagnetic field (EMF) exposure or noise complaints
- Sites located downwind of any heavy industry with airborne pollution that could be hazardous to personnel and potentially impact on the design life of the substation

Some of the other factors that may be considered in choosing a suitable site include the following:

- *Sufficient area for present and future needs*  
The substation site should be of sufficient size to accommodate the complete substation, including the substation itself, access routes for high-voltage and medium-voltage feeders, access routes for various services, and areas for driveway access, vehicle parking and landscaping, including a suitable buffer zone on the sides and rear of the substation.
- *Avoidance of adverse environmental conditions*  
The performance of the substation should not be unfavorably affected by the substation site condition during adverse environmental conditions (including defined disasters) specified for the substation. This includes secondary effects such as soil erosion and scouring during severe ice, snow, rain and flooding, and increased earth resistance during droughts. In addition, the site should not be located such that the substation may have an adverse impact on sensitive environmental zones.
- *Adequate access during construction and future operations and maintenance*  
Site access should enable access by staff, equipment and vehicles required for construction, operations and maintenance and plant replacement during substation design life. This access requirement should cover all aspects of the substation's operation, including for personnel and light and heavy vehicles. The access should be available in all weather conditions. Access roads, feeder routes and services access through private property must be covered by a suitable registered easement.
- *Allowance for vehicular traffic*  
The selected site should avoid potential adverse effects from road traffic. It should not be located on the outside bend of a heavily trafficked or high-speed road. The site should have at least one suitable vehicle access point from a public road. This access point should provide safe vehicle exit and entry to the public road. Access points on blind curves, close to the crest of hills and other locations with restricted vision or acceleration areas should be avoided. The access point should be suitable for development as a roadway for vehicles, including low loaders and cranes (to enable heavy plant such as power transformers to be transported to and from the substation). Relevant local government or road authority approval should be obtained for access if necessary.
- *Provision for vehicles*  
The site should be provided with adequate parking for maintenance vehicles immediately adjacent to

the substation building and outside the substation security enclosure. Sites with limited load-bearing capacity soils should be fitted with concrete pads for crane-stabilizing legs adjacent to the two power transformer locations.

- **Landscaping**  
The substation construction program should include landscaping the site. This should be arranged in agreement with the local authorities and may involve community consultation. Landscaping should incorporate aesthetic and security aspects. In some cases, land may be set aside for planting of flora or positioning of an architecturally designed substation building to limit the view and noise of outdoor high-voltage (HV) plant. On completion of the substation, the design and finish of the site should meet local council and community expectations with respect to aesthetics.
- **Avoidance of the risk of flooding**  
A typical requirement is that the substation site be located at least 300 mm above the *100-year* flood line and above the local tidal surge and tsunamis levels.
- **Avoidance of nearby cliffs**  
The site should be located away from cliffs and steep rocky slopes so that the risk of damage from slides, avalanche and, potentially, vandalism are reduced to an acceptable level.
- **Rock layers**  
Any site rock layers should be assessed to allow for the installation of standard foundations, stormwater drains, earthing, cables and other underground substation components.
- **Site security**  
consideration of nearby residential or industrial zone to reduce the risk of vandalism or unwanted intrusion.

In practice, no potential site is perfect, and a compromise is often required in the choice of the ideal location for a new substation.

### 11.2.3 Primary Equipment Layout

Many design decisions for substations are influenced or dictated by local standards, historical design approaches and past local practices [11.4]. There is good reason for conservatism in the design of layouts as operations and maintenance staff and designers become familiar with particular types of substation configurations. Any change to an alternative arrangement needs to be considered carefully, including consideration of the impact on operations and maintenance staff and contractors.

The basic objective of the primary plant layout is to facilitate the operational requirements of the substation within the overall electrical network. The key switching functions within the substation are carried out using circuit breakers, and in the past the types of technology used meant that frequent routine, preventive and corrective maintenance was required. Oil-filled breakers, air-blast breakers and the different types of operating mechanisms required regular and sometimes frequent maintenance. This maintenance requirement remains a key element of substation layout design.

Disconnectors were required to facilitate the safe performance of maintenance activities, allowing circuit breakers to be isolated from the network for maintenance. This requirement for disconnectors has had a strong influence on the design of historical substation layouts and many standard layouts include a proliferation of unnecessary disconnectors. Circuit breaker design has evolved so that maintenance requirements are significantly less than that required historically, but the *standard layout* adopted has remained unchanged in many utilities. In many utilities, disconnector maintenance is now the dominant driver of substation maintenance programs.

Substations are nodes or hubs for interconnections between regions, countries, etc., in the network, and also transform power between networks of different voltages and at infeed (generation) and load points of the network. The network characteristics together with a particular substation type lead to consideration of a range of different primary equipment layouts.

Primary equipment layouts are also called circuit arrangements, switching arrangements, circuit configurations or busbar schemes, busbar switching arrangements or busbar configurations, among others. The substation single-line diagram (SLD) provides an overview of the substation circuit arrangement and generally shows all switching and non-switching high-voltage equipment. It is the basic document required to begin the design of the remainder of a high-voltage substation.

The primary equipment layout defines the relative arrangement of required busbars and busbar sections, circuit breakers, disconnector/earthing switches, power transformers, instrument transformers and surge arresters. The choices made at this early stage of the design process have a major influence on the final operability, maintainability, flexibility of switching arrangements and other factors related to the primary functions of the substation. The equipment layout influences the design of the secondary and auxiliary systems for control and protection, and ultimately the reliability and availability and the whole-of-life cost of managing the substation.



The main broad requirements to be considered when choosing a primary equipment layout are as follows:

- **Security and redundancy**  
The capability of a power system at a given moment in time to perform its supply function in the case of a fault [11.5]
- **Maintainability**  
The ability of an item under given conditions of use to be retained in, or restored to, a state in which it can perform a required function when maintenance is performed under given conditions and using stated procedures and resources [11.6]
- **Flexibility**  
The ability for the substation to be reconfigured to meet operational requirements during credible contingency events.

Choosing an optimal layout for a particular substation situation requires consideration and comparative analysis of a range of factors specific to the application of the circuit breaker, its function within the network and local standards, and there are various multi-criteria analysis methods available to compare different options for a particular project. CIGRE Technical Brochure 585 [11.4] provides a simple method for comparing different layout options based on overall design requirements and preferences.

Apart from those mentioned previously, some additional considerations that might affect the final choice of layout for a particular substation may include:

- Extendibility of the layout for future needs
- Consideration of credible contingency events
- Existing operational familiarity with a particular layout used historically
- Physical arrangement, direction and location of incoming or outgoing lines or feeders
- The number of busbars and busbar sections required
- Physical location of busbars to avoid a single fault affecting two or more busbar sections
- Maintenance capability and equipment
- Environmental and aesthetic requirements.

Options for the layout of the substation can be analyzed and various factors considered depending on the application and location in the network of the substation. For example, substations designed for direct power station connection may have different layouts and arrangements because of the different emphasis (and analysis weightings) on the key criteria of security and redundancy, maintainability and operational flexibility when compared with

other substation applications such as in switching stations or step-down applications. CIGRE TB 585 [11.4] provides a method for conducting this analysis.

#### 11.2.4 Service Security, Redundancy and Reliability

One of the key drivers in the design of the primary substation layout is the requirement for network security and redundancy, and some explanation is given here. For the substation to achieve its functional objectives, it must be capable of effective operation following different credible contingency events, such as failure of a single or multiple network or substation components. This concept of substation design is referred to as service security and redundancy. Service security is defined as the analysis of the substation's configuration in terms of availability of supply to the network after internal (busbar side of circuit breaker) and external faults (line side of circuit breaker), assuming otherwise normal system configuration.

The service security or redundancy is commonly characterized by the terminology  $N-1$  criteria and  $N-2$  criteria (some jurisdictions use the terminology  $N+1$  and  $N+2$ ), defined as:

- $N-1$  security means that the security of supply to all connected customers is maintained in the event of failure of a single primary network element or associated secondary system.
- $N-2$  security means that the security of supply to all connected customers is maintained in the event of the failure of two primary network elements or associated secondary systems in the same event.

While these terms ultimately apply to overall network security, they can also be applied to the consideration of options and the arrangements of components within the substation.

Another key aspect of substation design is its inherent reliability. The functions of the substation are defined by the circuit arrangement comprising the various components including circuit breakers, disconnectors, busbars, transformers, and related control and protection systems. The failure rate and the typical repair rate of individual devices or the *mean time between failure* (MTBF) can be summated mathematically to determine an expected outage time per year for the overall substation by considering the interrelationships of the individual components in the substation. This enables a statistical approach and probabilistic calculations of overall substation reliability for comparison of various primary substation layouts.

Reliability analysis studies of the proposed substation layout can be undertaken using *failure mode and effects analysis* (FMEA) techniques.

Various references [11.7] are available to provide expected failure rates of different circuit arrangements and voltage levels. These values can be used to mathematically analyze the overall substation design reliability, including consideration of the reliability of modern high-voltage devices and switchgear components. In addition, maintenance strategies and philosophies should be taken into account, as these practices will influence the MTBF value of components and the reliability of the final substation design.

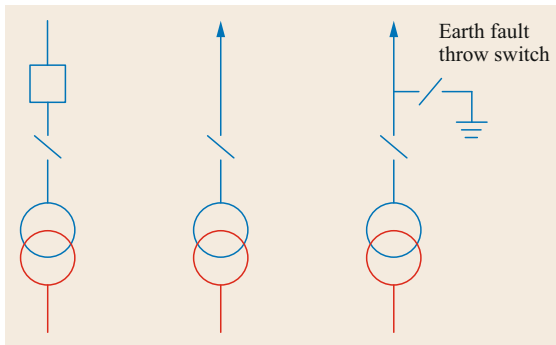


Fig. 11.10 Typical *no-busbar* substation layouts

### 11.2.5 Typical Substation Layouts

Utilities and regions often use a range of different primary layouts, and these layouts are often adopted as standard practice within that utility or region. Some of the more common layout options are listed in the following sections.

#### No Busbar

The most basic substation layout includes no high-voltage busbar at all. This type of layout may be considered for remote or end-of-line substations feeding a single consumer such as a mine site. If no circuit breaker is fitted, then high-speed communications may be required to trip the remote circuit breaker at the feeder substation in the event of a substation or transformer fault. Alternatively, an earth fault throwing switch may be used to deliberately apply a single-phase earth fault to the incoming line in the event of a transformer or other substation fault that requires the remote end to be tripped.

A *no-busbar* layout (Fig. 11.10) may be used as an interim substation development step, with a bus to be added at a later date as load grows or the security of supply becomes more important. In that case, space should be allocated in the yard layout to allow future expansion to add a circuit breaker or a single bus. This is an impor-

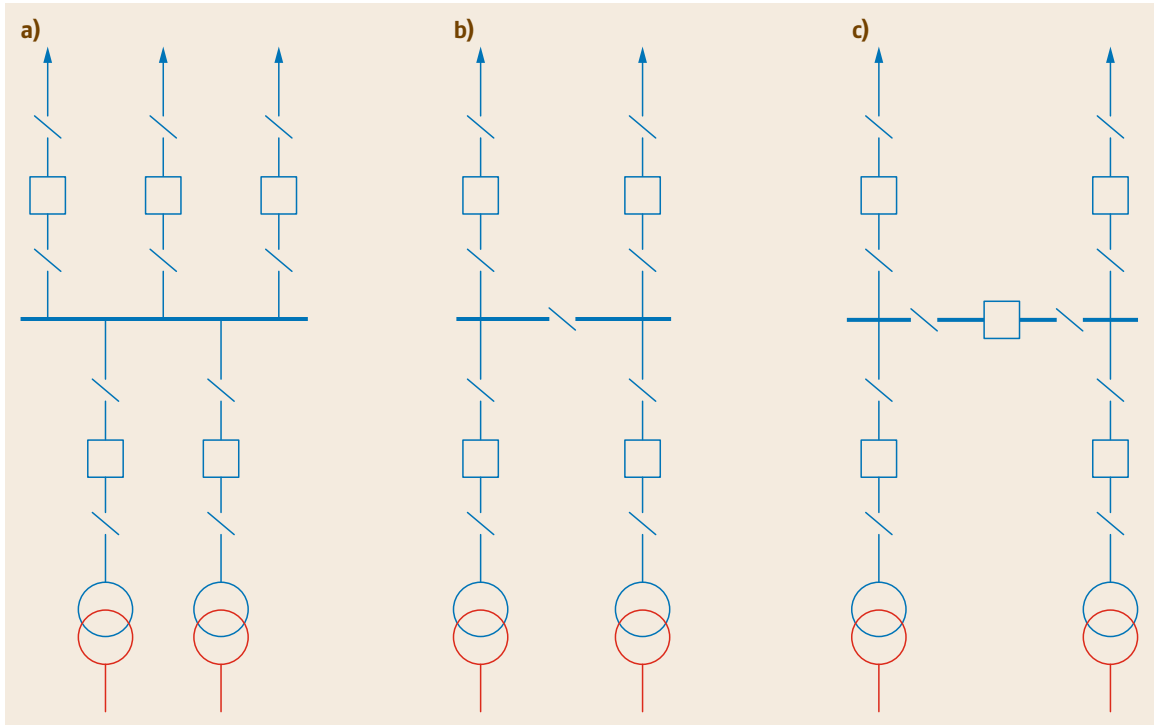


Fig. 11.11a–c Single-busbar variations. (a) No bus section, (b) bus section disconnector, (c) with bus section circuit breaker

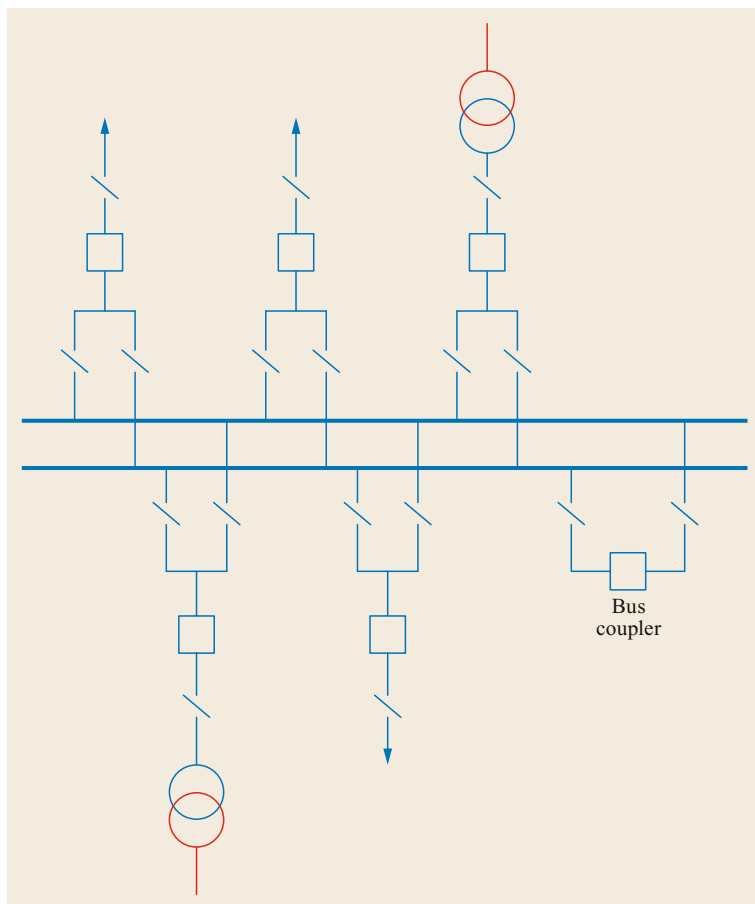


Fig. 11.12 Double-busbar layout

tant consideration to allow a low-cost initial design with allowance for future needs. It may be extremely difficult to add additional components if insufficient space is allocated at the initial design and layout stage.

### Single Busbar

Apart from the direct connection of the transformer to a line as described in the preceding section, the single-busbar layout is perhaps the simplest of substation layouts that can be selected. This is also called an *H-configuration*. There are a range of possible variations (some examples are shown in Fig. 11.11) depending on the level of security and flexibility that is required and the number of incoming and outgoing feeders or lines.

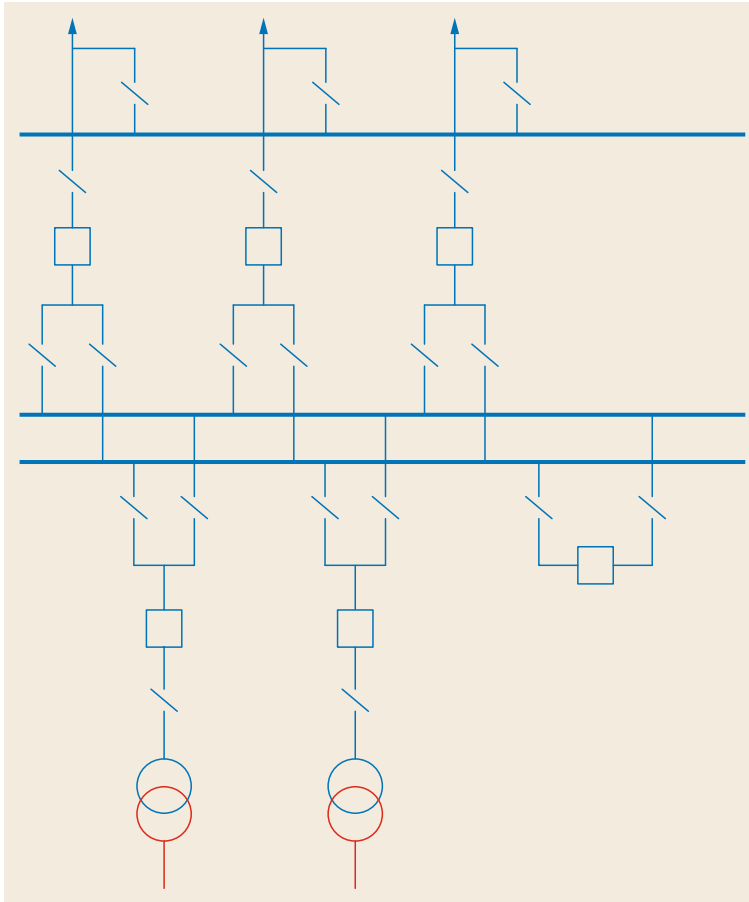
The single-busbar layout is generally the lowest-cost and easiest design option, providing a simple layout for operations. However, a fault on the busbar will generally cause loss of the entire substation unless a section circuit breaker is fitted. Maintenance of busbar disconnectors will typically require a complete substation outage (Fig. 11.11a,b). Using a single, sec-

tionized bus (Fig. 11.11c) offers benefits in terms of security and flexibility, enabling load to be transferred from one transformer to the other for maintenance.

### Double Busbar

In the double-busbar arrangement, lines and transformers may be connected to one of two busbars. This arrangement is often used in higher-security applications in well-interconnected networks, allowing for additional switching flexibility. The coupler circuit breaker provides the ability to join (or split) the two busbars, enabling a faulted line or a component being maintained to be isolated from the network. Circuits (lines or transformers) can be switched to either bus without interruption of supply.

In the double-busbar arrangement (Fig. 11.12), if the bus coupler is not closed, a single bus fault will most likely cause loss of the connected feeders but not the entire substation as in the single-bus layout. Feeders can be quickly switched to the healthy bus to restore the connection.



**Fig. 11.13** Double-busbar layout with transfer bus

A variant of the double-busbar arrangement provides a *third transfer bus* to enable circuits to be temporarily connected to a bus so that circuits can remain in service during maintenance or repair of the line circuit breaker (Fig. 11.13).

#### Triple Busbar

In a triple-busbar layout (Fig. 11.14), the connected lines and transformers can be switched to one or more of three busbars using disconnectors. This is used in some situations where reliability, security and flexibility are very important.

#### Breaker-and-a-Half

A *breaker-and-a-half* layout (or 1.5 breakers) is based on a double-busbar layout but is arranged so that two circuits (lines, transformer connections or generation source) share three circuit breakers (Fig. 11.15). This means that three circuit breakers connected between the two busbars (called a *diameter*) connect to two circuits

(line, transformer, generator). This provides a very flexible substation layout that is often used where there are a number of incoming lines and where the network requires a high degree of interconnectivity. This layout allows a single circuit breaker to be isolated for maintenance without affecting customer loads or transmission lines.

The normal state for this layout is for all circuit breakers and disconnectors to be closed at all times. The connection of various lines and transformers often depends on the physical layout of the site and the spatial position of the incoming lines in relation to the substation site.

The advantage of this layout is that a busbar fault in the substation will have only limited impact on reliability and may not cause loss of connection of any lines or transformers. A single line fault trips two circuit breakers in the diameter, but the other circuit remains connected via the remaining circuit breaker. If only two diameters are initially installed, the layout is similar to

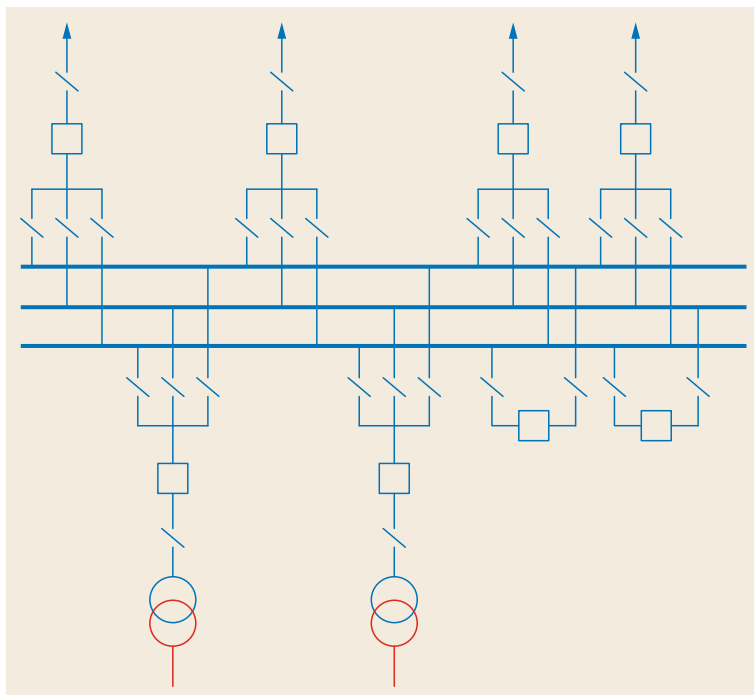


Fig. 11.14 Triple-busbar layout

the ring layout (see later section). If the initial development is only a small number of lines, the substation may be laid out geographically to suit a *breaker-and-a-half*, with some circuit breakers missing from the layout, to be added at a later date as new circuits are added in future years.

One of the disadvantages of the breaker-and-a-half layout cited by some designers is the added secondary circuit and protection complexity. Also, there are some protection considerations required to address possible protection *dead zones* within parts of the primary layout due to the relative position of current transformers (CT) and overlapping of CT summation zones.

#### Two-Circuit-Breaker Layout

Using two circuit breakers per circuit between busbars offers additional flexibility but with the disadvantage that additional primary components are required, adding to substation cost (Fig. 11.16).

#### Ring and Mesh Layouts

A Ring or mesh bus substation layout is a single-busbar station with a closed loop formed by each connected circuit breaker (Fig. 11.17). Circuits (lines or transformers) are connected between any two circuit breakers. The number of circuit breakers fitted equals the number of circuits (lines or transformers), and all circuit break-

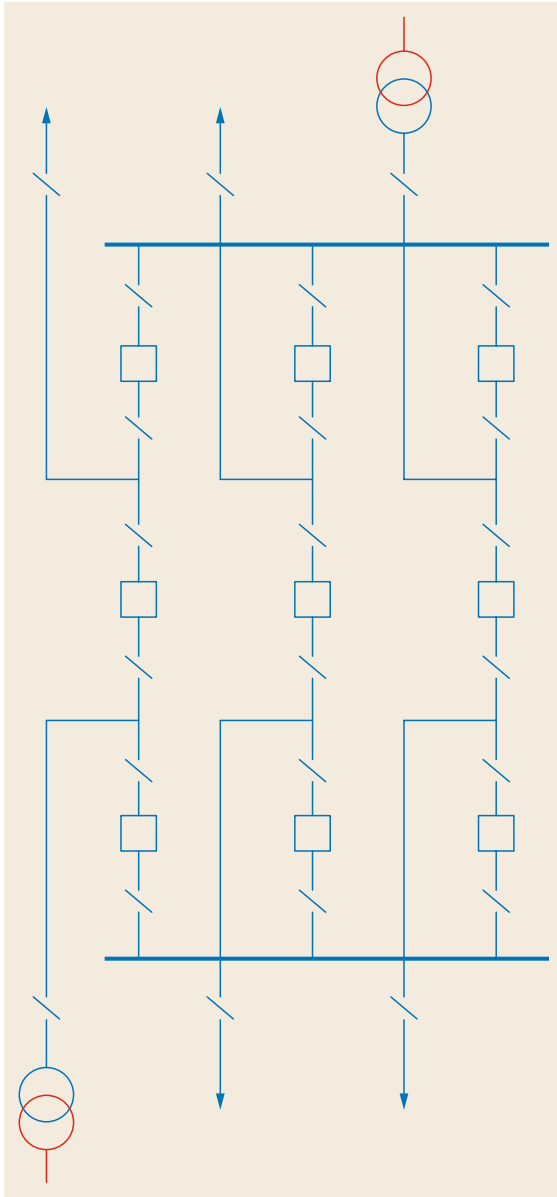
ers must be rated for the combined load current of each circuit with allowance for busbar current.

The ring or mesh bus layout may be used as a first step in the development of a breaker-and-a-half substation, and this may dictate the physical layout of the primary plant.

The preceding section does not cover all possible layout options for any particular project. There are many combinations of the basic and most common layouts that are represented here. The choice of layout for a new substation depends on the preferences of the utility and local standards and also the degree of weighting that the utility owner places on the criteria of security, redundancy, maintainability and flexibility for the substation application. The choice of layout will also be influenced by budget and future plans for the substation project.

#### Choosing the Right Substation Layout

Choosing the *right* substation layout for a new project is not a precise science. In some cases, the layout will be preselected based on regional standards or regulatory requirements. Where the layout is not predetermined, various methods of multi-criteria analysis can be used to compare the relative advantages and disadvantages of each proposed layout. The final decision will be based on the intended application of the substation (i.e., generator substation, interconnection, step-down, etc.), the

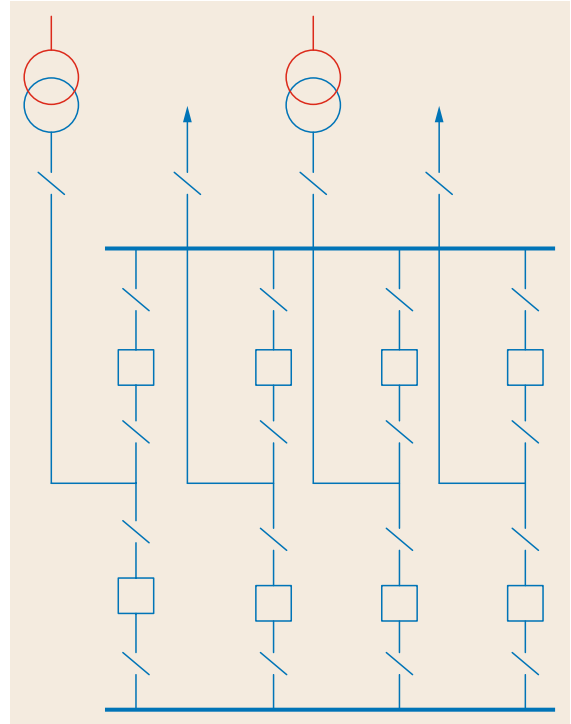


**Fig. 11.15** Three-diameter, breaker-and-a-half layout

cost involved and an acceptable balance of the criteria of security, redundancy, maintainability and flexibility as discussed in the previous section. CIGRE Technical Brochure 585 [11.4] provides a simple way to compare different layout options [11.8].

### 11.2.6 Primary Design Layout

Using the chosen busbar configuration, the chosen equipment and technology types and the construction



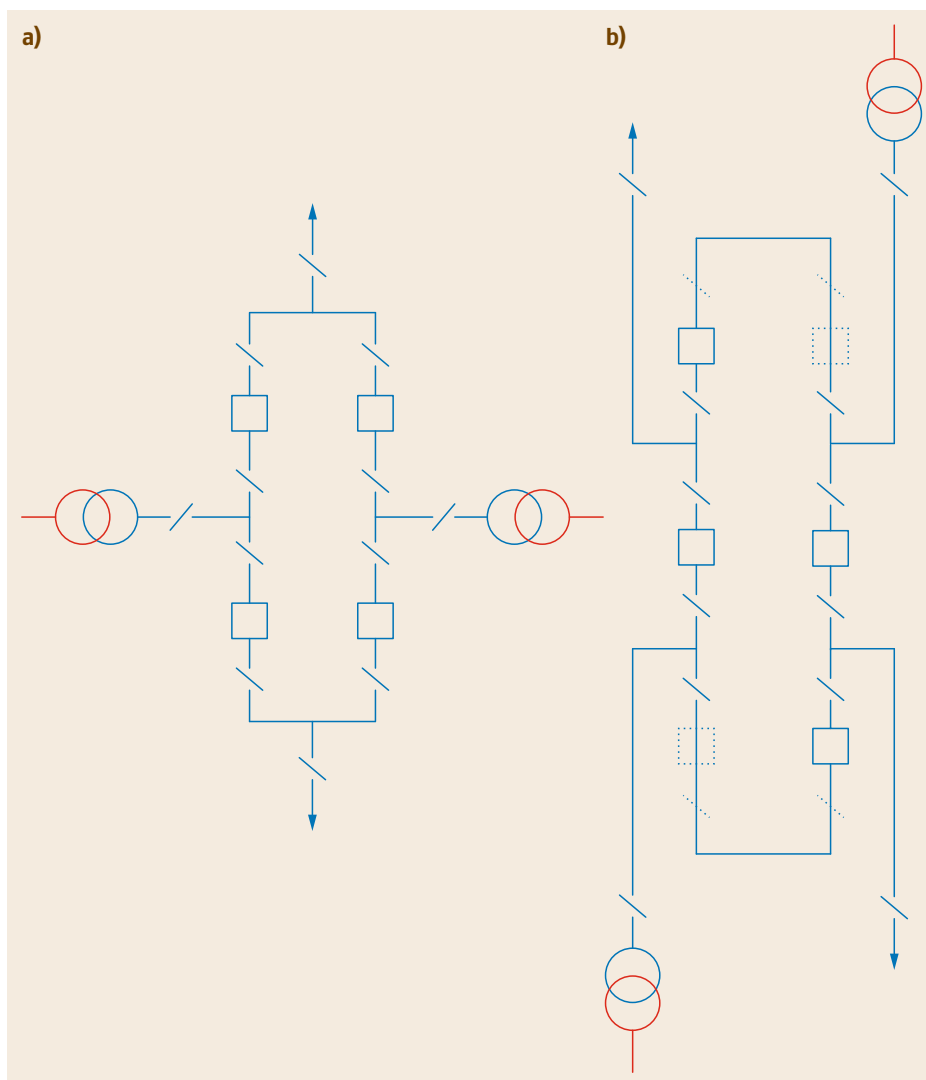
**Fig. 11.16** Two-circuit-breaker layout

method enables the designer to prepare the substation primary layout drawings, the primary design of the substation. Fig. 11.18 shows the typical layout of a 1.5-breaker (breaker-and-a-half) substation (one diameter shown). Fig. 11.19 shows a breaker-and-a-half layout under construction at Port Augusta, South Australia. Layouts can be difficult to identify from ground level.

### 11.2.7 Technology Types

Another important decision made at the planning or concept design phase of a substation project is the type or technology of primary equipment that will be used. The types can be broadly classified as either:

- *Air-insulated switchgear (AIS)*  
AIS is defined as switchgear and other high-voltage equipment where the insulation to earth and between phase conductors is provided mainly by air at atmospheric pressure and where some live parts are not enclosed.
- *Gas-insulated switchgear (GIS)*  
GIS comprises metal-enclosed switchgear and other high-voltage equipment where the insulation is obtained, at least partly, by an insulating gas other than air at atmospheric pressure. This gas is usually SF<sub>6</sub>



**Fig. 11.17a,b**  
Ring bus layouts considering later development into either a two-CB (a) or breaker-and-a-half CB layout (b). Future components shown as dotted lines

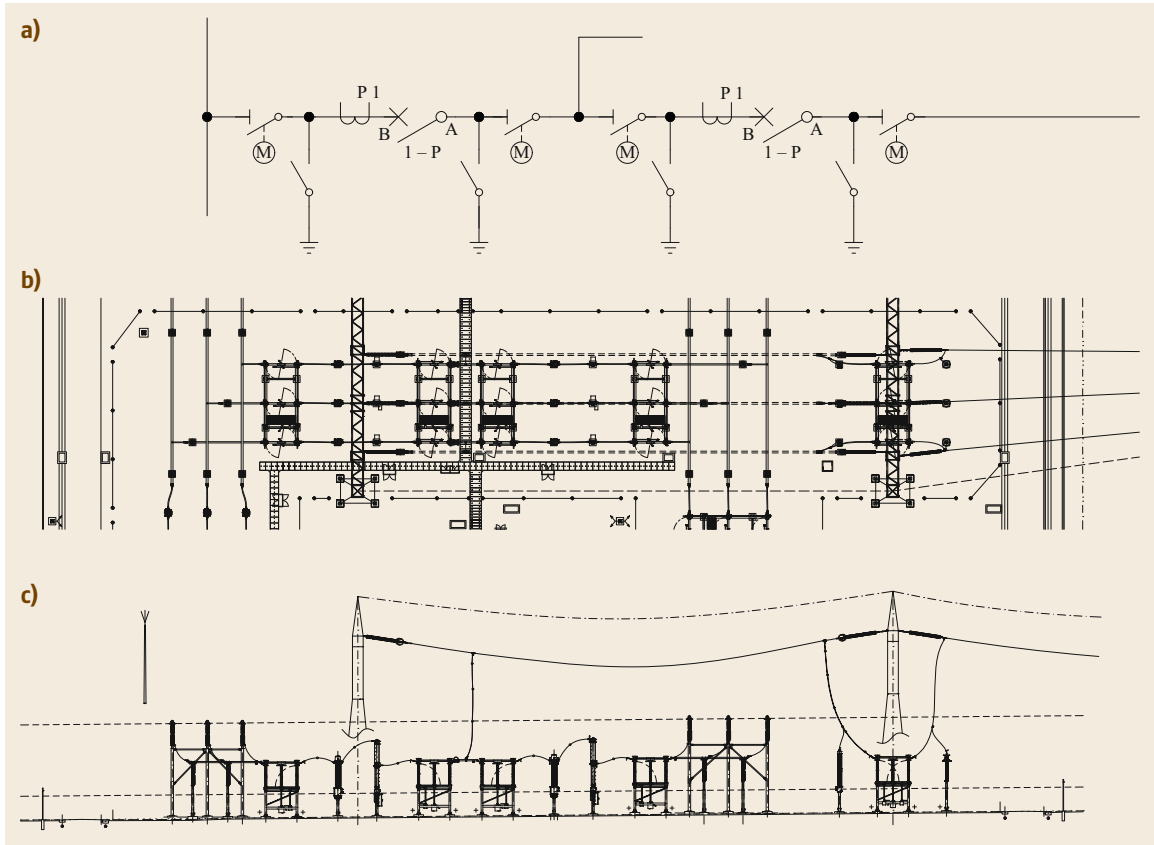
or an SF<sub>6</sub> mixture with other gases such as nitrogen, although a range of other alternative gas types are being considered [11.9]. IEC 62271-203 [11.10] provides requirements for substation design using GIS.

- **Mixed-technology switchgear (MTS)**  
MTS equipment has been developed from AIS or GIS into one of the combinations of AIS in compact and/or combined design GIS in combined design. Mixed technology may sometimes be referred to as hybrid-insulated switchgear (HIS), where bays are made from a mix of AIS and GIS technology components.

Choosing the type of technology for the primary equipment to achieve the configuration required in a substa-

tion project requires consideration of a range of factors. Some of these factors are related to the choice of site, the characteristics and size of the site, and the project economic factors.

AIS has the significant advantage that the equipment is generally initially the cheapest to purchase. However, its disadvantages include the requirement for more site space than other technologies to allow for the electrical clearances required in air. In addition, the primary equipment is exposed to the environment and subjected to animals and pollution. Where space is available and land cost is not prohibitively high, AIS will be the most suitable first solution for an extra-high-voltage (EHV) substation. AIS also has the advantage that it is relatively easy to extend and modify as the needs of the substation develop with time.



**Fig. 11.18a–c** Single diameter of a 1.5-breaker substation layout shown as (a) single line diagram (SLD), (b) plan view, (c) elevation



**Fig. 11.19** The author inspecting a 275 kV transmission substation extension (1.5-breaker layout) under construction, Port Augusta, South Australia (Courtesy Peter Burnell)

GIS equipment is usually initially more expensive to purchase than equivalent AIS substations but may have a lower overall whole-of-life cost if all

factors, including land cost, are considered. The substation will take up much less space than a comparable AIS substation with the same functionality. In locations where the cost of land is high, it may be necessary and advantageous to build using GIS technology that can be safely incorporated into an urban building design or even underground, avoiding large urban space requirements, pollution and other risks. GIS may also be advantageous from a safety perspective, with fewer exposed high-voltage components.

MTS (or HIS) shares some of the advantages of the compactness of GIS but with some AIS components, combining multiple functions and technologies. This design can enable a solution that is small in size while still generally cheaper than GIS, with some compromises. MTS can be used where the land costs are moderate and pollution is not a major issue, providing a compact and cost-effective solution. MTS can be used for new substations or the extension of existing AIS substations where space is limited, avoiding the need to procure more land.



CIGRE Brochure 390 [11.11] more fully describes the evaluation of different technology types and how these various factors can be compared.

### 11.2.8 Specifications and Contracting

There are many ways that a new substation may be acquired by the utility or asset owner. In some cases, in-house design and construction capability can be used, but often the design and construction, or the construction only is outsourced to another organization. In both the in-house and outsourcing situations, there is a need to specify the requirements for the new substation beyond the layout and technology type discussed above. This preparation of specifications, together with the required commercial terms and conditions, is used to procure the substation or to specify for internal design.

Specifications can be prescriptive (conventional), or they can define only the key functional requirements (functional). A function specification procurement method can be useful as a strategic approach to assist in the introduction of new technology and designs, but each specification style has both advantages and disadvantages.

#### Conventional Specifications

Using the conventional, generally more prescriptive approach to substation specification usually requires that all of the relevant information related to the site and the incoming circuits be predetermined and provided for the design and construction tender process. This information will most often include the following:

- *Site location details*  
The precise location and site constraints, usually in the form of a drawing or GPS (Global Positioning System) location.
- *Electrical and connection information*  
This includes the characteristics (voltage, current ratings), number and type (underground or overhead) of circuits to be connected to the substation. In the case of cable connection, this information may include the size and type of cables to be connected.
- *System parameters*  
This includes the nominal, highest and lowest system voltages together with the required basic impulse level (BIL) and switching impulse level (SIL). An important system characteristic is the short circuit level at that network location and the type of neutral earthing required.
- *Power transformers*  
including the open circuit voltage ratio, rating, cooling method, vector group (including tertiary if required), impedance, tap changer (on load, off load,

off circuit), tapping range and steps, noise level requirements termination details and capitalized value for losses.

- *Auxiliary supplies*  
Including the voltage and rating required for the low-voltage AC (LVAC) auxiliary supply and, importantly, the survival time and voltage level for DC batteries and any redundancy and segregation requirements.
- *Substation environmental conditions*  
This is to allow the designer to select appropriate equipment, design appropriate fittings, supports and buildings, and ensure adequate rating and plant performance.
- *Civil design constraints*  
This may include soil characteristics such as minimum ground-bearing pressure for footing design, and the earth resistivity and thermal resistivity of the soil for the earthing and electrical design, together with any site investigation reports and borehole results. The finished levels at the site and whether they are level, sloping or terraced may be included. The existence of contamination and any requirement for post-construction treatments may be included. The fencing and security requirements to be applied, together with necessary interface points with roads, water supplies and drainage. The detailed requirements for any buildings on the site including the dimensions of the rooms, heating, ventilating and air conditioning requirements as well as the finishing requirements. The locations of any known buried services existing within the site boundaries.
- *Secondary system requirements*  
This may include the details of the control center system to which the substation will interface, including the manufacturer and the protocol and software that will be used. In addition, the level of automation and control, both local and remote indications, and other control requirements.
- *Protection requirements*  
Including the requirements for each circuit, especially the required fault clearance time. Required redundancy and the protection philosophies to be applied for each circuit together with breaker failure and other requirements. Requirements for local test and other requirements to meet local maintenance requirements. Integration with remote end protection systems will need to be specified.
- *Communications requirements*  
Including the method communication available or to be supplied. This may be power line carrier (PLC), microwave radio, telephone line, pilot cable or optical fiber, or a combination. Communications will include a mix of voice, telephony, data and me-

tering, protection signaling and intertripping, and may include a mix of digital and analog signals to be communicated. The speed, redundancy and security of communications will usually be specified.

- **Standards and regulations**  
These may include local standards or other national or international standards and regulations applicable to the asset owner or to the site.
- **Health, safety and environmental requirements**  
This may include a range of local utility requirements. Environmental requirements may be local or regional regulations or standards including noise, EMF or EMC (electromagnetic compatibility) requirements, oil discharge limitations for the site, aesthetic requirements, and archaeological or other site constraints and considerations [11.12].
- **Other design requirements**  
These may include design life and the method for evaluating the design such as whole-of-life costing minimization and *safety in design* requirements.

Conventional prescriptive specifications are generally considered to have a lower level of commercial risk for the contractor and the owner.

### Functional Specifications

Increasingly, asset owners are finding that a conventional approach to specification delivers conventional outcomes, and many utilities have introduced a form of functional specifications that are aimed at defining the key outcomes required from the substation, without specifying the detail of *how* these outcomes might be achieved by a designer or builder. This type of specification is more appropriate when both design and construction are to be outsourced. Often, the aim for utilities who use this approach is to introduce new approaches to the design and introduce innovation that would not be possible using a conventional specification approach.

The principle of a functional specification is to specify the broad requirements (the *what* that is required, rather than the detail) and the objectives of the substation without specifying *how* this is to be achieved, leaving that to the designer. In some cases, this approach can be coupled with a contracting arrangement between the owner and outsource organization that provides a way to share the benefits (and penalties) if the overall objectives of the project can be achieved.

Functional specifications come with some commercial risk for both parties, and the associated terms and conditions are therefore important and must be aligned with the business requirements of both parties.

One approach for the specification of substations used in Australia and detailed in reference [11.13] involved articulating and documenting:

- The *design philosophy* for the new substation  
This is a relatively short document that establishes the key policies and philosophies that the design must adhere to.
- The *functional specifications* of the substation  
Including the key limitations and performance requirements. Present and future requirements should also be specified.
- The *concept design* detailing key design elements as a guide or template for the detailed full substation design documentation.

Using this three-stage approach, the asset owner can have more confidence that the new substation will meet present and future requirements, aligned with broader corporate objectives, without preparing detailed specification that might contain errors and inconsistencies.

### Standardization

One of the criticisms that manufacturers and suppliers have leveled against utilities is that they are often resistant to change and that the prescriptive procurement specification processes traditionally used by utilities limit the ability for suppliers to present new approaches and introduce new technology. The reader may wish to read [11.13] for more discussion on this issue.

On the utility side, there is good reason to be conservative in new projects and to avoid making substantial design changes that might ultimately cause reliability issues or add to whole-life costs in future years, long after the builder has completed the project and moved on. One fundamental factor is the capability of existing operations and maintenance staff and their ability to adapt to a change in design of controls, layouts or equipment. It is vital that any designer include a consideration of operations and maintenance staff capability and their opinions and preferences in designing new substations. There are safety and reliability as well as industrial risks in ignoring the corporate knowledge and capability of staff and operating equipment that will be required to operate and maintain the station. There are also considerations of the type and mix of spares kept, so there is often good reason to restrict the level and number of changes to primary equipment.

Utility standards often incorporate national and regional legislation and regulations regarding health and safety, environment and security, and can also extend to incorporating common standards to assist in reducing construction errors, outage time and cost, improving safety, ensuring knowledge sharing and simplify operating and maintenance procedures.

Utilities normally select standardized substation configurations using prescribed equipment for each substation layout together with the agreed method of

protection and control for each arrangement. High-value substation components, substation cables and other material may be predetermined according to corresponding procurement contracts in place.

However, for corporate strategic reasons, many utilities have an interest in exploring new technologies, not just repeating the same designs. Using the functional specification approach described in the previous section is one way to achieve this, but there are other ways to identify and incorporate innovation in new substation design.

The regulatory and commercial environment for many utilities means that there is often a need to reduce cost of delivery of new infrastructure, and rapid load growth may also mean that new infrastructure needs to be delivered more quickly than traditional processes have been required to deliver.

The utility needs to preserve the important aspects of past practices in relation to maintainability and operability, and to do this at lower cost and faster delivery times. There is often a corresponding strategic objective to not *lock out* new ideas and new approaches that might be available in the future and that align with the utility aims and objectives. One strategy that some companies have used to introduce innovation is to change from conventional, prescriptive approaches to substation specification by using a functional specification approach. That step change process can allow suppliers the freedom to introduce new technological approaches to an otherwise conservative organization. The processes associated with that change can be significant, involving change management among managers, designers, operations and maintenance staff. This process of change requires the utility to ask internally, *what is it that we really need to meet our corporate objectives*. The answer to that question is often much less than previously defined in prescriptive specifications and existing design standards.

Another approach that can be taken to address the need for faster delivery and lower costs is for the utility to determine a set of *standard designs* that can be adopted for future substations. These standard designs can be prepared as a concept design that articulates as much of the design of the future substation as is feasible, without the final step of a detailed design. The adoption of a standard design involves deciding upon the key elements that will be standardized for the future designs. These key elements may include limiting the range of transformer sizes, limiting the switchgear fault levels or technology types to be considered, and even developing standard primary and secondary drawings that can be tailored once the actual site and the specific design parameters for a specific project have been determined. In this way, significant savings can be achieved

in the development of the design for a new substation. The approach is compatible with a traditional design approach, and often previous design drawings may be adapted by a designer for a new substation design project. This process of adopting a *standard design* for use in future substations can have significant benefits, and from a utility standards perspective allows the important aspects of design to be standardized, predetermined and aligned with operations and maintenance needs, and spares and procurement requirements, with reduced project design time.

There is another major advantage to the adoption of standard designs to standardize the design approach, and that relates to staff knowledge and experience. Traditionally, a utility or organization's substation standards were developed over a longer time period and were intended to document key corporate requirements based on experience and knowledge with key design requirements, but with the need to capture every future application requirement. This type of standard development requires considerable expertise and usually long-term experience in order to understand the rationale for different design approaches and also future needs. The type of skill required to develop an organization's design standards is becoming increasingly difficult for many companies to secure, and in any case, the approach often lacks the ability to innovate and adopt new technologies as they emerge. However, the process for preparing a standard design does not require the same level of experience and is not so different from the effort and knowledge required for a single design project.

A *standard design* approach enables more precise specification and contracting and reduces the potential misunderstanding that may develop between the utility and its substation builder. Design time can be significantly reduced using a *standard design* approach through the development of concept design drawings that need only to be tailored to the specific requirements of a particular project, rather than the designer starting from a blank slate, and with basic design parameters.

*Case Study*—In 2005, Ergon Energy, a transmission and distribution utility in Queensland, Australia, was faced with the challenge of delivering a significantly increased and prolonged capital program requiring lower costs and shorter delivery times. The company decided on a *standard design* approach with more functional specifications and achieved significant savings in design and delivery times for a number of key projects. The targeted 80% reduction in design time was achieved for some substation design projects. The process of changing the standards approach from prescriptive to functional design achieved significant innovation and new technologies that had never been used before by that utility. The project to make the necessary internal

changes involved communication and consultation with staff across the organization, carried out over a 2-year period. A new range of internal processes was introduced to ensure that future innovation was not locked

out, while still aiming to achieve the design savings and the procurement and spares holdings benefits. The basic designs that were adopted during that period are still in use by that utility today.

## 11.3 Design

Design of substations [11.14] involves a range of considerations, from site selection, to substation layout with adequate redundancy, electrical clearances, insulation coordination, structural and civil design, and secondary and auxiliaries design.

Once a suitable site has been defined that provides adequate access and security, considering issues such as soil types and the risk of flooding, and with a design that is acceptable to the local community, the design of the actual substation can commence. Substations operate in harsh environmental conditions, and earthing and lightning protection is a major design consideration. The impact of the substation on the environment and the environmental footprint of the substation must be considered when designing a new installation and also in ongoing life management.

Substations can be built using a range of insulation technologies, each with their own advantages and disadvantages. The most common technology for primary equipment is air-insulated switchgear (AIS) although the use of gas-insulated switchgear (GIS) using either SF<sub>6</sub> or any of a range of other gases has evolved and has become common in many regions, particularly where limited space may be an issue. The use of overhead connections, underground cables and gas-insulated lines (GIL) may also be part of the consideration for substation designers.

In some cases, substations are built for offshore applications requiring particular design considerations. For mobile and modular substations, the risks associated with transportation and relocation are a consideration.

The substation is required to operate reliably and to require minimal maintenance, meeting the required performance objectives over a long lifetime. These design aspects necessitate a range of electrical, mechanical, civil and structural engineering skills.

The design process varies from organization to organization, but some common elements can be defined. Fig. 11.20 provides a summary of the key steps and interdependencies for a typical greenfield substation design. Addition, more detailed information is available in other references, including CIGRE Technical Brochure

740—Contemporary solutions for low cost substations in developing countries [11.15].

### 11.3.1 Sustainability

Sustainability is a key area of concern for the power network and for substation designers today. This chapter does not discuss sustainability in general, but some aspects of sustainability directly affect substation design and are discussed briefly in this section. Sustainability can be considered to be about people, planet and profit (3 Ps). The following sections consider some of these aspects in relation to substation design.

### 11.3.2 Designing for Safety

Design is often influenced by local codes, design standards and legislation. Experience with safety incidents and accidents has led many countries to adopt health, safety and environmental protection laws or rules with mandated requirements for designers of electrical infrastructure [11.16].

The aim of these rules is to protect employees, the public and the environment from harm over the life of the installation. These rules or legislation may be referred to as health safety, environment and quality (HSEQ) or occupational safety and health (OHS) guidelines. In some cases, specific legislation requires designers to follow a defined process to ensure that applicable safety and environmental considerations are addressed during the design process.

In general terminology, designing for safety involves the integration of hazard identification and risk assessment within the design process to eliminate or minimize the risk of injury throughout the life of a product being designed.

One of the design challenges for infrastructure such as substations is considering what hazards might exist over the life of the installation, and that may mean considering what may occur over more than 50 years of installation life. The design process (Fig. 11.20) refers only to the key steps, but any requirements for HSEQ considerations are embedded into the design process and design decision-making.

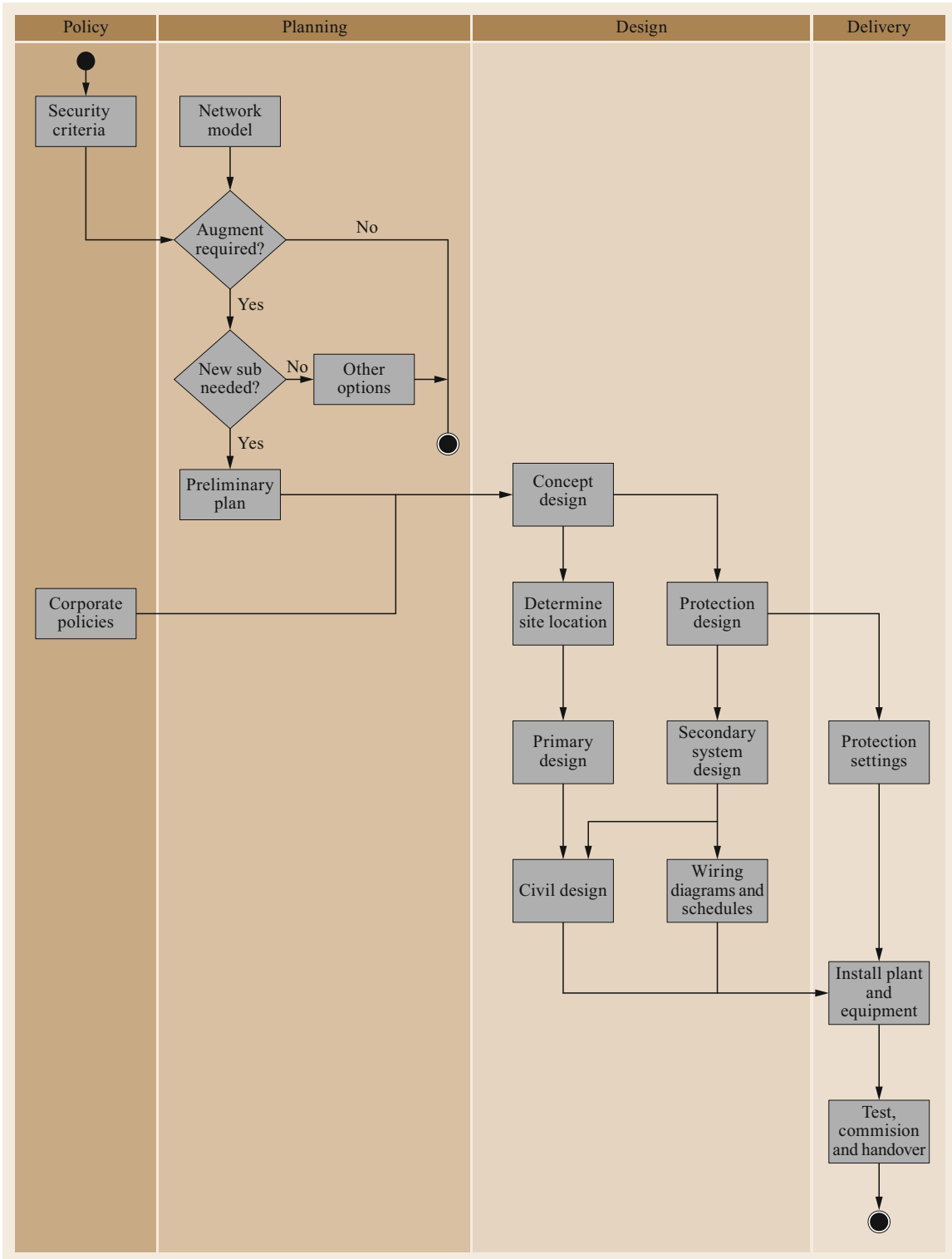


Fig. 11.20 Typical basic substation design process steps (summary only)

It is estimated that building inherently safe plant and equipment would save between 5–10% of their cost through reductions in inventories of hazardous materials, reduced need for protective equipment and the reduced costs of testing and maintaining the equipment.

The direct costs associated with unsafe design can be significant, for example retrofitting, workers' compensation and insurance levies, environmental cleanup and negligence claims. Since these costs have a greater impact on parties downstream in the life cycle who buy and use the product, the incentive for these parties to influence and benefit from safe design is also greater.

A safe design approach results in many benefits including:

- Prevention of injury and disease
- Improved usability of products, systems and facilities
- Improved productivity
- Reduced costs
- Better prediction and management of production and operational costs over the life cycle of a product
- Compliance with legislation
- Innovation, in that safe design demands new thinking.

Safety and environmental consideration is one of the fundamental requirements for all designers, whether it is legislated or not, for the particular utility or client.

### 11.3.3 Substations and the Community

Substations are designed to fulfill a set of functions within the electrical network, but they are often built adjacent to residential, business or industrial areas and other infrastructure, and are therefore required to meet community expectations for visual aesthetics, noise control and other factors, and in some cases mandatory regulatory requirements. In the past, substations could be designed to simply achieve their core electrical and mechanical functions, but increasingly utility owners need to consider the needs of the community in relation to electrical infrastructure. To this end, designers have often taken considerable effort to reduce the impact of the infrastructure on the community (Fig. 11.21). This can be justified on the basis that the utility can ultimately be shown to be a better community citizen, even if these measures add to the cost of the installation, which must be passed on to the shareholders and other stakeholders.

In some utilities, it is common practice to consider screening of the substation with trees, shrubs or other vegetation or by semi-sinking the substation into the ground, located behind a natural hill or artificial earth bank (Figs. 11.22 and 11.23) [11.17]. While from



**Fig. 11.21** The night lighting and facade of the Laura 110 kV Substation in Russia (Krasnaya Polyana—Sochi) is an example of design for aesthetics (Courtesy Electra)



**Fig. 11.22** Prinsenhage high-voltage substation in Breda Substation in the Netherlands (Courtesy TenneT/Movares)



**Fig. 11.23** Anneberg 400/220 kV Substation, Swedish National Grid (Courtesy Tennet/Movares)

a purely functional perspective the ideal substation location may be on the top of a prominent hill to achieve the best line approach direction and design, this would normally not be considered by the substation designer. One of the conflicting considerations for the designer in designing visual screening is to consider the needs of the substation security and to avoid creating locations where an intruder might be hidden from view.

A substation may also be located in a more urbanized area. In these cases, the landscape elements will often have an environmental added value as an urban recreation area. For example, the substation may have elements that serve as a visual or acoustic buffer, parking strip or cycling route.



**Fig. 11.24** Technical facilities with an attractive outer shell or fence in Dronten, Rotterdam, Liedsche Rijn, Utrecht (Courtesy Tennet)



**Fig. 11.25** 3-D visualization showing a proposed new substation in a suburban street in North Queensland, Australia (Courtesy Ergon Energy)

In some cases, attractive screening can be added to the substation façade (Fig. 11.24).

Three-dimensional visualization techniques can be used by the design team during a community engagement process to demonstrate how the design will integrate into the streetscape.

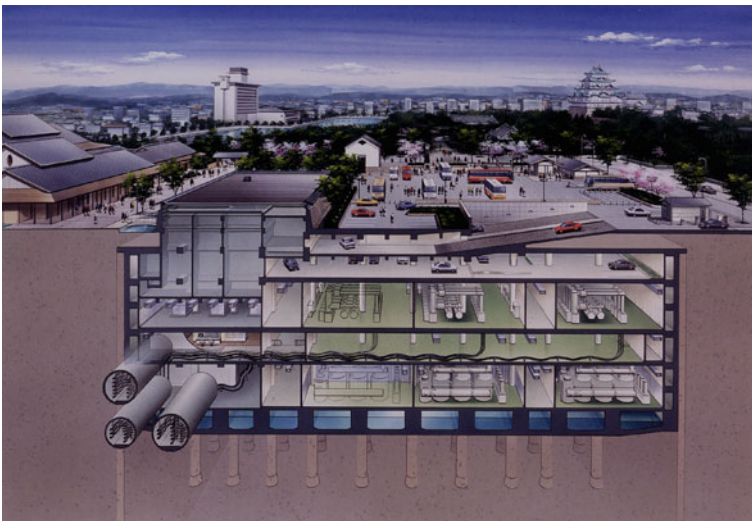
The example shown in Fig. 11.25 from Australia demonstrates how architectural additions to the substation can be used to modify the appearance of the substation building to adapt to the local street environment.

None of the examples above completely hide the substation, and ultimately the only way this can be achieved is by building the substation underground, as in the example from Japan in Fig. 11.26.

Increasingly designers need to consider how to integrate substations into the community. In some cases, mandatory requirements are enforced by local authorities as part of a project approval process, but in others these measures are to ensure that the substation gains community acceptance. There are many examples of practices around the world, and the requirements for the substation to be an accepted part of the local community should never be ignored.

#### 11.3.4 Key Components

Substations can be constructed with a number of different layouts and using a number of construction methods including indoor, outdoor, overhead or underground, on ground, on pylons or floating on the sea, and may be built using AIS, GIS or hybrid technologies or



**Fig. 11.26** Meijou Underground Substation design in Japan (Courtesy Chubu Electric)

a combination. Whatever the type and method of construction, a substation includes some or all of a number of high-voltage and low-voltage components that can be classified as:

- Primary power lines or cables
- Busbars and overhead conductors
- Instrument transformers including voltage and current transformers
- Disconnectors or isolating switches
- Circuit breakers
- Surge or lightning arresters
- Power transformers
- Reactive compensation devices including reactors and capacitor banks
- Support insulators and bushings
- Control buildings to house protection and control equipment
- Secondary control and protection systems
- Earthing system
- AC and DC auxiliary systems that may include an on-site emergency generator
- Environmental control systems
- Security fences
- Civil and structural supports.

### 11.3.5 Preliminary Design

The first step in the design of a substation is to confirm the busbar layout, often determined at an early planning stage. The busbar layout is usually defined by overall network requirements and the required substation function as described in Sect. 11.2. This design process step defines the single-line diagram of the substation and the key primary components that will be required.

The preliminary design, (or concept design), is part of the early stages of the overall design process and involves the development of the single-line diagram together with the chosen primary and secondary philosophies and technology decisions into a more coherent document that articulates how the substation will look and fit onto the selected site. The concept design normally considers the actual selected site characteristics. In most cases, the site will be predetermined because it has been already forward-purchased or allocated or otherwise defined, and so the concept design will incorporate those details.

Good practice approaches in design often include a collaborative approach to development of ideas for the concept design phase, as decisions made at the concept phase often have a major impact of the final design. Collaboration at this early stage with operations, maintenance and commissioning staff, as well as representatives from the various engineering disciplines

including primary, secondary, protection and civil design, can be a useful input to the design process.

The design standards of the organization or utility may define many of the key parameters that need to be addressed in the physical and electrical layout of the substation, but the concept design must include reference to:

- Primary design including maintenance access and electrical clearance requirements
- Insulation coordination requirements including lightning protection
- Structural and civil design including seismic requirements
- Earthing and lightning protection
- Reactive plant requirements
- Control and protection philosophy and automation
- Auxiliary system requirements
- Environmental requirements including the effects of the environment on the substation and the substation on the environment.

Many of these design aspects are interrelated and may require an iterative approach during the design process, particularly in the early stages. For example, the size of the site available may restrict the types of technology or the actual physical layouts that may be considered. It is unusual for a designer to have the luxury of first deciding on a bus layout, then defining a required space, and then finding suitable land or space.

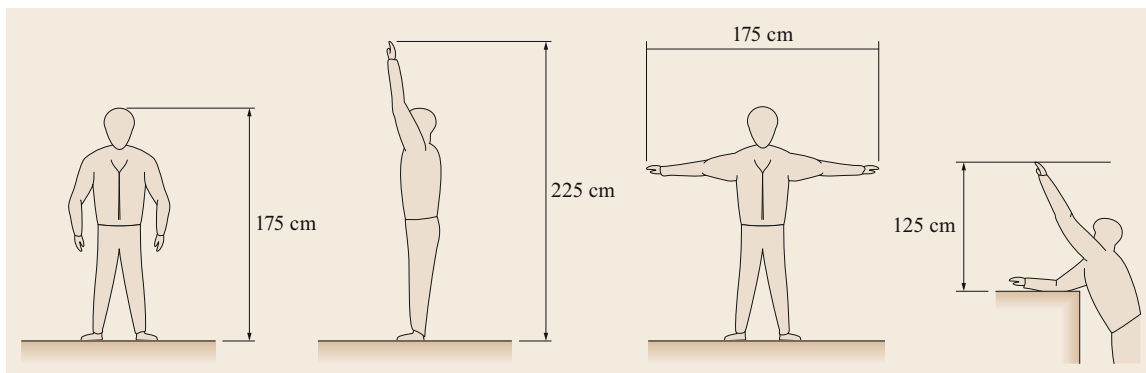
A range of aspects of the design phase are discussed in the following sections.

### 11.3.6 Electrical Clearances

Electrical clearances (or safety clearance distance) [11.18] are required to ensure adequate safety for operations, maintenance and other staff by establishing adequate distances between high voltages and accessible locations within the substation fence. Clearance distance is defined as the minimum distance to be maintained between live equipment or conductors in order for work to be safely carried out in the substation. These distances are used by the designer to arrange the equipment within the substation.

These standard clearance distances vary around the world and have been derived in many different ways, and not always logically in relation to the nominal voltages. Different methods have been adopted in each country or region to establish electrical safety clearance, based on the nominal voltage level of the substation. It should be noted that these safety distances are in air and do not relate to insulator length or creepage distance.





**Fig. 11.27** Typical human dimensions for determining safety clearance charts (Adapted from [11.19], © IEEE)

This *safety distance* is initially defined by the impulse withstand voltage rating of the substation, but is also intended to account for the expected physical size and movements of operations and maintenance staff within the substation. The design intention is always to reduce the risk of inadvertent contact by staff with live equipment during typical maintenance and operations tasks within the substation.

In most cases, safety clearance distances are defined by regional standards or legislation and are incorporated into the design by referring to tables and charts. However, in formulating such tables of safety clearance, the following are considered:

- The basic value aimed at ensuring no flashover from high voltage under the least favorable conditions. This basic value usually incorporates a safety factor.
- A safety zone is established to account for typical human activities.

The average dimensions of operations staff are used to determine an appropriate safety zone to be incorporated into the clearance distance. Fig. 11.27 shows typical human dimensions and activities that might be expected during substation operations and maintenance.

One of the difficulties in using *typical* dimensions is that no two individuals are the same, and the size of staff may vary considerably.

If there are no guards or safety screens in place, then the safety distance must allow for the free movement of staff beneath the high-voltage equipment. Based on the typical dimensions, the minimum distance to live equipment from ground access may be considered as 2.25 m; however, for simplicity and additional safety, a minimum of 3.0 m is commonly recommended, even though the impulse withstand distance for voltages under 380 kV may be much less than this distance.

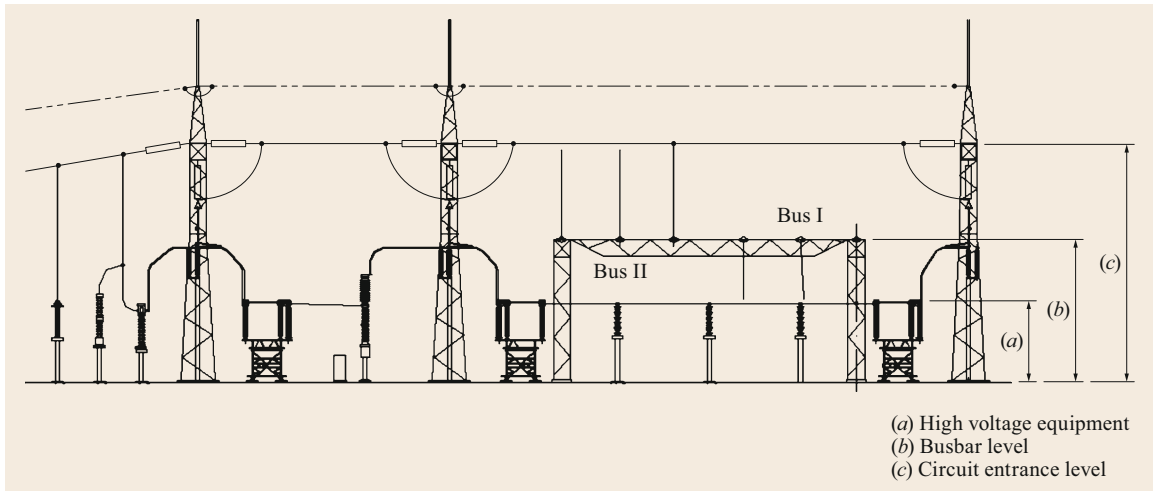
The minimum safety distance from the ground is considered as that measured from the highest accessible point on or near the ground level (without climbing supports or structures in the normal course of activities) and the nearest live conductor. Insulators are considered to be live conductors for the purposes of safety clearance measurement, even though the lower parts of the insulator may be at earth potential.

If safety clearance distances cannot be achieved by placement and design of support structures, then appropriate guards or screens will be required to prevent or limit free access by staff from the ground.

Safety clearances are also required to allow maintenance work on live components in relation to adjacent circuits. Similar principles to those used for ground clearance can be applied to determine horizontal and vertical distances to be added to the basic clearance distances to ensure adequate safety margins for maintenance staff using tools. To determine an appropriate clearance, the normal distance that a worker could be expected to reach (with light tools) is added to the basic non-flashover distance, with an appropriate safety margin. Typical values that may be used, in addition to the non-flashover distance, are:

- 1.75 m horizontally corresponding to a worker with arms outstretched
- 1.25 m vertically above the working plane corresponding to that part of the worker passing above the plane when their arms are outstretched.

Permanent visual means of identifying the defined safety zone may be incorporated into the design. Vehicle access barriers, for example, may be used to restrict movement of vehicles under live equipment where the vehicle height may encroach beyond the safe zone. When work is required within the substation, it is normal practice that a safe working area is defined using



**Fig. 11.28** Typical substation elevation showing different heights for conductors

ropes, chains, flags or other markers according to local safety regulations.

There is no design that can be made completely safe for all work tasks. For example, the common use of elevating work platforms and scissor lifts means that maintenance staff have significant reach within, above and outside the work area that is difficult to control by screens or guards. Training and adequate safety procedures are required to ensure that there is minimal risk of staff being injured during maintenance activity in a live substation by reaching outside the defined safe working area. The designer should aim to minimize risk to a level as low as reasonably practicable (ALARP) by ensuring adequate safety clearances and avoiding known risks such as *oversailing conductors*, which have been the cause of death in some countries. Appropriate screens and barriers should be used where appropriate.

### 11.3.7 Primary Design

The layout of the substation is driven primarily by the choice of busbar configuration allowing for the required clearances, the insulation type and voltage level, and the technology type allowing for the ongoing maintenance and security of the site [11.14]. The substation layout defines the disposition of the various items of high-voltage equipment (line or cable entry, switchgear, transformers, etc.) and their connection to achieve the busbar configuration within the site size and shape that has been chosen. Once a basic layout has been determined, the type of connection and busbars must be chosen to finalize the primary design.

For an air-insulated substation, different parts of the substation are usually arranged at different heights to

achieve adequate distance between parts of the circuit (Fig. 11.28).

Busbars and connections between the busbars and other components may be either rigid or flexible, or a combination of both. Often the choice of conductor type will depend on local practices and standards, but it is also dependent on the type of switchgear that will be installed. For either choice, the issues of safety, final layout complexity, ease of erection, short circuit forces, aeolian vibration/resonance and cost should be considered by the designer. Effective design solutions can be determined for either flexible or solid conductors.

The final layout must allow for adequate phase-to-phase and phase-to-ground (or other equipment) distances and provide adequate access for typical maintenance activities.

There are other considerations involved in finalizing the substation layout, including:

- Future expansion—consideration of the ultimate layout requirements and ease of extension and any future uprating requirements
- The direction of approach of incoming lines and feeders
- The risk of failure of flyover spans and overheads wires
- Physical security
- Storage, parking and laydown areas
- Environmental requirements.

Historically, substations have been designed to allow frequent circuit breaker maintenance, and consequently disconnectors are a major part of the primary design. Consideration may be given to the use of disconnect-

ing, rotating or withdrawable circuit breakers to reduce or even eliminate the need for disconnectors. The lower maintenance frequencies of modern circuit breakers means that electrical isolation for maintenance may be achieved by flexible leads with disconnectable links rather than actual disconnectors. The use of hybrid switchgear can also simplify substation layouts and reduce the physical dimensions required for bays.

Another considerations for the primary designer is visual impact and aesthetics. A low-profile layout may be preferred in order to reduce the visual impact of the site.

### 11.3.8 Insulation Coordination

Insulation coordination involves a series of design process steps to select the appropriate dielectric strength of substation equipment and to match this with appropriate protective measures to be incorporated into the substation design. It can be a complex subject, and only general considerations are given in this section [11.19–21].

Insulation coordination considers the expected overvoltages generated in the external network that affect the substation and overvoltages from within the substation itself. These overvoltages may consist of external overvoltages due to lightning, switching operations and other transitory conditions, and also overvoltages due to circuit resonance. There are some particular considerations for GIS substations including DC and AC voltage stressing and very-fast-front overvoltages.

The aim of insulation coordination is to reduce the risk of dielectric failure and to coordinate the insulation within the substation by considering:

- Equipment voltage ratings including lightning impulse withstand, switching impulse withstand and power-frequency voltages
- Insulation withstand levels
- Creepage distance of external insulators
- Clearances in air of various components
- Footing and earth resistances
- Ratings and energy dissipation characteristics of selected surge arresters.

Externally generated overvoltages are generally controlled by the use of overvoltage-limiting devices such as surge arresters and rod gaps. Internally generated overvoltages are controlled by the design of primary equipment and other precautions. The aim for the designer is to reduce the probability of insulation failure due to overvoltages, whether generated internally or externally. The risk cannot be totally eliminated, and

the objective is to achieve an economically and operationally acceptable risk level.

The majority of lightning overvoltages affecting substations enter as traveling waves on the overhead lines. Where a transmission line is shielded and its tower footing resistances are low (generally considered to be  $10\Omega$  or less), a lightning stroke to a shield wire or a tower will normally discharge safely to earth on the tower and not enter the substation. If the tower footing resistances are high or if shielding is not effective, a stroke to a shield wire or tower may raise the potential of the tower far above that of a phase, and depending on the current of the stroke may result in a *back flashover* from the tower to the phase conductor. This could result in accompanying power-frequency earth fault current in the ionized path formed, flowing in the opposite direction to that of the surge current.

A back flashover will typically initiate a traveling overvoltage wave of extremely high rate of rise on the phase conductor that travels along the conductor and ultimately enters the substation. Similarly, lightning strokes that occur close to the line may induce sufficient overvoltage in the phase conductor to generate a traveling wave.

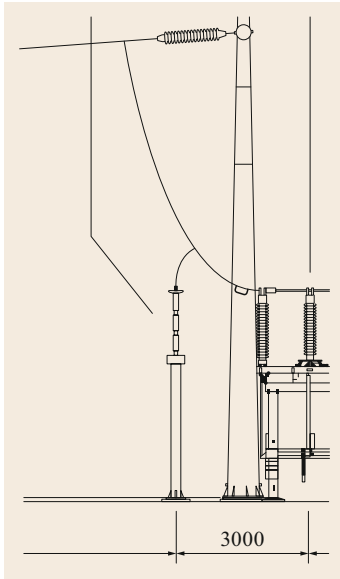
This type of induced overvoltage is usually not an issue at transmission voltages, but can have a severe impact on distribution equipment.

Traveling waves travel along the line in both directions away from the point of strike or back flashover, but are attenuated by the resistance of the phase conductor and so dissipate with distance. A strike or a flashover within 2–3 km of a substation is generally considered to be close enough to cause potential problems that must be considered in the insulation coordination study.

The main task in insulation coordination is to coordinate the expected overvoltage stress in the substation from various sources with the insulation strength of the insulating components of equipment installed in the substation.

Two methods can be used to assess the adequacy of insulation coordination. These are basically classified as:

- *Deterministic* method, which can be applied if there is little or no statistical information available. In this case, a set of values is determined or assumed and coordinated so that no breakdown will occur under this assumption. A safety factor is applied to allow for statistical scatter in assessing the expected level and frequency of occurrence of transient overvoltage.
- *Statistical* method, which can be used if the risk of failure can be fixed at an acceptable value and calcu-



**Fig. 11.29** Surge diverter fitted to incoming line in a 132 kV substation (Courtesy CPP, Australia)

lated using an overvoltage probability distribution and the breakdown probability of the insulation.

#### Achieving Adequate Insulation Coordination

The process of insulation coordination will usually result in the need for metal-oxide surge arresters fitted at each overhead line or cable entry point and at GIS, transformer and reactor interface points (Fig. 11.29).

For small, compact substations in moderate-risk lightning regions and with voltages up to 300 kV, surge arresters on the entry points are normally sufficient for protecting the substation and adjacent high-voltage equipment. For physically large substations in high-risk lightning regions or in substation arrangements with long busbars or bus ducts and for voltages higher than 300 kV, extra surge arresters mounted close to the transformers or reactors may be required.

#### Surge Arrester Selection

The selection of a surge arrester is a compromise between temporary overvoltage capability, level of protection and energy dissipation capability of the surge arrester. The surge arrester must be stable under system conditions and under short-duration power-frequency overvoltages. When these conditions are not known, a sufficient safety margin should be selected. The protection level should be selected as low as possible in order to achieve an economically sufficient margin between the protection level of the surge arrester and the insulation level of the equipment. The energy dissipation capability of the surge arrester must match the stress that the surge arrester will endure during switching and lightning overvoltages. Simpli-

fied calculations are normally sufficient to select the correct temporary overvoltage capability, protective level and energy dissipation capability of surge arresters.

The overvoltage protection of a substation is not only a question of which arrester to choose. For protection against lightning surges close to the station, it is even more important that the arrester be installed in the most effective way. The surge arrester should always be placed as close as possible to the equipment to be protected. An important aspect of all surge arrester mounting (especially in the vicinity of GIS) is that the length and inductance of the earth connection of the surge arrester should be minimized. The use of a normal stranded earthing conductor is not recommended for any GIS earthing, especially surge arresters, due to self-inductance of the conductor. The use of a flat square-, rod- or rectangular-section solid conductor is the preferred method of earthing in situations where fast rate-of-rise transients may be expected (such as lightning- or GIS-induced transients).

In addition to considering very-fast-front overvoltages, insulation coordination should also consider ferroresonance phenomena. Ferroresonance is a resonance between nonlinear inductance and some form of series capacitance associated with parts of the substation such as capacitive voltage transformers, long line connections, cables or capacitive coupling. It may occur where a transformer is lightly loaded and during single-pole switching procedures and can result in equipment damage under some circumstances.

### 11.3.9 Earthing and Lightning Protection

The substation earth mat or grid is an important aspect of the overall design of the substation, particularly in relation to the safety of personnel.

A substation earth grid has two main functions:

1. *Operational*  
Providing a path for current to the general body of earth in normal and fault conditions.
2. *Safety*  
For personnel, animals or equipment within the environs of a substation or in remote locations to avoid dangerous voltages during the flow of earth fault currents in the earth grid.

The earth grid also provides for the discharge of lightning and switching surges to earth and for the earthing of high-voltage equipment during maintenance.

The earth grid and the connections to it from the transformer neutral points must be rated for the most onerous prospective earth fault currents that might be

expected under worst-case conditions. The grid resistance to remote earth should be low enough to limit the earth fault current below a minimum value necessary for correct operation of the protective relays.

The earth grid and the connections to it from equipment, housings and structures should be such that touch and step voltages within or in the vicinity of the substation and transferred from the earth grid to external locations over telephone circuits or low-voltage power circuits or by any other means, are maintained within safe limits [11.22].

It is common practice to also connect the shield wires of overhead conductors and any metallic bare conductors entering or leaving the substation to the substation earth grid. This has the effect of further reducing the impedance of the earthing system to ground, particularly for smaller substations, but care must be taken so that the earth grid potential rise under fault conditions is not transferred to water pipes or telecommunications circuits or other metallic conductors that might be contacted by persons.

During earth-fault conditions, the flow of current to earth will produce voltage gradients within and around a substation, and it is therefore important that persons within the substation or in the vicinity are not exposed to dangerous voltage gradients.

There are a number of different types of hazardous potentials that may arise when an earth fault occurs:

- *Rise of earth potential or grid potential rise (GPR)*  
Due to a rise in voltage of a part of the earth system above true earth.
- *Step voltage*  
The voltage occurring between the feet of a person walking (or stepping) across the earthed system at the time a fault occurs.
- *Touch voltage*  
Between the hand of a person touching equipment (such as a metal support or an operating panel) at the time a fault occurs. Touch voltage can be considered the most serious because the expected path of the current may be through the heart from hand to feet, potentially causing ventricular fibrillation.
- *Mesh voltage*  
Voltage that occurs within the earth grid when a fault occurs.
- *Transferred voltage*  
Voltage that is transferred from a site with an earth fault to a remote location by conduction through screens, pipes or other conductors.

The effects of electric current passing through the parts of a human body depend on the physiology of the person and the duration, magnitude and frequency of the

current. The most dangerous consequence of such an exposure is a heart condition known as ventricular fibrillation, which may result in damage to the heart and loss of blood circulation.

The earth mat or grid is designed to limit these hazardous potentials to values that are not dangerous to personnel, animals or equipment. The supports and metallic frames of all high-voltage equipment within the substation are permanently connected to the earth grid.

### General Earth Grid Design

The typical substation earth grid is composed of suitably sized earthing conductors (usually copper) laid approximately 500 mm below the surface of the ground and covering the whole extent of the site. The fence may be connected to the substation earth mat, but may be earthed separately for a range of reasons. Earthing conductors are placed within the grid based on the calculation of expected hazardous voltages under fault conditions. It is important that earthing conductors are not subject to corrosion due to chemical interaction with the surrounding soil.

The size of conductors and the spacing of the earth grid is determined during the earthing design process.

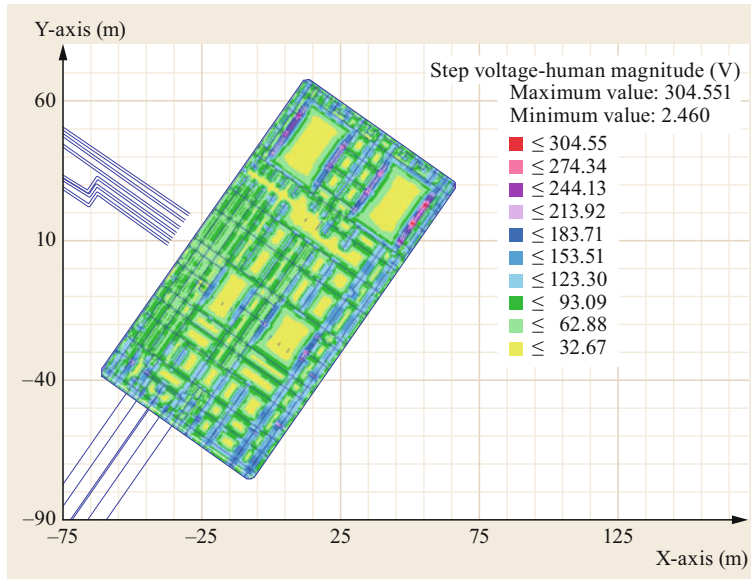
Calculations of expected hazardous voltages consider a range of factors including:

- Substation physical layout
- Soil characteristics including thermal and electrical resistivity
- Earth return paths via overhead line earth wires or cable sheaths
- Earth fault level due to network characteristics and the expected duration of faults based on protection design.

During earth-fault conditions, the flow of current to earth will produce voltage gradients within and around a substation. Because of this rise, there are voltage gradients across the earth grid and around the substation, which may be represented as surface voltage contours.

Calculations of earthing gradients and other earthing calculations are usually carried out using specialized earthing analysis software packages (e.g., the SES-CDEGS [11.23] or similar software packages). A typical outcome of a substation earthing design package for step voltages in a small substation is shown in Fig. 11.30.

Connection of the equipment frames to the earth mat should be made so that connections will not be physically damaged or easily removed as part of normal maintenance activities and are able to withstand expected fault current without damage. Often two con-



**Fig. 11.30** Typical output of a substation earthing design step voltage analysis in the form of a heat map showing expected transient human step voltages under fault conditions

ductors per structure are used to provide a level of redundancy and safety in case of removal or damage. Earth grids are designed to carry the maximum earth fault current for the duration of the expected earth fault. For the purpose of conductor sizing, fault durations are usually assumed to be one second for voltages in excess of 170 kV and three seconds for voltages below this, to allow for the unexpected failure of primary protection devices. Alternative worst-case clearing time assumptions may also be used as a design parameter for calculating the conductor size required.

#### Earth Grid Resistance Value

The earth grid resistance to remote earth should be kept as low as reasonably possible in order to fulfill the operational function of the earth grid. The earthing system should be designed to achieve safe touch and step voltages within the substation property for any person within the substation.

Maximum step and touch voltages are set to levels which will limit the current flowing through an exposed person to the safe current level.

The following factors influence the earth grid resistance:

- Soil resistivity
- Area covered by the earth grid
- Shape of the earth grid
- Mesh size of earth grid
- Burial depth of earth grid.

The characteristics of the earth grid conductor, including the cross-sectional area of the conductor and its

burial depth, also have a small effect on the earth grid resistance.

The equation is simplified from IEEE 80-2000 [11.24] and can be used to calculate approximate earth grid resistance

$$R_g = \frac{\rho}{4} \sqrt{\frac{\pi}{A}} + \frac{\rho}{L_T},$$

where  $R_g$  is the substation ground resistance ( $\Omega$ ),  $\rho$  the soil resistivity ( $\Omega \text{ m}$ ),  $A$  the area occupied by the grounding grid ( $\text{m}^2$ ), and  $L_T$  the total length of the conductors (m).

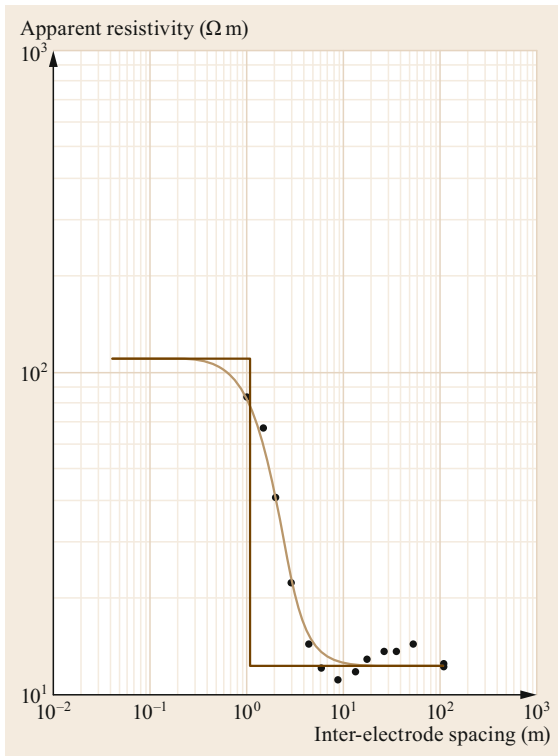
This equation assumes a simple grid arrangement and homogeneous soil resistivity, which is rarely the case in practice. This equation can be used to obtain an approximation of the earth grid resistance. In almost all cases, more complex analysis is needed.

The use of a suitable software package such as *SES-CDEGS* [11.23] or similar software is generally required to more accurately calculate grid resistance.

#### Soil Resistivity

Modeling of the expected performance of a substation earthing system requires knowledge of the soil characteristics and the determination of an equivalent electrical model of the surrounding soil and rock. This is achieved using the results of soil resistivity measurements in the vicinity of the site being studied and through careful interpretation of the results of such measurements.

Typically, soil resistivity measurements are taken using the *Wenner method* [11.25]. This method, which



**Fig. 11.31** Soil resistivity results for a large urban construction site

involves four measurement probes, enables the measurement of soil resistivity for different electrode spacing. Analysis by computer-aided methods is recommended to develop a soil model for the substation site. Typical soil model results are shown in the diagram below (Fig. 11.31).

In many cases, in analyzing the soil resistivity measurements it is possible to arrive at a simplified horizontally layered model of the soil structure around and below the earthing system. Occasionally, however, a more complex model will be required. Uniform or horizontal two-layer soil models can be used with manual calculations to determine the performance of an earthing system, but more complex soil models can be used only with computer-aided design.

#### Design for Touch and Step Voltage Limits

Design for touch and step voltage safety limits can be calculated using appropriate proprietary software or by simplified equations given in IEEE 80-2000 [11.24] and shown here based on a 50 kg body mass, 50 Hz frequency, a fault clearance time equal to the design earth fault clearance time selected and topsoil resistivity as

**Table 11.1** Typical soil resistivities—selected soil types

Soil type	Resistivity ( $\Omega$ m)
Clay, soft	50
Clayey sand	50–100
Soil, chalky	100–300
Limestone, fissured	500–1000
Granite	1500–10 000

indicated.

$$E_{\text{touch } 50} = (1000 + 1.5C_s\rho_s) \frac{0.116}{\sqrt{t_s}},$$

$$E_{\text{step } 50} = (1000 + 6C_s\rho_s) \frac{0.116}{\sqrt{t_s}},$$

$$C_s = 1 - \frac{0.09(1 - \frac{\rho}{\rho_s})}{2h_s + 0.09},$$

where  $E_{\text{touch } 50}$  = touch voltage in V,  $E_{\text{step } 50}$  = step voltage in V,  $C_s$  = surface layer derating factor,  $\rho_s$  = resistivity of the surface material ( $\Omega$  m),  $\rho$  = resistivity of the earth beneath the surface material ( $\Omega$  m),  $t_s$  = duration of shock current (s),  $h_s$  = thickness of the surface material (m).

In the absence of site-specific measured surface layer resistivity data, typical resistivities (as shown in Table 11.1) and thicknesses of surface layers can be assumed as a starting point for the calculation of the safety limits. However, it is always preferable to have actual site-specific data on soil characteristics available prior to the design.

The typical thickness of surface layers is 0.1–0.2 m for crushed rock or 0.05 m of tarmacadam. These materials can be used to reduce the risk of excessive or dangerous levels of step potentials within substation boundaries.

#### Transferred Voltages and Hot Zones

High ground potential rise (GPR) may cause problems outside the substation property, including:

- Hazardous step voltages
- Hazardous transferred touch voltages at fences and other metallic objects
- Equipment damage to infrastructure belonging to other utilities such as telecommunications cables and junction boxes.

Hazardous transferred touch voltages may occur where a metallic object, such as a fence, is earthed at a location and then traverses areas of different voltage levels. The metallic object is then at a different voltage from the ground over which it travels. A person touching such

**Table 11.2** Typical admissible voltages from ITU-T K.33 (International Telecommunications Union, 1996) [11.26]

Fault duration (s)	Admissible limit (V)
$t \leq 0.1$	2000
$0.1 < t \leq 0.2$	1500
$0.2 < t \leq 0.35$	1000
$0.35 < t \leq 0.5$	650
$0.5 < t \leq 1.0$	430

a metallic object is exposed to voltage difference in the form of a touch voltage.

Voltages may be transferred along the following metallic paths:

- Fences
- Shield wires
- Cable sheaths/screens
- LV neutrals
- Railway lines
- Gas pipe lines
- Other long metallic structures.

It is not always possible to model all of the mentioned metallic objects as part of an earth grid calculation. However, if any of the above are in the vicinity of the substation site, they should be tested using a current injection test.

Surface voltage contours are also used to define the *hot zone* of a substation or specific surface voltage safety limits agreed upon with the local authorities concerned.

A simplified calculation of the dimensions of specific surface voltage contours is given in IEEE 80-2000 [11.24] as

$$\varphi_e = \frac{\rho I_e}{2\pi d},$$

where  $\varphi_e$  = voltage on the surface of the earth (voltage level),  $\rho$  = soil resistivity,  $I_e$  = earth fault current,  $d$  = distance from the center of the grid.

This equation assumes a simple grid and uniform soil resistivity, which is rarely the case. This equation can be used to gain an approximate idea of the size of the hot zone contour. In nearly all cases, more complex analysis is needed.

One way of determining the extent of the hot zone is to use the voltage levels given in Table 11.2. These are the relevant voltage levels for different fault clearance times, and illustrate that the extent of the hot zone is dependent on fault clearance time.

Special design considerations may be required for transfer voltages associated with:

- Telephony and data cables entering the substation
- Distribution power cables for auxiliary or other supplies
- Adjacent traction or other power circuits
- LV systems and cables entering the substation
- Water and gas pipes.

### Earth Conductor Sizes

The earthing system comprises earth conductors, both underground and aboveground, including risers to connect aboveground equipment. Earth conductor size can be calculated using the Onderdonk formula or by consulting charts issued by conductor manufacturers

$$A = I \sqrt{\frac{t_c \alpha_r \rho_r 10^4 / \text{TCAP}}{\ln[1 + (T_m - T_a) / (K_0 + T_a)]}},$$

where  $A$  = area of the conductor ( $\text{mm}^2$ ),  $I$  = RMS current (kA),  $t_c$  = fault clearing time (s),  $\alpha_0$  = thermal coefficient of resistivity at  $0^\circ\text{C}$ ,  $\alpha_r$  = thermal coefficient of resistivity at reference temperature,  $T_m$  = maximum allowable temperature for the conductor type ( $^\circ\text{C}$ ),  $T_a$  = ambient temperature ( $^\circ\text{C}$ ),  $T_r$  = reference temperature for material constants used (typically  $20^\circ\text{C}$ ),  $\rho_r$  = resistivity of the earth conductor at reference temperature  $T_r$  ( $\mu\Omega/\text{cm}^3$ ),  $K_0 = 1/\alpha_0$ , TCAP = thermal capacity factor ( $\text{J}/(\text{cm}^3\ ^\circ\text{C})$ ).

### Earthing System Design

Earthing system design is an important aspect of the overall substation, and various analytical methods have been used in the past to achieve a safe earth system design. Previously, designers have generally used a deterministic approach to earthing design, but this often results in costly design solutions. Earthing design, as for other aspects of the substation, is a compromise between safety, risk and cost, and this balance can be optimized using quantified risk analysis techniques. CIGRE Working Group B3.35 surveyed the various analytical approaches in common use and examined the ways that designers could demonstrate due diligence in meeting their duty of care through risk and cost-benefit analysis using quantified risk techniques.

### Safety Earths or Portable Earthing Devices (PEDs)

Safety earthing is used to provide for personnel safety while working on otherwise live equipment. Typically, portable temporary earthing is applied on conductors on either side of the work area for protection of operating personnel against any improper re-energization of the work area due to error, transient effects, or induction from adjacent live circuits or from any other source.



Portable earthing devices must be rated for the maximum expected fault level and duration for that substation. Appropriate connection points and methods of connection are provided as part of the substation design.

In some cases, permanently installed earthing switches are provided to facilitate earthing of lines or other parts of the substation. Where ferroresonance of power transformers is likely, specially designed earthing switches may be installed to enable the quenching of the ferroresonance before re-energizing the circuit.

In designing the placement of portable earthing connection points, the designer should consider the height and the ability of the operator to apply the earth using operating sticks. Earthing connection points should be placed in the expected locations necessary to undertake typical maintenance activities. In applying earths, the normal operating procedure is to first prove that the circuit is dead, and then apply the earthing conductor. In applying earths, the operator will connect the earthed end first, before making the final connection to the device or conductor.

Special earth connection points or earthing spigots are fitted at the high-voltage end and connection points on the structures at the earth end. These points are designed to enable the type, size and number of portable earth connections required to carry the fault current to be easily attached.

### Earth Grid Testing

The earth grid at every substation should be checked and tested periodically to ensure that the performance of the earth grid is always capable of meeting the overall design requirements and the safety levels required for personnel in the vicinity of the substation.

Testing is important to verify the design calculations and to ensure that there have not been changes that might adversely affect the earthing system performance. Changes may include a change in fault level, removal of earth conductors (e.g., copper theft), degradation or damage due to corrosion, changes in soil characteristics and other changes.

Typical substation earthing system test frequencies are:

- Visual inspection annually
- Earth continuity testing every 5–7 years
- Remote injection testing every 12–15 years.

The test frequency for individual utilities depends on local policies and risk management practices.

### Lightning Protection

One of the issues for substations in some parts of the world is protection against lightning. Protection against

lightning can be problematic, as there are no measures that will provide 100% protection, and lightning itself is unpredictable. It is a phenomenon that has caused severe damage to life and property. Direct hits may cause structural failure, whereas indirect hits, through inductive or capacitive coupling, may affect the reliability and integrity of electronic equipment within the substation. Lightning can even affect substations built underground.

Although surge arresters are used to protect the substation against the effects of lightning striking lines and overvoltage surges entering the substation, it is also important to take steps to protect the substation against direct lightning strikes that may cause insulation flashover. The aim of the protection is to reduce the risk of injury to staff and equipment damage, and to prevent major outages. Even smaller lightning strikes that may not result in actual flashover have the potential to cause damage to substation equipment such as transformers.

The risk of lightning is defined by the frequency of the lightning strikes and by the ground flash density (GFD) or the keraunic level at the substation site. GFD is defined as the average number of strokes per unit area per unit time at a particular location. The keraunic level is defined as the average number of thunderstorm days or hours for a given locality. Maps are available in most regions that define the expected number of thunder-days per year and the expected severity.

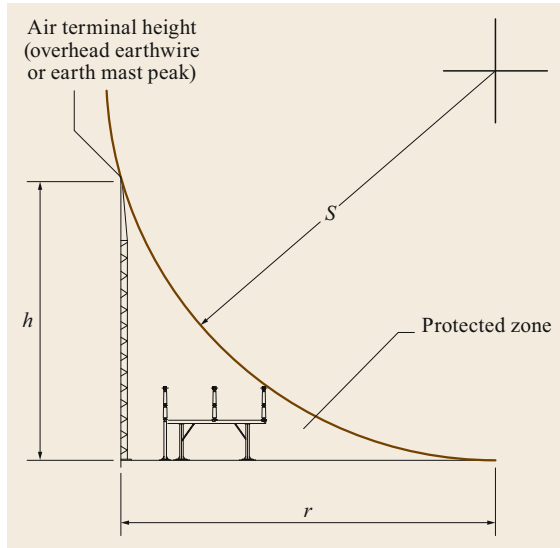
Protection from lightning can add significant costs to the substation, and a risk assessment is recommended to determine whether the cost versus risk is justified based on the criticality of the substation and the risk of lightning at that location. Three methods are typically used by designers for the analysis of lightning protection systems:

1. Classical empirical curves design approach using fixed protection angles and empirical curves
2. Electro-geometric model method (EGM), usually implemented as the rolling sphere method (RSM) as shown in Fig. 11.32
3. Collection volume method (CVM).

There are a range of other methods, but these three are the most commonly employed. The classical empirical approach was initially developed in the 1940s but is not recommended for higher-voltage substations.

Using the electro-geometric approach, an imaginary sphere of fixed radius is assumed to represent the risk of lightning strike distance and is *rolled* over the structure of the substation. Equipment that does not intersect with the rolling sphere is considered to be in the protection zone.

The radius of the sphere ( $S$ ) as shown in Figs. 11.32 and 11.33 represents the strike distance of the lightning



**Fig. 11.32** Rolling sphere method (Courtesy CPP, Australia)

stroke and is determined by the surge impedance and the allowable stroke current. Unlike the classical approach, the EGM takes account of the basic impulse level of the equipment being protected. However, one of the assumptions of this method is that the method assumes a fixed striking distance, regardless of the structure height.

The collection volume method, also known as Eriksson's attractive radius model, takes into account the physical features of the structure being protected. Based on this and on the intensification of the electric field created by different points of the structure, the CVM provides recommendations for the optimal placement of lightning rods or air terminals.

Protection against direct lightning strokes in the substation is carried out using either overhead earth wires or lightning rods, or a combination of both these protection methods. If overhead earth wires are to be used, then attention must be paid to the elimination of the risk of earth wires falling down onto busbars or other substation equipment. Overhead earth wires can be difficult to inspect and maintain in a live substation. Lightning rods may be mounted on freestanding structures or on vertical extensions of substation support structures.

As for earthing, lightning protection analysis is usually undertaken using specialized software and 3-D design methods.

For additional information about lightning protection and analysis methods for substations, see IEEE 998—Guide for Direct Lightning Stroke Shielding of Substations [11.18], IEC 62305-1 Protection against

Lightning [11.27] and IEC 61936-1 Power Installations exceeding 1 kV AC [11.28].

### 11.3.10 Reactive Plant

Reactive plant may be included in a substation for the purpose of network reactive compensation or voltage control. Network voltage and var control requirements may include both steady-state and dynamic system conditions, and will be dependent on the generation capabilities and the load characteristics of the network.

Reactive compensation is generally applied at the point in the network that is causing the effect, so that the substation affected will be the one that includes the new device. This means that a long line which would normally give rise to increased voltages (Ferranti effect) will normally be fitted with a line reactor at the receiving end to reduce the voltage. The line reactor may be switched or may be permanently connected to the line. Series capacitors can also be used to compensate for line inductance and to increase the power transfer capability of a line.

The most common forms of reactive plant in a typical substation are shunt-connected capacitor banks or line reactors. Shunt-connected capacitor banks are commonly used to control network voltages and are generally switched using an associated circuit breaker.

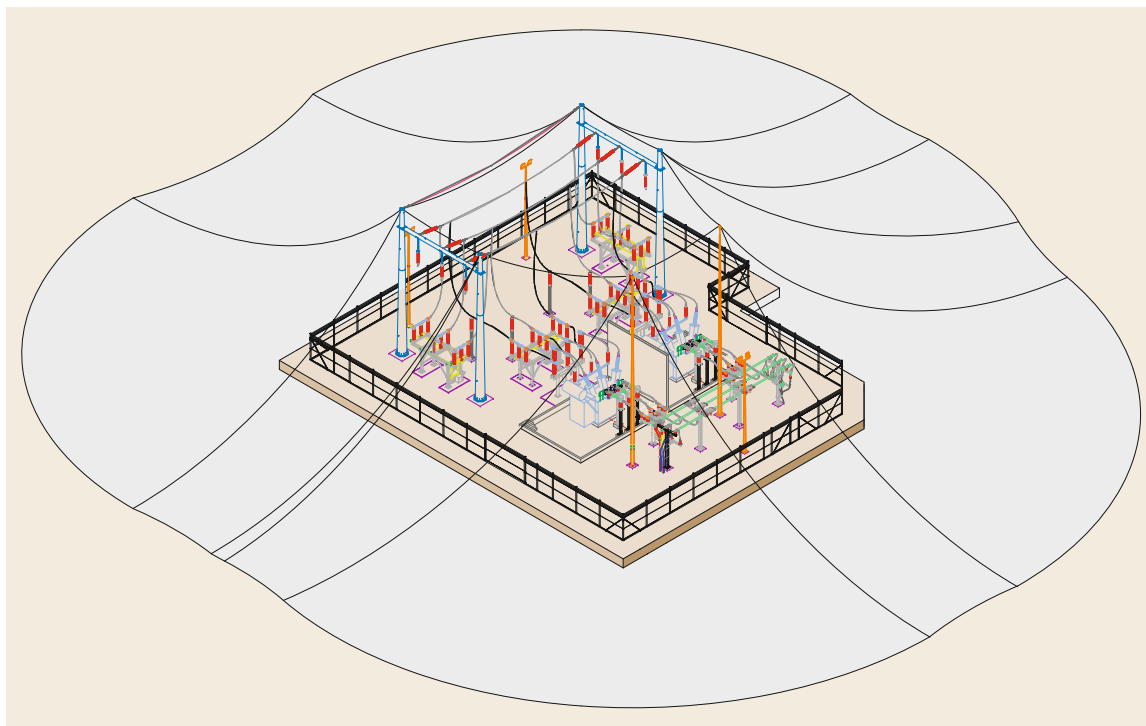
Reactive circuit breaker switching can be onerous, and the reactive switching capability of the circuit breaker should be considered in the design process.

Dynamic compensation or fast-acting reactive compensation such as static var compensators (SVCs) may be used to improve overall network stability, reduce harmonics and provide voltage and power factor correction. An SVC is a static device and generally comprises a switched capacitor element combined with a thyristor-controlled reactor to provide variable reactive compensation that is essentially stepless and fast-acting.

### 11.3.11 Substations and the Environment

One of the fundamental design considerations for a new substation is the environment. The environmental conditions that exist at the new site must be considered in designing the infrastructure, but the designer must also consider the impact of the new substation on the environment once built. This is often referred to as the substation *environmental footprint*. The objective for many utilities is to ensure that the substation has minimal impact on the local environment from any aspect of the design.

The environment in which the new substation is to be built is a major design consideration. Ambient tem-



**Fig. 11.33** Typical small substation lightning coverage 3-D model (Courtesy CPP, Australia)

perature, solar radiation, wind, rain, snow, ice and the likelihood of pollution all affect the selection of equipment supports, housing and insulation, and the design of the substation components, particularly where the substation is outdoors. Ambient temperatures have a major impact on loading and must be considered in equipment selection. Sporadic environmental conditions or risk factors such as floods, bushfires, hurricanes, earthquakes, volcanic eruptions and lightning all need to be taken into account by the designer.

The impact of the substation on the environment usually comprises a range of factors including:

- Spoil from construction activities
- Noise
- Visual amenity
- Archaeological or cultural heritage issues associated with the site
- EMF
- Oil and cleaning agent pollution of soil and in runoff
- Release of SF<sub>6</sub> and other gases into the atmosphere
- Water and other liquid site runoff.

Some of these factors can be controlled as part of the design; others are a matter of consultation, safe work practices and community awareness.

### Physical Environment

The design ratings of the substation are based on the expected operating environment of the site. This operating environment is sometimes referred to as the *physical rated environment* and can be derived from the service conditions used in the various high-voltage equipment specifications and reproduced in national and international standards. Typical rated physical environment specifications for a site in Australia are shown in Table 11.3.

### Animals

Another aspect of the substation physical environment is the effects of wildlife on substation reliability. The types of animals that typically cause reliability problems in substations are rodents, reptiles and small animals that are able to enter the substation through the fences or walls, and birds and bats, but frogs and snakes may also be a hazard in some regions. Snakes in particular may be not only a hazard to maintenance workers but also a danger to insulation.

Various forms of protection and barriers can be used to prevent bird, small animal and reptile damage, while appropriate baiting can be used to deter small rodents.

The use of composite insulators can cause problems in certain areas, especially on de-energized lines.

**Table 11.3** Typical rated physical environment specifications, Australia

Factor	Minimum	Maximum
Shaded air temperature (no solar radiation) (°C)	-5	+50
Solar radiation (horizontal surface) (W/m <sup>2</sup> )	Nil	1200
Wind speed (m/s)	0.7	50
Monthly rainfall (mm)	Nil	360
Maximum rainfall—100 years (mm/h)	-	347
Relative humidity—outdoor (%)	25	100
Altitude (m)	< 1000	
Ambient ground temperature at 900 mm (°C)	+20	+35
Soil thermal resistivity (K m/W)	1.0	1.5
Isokeraunic level	Up to 50 thunder days/year	
Minimum pollution severity	Level II—medium	

Certain parrot species peck the silicon rubber in de-energized composite insulators and can completely destroy a composite insulator in extreme cases, as in Fig. 11.34.

One solution is to place a protective sleeve over the composite insulator during installation. This sleeve is removed by pulling a cord at ground level before energization. Although sensitive to electric fields, birds in some cases will damage energized insulation, and this is much more difficult to combat. In extreme cases, some utilities have reverted to glass and/or porcelain insulators to avoid the issue.

#### Environmental Control Measures

Once the substation is constructed, the main environmental issues are oil/water control and noise control.

Generally, a substation site will be chosen to avoid the risk of damage to the surrounding environment, es-



**Fig. 11.34** Bird damage on a composite insulator (Courtesy TransGrid, Australia)

pecially to permanent watercourses and underground aquifers.

Utilities will generally ensure that care is taken during construction and during the life of the substation to avoid leakage of oil or other substances into groundwater or outside the substation boundary. Oil leaks from power and instrument transformers, switchgear, capacitors, coils, etc., are generally safely contained on-site. Oil retention pits are sometimes used for on-site storage of oil (or other contaminants) and also as a fire control measure. A central underground tank may be used to retain oil and contaminants on-site. The tank must be sized to contain the volume of the largest oil-filled equipment plus a margin that allows for rainwater and water from fire protection or control systems (where used).

The probability of an oil spill occurring in a substation is generally considered to be very low. However, when substations are located near sensitive areas such as lakes and reservoirs or wetlands, depending on the quantity of oil on-site, the consequences of discharge outside the substation are higher, requiring special attention.

Solutions that are required by regulation or legislation will vary from region to region, and specific solutions will be determined by the risk identified for a particular site and the type of equipment installed. Some common control methods include:

- Oil spill containment on-site using bund walls around power transformers, ditches around the substation, pits, dams or tanks. Adequate allowance for rainwater and fire control water should be included in the design. Care should be taken to ensure that overflow is managed so that there is no unwanted discharge from the site.
- Oil/water separator systems—there are a number of methods that are commonly used and a range of commercial products that separate water from the contaminated liquid. Generally, these systems rely on the difference in specific gravity between water and oil in order to separate contaminants from water.
- Oil-blocking systems—allow liquid to pass unless oil is detected, blocking the flow of oil and water.

CIGRE Technical Brochure 221 [11.28] contains more detailed information on this subject.

Noise from substations can be a significant issue for residents near the site. While at the design stage the distance to nearby residences may be large and the noise control adequate, housing built near the substation after construction and heightened awareness of acoustic noise can cause issues for the asset manager.

### 11.3.12 Structural and Civil Design

Civil and structural design is an important aspect of the overall substation design project. Civil and structural components include:

- Buildings
- Equipment and conductor supports
- Footings and ducts
- Drainage and oil control
- Noise control
- Fire barriers
- Security and fencing.

In a substation, a range of structural materials may be used, including wood, concrete, steel and aluminum. Structures are required to support high-voltage equipment, meeting the loads and forces imposed by the environmental conditions such as wind and the electrical forces associated with short circuit forces under fault conditions.

Substations have design lives of typically more than 40 years, and measures need to be taken so that corrosion is managed in order to ensure the life of steel and concrete supports and structures. Generally, steel used for supports is treated with hot-dip galvanizing, but other treatments and coatings may need to be considered in extremely hostile environments.

#### Foundations

Foundations or footings are required for the mounting of high-voltage equipment, and comprise a considerable proportion of the civil works for a substation. Footings are designed to the applicable national or regional standards by a civil engineer in conjunction with the substation primary designer, and some level of iteration between the two may be required to determine the most economical design solution to meet the required design loads. The design calculations will be based on the site geotechnical report detailing soil characteristics including the soil properties in relation to moisture content.

Based on the soil characteristics, different foundation designs may be used to achieve the required outcome, including shallow raft foundations, block foundations, rock anchors or deep foundations with pillars to mount the equipment. Selection can be based on factors such as ground conditions, installation cost for the different approaches or selected utility standard design approach.

Depending upon the type of soil and the loads, the foundation construction material is generally concrete, with or without steel reinforcement. In some cases, piles may be needed to achieve support requirements.

The finished level of the footings is used to align high-voltage equipment, which is usually fixed a small distance above the finished level to allow a degree of adjustment in aligning components. The space between the footing and the equipment is usually grouted or sealed to prevent water lodging in the interface, causing corrosion.

Equipment is mounted on the prepared footings using either cast-in threaded fixings or alternatively chemical or expansion anchor bolts. Chemical anchors have the advantage that the support structure can be located and the holes in the baseplate used as the drilling template. Cast-in bolts require considerable care during foundation installation to ensure that the anchor bolts are in the correct location. Some types of cast-in bolt do allow a degree of play in the position of the bolts, which can then be grouted into place when the support structure is in place.

Foundation design must also allow for the later installation of earth conductors and control cables to avoid the need for cutouts after the foundation is installed. In addition, ensuring that steel reinforcement is adequately connected to the substation earth grid and does not result in earth current loops in normal or fault conditions may be important in some installations, particularly in the vicinity of air-core reactors, where strong magnetic fields may exist.

Power transformers require a foundation to adequately support the static load plus oil containment and fire control facilities. Firewalls may be required between adjacent transformers, and in some cases may also act as noise control devices.

#### Buildings

Substation buildings are designed to applicable building codes or national standards. The main role of the substation control building is to provide physical protection for equipment, including control and protection equipment, SCADA (supervisory control and data acquisition) equipment and substation auxiliaries. In some cases, high-voltage switchgear may be located inside a building to provide environmental protection and security for the primary equipment, including AIS, GIS and hybrid (mixed technology) switchgear.

Although substations are generally designed to be unmanned on a continuous basis, some human amenities and workshop facilities may be required for periodic attendance by inspectors or operations and maintenance personnel.

Similar to other buildings, there are a range of approaches that can be used to design a substation building. The substation building may be a permanent brick or concrete construction, but there is a trend toward the use of modular, prefabricated and transportable build-

ings that have the advantage of off-site construction, including fitment of control and protection equipment, to reduce project cost and commissioning time.

While initial and lifetime costs for the particular country or individual location are the main basis for the construction type selected, security concerns must also be taken into account, which may result in requirements such as minimal or no windows (or protected windows), reinforced nonflammable roofs or reinforced doors.

The local climate and the environmental requirements of the installed equipment will determine the degree of climate control required in substation buildings. A common practice is to use a two-stage climate control system that maintains temperatures for the short times of worker occupation at one set point and reverts to a lower (or higher, depending on the climate) setting when unattended to reduce energy consumption. Some electronic equipment items generate heat and also have a limited environmental range, requiring some degree of continuous climate control. This also applies to batteries, where some types have an optimal temperature range and which also have ventilation requirements due to the emission of gases during charging.

Appropriately zoned security and fire alarm systems should be provided and connected to the SCADA system or local fire authority. A risk assessment should be used to determine the degree of security and fire detection and suppression to be provided.

#### Cable Trenches and Ducts

Cable trenches are a common method of providing adequate protection for secondary control cables between the individual items of HV equipment and for connection to the control building. Some equipment-to-equipment connections will typically be made by providing conduits for the necessary control cables, but for the connections to the control room, surface ducts with reinforced lids are the customary approach in substations. The advantage of surface ducts (although this may be the most expensive option) is the ease of access for later changes during the life of the substation. It is important that the choice of duct cover is carefully considered to ensure that the lid is strong enough to support vehicle loads in the substation during operations and maintenance.

#### 11.3.13 Seismic Considerations

Earthquakes can occur in any part of the world but are most common in the area described as the *Pacific rim*. Substations can be vulnerable to earthquakes, both from the risk of physical structural and equipment damage and from unwanted maloperation of equipment such as relays and other mechanical devices in the substation.

In areas where earthquakes are considered a foreseeable risk, a range of methods can be used to reduce the impact on reliability and to ensure that the power network can be rapidly restored following a major earthquake.

Different techniques can be used to model the expected behavior of equipment under earthquake conditions. A common approach is to use a shake table to simulate different earthquake scenarios and to validate design solutions. One of the most obvious areas of weakness in high-voltage electrical equipment is porcelain insulators, and various methods can be used to brace or strengthen structures with porcelain insulation.

Other measures to counteract earthquake issues in substations include:

- Removal of transport wheels on power transformers and solid fixing to avoid shifting in earthquakes
- Additional mechanical bracing and stiffening on support frames for conservators, piping and radiators on transformers
- Insulating rubber damper mountings used for sensitive relays and control devices.

Whatever procedures and solutions are adopted to reduce the risk of damage from earthquakes, it is important that the solutions are aligned with the earthquake risk for the particular substation and that region, and the expected characteristics of earthquakes in that location. The solutions adopted by the designer must be cost-effective and must not have an adverse impact on substation reliability, severability or maintainability.

#### 11.3.14 Fire Control

Fire in a substation is generally considered a rare occurrence, and the measures for the detection and suppression of fires in a substation vary depending on the risk appetite of the asset owner, the criticality of the substation, local standards, the type of construction and the equipment used. The most common approach for managing fire risk is to design layouts that ensure adequate physical separation between equipment such as power transformers to reduce the risk that a fire on one transformer will affect an adjacent unit.

The general objective in substation fire protection is to minimize the hazard, limit the damage and reduce the impact on overall substation reliability. When designing any aspect of the substation, including fire protection systems, the final design is a balance between risk and cost.

One of the most common fire suppression systems used in substations is a water spray system on power transformers. The key aim of such a system is to limit the conflagration, to cool the fire and to reduce the risk

of the fire spreading to other parts of the substation, particularly adjacent units. Gas systems including  $N_2$  or  $CO_2$  may also be used to attempt to smother the flames in the event of a transformer fire. An important aspect of the design of fire suppression for transformers is the need to contain the resulting oil/water mix from pollution of groundwater. Oil containment is designed to accommodate the transformer oil volume plus an allowance for rainfall collected in the containment and from firefighting.

Fires in substation control rooms are considered even more rare than transformer fires. However, it is common, usually due to building standard requirements, to have some type of fire detection system, and in some cases to have fire suppression in control rooms and switch rooms. Fire suppression may be some form of gas release or hypoxic system where oxygen levels are kept lower than normal. Any suppression system requires consideration for maintenance worker access and staff safety.

Fire detectors in substations are typically connected to control centers via SCADA systems to alert operations personnel to the fire, and may also be connected to local fire authorities. Local fire authorities who are not experienced in high-voltage substations and who enter to fight a fire may present a safety issue to be managed by the asset owner. There are cases where inexperienced firefighting personnel have entered substations to fight a fire, gaining access by cutting gate locks, without proper awareness of the hazard of high-voltage equipment. This type of issue is best managed by training and awareness and by adequate levels of consultation between the substation owners and the local fire authorities.

Fire control measures in substations vary depending on local standards, fire regulations, and the risk and criticality of the substation. Some utilities manage the risk by accepting that a substation fire is a risk but that the fire cannot be contained, and the loss of part of the substation is inevitable.

### 11.3.15 EMF and EMC Design

Substation equipment can be the cause but also may be susceptible to electromagnetic interference and electrical disturbances. Sources of disturbance include a range of electrical transient phenomena that might affect substation equipment:

- Electrical transients from high-voltage device switching of circuit breakers and disconnectors
- Electrical transients from some form of insulation breakdown
- Power-frequency electrical and magnetic fields

- Transient earth potential rises during faults
- Lightning and switching transients from outside the substation
- Geomagnetic disturbances.

Each of these potential sources of electrical disturbance can have a major effect on components within the substation, requiring special attention on the part of the substation designer and during the construction of the substation, to layout, shielding, earthing and screening practices in the substation.

#### Disconnecter-Induced Disturbances

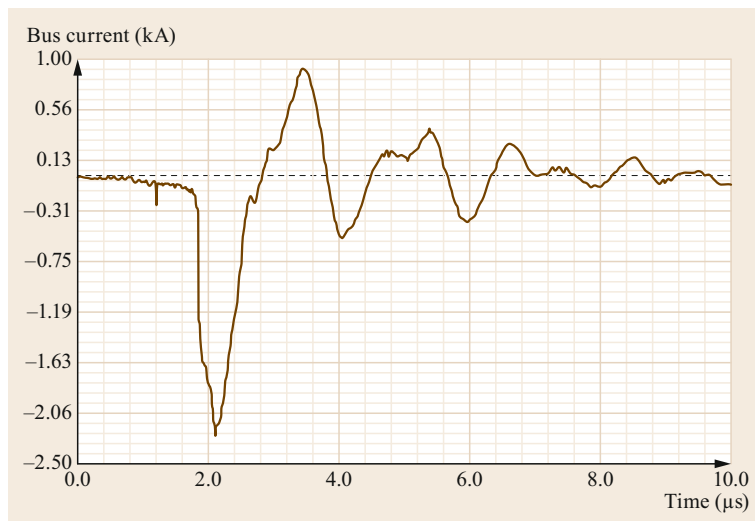
Switching of a disconnector occurs when the load current has been removed and disturbances result from the voltage collapse and multiple restrikes at the point of interruption of the primary arc. Typically for air-insulated substations, the transients that result are tens to hundreds of kilohertz; however, in the case of GIS, the transients have a far higher frequency, up to thousands of megahertz. The initial value of the peak current of these transients is proportional to the change in voltage at the arc point ( $\Delta V$ ) and the surge impedance, which is dependent only on the geometry and characteristics of the surge path. In general, this phenomenon can be significantly worse in substations where the rated voltage is 100 kV or higher. The effects can be a much more serious issue for GIS than for AIS, and can generally be observed as short-duration, steep-fronted transient pulses.

Fig. 11.35 shows a typical measured transient, although the reader should note that the measured waveform is limited by the capability of the measuring equipment, and the observed waveform may not be an accurate measure of the actual frequency or the level of the signal that is being generated. The actual signal frequency and rate of rise is likely to be much higher than can be measured by conventional measuring equipment.

While these transients are generally not a human safety issue (although some operators have reported shocks during manual operation), this transient phenomenon is observed in substations as short-duration electrical transients during disconnector switching that can have significant effects on electronic equipment. Although related transient phenomena can be observed during circuit breaker switching, the more serious (in terms of control systems) generally result from disconnector switching.

Power-frequency electric and magnetic fields are also a potential source of concern. However, as the field levels originate from high-voltage conductors, the typical distances from such conductors are usually sufficient for human safety and short-term exposure.

Insulation breakdown can also be a source of electrical disturbances and transients, and often these can be



**Fig. 11.35** Transient waveform (bus current) measured during opening of a 500 kV disconnector (Adapted from [11.29], © CIGRE)

detected with RF (radio frequency)-sensitive measuring equipment and used as a method for general condition assessment of a substation.

All of these disturbance sources can have a significant effect on electronic devices, causing maloperation and failure of components, and the proper design and treatment of cable screens and general substation earthing practices are important control methods.

### Geomagnetic Disturbances

Geomagnetic disturbances can have a serious effect on substations and the power system. Currents induced in power lines flow to ground through substation transformers, which can cause saturation of the transformer core and a variety of consequential problems. Increased heating due to geomagnetic interference has caused transformers to fail in the past. Increased harmonics generated in the transformer can result in unwanted relay operations, causing unwanted tripping of power lines.

Geomagnetically induced currents (GIC) are driven by the electric fields produced by the variation in the earth's magnetic field that occurs during a geomagnetic disturbance. These variations are driven mainly by solar activity, particularly solar flares and solar storms. Because of their low frequency compared with the AC frequency, the geomagnetically induced currents appear to a transformer as a slowly varying DC current. GIC flowing through the transformer winding produces extra magnetization which, during the half-cycles when the AC magnetization is in the same direction, can saturate the core of the transformer. This results in a non-sinusoidal, distorted AC waveform with increased har-

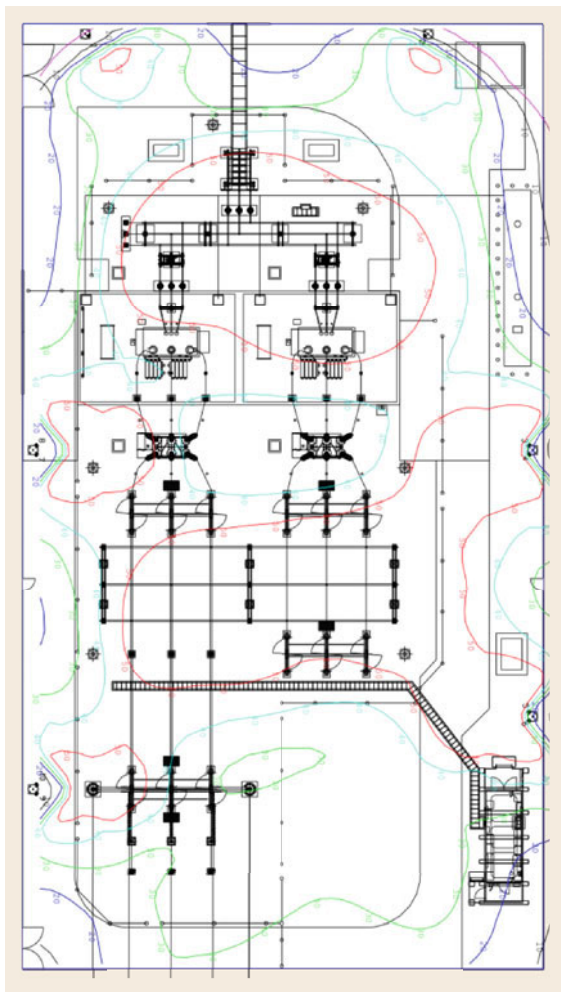
monic levels that can cause maloperation of relays and other equipment on the system. Transformers may be damaged thermally.

Saturation of the transformer core produces increased eddy currents in the transformer core and structural supports heating the transformer. The large thermal mass of a high-voltage power transformer means that this localized heating may not produce a major change in the overall transformer temperature but can cause damage to parts of the transformer windings.

### EMC Control Methods

In most cases, there is no treatment to eliminate the actual generation of electrical transients and geomagnetic disturbances, which are inevitable within a high-voltage substation environment. However, there are steps that can be taken by the substation designer to minimize the effect of the transients and other disturbances typically observed in substations, and this is commonly managed by earthing practices and secondary cable screening. Unlike conventional practice for power-frequency screening, the recommended practice for the earthing of most substation control cables is generally to earth all secondary cable screens at both ends of the cable (sending and receiving ends, with the screen suitably sized for fault current flow) or, ideally, double-screen cables with the inner screen earthed at one end and the outer screen or sheath at both ends. The exception to this practice of double-end screen earthing is small signal cables. This practice is sometimes accompanied by the installation of a large-diameter parallel earthing conductor in the same trench as the control cables to provide an alternative low-impedance path under fault





**Fig. 11.36** Lighting contours for a small substation, with contours showing lighting levels in lux (Courtesy CPP, Australia)

conditions. The latter measure is to bypass any circulating current that might occur due to transient potential rise in parts of the earthing system due to system or substation faults.

The other aspect of the control of transients is to ensure that there is a low-inductance path for transients to earth. A stranded earthing conductor may have significant self-inductance, presenting a high impedance to high-frequency or fast-rate-of-rise transients. The use of a flat bar, rod or zero-inductance cable should be considered for all major equipment earth connections to provide a low-impedance path for electrical transient pulses into the earthing system.

The reader should be aware that the information provided in this section is a summary only, and the topic of transient disturbance and EMC in substations is a specialized topic. CIGRE Technical Brochures 124 [11.30] and 535 [11.14] provide much more detailed information and coverage of this topic.

### 11.3.16 Lighting Design

The objective of substation lighting design is to provide sufficient light both within and outside the substation building for normal and emergency work activities, including operations and maintenance. Another consideration for the designer is the security aspect of substation lighting, which may include photoelectric cell or motion sensing.

Typically, a designer will work with lighting levels from local standards specified for internal surfaces and external work areas. External lighting must be adequate for the typical work activities that might be undertaken, with consideration for luminance level at key locations, glare rating, color rendering, spill and *sky glow* rating. DC emergency lighting, driven from substation auxiliary batteries, may be provided in case of system power outage.

Specified design light levels will vary from one region to another, but typical values are:

- Inside buildings: 160 lux at floor level
- Outside: 10 lux for operational or walking areas, 5 lux other areas.

These levels are typical requirements and may vary on a case-by-case basis or based on local standards.

A lighting study is usually undertaken using specialized lighting software to prepare a lighting contour plan based on the selected luminaires, selected location and mounting heights. An example of the outcome of a lighting study is shown in Fig. 11.36. Particular attention should be paid to light spillage to neighboring properties and shadows in operational areas. Color rendition can also be an issue for operations and maintenance. Generally, white color (color rendition index of 50 or higher) is considered preferable for substations.

Outside lighting should be mounted in a way that facilitates maintenance, reduces glare outside the substation, and does not require an outage of the high-voltage plant or the use of ladders or other equipment for access to lamps for replacement. This often requires the installation of separate swing-down light fittings rather than mounting on high-voltage structures and supports.

## 11.4 Construction and Commissioning

Once the design has been completed, there are various methods and contracting arrangements that can be used to facilitate the construction and commissioning of new substations or the enhancement of existing facilities. Each of these methods has challenges, advantages and disadvantages for the utility. Construction involves a range of challenges in ensuring that the works are adequately managed from the perspective of quality control and site logistics, to ensuring site safety. Commissioning the substation involves suitable testing and validation of the design to enable connection of the substation into the overall grid. Finally, training for operations and maintenance staff and documentation are vital functions for any new substation.

### 11.4.1 Methods

Construction of a new substation or major modifications can be undertaken in a number of ways, depending on the preferences of the owner. In some cases, the owner has internal staff who are able to specify, design, procure, construct and commission a new substation, but frequently, any part of that process may be undertaken by external contracted organizations. In some countries, this practice of outsourcing is common, while in others it is observed as an emerging trend.

The substation may be fully supplied by an external organization or different combinations of delivery retained in-house. In some cases, the owner organization will retain engineering in-house and construction services will be obtained from an external contractor. In others, the entire process is managed by external parties, apart from specifying the initial requirements.

All of these approaches can be managed with effective controls and delivery processes, and each has attendant commercial and operational risks, advantages and disadvantages. Whatever the method adopted, it is important that the construction process is managed methodically, using project management principles, to ensure that the work sequence is logical and aimed at minimizing delays and optimizing costs.

### 11.4.2 Site Logistics

The process of construction begins with site preparation and benching as required by the civil design. The delivery and storage of materials and equipment on-site will commence soon after the site is prepared, and should be coordinated so that the equipment is delivered in time for erection or appropriately unloaded and stored on or near the substation site. Transport delivery ideally should be arranged to deliver the equipment as it is

needed for construction, as storage on-site has attendant risks. For example, the largest items are usually power transformers, and these should be delivered only when the site is adequately prepared and when the arrival does not interfere with other works.

Each substation site and transport route is unique, and the challenges for the construction crew in logistics and transportation are different. A transport and logistics plan may be useful to ensure coordinated, just-in-time delivery of equipment and materials.

### 11.4.3 Quality Control

Quality control is one of the most important aspects in substation construction projects, and key to successful execution of the project. Contractors and suppliers should be required to submit a quality control plan that documents all the necessary procedures and steps to be undertaken for delivery of equipment, installation and construction work.

Once the layout has been established and footings are installed, the first task is usually heavy steelwork installation, followed by major primary equipment items and bus-work. In some cases, preassembly of equipment in the workshop in a controlled environment is advantageous, saving time on-site.

A good site construction manager is able to foresee issues and uses experience to ensure that works are coordinated and that appropriate quality control is applied for equipment delivery and at early construction and erection stage.

Although the early-works stages of substation construction are largely physical erection of plant, one of the important requirements at this stage is to ensure that the underground components of the earth grid are installed according to required specifications. This is difficult to assess once trenches are covered and conductors buried.

### 11.4.4 Documentation

Manuals, drawings and other documentation are an important aspect of substation construction and life management. The level of documentation is often related to the contracting approach (turnkey or in-house) and the degree of design standardization adopted by the utility. If substation design is highly standardized, then the level of design documentation may be less than that required for a new design supplied by an external supplier. It is important that various manufacturers' manuals are collected as the construction progresses for later documentation of the entire substation. The other

aspect of design documentation is ensuring that any departures from the design drawings are documented in *as-built* drawings, so that the final substation drawings reflect the actual installation on-site and not just the design intent.

Any test results related to tests carried out on equipment should be retained as a base for future condition monitoring and lifetime trending.

### 11.4.5 Commissioning and Testing

Substation commissioning is the process that takes the substation from construction and connects it to the power network to achieve the network function specified for the substation. It is an important process, as it represents the start of the life of the substation as an asset in the network. The records of the testing undertaken at commissioning become the base level for lifetime condition monitoring and trending.

The overall process of commissioning a new substation is usually considered a two-stage process:

- Precommissioning
- Connection of the substation to the network.

The commissioning process typically starts with workflow planning and determination of the required final connection date. The commissioning tasks are then assembled into a project workflow that ends at that date. Commissioning tasks are coordinated with construction activities to ensure that tasks are completed as soon as possible within the construction program, and sequenced logically to avoid overlap, interruption to construction, and waiting time. Commissioning a large substation is not a task for a graduate engineer and takes a degree of experience often gained working with other commissioning personnel or after long experience on smaller projects. The knowledge required to effectively commission a substation covers a wide area of substation design and plant technology, and an understanding of control and protection systems.

Commissioning activities are documented and the process controlled using preprepared *inspection and test plans* (ITP) and *test reports* that detail the key tasks completed and testing results obtained. This plan is used and the test results, when complete, become the main documentation of the commissioning process. ITPs and test plans are the main quality control documents specifying the testing.

#### Precommissioning

The general objective of precommissioning is the identification of drawings and equipment, confirmation of proper primary connection, correct orientation of equip-

ment, and functional testing of the assembled equipment to confirm correct operation of circuitry and components. Precommissioning assumes that the equipment installed has been previously type-tested in the factory or laboratory, and the tests carried out on-site for precommissioning are to confirm that the equipment is undamaged, functional, correctly assembled and erected, aligned and fully operational. Precommissioning generally does not involve the whole substation as an assembly, but treats the various components and circuits separately.

**Identification and Location of Equipment and Components.** The first step in precommissioning is to identify and locate all the primary components, check correct erection and orientation, check that design details on drawings are correct, and record serial and other information that might be required later.

**Preliminary Testing—General.** Pretesting is carried out at this stage to ensure that instrument transformers are undamaged in transport, have the correct polarity and that ratios are correct, and switchgear auxiliaries and mechanisms are working according to manufacturer's instructions. Pretesting is carried out before the primary circuit is connected to the network. Ideally, the entire substation is not connected, but in some case parts of the substation may be live, and extra care needs to be taken to avoid operational or safety issues during testing.

Switchgear is checked to ensure that fluid levels, settings and all adjustments are as per requirements, and functional testing is carried out to ensure that the disconnect or circuit breaker is fully operational. Timing tests on circuit breakers may be carried out at this stage.

Power transformers are often set up by the manufacturers who install the coolers, bushings and other auxiliary systems, fill the unit with oil, commission auxiliary systems and carry out basic testing. For power transformers, it may be useful to take an oil sample at this final setup stage, well before energization, to provide base levels for gas concentrations and to confirm oil quality and dryness.

Generally, all equipment can be tested in some way to make sure it is operational; however, full type testing generally will not be feasible on-site, and it is assumed that this is carried out before arrival. Factory test certificates should be reviewed and collected at this stage for later inclusion in the substation commissioning document set.

Instrument transformers are often tested on-site using a primary injection test set to confirm that available ratios are correct, leaving the selected ratio finally connected at the end of the pretesting ready for the next stage of testing.

Pretesting can be carried out on unconnected equipment, but it is important to carry out functional testing after all physical erection activities are completed. An important aspect of this first stage of precommissioning is to ensure that wiring within devices and between the devices and the control room is installed and labeled correctly according to the design drawings. This is typically carried out before DC or AC auxiliaries are switched on. A common technique before any energization of even auxiliary voltages is to first *bell-test* wiring to ensure correct connection as per the schematic wiring diagrams. It is important to confirm using both positive and negative testing, i.e., that low-resistance circuits exist where intended and that there is no path to adjacent cores. This can be difficult in some cases. Often visual inspections alone are used to identify correct wiring and the connection of the right cores of cables on terminals. Secondary cable insulation resistance to earth should be checked once all cables and connections have been confirmed.

Other aspects of precommissioning include:

- Checking the tightness of connections
- Inspection and validation of earthing and correct connection to all equipment
- Validation of cable screen earthing according to design
- Validation of drawings and asset records with nameplates
- Energizing and testing of AC and DC auxiliary circuits.

Pretesting is carried out in a sequential manner, so that testing occurs after erection and wiring, but once tested, equipment wiring is left undisturbed where possible. Generally, the first stage of pretesting is focused on the equipment itself, then the wiring and interconnections, and gradually as the equipment itself is confirmed as correctly wired, the assembly and the overall primary and secondary circuit functionality can be tested.

Finally, once all mechanical primary connections have been checked for tightness, and micro-ohm tests carried out on joints or sections in busbars or in flexible connections, high-voltage testing should be carried out on primary equipment to check for insulation problems. This high-voltage testing is typically not carried out to full working voltage level, but is rather used to identify any gross errors and problems as a last test before energization. Once resistance testing on conductors and insulation is complete, it is important that these connections are not disturbed again for other testing; hence planning for a proper sequence of tests is important.

In the pretesting stage, control and protection relay testing can commence. As for primary equipment, it is assumed that the relay has passed type testing in

the laboratory, and the site testing is focused more on the settings to be applied, confirming that these are correctly applied and that the relay performs as expected at those settings.

Records are kept as the pretesting progresses to indicate which circuits and equipment have been pretested. This may be in the form of notes, but a good approach is to retain a set of *commissioning drawings* that are colored or otherwise marked as the pretesting proceeds. This becomes a record of progress for the commissioning team. Documentation is maintained to the level agreed upon with the asset owner for eventual handover after commissioning is completed.

The following is a list of the generic checks and tests in the recommended order:

- Inspection of the plant and nameplate data
- Confirmation of basic plant operation where applicable
- Insulation resistance and polarization index testing of primary plant
- High-voltage pressure tests of primary plant
- Resistance measurements of primary circuit connections
- Insulation resistance testing of AC and DC control and protection circuits
- Secondary circuit insulation tests.
- CT and VT (voltage transformer) ratio and polarity tests by primary injection and wiring loop resistance or secondary burden tests
- CT magnetization tests
- Relay secondary injection tests
- Checking of control circuitry wiring
- Functional tests of local and remote control, closing, tripping and protection including intertripping
- Electrical and mechanical interlocking checks
- Functional tests of SCADA, controls, alarms, indications and analogs
- Testing of trip and blocking circuitry
- Final pre-energization checks.

**Building Services and Auxiliary Systems.** The building itself should be commissioned as early as possible and any auxiliary power and light circuits switched on and tested as required.

AC supply will be required as a first step, and so this is often tested and commissioned at the first stages of the commissioning or even construction phases. Automatic and manual changeover and interlocking should be checked together with diesel and other standby functionality.

DC supplies including batteries and chargers should be commissioned ready for progressive energization of secondary circuitry and further substation testing.

**Circuit Breakers.** Each circuit breaker should be tested after erection to ensure that it is fully operational. Primary, secondary and earthing connections should be checked. Primary insulation resistance and contact resistance tests should be carried out using a suitable test set. Any discrepancies should be investigated and corrected. The operation of any circuit breaker alarms, mechanisms, pumps, compressors, switches or interlocks should be verified. Gas pressure lockout circuitry and settings should be verified and set as required.

Once adjustments have been made and the circuit breaker proven operational, timing tests should be carried out to ensure the unit meets specified values, and any discrepancies, including differences between phases, investigated.

The mechanism energy storage capability should be verified on-site by simulating the O–CO–t–CO sequence according to specification. This is recommended for each unit in case of specific installation issues. The value of t, the recovery time between operations, will vary depending on the type of mechanism and the specification.

**Gas-Insulated Switchgear (GIS).** GIS needs to be considered carefully from a commissioning perspective. GIS cannot be fully assembled off-site, and the process of GIS erection on-site carries the risk of contamination of the gas spaces. High-voltage testing on the constructed sections is typically performed once they are assembled on-site. A one-minute power-frequency test or a longer operational voltage soak test are both commonly used and can be effective in checking that the sections have been cleaned and assembled without contamination by dust or metallic particles. Functional operation, timing tests and checks on the gas monitoring relays, lockout and alarms should also be undertaken.

**Power Transformers.** Following delivery on-site, one of the first checks undertaken is to check the shock recorder for any evidence of impact during transportation. Once the transformer is located on its foundation, then the oil filling/filtering process should be commenced. Samples of the oil should be taken and tested until a satisfactory moisture level and oil withstand test voltage is obtained (e.g., in excess of 50 kV across a gap of 2.5 mm). When the oil handling process is completed, the following checks should be done:

- Check that all oil levels are correct in conservator, diverter switch tank, bushing, etc.
- Check the operation of low-oil-level alarms
- Check that all valves are in the correct position—open or closed as required
- Check that thermometer pockets are filled with oil.

Insulation resistance (IR) and polarization index (PI) values should be checked preferably before the transformer connections are made so that the values can be compared with those taken in the factory. The insulation resistance of the core ground should be measured as well, as this can also give an indication of any damage in transit.

A ratio and vector group test will normally be carried out to verify that the phasing is correct for the network.

The following tests should be carried out at every tap:

- Ratio
- Winding resistance.

A magnetization current check can be carried out using an appropriate test set or by connecting an LV supply to the transformer HV terminals with the LV open circuit. The measurements should be carried out using an analog ammeter, and it should be confirmed that there is no break in current as the tap changer moves from one tap to another. If there is a short break, this can be seen when using an analog meter (rather than a digital instrument).

Other checks on the tap changer are manual operation, local electrical operation, remote electrical operation and automatic parallel operation, and a check of the limit switches at the ends of the range. Secondary injection of the automatic tap change scheme should be carried out to verify that settings and dead bands are operating correctly.

The cooling system should be checked by setting and confirming the temperature for operation of the fans and pumps and the winding temperature alarm and trip values. It must be confirmed that the pump filters are fitted correctly and the pump flow is in the correct direction. The winding temperature indicator should be checked by secondary injection and the oil temperature also checked.

The Buchholz alarm and trip should be tested by injection of air and operation of the relevant flag relays verified. Explosion vent functionality should be simulated to verify correct operation and connection of all associated secondary wiring.

On larger transmission system transformers, it is good practice to perform a frequency response analysis (FRA) test and a swept frequency response analysis (SFRA) test during the commissioning of the transformer. These tests are carried out using specialized test sets, applying a voltage to one end of a winding and analyzing the output voltage at the other end of the winding, the other windings being open circuit during the test. The voltage is kept the same, and the frequency of the applied

voltage is swept through a range of frequencies and the output voltages recorded and plotted on a graph. This effectively creates a *fingerprint* for the winding that can be compared against the result obtained in the factory. A change in the *fingerprint* will indicate any movement of the windings that may have occurred during transport. The commissioning *fingerprint* can also be used for comparison with later tests during the life of the transformer to detect whether any damage has occurred to the transformer while it has been in service.

**Power Cables.** Power cable testing is a specialized area and generally outside the scope of normal substation commissioning, but a series of visual checks can be undertaken to ensure correct connection to bushings and surge arrestors and phasing and connection of screens. Cable screens may be grounded at either both ends or a single end, but this should be according to the design requirements.

Insulation resistance (usually 15 kV), cable and screen continuity, and path resistance testing can be undertaken. Other testing that may be undertaken includes:

- Polarization index
- AC or DC testing (depending on cable type)
- Very low frequency (VLF) testing
- Oscillating wave test
- Partial discharge testing.

**Earthing Systems.** One of the most important aspects of substations and the safety of persons and equipment is the earthing system. Generally, the testing carried out on earthing systems can be summarized as follows:

- *Earth conductor resistance*  
Measurement of all joint resistances.
- *Earth bonding tests*  
Verification that all plant, towers and structures are correctly connected to the earthing system, and measurement of bonding resistance.
- *Earth grid resistance* to remote earth  
Verification that the design levels are achieved on-site.
- *Verification of separation* where applicable  
Checking that separately earthed structures or other earthing systems are isolated from the earth grid as per the design. A common example is the substation fence, which may or may not be connected, according to the particular earthing design requirements.

Much of the earthing system is buried and installed as part of the site initial works. It is good practice that the substation commissioning process include inspection of

earth grid trenching and installation to ensure adequate trench backfill.

**Instrument Transformers.** Current transformer ratio and polarity can be easily checked on-site. Polarity is checked using an instrument or a simple DC *flick test* and small battery. Where ratios match, differential current transformer connections (bus zone or similar) can be tested by current injection across the substation bus work to confirm correct connection of each of the CTs. Magnetization curves should be carried out using specialized test equipment. Finally, insulation resistance tests should be carried out and results recorded before connection of secondary wiring. Any earthing links should be temporarily removed during testing to ensure that a single earth is wired to the circuit.

The voltage transformer ratio can be checked by injection and measurement, and each secondary circuit insulation resistance measured and recorded, before secondary wiring connection. Checks of any deliberate circuit earths should confirm the single point of secondary earth connection.

**Reactive Compensation.** Reactors and capacitors are tested by measuring capacitance and inductance and also insulation resistance where applicable. All values are recorded for commissioning records.

**Surge Diverters.** Surge diverters are generally not able to be fully tested on-site, and simple functional tests should be carried out to ensure that the units are serviceable and have not been damaged in transit to site or in erection.

**Protection Relays.** As for other substation plant, the full functionality and type testing of protection relays is assumed to be undertaken off-site, and the philosophy for precommissioning is to verify the operation of the relay and the application and verification (by testing) of the assigned protection settings. The increasing complexity in functionality of relays means that full testing or even testing of the settings may be a major exercise, and automated test sets are useful to reduce testing time.

The verification of protection logic settings is important, as there are parts of the logic and in-service conditions that the protection engineer may not have considered when determining required settings, causing possible maloperation in service. Unused functions should be verified as disabled or isolated from basic functions.

Before applying DC auxiliary voltages, testing of the basic insulation resistance of the relay and the associated secondary circuits should be performed. This includes VT, CT and DC circuits, ensuring appropriate levels of insulation resistance.

Once DC is applied, secondary injection tests should be undertaken to measure the relay and the secondary wiring burden, and there are several ways that this can be done, depending on the circuitry and the CT secondary windings. Ideally, the burden applied to the CT should be measured with the rated nominal current injected. Secondary injection can be arranged and measured at the CT secondary terminals to ensure that the entire secondary circuit and the burden of the relay itself is included. In some cases, the CT may be constructed with an additional injection winding to enable secondary injection.

Secondary injection is also used to verify the operation of the relay at the required settings. The most basic injection test measures pick-up and drop-off levels, and these should be compared against the required settings. Specialized and automated test sets can be used to verify that the relay operates according to the selected settings. Testing should generally be carried out in accordance with the manufacturer's instructions and aimed at verification of the selected setting and the functionality selected for the application, rather than trying to test all relay functions and verify all setting ranges.

The correct operation of all output trips, alarms, and input and output signals should be verified using the associated initiating relays or contacts in the substations where possible. In some cases, testing of relay output trips or associated isolating points may require a large number of primary circuit breaker operations. The use of a *dummy circuit breaker*, simulating the CB characteristics, is recommended in order to reduce the wear and tear on the primary equipment, but final testing of the circuit breaker is essential to ensure that the protection scheme is fully operational. In all cases, where isolating links or switches are fitted, these links should be verified by both positive and negative testing. *Positive* and *negative* testing checks the conditions for both operation and non-operation when required.

An important part of secondary injection and relay testing is to verify operation, test functionality and settings, and record operating times for all relays.

**Overall Checks and Tests.** The earlier stages of pretesting described above are carried out mainly on individual equipment items, circuits and bays, and once these tests have been completed, additional overall tests can be undertaken that cover sections of the substation or even the entire substation. Examples of such testing include circuit breaker failure systems that trip multiple devices on failure of a single breaker, hard-wired interlocking systems that include multiple primary equipment items, bus protection circuits and other hard-wired protection circuits.

Overall testing of these types of systems may involve primary injection across large parts of the substation or functional tripping of several circuit breakers. Ideally, these types of tests are carried out when the entire substation is disconnected from the network. Extreme care from a safety and network reliability perspective is required when parts of the substation are live and the commissioning is being undertaken on a new bay or line.

**Final Commissioning Tests.** The testing undertaken in the precommissioning stage verifies that the equipment is set up and connected correctly and ready for energization. All testing is designed to identify and rectify problems, to enable the substation to be energized. However, there are a number of protection tests that can only be carried out by energization and loading. Before the next stage of commissioning commences, all test leads and temporary connections should be checked and removed. The substation should be placed in a condition ready to energize. All workers on-site should be briefed in regard to site safety prior to energization.

Typically, there are local administrative procedures required for this pre-energization stage, and documentation may be required to prepare for the substation's connection to the network.

A switching program will be prearranged and authorized in conjunction with the commissioning team to provide the necessary steps to finally confirm VT phasing or current transformer summation as required by the particular configuration of the network. It is important that the mind-set of the commissioning team changes at this point, and the substation is from this point considered to be energized.

The energization process will be managed using the defined switching steps and under the control of the network controller. Energizing the substation is carried out step-by-step to allow sufficient time to identify any issues and for safety in the event of primary equipment failure. At various steps, secondary voltages, currents and phase rotation are checked at relay terminals to ensure correct connection from the primary system. In some cases, commissioning may involve synchronizing parts of the network interconnected for the first time, and it is important that the commissioning team understand any identified differences in phase or voltage levels.

In some cases, temporary secondary connections may be made to verify CT balance in differential circuits or to verify the correct connection of directional relays. Soak testing is recommended for major equipment such as transformers, and staff should remain indoors and protected from any catastrophic equipment failures that might occur. It may be useful to take additional oil samples at various stages of the transformer

energization to assist in identifying any latent issues. Immediately after energization, after soak testing and after loading are typical points where additional samples are taken.

Thermographic inspection may also be useful to identify any hot spots in equipment or connections.

As the various tests are successfully completed, the temporary settings are removed and the final settings applied. Test connections and instruments are removed and the substation configured for full service.

Following successful commissioning and energization, the final documentation of the commissioning process, the various factory test certificates, manuals, as-built drawing set and test results can be finalized for handover to the network owner, completing the main commissioning process.

#### 11.4.6 Training

Substation training requirements depend on the training policies and practices of the asset owner and organizational philosophies. There are a range of employee interactions with substations, and this implies a range of training levels and requirements to support different activities. One of the more important aspects of training for substations follows from the commissioning process, and it relates to training for operations and maintenance staff who should be trained in the particular requirements of the new substation. Often, a commis-

sioning team will provide familiarization training for operators and inspection and maintenance staff at the time a new substation is connected to the system.

Other general training may include:

- Safety induction for visitors or nonaccredited staff
- General substation awareness training for new staff
- Specific training on new substation equipment for operations and maintenance staff

Some of the training on specific new substation equipment may be undertaken by the supplier as part of a procurement agreement.

In general, university and technical training for engineers and technical staff is more difficult to obtain. General industry courses are available in most countries, but with the diversity in skills required for the range of aspects of substation planning, design, asset management, maintenance, operations and other asset aspects, there is no simple solution for the provision of substation training. Manufacturers may be able to supply courses on their own products, but general training is more difficult to obtain. This book is aimed at addressing some of the training needs for the general industry.

In some countries, industry organizations have recognized the lack of appropriate university training and are working with universities to improve power sector and substation training for undergraduates.

## 11.5 Substation Asset Management

Substations are long-lived assets, and an operating substation site may exist for 100 years or more, with equipment, components and systems changing and evolving to meet the ongoing and changing needs of the grid.

Since the 1990s there has been more awareness within the power industry of the value of asset management, which has now been developed as a recognized discipline to become an agreed-upon global standard.

Asset management for substations includes the complete asset life cycle and includes risk management and the balancing of often conflicting objectives for asset owners. Asset management is applied to all aspects of the substation life cycle, including planning and design, construction, operations and maintenance, environmental management, performance and condition monitoring, security, spares management and, ultimately, decommissioning of the substation at end of life.

A formalized asset management process provides a means for asset owners and operators to demonstrate

to shareholders, regulators and a range of other stakeholders that assets are being managed in a way that is consistent with the highest level of objectives defined for the organization.

### 11.5.1 Asset Management Fundamentals

Asset management has various definitions, but is an important aspect of the management of inherently long-lived-asset high-voltage substations. Many of the preceding sections of this chapter have focused on the delivery of new substation infrastructure, but a network comprises mostly older substations, some reaching ages of over 80 years in certain regions of the world.

Successfully managing a large population of substations requires the interaction of many individuals within the owner's organization and a range of suppliers and service providers. Asset management invariably involves all levels of the business, from senior management through all levels of asset management activities.



While there are many definitions, asset management generally involves balancing risks, costs and performance to achieve agreed-upon asset objectives. These objectives are often defined at a high strategic level but involve activities at the lowest level of the organization. An important aspect of asset management is the asset life cycle, from conception to disposal.

Asset management is not new, and organizations have been managing all types of assets, including substations, for many decades. In the 1980s, however, the discipline of *asset management* began to be discussed, particularly in the UK, USA, Australia and New Zealand, and rapidly spreading to many other countries. Since that time, there has been significant development in international understanding of the best practice principles that underlie good asset management practice.

In 2004, the British Standards Institute (BSI), in collaboration with the Institute of Asset Management, released Publicly Available Specification (PAS) 55 in two parts, considered to be the first internationally recognized specification for asset management.

In 2014, the ISO 55000 series of standards [11.31] were issued, defining accepted global understanding of asset management principles. These standards detail agreed-upon best practice principles that have relevance for many assets, including high-voltage substations.

This section discusses some of the key principles that are part of the practice of asset management for substations.

### 11.5.2 Stakeholders

One of the reasons for the development of the discipline of asset management was the difficulty in providing assurance to stakeholders that an organization was effectively managing its assets. The introduction of PAS 55 in 2008 was driven by the need to demonstrate that privatized utilities and transport organizations in the UK were effectively managing their assets. In particular, there were concerns regarding the asset management systems in place to ensure the longer-term integrity and safety of the privatized assets.

Successful asset management requires the active participation of many individuals within an organization and its supply chain. It requires the understanding and support of internal and external stakeholders, such as shareholders and regulators, who may wish to exert influence on the utility.

### 11.5.3 Risk Management

Risk management a foundational principle of asset management. Risk is related to uncertainty but can be assessed in relation to the likelihood that an event may occur and the consequence of that event.

Risk management can be considered as a coordinated set of practices to identify and define hazards and inherent asset risk, to assess the risks and the consequences and compare these against other risks to determine priority, consider feasible mitigation methods for that risk, and determine and implement a solution.

Risk management often aims to reduce risk to a level *as low as reasonably practicable* (ALARP), particularly for safety-related risks. Many organizations develop an internal risk policy that defines what the organization accepts as tolerable risk, referred to as the organization's risk appetite. This is often represented as a risk–consequence matrix that includes several risk criteria, including:

- Safety
- Financial implications
- Reliability
- Market efficiency
- Relationships
- Organization and people
- Environment.

The matrix then defines the levels of consequence in each of those criteria to provide guidance for asset decision-making and prioritizing.

Risk management is an essential task for the asset manager, particularly in relation to optimizing the costs and reliability of infrastructure. The goal of risk management is to find the optimal solution from several options meeting broader organization objectives.

Broader organizational objectives may include:

- *System*: reliability and quality of supply
- *Equipment*: technical condition of the equipment to meet performance, regulatory and legislative objectives
- *Financial*: capital investment and whole-of-life costs
- *Societal*: public opinion, reputation, community acceptance.

There are many references to the practice of risk management, and the reader is encouraged to search for those to find more information on this topic.

### 11.5.4 Reliability

The reliability of substations is obviously a key concept and is related to risk management. The concepts of risk and reliability together can be used to develop an appropriate maintenance strategy for the organization. Consideration of risk in assets such as substations invariably involves a third concept, that of criticality. The introduction of criticality provides another way to prior-

itize activities including maintenance, replacement and refurbishment works.

### 11.5.5 Maintenance

Similar to risk management, there are many texts and references available on the topic of maintenance management.

Maintenance is defined in IEC 60300-3-14: 2004 [11.32] as

the combination of all technical, administrative and managerial actions during the lifecycle of an item intended to retain it in, or restore it to, a state in which it can perform the required function.

Part of the range of activities broadly described as asset management is maintenance management, and that is defined as

all the activities of management that determine the maintenance objectives or priorities, strategies and responsibilities, and implement[ing] them by means such as maintenance planning, maintenance control and supervision, and several [improvement] methods including [economic] aspects.

Maintenance management can be complex and may involve a range of disciplines within a company, including operations, engineering, information technology, economics, safety, risk, engineering and accounting.

A maintenance strategy can be broadly divided into two approaches:

1. Corrective maintenance (or defect maintenance)
2. Preventive maintenance.

There is no right or wrong approach, and different maintenance strategies may be appropriate for different components of the substation.

*Corrective maintenance:* Corrective maintenance can be otherwise described as a *run-to-failure* maintenance approach. Assets are repaired when they fail, either immediately or in some prioritized fashion. Repairs based on unpredictable equipment failure are inherently unplanned, and it is generally accepted that unplanned repairs can be up to ten times as expensive as planned and scheduled repairs carried out in a planned and scheduled manner. However, corrective maintenance may be appropriate for some asset types and may even be necessary if there is no feasible or cost-effective preventive maintenance that can be applied.

*Preventive maintenance:* Preventive maintenance is maintenance that is regularly performed on a piece of

equipment to maintain its condition and reduce the likelihood of failure. Preventive maintenance may be performed while the equipment is in service in order to avoid an unplanned failure. Preventive maintenance is generally time-based but can also be condition-based. Traditionally, substation maintenance was carried out by periodic preventive maintenance, but many utilities have progressed to a condition-based protocol, where maintenance is carried out when the condition of the equipment is such that maintenance is required. Condition-based preventive maintenance is generally considered the optimal approach in terms of cost and risk.

Maintenance that is initiated and triggered on the basis of time periods (time-based maintenance, TBM) is relatively easy to implement with modern maintenance management information systems. Work orders are issued at predetermined time intervals, allowing for forward resource planning and scheduling.

*Condition-based maintenance:* Condition-based maintenance (CBM) relies on the known condition of the asset and may be more difficult to implement than TBM unless a clear picture of the asset condition can be obtained and there are sufficient resources, skills and knowledge for the more complex planning of maintenance activities. Forward planning of the required resources is more difficult with CBM. Condition assessment often relies on inspections unless suitable condition monitoring techniques are available for the asset type.

In some asset types, the condition of the asset may be obtained by diagnostics, and some may be suitable for online condition monitoring techniques. However, in all cases, the speed of decay or the gestation period of typical faults from the first signs of a change in condition may be difficult to predict.

Condition monitoring is a well-accepted concept in substations, and a range of techniques for both offline and online monitoring can be employed. A number of techniques have been adopted by the power industry to enable the development of an optimized maintenance management approach, including:

*Reliability-centered maintenance (RCM)* is a structured approach that considers reliability in high-risk asset types and was originally conceived within the aircraft industry. It is a step-by-step approach that can yield good results, but its implementation can be time-consuming and resource-hungry.

*Risk-based maintenance (RBM)* is aimed at minimizing cost and risk in order to achieve an optimal maintenance solution using aspects of RCM, CBM, TBM and CM.

*Total productive maintenance (TPM)* is often considered to be more appropriate for the manufacturing industry. TPM aims at the most efficient and effective use of equipment (overall equipment effectiveness, OEE).

This method considers a range of factors including human and technical aspects; however, like RCM, it can be time-consuming and resource-hungry to implement.

Ultimately, the maintenance approach used by any organization depends on the nature and the condition of the assets and the risk appetite of the asset owner. The important progression for any utility is from a reactive to a proactive and preventive maintenance approach. The choice of technique to determine the optimal maintenance approach will be best determined by the broad objectives of the organization.

### 11.5.6 Strategy and Policy

The establishment of an asset management model in an organization is a common response to external drivers of better business performance including improved asset decision-making. Effective asset management provides the opportunity to align asset decision-making with broader organizational objectives. Optimizing asset decision-making usually relates to reliability, risk, and operational and capital investment costs.

The asset manager is required to meet corporate objectives including legislative and regulatory requirements.

This combination of potentially conflicting objectives requires the establishment of organizational policies and strategies to articulate how the various, and often conflicting, requirements will be balanced.

A powerful feature of good asset management practice is the alignment of asset activities throughout the organization, from the corporate objectives right through to the smallest asset inspection or maintenance task.

The establishment of appropriate policies and strategies becomes a tool for utilities to demonstrate this whole-of-business alignment. Examples of key asset management policies include:

- Risk management policy
- Safety policy
- Environmental policy
- Quality of supply and security policy
- Financial policy
- Procurement policy
- Employee conduct and equal opportunity policy.

Asset managers must be familiar with relevant internal company policies and understand how these affect asset management decision-making. In some cases, there may be specific asset management policies defining the approach to asset decision-making, maintenance and condition monitoring.

The usual definition of asset strategies is that they are high-level plans of action to achieve an objective

or asset policy. The development of strategy is often the responsibility of the asset manager (as is sometimes the development of policy). An asset strategy may contain the overall approach and may be complemented by more detailed asset action plans; such a strategy is important in articulating a plan for achieving a higher-level organizational objective.

### 11.5.7 Environmental Management

The general aim of substation environmental management from an asset management perspective is to reduce the environment footprint of the substation during its service life. Some of the environmental control measures are built in at the design stage and include oil/water separation systems, drainage measures and buffer zones. Other measures include ongoing site management, maintenance and operations in relation to conservation of natural resources, protection of habitats and control of hazards.

One of the challenges for substation asset owners may be older substations and equipment built to different standards than would be acceptable today. CIGRE Technical Brochure 221 provides a guide to reducing the environmental impact of substations at the design phase [11.33].

The broader movement toward the concept of sustainability means that a whole range of aspects of substation management may need to be considered, depending on organizational policy.

### 11.5.8 Whole-of-Life Management

The lifetime of a substation is typically considered to be more than 50 years, during which the substation can be expected to undergo significant changes with new (particularly secondary) equipment and expansion with new circuits and additional transformers. The substation becomes a mix of various technologies, and the age of installed equipment will range from brand-new to over 50 years.

Whole-of-life management and decision-making is an important aspect of asset management and affects the way maintenance is carried out, including refurbishment and replacements.

#### Life-Cycle Factors

A range of lifetime factors are considered when making asset decisions (such as life extension options) for substations and other assets, including:

- *Future needs*: Is the substation due for decommissioning or even complete substation replacement at some stage in the foreseeable future?

- *Fault levels:* Is the substation capable of managing current or predicted fault levels, and is the current equipment rating suitable?
- *Asset health and performance:* This usually entails a detailed assessment of the plant condition compared with network requirements.
- *Safety:* Is the equipment safe? Can life be extended safely according to current standards?
- *Costs and risk:* Are the costs and risk of life extension or refurbishment well understood?

### Asset Life-Cycle Phases

Asset life cycle includes all aspects of managing assets, from the initial concept to disposal. The substation life cycle can include up to seven phases:

1. Identification of need
2. Design
3. Construction
4. Commission
5. Operation and maintenance
6. Decommission
7. Manage residual liabilities.

Clearly, not all of these activities involve the same length of time, with the *operate-and-maintain* phase the predominant activity in terms of proportion of substation asset life. In many utilities, the aspect of substation life that attracts the most attention is the early stages of *design and construction*.

### Life-Cycle Cost Analysis

Life-cycle costing (LCC) is the most effective means of considering the financial aspects of asset management decisions. Consideration of not only the initial purchase cost but also the implications for the asset lifetime provides a more accurate picture of the value of a decision, whether a new substation purchase, implementation of new technology or a change in maintenance strategy. The general understanding of life-cycle costs is that the initial purchase price is only part of the cost of an item or project.

Life-cycle cost  
 = purchase cost  
 + installation and commissioning cost  
 + cost during asset life (including losses)  
 + cost of disposal at end of life .

The cost of operations and maintenance is a major component of the ownership cost of a long-lived substation asset. Refurbishment costs, maintenance costs including labor, tools and equipment, and spare parts and

consumables, and costs for outages, including costs associated with unavailability when an asset is out of service for maintenance or following a failure, must all be taken into account for a lifetime assessment. The initial purchase cost is relatively easy to assess and compare, whereas the lifetime and disposal costs may be more difficult to assess, particularly considering a 50-year time horizon.

The substation lifetime is also a matter of debate for any utility. There is usually a financial lifetime, typically 40–45 years determined for accounting purposes, whereas the technical lifetime may be much longer (or shorter) depending on the technology and the care taken during the life of the asset. Life-cycle cost analysis is strongly influenced by the organization's accounting approach and by the regulatory environment and the various strategies that are employed by the organization to achieve its objectives.

**Net Present Value Calculations.** Life-cycle costs can be analyzed and different options compared using discounted cash flow techniques based on the time value of money. Typically, each organization has an approach mandated by financial policies for such analysis. One common technique is to use the net present value (NPV) to analyze and compare option costs. This technique applies simple mathematics to account for the time value of money. The NPV technique can be applied in different ways. In the formula below, an initial purchase or capital investment can be compared with the savings that accrue from year to year.

$$NPV = \sum_{n=0}^T \frac{C_n}{(1+i)^n} - C_0 ,$$

where  $n$  = the year of the cash flow,  $T$  = total number of years being analyzed,  $i$  = the discount rate (determined by the organization, typically 5–10%),  $C_n$  = the net cash flow, benefit or cost in year  $n$ , and  $C_0$  = the total initial investment cost (at year 0) if applicable.

The costs should include all costs, including any disposal costs at the end of the period. If NPV is positive (or  $> 0$ ), this means that the investment adds value to the organization and the project may be justifiable from an accounting perspective. Another application for this formula is to compare a capital purchase with a lease cost, where the capital purchase is  $C_0$  and the lease costs are the costs per year ( $C_n$ ). If the NPV result is positive, it may be better financially to lease the asset rather than purchase outright.

This is an important technique for the asset manager and enables the comparison of long-term options and whole-of-life costing. There are many references

available on the application of NPV techniques for decision-making, including CIGRE TB 354 [11.34].

### 11.5.9 Condition Monitoring

One of the fundamental functions of asset management is the need to *manage risk* associated with assets. Achieving that function and actually *managing the risk* requires the manager to *understand* the level of risk, and this requires *knowledge* of the asset health or condition and taking appropriate actions in response (management) to achieve an overall objective. Condition monitoring is therefore an important function of asset management that must be undertaken for assets of any kind, and particularly in substations.

#### Goals of Condition Monitoring

One of the goals of condition monitoring is to reduce the likelihood of unplanned failure by applying tools and techniques to assess the ongoing condition of the asset and to detect changes to enable remedial actions in a timely manner. Other goals for condition monitoring include:

- Cost savings by reducing inspections or periodic monitoring
- Better utilization of staff (or working with reduced staff numbers)
- Asset risk reduction
- Better asset utilization by getting more performance out of the asset with better knowledge of the condition with time
- Asset life extension.

Condition monitoring can be periodic (diagnostic testing when needed or at predetermined intervals) or continuous, and there are now many techniques and devices available to cost-effectively monitor the condition online in a continuous manner.

#### Diagnostic Testing

The basis and the foundation of condition monitoring involves carrying out some type of diagnostic test that is appropriate for the asset type (e.g., an oil test on a power transformer). The results of this test may indicate the asset condition at the time the test was undertaken, if properly selected for that type of asset, but may require expert interpretation. An important aspect of condition monitoring is the process of taking diagnostic test results and using those results to provide an indication of asset condition and any changes with time. The condition may then be used as a trigger for remedial actions on an individual asset level (i.e., a repair or refurbishment) or to assess a group of assets to assist

decision-making for the entire population (e.g., deciding that the population needs to be replaced).

Effective condition monitoring enables the asset manager to take a more proactive rather than reactive role in managing the asset.

#### Information Management

Typically, an asset manager will manage not just one but a large number of substations, each substation with a large number of equipment items, and the condition information required to be managed effectively is extensive. Understanding the risk of the assets overall requires knowledge of the condition of all those components. The added complexity is the need to manage that information on a time basis so that a change in condition over time can be identified and action taken to avert a failure. This complexity requires the application of appropriate information management systems and business processes to manage the numerous data sources and to provide and present information so that asset decisions can be made. Information management is therefore core to an effective condition monitoring strategy for an organization. The processes of managing that information and using the information for asset decision-making are also important parts of effective asset management.

#### Capital Investments

One important aspect of condition monitoring is that online monitoring usually requires some capital investment for equipment up-front. This often includes the purchase, installation and ongoing maintenance of some type of electronic device, appropriate for the type of asset, measuring a quantity that is indicative of the asset condition or performance and fitted permanently to the asset. The NPV techniques described in the previous section may be useful for comparing options or evaluating benefits versus cost for such investment.

However, in some cases, condition monitoring can use already existing condition data sources without any new capital investment. An example of this is the use of applications such as *PI Historian* to access existing SCADA information and provide longer-term information on asset performance.

#### Condition Monitoring Strategy

A common mistake in investigating new technologies and implementing condition monitoring is failing to first consider the objectives of the organization and to establish adequate processes and systems to manage the outcomes after a decision to trial new technology is made. Some organizations have been slow to adapt to the availability of new technology and have failed to transition the organization to a new approach with

new online platforms and devices, new monitoring techniques and new information management processes. Industry best practice suggests the consideration of a *condition monitoring strategy* that articulates what the condition monitoring approach aims to achieve in terms of organizational objectives and how these processes will be implemented to achieve those objectives.

### Conclusions

Condition monitoring is core to effective risk management and ultimately to overall substation asset management. Whether continuously online, or offline and periodic, condition monitoring is necessary to fully understand the risk and performance associated with the asset fleet. A range of appropriate techniques are available for all key substation asset types, and many organizations have had good experiences with the introduction and application of online methods of continuous condition monitoring of substation equipment.

### 11.5.10 Substation Security

Substation owners have a responsibility to prevent unauthorized access to sites within their control, both to protect the infrastructure from harm and to ensure the safety of personnel who may deliberately or unwittingly attempt to enter the site. Security for substations must necessarily consider relevant local legislation, regulations, national standards and any other relevant documentation, including past legal proceedings. Physical security is fundamentally a risk management issue, and the particular security measures applied to each site will be managed according to the organization's risk assessment processes.

Physical security of substations is usually considered as three levels of control:

1. *Primary controls*  
The physical security such as fences, gates and equipment layouts to control or prevent access or contact with high-voltage equipment
2. *Secondary controls*  
Used to assist in the identification of persons, the detection of intrusion and generally to support primary control methods
3. *Procedural controls*  
Support primary and secondary controls to ensure ongoing effectiveness of controls including security policies, procedures, risk assessments, inspections and auditing.

Security for substations and other infrastructure is often considered based on the principle of *defense in depth*. The *defense-in-depth* principle is the consideration of

layers of protection to secure an asset from an external attack, with the rationale that these security layers provide an increasing barrier to penetration.

Physical security measures for new buildings and major refurbishment projects should be considered as early as possible in the predesign phase of the project.

Security risk assessments should be carried out early in the overall design process for greater effect and cost efficiency. The location and proximity of substation buildings may warrant special consideration regarding the placement of doors, locks and windows. Grounds design and vegetation can also have an impact on security.

When siting substations near roads, the likelihood of impact by vehicles should be assessed. Siting installations away from curves in roadways or behind natural vehicular barriers or the use of protective bollards will minimize the likelihood of unauthorized access following damage by vehicles.

The general security measures for the outer layer of substation security are often considered to be the substation fencing and gates, but natural barriers such as plants, rocks, moats and gullies may also provide an outer barrier to substation entry. Additionally, consideration should be given to *natural surveillance*, or the exposure of an individual trying to access the outer barrier of a substation. It is important to avoid providing natural hiding places adjacent to the substation boundary. Other measures include providing an outer lower fence and inner security fence to assist in observing unauthorized individual access in the space between the two fences (referred to as a *sterile* security space).

Fencing or walling are the primary means for preventing unauthorized access to high-voltage substations, and the design of the fence and the materials used for construction can have a major impact on the effectiveness of the fence as a security measure. An intruder-resistant fence should provide a degree of resistance to climbing or otherwise breaching by an opportunistic intruder. Obviously, a determined intruder with tools can breach any fence, and the security value may be measured by the amount of time such an intruder might take to breach the fence. Typically, the chain mesh fence with barbed wire that was often used in the past is being replaced by high-tensile-strength welded mesh or security-rated fencing materials, brick or masonry to resist unauthorized intrusion.

Fence height (including topping) is typically a minimum of 2.9 m. Tops should be barbed wire, barbed tape or razor wire with a concrete footing to limit the ability to dig underneath the fence. Electric fences with detection sensing may be considered in high-security applications. Various commercial fence types such as

palisade are available that are resistant to all but determined entry using tools.

Security measures to control the issue of locks are important, as is the selection of appropriate durable, high-security key systems and lock hardware.

Primary security may be reinforced with electronic detection systems as a secondary control measure at the substation boundary and for buildings within the substation. Closed-circuit TV, alarms and monitoring systems and various types of detection systems can be installed to detect intrusion attempts and enable a response. Adequate levels of lighting are also an important deterrent and may assist in positive identification of intruders for visual detection methods.

Public awareness of the risks of substation entry and the need to report unauthorized entry is an important aspect of substations security. Warning signs should be fitted at the boundary as a deterrent to less-determined intruders.

This section is intended to provide the reader with a general introduction to substation security, and more in-depth information is available from a variety of sources. An independent security consultant and an assessment of site security is often a useful tool in assessing the adequacy of existing security measures.

### 11.5.11 Spares Management

The effective management of risks associated with power system assets requires consideration of the level and availability of suitable spares. The spares strategy

affects the way the network and the substation are designed, particularly in regard to the level of redundancy to be included in the design.

Spares management is not just managing data and ensuring that there is a spare unit for every plant item in the substation. Substation spares management should be carried out at the network level and derived from the basic asset and risk management policies of the organization. Stock levels of essential spares should be based on the number and types of assets in the network, and must consider the strategic significance and criticality of the unit in the network, failure rate, procurement lead time and cost of the item.

Power transformers are arguably the most important and critical items within a substation. Sufficient spare transformers should be retained as spares in case of transformer failure in any substation within the network. The spare needs to be compatible with the range of locations for which it is applicable, with the appropriate fittings (bushings, connection type, shape and size) to enable replacement of a failed unit within the required replacement times.

One aspect of spares management that can be overlooked is the need to ensure that the spare equipment is adequately stored and maintained. In the case of spare power transformers, this may include periodic inspection and testing to ensure that the transformer is in good condition, and storage measures to prevent the ingress of moisture. Consideration may be given to keeping the spare energized to assist in managing moisture ingress.

## 11.6 Secondary Systems

Secondary systems are an important aspect of the overall substation performance and operations, and are used to control and monitor the operation of primary equipment, whether AIS, GIS or MTS technology. Secondary systems provide the intelligence that enables the substation to react to system demands and to safely isolate network faults external to the substation, as well as faults within the substation itself. Protection, monitoring and diagnostic functions provide ongoing assurance that the substation is healthy and operating effectively. Important functions of secondary systems include voltage and reactive plant control. Communications systems provide the necessary ability to send and receive data for control, metering and monitoring purposes.

Auxiliary systems in substations provide reliable and secure power supply in the event of extended network outages.

Condition and performance monitoring is also facilitated by secondary systems and is an important aspect of the ongoing management of the substation, especially as the majority of substations are unmanned and fully automated.

### 11.6.1 Auxiliary Systems

Auxiliary systems include the various low-voltage AC and DC power supplies required to power all of the substation equipment. The auxiliary supplies generally provide power for building and cabinet heating, lighting, battery chargers, transformer cooling fans and pumps, while the DC supplies are used for the control and protection of the plant and for tripping and closing of switchgear to clear faults. These systems need careful design to ensure reliable operation of the substation

and the ability to allow for future expansion of the substation.

### AC Auxiliary Systems

AC auxiliary systems in a substation typically consist of a transformer either connected to an external distribution system or from the tertiary of the main substation transformers. In high-criticality substations, a diesel backup generator is sometimes fitted to provide AC auxiliary in the event of a system outage. Typical AC auxiliary loads include:

- Building power and light and external switchyard lighting
- Battery charging
- Transformer tap-changer drives, cooling fans and pumps
- Cabinet heating
- Fire pumps.

The AC switchboard may be segregated to provide a more secure supply for *essential loads*, with appropriate changeover systems to allow for automatic changeover in the event of an outage of one or more incoming supplies.

### DC Auxiliary Systems

One of the most critical loads on the AC auxiliary system is the station battery chargers supplying the DC auxiliary systems. The majority of the control and protection systems within the substation are powered by the DC auxiliary system, which is designed to provide the appropriate levels of reliability and redundancy consistent with the criticality of the substation.

Battery bank nominal voltages vary according to local standards, but 50, 110, 125 and 220 V are commonly used within substations. Batteries are selected and sized to meet the *survival time* requirements of the substation. *Survival time* is defined as the length of time that the substation can perform its function in the absence of AC auxiliary supplies. Typically, this survival time is 10–12 h but may be 24 h or more in remote regions at long distances from maintenance workshops.

In smaller substations, one battery bank may be fitted, but the usual practice in most transmission substations is to install two completely separate battery banks with separate chargers and associated changeover systems. Each of these batteries feeds different sets of protection and control equipment to provide the appropriate level of redundancy for the substation. Transmission-level substations will typically have two battery banks for control and protection functions and possibly two more for communications equipment.

The most common technologies for batteries in substations are lead-acid or nickel-cadmium. Nickel-cadmium types are generally more expensive initially but have a longer life expectancy than the equivalent lead-acid types. The most common technology type currently used in new substations is *sealed* lead-acid (SLA) batteries or valve-regulated lead-acid (VRLA) batteries. Absorbed glass mat (AGM) batteries refer to a specific type of SLA/VRLA battery. Batteries are usually installed in separate battery rooms where temperature and ventilation can be controlled. The advent of sealed battery technology has meant that batteries can be safely installed in a control room and bay cabinets, but even with sealed batteries, adequate allowance for ventilation is required.

### DC Distribution in Substations

Substations can be physically large, with long DC auxiliary cable lengths, and one of the important considerations for the DC system designer is voltage drop. The nominal voltage of the bank is not the normal battery float voltage, and the designer needs to consider the rating and operating range of control and protection equipment, the effects of loss of AC power and the voltage drop during DC equipment operation at substation extremities. Typically, the DC system is arranged as a *floating* system, and neither the positive nor negative side is directly earthed, with relays arranged to detect unintentional earth faults and to raise an alarm. This isolation from earth provides a measure of safety for staff working on equipment in the substation.

Appropriate segregation of adjacent circuits is an important aspect of the planning for DC auxiliary cable routes within the substation.

## 11.6.2 Protection and Control

Protection systems are essential in ensuring that substation and external faults are detected and cleared in a discriminative manner and rapidly enough to ensure safety, maintain overall network stability and minimize equipment damage.

The design and provision of adequate protection to detect and isolate faults quickly and with discrimination is an integral aspect of the substation and, in turn, the overall power network. Protection systems incorporate many of the primary and secondary components of the substation including the instrument transformers, circuit breakers, DC auxiliary systems and the protection relays themselves.

### Basic Principles

Discrimination in protection means that when a fault is detected, the appropriate circuit breakers trip to clear



a fault, but only those necessary to isolate the fault. Appropriate discrimination in protection systems is achieved by one (or a combination) of three basic methods:

1. *Current-graded protection*  
Relies on the fact that current values under fault conditions will vary depending on the location of the fault because of the impedance between the source and the fault.
2. *Time-graded protection*  
Where relay operation may be time-delayed to allow other protection to operate first to clear the fault.
3. *Unit protection*  
Faults are detected within zones by comparison of two or more current quantities or phase angles. Unit protection does not need time grading to discriminate and can be fast-operating.

Protection systems and schemes are designed to ensure that the system will operate under all required conditions, but will *not operate* under conditions when not required to do so. Generally, this means that protection is designed to *not operate* for faults outside the protected zone. In designing a protection scheme, consideration must be given to the type and expected frequency and duration of faults that are likely, all relevant parameters of the power system and the characteristics of the protection equipment to be used. An appropriate grading margin is applied to allow for calculation and measurement errors and other variations.

Protection schemes are also designed to ensure a level of redundancy so that failure of a single protection element does not cause failure of the entire protection scheme. This can be achieved by duplication and the use of multiple sets of protection relays or overlapping zones of protection or a combination of both approaches.

The main types of protection in a substation broadly depend on the type of substation but generally include:

- Transformer protection including differential protection, thermal and other protection such as explosion and gas detection
- Busbar protection
- Feeder, line or cable protection.

An important aspect of protection schemes is current summation, where the secondaries of multiple current transformers are summated to represent the out-of-balance current (in magnitude or phase), a direct application of Kirchhoff's first law. In a busbar differential scheme, current balance is achieved when the current

into the busbar is equal to the current out. Any imbalance indicates a system fault. In other cases, the imbalance between two current transformers in a bay of a  $1\frac{1}{2}$  breaker substation may represent the line current of the circuit connected to that bay.

A direct example of current summation is power transformer differential protection. Current transformers on the primary and secondary sides of the protected transformer are usually connected to form a circulating current system. Imbalance between the primary and secondary currents, indicating a transformer fault, causes operation of the relay. Differential protection schemes are designed to allow for the transformer ratio differences between the primary and secondary, tap changer range and the vector arrangements of the transformer. Filtering is applied to unbalanced currents to allow for transient DC offset and harmonics due to transformer inrush current.

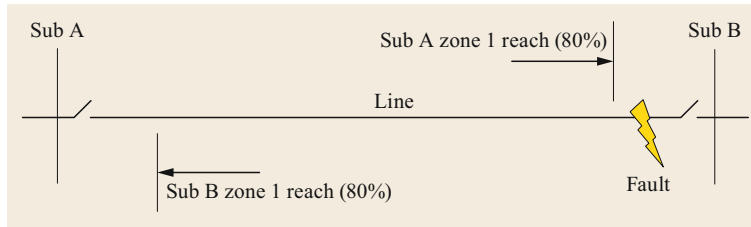
### Line Protection

Line protection schemes may also use the current summation or differential approach using current references from either end of the cable or line, although distance impedance protection is commonly used. Distance protection is a form of non-unit protection. Voltage and current references can be used to determine the apparent impedance of a line or cable as seen by voltage and current references, thus providing an indication of the location of a fault and its direction in relation to the relay. If the measured impedance is less than the reach setting and in the correct *direction*, this may indicate a fault on the protected line.

In distance protection, operating time varies depending on the apparent location of the fault providing discrimination in the protection scheme. By providing communication signals between remote ends of the line, in different scheme arrangements, high-speed relay operation and fault clearance can be achieved for line faults over the entire line section.

Typically, distance to fault (relay reach) is classified in zones, with a fault within the first 80% of the line generally considered to be in zone 1. Zone 2 reach may include the line and the remaining section of the line and beyond the next substation, or typically 120% of the protected line impedance. Zone 2 tripping is normally time-delayed to allow appropriate time discrimination for remote-end protection on adjacent lines to clear the fault.

Zone 3 is typically set to detect faults 120% beyond the second line section and is further delayed in relation to zone 2. Zone 1 tripping time is usually instantaneous, aimed at achieving overall fault clearance times as low as 1–2 cycles if possible.



**Fig. 11.37** Application of line protection between two substations (zone 1 only)

Distance relay setting can be complex, and modern relays have a large number of features and settings to be considered in each application. Protection schemes may include a number of arrangements incorporating remote-end intertripping and communications. For example, in a blocking distance protection scheme, the local relay may be set to detect distance faults beyond the remote-end substation, but a blocking signal initiated from the remote end if the fault is detected beyond the remote-end relay (seen as a fault *behind* the remote-end relay), is sent to block operation of the local relay.

In a permissive underreach transfer tripping scheme (referred to as PUP or PUTT), the relays for a line from substation A to substation B may be arranged so that a fault detected in the right direction in the remote-end relay (substation B detects a fault in the A direction) but in the zone 2 reach of the local relay (in Substation A) results in a permissive (or acceleration) signal to be sent from the substation B relay to the substation A relay giving *permission* to trip immediately, effectively accelerating the operation of the substation A relay. In Fig. 11.37 the relay at sub A has zone 1 reach set to 80% of the distance to sub B. A line fault at 90% of the line distance is within the zone 2 reach of the sub A relay, and a relay trip signal would normally be time-delayed. Using a PUTT scheme means that the relay at sub B operates when it *sees* the fault within its zone 1, trips in zone 1 time and sends a permissive signal to the relay at sub A to also trip.

This section is not intended to be a protection text, and the reader is encouraged to refer to many references for a more complete explanation of substation and line protection schemes.

### 11.6.3 Voltage and Reactive Control

Voltage on a transmission network is normally controlled by the dispatching of reactive power from generators connected to the network. Injecting more reactive power increases the system voltage, while reducing the injection or even absorbing reactive power reduces the voltage. Additional local steady-state voltage control is mainly achieved using either automatic tap changer

control on power transformers or automated reactor switching.

Automatic tap-change control schemes (ATCC) are used to control the voltage on the low-voltage side of transformers, using the busbar voltages on the low-voltage side of the transformers as a reference. Voltages outside the preset voltage limits (dead-band) initiate the operation of the transformer on-load tap changers, adjusting taps to bring the voltages within the specified limits. Tap-change timing is often coordinated using time delays to ensure that there is no interaction with other automatic tap changers, as that may cause *hunting* as multiple devices interact with each other.

Line drop compensation (LDC) may be incorporated into the automatic tap changer control system to control the voltage at the other end of a line by compensating for the voltage drop in the line.

ATCC was traditionally performed by dedicated schemes and relays. With the increasing use of computerized control systems, the ATCC function can be integrated into the control system by the use of suitable software, significantly reducing the amount of cabling on the site.

As networks become more complex, it is becoming increasingly necessary to install additional reactive plant at substations remote from major generation sources in order to control the voltage. This reactive plant may be either of the dynamic type, such as static var compensators (SVC) or static synchronous compensators (STATCOM), synchronous condensers or passive devices such as shunt capacitors or shunt reactors. When both dynamic and passive devices are connected, they are coordinated such that the steady-state voltage control is carried out by the passive devices, and the dynamic plant is kept in reserve to respond to incidents on the network such as tripping of circuits or load rejection.

### 11.6.4 Metering

Metering can be largely divided into two categories: operational metering and tariff metering. Operational metering provides the measurement of analog values such as voltage, current and frequency, and active and reactive power for the purpose of system operations,

while tariff metering ensures that the sale of electricity between different parties within the network can be performed. These two categories of metering are normally provided by separate measurement transformers and subject to different regulatory and operational requirements. In addition, there are many other monitoring functions that may be applied to improve the performance of the system including fault locators for overhead lines, fault recorders to give analog traces of fault conditions to aid in the analysis of faults, and event recorders to understand the sequence of events upon the occurrence of faults. In addition to these functions, there are cables, self-supervision of the devices and specialized condition monitoring equipment to optimize maintenance and indicate incipient faults before they become full-blown faults. Based on the measurement

scanning frequency, these monitoring functions can be divided into three categories: plant performance monitoring, fault recording and system dynamic monitoring.

### 11.6.5 Communications

The substation is part of an interconnected system for power system operations, and so there must be a means of communicating to and from the substation both between substations and to control centers. The types of information that need to be communicated include telephony for giving switching and permit information to the operators, data for providing the relevant information to the central control point, and signaling to enable the correct operation of protection. The speed and security required for each of these functions may differ.

## 11.7 Special-Purpose Substations

There are myriad different substation types used in the power industry, but there are some special design cases that have been introduced in recent years that are briefly discussed below.

The types of substations include transmission and distribution, switching stations, collector substations used for wind farms, DC substations or converter stations and traction substations. Within those broad classifications, a number of special-purpose substations have evolved to meet the needs of the industry. These include offshore substations associated with oil and gas or offshore wind farms. The remoteness of the locations for these substations and the associated difficulties in operations and maintenance means that special attention to design is required. Mobile and modular substations have been developed for fast deployment within networks or in mining or similar situations. The growth in demand and the development of megacities has led to the development of ever-increasing transmission voltages, and now UHV (ultra-high-voltage) AC and DC (> 800 kV) substations have been successfully developed and commissioned to meet the growing demand in some countries. All of these special-purpose substations require careful consideration in design and construction and in ongoing operations and management.

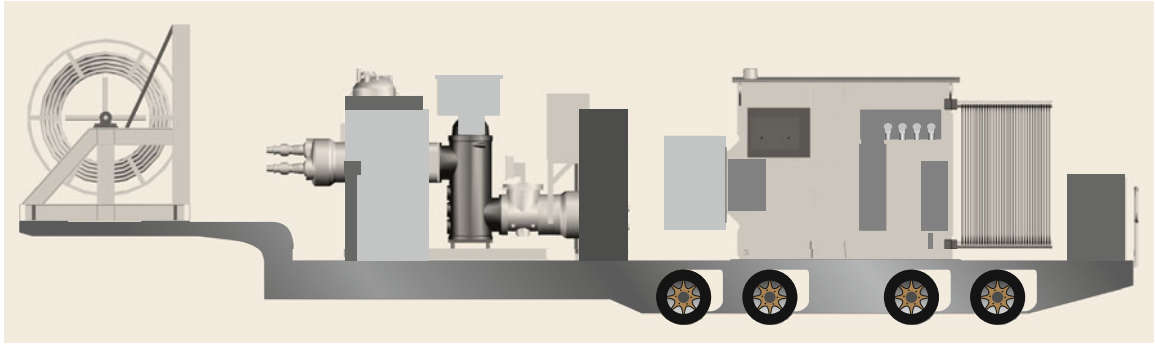
### 11.7.1 Mobile Substations

Mobile substations were initially developed in the mining industry. Electrical machinery for mining is often electrically driven and sometimes at high voltages. As the mining progressed, electrical loads including electrically supplied excavators, crushing equipment and

dump trucks moved to new areas of the mine. Frequently mines were depleted and the infrastructure relocated to new sites. A range of technologies were developed over time to provide the necessary portability, extending to mobile substations for the mining industry. It is believed that one of the first mobile substations was developed as early as 1937 in Italy.

Mobile substations can be broadly considered to be any transportable substation, but in this section, *mobile* refers to substations with permanently attached wheels and the ability to be towed on roads. Other types of substations that may be considered mobile are skid-mount substations and prefabricated substations.

Transmission and distribution utilities typically design networks to allow for relatively slowly changing network loads compared with the mining industry. Load forecasts enable the development of plans for new infrastructure, including new substations. If that planning is effective, then the substation is built just in time to meet the load growth requirements in a particular region. Substations are designed to provide redundancy or facilities for maintenance, so that customers are not unduly affected when a transformer or other substation plant item is removed for maintenance purposes. However, in some cases there is insufficient warning of load increases, and temporary augmentation of substation capability is required. There may not be sufficient justification or funding to permanently increase the transformer capability to allow for sufficient redundancy on a permanent basis. Also, it may be necessary to allow for emergency failures and a way to rapidly respond to an unplanned failure. In a single-transformer substation, there may be insufficient time or funding for a second transformer to provide



**Fig. 11.38** 66 kV substation using multi-voltage transformer and GIS switchgear (Courtesy Ergon Energy, Australia)

redundancy, and many utilities have implemented mobile substation technology.

A mobile substation such as the one shown in Fig. 11.38 is designed to match the requirements of the network and to provide the ability to be rapidly inserted into the substation to replace a transformer or a circuit breaker or switchboard. The design of a mobile substation requires consideration not only of the basic electrical requirements or road authority requirements for road transport, the ability of the supporting vehicle to be able to access the site within the appropriate response time. Consideration must also be given to how the mobile system will be connected, the transport restrictions and the effect of vibration and shock. A further challenge is the integration of the mobile substation into the existing substation control and protection system.

In some cases, mobile substations are built in multiple parts that must all be transported and connected on-site. In other applications, transformers are designed with multiple voltage ranges to suit a variety of substation applications, such as the one in Fig. 11.39. Mobile substations may be built using AIS, hybrid or GIS tech-



**Fig. 11.39** NOMAD mobile substation in Australia in 2006 (Courtesy Ergon Energy, Australia)

nologies. One of the significant challenges for a mobile substation designer is road authority weight and size restrictions. Mobile substations may be designed as containerized or *skid-mount*, or as fully articulated towable vehicles with permanently attached wheels, either for road or for rail. Mobile substations may also be designed for transport on planes, barges or ships.

The application of mobile substations can have significant benefits for restoration after catastrophic weather or disaster events, with the ability to rapidly replace damaged substation components. In addition, the ability to transfer customer load to a mobile substation to allow maintenance on a substation transformer may allow a utility to defer capital investment in enlarging an existing substation capability permanently or meeting temporary regional load increases.

One important aspect of the application of mobile substation design is the required connection time. If a very short connection time is required, then the site is often prepared by establishing defined connection points and spaces to allow quick installation. This may extend to the inclusion of plug and socket arrangements to enable fast connection and switched protection arrangements to readily integrate the mobile unit into the substation and the site.

### 11.7.2 Offshore Substations

The development of renewables, and wind power in particular, has spurred growth in offshore wind farms and the corresponding need to introduce more offshore substations and other transmission and distribution infrastructure. Wind farms are often located some distance from shore, and collector substations may be required to provide voltage transformation and switching to enable a reliable shore connection.

The design of offshore substations has some additional challenges for any designer beyond the basic electrical requirements that need to be addressed. The



**Fig. 11.40** A typical containerized substation being lifted off shore (Courtesy CIGRE [11.28])

most common shore connection is cable, and this may be AC- or DC-connected, often depending on the relative distance to shore and load centers.

In an offshore application such as the containerized substation module shown in Fig. 11.40, the substation is built on a platform that may be floating or fixed to the sea bottom. The designer needs to consider a range of additional issues including:

- Transport of the substation to its final resting place at sea.
- Transport of operations and maintenance staff to and from the substation—including how staff can access the site from boats.
- Emergency evacuation requirements—in the event of fire, explosion, accident or damage due to storms.
- Maintenance requirements—the frequency of maintenance may be dictated by how often staff can access the site. Daily inspections may not be feasible.
- Environmental issues associated with a marine location—marine environments have a range of hazards such as corrosion and salt spray. Potential pollution from substation operations, equipment failures and maintenance should also be considered.
- Navigation, security and other hazards associated with the remote location.

In an offshore application, the designer generally aims to reduce the size of substation assemblies, and in some cases, confined space issues may arise requiring special attention during maintenance and operations.

The remoteness of the substation and the difficulty in accessing for maintenance may create the need to consider inclusion of more condition monitoring equipment to provide early warning of problems and

planning or repairs. Further guidance on the development of off-shore substations can be found in CIGRE Technical Brochure 483 [11.35].

### 11.7.3 DC Substations

HVDC has seen an increased focus in electricity networks as the need for large power transmission grows within the interconnected power grid worldwide. New technological developments have enabled the development of higher-voltage DC systems, and more cost-effective HVDC transmission is now a feasible option along with traditional AC solutions. More substations around the world now incorporate both AC and DC; typically this has been for linear applications between two different transmission or distribution systems. The future challenge is the development of an HVDC grid and substations with DC buses or multi-circuit DC solutions.

#### Design Issues

Many of the basic substation design fundamentals are valid for both AC and DC technologies. However, the safe operation of the substation requires consideration of switching, isolation and making equipment safe for maintenance, considering issues such as management of DC current and associated electric and magnetic fields and trapped charge in DC conductors. New methods and strategies are needed to detect and clear faults, to achieve faster clearance time for DC systems (compared with AC) in order to prevent large system collapse events.

#### Standards

Work is under way on establishing standard voltages, electrical and safety distances for DC systems. This is necessary so that there is some consistency among different designs, and in the longer term, multi-vendor solutions can be safely operated together. This will also encourage competition and reduce costs, making DC more accessible and viable as a network choice.

This should also enable agreement on type tests, which will reduce the need for repeating type tests, leading to reduced costs over the longer term.

### 11.7.4 Modular Substations

Substations are traditionally built on-site using high-voltage and secondary components that are assembled, mounted, connected and tested on-site. This type of construction requires a construction team to undertake a range of on-site activities during the construction period. For remote sites, this often means that field personnel are required to live away from home in suitable accommodations, incurring attendant living and other costs. The industry is increasingly striving to achieve



**Fig. 11.41** Skid-mount substation example (Courtesy Ergon Energy, Queensland, Australia)

lower delivery costs for substations and faster delivery time, and there is a trend toward the use of modular, preassembled and tested components to reduce project costs and delivery times. Modularity is essential in some situations, such as offshore substations where it is not feasible to assemble components in the final site location, but the use of modular substations can also apply for tradition distribution and transmission scenarios in urban and rural locations.

The use of modular substation assemblies (e.g., pre-built switch rooms, switchgear bays, control rooms) and even entire substation solutions can reduce project delivery risks with respect to project management and such aspects as coordination of skilled resources and interfacing, reducing project costs. Modularity in substation design provides benefits in standardization of designs, saving design and installation time, and reducing spare parts requirements. Maintenance may also be simplified through the use of similar configurations and standardized components.

In the past, the concept of modular substations was seen as an acceptable emergency approach, but one that provided a less permanent or inferior design solution in the long term. However, with advanced design and modern materials and manufacturing techniques, modular substations can be designed to be situated in the most extreme environments, offering significant advantages over traditional construction methods, particularly in remote or challenging locations such as the skid design substation shown in Fig. 11.41.

Building substations or major parts of substations in a factory environment may eliminate many construction-related risk factors including weather, availability of skilled labor, remote access and the need for worker accommodations. Modular substations such as the one shown in Fig. 11.42 can be designed to suit a range of physical environments that may be applica-



**Fig. 11.42** Prefabricated substation example (Courtesy Ergon Energy, Queensland, Australia)

ble in high-wind, fire-risk or earthquake-prone regions. Substation components can be preassembled, prewired and pretested prior to transport to site, saving on-site assembly and testing time.

The use of modular components allows the designer to consider the application of *plug-and-play* solutions that provide the ability to add primary and secondary components as needed in future years. This may be achieved by replacing switch rooms with larger capacity on the same footprint or adding sections of preassembled components, such as a new control room with secondary equipment preinstalled, requiring only reconnection of external cabling that may be assembled using plug-and-socket connection.

A further advantage of the use of preassembled modular substations is the suitability of this method for single-supplier arrangements. Rather than dealing with a range of equipment suppliers, the use of a modular approach means that a utility can contract with one supplier for a complete turnkey solution.

Modular substations will not be suitable for every situation or voltage class, but for smaller substations, particularly distribution stations, complete substations in modular form are feasible. In larger transmission-level substations, sections such as switchgear bays or capacitor banks, control rooms or relay rooms may be suitable for this type of construction and delivery method. The modular construction and delivery approach is particularly well suited for remote and difficult locations.

### 11.7.5 UHV Substations

Ultrahigh voltage is defined as voltage levels greater than 800 kV (AC). UHV transmission has been in use to some extent since the 1980s, but mainly in research applications. The first commercial UHV transmission lines were installed in the former USSR in 1985



**Fig. 11.43** 1200 kV Bina National Test Substation, Madhya Pradesh (India), in 2013

(500 km line from Ekibastuz to Kokchetau, 400 km line from Kokchetau to Kostanay), but were later discontinued because of reliability and partial discharge issues. Further application of UHV has been carried out in China, and in 2009 the 1000 kV line between Jindongnan, Nanyang and Jinmen was placed in service. India successfully commissioned a 1200 kV substation and transmission line in 2012. Fig. 11.43 shows part of the 1200 kV Bina test station under construction.

The application of higher voltages and UHV AC and DC has been driven by an ever-increasing demand for electricity, and in some cases the development of megacities with high population densities. UHV transmission provides the ability to transmit high levels of electrical energy power efficiently over large distances using a minimum number of lines and substations.

#### Advantages and Disadvantages

UHV lines have some advantages, generally requiring less right of way to be approved for construction when compared with the equivalent energy capability and lower voltage levels. UHV has the ability to transmit large amounts of energy from one part of the electricity system to another, and this may have broad advantages as regards overall network stability, particularly in areas with a large proportion of intermittent or renewable energy sources.

However, there are also some disadvantages to be considered. For example, an air-insulated UHV substation requires a large site, and the space requirements are generally significantly higher than for lower voltages. The use of gas-insulated or hybrid insulation systems is common in UHV applications to reduce space requirements. The cost of a UHV substation is higher than that for the more conventional and common EHV, and so careful cost analysis is required to evaluate the whole-of-life cost benefits in using UHV.

#### Design of UHV Substations

One of the considerations for the design of UHV infrastructure is the need for reliability. As the UHV is used to transmit comparatively large amounts of energy, failure of a UHV component may have a significant effect on the substation and the overall network. And because UHV equipment is relatively new, there is limited experience with equipment failure and few global reliability statistics. Failure statistics for EHV equipment can be used to provide an indication of the expected reliability of UHV, enabling an assessment of the reliability of UHV equipment to assist the design process.

The UHV substation designer needs to consider adequate levels of redundancy to avoid a single failure causing a total system outage. The spares policy for the substation should consider the possible long replacement times for components that may not be *off-the-shelf* items.

The UHV substation may be designed using either AIS, GIS or some form of hybrid component insulation. Each of these options will need to be considered in relation to available land, the reliability and redundancy required, and the total project budget.

#### Transport and On-Site Testing

The components for a UHV substation are physically large, and transport to remote sites may be a challenge in the construction and installation stages of the project. Power transformers are generally the largest substation component, and a UHV transformer needs to be able to be transported to site using available roads and handling equipment. The mass and physical dimensions need to be considered.

Because of the size of the components, preassembly and pretesting of components is not feasible, as might be considered for lower voltages with comparatively small components. This means that on-site erection is required, and subsequent on-site testing is important to verify that assembly is complete and there is no transport damage.

#### Conclusions

The growth in demand for energy is expected to continue, together with a higher proportion of renewable generation sources. These trends will lead to increased application of UHV in more countries, to provide large energy transfer over greater distances.

#### 11.7.6 Railway Substations

Electric train traction systems require substations that may incorporate converters for DC traction or rotary converters for non-system frequency applications. These substations are often at distribution voltages (less than 50 kV), and apart from the AC-to-DC or

variable-frequency converters have comparable primary and secondary components to transmission and distribution substations.

A railway company may operate its own transmission and distribution network specifically to service its own power requirements for traction applications including substations, overhead lines and cables. The

nature and size of railway substations means that the application of modular buildings is feasible and is commonly used.

Protection systems and general earthing may be different from that used in traditional transmission and distribution substations, due to the nature of the power supply, the load and the rail system.

## 11.8 Trends in Substations

Substations will continue to evolve to meet changing needs. Growth in the use and application of digital techniques in substations will continue, eventually leading to better integration of components, improved reliability, higher functionality and, ultimately, lower costs. Higher levels of monitoring, artificial intelligence and increased automation will lead to *smarter substations*.

The availability of novel materials means that the design of insulation systems will continue to evolve. The advent of robotics will mean improvement in substation management and better utilization of limited human resources in managing the increasing complexity of the modern substation.

Ultimately substations are an investment for the community and still today there are many parts of the world that have no access to electricity. One of the more recent trends is to consider ways in which lower cost solutions, suitable for remote or rural communities can be implemented.

### 11.8.1 Digital Substations

One of the significant trends in substation development in recent years is the evolution from traditional substation design to the use of digital technologies. Substations are critical nodes in the overall transmission and distribution system, providing a link between generation sources and the consumers of energy. The entire network, and substations in particular, must be not only reliable but also adaptable to changing requirements as the network expands and develops to meet the needs of energy consumers. Although the lifetime of a substation site may be more than 100 years in some cases, the components inside the substation itself will change and will be replaced during that lifetime. Some components will be changed many times. In some cases, these changes will include increasing capacity to meet higher demand or increased fault levels, but changes will also include adding capability to meet new protection, automation and control requirements as the network itself becomes ever more complex.

One of the largest obstacles to the complete transition of substation design to a fully digital model is not the technology itself and the availability of expertise; it is the legacy of existing, older substations. Slow adoption of a radical new approach means that a hybrid approach is needed, with many old substations being gradually replaced with newer digital components integrated with the older technologies, and this can be challenging for designers and for ongoing operations and maintenance activities.

The advantages of digital substation technology include:

- Significantly reduced copper wiring and simpler installation
- Reduced design time and the use of design standardization
- Interoperability between devices from various suppliers
- Improved reliability
- Improved measurement accuracy and recording
- Simplified commissioning and testing
- Ease of future expansion.

Each utility is managing the transition to digital substations at their own pace and based on strategic and commercial objectives that are often different for each utility.

### Digital Components

Traditionally, substations have been constructed using individual components such as circuit breakers, instrument transformers and protection relays wired together with copper cabling. Using a digital approach, the components can be interconnected digitally using optical fiber as a communications path. IEC 61850 *Communication networks and systems in substations* [11.36] is a set of international standards governing communications, SCADA and automation systems within substations, and is the backbone and framework around which a digital substation may be built.



**Low-Power (LPIT) and Nonconventional Instrument Transformers (NCIT).** One of the most important parts of the digital substation is optical VTs and CTs used to directly convert analog primary quantities (volts and amperes) to digital signals. These are often referred to as low-power instrument transformers (LPITs), sensors or nonconventional instrument transformers (NCITs). Digital signals are not subject to secondary cabling voltage drop or to electromagnetic interference. Optical transducers may also have improved linear performance and frequency response compared with conventional instrument transformers, providing more accurate measurement of the characteristics of the primary signal. Conventional VTs and CTs can also be used in a digital substation, and a merging unit is used to convert the analog signals to digital.

**Intelligent Electronic Devices.** The core principle of a digital substation is a system of primary and secondary devices connected using optical fiber communications. In a digital substation, primary devices such as circuit breakers, tap changers, instrument transducers and secondary human-machine interfaces (HMIs), bay controllers and protection relays are all implemented as intelligent electronic devices (IEDs). IEDs communicate with each other via the 61850 communications network within the substation.

**GPS Time Clock.** An important aspect of the digital substation is accurate time synchronization between different devices and between substations. This ensures that protection functions operate correctly as part of the overall protection scheme and that event and alarm logs accurately report event timings. Time synchronization is achieved using a GPS clock transmitting time synchronization signals to all IEDs.

**Merging Units.** Merging units are used to combine signals from different measurement sources for transmission to other devices. They provide the interface between conventional analog measurement transducers and bay controllers and control and protection devices.

#### IEC 61850

The digital substation can be achieved using the principles embodied in various parts of International Standard IEC 61850 *Communication networks and systems in substations* [11.36]. This standard and its various parts defines the protocols for communications, SCADA and automation systems within substations, providing a framework from which to build the digital substation. IEC 61850 is designed to enable interoperability between different manufacturers and types of IEDs. It defines requirements for data that include protection,

automation, communication and condition monitoring functions within the substation.

#### Generic Object-Oriented Substation Event (GOOSE).

The IEC 61850 optical network within the digital substation operates using an Ethernet protocol in which traditional high-priority, time-sensitive digital signals (status, value) are transmitted (broadcast) in the form of generic object-oriented substation event (GOOSE) messages. GOOSE is a specific formatting of data enabling the fast transmission of protection status signals (less than 4 ms). The consistent high-speed transmission of signals is essential to ensuring the reliable and timely operation of interconnected IEDs (relays or circuit breakers).

#### System Architecture.

The initial implementation of IEC 61850 in the 1980s was mainly concerned with the station bus, which provided a way for various IEDs to communicate with each other. Primary devices under this scenario still used conventional instrument transformers, hard-wired to the protection relays. In 2005, IEC 61850 was enhanced to include what is referred to as the *process bus* to provide the connection between primary devices and bay controllers.

More recent standardization work within IEC 61850, in particular the harmonization with utility communications architecture (UCA), showed that this was not the only architecture that could be used. IEC 61850 therefore provides no specifications with regard to communication topology. As a consequence, IEC 61850 does not restrict any physical communication interfaces; it only specifies communication services that may be combined on a (physical) communication link according to requirements.

IEC 61850 is unique and is not a former serial link protocol adapted to TCP/IP-Ethernet. IEC 61850 was designed to operate over modern networking technologies and delivers significant levels of functionality not available from legacy communications protocols. These characteristics of IEC 61850 provide a benefit in relation to the cost to design, build, install, commission and operate power systems. IEC 61850 enables fundamental improvements in the substation automation process that is simply not possible with a legacy approach, with or without TCP/IP-Ethernet.

#### Conclusions

The technology to implement digital solutions is mature and available in the market, and will be the dominant trend in future digital substation designs. It can be expected that more manufacturers will offer primary equipment with embedded sensors and transducers. The challenge for designers is to harness

this trend economically and effectively while retaining the dependability and reliability required for a substation, and to find effective ways of integrating older technology as the transition to digital substations occurs.

There is vast potential to be realized from the existing capability of devices that form the digital substation to enable improved management of substation information and functionality, and wide area monitoring and control functions between network substations. The implementation of digital substations will provide higher reliability and enable better utilization of information regarding plant status and condition. Digital substation technology will assist in reducing the cost of infrastructure and will form an important part of the future Smart Grid.

### 11.8.2 Novel Materials

Significant step changes have occurred in the substation automation and communication aspects of substations, but the pace of change in basic primary equipment technologies has been slower. Utilities are often reluctant to be the first to try new technologies, and there must be a clear business objective in implementing changes to existing approaches.

There have been significant improvements in substation equipment technology that have come from the manufacturing industry, such as the improved reliability of circuit breakers. The key areas for future development of substations are expected to be in power electronics and energy storage.

Some of the key new technologies influencing substation equipment development are listed in the following sections.

#### Composites

Composite insulation materials in high-voltage equipment provide the opportunity to reduce weight and increase mechanical strength with more efficient fabrication techniques. This means that equipment can be safer and lower-cost, while still offer performance similar to that of *traditional* materials such as porcelain, glass, steel and concrete. A key driver for the use of composite insulation rather than porcelain is safety.

The lower mass of composite materials means that support insulators, bushings and prefabricated buildings are easier to handle and transport, resulting in faster construction times.

There is still a lack of experience with the longer-term issues associated with some types of composites, including whole-lifetime performance such as losses, maintenance burden, failure modes and effects, and compatibility with other substation materials.

#### Nanomaterials

Using nanomaterials, designers are able to optimize insulation design by eliminating unnecessary equipment components, reducing the physical footprint and reducing overall stress in service.

The use of nanomaterials provides the opportunity to enhance material performance to distribute current more effectively to reduce heating or losses, or profiling of the voltage grading to reduce the electrical stress seen on different parts during operation, enabling an overall reduction in the size, weight or functionality of the equipment. One of the earliest applications of nanomaterials was GIS spacers.

#### Superconductivity

The need to provide costly specialized auxiliary systems to support cryogenic cooling has slowed the adoption of superconductivity in mainstream electricity delivery when considered against alternative conventional technologies.

The application of superconductivity in substations worldwide has been largely associated with transformers, energy storage and fault current-limiting applications.

New risks associated with personnel handling and maintaining cryogenic material in terms of training, safety and work processes around handling will need to be considered.

### 11.8.3 Alternatives to SF<sub>6</sub>

Sulfur hexafluoride, or SF<sub>6</sub>, has been used extensively in the power industry since the 1960s in transmission and distribution systems [11.37]. SF<sub>6</sub> is a unique gas with exceptional electrical insulation and arc interruption capability. However, it also has high global warming potential (GWP) of 23 500 (100-year time horizon), and the industry has searched for alternatives, driven by environmental concerns.

The search for alternative gases [11.9] began with the establishment of the Kyoto Protocol in 1997. The characteristics of these alternative gases include:

- Lower GWP than SF<sub>6</sub>
- Low toxicity
- Nonflammable, high heat dissipation
- High dielectric strength and arc-quenching capability
- Stability and compatibility
- Availability and low cost.

The most promising naturally occurring alternative was found to be CO<sub>2</sub>, but with switching and dielectric per-



**Fig. 11.44** Patrol robot in Liantang 1000 kV Substation, China (Photo: Krieg)

formance far below SF<sub>6</sub>. Field experience has been obtained using CO<sub>2</sub>-filled switchgear, and units are commercially available for some voltages.

The most promising alternative gases appear to be fluorinated gas mixtures such as C5 perfluoroketone (CF<sub>3</sub>C(O)CF(CF<sub>3</sub>)<sub>2</sub> or C5-PFN) or iso-C4 perfluoronitrile ((CF<sub>3</sub>)<sub>2</sub>-CF-CN or C4-PFN). These gases are mixed with CO<sub>2</sub> or air as a buffer gas to achieve a sufficiently low boiling point for low-temperature requirements.

These gas mixtures appear to offer dielectric performance below that of SF<sub>6</sub> but may be feasible with derating and design modifications for use in switchgear.

An important aspect of gas alternatives is the toxicity of breakdown products. This is an issue with the

management of SF<sub>6</sub> and is also likely to be an issue for these alternative mixtures, although there is limited knowledge available to date.

The search for alternative gases as an insulating medium will continue. The identification and selection of a suitable alternative, without the disadvantages of SF<sub>6</sub>, is important to the power sector.

#### 11.8.4 Robotics

Traditional substation patrol, inspection and manual operations in substations require significant manpower, and there are issues with efficiency, consistency and quality. There are also potential safety problems for workers in severe climatic conditions such as rain, snow, fog, storm, heat and cold. With increasing demand for more intelligence in substations and unattended operation, new technologies have been developed for substation inspection and operation.

The development of robotics and drone technology in general industry has made it possible to apply this technology in the electric power industry. The robot may be used to replace or supplement human workers to complete security and equipment inspections, analysis and diagnosis, remote control, supplementary maintenance and live-line working, and other functions, to improve effectiveness and safety and thus reduce the cost and risk associated with operations and maintenance of in-service substations.

In the 1980s, a number of countries including Japan, Canada and China began research into the application of robotics in substations, and since that time there have been significant developments in robotics technology. Robots for substation inspection have become commercialized, and currently more than 900 substations in China are using robots to replace or assist human inspection (Fig. 11.44).

Given the current global business environment and heightened risk awareness, robots used in substations must meet many requirements, including functionality, environmental adaption, reliability and safety. The development of relevant standards in IEC and ISO is anticipated in the coming years, and the use of robots is expected to become more mainstream.

#### References

- |                                                                                                                                                                                                                                                                                                                                                           |                                                                                                                                                                                                                                                                                                                                |
|-----------------------------------------------------------------------------------------------------------------------------------------------------------------------------------------------------------------------------------------------------------------------------------------------------------------------------------------------------------|--------------------------------------------------------------------------------------------------------------------------------------------------------------------------------------------------------------------------------------------------------------------------------------------------------------------------------|
| <p>11.1 T. Krieg, J. Fin (Eds.): <i>Substations</i>, CIGRE Green Books (Springer, Cham 2019)</p> <p>11.2 Edison Tech Center: Lauffen to Frankfurt/Germany 1891, the beginning of modern electric power in the world, <a href="http://www.edisontechcenter.org/LauffenFrankfurt.html">http://www.edisontechcenter.org/LauffenFrankfurt.html</a> (2013)</p> | <p>11.3 J.J. O'Neill: <i>Prodigal Genius: The Life of Nikola Tesla</i> (Washburn, New York 1944)</p> <p>11.4 CIGRE: <i>Circuit Configuration Optimization</i>, JWG B3/C1/C2.14, TB 585 (CIGRE, Paris 2014)</p> <p>11.5 IEC: <i>IEV Ref. 603-05-03: Generation, Transmission and Distribution of Electricity—Power Sys-</i></p> |
|-----------------------------------------------------------------------------------------------------------------------------------------------------------------------------------------------------------------------------------------------------------------------------------------------------------------------------------------------------------|--------------------------------------------------------------------------------------------------------------------------------------------------------------------------------------------------------------------------------------------------------------------------------------------------------------------------------|

- tems Planning and Management, Section 603-05: Power System Reliability (IEC, Geneva 2019)
- 11.6 IEC: *IEV Ref. 60050-191:1990, Chapter 191: Dependability and Quality Of Service* (IEC, Geneva 1990), superseded by IEC 60050-192:2015
- 11.7 CIGRE: *Session Paper 33-04: The CIGRE Lightning Flash Counter: Australian Experience* (CIGRE, Paris 1974)
- 11.8 CIGRE: *General Guidelines for the Design of Outdoor AC Substations, WG 23.03*, TB 161 (CIGRE, Paris 2000)
- 11.9 CIGRE: Reference paper: Recent development and interrupting performance with SF<sub>6</sub> alternative gases, *Electra* **291**, 26–29 (2017)
- 11.10 IEC 62271-203, 3.102: *High-voltage Switchgear and Controlgear—Part 203: Gas-insulated Metal-enclosed Switchgear for Rated Voltages Above 52 kV* (IEC, Geneva 2011)
- 11.11 CIGRE: *Evaluation of Different Switchgear Technologies (AIS, MTS, GIS) for Rated Voltages of 52 kV and Above, WG B3.20*, TB 390 (CIGRE, Paris 2009)
- 11.12 CIGRE: Reference paper: living with electric fields (EMF), *Electra* **292**, 8 (2017)
- 11.13 CIGRE: *Combining Innovation with Standardisation, WG B3.11*, TB 389 (CIGRE, Paris 2011)
- 11.14 CIGRE: *EMC Within Power Plants and Substations, WG C4.208*, TB 535 (CIGRE, Paris 2013)
- 11.15 CIGRE: *Contemporary Solutions for Low Cost Substations, WG B3.43*, TB 740 (CIGRE, Paris 2018)
- 11.16 CIGRE: *The Effect of Safety Regulation on the Design of Substations*, *Electra*, Vol. 19 (CIGRE, Paris 1971)
- 11.17 United Power: *A Study of Models for Integrating High-voltage Substations into the Urban and Rural Landscape* (Tennet/Movares, Gouda 2013)
- 11.18 IEEE 998: *Guide for Direct Lightning Stroke Shielding of Substations* (IEEE, New York 2013)
- 11.19 IEC 60071-1: *Insulation Co-ordination—Part 1: Definitions, Principles and Rules* (IEC, Geneva 2019)
- 11.20 IEC 60071-2: *Insulation Co-ordination—Part 2: Application Guide* (IEC, Geneva 2018)
- 11.21 IEC 62271-1: *High-voltage switchgear and controlgear—Part 1: Common specifications for alternating current switchgear and controlgear* (IEC, Geneva 2017)
- 11.22 IEC EN 50522: *Earthing of Power Installations Exceeding 1 kV AC* (IEC, Geneva 2010)
- 11.23 SES: CDEGS Suite, <http://www.sestech.com/products/softpackages/cdegs.htm> (2019)
- 11.24 IEEE 80-2000: *IEEE Guide for Safety in AC Substation Grounding* (IEEE, New York 2015)
- 11.25 F. Wenner: A method of measuring earth resistivity, *Bull. Bur. Stand.* **12**, 469 (1915)
- 11.26 ITU-T Limits for people safety related to coupling into telecommunications system from a.c. electric power and a.c. electrified railway installations in fault conditions 10/1996 (withdrawn in 2008)
- 11.27 IEC 62305-1: *Protection Against Lightning* (IEC, Geneva 2006)
- 11.28 IEC 61936-1: *Power Installations Exceeding 1 kV AC* (IEC, Geneva 2010)
- 11.29 CIGRE: *EMC Within Power Plants, WG C4.208*, TB 535 (CIGRE, Paris 2013)
- 11.30 CIGRE: *Guide on EMC in Power Plants and Substations, WG 36.04*, TB 124 (CIGRE, Paris 1997)
- 11.31 ISO 55000: ISO 55000:2014 Asset management—Overview, Principles and Terminology, ISO 55001:2014 Asset Management—Management Systems—Requirements, ISO 55002:2014 Guidelines for the Application of ISO 55001 (2014)
- 11.32 IEC 60300-3-14: *Dependability Management—Part 3-14: Application Guide—Maintenance and Maintenance Support* (IEC, Geneva 2004)
- 11.33 CIGRE: *Improving the Impact of Existing Substations on the Environment, WG B3.03*, TB 221 (CIGRE, Paris 2003)
- 11.34 CIGRE: *Guidelines to Cost Reduction of Air Insulated Substations, WG B3.15*, TB 354 (CIGRE, Paris 2008)
- 11.35 CIGRE: *Guidelines for the Design and Construction of AC Offshore Substations for Wind Power Plants, WG B3.26, TB 483* (CIGRE, Paris 2011)
- 11.36 IEC 61850: *Communication Networks and Systems in Substations* (IEC, Geneva 2019), various parts
- 11.37 CIGRE: Reference paper: application of SF<sub>6</sub> in transmission and distribution networks, *Electra* **34**, 274 (2014)

### Terry Krieg

Power Network Consulting Pty. Ltd.  
Willaston, Australia  
terry.krieg@  
powernetworkconsulting.com.au



Terry Krieg was appointed Chairman of SC B3 (Substations) from 2012–2018. He received his Bachelor degree in Electrical Engineering from the University of South Australia, and is a Fellow of the Institute of Engineers Australia (FIEAust) and Registered Professional Engineer Queensland (RPEQ). A graduate of the Australian Institute of Company Directors (GAICD), he manages his own international consulting company, Power Network Consulting.

# HVDC and Power Electronics

Mohamed Rashwan, José Antonio Jardini

High voltage direct current (HVDC) is an economic alternative to alternating current (AC) transmission to transmit power over long overhead lines when the transmission distance exceeds 500–1000 km. It is practically the only solution for transmitting power with long underground/submarine cables or to connect two nonsynchronous systems.

Two types of converter technologies are available: the line-commutated converter (LCC) utilizing thyristor valves and the voltage-source converters (VSCs) utilizing insulated gate bipolar transistors (IGBTs).

In this chapter, these technologies are introduced together with the corresponding system architectures. Also direct current (DC) grids are introduced. DC grids will facilitate the interconnections between systems and the expansion in renewables integration in the grid.

12.1	<b>History of Power Transmission</b> .....	935	12.4.2	Two Converters in Series Per Pole.....	941
12.2	<b>Applications of HVDC</b> .....	937	12.4.3	Two Parallel Converters Per Pole.....	941
12.2.1	Long-Distance Transmission Using an Overhead Line.....	937	12.4.4	Staging.....	942
12.2.2	Transmission via Cables.....	937	12.5	<b>Line-Commutated Converter (LCC) Fundamentals</b> .....	942
12.2.3	Transmission Between Nonsynchronous AC Systems.....	938	12.5.1	LCC Operation (Rectifier Operation).....	942
12.2.4	Integration of Renewable Offshore Wind Resources.....	938	12.5.2	LCC Operation (Inverter Operation).....	944
12.3	<b>HVDC System Configuration</b> .....	939	12.5.3	Application Example and Basic Control.....	945
12.3.1	Bipolar System.....	939	12.5.4	Peak Rectification.....	946
12.3.2	Monopolar System.....	940	12.5.5	Changing the Power Direction in LCC Converters.....	946
12.4	<b>Converter Pole Configuration</b> .....	941	12.5.6	Harmonics.....	947
12.4.1	Single Converter Per Pole.....	941	12.5.7	Reactive Power.....	948
			12.5.8	Capacitor Commutated Converter (CCC).....	949
			12.5.9	AC System Strength.....	950
			12.5.10	Power Voltage Instability.....	950
			12.5.11	Multi-infeed.....	951
			12.5.12	LCC Control and Protection.....	951
			12.5.13	LCC Converter Startup (Deblock).....	952
			12.5.14	LCC Converter Faults and Disturbances.....	954
			12.5.15	Thyristors and Thyristor Valves.....	956
			12.6	<b>Voltage-Source Converter (VSC)</b> .....	958
			12.6.1	IGBTs.....	958
			12.6.2	VSC Design.....	959
			12.6.3	Modular Multilevel Converter.....	960
			12.6.4	Active and Reactive Power Control.....	964
			12.6.5	Full-Bridge Converter.....	966
			12.6.6	Symmetrical Monopole.....	968
			12.6.7	Bipolar Arrangement.....	968
			12.6.8	Converter Charging.....	969
			12.7	<b>DC Grid</b> .....	969
			12.8	<b>Future Trends</b> .....	971
			12.9	<b>Further Reading</b> .....	971
			<b>References</b> .....		972

## 12.1 History of Power Transmission

Electric power transmission was initially based on a DC system. Thomas Edison designed the world's first central electric station, which began operation in 1882 in New York. It supplied the region of the city within a radius of approximately 1.6 km from the station with DC power.

However, DC was soon replaced by AC for electricity generation and transmission because AC generators were considered to be simpler to use and it is easy to step AC up or down from one voltage level to another. These advantages made AC very convenient for trans-

mission and distribution. The development of three-phase AC further encouraged the widespread adoption of AC for power transmission.

In spite of this, some engineers remained convinced that DC could play an important role in power transmission. Those engineers soon realized the advantages of DC; for instance, the need for just one conductor instead of three simplifies the transmission line. In 1883, the French engineer René Thury developed and designed a high-voltage DC transmission system using DC generators connected in series at the sending end and a comparable number of DC motors connected in series at the receiving end. The DC motors drove low-voltage AC generators.

The most famous of Thury's plants was the Mouties to Lyon DC system. This system, commissioned in 1906, had a power rating of 4.5 MW, which was transmitted for a distance of 180 km at a DC voltage of 60 kV. The system was expanded around 1912 such that it transmitted 19.3 MW at a transmission voltage of 125 kV. The Thury system remained in operation until the mid thirties.

In 1922, a link across the Skagerrak between Norway and Denmark was discussed for the first time. A Thury system was considered for this link, at a rated power of 42 MW and a transmission voltage of 110 kV DC.

Research into HVDC transmission continued. Even though the principle of the Thury system had been proven, the conversion of AC to HVDC and vice versa was considered to be the most desirable approach.

Mercury arc valves for low-voltage applications became available in the late 1920s. In the early 1930s, Uno Lamm developed a mercury arc valve for high-voltage applications. This development led to the construction in 1954 of the first converter-station-based HVDC link, the Gotland HVDC link, which was rated at 100 kV DC.

The development of HVDC based on this converter technology led to an expansion in the use of HVDC. Between 1954 and 1972, eleven systems were constructed with a highest rating of 1800 MW and  $\pm 450$  kV in a bipolar configuration, all of which utilized mercury arc valves.

The first HVDC system using thyristor valves was constructed in 1972 between Hydro Quebec and New Brunswick (the Eel River back-to-back HVDC link) in Canada. The valves were air cooled and the scheme was rated for 320 MW. In 1978, the first water-cooled thyristor valve was introduced in the Nelson River HVDC system in Canada, with a DC voltage of  $\pm 500$  kV.

The introduction of thyristor valves encouraged the application of HVDC in power transmission projects. Since 1972, the DC voltage of a single bipolar HVDC link has increased to  $\pm 800$  kV, and the power rating to 8000 MW. Recently, HVDC at  $\pm 1100$  kV and 12 000 MW was introduced.

Until 1997, HVDC converter stations were based on line-commutated converter (LCC) technology. This technology utilizes the features of high-power, high-voltage thyristors, which do not have the ability to be

**Table 12.1** Characteristics of LCC and VSC systems

Function	LCC	VSC
Semiconductor device	Thyristor devices are presently 4, 5, and 6 inches in size, and have a rating of 8.5 kV and 6300 A	IGBTs with an antiparallel freewheeling diode and an ability to be turned off when desired. Current rating 4.5 kV and turn-off current of $\approx 2000$ A
DC transmission voltage	$\pm 1100$ kV with an overhead transmission line and up to $\pm 600$ kV with a mass impregnated polypropylene laminate (PPL-MI) cable	Up to $\pm 500$ kV with an overhead transmission line or a cross-linked polyethylene (XLPE) cable
DC power	Up to 12 000 MW on a single bipole and a DC voltage of $\pm 1100$ kV [12.1]	Up to 2000 MW at $\pm 500$ kV
Reactive power requirements	Consumes up to 60% of its rating reactive power at each terminal	Does not consume any reactive power, and each terminal can independently control its reactive power
Filtering	Requires large filter banks	Requires moderately-sized filter banks or no filters at all
Black start	Limited application	Capable of black starts and feeding passive loads
AC system short-circuit level	Critical to the design	Not critical
Commutation failure performance	Commutation fails in the event of AC and DC disturbances in a bipolar system	No commutation failure
Load rejection overvoltage	Large, and has to be mitigated because of the large reactive power support	Not large due to the small size of the filters (if required)
Footprint	Large due to the size of the filtering and reactive power support equipment	40–50% of the size of a LCC system with a similar rating
Power losses	Approximately 0.65–0.7% of the station rating	Approximately 0.85–0.9% of the station rating

turned off on demand. However, in 1997, the voltage-source converter (VSC) was used for the first time (in the Hellsjön experimental project, at a moderate rating of 10 kV and 3 MW). In contrast to thyristors, VSCs are semiconductor-based devices that can be turned off on demand, which has distinct advantages for certain ap-

plications. The VSC device of choice is presently the insulated-gate bipolar transistor (IGBT).

Therefore, the HVDC industry currently has two technologies to choose from: LCC and VSC systems. Each has its own characteristics that makes it suitable for specific applications, as shown in Table 12.1.

## 12.2 Applications of HVDC

There is a continuous debate in the industry whether to utilize HVDC or AC for a specific project. It is important to choose the most appropriate technical and economic solution (AC or HVDC) for a particular application [12.2]. We now consider some important applications of AC and HVDC.

### 12.2.1 Long-Distance Transmission Using an Overhead Line

This application can involve either the connection of two AC systems or the transmission of bulk power over a long transmission distance. AC and DC transmission systems are competitors for this application, and the transmission distance plays an important role in the analysis and selection of the most suitable technology.

A HVDC line utilizes only two conductors at plus and minus polarities for a bipolar system and is therefore cheaper to construct than an AC line of the same capacity, which requires three conductors. In HVDC, there is a need for converter stations at each end of the transmission line, so the total cost of the scheme consists of the cost of the transmission line plus that of the converter stations. Even at a transmission distance

of zero, the cost of the converter stations must still be factored in for HVDC; however, due to the lower cost of the HVDC line than the AC line, the cost of the HVDC system does not increase as rapidly with transmission distance than the AC system. This is because the HVDC has less conductors and the AC lines require compensation elements when the transmission distance is sufficiently large, and these elements must be factored into the costs of the system. Therefore, HVDC will begin to be economically advantageous compared to AC beyond a certain distance, referred to as the breakeven distance (Fig. 12.1). This distance depends on the cost of the line in a particular jurisdiction. The comparison is even more complicated if the AC line needs to be series and shunt compensated, as depicted in Fig. 12.1.

The CIGRE technical brochure TB 388 (published in 2009), which discusses the impacts of HVDC lines on the economics of HVDC projects, is a valuable document in this regard [12.3].

Figure 12.2 shows a comparison of the tower dimensions of a 500 kV HVDC bipolar line with those of a 500 kV double-circuit AC line.

When utilizing HVDC to transmit bulk power from a remote isolated generator that has no local load connected to its busbar, it is possible to select the generation frequency independent of the typical system frequency. In addition, larger frequency excursions can be accepted at the generating station. Such a system is shown in Fig. 12.3.

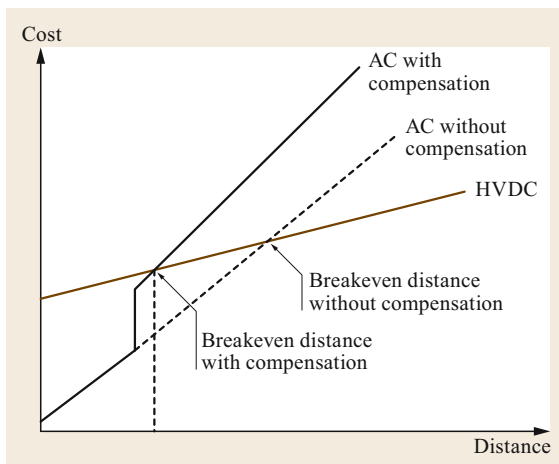


Fig. 12.1 Cost comparison of AC versus DC systems

### 12.2.2 Transmission via Cables

Due to the structure of an insulated cable, it exhibits a high capacitance and low inductance compared to an overhead line. Under AC conditions, this high cable capacitance results in an increased reactive charging current that increases with the transmission voltage. Obviously, the cable capacitance also increases with transmission distance. All of these factors limit the power that can be transmitted by cables.

HVDC has the advantage that there is no further charging current once the cable capacitance is charged.

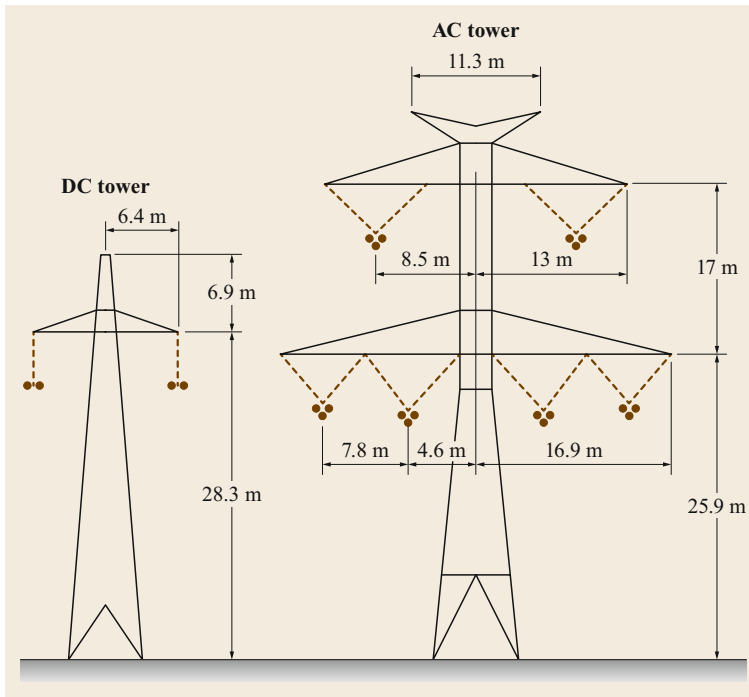


Fig. 12.2 Tower dimensions

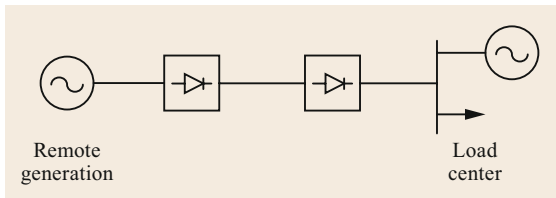


Fig. 12.3 Point-to-point transmission

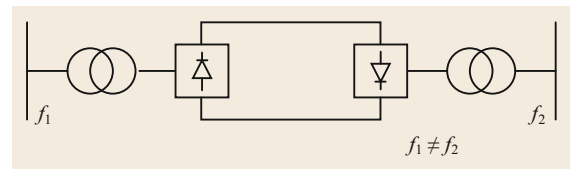


Fig. 12.5 Connecting systems with different frequencies

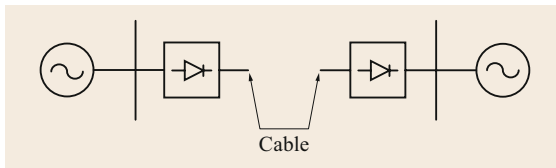


Fig. 12.4 HVDC transmission using cables

This means that there is no limitation on either the voltage or the transmission distance (Fig. 12.4).

### 12.2.3 Transmission Between Nonsynchronous AC Systems

When it is necessary to connect two nonsynchronous AC systems (e.g., a 50 Hz system to a 60 Hz system), the only technical practical way to achieve this is via HVDC, as shown in Fig. 12.5.

### 12.2.4 Integration of Renewable Offshore Wind Resources

There seems to be a drive to position wind power plants further offshore (Fig. 12.6) [12.5]. This means that increasingly long power cables are being used to connect these offshore wind power plants to the shore. As described earlier, long AC cables are not a practical solution. Therefore, HVDC is a practical alternative for bulk power transmission from offshore wind plants. There are challenges in this regard relating to the efficient use of space on the offshore platforms (Fig. 12.6) as well as the interactions of the HVDC controls with the wind farm controllers. Further, special measures are needed to deal with mechanical stresses caused by the sea conditions, wind, and corrosion out on the open water. Having said that, many projects based on offshore platforms have been already implemented.



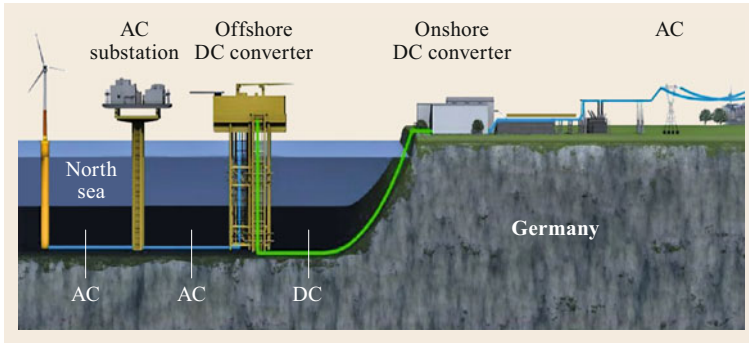


Fig. 12.6 Offshore arrangement [12.4]

## 12.3 HVDC System Configuration

Both LCC and VSC HVDC systems can be configured in many ways depending on the application and the economics involved.

### 12.3.1 Bipolar System

In this configuration, a positive pole and a negative pole are connected to a bipolar transmission circuit [12.6]. The transmission circuit can be an overhead line, a HVDC cable, or a combination of both. The bipolar configuration can use LCCs or VSCs. It can also be implemented with one LCC pole and one VSC pole. In a bipolar configuration, the high-voltage (HV) terminal of each converter is connected to the transmission circuit, and the neutral terminal is connected to an electrode via an electrode line or a low-voltage metallic return conductor.

The electrode can be a ground electrode or a sea or shore electrode, as shown in Fig. 12.7. Another alternative is to connect the neutral (N) terminal to a dedicated metallic return (DMR) conductor, as shown in Fig. 12.8. Such an arrangement is considered if electrodes are not an acceptable solution either technically or for environ-

mental reasons. In a typical bipolar scheme, the DC current is the same at the two poles. Therefore, no DC current will flow in either the electrodes or the DMR. When the currents at the two poles are unbalanced, the difference in current will flow in the electrodes or the DMR.

Obviously, if only one pole is in operation, the other pole can still operate at full DC current and DC voltage capacity, and the DC current return path involves either the electrodes or the DMR. This is referred to as monopolar operation.

During monopolar operation of a bipolar HVDC system with electrodes, the full DC current will flow continuously in the electrodes. This mode of operation was allowed in many early HVDC systems, but monopolar operation with DC current flowing in the electrodes for a prolonged duration is avoided in most modern HVDC systems. This is achieved by adding a switching arrangement at the neutral end of the bipole to divert the DC return current to the other pole conductor. This is referred to as metallic return operation.

The switching arrangement is shown in Figs. 12.9 and 12.10. Figure 12.9 depicts normal bipolar opera-

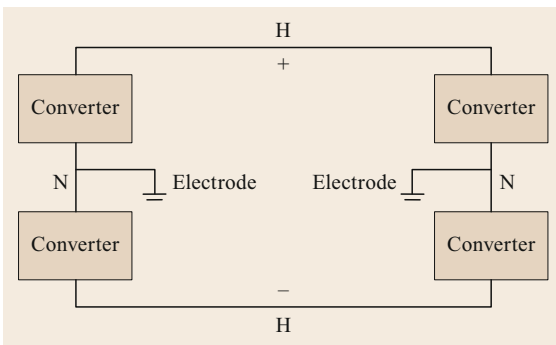


Fig. 12.7 Bipolar HVDC system with ground return

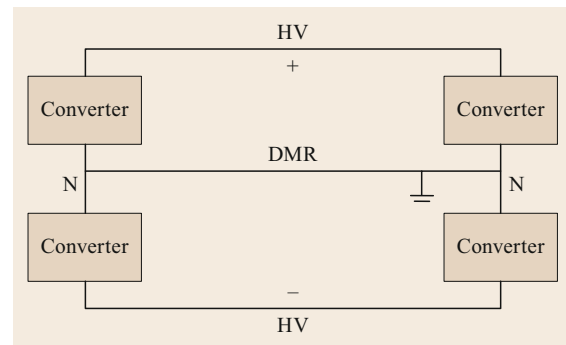


Fig. 12.8 Bipolar HVDC system with metallic return

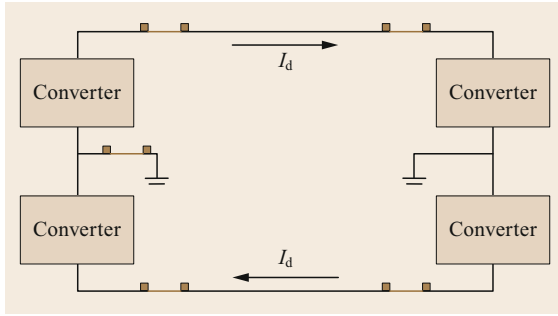


Fig. 12.9 Bipolar transmission

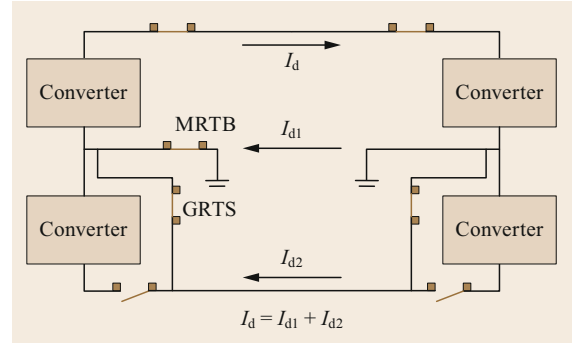


Fig. 12.12 Closed GRTS and MRTB switches

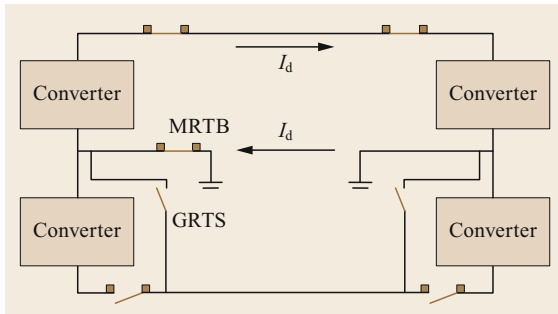


Fig. 12.10 Monopolar transmission

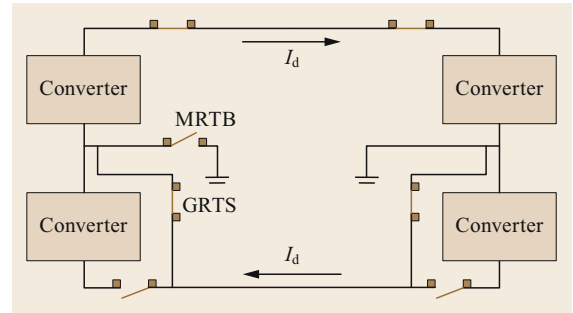


Fig. 12.13 Open MRTB. Monopolar transmission with metallic return

tion with equal DC currents at the two poles, whereas Fig. 12.10 shows bipolar operation with just one pole and DC current flowing in the electrodes.

The additional switches required to shift from monopolar operation with electrode return to monopolar operation with metallic return are shown in Fig. 12.10. Two types of switches are required, the metallic return transfer breaker (MRTB) and the ground return transfer switch (GRTS). These two switches are not DC breakers but commutating switches, as shown in Fig. 12.11. In principle, when the switch is closed, a DC current  $I$  is flowing through breaker  $S$ . When the switch is commanded to open, breaker  $S$  opens and draws an arc that excites the series combination of  $L$  and  $C$  into oscillation at a specific frequency and forces the current in  $S$  to zero. The current is diverted to the absorber  $Z$  (ZnO), which must dissipate the energy.

Upon closing the GRTS, the metallic conductor at the pole is connected in parallel with the electrodes, and

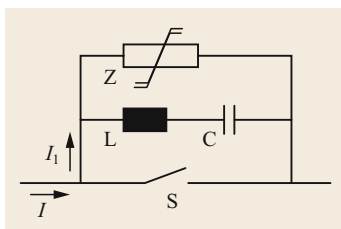


Fig. 12.11 Metallic return transfer breaker (MRTB)

the DC current is shared according to the relative resistances (Fig. 12.12).

Upon opening the MRTB, the full DC current at the pole flows in the metallic return at the pole (Fig. 12.13).

### 12.3.2 Monopolar System

In this configuration, the system contains only one pole of either polarity. The transmission circuit can be an overhead line, a HVDC cable, or a combination of both. This configuration can be used with LCCs and VSCs. In this configuration, the HV terminal of each converter is connected to the transmission circuit and the neutral (N) terminal is connected to an electrode via an electrode line (Fig. 12.14). The electrode can be a ground electrode or a sea or shore electrode.

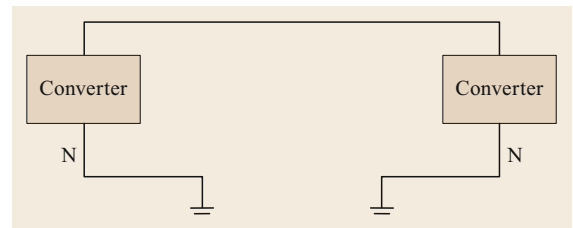


Fig. 12.14 Monopolar transmission with earth return

## 12.4 Converter Pole Configuration

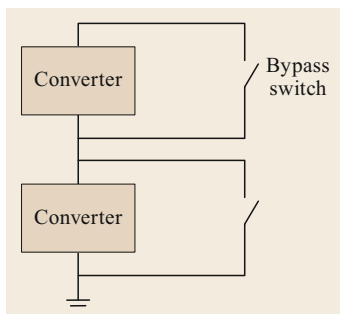
There are many ways to arrange the converters in a HVDC station. The choice of a particular converter arrangement is dictated by the rating of the HVDC system as well as reliability and availability requirements.

### 12.4.1 Single Converter Per Pole

Here, in principle, there will be only one converter per pole at each end of the transmission. This converter can be either a LCC or a VSC. This configuration can also be realized with a LCC at one station and a VSC at the other station. The single converter per pole concept is utilized in many LCC- and VSC-based HVDC systems. It is clear that, in such a configuration, any converter outage will result in a pole outage. However, this issue can be overcome by utilizing the built-in capacity for converter overload at the healthy pole in a bipolar system.

### 12.4.2 Two Converters in Series Per Pole

In this case, two converters in each station are connected in series at each pole, as shown in Fig. 12.15. The typical arrangement is that the two converters in series have the same voltage rating, but unequal voltage ratings are also possible. The DC current is the same in the two converters; therefore, in the equal voltage rating case, each converter is rated for half the pole power, and in a bipolar system it represents 25% of the bipole rating. An outage of a converter at any pole will cause the pole to operate at only 50% of the DC voltage. In an arrangement with converters in series, additional equipment (such as bypass switches) is needed to allow the operation of a single converter at the pole. Such an arrangement is utilized in ultrahigh-voltage direct current (UHVDC) to achieve the high DC voltage;



**Fig. 12.15** Two converters connected in series per pole

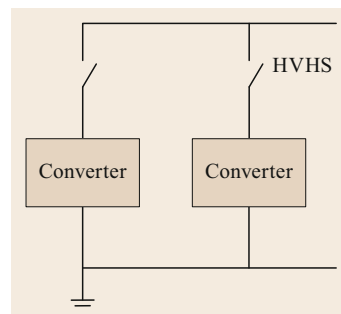
for example, at  $\pm 800$  kV, each converter will be rated for 400 kV [12.7–9]. It is also utilized in some HVDC systems at lower voltages ( $\pm 500$  kV) when the contingency of a pole outage based on a single converter per pole design is not acceptable. In addition, this type of arrangement can be utilized to construct a HVDC project in several stages in order to spread the development costs or if the full rating is not required from the start. The converters connected in series can be LCCs, VSCs, or a LCC and a VSC.

The bypass switches employed in series converters are not DC circuit breakers; they are typically high-speed switch with no DC current interruption capability. Therefore, a special control process to allow the bypass switch to open at zero DC current is required when starting up the series-connected converters.

### 12.4.3 Two Parallel Converters Per Pole

In this arrangement, two converters in each station are connected in parallel at each pole, as shown in Fig. 12.16. The two converters will have the same DC voltage rating but can have equal or unequal DC current ratings. In this configuration, an outage of the converter will lead to a loss of only 50% of the pole power or 25% of the bipole rating in the equal ratings scenario.

An outage of a converter at a pole will lead to the pole operating at full voltage but reduced DC current. Such an arrangement is utilized in UHVDC to achieve high DC current ratings at the maximum possible DC voltage if the current required is higher than the rating of a single converter per pole. High-voltage, high-speed switches (HVHS) are typically connected in series to each converter to enable the rapid isolation of one converter and continued pole operation with a single converter.



**Fig. 12.16** Two parallel converters per pole

This type of arrangement can be also utilized to construct a HVDC project in several stages to spread the development costs or if the full rating is not required from the start. In this case, each stage is operating at the nominal pole voltage. The parallel converters can be LCCs, VSCs, or a LCC and a VSC.

#### 12.4.4 Staging

One advantage of HVDC is that the project can be constructed in stages. Staging is useful if there is no need

for the full HVDC rating from the start. Typical staging options are as follows:

- In a bipolar HVDC system with a single converter per pole, one pole is constructed first and the second pole is added at a later stage.
- There are many options for a bipolar system with series- or parallel-connected converters at each pole. For example, a single converter could be used per pole initially, and other converters could then be added to the poles in stages.

### 12.5 Line-Commutated Converter (LCC) Fundamentals

In Fig. 12.17, the DC current in the circuit is only a function of the difference between the two DC voltages  $U_{d1}$  and  $U_{d2}$  of the rectifier and the inverter, respectively, as well as the ohmic resistance of the line  $R$ . Thus,

$$I_d = \frac{U_{d1} - U_{d2}}{R}.$$

The DC power  $P_r$  at the sending end (rectifier) =  $I_d U_{d1}$ .

The DC power  $P_i$  at the receiving end (inverter) =  $I_d U_{d2}$ .

The difference between  $P_r$  and  $P_i$  is the loss in the transmission circuit.

It will be shown later that neither  $U_{d1}$  nor  $U_{d2}$  are dependent on the frequency or the phase angle between the two AC systems, which is a significant advantage when connecting two asynchronous systems.

Reactive power cannot be transmitted over the HVDC link. Therefore, one AC network does not contribute short-circuit power to the other AC network.

#### 12.5.1 LCC Operation (Rectifier Operation)

LCC technology is based on the six-pulse bridge shown in Fig. 12.18 [12.2, 10].

As shown in Fig. 12.18, there are six controlled thyristor valves in the bridge. These valves can be turned on but not off, and they act as unidirectional switches. Each valve can only turn on if its anode is more positive than its cathode and a trigger pulse is ap-

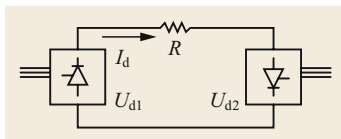


Fig. 12.17 Electrical circuit of a LCC

plied to the thyristors. There are two valves for the R phase and two for each of the other two phases.

The valves are arranged in two groups. The cathodes (C) of three of the valves are connected together and are referred to as the cathode valves; the other three have their anodes (A) connected together, and are referred to as the anode valves.

In this six-pulse bridge, the valves are turned on (triggered) sequentially, with two valves conducting at any particular moment in time to complete the current path, as shown in Fig. 12.19. The six valves are

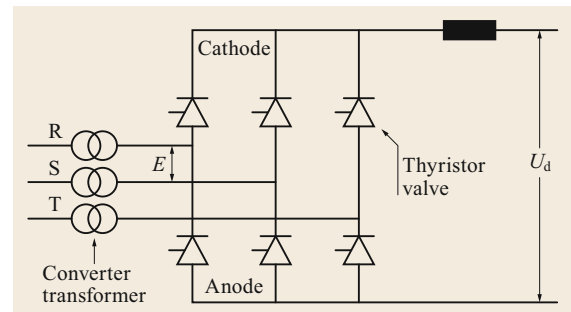


Fig. 12.18 Rectifier operation

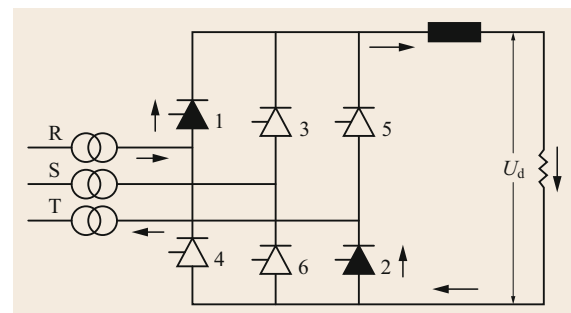
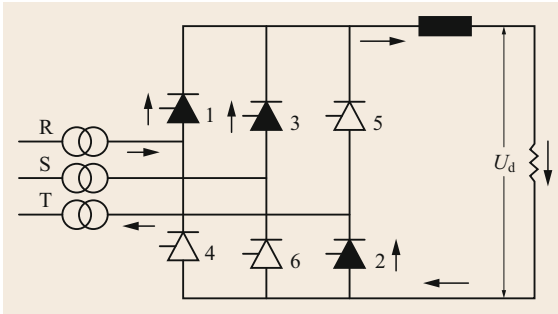
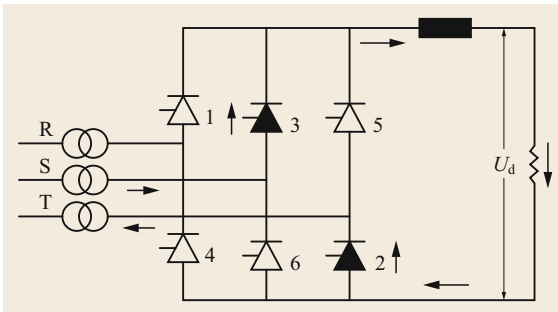


Fig. 12.19 Two of the valves (1 and 2) in the six-pulse bridge conducting at a particular instant


**Fig. 12.20** Commutation of valve 1 to valve 3

**Fig. 12.21** Valves 2 and 3 conducting

triggered once per fundamental frequency cycle, which means that the six-pulse bridge operates at a frequency of six times the fundamental frequency of the AC system. One valve is triggered every  $60^\circ$ . This means that if we start with valve 1, valve 2 will be triggered  $60^\circ$  later, and so on. Each of the valves will carry the current for  $120^\circ$ .

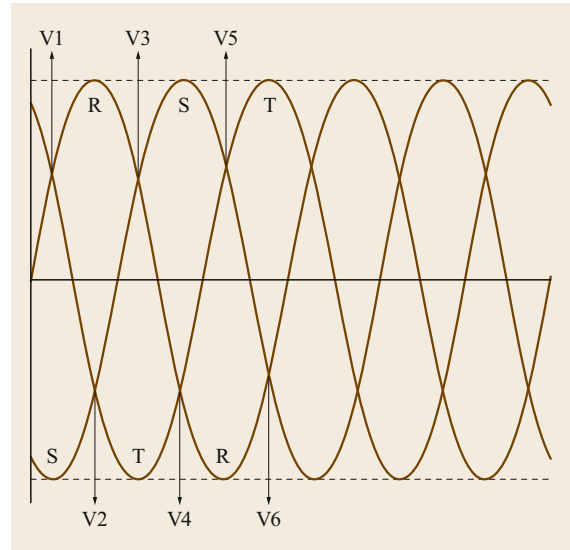
The current for the cathode valves shifts between valves 1, 3, and 5. The current for the anode valves shifts between valves 2, 4, and 6. Under normal operating conditions, no two valves in the same phase (e.g., valves 1 and 4) can conduct at the same time, as this would produce a short circuit at the DC terminals and result in  $U_d = 0$ .

When valve 1 is conducting, the current is flowing in the R phase to the load. It returns through valve 2 to the T phase, and the voltage RT is applied to the DC line. When valve 3 is triggered, the current is passed as shown in Fig. 12.20. The sharing of the current between valves is referred to as the commutation process.

When the current in valve 1 is completely commutated to valve 3, valve 3 carries all of the current, as shown in Fig. 12.21. Note that the voltage in the DC line is then ST.

The same commutation process occurs between valves 2 and 4 and the remaining valve.

By controlling the moment that a valve is triggered relative to the zero crossing, the DC voltage  $U_d$  can be


**Fig. 12.22** Commutation instants at phase-to-phase zero-voltage crossings

controlled. As shown in Fig. 12.22, zero voltage crossings occur for each valve as follows:

- Valve 1 is connected between phases R and T
- Valve 2 is connected between phases S and T
- Valve 3 is connected between phases S and R
- Valve 4 is connected between phases T and R
- Valve 5 is connected between phases T and S
- Valve 6 is connected between phases R and S.

Therefore, individual valves can be triggered at zero crossings. If valve triggering is delayed by a time (also known as a firing or delay angle)  $\alpha$ , as shown in Fig. 12.23, the average voltage (taking  $I_d = 0$ ) on the DC side is

$$U_d = \frac{3\sqrt{2}}{\pi} E \cos \alpha = 1.35E \cos \alpha,$$

where  $E$  (Fig. 12.18) is the line-to-line AC voltage applied to the valve.

It is clear that the DC voltage can be modified by changing  $E$ ,  $\alpha$ , or both. The maximum DC voltage is obtained at  $\alpha = 0$ , and the average DC voltage is zero at  $\alpha = 90^\circ$ .

The term  $(3\sqrt{2}/\pi)E$  is referred to as the ideal no-load direct voltage or the open circuit voltage of the converter  $U_{dio}$ .

Earlier in the discussion, we introduced the commutation process, which was assumed to occur instantaneously. However, this is not realistic, as it would disobey the laws of physics due to the inductance in

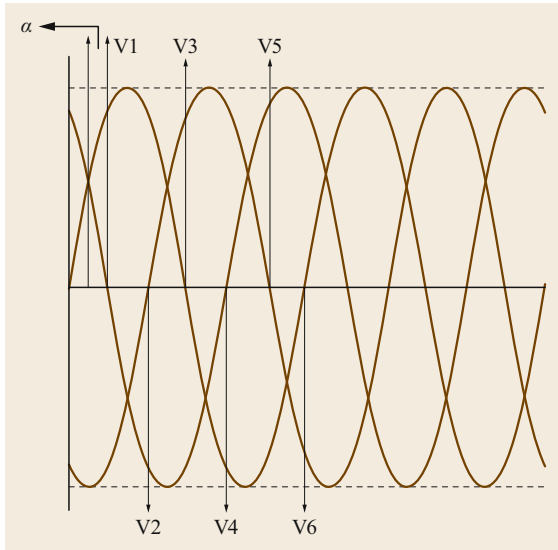


Fig. 12.23 Commutation instants with a firing angle of  $\alpha$

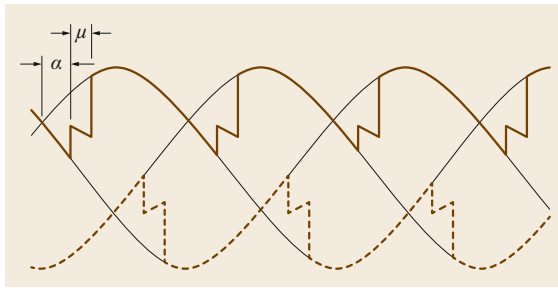


Fig. 12.24 Overlap and firing angles for rectifier DC voltages

the circuit. Because of the inductance in the commutation path, the commutation of the current from, say, valve 1 to valve 3 will take a finite amount of time. There will then be an overlap where the current will decay to zero in one path (for valve 1) and rise to its steady-state value in the other path (for valve 3). This period is referred to as the overlap angle  $\mu$  (Fig. 12.24).

This angle depends on the inductance in the circuit. There are several inductances in the circuit, but the transformer reactance dominates. The inductance in the circuit is referred to as the commutating reactance  $X_C$ . Naturally, the overlap angle  $\mu$  is also a function of the value of the DC current. The higher the DC current in the circuit, the longer it takes to commutate from one valve to another.

The impact of the commutation process and the overlap angle  $\mu$  is to reduce the output DC voltage  $U_d$  of the converter, as shown in Fig. 12.24. If  $\mu$  is zero, which means that  $X_C$  is zero too, the DC voltage only depends on  $\alpha$  in Fig. 12.24.

From Fig. 12.24, it is clear that during the period  $\mu$ , the voltage at the upper pole is

$$\frac{\dot{V}_R + \dot{V}_S}{2} = -\frac{\dot{V}_T}{2}.$$

The commutation process and the resulting  $\mu$  reduces the DC voltage of the converter during rectifier operation according to the following

$$\begin{aligned} U_d &= \frac{3\sqrt{2}}{\pi} E \cos \alpha - \frac{3I}{\pi} X_C \\ &= \frac{1}{2} U_{\text{dio}} [\cos \alpha + \cos (\alpha + \mu)], \end{aligned}$$

$$U_d = U_{\text{dio}} \cos \alpha - \frac{3I}{\pi} X_C.$$

The above equations can also be written as

$$U_d = U_{\text{dio}} \left( \cos \alpha - d_x \frac{I_d}{I_{dN}} \frac{U_{\text{dio}N}}{U_{\text{dio}}} \right),$$

where  $N$  refers to rated values and  $d_x$  is the commutation reactance (p.u.)

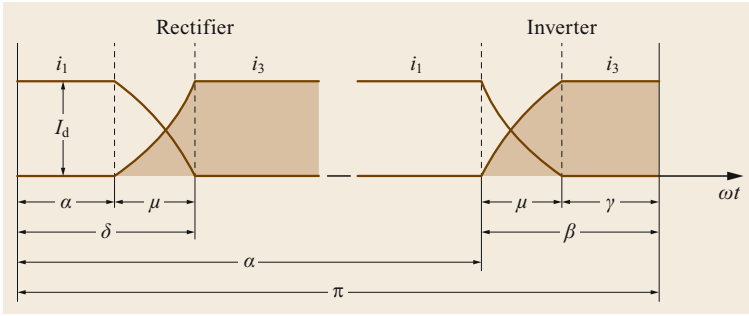
$$d_x = \frac{3I}{\pi} X_C \frac{I_{dN}}{U_{\text{dio}N}}.$$

### 12.5.2 LCC Operation (Inverter Operation)

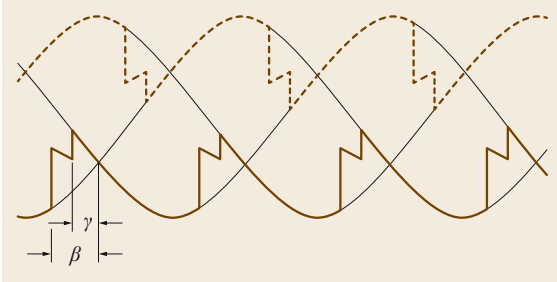
As discussed earlier, the DC voltage is zero at a delay angle of  $90^\circ$ . If we increase the delay angle  $\alpha$  beyond  $90^\circ$ , the resulting DC voltage will be negative.

During inverter operation, both  $\alpha$  and the overlap angle  $\mu$  have the same definitions as before, but there is another angle  $\gamma$ , the extinction angle, that is important too. In order to define this angle, it is necessary to understand phenomena associated with the valve conducting current.

The valve turns off when the current in the thyristors falls below a critical level referred to as the holding current. The anode current falls at a certain  $dI/dt$  to zero and then continues to move to a negative value in the reverse direction by the application of a reverse voltage. A reverse current will continue to flow until all of the excess stored charge is removed from the thyristors. If a forward voltage is reapplied to the valve soon after the current has passed zero, the thyristor will turn on again. However, if sufficient time is allowed for all of the stored charge to be removed by the reverse voltage, the forward voltage can be reapplied. It is important to note that the voltage distribution across the series-connected thyristors is not ideal under such conditions. The turn-off time is defined as the time taken for the voltage across the thyristor to turn positive after the anode current has passed through zero. For defining the extinction angle  $\gamma$  it is necessary to take into consideration the turn-off time of the thyristors and any sudden



**Fig. 12.25** Firing, overlap, and extinction angles during commutation from valve 1 to valve 3



**Fig. 12.26** Inverter operation and the resulting DC voltage of the converter

increase in the DC current as well as any sudden drop or shift in the AC voltage due to AC disturbances.

The angle between the end of the current in the valve and the start of the voltage going positive is referred to as the deionization period or extinction angle  $\gamma$ . The angles  $\alpha$ ,  $\mu$ , and  $\gamma$  are related in the following manner

$$\alpha + \mu + \gamma = \pi,$$

and  $\gamma + \mu = \beta$ , as shown in Fig. 12.25.

The following inverter equations can be defined in a similar way to the rectifier equations

$$\begin{aligned} U_d &= \frac{3\sqrt{2}}{\pi} E \cos \alpha - \frac{3I}{\pi} X_c \\ &= \frac{1}{2} U_{dio} [\cos \alpha + \cos (\alpha + \mu)], \\ U_d &= \frac{3\sqrt{2}}{\pi} E \cos \alpha - \frac{3I}{\pi} X_c \\ &= \frac{1}{2} U_{dio} [\cos \alpha + \cos (\alpha + \mu)], \\ U_d &= \frac{1}{2} U_{dio} \{ \cos [\pi - (\mu + \gamma)] + \cos (\pi - \gamma) \} \\ &= \frac{1}{2} U_{dio} [\cos (\gamma) + \cos (\mu + \gamma)], \\ U_d &= \frac{3\sqrt{2}}{\pi} E \cos \gamma - \frac{3I}{\pi} X_c = U_{dio} \cos \gamma - \frac{3I}{\pi} X_c. \end{aligned}$$

Or

$$U_d = U_{dio} \left( \cos \gamma - d_x \frac{I_d}{I_{dN}} \frac{U_{dioN}}{U_{dio}} \right).$$

The rectifier and inverter DC voltage equations are similar except that  $\alpha$  is replaced with  $\gamma$  (Fig. 12.26).

### 12.5.3 Application Example and Basic Control

The equations used to determine the conditions in a LCC HVDC system were listed earlier but are repeated here for the sake of clarity.

#### Combined Equations

For the rectifier,

$$U_{dR} = U_{dioR} \left( \cos \alpha - d_x \frac{I_d}{I_{dN}} \frac{U_{dioN}}{U_{dioR}} \right).$$

For the inverter,

$$U_{dI} = U_{dioI} \left( \cos \gamma - d_x \frac{I_d}{I_{dN}} \frac{U_{dioN}}{U_{dioI}} \right).$$

For the line,

$$I_d = \frac{U_{dR} - U_{dI}}{R}.$$

Additional equations to determine other values are now presented.

For the overlap angle,

$$\begin{aligned} \mu_R &= \arccos [\cos (\alpha_R) - 2d_{xR}] - \alpha_R, \\ \mu_I &= \arccos [\cos (\gamma_I) - 2d_{xI}] - \gamma_I. \end{aligned}$$

For reactive compensation,

$$\tan (\varphi_R) = \frac{2\mu_R + \sin (2\alpha_R) - \sin (2\delta_R)}{\cos (2\alpha_R) - \cos (2\delta_R)},$$

$$\begin{aligned} \delta_R &= \alpha_R + \mu_R, \\ Q_R &= P_R \tan (\varphi_R), \end{aligned}$$

$P$  and  $Q$  represent the active and reactive power, respectively, while the subscripts R and I correspond to the rectifier and inverter, respectively.

The remaining variables are the same as those described previously

$$\tan(\varphi_I) = \frac{2\mu_1 + \sin(2\gamma_1) - \sin(2\delta_1)}{\cos(2\gamma_1) - \cos(2\delta_1)},$$

$$\delta_I = \gamma_1 + \mu_1,$$

$$Q_I = P_I \tan(\varphi_I).$$

### Example

Consider the following example based on the Brazilian Rio Madeira HVDC project:

- Power per bipole: 3000 MW (in the rectifier)
- One 12-pulse bridge per pole
- Rated voltage:  $\pm 600$  kV
- Rated rectifier angle:  $\alpha = 15^\circ$
- Minimum rectifier angle:  $\alpha = 5^\circ$
- Rated inverter minimum angle:  $\gamma = 17^\circ$
- $d_x = 0.09$  p.u.
- Line resistance:  $15 \Omega$
- AC system voltage: 500/550 kV (both sides)
- Rated current:  $3000/(2 \times 600) = 2.5$  kA

The aim is to calculate the rated condition values.

In a point-to-point LCC system, one converter (generally the inverter) controls the DC voltage, and the other controls the DC current.

On the rectifier side, for a six-pulse bridge, the values are

$$U_{dR} = U_{dioR} \left( \cos 15 - 0.09 \frac{1}{1} \right),$$

$$U_{dioR} = 342.5 \text{ kV} = 1.35 E_R,$$

$$E_R = 253.7 \text{ kV}.$$

The nominal ratio of the transformer should therefore be 500/253.7.

Note that an on-load tap changer (OLTC) should be included to take care of loading variation at the high-voltage side of the transformer. This should have an appropriate tap range, which can be achieved using a small step:

The overlap angle  $\mu = 23.19^\circ$ .

The reactive power is 1606 MVAR.

The voltage in the inverter and other values are as follows

$$600 - 15 \times 2.5 = 526 \text{ kV per pole},$$

$$P_I = 2812 \text{ MW},$$

$$U_{dioI} = 324.7 \text{ kV},$$

$$E_I = 240.5 \text{ kV}.$$

The overlap angle  $\mu = 22.08^\circ$ .

The reactive power is 1583 MVAR.

### Working Principle

In a point-to-point LCC system, one converter controls the DC voltage (typically the inverter) while the other (the rectifier) controls the DC current. The general principle is shown in Fig. 12.27.

In the steady state, the insertion of  $I_{\text{margin}}$  ( $\Delta I_d = 10\%$ ) into the inverter loop control leads to the requirement that  $\gamma_d$  is larger than  $\gamma_{\text{min}}$ . The value of the latter is chosen and thus defines  $U_{dI}$ . Consequently, the inverter voltage can be controlled.

Now, suppose that the AC voltage of the rectifier is reduced for any reason. This will cause a reduction in  $U_{dR}$ , so  $\alpha_r$  will decrease to compensate provided that it is not below  $\alpha_{\text{min}}$ , in which case the OLTC will act to increase the AC voltage in the rectifier, pulling  $\alpha_r$  up to the rated value.

Conversely, suppose that the AC voltage in the inverter drops. The value of  $U_{dI}$  will then decrease, so  $I_d$  will tend to rise and  $\alpha_r$  will increase to maintain the current.

These two operational assumptions are just examples, and it should be noted that the LCC control system has other features that will be described later.

### 12.5.4 Peak Rectification

Peak rectification, also referred to as amplitude rectification, occurs in any converter with no load [12.10]. The ideal no-load voltage was defined earlier as  $U_{dio} = (3\sqrt{2}/\pi)E$ . However, the true no-load voltage will be higher because the converter can charge the circuit capacitance on the DC side during an open circuit. While it is being charged, the capacitance will also discharge through the high leakage resistance in the DC circuit. If the time constant for the discharging of the capacitance is longer than the time between converter voltage peaks, the circuit capacitance will recharge to a higher value, which explains why this behavior is referred to as peak or amplitude rectification. The circuit capacitance discharges in an exponential manner.

Peak or amplitude rectification will occur in any open-circuited converter, even at firing angles that are slightly higher than  $90^\circ$ . This phenomenon is utilized in HVDC systems during open-circuit testing of the converter station or DC transmission circuit. It can also be used for the precharge function in multiterminal HVDC systems.

### 12.5.5 Changing the Power Direction in LCC Converters

In LCC technology, the DC current direction is always the same because thyristor valves can only carry cur-



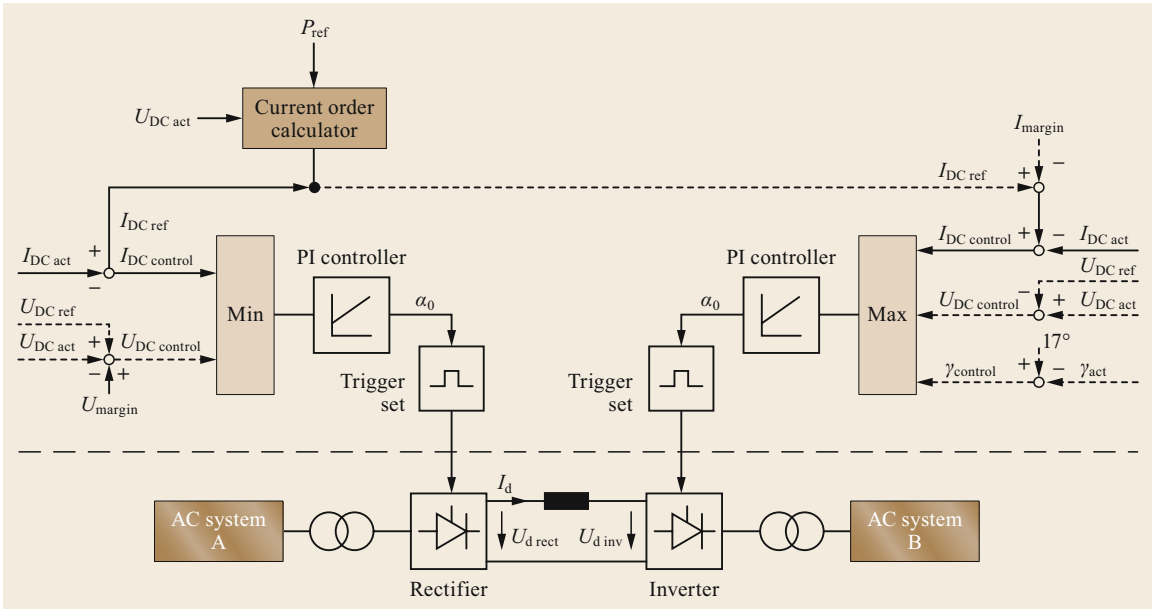


Fig. 12.27 Working principle of a point-to-point LCC HVDC system

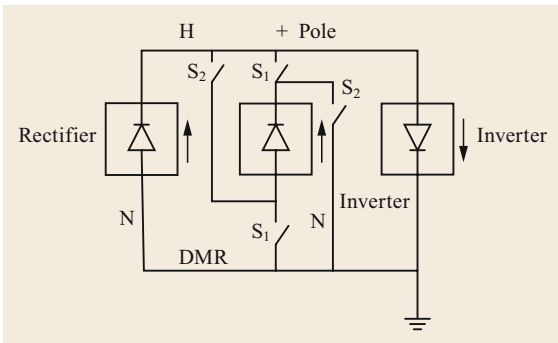


Fig. 12.28 Reversing power to the negative pole in an intermediate converter. During the reversing process, the  $S_1$  switches are closed while the  $S_2$  reversing switches are open; the  $S_1$  switches are then opened and the  $S_2$  reversing switches are closed

rent in one direction. Therefore, in order to reverse the power direction in a two-terminal HVDC system, the DC voltage polarity is reversed but the direction of the DC current remains the same. In a multiterminal HVDC system, if all of the terminals reverse their power directions, then the direction of the current remains the same but the voltage polarity is reversed.

However, if only one terminal in a multiterminal system changes its power direction, it must still change its voltage polarity [12.11]. Since it is connected to a pole of opposite polarity, reversing switches are required, and the converter will have full insulation at both of its terminals, as shown in Fig. 12.28.

### 12.5.6 Harmonics

#### Characteristic Harmonics

Cyclic triggering of the valves in a six-pulse bridge produces harmonics [12.2, 10]. Both the output DC voltage and the currents that appear in the valve-side phases of the transformer contain certain characteristic harmonics that are produced whether the converter is operating as a rectifier or an inverter.

#### AC Current Harmonics

Assuming that the AC system is perfectly symmetrical, there is no imbalance in the commutating reactor  $X_C$ , or equidistant triggering (firing) of the valves. For a six-pulse bridge, the harmonics produced in the current on the valve side of the transformer are of order  $6n \pm 1$ , where  $n$  is an integer that takes values from 1 to  $n$ . Therefore, the current harmonics are as follows:

- 5th and 7th harmonics for  $n = 1$
- 11th and 13th harmonics for  $n = 2$
- 17th and 19th harmonics for  $n = 3$
- Higher harmonics for higher values of  $n$ .

The magnitude of the  $n$ -th harmonic current is given by

$$I_n = \sqrt{6} \frac{I_d}{n\pi},$$

where  $I_d$  is the DC current.

### Voltage Harmonics

Assuming that the AC system is perfectly symmetrical, there is no imbalance in the commutating reactor  $X_C$ , or equidistant triggering (firing) of the valves. The six-pulse bridge harmonics produced in the DC voltage are of order  $6n$ , where  $n$  is an integer that takes values from 1 to  $n$ . Therefore, the voltage harmonics are as follows [12.12, 13]:

- 6th for  $n = 1$
- 12th for  $n = 2$
- 18th for  $n = 3$
- Higher harmonics for higher values of  $n$ .

### Twelve-Pulse Bridges

The previous discussion considered the characteristic harmonics of a six-pulse bridge. However, we can take advantage of the design and winding configuration of a converter transformer to eliminate some of these harmonics.

In a converter consisting of two six-pulse bridges connected in series on the DC side (one with a wye–wye transformer and the other with a wye–delta transformer) the voltages of the bridges will be  $30^\circ$  out of phase, so that their harmonics will also be out of phase. Since  $30^\circ$  of the main frequency correspond to half a cycle of the 6th harmonic, the 6th harmonic will be in phase opposition in the two bridges, and the two bridges will be in phase for the 12th harmonic.

A similar effect is also seen for the AC current harmonics (Fig. 12.29). These harmonics will be of order  $12n \pm 1$ ; in other words:

- 11th and 13th harmonic for  $n = 1$
- 23rd and 25th harmonic for  $n = 2$ .

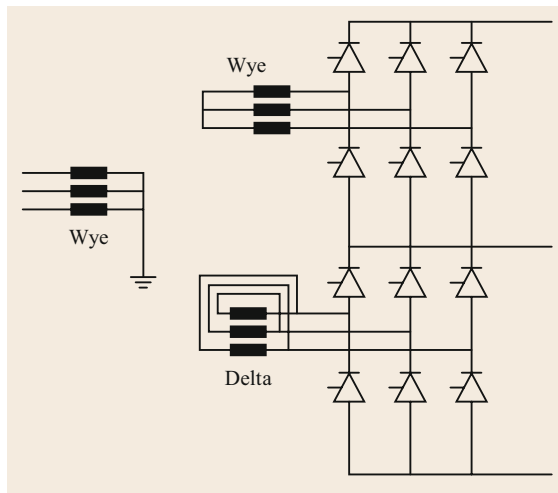


Fig. 12.29 Arrangement of a twelve-pulse bridge

The DC voltage harmonics will be of order  $12n$ , implying:

- 12th harmonic for  $n = 1$
- 24th harmonic for  $n = 2$ .

Thus, it is clear that the use of a twelve-pulse bridge eliminates certain harmonics.

### Noncharacteristic Harmonics

As mentioned earlier, the characteristic harmonics are based on ideal conditions. In reality, however, the following issues will influence the harmonics [12.2]:

- Firing error
- AC voltage unbalance or distortion
- Direct current modulation from the remote station
- Imbalance between converter components
- Imbalance between the applied voltages of the wye–wye and wye–delta transformers
- Imbalance between the firing angles of the wye–wye and wye–delta transformers
- Induced harmonics due to parallel AC lines sharing the same right-of-way as the DC line or in some cases both the DC and the AC lines on the same tower.

This will result in the generation of noncharacteristic harmonics of all orders. Such harmonics should be taken into consideration when designing the equipment, especially the AC and DC filters.

### 12.5.7 Reactive Power

The operation of the converter results in a phase angle between the fundamental component of the currents and the phase voltages. In principle, this phase angle is similar to a power factor. This means that the converter (a rectifier or an inverter) will consume reactive power. A rule of thumb is that a typical converter at nominal firing angles will consume approximately 50–60% of its rating in reactive power. More precisely, the reactive power consumption is a function of the delay angle  $\alpha$ , the overlap angle  $\mu$ , and the converter power at that point of operation.

The converter power factor

$$\cos \varphi = \frac{U_d}{U_{dio}},$$

$$\cos \varphi \approx \frac{1}{2} [\cos \alpha + \cos (\alpha + \mu)].$$

$$P_{dc} = U_d I_d = EI \cos \varphi,$$

where  $U_d$  is the DC voltage of the converter and  $I_d$  is its DC current

$$EI = \frac{P_{dc}}{\cos \varphi},$$

$$Q = EI \sin \varphi = P_{dc} \tan \varphi.$$

The consumption of reactive power by the converter is compensated by using either shunt capacitor banks or a combination of shunt banks and shunt AC filters. This is the typical approach that is used to provide reactive compensation for a converter. However, the reactive power compensation must be managed together with the reactive power consumption of the converter as well as the filters needed to meet the harmonic performance of the DC system.

In practice, as the DC power of the converter is ramped upwards, its consumption of reactive power increases. Therefore, shunt elements must be switched on to avoid excessive reactive power consumption from the AC system. Reactive power exchange with the AC system should be controlled. The magnitude of the steps due to the switching of the shunt bank are a function of the robustness of the AC system and are determined through system studies. Figure 12.30 shows how reactive power exchange with the AC system can be maintained in a band between  $+Q$  and  $-Q$  using this approach.

As the DC power of the converter is increased, the reactive power requirements of the converter  $Q_{\text{Converter}}$  will also increase. If the reactive power demand of the converter minus the reactive power supplied by the shunt banks  $Q_{\text{Shunt}}$  exceeds  $+Q$  (i.e.,  $Q_{\text{Converter}} - Q_{\text{Shunt}} > +Q$ ), then another shunt element must be switched on to ensure that the reactive power remains between  $+Q$  and  $-Q$ .

Similarly, as the converter DC power is reduced, its reactive power requirements will also decrease. If the reactive power demand of the converter minus the reac-

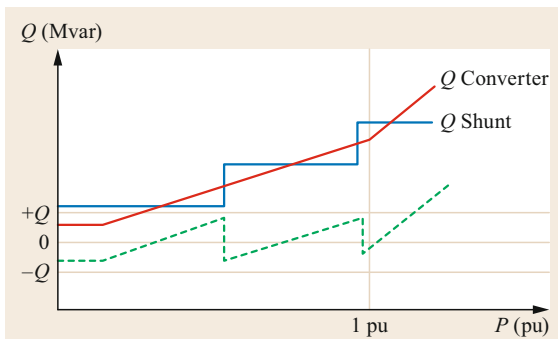


Fig. 12.30 Reactive power management in a conventional converter

tive power supplied by the shunt banks falls below  $-Q$  (i.e.,  $Q_{\text{Converter}} - Q_{\text{Shunt}} \leq -Q$ ), then a shunt bank must be switched off. For all the bank switchings one should take into consideration the harmonic performance specified.

### 12.5.8 Capacitor Commutated Converter (CCC)

In this circuit, series capacitors are connected between the converter and the AC bus on the valve side of the converter transformer (Fig. 12.31) [12.14]. It is clear that the capacitors are insulated at the full DC voltage from ground. Because of the presence of the capacitors on the valve side, the CCC typically has higher voltage applied at the valve side than a conventional converter, resulting in higher stress design requirements for the snubber circuits and an increased voltage rating for the arrester. Depending on the design, and considering a typical capacitor size of 20–25% of the rating, the increase in the voltage stress is around 10%. On the other hand, the short-circuit current due to a valve short circuit is lower than that for a conventional valve. This is due to the fast charging of the capacitors, which produces a counter voltage that limits the peak value.

The typical protective process applied during a valve short-circuit fault is to block the valves with no bypass action. However, it is standard in such a design to assume that the blocking may fail and that three or four loops of fault current will continue, depending on the speed of the circuit breaker trip. The capacitor counter voltage will certainly reduce the loop peak. The capacitor counter voltage will also reduce the blocking voltage seen by the valve involved in the short circuit.

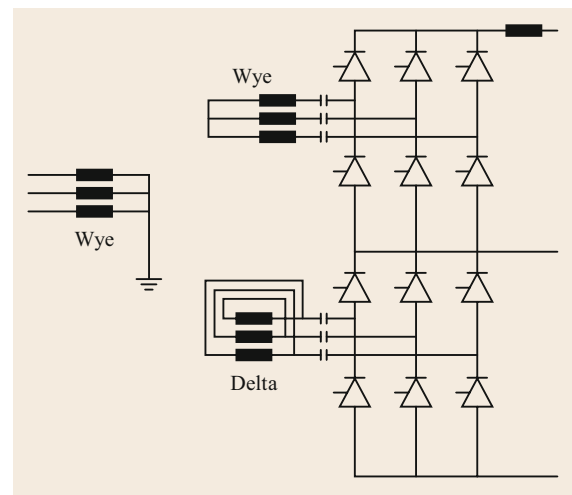


Fig. 12.31 Capacitor commutated converter (CCC)

The phase currents of a CCC are very similar to the phase currents of a conventional converter. The only difference is that the currents during the overlap interval include not only the sine wave of fundamental frequency but also a component with the natural frequency of the capacitor/inductor circuit. As explained earlier, because the capacitor voltage supports the commutation of current from one valve to another, the overlap angle is reduced. This reduction will lead to a slight increase of 1–2% in the AC harmonics.

In a CCC, the rating of the converter transformer is reduced because the reactive power that flows through the transformer is reduced. The no-load losses of the converter transformer are lowered by the reduced rating of the unit, but the load losses are increased due to increased harmonic currents and commutation jumps.

The presence of the capacitor provides an additional commutation margin proportional to the direct current. This results in improved commutation failure performance.

### 12.5.9 AC System Strength

The strength of the AC system—the short-circuit MVA—plays an important role in the operation of a HVDC system. The interaction between the DC and AC systems is a very important consideration in the system studies performed before implementing a HVDC project [12.15].

Such interactions and the overall stability of the system can only be determined through studies carried out during the planning stage, the design phase, and when the system is operational (as the AC system changes). Such studies can determine the viability of integrating a HVDC into an AC network, as well as any enhancement that may be required to achieve this. Figure 12.32 shows how an inverter is typically connected to the AC network.

The inverter supplies DC power ( $P_{dc}$ ) to the AC system and consumes reactive power ( $Q_C$ ). Most of the reactive power is supplied by the shunt banks ( $Q_S$ ).

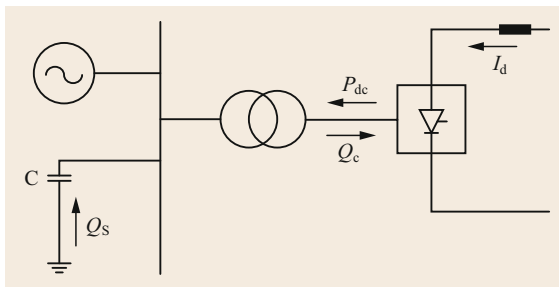


Fig. 12.32 Connecting an inverter to the AC network

We now need to define some very important quantities

Short-circuit ratio (SCR)

$$= \frac{\text{System (short circuit) MVA } (S)}{\text{DC power } (P_{dc})}$$

Effective short-circuit ratio (ESCR)

$$= \frac{\text{System MVA } (S) - \text{Capacitor MVA } (Q_s)}{\text{DC power } (P_{dc})}$$

Both the SCR and the ESCR are quantities that can be utilized to explore the difficulties that may be encountered. An ESCR of less than 2.5 is often said to indicate a weak network that may require some mitigation measures to overcome any performance issues.

### 12.5.10 Power Voltage Instability

HVDC systems, especially those utilized for bulk power transmission, are operated with constant DC power control [12.16].

The principle of constant power control means that, for a given operating point, the system is set to transmit a certain power order  $P_{dc}$ . The DC current reference is calculated as

$$I_{dref} = \frac{P_{dc}}{U_d}$$

where  $U_d$  is the DC voltage.

This means that  $I_{dref}$  would be expected to be constant at any operating point since both  $P_{dc}$  and  $U_d$  are constant. However,  $U_d$  is dependent on the AC system voltage. If the AC system voltage  $V$  decays due to problems relating to voltage control in the AC network, the output of the shunt capacitors connected to the converter bus bar will fall in proportion to  $V^2$ , which will in turn lead to a further decline in the system voltage  $V$ . Thus,  $U_d$  will also decrease and, based on the above equation,  $I_{dref}$  will increase, resulting in greater demand from the converter for reactive power. This will prompt a further reduction in  $V$ , and in some cases will lead to a complete collapse of the system.

The power voltage instability depends on:

- The operational control mode of the DC system (e.g., constant power control or constant current control)
- The AC system strength ESCR
- The AC system operating bus voltage criterion
- The method of regulating the voltage at the inverter bus
- The inverter control mode.

The maximum available power (MAP) of a HVDC is the maximum power that the system can transmit without incurring a system collapse. This can be evaluated by considering all of the above factors in system studies.

### 12.5.11 Multi-infeed

In the above analysis, the ESCR is based on the use of one HVDC link to feed an AC system. However, in many situations, there are several HVDC links that terminate in close vicinity (electrically speaking) in an AC system. Therefore, the performance of each HVDC link (inverter) will be affected by the presence of the other DC links. Such interactions are referred to as multi-infeed interactions. The degree of interaction will depend on how close the AC buses are to where the DC links terminate. The following phenomena associated with multi-infeed interactions are discussed in detail in CIGRE TB 364 [12.17], published in 2008:

- Transient overvoltages
- Commutation failures
- Harmonic interaction
- Power voltage instability and control interaction.

Although tuning the control system can help to mitigate these interactions, it is first necessary to study and determine such interactions.

CIGRE TB 364 introduces a first-level indicator of the degree of interaction between two HVDC links, which it terms the multi-infeed factor (MIF). This is defined mathematically for AC systems  $e$  and  $n$  as

$$\text{MIF}_{e,n} = \frac{\Delta V_e}{\Delta V_n},$$

where  $\Delta V_e$  is the observed voltage change at bus  $e$  for a small induced voltage change at bus  $n$ . A MIF value of zero implies that the buses are far apart and there is no interaction, whereas a MIF of 1 means that the two buses are very close and there will be an interaction. The brochure suggests that a MIF of more than 0.15 is indicative of a possible interaction. It also states that for interactions between AC systems with many HVDC systems, a matrix of MIF values can be derived. MIF values can be evaluated using transient stability or short-circuit studies.

### 12.5.12 LCC Control and Protection

The control and protection of an LCC HVDC is achieved using various functions. These can be categorized into:

- The HVDC controls
- The measurement system

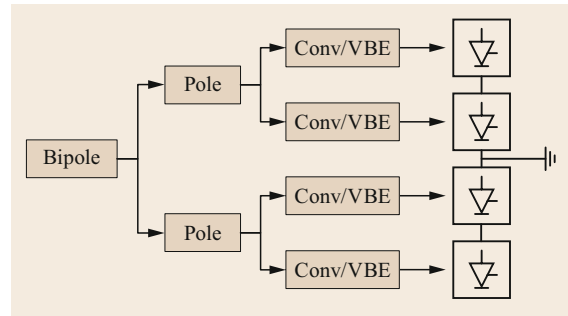


Fig. 12.33 LCC control system hierarchy

- The sequence controls
- The slow control functions (tap changer control)
- The protection.

The steady-state DC voltages of the rectifier and the inverter were presented in Sects. 12.5.1 and 12.5.2. It is clear that the DC voltages are dependent on the converter delay angle/extinction angle and the line-to-line AC voltages applied to the converter valves. The valve voltages are governed by the AC system voltage and the turns ratios of the converter transformers. However, the valve voltage can be regulated via the on-load tap changer. Therefore, LCC converter control can be achieved by controlling either the delay angle  $\alpha$  or the AC voltage of the valve  $E$ . Delay angle control is fast and can be relied upon to respond rapidly, whereas  $E$  control is slow and is typically used to keep the delay angle within certain margins.

The following control loops are used in a LCC control system:

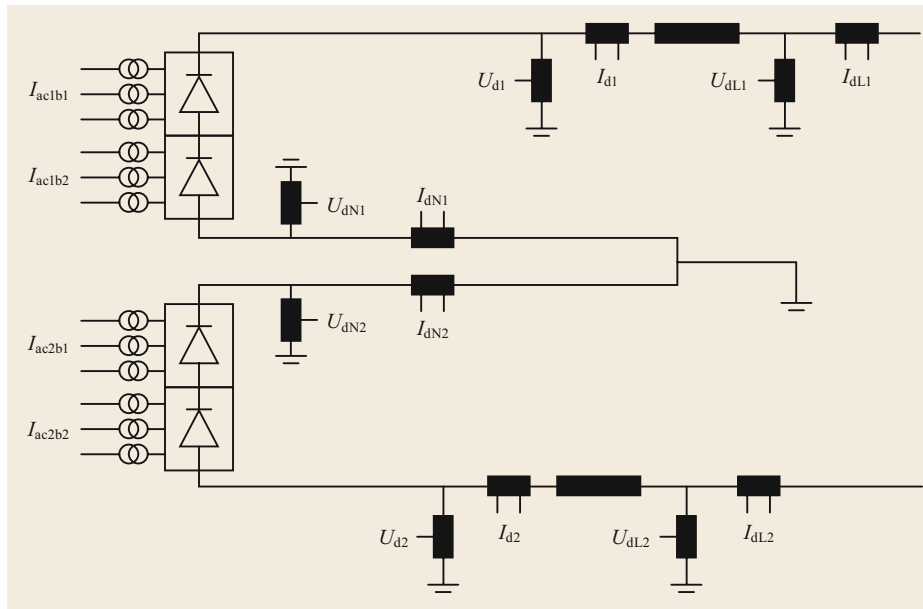
- DC power control (an open or closed loop)
- DC current control
- DC voltage control
- Minimum extinction angle  $\gamma$  control
- Reactive power control
- AC voltage control.

The control strategy used for a particular terminal is not chosen in isolation; the aim is to identify the most suitable and reliable way of operating the entire HVDC system. Indeed, several modes of control are actually assigned to each terminal, with smooth transitions between them.

A typical LCC control system hierarchy is shown in Fig. 12.33.

Different control functions may be assigned to the different levels. This assignment process is part of the design strategy of any supplier.

To understand the concept of LCC controls, it is important to note that the aim is to translate a power



**Fig. 12.34**  
Equipment used and measurements performed in a bipolar system

demand into control pulses that are supplied to the thyristor valves.

Before we examine the control system, we should consider where measurements are performed in a typical converter station, as shown in Fig. 12.34.

The quantities and the measurement locations indicated are typical and can therefore vary for different projects. The following quantities are measured:

- The DC line current at each pole,  $I_{dL}$
- The DC line voltage at each pole,  $U_{dL}$
- The DC pole current at each pole,  $I_{d1}$
- The DC pole voltage at each pole,  $U_{d1}$
- The neutral DC bus voltage at each pole,  $U_{dN}$
- The neutral bus DC current at pole 1,  $I_{dN1}$
- The AC currents in the converter transformers on the valve side,  $I_{acb1}$  and  $I_{acb2}$ .

In Fig. 12.35, the DC reference power (power order)  $P_{ref}$  is an input for the power controls. Dividing  $P_{ref}$  by the sum of the two DC pole voltages  $U_{d1}$  and  $U_{d2}$  in a bipolar HVDC system yields  $I_{ref1}$ . This equation still applies if the system is monopolar (i.e., there is only one  $U_d$ ) and if one pole in a bipolar system is not in service (i.e.,  $U_{d1}$  is equal to zero). This is an important feature of bipolar HVDC systems, as the remaining pole can compensate for the loss of power at one pole up to its rating plus any overload.

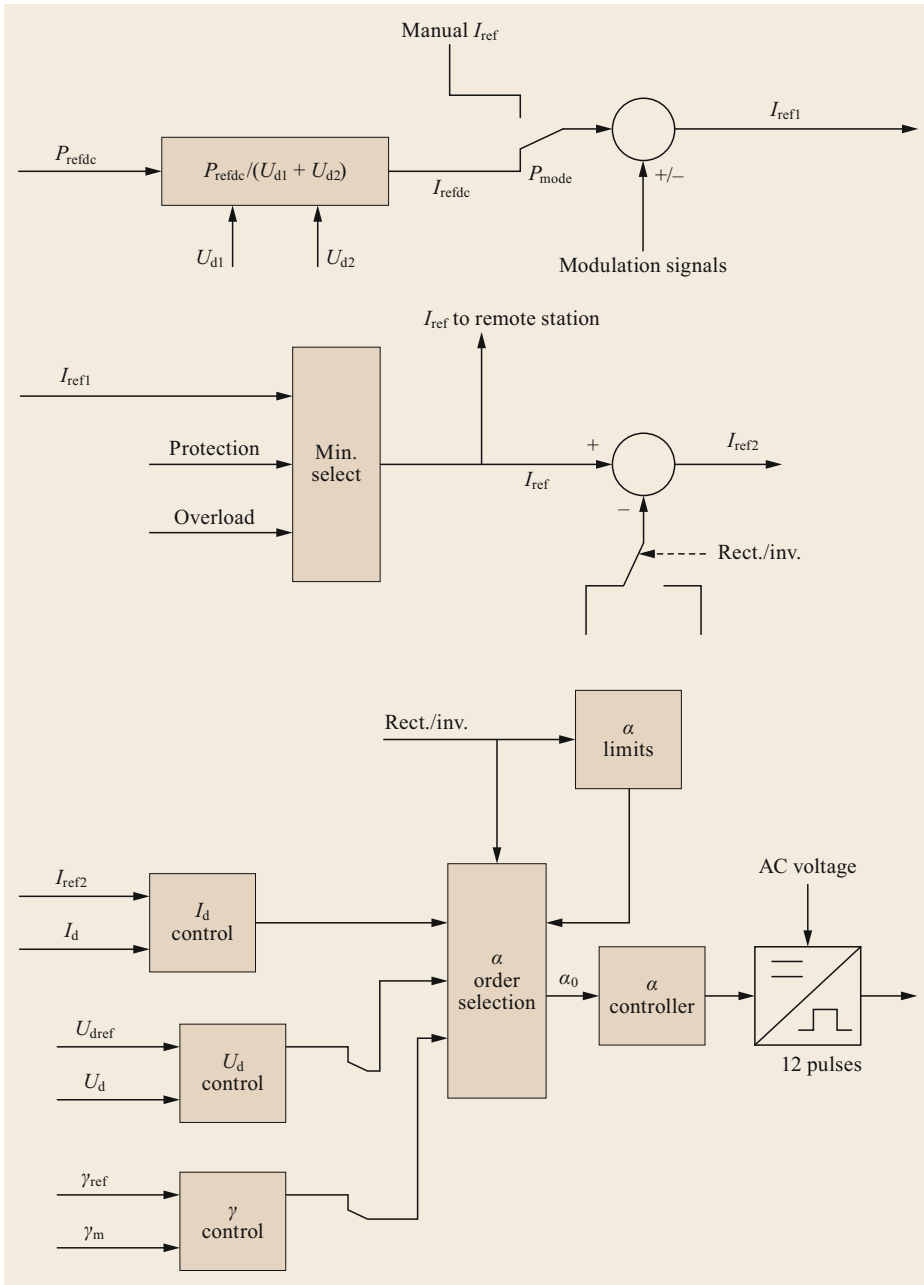
If power modulation controls are needed for damping purposes in the AC systems, the relevant inputs and signals are taken into consideration as modulation signals to the current reference. The current reference  $I_{ref1}$  is sent to both the local station and the remote station

via the communication system. To prevent any interaction between the DC current controllers for the two stations, a small current margin (typically 10% of the rated current) is subtracted from the current reference at the inverter station. The signal  $I_{ref2}$  is fed to the DC current controller. Depending on the control strategy applied, other controllers such as a DC voltage controller ( $U_d$  control) and a gamma controller ( $\gamma$  control) may also be active or inactive. However, only the firing angle ( $\alpha$  order) of a particular controller is selected at a given time, which in turn affects the output of firing pulses during the final stage. Controllers are selected and deselected dynamically, and the transition or control mode switchover must be smooth.

### 12.5.13 LCC Converter Startup (Deblock)

The term *deblock* refers to converter startup. In the configuration with a single converter per pole, as shown in Fig. 12.36, deblocking is very straightforward. The firing pulses for the converter are released at a firing angle ( $\alpha$ ) of  $150^\circ$ , which is referred to as force retard. The inverter is typically deblocked before the rectifier. Because the inverter starts first, it needs to send a signal to the rectifier via the communication system. Thus, the rectifier is released after a telecommunication time delay. Following successful deblocking, the firing angle for the converter ( $\alpha$ ) is determined by the appropriate controller at that station, e.g., the gamma ( $\gamma$ ) controller at the inverter or the DC current ( $I_d$ ) controller at the rectifier.

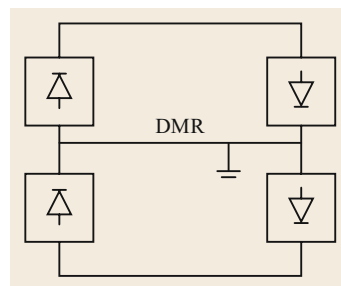
The deblocking of series-connected converters per pole is a little more involved than for a single converter



**Fig. 12.35**  
Converter control loops

per pole. There are many possible scenarios. Converters in series are shown in Fig. 12.37.

If pole 1 is out of operation and pole 2 is in operation, the bypass switches at pole 2 will be in the open position and the DC current will pass through the converters at pole 2. On the other hand, the converters at pole 1 are in the blocked state and the bypass switches at pole 1 will be in the closed position, so DC current will flow through the bypass switches at pole 1. This DC current is referred to as the spill current from pole 2,



**Fig. 12.36** Single converter per pole

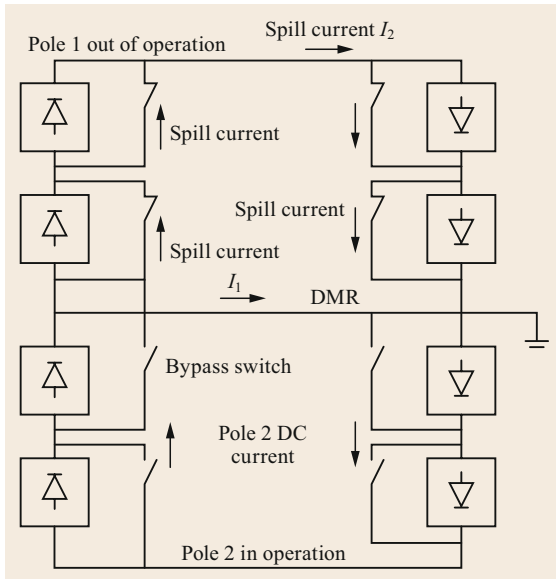


Fig. 12.37 Configuration of converters in series

and is divided between the DMR and pole 1 according to the relative resistances of the DMR and the pole 1 DC circuit, which includes the DC line or cable.

Bear in mind that the bypass switches are normal breakers with no ability to interrupt the DC current. Therefore, zero current must be present in the bypass switch before it will open and extinguish the arc. In a typical sequence, the converter is allowed to deblock at a delay angle  $\alpha$  in the rectifier region. By deblocking at such  $\alpha$ , the converter will produce a current opposite to the spill current, leading to zero current in the switch, which in turn extinguishes the arc. The value of  $\alpha$  is dependent on the switch characteristics as well as the speed of separation of the contacts. Delay angles  $\alpha$  of between  $45^\circ$  and  $75^\circ$  have been utilized.

The second mode of operation involves deblocking the second converter at a pole. In this case, one converter is deblocked and the second converter is blocked with a closed bypass switch. Therefore, the closed switch will carry the actual pole current. This current can be the full load current of the pole, which is much higher than the spill current. However, the same sequence described above for deblocking with a spill current will also apply.

There are several variations of the above sequence, but the aim is always to create zero current in the switch.

#### 12.5.14 LCC Converter Faults and Disturbances

Although there are a wide variety of converter faults and disturbances that can occur in a HVDC converter station, we only discuss some of them here.

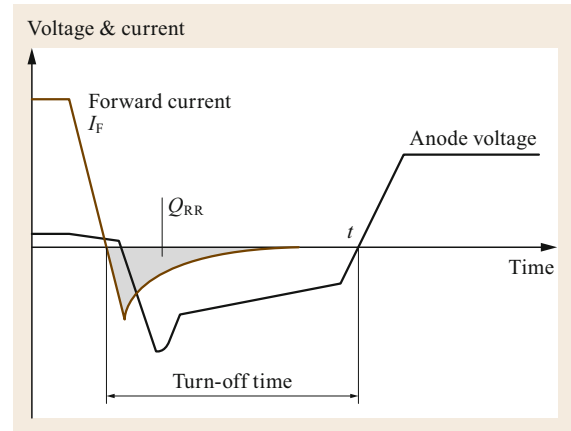


Fig. 12.38 Turn-off process

#### Inverter Commutation Failure

Inverter commutation failures can occur due to [12.18]:

- AC system faults and disturbances
- DC faults or disturbances
- Equipment failure.

Among the above causes, equipment failure can usually be excluded due to the redundancy built into the control equipment. Therefore, we will concentrate here on AC faults and disturbances. An AC fault at the converter busbar will lead to a commutation failure. The severity of the converter AC bus fault will determine how fast the inverter will recover from a commutation failure. A remote AC fault that results in either a reduction, a phase shift, or a distortion of the inverter commutating voltage will also induce a commutation failure. A drop in the valve voltage to approximately 80% for one of the phases will typically lead to a commutation failure. However, it is expected that the control system will help the inverter to recover and resume normal operation at a reduced AC bus voltage. The stronger the AC system, the lower the probability that a commutation failure will occur due to a remote AC fault.

A commutation failure occurs due to the physical characteristics of the thyristor valves in a LCC. Therefore, in order to understand commutation failures, it is necessary to examine the turn-off process for thyristors (Fig. 12.38).

Thyristor turn-off occurs when the current drops below a certain value (known as the holding current). During the commutation process, the current falls to zero, but current will continue to flow in the reverse direction in the thyristors when a reverse voltage is applied to them. This reverse current will continue to flow until all of the excess stored charge is drained from the thyristors.



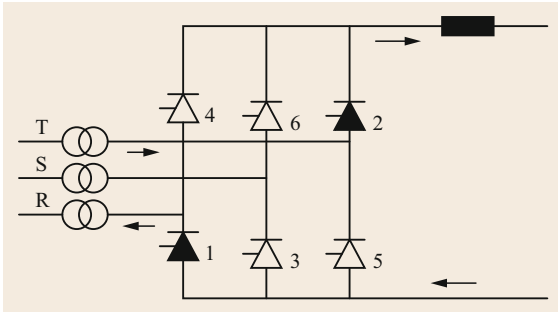


Fig. 12.39 Normal commutation

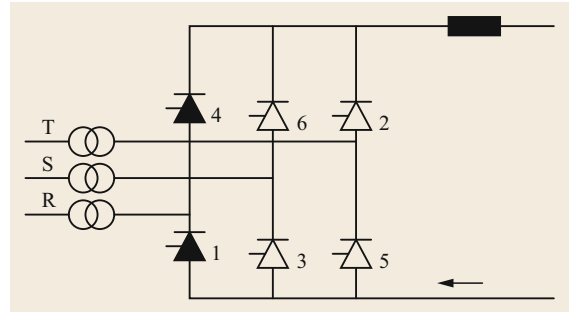


Fig. 12.41 Commutation failure

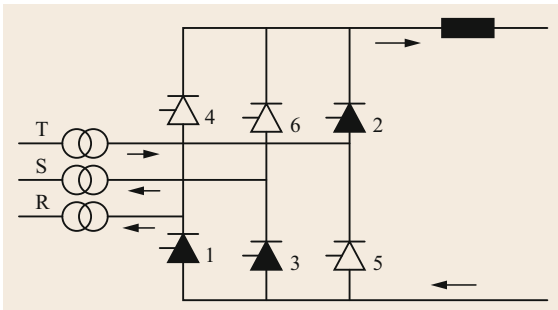


Fig. 12.40 Commutation of valve 1 to valve 3

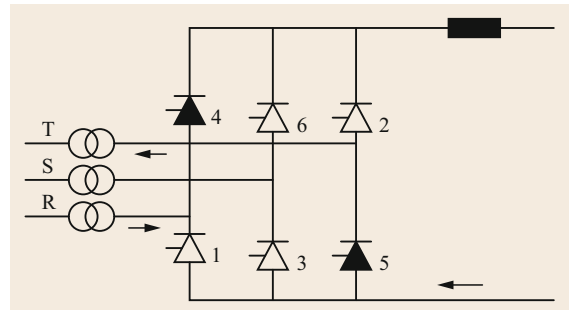


Fig. 12.42 Recovery from commutation failure

If a forward voltage is reapplied before this excess reverse charge is removed, the thyristor will turn on again. The turn-off time is defined as the time from the point at which the current reaches zero to the point at which the thyristor voltage turns positive.

The reverse recovery charge  $Q_{RR}$  is an important parameter of thyristors.

The impact of the AC system fault/disturbance is that insufficient charge is removed from the thyristors before a positive voltage is reapplied. Since it is a statistical phenomenon, some thyristors will be more affected than others. However, even if only a few thyristors turn on because of this phenomenon, the whole valve will be triggered to turn on to protect the thyristors. This results in out-of-turn conduction and thus a commutation failure. Commutation failure is therefore related to a lack of time for the outgoing valve to fully deionize following an AC disturbance.

In principle, this is due to a decrease in the extinction angle  $\gamma$ . Because of the statistical nature of thyristor characteristics, the  $\gamma$  of the whole valve is set to be larger than the actual time needed to deionize the thyristors.

When a commutation failure occurs, it creates a bypass at the DC terminals of the bridge, which results in an increased DC current and an average DC voltage of zero, so the DC power during the commutation fail-

ure is momentarily zero. In Fig. 12.39, valves 1 and 2 are conducting normally. When valve 3 is prompted to fire, the commutation process starts, as shown in Fig. 12.40.

If an AC fault or disturbance occurs, valve 1 may not have enough time to fully turn off after commutating the current to valve 3, so it can conduct current as soon as a positive voltage is reapplied to it. This out-of-turn conduction of valve 1 causes valve 3 to extinguish. When valve 4 is commanded to fire, a short circuit develops on the DC side, as shown in Fig. 12.41.

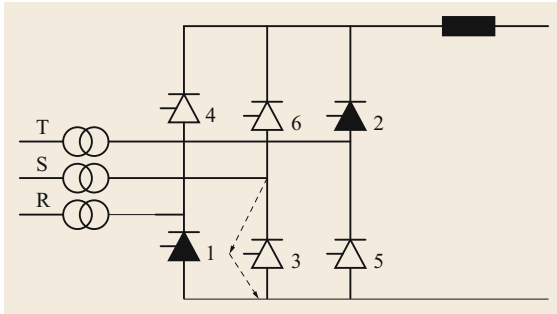
When valve 5 is commanded to fire (Fig. 12.42), the bypass is extinguished and recovery takes place so long as faults do not continue to occur.

If the commutation failure persists, the converter is removed from service. The commutation failure protection usually commands a block of the converter.

#### Valve Short Circuit

This type of fault can be the result of a flashover across any valve that is not conducting at the time. This will cause a short circuit between two AC phases of the transformer on the valve winding side.

Let us suppose that a flashover occurs between the terminals of valve 3 in Fig. 12.43 while valve 1 is conducting. This results in a short circuit between the R and S phases.



**Fig. 12.43** Valve short circuit

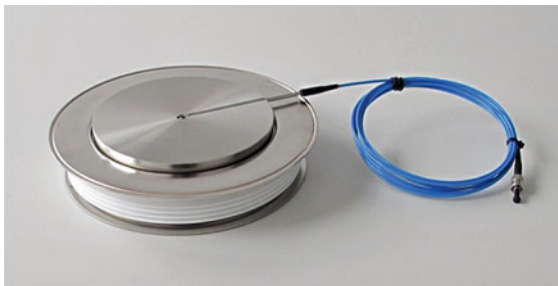
The valve short-circuit current is calculated based on the following:

1. The maximum short circuit level of the AC system
2. The minimum commutating reactance
3. The minimum frequency
4. The maximum DC voltage
5. The minimum permissible delay angle  $\alpha$ , which is typically  $5^\circ$ .

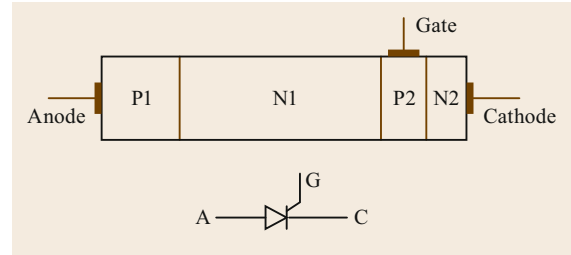
Two calculations are performed. The first is for the single loop (pulse) of short-circuit current. Because the converter is blocked, the valve must withstand the AC voltage, including the overvoltage resulting from the load rejection due to the blocking of the converter. The second is for multiple loops (typically three loops) in which the AC breaker trips and clears the fault. This multiple loop scenario will occur if converter blocking fails. However, no forward voltage is reapplied to the valves in the multiple loops.

### 12.5.15 Thyristors and Thyristor Valves

The backbone of HVDC LCC technology is the high-voltage, high-power thyristor. Active silicon thyristors that are six inches in diameter and have a current rating of 6.3 kA per device (Fig. 12.44) are currently available [12.19]. Thyristors with a flat-pack design are the



**Fig. 12.44** 6-inch light-triggered thyristor with a DC current rating of 6.3 kA (© Siemens/Infineon Bipolar)



**Fig. 12.45** The four layers and three terminals of a thyristor

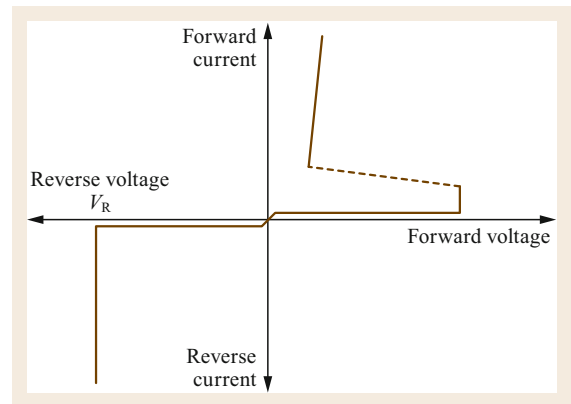
norm in HVDC valve applications. This type of device is easy to manipulate mechanically within the valve and easy to cool. In principle, a thyristor should be sandwiched between water-cooled heat sinks.

A thyristor is a semiconductor device with four layers and three terminals, as shown in Fig. 12.45. The anode is connected to the P1 layer, the cathode to the N2 layer, and the gate to the P2 layer.

In the forward blocking mode, when the anode is positive with respect to the cathode, the thyristor will conduct a small leakage current, as shown in Fig. 12.46. If the forward voltage is increased beyond a specific value, referred to as the breakover voltage (VBO), the thyristor will turn on. However, this kind of activation is not desirable as it is not a gated turn-on and it is not possible to control how the current spreads in the device. This type of activation can lead to thyristor failure.

In the reverse blocking mode, when the anode is negative with respect to the cathode, a small leakage current will flow. However, if the voltage is increased above the breakdown voltage  $V_R$  of the junction between P1 and N1 (see Fig. 12.46), the current increases rapidly. This breakdown is due to avalanche effects.

The leakage current that flows in both forward and reverse blocking is temperature dependent, and when a temperature of  $125^\circ\text{C}$  is exceeded the leakage current can increase rapidly and failure can occur.



**Fig. 12.46** Current–voltage characteristic of a thyristor



Fig. 12.47 500 kV thyristor valves (© Siemens)

When a gate pulse is applied to a thyristor and the anode is positive with respect to the cathode, the thyristor is turned on. Thyristor gating can be achieved using either an electrical pulse (i.e., an electrically triggered thyristor, ETT) or a light pulse (i.e., a light-triggered thyristor, LTT).

The power dissipation is high during turn-on. The allowable rate of increase in the anode current  $dI/dt$  is a critical parameter. If the anode current increases too rapidly it will lead to high power loss in a small area and the device may fail due to localized heating. This is mainly due to the increased current density: the current increases very quickly, meaning that it does not have sufficient time to spread.

### Thyristor Valves

Modern thyristor valves (Fig. 12.47) have the following features:

- A modular design with stacked thyristors and heat sinks
- Deionized water cooling of the thyristors, valve reactors, and snubber resistors
- The use of fiber optics for signal transmission between the thyristor levels and the valve control via the valve base electronics (VBE).
- On board thyristor protection, either electronic or integrated.

A thyristor valve consists of multiple thyristor levels, where a thyristor level consists of a thyristor, its heat sinks, snubber circuits, DC grading resistors, and the associated electronics (see Fig. 12.48) [12.20].

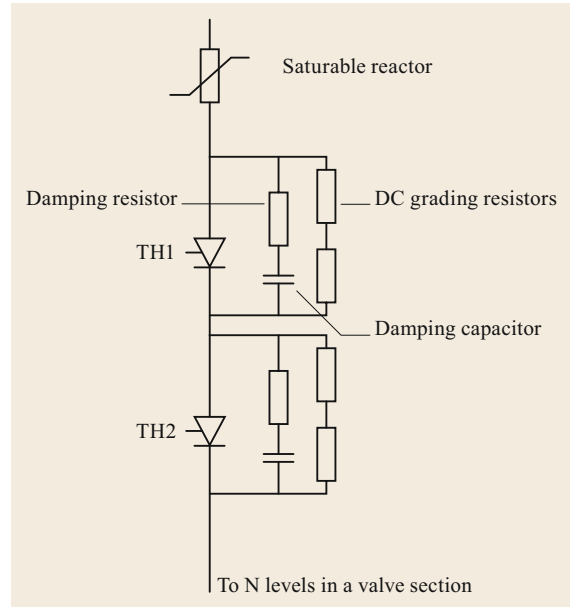


Fig. 12.48 Typical thyristor levels

There may be one saturable reactor per thyristor level, or a saturable reactor may serve multiple thyristor levels in series. The thyristor levels are connected in series, which is achieved mechanically by including a number of levels in a module or valve section together with the necessary cooling manifold and piping. The valve sections or modules are assembled into a valve structure together with fiber optic cables, cooling pipes, and insulators. The valve structure can include a single valve, a double valve, or a quadruple valve.

For thyristor valves that use ETT (Fig. 12.49), each thyristor level is equipped with thyristor electronics that are termed the gate electronics. The gate electronics receive trigger pulses in the form of light pulses from the VBE. These pulses are converted into electrical pulses that are processed by the gate unit and delivered to the thyristor gate as electrical signals. The status and condition of each thyristor level are also reported by the gate electronics to the VBE, and the gate electronics protect the individual thyristors against forward overvoltage and steep front voltages  $dv/dt$  that may occur during the thyristor recovery period.

Forward overvoltage can occur during faults or due to the loss of a firing pulse. Forward overvoltage protection is referred to as breakover diode protection (BOD). In most designs, this is a passive element that triggers the thyristor into conduction based only on the forward voltage of the forward thyristor. The gate electronics require power, which is obtained from the voltage across the thyristor in the off state.

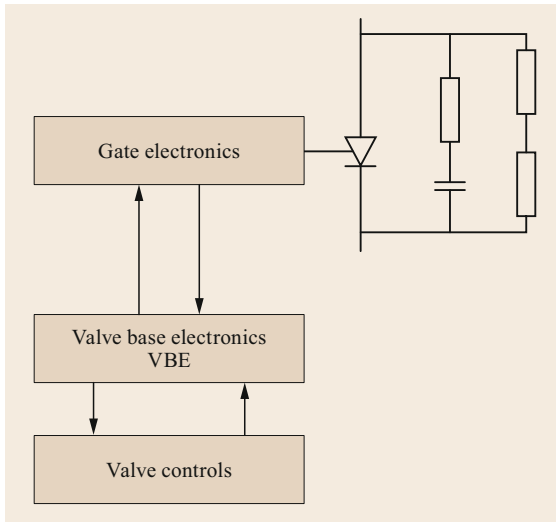


Fig. 12.49 Thyristor level concept for an ETT

For a light-triggered thyristor (Fig. 12.50) with integrated self-protection (LTT), the trigger pulses are transmitted from the VBE as light pulses. Since the thyristor is triggered by light energy there is

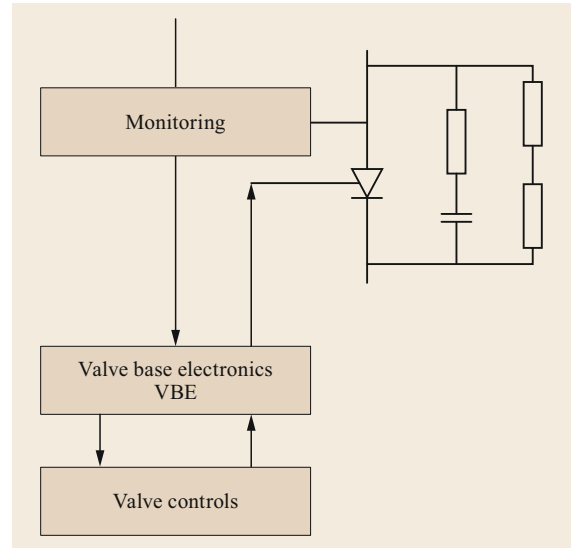


Fig. 12.50 Thyristor level concept for a LTT

no need to convert the pulses to electrical signals, so the need for gate electronics is eliminated.

## 12.6 Voltage-Source Converter (VSC)

The voltage-source converter was introduced in 1997, when it was used at a very low rating ( $\pm 10$  kV and 3 MW) in the Hellsjön project, together with a HVDC XLPE cable. However, this does not mean that VSC technology can only be used with HVDC XLPE cables. VSCs can also be applied to overhead lines, mass-impregnated (MI) cables, or combinations of HVDC cables and overhead lines. The semiconductor device usually employed in VSCs is the insulated gate bipolar transistor (IGBT). A VSC can control the active and reactive power exchanged with the AC system separately.

### 12.6.1 IGBTs

The IGBT is a three-terminal, four-layer (p-n-p-n) semiconductor (Fig. 12.51) device with a metal oxide

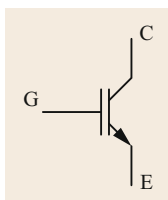


Fig. 12.51 The symbol for an IGBT

semiconductor (MOS) gate structure and a high input impedance. It has a very low on-state voltage drop due to conductivity modulation, and has superior on-state current density.

It has a wide safe operating area (SOA), which is the current-voltage region within which a power switching device can be operated without destructive failure. For the IGBT, this region is defined by the maximum collector-emitter voltage  $V_{CE}$  and collector current  $I_C$  below which the IGBT must be operated to protect it from damage.

An IGBT can be easily turned on or off. To turn it on, a positive signal is applied between the gate and the emitter, and to turn the device off, the signal between the gate and the emitter must be zero or



Fig. 12.52 Wire-bonded IGBT [12.21]



**Fig. 12.53** Stakpak module [12.22]

slightly negative. When a positive voltage is applied from the collector terminal (C) to the emitter terminal (E), the device is in the forward-blocking mode. Applying a positive voltage of sufficient level to the gate (G) will then cause the device to conduct. On the other hand, when a negative voltage is applied from C to E, the device becomes reverse biased.

A very important feature of an IGBT is the ability to limit the short-circuit current that passes through the device when a short circuit occurs at its terminals. The IGBT collector current  $I_C$  is a function of the gate-emitter voltage  $V_{GE}$  and the temperature. The device will have to be turned off to protect it.

Two types of IGBTs are currently available for HVDC applications: wire-bonded IGBTs (Fig. 12.52) with low losses and press-pack IGBTs (Fig. 12.53). The type of IGBT used in a HVDC converter will impact the converter design.

### 12.6.2 VSC Design

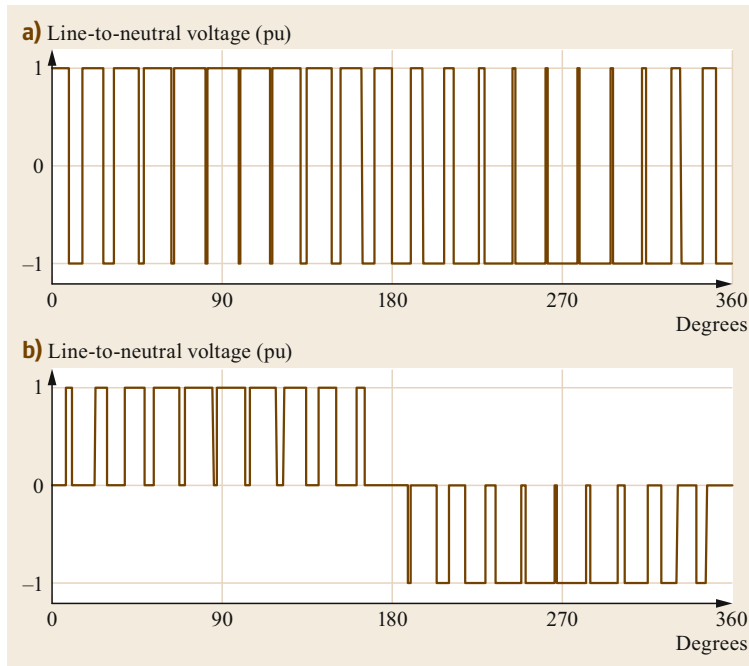
VSCs for HVDC applications include many IGBTs connected in series. Many issues must therefore be considered during VSC design:

- The mechanical design of the converter valves
- The cooling requirements within the valve
- The control of many IGBTs in the same valve
- Minimizing losses
- Equipment reliability
- The voltage distribution under both transient and steady-state conditions.

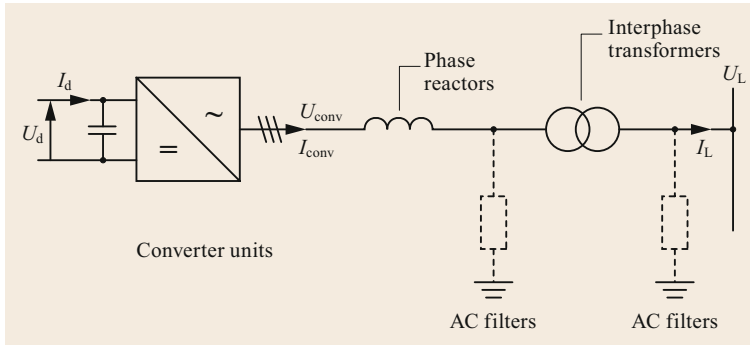
Following the introduction of VSCs for HVDC applications, a number of converter topologies were utilized in early HVDC projects. All of these topologies (Fig. 12.54) utilized two- or three-level converters with pulse width modulation (PWM) [12.24, 25].

As shown by Fig. 12.55, the VSC generates an AC waveform that has a fundamental frequency and harmonics. The harmonics can be filtered.

The converter controls the angle of the voltage by starting with square waves, and it controls the mag-



**Fig. 12.54** (a) Two- and (b) three-level VSCs [12.23]



**Fig. 12.55** Simplified circuit diagram for a VSC. Here,  $U_{conv}$  is the rms line-to-line AC voltage of the converter unit(s) including harmonics,  $U_{conv-ph}$  is the rms phase-to-phase AC voltage of the converter unit(s) including harmonics, and  $I_{conv}$  is the rms alternating current of the converter unit(s) including harmonics [12.23]

nitude of the voltage by controlling the pulse width. Therefore, a VSC can be represented as the simple circuit depicted in Fig. 12.55. The VSC electrical circuit can also be represented as shown in Fig. 12.56.

The rms value of the fundamental frequency component of the phase voltage  $U_{conv-ph}$  on the valve side of the interface reactance for the VSC in square-wave operation can then be defined as

$$U_{conv-ph(1)} = \frac{\sqrt{2}}{\pi} K_{\gamma} U_d e^{-j\delta},$$

where:

$\delta$  is the phase angle between the converter voltage  $U_{conv}$  and the AC voltage  $U_L$   
 $K_{\gamma}$  is the voltage ratio factor [0 ... 1].

Ignoring the resistance, the corresponding phase current in phase (a) can be expressed as

$$I_{conv-a(1)} = \frac{U_{conv-ph(1)} - U_{L(1)}}{Z}$$

$$= \frac{\frac{\sqrt{2}}{\pi} K_{\gamma} U_d e^{-j\delta} - U_{L(1)} e^{-j0}}{jX};$$

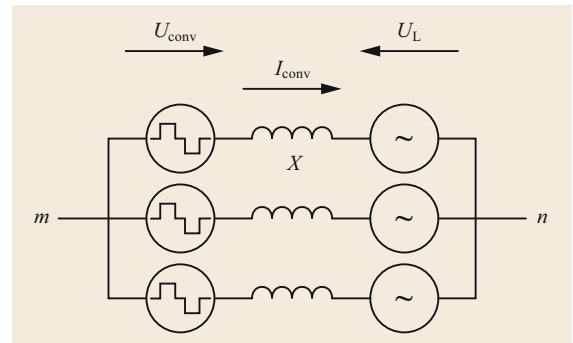
$$P = \frac{U_{conv(1)} U_{L(1)}}{X} \sin \delta,$$

$$Q = \frac{U_{L(1)} (U_{L(1)} - U_{conv(1)} \cos \delta)}{X}.$$

The direct current of the converter bridge  $I_d$  can also be derived using the equality of power on the AC and DC sides

$$I_d = \frac{\sqrt{6}}{\pi} \frac{U_{L(1)}}{X} \sin \delta.$$

As can be seen from the  $I_d$  equation, the active power is mainly determined by the phase angle between  $U_{L(1)}$  and  $U_{conv(1)}$ . At any given operating point, an increase



**Fig. 12.56** Representation of a VSC circuit [12.23]

in the phase delay of  $U_{conv(1)}$  would decrease the active power delivered to the AC system. Similarly, at any given operating point, a decrease in the phase delay of  $U_{conv(1)}$  would increase the active power delivered to the AC system.

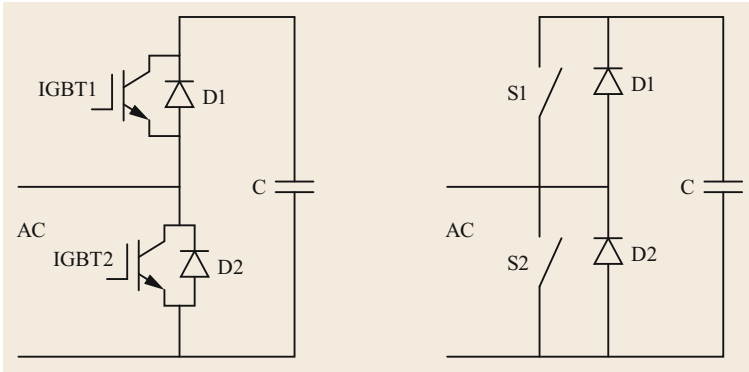
The reactive power is defined by the converter voltage magnitude ( $U_{con(i)}$ ).

### 12.6.3 Modular Multilevel Converter

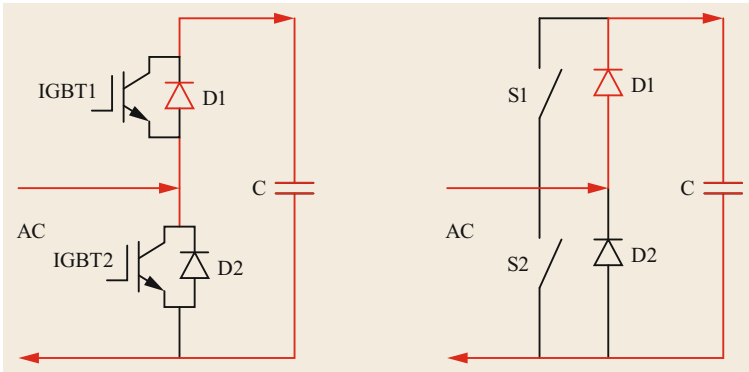
Although the solution discussed above certainly works, converter losses are high due to the switching losses from the IGBTs at a PWM frequency of 1260 Hz (using the Cross-Sound Cable project as an example). However, in 2006, the modular multilevel converter (MMC) was introduced. The advantages of the MMC are as follows [12.26, 27]:

- Low converter losses as there is no high-frequency switching
- No AC filter requirements
- Low  $dv/dt$  upon switching due to small switching steps.

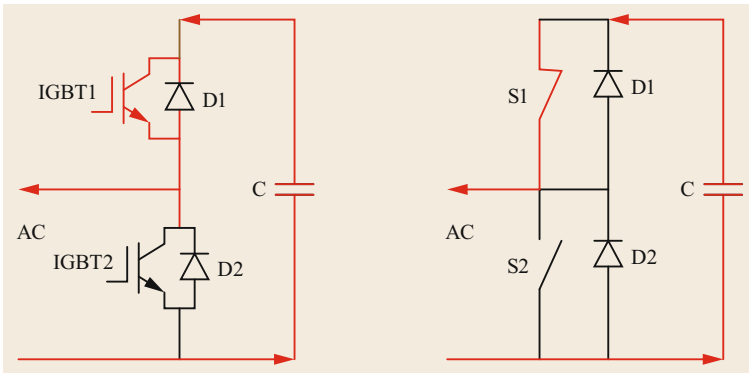
The smallest block in a MMC configuration, which is referred to as a submodule (Fig. 12.57), contains two main components:



**Fig. 12.57** MMC submodule (half bridge)



**Fig. 12.58** IGBT1 and IGBT2 in the off state

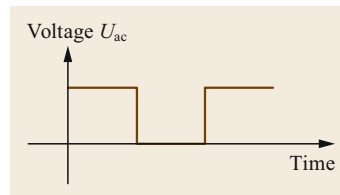


**Fig. 12.59** IGBT1 triggered into conduction

- A DC capacitor
- Two IGBTs connected across the capacitor.

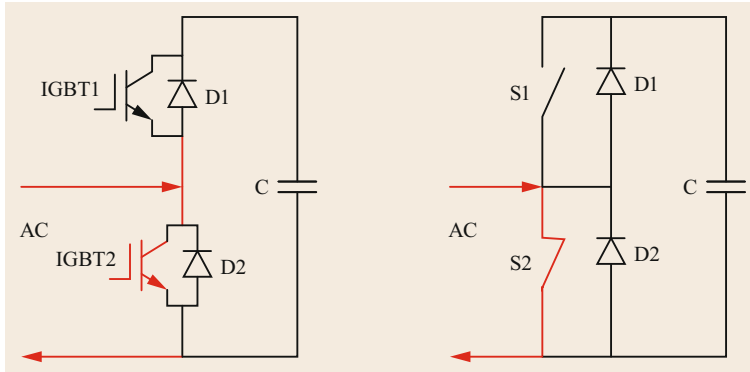
The AC connection is located at the midpoint of the two IGBTs, IGBT1 and IGBT2, which are similar to the controlled switches S1 and S2. When IGBT1 and IGBT2 are in the off state, capacitor C is charged through diode D1, as shown in Fig. 12.58.

When IGBT1 is triggered into conduction (similar to S1 being closed), capacitor C will discharge through IGBT1 to the AC side, as shown in Fig. 12.59.



**Fig. 12.60** AC voltage using a MMC

The resulting AC voltage is as shown in Fig. 12.60. Basically the output voltage consists of many capacitor voltages inserted when IGBT1 is conducting.

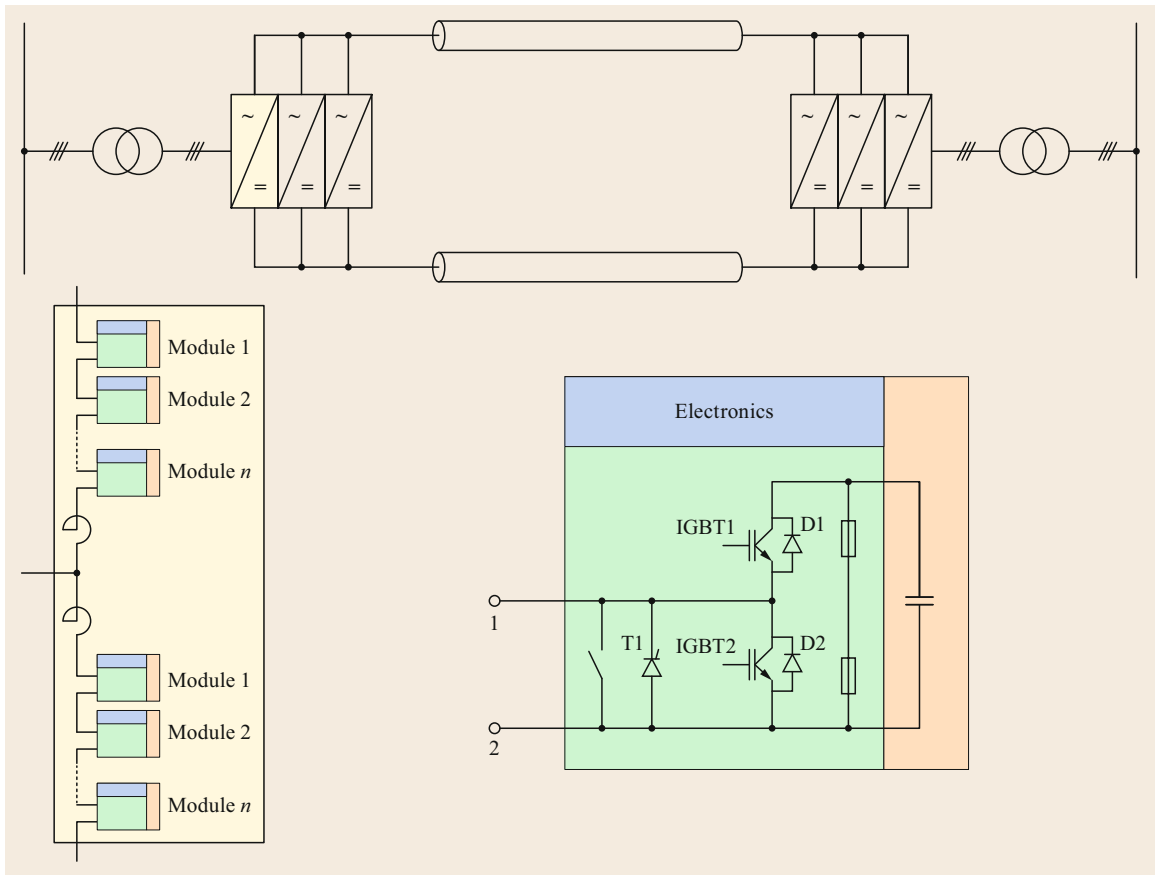


**Fig. 12.61** IGBT2 triggered into conduction

If IGBT2 is switched on (i.e., switch S2 is closed), then the submodule is bypassed and no voltage builds up on the capacitor, as shown in Fig. 12.61.

It is important to define the terminology of a multi-module VSC:

- A *submodule* is the smallest single phase unit; it consists of two IGBTs and their associated equipment
- A *phase module* is obtained by connecting  $N$  sub-modules in series along with one phase reactor to form either the positive or the negative side of an AC phase, as shown in Fig. 12.62
- A *phase arm* is obtained when two phase modules are connected to obtain a complete phase, as shown in Fig. 12.63
- A *converter* comprises of three phase arms.



**Fig. 12.62** MMC concept (© Siemens)



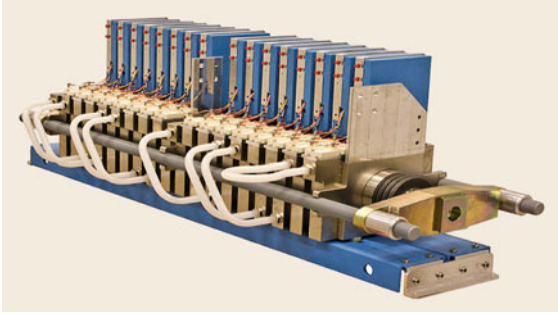


Fig. 12.63 Power module (courtesy of ABB) [12.28]



Fig. 12.64 VSC converter (courtesy of Siemens)

Some photos of physical parts of a VSC converter are depicted in Figs. 12.63 and 12.64.

If more than one submodule, for example  $N$  submodules, are connected in series, then each submodule can be either:

- Off, where IGBTs 1 and 2 are both in the off state
- On, where IGBT1 is conducting (on state) and the capacitor voltage is applied at the terminals
- Bypassed, where IGBT2 is conducting (on state).

In principle, a voltage is generated in steps (which depend on the number of submodules connected in series and the individual status of each submodule) at the terminals of the phase arm. The switching process of a submodule is not performed at high frequency, so the switching losses of the IGBTs are reduced, as are the total losses of the converter. Figure 12.65 shows the resulting waveform of the MMC VSC converter. From the VSC electrical scheme, it is apparent that the phase voltages are built from the positive and negative terminals with the addition of a variable source, the capacitor voltages (Fig. 12.65). Increasing the number of capacitors leads to a better and smoother AC waveform.

A back-to-back VSC converter is shown in more detail in Fig. 12.66. In Fig. 12.66a the single line diagram of the back-to-back system is shown. In the Fig. 12.66b the back-to-back alone is shown with the details of the modules. The positions of the switches at a particular instant are presented in Fig. 12.67. Note that six arms with six capacitors per arm are depicted in Fig. 12.67. Some capacitors are inserted and some are bypassed. Taking as an example the two arms in series on the right-hand side of Fig. 12.68, it is clear that the voltage  $V_c$  is obtained through both arms: one (the lower arm) includes half the DC voltage plus the voltage of six capacitors and the other (the upper arm) includes half of the DC voltage plus the voltage of zero capacitors.

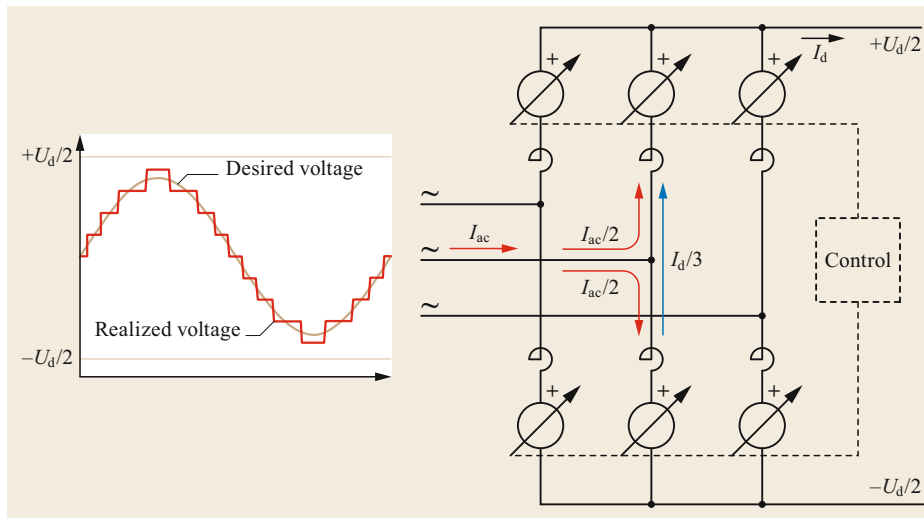


Fig. 12.65 Overview of the MMC concept by CIGRE [12.29]

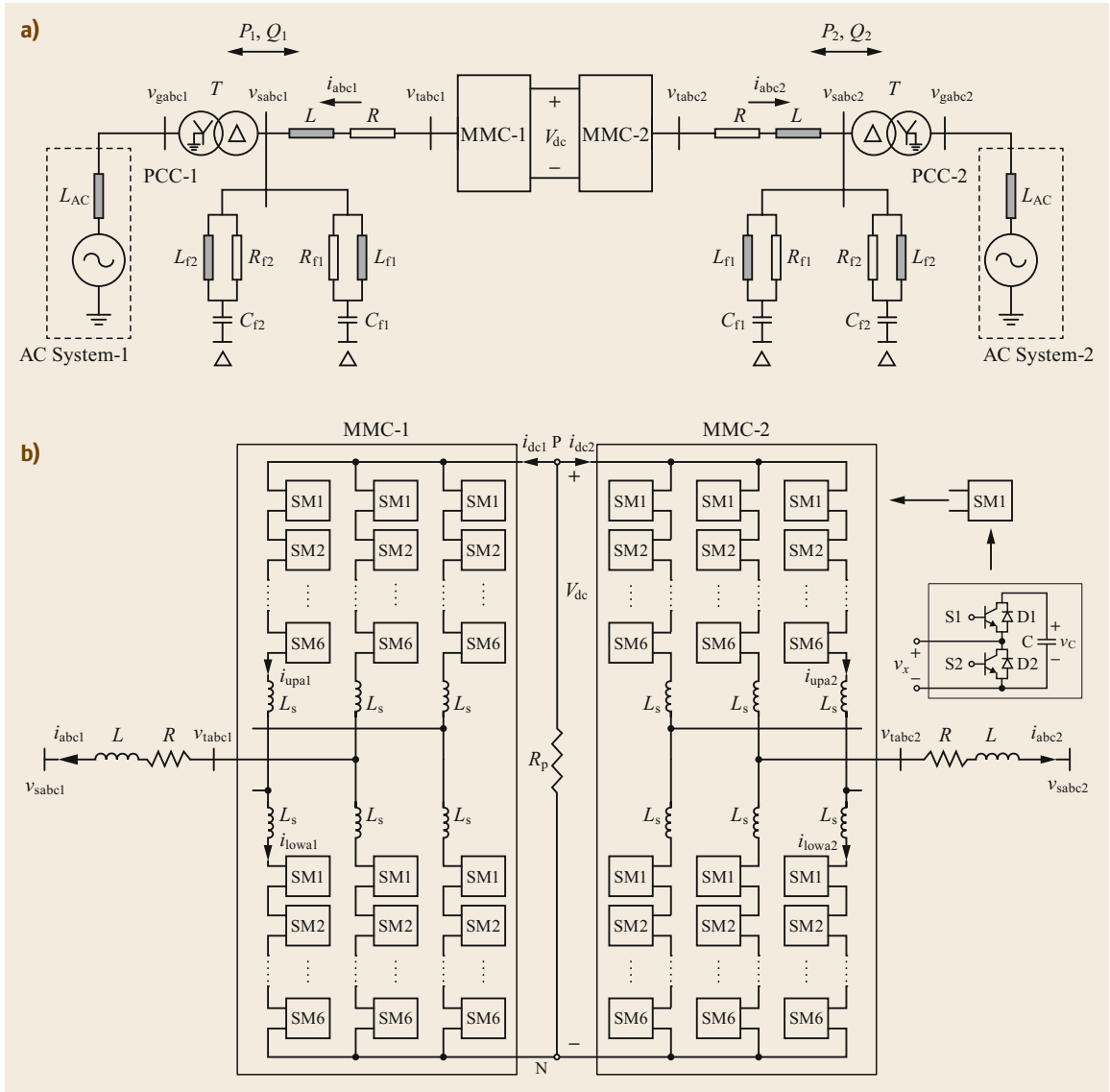


Fig. 12.66a,b Back-to-back VSC [12.27]

Therefore,

$$V_{tc} = -\frac{V_{dc}}{2} + nlV_{cap} = \frac{V_{dc}}{2} - nuV_{cap} ,$$

where  $nl$  and  $nu$  are the number of capacitors in the lower and upper arms, respectively.

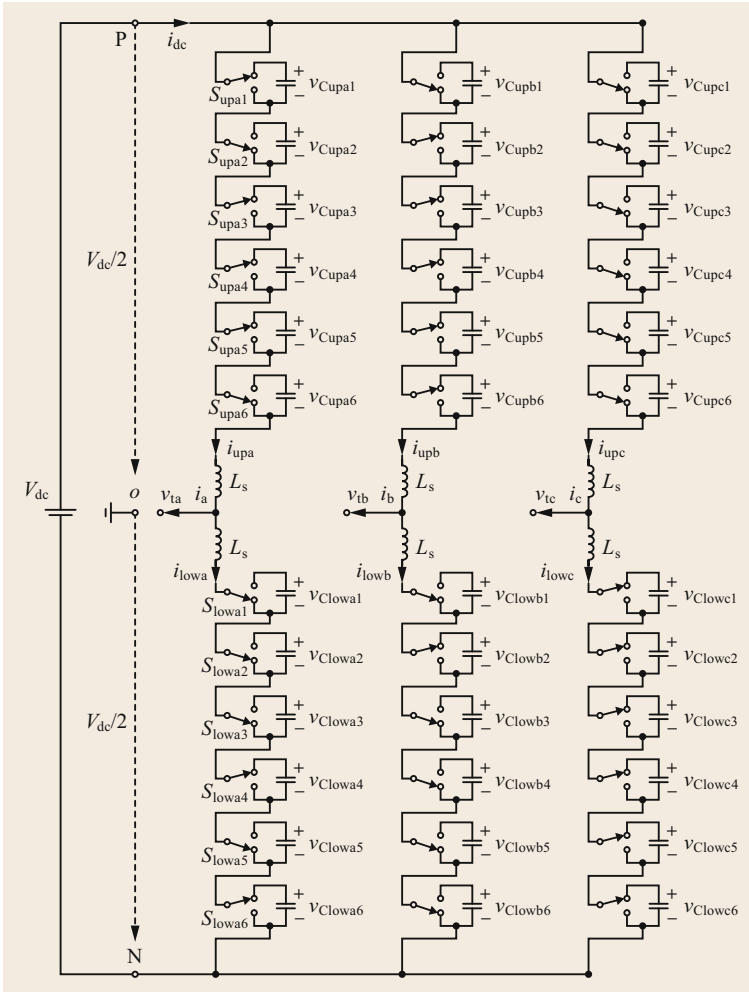
Note that Fig. 12.67 indicates that there are  $nl + nu = 6$  voltage components in each of the three voltage pass. The voltage of each capacitor is  $V_{dc}/6$ .

### 12.6.4 Active and Reactive Power Control

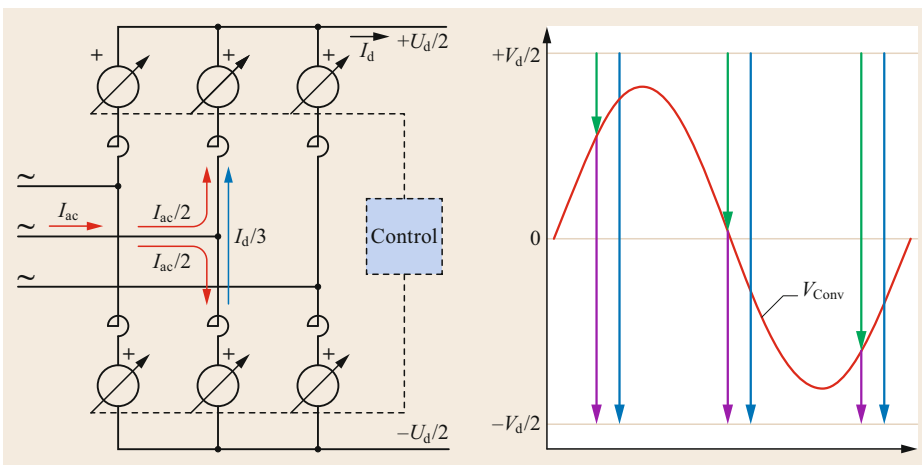
As mentioned earlier, a VSC converter can independently control active and reactive power and exchange them with the AC system (Fig. 12.69) [12.23].

The converter can control the output power by modifying the magnitude and phase of the generated voltage.

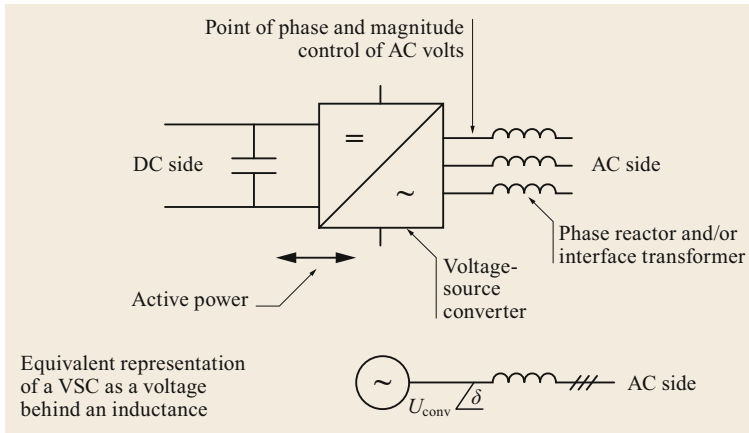
The VSC can control the active power or  $U_d$  using  $\delta$  or the AC voltage, and the reactive power can be controlled via  $\lambda$  (Figs. 12.70 and 12.71).



**Fig. 12.67** Positions of the switches in a MMC at a specific instant [12.27]



**Fig. 12.68** Voltage build-up



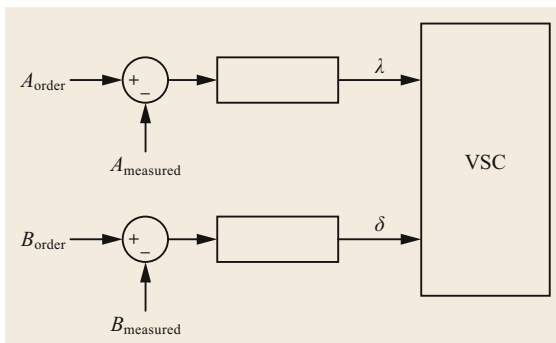
**Fig. 12.69** Converter control components [12.23]

Consider a VSC converter that has an output of  $U_C$  (or  $U_{conv}$  in Fig. 12.55) and is connected through an impedance  $X$  to the AC system. This converter will supply or absorb reactive power based on whether the converter voltage  $U_C$  is higher or lower than the system voltage  $U_S$  (or  $U_L$  in Fig. 12.55), as shown in Figs. 12.72, 12.73, and 12.74.

The active power is a function of the angle  $\delta$  between the converter voltage  $U_C$  and the system voltage  $U_S$ , as shown in Figs. 12.75 and 12.76.

### 12.6.5 Full-Bridge Converter

In the preceding discussion, the converter was arranged in a half-bridge configuration. Such an arrangement works adequately in most VSC applications, but in a bipolar DC system configuration, where there is a ground connection on the DC side, large short-circuit currents are driven to the DC side through the diodes during a DC-side ground fault (similar to a pole-to-pole fault in a symmetrical monopole). Such currents can-



**Fig. 12.70** Direct control of  $\lambda$  and  $\delta$  using parameters  $A$  and  $B$  [12.23]

not be controlled by a half-bridge converter, so a full-bridge converter (see Fig. 12.77) can be utilized instead. In a full-bridge converter, the current can be controlled in four quadrants, as shown in Fig. 12.78. The AC side voltage of the full bridge is basically symmetrical, as shown in Fig. 12.78.

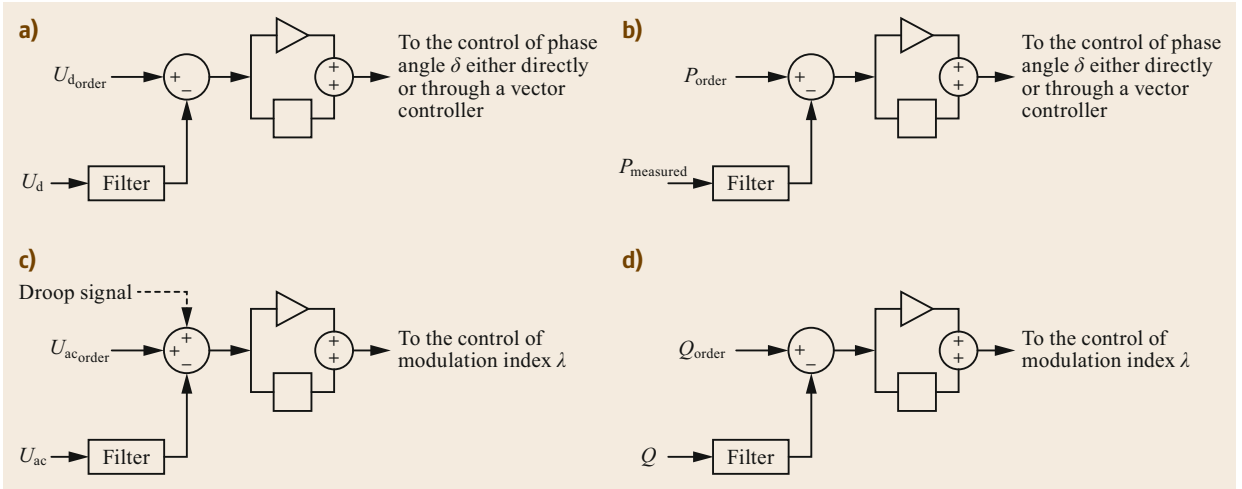
During a DC fault (pole to ground in a bipolar system or pole to pole in a symmetrical monopole system), the module capacitors in both half- and full-bridge converters can discharge, producing very large DC currents. The rate of change in these currents can be very large, so fast detection and interruption of fault currents is needed to protect converters. Fast detection of DC faults is possible by measuring the rates at which DC currents and voltages increase. Once a fault has been detected, the fault currents can be interrupted in several ways in full-bridge MMC converters [12.30].

#### DC Fault Current Interruption Through Blocking

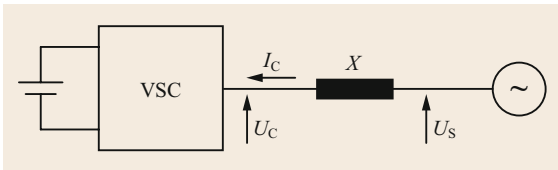
The most popular DC fault-current interruption mechanism used in full-bridge MMC converters is blocking. As soon as the converter is blocked, all of the converter module capacitors are inserted via freewheeling diodes in the direction opposite to that of the fault current. This can momentarily yield voltages of opposite polarity that are more than 2 p.u. at the faulted DC pole, which quickly reduce the fault current.

#### Active DC Fault Current Control

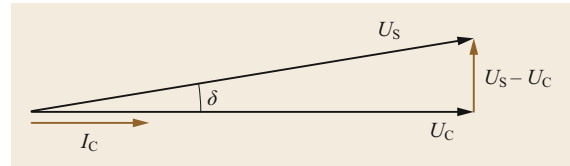
One of the main advantages of full-bridge converters over half-bridge converters is the ability to control both the AC internal voltage and the DC voltage independently (i.e., an extra degree of freedom) over the full range of DC voltages. If required, the DC pole voltage can be instantly reversed by inserting the modules in the opposite direction while maintaining the AC voltage.



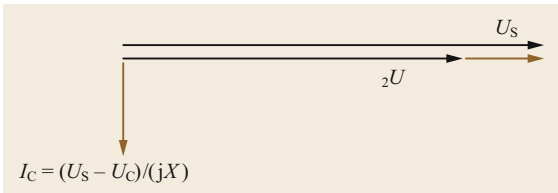
**Fig. 12.71a-d** VSC controller. (a) DC voltage controller, (b) active power controller, (c) AC voltage controller, (d) reactive power controller [12.23]



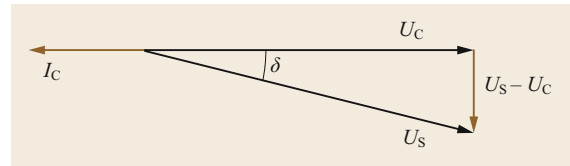
**Fig. 12.72** Single-line scheme



**Fig. 12.75** The converter is absorbing active power



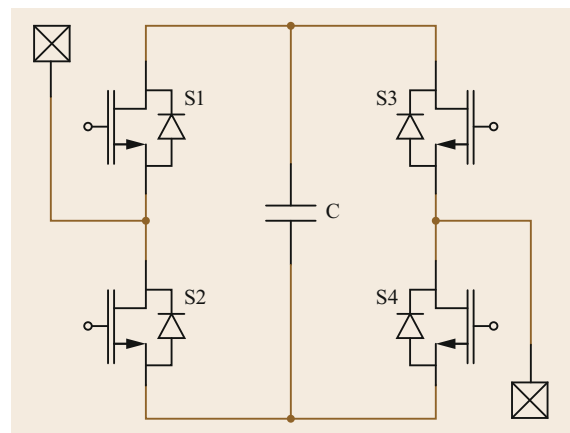
**Fig. 12.73**  $U_s > U_c$ : the converter is absorbing reactive power



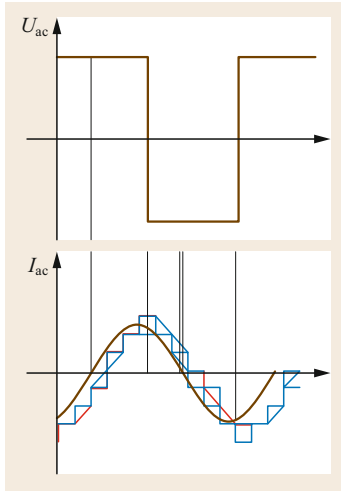
**Fig. 12.76** The converter is supplying active power



**Fig. 12.74**  $U_s > U_c$ : the converter is supplying reactive power



**Fig. 12.77** Full-bridge converter



**Fig. 12.78**  
Current path in four quadrants

- It can be built from half-bridge converters, as described earlier. It can be also constructed with full-bridge converters, although there is no technical advantage to doing so if it is a cable-based application (the probability of a pole-to-pole fault is small).
- Since the system is floating with no intentional ground connection in a symmetrical monopole, the DC voltages of the two poles may drift. However, leakage currents due to the high resistance to ground (e.g., the DC voltage dividers) on the DC side prevent excessive DC voltage drift.
- Another approach that is used to address the problem is to connect a high impedance (a reactor plus a resistor) between the transformer and the converter at one station, as shown in Fig. 12.80. Under normal conditions, the current in the L1 reactor is negligible. The stress during a DC-side ground fault should be considered when selecting R2 (Fig. 12.80).

### 12.6.6 Symmetrical Monopole

The symmetrical monopole (Fig. 12.79) is one of the configurations used in VSC converters.

In this configuration, the VSC converter is connected to the positive and negative poles but not to ground. The main features of this configuration are as follows:

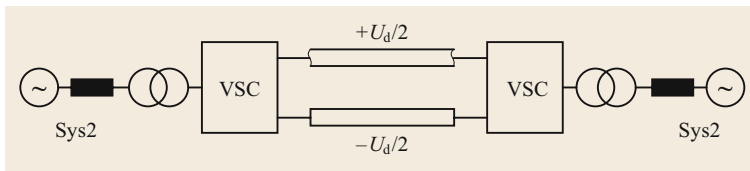
- The transformer is not exposed to DC voltage, so it is a regular AC power transformer.
- It is implemented with two XLPE cables in most applications.
- A DC ground fault does not result in short-circuit currents, but it does expose the healthy pole to very high voltages that can be as high as twice the rated voltage.
- There is no power transfer during any outage.

### 12.6.7 Bipolar Arrangement

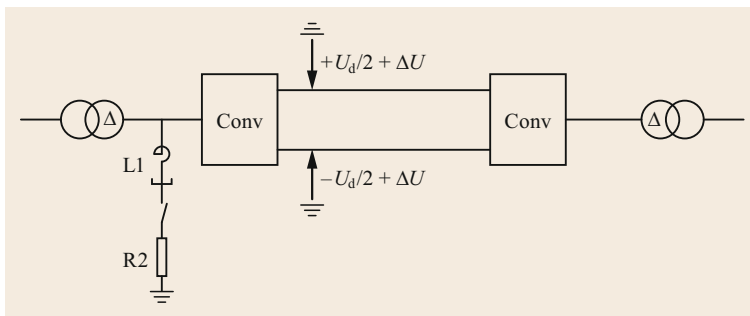
In a bipolar arrangement, just as in a LCC, there are two independent poles arranged in a bipolar configuration with either a ground return or a dedicated metallic return (Fig. 12.81).

In a bipolar arrangement:

- The transformer is a converter transformer subjected to DC stress.
- A ground fault on the DC side is characterized by high short-circuit currents that impact the AC system. These occur because, in addition to the DC current, an AC current component feeds the fault through the diodes from the AC side.



**Fig. 12.79** Symmetrical monopole



**Fig. 12.80** Control of voltage drift

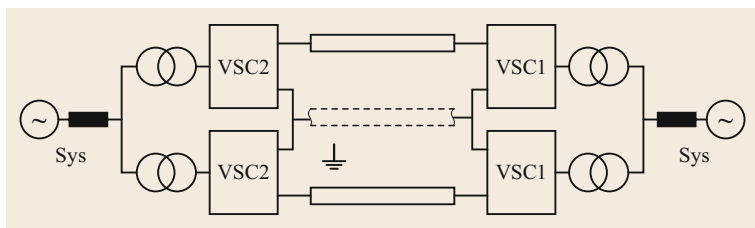


Fig. 12.81 Bipolar arrangement

- Half-bridge or full-bridge converters can be utilized. However, in the event of a DC-side fault in either the cable or the overhead transmission line, a half-bridge converter requires the breaker on the AC side to be tripped. This is not a problem if cable-based transmission is used. However, in the case of an overhead line (which can frequently suffer weather-induced DC line faults), AC breaker tripping is problematic. This is because a restart is performed following a DC line deionization period in HVDC. A full-bridge converter is capable of deionizing the DC line without the need to trip the AC circuit breaker.

### 12.6.8 Converter Charging

In a typical MMC, the capacitors and (if present) DC cables are charged through the diodes before the converter is started. The capacitors and the cables are charged as soon as the AC breaker is closed. A preinsertion resistor (charging resistor) is utilized to limit the charging current. When a half-bridge converter is used, the capacitors and the cables are charged to approximately the peak of the line-to-line-to-line voltage.

## 12.7 DC Grid

As converter technologies (especially MMC technology) are now mature, researchers are considering a configuration in which converters are connected via a meshed grid. This would increase the reliability of the HVDC transmission system. Studies of this configuration have been carried out by CIGRE, which has created specific working groups to discuss issues such as:

- HVDC feasibility [12.31]
- The preparation of connection agreements or grid code for multiterminal schemes and DC grids [12.32]
- The development of HVDC converter models for a HVDC grid [12.33]
- Control methodologies for direct voltage and power flow in a meshed HVDC grid [12.34]
- Protection and local control of DC grids [12.35]
- The design of HVDC grids for optimal reliability and availability performance [12.36].

The aim is to bring knowledge of DC grid technology up to the same level as that for AC grids.

Figure 12.82 shows an example of the CIGRE test system, which integrates offshore and onshore renewable generation into AC power systems [12.33].

The test system consists of two onshore and four offshore AC networks (the buses labeled Ba) and three DC systems (DCS1, DCS2, and DCS3). System DCS1

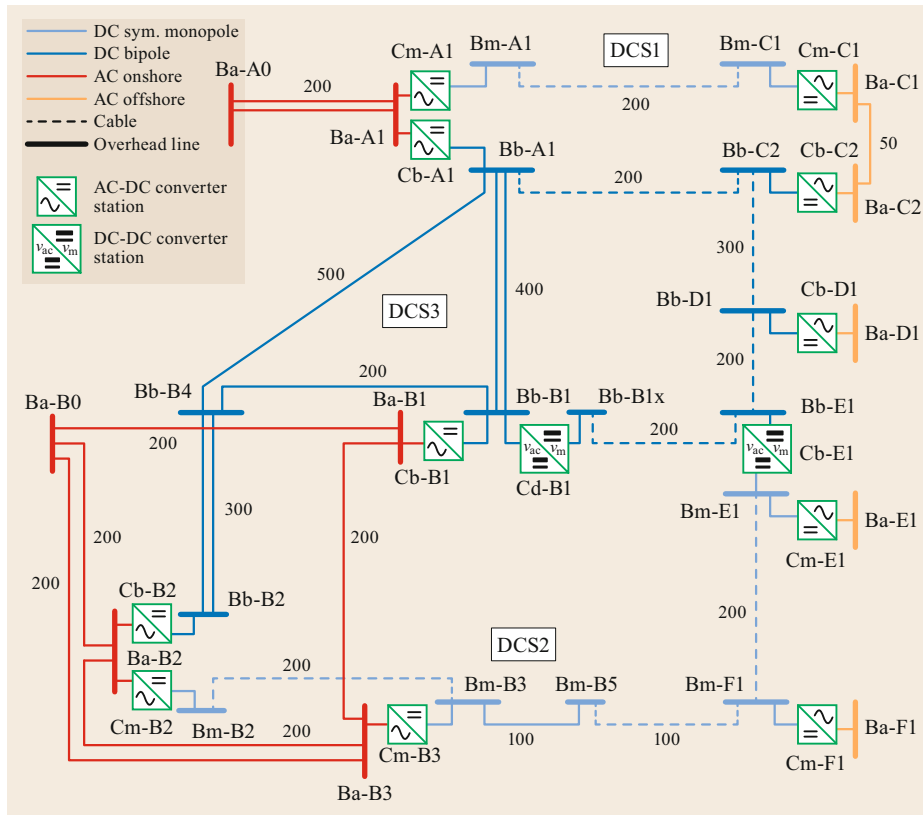
utilizes point-to-point cable transmission,  $\pm 200$  kV, and employs a symmetrical monopole configuration. System DCS2 is a  $\pm 200$  kV multiterminal system with symmetrical monopoles. System DCS3 is a DC meshed grid,  $\pm 400$  kV, that uses a bipolar configuration, overhead lines, and cables.

There are many VSC AC/DC converters and two DC/DC converters in the test system. One of the DC/DC converters (Cd-B1) causes small changes in the Bb-B1x bus to control the power in the Bb-B1x to Bb-E1 circuit. The other DC/DC converter (Cd-E1) connects the 400 and 200 kV DC systems.

In a symmetrical monopole configuration, the need for or the occurrence of an outage in one pole (converter or line) causes both poles to disconnect. In a bipolar configuration, the system can remain in operation with only one pole; this type of operation is usually termed an asymmetrical configuration.

The interconnection of systems (AC and DC) is achieved through converters (controllable devices), which allows the systems to be independent. Therefore, the power flow can be calculated separately for each system.

There are many challenges that must be overcome in order to develop a system like the one described. For instance, as of 2018, the capacity of a VSC was below 2000 MW, whereas the capacity of a LCC was about 6000 MW at  $\pm 800$  kV. Also, a DC cable with ethylene-



**Fig. 12.82** CIGRE DC grid test system [12.33]

propylene-rubber (EPR) insulation is limited to 320 kV, although 500 kV cables may become available soon. Indeed, some 500 kV high-capacity oil-filled cables are already on the market.

DC/DC converters (buck–boost configuration) are in use in industrial systems with low power ratings. The use of a combination of components (DC/AC converter, transformer, and AC/DC converter) in DC/DC converters such as Cd-E1 has been proposed. The transformer may be single-phased and designed for a specific frequency (not necessarily 50 or 60 Hz).

The main challenge, however, is to develop fast-acting DC breakers. Some engineers believe that, if the transient current capability of an IGBT is taken into account, the fault clearing time (i.e., the time from the instant the fault is detected until the current is interrupted) should be less than about 5 ms to avoid system collapse. A protection relay in an AC system can detect a fault in 8–15 ms, and the breaker will open in about 20–40 ms. Thus, new devices (based on power electronics) will need to be developed for DC grid applications [12.31].

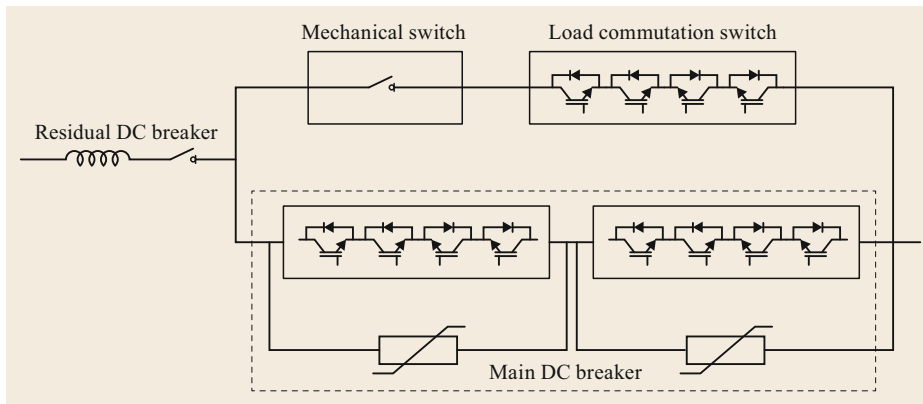
Some manufacturers have, however, developed prototypes of a hybrid DC breaker; see, for example, Fig. 12.83. During steady-state operation, the mechanical and load commutation switches are closed. When

a fault is detected, the commutation switch opens and the current is rerouted to the main DC breaker. The mechanical switch also opens (there is no arcing). The main breaker then trips and the current is rerouted to the varistor branch. The current decreases to zero and the residual DC breaker is opened. To reconnect the line, the reverse procedure is carried out. Note that mechanical and load commutation switches are also employed to reduce losses, which are high in the main circuit breaker.

Other manufacturers believe that for DC grid applications, a full-bridge architecture must be used in the VSC. A half-bridge architecture is generally used in the bipolar configuration. When a pole-to-ground fault occurs, the short-circuit current circulates through the diodes (see Fig. 12.57), which may damage the converter. In a point-to-point transmission system, this threat (damage) is prevented by opening the AC breaker sufficiently rapidly (this approach is used in the Caprivi Link HVDC Scheme). Although the use of the full-bridge architecture may result in greater reliability, it is also more expensive.

One of the CIGRE working groups (B4-72) is considering possible applications of DC grids and is producing benchmark models that include VSCs, LCCs, breakers, and other related devices.





**Fig. 12.83** Hybrid DC breaker

Finally, it is important to mention that the increasing generation of renewable energy will have an impact on new HVDC systems. Some wind power plants (specifically those that use type 4 wind turbines) employ the full converter architecture to connect them to AC feeders. Photovoltaic power plants generate DC voltage and are connected to AC feeders through inverters. In

all of these cases, a voltage and frequency transient ride-through capability is required, and this is easily obtained with VSC converters. Offshore wind farms located far (e.g., 100 km) from the shore must be connected to the grid via DC cables.

All of these factors will enhance the application of DC grids in a meshed configuration.

## 12.8 Future Trends

As discussed above, future developments in this field are likely to include (among others):

- EPR insulated cables with a voltage rating of 500 kV or more.
- VSCs with high power rating capacities.
- The development of economic full-bridge converters.
- The development of fast DC circuit breakers based on power electronics.
- Offshore DC grids. When developing an offshore DC grid, it is important to identify the required converter characteristics, determining the operating points, DC voltage level, amount of reserve, DC grid fault behavior, type of testing, and the DC grid behavior during AC faults.

## 12.9 Further Reading

- M. Erimia, C.C. Liu, A.A. Edris: *Advanced Solutions in Power Systems* (Wiley-Blackwell, New York 2016)
- CIGRE TB 590: *Protocol for Reporting the Operational Experience of HVDC Transmission Systems* (CIGRE, Paris 2014)
- CIGRE TB 675: *General Guidelines for HVDC Electrode Design* (CIGRE, Paris 2017)
- CIGRE TB 508: *HVDC Environmental Planning Guidelines*, WG B4-44 (CIGRE, Paris 2012)
- CIGRE TB 536: *Influence of Embedded HVDC Transmission on System Security and AC Network Performance* (CIGRE, Paris 2013)
- CIGRE TB 97: *System Tests for HVDC Installations* (CIGRE, Paris 1995)
- CIGRE TB 609: *Study of Converter Transients Imposed on the HVDC Converter Transformers* (CIGRE, Paris 2015)
- CIGRE TB 583: *Guide to the Conversion of Existing AC Lines to DC Operation* (CIGRE, Paris 2014)
- CIGRE TB 202: *HVDC Station Audible Noise*, WG 14.26 (CIGRE, Paris 2002)
- CIGRE TB 536: *Influence of Embedded HVDC Transmission on System Security and AC Network Performance* (CIGRE, Paris 2013)
- CIGRE TB 113: *Test Circuits for HVDC Thyristor Valves* (CIGRE, Paris 1997)
- CIGRE TB 649: *Guidelines for Life Extension of Existing HVDC Systems* (CIGRE, Paris 2016)

- CIGRE TB 127: *Guide for Upgrading Transmission Systems with HVDC Transmission* (CIGRE, Paris 1998)
- D. Wu, U. Astrom, L. Arevalo, R. Montano, B. Jacobson: *Selection Between Indoor or Outdoor DC Yards*, Paper B3-115 (CIGRE, Paris 2014)
- CIGRE TB 447: *Components Testing of VSC Systems for HVDC Applications*, WG B4.48 (CIGRE, Paris 2010)
- S. Johansson, G. Asplund, E. Jansson, R. Rudervall: *Power System Stability Benefits with VSC DC-Transmission Systems*, Paper B4-204 (CIGRE, Paris 2004)
- M. Hyttinen, J.O. Lamell, T. Nestli: *New Application of Voltage Source Converter (VSC) HVDC to be Installed on the Gas Platform Troll A*, Paper B4-210 (CIGRE, Paris 2004)
- P. Sorensen, B. Franzen, J.D. Wheeler, R.F. Bonchang, C. Barker, R. Preedy, M. Baker: *Konti-Skan I HVDC Pole Replacement*, Paper B4-207 (CIGRE, Paris 2004)
- P. Esmeraldo, E. Araujo, D. Souza, D. Menzies, L. Carijo, M.G. Sereno, N. Macedo, S. Vidigal, A. Leite, A.R.C.D. Carvalho, V. Simões: *Feasibility Studies for Madeira Transmission System Technical and Economic Analysis*, Paper B4-103 (CIGRE, Paris 2008)
- J.P. Kjaegaard, C. Rasmussen, K. Sobrink, J. Nacker, R. Rossel, E.M. Leutner, S. Nyberg: *The New Storebaelt Project for Interconnecting Eastern and Western Denmark*, Paper B4-104 (CIGRE, Paris 2008)
- M. Haeusler, H. Huang, K. Papp: *Design and Testing of 800 kV HVDC Equipment*, Paper B4-115 (CIGRE, Paris 2008)
- E. Stern, J. Nash, C. Schoeniger, C. Bartzsch, G. Acquavotta, M. Bacchini, A. Orini: *The Neptune Regional Transmission System 500 kV HVDC Project*, Paper B4-118 (CIGRE, Paris 2008)
- D. Trainer, C. Davidson, C.D. Oates, N.M. Macleod, D.R. Critchley, R.W. Crookes: *A New Hybrid Voltage Sourced Converter for HVDC Power Transmission*, Paper B4-111 (CIGRE, Paris 2010)
- S. Dodds, B. Railing, K. Akman, B. Jacobson, T. Worzyk, B. Nilsson: *HVDC VSC (HVDC Light) Transmission-operating Experiences*, Paper B4-203 (CIGRE, Paris 2010)
- J. Prieto, R. Grandino, C. Velazquez, C. Gaebler, E. Betten, G. Curtotti, H. Weinkauff, S. Achenbach, A. Galarza: *The Romulo Project, Spanish Peninsula-Mallorca (243 Km, 250 kV, 2X200 MW): First Spanish HVDC Link*, Paper B4-204 (CIGRE, Paris 2010)
- N. Macleod, S. Chackravorty, B.T. Barrett: *Design Studies for the 3150 MW,  $\pm 600$  kV UHVDC Bipole 2 of the Rio Madeira Long Distance Transmission Project in Brazil*, Paper B4-208 (CIGRE, Paris 2010)
- D. Jacobson, P. Wang, C. Karawita, R. Ostash, M. Mohaddes, B. Jacobson: *Planning the Next Nelson River HVDC Development Phase Considering LCC vs. VSC Technology*, Paper B4-103 (CIGRE, Paris 2012)
- T.D. Ingemansson, T. Kiiveri, H. Nurminen, B. Pajarvi, K.G. Dannielsson: *New Fenno-Skan HVDC Pole with an Upgrade of the Existing Fenno-Skan I Pole*, Paper B4-105 (CIGRE, Paris 2012)
- J. Graham, T. Holmgren, P. Fischer, N.L. Shore: *The Rio Madeira System-Design Aspects of Bipole I and the Connector to Acre-Rondonia*, Paper B4-111 (CIGRE, Paris 2012)
- L. Zehong, G. Liying, W. Zuli, Y. Jun, Z. Jin, L. Licheng: *R&D Progress of  $\pm 1100$  kV Technology*, Paper B4-201 (CIGRE, Paris 2012)
- C. Barker, C. Davidson, D. Trainer, R. Whitehouse: *Requirements of DC-DC Converters to Facilitate Large DC Grids*, Paper B4-204 (CIGRE, Paris 2012)
- V. Hussennether, J. Rittiger, A. Barth, D. Worthington, G. Dell'Anna, M. Rapetti, B. Huehnerbein, M. Siebert: *Projects BorWin2 and HelWin I—Large Scale Multilevel Voltage Sourced Converter Technology for Bundling of Offshore Wind Power*, Paper B4-306 (CIGRE, Paris 2012)
- E.W. Kimbark: *Direct Current Transmission*, Vol. I (Wiley, Chichester 1971)

## References

- |                                                                                                                                                                                                                                                                                                                                                                                                                                                                                |                                                                                                                                                                                                                                                                                                                                                                                                                                          |
|--------------------------------------------------------------------------------------------------------------------------------------------------------------------------------------------------------------------------------------------------------------------------------------------------------------------------------------------------------------------------------------------------------------------------------------------------------------------------------|------------------------------------------------------------------------------------------------------------------------------------------------------------------------------------------------------------------------------------------------------------------------------------------------------------------------------------------------------------------------------------------------------------------------------------------|
| <p>12.1 R. Nayak, R.P. Sasmal, Y.K. Sehgal, M. Rashwan, G. Flisberg: <i>Technical Feasibility and Research &amp; Development Needs for <math>\pm 1000</math> kV and Above HVDC System</i>, Paper B4-105 (CIGRE, Paris 2010)</p> <p>12.2 J. Arrillaga: <i>High Voltage Direct Current Transmission</i>, IET Power Series, Vol. 29, 2nd edn. (IET, London 2008)</p> <p>12.3 CIGRE TB 388: <i>Impacts of HVDC Lines on the Economics of HVDC Projects</i> (CIGRE, Paris 2009)</p> | <p>12.4 CIGRE B4-132: <i>Design Consideration Associated with DoIWin3 and Evolution of GE's Grid Solutions Business VSC Solution</i> (CIGRE, Paris 2016)</p> <p>12.5 CIGRE TB 619: <i>HVDC Connection of Offshore Wind Power Plants</i> (CIGRE, Paris 2015)</p> <p>12.6 W. Breuer, V. Hartmann, D. Povh, D. Retzmann, E. Telsch: <i>Application of HVDC for Large Power System Interconnection</i>, Paper B4-106 (CIGRE, Paris 2004)</p> |
|--------------------------------------------------------------------------------------------------------------------------------------------------------------------------------------------------------------------------------------------------------------------------------------------------------------------------------------------------------------------------------------------------------------------------------------------------------------------------------|------------------------------------------------------------------------------------------------------------------------------------------------------------------------------------------------------------------------------------------------------------------------------------------------------------------------------------------------------------------------------------------------------------------------------------------|

- 12.7 CIGRE TB 417: *Technological Assessment of 800 kV HVDC Applications*, WG B4-45 (CIGRE, Paris 2010)
- 12.8 CIGRE TB 215: *HVDC Converter Stations for DC Voltages Above +/- 600 kV*, WG B4-32 (CIGRE, Paris 2002)
- 12.9 R. Adapa, N. Hingorani, S. Maruvada, M. Szechtman, M. Rashwan, R. Nayak: *Revised Needs for UHVDC at 800 kV and Above*, Paper B4-114 (CIGRE, Paris 2008)
- 12.10 E. Uhlman: *Power Transmission by Direct Current* (Springer, Berlin, Heidelberg 1975)
- 12.11 A. Kumar, V. Lescale, L.E. Juhlin, R.K. Chauhan: *Concept to Design—Multiterminal at 800 kV HVDC:NER/ER-NR/WR Interconnector-I Project in India*, Paper B4-103 (CIGRE, Paris 2010)
- 12.12 CIGRE TB 92: *DC Side Harmonics and Filtering in HVDC Transmission Systems* (CIGRE, Paris 1994)
- 12.13 CIGRE TB 139: *Guide to the Specification and Design Evaluation of AC Filters for HVDC Systems* (CIGRE, Paris 1999)
- 12.14 CIGRE TB 352: *Technical Report Capacitor Commutated Converters HVDC Interconnections Digital Modeling and Benchmark Circuit*, WG B4-34 (CIGRE, Paris 2008)
- 12.15 CIGRE TB 115: *Guide for Planning DC Links Terminating at AC System Locations Having Low Short Circuit Capacity* (CIGRE, Paris 1997)
- 12.16 CIGRE TB 222: *On Voltage and Power Stability in AC/DC Systems* (CIGRE, Paris 2003)
- 12.17 CIGRE TB 364: *Systems with Multiple DC Infeed* (CIGRE, Paris 2008)
- 12.18 CIGRE TB 103: *Commutation Failures Causes and Consequences* (CIGRE, Paris 1995)
- 12.19 P.D. Taylor: *Thyristor Design and Realization* (Wiley, Chichester 1987)
- 12.20 CIGRE TB 136: *Fire Aspects of HVDC Thyristor Valves and Valve Halls* (CIGRE, Paris 1999)
- 12.21 H. Huang: Multilevel voltage source converters for HVDC and FACTS applications. In: *Paper 401* (SC B4 Colloquium, Bergen 2009)
- 12.22 CIGRE B4-302: *The Bimode Insulated Gate Transistor (BIGT), an Ideal Power Semiconductor for Power Electronics Based DC Breaker Applications* (CIGRE, Paris 2014)
- 12.23 CIGRE TB 269: *VSC Transmission Part 1*, WG B4-37 (CIGRE, Paris 2005)
- 12.24 B.D. Railing, J.J. Miller, P. Steckley, G. Moreau, P. Bard, L. Ronstrom, J. Lindberg: *Cross Sound Cable Second Generation VSC Technology for HVDC*, Paper B4-102 (CIGRE, Paris 2004)
- 12.25 I. Mattson, A. Ericsson, B.D. Railing, J.J. Miller, B. Williams, G. Moreau, C.D. Clarke: *Murraylink, the Longest Underground Cable in the World*, Paper B4-103 (CIGRE, Paris 2004)
- 12.26 T. Westerweller, K. Friedrich, U. Armonis, A. Orini, D. Parquet, S. When: *Trans Bay Cable—World's First HVDC System Using Multilevel Voltage-sourced Converter*, Paper B4-101 (CIGRE, Paris 2010)
- 12.27 M. Saeedifard, R. Iravani: Dynamic performance of a modular multilevel back-to-back HVDC system, *IEEE Trans. Power Deliv.* **25**(4), 2903–2912 (2010)
- 12.28 B. Jacobson, P. Karlsson, G. Asplund, L. Harnefors, T. Jonsson: *VSC-HVDC Transmission with Cascaded Two-level Converters*, Paper B4-110 (CIGRE, Paris 2010)
- 12.29 J. Doran, H. Huang, D. Retzmann: *A New Multilevel Voltage Sources Converter Topology for HVDC Applications*, Paper B4-304 (CIGRE, Paris 2008)
- 12.30 C. Karawita, D.H.R. Suriyaarachchi, M. Mohaddes: A controlled DC fault clearance mechanism for full bridge MMC VSC converters. In: *CIGRE Lund Symposium*, ed. by CIGRE (CIGRE, Paris 2015)
- 12.31 CIGRE TB 533: *HVDC Feasibility Study*, WG B4-52 (CIGRE, Paris 2013)
- 12.32 CIGRE TB 657: *Guide Lines for the Preparation of Connection Agreements or Grid Code for Multiterminal Schemes and DC Grids*, WG B4-56 (CIGRE, Paris 2016)
- 12.33 CIGRE TB 604: *Guide for the Development of Models for HVDC Converters in a HVDC Grid*, WG B4-57 (CIGRE, Paris 2014)
- 12.34 CIGRE TB 699: *Control Methodologies for Direct Voltage and Power Flow in a Meshed HVDC Grid*, WG B4-58 (CIGRE, Paris 2017)
- 12.35 CIGRE TB 739: *Protection and Local Control of DC Grids*, WG B4/B5-59 (CIGRE, Paris 2018)
- 12.36 CIGRE TB-713: *Designing HVDC Grids for Optimal Reliability and Availability Performance*, WG B4-60 (CIGRE, Paris 2017)

### Mohamed Rashwan

TransGrid Solutions  
Winnipeg, Canada  
mrashwan@tgs.biz



Mohamed Rashwan is the president of Transgrid Solutions (TGS) and has been involved in numerous HVDC and FACTS projects worldwide, working with utilities, suppliers, and developers. He is a Life Fellow of IEEE and a distinguished member of CIGRE. In 2010 he received the prestigious IEEE HVDC Uno Lamm Award for contributions to the field. Dr. Rashwan is the current chair of CIGRE SC B4 (DC and Power Electronics).

### José A. Jardini

Energy and Automation Department  
Sao Paulo University  
Sao Paulo, Brazil  
jose.jardini@gmail.com



José A. Jardini received a PhD from São Paulo University in 1973. He has worked for Themag Engineering and São Paulo University. His work focuses on power systems and electrical system automation, and he has participated in many important Brazilian AC and DC system studies. He is a Fellow of IEEE and a member of CIGRE, and contributes to the CIGRE Transmission Line and HVDC System Working Group.

# Power System

## 13. Power System Protection

Peter Schegner

A protection system is an essential requirement for the safe and reliable operation of an electric power system. An electric power system is part of an infrastructure that covers a large area and in which faults cannot be avoided in general. The protection system must guarantee that faulty equipment is disconnected from the system as quickly as possible in order to ensure the continued operation of the rest of the electric power system.

At the beginning of this chapter, the general requirements for a selective protection system and its basic concepts are presented. This is followed by a description of the criteria that can be used to detect faults in electric power systems. Current and voltage transformers are required to measure high voltages and currents. The selection and dimensioning of these are described in the following. The basic selective protection functions are explained and their implementation is described in the following section. Additional functions that are used to increase the performance and selectivity of the protection system are also presented. At the end of this chapter, some examples are presented to illustrate the structure of the protection system for selected electric equipment.

13.1	<b>Background</b> .....	975
13.1.1	General Requirements .....	975
13.1.2	General Protection Concepts .....	977
13.2	<b>Protection Criteria</b> .....	979
13.2.1	Electric Protection Criteria .....	979
13.2.2	Nonelectric Criteria .....	985
13.2.3	Notes on Protection Criteria .....	985
13.3	<b>Requirements on Current and Voltage Transformers</b> .....	987
13.3.1	Inductive Current Transformers .....	987
13.3.2	Inductive Voltage Transformers .....	991
13.4	<b>General Protection Functions</b> .....	992
13.4.1	Introduction to Protection Functions ...	992
13.4.2	Overcurrent Protection .....	996
13.4.3	Transformer Differential Protection .....	999
13.4.4	Busbar Differential Protection .....	1003
13.4.5	Distance Protection .....	1006
13.4.6	Additional Functions .....	1011
13.5	<b>Outlook on Protection Systems</b> .....	1012
13.5.1	Changes in the Electrical Power System .....	1012
13.5.2	Technological Drivers .....	1013
13.5.3	General Requirements .....	1013
	<b>References</b> .....	1013

### 13.1 Background

Fault and hazard conditions cannot be avoided in broadly distributed electric power systems, so their impact on the electric power system has to be minimized by using a selective protection system. The essential task of the protection system is to switch off faulty equipment very quickly and selectively [13.1]. The objectives are to significantly reduce the damage to the faulty equipment, to protect equipment exposed to short-circuit currents from overloading, and to ensure the safety of people and animals against step and touch voltages. The protection system must ensure that the fault does not extend and that the function and stability of the entire electric power system are guaranteed.

#### 13.1.1 General Requirements

In addition to the requirements applicable to all technical systems, such as small size, low maintenance, easy operation, and reasonable price, the following additional requirements must be met by protection systems:

##### Selectivity of Protection

According to [13.2], selectivity is the ability of a protection system to identify the faulty section and phase of an electric power system. The term *selectivity* includes the identification of the faulty equipment and its position inside the electric power system, as well as the detailed

state of the fault, characterized by its type and behavior. The requirement for selectivity is of fundamental importance to ensure that only faulty equipment is disconnected from the electric power system and that the actions of the protection system are appropriate for each fault situation.

#### Sufficiently Fast Response Time

The requirement for a sufficiently fast response time of the protection system results from two important facts: on the one hand, the amount of damage depends on the duration of the fault, while on the other hand, the stability of the overall electric power system is also directly affected by the duration of the fault. This applies, for example, to arc faults, which lead to a rapid increase of the temperature in the surroundings of the arc. This may result in an explosion of encapsulated equipment as well as thermal and mechanical overload of all current-carrying components. In addition, loss of stability of generators and other consequences could arise.

When determining the response time, a trade-off must be achieved between technical requirements and economic expenditure. In practice, the response time required for a protection system depends on the electric equipment to be protected, ranging from a few milliseconds (e.g., for trolley wires of electric railways) to a few minutes for overload protection (e.g., for transformers).

#### Reliability of Protection

Reliability is an important feature of any technical system. Commonly, reliability requirements are subdivided into different aspects, as the technical approaches used to improve reliability in different fields can vary greatly and even be contradictory. Often, reliability is divided into dependability and security. In order to increase the dependability (functional reliability), i.e., to reduce the probability of outage of the technical system, several redundant and diverse devices may be operated in parallel at the same time. Finally, a one-of- $n$  decision is implemented. On the other hand, to increase the safety against malfunctions, several devices may be connected in series, meaning that  $n$  devices must reach the same decision to cause a response of the technical system. This illustrates the contradictory solutions to increasing the reliability of any technical system. The objective must be a technically reasonable solution.

The reliability of a protection system is strongly related to the definition of incorrect operation of protection. In [13.2], incorrect operation of protection is defined as the failure to operate or an unwanted operation. Failure to operate means that there is a fault in the

electric power system but the protection system does not operate or misoperates. An unwanted operation of the protection system is the activity of the system during normal network operation or during a fault in the energy system that lies outside the zone of the protection system.

For protection systems, any unnecessary intervention in the form of switching off fault-free primary equipment is an undesirable event. A malfunction, i.e., the misoperation of the protection system during a primary fault, is extremely critical. In any case, the protection system must be, in principle, more reliable than the protected system, i.e., the primary equipment of the electric power system.

#### Accuracy and Sensitivity of Protection

These requirements are related to the implementation of the protection function, including both its measuring accuracy and timing.

The timing is important for the selectivity of the protection system. In modern numerical protective devices, the timing depends only on the runtime of the software. Therefore, nowadays there are in general no timing problems associated with aging of hardware or other environmental effects such as temperature.

However, timing may still vary, even for numerical protective devices. This variation depends on the software implementation and the calculation time of the protection algorithm, which defines the cycle time of the software. These fluctuations should lie in the range of a few milliseconds.

An additional challenge is the measurement accuracy of the protection system. On the one hand, currents in the range of 10% of the rated current have to be measured with high accuracy in order to start, for example, impedance calculations. On the other hand, the short-circuit current could be more than 50 times the rated current, and this high current should also be measured with high accuracy. The measurement range of the current path should be 1–100, with an error below 1%.

Only if these requirements are fulfilled is selective and accurate fault location realizable.

#### Economic Adequacy of Protection

The costs of the protection system must be reasonable in relation to the value and importance of the primary equipment to be protected; for example, the protection system for a low-voltage network with a small number of customers should be simpler and cheaper than the protection system for a transmission transformer. As a rule of thumb, the price of the protection system should lie in the range of 2–5% of the value of the primary equipment.

### 13.1.2 General Protection Concepts

The protection system is part of the secondary equipment of any electric power system. The main parts of the secondary equipment are the control and protection systems [13.3]. One of the special challenges faced by the protection system is that it must function automatically in critical network conditions without support from operating personnel. Furthermore, it is expected that the protection system will work properly even if extreme voltage and current conditions are present in the electric power system.

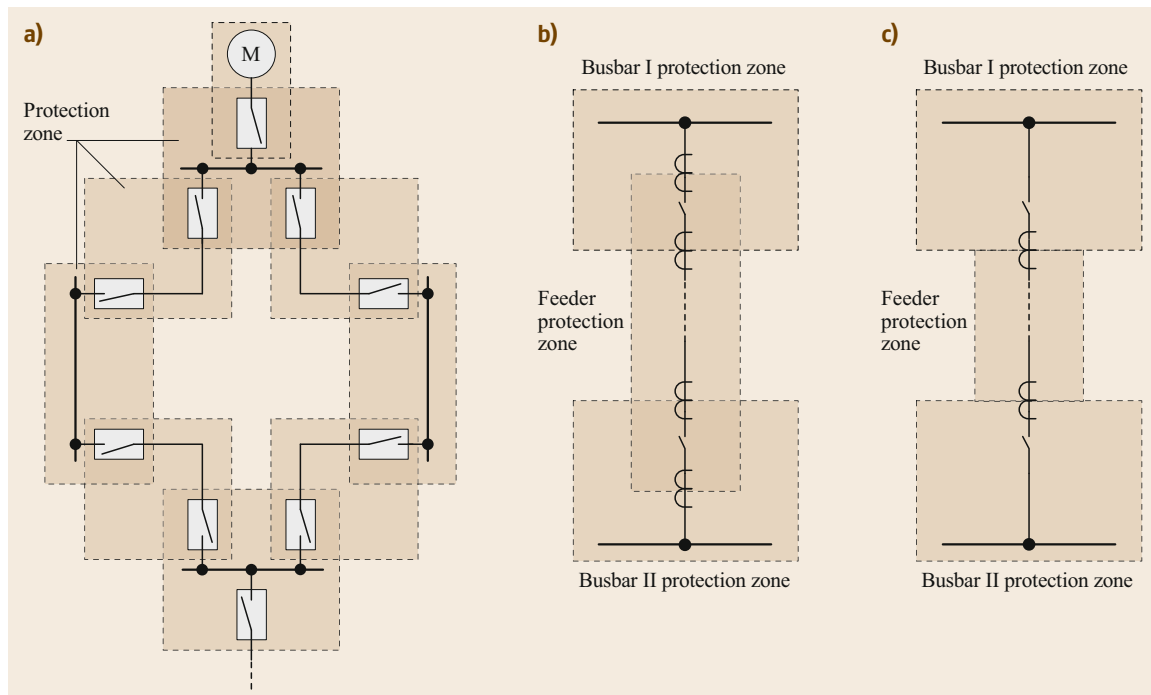
#### Protection Zones

In order to meet the general requirements described above, the entire electric power system is divided into so-called protection zones. Figure 13.1a shows an example of an electric power system, which is divided into several protection zones. The borders of the protection zones are defined by the current measurements, i.e., the position of the current transformers installed in the electric power system. Theoretically, each piece of electric equipment should be assigned to a separate protection zone. Therefore, to achieve overlapping of the protection zones, theoretically, two current measurements should be carried out at the interface between protection zones. This is shown in Fig. 13.1b. However, this

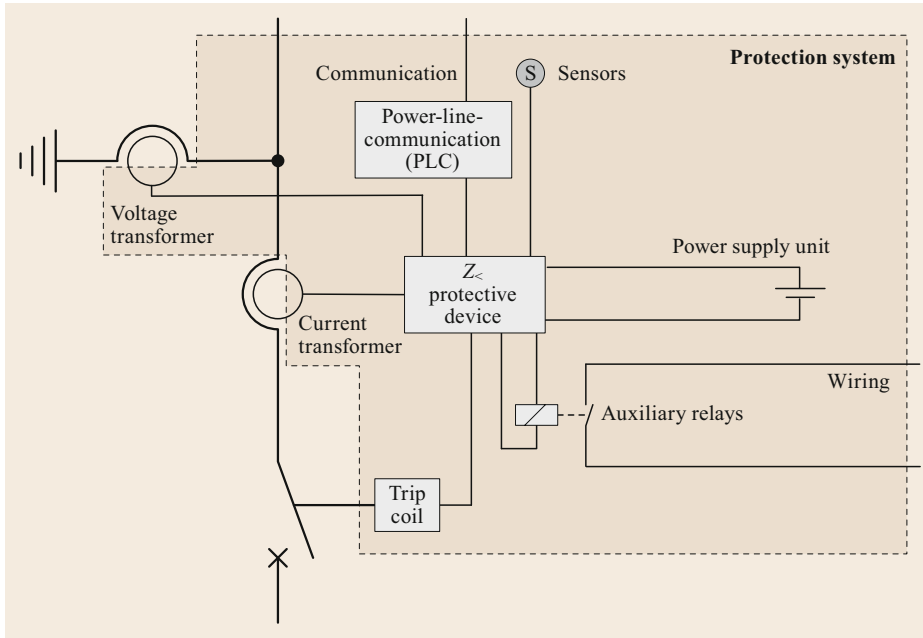
theoretical requirement of overlapping protection zones is not implemented in practice due to the high costs involved; rather, the current measurement is carried out at only one place. In order to implement two independent protection systems for adjacent protection zones, two separate secondary windings of the current transformer are used, resulting in the arrangement shown in Fig. 13.1c. The adjacent protection zones no longer overlap, but only touch each other. In the event of a fault in the small area between the current transformer and circuit-breaker, the busbar is switched off unnecessarily while the fault will still be transmitted via the line. The fault is switched off by the backup protection system, which is explained below. The small, nonselective area described above is therefore acceptable.

#### Backup Protection System

In order to achieve the necessary reliability of the protection system, a backup protection system is provided for each protection zone. A backup protection system is a fully redundant protection system. According to [13.2], a protection system consists of at least a protective device, a separate secondary winding of the instrument transformer, independent wiring, independent tripping circuits, its own auxiliary supply, and where provided its own communication system. The circuit-breakers are excluded. This is illustrated in Fig. 13.2.



**Fig. 13.1a–c** Layout of protection zones. (a) Electric power system with protection zones, (b) ideal protection zone, (c) real protection zone



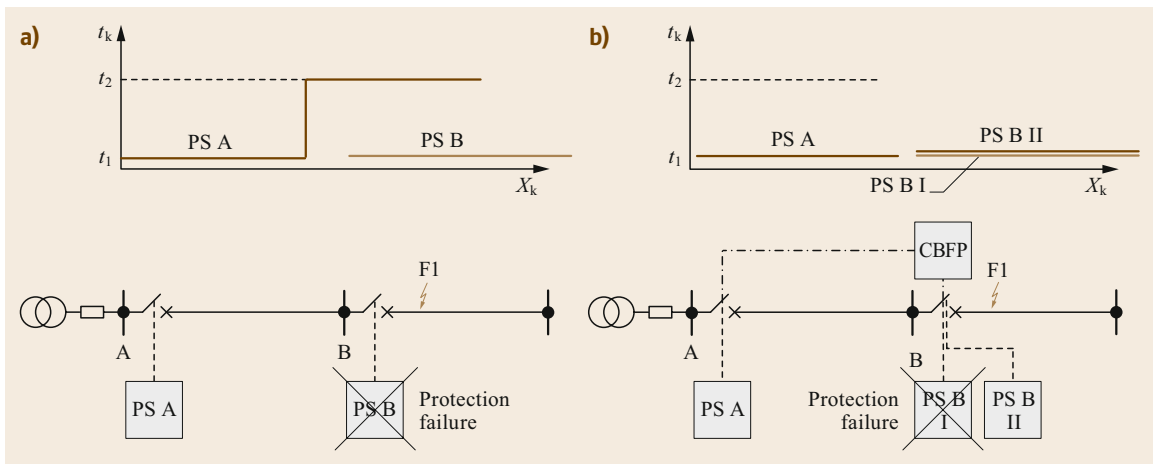
**Fig. 13.2** Elements of a protection system (adapted from [13.2])

In the past, there was a distinction between the so-called main and backup protection systems. However, today, there is no such prioritization between the two protection systems, indicating that both work on an equal and independent basis.

It should be noted that the possibility of a failure of the circuit-breaker must also be taken into account when designing the backup protection, although by definition the circuit-breaker is not part of the protection system.

There are two fundamentally different concepts for implementing backup protection systems, viz. remote backup protection and local backup protection.

In the case of remote backup protection, the faulty equipment is switched off by the protection system of an adjacent protection zone, as illustrated in Fig. 13.3a. To achieve this, all the protection systems in the electric neighborhood of the fault should also detect faults in adjacent protection zones. If the fault is not switched off within a specified time, the reach of all the protection zones is extended. These extended protection zones now also include the electric equipment of the neighboring protection zones. If the short circuit is located in this extended protection zone, a trip is triggered. When using this type of backup protection, a malfunction of the protection system leads to a nonselective



**Fig. 13.3a,b** Backup protection schema. (a) Remote backup protection. (b) Local backup protection with additional circuit-breaker failure protection (CBFP)

trip with an additional time delay. Remote backup protection covers the malfunction of both the protection system and the circuit-breaker. The concept of remote backup protection is typically used in distribution networks.

In contrast, local backup protection is characterized by the local duplication of the entire protection system. According to Fig. 13.3b, this duplication affects not only the actual protected device but also the complete wiring and power supply up to the tripping coil of the circuit-breaker. To prevent systematic faults in protective devices from failure to operate, devices from different manufacturers are normally used, and

optimally different protection principles should also be used.

Since the malfunction of the circuit-breaker is not included in this concept, circuit-breaker backup protection must always be installed in addition. This can be achieved, for example, by an additional communication link to the next circuit-breaker with corresponding logic. Such local backup protection is used in high-voltage and extrahigh-voltage networks. The expense is considerably higher, but significant shorter fault clearance times can be achieved in the event of protective or power switch malfunctions [13.4], which is necessary for the stability of such networks.

## 13.2 Protection Criteria

In this section, physical quantities that can be used to identify faults in electric power systems, i.e., so-called protection criteria, are presented. These protection criteria should be able to discriminate between operating, fault, and hazard status in the electric power system. In the simplest case, a physical quantity (e.g., current, temperature, or pressure) is compared with an adjustable threshold value. In addition, a special tripping characteristic (depending on a physical quantity) or sets of tripping characteristic (e.g., depending on several physical quantities) can be used to classify the network status.

These protection criteria can be divided into electric and nonelectric categories.

### 13.2.1 Electric Protection Criteria

The voltage and current, as well as values derived therefrom, can be used as protection criteria. Such derived values can include, for example, the impedance, admittance, and active, reactive, or apparent power. In addition, the phase angle between the voltage and current can also be used as a criterion for the fault condition of an electric power system. Not only the voltage and current of the natural system (e.g., line currents and phase-to-earth voltage or phase-to-phase voltages) but also the voltages and currents of the symmetrical components are evaluated. In addition, dielectric and magnetic fields or electric charges can also be used as protection criteria for special applications.

Selected electric protection criteria are described in more detail below. For this purpose, the measuring circuits are shown schematically, the typical range of values is explained, then a statement on selectivity is made.

### Overcurrent Criterion

Figure 13.4a shows the basic measuring diagram for the overcurrent criterion. The overcurrent protective device is typically connected by a current transformer. The tasks of the current transformer are explained in the following section. In the simplest case, the circuit-breaker is actuated when a preset current threshold is exceeded.

In order to guarantee reliable and secure discrimination between operational and failure status based on the overcurrent criterion, the following conditions must be observed

$$I_{\text{pi}} < c I_{\text{sc min}}; \quad c < 1, \quad (13.1)$$

$$I_{\text{do}} < \frac{1}{c} I_{\text{o max}}; \quad c < 1, \quad (13.2)$$

with:

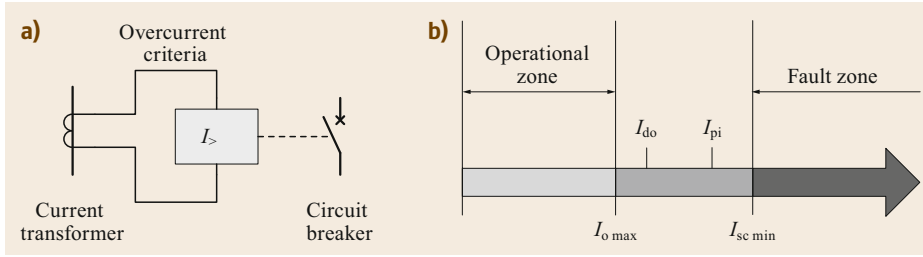
$I_{\text{pi}}$	pick-up current
$I_{\text{do}}$	drop-off current
$I_{\text{sc min}}$	minimum short-circuit current
$I_{\text{o max}}$	maximum operation current
$c$	constant factor.

This relation between the different current levels is additionally illustrated in Fig. 13.4b. The necessary difference between the pick-up and drop-off current is explained at the end of this chapter.

For the overcurrent criterion, the following conditions must be observed:

The security factor  $c$  takes into account the measurement accuracy of the current transformers and the protective device itself, as well as the inaccuracy in determining the current settings. It must be considered that the maximum operating current at particular times,





**Fig. 13.4a,b** Overcurrent criterion with the connection to the primary system. (a) Measurement diagram, (b) range of application

e.g., during start-up processes, may be significantly higher than the rated current of the equipment. The calculation of the minimum short-circuit current must take into account, in addition to the specifications of [13.5], the most unfavorable switching condition (weakest supply) and the most critical fault location, as well as the most unfavorable fault conditions (high equipment temperature, fault transition resistance).

Selective short-circuit clearing based on the overcurrent criterion can only be achieved by introducing an additional delay time. This may lead to conflicts between the requirement for short fault clearing time and the selectivity of the protection system. In addition, the maximum fault clearing time prescribed by the upstream network operator must be observed.

Depending on the application, the overcurrent criterion can be applied directly to the line currents as well as the positive-, negative-, and zero-sequence currents of the symmetrical components. In some cases, the levels of single harmonics of the current are used as criteria.

In addition, it is important to consider whether the rms value, the maximum amplitude, or only the fundamental value of the current will be rated. Especially in critical borderline cases, this choice can lead to very diverse reactions of the protection system.

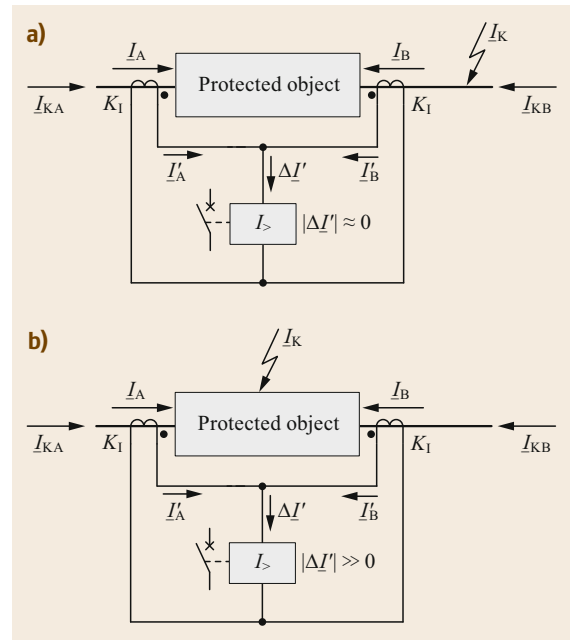
### Differential Current

The basic principle of differential protection has been known for a long time. In differential protection, the measured values are compared according to their magnitude and phase position. This can be done, for example, by a direct comparison of instantaneous values. It is also possible to compare the magnitude and phase angle of the current.

Differential current protection is the simplest and most commonly used form of differential protection. From a theoretical point of view, the procedure is based on Kirchhoff's circuit law, which states that the geometric sum of the currents at a node must be zero at all times.

The principal circuit used for unstabilized current differential protection is shown in Fig. 13.5.

Current transformers are connected at the ends of the protected object, thereby defining the differential



**Fig. 13.5a,b** Basis of the unstabilized current differential criterion. (a) Current differential protection with an external fault, (b) current differential protection with an internal fault

protection zone. The measuring direction of the current transformers is of great importance here. Usually, the measuring direction is oriented towards the protected object. This is indicated in the figure by the points on the current transformers and the counting direction of the current arrows. However, the direction of the current arrows on the current transformers thus does not correspond to the physical direction of the current, which depends on the position of the fault and of the power source. This representation of the principle is based on the assumption that the current transformers have an identical ratio.

The secondary windings of the current transformers are connected in series. The following relationship applies to the differential current

$$|\Delta I'| = |I'_A + I'_B|, \tag{13.3}$$

with:

$|\Delta I'|$  absolute value of the differential current on the secondary side

$I'_{\underline{A}}$  secondary current from side A  
 $I'_{\underline{B}}$  secondary current from side B.

The current split for an external fault is shown in Fig. 13.5a. In this case, the measured currents and the differential current are as follows

$$I'_{\underline{A}} = K_I I_{\underline{A}} = K_I I_{\underline{K}A}, \quad (13.4)$$

$$I'_{\underline{B}} = K_I I_{\underline{B}} = -K_I I_{\underline{K}A}, \quad (13.5)$$

$$|\Delta I'| = |K_I I_{\underline{K}A} + (-K_I I_{\underline{K}A})| = 0, \quad (13.6)$$

with:

$K_I$  transformation ratio of the current transformer

$I_{\underline{A}}$  primary current from side A

$I_{\underline{B}}$  primary current from side B

$I_{\underline{K}A}$  short-circuit current from side A.

It can be seen that, if a fault occurs outside the protected object, the measured currents cancel each other and no differential current flows via the differential branch.

Figure 13.5b illustrates a fault within the protected object, resulting in the following current distribution

$$I'_{\underline{A}} = K_I I_{\underline{A}} = K_I I_{\underline{K}A}, \quad (13.7)$$

$$I'_{\underline{B}} = K_I I_{\underline{B}} = K_I I_{\underline{K}B}, \quad (13.8)$$

$$|\Delta I'| = |K_I I_{\underline{K}A} + K_I I_{\underline{K}B}| \neq 0, \quad (13.9)$$

with:

$K_I$  transformation ratio of the current transformer

$I_{\underline{A}}$  primary current from side A

$I_{\underline{B}}$  primary current from side B

$I_{\underline{K}B}$  short-circuit current from side A.

The short-circuit current components ( $I_{\underline{K}A}$  and  $I_{\underline{K}B}$ ) of both sides depend on the short-circuit power of the respective connected networks. If no feeding network is connected to one of the sides, this portion of the short-circuit current may become zero. However, it is important that none of the short-circuit current components be negative in relation to the defined counting direction. This ensures that, in the case of a fault within the differential protection zone, a differential current always occurs.

As explained above, this principle is referred to as unstabilized current differential protection. This criterion is applicable to all spatially concentrated protected

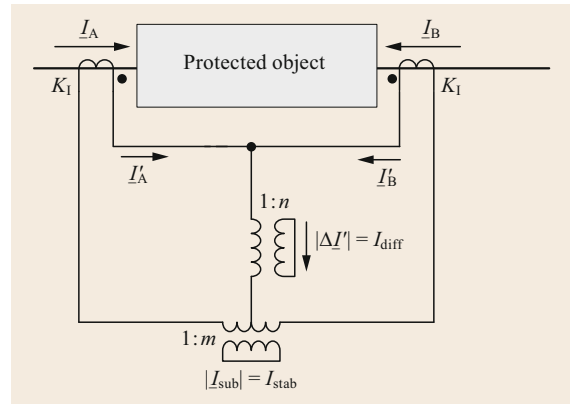


Fig. 13.6 Basis of the stabilized current differential criterion

objects. In this basic form, current differential protection is not used, since even the slightest inaccuracies in the current transformers can lead to considerable differential currents in the event of high short-circuit currents outside the protection zone, in which case nonselective tripping could occur.

In practice, the so-called stabilized differential protection function is used, as shown in Fig. 13.6.

In addition to the differential current, the through current or stabilizing current  $I_{stab}$  is also measured in this case. According to Fig. 13.6, this current can be simply determined using the following relationship

$$I_{diff} = |I'_{\underline{A}} + I'_{\underline{B}}| n, \quad (13.10)$$

with  $I_{diff}$  is the secondary differential current,  $n$  is the ratio of the secondary current transformer,

$$I_{stab} = |I'_{\underline{A}} - I'_{\underline{B}}| m, \quad (13.11)$$

with  $I_{stab}$  being the secondary stabilizing current and  $m$  the ratio of the secondary current transformer.

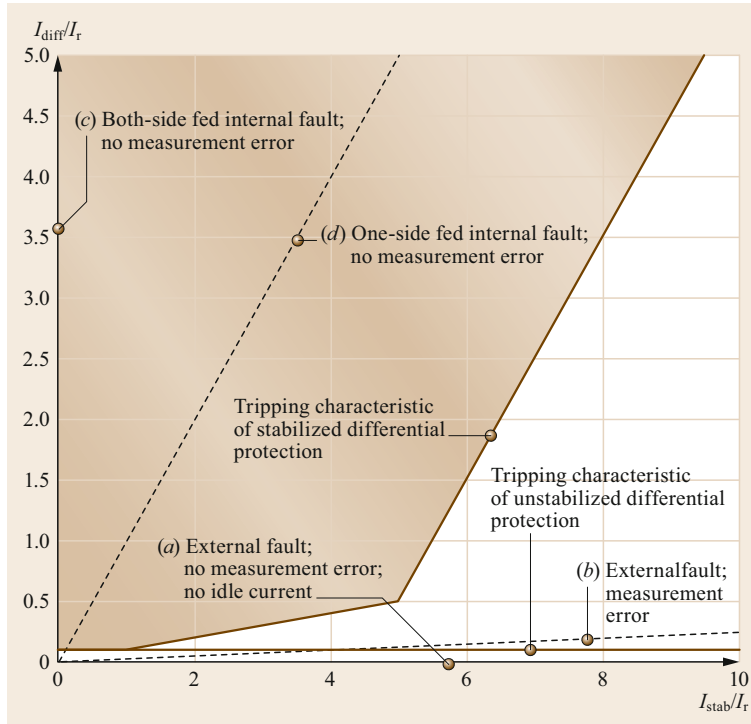
In modern numerical protective devices, other definitions of the stabilizing current are also used, for example,

$$I_{stab\ alt} = |I'_{\underline{A}}| + |I'_{\underline{B}}|. \quad (13.12)$$

Based on this definition, the stabilizing current can be calculated more easily, and the definition is also applicable for three-winding power transformers.

Figure 13.7 shows a diagram of the differential and stabilizing current for various faults and network situations. All currents are referred to the rated current  $I_r$  of the primary terminal of the power transformer. The stabilizing current is estimated according to (13.11).

Curve (a) shows the resultant correlation between the differential and stabilizing current for a short-circuit



**Fig. 13.7** Basis of the stabilized current differential characteristic

outside the protection zone. It is assumed that the two current transformers on both sides of the protected object work without measuring errors. Curve (b) results if it is assumed that the current transformers have a relative measurement error of  $\pm 2.5\%$ . This measurement error is still within the accuracy definition of the current transformer. It can be seen that a significant differential current already occurs.

Curve (c) is obtained in the case of a short circuit within the protected object that is supplied from both sides with identical short-circuit power. If only one network feeds the fault, the curve (d) applies.

This results in the tripping characteristic for stabilized differential protection shown in Fig. 13.7. Such a multistage tripping characteristic is used very often and can be applied to achieve high sensitivity for low short-circuit currents and increased stability for high through currents due to short circuits outside the protected zone.

The principle of stabilized differential protection is state of the art today. Differential protective devices differ in their definition of the differential and stabilization currents.

#### Further Current Criteria

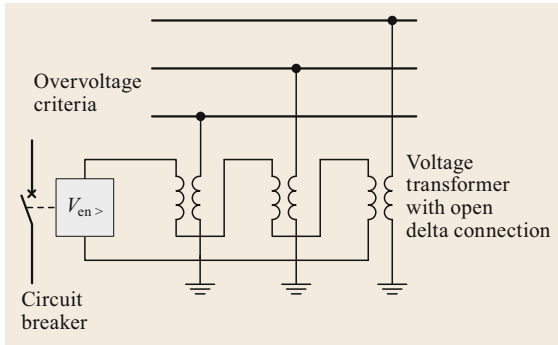
In addition to the overcurrent criterion described above, the current rise can also be used as a criterion. In mathematical terms, the derivative of the current  $di/dt$  is

monitored. In this way, the maximum current value can be determined before it reaches its maximum value. This is a very fast method, but it is not a fault location selective criterion. An additional delay time to achieve a selective reaction does not make sense, because it reduces the fast operation time of this criterion. Therefore, this criterion can only be used for clearly spatially delimited electric equipment that requires a very fast fault clearing time. A typical application for this criterion is the protection of the contact wire of electric railway systems.

A further criterion is the so-called off-system current. This criterion can only be applied to clearly spatially delimited electric equipment that is completely isolated from the earth potential. Via a coupling device, such as a capacitor, an external current is injected with a frequency that does not match the system frequency. The external current circuit is closed via the parasitic capacitance of the primary electric equipment. If a galvanic connection appears between the primary electric equipment and earth, e.g., when an earth fault occurs, the current in the external circuit increases. This off-system current criterion is very sensitive. In Germany, it is used to monitor the windings of large generators.

#### General Voltage Criteria

Figure 13.8 shows the basic measuring diagram of the zero-sequence voltage. The open-circuit voltage at the



**Fig. 13.8** Zero-sequence overvoltage criterion with the connection to the primary system

delta winding of the three voltage transformers is proportional to the zero-sequence voltage. If this voltage exceeds a defined threshold, there is an earth fault in the electric power system. This can be used for signaling or disconnection, depending on the type of star point treatment of the electric power system.

This criterion cannot be used to determine the location of the earth fault, which implies that it can only be used in a nonunit protection schema. This criterion is used in conjunction with other criteria for the detection of earth faults in all electric equipment.

#### Further Voltage Criteria

In addition to the aforementioned overvoltage criterion, there are also undervoltage criteria. Both types of voltage criteria are often used together with other criteria.

The phase-to-earth and phase-to-phase voltages as well as the positive-, negative-, and zero-sequence voltages can be used as inputs for the voltage criteria. For special applications, single harmonics of the voltage may also be used as criteria.

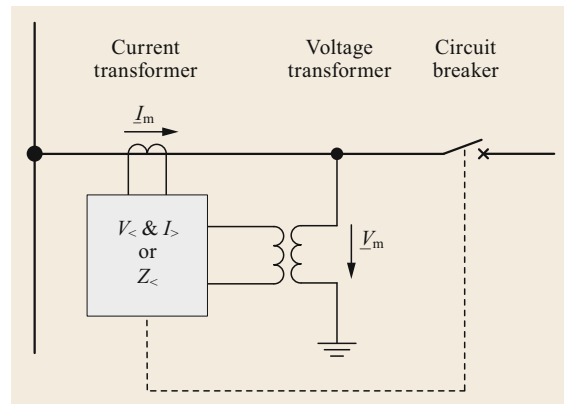
#### Derived Characteristic Criteria

Both the voltage and current can be used as input signals for the mentioned criteria. These electric signals are used to calculate the impedance, admittance, but also the active, reactive, or apparent power. In addition, the angle between the current and voltage can also be calculated as a criterion. The simplest case is a logical combination of an undervoltage and overcurrent criterion.

The basic connection for measuring voltage and current is shown in Fig. 13.9.

The undervoltage/overcurrent derived criterion is a logical combination of voltage and current thresholds. It can be formulated as

$$[(|V_m| < V_<) \wedge (I_m > I_b)] \vee [ |I_m| > I_> ], \quad (13.13)$$



**Fig. 13.9** Measurement of voltage and current for derived characteristic criteria

with:

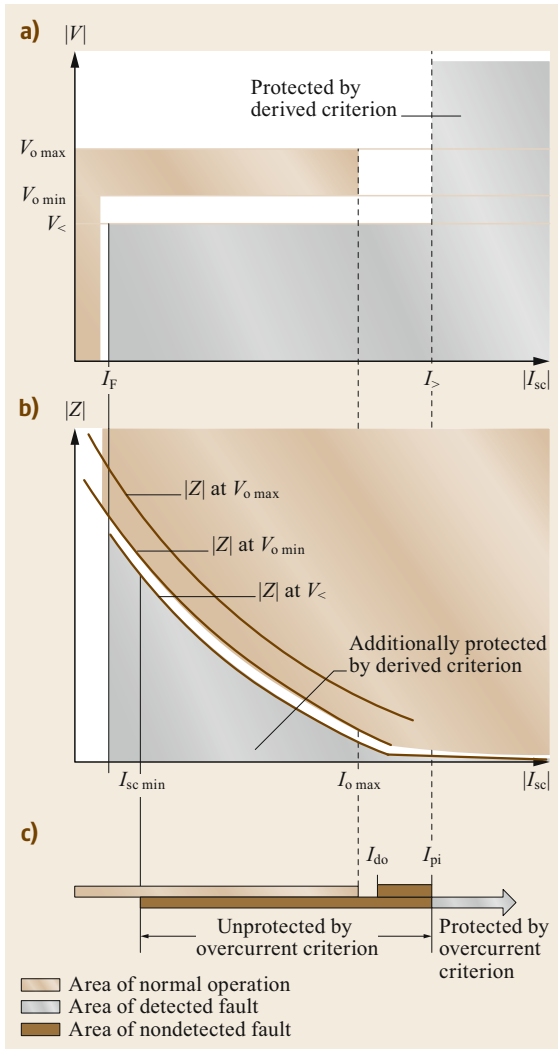
- $|V_m|$  absolute value of the measured voltage
- $|I_m|$  absolute value of the measured current
- $V_<$  threshold for minimum operational voltage
- $I_b$  threshold for base point current
- $I_>$  threshold for overcurrent.

Figure 13.10a illustrates a situation in which the maximum operating current  $I_{o,max}$  is greater than the minimum short-circuit current  $I_{sc,min}$ . In this case, the relations defined in (13.1) and (13.2) cannot be fulfilled. Therefore, the pick-up and drop-off current must be set above the maximum operation current. The lower part of the figure clearly shows that there is a wide current range in which a fault will not be detected by the overcurrent criterion.

The logical combination of the undervoltage and overcurrent criteria according to (13.13) is illustrated in the top of Fig. 13.10. The value of the base point current could be 10% of the rated operation current. Based on the logical operation, the fault situation is identified. It can be clearly seen that, based on this logical operation, faults with current below the rated current can also be detected.

Figure 13.10b additionally illustrates the corresponding fault detection area in the impedance versus current diagram. The three curves in the middle represent the absolute value of the measured impedance at the maximum and minimum operational voltage ( $V_{o,max}$  and  $V_{o,min}$ ). The lowest curve shows the lowest acceptable impedance during normal operation as a function of the current; this corresponds to the  $V_<$  threshold. The area below this curve represents the additional protected impedance region.

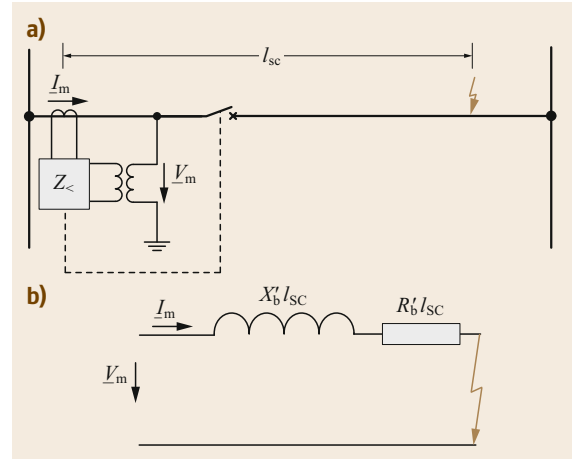
Another derived criterion is the underimpedance criterion. The basis of this criterion is the assumption



**Fig. 13.10a-c** Discrimination between fault and normal operation by derived electric criteria. (a) Derived criterion: undervoltage and overcurrent criterion, (b) resulting fault detection area, (c) simple criterion: overcurrent criterion

that there is a correlation between the impedance measured during a short circuit and the distance to the short circuit. In this way, the location of the fault can be calculated directly from the impedance value, if the impedance per length of the electric line is known. The single line diagram in Fig. 13.11a illustrates this situation. The second part of this figure shows the electric circuit. It can be clearly seen that the impedance measured at the start of the line indicates the distance between the measurement and the fault location.

Based on the voltage loop in Fig. 13.11b, the fault impedance can be calculated from the measured voltage  $\underline{V}_m$  and current  $\underline{I}_m$  as



**Fig. 13.11a,b** Relation between fault impedance and fault location. (a) Single line diagram, (b) electric circuit

$$\underline{Z}_m = \frac{\underline{V}_m}{\underline{I}_m} = (R'_1 + jX'_1) l_{sc} \quad (13.14)$$

with:

$\underline{Z}_m$  complex value of the calculated impedance

$\underline{V}_m$  complex value of the measured voltage

$\underline{I}_m$  complex value of the measured current

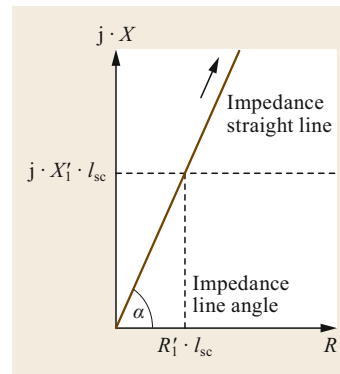
$R'_1$  length-related positive-sequence resistance of the line

$X'_1$  length-related positive-sequence reactance of the line

$l_{sc}$  distance between measurement point and fault location.

Figure 13.12 illustrates (13.14) in the complex  $X/R$ -plane. The impedance straight line represents the constant  $X/R$ -ratio of the transmission line. The position along this straight line changes depending on the fault distance  $l_{sc}$ .

Figure 13.12 illustrates how either the reactance or resistance of the fault loop can be used to deter-



**Fig. 13.12** Fault distance in the complex plane

mine the fault distance. This is only valid for an ideal fault without additional contact or arc resistance. In real applications of this criterion, the fault distance is determined based on the reactance. The mentioned contact resistance does not considerably disturb the reactance. The underimpedance criterion is used to protect overhead transmission lines, cables, transformers, and generators. It is a universal criterion.

### 13.2.2 Nonelectric Criteria

The following list presents the numerous nonelectric physical variables that can also be used to detect faults in electric power systems:

- **Temperature**  
Temperature measurements are used for transformers, electric machines, generator cables, and overhead lines. Such temperature measurements are partly carried out using simple sensors (e.g., PT100 resistance thermometers), but also with the help of infrared temperature measurement instruments.
- **Gas pressure**  
The pressure of the gas can be used as a fault indicator for air- and gas-insulated switchgear (GIS) or gas-insulated lines (GILs). Very different techniques for measuring the pressure of the gas are available, including simple pressure equalization flaps up to modern temperature-compensated pressure sensor technology.
- **Light**  
Light is often used for the identification of arcs in closed or encapsulated switchgear. Either simple point-based light sensors or fiber-optic cables can be used as sensors.
- **Structure-borne noises**  
Noise can be used to detect partial discharges in gas-insulated switchgear. Special microphones for structure-borne sound can be used for this purpose.
- **Oil flow rate and oil level**  
The oil flow rate is often used for oil-filled electric equipment. The oil flow rate between the electric equipment and oil storage is measured. During normal operation, this flow rate is determined by the thermal behavior of the equipment. If a fault occurs, the resulting decomposition of the oil results in a very high flow rate.

This list presents only a small selection of the nonelectric criteria, which are often used as additional diverse criteria for the protection of electric equipment.

### 13.2.3 Notes on Protection Criteria

Below, general information related to the protection criteria is given. First, a classification of the protection criteria is presented, based on the underlying characteristics of each which define the overall behavior.

All set points must include hysteresis in order to achieve a stable and predefined response according to the chosen protection criterion. Before implementation of such criteria in hardware, this behavior was achieved based on the physical effect itself. In modern software implementations, this behavior must be implemented as a software function. Additionally, general information about the treatment of the settings of protective devices are given. The final note relates to the determination of direction.

#### Classification of Protection Criteria

In general, protection criteria can be categorized into absolute selective criteria (unit protection) and relative selective protection criteria (nonunit protection).

Absolute selective criteria are characterized by the fact that faulty equipment can be identified unambiguously. Absolute selective criteria enable fault location determination without additional information or equipment. When using these criteria, faults outside the considered protection zone cannot be detected, thus these criteria are not suitable for remote backup protection.

Relative selective criteria detect a fault in the electric power system but identify the faulty equipment only ambiguously. As a rule, a time delay is used to achieve selective identification of faulty equipment. These criteria are always suitable for remote backup protection.

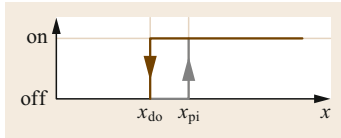
Table 13.1 illustrates the different types of protection criteria and provides additional examples.

#### Hysteresis of Set Points

All set-point values or tripping characteristics are executed with hysteresis, as shown in Fig. 13.13. In this regard, a so-called disengaging ratio is defined. This disengaging ratio is necessary to ensure stable operation of the protective device (without *chattering*). In the case

**Table 13.1** Comparison of absolute and relative selective protection criteria

Type of protection criteria	Example	Remote backup protection	Supplementary measures to achieve selectivity
Absolute selective	$\Delta I, \Delta \varphi$	Not suitable	Stabilization
Relative selective	$Z <, I >$	Suitable	Time graduation



**Fig. 13.13**  
Threshold with hysteresis

of electromagnetic protective devices, this function is included in the design. In the case of modern numerical protective devices, this function must be implemented in the software.

The disengaging ratio is defined as

$$f_{dr} = \frac{x_{do}}{x_{pi}}, \quad (13.15)$$

with:

$f_{dr}$  disengaging ratio  
 $x_{pi}$  pick-up value  
 $x_{do}$  drop-off value.

The disengaging ratio  $f_{dr}$  is smaller than 1 for all protection criteria that monitor the exceeding of a threshold, e.g., the overcurrent threshold. Depending on the application, this disengaging ratio should lie between 0.75 and 0.99.

When monitoring whether a quantity falls below a threshold, the disengaging ratio must be higher than 1, e.g., for undervoltage monitoring.

### Settings of Protective Devices

Protective devices, with rare exceptions, are designed as so-called secondary devices, meaning that they are connected to the electric power system via current and voltage transformers. For this reason, protective devices are always set in relation to these secondary values.

With the introduction of numerical protective devices, it becomes possible in principle to carry out the setting using primary values, if the ratio of the voltage and current transformers is specified. However, in order to be backwards compatible and to avoid confusion, the setting of protective devices remains based on secondary values today.

This results in the following setting calculation for current values

$$I_{s\text{set}} = \frac{I_{srCT}}{I_{prCT}} I_{p\text{set}} = \frac{1}{w_{rCT}} I_{p\text{set}}, \quad (13.16)$$

with:

$I_{s\text{set}}$  secondary set value of the current  
 $I_{srCT}$  secondary rated current of the current transformer  
 $I_{prCT}$  primary rated current of the current transformer  
 $I_{p\text{set}}$  primary set value of the current.

Here, the currents  $I_{prCT}$  and  $I_{srCT}$  are the primary and secondary rated values of the current transformers, while the calculated secondary set value is  $I_{s\text{set}}$ . In practice, the setting is often determined based on the nominal input value of the protective device.

The secondary impedances are calculated as

$$Z_{s\text{set}} = \frac{\frac{I_{prCT}}{I_{srCT}} Z_{p\text{set}}}{\frac{U_{prVT}}{U_{srVT}}} = \frac{1}{w_{rCT} w_{rVT}} Z_{p\text{set}}, \quad (13.17)$$

with:

$Z_{s\text{set}}$  secondary set value of the impedance  
 $U_{srVT}$  secondary rated voltage of the voltage transformer  
 $U_{prVT}$  primary rated voltage of the voltage transformer  
 $Z_{p\text{set}}$  primary set value of the impedance.

The voltages  $U_{prVT}$  and  $U_{srVT}$  are the primary and secondary values of the voltage transformer.

### Directional Decision

All relative selective protection criteria generally require a directional decision in meshed electric power systems or electric power systems with changing flow directions. In these cases, it must be determined whether the fault is in the direction of the protected object or not.

In addition to the current, the voltage is also required to determine the short-circuit direction. The short-circuit direction is derived from the angle between the current and voltage. Such directional determination can be negatively influenced by numerous factors, including, for example, the resistance/reactance ratio of the short-circuit loop, the level of the load current, and the compensation of overhead lines. The following description illustrates only the general principles of directional estimation; for detailed information, see [13.6].

In principle, the short-circuit direction could be determined from the sign of the short-circuit impedance or admittance. However, this method is not used, because this information is not reliable in critical short-circuit situations, e.g., nearby three-phase fault conditions. Therefore, a separate directional determination function is always implemented.

There are different technical solutions for determining the direction. In Europe, short-circuit loops in the natural system are usually evaluated. This means, for example, that in the case of a single phase-to-earth fault, the phase-to-earth voltage and the phase current of the faulty conductor are compared. However, this method becomes problematic with very small fault voltages, which is typical of nearby faults.

To determine the fault direction correctly even in these cases, the directional decision is often based on nonfault voltages, particular in overcurrent protection devices. In this case, the voltage of a loop, which is not affected by the fault, is used as a reference. An additional angle correction must be applied. It should be noted that, for all protection devices in electric power systems, the selection of the nonfault voltage must be made according to the same principle, which is normally the set point of each protective device.

In the case of a nearby three-phase fault, all voltage loops will have very low values. Therefore, the above-described procedure based on the nonfault voltage cannot be used. With the introduction of numerical protective devices, a so-called voltage storage function can be implemented. In this case, the shape of the voltage before the fault is repeated periodically. The prerequisites for this are, on the one hand, a high-precision frequency measurement, and on the other hand, that the network frequency changes only slightly

during a short circuit. The use of the voltage storage function has been tested in modern numerical selective protective devices and is state of the art today. This function correctly determines the direction of the short circuit, even if there is no voltage at all.

If the fault direction cannot be determined, for example, in the case when the voltage storage is empty and this function is not available, a preorientation is usually specified. This preorientation is typically set to the protected object, which normally leads to tripping.

Fault direction estimation in Anglo-American countries is often based on the direction evaluation of the symmetrical components. In the simplest case, the short-circuit direction is calculated based on the positive-sequence system. Since it is necessary to increase the reliability of directional estimation in the case of critical faults, procedures which additionally consider the directional decision in the negative- and zero-sequence systems can be applied.

## 13.3 Requirements on Current and Voltage Transformers

Only a few primary protective devices directly analyze the primary voltage and current values. These are usually limited to low and medium voltage levels.

Due to the huge amplitudes and high potentials of the voltage and current signals, they cannot be directly processed by secondary protective devices. The signals must therefore be adapted by voltage and current transformers or corresponding dividers.

The main tasks of the current and voltage transformers are:

- conversion of standardized primary values to standardized secondary values
- electric insulation of the protective devices against the high-voltage potential of the protected object
- exact instantaneous transformation of the primary values of current and voltage over the entire working range of the protective device
- supply of auxiliary power for transformer-powered protective devices.

A distinction is made between transformers for protection or measurement applications in terms of their accuracy and transformation characteristics. The following information is focused on the requirements for protection applications.

### 13.3.1 Inductive Current Transformers

Inductive current transformers are inductive transformers that are operated in short circuit. The primary side

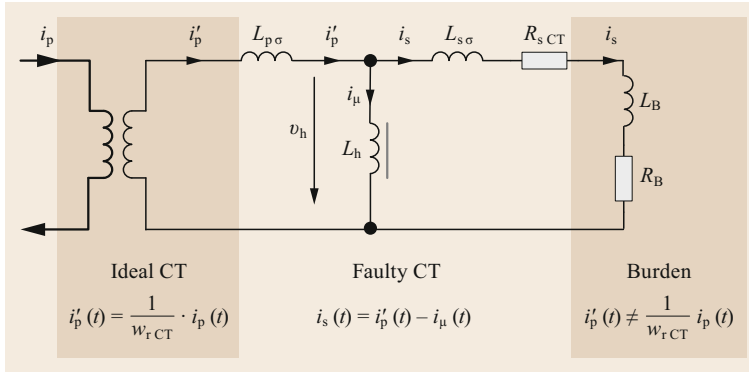
has only a few turns (in extreme cases only one), while the secondary side has a large number of turns. The primary side is operated in series with the electric power system, thus the current is impressed. With an ideal current transformer, the secondary current is therefore completely independent of the load. The secondary side acts as a theoretically ideal controlled current source. If the short circuit on the secondary side of the current transformer is opened during operation, large and dangerous overvoltages can occur.

A fundamental distinction is made between current transformers for measuring and protection purposes. Current transformers for measuring purposes must exhibit very high accuracy up to their rated current. These types of current transformers are used for billing. If the flowing current exceeds the rated value, the current transformer should saturate to protect the connected secondary devices. Current transformers for protection purposes must have a very wide measuring range, i.e., from 1% up to 100 times the rated current. The ratio of the measurement range is 1–1000.

The characteristics of current transformers for protection purposes are explained in more detail below. The international standard [13.7] specifies a number of standardized nominal values for the primary and secondary rated currents of such current transformers.  $I_{sT} = 1 \text{ A}$  has become established worldwide as the standardized secondary rated current, although sometimes the value  $I_{sT} = 5 \text{ A}$  is used.

Due to the necessary magnetizing current and the nonlinear behavior of the iron core, real current trans-





**Fig. 13.14** Simplified equivalent circuit of an inductive current transformer

formers do not exhibit ideal transfer behavior [13.8]. Measurement errors occur, depending on the one hand on the load (burden) and on the other on the setup of the iron core. A current transformer is dimensioned by the manufacturer for the rated burden, but in normal operation, it is loaded with a different burden. In addition, the exponentially decaying part of the short-circuit current at the installation site must also be taken into account. Therefore, it is necessary to dimension current transformers for each installation site.

As the stationary and transient magnetic flux can be superimposed in the magnetic circuit, the sizing of current transformers can also be divided into a stationary and transient dimension step. This requires that current transformers must always be dimensioned for the stationary and transient short-circuit current, taking into account the operational burden of the current transformer when connected.

Such dimensioning is achieved by calculating a stationary dimension factor  $K_{ost}$  and a transient dimension factor  $K_{tfdc}$ . The maximum secondary short-circuit current that can be transferred for an accuracy limit time of  $t'_{al}$  by the current transformer without saturation can then be calculated using the equation

$$I_{s\max} = \frac{K_{ost}}{K_{tfdc}} I_{sr} \tag{13.18}$$

$$I_{p\max} = \frac{K_{ost}}{K_{tfdc}} I_{pr} \tag{13.19}$$

with:

$K_{ost}$  stationary dimension factor

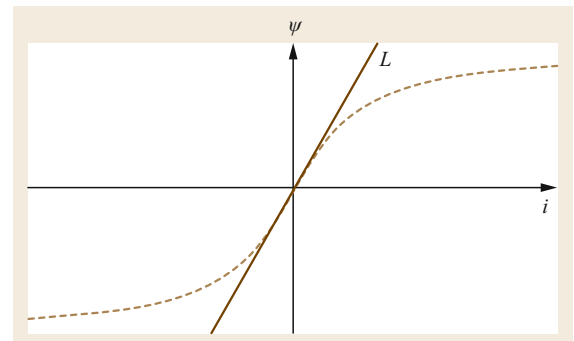
$K_{tfdc}$  transient dimension factor

$$w_{rCT} = \frac{I_{prCT}}{I_{srCT}} \tag{13.20}$$

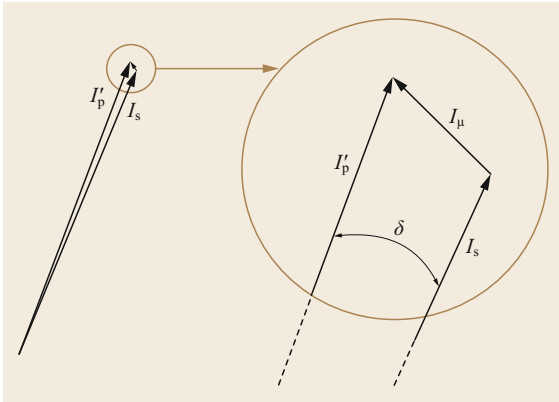
is the rated transformation ratio of the current transformer.

The method for dimensioning of current transformers relies on the equivalent circuit diagram shown in Fig. 13.14, divided into three parts. The first part is an ideal current transformer with a theoretical ideal transformation ratio. This means that all further currents, voltages, and impedances are referred to the secondary side of the current transformer. The second part represents the nonlinear behavior of the real current transformer. This includes the leakage inductance of the primary and secondary winding, the resistance of the secondary winding, and the nonlinear and stray magnetization impedance. The third part is a model of the burden of the current transformer at the installation site. This burden includes both the wiring and the input impedances of the connected protective devices or other secondary equipment.

The nonlinear physical behavior is very difficult to describe, so simplifications are necessary. First, hysteresis is neglected and the magnetizing characteristic is simplified to the original curve with saturation [13.9], as shown by the dashed line in Fig. 13.15. In the next step, the linear part of this curve is represented by a single, constant inductance  $L_h$ , corresponding to the slope of the magnetizing curve in Fig. 13.15. In this case, the saturation is neglected too.



**Fig. 13.15** Simplified model of the nonlinear inductance  $L_h$



**Fig. 13.16** Phasor diagram of current transformer in the linear range

With this simplified linear analytical model, the magnetic behavior is only described correctly for a demagnetized current transformer. There should be no remanence present in the iron core, therefore the current transformer should be slotted to significantly reduce the remanence. This model is only valid up to the first saturation of the iron core, the so-called accuracy limit time  $t'_{al}$ .

**Stationary Dimension**

For steady-state dimensioning of current transformers, it is assumed that both the primary and secondary currents are sinusoidal. The current transformer is only operated up to the saturation limit. The error occurs due to the magnetizing current of the inductance  $L_h$ . Based on some assumptions, the resulting measurement error is illustrated as a vector diagram in Fig. 13.16, revealing that the measurement error of the current transformer results from the magnetizing current  $i_\mu$ . The secondary current is obtained by phasor subtraction of the magnetizing current from the ideally transferred primary current. The resulting secondary current has an error on the absolute value and angle in the linear operating range of the current transformer.

The magnetizing current is very small compared with the nominal current of a current transformer in this range. The accuracy of the current transformer for protection purposes is defined by the accuracy classes presented in Table 13.2. The calculation of the magnitude of errors at the rated current and at the rated

accuracy limit current are calculated according to [13.7] in two different ways. The first calculation method assumes a sinusoidal primary and secondary current. Therefore, this calculation is based on rms values. The second method assumes a small distortion of the secondary current. The calculation of the accuracy is carried out in the time domain.

Assuming that the current transformer is operated in the linear range, there is no saturation and all currents and voltages are sinusoidal. In this case, the calculation for an inductive current transformer represented by the equivalent circuit diagram shown in Fig. 13.14 can be carried out using phasors.

To a first approximation, the main field voltage  $V_h$  in Fig. 13.14 is identical to the voltage on the burden and the voltage on the secondary winding. If this main field voltage  $V_h$  at the magnetizing inductance  $L_h$  exceeds the so-called knee-point voltage  $V_{h\,sat}$ , the current transformer leaves its linear range, causing an abrupt increase of the magnetizing current. The current transformer goes into saturation and can no longer be described using phasors. From the equivalent circuit diagram, it is immediately visible that, with a lower burden (lower resistance), a greater current can flow until the knee-point voltage is reached. There are different approaches for determining the knee-point voltage. Unfortunately, these also give different results, so the method used to determine the knee-point voltage must always be known.

The manufacturer designs the current transformer in such a way that it reaches the saturation point at the rated accuracy limit current, when the rated burden is applied to the current transformer. According to standards, the rated burden occurs at  $\cos(\varphi) = 0.8$ , resulting in

$$V_{h\,sat} = K_{rst} I_{sr} |(R_{sCT} + R_{rB}) + j\omega (L_{s\sigma} + L_{rB})|, \tag{13.21}$$

with:

- $R_{sCT}$  resistance of secondary winding
- $L_{s\sigma}$  leakage inductance of secondary winding
- $R_{rB}$  rated resistance of the burden
- $L_{rB}$  rated inductance of the burden
- $I_{sr}$  secondary rated current
- $K_{rst}$  rated stationary accuracy limit factor
- $U_{h\,sat}$  saturation voltage of magnetizing inductance.

**Table 13.2** Accuracy classes of current transformers for protection applications according to [13.7]

Accuracy class	Measurement error at the primary rated current (%)	Phase displacement at the primary rated current (min)	Measurement error at the primary rated accuracy limit current (%)
5P	1	60	5
10P	3	–	10

Normally, the current transformer is not operated at its rated burden, as the burden in the application depends on the wiring and the connected protective devices. Normally, the operational burden is lower than the rated burden, but the knee-point voltage is the same. The following equation is therefore valid for the operation mode

$$V_{h\text{sat}} = K_{\text{ost}} I_{\text{sr}} |(R_{\text{sCT}} + R_{\text{oB}}) + j\omega (L_{\text{s}\sigma} + L_{\text{oB}})|, \quad (13.22)$$

with:

- $R_{\text{oB}}$  operation resistance of the burden
- $L_{\text{oB}}$  operation inductance of the burden
- $K_{\text{ost}}$  operation stationary accuracy limit factor.

Combining (13.21) and (13.22), the stationary accuracy limit factor can be calculated as

$$K_{\text{ost}} = K_{\text{rst}} \frac{|(R_{\text{sCT}} + R_{\text{rB}}) + j\omega (L_{\text{s}\sigma} + L_{\text{rB}})|}{|(R_{\text{sCT}} + R_{\text{oB}}) + j\omega (L_{\text{s}\sigma} + L_{\text{oB}})|}. \quad (13.23)$$

The leakage inductance of the secondary winding is very small and can be neglected, thus

$$K_{\text{ost}} = K_{\text{rst}} \frac{|R_{\text{sCT}} + \underline{Z}_{\text{rB}}|}{|R_{\text{sCT}} + \underline{Z}_{\text{oB}}|}. \quad (13.24)$$

The impedance angle of the operating burden is often not known, therefore only the resistance of the operating burden is used. To avoid oversizing, the absolute value of the rated burden is simply used. This leads to the following simplified equation for the calculation of the stationary operational accuracy limit factor

$$K_{\text{ost}} = K_{\text{rst}} \frac{R_{\text{sCT}} + |\underline{Z}_{\text{rB}}|}{R_{\text{sCTs}} + R_{\text{oB}}}. \quad (13.25)$$

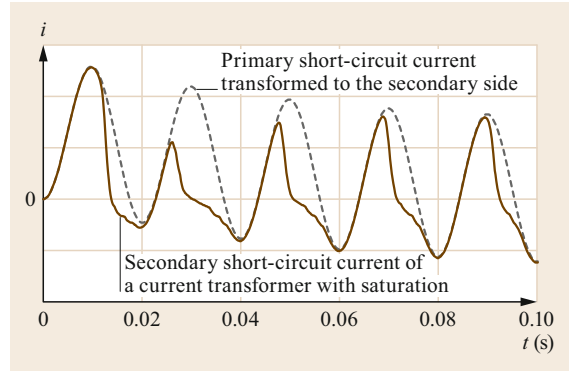
### Transient Dimension

Depending on the inception time of a short-circuit fault, an exponentially decaying direct-current component results in the primary short-circuit current. This short-circuit current can be expressed as (13.26)

$$i_{\text{p}} = \sqrt{2} I_{\text{SC}}'' \left[ e^{-\frac{t}{T_{\text{p}}}} \cos(\theta) - \cos(\omega t + \theta) \right], \quad (13.26)$$

with:

- $T_{\text{p}} = L_{\text{p}}/R_{\text{p}}$  primary time constant
- $\theta = \gamma - \vartheta$  fault angle
- $\gamma$  switching angle or fault inception angle
- $\vartheta = \arctan(X_{\text{p}}/R_{\text{p}}) = \arctan(\omega T_{\text{p}})$  phase angle of the short-circuit impedance.



**Fig. 13.17** Primary and secondary currents of current transformer with exponentially decaying direct-current component

The primary time constant of the short-circuit current  $T_{\text{p}}$ , also referred to as the network time constant, is determined by the  $R/X$  ratio of the primary network at the installation point of the current transformer. This time constant depends mainly on the voltage level and the structure of the network. It can take values from a few tens to several hundreds of milliseconds. This time constant must be determined by the network operator.

Figure 13.17 shows the transient transfer behavior of a current transformer. The primary short-circuit current has a time constant of  $T_{\text{p}} = 100$  ms. This is typical for medium-voltage networks. The secondary time constant of the converter is  $T_{\text{s}} = 300$  ms. The second curve shows the current transformer's transfer behavior. In this case, the current transformer saturates after 12 ms.

On the secondary side of the current transformer, the time constant of the short-circuit current and the time constant of the current transformer  $T_{\text{s}}$  itself superimpose.

The magnetic flux resulting in the current transformer is the integral of the main field voltage over time. For a purely sinusoidal main field voltage, the magnetic flux reaches its maximum after a half-wave, since the current transformer is magnetized with opposite polarity in the next half-wave. This balance is lost due to the direct-current (DC) component of the short-circuit current. The current transformer is additionally magnetized by the DC component until the saturation flow is reached.

In addition, the duty cycle must be taken into account. If the short-circuit current is only a switch-off, viz. the so-called C-0 cycle, there is no additional magnetization. In combination with the auto-reclosing function, the duty cycle would be C-0-C-0. After a short interruption, the short-circuit current could flow again, and an additional magnetization would occur.

**Table 13.3** Different types of current transformers for protection according to [13.7, 10]

Type of current transformer	Threshold for remanence flux	Description
P	No	Definition of the accuracy by rated accuracy factor for symmetrical short-circuit current
PR	Yes	
PX	No	Definition of current transformer behavior by parameters of the magnetizing curve
PXR	Yes	
TPX	No	Closed-core current transformer for specified transient duty cycle
TPY	Yes	Gapped (low-remanence) current transformer for specified transient duty cycle
TPZ	Yes	Linear current transformer (no remanence)

This leads to additional requirements on current transformers.

In the following, a C–0 cycle is assumed. The calculation of the transient dimension factor is based on the differential equation for the simplified equivalent circuit of an inductive current transformer shown in Fig. 13.14. The transient factor is obtained from the ratio  $K_{tf}(t)$  between the time-dependent magnetic flux and the peak value of the sinusoidal component

$$K_{tf}(t) = \frac{\psi(t)}{\hat{\psi}_{\text{sinus}}} = \frac{L_h i_{\mu}(t)}{\hat{\psi}_{\text{sinus}}}, \quad (13.27)$$

with:

- $K_{tf}(t)$  time-dependent ratio of the magnetic flux
- $\psi(t)$  time-dependent magnetic flux
- $\hat{\psi}_{\text{sinus}}$  peak value of the sinusoidal magnetic flux.

The calculation of this time-dependent factor is illustrated in detail in [13.11]. Taking into account some simplifications and the worst-case assumption, the following equation published in [13.10] results

$$K_{\text{tf dc}}(t'_{\text{al}}) = \frac{\omega T_P T_S}{T_P - T_S} \left( e^{-\frac{t'_{\text{al}}}{T_P}} - e^{-\frac{t'_{\text{al}}}{T_S}} \right) + 1, \quad (13.28)$$

with:

- $K_{\text{tf dc}}(t'_{\text{al}})$  transient dimension factor as a function of the accuracy time
- $t'_{\text{al}}$  accuracy limit time.

The entire dimensioning of the current transformer for the C–0 cycle can now be carried out according to (13.28).

For the dimensioning of a current transformer for a C–0–C–0 cycle, the demagnetization during the idle period and the remanence of the current transformer must be taken into account. It is assumed that the short-circuit current after the reclosing maintains the same polarity as immediately before switching off, i.e., the

worst-case situation,

$$K_{\text{tf dc}}(t'_{\text{al}}, t''_{\text{al}}) = \left[ \frac{\omega T_P T_S}{T_P - T_S} \left( e^{-\frac{t'_{\text{al}}}{T_P}} - e^{-\frac{t'_{\text{al}}}{T_S}} \right) + 1 \right] e^{-\frac{(t_{\text{dt}} + t''_{\text{al}})}{T_S}} + \left[ \frac{\omega T_P T_S}{T_P - T_S} \left( e^{-\frac{t''_{\text{al}}}{T_P}} - e^{-\frac{t''_{\text{al}}}{T_S}} \right) + 1 \right], \quad (13.29)$$

with:

- $t_{\text{dt}}$  dead time during auto-reclosing
- $t''_{\text{al}}$  accuracy limit time for the second current flow.

The remanence is taken into account by the definition of different types of current transformers, as listed in Table 13.3 according to standards [13.7] and [13.10].

### 13.3.2 Inductive Voltage Transformers

Inductive voltage transformers are inductive transformers that are operated in almost no-load condition. The primary side has a large number of windings, while the secondary side has a small number of windings. A short-circuit on the secondary side of the voltage transformer can lead to overload and thermal damage of the voltage transformer. Therefore, voltage transformers must be protected against overload.

The standard [13.12] specifies a number of fixed values for the primary and secondary rated voltages.  $V_{\text{sr}} = 100 \text{ V}$  has become established as the secondary rated voltage in many countries. The standard [13.12] defines different accuracy levels for voltage transformers depending on their application. This includes not only the accuracy levels but also the ranges of the nominal voltage at which these accuracy levels apply. Table 13.4 lists the requirements for voltage transformers for protection applications. The given accuracy values must be guaranteed in the voltage range from 5% of the rated voltage up to the rated voltage multiplied by the rated voltage factor to be selected by the customer (typically 1.2, 1.5, or 1.9). A range of burdens

**Table 13.4** Different types of voltage transformers for protection applications according to [13.12]

Accuracy class	Measurement error at the primary rated voltage (%)	Phase displacement at the primary rated voltage (min)
3P	3	120
6P	6	240

over which these values must be guaranteed is also defined in the standards.

In contrast to a current transformer, no further dimensioning is required for a voltage transformer with

regard to the transfer behavior as long as it is burdened with a load identical to or below its rated burden. A small burden for a voltage transformer implies a small current at a large voltage, which corresponds to a large impedance on the secondary side.

Because voltage transformers must not be overloaded, they must be protected with a fuse or voltage transformer automatic fuse. It is important that the tripping of this automatic fuse be signaled to the protective devices, in particular to distant protection; otherwise, there is the danger of overfunctioning, as zero impedance will be calculated in the absence of a voltage.

## 13.4 General Protection Functions

This section illustrates the three main and most widely used protection functions. When implementing these protection functions in devices, there are minor differences between manufacturers. These minor differences are not illustrated, but only the basic functional concept. In order to obtain an understanding of the detailed differences, manufacturers' manuals must be studied in detail.

Initially, the protection function was implemented using mechanical relays. Therefore, even today, protective devices are often called protection relays. However, modern protective devices are based on microprocessors, and the functions are implemented using highly complex signal-theoretical algorithms. For this reason, the term *protective device* is increasingly being used.

### 13.4.1 Introduction to Protection Functions

#### Function Numbers

Individual protection functions are often identified using the ANSI device number system [13.13]. Device numbers are used to identify the functions of devices shown on a schematic diagram. Some examples of device numbers are shown in Table 13.5. One physical device may correspond to one function number or may have many function numbers associated with it, as is the case with new, numerical protective devices.

**Table 13.5** Example ANSI device numbers according to [13.13]

Device number	Description
50	Instantaneous overcurrent relay
51	AC time overcurrent relay
51N	AC time neutral overcurrent
51P	AC time phase overcurrent
59	Overvoltage relay
59N	Neutral overvoltage
59P	Phase overvoltage

A suffix letter or number may be used with the device number; for example, the suffix *N* is used if the device is connected to the neutral (e.g., 59*N* indicates protection against neutral voltage displacement), whereas the suffixes *X*, *Y*, and *Z* are used for auxiliary devices.

#### Starting

As illustrated above, a distinction is made between absolute and relative selective protection criteria. It has been illustrated that relative selective protection criteria need a time delay for selective fault clearing and the back-up functionality. To implement this time delay, a common time base for all protective devices in the same network is needed. This is achieved by the so-called starting element.

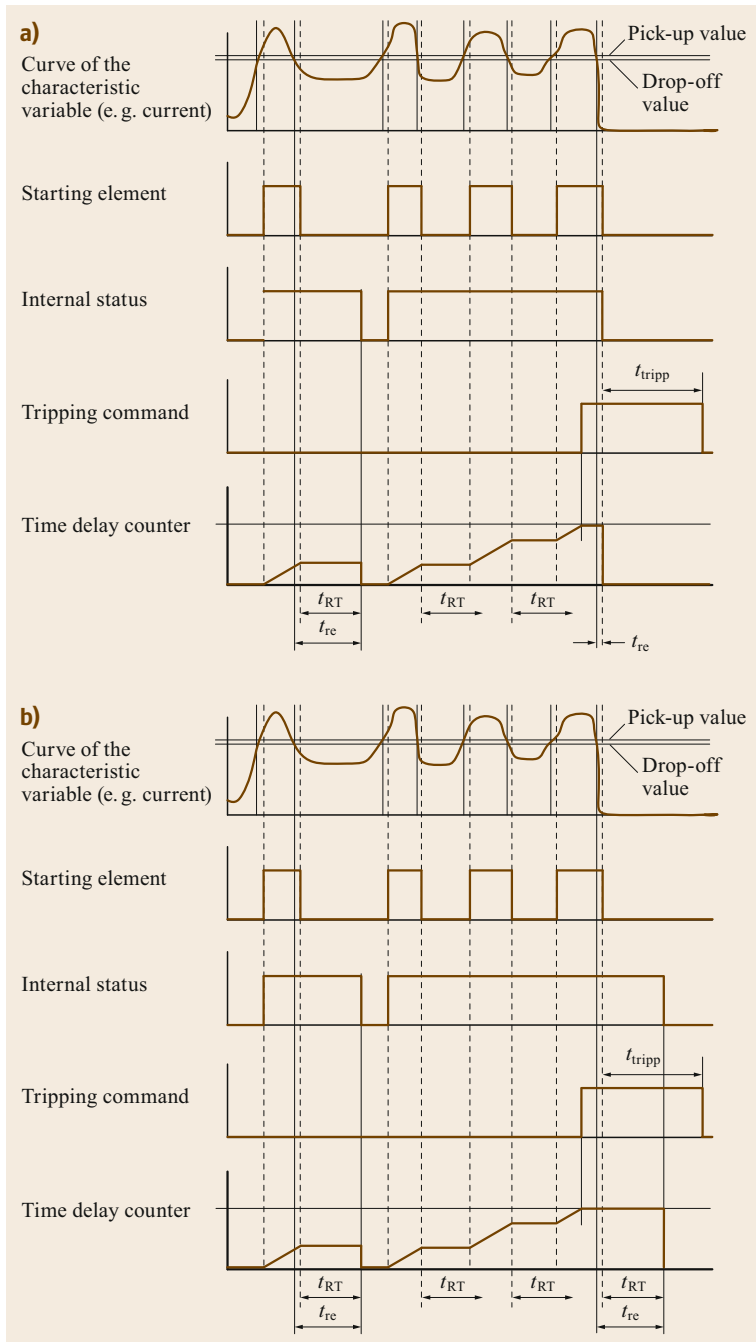
The main task of the starting element is to detect short circuits in the electric power system, independent of their location, aiming to detect short circuits in not only its own but also distant protection zones.

The starting element has the task of starting the internal time base for all protective devices. In this way, the starting element defines a common reference time point for all protective devices. There are also protective functions where the starting element has additional functions.

Depending on the protection criterion applied, different methods can be used to implement the starting element. In some cases, the procedures are very simple, to ensure the starting of the protective devices and avoid the requirement for additional setting parameters. However, there are also very complex algorithms. The individual methods for implementing the starting elements are explained in detail when the respective protective function is described.

#### Release Characteristic

Special release characteristics apply to achieve a defined behavior of protective devices in case of repeated



**Fig. 13.18a,b** Function of the independent reset time: **(a)** Immediate release after switch-off command, **(b)** delayed release after switch-off command (adapted from [13.14])

intermittent faults or faults occurring in rapid succession. A fundamental differentiation is made between instantaneous, independent, and dependent release behavior.

**Instantaneous Release.** If no intended delay is foreseen, the protective device must release itself when the

drop-off value  $I_{do}$  of the input quantity is reached. This applies for both types of overcurrent protective devices described below.

**Independent Release.** With this method, the protective device must remain active for a fixed reset time after the value of the characteristic quantity falls below

**Table 13.6** Examples of inverse time characteristic functions (adapted from [13.14])

Typ	Trip time			Release time		Description
	$t_{TT} = T_P \left[ \frac{k}{\left(\frac{I}{I_S}\right)^\alpha - 1} + c \right]$			$t_{RT} = T_P \frac{t_r}{1 - \left(\frac{I}{I_S}\right)^\alpha}$		
	$k$ (s)	$c$ (s)	$\alpha$	$t_r$ (s)	$\alpha$	
A	0.14	0	0.01	a	a	Inverse
B	13.5	0	1	a	a	Very inverse
C	80	0	2	a	a	Extremely inverse
D	0.0515	0.1140	0.02	4.85	2	IEEE moderately inverse
E	19.61	0.491	2	21.6	2	IEEE very inverse
F	28.2	0.1217	2	29.1	2	IEEE extremely inverse

<sup>a</sup> To be defined by the manufacturer

the drop-off value; the starting element is set to zero. All other internal functions of the protective device remain at the reached operating states, but without being reset. This also applies to the time delay counter of the time zones, which remain active and stop counting, but are not set to zero.

The basic behavior is shown in Fig. 13.18. If the characteristic quantity, e.g., the current, exceeds the pick-up value, the protective device is triggered after an internal response time. The starting signal and the active status are set. If these two signals are active, all functions of the protective devices work; in particular, the internal time zones are started. If the characteristic quantity falls below the drop-off value, the starting signal is reset after an internal release time, and the adjusted reset time  $t_{RT}$  is started. Only the active status is now present. The internal protection functions are stopped but not reset. After the release time has elapsed, the internal active state and thus all internal protective device functions are reset  $t_{re}$ . It is assumed that the adjusted delay time to switch off the circuit-breaker  $t_{tripp}$  has not yet been reached. As seen in the first part of Fig. 13.18a,b, the actual release time consists of the internal response time and the adjusted release time setting.

The second part of Fig. 13.18a,b explains the behavior when a starting signal occurs again within the release time. Whenever the starting signal is set, all internal protective device functions continue to run from the previously stored state, since the starting and active signal are present. This applies in particular to all time zones. If the adjusted delay time to switch off is reached, the protective device issues the switch-off command.

If the characteristic quantity falls below the drop-off threshold after the switch-off command, the starting signal is reset after an internal response time. The manufacturer of the protective device can now specify in which way the protective device behaves: either the adjusted release time is started again, as shown in Fig. 13.18b, or as shown in Fig. 13.18a, the protective device is immediately released.

**Dependent Release.** The logic of dependent release is identical to that of independent release. The difference is that the release time does not correspond to a fixed adjusted time value but is dependent on the value of the time delay counter and the current flowing after the reset of the starting element. The time delay counter will be integrated upward while the starting element is active and downward after the reset of the starting element. The speed of these upward and downward integrations depends on the actual flowing current and the selected delay function according to Table 13.6. The logic is shown in Fig. 13.19. Again, there are the two different behaviors after a switch-off command, which is explained in the independent release function.

The release time can be calculated using

$$\int_0^{t_p} \frac{1}{t_{TT}(G)} dt - \int_0^{t_{RT}} \frac{1}{t_P(G)} dt = 0. \tag{13.30}$$

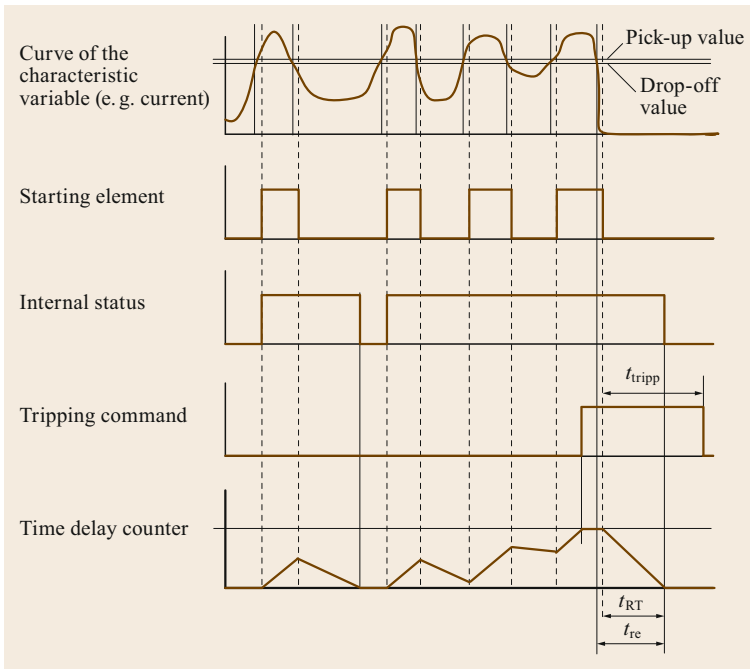
In this case,  $t_p$  is the time during which the starting signal is active. It is assumed that this time is shorter than the switch-off command time  $t_{tripp}$ . The resulting release time is  $t_{RT}$ . These relations are very easy to understand for two constant currents during and after the starting signal.

**Grading Time**

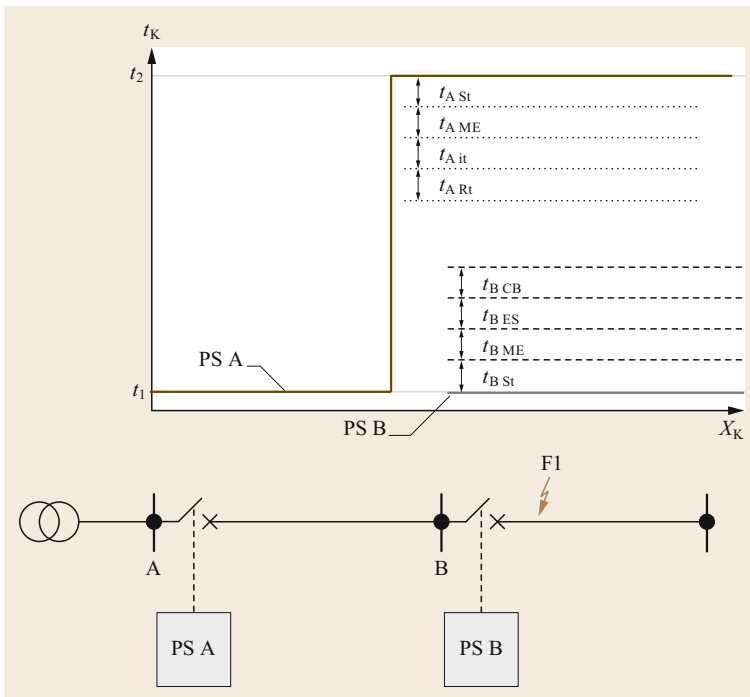
All relative selective protection criteria require a delay time to achieve selectivity. The aspects to be taken into account when determining the delay time are explained below.

Figure 13.20 shows two protective devices in neighboring protection zones. The short circuit is to be switched off by protective device B, whereas protective device A supplies backup protection for protective device B.

Protective device B requires the following times until the short circuit is cleared:



**Fig. 13.19** Function for the dependent reset time (adapted from [13.14])



**Fig. 13.20** Explanation of definition of the grading time

- $t_{B St}$  is the internal starting time of protective device B. This time depends on the implementation of the algorithms used.
- $t_{B ME}$  is the delay time caused by the error of the internal time measurement of protective device B. This value is particularly critical for electronic and electromechanical protective devices.
- $t_{B DI}$  is the adjusted delay time of protective device B. This delay time is assumed to be zero to estimate the grading time.
- $t_{B ES}$  is the delay time due to external switching relays for controlling the circuit-breaker.



- $t_{BCB}$  is the circuit-breaker opening time. This is the time from the switch-off command to the interruption of the current. This includes not only the time to open the power switch contacts but also the arc extinguishing time.

In addition to the delays caused by protective device B, the delays caused by protective device A must also be taken into account:

- $t_{ASt}$  is the internal starting time of protective device A. This time depends on the implementation of the algorithms used.
- $t_{AME}$  is the delay time caused by the error of the internal time measurement of protective device A. This is particularly critical for electronic and electromechanical protective devices.
- $t_{Ait}$  is the internal release time of protective device A. This time depends on the implementation of the algorithms used.
- $t_{ARt}$  is the additional adjusted release time of protective device A.

The required grading time  $\Delta t_{gt}$  is estimated as the sum of the times listed above. The worst-case times, meaning the maximum times, must always be selected

$$\Delta t_{gt} = t_{BSl} + t_{BME} + t_{BES} + t_{BCB} + t_{ASl} + t_{AME} + t_{Ait} + t_{ARt} \quad (13.31)$$

The required grading time thus depends largely on the technology used. Numerical protective devices have considerably shorter starting times than electromechanical protective devices. Additionally, the accuracy of the internal measurement time is considerably higher and independent of the temperature and age of the protective device. This also applies to circuit-breakers.

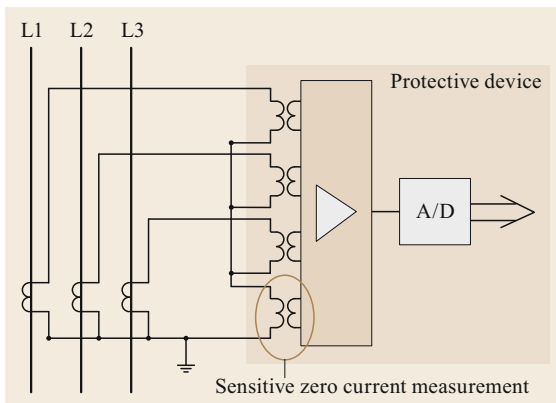


Fig. 13.21 Connection schema for overcurrent protection

Modern circuit-breakers have a short opening time. In addition, the variation of the switch-off times, depending on the temperature, is considerably smaller.

Typical grading times range from 200 to 600 ms. The shorter time applies exclusively to stations which are equipped with numerical protective devices and modern circuit-breakers. The longer times apply to stations with electromechanical protective devices and old circuit-breakers.

Usually, grid operators consider the issues described above only once when calculating the grading time. A grading time that is valid for the entire network is then defined and applied, with modifications being made only in exceptional cases.

### 13.4.2 Overcurrent Protection

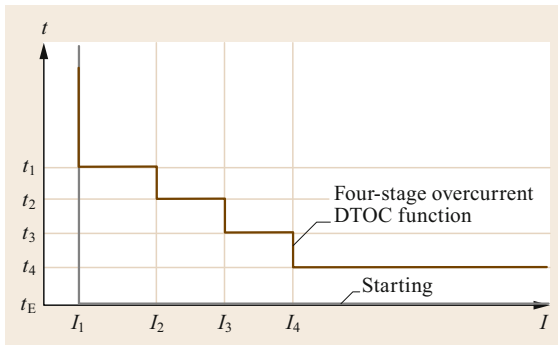
In the case of overcurrent protection, a basic distinction is made between independent and dependent overcurrent protection.

As shown in Fig. 13.21, overcurrent protective devices are connected in the same way regardless of the type of overcurrent protection function. Overcurrent protection devices have at least three current inputs for the phase currents. Often, a fourth current input is used for the zero-sequence current measurement. The zero-sequence current can theoretically also be calculated internally from the measured phase currents, but direct measurement is always more accurate. Therefore, overcurrent protective devices often have these fourth current inputs. In distribution networks with isolated star point or resonance star point earthing, a ring-type current transformer with a more sensitive transformation ratio is often used. Therefore, versions of overcurrent protective devices with a fifth current input are also available.

The inputs of all types of protective devices are completely galvanically isolated. Different technical solutions are available to achieve this, such as the use of current transformers inside each protective device. The feasible measuring ranges of protective devices are specified in the standard [13.15], with 1 A and 5 A being typically preferred.

#### Instantiations of Overcurrent Protection

The instantaneous overcurrent (IOC) or definite time overcurrent (DIOC) function is typically used by European electric distribution network operators. Modern DIOC devices offer multistage overcurrent protection functions. Figure 13.22 illustrates a four-stage overcurrent function. There are four independent settings for the current thresholds and related delay times. The smallest current threshold automatically gives the



**Fig. 13.22** Current–time characteristic of four-stage definite time overcurrent device

threshold for the starting function. There is no additional setting for the starting function. This results in simple handling for this type of protection function. If the flowing current is above this smallest threshold, almost all the internal timers are started.

Modern numerical DTOC protective devices have up to six overcurrent stages. On the one hand, this large number of overcurrent stages makes it possible to implement short tripping times for high-current faults within their own protection zone, while on the other hand, it is possible to implement multistage backup protection. This large number of overcurrent stages can be easily and cheaply implemented in numerical overcurrent protective devices, since the same programming code is called for each stage. The number of useful overcurrent stages depends on the topology of the electric power system.

The calculation of the flowing current from the sampled values can be achieved using different types of algorithms. It is possible to estimate the rms value, the amplitude of the fundamental value, or the peak value. Depending on the manufacturer, different solutions are offered. There are overcurrent protective devices where one of the above-mentioned algorithms is fixed, but also devices where the customer can select the calculation algorithm.

In addition to the analysis of the phase currents, overcurrent protective devices also include the zero-sequence and negative-sequence current. The evaluation of the zero-sequence current is used for the detection of single phase-to-earth faults, whereas the evaluation of the negative-sequence current is used for the detection of an imbalance in the network.

In addition to the classic overcurrent functions, modern numerical overcurrent protective devices now offer other functions that improve the selective short-circuit detection. These include, for example, trans-

former inrush detection and power-on stabilization for protection of capacitor banks.

To achieve selective short-circuit clearance in networks with ring structures, the short-circuit direction is additionally required. To determine the short-circuit direction, voltage information is also needed. Therefore, overcurrent protective devices that are additionally equipped with voltage inputs are also available. Based on the voltage information, various further functions, such as overvoltage protection, are implemented.

The focus of the further explanations presented below will be on the basic function of overcurrent protection. Further information on the mentioned additional function is available in the book [13.16].

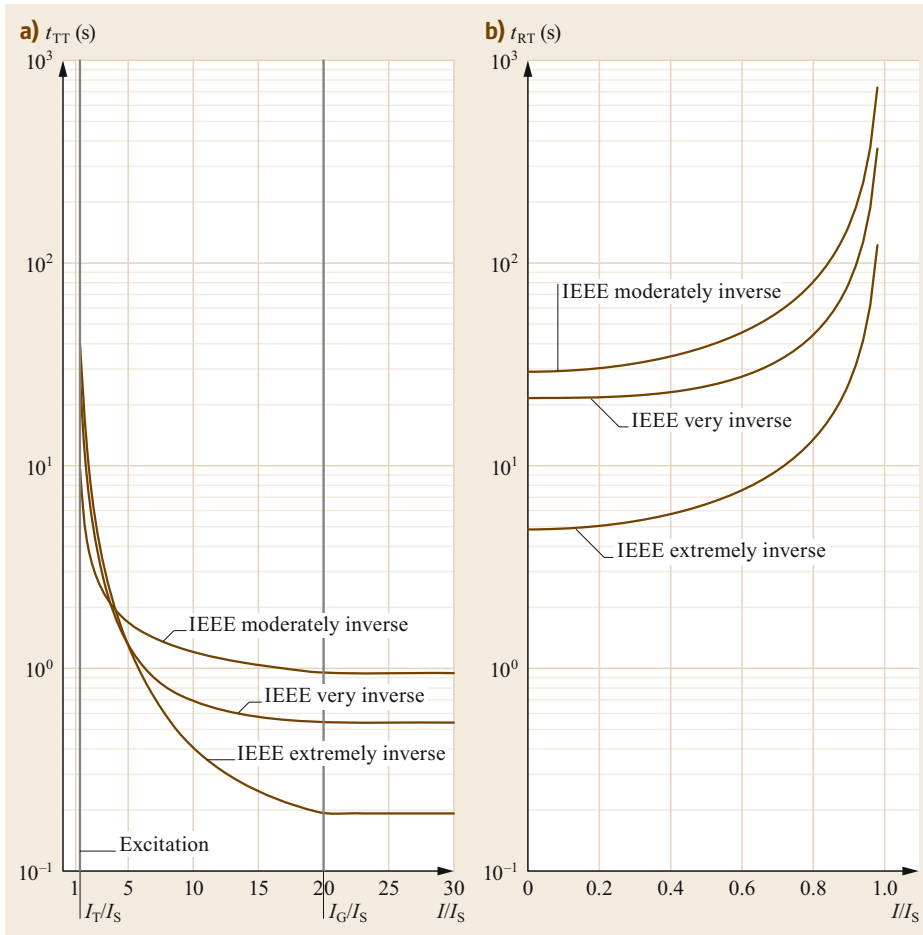
### Inverse Time–Delay Overcurrent Protection

Inverse time-delay overcurrent protection or inverse definite minimum time (IDMT) devices are typically used in North and South America for the protection of distribution lines [13.17]. With this overcurrent function, the tripping time is inversely proportional to the short-circuit current. Numerous different tripping time characteristics and reset time characteristics are defined in different standards, the best known being [13.14].

The basic parameters of these current–time characteristic curves are the so-called reference setting current ( $I_S$ ) or pick-up current and the time factor  $T_P$  or time multiplier setting (TMS). The current–time characteristic is always defined in relation to the reference setting current. In addition, the starting signal is seeded when the reference setting current is reached, implying that the overcurrent device starts operating. The TMS factor defines the general behavior of the overcurrent device. When this multiplier is adjusted to below 10, an inverse time characteristic is obtained. Multiplier factors between 10 and 20 result in a DTOC-like time characteristic. In Table 13.6, the most often-used inverse-time characteristics according to [13.14] are defined.

The time-dependent characteristic curves must be observed by the protective devices in a range from  $I_T$  to  $I_D$ .  $I_T$  is the lowest current value at which the protective device is guaranteed to operate. The determination of the delay time starts from this value. The ratio  $I_T/I_S$  must be less than 1.3. This implies that the protective device must operate correctly at a maximum of 30% above the reference value  $I_S$ .

All protective devices with a dependent characteristic curve must guarantee a shortest tripping time starting from a current value  $I_D$ . From this current onwards, the protective device can operate with a constant tripping time. This means that, from this current value onwards, dependent overcurrent time protection becomes



**Fig. 13.23a,b** Examples of current–time characteristic of inverse time–current protective devices (adapted from [13.14]).  
**(a)** Tripping time, **(b)** release time

independent overcurrent time protection. The shortest guaranteed tripping time must be calculated using

$$t_c(I_D) = T_P \left[ \frac{k}{\left(\frac{I_D}{I_S}\right)^\alpha - 1} + c \right], \tag{13.32}$$

with:

- $k$  parameter of the IDMT function [13.14]
- $\alpha$  parameter of the IDMT function [13.14]
- $c$  parameter of the IDMT function [13.14]
- $I_D$  highest current value at which the IDMT function is guaranteed to operate
- $I_S$  reference current value of the IDMT function
- $T_P$  time factor of the IDMT function.

For clarification, the different time dependences are represented graphically in Fig. 13.23a,b. In Fig. 13.23a, the three IEEE [13.14] inverse time tripping curves are shown. The TMS is set to 1 for this illustration. Depend-

ing on the flowing short-circuit current, the tripping time lies in the range from 100 s down to a few milliseconds. The advantage is that faults with a very high short-circuit current will be switched off in a very short time. This reduces the damage to the faulty equipment and the mechanical and thermal stresses on the devices carrying the short-circuit current. This figure shows the limits for the currents  $I_T/I_S$  and  $I_D/I_S$ . It can be seen that, from the current ratio  $I_D/I_S$  onwards, the protective device operates with a constant time delay.

Figure 13.23b illustrates the dependence between the current and the release time according to IEEE [13.14]. If the current ratio  $I/I_S$  is near 1, then the release time is above 100 s.

Just as for the DTOC function, not only the phase currents but also the zero- and negative-sequence currents are evaluated.

The right of Fig. 13.23 illustrates the reset time for the IEEE inverse time characteristic. Again, the TMS is set to 1. It can be seen that, for small fault currents, the reset time could be in the range of 100 s. This feature

stabilizes the protection function against intermittent faults with weak currents.

### 13.4.3 Transformer Differential Protection

The basic principle of differential protection was explained in Sect. 13.2. As described above, only the stabilized differential protection function is used today. In order to achieve a reliable and stable behavior of the differential protection, each modern differential protective device has a number of additional functions, as explained below.

#### Saturation Discriminator

High short-circuit through currents can cause the saturation of one of the two current transformers. This results in a differential current and will lead to tripping of the differential protective device. This should be avoided by correct dimensioning of the current transformers. In addition, it is generally required that identical current transformers be used on both sides of the protected object, where possible. Since, despite the above-mentioned measures, one-sided current transformer saturation can occur, a saturation discriminator is used to stabilize the differential protection.

The principal function of the saturation discriminator is based on the assumption that all current transformers operate saturation free in the first milliseconds. In this case, the differential current  $I_{\text{diff}}$  will be small but the stabilization current  $I_{\text{stab}}$  will be high.

This behavior is illustrated in the bottom of Fig. 13.24. From the starting operating point (P1), the

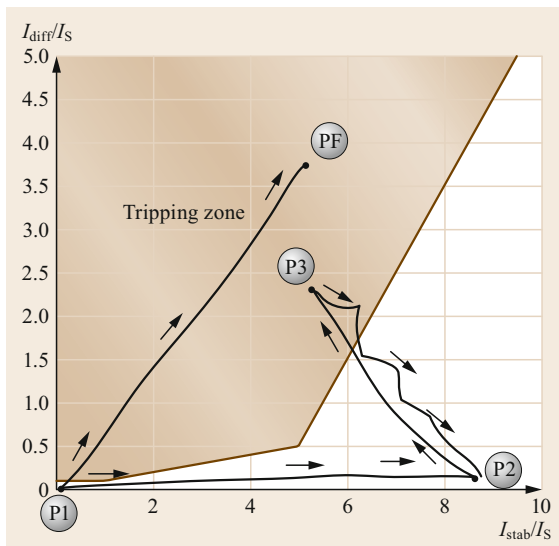


Fig. 13.24 Explanation of the saturation discriminator function

differential/stabilization current trajectory jumps to P2. This point indicates a high stabilization but low differential current. If one of the current transformers starts to saturate, the trajectory moves from point P2 to P3 inside the tripping zone, because the differential current increases. In this case, the switching off is blocked. If the saturation of the current transformer drops, the trajectory moves in steps back to point P2. If the external fault is switched off, the trajectory jumps back to the operational point P1.

In the case of an internal fault, the differential/stabilization current trajectory jumps directly from the operation point P1 to the fault point PF. In this case, switching off by the circuit-breaker is initiated.

This saturation discriminator analysis explains the movement of the differential/stabilization current trajectory. In this way, any external or internal fault with saturation of the current transformer can be discriminated.

#### Inrush Detection

A high transient current can occur when switching on transformers or other electric equipment with an iron core. The reason is the saturation of the iron core, which depends on the remanence and the switching instant. These so-called inrush currents with amplitude up to 10 times the nominal current can occur for several 100 ms. This is illustrated in Fig. 13.25.

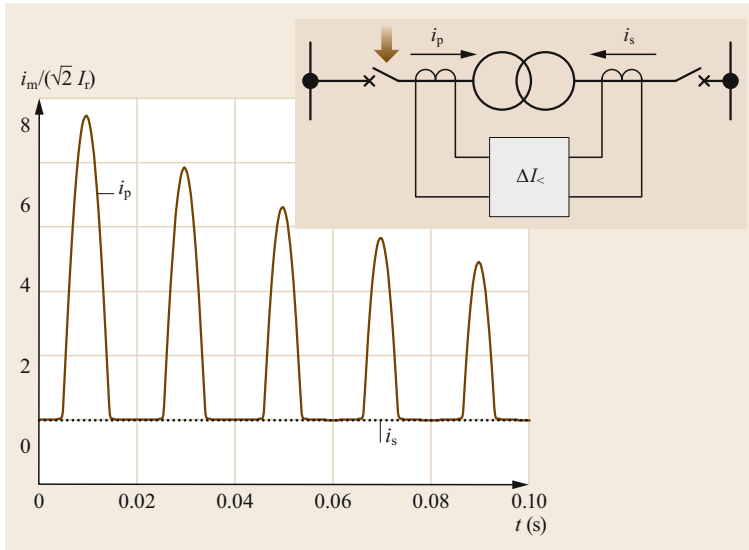
The unsymmetrical inrush current leads to an unsymmetrical voltage drop across the long connection lines. This results in an unsymmetrical voltage at the connection point, which is comparable to a small DC voltage offset. This DC voltage offset leads to saturation of other electric equipment with an iron core that has not been switched, an effect called sympathetic inrush.

The inrush current only flows from one side into the electric equipment. From the point of view of the differential protection function, this current therefore always indicates an internal fault. To avoid malfunction, the inrush stabilization function is necessary for the differential protection function.

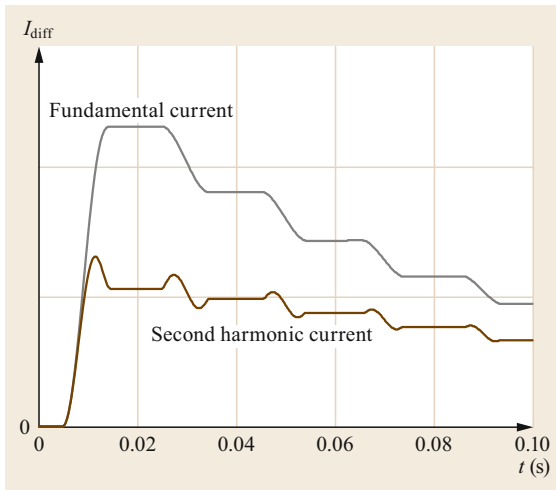
Inrush stabilization is based on an analysis of the frequency spectrum of the differential current. Figure 13.26 shows a typical frequency spectrum for an inrush current. The second harmonic reaches values up to 50% of the fundamental current. A typical threshold to identify the inrush current is 20–30% of the fundamental current. During normal operation, the second harmonic will never reach this level.

#### Additional Functions for Power Transformers

Additional functions are required to provide differential protection for transformers. Very often, the rated cur-



**Fig. 13.25** Example of an inrush current



**Fig. 13.26** Frequency spectrum of an inrush current

rent of a power transformer and a current transformer are not identical. In addition, three-phase transformers may exhibit a phase shift between the different terminals of the transformer. Both effects have to be considered for the application of a differential protection schema.

#### Normalization of the Measured Currents

The rated current at each terminal of a power transformer is determined by the rated voltage at this terminal and the rated power of the winding of the terminal. Therefore, the values of the rated current of a power transformer are not compatible with the standard values for current transformers according to [13.7]. In order to reduce the reserve requirement, grid operators some-

times use selected values of the rated currents defined in the standard. There is always a mismatch between the rated current of the power transformer, current transformer, and protective device.

Previously, an adjustment transformer was used to interconnect the current transformer and protective device. This adjustment transformer was individually dimensioned and built, and this approach was not very flexible and was prone to errors.

Normalization of the measured currents includes two steps. First, all the currents are transformed to the primary terminal of the power transformer, taking into account the transformer ratio of the current transformers and the power transformer itself. In the second step, these currents are referred to the rated current of the primary terminal of the power transformer. Today, modern numerical differential protective devices calculate an internal adjustment factor  $k_x$  based on the parameters of the power and current transformers. The measurements of the protective device are then scaled internally using this adjustment factor. The superscript symbol (") is used to indicate that the current is normalized.

The calculation of the adjustment factor is explained below.

To estimate the currents at each terminal of the power transformer, the measured currents must be multiplied by the current transformation ratio of the used current transformers. The current on the primary terminal of the power transformer can be calculated as

$$I_{pPT} = I_{pm} \frac{I_{prCTP}}{I_{srCTP}}, \tag{13.33}$$

with:

- $I_{pPT}$  current at the primary terminal of the power transformer  
 $I_{pm}$  measured current at the primary terminal of the power transformer  
 $I_{prCTP}$  primary rated current of the current transformer on the primary terminal of the power transformer  
 $I_{srCTP}$  secondary rated current of the current transformer on the primary terminal of the power transformer.

A related calculation can be done for the secondary terminal of the power transformer using

$$I_{sPT} = I_{sm} \frac{I_{prCTS}}{I_{ssCTS}}, \quad (13.34)$$

with:

- $I_{sPT}$  current at the secondary terminal of the power transformer  
 $I_{sm}$  measured current at the secondary terminal of the power transformer  
 $I_{prCTS}$  primary rated current of the current transformer on the secondary terminal of the power transformer  
 $I_{srCTS}$  secondary rated current of the current transformer on the secondary terminal of the power transformer.

The calculations of the differential and stabilizing currents are carried out at the primary terminal of the power transformer. Therefore, all the currents must be converted to this side of the power transformer. The current transformation ratio of the power transformer can be calculated as

$$u_{vpsPT} = \frac{V_{prPT}}{V_{srPT}} = \frac{S_{prPT} \sqrt{3} I_{srPT}}{S_{srPT} \sqrt{3} I_{prPT}}, \quad (13.35)$$

with:

- $u_{vpsPT}$  voltage transformation ratio between the primary and secondary terminal of the power transformer  
 $V_{prPT}$  rated voltage at the primary terminal of the power transformer  
 $V_{srPT}$  rated voltage at the secondary terminal of the power transformer  
 $S_{prPT}$  rated apparent power at the primary terminal of the power transformer  
 $S_{srPT}$  rated apparent power at the secondary terminal of the power transformer  
 $I_{prPT}$  rated current at the primary terminal of the power transformer  
 $I_{srPT}$  rated current at the secondary terminal of the power transformer.

Usually, the apparent powers of the primary and secondary terminal of a power transformer are identical. However, power transformers with three terminals often have different apparent powers at each terminal. Therefore, this general equation is selected to calculate the transformation ratio of a power transformer.

The secondary current referred to the primary side of the power transformer is calculated as

$$I'_{sPT} = I_{sPT} \frac{1}{u_{vpsPT}} = I_{sPT} \frac{S_{srPT} I_{prPT}}{S_{prPT} I_{srPT}}, \quad (13.36)$$

with:

- $I'_{sPT}$  secondary current referred to the primary side of the power transformer

Normally, the currents are scaled by the rated current of the primary terminal

$$\begin{aligned} I''_s &= I_{sPT} \frac{1}{u_{vpsPT}} \frac{1}{I_{prPT}} = I_{sPT} \frac{S_{srPT}}{S_{prPT}} I_{srPT} \\ &= I_{sm} \frac{I_{prCTS}}{I_{srCTS}} \frac{S_{srPT}}{S_{prPT}} I_{srPT} = I_{sm} k_s, \end{aligned} \quad (13.37)$$

with:

- $I''_s$  normalized secondary current on the primary terminal of the power transformer  
 $k_s$  internal adjustment factor for the secondary terminal.

This results in the general internal adjustment factor  $k_x$ ,

$$k_x = \frac{I_{prCTx}}{I_{srCTx}} \frac{S_{rxPT}}{S_{prPT} I_{rxPT}}, \quad (13.38)$$

with:

- $k_x$  general internal adjustment factor, where x stands for s (secondary), p (primary), or t (tertiary)  
 $I_{prCTx}$  primary rated current of the current transformer on terminal x of the power transformer  
 $I_{srCTx}$  secondary rated current of the current transformer on terminal x of the power transformer  
 $S_{prPT}$  rated apparent power at the primary terminal of the power transformer  
 $S_{xPT}$  rated apparent power at terminal x of the power transformer  
 $I_{xPT}$  rated current at terminal x of the power transformer.

Depending on the design of the numerical differential protective device, the adjustment factor can only be calculated for a defined ratio of the rated currents.

If there is a large mismatch between the rated current of the power transformer and the rated primary current of the current transformer, the signal at the input of the protective device will be very low and noisy. This inaccuracy would be increased by multiplication with a huge adjustment factor, so depending on the manufacture, the adjustment factor is limited.

### Vector Group Adjustment

Power transformers are built with different types of connection of the windings. Typical winding connections are delta and star connection. Depending on the connection type and winding scheme applied, a phase shift appears between the currents at the terminals of the power transformer. This is defined by the vector group of the transformer.

Previously, phase adjustment transformers were interconnected between the current transformer and protective device to eliminate this phase shift. However, the phase adjustment transformer must be individually dimensioned and built. This was not very flexible and was prone to errors.

Modern numerical differential protective devices use a so-called vector group adjustment matrix. The structure and calculation of this matrix are explained below.

The calculation of the transformer differential current is based on the winding currents. The winding currents are calculated by means of the measured terminal currents. It is assumed that all the terminal currents are normalized. For windings with star connection, the measured terminal currents are identical to the winding currents. For windings with delta connection, it must be considered that the voltage ratios and winding ratios are not identical. For delta winding, the currents can be calculated by

$$\underline{I''_{s a W}} = \frac{1}{\sqrt{3}} \underline{I''_{p a}}, \quad (13.39)$$

$$\underline{I''_{s b W}} = \frac{1}{\sqrt{3}} \underline{I''_{p b}}, \quad (13.40)$$

$$\underline{I''_{s c W}} = \frac{1}{\sqrt{3}} \underline{I''_{p c}}, \quad (13.41)$$

with:

- $\underline{I''_{p a}}$  normalized primary terminal current of phase a
- $\underline{I''_{p b}}$  normalized primary terminal current of phase b
- $\underline{I''_{p c}}$  normalized primary terminal current of phase c
- $\underline{I''_{s a W}}$  normalized secondary winding current of the delta winding phase a
- $\underline{I''_{s b W}}$  normalized secondary winding current of the delta winding phase b
- $\underline{I''_{s c W}}$  normalized secondary winding current of the delta winding phase c.

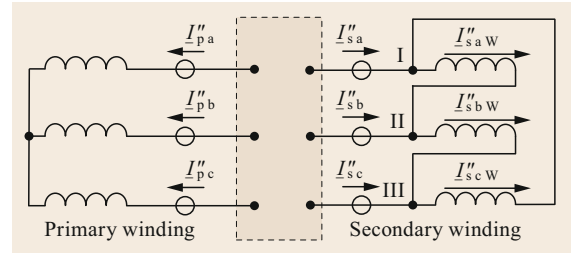


Fig. 13.27 Example for the calculation of the vector group adjustment matrix

According to Fig. 13.27, the measured terminal currents do not correspond to the winding currents. There is one branching point (node) between these two currents. The following current equations result at these branching points, where the calculation is performed using the currents whose values have already been adjusted to the rated current of the current transformers

$$\text{Node I: } \underline{I''_{s a}} = \underline{I''_{s a W}} - \underline{I''_{s c W}}, \quad (13.42)$$

$$\text{Node II: } \underline{I''_{s b}} = \underline{I''_{s b W}} - \underline{I''_{s a W}}, \quad (13.43)$$

$$\text{Node III: } \underline{I''_{s c}} = \underline{I''_{s c W}} - \underline{I''_{s b W}}, \quad (13.44)$$

with:

- $\underline{I''_{s a}}$  normalized secondary terminal current of phase a
- $\underline{I''_{s b}}$  normalized secondary terminal current of phase b
- $\underline{I''_{s c}}$  normalized secondary terminal current of phase c.

Using this equation system alone, the winding currents cannot be calculated; An additional equation is needed:

Node I minus node II results in

$$\underline{I''_{s a}} - \underline{I''_{s b}} = \underline{I''_{s a W}} - \underline{I''_{s c W}} - \underline{I''_{s b W}} + \underline{I''_{s a W}}, \quad (13.45)$$

$$\underline{I''_{s a}} - \underline{I''_{s b}} = 2\underline{I''_{s a W}} - (\underline{I''_{s c W}} + \underline{I''_{s b W}}) + \underline{I''_{s a W}} - \underline{I''_{s a W}}, \quad (13.46)$$

$$\underline{I''_{s a}} - \underline{I''_{s b}} = 3\underline{I''_{s a W}} - (\underline{I''_{s c W}} + \underline{I''_{s b W}} + \underline{I''_{s a W}}). \quad (13.47)$$

The sum of the three winding currents corresponds to three times the zero-sequence current in the transformer of the rate current adjustment and normalized currents. Due to the rate current adjustment and normalization of all currents, the current in the secondary winding is equal to the current in the primary winding, yielding

$$\begin{aligned} \frac{1}{3} (\underline{I''_{s a}} - \underline{I''_{s b}}) &= \underline{I''_{s a W}} - \underline{I''_{0 W}} \\ &= \frac{1}{\sqrt{3}} (\underline{I''_{p a}} - \underline{I''_{0}}). \end{aligned} \quad (13.48)$$

This calculation is repeated also for node II minus node III and node II minus node I.

Finally, the following matrix equation results

$$\underbrace{\begin{pmatrix} I''_{pa} \\ I''_{pb} \\ I''_{pc} \end{pmatrix}}_{\mathbf{i}_p^{''*}} - I''_0 = \frac{1}{\sqrt{3}} \begin{pmatrix} 1 & -1 & 0 \\ 0 & 1 & -1 \\ -1 & 0 & 1 \end{pmatrix} \underbrace{\begin{pmatrix} I''_{sa} \\ I''_{sb} \\ I''_{sc} \end{pmatrix}}_{\mathbf{i}_s''}. \quad (13.49)$$

This equation can be written as

$$\mathbf{i}_p^{''*} = f_{vs} \mathbf{S}_s \mathbf{i}_s'', \quad (13.50)$$

with:

- $f_{vp}$  winding factor of secondary terminal
- $\mathbf{S}_s$  vector group adjustment matrix
- $\mathbf{i}_s''$  vector of the measured and normalized current of the secondary terminal
- $\mathbf{i}_p^{''*}$  vector of the measured and normalized current of the primary terminal without the zero-sequence current.

#### 13.4.4 Busbar Differential Protection

Different protection criteria (Sect. 13.2.1) are used for busbar protection. For applications in distribution networks, only the binary starting signals from other protection devices, e.g., for overcurrent protection of the feeders, are logically linked to detect busbar faults. For a single-busbar substation with only a single feed-in and a small number of outgoing feeders, without feed-in, so-called backward interlocking is used. This is an effective, fast, and inexpensive busbar protection solution for simple busbar systems [13.18]. In general, no additional equipment is required. As described above, a definite direction of the energy flow—from the transportation to the distribution network—is necessary.

In the past, power differences or phase shifts of the currents between all the feeders of a busbar were used to detect busbar faults [13.19]. In addition, so-called high-impedance differential busbar protection devices are also used outside of Europe [13.20]. This type of busbar protection is usually recommended for small busbar systems with few feeders. The advantage of this technology is its good performance, immunity to current transformer saturation, and relatively low cost [13.21]. With the introduction of numerical protection devices, the significance of this type of busbar differential protection has decreased.

In modern low-impedance differential busbar protection, the currents are digitized immediately at the current transformers and then processed numerically. This principle is a lot more flexible [13.22]; for example, current transformers with different transformation ratios and transmission behavior can be used. In addition, it is much easier to extend the protection system [13.23]. Such low-impedance differential busbar protection is described in detail below.

Modern busbar protection devices are based on the stabilized current differential principle (Sect. 13.2.1). For larger busbar substations with several busbar sections or reverse busbars, a subdivision into discriminating zones is implemented [13.24]. The current sum is calculated for each independently operated discriminating zone and is zero under normal operation conditions or if a fault occurs outside the discriminating zone. The described procedure is physically based on Kirchhoff's current law, which states that the currents flowing into a node must be equal to the current flowing out of it. This means that the sum of all the currents flowing into a node is zero if the direction of the currents is taken into account. This natural law is valid for alternating currents at any time or to the complex current phasor with the correctly calculated phase.

The principle of low-impedance differential busbar protection is illustrated in Fig. 13.28, which shows a double busbar system. The number and structure of discriminating zones are defined by the position of the disconnectors. Ideally, the discriminating zones should correspond to the protection zones (Sect. 13.1.2). However, this is not feasible technically, since the protection zones are bordered by the current transformers and not by the disconnectors and circuit-breakers. If a short circuit occurs between the current transformer and circuit-breaker of an outgoing feeder, it is no longer located within the protection zone but lies in the corresponding discriminating zone. Nonselective tripping occurs for this small area of the busbar system.

The equations presented below apply to the protection zones within the two discriminating zones (DZs) of the double busbar substation considering the position of the disconnectors illustrated in Fig. 13.28. During normal operation, the following sum of the primary currents applies to each discriminating zone

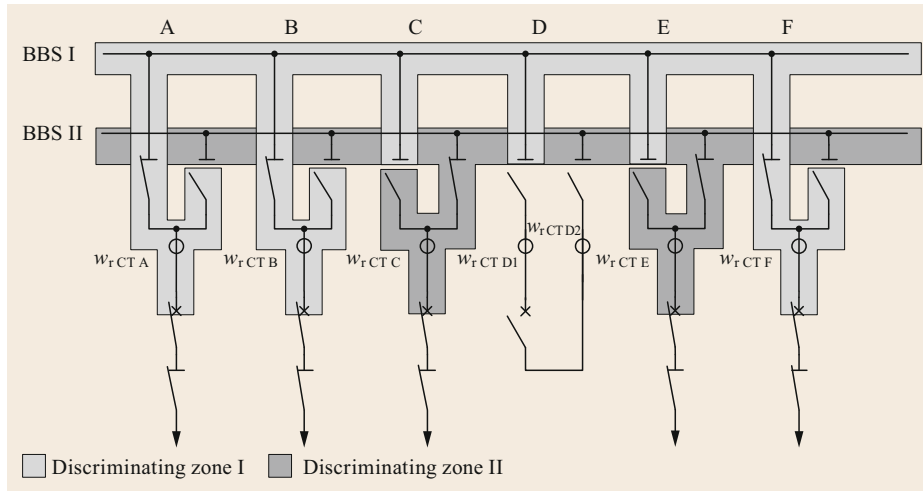
DZ I (normal operation):

$$I_{pDZIA} + I_{pDZIB} + I_{pDZIF} = \Delta I_{pDZI} = 0, \quad (13.51)$$

DZ II (normal operation):

$$I_{pDZIC} + I_{pDZIE} = \Delta I_{pDZII} = 0. \quad (13.52)$$





**Fig. 13.28** Double busbar substation with two busbar sections (BBS I and BBS II) and two discriminating zones (DZs)

The total primary current for the entire busbar substation can be calculated for normal operation as

$$\text{Total busbar system (normal operation):} \\ \Delta I_{p,DZI} + \Delta I_{p,DZII} = 0. \quad (13.53)$$

A prerequisite for the correct calculation of the primary current sum is a standardized measuring direction for the current transformers. This must be ensured during the installation of the current transformers. It could be decided, for example, that currents flowing into the busbar are positive while currents flowing out of it are negative.

If one of (13.51)–(13.53) is not fulfilled, there is a fault within the busbar system. These simple relations form the basis for low-impedance busbar differential protection. Theoretically, only the current sum can be used to differentiate between the faultless and faulty states within the discrimination zone. The current sum can be calculated by using either the instantaneous values of the currents or the complex current phasor, mentioned above. In these equations, the representation of the current phasors is used. In numerical busbar differential protection systems, the current sum is calculated on a phase-selective basis. In the event of a short circuit within a discrimination zone, all the circuit-breakers assigned to this discrimination zone are selectively opened. The goal is to disconnect from the faultless network only the part of the busbar that is affected by the fault.

However, numerous inaccuracies in the measurement system must be taken into account when implementing busbar protection systems, e.g., the deviations of the transmission ratio of the used current transformers within their fault tolerances, the stationary and dynamic transmission behavior of the current

transformers, and the measurement errors of the entire measurement chain.

### Normalization of the Measured Secondary Currents

In this straightforward form, the calculation of the current sum applies only to the primary currents in the substation. Like all protective devices, the busbar protection system is connected to the primary system via current transformers. The current transformers reduce the currents according to their transmission ratio true to scale. The phase angle of the currents is retained. The following equation corresponds to the current sum of discriminating zone I (DZ I) for the secondary measured currents, where the nominal transmission ratios of the current transformers are considered (Sect. 13.3.1)

$$I_{sIA} w_{rCTA} + I_{sIB} w_{rCTB} + I_{sIF} w_{rCTF} = 0. \quad (13.54)$$

The equation for the current sum calculation based on the currents measured on the secondary side of the current transformers and their nominal transformation ratios is mathematically accurate, but can suffer from numerical problems if implemented in numerical protection devices. For this reason, manufacturers of protective devices internally convert the current to a fictitious uniform busbar reference current, similar to the implementation in transformer differential protection devices.

### Stabilization of Busbar Differential Protection

If a busbar protection algorithm were to be based only on the calculation of the current sum, measurement errors in the current transformers, for example, could already lead to unwanted tripping. If the short circuit occurs near the busbar, the outgoing short-circuit cur-

rent is divided between several feeders. These parts of the short-circuit currents are considerably smaller. Due to the percentage errors of the current transformers, this can result in significant residual currents. For this reason, busbar differential protection also works with stabilization. Further details can be found in Sect. 13.2.1. This implies that, for busbar differential protection, a stabilization characteristic similar to that for transformer differential protection must be set.

#### Synchronized Data Acquisition

Due to the spatial extent of large busbar systems, the current signals cannot be transmitted as analog values to a central data acquisition system. Therefore, modern busbar protection devices work with decentralized data acquisition units. In addition to the analog signals, the feeder-related binary input and output are also recorded there. For the current sum calculation explained above, however, it is a precondition that all analog information be acquired synchronously. Today, manufacturers of busbar protection devices use proprietary communication protocols to guarantee this. Physically, fiber-optic connections to the central device are often used. These enable very high data rates and can ensure electromagnetic compatibility at the same time.

#### Discriminating Zone

As explained above, large busbar systems will be divided into discriminating zones. The discriminating zones are defined by the position of the disconnectors within the topology of the busbar system and the current position of these disconnectors. When the disconnectors are switched on, the downstream circuit-breakers form the physical border of the discriminating zone. The discriminating zone defines which measured current values are merged to become a current node. The structure of the discriminating zone can be determined by logical operations or by a topological calculation algorithm. Both methods are used in practical applications.

Due to the long operation times of disconnectors, which can extend several tens of seconds, the following states of the disconnector have to be taken into account: switched on, switched off, and fault/intermediate position. There are different strategies for handling the fault/intermediate position of a disconnector. The discriminating zone can be completely blocked. A busbar fault occurring at that time results in a complete switch-off of all circuit-breakers of this busbar system by the comprehensive check zone. Alternatively, the fault/intermediate position of the disconnector can be substituted by a predefined switch position. This substitute value is selected such that reliable tripping occurs in an extended discriminating zone. Within very large busbar systems with a large number of discriminating

zones, this prevents the protection system from completely switching off the whole busbar system if a short circuit occurs during this transition period.

#### Check Zone

In the check zone, the actual positions of the disconnectors are not taken into account. The sum of all the measured currents of the entire busbar substation is calculated. In the case of an internal short circuit, this leads to a nonselective switch-off of the entire busbar system. The check zone acts as a backup function for when an internal short circuit in a busbar is not detected within the associated discriminating zone.

The check zone could also be used to stabilize the operation of the busbar protection device. If an internal short circuit is detected in one of the discriminating zones but not within the check zone at the same, the tripping is blocked. Such miscalculation of the current sum within the discriminating zone could be caused, for example, by an incorrect assignment of a feeder to this discriminating zone.

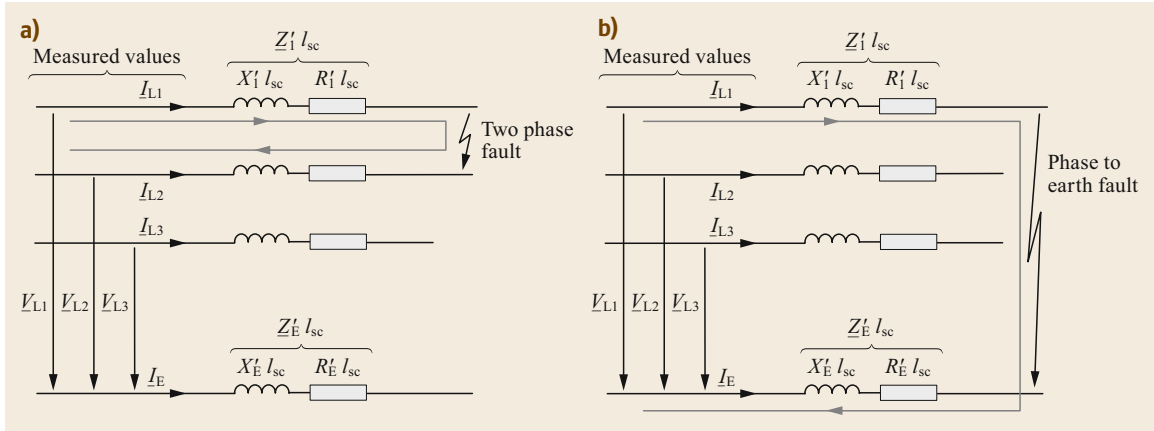
#### Saturation Discriminator

In the event of a high-current short circuit near the busbar substation, current transformer saturation may occur. A saturation discriminator is used in order to achieve a stable behavior of the busbar differential protection system, similar to the one used in transformer differential protection systems. The functionality of the saturation discriminator is explained in Sect. 13.4.3. The detailed technical realization of the saturation discriminator depends on the manufacturer of the busbar protection device. In addition, it depends on whether the current sum is calculated using instantaneous values or phasors.

#### Additional Functions

The busbar protection device records a large amount of information from the whole busbar system. It is aware of the current switching status of disconnectors and circuit breakers and can respond very quickly. Therefore, a number of additional functions are integrated into numerical busbar protection systems today; these are not busbar protection functions in the strict sense, but they improve the selectivity and reaction time of the overall protection system.

**Circuit-Breaker Failure Protection.** If a fault occurs within the discriminating zone, all circuit-breakers which border this discriminating zone receive the switch-off command. The circuit-breaker failure protection function checks whether the current flowing through these circuit-breakers is very small within an adjustable time after a trip command. If the current does



**Fig. 13.29a,b** Illustration of calculation loop depending on the fault type. (a) Phase-to-phase calculation loop, (b) phase-to-earth calculation loop

not drop below a minimum value, a trip signal is sent to the circuit-breaker at the other end of the connected line. This enables quick identification of a busbar fault in case of a malfunction of the circuit-breaker of a busbar feeder. This function improves the stability of the electrical power transmission system.

**Direct Tripping of a Discriminating Zone Through External Signals.** This fallback function is used in the case of a circuit-breaker malfunction in the event of a short circuit on the line. The short circuit on the line is detected by the line protection device. The line protection device sends an off command to the corresponding circuit-breaker. If this circuit-breaker malfunctions, the short-circuit current can only be interrupted by opening all of the circuit-breakers which belong to the same discriminating zone. An external trip signal at the corresponding feeder is used to notify the busbar protection system that all circuit-breakers assigned to this discriminating zone should be switched off. As this is a very critical function—as a major part of a busbar system is switched off—this function is ensured by secondary information, which can be either an additional binary enable signal or an internal current threshold. The external trip signal is only accepted if the current threshold is exceeded or a binary enable signal is present at the same time. In addition, the time sequence of the trip and enable signals is usually monitored to avoid overfunctions.

### 13.4.5 Distance Protection

The distance protection criterion was explained in Sect. 13.2.1 based on a single-phase example. Real distance protection devices have at least three current inputs for the phase currents and three voltage inputs

for the phase-to-earth voltages. Further technical specifications are described in [13.25]. Depending on the additional functions, for example, a sensitive earth fault detection or so-called zero-current compensation for double circuit lines, additional current and/or voltage inputs may also be present. However, only the three current and voltage inputs mentioned above are required for the basic distance protection function. For the connection and dimensioning of the current transformers, the information given for overcurrent protection and the current transformer apply.

#### Calculation of the Loop Impedance in a Three-Phase System

Depending on the type of short circuit, different calculation loops have to be used. Figure 13.29 shows an example of a single-phase fault and a two-phase fault. The first case results in a single phase-to-phase calculation loop, for which the following equation can be applied

$$I_{L1}Z'_{sc} - I_{L2}Z'_{sc} = V_{L1} - V_{L2} \quad (13.55)$$

The equation for calculating the fault impedance of a phase-to-phase calculation loop can thereby be obtained. To calculate the fault distance, only the positive-sequence reactance per unit length has to be known

$$\frac{V_{L1} - V_{L2}}{I_{L1} - I_{L2}} = Z'_{sc} = R'_{sc} + jX'_{sc} \quad (13.56)$$

A phase-to-earth fault results in a phase-to-earth calculation loop, for which the following equation can be applied

$$I_{L1}Z'_{sc} - I_E Z'_E = V_{L1} \quad (13.57)$$

The positive-sequence reactance per unit length and the earth reactance per unit length have to be known for the further calculation. The goal is to obtain identical equations to calculate the fault distance independent of the fault type. Therefore, the equation is converted and the so-called complex  $\underline{k}_E$ -factor introduced

$$\begin{aligned} \underline{Z}'_1 l_{sc} \left( I_{L1} - I_E \frac{\underline{Z}'_E}{\underline{Z}'_1} \right) &= \underline{Z}'_1 l_{sc} (I_{L1} - I_E \underline{k}_E) \\ &= \underline{V}_{L1} . \end{aligned} \quad (13.58)$$

This results in

$$\frac{\underline{V}_{L1}}{I_{L1} - I_E \underline{k}_E} = \underline{Z}'_1 l_{sc} = R'_1 l_{sc} + jX'_1 l_{sc} , \quad (13.59)$$

$$\underline{k}_E = \frac{\underline{Z}'_E}{\underline{Z}'_1} = \frac{\underline{Z}'_0 - \underline{Z}'_1}{3\underline{Z}'_1} . \quad (13.60)$$

From (13.60), it can be seen that the complex factor  $\underline{k}_E$  can be interpreted as a weighting factor for the earth return current, which is constant for specific cables or overhead line arrangements. It should be pointed out that the factor  $\underline{k}_E$  depends on the zero-sequence impedance. This includes not only the conductivity of the earth itself, but also all conductive material in the earth. The calculation of this impedance is therefore problematic, especially in cities, and it has to be measured.

There are different definitions for the  $\underline{k}_E$  factor depending on the manufacturer. However, all the definitions are based on (13.57); For example, this equation can be split into real and imaginary parts to get a real  $k_R$  factor for the resistance and a real  $k_X$  factor for the reactance. A common feature of all the methods is that the positive-sequence reactance per unit length is always used to calculate the fault distance.

Functionally, a distinction is made between a switched or full distance protection schema. In the case of a multiphase fault, the fault distance can be calculated in all fault-affected phase-to-earth and phase-to-phase loops. In the case of a two-phase-to-earth fault (Fig. 13.30), there are two phase-to-earth loops and one phase-to-phase loop, for which the fault distance can be calculated. In the case of the switched distance schema based on complex logic, one of these loops is selected. This should be the same loop for all the distance protection devices in a physically connected electrical network. In Europe, the switched distance protection schema is typically used in medium- and high-voltage networks [13.26]. The full distance protection schema is applied worldwide in extrahigh-voltage networks. A mixture of the two different distance protection schemas should be avoided, as complex short-circuit sequences may result in nonselective tripping.

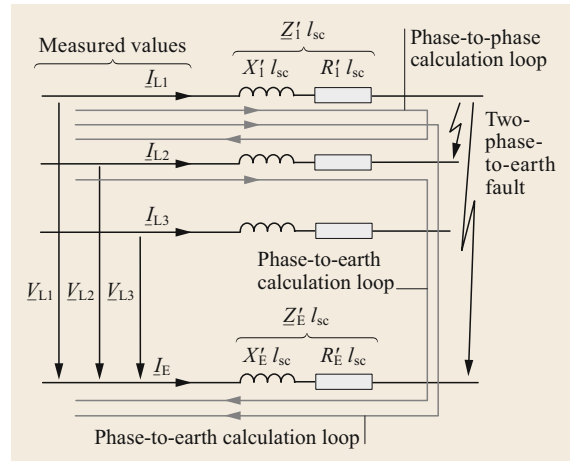


Fig. 13.30 Illustration of switched and full distance protection schemas

The differentiation between switched and full distance protection schemas has its origin in electromechanical and analog protection devices. When using these technologies, each measurement loop was implemented in separate hardware. For the switched distance protection schema, only one measurement unit and simple switching logic were needed.

Figure 13.31 shows the main functions of a switched distance protection system. In comparison with overcurrent protection, significantly more subfunctions must be configured by the user. This increases the complexity of distance protection applications.

Switch distance protection calculates the fault direction and distance, then selects a distance zone based on the selected calculation loop.

#### Distance Measuring System

The concept of distance protection was explained in Sect. 13.2.1. The measured reactance is used to determine the distance between the measuring point and the short-circuit location. This is done because the measured resistance could be biased by a short-circuit resistance at the fault location and additionally, in the case of an arc fault, by the arc fault resistance. The realization of the impedance measurement function by electromechanical relays or analog circuits does not allow separate evaluation of the resistance and reactance, as should be done ideally.

The tripping characteristic of electromechanical or analog technology-based distance protection [13.27] in the complex  $R$ - $X$  plane results in circles or a so-called mho characteristic (admittance circle) [13.6]. This is illustrated in Fig. 13.32. The introduction of modern numerical protection devices enabled an optimized design of the tripping characteristic. The goal was to achieve

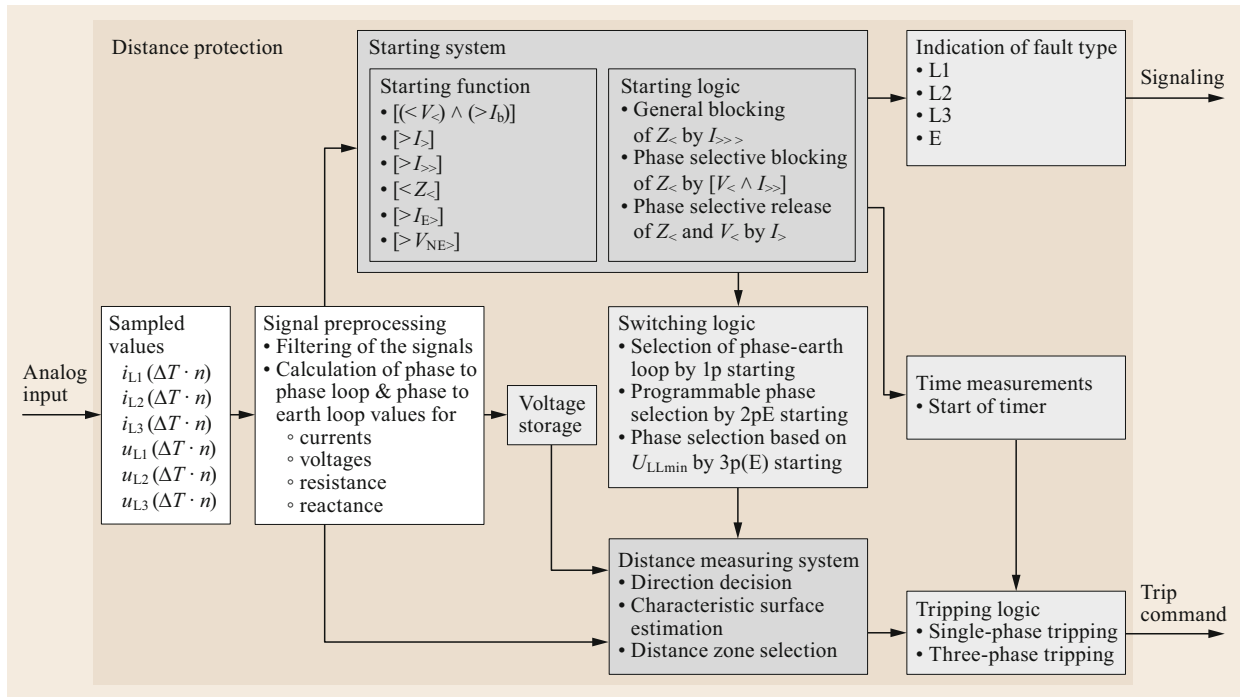


Fig. 13.31 Functions of a switched distance protective device

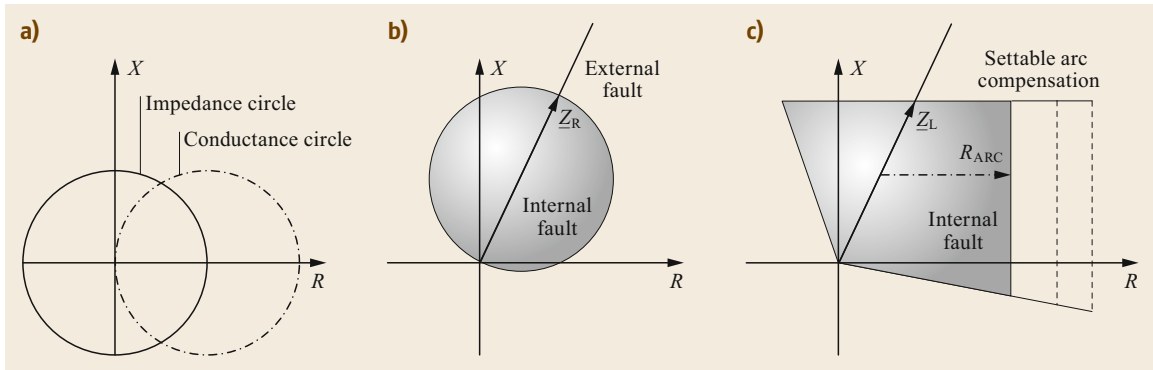


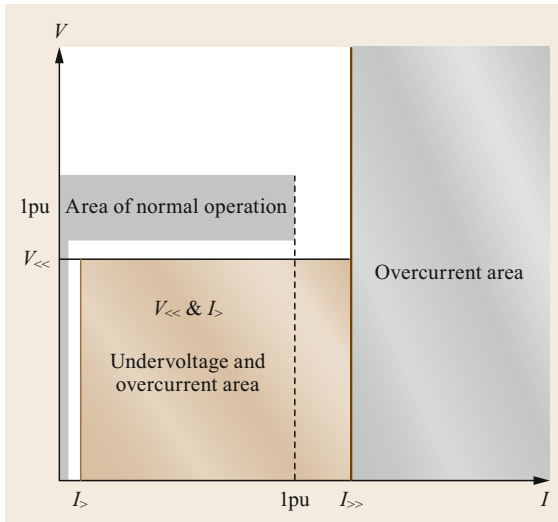
Fig. 13.32a–c Illustration of various tripping characteristics. (a) Tripping characteristic of an electromechanical device. (b) Mho characteristic (admittance circle). (c) Polygonal tripping characteristic

the largest possible and user-adjustable arc resistance reserve or compensation. This leads to the polygonal tripping characteristic curves which are typical today. The mixed use of distance protection devices with mho and polygonal tripping characteristics is possible, but problematic. In Europe, the use of the polygonal tripping characteristic curve has been established on all voltage levels due to its many advantages.

#### Starting System

The goal of the starting system is to differentiate between the fault condition and the normal operation

status. In contrast, the focus of the described distance measuring system is only on the protected object, e.g., an overhead line, and not on the overall electrical energy system. This starting function should detect all abnormal states in the complete electrical energy network. A distinction from the permitted load range has to be made. In general, a distinction is made between the overcurrent, undervoltage, and underimpedance starting functions. Numerical distance protection devices today work in parallel with all three types of starting functions. In detail, these functions can have different specifications depending on the manufacturer.



**Fig. 13.33** Illustration of the overcurrent and undervoltage starting function

#### Overcurrent and Undervoltage Starting Function.

The overcurrent and undervoltage starting function is illustrated in Fig. 13.33. The permissible operating range is marked in the current–voltage plane by a gray area. This operation range is limited by the permissible voltage range and the maximum permissible operating current, taking into account a temporary overload. It has to be considered that the switched-off line is also a permissible operating state. Here, the voltage and current are zero, or very small for measuring reasons. These effects result in the gamma-shaped permissible operating range displayed.

It can be seen that a simple overcurrent starting threshold  $I_{\gg}$  does not optimally adapt to the permissible operating range. In the case of a weak in-feed, the voltage drops below the permissible operating voltage but the short-circuit current does not reach the overcurrent starting threshold, so the fault would not be detected.

The undervoltage starting function ( $V_{\ll}$ ) with an additional enabling current threshold ( $I_{\gg}$ ) provides a much better adaptation to the permissible operating range. The enabling current threshold is necessary to identify the switched-off status. This is illustrated in Fig. 13.33.

**Underimpedance Starting Function.** In the case of underimpedance starting, the actual measured impedance is compared with the permissible load impedance. The principle is shown in Fig. 13.34. It is assumed that the permissible load always has a very large ohmic component. A pure reactive load is not regarded as a permissible operating condition.

In the case of electromechanical and electronic distance protection devices, the shape of the starting char-

acteristic in the  $R$ – $X$  plane is often a technology-based circular characteristic or one of its variants, similar to the distance measurement system.

With today's numerical distance protection devices, the characteristic of the starting area depends on the manufacturer. Different variants are shown in Fig. 13.35. The goal is to approximate as closely as possible the impedance characteristic of the permissible load.

**Starting Logic.** The different presented starting functions must be logically combined to reach an overall decision. Among other features, the type of neutral point treatment of the electrical network has to be taken into account. In addition, its function should eliminate implausible decisions of the underimpedance, overcurrent, or undervoltage starting functions. Such implausible decisions of these functions may result from incorrect settings. The goal of the starting logic is to ensure a clear identification of the fault type and the faulty phases.

One of these logical criteria is explained in the following. Figure 13.36 shows a phase-to-earth fault. The underimpedance starting function does not know which type of fault occurred. Therefore, the impedances of all three phase-to-earth calculation loops are calculated by

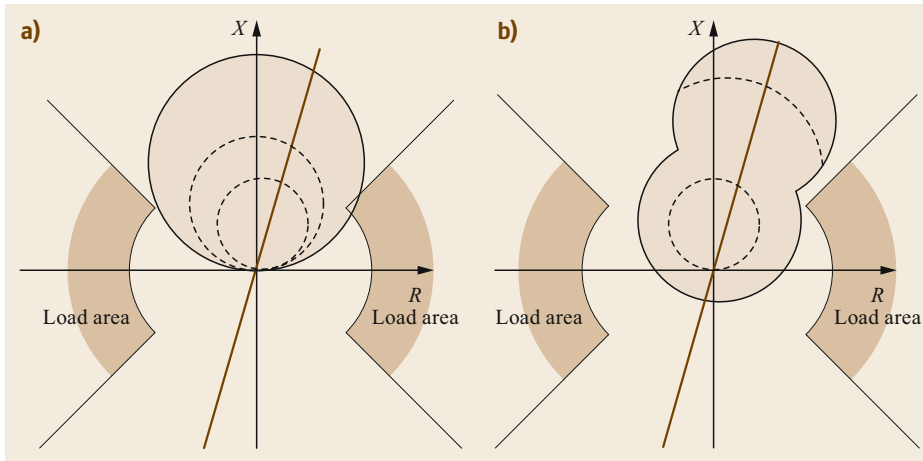
$$\frac{V_{L1}}{I_{L1} - I_E k_E} = Z'_1 I_{sc} = Z_{L1-E}, \quad (13.61)$$

$$\frac{V_{L2}}{I_{L2} - I_E k_E} = Z'_1 I_{sc} = Z_{L2-E}, \quad (13.62)$$

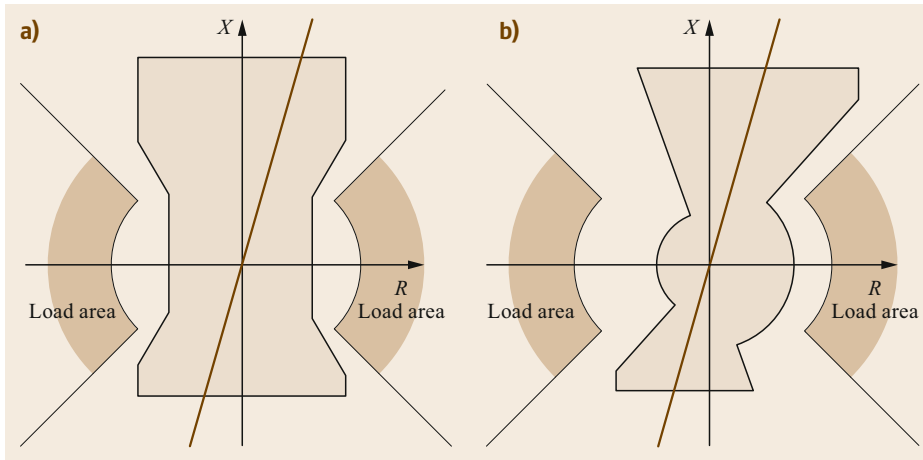
$$\frac{V_{L3}}{I_{L3} - I_E k_E} = Z'_1 I_{sc} = Z_{L3-E}. \quad (13.63)$$

The impedances calculated in phase-to-earth loop L2–E and phase-to-earth loop L3–E do not make sense physically. Since the earth return current is included in (13.62) and (13.63), small impedances are calculated. For a selected situation, the calculated phase-to-earth impedances are given in Fig. 13.36. It can be seen that there are two phase-to-earth loop impedances (L1–E, L2–E) within the underimpedance starting characteristic. To avoid a wrong decision of the starting function, the starting logic selects the smallest phase-to-earth loop impedance and rejects all loop impedances that are 1.5-times higher. The result is a correct detection of the single phase-to-earth fault in the phase L1–E.

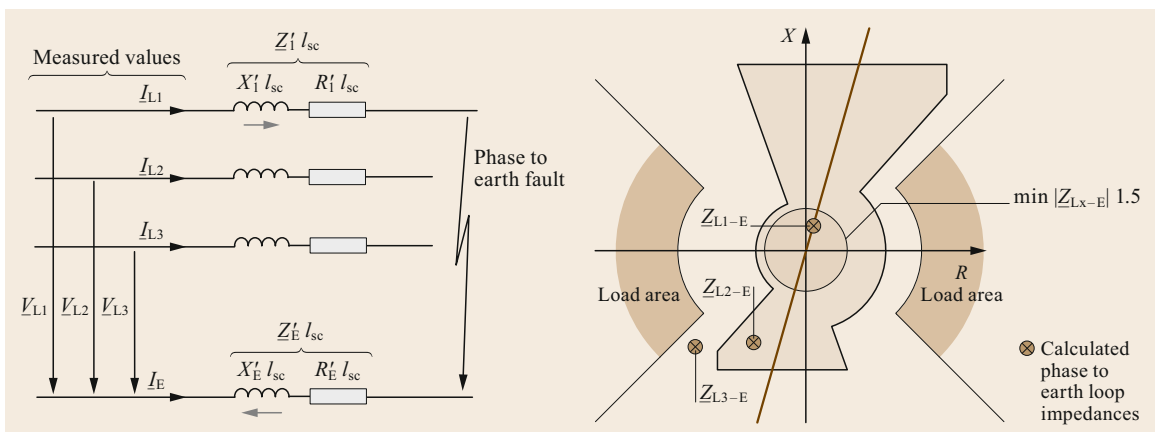
**Switching Logic.** The switching logic is only necessary for switched distance protection schemas. Based on the final decisions of the starting logic and on given rules, which have to be selected by the user, the measuring loop is determined. This measuring loop is used by the distance measuring system to calculate the fault distance.



**Fig. 13.34a,b** Underimpedance starting characteristic of electromechanical and electronic distance protection devices. (a) Offset mho-circle, (b) eight (peanut) (adapted from [13.6])



**Fig. 13.35a,b** Underimpedance starting characteristic of numerical distance protection devices. (a) Starting characteristic for manufacturer A, (b) Starting characteristic for manufacturer B (adapted from [13.6])



**Fig. 13.36** Illustration of the elimination of implausible decisions of underimpedance starting

### General Information on the Application of Distance Protection

These illustrations show that the complexity of distance protection is considerably higher in comparison with overcurrent protection. On the other hand, distance protection significantly improves the quality of short-circuit detection and clearing. Especially in critical fault situations, e.g., weak in-feed situations, the distance protection still ensures a high degree of selectivity in the clarification of short circuits. This is the reason why distance protection is very often used in extrahigh-voltage networks. In these networks, distance protection is the standard protection schema.

Due to the growing number of decentralized generation plants in the distribution network, it will become necessary to use distance protection at this voltage level increasingly as well. One challenge here is the high parameterization demands mentioned above.

#### 13.4.6 Additional Functions

With the aid of so-called additional functions, the command time of the protection system should be reduced, its selectivity increased, and the interruption time shortened. In addition, there are special functions for detecting critical conditions of selected equipment or the entire electric power system that are not directly caused by a short circuit, e.g., overloads, earth faults, power swings, and frequency deviations. The most important additional functions are briefly described below.

##### Auto-Reclosing

A large fraction of the short circuits that occur in an overhead line network are arc faults, caused by atmospheric or switching overvoltages. After the fault has been switched off, these arcs extinguish themselves and the overhead line can be reconnected. Especially at the extrahigh-voltage level, more than 90% of faults that occur can be eliminated immediately in this way.

In principle, the automatic reclosing (AR) function gives the circuit-breaker an on command at the end of the dead time. However, additional requirements must be met before this function can be implemented; For example, the drive of the circuit-breaker must be able to operate the switching sequence off–on–off, it must be ensured that the type of fault is suitable for automatic reclosing and that the short circuit has been completely switched off. Depending on the length of the dead time, it may be necessary to check the synchronicity of the power system before switching on.

One-, two-, or three-pole automatic reclosing can be carried out in high- and extrahigh-voltage networks.

A precondition is that each pole of the circuit-breaker has its own drive.

##### Signal Comparison

Signal comparison methods are used for the following applications:

- protection of the total line length of an overhead line or cable within the time first zone
- protection of short transmission lines with distance protection (where the impedance of the line is smaller than the smallest possible setting)
- reduction of the operation time for a fault near the far-end station (reducing stability problems).

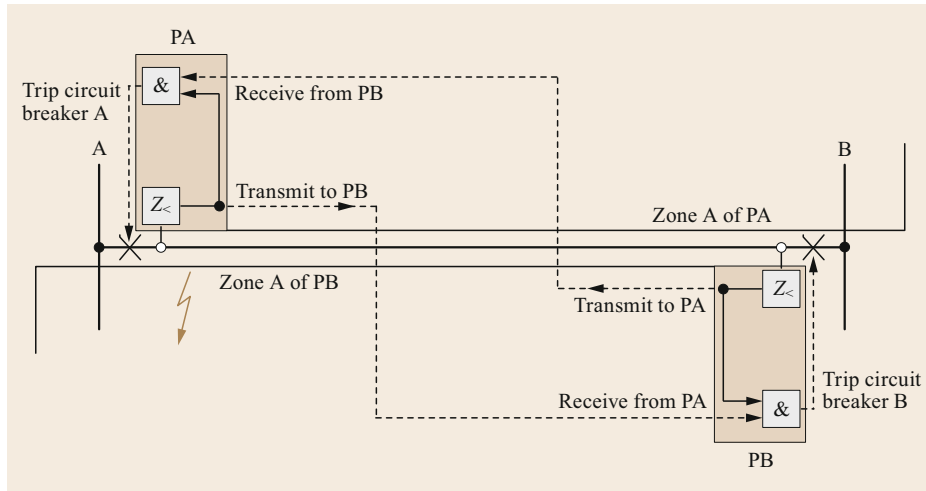
In general, the selectivity and response time of the protective device are increased with the help of such signal comparison methods. For this purpose, binary information is exchanged between the protective devices installed at both sides of the protection object, which could be an overhead transmission line or transformer but also switchgear. There is no exchange of measured values or other analog information.

To avoid the unwanted operation of a protective device, the received binary information is always linked to local information, to give permission or block a local decision. The advantage of signal comparison is that the requirements for signal transmission in terms of speed and bandwidth are very low.

Regarding signal comparison methods, a fundamental distinction is made between unblocking and blocking methods. The unblocking methods are more oriented towards avoiding unwanted operation. If, for example, the expected binary signal is not received due to a transmission fault, there is no unblocking and the backup function of the protective device is activated, leading to delayed but selective fault tripping. This type of signal comparison is often used in Central Europe. The basic decision of the blocking method is based on local information, e.g., an impedance measurement. If no blocking signal arrives within a short delay time, the protective device trips the fault. These methods guarantee a short fault clearing time, albeit with the danger of unwanted or unnecessary tripping. This method is often used in the USA.

The permissive overreach distance protection schema is now explained. This schema belongs to the unblocking methods. It is illustrated in Fig. 13.37. The line is protected by a distance protective device. The so-called overreach zone A is set between 120–150% of the total line length on both sides of the line. A binary signal is transmitted if a fault is detected within this overreach zone A. There is no direct tripping of





**Fig. 13.37** Example of signal comparison with permissive overreach distance protection (adapted from [13.28])

the line, because a short circuit in this zone will also be signaled if a real fault occurs beyond the next station.

When the distance protective device receives a binary signal, a logical link to the local decision of zone A will be performed. If both conditions are fulfilled, the

circuit-breaker will be tripped. This method guarantees a short operation time independent of the location of the short circuit. The permissive overreach distance protection schema is often used for the protection of short transmission lines. A reliable communication channel is necessary.

## 13.5 Outlook on Protection Systems

The development in the field of selective protection systems is characterized by the changing requirements of electrical power systems and by developments in the fields of communications and computer technology.

### 13.5.1 Changes in the Electrical Power System

Due to the increased integration of small and decentralized generation units into the electrical power system, new requirements for protection arise.

#### Reduction of Short-Circuit Current

Small and decentralized generation units, e.g., wind power plants or photovoltaic systems, are often connected to the grid via power electronics. The maximum short-circuit current of these devices is restricted by the thermal limits of the electronic components and normally lies in the range of the rated load current. Therefore, overcurrent protective devices can no longer differentiate between the normal load and the fault situation. Thus, additional criteria are needed. One solution could be the application of distance protection. The drawback is the high complexity and price of this protection schema. Due to the increasing availability of

high-speed communication links, differential protection schemas could be implemented more easily. The disadvantage of this solution is the lack of a backup function and its high dependency on the reliability of the communication link.

#### Changing Short-Circuit Current Direction

Decentralized generation units are often based on renewables, thus the in-feed is heavily feature dependent [13.29]. This results in a high dynamic in the magnitude and rapid direction changes of the short-circuit current. This makes it very difficult to determine the settings for protection devices. Today, one option is to adapt the settings of protection devices remotely, depending on the load situation. Generally, precalculated settings are used. Another idea is so-called adaptive protection [13.30], where each protection device estimates its own settings automatically based on the actual situation of the electrical grid [13.31].

#### Heavily Loaded Transport Lines

Another challenge is the transportation of huge amounts of electrical energy over long distances. In some cases, so-called high-temperature low-sag (HTLS) conductors are used to increase the transmission capacity. The clear

distinction between the load and the short-circuit areas shown in Sect. 13.4.5 is then often no longer possible. It may happen that the maximum permissible transmission power is limited by the protection system and not by the physics of the overhead line. This is not acceptable, so new protection schemas have to be developed.

### Overall System Protection

The protection system was originally designed to detect faulty equipment in the electrical system based on locally available information (e.g., voltage, current) and to switch off faulty equipment as fast as possible. Due to the presented challenges in secure and reliable detection of faults in electrical networks, this equipment-based approach of classical protection schemas is critically discussed. The idea is to complement the equipment-based approach by an overall system protection schema. Such concepts are technically possible today due to the availability of fast communication links and powerful computers.

The advantage of overall system protection is that not only equipment-based faults but also critical system status (e.g., power swings, resonances) can be detected and eliminated. New algorithms must be developed for this purpose.

### 13.5.2 Technological Drivers

In the case of electromechanical protective devices, the individual functions of a protection system were usually separate boxes. With the introduction of analog circuit technology, the protective functions were implemented on printed circuit boards. In numerical protection devices, the protection functions are only software modules. To date, protective devices remain

individual, dedicated pieces of equipment; they fulfil all the necessary protection functions related to [13.13].

### Common Protection and Communication Devices

The increased use of communications technology also within switchgear, for example, to transmit sampled values from current and voltage transformers, enables new system architectures for protective devices. One approach that has been discussed is thus to implement the protective function as a subfunction on the communication controller, where the necessary local information (e.g., voltage, current) is already available. The reliability and availability of the protective function based on such a concept must be critically evaluated.

### Protection in the Cloud

Another idea is the implementation of virtual protective devices in the cloud. New communication technologies such as 5G guarantee low latency. Therefore, this standard will be used in industry automation. The possible application of this technology for protection systems is also being investigated in initial research projects. The very high computing power required for 5G technology meets the requirements for protection technology.

### 13.5.3 General Requirements

As described above, protection technology is developing very rapidly. However, it has to be taken into account that protection systems play an essential role in the safe and reliable supply of electrical energy. Compliance with the basic requirements for protection systems outlined in Sect. 13.1.1 must be critically reviewed before new technologies can be introduced in this field.

## References

- |                                                                                                                                                                                                                                                                                                                                                                                                                                                                                                                                                                                                                                                                                                                                                                            |                                                                                                                                                                                                                                                                                                                                                                                                                                                                                                                                                                                                                                                                                                                                                                                                            |
|----------------------------------------------------------------------------------------------------------------------------------------------------------------------------------------------------------------------------------------------------------------------------------------------------------------------------------------------------------------------------------------------------------------------------------------------------------------------------------------------------------------------------------------------------------------------------------------------------------------------------------------------------------------------------------------------------------------------------------------------------------------------------|------------------------------------------------------------------------------------------------------------------------------------------------------------------------------------------------------------------------------------------------------------------------------------------------------------------------------------------------------------------------------------------------------------------------------------------------------------------------------------------------------------------------------------------------------------------------------------------------------------------------------------------------------------------------------------------------------------------------------------------------------------------------------------------------------------|
| <p>13.1 M.A. Ibrahim: <i>Protection and Control for Power System</i> (CreateSpace Independent Publishing Platform, North Charleston 2016)</p> <p>13.2 IEC: <i>IEC International Electrotechnical Vocabulary (IEV) Part Power System Protection; IEC 60050, Part 448</i> (IEC, Geneva 2017)</p> <p>13.3 P.M. Anderson: <i>Power System Protection</i> (McGraw-Hill, New York 1998)</p> <p>13.4 GEC ALSTHOM: <i>Protective Relays—Application Guide</i> (GEC ALSTHOM Measurements Limited, Stafford 1987)</p> <p>13.5 IEC: <i>IEC 60909-0 Short Circuit Current in Three-phase a.c. Systems; Part 0: Calculation of Currents</i> (IEC, Geneva 2016)</p> <p>13.6 G. Ziegler: <i>Numerical Distance Protection—Principles and Applications</i> (Publicis MCD, Munich 1999)</p> | <p>13.7 IEC: <i>IEC 61869-2 Instrument Transformers; Part 2: Additional Requirements for Current Transformers</i> (IEC, Geneva 2012)</p> <p>13.8 A. Wright, C. Christopoulos: <i>Electrical Power System Protection</i> (Chapman &amp; Hall, London 1993)</p> <p>13.9 C. Prévê: <i>Protection of Electrical Networks</i> (ISTE, London 2006)</p> <p>13.10 IEC: <i>IEC 60044-6 Instrument Transformers; Part 6: Requirements for Protective Current Transformers for Transient Performance</i> (IEC, Geneva 1992)</p> <p>13.11 IEC: <i>IEC 61869-100 Guide for Application of Current Transformer in Power System Protection</i> (IEC, Geneva 2007)</p> <p>13.12 IEC: <i>IEC 61869-3 Instrument Transformers; Part 3: Additional Requirements for Inductive Voltage Transformers</i> (IEC, Geneva 2011)</p> |
|----------------------------------------------------------------------------------------------------------------------------------------------------------------------------------------------------------------------------------------------------------------------------------------------------------------------------------------------------------------------------------------------------------------------------------------------------------------------------------------------------------------------------------------------------------------------------------------------------------------------------------------------------------------------------------------------------------------------------------------------------------------------------|------------------------------------------------------------------------------------------------------------------------------------------------------------------------------------------------------------------------------------------------------------------------------------------------------------------------------------------------------------------------------------------------------------------------------------------------------------------------------------------------------------------------------------------------------------------------------------------------------------------------------------------------------------------------------------------------------------------------------------------------------------------------------------------------------------|

- 13.13 ANSI, IEEE: *C37.2, ANSI/IEEE Standard for Electric Power System Device Function Numbers and Contact Designations* (IEEE, Piscataway 2008)
- 13.14 IEC: *IEC 60255-151 Measuring Relays and Protection Equipment; Part 151: Functional Requirements for Over/Under Current Protection* (IEC, Geneva 2009)
- 13.15 IEC: *IEC 60044-1 Instrument Transformers; Part 1: Current Transformers, A1:1996+ A1:2000 +A2:2002* (IEC, Geneva 2002)
- 13.16 M.A. Anthony: *Electric Power System Protection and Coordination: a Design Handbook for Overcurrent Protection* (McGraw-Hill, New York 1995)
- 13.17 S.H. Horowitz, A.G. Phadke: *Power System Relaying* (Research Studies, Somerset 1995)
- 13.18 ABB: Applying High Impedance Differential Protection with IED 670 (2007) p. 9, Document ID: SA2007-000725
- 13.19 K. Rothe, H. Clemens: *Schutztechnik in Elektroenergiesystemen* (Verlag Technik, Berlin 1991)
- 13.20 ALSTOM T&D: *Network Protection and Automation Guide* (Alstom, Levallois-Perret 2002)
- 13.21 Valence Electrical Training Services: High Impedance Busbar Differential Protection, <https://relaytraining.com/high-impedance-busbar-differential-protection/> (2019)
- 13.22 B. Kasztenny, L. Sevov, G. Brunello: Digital Low-Impedance Bus Differential Protection—Review of Principles and Approaches, <https://store.gegridsolutions.com/FAQ/Documents/B30/GER-3984.pdf> (2002)
- 13.23 K. Behrendt, D. Costello, S.E. Zocholl: Considerations for using high-impedance or low-impedance relays for bus differential protection. In: *63rd Annu. Conf. Prot. Relay Eng.* (2010), <https://doi.org/10.1109/CPRE.2010.5469509>, revised February 2016
- 13.24 A.R. v. Cortlandt Warrington: *Protective Relays Their Theory and Practice*, Vol. 1 (Springer, New York 1968)
- 13.25 IEC: *IEC 60255-121 Measuring Relays and Protection Equipment; Part 121: Functional Requirements for Distance Protection* (IEC, Geneva 2014)
- 13.26 J.M. Gers, E.J. Holmes: *Protection of Electricity Distribution Networks* (IET, London 2011)
- 13.27 D. Robertson: *Power System Protection Reference Manual* (Oriel, Northumberland 1982)
- 13.28 CIGRÉ: Protection Using Telecommunications – Final Report. CIGRÉ Joint Working Group 34/35.11 (CIGRÉ, Paris 2001)
- 13.29 B. Hadzi-Kostova: *Protection Concepts in Distribution Networks with Decentralised Energy Resources* (RES Electricae Magdeburgenses, Magdeburg 2005)
- 13.30 I. Bielchev: *Adaptiver Distanzschutz im Standard IEC 61850* (RES Electricae Magdeburgenses, Magdeburg 2016)
- 13.31 S.M. Madani: *Analysis and Design of Power System Protection Using Graph Theory*, Dissertation (Technische Universiteit Eindhoven, Eindhoven 1999)

**Peter Schegner**

TU Dresden  
Dresden, Germany  
[peter.schegner@tu-dresden.de](mailto:peter.schegner@tu-dresden.de)



Peter Schegner studied electrical power engineering, then worked as a system engineer in power system control and joined the scientific staff at Saarland University, receiving his PhD with a thesis on earth-fault distance protection. He then worked as Head of the Development Department of Protection Systems at AEG, Frankfurt, later becoming Full Professor and Head of the Institute of Electrical Power Systems and High Voltage Engineering of TU Dresden.

# 14. Information Systems and Telecommunications

# Information

Carlos Samitier 

Since the very beginnings of the power grid, telecommunications has been a necessary component to operate the system. The evolution of information technology and the improvement of its capabilities open new opportunities to improve system operation, which evolved from a manual operation to a more automated one and is presently a fully automated system that is paving the way to the deployment of smart grids and the future use of artificial intelligence. This chapter depicts the working principles and technologies used to manage and operate the power grid. The first part is devoted to operational applications. These are the *brain* of the system and gather information from the field and make decisions to automatically control the grid and take the required actions to protect its components from fault or other events that may impair the stability of the system. The most important applications and analyses of their telecommunications requirements are identified. These requirements will be the input for telecommunications technology selection and network design. The second part of this chapter is focused on telecommunications technologies and networks. A review of telecommunication technologies used to implement power utilities operational services is given. Telecom services are classified, and their attributes are described in order to give an understanding of further classifications and their operational applications. Network design is introduced in order to highlight the key differentiated aspect of power-system automation telecom networks. Finally, cybersecurity aspects are introduced, providing key aspects and a reference to international standards that should be applied. Smart grid architecture and components are also briefly described.

14.1	<b>The Role of Information and Communication (ICT) in a Power Grid</b>	1016
14.2	<b>Operational Applications</b>	1018
14.2.1	Energy Management System	1018
14.2.2	Distribution Management System	1019
14.2.3	SCADA	1020
14.2.4	Asset Management and Condition Monitoring	1022
14.2.5	System Protection Schemes and the Protection Management Center	1022
14.2.6	Energy Market	1023
14.2.7	ICT Management and Maintenance	1024
14.2.8	Control Center Application Architecture	1024
14.2.9	Substation Applications Architecture	1029
14.2.10	Standards	1042
14.2.11	Technologies	1045
14.2.12	Design Principles	1048
14.3	<b>Telecommunications Services</b>	1049
14.3.1	Basic Concepts	1052
14.3.2	Service Classes and Applications	1053
14.3.3	Service Attributes	1057
14.3.4	Service Provisioning and Service Level Agreement	1060
14.3.5	Telecommunications Technologies	1062
14.3.6	Networking Technologies: The Network Layer	1069
14.3.7	Network Architecture	1073
14.3.8	Network Design	1074
14.3.9	Network Management	1078
14.3.10	Business Continuity Management	1081
14.4	<b>Cybersecurity</b>	1084
14.4.1	Basic Principles	1084
14.4.2	International Standards	1085
14.4.3	Cybersecurity Control Center	1087
14.5	<b>Smart Grid</b>	1087
14.6	<b>Outlook of Future Technologies</b>	1090
14.7	<b>Further Reading</b>	1091
	<b>References</b>	1092

## 14.1 The Role of Information and Communication (ICT) in a Power Grid

As explained in previous chapters, a power grid is a complex distributed system, whose main function is the supply of electricity to customers distributed in over a wide area, the technical difficulty being the requirements for maintaining almost constant voltage and frequency. To achieve this, a balance between generation and consumption must be maintained. As the consumption changes continuously, generation must be accommodated in realtime.

This functionality is implemented by a number of applications, some of them working at the system level, several supporting grid nodes functionality, substations, generation plants, etc., and others directly related to primary equipment and other field devices.

As these applications require data interchange between them, as well as remote data access, telecommunications is required, thus becoming a necessary component to assure grid functionality. Applications and telecommunications infrastructure form a distributed system, whose key function is to maintain the stability and continuity of the system by providing services to operate and protect the grid. This system can be considered

as the brain and nervous system of a power grid. Without its functionality, a grid cannot maintain its operation.

Figure 14.1 shows the main ICT components. Control centers gather field information, process it, and provide the interfaces for human interaction. To implement such functionality, a telecommunications infrastructure providing specialized operational services is required, as shown in Fig. 14.1.

This generic structure is replicated in every site, so every substation or generation plant is equipped with a site control application that allows operations to be carried out on site. Similarly, every substation bay has a local controller with similar functionality to supervise and operate the bay's primary devices. Substations and generation plants require a local communications infrastructure that is, nowadays, implemented using a local area network (LAN) that connects intelligent electronic devices (IED) that carry out operation functions in the local environment. Their communications capabilities together with the wide area network (WAN) allow local information to be consolidated by control center applications.

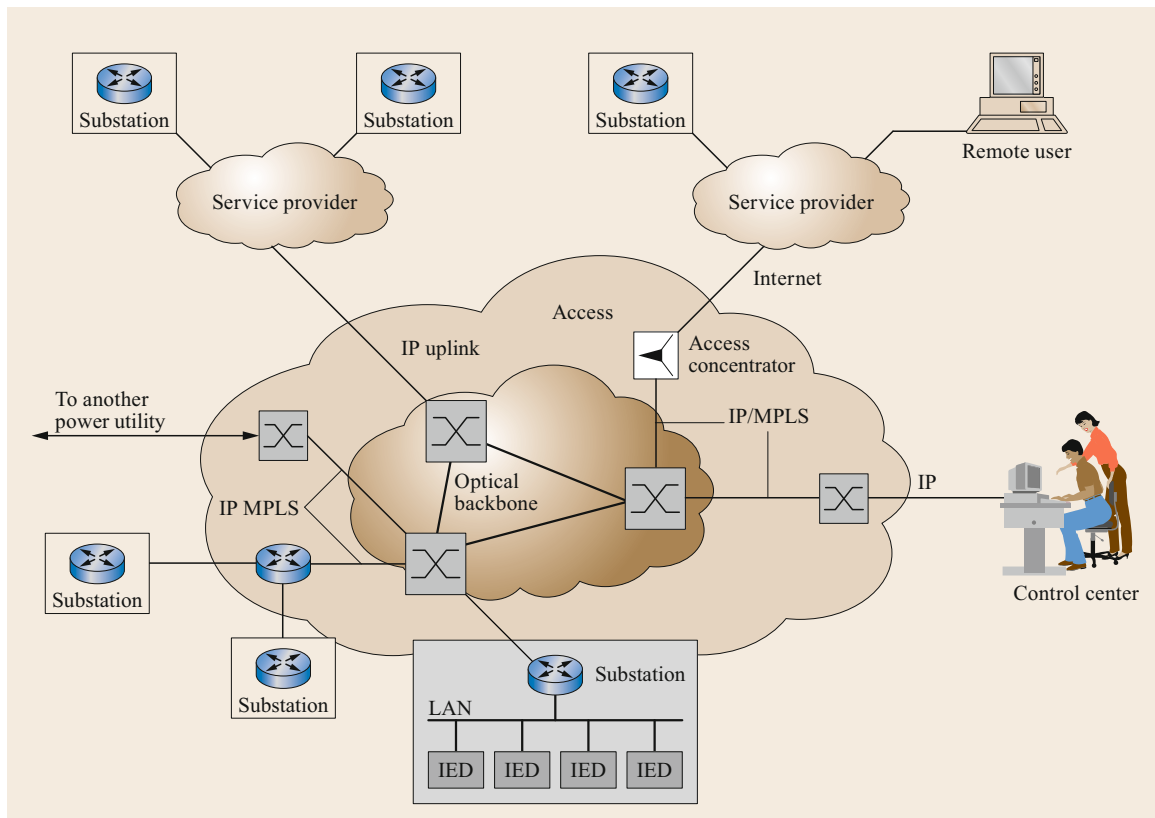


Fig. 14.1 ICT overview

ICT provides a logical view of the power grid. Primary devices components, values, status, etc., are stored and processed by local operational applications and transmitted to control centers

Both applications and telecom infrastructure need to fulfil very demanding performance requirements, the most critical being the realtime response together with a very high availability and dependability.

The term *realtime* has a specific meaning for operational applications; it applies to service latency or application response time. It can be understood in different manners, and it is not only matter of time but also of the reliability of the response time. That is to say, performance measurements based on statistics cannot be used for critical functions, as once the maximum delay is exceeded, the operation is considered faulty. In the operational environment, every operation has to be carried out before the maximum accepted delay.

The maximum response time depends on every operational application and can range from 1 s to 3 ms. The requirements for time synchronization functions are expressed in functions of the synchronization error. Some precision time synchronization applications require a synchronization error lower than a tenth of a microsecond.

Some applications require a quite deterministic latency, whereas others accept some latency variation, but all of them require a bounded delay. Consequently, mission-critical applications and telecom services will need to be implemented to achieve these operational requirements.

These application requirements impose tough design conditions for the telecommunications infrastructure. Telecommunications networks as well as internal substation communications should be as reliable as operational application requirements. Due to this, even using the same technology as telecom operators, design, configuration, and operation are rather different, as is explained later in the telecommunications section (Sect. 14.3).

The aforementioned characteristics of operational applications made them quite different from the information technologies used in business applications, not only in the way technologies are used but also with respect to the application design. The main differences are:

- IT systems are focused on information, whereas operational applications are focused on the process. Their functionality is to optimize and maintain the operation of the process; information is only required to achieve their functionality.
- IT reliability and dependability requirements are not as high as for operational applications, which can

be considered mission critical, as their reliability and dependability requirements are several orders of magnitude higher than IT applications.

- Short service interruptions used to be accepted for IT applications, but service interruption of some critical operational applications may lead to catastrophic situations, so these applications should be designed to be fault tolerant.

The operation of the power grid is carried out using a number of collaborative applications, some working in a centralized way, and others being distributed along the grid. Applications working at system level are normally located at control centers. These applications interact with operational applications located at every site using the telecommunications services provided by a telecommunications infrastructure.

Primary ICT goals have evolved over time. The first use of operational applications was focused on the remote control of field devices. Simple telecom services using point-to-point telecommunications channels were used to support this functionality.

This approach evolved towards the control of the power grid as a system. New applications were developed to provide a view of the grid and optimize its performance. This approach required enhancing the telecommunications infrastructure both to improve communications with grid sites and also between applications at control centers.

The next step was focused on business performance, that is to say, how grid operations, asset-management, condition monitoring of primary equipment, other field devices, etc., impact on business performance. New applications were developed, and interchange of information with IT applications became a must. This led to the development of new control center architecture and data modeling requirements, which paved the way to the latest development, the smart grid concept.

Smart grid implies *total interoperability*, which is achieved by standardizing the following key concepts:

- Information modeling. Object modeling and standardized semantics are applied to every component of the power grid.
- Information services. Information interchange is standardized considering data modeling properties.
- Communications services. Object communications, which is implemented using message interchange, is defined using abstract communications services, which provides isolation from actual telecom technology. Consequently, many different telecommunications technologies can be used, thereby allowing optimization of cost and performance.
- Application interface allowing integration at the business level.

Following this trend, modern applications model all primary equipment in a standardized way, thereby simplifying information interchange between applications, and use standard communications interfaces. This new architecture is defined by the IEC 61850 series of standards and is the foundation of modern operational ICT systems.

The use of standard protocols and the increased need for information interchange between operation and IT systems, the use of public telecommunications

infrastructures, and the Internet introduced a number of opportunities for cybersecurity attacks. The number of attacks are growing day by day. Therefore, there is a need to take protection measures to reduce the risk of successful cyberattacks.

Cybersecurity is a necessary component in all modern operational systems. Cybersecurity protection measures must be considered from the design phase throughout the system's life cycle, as explained in the cybersecurity section (Sect. 14.4).

## 14.2 Operational Applications

This section identifies operational applications, shows its functionality and develops architectural details, and describes information interchange. The focus of this section is on identifying operational applications' functionality, and how they interact each other to support power-grid operations.

Therefore, architecture, data modeling, information interchange, interfaces, and interoperability are of primary interest to understand how they form an integrated system. Furthermore, these subjects are a primary source of information to define telecommunications requirements.

These applications are implemented using proprietary algorithms; consequently, they are different for each system supplier. Nevertheless, data modeling semantics and protocols are standard in order to assure interoperability, as will be explained in following sections. The description and working principles of these algorithms are out of the scope of this chapter, since our focus is on information structure and the required telecommunications services. Operational applications are distributed along the grid forming subsystems, systems, and systems of systems.

Legacy ICT technologies were based on a set of independent applications unable to share information; due to this, the same piece of information acquired in the field was coded in different ways and transmitted to different applications using different protocols. The use of object-oriented technologies paved the way to the implementation of a common information bus that enables application integration. This evolution started in two parts, at control centers for enterprise application integration and at fields for substation automation systems.

In a modern grid, including the smart grid, applications are designed using standard data modeling and communications services, so they can share and interchange information, thereby forming an integrated system that provides the functionality to operate, man-

age, and maintain the grid and its relations with IT applications and the energy market.

Operational applications provide operational services implemented using the following components:

- Applications running on servers and other devices with communications and processing capabilities called intelligent electronic devices (IEDs).
- Operator interfaces implemented by terminals that provide the human-machine interface (HMI) or by IEDs displays.
- Communications infrastructure providing telecommunications services. These services can be based on internet protocol (IP) connectivity or merely on bit transport services to connect legacy devices.

The most important system used to operate the grid are the energy management system (EMS) and the distribution management system (DMS). EMS and DMS include a number of operational applications, each with its own application domain with specific working modes and performance requirements.

### 14.2.1 Energy Management System

The energy management system (EMS) is a realtime high-performance distributed set of applications and tools used by the operators of a power grid to monitor, control, and optimize the performance of the generation and transmission system.

EMS is composed of the following applications.

#### Realtime Supervisory Control and Data Acquisition (SCADA)

SCADA provides data acquisition and supervisory control of field information and devices. It includes alarm and event logging, control operation, and other facilities to operate the grid. Further information and architecture are provided later on.

### Generation Dispatch and Control

This provides the functions required to dispatch generators according to the criteria settled by grid operator with the aim of maintaining grid stability.

### Energy Scheduling and Accounting

This provides the functionality to interact with the energy market, including interchange scheduling, accounting, and weather demand forecast.

### Transmission Security Management

This provides facilities and advanced functions to analyze and optimize the use of grid assets in a reliable and secure manner. State estimation is the most important function. The state estimator (SE) uses data provided by SCADA and other field devices to create a realtime model of the grid, which is used to optimize power flows. The reliability of SE depends to a great extent on the precision of phasor measurement units (PMU). Modern PMUs take 30 or more samples of the current and voltage values and time stamp them with a common reference clock synchronized with the global positioning system (GPS) universal clock. This provides time-coherent information of the values in all the grid nodes. The higher the number of samples, the higher precision and realtime performance of the calculation results. Nevertheless, this introduces a considerable traffic load on the telecommunications infrastructure and an increasing processing strain on the data processing infrastructure.

### Operator Training Simulator

This provides a number of functions to check different network operations using a realistic interface with the same models, icons, and functionality as the real EMS application. This application allows testing the effect of different operations on the functioning of the network status.

## 14.2.2 Distribution Management System

A distribution management system (DMS) is a set of applications that provides services to monitor and control the distribution grid in a reliable and efficient manner.

The key advantages brought about by DMS are:

- Reduction in the duration of outages
- Improvement of the operational efficiency
- Determination the resources required to restore faults quickly and efficiently
- Improvement of outage communications to customers with more accurate information and estimated restoration time

- Improvement of service reliability by reducing the outage effect through a more accurate grid configuration and state.

DMS uses the services and information provided by SCADA to implement a number of functions described in following paragraphs.

### Network Connectivity Analysis

Distribution grids usually include a large number of customers and field equipment with changing configurations, so it may be difficult for the operator to identify functionality from a graphical connectivity display. Network connectivity analysis is a function that provides connectivity information obtained from the information of the position of switches and breakers, which determine the feeding point of a due load. Network connectivity function informs the operator about the operating state of the distribution grid, indicating working schemes such as radial mode, loops, or parallel configurations.

### Maintenance Schedule and Safety Management

Safety measures to protect field personnel is a key issue for power utilities. Grid operators schedule grid reconfiguration to isolate a section of the network to make it safe before work can be carried out. Schedules must be validated before implementation to verify their suitability and effect on network stability. Switching operations can combine telecontrol commands with manual operations of nonautomated apparatus. When a section has been secured, a working order is issued. Once the work has been finished, this function will facilitate the restoration of the working configuration by controlling the order of commands and manual operations.

### Power Flow

Power flow, or load flow, is an application that calculates voltage and currents at different parts of the power grid in normal steady-state conditions. It is very important to know the working conditions of grid elements in order to analyze whether they can withstand stress without any damage or degradation of their life span. Furthermore, from economical point of view, losses should be kept as low as possible when considering system constraints and the risk that the system falls in an unstable mode should be limited.

Power-flow calculation is carried out from the voltages of every power bus of the grid. As power-flow calculation is a nonlinear problem, numerical methods are employed. Market products implement proprietary algorithms.



Modern power flow algorithms consider nonlinearities and a set of constraints to determine the optimal power flow. Operational limits can also be calculated using these algorithms. Limits such as active or reactive power of a generator, current and voltage upper limits, tap position of a power transformer, etc., can be determined by power-flow algorithms.

### Voltage and Reactive Power Control

Voltage and reactive power control application manage voltage levels and reactive power throughout the grid. There are two primary mechanisms to control voltage across the grid, load tap changers in power transformers and capacitor banks. Voltage and reactive power control applications interact with tap changers and capacitor bank local controllers to maintain voltage levels in selected power bus. This interaction is normally implemented using SCADA, which gathers voltage information from the field and issues control commands to field devices, as explained in the following sections. In fact, regulation of apparatus to achieve the set point level sent by the control center application is implemented by a local automatic control system that modifies the working point of the apparatus to achieve the desired voltage level. Ampacity of power lines and feeders can also be controlled by this application, with the advantage that the effect of the reactive power is considered in the calculation of the current flow.

### Load Balancing

Load balancing using feeder configuration is essential to manage load-congested areas. A load-balancing application monitors the status of the distribution grid, identifies overload areas, and allows the operator to reroute the loads to other parts of the network. Load balancing can also be used for loss minimization. The load balancing application uses optimal power-flow algorithms and switching plans to minimize losses.

### Distribution Load Forecasting

A load forecast is essential to the operation and planning of a distribution grid. The load forecasting application helps the grid operator make important decisions with respect to grid configuration planning and load switching, as well as identifying the need for future grid development.

Load forecasting is carried out both in the short term – up to one day – and in the long term – up to one year to forecast the load in the long term; external factors such as weather, holidays, etc., should be considered.

Several mathematical models have been developed for load forecasting based on different techniques such as multiple regression, exponential smoothing, stochas-

tic time series, fuzzy logic, neuronal networks, and knowledge-based systems. None of them have been standardized, so each power utility requires that algorithm that better suits its topology and operation modes.

### Fault Location and Restoration

The reliability of the power supply depends to a great extent on the number of outages and their duration. Reducing the outage time duration is, therefore, important to fulfil reliability requirements.

The fault locator and system restoration application reduces outage time by helping the operator locate the fault and suggesting a switching plan or, in some cases, automating service recovery. SCADA provides the information to locate the fault. Once located, a switching action plan is implemented. The switching operation can be carried out manually or automatically. In any case, switching is implemented using SCADA services.

### Load Shedding

Unexpected changes in network conditions may lead to instabilities and critical failures. A load shedding scheme detects predetermined network conditions and performs a predefined set of control actions to re-establish normal conditions.

Load shedding is a component of a wide area protection scheme, the remedial action scheme (RAS). Consequently, it may act by tripping loads in response to some condition detected in the wide area protected by RAS or due to some condition detected in the distribution network.

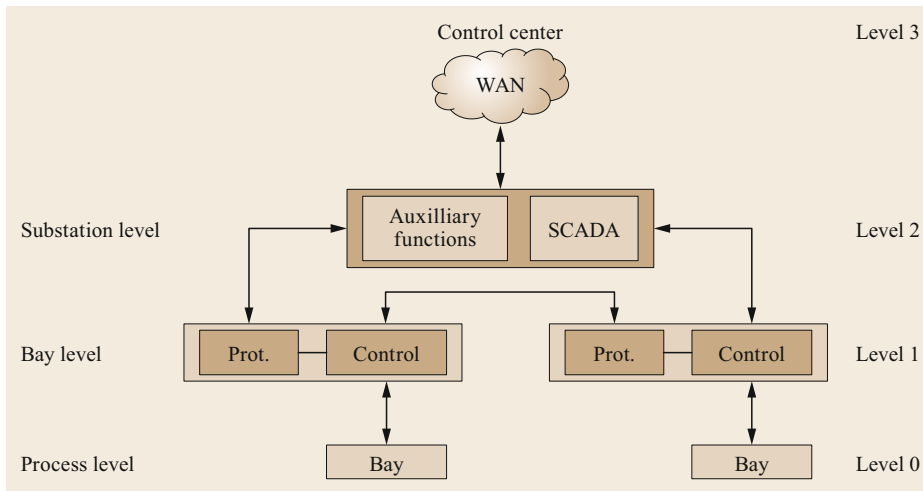
## 14.2.3 SCADA

Supervisory control and data acquisition is a distributed control system that uses intelligent electronic devices (IEDs) and networked data communications to supervise and control different aspects of a power grid. SCADA services and functionality are provided through a graphical operator interface that shows the grid status of supervised elements and allows process commands to be issued.

SCADA architecture and implementation evolved from monolithic proprietary solutions to distributed systems using standard communications protocols to the latest architecture based on IEC 61850 series of standards, which defines protocols, communications services, data models, and object semantics.

Figure 14.2 shows the SCADA architecture. The SCADA system is structured as levels that perform different processes.

Level 0: field level. This includes primary equipment and other field apparatus. This level provides field information such as voltages, current, status, alarms, etc.



**Fig. 14.2** SCADA architecture

**Level 1: bay level.** This comprises bay control and supervision functionality. These functions are carried out by an IED, the bay control unit, which gathers field information, and execute commands whether issued locally or remotely. It can also perform logic functions related to bay operation.

**Level 2: substation level.** This includes all the functions to supervise and control the whole substation or plant. These functions are implemented by a substation controller, which in fact is a local SCADA system that gathers substation information, execute commands, log system activity, carry out logical functions, and provide a graphical operator interface that allows local supervision and operation of the substation, as well as the substation information display.

**Level 3: control center level.** The SCADA application located at control center servers provides supervision and control services of the power grid and gathers grid information and shares it with other control center applications.

SCADA typically uses a database that contains data elements called *points*, which represent each specific field element. Points may hold field values such as analogue magnitudes or status, or can be used to issue commands. Modern architecture based on IEC 61850 standard uses objects instead of points. Objects provide a powerful functionality and a richer information structure, which enables interoperability with other applications, as explained in following sections.

SCADA functionality at substation level works in a similar way. It gets all the information from the substation field and filters and groups this information before sending it to the control center. Furthermore, using this information implements some local logical functions related to supervision of the operation and status of substation devices. Substation SCADA is configured

to filter and process field information before send it to the control center. Some legacy SCADA implementations use different protocols inside the substation and from substation to control center. Modern approaches unify protocols and data models at all SCADA levels.

The man-machine interface (MMI) or the human-machine interface (HMI) provides the view of the system and the interaction interface to the SCADA operator. Grid and substation information is presented to operating personnel in a graphical way in the form of mimic diagrams, which are a schematic representation of the grid or a particular site. Alarms, status, values, etc., are presented in realtime on the MMI display.

Mimic diagrams consist of line diagrams, symbols, and icons that represent the grid structure and process elements. Status and values of mimic elements are updated in realtime.

MMI is also used to host the graphical interface of other SCADA functions, such as the historian that stores time-stamped data, events, and alarms in a database. Historian database information can be retrieved to analyze faults or unusual events. This information can be shown as a text list or in a graphical way. Alarm handling is a very important SCADA functionality that uses MMI to present its events. It classifies alarms according to their severity and provides facilities for alarm management according to the operator's criteria.

SCADA monitors field values to determine when an alarm condition is present. Once an alarm or other event occurs, actions will be taken depending on the logic implemented at any SCADA level from 0 to 4. This event can be generated directly by a change in the status of a field signal or indirectly when is the result of a calculation carried out from several signals, like in

the case of analogue ones or a result of a logic function. The activation of an alarm rises and an indicator generates an alarm report, etc. This event can be presented and processed at any SCADA level, but in any case, it is presented to the SCADA operator using the MMI. Alarms can be classified into different levels of severity and can have a different status, such as pending, recognized, and cleared. The level of severity and the status are clearly identified by color codes, font type, blinking text, etc.

SCADA provides services to other control center applications. Data interchange was formerly proprietary, later based on generic standards, and finally, fully standardized in an open and distributed power utility architecture, as described in following sections.

To perform all the above-mentioned functions, SCADA requires a telecommunications infrastructure that becomes a key component to guarantee system performance and reliability. Two different types of communications infrastructure are required: local communications inside substations and plants and wide area network communications to connect substations to the control center. The most important requirements for SCADA communications are availability and reliability. Nowadays, SCADA uses standard communications protocols that have been specifically designed for this application, efficiency and reliability being its most important characteristics. Details on communications technologies and SCADA protocols can be found in the telecommunications section (Sect. 14.3).

#### 14.2.4 Asset Management and Condition Monitoring

Asset management applications provide the functionality to guarantee the service level of physical assets in the most cost-effective manner with an acceptable and manageable risk. Although the concept includes the entire life cycle of the asset, from design to disposal, asset management applications are focused on operating conditions, maintenance, repair, and refurbishing.

Asset management is a centralized application that provides functionality to support risk-based management decisions. The decision process is rather complex due to the fact that both short-term and long-term decisions should be supported on the grounds of a holistic approach.

The decision-making process must consider aspects such as:

- System development plans
- System performance impact
- Economic aspects such as price, cost, and benefit
- Impact on safety and society.

An asset management application should integrate data related to primary equipment, secondary equipment, and IT infrastructure. This integration simplifies the two key challenges, the integration and correlation of heterogeneous operational systems and integration with other business applications such as enterprise resource planning (ERP), customer relationship management (CRM), etc. A new power-system operational architecture and associated technologies make this integration possible, as will be explained later in this section.

Using the information provided by SCADA and other field devices, an asset management application extracts key information from the huge amount of data gathered from the grid. These data are linked with other relevant information related to economic aspects, social and environmental information, etc., to make decisions to improve asset management.

Condition monitoring is a complementary tool of asset management. Condition monitoring is the process that monitors parameters that provide information about the working condition of an apparatus in order to identify a significant change that is indicative of a developing fault. Condition monitoring is a key component of predictive maintenance and provides very relevant information to the asset management application.

Condition monitoring information allows maintenance to be scheduled and other actions be taken to prevent failure and avoid its consequences. Condition monitoring is normally applied to primary equipment such as power transformers, breakers, rotating machines, etc. Traditional architecture consists of specialized equipment associated with the primary device and located in the same location. This device processes specific parameters such as pressures, gases, etc., to identify anomalous conditions. A summary of the findings is transmitted to the asset management application. Nowadays, modern implementations based on IEC 61850 architecture models this monitoring function in a standardized way, so most sophisticated applications able to correlate information of different nature can be implemented. For further details, see Sect. 14.3.9.

#### 14.2.5 System Protection Schemes and the Protection Management Center

Protection of power system is a very important function to detect and isolate faults in order to protect the equipment and limit their effect on the grid. Chapter 13 has already presented different protection schemes that are specialized in clearing faults related to substation equipment, power lines, or cables.

In addition to these schemes, there are other schemes specialized in protecting the system as a whole. These

schemes combine protection and control functionality and rely on telecommunications services to perform their task.

A system protection scheme (SPS) is defined according to the North American Electricity Reliability Council (NERC) as follows.

An automatic protection system designed to detect abnormal or predetermined system conditions, and take corrective actions other than and/or in addition to the isolation of faulted components to maintain system reliability. Such action may include changes in demand, generation or system configuration to maintain system stability, acceptable voltage, or power flows.

SPS is normally designed to cope with the following phenomena:

- Transient angle instability
- Small signal angle instability
- Frequency instability
- Short-term voltage instability
- Long-term voltage instability
- Cascaded tripping.

A vast number of SPS are in operation worldwide; the most common actions are:

- Adaptive protection – changing protection settings based on system conditions
- Generator control and rejection
- Actions on automatic generation control
- Load shedding due to both underfrequency or undervoltage
- Out of step protection
- Load rejection – transmission line removal
- Reactive power compensation
- System split/separation
- Tap changer blocking.

SPS architecture can be local or system wide. Local implementation involves field information and control devices located at a substation or generation plant. System wide SPS involves collecting information from multiple sites. Decision-making and logic functions can be performed at one location or distributed among several places. Telecommunications facilities are required in all the cases to collect information and to initiate remote corrective actions. System wide SPS can encompass an area or the whole grid. Telecommunications service is a key component of a SPS system. Latency and service reliability have a direct influence on SPS performance. In fact, internal SPS algorithms

should consider telecom service performance and failure modes.

SPS can be deployed with different scopes namely:

- *Substation*: Information obtained locally within the substation and used to control substation devices
- *Regional area*: Information gathered from several nearby substations which have a greater but limited impact on power system
- *Wide area*: Information gathered from most of network sites to monitor the network with a complete geographical span having the greatest impact on power system.

The working principle of the SBS is based on a centralized working mode, that is to say, information is obtained from the field and transmitted to a central point where it is processed and analyzed to obtain relevant information about power system status. The result of this evaluation can be passed to an operator for manual action according to the operator's criteria, or a command can be automatically issued to start an automatic action in the field. Every scheme has different telecommunications requirements in terms of bandwidth, reliability, and latency. The telecommunications network is a critical component of every SPS. Therefore, the telecommunications service used by any SPS application should be tailored accordingly to application requirements, as will be discussed later in this chapter.

The use of Ethernet-based telecommunications with a large bandwidth capacity allows IEC 61850 GOOSE (generic object-oriented substation event) and sample values messaging to be used to transmit data from the field back to the central control application. This approach will simplify implementation while reducing the response time of SPS, thus improving its performance. Most SPS applications can provide a better accuracy when measurements coming back from different parts of the system are synchronized.

Current implementations use phasor measurement technology to correlate information obtained from different network locations, as this method can be synchronized using different precise-time synchronization methods to improve accuracy. Due to this, control actions can be taken faster and with more accuracy. Phasor measurement units (PMUs) provide synchronized vectors using GPS time synchronization. This information is transmitted to processing units using standardized protocols such as IEEE C37.118 or IEC 61850-90-5.

### 14.2.6 Energy Market

As was already explained in previous chapters, the energy market, or the electricity market, is a system that

enables electricity to be traded through bids to buy and offers to sell. Bids and offers are cleared by the market operator, which is an independent entity. Trade clearing considers internal market rules, load forecast, and grid conditions in order to maintain generation and load balance.

Power utilities, whether generators, transmission, or distribution ones, are actors in the electricity market. Therefore, they have to be connected to market operators to send offers, receive generation orders, etc. This connection must be implemented using standard data modeling and protocols with a near realtime performance. Consequently, deregulated markets should be implemented using communications standards. IEC has developed the IEC 62325 set of standards, which defines an energy market framework that includes semantics, data modeling, market operations, and application messaging process. IEC 62325 is an extension of the common information model (CIM); it defines the business process and operations, as well as semantics and data modeling. The most relevant functions required to interact in the energy market are:

- Auctioning. Sending bidding and buying offers.
- Acknowledgment. Functional and technical acknowledgment of documents.
- Scheduling. Process of exchanging information related to generation schedules, load schedules, and other schedules supported by the market.
- Settlement. Interchange of information to settle the electricity market such as differences between scheduled energy and meter values.
- Managing reserves. The process of managing spare generation units and dispatchable loads for balancing purposes.

Participation in the energy market requires the integration of operational applications in a common framework, since interaction with operational applications are required to implement scheduling actions and manage reserve assets. Therefore, EMS, DMS, and SCADA applications should share information using standard data models, as is discussed in Sect. 14.3.8

Cybersecurity is an issue of most concern for energy-market actors. Market transactions should be protected against cyberattacks, as these operations can compromise system stability and may involve important economic losses. IEC 62351 is the set of standards recommended to protect energy-market information. Cybersecurity details are discussed in Sect. 14.5.

### 14.2.7 ICT Management and Maintenance

As we saw in the previous section, ICT infrastructure has a capital role in the operation of a power grid.

Therefore, it is very important to manage and maintain it properly to assure service reliability and availability, as these have a direct impact on power-system reliability.

The scope considered does not only include the telecommunications networks, but also information processing platforms and system components, as well as IEDs implementing substation automation systems. Managing such a complex infrastructure is a challenge due to the need for integration of different technologies to provide a system view.

The following aspects must be considered:

- The need for a unified view of ICT systems. This can only be achieved by implementing a network management center.
- The technology integration challenge. Many different technologies working together to support operational services. Monitoring them is difficult due to the need for information integration, as every technology uses different semantics, data modeling, and protocols.
- Information presentation. The challenge here is how to present information in such a way that it becomes useful for the customer, that is to say, other operational applications.

These challenges should be overcome by the network management center, which provides both a console-supporting HMI, as well as a middleware layer that allows information to be interchanged with other applications. HMI provides the interface for day-to-day operation, administration, maintenance, and security monitoring of the network. These facilities are provided by management services that are implemented using a distributed infrastructure that involves every single device and application participating in the support of operational services and applications. On the other hand, middleware provides information and services to high-order management and business applications. Details on management architecture and functionality can be found in Sect. 14.3.9.

### 14.2.8 Control Center Application Architecture

We have seen how a power grid is operated and managed using quite a large number of applications, some local and some distributed, which gather information from the field to provide services and facilities that guarantee electricity delivery with the required level of quality and reliability. These applications should share information with business management IT applications to empower business management. They must support a number of different user groups and organizational

functions, including operators, supervisors, operator training, operation planning, and maintenance tasks.

Legacy systems were implemented in such a way that each application gathered field information using its own data format and protocol. For this reason, the same piece of information was coded in different ways and transported to the central application using different protocols and stored in different data bases with different formats. It was really difficult to share information between applications, so information interchange was very limited. Therefore, system view was poor and rather limited, which prevented an optimal use of grid resources.

This architecture was not scalable, so new technologies and system architecture have been developed and adopted. Nowadays, the goal is to implement integrated systems, that is to say, systems formed by applications able to share information and be fully interoperable.

Integrated systems require a high level of interoperability between applications. This implies that interoperability must be guaranteed at different levels:

- Connectivity. An open and standard communications interface must be used. Ethernet technology is the communications interface used in control centers.
- Protocols. A suite of protocols including all the layers needs to be defined. Not only the protocols, but also the profile or selected options must be standardized to guarantee interoperability at protocol level. Manufacturing message specification (MMS) and transport control protocol (TCP)/IP is the protocol stack used in modern control centers.
- Middleware. This is a software layer that supports transparent communications between distributed applications. Different technologies can be used to implement this functionality; all of them provide the facility of distributing applications in different servers in a transparent way.
- Application interface. This provides communications services with other applications.
- Object modeling and semantics. These specify data format and properties, as well as naming.

Integration technology should fulfil the following requirements:

- Open communications. These allow system components to exchange any kind of information of arbitrary complexity.
- Technology independence.
- Provide an information exchange model.
- Publishing independence. Any subscriber should be able to be configured to receive a message without modifying the publisher configuration.

- Open expansion. New publishers and subscribers can be deployed regardless of existing ones.

As we saw before, the two key aspects to implementing an integrated system is to use a common data model and semantics, as well as a common application interface able to provide communications services between distributed applications. This application interface is implemented using middleware that provides those services required to support what may be seen as the *application bus*, that is to say, a communications bus that provides transparent communications between any application connected to this bus.

This new architecture was designed to fulfil a key requirement: interoperability between applications. Consequently, two generic components have been standardized, the application programming interface (API) that defines communications services and data interchange methods, and a common information model (CIM) that unifies semantics and data object modeling.

This architecture facilitates application integration. Several scenarios can be envisaged:

- Integration of applications developed by different suppliers running on the same system
- On-line data exchange between independent systems
- Sharing of engineering data between different systems
- Exchange of data between the similar applications working in different systems.

This new architecture is defined by the IEC 61970 standard series for EMS and IEC 61968 series for DMS. Two fundamental components are defined by these sets of standards; the API is referred to in these standards as the component interface specification (CIS) and the common information model (CIM).

### CIM Architecture

The common information model is an abstract model that represents every power utility object related to grid operation. It provides a standard way of representing devices and resources as object classes and their attributes. CIM also defines a common language including semantics and syntax, so data can be published and interchanged independently of how it is represented inside the applications.

Due to the huge number of objects defined by CIM, the object classes are grouped into logical packages containing a set of objects related to a specialized function. The CIM model is described using the Unified Modeling Language (UML). Figure 14.3 shows a class diagram of top packages' dependencies.

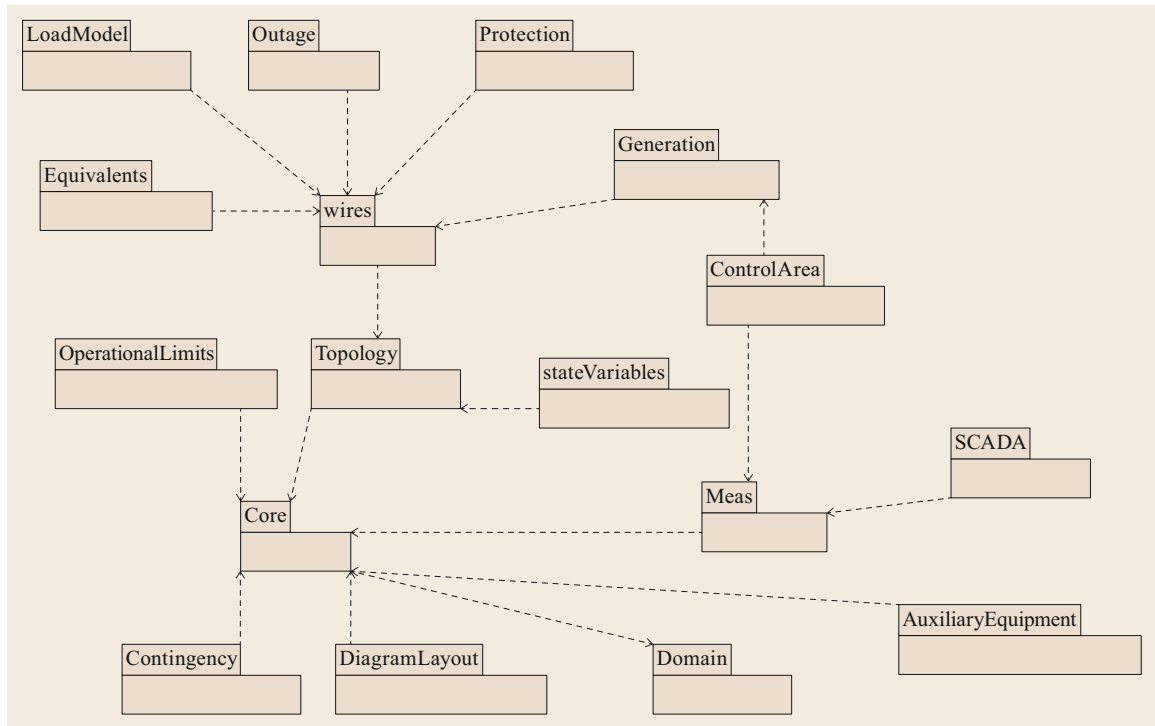


Fig. 14.3 CIM class diagram showing dependencies

The package *Domain* defines data types used by classes in other packages. The following types are defined (Fig. 14.3):

- *CIMDatatype*. A data type that contains a value attribute and optional unit of measure and multiplier.
- *Primitive*. The most basic data type such as Boolean, integer, etc.
- *Enumeration*. A list of constant values.
- *Compound*. A set of data of any of previous types.

The package *Core* contains the models of power-system resources including conducting equipment. This package only depends on the *Domain*, but most other packages have associations that depend on it.

The package *Diagram Layout* describes how objects are arranged to form a coordinated system.

The package *Operational Limits* models the working limits of operational system devices.

The package *Topology* describes how equipment is connected and models grid topology, which is the result of the state of switches and breakers.

The package *wires* models the electrical characteristics of transmission and distribution networks. This package is used by several applications, such as the state estimator, load flow, etc.

The package *Generation* contains other packages that model load forecasting, automatic generation control, economic dispatch, and unit commitment.

The package *Load Model* is responsible for modelling energy consumption and system load. Related information that may affect load, such as seasons and day types, are also included.

The package *Outage* is an extension of the packages *core* and *wires* and models current and planned network configuration.

The package *Auxiliary Equipment* models other types of equipment that is not related to topological connections such as sensors, fault locators, etc.

The package *Protection* is an extension of the packages *core* and *wires* and models protection equipment. It is also used by fault location applications.

The package *Equivalents* models equivalent networks that are the result of network reduction, considering actual connectivity in the functioning of switches and breaker position.

The package *Meas* describes data exchanged between applications. Data types for measurements can be:

- Control information
- Set points
- Analogue information
- Digital information, such as position, alarms, etc.

The package *SCADA* models information used by SCADA applications, including communications status.

The package *Control Area* models the operational specification of a grid area including actual generation,

actual area load, load forecast, and power flow. A control area gathers generators, loads, and a set of tie lines for the connection to other areas to implement different functionalities such as automatic generation control, power flow area interchange, etc.

The package *Contingency* models information related to contingency situations, including equipment status and contingency plans.

The package *State Variables* models variables for analysis solutions, including short circuits, power injection, power flow, voltages, and conducting equipment status.

### API Architecture

The application programming interface (API) is the tool used by applications to interchange information. API provides communications services to applications. In the context of CIM/CIS standards, these services should be independent of the implementation of the components supporting them and of the underlying protocols. This approach is aligned with service-oriented architecture (SOA). The SOA paradigm provides a uniform means to offer, discover, and interact with capabilities provided by other applications. Its central concept is *service*, which is defined as a mechanism to enable access to capabilities, where the access is provided by an interface used according to constraints and policies specified by the service description.

An integrated system should be based on services with the following characteristics:

- Explicitly defined interfaces. Interfaces should be declared and known using a formal and clear definition.
- Loosely coupled. Service should have dependency to standard interfaces only but never with internal interfaces or any other dependency.
- Use abstraction. Services should be independent of implementation technology.
- Reusability. Services should be reusable in different business contexts. This is very important, as it has a direct impact on cost and improves system consistency.
- Autonomy. Services should have control of their environment in order to be able to provide the required service level.
- State control. Services should be able to control their internal state. Services should always be in a known state that can be requested by a third party.
- Self-descriptive. Services should be understandable and can be found at design and run time.
- Manageable. A service can be started and initialized by a well-defined interface.
- Testable. Services should be testable without the use of the rest of the system.

In order to understand interface concept and implementation, it is broken down into its components. This component-based approach also facilitates the use of systems and software of different sources. It is important to mention that this approach is independent of any particular middleware services or technology. Consequently, service interface does not depend on middleware technology just uses it internally.

The reference model is shown in Fig. 14.4. Rather than showing the functional layer, the model shows the components required to create a reusable framework.

The model is intended to be applied to control center environments, which are typically based on a number of servers connected by a local area network (LAN). Since a control center includes a variety of systems to support operational applications, it is important that applications can be used in multiple contexts. This is achieved due to the properties associated with each component interface.

A component is a reusable building block. It shall provide a standard interface that allows other applications to invoke its functions and to access internal data component. Components expose methods, properties, and events. The model of a component defines its basic architecture and specifies the structure of the interface and the way it interacts with other components. Components are executed within a *container*. A container provides an operating-system process in which the component can be executed. The container isolates the component from the runtime platform. The component adapter is a piece of software that links the component and its container. The adapter can implement protocol and data translation. The component

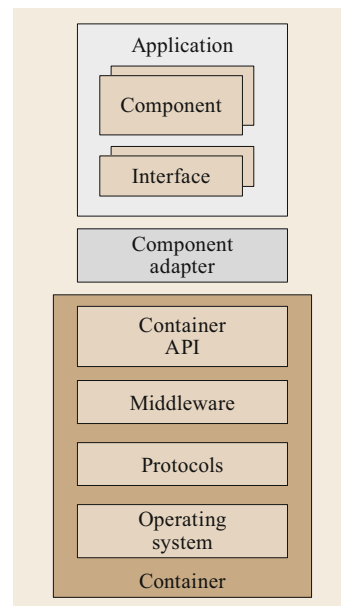


Fig. 14.4  
Functional layers



adapter deals with the differences between component interfaces and container technologies. The application interface is completed with two more components, the middleware and the communications protocol stack.

There are several technologies and different middleware implementations, as is described in technology section. The power utility should select the technology and define a middleware implementation profile, as well as a communications profile. Profiling is a necessary step to guarantee interoperable solutions, as standards are normally opened so they offer many implementation approaches.

### Hardware Architecture

Although every supplier implements different solutions, the most common approach is the use of a redundant fault-tolerant architecture implementing a layered model.

The computing platform comprises the following components:

- Local communications implemented using an Ethernet LAN
- Servers hosting applications
- Storage units built into servers and external ones holding a backup image of the system
- Backup units
- A user interface.

The hardware architecture should provide the following features:

- *Fault-tolerant architecture.* This implies the use of two disjoint LANs and, in general, redundant communications and cyber-protection infrastructure. The connection with the WAN is normally implemented through two routers and two firewalls, each connected to a different LAN. Every device has two Ethernet ports each connected to one LAN.
- *Server redundancy.* This includes data storage and power supply redundancy.
- *Resiliency.* The architecture should assure continuous operations in spite of local anomalies and planned maintenance, including installation of updates and patches.
- *Disaster recovery.* In the case of major failure or local disaster, a minimum functionality should be guaranteed.

Layering architecture implies that communications, applications, and data are supported by different servers that can only communicate through firewalls. The minimum architecture comprises the following layers:

- *Communications layer.* Supported by the front-end servers that have IP connectivity with field IEDs through a firewall and a wide area network. These servers implement communications protocols and data conversion when needed.
- *Application layer.* Control center applications are installed in servers allocated to the same layer. Sub-layering is also possible.
- *Data layer.* Data are stored in a different layer to protect their integrity.

The number of servers and layers depends to a great extent on the size of the system. Regardless of the number of servers, data modeling and API should be implemented according to the above-mentioned standards.

### Service Continuity

Control center host-operational applications are capital to guarantee electrical supply continuity. Consequently, business continuity and disaster recovery plans should be implemented. The implementation of these plans affects not only every aspect of both hardware and software architecture, but also the fact that a complete backup control center is usually implemented in a different location.

To support these specific requirements, control center platform architecture has to be designed to provide redundancy to support continuous operations while providing flexibility to react to system component failures or disaster scenarios. This performance has to be maintained even during maintenance or system upgrades.

The most relevant requirements related to business continuity are:

- *Flexibility of operation.* The architecture should support different operation modes between the main and redundant system:
  - Main–main. Both systems are active and synchronized.
  - Split mode. Some functions are segregated to one of the systems during maintenance or upgrades.
  - Main–backup. One system acts as primary and becomes synchronized with the other.
- *Synchronization.* Functions and services must be synchronized between systems. The transfer time of applications and services should be optimized.
- *Storage.* Data backup facilities must be provided.
- *Maintenance facilities.* System architecture should support the upgrade or maintenance of applications, the operating system, and hardware components carried out in one of the system images.

Continuity of operations is closely related to the continuity of telecommunications services, both inside the control center and at the wide area network, since communications between system images will usually require telecommunications services. Consequently, a contingency and business continuity plan should embrace all ICT aspect and components. Business continuity and disaster recovery techniques are developed in the telecommunications section (Sect. 14.3.10).

### The User Interface

The user interface is a very important functionality in a control center, since it supports the interaction between system operator and operational applications. A control center user interface is not limited to a screen to present data but a complete framework that provides flexibility and enables integration and expansion of multivendor solutions into a system that looks like a large, single application. Visualization devices are the primary interface between the control room operator and grid operational application. Typically, they consist of operator consoles and electronic wall displays.

Consequently, the most important requirement for a user interface framework are:

- *Common look and feel.* Common presentation and navigation perspective, regardless of the underlying applications.
- *Task-oriented displays.* Capabilities to define user displays according to business rules regardless of the origin of the data.
- *Flexibility.* The ability to customize the user displays consistently with the enterprise business practices and style guides.
- *Technology independence.* Capability to define user displays regardless of application technology and data format.
- *Multi-vendor console management.* The ability to enable displays from multiple vendors within a shared user interface framework.
- *CIM support.* The display process should be integrated in the CIM data model.
- *Cybersecurity support.* User interface must implement cybersecurity measures in accordance with IEC 62351 to implement access control to applications and data.

The user interface framework includes the components:

- *Visualization environment.* The control-room visualization environment controls visualization devices that are the primary interface between the control-

room operator and the grid. Typically, they consist of operator consoles and electronic wall displays.

- *Visualization management.* This implements the visualization of several applications on the same display at the same time.
- *Display editor.* This includes the tools for display configuration.
- *Rendering engine.* This generates the display content from the application data.

Although the display format and content can be configured, displays shown on user interfaces can be classified into three major categories:

- *Operator displays.* These present the state of the power grid and allow the operator to operate the system. They include one-line diagrams, geographic displays, alarms, etc.
- *Engineer displays.* These are used for engineering and maintenance tasks. They are nonoperational displays and so less critical than operator displays.
- *Management displays.* These dashboard-type displays are used by management or nonoperator personnel. They may also be available externally to the operational environment.

### 14.2.9 Substation Applications Architecture

IEC 61850 architecture and technology is the cornerstone of modern power-utility operational systems. The first edition of the IEC 61850 series was focused on the substation automation system (SAS), which includes all the functions implemented by IEDs to control, monitor, and protect the substation equipment and its power supplies. In addition, there are other functions that maintain the SAS, such as system configuration, IEDs management, and communications monitoring, or software management and cybersecurity.

This section is focused on understanding the way IEC 61850 models devices, and the way IEDs communicate to implement an automation function. This has an important impact on the way Ethernet and IP are used in the application domain which, correspondingly, affects the design and configuration principles.

#### Relevant Aspects of the IEC 61850 Standard

The fundamental goal of the IEC 61850 standard (Communications Networks and Systems in Substations, Edition 1) – published at the end of 2004 –, which applies to SAS, is to standardize the communications between intelligent electronic devices (IEDs) from different manufacturers inside the substation. In other words, the objective is to define a substation automation

system (SAS) which allows interoperability between IEDs from different manufacturers; or more precisely, between functions that are carried out by equipment installed in the substation. In this scenario, interoperability is the capability for two or more IEDs of interchanging information, and of using that information for a correct cooperation regardless of the model or manufacturer of the devices. Interoperability should not be confused with *interchangeability*, which corresponds to a wider concept and is out of the scope of the standard. It is important to highlight that the standard does not have as an objective to achieve interchangeability between IEDs nor the complete configuration of the equipment in a substation, but just interoperability with respect to the communications between devices.

To achieve this, the standard defines:

1. A *suite* or set of well-proven protocols and the way to use them to fulfil operational requirements.
2. Data models and semantics that will be used to interchange information between SAS functions.
3. Communications services specified in such a way that they become independent of the communications protocols.
4. The language and format used to describe IEDs and SAS configuration and capabilities.

Due to these features, a very important capability is achieved; the specification is not related to its implementation. That is to say, a SAS can be specified using IEC 61850 architecture and features, and the final performance of the system is independent of its implementation. This provides a very high degree of flexibility and reutilization of proven solutions regardless of their final implementation.

Another relevant feature introduced by IEC 61850 is the standardization of IEDs configuration files using the common language Substation Configuration Language (SCL) that is used to interchange IEDs configuration information files among the different engineering tools and from these tools to IEDs.

After some years of positive experiences using IEC 61850 technology, it was proposed to extend this technology and concepts outside of the substation. By the end of 2012, most of the IEC 61850 Edition 2 was approved. This new edition extends the use of this technology to the whole power system from the control center to every single device of the power grid. In 2017, some parts are still under discussion. A summary of related standards and their status is summarized later in this section.

Historically, in order to carry out these functions, serial protocols have been used in point-to-point or point-to-multipoint configurations. These approaches needed to differentiate services or subsystems in differ-

ent networks, and for this reason, the communications architecture, although being simple, ended up becoming inflexible and complicated to maintain topology. Furthermore, nowadays, more and more substation devices have communications capabilities, so legacy solutions are not appropriate, as they do not provide flexibility or scalability. Consequently, Ethernet technology has become the standard communications interface due to its flexibility, as it can carry any protocol or data format, and its scalability that ranges far higher than what is required by power automation systems.

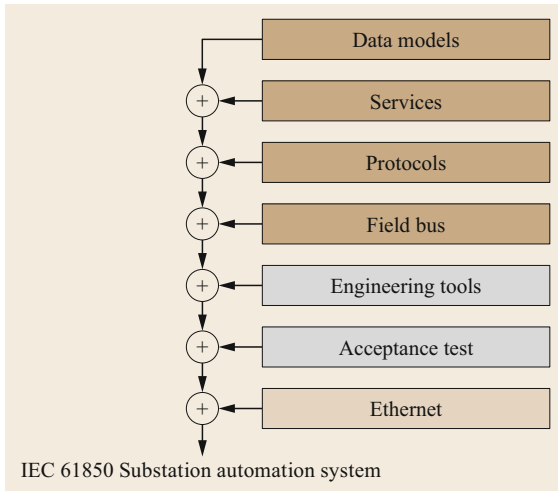
The scope of the IEC 61850 series is not limited to interoperability, but it is much broader, as it proposes not only a new concept of automation of substations – based upon a new architecture for communications – but also defines models of information and configuration languages based on the Extensible Markup Language (XML). Likewise, IEC 61850 standardizes the use of Ethernet networks with priority, and it defines the interchange of critical messages called generic object-oriented substation events (GOOSE), as well as sampled value (SV) messages, for the transmission of the measurements of current and voltage transformers. These measurements can be carried out by means of new models of measuring transformers whose output values are digital, or by means of specific units that convert the conventional analog measurements into digital information, called *merging units*.

The models of information and the communications services are independent of the protocol, and the use of the manufacturing message specification (MMS) protocol in the application and Web service layers will allow the growth and validity of this standard, as they make the use of new technologies of communications feasible.

Edition 1 of the standard is made up of 14 parts; it was a great innovation not only with regard to the approach of using object-oriented modeling techniques, but also with respect to communications modeling that allows services to be isolated from the protocols supporting them. Edition 2 is made up of a larger number of parts, as it covers the whole power utility grid from control centers to customer premise devices. For further details of both editions, see the standards section (Sect. 14.2.10).

Figure 14.5 shows the components that make up an IEC 61850 substation automation system. The most generic component is data modeling; this part models every substation device and in Edition 2 also every power grid device. Models use services that have been defined in an abstract mode, so they are independent of underlying protocols. Protocols used by IEC 61850 are well known and proven, e.g., MMS and IP. The standard defines protocol profiles to ensure service performance.

A field bus or process bus defines how primary equipment with communications capabilities can send



**Fig. 14.5** IEC 61850 components

and receive their status, as well as voltage and currents in the form of samples.

The definition of the Substation Configuration Language (SCL) based on XML defines the format of configuration files, and how these file can be interchanged between configuration tool and IEDs. Finally, the standard includes the specification of conformity test procedures. All the above-mentioned components rely on Ethernet as the communications interface and technology to implement a communications network inside the substation. Communications outside substations can be implemented using Ethernet or IP according to the service and application. Therefore, to fully understand this technology and to make the most of it, technologies involved in every component must be well understood; namely, Ethernet, IP, XML, and object-oriented technology, including UML.

### IEC 61850 SAS Architecture

Legacy technologies had fewer resources to implement a well-structured SAS. Communications were not as widely used as in modern systems, so it was difficult to implement redundant systems, and consequently, they were less reliable and had poor flexibility.

IEC 61850 defines a hierarchical SAS architecture made up of four levels using the same concept shown in Fig. 14.2. Although the concept is similar to the legacy architecture, the big difference is that it is fully implemented using communications devices.

Level 0 comprises the process level, which includes primary equipment with communications capabilities and any other associated IED. Communications between this level and upper levels is implemented using process bus technology, which uses fast messages to transmit status and sample values.

Level 1 comprises IEDs that implement protection, control, and measurement at the bay level. This level obtains information from level 0, processes it, and generates information to the field level, upper levels, and to other bays. Edition 2 of the standard includes the interaction with bays of other substations, mainly for protection and automation functions.

Level 2 is the substation level. This level includes the functions related to the whole SAS, such as substation automation logic, local SCADA, and gateway or proxy devices. Level 2 communicates with the bay level and gathers information to be interchanged with the control center.

Level 3 is the control-center level. This level was out of the scope of Edition 1 but was included in Edition 2. Control-center communicates with substation level 2 IEDs to update the status of LN objects and map them to CIM objects, which are, in fact, accessed by control-center applications.

In order to avoid the legacy SAS limitations introduced by several of the above factors, the new IEC standard suggests building the automation system on top of an Ethernet-based LAN. This allows virtualization of a large number of peer-to-peer connections over the same physical infrastructure, ensuring a high degree of redundancy, bandwidth, very low latency, and higher reliability.

A number of different network topologies are possible using Ethernet technology; this standard can integrate over the same network, multiple communications services, and protocols, such as MMS, GOOSE, FTP, SNMP, etc., ensuring redundancy and reliability. Furthermore, Ethernet can provide several mechanisms to implement fast and even bumpless communications recovery, as is described in the communications section (Sect. 14.3.5).

### Function Modeling

SAS is implemented by several functions, such as protection, control, automation, etc. IEC 61850-5 defines each SAS function and depicts how it can be implemented and how information is interchanged. The implementation of every function is expressed by means of the LNs and the messages interchanged between them.

The concepts involved in function modeling are:

- Functions are implemented using *logical nodes* (LN). A LN is the most basic function with communications capabilities. It is defined by means of an object class.
- LNs are grouped into *logical devices* (LD) that model the functionality associated with a device. This concept is no longer used in most IEC 61850 device implementations, as LD is a mere LN container.

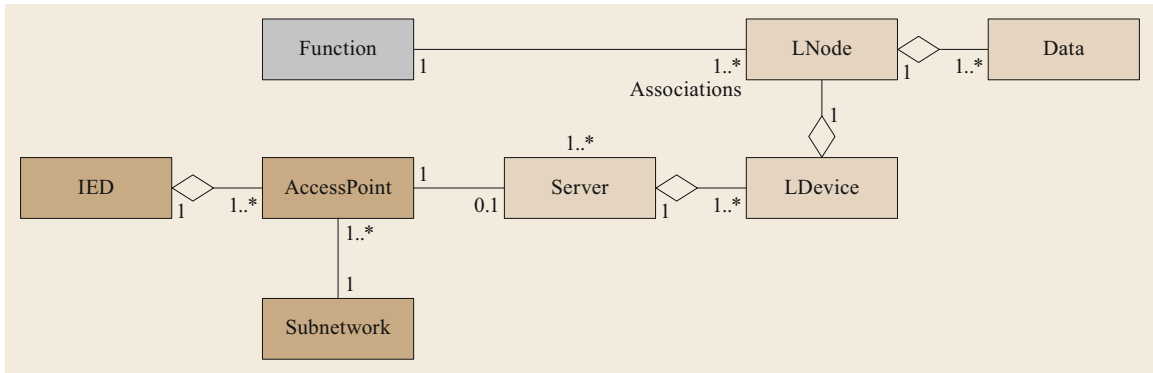


Fig. 14.6 UML diagram of a function

- LDs are contained in a *server* that is associated with a communications access point, which is implemented using an Ethernet interface.

Figure 14.6 shows the UML diagram of a function.

This diagram shows the composition of an IEC 61850 IED and the relation of its internal components from the communications interface to LNs. It is important to mention that SAS functions are only related to LNs.

#### Data Structure

A very important aspect introduced by the IEC 61850 standard is the structure of the data. While classical protocols typically operate under the concept of numerical and linear addressing and data coding, IEC 61850 works with a structured data model based on the object principle. Linear approximation is simple is difficult to maintain; it is not scalable and does not provide interoperability. With the old approach, each control point requires an arbitrary and individual address.

The IEC 61850 standard models substation devices using object modeling techniques. In fact, modeling is not limited to physical devices as it also includes SAS functions.

Object-oriented techniques provide three important features:

- *Abstraction*. An object is the abstraction of a real device. It represent the features required to implemented SAS functions. These features are expressed by means of a data structure and a communications interface that support the interaction with other objects and define how to use object functionality.
- *Encapsulation*. Every object performs an internal function using its own data and algorithms. These internal data and algorithms are hidden from other objects, so every implementation can be differ-

ent yet still compatible, as they all use the same standard communications interface that is used to transmit messages with information related to the public part of the object.

- *Inheritance*. Hierarchical relations between object can be defined in order to establish relationships between the most general objects to other more particular ones that provide details. Inheritance enables that a class receives or inherits the properties and methods of another class. This creates an object class hierarchy, so the *children* class inherits features and properties from the superclass. This feature allows detailed object classes to be reused in the definition of more complex ones.

Consequently, the IEC 61850 standard is based on the following hierarchy of concepts that are expressed as objects:

- *FUNCTION*. Every SAS basic function that is implemented using objects that interchange messages to execute the action of the function.
- *LOGICAL NODE (LN)*. A logical node is the most basic function. It is implemented as an object form by data, internal methods that implement its functionality, and a communications interface that allows messages to be interchanged with other LNs and expose the service supported. Methods are encapsulated and can only be used through interface communications services. LN data are objects, so its content is not a simple value but an object that has a complex structure.
- *COMMON DATA CLASS (CDC)*. Data included in LNs are modeled using CDC objects. A CDC is an object that models data and – as any other data – is formed by data that are attributes of the CDC and are expressed using basic data. Attributes contain values and properties of the generic data concept expressed by the CDC.

- **BASIC DATA.** These define the coding format of the attribute information.

This data modeling methodology is based on a structured information format that, together with standardized object semantics, provides self-descriptive objects so any application can interact without previous knowledge of the data structure. This provides flexibility and expandability, facilitating future retrofitting.

### Logical Nodes – General Concepts

A logical node is the abstract representation of a specific functionality for substation automation. Its main feature is that this function cannot be decomposed into more basic functions. It can be said that it is an atomic function.

LN are modeled using object classes. This is a concept used in object-oriented programming, which allows real objects to be modeled and thus implemented in a program in such a way that this program resembles the properties of the real object.

An object class is defined by:

- **Name.** This identifies the class. IEC 61850 identifies LNs by four capital letters.
- **Data structure.** This is the information content in the class. In IEC 61850, data are object classes named common data class (CDC) with the structure of an object class.
- **Interface.** This is a communications service that supports the interaction with other class by means of messages.
- **Methods.** These implement the services offered by the interface.

Methods and private data are encapsulated, which means that they are hidden to other objects and, consequently, not specified by the standard. The scope of the standard is limited to public parts, name, public data, and interface. For this reason, each implementation can be different and still compatible.

LN classes, as any other object class, are specified by means of a table that contains the LN name, data objects, and services. Data objects contained in LNs are defined using CDC object classes. The CDC data structure is formed by attributes. Each attribute contains the following fields:

- **Name.** This identifies the attribute. Names are standardized by IEC 61850-7-3.
- **Type.** This defines the data type of the attribute.
- **Functional constraint (FC).** This defines the use of the attribute, as described later this section.

- **Trigger options.** These specify whether this attribute can generate a trigger condition. Three conditions may generate a trigger: data change, quality change, and data update. Triggers are used to generate spontaneous messages, such as GOOSE and reports.
- **Value.** This contains the value of the attribute.

The FC defines functionality associated with the attribute. As specified by IEC 61850-7-3, FC types are coded with two letters with the following use:

- **ST** refers to attributes related to a *status* information, whose value may be read, substituted, reported, and logged, but not written. It can also be included in a dataset.
- **MX** refers to an analogue *measure* information, whose value may be read, substituted, reported, and logged, but not written. It can also be included in a dataset.
- **CO** refers to *control* information the value of which can be operated using the control model service and read.
- **SP** refers to a *set-point* information, whose value can be operated using the control model service and read.
- **SV** refers to a *substitution*, whose value can be written.
- **CF** refers to a *configuration* information, whose value can be written and read.
- **DC** refers to a *description* information, whose value can be written and read.
- **SG** refers to a *setting group* and identifies the active setting group. It cannot be written.
- **SE** refers to *setting group editable* and uses the setting group control block service.
- **EX** identifies *extension* information providing a reference to the namespace.

FC relates attributes to services. That is to say, an attribute can be accessed using the service identified by its FC. This provides an extra verification of the coherency of the use of LN objects and attributes. LN classes are defined by IEC 61850-7-4. CDCs are defined by IEC 61850-7-3 and the service interface is specified by IEC 61850-7-2.

### IED Structure

An IED is a physical device, a physical entity with specific properties like serial number, status, health, etc. An IED implementing server functionality should have a data structure in accordance with the UML diagram of Fig. 14.5. This implies that the access point must have at least one logical device that contains LNs. An IED may contain multiple logical devices. A logical device must

contain at least two logical nodes that support generic IED functions.

**LLN0:** logical node zero. This logical node contains information about the logical device and its communications control blocks that configure how GOOSE, SV, reports, and log messages will be constructed. Usually, it also contains the data sets associated with control blocks. Therefore, it is a container for all the information and data necessary for the operation of the LN included in its LD. LLN0 also controls local/remote working mode and testing facilities. LLN0 configuration of these features affects all LNs inside the same LD.

**LPHD:** contains information about the physical device. Serial number, description, health, etc.

### Naming

LN objects and attributes are addressed according to the structure

```
<IEDName>/<AccessPoint>/<LDName>/
<LNName>.<DataObject>.<DataAttribute>
```

IEDName, Accespoint identification, and LD name are not defined by the standard.

The LN name is formed by three fields:

- **Prefix:** Optional identifier.
- **LN class name:** A four-letter code that identifies its functionality.

- **Instance:** Optional ordinal number used when more than one instance of the same class is included in an LD.

Finally, in order to exchange communication information between different devices, configuration file content and syntax are defined by an XML schema. This file contains naming of objects, specification of mandatory and optional parameters, data types of every attribute, and value ranges. Since naming and object content rules are defined by this file, it can be used to validate other SCL files, such as IED configuration files and substation configuration files.

### Communications Interfaces

IEC 61850 defines the communications interfaces between substation levels. Figure 14.7 shows the reference architecture of an IEC 61850 substation including communications interfaces shown as numbers in circles.

The numbers in Fig. 14.7 identify different types of interfaces, which support different services and, therefore, have different communications requirements. Interface types are:

1. Protection data between station level and bay level
2. Protection data between bay level and remote protection device
3. Data exchange between bay level devices

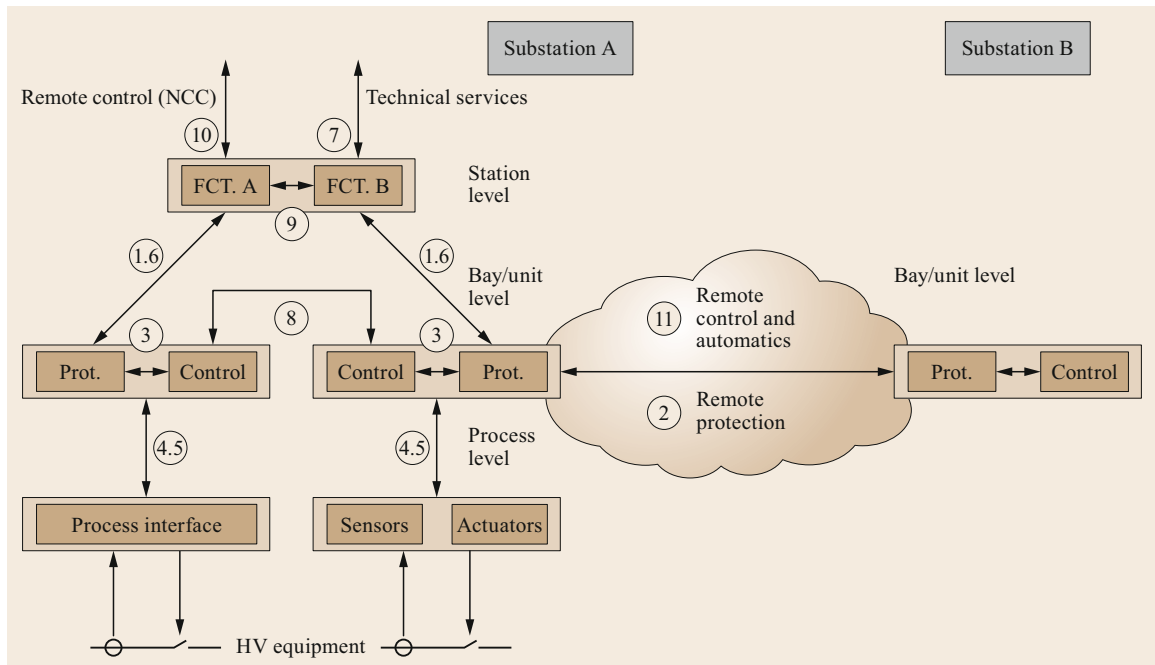


Fig. 14.7 Logical interfaces. (Adapted from IEC 61850-1)

4. Data exchange between process level and bay level of instantaneous samples of current and voltage
5. Control data between process level and bay level
6. Control data between station level and bay level
7. Remote configuration and monitoring data
8. Direct data exchange between bays for fast functions, such as protection and interlocking
9. Internal control data in the substation level
10. Control data between station level and control centers
11. Control data exchange between different substations.

IEC 61850 Edition 1 did not implement interfaces 2, 7, 10, and 11, whereas Edition 2 includes all of them.

It is important to explain the interface concept. In this context, every interface is related to a specific communications service that has a performance requirement. Several interfaces can share the same physical interface but use it in a different way with different protocols and settings.

As shown in Fig. 14.7, by using a wide area network – typically an IP network – the remote system can be connected to several control centers or engineering facilities. For those legacy facilities that typically communicate using IEC 60870-5-101, IEC 60870-5-104 (TCP/IP), or DNP 3.0 protocols, information interchange between control center and substations a *protocol interpreter* or *gateway* must be provided to *translate* the information from IEC 61850 to the protocols and formats used by the control center. The standardization of this communication involves not only communication between the two levels but also an adaptation of the data models used in the control center. IEC 61850-80-1 specifies the mapping of IEC 60870-5 series, whereas IEC 61850-80-2 the mapping to DNP 3.0.

Information interchange with modern control centers can be implemented using the new standard IEC 61850-90-2. This standard defines two communications models, the direct information interchange and the use of a proxy device. The first model allows control centers to access any object of the SAS. This approach provides transparency and flexibility but puts heavier workload on the control center. The second model uses a proxy to mirror the information required by the control center. Proxies do not modify information or protocols.

#### Communication Between LNs

As LNs are modeled using object classes; their communication is implemented using messages sent and received through their communications interface. There are two types of communications, client–server and peer-to-peer messaging. Client–server communications are based on the connection-oriented paradigm us-

ing MMS protocol over TCP. This kind of messages is mainly used for SCADA applications. Peer-to-peer messages are instantaneous multicast messages that, in fact, do not use any protocol, as the information is encapsulated in multicast Ethernet frames. There are two type of messages, event oriented and sampled values of current and voltages. Event information is transmitted using generic object-oriented substation events or GOOSE messages.

The IED sending GOOSE messages is called the *publisher*, and the IEDs listening to GOOSE messages are called *subscribers*. There is no protocol or communication between publisher and subscribers. Configuration of this messaging communication is carried out at configuration time before the system is in operation and can only be modified by changing configuration.

IEC 61850-5 defines seven different types of messages. Each message is associated with a service, to one or several interfaces, and to a protocol:

- *Type 1A*. Trip. Used for protection applications. Associated with interfaces 2, 3, 5, 8, and 11. Implemented by a GOOSE message carried over a multicast Ethernet frame.
- *Type 1B*: Used for protection automation applications not related to direct tripping. Associated with interfaces 2, 3, 5, and 8. Implemented by a GOOSE message carried over a multicast Ethernet frame
- *Type 2*. Medium-speed SCADA messages, such as status and tripping information. Associated with interfaces 1 and 6. Implemented using MMS over TCP/IP.
- *Type 3*. Low-speed SCADA messages, such as alarms and measured values. Associated with interfaces 6, 10, and 11. Implemented using MMS over TCP/IP.
- *Type 4*. Raw data. Associated to process bus sample values. Associated with interface 4. Implemented by an SV message carried over a multicast Ethernet frame.
- *Type 5*. File transfer. Associated with interfaces 6 and 7. Implemented using FTP over TCP/IP
- *Type 6*. Time synchronization. Used for IED time synchronization and phasors and sample-value time stamping. Associated with all the interfaces. It can be implemented using SNTP over IP for IEDs time synchronization or IEEE 1588 over Ethernet for phasors and sample values.
- *Type 7*. Commands. Used to issue control commands. Associated with interfaces 6 and 10. Implemented using MMS over TCP/IP.

To adapt to different requirements of different applications message types are subdivided into performance



classes. Different groups of performance classes are specified for control and protection and for time synchronization. Control and protection classes identified as TT0 to TT6 specify the maximum transfer time that ranges from 3 ms to 1 s. Time synchronization classes identified as T0 to T5 specify synchronization accuracy that ranges from 1  $\mu$ s to 1 ms. IEC 61850 specifies two types of communication requirements: static and dynamic. Static requirements refer to properties not related to latency or transmission capacity. Static requirements are:

- *Ubiquity*. Any function or LN may be allocated in any IED without limitations imposed by communications.
- *Abstraction*. SAS function and their characteristics must be specified without referring to their implementation and the communications infrastructure.
- *Standardization*. Interaction between functions should be described using logical interfaces. Those interfaces must be independent of their physical implementation.

Dynamic requirements refer to latency or transfer time. In this context, latency refers to the maximum transmission time. The average latency should be used in the context of operational realtime services. Transmission time refers to the time required by an LN to transfer a message to another application or an LN located in a different IED. Therefore, it includes not only the communications latency in the LAN but also the processing time in both IEDs required to convert this message in an Ethernet frame and decode it at the receiver side. Latency is specified by performance classes as explained above.

#### Communications Methods

Legacy SAS were implemented using the master–slave communication method. This method is neither flexible nor scalable, so it has been abandoned in modern operational communications. IEC 61850 is based on the client–server paradigm, which is complemented with peer-to-peer messaging communications for fast information transfer.

*Client–Server*. By definition, a server is a device that offers a service using internal data, and a client is a device that requests a service that interacts by getting or interchanging data with the server. As a typical example of a client we can mention an Internet browser that connects to a Web server to get information or interchange data. This communications principle is connection-oriented, which implies that client and server should establish a connection prior to information interchange.

A server can accept a connection from any client without previous configuration and from several clients at the same time, the maximum number of clients being limited by hardware capabilities. For this reason, this method provides flexibility and scalability. LNs can be associated with a client or a server functionality. An IED can have server or client functionality and in some cases both functionalities, client and server, at the same time. In any case, it is only the client the one that gathers information from other IEDs.

As IEC 61850 servers support directory services, which implies autodescription and discovery functionality, clients can discover server data structure and functionality, and consequently, they can interact with any server without previous knowledge of the server capabilities. For this reason, an object's database is no longer required, as clients can dynamically create the internal image of the server's data structure. Furthermore, as explained later this section, IEC 61850 specifies how a substation configuration file can be created. This file contains the data model and services of all the IEDs of the SAS. Clients can also use this file to learn server's information structure.

*Control Command Service*. Control commands can be executed in different ways. The supervision of the expected state change produced by a command is the factor used to differentiate command types. Commands can be classified as normal or not monitored and with enhanced security when the status change is monitored to inform of the result of the command and with or without the previous selection of the device.

Then there are four different types of commands:

1. Direct commands with normal security
2. Select before operate (SBO) commands with normal security
3. Direct commands with enhanced security
4. SBO commands with enhanced security.

The best choice is probably the last one due to the following:

1. Data integrity requirements: As specified by IEC 60870-4, commands require integrity class 3, which under certain conditions can only be reached by using a SBO procedure.
2. The standard IEC 61850-80-1 specifies the mapping of IEC 60870-5-101 and IEC 60870-5-104 to IEC 61850; only enhanced security commands are supported.

It must be considered that an SBO control command is a completed process that starts when the device

is selected and has finished delivering the result of the process, so it is not necessary to read the status of the device afterwards, as the command delivers complete information about the result.

**Origin of Commands.** The hierarchy of control command is implemented using the origin attribute. This attribute is used to identify the origin of commands in order to enable or disable command execution considering their origin and the status of the local mode data attribute value.

The philosophy is that commands can be generated manually or automatically whether from any automatic process or application. In any case, the command source can be:

- A control center
- Local SCADA
- A bay.

IEC 61850 local control model is hierarchical. This means that when a local mode is active within a SAS level commands are only accepted from the same level.

Note that in order to apply the behavior of local command, it is necessary to distinguish between commands coming from an automatic process or from an application. Commands from automatic processes may not be subject to local command blocking.

The different command origins types are:

- *Bay control.* The command comes from a bay-level device.
- *Station control.* The command comes from a station-level device.
- *Remote control.* The command comes from the control center.
- *Automatic bay.* The command comes from a bay-level automatic process.
- *Automatic station.* The command comes from a station-level automatic process.
- *Automatic remote.* The command comes from an automatic process from the control center.
- *Maintenance.* The command comes from maintenance tools.
- *Process.* The command comes from spontaneous state change.

**Remote/Local Mode.** With regard to local modes, the generic working principle is as follows: each level – station, position, and process – has its own local mode attribute. When a level is in local mode, it only accepts commands from that level and not from upper levels. Local mode is controlled by the attribute *Loc* in LNs related to control functions. LLN0 also has this attribute;

consequently, as for other functionality, setting LLN0 in local mode automatically sets all LNs inside the LD to local mode too.

### Proxies and Gateways

Proxy functionality is required when not every piece of information of the SAS needs to be available for some external clients. In this case, a proxy device gathers information from different SAS servers and presents it in the form of LNs. By doing this, a summary of SAS information is available for any client, whether internal, such as local SCADA, or external, such as a maintenance center.

When the external client does not support IEC 61850, a gateway device is required to map the information and translate to the client's protocol. A gateway is a device that works at the application layer. This means that has to decode all the information interchanged in one side and map it to an internal database and process this information to adapt it to the format and protocol of the other side. Typically, a gateway is installed at the substation level for translating from IEC 61850 protocols at new substations and IEC 60870-5-101 or IEC 60870-5-104 in current control centers.

The recommendations to implement a device of this type are included in the technical specification IEC 61850-80-1. Basically, it is a guide that addresses the information-exchange model based on CDC data using IEC 60870-5-101 or IEC 60870-5-104 and includes the following items [14.1]:

1. Conceptual model of the gateway.
2. Command mapping to IEC 60870-5-104 IEC 61850.
3. Mapping of CDC (common data classes) of IEC 61805 to ASDUs (application service data unit) IEC 60870-5-104.
4. Mapping of data attributes to CDC data types in IEC 60870-5-104. An example can be seen in Fig. 14.8.
5. Mapping from IEC 61850 services to IEC 60870-5-104 services.
6. Extension of SCL file syntax in private sections in order to include the association between IEC 61850 data attributes and IEC 61870-5-101/104 information object addresses (IOAs).

### Communications Interface ACSI

LNs communicate using the abstract communications service interface (ACSI). The term *abstract* means that the interface is specified without implementation details, so it is not related to a particular application interface and, therefore, it can be used over any application protocol. Actually, ACSI can be implemented using MMS protocol or Web services without any change in the LN interface being required.

Services provided by ACSI are listed here:

- *Directory services.* These provide the capabilities to browse the content of an IEC 61850 server. By using this service, a client can obtain all the information trees of a server. This includes a list of LDs on the server; in every LD, LNs include a list of data objects and their attributes included in every LN. This service provides an autodescription of the IED data model.
- *Get, set, and substitution.* This group of services implements read and write operation over data, attributes, or datasets. Substitution is a more complex service, which includes two actions. First, write the value to be shown when substitution is activated. Second, activate substitution, so that when a client reads data or an attribute, the delivered value provided will be the substitute instead of the value read from the field. The substitution state is indicated when providing a substituted value in a reading operation.
- *Select active setting group.* This service allows the selection of a particular setting group among those previously loaded into LLN0.
- *Report control subscribe.* This service establishes the relation between a client and a report control block already configured on a server. When the client subscribes to a report, the report is sent to the client using this service. Transmission of a report as well as its content depends on the configuration of the report control block. It can be event driven or periodic.
- *Query log control.* This service allows querying the content of the log. It can also be used to clear log content.
- *Control.* This service issues control commands. It includes the entire process of selection and execution, as well as getting the final result of the command.
- *GOOSE.* This service supports GOOSE message publication and subscription.
- *Sampled values.* This service supports publication and subscription of sample values.

ACSI services are mapped to the application protocol using the specific communication service mapping (SCSM). There is one SCSM for each application protocol, including Ethernet encapsulation for GOOSE and SV messages. SCSM specifies how every abstract service is defined depending on the application protocol. Details are included in following sections.

#### IEC 61850 Protocol Stack

The IEC 61850 standard defines a LAN Ethernet as the physical communications technology to implement

a SAS. The LAN architecture and topology are not specified by the standard. In fact, every solution can adopt the topology required to achieve performance and availability objectives. The telecommunications section (Sect. 14.3) discusses the aspects that affect performance and topologies, and features that may improve availability.

*Message Types.* In an IEC 61850 substation, there exist two different ways of communicating for the different types of messages involved. One way is vertical, from the substation controller to the IEDs and vice versa; and the second way is horizontal, between IEDs. In the case of vertical communication, a client-server is used. In the case of horizontal communication, the transmission is based on the peer-to-peer principle.

In any case, the standard distinguishes between different types of messages depending on the intrinsic characteristics of their nature and classifies them into performance classes, as was already introduced in previous section.

As has been mentioned, there are messages whose transfer time must be very fast, such as GOOSE messages, for which the standard defines a simplified protocol stack or *shortened* path, in comparison with that of the full OSI/ISO reference model. The principle followed by these messages that circulate through a *shortened* path is, in certain way, similar to that used in the protocols of the IEC 60870-5 series, which make use of the EPA model (enhanced protocol architecture), based only upon three layers or levels with the aim of reducing the times required for communication between two devices. It is in this way that *peer-to-peer* messages or GOOSE do not pass through the different levels in the model but are delivered directly to the link layer.

*Suite of Protocols.* The IEC 61850 standard adopts a set of existing protocols widely used in order to carry out the different functions that implement ACSI services. Figure 14.8 shows more specifically different approaches according to the type of messages and the service supported. Messages with high requirements regarding transfer time, by virtue of their *mission-critical* nature, are directly mapped to the data-link layer as this procedure reduces message processing workload.

*Profile for Peer-to-Peer Communications.* In *GOOSE* (generic object-oriented substation event) messages, the information published is defined by the dataset content. Trigger conditions of dataset components generates the event. Please note that former generic substation status event (GSSE) messages that only support fixed state information has been deprecated by Edition 2. GOOSE messages are sent

Message type	Events	Samples	Synchronization		SCADA
	1, 1A	4	6	6	2, 3, 5
	GOOSE	SV	PTP	SNTP	MMS
				UDP/IP	TCP/IP
Ethernet ISO/IEC 8802-3					

Fig. 14.8 IEC 61850 protocols

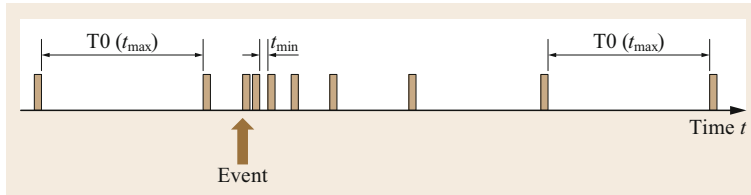


Fig. 14.9 GOOSE message transmission procedure

periodically with a cadence that can be configured independently for every GOOSE message. When an event associated with a trigger condition is generated, a burst of messages is generated. This mechanism improves dependability because if a message is lost, the following one will be processed. Figure 14.9 shows the transmission pattern of a GOOSE message.

$T_0$  indicates the retransmissions cadence of messages when there is no event that produces a trigger condition. This is the rest condition. The continuous retransmission of messages is also used to check that publisher IED and LAN are working properly.

$T_1$  is the smallest retransmission time of an event. As can be appreciated, the message is immediately sent after a trigger condition.

$T_2$  and  $T_3$  are the retransmission times that become duplicated until the rest retransmission time ( $T_0$ ) is reached.

*Sampled-value* messages use the same protocol profile but a different transmission mechanism, as these messages are sent periodically. SV messages are not related to trigger conditions. They carry a dataset containing time-tagged samples of voltage and/or current. The cadence of transmission depends on the sampling rate and the number of samples contained in the dataset. For these messages, latency is not as critical as with GOOSE, but it must be bounded. What is more critical in this case is the delay variation that is a specific requirement, since if not bounded, it may affect relay performance.

**Profile for Time Synchronization.** In the substation bus, time synchronization is implemented by means of the Simple Network Time Protocol (SNTP). The SNTP protocol is transported over UDP connectionless transport protocol. SNTP is generated by an IED that acts as a master clock. This IED uses a global positioning

system (GPS) receiver to synchronize its internal clock. SNTP can provide a synchronization accuracy better than 1 ms, which is adequate for SCADA time stamping.

The process bus requires a more accurate time synchronization. IEC 61850-9-3 specifies that the process bus should be synchronized using the IEEE 1588v2 or Precision Time Protocol (PTP). PTP can provide a synchronization accuracy better than 1  $\mu$ s. Details of PTP applications can be found in Sect. 14.2.

**Profile for Client–Server Communications.** For client–server communication mode, an MMS application protocol together with the profile of the transport type or the  $T$  profile is used. As mentioned, the IEC 61850 standard adopts widely spread standardized protocols, which as a consequence are very well tested, on the several levels of its model – this being structured and presented in a similar way to how the OSI/ISO model of reference is conceived and usually presented –, as is explained in more detail in the telecommunications section (Sect. 14.3).

#### Manufacturing Message Specification (MMS) Protocol

The specification of messages for manufacturing consists of the application-level specification of the services and procedures necessary for the purpose of interchanging information between devices of the type of those installed in production chains. MMS is an application protocol that was initially defined for industrial process control that later found application for realtime SCADA. Its first use in this field was as the application protocol for ICCP/TASE.2 IEC 60870-6 for interconnection of control centers. Later, it was adopted by the utility communications architecture and finally by IEC 61850.

One key feature of MMS particular architecture is its capability of simultaneously providing client and

server functionality. This feature is supported by the *virtual manufacturing device* that implements the following functionalities:

- Access to object contained on the server
- Services used by the client to access those objects
- Server behavior.

Basically, the services that can be performed by MMS are writings, readings, and descriptions of variables (directories), which in our case will consist of sets of attributes of logical nodes and of files or folders (transparent transfers of blocks of bytes without specifying their sizes). These services, taken to our particular case, can be translated into alarm reports, control and instructions executions, autodescription of the objects, and transfers of files.

The MMS standard was published in 1986. It is considered a very reliable and extremely secure protocol. Nevertheless, its technology is becoming cumbersome for some lightweight applications, so other middleware solutions and application protocols based on XML, such as XMPP, will gradually replace MMS. Consequently, we will not develop any further detail of the MMS architecture.

The MMS application protocol is transported using the so-called *T* profile, which is based on TCP for connection-oriented transport and IP. Further details of this profile and protocols' working principles can be found in the telecommunications section (Sect. 14.3).

### Configuration

Legacy SAS lack the concept of the *legacy system*; each device performs a function depending on the values of its input without any knowledge of internal process of other devices. For this reason, the configuration of every device was carried out using proprietary vendor tools that do not need information from other devices to create the configuration. Consequently, it was not possible to share that configuration information between the different engineering tools, and IEDs have no information about the configuration of other IEDs of the SAS.

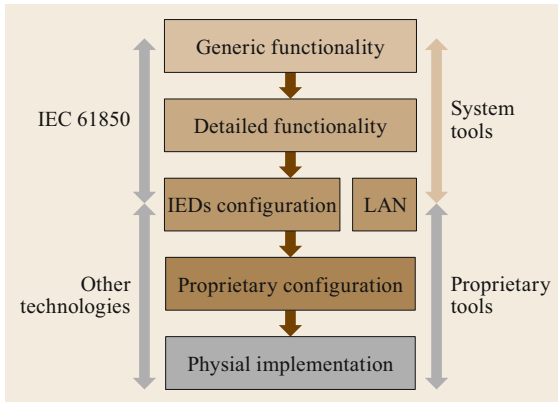
IEC 61850 defines a method for SAS configuration with a system view approach, so every device has the configuration information of other IEDs required to perform their functions, so that they can collaborate to implement more complex tasks. IEC 61850-6 defines the Substation Configuration Language (SCL). This language allows the interchange of specification and configuration files between system configuration tools, IED configuration tools, and IEDs. Due to this, it is possible to automatically create a SAS configuration file that contains data models, service capabilities, communication information, and private data.

The standard defines the following file types. The content and use of the files is identified by the file extension:

- *System specification description. File type .ssd.* This file contains an XML description of the single line diagram of the substation and the LNs associated with every primary device, bay, voltage level, or substation level. It also includes the data model of LNs. It is used to specify SAS projects.
- *IED capability description. File type .icd.* This file describes the functional and engineering capabilities of and IED type. The IED name is the *TEMPLATE*. The file describes services supported by the IED as well as its data model. It can contain a communications part with preconfigured information. There is one icd file per every IED model.
- *Instantiated IED description. File type .iid.* This file contains all the information of a single instance file of an IED preconfigured specifically for a project. Configuration data may not be completed and may change during the engineering process.
- *Configured IED description. File type .cid.* This file describes the final configuration of an IED in a project. There is an icd file for each IED in a project. This files contains all the information needed by the IED to perform its function. In Edition 2, the cid file is a subset of the scd file.
- *System configuration description. File type .scd.* This file contains all the IEDs of a project, including communication and data flow information.
- *System exchange description. File type .sed.* This file describes the interfaces of one project to be used by other project. It is a subset of the scd file containing all the information required by other project to connect external information. This file is required to automatically configure GOOSE subscriptions between substations.

IEC 61850 defines a novel configuration process that is very flexible and well structured. As shown in Fig. 14.10, the configuration process starts from the most generic specification to construction details. SCL language and the files described above are used in most parts of the process both to create the files and also to interchange files between tools, and to download the cid configuration files to IEDs.

The process starts using a *system tool* that is able to generate the *ssd* file, and from this file the rest of the process, including the specific IEC 61850 engineering process. As an IEC 61850 SAS is a distributed system made of basic functions, it is important to star design the SAS from the system view. From this information further details can be added, and when the actual im-



**Fig. 14.10** Configuration process

plementation level is reached, proprietary tools must be used, as information and configuration that are out of the scope of the standard must be defined.

### Specification Process

The main goal of an IEC 61850 specification is to assure functionality and interoperability. The specification process comprises the following steps:

- *Data profile definition.* This is a key step to achieve interoperability. A formal definition of the data model removes any ambiguity and select which options will have to be implemented to guarantee SAS functionality and performance.
- *SAS functions.* Selection of required functions.
- *Logical node selection.* List of logical nodes required for the implementation of SAS functionality.
- *LN communications.* Logical nodes interchange information by means of messages that are specified using the concept of PICOM (piece of information for communication). This process provides detailed information on how logical nodes interact to implement every SAS function.

Once the whole process is completed, a generic specification that guarantees functionality is obtained. It is important to mention that this specification guarantees the functionality regardless of how SAS will be implemented. Any specification tool is able to generate the *ssd* file according to the standard, but as this file does not include all the required specification information, only advanced tools can complement this file with the rest of the specifications, such as *picoms* or even wired signals. Implementation constraints can also be defined in the specification. For instance, it can be defined that some logical nodes should be included in the same device. By doing this, we can obtain a generic

specification of the devices that will implement the project.

Finally, by gathering logical nodes in a specification IED, a specification *scl* file is automatically created. This file specifies the IED data model and capabilities in very similarly to how an *icd* file does it for real devices. The specification file can be checked against a real IED *icd* file to verify compliance.

### IEC 61850 Engineering Process

A completed IEC 61850 engineering project should not only contain IEC 61850-related information, such as logical nodes and how they interchange information but also wired signals and legacy devices. As the main function of an engineering tool is to describe functionality, it is very important that the tool seamlessly relates wired signals with IEC 61850 functionality providing a clear view of system functionality regardless of the technologies used to implement it. As IEC 61850 includes a number of facilities that allow SAS functionalities to be implemented in different ways, the system tool should support all of them, providing the required capabilities to choose the working mode freely. Namely, some functions can be implemented whether by using sequential interrogations or by means of trigger conditions and reports, or GOOSE messages.

Figure 14.11 shows the engineering process step by step. The engineering tool provides the required functionality to assure coherency of the process. The results of the process are *scl* files according to the standard, as well as drawings, connection lists, and other documents not shown in the figure.

The use of signals based on reports or GOOSE messages requires some specific functions to support the generation of a list of signals, as well as the generation of drawings showing the implemented functionality in a classical way.

### Configuration

The configuration process is different depending on the edition of the standard. Edition 1 lacks many functionalities and information in the configuration files, so it is not possible to directly configure an IED from the files defined by the standard and, therefore, the IED configuration tool of the IED manufacturer has to be used. On the other hand, Edition 2 included these missing data, so IED can be directly configured from the system tool by downloading the *cid* file.

This is possible due to the definition of a new type of file, the *iid*, which includes settings and other private parameters. Nevertheless, there are a number of parameters that are not included in *scl* files yet, being the most important logical functions configuration and relay setting.

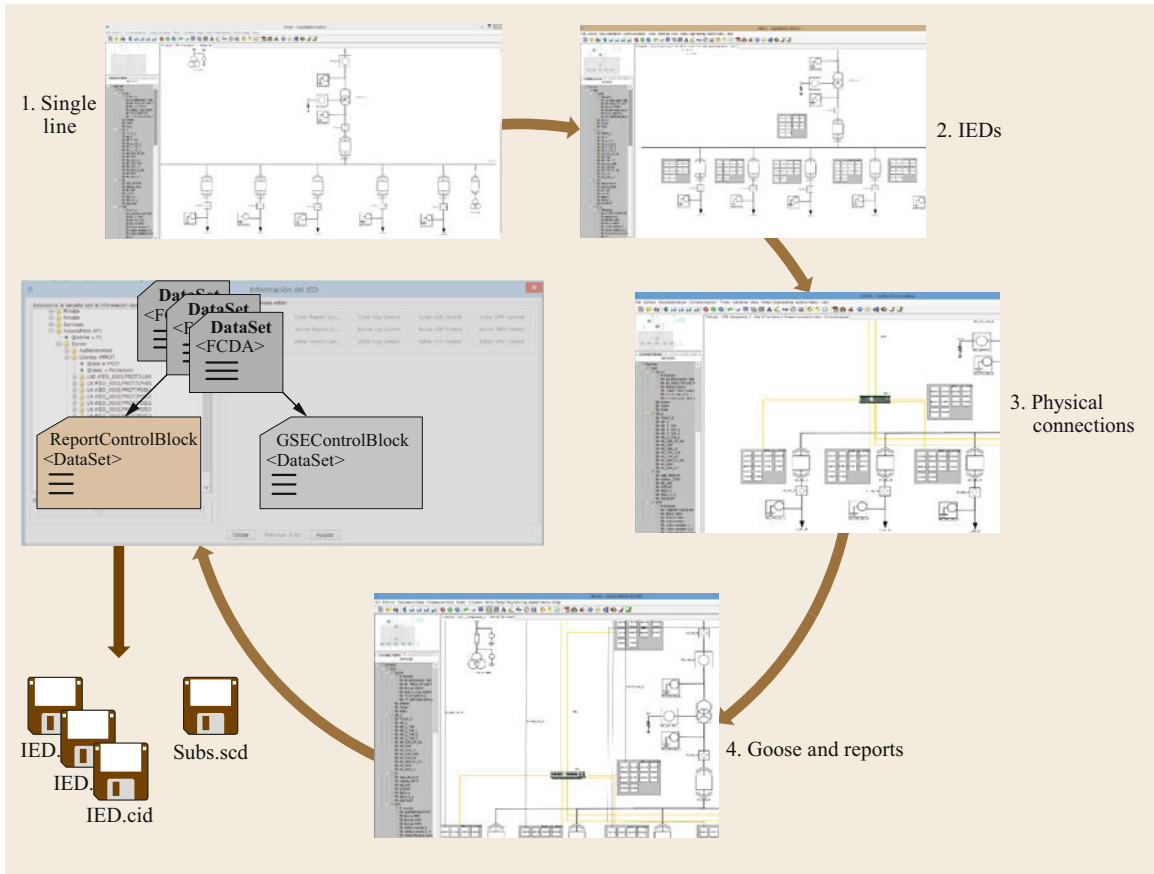


Fig. 14.11 Engineering process

Section 14.2

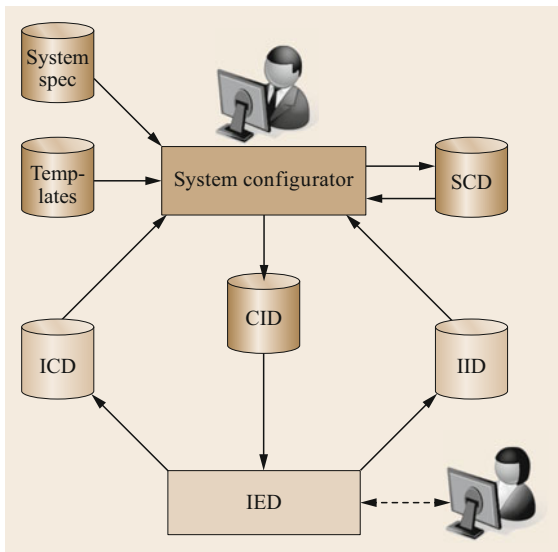


Fig. 14.12 Configuration options

### 14.2.10 Standards

The International Electrotechnical Commission (IEC) is the standardization body in charge of the preparation of international standards in the electrotechnical field. Its Technical Committee 57 (TC57) is in charge of the set of standards related to operational systems, including the smart grid. This section names the different families of standards with the aim of providing a relation of the standards that should be considered when specifying or designing an operational system. The applications and the key concepts included in these standards are developed throughout the entire chapter.

#### Control Center Standards

Control centers comprise a set of applications that are specified by the following standards.

**IEC 61968.** Application integration at electrical utilities – system interfaces for distribution management.

The IEC 61968 series is intended to facilitate integration of distributed applications that communicate each other using middleware.

- IEC 61968-1. Interface architecture and general recommendation.
- IEC 61968-2. Glossary of terms.
- IEC 61968-3. Interface for network operation.
- IEC 61968-4. Interface for records and asset management.
- IEC 61968-5. Interface standard for operational planning and optimisation.
- IEC 61968-6. Interface for maintenance and construction.
- IEC 61968-7. Interface standard for network extension planning.
- IEC 61968-8. Interface standard for customer support.
- IEC 61968-9. Interface for meter reading and control.
- IEC 61968-11. Common information model (CIM) extensions for distribution.
- IEC 61968-13. CIM resource description framework (RDF) model exchange format for distribution.
- IEC 61968-100. Implementation profiles.

*IEC 61970.* Energy management system application program interface (EMS-API). The IEC 61970 series develops a set of guidelines and standards to facilitate distributed application integration and information interchange with systems external to the control center.

- IEC 61970-1. Guidelines and general requirements.
- IEC 61970-2. Glossary of terms.
- IEC 61970-301 Edition 6. Common information model (CIM) base.
- IEC 61970-302. Common information model (CIM) for dynamics specification. Extension of IEC 61970-301 to specify exchange models representing the dynamic behavior of power-system components to facilitate system simulation studies for system dynamic assessment and planning.
- IEC 61970-401. Component interface specification (CIS) framework.
- IEC 61970-402. Common services.
- IEC 61970-403. Generic data access.
- IEC 61970-404. High-speed data access (HSDA).
- IEC 61970-405. Generic eventing and subscription (GES).
- IEC 61970-407. Time-series data access.
- IEC 61970-452. CIM static transmission network model profiles.
- IEC 61970-453. CIM-based graphics exchange.

- IEC 61970-456. Solved power system state profiles.
- IEC 61970-552 Edition 2. CIMXML model exchange format.
- IEC 61970-555. CIM-based efficient model exchange format (CIM/E).
- IEC 61970-556. CIM-based graphic exchange format.
- IEC 61970-600-1. Common grid model exchange specification (CGMES) – Structure and rules.
- IEC 61970-600-2. Common grid model exchange specification (CGMES) – Exchange profiles' specification.

*IEC 62325.* The framework for energy market communications. The IEC 62325 series facilitates the integration of market application software in the CIM framework. IEC 62325 standards are associated with IEC 61968 and IEC 61970 series and complement them with market information exchange and modeling aspects.

- IEC 62325-301. Common information model (CIM) extension for markets.
- IEC 62325-351. Edition 2. CIM European market model exchange profile.
- IEC 62325-450. Profile and context modeling rules.
- IEC 62325-451-1. Edition 2. Acknowledgement business and contextual model for the CIM European market.
- IEC 62325-451-2. Scheduling business process and contextual model for the CIM European market.
- IEC 62325-451-3. Transmission capacity allocation business process (explicit or implicit auction) and contextual models for the European market.
- IEC 62325-451-4. Edition 2. Settlement and reconciliation business process, contextual and assembly models for the European market.
- IEC 62325-451-5. Problem statement and status request business processes, contextual and assembly models for the European market.
- IEC 62325-451-6. Publication of information on market, contextual, and assembly models for the European style market.
- IEC 62325-503. Market data exchange guidelines for the IEC 62325-351 profile.
- IEC 62325-504. Utilization of Web services for electronic data interchange on the European energy market for electricity.

### OASIS

The Organization for the Advance of Structured Information Standards (OASIS) is a nonprofit consortium that drives the development, convergence, and adoption of open standards for the global information society. OASIS promotes the development of industrial



standards for security, the Internet of Things, cloud computing, energy, content technologies, emergency management, and other areas. OASIS has defined the SOA framework that is used in control centers to implement CIM architecture. The OASIS reference model for service-oriented architecture 1.0 standard was released in 2006.

#### IEC 61850 Standards Series

As we saw before, IEC 61850 has become the common technology and architecture for the power grid. This technology allows a common platform for all the operational applications to be established, thereby finding applicability in the whole power system. The standards that specify this new architecture are shown in the following list.

*IEC 61850 Edition 1.* Comprises the following parts:

- IEC 61850-1. Introduction and overview. Technical report, 2004.
- IEC 61850-2. Glossary of terms, 2003.
- IEC 61850-3. General requirements, 2002.
- IEC 61850-4. System and project management, 2002.
- IEC 61850-5. Communication requirements for functions and models, 2003.
- IEC 61850-6. Configuration description language for communications in electrical substation related to IEDs, 2004.
- IEC 61850-7-1. Basic communication structure for substation and feeder equipment – Principles and models, 2003.
- IEC 61850-7-2. Basic communication structure for substation and feeder equipment – Abstract communication service interface (ACSI), 2003.
- IEC 61850-7-3. Basic communication structure for substation and feeder equipment – Common data classes, 2003.
- IEC 61850-7-4. Basic communication structure for substation and feeder equipment – Compatible logical node classes and data classes, 2003.
- IEC 61850-8-1. Specific communication service mapping (SCSM) – Mappings to MMS (ISO 9506-1 and 9506-2) and to ISO/IEC 8802-3, 2004.
- IEC 61850-9-1. Specific communication service mapping (SCSM) – Sampled values over serial unidirectional multidrop point to point link, 2003.
- IEC 61850-9-2. Specific communication service mapping (SCSM) – Sampled values over ISO/IEC 8802-3, 2004.
- IEC 61850-10. Conformance testing, 2005.

Edition 1 was deprecated by Edition 2.

*IEC 61850 Edition 2.* Comprises the following parts related to SAS:

- IEC 61850-1. Introduction and overview. Technical report, 2013.
- IEC 61850-3. General requirements, 2013.
- IEC 61850-4. System and project management, 2011.
- IEC 61850-5. Communication requirements for functions and models, 2013.
- IEC 61850-6. Configuration description language for communications in electrical substation related to IEDs, 2009.
- IEC 61850-7-1. Basic communication structure for substation and feeder equipment – Principles and models, 2011.
- IEC 61850-7-2. Basic communication structure for substation and feeder equipment – Abstract communication service interface (ACSI), 2010.
- IEC 61850-7-3. Basic communication structure for substation and feeder equipment – Common data classes, 2010.
- IEC 61850-7-4. Basic communication structure for substation and feeder equipment – Compatible logical node classes and data classes, 2010.
- IEC 61850-7-410. Hydroelectric power plants – Communication for monitoring and control, 2007.
- IEC 61850-7-420. Basic communication structure – Distributed energy resources logical nodes, 2009.
- IEC 61850-7-510. Basic communication structure – Hydroelectric power plants – Modeling concepts and guidelines. Technical report, 2012.
- IEC 61850-8-1. Specific communication service mapping (SCSM) – Mappings to MMS (ISO 9506-1 and 9506-2) and to ISO/IEC 8802-3, 2011.
- IEC 61850-9-2. Specific communication service mapping (SCSM) – Sampled values over ISO/IEC 8802-3, 2011.
- IEC 61850-9-3. Precision Time Protocol profile for power-utility automation, 2015.
- IEC 61850-10. Conformance testing, 2012.
- IEC 61850-80-1. Guidelines to exchanging information from CDC-based data models using IEC 60870-5-101 or IEC 60870-5-104. Technical specification, 2016.
- IEC 61850-80-2. Exchange of information between networks implementing IEC 61850 and DNP3. IEEE 1815.1 standard.
- IEC 61850-80-3. Mapping to Web protocols – Requirements and technical choices. Technical report, 2015.
- IEC 61850-80-4. Translation from the COSEM object model (IEC 62056) to the IEC 61850 data model. Technical specification, 2016.

- IEC 61850-85-1. Standard for  $N$  times 64 kb per second optical fiber interface between teleprotection and multiplexer equipment. IEEE C37.94 standard.
- IEC 61850-90-1. Use of IEC 61850 for communication between substations. Technical report, 2010.
- IEC 61850-90-2. Use of IEC 61850 for communication between substations and control centers. Technical report, 2016.
- IEC 61850-90-3. Use of IEC 61850 for condition monitoring diagnosis and analysis. Technical report, 2016.
- IEC 61850-90-5. Use of IEC 61850 to transmit synchrophasor information according to IEEE C37.118. Technical report, 2012.
- IEC 61850-90-7. Object models for power converters in distributed-energy resource (DER) systems. Technical report, 2013.
- IEC 61850-90-12. Wide area network engineering guidelines. Technical report, 2015.
- At the time of writing this text the following standards were in development.
- IEC 61850-7-6. Guideline for definition of basic application profiles (BAPs) using IEC 61850. Technical report.
- IEC 61850-7-500. Use of logical nodes for modeling application functions and related concepts and guidelines for substations. Technical report.
- IEC 61850-7-520. Distributed energy resources modeling concepts and guidelines. Technical report.
- IEC 61850-8-2. Specific communication service mapping (SCSM) – Mappings to extensible messaging presence protocol (XMPP).
- IEC 61850-80-5. Guideline for mapping information between IEC 61850 and IEC 61158-6 (Modbus). Technical specification.
- IEC 61850-90-4. Network engineering for substations. Technical report.
- IEC 61850-90-6. Use of IEC 61850 for distribution automation systems. Technical report.
- IEC 61850-90-8. Object model for E-mobility. Technical report.
- IEC 61850-90-9. Use of IEC 61850 for electrical energy storage systems. Technical report.
- IEC 61850-90-10. IEC 61850 objects for scheduling. Technical report.
- IEC 61850-90-11. Methodologies for modeling of logics for IEC 61850 based applications. Technical report.
- IEC 61850-90-14. Using IEC 61850 for FACTS data modeling. Technical report.
- IEC 61850-90-17. Using IEC 61850 to transmit power-quality data. Technical report.
- IEC 61850-10-210. IEC 61850 interoperability test – Hydro profile. Technical specification.

### 14.2.11 Technologies

Control centers and substation automation systems are designed using specific application design methodologies and architecture. Furthermore, IT and telecom technologies are configured in a specific manner. This section is focused on the solutions commonly used by power utilities to implement their operational services. Both control center and SAS are built using distributed applications running in different devices that are connected in the same LAN or through a WAN with IP connectivity. For this reason, application architecture has to fulfil two key requirements: scalability and ubiquity. To achieve this, middleware and application architecture are very important. This section explains the working principles and properties of different middleware solutions, as well as the distributed application solution currently used for control center implementation.

#### Middleware

Middleware is a software layer that enables communications and management of data among distributed applications. It is typically a layer above the transport layer and below the application layer. Using a middleware layer, distributed applications interact as if they were running on the same computer. Middleware is used to provide other facilities such as object location and service description. CORBA and Web services are examples of middleware solutions.

#### CORBA

Many industries face the need to integrate distributed processes. Different technologies have been developed to respond to these requirements. The common object request broker architecture (CORBA) was the first to have a wide acceptance and is still used in many power utility distributed applications.

The deployment of TCP/IP networks simplifies data interchange between computers, paving the way to the implementation of distributed systems. Nevertheless, data communications are not enough to implement an open distributed system, the location to distributed processes and objects, as well as the access interface, must be standardized in order to achieve interoperability. Furthermore, in order to support mission-critical applications real-time constraints must be considered.

As we saw in the previous sections, power system operation has evolved from a centralized system to a distributed one able to integrate any kind of information. This evolution started when IP technology was adopted, since it provides open connectivity, the following step being the implementation of distributed systems using the concept of a middleware layer. A middleware layer provides services to the applications.

These services implement access to data, applications, and objects that are connected through a TCP/IP networks, thus hiding the fact that these objects are not located in the computer where the application is running. CORBA became the first standard middleware architecture. It simplifies information interchange and interaction between applications and processes developed by different manufacturers. CORBA was formerly used in network management systems and later adopted in other process applications, mainly at high-level applications. Nowadays, CORBA is being replaced by other technologies, as is explained in this section.

The CORBA environment opens the door to a distributed object environment able to host any kind of application. CORBA technology is being developed and standardized by the object management group (OMG). CORBA 2.0 was introduced in 1994 and is still evolving, since the latest technologies of objects are being incorporated to it. Despite this evolution, there is a stable nucleus based on an open and standard set of services that allows distributed application to be implemented in heterogeneous environments, with the advantage that the objects defined in this architecture can be reused. For these reasons, it has been adopted by the ITU-T (International Telecommunication Union – telecommunication standardization sector) as the basis of the management system of the telecommunications networks and by IEC as a middleware technology to implement operational applications based on CIM/CIS architecture.

The communications between the client application and the objects in a CORBA implementation is supported by the object request broker (ORB) bus. The main function of the ORB is to provide transparency over the infrastructure that provides communications between the clients or users and the objects. The functionality provided by ORB comprises:

- *Object location.* There is no need to know where an object is located to invoke it.
- *Object implementation.* There is no need to know how the object is implemented, nor the operating system or the hardware platform in which the object is executed.
- *Object execution state.* There is no need to know the actual object state before using it.
- *Object communication mechanisms.* There is no need to know how the communication with the object is implemented, shared memory, a LAN, an IP WAN, etc.

The connection between the client and the ORB and the object and the ORB is carried out by means of a standard interface implemented using the Interface Definition Language (IDL). Since the ORB manages

the location of objects and applications solving all the issues related to the network layer, it is possible to move an object or an application without introducing any modification of the elements that interact with it. Hence, CORBA is the first step to achieve mobility, ubiquity of a server, or an object collection, thereby simplifying the implementation of distributed processing and data gathering systems.

CORBA standards define how objects are invoked and how clients send requests to servers. Due to the use of the IDL, it is possible to modify the actual implementation of a server without notifying any of its users of this change. This is a great help in achieving modern architecture requirements, as was stated in previous sections.

The services provided by the ORB are directly available at the network domain, where the objects and clients are located by simply using the IDL interface. The integration of two ORB buses of two different domains requires the use of the Inter-ORB Protocol. For the specific case of IP networks, the Internet Inter-ORB Protocol (IIOP) is used.

The CORBA application programming interface (API) has been updated with a quality of service (QoS) parameters definition, so that it is possible to request a quality service level to the ORB in the interaction with any object. Since the specification is quite open, the key issue is to design an ORB able to process QoS requests and map them into the QoS architecture of the underlying IP network. The use of static priorities to map QoS requests and differentiate services with higher priority is the simplest approach to achieve a level of QoS bounded into the limits required by control systems. Nevertheless, to achieve a bounded delay, which fulfils the requirements of the protection systems, will require further research that follows out of the scope of the present project but that will have to be implemented in order to obtain a platform able to support both control and protection in the substation environment.

The details of how an IP network provides QoS are described in the telecommunications section (Sect. 14.3.6). The key issue in this case is how to assign the right QoS parameters to every user, since they are not hosts or IEDs but objects and clients using objects. In other words, when an application invokes a certain remote object, this invocation and all the related information must experience a determined QoS. The way to achieve this dynamic QoS assignation is by using the Lightweight Directory Access Protocol (LDAP). LDAP is an Internet standard originally developed to simplify the ITU-T X.500 directory service recommendation that allows a tree-like directory to be implemented in a distributed way amongst several servers located at different sites. By using LDAP, it is possible to define the user profile of every service and even define the QoS

required by a transaction like the use of certain object, application, or server. Hence, by defining the service directory, different QoS will be defined for every object invocation in such a way that it is possible to adapt the network performance to the requirements of a particular object, even in the case when several objects with different requirements have been installed in the same object repository. The use of a communications protocol based on TCP/IP extends the *ORB object bus* to remote platforms in such a way that they can be controlled and executed remotely without limitations.

The use of CORBA or any other middleware technology changes the concept of a control center as a system confined into a building, as by using a middleware the scope of the control center is only limited by IP connectivity. These technologies represent the first step towards virtualization.

### Web Services

One of the latest advances in Internet applications standardization is the Web services architecture. Web services are modular applications that can be described, located, and invoked using standard Internet protocols and XML messaging. The entire new architecture is a new industrial standard defined by the Web Consortium W3C.

The use of the Web services allows a standard and distributed application environment to be deployed using common Internet technologies. This is the component that was missing in a management system to be able to integrate new and existing devices under a common management environment.

A Web service application is self-contained, self-describing, modular, and can be published, located, or invoked across the IP network that connects clients and application repositories. This is achieved due to the standardization of objects and services using standard specification and description languages, UML and Web Services Description Language (WSDL), and the provision of an application discovery service, the Universal Description Discovery and Integration (UDDI) service to implement directory-like application discovery agencies and the use of the Simple Object Access Protocol (SOAP) to access distributed objects.

Web services provide an advanced Web middleware where services can be distributed, legacy data and database information can be accessed using standard interfaces, service provision is independent of network topology and architecture, and the user interface is unified for all the applications. When using the proper implementation architecture, scalability and fault tolerance can be obtained, thus configuring the right approach to support operational power system services.

The SOAP protocol specifies how two processes running on different devices or containers interchange

structured information through an IP network. SOAP is a message-oriented protocol; information is interchange using messages coded in XML.

SOAP consists of three parts:

- The SOAP envelope construct is the root of the message. It describes *what* is in a message, *who* should process it, and *whether* it is optional or mandatory. It contains the *header* and the *body*. The header is optional, it can contain ancillary or complementary information, as well as advanced control directives. The body is mandatory and contains the XML message.
- The SOAP encoding rule defines a *serialization mechanism* that should be used to exchange instances of objects.
- The SOAP RPC defines *procedures* to use remote procedure calls (RPC) and their responses.

These parts are fully decoupled, which provides the following advantages:

- Extensibility
- Protocol independence
- Programming language independence.

### Service-Oriented Architecture (SOA)

SOA is way of implementing distributed applications based on distributed components that provide capabilities and functionalities to others that use them. The SOA principle is independent of the technology or the product implementing it. SOA is not a programming technology or a middleware, it is a paradigm or a guideline to design a system from a set of distributed applications able to provide services and collaborate with each other to perform their task. SOA is based on a central concept – the service. The service concept can be defined as *the performance of a function or work by one entity for another*. The service concept embraces the following ideas:

- The capability to carry out work for another entity.
- The specification of the work offered to another entity.
- The need for work to be carried out by another entity.

SOA is a powerful framework that matches needs and capabilities, including the combination of capabilities to fulfil a complex need. It facilitates scalability and interoperability.

A service is used or accessed by means of its service interface. It defines how to access the functionalities provided by the service. Invoking a service may pro-

vide information as a response to a request or change the internal status of the entity providing the service or both things at the same time.

Visibility, interaction and effect or outcome are key concepts describing SOA framework.

*Visibility* refers to the capacity for those that need a service and those with capabilities to provide it to see each other. *Visibility* requires *awareness*, *willingness*, and *reachability*. In other words, the service requester must be aware of service availability, the provider must be willing to provide the service, and parties must have connectivity to interchange messages.

To implement the visibility description of service functionality, technical requirements, constraints, use policies, and access and response mechanisms must be provided. The service description must be implemented with a self-description syntax and semantics language such as XML, for instance.

*Awareness* of service offerings requires discovery mechanisms. The service provider must be able to describe its service and its policies. Service awareness requires that service description and policy be available to potential consumers.

*Willingness* is the act of initiating and participating in a service interaction.

*Interaction* is the actual use of a service. This is implemented by exchanging messages. A prerequisite for interaction is reachability.

*Outcome* is the result of using a service. The result may imply a state change that may produce a returned information to be sent to the service requester.

The information model is an important characteristic of a service. It determines which information can be exchanged when using the service. The information model has a structure that defines data coding, format, and structure data included in the model. Another important property of the information is the semantics. A critical issue is the interpretation of data, as it must be consistent between the participants in a service interaction. A formal description terms and their relationships provides the basis for the definition of semantics and ontology that in turn facilitates the correct interpretation of information exchanged.

The behavioral model is the other aspect that has to be known to successfully use a service. It defines the sequence of actions and temporal aspects of interacting with a service.

Nowadays SOA is implemented using Web services, but in fact it is independent of technology and implementation, so any other solution can be used in the future. SOA can be seen as the evolution of object-oriented technology. The trend is to evolve SOA to a virtualization of services, as is explained in Sect. 14.6.

## 14.2.12 Design Principles

The way applications and their functions are distributed will determine their performance and telecom requirements. Therefore, it is important to define design principles that may optimize cost and performance of the overall system. This section will focus on application and control-center architecture, telecom network design issues will be covered in the subsequent section.

### Control-Center Architectural Objectives

The main architectural requirements are the following:

- *Lower total cost of ownership (TCO)*. The deployment of a new control center is a big investment, where the cost of the product is not the only aspect to be considered. TCO includes the following concepts:
  - Project implementation costs
  - Multivendor integration costs
  - Model development and maintenance costs
  - Graphical interface development and maintenance costs
  - Migration costs
  - Training and skill requirements.
- *Improved business continuity*. This includes minimizing the impact of outages for any reason, including cyber-attacks.
- *Improved user interface*. This establishes a common, role-based, and customizable task-oriented interface independent of underlying applications, thus eliminating multiple application-specific user interfaces.
- *Improved standardization*. Absolute compliance with IEC standard series.
- *Interoperability*. This includes the straightforward integration of multivendor solutions.
- *Reuse of software components*. This implies the ability to share components in multivendor solutions.

The control-center architecture can be evaluated according to its architectural qualities, which describe the degree of achievements of the above-mentioned architectural objectives. Although these qualities are difficult to evaluate, it is important to consider them during specification and design phases. The most relevant qualities are:

- *Scalability*. This is the ability of a system to grow several orders of magnitude in response to increased work load or expansion of its functionality. Scalability is a very important quality, since it will extend the lifespan of the system as long as it can keep being upgraded. Scalability may involve adding more servers, increasing bandwidth, etc. It is, therefore, important to check the scalability of all technology, as well as of the system architecture.

- *Flexibility*. This is determined by the capacity of a solution to adapt to business requirement changes. Flexibility may impact the system performance.
- *Platform independence*. This includes the following aspects:
  - Operating system independence
  - Middleware independence
  - Management system independence.
- *Maintainability*. This determines the effort required to identify and isolate problems, replace components, and implement system modifications. It has a direct influence on TCO.
- *Security*. Protection against cyber-attacks is a capital quality of a system. The system architecture must be designed to minimize vulnerabilities. Security design principle should be aligned with the IEC 62351 series of standards, as is explained in Sect. 14.4.
- *Availability*. This is the percentage of the total up-time during which the system is available to the users performing according to its operational requirements. Availability is related to the service not only to hardware; consequently, software quality has a relevant impact on system availability.
- *Business continuity*. This is the ability to recover from a system failure. It is closely related to availability. Business availability requirements together with components' failure rate determine the degree of redundancy of the system and the algorithms that should be implemented to use them efficiently.
- *Usability*. This measures how well the human-machine interface responds to business functions and activities that should be carried out by the system operators. A user-friendly interface and consistent look and feel are common usability requirements.

## 14.3 Telecommunications Services

We have seen in previous paragraphs that different operational applications require sharing information to perform their tasks. Communications between distributed applications is supported by communications services. A service represents a set of functions offered to a user by a provider. The service is made available through service access points (SAP). In fact, the qualities and capabilities of a service are completely defined by the interface of the SAP. Consequently, the provider becomes an abstract entity, whose implementation is hired from service users. For this reason, a service provider may be composed of smaller entities that may be using underlying services providers. This implementation concept is known as *layering*. A service can be upgraded by using underlying services that are more powerful. This process can be nested until the desired service functionality is achieved. Services provided by a SAP are invoked using service primitives. These primitives, which are similar to programming sentences, are issued by the user to ask the service to perform some action. The result of the action is reported to the user.

Three different types of interactions can be distinguished:

1. **CONFIRMED SERVICES**. These involve a handshake between the user requesting the service and the remote user accepting the interaction. This type of service provides sequence control, and it is normally used for connection-oriented communications; it involves four primitives:
  - **Service.REQUEST**, invoked by the requesting user

- **Service.INDICATION**, delivered to the remote accepting user
  - **Service.RESPONSE**, an answer sent by the remote accepting user
  - **Service.CONFIRMATION**, delivered to requesting user.
2. **UNCONFIRMED SERVICES**. This type of service does not require a handshake. It does not provide sequence control or information synchronization; it is normally used for connectionless services. They involve two primitives:
    - **Service.REQUEST**, invoked by the requesting user
    - **Service.INDICATION**, delivered to the remote accepting user.
  3. **PROVIDER-INITIATED SERVICE**. This service is generated by the service provider due to an internal condition. It is used by the service provider to inform its users about changes in service conditions; it involves a single primitive:
    - **Service.INDICATION**, sent to both users upon an internal condition of the service.

From the above list we can identify two types of services, connection-oriented services and connectionless services. Connection-oriented services are implemented through three phases:

- **Connection establishment**. During this phase, user and service provider negotiate the service working mode and requirements. If successful, a connection is established.

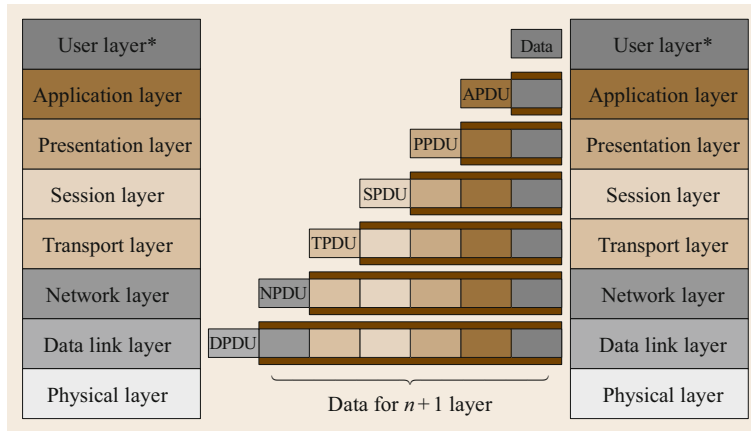


Fig. 14.13 Seven-layer model

- Data transfer. During this phase, data is transferred, since the service is operative as agreed in previous phase.
- Connection release. The service is terminated and users binding is released.

A connectionless service has one phase, data transfer. Each time data is transferred, different options may be requested to the service provider. There is no explicit relationship between service users.

Service information interchange is implemented using protocols. A protocol defines a sequence of messages called protocol data units (PDU) and a finite state machine that implement the way a service is used. When an application wants to transfer some data to a remote user, the service interface must be used. Data to be transferred is called *service data unit* (SDU). The service provider attaches protocol control information (PCI) to form the PDU. PCI identifies the data and their nature. When the service is implemented using the layering concept, that is to say, using an underlying service, the original PDU becomes the SDU of the underlying service interface.

In order to clarify these abstract concepts, we can establish the following association to clarify the above-mentioned terms:

- SDU can be understood as user data.
- The PCI concept can be associated with the protocol header.
- The PDU concept can be associated with a packet.

The open system interconnection (OSI) reference model defines communications tasks in terms of seven functional layers. Altogether, they implement the communications service offered at the application SAP.

The seven functional layers perform the following functions:

- *Application layer*. This provides the SAP to applications and implements information transfer using the underlying services provided by the rest of the functional layers.
- *Presentation layer*. This adds structure to SDUs in order to assure a common understanding of the information exchanged.
- *Session layer*. This adds control mechanisms to information exchange.
- *Transport layer*. This is responsible for the reliable end-to-end data transfer across the network.
- *Network layer*. This is responsible for the delivery of data to the remote user regardless of the network topology.
- *Data link layer*. This is responsible for the transmission, framing, and error control over a single link.
- *Physical layer*. This implements the physical interface to the communications media.

As shown in Fig. 14.13, every functional layer implements its service using its own protocol. The transmission of every functional layer PDU is implemented using the services provided by the underlying layer. For this reason, every layer establishes communications with its peer to implement its service. This process is repeated until the physical layer generates a physical signal suitable for transmission through a communications medium.

It is important to note that each layer introduces its own protocol header, which means a considerable overhead. This effect must be considered when a critical realtime service must be implemented. For this reason, some realtime operational services use a simplified protocol stack to optimize response time and overhead. The functional layers are divided into two blocks. The upper three layers provide the information transfer service to applications. The four lower layers provide end-to-end data transfer service.

Services provided by the application layer are structured into application service elements (ASE) that are specialized in specific service formats like remote connection, file transfer, etc. Every ASE has an association control service element (ACSE) that implements the task related to the relation establishment and releases with the peer application layer. An association is a binding between two entities, the initiator and the responder. The primary task of the ACSE is to bind to application processes.

Every ASE uses the service provided by the presentation layer to implement its service. ASE PDUs are abstract in nature, which means that every implementation is free to code them in their preferred format, depending on the programming language and the operation system. The presentation layer unifies these formats, defining a concrete representation that results in an unambiguous format that can be understood by any receiver. The presentation layer uses the abstract syntax notation one (ASN.1) (ISO/IEC 8825-1). ASN.1 uses the basic encoding rules (BER) to define how information has to be coded.

BER is based on the *tag-length-value* paradigm. That is to say, every object is coded using this principle, so that three fields are generated for every object, the tag that defines the type of data, the length of the data, and the value. The tag is a code that identifies data types such as boolean, integer, real, string, etc. ASN.1 is the common encoding method or presentation layer used in operational applications, including control centers and IEC 61850.

The session layer controls and synchronizes data transfer during the binding of the processes. Unlike the transport layer that provides a reliable communications circuit, the session layer supervises data stream transmission and establishes and maintains the connection with the peer session entity.

The application profile is usually embedded into the application, whereas the transport profile can be included in the operating system or become a specialized library. Telecommunications network design is focused on the transport profile or T-profile. The application profile must match application service requirements. These requirements are mainly focused on functionality but may also include quality of service and performance issues. In fact, performance requirements are transferred to lower layers that are control the working modes that can fulfil those requirements. Telecom service provision is based on the T-profile. From the point of view of telecommunications implementation, the SAP is provided by the transport layer. The transport layer provides end-to-end transport services. The most important task of the transport service is to provide transparency over network topology and

the changing reliability conditions of the underlying infrastructure.

Two types of transport services can be distinguished, connection-oriented and connectionless. The connection-oriented transport service provides a reliable end-to-end data transport. The service is implemented in three phases: connection, data transfer, and release. This service is normally implemented using the TCP protocol. TCP provides data segments' fragmentation and reassembly, end-to-end flow control, and errored or lost-frame retransmission.

The connectionless service provides unreliable transport. It only comprises the data transfer phase. The connectionless service is normally implemented using the UDP Protocol.

The network layer service is responsible for data transfer regardless of the network topology and transmission media. Consequently, it provides transparency over the topology of the network and transparency over the transmission media of every traversed link. To achieve this, the network layer must include the following functions:

- *Addressing*. This is a uniform mechanism to identify nodes, and users must be provided. Addressing should be independent of network topology and from any media-specific addressing scheme.
- *Routing*. The process of finding the shortest route between origin and destination is the key routing functionality. To achieve this, connectivity and topology discovery are required.
- *Quality of service*. Different applications may have different performance requirements. This information must be considered when applications' binding is established. The network layer should provide the functionality to guarantee performance requirements.

The link layer service is responsible for the reliable transmission of data over point-to-point links. To achieve this, error detection or correction codes may be added, and frame retransmission may be used, depending on the technology of the link. For multicast links, a specific link layer address may be required, as in the case of Ethernet. In those cases, a mapping between network layer and link layer addresses must be provided. The physical layer service adapts the bits of the messages to the physical interface generating the signal required by the telecommunications media.

Due to the diversity of telecommunications media and the different performance requirements of operational applications, it is important to define a detailed profile. The profile defines the specific configuration of every layer required to fulfil specific service require-



ments and considers the capabilities of the underlying layers. Further details on the working principles of the T-profile layer are given in the following sections. Section 14.3.5 is focused on depicting operational telecom requirements and suitable technologies supporting operational services, including how networks should be designed to achieve those requirements.

### 14.3.1 Basic Concepts

As presented in the previous sections, power-system operation requires the interaction of multiple applications distributed through the system. The implementation of a telecommunications network to support operational services must consider quite a large number of aspects, both internal to the network such as size and architecture and others external due to the requirements and specific working modes of the applications using its services.

The internal network factors to be considered are geographical scope, infrastructure availability, site locations, etc. External requirements that impose design constraints are normally associated with the criticality of operational applications and the volume, type, and scope of information exchange across the power system.

Figure 14.14 shows the interaction model between application and telecommunications infrastructure. Applications have telecommunications service requirements that are expected to be offered at the service access point (SAP). The telecom infrastructure has a set of service capabilities that are a function of the technology and implementation of the telecom infrastructure. A match must be achieved between requirements and capabilities. This agreement is expressed by means of a so-called service-level agreement (SLA), as is explained later in this section.

When a match between requirements and capabilities cannot be found, a redesign of the telecom

infrastructure is the only solution due to the criticality of operational applications. Telecommunications service can be implemented using a dedicated telecom infrastructure or using a service provided by an external telecom operator. The former provides an easier match between requirements and capabilities, whereas the latter does not allow specific service matching, as it is normally based on services implemented using a limited number of standard levels of quality and performance. Communications service requirements are related to the applications they serve (e.g., SCADA or protection communications services). We will focus on operational application telecom requirements that are defined considering application-specific working modes and the degree of criticality.

There are other applications related to maintenance and support of the power system, such as voice and data communications for field maintenance staff, which have an indirect impact on the operation, so they should be also treated as *operational*, even if their service performance requirements are not so demanding.

The criticality of communications services in the power-utility environment can be assessed through the consequences of service loss and degradation. The operation-support services are the most critical ones, and so financial consequences of a loss of communications in utility business and market activities can be much higher. *Nonoperational* communications are, however, more tolerant of transient or programmed service unavailability, allowing IT-type procedures for service restoration and maintenance to be used.

Power-utility operational applications can be grouped into different categories according to their information exchange scope:

- *Substation-to-substation applications.* These applications comprise fast automation systems providing

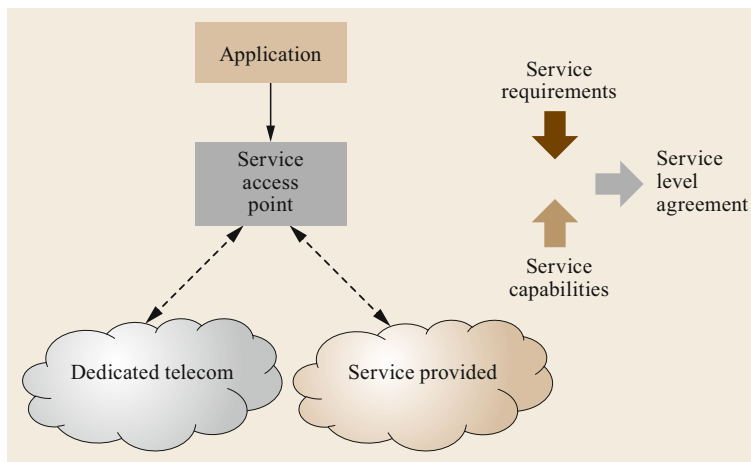


Fig. 14.14 Application and telecom interface

protection and control of power-system primary assets and prompt detection and isolation of electrical faults. The most critical requirement is latency, the limits of which may range from 200 to 10 ms. These applications are also used in bulk generation plants, energy farms, and energy-related process sites. These applications have critical requirements that constitute one of the main drivers for implementing dedicated telecommunications infrastructures in electrical power utilities.

- *Field device-to-control center applications.* These applications present status and measurement data from the grid or bulk generators to control center applications. SCADA and wide area monitoring systems are realtime mission-critical applications, but their latency requirements are not as high as those of protection applications, since their latency requirements are in the range of 1–5 s.
- *Interplatform applications.* These applications comprise the synchronization or coordination of databases in geographically remote platforms, whether for redundant processing or to gather information in a hierarchical architecture, such as between regional and national levels, or in a functionally distributed system implementing monitoring and control platforms. They generally require a sporadic transfer of much larger volumes of data. The time constraints here are around a few seconds. It should, however, be noted that cybersecurity constraints in this case become more severe, in particular when more than one company and one dedicated network are concerned.
- *Office-to-field applications.* These can be considered as *IT-to-OT* applications. They cover the access requirements from an engineering office located in the corporate enterprise environment of the power utility to devices, data, or staff located on field sites. Remote configuration, maintenance, and parameter settings of intelligent devices in the substation, as well as field worker mobile data access to support platforms are among these types of applications. Cybersecurity of remote access is of major concern here.

One of the most relevant characteristics of operational applications are their sensitivity to time delays. Deterministic and controlled time behavior is one of the major requirements that drives utilities to deploy and maintain dedicated telecommunications networks. In these networks, the time performance, as well as availability and fault tolerance, can be adapted to the requirements of each application through the appropriate choice of technologies and proper topological structuring. On the other hand, when public telecom services are used, bounded latency is rarely part of the service-level agree-

ment (SLA) of the service provider. Generally, the service provider cannot commit contractually to anything better than an *average communications delay* and is, therefore, to be excluded when time-sensitive applications are to be carried, as this kind of service performance cannot guarantee a bounded delay.

### 14.3.2 Service Classes and Applications

The concept of service classes was introduced to allow quality of service (QoS) requirements to be broadly determined for each application type. This reduces the number of different service types as one class can be used by several applications. From the generic point of view, service classes can be associated with two generic groups: nonelastic and elastic. The nonelastic service class is used to support those applications that are not tolerant to uncontrolled delays and/or losses. Elastic applications are those that can control the traffic flow that they are offering to the network and can, therefore, tolerate some changes in delay and throughput.

In order to better understand application requirements, they can be classified as elastic and nonelastic according to their tolerance to delay variation and packet losses. This classification is rather generic, as several different subcategories can also be identified. However, it is very important to understand application behavior and requirements in order to identify the proper service model, as this will determine the protocol stack to be used and will also influence the choice of technology.

#### Nonelastic Applications

Nonelastic applications are an important class of realtime applications they are also called *playback* applications, such as voice, video, or circuit emulation services over packet networks, as well as the delivery of IEC 61850 sample value messages. These applications must deliver information at a constant rate, so they should be able to cope with delay variations introduced by packet networks and reduce or compensate them.

These kind of applications handle information that is changing continuously. The source processes and packetizes the information and sends the packets to the network, normally at a constant rate, generating a continuous flow of packets. Packet networks, whether Ethernet or IP, introduce a variable delay, so packets are delivered to the destination with a continuously changing latency. The receiver must deliver the information at the same bit rate as it was generated, so it must include some mechanism to compensate the delay variation introduced by the network. This is implemented by buffering the incoming packets and delivering the packets with a fixed offset delay, which corresponds to

the average delay, whereas the size of the buffer is related to the maximum delay variation introduced by the network. The total offset delay of the service is related to the buffer size and, therefore, this is a key requirement to be considered when designing a network, as this kind of application requires a service with reduced delay variation.

Some applications like video playback are not affected by offset delay, others like video or voice conferencing can accept some average delay variation due to network overload, as they can measure the actual delay and dynamically modify their behavior. Nevertheless, other applications like sample value messages offset delay directly, which affects their functionality, as some protection application are not able to measure delay and, in any case, this delay will be added to the tripping time. Network design must consider performance requirements and delay variation tolerance of the application using telecom services. This is a very limiting requirement that may affect the choice of network architecture and the technologies used to implement it. The implementation of a service providing guaranteed upper bound delay implies having a quite deterministic one that requires the use of network technologies able to reserve bandwidth and with the proper queue scheduling procedures.

### Elastic Applications

While nonelastic realtime applications do not wait for late packets to arrive, elastic applications have a greater tolerance, which is a function of the transport protocol and the application itself. The fact that elastic applications can wait for a packet to arrive does not mean that the application's performance will not be affected. There is a direct relation between service latency and application performance but unlike nonelastic applications, a packet arriving too late is not a lost packet.

Elastic applications process packets as they arrive. The application will wait for received packets rather than continue execution without the information. IT applications such as Web browsing, file transfer, etc., do not require service characterization but protection-related application, i.e., different types of teleprotection schemes require a guaranteed bounded delay. Packets arriving later than this bound will be considered lost and thus also the associated command. The teleprotection service is an example of an elastic service with some constraints similar to nonelastic applications. That is to say, delay variation does not affect application performance if it is lower than the upper bound. A delay higher than the bound implies a loss of information. Other elastic applications does not have this constraint but, in fact, there is always a limit on the accepted packet delay. For IT applications, if the delay

is higher than session or application timeout, the application will consider that communication to have been lost. Upper bound delay requirements vary from very demanding ones, such as teleprotection that requires a few ms, or SCADA applications that require a few seconds to the less demanding requirements of IT applications. An appropriate service model for interactive burst elastic applications requires throughput commitment provision, whereas other service, like file transfer, can be supported by a best-effort service.

Now that we have discussed the generic application requirement types, we will analyze specific communications service requirements for every operational application.

### IEC 61850 Service Classes

As we saw in the previous section, IEC 61850 functionality is implemented using different services with different performance requirements, the most critical being time transfer or latency and availability. The standard distinguishes three types of performance classes that apply to sample values, control and protection signals, and time synchronization. The service used by sampled values should introduce a delay so small that it does not influence the operation time.

Table 14.1 shows IEC 61850 transfer-time classes. A communications network must be designed to guarantee the required performance for every application type.

Time synchronization is an important service to obtain a correct sequence of events and be able to process sample values of different sources in a coherent way. Table 14.2 shows IEC 61850 time-synchronization service classes.

The time class determines the synchronization protocol to be used. For instance, to achieve T1 requirements, SNTP can be used, whereas for T4, the Precision Time Protocol IEEE 1588V2 must be used.

### Teleprotection Signaling

Protection application services require the most demanding performance of telecom services. Their key function is to improve the performance of protection

**Table 14.1** Transfer-time requirements

Transfer-time class	Transfer time (ms)	Application examples: Transfer of
TTO	> 1000	Files, events, log contents
TT1	1000	Events, alarms
TT2	500	Operator commands
TT3	100	Slow automatic interactions
TT4	20	Fast automatic interactions
TT5	10	Releases, status changes
TT6	3	Trips, blockings

**Table 14.2** Time synchronization classes

Time-synchronization class	Accuracy ( $\mu$ s) synchronization error	Application
TL	> 10 000	Low time synchronization accuracy – miscellaneous
TO	10 000	Time tagging of events with an accuracy of 10 ms
T1	1000	Time tagging of events with an accuracy of 1 ms
T2	100	Time tagging of zero crossings and of data for the distributed synchrocheck. Time tags to support point on wave switching
T3	25	Miscellaneous
T4	4	Time tagging of samples and synchronized sampling
T5	1	High-precision time tagging of samples and highly synchronized sampling

devices by sending information of the remote end of the power line. The term *teleprotection* refers to the communications interface of the protection system. Teleprotection signaling transforms the state information transmitted by the protection relay into a signal suitable for transmission over a telecommunications channel and restitution to the remote protection relay or remote circuit breaker in a secure and prompt manner. It may be integrated into the protective device, into the telecommunications access equipment, or more generally, it may constitute a stand-alone device. This often supplements locally available data, confirming that a fault detected by at least one end, is, in fact, internal to the line, such that otherwise time-delayed operations may be accelerated.

In accordance with previously defined protection performance parameters, the operational performance of a teleprotection signaling system can be defined through the following parameters:

- *Security* is the ability to prevent communications service anomalies from issuing a command at the remote end when no command has been sent. Security is expressed as the probability  $P_{uc}$  of *unwanted commands*. Security is related to the communications service integrity (error performance) and the teleprotection signaling system's error detection capability.
- *Transmission time* is the maximum time ( $T_{ac}$ ) for the delivery of the command at the remote end, after which it is considered as having failed to be delivered. This is a constraint to the time performance of the communications service, not only in terms of nominal value but also as a guaranteed limit.
- *Dependability* is the ability to deliver all issued commands at all times. It is expressed as the probability  $P_{mc}$  of *missing commands*. This sets a very severe constraint on the availability and error performance of the communications service, challenging such telecom service concepts as *errored seconds* and *degraded minutes* being counted in the available time of a communications service.

In this context, *security* is not related to cybersecurity, as is explained by its definition. Cybersecurity attacks may impair any of the three parameters that determine teleprotection performance. The term *command* refers to a tripping or blocking order that is a binary signal. Teleprotection services can be used to transmit *state* information or analogue information. Teleprotection services can be understood as specialized telecommunications services used by some protection schemes, as is described in the following paragraphs.

#### State Comparison Protection Schemes

State comparison protection schemes use communication channels to share logical status information between protective relay schemes located at each end of a transmission line. This shared information permits high-speed tripping for faults occurring on 100% of the protected line. The logical status information shared between the relay terminals typically relates to the direction of the fault, so the information content is very basic and, generally, translates into a *command* requiring very little communication bandwidth. Additional information such as *transfer tripping* of a remote breaker to isolate a failed breaker and block recloser function may also be sent to provide additional control. The *command transmission time* is of great importance because the purpose of using communications is to improve the tripping speed of the scheme. Transmission-time variation is tolerated when it is below the maximum transmission time. Commands received later than the maximum transmission time are considered lost.

Communication-channel security is essential to avoid false signals that could cause incorrect tripping, and communication-channel dependability is important to ensure that the proper signals are communicated during power system faults, the most critical time during which the protection schemes must perform their tasks flawlessly.

Communications for state-comparison protection schemes must, therefore, be designed to provide safe, reliable, secure, and fast information transfer from one relay scheme to another. The communications scheme

must – for the vast majority of protection schemes – also be able to transmit information in both directions at the same time. The amount of information required to transfer between relay schemes depends on the relay scheme logic.

The terminology used to describe these state comparison protection schemes is presented below:

- Directional comparison blocking schemes (also called blocking overreach, BO)
- Directional comparison unblocking schemes (DCUB)
- Permissive overreaching transfer trip schemes (POTT)
- Permissive under-reaching transfer trip schemes (PUTT)
- Direct transfer tripping (DTT).

#### Current Differential Protection Schemes

Current differential protection, extensively used on high-voltage transmission lines, compares the amplitude and phase of the local terminal currents with the amplitude and phase of the currents received from the remote terminal through a communications channel. The currents at each line terminal are sampled, quantified, and transmitted to the remote end of the protected line for comparison. Current samples collected from a remote point must be compared with those measured locally at the same instant of time. An error in the delay compensation mechanism results in a differential current measurement error that increases the risk of unwanted tripping.

Delay compensation in differential protection relies on the existence of a common time reference. Originally, and still in the great majority of installed and operational devices, this is achieved using a *ping-pong* technique to evaluate the *round-trip* transfer time and performance delay compensation assuming equal send and receive path delays. This creates a great sensitivity of the system to latency asymmetry and variability and, therefore, and has become a very important communications requirement.

Modern protection systems can receive an external time reference such as a GPS clock to provide global time-stamping of samples, enabling them to tolerate

switched networks. Once the system is synchronized, a loss of GPS signal can be tolerated on a switched communications network using various techniques provided that the communications path does not change too often. There is, however, some reticence to render the protection system dependent upon an *externally provided* synchronization service such as a GPS satellite.

New-generation current differential relays using the IEC 61850 network interface and Precision Time Protocol (IEEE 1588v2) are expected to receive self-provisioned time coherence through the network, which will perform the necessary ping-pong action from switch to switch to determine the travel time from relay to relay. It is expected that precision time distribution will itself become a critical *substation-to-substation* service in future utility telecommunications networks.

Due to latency variation and symmetry requirements of existing relays, fixed path and nonqueued communications are used. Direct fiber and multiplexed communications are frequently employed. Packet-switched Ethernet communications with deterministic routing and time delay are presently being tested. It must be emphasized that the availability of current differential relays depends upon the availability of the communications channel. Consequently, it is required to have the capability of quickly detecting any loss of communications or inadequate quality of a channel in order to disable the differential scheme and employ another means of protection, such as distance and over-current backup. Path delay increases tripping time. For very high voltage levels, the overall communication-path delay should be lower than 6 ms. Table 14.3 summarizes the teleprotections service requirements.

#### System Protection Schemes

As described in the previous section, system protection schemes (SPS) involve a number of wide area protection schemes, the function of which is to maintain power-system stability. SPS requires telecommunications services to carry out their tasks. SPS perform its functions by comparing data acquired across the controlled system. Telecom service requirements involves a high-resolution capture and tight time imperatives which imply high bandwidth and low latency deterministic communications requirements. The completeness

**Table 14.3** Summary of line protection schemes and their communications requirements

Protection scheme		Main communications attributes
Directional comparison blocking (blocking overreach)	BO	High dependability (on healthy lines), very low transfer time
Permissive overreaching transfer trip	POTT	High dependability, controlled time
Directional comparison unblocking	DCUB	(Special case of POTT)
Permissive underreaching transfer trip	PUTT	High dependability, controlled time
Direct transfer tripping	DTT	Very high security, high dependability, controlled time
Current differential protection	CDP	Time synchronization of samples, bandwidth for transport of samples

**Table 14.4** Telecom requirements of system protection schemes

Factor	Reporting rate range	End-to-end latency	Measurement timing error ( $\mu$ s)	Sensitivity to message transfer delay variations	Sensitivity to lost packets	Currently covered in 61850
Sync-check	$\geq 4$ 1/s	100 ms	50	Medium	High	SV service
Adaptive relaying	$\geq 10$ 1/s	50 ms	50	Low	Medium	SV service
Out-of-step protection	$\geq 10$ 1/s	50–500 ms	50	Medium	Medium	SV service
Situational awareness	1–50 1/s	5 s	50	Low to medium	Low to medium	Periodic reporting, SV service
State-estimation and security assessment	1/300–10 1/s	5 s	50	Low	Medium	Periodic reporting, SV service
Data archiving	Any	N/A	50	Low	Medium	All as needed
Wide area control	$\geq 10$ 1/s	50–500 ms	50	Medium	High	SV service

of data sets is to be assured through the reliability and integrity of the communications system. This cannot be fulfilled by an acknowledged exchange and retransmission upon error detection due to time imperatives of the closed-loop system. IEC 61850-90-5 describes the communications requirements for many protection schemes based on synchrophasors. Table 14.4 summarizes these requirements.

### 14.3.3 Service Attributes

The performance of a telecommunication depends on a set of attributes that have a direct impact on its capability to fulfil operational services performance requirements. These attributes cover three main aspects: connectivity, capacity, and timing.

#### Connectivity

Every operational site needs to have access to telecom services. Substation and power plants can be connected to telecom facilities using optical fibers over power lines or power line carriers for some applications that can work over narrow band channels. Utility offices that are located in urban sites cannot be accessed using the dedicated telecom network. Connection to a utility site can be achieved using microwave links, which is not always feasible. The most common solution is to use telecom services offered by a public telecom operator.

The topology of the network infrastructure also has direct influence on the performance and fault tolerance that can be expected from the communications service. The number of switching nodes to be crossed determines the dependability of the connection; consequently, direct links based on dedicated fibers are preferred for critical applications such as teleprotection or other protection applications. Mission-critical applications require fault-tolerant telecommunications infrastructure. To achieve this, two physically independent routes between ingress and egress points are required. This imposes some constraints on the network

topology design, as will be explained later in this section.

#### Throughput (Capacity)

The term *throughput* refers to the service or channel capacity, that is to say, the amount of information, bits, or packets per second that can be transferred using this channel or service. This is a major criterion for selecting a telecom solution. Throughput is, indeed, related to an overall communications system capacity, which itself is related to the allocated bandwidth across the telecom media. However, throughput is not directly related to the channel bit rate, since there are other factors, such as protocol overhead, information coding, among others, that may reduce the effective transfer capacity of a communications interface. Service throughput is also related to other factors, such as application traffic profiles, transport protocols, and network dynamics, as will be explained in subsequent sections.

#### Latency (Delay)

Latency is the absolute delay introduced by the communications network into an application. Time latency is an important constraint for applications requiring a bounded delay. Time latency also matters where a bidirectional exchange is to be established with limited response waiting time. Service latency is a critical requirement of protection applications. Transfer time across the communications infrastructure or latency is added to the fault clearing time, so it is important that latency be bounded to a quite low limit. From 8 to 10 ms is the maximum allowed latency for protection applications, be they analogue or state comparison schemes. Although SCADA is a realtime application, its latency requirements are less strict, as delay in the range of seconds can be tolerated. On the other hand, voice communications can be seriously degraded by latency higher than 150 ms. Absolute time-latency problems may be avoided through appropriate topology design and proper selection of technologies, minimizing the number of nodes

crossed to reduce the delay introduced by store-and-forward and traffic queues. It is important to consider that bounded delay is not an average value but a maximum absolute one that has to be guaranteed in all cases.

### Delay Variation

Delay variation is produced by a lack of determinism in the telecommunications service. That is to say, the information is delivered to the remote end with a latency that changes continuously. This effect can be produced by the queues of a packet network and by a change of propagation delay. The amount of variation depends on the number of nodes crossed and the presence of interfering traffic that shares some communications links, thus increasing the traffic load in some parts of the path. Time predictability is achieved by imposing constrained routing (e.g., maximum number of hops, predetermined backup route, etc.) and adding a jitter buffer to absorb delay variation at the expense of adding an extra absolute delay. This mechanism is normally used to emulate a constant bit-rate connection over a packet network.

Time-division multiplexing (TDM) networks are deterministic. Delays tend to be constant and depend on the propagation delay of the signal and the number of hops. Delay variation in TDM systems can only occur after a route change following an automatic restoration. Transmission-delay variation can affect the performance of current differential relays. An excess of variation may block or even produce a false trip. Teleprotection services can accept delay variation if the total delay does not exceed the maximum transmission time.

### Delay Asymmetry (Path Asymmetry)

Delay asymmetry may be caused by two factors, path symmetry and different traffic load in the go-and-return path. The former is the most relevant factor, which may appear both in TDM and packet networks. Services supporting applications sensitive to delay asymmetry need to be configured with routing or connection establishment algorithms that guarantee path symmetry.

### Service Recovery Time

Mission-critical operational applications require a fault-tolerant service provision, which implies that in the event of a service outage, it can be restored in a very short time. In fact, most operational applications require a bounded restoration time, and for some critical services hitless, even switching is required, which implies no loss of service during the switchover from the faulty channel to the backup one.

Restoration time depends upon the communications technologies and network topology employed. Different methods can be used to implement service

restoration. The selection of any of the above methods depends on the criticality of the service:

- End-to-end alternate route switch-over for each critical service is very fast but not scalable.
- Ring protection across an SDH network can restore a connection in less than 50 ms.
- Ethernet Rapid Spanning Tree Protocol (RSTP) has a convergence time that depends upon the complexity of the network and can range from few to some hundred ms.
- Routing in an IP network is based on different algorithms that re-establish the routing table in each node after any network configuration or status change. Typically, RIP-based routing requires less than 1 min to restore communications, while an OSPF-based system can restore communications in 5–10 s.
- Transport profile multiprotocol label switching (MPLS-TP) enables the network to restore services using pre-established alternate paths for each data tunnel and can, in this way, provide restoration times similar to SDH.

### Service Integrity and Data Loss

Service integrity is the aptitude of the communications network to deliver the transmitted information without degradation, without loss, and without on-purpose alteration. The present section deals with degradation and loss of information due to channel impairments, on-purpose alteration being covered in the cybersecurity section (Sect. 14.4).

Service integrity depends on the performance of every one of the lower layers. Consequently, it depends on the channel integrity as well as the network and transport layers, which may produce loss of packets. We will focus our analysis on aspects that may impair operational service performance.

Focusing in the transmission aspects, data-channel integrity is characterized by its error performance. This is the capability of the network to deliver error-free data between network user interfaces. Error performance depends upon the error-generating behavior of the network, generally characterized by an average bit error rate (BER) measured over a 24 h time period, excluding 1 s intervals where the BER is worse than  $10^{-3}$ .

Long-term average BER, however, does not contain any information regarding the distribution of errors in time and is, hence, meaningful only if we assume a fully random distribution of errors, which is normally far from being the case. It is, therefore, useful to specify different thresholds of error behavior (e.g., BER) measured over shorter time intervals and then to

characterize the communications channel through the statistical distribution of these error behaviors.

Three parameters are defined by ITU-T G.821 to describe the error performance of a 64 kb/s connection:

1. *Errored second (ES)* is a 1-s period that contains one or more errors. For data services, the information is commonly transmitted in blocks containing error detection mechanisms. Blocks received with one or more transmission errors are subject to retransmission. In order to have a high throughput, it is necessary to minimize the number of errored blocks. The 1-s period was historically adopted as a compromise value for data block size.
2. *Severely errored second (SES)* is a 1-s period where the short-term bit error rate evaluated over 1 s exceeds  $10^{-3}$ . An SES can lead to a loss of synchronization, and it is considered that the connection is unusable during the time interval.
3. *Degraded minute (DM)* is a 1 min period where the short-term error ratio exceeds  $10^{-6}$ . The degraded minute was devised principally for digital telephony for which the mentioned error rate is the subjectively perceived boundary of virtually unimpaired transmission.

These parameters are to be derived from averaged data over at least a 1-month period. However, in practice, channels are tested for 4 h to assess ITU-T G.821 compliance.

The network and transport layers work in packet mode. Packets may be lost at the network layer for several reasons:

- Packets are discarded due to transmission errors detected by the link layer error-detection mechanism.
- Packets are discarded by the network protocol due to undetected errors that corrupt the network protocol format.
- Packets are lost due to queue overload because of network congestion.

The packet-loss rate is the addition of these three effects. Errors are not recovered by the network layer.

The transport layer recovers errors by packet retransmission when the TCP transport protocol is used. The Fletcher checksum added to the TCP information segment allows undetected network layer errors to be detected and corrected using retransmission procedure. UDP connectionless transport protocol does not provide a correction mechanism, so the application should take care of error detection and correction when required. A marginal amount of transmission er-

**Table 14.5** Availability objectives

Availability objective	Service down-time in min/y (h/y)	Example of service
99.999%	5.25 ( $\approx 5/57$ )	Protection communications
99.99%	52.5 ( $\approx 5/5.7$ )	SCADA, operational voice
99.9%	525 ( $\approx 5/0.57$ )	Data service

rors, called *residual errors*, are undetected by the error detection mechanism and handed over to the user. Operational applications may have a specified objective for the *residual error probability*;  $10^{-12}$  is the most common figure whatever be the channel bit error rate for control commands. Furthermore, an information packet that arrives with a delay outside the application time constraints is considered as lost information.

### Availability and Dependability

Availability is a service-related statistical parameter that can be defined as the probability of proper operation of the network for a given information exchange. It is normally quoted as a percentage of *up* time of the service, or the percentage of time that the network can effectively forward traffic (e.g., 99.999%). It can be estimated theoretically and measured practically on a network-wide or per-circuit basis.

Service availability can be expressed as

$$A_{\text{Service}} = 1 - \left( \frac{\text{Mean.Time.To.Restore.Service}}{\text{Mean.Time.Between.ServiceOutages}} \right).$$

Some currently used values are given in Table 14.5.

However, this statistical parameter, widely used in public telecommunications, in computer systems and networks, and in defining SLAs, must be used with precaution when applied to operation-critical services with an extremely low *service-to-idle* time ratio.

As an example, consider a managed service with an apparently high contractual availability of 99.999%. This gives an unavailability figure of  $10^{-5}$  and an unavailable time of 311 s/y.

**A protection relay system sending 50 trip commands in 1 year can be unavailable during 6 s each time a trip must be transmitted and still respect 99.999% availability!**

For low-duty cycle operation-critical services, it is more appropriate to use *service dependability* defined as the conditional probability of a service being available when it is solicited. It is important to consider the correlation between power faults and service availability. In fact, there is a correlation between them due to the fact that a power-system fault is a situation that ini-



tiates an extensive exchange of information, but it also induces impairments in the operation of the communications system.

### Electromagnetic and Environmental Constraints

Most access points are located at high voltage sites, so communications equipment should work under harsh electromagnetic conditions. Consequently, wired-access interface must be adequately protected to avoid disturbances that may produce errors, loss of information, or even interface damage that will downgrade service availability. It should be noted that adopting services provided by a public telecom operator does not remove the need for taking these measures, since access equipment must be installed at utility sites.

### Service Survivability

*Survivability* is defined as the ability of the communications service to continue during and after a disturbance (network infrastructure fault). Many operation-critical communications services do not tolerate service interruption and downtime. In addition to the statistical concept of availability, it is essential to assure that, as a minimum, no single fault in the reliability chain will jeopardize the application. The concept of service survivability perceived at the user end translates into *resilience* in the telecom service provider's infrastructure. Resilience is the ability to provide and maintain an acceptable level of service in the presence of faults.

This is achieved through a multilevel resilience model comprised of the following:

- Fault tolerant network elements with duplicated core components and duplication of access equipment at critical sites
- Survivable topology (e.g., ring and mesh structures allowing alternate routing)
- Disruption-tolerant end-to-end transport through protection switching and service restoration mechanisms like SDH MSP ring protection, Ethernet Spanning Tree Protocol (RSTP), MPLS alternate paths, IP routing mechanisms (e.g. OSPF), etc.
- Fault-tolerant and adaptive applications and overlays
- Adapted management strategy and system supervision through appropriate fault management tools dedicated to the operational services.

Some points need to be kept in mind concerning service survivability and the design of resilience:

- *Service restoration time.* Different levels of network resilience operate at different time scales that may

or may not be compatible with different applications' maximum acceptable outage duration.

- *Routing control.* Designing resilience into the network generally signifies injecting a degree of uncertainty into the routing of information and the resources that are used for delivering the service. This in turn, impacts the absolute time latency of the network and generates delay variation. In the most time-sensitive applications, resilience is restricted to the application itself (main/backup end-to-end routes). The two communication channels for these applications must be disjoint, that is to say, they should not have any common path, common node or common equipment, in order to avoid a single failure disrupts the application. To achieve this, a controlled routing algorithm is required.
- *Underlying infrastructure.* Where the telecom service provider network employs a contracted lower layer infrastructure, it becomes difficult or impossible to guarantee the independence of main and backup routes. Tracking the full routing of connections can become extremely difficult.
- *Coordination of resilience.* Applying different layers of resilience in the network to the same service without adequate coordination may cause unnecessary cost and complexity. As an example, main/backup end-to-end application-level fault-tolerance, spanning tree protection on the Ethernet connectivity, and ring protection in the underlying SDH network may all operate on the same network fault with different time scales to switch the traffic from the same topological path to another unique topological path.
- *Dormant faults.* An important issue in assuring service survivability is the capability to detect latent faults in the backup routes. A classical strategy adopted in power system telecommunications networks, is the crossover of main and backup routes for different applications. This approach uses each of the two paths and its associated resources for one main and one backup route, and, therefore, continuously checks each path to detect any anomalies.

### 14.3.4 Service Provisioning and Service Level Agreement

It is important that operational services used by time-sensitive applications be contractually committed through a service-level agreement (SLA) to assure that every aspect of the service will comply with critical operational requirements, such as time constraints and dependability. Whether the service be provided by a public operator or internally provided using power-utility telecommunications infrastructure, the SLA is

useful to formally specify requirements and assess capabilities of the service to be provided.

The electrical power utility's decision on the way a communications service is implemented depends upon several factors, the most important of which are listed here:

- Service quality and reliability requirements
- Service accessibility at sites where communication is required
- Cost of deployment and maintenance of the service during the required operation period
- Commercial availability (or nonavailability) and cost
- Number and dispersion of sites to cover and their communications traffic
- Company policy and regulatory issues concerning capital and operation expenditure (CAPEX/OPEX)
- Disaster recovery/business continuity and security constraints
- Company policy and regulatory position on recovering investments through nonoperational telecom services (e.g., recovering the cost of optical infrastructure through leasing of dark fibers)
- Organizational issues including in-house availability of skilled staff.

Service provisioning can be performed through a public multicustomer operator, in which case the power utility effort is mainly focused on adequately defining the service, contracting the provider's agreement on the quality of the delivered service, and assuring that the provider delivers the contracted service level.

The power utility can also decide that the most adequate manner to provision the service is to use a dedicated telecom infrastructure through its own service delivery process and organization, in which case the network is generally shared with other utility communications services in order to optimize the investment.

Different intermediate solutions may exist between the purely procured and fully in-house service provision using different extents of outsourced operations, field intervention, or maintenance support. Moreover, services of different kinds or in different parts of the network may be provisioned through different modes.

The performance objectives and the quality of service are also different among these different service types. Many operational services, such as protection relay applications, have extremely severe time delay and communication-integrity constraints, whereas the other communications service types are mainly transactional with less severe time sensitivity. On the other hand, business and market communications services implicate access beyond the perimeter of the

power company and may raise more severe security issues.

Considering the organizational diversity of electrical power utilities and their different sizes, activities, and regulatory constraints, the exact perimeters can vary to some extent and may evolve with organizational changes. Some of the factors that influence service provisioning are:

- *Security policy.* The definition of separate security domains across the company and the consequent allocation of applications to these different security domains can result in communications infrastructure segmentation.
- *Organization.* The organizational entity in charge of a group of applications may require exclusive usage of a service or a same group of communications services.
- *Company strategy.* Grouping of communications services may depend upon the company's strategy, for example to merge corporate and operation-related IT and telecoms, or to merge corporate and market related applications' communications provision, etc.
- *Regulatory issues.* Regulation authorities may prevent operational applications to share communications services with nonoperational ones.

When the telecom service-providing entity is tightly related to the *service user* entities, there is a one-to-one correspondence between applications and communications services resulting in an *application-oriented* definition of the communications service (e.g., SCADA or protection circuits). The communications service provider is assumed to be sufficiently familiar with the applications to apply the necessary precautions in the delivery of the required service. However, when a new application is introduced or the requirements of an application change in time, then the user and provider must seek a new common understanding of the service requirements.

On the other hand, where communications service is provided by an external telecom operator, then the service provision contract defines the service attributes according to the provider's *service catalogue* (interface type, throughput, availability, delay, etc.). In this case, the utility user must decide upon the suitable service category for his application *out of the provider's catalogue*.

The service provision contract is known as a *service-level agreement* (SLA), which can be explicit in the case of externally provisioned services or implicit, based on common understanding, for internally provisioned services. SLA is an essential mechanism to ensure the successful provision and operation of net-

work services from an external provider. SLA expresses application requirements in terms of service parameters. The most important parameters that should be included in an SLA are:

- *Service availability.* The frequency, duration, and timing of service failures need to be determined for each service.
- *Bandwidth.* This is the bandwidth available to the different services and may include some flexibility in how this is applied.
- *Delay and delay variation.* It will be necessary to specify this for each application.
- *Data security.* Again, this will be specific to different applications.
- *Power fault correlation.* For services that are critical during power system disturbances, it may be important that specific additional precautions be specified.
- *Penalties.* While penalties may not compensate for loss of critical services, they do focus a service provider's attention on the need to monitor SLA guarantees.
- *Mean time to repair (MTTR).* It is important that there is adequate confidence in the service provider's ability to respond to service failures and carry out the necessary repairs in an acceptable time.
- *Service isolation guarantees.* This refers both to isolation between internal and external traffic, as well as between different internal services.
- *Physical redundancy check (reliability).* This may specify the level of redundancy required, for example, at a network level, an equipment level, or at specific locations.
- *Power backup.* This is critical for those services required during power-system disturbances. It is important to ensure that rural switching locations have sufficient standby arrangements.
- *Performance reports specification.* It is important that meaningful and comprehensible information is provided in a timely fashion. There is very little use in providing vast amounts of data but very little information.
- *Qualified workforce availability.* Obtaining and holding on to qualified personnel is an increasing difficulty for service providers. It is important to ensure that a potential service provider has sufficient depth in their workforce. It is also worth examining that they have the right number of personnel in the right locations in order to ensure that response time guarantees are realistic.
- *Reporting.* This pertains to how service performance will be evaluated including measurement methods, parameters to be controlled, and reporting frequency and format.

Adopting a particular telecom service-provisioning model is not an irrevocable decision. It is often re-examined and reviewed in the light of new situations, some of which are:

1. New company policy and orientation
2. New regulatory issues and requirements
3. Emergence or abandonment of adequate telecom services to be procured
4. New applications or change of scale incompatible with the present provisioning model
5. Lack of satisfaction from the services obtained through the existing provisioning mode
6. Major capital investments and running costs required for refurbishment and extension of existing facilities
7. Technological changes in telecommunications and in power-system technology
8. Lack of qualified staff and the ageing of the technical workforce concerned.

### 14.3.5 Telecommunications Technologies

Operational telecom networks are built using a variety of technologies. The focus of this section is to introduce working principles and specific ways telecom technologies are used. A detailed analysis of the working theory can be found in a quite large number of publications and books.

In order to optimize investment, telecom resources are usually shared by several services. This is accomplished through the use of multiplexing techniques, which will be presented later this section.

Telecom working principles can be grouped into three categories associated with different working modes:

- *Transmission technologies.* Their function is to deliver bits at the remote end of the link. This concept applies mainly to point-to-point links, although some wireless technologies can provide point-to-multipoint transmission services.
- *Transport technologies.* Their function is to deliver bits to a far end, crossing several intermediate nodes. These technologies are able to establish a point-to-point link over a digital network providing bit transparency. They can use a mix of transmission technologies in every one of the point-to-point links used to establish the path.
- *Networking technologies.* Their function is to transport packets between two access points. Packets delivered at the ingress access point can be delivered to any egress access point of the network, so they can establish multiple virtual links using the same access interface.

From the working modes described above, we can summarize that communications can be implemented using the *circuit* or the *packet* paradigm. Both have advantages and disadvantages, as is shown later in this section. Although most existing communications networks are based on circuit technology, power utilities are migrating towards packets due to their higher flexibility, scalability, and cost-effectiveness. Furthermore, the IEC 61850 family of standards specify the use of Ethernet and IP to implement operational communications services form control centers to the other power grid actors. This means that in the near future, the packet paradigm will be the only technology considered to implement operational services. Nevertheless, we will analyze existing technologies, as the migration to a packet-only system will take many years.

Considering the way physical communications links are used, most technologies allow communication-resource sharing or information multiplexing. Multiplexing is normally used to optimize the use of communications resources by integrating operational and sometimes nonoperational services over common infrastructure. This includes multiplexing of dedicated frequency bands, optical wavelengths, time intervals in a high-speed data stream, or dedicated packets in a high-capacity data link.

Circuit technology uses a fixed path or a *circuit* through the network. This path – once established – offers a fixed bandwidth and a fixed and deterministic latency to the service. For the simultaneous transmission of a multitude of services (i.e., many data, voice, or video signals) sharing the same medium, these signals are combined using *time-division multiplexing (TDM)*, where each signal is cyclically allocated a time slot with a time gap short enough to be unnoticed by the user.

The disadvantage of this technology is that the network resources are inefficiently used by sporadic burst traffic, like voice or video. For example, the bandwidth allocated to a voice channel is permanently occupied even during speech pauses or when not used at all. The advantage is that each service receives its dedicated network resource with fixed bandwidth and stable end-to-end delay. The PDH and SDH technologies described in the following sections are examples of TDM networks.

The disadvantage of poorly exploiting network resources has been tackled by the so-called *packet switched* technology. Simply speaking, the data to be transmitted is split into packets (which can be of various sizes) and are labeled with a source and destination address. The packets enter a queue at the ingress of the network, and as network resources become available, the packets are forwarded by switches and routers through the network, normally following the shortest or

the fastest available path. This technology is employed in wide area networks (WAN) based on Ethernet or IP packets.

Marketization, queuing, and competing for network resources like bandwidth, inherently generate the risk of a nondeterministic service delivery that is a potential problem for time-critical signals such as protection. Bandwidth overprovisioning combined with advanced techniques, such as service prioritization, traffic engineering and bandwidth reservation, time distribution protocols, data buffering, and synchronous Ethernet contribute to gradually overcoming or reducing most of the undesired statistical behavior of packet-switched technologies.

*Frequency division multiplexing (FDM)* is a multiplexing technique used at the transmission level. It is based on using separate frequency bands for each service, as is done in power-line carriers or in radio systems. The same principles apply to *wavelength division multiplexing (WDM)*, which is employed over optical fibers. In these systems, the interaction between different services is only through potential crossband interferences. It should be noted that resource allocation through TDM and FDM – or WDM – may be simultaneously used in different hybrid configurations.

Optical communications is the most reliable and powerful transmission technology available nowadays. Optical fibers are widely deployed in power-utility communications networks and constitute the preferred communications medium between substations, as well as for the substations' internal automation networking. Fibers can be dedicated to a single application (e.g., protection relays) or may be shared for the use of many applications.

Power-utility communications networks employ single-mode (SM) fibers due to their better transmission characteristics, such as attenuation, dispersion, and bandwidth. Multimode (MM) fibers are limited in their application to short distances inside the substation (protection relays, actuators, metering devices, etc.), to assure galvanic isolation at low installation and maintenance costs.

Power-utility optical fiber cables are generally deployed along overhead, underground, or undersea power lines. The fibers are illuminated by laser emitters and can be used in single-wavelength or multiple-wavelength modes. In the latter case, every wavelength acts as an independent carrier of information, increasing the fiber capacity or reinforcing service separation. Many optical cable technologies are presently in use, depending on the nature and voltage level of the power transmission lines. In the case of overhead power transmission lines, the optical cable may be incorporated into the protection ground wire, OPGW, or wrapped around it.

Alternatively, the optical cable may be *self-supported*, attached to transmission towers or distribution poles. All-dielectric self-supporting (ADSS) optical cables are generally used for existing line retrofitting when the line voltage is below 150 kV, and where the line is not equipped with protective ground wires with full continuity. This is often the case of medium-voltage distribution lines.

However, above 150 kV, the presence of electric fields affects the transmission characteristics of the fiber, increasing its birefringence effects. Moreover, at higher voltages, ADSS is generally not employed due to the effects of the electrical field on the dielectric sheath. For these systems, the preferred technology is OPGW with the optical fibers placed inside steel, aluminum, or plastic tubes to protect 12, 24, 48, and 96 optical fibers, according to different cable designs.

The available capacity of optical fibers is often assumed to be almost limitless based on advances in optical communications although factors such as temperature change, mechanical stress, and strong electrical fields may limit these capabilities at very high communication speeds far higher than required by operational and IT services.

Wavelength division multiplexing (WDM) is increasingly in use in power-utility communications networks to provide separation between different types of services (operational and corporate networks, legacy and new-packet core networks, fiber-based protection relays, and other communications, etc.). This is particularly true where extra fibers are not available or cannot be provisioned economically. WDM allows multiple optical beams from different optical communications systems, each at a different optical wavelengths, to be combined through an optical multiplexer and injected into the same fiber. At the reception side, the different wavelengths are separated by a passive optical filter bank and treated by different optical receivers. WDM provides full isolation of telecom services that only share the fiber and possible optical amplification.

Coarse-wavelength division multiplexing (CWDM) is defined by the ITU-T Rec. G.671 standard. It allows implementing reliable and cost-effective systems, through a combination of uncooled lasers, relaxed laser wavelength selection tolerances, and wide pass-band filters. CWDM systems can be used in transport networks for a variety of architectures, delivering a very cost-effective solution. Figure 14.15 presents the channeling structure for CWDM together with fiber attenuations.

It is worth noting that the water absorption peak around 1400 nm is no longer present in more recent fiber designs (ITU-T G.652-C or G.652-D) in which the OH ions inside the crystal structure have been removed through a modified manufacturing process.

The dense-wavelength division multiplexers (DWDM) on the other hand, is a technology used to further increase the capacity of the fiber by adding more channels (ITU-T G.694.1). DWDM systems, mainly used by public telecom operators, can multiplex from 32 to more than 100 channels in the range of 1530–1624 nm. With a channel spacing of 1 nm (or below), DWDM operation requires extremely precise optical sources with laser-temperature stabilization resulting in significantly higher complexity and cost. With a channel spacing that is ten times larger, CWDM systems tolerate temperature drift over the whole industrial temperature range of the laser emitters without leaving their allocated channel. This ruggedness, in addition to a considerably lower cost, constitutes significant advantages in the utility communications network where wavelength multiplexing is not often used to attain maximum bandwidth but rather to separate networks. For the use of optical amplification systems in long spans, CWDM systems should be limited to four channels (C- and L-bands) to make them compatible to the limited bandwidth of these devices.

#### Time-Division Multiplexing (PDH and SDH)

*Time-division multiplexing (TDM)* was the prevailing transport technology of power-utility telecom networks, but nowadays it is being replaced by Ethernet and IP technologies. Nevertheless, we will include a brief description of its working principles. Historically, the *elementary digital stream* was fixed at 64 kb/s (56 kb/s in North America) corresponding to 8000 analogue samples/s with each sample coded over 8 bits (8000 sample/s required to convert a 4 kHz analogue voice signal to digital and reconvert back to analogue after transmission across a link without loss of information).

In order to exploit a much higher digital-transmission capacity of transmission systems, the digital bit-stream was used to continuously transport cyclic frames of fixed length, which are partitioned into equal *time slots (TS)*. Using the same TS in each frame, one can transport an elementary digital stream, time-domain multiplexed with other digital streams. A frame header sequence allows synchronizing both ends of the link and, therefore, to separate multiplexed characters at the receiving end.

Time-multiplexing of 32 elementary digital streams (30 useful streams plus slot 1 for header sequence and slot 16 normally reserved for signaling) has yielded a multiplex system with an aggregate bit rate of 2048 kb/s (currently referred to as 2 Mb/s or *E1*). A slightly different constitution in North American and Japanese systems gives a 24-channel multiplex at 1544 kb/s (referred to as *T1 and J1*).

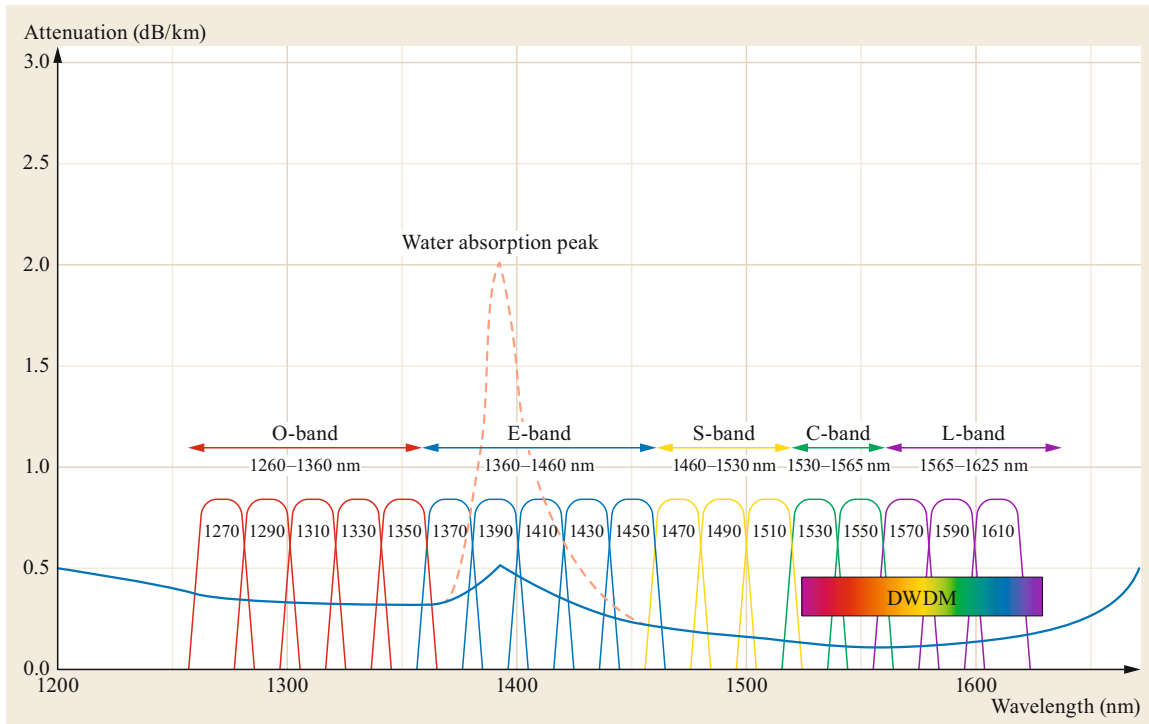


Fig. 14.15 WDM channeling. (Adapted from [14.1])

The E1 system is byte-multiplexed (8 bit per time interval), has a frame length of 256 bit, and a periodicity of 125  $\mu$ s. This system is referred to as a *primary multiplex system* (ITU-T G.703) and can carry voice or legacy data at speeds ranging from 0.3 to  $N \times 64$  kb/s. A primary multiplex system is purely synchronous: at the receiving end, the system must reconstitute clocks from the received signal for bit reception and for frame synchronization. Frame synchronization is performed through initial searching of the frame-header sequence and multiple successive reception of the same pattern at the right time. Synchronization is lost when the pattern is not found at the right place a determined number of times, and a new search for headers is initialized. The loss of synchronization and the consequent time of resynchronization can lead to periods of unavailability, which can affect the performance of certain utility-operational applications, such as protection signaling if no special measure is taken.

However, when multiple E1 streams from different primary multiplexers are to be combined together to use a higher capacity transmission resource, the clocks of the different primary multiplex systems, although at the same nominal frequency, are never identical. Clocks at the same nominal frequency are called *plesiochronous*.

Higher-level combination of primary multiplex data streams is performed through bit multiplexing (com-

binning four 2 Mb/s to constitute an 8 Mb/s stream and then combining by four to constitute a 34 Mb/s, etc.). Successive multiplexing produces a *digital hierarchy* known as a *plesiochronous digital hierarchy* (PDH).

PDH multiplexing was devised – and was well suited – for the connection of telecom switching centers (central office, CO). It is not appropriate for adding and dropping of *containers* at intermediate stations across the network. This means that the whole load of channel groups in the hierarchy need to be *unfolded* whenever some load needs to be *dropped or added*. This method results in unreasonable time delay, complexity, costly equipment, and excessive crossconnect wiring. This drawback has been overcome by the implementation of *synchronous* digital networks. *Synchronous digital hierarchy* (SDH) was designed to deploy digital transport networks able to establish digital channels of different bit rates between any two points of a wide area network. This was achieved by implementing a synchronous digital network that provides intrinsic cross connections and add-drop facilities. The synchronous digital hierarchy is composed of multiplexed digital rates of 155 Mb/s (STM-1), 622 Mb/s (STM-4), 2.5 Gb/s (STM-16), and 10 Gb/s (STM-64). Power-utility telecom networks employ currently STM-1, STM-4, and STM-16.

Unlike PDH, SDH is a network-based system using *add-drop multiplexers* (ADM) at each node loading and

unloading data streams in previously reserved *virtual containers (VC)* to connect to different destinations. The data capacity available is partitioned into a pointer domain and a payload domain. Each VC in the SDH payload corresponds to a specific pointer indicating the location of the VC in the payload. The VCs in the same payload can have different sizes (the number of reserved bytes in the payload), depending on the capacity of the data stream (2, 34 Mb/s, etc.). The minimal size of the VC is 2 Mb/s (VC12) allowing the transport of an E1.

Different levels of overhead (segment, path, etc.) allow more elaborate management and end-to-end recovery of connections across the network. In particular, the *SNCP (subnetwork connection protection)* protects each tributary data stream in a differentiated manner through an alternate path around a ring.

Transport of data across an SDH network is performed through previously reserved capacity and centrally controlled deterministic routing, thus leading to a highly predictable transmission delay. Furthermore, the management information accompanying each virtual container enables very fast data-traffic recovery on network fault conditions (< 50 ms). However, the self-healing mechanisms of SDH are not implicitly bidirectional and may lead to different go and return paths and, consequently, delay differences causing anomalous operation of differential line relays or other devices using an echo method for time synchronization. Precise network design or specific mechanisms are required to avoid such asymmetry in the network.

The SDH systems deployed in the 1990s were focused on the transport of circuit-switched traffic (E1, etc.) with only limited and proprietary facilities for Ethernet packet transport. New-generation SDH (NG-SDH) has since been completed with a set of standards for optimized mapping and control of Ethernet traffic (*Ethernet over SDH or EoS*), as is described in Sect. 14.3.6. This allows power utilities to combine at a control bandwidth granularity, the more efficient and flexible bandwidth sharing packet networks with the deterministic behavior, low delay, and fast healing of SDH.

### Layer 2 Networks – ETHERNET Technology

As we already introduced, Ethernet has become the standard telecommunications interface. Ethernet technology implements the physical layer and link layer functionality, which allow layer 2 networks to be implemented using this sole technology. A layer 2 network is network formed by a limited number of physical devices connected by means of a communications medium able to provide full connectivity. The communications media can be formed by a bus implemented by physical wires, a point-to-multipoint radio, a satellite

system, or an Ethernet LAN. A layer 2 network based on Ethernet technology is a network formed by Ethernet switches and bridges able to forward Ethernet frames to its destination host, thus providing Ethernet service in all of its access ports.

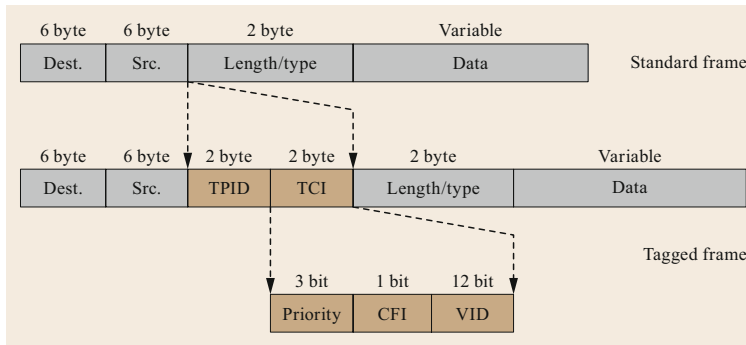
Layer 2 networks do not have routing procedures. There is no need, since layer 2 networks provide broadcast to all their members. Nevertheless, Ethernet switches provide mechanisms to find where every host is connected and, therefore, deliver the frames to its right destination without using broadcast forwarding. This mechanism is not based on the routing principles but on dynamic the Address Resolution Protocol (ARP) table built from the switched traffic. Frames addressed to unknown destinations are broadcasted to all the destinations. Every time an Ethernet switch receive a frame with a new address, this address is automatically added to the ARP table, so as traffic is forwarded, spontaneous broadcast decreases.

Layer 2 addresses are unique and randomly assigned. Unlike layer 3 addresses, they do not identify the location where the host is connected. They are just used to identify the host. Due to the random distribution of Ethernet addresses, the address of every host must be stored in every Ethernet switch and, therefore, it is not possible to implement a routing procedure like in layer 3. Layer 2 networking is a cost-effective approach that presents some scalability limitations mainly due to the random address allocation and the lack of routing procedure. For this reason, large WANs usually require a backbone and more scalable assignment capability.

The concept of *virtual networking* can be applied to both the link layer or LAN and the network layer. In order to segment traffic and improve scalability, mechanisms to implement virtualization of local-area networks have been defined. Virtual networking allows network connections to share common physical media with other data while remaining logically isolated to and from other users. Virtual networking can be set up at different levels in the OSI layer model, from layer 1 to layer 3.

Virtual LANs or VLANs (IEEE 802.1Q) are the mechanism used over Ethernet networks. Upper-layer technology virtual private networks (VPN), such as IPSec, are used at the network layer. The main advantages are the following:

- *Expandability.* Once the network is in place, it can be easily expanded to other sites or higher capacities just contracting new capacity from public network operators.
- Lower cost compared to private or leased communications means, as infrastructure maintenance costs are much lower.



**Fig. 14.16** VLAN frame format. (Adapted from [14.2])

- *Simplified network topology.* Virtually connected LANs can be seen as a single network from the end user/application perspective.

A VLAN defines a logical segment that comprises several LAN resources, including cables, equipment, and some of their ports. Each VLAN becomes a new broadcast domain. Since the broadcast domain defines the scope of a LAN, any host attached to a VLAN can only reach other hosts of the same VLAN due to the limitation of broadcast messages. This provides traffic isolation and a very powerful security mechanism, as there is no way two hosts of different VLANs send information directly. In order for hosts of different VLANs to communicate, a router must be added. In this case, the router controls traffic flows and set communication rules between VLANs.

The IEEE 802.1Q standard defines a 4-byte extension to the Ethernet frame header that allows traffic from one VLAN to be distinguished from another VLAN, as is shown in the following Fig. 14.16.

The tag includes a 12 bit field used as VLAN identifier (VID). VID allows 4096 different VLANs to be defined in a LAN. Whereas trunk ports that interconnect switches carry tagged frames, edge ports can accept tagged or untagged frames. In fact, there are two generic types of VLANs, the ones generated by the switches, normally associated with a set of ports, or a MAC address, IP network, etc., and the ones generated by the IEDs, like in the case of IEC 61850 GOOSE and sample-value messages, where the IED generate the tagged frame. The simplest way to implement Ethernet connectivity with local or limited coverage is to use unshielded twisted-pair (UTP) copper wires or optical fibers through the appropriate Ethernet transceivers incorporated into the Ethernet LAN switches. Due to the harsh electromagnetic environment of power plants and substations, the use of copper interfaces should be limited to connections between equipment located in the same cabinet. Currently, Ethernet has many different interface types; copper interfaces can run from 10

to 1000 Mb/s, whereas fiber interfaces can run from 0.1, 1, 10, and even 40 and 100 Gb/s. Optical Ethernet interfaces – in particular gigabit Ethernet – can be implemented over a wavelength, this way sharing the fiber capacity with other traffic through wavelength division multiplexing (WDM).

Although fiber optic variants of Ethernet were initially designed to connect devices in different floors of a building or even between nearby buildings, the extremely long range of optical interfaces ranging up to 180 km at 1 Gb/s without repeaters allows a LAN to be extended outside the substation becoming a single distributed LAN that works like a LAN but without being local. The implementation of a WAN using Ethernet is simply the interconnection of Ethernet switches using medium and long-range optical interfaces. Furthermore, the increased capacity of new Ethernet standards ranging up to 10 Gb/s allows the capacity of the optical fiber to be used, thus providing a simpler alternative to other transport technologies. Nevertheless, despite its broadband performance, these new Ethernet standards maintain the same working principle, which means that they also suffer from the same technical limitations. In particular, the lack of native quality of service support, routing limitations, and lack of traffic engineering control.

### Radio Communications

Radio communications covers a very large spectrum of systems and solutions used in power utilities to various extents. In general, they present the advantages of fast deployment, where no existing wires can be used and the potential mobility of the communicating peers. On the other hand, they have implicit limitations in service availability (propagation conditions, obstacles, fading due to multipath propagation, etc.), bandwidth limitations compared to wired solutions, frequency allocation and licensing issues, as well as their associated tower and mast infrastructures to assure long coverage.

Some particularly useful applications of radio communications in the power utility are as follows:



- Line-of-sight microwave radio systems (2–13 GHz) are often used to complete optical networks to cover spans that are impossible or difficult to implement in optical fibers (e.g., crossing main motorways, rivers, etc.) or connecting the network to nonelectrical sites (e.g., control centers, office buildings, etc.). Frequency bands are increasingly difficult to obtain in the low end and are constantly pushed to 10–13 GHz or higher, with increased difficulty in assuring path clearance (Fresnel zone clearance) and, hence, requiring more costly tower infrastructure (when not installed on the top of a building) whose height is proportional to line-of-sight constraints. Microwave links, through their high frequency and high directivity are allocated large bandwidths, enabling them to transport high-capacity data flows (e.g., 155 Mb/s TDM or 100 Mb/s Ethernet). However, unlike fiber systems, their capacity cannot be increased with growing requirements beyond the allocated frequency bandwidth. WiMAX technology, defined by IEEE 802.16x standards, is still in use mainly in North America and provides a point-to-multipoint microwave solution with around 70 Mb/s capacity. Line-of-sight radio systems are also used in UHF radio bands with lower capacity (according to different national frequency regulations) but lighter infrastructure (less directional antenna systems, partial clearance of Fresnel zones leading to lower antenna heights). These are frequently used in industrial radio systems deployed in distribution grids.
- Broadband packet-based wireless network IEEE 802.11 (WiFi) is mainly used in the distribution grid to provide a high-throughput network to cover the emerging smart distribution applications. IEEE 802.11, in particular, enables the implementation of broadband wireless mesh infrastructures with ad-hoc network configuration algorithms to cover a distribution network perimeter. A network capacity of around 400 Mb/s can be attained through aggregating multiple channels. Powerful encryption algorithms overcome the security issues often associated with the usage of wireless technology to support operational networks applications.
- Narrowband industrial UHF radio systems provide up to around 20 kb/s over 12.5 kHz allocated frequency bands. These systems are widely used in distribution grid automation and SCADA applications. In some countries, allocated bandwidths of 25 kHz or more allow higher link rates.
- Private mobile radio (PMR) systems also known as land mobile radio (LMR) systems are UHF/VHF radio systems allowing the communications of the utility mobile work force. One or several radio

channels are shared among multiple mobile terminals. Different trunking protocols, such as TETRA or MPT-1327, are used by a central station to control channel access, network signaling, and some specific closed network functions. Implementing an adequate coverage through a PMR is costly compared to public alternatives, considering the area to cover (number of base stations) and, generally, small number of mobile terminals using the network. The major advantage over public cellular service is the higher availability.

- Private cellular radio systems cover different technologies, such as GSM-R (used mainly in transportation), and LTE (4G) are trunked cellular solutions that can be implemented in a private utility operations network to provide very high communication capacities. These technologies can find their place in the future smart distribution network integrating a large number of bandwidth-consuming applications (large-scale realtime metering and demand response), although procuring frequency licenses may be hard to justify for a power utility.
- Satellite communications is radio communications that uses an artificial satellite located in a geostationary orbit to relay and amplify radio signals using a transponder. This is commonly used for TV or any other type of signal broadcasting. A special type of satellite communications is the very-small-aperture terminal (VSAT). This system uses a very small dish antenna and implements a point-to-multipoint bidirectional communications channel. Its use is common for operational applications that can tolerate rather high latency such as data acquisition or even SCADA applications to remote places, where deploying radio or fiber communications is not possible or very expensive. In most cases, the data rate can range up to 16 Mb/s or even higher. Modern implementations use the  $K_a$  band ranging from 26.5 to 40 GHz.

#### Power-Line Carrier

Narrowband power-line carriers (PLC) allows the transmission of communications signals, in particular protection relay communications, over power transmission lines. This technique, which has been in use for a long time, still provides a dedicated infrastructure fully incorporated into the substation with a signal path that implicitly follows substation-to-substation connections over long distances without any repeaters (> 500 km) and, therefore, an interesting solution for transmitting small bits of information such as teleprotection signaling, low-speed data, and speech over long distances. Channels for different applications are aggregated together through frequency multiplexing (FDM)

and transposed to a carrier frequency (roughly 25–500 kHz) or time-multiplexed to construct a digital data stream that is translated in frequency through digital modulation schemes.

Power-line carriers are used when no fiber is available or as a second path to secure the operation of a protection system. The availability of the communications channel being strongly correlated with power transmission line fault conditions, PLC is unsuitable for transmitting current differential protection, coded-sampled values (e.g., IEC 61850), or digital stream teleprotection signaling (due to potential synchronization loss on line faults). They are employed to transmit voice-frequency command type teleprotection, speech signals, and data.

Power-line communications are also used in power distribution grids for building advanced metering infrastructure (AMI) covering smart meters in customer premises, public lighting control, and different distribution automation and SCADA applications. These systems range from lower bandwidth PRIME, G3 and IEEE 1901.2 solutions with a capacity below 120 kb/s, to broadband power-line (BPL) solutions allowing building a packet network over medium-voltage or low-voltage distribution network conductors. Different techniques are used to cross open breakers, eliminate band-limited noise and disturbances, and to operate over variable grid topology and signal transmission characteristics. The system can typically provide 10–100 Mb/s capacity with a span of 3–4 km between nodes. BPL solutions can integrate multiple applications, each of which allocated a distinct VLAN, and may be used for higher data volume and resolution metering applications (e.g., for demand response), backhauling of smart metering, grid automation, SCADA, and other distribution grid applications.

### 14.3.6 Networking Technologies: The Network Layer

The network layer is implemented using the datagram paradigm that offers a connectionless packet service using the Internet protocol, IP. The IP protocol is widely known, so we will not explain its working details. IP has been used for SCADA applications for many years, since the beginning of this century. In 2004, IEC 61850 was approved and, as was previously explained, it is based on IP. Furthermore, in 2012, Edition 2 of the IEC 61850 standard was released, which extends the use of Ethernet and IP to every application involved in power-system operation. Basic IP technology does not provide quality of service (QoS). An IP QoS architecture was defined providing bounded delay, but this architecture was focused on multimedia services and was not specialized in

specific operational requirements. The provision of committee QoS over and IP networks was a problem until the advent of multiprotocol label switching technology, as is explained in the following paragraphs.

#### Multiprotocol Label Switching (MPLS)

Multiprotocol label switching (MPLS) is a packet forwarding technique that was specified by the Internet engineering task force (IETF) in the 1990s in order to implement IP over ATM in a scalable way. This also simplified the provision of IP quality of service and allowed a symmetric path to be established. In fact, it converts connectionless IP into a *connection-oriented* service one, thus simplifying traffic-engineering procedures.

MPLS operates through the insertion of a label at the ingress port of the network and associates a forwarding equivalence class (FEC) to the label. Each FEC defines the manner in which the packet is to be treated in each MPLS node. The label is removed at the egress port of the network. A connection established this way is called a label-switched path (LSP). Labels are swapped at intermediate nodes according to a plan defined through a distributed control plane using a Label Distribution Protocol (LDP). This exchange of control information between the network nodes, each of which takes part in the definition of paths, is a great force giving scalability to very large systems but is also a source of substantial complexity, which may often be found unnecessary in the scale and size of an electrical power utility dedicated network.

The MPLS labels are replaced at each switching node. This provides high flexibility and a dynamic routing capability but it requires network-wide intelligence, implying permanent exchange of control information across the network. This is known as a *distributed control plane*. Moreover, in order to enable each node to allocate capacity for each traffic stream, some traffic rule or policy must be given to the node. A distributed control plane generates critical control traffic across the network, and traffic engineering implies some prior knowledge of traffic classes and attributes. The IP protocol control traffic is transported using a resource reservation protocol, RSVP. Such an operation is suitable for extremely large networks with large variations of traffic volumes and source-to-destination paths, but well characterized traffic models. This is typically the case for telecom operator networks. Adjusting traffic engineering parameters in such a system is complex but far less laborious than configuring thousands of predetermined data paths, which, moreover, can change with time-of-day and with seasons according to network users' bulk movements. The technique is known as MPLS-TE, where TE stands for traffic engineering.

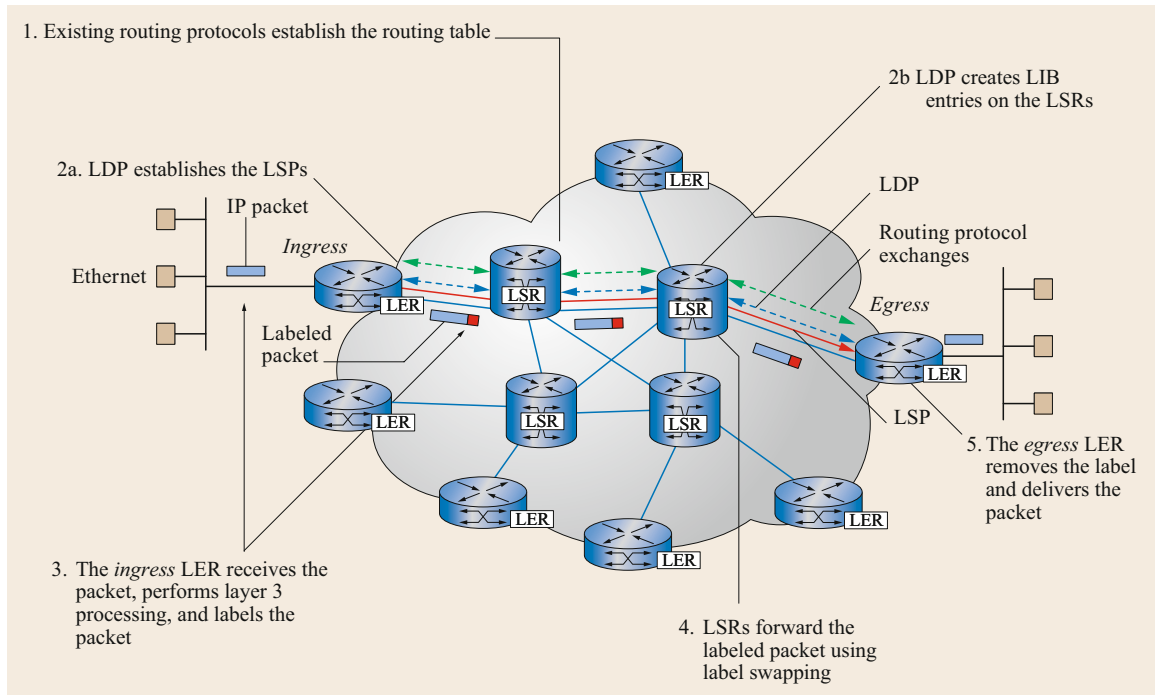


Fig. 14.17 MPLS working principle. (Adapted from [14.3])

IP-MPLS, in its simplest form, uses no traffic engineering but simple priority assignment, as in native Ethernet. The most time-sensitive traffic will only have a better delay variation than lower priority traffic. Such a system provides the traffic isolation advantages of MPLS, dynamic routing through a distributed control plane, but no guarantee on resource allocation to each service (except for the control plane exchanges using RSVP). It suits multisite enterprise networks such as utility nonoperational networks with no tight time and quality of service imperatives.

Transport profile MPLS, or MPLS-TP, is a variant of the MPLS technology simplified for transport-type networks providing predefined tunnels between service access points. It is an adaptation of MPLS to support traditional transport network requirements, such as high availability and QoS support, presently fulfilled by SDH transport technologies. MPLS-TP data traffic is forwarded across the network according to labels, which are added at the network ingress and removed at the network egress point without being changed at intermediate switching nodes. This provides a predetermined tunnel with no *distributed control plane*.

Packet forwarding tables at each node are provided by a central control platform in the same way as in SDH. The centralized control, moreover, allows predetermined end-to-end alternate routes and simple resource allocation. The control platform can allocate

a maximal capacity (peak information rate or PIR) and, if necessary, a minimal capacity (committed information rate or CIR) to each data stream, hence assuring SDH-like quality of service for time-critical services and IP-type flexible bandwidth for non-time-critical services.

MPLS-TP decouples the *end user-to-end user* network into distinct segments of the customer network (application network) and transport network. The latter segment essentially requires point-to-point services known as *pseudowires* (PW) transporting Ethernet (E-line or E-LAN carrier Ethernet services) and legacy TDM circuits upon the packet switched network. Moreover, the focus on transport domain allows MPLS-TP to use only a subset of MPLS, removing nonrelevant features and their corresponding complexity while adding some missing functions necessary for transport networks and existing in SDH/SONET, such as implicit operation, administration, and maintenance (OAM) signals exchanged at different levels of connectivity. MPLS-TP is a nonscalable solution for a telecom operator due to its fixed *tunnel* approach that makes it a nonfeasible approach to manage a very large number of connections. Conversely, it offers many advantages for the implementation of operational services, since MPLS-TP provides very similar features to existing SDH, thus simplifying technology migration and delivering new capabilities with similar management

processes and skills than the ones already existing in the power company.

The obsolescence of SDH technology is forcing the migration to MPLS. In the power-utility context, deploying MPLS is not *build from scratch* but part of an evolutionary transformation plan that should define the migration strategy. This plan should consider mission-critical time-sensitive services that require deterministic and symmetric circuits that would have to be emulated across the packet core. Moreover, the utility controls its telecom network from a central network management platform with processes and skills that are adapted to such an operation. In this context, MPLS-TP is a more appropriate technology than IP-MPLS, with or without traffic engineering. Some of the main reasons for this are summarized below:

- *Maintaining full control of the network.* In MPLS-TP, forwarding labels are produced by a central network management system (NMS) allowing end-to-end main and alternate route definitions, as is presently done through SDH. In IP-MPLS on the other hand, the proper operation of the network depends upon control plane communications. Moreover, if a deterministic behavior is necessary for some data streams, then adequate traffic engineering must be introduced to govern routing nodes decision. Adjusting traffic engineering parameters in an IP-MPLS network (MPLS-TE) is complex and requires tuning and adjustments rendering the network subject to nonoptimal settings.
- *Quality of service and deterministic behavior.* Some utilities using dedicated resources, such as separate fibers for protection, may imagine that these constraints are definitively out of their shared network. In reality, other protection-like applications with network-wide coverage will be deployed in the coming years, and dedicated fibers used between adjacent substations can no longer be the solution (e.g., system integrity protection schemes SIPS). Being able to implement time-sensitive applications remains a *must* in an operational network.
- *Size of network and type of traffic.* By its SDH-like behavior, MPLS-TP responds to all existing service requirements, as well as new packet-based services in utility-sized networks. Deploying MPLS-TE on the other hand, is suitable for public networks with highly dynamic data traffic characteristics and too many nodes for centralized control; traffic rules are, hence, given to nodes so that they can build the forwarding labels at any moment (TE).
- *Capability versus complexity.* IP-MPLS provides numerous technical capabilities but with increasing

complexity. Implementing QoS through dynamic resource reservation (RSVP) can be done in IP-MPLS but making it for hundreds of connections is far from being trivial. This level of dynamic complexity for a *static-by-substance* service seems unnecessary. Similarly, performing any meaningful traffic engineering in IP-MPLS (MPLS-TE) requires fairly good knowledge of the traffic shapes and characteristics, which is far from being the case for many new coming and future services over the operational network.

- *Migration from SDH.* Transition to packet for power utility networks with extensive SDH infrastructure, management tools, and skills is almost smooth for MPLS-TP because of its SDH-like behavior and network management. IP-MPLS is a jump into another type of network operation. With a large telecom network, utilities will become entirely dependent on their supplier. IP-MPLS suppliers provide specific tools and features to overcome some of the basic problems but in a nonstandard manner causing further dependence on a single supplier.

As transport functionality is migrating from SDH to MPLS, and Ethernet is the universal service access interface, it is important to consider that Ethernet will have to be transported over MPLS in most of the cases. In fact, we can identify three possible Ethernet transport solutions:

- Ethernet transported over SDH
- Native Ethernet transported over optical links
- Ethernet transported over MPLS.

As was mentioned in the previous paragraph, SDH has been complemented with specific protocols to integrate Ethernet packet traffic to the virtual containers (VC) constituting the SDH payload. Ethernet encapsulation over SDH is defined by the Generic Framing Protocol (GFP), virtual concatenation (VCAT), and the link capacity adjustment scheme (LCAS). However, matching asynchronous data streams such as Ethernet packets to a constant rate container system such as SDH becomes complicated, inefficient, and expensive as the proportion of packet to TDM traffic grows.

Native optical Ethernet transport between substations becomes a candidate solution, as the extent of legacy traffic decreases in quantity and importance as compared to natively Ethernet-interfaced applications. This is, indeed, to be thought of in the present context of IEC 61850 substation communications architecture and gradual migration of substation intelligent electronic devices (IED) into a networked environment. Native

optical Ethernet can use dedicated fibers or dedicated wavelengths (C- or D-WDM).

Native optical Ethernet transport, however, suffers a number of shortcomings:

- Ethernet protocols include mechanisms for restoring connectivity across a meshed network of switches when one or multiple nodes or links become unavailable due to faults (Rapid Spanning Tree Protocol). The time needed for such restoration, depends on several factors, such as network topology, number of nodes, and implementation of the algorithms, so it can range from 20 ms for small and simple networks to hundreds of milliseconds for larger networks.
- *Aggregating services and delay issues.* When multiple communications services are to be transported together, TDM (e.g., SDH) allocates a predetermined communications capacity to each application, therefore guaranteeing a fixed and predetermined transfer time across the network (L1 separation). Native Ethernet, on the other hand, uses the principle of packet queuing. Data packets belonging to different applications are stored in a queue and processed sequentially at each node. Ethernet switches may have the capability to distinguish packets belonging to different applications by associating specific tags to data frames belonging to each connection (L2 separation). Each group of similarly tagged frames constitutes a *virtual local-area network (VLAN)*. Different levels of priority (different queues) may be assigned to different VLANs (IEEE 802.1P and Q). However, priority assignment does not guarantee a fixed delay.
- *Scalability.* As the number of virtual connections to be deployed across the network grows, VLAN allocation proves to be complex and not scalable. Cascaded tagging (stacked tagging) mechanisms have been added to Ethernet to overcome this issue. IEEE 802.1ah, also called mac-in-mac, is a native Ethernet mechanism (L2) that overcomes the scaling limitation of VLANs by re-encapsulating the traffic with an outer Ethernet header carrying input and output addresses of the Ethernet transport network. This way, the provider's Ethernet switches no longer need to learn the large number of end-user MAC addresses. This technique is called provider backbone bridging and separates Ethernet transport from Ethernet LANs of end-users.

The use of MPLS facilities allows deploying virtual private networks (MPLS VPNs) in a unified multiservice network. A VPN is a group of network access nodes

using the same label and is, hence, capable of exchanging data packets in a closed manner across an otherwise public multiservice network. The VPN concept can be applied at layer 2 or layer 3. The first case is a solution for Ethernet transport over MPLS, and the second is the way IP VPN can be implemented across an MPLS backbone.

Implementing separate Ethernet virtual LANs (VLAN) through layer 2 tagging, as described in the previous sections, provides a simple, but not a scalable solution. As the number of VLANs grows, the size of the MAC address table can become extremely large, and the switches constituting the network will have to *learn* MAC addresses per port for the whole network, and VLAN management may become complex.

Transporting Ethernet over MPLS provides the technology for the creation of a core layer overcoming the problem of scalability, while maintaining the end-to-end Ethernet service provision. MPLS can be used to transfer encapsulated data from different technologies over a certain network. An additional label is inserted in the data for the encapsulation purpose, and this label is used for forwarding and classification inside the MPLS network. This additional label can be used to encapsulate layer 2 frames, e.g., Ethernet frames. This solution, called layer 2.5 MPLS or L2 VPN, is very scalable but can be quite complex.

Ethernet service over MPLS can be point-to-point (P2P) or multipoint-to-multipoint (MP2MP):

- The P2P Ethernet service or E-line, also called the pseudowire (PW), is based on a *packet-leased line* concept and can be implemented using the L2 Tunneling Protocol (L2TP).
- The MP2MP Ethernet service (E-LAN) implemented over an MPLS infrastructure is generally referred to as a virtual private LAN service (VPLS).

The Ethernet frame received at the MPLS edge is encapsulated without any modifications. The MPLS label is inserted directly in front of the old destination MAC address, and then a new Ethernet header is added in front of the MPLS label. Two labels are used:

- *Tunnel label.* The tunnel label is used to carry frames across the MPLS network. Core label switch routers (LSR) only look at this label. The tunnel label is removed by the penultimate hop prior to the egress node.
- *Virtual circuit (VC) label.* The virtual circuit label is used by the egress node and determines how to process the frame and where to deliver the frame on the destination network.

### Virtual Private LAN Service (VPLS)

The virtual private LAN service (VPLS) provides a scalable, switched Ethernet LAN over an IP/MPLS network. It uses MPLS layer 2 encapsulation to create an L2VPN. VPLS provides the transport of any type of Ethernet traffic (unicast, broadcast, and multicast) from a source 802.1Q VLAN to a destination 802.1Q VLAN over an MPLS network. VLAN tags are mapped to MPLS label switched paths (LSP). Ethernet over MPLS uses the Label Distribution Protocol (LDP) to dynamically set up and tear down LSPs paths over the MPLS network, which facilitates the implementation of dynamic service provisioning. When MPLS-TP is used, the association between source and destination is established manually and remains fixed during the connection lifetime. VPLS allows us to profit from the implicit service security and availability features of MPLS-TP.

### 14.3.7 Network Architecture

As discussed in the previous sections, substation-to-substation applications require information exchange between fixed peers that are generally adjacent or a small number of links away in terms of telecom network connectivity. They require little or no network routing resilience but tight constraints on time behavior. This pleads in favor of *more physical* – transmission-like – communications architectures providing latency control and implicit security. Service continuity in this case is to be assured through fast and simple preprogrammed switching of end-to-end normal and backup paths.

Network-wide applications, in particular those concerning human operators at undetermined locations and remote processing platforms on the other hand, require flexibility and high-level resilience, as well as a more elaborate security protection, such as access filtering, encryption, authentication, etc. This pleads in favor of *more logical* communications architectures managing topologies and data routing automatically.

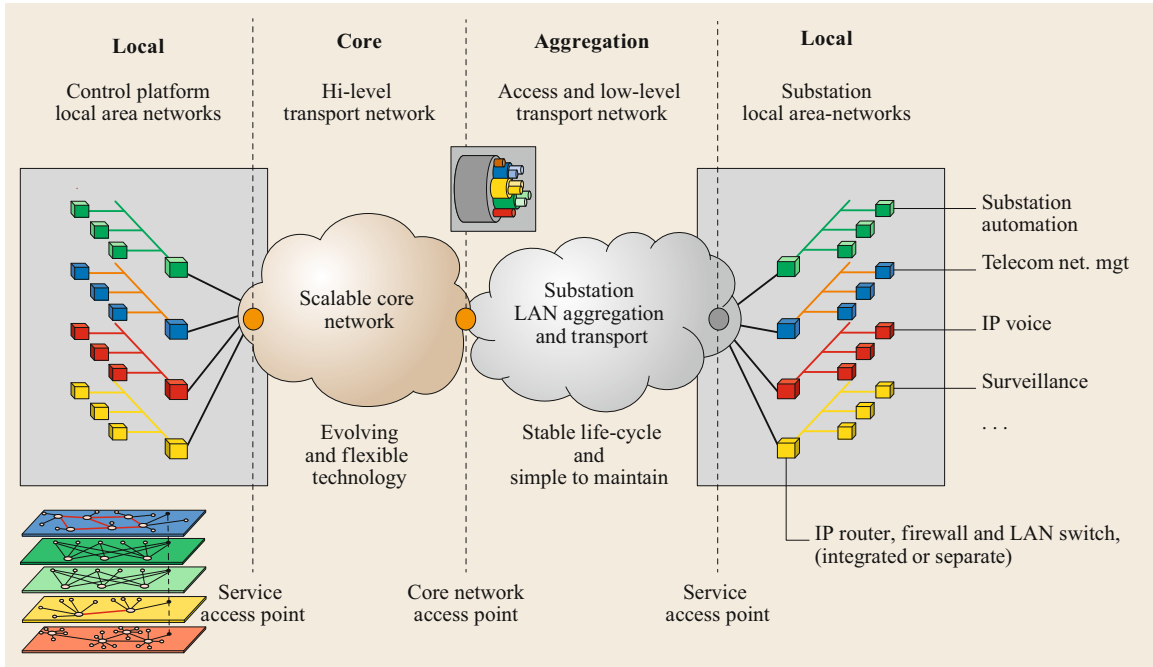
Adopting a hierarchical architecture not only combines these diverging requirements but simplifies network deployment, service migration, trouble-shooting and testing, network extensions and upgrades and future technology migrations.

In comparison to public networks that have three well-differentiated areas, last-mile, access, and core, power utility network architecture has the particularity that final users and network nodes are located at the same sites, substations, power plants, or offices. Consequently, network architecture tends to be simpler. In addition to this, some protection applications require pure transmission services that are almost not related

to the rest of the network. This makes the integration of services over a single technology almost impossible, requiring a multilayered approach that combines several technologies such as fiber optical network, Ethernet, MPLS-TP, etc.

The architecture of the network depends on several factors:

- *Power utility type.* The type of utility is a factor that influences network architecture:
  - Transmission utilities usually have their own fiber infrastructure, so they can implement mission-critical services using their private infrastructure. Furthermore, all their users, out of control centers, are located in substations, so the use of public telecom services are very limited.
  - Generation companies do not have telecom infrastructure and should normally share their operation information with the transmission company and with the system operation authority, so their telecommunications infrastructure is limited to the use of access connections.
  - Distribution companies have a mix of locations, some are in their facilities and some are in the field, or even on the customer's premises. The implementation of operational services requires a mix of technologies and, in most cases, the use of public telecom operators services.
- *Size of the network.* The number of nodes, or sites, is a factor that has a strong influence on the network architecture. Less than 50 nodes does not require a complex architecture, so operational services can be implemented using no more than two different technologies, an optical layer for transmission and transport and a MPLS-TP or plain IP for less time-critical services. For a higher number of nodes, a core network and an access or aggregation network using segmentation techniques must be implemented.
- *Geographical expansion.* The physical distance between nodes is a factor that has an influence in the transmission technology that can be used.
- *Availability of internal communications infrastructure.* The internal communications resources such as fibers, radio links, PLC, etc., will determine the architecture of the network, since their use will be a priority. Sharing these resources with other companies or for IT services is also a factor that must be considered.
- *Internal organization and telecom assets policy.* How IT applications and operational application use telecommunications resources is a key aspect for architecture design, as this will determine the need for virtualization of several services.



**Fig. 14.18** Network architecture with service segregation. (Adapted from [14.1])

Figure 14.18 shows a generic architecture where several services are segregated using different LANs including the core network and the aggregation or access network. Requirements and constraints in the two parts of the network are different, as summarized in Table 14.6.

This approach results in a hierarchical network in which different technologies and different evolution plans can be applied to each part. Moreover, the network may be further partitioned into larger networks, and different technologies may be used in different substation aggregation networks to build a gradual migration plan or to fulfil diverging requirements.

Another concept currently used in power utility telecom network architectures is that of *network overlay*. Network topology is strongly influenced by the power

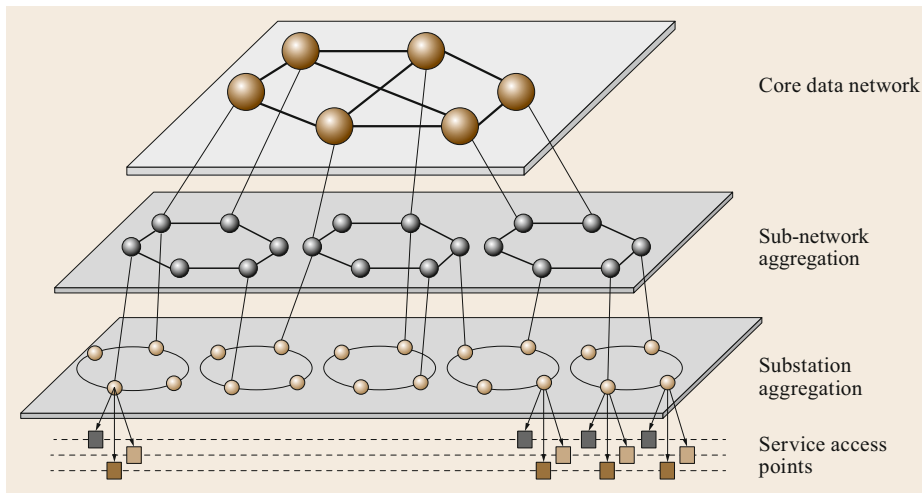
system layout, but this may not be the optimal topology for telecom service deployment. A transmission layer allows us to change the physical topology by establishing circuits between nonadjacent nodes, so switching nodes may work in an optimal topology. In legacy networks, it is rare to find a single user interface or a single transmission technology, but in modern IEC 61850 systems, the trend is to use Ethernet interface only and fiber optics infrastructure due to the high bandwidth demand of modern operational services.

### 14.3.8 Network Design

Network design may be a complex task, depending on the network size and the number and type of services supported. Complex mathematics is involved in net-

**Table 14.6** Substation aggregation/access and core network requirements

Substation aggregation/access network	Core network
Long life-cycle power applications such as protection requires fixed configurations	Frequent upgrades to keep up with release, bandwidth and technology evolution may be required
Must be easy to deploy and easy to maintain, considering large number of sites and the low level of specialized telecom skills of field staff	Can tolerate more complexity considering the relatively smaller number of sites and usage of more specialized telecom staff
Migration is extremely slow due to number of sites and applications. Must coexist with legacy technologies in many sites with gradual service switch-over	Can be quickly deployed on separate fibers or wavelengths and can be used as a support structure for the more gradual deployment of substation networks
Time-critical applications, such as protection, are often confined to the same substation network	Enterprise networks, if transported over the same network, are confined to core network only



**Fig. 14.19** Multi-level hierarchical transport network. (Adapted from [14.1])

work design and, generally, cannot be achieved without the use of appropriate algorithms. Common sense and experience are also a necessary component to achieve a good network design.

Furthermore, green field network design is a very unusual case, since every power utility already has a communications infrastructure, so the most usual case is usually a migration scenario where some of the existing resources are reused. Telecom technologies and services' life-cycles are issues to be considered when designing a network.

Utility operational applications and substation assets have, in general, a much higher service lifetime than telecommunications services. A newly deployed substation application is expected to operate 10–15 years before being replaced. The adopted communications services for such an application are, moreover, expected to be *stable and field-proven* at the time of deployment. The communications solution, service, or technology must, therefore, be sustainable well beyond the expected lifetime of any new generation, mass-market, consumer-oriented service or technology. If a public operator service is employed, the service may disappear before the end-of-life of the power system application. If a dedicated telecom service is used, the interfacing units or equipment may no longer be supported by the manufacturer. Furthermore, the upgrade of communications system software releases or core components, which is a current operation in most communications networks, may be extremely difficult and may require long-term intervention planning, if critical applications such as power-system protection relaying are to be carried over the network.

Similarly, implementing a new communications infrastructure requires the ability to connect many gener-

ations of power-system applications rendering the issue of legacy interfacing essential. A new communications solution must provide a way to serve existing applications, which may coexist with the systems replacing them for a very long time. In order to assure future upgrade and legacy openness, communications solutions and the corresponding service delivery scheme must not depend upon the use of any proprietary interfaces or technologies and must be technology-independent as far as possible.

Network design is a tradeoff between the four main characteristics:

- Requirements
- Cost
- Performance
- Reliability.

The best design is the one that at the lowest cost can achieve the performance and reliability requirements. The starting point is service requirements. This information is used to define application layer and the underneath layers.

Network design implies the definition of every aspect of the network from its topology to links and node capacity, as well as the choice of the algorithms that support the services. Based on the business policy, the company's financial strength, and its competence in communications, an organization must decide whether to operate the services or network itself, or whether total or partial outsourcing is a more desirable option. An organization must also define its external service plan in order to define the interconnection with other networks or service providers. The plan will regulate the relation between the company and the external commu-



communications customers and/or external service providers. The external plan will also define to which degree its services will provide full interoperability across service borders and across network borders. Based on the business objectives that define the overall communications performance required by the company, the design of any network must start with an investigation of existing and potential users to produce a listing of the required services. These services must be quantified and broken down to produce a quality of service (QoS) specification. This specification should be expressed by means of the corresponding QoS parameters, such as availability, capacity profile, accepted error tolerance and delay parameters. A requirement specification based on these parameters will make up the basic specification for the network design.

This specification will include, amongst others, the following information:

- Number of services to be integrated in the network
- Class of service specification
- QoS objectives for every service including availability level
- Traffic profiles of every service
- Budget
- Any existing constraint such as:
  - Topological constraints
  - Reuse of existing equipment
  - Technological limitations, etc.

The choice of service-network technology depends on the type of service to be offered by the network and on the service-integration architecture chosen. Realtime services, such as SCADA, telecontrol, and teleprotection, are fundamental to power-utility operations.

Public networks are often dimensioned according to the statistical data traffic and some rough empirical guidelines to make the most of the transmission resources. These methods work well for networks based on noncritical services. For mission-critical services, the design of the network should guarantee availability and serviceability and should comply with a number of characteristics typically required to achieve mission-critical performance, such as reliability and security. This cannot be achieved with a design based on statistical approximation but with one based on firm guarantee that consider the worst case and incorporate cybersecurity measures at the design phase.

The implementation of a network supporting different services requires carrying out a complete project baseline. Some generic data, as well as some service-specific data must be gathered into complete project requirements.

The following are required for the implementation of a network supporting mission-critical services:

- Make an overview of all data applications needing communications.
- Define what applications/users require communications. Make an overview of what resources are in use and their traffic profiles.
- Define service requirements, considering availability, resiliency, and cybersecurity.
- Find the load during the busiest hour of the day and in the worst case, like alarm avalanche.
- Build a table to show how the traffic flows between the various nodes.
- Estimate the capacity needed for routing information and other administrative traffic.
- Dimension links and node capacity so that the average load over any one period never exceeds 50% of the total capacity.
- For critical applications or large networks, add resources to give sufficient resilience.
- Identify maximum end-to-end delays.
- Assess the additional capacity required for expected future growth.

To dimension networks with mixed services, the following information is required:

- The number of traffic sources
- Individual capacity requirements – both average and peak
- The delay requirements of each service
- Availability requirements of each service
- Capacity of routers and switches
- Capacity of transport links
- Error performance of these links
- Availability requirement of each network component.

Once the design process starts, it may be possible that the design requirements together with the constraints applied to the selected network technology do not result in a possible implementation, so a renegotiation of the requirements must be carried out. After the monitoring process, which verifies the correctness of the actual network implementation, the network-management information gives an indication to evaluate whether the network covers the business expectations. The analysis of this information, together with any change introduced at the business level, is used to decide whether the whole process must be started again.

It is widely accepted that the best choice for the design of a network that integrates several services is an

overlaid solution. This approach makes the design process even more difficult to accomplish, since the best solution is the one that combines different networking and transport technologies to obtain the cheapest solution that fulfils the design goals. Although IEC 61850 reduces the number of technologies and protocols, we cannot forget that legacy technologies must be integrated in the same infrastructure, so the complexity will remain until legacy technology is discontinued. Although there are design tools that could help in this process, there are no accepted rules for the design, as it is a multidimensional problem without a mathematical solution. That is to say, it cannot be proved that a network is an optimum design but it can only be stated that it is better than another one. For this reason, the objective of the network design process is to achieve the objectives set in the network design specification.

The main points to be considered are:

- *Scalability.* A well-designed network should be scalable with the potential to grow with increasing requirements.
- *Open standards.* The entire design and the components that build the network should be based on open standards.
- *Availability.* The application requirements assuredly demand a level of availability and reliability of the network, including QoS.
- *Modularity.* An important concept to adopt is the modular design approach in building a network.
- *Security.* Considering security risks and taking care of them in the design stage of the IP network is essential for complete certitude in the network.
- *Network management.* Implementing network management should be integrated into the design of the network from the beginning.
- *Performance.* There are two key forms of performance measures, throughput requirement and response time, which should be considered for the network.

The most important steps of the design process are:

- The preparation of the design specification documents, which gathers information from service requirements, company policies, as well as site locations and asset availability.
- The topology design that will lead to the definition of the network architecture, which implies the selection of the technology of every one of the layers that will form the model.
- Service integration and mapping.
- The definition of the management architecture including that of the management centers.

- Cybersecurity architecture.
- Routing design and setup as a function of the naming and addressing and the service mapping.
- Traffic engineering techniques and tools to assure the service level specified as a function of the topology network architecture and routing design.
- Finally, once the final network design has been obtained, a simulation of some services or a part of the network may be advisable as a function of the technology, network size, and architecture selected.
- Once the design has been fully validated, the network can be implemented.
- Using network management tools, a report about service performance can be obtained to check the need for a network redesign.

The above-mentioned issues work together to achieve the three key features of a mission-critical service: dependability, performance, and security. Altogether they provide service *trustworthiness*, which measures the degree of assurance that a service will perform as expected.

In this context, dependability quantifies service reliance, which is a function of the following factors:

- *Reliability.* Measure the continuity of the service when needed.
- *Availability.* Measure the time the service performs according to requirements.
- *Maintainability.* Measure the capability of maintaining the service during maintenance operations.
- *Integrity.* Measure that the service provides information that has not been altered.

Network design processes should be carried out considering these features.

The design of a network that supports operational services using packet technology requires an accurate evaluation of the latency. End-to-end network delay is composed of:

- *Packetization delay (PD).* This is time delay introduced by buffering of data before transmitting them as Ethernet packets. The more data we pack into an Ethernet frame, the higher the PD will be, but the higher the bandwidth efficiency will also be. On the other hand, we can pack very little protection data into each Ethernet frame so that it can be expedited faster, but in this case, the remaining capacity of the Ethernet frame is wasted and, therefore, a lot of Ethernet bandwidth is required for each communications service.
- *Network delay (ND).* This is the time taken for a packet to cross the network. ND is composed of

signal propagation time ( $5 \mu\text{s}/\text{km}$ ) and intermediate node processing, which includes switching and buffering. When the bit rate of the links is much higher than the traffic delivered by a user, it can be assumed that intermediate nodes operate at much faster rates with reduced buffering and processing times. Buffering delay or queuing delay are normally estimated using stochastic methods that consider traffic profile, queue length, and packet size. Realtime mission-critical services cannot use this statistical approach, since the service should guarantee the performance even in the worst case. Network capacity must be dimensioned to guarantee end-to-end delay in the worst case. Queues in the network nodes must be dimensioned to assure that packet loss probability is lower than required.

- *Jitter buffer delay (JBD)*. JBD is the absolute delay generated by dejittering, that is to say, absorbing delay variations of the network through a buffer. The size of the buffer (in packets) depends upon the amplitude of delay variation that must be absorbed. Needless to say, the larger the buffer, the more it introduces absolute delay. This buffer is used only for circuit-emulation services.

For delay-critical services delivered over IP, pre-established static routes are preferred to ensure end-to-end performance.

Migration and integration of legacy technologies in a new network design is a challenge that may introduce a number of difficulties and even some design limitations. The most relevant aspects that may impact the behavior of mission-critical realtime services are given below:

- *TDM to packet network*. The migration from conventional TDM networks towards Ethernet and IP increases the network's bandwidth efficiency considerably due to statistical multiplexing, flexibility, and resilience. However, it can also be a major source of concern for the control of time behavior. Assembling data packets before transmission and store-and-forward of the packet at each intermediate node causes additional buffering delay, which increases with the packet size and with the number of queues. Dynamic data routing gives rise to delay variation and lack of time predictability. These extra delays are not present in TDM networks, so they should be considered to limit the number of hops and allocate the required bandwidth to control the maximum path latency.
- *Multiservice integration*. Bandwidth efficiency in packet networks is achieved through integrating multiple traffic streams into the same packet net-

work. Queuing scheduling mechanisms are often employed to assure a bounded delay for more critical services. It is important to implement reliable service-segmentation mechanisms to isolate traffic flow and prevent service interference. This issue is sometimes masked through overdimensioning of the network an *order of magnitude*, which reduces the interference effect to a negligible level.

- *Network resilience versus fixed routing*. Network resilience ensures the continuity of service in the presence of network faults, but at the same time, renders indeterminate the routing of communications. Time predictability is generally sacrificed for improved resilience. Traffic streams that are sensitive to delay variations must generally be treated separately with fixed routing.
- *L1/L2/L3 partitioning and topological structuring*. In order to provide adequate time performance to critical services while maintaining bandwidth efficiency, flexibility, cost, and resilience, it is necessary to design the network with an adequate level of *information forwarding* at physical, link, and network layers.
  - Direct transmission connections for best time performance but at low bandwidth efficiency (except for services requiring continuous data flows like SV), flexibility, and resilience.
  - Ethernet switching with virtual networking (VLAN) and priority assignment for fast transfer of information packets.
  - IP routing for maximum resilience and multiservicing.

This way, different network topologies can be obtained for different services over the same telecom infrastructure, leading to different numbers of intermediate nodes at each layer.

### 14.3.9 Network Management

Operational information exchange in power utilities is undergoing tremendous growth, which is leading to an ever more complex and extensive communications network, as described in the previous sections. The corresponding operation and maintenance demand specific processes and tools well beyond the ad-hoc management previously employed in most cases. The new operational communications network also employs a new range of technologies, which, moreover, are evolving much faster than before, and hence, require a great diversity of skills; the field worker can no longer be considered as autonomous and increasingly needs to be supported remotely by a wide range of technology experts. These experts can be located in one central facility or increas-

ingly dispersed across the wide footprint of the communications network. They can be in-house or part of an external contractor or vendor organization. Processes and tools need to be adjusted accordingly. The adopted processes, tools, and field communications systems also depend on the organizational aspects of the power company: fusion or separation of operational and corporate enterprise services, of IT and telecom systems, and of local and wide area communications, as well as the adoption of in-house or contracted operation and maintenance services with specific security issues in the latter case.

To provide a better understanding of the operation and maintenance process for telecom networks and services in power utilities, we will analyze the most relevant points:

*Assessment of service provisioning.* Power utilities in the new liberalized market are constantly in quest for cost reduction. Reliability of operational communications services and their cost of achievement are increasing challenged by alternative service-provisioning modes. It is essential to have an O&M process and associated key performance indicators (KPI) to meet operational service imperatives:

- For fair assessment of alternatives (in-house/external)
- For determination of the market's capability to deliver appropriate O&M services
- For consequent partitioning and interfacing of in-house and external service provision.

These processes contribute to network redesign and optimization.

*Increased scope and change of scale.* New power-system applications are bringing a great number of new communications service requirements in substations and across the grid. These applications range from the control and maintenance of the distribution grid, the integration of renewables, and outage prevention, as well as grid stability control and new system protection schemes. This explosion of communications-based intelligent applications is changing the scope and scale of O&M activities. It is also accompanied by the introduction of new communications technologies and the evolution of the telecom networks necessitating multiple skills and tools to maintain the system.

*New rules.* Another major on-going change concerns external regulating authorities and legislation on efficiency of network operation. The power utility is expected to keep its infrastructure in good operating condition and its operational expenditure, including that related to O&M, needs to be precisely determined and justified in order to be able to reflect it in the price of the electrical power delivered. Moreover, the increased

weight of the electrical power utility as a critical national infrastructure, due to the increasing dependence upon power supply, increasingly results in sanctions and penalties for delivery failure. This, in turn, increases the importance of communications reliability and, consequently, the promptness of the O&M.

*New actors and players.* From an incumbent model of vertical power utility, where all components of the power production and delivery were part of a same company (and, therefore, all related communications were internal), the power industry is moving to a partitioned scheme leading to the multiplication of partners requiring exchange of information and consequent multiplicity of technical issues and solutions. The O&M process must now cover such issues as cybersecurity and protocol compatibility for external communications.

*New workforce constraints.* In-house capability of electrical power utilities is shrinking due to an aging workforce, downsizing policies and economic constraints of organization, multiplicity of technologies, and technical issues due to the fact that legacy technologies persist, while new ones are introduced into the network, and the difficulty to attract and maintain appropriate skills. The multiplication of technical issues and solutions, the fast rate of change of technologies, and the fast turnover of technical teams both in-house and outsourced, is leading to a reduced grasp of the network and its potential problems. It is increasingly important to have a formal and specified manner to operate and maintain the network.

*New tools and process automation.* Mainstream telecom and the IT world is proposing a wide range of tools to the utility telecom networks for automating the processes of network and service management. These tools are designed and optimized for public service providers and enterprise networks. Rather than modifying O&M processes according to market tool capabilities, an assessment of O&M practice in the operational context and its required evolution allows the implementation of more suitable and cost-effective tools according to operational requirements.

*O&M cost.* The growing complexity of telecom networks is increasing the cost of the O&M process, and tools are becoming a relevant cost factor in the full life-cycle cost of the system. Proper modeling and implementation of O&M service allows cost optimization.

The above-mentioned issues show the relevance of O&M functionality. In fact, O&M must be considered, planned, and implemented as another service of the telecom network. A network supporting mission-critical services cannot guarantee performance without a well-planned and implemented O&M service. The rest of this section will describe the minimum infrastructure required to implement an O&M service.

### Management Architecture

The management services are organized into a four-layer hierarchical architecture by the ITU-T, as described hereafter. Even if the four-layer – business, service, network, and element – management-layer model (BSNE-ML) has been devised for telecommunications network management services, the conceptual model can be adopted for other information related infrastructure management in the power-utility environment.

*Element management layer (EML).* This layer implements the management of individual equipment. It covers the different tasks related to the maintenance, administration, logging of usage, and statistics of the events recorded from this equipment.

*Network management layer (NML).* This layer implements the management of a group of interconnected equipment performing a particular task. It can be assimilated to system management with end-to-end overall functional and performance requirements. The task of this management layer is, therefore, to interact with each component of the system, whether aggregated together or geographically dispersed, in order to control and coordinate their operation for the proper functioning of the system, to assess the utilization of the system by authorized users and to reconfigure it if necessary in order to fulfil the system's requirements.

*Service management layer (SML).* This layer manages a service delivered to a group of users, e.g., switched voice service or SCADA service, through the monitoring of one or many different systems or networks. It manages the interfacing between the service users and service providers through personalized service availability indications, the measurement of the quality of service, the monitoring of service level agreements taking necessary measures in order to meet the pre-established SLA, and the billing of the services.

*Business management layer (BML).* This layer manages business aspects, which may comprise multiple services, e.g., operational communications, third-party communications, corporate IT infrastructure, or control center facilities, with overall management and/or enterprise responsibility. Business-oriented statistics for system and human resource planning and budgeting, and for the elaboration of executive master plans are typically at this layer.

In a similar manner to the four-layer BSNE management service architecture, the model for management functions to be performed was derived from the world of telecommunications and adapted to the requirements of the power utility's information infrastructure management. The fault, configuration, accounting, performance, and security model (FCAPS) covers the different functions that may have to be implemented for information infrastructure management:

- *Fault management (FM):*
  - Alarm collection and processing
  - Fault-event indication to users
  - Trouble ticketing
  - Maintenance organization and fault escalation
- *Configuration management (CM):*
  - Addition, suppression, and modification of equipment, systems, and channels
  - Provisioning and configuration of new services
- *Accounting management (AM):*
  - Ticketing and billing for the utilization of equipment, systems, network, or services by different categories of internal and external users
- *Performance management (PM):*
  - Monitoring of performance parameters for each service, system, or equipment
  - Statistics and trends for planning purposes and proactive measures
- *Security management (SM):*
  - Access control to facilities, services, devices, etc.

A nonexhaustive list of management functions organized according to the service architecture described is presented in Table 14.7.

Since the implementation of O&M services requires a system view, a management center is required to gather and process network and element information. The network management center (NMC) constitutes the core entity for day-to-day operation, administration, maintenance, and security monitoring of the network, medium-term extension and enhancement planning, as well as an advisory entity for long-term and strategic decision-making through a synthetic and statistical view of the information network, systems, and services.

The technological evolution has widened the scope of the network beyond the limits of telecommunications equipment. The information exchange system includes all communicating entities from the substation IED to the different management platforms of the power utility (power-network management, energy management, enterprise applications, etc.). A more general concept of integrated management information can, therefore, become attractive. In this case, the NMC need not be a single geographical entity but a distributed platform serving the different functional layers of the infrastructure and the different functions in the utility organization.

The following tasks are to be performed through the NMC:

- Control, operate, and manage in a unified manner all elements constituting the telecommunications network including auxiliary systems.

**Table 14.7** Management functions

	<b>Fault</b>	<b>Configuration</b>	<b>Accounting</b>	<b>Performance</b>	<b>Security</b>
Element	Maintenance, supervision, spare management	Parameter setting and recording of equipment, change management	Monitoring of equipment usage	Equipment perf. monitoring, condition monitoring, preventive maintenance	Equipment access monitoring, password management
Network (system)	Network management, end-to-end system analysis,	Group configuration of multiple elements constituting a system/network	Billing of the usage of a system or a network	Network or system performance monitoring, QoS monitoring	System and site-access monitoring
Service	Service availability, QoS monitoring, service impact analysis	Service provisioning, configuration of new services into the network	Billing of voice and data processing, storage and exchange services	Service monitoring	Operational and corporate IT platform security management
Business	Fault statistics, OPEX estimation, SLA monitoring	–	Utility-wide internal IT service billing	Service contract management, SLA monitoring,	Utility-level security engineering

- Supervise, locate, and isolate faults in the system through monitoring of the different elements in a permanent manner (24 h/7 d).
- Supervise IT platforms (servers, workstations, LAN components, etc.) associated with the operation of the system.
- Track all fault management tasks through to conclusion, including restoration of services, replacement of faulty units, return of faulty units to the manufacturer, and restoration of spares to the required level.
- Assign maintenance and problem-solving to appropriate staff, who may be geographically remote and dispersed, or even to an external contractor.
- Supervise network, system, and data security against cyber-attacks, intrusions, and viruses.
- Monitor the performance of the different elements through the measurement of traffic, loss rates, service times, and overall delays in the system. In particular, switching networks and IP infrastructure must be monitored.
- Determine the service impact of infrastructure faults and take appropriate action.
- Produce business-oriented dashboards and management reports with dedicated synthetic information for maintenance management, overall system management, network engineering and planning, cybersecurity management, power-system communications management, and dedicated service-provider business management.
- Perform asset management and inventory activities for the whole system and produce up-to-date network documentation available online to all parties concerned.
- Perform network and system documentation including physical and logical resource management. The documentation must include enough information to identify:
  - Channels multiplexed over a certain higher-level container, through certain equipment or over a certain communications medium.
  - Processes using a particular processing resource.
  - Services carried over a certain network resource.
  - Users affected by the failure of a particular resource.
- Perform directory services, IP address management, priority management, and user inventory functions in general.
- Perform service-oriented and business-oriented management tasks for both internal (the utility) and external customers. In particular, provide customer relationship management (CRM), including service usage monitoring, billing, and service notification for each customer and each category of service, as well as service-level agreement (SLA) monitoring for each customer contract.

### 14.3.10 Business Continuity Management

An extraordinary situation or disaster occurs when the nature of an incident is such that it actually interferes with or poses a significant risk to the operation of the power system and affects critical business objectives. Business continuity management (BCM) provides the availability of processes and resources in order to ensure the continued achievement of the critical objectives.

The telecom infrastructure and service must, therefore, be implemented to:

1. Tolerate the loss of infrastructure in a node, in a link or in a region
2. Tolerate the loss of mains power supply for a relatively long duration
3. Redirect all substation communications (SCADA and voice) to a backup control center when required

(e.g., in the case of destruction or major damage of the control center)

4. Include fast deployment communications systems (e.g., radios, satellites) to implement temporary communications links and networks to replace the damaged or nonoperating facilities or to constitute temporary relays for the EPU's restoration staff
5. Provide specific information exchange facilities for disaster warning, staff coordination, and recovery team communications.

It is important to distinguish between faults and disasters. Operational services should be *fault-tolerant*, which implies that the service is maintained without any degradation of its performance in the event of a fail of a single component, e.g., one link, one node, etc. In the event of a disaster with massive failures, some services may be discontinued and others maintained with a reduced performance, which should be enough to support recovery system operations.

Disaster recovery is not a concept specific to telecommunications but a general plan covering all aspects of the power utility. As such, if telecom assets, infrastructure, and staff are located within the perimeter of utility's premises, then they are integrated into the utility's disaster recovery and business continuity plan (DR/BCP). However, if telecommunications services are provided by a different entity, with staff and assets at other sites, then the coherence of the telecom service provider's DR/BCP with that of the utility must be assured and periodically audited. In the former case, DR/BCP is a very important input for telecommunications network design and must be considered during the entire network life-cycle to verify its feasibility and avoid common mode failures.

Business continuity planning (BCP) is based on:

- Maintaining, resuming, and minimizing the impact of a disaster and recovering the business. It is more than a recovery of the technology.
- It is based on business impact assessment (BI) and risk assessment.
- Regular validation testing.

The disaster recovery plans are generally written to the base of the recovery after a major event: the loss of a plant through fire or flood or the loss of computer or telecommunications systems across the enterprise.

The goal of BCM is to minimize the effects of a disaster with preventive actions. It seeks to establish a culture within organizations to generate greater resilience to ensure continuity of service delivery. The BCM process is defined on different levels within the organization:

- *Strategic level.* Policies, scope, and preconditions are defined here. The process is formalized, and its organization is agreed upon. Responsibility and ownership of BCM is part of this level.
- *Tactical level.* The decisions taken at the strategic level are the framework for the structure of BCM.

Tactical level responsibilities include risk assessments process and the definition of requirements and guidelines. The operational level is responsible for the implementation of predefined tactical actions in order to assure the agreed-upon service levels.

### Evaluating Threats to Critical Activities

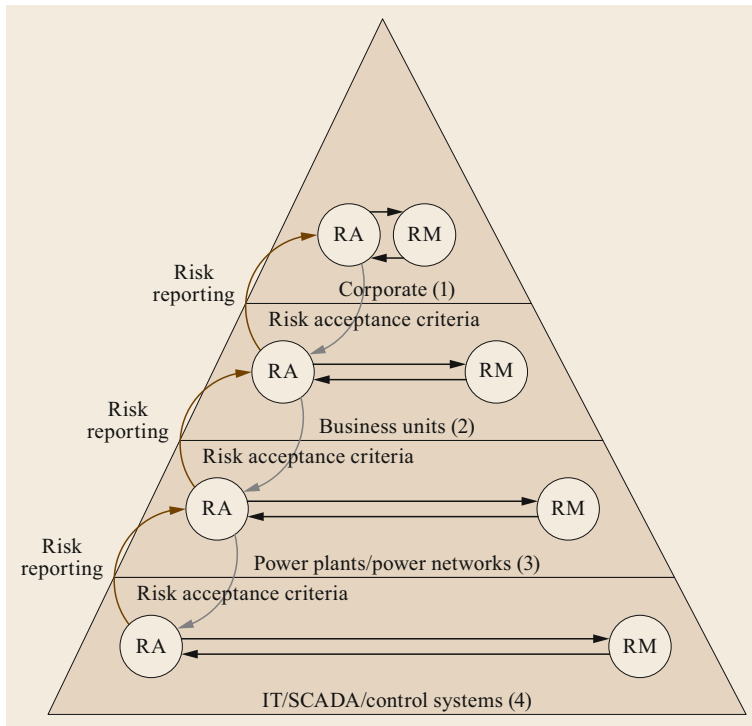
Telecommunications services can be negatively affected by many different threats of different origins, whether natural or intentional acts. Recovery mechanisms must be defined in order to cope with these threats and minimize their impact on the overall service performance. The definition of a recovery procedure requires a risk assessment to be carried out to determine the source of threats and their impact on operational service performance. In fact, this risk assessment study should be part of a company risk assessment process in order to correlate the risk of ICT infrastructure with company operations.

The risk assessment process relies on two inputs, the estimated likelihood of every type of threat and internal vulnerability assessment. The result is a matrix that provides information about the likelihood of a risk and its impact compared with the cost of mitigating it. The company should make a decision about the level of risk that can be accepted, so this will determine the measures to be taken to overcome and minimize the effect of those threats.

Threats faced by a utility can be disasters, failures, or other disruptive events; the most common are included in the following list:

- Natural disasters like floods, earthquakes, rainstorms, typhoon, snowstorm, landslides etc.
- Fire
- Power failure
- Terrorist attacks
- Organized or deliberate disruptions
- Theft
- Major system and/or equipment failures
- Human error
- Cyberattacks or computer viruses
- Legal issues
- Worker strikes.

One important outcome of risk evaluation is the correlation between generic company risks and their effect



**Fig. 14.20** Risk management and risk assessment model. (Adapted from [14.4])

on telecommunications infrastructure. In order to thoroughly analyze every risk and make the right decision in terms of risks accepted and cost of mitigating other risks, a risk management framework has to be used as shown in Fig. 14.20. Layering risk assessment and management process is very important to include every aspect and detail of different functions and technologies included in the company.

The four layers in Fig. 14.20 show the hierarchical levels of the operation's part of a typical power utility. Every level of the organization or layer must carry out its own risk assessment process, inform the upper level, and manage its risks according to the directives set by the upper level. These risk-management objectives are related to the risk-management policy of the company. Each level of the organization has a different set of objectives, as it is exposed to different sets of risks. Nevertheless, it is important to take into account that there are also risk dependencies between levels, so in order to determine global company risk exposure, these dependencies should be considered. On the other hand, these dependencies influence risk assessment and management of a particular layer, since dependencies with other layers must be taken into account. Due to these dependencies, a common framework and language must be used for the identification and management of risks.

The business continuity plans of power utilities should consider the effect of the disruption of critical activities due to external or internal threats. To carry out

this analysis it is important to consider the resources required to support these critical activities and, thus, consider specific threats and their particular vulnerabilities in order to achieve a comprehensive risk assessment. The risk-assessment method chosen depends on the organization, and it is important that the approach is adequate to meet the organization's needs and its own context, also politically, in terms of legislation and geographical location, considering specific risk factors such as flooding, earthquakes, etc. It is important to consider that a BCP must be managed and maintained. The use of new technologies requires a detailed risk analysis and may require the reformulation of the BCP. Some of the more relevant aspects of business continuity management for a power utility are the following:

- Risk and vulnerability analysis. Risk assessment must be updated regularly to identify new vulnerabilities introduced by changes in the implementation of services and system reconfiguration.
- Business impact analysis.
- Response strategies.
- Planning documentation and maintenance.
- Staff training and awareness.

BCP should consider technology failure modes, common failure modes of different systems using the same technology, as well as the risks introduced by cybersecurity attacks, which may have a much higher impact than a natural disaster.



## 14.4 Cybersecurity

Information security is a very important issue affecting the entire information and communications system. It is treated as a full end-to-end process through an appropriate security policy identifying security domains, taking measures to mitigate risks, and devising periodic audit schemes to assess the effectiveness. The scope of information security must cover the system specification phase to the dismantling phase.

### 14.4.1 Basic Principles

This section focuses on the influence of cybersecurity on operational services and its related information. A cybersecurity attack has a direct impact on service reliability or, in a more generic way, on the reliability of the operational system.

The design of a mission-critical operational system is implemented with an architecture and redundancy to be tolerant to a single failure. Up to now, the effect of a cybersecurity attack was not considered in the evaluation of system availability, but this kind of attack may have a much wider influence than device faults. Some types of attacks can affect the reliability of an operation without a total breakdown of the system. Consequently, cybersecurity is becoming a capital aspect of operational system design. Large efforts have been made by the international community to develop standards and recommendations to better protect operational systems.

One aspect that cannot be denied when analyzing the cybersecurity of operational services is its specificities and the big differences that can be identified in comparison with that of information technology systems. Table 14.8 shows the most relevant differences.

In addition to these differences, there are other differences to consider:

- *Architecture.* SAS architecture is rather different from office or data center architecture. In an office, there is a limited number of servers and a large number of hosts working as clients, whereas in a SAS, every IED is a server, and there is only one client, the SAS controller. Furthermore, in an SAS, con-

figuration is static, so there are no DHCP or DNS servers but in an office configuration it is dynamic.

- *Source of attacks.* Office protection from cyberattacks is designed to prevent attacks from outside the LAN. Nevertheless, attacks to a SAS LAN coming from outside the substation are extremely unlikely, as there the connection comes from the control center, which is the most secure domain in a power utility. Attacks to SAS may come from inside the LAN because of uncontrolled or unauthorized work and from remote access. In fact, remote access is the most critical connection from the point of view of cybersecurity. Its protection must be thoroughly analyzed to achieve the required protection level.
- *Types of attacks.* Hosts used in office environment are prone to suffer from virus and malware attacks, whereas IEDs are much less susceptible to these types of attacks. IEDs may suffer other attacks, such as denial-of-service, unauthorized access to gain control of a function or change settings that may produce considerable damage.
- *Configuration principles.* Due to the above-mentioned issues, security configuration must be implemented in a rather specific way in order to protect from internal attacks and from specific attacks that affect the availability and reliability of the SAS. These principles are described by the IEC 62351 family of standards.

Attacks to operational systems or functions are not focused on copying or stealing information but on blocking or gaining control of operational functions, such as control to operated breakers or generators and protection to disconnect loads.

For an attack to be successful, it has to exploit a vulnerability of one or several IEDs. Vulnerabilities may be brought about by several reasons:

- *Poor software quality.* Errors and weakness in operating system and applications.
- *Legacy devices.* Legacy devices have well-known vulnerabilities that cannot be avoided, since these

**Table 14.8** IT versus OT differences

Topic	Information technology	Operational systems
Basic goal	Information	Maximize process availability
Primary risk impact	Access to information	Availability of operation
Security focus	Centralized. Security of servers, Internet access	Decentralized. Security of P&C functions. Minimize Internet access
Availability	95–99%	99.9–99.999%
Patch management	Regular updated. Service disruption	Selective updates. Minimize service disruptions
Mode of operation	Interactive, transactional	Interactive, real time, event driven
Reliability	Depends on staff	Depends on system design and IEDs

devices cannot be updated due to lack of software support from the vendor.

- *Configuration mistakes.* Incomplete configurations may let backdoors be opened or disable protection mechanisms, thus facilitating attacks.
- *Password management.* Changing default passwords, using nonstandard ones, and managing them properly helps to protect from *dictionary* attacks that may gain control of IEDs.
- *Documentation.* Incomplete or errored documentation may lead to operation and maintenance mistakes that are considered as nonmalicious internal attacks.

In the above list, we can notice that technology is not the only factor that determines the degree of protection. In fact, cybersecurity depends on the balance of three major factors:

1. *Technology.* Cybersecurity aspects related to technology involve not only the equipment required to protect operational systems, such as firewalls, but also the proper configuration of every IED. Configuration plays a capital role in achieving a good protection level.
2. *Procedures.* An organization must be aware of cybersecurity risks and, consequently, cybersecurity measures should be included in every operational procedure. Furthermore, specific procedures for cybersecurity management, like passwords, access rights, or certificate management, must be defined.
3. *Human resources.* Company staff need to be trained on cybersecurity. Responsibilities related to cybersecurity must be clearly stated. Security policy and procedures must be known and used by the staff.

To protect an operational system in a cost-effective way it is necessary to carry out a vulnerability assessment analysis. Knowing the vulnerabilities is the starting point of safe system design. Not all the vulnerabilities may be exploited if a corresponding vector attack cannot be used in the operational environment. For instance, if a vulnerability can only be exploited using an email, and this service is not available in our SAS, there is no risk associated with this particular vulnerability.

The following step is to determine the risk introduced by every vulnerability. The risk level is a function of the likelihood of an attack able to exploit this vulnerability. The impact of a successful attack on the availability of the system and on business operation should also be considered. Once risks have been identified and quantified in terms of probability, we produce a risk matrix that will help us to determine how cyber-protection is to be implemented and configured in order to reduce

the probability of a successful attack and assure that its impact on the system will not reduce system availability and reliability below performance objectives.

## 14.4.2 International Standards

There is a large number of standards related to cybersecurity. We will focus on international standards developed for the protection of operational systems. Figure 14.21 shows a hierarchy of cybersecurity standards. The most generic family of standards is the ISO/IEC 27000 series that deals with the implementation and management of cybersecurity in a company. This standard should be applied in any type of organization and has no specific requirements for operational systems.

*IEC 62433* is a series of standards that deals with the cybersecurity aspects of industrial automation and control systems, including power-utility automation systems. It comprises a total of 13 volumes that are grouped into four parts:

- *General part.* This includes generic concepts, conformance metrics and product development requirements.
- *Policies and procedures.* This comprises security management considerations, implementation guide, patch management, and security requirements for service providers.
- *System aspects.* This includes security technologies, risk assessment, and system security requirements.
- *Components.* This includes product development, life-cycle requirements, and security requirements for components.

This standard provides an overview of cybersecurity in the context of operational applications. The role of the three main factors required to build a secure system (procedures, persons, and technology) are presented. Their associated functions along the system life-cycle are developed.

The security domain and the zone design are also relevant contributions of this standard. In this context,

IEC 27000	• Cybersecurity management system
IEC 62443	• Cybersecurity of industrial control systems
IEC 62351	• Cybersecurity of operational systems and control centers
IETF	• Internet standards

Fig. 14.21 International standards

a security domain is a set of devices and applications that share the same security policy. Domains are divided into security zones. A security zone gathers elements that implement one or several functions and are protected by a set of cybersecurity measures that guarantee information confidentiality. In the context of operational systems, security zones are associated with SCADA or SAS functions.

A security zone is defined by:

- Scope: number and location of devices
- Associated risks due to vulnerabilities and threats
- Functions inside the zone
- Access-control methods and rights
- Technologies allowed to implement the zone.

Zones interchange information using *conduits*. A conduit is a communications channel protected by a set of cybersecurity measures. Conduits are treated in a similar way to security zones. Vulnerabilities are associated with telecommunications technologies, and it is usual to forbid some technologies, depending on the type and criticality of the information carried by this conduit. For the technologies allowed, protection measures should be specified, it can range from segmentation using tunnels to encryption.

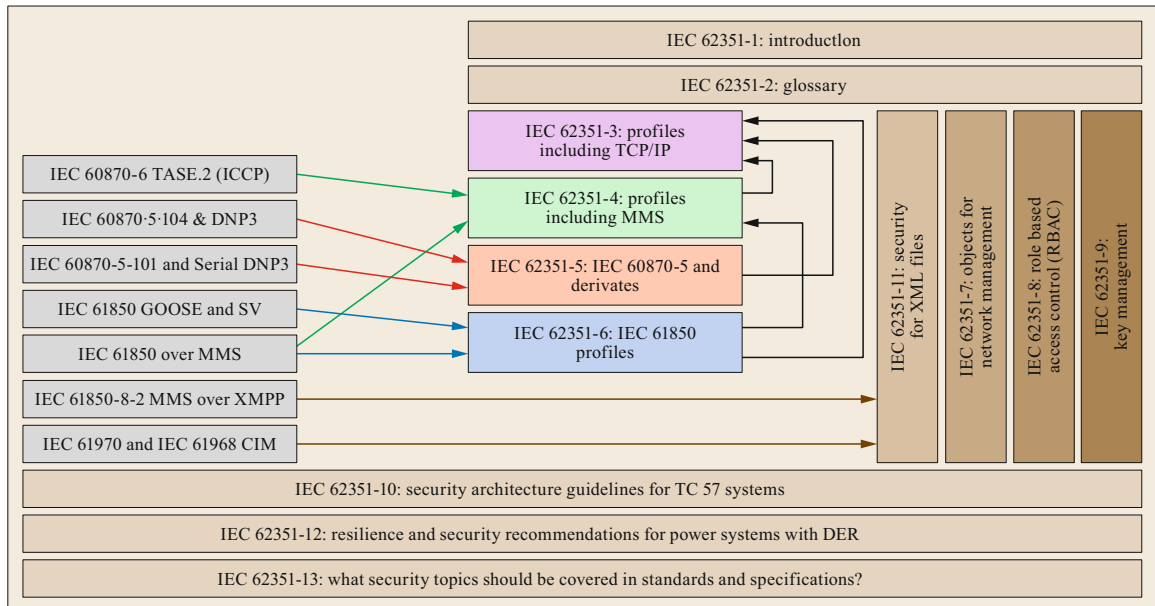
*IEC 62351* is a series of standards focusing on the protection of the SCADA domain. This family of standards provides a clear and simple way of protecting the SCADA infrastructure against almost any type of attack.

The advantage of IEC 62351 is the use of existing resources to implement cybersecurity protection measures. The standard focuses on the key security measures:

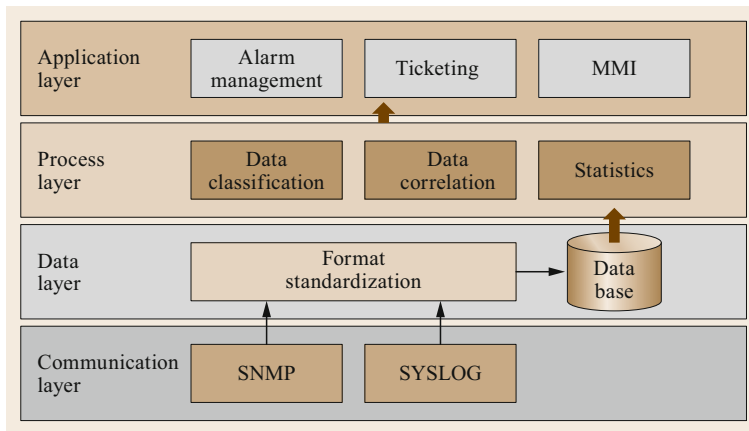
- *Authentication*. This is the most important cybersecurity function. There is no security without authentication. It is required to verify a user's identity and prevent nonauthorized access.
- *Confidentiality*. This has to be used when the communications channel is not reliable to prevent eavesdropping, listening, media playback, etc.
- *Auditing*. It is very important to detect security anomalies and to prevent denial of action or false claim of action.

These functions are implemented using Internet standards or recommendations. Internet standards are prepared by the Internet engineering task force (IETF) that produces a *request for comments* (RFC), which is a document that specifies protocols, formats, and methods to be used to implement services over the Internet; RFCs may become Internet standards, but even in this early stage, they are being used by other standardization bodies.

As mentioned before, access control and use control are the most important cybersecurity functions. IEC 62351 has standardized the role-based access-control (RBAC) method to implement this functionality. IEC 61850 has also adopted this method, which is now



**Fig. 14.22** IEC 62351 architecture. (Adapted from IEC 62351-1)



**Fig. 14.23** Cybersecurity control-center architecture

mandatory for this technology and will become the most common access control method for power-utility operational functions in the near future.

When a person or an entity wants to use a service protected by RBAC, it needs to specify its identity and the role it wants to play in its interaction with the service. This provides a higher level of protection, as the user needs to have a valid identification, and the assigned role limits the possible actions that the user can do within the system. Identity, roles, and properties of RBAC can be expressed using the XACML language that generates XML security configuration files, the format of which is defined with an XML schema.

### 14.4.3 Cybersecurity Control Center

Operational systems can suffer sophisticated attacks that are not addressed to a single IED or function but to a large number of them. These types of attack aim to destroying assets or produce a blackout. These distributed and sophisticated attacks cannot be detected or prevented from a single point of the network. A global view is necessary to detect a collection of anomalies,

which, once correlated, can identify these types of advanced attacks. This dispersed information must be gathered in a cybersecurity control center to be able to process it and produce indications and alarms.

Figure 14.23 shows an example of the functional architecture of such a type of control center.

Information is gathered using standard protocols, such as the Simple Network Management Protocol (SNMP) or syslog. This information is converted to a standard format and stored in a database for later processing. The process layer is where intelligence is implemented to detect sophisticated attacks and produce statistics and reports for auditing purposes. Finally, some applications present the information to the user and generate alarms and working orders.

The cybersecurity control center is a very important component to support active security auditing, which is a key component of a secure system.

Depending on the number of devices connected in the operational network, the size of the cybersecurity control center may range from a single host to an architecture made of several servers that may be physical or virtualized.

## 14.5 Smart Grid

The smart grid is the evolution of the traditional power system based on a hierarchy of bulk generation power transmissions and distributions. This new architecture uses advanced ICT technologies to connect dispersed generators and consumers in an optimal way to obtain economic efficiency.

The most relevant objectives of a smart grid are:

- To support new business models to promote the presence of active users to make the most of electricity.
- To facilitate the use of renewable energies, improving energy efficiency.

- To provide the required level of resilience complying with the established reliability objectives.
- To facilitate the integration of legacy technologies and the migration of existing systems.
- To ensure interoperability to support multivendor solutions.
- To use scalable and modular technologies able to cope with the much higher volume of information and able to adapt to technology evolution.

The smart grid is a very good example of a totally distributed grid, whose working principle is based on ICT.

Consequently, this section is focused on ICT-specific aspects of a smart grid, since this is the key component to implement the *smart* part of the grid.

There are three key factors to implementing a reliable smart grid:

1. *Telecommunications infrastructure.* The deployment of a private telecom infrastructure is not economically feasible, so public telecom services need to be used together with already existing private infrastructure. The fact that public services do not comply with mission-critical services requirements, introduces a drawback that can only be solved by re-designing critical applications and accepting some limitation in the reliability of those critical services.
2. *Applications.* New applications are required to support new operational decentralized principles, for protection, control, and other new functions such as demand response, etc. A large number of new applications is planned and will be gradually deployed to allow the interaction of the power company with dispersed energy consumers, producers, and storage facilities. These applications comprise smart metering at the energy customer's point of delivery, but also the control of electrical loads and distributed power generators, public facilities, such as electrical vehicle chargers and public lighting, as well as industrial and commercial/residential microgrids. This mix of revenue management and operational information exchange is still under research.
3. *Cybersecurity.* Smart grid cybersecurity has to face very important challenges that will require a thorough study starting from the specification phase. The key aspects are:
  - The use of public unreliable communications channels, such as wireless links, channels provided by public telecom operators, and the Internet.
  - The need to protect critical assets located at public sites and, therefore, without physical protection.
  - Extremely large and distributed infrastructure with a large number of different types of IEDs.
  - Public services that imply the interaction of customers with some devices and services using the Internet or directly connected to some IED.

Figure 14.24 shows the smart-grid architecture as defined by [14.5].

Two important aspects must be noted: the model covers all the actors involved in a smart grid distributed into domains and zones. The second and most important aspect is the definition of interoperability at every one of the layers. At the component, the communications and

information layer is achieved by using IEC 61850 standards, and the upper layer is defined by the smart-grid user interface specified by the standard IEC 62939-1.

There are three technologies required to implement a smart grid: the common information model for the implementation of control centers, IEC 61850 for substations, generating plants and field devices, including distributed-energy resources (DER) and the IEC 62351 to provide cybersecurity protection to the whole system. As has already been mentioned, these technologies used Ethernet as the physical access interface and IP as the network protocol.

The design of a smart grid should consider most of the issues already developed in the previous sections. The reader is referred to Sect. 14.3 for topics related to telecommunications network design, IEC 61850 and cybersecurity.

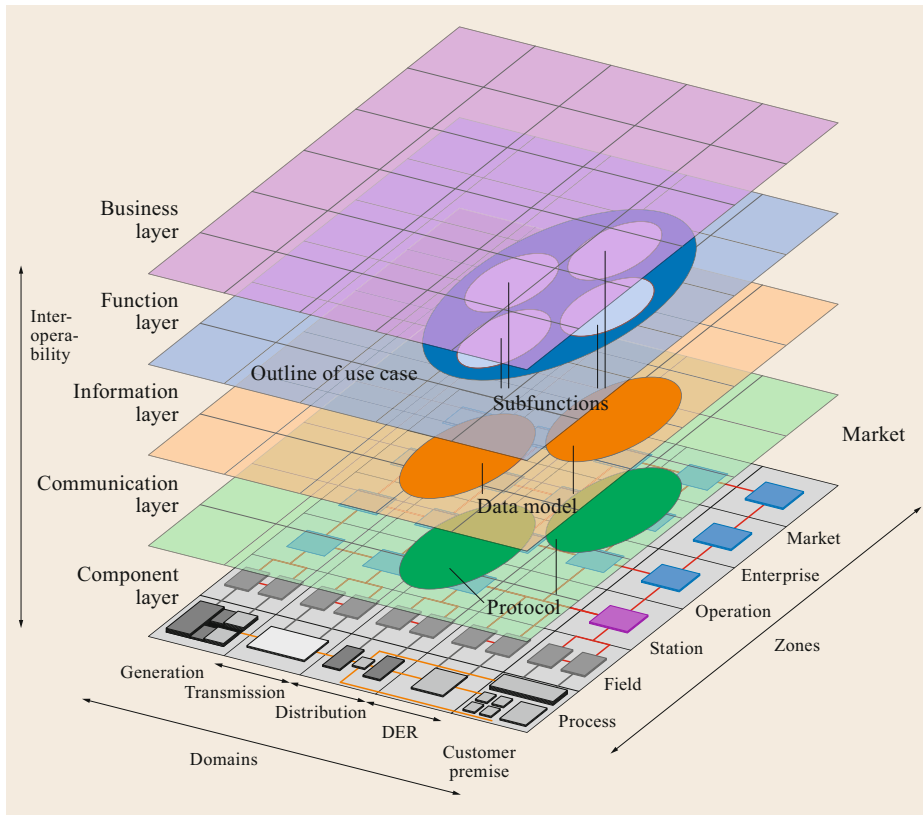
ICT challenges that smart-grid design are faced with are related to the following issues:

- *Scalability.* The expected massive deployment of the smart grid requires scalable solutions and technologies. Nevertheless, this may be a drawback, as high-end technology may be too expensive to justify the initial investment. The use of less-scalable solutions may require frequent retrofitting, which may put the return of the investment at risk.
- *Network management.* Management and operation of a heterogeneous telecom network requires complex management procedures that should be implemented using management centers able to cope with many different technologies as well as the use of externally provided services.
- *IT governance.* The smart grid involves many different applications, some of them devoted to grid operations and others to support customer interaction, and even, in the near future, some IT infrastructure used to provide services to third parties. These issues together with the growing virtualization will require new IT-governance principles.

Although many successful experiences have already been deployed, the complete migration from the *traditional* power system to a new smart-grid architecture will take several years. There are a number of new standards – most of them already approved – that will pave the way to this evolution, thus providing the necessary guarantees of feasibility of this new approach.

The following paragraphs shows the most relevant standards related to smart grids:

- *ISO/IEC 15067-3.* Smart grid application specifications for demand response, distributed-energy resources, and local storage. This standard specifies



**Fig. 14.24** Smart-grid architecture. (Adapted from IEC TR 63097)

a framework to align residential needs to available supplies.

- *ISO/IEC 15045 series*. Gateways to link a home network to the smart grid.
- *ISO/IEC 14543 series*. Residential communications architecture, protocols, network configuration, and network management that carry smart-grid signals.
- *ISO/IEC 29145 series*. Wireless beacon-enabled energy-efficient mesh networks.
- *IEC 61400-25 series*. Communications for monitoring and control of wind power plants. It is considered an expansion of IEC 61850, as it uses the same data modeling, ACSI services, and the same protocol stack.
- *IEC 61588/IEEE 1588*. Precision clock-synchronization protocol for networked measurement and control systems.
- *IEC 61850-90-7*. Object models for power converters in distributed-energy resources, as mentioned in the previous sections.
- *IEC 61850-90-8*. Object models for electric mobility, as mentioned in the previous sections.
- *IEC 61968 series*. System interfaces for distribution management, as mentioned in the previous sections.
- *IEC 61970*. Energy-management system application programming interface, as already mentioned in the previous sections.
- *IEC 62056 series*. Data exchange for meter reading, tariffs, and load control. This standard defines methods, object identity, object modeling and services, communications, and media-access methods to establish instrument interfaces.
- *IEC 62325*. Framework for energy-market communications.
- *IEC 62351 series*. Data and communications security. This series of standards identifies threats to operational systems, including smart grids, and specifies protection methods.
- *IEC 62448*. Power-line communications systems for power-utility applications. Establishes the planning of service and performance parameters for operational requirements.
- *IEC 62746*. System interface between the customer's energy-management system and the power management system. It defines system interfaces, profiles, and communications protocols.
- *IEC 62872*. System interface between industrial facilities and the smart grid.

- *OASIS Energy Interoperation 1.0*. Information model and messages to enable standard communications of energy interoperation, such as demand response events, realtime price, etc.
- *OASIS Energy Market Information Exchange*. Defines an information model and XML vocabulary for the interoperable and standard exchange energy-market-related information.
- *OASIS WS-CALENDAR*. Information model and XML vocabulary for communications schedules generating orders.
- *IEEE P203.5 Smart Energy Profile 2.0*. Standard-based application profile for use in smart-grid home-area networks (HAN) based on IEC CIM (IEC 61968) using the IP Protocol.
- *IEEE 1547.3*. Guide for monitoring, information exchange, and control of distributed resources interconnected with electric power systems. This standard provisions information modeling and case analyses.

## 14.6 Outlook of Future Technologies

The massive deployment of the smart grid, which implies the integration of distributed-energy resources, most of them based on intermittent generating units, will require the use of new technologies that allow new and more advanced services to be supported.

Operational services must maintain or even improve their performance. Although the technologies to come will introduce a number of advantages, they will also present a number of challenges. The most relevant changes that must be considered are:

- *Virtualization*. Telecommunications and virtualization of applications is becoming common practice for the implementation of IT solutions. It brings many advantages and cost reduction. Nevertheless, for mission-critical operational applications, and this is related to telecom services, these solutions bring about many doubts about their reliability and availability, as well as their lack of transparency on how the service is being implemented. Performance assessment is not a guarantee, since service configuration and implementation modes can change without the user being informed. Not to mention cybersecurity concerns, as it is not possible to know the level of protection offered by the service. Internally provided virtual services may be a feasible solution, as power utility can verify which technologies are being used, as well as the proper configuration to prevent a loss of service reliability.
- *Clouds*. Clouds are another way of service virtualization that present similar advantages and drawbacks to those mentioned in the previous paragraph.
- *Big data*. The massive and exponential growth of information gathered by new intelligent devices and new applications will require the use of big-data technology to extract useful information. This information will be used to improve the efficiency and performance of the power system.
- *Wireless communications*. Last-mile communications technologies are evolving towards wireless solutions. Consequently, wired-access interfaces will be used less and less in the future. The transmission capacity of wireless technologies is continuously growing, putting wired solutions aside. These technologies provide great flexibility and mobility and simplify installation procedures, but wireless service reliability is lower than wired solutions, and, in many cases, is not suitable for mission-critical operational applications. The use of wireless solutions has to be thoroughly studied due to their higher latency and lower service reliability.
- *Cybersecurity*. The use of standard and opened technologies enables new attacks. The secure deployment of new technologies requires implementing cybersecurity-protection methods using an engineering approach. That is to say, assessing new vulnerabilities and implementing the right protection measurements. New tools and technology are being implemented to facilitate this new engineering process.

If we focus on telecom technologies, the transmission capacity of fiber optics is far higher than that required for any operational or added-value application. On the other hand, new network technologies will need to be used to cope with the scalability requirements. Among other solutions software-defined networks (SDN) are expected to be the next technology wave.

SDN is a set of techniques used to facilitate the design, delivery, and operation of network services in a deterministic, dynamic, and scalable manner. SDN is a technology currently used in data centers because of its flexibility, scalability, and virtualization.

The SDN architecture is an evolution of traditional connection-oriented networks, that is to say, there is a control plane that set ups connections – or in this case,

data-flow paths – and a forwarding plane that switches packets through pre-established paths.

Forwarding and control planes are decoupled and defined using abstract definition methods. Due to this, applications can specify services and control a network dynamically, accordingly using implementation criteria that better suits the application requirements. The separation between control and forwarding planes is implemented with the goal of reducing complexity and providing flexibility to allow for a faster innovation.

SDN includes four functional layers:

- *Device and resource functional layer.* The resources of the control and management planes of devices are mapped to control and management planes using abstraction techniques. The forwarding plane, which implements the *data path*, is responsible for handling and forwarding packets. It provides switching, routing, packet transformation, and filtering functions. The operational plane controls the operational state of the network device, including the information of the device.
- *Control layer.* The control plane can be distributed among SDN nodes. Its main functionality is the configuration of the forwarding plane by setting the rules to handle network packets. Communications between control-plane entities is implemented using gateway protocols, such as the Border Gateway Protocol (BGP) or other protocols, such as the Path Computation Element (PCE) Communications Pro-

ocol (PCEP). Control-plane functionalities usually include:

- Topology discovery
- Maintenance services
- Packet route setup
- Path failover mechanisms.
- *Management layer.* The management plane is centralized. It implements network-configuration functions as well as fault and monitoring management.
- *Network services layer.* This provides a service-abstractions interface to be used by applications and other services.

When the control plane is centralized, the OpenFlow Protocol is used to communicate the control plane with the forwarding plane.

OpenFlow defines the protocol used by a centralized network controller to control OpenFlow switches. Each OpenFlow-compliant switch maintains one or more flow tables, which are used to perform packet lookups. Tables define packet forwarding actions.

The use of SDN to support operational applications must be assessed. It offers many advantages, but availability, reliability, and implementation architecture must be checked in order to verify the fulfilment of mission-critical operational application requirements.

*Reference note:* this chapter relies on [14.1], edited by the author of this chapter as a result of the compilation and update of several works produced by CIGRE study committee D2.

## 14.7 Further Reading

- CIGRE: Telecommunication Service Provisioning and Delivery in the Electrical Power Utility, CIGRE Technical Brochure 461, Working Group D2.26 (2011)
- CIGRE: The Use of IP Technology in the Power Utility Environment, CIGRE Technical Brochure 153, Working Group 35.07 (2000)
- CIGRE: Line and System Protection Using Digital Circuit and Packet Communications, CIGRE Technical Brochure 521, Working Group D2/B5.30 (2012)
- CIGRE: Operation and Maintenance of Telecom Networks and Associated Information Systems in the Electrical Power Utility, CIGRE Technical Brochure 588, Working Group D2.33 (2014)
- CIGRE: Communication Architecture for IP-Based Substation Applications, CIGRE Technical Brochure 507, Working Group D2.28 (2012)
- CIGRE: Scalable Communication Transport Solutions over Optical Networks, CIGRE Technical Brochure 618, Working Group D2.35 (2015)
- CIGRE: Security Architecture Principles for Digital Systems in Electric Power Utilities. CIGRE Technical Brochure 615, Working Group D2.31, 2015
- CIGRE: EMS for the 21st Century – System Requirements. CIGRE Technical Brochure 452, Working Group D2.24 (2011)
- CIGRE: System Protection Schemes in Power Networks, CIGRE Technical Brochure, Task Force 38.02.19 (2001)
- CIGRE: Integrated Management Information in Utilities, CIGRE Technical Brochure 341, Working Group D2.17 (2008)
- CIGRE: IP cost versus risk. In: *CIGRE Study Comm. 35 Meet., Paris* (2000)



- C. Samitier: The new IEC 61850 architecture for substation automation. In: *Proc. XI ERIAC, Ciudad del Este* (2005)
- C. Samitier, J. Darne, R. Pellizzoni: Using ethernet service to improve resiliency and performance. In: *CIGRE Study Comm. D2 Colloq., Lucerne* (2007)
- S. Gonzalez, C. Samitier: Application of peer-to-peer networks in power system control. In: *CIGRE Study Comm. D2 Colloq., Cuernavaca* (2005)
- C. Samitier, A. Lichtig: Cybersecurity for IEC 61850 substations. In: *Proc. XVII ERIAC, Ciudad del Este* (2017)
- C. Samitier, R. Pellizzoni, J. Darne: New architecture for protection and control networks. In: *CIGRE Study Comm. D2 Colloq., Fukuoka* (2009)
- A. Trullos, C. Samitier, J. Sorribas, J. del Rio: CORBA for distributed measurements. In: *6th World Multiconf. System. Cybern. Inform./8th Int. Conf. Inf. Sys. Anal. Synth. (SCI/ISAS)* (2002)
- A. Trullos, C. Samitier, J. Sorribas, A. Manuel, R. Palomera, J. del Rio: LabVir: A virtual distributed measurement system. In: *Instr. Meas. Technol. Conf.* (2003), <https://doi.org/10.1109/IMTC.2003.1208261>
- C. Samitier, E. Trullos, A. Manuel: Virtual distributed instrumentation in the substation environment. In: *CIGRE Study Comm. 35 Sess., Paris* (2002)
- C. Samitier, J. Bembibre: Web services, a new approach to substation management. In: *CIGRE Study Comm. D2 Meet., Rio de Janeiro* (2003)
- World Wide Web Consortium: <http://www.w3c.org>
- Organization for the Advance of Structured Information Standards (OASIS): <http://www.oasis-open.com>
- OASIS: Reference model for service oriented architecture (SOA-RM) v1.0, <http://docs.oasis-open.org/soa-rm/v1.0/> (2006)
- JWG 61850 RIAC CIGRE: Technologies required for implementing IEC 61850 substations (2010)
- E. Handschin, A. Petroianu: *Energy Management Systems: Operation and Control of Electric Energy Transmission Systems* (Springer, Berlin, Heidelberg 2011)
- A. Phadke, J. Thorp: *Synchronized Phasor Measurements and Their Applications* (Springer, New York 2017)
- R. Perlman: *Interconnections. Bridges and Routers* (Addison-Wesley, Boston 1992)
- D.E. Comer: *Interworking with TCP/IP, Volume 1: Principles, Protocols and Architecture*, 6th edn. (Pearson, London 2015)
- S. Keshav: *An Engineering Approach to Computer Networking* (Addison-Wesley, Boston 1997)
- R.S. Cahn: *Wide Area Network Design* (Morgan Kaufmann, San Francisco 1998)
- T.G. Robertazzi: *Planning Telecommunication Networks* (IEEE, Piscataway 1998)

## References

- 14.1 C. Samitier (Ed.): *Utility Communication Networks and Services*, CIGRE Green Books (Springer, Cham 2017)
- 14.2 CIGRE: The Use of Ethernet Technology in the Power Utility Environment, CIGRE Technical Brochure 460, Working Group D2.23 (2011)
- 14.3 CIGRE: Integrated Service Networks for Utilities, CIGRE Technical Brochure 249, Working Group D2.07 (2004)
- 14.4 CIGRE: Telecommunication and Information Systems for Assuring Business Continuity and Disaster Recovery, Technical Brochure 668, Working Group D2.34 (2016)
- 14.5 IEC TR 62357-1:2016: Power Systems Management and Associated Information Exchange – Part 1. Reference Architecture (2016)

### Carlos Samitier

Pullnet Technology  
Mexico City, Mexico  
[carlos.samitier@smart61850.com](mailto:carlos.samitier@smart61850.com)



Carlos Samitier holds a degree on Telecommunication and an MBA by the University of Madrid. He has been working for more than 30 years in the field of Power Utility Control Networks. Carlos Samitier has been serving CIGRE since 1997. In 2010 he was appointed as Chairman of Study Committee D2 of CIGRE. In 2016 he was appointed CIGRE Honorary Member. He works as an independent consultant in the field of Power System automation.

# Distribution Systems

Nikolaos C. Koutsoukis , Pavlos S. Georgilakis , George N. Korres , Nikos D. Hatziargyriou 

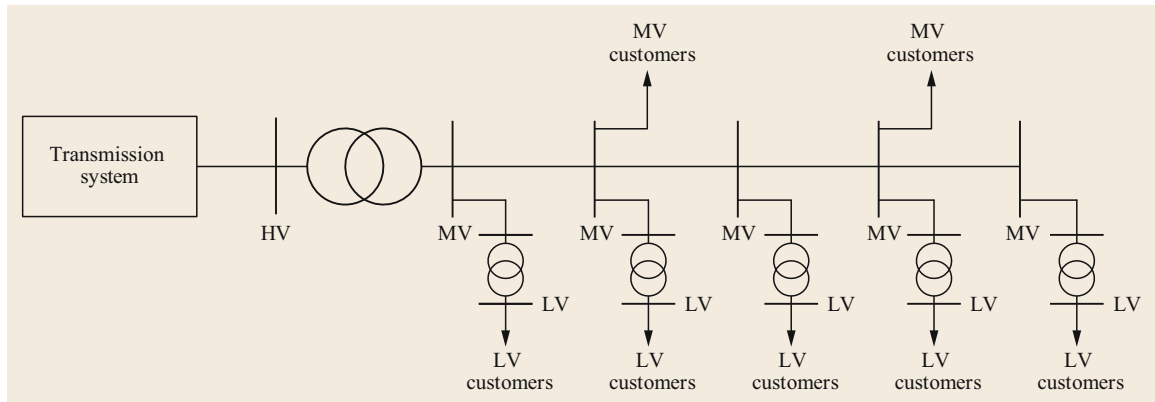
This chapter presents an overview of power distribution networks. The description of the main components of a distribution network are given and various power flow models for the steady state analysis of distribution networks are formulated. The increasing penetration of distributed energy resources into the distribution level has transformed distribution networks into active ones. The basic functions of an advanced distribution management system for the control and monitoring of a distribution network are presented. Furthermore, methods for the operation of the network under normal and emergency operating conditions and for distribution network planning are presented.

15.1	<b>Power Distribution Networks</b> .....	1093
15.2	<b>Network Components Modeling</b> .....	1095
15.2.1	Transformers .....	1096
15.2.2	Distribution Lines .....	1096
15.2.3	Load Models .....	1097
15.2.4	Shunt Capacitors .....	1097
15.2.5	Voltage Regulators .....	1098
15.3	<b>Power-Flow Analysis of Distribution Networks</b> .....	1099
15.3.1	Branch-Flow Equations .....	1099
15.3.2	Linear Approximation of Branch-Flow Equations .....	1100
15.3.3	Quadratically Constrained Approximation of Branch-Flow Equations .....	1100
15.3.4	Conic Approximation of Branch-Flow Equations .....	1100
15.3.5	Simulation Results .....	1101
15.3.6	Three-Phase Power-Flow Analysis of Unbalanced Distribution Networks ..	1101
15.4	<b>Active Distribution Networks</b> .....	1103
15.4.1	Distributed Energy Resources .....	1103
15.4.2	Demand Response .....	1105
15.4.3	From Passive to Active .....	1106
15.4.4	Active Network Management .....	1106
15.5	<b>Distribution Network Monitoring and Control</b> .....	1107
15.6	<b>Operation of Active Distribution Networks</b> .....	1115
15.6.1	Operation of Active Distribution Networks Under Normal Operating Conditions .....	1115
15.6.2	Operation of Active Distribution Networks Under Emergency Operating Conditions .....	1117
15.7	<b>Distribution Network Planning</b> .....	1120
15.8	<b>Summary</b> .....	1123
15.A	<b>Appendix: Load and Line Data of Distribution Networks</b> .....	1123
	<b>References</b> .....	1126

## 15.1 Power Distribution Networks

*Power distribution systems* are responsible for delivering electric power from high-voltage transmission or subtransmission systems to the end customers. As shown in Fig. 15.1, the distribution system starts from the primary distribution substation, where a power transformer decreases the high voltage (HV) of the transmission system (35–230 kV) to medium voltage (MV) (1–35 kV) [15.1]. Primary *distribution feeders*, which are MV circuits, connect the primary distribution substation with the secondary distribution substations. The power transformers in the secondary dis-

tribution substations decrease the MV to low voltage (LV) (100–1000 V) [15.1], where residential and commercial end users are connected to the system using secondary distribution lines. Most distribution systems (both primary and secondary) operate in radial configuration, which means that there is only one path from the distribution substation to each end customer. However, operation of meshed MV distribution networks also exists in some countries, feeding major urban areas. The main advantages of the operation of radial distribution networks over meshed ones [15.2, 3] are:



**Fig. 15.1** An example of a distribution network

- Network planning is easier and with lower investment cost.
- Network operation, which includes voltage control and power flow management, is less complex.
- Protection coordination is simpler.
- Short circuit currents are lower.

Distribution networks can be either overhead or underground. Overhead distribution networks have lower investment cost than underground ones, and they are very common in rural areas, where load density is low. Underground distribution networks are usually found in urban areas with high load density, for aesthetic reasons and due to space limitations. Their reliability is higher, since they are not directly affected by weather conditions, e.g., lightning, wind, and freezing. Furthermore, in some areas, distribution networks are designed to be partially overhead and partially underground.

The *infrastructure of distribution systems* is extensive, and its main components are [15.4]:

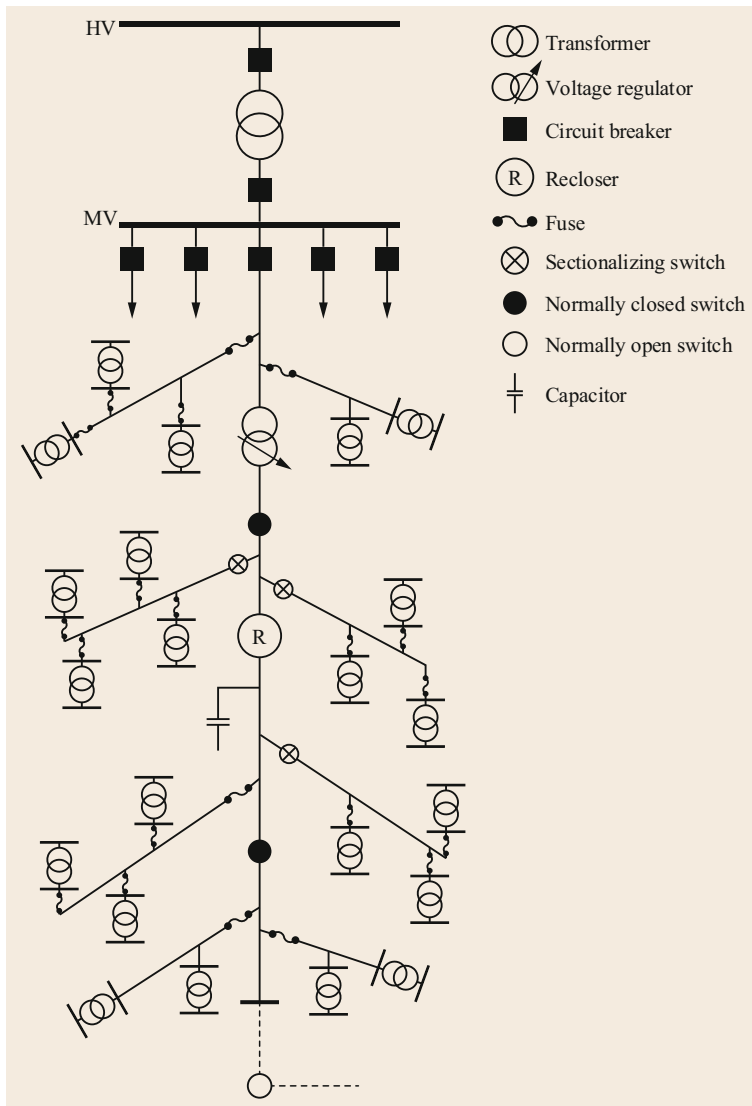
- Distribution substations
- Primary distribution feeders
- Distribution transformers
- Secondary distribution lines
- Voltage regulators
- Shunt capacitors
- Switchgears
- Metering equipment.

The configurations and lengths of distribution networks vary depending on the country, area (urban or rural) and the type of customers they serve. However, most of them share similar characteristics. Figure 15.2 presents the one-line diagram of a *typical* distribution network configuration and its major components. The distribution network comprises one or more feeders (lines) originating from the main substation. The main feeder

is a three-phase circuit, which usually consists of conductors with an ampacity of 400 A and above, and it is considered as the backbone of the distribution network. The distribution lines branching of the main feeder are called laterals, and they connect secondary distribution transformers or other sublaterals. Even though distribution networks are designed to operate as perfectly balanced three-phase power systems, they are inherently unbalanced, mostly due to the uneven connection of single-phase loads or distributed generators along the feeder.

A circuit breaker is placed at the origin of the feeder to protect it from excess current caused by an overload or a short circuit and prevent its damage. A recloser, which is a circuit breaker equipped with relays, is usually placed in the main feeder of overhead lines. Switches and/or disconnectors are also placed along the feeder to sectionalize it for maintenance and restoration purposes. Note that a switch can carry and break current under normal circuit conditions only, and a disconnector can open or close only when the current is negligible. In the case of faults, fuse cutouts or sectionalizing switches, which are disconnectors equipped with a tripping mechanism, are used in the laterals to isolate them from the distribution network. The sectionalizing switches cooperate with the upstream recloser, since they are not rated to interrupt fault currents. Most feeders are connected with at least one other feeder or substation via a line with a normally open switch (tie line). In the case of permanent faults, this switch can be closed to partially restore the load.

Voltage regulators and shunt capacitors are the primary devices for voltage control in distribution networks. Shunt capacitors can be used for reactive power support and power factor correction. Voltage regulators can be placed in the distribution substation and along the feeder to maintain the voltage within its nominal limits.



**Fig. 15.2** A typical distribution network configuration

The main goal of distribution systems is to ensure the continuity of service to load demand at minimum cost. Moreover, they are responsible for integrating distributed energy resources (DER) ensuring certain standards of power quality. DER include distributed generators, mostly based on renewable energy resources (RES), active demand, and storage. Therefore, the role

of distribution systems has become more *active*, creating new challenges. The key to achieving these goals is the optimal operation of the existing network and optimal distribution network planning. Due to the complexity and the large number of components in the distribution network, its optimal operation and planning are complex tasks, which are affected by many factors.

## 15.2 Network Components Modeling

The *steady-state analysis of power distribution networks* requires the effective modeling of various network components. The *equivalent circuit* of each component is necessary to perform technical calculations,

and their combination enables the representation of the actual distribution network. The main components of the power distribution network and their modeling are presented in the following sections.

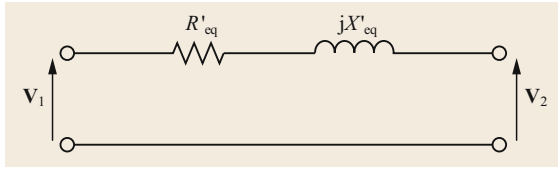


Fig. 15.3 Single-phase equivalent circuit of a transformer

### 15.2.1 Transformers

Power transformers are static devices that transfer power from one alternating voltage to another through electromagnetic induction. They are the basic components of distribution substations and they are generally used to reduce (i) high voltages (< 230 kV) to primary system voltages (1–35 kV) and (ii) primary system voltages to utilization voltages (120–600 V). The simplified transformer model referred to the primary side is presented in Fig. 15.3. As is shown in Fig. 15.3, transformers can be represented by a series impedance. Distribution transformers with low capacity (rated power) have a larger series resistance than reactance. On the contrary, the resistance of high-capacity transformers can be considered negligible compared to their reactance. For simplification purposes, transformers are sometimes considered ideal, having zero losses and 100% efficiency.

Given the specifications of a transformer, the equivalent transformer impedance referred to the primary winding ( $Z'_{eq}$ ) is calculated as follows

$$Z'_{eq} = R'_{eq} + jX'_{eq}, \quad (15.1)$$

$$R'_{eq} = R_1 + R'_2 = R_1 + a^2 R_2, \quad (15.2)$$

$$X'_{eq} = X_1 + X'_2 = X_1 + a^2 X_2, \quad (15.3)$$

$$a = \frac{N_1}{N_2} = \frac{V_1}{V_2}, \quad (15.4)$$

where,  $R_1$  and  $R_2$  represent the resistance of the primary and secondary winding, respectively;  $X_1$  and  $X_2$  represent the reactance of the primary and secondary winding, respectively; and  $a$  denotes the transformer turns ratio or voltage ratio. Note that complex numbers are marked with bold font. Tables 15.1 and 15.2 present the technical characteristics of single-phase and three-phase distribution transformers [15.5], respectively.

### 15.2.2 Distribution Lines

Distribution lines can be divided into two categories:

- Overhead lines: these have one or multiple conductors (usually three or four), and they are mounted in

Table 15.1 Technical characteristics of single-phase distribution transformers with primary voltage 20 kV and secondary voltage 0.231 kV [15.5]

Rated power (kVA)	R (%)	X (%)	Z (%)
5	2.16	3.37	4.00
10	2.23	3.32	4.00
15	1.87	3.53	4.00
25	1.95	3.49	4.00
50	1.58	3.67	4.00

Table 15.2 Technical characteristics of three-phase distribution transformers with primary voltage 20 kV and secondary voltage 0.4 kV [15.5]

Rated power (kVA)	R (%)	X (%)	Z (%)
250	1.13	3.84	4.00
400	1.00	3.87	4.00
500	0.95	3.89	4.00
630	0.90	3.90	4.00
800	0.97	5.92	6.00
1000	0.94	5.93	6.00
1250	0.96	5.92	6.00
1600	0.96	5.92	6.00

poles made of wood or concrete. Their cost is generally low, since their insulation is provided mostly by air. Conductors are generally made of aluminum (all-aluminum or steel-reinforced) and copper.

- Underground lines: their cost is several times higher than the cost of overhead lines. They are preferred for aesthetic and environmental reasons in urban environments. They are less susceptible to outages due to weather conditions (e.g., lighting, wind, freezing, etc.).

The relatively short length of MV and LV distribution lines, compared to transmission lines, allows simplified modeling. Overhead distribution lines are usually represented by a series impedance circuit ignoring its shunt capacitance. In the modeling of underground distribution lines, the line's shunt capacitance needs to be considered, and the  $\pi$  equivalent line model is used. The typical electrical characteristics of a distribution line are:

- Type (overhead or underground)
- The conductor's material and cross-sectional area
- Series impedance per unit of line length
- Ampacity
- Nominal operating voltage.

Table 15.3 presents the typical electrical characteristics of several overhead lines. In Table 15.3, ACSR stands for aluminum conductor steel reinforced, Cu stands for copper, and Al stands for aluminum.

**Table 15.3** Typical electrical characteristics of various overhead distribution lines

Material and cross-sectional area (mm <sup>2</sup> )	R (Ω/km)	X (Ω/km)	Ampacity (A)	Voltage (kV)
ACSR-16	1.268	0.422	136	20
ACSR-95	0.215	0.334	448	20
Cu-95	0.220	0.358	352	20
Cu-16	1.274	0.334	115	0.4
Cu-35	0.596	0.309	185	0.4

### 15.2.3 Load Models

The term *load* is defined as the aggregation of multiple single devices, such as electrical appliances, lighting, and motors, which consume power and are connected to the system [15.4, 6]. A *load model* is a mathematical representation of the changes in load demand (active and reactive power), usually as a function of the changes in the bus voltage and, in some cases, frequency. Load models can be divided into two categories: dynamic and static [15.7]. Dynamic models represent load demand at any instance of time as a function of voltage, frequency, and time. Dynamic models are typically represented in the form of differential equations and are used in voltage stability studies. Static models represent the power demand of the load (active and reactive) as a function of voltage magnitude and frequency at a particular instant in time (*snapshot*). For power-flow applications, static models that incorporate only the voltage dependence characteristics are used [15.6].

The most common static load models are:

- *Constant impedance load model.* The active and reactive power of constant impedance loads vary proportionally to the square of the voltage magnitude.
- *Constant current load model.* The active and reactive power of constant current loads vary in direct proportion (linearly) to the voltage magnitude.
- *Constant power load model.* Constant power loads draw constant active and reactive power, irrespective of the changes in the bus voltage magnitude.
- *Polynomial load model.* This model represents the active ( $P$ ) and reactive ( $Q$ ) power of the load in relationship to voltage magnitude as follows

$$P = P_0 \left[ c_1 \left( \frac{V}{V_0} \right)^2 + c_2 \frac{V}{V_0} + c_3 \right], \quad (15.5)$$

$$Q = Q_0 \left[ c_4 \left( \frac{V}{V_0} \right)^2 + c_5 \frac{V}{V_0} + c_6 \right], \quad (15.6)$$

where  $c_1$ – $c_6$  are the polynomial model coefficients,  $V$  is the actual voltage magnitude,  $V_0$  is the nominal voltage, and  $P_0$  and  $Q_0$  are the nominal active

and reactive power of the load. This model is often referred to as the *ZIP model*.  $Z$  stands for constant impedance,  $I$  represents constant current and  $P$  refers to constant power.

- *Exponential load model.* This model expresses the relationship between active/reactive power demand and system voltage with an exponential equation, as

$$P = P_0 \left( \frac{V}{V_0} \right)^{np}, \quad (15.7)$$

$$Q = Q_0 \left( \frac{V}{V_0} \right)^{nq}. \quad (15.8)$$

The exponents  $np$  and  $nq$  can be set to any value in order to represent the desired load characteristic. Setting  $np = nq = 2$ , the load is a constant impedance load; setting  $np = nq = 1$ , the load is a constant current load, and setting  $np = nq = 0$ , the load is a constant power load.

- *Frequency-dependent load model.* This is a model that includes frequency dependence on either exponential or polynomial load models. This is achieved by multiplying the relevant exponential or polynomial load model with the frequency factor given by

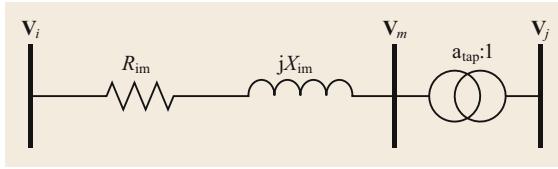
$$1 + a_f (f - f_0), \quad (15.9)$$

where  $f$  is the actual frequency of the bus considered,  $f_0$  is the nominal frequency, and  $a_f$  is the frequency-sensitivity parameter of the model.

### 15.2.4 Shunt Capacitors

*Shunt capacitors* are used extensively in distribution networks to regulate the voltage and to provide reactive power support. Shunt capacitors are installed at (i) the MV side of the HV/MV substation to provide reactive power support to the transmission system and (ii) along the distribution feeder for voltage support and power factor correction. Based on their installation type, capacitors are categorized as follows:

- *Fixed capacitors:* these are the most common type of capacitor banks, and their connection is permanent. They provide voltage support, but their effect



**Fig. 15.4** Voltage regulator model

on voltage fluctuation along the feeder is limited. Their installation cost is relatively low.

- **Switched capacitors:** these can be switched as a block or in discrete consecutive steps. They are operated manually or by automated control. They reduce the voltage drop and fluctuations along the feeder. However, their investment cost is higher than that of fixed capacitors.

Similarly to the load model, shunt capacitors can be modeled as purely reactive constant impedance or power load.

### 15.2.5 Voltage Regulators

The *voltage regulator* is used to automatically maintain voltages constant along the entire feeder for varying load demand. It consists of an autotransformer with a tap (step) changer in the series winding. Most voltage regulators installed in MV distribution networks enable voltage regulation in a range of  $\pm 10\%$  of the nominal voltage in 32 steps, with voltage change per step equal to 0.625% of the nominal voltage. The voltage regulator is usually modeled as an ideal transformer in series with the distribution line, as shown in Fig. 15.4. The regulated voltage of bus  $j$  ( $V_j$ ) is calculated as a func-

tion of the tap position as

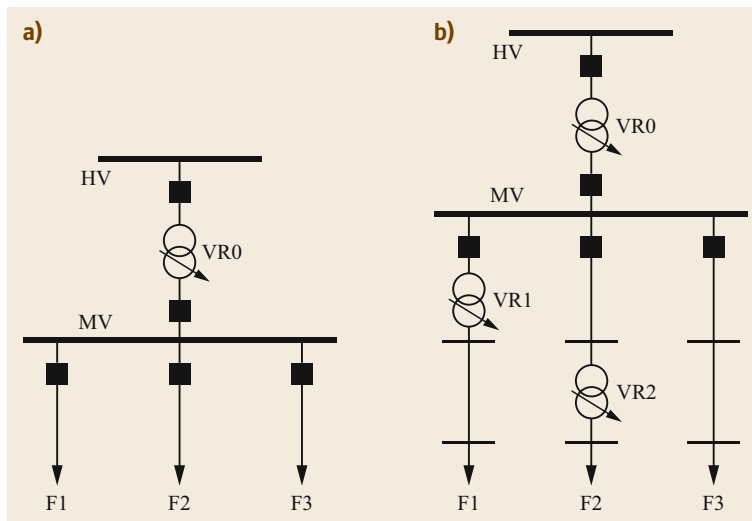
$$V_j = \frac{V_m}{\alpha}, \tag{15.10}$$

$$a_{\text{tap}} = 1 \pm \text{Step tap}_{ij}, \tag{15.11}$$

where  $V_m$  is the voltage of bus  $m$ ,  $a_{\text{tap}}$  is the voltage regulator's ratio, Step is the voltage regulator's step voltage (per unit, p.u.), and  $\text{tap}_{ij}$  is the tap position of the voltage regulator.

The tap position of the voltage regulator is controlled by the line-drop compensator (LDC). The LDC changes the tap position of the voltage regulator in order to maintain the voltage at a regulation point that is located between the voltage regulator and the end of the feeder. The LDC boosts the voltage during heavy load and lowers it during light load. Thus, the range of the voltage fluctuation along the feeder remains relatively small throughout the day.

Most of the HV/MV substations are equipped with a voltage regulator with an on-load tap changer. In this case, voltage regulation is performed simultaneously in all distribution feeders connected to this substation. As is shown in Fig. 15.5a, VR0 regulates the voltage of feeders F1, F2, and F3. The simultaneous voltage regulation is effective when the load variation of all feeders is similar throughout the day, e.g., all feeders serve residential loads. Otherwise, individual voltage regulators are installed along each feeder, which serve customers with different load behaviors. As is shown in Fig. 15.5b, VR0 provides voltage regulation in all feeders; VR1 individually regulates the voltage of feeder F1 in coordination with VR0; VR2 individually regulates the voltage of feeder F2 in coordination with VR0.



**Fig. 15.5a,b** Voltage regulator placement. (a) VR0 regulates the voltage of the three feeders, (b) VR1 and VR2 individually regulates the voltage of feeders F1 and F2, respectively, in coordination with VR0

## 15.3 Power-Flow Analysis of Distribution Networks

*Power-flow analysis* is fundamental for the operation and planning of power distribution systems. The loading of a distribution feeder is inherently unbalanced due to a large number of unequal single-phase loads and the nonsymmetrical conductor spacing of three-phase distribution lines. However, in several cases, it is assumed a perfectly balanced system so that a single-phase equivalent can be used. Sections 15.3.1–15.3.5 present power-flow models for the analysis of balanced distribution networks, while Sect. 15.3.6 presents the analysis of three-phase unbalanced distribution networks. It should be noted that complex numbers are marked in bold font.

### 15.3.1 Branch-Flow Equations

The *AC power-flow problem* is inherently a nonlinear and nonconvex problem. The power flow models presented in Sects. 15.3.1–15.3.5 are based on the branch-flow equations that were first used in [15.8, 9]. The single-phase equivalent circuit of a branch of a distribution system is shown in Fig. 15.6. For the line of Fig. 15.6 that connects bus  $i$  with bus  $j$ ,  $\mathbf{V}_i$  and  $\mathbf{V}_j$  are the complex voltage of bus  $i$  and bus  $j$ , respectively;  $\mathbf{I}_{ij}$  are the complex current on line  $i$ – $j$ ;  $P_{ij}$  and  $Q_{ij}$  are the real and reactive power flows from bus  $i$  to bus  $j$ , respectively;  $\mathbf{z}_{ij} = r_{ij} + jx_{ij}$  is the complex impedance of line  $i$ – $j$ ;  $P_j$ , and  $Q_j$  is the injected active and reactive power at bus  $j$ , respectively, calculated as the load power minus the power generated at bus  $j$ . According to Ohm's law, the voltage drop of branch  $i$ – $j$  can be written as

$$\mathbf{V}_i - \mathbf{V}_j = \mathbf{I}_{ij} \mathbf{z}_{ij}. \quad (15.12)$$

The branch-flow on line  $i$ – $j$  is calculated as

$$\mathbf{S}_{ij} = \mathbf{V}_i \mathbf{I}_{ij}^*. \quad (15.13)$$

To simplify the notation, let  $|\mathbf{V}_i|^2 = U_i$  and  $|\mathbf{I}_{ij}|^2 = I_{ij}^{\text{sqqr}}$ . Then, taking the magnitude squared of (15.12), we have

$$\begin{aligned} |\mathbf{V}_j|^2 &= |\mathbf{V}_i - \mathbf{I}_{ij} \mathbf{z}_{ij}|^2 \\ \Rightarrow U_j &= (\mathbf{V}_i - \mathbf{I}_{ij} \mathbf{z}_{ij}) (\mathbf{V}_i - \mathbf{I}_{ij} \mathbf{z}_{ij})^* \\ \Rightarrow U_j &= |\mathbf{V}_i|^2 - \mathbf{V}_i \mathbf{I}_{ij}^* \mathbf{z}_{ij}^* - (\mathbf{V}_i \mathbf{I}_{ij}^* \mathbf{z}_{ij}^*)^* + |\mathbf{I}_{ij}|^2 |\mathbf{z}_{ij}|^2 \\ \stackrel{(11)}{\Rightarrow} U_j &= U_i - \mathbf{S}_{ij} \mathbf{z}_{ij}^* - (\mathbf{S}_{ij} \mathbf{z}_{ij}^*)^* + I_{ij}^{\text{sqqr}} (r_{ij}^2 + x_{ij}^2) \\ \Rightarrow U_j &= U_i - 2\text{Re}(\mathbf{S}_{ij} \mathbf{z}_{ij}^*) + I_{ij}^{\text{sqqr}} (r_{ij}^2 + x_{ij}^2) \\ \Rightarrow U_j &= U_i - 2(P_{ij} r_{ij} + Q_{ij} x_{ij}) + I_{ij}^{\text{sqqr}} (r_{ij}^2 + x_{ij}^2), \end{aligned} \quad (15.14)$$

where  $\text{Re}(z)$  is the real part, and  $z^*$  is the complex conjugate number  $z$ , respectively.

Using the branch-flow equations, the power-flow balance at each bus can be expressed in terms of voltage square magnitude, current square magnitude, active power branch flow and reactive power branch flow, assuming that all system loads are constant power loads. Assuming radial distribution network operation, let  $W = (N, E)$  be the directed graph that represents the network, in which  $N$  represents the set of buses, and  $E$  represents the set of the distribution lines. Due to its radial configuration, graph  $W$  is a spanning tree, and the root of the tree is the substation bus. Let  $N_{\text{ss}} \subseteq N$  be the set of the substation buses. The direction of the spanning tree  $W$  can be arbitrarily defined with the connection  $(i, j)$  denoting a direction from bus  $i$  to bus  $j$ . For each connection  $(i, j) \in E$ , it is considered that bus  $i$  is the parent of bus  $j$ , or bus  $j$  is the child of bus  $i$ . Let  $N_p(j) \subseteq N$  be the bus set of the parent of bus  $j$  and let  $N_c(j) \subseteq N$  be the bus set of all the children of bus  $j$ . Note that in radial distribution networks, each bus can only have one parent, except for the substation bus, which has no parents. The power-flow analysis variables and parameters are illustrated in Fig. 15.7. Therefore, the power-flow problem can be formulated as

$$\sum_{i \in N_p(j)} (P_{ij} - I_{ij}^{\text{sqqr}} r_{ij}) - \sum_{k \in N_c(j)} P_{jk} = P_j, \quad \forall j \in N \setminus N_{\text{ss}}, \quad (15.15)$$

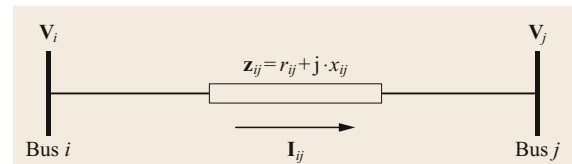
$$\sum_{i \in N_p(j)} (Q_{ij} - I_{ij}^{\text{sqqr}} x_{ij}) - \sum_{k \in N_c(j)} Q_{jk} = Q_j, \quad \forall j \in N \setminus N_{\text{ss}}, \quad (15.16)$$

$$P_{\text{ss},i} = \sum_{j \in N_c(i)} P_{ij}, \quad \forall i \in N_{\text{ss}}, \quad (15.17)$$

$$Q_{\text{ss},i} = \sum_{j \in N_c(i)} Q_{ij}, \quad \forall i \in N_{\text{ss}}, \quad (15.18)$$

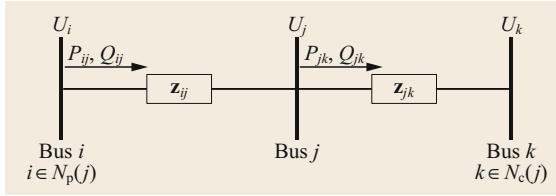
$$U_i I_{ij}^{\text{sqqr}} = P_{ij}^2 + Q_{ij}^2, \quad \forall (i, j) \in E, \quad (15.19)$$

$$\begin{aligned} U_j &= U_i - 2(P_{ij} r_{ij} + Q_{ij} x_{ij}) + (r_{ij}^2 + x_{ij}^2) I_{ij}^{\text{sqqr}}, \\ &\forall (i, j) \in E. \end{aligned} \quad (15.20)$$



**Fig. 15.6** Single-phase equivalent circuit of a branch connecting bus  $i$  with bus  $j$





**Fig. 15.7** Power-flow analysis variables of a radial distribution network

The active and reactive power-node balances are given by (15.15) and (15.16), respectively. The active ( $P_{ss,i}$ ) and reactive ( $Q_{ss,i}$ ) power supplied by the substation at bus  $i$  are calculated by (15.17) and (15.18), respectively. The apparent power flow of line  $i$ – $j$  is given by (15.19). The voltage drop between buses  $i$  and  $j$  is presented in (15.20). The power-flow problem described by (15.15)–(15.20) is a nonlinear programming (NLP) problem due to the nonlinear constraint (15.19). The number of equations is equal to  $2|N| + 2|E|$ , where  $|N|$  and  $|E|$  are the orders of the set of buses and distribution lines, respectively. For radial distribution networks, it is known that  $|E| = |N| - |N_{ss}|$ , where  $|N_{ss}|$  is the order of the set of the substation buses. Hence, the total number of equations is equal to  $4|N| - 2|N_{ss}|$ .

### 15.3.2 Linear Approximation of Branch-Flow Equations

The linearized model of the power-flow equations (15.15)–(15.20) is obtained by eliminating the active and reactive power losses of the lines and considering that all bus voltages are equal to 1.0 p.u. Therefore, the linearized power flow model [15.10] is formulated as

$$\sum_{i \in N_p(j)} P_{ij} - \sum_{k \in N_c(j)} P_{jk} = P_j, \quad \forall j \in N \setminus N_{ss}, \quad (15.21)$$

$$\sum_{i \in N_p(j)} Q_{ij} - \sum_{k \in N_c(j)} Q_{jk} = Q_j, \quad \forall j \in N \setminus N_{ss}, \quad (15.22)$$

$$P_{ss,i} = \sum_{j \in N_c(i)} P_{ij}, \quad \forall i \in N_{ss}, \quad (15.23)$$

$$Q_{ss,i} = \sum_{j \in N_c(i)} Q_{ij}, \quad \forall i \in N_{ss}. \quad (15.24)$$

The power-flow problem described by (15.21)–(15.24) is a linear programming (LP) problem. The number of equations is equal to  $2|N|$ , which is considerably lower compared to the model of Sect. 15.3.1. Using this model, the active and reactive power flow of distribution lines and the active and reactive power supplied by the substation(s) can be calculated approximately.

### 15.3.3 Quadratically Constrained Approximation of Branch-Flow Equations

The NLP power-flow problem described by (15.10)–(15.15) can be simplified to a quadratically constrained programming (QCP) problem. This approximation is achieved by considering that all bus voltages are equal to 1.0 p.u. Thus, the QCP power flow model is formulated as

$$\sum_{i \in N_p(j)} [P_{ij} - (P_{ij}^2 + Q_{ij}^2) r_{ij}] - \sum_{k \in N_c(j)} P_{jk} = P_j, \quad \forall j \in N \setminus N_{ss}, \quad (15.25)$$

$$\sum_{i \in N_p(j)} [Q_{ij} - (P_{ij}^2 + Q_{ij}^2) x_{ij}] - \sum_{k \in N_c(j)} Q_{jk} = Q_j, \quad \forall j \in N \setminus N_{ss}, \quad (15.26)$$

$$P_{ss,i} = \sum_{j \in N_c(i)} P_{ij}, \quad \forall i \in N_{ss}, \quad (15.27)$$

$$Q_{ss,i} = \sum_{j \in N_c(i)} Q_{ij}, \quad \forall i \in N_{ss}. \quad (15.28)$$

The number of equations of the model described by (15.25)–(15.28) is  $2|N|$  as in the model of Sect. 15.3.2. Moreover, the use of the quadratic constraints (15.25) and (15.26) instead of the linear constraints (15.21) and (15.22) increases the accuracy of the model. Similarly to the model of Sect. 15.3.2, the QCP model calculates approximately the active and reactive power flow of distribution lines and the active and reactive power supplied by the substation(s).

### 15.3.4 Conic Approximation of Branch-Flow Equations

The power-flow problem described by the equality constraints (15.20)–(15.25) is, in general, nonlinear due to the nonlinear constraint (15.19). Relaxing the equality constraint (15.19) to inequality, a second-order cone programming (SOCP) approximation of the branch flow can be derived [15.10, 11]. The branch-flow equations are further simplified by dropping the last quadratic term of (15.20), since its value is negligible compared to the values of the remaining terms. Hence, the SOCP approximation of the branch-flow equations is formulated as

$$\sum_{i \in N_p(j)} (P_{ij} - I_{ij}^{\text{sqtr}} r_{ij}) - \sum_{k \in N_c(j)} P_{jk} = P_j, \quad \forall j \in N \setminus N_{ss}, \quad (15.29)$$

$$\sum_{i \in N_p(j)} (Q_{ij} - I_{ij}^{\text{sqtr}} x_{ij}) - \sum_{k \in N_c(j)} Q_{jk} = Q_j, \quad \forall j \in N \setminus N_{ss}, \quad (15.30)$$

$$P_{ss,i} = \sum_{j \in N_c(i)} P_{ij}, \quad \forall i \in N_{ss}, \quad (15.31)$$

$$Q_{ss,i} = \sum_{j \in N_c(i)} Q_{ij}, \quad \forall i \in N_{ss}, \quad (15.32)$$

$$U_i I_{ij}^{\text{sqf}} \geq P_{ij}^2 + Q_{ij}^2, \quad \forall (i,j) \in E, \quad (15.33)$$

$$U_j = U_i - 2(P_{ij}r_{ij} + Q_{ij}x_{ij}), \quad \forall (i,j) \in E. \quad (15.34)$$

SOCP [15.12] problems are convex optimization problems, and they can be solved in polynomial time using primal-dual interior point algorithms. It should be noted that their mixed integer counterparts [15.10] can be efficiently handled by commercial branch and bound solvers, and they can be widely applicable to power engineering problems. The SOCP model approximately calculates the active and reactive power flow of distribution lines; the active and reactive power supplied by the substation(s); and the voltage square magnitude of all buses.

### 15.3.5 Simulation Results

This section evaluates the performance of the aforementioned models of the branch-flow equations using 33-bus, 83-bus, and 135-bus distribution test systems. The bus load data and the technical characteristics of the distribution lines of the 33-bus, 83-bus, and 135-bus distribution test systems can be found in Tables 15.11–15.13 of Appendix 15.A. The following power flow models are analyzed:

- *LP*: this model is described by (15.21)–(15.24).
- *QCP*: this model is described by (15.25)–(15.28).
- *SOCP*: this model is described by (15.29)–(15.34).
- *NLP*: this model is described by (15.15)–(15.20).

The voltage magnitude of the primary substation(s) is equal to 1.0 p.u. in all simulations for each test system. The aforementioned branch-flow models were implemented in the GAMS (general algebraic modeling system) [15.13], and the CONOPT [15.14] solver was used for the solution of LP, QCP, SOCP, and NLP models. All simulations were carried out on a PC with an Intel Core i7 CPU at 3.40 GHz and 4 GB of RAM.

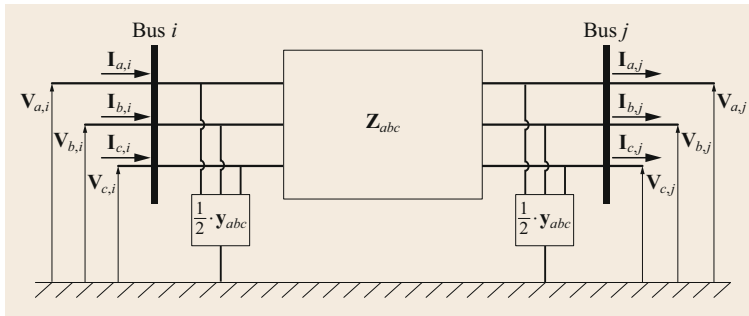
The simulation results of power flow for the aforementioned test systems are presented in Table 15.4. As is shown in Table 15.4, the simulation results of the SOCP model are almost identical to the results of the NLP model, which represents the original branch-flow equations. However, the computation performance of the SOCP model is better than that of the NLP model. Furthermore, the solution of the QCP model derives similar results to the SOCP and NLP models in shorter computation time. As expected, the least accurate power-flow model is the LP model, since it neglects the active and reactive power losses and it considers that the voltage magnitude of all buses is equal to 1.0 p.u. In terms of accuracy and computation performance, the QCP model is more attractive than the LP, SOCP, and NLP models. However, it cannot be used for planning or operation methods that require the calculation of bus voltages or need to consider voltage constraints. In this case, the SOCP model is the most reliable choice.

### 15.3.6 Three-Phase Power-Flow Analysis of Unbalanced Distribution Networks

The model of a three-phase distribution line is presented in Fig. 15.8. The bus voltage and line current are represented by  $3 \times 1$  matrices, while the line's series impedance and shunt admittance matrices are repre-

**Table 15.4** Power-flow analysis results of the 33-bus, 83-bus, and 135-bus distribution systems

33-bus distribution system				
	LP	QCP	SOCP	NLP
Active power injected from substation (MW)	3.715	3.901	3.913	3.913
Reactive power injected from substation (Mvar)	2.300	2.423	2.432	2.432
Minimum voltage magnitude (p.u.)	–	–	0.914	0.914
Computation time (s)	0.063	0.063	0.078	0.140
83-bus distribution system				
	LP	QCP	SOCP	NLP
Active power injected from substation (MW)	28.350	28.852	28.868	28.868
Reactive power injected from substation (Mvar)	20.700	21.998	22.037	22.037
Minimum voltage magnitude (p.u.)	–	–	0.929	0.930
Computation time (s)	0.109	0.125	0.219	0.265
135-bus distribution system				
	LP	QCP	SOCP	NLP
Active power injected from substation (MW)	18.314	18.619	18.628	18.627
Reactive power injected from substation (Mvar)	7.935	8.605	8.623	8.623
Minimum voltage magnitude (p.u.)	–	–	0.932	0.933
Computation time (s)	0.218	0.249	0.749	1.155



**Fig. 15.8** Three-phase distribution line model

sented by  $3 \times 3$  matrices, as follows

$$[\mathbf{V}_{abc}] = \begin{pmatrix} \mathbf{V}_a \\ \mathbf{V}_b \\ \mathbf{V}_c \end{pmatrix}, \quad (15.35)$$

$$[\mathbf{I}_{abc}] = \begin{pmatrix} \mathbf{I}_a \\ \mathbf{I}_b \\ \mathbf{I}_c \end{pmatrix}, \quad (15.36)$$

$$[\mathbf{Z}_{abc}] = \begin{pmatrix} \mathbf{z}_{aa} & \mathbf{z}_{ab} & \mathbf{z}_{ac} \\ \mathbf{z}_{ba} & \mathbf{z}_{bb} & \mathbf{z}_{bc} \\ \mathbf{z}_{ca} & \mathbf{z}_{cb} & \mathbf{z}_{cc} \end{pmatrix}, \quad (15.37)$$

$$[\mathbf{y}_{abc}] = \begin{pmatrix} \mathbf{y}_{aa} & \mathbf{y}_{ab} & \mathbf{y}_{ac} \\ \mathbf{y}_{ba} & \mathbf{y}_{bb} & \mathbf{y}_{bc} \\ \mathbf{y}_{ca} & \mathbf{y}_{cb} & \mathbf{y}_{cc} \end{pmatrix}, \quad (15.38)$$

where,  $\mathbf{V}_a$ ,  $\mathbf{V}_b$  and  $\mathbf{V}_c$  are the complex voltages of phase  $a$ ,  $b$ , and  $c$ , respectively;  $\mathbf{I}_a$ ,  $\mathbf{I}_b$  and  $\mathbf{I}_c$  are the complex currents of phase  $a$ ,  $b$ , and  $c$ , respectively;  $\mathbf{z}_{mm}$  is the series self-impedance of phase  $m$  for  $m = \{a, b, c\}$ ;  $\mathbf{z}_{mn}$  is the series mutual impedance between phases  $m$  and  $n$  for  $\{m, n\} = \{a, b, c\}$  and  $m \neq n$ ;  $\mathbf{y}_{mm}$  is the shunt self-admittance of phase  $m$  for  $m = \{a, b, c\}$ ;  $\mathbf{y}_{mn}$  is the shunt mutual admittance between phases  $m$  and  $n$  for  $\{m, n\} = \{a, b, c\}$  and  $m \neq n$ .

Applying the Kirchhoff's laws, the voltages and currents at bus  $i$  in terms of the voltages and currents

of bus  $j$  are calculated by (15.39)–(15.41) as

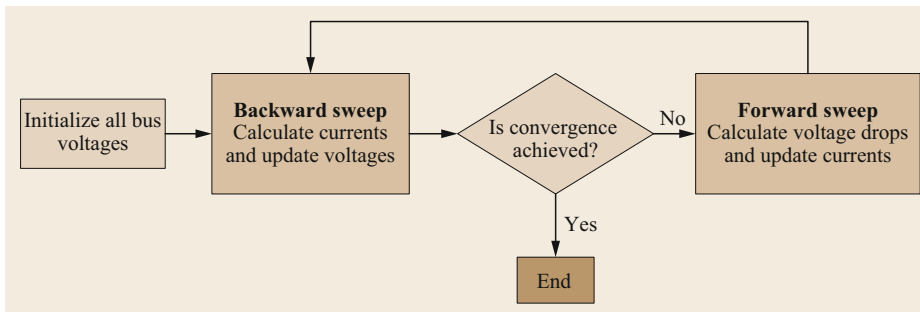
$$[\mathbf{V}_{abc}]_j = [\mathbf{V}_{abc}]_i + \mathbf{Z}_{abc} \left( \frac{1}{2} \mathbf{y}_{abc} [\mathbf{V}_{abc}]_i - [\mathbf{I}_{abc}]_i \right), \quad (15.39)$$

$$[\mathbf{V}_{abc}]_i = [\mathbf{V}_{abc}]_j + \mathbf{Z}_{abc} \left( \frac{1}{2} \mathbf{y}_{abc} [\mathbf{V}_{abc}]_j + [\mathbf{I}_{abc}]_j \right), \quad (15.40)$$

$$[\mathbf{I}_{abc}]_j = \frac{1}{2} \mathbf{y}_{abc} ([\mathbf{V}_{abc}]_i + [\mathbf{V}_{abc}]_j) - [\mathbf{I}_{abc}]_i. \quad (15.41)$$

An efficient method to solve the three-phase power-flow problem is the *backward/forward sweep method* [15.4]. This method consists of three basic steps, and its flowchart is presented in Fig. 15.9. The method comprises an iterative process, which is terminated when a convergence criterion is satisfied. Figure 15.10 shows a simple distribution network example, which helps describe the backward and forward sweep steps. The indexing of the buses is performed using the reverse breadth-first (RBF) and breadth-first (BF) sorting methods [15.15].

The method starts by initializing all the bus voltages. The selected initial values of the bus voltages are



**Fig. 15.9** Flowchart of the backward/forward sweep method

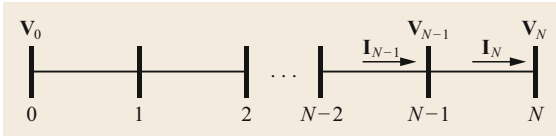


Fig. 15.10 Distribution network example

usually equal to their nominal values. Afterwards, the distribution network is traversed processing the buses and the laterals in the RBF order. For example, in Fig. 15.10, the distribution network will be traversed from the end bus, i.e., bus  $N$ , towards the first bus, i.e., bus zero. In every bus, the currents injected by the load or the shunt capacitor are calculated based on the bus voltage of the current iteration. Then, Kirchhoff's current law is applied in order to determine the incoming injected current ( $I_N$ ). After computing the incoming injected current at bus  $N$ , the voltage of bus  $N-1$  ( $V_{N-1}$ ) is calculated. Hence, all bus voltages and line currents are determined in RBF order and moving the process towards the source bus. Thus, the last examined lateral, which is in fact the main feeder, is processed, and

the bus voltage of the source bus is determined completing the backward sweep step. The voltage of the source bus ( $V_0$ ) is given, and the error between the calculated value of the backward sweep step, and the given value of source bus voltage is computed. If the error is smaller than a given threshold, the power-flow analysis is terminated. Otherwise, the forward sweep step is executed. The selection of the error threshold value is critical because a relative high value may lead to inaccurate results, while a relative small value may lead to multiple iterations.

If the error does not have a value lower than the defined threshold, then the execution of the forward sweep step is necessary. In this step, the currents that were calculated in the backward sweep step are taken as granted, and the bus voltages of the network are calculated considering that the source bus voltage is equal to its given value. The distribution network is, now, traversed processing the buses and the laterals in BF order. For example, in Fig. 15.10, the distribution network will be traversed from the first bus, i.e., bus zero, towards the end bus, i.e., bus  $N$ .

## 15.4 Active Distribution Networks

The increasing penetration of distributed generation (DG) [15.16], the integration of energy storage systems (ESSs) [15.17], and the participation of the consumers in demand-response (DR) mechanisms [15.18] have reshaped the planning and operation of modern distribution networks. The advancements of information and communication technologies (ICT) and the extensive deployment of smart meters and advanced metering infrastructure (AMI) enable the management of DERs transforming the distribution networks from passive to *active distribution networks* (ADNs).

The definition of ADNs, as formulated by CIGRE 2008 WG C6.11 [15.19] is:

ADNs have systems in place to control a combination of DERs, defined as generators, loads and storage. Distribution system operators (DSOs) have the possibility of managing the electricity flows using a flexible network topology. DERs take some degree of responsibility for system support, which will depend on a suitable regulatory environment and connection agreement.

The main goals of the ADN concept can be summarized as follows:

- Increased penetration of DG and storage
- Participation of consumers in DR mechanisms
- Asset management optimization and cost-efficient network operation
- Enhancement of the self-healing capability of the network during an outage
- Power quality improvement
- Ancillary service provision to DSO and transmission system operator (TSO)
- Security improvement from physical and cyber-attacks.

### 15.4.1 Distributed Energy Resources

This section gives a brief overview of the various *distributed energy resources* (DERs) most commonly met in ADNs [15.20]. It should be noted that the section intends to describe small dispersed resources, while larger installations are beyond its scope.

#### Photovoltaic Systems

Photovoltaic (PV) systems directly convert solar energy into electricity [15.21]. They consist of an arrangement of several components, which include solar panels, solar inverters, and mounting and cable equipment.



**Fig. 15.11** A rooftop PV system installed at the Electric Energy Systems Laboratory of the National Technical University of Athens (Courtesy Authors)

A solar panel comprises multiple solar cells, which are made of semiconductor materials and are connected together in various series and parallel configurations. The output direct current of the solar panels is converted into utility frequency alternate current by the solar inverter. Due to the fact that the solar irradiation has a nonlinear effect on the output power of a PV system, a maximum power-point tracking (MPPT) mechanism is employed by the inverter to determine its optimal operating point [15.22].

The main advantage of the PV systems is that their installation and operation do not cause environmental pollution or greenhouse gas emissions. Their main disadvantage is that they are an intermittent source of energy, since they are dependent on a stochastic primary source. Other disadvantages are their relatively low efficiency, e.g., 10–24% and the fact that their output power drops dramatically when even a small portion of the solar panel is shaded. A way to improve their efficiency is the installation of solar trackers, which orientate the solar panels toward the sun. PV systems can be rooftop, pole, or ground mounted. The capacity of the rooftop mounted PV systems ranges from few to several tens of kW. A rooftop-mounted PV system is shown in Fig. 15.11. PV systems with a larger capacity that ranges from few hundreds of kW to few MW are pole or ground mounted.

#### Wind Turbines

Wind turbines convert the kinetic energy of the wind into electricity [15.23, 24]. The output power of a wind turbine depends on wind speed. The wind speed at which the turbine starts to generate power is called cut-in speed, and it is typically equal to 3–4 m/s. The turbine does not generate electric power below the cut-in speed. As the wind speed rises above the cut-in speed, the output power of the wind turbine increases rapidly until it reaches the rated wind speed of the

turbine, which typically ranges from 12–17 m/s. At higher wind speeds, the wind turbine generates its rated output power. The wind turbine is forced to shut down when the wind speed exceeds the cut-out speed, typically around 25 m/s, in order to prevent its damage.

Wind turbines can be classified into (i) horizontal-axis and (ii) vertical-axis wind turbines, with the former being the most common. Horizontal-axis wind turbines have the rotor shaft and generator arranged horizontally at the top of a tower. A small horizontal-axis wind turbine is shown in Fig. 15.12. Vertical-axis wind turbines



**Fig. 15.12** A small horizontal-axis wind turbine installed at the Electric Energy Systems Laboratory of the National Technical University of Athens (Courtesy Authors)

have the rotor shaft and generator arranged vertically to the ground. Similarly to PVs, the main advantage of the wind turbines is that they are a clean source of energy, available worldwide. The main disadvantage is that they are an intermittent power source and, if not properly designed, they can create noise. Larger sized wind turbines are accused of aesthetic problems.

### Small Hydro Turbines

Small hydro stations produce hydroelectric power [15.25]. Hydro turbines convert water pressure into mechanical shaft power, which is used to rotate an electrical generator. Even though there is no global definition of small hydro turbines, their generating capacity usually ranges from 1–25 MW. Installations with a generating capacity from 100 kW to 1 MW are termed mini hydro turbines; installations from 10–100 kW micro hydro turbines, and installations below 10 kW are termed pico hydro turbines. In most cases, small hydro is *run-of-the-river*, which means that there is a small or no water reservoir capacity. Therefore, they have a small environmental impact.

### Microturbines

Microturbines are small combustion turbines, which can be used as small-scale distributed power generation, often in combined heat and power (CHP) applications [15.26]. Their generating capacity ranges from 25–500 kW. The operation of a microturbine is similar to that of conventional gas turbines. They use most commercial fuels, such as natural gas, petrol, propane, and diesel, and their typical efficiency ranges from 20–35%. However, when they are used in CHP applications, their efficiency can exceed 80%. The main advantages of microturbines are that they have a compact size, a small number of moving parts, and low emissions.

### Electrical Energy Storage Technologies

Electrical energy storage systems are recognized to have great potential in meeting challenges for the efficient management of the power systems, created by the intermittency of the generation of renewable power [15.27]. Electrical energy storage systems convert electrical energy to chemical, mechanical, or another storable forms of energy. Then, they can convert this stored energy back to electrical energy, when needed. They can provide various services at the distribution-system level, like load leveling and peak shaving, ancillary services (e.g., voltage and frequency regulation, power quality improvement, and spinning reserves), balancing (firming up) renewable energy power variations, resiliency to ride through blackouts, etc.

There are several energy storage technologies, such as battery energy storage systems (BESS), flywheels, pumped-storage hydroelectricity, compressed air energy storage (CAES), and superconducting magnetic energy storage (SMES) [15.28]. BESS use rechargeable batteries to convert electrical energy to chemical energy. They provide fast response times and, due to their compact size and quiet operation, they can be placed inside or close to buildings, household facilities, or wherever they are needed. The most common technologies use lead-acid, lithium-ion (Li-ion), sodium-sulfur (NaS), and nickel-cadmium (NiCd).

Pumped-storage hydroelectricity facilities pump water from a reservoir at low altitude to another one at a higher altitude during off-peak electricity periods. During periods of high demand, the stored water is released to generate electricity through turbines. Pumped storage enables the use of surplus energy from RES during periods with high load demand.

Flywheels store electricity in kinetic energy by accelerating a rotor. They have a longer lifespan than batteries and they can be used as an uninterrupted power supply, frequency regulation, or for smoothing wind power fluctuations.

CAES systems compress air into a storage vessel, e.g., an underground cavern, during periods of low demand. During periods of high demand, the air is released, heated and used to drive a turbine in order to generate electricity. SMES systems store energy within the magnetic field of a superconducting coil, which has been cryogenically cooled to a temperature below its superconducting critical temperature. They have small power losses and short time delays during charge and discharge.

## 15.4.2 Demand Response

*Demand response* (DR) is defined as:

Changes in electric usage by end-use customers from their normal consumption patterns in response to changes in the price of electricity over time, or to incentive payments designed to induce lower electricity use at times of high wholesale market prices or when system reliability is jeopardized [15.29].

DR programs provide mutual financial benefits to both utilities and end customers, improve reliability, and can reduce a network's peak load in the long term. Customers who participate in DR can change their energy consumption by partial load curtailment or load shifting from on-peak to off-peak time periods (valley filling). The efficient implementation of DR requires advanced

ICT to enable communication between utility and customers, installation of smart meters, and load control devices. Load control devices are used to remote control specific loads, e.g., motors, compressors, and thermostatic loads, e.g., space/water heating, and refrigeration.

### 15.4.3 From Passive to Active

The configuration of the distribution network has a direct impact on its operation and performance. Traditionally, distribution networks have been planned based on load forecasting, whereas distributed generation is often excluded. The network configurations derived from these planning studies consider maximum load demand and one-directional power flows (from substation to the consumers). Voltage regulation is provided by the on-load tap changers (OLTCs) at the HV/MV substations, in-line voltage regulators, and capacitors. Loss minimization studies involve the reconfiguration of distribution networks on a seasonal or monthly basis. Control actions in these *passive* distribution networks are limited, since all the potential operational issues are solved at the planning stage.

Offline power system analysis is performed to estimate the feasibility of the DG units' connection in order to avoid overvoltages and feeder overloads. These studies consider worst-case load/generation conditions, i.e., maximum load/no generation and minimum load/maximum generation. DG is modeled as a negative load with a constant power factor. This approach, known as the *fit and forget* approach, is acceptable, if DG connections to the network are relatively rare and geographically scattered, and thus do not have a negative impact on network operation and planning. At higher levels of DG penetration, however, the *fit and forget* approach can become a barrier, or it can lead to costly investments of the distribution infrastructure. To deal with these challenges in a reliable and cost-effective way, a more *active* approach is needed.

### 15.4.4 Active Network Management

*Active network management* (ANM) enables the coordinated control of distribution network components, such as OLTCs, voltage regulators, switched capacitors and switches, DG active and reactive output powers, energy storage systems, and flexible loads in an integrated manner. The objective of ANM schemes is to optimize the network operation considering single or multiple criteria. The fundamental difference between passive and active distribution networks is that ANM exploits the capacity and control capabilities of the DERs at distribution level, in order to optimize the network's planning and operational costs.

The large-scale integration of variable RES brings significant challenges to grid operation, which requires new and more complex tools for the distribution management system (DMS), however ANM techniques can exploit the inherent flexibility of the DER to provide cost-effective and efficient solutions for voltage and power-flow management in distribution systems.

The most common ANM schemes can be grouped as follows [15.30, 31]:

- *Coordinated voltage control*: voltage regulation devices are operated in a coordinated way with all available DERs active and reactive power-control capabilities.
- *Adaptive power factor*: the power factor of DG units is adapted in order to absorb or supply reactive power, in coordination with other voltage control devices.
- *Active power curtailment*: DG active power is curtailed due to technical constraint violations. This is usually a last resort scheme, since it has financial implications for the DG operators.
- *Energy storage management*: energy storage used for valley filling and peak power shaving to optimize the operation of the network in a technical and economic way. Energy storage operation can provide several benefits in distribution system operation, but it potentially affects the local energy market.
- *Demand side participation*: modification of the consumers' loads (load reduction, load shifting) either by direct control actions or individual consumer actions through financial incentives, is a great source of flexibility.
- *Distribution network reconfiguration*: the online reconfiguration of distribution networks through remotely controlled switching during normal and emergency conditions.

Table 15.5 summarizes passive and active network solutions to current distribution network problems.

The implementation of ANM requires an advanced communication infrastructure that is more flexible and more demanding than that of traditional distribution networks. The communication infrastructure is a substantial part of ADN, since ANM is highly dependent on real-time information about the network. Simultaneous analysis of power and communication systems is necessary to properly assess the reliability, availability, and security requirements of ADNs [15.32].

In the smart grid era, DMSs could provide real-time monitoring and control in order to improve a network's performance. The management system of an ADN consists of two functional blocks: state estimation and

**Table 15.5** Passive and active network management solutions to the technical challenges of distribution networks

Technical challenges	Passive distribution network	Active distribution network
Feeder overload	<ul style="list-style-type: none"> <li>● Network reinforcement (e.g., reconductoring of feeder segments)</li> <li>● Network reconfiguration</li> </ul>	<ul style="list-style-type: none"> <li>● DG active/reactive power control</li> <li>● ESS integration</li> <li>● DR schemes</li> <li>● Online reconfiguration</li> </ul>
Voltage drop/rise	<ul style="list-style-type: none"> <li>● Capacitor/voltage regulator placement</li> <li>● Network reinforcement</li> <li>● Network reconfiguration</li> </ul>	<ul style="list-style-type: none"> <li>● Coordinated voltage control</li> <li>● DG active/reactive power control</li> <li>● ESS integration</li> <li>● DR schemes</li> <li>● Online reconfiguration</li> </ul>
Loss minimization	<ul style="list-style-type: none"> <li>● Capacitor placement</li> <li>● Network reinforcement</li> <li>● Network reconfiguration</li> </ul>	<ul style="list-style-type: none"> <li>● Coordinated voltage control</li> <li>● DG active/reactive power control</li> <li>● ESS integration</li> <li>● DR schemes</li> <li>● Online reconfiguration</li> </ul>
Reactive power support	<ul style="list-style-type: none"> <li>● Capacitor placement</li> <li>● Transmission system</li> </ul>	<ul style="list-style-type: none"> <li>● DG units</li> <li>● ESS</li> </ul>
Protection	<ul style="list-style-type: none"> <li>● Recloser/fuse coordination</li> </ul>	<ul style="list-style-type: none"> <li>● Adaptive protective schemes</li> </ul>
Fault location	<ul style="list-style-type: none"> <li>● Trouble call system</li> <li>● Impedance-based methods</li> </ul>	<ul style="list-style-type: none"> <li>● Fault passage indicators</li> <li>● Smart meters</li> <li>● Automated outage mapping</li> </ul>
Service restoration	<ul style="list-style-type: none"> <li>● Technical crew dispatch</li> <li>● Manual switches operation</li> </ul>	<ul style="list-style-type: none"> <li>● Self-healing schemes</li> <li>● Remote controlled switches operation</li> </ul>

control scheduling. A distribution system state estimator (DSSE) receives real-time measurements from the advanced metering infrastructure installed in the distribution network, and with the proper deployment of pseudomeasurements and the use of network topology, the network status, i.e., nodal voltage magnitude and angle, is estimated. Based on the output values of the DSSE, an operation framework calculates the control values for the devices connected to the network. The set of control values aims at optimizing the power flow in the network and mitigating eventual voltage problems

that may arise in the operation of the grid, resulting from the variability of RES. Furthermore, a short-term load and RES forecasting function is required by the management systems of ADNs that incorporate optimization functions for the grid operation under normal and emergency conditions.

The main goal of ADNs is also to increase renewable DG penetration in existing distribution networks, which have been designed assuming HV/MV substation is the sole power source, while certain technical constraints are kept within their limits.

## 15.5 Distribution Network Monitoring and Control

Electric distribution utilities need to efficiently manage their distribution assets, with the aid of an *advanced distribution management system* (ADMS), in order to ensure higher reliability, improved power quality, data security, and resiliency to natural disasters for the customers [15.33–35]. ADMS is a collection of applications designed to continuously monitor and control, in an optimal manner, the various devices at substations and feeders of the distribution network (circuit breakers, reclosers, line switches, capacitor bank switches, voltage regulators, etc.), acting as a decision support system to the field operating personnel. ADMS includes the network applications, an outage management

system (OMS), and the Supervisory Control and Data Acquisition (SCADA) system.

SCADA gathers the real-time data from various remote locations or plants, presents the data on various HMIs, and records and logs the data on SCADA database management system [15.35, 36]. Figure 15.13 depicts the configuration and components of a SCADA system.

As can be seen from Fig. 15.13, a SCADA system consists of the following main elements:

- *Supervisory computer system*: This is responsible for communicating with the field-level controllers



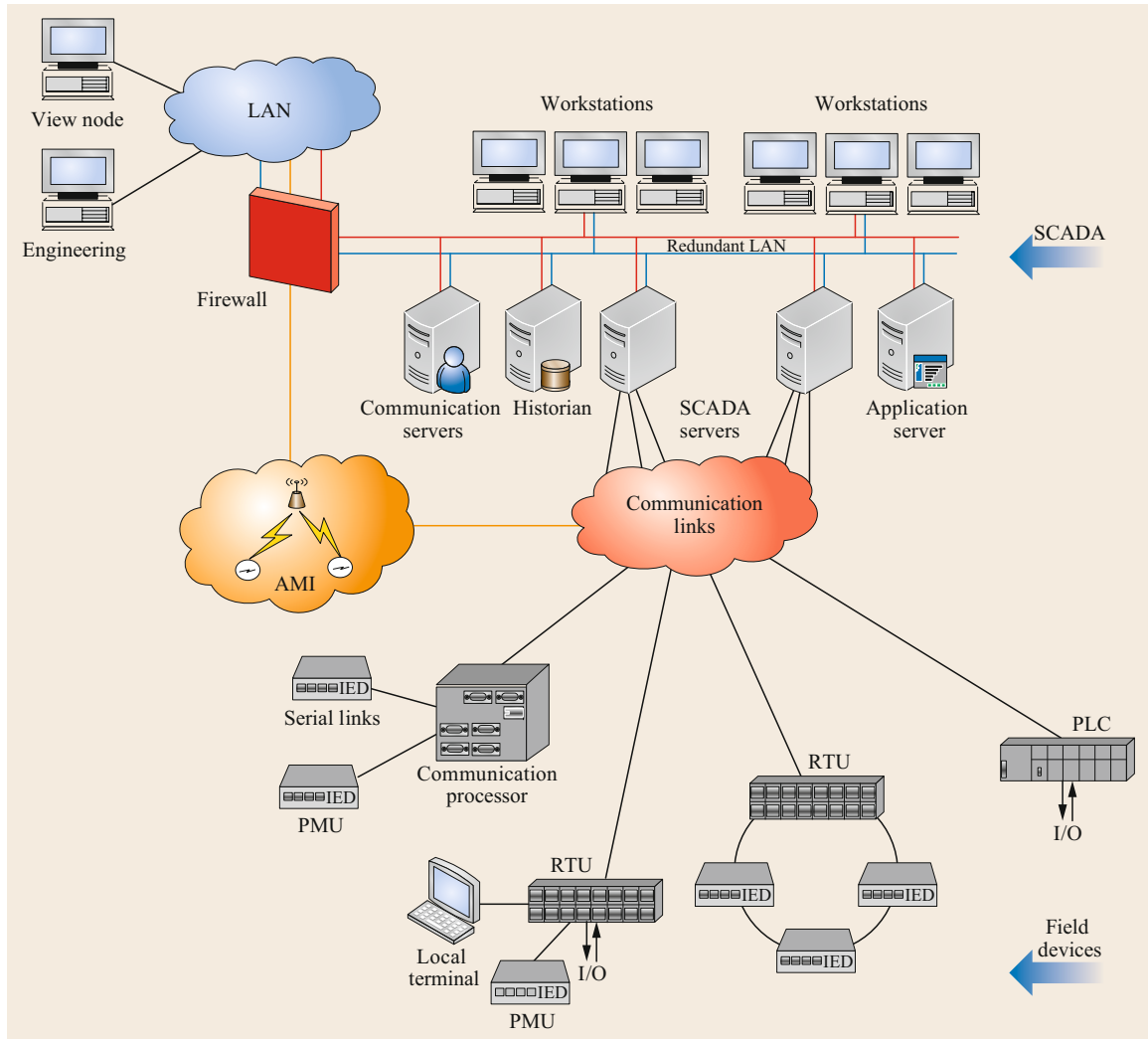
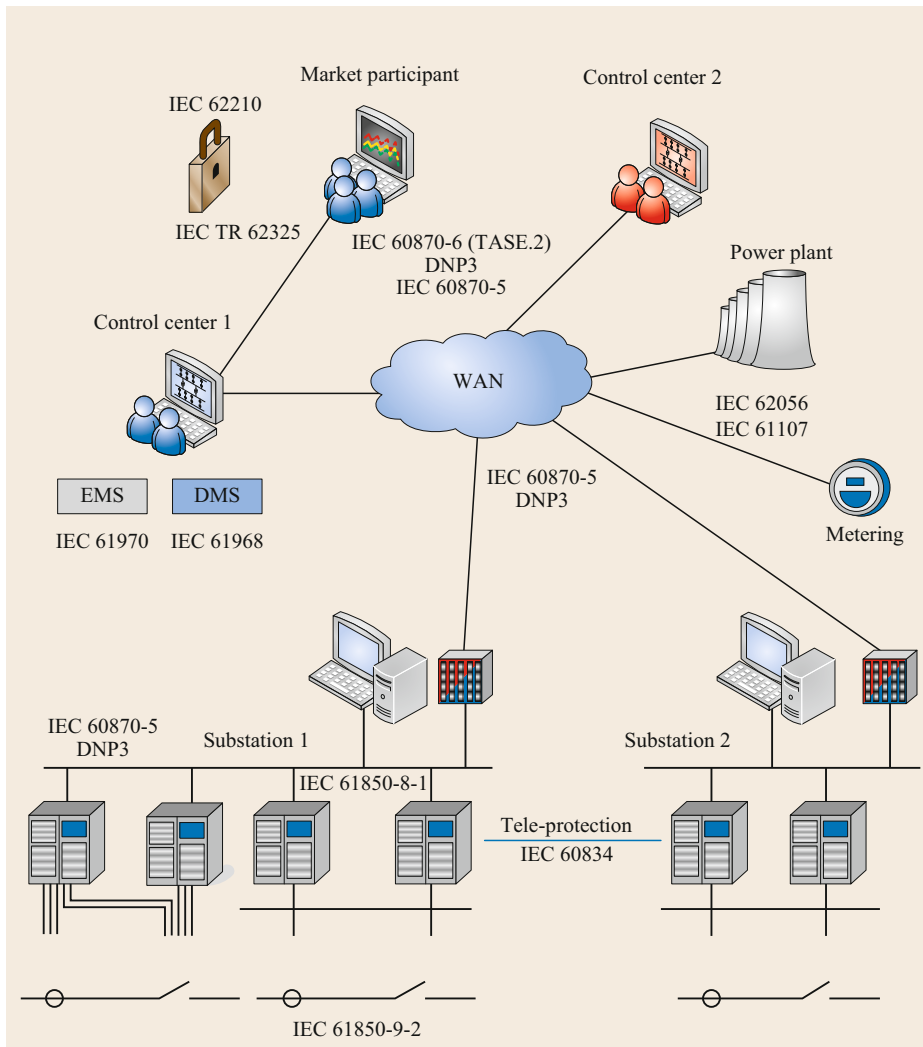


Fig. 15.13 Configuration of a SCADA system

(RTUs and PLCs). The remote terminal units (RTUs) and the programmable logic controllers (PLCs) are connected to sensors and actuators in the process and are networked to the supervisory computers. An RTU is a microprocessor-controlled electronic device that interfaces objects in the physical world to the control system by using messages from the master supervisory system to the control connected objects [15.37, 38]. A PLC is a digital computer used for automation of typically industrial electromechanical processes, such as control of machinery on factory assembly lines, amusement rides, or light fixtures [15.39]. PLCs have more sophisticated embedded control capabilities than RTUs and are programmed in one or more IEC 61131-3 programming languages [15.39]. PLCs are often used

in place of RTUs as field devices because they are more economical, versatile, flexible, and configurable.

- *Communication infrastructure*: This connects the supervisory computer system to the RTUs and PLCs, and may use industry standard or manufacturer proprietary protocols [15.40, 41]. Both RTUs and PLCs operate autonomously on the near-real-time control of the process, using the last command given from the supervisory system. Figure 15.14 depicts the most common communication protocols used in distribution network control.
- *Human-machine interface (HMI)*: This presents information to the system operators graphically in the form of mimic diagrams, which are a schematic representation of the network being controlled, and



**Fig. 15.14** Typical communication protocols used in a power system

alarm and event logging pages. The HMI is linked to the SCADA supervisory computers to provide live data to drive the mimic diagrams, alarm displays, and trending graphs.

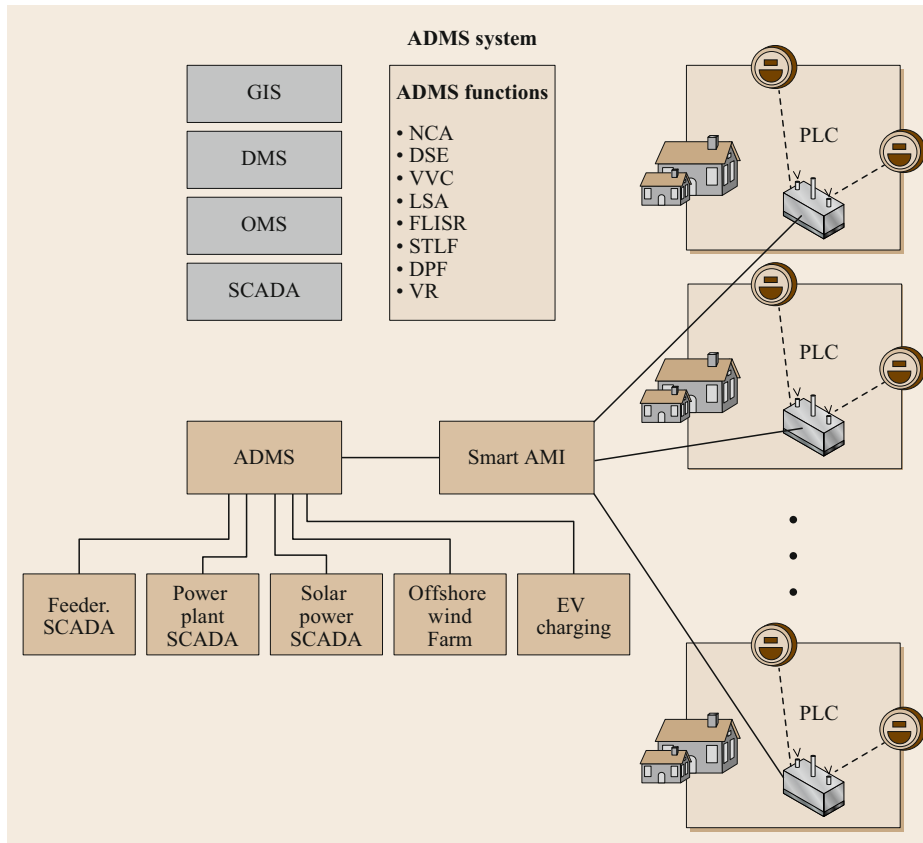
- **Alarm handling:** This checks whether certain alarm conditions are satisfied, to determine when an alarm event has occurred. Once an alarm event has been detected, one or more actions are taken (such as the activation of one or more alarm indicators, and perhaps the generation of email or text messages, so that management or remote SCADA operators are informed).

Figure 15.15 shows the structure of an ADMS system. The OMS includes trouble call, fault detection, fault location, isolation and supply restoration, crew management and outage reporting. The geographic in-

formation system (GIS) integrates hardware, software, and data for capturing, managing, analyzing, and displays all forms of geographically referenced information. GIS manages and maps the location of millions of miles of overhead and underground transmission lines, enabling the distribution utilities to identify vulnerabilities that cause outages, to weigh asset investments, to understand customer satisfaction, and to determine the right location for new facilities and new technology, such as smart grid sensors and smart meters.

The different functions of an ADMS system are briefly analyzed here:

- **Network connectivity analysis (NCA)**  
This helps the operator to identify or locate the feeding point of the various network components. Based on the status of all switching devices, such as circuit



**Fig. 15.15** ADMS functional structure

breakers (CBs), ring main units (RMUs), and isolators, NCA determines the topology and the radial or loop mode of the network.

- **Distribution state estimation (DSE)**  
 DSE is used for estimating the distribution network state and represents the basic DMS function, with all other DMS analytes based on its results. The state estimation (SE) function is based on algorithms especially oriented towards distribution networks, with low availability of real-time data, which must be compensated with historical data. The historical data of the network consist of daily load profiles—current magnitudes and power factors, or active and reactive power for all load classes (industrial, commercial, residential), for all seasons (winter, spring, summer, autumn), for types of days (weekday, Saturday, Sunday, and holidays)—and peak loads for all distribution transformers and/or consumers (peak currents and/or peak powers), and/or monthly electric energy transfers across all distribution transformers.
- **Volt/VAR control (VVC)**  
 This refers to the process of managing the voltage levels and the production, absorption, and flow of re-

active power at all levels in the distribution system. The VVC application helps the operator to mitigate such conditions by suggesting the required tap positions and capacitor switching to ensure the voltage to its limit and, thus, optimize Volt/VAR control.

- **Load shed application (LSA)**  
 The LSA automates and optimizes the process of selecting the best combination of switches to be opened and controlling in order to shed the desired amount of load.
- **Fault location isolation and service restoration (FLISR)**  
 This works in conjunction with SCADA, telecommunications, and distribution automation devices to decrease the number of customers affected by a power outage by automatically opening and closing switches to isolate compromised sections of line and to re-energize healthy sections of the system to restore energy distribution.
- **Short-term load forecasting (STLF)**  
 Short-term load forecasting is an important tool for planning, triggering load management strategies, and for determining unit commitment schedules. It can produce three types of forecasts based on full

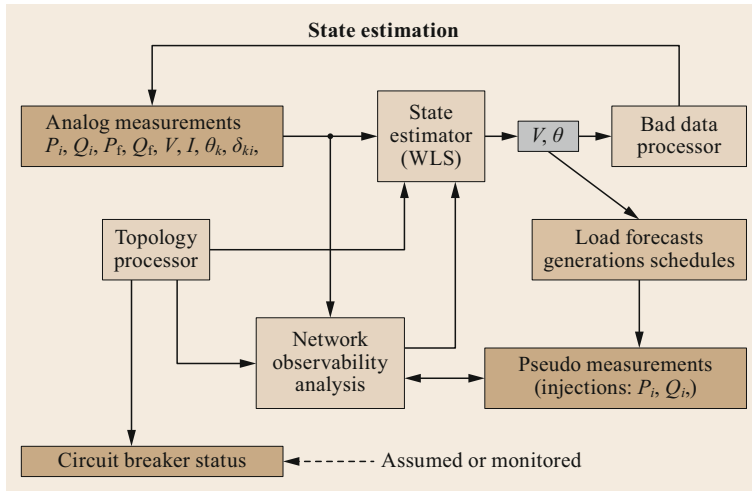


Fig. 15.16 Functionality of DSSE

historical load and weather data: 24-hour forecast, 7-day forecast, and 24-hour forecast, also producing interpolated predictions for 15, 30, 45, and 60 min into the upcoming hour.

- **Distribution power flow (DPF)**  
This provides a power-flow solution that best fits the power system model and the SCADA feeder measurements in the substations, and offers benefits, such as improved detection of system problems, including overloads and voltage violations, and accurate assessment of line losses.
- **Voltage reduction (VR)**  
This helps the operator to reduce, maintain, or restore system voltage in response to event triggers.

The DSSE, which is the key function in the ADMS, will be further described in the following. DSE is carried out based on measurements of electrical variables and calculates the state estimates (all node voltage magnitudes and phase angles) at a specified time. The functionality of state estimation is shown in Fig. 15.16.

In order to derive consistent and qualified state estimates, it is necessary to use all the information available for the distribution network and not only real-time measurements, whose availability is very limited in practice [15.42]. Therefore, the DSSE functionality includes information from different sources, namely: automated meter reading (AMR)/advanced metering infrastructure (AMI), RTUs, and phasor measurement units (PMUs) synchronized by the Global Positioning System (GPS) signal [15.43–55]. Furthermore, smart meters connected to LV nodes can make time-synchronized measurements of active and reactive loads, as well as voltage magnitudes, at predefined time intervals (usually every 15 min), transmitting them to a database server periodically (for instance, daily). This

ensures that the DSE will have, at least, measurements from the previous day of all the loads [15.46, 50]. Based on these measurements a set of pseudomeasurements will be generated and used together with near real-time information, for instance from DGs [15.43, 47], to make the network fully observable and guarantee an adequate degree of redundancy for running the state estimator. This can be accomplished by one of the proposed load estimation models in the literature [15.56–62], which utilize previous-day metered LV consumption data as well as same-day dependent variables, such as temperature, day type (weekday or weekend), humidity, etc. The upstream MV/LV substation load is estimated by aggregating all the downstream LV loads.

Figure 15.17 shows the components of the distribution network control architecture.

The mathematical formulation of the DSSE is based on the following nonlinear measurement model [15.42, 63]

$$z = \mathbf{h}(\mathbf{x}) + \mathbf{e}, \quad (15.42)$$

where  $\mathbf{z}$  is the measurement vector,  $\mathbf{h}(\mathbf{x})$  is the vector of nonlinear functions relating measurements to states,  $\mathbf{x}$  is the true state vector consisting of nodal voltages (magnitudes and phase angles), and  $\mathbf{e}$  is the vector of measurement errors. The class of estimators discussed in this section is based on the maximum likelihood theory and relies on a-priori knowledge of the distribution of the measurement error (normal), with  $E(\mathbf{e}) = 0$  and  $E(\mathbf{e}\mathbf{e}^T) = \mathbf{R} = \text{diag}(\sigma_i^2)$ , where  $\sigma_i^2$  is the variance of the  $i$ -th measurement error. A node is arbitrarily selected as the reference node, and its voltage angle is set to zero.

Measurements can be classified as *critical (nonredundant)* and *noncritical (redundant)*. A critical measurement is one whose elimination from the measurement set makes the network unobservable [15.64]. Crit-

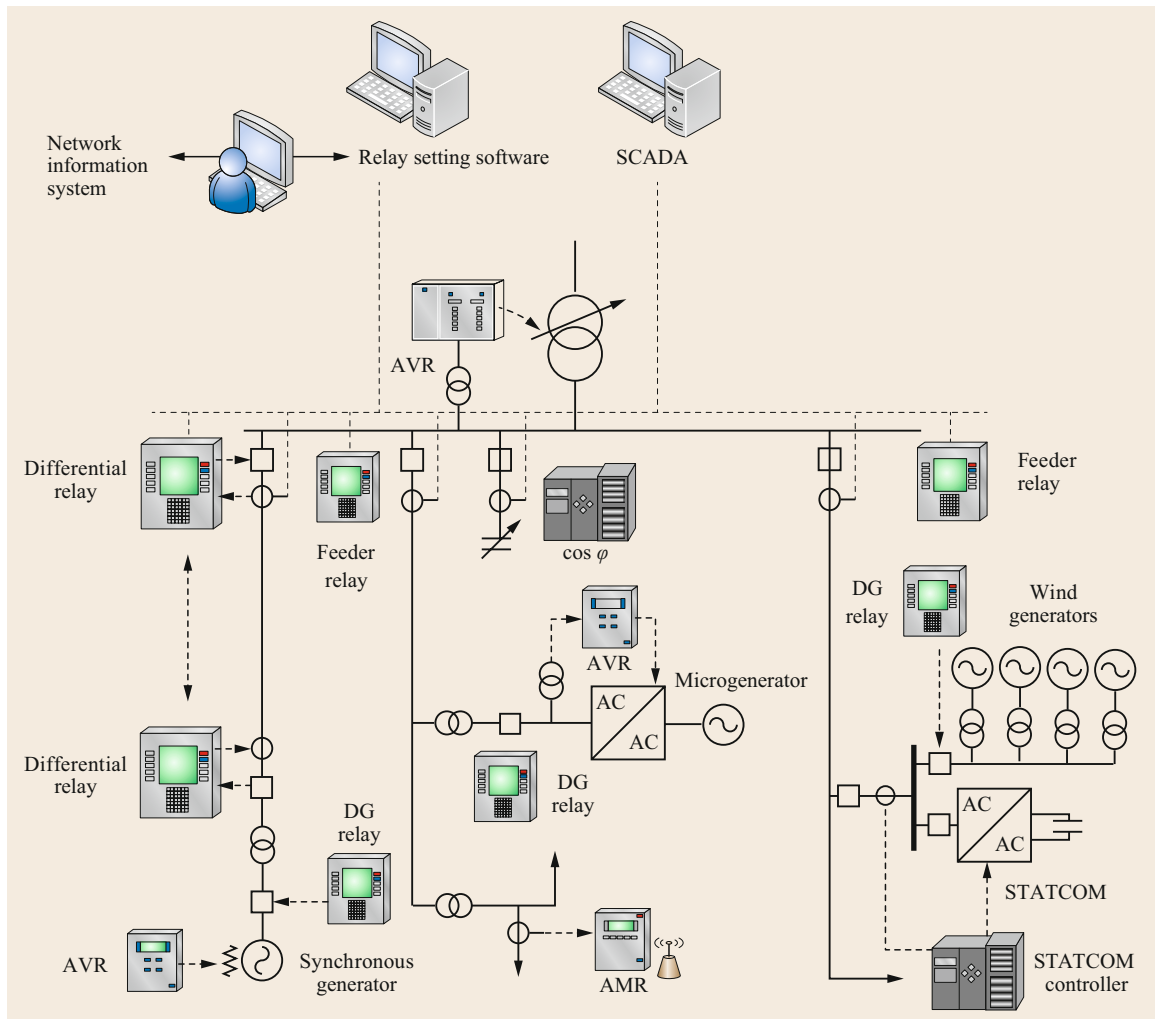


Fig. 15.17 Distribution network control architecture

ical measurements have zero residuals and, therefore, their errors cannot be detected. Noncritical measurements have nonzero residuals, allowing detection and possibly identification of their errors. A minimally dependent set of measurements has the property that elimination of any measurement from this set makes the remaining measurements critical. All the measurements of a minimally dependent set have equal absolute values of their normalized residuals [15.64]. As a consequence, gross error on one or more measurements of a minimally dependent set can be detected but not identified. Since the measurement redundancy is low in distribution networks, a few critical measurements and minimally dependent sets may occur, making the error filtering process rather difficult. This is the reason why forecast load (pseudo) measurements should be as accurate as possible.

The following input information should be available to the state estimator:

- Network electrical parameters
- Network configuration (topology) based on the status of switching devices and the position of transformer taps
- Actual (real-time) measurements subject to errors, due to metering inaccuracies and communication system (voltage magnitudes  $V$ , active and reactive branch power flows  $P_f$  and  $Q_f$ , active and reactive injections  $P_i$  and  $Q_i$  at load and generation nodes, and branch currents  $I$  at primary or distribution substation transformers and often at feeder heads)
- Pseudo measurements subject to errors (forecasted or historical active and reactive load injections  $P_i$

and  $Q_i$  or manually entered measurements of any type)

- Virtual measurements that contain no error (zero injections  $P_i$  and  $Q_i$  at network nodes that have neither load nor generation, zero voltage drops  $V_{ki}$  and  $\delta_{ki}$  at closed switching devices  $ki$ , and zero active and reactive power flows  $P_f$  and  $Q_f$  at open switching devices).

After the execution of the SE algorithm, the voltage magnitudes  $V$  and phase angles  $\Theta$  of the network nodes are estimated. The following output information is provided:

- Voltage magnitudes and phase angles at all nodes
- Active and reactive injected power at each generation and load node
- Active and reactive power flows at both sides of each line, transformer, and switch
- Current flows at both sides of each line, transformer, and switch
- Detection and removal of bad and conflicting data.
- Status of the switching devices with unknown or wrong status.

The problem is finding an estimate  $\hat{x}$  of the state vector that minimizes the following objective function [15.42]

$$J(x) = \sum_{i=1}^m \rho(r_i), \tag{15.43}$$

where  $r_i \approx N(0, 1)$  is the weighted residual of the  $i$ -th measurement

$$r_i = \frac{z_i - h_i(x)}{\sigma_i}. \tag{15.44}$$

Table 15.6 summarizes the approaches adopted for state estimation solution. The different estimators can be characterized based on the choice of the  $\rho$  function.

Performance evaluation of the SE techniques has shown that WLAV and SHGM methodologies cannot be applied to distribution systems [15.44]. The WLS method gives consistent and better quality performance when applied to distribution systems. Hence, WLS is

found to be the suitable solver and is used in this project.

The solution  $\hat{x}$  can be found by the normal equations' (NE) iterative procedure as follows

$$G(x^k) \Delta x^k = H^T(x^k) R^{-1} \Delta z^k, \tag{15.45}$$

where,  $\Delta x^k = x^{k+1} - x^k$ ,  $\Delta z^k = z - h(x^k)$ ,  $H = \partial h / \partial x$ , and  $G = H^T R^{-1} H$  is the Jacobian matrix, respectively, evaluated at  $x = x^k$ , and  $k$  is the iteration index.

Since real-time measurements of node injections (loads) are not available in practical distribution networks, a kind of load modeling is necessary to generate the required load data for the DSSE execution. The load information can be modeled considering one of the following sources [15.53–62]:

- Historical samples obtained for different seasons, days, and times, are stored separately for different load types (residential, industrial, and commercial), based on some monitoring and energy bill data.
- AMI, which transfer customer load information to the utility DMS in a bidirectional way.
- AMR systems, which transmit energy consumption data to the utility for billing, between defined time intervals (minutes to hours), in a unidirectional way.
- Advanced AMR meters, which work as intelligent monitoring devices and utilize the communication infrastructure to provide vital information on low voltage levels.
- Smart GPS synchronized PMU devices, located at strategic nodes of the network, to measure voltage and current phasors.

It is assumed that domestic smart meters connected to a node take synchronized measurements of active ( $P$ ) and reactive ( $Q$ ) consumption of the loads at predefined time intervals. These measurements are transmitted to a database server periodically. In any case, DSE will have the previous day's measurements of all the loads. The proposed SE will reliably estimate the node voltages of a distribution network by using the previous day's measurements (while considering whether the day is a weekday, Saturday, or Sunday).

**Table 15.6** State estimation approaches

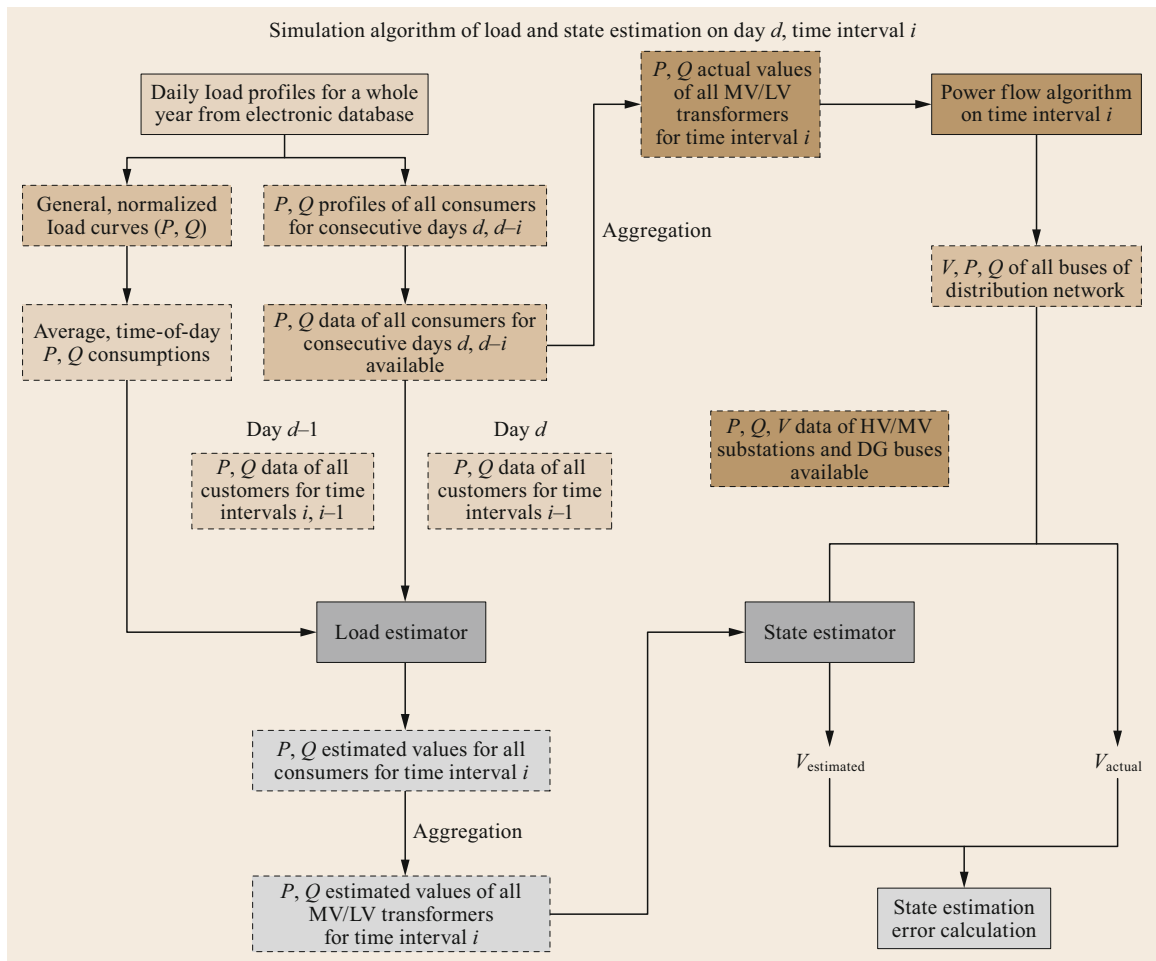
Approach	$\rho(r_i)$	Solution method
Weighted least squares (WLS)	$\frac{1}{2}r_i^2$	Newton iterative
Weighted least absolute value (WLAV)	$ r_i $	Linear programming (LP) or interior point (IP)
Schweppe–Huber generalized-M (SHGM)	$\begin{cases} \frac{1}{2}r_i^2 & \text{if }  r_i  \leq \alpha w_i \\ \alpha w_i  r_i  - \frac{1}{2}\alpha^2 w_i^2 & \text{otherwise,} \end{cases}$ where $w_i$ is the iteratively modified weighting factor and $\alpha$ is a tuning parameter	Iteratively reweighted least squares (IRLS)

**Table 15.7** Required data for state estimation execution

LV network	<ul style="list-style-type: none"> <li>● <math>P/Q</math> power consumption and <math>V</math> magnitude at every LV load bus</li> <li>● <math>P</math> power production and <math>V</math> magnitude at every LV production bus.</li> </ul>
MV network	<ul style="list-style-type: none"> <li>● <math>P/Q</math> power consumption at MV consumption bus, if available.</li> <li>● <math>P/Q</math> power production and <math>V</math> magnitude and phase at MV production bus, if available.</li> <li>● <math>P/Q</math> power flow in the MV lines with RTU or PMU.</li> </ul>
MV/LV (secondary) substations	<ul style="list-style-type: none"> <li>● <math>P/Q</math> power consumption, <math>V</math> magnitude and/or <math>I</math> magnitude and power factor, in the primary or secondary of the transformer, if available.</li> </ul>
HV/MV (primary substation)	<ul style="list-style-type: none"> <li>● <math>P/Q</math> power consumption, <math>V</math> magnitude and/or <math>I</math> magnitude and power factor, in the primary or secondary of the transformer, if available.</li> </ul>

**Table 15.8** Transmission frequency for each data level

Past data of the LV network	It should be available once a day with 24 h of delay (i.e., from $d - 1$ ).
Dynamic data of the LV network	The data of some reference DG and load units (by distribution transformer controllers—DTC) should be available every 15 min with a maximum delay of 1 min.
MV network	It should be available in real time (e.g., on a 1 min time basis).



**Fig. 15.18** Data flow chart of the load and state estimation

The AMR meters installed at distributed generators (DG) will measure the net active power  $P$ , the net reactive power  $Q$ , and the voltage magnitude  $V$  at predefined time intervals and communicate immediately to the server. The SE will also read the  $P/Q$  consumption of the loads connected to each transformer, which will be summed up (as the measurements are time synchronized) to calculate the load of the transformer (and the node). The previous day's loads of the nodes and near real-time power measurements from distributed generators will be used as power injection measurements. Summarizing, the required data for state estimation execution are shown in Table 15.7 [15.42].

The transmission frequency for each data level is shown in Table 15.8 [15.42].

A general framework for the combined simulation of load and state estimation is presented in Fig. 15.18.

The *load estimation algorithm* uses data provided by LV or MV smart meters and deploys a simple time series model [15.62] using basic class-specific load curves associated to each consumer type (e.g., domestic, commercial etc.) to improve the accuracy of individual customer load estimates. Load estimates can be obtained hourly, half-hourly, or at shorter time intervals. Then, all individual load estimates are aggregated, based on topology and connectivity data, to extract load estimates per MV/LV distribution transformers. These values are treated as pseudomeasurements and used as inputs to the state estimation algorithm along with (near) real-time data collected from other points of the power network [15.62]. The time delay in data transmissions from smart meters to data management centers is a parameter that significantly affects the load estimation algorithm performance.

## 15.6 Operation of Active Distribution Networks

Distribution system operation aims at satisfying the load demand in a safe and economical way. The security, quality, and economy of the power supply depend on the control capabilities of the network's equipment. The *operation functions of power distribution networks* can be divided into two categories, each corresponding to different time horizons:

- *Realtime operation*, in which control actions are applied in a short time period; they are calculated based on real-time measurements and state estimation techniques.
- *Day-ahead or schedule operation*, in which control actions of one or more days are calculated based on forecasted values of load demand and renewable generation. Realtime operation management consists of state estimation and control scheduling.

A DSSE receives real-time measurements from the metering infrastructure installed in the distribution network and with the proper deployment of pseudomeasurements and the use of network topology, the network status, i.e., nodal voltage magnitude, and angle, is estimated. Based on the output values of the DSSE, an operation framework calculates the control values for the devices connected to the network. The set of control values aims at optimizing the power flow in the network and mitigating eventual voltage problems that may arise in the grid operation. For the management of ADNs, short-term load and RES forecasting functions that incorporate optimization functions for the grid operation under normal and emergency conditions might be required.

### 15.6.1 Operation of Active Distribution Networks Under Normal Operating Conditions

Under normal operating conditions, control actions aim at the safe and optimum operation of the network, considering variable demand and renewable generation. Control actions in passive distribution networks were limited in the control of network components such as OLTC, switches, and switched capacitors. However, ANM enables the coordinated control of network components and DER to ensure the safe operation of the network. Thus, the network operation becomes more complex with more sophisticated optimization criteria and operational constraints.

The operation of the distribution network depends on the regulatory framework and the level of automation, which differ from one country to another. *The optimal operation of ADNs under normal operating conditions* requires the optimization of several objectives. Some of these can be summarized as follows [15.31, 65]:

- *Minimization of energy losses*: energy loss cost constitutes a substantial part of the network's operational cost, and its minimization improves the network's performance.
- *DG curtailment minimization*: curtailment of DG active power is usually employed to prevent line overload and/or voltage rise along the feeder. DG curtailment has financial consequences for the owners of the DG units, and it can be a barrier for further DG penetration.



- *Minimization of OLTC tap position changes:* frequent operation of OLTCs will shorten their lifetime.
- *Minimization of switch operations:* the reconfiguration of ADNs should be based on a limited number of switch operation. Extensive operation of the switches and switched capacitors will shorten their lifetime.

The aforementioned optimization criteria are not necessarily conflicting and of equal importance. Their priority is determined based on the regulatory framework and the existing infrastructure of the distribution network.

The optimal operation of ADNs is subject to the network's technical constraints. As shown in Sect. 15.3, power-flow balance should be ensured at all system buses. Due to the variability of load demand and renewable generation, voltage constraints need to be considered in order to ensure that bus voltages are kept within their limits for every applied control action. Similarly, line capacity limits should be considered. In the case when reconfiguration is applied, the radiality of the network configuration needs to be maintained. The DG units can absorb or supply reactive power via their inverter interface. The limits of the active and reactive power output of a DG unit are expressed as

$$Q_{DG,i,t} \leq (P_{DG,i,t} - P_{DG,i,t}^{curt}) \tan \varphi_{DG}, \quad (15.46)$$

$$Q_{DG,i,t} \geq -(P_{DG,i,t} - P_{DG,i,t}^{curt}) \tan \varphi_{DG}, \quad (15.47)$$

$$0 \leq P_{DG,i,t}^{curt} \leq P_{DG,max,i}^{curt}, \quad (15.48)$$

$$P_{DG,max,i}^{curt} \leq P_{DG,i,t}, \quad (15.49)$$

$$(P_{DG,i,t} - P_{DG,i,t}^{curt})^2 + Q_{DG,i,t}^2 \leq S_{DG,max,i}^2, \quad (15.50)$$

where  $P_{DG,i,t}$  and  $Q_{DG,i,t}$  are the active and reactive power output of the DG unit at bus  $i$  at period  $t$ ,  $P_{DG,i,t}^{curt}$  is the active power curtailment of the DG unit at bus  $i$  at period  $t$ ,  $\varphi_{DG}$  is the maximum power angle of the DG unit of bus  $i$ ,  $P_{DG,max,i}^{curt}$  is the maximum active power curtailment of the DG unit at bus  $i$  at period  $t$ , and

**Table 15.9** Load data of the 30-bus distribution system

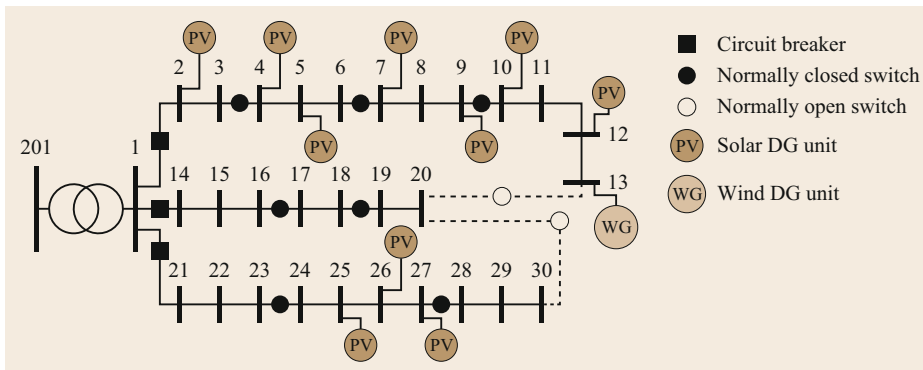
Bus	Load (kVA)
3, 4, 5, 8, 9, 10, 12, 13, 15, 16, 18, 23, 24, 27, 30	50
2, 6, 7, 11, 14, 17, 20, 21, 22, 25, 26	350
19, 28, 29	675

$S_{DG,max,i}$  is the maximum apparent power of the DG unit at bus  $i$ . The maximum and minimum DG reactive power injection limits are given by (15.46) and (15.47), respectively. Note that  $P_{DG,i,t}^{curt}$  is greater than or equal to zero and is limited by (15.48) and (15.49). The apparent DG power output is lower than the apparent power limit of the DG inverter according to (15.50).

**Example 15.1**

Consider the 30-bus distribution of Fig. 15.19, which is a 20kV system with 3 feeders, 29 load buses, 7 normally closed switches, and 2 normally open switches. Each feeder is equipped with a circuit breaker. The length of each feeder segment is 2 km; the length of the tie lines is 3 km and the conductor of the feeders and tie lines is ACSR-95 mm<sup>2</sup> (Table 15.3). The bus load data are presented in Table 15.9; their power factor is 0.95 lagging. The network accommodates 100kW of solar DG at buses 2, 9, 10, 25, 26, and 27; 300kW of solar DG at buses 4 and 12; 500kW of solar DG at bus 7; 600kW of solar DG at bus 5; and 5 MW of wind DG at bus. In this example, the voltage limits are set to ±5% of the nominal voltage.

For the hourly load, and the solar and wind profile of Fig. 15.20, the day-ahead operation of the network is simulated considering two ANM schemes in order to minimize the DG curtailment. The first ANM involves the active power curtailment (APC) of all DG units, while the second ANM scheme involves the APC and the active distribution network reconfiguration (ADNR). As shown in Fig. 15.21, in the first ANM scheme, the DG energy curtailment is equal to 3.812 MWh, while in the second ANM scheme, there is no need for DG curtailment. Note that in the sec-



**Fig. 15.19** The 30-bus distribution system

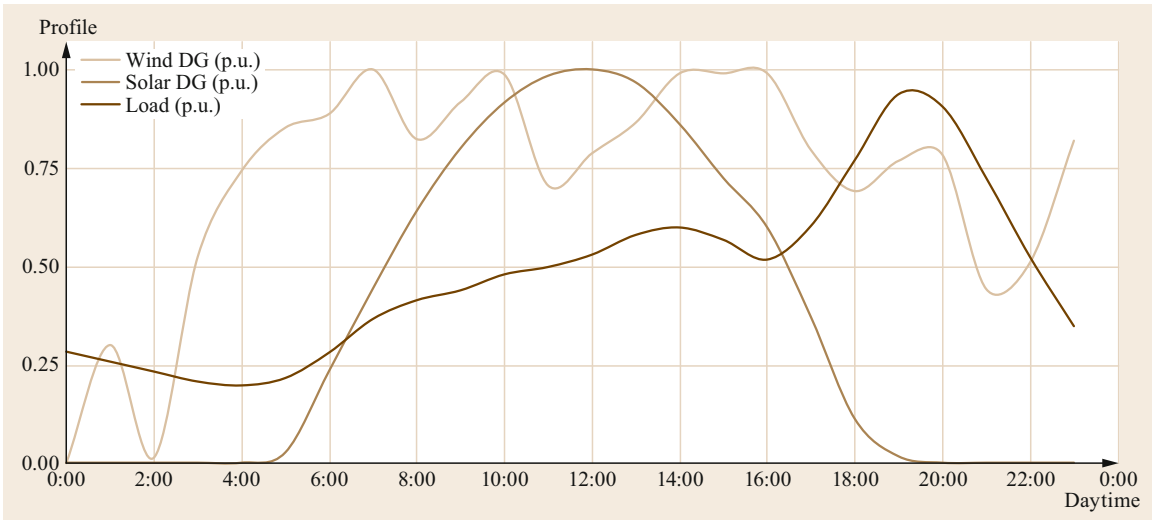


Fig. 15.20 Hourly load, solar DG and wind DG profiles (p.u.)

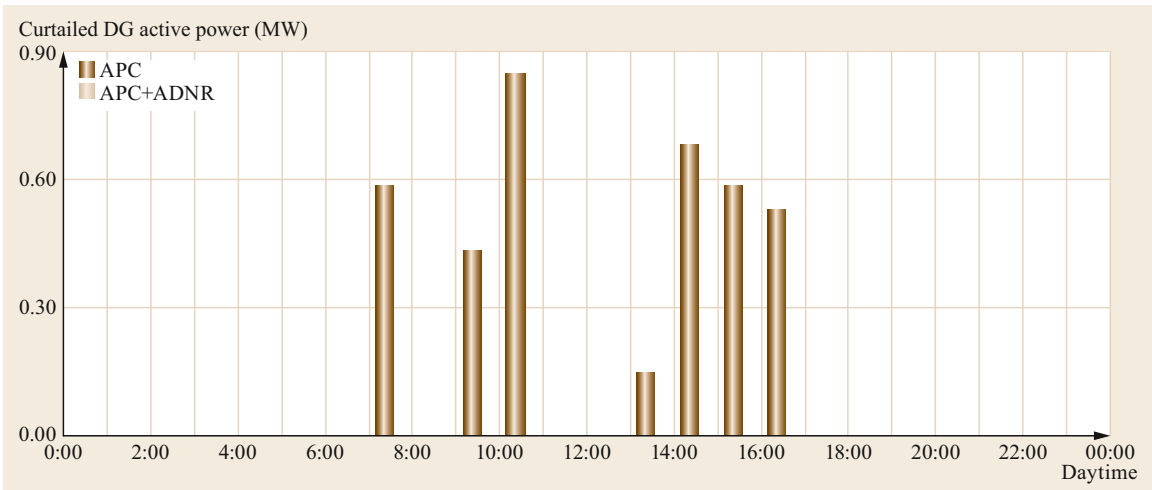


Fig. 15.21 Curtailed DG active power

and ANM scheme, the normally closed switch in line 16–17 is opened, and the normally open switch in line 13–20 is closed. Furthermore, the necessity of ANM is highlighted in Fig. 15.22. As shown, if passive management is adopted, the voltage limits at bus 13 will be violated. Hence, the distribution network will operate outside its technical limits for a considerable time.

### 15.6.2 Operation of Active Distribution Networks Under Emergency Operating Conditions

Distribution networks are designed with a meshed structure, and they are equipped with normally open

and normally closed switches. However, they operate in radial configuration to simplify protection coordination. Hence, a network component failure will interrupt the power supply to all buses downstream of the faulted area. Network component failures can occur for various reasons, such as extreme weather conditions, component ageing, or an accident. Under these emergency conditions, an OMS aims at resolving the outage and restoration of power supply to customers. As is shown in Fig. 15.23, after the outage alert, the three stages of the *outage management* are [15.66]:

- Fault location
- Fault isolation
- Service restoration.

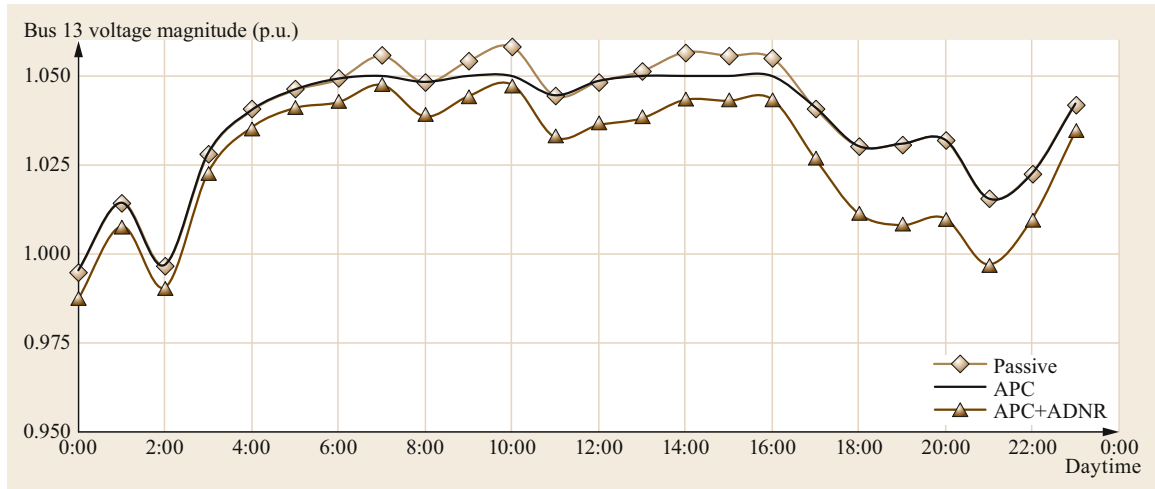


Fig. 15.22 Bus 13 voltage magnitude (p.u.)

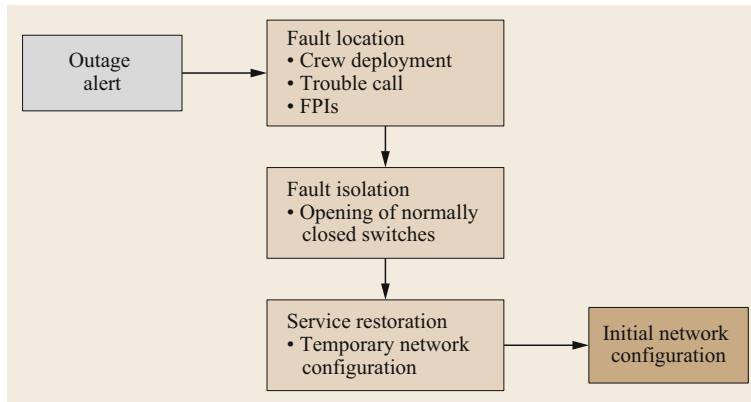


Fig. 15.23 The stages of the FLISR process

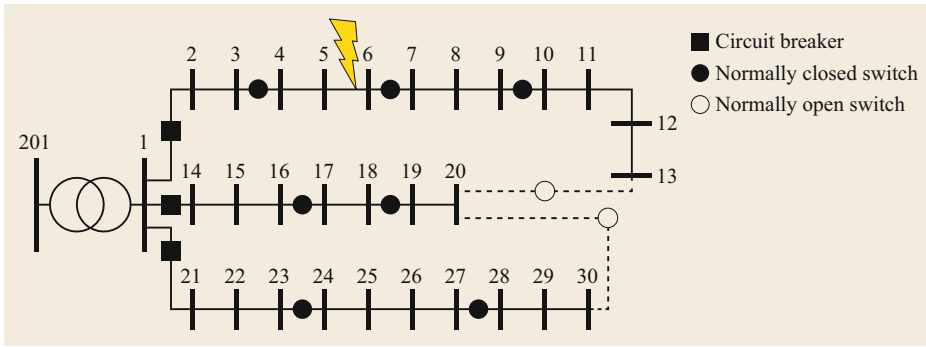
The fault location, isolation, and service restoration (FLISR) process needs to be implemented as fast as possible to decrease restoration time and potential lost revenues. Most distribution systems are not fully automated, and some required control actions of the FLISR process need manual operation. Hence, a self-healing distribution system is important, with social and economic benefits. Self-healing can be described as the capability of the distribution system to perform all phases of the FLISR process automatically, without human intervention.

When a fault occurs, the circuit breakers, which are installed at the source of the feeder, or reclosing devices trip, and the power supply to the downstream buses is interrupted. After identifying the faulted feeder, the exact location of the faulted section needs to be determined. Several approaches have been implemented to identify the *fault location*; they are summarized as follows [15.67]:

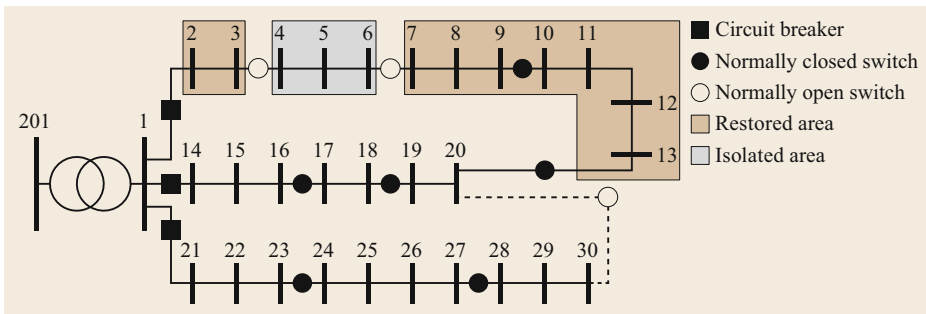
- Crew deployment to visually identify the faulted area and repair it. This approach may prove time consuming, leading to extended interruption periods.
- Direct three-phase circuit analysis-based methods.
- Impedance-based methods.
- Traveling-wave methods.
- Data collected from fault passage indicators (FPIs).

The main drawback of the direct three-phase circuit methods and impedance-based methods is the multiple estimations of fault location. The traveling wave methods may yield inaccurate fault locations due to the presence of laterals and sublaterals.

After fault isolation, *service restoration* aims at determining the appropriate switch operations to restore power supply to the nonfaulted part of the distribution feeder. To achieve this, loads of the nonfaulted part of the distribution feeder are transferred to the neighboring, healthy distribution feeders. Service restoration



**Fig. 15.24** The 30-bus distribution system



**Fig. 15.25** Topology of the 30-bus distribution system after service restoration due to fault in line 5–6

needs to satisfy multiple objectives in a very short time. The objective with the foremost importance is the minimization of the nonsupplied loads. Minimization of the number of switch operations has the second priority. When a service restoration plan is determined, the priority of critical loads, e.g., hospitals, needs to be considered along with the network's technical constraints. There are several methods implemented for the solution of the service restoration problem; they are summarized as follows [15.67]:

- Expert system methods based on knowledge-based if-then-else rules [15.68–70].
- Heuristic methods based on artificial intelligence [15.71–74].
- Mathematical programming methods that formulate the service restoration problem as an optimization problem utilizing global optimization techniques [15.75–77].

Expert-system methods are the most widely used methods for the solution of service restoration. However, they tend to be problem specific, and their rules are normally different among distribution networks. Heuristic

methods require the incorporation of a power-flow model, and they may require multiple iterations to converge to an optimal solution. Mathematical programming methods may require high computation times for large-scale distribution systems.

#### Example 15.2

Consider the 30-bus distribution system of Example 15.1 (Sect. 15.6.2). As is shown in Fig. 15.24, it is assumed that a permanent fault occurs in line 5–6. In this case, the circuit breaker in line 1–2 trips, and the power supply of load buses 2–13 is interrupted. After the fault location has been identified, the normally closed switches in line 3–4 and in line 6–7 are opened to isolate the faulted area. The load buses 4, 5, and 6 will stay out of service until the damaged line is repaired or replaced. Service restoration needs to determine the minimum switch operations to restore power supply to buses 2 and 3, and 7–13. Thus, the circuit breaker in line 1–2 and the normally open switch in line 13–20 are closed, and the power supply of the non-faulted area is restored. The network topology after the implementation of the service restoration plan is shown in Fig. 15.25.

## 15.7 Distribution Network Planning

*Distribution network planning* (DNP) aims at determining the location, capacity, and time period of network investments at minimum cost, in order to serve the load growth and the new loads, while ensuring the safe operation of the distribution network. Depending on the duration of the planning period, the DNP can be classified as short term (1–5 years) or long term (5–20 years). Short-term planning considers network reinforcement or line reconductoring, reconfiguration schemes, and reactive power support options, while long-term planning considers the reinforcement of existing network components, e.g., substation, lines, and the addition of new ones. There are two DNP models [15.78]:

- *Static distribution network planning*, wherein the DNP problem is solved in a single stage considering only the conditions of the final stage of the planning period. In this model, the investment decisions are decoupled from time, and they are implemented at the beginning of the planning period.
- *Multistage distribution network planning*, wherein the DNP problem is solved considering the multiple stages of the planning period. Hence, the investment variables are determined over successive planning stages based on the requirements of each stage.

The multistage DNP formulation is more efficient than the static formulation, since the investment decisions are implemented over the planning period. Thus, the investment decisions required at the first stages of the planning can be implemented immediately, while the ones determined for the later stages of the planning period can be reexamined using updated values of the load forecast. Obviously, the formulation and solution of the multistage DNP model are more complicated than the static ones.

The planning of a distribution network is affected by a large number of miscellaneous factors, such as load growth, the necessity to increase the level of distribution automation, and the increasing DG penetration. The most important of these factors is the forecasted load growth rate of the geographical area that the distribution network serves. Load growth depends on the area development, load density, population growth, customer behavior, and geographical limits. Apart from load growth, modern power distribution systems are facing the challenge to accommodate an increasing amount of DG. Consequently, DNP should also consider future connections of DG units and their increase rate.

The determination of the maximum stress conditions of a planning period is essential for the calculation of the planning requirements. The maximum stress conditions consider load/generation scenarios

with: (i) maximum load/no generation and (ii) minimum load/maximum generation. Furthermore, the determination of representative load/generation scenarios that represent the stochastic behavior of load demand and renewable generation is essential to calculate the cost of energy losses, which is the largest part of the network's operational costs. To derive these representative load/generation scenarios, it is necessary to process historic and statistical data.

The main objective of every DNP formulation is the minimization of the net present value of the investment and operational cost of the network for a planning period. The investment cost is the sum of the costs for the reinforcement and/or addition of network components, and they can be summarized as follows:

- Investment cost for the reinforcement and/or addition of distribution substation (IS)

$$IS = \sum_{i \in \Omega_{SR}} \sum_{a \in \Phi_{SS}} C_{SS,a} y_{i,a,t}^{SR} + \sum_{i \in \Omega_{SA}} \sum_{a \in \Phi_{SS}} C_{SS,a} y_{i,a,t}^{SA}, \quad (15.51)$$

where  $\Omega_{SR}$  and  $\Omega_{SA}$  are the sets of the candidate substations to be reinforced and added, respectively;  $\Phi_{SS}$  is the set of the available types of substations;  $C_{SS,a}$  is the cost of type  $a$  substation; and  $y_{i,a,t}^{SR}$  and  $y_{i,a,t}^{SA}$  are the decision variables for the reinforcement and addition of substation at bus  $i$  using type  $a$  substation at period  $t$ , respectively.

- Investment cost for the reinforcement and/or addition of distribution lines (IL)

$$IL = \sum_{ij \in \Omega_{LR}} \sum_{b \in \Phi_L} C_{L,b} l_{ij} y_{ij,b,t}^{LR} + \sum_{ij \in \Omega_{LA}} \sum_{b \in \Phi_L} C_{L,b} l_{ij} y_{ij,b,t}^{LA}, \quad (15.52)$$

where  $\Omega_{LR}$  and  $\Omega_{LA}$  are the sets of the candidate distribution lines to be reinforced and added, respectively;  $\Phi_L$  is the set of the available types of conductors;  $C_{L,b}$  is the cost per distance of type  $b$  conductor;  $l_{ij}$  is the length of line  $i$ – $j$ ; and  $y_{ij,b,t}^{LR}$  and  $y_{ij,b,t}^{LA}$  are the decision variables for the reinforcement and addition of line  $i$ – $j$  using type  $b$  conductor at period  $t$ , respectively.

- Investment cost for the placement of capacitor banks (IC)

$$IC = \sum_{i \in \Omega_{CB}} \sum_{c \in \Phi_{CB}} C_{CB,c} y_{i,c,t}^{CB}, \quad (15.53)$$

where  $\Omega_{CB}$  is the set of the candidate buses for the placement of capacitors;  $\Phi_{CB}$  is the set of the types

of capacitors available;  $C_{CB,c}$  is the cost of type  $c$  capacitor;  $y_{i,c,t}^{CB}$  is the decision variable for capacitor placement at bus  $i$  using type  $c$  capacitor at period  $t$ .

- Investment cost for the placement of voltage regulators (IVR)

$$IVR = \sum_{ij \in \Omega_{VR}} \sum_{d \in \Phi_{VR}} C_{VR,d} y_{ij,d,t}^{VR}, \quad (15.54)$$

where  $\Omega_{VR}$  is the set of the candidate lines for the placement of voltage regulators;  $\Phi_{VR}$  is the set of the available types of voltage regulators;  $C_{VR,d}$  is the cost of type  $d$  voltage regulator; and  $y_{ij,d,t}^{VR}$  is the decision variable for the voltage regulator placement at line  $i$ – $j$  using type  $d$  voltage regulator at period  $t$ .

For an optimal network reinforcement and expansion plan, it is required to examine as many as possible of the planning alternatives presented in (15.51)–(15.54) in order to achieve the optimal budget allocation. The operational cost consists of several terms, such as the cost for energy losses, reliability costs, and maintenance costs.

The constraints of the DNP can be classified into two categories: (i) the operational constraints and (ii) the constraints associated with the investment decision variables. For a given load forecast and generation, the operational constraints need to ensure that the bus voltages are kept within their limits, the thermal capacity of lines and substations are not violated, and the configuration of the network is radial during the whole planning period. If the investment decision variables of (15.51)–(15.54) are formulated as binary variables, the investment constraints are formulated as

$$\sum_{t \in T} \sum_{a \in \Phi_{SS}} y_{i,a,t}^{SR} \leq 1, \quad (15.55)$$

$$\sum_{t \in T} \sum_{a \in \Phi_{SS}} y_{i,a,t}^{SA} \leq 1, \quad (15.56)$$

$$\sum_{t \in T} \sum_{b \in \Phi_L} y_{ij,b,t}^{LR} \leq 1, \quad (15.57)$$

$$\sum_{t \in T} \sum_{b \in \Phi_L} y_{ij,b,t}^{LA} \leq 1, \quad (15.58)$$

$$\sum_{t \in T} \sum_{c \in \Phi_{CB}} y_{i,c,t}^{CB} \leq 1, \quad (15.59)$$

$$\sum_{t \in T} \sum_{d \in \Phi_{VR}} y_{ij,d,t}^{VR} \leq 1. \quad (15.60)$$

Constraints (15.55) and (15.56) ensure that there will be at most one change in the capacity of the substations that are candidates for reinforcement and addition, respectively. Constraints (15.57) and (15.58) are applied in order to avoid more than one conductor change during the planning period, for the distribution lines

that are candidate to be reinforced or added. According to (15.59) and (15.60), investments in capacitors and voltage regulators can be made at most once in each candidate bus and branch during the planning period.

The advent of ADNs modifies the objectives and the requirements of the planning process [15.79]. Solution methods and concepts that were used extensively for transmission systems are adapted for distribution systems to deliver more cost-effective planning solutions that rely less on traditional network investments and exploit the active management of the DER available [15.80]. Thus, the incorporation of the operational aspects of DER control into the planning process is essential. For example, the control of the active and/or reactive power of the DG units can be considered in the planning process in order to cope with the voltage rise effect caused by DG penetration, alleviate line congestion, and decrease power losses. Energy storage systems can be used to inject energy into the network during periods of low demand; the energy stored in this manner can be returned to the grid at a later time, when load demand is higher. This load shifting effect can eliminate line overloads and/or violation of bus voltage limits, while the cost for network reinforcement can be deferred. Similarly, demand response schemes can be employed, when customers' consumption leads to violation of network's technical characteristics. The way that the most common technical challenges found in distribution networks can be solved considering active management of the distribution network is presented in Table 15.5.

### Example 15.3

Consider the 20 kV distribution network of Fig. 15.26 with two substations, 20 load buses, and a planning period that is divided into three stages; the candidate

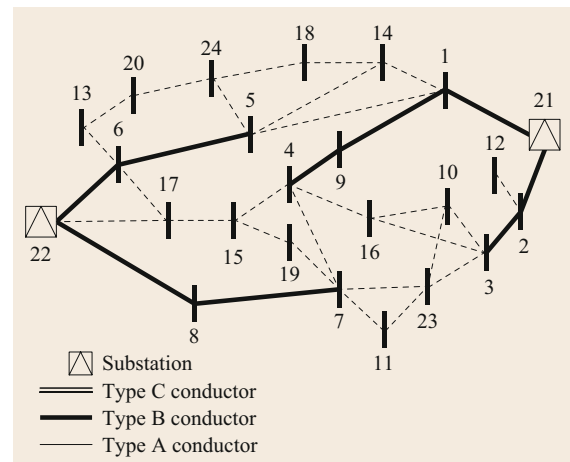
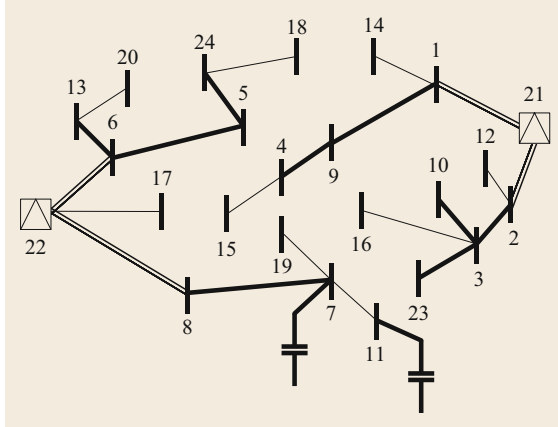


Fig. 15.26 The initial topology of the 24-bus distribution system

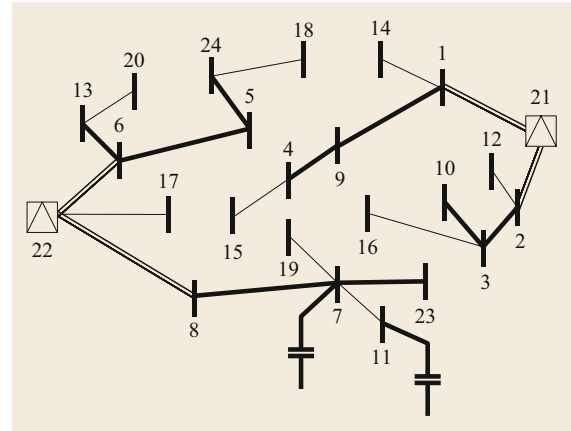
**Table 15.10** Technical and economic characteristics of the available conductors

Type	$R$ ( $\Omega/\text{km}$ )	$X$ ( $\Omega/\text{km}$ )	Ampacity (A)	Cost (\$/km)
A	1.268	0.422	136	12 000
B	0.576	0.393	261	25 000
C	0.215	0.334	445	56 000

**Fig. 15.27** The reinforcement and expansion plan of the 24-bus distribution system considering passive management

lines for expansion are depicted with dashed lines. The branch and load data can be found in Table 15.11 of Appendix 15.A. The technical and economic characteristics of the conductors available are shown in Table 15.10. The investment cost of a capacitor with a 1.2 Mvar capacity is equal to 8k\$, while the investment cost of a voltage regulator is 42k\$. The capacity of the existing substations is 25 MVA, and the voltage limits are  $\pm 5\%$  of the nominal voltage. The inflation and interest rates are 2% and 8%, respectively. At the first stage, it is planned to install three wind DG units: 5 MW at bus 7; 6 MW at bus 23; and 7 MW at bus 24. Furthermore, it is planned to connect one solar DG unit of 100 kW at each future load bus. Capacitors and voltage regulators can be installed at every corresponding part of the initial network configuration. The optimal reinforcement and expansion plan is determined for two cases: (i) considering the passive management of DG units and (ii) considering the control of the active and reactive power of the DG units.

Figure 15.27 presents the network topology of the 24-bus distribution system at the end of the planning

**Fig. 15.28** The reinforcement and expansion plan of the 24-bus distribution system considering ANM

period considering DG passive management. The total investment cost of the network topology of Fig. 15.20 is 652.09k\$. At the first stage, the distribution line 22–6 is reinforced with a type C conductor to meet renewable DG; lines 3–10, 5–24, and 3–23 are constructed with a type B conductor to connect the new load and the DG points. At the second stage, line 21–1 is reinforced with a type C conductor to meet load demand; line 6–13 is constructed with a type B conductor to connect the load at bus 13; lines 7–11, 2–12, 1–14, 4–15, and 22–17 are constructed with a type A conductor to connect the future load buses. At the third stage, lines 21–2 and 22–8 are reinforced with a type C conductor to meet load demand; lines 3–16, 24–18, 7–19, and 13–20 are constructed with type A conductor. One capacitor is installed at bus 11 at stage two, and another one is installed at bus 7 at the third stage of the planning period to deal with the voltage drop issues.

Figure 15.28 presents the network topology of the 24-bus distribution system at the end of the planning period, incorporating ANM aspects into the planning process. The ANM scheme assumes that the power factor of the DG units can vary from 0.95 lagging to 0.95 leading, and the maximum allowable DG active power curtailment is 5% of the DG rated power. The total investment cost of this topology is 629.58k\$. The difference between the investment cost of Figs. 15.20 and 15.21 is due to the fact that the reinforcement of line 22–6 is deferred to the third stage, and line 7–23 is constructed to connect the wind DG unit of bus 23 instead of line 3–23. Note that the length of line 3–23 is longer than the length of line 7–23.

## 15.8 Summary

This chapter presents the basic principles of power distribution systems and the modeling of their components. Different models for the power-flow analysis of radial distribution networks are given, and results on various distribution test systems demonstrate their accuracy and computational performance. The new challenges faced by modern distribution networks due to the increasing penetration of DER, including renewable DG, are discussed. The principles and functions of an advanced distribution management system for the control and monitoring of the distribution network are presented. The coordinated control

of DERs and network components leads to the transformation of passive distribution networks to active distribution systems. It is shown that the adoption of ANM to the operation of distribution networks under normal and emergency conditions increases the network's efficiency, deals with voltage rise/drop issues, and alleviates line congestion in a cost-effective way. Furthermore, the incorporation of ANM into distribution network planning exploits all network components and DER control capabilities, leading to reinforcement and network expansion planning at lower investment costs.

## 15.A Appendix: Load and Line Data of Distribution Networks

**Table 15.11** Load and line data of the 33-bus distribution network

Nominal voltage: 12.66 kV					
From $i$	To $j$	$R$ ( $\Omega$ )	$X$ ( $\Omega$ )	$P_j$ (MW)	$Q_j$ (Mvar)
1	2	0.092	0.047	0.100	0.060
2	3	0.493	0.251	0.090	0.040
3	4	0.366	0.186	0.120	0.080
4	5	0.381	0.194	0.060	0.030
5	6	0.819	0.707	0.060	0.020
6	7	0.187	0.619	0.200	0.100
7	8	0.711	0.235	0.200	0.100
8	9	1.030	0.740	0.060	0.020
9	10	1.044	0.740	0.060	0.020
10	11	0.197	0.065	0.045	0.030
11	12	0.374	0.124	0.060	0.035
12	13	1.468	1.155	0.060	0.035
13	14	0.542	0.713	0.120	0.080
14	15	0.591	0.526	0.060	0.010
15	16	0.746	0.545	0.060	0.020
16	17	1.289	1.721	0.060	0.020
17	18	0.732	0.574	0.090	0.040
2	19	0.164	0.157	0.090	0.040
19	20	1.504	1.355	0.090	0.040
20	21	0.410	0.478	0.090	0.040
21	22	0.709	0.937	0.090	0.040
3	23	0.451	0.308	0.090	0.050
23	24	0.898	0.709	0.420	0.200
24	25	0.896	0.701	0.420	0.200
6	26	0.203	0.103	0.060	0.025
26	27	0.284	0.145	0.060	0.025
27	28	1.059	0.934	0.060	0.020
28	29	0.804	0.701	0.120	0.070
29	30	0.508	0.259	0.200	0.600
30	31	0.974	0.963	0.150	0.070
31	32	0.311	0.362	0.210	0.100
32	33	0.341	0.530	0.060	0.040

**Table 15.12** Load and line data of the 83-bus distribution network

Nominal voltage: 11.4 kV					
From $i$	To $j$	$R$ ( $\Omega$ )	$X$ ( $\Omega$ )	$P_j$ (MW)	$Q_j$ (Mvar)
501	1	0.194	0.662	0.000	0.000
1	2	0.210	0.430	0.100	0.050
2	3	0.236	0.484	0.300	0.200
3	4	0.092	0.188	0.350	0.250
4	5	0.210	0.430	0.220	0.100
5	6	0.039	0.081	1.100	0.800
6	7	0.041	0.138	0.400	0.320
7	8	0.105	0.215	0.300	0.200
7	9	0.236	0.484	0.300	0.230
7	10	0.105	0.215	0.300	0.260
501	11	0.079	0.161	0.000	0.000
11	12	0.341	0.694	1.200	0.800
12	13	0.026	0.054	0.800	0.600
12	14	0.079	0.161	0.700	0.500
501	15	0.113	0.386	0.000	0.000
15	16	0.052	0.108	0.300	0.150
16	17	0.052	0.108	0.500	0.350
17	18	0.157	0.323	0.700	0.400
18	19	0.039	0.081	1.200	1.000
19	20	0.170	0.350	0.300	0.300
20	21	0.236	0.484	0.400	0.350
21	22	0.157	0.323	0.050	0.020
21	23	0.197	0.404	0.050	0.020
23	24	0.131	0.269	0.050	0.010
501	25	0.057	0.193	0.050	0.030
25	26	0.105	0.215	0.100	0.060
26	27	0.249	0.511	0.100	0.070
27	28	0.049	0.166	1.800	1.300
28	29	0.131	0.269	0.200	0.120
501	30	0.197	0.396	0.000	0.000
30	31	0.131	0.269	1.800	1.600
31	32	0.131	0.269	0.200	0.150



**Table 15.12** (continued)

Nominal voltage: 11.4 kV					
From <i>i</i>	To <i>j</i>	<i>R</i> (Ω)	<i>X</i> (Ω)	<i>P<sub>j</sub></i> (MW)	<i>Q<sub>j</sub></i> (Mvar)
32	33	0.026	0.054	0.200	0.100
33	34	0.170	0.350	0.800	0.600
34	35	0.052	0.108	0.100	0.060
35	36	0.498	1.022	0.100	0.060
36	37	0.039	0.081	0.020	0.010
37	38	0.039	0.081	0.020	0.010
38	39	0.079	0.161	0.020	0.010
39	40	0.210	0.430	0.020	0.010
38	41	0.197	0.404	0.200	0.160
41	42	0.210	0.430	0.050	0.030
501	43	0.049	0.166	0.000	0.000
43	44	0.039	0.081	0.030	0.020
44	45	0.131	0.269	0.800	0.700
45	46	0.236	0.484	0.200	0.150
502	47	0.243	0.828	0.000	0.000
47	48	0.066	0.135	0.000	0.000
48	49	0.066	0.135	0.000	0.000
49	50	0.039	0.081	0.200	0.160
50	51	0.079	0.161	0.800	0.600
51	52	0.039	0.081	0.500	0.300
52	53	0.079	0.161	0.500	0.350
53	54	0.052	0.108	0.500	0.300
54	55	0.131	0.269	0.200	0.080
502	56	0.227	0.773	0.000	0.000
56	57	0.537	1.103	0.030	0.020
57	58	0.052	0.108	0.600	0.420
58	59	0.041	0.138	0.000	0.000
59	60	0.039	0.081	0.020	0.010
60	61	0.026	0.054	0.020	0.010
61	62	0.105	0.215	0.200	0.130
62	63	0.236	0.484	0.300	0.240
63	64	0.024	0.083	0.300	0.200
502	65	0.049	0.166	0.000	0.000
65	66	0.170	0.350	0.050	0.030
66	67	0.122	0.414	0.000	0.000
67	68	0.219	0.745	0.400	0.360
68	69	0.049	0.166	0.000	0.000
69	70	0.073	0.248	0.000	0.000
70	71	0.057	0.193	2.000	1.500
71	72	0.026	0.053	0.200	0.150
502	73	0.324	1.104	0.000	0.000
73	74	0.032	0.110	0.000	0.000
74	75	0.057	0.193	1.200	0.950
75	76	0.049	0.166	0.300	0.180
502	77	0.251	0.856	0.000	0.000
77	78	0.130	0.442	0.400	0.360
78	79	0.049	0.166	2.000	1.300
79	80	0.131	0.264	0.200	0.140
80	81	0.131	0.264	0.500	0.360
81	82	0.092	0.188	0.100	0.030
82	83	0.314	0.646	0.400	0.360

**Table 15.13** Load and line data of the 135-bus distribution network

Nominal voltage: 13.8 kV					
From <i>i</i>	To <i>j</i>	<i>R</i> (Ω)	<i>X</i> (Ω)	<i>P<sub>j</sub></i> (MW)	<i>Q<sub>j</sub></i> (Mvar)
1	2	0.332	0.767	0.000	0.000
2	3	0.002	0.004	0.048	0.019
3	4	0.223	0.515	0.043	0.017
4	5	0.099	0.230	0.087	0.035
5	6	0.156	0.359	0.311	0.124
6	7	0.163	0.377	0.149	0.059
7	8	0.114	0.264	0.239	0.095
7	9	0.057	0.057	0.062	0.025
9	10	0.521	0.274	0.125	0.050
9	11	0.109	0.109	0.140	0.056
11	12	0.398	0.209	0.117	0.046
11	13	0.917	0.315	0.249	0.099
11	14	0.118	0.118	0.291	0.116
14	15	0.502	0.264	0.304	0.121
14	16	0.057	0.057	0.215	0.086
16	17	0.294	0.155	0.199	0.079
1	18	0.332	0.767	0.000	0.000
18	19	0.002	0.004	0.000	0.000
19	20	0.223	0.515	0.000	0.000
20	21	0.109	0.251	0.030	0.015
21	22	0.711	0.374	0.231	0.113
21	23	0.182	0.420	0.060	0.029
23	24	0.303	0.160	0.231	0.113
23	25	0.024	0.056	0.121	0.059
25	26	0.045	0.104	0.000	0.000
26	27	0.019	0.043	0.057	0.028
27	28	0.118	0.118	0.365	0.178
28	29	0.024	0.024	0.000	0.000
29	30	0.190	0.100	0.125	0.061
30	31	0.398	0.209	0.057	0.028
29	32	0.057	0.057	0.000	0.000
32	33	0.095	0.050	0.085	0.042
33	34	0.417	0.219	0.000	0.000
34	35	0.114	0.060	0.397	0.194
32	36	0.076	0.076	0.000	0.000
36	37	0.370	0.194	0.181	0.089
37	38	0.265	0.140	0.242	0.118
36	39	0.057	0.057	0.075	0.037
1	40	0.332	0.767	0.000	0.000
40	41	0.118	0.273	0.001	0.001
41	42	2.963	1.016	0.006	0.003
41	43	0.002	0.004	0.000	0.000
43	44	0.069	0.160	0.118	0.050
44	45	0.815	0.429	0.063	0.027
44	46	0.064	0.147	0.172	0.073
46	47	0.131	0.303	0.459	0.194
47	48	0.062	0.143	0.263	0.111
48	49	0.114	0.264	0.236	0.100
49	50	0.284	0.283	0.000	0.000
50	51	0.284	0.283	0.109	0.046

**Table 15.13** (continued)

Nominal voltage: 13.8 kV					
From <i>i</i>	To <i>j</i>	<i>R</i> (Ω)	<i>X</i> (Ω)	<i>P<sub>j</sub></i> (MW)	<i>Q<sub>j</sub></i> (Mvar)
49	52	0.045	0.104	0.000	0.000
52	53	0.026	0.061	0.073	0.031
53	54	0.060	0.139	0.258	0.110
54	55	0.030	0.069	0.069	0.029
55	56	0.021	0.048	0.022	0.009
53	57	0.109	0.251	0.000	0.000
57	58	0.256	0.135	0.021	0.009
58	59	0.417	0.219	0.151	0.064
59	60	0.502	0.264	0.221	0.094
60	61	0.332	0.174	0.092	0.039
61	62	0.208	0.110	0.000	0.000
48	63	0.139	0.320	0.227	0.096
1	64	0.008	0.017	0.000	0.000
64	65	0.270	0.624	0.294	0.117
65	66	0.383	0.883	0.083	0.033
66	67	0.330	0.762	0.083	0.033
67	68	0.328	0.758	0.104	0.041
68	69	0.171	0.394	0.176	0.070
69	70	0.559	0.294	0.083	0.033
69	71	0.058	0.134	0.218	0.087
71	72	0.701	0.369	0.023	0.009
72	73	1.024	0.538	0.005	0.002
71	74	0.068	0.156	0.073	0.029
74	75	1.324	0.454	0.406	0.162
1	76	0.011	0.026	0.000	0.000
76	77	0.730	1.685	0.100	0.042
77	78	0.225	0.520	0.143	0.060
78	79	0.208	0.481	0.096	0.041
79	80	0.047	0.108	0.300	0.127
80	81	0.620	0.619	0.141	0.060
81	82	0.340	0.340	0.280	0.119
82	83	0.569	0.299	0.087	0.037
82	84	0.109	0.109	0.244	0.103
84	85	0.569	0.299	0.248	0.105
1	86	0.011	0.026	0.000	0.000
86	87	0.418	0.966	0.090	0.038
87	88	0.105	0.136	1.137	0.482
87	89	0.439	1.013	0.458	0.194
89	90	0.075	0.026	0.385	0.163
90	91	0.077	0.178	0.000	0.000
91	92	0.332	0.767	0.080	0.034
92	93	0.084	0.195	0.087	0.037
93	94	0.133	0.307	0.000	0.000

**Table 15.13** (continued)

Nominal voltage: 13.8 kV					
From <i>i</i>	To <i>j</i>	<i>R</i> (Ω)	<i>X</i> (Ω)	<i>P<sub>j</sub></i> (MW)	<i>Q<sub>j</sub></i> (Mvar)
94	95	0.293	0.293	0.074	0.031
95	96	0.218	0.217	0.232	0.098
96	97	0.265	0.264	0.142	0.060
94	98	0.103	0.238	0.000	0.000
98	99	0.135	0.312	0.076	0.032
1	100	0.009	0.022	0.000	0.000
100	101	0.169	0.390	0.051	0.022
101	102	0.118	0.273	0.060	0.025
102	103	2.286	0.784	0.009	0.004
102	104	0.456	1.052	0.002	0.001
104	105	0.696	1.607	0.017	0.007
105	106	0.458	1.057	1.507	0.639
106	107	0.203	0.264	0.313	0.133
107	108	0.213	0.277	0.080	0.034
108	109	0.550	0.289	0.051	0.022
109	110	0.540	0.284	0.000	0.000
108	111	0.046	0.059	0.202	0.086
111	112	0.474	0.249	0.061	0.026
112	113	0.862	0.454	0.046	0.019
113	114	0.569	0.299	0.000	0.000
109	115	0.777	0.409	0.157	0.067
115	116	1.080	0.568	0.000	0.000
110	117	1.099	0.578	0.250	0.106
117	118	0.474	0.249	0.000	0.000
105	119	0.323	0.745	0.070	0.030
119	120	0.146	0.338	0.032	0.014
120	121	0.124	0.286	0.061	0.026
1	122	0.011	0.026	0.000	0.000
122	123	0.649	1.498	0.095	0.046
123	124	0.045	0.104	0.050	0.024
124	125	0.526	0.181	0.123	0.060
124	126	0.021	0.048	0.078	0.038
126	127	0.531	0.279	0.145	0.071
126	128	0.098	0.225	0.021	0.010
128	129	0.118	0.273	0.075	0.037
128	130	0.139	0.320	0.228	0.111
130	131	0.043	0.100	0.036	0.017
131	132	0.092	0.212	0.249	0.122
132	133	0.161	0.372	0.317	0.155
133	134	0.378	0.378	0.334	0.163
134	135	0.397	0.397	0.249	0.122
135	136	0.293	0.293	0.000	0.000

**Table 15.14** Load and line data of the 24-bus distribution network

Nominal voltage: 20 kV								
Line data								
From <i>i</i>	To <i>j</i>	Length (km)	From <i>i</i>	To <i>j</i>	Length (km)	From <i>i</i>	To <i>j</i>	Length (km)
1	5	2.22	4	9	1.20	7	23	0.90
1	9	1.20	4	15	1.60	8	22	1.90
1	14	1.20	4	16	1.30	10	16	1.60
1	21	2.20	5	6	2.40	10	23	1.30
2	3	2.00	5	24	0.70	11	23	1.60
2	12	1.10	6	13	1.20	14	18	1.00
2	21	1.70	6	17	2.20	15	17	1.20
3	10	1.10	6	22	2.70	15	19	0.80
3	16	1.20	7	8	2.00	17	22	1.50
3	23	1.20	7	11	1.10	18	24	1.50
4	7	2.60	7	19	1.20	20	24	0.90
Load data								
Bus <i>i</i>	Initial		Stage 1		Stage 2		Stage 3	
	$P_i$ (MW)	$Q_i$ (Mvar)	$P_i$ (MW)	$Q_i$ (Mvar)	$P_i$ (MW)	$Q_i$ (Mvar)	$P_i$ (MW)	$Q_i$ (Mvar)
1	4.167	2.018	3.645	1.765	4.262	2.064	4.878	2.363
2	0.648	0.314	0.702	0.340	0.896	0.434	1.089	0.527
3	3.033	1.469	2.322	1.125	3.042	1.473	3.582	1.735
4	0.369	0.179	0.288	0.139	0.369	0.179	0.441	0.214
5	0.234	0.113	0.252	0.122	0.333	0.161	0.423	0.205
6	0.963	0.466	1.053	0.510	1.175	0.569	1.296	0.628
7	3.690	1.787	3.636	1.761	3.780	1.831	3.924	1.900
8	0.585	0.283	0.648	0.314	0.747	0.362	0.846	0.410
9	0.000	0.000	1.026	0.497	1.310	0.634	1.593	0.772
10	0.000	0.000	1.404	0.680	1.836	0.889	2.160	1.046
11	0.000	0.000	0.000	0.000	1.719	0.833	2.520	1.220
12	0.000	0.000	0.000	0.000	0.837	0.405	1.161	0.562
13	0.000	0.000	0.000	0.000	1.035	0.501	1.215	0.588
14	0.000	0.000	0.000	0.000	2.745	1.329	2.844	1.377
15	0.000	0.000	0.000	0.000	1.458	0.706	1.458	0.706
16	0.000	0.000	0.000	0.000	0.000	0.000	1.098	0.532
17	0.000	0.000	0.000	0.000	1.944	0.942	2.160	1.046
18	0.000	0.000	0.000	0.000	0.000	0.000	1.890	0.915
19	0.000	0.000	0.000	0.000	0.000	0.000	1.620	0.785
20	0.000	0.000	0.000	0.000	0.000	0.000	3.411	1.652

## References

- 15.1 IEC 60038: *IEC Standard Voltages*, 6.2 edn. (IEC, Geneva 2002)
- 15.2 E. Lakervi, E.J. Holmes: *Electricity Distribution Network Design*, IEE Power Engineering Series, Vol. 21 (Peter Peregrines, London 1995)
- 15.3 T.A. Short: *Electric Power Distribution Equipment and Systems* (CRC, Boca Raton 2005)
- 15.4 W.H. Kersting: *Distribution System Modeling and Analysis* (CRC, Boca Raton 2012)
- 15.5 Schneider Electric: *Use and Maintenance of ELVIM Oil-immersed Distribution Transformers* (Schneider Electric, Rueil-Malmaison 2002)
- 15.6 IEEE: Load representation for dynamic performance analysis, *IEEE Trans. Power Syst.* **8**(2), 472–482 (1993)
- 15.7 L.L. Grigsby: *Electric Power Generation, Transmission and Distribution* (CRC, Boca Raton 2006)
- 15.8 M.E. Baran, F.F. Wu: Network reconfiguration in distribution systems for loss reduction and load balancing, *IEEE Trans. Power Del.* **4**(2), 1401–1407 (1989)
- 15.9 M.E. Baran, F.F. Wu: Optimal sizing of capacitors placed on a radial distribution system, *IEEE Trans. Power Del.* **4**(1), 735–743 (1989)

- 15.10 J.A. Taylor, F.S. Hover: Convex models of distribution system reconfiguration, *IEEE Trans. Power Syst.* **27**(3), 1407–1413 (2012)
- 15.11 M. Farivar, C.R. Clarke, S.H. Low, K.M. Chandy: Inverter VAR control for distribution systems with renewables. In: *Proc. 2nd IEEE Int. Conf. Smart Grid Commun.* (2011) pp. 457–462
- 15.12 M.S. Lobo, L. Vandenbergh, S. Boyd, H. Lebre: Applications of second-order cone programming, *Linear Algebra Appl.* **284**, 193–228 (1998)
- 15.13 B.A. McCarl: *GAMS User Guide, Version 23.8* (GAMS Corp, Fairfax 2012), available from <http://www.gams.com>
- 15.14 A. Drud: CONOPT: a GRG code for large sparse dynamic nonlinear optimization problems, *Math. Program.* **31**(2), 153–191 (1985)
- 15.15 R. Zimmerman: *Comprehensive Distribution Power Flow: Modeling, Formulation, Solution Algorithms and Analysis*, Ph.D. Dissertation (Cornell Univ., Ithaca 1995) pp. 57–83
- 15.16 P.S. Georgilakis, N.D. Hatziargyriou: Optimal distributed generation placement in power distribution networks: models, methods, and future research, *IEEE Trans. Power Syst.* **28**(3), 3420–3428 (2013)
- 15.17 CIGRE TB 458: *Electric Energy Storage Systems, Working Group C6.15* (CIGRE, Paris 2011)
- 15.18 CIGRE TB 475: *Demand Side Integration (DSI), Working Group C6.09* (CIGRE, Paris 2011)
- 15.19 CIGRE TB 457: *Development and Operation of Active Distribution Networks, Working Group C6.11* (CIGRE, Paris 2011)
- 15.20 M.F. Akorede, H. Hizam, E. Pouresmaeil: Distributed energy resources and benefits to the environment, *Renew. Sustain. Energy Rev.* **14**(2), 724–734 (2010)
- 15.21 A. Labouret, M.I. Villos: *Solar Photovoltaic Energy*, 4th edn. (IET, London 2009)
- 15.22 T. Markwart, L. Castañer: *Practical Handbook of Photovoltaics: Fundamentals and Applications* (Elsevier, Amsterdam 2003)
- 15.23 S. Heier: *Grid Integration of Wind Energy Conversion Systems* (Wiley, Chichester 1998)
- 15.24 T. Ackermann: *Wind Power in Power Systems* (Wiley, New York 2005)
- 15.25 O. Paish: Small hydro power: technology and current status, *Renew. Sustain. Energy Rev.* **6**(6), 537–556 (2002)
- 15.26 Y. Zhu, K. Tomsovic: Development of models for analysing the load-following performance of microturbines and fuel cells, *Electr. Power Syst. Res.* **62**(1), 1–11 (2002)
- 15.27 X. Luo, J. Wang, M. Dooner, J. Clarke: Overview of current development in electrical energy storage technologies and the application potential in power system operation, *Appl. Energy* **137**, 511–536 (2015)
- 15.28 A. Evans, V. Strezov, T.J. Evans: Assessment of utility energy storage options for increased renewable energy penetration, *Renew. Sustain. Energy Rev.* **16**(6), 4141–4147 (2012)
- 15.29 P. Siano: Demand response and smart grids—a survey, *Renew. Sustain. Energy Rev.* **30**, 461–478 (2014)
- 15.30 J.A.P. Lopes, N. Hatziargyriou, J. Mutale, P. Djapic, N. Jenkins: Integrating distributed generation into electric power systems: a review of drivers, challenges and opportunities, *Electr. Power Syst. Res.* **77**(9), 1189–1203 (2007)
- 15.31 V.A. Evangelopoulos, P.S. Georgilakis, N.D. Hatziargyriou: Optimal operation of smart distribution networks: a review of models, methods and future research, *Electr. Power Syst. Res.* **140**, 95–106 (2016)
- 15.32 CIGRE TB 678: *Smart metering, regulatory aspects, standards and development status, Working Group C6.21* (CIGRE, Paris 2017)
- 15.33 U.S. DoE: *Voices of Experience—Advanced Distribution Management Systems* (2015)
- 15.34 S. Grillo, S. Massucco, F. Silvestro: A smart grid approach to distribution management systems (DMS) for electric networks. In: *CIGRE Workshop* (2010)
- 15.35 M. Thomas, J. McDonald: *Power System SCADA and Smart Grids* (CRC, Boca Raton 2015)
- 15.36 D. Bailey, E. Wright: *Practical SCADA for Industry* (Oxford, Newnes 2003)
- 15.37 R.P. Gupta, S.C. Srivastava, R.K. Varma: Remote terminal units for distribution automation: development and commissioning experience, *Int. J. Comput. Appl.* **30**(2), 80–91 (2008)
- 15.38 W. Jusoh, M. Ghani, M. Hanafiah, S. Raman: Remote terminal unit (RTU) hardware design and development for distribution automation system. In: *Proc. 2014 IEEE Innov. Smart Grid Technol. Asia (ISGT ASIA)* (2014) pp. 572–576
- 15.39 W. Bolton: *Programmable Logic Controllers* (Oxford, Newnes 2009)
- 15.40 G. Clarke, D. Reynders: *Practical Modern SCADA Protocols—DNP3, 60870.5 and Related Systems* (Newnes, Oxford 2004)
- 15.41 S. Mohagheghi, J. Stoupi, Z. Wang: Communication protocols and networks for power systems—current status and future trends. In: *Proc. IEEE/PES Power Syst. Conf. Expo. (PSCE)* (2009) pp. 1–9
- 15.42 CORDIS: Smart distribution System operation for maximizing the integration of renewable generation (SuSustainable), funded under: FP7-ENERGY-2012-7.1.1, grant agreement number 308755, start date: 01 Jan. 2013, end date: 31 Mar. 2016, available from <https://cordis.europa.eu/project/id/308755>
- 15.43 I. Cobelo, A. Shafiu, N. Jenkins, G. Strbac: State estimation of networks with distributed generation, *Eur. Trans. Electr. Power* **17**, 21–36 (2007)
- 15.44 R. Singh, B.C. Pal, R.A. Jabr: Choice of estimator for distribution system state estimation, *IET Gener. Transm. Distrib.* **3**(7), 666–678 (2009)
- 15.45 G.N. Korres, N.D. Hatziargyriou, P.J. Katsikas: State estimation in multi-microgrids, *Eur. Trans. Electr. Power* **21**(2), 1178–1199 (2011)
- 15.46 K. Samarakoon, J. Wu, J. Ekanayake, N. Jenkins: Use of delayed smart meter measurements for distribution state estimation. In: *Proc. IEEE Power Energy Soc. General Meet.* (2011), <https://doi.org/10.1109/PES.2011.6039384>
- 15.47 F. Shabaninia, M. Vaziri, S. Vadhva, J. Vaziri: A novel state estimation formulation for distribution grids with renewable energy sources. In:

- Proc. IEEE Power Energy Soc. General Meet.* (2012), <https://doi.org/10.1109/PESGM.2012.6345067>
- 15.48 G.N. Korres, N.M. Manousakis: A state estimation algorithm for monitoring topology changes in distribution systems. In: *Proc. IEEE Power Energy Soc. General Meet.* (2012), <https://doi.org/10.1109/PESGM.2012.6345126>
- 15.49 D. Atanackovic, V. Dabic: Deployment of real-time state estimator and load flow in BC Hydro DMS—Challenges and opportunities. In: *Proc. 2013 IEEE Power Energy Soc. General Meet.* (2013), <https://doi.org/10.1109/PESMG.2013.6672408>
- 15.50 M.Z. Degefa, R.J. Millar, M. Koivisto, M. Humayun, M. Lehtonen: Load flow analysis framework for active distribution networks based on smart meter reading system, *Engineering* **5**, 1–8 (2013)
- 15.51 S. Lefebvre, J. Prevost, L. Lenoir: Distribution state estimation: a necessary requirement for the smart grid. In: *Proc. IEEE PES General Meet. Conf. Expo* (2014), <https://doi.org/10.1109/PESGM.2014.6939030>
- 15.52 A. Primadianto, C.-N. Lu: A review on distribution system state estimation, *IEEE Trans. Power Syst.* **32**(5), 3875–3883 (2017)
- 15.53 Y. Gao, N. Yu: State estimation for unbalanced electric power distribution systems using AMI data. In: *Proc. 8th IEEE Int. Conf. Innov. Smart Grid Technol. (ISGT)* (2017), <https://doi.org/10.1109/ISGT.2017.8085999>
- 15.54 M. Wache, D.C. Murray: Application of synchrophasor measurements for distribution networks. In: *Proc. IEEE Power Energy Soc. General Meet.* (2011), <https://doi.org/10.1109/PES.2011.6039337>
- 15.55 M. Paolone, A. Borghetti, C.A. Nucci: On the measurement of synchrophasors in active distribution power networks. In: *Proc. IEEE Int. Conf. Innov. Smart Grid Technol. (ISGT)* (2011)
- 15.56 A.K. Ghosh, D.L. Lubkeman, R.H. Jones: Load modeling for distribution circuit state estimation, *IEEE Trans. Power Del.* **12**(2), 999–1005 (1997)
- 15.57 R. Arritt, R. Dugan: Comparing load estimation methods for distribution system analysis. In: *Proc. 22nd Int. Conf. Exhib. Electr. Distrib.* (2013), <https://doi.org/10.1049/cp.2013.0869>
- 15.58 E. Manitsas, R. Singh, B.C. Pal, G. Strbac: Distribution system state estimation using an artificial neural network approach for pseudo measurement modeling, *IEEE Trans. Power Syst.* **27**(4), 1888–1896 (2012)
- 15.59 V. Miranda, J. Pereira, J.T. Saraiva: Load allocation in DMS with a fuzzy state estimator, *IEEE Trans. Power Syst.* **15**(2), 529–534 (2000)
- 15.60 J. Wan, K.N. Miu: Weighted least squares methods for load estimation in distribution networks, *IEEE Trans. Power Syst.* **18**(4), 1338–1345 (2003)
- 15.61 A.T. Saric, A. Rankovic: Load reallocation based algorithm for state estimation in distribution networks with distributed generators, *Electr. Power Syst. Res.* **84**, 72–82 (2012)
- 15.62 T.C. Xygkis, G.D. Karlis, I.K. Siderakis, G.N. Korres: Use of near real-time and delayed smart meter data for distribution system load and state estimation. In: *Proc. 9th Mediterr. Conf. Power Gener. Transm. Distrib. Energy Convers.* (2014)
- 15.63 A. Abur, A.G. Exposito: *Power System State Estimation—Theory and Implementation* (Marcel Dekker, New York 2004)
- 15.64 G.N. Korres, G.C. Contaxis: Identification and updating of minimally dependent sets of measurements in state estimation, *IEEE Trans. Power Syst.* **6**(3), 999–1005 (1991)
- 15.65 N.C. Koutsoukis, D.O. Siagkas, P.S. Georgilakis, N.D. Hatziaargyriou: Online reconfiguration of active distribution networks for maximum integration of distributed generation, *IEEE Trans. Autom. Sci. Eng.* **14**(2), 437–448 (2017)
- 15.66 J. Northcote-Green, R.G. Wilson: *Control and Automation of Electrical Power Distribution Systems* (CRC, Boca Raton 2007)
- 15.67 A. Zidan, M. Khairalla, A.M. Abdrabou, T. Khalifa, K. Shaban, A. Abdrabou, R. El Shatshat, M. Gaouda: Fault detection, isolation, and service restoration in distribution systems: state-of-the-art and future trends, *IEEE Trans. Smart Grid* **8**(5), 2170–2185 (2017)
- 15.68 C.S. Chen, C.H. Lin, H.Y. Tsai: A rule-based expert system with colored Petri net models for distribution system service restoration, *IEEE Trans. Power Syst.* **17**(4), 1073–1080 (2002)
- 15.69 M.-S. Tsai: Development of an object-oriented service restoration expert system with load variations, *IEEE Trans. Power Syst.* **23**(1), 219–225 (2008)
- 15.70 M.R. Kleinberg, K. Miu, H.-D. Chiang: Improving service restoration of power distribution systems through load curtailment of in-service customers, *IEEE Trans. Power Syst.* **26**(3), 1110–1117 (2011)
- 15.71 R. Pérez, G. Heydt, N. Jack, A. Castelhana: Optimal restoration of distribution systems using dynamic programming, *IEEE Trans. Power Del.* **23**(3), 1589–1596 (2008)
- 15.72 D.S. Sanches, J.B.A. London Jr, A.C.B. Delbem: Multiobjective evolutionary algorithm for single and multiple fault service restoration in large-scale distribution systems, *Electr. Power Syst. Res.* **110**, 144–153 (2014)
- 15.73 A. Augugliaro, L. Dusonchet, E.R. Sanseverino: Multiobjective service restoration in distribution network using an evolutionary approach and fuzzy sets, *Electr. Power Energy Syst.* **22**, 103–110 (2000)
- 15.74 A. Botea, J. Rintanen, D. Banerjee: Optimal reconfiguration for supply restoration with informed A\* search, *IEEE Trans. Smart Grid* **3**(2), 583–593 (2012)
- 15.75 P.L. Cavalcante, J.C. López, J.F. Franco, M.J. Rider, A.V. Garcia, M.R.R. Malveira, L.L. Martins, L.C.M. Direito: Centralized self-healing scheme for electrical distribution systems, *IEEE Trans. Smart Grid* **7**(1), 145–155 (2016)
- 15.76 R.A. Romero, J.F. Franco, F.B. Leão, M.J. Rider, E.S. Souza: A new mathematical model for the restoration problem in balanced radial distribution systems, *IEEE Trans. Power Syst.* **31**(2), 1259–1268 (2016)
- 15.77 N.C. Koutsoukis, P.A. Karafotis, P.S. Georgilakis, N.D. Hatziaargyriou: Optimal service restoration of

- power distribution networks considering voltage regulation. In: *Proc. IEEE PowerTech Conf.* (2017)
- 15.78 P.S. Georgilakis, N.D. Hatziaargyriou: A review of power distribution planning in the modern power systems era: models, methods and future research, *Electr. Power Syst. Res.* **121**, 89–100 (2015)
- 15.79 CIGRE TB 591: *Planning and optimization methods for active distribution systems*, Working Group C6.19 (CIGRE, Paris 2013)
- 15.80 N.C. Koutsoukis, P.S. Georgilakis, N.D. Hatziaargyriou: Multistage coordinated planning of active distribution networks, *IEEE Trans. Power Syst.* **33**(1), 32–44 (2018)

---

### Nikolaos C. Koutsoukis

School of Electrical and Computer Engineering  
National Technical University of Athens  
Athens, Greece  
[koutsoukis@power.ece.ntua.gr](mailto:koutsoukis@power.ece.ntua.gr)



Nikolaos C. Koutsoukis received the Diploma in Electrical and Computer Engineering from the National Technical University of Athens (NTUA), Greece, in 2012, where he is currently pursuing a PhD in active distribution networks. His research interests include power system planning, distributed generation, and power distribution system control, and automation. He is a member of the Technical Chamber of Greece.

---

### Pavlos S. Georgilakis

School of Electrical and Computer Engineering  
National Technical University of Athens  
Athens, Greece  
[pgeorg@power.ece.ntua.gr](mailto:pgeorg@power.ece.ntua.gr)



Pavlos S. Georgilakis received his Diploma in Electrical and Computer Engineering and his PhD from the National Technical University of Athens (NTUA), Athens, Greece in 1990 and 2000, respectively. He is currently Assistant Professor at the School of Electrical and Computer Engineering of NTUA. His research interests include power systems optimization, smart grids, and distributed energy resources.

---

### George N. Korres



School of Electrical and Computer Engineering  
National Technical University of Athens  
Athens, Greece  
[gkorres@cs.ntua.gr](mailto:gkorres@cs.ntua.gr)

George N. Korres received his Diploma in Electrical and Computer Engineering and his PhD from the National Technical University of Athens (NTUA), Athens, Greece in 1984 and 1988, respectively. He is currently Professor at the School of Electrical and Computer Engineering of NTUA. His research interests include power system state estimation, power system protection, and industrial automation.

---

### Nikos D. Hatziaargyriou



School of Electrical and Computer Engineering  
National Technical University of Athens  
Athens, Greece  
[nh@power.ece.ntua.gr](mailto:nh@power.ece.ntua.gr)

Nikos D. Hatziaargyriou is Professor at the National Technical University of Athens (NTUA) and Chairman and CEO of the Hellenic Electricity Distribution Network Operator (HEDNO). He is Chair of the EU Technology and Innovation Platform on Smart Networks for Energy Transition. He is author of more than 200 journal publications and 500 conference papers. His research interests include smart grids, distributed energy resources, microgrids, renewable energy sources, and power system security.

# Energy Storage

## 16. Energy Storage

Alfred Rufer

This chapter provides an overview on classical and innovative storage solutions and systems. The historical context and today's motivation for the development and application of energy storage are presented, together with methods and definitions for quantitative and qualitative comparison of different energy storage means. An energy-efficiency-based description method called *The Theory of Ragone Plots* is included.

From the classical pumped storage and its recent evolution as flexible speed-variable pump-turbines to the most recent high-power and high-energy density batteries coupled to smart grid configurations, the chapter will present the main characteristics and properties of each component. In addition, compressed-air technologies, flywheels, as well electrical magnetic and capacitive storage components are introduced. For large-capacity and so-called seasonal storage, the hydrogen storage principle is described.

Finally, system arrangements and applications are described as storage as a grid component, storage for renewable energies, hybrid power plants, or uninterruptible power sources.

Examples of recent realizations of large-scale storage plants complete the chapter.

Additional information and supplementary exercises for this chapter are available online.

16.1	<b>The Context of Use of Energy Storage</b>	1132
16.2	<b>General Definitions of Energy Storage</b>	1135
16.2.1	Energy and Power	1135
16.2.2	System Ratings	1136
16.2.3	The Ragone Chart	1138
16.3	<b>Technical Definitions</b>	1138
16.3.1	General Parameters	1138
16.3.2	Round-Trip Efficiency Under Normal, Ideal, and Real Conditions	1139
16.3.3	The Round-Trip Efficiency	1140
16.3.4	The Theory of Ragone Plots	1141
16.4	<b>Electric Power and Energy Storage</b>	1143
16.4.1	Storage Forms of Energy	1143
16.4.2	The Intermediary Conversion	1143
16.4.3	Control and Diagnostics	1143
16.5	<b>Energy Storage Systems</b>	1144
16.6	<b>Storage Systems Based on Physics</b>	1144
16.6.1	Gravitational Hydro-Pumped Storage	1144
16.6.2	Compressed-Air Energy Storage	1151
16.6.3	Rotational Kinetic Energy (Flywheels)	1152
16.7	<b>Electrical Systems</b>	1154
16.7.1	Superconductive Magnetic Energy Storage Systems (SMES)	1154
16.7.2	Capacitive (and Supercapacitive) Systems	1154
16.8	<b>Electrochemical Systems</b>	1156
16.8.1	Electrochemical Principles and Properties	1156
16.8.2	Different Types of Accumulators	1157
16.9	<b>Fuel Cells and Hydrogen Storage</b>	1163
16.9.1	Main Properties of Hydrogen Storage	1163
16.9.2	The Power-to-Power Storage System Based on Hydrogen	1164
16.9.3	Producing Hydrogen Through the Electrolysis of Water	1164
16.9.4	Conversion from Hydrogen to Electricity	1165
16.9.5	Efficiency Considerations	1165
16.10	<b>System Arrangements and Applications</b>	1166
16.10.1	Storage as a Grid Component	1166
16.10.2	Renewable Energies and the Hybrid Power Plant	1166
16.10.3	UPS Technologies	1167
16.11	<b>Examples of Large-Scale Energy Storage Plants</b>	1168
16.11.1	Nant-de-Drance, Switzerland	1168
16.11.2	Hyundai and the Korea Zinc Energy Storage System	1168
16.11.3	Hornsedale Power Reserve, South Australia, Jamestown	1168
16.11.4	NGK Sodium-Sulfur (Na-S) Battery	1168
16.11.5	Dalian VFB-UET/Rongke Power	1168
16.11.6	Clear Creek Flywheel Wind Farm Project	1169
16.11.7	Huntorf CAES Plant	1169
	<b>References</b>	1169

Energy storage is an important area of the domain of electric power systems in general. It comprises classical solutions used for a longer time, with the example of large hydropower facilities, and also new technologies issued from the evolution of material sciences, such as the modern lithium-ion-based accumulators. While the principle of centralized power generation is moving slowly into the direction of distributed and renewable sources, energy storage is expected to play a new role in this context, principally due to the variability of the new sources.

Portable or mobile applications are based on batteries and concern lower energy capacity and lower power levels. Essentially, energy density and also power density are in the center of interest of many academic and industry research and development projects and are motivated by increasingly more performance.

Energy storage technologies, components, and systems are described in [16.1], together with the necessary tools and methodologies allowing their proper modeling and design.

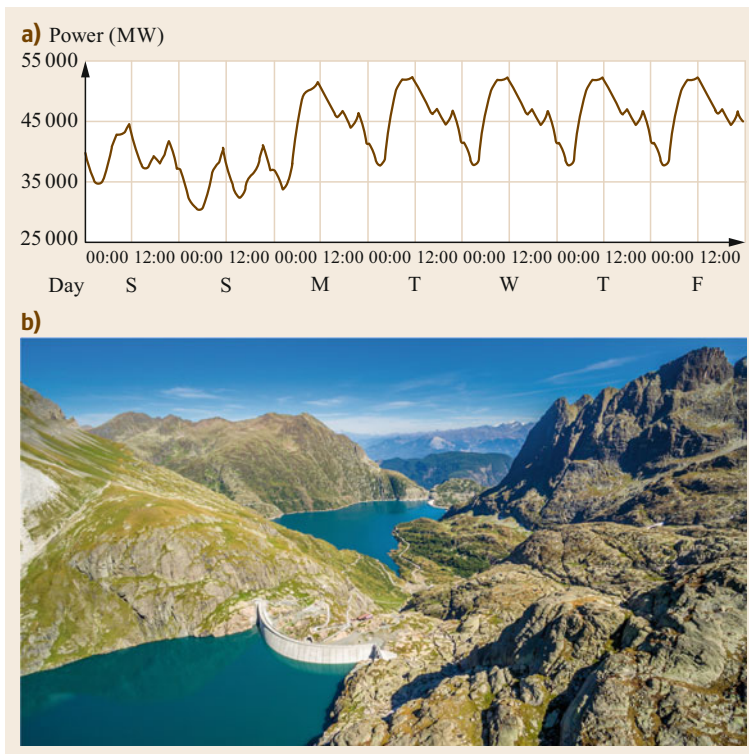
## 16.1 The Context of Use of Energy Storage

Large facilities for electrical energy storage have been built in the second half of the twentieth century, in the context of matching the variable power demand (daily cycles) with the installation of nuclear power plants, known for their mostly constant power production. Figure 16.1a shows the typical power profile of weekly consumption, and Fig. 16.1b illustrates one of the newest pump-storage facilities, built in the Swiss Alps, the Nant-de-Drance project. Many facilities have been realized with the motivations of compensating daily variations, such as the examples of the Hongrin–Leman facility in Switzerland, the Raccoon Mountain

Pumped-Storage Plant, west of Chattanooga, TN, US, or the Yagisawa Power Station in Japan.

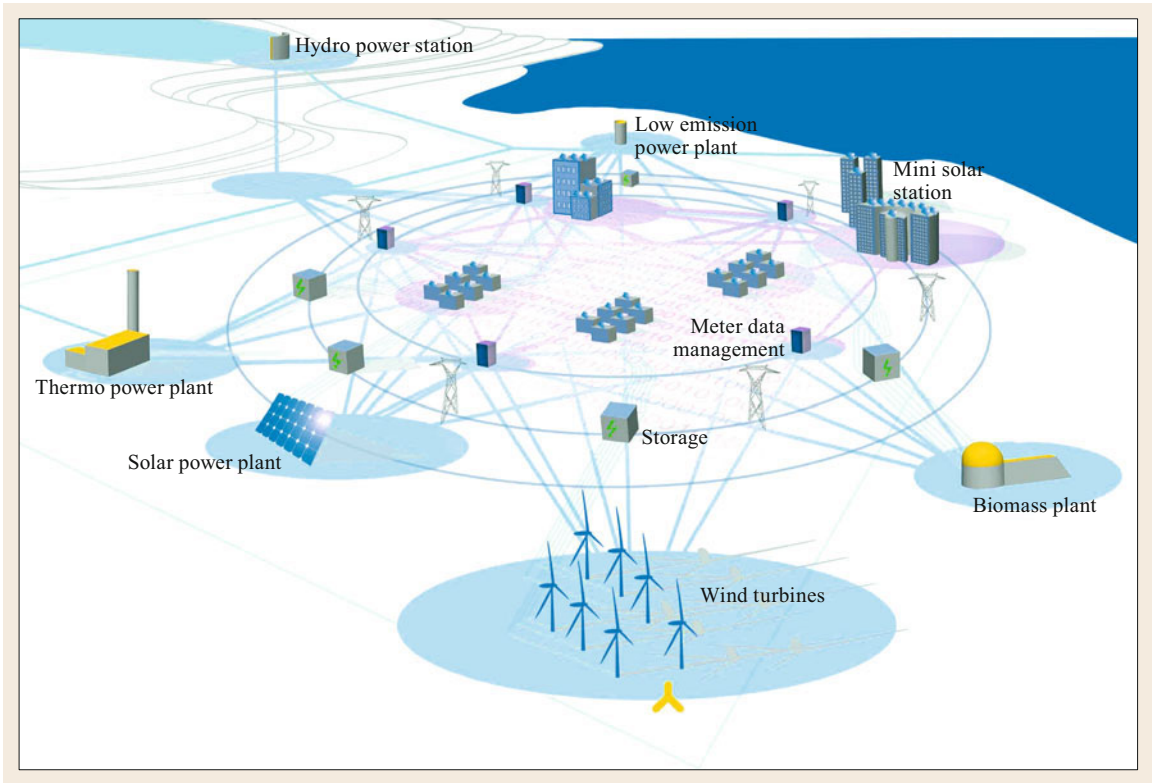
From the end of the twentieth century, another tendency appeared in the context of the development of renewable energy sources. From the classical centralized utility of today, there is a clear movement in the direction of the distributed utility of tomorrow, together with the appearance of so-called smart grids (Fig. 16.2).

Renewable energy sources are known for their variation in time or available power related to meteorology conditions. This is clearly a new motivation for the development and realization of energy storage systems.

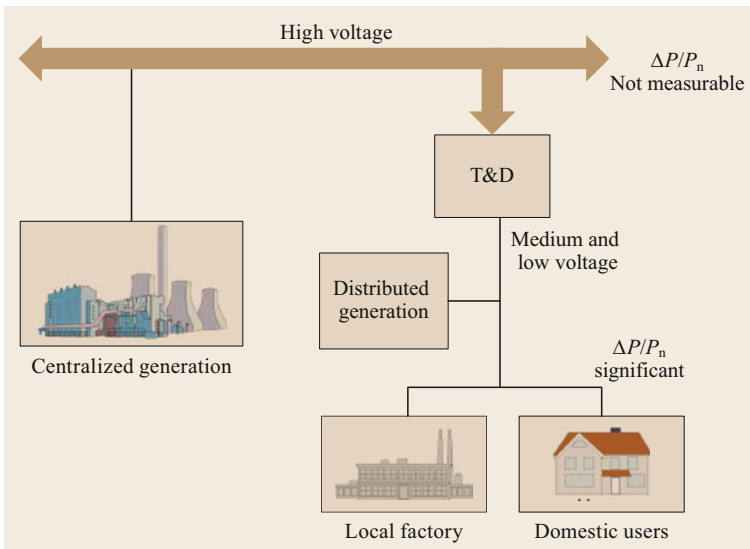


**Fig. 16.1a,b** Daily variations of power demand. **(a)** Profile of demand over a week. **(b)** Pumped-storage plant Nant-de Drance (Switzerland). **(b)** Reprinted with permission from JBcomm, 2019





**Fig. 16.2** From the centralized utility of today to the distributed utility of tomorrow (reprinted with permission from Mario Paolone, 2019)



**Fig. 16.3** Power fluctuations ( $\Delta P/P_n$ ) in centralized and decentralized power generation systems

An additional reason can be found in the principle itself of decentralizing energy production. This concerns power matching between decentralized generators and their loads nearby, which can generate significant and fast variations of the local power demand in local net-

works. Figure 16.3 illustrates the principle of *losing* the averaging effect of the power due to decentralization of production.

A general tendency towards an increasing use of energy storage can be observed.

**Table 16.1** Categorization of energy storage scales and their applications [16.2]

Category	Applications	Storage duration
Power quality and regulation	Fluctuation suppression/smoothing Dynamic power response Low-voltage ride through Line-fault ride through Uninterruptible power supply Voltage control support Reactive power control Oscillation damping Transient stability	< 1 min
Bridging power	Spinning/contingency reserves Ramping Emergency backup Load following Wind power smoothing	1 min–1 h
Energy management	Peak shaving/generation/time shifting Transmission curtailment Energy arbitrage Transmission and distribution deferral Line repair Load cycling Weather smoothing Unit commitment Load leveling Capacity firming Renewable integration and backup Seasonal storage Annual smoothing	5–12 h  Hours to days  > 4 months

Four different aspects are considered:

- First, the use of storage technology in order to solve the problem of availability of renewable energy sources (RES) (day-to-night shift for photovoltaic plants as a first example) or the bridging of a lack of production of fluctuating sources. In many decentralized places where PV (photovoltaic) installations are used, night power is often produced by diesel generators. For ecological reasons, these generators can be replaced by storage techniques and increased PV collectors.
- Second, the potential for enhancing market participation, such as energy or capacity balancing, also ancillaries markets.
- Third, the use of energy storage technology in order to assist some problematic consumers characterized by strong and fast demand, which are not compatible with the local grid-access codes.
- Fourth, a high smart-grid-related potential with diverse innovative functions as final prosumer applications related to sustainable energy concepts.

- A fifth category of use is more related to economic aspects, as in the case of generation using fuel cells. The design of such systems for maximum peak power can lead to unacceptable costs. The design for the *mean value* is more realistic, and the highest power demand can be taken out of a storage device. Also, in the category of economic advantages, storage techniques could allow us to practice the strategy of buy low, sell high.

Table 16.1 gives a further view of the categorization of energy storage scales and their applications in relation to grid applications.

Regarding the applications of voltage support and reactive power control, it must be known that modern power electronic circuits such as VSCs (voltage source converters) used for the interface between storage components and the grid have the inherent property that the active and reactive currents can be controlled separately. As a consequence, such applications can be operated for an unlimited time, if the design of current and thermal capacity is adapted.

## 16.2 General Definitions of Energy Storage

### 16.2.1 Energy and Power

An engineering approach to the topic of energy storage is clearly based on a quantitative characterization. First of all, energy quantities should be clearly defined, as well as all energy transformations. Energy transformations, and this is also valid for a storage process, are characterized by well-defined efficiencies. The quality or efficiency of the process does not only depend on the process type itself, but on the conditions that this process is applied. More explicitly, these conditions can be characterized by what is called power. As a consequence, one has to first properly define what is energy and what is power.

#### Definitions of Energy

The general definition of energy is provided by the conventions of a thermodynamic system in combination with the description of the macroscopic forms of energy of the system. The sum of all energies forms of a system is called the *total energy*.

*Macroscopic energy* of a system is related to its movement and to external effects such as gravity, magnetism, or electricity.

*Microscopic energy* is related to the molecular activity of a system and is often called the *internal energy*.

A simple definition of the total energy is given by the sum of the internal energy  $U$ , the kinetic energy KE, and the potential energy PE, leading to the expression of (16.1) [16.3].

$$E = U + \text{KE} + \text{PE} = U + m\frac{V^2}{2} + mgz, \quad (16.1)$$

where  $m$  is the mass,  $V$  is the velocity of the mass from a given reference point,  $g$  is the gravitational acceleration, and  $z$  is the height of the mass center related to a reference point.

For a system with a rotating mass, the term for the kinetic energy becomes

$$\text{KE}_{\text{rot}} = J\frac{\omega^2}{2}, \quad (16.2)$$

where  $J$  is the moment of inertia, and  $\omega$  is the angular velocity.

When (16.1) is valid for closed systems, it must be completed for so-called open systems by a term corresponding to the energy associated with the flow of material. This energy is characterized through the mass flow rate

$$\dot{m} = \rho \dot{v} = \rho A v_{\text{mean}}, \quad (16.3)$$

$\dot{v}$  being the volumetric flow rate,  $\rho$  the density,  $A$  the section of the flow, and  $v_{\text{mean}}$  the average velocity of the flow.

The energy flow rate associated with the flow of material is given by

$$\dot{E} = \dot{m}e, \quad (16.4)$$

where  $e$  is the specific energy of the material.

Magnetic and electric effects can play a major role in the energy of given systems like inductors or capacitors. These amounts are considered as macroscopic energy and can be calculated as

$$E = E_{\text{mag}} + E_{\text{cl}} = \frac{1}{2}LI^2 + \frac{1}{2}CU^2. \quad (16.5)$$

In (16.1),  $U$  is the internal energy of a system and includes all forms of microscopic energy at the level of the molecular and atomic scale. It corresponds to kinetic and potential energy of molecules and atoms, of nucleons and electrons, and to the energy that binds them together. In the case of energy storage devices, the variation of the internal energy is generally considered and it can be described through (16.6) [16.3]

$$dU = -pdV + TdS + \sum_i \mu_i dn_i. \quad (16.6)$$

The first term on the right-hand side of (16.6) is the work done on the system, where  $p$  is the pressure and  $V$  the volume. The second term corresponds to the heat transferred into the system in terms of temperature  $T$  and entropy  $S$ .

The third term represents the chemical energy and is the form of the internal energy related to the cohesion between the positively charged nucleus of the atoms and their negative electrons. The chemical energy also binds the atoms in the molecule;  $\mu_i$  is the chemical potential of a species  $i$ , and  $n$  corresponds to the number of moles considered.

In the case of an electrochemical battery, the internal energy is expressed through the Gibbs energy  $\Delta G$ . This energy is related to the standard redox potential by the known Nernst law

$$E_{\text{SHE}} = -\frac{\Delta G}{nF} = \left(E_{\text{ox/red}}^0\right)_{\text{SHE}} + \frac{RT}{nF} \ln\left(\frac{\text{ox}}{\text{red}}\right), \quad (16.7)$$

where (ox) and (red) designate the concentrations of the oxidized and reduced forms of the redox couple,  $R = 8.32 \text{ J}/(\text{K mol})$ ,  $T$  is the absolute temperature,  $n$  is the number of electrons implicated in the reaction, and  $F$  is Faraday's constant, as will be explained later in

Sect. 16.8. In (16.7), the index SHE denotes that the potential is referred to the standard hydrogen electrode.

### Power or Energy Flow Rate

The power can be defined as the *energy flow rate* to or from a given system

$$P(t) = \frac{dE}{dt}, \quad (16.8)$$

where:

$P$  (power) is expressed in watt

$E$  (energy) is expressed in joule, or kW h

$t$  (time) in seconds (s), hours (h),

$$1 \text{ J} \hat{=} 1 \text{ W s} \hat{=} 1 \text{ N m}.$$

Example: transformation of electric power into heat

Energy: heating up 100 L of water from 20 to 60 °C needs 4.6 kW h (4.18 J/°C and per gram gives 16.7 MJ or 4.6 kW h).

Power: to do this heating up within 4 h, a 1.15 kW heater is needed; within 1 h, a 4.6 kW heater is needed.

## 16.2.2 System Ratings

In order to design an appropriate storage device and to choose the right solution in relation to a given application, it is important to have a comparative evaluation of the possible capacity and performance. First, the

power range must be defined. Then, with respect to the expected time autonomy, the energy capacity can be defined. Figure 16.4 is a representation of a high number of possible storage solutions over a large power range of 6 decades, starting from the 1 kW level up to the GW level. Different storage technologies are represented, from electrochemical batteries to large-scale pumped hydro storage. CAES (compressed-air energy storage), superconductive magnet energy storage SMES, as well as flywheels are compared. The vertical axis of the figure illustrates the system autonomy, in powers of 10 h. The product of the power multiplied by the time gives the energy capacity. This parameter corresponds to the surface delimited by the horizontal and vertical lines of the values represented in the diagram.

Power bridging means the action to bridge the downtime during a switching transition by carrying the critical load away from a failing power source to a stable alternate source immediately. Energy management should be understood as the task of the planning and operation of larger energy production and energy consumption units connected to the grid. For batteries, the values indicated reflect some of the most important realizations, but in relation to the increase of the possible performance, capacity, and costs, the different fields are expected to evolve continuously.

Regarding time autonomy, a conventional approach considers real systems related to up to several tens of hours. These technologies are represented in the lower half of Fig. 16.4. For longer storage times, such as the so-called seasonal storage, several possibilities exist, which are based on complex transformations. In

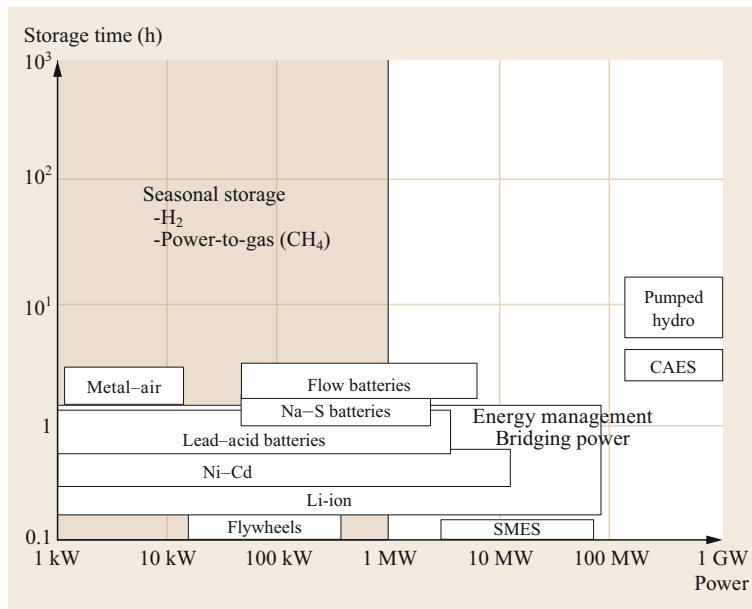


Fig. 16.4 Overview on storage systems

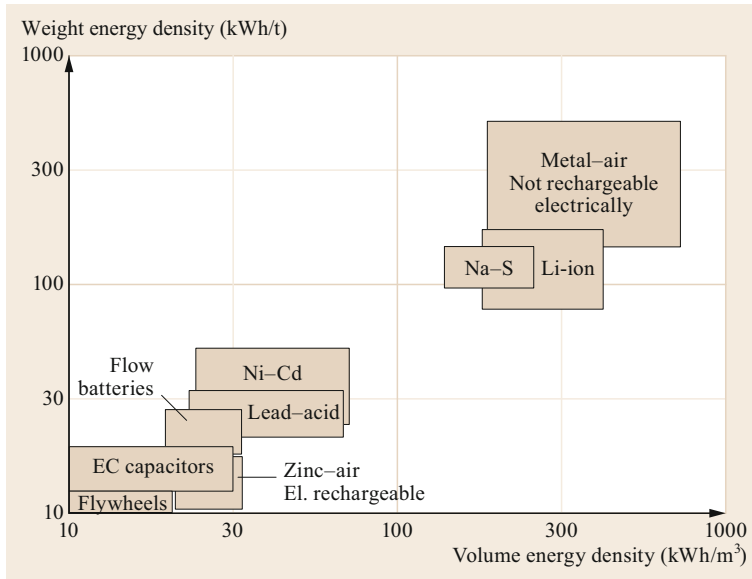


Fig. 16.5 Weight and volume energy density

Fig. 16.4, the long-term storage is represented by up to  $10^3$  h. This indicative value could correspond to a transformation from solar power to hydrogen defined over 3 months (100 d) and with a collection of up to 10 h/d. The 1 MW value indicated for this seasonal storage is chosen arbitrarily.

### Energy Density

One important parameter related to a given technology is the energy density. In Fig. 16.5, the energy densities of several techniques are indicated. On the vertical axis, the *weight energy density* is indicated.

The symbol used for the weight energy density is:  $e_m$  (Wh/kg); this parameter is generally indicated in Wh/kg, or in kWh/t. Another parameter for the energy density is the *volume energy density*. The symbol used for the volume energy density is:  $e_v$  [Wh/dm<sup>3</sup>]; this parameter is indicated in kWh/m<sup>3</sup>, or in Wh/dm<sup>3</sup>. These symbols are chosen according recommendations of the IEC [16.4].

The parameters on energy density are important with respect to the choice of technology for a given application. Mobile applications are the most concerned with the weight energy density. In this context, an extreme case of application is the *Solarimpulse* project, which uses modern high-performance batteries in order to fly overnight with energy accumulated during the day by PV cells placed on the airplane wings [16.5].

In opposition to what will be demonstrated in Sect. 16.3.4, the values indicated by the manufacturers of storage components related to energy density generally do not consider any energy efficiency or losses during charging or discharging, nor do they consider any

self-discharging losses. In reality, the internally-stored energy corresponds to a given value that is neither equal to what was supposed to be stored initially, nor to what can be recovered. These values depend on the power level of the energy exchange. A schematic representation of the energy quantities and the related losses is given in Fig. 16.6.

### Power Density and Specific Power

A second possibility to compare storage devices is to quantify their power capability. This is often given by the power density or by the specific power. The power density is the amount of power (the time rate of energy transfer) per unit volume. It is also called the *volume power density*. The symbol used for the power density is  $p_v$  (W/dm<sup>3</sup>). It is expressed in W/dm<sup>3</sup> or in kW/m<sup>3</sup>. It is also possible to give the value of the volume power

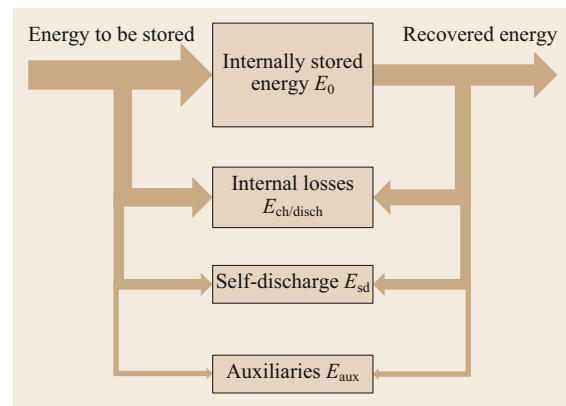


Fig. 16.6 Energy stored and recovered with losses

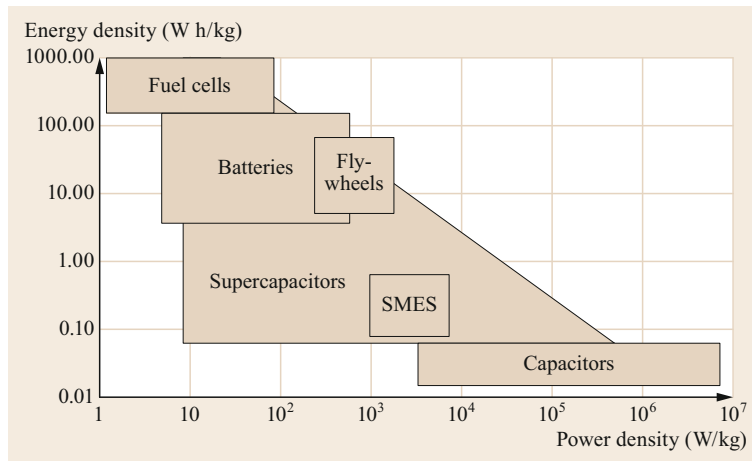


Fig. 16.7 The Ragone chart

density in  $\text{W}/\text{m}^3$ , as can be seen in some scientific tables [16.5].

The *power-to-weight ratio*, or *specific power*, is the power generated by a source divided by the mass. The symbol used for the *power-to-weight ratio* is  $p_m$  ( $\text{W}/\text{kg}$ ). This parameter is given in  $\text{W}/\text{kg}$  or in  $\text{kW}/\text{t}$ . For powerful devices, such as supercapacitors or thermal generators, the specific power is often given in  $\text{kW}/\text{kg}$ . As was said before for the energy density, these parameters are only an indication given by the manufacturer to define what is possible or admissible for their use. The values indicated cannot be interpreted in the sense of energy efficiency.

## 16.3 Technical Definitions

To define the application of a given storage device correctly and in order to have clear parameters for the design, technical definitions are needed [16.6].

### 16.3.1 General Parameters

#### Capacity

The capacity is the quantity of electricity to be recovered from an accumulator. It is generally expressed in  $\text{A h}$  and corresponds to the time integral of the current

$$C = \int_0^t i(t) dt. \quad (16.9)$$

#### Depth of Discharge

This is the indication of the quantity of electricity already extracted from an accumulator related to its maximum capacity  $C$ ,

$$\text{DoD} = \frac{\int_0^t i_{\text{dis}}(t) dt}{C}. \quad (16.10)$$

### 16.2.3 The Ragone Chart

The Ragone chart is used for the performance comparison of various energy storage devices. The values represented on a Ragone chart are the specific energy or weight energy density  $e_m$  (in  $\text{W h}/\text{kg}$ ) versus the specific power or power-to-weight ratio  $p_m$  (in  $\text{W}/\text{kg}$ ). The axes of a Ragone chart are logarithmic, which allows comparing the performance of very different devices (for example, extremely high and extremely low power). Figure 16.7 gives an example of a Ragone chart used by one manufacturer for the positioning of a given technology in a general context of energy storage devices.

#### State of Charge

This is an indication of the remaining quantity of electricity available from an accumulator, related to its maximum available capacity

$$\text{SoC} = \frac{\text{Amount of remaining charge}}{\text{Practical capacity of an accumulator}},$$

$$\text{SoC} = \frac{C - \int_0^t i_{\text{dis}}(t) dt}{C}. \quad (16.11)$$

The state of charge (SoC) and depth of discharge (DoD),

$$\text{SoC} = 1 - \text{DoD} \quad \text{or} \quad \text{DoD} = 1 - \text{SoC}. \quad (16.12)$$

The SoC and DoD are related to electric charges as current integrals. They are usually applied to electrical and electrochemical accumulators. By analogy, the state of charge can be replaced by the state of energy (SoE), corresponding to the ratio between the remaining amount of energy available ( $E$ ) and the total amount of stored

**Table 16.2** Charging/discharging rates

Battery capacity: $n \text{ A h}$		
C-rate	Time (min)	Current (A)
5 C	12	$5n$
2 C	30	$2n$
1 C	60 (= 1 h)	$n$
0.5 C (or C/2)	120 (= 2 h)	$n/2$
0.1 C (or C/10)	600 (= 10 h)	$n/10$

energy ( $E_{\text{sto}}$ ). SoE is a more universal parameter and can be used for any storage device,

$$\text{SoE} = \frac{E}{E_{\text{sto}}} . \quad (16.13)$$

### Charge and Discharge Rates (C-Rates)

The charge and discharge rates of an accumulator are generally defined through C-rates. With the definition of Sect. 16.3.1, the capacity of an accumulator is usually given at 1 C, which means that a battery rated  $n \text{ A h}$  should deliver  $n \text{ A}$  for 1 h. Choosing different values for the C-rate of the same battery corresponds to a charge or discharge with different times and different currents, as shown in Table 16.2.

The values given in Table 16.2 correspond to an idealized battery without charging/discharging losses. The internal losses can strongly reduce the discharge time or affect the charging time of a given battery.

### 16.3.2 Round-Trip Efficiency Under Normal, Ideal, and Real Conditions

Energy efficiency values are, in a very broad context, highly sensitive parameters. It is, therefore, of great importance to specify the exact conditions of their evaluation in a pragmatic way.

The energy storage cycles considered correspond to a series of charges, discharges, and idle modes. To define the round-trip efficiency properly, it is necessary to first have identical states of energy at the end and at the beginning of the cycle. Even if the storage systems are of huge complexity and of diverse technologies, the energy loss can be divided into two main categories, namely, the loss due to the power transfer  $P_{\text{ch}}$  (charge and discharge) and the loss due to the self-discharge  $P_0$ .

For the round-trip efficiency (index c), one new definition and notation is defined that concerns the ratio between the charging and discharging power. In many references, such as [16.7], the assumption is made that the charge and discharge powers are identical. Such conditions are called *normal*, and this condition will be indicated through the index n. Thus, a first symbolic is proposed: *the normal round-trip efficiency is  $\eta_{\text{cn}}$*  as a general definition.

Further, one should know through the definition of the symbol used for the round-trip efficiency, whether or not it includes the self-discharge loss  $P_0$ . As a consequence, the second proposal is to add the index 0 to the general symbol, if it describes *the ideal normal round-trip efficiency  $\eta_{\text{cn}0}$* .

Finally, if the self-discharge losses are included, the symbol is completed by the letter t, leading to *the real normal round-trip efficiency  $\eta_{\text{cnt}}$* , where the additional index t is an indication that the storage time influences the final value of the energy balance due to self-discharge.

### Charge and Discharge Losses

One can suppose the charge and discharge losses are of the form

$$P_{\text{ch}} \cong \alpha P^2 , \quad (16.14)$$

with  $P$  being the charge or discharge power.

In the case of an electrochemical battery, the parameter  $\alpha$ , which is related to the internal resistor, is dependent on the SoE and also on the direction of the energy transfer. In an electrochemical battery, it can be assumed that the power is proportional to the current (voltage approximatively constant). This is not the case for other storage elements, like capacitors (supercapacitors), where the voltage varies strongly with the state of energy.

### Losses Due to Self-Discharge

Self-discharge losses are generally an increasing function of the state of energy. They are noted as  $P_0(\text{SoE})$ .

### Total Losses

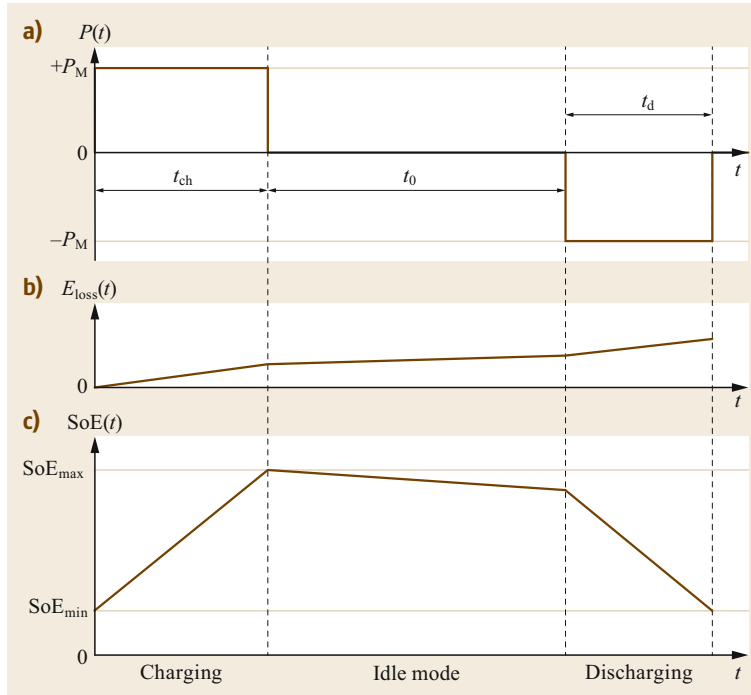
Considering one operating cycle of the storage device that is characterized by one specific power profile  $P(t)$  and by one state of energy  $\text{SoE}(t)$ , the total losses  $P_{\text{loss}}$  are equal to the sum of the charge/discharge losses added to the self-discharge losses

$$P_{\text{loss}} = \alpha P^2(t) + P_0[\text{SoE}(t)] . \quad (16.15)$$

Further, the dissipated energy  $E_{\text{loss}}$  over one complete cycle can be calculated as

$$E_{\text{loss\_cyc}} = \int_0^{t_{\text{cyc}}} \{ \alpha P^2(t) + P_0[\text{SoE}(t)] \} dt . \quad (16.16)$$

By convention, the energy storage device is defined as an *energy sink* and, consequently, the power  $P(t)$  is positive during the charge phase and negative during the



**Fig. 16.8a–c** Successive phases of the round-trip cycle of a storage device. (a) Charging and discharging power  $P(t)$ , (b) energy losses  $E_{loss}(t)$ , (c) state of energy  $SoE(t)$

discharge phase. The profile of the state of energy  $SoE$  is given by

$$SoE(t) = SoE(t_0) + \frac{\int [P(t) - P_{loss}(t)] dt}{E_{sto}}, \quad (16.17)$$

where  $E_{sto}$  is the energetic capacity of the storage device.

As a standard example, Fig. 16.8 shows a specific power profile consisting of three successive phases. First, a charging phase at constant power  $P_M$  during one charging time of  $t_{ch}$ , then an idling phase characterized by a low self-discharge, and finally, a discharging phase at an identical power as during the charging phase, but of a slightly reduced duration  $t_d$  due to the fact that the energy amount recovered during discharging can only be smaller than the amount transferred during the charging phase.

The schematic power profile of Fig. 16.8 illustrates the importance of the specific characteristics of the charge/discharge cycle, the intensity of the charging and discharging power, as the ratio of the different phase durations, especially the duration of the idling mode. The evolution of the energy losses is indicated. Finally, the state of energy  $SoE(t)$  is also represented.

### 16.3.3 The Round-Trip Efficiency

The round-trip efficiency  $\eta_c$  is the ratio of the energy  $E_d$  recovered during the discharge to the energy spent

$E_{ch}$  for the charging process, calculated as a mean value over one charging/discharging cycle. Such a cycle can be chosen arbitrarily, but the  $SoE$  after discharge must be identical to the  $SoE$  before the charging process.

For the ideal example of Fig. 16.8, the ideal normal round-trip efficiency where the self-discharge losses are neglected is calculated according the definitions of Sect. 16.3.2

$$\eta_{cn0} = \frac{E_d}{E_{ch}} = \frac{P_M t_d}{P_M t_{ch}} = \frac{t_d}{t_{ch}}. \quad (16.18)$$

The round-trip efficiency can also be expressed by

$$\begin{aligned} \eta_{cnt} &= \frac{E_{ch} - E_{loss}}{E_{ch}} \\ &= \frac{P_M t_{ch} - \alpha P_M^2 (t_{ch} + t_d) - \int P_0 [SoE(t)] dt}{P_M t_{ch}}. \end{aligned} \quad (16.19)$$

Substituting  $t_d$  by  $t_d = \eta_{cnt} t_{ch}$  leads to

$$\eta_{cnt} = \frac{1 - \alpha P_M}{1 + \alpha P_M} - \frac{\int P_0 [SoE(t)] dt}{P_M t_{ch} (1 + \alpha P_M)}. \quad (16.20)$$

The round-trip efficiency can be expressed in dependency of each phase of the cycle, more precisely through consideration of the *instantaneous power effi-*



ciencies during charging  $\eta_{\text{ch}}$  and discharging  $\eta_{\text{d}}$

$$\eta_{\text{ch}} = \frac{P_{\text{M}} - \alpha P_{\text{M}}^2}{P_{\text{M}}} = 1 - \alpha P_{\text{M}}, \quad (16.21)$$

$$\eta_{\text{d}} = \frac{P_{\text{M}}}{P_{\text{M}} + \alpha P_{\text{M}}^2} = \frac{1}{1 + \alpha P_{\text{M}}}. \quad (16.22)$$

Finally, considering the *self-discharge energy factor*

$$\eta_0 = \frac{\int P_0[\text{SoE}(t)]dt}{P_{\text{M}}t_{\text{ch}}},$$

$$\text{we get } \eta_{\text{cnt}} = (\eta_{\text{ch}} - \eta_0)\eta_{\text{d}}. \quad (16.23)$$

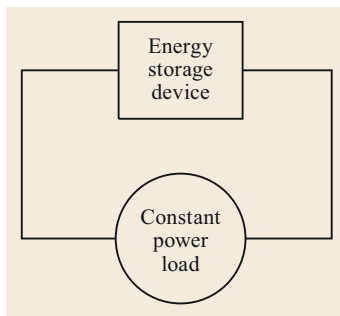
This expression highlights the influence of the individual efficiencies of charging, discharging, and idling (self-discharge) very well. It must be noted that the same expression is obtained for any profile of the charging power ( $P_{\text{ch}}$ ) and the discharging power ( $P_{\text{d}}$ ).

### 16.3.4 The Theory of Ragone Plots

As was described in Sect. 16.3.3, the energy efficiency of a storage device is related to the different losses. Charging and discharging losses, as well as self-discharge losses, directly influence the round-trip efficiency. As a consequence, the amount of energy that can really be recovered from a fully charged storage device must be defined in dependency of the instantaneous power of the energy transfer. This principle of interdependency between the energy density and the power density was described in [16.8].

In [16.8], a general circuit is associated with Ragone plots (Fig. 16.9). The energy storage device (ESD) feeds a load with constant power  $P$ . The ESD contains elements for energy storage. Due to constant power, energy supply occurs only for a finite time  $t_{\text{inf}}(P)$ . The energy amount  $E$  available for the load in dependence of the power  $P$  defines a Ragone plot.

With reference to the general circuit of Fig. 16.9, the ESD may, for example, consist of a voltage source,



**Fig. 16.9** General circuit associated with Ragone plots (adapted from [16.8])

$U(Q)$ , depending on the stored charge  $Q$ , an internal resistor  $R$ , and an internal inductance  $L$ . In reality, this ESD can describe many kinds of electric power sources. The ESD feeds an active load where the power is maintained constant  $P \geq 0$ . Such a load can be realized with an electronically controlled power converter feeding an external user. The current  $I$  and voltage  $U$  at the load are then related nonlinearly by  $U = P/I$ . With reasonable initial conditions

$$Q(0) = Q_0 \quad \text{and} \quad \dot{Q}(0) = \dot{Q}_0,$$

the evolution of the electrical variables is governed by the following differential equation,

$$L\ddot{Q} + R\dot{Q} + U(Q) = -\frac{P}{Q}, \quad (16.24)$$

where

$$\ddot{Q} = \frac{d}{dt}(\dot{Q}) = \frac{d}{dt} \left[ \frac{d}{dt}(Q) \right].$$

Without making reference to a specific physical interpretation of (16.24), the Ragone curve can be defined as follows. At time  $t = 0$ , the device contains the stored energy

$$E_0 = \left( \frac{L\dot{Q}_0^2}{2} \right) + W(Q_0). \quad (16.25)$$

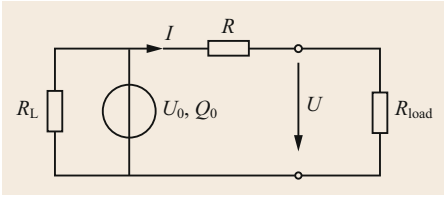
For  $t > 0$ , the load imposes a constant power  $P$  such that  $Q(t)$  satisfies the relation (16.24). For finite  $E_0$  and  $P$ , the ESD is able to supply this power only for a finite time:  $t_{\text{inf}}(P)$ . Starting with the initial stored energy  $E_0$ , the feeding of the load ends when the storage device reaches its state of energy  $\text{SoE} = 0$ . Since the power is time-independent, the amount of energy transferred to the load is

$$E(P) = Pt_{\text{inf}}(P). \quad (16.26)$$

The curve  $E(P)$  versus  $P$  corresponds to the Ragone plot.

#### The Ragone Plot of a Battery

The particular case of an ideal battery is studied based on a simple equivalent circuit as represented in Fig. 16.10. First, and regarding the model leading to (16.24), we assume the condition  $L = 0$ . Then, the ideal battery with a capacity of  $Q_0$  is characterized by a constant cell voltage  $U = U_0$  if  $Q_0 \geq Q > 0$ , and  $U = 0$  if  $Q = 0$ . In a first approach, the leakage resistor  $R_L$  is neglected.



**Fig. 16.10**  
Equivalent scheme of the ideal battery

Equation (16.24) then reads

$$P = UI = (U_0 - RI)I,$$

where  $U$  is the terminal voltage, and  $I = \dot{Q}$  is the current.

The solutions of the quadratic equation are

$$I_{\pm} = \frac{U_0}{2R} \pm \sqrt{\frac{U_0^2}{4R^2} - \frac{P}{R}}. \quad (16.27)$$

At the limit  $P \rightarrow 0$ , two different values of the discharge current are

$$I_+ \rightarrow \frac{U_0}{R} \quad \text{and} \quad I_- \rightarrow 0.$$

For the ideal battery, the constant power sink can also be represented by a constant load resistance  $R_{\text{load}}$ .

The two limits then belong to  $R_{\text{load}} \rightarrow 0$  (short circuit) and  $R_{\text{load}} \rightarrow \infty$  (open circuit), respectively. Considering realistic energy and power conditions, the second solution (open circuit) for the zero power is retained. This corresponds to the solution of (16.27) with the minus sign,  $I \equiv I_-$ .

Now, the battery is empty at time  $t_{\text{inf}} = Q_0/I$ , where the initial charge  $Q_0$  is related to the initial energy  $E_0 = Q_0 U_0$ . The leakage current in the resistor  $R_L$  is taken into account. This current increases the discharge current  $I$  by  $U_0/R_L$ .

The energy being available for the load becomes

$$E_b(P) = Pt_{\infty} = \frac{2RQ_0P}{U_0 - \sqrt{U_0^2 - 4RP + \frac{2U_0R}{R_L}}}. \quad (16.28)$$

Equation (16.28) corresponds to the Ragone curve of the ideal battery. In the presence of leakage,  $E_b(0) = 0$ .

For the extracted energy, there exists a maximum at

$$P = \frac{U_0^2}{\sqrt{2RR_L}}.$$

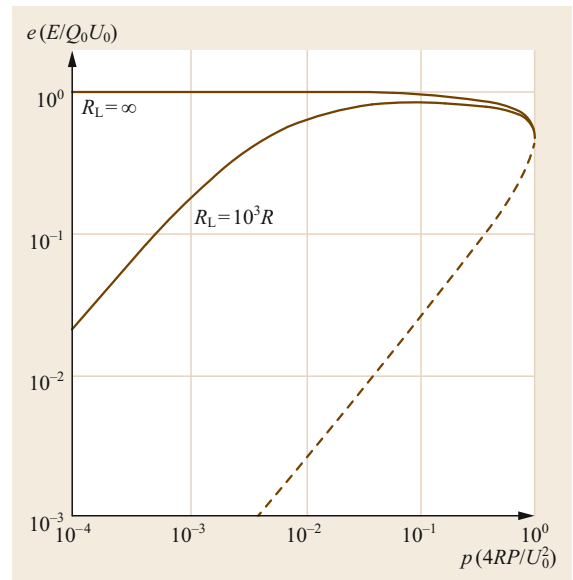
Without leakage  $R/R_L \rightarrow 0$ , the maximum energy is available for vanishing low power  $E_b(P \rightarrow 0) = E_0$ . From (16.28), one concludes that there is a maximum power  $P_{\text{max}} = U_0^2/4R$  associated with an energy  $E_0/2$  (a small correction due to leakage is neglected). This point is the endpoint of the Ragone curve of the ideal battery, where only half of the energy is available, while the other half is lost at the internal resistance.

Finally, the expression of the Ragone plot is given in dimensionless units using

$$e_b = \frac{E_b}{Q_0 U_0} \quad \text{and} \quad p = \frac{4RP}{U_0^2},$$

$$e_b(p) = \frac{1}{2} \frac{p}{\left(1 - \sqrt{1-p} + \frac{2R}{R_L}\right)}. \quad (16.29)$$

The Ragone curves according to (16.29) with and without leakage are shown in Fig. 16.11 for the ideal battery. The branch belonging to  $I_+$  is shown by the dashed curve.



**Fig. 16.11** Ragone curve of the ideal battery (adapted from [16.8])

## 16.4 Electric Power and Energy Storage

Energy systems tend to become *electrically controllable* systems or to somewhere integrate the *electric vector*, because the most convenient and most efficient way to transport, convert, or control the power is in its electric form.

On such a basis, the scheme represented in Fig. 16.12 will be valid for most energy storage systems [16.7]. The input source on the left-hand side is interfaced with a power electronic converter circuit that allows the control of the power flow to the storage means (right-hand side). In the middle, one or more additional conversions can be involved as electromechanical, electro-thermal, or electrochemical conversions.

### 16.4.1 Storage Forms of Energy

In Fig. 16.12, the real storage element shown indicates the *storage form of energy*, representing, in fact, the energy reservoir. This block corresponds to one unit, where the change of the internal state is directly related to the change of the energy content with a high reversibility.

The storage forms of energy can be of different nature, such as:

- The potential energy associated to the earth's gravity when one mass is moved from one altitude to another (for example, water in a pumped storage plant)
- The kinetic energy of a mechanical system in rotation (flywheels)
- The pressure of a compressible fluid (compressed air)
- Covalent bonds of given molecules (electrochemicals)
- Electric or magnetic state variables (electrical field, magnetic field, capacitors, superconducting inductors).

### 16.4.2 The Intermediary Conversion

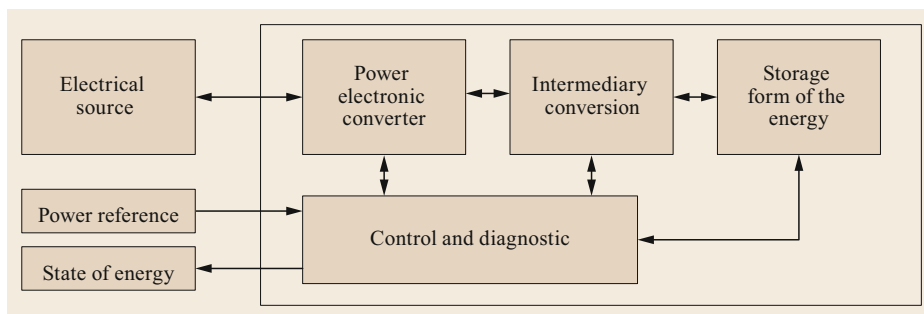
The interface between the storage form unit and the electrical level (output of the power electronic converter) may need the so-called intermediary conversion also shown in Fig. 16.12. The intermediary conversion can be of different nature. For example, it includes the electric motor-generator and the hydraulic pump/turbine in a pump storage plant, or it is simply the electric driving machine of a flywheel. In the case of compressed-air energy storage, the intermediary conversion can involve several successive conversions, such as a water pump in a liquid piston system or a simple motor and compressor.

### 16.4.3 Control and Diagnostics

The control and diagnostic device is essential for the numerous different conversion functions, such as controlling the torque and speed of the driving machine or simply to control the current or voltage. The control quantities are generally related to the power level exchanged during charge and discharge of the storage device.

The value of the instantaneous charge and discharge power level must be related to the typical power density ( $\text{kW}/\text{dm}^3$ ) or specific power ( $\text{kW}/\text{kg}$ ) of the energy storage device itself, according the definitions given above.

The control and diagnostic unit must provide information on SoC, or SoE. The parameter of the depth of discharge (DoD) is also used. In some sensitive cases, the diagnostic unit can give information about the state of health (SoH).



**Fig. 16.12** Electrical energy storage system (ESS)

## 16.5 Energy Storage Systems

In the following chapters, the most well-known storage systems will be presented. They are classified according to a scheme where their main characteristics appear, corresponding to their structure and basic phenomena.

The first category describes storage systems based on physical principles, like gravitational potential forces, air compression, or rotational kinetic energy. The next category encompasses purely electrical systems, like superconductive magnets and capacitors.

Finally, storage systems using electrochemical transformations are presented. Classical battery-energy storage systems and technologies are described, as well as so-called flow batteries. Fuel cells and hydrogen storage are briefly introduced.

For all systems introduced in this chapter, the elementary rules for the quantified storage of energy are given. Another aspect of the descriptions is the presentation of the power electronic circuits and architectures that are needed for a continuously controllable power flow to and from the different storage means.

## 16.6 Storage Systems Based on Physics

Storing energy is usually a repetitive task with a very high number of expected cycles. Contrary to classical electrochemical batteries, where the expected number of cycles is limited due to degradation phenomena, physical systems based on reversible mechanisms of various natures can be used with much higher life cycles. One good example can be found in the hydraulic sector, with classical pumped-hydropower plants. Such systems can, in addition, be realized for very high power levels in the hundreds of MW range.

Another principle is based on gas compression and expansion and is known as CAES (compressed-air energy storage) [16.9–11]. Further mechanical systems are also used based on rotational kinetic energy and are known as flywheels [16.12]. Electrical components like capacitors or inductors are also candidates for energy storage, even if their specific energy capacity is limited. Such systems are generally used for their ability to provide high levels of instantaneous power [16.13–15].

### 16.6.1 Gravitational Hydro-Pumped Storage

#### General Properties

Hydraulic, pumped storage facilities allow storing tremendous amount of energy, allowing supply of the network over several days or months, or, in some cases, compensating seasonal demand.

The ratings of hydropower have been shown comparatively in Sect. 16.2.2. Pumped-storage power plants have used conventional machinery for a longer time, where the electric motor-generator is directly connected to the grid. For such facilities, even when the power level in the generation mode can be controlled through the governor, the variation of the power in the pumping mode is not possible due to the fixed rotational speed of the equipment.

Controlling power in pumping mode is the main reason that modern pumped-storage equipment features variable speeds of the rotating machinery. Furthermore, variable-speed technology has made possible to cope with larger variations of headwater and tailwater reservoir levels to optimize plant performance and to solve specific problems [16.16].

Pumped-storage facilities benefit from good conditions with respect to energetic efficiency and can be operated over several decades as far as the machinery is concerned, even if some periodic revisions are needed. With respect to dams, the lifetime is in the range of centuries.

#### Components of a Hydropower Plant

Figure 16.13 represents a classical pumped-storage facility, where water flows from the lower reservoir (tailwater reservoir) to the upper one (headwater reservoir) in the pumping mode, and in the inverse direction for the generating mode [16.17].

From the headwater reservoir, the water flows through a tunnel and a penstock to the hydraulic machine. This hydraulic machine, which is generally a reversible machine (pump/turbine), is coupled to the electric motor-generator, which is generally a synchronous machine.

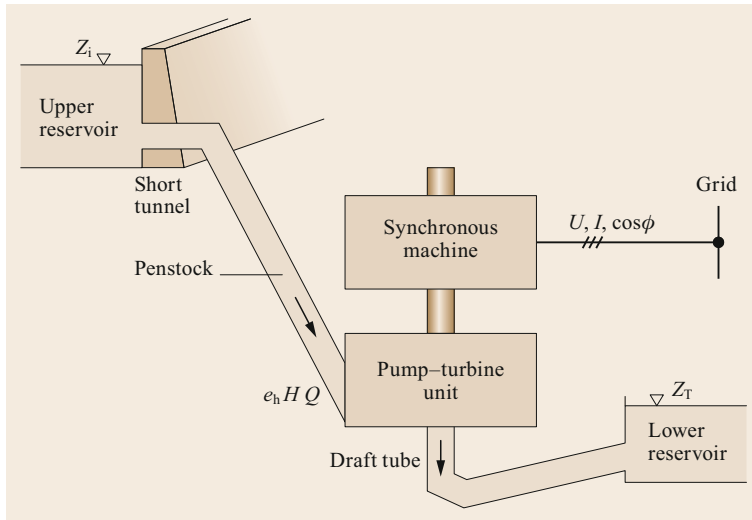
#### Water Power: Definitions

From Fig. 16.13, the following definitions are deduced

$$\text{Head: } H = H_1 - H_2 \quad (\text{m}), \quad (16.30)$$

where head is derived from the headwater and tailwater reservoir levels  $Z_i$  and  $Z_T$ , respectively, as follows

$$\begin{aligned} \text{in generating mode: } H &= H_1 - H_2 \\ &= (Z_i - Z_T) - H_i^{\text{Gen}}. \end{aligned} \quad (16.31)$$


**Fig. 16.13** Schematics of a pumped-storage facility

with  $H_r^{\text{Gen}}$  the head loss in the hydraulic circuit in turbine mode;

$$\begin{aligned} \text{in pumping mode } H &= H_1 - H_2 \\ &= (Z_i - Z_T) + H_r^{\text{Pump}}, \quad (16.32) \end{aligned}$$

with  $H_r^{\text{Pump}}$  the head loss in the hydraulic circuit in pumping mode.

Throughout this document, head losses are considered negligible.

Discharge:  $Q$  ( $\text{m}^3/\text{s}$ )

$$\text{Specific hydraulic energy } e_h = gH = g(H_1 - H_2). \quad (16.33)$$

The dimension of the specific hydraulic energy is  $(\text{m}/\text{s}^2)\text{m} = \text{J}/\text{kg}$ .

Further parameters used are:

- Water density  $\rho$  ( $\text{kg}/\text{m}^3$ )
- Acceleration due to gravity  $g = 9.81$  ( $\text{m}/\text{s}^2$ ).

#### Elementary Relations of Hydropower Generation

**Potential Energy.** The potential energy of a mass of water accumulated through elevation is described ideally by the following relation

$$E = me_h = mgh, \quad (16.34)$$

where  $e_h$  is the specific hydraulic energy, as defined before.

Example: a mass of water of 1000 kg ( $1 \text{ m}^3$ ) at a height of 1000 m has a potential energy of

$$\begin{aligned} E &= 1000 \text{ kg} \cdot 9.81 \text{ m}/\text{s}^2 \cdot 1000 \text{ m} = 9.81 \times 10^6 \text{ Ws} \\ &= 2.73 \text{ kWh}. \quad (16.35) \end{aligned}$$

**Kinetic Energy.** If a mass of water begins to be set in motion (friction free), its accumulated potential energy is converted into kinetic energy according to

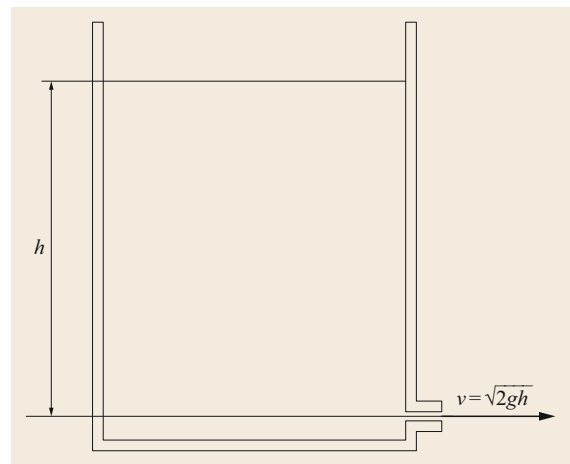
$$E = \frac{mv^2}{2}. \quad (16.36)$$

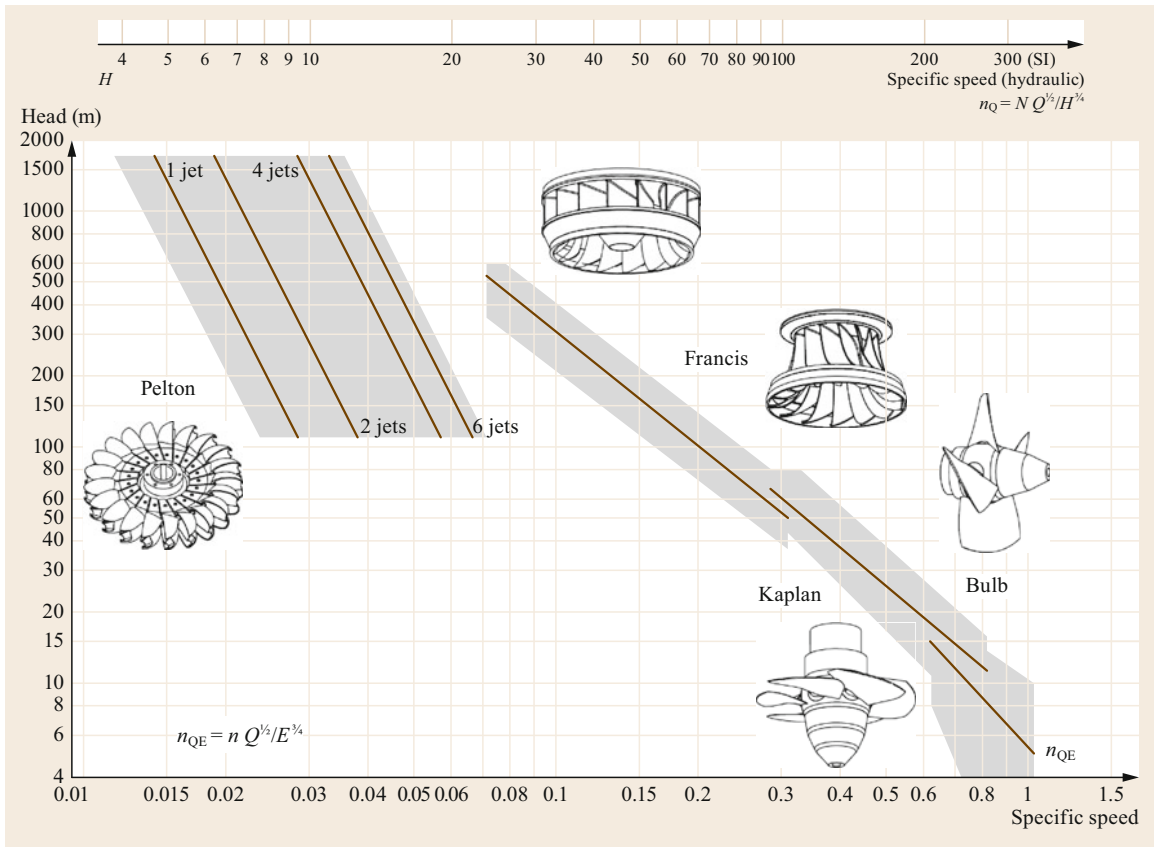
So, the velocity reached by one mass of water through conversion from the potential fall energy into kinetic energy is ideally calculated from

$$mgh = \frac{mv^2}{2}, \quad (16.37)$$

leading to (Fig. 16.14)

$$v = \sqrt{2gh}. \quad (16.38)$$


**Fig. 16.14** Conversion from potential to kinetic energy



**Fig. 16.15** Head versus specific speed for hydraulic turbines and the corresponding shape of the runners. (Reprinted by permission from François Avellan, 2019)

**Pressure.** Considering one reservoir as represented in Fig. 16.14, the pressure at the bottom of the reservoir can be calculated according to

$$p = \rho gh . \tag{16.39}$$

**Power.** A turbine ideally converts the potential energy  $mgh$  of the water into mechanical energy in a given time unit  $t$ . Its power (friction is not considered) is defined as the per-second converted amount of energy

$$P = \frac{m}{t} gh . \tag{16.40}$$

For the same example (16.35), the power becomes

$$\begin{aligned} P &= \frac{1000 \text{ kg}}{1 \text{ s}} \cdot 9.81 \text{ m/s}^2 \cdot 1000 \text{ m} \\ &= 9.81 \times 10^6 \text{ N m/s} = 9.81 \times 10^6 \text{ W} \\ &= 9.81 \text{ MW} . \end{aligned} \tag{16.41}$$

The power can be further calculated by

$$P = \frac{m}{t} gh = \rho Q e_h . \tag{16.42}$$

For a real turbine, the converted power is affected by the turbine efficiency

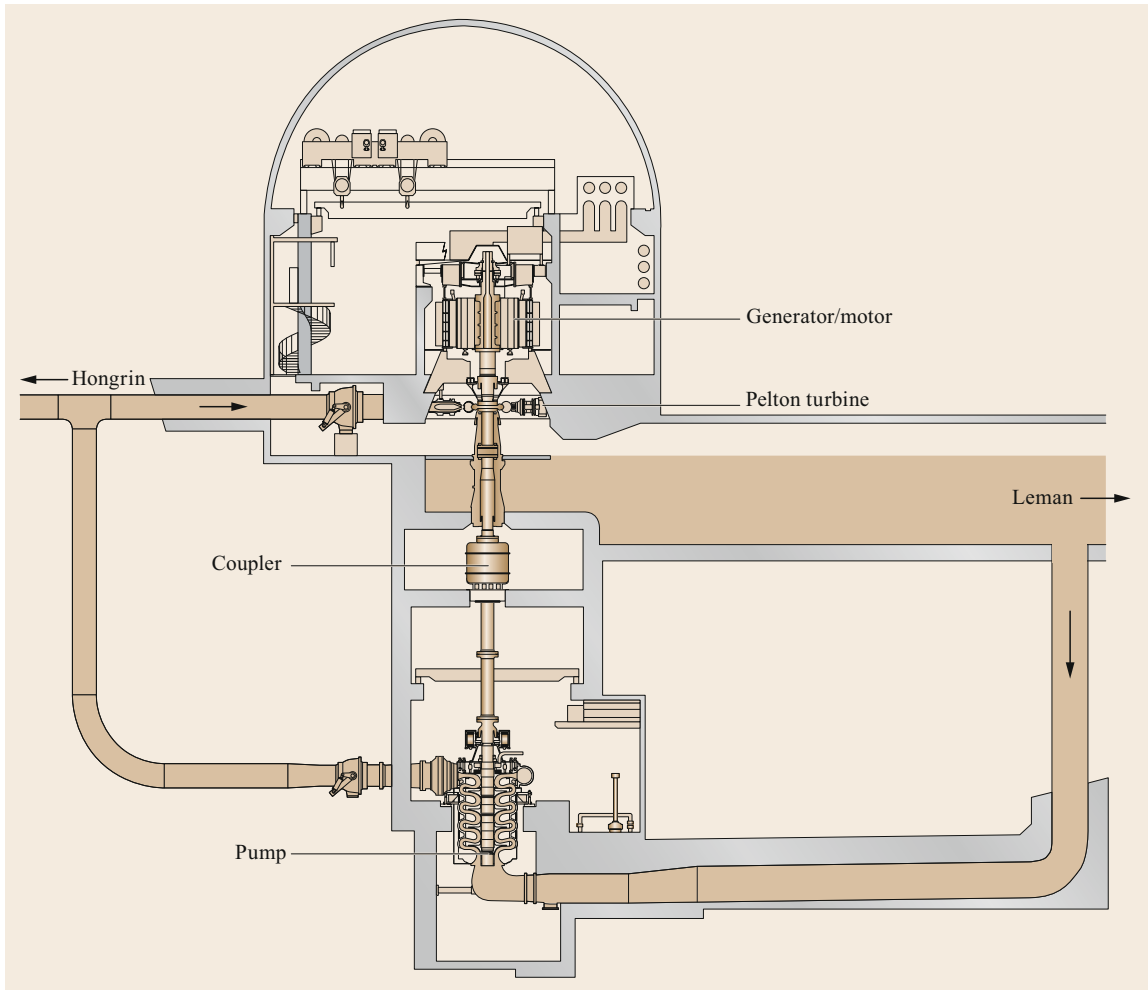
$$P = \eta \rho Q e_h . \tag{16.43}$$

### Classification of Turbines

There are three main types of hydraulic machines:

- The *Pelton* turbine is an impulse turbine with tangential flow and is suited for high-head applications.
- The *Francis* turbine is a reaction machine with radial flow and is suited for medium-head applications.
- The *Kaplan* turbine is another reaction machine but with axial flow. It is suited for low-head applications.

The various types of hydraulic machines are represented in Fig. 16.15. The classification is made using a specific parameter of hydraulic machines, the specific speed. The specific speed is a dimensionless quantity used to characterize hydraulic turbomachines [16.18].



**Fig. 16.16** Example of the 120 MW pump–turbine ternary arrangement of FMHL (Forces Motrices Hongrin Leman, Switzerland)

According to the IEC standard,  $n_{QE}$  is given by

$$n_{QE} = \frac{nQ^{1/2}}{e_h^{3/4}}, \quad (16.44)$$

where  $n_{QE}$  is the specific speed (dimensionless),  $n$  is the runner/impeller rotational speed (Hz),  $Q$  is the flow rate ( $\text{m}^3/\text{s}$ ) at the point of best efficiency, and  $e_h$  is the specific hydraulic energy.

Alternately, hydraulic engineers often use the unit specific speed  $n_Q$  defined as

$$n_Q = N \frac{Q^{1/2}}{H^{3/4}}, \quad (16.45)$$

where  $n_Q$  is the specific speed (not dimensionless),  $N$  is the runner/impeller rotational speed (1/min),  $Q$  is the flow rate ( $\text{m}^3/\text{s}$ ) at the point of best efficiency, and  $H$

is the head (m) per stage at the point of best efficiency. The specific speed value for a turbine is the speed of a geometrically similar turbine that would produce unit power (1 kW) under unit head (1 m).

### Ternary Pump–Turbine Units

A ternary set consists of a motor–generator, a separate turbine, and a pump set. Pump-turbine units based on the use of Pelton machines do not benefit from the reversibility of this type of turbine. As a consequence, the train must be completed by a separated pump. The drawback of this solution is evidently the higher length of the rotating train. However, the train can be started by the turbine without an additional start-up machine. The rotating train has only one direction of rotation, and a changeover from turbine mode to pump mode is possible without changing the direction of rotation.

Figure 16.16 shows an example of a ternary unit as is realized in the FMHL plant in Veytaux Switzerland [16.19]. The FMHL plant uses an upper basin called *Lac de l'Hongrain*, and the lower basin is the lake of Geneva (Lac Léman). One of the characteristics of the plant is the pump submerged under the level of the lake.

### Reversible Pump–Turbine Units

Figure 16.17 illustrates an example of a reversible Francis machine, a 250 MW pump–turbine of a 500 rpm facility.

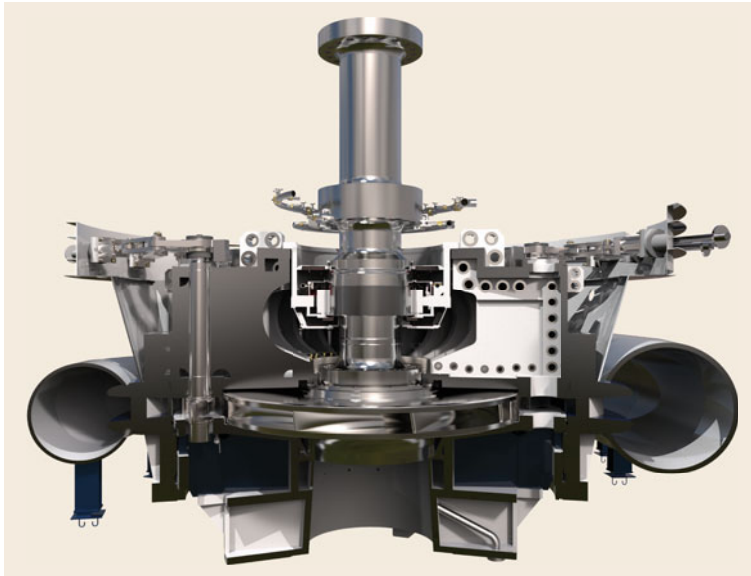
With reversible pump–turbine sets, the direction of rotation must be inverted for the changeover from turbine mode to pump mode. This can be achieved using a so-called pony motor for the acceleration of the train from standstill to the synchronous rotational speed.

Other solutions exist, where the start-up is realized in the pump mode through a static frequency converter feeding the synchronous machine with variable frequency.

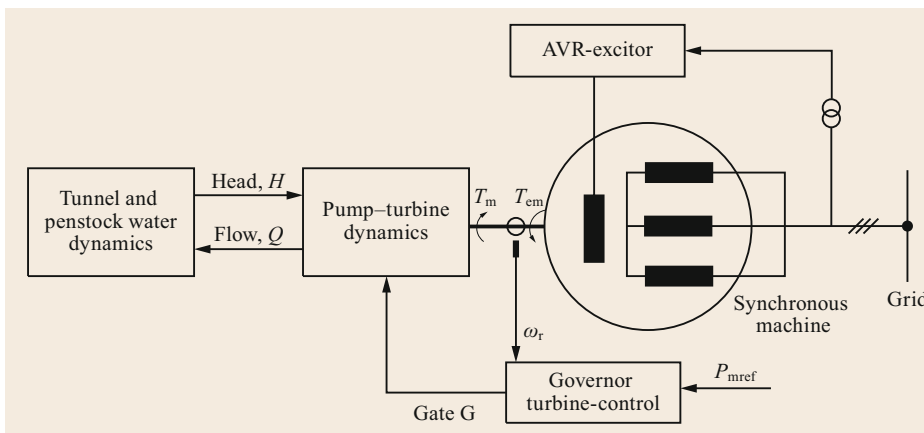
Reversible pump–turbines are traditionally operated with constant speed, but they can also be operated with variable speed. Two solutions are described in [16.1], namely the doubly-fed asynchronous motor generator and the synchronous motor generator with the full-conversion principle, where the static frequency converter is designed for the full power of the motor generator. For both solutions, the reversal of the train is achieved through the main frequency converter.

### Fixed-Speed Pumped Storage

In Fig. 16.18, the structural diagram of a fixed-speed pumped storage plant is shown. The synchronous machine also serves as a motor in the pump mode, as

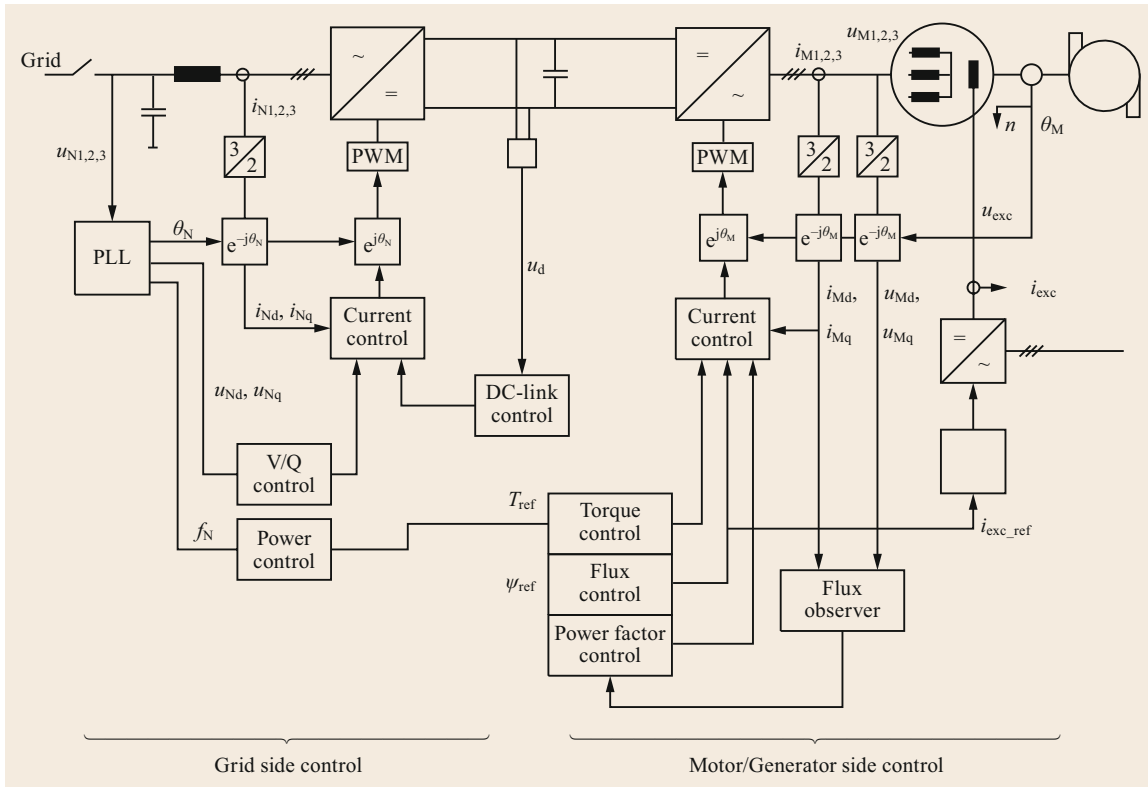


**Fig. 16.17** Reversible pump–turbine unit of 250 MW/500 rpm (courtesy of GE/Alstom)



**Fig. 16.18** Fixed speed pump–turbine system





**Fig. 16.19** Structural diagram of a full-conversion, variable-speed pumped-storage system

a generator for the turbine mode. The synchronous machine is connected to the grid by its armature and is coupled to the reversible hydraulic machine.

The active power is controlled through the governor and turbine control. The imposition of the voltage, as well as the control of the reactive power, is achieved through the machine's excitation system. Because the pump discharge (water flow rate) is linked to the rotation speed of the machines, the level of the power in the pump mode cannot be varied when the motor runs at the synchronism of the grid frequency. This limitation is one of the motivations to realize variable speed pump storage facilities.

### Variable-Speed Pumped Storage

In order to be able to vary the power in the pumping mode, and also to optimize the turbine mode, variable speed-pump-storage plants have been realized [16.20]. For such systems, two different solutions are used for energy conversion from the mechanical shaft to the electric grid.

The simplest method for the adaptation of the variable frequency of the synchronous motor-generator to the grid frequency is to use a static frequency converter. This frequency converter transforms the entire

electric power from the stator side of the machine, where the stator frequency is linked to the rotation speed of the machines, to the electrical grid with its constant frequency. The principal scheme of a variable speed-pumped storage system with full conversion is represented in Fig. 16.19, which shows the complexity of the control needed at the grid and machine sides.

A second possible solution for variable pump storage plants is the so-called doubly-fed induction motor-generator. In such a system, the electric machine is of the asynchronous type, where the wound rotor is interconnected to a frequency converter via slip rings and brushes. The machine's stator is directly connected to the grid. The bidirectional active feeding of the machine's rotor winding makes it possible to cover significant speed excursions in the hyper and hypynchronous domain. A doubly-fed induction motor-generator is shown in Fig. 16.20.

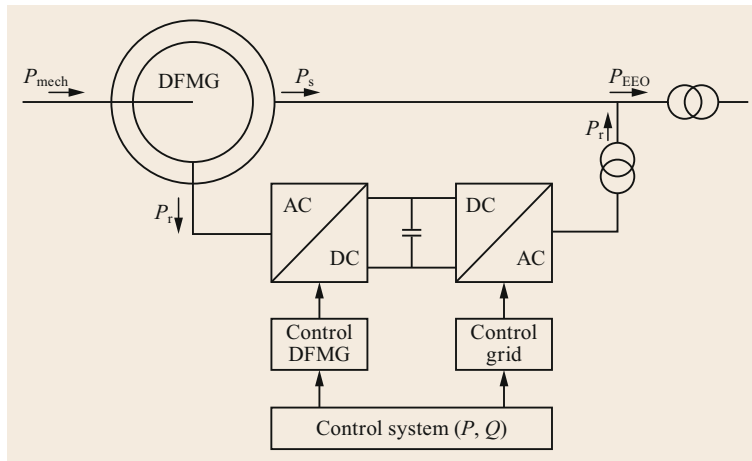
### Example of a Very High Power Variable-Speed-Pumped Storage Plant

An example of a large pumped storage plant is given by the Grimsel 2 facility of the KWO plant (Kraftwerke Oberhasli) in the Bernese Oberland of the Swiss Alps. The variable frequency operation of the 100 MW syn-

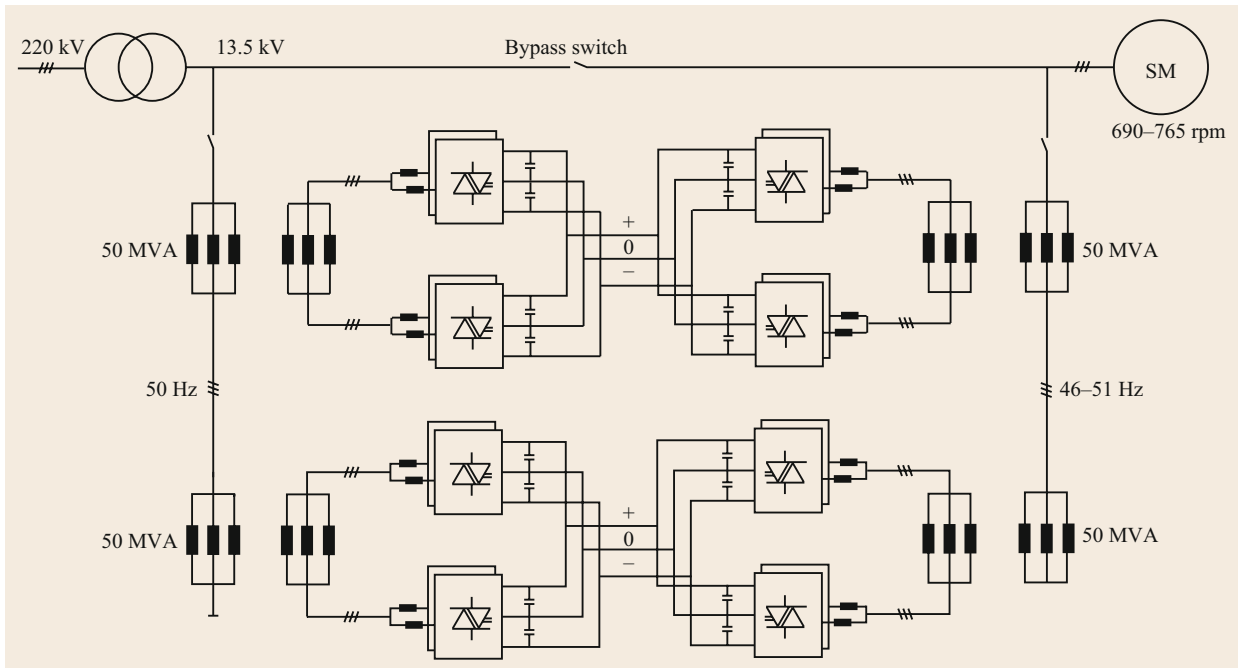
chronous machine is possible through the use of a high-end power electronics converter. The very high power VSC (voltage source converter) used for the synchronous machine is realized through the coupling of submodules with transformers (Fig. 16.21). Two line side transformers feed two line side converters. They are connected to the machine side converters and transformers via two separated DC (direct current) links. The so-called three-level technology is based on a positive and a negative voltage intermediary DC circuit. The

schematic of the complete installation of the Grimsel 2 facility is represented in Fig. 16.21. The full-conversion variable-speed operation range is defined from 690 to 765 rpm, corresponding to stator frequencies between 46 and 51 Hz.

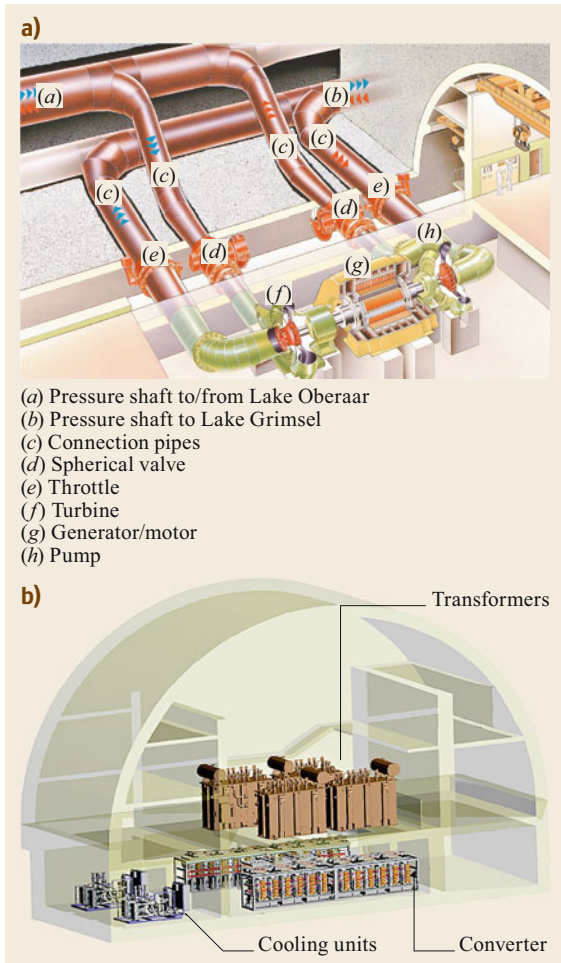
Figure 16.22 shows more details of the KWO 100 MW facility, with Fig. 16.22a showing the variable speed rotating machinery, and Fig. 16.22b the volume occupied in the cavern by the transformers and the frequency converter.



**Fig. 16.20** Block diagram of a doubly-fed induction motor generator (DFIMG)



**Fig. 16.21** The 100 MW pumped-storage facility of KWO/Grimsel 2 plant



**Fig. 16.22a,b** Rotating machinery and frequency converter with transformers of the 100 MW facility of KWO; (a) variable-speed rotating machinery; (b) volume occupied in the cavern by the transformers and the frequency converter. (Courtesy ABB Review [16.21])

## 16.6.2 Compressed-Air Energy Storage

Compressed-air energy storage CAES is based on the compression and expansion of air. Such systems generally use a compression stage comprising an electric motor driving a compression machine. The compressed air is then stored in a reservoir. For the recovery of the stored energy, an expansion system is provided. This expansion machine is composed of a volumetric expander driving an electric generator. The general scheme of CAES is represented in Fig. 16.23.

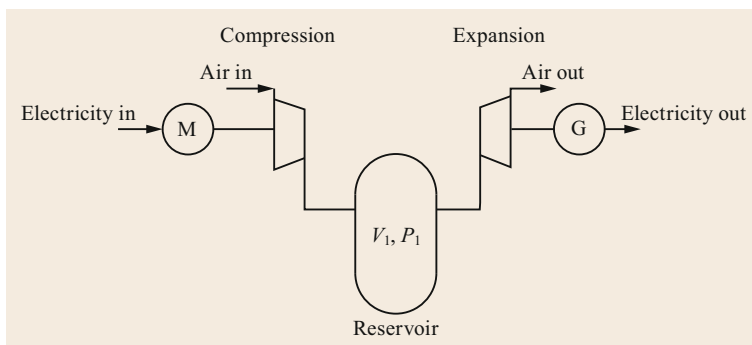
The amount of energy stored in a reservoir of volume  $V_1$ , pressurized at a pressure level  $P_1$  and stabilized at the same temperature as the surroundings, can be calculated through the expression (16.46) [16.1, 22]

$$E = P_1 V_1 \left[ \ln \left( \frac{P_1}{P_a} \right) - 1 + \frac{P_a}{P_1} \right]; \quad (16.46)$$

$P_a$  is the pressure of the surrounding (atmosphere). The expression gives the value of the maximum amount of energy that can be recovered from the reservoir that corresponds to a full expansion under isothermal conditions.

CAES systems, dedicated to diverse applications in industry, house-delivered energy, or in transportation have been built over the decades [16.23, 24]. The first utility CAES system was developed in Germany as a 290 MW plant in Huntorf [16.9]. Other systems have been realized, such as the McIntosh facility (Alabama, USA) [16.10].

Figure 16.24 shows the CAES plant in Huntorf Germany. The facility stores energy in an underground cavern, using the compressor stage of a gas turbine (7) and (9) for loading and its turbine in the discharge sequence (3) and (5) (Fig. 16.24). In order to compensate the decrease of the air temperature during the discharge



**Fig. 16.23** General scheme of CAES

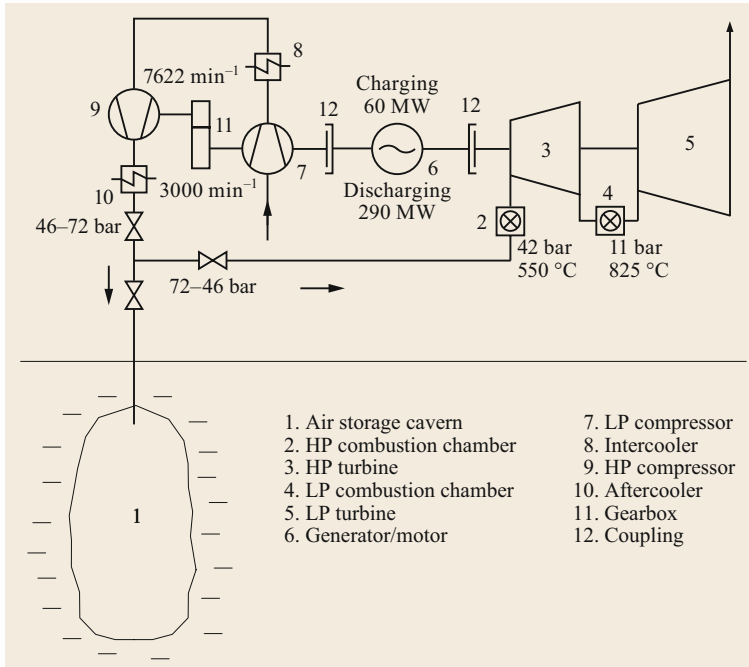


Fig. 16.24 The CAES plant at Huntorf

sequence, the burners of the gas turbine are maintained, (2) and (4) (Fig. 16.24).

### 16.6.3 Rotational Kinetic Energy (Flywheels)

Another possibility to store energy is given through rotational kinetic energy. Such systems also belong to the category of reversible physics phenomena. A flywheel system is generally composed of an electric machine coupled to a rotating mass. With the help of a power electronic converter, the driving torque of the variable-speed machine (positive torque for charging and negative for discharging) can be imposed precisely and makes the control of the exchanged power level possible. Flywheels were for a long time realized based on normal steel and limited speed, but modern equipment benefits from advanced materials like carbon composites and fast-running permanent magnet motors, which

can rotate at several hundred thousands of revolutions per minute (rpm). Partially evacuated encapsulations reduce the aerodynamic losses of the flywheel and motor. A schematic representation of a flywheel system is given in Fig. 16.25.

The amount of energy stored in a rotating mass running at a speed  $\Omega$  is given by

$$E = \frac{1}{2} J \Omega^2, \quad (16.47)$$

where  $J$  is the moment of inertia.

The auxiliaries of a flywheel system provide the partial vacuum needed to reduce aerodynamic losses, and they often include the control of special bearings (magnetic, air). The principle of the flywheel storage, together with detailed models for high performance can be found in [16.12].

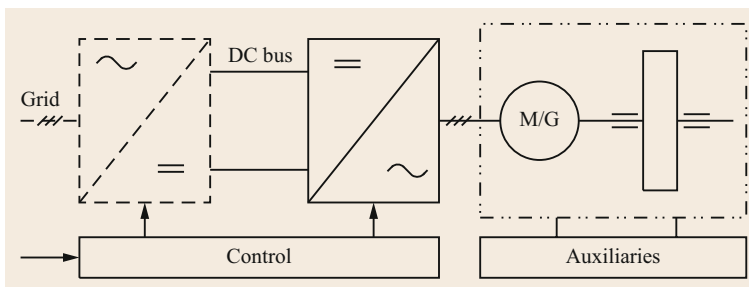


Fig. 16.25 Flywheel system

**Table 16.3** Flywheel shape factors

Flywheel shape	$K$
Constant stress disk	0.931
Flat unpierced disk	0.606
Thin rim	0.5
Rod or circular brush	0.333
Flat pierced disk ( $r_{ext}/r_{int} = 1.1$ )	0.305

### The Specific Energy of a Flywheel

The maximum specific energy of a flywheel rotor is mainly dependent on the rotor's geometry and on the properties of the material used. For an isotropic rotor, the expression of the specific energy  $e_{fw}$  can be expressed by (16.48).

$$e_{fw} = \frac{E}{m} = K \left( \frac{\sigma}{\rho} \right), \quad (16.48)$$

where  $E$  is the kinetic energy of the rotor (J),  $m$  the mass of the rotor (kg),  $K$  the geometric form factor (dimensionless),  $\sigma$  the tensile strength of the material (Pa), and  $\rho$  the density of the material used ( $\text{kg}/\text{m}^3$ ).

The form factor  $K$  depends on the geometry of the flywheel and is also called the flywheel shape factor [16.12]. Essentially, the value of  $K$  comes from the expression of the moment of inertia. Values of  $K$  for different flywheel shapes are given in Table 16.3.

The tensile strength of the material dictates the upper limit of angular velocity

$$\sigma_t = \rho r^2 \omega^2. \quad (16.49)$$

The expression (16.49) can be simplified using the specific tensile strength  $\sigma_t/\rho$  and the tangent velocity  $v_t$ ,

$$\frac{\sigma_t}{\rho} = v_t^2. \quad (16.50)$$

### Aerodynamic Drag of a Flywheel

A flywheel with a high value of specific energy is characterized through the high rotational speed and further through the tangential velocity of the rotor. The friction losses due to the interaction with the surrounding air, even if the rotor runs inside a partial vacuum chamber, should not be underevaluated.



**Fig. 16.26** Example of 600 kW/100 kWh flywheel energy storage system (courtesy of Stornetic [16.25])

The drag force causing the aerodynamic losses can be calculated in a general case through [16.26],

$$F_D = \frac{C_D \rho_g V^2 A}{2}, \quad (16.51)$$

where  $\rho_g$  is the density of the air,  $V$  is the velocity of the undisturbed fluid (m/s), and  $A$  is the projected area of objects as spheres, disks, or plates with axes perpendicular to the flow ( $\text{m}^2$ );  $C_D$  is a constant depending essentially on the Reynolds number.

The problem of the aerodynamic drag force is at the base of a general choice of flywheel manufacturers to operate the rotors under partial vacuum. An example of a recently developed product of a flywheel is given in Fig. 16.26.

## 16.7 Electrical Systems

### 16.7.1 Superconductive Magnetic Energy Storage Systems (SMES)

On the basis of a purely electric/magnetic component like the inductor, energy can also be stored. The energy stored in an inductor can generally be expressed by

$$E = \frac{1}{2}LI^2, \quad (16.52)$$

with  $L$  being the value of the inductance and  $I$  the circulating current. The maximum power  $P_{\max}$  during charging and discharging is given by the values of maximum current in the coil and the maximum voltage delivered by the power electronic converter used for the control of the charging and discharging process. This converter applies a positive voltage while increasing the current (charging) and a negative one while decreasing it (discharging)

$$P_{\max} = U_{\max}I_{\max}. \quad (16.53)$$

SMES systems use superconductivity in order to increase the energy density (higher current in the same support) and in order to reduce the ohmic losses to a minimum value [16.27]. A general scheme of an SMES system is represented in Fig. 16.27.

The power electronic converter provides a positive voltage during the charge process (an increase of the current) and a negative one during discharge.

One must note that during the charged state of an SMES system, the inductor current must always flow. Even if there are no variations of this current (idle mode), and even if the conduction losses in the superconducting coil can be neglected, there are still losses in the interconnections and in the freewheeling paths of the converter. For a long-term idling mode, and also for security reasons, a by-pass switch is generally provided (Fig. 16.27).

### 16.7.2 Capacitive (and Supercapacitive) Systems

The dual element of the inductor is the electric capacitor. It can be used for energy storage according to the

relation giving its energy content

$$E = \frac{1}{2}CU^2, \quad (16.54)$$

with  $C$  being the capacitance and  $U$  the voltage across the capacitor. The charging and discharging of a capacitor is realized by using a power electronic converter. The general scheme of a capacitive energy storage device is represented in Fig. 16.28. Classical high-voltage capacitors can be used for energy storage [16.13] and also more recently-developed supercapacitors characterized by their high capacity value [16.28].

In the case of a capacitive storage system, the power electronic converter must be able to control the capacitor current. A positive current charges the capacitor, while a negative current causes its discharge. A steady-state idling mode is characterized through the flow of a zero current. This is an interesting property with respect to the energy efficiency.

An example of an application of high-power capacitive storage is described in [16.13]. The equipment is dedicated to the smoothing of the power demand of the supply of the magnets of a particle accelerator (CERN). The capacity is around 20 MJ, and the maximum power is at 60 MW (Fig. 16.29).

Since the beginning of the twenty-first century, the capacitive storage has, in general, received higher interest due to the appearance on the market of new components called supercapacitors or double-layer ca-

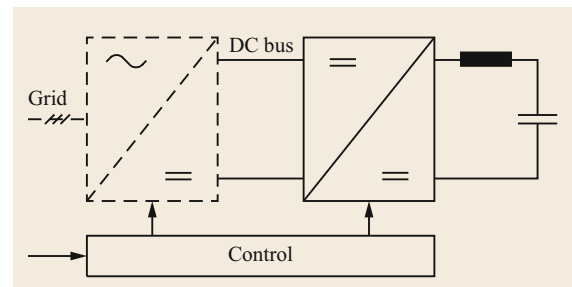


Fig. 16.28 Capacitive energy storage system

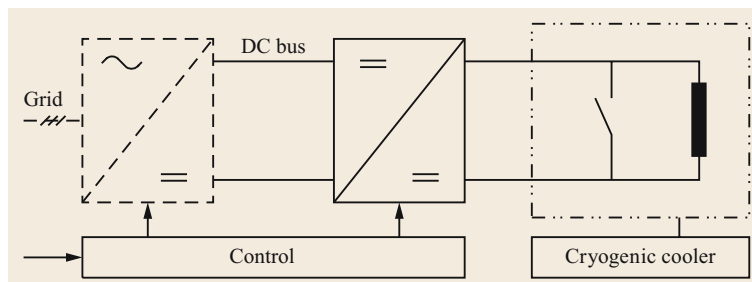
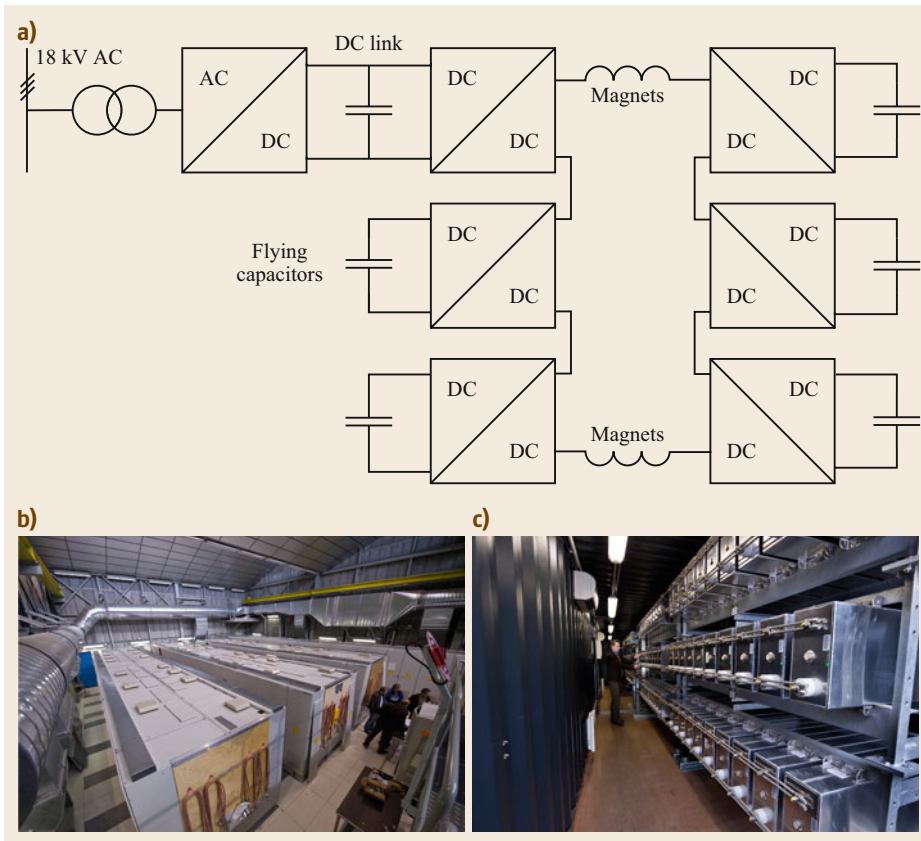


Fig. 16.27 SMES superconductive magnetic energy storage system



**Fig. 16.29a–c** Capacitive energy storage of 60 MW/20 MJ used for the supply of the magnets of a particle accelerator (CERN). **(a)** Schematics; **(b)** converter cubicles; **(c)** storage capacitors. (Reprinted with permission from Jean-Paul Burnet, CERN, 2019)



**Fig. 16.30** Samples of supercapacitors, single components, and modules

capacitors [16.29]. Examples of such components, which are characterized by capacity values in the thousands of farads, are represented in Fig. 16.30. However, the voltage of supercapacitors is generally  $\approx 2.7$  V, and

powerful storage equipment must use the series connection of a large number of components.

There are applications of supercapacitors in many different sectors where a relative high power demand

during limited time is specified. The applications comprise grid services as voltage support and power buffering, electric vehicle (EV) charging facilities, street lightning, automotive, and bus/tram transportation, or

energy recovery. Industrial applications such as forklifts, cranes, or tractors have been realized as energy-saving and pollution-free alternatives to diesel-powered systems for the lifting and transportation of containers.

## 16.8 Electrochemical Systems

There is a high diversity of electrochemical technologies as potential solutions in the area of energy storage. Many of them are well established, especially in the domain of mobile applications. Larger systems are currently developed for their utilization in connection with public grids [16.30–32].

Nowadays, an increasing number of modern materials are emerging, which often have promising characteristics. This progress is also being made in the direction of higher energy densities and also with respect to power density. Additionally, deeper studies on failure and aging mechanisms aim to reach an increasingly higher number of cycles or longer lifetimes of batteries [16.33].

From the system approach point of view, an electrochemical battery can be seen as a voltage source, the charging and discharging variable being the battery current. Figure 16.31 gives a simplified scheme of a BESS (battery-energy storage system).

The principal scheme of a BESS is very similar to that of a capacitive storage device. Principally, the positive and negative DC current is provided by a DC–DC converter. The interface to the external world can be defined at the DC bus level or through a front-end converter to the AC (alternating current) grid.

A so-called battery management system (BMS) is represented on the right-hand side of Fig. 16.31. This unit has the role of balancing the different elements of the series connection but also has the task of supervising and protecting the overall system.

### 16.8.1 Electrochemical Principles and Properties

Electrochemical storage components, often called electrochemical batteries, are closed systems able to per-

form a reversible conversion from chemical energy to electrical energy. Such transformations can be made with a good efficiency, depending on the operating conditions. Usual values of the energy efficiency are situated around 80–90%.

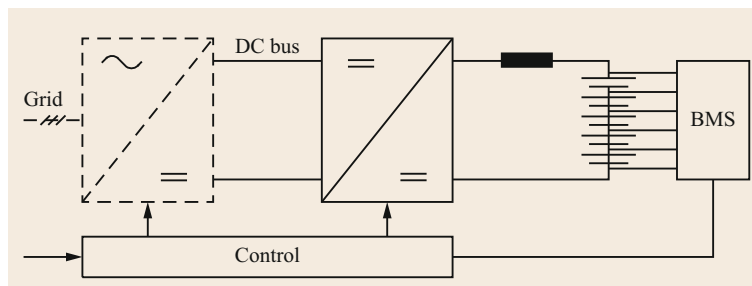
Like other storage components, electrochemical batteries are characterized by their energy density, which is between 30 and 200 Wh/kg. As a comparison, hydrocarbon-based sources present a much higher value of the energy density, of the order of 10 kWh/kg. Contrary to primary cells like the ordinary flashlight batteries, storage batteries are also called secondary batteries and can be recharged. Their electrode reactions can be processed in either direction.

#### The Structure of an Electrochemical Accumulator

Electrochemical accumulators are charged by converting electrical energy into chemical energy and are discharged by an inverse transformation. Each element of a battery is made of a so-called negative active mass able to provide electrons to the external circuit during discharge and a positive active mass able to accept the electrons from the return path of the external circuit.

Figure 16.32 is a schematic representation of an electrochemical cell. The indicated direction of electrons and ion flows corresponds to the battery discharge process.

The transfer of electrons from the active masses to and from the external circuit is possible due to the presence of current collectors assuming the electronic conduction. The positive and negative active masses are of different chemical compositions and have an electric separator in between that prevents the passage of elec-



**Fig. 16.31** Battery-energy storage system (BESS)



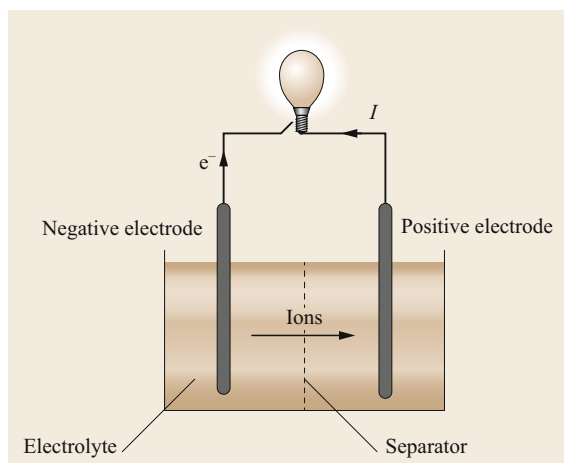


Fig. 16.32 Electrochemical cell connected to a load

trons from the positive to the negative side. The internal flow of the electric current is possible due to the displacement of electric charges in the form of ion transfer from one active mass to the other. The separator must be an ionic conductor. Current collectors are generally metallic, and the active masses are porous solids, made from powders, and are soaked by a liquid ion conductor.

### Elementary Principles

The active masses of an electrochemical cell each contain a couple of redox reactants, namely a set of chemical species in reduced form (red) able to provide electrons and to be transformed into another set of chemical species (ox), able to accept electrons. A redox couple is characterized through its potential determined by the Nernst law [16.34]

$$E = E^0 + \frac{RT}{nF} \ln \frac{\text{ox}}{\text{red}}. \quad (16.55)$$

In this relation, (ox) and (red) designate the concentrations of the oxidized and reduced forms of the redox couple,  $R = 8.32 \text{ J}/(\text{K mol})$ ,  $T$  is the absolute temperature, 298 K at 25 °C,  $n$  is the number of electrons implicated in the reaction, and  $F$  is the Faraday constant: 96 500 C/mol.

An electrochemical generator transforms the chemical energy (free enthalpy) into electrical energy provided to the external system in the form of an electrical current.

The negative terminal of an elementary cell is connected to the negative active mass that contains a reducer material (electron source)  $\text{red}_1$ , capable of undergoing an electrochemical oxidation

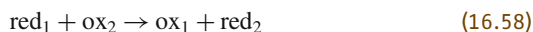


At zero current, the  $E_1$  potential of the negative terminal is controlled by the Nernst equation related to the  $\text{red}_1/\text{ox}_1$  couple. Symmetrically, the positive terminal is connected to the positive active mass containing an oxidant material (electron acceptor),  $\text{ox}_2$ , capable of undergoing an electrochemical reduction



At zero current, the potential  $E_2$  of the positive terminal is controlled by the Nernst equation related to the  $\text{red}_2/\text{ox}_2$  couple.

The global chemical reaction is then



The voltage of the elementary cell is equal to the difference of the positive and negative potentials.

The transformation of 1 mole of reactant in these conditions releases an electrical energy of  $n$  Faraday, namely a maximum of  $n \times 96\,500 \text{ C} \times (E_2 - E_1) \text{ J}$ . This maximum corresponds to the variation of the standard free enthalpy of the reaction [16.35]. In a general manner, the electrode where the reduction takes place is called the cathode. The electrode where the oxidation takes place is called the anode. In the case of a cell working as a generator (discharge), the cathode will be the positive terminal and the anode the negative terminal. On the contrary (charge), the cathode will be the negative terminal and the anode the positive terminal.

## 16.8.2 Different Types of Accumulators

Several possibilities exist for accumulators like the ones in an aqueous, acid, or alkaline medium, hot accumulators, or accumulators in an organic medium. The aqueous medium presents the advantage of a higher ionic conductivity, but the possible choices for the active masses are limited. Nonaqueous media permit higher cell voltages and a higher number of possible active masses.

### Accumulators with Aqueous Electrolytes

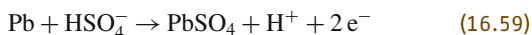
The acid or alkaline aqueous electrolyte is a medium with a relatively good ionic conduction, but the cell voltage is limited by the possible decomposition of water into oxygen and/or hydrogen produced through the oxidant (or reductant) character of the active masses.

**Lead–Acid Accumulators.** Invented by Gaston Planté in 1858, the lead–acid accumulator is today one of the most-used accumulators and must be considered as the cheapest electrochemical storage solution. In the lead–acid battery, both the positive and the negative plates

become lead sulfate ( $\text{PbSO}_4$ ) in the discharged state, and the electrolyte loses much of its dissolved sulfuric acid and becomes primarily water. In the fully charged state, the negative plate consists of lead, and the positive plate consists of lead dioxide. The electrolyte is of concentrated sulfuric acid.

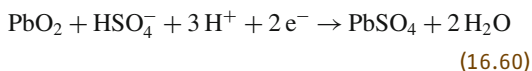
During discharge, the  $\text{H}^+$  ions produced at the negative plate move into the electrolyte solution and are then consumed at the positive plate;  $\text{HSO}_4^-$  is consumed at both plates. The reverse occurs during charge. The discharge process is driven by conduction of electrons from the negative plate back into the cell at the positive plate through the external circuit.

The negative active mass contains a redox couple as



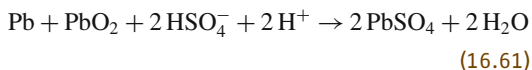
The negative active mass potential is equal to  $E^0 = -0.356\text{ V}$ .

With the positive active mass, another redox couple corresponds to



The potential on the positive side is  $E^0 = 1.685\text{ V}$ .

The global reaction is



The cell voltage corresponds to the difference of potentials and is equal to  $E^0 = 2.05\text{ V}$ .

The sum of the molecular masses of the reactants is  $642\text{ g/mol}$ , so, theoretically a cell can produce  $2\text{ F}$  of charge ( $2 \times 96\,500\text{ C} = 193\,000\text{ C}$  from  $642\text{ g}$  of reactants, or  $83.5\text{ A h/kg}$ ). For a  $2\text{ V}$  cell, this comes to a theoretical value of  $167\text{ Wh/kg}$  of reactants. In reality, a lead–acid cell gives only  $30\text{--}40\text{ Wh/kg}$ , due to the mass of the water and other constituent parts.

During charge and discharge, the potentials of the active masses vary in dependency on the state of chemical conversion. This leads to a variation of the cell voltage in the open-circuit state. In the real case of a lead-sulfuric acid battery, the cell voltage varies from  $2.15\text{ V}$  when fully charged to  $1.6\text{ V}$  when discharged (open circuit).

The acid concentration of the electrolyte brings the maximum of conductivity in the fully charged state of the cells. This brings a high availability of power with up to 10 times the rated current (a  $30\text{ A h}$  battery can deliver  $300\text{ A}$ , delivering  $3.6\text{ kW}$  when the battery voltage is of  $12\text{ V}$ ).

In its discharged state, the lead–acid battery has a relatively weak acid concentration, which limits the available power. By each discharge, lead sulfate is accumulated on the electrodes and is normally dissolved by the next charge. With a too-long discharge or in a too-low state of charge or operation at a too-high temperature, crystals of lead sulfate appear and are no longer dissolved by the charge. The capacity of the battery and its power level are strongly reduced.

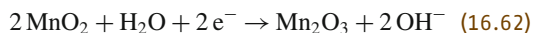
In practice, five main categories of lead–acid batteries are available:

- Starter batteries (with grating): these are developed and produced for the automotive industry for the start-up of internal combustion engines. They are designed to be kept permanently charged and to deliver high currents rapidly. They are widely available and at very low costs ( $0.2\text{ EUR}/(\text{Wh})$ ).
- Drive batteries (flat plates): these are similar to starter batteries but present a larger capacity. They are used in small electric vehicles, like autonomous carts or forklifts. They are designed to be charged and discharged on a daily basis and can be operated in low state of charge. Their costs are around  $0.5\text{ EUR}/(\text{Wh})$ .
- Batteries with gel electrolytes (flat plates): these batteries do not need any maintenance and can be operated in any position. They are typically used in small professional equipment (radio communication, shining buoys, etc.). Their capacity is of the order of  $100\text{ A h}$ . Their costs are around  $0.6\text{ EUR}/(\text{Wh})$ .
- Absorbent glass mat (AGM) batteries: in AGM batteries, the sulfuric acid is absorbed by a very fine fiberglass mat, making the battery spill-proof. AGM batteries have a very low internal resistance, are capable of delivering high currents on demand, and offer a relatively long service, even when deep cycled.
- Stationary batteries (tubular plates): these are used in security supply technology. They use a frame structure consisting of a series of vertical spines connected to a common bus bar. The tubular design keeps the active material together and presses it onto the collecting grid. The active lead-oxide mass is held in microporous, nonconductive tubes (gauntlets), which are placed over the individual spines.

**Alkaline Accumulators.** Nonacid electrolyte batteries were initially proposed by Waldemar Junger in 1899 and by Thomas Edison in 1901. These alkaline accumulators were primary batteries and based on a zinc/manganese pair of active materials.

The chemical reactions in the alkaline batteries produce electricity when the manganese dioxide cathode is reduced and the zinc anode becomes oxidized. At the

MnO<sub>2</sub> cathode, water (H<sub>2</sub>O) is consumed, and hydroxyl ions (OH<sup>-</sup>) are produced by the following reaction



At the same time, the anode consumes hydroxyl ions and produces water,



The overall reaction is

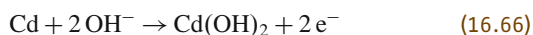


The evolution of alkaline batteries has gone through the use of other metals like nickel (Ni), a totally insoluble metal in an alkaline medium. Its oxyhydroxide form NiOOH-layer is used on its positive electrode. The electrochemical reaction at the positive active mass side is



The mode of operation of the positive electrode can be considered as a proton intercalation into the layered crystalline structure of the NiOOH during discharge and disinsertion during charge. The negative active mass is primarily based on zinc metal soaked in a potassium hydroxide solution, like in the original zinc/manganese battery.

**Nickel-Cadmium Accumulators.** Due to the corrosion effects of zinc in the basic solution, the Zn/NiOOH elements were soon replaced by Ni-Cd elements, which rapidly became high-performance rechargeable alkaline batteries. The electrochemical reactions of Ni-Cd batteries are (discharge)

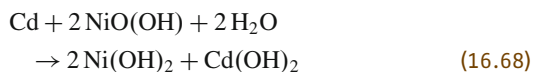


at the negative electrode and

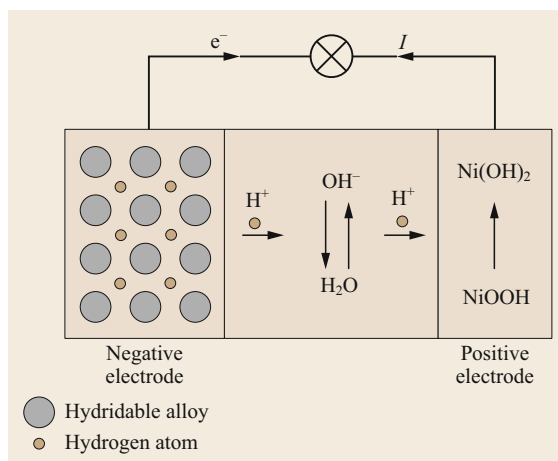


at the positive electrode.

The overall reaction is



Ni-Cd batteries have a specific energy of 40–60 Wh/kg and can easily overcome deep discharge and recharge. They have a nominal voltage of 1.2 V per cell and can be stored in their discharged state. One of the most interesting parameters is the high power capability up to 1 kW/kg. Ni-Cd batteries can be recycled but present



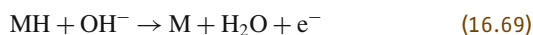
**Fig. 16.33** Discharge of an Ni-MH cell (adapted from [16.34])

the disadvantage of the toxicity of cadmium, which has made this technology obsolete. Another typical behavior of Ni-Cd cells is their memory effect. This effect corresponds to situations where the battery gradually loses its maximum energy capacity if it is repeatedly recharged after being only partially discharged.

**Ni-MH Accumulators.** In Ni-MH accumulators, the problematic cadmium in the cell has been replaced by a metallic alloy capable of storing hydrogen. It works similarly to the Ni-Cd accumulator and has the following characteristics:

- 1.2 V cell voltage
- 40% higher energy density than that of Ni-Cd cells
- A very low memory effect.

The electrochemical reactions in a Ni-MH cell are (discharge)



at the negative electrode and



at the positive electrode. The structure of an Ni-MH element is represented schematically in Fig. 16.33.

The application domain of Ni-MH batteries ranges from portable tools and toys (replacement of Ni-Cd batteries) to the automotive industry (hybrid cars).

#### Accumulators with Nonaqueous Electrolytes

In the beginning of the 1980s, the idea of utilizing lithium (Li), one of the highest electropositive elements

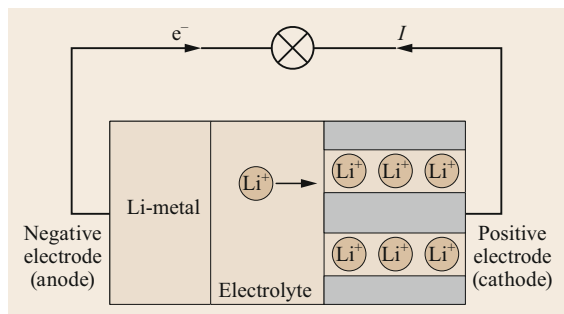


Fig. 16.34 Lithium-metal cell (adapted from [16.37])

( $-3.02\text{ V}$ ), led to the development of chemical compounds able to insert and disinsert Li at the negative electrode. Because of the high reactivity of Li versus  $\text{H}_2\text{O}$ , these developments induced the change from aqueous to nonaqueous electrolytes. Such electrolytes consist of lithium salts dissolved in an organic solvent [16.36]. One should distinguish the lithium metal technology, where the negative electrode is composed of metallic lithium from lithium-ion technology, where lithium remains in ionic state due to the use of insertion/disinsertion compounds at both the negative and the positive electrodes.

**Lithium-Metal Accumulators.** In lithium-metal batteries, the negative electrode (the anode) is made of metallic lithium. During discharge, the lithium ions migrate from this electrode through the electrolyte to the cathode, where they mix with a host material (for example,  $\text{LiMn}_2\text{O}_4$ ). The electrons produced at the anode supply the external circuit and return to the cathode. During charging, the  $\text{Li}^+$  ions migrate in the opposite direction, while electrons are supplied by the external circuit (Fig. 16.34).

**Lithium-Metal Polymer Cells.** Lithium-metal polymer technology uses a lithium-metal electrode at the negative side. The positive electrode is based on vanadium oxide. The electrolyte is a (ion)-conductive polymer membrane based on POE (polyoxide ethylene). A lithium polymer battery costs around  $0.1\text{ EUR}/(\text{Wh})$ , and its energy density is given as  $110\text{ Wh/kg}$  (Batscap). The temperature range for good performance is between  $60$  and  $150^\circ\text{C}$  without security problems.

**Lithium-Ion Accumulators.** A lithium-ion cell is different from a lithium-metal cell at the side of the negative electrode, where pure lithium is replaced by a compound capable of inserting and disinserting lithium ions (Fig. 16.35). The lithium-ion concept uses two materials that allow the reversible exchange of lithium

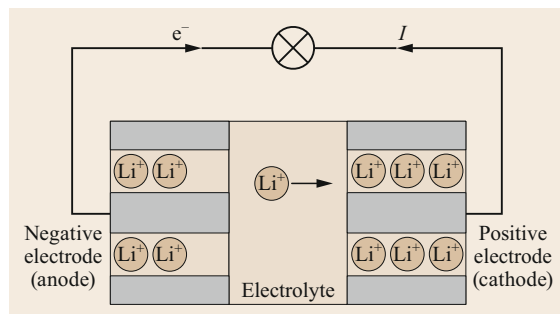


Fig. 16.35 Lithium-ion cell (adapted from [16.37])

ions. The negative electrode (anode) is a thin layer of graphite in which atoms of lithium have been inserted ( $\text{LiC}_6$ ). For the positive electrode (cathode), a lithium-oxide of a transition metal such as  $\text{LiCoO}_2$  can be used. The liquid electrolyte is usually a hexafluorophosphate of lithium ( $\text{LiPF}_6$ ) mixed with a solution (carbonate mixture) [16.36].

Lithium-ion cells present a very high energy density up to  $200\text{ Wh/kg}$ . Their typical potential is  $3.7\text{ V}$ .

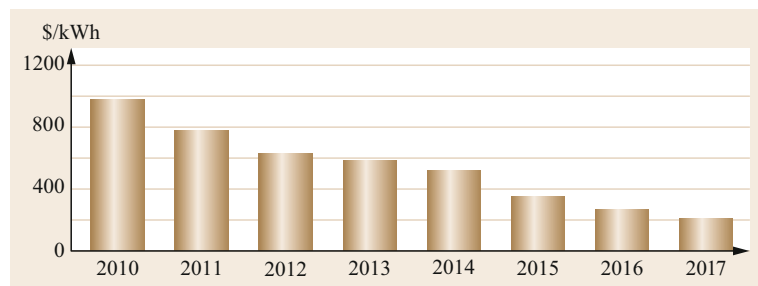
**Lithium-Iron Phosphate (LFP) Cells.** Lithium-iron phosphate is a widely spread lithium-ion technology. The positive electrode active material ( $\text{LiFePO}_4$ ) is associated with a negative graphite electrode. These cells are currently the most wide-spread and have replaced classical Li-ion cells based on lithium cobalt dioxide ( $\text{LiCoO}_2$ ). The energy density and the potential of these cells are slightly lower than those of classical Li-ion cells ( $130\text{ Wh/kg}$ ,  $3.3\text{ V}$ ). These batteries need a BMS system (battery management system).

**Lithium-Ion Polymer (Li-Po) Cells.** The mode of operation of these cells is similar to that of other lithium-ion cells. The electrolyte is made of gelled polymer. Their energy density is higher than that of other Li-ion cells, but their supervision and balancing circuits are more complex. The maximum cell voltage ( $> 4\text{ V}$ ) and also the minimum cell voltage ( $\approx 2.7\text{ V}$ ) must be monitored carefully.

**Lithium Titanate Cells (LTO).** LTO batteries are also called SCiB (super-charge ion battery). This technology is characterized by high charging and discharging rates. It is based on the use of a nanocrystalline technology. The specific energy is given as being between  $30$  and  $110\text{ Wh/kg}$ , and the cell voltage is between  $1.9$  and  $2.4\text{ V}$ . The specific power can reach  $5000\text{ W/kg}$ . These batteries can operate between  $-40$  and  $+55^\circ\text{C}$ . The durability cycle is given to be  $6000$  cycles, some manufacturers even indicate  $10\,000$ – $20\,000$  cycles.

**Table 16.4** Common characteristics of different types of batteries

Characteristics	Conventional batteries			Li-ion batteries	
	Lead–acid	Ni–Cd	Ni–MH	Graphite/NMC	LTO
Specific energy (Wh/kg)	40	40–60	30–80	120–200	70–80
Initial costs (EUR/kWh)	150	500	600	120–250	400–800
Life cycle	200–300	1000–1500	300–800	500–4000	15 000–25 000
Cost per life cycle (EUR/kWh)	0.15–0.7	0.3–0.5	0.75–2.0	0.35–0.04	0.024–0.04
Disch. cond. for low ageing	C/3	C/2	C/5	1 C	2 C
Charging rate	C/4–C/8	–	C/10	C/2	2 C
DoD window (%)	50	–	80–100	80	80

**Fig. 16.36** Evolution of lithium-ion battery prices over the past years (adapted from the Bloomberg New Energy Finance survey of more than 50 companies)

### Choosing Between Competitive Battery Technologies

The constant evolution in battery technology and performances addresses the question of the adequate choice to be made by the design of an application. A very general principle produces competition between proved techniques and innovative ones, where even if the performance advantages are evident, the life cycle and ageing phenomena cannot be evaluated due to the lack of hindsight and experience. A common example is given by classical lead–acid batteries, which have been used for decades and can be considered as tried-and-true technology. Especially solar photovoltaic off-grid applications are currently in competition with lighter, smaller lithium-ion batteries, which, in addition, have longer life cycles [16.38].

Several comparison criteria can be used:

- The specific energy
- The initial costs
- The life cycle
- The cost per life cycle
- The state of charge window for low ageing
- The available power for low ageing
- The recommended charging time

All batteries are sensitive to excessive discharging and extreme temperature. Lead–acid batteries lose potential cycles if they are discharged below 50% of their state of charge (SoC) or if discharged faster than C/8. On the other hand, lithium-ion batteries can be discharged to  $\approx 80\%$  SoC and at a rate of C/2 without any long-term

damage. Table 16.4 shows common characteristics of different types of batteries: lead–acid, Ni–Cd, Ni–MH, and two different types of lithium-ion, graphite/NMC (nickel mangan cobalt) and LTO technologies.

The values given in Table 16.4 are indicative values obtained from different sources. They show the available values of specific manufacturers. A more global figure of the evolution of the price of lithium-ion batteries is given in Fig. 16.36.

### High-Temperature Batteries

**Sodium–Sulfur (Na–S) Batteries.** Na–S battery technology is known for its very high energy density, excellent life cycle, low-cost materials, and high efficiency. However, these cells need high temperatures to operate due to the use of molten sodium. Na–S batteries have been developed since the middle of the 1960s (Ford Motor Company USA, Brown Boveri Germany, and NGK in Japan). The packaging of the battery consists of a high-performance thermal insulation enclosure (operating temperature  $\approx 350^\circ\text{C}$ ). Other difficulties of realization are related to the quality of the insulator (brittle ceramics). Safety concerns stem from the need to protect the highly reactive sodium from moisture.

The specific energy is between 150 and 760 Wh/kg (high-temperature version), the volume energy density is  $\approx 150\text{ Wh/L}$ , the specific power is given at 200 W/kg, the nominal cell voltage is 2 V. These batteries have a very good cycle durability (4000–5000 cycles). Very large facilities have been realized (50 MW/300 MW h NGK, [16.39]). The electrolyte of a Na–S cell consists of a beta alumina tube and con-

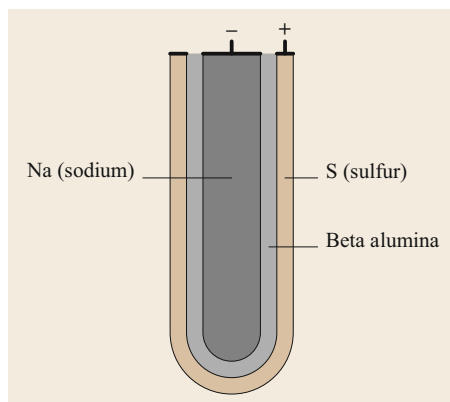


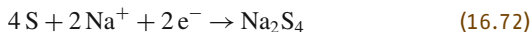
Fig. 16.37 Sodium–sulfur cell

tains the liquid sodium. The external envelope is made of sulfur (Fig. 16.37). During discharge, sodium ions converted from sodium in the negative electrode pass through the electrolyte and combine with sulfur in the positive electrode to form sodium polysulfide. The electrons flow through the external path. The structure and reactions in a Na–S cell are represented in Fig. 16.38.

The electrochemical reactions in an Na–S cell are (discharge) at the negative electrode



At the positive electrode



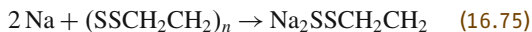
The global reaction is



Other chemistries are possible



or



for lower melting temperatures (90–100 °C). An example of a large energy storage plant based on Na–S batteries is shown in Fig. 16.39.

### Flow Batteries

Flow batteries are a new type of electrochemical accumulator composed of two electrodes separated by a proton exchange membrane, as can be found in fuel cells or in electrolyzers. In such flow batteries, the energy storage occurs within the change of concentration of ions at the level of two liquids, an anolyte and a catholyte, circulating from two separated reservoirs [16.40, 41].

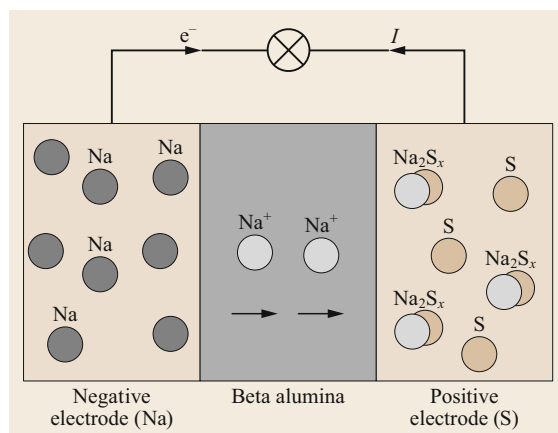


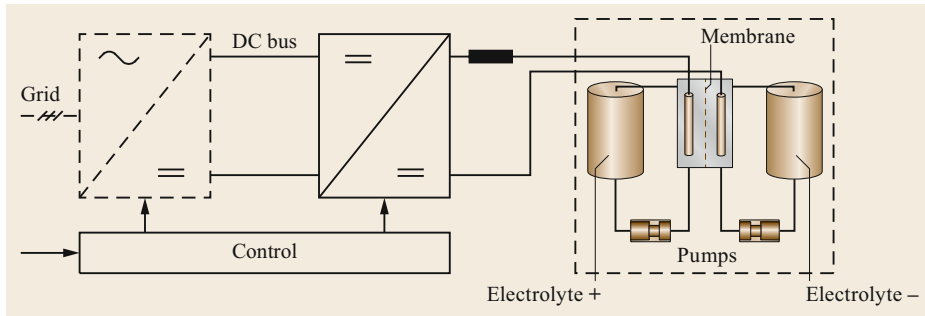
Fig. 16.38 Discharge in an Na–S cell



Fig. 16.39 A 34 MW Na–S storage facility in Japan (courtesy of JWD and NGK)

Flow batteries allow skirting some limitations of classical electrochemical batteries, where the electrochemical reactions create solid composites accumulated on the electrodes where they are generated, and where the mass that can be accumulated is perforce limited. The generation of internal stresses on the electrodes due to variations of the volumetric density of the active materials is another cause of battery ageing phenomena. In flow batteries, the chemical compounds that represent the state of charge are in liquid form and are in solution in the two electrolytes. These electrolytes are pumped from separated reservoirs to the *reactor*, which is composed of the electrodes and the membrane. One main characteristic of flow batteries is that the electrochemical converter (the reactor) is designed for the power level of the accumulator, while the energy capacity is only related to the volume (and mass) of the liquid electrolytes. An example of a flow battery is presented in Fig. 16.40.

Near the main elements of the flow battery, namely the electrolyte reservoirs and the membrane in the reactor, the system comprises electrolyte circulating pumps.



**Fig. 16.40** Redox flow-battery storage system

These auxiliary components need some electric power, which must be included in the calculation of the global efficiency. Dedicated control strategies for circulating

pumps have been proposed [16.42, 43] in order to reach good efficiency, even if the power level of the charge and discharge process is low.

## 16.9 Fuel Cells and Hydrogen Storage

Hydrogen can be used for energy storage as an energy carrier, due to its high energy density of 33 kWh/kg. This high value makes hydrogen a possible candidate for mid and long-term storage, typically such as the so-called seasonal storage in the context of renewable energy sources [16.1].

### 16.9.1 Main Properties of Hydrogen Storage

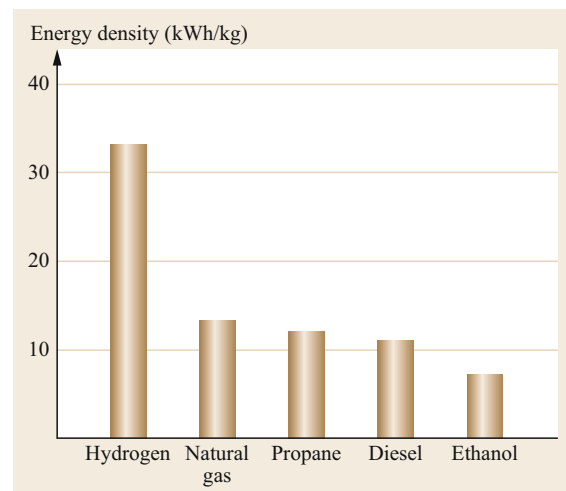
Compared to other fuels, hydrogen contains three times more energy than diesel fuel, and 2.5 times more than natural gas. Hydrogen can be produced from electricity using electrolyzers, and the reverse transformation from hydrogen to electricity can be realized using a fuel cell. However, hydrogen is difficult to store due to its very low weight density. At atmospheric pressure and ambient temperature, 1 kg of hydrogen needs a storage volume of 11 m<sup>3</sup>. As a consequence, hydrogen is usually compressed at a high pressure level between 350 and 700 bar. This high pressure addresses the question of the volume and weight needed for the reservoir, as well as the energy needed for the compression. Figure 16.41 shows the different energy densities of important energy vectors such as hydrogen, natural gas, propane, diesel fuel, and ethanol.

In the previous sections, the energy densities of different storage means were presented, where typically a powerful Li-ion battery appears with *only* 0.15 kWh/kg. As was mentioned above, hydrogen must be conditioned in order to reach a valid energy density corresponding to a real application, in the sense that the storage volume can be reduced.

Three main techniques can be used for the volume reduction, namely:

- Storage of hydrogen as compressed gas (350–700 bar)
- Storage of hydrogen in its liquid phase (–253 °C)
- Storage of hydrogen in a solid form.

The solid form of hydrogen corresponds to a metallic hydride, where different metals can be used, such as Mg, Al, or other metallic alloys. Table 16.5 indicates the amount of hydrogen mass that can be stored in these three forms.



**Fig. 16.41** Energy densities of important energy vectors

**Table 16.5** Various forms of hydrogen

Technique	Parameters	Amount of hydrogen (kg/m <sup>3</sup> )
Compressed hydrogen	700 bar	42
Liquid hydrogen	-253 °C	70
Metal hydride MgH <sub>2</sub>	Atmospheric pressure, ambient temperature	106

### 16.9.2 The Power-to-Power Storage System Based on Hydrogen

In Sect. 16.4, an electrical energy storage system (ESS) was defined. In such a system, the input and output of the storage system is interfaced to an electrical source, an electrical distribution system or grid. The storage form of energy, as well as the intermediate conversions are mentioned. An ESS or power-to-power storage system based on hydrogen can be realized using a water electrolyzer and a fuel cell for the intermediate conversions. In addition to these intermediate conversions, hydrogen (and sometimes oxygen) conditioning systems are needed in order to elevate the volumetric energy density. Figure 16.42 shows the elementary structure of an ESS based on hydrogen.

In Fig. 16.42, the basic components of the system are the electrolyzer, the hydrogen storage, and the fuel cell. Between the electrolyzer and the storage reservoir, a hydrogen conditioning device is represented ( $C_{H_2s}$ ), as well as between the storage reservoir and the fuel cell ( $C_{H_2r}$ ). The electrolyzer also produces oxygen that can be stored. In Fig. 16.43, the oxygen path is represented by dotted lines due to the fact that in a large number of modern fuel cells, the oxidation is achieved using ambient air. For this purpose, an air compressor is used (K). For the case of using stored oxygen, conditioning blocks are used ( $C_{O_2s}$ ,  $C_{O_2r}$ ).

The conditioning devices for the storage process ( $C_{H_2s}$ ,  $C_{O_2s}$ ) are generally compressors or liquefiers, while the recovery conditioning devices ( $C_{H_2r}$ ,  $C_{O_2r}$ ) are

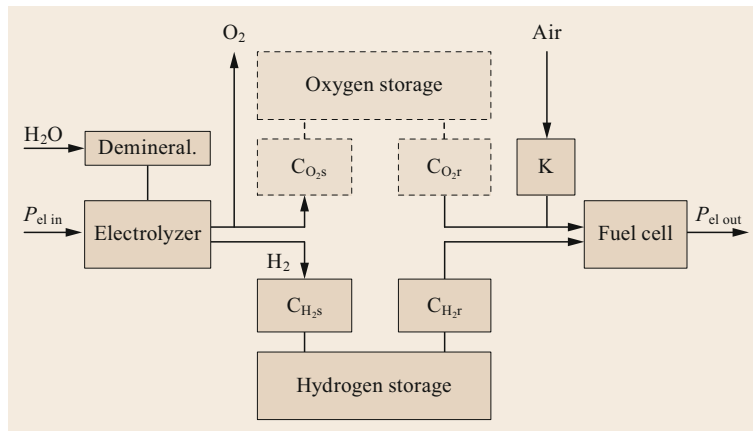
simple relieve valves. In the case of solid storage of hydrogen in the form of metal hydrides, the conditioning processes are more complex.

### 16.9.3 Producing Hydrogen Through the Electrolysis of Water

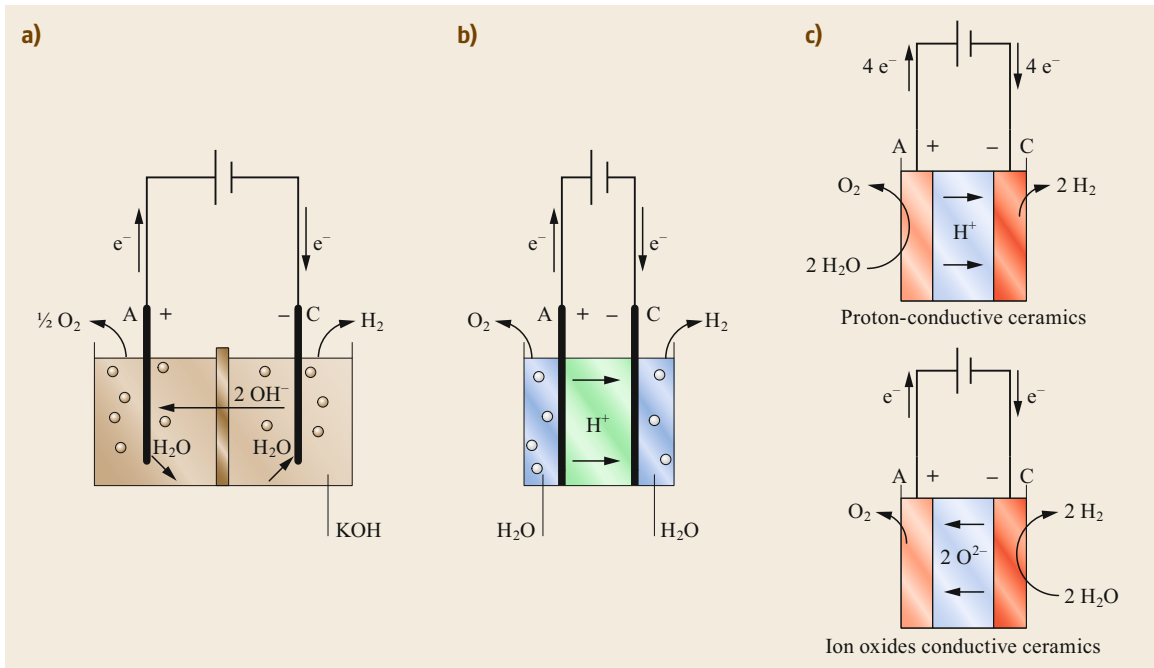
Nowadays, around half of the hydrogen produced around the world is obtained by reforming natural gas, which represents the most economic source. The other half of the hydrogen produced is from coal or oil. Electrolysis of water is a more expensive process and currently represents only a few percent of the total amount of hydrogen produced. However, it allows to convert electrical power into a chemical carrier characterized by a high specific energy. Recently, there has been a growing interest in this conversion, such as the example of recently-built power-to-gas plants [16.44]. Electrolysis of water is a well-known process in the industry for the production of hydrogen and has been developed for the production of hydrogen of high purity.

An electrolyzer is a device for the chemical decomposition of water by circulation of an electric current. It comprises two electrodes, the anode and the cathode, separated by an electrolyte. The electrodes are connected to a DC current source, which allows the circulation of the current, and the electrolyte is the internal ionic conductive means.

Three types of water electrolyzers have been developed or are under research. The most-used system is the alkaline electrolyzer. Then there are solid polymer elec-

**Fig. 16.42** Structure of a storage system based on hydrogen





**Fig. 16.43a–c** Three types of electrolyzers. (a) Alkaline electrolysis, (b) PEM electrolysis, (c) high-temperature steam electrolysis

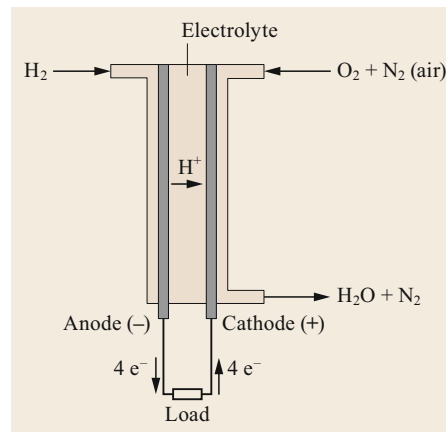
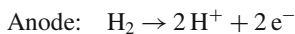
trolyzers (SPEs), where a proton exchange membrane is used, like in a PEM fuel cell. Finally, a younger technique is based on the electrolysis of water vapor at high temperature, utilizing solid oxide electrolytes (SOEs). Figure 16.43 illustrates the three electrolyzers according to the principles described in the next section.

### 16.9.4 Conversion from Hydrogen to Electricity

In the structural diagram of Fig. 16.42, the output stage of the system that converts the stored hydrogen into electrical power is a fuel cell. A fuel cell allows the direct conversion of hydrogen into current, by chemical reaction between the hydrogen and oxygen. In conventional fuel cells, the oxidant is generally taken from the ambient air.

The schematic diagram shown in Fig. 16.44 shows the main components of a classical PEM (polymer electrolyte membrane) fuel cell with hydrogen and air supply. For such a fuel cell, the energetic balance must be evaluated in detail, taking into account the power necessary for the air compressor when it is operated at partial load [16.45]. Load-current proportional airflow can be a well-adapted control method.

The chemical reactions at anode and cathode side are



**Fig. 16.44** Standard structure of a PEM fuel cell

### 16.9.5 Efficiency Considerations

The overall efficiency of the hydrogen storage defined as the ratio of the electrical output energy to the electrical input energy can be evaluated as the product of the individual part efficiencies, namely the efficiencies of the electrolyzer  $\eta_{\text{elys}}$ , the conditioning or compression stage  $\eta_{\text{con}}$ , and the fuel cell  $\eta_{\text{fc}}$ ,

$$\eta_{\text{global}} = \eta_{\text{elys}} \cdot \eta_{\text{con}} \cdot \eta_{\text{fc}} = 0.55 \cdot 0.9 \cdot 0.5 = 0.247.$$

The use of electrolyzers directly producing hydrogen under pressure or high temperature electrolyzers that

can re-use the thermal dissipation of the fuel cell will lead to a higher energy efficiency of hydrogen storage. Additionally, the storage of hydrogen or simply the use

of fuel cells in the context of CHP (combined heat and power) will increase the benefits of the use of hydrogen in energetic chains based on RES.

## 16.10 System Arrangements and Applications

This section describes system arrangements and applications of energy storage. Different configurations are presented as storage as a grid component, storage in combination with a photovoltaic system, and a more general configuration, such as a hybrid power plant [16.46]. Future applications, such as power buffers dedicated to the fast charging of electric vehicles, are currently the subject of much research and development [16.47, 48].

With most classical applications of battery energy storage, there are so-called uninterruptible power supplies (UPS), with their standard architectures, off-line systems, line-interactive systems, and online double-conversion UPS.

### 16.10.1 Storage as a Grid Component

The application consists of the connection of storage capacity to the private grid. The storage means serves to stabilize the load profiles, to cover power peaks, and to limit the power consumption from the public grid. The system offers grid services as primary and secondary control power. The different components needed for storage as a grid component are represented in the general representation of Fig. 16.45.

As shown in Fig. 16.45, connection to the public grid (1) needs a bidirectional counter (2) where not only the fluctuating power consumption (3) is measured, but also the possible power injection from the battery (4). The

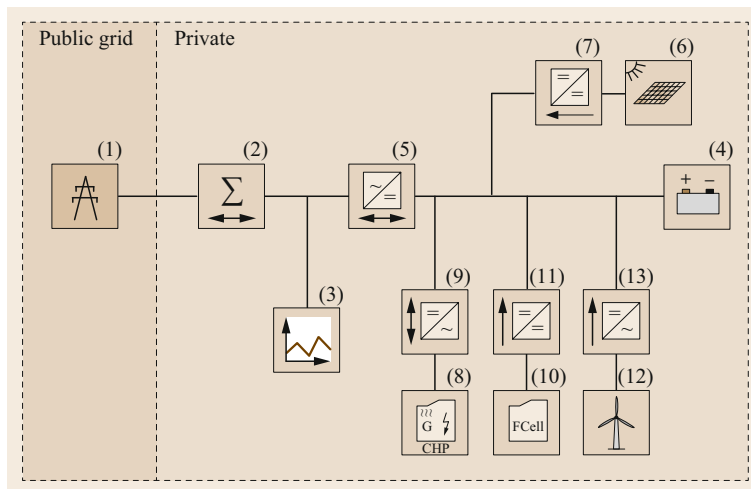
conversion from DC current to AC is achieved through a voltage-source converter (5). Such a device makes it possible to impose positive and negative current injection, as well as capacitive or inductive reactive current.

In Fig. 16.46 the results that can be achieved with storage as a grid component are illustrated. By profiling the power demand it is possible to manage peak demand using power stored during low utilization periods.

The values indicated by blue bars represent the difference of power provided by the storage equipment in addition to the constrained utility value (black dotted line). The light blue values correspond to the additional power taken from the external grid for the compensation of the energy extracted from the battery during peaks.

### 16.10.2 Renewable Energies and the Hybrid Power Plant

The hybrid power plant consists of various producer structures on a shared medium or low-voltage DC bus. Near PV panels they can include generators driven by ICE (internal combustion engine), where low-grade heat is used for house or district heating (CHP) (combined heat and power) ((8) in Fig. 16.45). The producers can also be fuel cells (10) or other sources such as wind generators (12). The different sources are interfaced through dedicated power electronic converters (9), (11), and (13) (as shown in Fig. 16.45). There are many more



**Fig. 16.45** Storage as a grid component and combination with renewable energy sources: the hybrid power plant

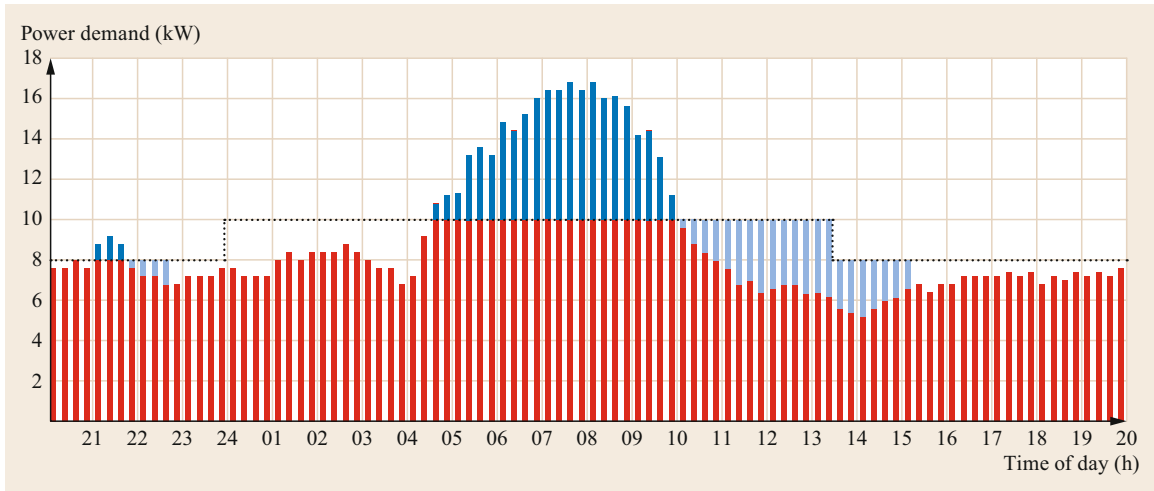


Fig. 16.46 Profiled power demand using storage (adapted from [16.46])

examples of hybrid plants with energy storage, where the emissions of diesel generators can be strongly reduced due to the day-to-night shift principle based on electrochemical storage [16.49].

### 16.10.3 UPS Technologies

Various types of uninterruptible power supplies systems have been developed during the past decades, and they currently exist on the market as highly standardized products. In general, there are three different types of arrangements [16.50].

#### Off-Line Topology

When the input mains supply is available, the load is connected to it through a commutation device or switch. The output switch commutates the load to the output of the inverter when the input voltage disappears, and the power is provided by the batteries. The system configuration of an off-line UPS is shown in Fig. 16.47.

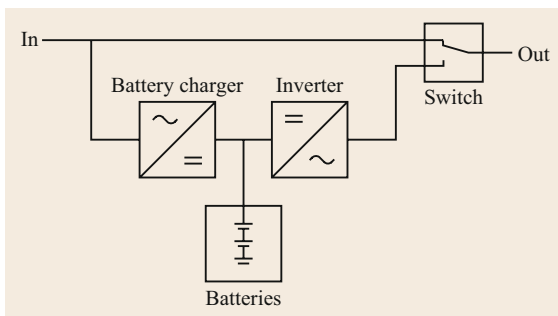


Fig. 16.47 Off-line UPS

#### Line-Interactive Topology

When the input voltage is available, the load is connected to it through an automatic voltage regulator (AVR). This circuit filters and stabilizes the input voltage using passive components and, in many cases, a controlled multi-tap variable-voltage autotransformer. Similarly to the off-line circuit, the load is connected to a battery powered inverter when the input supply fails. The circuit is represented in Fig. 16.48.

#### The On-Line Double Conversion Topology

The input voltage is rectified and reconverted into alternating current. This way, the output voltage waveform is totally independent of the input. All mains disturbances are eliminated, and there is no transient time-switching from the mains to the battery, as the output is always powered by the inverter. In the event of overloads or other possible problems, this type of UPS has an automatic bypass that ensures that the load is powered by the input mains.

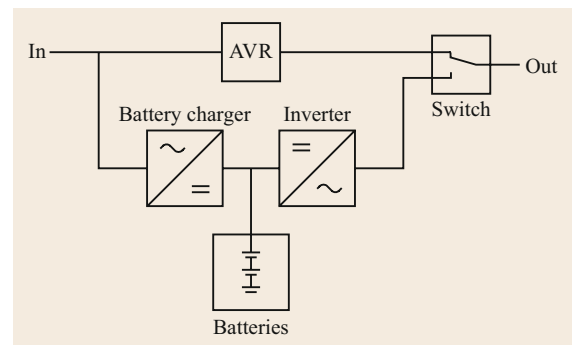
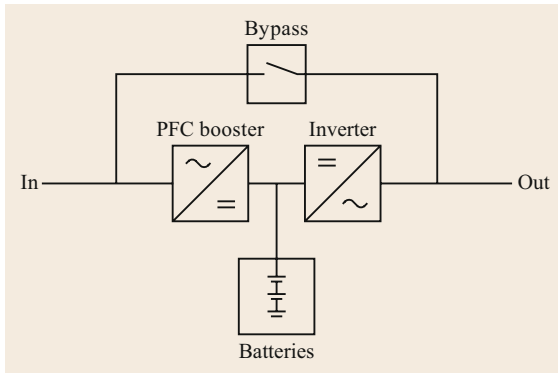


Fig. 16.48 Line-interactive UPS



**Fig. 16.49** On-line double conversion UPS

ered by switching it directly to the input. The on-line double-conversion UPS has the disadvantage that the

power is continuously affected by rectifier and inverter losses, resulting in a lower energy efficiency. The circuit of the on-line double conversion UPS is represented in Fig. 16.49.

For the off-line and line-interactive systems, the battery charger is generally realized with simpler diode rectifiers. The distorted input current of this rectifier circuit is only of a limited impact due to the fact that for normal operating conditions, the input current corresponds to the load current, and the fully charged battery imposes a negligible rectifier current. For the on-line double-conversion UPS, more sophisticated rectifier circuits are used, such as so-called PFC (power factor corrected) rectifiers or active rectifiers with PWM (pulse width modulated) conversion circuits with high power factors or low THD (total harmonic distortion) factors.

## 16.11 Examples of Large-Scale Energy Storage Plants

This section gives some examples of large-scale energy storage facilities in different parts of the world. These examples are a good illustration of the needs for local storage capacities in the context of the change of paradigm in electric power supply generally. Day-to-night shifting functions of photovoltaic generation, also assuming the reliable operation of the local distribution infrastructure, are the main motivations of these new realizations. These new projects further play the role of showcases for the fast-developing battery storage technologies and industry, and also for the evolution of classical techniques like the variable-speed pumped storage with high-capacity power electronics in the range of several hundred megawatt.

### 16.11.1 Nant-de-Drance, Switzerland

A variable-speed pumped storage plant is under construction in the alpine region in western Switzerland. The innovative plant is composed of six doubly-fed induction motor generators, each of 150 MW. The plant has a capacity of 18 400 MW h and a total rated power of 900 MW.

### 16.11.2 Hyundai and the Korea Zinc Energy Storage System

Korea Zinc, a metals melting company, has ordered an industrial energy storage system (ESS) to be installed in Ulsan, Korea in a refinery. The project will be the largest electrochemical battery system in the world and was expected to be commissioned in February 2018.

The technology used is lithium-ion, and the rated power is 150 MW.

### 16.11.3 Hornsdale Power Reserve, South Australia, Jamestown

A lithium-ion-based storage plant (Tesla Powerpack Technology) is under construction in South Australia and will be connected to the South Australian electrical infrastructure. The plant is expected to be charged from renewable energy sources and to support the grid during peak hours, maintaining reliable operation of the electrical infrastructure. The plant will provide up to 100 MW peak power with a capacity of 129 MW h.

### 16.11.4 NGK Sodium–Sulfur (Na–S) Battery

A large sodium–sulfur (Na–S) battery has been installed in the village of Rokkasho, Aomori, Japan and is used for the stabilization of a 51 MW wind power plant. The plant has a rated power of 34 MW and can deliver the rated value during 7 h (238 MW h). The battery is charged at night, when the power demand is low. The battery supplies the national power grid; it has been in operation since 2008.

### 16.11.5 Dalian VFB–UET/Rongke Power

A very large battery-storage plant is expected to be built in the city of Dalian, China. The battery system will be realized on the basis of vanadium redox flow-battery arrays made up of ten (10×) 20 MW/80 MW h

VFB units. The battery system will be connected to the main grid of Liaoning Province, which has experienced stress during extreme weather events. When completed (200 MW/800 MW h), the storage facility will have the capacity to peak-shave  $\approx 8\%$  of Liaoning Province's expected peaking capacity in 2020. Further, the large-scale battery will form an additional load center, which will enhance grid stabilization including securing the power supply and providing black-start capabilities in the event of emergency.

### 16.11.6 Clear Creek Flywheel Wind Farm Project

Ontario's Hydro One Networks Inc. intends to realize a 10-flywheel 5 MW flywheel energy storage (FES) installation. The system will provide local power quality support, by compensating real and reactive power flows from a 20 MW-wind farm technology.

### 16.11.7 Huntorf CAES Plant

The first commercial CAES plant is in operation since 1978 in Huntorf, Germany. The system is fed from thermal and nuclear night-time power to compress and inject the air into two caverns of 310 000 m<sup>3</sup> total volume. The 600 m cavern depth ensures the air's stability through seasonal temperature changes, and guarantees the specified maximum pressure of 100 bar. The compression operation is characterized by a power of 60 MW and lasts 12 h. The turbine operation allows the power generation at 290 MW during 3 h.

#### Additional Information and Exercises

Additional information and supplementary exercises relating to this chapter can be found at [https://go.sn.pub/SHb\\_PowerSystems\\_Rufer\\_EnergyStorage](https://go.sn.pub/SHb_PowerSystems_Rufer_EnergyStorage).

## References

- 16.1 A. Rufer: *Energy Storage—Systems and Components* (CRC, Boca Raton 2017)
- 16.2 P. Swain, A. Shyamaprasad: Energy storage technologies: Past, present and future. In: *Int. Conf. Exhib. Smart Util.* (Smart Cities, New Delhi 2019)
- 16.3 Y.A. Cengel, M.A. Boles: *Thermodynamics – An Engineering Approach*, 6th edn. (McGraw-Hill, New York 2008)
- 16.4 IEC 60027-2: *Letter Symbols Including Conventions and Signs for Electrical Technology* (IEC, Geneva 2005)
- 16.5 B. Piccard, A. Borschberg: *Objectif Soleil: L'Aventure Solarimpulse* (Stock, Paris 2017)
- 16.6 C. Glaize, S. Geniès: *Les Accumulateurs Electrochimiques au Lithium, Haute Temperature et à Circulation d'Électrolyte* (Hermes, Lavoisier, Paris 2013)
- 16.7 B. Multon, J. Aubry, P. Haessig, H. Ben Ahmed: *Systèmes de Stockage d'Énergie Électrique BE 8 100* (Techniques de l'ingénieur, Saint-Denis, 2013)
- 16.8 T. Christen, M.W. Carlen: Theory of Ragone plots, *J. Power Sources* **91**, 210–216 (2000)
- 16.9 J. Lehmann: Air storage gas turbine power plants, a major distribution for energy storage. In: *Int. Conf. Energy Storage* (BHRA Fluid Engineering, Cransfield 1981) pp. 327–336
- 16.10 D.R. Mack: Something new in power technology, *IEEE Potentials* (1993), <https://doi.org/10.1109/45.283812>
- 16.11 S. Van der Linden: CAES for today's market. In: *EESAT 02 Conf. Electr. Energy Appl. Technol., San Francisco* (2002), [https://www.sandia.gov/ess-ssl/EESAT/2002\\_papers/00003.pdf](https://www.sandia.gov/ess-ssl/EESAT/2002_papers/00003.pdf)
- 16.12 G. Genta: *Flywheel Energy Storage: Theory and Practice of Advanced Flywheel Systems* (Butterworth, Cambridge 1985)
- 16.13 C. Fahrni, A. Rufer, F. Bordry, J.P. Burnet: A novel 60 MW pulsed power system based on capacitive energy storage for particle accelerators. In: *Eur. Conf. Power Electron. Appl.* (EPE Association, Brussels 2007)
- 16.14 A. Rufer, P. Barrade: A supercapacitor-based energy-storage system for elevators with soft commutated interface, *IEEE Trans. Ind. Appl.* **38**(5), 1151–1159 (2002)
- 16.15 M.H. Ali, B. Wu, R.A. Dougal: An overview of SMES applications in power and energy systems, *IEEE Trans. Sustain. Energy* **1**(1), 38–47 (2010)
- 16.16 Europump, Hydraulic Institute: *Variable Speed Pumping: A Guide to Successful Applications* (Elsevier, Amsterdam 2005)
- 16.17 J. Liang, R.-G. Harley: Pumped storage hydro-plant models for system transient and long-term dynamic studies. In: *IEEE Power Energy Soc. General Meet.* (2010) pp. 1–8
- 16.18 CEI-IEC 60193: *Hydraulic Turbines, Storage Pumps and Pump-Turbines* (IEC, Geneva 1999)
- 16.19 C. Nicolet, J.-P. Taulan, J.-M. Burnier, M. Bourrilhon, G. Micoulet, A. Jaccard: Transient analysis of FMHL and pumped-storage power plant and new surge tank design. In: *Proc. Congr. SHF Grenoble* (SHF, Paris 2014)
- 16.20 H. Tanaka: An 82 MW variable speed pumped-storage system, *Water Power Dam Constr.* **43**(11), 25 (1991)
- 16.21 P. Steimer, O. Senturk, S. Aubert, S. Linder: Converter-fed synchronous machine for pumped hydro storage plants. In: *Proc. IEEE Energy Convers. Congr. Expo* (2014) pp. 4561–4567
- 16.22 S. Lemoufouet: *Investigation and Optimisation of Hybrid Electricity Storage Systems Based on Compressed Air and Supercapacitors*, Dissertation (Ecole

- Polytechnique Fédérale de Lausanne, Lausanne 2006)
- 16.23 Wikipedia: *The Mekarski system* (2019), [https://en.wikipedia.org/wiki/Mekarski\\_system](https://en.wikipedia.org/wiki/Mekarski_system)
- 16.24 Motor Development International: *Homepage* (2020), <http://www.mdi.lu>
- 16.25 STORNETIC GmbH: *Powerful Storage System for Grid Services* (STORNETIC GmbH, Jülich 2018), [https://stornetic.com/assets/downloads/stornetic\\_general\\_presentation.pdf](https://stornetic.com/assets/downloads/stornetic_general_presentation.pdf)
- 16.26 National Council of Examiners for Engineering and Surveying: *Fundamentals of Engineering Supplied Reference Handbook*, 7th edn. (National Council of Examiners for Engineering and Surveying, Clemson 2005), [www.ncees.org](http://www.ncees.org)
- 16.27 S. Nomura, H. Chikaraishi, R. Shimada: Design study on series compensated thyristor converters for large scale SMES. In: *Proc. 15th Eur. Conf. Power Electron. Appl. (EPE)* (2013) pp. 1–10, <https://doi.org/10.1109/EPE.2013.6634613>
- 16.28 P. Barrade, A. Rufer: Current capability and power density of supercapacitors: Considerations on energy efficiency. In: *Proc. Eur. Conf. Power Electron. Appl.* (2003)
- 16.29 B.E. Conway: *Electrochemical Supercapacitors Scientific Fundamentals and Technological Applications* (Springer, New York 1999)
- 16.30 N.W. Miller, R.S. Zrebiec, G. Hunt: Design and commissioning of a 5 MVA, 2.5 MWh battery energy storage system. In: *Proc. IEEE Transm. Distrib. Conf.* (1996) pp. 339–345
- 16.31 N.W. Miller, R.S. Zrebiec, R.W. Delmerico, G. Hunt: Battery energy storage systems for electric utility, industrial and commercial applications. In: *Battery Conf. Appl. Adv.* (IEEE, New York 1996) pp. 235–240
- 16.32 Tesla: *Energy Storage for a Sustainable Home* (Tesla Powerwall, Athens 2015)
- 16.33 J.-M. Timmermans, N. Alexandros, J. De Hoog, R. Gopalakrishnan, S. Goutam, N. Omar, J. Van Mierlo, A. Warnecke, D. Sauer, M. Swierczynski, D.I. Stroe, E. Martinez-Laserna, E. Sarasqueta-Zabala, J. Gastelurrutia, N. Nerea: Batteries 2020—Lithium-ion battery first and second life ageing, validated battery models, lifetime modelling and ageing assessment of thermal parameters. In: *Proc. Eur. Conf. Power Electron. Appl.* (2016)
- 16.34 P. Odrú: *Le Stockage de l'Énergie* (Dunod, Paris 2013)
- 16.35 Wikipedia: *Gibbs free energy* (2020), [https://en.wikipedia.org/wiki/Gibbs\\_free\\_energy](https://en.wikipedia.org/wiki/Gibbs_free_energy)
- 16.36 F. Fusalba, S. Martinet: Electrochemical storage, cells and batteries. In: *Energy Storage*, ed. by Y. Brunet (Wiley, New York 2011)
- 16.37 H. Girault: *Analytical and Physical Electrochemistry* (CRC, Boca Raton 2004)
- 16.38 J.P. O'Connor: *Off Grid Solar—A Handbook for Photovoltaics with Lead-Acid or Lithium-Ion Batteries* (Createspace, North Charleston 2016)
- 16.39 N. Kawakami, Y. Iijima, M. Fukuhara, M. Bando, Y. Sakanaka, K. Ogawa, T. Matsuda: Development and field experiences of stabilization systems using 34 MW NAS batteries for a 51 MW wind farm. In: *2010 IEEE Int. Symp. Ind. Electron.* (IEEE, Bari 2010) pp. 2371–2376
- 16.40 M. Skyllas-Kazacos, C. Menictas: The vanadium redox battery for emergency back-up applications. In: *Proc. Power Energy Syst. Conv. Mark.* (IEEE, New York 1997)
- 16.41 M. Bartolozzi: Development of redox flow batteries. A historical bibliography, *J. Power Sources* **27**(3), 219–234 (1989)
- 16.42 C. Blanc, A. Rufer: Multiphysics and energetic modelling of a vanadium redox flow battery. In: *Proc. IEEE Int. Conf. Sust. Energy Technol.* (IEEE, New York 2008)
- 16.43 C. Blanc: *Modeling of a Vanadium Redox Flow Battery Electricity Storage System*, Dissertation 4277 (EPFL, Lausanne 2009), [https://infoscience.epfl.ch/record/129758/files/EPFL\\_TH4277.pdf](https://infoscience.epfl.ch/record/129758/files/EPFL_TH4277.pdf)
- 16.44 G. Gähleitner: Hydrogen from renewable electricity: An international review of power-to-gas pilot plants for stationary applications, *Int. J. Power Hydrog. Energy* **38**, 2039–2061 (2013)
- 16.45 F. Grasser, A. Rufer: PEMFC system efficiency optimization through model based control strategies. In: *IEEE Veh. Power Propuls. Conf.* (IEEE, Windsor 2006)
- 16.46 ADS-TEC GmbH: *StoraXe, Industrial and infrastructure scalable large-scale storage solutions* (2014), [https://www.ads-tec.de/fileadmin/download/doc/brochure/Brochure\\_Energy\\_Industrial\\_EN.pdf](https://www.ads-tec.de/fileadmin/download/doc/brochure/Brochure_Energy_Industrial_EN.pdf)
- 16.47 H. Hõimoja, M. Vasiladiotis, S. Griani, M. Capezzali, A. Rufer, H.B. Püttgen: Towards ultrafast charging solutions of electric vehicles. In: *CIGRE Session 44* (CIGRE, Paris 2012)
- 16.48 M. Vasiladiotis, A. Rufer: A modular multiport power electronic transformer with integrated split battery energy storage for versatile ultrafast EV charging stations, *IEEE Trans. Ind. Electron.* **62**(5), 3213–3222 (2015)
- 16.49 V. Franzitta, D. Curto, D. Rao: Energetic sustainability using renewable energies in the Mediterranean Sea, *Sustainability* **8**, 1164 (2016), <https://doi.org/10.3390/su8111164>
- 16.50 Legrand: *Uninterruptible power supply UPS, technical guide* (2012), [https://www.legrand.co.za/download/products\\_tobe%20deleted/ups-technical-guide.pdf](https://www.legrand.co.za/download/products_tobe%20deleted/ups-technical-guide.pdf)

### Alfred Rufer

STI-DO  
EPFL, Ecole Polytechnique Fédérale de  
Lausanne  
Lausanne, Switzerland  
[alfred.rufer@epfl.ch](mailto:alfred.rufer@epfl.ch)



Alfred Rufer received his BS and MS degrees from EPFL (Ecole Polytechnique Fédérale de Lausanne Switzerland) in 1976. In 1993 he became Assistant Professor at EPFL and Full Professor in 1997. He became the Director of the Industrial Electronics Lab at EPFL. Alfred Rufer has published more than 300 conference and journal papers, as well as several patents. He is now Professor emeritus.

# Power Quality

## 17. Power Quality

Oscar Lennerhag , Math Bollen

Power quality concerns the electrical interaction (through voltages and currents) between the electricity grid and equipment connected to it. The field of power quality is subdivided into different types of disturbances, each of which represent one specific deviation from the ideal voltage and/or current. Section 17.1 will introduce the power-quality field, including terminology and a brief history. One of the disturbance types, waveform distortion, or harmonics, is discussed in detail in Sect. 17.2. Other types of disturbances are discussed briefly in Sect. 17.3.

17.1	<b>Terminology of Power Quality</b> .....	1171
17.1.1	Origin of the Term Power Quality .....	1171
17.1.2	Disturbances and Interference.....	1172
17.1.3	Events and Variations .....	1173
17.1.4	History of Power Quality .....	1174
17.1.5	Power Quality Standards and Regulation .....	1175
17.1.6	Limits and Interference.....	1176
17.1.7	Power Quality Monitoring .....	1176

17.2	<b>Harmonics</b> .....	1177
17.2.1	Sources of Harmonics .....	1177
17.2.2	Impacts of Harmonics .....	1180
17.2.3	Spread of Harmonics .....	1181
17.2.4	Mitigation of Harmonics .....	1183
17.2.5	Harmonic Measurements .....	1183
17.2.6	Standards and Regulation.....	1186
17.3	<b>Other Power-Quality Disturbances</b> ....	1187
17.3.1	Voltage Dips.....	1187
17.3.2	Voltage Swells.....	1189
17.3.3	Long Interruptions .....	1190
17.3.4	Short Interruptions.....	1191
17.3.5	Transients.....	1193
17.3.6	Interharmonics .....	1194
17.3.7	Supraharmonics .....	1194
17.3.8	Slow Voltage Variations.....	1195
17.3.9	Fast Voltage Variations.....	1197
17.3.10	Voltage Unbalance .....	1197
17.3.11	Frequency Variations .....	1198
17.4	<b>Power Quality in Microgrids</b> .....	1199
17.5	<b>Conclusions</b> .....	1200
	<b>References</b> .....	1200

### 17.1 Terminology of Power Quality

This section introduces some of the basic terminology related to power quality and a brief historical introduction. The term *power quality* is commonly used in electric power system studies and it covers a range of phenomena. Some of those phenomena will be discussed in this chapter. For other phenomena and more details on the phenomena described here, the reader is referred to the extended literature on power quality. Some reference books on power quality include [17.1–4].

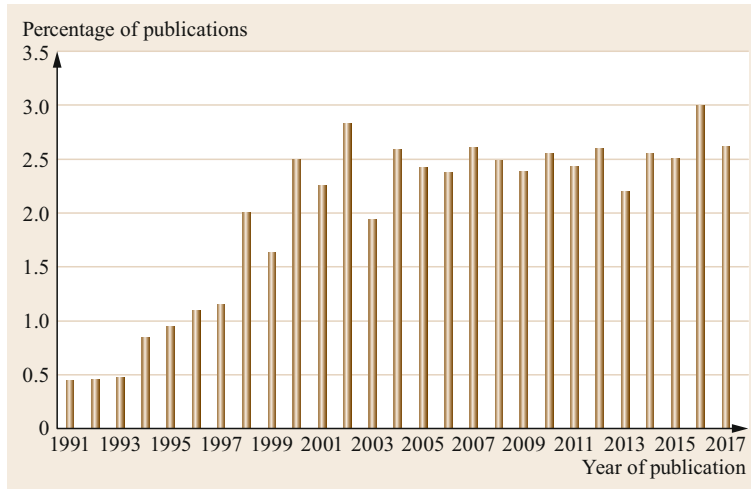
#### 17.1.1 Origin of the Term Power Quality

A search in IEEE Xplore (19 February 2019) resulted in 21 127 hits for the term *power quality*, 3732 of those were journal papers and 100 were standards. Power quality is a research field with a high amount of standards. This makes power quality a relatively large part

of applied research. A search on Google scholar (on the same date) resulted in about 357 000 hits.

The term *power quality* was first mentioned in an IEEE publication in June 1962 [17.5]: power quality was mentioned as one of the most important parameters for aerospace applications. The early papers on power quality were mainly on aerospace applications. The first use of the term *power quality* in its modern meaning was in a paper by *Alexander Kusko* in 1967 [17.6]. The paper was appropriately named *quality of electric power* and it introduced the *voltage tolerance curve* for voltage dips and voltage swells that would become widely used some 30 years later.

Although the term *power quality* only came into use in the 1960s, the phenomena that are part of the field have been studied for much longer. For example, in a discussion at a meeting of the American Institution



**Fig. 17.1** Number of papers on power quality as a percentage of the number of papers on power engineering in IEEE Xplore

of Electrical Engineers in January 1899, reference was made to the *existence of higher harmonics* [17.7].

The number of publications on power quality has shown a steady growth since about 1995. This is in part due to the general growth in the number of publications. A comparison is therefore made with the total number of publications on *power*. Figure 17.1 shows the percentage of the publications on *power* that are about *power quality* for each year between 1991 and 2017. The figure shows the appearance of power quality as a respected research field between 1995 and 2000. Since the year 2000, about 2.5% of the papers on *power* are about *power quality*. The value in the figure was obtained as the ratio of the number of hits on *power quality* in IEEE Xplore and the number of hits on *power* for each year.

Power quality concerns the (electrical) interaction between the grid and equipment or installations connected to it. Power quality is important for several of the stakeholders in electric power systems. The importance for network customers (consumers, producers and those that are both) is that voltage disturbances can affect electrical equipment connected to the grid. The importance for the network operator is somewhat more complicated. Both current disturbances and voltage disturbances can affect the grid and components in the grid. Information on power quality is also important for the network operator as feedback for investment decisions. Under the regulatory regime in most countries, the network operator is responsible for maintaining sufficient power quality. The network operator in turn can put requirements on the customers to be able to maintain sufficient power quality.

There are different definitions of power quality and the reader is referred to the literature to find out more about them. The authors use the term *power quality* as a combination of *voltage quality* and *current quality*. Voltage quality concerns deviation from the ideal volt-

age; current quality concerns deviations from the ideal current.

In power-quality regulation, the general term *quality of supply* is used to describe how the electricity grid affects the customer. A distinction is thereby made in [17.8] between:

- Continuity of supply: *availability of electricity*; short and long interruptions.
- Voltage quality: *the technical properties of the electricity*, or (using the terminology in this chapter) all other voltage disturbances apart from short and long interruptions.
- Commercial quality: the speed and accuracy with which customer requests are handled.

A term commonly used in standardization is *electromagnetic compatibility* (often abbreviated as EMC). It is defined [17.9] as the

ability of equipment or a system to function satisfactorily in its electromagnetic environment without introducing intolerable electromagnetic disturbances to anything in that environment.

Note that the terms *voltage quality* and *current quality*, that are part of our definition of power quality, are embedded in this definition.

### 17.1.2 Disturbances and Interference

The earlier-mentioned deviations from ideal voltage or current are referred to as *disturbances*: voltage disturbances and current disturbances, respectively. Based on the kind of disturbance, different terms are used like *voltage dips*, *transients* or *even order harmonics*. In reality, there is no such thing as a pure voltage dis-



turbance, or a pure current disturbance. Voltage and current in the power system are strongly linked. For some types of disturbances, like *voltage dips*, it is obvious from the name that it is mainly treated as a voltage disturbance. For other types of disturbances, like *harmonics*, both voltage and current are of interest.

A *power quality disturbance* is, as reasoned above, any deviation from the ideal voltage or current waveform, magnitude or frequency.

Even if the deviation is very small, we refer to it as a disturbance. The term is somewhat confusing because the disturbance does not actually have to disturb anything. The interest in power quality is however in disturbances that do have an adverse impact. This is where we use the term *interference*.

Interference occurs when a power quality disturbance adversely affects equipment. This can be equipment with end-users, but also equipment in the grid. Examples of interference are:

- Equipment trips or mal-functions
- Equipment suffers permanent damage immediately
- Equipment suffers from loss-of-life.

Almost all the studies, measurements, standards and regulation within power quality are related to voltage or current disturbances. However, only the occurrence of interference matters. The ultimate aim of all the work on power quality should be to reduce the probability of interference. In the IEC standards on electromagnetic compatibility, this is formulated as *guaranteeing a high probability of electromagnetic compatibility*.

### 17.1.3 Events and Variations

We saw earlier that power quality disturbances are deviations from the ideal voltage or current. Not all power-quality disturbances are treated equally, and a further classification is needed to understand for example some of the details of standardization and power-quality monitoring. Based on the way they are treated, two groups are distinguishable: *power quality variations* and *power quality events*. This terminology is certainly not unique, but the division in these two types of disturbances is common in many works on power quality.

Variations, are slow and small deviations from the ideal voltage or current. They can be measured at any instant in time or over a pre-defined period. When one is interested in the voltage magnitude (expressed typically as the RMS voltage over a certain period), one has just to go to a wall outlet (or to a voltage transformer in the substation), connect a measurement instrument and obtain the value.

Events, are sudden and large deviations from the ideal voltage or current. To measure events, one has to wait until one occurs. This requires some kind of triggering mechanism.

One of the first documents that listed and described power-quality disturbances is the European standard defining voltage characteristics, EN 50160 [17.10]. The list of disturbances below is largely based on that document. The following types of variations (referred to as *continuous phenomena* in EN 50160) are distinguished:

- Power frequency variations.
- Supply voltage variations.
- Flicker severity.
- Supply voltage unbalance.
- Harmonic voltage.
- Interharmonic voltage.
- Mains signaling voltage.

The following types of events are distinguished:

- Interruptions of the supply voltage.
- Voltage dips.
- Voltage swells.
- Single rapid voltage changes.
- Transient overvoltages.

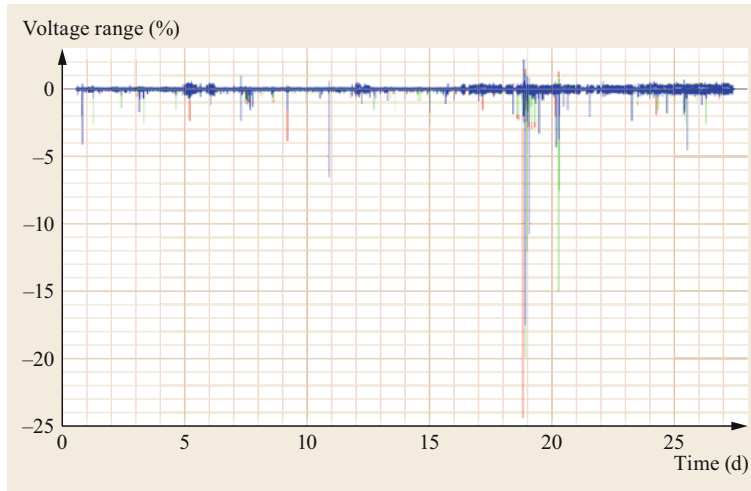
Differences in terminology are a common feature of power quality and despite several attempts to solve this, the confusion remains. In this book, we will use a certain terminology, but we do not claim that this is the correct or the best terminology. The reader is strongly advised to be careful with terminology, check the meaning of the terms used by others, and explain the used terminology in their own documents. Where possible, commonly used terminology is preferred, but even in this case it is important to explain the meaning of the terms, to avoid confusion.

The definition of variations and events distinguishes between small and large deviations from the ideal. There is no unique distinction between small and large as per the *sorites paradox* [17.11] from the classical Greek period. In power quality monitoring, this paradox is better known as the *triggering problem* and more generally as *what is normal?*

The triggering problem is illustrated in Fig. 17.2. This figure is obtained from a 28 day voltage measurement in a medium-voltage grid. For every 1 min interval, the following two values are plotted (both expressed in percent of the nominal voltage)

$$\max(V_{1\text{cycle}}) - V_{1\text{min}} \quad (17.1)$$

$$\min(V_{1\text{cycle}}) - V_{1\text{min}} \quad (17.2)$$



**Fig. 17.2** Example of voltage variation and possible thresholds. The different colors refer to the three phase-to-neutral voltages

where  $V_{1\min}$  is the RMS voltage over the 1 min window;  $\max(V_{1\text{cycle}})$  and  $\min(V_{1\text{cycle}})$  are the highest and lowest 1-cycle RMS voltages during the same 1 min window.

Consider a hypothetical event that is triggered when one or both values exceed, in absolute value, a certain threshold. As can be seen from the figure, the number of such events detected depends strongly on the threshold setting. For thresholds above 25% of the nominal voltage, not a single event would be detected. For thresholds below 1%, many events would be detected. There is no correct or incorrect threshold setting, although research is ongoing about how to optimize between *fail to detect* and *incorrect detection*. Such studies require detailed insight in the underlying event behind the power-quality event and there is no obvious solution to the triggering problem.

Note that the hypothetical event discussed here is not among the standard list of power-quality events. There are however strong similarities with voltage dips (Sect. 17.3.1) and voltage swells (Sect. 17.3.2).

#### 17.1.4 History of Power Quality

It was already mentioned before that the term *power quality* was first used in aerospace engineering. Through the years, power quality has seen several different drivers. Some of these had to do with certain challenges that occurred. Sometimes, a new solution resulted in renewed interest in power quality.

Some of the drivers for interest in power quality, through the years, are listed here:

- HVDC (high voltage DC) links and large power-electronic converters were a major source of harmonic currents. Much of the work on harmonics

was developed to be able to study the connection of such devices. The harmonic voltage limits in IEEE 519 [17.12], including the fact that they are frequency independent, can be traced back to the connection of large power-electronic converters.

- Arc furnaces and some other large industrial installations are a major source of fast voltage variations. The main impact of this was light flicker, a phenomenon that was common for candle light but that was supposed to have disappeared with the introduction of the incandescent lamp. Once electrical motors were connected to the grid, voltage drops occurred and light flicker reappeared. The *general electric flicker curve* [17.13], developed in the 1930s, allowed for a compromise where a certain level of fast voltage variations were allowed. This curve later resulted in the flickermeter and IEC 61000-4-15 [17.14]. The work on fast voltage fluctuations was driven not just by the need to connect large arc furnaces, but also by the development of the static var compensator (SVC) that allowed for the mitigation of fast voltage variations without the need to increase the fault level. The SVC was based on the same technology as HVDC and large drives, which were the drivers behind much of the work on harmonics.
- The widespread use of televisions in households resulted in a significant source of harmonics at millions of locations in the grid. Cathode ray tubes required a high DC voltage. A diode rectifier directly connected to the 220 or 120 V supply was used. The earliest television used a single diode, with high second harmonic currents as a result. Later designs, with four diodes, resulted in low-order odd harmonics (3, 5, 7, etc.). All televisions

had almost the same current waveform so that they all together resulted in the typical *television peak* in the early evenings for those harmonics.

- Adjustable-speed drives and process control were, upon their introduction in the 1990s, very sensitive to voltage dips [17.15]. This resulted in a shift of emphasis within power quality research from harmonics to voltage dips, with many technical papers and a number of textbooks produced as a result. The same power electronics that has resulted in HVDC and SVC were used to come up with a solution for voltage dips: the *dynamic voltage restorer* (DVR) [17.16]. Many technical papers were written on the DVR and on different control algorithms for the DVR.
- The availability of measurement instruments, data storage and data processing allowed for much more monitoring of the voltage and currents in the grid than with traditional instruments like oscilloscopes and multimeters. With more data becoming available, the need for data analysis appeared almost immediately. Signal processing of power-quality data became a major subject of publications. On the standardization side, the IEC power-quality monitoring standard, IEC 61000-4-30 [17.17], resulted from this.
- Modern equipment contains almost exclusively a power-electronic interface with the grid. Almost all these devices inject harmonics or supraharmonics into the grid. This is one of the reasons for the recent increased interest in waveform distortion.
- Distributed generation has resulted in a significant increase in interest in power quality. Some types of distributed generation are a source of disturbances, e.g., voltage variations, unbalance and waveform distortion. Distributed generation is also susceptible to voltage disturbances at its terminals. The issue that has received most attention in the literature and among transmission system operators is the potential massive tripping of distributed generation. The disturbances most studied in this context are frequency variations and voltage dips. The term *fault-ride-through* is commonly used in the literature.
- The replacement of incandescent lamps with compact fluorescent and LED (light emitting diode) lamps triggered a concern about large increases in harmonic distortion [17.18]. The concern did not (yet) materialize [17.19–21], but certain aspects remain unclear and the research is ongoing. It is for example not clear why the modeling and measurement results differ significantly. The introduction of, especially, LED lamps has also resulted in a renewed interest in light flicker.

### 17.1.5 Power Quality Standards and Regulation

Compared to most other fields within electric power engineering, power quality has a rather large number of standards. Some of those standards are of a mere technical nature, but many of them are of a legal nature. For the latter ones, the contents are still mainly technical, but the document defines obligations for different stakeholders.

Before discussing standards and regulation, it is important to clarify the difference between standardization and regulation. Standardization is a consensus process, where the different stakeholders sit together and discuss different proposals to come to an agreement. It is not always an agreement that everybody is happy with, but all stakeholders at least accept the compromise. Because it is a consensus process, it is also difficult to make changes to standards and an old standard could stay in place because there is no agreement among the stakeholders on a better version. For the same reason, standardization is a slow process. Making even a small change can easily take five years. However, despite that, standards do change and before using a standard, it is good to check the latest version.

Regulation on the other hand is not a consensus process; the regulator gets certain powers under the local law and that allows the regulator to set and/or enforce certain detailed rules. In most countries, the regulator will do this in close collaboration with the different stakeholders. However, in the end the regulator decides, whether the other stakeholders agree or not. Within power quality, the regulation in most countries is strongly related to national or international standards, so that the general discussion on standardization below also holds for regulation.

Where it concerns the detailed standardization for different types of disturbances, standardization has come a long way for long and short interruptions, for slow voltage variations, harmonics, and fast voltage variations that potentially result in light flicker. More work is needed on voltage dips, interharmonics, supraharmonics, fast voltage variations not resulting in light flicker, and on transients.

There are two different types of power-quality standards. The first type is those that define certain types of disturbances, disturbance characteristics or measurement methods. The IEC power-quality measurement standard (IEC 61000-4-30 [17.17]) plays an important role here. The second type are standards that define acceptable limits. These can be limits for the network operator, where EN 50160 [17.10] has become the leading document, but also limits for installations

or individual devices. A large number of IEC product standards set performance requirements for individual devices. Some standards set limits on emissions from equipment, others set limits on the immunity of equipment against voltage disturbances. A big challenge in standardization is to ensure that there is a correct balance between emission and immunity requirements.

We will further discuss the different standards and regulations together with the different types of disturbances in Sects. 17.2 and 17.3.

### 17.1.6 Limits and Interference

The difference between *disturbance* and *interference* was discussed in Sect. 17.1.2. Next to that, a distinction is often made between *acceptable disturbance levels* and *unacceptable disturbance levels*. Whether the level is acceptable or unacceptable is determined not by the presence or absence of interference but by comparing the level with a limit. For example, the voltage distortion is considered unacceptable when the total harmonic distortion (THD) is above a limit set in a standard or by regulation.

The relations between *exceeding the limit* and *occurrence of interference* are shown in Fig. 17.3, where all four combinations occur in reality. The top right relates to cases where the limits are exceeded and where equipment is adversely impacted (where there is interference). This is why there are limits: to avoid interference. The responsibility for the interference is easy to allocate, it is with the one that exceeds the limit. Cases that end up on the bottom left are also easy: this is where the limits are not exceeded and where everything works correctly, i.e., where there is no interference.

The other two blocks in the figure require some further discussion and cases that end up here often result in much discussion. For the block on the upper left, interference occurs while none of the limits are exceeded. Researchers and others that want to promote power quality often use cases like this to show that *the standards do not work* or that *the standards need to*

*be improved*. This is an oversimplification. The aim of standardization is to ensure a small probability of interference, at reasonable costs to society as a whole. As long as cases like this are small in numbers, there is no need for making changes in standardization. When the number of cases increases, or is expected to increase, changes are obviously needed. Even when individual cases do not warrant changes in the standards, it remains worthwhile to study such cases to learn more about the different phenomena and about which specific aspect or characteristic of a disturbance leads to interference. The occurrence of individual cases here may also possibly indicate a larger number of cases in the future.

The cases on the bottom right are the ones where one or more limits are exceeded but there is no interference. These should actually not be of any concern, as there is no interference. When cases like this occur too often, this could be an indication that the limits are too strict. The stakeholder that is responsible for keeping that limit may request for a lessening of the requirements. Two examples of this are:

- The regulator requirements on voltage are not fulfilled, but no equipment is adversely impacted. In that case, the question arises if the network operator (the stakeholder responsible for the voltage under the regulation) should take mitigation measures or not. This differs between countries and there are arguments to be given for both.
- Requirements for the connection of wind power plants often contain very strict conditions on harmonic currents. Especially the ones on higher-order even harmonics are hard to comply with in many cases. However, the choice of those limits is more based on existing levels many years ago than on possible interference.

### 17.1.7 Power Quality Monitoring

There are different types of power-quality monitoring, where the main difference is between short-duration

	Limits not exceeded	Limits exceeded
Equipment impacted	Investigation typically triggered by the owner of the equipment impacted	Measures have to be taken by the network operator or by the source of the emission
Equipment not impacted	Everybody is happy	Measures are actually not needed, but still often required under regulation or contracts

**Fig. 17.3** Relations between interference and exceeding of acceptable limits

manual measurements and long-duration automatic measurements. The latter are ruled by IEC 61000-4-30 [17.17], where so-called *class A instruments* are preferred. Such instruments continuously perform two types of calculations, related to variations and events (Sect. 17.1.3).

For variations, a number of characteristics are calculated and stored over pre-defined periods. Two simple examples are:

- The frequency of the voltage is calculated every 10 s from the number of zero crossings within the preceding 10 s interval.

- The voltage magnitude is calculated every 10 min as the RMS voltage over the preceding 10 min interval.

To detect events, a number of characteristics are calculated continuously and compared with pre-set threshold values. These characteristics are not stored, but once a threshold is exceeded, an event is detected, and the recording and characterization of the event is triggered.

A simple example: a voltage dip is detected when the 1-cycle RMS voltage becomes lower than 90% of the nominal voltage. Once the event is detected, single-event characteristics are calculated from the voltage and/or current waveform.

## 17.2 Harmonics

Harmonic distortion refers to components of the voltage or current at integer multiples of the fundamental frequency. A distinction is typically made between even harmonics, odd harmonics, and DC-components, where DC-components are usually treated differently since their consequences and measurement techniques differ.

A voltage or current waveform containing harmonic distortion (i.e., a periodic but non-sinusoidal waveform) can be decomposed into a sum of harmonic components according to

$$v(t) = V_{DC} + \sum_{h=1}^N \sqrt{2}V_h \sin(h\omega_0 t + \theta_h). \quad (17.3)$$

Harmonic distortion is typically presented in the form of a harmonic spectrum, as is exemplified in Fig. 17.4, for the voltage at the wall-outlet in a low-voltage installation. The bars represent individual harmonics, expressed as percent of the fundamental.

### 17.2.1 Sources of Harmonics

Harmonics are mainly caused by non-linear loads, such as variable speed drives, arc furnaces, computers, LED lamps, etc. Other power system elements that present a non-linear behavior include transformers and power electronic devices in the grid such as FACTS (flexible AC transmission system) and HVDC.

A non-linear device will draw a non-sinusoidal current even when fed by a sinusoidal voltage. Figure 17.5 shows an example of the current drawn by a computer, and its corresponding harmonic spectrum.

Different types of converters (e.g., single- or three-phase, current or voltage source, passive or active) behave differently with regard to the generation of harmonics. Figure 17.6 shows the harmonic current spectrum for a single- and three-phase DC current source (diode rectifier), as well as the corresponding mathematical expression for the generated harmonics,

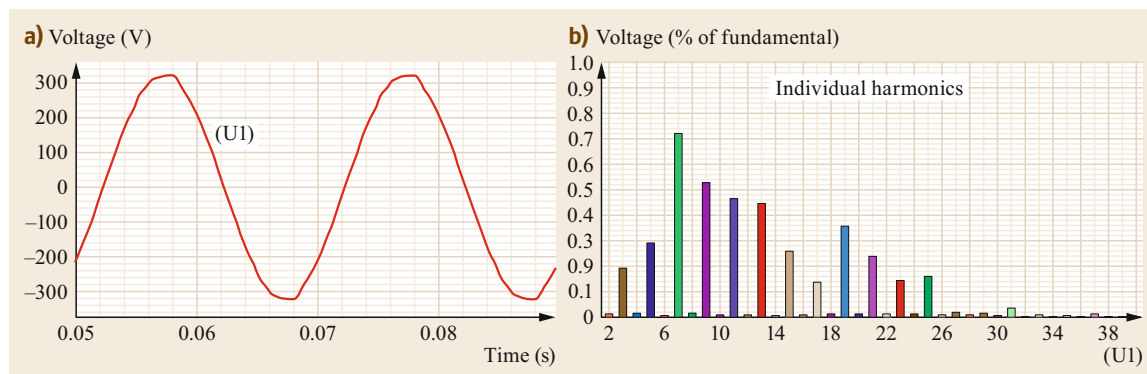


Fig. 17.4a,b Voltage waveform (a) and its corresponding harmonic spectrum (b). Measurement by Metrum PQSmart

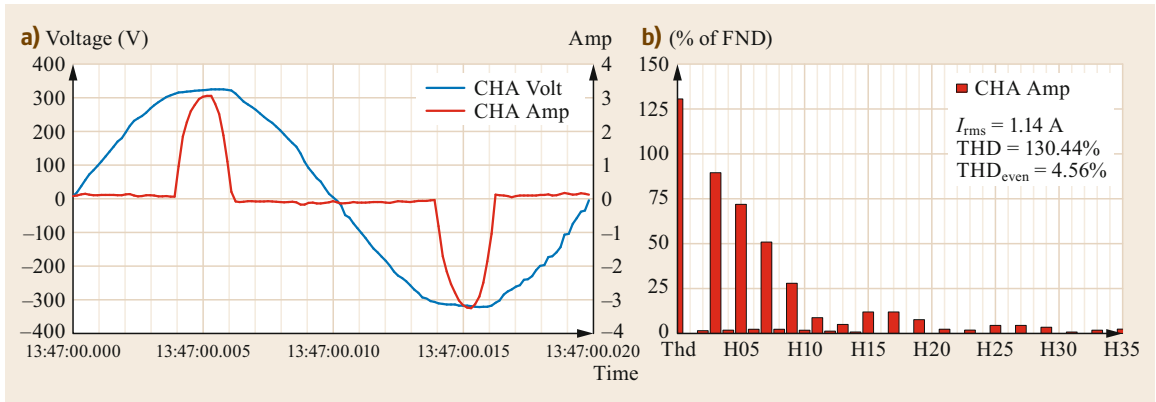


Fig. 17.5a,b Current to a computer (a) and the corresponding spectrum (b). Measurement by Dranetz PP1

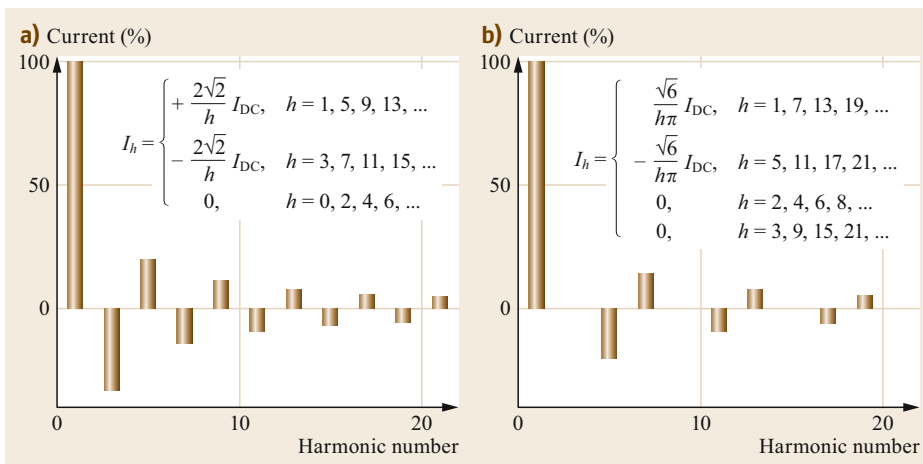


Fig. 17.6a,b Current spectrum of a single-phase DC current source (a) and a three-phase DC current source (b)

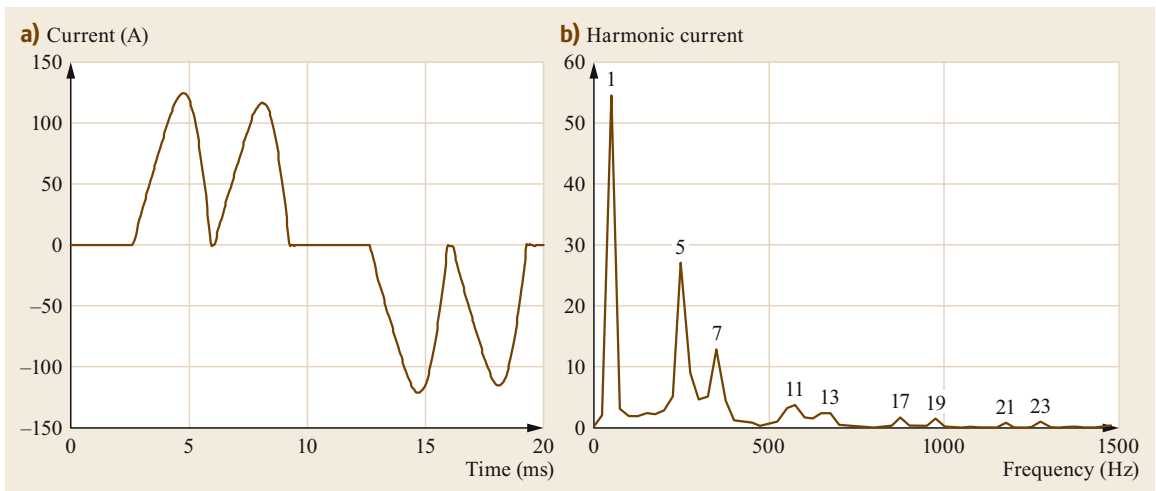
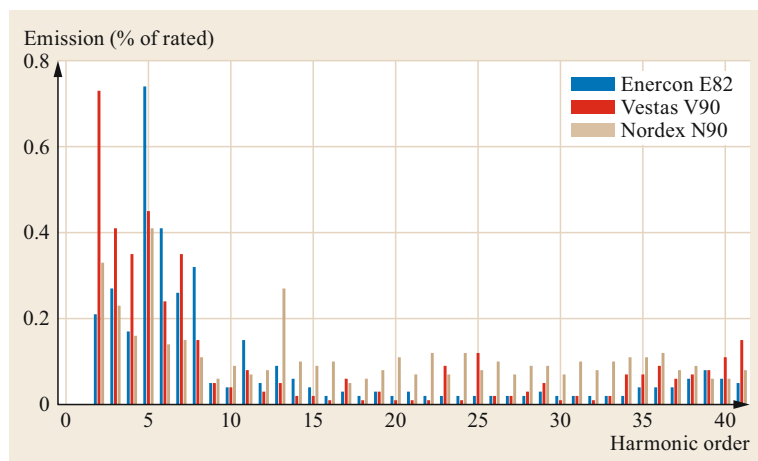


Fig. 17.7a,b Current waveform (a) and spectrum (b) of a three-phase DC voltage source



**Fig. 17.8** Emission from three different wind turbines; 95th percentile of the 10 min value of a period of one to three weeks

where  $h$  is the harmonic order,  $I_{DC}$  the DC current and  $I_h$  the resulting harmonic current of order  $h$  [17.4]. A negative value means that the emission is in phase opposition with the fundamental.

Figure 17.7 shows the current waveform and spectrum of a three-phase DC voltage source: a three-phase diode rectifier powering an adjustable-speed drive [17.22].

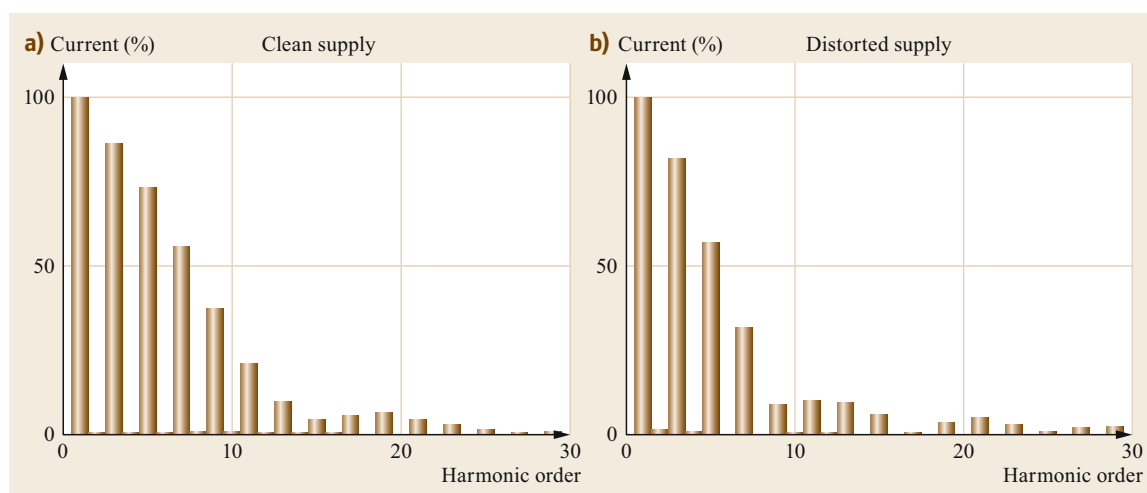
Modern types of power electronic converters used e.g., in HVDC applications or wind farms utilize an active switching scheme, which results in a less predictable spectrum compared to the spectrum of passive diode rectifiers. While such modern devices perform well regarding low-order harmonics, they instead act as a source of high-frequency harmonics (also known as *supraharmonics*). Figure 17.8 shows an example of harmonic emission from three modern wind tur-

bines [17.23]. When compared to IEEE 519 [17.12], harmonic orders 36 and 40 are exceeded by some of the turbines.

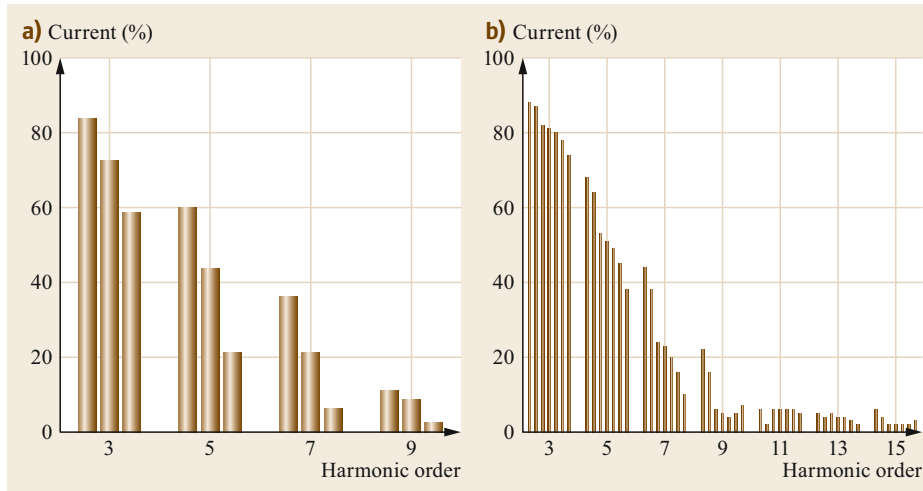
#### Impact of Background Distortion and the Number of Devices

The emission from a non-linear device is affected by the voltage distortion at its terminals. Figure 17.9 shows a comparison of the current to a personal computer when supplied from a clean supply and from a distorted supply [17.24]. When it is fed by the distorted supply, there is a reduction in harmonic currents, especially at higher frequencies.

Similarly, the current emission per device will be reduced as more equipment (computers, televisions, etc.) is added to the same node. Two examples are shown in Fig. 17.10. In Fig. 17.10a, the current spectrum



**Fig. 17.9a,b** Current spectrum of a computer (DC voltage source) when connected to a clean (a) and a dirty supply (b)



**Fig. 17.10a,b**  
Spectrum for 1, 10 and 80 televisions (a), and for an increasing number of computers (b)

for 1, 10 and 80 televisions is compared [17.24], and in Fig. 17.10b, the current spectrum per computer is shown for an increasing number of computers [17.25].

For active converters, the impact of voltage distortion on the emission is more complicated and the emission can increase or decrease with increasing voltage distortion.

### 17.2.2 Impacts of Harmonics

Due to regulation and standardization harmonics are typically not a problem for customers, but occasional problems do occur, typically because of amplification due to resonances. The consequences of high levels of harmonic distortion include increased heating of transformers, capacitors and rotating machines, malfunction of electronic equipment that relies on detecting the voltage zero-crossing, unwanted operation of relays, etc. The following sections describe some of the consequences in more detail [17.4].

#### Transformers

For transformers, the main issue is heating, mainly due to additional losses caused by harmonic currents. The losses are not uniformly spread through the transformer, which can lead to hot spots forming. The heating effect becomes more severe with increasing frequency. Another consequence of harmonics in transformers is audible noise.

#### Cables and Lines

Cables and lines are also impacted in the form of additional heating, but the effect is not as pronounced as for transformers. For cables, there is a risk of hot spots forming in cable joints, especially in the case of higher frequencies.

#### Neutral Conductors

The neutral conductor normally does not carry a significant current in a three-phase system. However, triplen harmonics present in the phase conductors will add in the neutral conductor. In some cases, this can lead to the current in the neutral exceeding the phase current. Consequently, there is a risk of overheating of the neutral conductor, without the overload protection removing the overload.

#### Electronic Equipment

Waveform distortion may cause a shift in the zero crossing or multiple zero-crossings, which will affect equipment that utilizes the voltage zero-crossing to determine the phase-angle.

Indirect effects of waveform distortion on electric equipment include e.g., malfunctions related to the coupling of high-frequency distortion through the power supply circuit.

#### Signaling

Waveform distortion may cause difficulties for signaling, since the distortion may be confused with the control signal. If passive filters are installed to mitigate harmonics this may have the indirect consequence of damping the control signals.

#### Telephone Interference

The inductive coupling of harmonic currents to telephone lines may cause audible telephone interference. A related issue is the appearance of audible noise on hearing loops (*audio induction loops*).

#### Magnetic Fields

A consequence of harmonic currents are magnetic fields at harmonic frequencies. The main magnetic field of



three-phase lines at a certain distance from the line is caused by the zero-sequence current, which is mainly caused by triplen order (3, 9, 15, etc.) harmonic current.

#### Capacitors

High-frequency harmonic currents may cause overheating, fuse blowing and damage to capacitor banks.

#### Rotating Machines

Low-order harmonics may lead to the forming of hot spots in rotating machines. Other effects include torque oscillations and audible noise.

#### Insulation

A high crest factor (caused e.g., by notching or resonances causing amplification of certain harmonics) leads to additional stress on insulation.

#### Protection

High harmonic distortion may cause incorrect operation of relays; this is especially a concern for solid-state relays.

#### Reactance-Earthed Networks

High harmonic distortion may cause detuning of Petersen coils, and may increase the earth-fault current.

#### Lighting and Other Electronics

The main impact on lighting is the destruction of the input capacitor, caused by high harmonic distortion. It has been shown recently that supraharmonics (in the range from 2–150 kHz) can result in light flicker [17.26].

#### Digital Energy Meters

Digital energy meters may give incorrect values because of supraharmonics.

### 17.2.3 Spread of Harmonics

The flow of distorted currents will cause voltage distortion throughout the network. In case of resonances the distortion may be amplified, leading to high distortion levels at nodes some distance away from the harmonic source.

Harmonic studies may involve the calculation of source and transfer impedances, or calculation of harmonic distortion in the network. Several software packages for performing harmonic calculations are available and a comprehensive source on network modeling for harmonic studies can be found in [17.27].

A simple and often used approach to assess the voltage distortion caused by the emission from a certain device is by modeling it as a current source. The system impedance  $Z_h$  is calculated for each harmonic order  $h$

and Ohm's law is used to calculate the voltage distortion  $V_h$

$$V_h = Z_h I_h . \quad (17.4)$$

This model assumes that the current injection is independent of the voltage. In reality, this is not the case, but the model may still be acceptable depending on the type of device that is being considered.

For modern sources of harmonic distortion, including converters used in wind farms, etc., the pure current source model is not suitable. Typically, a Thévenin or Norton equivalent model is used instead, with different values for the source and impedance, depending on the operating point.

#### Harmonic Transfer Impedance

The harmonic transfer impedance relates the voltage at a certain node with the current injected at another node. It can be used to assess the voltage distortion at a remote node following current injection at the local node, and vice versa [17.28, 29]

$$V_r^h = Z_{sr}^h I_s^h . \quad (17.5)$$

Here,  $r$  represents the receiving node, and  $s$  the sending node. In case of several sources, the total harmonic voltage at location  $r$  can be calculated using the superposition principle

$$V_r^h = \sum_{i=1}^N Z_{ri}^h I_i^h . \quad (17.6)$$

#### Study Domain

Harmonic studies are typically performed in the frequency or time domain, depending on the purpose of the study.

*Frequency-domain methods* are robust and allow for a simple definition of harmonic sources, but non-linear devices in the study have to be linearized. Typical applications include frequency scans in order to evaluate resonances, filter design studies and harmonic propagation studies.

*Time-domain methods* allow for modeling of non-linear devices in any level of detail and time-varying properties, including power electronic converters and their control. However, significant effort is often required to incorporate such models correctly, and time-domain simulations can be computationally heavy. Typical applications include studies involving transformer saturation and studies where detailed modeling of power electronic converters is required.

More information on study domains can be found in [17.27].

**Table 17.1** Harmonics and symmetrical components

	1	2	3	4	5	6	7	8	9	10	11	12	13	14	15
Positive sequence	+			+			+			+				+	
Negative sequence		-			-			-			-				-
Zero sequence			0			0			0			0			0

**Harmonics and Symmetrical Components**

In the same way as for the fundamental frequency, harmonics can be transformed into symmetrical components. In a balanced system, each harmonic frequency belongs to one of the sequences, as illustrated in Table 17.1.

Special attention should be given to zero-sequence harmonics due to the way they propagate in the system:

- Zero-sequence harmonics in the three phases will add in the neutral conductor, which may lead to overheating of the neutral.
- Zero-sequence harmonics circulate in the delta windings in transformers, meaning that they will not propagate through the transformer. Thus, any 3<sup>rd</sup> harmonic distortion originates locally.

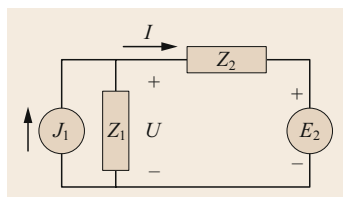
**Primary and Secondary Emission**

When assessing the contribution of a device to the harmonic distortion, a distinction should be made between primary emission, which refers to any emission originating from the device itself, and secondary emission, which originates from outside of the device. The concept of primary and secondary emission can be explained using Fig. 17.11 [17.28].

In this case, the primary emission is driven by the current injected by  $J_1$ , and the secondary emission is driven by  $E_2$ . It is not straightforward (or even possible, depending on the assumptions made) to distinguish between primary and secondary emission through field measurements alone.

**Resonances**

Resonances are often the cause of high harmonic distortion and interference.



**Fig. 17.11** Primary and secondary emission.  $I$ : emission,  $J_1$ : internal emission,  $Z_1$ : device impedance,  $Z_2$ : grid impedance,  $E_2$ : background voltage

A *parallel resonance* is characterized by a large impedance at the resonance frequency. If a parallel resonance is excited by a harmonic current, there is a risk of significant voltage distortion, even for moderate levels of current distortion. Consider a simple system with source impedance  $L$  and shunt capacitance  $C$ . The impedance seen from the harmonic source will be

$$Z(\omega) = \frac{j\omega L}{1 - \omega^2 LC} \tag{17.7}$$

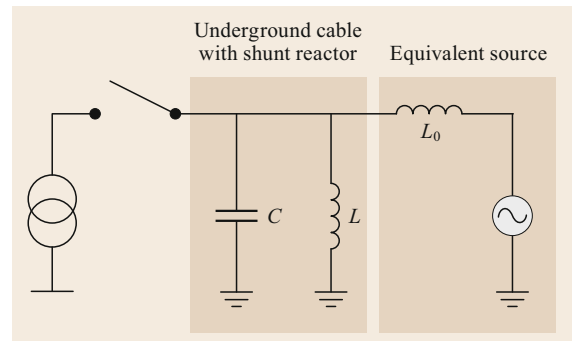
At the resonance frequency, the impedance becomes infinite. The resonance frequency is determined by

$$f_{res} = \frac{1}{2\pi\sqrt{LC}} \tag{17.8}$$

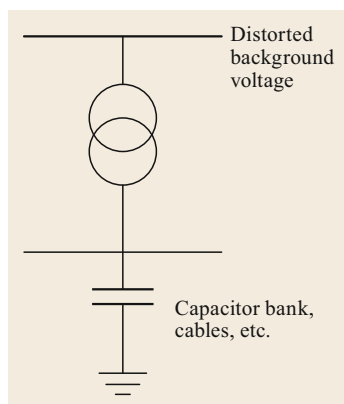
Figure 17.12 shows a typical parallel resonance circuit, where a transformer is energized in the presence of a cable. The cable capacitance and source inductance form a parallel resonance circuit, and the transformer acts as a source of harmonic currents.

A *series resonance* is characterized by a small impedance at the resonance frequency. Figure 17.13 shows an example of a series resonance circuit, which consists of a transformer with a capacitance connected to its secondary side. In case of high background distortion on the primary side of the transformer, this may lead to high harmonic distortion on the secondary. The relation between the voltage at the secondary side,  $V_{sec}$ , and the primary side  $V_{prim}$ , is

$$\frac{V_{sec}(\omega)}{V_{prim}(\omega)} = \frac{1}{1 - \omega^2 LC} \tag{17.9}$$



**Fig. 17.12** Parallel resonance circuit



**Fig. 17.13** Series resonance circuit

The impedance at the resonance frequency will depend on the damping (series and shunt resistances in the grid). However, the damping is typically not known, especially at higher frequencies. Resonances are generally not a problem if the damping is high or if there is no emission around the resonance frequency.

#### 17.2.4 Mitigation of Harmonics

Harmonics can be mitigated by limiting the emission from equipment, by the use of harmonic filters or by strengthening the network. The latest developments focus on the use of power electronics and active filtering to mitigate harmonics. A comprehensive source on harmonic mitigation can be found in [17.30].

##### Passive Filters

Passive filters are cheaper and more commonly used than active filters. A passive filter consists of a combination of inductances, capacitances and resistances arranged in specific ways to suppress certain harmonics. There are several types of passive filters, with the single-tuned *notch* type filter being the most common. At the resonance frequency, the filter acts as a current sink, meaning that all harmonic current passes through the filter. The sharpness of the filter is determined by its  $Q$ -value, where a high  $Q$  means it is sharply tuned to a certain frequency and a low  $Q$  means it has a low impedance over a wide range of frequencies. A filter bank consists of a combination of filters, such as 5th and 7th, 11th and 13th, and high-pass filters.

##### Active Filters

Active filters are power electronics-based devices that aim to reduce the harmonic distortion through dedicated control algorithms. The reduction can be achieved either by compensating the harmonic currents or through impedance shaping. Active filters are more flexible than

passive filters, but also more complicated and more expensive.

#### 17.2.5 Harmonic Measurements

Harmonic measurements deal with the monitoring of voltages and currents in the power system. Captured voltages and currents are transformed into the frequency domain and processed in order to obtain suitable indices for quantifying the harmonic distortion.

IEC 61000-4-7 [17.31] and IEC 61000-4-30 [17.17] provide guidelines for harmonic and interharmonic measurements and instrumentation.

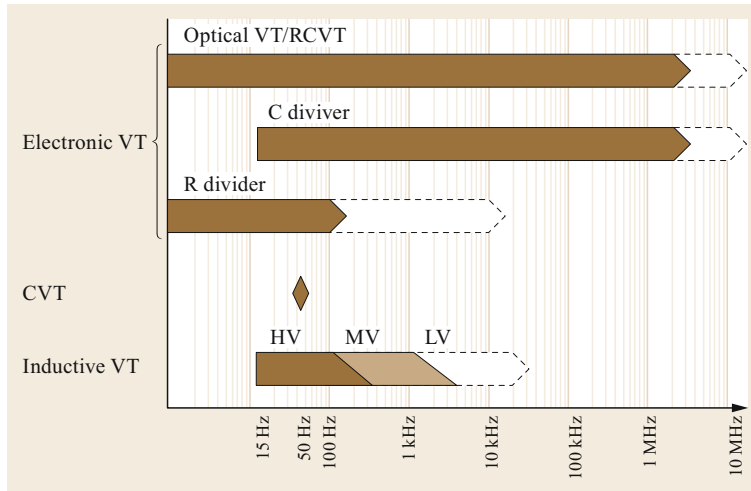
##### Measurement Transformers

In cases where a direct connection is not possible, measurement transformers are used to provide a signal level that is compatible with the measurement equipment. Although the behavior of measurement transducers at the fundamental frequency is well-defined, their suitability for measurements of higher frequencies may be limited.

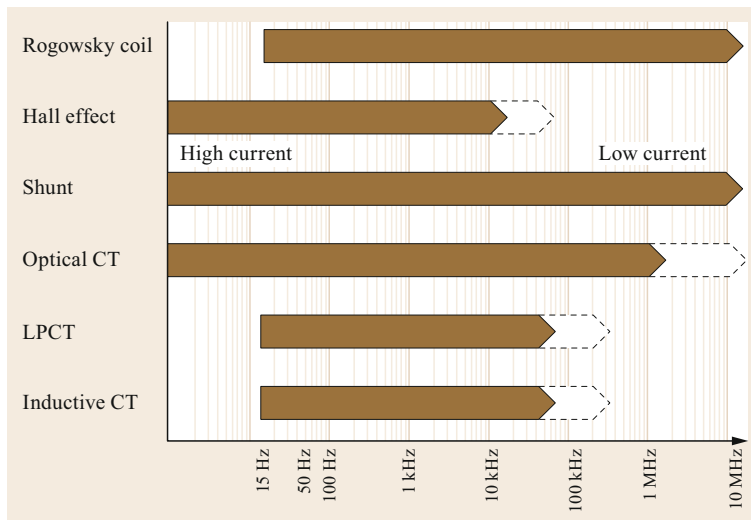
**Voltage Transformers.** For low-voltage measurements, it is possible to connect the measurement equipment directly to the terminals. For measurements at higher voltage levels, a voltage transformer is required. There are several types of voltage transformers available, the most common being inductive voltage transformers (IVTs) and capacitive voltage transformers (CVTs).

IVTs are designed to have a mostly linear behavior around the fundamental frequency. Due to their construction, resonances between the winding inductances and stray capacitances may introduce large phase and magnitude errors at frequencies above the fundamental. Based on performed tests, IVTs applied in medium voltage networks have been deemed suitable up to 1 kHz (60% of the tested units manage to cover the entire harmonic spectrum up to 2 kHz). However, this is without consideration of requirements on the accuracy of the measured phase angle. As the system voltage increases, resonances may appear at lower frequencies, and IVTs used for high voltage are deemed suitable only up to a few 100 Hz [17.32].

CVTs consist of a capacitive voltage divider (CVD) and an electromagnetic unit (EMU). The CVD and the EMU are tuned so that they are in resonance at the fundamental frequency. This means that a small shift in frequency will cause large errors in magnitude and phase, with resonance frequencies as low as 200 Hz reported. Thus, CVTs are generally considered unsuitable for measuring harmonics [17.32, 33]. There are ways to improve the performance of CVTs for harmonic



**Fig. 17.14** Overview of frequency range of different voltage transformer technologies



**Fig. 17.15** Overview of the frequency range of different current transformer technologies

measurements, e.g., by utilizing current measurements immediately after the LV capacitance and at the earth connection.

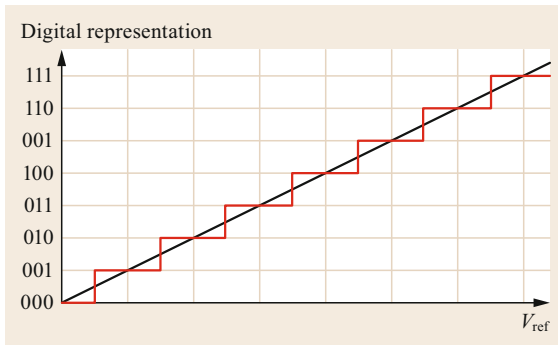
Other types of voltage transformers include CVDs, resistive voltage dividers (RVDs) and resistive-capacitive voltage dividers (RCVDs). RVDs are impacted regarding magnitude and phase above 800 Hz. CVDs and RCVDs are able to accurately monitor transients up to 1 MHz or higher, meaning they are suitable for harmonic measurements even in the supraharmic range. A summary of the suitability of different voltage transformers is given in Fig. 17.14 [17.32].

**Current Transformers.** Inductive current transformers with a toroidal and ferromagnetic core are most commonly used in the power system today. Their frequency

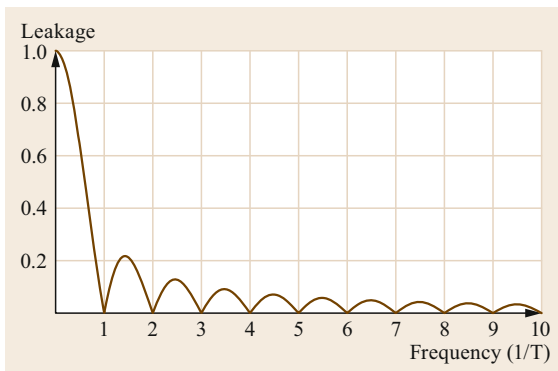
response is determined by the transformer inductances and capacitances. While the capacitances may have a significant effect on the measurements at high frequencies, the impact is deemed negligible for the traditional harmonic range [17.32, 33]. In cases where a DC-component may be present, air-gap current transformers should be used to avoid offsets in the core flux. Aside from inductive current transformers, there are several other options, such as Rogowski coils or optical current transformers. A summary of the suitability of different current transformers is given in Fig. 17.15 [17.32].

#### Signal Processing

After the signal has been sampled, a discrete Fourier transform (DFT) is used to obtain the harmonic spec-



**Fig. 17.16** Example of quantization (conversion to digital representation)



**Fig. 17.17** Fourier transform of rectangular window

trum of the sampled waveform. However, this process results in different unavoidable artefacts.

**Aliasing.** When sampling an analogue signal with a sampling frequency  $f_s$ , the highest frequency component in the digital signal will be equal to half of the sampling frequency. This frequency is referred to as the Nyquist frequency. Frequencies above the Nyquist

frequency in the sampled signal will appear in the spectrum at lower frequencies. This is referred to as aliasing.

Aliasing is mitigated by use of an anti-aliasing filter (analogue low-pass filter) before the analogue-to-digital converter (ADC).

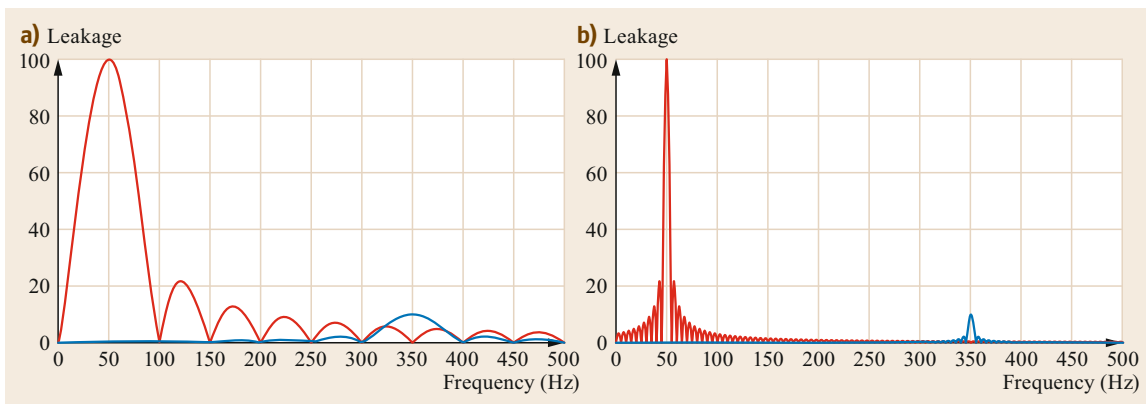
**Quantization Noise.** When a continuous signal is converted to its digital representation through an ADC, a range of discrete values are used to represent the signal, as shown in Fig. 17.16. The difference between the signal and its digital representation is called the quantization error. This error will appear in the frequency domain as a form of broadband noise.

Quantization noise can be reduced by utilizing a higher bitrate in the A/D conversion or by using a higher sampling frequency.

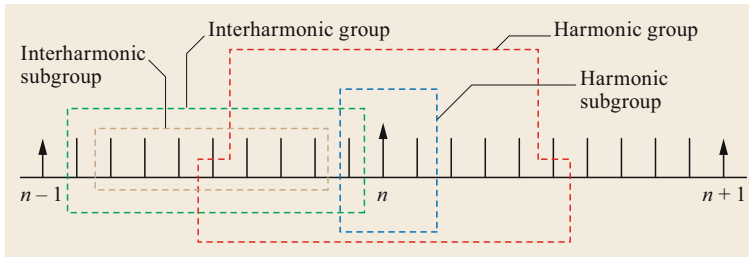
**Spectral Leakage.** When analyzing a continuous signal, only a small portion of the signal is observed. This is done through a process referred to as windowing. When a DFT is applied to a windowed signal, this will result in *leakage* to frequencies other than the actual frequency content of the signal. Consequently, it may be difficult to distinguish actual and leaked frequency components from each other. Spectral leakage can be demonstrated by examining the Fourier transform of a rectangular window, shown in Fig. 17.17.

The window length determines the width of the main lobe. As an example, Fig. 17.18 shows the same signal for window lengths of 20 and 200 ms, respectively. The signal consists of a 50 Hz component and a 350 Hz component.

The impact of spectral leakage can be reduced by choosing an appropriate window function. IEC prescribes a rectangular window, but when analyzing interharmonics, e.g., Hanning or Hamming windows may be more appropriate.



**Fig. 17.18a,b** Fourier transform of 50 Hz (red) and 350 Hz (blue) signal with a window length of 20 ms (a) and 200 ms (b)



**Fig. 17.19** Harmonic groups and subgroups as defined in IEC 61000-4-7

### Quantifying Harmonic Distortion

IEC 61000-4-30 [17.17] prescribes the use of a 10 cycle (200 ms) window in a 50 Hz system. After applying the DFT, this results in a frequency spectrum with a resolution of about 5 Hz (one tenth of the power-system frequency). The results can be presented e.g., as the absolute value of the harmonic components, or by aggregating the harmonic components into groups.

**Groups and Subgroups.** For assessment of harmonics, IEC 61000-4-30 [17.17] prescribes the use of harmonic groups and subgroups, as defined in IEC 61000-4-7 [17.31]. An overview of the concept of harmonic groups and subgroups is shown in Fig. 17.19 for a 50 Hz system, where  $n$  represents the harmonic order [17.4].

**Total Harmonic Distortion (THD).** THD is commonly used to quantify waveform distortion. It is defined as the relative signal energy at frequencies other than the fundamental

$$\text{THD} = \frac{\sqrt{\sum_{h=2}^H V_h^2}}{V_1} \quad (17.10)$$

Since THD is given in relation to the fundamental, care should be used when evaluating current THD. As an

alternative, total demand distortion (TDD) can be used, which instead relates the distortion to the maximum or rated current

$$\text{TDD} = \frac{\sqrt{\sum_{h=2}^H I_h^2}}{I_{1, \max}} \quad (17.11)$$

### 17.2.6 Standards and Regulation

A distinction should be made between power-quality standards that define types of disturbances, disturbance characteristics or measurement methods, and those that define acceptable limits.

IEC 61000-4-7 [17.31] defines measurement instrumentation for testing equipment against applicable emission limits as well as for measurement of harmonic voltages and currents in the power system.

IEC 61000-4-30 [17.17] defines measurement methods and methods to interpret results for various power quality parameters, including harmonics, flicker, dips, etc.

IEEE 519 [17.12] provide recommendations for voltage limits (applicable to the network operator) and current limits (applicable to network users) referred to the point of common coupling (PCC). As an example, Table 17.2 presents the current distortion limits

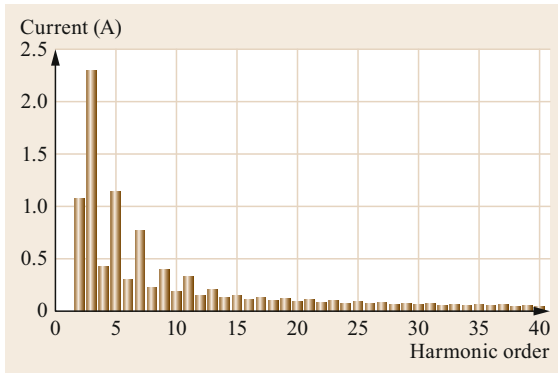
**Table 17.2** IEEE 519: Current distortion limits for systems rated 120 V through 69 kV

Maximum harmonic current distortion in percent of $I_L$						
Individual harmonic order (odd harmonics) <sup>a,b</sup>						
$I_{sc}/I_L$	$3 \leq h < 11$	$11 \leq h < 17$	$17 \leq h < 23$	$23 \leq h < 35$	$35 \leq h \leq 50$	TDD
< 20 <sup>c</sup>	4.0	2.0	1.5	0.6	0.3	5.0
20 < 50	7.0	3.5	2.5	1.0	0.5	8.0
50 < 100	10.0	4.5	4.0	1.5	0.7	12.0
100 < 1000	12.0	5.5	5.0	2.0	1.0	15.0
> 1000	15.0	7.0	6.0	2.5	1.4	20.0

<sup>a</sup> Even harmonics are limited to 25% of the odd harmonic limits

<sup>b</sup> Current distortions that result in a DC offset are not allowed

<sup>c</sup> All power generation equipment is limited to these values of current distortion

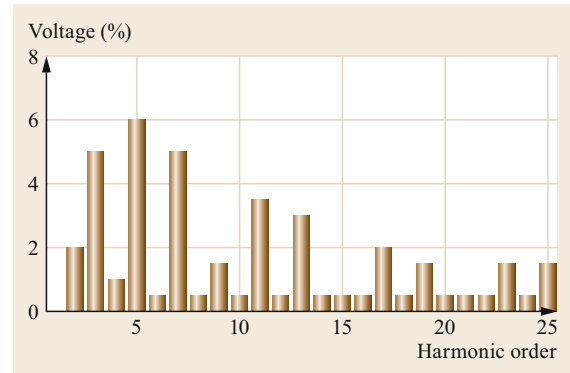


**Fig. 17.20** Reference levels of harmonic current emission for low-voltage equipment according to IEC 61000-3-2

given in IEEE 519 for systems rated 120 V through 69 kV.

$I_{SC}$  refers to the maximum short-circuit current at the PCC and  $I_L$  the maximum demand load current at the PCC under normal operating conditions.

IEC 61000-3-2 [17.34] specifies current emission limits for equipment rated  $\leq 16$  A per phase. An example is given in Fig. 17.20.



**Fig. 17.21** Voltage distortion limits given in EN 50160 up to 1 kV

EN 50160 [17.10] defines voltage distortion limits that the network operator should comply with. Figure 17.21 presents the permissible harmonic levels (given as percent of the fundamental) for voltages up to 1 kV.

IEC 61000-2-4 [17.35] defines compatibility levels for conducted disturbances in industrial installations in the frequency range 0–9 kHz.

## 17.3 Other Power-Quality Disturbances

### 17.3.1 Voltage Dips

Voltage dips are short duration reductions in voltage magnitude. Different documents give different values for the range of durations and residual voltage of a voltage dip. Generally, a drop below 90% of the nominal voltage for up to about a minute is considered a voltage dip.

#### Description and Characterization

Voltage dips are, in standards, described by two single-event characteristics: residual voltage (*dip magnitude*) and dip duration. These two characteristics are defined in IEC 61000-4-30 [17.17] and in IEEE 1564 [17.36]:

- The dip duration is defined as the length of time during which the 1-cycle RMS voltage is less than the voltage-dip threshold in at least one of the measurement channels.
- The residual voltage is defined as the lowest 1-cycle RMS voltage in any of the measurement channels.

Next to the standard characteristics, a number of additional single event characteristics have been discussed in the scientific literature. Most emphasis has been on

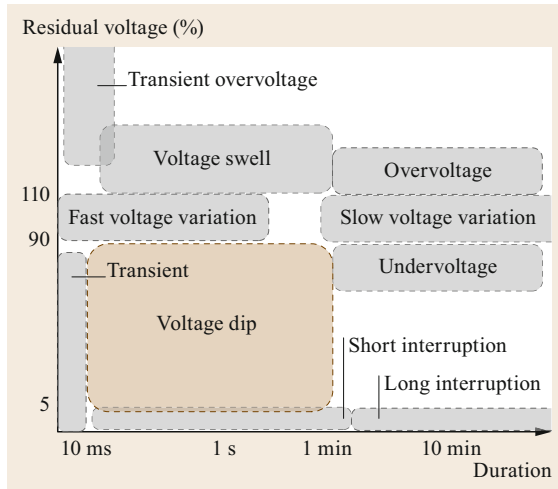
three-phase unbalance, where an early classification in dip types [17.37] still receives a lot of attention. Phase-angle jump [17.38, 39] and point-on-wave [17.40] have been discussed in the literature by different authors as well.

It was mentioned before that different documents give different values for the range of duration and residual voltage of voltage dips. When one of these single-event characteristics is beyond the indicated range, the disturbance should strictly speaking not be referred to as a voltage dip. There is, however, no reason for a hard limit and the same disturbance may be referred to in different ways. The different types of disturbances, in relation to voltage dips, are summarized in Fig. 17.22 as a function of residual voltage and duration.

#### Origins and Impacts

Voltage dips are due to short-duration increases in current magnitude, typically at another location than where the dip is measured. The main causes of voltage dips are:

- High currents during short-circuits and earth faults.
- High currents during transformer energizing.
- High currents during motor start or start of other equipment with a high starting current.



**Fig. 17.22** Different types of voltage disturbances separated by voltage and duration

The drops in voltage due to high currents with capacitor energizing could also be treated as voltage dips, but these events are generally considered as voltage transients and not as dips.

A number of different aspects of voltage dips have a direct impact on the performance of equipment connected to the grid:

- The actual drop in voltage results in a reduced energy flow between the grid and the device. For consumption equipment, this results in a shortage of energy, leading, for example, to a drop in speed for an electrical motor. For production equipment, it results in a surplus of energy with the device connected to the grid. This same disruption of the energy flow results in angular instability after a fault. This impact of the voltage dip is most severe for balanced dips (due to three-phase faults) and is dependent on both residual voltage and duration.
- The change in magnitude and phase angle of the voltage at the start of the dip affects the operation of equipment. For example, high currents on the rotor-side of the converter with a double-fed induction generator. Not only the residual voltage (the drop in voltage) is of importance here, but also the phase-angle jump and the point-on-wave of dip starting.
- The unbalance or distortion during the dip affects the operation of equipment. High current unbalance and overcurrent through diode rectifiers could result in tripping of the rectifier. High harmonic voltage distortion (for a dip due to transformer energizing) could affect the control system of large converters.

To quantify this kind of impact, additional characteristics are needed, like type of unbalanced dip or the spectrum of the voltage during the dip.

- The change in magnitude and phase angle of the voltage at the end of the dip affects the operation of equipment. Many grid-connected devices contain a capacitor, on the AC side, or the DC side, or both. The sudden rise in voltage at the end of the dip gives a high inrush current that could result in tripping of fuses or overcurrent protection.

Additional characteristics like point-on-wave of dip ending, phase-angle jump, and the details of the voltage recovery are also important in quantifying this impact [17.41].

All of these impacts can result in tripping of the device or otherwise malfunctioning. In industrial installations, this can easily result in an interruption of a complicated production process. Such a process can take a long time to restart; a voltage dip as short as 100 ms can result in several hours of lost production.

Repetitive dips can result in long-term equipment damage. The overcurrent for each individual dip may not lead to the device tripping, but many of them over a longer period cause damage to the device.

#### Standards and Regulation

There is no consistent set of standards or regulation for voltage dips, but some individual standards do exist.

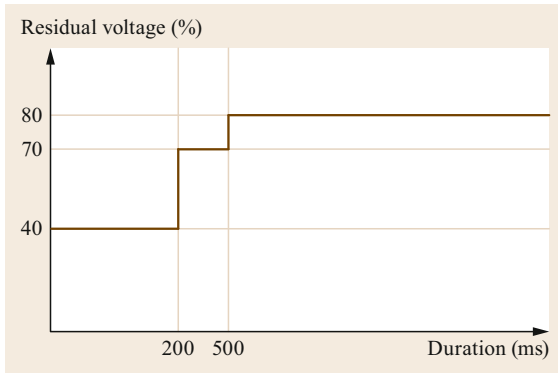
Methods for immunity testing are defined in IEC 61000-4-11 [17.42], IEC 61000-4-34 [17.43] and IEEE 1668 [17.44]. The IEC standards only define tests for unbalance dips; the IEEE standard also includes tests for balanced dips. The definition of residual voltage and duration in IEC 61000-4-30 [17.17] and IEEE 1564 [17.36] is however only relevant for balanced dips.

Immunity requirements are part of some IEC product standards, like IEC 61800-3 [17.45] for adjustable-speed drives. For equipment without immunity requirements in a specific product standard setting, the generic immunity standards IEC 61000-6-1 [17.46] and IEC 61000-6-2 [17.47] hold. The immunity requirements aim at avoiding damage to equipment, not to ensure that equipment remains connected to the grid during a voltage dip.

Some industry standards contain immunity requirements for equipment as well. The ones published by ITIC and SEMI are the ones most commonly used and cited. A general discussion on immunity of equipment and installations against voltage dips has been published by an international group of experts [17.48].

Voltage-dip regulation is based on the definition of a *responsibility-sharing curve* in the voltage-duration





**Fig. 17.23** Voltage-tolerance curve (indicative compatibility curve) recommended by the Council of European Energy Regulators

plane. An example is shown in Fig. 17.23. The customer or owner of the installation is responsible for dips above the curve; the network operator is responsible for dips below the curve. The responsibility does in this case not imply that the network operator is responsible for all costs and consequences of dips below the curve. Instead, a regulatory agency can put limits on the number of dips below the curve. Hence the use of the term *indicative compatibility curve* as a synonym. The curve shown in Fig. 17.23 is the one recommended by the European energy regulators [17.49]. Voltage-dip regulation is in place in a few countries only, where different countries use different responsibility-sharing curves, and with significant differences in the regulations.

#### Trends and Unsolved Issues

An important reason for continued interest in voltage dips is the susceptibility of production units to voltage dips. A serious concern for transmission-system operators is the potential mass tripping of production units due to a voltage dip. A serious fault at transmission level could result in the tripping of production units over a large geographical area. The resulting shortage of production could cause frequency, voltage and/or angular instability of the transmission system. Instead of *voltage dip immunity*, the term *fault-ride-through requirements* is often used. The basic phenomenon remains the voltage dip at the terminals of the production unit. The main interest in literature has been on the fault-ride-through of wind turbines [17.50, 51], but more recently also photovoltaic (PV) installations have received attention [17.52].

Voltage dips remain an important issue for industrial installations. In the scientific literature, there is only limited interest in the impact of voltage dips on industrial equipment and installations. After a large number

of publications on this subject up to about 2005, interest in the subject diminished. Modern industrial equipment is often of another type than that of 20 years ago (with *active front end* instead of *diode rectifier*) and it may react differently to voltage dips.

The definition of additional characteristics for voltage dips remains of interest for research and for standardization. The next step in standardization, after residual voltage and dip duration, is likely to be unbalance (often referred to as *dip type*), and phase-angle-jump. Standard methods for defining point-on-wave require a serious amount of further development [17.53].

The treatment of large amounts of voltage-dip data is another emerging subject. Some work was also done here up to 2005, but recently, research has been taken up again [17.54]. Both the availability of increasing amounts of data (*big data*) and a new generation of algorithms (*deep learning*) have contributed to this.

### 17.3.2 Voltage Swells

Voltage swells are short-duration increases in voltage magnitude. Swell durations are up to about 1 min. A voltage exceeding 110% of nominal is generally considered a voltage swell.

#### Description and Characterization

Voltage swells are characterized by two single-event characteristics, both defined in IEC 61000-4-30 [17.17]: *maximum swell voltage* and *swell duration*. The definition of these characteristics is very similar to the definition of dip characteristics.

The definitions of swell and dip in IEC 61000-4-30 are such that the same event can be classed as a dip and as a swell. That occurs with a three-phase measurement when one of the phase-to-neutral voltages is above the swell threshold and another one below the dip threshold. Such events can occur due to single-phase faults.

#### Origins and Impacts

Voltage swells are often presented as the opposite phenomenon to voltage dips. That is an oversimplification as there are differences in both the origin and impact of the two phenomena. A number of causes for voltage swells can be distinguished:

- A single-phase fault can result in a voltage rise in the non-faulted phases. The severity of the voltage rise depends on the location of the fault and on the ratio between zero and positive-sequence source impedance. There is also a significant difference here, depending on the system grounding at the voltage level where the fault occurs.

- The starting of a large single-phase load can result in a voltage rise in the other two phases. Like with swells due to single-phase faults, the voltage rise increases for an increasing ratio between zero and the positive-sequence impedance. These swells are of lower magnitude (less voltage rise) than the first kind, but they are of longer duration.
- The sudden loss of a large load will result in a voltage rise. When the loss of load occurs in the low or medium-voltage network, the voltage rise will be long term. In that case the phenomenon is more typically referred to as a (long-duration or sustained) overvoltage. When the loss of load occurs at a higher voltage level, the on-load tap-changer will bring the voltage back to within its normal range. As a result, the customers will see a voltage rise of a few minutes' duration.
- A broken neutral conductor can, under some conditions, result in an overvoltage over the terminals of single-phase connected low-voltage equipment. These overvoltages can be high, up to the line voltage (170% of the normal voltage) resulting in permanent damage to the equipment. The broken conductor can result in overvoltage or in undervoltage depending on the load balancing between the three phases [17.55].
- Making an incorrect connection in the low-voltage network could expose end-user equipment to the line voltage. This will almost immediately result in permanent damage to end-user equipment.

As was mentioned before, the system grounding plays an important role in the occurrence of voltage swells during single-phase faults. Two types of grounding should be distinguished here: solid grounding versus all methods where there is some kind of impedance between the neutral and ground. The latter aims at limiting the fault current, but a consequence is the occurrence of voltages up to about 180% in the non-faulted phases. Those voltages occur only between phase and ground, not between the phases. Equipment connected to such a system will either be connected phase-to-phase or through a delta-wye-connected transformer. In both cases, the equipment will experience at most a minor dip or swell during the fault.

High voltage in the non-faulted phases also occurs in solidly grounded systems. For locations further away from the transformer, the zero-sequence source impedance becomes significantly bigger than the positive-sequence one. The result is that the voltage in the non-faulted phases rise during a single-phase-to-ground fault. Equipment, which is typically connected phase-to-neutral in such a system, will be exposed to this voltage rise. In other words, the equipment experiences a swell.

### Standards and Regulation

There are limited standards on the immunity of equipment against voltage swells. The ITIC curve includes a part on voltage swells, but no IEC standards set any requirements.

The power-quality regulation in Sweden defines two responsibility-sharing curves for voltage swells in low-voltage networks.

### Trends and Unsolved Issues

There is very limited research work going on about voltage swells. The general rise of the voltage magnitude with an increased connection of small-scale photovoltaics could result in an increased number of voltage swells. Insufficient data is available to know if this would be a serious concern.

There is also some interest in voltage swells, because of the overvoltage ride-through requirements for production units in some countries.

### 17.3.3 Long Interruptions

Long interruptions are characterized by the complete absence of voltage for more than a few minutes.

#### Description and Characterization

Long interruptions are a concern for all customers connected to the grid. The statistical properties of long interruptions are discussed within the field *power system reliability* and details of this can be found in some of the textbooks on reliability [17.56–58].

Long interruptions are not commonly treated as a power quality issue. In fact, the terminology used by the European energy regulators distinguishes between continuity of supply (long and short interruptions) and voltage quality (all other voltage disturbances).

Long interruptions are characterized through their duration. This duration is defined in the IEC power quality measurements standard, IEC 61000-4-30, [17.17] as the time that the one-cycle RMS voltage is below the interruption threshold (for example 10% of the nominal voltage). For reliability statistics, and in regulation, the duration of an interruption is defined more commonly as the time elapsed between the opening and closing of an interrupting device.

Statistics on long interruptions are gathered by most network operators, either for internal use or on request of the regulator. What is reported and published are typically only a small number of system indices. These are defined in IEEE 1366 [17.59]; the ones most commonly used are SAIFI (system average interruption frequency index) (also known as *interruption frequency*), SAIDI (system average interruption duration index) (*unavailability*) and CAIDI (customer average

interruption duration index) (*average interruption duration*). Such average values are a suitable performance index for the network as a whole but have limited value for individual customers. Few network operators publish data on the number of interruptions experienced by individual customers.

### Standards and Regulations

Many countries have limits on the number and duration of long interruptions. An up-to-date overview on this is produced every few years by the *Council of European Energy Regulators (CEER)* [17.8]. For details, the reader is referred to those reports. Different types of standards and regulations are used in different countries:

- Limits on system indices (SAIFI, SAIDI). These are typically used as a quality adjustment to the tariffs that the network operator is allowed to charge to its customers. A minor adjustment in tariff can result in a large change in the financial result of the company. Such quality adjustments are thus an important regulatory instrument.
- Limits on the number or duration of interruptions for individual customers. The enforcement could be in the form of compensation that the network operators have to pay to the impacted customers.

### Trends and Unsolved Issues

Regulation and gathering of statistics on long interruptions considers them as events with a sudden start and a sudden end. Details of the start or end of an interruption are not considered in the statistics or in the regulations. Measurements show large differences between interruptions in the way the voltage disappears and the way in which the voltage recovers when the supply is reconnected. The start of the interruption could be due to a fault followed by protection clearing. The customer will experience a dip followed by a complete disappearance of the voltage. A large part of the different dip characteristics discussed in the literature (Sect. 17.3.1) will also apply here.

When an interruption is due to an incorrect tripping of the protection, or due to manual switching, the voltage will disappear immediately. Several measurements show transient overvoltages during the start of such an interruption. The impact of this on equipment has never been systematically studied. The increased presence of small-scale production units (specifically solar power) has put this subject on the agenda again. The emphasis in the research is very much on methods to avoid uncontrolled island operation, not on the potential impact on equipment connected to the uncontrolled island.

When the voltage recovers, this can occur suddenly, it can occur slowly, or there can be oscillations after the interruptions for a while. A specifically complicated and potentially disruptive case is the saturation of transformers due to the voltage recovery. This results in high levels of harmonic voltage distortion. Especially for unloaded transformers the distortion can continue for several seconds. Harmonic resonances could further amplify the voltage distortion resulting in temporary overvoltages.

### 17.3.4 Short Interruptions

Short interruptions (*momentary interruptions* in many publications and in IEEE documents) are events during which the voltage has completely disappeared for a few minutes.

#### Description and Characterization

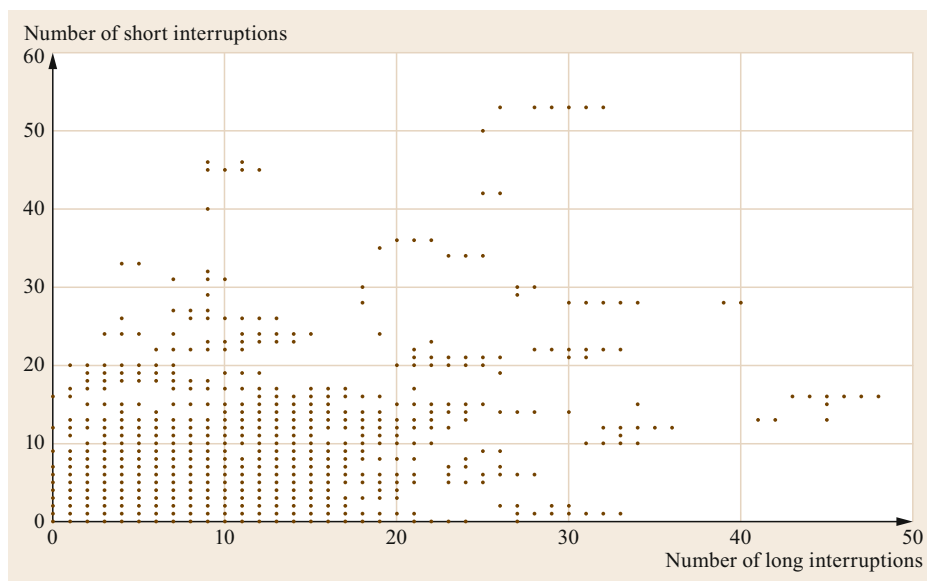
The term *short interruption* or *momentary interruption* refers to interruptions with a duration of a few minutes. There is no difference in the start (or cause) of short and long interruptions. The difference is in the speed with which the supply is restored. With short interruptions, the restoration is typically automatic, whereas it is manual with long interruptions.

In some countries, the term *transient interruption* is used for durations of a few seconds or less. The terminology used within IEEE is rather confusing, with different standards using different terms. In an important power-quality standard, IEEE 1159 [17.60], the following terms are used:

- Momentary interruption: up to 3 s
- Temporary interruption: between 3 s and 1 min
- Sustained interruption: longer than 1 min.

The standard that defines reliability indices, IEEE 1366 [17.59], defines a momentary interruption as an interruption with a duration up to 5 min. Interruptions lasting longer than 5 min are sustained interruptions. In most European countries, any interruption with a duration longer than 3 min is a long interruption; a duration lasting up to 3 min is a short interruption.

Following the IEC power-quality monitoring standard, IEC 61000-4-30 [17.17], an event should only be called an interruption when all three voltages are below the interruption threshold. An event with only one or two voltages below that threshold would be classed as either a voltage dip or an undervoltage. In regulation, an event might be considered as an interruption already when one of the voltages is below the threshold.



**Fig. 17.24** Correlation between number of long interruptions and number of short interruptions for about 100 000 low-voltage customers connected to a Swedish network operator

### Origins and Impacts

Short interruptions are a concern for industrial customers and for some domestic customers. The impact is in between the impact of a voltage dip and the impact of a long interruption.

The impact of a short interruption is in almost all cases less than the impact of a long interruption. Automatic (fast) restoration is thus generally an improvement compared to manual (or slow) restoration. Automatic reclosing is however combined typically with so-called *fuse-saving*. This combination results in a reduction of the number of long interruptions and an increase in the number of short interruptions. The total number of (short and long) interruptions increases, however. When the impact (economic consequences) of a short interruption is much less than for a long interruption, such a scheme is an improvement. When the impact is about similar, it is a deterioration. The latter is the case for many industrial installations. The appropriateness of such schemes has therefore been under discussion for many years.

### Standards and Regulation

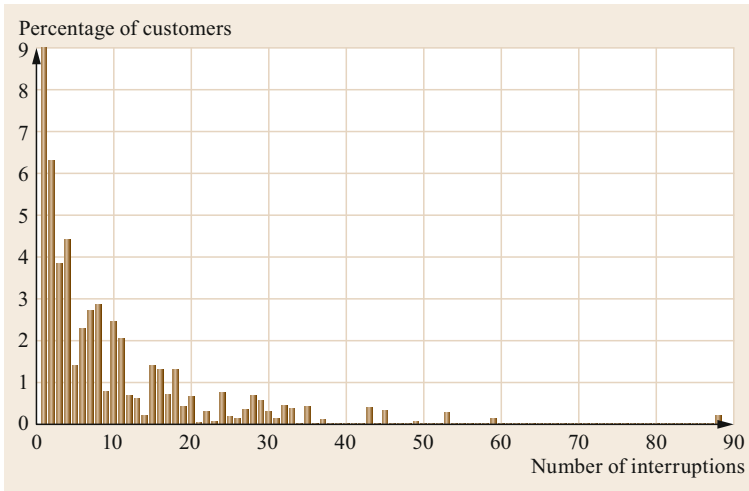
There are limited requirements in standards and regulation on the number and duration of short interruptions. Some countries require network operators to report the number of short interruptions. Like with long interruptions, statistics can be averages over all customers or data at the individual customer level. In Sweden, network operators have to provide data on the number of short and long interruptions for each individual customer. This data has been used in [17.61] to obtain the required density of monitoring to estimate high-order statistics.

Some further statistics are shown in Figs. 17.24 and 17.25. Both figures are based on the number of interruptions for about 100 000 individual customers with a network operator in the middle of Sweden. The former figure shows that there is very little correlation between the number of short interruptions and the number of long interruptions for individual customers. Regulation of long interruptions does thus not automatically result in a reduction of the number of short interruptions as well. Figure 17.25 shows that the number of short interruptions varies a lot between individual customers, even when they are in a limited geographical area (in this case, connected to the same network operator). The average number of short interruptions over all customers was 5.1 for that year. However, almost all customers experienced a different number, with some experiencing only one or two and some experiencing 10 or more short interruptions. The average number of short interruptions does not provide any information for the number of short interruptions experienced by an individual customer.

### Trends and Unresolved Issues

There is limited interest for short interruptions in regulation and in research. Short interruptions are mainly an issue for remote rural customers. The average number of short interruptions that customers experience is small, but some customers can experience several tens of them per year, which would be a serious issue for those customers. See [17.61] for a discussion of some statistics about short interruptions.

An unresolved issue is the impact of multiple short interruptions on equipment. There have been consistent



**Fig. 17.25** Density function of the number of interruptions for customers connected to a Swedish network operator

(mainly oral) reports of equipment damage due to the occurrence of two short interruptions briefly after each other, for example as part of a non-successful auto-reclosing sequence. There has never been a systematic study to find out if there is an increased probability of equipment damage because of a second short interruption.

A related issue is the impact of transient interruptions (with a duration of less than a few seconds) on equipment. Regulation on the number and duration of short interruptions could result in an increase in the number of transient interruptions. This could actually result in an increased impact on end-user equipment, especially in an increased number of cases where equipment is damaged.

### 17.3.5 Transients

#### Description and Characterization

Transients are large and sudden deviations from the ideal voltage lasting less than one cycle of the power-system frequency. The term *transients* covers a range of phenomena and several different classification schemes for transients have been introduced. None of these schemes has reached broad acceptance.

A list of possible characteristics for transients is given in an informative annex with IEC 61000-4-30 [17.17]. The standard does not give any definition or guidance on how to calculate the values of these indices. Although many power-quality monitors detect, record, and characterize transients, there is no commonly accepted standard method for this. A consequence of this is for example that there is limited data available on voltage transients. Another consequence is that the subject is not part of any regulatory document. This results

in no pressure or incentives to develop standard characterization methods.

#### Origins and Impacts

Three major types of transients can be distinguished, based on their origin:

- Normal switching transients, where capacitor energizing gives the most severe transient. Peak voltages during normal switching transients are up to about 180% of the nominal peak voltage (square root of two times the nominal RMS voltage). Higher peak voltages can occur when other capacitor banks are located nearby.
- Abnormal switching transients are associated with phenomena like pre-strike, restrike and current chopping. Oscillations of high amplitude and high frequency occur close to the element being switched. This is especially a concern for the switching elements and the subject of several books on switching transients [17.62–65]
- Lightning transients cause the highest voltage magnitudes, up to megavolts where the lightning strikes.

The impact of transients depends strongly on the kind of transient, in terms of duration, frequency, and magnitude. Switching transients are some concern for industrial customers. Transient overvoltages are a serious concern for low-voltage customers, especially those supplied from overhead distribution lines.

#### Standards and Regulation

A range of standards exists that define the testing of equipment against switching and lightning overvoltages, e.g., IEC 60060-1 [17.66].

### Trends and Unsolved Issues

The replacement of overhead transmission lines by underground cables will result in lower resonance frequencies of the transmission grid. Operational states with high amounts of renewable electricity production (and hence less conventional production connected to the transmission grid) will also result in lower resonance frequencies than traditionally occur.

The main unresolved issue is the lack of standards or commonly-accepted methods for characterizing transients.

### 17.3.6 Interharmonics

#### Description and Characterization

The term *interharmonics* refers to frequency components that are not an integer multiple of the power-system frequency, e.g., 170 Hz in a 50 Hz system.

#### Origins and Impacts

Sources of interharmonics include cyclo-converters and other frequency converters, arc furnaces, power electronic converters used for solar or wind power, etc. Mechanisms for the origin of interharmonics are often complicated, but the case of frequency conversion is well understood. When two systems with different operating frequencies are connected to each other, interharmonics can occur on both sides of the frequency converter.

In the case of wind power, conversion from the turbine-side frequency  $f_{in}$  to the power-system frequency  $f_{out}$  results in the generation of additional frequency components. The generated harmonics by a wind turbine with a 6-pulse rectifier on the turbine side together with a voltage source converter (VSC) on the grid side can be described by [17.67]

$$f = 6kf_{in} \pm (6n \pm 1)f_{out} \quad (17.12)$$

Table 17.3 shows the resulting frequency components for a selection of values of  $k$  and  $n$ .

As can be seen, the generated interharmonics will appear in pairs, which is exemplified in Fig. 17.26 and which was verified through measurements at the terminals of a wind-turbine transformer in [17.67]. The turbine-side frequency was varied, and the power-system frequency was kept constant at 50 Hz.

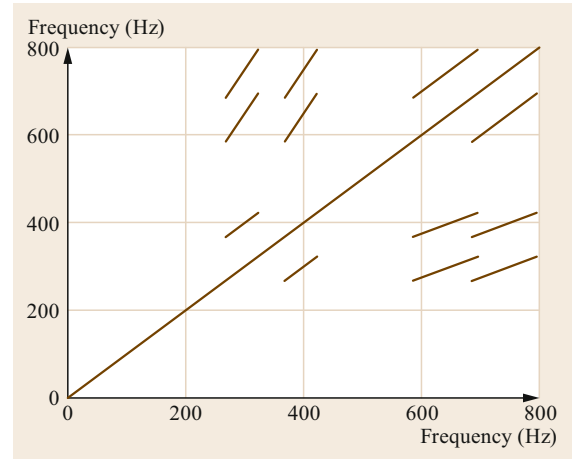
Several of the impacts of interharmonics are similar to those of harmonics, including e.g., additional heating of components. Other consequences include light flicker and interference with power-line communications.

#### Standards and Regulation

IEC 61000-4-7 [17.31] and IEC 61000-4-30 [17.17] define measurement instrumentation and methods for

**Table 17.3** Example of generated frequency components for  $k = 1, 2, 3$  and  $n = 0, 1$

	$n = 0$	$n = 1$	
$k = 1$	$6f_{in} \pm f_{out}$	$6f_{in} \pm 5f_{out}$	$6f_{in} \pm 7f_{out}$
$k = 2$	$12f_{in} \pm f_{out}$	$12f_{in} \pm 5f_{out}$	$12f_{in} \pm 7f_{out}$
$k = 3$	$18f_{in} \pm f_{out}$	$18f_{in} \pm 5f_{out}$	$18f_{in} \pm 7f_{out}$



**Fig. 17.26** Correlation between interharmonic frequencies

measuring interharmonics. A similar aggregation into groups and subgroups is defined for interharmonics as for harmonics.

With regards to standardization, there is no consensus on interharmonic limits. Some standards such as IEEE 519 [17.12] suggests interharmonic limits with the goal of preventing light flicker, but only in the range 0–120 Hz.

#### Trends and Unsolved Issues

While the traditional interharmonic sources are well understood, there is a lack of understanding of modern sources of interharmonics. Little is also known about existing levels of interharmonics, and it is unclear what levels would be acceptable.

There is ongoing research on light flicker in modern types of lighting, one potential cause being interharmonics above 100 or 120 Hz [17.68].

### 17.3.7 Supraharmonics

Supraharmonics refer to waveform distortion in the frequency range of 2–150 kHz.

#### Description and Characterization

Fig. 17.27 shows the current waveform of a modern television and Fig. 17.28 shows the corresponding current spectrum [17.69]. Emission can be seen up to around 70 kHz.

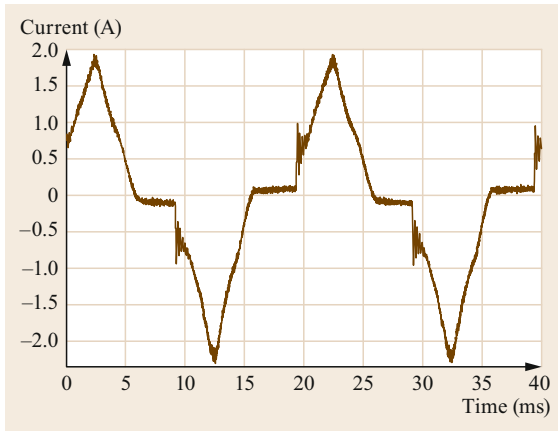


Fig. 17.27 Current waveform of a modern television

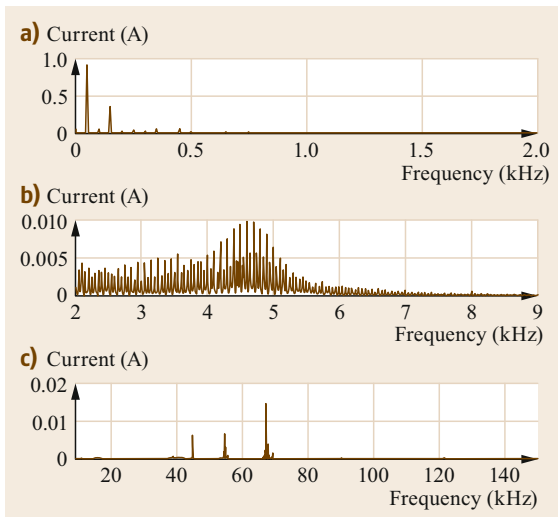


Fig. 17.28a–c Current spectrum of a modern television, showing harmonics (a), and supraharmonics (b,c)

### Origins and Impacts

The main sources of supraharmonics are power-electronic converters (active or passive) and transmitters used for power-line communication. Several studies have been done on emission from new types of equipment, including LED lamps, PV inverters and wind turbines [17.69–71]. It was found that while there is a reduction of low-order harmonics, there is instead emission at higher frequencies. It was further shown that a substantial amount of devices emit supraharmonics.

Similarly for harmonics, resonances play an important part in the propagation of supraharmonics. A well-known example concerns the Eagle-Pass HVDC light installation where 13–40% of the fundamental voltage could be seen at 12.4 kHz (approx. 10 times the switching frequency) due to resonance conditions [17.72]. The

propagation of supraharmonics has been studied e.g., in [17.73] and [17.74], where it was found that the current is mainly flowing between devices, rather than towards the grid.

Several cases of interference due to supraharmonics can be found in the literature, including e.g., [17.75]:

- Interference with power-line communication
- Interference with electrical equipment, such as light dimmers or medical equipment
- Audible noise

Many more cases have been reported informally that never appear in the technical literature.

### Standards and Regulation

While some standards exist already, EN 50065-1 [17.76] and IEC 61000-3-8 [17.77] for power-line communication, IEC 61000-2-2 [17.78] for compatibility levels, IEC 61000-4-19 [17.79] for certain immunity requirements, there is no accepted framework covering the entire supraharmonic range. Work is ongoing within the IEC, IEEE and CENELEC to develop standards, including limits, compatibility levels and test methods.

### Trends and Unsolved Issues

There are several gaps in the understanding of the origin and spread of supraharmonics, but due to needs for standardization and an increase in emission, the supraharmonic range has gained significant attention by researchers. One of the driving factors is that the supraharmonic range coincides with the frequencies used for power-line communication.

The impact of supraharmonics on equipment need to be studied further, and there is a need for models that are suitable for the supraharmonic range.

Measurements in the supraharmonic range are not trivial; they require measurement transducers and measurement equipment with a high accuracy for both amplitude and phase angle over a wide frequency range.

### 17.3.8 Slow Voltage Variations

Slow voltage variations are variations of the voltage magnitude on a time scale of minutes or longer. The term *supply voltage variations* is used in EN 50160 [17.10].

#### Description and Characterization

The most-common way of characterizing slow voltage variations is through the 10 min value as defined in IEC 61000-4-30 [17.17]. That standard however also allows for calculation over other period lengths (like 1 min) as well as the so-called *very-short value* over 150 or 180 cycles of the power-system frequency (about 3 s).

There is no standardized method to characterize slow voltage variations in a three-phase system, apart from characterizing them as three individual values. The most obvious approach would be to quantify the slow voltage variations by means of the positive-sequence voltage. Negative-sequence and zero-sequence voltage can be treated as part of the voltage unbalance (Sect. 17.3.10).

### Origin and Impact

Limiting slow voltage variations is an important part of the design of distribution networks, especially for rural distribution networks. In such networks, the voltage drop determines the maximum feeder length. Traditionally, the voltage drop during high load has been the main limitation.

The main impact of slow voltage variations is on equipment with low-voltage customers. The actual variations in voltage are normally not of concern. Instead, the concerns are high or low values of the supply voltage, referred to as *overvoltage* and *undervoltage*, respectively.

Both too low and too high voltages could result in equipment damage. Overvoltage could lead to reduced lifetime of equipment. Complaints about premature failure of incandescent lamps used to be a warning flag for the network operator that the voltage was too high. With most equipment it is not the high supply voltage (a high 10 min value) that makes the equipment fail. The high average value will make fast voltage variations and transients start from a higher voltage. These short duration overvoltages and transients result in a reduction in equipment lifetime.

High operating voltage at higher voltage levels (medium voltage or higher) will result in increased magnetizing current for transformers. This current has a high harmonic content, causing increased harmonic voltage distortion. This relation between high operating voltage and harmonic voltage distortion is one of the many relations between types of power-quality disturbances. The historical compartmentalization of power quality into different types of disturbances has limited the attention these relations attract [17.80].

Low supply voltage can result in mal-functioning of electronic equipment. It will also make equipment more susceptible to voltage dips. Some equipment, like many electrical motors, take a higher current when the voltage is lower. A sustained low voltage will thus result in a sustained high current, causing increased heating and reduced lifetime.

### Standards and Regulation

Limits on slow voltage variations are in place in many countries. The voltage characteristics in EN 50160

[17.10] are the base for power-quality regulation in most European countries and in several countries outside of Europe. According to EN 50160, the 10 min RMS value of the voltage shall be between 90 and 110% of the nominal voltage for at least 95% of the week. Beyond that, the voltage shall be between 90 and 115% of nominal all of the time. This holds for customers connected to the low-voltage network; other requirements hold for other voltage levels. The regulatory requirements in most European countries are stricter than this. Either the limits shall be kept for more than 95% of the time, or lesser deviations are allowed. Some examples for European countries are listed here:

- In Spain, the 10 min RMS voltage shall be between 93 and 107% of the nominal voltage for 95% of the week.
- In Hungary, the 10 min RMS voltage shall be between 92.5 and 107.5% of the nominal voltage for 95% of the week.
- In Norway, the 1 min RMS voltage shall be between 90 and 110% of the nominal voltage, all of the time.
- In Sweden, the 10 min RMS voltage shall be between 90 and 110% of the nominal voltage, all of the time.

There are no immunity standards setting requirements on equipment for long-term overvoltage or undervoltage. IEC 61000-4-14 [17.81] defines a set of tests for fast variations in voltage. Those variations come in three groups:

- Stepwise increase and decrease by 8 or 12% of nominal starting from the nominal voltage.
- Stepwise decrease by 8 or 12% starting from 110% of nominal
- Stepwise increase by 8 or 12% starting from 90% of nominal

The 12% steps are for equipment to be used in industrial environments (so-called class 3 environments). The voltage is constant for about 2 s, the increase or decrease takes about 100 ms, and a number of stepwise increases and decreases should be considered.

### Trends and Unsolved Issues

The hosting capacity [17.82, 83] is the amount of new production or consumption that can be connected to the grid without unacceptably deteriorating the reliability or power quality [17.84]. The voltage rise is commonly setting the limit for small-scale solar power. This has put slow voltage variations back on the agenda again.

The (expected) appearance of electric vehicle charging and electric heating makes slow voltage variations



of further importance. The classical solution against excessive slow voltage variations (i.e., overvoltage or undervoltage) has been to add more transformers and in that way reduce the feeder length. Many research teams study alternative methods, where curtailment of production and consumption appears the most effective one. Reactive-power control is also often mentioned as a solution, but in low-voltage networks, it is more likely to make the situation worse. For remote customers, the ones where voltage drop or rise becomes an issue first, the source impedance is mainly resistive. Injecting reactive power will not have much impact in the voltage drop or rise over the low-voltage cable or line, but instead will mainly impact the voltage on LV side of the distribution transformer. By mitigation, for example, for an overvoltage with one customer, an undervoltage is created for other customers.

For larger installations, connected to the medium-voltage network or for installations connected directly to the distribution transformer, reactive-power control may be a possible solution.

### 17.3.9 Fast Voltage Variations

Fast voltage variations are changes in voltage magnitude at time scales up to a few minutes.

#### Description and Characterization

The term *fast voltage variations* refers to variations in the RMS voltage that occur faster than slow voltage variations. Most of the attention is given to time scales up to a few seconds, the voltage variations that traditionally resulted in light flicker with incandescent lamps. This is also referred to as *voltage flicker* or (rather confusingly) simply *flicker*. The European standard EN 50160 [17.10] uses the term *rapid voltage changes*, which is not fully free of confusion either. Two types of rapid voltage changes are distinguished in the standard: *continuous rapid voltage changes* and *individual rapid voltage changes*. The latter ones are actually commonly referred to as simply *rapid voltage changes*.

#### Origins and Impacts

Fast variations in RMS voltage are mostly due to fast variations in current taken by installations. The kind of voltage variations that result in light flicker are mainly due to large industrial installations, like arc furnaces. Individual rapid voltage changes are due to tap-changer operations or switching of capacitor banks. In weak parts of the grid (like remote rural networks), load switching can also result in rapid voltage changes.

The main consequence of fast voltage variations is light flicker. Modern lamps are typically less sensitive to voltage variations than the classical incandescent

lamps, but some compact fluorescent or LED lamps are more sensitive than incandescent lamps [17.68].

#### Standards and Regulation

The standards and regulation on fast voltage variations are all based on the incandescent lamp. An eye-brain-lamp model has been developed that formed the base for the flickermeter in IEC 61000-4-15 [17.85]. The level of fast voltage variations is characterized using short-term and long-term flicker severity (Pst and Plt, respectively). Contrary to its name, this characteristic quantifies voltage variations, it does not quantify light flicker. However, for the voltage at the terminals of an incandescent lamp it is an indicator of light flicker as well. The definition of Pst and Plt is such that 1.0 is a natural limit in regulation and standards.

#### Trends and Unsolved Issues

The transition from incandescent lamps to LED lamps has resulted in an increased interest for light flicker and hence for fast voltage variations. One of the conclusions from the early work on that subject is that light flicker with LED lamps is much more complicated than with incandescent lamps. Not only fast voltage variations, but also other voltage disturbances, can result in light flicker.

Medium-timescale voltage variations (less than a few minutes, but more than a few seconds) are becoming important because variations in solar-power production occur on this timescale. There is however very little information on the existing levels of these variations [17.86, 87].

### 17.3.10 Voltage Unbalance

The term *voltage unbalance* refers to the situation in which the three voltages do not form a balanced three-phase system.

#### Description and Characterization

There are two fundamentally different ways to quantify voltage unbalance: through the negative-sequence voltage; or through the difference between the three RMS voltages.

The characterization method prescribed by IEC defines the voltage unbalance as the ratio between the negative-sequence and positive-sequence voltage. Like for slow voltage variations and harmonics, the basic measurement window is 10 or 12 cycles of the power-system frequency (in a 50 or 60 Hz system, respectively). These values are next aggregated into 10 min values.

Although not defined in any standard, the zero-sequence unbalance can be defined in an equivalent way.

In fact, this definition is used by some manufacturers of power-quality monitors.

The IEEE, next to the IEC definition, defines the unbalance as the relative difference between the highest and the lowest RMS voltage. See [17.88] for a comparison between the IEC and IEEE characterization methods.

### Origins and Impacts

Voltage unbalance is due to either unbalance in the grid or unbalance in equipment connected to the grid [17.89]. The latter is the one that gets most attention in the literature and in connection studies. Large single-phase loads (railway power supplies, certain furnaces in the steel industry) can cause a voltage unbalance over a wide geographical area. Smaller single-phase loads connected to weak parts of the grid, like in agricultural installations, can result in high unbalance locally.

The unbalance of the grid, non-transposed transmission lines, and transformers, do actually make a large contribution to the voltage unbalance as well. At transmission level, this contribution could be the dominating one.

In distribution networks with single-phase laterals, voltage unbalance can occur on the main feeder when the load is unevenly distributed over the laterals.

The negative-sequence voltage impacts three-phase equipment connected to the grid. The main studied impact is on directly connected rotating machines, both synchronous and induction machines. The negative-sequence voltage results in a high negative-sequence current through the machine. When the machine is lightly loaded, it can easily cope with the additional heat generated by the negative-sequence currents. However, the machine cannot operate at its rated power because it would get too hot. The motor or generator will have to be derated. This could be expensive for large industrial motors; the motor may have to be replaced by a motor of higher rating. For large synchronous machines, the solution is to reduce the produced power.

With three-phase converters, voltage unbalance also results in large current unbalance. This holds both for converters with active front-end and for diode rectifiers. The currents during voltage unbalance can become much higher than during balanced operation. This can result in damage to the diodes or in protection operations tripping the rectifier.

### Standards and Regulation

Limits on voltage unbalance are given in several national and international documents. Standardization and regulation for voltage unbalance is very similar to the standardization and regulation for harmonic voltages.

### Trends and Unsolved Issues

There is an increased interest in voltage unbalance because of the expected high penetration of single-phase PV installations [17.90] and electric vehicle charging.

An unsolved issue is the impact of high levels of voltage unbalance on the currents with three-phase converters. The impact on voltage-source converters is probably easy to formulate. The impact on three-phase diode rectifiers may turn out to be more complicated.

### 17.3.11 Frequency Variations

The ideal frequency in the power system is normally 50 or 60 Hz, the so-called nominal frequency. The frequency is however not constant and small variations occur due to unbalances between production and consumption of electrical energy. Frequency variations are very much a transmission system issue and frequency deviations are rarely so much that they have any effect on equipment connected to the grid.

#### Description and Characterization

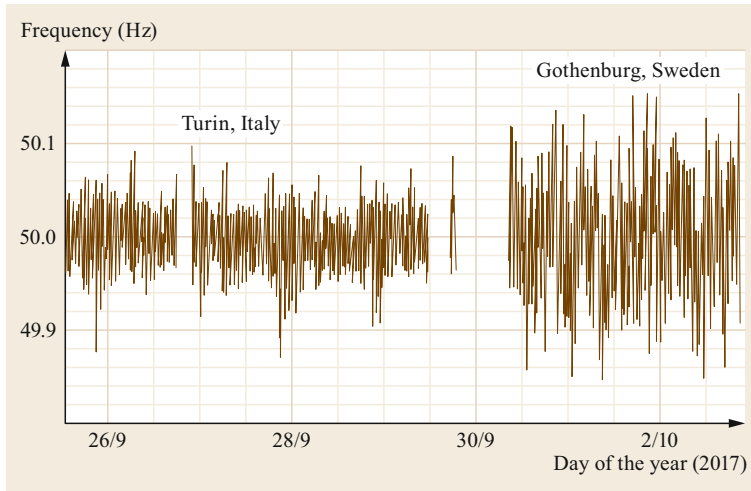
An example of frequency variations is shown in Fig. 17.29. The figure shows the variations in 10 s frequency values measured by a portable monitor during a period of slightly more than one week. During the first part of the measurement, the monitor was located to a wall-outlet in Turin, Italy, part of the central European interconnected grid. The second part of the measurement was done in Gothenburg, Sweden, part of the Northern European interconnected grid. Because the central European grid is much bigger, the frequency variations are smaller. This rule does not hold generally, as for example the frequency on the Swedish island of Gotland is more constant than on the Scandinavian mainland.

#### Standards and Regulation

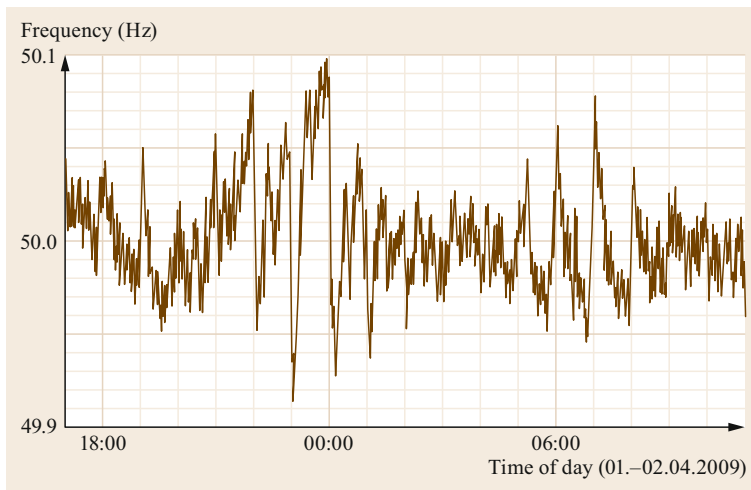
The frequency, at most locations in the world, rarely comes out of the range 49.5–50.5 Hz (or, 59.5–60.5 Hz in a 60 Hz system). The impact of frequency on equipment in that range can be neglected. During major events on the transmission system (like system splitting or island operation), the frequency may deviate more. Under-frequency load shedding or tripping on under/over frequency could result in installations being affected. One may argue on whether this is a power-quality or a system-operational issue, but the impact on end users is the same, nevertheless.

#### Trends and Unsolved Issues

With the predicted growth in island operation of microgrids, frequency variations may become a power-quality issue in the future. Recent studies in a single-house microgrid [17.91] have shown that the frequency



**Fig. 17.29** Frequency variations in the Central European interconnected grid (*left*) and in the Northern European Interconnected Grid (*right*). The measurements were performed using Metrum PQsmart



**Fig. 17.30** Fast frequency shifts measured in the central European interconnected system

in that microgrid regularly gets out of the band from 49 to 51 Hz. Further studies are needed on frequency variations in microgrids.

Deviations from the ideal frequency are normally described as a variation, but certain phenomena could better be described as events. Examples are the sudden

drop in frequency due to the disconnection of a large production unit (a well-known phenomenon) and the fast shifts in frequency that happen around the start of the hour due to the operation of the electricity markets (a generally unknown phenomenon). An example of the latter is shown in Fig. 17.30.

## 17.4 Power Quality in Microgrids

In recent years there has been a rising interest in microgrids, e.g., as alternatives to grid expansion in rural areas. Microgrids may be operated as grid-connected or as islands. When operated as grid-connected they behave, from a power-quality viewpoint, in the same way as other grid-connected installations. It is during island operation that large differences occur.

Microgrids typically contain a large share of power electronics, e.g., battery storage systems and PV, and generally have a larger system impedance compared to the centralized grid. This has led to concerns e.g., regarding voltage variations and distortion levels when in islanded operation. However, there is a lack of experience regarding power quality in existing microgrids

and while there are some recent publications on the subject [17.91–93], more research is needed. There is especially a lack of measurements of power quality in real-world microgrids during island operation.

Microgrids are also presented by several authors as a way of improving power quality, as any distur-

bances originating elsewhere in the grid are avoided during island operation. By properly switching between grid-connected and island operation, the optimal power quality can be selected [17.94, 95]. Even here, there is a lack of experience from real-world microgrids.

## 17.5 Conclusions

Power quality concerns the interaction between the electricity network and the customer (network user) or between the network and equipment connected to it. Power quality is a broad subject covering a wide range of phenomena, so called *power-quality disturbances*. Different types of phenomena affect different customers and often the network operator. Different types of disturbances require different analysis tools and different mitigation methods. An important distinction is the one between variations and events.

A large part of the power-quality field has become classical knowledge, where little new research is being done. Some of the new developments in electric power engineering, like solar power and LED lamps, have resulted in renewed interest in some power-quality disturbances. The other types of disturbances and the impact on more classical equipment require further research and knowledge gathering.

## References

- 17.1 R. Dugan, M.F. McGranaghan, H.W. Beaty, S. Santosa: *Electrical Power Systems Quality* (McGraw-Hill, New York 1996)
- 17.2 M.H.J. Bollen: *Understanding Power Quality Problems* (Wiley-IEEE, Piscataway 2000)
- 17.3 J. Arrillaga, N.R. Watson, S. Chen: *Power System Quality Assessment* (Wiley, Chichester 2000)
- 17.4 M.H.J. Bollen, I.Y.H. Gu: *Signal Processing of Power Quality Disturbances* (Wiley-IEEE, Piscataway 2006)
- 17.5 J.T. Duane: Dynamic converters for aerospace use, *Electr. Eng.* **81**(10), 776–783 (1962)
- 17.6 A. Kusko: Quality of Electric Power, *IEEE Trans. Ind. Gen. Appl.* **IGA-3**(6), 521–524 (1967)
- 17.7 L. Bell: Discussion, *Trans. Am. Ins. Elec. Eng.* **XVI**, 297–301 (1899)
- 17.8 CEER: 6th CEER benchmarking report on the quality of electricity and gas supply (CEER, Brussels 2016)
- 17.9 International Electrotechnical Commission: *Electropedia*, Definition 161-01-07, (IEC, Geneva 2007) <http://www.electropedia.org>
- 17.10 EN 50160:2010: Voltage characteristics of electricity supplied by public electricity networks
- 17.11 K. van Deemter: *Not Exactly: In Praise of Vagueness* (Oxford Univ. Press, Oxford 2010)
- 17.12 IEEE 519-2014: IEEE recommended practice and requirements for harmonic control in electric power systems (IEE, Piscataway 2014)
- 17.13 M.K. Walker: Electric utility flicker limitations, *IEEE Trans. Ind. Appl.* **IA-15**(6), 644–655 (1979)
- 17.14 IEC 61000-4-15:2010: Electromagnetic compatibility (EMC) – Part 4-15: Testing and measurement techniques – Flickermeter – Functional and design specifications (IEC, Geneva 2010)
- 17.15 L. Conrad, K. Little, C. Grigg: Predicting and preventing problems associated with remote fault-clearing voltage dips, *IEEE Trans. Ind. Appl.* **27**(1), 167–172 (1991)
- 17.16 N.H. Woodley, L. Morgan, A. Sundaram: Experience with an inverter-based dynamic voltage restorer, *IEEE Trans. Power Deliv.* **14**(3), 1181–1186 (1999)
- 17.17 IEC 61000-4-30:2015: Electromagnetic compatibility (EMC) – Part 4-30: Testing and measurement techniques – Power quality measurement methods (IEC, Geneva 2010)
- 17.18 N.R. Watson, T.L. Scott, S.J.J. Hirsch: Implications for distribution networks of high penetration of compact fluorescent lamps, *IEEE Trans. Power Deliv.* **24**(3), 1521–1528 (2009)
- 17.19 S.K. Rönnberg, M.H.J. Bollen, M. Wahlberg: Harmonic emission before and after changing to LED and CFL—Part I: Laboratory measurements for a domestic customer. In: *Proc. 14th Int. Conf. Harmon. Qual. Power* (ICHQP, Bergamo 2010)
- 17.20 S.K. Rönnberg, M. Wahlberg, M.H.J. Bollen: Harmonic emission before and after changing to LED and CFL—Part II: Field measurements for a hotel. In: *Proc. 14th Int. Conf. Harmon. Qual. Power* (ICHQP, Bergamo 2010), <https://doi.org/10.1109/ICHQP.2010.5625413>
- 17.21 S.K. Rönnberg, M. Wahlberg, M.H.J. Bollen: Harmonic emission before and after changing to LED lamps—Field measurements for an urban area. In: *Proc. 2012 IEEE 15th Int. Conf. Harmon. Qual. Power* (ICHQP, Hong Kong 2012) pp. 552–557

- 17.22 J. Lundquist: On harmonic distortion in power systems, Licentiate of Engineering Thesis (Chalmers University of Technology, Gothenburg 2001)
- 17.23 M. Bollen, K. Yang: Harmonics – another aspect of the interaction between wind-power installations and the grid. In: *Proc. Int. Conf. Electr. Distrib (CIRED, Stockholm 2013)*
- 17.24 J. Arrillaga, D.A. Bradley, P.S. Bodger: *Power System Harmonics* (Wiley, Chichester 1985)
- 17.25 A. Mansoor, W.M. Grady, P.T. Staats, R.S. Thallam, M.T. Doyle, M.J. Samotyj: Predicting the net harmonic currents produced by large numbers of distributed single-phase computer loads, *IEEE Trans. Power Deliv.* **10**(4), 2001–2006 (1995)
- 17.26 S. Sakar, S. Rönnberg, M. Bollen: Interferences in AC-DC LED drivers exposed to voltage disturbances in the frequency range 2 kHz–150 kHz, *IEEE Trans. Power Electron.* (2019), <https://doi.org/10.1109/tpele.2019.2899176>
- 17.27 CIGRE TB 766: CIGRE JWG B4/C4.38, Network modeling for harmonic studies (CIGRE, Paris 2019)
- 17.28 D. Schwanz: On transfer functions for power quality studies in wind power and solar PV plants, Ph.D. Thesis (Luleå University of Technology, Skellefteå 2019)
- 17.29 T. Busatto, A. Larsson, S.K. Rönnberg, M.H.J. Bollen: Including uncertainties from customer connections in calculating low-voltage harmonic impedance, *IEEE Trans. Power Deliv.* **32**(2), 606–615 (2019)
- 17.30 J.C. Das: *Power System Harmonics and Passive Filter Designs* (Wiley-IEEE, Piscataway 2015)
- 17.31 IEC 61000-4-7: Electromagnetic compatibility (EMC) – Part 4-7: Testing and measurement techniques – General guide on harmonics and interharmonics measurements and instrumentation, for power supply systems and equipment connected thereto (IEC, Geneva 2010)
- 17.32 IEC TR 61869-103: Instrument transformers – The use of instrument transformers for power quality measurement (IEC, Geneva 2010)
- 17.33 J. Arrillaga, N.R. Watson: *Power System Harmonics* (Wiley, Chichester 2004)
- 17.34 IEC 61000-3-2: Electromagnetic compatibility (EMC) – Part 3-2: Limits – Limits for harmonic current emissions (equipment input current  $\leq 16$  A per phase) (IEC, Geneva 2010)
- 17.35 IEC 61000-2-4: Electromagnetic compatibility (EMC) – Part 2-4: Environment – Compatibility levels in industrial plants for low-frequency conducted disturbances (IEC, Geneva 2010)
- 17.36 IEEE 1564-2014: IEEE Guide for Voltage Sag Indices (IEEE, Piscataway 2014)
- 17.37 M.H.J. Bollen: Characterisation of voltage sags experienced by three-phase adjustable-speed drives, *IEEE Trans. Power Deliv.* **12**(4), 1666–1671 (1997)
- 17.38 Y. Wang, M.H.J. Bollen, X.-Y. Xiao: Calculation of the phase-angle-jump for voltage dips in three-phase systems, *IEEE Trans. Power Deliv.* **30**(1), 480–487 (2015)
- 17.39 H.-S. Song, K. Nam: Instantaneous phase-angle estimation algorithm under unbalanced voltage-sag conditions, *IEE Proc. Generat. Transm. Distrib.* **147**(6), 409–415 (2000)
- 17.40 S.Ž. Djokić, J.V. Milanović, S.M. Rowland: Advanced voltage sag characterisation II: point on wave, *IEE Trans. Generat. Transm. Distrib.* **1**(1), 146–154 (2007)
- 17.41 M.H.J. Bollen: Voltage recovery after unbalanced and balanced voltage dips in three-phase systems, *IEEE Trans. Power Deliv.* **18**(4), 1376–1381 (2003)
- 17.42 IEC 61000-4-11:2004: Electromagnetic compatibility (EMC) – Part 4-11: Testing and measurement techniques – Voltage dips, short interruptions and voltage variations immunity tests (IEC, Geneva 2010)
- 17.43 IEC 61000-4-34:2005: Electromagnetic compatibility (EMC) – Part 4-34: Testing and measurement techniques – Voltage dips, short interruptions and voltage variations immunity tests for equipment with mains current more than 16 A per phase (IEC, Geneva 2010)
- 17.44 IEEE 1668-2014: IEEE Trial-use recommended practice for voltage sag and short interruption ride-through testing for end-use electrical equipment rated less than 1000 V (IEEE, Piscataway 2014)
- 17.45 IEC 61800-3:2017: Adjustable speed electrical power drive systems – Part 3: EMC requirements and specific test methods (IEC, Geneva 2010)
- 17.46 IEC 61000-6-1:2016: Electromagnetic compatibility (EMC) – Part 6-1: Generic standards – Immunity standard for residential, commercial and light-industrial environments (IEC, Geneva 2010)
- 17.47 IEC 61000-6-2:2016: Electromagnetic compatibility (EMC) – Part 6-2: Generic standards – Immunity standard for industrial environments (IEC, Geneva 2010)
- 17.48 CIGRE TB 412: CIGRE/CIRED/UIE JWG C4.110, Voltage dip immunity of equipment and installations (CIGRE, Paris 2010)
- 17.49 CEER: 5th CEER benchmarking report on the quality of electricity supply (CEER, Brussels 2012)
- 17.50 D. Xiang, L. Ran, P.J. Tavner, S. Yang: Control of a doubly fed induction generator in a wind turbine during grid fault ride-through, *IEEE Trans. Energy Convers.* **21**(3), 652–662 (2006)
- 17.51 C. Wessels, F. Gebhardt, F.W. Fuchs: Fault ride-through of a DFIG wind turbine using a dynamic voltage restorer during symmetrical and asymmetrical grid faults, *IEEE Trans. Power Electron.* **26**(3), 807–815 (2011)
- 17.52 M. Mirhosseini, J. Pou, V.G. Agelidis: Single- and two-stage inverter-based grid-connected photovoltaic power plants with ride-through capability under grid faults, *IEEE Trans. Sustain. Energy* **6**(3), 1150–1159 (2015)
- 17.53 A.F. Bastos, K.W. Lao, G. Todeschini, S. Santoso: Accurate identification of point-on-wave inception and recovery instants of voltage sags and swells, *IEEE Trans. Power Deliv.* **34**(2), 551–560 (2018)
- 17.54 A. Bagheri, I. Gu, M. Bollen, E. Balouji: A robust transform-domain deep Convolutional network for voltage dip classification, *IEEE Trans. Power Deliv.* **33**(6), 2794–2802 (2018)

- 17.55 M.H. Xivambu: Impact of floating neutral in distribution systems. In: *Proc. Int. Conf. Electr. Distrib.* (CIRED, Vienna 2007)
- 17.56 R. Billinton, R. Allan: *Reliability Evaluation of Electric Power Systems* (Springer, New York 2013)
- 17.57 R.E. Brown: *Electric Power Distribution Reliability* (CRC, Boca Raton 2008)
- 17.58 A. Chowdhury, D. Koval: *Power Distribution System Reliability – Practical Methods and Applications* (Wiley-IEEE, Piscataway 2009)
- 17.59 IEEE 1366–2012: IEEE Guide for electric power distribution reliability indices (IEE, Piscataway 2014)
- 17.60 IEEE 1159–2009: IEEE Recommended practice for monitoring electric power quality (IEE, Piscataway 2014)
- 17.61 S.K. Rönnerberg, M.H.J. Bollen: Estimating system indices for short interruptions from data obtained by a limited number of monitors, *Electr. Power Syst. Res.* **146**, 63–70 (2017)
- 17.62 A. Greenwood: *Electrical Transients in Power Systems* (Wiley, Chichester 1991)
- 17.63 L. van der Sluis: *Transients in Power Systems* (Wiley, Chichester 2001)
- 17.64 R. Smeets, L. van der Sluis, M. Kapetanonic, D. Peelo, A. Janssen: *Switching in Electrical Transmission and Distribution Systems* (Wiley, Chichester 2014)
- 17.65 R. Rudenberg: *Transient Performance of Electric Power Systems: Phenomena in Lumped Networks* (MIT Press, Cambridge 1969)
- 17.66 IEC 60060–1: High-voltage test techniques – Part 1: General definitions and test requirements (IEC, Geneva 2010)
- 17.67 K. Yang, M.H.J. Bollen: Interharmonic currents from a type-IV wind energy conversion system, *Electr. Power Syst. Res.* **143**, 357–364 (2017)
- 17.68 A. Gil de Castro, S. Rönnerberg, M. Bollen: Light intensity variation (flicker) and harmonic emission related to LED lamps, *Electr. Power Syst. Res.* **146**, 107–114 (2017)
- 17.69 S. Rönnerberg: Emission and interaction from domestic installations in the low voltage electricity network, up to 150 kHz, Ph.D. Thesis (Luleå University of Technology, Skellefteå 2013)
- 17.70 A. Varatharajan, S. Schoettke, J. Meyer, A. Abart: Harmonic emission of large PV installations – case study of a 1 MW solar campus. In: *Proc. Int. Conf. Renewable Energy and Power Quality* (ICREPQ, Córdoba 2014)
- 17.71 N. Uribe-Pérez, I. Angulo, L. Hernández-Callejo, T. Arzuaga, D. de la Vega, A. Arrinda: Study of unwanted emissions in the CENELEC-A band generated by distributed energy resources and their influence over narrow band power line communications, *Energies* **9**(12), 1007 (2016)
- 17.72 L. Paulsson, B. Ekehov, S. Halen, T. Larsson, L. Palmqvist, A.-A. Edris, D. Kidd, A.J.F. Keri, B. Mehraban: High-frequency impacts in a converter-based back-to-back tie; the eagle pass installation, *IEEE Trans. Power Deliv.* **18**(4), 1410–1415 (2003)
- 17.73 S. Rönnerberg, A. Larsson, M. Bollen, J. Schanen: A simple model for interaction between equipment at a frequency of some tens of kHz. In: *Proc. 21st Int. Conf. Electr. Distrib.* (CIRED, Frankfurt 2011)
- 17.74 A. Larsson, M. Bollen: Measurement result from 1 to 48 fluorescent lamps in the frequency range 2 to 150 kHz. In: *Proc. 14th Int. Conf. Harmon. Qual. Power* (ICHQP, Bergamo 2010), <https://doi.org/10.1109/ICHQP.2010.5625395>
- 17.75 S.K. Rönnerberg, M.H.J. Bollen, H. Amaris, G.W. Chang, I.Y.H. Gu, L.H. Kocewiak, J. Meyer, M. Olofsson, P.F. Ribeiro, J. Desmet: On waveform distortion in the frequency range of 2 kHz–150 kHz – Review and research challenges, *Electr. Power Syst. Res.* **150**, 1–10 (2017)
- 17.76 EN 50065–1: Signalling on low-voltage electrical installations in the frequency range 3 kHz to 148,5 kHz – Part 1: General requirements, frequency bands and electromagnetic disturbances
- 17.77 IEC 61000–3–8: Electromagnetic compatibility (EMC) – Part 3: Limits – Section 8: Signaling on low-voltage electrical installations – Emission levels, frequency bands and electromagnetic disturbance levels (IEC, Geneva 2010)
- 17.78 IEC 61000–2–2/AMD2:2018: Electromagnetic compatibility (EMC) – Environment – Compatibility levels for low-frequency conducted disturbances and signaling in public low-voltage power supply systems (IEC, Geneva 2010)
- 17.79 IEC 61000–4–19: Electromagnetic compatibility (EMC) – Part 4–19: Testing and measurement techniques – Test for immunity to conducted, differential mode disturbances and signaling in the frequency range 2 kHz to 150 kHz at A.C. power ports (IEC, Geneva 2010)
- 17.80 M.H.J. Bollen, P. Ribeiro, I.Y.H. Gu, C.A. Duque: Trends, challenges and opportunities in power quality research, *Int. Trans. Electr. Energy Systems* **20**(1), 3–18 (2010)
- 17.81 IEC 61000–4–14:1999: Electromagnetic compatibility (EMC) – Part 4–14: Testing and measurement techniques – voltage fluctuation immunity test (IEC, Geneva 2010)
- 17.82 M. Rylander, J. Smith, W. Sunderman: Streamlined method for determining distribution system hosting capacity, *IEEE Trans. Ind. Appl.* **51**(1), 105–111 (2016)
- 17.83 CIGRE TB 672: CIGRE JWG C4/C6.29, Power quality aspects of solar power (CIGRE, Paris 2016).
- 17.84 M.H.J. Bollen, F. Hassan: *Integration of Distributed Generation in the Power System* (Wiley, Chichester 2011)
- 17.85 UIEPQ–9715: Guide to quality of electricity supply for industrial installations, Part 5. Flicker and voltage fluctuations (UIE 1999)
- 17.86 M.H.J. Bollen, M. Häger, C. Schwaegerl: Quantifying voltage variations on a time scale between 3 seconds and 10 minutes. In: *Proc. 18th Int. Conf. Exhib. Electr. Distrib.* (CIRED, Turin 2005) pp. 1–5
- 17.87 M.H.J. Bollen, I.Y.H. Gu: Characterization of voltage variations in the very-short time-scale, *IEEE Trans. Power Deliv.* **20**(2), 1198–1199 (2005)

- 17.88 M.H.J. Bollen: Definitions of voltage unbalance, IEEE Power Eng. Review **22**(11), 49–50 (2002)
- 17.89 A. von Jouanne, B. Banerjee: Assessment of voltage unbalance, IEEE Trans. Power Deliv. **16**(4), 782–790 (2001)
- 17.90 D. Schwanz, F. Möller, S.K. Rönnerberg, J. Meyer, M.H.J. Bollen: Stochastic assessment of voltage unbalance due to single-phase-connected solar power, IEEE Trans. Power Deliv. **32**(2), 852–861 (2017)
- 17.91 J. Nömm, S.K. Rönnerberg, M.H.J. Bollen: An analysis of frequency variations and its implications on connected equipment for a nanogrid during islanded operation, Energies **11**(9), 2456 (2018)
- 17.92 S. Rönnerberg, M. Bollen, J. Nömm: Power quality measurements in a single-house microgrid. In: *Proc. 24th Int. Conf. Exhib. Electr. Distrib.* (CIRED, Glasgow 2017), <https://doi.org/10.1049/oap-cired.2017.0240>
- 17.93 J. Nömm, S. Rönnerberg, M. Bollen: An analysis of voltage quality in a nanogrid during islanded operation, Energies **12**(4), 614 (2019)
- 17.94 B. Lasseter: Microgrids (distributed power generation). In: *Proc. 2001 IEEE Power Eng. Society Winter Meeting* (IEEE, Columbus 2001) pp. 146–149
- 17.95 J.M. Guerrero, P.C. Loh, T. Lee, M. Chandorkar: Advanced control architectures for intelligent microgrids—Part II: power quality, energy storage, and AC/DC microgrids, IEEE Trans. Ind. Electron. **60**(4), 1263–1270 (2013)

### Oscar Lennerhag

Independent Insulation Group  
Ludvika, Sweden  
[oscar@i2group.se](mailto:oscar@i2group.se)



Oscar Lennerhag received his M.Sc. from Chalmers University of Technology in 2013. He is working for the Independent Insulation Group, Ludvika, Sweden, and as a PhD student at the Luleå University of Technology, Skellefteå, Sweden. He has published several papers on power quality and is involved in several CIGRE working groups within the topics of harmonic analysis and transient overvoltages.

### Math Bollen

Luleå University of Technology  
Skellefteå, Sweden  
[math.bollen@ltu.se](mailto:math.bollen@ltu.se)



Math Bollen is a professor of electric power engineering at Luleå University of Technology, Skellefteå, Sweden. He is a leading researcher on power quality, with extensive experience on a range of subjects, both in academia and industry. Math Bollen has worked for the Swedish energy regulator as a consultant, and at universities in Sweden, the United Kingdom and the Netherlands.

# 18. Electricity Markets and Regulation

Philip Southwell, Gregory H. Thorpe, Alex Cruickshank, Colin Ray

The reliability and cost of electricity is critical to the success of modern economies. Infrastructure needed to provide the desired services requires large amounts of capital expenditure and governments are keen to ensure prices are kept to a minimum while maintaining the required reliability. To this end, electricity markets have been introduced to allow electricity generating and retailing companies to compete. At the same time regulations have been put in place to minimize anticompetitive activities and ensure that any monopoly services are charged at fair and reasonable rates.

This chapter explores the design and operation of electricity markets and regulation in relation to power systems. It briefly considers the evolution of the electricity industry and provides a general description of the range of market models used and the associated regulation applied to assist their efficient operation. Practical examples from various countries around the world are also provided.

18.1	<b>Electricity Industry Structure</b>	1207	18.4.6	Retail Competition	1214
18.2	<b>Industry Organization</b>	1208	18.4.7	Market for Transmission Expansion	1214
18.3	<b>Electricity Markets</b>	1209	18.5	<b>Market Structures Around the World</b>	1215
18.3.1	Supply and Demand	1209	18.5.1	Europe	1215
18.3.2	The Role of Markets	1210	18.5.2	Australia	1218
18.4	<b>Market Models</b>	1211	18.5.3	North America	1221
18.4.1	Vertically Integrated Utility	1211	18.5.4	Brazil Market Overview	1224
18.4.2	Vertically and Horizontally Disaggregated Utility with only Utility Plant Connected	1211	18.6	<b>Regulation</b>	1224
18.4.3	Competitive Market at Time of Investment Only	1212	18.6.1	Electricity as an Essential Service	1224
18.4.4	Separate Capacity Management Combined with Central Dispatch of Energy	1213	18.6.2	Vertical Integration and Disaggregation	1225
18.4.5	Energy-Only Markets	1213	18.6.3	Transmission and Distribution as Natural Monopolies	1225
			18.6.4	Economic Regulation of Monopolies	1225
			18.6.5	Rate of Return Regulation	1226
			18.6.6	Price Control	1226
			18.6.7	Revenue Determination	1226
			18.6.8	Revenue Cap	1226
			18.6.9	Price Cap	1226
			18.6.10	Pricing Methods	1227
			18.6.11	Performance Reporting	1228
			18.6.12	Regulated Versus Non-Regulated Services	1229
			18.6.13	Treatment of Losses	1229
			18.6.14	Metering/Smart Meters	1230
			18.6.15	Technical Regulation	1230
			18.6.16	Technical Rules	1231
			18.6.17	Service Standards	1232
			18.6.18	Environmental Regulation	1232
			18.6.19	Climate Change	1232
			18.6.20	Energy Efficiency	1232
			18.6.21	Visual Impact	1233
			18.7	<b>Regulation Models Around the World</b>	1233
			18.7.1	United States	1234
			18.7.2	Great Britain	1234
			18.7.3	Australia	1235
			18.7.4	Nordic Countries	1236
			18.8	<b>Conclusion</b>	1236
			<b>References</b>		1237

The design and application of the various market models continues to evolve and it is recommended that the reader access current information to stay aware of the

latest developments. A useful source is work by Study Committee C5, which can be found at the e-cigre web site (<https://e-cigre.org>). Other sites include those that



have a regulatory or government sponsored oversight of the operations of the parties. Examples include Ofgem in the UK (<https://www.ofgem.gov.uk/about-us/who-we-are/gas-and-electricity-markets-authority>), ENTSOE in Europe (<https://www.entsoe.eu>), AEMC in Australia (<https://www.aemc.gov.au>) and FERC in the US (<https://www.ferc.gov/market-oversight/market-oversight.asp>).

One area that is in its infancy at the time of writing relates to developments such as micro-grids with distributed generation, battery storage and smart load control. These are now becoming viable and are likely to operate both as local micro-markets and as participants in the larger markets.

This chapter addresses the design and operation of markets and regulation in relation to power systems. The discussion will cover the topic at a reasonably high level and provide references where appropriate to a more detailed examination.

There are many texts that can provide a detailed description of markets, their structure and their benefits and failings. It is however useful to give a brief overview in order to set the context for a discussion of electricity markets.

Any mechanism that brings buyers and sellers together to trade by establishing prices for a quantity of product or service is a market. The concept of trading has been around since very early civilization. Trading can occur by direct negotiation between a seller and a buyer or an organized market where buyers and sellers compete to achieve a trade that produces the best commercial return.

Markets are beneficial when the competitive pressures on the players lead to higher efficiency than the alternative (e.g., a central utility) but only if the costs of running the market are less than the benefits gained. Markets need to be *workably competitive* to deliver value. When there is a risk of inefficient outcomes because of insufficient competition leading to the exercise of market power, regulators or governments often apply rules or place limits on commercial behaviors. It is always a difficult trade-off between rules to limit market behaviors and the reduced efficiency that can result. However, potentially distorted outcomes are better than allowing excessive market power. One way to achieve this balance is to limit the periods or conditions where one or more players can dominate but allow sufficient time to signal an opportunity for new investment. An often forgotten aspect of market power is that it can either raise or lower prices. For example, a strong player can force prices down until its competitors are forced out of the market. This enhances the market power of the strong player who is then free to raise prices.

Throughout history there have been examples of market failure. In recent times, the sub prime mortgage disaster that led to the global financial crisis and the collapse of Lehmann Brothers in the US are good examples [18.1]. An example related to electricity is the California market in the US where, amongst other things, market failure led to widespread interruptions to supply, bankruptcy of Enron and near bankruptcy of other utilities. This is discussed in more detail in the section on North America.

In some cases, a product or service can be a natural monopoly. For example, electricity network infrastructure can be viewed as a monopoly as it is normally difficult to duplicate. This is because of economic and environmental barriers for construction of a second transmission line in competition with an existing one. In these situations, prices, behaviors and service levels are often regulated, or otherwise managed. An industry regulator is often charged with overseeing the activities of monopolies but other solutions are also used such as by the auctioning of a license to build and operate the network infrastructure, as is done in Brazil.

Regulation often appears in conjunction with competitive arrangements in order to ensure some level of protection for the participants in the market. Electricity has been subjected to some form of regulation for many years, particularly in relation to transmission and distribution. This has included regulation of customer tariffs, monitoring and approval of expenditure and, various aspects of technical and safety performance.

In order to minimize conflicts of interest, transmission and distribution systems are often separated from generation and retailing. However, many arrangements have also evolved where distribution and retailing are combined, or remain combined when a previously vertically integrated utility is disaggregated. In these systems regulators often require the commercial arrangements to be ring-fenced from each other.

Third party access to transmission and distribution is central to competitive electricity markets. Access involves a set of rights and obligations that allow new entrants to connect to the network in order to compete. Over the last 30 years, access and market or competition-oriented reforms have been introduced to the electricity sector in many countries.

This chapter examines the foundations of the electricity industry and how competitive markets can enhance its economic efficiency and therefore assist in minimizing costs to end users. The chapter introduces a number of the different forms of electricity trading that have emerged as the industry has matured technically and economically. The description starts by very briefly tracing the evolution of the industry from a small

disaggregated service through to a large central commodity and most recently back towards a more disaggregated, market-oriented industry driven by dramatic changes in technology and cost. Current electricity markets have evolved around larger power systems and the discussion that follows will mainly focus on these. Developments such as microgrids with distributed generation, battery storage and smart load control are now becoming viable and it is likely that these systems will

participate in the larger markets and internal *micro-markets* will develop within the microgrids. A number of examples of markets that have been implemented across the world are briefly described, together with some particular challenges that have been faced as they have evolved. The second half of the chapter focuses on key aspects of regulation of electricity businesses, together with a high level description of the regulation implemented in a number of countries.

## 18.1 Electricity Industry Structure

Electricity has two challenging characteristics. Firstly there must be equilibrium between the quantity dispatched and that consumed by loads and storage mediums at any instant (net of losses incurred in transport across networks). Until recently the only loads that were material were those of end use customers, including relatively inflexible hydro pumped storage, and this required flexible generation facilities to track variations in customer load. More recently, large flexible chemical storage technology has emerged. As the following sections will explain, the development of flexible storage is reducing the need for flexible generation and also counteracting the introduction of intermittent generation technology. Secondly the laws of physics govern the physical operation of the power system and these determine the path electricity will flow, rather than any commercial or regulated mechanism.

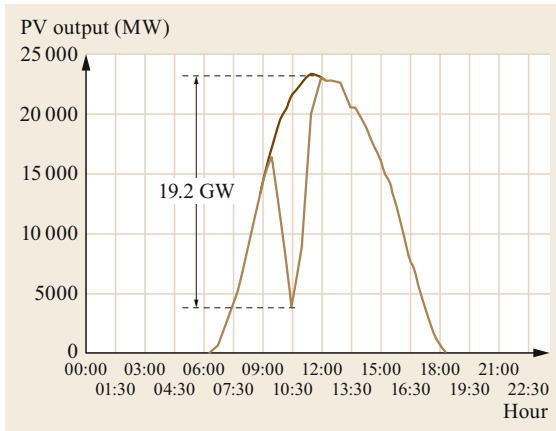
Power systems are the interconnection of a number of generators and end users located over a wide area. The earliest power systems from the late 1800s and into the first half of the twentieth century were township systems with local generation. Over time the systems of separate townships were linked together to share costs with generation distributed across the townships and eventually connecting very large areas. In the second half of the twentieth century as the size of the consumer demand grew, larger and larger generators were built. Eventually most of the township generation was retired leading to the era of central generation. This development led to industry structures based on specific functions for generation, transmission, distribution and the interface with end consumers (retailing).

From the late twentieth century the cost of small and distributed generation fell dramatically reducing the benefits of scale and leading to a shift in the mix of generation back towards a combination of central and distributed generation. Much of the distributed generation of today utilizes wind and solar-photovoltaic (PV) technologies, which also bring benefits of low

emissions of carbon dioxide. This shift is blurring the distinction between generation, transmission, distribution and retailing. For example, individual consumers may now host solar-PV on their household rooftop and export to their neighbors via the distribution network. Retailers may facilitate this transfer or simply be bypassed.

The newer technologies have different technical characteristics. Wind, solar-PV, wave and tidal generation technologies are generally non-synchronous in that they are usually connected via power electronics in contrast with spinning AC machines that are directly connected. They exhibit low (or no) inertia, which is important as this affects the rate at which power system frequency can deviate from the level needed for the power system to remain stable. Where the percentage of this form of generation is significant, it can change the dynamic performance of power systems. In some power systems, this shift is already requiring a major change in their operation. For example, where previously high fault currents due to short circuits may have restricted operation, the newer technologies create fault currents that may be too low to be detected by existing protection equipment.

Sitting between pure supply and pure consumption, large scale battery storage technology is reshaping the operation of power systems. Hydro pumped storage along with limited numbers of flywheels and compressed air energy storage have been in use for many years but limited by cost or suitable location. Recent technological developments and lower costs of chemical battery storage are allowing deployment of storage devices across the entire supply chain. Batteries are being installed in conjunction with intermittent technologies connected to major transmission facilities and *behind the meter* in households to better match the requirements of end customer demand. Storage devices such as batteries or flywheels can also counteract the effects of low inertia from other new technologies. While the cost and performance of batteries are constantly im-



**Fig. 18.1** Impact of solar eclipse on PV generation in Germany, 20.03.2015. (reprinted by permission, © Amprion)

proving, they are currently more suitable for short term back up which allows time for longer-term support such as gas turbines or hydro storage to be brought into service.

Rooftop solar-PV, micro-generators and some small wind farms are typical examples of small generators, embedded in the distribution system. As the development of these technologies grows quite rapidly around the world, their effect is becoming more pronounced. For example, large-scale application of rooftop solar-PV may reduce the power flows from higher voltage levels of the system at a particular substation to zero. It could even result in power flows from lower to higher voltage levels of the system at the substation. Power flows can also swing dramatically as intermittent clouds appear and screen the PV cells. While, in parts of the world the majority of current rooftop solar-PVs are not yet metered, recent technological innovations in measurement, communications and trading, including through the application of block-chain concepts, are resulting in these widely distributed resources being more closely monitored and controlled. This also makes possible *peer to peer* trading arrangements with potentially strong effects on the physical and commercial operation of the broader system and any market operating on it.

## 18.2 Industry Organization

While the physics of the electricity supply process is the same everywhere, there are many ways the industry can be organized commercially and functionally.

Historically, the dominant organizational model was a utility that owned all elements of the supply chain

An extreme example of the variability of solar can be seen from the impact of the solar eclipse that occurred in Europe in March 2015.

At the time of the eclipse the installed solar-PV capacity in the Continental European synchronous system was approximately 89 GW, and the potential solar-PV reduction was expected to be as high as 34 GW. The effect in Germany is shown in Fig. 18.1. The gradient of the steep ramp that shows the sudden loss of solar-PV generation was estimated to be 2–4 times higher than normal daily ramping, while the short morning peak caused a significant increase in demand for flexible power plants. While the actual reduction in solar-PV output was lower on the day (19.2 GW), due to more than expected cloud cover, there was still a substantial change. The event was anticipated, however, and adequate reserves were scheduled, ensuring there was no risk to power system security. The key points are that there needs to be adequate back up to cover the significant loss of generation that can occur and the solar event may cause a much more rapid ramp rate than would normally occur.

Utilities in the US also undertook contingency planning and scheduled additional generation for the solar eclipse in the US in August 2017. However, it had a fairly minimal impact, partly due to the lower than expected temperatures and some cloud cover [18.2].

Large-scale wind and solar-PV farms have also been constructed to take advantage of economies of scale and the benefits of being close to strong wind and solar resources. While it is possible to predict the timing and size of the outputs of these intermittent sources over the short term with reasonable accuracy, wind strength does not always align with the demand of customers. In addition, local cloud cover can affect the output of large-scale solar facilities (which is less of an issue with distributed small-scale solar-PV). Fast acting and flexible generation, storage systems and transmission interconnectors can be used to counter the effect of variations (and any inaccuracies). Renewable energy technologies with substantial inherent storage, in particular solar-thermal, have a dispatchability advantage over technologies without storage. Solar-thermal also brings significant inertia, accentuating its advantage, although at significantly higher cost for now.

or contracted specific activities such as individual generators. The internal operations of these utilities were based on a management hierarchy. The entities typically had a franchise to supply end-consumers in defined geographic areas and government-appointed bodies regu-

lated prices charged to end consumers. A variation of this model was where local supply boards took bulk supply from central generators.

In the early years, there was massive growth of the power systems driven by strong social objectives. Governments took a lead role; either directly through government owned entities or regulated private companies. As the systems grew, the efficient size of generating units also increased and the number of generating companies within a particular power system remained relatively small. In addition, the IT and communications systems were not yet suitable to host real time competition. These circumstances tended to make monopoly ownership and control of generation the natural path.

As the power systems evolved, major utilities interconnected their networks forming large power systems across different government boundaries and between countries, continuing the earlier pattern of interconnection between townships. Interconnected utilities established agreements and sometimes, common control facilities to coordinate the operation of their power systems.

Since the early 1990s, many utility-based arrangements have been amended to introduce third party

access to the networks and competitive market mechanisms with the aim of reducing the cost to the end customer by:

- Providing end consumers with a choice of supplier
- Introducing short term competition into day-to-day operation of power systems and, in particular
- Devolving many decisions including investment decisions to individual generators, retailers and customers, i.e., away from a command and control based central management by system controllers.

The short-term competitive day-to-day operations of power systems have been enabled by advances in communication, supervisory control and data acquisition technologies that have allowed the vast amount of data needed to manage a power system this way. The devolution of decisions required a dramatic move away from the centralized hierarchy model of managing a power system. In particular, the power system operators became managers of system security and service providers to competing generation and retailing businesses, which all depend on the neutrality of the network businesses to reach their customers.

## 18.3 Electricity Markets

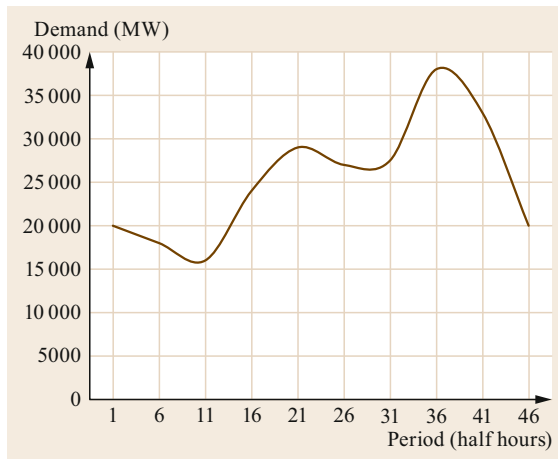
Specific technical characteristics of electricity are that it is invisible and, when supplied via a shared alternating current network, it is also indivisible. In addition, supply and demand must be balanced on a second-by-second basis. Together, these factors restrict the form a market can take for trading of the physical product. Forward sales for electricity, however, can be transacted much like any other commodity. For example, this could be in a financial exchange or by direct negotiation in *over the counter* sales. The need to balance real time supply and demand will generally mean delivery does not perfectly match forward sale volumes and some form of real time balancing or spot market is needed in parallel with the forward market.

In order for disaggregated entities to collectively make economically efficient decisions that also maintain security and reliability, they require timely information about supply, demand and cost. A number of market models have evolved to provide a platform for a central market and system operators have been allocated the task of receiving and publishing this information. The various models employ a different mix of central control and disaggregated decision-making, where the separate generators and retailers are responsible for their own commercial wellbeing.

### 18.3.1 Supply and Demand

To run a power system effectively there needs to be adequate capacity to meet total demand and an ability to match variations in demand across each day. The total customer demand varies across the day and across the year in most systems. The variation is generally more pronounced in countries located away from the equator and varies with the season and use of heating and cooling. Figure 18.2 presents a typical winter demand curve for a day in a cool climate and shows overnight load is low and there is a peak that occurs for a short period in the early evening, generally driven by domestic cooking, lighting and in some cases, heating.

Traditionally, generation plant has been characterized by the role it plays. Generation plant that runs most hours of the day is termed base load. Plant that is used only occasionally, or for limited hours per day to follow variations in demand, is termed peaking plant, with intermediate load plant running for part of the time. The most cost effective mix of technologies will depend on the capital and operating cost of available technologies and fuels and can only be assessed over the long term. Decisions about which technology is best to run within a day depend on the controllable cost of operation, the



**Fig. 18.2** A cool climate winter daily demand curve

variable operating cost of plant that has been built (i.e., excluding sunk capital cost) and the shape of the daily demand curve. The demand in Fig. 18.2 would be met using the lowest cost plant across the entire day (making this plant base load) and higher cost plant for less time during the peaks.

Historically, in large power systems, coal, nuclear, hydro or combined cycle gas fired generation generally operated near to 24 h a day (base load). These generators typically have high capital costs and low operating costs and, with the possible exception of hydro, are not designed to be turned on and off on a regular basis. On the other hand, peaking plant such as open cycle gas turbines have a much lower capital cost but higher operating costs and are much easier to turn on and off. In a market system where generators offer a price to the system operator for dispatch you would expect the lowest cost generators to offer low prices at low load times to ensure that they run all the time.

More recently there has been a substantial increase in wind and solar generation in many countries. The operating costs of these technologies are low as there is no fuel cost. So, they will want to run as often as the wind blows or the sun shines. In bid based market arrangements they will also tend to bid lower prices to ensure they run when they can. This will be in direct competition with traditional base load plants and will put pressure on their revenue streams. While this may drive efficiency, it can also impact on the overall financial viability of the generator.

As the penetration of wind and solar generation continues to increase, markets have to increase flexibility to balance surpluses and deficits both within a particular power system and across the interconnections between the systems. In many cases this will be across international borders and this is driving the need to standardize

market structures and systems where these interconnections can and do occur.

Variable operating and maintenance costs of offshore wind farms can be more substantial, and potentially be above the prevailing market price. Operators should therefore aim to run the wind farms as much as possible whenever the market price is above their variable operating and maintenance costs, while scheduling outages at times that have the lowest impact on revenue.

As discussed above, the growth of distributed generation, mostly in the form of rooftop solar-PVs and, more recently, associated storage, is opening up opportunities for customers to participate in the market, both in terms of sale of surplus generation and demand management.

### 18.3.2 The Role of Markets

A market is only useful if it ensures generation capacity is introduced and withdrawn in a timely manner. Markets may signal the right time through prices rising or falling as demand grows. For example, higher prices will encourage higher cost generators to run more often or, if a new lower cost source of power is available, it may undercut operation of an incumbent technology. On the other hand, reducing customer demand may cause prices to fall. Entry and exit of capacity may also be centrally managed in terms of price or volume and market arrangements will focus on efficient use of incumbent capacity. Given the significance of electricity in most countries, if new entry does not occur in a timely manner, reliability of supply will fall suggesting market failure and this will usually lead to government intervention.

A centrally managed process to determine the level of capacity may be used where markets pay for capacity or availability, separately to dispatched energy. In this case, generators are paid to guarantee that their plant will be available at times of system stress even if they otherwise do not run often or at all.

In order to design or understand a market for electricity, it is important to be clear about the definition of the product or products that are being traded, be it capacity, energy, availability, frequency keeping services or network support. Electricity systems are highly integrated and market arrangements for one or more products generally affect others. As noted, transmission and distribution networks are often regulated, even if there is a market in operation for other parts of the industry such as generators and retailers. Network costs can be optimized, and therefore the combined costs of generation and networks charged through to users reduced, by lowering infrastructure investment to optimum levels and by leveling demand to reduce the size

of peaks and troughs. Subsidies have been provided to some market participants as part of a (legitimate) social policy agenda of governments. A technology specific subsidy can also impact the operation of markets and ironically, market design activities usually need to consider how these non-market subsidies are applied.

There may also be constraints in the transmission and distribution systems, which may limit the amount of electricity that an individual generator can sell. These constraints can impact on the returns to the affected generators as well as the reliability of supply for some end customers. Examples of these constraints are thermal capacity limitations or operational restrictions in relation to system security or stability. In a market situation these constraints need to be clearly identified to

minimize the likelihood of contractual disputes at a later date.

In summary, the overall goal of a market is to achieve market efficiency in both the short term and the long term. In the short term, output should be produced in the right quantities by the lowest cost generators and consumed by those that are prepared to pay the most. In order to achieve this, generators are dispatched to achieve the best economic outcome starting with the lowest short run marginal cost. In the long term the market must provide signals to trigger the timely investment in appropriate quantities of new generation. It must also generate confidence that investors will receive a reasonable return on their investment considering the risks involved.

## 18.4 Market Models

This section introduces a number of the market models that have evolved around the world. Specifically, the following models are described:

- A vertically integrated utility
- A vertically and horizontally disaggregated utility with only utility plant connected
- A competitive market only at the time of investment
- Separate capacity management combined with central dispatch of energy
- A general overview of energy-only markets and specific descriptions of:
  - A pool system with a marginal system price
  - A pool system with pay as bid.

The section then continues to discuss the operation of retail competition and a brief overview of using a market for transmission expansion.

One way to understand the differences in the models is to consider where each sits on a spectrum of central disaggregated control and the allocation of risk. This is illustrated in Table 18.1. Generally, the more centralized the control the more the risk is retained by central entities and ultimately passed through to the end consumers in the form of fees and tariffs. Conversely, the more devolved the decision-making; the more the individual generators and retailers carry the commercial risks (and rewards) of decisions in the industry.

Prior to the introduction of markets, the traditional function of a system operator was to manage system security, physical dispatch, system reserves and network loading. To manage the commercial interactions with buyers and sellers a new function emerged – market operator or power exchange. Around the world the activities involved in managing security, dispatch, network

loading, network switching, metering, market registration and settlement are combined in a number of ways. A range of labels has emerged for the different activities and combinations, for example system operator, market operator or transmission system operator. The label independent is generally applied when independence of the system operator or transmission operator is required. For the market operator or power exchange, this level of independence is always assumed regardless of the label. The role varies from market to market but can be seen as the entity that runs the trading activities that are not handled by the traditional system operator.

### 18.4.1 Vertically Integrated Utility

The traditional utility, operated under a centralized hierarchy model, sits in column 1 at the left hand end of the spectrum in Table 18.1. In this model, individual generators are generally owned by or contracted to the utility and carry little risks other than for their own performance. Any errors in forecasting, in the choice of which units to dispatch, in the fuel to purchase or the trades with adjacent networks, stay with the central utility and are ultimately paid for by its owners – be they end consumers or private investors.

### 18.4.2 Vertically and Horizontally Disaggregated Utility with only Utility Plant Connected

The next step along the spectrum is in column 2 of Table 18.1. Here, vertical and horizontal disaggregation has been used to allow financial separation of the generators and network components of the electricity supply. However, there is no commercial market and the

Table 18.1 Spectrum of market options

1. Vertically integrated utility		2. Vertically and horizontally disaggregated utility. Only utility plant connected		3. Competitive market at time of investment/tendering only. Only successful tenderers can connect.		4. Competitive market third party access		
Direct management control	Direct management control	Transfer pricing	Utility tenders for PPA (power purchase agreement)	Independent single buyer tenders for PPA	Separate capacity management combined with central dispatch of energy	Investment to centrally administered capacity. Balancing or spot price market used for dispatch	Investment based on price. Balancing or spot price market used for dispatch	Energy only (combined investment and operating price incentive)
				Investment based on physical standard. Operations under utility control				Back up intervention (e.g. strategic reserve)
								No intervention

Low market influence

Strong market influence

Level of administrative control

Level of competition

generators are still under direct management control or a form of transfer pricing is introduced.

### 18.4.3 Competitive Market at Time of Investment Only

This is illustrated in column 3 of Table 18.1 and can be described as a single-buyer/power purchase agreement (PPA) model. Traditionally, many utilities operated with a combination of owned generation and other contracted generators. In a single buyer model, competition occurs only at the time of contracting. In this case, the buyer would normally tender for a generator supply and enter into a long-term contract or PPA with the successful bidder. At the simplest level, the buyer may be the utility but there may be concerns that it has some level of vested interest in the outcome. A more sophisticated model is where the entity assigned the role of single buyer is commercially independent. It has no allegiance to any particular generation business. The single buyer will liaise with or be integrated with a market operator.

The model does not readily allow any choice of supplier to end consumers. In principle it does allow for multiple retailers to buy from the single buyer and compete on retail margin and service offering but the benefits of this form of competition are small. A single buyer is often seen as a transitional step to greater levels of competition.

A variation on the single buyer is a PPA market where individual blocks of demand enter into contracts with generators under long term PPAs. This arrangement differs from a single buyer in that it is demand or customer focused as it is the demand side or customers who decide to purchase, typically in the form of large industrial loads or retailers. A similar mechanism to a single buyer market is often used as a means to coordinate the operation of the contracted generators.

Single-buyer/PPA arrangements need a mechanism to commercially account for times when generators produce more or less than their contracted amounts and this is often termed out of balance. Out of balance can be calculated and priced in a number of ways. For example, all contracted generators may be required to inform the market operator of their intended outputs in advance. Uncontracted or partially contracted sellers may be required to bid to the market operator their willingness to raise or lower output at various quantities and prices. Depending on the needs of the balancing market and the competitiveness of their bids, these uncontracted or partially contracted sellers may or may not physically run.

As the arrangements become more sophisticated, they begin to look more and more like the shared or

pooled price arrangements that sit further along the spectrum of industry structures.

#### 18.4.4 Separate Capacity Management Combined with Central Dispatch of Energy

A widely used structure for competitive participation provides for a payment for capacity separate from payment for dispatched energy. This arrangement is often described as a capacity market but is more correctly a capacity plus energy structure. It falls within column 4 of the spectrum in Table 18.1. The arrangement reflects the typical structure of earlier PPA contracts that cover availability plus dispatch payments and provide for close management of the level of capacity present in the market [18.3].

In these market arrangements, one (but rarely both) of the amount of capacity or the price of capacity is set administratively. For example:

- The amount of capacity considered to be needed to meet a reliability standard is calculated and a competitive process run to acquire that amount, with the price being determined by the market responses; or alternatively
- The price that will be paid for capacity is announced and calls for parties to provide capacity at that price are made.

The acquisition process can be a tender, subscription or auction.

These markets typically arrange dispatch on the basis of prices submitted by generators rather than costs of production that are used in PPA and single buyer arrangements. Prices provide much greater flexibility and competitive tension in the market than a cost based regime. However, the typical objective is that sufficient competition will drive prices down to costs and, in the process, create incentives for an economically efficient mix of generation and continual pressure for improvement. Later sections discuss the common situation where this assumption about adequate competition is not valid and measures to control market power are overlaid on the operation of the market.

Typically a central or pool price is derived from the prices of the generators that are dispatched. This real time market price is most commonly set by the marginal value of generation to the system (often approximated by the price of the highest priced generation dispatched). All generation dispatched is paid at this market price.

Different implementations of this design include day-ahead, intra-day and longer-term markets, which set a price for agreed volumes of electricity in advance of dispatch. These markets can be for physical quanti-

ties or they can be financial contracts that settle against the real time price. The real time price is then applied only for the volumes not covered by advance markets.

The real time price can thus be seen to be equivalent to the out of balance price of PPA arrangements and the day-ahead markets or the price paid for *unders and overs* of actual compared to contracted volumes.

In these designs it is usual that a central government or other regulated body determines the amount of capacity or the price that is to be paid for capacity that is passed through to customers. Customers therefore bear the risk to the extent that the central body over or under-estimates demand, the flexibility or price elasticity of demand, or the availabilities of installed generation equipment.

#### 18.4.5 Energy-Only Markets

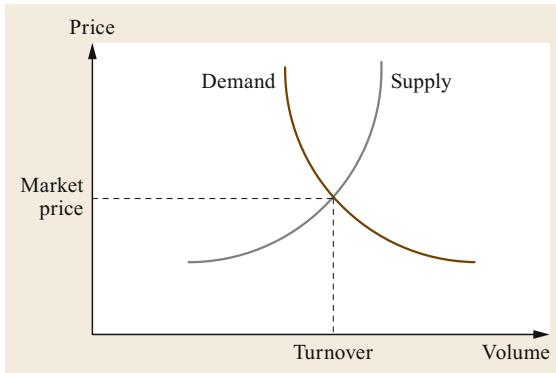
At the right hand end of the spectrum in column 4 of Table 18.1, a market arrangement that pays only for energy dispatched on the basis of a price offered for dispatch transfers the commercial risk to the industry players. Critically, this relies on competition between these players to contain prices, as without sufficient competition there is a risk of uncompetitive prices. These markets have an energy market that operates along similar price based lines to that of a capacity market, but with quite different price outcomes. Generators earn revenue from the market only when dispatched. This type of market relies on price incentives to ensure sufficient capacity is available. As a result price must rise above the short run cost of generation for long enough for the efficient amount of generators to recover all costs. In principle the price will reflect the cost of generation and the risk of scarcity of supply to customers. When generation reserves are very low the price will approach or reach the value of customer scarcity. This price can be politically unacceptable prompting the use of low price caps but creating a risk of 'missing money', whereby potential investors do not have confidence that they will achieve an acceptable return on investment, aside from other risks such as plant performance and the level of demand.

Typically, day-ahead, intra-day and longer-term markets also operate in conjunction with the real time market.

In these designs, far more of the investment risk of the industry initially sits with generators. Generators and retailers may, however, enter into hedging or other longer term contracts to reallocate that risk in return for price certainty.

There are many variants of each of the basic forms. Within energy only markets, two specific examples are *pool system with marginal system price* and *pool system with pay as bid*.





**Fig. 18.3** Supply–demand curve

#### Pool System with Marginal System Price

For this system, the sellers bid (confusingly analogous to offers to sell in most financial markets) to the market operator their willingness to sell various quantities at nominated prices. All the energy that they wish to sell is bid into the market and for this reason the market is sometimes described as a gross pool. One form of this design sees the bid quantities accumulated to form an aggregate supply curve. Buyers bid to the market operator their willingness to buy at various quantities and prices. These are accumulated to form an aggregate demand curve. This demand curve has traditionally been relatively inelastic as most customers are currently unable to respond to price signals. The quantity traded is at the intersection of these curves. The price is also at the intersection of these curves. The clearing price is the rate for all bidders for all quantities. This is illustrated in Fig. 18.3.

The system marginal price is the price set by the most expensive unit needed to meet the demand quantity. Only sellers that bid below this price will physically run.

A more sophisticated version is based on a mathematical optimization. Generators and any demand blocks that choose to participate in the wholesale market, offer their prices. The market operator then determines the economically efficient combination of generation and demand needed to meet customer needs, accounting for network losses and security constraints. The market price is one of the outputs of the mathematical optimization.

#### Pool System with Pay as Bid

Pay as bid arrangements differ from pay at marginal price described in the previous section in the way the market price is determined, but are otherwise very similar.

For this system, sellers bid to the market operator their willingness to sell at various quantities and prices. These are accumulated to form an aggregate supply curve. Buyers bid to the market operator their willingness to buy at various quantities and prices. These are accumulated to form an aggregate demand curve. The quantity traded is at the intersection of these curves. Only sellers that bid below this intersection physically run.

Each generator that is dispatched is paid at the price it offered and each block of load pays at the price they offered to buy at. Experience shows, and many commentators note, that in practice the price in pay as bid arrangements often trends towards the marginal price, as participants learn that their dispatch is unchanged until they bid above the marginal price.

#### 18.4.6 Retail Competition

While an objective of wholesale market reform is to facilitate competition amongst suppliers, choice of supplier (retailer) for end customers is very often a key objective. The competition that then results between retailers can put downward pressure on profit margins and encourage the improvement of service standards. Retail margins are generally quite low and there is a need to spread the costs over several products with similar metering and billing requirements. Large companies can achieve economies of scale that tend to encourage the amalgamation of smaller retailers. However, too few retailers may hamper competition and lead to monopolistic behavior. Customers are given freedom of choice over their preferred retailer.

#### 18.4.7 Market for Transmission Expansion

There have been attempts to use a market mechanism to drive down the costs of transmission infrastructure rather than to rely on regulatory oversight. An example of this is in Brazil. In this case, a planning process is used to assess future transmission requirements. The federal regulatory agency then holds auctions for bidders who will build, own and operate the facilities. The winner of this auction is the one who requires the lowest annual revenue over thirty years. While initially successful, recent auctions have failed to attract significant competitive bidders. To some extent this is due to regulatory uncertainty caused by rule changes and the forcing of companies who are renegotiating expiring contracts to substantially reduce prices by placing a ceiling on allowed revenues.

## 18.5 Market Structures Around the World

This section provides some practical examples of electricity markets around the world. It draws on a recent CIGRE technical brochure number 626 [18.4], which has surveyed the current status of electricity markets in selected countries. In some cases other sources from the various countries have also been used. These markets are evolving and some may look quite different in the future. They do, however, provide concrete examples that relate to the theory discussed earlier. One significant change that is occurring relates to the growing penetration of wind and solar generation coupled with growing opportunities for demand response, demand flexibility and energy storage. These present particular challenges to the current market arrangements due to the variable nature of wind and solar energy. Government policies and a range of direct and indirect subsidies are also driving the growth in these forms of generation.

### 18.5.1 Europe

While a form of trading of electricity commenced in Norway in 1971, for the rest of Europe, market liberalization began in England and Wales and the remaining Nordic countries in the early 1990s. These early markets, while still visible, are now incorporated into a pan-European market that covers energy and the implicit trading of network capacity.

European directives have been enacted since 1996 to establish a common internal electricity market in Europe, which is still evolving. These directives have established common rules for the generation, transmission and distribution of electricity both for the organization and functioning of the sector and for the operation of the market. Key outcomes have been:

- Unbundling of monopoly activities – i.e., separation of generation from transmission
- Third party access to all electricity networks
- Entry of new suppliers or load serving entities into markets
- Customer rights to choose their supplier
- Establishment of a National Regulatory Authority for each member state and
- Establishment of network codes or rules, derived from a common European root, which address issues such as connection to the network, operation of the market and operation of the power system.

In many cases, trading in electricity is by bilateral contracts, but in some cases, a market operator or power exchange has been created. These power exchanges take various forms across Europe, some of which are

private entities. For example, the European Energy Exchange (EEX) in Leipzig, operates spot and derivatives markets and EPEX SPOT operates a spot market. German EEX AG and French Powernext SE own this latter market. There is a forward market for deliveries up to six years in advance and a spot market for day-ahead and intra-day trades. Buyers and suppliers submit their bids by midday on the day before as part of electricity auctions in the day-ahead market. After the day-ahead auction closes further bids can be made in the intra-day market. This trading closes 45 min before delivery. Finally, TSOs procure balancing capacity to cover unforeseeable imbalances through a competitive bidding process in a balancing market.

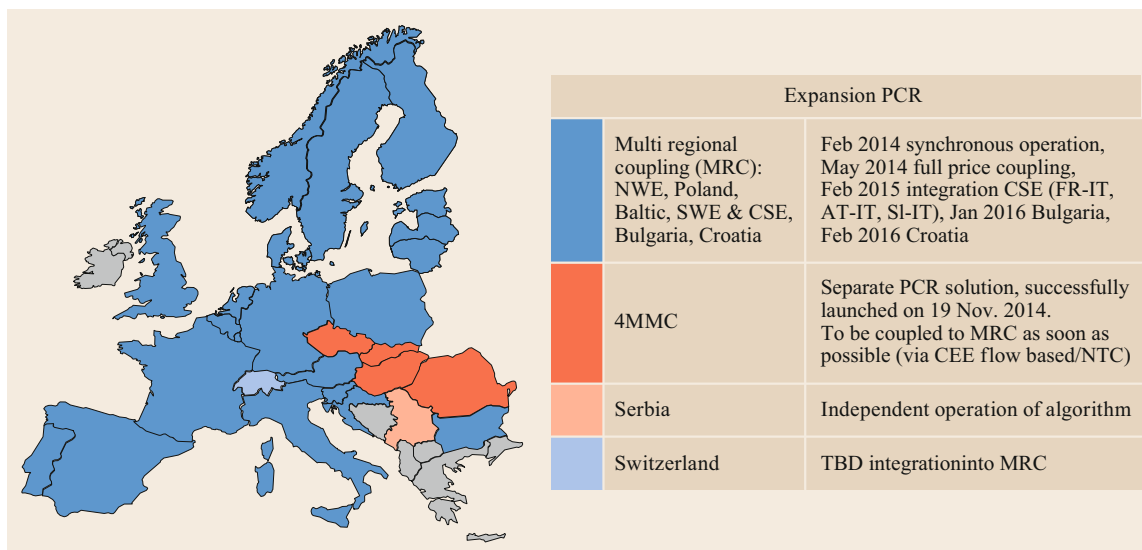
As these markets have evolved moves have been initiated to couple the various markets. In some cases this has been enhanced by the installation of new physical interconnections, for example across the Baltic and North Seas. The stronger these interconnections are, the less the physical constraints will impede the competitive pressures and the more opportunities there will be to dispatch the lowest cost generation. In the move to an integrated European market, work has been undertaken to develop a common approach to calculating cross-border transmission capacity, defining bidding areas and creating efficient trading mechanisms.

In May 2014, two regions, the north west region and the south west region were price coupled with common synchronized operation as shown in Fig. 18.4. The price coupling of regions (PCR) now includes Belgium, Denmark, Estonia, Finland, France, Germany, Austria, Great Britain, Latvia, Lithuania, Luxembourg, the Netherlands, Norway, Poland, Sweden, Italy, Bulgaria, Croatia, Portugal and Spain. The coupling of the day-ahead markets has enabled more efficient allocation of interconnection capacities of the involved countries. Market prices are calculated simultaneously, operational procedures are harmonized and offers are made to the market in a coordinated way. In addition, other countries are being brought into the PCR as soon as possible.

#### Nordic Market Overview

A market for electricity trading in Norway commenced in 1971. This took the form of a power pool, which allowed generators to trade surpluses and deficits of power through a central grid. Virtually all power generation in Norway is by hydroelectricity whereas the other Scandinavian countries have a mix of hydro, nuclear, coal and other fuels.

Electricity market liberalization in the Nordic countries commenced in 1991 and now includes Norway, Sweden, Finland, Estonia, Latvia, Lithuania and Den-



**Fig. 18.4** Developments for price coupling of regions. (Source: ENTSOE, PCR Status report, Q3, 2017 [18.5])

mark. As part of the process, a regulator and a transmission system operator were established in each country. All networks were separated from competitive activities and are now open to third party access by all customers.

Trading of electricity is by direct physical contracts between generators, retailers and customers, with all having the option to access the power pool to trade at the margin. For the pool, buyers nominate the energy needed and the price they are prepared to pay each hour and sellers nominate how much they can deliver each hour and for how much. The hourly price is set for where the sell and buy prices meet. There is no capacity payment unless there is a transmission constraint. Within NordPool there is a spot market (ELSPOT) that settles quantities and price nine hours before delivery, taking into account interconnection limitations. There is also another spot market (ELBAS) that operates in Sweden and Finland and settles two hours before delivery. Both require physical delivery. Each transmission system operator operates a balancing market to enable physical balance in real time. There is an organised futures market for financial hedging up to three years in advance.

There is no capacity market although this may be considered in the future if there is concern that the market does not trigger timely investment in new generation. Stagnating load growth, a rapid increase in renewable generation and high penetration of hydro are mitigating the risk of insufficient generation investment. Most of the recent renewable generation has been intermittent wind generation, however, and the capability to manage dispatch is being compromised. While not a capacity market, Sweden maintains

a strategic reserve. This is a capacity remuneration mechanism as discussed in more detail in the CIGRE technical brochure 647 [18.3], which describes the capacity mechanisms used in the various countries.

#### UK Market Overview

The United Kingdom (UK) comprises Great Britain (GB) and Northern Ireland. GB encompasses England, Wales and Scotland. The system in Northern Ireland became part of the single electricity market in 2007. Liberalization in GB was first instituted in 1990 with, initially; different market arrangements in Scotland separate from those in England and Wales.

Historically, fuel for power generation in GB has been dominated by coal, gas, and nuclear. Recent years have seen a growing percentage of renewable generation mostly in the form of wind turbines but also, increasingly, from solar PV. At the time of writing there are interconnections with France, the Netherlands and Ireland with further interconnections under development to Belgium and Norway and still others under consideration. In 2016, the GB system was run for some hours without any coal generation for the first time ever and coal fired power stations are predicted to close completely by 2025.

The first England and Wales market required all electricity to be bought and sold through a common pool. For each trading period there was a single input and a single output price. The pool input price was set by the last bid accepted to fill the quota of capacity for each half hour. Bidding into the market was optional. There was also a capacity payment made to encourage generators to offer capacity. This payment was based

on estimates of the value of lost load (VOLL) and loss of load probability (LOLP). Concerns with this mechanism included that it rewarded shortages rather than new investment and that generators could manipulate the pool price by withdrawing generation plant at critical times.

Scotland did not enter into this market. It retained two vertically integrated utilities with contracts in place between them to allow the mix of power plants to be optimum for both companies. Due to the lack of competitive pressure, the businesses were heavily regulated with prices linked to the England and Wales pool price. A similar process was adopted in Northern Ireland. The wholesale market in Scotland was merged with that in England and Wales in 2005 to form a single GB market with a single GB system operator adopting the structure that was put in place in England and Wales in 2001.

Amongst other things, concerns over excessive pool prices, potential gaming of the complex pool rules and the lack of demand side participation led the government to change the market. In March 2001, new electricity trading arrangements (NETA) were introduced. Under these new rules, encouragement was given to the decentralized trading of energy via bilateral contracts between generators and suppliers acting on behalf of end customers. To cover any remaining imbalances, there was also access to an optional power exchange to cover contractual imbalances and a balancing mechanism (BM). For the BM, participation is compulsory for larger generating units and suppliers and optional for others. The resulting market is similar to that operating in the Nordic power pool. The BM accepts bids and offers up to *gate closure* at 1 h ahead of delivery. The BM is managed by the system operator part of National Grid, which in 2018 is being separated from the transmission company that owns the transmission network in England and Wales. (There are two further transmission owners covering the north and south of Scotland).

The general view by Ofgem, the GB regulator, was that the NETA reforms had performed well alongside other factors such as falling fuel prices, a generous capacity margin and increased competition in generation with significant reductions in wholesale prices [18.6].

In 2013, the government introduced further reform with the objective of providing incentives to invest in secure, low carbon electricity; improving the security of Great Britain's electricity supply; and improving affordability for customers. A key aspect of this reform was the introduction of a capacity market to ensure sufficient reliable capacity during periods of higher risk such as when high demand coincides with low wind power generation. The market operates as two auctions, one for year-ahead capacity and the other for capacity four years ahead. The successful bidders enter into

capacity agreements that allocate payments for guaranteed capacity availability.

A further support to renewable generation providers is in the form of long term contracts for difference that provide stable and predictable revenue streams for investors. If the wholesale market price is higher than the contract price, the generator makes a payment and if the price is lower, it receives a payment.

The reform also introduced an offtaker of last resort scheme, which facilitates a contract between a renewable generator and a licensed supplier through a competitive auction where the contract must be at a discount below the market reference price. This process is used where the renewable generator cannot secure a contract via usual commercial means.

### German Market Overview

The electricity market in Germany is Europe's largest with an installed generation capacity of 184 GW. Full deregulation of the domestic electricity market occurred in 1998. There are four transmission companies that own and operate their respective transmission systems Amprion, ENBW Transportnetze, TenneT and 50 Hz transmission. Transmission is legally unbundled with defined rules for non-discriminatory third party access. Power generation and distribution is provided by a few large companies and a large number of small distribution companies. The larger companies are RWE, E.ON, innogy SE, Uniper, EnBW and Vattenfall.

As mentioned earlier, the German market is coupled with 15 neighboring countries and the exchange price for the day-ahead market is calculated jointly for the coupled markets. The coupled market determines the lowest price from any market zone until the cross-border interconnections are fully utilized and then it reverts to the lowest price in the particular market zone where the load is being served.

In June 2016, the German Federal Parliament approved a number of reforms to the power market and agreements about transferring existing lignite power stations into an emergency reserve. Ultimately these generators will be phased out permanently.

The main driver of the reforms is to ensure efficient power station operation and overall security of supply as the amount of renewable generation continues to grow. The main reforms include [18.7]:

- Strengthen the price signal to investors – in times of supply scarcity, peak prices will not be capped and may increase substantially which should signal investment opportunities to power station investors. They may choose to invest in peaking plant such as open cycle gas turbines, load management or storage.

- Penalties for insufficient power delivery – traders must ensure they buy sufficient power to supply their customers and not rely on grid operators to make up the difference.
- Increased competition for flexible power options or peaking plant – providers of flexible options, including electric vehicles in the future, will have access to the balancing market.
- Reduce network costs – firm access to all renewable generation will no longer be required and network charges across the country will be harmonized.
- Provide a capacity reserve – similar to the strategic reserve in Sweden, this will ensure adequate capacity is retained in constrained network regions and support power system security for extreme events. This plant will not be part of the power market to ensure there is no distortion of the competitive elements of the market.
- Mothballing of inefficient lignite power plants – these will be put on temporary standby for a period of four years before being permanently closed.
- Smart meters will be rolled out – this will commence with the largest customers and be governed by a cost benefit ceiling and strict data security.

### 18.5.2 Australia

The National Electricity Market (NEM) encompasses eastern and southern Australia (Fig. 18.5 [18.8]). It is geographically one of the largest interconnected AC systems in the world covering 5 200 km from tropical Queensland to western South Australia. The maximum demand of the NEM is now (2017) approximately 37 GW.

Economic reform of the electricity sector began in the early 1990s. Victoria was the first to establish a market within the state, followed by NSW and later still a form of market arrangement in South Australia. The states collaborated and designed the National Electricity Market (NEM), which commenced December 1998. The NEM covers all of the east coast of Australia but not Western Australia or the Northern Territory, which are not interconnected with the east coast system.

At the time of writing the NEM consists of five major and two minor transmission companies, seventeen distribution companies, twenty-five major and twenty-five smaller retailers and individual market customers as well as eighty-one generators.

The market design is similar in some ways to early versions of the UK model. The participants in the NEM are a mixture of private and government owned utilities. A key industry change was the disaggregation of generation, transmission, distribution and retail during the early 1990s in the lead up to the start of the NEM.

Western Australia followed later with disaggregation into generation, retail and a combined transmission distribution business occurring in 2006. More recently the disaggregated generator has been re-combined with the retailer and this larger business is intended to compete with other smaller combined generator retailers. The size of the market and the lack of diversity limit the extent of the competition that can occur.

The current market model in the NEM is consistent with the above description of a pool system with a marginal system price [18.9]. It is a gross pool, trading in energy only and it is broken down into regions, which follow state boundaries and each has its own spot price. There are no capacity payments. The intention is that as the spot prices increase, or rather forecasts of future spot prices increase, this signals to investors that the addition of new generation will be a profitable venture. While the visible trading in the market is seen as a spot price, behind the scenes there is extensive bilateral contracting to reduce the risk from short-term price variations. Today, many of the separate generation and retailing businesses have merged into a few very large gen-tailers. There is a reliability and emergency reserve trader, which is a function available to the market operator to contract for electricity reserves ahead of a period where there is a predicted shortage of generation. This is a form of strategic reserve as described for Sweden and Germany and discussed in more detail in [18.3].

In the NEM, the Australian energy market operator (AEMO) is both the market and system operator and is required to be independent of market participants. The market is intended to operate commercially at all times. AEMO has powers of direction to maintain reserve margins and ensure secure operation of the transmission network. There is also a spot market for frequency control services.

A snap shot of the data dashboard for Queensland in the Australian national electricity market is shown in Fig. 18.6 [18.10]. The chart shows 30 min data including current and historical spot prices, forecast spot prices, current and historical scheduled demand and forecast scheduled demand for a twenty-four hour period. Figure 18.6 is regularly updated. To obtain the latest figure, go to: <https://www.aemo.com.au/energy-systems/electricity/national-electricity-market-nem/data-nem/data-dashboard-nem>. Then select price and demand and QLD.

The spot market is used to instantaneously match wholesale electricity supply and demand in real time. AEMO centrally coordinates the dispatch process and determines which generators will meet the demand based on 5 min bids from the generators for quantity and price. AEMO then arranges the dispatch of the generation accordingly.

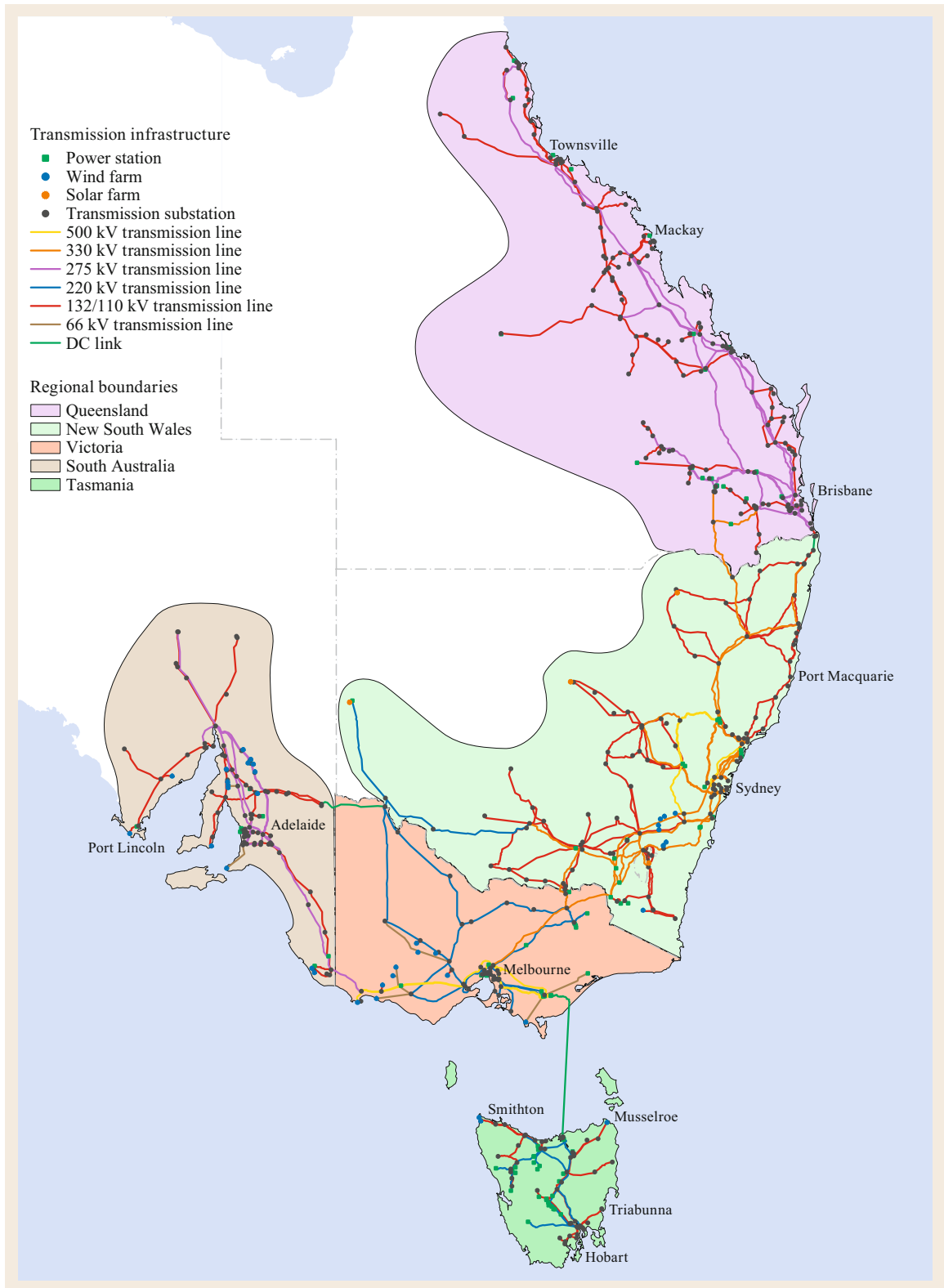
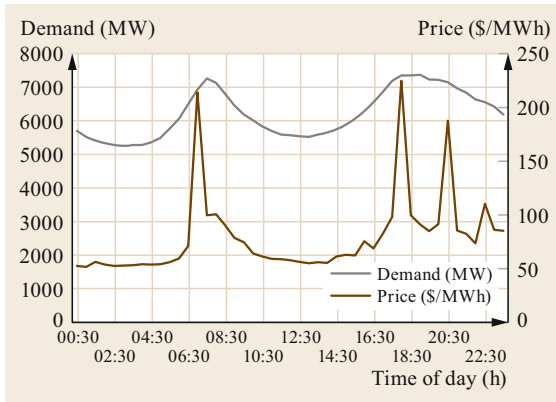


Fig. 18.5 The Australian national market (reprinted by permission from [18.8], ©AEMO 2016)



**Fig. 18.6** 30 min data for Queensland in the Australian national market: Electricity price and demand, Queensland, 01.06.2018 (reprinted by permission from [18.10], ©AEMO 2018)

Currently, every 5 min, participant bids are used to determine a dispatch price and the average of six consecutive bids is used to determine the spot price for each half hour of trade. Prices are submitted the day ahead for each trading interval but can be varied with around 10 min notice. The dispatch system assesses the demand and constraints at the start of each 5 min interval and then calculates the dispatch solution and price. The spot prices are used for financial settlement of all energy traded. From 2021 the spot price for settlement of trades will be moved to the 5 min price.

During times of generator shortage, where there may be inadequate reserves of generation to meet the customer demand, the bid prices may go very high. In order to protect the customers, the spot price is capped to nearly 15 000 \$ (AUD)/MWh (2019–20) [18.11]. This cap is periodically reviewed and is set to create incentives for sufficient capacity to meet the market reliability standard. A temporary lower cap is set if the spot price is consistently high over a rolling seven day period.

The NEM has now been in operation for nearly twenty years. It was introduced at a time of excess generation capacity in most regions followed by a period of stagnating demand coupled with a significant surge of investment in renewable generation in the form of wind and solar-PV.

As in most parts of the world, electricity is considered to be an essential commodity and loss of supply due to a major system blackout or a sudden surge in electricity prices are guaranteed to receive intense political focus. Both of these events coincided recently in Australia, mainly focused in South Australia, which experienced a statewide blackout at a time when electricity prices have been rising excessively. To some this

is an indication that the electricity market is not working very well.

On Wednesday September 28, 2016 a major storm in South Australia, including two tornadoes, brought down transmission towers and caused a number of transmission lines to trip, including the primary interconnector to the adjoining state of Victoria. During this period, a large number of voltage dips caused a number of wind farms to power down. The sudden loss of this generation, coupled with the loss of transmission lines and the input from interconnection, caused frequency drops in excess of those allowed for in the under frequency load shedding schemes. This led to a state wide blackout. At the time of the event, wind power was supplying almost half of the state's power needs.

Analysis of the event by AEMO [18.12] determined that settings on the wind farms coupled with a large number of network outages due to the storm exceeded the systems ability to deal with the resultant rapid fall in frequency. To some extent this can be remedied by modifying the wind farm settings. However, there is a longer-term issue developing due to the changes to the nature of the grid where less synchronous generation is leading to more periods with low inertia and low fault levels. This has been exacerbated by the unexpected size of withdrawal of older coal and gas fired generation. AEMO is recommending that frequency response services traditionally provided by synchronous generators should be procured from non-synchronous generators where feasible or from services such as demand response or synchronous compensators.

As a result of this blackout and the rapidly rising prices across the NEM, the government initiated a review into the future security of the NEM. This has led to the recent publication of the review report by the chief scientist in Australia, Dr. Alan Finkel. Of direct relevance to this chapter is a recommendation that all new generators must meet technical requirements to contribute to fast frequency response and system strength and that there must be a minimum level of inertia maintained within each region. In the future it recommends a move to a market based mechanism for procuring fast frequency response if there is a demonstrated benefit. It also recommends an orderly transition to a clean energy target via an emissions reduction trajectory. All large generators should provide at least three years notice of closure. The need for a strategic reserve to act as a safety net in exceptional circumstances should be considered. In addition, an integrated grid plan should be developed to promote the development of renewable energy zones. There should also be greater transparency and clarity associated with the setting of retail prices, together with stronger governance over the NEM. For consumers, issues associated

with demand management, distributed energy resources and improved energy efficiency should be examined. If adopted the review panel believes its recommendations will lead to lower costs, greater security and reliability coupled with lower emissions. We can expect there to be a number of changes to the NEM over the next few years as the industry grapples with these recommendations.

Another recommendation of that report was to establish an energy security board (ESB) comprising the three peak regulatory bodies (the Australian Energy Market Commission – the rule maker, AEMO – the System and Market Operator and the Australian Energy Regulator – the economic regulator and market surveillance entity). The ESB proposed the development of a National Energy Guarantee (NEG) which would combine a requirement to contract capacity that is able to be dispatched with a requirement to contract low emissions plant. This simultaneous requirement on retailers was in response to reliability problems that were then plaguing the market. The problems had developed as a result of uncertainty and extended policy inertia that placed future investment at risk. The lack of investment hampered responses to the operating challenges of the NEM due to the change in technology mix in the market and the withdrawal of coal fired plant. In the event,

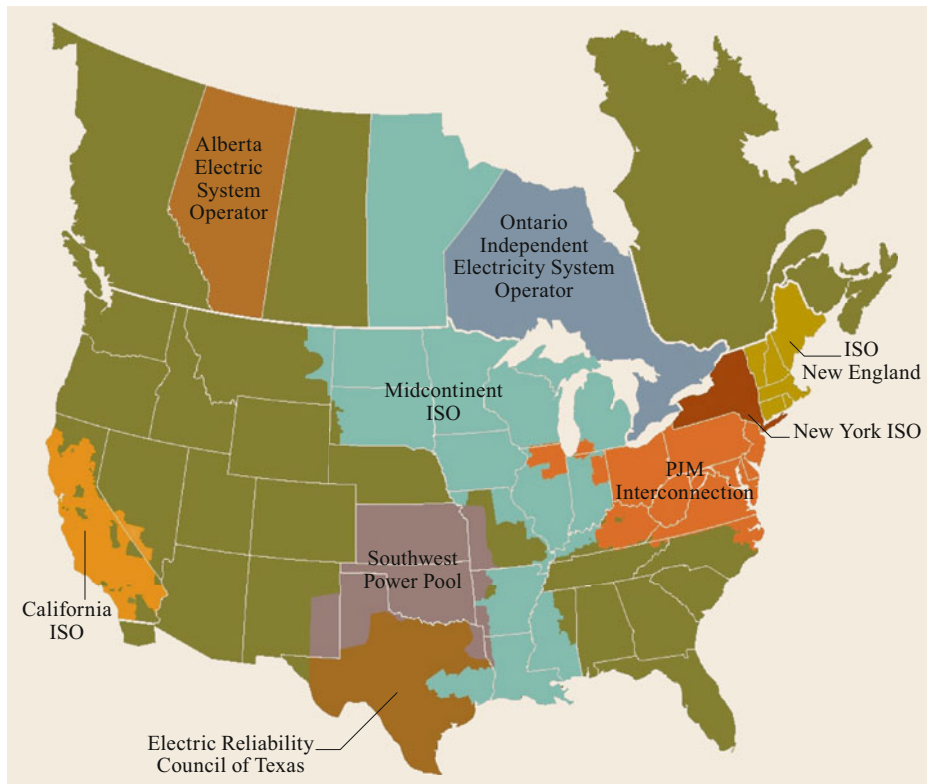
only the obligation on retailers to contract plant that could be dispatched to meet their loads, the Retailer Reliability Obligation, was implemented (in July 2019). Mechanisms to limit emissions are still being debated by governments.

### 18.5.3 North America

Market liberalization in North America began when the US federal energy regulatory commission (FERC) mandated transmission open access across the US in the late 1990s. At this time, wholesale trading was permitted between all utilities with some basic rules governing use of the transmission system; there were no rules for an electricity market.

More formal markets began to evolve by the early 2000s with rules in place to govern how the trading should occur. In parallel with this, parts of Canada also established markets to allow trading with their US neighbors.

There are now nine markets as illustrated in Fig. 18.7. Each has an independent system operator (ISO) or regional transmission operator (RTO), which manage both the market trading and the system operation. These organizations are independent of the generator or network functions.



**Fig. 18.7** Markets in North America (reprinted by permission from IRC)



### Pennsylvania, New Jersey, Maryland (PJM)

The PJM interconnected power pool was formed in 1927 and is one of the oldest and largest centrally coordinated power systems in the world. It now operates as an independent regional transmission organization operating the wholesale electricity market and managing the high voltage transmission grid. In 1997, PJM began to expand from the long standing group of eight investor owned utilities and now has members operating in all or parts of Delaware, Illinois, Indiana, Kentucky, Maryland, Michigan, New Jersey, North Carolina, Ohio, Pennsylvania, Tennessee, Virginia, West Virginia, and the district of Columbia and supplying more than 65 million people.

In 2018, PJM had an installed generation capacity of 180.086 GW with approximately 10 GW of demand side management also available [18.13, 14]. PJM operates a day ahead spot market with energy only prices and a real time (5 min) market, also with energy only prices. The major portion of electricity is traded via bilateral contracts between generators and customers or is self generated and consumed within vertically integrated utilities. There is also an ancillary services market.

FERC oversees the PJM market and loads or retailers are required to have or contract for capacity plus a reserve margin or pay a penalty. There are a number of points of congestion across PJM and a system of financial transmission rights (FTR) is applied within a number of zones that allows market participants to cover potential losses related to delivering energy to the grid. The FTR holder collects revenue based on the day ahead hourly congestion price difference across an energy path. These FTRs are traded along with the energy produced.

### California

It is informative to examine the market evolution in California, as there were some significant challenges with the initial set up. California started deregulation in March 1998 and intended to complete the transition by 2002. Before deregulation, eighty percent of electricity was supplied by three vertically integrated utilities. These were Pacific Gas and Electric (PG&E), Southern California Edison (SCE) and San Diego Gas and Electric (SDG&E). The remainder of power was supplied by a number of municipalities and public power utilities. At this time, peak demand was about 45 GW and installed generation was about 44 GW with the remainder being imported, mostly from the Pacific North West region. The generating resources are a mixture of gas, nuclear, hydroelectric, coal and renewables.

The California market was initially modeled on the one established in the UK and was established roughly

at the same time as the one in Australia. As part of the market development, vertically integrated utilities had to divest most of their generation. There was a short-term day-ahead market, which closed sixteen hours before delivery and a day of market that closed eight hours before delivery. In addition there was a real time market for imbalances 45 min before delivery and an extensive ancillary services market.

About eighty-five percent of the energy was traded through the market. In the original design, most of the energy was bilaterally traded and settled via the power exchanges. Like PJM, there were two stages; the development of the dispatch schedules a day ahead and then the on the day balancing. Initially, only one power exchange was developed, CALPX, and so there was only one day-ahead schedule.

The day-ahead schedule was driven by the planned dispatch and usage of participants, which were lodged with CALPX – based on bilateral agreements and adjustments bid into the day-ahead process. A feasible solution was developed, with a day-ahead price, which was given to the operator. On the day the market ran, the programmed schedule was varied to match changes in load and generation.

There was a cap on the price for the day-ahead market, which was to be the main price. While there was no formal limitation on financial products for the balancing pool, the existence of the power exchanges meant that risk management was not required for the (expected) low amounts of energy to be settled in the pool.

A further complication was that there was a separation of the physical and market functions. An independent system operator (ISO) was established to deal with the actual technical management of the power system and generation dispatch and to financially deal with occasional imbalances in the real time market. The market functions were incorporated into a power exchange, which dealt with the actual financial energy transactions. The market only traded in energy and not capacity and there was a cap on the market price.

Concerns about pollution in California had increased the reliance on power imports from other states but the transmission infrastructure had not kept pace with this leading to transmission congestion with other states and within the state. Customers were allowed full retail choice from day one, however, some of the investments in generation were considered uneconomic in a competitive environment and the retail rates were frozen until the stranded assets were paid off. The general expectation was that lower prices would eventuate over time, particularly due to the entry of new high efficiency gas turbines. The pool was designed to be compulsory, where generators lodged hourly bids to meet demand at prices of their choosing and a common

pool price was set by the last generator to be loaded in that hour.

There were a number of issues worth noting which would later prove to be of concern. None of the markets were physically binding. Ultimately, real time dispatch compliance was purely voluntary which resulted in difficulty maintaining system stability and reliability. There was a lack of a single unambiguous price for electricity to be used for hedging and investment decisions. There was some concern about the use of the fixed cap in that it may have sent adverse signals to participants for investment decisions and could also act as a target for bidders when prices are on the rise. There were long lead times on approvals for new transmission lines and generators.

California is a summer peaking area and in the 1998 and 1999 summers, temperatures were typically average. There was above average runoff into the hydroelectric dams of the Pacific North West and California was allowed to import low cost hydropower from these areas. The three major utilities PG&E, SCE and SDG&E were starting to divest their generators but still owned most of them. Natural gas prices were low to moderate, averaging around 2 \$US/GJ. Wholesale electricity prices generally remained in the 20–30 \$US/MWh range. Electricity pool prices were well below the levels of wholesale prices previously embedded into the tariffs that had been frozen for the major utilities. These utilities were therefore quite profitable at this time and were able to pay off the stranded asset charges more quickly than expected.

All this changed in the summer of 2000. Average temperatures were higher than normal with several heat waves. Water inflows in the Pacific North West returned to their long-term averages and reduced the amount of hydropower available. Natural gas prices increased to 10 \$US/GJ, a five fold increase and gas transport capacity reached its limits. In California, all gas fired generators needed to purchase nitrous oxide emission credits when operating and the price of those credits increased. The marginal cost of operation of an open cycle gas turbine exceeded 150 \$US/MWh. As a result of all these coincident events, price spikes began to occur in May and by June prices had reached record levels.

In reaction to these events, the California ISO lowered its wholesale price cap from 750 to 500 \$US/MWh and then a month later to 250 \$US/MWh. However, there was no noticeable effect on the pool prices. At this time, SDG&E had moved out of the rate freeze. The average monthly residential bill in San Diego went from 40 to 68 and then to 130 \$US from June to July 2000—more than trebling over the summer months. General price levels throughout the western states, caused ma-

nor energy intensive industries, including most of the aluminum smelters in the Pacific North West, to curtail output or cease production.

Not surprisingly, there was considerable anger amongst customers who forced the state government to cap residential prices around pre existing levels. Price caps were also implemented at the wholesale level leading to almost 12 billion \$US of costs that retailers were unable to recover from customers. These retailers were forced into bankruptcy (or would have been without government support) while owners of generators reported record profits.

A number of factors in the design of the market can be identified as contributing to the surge in prices. There was limited demand side response. The rate freeze prior to the sudden increase in prices had given no signal to conserve energy or in fact develop strategies to manage varying prices. There was a sudden increase in power production costs coincident with an unexpected increase in demand due to unusually high temperatures. The fact that the three major utilities had to buy and sell all their energy needs through the California Power Exchange, coupled with restrictions on their ability to forward contract, removed their ability to mitigate price volatility. There was also withdrawal of large capacity from the market close to days of high prices indicating a possible abuse of market power. This last issue was a practice extensively used by Enron, an aggressive market trader at the time.

Traders looked for ways to maximize profits within a market structure that was new, complex and had little oversight or governance. Enron found a way to play the California power exchange off against the California ISO. The ISO was only meant to deal with occasional imbalances in a real time market. Daily schedules of load and generation were expected to be more or less equal. However, Enron and others would deliberately overstate expected customer loads, leading the ISO to pay a premium for delivering more power and a premium for removing load from the grid.

Ultimately Enron filed for bankruptcy in December 2001 becoming the largest bankruptcy in US history at that time. This was driven by illegal corporate practices and most of their top executives were tried for fraud after it was revealed that Enron's earnings had been overstated by hundreds of millions of dollars. The risks inherent in the market design had ultimately captured one of its most aggressive players who tried to hide their financial position with the hope that they could trade their way out of trouble.

A number of changes were put in place to address the problems. There was a move from compulsory spot market trading to bilateral trading as used in the other electricity markets in the US. FERC was given the au-

thority to investigate abuse of market power where any bids over 150 \$US/MWh need to be justified and may be investigated. New generation was fast tracked. The oversight of the California ISO was changed from one representing stakeholder interests to an expert panel appointed by the governor. Finally, the California power exchange was dissolved and the market and operational roles were combined into the ISO.

#### 18.5.4 Brazil Market Overview

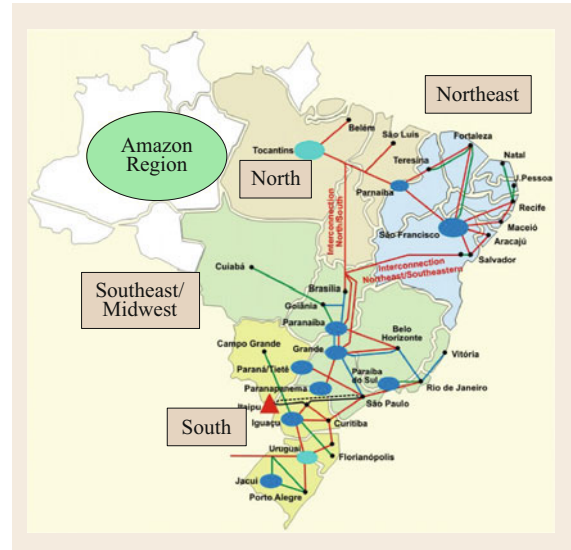
Brazil has the largest electricity market in South America with a generation capacity of more than 137 GW, dominated by hydro power with most of the remainder supplied by fossil fuels, biomass and small amounts of wind and solar. There is limited interconnection with neighboring countries. Unbundling of generation, transmission, distribution and retailing occurred in the 1990s, although generators and retailers may be integrated. Third party access to the transmission is available to all parties on commercial terms.

There are two market environments. The first requires bilateral energy contracts to be established between generators and retailers that are considered to have captive customers. These are conducted by auctions in a regulated environment. The second allows unregulated contracts to be established between generators, uncontracted customers (generally if the load is greater than 3 MW), retailers and traders.

Generators, through long and medium term contracts, must supply 100% of the total demand of each retailer. A spot market allows for short term contracts to cover the difference between longer term contracts and real demand.

Auctions for new and existing generation capacity are carried out annually with new generation offered long term contracts. The regulator sets a ceiling price for these auctions.

There is a separate market operator and system operator. The market operator manages the long term and spot markets, with the marginal cost for the spot market



**Fig. 18.8** The Brazilian subsystems and regions (reprinted by permission from [18.4], ©CIGRE 2015)

provided by the system operator used as a reference for the spot market. The system operator is responsible for generation dispatch, power balance management and the coordination of ancillary services. The regulator oversees both operators.

There are four large subsystems as shown in Fig. 18.8 and there is a procedure to deal with transmission congestion within and between these regions where this impacts on lowest cost dispatch and contractual arrangements.

There are some specific market challenges that are currently being reviewed. These include the timely development of adequate transmission for sufficient generator competition and cross border flows. This is coupled with the growing interconnection of renewable energy sources, particularly when these occur as distributed generation that is not under the control and monitoring of the system operator.

## 18.6 Regulation

This section will examine the role of regulation in the operation of power systems.

### 18.6.1 Electricity as an Essential Service

Electricity is unique in that it must be available the instant it is required and must be consumed or stored the instant it is produced. Failure to meet these require-

ments results in a disruption to the power system where loads or generators may be tripped and, in the extreme, major power blackouts may occur. There have been examples of these blackouts in virtually all developed countries. They often lead to front-page news and government led inquiries.

There is no doubt that electricity is now considered an essential service in all developed economies. Fre-

quent loss of power or loss of power to customers for extended periods can lead to significant economic loss and have major political implications. Customers rely on electricity in almost every aspect of daily life from lighting and air conditioning through to the operation of most appliances as well as most aspects of manufacturing. It is becoming more and more important for transport and electric vehicles are predicted to overtake petrol and diesel fuelled vehicles as the preferred form of transport within the next twenty years. A number of countries have announced plans to phase out petrol and diesel vehicles including France, Germany, UK, China, India and Norway. While the timing for some countries is still being finalized, some have already declared a target year. For example, France has recently announced that it will outlaw the sale of petrol or diesel vehicles by 2040 [18.15]. China is currently studying the timing of a move to phase out fossil fuel vehicles and has commenced using incentives and subsidies to guide this outcome. It is currently the world's largest manufacturer of electric vehicles [18.16]. This has been driven partly by the growing smog problem in the major cities, partly by industrial policy and by commitments to acting on climate change.

Electric vehicles and a growing number of appliances rely on battery power as their energy source. While this is generally not the case at the moment, there is the opportunity to control the timing of charging of these devices so that the power demand is aligned to the capacity of the power system. There is also the possibility to use the electric vehicles as a source of ancillary services to the electricity system in the future. Accommodation of large scale charging of electric vehicles will require changes to industry operation practices and installed infrastructure capacity. A recent study by Vector in New Zealand estimates that power demand per dwelling could increase between 100% for slow trickle charging and 2000% for rapid charging [18.17]. Minimization of peak power increases and optimization of infrastructure usage will require a range of market design changes coupled with effective regulatory controls on both the utilities and the electric vehicle industry.

### 18.6.2 Vertical Integration and Disaggregation

As previously discussed, power system industry structures have evolved to take advantage of economies of scale, with large interconnected transmission systems allowing the shared use of generation reserves and larger, more efficient generators. In many cases this has resulted in vertically integrated business structures where the utility generates, transmits, distributes and sells the electricity. As discussed below, the introduc-

tion of competition between interconnected generators and also between retailers has placed more attention on the interconnecting networks. In some cases this has led to rules that financially ring fence the networks from the rest of the business. In others it has led to complete separation of the businesses.

### 18.6.3 Transmission and Distribution as Natural Monopolies

The transmission and distribution or network components of the utilities are considered natural monopolies as it is not economic to duplicate these components, and even if it were, it would be unlikely to be publicly or environmentally acceptable. As a result, the networks are in a privileged position and able to charge monopoly rents for the use of their services. It could be argued that too high a charge for service would result in the end customer going elsewhere for their power. However, this would almost certainly be at a much higher incremental cost and result in inefficient use of assets. Governments are well aware of this problem and in most countries have installed a regulator to oversee the investment in new assets and the allowed return on any investment in those assets. In other countries such as Brazil and Chile, competitive auctions are used to try to ensure the lowest cost provision, operation and maintenance of transmission infrastructure.

### 18.6.4 Economic Regulation of Monopolies

It is difficult for an external party to fully understand the internal costs of a utility or the link between investment and the quality of service provision. Attempts to build this understanding could lead to extensive duplication of resources, add significant costs to the process of oversight and therefore limit the benefits of regulation. The overall aim of regulation is to drive the business to deliver the desired quality of service at the lowest cost that is sustainable over the long term. Regulators therefore tend to focus on the outputs in terms of cost of service and delivery against prescribed service standards. At the simplest level, this may be a monitoring of the prices charged for the service, any annual increases relative to inflation and the performance against agreed service level targets. In addition, benchmarking with other similar organizations may be used to assess their relative efficiency.

While this may result in a lower cost of regulation, there may be a concern that the initial prices at the start of the regulation process may be too high. While benchmarking can help here, it is difficult to ensure a level playing field when comparing organizations. The historical timing of large investments and past decisions

on technical issues are linked to the perspective on future conditions at the time the investment decisions were made. For example, an expectation of a high load growth may lead to a choice of a higher standard voltage level and the use of larger standard transformers. Accurate load forecasting is notoriously difficult and this may lead to the investment appearing inappropriate in hindsight. In addition, utilities vary in size and small utilities have fewer opportunities to enjoy the benefits of economies of scale.

Services are normally classified as regulated or non-regulated services. Regulated services are those not subject to adequate competition to drive lower prices and are normally classed as monopoly services. Conversely non-regulated services are those that are subject to competition (say by means of an auction) or can be provided by a number of entities. Classification of these services can be complicated further when the utility is vertically integrated. In this case it is possible for the utility to load additional costs into the network part of the business, which has the added benefit of allowing the utility to charge lower prices or make larger profits in the unregulated generation or network parts of the business. To some extent this can be overcome by requiring financial ring fencing of the regulated network components of the business but this still carries the risk associated with the regulator having less information on the internal workings of the business. In a number of cases, this has led to a requirement for the vertically integrated business to sell its network assets.

### 18.6.5 Rate of Return Regulation

For this form of regulation, the regulator scrutinizes the utility investment to ensure that the investment is required and efficient. It then allows sufficient revenue to ensure the utility fully recovers its costs. This form of investment is popular with investors as it allows a consistent return despite fluctuations in the economy. However, it does not provide strong incentives for the utility to operate efficiently.

### 18.6.6 Price Control

To reflect the information asymmetry between the regulator and the utility, regulators often choose to use incentives to drive the business to improve its efficiency. In this case, if the utility spends less than forecast for the regulatory period, it will be allowed to keep a portion of the difference between actual and forecast revenue as a reward. Conversely, if the utility spends more than forecast, a portion of the difference between actual and forecast revenue will be applied as a penalty. In both cases, this will then be taken into account when setting

desired revenue and consequent price settings for the next regulatory period.

### 18.6.7 Revenue Determination

A more intrusive regulatory model is to require the network business to propose and justify its required revenue for a regulatory period that could typically be five years. This revenue would be determined based on the total anticipated efficient capital, operating and maintenance costs over the regulatory period together with asset depreciation, tax liabilities and a commercial return on the capital investment. To determine the capital costs, an asset valuation of all existing and proposed new primary and secondary assets would be required. Then a rate of return on this capital would need to be proposed based on identified risks and known costs of capital. This would typically be based on allowing a reasonable return on equity to reflect efficient equity finance costs and a return on debt that reflects the costs of regularly sourcing debt within the regulatory period. As part of the revenue determination model, revenue cap or price caps are usually applied for the regulatory period to apply incentives to the utilities and provide price certainty.

### 18.6.8 Revenue Cap

Revenue cap regulation fixes the revenue that the utility can receive regardless of actual output or demand. Prices are set based on the allowed revenue and forecast electricity consumption but if actual consumption differs from forecast consumption, the allowed revenue is corrected in the following year. There is therefore no incentive to incorrectly forecast the expected consumption. In this model, prices may be more volatile if demand is less predictable. It is also possible to apply an incentive in the form of  $CPI - X$ , where  $CPI$  is the general inflation rate in the economy and  $X$  is an estimation of the utility's expected efficiency gains. This provides a very strong incentive to find efficiency gains.

### 18.6.9 Price Cap

For price cap regulation, prices are regulated rather than the revenue. The initial starting price is set and then it is adjusted each year by  $CPI - X$  as described for revenue cap regulation. If electricity consumption rises in the regulatory period, revenue will increase and if it falls, revenue will reduce. This should encourage the utility to adjust the timing of investments to suit changing load expectations and to drive efficiencies harder when consumption falls. On the other hand the  $X$  is known in

advance of the regulatory period, which allows the utility to plan and deliver efficiencies over the period.

In reality there may be limited opportunities to take action on investment timing, as is the case for transmission, which usually has long lead-time projects. It is therefore more common to use price cap regulation for distribution investments, as these are usually more short term.

### 18.6.10 Pricing Methods

The subject of electricity pricing is complex and varies from country to country. This section will provide a high level overview of this topic. More detailed information can be found in the reference documents referred to in Sect. 18.7.

Ideally pricing should be efficient in that it recovers all the required revenue of the utilities while providing signals to customers that support the efficient use of electricity. Unfortunately, many practical issues may interfere to tarnish this objective. Governments are well aware that any large increase in electricity prices can cause headaches for them and therefore often place controls on the actual prices that can be applied. In some cases the government will subsidize the end price in order to deliver on social issues. In addition, ambitious renewable energy targets have been set by governments to combat climate change. To help increase the rate of installation of the renewable generators, subsidies have been applied either as payments for the surplus energy generated or by direct government payments that effectively reduce the capital cost of the renewable generator installation. As the efficiency of both the technologies involved and the production processes have improved and significant economies of scale have been achieved, the level of subsidy has been reduced.

The cost components of the pricing are driven by the wholesale prices from the generators, the network prices from the transmission and distribution companies and by a charge from the retailers. All of the participants will need to recover fixed and variable costs. However, accurately modeling the end charges on each of the total fixed and total variable costs will not necessarily produce the ideal result. For example, one could argue that the majority of costs incurred by a network business will be fixed costs as they are either incurred as a result of capital investment in the infrastructure or maintenance costs incurred to support the infrastructure. Once the investment decisions are made, neither of these costs varies over time. Network costs generally make up a proportion of between 30 and 50% of total costs.

Fossil-fuelled generators will have a higher proportion of variable costs. While they still need to recover

the capital costs of the generator, the dominant cost will be the fuel. In the case of renewable generators such as wind and solar, the majority of the costs are fixed as the fuel is free leaving only maintenance as a variable cost. However, maintenance costs can be substantial for offshore wind turbines. Hydro is also dominated by fixed costs and nuclear is mostly a fixed cost, as it must continue to operate regardless of the demand from the end customer. If these costs were all passed through directly to the end consumer, the main component would be a fixed charge. There would then only be a small price signal to the end customer to vary their consumption at various times of the day.

variable prices can be used to encourage customers to apply demand management to reduce the peaks and troughs of daily load consumption. This should reduce the need for investment in new generation and network capacity as well as improve the utilization of existing infrastructure. Despite the difficulties in accurately providing cost reflective pricing, variability in pricing is a useful tool to encourage customer behavior that will lower overall costs.

Generators would prefer to operate at their maximum output whenever they are available, particularly in the case of base load generators such as coal, nuclear and combined cycle gas turbines. Open cycle gas turbines and large storage hydro generators are generally more flexible but are still keen to maximize their revenue, whereas solar and wind want to operate at their maximum possible output whenever the sun shines or the wind blows. In a market context, these parties are likely to price their output to ensure optimum output. This price will also be influenced by any longer term bilateral or hedging contracts that are in place.

End customers, on the other hand would like the electricity to be available at all times of the day and night at 100% reliability. They are however open to price signaling and, in many cases, would be prepared to vary their consumption to reduce their overall costs. This is becoming more and more possible with the advent of new technologies such as smart metering and remote appliance switching. Many household appliances are now available with batteries and some industries may be prepared to reduce demand occasionally for a fee.

Tariffs are determined by considering each class of customer. For example, domestic and other low use customers require more infrastructure and their peak loads are concentrated at times of the day that match system peak loads. On the other hand, industrial loads are generally fed by less network infrastructure and consume a more uniform load throughout the day. They can therefore be charged a lower tariff. Usually the tariff will have demand (\$/kW) and energy (c/kWh) compo-

nents with the demand charge higher for more peaky loads. Where meters have suitable capability, time of use tariffs are used to try to influence demand and reduce the overall system peak or to shift demand to times when renewable energy is abundant. Overall the setting of tariffs is partly political and social and is not an exact science. However, as technology improves, there are increasing opportunities to provide customers with more choice about the reliability and cost of their electricity and suppliers with a greater understanding of the impact of price signals.

Electricity pricing is set to try to achieve a balance between adequate signaling of the generator's desired mode of operation and meeting the end customer's needs for electricity availability at the best possible price. This applies regardless of whether the generators signal their requirements through a market structure or as regulated entities. Governments often intervene in the price setting to meet social objectives, particularly at the domestic customer level. For example, they may apply a uniform tariff across the entire customer supply area so that customers in the central business district pay the same price as those in remote country areas despite the fact that it costs much more to supply the remote customers. If the remote customers were to be charged based on the real costs to supply them they may choose an alternative such as a stand-alone supply.

The approach to pricing across the world varies depending on a range of factors, particularly related to the level of power industry restructuring. CIGRE Working Group C5.16 [18.18] has surveyed a number of countries to determine the types of costs that impact on end user billing and the methods and trends for practically allocating costs in both regulated and competitive market environments. The survey concluded that the main electricity cost drivers are a mix of fixed costs, capacity costs and variable energy costs. The retail billing components therefore include a balanced mix of fixed charges for common shared customer costs, demand charges for capacity, energy charges for fuel and other operating costs and policy charges for taxes and other externally imposed costs. The survey revealed that the extent of using demand charges varied widely, driven to some extent by the desire for rate simplicity, metering limitations and historical perspectives on electric service.

Large scale embedded generation has a significant impact on the use of the network. When combined with storage and smart meter enabled load control, the use of the network can be reduced to zero for extended periods. This has significant implications for transmission and distribution pricing. Most domestic electricity consumption is measured in kilowatt-hours and virtually all network costs are fixed, based on a return

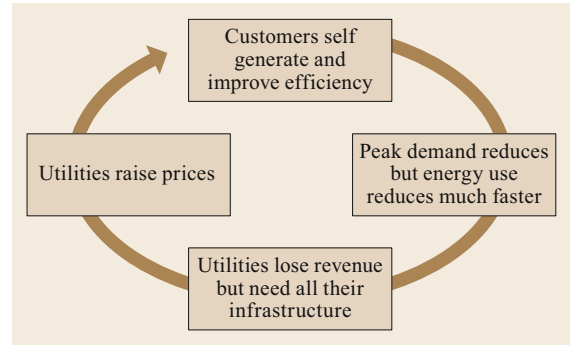


Fig. 18.9 The death spiral

on the large capital investment and operating costs to operate and maintain the infrastructure regardless of the energy that flows through the system. To maintain the required revenue to service the network costs when energy consumption is falling requires the price on a unit of energy to be increased. This may lead to more customers investing in distributed generation with consequent higher energy delivery prices. This leads to what has been termed a *death spiral*, where the rising costs increase exponentially as the energy reduces (Fig. 18.9). Ultimately this could lead to prices for connection to the network being so high that no one can afford to connect.

Rapidly increasing prices is one possibility and will depend on the responses of the network utilities and the development of new technologies. While significant installations of roof top solar are likely to continue, helping to exacerbate the above problem, large-scale renewable generators are still more economic than small-scale generators and these will require transmission lines to bring this energy from remote locations to load centers. This may encourage greater use of the network resulting in lower per kWh customer charges. In addition, individual houses that have surplus generation may want to trade this with others in the neighborhood. This will again require greater use of the network and will exert downward pressure on network prices. Electric vehicles and electrification of heating are also likely to increase demand on the networks. Ideally incentives will be placed on this increasing load to minimize the impact on peak loads. A key factor will relate to how the pricing structures adapt and how the customers respond to these changing opportunities.

### 18.6.11 Performance Reporting

While keeping the end price of electricity as low as sustainably possible is a key focus of regulators, it is also important to ensure technical performance is maintained or, in some cases, improved. One of the ways that

regulators can keep tabs on the relative performance of monopoly network businesses is to require performance reporting. As discussed earlier there may be some difficulties comparing different organizations, particularly if they have different histories and current environments. However, comparisons will provide some useful information and the tracking of performance of a particular utility from one year to the next is certainly an effective model.

Utilities will generally use a number of both financial and technical performance indicators to help drive performance improvement in the organization. A number of these are likely to end up in the utility annual report as direct feedback to staff, stakeholders and shareholders. The regulator may use the annual report or even ask the utility to nominate certain indicators. They may also have additional requirements, especially where there is required ring fencing of monopoly components within the organization.

Regulators may also use a financial reward and penalty scheme to provide an incentive for the utility to improve performance. For this to work well, it is important to ensure that performance targets are reasonable and the rewards are sufficient without being excessive. Incentives may also be provided to drive innovation. Network utilities are necessarily conservative in their operations as large scale extended black outs can be catastrophic for both the utility and the country. With this rider, it is important that the regulatory controls do not stifle innovation, which can improve performance or reduce costs. In some cases, a value of loss of load may be used to justify network investments. This is often based on survey results to determine the value of the electricity to the customer at a particular time of day. This perceived value would tend to vary depending on how recently the respondents have experienced a black-out. Regulators therefore tend to prefer a lower value for this, although it is still usually significantly greater than the normal energy charge and will vary depending on, amongst other things, whether the supplied area is the central business district, a commercial area or a suburban domestic load area. Smart meters and dynamic pricing may also provide useful data for the customer electricity valuation adopted by the regulator.

### 18.6.12 Regulated Versus Non-Regulated Services

Within the transmission or distribution business there may be services that the utility provides that are not obligatory and can be provided on a contestable basis from a range of suppliers. These are not regulated but need to be ring fenced from the regulated business to ensure no cross subsidies. In some cases, transmission

and distribution connections are not part of the regulated income and the connection can be either built by the user in accordance with prescribed standards or be subject to a separate competitive tender.

Similarly a utility may choose to build a transmission interconnector as an unregulated asset or merchant line. In this case, it would not have a regulated income but derive its revenue from users that wish to utilize the asset on a pay for service basis. These kind of interconnectors are not common but have generally been used to link power systems where the price in one system is different to the price in the adjacent system. The transmission business then leverages this difference to fund the cost of the interconnector. These types of interconnector are less popular due to the much higher risks involved as the price differentials between the adjacent systems can vary over time and investors tend to prefer the long term certainty of a regulated return on the asset.

### 18.6.13 Treatment of Losses

Electricity is produced and used at many different locations and there are product losses as it is transported to the loads. Generation must make up these losses at all times, which, on a typical system, tend to be on average in the order of four to five percent. The value of these losses will vary from one location to another, depending on the distance and transmission or distribution voltage. These losses have an economic and environmental cost. Network businesses may have an incentive within their revenue or price control to reduce the losses. However, these are not always under their control. As dispatch of the generators in different locations changes so too will the current flows in the network and the losses will increase or decrease with the square of the current. This may occur in relation to large generators connected at transmission level or for distributed generators such as rooftop solar. In some countries the penetration of rooftop solar is so significant that at some times of the day the current flow reverses away from the load back into the transmission system. A useful discussion on the management of network losses can be found in a recently published CIGRE reference paper [18.19].

There are some losses that can be controlled by the network businesses but for this to be meaningful there needs to be accurate metering at the points of connection of loads or generators. While the end customer load will have tariff quality metering, the generators may not. Certainly, many rooftop solar systems will not currently have metering and their input will simply be seen by the customer tariff metering as a reduction in load.

Where the metering issue can be resolved, there may still be issues such as electricity theft and the re-



duced accuracy of meters as they age to deal with, although this latter aspect is less of an issue for digital meters. It may therefore be more practical to provide a reward for the utility that reduces losses when it provides specific evidence of the cost benefit for the particular location where the action has been taken. For example a transmission line voltage could be increased or a high loss transformer could be replaced with a low loss transformer.

#### 18.6.14 Metering/Smart Meters

As mentioned in the above section on losses, tariff meters provide a very important role in the management of the power system. They ensure that customers are paying the correct amount for their service and that the utilities receive the required recompense for the service they provide.

In recent times, smart meters have been introduced into an increasing number of countries. A smart meter may vary in complexity but fundamentally it consists of a tariff meter that records electricity consumption in intervals of one hour or less and is able to communicate with a central control system. In some cases the meters have been introduced to combat theft and in other cases for a range of technical solutions that enable customers to manage their load and reduce their cost based on price signals provided by the utility.

For example there may be a shortage of generation resulting in a very high wholesale price. The smart meter could be sent a signal from the retailer, the supplier or the load aggregator asking for load to be reduced. This would normally be based on the contractual relationship between the company and the customer. One input to the company's decision-making could be scarcity price signals from a power exchange or congestion price signals from a system operator. The smart meter could then send a signal to various appliances either switching them off or reducing their load. One of these could be a non essential load such as a pool pump or an air conditioner that could be switched to run with a fan only for say 15 min in the hour. The customer would receive a reduced tariff to compensate for the inconvenience of the power reduction. Various appliances can also be set in advance to operate at times of low demand. Ultimately, with the use of batteries at the load point, it would be possible to match the load to the ideal generation profile. In the case of wind and solar, this would be when the sun shines or the wind blows. While some countries have taken major steps to roll out smart meters to all or most customers, the technology is still considered expensive by some, especially if it requires the replacement of perfectly good meters that are already installed at the load points. Evaluating the full

costs and benefits is complex and the subsequent large capital investment may prove difficult to justify without some overriding government policy directive.

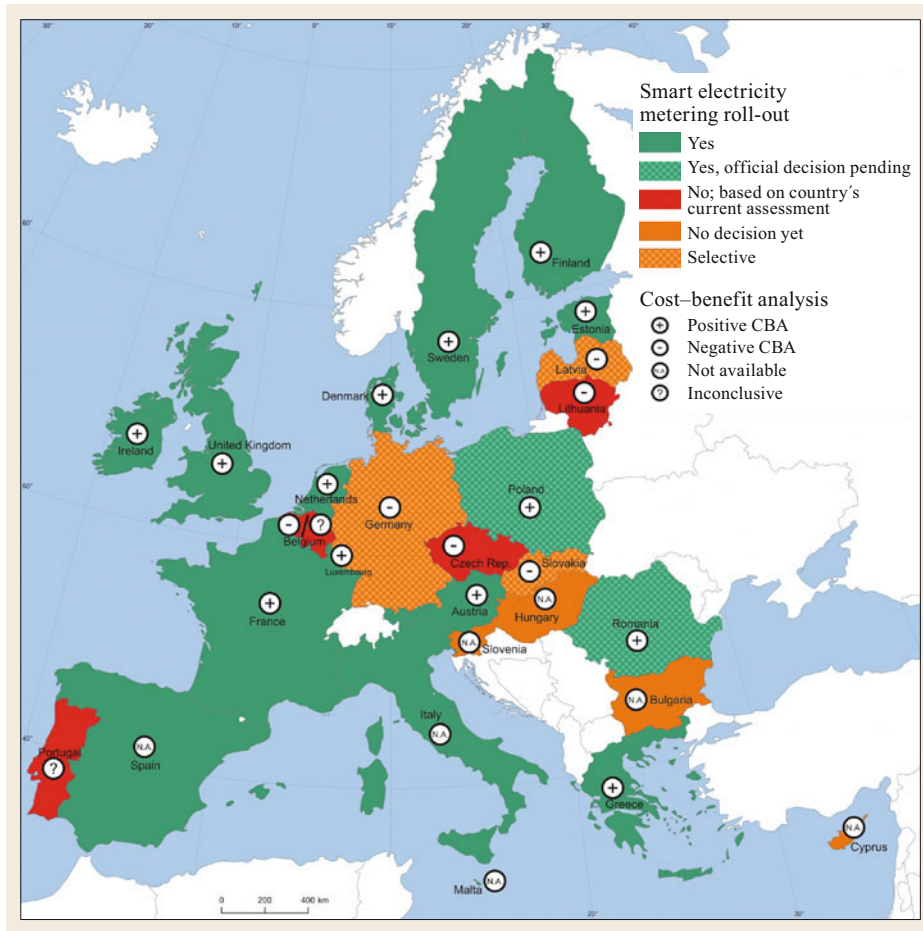
The European Commission has directed that 80% of customers should have smart meters by 2020, providing an incentive for member states. Some countries (e.g., Italy and Spain) had already rolled out smart meters and other countries are well on the way (e.g., France and the Netherlands) but others are well behind (e.g., UK and Germany) [18.20]. Figure 18.10 shows the current (2017) responses from member countries, as reported by the EC Joint Research Center Website.

Other parts of the world have also made progress with the installation of smart meters. For example, in Australia, Victoria has achieved a 96% rollout and there has also been a significant rollout in South Australia and New South Wales. A national electricity market rule now requires smart meters for new and replacement meters. In China more than 400 million meters had been rolled out by 2017 whereas in other parts of the world such as Eastern Europe, Latin America, the Middle East and Africa, the rollout has been quite limited [18.22].

#### 18.6.15 Technical Regulation

In parallel with economic regulation it is also desirable to monitor the technical aspects to ensure the power system delivers the required reliability and quality. Instantaneous matching of supply and demand is required if the power system is to meet the required standards. It must also withstand sudden disturbances such as system faults and deliver electricity within prescribed bands of voltage and frequency. In addition, interference such as harmonic distortion must be managed to ensure customer equipment does not mal-operate or become damaged. In order to manage these impacts, power systems are designed with a level of redundancy, installed equipment must meet prescribed standards and steps are taken to reduce power quality issues such as harmonic distortion to within prescribed limits. The level of reliability and quality is usually chosen to meet customer needs and will usually vary from major city central business districts where high levels of redundancy and power quality are required to remote rural loads, which would normally have lower standards. The chosen standards are also limited by economic limitations.

It is also important that customers that connect to the network meet required standards as they may impact on other customers that are connected. These standards are designed to assist the system and network operators to meet system standards. For example, the sudden switching of a large load onto a network that is not rated to take it may result in large unacceptable voltage swings for nearby customers and in the extreme, may cause the



**Fig. 18.10** Smart metering rollout (EC Joint Research Centre, 2017) [18.21]

supply circuit to trip causing loss of supply to other customers on the same feeder. There are also safety standards that must be met to ensure public safety.

While the power systems are designed and built to meet the prescribed standards, they must also be operated within defined rules to ensure the required power system performance is delivered. Prior to the deregulation of the electricity industry and the introduction of electricity markets, many of the technical issues were managed internally by the various electricity businesses. Open competition amongst generators and amongst retailers has meant that the technical rules and standards are required to be public. This ensures clear accountability and avoids accusations of bias, particularly if vertically integrated utilities are involved.

### 18.6.16 Technical Rules

Published technical rules or grid codes now governs many utilities. These documents may have been produced by utilities but they will normally have been

subject to review and public consultation by regulators prior to publication. It is beyond the scope of this chapter to go into detail on the technical rules; however, the section on regulation models around the world will highlight some of the differences between countries and provide references to the various documents that are applicable in those countries.

A recent CIGRE publication on the review of drivers for transmission investment decisions [18.23] has established that the main reason for expansion or new build projects is security of supply followed by new connections, generation integration and economically motivated projects. The report also noted that compliance with technical planning criteria is the primary determinant of reinforcement and that most transmission investments are made on a long-term basis. In a number of cases, changes to planning criteria are being made to reflect the changing industry, particularly in relation to integration of high levels of renewable energy sources. In addition, changes are also being made to accommodate new technology or industry wide prac-

tices. In many cases, economic principles such as the cost of unserved energy and societal impacts are considered as part of the review of the planning criteria.

### 18.6.17 Service Standards

The earlier section on performance reporting referred to the technical performance indicators that regulators monitor to ensure that cost cutting does not result in poor service outcomes for customers. This requires the relevant utility to publish its performance against the various service standards. These service standards may relate to the frequency of interruptions to supply or the duration of the outages.

### 18.6.18 Environmental Regulation

In addition to all the technical requirements necessary to deliver a sustainably reliable power supply at a reasonable cost, many countries have imposed additional environmental requirements on the electricity utilities and their customers. These may be at a local level, say for an individual town, a region or state level, an individual country or for an entire continent. While the various political leaders may agree these at a high level, the detailed interpretation and implementation of the requirements is left to individual areas. In most cases, satisfying these additional requirements will add costs to the delivery and consumption of power. While some attempts have been made to quantify the costs of inaction on these issues, they are not yet universally accepted.

### 18.6.19 Climate Change

Climate change is an issue that has maintained considerable global attention for a number of years. In December 2015, 195 countries agreed to a global climate deal that is legally binding [18.24]. This agreement aims to limit the increase in CO<sub>2</sub> emissions from those countries to a level that scenarios indicate would restrain the increase in average global temperatures to significantly less than 2 °C above pre industrial levels and ideally as low as 1.5 °C above. While the global commitment has remained resolute for most signatories, at the time of writing the US appears to be reducing some of the previously committed actions where it believes they will have a negative impact on its economy [18.25] and, it is reported that many countries are expected to fail to meet their commitments.

The actions taken by countries in relation to these climate change commitments will directly impact on the electricity sector, particularly where they are reliant on fossil fuels. Common actions to be taken relate to

use of less fossil fuels, an increase in renewable energy, control of CO<sub>2</sub> production and a drive to improve energy efficiency. Each of these actions can have a direct impact on costs of electricity and interfere in the pure economic drivers in a commercial market. Regulatory oversight is required to ensure actions and related cost impacts are clear, open and accountable.

### 18.6.20 Energy Efficiency

Energy efficiency refers to the ability to produce more for the consumption of less energy. The World Energy Council has produced a useful report on the current status of energy policies around the world [18.26]. It considers the policies and trends that are occurring in relation to this topic. Energy efficiency is one of the simplest ways to reduce the impact of fossil fuels on the environment as well as ensuring a more sustainable approach to the use of the world's scarce resources. Often it can pay for itself in a relatively short period. Some countries have set aspirational targets and others have legislated to eliminate some of the less efficient plant, equipment and appliances. Others use labels to advise consumers of the appliance efficiency at the time of purchase.

A key problem in relation to energy efficiency relates to the disaggregated nature of the supply chain. If the maximum end customer benefits are to be achieved, the reward must be spread appropriately across all parties that contribute to the efficiency. This will require clear price signals and profit incentives that encourage an integrated approach to the problem.

Within the electric power system, efficiencies can be gained by modifying the design, construction and operation of the system components, reduction of network losses (while avoiding suboptimal generator dispatch) and the use of energy storage. The use of smart meters and intelligent devices allows the ability to control and influence consumption rates and timing, which can improve efficiency of the whole system. Choosing the optimum mix of these factors will determine the ultimate system efficiency.

The various aspects can be described as shown in Fig. 18.11 as presented at the CIGRE symposium in Bologna [18.27].

Various approaches can be used to encourage energy efficiency. The electricity market can send signals and reward efficient operators; although to work well, this would require access to storage and demand side management together with clear price signals. Regulatory targets can be set, although this can be distortionary as it may lead governments to back politically attractive technologies. International standards can improve interoperability as long as they don't stifle innovation and competition.

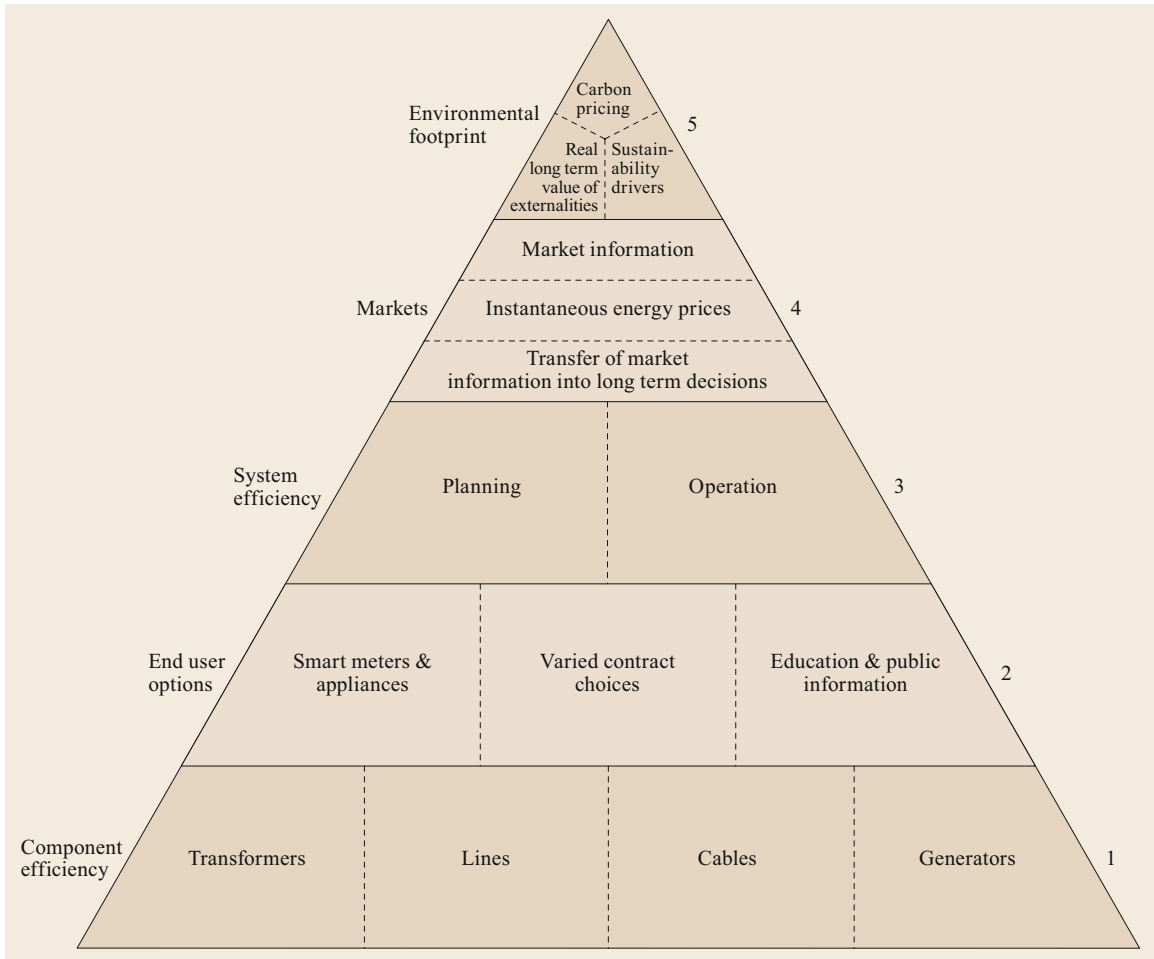


Fig. 18.11 Energy efficiency pyramid (reprinted by permission from [18.27])

### 18.6.21 Visual Impact

As power consumption around the world has increased so have the number, size and density of transmission lines and substations. In addition the growing number of large-scale renewable energy projects that are adding to and sometimes displacing existing fossil fuel generators are driving further construction of new transmission lines. In some cases transmission interconnectors are being built to connect the diverse generation and load portfolios of adjacent countries in order to lower the overall cost to customers. Line routes to supply the cen-

tral business districts of large cities are also becoming more difficult and expensive to procure. In many of these cases there is considerable public opposition to the construction of these assets due to the visual impact. As a result, more lines are being placed underground or, at the very least, suboptimal line routes are being used to avoid contentious areas. These changes will generally lead to increased construction costs, which will need special consideration by the regulator. Evidence needs to show that the chosen route was the lowest practical cost for the service provided and that the utility has not simply taken the easy way out.

## 18.7 Regulation Models Around the World

This section considers a few examples of the regulation models applied across the world. There are similarities between them as well as an overall consistency

with the descriptions above. Some detail has been provided to demonstrate the differences between the countries that often reflect the history of evolution of

electricity markets and deregulation within the different regions.

### 18.7.1 United States

In general the US follows the methodologies discussed above although this varies between states, unless it falls under the jurisdiction of the federal regulatory body. The following discussion highlights a few general points in relation to the US. One source of a more detailed examination can be obtained from [18.28].

The majority of utilities are privately owned with the remainder mostly owned by government entities or local communities. Electricity generation is generally fuelled by coal, gas and nuclear with some hydro and a growing proportion of solar and wind.

In recent times there has been a huge surge in gas generation, which has coincided with the rapid expansion of the use of shale gas. This has resulted in the replacement of a large number of aging coal fired generators. The US is now considered to be the world's leading natural gas producer. When operated in parallel with intermittent generation from wind and solar, open cycle and to a lesser extent combined cycle gas turbines are more able to follow rapid changes in generator output than coal and nuclear and gas has the added advantage of emitting lower greenhouse gases than coal.

Some states have unbundled their transmission and distribution monopoly components from the contestable generation components.

Regulation generally occurs at a state level unless it relates to interstate transmission. This will include any part of the state system that has an impact on the interstate transmission as well as the transmission interconnector itself. The federal regulatory body is known as the Federal Energy Regulatory Commission (FERC). Third party access is allowed to the transmission system by law and the tariff for access is approved by FERC. The North American Electric Reliability Council (NERC) oversees reliability and the adopted standards are legally binding.

Generally in the US, rate of return regulation is used and this provides a steady stream of revenue to cover the costs to the utility of producing, transmitting and distributing electricity. Electricity regulation is used to protect public interest and allow access to all at an approved price.

The scope of regulation in the US generally follows the principles described earlier in Sect. 18.6. This includes revenue determination and the setting of prescribed service standards and prices to customers. Many states are being influenced by legislated environmental requirements, particularly in relation to the use of renewable energy. The costs of implementation of these

requirements fall under the jurisdiction of the regulators assuming the utilities wish to recover these costs as regulated revenue. There is also some oversight of the boundary between regulated and unregulated revenue to ensure no cross subsidies. This may require the use of subsidiary companies.

In general there is no prescription on the timing of when a utility should seek regulatory approval of a major review of prices and service standards. However, this normally occurs every two to five years.

The review process generally involves a hearing where the utility presents evidence to justify the requested changes. A process of interrogation then follows where the utility may present expert witnesses and, in some cases, other affected parties may provide evidence. There is also usually an opportunity for the general public to provide comment or evidence. Negotiations then commence with the goal of achieving an agreed settlement on the final outcome. Ultimately this leads to a final order by the regulator.

Annual costs are determined based on analysis of actual expenditure and revenue in a past year, taking into account the effects of weather and any other significant disruptions and expenditure forecast for a future year. The process requires the utility to submit these costs as evidence to support any required rate increase.

Utilities are allowed to earn a reasonable rate of return on their regulated asset base considering the level of risk they are facing. Traditionally this would have been a relatively low risk, although there may be some argument that this risk is changing with the rapid growth of renewable and gas generation leading to a lower demand for existing coal generation. This new generation may be installed at different locations to the existing facilities leading to some level of stranding of transmission assets. The rate of return is normally calculated as a weighted average cost of capital taking account of the varying rates for equity and debt.

While traditional costs are relatively consistent each year, significant events such as major storms or the closing of a nuclear power station are usually considered separately.

Tariffs are determined by considering each class of customer as described in Sect. 18.6. Charges for connection to the electricity network are subject to regulation and may include cross subsidies if this is considered an economically efficient way of recovering costs. The charges are required to have reasonable terms and conditions set at a fair price.

### 18.7.2 Great Britain

In Great Britain, generation assets were split from network assets as part of major reforms to the electricity

sector in 1990. Transmission was divided into three parts each of which is now privately owned. One sector was a combination of England and Wales, another was northern Scotland and the third was a combination of southern and central Scotland. There is one system operator for the whole of Great Britain, National Grid Electricity Transmission plc (NGET), which is also the owner of the England and Wales transmission system. There are 14 licensed distribution companies, which are owned by six different groups. There are also a number of smaller distribution network operators.

All of these transmission and distribution companies are considered natural monopolies and are regulated by Ofgem that also has a role to oversee the operation of the markets.

The transmission and distribution networks are regulated by an RIIO framework where revenue = incentives + innovation + outputs. This model is intended to drive improvements in performance in relation to both safety and reliability and lower costs for customers by providing incentives for the network businesses. It is also intended to encourage addressing wider environmental objectives such as those associated with climate change. To this end it encourages innovation, recognizing that this may have a higher risk than traditional investment. The framework is used to set price controls for a period of eight years.

While Ofgem requires each network business to submit proposals on how it will deliver within the RIIO framework, it also provides a number of documents on how the submissions should be structured and the information that should be provided. Amongst other things, these include comment on expected content in relation to the environment, stakeholder consultation, losses and innovation. Network businesses are required to propose for approval, performance targets with financial penalties and rewards, an allowed revenue requirement and mechanisms that would be used to cover unforeseen developments that may require changes to the allowed revenue.

The success of the latest scheme may not be fully understood until the next regulatory period is reviewed in 2021; however, Ofgem is already proposing that a more onerous scheme will apply in the next review. It is claiming that there have been significant improvements in reliability, costs to customers and customer satisfaction under Ofgem's current and past regulation [18.29].

The framework also gives an incentive for the network businesses to reduce losses, which are the main opportunity to improve energy efficiency, provided the solutions do not lead to suboptimal generator dispatch. Losses include theft as well as those on the network. Network businesses are required to publish their strategies

to reduce their losses as part of their compliance with the RIIO framework. A useful reference has been published by Ofgem titled *Energy efficiency directive: An assessment of the energy efficiency potential of Great Britain's gas and electricity infrastructure* [18.30].

As regulation has developed in the UK, so has its complexity with regulatory submissions running into hundreds of pages that provide considerable detail on how they propose to deliver on their expenditure and performance targets.

One of the changes made under the new regime is to consider the total proposed expenditure rather than separately considering operating and capital expenditure. This reflects a view that there has been cost shifting between the two categories in the past.

A further change is the eight-year period rather than the previous five-year duration. Longer time frames are possible as the industry and Ofgem are now more mature and both sides have considerable experience. It also reflects the fact that transmission and distribution investments are generally long term. There is still some risk that technological change will accelerate the transformation to alternative forms of energy provision and produce an unforeseen risk on the network companies. However, this can be dealt with to some extent by the change mechanisms that are built into the regulatory process.

### 18.7.3 Australia

The Australian Energy Regulator (AER) [18.31] carries out regulation of the electricity sector in Australia other than in Western Australia. This includes monitoring the operation of the electricity market and the allowed revenue of the network businesses. In Western Australia the Economic Regulation Authority (ERA) [18.32] carries out a similar but independent role. Consideration was recently given to moving the role to the AER, but it remains with the ERA at the time of writing. Network businesses are considered natural monopolies and have to submit proposals to the AER on their required revenue in accordance with a prescribed framework and timeline. This framework is set out in national electricity law and rules. The approach is similar to the RPI – X incentive regime that was used in the UK prior to the implementation of the new RIIO regime. In this case, the X is an efficiency factor and the regulator expects the business to find a range of efficiencies that exceed those driven by this framework. As the revenue is approved for a five-year period, there is an incentive for the network business to reduce expenditure by more than the regulated X factor over the period and therefore increase its profits. The regulator can also look at these found efficiencies and factor them into the next review.

During the review process, factors considered include the projected electricity demand, the age of the infrastructure, operating and financial costs and network reliability and safety. Decisions usually apply for five years. Under the prescribed framework, the AER determines the allowed revenue for the business that covers its efficient costs by using a building block model. These building blocks include capital expenditure, operating and maintenance costs, asset depreciation and taxation liabilities. The AER also determines an allowed rate of return on capital taking into account debt, equity and risk issues amongst other things. The incentive to defer cost savings towards the end of the regulatory period that may occur in a traditional CPI – X regime is counteracted by an efficiency carryover mechanism in the building block approach.

The AER also reports on the performance of the market and electricity businesses including customer issues relating to affordability and disconnection of customers for non-payment of bills. It also administers a retailer of last resort scheme as a protection for customers in case an electricity retailer fails.

As for the UK model, the Australian regime is evolving. The current rules are quite prescriptive and revenue submissions run into many hundreds of pages. The prescriptive nature of the regime makes it quite difficult to make changes that may produce more favorable outcomes for the customer. Under the original process, the network business could appeal if it perceived the regulator's decision to be unreasonable. On the surface, this appears acceptable as the regulator is attempting to strike the correct balance between the long-term interests of the customer and those of the network business and various decisions may therefore be subject to challenge. Also, an appropriate return is necessary to ensure that the network business owner will continue to invest its capital. However, there were a number of concerns raised that, amongst others, the process produced unjustifiably higher prices for cus-

tomers, the long process led to significant regulatory and price uncertainty and that the appeals may be related to procedural correctness rather than the merits of the outcome. As a result, the appeal process has been removed, except for decisions related to the disclosure of confidential or protected information. The lawfulness of the regulator's decision can, however, still be subject to a judicial review in the Federal Court. This limits the review to breaches of the rules of natural justice or errors of law rather than the merits of the regulator's decision.

#### 18.7.4 Nordic Countries

Deregulation in the Nordic countries started in Norway in 1991 followed by Finland in 1995 and Denmark and Sweden in 1996. There is one transmission system operator in each country and a large number of distribution companies (varying from 84 in Denmark to 380 in Sweden). Consistent with previously discussed models, revenue cap electricity regulation is now used in all the Nordic countries.

Differences in approaches in each of the Nordic countries are in the detail. For example different models are used for deciding the allowed rate of return. In addition, the assessment of the regulatory asset base varies leading to large differences in the applied revenue caps. Similarly, benchmarking and efficiency targets may be applied differently. The regulatory period is one year in Denmark, four years in Finland, five years in Norway and four years in Sweden.

Incentives are provided to ensure reliability is maintained despite incentives to lower costs. These vary between countries, but in all cases attempts are made to relate the rewards and penalties to the customer value of the reliability.

NordREG, the Nordic energy regulator, has produced a detailed overview of the economic regulation of electricity grids in Nordic countries [18.33].

## 18.8 Conclusion

This chapter has provided an overview of the current state of electricity markets and associated regulation. This has included the development of the electricity industry structure and its organization. A more detailed explanation of electricity markets and the various models that have been adopted to facilitate competition then follow, as well as some examples from around the world. A similar approach has been used to explain the use of regulatory oversight.

The chapter is necessarily at a reasonably high level and the reader is encouraged to further explore at a more detailed level to view the latest developments and in depth explanations regarding the design and operation of market and regulatory schemes that are used across the world. Widespread adoption of electricity markets is relatively recent, occurring over the last twenty-five to thirty years and the models used continue to be developed and refined.

The drive to reduce the carbon footprint of electricity supply while ensuring the end price to customers remains affordable is ongoing. To some extent this is dependent on the evolution of existing and the development of new technologies. This includes storage mechanisms such as batteries, new distributed generations and a range of new smart load control processes. Some of these will increase the number of competitive generators and loads in the market as well as change the nature of their operation. In some cases this may put pressure on the traditional monopoly

status of the network businesses. Electricity markets will need to evolve to facilitate the new forms of trading and customer expectations. In addition, regulatory oversight will need to change to ensure it supports market developments that benefit the end customers.

**Acknowledgments.** The Authors would like to thank Keith Bell, Scottish Power Professor of Smart Grids at the University of Strathclyde, for his valuable feedback on the market in the United Kingdom.

## References

- 18.1 L. McDonald: *A Colossal Failure of Common Sense, The Incredible Inside Story of the Collapse of Lehman Brothers* (Ebury Press, London 2009)
- 18.2 R. Munoz: Solar eclipse's effect on power demand proved a yawn for utilities, <https://www.reuters.com/article/us-solar-eclipse-usa-grid-idUSKCN1B221P> (2017)
- 18.3 CIGRE: Capacity mechanisms: needs, solutions and state of affairs, <https://e-cigre.org/publication/647-capacity-mechanisms-needs-solutions-and-state-of-affairs> (2016)
- 18.4 CIGRE: Market operators – Their evolution, current organization and future structure, [https://e-cigre.org/publication/ELT\\_282\\_3-market-operators--their-evolution-current-organisation-and-future-structure](https://e-cigre.org/publication/ELT_282_3-market-operators--their-evolution-current-organisation-and-future-structure) (2015)
- 18.5 PCR: PCR status report Q3 2017, [https://www.entsoe.eu/network\\_codes/cacm/implementation/sadc/](https://www.entsoe.eu/network_codes/cacm/implementation/sadc/) (2017)
- 18.6 Ofgem: New electricity trading arrangements (NETA) – One year review, <https://www.ofgem.gov.uk/ofgem-publications/76199/1109-factsheet110224july.pdf> (2002)
- 18.7 S. Amelang, K. Appunn: Germany's new power market design, <https://www.cleanenergywire.org/factsheets/germanys-new-power-market-design> (2016)
- 18.8 AEMO: Regional boundaries for the national electric market, [https://www.aemo.com.au/-/media/files/electricity/nem/planning\\_and\\_forecasting/maps/2016-nem-regional-boundaries-map-web.pdf?la=en&hash=463EE44B46732E705C4EFA5748F87DD](https://www.aemo.com.au/-/media/files/electricity/nem/planning_and_forecasting/maps/2016-nem-regional-boundaries-map-web.pdf?la=en&hash=463EE44B46732E705C4EFA5748F87DD) (2016)
- 18.9 AEMO: General information about the Australian Electricity Market, <https://www.aemo.com.au> (2010)
- 18.10 AEMO: AEMO energy live: Queensland, June 1, 2018, <https://aemo.com.au/> (2018)
- 18.11 AEMC: Schedule of reliability settings, <https://www.aemc.gov.au/news-centre/media-releases/aemc-publishes-schedule-reliability-settings-2019-20> (2018)
- 18.12 AEMO: Black system South Australia, 28 September 2016, [https://www.aemo.com.au/-/media/Files/Electricity/NEM/Market\\_Notices\\_and\\_Events/Power\\_System\\_Incident\\_Reports/2017/Integrated-Final-Report-SA-Black-System-28-September-2016.pdf](https://www.aemo.com.au/-/media/Files/Electricity/NEM/Market_Notices_and_Events/Power_System_Incident_Reports/2017/Integrated-Final-Report-SA-Black-System-28-September-2016.pdf) (2017)
- 18.13 PJM: Annual report, <https://www.pjm.com/about-pjm/who-we-are/annual-report.aspx> (2020)
- 18.14 PJM: 2019 Demand response operations market activity report: January 2020, <https://www.pjm.com/-/media/markets-ops/dsr/2019-demand-response-activity-report.ashx?la=en> (2020)
- 18.15 A. Gray: Countries are announcing plans to phase out petrol and diesel cars. Is yours on the list?, <https://www.weforum.org/agenda/2017/09/countries-are-announcing-plans-to-phase-out-petrol-and-diesel-cars-is-yours-on-the-list/> (2017)
- 18.16 C. Clover: Electric cars: China's highly charged power play, <https://www.ft.com/content/00b36a30-a4dd-11e7-9e4f-7f5e6a7c98a2> (2017)
- 18.17 Vector: EV network integration, Green paper, <https://vectorwebstoreprd.blob.core.windows.net/blob/vector/media/the-spin-off/ev-network-integration.pdf> (2018)
- 18.18 A. Chuang, A. Cruickshank, T. Njuguna, J. Wright: International perspectives on the alignment of electric service costs and retail costs and retail rate structures. In: *CIGRE Symp., Dublin* (2017)
- 18.19 CIGRE: Management of network losses, [https://e-cigre.org/publication/RP\\_293\\_1-management-of-network-losses](https://e-cigre.org/publication/RP_293_1-management-of-network-losses) (2017)
- 18.20 Modern Power Systems: European smart metering rollout progresses – slowly, <https://www.modernpowersystems.com/features/featureeuropean-smart-metering-rollout-progresses-slowly-5886908/> (2017)
- 18.21 European Commission: Smart metering deployment in the European Union, <http://ses.jrc.ec.europa.eu/smart-metering-deployment-european-union> (2019)
- 18.22 Smart Energy International: US utility expands smart meter rollout, <https://www.smart-energy.com/industry-sectors/smart-meters/smart-electric-meters-programme/> (2017)
- 18.23 CIGRE: Review of drivers for transmission investment decisions, <https://e-cigre.org/publication/>



- 701-review-of-drivers-for-transmission-investment-decisions (2017)
- 18.24 European Commission: Paris Agreement, <https://ec.europa.eu/clima/policies/international/negotiations/paris> (2020)
- 18.25 C. Davenport, A.J. Rubin: Trump signs executive order unwinding Obama climate policies, <https://www.nytimes.com/2017/03/28/climate/trump-executive-order-climate-change.html> (2017)
- 18.26 World Energy Council report on energy efficiency: a straight path towards energy sustainability, <https://www.worldenergy.org/publications/entry/energy-efficiency-a-straight-path-towards-energy-sustainability> (2016)
- 18.27 P. Southwell, A. Negri: Power system component efficiency and energy delivery effectiveness designed for minimal environmental impact. In: *CIGRE Symp., Bologna* (2011)
- 18.28 J. Lazar: *Electricity Regulation in the US: A Guide*, 2nd edn. (RAP, Montpellier 2016), Available at: <https://www.raponline.org/knowledge-center/electricity-regulation-in-the-us-a-guide-2/>
- 18.29 Ofgem: Energy networks should prepare for tougher price controls, <https://www.ofgem.gov.uk/publications-and-updates/energy-networks-should-prepare-tougher-price-controls> (2017)
- 18.30 Ofgem: Energy efficiency directive: An assessment of the energy efficiency potential of Great Britain's gas and electricity infrastructure, [https://www.ofgem.gov.uk/sites/default/files/docs/2015/06/energy\\_efficiency\\_directive\\_report\\_-\\_final\\_for\\_publication.pdf](https://www.ofgem.gov.uk/sites/default/files/docs/2015/06/energy_efficiency_directive_report_-_final_for_publication.pdf) (2015)
- 18.31 Australian Energy Regulator: <https://www.aer.gov.au>
- 18.32 Economic Regulation Authority (ERA) of Western Australia: <https://www.erawa.com.au/electricity> (2020)
- 18.33 NordREG: Economic regulation of electricity grids in Nordic countries, [http://www.nordicenergyregulators.org/wp-content/uploads/2013/02/Economic\\_regulation\\_of\\_electricity\\_grids\\_in\\_Nordic\\_countries.pdf](http://www.nordicenergyregulators.org/wp-content/uploads/2013/02/Economic_regulation_of_electricity_grids_in_Nordic_countries.pdf) (2011)

### Philip Southwell

Southwell Power System Consulting  
Shenton Park, WA, Australia  
[phil.southwell.cigre.ci@gmail.com](mailto:phil.southwell.cigre.ci@gmail.com)



With degrees in Electrical Engineering and Management, Phil has over 40 years experience in power system planning, design and regulation, including several years as a senior executive of Western Power in Australia. He was Chair of CIGRE Study Committee C1 on System Development and Economics, is a Fellow of Engineers Australia and a Fellow and Honorary Member of CIGRE.

### Gregory H. Thorpe

Executive  
Oakley Greenwood Pty Ltd  
Margate Beach, QLD, Australia  
[gthorpe@oakleygreenwood.com.au](mailto:gthorpe@oakleygreenwood.com.au)



Greg holds qualifications in Electrical Engineering, Business and Alternative Dispute Resolution. He advises on industry and competitive market design and operation across Asia-Pacific. He has held positions with regulators, market operators and utilities. He sits on industry dispute panels in Australia and Singapore and has provided testimony in Court and arbitrations for commercial and market rule matters.

### Alex Cruickshank

Energy Consulting  
Oakley Greenwood Pty Ltd  
Margate Beach, QLD, Australia  
[acruickshank@oakleygreenwood.com.au](mailto:acruickshank@oakleygreenwood.com.au)



Alex Cruickshank received his BSc in 1974 and an MBA in 1990. He has worked for energy utilities, regulators and government advising on markets and rules in relation to the energy industry and the Australian National Electricity Market. He is on international study and working groups as part of CIGRE and chairs Study Committee C5 on Electricity Markets and Regulation.

### Colin Ray

Colin Ray Consulting  
Stratford on Avon, Warwickshire, UK  
[colin@colinray.org.uk](mailto:colin@colinray.org.uk)



Colin has more than 40 years experience in the electricity industry including privatization within England and Wales. He was chairman of the CIGRE committee on System Development and Economics and a member of a World Energy Council Task Force on transmission interconnectivity. He was awarded the CIGRE Gold Medal honor in 2012 for services to CIGRE and the industry.

## Subject Index

5G 1013

2000 W-society 32

### A

abnormal switching transient 1193

absolute

– delay 1057, 1058, 1078

– selective criterion 985

absorbed glass mat battery 922

absorbent glass mat (AGM) 922,  
1158

abstract communications service  
interface (ACSI) 1037

AC

– auxiliary system 922

– current harmonics 948

– fault current 968

– insulation test 841

– measurement 264

– method 297

– system strength 950

– test on-site 494

– transformer 164, 165

– transmission 512, 784

– voltage 163

– voltage test 841

accessory

– component 821

– failure 845

accounting management (AM)  
1080

accuracy classes 989

acoustic noise (AN) 637

active

– and reactive power control 964

– decoupling 297

– filter 1183

– mass 1156

– network management (ANM)  
1106

– parts of a transformer 466

– power (MW) 284, 295, 399

active DC fault current 966

– control 966

active distribution network (ADN)  
1103

– econfiguration (ADNR) 1116

– optimal operation 1115

active power

– curtailment (APC) 1116

– flow 297

adaptive protection 1012

add-drop multiplexer (ADM) 1065

address resolution protocol (ARP)  
1066

adequacy of insulation coordination  
893

adjustment transformer 1000

admittance

– circle 1007

– matrix 289

ADMS system structure 1109

advanced

– distribution management system  
(ADMS) 1107

– gas cooled reactor (AGR) 86

– metering infrastructure (AMI)  
1069, 1103, 1111

aerial photogrammetry 734

aerial-based robot 744

aerodynamic

– damping 663

– drag of a flywheel 1153

– galloping controller (AGC) 670

– loss 1152

aesthetic 875

AFC (alkaline fuel cell) 125

aged fitting 742

aggregated

– load 338

– system 338

aging

– chemical corrosion 252

– experiment 258

– force reduction 258

– fretting 258

– mechanism 1156

– of cable insulation 785

air compression 1144

air-blast

– breaker 874

– circuit breaker 528

aircraft warning marker (AWM)  
704

airfoil theory 101

air-gap torque 331

air-insulated

– switchgear (AIS) 573, 880

– termination 829

alarm handling 1109

aliasing 1185

alkaline

– accumulator 1158

– fuel cell (AFC) 125

all aluminum

– alloy conductor (AAAC) 641

– conductor (AAC) 619, 641

all-dielectric self-supporting (ADSS)  
656, 1064

allowable bending strain 668

alternating current (AC) 131, 199,  
273, 373, 379, 449, 512, 612, 759,  
858, 868, 935, 1156

aluminum (Al) 774

– trihydrate (ATH) 689

aluminum conductor 185

– alloy reinforced (ACAR) 667

– steel-reinforced (ACSR) 614,  
640, 641, 1096

– steel-supported (ACSS) 657

aluminum conductor composite

– core (ACCC) 658

– reinforced (ACCR) 658

American

– Electric Power (AEP) 568

– wind turbine 95

amorphous silicon solar cell 116

amplitude factor 572

Ampère's law 446, 448

analogue-to-digital converter (ADC)  
1185

analysis 623

anchor foundation 731

anchoring of leg member 733

angle tower 722

annealing 657

annual

– expenditures 622

- water volume 49
- anode 1157
- apparent power (MVA) 370
- application
  - example and basic control 945
  - programming interface (API) 1025
  - service element (ASE) 1051
- applied voltage test 493
- appropriate technology index (ATI) 616
- aqueous electrolyte 1157
- arc
  - current 536
  - fault 976
  - interrupting process 537
  - interruption 536
  - plasma injector (API) 524
  - protection fitting 707
  - resistance 597
- arc-furnace transformer 501
- arch dam 55
- arcing
  - distance 527, 673
  - horn 705
- arc-quenching arrangement 535
- area control error (ACE) 342
- armature
  - current limit 292
  - reactance 315
- armored cable 777
- Armor-Grip Suspension (AGS) 700
- armour wire, tensile stress in 825
- artificial intelligence 930
- as low as reasonably practicable (ALARP) 892, 915
- asset
  - investment 1109
  - management process 623
  - manager 919
- association control service element (ACSE) 1051
- asymmetrical load 459
- asynchronous
  - interconnection 871
  - swing 632, 633
- ATI 618
- atmospheric correction factor 149
- atomic absorption spectrometry (AAS) 697
- attenuation constant 279
- audible noise (AN) 654
- augmentation 872
- augmented network 332

- Australian blackout in 2016, market implications 1220
- automated
  - continuous injection molding (ACIM) 691
  - meter reading (AMR) 1111
- automatic
  - control system 339
  - generation control (AGC) 336, 341
  - reclosing (AR) 1011
  - tap-change control (ATCC) 924
  - voltage regulator (AVR) 321, 1167
- auto-reclosing 1011
- autotransformer 499
- auxiliary system 871
- availability 1059
- available primary energy type 4
- average failing load 686
- axial magnetic field (AMF) 540

## B

- back flashover 893
- backfilling 735
- back-flashover 728
- backup protection 977, 978
  - local 978, 979
  - remote 978
- backward interlocking 1003
- backward/forward sweep method 1102
- balancing mechanism (BM) 1217
- basic
  - application profile (BAP) 1045
  - encoding rules (BER) 1051
  - impulse level (BIL) 883
  - insulation level (BIL) 770
- basket grip 738
- battery
  - energy storage system (BESS) 1105, 1156
  - management system (BMS) 1156
- battle of currents 444
- bearing pressure 726
- Belleville washer 710
- bending
  - amplitude 666
  - stiffness 662
- Bernoulli equation 57
- Betz's law 97
- bimetallic conductor 646
- binary
  - enable signal 1006
  - information 1011
- bio-fuel 36
- biological conversion 9
- biomass 9
  - energy 36
- bipolar
  - arrangement 968
  - system 939
- bipolar transmission 940
  - circuit 939
- bird streamer 675
- blade profile 100
- Bloch wall 461
- blocking
  - distance protection 924
  - method 1011
  - overreach (BO) 1056
- boiler control 84
- boiling water reactor (BWR) 86
- bolt shearing 726
- bolted
  - connection 239
  - dead-end 701
  - joint 245
- bonding arrangement 806
- Bonneville Power Administration (BPA) 568
- border gateway protocol (BGP) 1091
- bore across an intersection 834
- boundary element method (BEM) 636
- brace arrangement 721
- branch-flow 1101
- branching point 1002
- breadth-first (BF) 1102
- breakdown 143
  - fluid 150, 151
  - gas 144
  - gases 145
  - parameter 149
  - probability 144
  - relative water content 151
  - SF<sub>6</sub> 147
  - solid 152
  - statistics 143
  - streamer mechanism 147
  - thermal 153
  - time 785
  - Townsend mechanism 146
- breaker-and-a-half 878, 879

- breakeven distance 937
  - break-even distance 764
  - breaking
    - capacity 301
    - current 601
    - strength 645
  - breakover
    - diode protection (BOD) 957
    - voltage (VBO) 956
  - bridging 1134
  - broadband power-line (BPL) 1069
  - Buchholz relay 484
  - buckling curve 725
  - building 903
  - built-in transformer voltage sensor 585
  - bulb turbine 51
  - bundle arrangement 655
  - buried cable 777
  - bus
    - admittance matrix 332
    - coupler 877
    - terminal fault (BTF) 544, 545, 566
  - bushing voltage sensor 586
  - business
    - impact (BI) 1082
    - management layer (BML) 1080
  - business continuity
    - management (BCM) 1081
    - planning (BCP) 1082
  - bypass
    - disconnecter 525
    - switch (BPS) 606, 941
- 
- C**
- cable 894, 1180
    - accessory workmanship 821
    - capacitance 770, 801
    - chamber 830
    - damage 800
    - design 789, 803
    - fluid reservoir 809
    - installation work 831
    - insulation 785, 804
    - layout 779
    - line 280, 285
    - manufacturing 803
    - pressure 812
    - rating 789
    - repair procedure 846
    - sheath bonding 805
    - transposition 778
    - trench 904
  - cable fault location
    - method 844
    - procedure 844
  - cable in
    - ducts 777
    - tunnels 777
  - cable route
    - monitoring 844
    - planning 803
  - cable system 768, 771, 773
    - failure 804
    - life expectancy 849
    - performance 848
  - cables and lines 1180
  - CAES 1151
  - calculation of tower member forces 723
  - cantilever failing load (CFL) 688
  - capability
    - curve 293
    - limit 292
  - capacitive
    - switching capability 567
    - system 1154
    - termination 351
  - capacitive voltage
    - divider (CVD) 1183
    - transformer (CVT) 519, 1183
  - capacitor 1144
    - bank 285, 524, 1181
    - bank switching 554
    - commutated converter (CCC) 949
    - voltage transformer (CVT) 519, 521
  - capacity 1138
    - market 1213
  - capital
    - expenditure (CAPEX) 795
    - investment 919
  - carbon capture and storage (CCS) 5, 46
  - carcinogenicity 638
  - Carpentier's
    - approximation 295
    - method 297
  - cart for in-span work 739, 742
  - cascade flashover 680
  - catenary 647, 648
    - catenary constant 648
    - length 648
  - cathode 1157
  - CCS (carbon capture and storage) 46
  - cell voltage 1158
  - cellulose 162
    - molecule 162
  - center of inertia (COI) 337
  - Central European Time (CET) 119
  - centralized utility 1132
  - chain matrix parameter 283
  - changing the power direction in LCC converters 946
  - characteristic
    - harmonics 947
    - impedance 279, 282
  - characteristics of LCC and VSC systems 935, 937
  - charge and discharge loss 1139
  - chattering 985
  - check zone 1005
  - chemical
    - anchor 903
    - energy 1135
    - species 1157
  - childhood leukemia 638
  - chlorinated fluorocarbon (CFC) 11
  - Chubu Electric 870
  - CIGRE
    - DC grid test system 970
    - investigation 569
    - life expectancy estimation 669
  - circuit breaker (CB) 301, 512, 513, 581, 598, 802, 871, 977, 996, 1110
    - air 532
    - bulk-oil 529
    - DC 591, 604
    - development 528
    - double-pressure gas 530
    - failure protection (CBFP) 978, 1005
    - gas 598
    - high-voltage 563
    - hybrid 604
    - Kelman's oil 529
    - oil 532
    - oil-immersed 529
    - type 528
    - UHV 574
  - circumferential
    - compression 246
    - speed 58
  - civil engineering 871
  - clamp connection 245
  - class A instrument 1177

- Clean Energy Package (CEP) 363
- cleated cable installation
  - arrangement 837
- climate change 872
- closing resistor 590
- CO<sub>2</sub>
  - capture utilisation and storage (CCUS) 36
  - emission 27
- CO<sub>2</sub> emission 19
- CO<sub>2</sub>-free electricity production 38
- coal 5
- coarse-wavelength division
  - multiplexing (CWDM) 1064
- coating 679
  - material 253, 257
- coefficient of linear expansion 647
- collection volume method (CVM) 899
- color rendition 907
- combination of wind and ice loads 630
- combined design (CD) 816
- combined heat and power (CHP) 76
- combined heat and power generation (CHP) 46
- combined heat and power plant (CHP) 42, 45, 1105, 1166
- commercial quality 1172
- commissioning 908
  - test 841
- common
  - data class (CDC) 1032
  - grid model exchange specification (CGMES) 1043
  - information model (CIM) 1024
  - object request broker architecture (CORBA) 1045
  - rules across Europe 1215
- communication 872
  - cable duct 835
  - infrastructure 1108
  - protocol 1109
- commutation
  - failure 954
  - path 944
  - process 943
- compact line 692
- compensated line switching 589
- compensation 764
- complete cable system test 840
- component
  - failure 740
  - interface specification (CIS) 1025
- composite
  - insulator 683
  - joint 819
  - post insulator 526
- compressed gas-insulated cable (CGIC) 854
- compressed-air energy storage (CAES) 1105, 1136, 1151
- compression and expansion of air 1151
- compression clamp 700
- compressor stage 1151
- concentrating collectors 10
- concept
  - design 890
  - of capability curves 292
- concrete pole damage 743
- condenser 78
- condition
  - monitoring 838, 842
  - reliability maintenance (CRM) 843
- condition monitoring 919
  - technique 842
- condition-based maintenance (CBM) 916
- conductor 630
  - aluminum conductor composite core (ACCC) 658
  - aluminum conductor composite reinforced (ACCR) 658
  - bundle 655
  - bundled 238
  - connections 185
  - current 824
  - design 640, 823
  - endurance limit 665
  - fabrication 640
  - factor  $k$  664
  - fastening 189
  - flexible 238
  - G(Z)TACSR or gap-type 658
  - galloping 661
  - HTSL 247
  - load 646
  - manufacture 643
  - material 184, 243, 774
  - mechanical characteristics 651
  - mechanical properties 646
  - parallel 223
  - sag adjustment 700
  - size 767, 798
  - stranded 247
  - structure 185
- surface gradient 654
- swing 630
- test 645
- thermal state 652
- weight 628
- wire test 643
- cone penetration test (CPT) 730
- configuration management (CM) 1080
- connecting land cable 828
- connection
  - length 673
  - long-term behavior 250
  - technique 778
- connector 701
- constant
  - current load 1097
  - inductance 988
  - stress 1153
- constriction resistance 238
- construction 872
  - method 777
- consultation model 639
- contact
  - aging 250
  - area 239
  - electric 238
  - finger 245
  - model 238
  - resistance 238
  - surface 238
- contamination uniformity ratio (CUR) 676
- continuity of
  - service 1095
  - supply 1172
- control and
  - diagnostics 1143
  - management of loss 1229
  - protection 872
- control gear 192, 193
- controlled
  - closing 577
  - opening 577, 582
  - sliding clamp 722
  - thyristor valve 942
- controlled switching 523, 576, 579
  - system (CSS) 576
- conventional
  - heating 41
  - specification 883
- converter
  - bank 606
  - charging 969

- control loop 953
  - firing angle 952
  - in series 941, 954
  - outage 941
  - pole configuration 941
  - staging 942
  - station (C/S) 502, 600
  - substation 869
  - coolant flow 210
  - cooling
    - fluid 483
    - tower 80
    - type 482
  - copper
    - conductor 185, 771
    - wire 614
  - core
    - clamp 464
    - clamping (CC) 465
    - lamination (CL) 465
    - loss 450
    - material 461
    - sheet material 467
  - corona
    - effect 637
    - loss (CL) 654
  - corrective maintenance 916
  - corrosion 677, 741
    - protection 721
  - corrugated aluminum sheath (CAS) 807
  - cost
    - comparison AC × DC systems 937
    - reflective pricing 1227
  - cost of
    - investments 622
    - normal operations 622
    - unserved energy 1231
  - Coulomb damping 663
  - Council of European Energy Regulators 1189, 1191
  - counterpoise conductor 728
  - credible contingency 875
  - creep 646
    - curve 646
    - strain 646
    - test 646
  - creepage
    - distance 673, 674, 676, 893
    - factor (CF) 677
  - crimping 686
  - C-ring 706
  - critical measurement 1111
  - cross-bonded cable system 800
  - cross-bonding
    - joint 830
    - method 780
    - system 806
  - crosslinked polyethylene (XLPE) 141, 154, 764, 788, 815, 823, 936
  - cryogenic
    - envelope 852
    - material 932
  - current
    - capacity 849
    - density 197
    - differential protection 1056, 1069
    - harmonics 947
    - injection scheme 592
    - interruption process 537
    - measurement 175
    - overflow 219
    - overload ability 217
    - quality 1172
    - return path 939
    - rise 982
    - source inverter (CSI) 435
    - summation 923
  - current transformer (CT) 517, 879, 1184
    - type 520, 991
  - current zero
    - creation scheme 591, 601
    - scheme 596
  - current-carrying
    - capability 568
    - capacity 191, 747
  - current-conducting device 184
  - current-graded protection 923
  - current–voltage characteristics 113
  - customer average interruption duration index (CAIDI) 1190
  - customer relationship management (CRM) 1022
  - cut-in speed 1104
  - cyclic
    - load 660
    - triggering of the valves 947
- 
- D**
- daily-storage facility 53
  - damage
    - during installation 831
    - limit 626
  - limit load (DLL) 686
  - damped AC (DAC) 804
  - damper
    - design 708
    - fatigue test 708, 711
    - impedance 709
    - placement 709
    - test 711
  - damper clamp 710
    - materials and construction 710
  - damping
    - by resistance 802
    - elastomer 712
  - Danube-type tower 636
  - Darrieus 95
    - rotor 99, 101
  - day-to-night shift 1167
  - DC
    - approximation 297
    - auxiliary system 922
    - cable 142
    - circuit breaker 604
    - current interruption 593, 605
    - fault current 966
    - grounding fault 598
    - insulator 676
    - measurement 264
    - oversheath test 842
    - substation 927
    - system fault 592
    - transmission 512, 784
  - DC fault 598
    - currentes interruption through blocking 966
  - DC grid 969
    - test system 970
  - DC voltage 166
    - harmonics 948
    - rating 941
    - test 804
  - dead-end
    - clamp 700
    - insulator 672
    - or terminal tower 722
  - decentralized
    - data acquisition 1005
    - generation units 1012
  - decommissioning 872
  - decoupled load flow 296
  - dedicated metallic return (DMR) 939
  - deenergization 578
  - deenergizing cables 513
  - defense in depth 920

- definite time overcurrent (DTOC)
  - 996, 998
- definition of
  - energy 1135
  - the electricity product 1210
- degraded minute (DM) 1059
- de-jittering 1078
- delay
  - angle 943, 944
  - asymmetry 1058
  - time 980
  - variation 1058
- delayed maintenance 740
- delta
  - connection 457, 1002
  - winding 983
- demagnetized current transformer 989
- demagnetizing effect 312
- demand response (DR) 1103, 1105
- dense-wavelength division multiplexer (DWDM) 1064
- Denver study 637
- dependability 1055, 1059
- dependent
  - overcurrent 996
  - release 994
- depth of discharge (DoD) 1138
- design
  - insulation level (DIL) 470
  - life 872
  - parameter 621
- detailed design 616
- detect defects 741
- deterministic 893
  - method 626
- Deutsches Reichspatent (DRP) 444
- development testing 839
- device
  - number system 992
  - under test (DUT) 498
- diagnostic
  - method 697
  - test (DT) 486
  - testing 919
- diameter 878
  - correction factor 677
- dielectric
  - dissipation factor 489
  - interrupting capability 566
  - loss 200
  - measurement 179
  - recovery characteristics 539
  - stress factor 558
- test 492
- diesel fuel 39
- differential
  - current 980, 981
  - protection 800, 980, 999, 1012
  - scanning calorimetry (DSC) 697
  - transformer 504
- diffuser 59
- digital
  - position (DP) 846
  - substation 930
- direct
  - current (DC) 131, 262, 274, 382, 403, 447, 512, 613, 760, 858, 868, 935, 990, 1150
  - methanol fuel cell (DMFC) 125
  - torque control (DTC) 433
  - transfer tripping (DTT) 1056
  - wave 281
- directional
  - comparison unblocking (DCUB) 1056
  - decision 986
  - drilling 832
- directly buried cable 833
- disadvantage 1012
- disc winding 476
- discharge 1145
  - pattern 49
- disconnecting switch (DS) 514, 606
- disconnecter 874
- discrete Fourier transform (DFT) 1184
- discriminating zone (DZ) 1003, 1005
- disengaging ratio 985
- disperse 869
- disruptive failure 842
- dissolved gas analysis (DGA) 179, 485
- distance
  - measuring system 1007
  - protection 1006
  - protection criterion 1006
- distflow method 333
- distortion constant 279
- distributed
  - energy resources (DER) 1045, 1095, 1103
  - generation (DG) 277, 360, 1103, 1115
  - temperature sensing (DTS) 792, 799
- distribution
  - feeder 1093
  - management system (DMS) 1018, 1106
  - network 1102
  - power flow (DPF) 1111
  - state estimation (DSE) 1110
  - substation 869, 870, 1096
  - transformer controller (DTC) 1114
- distribution line 704, 1096
  - electrical characteristics 1096
- distribution network
  - backbone 1094
  - control 1111
  - planning (DNP) 1120
- distribution system
  - infrastructure 1094
  - operator (DSO) 1103
  - power flow management 1106
  - state estimator (DSSE) 1107, 1115
- disturbance 337
- donut device 659
- doping 107
- dormant faults 1060
- double
  - busbar 877
  - busbar layout 877
  - shear connection 726
  - tension string 672
- double-circuit network 555
- doubly-fed induction motor generator (DFIMG) 1150
- drag
  - factor 630
  - turbine 102
- drainage 903
- drehstrom (rotary current) 444
- drilled shaft foundation 732
- drive battery 1158
- drop-off current 979
- dry-type transformer 480, 484
- duration line 49
- duty cycle 990
- Dy5 transformer 459
- dynamic
  - cable rating 799
  - model 233
  - rating system (DRS) 792
  - voltage restorer (DVR) 1175

## E

- earth
  - conductor size 898
  - continuity conductor (ECC) 835
  - fault 895, 983
  - resistance 893
  - wire 656
- earth grid
  - design 895
  - resistance 896
  - testing 899
- earthed transformer 584
- earthing 716
  - joint 830
  - rod 728
  - switch (ES) 606
  - system design 898
- economic adequacy 976
- economies of scale 1213
- eddy current loss 200, 461, 474
- Edison 868
- effective
  - buckling length 721
  - cross section 725
  - modeling 1095
  - short-circuit ratio (ESCR) 950
- elastic
  - deformation 230
  - pressure surge 69
- elastomer bushing 712
- elastomeric
  - sleeve 818
  - suspension (ES) 699, 700
- electric
  - capacitor 1154
  - motor-generator 1144
  - separator 1156
  - strength 142
  - transportation technology 360
  - vector 1143
  - vehicle (EV) 1156
- electric field (EF) 137, 138, 637
  - basics 137
  - coaxial arrangement 141
  - DC cable 142
  - gradient 654
  - homogenous field 138
  - inhomogeneous field 140
  - layered dielectrics 138, 139
  - utilization factor 140
- electric power system 277
  - faults 300
- electrical
  - characteristic of cables 772
  - clearance 890
  - connector, plug-in-type 248, 258
  - equipment 218
  - heat loss 199
  - operating behavior 248
  - stress 786
- electrical connection 238, 240
  - aging 190
  - assembling 244
  - bimetallic 253
  - bolted 239
  - clamp 245
  - design and dimensioning 243
  - function 241
  - installation 245
  - moving 241
  - plug-in-type 242, 244
  - requirements 241
  - resistance measurement 264
  - standard for testing 243
  - stationary 241
- electrically triggered thyristor (ETT) 957
- electricity
  - as an essential service 1224
  - production worldwide 36
- electrochemical
  - accumulator 1156
  - battery 1135
  - oxidation 1157
  - principle 1156
  - reduction 1157
  - system 1156
  - transformation 1144
- electrode 1162
- electrodynamic stress 301
- electro-geometric model (EGM) 899
- electrolyte 124
- electrolyzer 1162
- electromagnetic
  - compatibility (EMC) 884, 1172, 1173
  - energy converter 445
  - field (EMF) 611, 632, 634, 873
  - force 222, 251
  - interference (EMI) 654
  - transient program (EMTP) 345
  - transient program (EMTP-RV) 295
  - unit (EMU) 1183
- electromagnetic transient (EMTP) 273
- electromotive force (EMF) 126, 301, 373
- electron 1156
- electronic
  - control equipment 577
  - converter 1143
  - current transformer (ECT) 517
  - equipment 1180
  - voltage transformer (EVT) 520
- element management layer (EML) 1080
- elevator transformer 297
- elliptical contact 664
- embedded generation 1208
  - impact on cost of service and price behavior 1228
- EMC 905
- emergency restoration 740
- EMF 905
- emission target impact 1232
- EN
  - 50065-1 1195
  - 50160 1173, 1175, 1187, 1197
- EN 50160 1195, 1196
- encapsulation 1071
  - loss 199
- end
  - fitting 686
  - of life of cable 851
  - region 292
- energization 578
  - strategy 583
  - test 580
- energizing cable 513
- energy
  - and loss 13, 19
  - balance principle (EBP) 664
  - consumption per capita 15
  - content 5
  - cost 39
  - dissipation capability 894
  - efficiency 360
  - flow rate 1136
  - indicator, worldwide 32
  - intensity 19, 21
  - intensity of GDP 24
  - management system (EMS) 1018
  - storage 1207
- energy sector 20
  - Asia/Oceania 31
  - of the economy 1
- energy storage
  - device (ESD) 1141
  - system (ESS) 1103, 1143, 1144



engagement 639  
 enterprise resource planning (ERP) 1022  
 environmental  
 – impact 639  
 – impact assessment (EIA) 616, 638  
 – performance 527  
 – protection 7, 50  
 – test 839  
 epoxy resin 163, 684  
 EPR (European pressurized reactor) 86  
 EPRI endurance limits 668  
 equal area criterion 329  
 equilibrium point (EP) 328  
 equipment  
 – design 773  
 – parameter 770  
 equivalent  
 – circuit 988  
 – diameter 630  
 – salt deposit density (ESDD) 675  
 Ergon Energy 885  
 Eriksson's attractive radius model 900  
 errored second (ES) 1059  
 ethical aspect 7  
 ethylene propylene  
 – diene monomer (EPDM) 689  
 – monomer (EPM) 689  
 – rubber (EPR) 160, 772, 970  
 Euler load 694  
 Euroelectric 362  
 European  
 – electric grid 361  
 – Machinery Directive 445  
 – pressurized reactor (EPR) 86  
 – price coupled region 1215  
 – supergrid 361  
 event trigger 1111  
 everyday stress (EDS) 619, 666  
 exceptional load 628  
 exciter 331  
 exergy comparison 40  
 expanded bundle 655  
 experimental plastic elongation (EPE) 649  
 – model 649  
 exposure limit 638  
 extendibility 875  
 extensible messaging presence protocol (XMPP) 1045  
 external

– clearance 634  
 – constraint 290  
 – current 982  
 – network 290  
 extracted energy 1142  
 extrahigh voltage (EHV) 276, 513, 751, 759, 881  
 extraterrestrial  
 – irradiation 121  
 – radiation intensity 117  
 extruded  
 – insulation 788  
 – submarine cable 822  
 extruded cable 773, 801  
 – accessory 817  
 – lifetime 786  
 – new trends in the design 816

## F

facilitation of competition 1213  
 factory joint 826  
 failure  
 – limit 627  
 – mechanism 1156  
 failure mode  
 – and effects analysis (FMEA) 876  
 – composite insulator 685, 687  
 Faraday rotation 519  
 fast  
 – breeder reactor 88  
 – contact (FC) 524  
 – Fourier transformation (FFT) 174  
 – protective device (FPD) 524  
 – voltage variation 1197  
 fast-acting DC breaker 970  
 fatigue test 665  
 fault  
 – analysis 300  
 – clearance 770  
 – clearance time 872  
 – clearing 557  
 – clearing time 980  
 – condition 979  
 – countermeasure 301  
 – detection 847  
 – location 1118  
 – management (FM) 1080  
 – passage indicator (FPI) 1118  
 fault current 311, 544, 841, 949  
 – calculation 301  
 – during a failure 780  
 fault location 301, 545, 844, 847  
 – isolation, and service restoration (FLISR) 1110, 1118  
 fault, configuration, accounting, performance, and security model (FCAPS) 1080  
 fault-detection technique 743  
 fault-ride-through 1175, 1189  
 faulty phase 802  
 feasibility condition 333  
 fencing 903  
 Fermi–Dirac distribution 106  
 Ferranti effect 284, 900  
 ferroresonance 521, 894  
 fiber reinforced plastic (FRP) 683  
 fiber-optic connection 1005  
 fictitious 1004  
 field current limit 292  
 fill factor 114  
 filling  
 – fluid 840  
 – material test 841  
 final  
 – acceptance test (FAT) 484  
 – commissioning 913  
 – energy 1  
 financial transmission rights (FTR) 1222  
 finite element method (FEM) 194, 636, 722  
 fire barrier 903  
 firing angle 944  
 first telegrapher's equation 346  
 first-pole-to-clear 557  
 – factor 546  
 fissile materials 5  
 fittings for  
 – distribution line 704  
 – HTLS conductors 703  
 five-limb core 464  
 fixed-speed pumped storage 1148  
 flashunder 692  
 flat  
 – collectors 10  
 – plate 1158  
 flexible alternating current transmission system (FACTS) 566, 1177  
 flexible installation 837  
 flick test 912  
 flickermeter 1197  
 flooding 874  
 flow  
 – battery 1162

- chart cable system 769
  - rate 61
  - through hysteresis 462
  - fluid 157
  - fluid-filled (FF) 773
    - cable 838
  - flywheel 1152
    - energy storage (FES) 1169
  - footing 903
  - forced interruption 581
  - form locking 702
  - Fortescue
    - theory 301
    - transformation 303
  - forwarding equivalence class (FEC) 1069
  - forward-traveling voltage wave 348
  - foundation 903
    - design 729, 730
    - test 733
    - type 730
    - work 735
  - Fourier-transform infrared (FTIR) 697, 841
  - four-stage overcurrent function 996
  - FRA measurement 558
  - Francis turbine 51, 60, 1146
  - Frankfurt Electro-Technical Exhibition 868
  - frequency
    - bias factor 343
    - control 336
    - converter 1148
    - division multiplexing (FDM) 1063
    - stability 321
    - variation 1198
  - frequency response 488
    - analysis (FRA) 558, 911
  - frequency response analysis (FRA) 487
  - frequency-domain
    - method 1181
    - reflectometry (FDR) 847
    - spectroscopy (FDS) 487
  - freshwater cooling 79
  - fretting fatigue 665
  - frictional locking 702
  - FRP (fiber reinforced polymer) 719
    - rod 684
  - fuel cell 39, 124, 1162, 1163, 1166
    - efficiency 126, 127
    - grid-connected 128
    - structure 124
  - system technology 128
  - technology 127
  - fuel cycle 89
  - full distance protection schema 1007
  - full-bridge converter 966
  - function of a substation 868
  - functional
    - constraint (FC) 1033
    - specification 884
    - test 488
  - fuse 992
  - future
    - trends 971
    - work on HTS cable testing 853
- ## G
- Gallium arsenide (GaAs) solar cell 116
  - galloping 669
    - control device (GCD) 670
  - galvanic corrosion 712
  - gas 157
    - circuit breaker 514, 536
    - production 785
    - turbine plant 77
  - gas-filled (GF) 773
    - paper cable transition joint 821
  - gas-insulated
    - line (GIL) 140, 221, 760, 854, 857, 886, 985
    - switchgear (GIS) 140, 221, 517, 829, 880, 985, 1109
    - transmission line (GITL) 854
  - gas-to-liquid (GTL) 483
  - gate turn-off thyristor (GTO) 430
  - gel electrolyte 1158
  - general
    - algebraic modeling system (GAMS) 1101
    - electric flicker curve 1174
  - General Electric 868
  - generating mode 1144
  - generation
    - bus 290
    - frequency 937
    - of electricity 34
  - generator
    - step-up (GSU) 497
    - substation 872
  - generic
    - bus 286
    - eventing and subscription (GES) 1043
    - framing protocol (GFP) 1071
    - object-oriented substation event (GOOSE) 931, 1023
    - substation status event (GSSE) 1038
  - geomagnetic disturbance 906
  - geomagnetically induced current (GIC) 906
  - geometric
    - form factor 1153
    - mean radius 655
  - George Westinghouse 868
  - geothermal energy 7, 36
  - GIL
    - configuration 854
    - laying type 856
  - GIS termination 820
  - glass
    - fiber 684
    - insulator, manufacturing process 682
    - reinforced plastic (GRP) 683
  - global
    - positioning system (GPS) 734, 883, 1019, 1111
    - power grid 360
    - warming potential (GWP) 932
  - grading time 994
  - graphite-moderated reactors 86
  - Grätzel cell 117
  - gravitational potential force 1144
  - gravity
    - dam 55
    - fluid tank 809
  - gray energy 35
  - greenhouse
    - effect 11
    - gas emission 360
  - grid
    - code 1231
    - load 805
    - potential rise (GPR) 895
    - service 1166
  - gross domestic product (GDP) 15
  - gross energy
    - demand 13
    - intensity 35
  - ground
    - flash density (GFD) 899
    - investigation method 730
    - potential rise (GPR) 897

- return 939
- return transfer switch (GRTS) 940
- wire 656
- ground-based robot 744
- grounding 716
- system 301
- groundwater 902

## H

- half-bridge converter 962, 966
- hardness 238
- hardware in the loop (HIL) 363
- harmonic
  - level 906
  - spectrum 1177
- harmonics 947, 1172, 1177
  - impact 1180
- hauling machine 838
- hazard status 979
- head 1144
  - loss 1145
- headwater (OW) 56
  - reservoir 1144
- health issue 637
- health safety, environment and quality (HSEQ) 886
- healthy worker effect 638
- heat
  - extraction 76
  - pump 8, 39
  - run test 496
  - test 212
  - transfer 204, 206
- heating 39
  - for comfort 39
- heat-power cogeneration 76
- heat-pump heating 42
- Heaviside condition 282
- heavy water reactor (HWR) 86
- Heffron–Phillips model 329
- helical
  - termination 701
  - winding 476
- helically attached elastomeric suspension (HAES) 699, 700
- helicopter method 737
- Hellsjön project 958
- hexahydrophthalic anhydride (HHPA) 160
- high
  - dynamic 1012
  - voltage (HV) 276, 449, 513, 612, 759, 874, 939, 1093
  - voltage DC 1179
- high-current bushing 481
- high-density polyethylene (HDPE) 159, 835
- higher harmonic current 802
- high-frequency (HF) 556
  - overvoltage 805
- high-impedance differential 1003
- high-performance MOSA 569
- high-pressure (HP) 83
  - fluid-filled (HPFF) 772, 809
  - gas-filled (HPGF) 772, 787
  - oil-filled (HPOF) 787
- high-speed
  - data access (HSDA) 1043
  - grounding switch (HSGS) 576
  - mechanical switch 592
- high-temperature
  - reactor (HTR) 87
  - superconductor (HTS) 414, 852
- high-temperature low-sag (HTLS) 194, 614, 640, 1012
  - conductor 656
- high-temperature vulcanized (HTV) 689
  - silicone rubber 690
- high-voltage
  - alternating current (HVAC) 501, 511
  - bushing 481, 482
  - connection 802
  - distribution network 277
  - equipment 856
  - insulated gate bipolar transistor (HVIGBT) 435
  - test system 494
- high-voltage direct current (HVDC) 11, 274, 277, 403, 501, 511, 617, 871, 935, 1174
  - research 935
- high-voltage, high-speed switches (HVHS) 941
- history of electric power transmission 935
- hollow-core design 526
- home-area network (HAN) 1090
- homopolar
  - sequence 308
  - sequence current 301
- horizontal directional drilling (HDD) 766
- horsepower (HP) 410
- hosting capacity 1196
- hot
  - line washing 679
  - zone 898
- hot spot 1180, 1181
  - calculation 473
- hourly cost 300
- HTLS (high-temperature low-sag) 656, 745
  - conductor 248
- HTS cable
  - installed 853
  - tested 853
- HTV stepping 691
- human–machine interface (HMI) 931, 1018, 1108
- HV
  - cable trench 835
  - compensation 804
  - termination 766
- HV/EHV cable accessory 829
- HVDC
  - circuit breaker 600
  - installation 764
  - system configuration 939
  - transmission 764
- HVDC line 617, 937
  - bundle selection 617
- hybrid
  - connection 800
  - DC breaker 971
  - line 746, 798
  - link 800
  - power plant 1166
- hybrid-insulated switchgear (HIS) 881
- hydraulic
  - design 809
  - efficiency 59
  - machine 1144
- hydraulic system 68, 72
  - transfer function 72
- hydroelectric
  - plant model 72
  - power 1105
- hydrogen 1163
  - as compressed gas 1163
  - conditioning 1164
  - in a solid form 1163
  - in its liquid phase 1163
  - storage 1163
- hydrophobicity 671, 690
  - transfer (HT) 690, 697

- transfer material (HTM) 676
  - hydropower 37
    - generator 591
  - hydropower plant 67, 73, 1144
    - capacity of 65
  - hydro-pumped storage 1144
  - hyper and hyposynchronous 1149
  - hypoxic system 905
  - hysteresis 985, 988
    - curve 461
    - loop 518
- 
- I
- ice
    - load 628
    - on conductors 628
  - ideal
    - battery 1142
    - generator 301
    - making instant 585
    - normal round-trip efficiency 1139
    - transformer 448
  - IEC
    - 61000-2-2 1195
    - 61000-2-4 1187
    - 61000-3-2 1187
    - 61000-3-8 1195
    - 61000-4-7 1183, 1186, 1194
    - 61000-4-11 1188
    - 61000-4-14 1196
    - 61000-4-15 1197
    - 61000-4-19 1195
    - 61000-4-30 1175, 1183, 1186–1191, 1193–1195
    - 61000-4-34 1188
    - 61000-6-1 1188
    - 61000-6-2 1188
    - 61800-3 1188
    - 61850 1069
    - Technical Specification (IEC TS) 488
  - IEEE
    - 519 1186, 1194
    - 1366 1190
    - 1564 1187, 1188
    - 1588v2 1056
    - maximum allowable bending strain 668
  - IGBT 958
  - impact of
    - electric vehicles 1225
  - EMFs 637
  - impedance
    - matrix 311
    - relay 798
  - impeller 1147
  - impregnated solid 162
  - impulse 891
    - current 134, 167
    - current method (ICM) 845
    - generator 167
    - test system 497
    - turbine 57, 1146
  - impulse voltage 133, 167
    - chopped lightning impulse 133
    - full lightning impulse 133
    - switching impulse 133, 134
  - impurity
    - conduction 107
    - film resistance 238
  - incident solar radiation 122
  - independent
    - overcurrent 996
    - release 993
  - induced voltage test 493
  - inductance 1154
  - induction–capacitance (LC) 802
  - inductive
    - current transformer 987
    - load 312
    - reactance 450
    - switching capability 567
    - termination 351
    - voltage transformer (IVT) 521, 1183
  - inductor 1154
  - industrialized society 4
  - inert gas configuration 146
  - infinite power
    - bus 308, 327
    - machine 328
  - information
    - and communications technology (ICT) 362, 1016, 1103
    - management 919
    - object addresses (IOA) 1037
  - infrared (IR) 743
    - measurement 270
  - initial
    - cost (IC) 618
    - transient recovery voltage (ITRV) 551
  - injection molding 690
  - inrush
    - current 451, 553, 580, 999, 1000
  - detection 999
  - stabilization 999
  - insertion/disinsertion 1160
  - in-service maintenance 803
  - inspection
    - and test plan (ITP) 909
    - report 624
    - technique 743
  - installation
    - technique 803
    - trend 828
  - instantaneous
    - overcurrent (IOC) 996
    - release 993
  - instrument transformer 515, 516
  - Insulated Cables Study Committee 762
  - insulated-gate bipolar transistor (IGBT) 430, 495, 591, 935, 958
  - insulating
    - fluid 482, 483
    - material 156, 474, 816
  - insulation 775
    - arrangement 187, 189
    - coordination 132, 345, 893
    - design 787
    - material 187, 189, 474, 525
    - resistance (IR) 489, 911
    - screen 803
    - system 823
    - withstand 893
  - insulator 671
    - arcing distance 673
    - cap and pin 680
    - connection length 673
    - corrosion 677
    - creepage or leakage distance 673
    - fitting 677
    - geometry 673
    - material 671
    - polymer longrod 672
    - porcelain 680
    - puncture proof 671
    - reuse 639
    - shape 671
    - surface 674
    - under pollution 674
  - Insulator News and Market Report (INMR) 688
  - insulator protection fitting 705
    - material 706
  - integrated
    - condensate accumulation 82

- gate commuted thyristor (IGCT) 436
- integration of renewable offshore wind resources 938
- intelligent electronic device (IED) 931, 1071
- IntelliGrid 362
- intensified testing 694
- interconnected power system 803
- interconnection 874
  - substation 869
- interface
  - between cable and accessories 821
  - definition language (IDL) 1046
- interference 1173, 1176
- interharmonics 1185, 1194
- interior point (IP) 1113
- intermediary conversion 1143
- intermetallic phase (IMP) 258
- intermittent 869
- internal
  - clearance 632
  - combustion engine (ICE) 1166
  - conductor mechanics 668
  - electrical power 126
  - energy 1135
  - structure of a GIL 855
- internally-stored energy 1137
- international efficiency (IE) 429
- International Telecommunication Union – telecommunication standardization sector (ITU-T) 1046
- internet
  - engineering task force (IETF) 1069
  - inter-ORB protocol (IIOP) 1046
  - protocol (IP) 1018
- interphase
  - flashover 693
  - spacer (IPS) 693
- interrupting
  - capability 552
  - medium 542
  - performance 543
  - process 541
- interruption current 597
- inverse
  - definite minimum time (IDMT) 997
  - standing wave ratio (ISWR) 711
  - time characteristic functions 994
  - time-delay overcurrent 997

- wave 280, 281
- inverter
  - commutation failure 954
  - equation 945
  - operation 944
- investment 871
  - constraint 1121
- ionization inside the insulation 806
- iron core 987
- ISO 55000 serie 915
- isolated neutral transformer 583
- isothermal condition 1151
- iteratively reweighted least squares (IRLS) 1113
- ITU-T G.821 1059

---

## J

- Jantzen principle 479, 480
- jet deflectors 69
- jitter buffer delay (JBD) 1078
- joint
  - assembly 828
  - failure 702, 805
  - handling 828
  - resistance 238, 702
- Joule loss 652

---

## K

- Kaplan turbine 51, 60, 1146
- Kapp
  - diagram 453
  - triangle 452
- $k_E$ -factor 1007
- keraunic level 729, 899
- key performance indicator (KPI) 1079
- $k$ -factor 169
- Kihoku C/S 606
- kinetic energy 1135, 1145
- Kirchhoff's
  - circuit law 980
  - current law 1003
- knee-point
  - temperature (KPT) 649
  - voltage 989
- Károly Zipernowsky 444
- $k_R$  factor 1007

---

## L

- La Cour wind turbine 95
- label
  - distribution protocol (LDP) 1069
  - switch router (LSR) 1072
- label-switched path (LSP) 1069
- laminated covering 816, 817
- lamination 462
- Lamm, Uno 936
- land
  - cable 777
  - mobile radio (LMR) 1068
- land and
  - sea AC cable 773
  - sea cable 774
  - submarine application 771
- landscaping 874
- lapped cable 806
- large
  - generator 322
  - line reactance 565
  - scale energy storage 1168
- laser scanning method 734
- last point of contact (LPC) 666
- Lauffen am Neckar 612
- lay
  - angle 641
  - length 640
  - ratio 641
- layer winding 475
- LCC
  - control and protection 951
  - operation (inverter operation) 944
  - operation (rectifier operation) 942
- LCC converter
  - faults and disturbances 954
  - startup (deblock) 952
- lead–acid accumulator 1157
- leakage
  - current 114
  - flux 450, 468
  - inductance 988
  - reactance 312
- leaktight GIL system 856
- LED lamp 1197
- life cycle
  - assessment (LCA) 635, 639, 850
  - cost (LCC) 618, 918
  - cost analysis 918
  - cost-benefit ratio 35
  - factor 917
- life time 153
- lifetime curve for cables 786

- light
    - detection and ranging (lidar) 734
    - emitting diode (LED) 1175
    - flicker 1175, 1194
    - water reactor 86
  - light angle (LA) 722
    - tower 722
  - lightning 135, 893
    - development 136
    - fault 600
    - generation 135
    - impulse (LI) 492, 893
    - protection 137, 899
    - stroke 515, 656, 728
    - transient 1193
  - lightning impulse
    - protection level (LIPL) 570
    - withstand voltage (LIWV) 569
  - light-triggered thyristor (LTT) 957, 958
  - lightweight directory access protocol (LDAP) 1046
  - line 1180
    - component cost 620
    - conductor 345
    - deviation angle 722
    - discontinuity 349
    - fault 800
    - inductance 346
    - length limitation 764
    - of finite length 352
    - parameter 621
    - protection 1056
    - start permanent magnet (LSPM) 415
    - uprating technology 745
  - linear
    - analytical model 989
    - impedance 800
    - induction motor (LIM) 439
    - programming (LP) 1100, 1113
  - linear elastic (LE) 649
    - model 649
  - line-commutated converter (LCC) 591, 935
    - fundamentals 942
  - line-drop compensation (LDC) 924, 1098
  - line-interactive topology 1167
  - line-of-sight 1068
  - line-switching overvoltage 588
  - link capacity adjustment scheme (LCAS) 1071
  - liquid
    - electrolyte 1162
    - form 1162
    - insulation 486
    - silicone rubber (LSR) 689
  - liquid-filled
    - power transformer 449
    - transformer 484
  - lithium titanate oxide (LTO) 1160
  - lithium-ion
    - accumulator 1160
    - polymer (Li–Po) 1160
  - lithium-iron phosphate (LFP) 1160
  - lithium-metal accumulator 1160
  - lithium-metal polymer
    - cell 1160
    - technology 1160
  - live line work (LLW) 743
  - live-line maintenance 698
  - load 186, 188, 190, 230
    - bus 286
    - capacitance 575
    - case 722
    - consumption 334
    - control device (LCD) 699
    - flow calculation 310
    - model 1097
    - shed application (LSA) 1110
  - load estimation
    - algorithm 1115
    - model 1111
  - loaded cable, magnetic field from 824
  - load-flow
    - calculation 298
    - problem 295
  - local
    - area network (LAN) 1016
    - energy community (LEC) 363
  - localized effect 11
  - lockout system performance 800
  - logical
    - device (LD) 1031
    - node (LN) 1031
  - logically combined 1009
  - long
    - interruption 1190
    - line faults (LLF) 572
    - transmission line 587
  - long-distance transmission using an overhead line 937
  - longitudinal
    - armor 813
    - impedance 279
    - profile of the line route 734
    - reactance 297
  - longrod 680
    - insulator 673
  - loop
    - bridge measurement 847
    - impedance 1006
  - loss
    - dielectric 200
    - eddy current 200
    - encapsulation 201
    - factor 152, 160, 180
    - of load probability (LOLP) 1217
  - losses and energy 26
  - lossless
    - line 281, 345
    - overhead line 281
  - low
    - molecular weight (LMW) 690
    - voltage (LV) 277, 449, 513, 671, 1093
  - low-density polyethylene (LDPE) 764
  - low-impedance
    - busbar differential protection 1004
    - differential 1003
  - low-power instrument transformer (LPIT) 931
  - low-pressure (LP) 83
    - oil-filled (LPOF) 772, 786
    - system 51
  - low-temperature superconducting (LTS) 852
  - low-voltage
    - AC (LVAC) 883
    - bushing 480
  - low-weight conductor (LWC) 747
- 
- ## M
- 
- macroscopic energy 1135
  - magnetic
    - circuit 312, 582
    - field (MF) 637, 1180
  - magnetization 517
    - curve 912
  - magnetizing
    - current 987, 989
    - effect 312
  - magnetomotive force (MMF) 375
  - magnetostriction 461
  - main

- field voltage 989, 990
- switching duty 606
- maintenance 837, 874, 1094
  - guideline 843
  - management 916
  - operation 743
  - strategy 740
- majority carrier 107
- malfunction 976
- man–machine interface (MMI) 1021
- manufacturing 829
  - message specification (MMS) 1025, 1030
- market
  - benefit 1206
  - operator 1211
  - opportunity for customers 1210
- Marx generator 492
- mass-impregnated (MI) 788, 807, 958
  - cable 807, 838
  - paper cable 807
- material
  - aging 841
  - insulating 674
  - property 626
- maximum
  - available power (MAP) 951
  - credible accident (MCA) 90
  - design cantilever load (MDCL) 688
  - efficiency of solar cells 115
  - fault clearing 980
- maximum power point (MPP) 111
  - tracking (MPPT) 1104
- Maxwell's equations 446
- Mayr arc model 596
- MCFC (molten carbonate fuel cell) 124
- mean time
  - between failure (MTBF) 875
  - to repair (MTTR) 1062
- mean water speed 67
- measurement
  - accuracy 976
  - error 989
  - standard of power-quality 1175
- measuring technique 171
- mechanical
  - consideration 814
  - property 189
  - protection 809
  - work 3
- medium voltage (MV) 277, 513, 671, 762, 795, 1093
- medium-pressure (MP) 83
- medium-term planning 286
- megajoule (MJ) 410
- megavolt ampere (MVA) 950
- membrane 1162
- Mercedes tower 722
- mercury arc valve 936
- merging units 931
- mesh 879
  - voltage 895
- meshed underground network 794
- metal
  - hydride  $MgH_2$  1164
  - oxide (MO) 516
  - oxide semiconductor (MOS) 958
  - screen 776
  - screen/sheath 824
  - wire armor 824
- metallic pole
  - flange joint 718
  - slip joint 718
- metallic return
  - line 600
  - transfer breaker (MRTB) 592, 940
- metallic sheath 803
- metallurgical creep 646
- metal-oxide surge arrester (MOSA) 515
- metal-oxide-semiconductor field effect transistor (MOSFET) 430
- metering 924
- method of symmetrical components 491
- methylhexahydrophthalic anhydride (MHHPSA) 160
- mho 1008
  - characteristic 1007
- microgrid 363
- micromorph solar cell 117
- micro-ohmmeter 263, 265
- microporous 1158
- microscopic energy 1135
- microtunnel boring machine (MTBM) 834
- microtunneling 834
- microturbine 1105
- mid span clearance 633
- Mikhail Dolivo-Dobrovolsky 868
- Miksa Déri 444
- Milliken
  - conductor 775
  - copper conductor 808
- mineral oil 5, 163
- minimum
  - impedance setting 800
  - operational voltage 983
  - ‘missing money’ 1213
- mixed-technology switchgear (MTS) 574, 881
- MMC
  - concept 962, 963
  - submodule 963
- mobile substation 925
- mock-up test 494
- model of power transmission 564
- modern electric power system 278
- modular
  - manufacturing process 691
  - multilevel converter (MMC) 960
  - substation 927
- modulus of elasticity 647
- molded case circuit breaker (MCCB) 594
- molten carbonate fuel cell (MCFC) 124, 127
- momentary interruption 1191
- monitoring
  - standard 1175
  - system replacement 803
- monoblock foundation 718
- monopolar
  - system 940
  - transmission 940
- motor generator (MG) 56
- motor-driven roller 838
- moving wind turbine 96
- MPLS-TP 1058
- MPP maximum power point 112
- multibundle conductor 550
- multi-criteria analysis 875
- multi-infeed 951
  - factor (MIF) 951
- multi-machine stability 331
- multimode (MM) 1063
- multiple
  - hydraulic sections 811
  - impulse method (MIM) 845
  - reignition 557
- multiprotocol label switching (MPLS) 1069
- multipurpose tunnel 837
- multistage distribution network planning 1120
- mussel diagram 64
- mutual

– admittance 289  
 – induction 447  
 MV distribution network 1093

## N

N-1 security 875  
 N-2 security 875  
 Nagoya, Japan 870  
 nanomaterial 932  
 Na–S 1162  
 natural  
 – frequency 661  
 – gas 5, 1163  
 – power 282  
 nature of cable failures 846  
*n*-bus system 290  
*n*-conductivity 107  
 negative  
 – active mass 1157  
 – corona 654  
 negative-sequence 983, 997  
 Nernst equation 1157  
 net present value (NPV) 621, 918  
 – calculation 918  
 network 768  
 – capacity increase 745  
 – connectivity analysis (NCA) 1109  
 – delay (ND) 1077  
 – overlay 1074  
 – parameter 770  
 – planning 872  
 – stability 869  
 – time constant 990  
 network management  
 – center (NMC) 1080  
 – layer (NML) 1080  
 – system (NMS) 1071  
 neutral conductor 1180  
 Newton–Raphson’s method 293  
 nickel mangan cobalt (NMC) 1161  
 nickel–cadmium accumulator 1159  
 Nikola Tesla 868  
 Ni–MH accumulator 1159  
 nitrile butadiene rubber (NBR) 712  
 no busbar 876  
 Noda model 566  
 nodal  
 – analysis 286  
 – voltage 310  
 node 868

no-fuse breaker (NFB) 591  
 noise control 903  
 no-load  
 – current 490  
 – line energization 553  
 – lines and cables 554  
 – loss 453, 490  
 – operation 451  
 nominal water quantity 67  
 non soluble deposit density (NSDD) 675  
 nonaqueous electrolyte 1159  
 nonceramic insulator (NCI) 671  
 noncharacteristic harmonics 948  
 nonconventional instrument transformer (NCIT) 931  
 nonelectric criterion 979  
 nonfault voltages 987  
 nonlinear programming (NLP) 1100  
 nonmagnetic core 462  
 non-renewable energy source 5  
 nonsalient  
 – pole (NSP) 384  
 – pole (NSPL) 411  
 nonsalient-pole  
 – generator (NSPG) 394  
 – machine (NSPM) 388  
 nonselective 978  
 non-sinusoidal waveform 906  
 nonsynchronous AC systems 938  
 nonunit protection 985  
 normal  
 – equation (NE) 1113  
 – operating conditions 1115  
 – round-trip efficiency 1139  
 – switching transient 1193  
 normalization 1000, 1004  
 North and South (NS) 375  
 Norton equivalent circuit 350  
 not in my backyard (NIMBY) 615  
 nuclear  
 – energy 4  
 – power plant (NPP) 47, 89

## O

object  
 – management group (OMG) 1046  
 – request broker (ORB) 1046  
 occupational safety and health (OHS) 886

OECD countries 25  
 off-line topology 1167  
 offshore  
 – high-voltage substation (OHVS) 796  
 – platform 771  
 – substation 796, 926  
 – wind farm 591  
 off-system current 982  
 ohmic loss 114, 450  
 oil  
 – flow 985  
 – leak 902  
 – resin compound 807  
 – spill containment 902  
 oil/water separator system 902  
 oil-blocking system 902  
 oil-directed (OD) 498  
 – cooling 477  
 oil-filled (OF) 762  
 – breaker 874  
 – cable 787  
 oil-forced (OF) 498  
 oil-impregnated paper (OIP) 481  
 oil-insulated transformer 445  
 oil-natural (ON) 498  
 Onderdonk formula 898  
 one-dimensional (1-D) 347  
 on-line  
 – double conversion topology 1167  
 – monitoring 842  
 on-load tap changer (OLTC) 449, 498, 499, 946, 1106  
 onshore station 501  
 open  
 – cut trench 831  
 – drip-proof (ODP) 416  
 – system interconnection (OSI) 1050  
 open-circuit (OC) 388  
 – characteristic (OCC) 386  
 – voltage 113  
 – voltage of the converter 943  
 operating  
 – current 979  
 – temperature 814  
 operation  
 – current 979  
 – day-ahead 1115  
 – function 1115  
 operation, administration, and maintenance (OAM) 1070  
 operational expenditure (OPEX) 795



- optical
    - ground wire (OPGW) 656, 739
    - time-domain reflectometry (OTDR) 847
  - optimal
    - DC voltage 619
    - load flow (OPF) 299
    - span length 619
  - optimization procedure 617
  - optimum transmission voltage 616
  - ordinary transformer 805
  - oscillating wave system (OWS) 804
  - Oskar von Miller 613
  - Ottó Bláthy 444
  - outage
    - management 1117
    - management system (OMS) 1107, 1109
  - outdoor link box 844
  - outer sheath test 843
  - out-of-phase
    - recovery voltage 563
    - switching 560
  - out-of-phase (OP) 572
  - overall
    - energy efficiency 76
    - equipment effectiveness (OEE) 916
    - system protection 1013
  - overcurrent
    - criterion 979
    - protection 996
    - starting 1009
    - starting function 1009
  - overexcitation limiter (OEL) 405
  - overhead 283
  - overhead line (OHL) 280, 285, 554, 613, 761, 794, 799, 858, 1096
    - corrosion detector (OHLCD) 741
    - cost 619
    - upgrade 749
  - overhead transmission line 969
  - overvoltage
    - problem 779
    - temporary 134
    - transient 134
  - overvoltage (OV) 134, 405, 515, 841, 893
  - oxidant 1157
- P**
- 
- packet switched 1063
  - packetization delay (PD) 1077
  - PAFC (phosphoric acid fuel cell) 124
  - paper insulation 807
  - parallel
    - capacitance 597
    - contact point 243
    - converter 942
    - groove clamp 703
    - reactance 597
    - resonance 1182
  - parallel-connected transformers 460
  - Park's transformation 312
  - parrot bill 701
  - partial discharge (PD) 143, 176, 469, 695, 759, 912
    - inception voltage (PDIV) 152
    - measuring circuit 178
    - testing 804
  - partial factor for
    - actions 632
    - materials 627
  - partial vacuum 1152
  - Paschen curve 148
  - passive
    - distribution network 1106
    - filter 1183
    - management 1122
  - path computation element (PCE) 1091
  - p-conductivity 107
  - peak
    - demand 1166
    - energy 53
    - rectification 946
    - short-circuit current 225
  - pedestal post insulator 526
  - Peek's formula 654
  - peer to peer trading including
    - blockchain 1208
  - PEFC (polymer electrolyte fuel cell) 124
  - Pelton turbine 57, 1146
  - penstock 1144
    - diameter 59
    - model 68, 70
  - per capita GDP 16
  - perfluoroalkoxy (PFA) 159
  - perfluoroketone 933
  - perfluoronitrile 933
  - performance
    - evaluation 1113
    - factor 246, 252
    - figure 76
    - management (PM) 1080
  - peripheral speed 96
  - permanent
    - deformation 192
    - elongation 646
    - fault 1094
    - magnet (PM) 415
    - magnet generator (PMG) 404
  - permissible strain 824
  - permissive
    - overreaching transfer trip (POTT) 1056
    - underreach transfer tripping scheme (PUP) 924
    - underreach transfer tripping scheme (PUTT) 924
    - under-reaching transfer trip (PUTT) 1056
  - Perrine–Baum diagram 284
  - Petersen coil 557
  - phase
    - angle 948
    - voltage 302
  - phase-angle regulator (PAR) 500
  - phase-shifting transformer 500
  - phase-to-ground fault 727
  - phase-to-phase
    - calculation loop 1006
    - fault 237
  - phasor
    - diagram 284, 312, 452
    - measurement unit (PMU) 1019, 1111
  - phosphoric acid fuel cell (PAFC) 124
  - photoconductivity 106
  - photocurrent 109, 110
  - photon loss 110
  - photovoltaic
    - geographical information system (PVGIS) 123
    - plant 1134
    - system 1103
  - photovoltaic (PV) 124, 1103, 1134, 1189
  - photovoltaics 11, 36, 336
  - phthalic anhydride (PSA) 160
  - physical
    - bioconversion 9
    - principle 1144

- pick-up current 979
- piece of information for
  - communication (PICOM) 1041
- pilot line 737
- pin insulator 671
- planning
  - criteria 1231
  - repair operation 847
  - stage 616
- plastic
  - deformation 230
  - elongation 646
- plesiochronous 1065
  - digital hierarchy (PDH) 1065
- plug-in-type connector 248
- Poffenberger–Swart formula 668
- point of common coupling (PCC) 1186
- point-to-point transmission 938
- polarization index (PI) 489, 911, 912
- pole
  - carbon steel 718
  - spun concrete 717
- political initiative 12
- polluter 15
- pollution flashover 674
- polyamide (PA) 160
- polychlorinated biphenyl (PCB) 483
- polydimethylsiloxane (PDMS) 689
- polyethylene (PE) 772, 788, 816
- polygonal tripping 1008
- polyimide (PI) 160
- polymer
  - housing 689
  - insulation 159
- polymer electrolyte
  - fuel cell (PEFC) 124
  - membrane (PEM) 1165
- polymeric
  - anticorrosion 824
  - extruded cable 820
- polymer-insulated cable 776
- polyoxide ethylene (POE) 1160
- polypropylene
  - laminate, mass impregnated (PPL-MI) 936
  - paper laminate (PPL) 786, 809
- polytetrafluoroethylene (PTFE) 159, 535, 689
- polyurethane (PU) 162
- polyvinyl chloride (PVC) 159, 835
- porcelain
  - bell type insulator 671
  - post insulator 526
- Port Augusta 882
- portable earthing device (PED) 898
- positive
  - active mass 1157
  - corona 654
- positive-sequence 983
  - reactance 1007
  - system 987
- post insulator 525, 527, 673
- post-event data 624
- potential
  - energy 1135, 1145
  - transformer (PT) 519
- power 1146
  - active 964
  - angle curve 328
  - arc 706
  - cable 807
  - capability 764
  - coefficient 96
  - compensation 801
  - decoupling 295
  - density 1137
  - direction 947
  - electronics 39
  - flashover 671
  - flow 292
  - flow calculation 332
  - fluctuation 1133
  - generator output 795
  - imbalance 336
  - load 1097
  - management 949
  - network 868
  - plant safety 90
  - purchase agreement (PPA) 1212
  - quality 336, 1171
  - range 1136
  - reactive 964
  - swing 1013
  - to gas (PtG) 46
  - transformer 307, 484, 1096
- power cable 789, 912
  - protection 800
- power distribution
  - network 1115
  - network, steady-state analysis 1095
  - system 1093
- power electronic
  - converter 360
  - switch 602, 603
- power factor (PF) 334, 489
  - corrected (PFC) 1168
- power frequency (PF) 567, 696
  - model 773
- power line
  - carrier (PLC) 883, 1068
  - model 805
- power quality
  - disturbance 1173
  - event 1173
  - variation 1173
- power station
  - chain 49
  - run-of-river 50
- power system 276
  - development 1207
  - element 307
  - reliability 1190
  - stabilizer (PSS) 329
  - technical standards and accountability 1230
- power system stability 320, 564
  - classification 320
- power voltage (PV) 334
  - instability 950
- power-flow
  - analysis 1099
  - equation 1100
  - problem 1100
- power-heat ratio 76, 77
- power-node balance 1100
- power-on stabilization 997
- power-to-weight ratio 1138
- precision time
  - protocol (PTP) 1039
- precision time protocol (PTP) 1056
- predictable event 622
- preliminary design 890
- premolded
  - one-piece joint 819
  - three-piece joint 819
  - two-piece joint 819
- prepressurized
  - feed tank 810
  - fluid tank 810
- prequalification test 840
- pressure 1146
  - coefficient 61
  - line (DL) 56
  - pipe 54
  - tunnel 54
- pressure-tunnel model 67
- pressure-wave model 70

pressurized water reactor (PWR) 86, 87  
 preventative maintenance 842  
 preventive maintenance 740, 916  
 price coupling of regions (PCR) 1215  
 price impact on customer behavior 1227  
 primary  
 – and secondary control power 1166  
 – cell 1156  
 – control 339  
 – emission 1182  
 – energy 4  
 – energy consumption 22  
 – equipment layout 874  
 – terminal 1000  
 – time 990  
 prime mover limit 292  
 primer 692  
 priority assignment 1070  
 private  
 – cellular radio 1068  
 – mobile radio (PMR) 1068  
 probabilistic method 626  
 probability of failure 626  
 programmable logic controller (PLC) 1108  
 propagation  
 – constant 279  
 – speed 281  
 – velocity 662  
 propeller turbine 60  
 proportional integral (PI) 84, 342, 433  
 protected connection 818  
 protection 871  
 – against corrosion 818  
 – criterion 979  
 – equipment 801  
 – system 799, 977  
 – zone 977, 1003  
 protocol  
 – control information (PCI) 1050  
 – data unit (PDU) 1050  
 prototype test 726  
 pseudowire (PW) 1070, 1072  
 public hearing 639  
 pulling machine 833  
 pulse width  
 – modulated voltage source inverter (PWM-VSI) 435  
 – modulation (PWM) 434, 959

pump turbine (PT) 56  
 pump/turbine 1144  
 pumped-storage plant 56  
 pumping  
 – mode 1144  
 – plant schematic 814  
 pump-storage 1132  
 purchasing power  
 – adjusted (PPA) 15  
 – parity (PPP) 15, 809  
 PV panel 1166

## Q

quadratically constrained programming (QCP) 1100  
 quality  
 – assurance test 250  
 – control 908  
 – of service (QoS) 1046  
 – of supply 1172  
 quantization noise 1185

## R

radial distribution network 333, 1093, 1099  
 radiation intensity 117  
 radiative heat transfer 653  
 radio  
 – frequency (RF) 906  
 – interference (RI) 637, 654  
 – interference voltage (RIV) 695  
 radioactivity 91  
 radius of gyration 725  
 Ragone  
 – chart 1138  
 – curve 1142  
 – plot of a battery 1141  
 rapid  
 – direction changes 1012  
 – spanning tree protocol (RSTP) 1058  
 raster electron microscope (REM) 697  
 rate of  
 – change of the frequency (ROCOF) 338  
 – decrease of dielectric strength (RDDS) 577  
 rate of rise

– in recovery voltage (RRRV) 539  
 – of dielectric strength (RRDS) 577  
 – of TRV (RRRV) 547, 558  
 rated  
 – accuracy limit current 989  
 – tensile strength (RTS) 627, 645  
 reactance 307  
 reactance-earthed network 1181  
 reaction  
 – machine 1146  
 – turbine 57  
 – turbine plant 61  
 reactive  
 – compensation bus 285  
 – compensator 805  
 – decoupling 297  
 – plant 900  
 reactive power 284, 295, 924, 948  
 – control 522  
 – exchange 949  
 reactor 285  
 – safety 88  
 reaktor bolshoy moshchnosti kanalnyy (RBMK) 86  
 real  
 – normal round-trip efficiency 1139  
 – power derivative 296  
 real-time  
 – monitoring (RTM) 659  
 – operation 1115  
 recombination loss 110  
 recovery voltage (RV) 552  
 rectifier  
 – equation 945  
 – transformer 503  
 recycled material 850  
 Redlands, California 868  
 redox 1157  
 reducer material 1157  
 redundancy 872  
 reference  
 – bus 286  
 – conductor (VL) 243  
 – unified specific creepage distance (RUSCD) 676  
 regenerative preheating 83  
 regulating winding (RW) 475  
 regulation 1175  
 regulation of outcomes and service standards 1225  
 regulator financial reward and penalty 1229  
 regulatory requirement 872

- relative selective protection criterion 985
  - relay reach 923
  - release 992
    - time 998
  - reliability 868, 915, 976
    - level 626
    - requirement 625
  - reliability-centered maintenance (RCM) 916
  - remanence 989, 991
  - remedial action scheme (RAS) 1020
  - remote
    - procedure call (RPC) 1047
    - short-circuit 224
    - terminal unit (RTU) 1108
  - remotely operated vehicle (ROV) 846
  - renewable energy 4, 360, 869, 1166
    - resources (RES) 1106
    - source (RES) 277, 360, 635, 692, 770, 1095, 1132, 1134
  - repair
    - execution 848
    - joint extension 827
    - sleeve 703
    - work 845
  - request for comments (RFC) 1086
  - required grading 996
  - reserves and resources 5
  - reset time 998
  - residual
    - error probability 1059
    - flux 586
    - phase flux 587
    - static load (RSL) 722
  - resin-bonded paper (RBP) 163, 481
  - resin-impregnated
    - paper (RIP) 163, 481
    - synthetics (RIS) 481
  - resistance
    - constriction 238
    - contact 238
    - impurity film 238
    - joint 238
  - resistive
    - end 353
    - voltage divider (RVD) 1184
  - resistive-capacitive voltage divider (RCVD) 1184
  - resonance 1013, 1180, 1181
    - earthing 557
  - resource
    - description framework (RDF) 1043
    - reservation (RSVP) 1071
  - responsibility-sharing curve 1188
  - restoration time 1058
  - restriction voltage 601
  - reverse breadth-first (RBF) 1102
  - reversible pump–turbine unit 1148
  - revolutions per minute (rpm) 1152
  - right of way (ROW) 616, 632, 845
  - right-hand rule 223
  - rigid penstock 68
  - ring 879
    - and mesh layout 879
    - main unit (RMU) 1110
  - rise in wind and solar generation 1210
  - risk management 621, 915
  - risk-based maintenance (RBM) 916
  - Ritter method 723
  - RMS line-to-line (RMSLL) 313
  - rms value 997
  - robot conductor deicing 744
  - robotic 930, 933
  - rock 874
    - dumping 813
  - Rogowski coil 518
  - role of generators to meet demand 1209
  - role-based access control (RBAC) 1086
  - rolling sphere method (RSM) 899, 900
  - room-temperature vulcanized (RTV) 679, 689
  - root mean square (rms) 132, 377, 636
  - rotating mass 1152
  - rotation
    - per second (rps) 370
    - speed 65
  - rotational kinetic energy 1144, 1152
  - rotor angle stability 321
  - round rotor synchronous machine 323
  - round-trip
    - cycle 1140
    - efficiency 1139, 1140
  - route planning 803
  - routine
    - mechanical load (RML) 686
    - test (RT) 486, 841
  - runner 1147
  - R–X plane 1009
- 
- ## S
- 
- S/N curve 665
  - sacrificial zinc sleeve 679
  - safe failure mode 688
  - safe operating area (SOA) 958
  - safe operation 798
  - safety 869
    - clearance distance 890
    - distance 891
    - factor 891
    - load 631
    - margin 894
    - of personnel 767
    - requirement 625
    - zone 891
  - sagging 739
    - condition 650
    - thermometer 739
  - sag–tension calculation 649
  - salient-pole
    - generator (SPG) 393
    - machine (SPM) 388
    - synchronous machine 322
  - sample test 841
  - sampled value (SV) 1030
  - saturation 906
    - discriminator 999, 1005
    - limit 989
  - Savonius rotor 95, 101
  - SCADA 905
    - system components 1107
  - Schering bridge 180, 489
  - Schweppe–Huber generalized-M (SHGM) 1113
  - sea/land transition joint 828
  - sealed lead-acid (SLA) 922
    - battery 922
  - seasonal
    - pump storage 56
    - storage 1137
  - second telegrapher’s equation 347
  - secondary
    - battery 1156
    - current 1001
    - devices 986
    - emission 1182
    - impulse method (SIM) 845
    - system 921

- second-order cone programming (SOCP) 1100
- security 872, 1055, 1084
  - factor 979
  - load 631
  - management (SM) 1080
  - requirement 625
- seismic consideration 904
- select before operate (SBO) 1036
- selectivity 975
- self-admittance 289, 298
- self-contained
  - fluid-filled (SCFF) 770, 787, 809
  - fluid-filled (SCFF) cable system 807
  - fluid-filled (SCFF) cable systems 807
  - liquid-filled (SCLF) 787
- self-damping 663, 664
  - spacer 237
- self-discharge 1139
  - energy factor 1141
- semiconductive layer 776
- semiconductor device 956
- separate
  - design (SD) 816
  - semiconductive design (SscD) 817
- sequence 307
  - network 302
- series
  - and shunt reactive power compensation (SSC) 764
  - capacitor 524
  - compensation 524
  - reactor 798
  - resonance 1182
- service
  - access point (SAP) 1049
  - data unit (SDU) 1050
  - integrity 1058
  - level agreement (SLA) 1052, 1053, 1061
  - life 831
  - management layer (SML) 1080
  - restoration 1118
- service-oriented architecture (SOA) 1027
- SES-CDEGS 896
- severely errored second (SES) 1059
- SF<sub>6</sub>
  - decomposition 533
  - electrical conductivity 534
  - property 532
- SF<sub>6</sub>-insulated switchgear 829
  - shape 1153
- shared structure 766
- sheath
  - damage 805
  - overvoltage 779
- sheath voltage 805
  - limiter (SVL) 830, 843
- sheath voltage limiter (SVL) 806
- shed profile 677
- shell-type core 464
- shielding angle 729
- short
  - interruption 1191
  - line fault (SLF) 544, 547
  - transmission line 284
- short circuit 301, 955, 1094
- short-circuit 980, 981
  - characteristic (SCC) 388
  - current 309, 454, 542, 979
  - direction 986
  - force 472
  - load 631
  - loss 453, 469
  - operation 501
  - power 126, 981
  - range 112
  - ratio (SCR) 388, 950
  - test 841
  - voltage 453, 455
- short-circuited end 349, 350
- short-term load 197
  - forecasting (STLF) 1110
- short-term planning 286
- shunt
  - capacitance 1096
  - capacitor 522, 553, 1097
  - reactance 297
- shunt reactor 505, 523, 555
  - bank 523
  - switching 581, 582
- Siemens 868
- signal comparison 1011
- signaling 1180
- SIL (surge impedance loading) 747
- silicone rubber (SR) 689
  - housing 689
- similarity law 664
- simple network
  - management protocol (SNMP) 1087
  - time protocol (SNTP) 1039
- simple object access protocol (SOAP) 1047
- simplified plastic elongation (SPE) 649
- simplified plastic elongation (SPE) model 649
- single
  - area system 345
  - converter per pole 941
  - core 772
  - shear connection 726
- single busbar 877
  - substation 1003
- single-bus power system 299
- single-conductor cable 777
- single-core cable 774
  - design 822
- single-line diagram (SLD) 874, 882
- single-mode (SM) 1063
- single-phase
  - autoreclosure (SPAR) 576
  - core 456
  - fault 308
  - transformer 449, 455
- single-point bonding 779
  - system 806
- site
  - equivalent salinity (SES) 676
  - investigation 729
  - pollution severity (SPS) 675
  - selection 872
- six-jet turbine 59
- six-pulse bridge 942
- skin effect 199, 774
- slack 648
  - bus 290
- slenderness ratio 725
- sliding-pressure control 82
- slotted 989
- slow voltage variation 1195
- small
  - inductive switching 556
  - line reactance 565
- smart
  - grid sensor 1109
  - meter 1109
- meters and customer behavior 1230
- snaked cable installation arrangement 837
- snaking design 837
- soak
  - test 842
  - testing 913
- societal 915
- sodium 1162

- sodium–sulfur (Na–S) battery 1161
- SOFC (solid oxide fuel cell) 124
- software-defined network (SDN) 1090
- soil
  - backfill 766
  - parameter 732
  - resistivity 728, 896
  - thermal conductivity 768
- solar
  - eclipse, impact of 1208
  - gas 38
  - heating 653
  - power 1197
  - radiation 10, 203
  - thermal power stations 10
- solar cell 108
  - cadmium telluride CdTe 117
  - characteristic curve 108
  - copper indium diselenide CuInSe<sub>2</sub> 117
  - type 116
- solar energy 7
  - balance 8
- solid 158
  - balanced fault 311
  - bonding 780, 806
  - conductor 774
  - polymer electrolyzer (SPE) 1165
- solid oxide
  - electrolyte (SOE) 1165
  - fuel cell (SOFC) 124, 128
- solid-core design 526
- solidity ratio 631
- sorites paradox 1173
- sound level 490
- spacer 711
- spacer damper 711
  - clamp 713
  - clamp type 713
  - short-circuit 713
- span
  - factor 631
  - length 648
- spares management 921
- spark gap 524
- special test (ST) 486
- specific
  - communication service mapping (SCSM) 1038
  - hydraulic energy 1145, 1147
  - power 1137, 1138
- specific energy
  - consumption 34
  - of a flywheel 1153
- specific speed 1146
  - of rotation 58
- specified
  - cantilever load (SCL) 688
  - mechanical load (SML) 686
- spectral
  - efficiency 110
  - leakage 1185
  - radiation distribution 110
- spread foundation 732
- spun concrete pole 717
- SSC 764
- stability limit 292
- stabilized
  - current differential 1003
  - differential 982
  - differential protection 981
- stabilizing current 981
- stakeholder 915
  - engagement strategy 639
- standard
  - design 885
  - free enthalpy 1157
  - oil test (SOT) 487
- standardization 1175
- star connection 457, 1002
- starting
  - element 992
  - system 1008
- state
  - comparison protection 1055
  - equilibrium point (SEP) 329
  - estimation (SE) 1019, 1110
  - of charge (SoC) 1138
- state of
  - energy (SoE) 1138
  - health (SoH) 1143
- state-change equation 649
- static
  - distribution network planning 1120
  - frequency converter (SFC) 495
  - load model 1097
  - synchronous compensator (STATCOM) 414, 523, 924
- static VAR
  - compensator (SCV) 900
  - compensator (SVC) 414, 523, 900, 924, 1174
- stationary dimension factor 988
- stationary operational accuracy limit factor 990
- statistical 893
- stator overcurrent limiter (SCL) 405
- steady-state short-circuit current 224
- steam
  - extraction 76
  - generator 78
  - power plant 79, 81
- steam turbine 78
  - plant 83
- steel
  - core 641
  - tower inspection 743
- step voltage 895
- step-by-step
  - approach 781
  - methodology for upgrading a cable 849
- step-down substation 869
- step-lap 464
- step-up transformer 498
- Stockbridge damper 667, 707
- storage 1144
  - as grid component 1166
  - forms of energy 1143
- store-and-forward 1078
- storm damage 740
- Stott's approximation 296
- strain tower 722
- stranding process 643
- stray
  - field distribution 472
  - flux distribution 469
  - resistance 597
  - voltage 467
- strength 186, 188, 192, 230
  - function 626
- strength-to-weight ratio 641
- stress 186, 188, 190, 230
  - time 153
- stress–strain test 645
- string fittings 704
- stringing
  - block 739
  - method 737
  - wheel 738
- Strouhal frequency 661
- structural
  - and civil design 903
  - diagram 1148
  - resonance factor 630
- submarine
  - fluid-filled cable 813
  - joint design 825

- submarine cable 771, 813
    - maintenance guideline 846
    - mechanical test 824
    - outer protection 825
    - pumping plant 814
  - subnetwork connection protection (SNCP) 1066
  - subspan oscillation 669
  - substation 514, 868
    - asset management 914
    - automation system (SAS) 1029
    - component 871
    - configuration language (SCL) 1030
    - earth grid 894
    - environmental footprint 900
    - equipment 511–513, 570
    - layout 876
    - planning 872
    - post insulator 527
    - security 920
    - transformer 498
    - type 869
  - substructure 231, 234
  - subsynchronous resonance (SSR) 524
  - subtransmission network 277
  - sunlight 110
  - sunrise (SA) 118
  - sunset (SU) 118
  - supercapacitive system 1154
  - supercapacitor 1154, 1155
  - super-charge ion battery (SCiB) 1160
  - superconducting
    - cable 772, 852
    - magnetic energy storage (SMES) 1105
  - superconductive
    - magnet 1144
    - magnet energy storage (SMES) 1136
    - magnetic energy storage system (SMES) 1154
  - superconductivity 932
  - superconductor synchronous
    - compensator (SSC) 414
    - generator (SSG) 413
  - supervisory control and data acquisition (SCADA) 903, 1018, 1107
  - support 226, 233
    - insulator 233
    - type 716
  - supraharmonics 1179, 1181, 1194
  - surface
    - coating 243
    - preparation 246
    - state coefficient 654
  - surge arrester 172, 515, 830, 894
    - selection 894
  - surge chamber 54
    - model 68
  - surge impedance 282, 283, 348, 572
    - load (SIL) 655
    - loading (SIL) 617
  - surge wave reflection 349
  - survivability 1060
  - survival time 922
  - susceptance matrix 298
  - suspension clamp 698
    - contact length 698
    - metacentric 699
  - sustainability 12, 19, 886
  - sweep method 1102
  - sweep step
    - backward 1102
    - forward 1102
  - swept frequency response analysis (SFRA) 911
  - swing equation 327
  - switched
    - capacitor 1098
    - distance protection schema 1007
    - reluctance (SR) 415
  - switchgear 192, 193
  - switching 868, 869
    - action 802
    - arrangement 939
    - equipment 513
    - overvoltages 798
    - phenomenon 542
    - program 913
    - station 872
    - transient 523
  - switching impulse (SI) 492
    - level (SIL) 883
    - protection level (SIPL) 570
    - withstand voltage (SIWV) 570
  - symmetrical
    - component 1182
    - monopole 968
  - synchronization 1065
  - synchronized data acquisition 1005
  - synchronous
    - digital hierarchy (SDH) 1065
    - Ethernet 1063
  - generator 292, 311
  - impedance 312
  - machine 327, 1144
  - reactance 312
  - synthetic rope 738
  - system
    - application 1166
    - arrangement 1166
    - based on physics 1144
    - operator 1211
    - planning 773
    - protection scheme (SPS) 1023
    - rating 1136
    - short circuit MVA 950
    - state classification 320
    - support 1103
    - voltage distribution 522
  - system average interruption
    - duration index (SAIDI) 1190
    - frequency index (SAIFI) 1190
- 
- ## T
- 
- tailwater (UW) 56
  - tailwater reservoir 1144
    - level 1144
  - technical
    - brochure (TB) 763, 864
    - lifetime 803
  - technology, impact of new 1207
  - teleprotection signaling 1054
  - television interference (TVI) 654
  - temperature distribution 199
  - temperature-rise
    - limit 193
    - test 491
  - temple core 445
  - temple-type core 463
  - tennis racket tower 693
  - tensile strength 1153
  - tension method 737
  - tension-induced compression 664
  - terminal fault 547
  - termination 819
    - design 819
  - ternary pump–turbine unit 1147
  - terrain factor 630
  - tertiary voltage (TV) 475
  - test
    - equipment 494
    - on-site 494
    - technique 163

- transformer 479, 505
- testing
  - AC voltage 164
  - after installation 801
  - connector 839
  - DC voltage 165
  - extruded cable 843
  - procedure 838
  - transition joint 820
- tetrafluoroethylen-hexafluoropropylene (FEP) 159
- theoretical wind power 93
- theory of Ragone plot 1141
- thermal
  - balance 194
  - capacity factor (TCAP) 898
  - condition 799
  - conductivity 195
  - current 197
  - energy 36
  - expansion 219, 647
  - load 196
  - local constant 199
  - network method 210
  - radiation 195
  - reactor 85
  - reignition 550
  - storage 195, 204
  - time constant 197
  - transfer 195
- thermal interrupting
  - capability 566
  - process 538
  - region 538
- thermal power
  - plant 299
  - station 78
- thermal rating 660
  - calculation 652
- thermally stable cable 807
- thermochemical bioconversion 9
- thermographic inspection 914
- thermogravimetric analysis (TGA) 697, 841
- thermoplastic insulating material 850
- Thévenin
  - circuit 310
  - equivalent impedance 311
  - network 301
- Thévenin's theorem 310, 349
- thin-film solar cell 116
- third party access 1209
- third-pole-to-clear 557
- three-bus power network 288
- three-core
  - cable 774, 777
  - cable design 822
  - transformer 583
- three-dimensional (3-D) 468
- three-leg core 456
- three-limb core 464
- three-phase
  - (alternating) current 445
  - energization 587
  - fault 237, 308
  - high-speed reclosure (TPHSR) 576
  - line 279
  - network 302
  - system 444
  - transformer 455
- three-phase distribution line 1099
  - model 1101
- three-pole short circuit 229
- three-stage turbine 83
- three-winding transformer 308
- threshold 979
- thyristor 956
  - valve 606, 956, 957
- thyristor-controlled series capacitor (TCSC) 524
- thyristor-protected series compensation (TPSC) 524
- tidal energy 7
- tie-off tower 722
- tilting method 736
- time
  - autonomy 1136
  - duration for repair works 848
  - latency 1057
  - multiplier setting (TMS) 997, 998
  - slot (TS) 1064
- time-based maintenance (TBM) 916
- time-dependent characteristic 997
- time-division multiplexing (TDM) 1058, 1063
- time-domain
  - method 1181
  - reflectometry (TDR) 844, 847
- time-graded protection 923
- timing 976
- top
  - deflection 719
  - power station 56
- torsional
  - control device (TCD) 670
  - damper and detuner (TDD) 670
- total
  - cost of ownership (TCO) 1048
  - demand distortion (TDD) 1186
  - energy module (TOTEM) 76
  - harmonic distortion (THD) 437, 1168, 1176, 1186
  - loss 1139
  - productive maintenance (TPM) 916
- totally-enclosed
  - fan-cooled (TEFC) 416
  - nonventilated (TENV) 416
- touch
  - and step voltage 897
  - voltage 301, 895
- tower
  - cooling 80
  - earthing resistance 728
  - erection 735
  - member, bending of 726
  - shape 720
  - spotting 734
  - teststation 726
  - type 721
- traction transformer 503
- trade off between open market and central control 1212
- traffic engineering (TE) 1069, 1071
- transadmittance 298
- transfer
  - bus 878
  - function 68
- transferred voltage 895
- transformer 285, 443, 444, 802, 871, 1180
  - equation 448
  - failure 459
  - inrush 997
  - model 560
  - secondary fault (TSF) 557
  - supply 795
- transformer limited
  - fault (TLF) 557, 572
  - fault interruption 544
- transformer-fed fault (TFF) 557
- transient 894, 1193
  - analysis 345
  - dimension factor 988
  - internal voltage 332
  - interruption 1193
  - overvoltage (TOV) 476, 802, 805
  - recovery voltage (TRV) 523



transition joint 820  
 transmission  
 – between nonsynchronous AC systems 938  
 – capacity 564, 798  
 – loss 639  
 – network 277, 285, 297, 513  
 – ratio 499  
 – substation 870  
 – time 1055  
 – via cables 937  
 transmission line 308, 345, 522, 589, 937  
 – robotics 744  
 – switching 552  
 – tower 722  
 transmission system  
 – cost 132  
 – impedance 546  
 – operator (TSO) 360, 795, 1103, 1211  
 – voltage level 132  
 transport  
 – control protocol (TCP) 1025  
 – generated power 795  
 transportation limitation 765  
 transposed conductor 474  
 transversal admittance 297  
 transverse  
 – admittance 279  
 – electromagnetic mode (TEM) 345  
 – magnetic field (TMF) 540  
 trapezoidal wire (TW) 657  
 traveling  
 – arc 541  
 – wave 345, 893  
 trigatron 524  
 triple busbar 878  
 triplen harmonics 1180  
 tripping  
 – characteristic 1007  
 – time characteristic 997  
 true local time (WOZ) 203  
 tubular design 1158  
 tuned mass damper (TMD) 707  
 tunnel  
 – boring machine (TBM) 834  
 – design 767  
 turbine  
 – design 62  
 – efficiency 64  
 – equations 74  
 – output 75

– power controller 340  
 – selection 65  
 turbine-alternator group 336  
 turbulence 662  
 – intensity 630  
 twisted winding 475  
 two- and three-level VSCs 959  
 two-area system 341, 345  
 two-circuit-breaker layout 879  
 two-dimensional (2-D) 468  
 two-limb core 464  
 type  
 – of joint 818  
 – of transformer 497  
 – test (TT) 486, 840

## U

UHV substation 928  
 ultimate tensile load of composite insulator 687  
 ultrafast disconnecter 602  
 ultrahigh  
 – frequency (UHF) 179, 485  
 – voltage (UHV) 132, 513, 751, 762, 925  
 ultrahigh-voltage direct current (UHVDC) 941  
 ultraviolet (UV) 160, 484  
 unblocking method 1011  
 uncompensated line 588  
 uncontrolled system 339  
 underexcitation limiter (UEL) 405  
 underground (UG) 764  
 – cavern 1151  
 – line 779, 1096  
 – option 769  
 – transmission 772  
 underground cable (UGC) 763, 859  
 – connection 769  
 – life cycle 851  
 – rating 790  
 – system 838  
 underimpedance 983, 985  
 – starting function 1009  
 undersea cable 501  
 undervoltage starting 1009  
 – function 1009  
 unexploded ordnance (UXO) 847  
 unified modeling language (UML) 1025

uninterruptible power supply (UPS) 1166, 1167  
 unit  
 – control principle 81  
 – protection 923, 985  
 universal description discovery and integration (UDDI) 1047  
 unmanned aerial vehicle (UAV) 744  
 unpredictable event 622  
 unregulated asset 1229  
 unshielded twisted pair (UTP) 1067  
 unstabilized current differential 980  
 unstable equilibrium point (UEP) 329  
 unsymmetrical load 457  
 unwanted operation 976  
 upgrading 848  
 – case study 749  
 – increase availability 747  
 – method 749  
 uprating 848  
 – mechanism 746  
 – option 746  
 UPS technology 1167  
 uranium  
 – fission 85  
 – reserve 7  
 useful energy 1  
 utility communications architecture (UCA) 931

## V

vacuum  
 – arc 540  
 – circuit breaker 539  
 – interrupter 529, 540  
 value of lost load (VOLL) 1217  
 valve  
 – base electronics (VBE) 957  
 – short circuit 955  
 valve-regulated lead-acid (VRLA) 922  
 variable  
 – frequency 1148  
 – power demand 1132  
 variable-speed  
 – drive (VSD) 415, 434  
 – pumped storage 1149  
 – technology 1144  
 variations of headwater 1144  
 vector

- group 456
- group adjustment 1002
- very
  - fast transient overvoltage (VFTO) 568
  - long submarine connection 815
  - low frequency (VLF) 912
- very-fast-front overvoltage 893
- very-small-aperture terminal (VSAT) 1068
- vibration
  - analysis 660
  - damper 707
  - recorder 666
  - safe design 667
- virtual
  - circuit (VC) 1072
  - concatenation (VCAT) 1071
  - container (VC) 1066
  - local-area network (VLAN) 1072
- virtual private
  - LAN service (VPLS) 1072
  - network (VPN) 1066
- visual inspection 696
- VLAN identifier (VID) 1067
- volt/var control (VVC) 1110
- voltage
  - control system 331
  - criterion 982
  - dip 1171, 1187
  - flicker 1197
  - harmonics 948
  - limit 1122
  - peak energization 578
  - quality 1172
  - ratio 488
  - reduction (VR) 1111
  - regulation 478
  - regulator 1098
  - source converter (VSC) 591, 935, 958, 1134, 1194
  - stability 321, 333
  - storage 987
  - swell 1171, 1189
  - tolerance curve 1171
  - transformer (VT) 517, 894, 910, 1183
  - unbalance 1197
  - wave 349
- voltage measurement 172, 173
  - AC voltage 173, 174
  - DC voltage 173
  - impulse 174
- volume

- effect 154, 156
- energy density 1137
- power density 1138
- vortex shedding 661
- VSC circuit
  - diagram 960
  - representation 960
- VSC submodule 962

---

## W

- war of the currents 276
- waste disposal 91
- water
  - flow rate 51
  - management 51
  - management planning 50
  - power 9
  - tightness 822
- water-forced (WF) 498
- wave
  - equation 661
  - impedance 662
- wavelength division multiplexing (WDM) 1063
- wax-filled compound 807
- W-clip 681
- weakest supply 980
- web services description language (WSDL) 1047
- wedge-type clamp 700
- Weibull distribution 94, 785
- weight energy density 1137
- weighted least
  - absolute value (WLAV) 1113
  - squares (WLS) 1113
- Weiss area 461
- Wenner
  - four-point method 728
  - method 896
- wet cooling tower 80
- wide area network (WAN) 1016
- wind
  - action on insulators 630
  - and ocean power 9
  - energy 36
  - farm 797
  - frequency 94
  - generator 1166
  - measurements 95
  - pressure 629
  - span 630
- turbine 1104, 1179
- velocity 629
- wind load 628
  - on poles 631
- wind power
  - input 662
  - plant 103, 938
- wind-induced
  - damage 741
  - vibration 660
- winding
  - block assembly 477
  - conductor 474
  - loss 469
  - noise 490
  - pressure 471
  - resistance 489
  - type 467, 475
- wing element 100
- wire 663
  - armor 809
  - residual stress 644
  - rope 738
  - test 643
  - welding 644
- withstand 891
  - strength 556
- wood pole 716
  - damage 743
- worker safety 873
- working group (WG) 637
- working principle 946
  - of a point-to-point LCC HVDC system 947
- world population 23, 33
  - growth since 1950 33
  - increase 33

---

## X

- x-ray
  - diffraction (XRD) 697
  - fluorescence (XRF) 697

---

## Y

- Yy6 transformer 459
- Yz5 transformer 460

**Z**

---

- zero carbon economy 360
- zero-miss effect 802
- zero-power factor characteristics (ZPFC) 392
- zero-sequence 983, 997
  - current 996
  - harmonics 1182
  - impedance 491
- zigzag connection 457
- zinc collar 679
- ZIP model 1097
- zone 923